

 CRC Press  
Taylor & Francis Group

# *Handbook of* **Membrane Separations**

**Chemical, Pharmaceutical, Food,  
and Biotechnological Applications**



Edited by  
**Anil K. Pabby**  
**Syed S.H. Rizvi**  
**Ana Maria Sastre**

*Handbook of*  
**Membrane  
Separations**

**Chemical, Pharmaceutical, Food,  
and Biotechnological Applications**



*Handbook of*  
**Membrane  
Separations**

**Chemical, Pharmaceutical, Food,  
and Biotechnological Applications**

**Edited by**

**Anil K. Pabby**

**Syed S. H. Rizvi**

**Ana Maria Sastre**



**CRC Press**

Taylor & Francis Group

Boca Raton London New York

---

CRC Press is an imprint of the  
Taylor & Francis Group, an **informa** business

CRC Press  
Taylor & Francis Group  
6000 Broken Sound Parkway NW, Suite 300  
Boca Raton, FL 33487-2742

© 2009 by Taylor & Francis Group, LLC  
CRC Press is an imprint of Taylor & Francis Group, an Informa business

No claim to original U.S. Government works  
Printed in the United States of America on acid-free paper  
10 9 8 7 6 5 4 3 2 1

International Standard Book Number-13: 978-0-8493-9549-9 (Hardcover)

This book contains information obtained from authentic and highly regarded sources. Reasonable efforts have been made to publish reliable data and information, but the author and publisher cannot assume responsibility for the validity of all materials or the consequences of their use. The authors and publishers have attempted to trace the copyright holders of all material reproduced in this publication and apologize to copyright holders if permission to publish in this form has not been obtained. If any copyright material has not been acknowledged please write and let us know so we may rectify in any future reprint.

Except as permitted under U.S. Copyright Law, no part of this book may be reprinted, reproduced, transmitted, or utilized in any form by any electronic, mechanical, or other means, now known or hereafter invented, including photocopying, microfilming, and recording, or in any information storage or retrieval system, without written permission from the publishers.

For permission to photocopy or use material electronically from this work, please access [www.copyright.com](http://www.copyright.com) (<http://www.copyright.com/>) or contact the Copyright Clearance Center, Inc. (CCC), 222 Rosewood Drive, Danvers, MA 01923, 978-750-8400. CCC is a not-for-profit organization that provides licenses and registration for a variety of users. For organizations that have been granted a photocopy license by the CCC, a separate system of payment has been arranged.

**Trademark Notice:** Product or corporate names may be trademarks or registered trademarks, and are used only for identification and explanation without intent to infringe.

---

**Library of Congress Cataloging-in-Publication Data**

---

Handbook of membrane separations : chemical, pharmaceutical, food, and biotechnological applications / editor(s), Anil Kumar Pabby, Syed S.H. Rizvi, and Ana Maria Sastre.

p. ; cm.

Includes bibliographical references.

ISBN-13: 978-0-8493-9549-9 (hardcover : alk. paper)

ISBN-10: 0-8493-9549-6 (hardcover : alk. paper)

1. Membrane separation--Handbooks, manuals, etc. I. Pabby, Anil Kumar. II. Rizvi, S. S. H., 1948- III. Sastre, Ana Maria.

[DNLM: 1. Membranes, Artificial. 2. Biotechnology--methods. 3. Ultrafiltration. TP 159.M4 H236 2008]

TP248.25.M46H35 2008  
660'.2842--dc22

2008009730

---

Visit the Taylor & Francis Web site at  
<http://www.taylorandfrancis.com>

and the CRC Press Web site at  
<http://www.crcpress.com>

---

# Contents

Foreword .....	ix
Preface .....	xi
Editors .....	xiii
Contributors .....	xv

## **SECTION I Membrane Applications in Chemical and Pharmaceutical Industries and in Conservation of Natural Resources**

<b>Chapter 1</b> Membrane Applications in Chemical and Pharmaceutical Industries and in Conservation of Natural Resources: Introduction.....	3
<i>Ana Maria Sastre, Anil Kumar Pabby, and Syed S.H. Rizvi</i>	
<b>Chapter 2</b> Application of Membrane Contactors as Mass Transfer Devices.....	7
<i>A. Sengupta and R.A. Pittman</i>	
<b>Chapter 3</b> Membrane Chromatography .....	25
<i>M.E. Avramescu, Z. Borneman, and M. Wessling</i>	
<b>Chapter 4</b> Membranes in Gas Separation.....	65
<i>May-Britt Hägg</i>	
<b>Chapter 5</b> Pervaporation: Theory, Practice, and Applications in the Chemical and Allied Industries.....	107
<i>Vishwas G. Pangarkar and Sangita Pal</i>	
<b>Chapter 6</b> Current Status and Prospects for Ceramic Membrane Applications.....	139
<i>Christian Guizard and Pierre Amblard</i>	
<b>Chapter 7</b> Membrane Technologies and Supercritical Fluids: Recent Advances .....	181
<i>D. Paolucci-Jeanjean, G.M. Rios, and S. Sarrade</i>	
<b>Chapter 8</b> Techniques to Enhance Performance of Membrane Processes .....	193
<i>A.G. Fane and S. Chang</i>	
<b>Chapter 9</b> Separation and Removal of Hydrocarbons Using Polymer Membranes .....	233
<i>S.I. Semenova</i>	
<b>Chapter 10</b> Zeolite Membranes: Synthesis, Characterization, Important Applications, and Recent Advances .....	269
<i>M. Arruebo, R. Mallada, and M.P. Pina</i>	

<b>Chapter 11</b>	Membrane Fouling: Recent Strategies and Methodologies for Its Minimization.....	325
	<i>Matheus F.A. Goosen, S.S. Sablani, and R. Roque-Malherbe</i>	
<b>Chapter 12</b>	Membrane Extraction in Preconcentration, Sampling, and Trace Analysis.....	345
	<i>Jan Åke Jönsson</i>	
<b>Chapter 13</b>	Hybrid Liquid Membrane Processes with Organic Water-Immiscible Carriers (OHLM): Application in Chemical and Biochemical Separations .....	371
	<i>Vladimir S. Kislik</i>	
<b>Chapter 14</b>	Advancements in Membrane Processes for Pharmaceutical Applications.....	409
	<i>Ralf Kuriyel, Masatake Fushijima, and Gary W. Jung</i>	
<b>Chapter 15</b>	Membranes in Drug Delivery .....	427
	<i>Mario Grassi</i>	
<b>Chapter 16</b>	Bio-Responsive Hydrogel Membranes.....	473
	<i>John Hubble and Rongsheng Zhang</i>	

## **SECTION II Membrane Applications in Biotechnology, Food Processing, Life Sciences, and Energy Conversion**

<b>Chapter 17</b>	Membrane Applications in Biotechnology, Food Processing, Life Sciences, and Energy Conversion: Introduction .....	495
	<i>Syed S.H. Rizvi</i>	
<b>Chapter 18</b>	Ultrafiltration-Based Protein Bioseparation.....	497
	<i>Raja Ghosh</i>	
<b>Chapter 19</b>	Membrane Distillation in Food Processing .....	513
	<i>Sanjay Nene, Ganapathi Patil, and K.S.M.S. Raghavarao</i>	
<b>Chapter 20</b>	Applications of Membrane Separation in the Brewing Industry .....	553
	<i>Carmen I. Moraru and Ernst Ulrich Schrader</i>	
<b>Chapter 21</b>	Developments of Bipolar Membrane Technology in Food and Bio-Industries.....	581
	<i>Gerald Pourcelly and Laurent Bazinet</i>	
<b>Chapter 22</b>	Applications of Membrane Technology in the Dairy Industry .....	635
	<i>Philipina A. Marcelo and Syed S.H. Rizvi</i>	
<b>Chapter 23</b>	Microporous Membrane Blood Oxygenators .....	671
	<i>S.R. Wickramasinghe and B. Han</i>	

<b>Chapter 24</b>	Transporting and Separating Molecules Using Tailored Nanotube Membranes .....	693
	<i>Punit Kohli and Charles R. Martin</i>	
<b>Chapter 25</b>	Use of Emulsion Liquid Membrane Systems in Chemical and Biotechnological Separations .....	709
	<i>Jilska M. Perera and Geoff W. Stevens</i>	
<b>Chapter 26</b>	Membrane Electroporation and Emerging Biomedical Applications.....	741
	<i>K.P. Mishra</i>	
<b>Chapter 27</b>	Proton-Conducting Membranes for Fuel Cells.....	759
	<i>Vineet Rao, K. Andreas Friedrich, and Ulrich Stimming</i>	

### **SECTION III Membrane Applications in Industrial Waste Management (Including Nuclear), Environmental Engineering, and Future Trends in Membrane Science**

<b>Chapter 28</b>	Membrane Applications in Industrial Waste Management (Including Nuclear), Environmental Engineering, and Future Trends in Membrane Science: Introduction .....	823
	<i>Ana Maria Sastre and Anil Kumar Pabby</i>	
<b>Chapter 29</b>	Treatment of Radioactive Effluents: Introduction, Fundamentals, and Scope of Different Membrane Processes .....	827
	<i>B.M. Misra and V. Ramachandhran</i>	
<b>Chapter 30</b>	Radioactive Waste Processing: Advancement in Pressure-Driven Processes and Current World Scenario.....	843
	<i>Grazyna Zakrzewska-Trznadel</i>	
<b>Chapter 31</b>	Liquid Membrane-Based Separations of Actinides.....	883
	<i>P.K. Mohapatra and V.K. Manchanda</i>	
<b>Chapter 32</b>	Reverse Osmosis-Based Treatment of Radioactive Liquid Wastes Generated in Hospital Facility and in Steel Industry: Case Studies .....	919
	<i>M. Sancho, J.M. Arnal, G. Verdú, and J. Lora</i>	
<b>Chapter 33</b>	Evaluation of Membrane-Based Processing of Radioactive Nuclear Plant Waste: Case Studies .....	933
	<i>Anil Kumar Pabby, S.K. Gupta, S.R. Sawant, N.S. Rathore, P. Janardan, R.D. Changrani, and P.K. Dey</i>	
<b>Chapter 34</b>	Application of Donnan Membrane Process for Recovery of Coagulants from Water Treatment Residuals .....	945
	<i>Prakhar Prakash and Arup K. SenGupta</i>	
<b>Chapter 35</b>	Utilization of Membrane Processes in Treating Various Effluents Generated in Pulp and Paper Industry .....	981
	<i>Mika Mänttari and Marianne Nyström</i>	

<b>Chapter 36</b>	Membrane Bioreactors for Wastewater Treatment.....	1007
	<i>Eoin Casey</i>	
<b>Chapter 37</b>	Membrane-Assisted Solvent Extraction for the Recovery of Metallic Pollutants: Process Modeling and Optimization.....	1023
	<i>Inmaculada Ortiz and J. Angel Irabien</i>	
<b>Chapter 38</b>	Membrane Contactors for Gaseous Streams Treatments .....	1041
	<i>Alessandra Criscuoli and Enrico Drioli</i>	
<b>Chapter 39</b>	Strip Dispersion Technique: Application for Strategic and Precious Metal Separation and Treatment of Wastewater Streams.....	1057
	<i>Anil Kumar Pabby, S.C. Roy, J.V. Sonawane, F.J. Alguacil, and Ana Maria Sastre</i>	
<b>Chapter 40</b>	Electrically Enhanced Membrane Separations and Catalysis.....	1071
	<i>V.M. Linkov, B.J. Bladergroen, and A.M. Maluleke</i>	
<b>Chapter 41</b>	Membrane Processes for Treatment of Industrial Tannery Effluents: A Case Study .....	1087
	<i>A. Bódalo, E. Gómez, and A.M. Hidalgo</i>	
<b>Chapter 42</b>	New Developments in Nanofiltration Technology: A Case Study on Recovery of Impurity-Free Sodium Thiocyanate for Acrylic Fiber Industry.....	1101
	<i>S. Sridhar and B. Smitha</i>	
<b>Chapter 43</b>	Future Progresses in Membrane Engineering.....	1131
	<i>Enrico Drioli and Enrica Fontananova</i>	
<b>Index</b> .....		1147

---

# Foreword

During the middle of the last century, when the first synthetic membrane with tailor-made separation properties became available, a multitude of technically and commercially interesting applications were identified. Today, 50 years later, membranes and membrane processes have indeed become valuable tools for the separation of molecular mixtures. They are the key components in artificial organs and in devices for the controlled release of active agents, or in energy conversion and storage systems. Seawater and brackish water desalination using reverse osmosis and electrodialysis are energy efficient and highly economic processes for large-scale production of potable water. Micro- and ultrafiltration are used for the production of high-quality industrial water and for the treatment of industrial effluents. Blood detoxification by hemodialysis and hemofiltration improves the quality of life for more than 1.3 million people suffering from acute and chronic renal failure. Membrane processes have found a multitude of applications in chemical and pharmaceutical industries as well as in food processing and biotechnology. They are used on a large scale in gas separation and as tools in analytical laboratories. Today's membrane-based industry is serving a rapidly growing multibillion euro market with a large number of products and processes. The development of membranes with improved properties will most likely increase the importance of membranes and membrane processes in a growing number of applications for the sustainable growth of modern industrial societies.

The term "membrane" refers not to a single item, but covers a large variety of structures and materials with very different properties. The same is true for membrane processes, which can be very different in the way they function. However, all membranes and membrane processes have one feature in common, i.e., they can perform the separation of certain molecular mixtures effectively and economically at ambient temperature, and without any toxic or harmful reaction by-products.

In the early days of membrane science and technology, research was mainly concentrated on elucidating the membrane mass transport mechanism and on developing membrane structures with specific mass transport properties. The fundamentals of most membrane processes and membrane preparation procedures are described in great detail in a large number of publications in various scientific journals and in several excellent textbooks. However, the application of membranes and membrane processes is much less comprehensively covered in today's literature. Only a relatively small number of applications of membrane processes such as reverse osmosis, micro- and ultrafiltration, and gas separation and pervaporation are treated in textbooks and reference books. A large number of interesting membrane applications in the food and drug industry, in chemical and electrochemical synthesis, and in artificial organs are often not adequately treated in the membrane-related literature, but are published in journals specific for certain industries, which are outside of the interest of many membrane scientists. Furthermore, application-oriented membrane studies that are often carried out in industrial enterprises are described only as patents, or are not published at all. Therefore, it is difficult to obtain a reasonably complete overview of the very large and heterogeneous field of membrane applications without reading a number of very different journals and patents where most of the publications are not really membrane related.

The aim of *Handbook of Membrane Separations: Chemical, Pharmaceutical, Food, and Biotechnological Applications* is to fill the gap in the presently available membrane literature by providing a comprehensive discussion of membrane applications in the chemical, food, and pharmaceutical industries, in biotechnology, and in the treatment of toxic industrial effluents. The applications of membranes in different areas are described by scientists and engineers who not only are experts in membrane science and technology but also have extensive experience in the specific field of membrane application. This book is not competitive, but rather complementary to other textbooks and handbooks on membrane science and technology presently available in the market. It provides enough background information on the various membrane components and processes to evaluate their potential applications without a detailed treatment of the fundamental aspects of membrane mass transport theories and membrane structure development. The book should, therefore, be of great value to scientists and engineers who are not necessarily membrane experts but are interested in using membrane processes in solving specific separation and mass transport problems. It is equally suited for the newcomers in the field of membrane science as for engineers and scientists, who do have basic knowledge in membrane technology but are interested in obtaining more information on specific present and potential future membrane applications. It also provides an excellent base for courses and lectures in postgraduate education.

**Professor Heiner Strathmann**  
*University of Stuttgart*  
*Germany*



---

# Preface

During the past two decades, membrane technology has grown into an accepted unit operation for a wide variety of separations in industrial processes and environmental applications. Tighter environmental legislation calls for equipment that is able to deal with the removal of components across a wide range of concentration levels and that offers considerable flexibility and efficiency. Membrane technology first became important during the 1960s and 1970s in water treatment and in processes such as reverse osmosis, ultrafiltration, dialysis, electrodialysis, and microfiltration. During the 1980s, membrane technology began to be applied on a large scale in the field of gas purification. The successful introduction of membrane technology in these fields was mainly the result of the development of reliable and selective polymeric membranes.

There are a number of reference publications in the field of membrane technology, such as handbooks, monographs, and compendia of conference and workshop proceedings. The relative abundance of such works begs the questions, “Why another?” and “How will this one be different?” These questions are probably best answered by considering what the *Handbook of Membrane Separations: Chemical, Pharmaceutical, Food, and Biotechnological Applications* has to offer. The handbook covers the full spectrum of membrane technology and discusses its advancement and applications in a series of chapters written by experts, prominent researchers, and professionals from all over the world.

The handbook is divided into three main sections: The first section deals with membrane applications in chemical and pharmaceutical industries, and in conservation of natural resources; the second section covers membrane applications in biotechnology, food processing, life sciences, and energy conversion. Finally, the third section deals with membrane applications in industrial waste management (including nuclear), environmental engineering, and future trends in membrane science. Each section is divided into chapters that deal with the subject matter in depth and focus on cutting-edge advancements in the field. Several authors were commissioned to write the chapters under the supervision of the editors, and each chapter was peer-reviewed for content and style before it was accepted for publication. The aim was to maintain the perspective of a practical handbook rather than merely a collection of review chapters.

The editors would like to acknowledge the contributions of a number of authors and institutions that have played a major role in drafting the handbook from conception to publication. The handbook would not have been possible without their input. These contributors are leading experts in their fields and bring a great wealth of experience to this book. The editors would also like to acknowledge the efforts of the reviewers who devoted their valuable time to revising the chapters before the deadlines and suggested improvements to maintain the high standard of the handbook. Finally, we would like to acknowledge the support of our home institutions at every stage in the handbook’s conception: the Bhabha Atomic Research Centre, Mumbai, India; Cornell University, Ithaca, New York; and the Universitat Politècnica de Catalunya, Barcelona, Spain.

**Anil Kumar Pabby**  
**Syed S.H. Rizvi**  
**Ana Maria Sastre**



---

# Editors



**Anil Kumar Pabby** is affiliated with one of the pioneering research centers of India, the Bhabha Atomic Research Centre (Department of Atomic Energy), Tarapur, Mumbai, Maharashtra. He received his PhD from the University of Mumbai and subsequently completed his postdoctoral research at the Universitat Politècnica de Catalunya, Barcelona, Spain. Dr. Pabby has more than 150 publications to his credit including 4 book chapters and a patent on nondispersive membrane technology. He was invited to join the team of associate editors at the *Journal of Radioanalytical and Nuclear Chemistry* during 2002–2005. He has also served as consultant to the International Atomic Energy Agency (IAEA) for developing a technical document on the application of membrane technologies for liquid radioactive waste processing. Dr. Pabby has been a regular reviewer for several national and international journals and also serves on the editorial board of various journals. His research interest includes pressure-driven membrane processes, nondispersive membrane techniques, extraction chromatography, solvent extraction, and macrocyclic crown compounds. In 2003,

Dr. Pabby was elected fellow of the Maharashtra Academy of Sciences (FMASc) for his contribution to membrane science and technology. In 2005, he received the prestigious Tarun Datta Memorial Award (instituted by Indian Association for Nuclear Chemists and Allied Scientists) for his outstanding contribution to nuclear chemistry and radiochemistry.



**Syed S.H. Rizvi** is an international professor of food process engineering and has served as director of graduate studies at the Cornell Institute of Food Science, Cornell University, Ithaca, New York. He has a PhD from Ohio State University, an MEng (chemical engineering) from the University of Toronto, and a BTech from Panjab University, India. Dr. Rizvi teaches courses devoted to engineering and processing aspects of food science and related biomaterials. His laboratory is engaged in research on experimental and theoretical aspects of bioseparation processes using supercritical fluids and membranes, high-pressure extrusion with supercritical carbon dioxide, physical and engineering properties of biomaterials, and novel food processing technologies. An invention of Cornell researchers, and subsequently patented, supercritical fluid extrusion offers several advantages over the conventional high-shear cooking extrusion and is being used to investigate the dynamics of the process and the mechanics of the microcellular extrudates generated for both food and nonfood applications. A major long-term goal is to

develop new and improved unit operations for value-added processing of food and biomaterials. Derivative goals include new techniques for measurement and control of processes and properties for industrial applications. Dr. Rizvi has published more than 140 technical papers, coauthored/edited 6 books, served on the editorial board of several journals, and holds 7 patents.



**Ana Maria Sastre** is a professor of chemical engineering at the Universitat Politècnica de Catalunya (Barcelona, Spain), where she has been teaching chemistry for more than 28 years. She received her PhD from the Autonomous University of Barcelona in 1982 and has been working for many years in the field of solvent extraction, solvent impregnated resins, and membrane technology.

She was a visiting fellow at the Department of Inorganic Chemistry, the Royal Institute of Technology, Sweden, during 1980–1981 and carried out postdoctoral research from October 1986 to April 1987 at Laboratoire de Chimie Minerale, Ecole Europeenne des Hautes Etudes des Industries Chimiques de Strasbourg, France. Professor Sastre has more than 190 journal publications and more than 80 papers in international conferences. Dr. Sastre also holds four patent applications, guided 11 PhD and 16 master thesis students, and is a

reviewer of many international journals. In 2003, she was awarded the Narcis Monturiol medal for scientific and technological merits, given by the Generalitat de Catalunya for her outstanding contribution to science and technology.

Professor Sastre was the head of the chemical engineering department from 1999 to 2005 and is presently vice rector (vice chancellor) for academic policy at the Universitat Politècnica de Catalunya.

---

# Contributors

**F.J. Alguacil**

Centro Nacional de Investigaciones Metalúrgicas  
Consejo Superior de Investigaciones Científicas  
Ciudad Universitaria  
Madrid, Spain

**Pierre Amblard**

Techno-Membranes  
Parc Scientifique Agropolis  
Montpellier, France

**J.M. Arnal**

Chemical and Nuclear Engineering Department  
Polytechnic University of Valencia  
Valencia, Spain

**M. Arruebo**

Department of Chemical and Environmental  
Engineering  
University of Zaragoza  
Zaragoza, Spain

**M.E. Avramescu**

Membrane Technology Group  
Faculty of Science and Technology  
University of Twente  
Enschede, the Netherlands

**Laurent Bazinet**

Institute of Nutraceuticals and Functional Foods  
Department of Food Sciences and Nutrition  
Laval University  
Laval, Québec, Canada

**B.J. Bladergroen**

South African Institute for Advanced  
Materials Chemistry  
University of the Western Cape  
Bellville, South Africa

**A. Bódalo**

Departamento de Ingeniería Química  
Universidad de Murcia, Campus de Espinardo  
Murcia, Spain

**Z. Borneman**

Membrane Technology Group  
Faculty of Science and Technology  
University of Twente  
Enschede, the Netherlands

**Eoin Casey**

School of Chemical and Bioprocess Engineering  
University College Dublin  
Dublin, Ireland

**S. Chang**

Global Product Development, UF/MBR Technology  
GE Water & Process Technologies  
Oakville, Ontario, Canada

**R.D. Changrani**

Nuclear Recycle Group  
Bhabha Atomic Research Centre  
Tarapur, Mumbai, Maharashtra, India

**Alessandra Criscuoli**

Research Institute on Membrane Technology  
University of Calabria  
Rende, Cosenza, Italy

**P.K. Dey**

Nuclear Recycle Group  
Bhabha Atomic Research Centre  
Tarapur, Mumbai, Maharashtra, India

**Enrico Drioli**

Research Institute on Membrane Technology  
University of Calabria  
Rende, Cosenza, Italy  
and  
Department of Chemical Engineering and Materials  
University of Calabria  
Rende, Cosenza, Italy

**A.G. Fane**

UNESCO Centre for Membrane Science and Technology  
University of New South Wales  
Sydney, New South Wales, Australia  
and  
Singapore Membrane Technology Centre  
Nanyang Technological University  
Singapore

**Enrica Fontananova**

Research Institute on Membrane Technology  
University of Calabria  
Rende, Cosenza, Italy  
and  
Department of Chemical Engineering and Materials  
University of Calabria  
Rende, Cosenza, Italy

**K. Andreas Friedrich**

German Aerospace Center  
Electrochemical Energy Technology  
Stuttgart, Germany

**Masatake Fushijima**

Crossflow Technology, SLS  
Pall Corporation  
Port Washington, New York

**Raja Ghosh**

Department of Chemical Engineering  
McMaster University  
Hamilton, Ontario, Canada

**E. Gómez**

Departamento de Ingeniería Química  
Universidad de Murcia  
Campus de Espinardo  
Murcia, Spain

**Mattheus F.A. Goosen**

Office of Research  
Alfaisal University  
Riyadh, Saudi Arabia

**Mario Grassi**

Department of Chemical, Environmental, and Raw  
Materials Engineering  
University of Trieste  
Trieste, Italy

**Christian Guizard**

Laboratoire de Synthèse et Fonctionnalisation des  
Céramiques  
Saint Gobain CREE  
Cavaillon, France

**S.K. Gupta**

Nuclear Recycle Group  
Bhabha Atomic Research Centre  
Tarapur, Mumbai, Maharashtra, India

**May-Britt Hägg**

Department of Chemical Engineering  
Norwegian University of Science and Technology  
Trondheim, Norway

**B. Han**

Department of Chemical and Biological Engineering  
Colorado State University  
Fort Collins, Colorado

**A.M. Hidalgo**

Departamento de Ingeniería Química  
Universidad de Murcia  
Campus de Espinardo  
Murcia, Spain

**John Hubble**

Department of Chemical Engineering  
University of Bath  
Bath, United Kingdom

**J. Angel Irabien**

Departamento de Ingeniería Química y Química Inorgánica  
Universidad de Cantabria  
Santander, Spain

**P. Janardan**

Nuclear Recycle Group  
Bhabha Atomic Research Centre  
Tarapur, Mumbai, Maharashtra, India

**Jan Åke Jönsson**

Analytical Chemistry  
Lund University  
Lund, Sweden

**Gary W. Jung**

Membrane Technology Consultant  
Daytona Beach, Florida

**Vladimir S. Kislik**

Casali Institute of Applied Chemistry  
The Hebrew University of Jerusalem  
Jerusalem, Israel

**Punit Kohli**

Department of Chemistry and Biochemistry  
Southern Illinois University  
Carbondale, Illinois

**Ralf Kuriyel**

Biopharm Applications R&D  
Pall Life Sciences  
Pall Corporation  
Northborough, Massachusetts

**V.M. Linkov**

South African Institute for Advanced Materials Chemistry  
University of the Western Cape  
Bellville, South Africa

**J. Lora**

Chemical and Nuclear Engineering Department  
Polytechnic University of Valencia  
Valencia, Spain

**R. Mallada**

Department of Chemical and Environmental  
Engineering  
University of Zaragoza  
Zaragoza, Spain

**A.M. Maluleke**

South African Institute for Advanced Materials Chemistry  
University of the Western Cape  
Bellville, South Africa

**V.K. Manchanda**

Radiochemistry Division  
Bhabha Atomic Research Centre  
Tarapur, Mumbai, Maharashtra, India

**Mika Mänttari**

Laboratory of Membrane Technology and Technical  
Polymer Chemistry  
Lappeenranta University of Technology  
Lappeenranta, Finland

**Philipina A. Marcelo**

Department of Chemical Engineering  
The Research Center for the Natural Sciences  
University of Santo Tomas  
Manila, Philippines

**Charles R. Martin**

Department of Chemistry  
Center for Research at the Bio/Nano Interface  
University of Florida  
Gainesville, Florida

**K.P. Mishra**

Radiation Biology and Health Sciences Division  
Bhabha Atomic Research Center  
Tarapur, Mumbai, Maharashtra, India

**B.M. Misra**

Nuclear Desalination Unit  
Division of Nuclear Power  
Nuclear Power Technology  
Development Section  
Department of Nuclear Energy  
Vienna, Austria

**P.K. Mohapatra**

Radiochemistry Division  
Bhabha Atomic Research Centre  
Tarapur, Mumbai, Maharashtra, India

**Carmen I. Moraru**

Department of Food Science  
Cornell University  
Ithaca, New York

**Sanjay Nene**

Biochemical Engineering Group  
Chemical Engineering and Process Development Division  
National Chemical Laboratory  
Pune, Maharashtra, India

**Marianne Nyström**

Laboratory of Membrane Technology and Technical  
Polymer Chemistry  
Lappeenranta University of Technology  
Lappeenranta, Finland

**Inmaculada Ortiz**

Departamento de Ingeniería Química y Química  
Inorgánica  
Universidad de Cantabria  
Santander, Spain

**Anil Kumar Pabby**

Nuclear Recycle Group  
Bhabha Atomic Research Centre  
Tarapur, Maharashtra, India

**Sangita Pal**

Department of Chemical Engineering  
Institute of Chemical Technology  
Mumbai University  
Mumbai, Maharashtra, India

**Vishwas G. Pangarkar**

Department of Chemical Engineering  
Institute of Chemical Technology  
Mumbai University  
Mumbai, Maharashtra, India

**D. Paolucci-Jeanjean**

European Membrane Institute  
Université Montpellier  
Montpellier, France

**Ganapathi Patil**

Department of Food Engineering  
Central Food Technological Research Institute  
Mysore, Karnataka, India

**Jilka M. Perera**

Department of Chemical and Biomolecular  
Engineering  
University of Melbourne  
Parkville, Victoria, Australia

**M.P. Pina**

Department of Chemical and Environmental  
Engineering  
University of Zaragoza  
Zaragoza, Spain

**R.A. Pittman**

Membrana-Charlotte  
Celgard  
Charlotte, North Carolina

**Gerald Pourcelly**

European Membrane Institute  
Université Montpellier 2  
Montpellier, France

**Prakhar Prakash**

Chevron Energy Technology Company  
Richmond, California

**K.S.M.S. Raghavarao**

Department of Food Engineering  
Central Food Technological Research Institute  
Mysore, Karnataka, India

**V. Ramachandhran**

Desalination Division  
Bhabha Atomic Research Centre  
Tarapur, Mumbai, Maharashtra, India

**Vineet Rao**

Department of Physics  
Technische Universität München  
Garching, Germany

**N.S. Rathore**

Nuclear Recycle Group  
Bhabha Atomic Research Centre  
Mumbai, Maharashtra, India

**G.M. Rios**

European Membrane Institute  
Université Montpellier  
Montpellier, France

**Syed S.H. Rizvi**

Food Process Engineering  
Institute of Food Science  
Cornell University  
Ithaca, New York

**R. Roque-Malherbe**

School of Science and Technology  
University of Turabo  
Gurabo, Puerto Rico  
and  
Institute of Chemical  
and Biological Technology  
University of Turabo  
Gurabo, Puerto Rico

**S.C. Roy**

Nuclear Recycle Group  
Bhabha Atomic Research Centre  
Tarapur, Maharashtra, India

**S.S. Sablani**

Department of Biological Systems Engineering  
Washington State University  
Pullman, Washington

**M. Sancho**

Chemical and Nuclear Engineering Department  
Polytechnic University of Valencia  
Valencia, Spain

**S. Sarrade**

Waste Management Division  
French Atomic Energy Commission  
Bagnols sur Ceze, France

**Ana Maria Sastre**

Chemical Engineering Department  
Universitat Politècnica de Catalunya  
Barcelona, Spain

**S.R. Sawant**

Nuclear Recycle Group  
Bhabha Atomic Research Centre  
Tarapur, Maharashtra, India

**Ernst Ulrich Schrader**

Beverage Engineering Inc.  
Concord, Ontario, Canada

**S.I. Semenova**

Vladimir State University  
Vladimir, Russia

**A. Sengupta**

Membrana-Charlotte  
Celgard  
Charlotte, North Carolina

**Arup K. SenGupta**

Department of Civil and Environmental  
Engineering  
Fritz Engineering Laboratory  
Lehigh University  
Bethlehem, Pennsylvania

**B. Smitha**

Membrane Separation Group  
Chemical Engineering Division  
Indian Institute of Chemical Technology  
Hyderabad, Andhra Pradesh, India

**J.V. Sonawane**

Nuclear Recycle Group  
Bhabha Atomic Research Centre  
Tarapur, Maharashtra, India

**S. Sridhar**

Membrane Separation Group  
Chemical Engineering Division  
Indian Institute of Chemical Technology  
Hyderabad, Andhra Pradesh, India

**Geoff W. Stevens**

Department of Chemical and Biomolecular Engineering  
University of Melbourne  
Melbourne, Victoria, Australia

**Ulrich Stimming**

Department of Physics  
Technische Universität München  
Garching, Germany  
and  
ZAE Bayern, Division 1  
Garching, Germany

**G. Verdú**

Chemical and Nuclear Engineering Department  
Polytechnic University of Valencia  
Valencia, Spain

**M. Wessling**

Membrane Technology Group  
University of Twente  
Enschede, the Netherlands

**S.R. Wickramasinghe**

Department of Chemical and Biological Engineering  
Colorado State University  
Fort Collins, Colorado

**Grazyna Zakrzewska-Trznadel**

Department of Nuclear Methods in Process Engineering  
Institute of Nuclear Chemistry and Technology  
Warszawa, Dorodna, Poland

**Rongsheng Zhang**

Department of Chemical Engineering  
University of Bath  
Bath, United Kingdom



# *Section I*

---

*Membrane Applications in Chemical  
and Pharmaceutical Industries  
and in Conservation of Natural Resources*



---

# 1 Membrane Applications in Chemical and Pharmaceutical Industries and in Conservation of Natural Resources: Introduction

*Ana Maria Sastre, Anil Kumar Pabby, and Syed S.H. Rizvi*

## CONTENTS

References .....	5
------------------	---

In the last 40 years, membranes have developed from a research topic to a mature industrial separation technology. This increase in the use of membrane technology is driven by spectacular advances in membrane development, the wider acceptance of the technology in preference to conventional separation processes, increased environmental awareness and, most importantly, strict environmental regulations and legislation. Various membrane processes are currently applied in the chemical (including petrochemicals), pharmaceutical, and food and beverage industries. Particularly, strong development and growth of membrane technology can be observed in the purification of wastewater and the production of drinking water.

This statement summarizes the discussions at a conference on the “Exploration of the potential of membrane technology for sustainable decentralized sanitation” held in Italy (at Villa Serbelloni, Bellagio) on 23–26 April 2003 [1].\*

Due to plummeting costs and dramatically improving performance, water-treatment applications based on membranes are blossoming. In particular, membrane bioreactors (MBRs) are today robust, simple to operate, and ever more affordable. They take up little space, need modest technical support, and can remove many contaminants in one step. These advantages make it practical, for the first time, to protect public health and safely reuse water for non-potable uses. Membranes can also be a component of a multi-barrier approach to supplement potable water resources. Finally, decentralization, which overcomes some of the sustainability limits of centralized systems, becomes more feasible with membrane treatment. Because membrane processes make sanitation, reuse, and decentralization possible, water sustainability can become an achievable goal for the developed and developing worlds.

A membrane can essentially be defined as a barrier that separates two phases and selectively restricts the transport of various chemicals. It can be homogenous or heterogeneous, symmetric or asymmetric in structure, solid or liquid, and can carry a positive or negative charge, or be neutral or bipolar. Transport across a membrane can take place by convection or by diffusion of individual molecules, or it can be induced by an electric field or concentration, pressure or temperature gradient. The membrane thickness can vary from as little as 100  $\mu\text{m}$  to several millimeters.

A membrane separation system separates an influent stream into two effluent streams known as the permeate and the concentrate. The permeate is the portion of the fluid that has passed through the semipermeable membrane, whereas the concentrate stream contains the constituents that have been rejected by the membrane.

The correct choice of membrane should be determined by the specific objective, such as the removal of particulates or dissolved solids, the reduction of hardness for the production of ultra pure water or the removal of specific gases/chemicals. The end use may also dictate the selection of membranes in industries such as potable water, effluent treatment, desalination, or water supply for electronic or pharmaceutical manufacturing.

Membrane technology covers various chemical technology disciplines, such as material science and technology, mass transport and process design. By manipulating material properties, membranes can be tailor-made for particular separation tasks

---

\* From Fane, A.G., Editorial, *J. Membr. Sci.*, 233, 127, 2004. With permission.

to be performed under specific separation conditions. Membranes are manufactured as flat sheets, capillaries, or in tubular shapes and are applied in various module configurations. The following membrane modules are commonly used for industrial applications: (a) the plate and frame module; (b) the spiral wound module; (c) the tubular membrane module; (d) the capillary membrane module; and (e) the hollow fiber membrane module.

Membrane separation processes have numerous industrial applications and provide the following advantages: They offer appreciable energy savings; they are environmentally benign; the technology is clean and easy to operate; they replace conventional processes like filtration, distillation, and ion exchange; they produce high-quality products; and they offer greater flexibility in system design. Pressure-driven processes such as ultrafiltration, nanofiltration, and microfiltration are already established and various applications have been commercialized in the fields of pharmaceutical and biotechnology. Recently, the development of a means of characterizing, controlling, and preventing membrane fouling has been proved vital. The development of tailored membranes, fouling prevention, and optimization of chemical cleaning will ensure a high level of membrane process performance. In the last five years, the development of new techniques for membrane characterization and the improvement of existing techniques have increased our knowledge of the mechanisms involved in membrane fouling. More advanced techniques, such as environmental scanning electron microscopy (ESEM), have been used to study membrane fouling during the microfiltration of high metal content solutions with aluminum oxide membranes [2]. This will provide not only useful insight into the fouling mechanism but also a better understanding of the factors that affect membrane fouling.

The combination of molecular separation with a chemical reaction, or membrane reactors, offers important new opportunities for improving the production efficiency in biotechnology and in the chemical industry. With regard to the future of biotechnology and pharmaceutical processes, the availability of new high-temperature-resistant membrane contactors offers an important tool for the design of alternate production systems appropriate for sustainable growth.

Membrane technology has widespread applications in chemical and pharmaceutical industries and its use in various other fields is increasing rapidly. It has established applications in areas such as hydrogen separation, the recovery of organic vapors from process gas streams, and the selective transport of organic solvents, and it is creating new possibilities for catalytic conversion in membrane reactors. It provides a unique solution for industrial waste treatment and for the controlled production of valuable chemicals. Since it deals with the smallest penetrants in the size spectrum, gas separation requires extremely precise discrimination of size and shape—often in the range of 0.2–0.3 Å—between permeated and rejected species. Such demands truly push the state of the art in materials science for these specific applications. In addition to polymeric media, ceramic, carbon, zeolite, and metal membranes are attractive options as they provide both precise separation and robustness. Vision and commitment are required to make the most of the large energy savings (and CO<sub>2</sub> emission reductions) offered by membranes when compared with traditional, thermally driven separations and energy conversion. The use of membranes for extraction in analytical chemistry has increased recently. The main aim is to selectively extract and enrich the compounds to be determined (analytes) from samples of varying chemical complexity. In contrast to many technical uses of membranes, in analytical applications it is essential to recover the extracted analytes as efficiently as possible so that they can be transferred to suitable analytical instruments for the final quantitative determination.

Similarly, membrane contactors have proved to be efficient contacting devices, due to their high area per unit volume that results in high mass transfer rates. They are not only compact but also eliminate several of the problems faced in conventional processes such as ion exchange, solvent extraction, and precipitation. Membrane contactor processes, in which phase contacting is performed or facilitated by the structure and shape of the porous membrane, provide new dimension to the growth of membrane science and technology and also satisfy the requirements for process intensification. In addition, membrane contactors represent a significant step forward from the initial success of blood oxygenators. Their integration with other membrane systems, including membrane reactors, could lead to the redesign of membrane-based integrated production lines.

This introductory section outlines several established applications of membranes in the chemical and pharmaceutical industries, reviews the membranes and membrane processes available in this field, and discusses the huge potential of these technologies. In addition, other important topic dealing with conservation of natural resources (zeolite membranes) is also presented in this section. Each chapter has been written by a leading international expert with extensive industrial experience in the field.

Chapter 1 (the current chapter) presents an overview of different membrane processes and a description of all of the chapters presented in Section I. Chapter 2 explains the potential of hollow fiber contactors in the field of chemical technology and how they have changed industrial preferences regarding contacting devices. This chapter gives an introduction to membrane contact technology, its principles of operation, and the benefits obtained from the use of membrane contactors. Important applications, new product development requirements, and future directions are also discussed. Chapter 3 deals with membrane chromatography. This chapter discusses the latest developments in membrane-based stationary phases (affinity membranes and mixed matrix membrane adsorbers) and monolithic separation media (organic and inorganic). It also provides information on new types of chromatographic support, focusing on membrane materials, properties, and preparation. Finally, it considers possible applications of chromatographic membranes in various process conditions. Chapter 4 focuses on the important aspects of membrane application in gas separation. It deals with the subject comprehensively, providing an

introduction and discussing transport mechanisms, different membrane materials for gas separation, module design, current and potential applications, and novel developments in this field. Chapter 5 presents developments in pervaporation (PV). It first gives a brief introduction to the theory of pervaporation and then discusses sorption thermodynamics in polymers, the solution diffusion model, the criteria for membrane polymer selection, and important applications of PV in different cases of aqueous and organic separation. Chapter 6 focuses on advances in the field of ceramic membranes, covering interesting applications in this area. Chapter 7 describes important developments in the fields of supercritical fluids and membrane technology. Chapter 8 presents the various methodologies or techniques for improving the membrane performance of microfiltration, ultrafiltration, nanofiltration, and reverse osmosis. The aim is to present the techniques that attempt to minimize concentration polarization (and fouling) and allow the membrane to perform closer to its intrinsic capability. The methods range from the critical flux approach to the suite of hydrodynamic techniques and other potential strategies. Chapter 9 records important developments in the field of polymeric membranes for the separation and removal of hydrocarbons. It provides an introduction to the subject, discusses the background and physicochemical regularities of hydrocarbon permeation in membrane-based glassy and rubbery polymers, and lists some important applications. Chapter 10 describes some of the main characteristics of the use of zeolite membranes in separation applications. Zeolite membranes separate molecules based on the differences in their adsorption and diffusion properties. They are therefore suitable for separating gas and liquid phase mixtures by gas separation and pervaporation, respectively. This chapter reviews the basic mechanisms of gas separation and pervaporation through zeolite membranes and presents examples of industrial applications. Chapter 11 focuses on membrane fouling and the strategies used to reduce it relative to pressure-driven processes. This chapter highlights recent strategies for minimizing membrane fouling. In particular, it discusses the literature on fouling phenomena in reverse osmosis and ultrafiltration membrane systems, the analytical techniques employed to quantify fouling, preventive methods, and membrane cleaning strategies. Specific recommendations are also made on how scientists, engineers, and technical staff can help to improve the performance of these systems by minimizing membrane fouling phenomena. Chapter 12 describes membrane extraction and its use in preconcentration, sampling, and trace analysis. Chapter 13 presents applications of aqueous hybrid liquid membranes (AHLM) and organic hybrid liquid membranes (OHLM) in the separation of organic and metal species, respectively.

Chapter 14 provides an introduction to membrane applications in the pharmaceutical industry, its current status, and future potential in this very important area. Chapter 15 is devoted to membrane applications in the drug delivery field with emphasis on the mechanisms governing mass transport to modulate the release kinetics. Hydrogel membranes, as a derivative construct of hydrogels, have become increasingly attractive for precisely controlling the drug delivery rate via chemical sensing and triggering. Their current status, challenges, and opportunities are highlighted in Chapter 16.

## REFERENCES

1. Fane, A.G., Editorial, *J. Membr. Sci.*, 233, 127–128, 2004.
2. Skerlos, S.J., Rajagopalan, N., DeVor, R.E., Kapoor, S.G., and Angspatt, V.D., Microfiltration polyoxyalkylene metalworking fluid lubricant additives using aluminum oxide membranes, *J. Man. Sci. Eng. Trans.*, 123, 692–699, 2001.



---

# 2 Application of Membrane Contactors as Mass Transfer Devices

*A. Sengupta and R.A. Pittman*

## CONTENTS

2.1	Introduction .....	7
2.2	Scope of This Chapter.....	7
2.3	Description of Membrane Contactor.....	8
2.4	Principle of Operation .....	8
2.5	Benefits of Membrane Contactor Technology .....	10
2.6	Mass Transfer Process in Membrane Contactor .....	10
2.7	Literature Review on Membrane Contactor Applications .....	12
2.8	Use of Gas–Liquid or Liquid–Gas–Liquid Contact.....	12
2.9	Use of Liquid–Liquid Contact .....	13
2.10	Review of Membrane Contactor Design Options.....	14
2.11	Commercial or Precommercial Installations of Large-Scale Membrane Contactors.....	15
	References .....	20

## 2.1 INTRODUCTION

Membrane contactors as a type of membrane device have been known for quite a few years now [1–2]. They involve a unique class of membrane-based mass transfer and separation technologies, which have grown beyond academic curiosity and found commercial applications across various industries and markets. It has been found to be a cost-effective technology and is therefore used to supplant or replace other technologies that might or might not be based on membranes. In some situations, membrane contacting has emerged as an enabling technology that is filling some previously unmet commercial needs.

By the standard of business size, membrane contactor technology is currently a minor player compared to other much better-known membrane separation technologies such as reverse osmosis (RO), membrane filtration, membrane gas separation, diffusion dialysis, and electrodialysis. By its very nature, the membrane contactor does not function or compete with the other membrane devices, and the capability and functionality of contactors are significantly different from the other devices. But membrane contactor technology seems to have the potential to be applicable over a much wider array of industries. Use of membrane contactor devices in various forms is growing continuously. In many applications the contactor is not even called a contactor but is referred to by other names depending on the specific application it is deployed in. Examples include blood oxygenator (the earliest use of membrane contactor), gas transfer membrane, membrane degasifier, membrane deaerator, membrane distillation device, osmotic distillation device, membrane gas absorber, membrane extractor, and membrane humidifier.

## 2.2 SCOPE OF THIS CHAPTER

Considering the wide applications of membrane contactors and the evolving nature of this technology, it is difficult to cover every aspect in a monograph. The intent of this article is to first explain the technology and the principles of operation, with some remarks on the mass transfer process in membrane contactors. This is followed by description of various types of contacting possibilities and review of a wide sampling of literature on the technology to date. Design options of membrane

---

The authors' references to the various patents mentioned in this article do not constitute a grant of a license to practice any of these technologies, nor do they imply the authors' acknowledgment of the validity of any of the referenced patents.

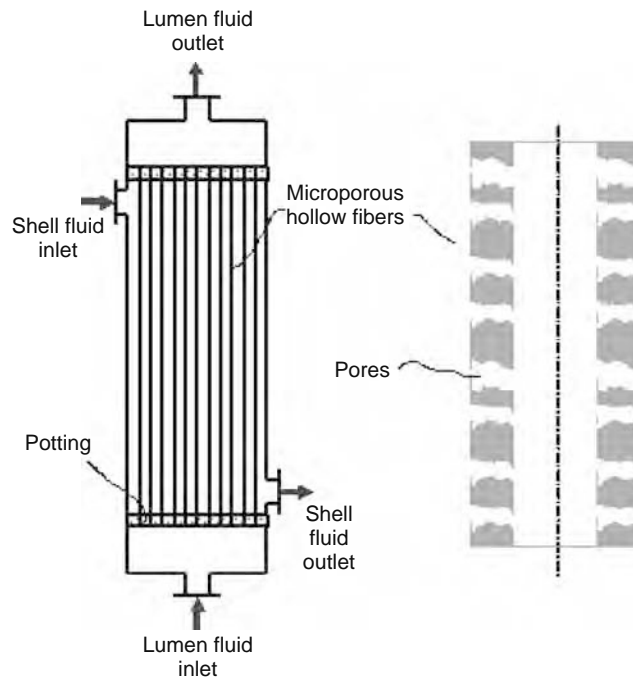


FIGURE 2.1 Microporous hollow fiber membrane in a membrane contactor.

contactors are then reviewed. Finally, some current and emerging commercial applications at different stages of development are discussed in detail.

### 2.3 DESCRIPTION OF MEMBRANE CONTACTOR

From outward appearance membrane contactors look similar to other membrane devices. However, functionally the membranes used in contactors are very different. They are mostly nonselective and microporous. Membrane contactors can be made out of flat sheet membranes and there are some commercial applications. Most common commercial membrane contactors are, however, made from small-diameter microporous hollow fiber (or capillary) membranes with fine pores (illustrated in Figure 2.1) that span the hollow fiber wall from the fiber inside surface to the fiber outside surface. The contactor shown as an example in Figure 2.1 resembles a tube-in-shell configuration with inlet/outlet ports for the shell side and tube side. The membrane is typically made up of hydrophobic materials such as Polypropylene, Polyethylene, PTFE, PFA, and PVDF.

The membrane in a contactor acts as a passive barrier and as a means of bringing two immiscible fluid phases (such as gas and liquid, or an aqueous liquid and an organic liquid, etc.) in contact with each other without dispersion. The phase interface is immobilized at the membrane pore surface, with the pore volume occupied by one of the two fluid phases that are in contact. Since it enables the phases to come in direct contact, the membrane contactor functions as a continuous-contact mass transfer device, such as a packed tower. However, there is no need to physically disperse one phase into the other, or to separate the phases after separation is completed. Several conventional chemical engineering separation processes that are based on mass exchange between phases (e.g., gas absorption, gas stripping, liquid-liquid extraction, etc.) can therefore be carried out in membrane contactors.

### 2.4 PRINCIPLE OF OPERATION

Principle of membrane contactor operation is based on the natural phenomenon of capillary force. When one side of a hydrophobic microporous membrane is brought in contact with water or an aqueous liquid, the membrane is not “wetted” by the liquid, i.e., the liquid is prevented from entering the pores, due to surface tension effect. The interface between a liquid and a solid substrate can be characterized by the parameter “contact angle” (Figure 2.2). The wettability of a solid surface by a liquid surface decreases as the contact angle increases. A contact angle of less than  $90^\circ$  implies that the liquid will tend to wet the substrate (hydrophilic), whereas if contact angle is greater than  $90^\circ$  the liquid will not tend to wet the surface (hydrophobic). Table 2.1 lists the contact angle values for few different materials in water at ambient temperature.

If a dry microporous hydrophobic hollow fiber membrane with air-filled pores was surrounded by water there would not be any penetration by water into the pores until the water pressure exceeds a certain critical breakthrough pressure. The magnitude

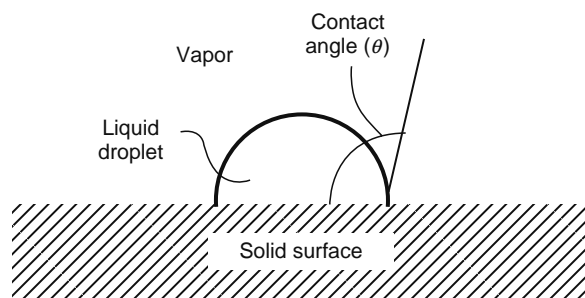


FIGURE 2.2 Representation of contact angle.

of this critical breakthrough pressure “differential” (water pressure minus air pressure)  $\Delta P_C$  has been mathematically derived, and is expressed [3] by the following equation that is often referred to as the Young–Laplace equation:

$$\Delta P_C = -\frac{4\lambda \cos \theta}{d} \quad (2.1)$$

where

$\lambda$  is the surface tension of water

$\theta$  is the contact angle for the system air–water–membrane in degrees

$d$  is the effective diameter of the membrane pore, assuming pores are circular in shape

For a hydrophobic porous material with contact angle greater than  $90^\circ$ , the  $\Delta P_C$  is  $>0$  and depends on the liquid surface tension and the membrane pore size. As an example, considering water–air–polypropylene system, one can calculate that for a dry membrane with a pore size of  $0.03 \mu\text{m}$  (30 nm) the critical entry pressure of water is more than 300 psi ( $>20$  bar).

Since the liquid phase does not enter the pores, a stable gas–liquid phase interface can be created and maintained (as illustrated in Figure 2.3) as long as the liquid phase pressure is higher than the gas phase pressure and the phase pressure differential  $\Delta P$  is between 0 and  $\Delta P_C$ . The pores remain air filled at this condition. The liquid and the gas phases could be flowing at different flow rates on either side of the membrane wall, but the phase interface remains stable all along the membrane. Thus, by proper control of pressures, the two immiscible phases come in constant contact without a need to disperse one into the other. This allows mass transfer or mass exchange between phases [4–5], such as gas absorption or gas stripping (desorption).

The same principle of operation as described above is applicable also to liquid–liquid extraction where an aqueous liquid and an organic liquid contact each other inside the contactor for extraction of a solute selectively from one phase to another [6–8]. The critical breakthrough pressure for liquid–liquid system could be calculated by Equation 2.1, except that the term  $\lambda$  would now be the interfacial tension between the two liquids. Further variation of membrane contacting technology is called gas membrane or gas–gap membrane where two different liquid phases flow on either side of the membrane, but the membrane pores remain gas filled [9–10]. In this situation two separate gas–liquid contact interfaces are supported on each side of a single membrane.

**TABLE 2.1**  
**Contact Angle for Various Materials in Water**  
**at Ambient Temperature**

Substrate	Contact Angle (In degrees)
Ordinary glass	20
Platinum	40
Anodized aluminum	60
PMMA	74
Nylon	79
Polyethylene	96
Polypropylene	108
Teflon	112

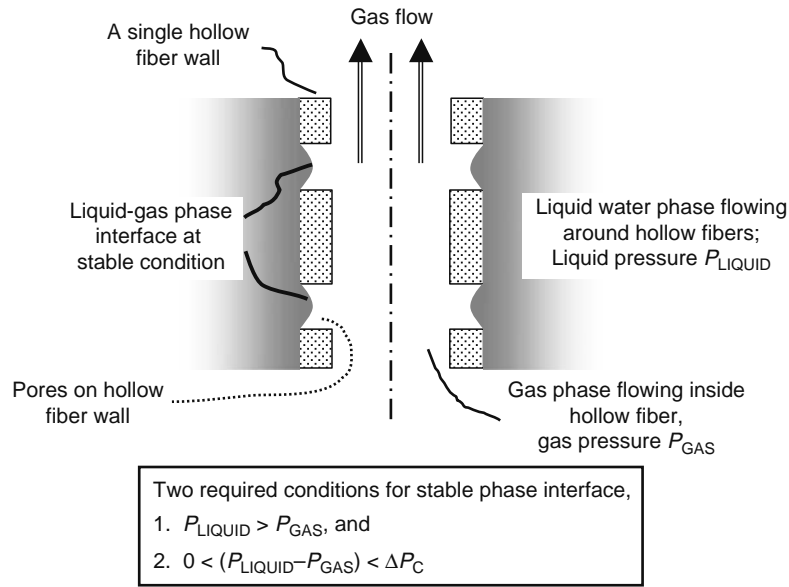


FIGURE 2.3 Liquid–gas interface in a membrane contactor.

## 2.5 BENEFITS OF MEMBRANE CONTACTOR TECHNOLOGY

Primary list of features and resulting benefits for the technology are shown in Table 2.2.

## 2.6 MASS TRANSFER PROCESS IN MEMBRANE CONTACTOR

In gas–liquid, liquid–liquid, or liquid–gas–liquid contactors there is no convective flow of any phase across the membrane. Mass transfer occurs only by diffusion across the immobilized phase in the pores. The direction of mass transfer of any molecular species depends on the concentration driving force maintained across the membrane for that species. The presence of the stationary phase in the membrane pore creates an extra diffusional mass transfer resistance. However, it can be shown that in many cases the membrane resistance is negligible, and that in most cases the high active mass transfer area created inside a membrane contactor more than compensates for any additional mass transfer resistance [4–5].

Mass transfer resistance in a continuous-contact separation device is the inverse of the mass transfer coefficient. In membrane contactors, the total resistance could be expressed as three resistances in series. These include the individual resistances in each flowing phase and the membrane resistance (Figure 2.4). For a liquid–gas contact system Equation 2.2 could be written for each diffusing species:

$$\frac{1}{d_{\text{OUT}}K_{\text{TOTAL}}} = \frac{1}{d_{\text{OUT}}k_{\text{SHELL}}} + \frac{1}{Hd_{\text{AVG}}k_{\text{M}}} + \frac{1}{Hd_{\text{IN}}k_{\text{TUBE}}} \quad (2.2)$$

where

$K$  is the overall coefficients

$k$  is the individual mass transfer coefficients

**TABLE 2.2**  
**Benefits of Membrane Contactor Technology**

Features	Benefits
High concentration of active phase contact area	Profile or footprint of membrane contactor systems are small; fit into existing building; no additional structure needed
Flow rates of phases in contact can be controlled independently	No physical limitations such as flooding or loading; contact area constant irrespective of phase flow rates; process more flexible
Modular in nature	Easier to add system capacity incrementally; can often be retrofitted into existing systems; easier scale-up
Mass transfer does not depend on gravity	Contactor can be mounted vertically or horizontally; will also work in microgravity; able to process two fluid phases of same densities
No need to disperse or coalesce phases	Eliminates extra steps; more efficient utilization of device volume
Can be operated with high fluid outlet pressures	Eliminates or reduces need for transfer pumps or booster pumps after contactor

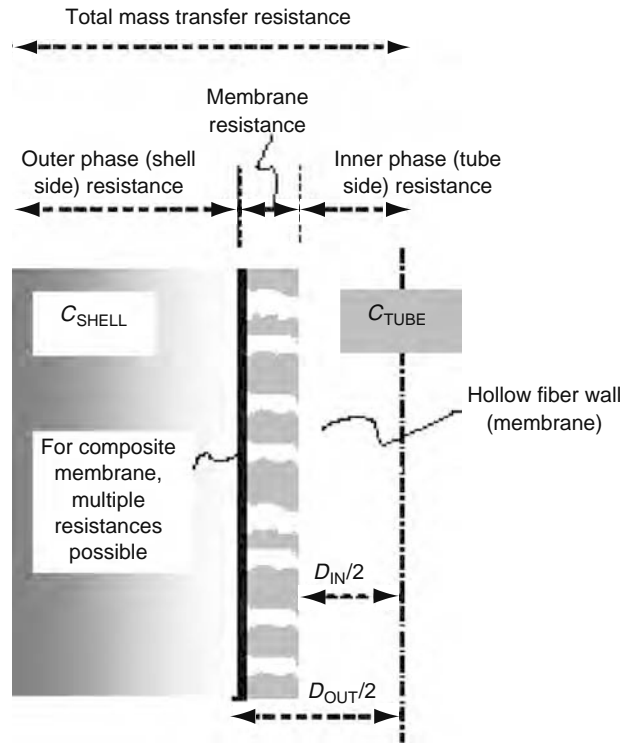


FIGURE 2.4 Mass transfer resistances in membrane contactor.

Each term on right side of Equation 2.2 represents an individual resistance as depicted in Figure 2.4. Hollow fiber diameters are  $d_{OUT}$  and  $d_{IN}$ . The term  $H$  is the Henry coefficient (liquid–gas equilibrium constant) for the species in question. In the case of liquid–liquid contact, the term  $H$  in Equation 2.2 should be replaced by  $m_D$ , the equilibrium distribution coefficient between tube side liquid and shell side liquid.

The membrane transfer coefficient  $k_M$  is a function of (1) the diffusion coefficient in the phase occupying membrane pores and (2) various membrane geometric parameters. Assuming pure Fickian diffusion in a symmetric microporous membrane,  $k_M$  can be shown as [5]

$$k_M = \frac{2D\varepsilon_M}{\tau_M(d_{OUT} - d_{IN})} \quad (2.3)$$

where

$D$  is diffusivity in the pore phase

$\varepsilon_M$  and  $\tau_M$  are membrane porosity and tortuosity factors, functions of the membrane morphology

In case of complex membrane morphology such as asymmetric or composite membranes, or when Fickian diffusion is not valid, evaluating  $k_M$  will be more complex. Individual mass transfer coefficients in Equation 2.2 depend on multiple factors such as temperature, pressure, flow rates, and diffusion coefficients and could often be estimated from empirical correlations available in literature [1,2,6].

The rate of mass transfer,  $R$ , for each species from shell side to tube side at any point inside the contactor is given as

$$R = K_{TOTAL} A [C_{SHELL} - C_{TUBE}] \quad (2.4)$$

where

$A$  is the membrane transfer area based on outside diameter of the hollow fiber

$C_{SHELL}$  and  $C_{TUBE}$  are bulk concentrations of the species in shell side and tube side, respectively

Strictly speaking Equations 2.2 and 2.4 are valid only locally within the contactor. The concentrations in each phase could change continuously inside the contactor. It is also possible for one of the mass transfer coefficients to change within the contactor. In such cases rate of mass transfer will be varying continually within the contactor, and the average overall mass transfer will be obtained by integrating over the entire contactor.

Useful simplifications are often made in Equation 2.2. We will use gas–liquid contact as an example, and assume gas-filled homogeneous membrane of high porosity, thin wall, and low tortuosity. Since diffusion in gas phase is generally of three orders of magnitude faster than in liquid phase, one can show that  $k_M$  and  $k_G$  are quite high in this case compared to  $k_L$ , and so the controlling resistance to mass transfer is in the liquid phase. This means  $K_{TOTAL}$  is essentially the same as  $k_L$ . If  $k_L$  is constant within the contactor the total mass transfer rate in Equation 2.4 can be approximated for the entire contactor as

$$R = k_L A_{TOTAL} \Delta C_{LOG-MEAN} \quad (2.5)$$

$\Delta C_{LOG-MEAN}$  is the log mean of the concentration differential ( $C_{SHELL} - C_{TUBE}$ ) from one end of the contactor to the other.

## 2.7 LITERATURE REVIEW ON MEMBRANE CONTACTOR APPLICATIONS

Over the years many research and development groups, both academic and industrial, have investigated membrane contactor technology and suggested or developed a wide range of possible applications. There is quite a spectrum of patent and published literature on this subject. Markets and industries that benefit from the development of this technology include medical, biotechnology, pharmaceutical, semiconductor and electronics, food and beverage, environmental, and other special process industries that are finding new uses. It is impossible to mention all the work done to date.

## 2.8 USE OF GAS–LIQUID OR LIQUID–GAS–LIQUID CONTACT

As mentioned earlier, membrane blood oxygenators probably would qualify as the earliest form of membrane contactors. Reference [11] is a good illustration of a hollow fiber device. However, most work on liquid–gas membrane contactor over the years has focused mainly on two categories: (1) separation, purification, and treatment of water or aqueous media and (2) absorption of gaseous species from air either for purification or for recovery, which will be discussed separately. Applications in multiple markets and industries have been investigated in each category.

An early example of a patent on membrane contactor for gas transfer is in Ref. [12]. Harvesting of oxygen dissolved in water and discharging of  $CO_2$  to the water is presented in Ref. [13]. A membrane device to separate gas bubbles from infusion fluids such as human-body fluids is claimed in Ref. [14]. A hollow fiber membrane device for removal of gas bubbles that dissolve gasses from fluids delivered into a patient during medical procedures is disclosed in Ref. [15]. Membrane contactors have also found application in dissolved gas control in bioreactors discussed in Refs. [16–17].

Application of membrane contactors for water degasification has been thoroughly investigated and reported in Refs. [18–21]. During the last few years this has been one of the most successful applications of membrane contactors on large commercial scale. Specifically, oxygen removal and gas transfer from ultrapure water for semiconductor industry have been discussed in Refs. [22–27]. Deaeration process for beverage water is discussed in Ref. [28]. Oxygen removal from boiler feed water as substitute for steam deaerator or oxygen scavenger is presented in Ref. [29]. Membrane contactors have also been used to carbonate water [30], to nitrogenate beer [31], to simultaneously nitrogenate and decarbonate beer, to control  $CO_2$  level in beer, and to control dissolved gas profile in beverages using mixed sweep gases of  $CO_2$  and  $N_2$  [32–33].

Removal of dissolved volatile organic compounds (VOC) from water in membrane contactors has been the subject of several investigations. VOC can be separated from water by applying a vacuum, the process is often termed vacuum membrane distillation [34–36]. Alternately, air can be used as a sweep gas to strip VOCs from water across the membrane [37]. Air stripping of water in packed or spray columns is a widely accepted process for ground water or process water treatment. If membrane contactors were used broadly for this purpose, the market potentials are certainly high. A variation of membrane air stripping process is discussed in Ref. [38] where the driving force for VOC stripping of water is established using methanotropic bacteria. Total organic carbon (TOC) reduction from ultrapure water during membrane degassing has been reported in Ref. [39]. Removal of tri-halo methane (THM) compounds, a chemical class of undesirable species, from ultrapure water has been discussed in Ref. [40]. Use of microporous membranes in combination with RO to separate dissolved gases from water is disclosed in Ref. [41]. Study on removal and recovery of volatile aroma compounds from water was presented in Ref. [42].

Adding oxygen or other beneficial gas species to water without forming gas bubbles is another application of membrane contactors. This subject has been discussed in Refs. [43–46]. Membranes in module form and hollow fibers in unconfined form have been investigated. Use of membrane contactors for supplying oxygen to a biofilm is claimed in Ref. [47]. A similar process where gaseous hydrogen is added to aqueous liquid without bubble formation is disclosed in Ref. [48]. The purpose for such a process would be to use dissolved hydrogen to biologically or catalytically remove oxygen, nitrite, or nitrate from water. Membrane contactors are also used to add trace quantity of  $CO_2$  into ultrapure water to control water resistivity and prevent formation of static electricity [49]. A more recent and significant application of membrane contactors is the addition of gaseous ozone to water for the purpose of disinfection and removal of organic contamination, such a process is disclosed in Ref. [50].

A number of applications of the previously termed gas membrane have also been studied over the years to remove or recover volatile species from water or other aqueous media. The primary drivers for these investigations are the intriguing and

creative possibilities of the gas membrane, which in effect combines two gas–liquid contact processes (stripping and absorption) within a single microporous membrane. Some of the early-published studies include recovery of bromine [51], cyanide [52], ammonia [53–55], and ethanol [56]. Applications of this technology for commercial purposes are in various stages of development [57].

Membrane processes termed as osmotic distillation or membrane distillation could be shown to be applications of membrane contactor technology also. Both of these processes are based on gas membranes. Osmotic distillation, sometimes called osmotic evaporation, involves transfer of water vapor across a gas-filled membrane, the process is driven by a difference in water vapor pressure maintained across the membrane [58–59] by separate aqueous liquids. Membrane distillation is a process where water vapor transfer is driven solely by a temperature difference across the gas-filled membrane [60–61]. Water evaporates from a hot aqueous phase and condenses on a cooler surface. This process may be useful in desalinating water or producing pure water if a good natural source of warm water is available, such as in a geothermal process.

As mentioned in Table 2.2, one unique feature of membrane contactors is the ability to operate without the aid of gravity. This, along with the advantage of smaller sizes for contactor systems, has led to the interest in possible use of this technology in microgravity and confined spaces such as spacesuits, manned spacecrafts, and space station. Primary applications are (1) separating gas and liquid phases in microgravity and (2) removal of unwanted gas species from liquids [62–64].

We now discuss the second category of applications that focus on treatment and conditioning of air or gas streams. This is done either (1) by capturing (absorbing) gaseous species from air or other gases into water or aqueous liquids or (2) by controlling the properties of air or gas phase by other means of heat and mass transfer across membrane in a contactor. The first detailed investigation of absorption of a gas species ( $\text{CO}_2$ ) in a liquid using a membrane contactor was discussed in detail in Refs. [4,5]. The mass transfer analysis in these early papers has been most influential for understanding the technology.

Absorption of various gases such as  $\text{CO}_2$ ,  $\text{SO}_2$ ,  $\text{NH}_3$ , and carbon monoxide in water using membrane contactors was studied by many other research groups and reported in Refs. [65–70]. Removal of  $\text{CO}_2$  as a greenhouse gas from air and bulk removal of  $\text{CO}_2$  from air in contactors using conventional absorbents have been reported in Refs. [71–73]. The topic of scrubbing  $\text{CO}_2$  from air for self-contained breathing systems using microporous membrane is discussed in Ref. [74]. Capturing  $\text{CO}_2$  from atmosphere using membrane contactors, as part of a hydrogen storage process, was suggested in Ref. [75]. Use of membrane contactors for recovery of VOCs from air was reported in Ref. [76]. A hollow fiber membrane bioreactor, for the purpose of destroying toxic compounds from air, is shown in Ref. [77].

Controlling temperature and humidity of process air or ambient air is another unique application of membrane contactors. Membranes are used to humidify or dehumidify air by bringing air in contact with water or a hygroscopic liquid. Mass transfer in such processes is very fast since mass transfer resistance in the liquid phase is negligible. Heat transfer and mass transfer are directly related to these processes, since latent heat of evaporation (or condensation) creates temperature profiles inside the contactor. Some of the references in Literature are shown in Refs. [78–79]. Application of such processes has been proposed for conditioning air in aircraft cabins [80], in buildings or vehicles [81], or in containers to store perishable goods [82].

## 2.9 USE OF LIQUID–LIQUID CONTACT

A historical perspective on aqueous–organic extraction using membrane contactor technology is available in Refs. [1,6,83]. The mechanism of phase interface immobilization was first explored in Ref. [84], while application of membrane solvent extraction for a commercial process was first explored in Ref. [85]. Two aspects of liquid–liquid contact in membrane contactors that are different from typical gas–liquid contact are (1) the membrane used could be hydrophobic, hydrophilic, or a composite of both and (2) the membrane mass transfer resistance is not always negligible. Ensuring that the right fluid occupies the membrane pores vis-à-vis the affinity of the solute in the two phases can minimize membrane resistance. These aspects have been discussed in detail in Refs. [6,86,87].

Membrane contactor applications in the liquid–liquid extraction field fall in two categories: (1) removal of unwanted species from water and (2) removal and recovery of valuable species from water. Many investigations have been conducted over the year by academia as well as by industry. Below we are providing some samples from the wide range of applications reported in literature. The examples presented are divided roughly into three sections: (a) biotech and pharmaceutical products, (b) industrial chemicals and VOC, and (c) metals.

Processes for production of ethanol and acetone–butanol–ethanol mixture from fermentation products in membrane contactor devices were presented in Refs. [88,89]. Recovery of butanol from fermentation was reported in Ref. [90]. Use of composite membrane in a membrane reactor to separate and recover valuable biotechnology products was discussed in Refs. [91,92]. A case study on using membrane contactor modules to extract small molecular weight compounds of interest to pharmaceutical industry was shown in Ref. [93]. Extraction of protein and separation of racemic protein mixtures were discussed in Refs. [94,95]. Extractions of ethanol and lactic acid by membrane solvent extraction are reported in Refs. [96,97]. A membrane-based solvent extraction and stripping process was discussed in Ref. [98] for recovery of Phenylalanine. Extraction of aroma compounds from aqueous feed solutions into sunflower oil was investigated in Ref. [99].

Extraction of phenol from aqueous solution using hollow fiber membrane contactor was first investigated in Ref. [100]. However, the membrane used was not completely microporous. Instead, it was a dialysis-type membrane. A commercial plant to separate phenol from hydrocarbon fraction using microporous membrane contactors was reported in Ref. [101]. Soda lye was used to react with the phenol transferred from the feed phase to create and maintain the driving force for separation. This industrial-scale application enabled the processing of hydrocarbon fraction to a full-value raw material for phenol and acetone synthesis.

The first known commercial membrane-based liquid–liquid extraction system involved extraction of by-products from a wastewater stream using an aromatic solvent [102]. Before the membrane system was installed, the entire wastewater stream had to be incinerated leading to high costs for the gas fired incinerator per year. The membrane system lowered the contaminant concentration to adequate levels before the biological wastewater treatment plant, and saved significant operating cost.

A process to separate naphthenes from paraffins is claimed in Ref. [103]. It involves the use of a polar solvent for separation in a microporous membrane device. Use of membrane extraction to remove *p*-nitrophenol in wastewater from dye and pesticide synthesis was investigated in Ref. [104]. Removal of nonvolatile pesticide components from water is presented in Ref. [105]. Removal of several important organic pollutants such as phenol, chlorophenol, nitrobenzene, toluene, and acrylonitrile from wastewater was investigated in Ref. [106].

Removal of VOC contaminants from water was discussed in Ref. [107]. This particular process used sunflower oil to absorb the VOC compounds transferred from water across a gas-filled microporous membrane. However, to prevent any possibility of liquid breakthrough, a plasma-polymerized di-siloxane coating was applied on the oil side of the membrane. Report [108] presents results from a pilot trial where organic pollutants such as chlorinated organic compounds and aromatic organic compounds were removed from plant wastewaters.

Various investigators have also explored removal or recovery of metals from aqueous process or waste streams. Liquid–liquid extraction is particularly useful for metal removal since alternate technologies such as distillation are not feasible. A process to separate molybdenum from tungsten leachate using a microporous membrane was disclosed in Ref. [109]. Copper extraction in a membrane contactor using metal chelating agent was presented in Ref. [110]. Other applications suggested in literature include extraction of gold from aqueous solutions [111], removal of copper from edible oil [112], separation of yttrium from heavy rare-earth metals [113], removal of copper and chromium from wastewater [114], and extractions of mercury, copper, and nickel from water [115].

## 2.10 REVIEW OF MEMBRANE CONTACTOR DESIGN OPTIONS

Although membrane is the heart of the membrane contactor technology, appropriate internal design of the contactor device or module is critical for any commercial advancement of the technology. Internal design dictates how the two phases flow inside the contactor and how the hydrodynamics in each phase is managed. As shown in Equation 2.2, the rate of mass transfer is directly dependent on the mass transfer coefficients in each of the phases, which in turn is dependent on the internal hydrodynamics. As the devices become larger to serve large commercial-scale process capacities, dependence on internal flow management becomes more critical. The device design is also important in developing the processes for large-scale manufacturing of the contactors. In the following section, we are reviewing various design options investigated over the years.

Designs of membrane contactors with hollow fiber membranes fall in one of the two categories: (1) the primary fluid being treated flows through the inside (lumen) of the hollow fibers and (2) the primary fluid being treated flows on the outside (shell) of the hollow fibers. Another consideration is the flow direction of the fluid in each phase with respect to the axis of the membrane and with respect to each other. In most membrane contactors of early commercial designs, the contactor housing was of cylindrical shape with tube-in-shell configuration (as in tubular heat exchangers) where the primary fluid flows on the lumen side from one end of the fiber to the other and the other fluid flows on the shell side in parallel direction. This design is generally called the parallel-flow design and is illustrated schematically in Figure 2.5a. The contactors of such a design are relatively easy to manufacture. However, the main drawback of the parallel-flow design is the nonuniform spacing of hollow fibers and the resulting poor flow distribution or flow channeling on the shell side, particularly as the contactor diameter increases.

A significant improvement over this parallel-flow design is the transverse-flow design where the primary fluid flows on outside of the hollow fiber membrane at a transverse direction to the fiber axis, while the other fluid flows on lumen side of the hollow fibers. The relative merits of the two designs were first analyzed comprehensively in Ref. [116]. It determined that transverse flow on shell side significantly improves the mass transfer coefficient compared to the parallel-flow design. However, it was still difficult to ensure that the transverse flow on shell side is completely uniform along the fiber length. Most investigations on membrane contactors continued to focus on parallel-flow design, since they are easier to fabricate on small scale. The effect of shell side hydrodynamics in parallel-flow contactors was investigated and reported in Ref. [117].

The twin problems of (1) ensuring transverse flow uniformly along the length of fibers and (2) ensuring even flow distribution on shell side were solved largely by adopting the concept of hollow fibers in fabric array form that was wound around a central hollow mandrel with porous wall. The shell side fluid could be introduced in the membrane contactor through the central distribution mandrel. It could then flow radially outward, in a direction transverse to hollow fiber axes. The central

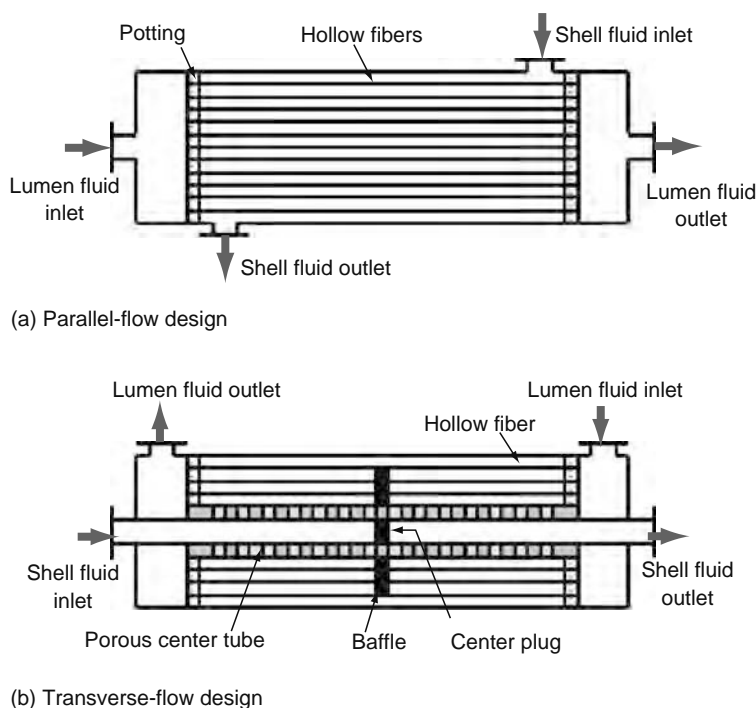


FIGURE 2.5 Primary design options for membrane contactors.

hollow mandrel ensures axial uniform flow distribution whereas the hollow fiber array ensures constant fiber-to-fiber distances and uniform transverse-flow distribution. A further improvement was the use of one or multiple flow-directing baffle inside the shell, just as practiced in commercial heat exchangers, which made the contactor more efficient and facilitated commercial production. Figure 2.5b schematically illustrates a transverse-flow contactor with flow-directing baffle. Detail investigations of this design are shown in Refs. [118–120], and both cylindrical and rectangular contactors are investigated in Ref. [118].

An interesting variation of the contactor design with baffle is disclosed in Ref. [121] for a degassing application. This shows a spiral-wound contactor similar to that shown in Ref. [120], but the baffle was placed on the gas side of the device and the water flow was on lumen side. Since most of the mass transfer resistances in liquid degassing process are essentially in the liquid phase, it is not clear how such a design would improve the hydraulic efficiency of the device.

In addition to what was discussed above, there have been many other contactor designs proposed over the years. A membrane contactor of rectangular design is disclosed in Ref. [122] made by laminating hollow fiber fabric sheets, and preventing flow channeling by specifying the densities of the hollow fibers and the warp fiber of the fabric. A similar structure of membrane contactor apparatus is claimed in Ref. [123]. Reference [124] discloses a contactor with multiple frames of square, polygonal, or circular, where the longitudinal directions of the fibers or tubes of adjacent frames are substantially perpendicular to each other. Stackable sub-modules with multiple frames of hollow fiber membranes in each sub-module were suggested in Ref. [125]. A rectangular contactor was also suggested in Ref. [75]. A tubular hollow fiber membrane contactor of parallel-flow design, with special spacers on shell side to reduce flow channeling, was disclosed in Ref. [50]. A radial-flow transverse-flow membrane contactor without any flow-directing baffle was shown in Ref. [126]. In some applications, particularly in degassing processes using deep vacuum, it has been shown that presence of flow-directing baffle such as claimed in Ref. [119] could actually be detrimental to performance because of internal diffusion in the gas phase. A hollow fiber membrane contactor that does not use a shell at all has been disclosed in Ref. [127].

## 2.11 COMMERCIAL OR PRECOMMERCIAL INSTALLATIONS OF LARGE-SCALE MEMBRANE CONTACTORS

Applications of membrane contactor technology in commercial processes are in various stages of development. Early success has come mainly in water degassing or gas addition applications. Membrane contactor systems of a wide range of flow capacities are currently in operation in various parts of the world. Systems with large capacities were possible only after membrane contactors of sufficiently large size and cost competitiveness could be produced commercially on a routine basis. Currently, the largest known commercially produced membrane contactor module has an active contact area of about 220 m<sup>2</sup> [128]. Commercial availability of such products has greatly facilitated the large-scale acceptance of this technology. A few examples of various installed contactor systems are provided below.

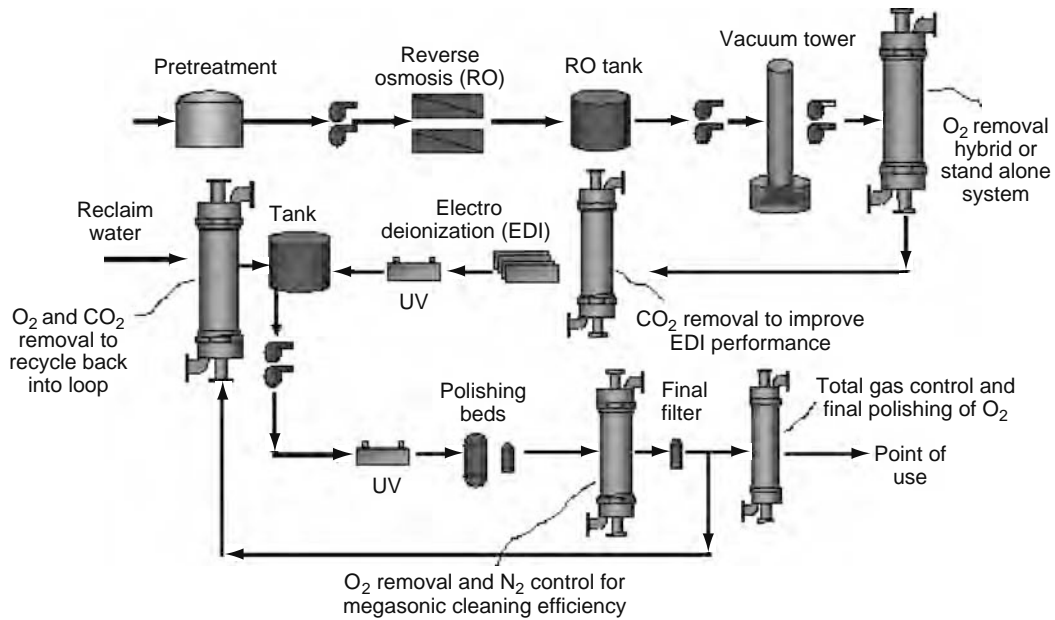


FIGURE 2.6 (See color insert following page 588.) Part of semiconductor plant ultrapure water production process.

Figure 2.6 schematically illustrates sections of a typical semiconductor ultrapure water (UPW) production process in a semiconductor plant. The water circuit consists of two main sections: (1) makeup (or central) system and (2) polishing loop, which provides water at the point of use. There are multiple locations in such a water process where membrane degassing could be needed as shown in the figure. Reverse osmosis is mostly used in makeup line as the primary purification means in such processes. In the past, large and inflexible vacuum towers were frequently used after RO to remove dissolved gases, such as O<sub>2</sub>, N<sub>2</sub>, and CO<sub>2</sub>. Membrane contactors are the norm today for replacement or supplement to vacuum towers in makeup lines, as shown in Figure 2.6.

A second place where membrane contactors are often used is before the electro deionization (EDI) step in UPW plants to remove residual CO<sub>2</sub> gas. Removal of CO<sub>2</sub> improves efficiency of EDI unit. Membrane contactors allow the opportunity to decarbonate water inline and under pressure just prior to EDI.

Contactors are also used in polishing loop for final degassing and to treat recycled or reclaimed water (Figure 2.6). The exact UPW process configuration depends on the specific needs in the plant and on quality of water supply to the plant. But no

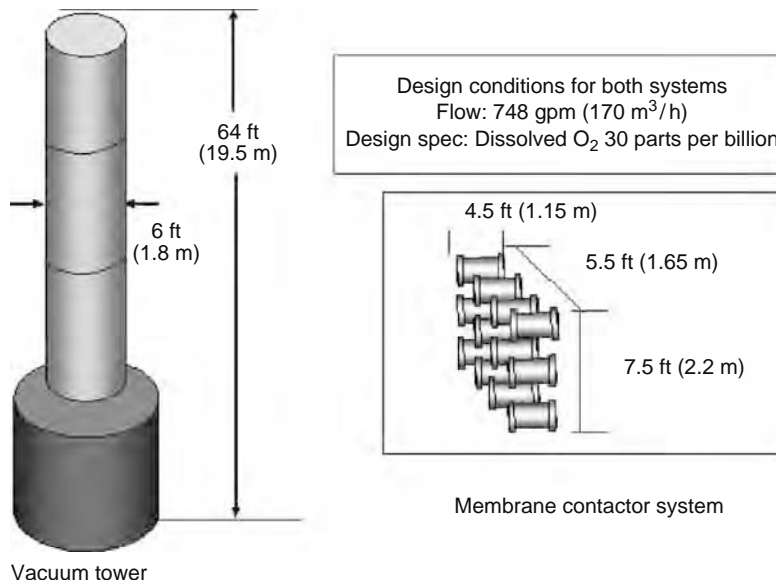
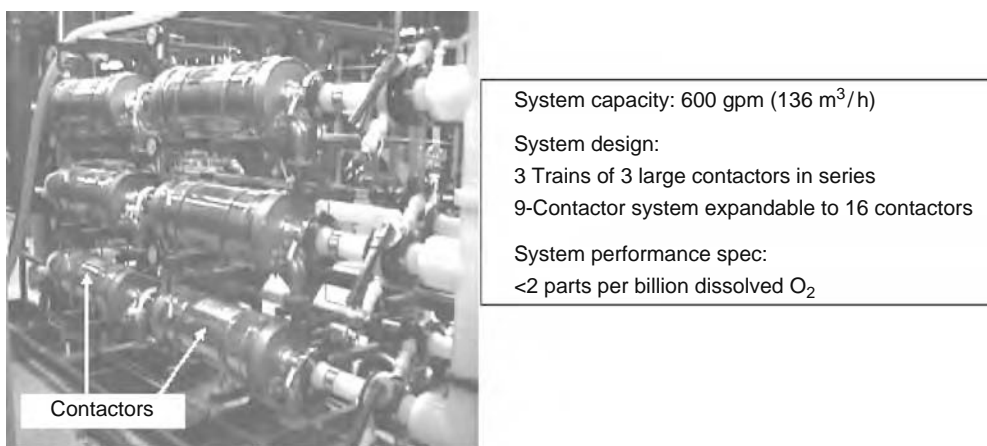


FIGURE 2.7 Relative system sizes of vacuum tower and membrane contactors.



**FIGURE 2.8** Central ultrapure water degasification system.

matter what configuration is adopted, membrane contactors are used in most of the modern plants because of their various advantages (smaller footprint, flexibility, and cost). As Figure 2.7 shows membrane systems occupy much smaller space and eliminate need for ground preparation or a permanent structure.

Figures 2.8 and 2.9 show photographs of commercially installed membrane contactor systems. Figure 2.8 shows that of a central UPW degasification system and Figure 2.9 that of a polishing loop degasification system in a DRAM facility. Each system is built from large membrane contactor modules. As explained earlier, one advantage of a membrane contactor system is the modularity. Similar size contactors could therefore be used in large or small UPW research degasification systems. Figure 2.10 shows the photo of a smaller capacity water supply system used in a research facility.

Another frequent use of membrane contactors is to help optimize the deionization step in water purification systems. The contactor is placed between the cation exchange bed and anion exchange bed (Figure 2.11). The pH after the cation bed is very low, which favors formation of gaseous CO<sub>2</sub> from bicarbonates present in water. By using a membrane contactor, most of the bicarbonate alkalinity can be removed from water as CO<sub>2</sub>, thus significantly reducing the load on the anion exchange bed that follows the contactor. The life of the anion bed can be doubled or tripled using contactor, resulting in large cost savings. In addition, sizes of the cation and anion beds could be equalized, helping in cost savings. Compared to existing technology, the membrane contactor is less expensive to operate and can operate in a closed system with little minimal chance of external contamination.

Boiler feed water is another excellent application for membrane degasification. Dissolved oxygen is unwanted in boiler feed water. Lowering dissolved oxygen level saves chemical costs and reduces blow down costs and energy costs. Figure 2.12 shows a typical schematic flow diagram in a boiler plant. As shown in this figure, degassing steps can be implemented in more than one location in such plants. A photograph of an actual installed membrane degasifier system is shown in Figure 2.13.

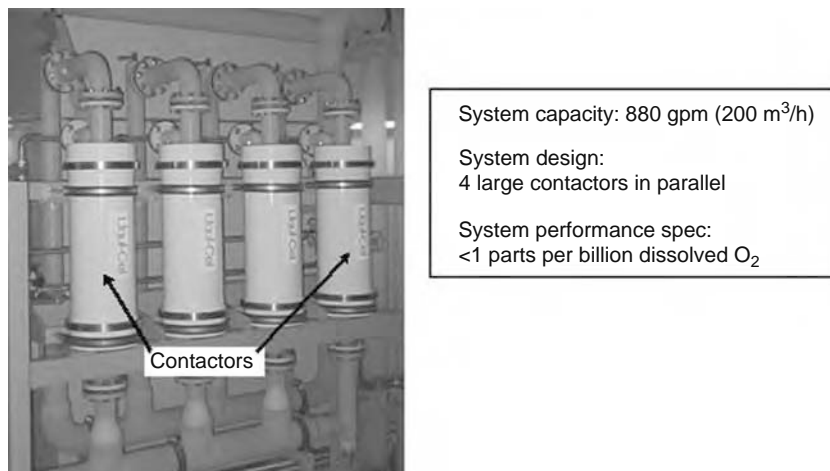


**FIGURE 2.9** (See color insert following page 588.) Polishing loop degasification system.

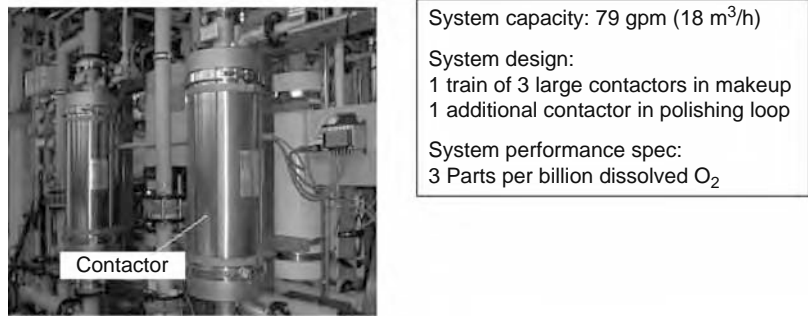


FIGURE 2.10 (See color insert following page 588.) Small-scale ultrapure water supply system.

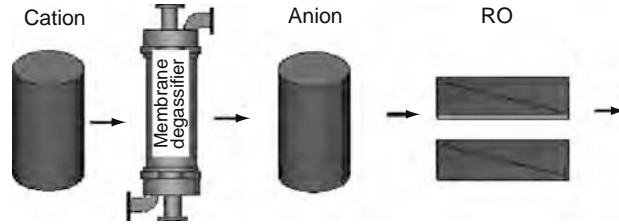


FIGURE 2.11 Membrane contactor to reduce size of anion exchange bed.

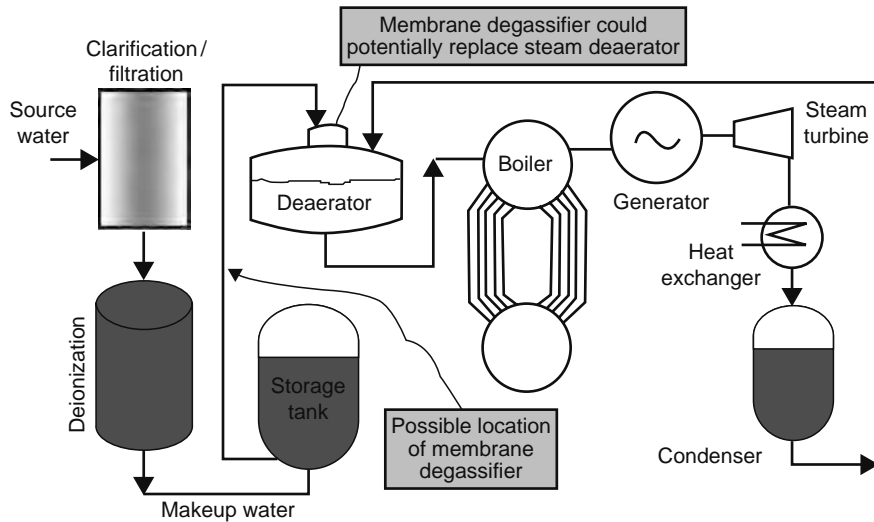


FIGURE 2.12 Schematic diagram of a boiler plant.

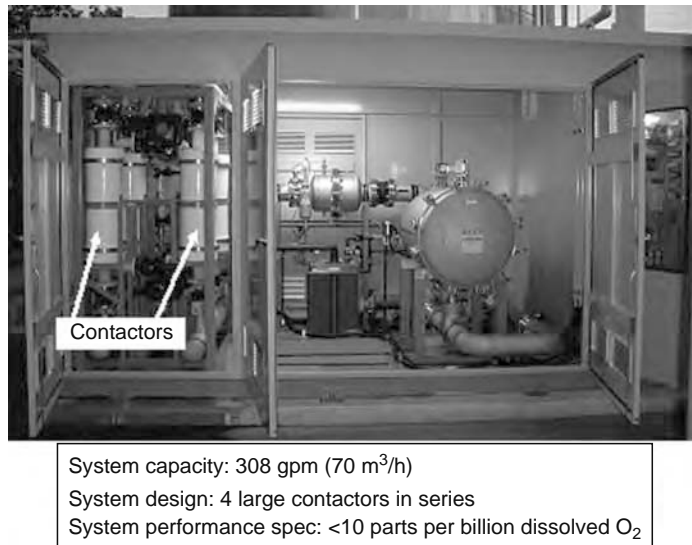
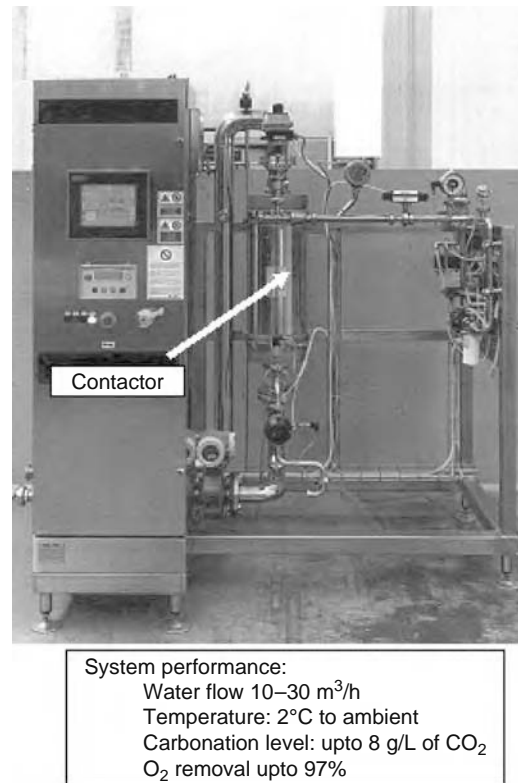


FIGURE 2.13 (See color insert following page 588.) Boiler water degasification system using membrane contactors.



**FIGURE 2.14** Membrane contactor for simultaneous carbonation and deoxygenation.

A photo of a small-scale membrane contactor system that could be used to simultaneously carbonate and deoxygenate water is shown in Figure 2.14. This is accomplished by passing CO<sub>2</sub> gas stream under pressure as a sweep on the lumen side of the contactor while water flows through the shell side. Water absorbs CO<sub>2</sub> under pressure and becomes carbonated while the presence of excess CO<sub>2</sub> gas creates a driving force for removing dissolved oxygen from the water.

Membrane contactors can be used in osmotic distillation process to transfer water vapor, as discussed in Section 2.8. Such a process has been investigated as a means of concentrating fruit juice [58] using concentrated brine as the receiving phase for water vapor. A photograph of a pilot system is shown in Figure 2.15.

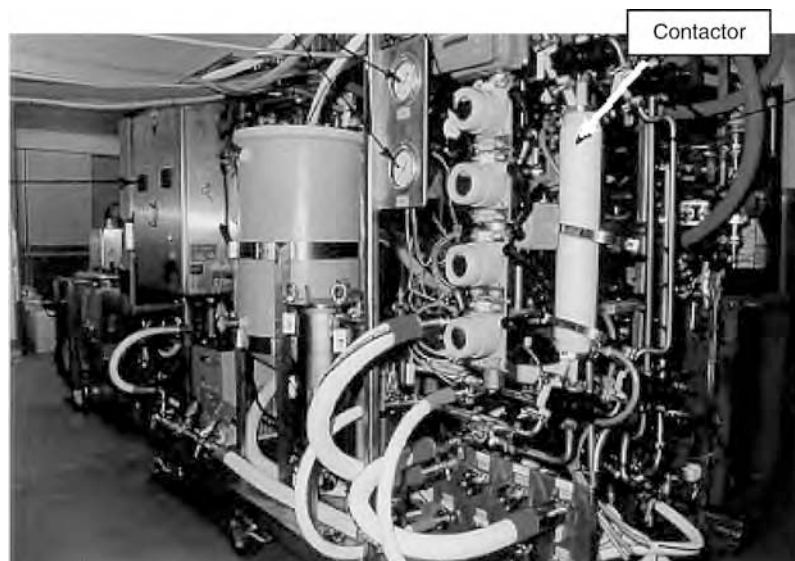


**FIGURE 2.15** (See color insert following page 588.) Membrane contactor for fruit juice concentration using membrane distillation process.

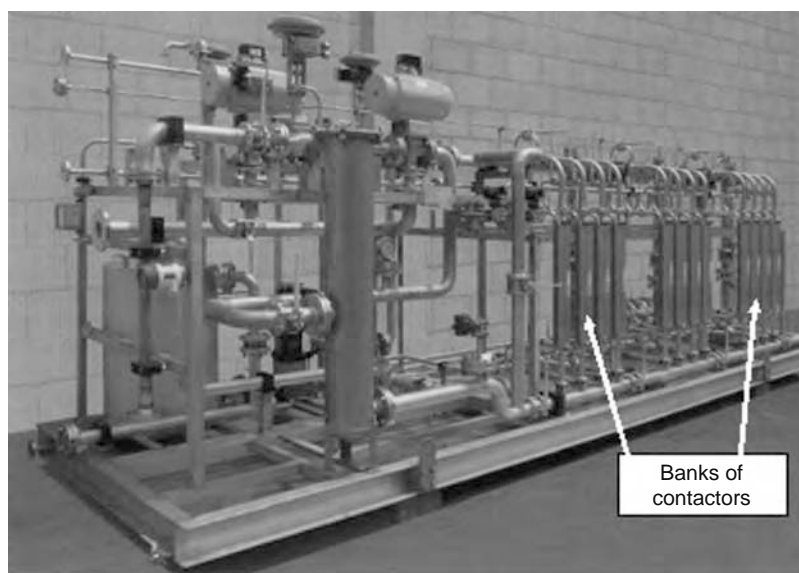


FIGURE 2.16 (See color insert following page 588.) Membrane contactors for liquid–liquid extraction.

Infusion of ozone into ultrapure water has become an excellent application of membrane contactors, as mentioned earlier. Ozone is generated in gas phase from air or oxygen, and the ozone-containing gas and ultrapure water are brought in contact with each other in the membrane contactor [50].

As mentioned in Section 2.9, liquid–liquid extraction has also been employed on a commercial scale in membrane contactors to remove environmentally toxic species from wastewater before incineration. Photograph of such a system is shown in Figure 2.16. Multiple banks of contactors are used in the system. The solvent used for extraction is returned to the chemical process that produces the toxic compounds.

In conclusion, membrane contactor technology has been creating a distinct application base for itself in recent years. The installed base of membrane contactors is still small compared to other membrane technologies. However, use of this technology cuts across diverse industries and markets, and in many instances membrane contactors are enabling customers with new opportunities that did not exist before. Many well-known producers of membrane and membrane modules today offer commercial membrane contactors as part of their product portfolio. It is our belief that new installations of membrane contactors will continue and new applications of this technology will be found in coming years.

## REFERENCES

1. Sirkar KK, Other new membrane processes, in Ho WSW and Sirkar KK, eds, *Membrane Handbook*. Van Nostrand Reinhold, New York 1992, 885–912.
2. Reed BW, Semmens MJ, and Cussler EL, Membrane contactors, in Noble RD and Stern SA, eds, *Membrane Separation Technology—Principles and Application*. Elsevier, Amsterdam 1995, 467–498.
3. Kim BS and Harriott P, Critical entry pressure for liquids in hydrophobic membranes, *Journal of Colloid and Interface Science* 1987, 115(1), 1–8.
4. Qi Z and Cussler EL, Microporous hollow fibers for gas absorption—I. Mass transfer in the liquid, *Journal of Membrane Science* 1985, 23, 321–332.
5. Qi Z and Cussler EL, Microporous hollow fibers for gas absorption—II. Mass transfer across the membrane, *Journal of Membrane Science* 1985, 23, 333–345.
6. Prasad R and Sirkar KK, Membrane-based solvent extraction, in Ho WSW and Sirkar KK, eds, *Membrane Handbook*. Van Nostrand Reinhold, New York 1992, 727–741.
7. Callahan RW, Novel uses of microporous membranes—a case study, in Sirkar KK and Lloyd DR, eds, *Membrane Materials and Processes for Separation*. American Institute of Chemical Engineers (AIChE) Symposium Series No. 261, 1988, 84, 54–63.
8. Sirkar KK, Immobilized-interface solute transfer process, US Patent 4,997,569, 1991.
9. Masano I, Furusaki S, and Miyauchi T, Separation of volatile materials by gas membrane, *Industrial Engineering Chemistry—Process Design and Development* 1982, 21, 421–426.
10. Qi Z and Cussler EL, Hollow fiber gas membranes, *AIChE Journal* 1985, 31(9), 1548–1553.
11. Skiens WE, Lipps BJ, Clark ME, and McLain EA, Hollow fiber membrane oxygenator, *Journal of Biomedical Materials Research Symposium*, 1971, 1, 135–148.
12. Shindo M, Yamamoto T, and Kanada K, Gas transfer process with hollow fiber membrane, US Patent 4,268,279, 1981.

13. Yang MC and Cussler EL, Artificial gills, *Journal of Membrane Science* 1989, 42, 273–284.
14. Baurmeister U and Pelger M, Device for separating gas bubbles from fluids, US Patent 4,828,587, 1989.
15. Kirsch CFE and Reed BW, Device for removal of gas bubbles and dissolved gases in liquid, US Patent 6,503,225, 2003.
16. Robinson JR, New developments in hollow fiber diffusional gas transfer for bioreactors. Bioprocess Engineering symposium, ASME Meeting, Chicago, IL, Nov 27–Dec 2, 1988.
17. Kang W, Shukla R, Frank GT, and Sirkar KK, Evaluation of O<sub>2</sub> and CO<sub>2</sub> transfer coefficients in a locally integrated tubular hollow fiber bioreactor, *Applied Biochemistry and Biotechnology* 1988, 18, 35–51.
18. Sengupta A, Sodaro RA, and Reed BW, Oxygen removal from water using process-scale extra-flow membrane contactors and systems. Seventh Annual Meeting of the North American Membrane Society, Portland, OR, May 21–24, 1995.
19. Macklin SH, Haas WE, and Miller WS, Carbon dioxide and dissolved oxygen removal from makeup water by gas transfer membranes. International Water Conference, Pittsburgh, PA, Oct 30, 1995.
20. Wiesler FE and Sodaro RA, Degasification of water using novel membrane technology, *Ultrapure Water* 1996, 35, 53.
21. Kosmella HJ, Schossig-Tiedemann M, Nitsche V, and Kneifel K, Degassing of water with membranes. Euromembrane 97, University of Twente, Enschede, The Netherlands, June 26, 1997.
22. Yagi Y, Imaoka T, Kasama Y, and Ohmi T, Advanced ultrapure water systems with low dissolved oxygen for native oxide free wafer processing. *IEEE Transactions on Semiconductor Manufacturing* 1992, 5(2), 121–127.
23. Mashimo N and Okumura K, Method of cleaning semiconductor wafers using mixer containing a bundle of gas permeable hollow yarns, US Patent 5,261,966, 1993.
24. Tai MSL, Chua I, Li K, Ng WJ, and Teo WK, Removal of dissolved oxygen in ultrapure water production using microporous membrane modules, *Journal of Membrane Science* 1994, 87, 99–105.
25. Bujedo J and Peterson PA, Removing dissolved oxygen from ultrapure water, *Semiconductor International* 1997, October.
26. Sengupta A, Peterson PA, Miller BD, Schneider J, and Fulk CW, Large-scale application of membrane contactors for gas transfer from or to ultrapure water, *Separation and Purification Technology* 1998, 14, 189–200.
27. Wiesler F and Kao CT, Meeting water quality specifications for 300 mm processing. SEMICON China, Beijing, China, March 28–29, 2001.
28. Breitschopf F, Brau W, Dittrich S, and Koukol R, A new kind of water deaeration based on hollow fiber membranes, *Brauwelt International* 1997, 5, 431–433.
29. D'Angelo P, Oxygen removal—theory and potential use of deoxygenation membranes in the utility industry, *Ultrapure Water* 1995, July/August, 60–63.
30. Mackey J and Mojonner J, CO<sub>2</sub> injection using membrane technology. Presented at the Eighth Annual Conference on the Operation of Technologically Advanced Beverage Plants and Warehouses, March 21–23, 1995.
31. Anonymous Technical Feature Article, Non-dispersive diffusion for nitrogenation, *Brauwelt International* 2000, 18(2), 129–130.
32. Page JKR and Kalthod DG, Control of dissolved gases in liquids, US Patent 5,565,149, 1996.
33. Gill CB and Menneer ID, Advances in Gas Control Technology in the Brewery, *The Brewer* 1997, 83(987), 77–84.
34. Bandini S, Gostoli C, and Sarti GC, Separation efficiency in vacuum membrane distillation, *Journal of Membrane Science* 1992, 73, 217–229.
35. Sarti GC, Gostoli C, and Bandini S, Extraction of organic components from aqueous streams by vacuum membrane distillation, *Journal of Membrane Science* 1993, 80, 21–33.
36. Wu B and Teo WK, Preparation and application of PVDF hollow fiber membranes in vacuum membrane distillation to remove TCE and TCA from aqueous solutions. Euromembrane 2004, Hamburg, Germany, September 28–October 1, 2004.
37. Semmens MJ, Qin R, and Zander A, Using a microporous hollow fiber membrane to separate VOCs from water, *Journal of the American Water Works Association* 1989, April, 162–167.
38. Aziz CE, Fitch MW, Linnquist LK, Pressman JG, Georgiou G, and Speitel GE, Methanotropic biodegradation of trichloroethylene in a hollow fiber membrane bioreactor, *Environmental Science and Technology* 1995, 29(10), 2574–2583.
39. Schwarz D, TOC reduction using membrane technology, *Ultrapure Water* 2000, 60–63.
40. Dey A, Thomas G, Kekre KA, and Guihe T, Removing THMs by membrane contactors in a UPW plant—a case study, *Water Conditioning and Purification* 2002, February, 120–123.
41. Colletto WV and Colletto AW, Purification of gases from water using reverse osmosis, US Patent 5,670,053, 1997.
42. Gascons VF, Souchon I, Athes V, and Martin M, Air stripping membrane contactor applied to aroma compounds extraction: Influence of heat and water transfers on aroma transfer. Euromembrane 2004, Hamburg, Germany, September 28–October 1, 2004.
43. Cote P, Bersillon JL, and Huyard A, Bubble-free aeration using membranes: Mass transfer analysis, *Journal of Membrane Science* 1989, 47, 91–106.
44. Semmens M, Bubbleless aeration, *Water Engineering and Management* 1991, April, 18–19.
45. Johnson DW and Semmens MJ, The performance of unconfined hollow fiber membranes as pipe flow and mixed flow aerators, Proceedings of the 1994 National Conference on Environmental Engineering, Sponsored by American Society of Civil Engineers, Boulder, CO, July 11–13, 1994.
46. Voss MA, Ahmed T, and Semmens MJ, Long-term performance of parallel-flow bubbleless hollow fiber membrane aerators, *Water Environment Research* 1999, 71(1), 23–30.
47. Cote P, Pedersen S, Behmann H, Husain H, and Phagoo D, Membrane module for gas transfer and membrane supported biofilm process, US Patent 6,645,374, 2003.
48. Sell M, Bischoff M, Mann A, Behling RD, Peinemann KV, and Kneifel K, Method of introducing hydrogen into aqueous liquids without forming bubbles, US Patent 5,523,003, 1996.

49. Sakai K, Kato H, and Kanbe T, Method and device for controlled resistivity of ultrapure water, Japanese Patent Publication Number 11057707, 1999.
50. Wikol MJ, Kobayashi M, and Hardwick SJ, Application of PTFE membrane contactors to the infusion of ozone into ultra-high purity water, The ICCS 14th International Symposium on Contamination Control, Phoenix, AZ, April 26–May 1, 1998.
51. Qi Z and Cussler EL, Bromine recovery with hollow fiber gas membrane, *Journal of Membrane Science* 1985, 24, 43–57.
52. Kenfield CF, Qin R, Semmens MJ, and Cussler EL, Cyanide recovery across hollow fiber gas membrane, *Environmental Science and Technology* 1988, 22(10), 1151–1155.
53. Hecht V, Bischoff L, and Gerth K, Hollow fiber supported gas membrane for in situ removal of ammonium during an antibiotic fermentation, *Biotechnology and Bioengineering* 1990, 35, 1042–1050.
54. Semmens MJ, Foster DM, and Cussler EL, Ammonia removal from water using microporous hollow fibers, *Journal of Membrane Science* 1990, 51, 127–140.
55. Marr R and Koncar M, Recovery of ammonia from industrial wastewater, *International Chemical Engineering* 1993, 33(3), 416–425.
56. Gostoli C and Bandini S, Gas membrane extraction of ethanol by glycols: Experiments and modeling, *Journal of Membrane Science* 1995, 98, 1–12.
57. Anonymous, Technical Brief volume 43, Successful ammonia removal from wastewater using liqui-cell membrane contactors at a European manufacturing facility, Membrana, January, 2005.
58. Hogan PA, Canning RP, Peterson PA, Johnson RA, and Michaels AS, Osmotic distillation: A novel athermal membrane-separation process for the food, pharmaceutical, and chemical industries, *Chemical Engineering Progress* 93, August 1997.
59. Alves VD and Coelho IM, Low temperature membrane processes for fruit juice concentration. Euromembrane 2004, Hamburg, Germany, September 28–October 1, 2004.
60. Lawson KW and Lloyd DR, Membrane distillation, *Journal of Membrane Science* 1997, 124, 1–25.
61. Cath T and Childress A, Experimental study of desalination using direct contact membrane distillation: A new approach to flux enhancement. 14th Annual Meeting of North American Membrane Society, Jackson Hole, WY, May 17–21, 2003.
62. Noyes G, A mobile liquid venting membrane separator for carbon dioxide, humidity, and waste heat removal from spacesuits and manned spacecraft. 23rd International Conference on Environmental Systems, Colorado Springs, CO, July 12–15, 1993.
63. Noyes G, Microporous hydrophobic hollow fiber modules for gas–liquid phase separation in microgravity, 23rd International Conference on Environmental Systems, Colorado Springs, CO, July 12–15, 1993.
64. Leimkuehler TO, Spelbring C, Reeves DR, and Holt JM, Development of the next generation gas trap for the space station internal thermal control system, Report number 2003-01-2566, SAE International, 2003.
65. Cooney DO and Jackson CC, Gas absorption in a hollow fiber device, *Chemical Engineering Communications* 1989, 79, 153–163.
66. OgunDIRAN SO, LeBlanc SE, and Varanasi S, Membrane contactors for SO<sub>2</sub> removal from flue gases. Sixth Annual International Pittsburgh Coal Conference, Pittsburgh, PA, September 25–29, 1989.
67. Kreulen H, Smolders CA, Versteeg GF, and van Swaaij WPM, Microporous hollow fiber membrane modules as gas–liquid contactors, Part I, Physical mass transfer processes, *Journal of Membrane Science* 1993, 78, 197–216.
68. Kreulen H, Smolders CA, Versteeg GF, and van Swaaij WPM, Microporous hollow fiber membrane modules as gas–liquid contactors, Part II, Mass transfer with chemical reactions, *Journal of Membrane Science* 1993, 78, 217–238.
69. Ghosh AC, Borthakur S, and Dutta NN, Absorption of carbon monoxide in hollow fiber membranes, *Journal of Membrane Science* 1994, 96, 183–192.
70. Rangwala HA, Absorption of carbon dioxide into aqueous solutions using hollow fiber membrane contactors, *Journal of Membrane Science* 1996, 112, 229–240.
71. Feron PHM, Jansen AE, and Klaassen R, Membrane technology in carbon dioxide removal, TNO Environmental and Energy Research, Publication No. 92-075, 1992.
72. Dindore Y, Brilman DWF, Feron, PHM, and Versteeg GF, CO<sub>2</sub> absorption at elevated pressures using a hollow fiber membrane contactor, *Journal of Membrane Science* 2004, 235, 99–109.
73. Hoff KA, Juliassen O, Falk-Pedersen O, and Svendsen HF, Modeling and experimental study of carbon dioxide absorption in aqueous alkanolamine solutions using a membrane contactor, *Industrial and Engineering Chemistry Research* 2004, 43(16), 4908–4921.
74. Li K, Tai MSL, and Teo WK, Design of a CO<sub>2</sub> scrubber for self-contained breathing systems using a microporous membrane, *Journal of Membrane Science* 1994, 86, 119–125.
75. Stucki S, Schuler A, and Constantinescu M, Coupled CO<sub>2</sub> recovery from the atmosphere and water electrolysis: Feasibility of a new process for hydrogen storage, *International Journal of Hydrogen Energy* 1995, 20(8), 653–663.
76. Wijmans JG, Goakey S, Wang X, Baker RW, and Kaschemekat JH, Membrane system for recovery of volatile organic compounds from remediation off-gases, Topical report for United States Department of Energy, April 1997.
77. Pressman JG, Georgiou G, and Speitel GE, A hollow fiber membrane bioreactor for the removal of trichloroethylene from the vapor phase, *Biotechnology and Bioengineering* 2000, 68(5), 548–556.
78. Bonne U, Deetz DW, Lai JH, Odde DJ, and Zook JD, Membrane dehumidification, US Patent 4,915,838, 1990.
79. Anonymous, Technical Brief volume 23, Humidification of gas streams using liqui-cell membrane contactors, Membrana, February 2002.
80. Wagner B, Jehle W, Steinwandel J, Staneff T, and Herczog J, Continuous membrane supported cabin air dehumidification process. Euromembrane 97, University of Twente, Enschede, The Netherlands, June 26, 1997.
81. Nowak S, Kneifel K, Waldemann R, Wind J, Albrecht W, Hilke R, Just R, and Peinemann KV, Hollow fiber membrane contactor for air humidity control. Euromembrane 2004, Hamburg, Germany, September 28–October 1, 2004.

82. Willemsen JHA, Dijkink BH, Kneifel K, Nowak S, and Peinemann KV, Application of dedicated membrane contactors for humidity control during storage of perishable goods. Euromembrane 2004, Hamburg, Germany, September 28–October 1, 2004.
83. Reed BW and Sengupta A, Beyond dispersion: A perspective on membrane contactors, AIChE Annual Meeting, Miami Beach, FL, November 12–17, 1995.
84. Kiani AK, Bhave RR, and Sirkar KK, Solvent extraction with immobilized interfaces in a microporous hydrophobic membrane, *Journal of Membrane Science* 1984, 20, 125–145.
85. Kim BM, Membrane-based solvent extraction for selective removal and recovery of metals, *Journal of Membrane Science* 1984, 21, 5–19.
86. Prasad R and Sirkar KK, Solvent extraction with microporous hydrophilic and composite membranes, *AIChE Journal* 1987, 33(7), 1057.
87. Cussler EL, Callahan RW, and Alexander PR, Liquid/liquid extractions with microporous membranes, US Patent 4,966,707, 1990.
88. Frank GT and Sirkar KK, Alcohol production by yeast fermentation and membrane extraction, Biotechnology and Bioengineering Symposium No. 15, John Wiley & Sons, New York, 1985, pp. 621–631.
89. Shukla R, Kang W, and Sirkar KK, Acetone–butanol–ethanol (ABE) production in a novel hollow fiber fermentor-extractor, *Biotechnology and Bioengineering* 1989, 34, 1158–1166.
90. Groot WJ, Soedjak HS, Donck PB, van der Lans RGJM, Luyben KCAM, and Timmer JMK, Butanol recovery from fermentations by liquid–liquid extraction and membrane solvent extraction, *Bioprocess Engineering* 1990, 5, 203–216.
91. Haggin J, Membranes play growing role in small-scale industrial processing, *Chemical and Engineering News* 1988, July 11, 25–32.
92. Wald SA, Lopez JL, and Matson SL, Membrane-mediated antibiotic extraction using liquid ion exchangers. North American Membrane Society (NAMS) Meeting, 1989.
93. Prasad R and Sirkar KK, Hollow fiber solvent extraction of pharmaceutical products—a case study, *Journal of Membrane Science* 1989, 47, 235–259.
94. Dahuron L and Cussler EL, Protein extractions with hollow fibers, *AIChE Journal* 1988, 34(1), 130–136.
95. Ding HB, Carr PW, and Cussler EL, Racemic leucine separation by hollow-fiber extraction, *AIChE Journal* 1992, 38(10), 1493–1498.
96. Vatai G and Tekic MN, Membrane-based ethanol extraction with hollow fiber module, *Separation Science and Technology* 1991, 26(7), 1005–1011.
97. Wang CJ, Bajpai RK, and Iannotti EL, Nondispersive extraction for recovering lactic acid, *Applied Biochemistry and Biotechnology* 1991, 589–603.
98. Kertesz R, Schlosser S, and Simo M, Membrane bases solvent extraction and stripping of Phenylalanine in HF contactors. Euromembrane 2004, Hamburg, Germany, September 28–October 1, 2004.
99. Baudot A, Flourey J, and Smorenburg HE, Liquid–liquid extraction of aroma compounds with hollow fiber contactor, *AIChE Journal* 2001, 47(8), 1780–1793.
100. Cooney DO and Jin CL, Solvent extraction of phenol from aqueous solution in a hollow fiber device, *Chemical Engineering Communications* 1985, 37, 173–191.
101. Porebski T, Tomzik S, Ratajczak W, Wieteska A, Zebrowski M, and Karabin M, Industrial application of hollow fiber modules in the process of phenol extraction from the hydrocarbon fraction. Proceedings International Conference PERMEA 2003, Tatranske Slovakia, September 7–11, 2003.
102. *VNCI (Dutch Chemistry Industry Organization) Magazine*, April 14, 11, 1999.
103. Chen TJ and Sweet JR, Selective separation of naphthenes from paraffins by membrane extraction, US Patent 5,107,056, 1992.
104. Tompkins CJ, Michaels AS, and Peretti SW, Removal of *p*-nitrophenol from aqueous solution by membrane-supported solvent extraction, *Journal of Membrane Science* 1992, 75, 277–292.
105. Zander AK, Chen JS, and Semmens MJ, Removal of hexachlorocyclohexane isomers from water by membrane extraction into oil, *Water Research* 1992, 26(2), 129–137.
106. Yun CH, Prasad R, and Sirkar KK, Membrane solvent extraction of priority organic pollutants from aqueous waste streams, *Industrial and Engineering Chemistry Research* 1992, 31, 1709–1717.
107. Zander, AK, Qin R, and Semmens MJ, Membrane/oil stripping of VOCs from water in hollow fiber contactor, *Journal of Environmental Engineering* 1989, 115, 768–784.
108. Klaassen R, Jansen AE, Oesterholt FIHM, and Bult BA, Pextraction of hydrocarbons from wastewater streams, Final Report 94–039, TNO Environmental and Energy Research, March 1994.
109. Kim BM, Process for separation of molybdenum from tungsten leachate, US Patent 4,443,414, 1984.
110. Matsumoto M, Shimauchi H, Kondo K, and Nakashio F, Kinetics of copper extraction with Kelex-100 using a hollow fiber membrane extractor, *Solvent Extraction and Ion Exchange* 1987, 5(2), 301–323.
111. Alexander PR and Callahan RW, Liquid–liquid extraction and stripping of gold with microporous hollow fibers, *Journal of Membrane Science* 1987, 35, 57–71.
112. Keurentjes JTF, Bosklopper TGJ, van Dorp LJ, and van't Rief K, The removal of metals from edible oil by a membrane extraction procedure, *Journal of the American Oil Chemists Society* 1990, 67(1), 28–32.
113. Goto M, Kubota F, Miyata T, and Nakashio F, Separation of yttrium in a hollow fiber membrane, *Journal of Membrane Science* 1992, 74, 215–221.
114. Yun CH, Prasad R, Guha AK, and Sirkar KK, Hollow fiber solvent extraction removal of toxic heavy metals from aqueous waste streams, *Industrial and Engineering Chemistry Research* 1993, 32(6), 1186–1195.
115. Raghuraman B and Wincek J, Extraction with emulsion liquid membranes in a hollow-fiber contactor, *AIChE Journal* 1993, 39(11), 1885–1889.

116. Yang MC and Cussler EL, Designing hollow fiber contactors, *AIChE Journal* 1986, 32(11), 1910–1916.
117. Costello MJ, Fane AG, Hogan PA, and Schofield RW, The effect of shell side hydrodynamics on the performance of axial flow hollow fiber modules, *Journal of Membrane Science* 1993, 80, 1–11.
118. Wang KL and Cussler EL, Baffled membrane modules made with hollow fiber fabric, *Journal of Membrane Science* 1993, 85, 265–278.
119. Prasad R, Runkle CJ, and Shuey HF, Method of making spiral-wound hollow fiber membrane fabric cartridges and modules having flow-directing baffles, US Patent 5,264,171, 1993.
120. Prasad R, Runkle CJ, and Shuey HF, Spiral-wound hollow fiber membrane fabric cartridges and modules having flow directing baffles, US Patent 5,352,361, 1994.
121. Yamamura H, Ikada H, Toyoda Y, Nishimura K, and Imai K, Spiral wound gas permeable membrane module and apparatus and method for using the same, US Patent 5,154,832, 1992.
122. Akasu H, Mimura R, Migaki T, Yamauchi T, and Kusachi M, Fluid treating apparatus and method of using it, US Patent 4,911,846, 1990.
123. Aanazawa T, Miyashita M, Murata K, Akasu H, and Mimura S, Hollow fiber membrane type phase contact apparatus, Japanese Patent 2,725,311, 1997.
124. Meulen T and Berend P, Transfer device for the transfer of matter and/or heat from one medium flow to another medium flow, US Patent 5,230,796, 1993.
125. Mitrovic MV and Vladislavljevic GT, Membrane multi-phase contactors. Euromembrane 97, University of Twente, Enschede, The Netherlands, June 26, 1997.
126. Sengupta A, Degassing a liquid with a membrane contactor, US Patent 6,402,818, 2002.
127. Peterson PA, Runkle CJ, Sengupta A, and Wiesler FE, Shell-less hollow fiber membrane fluid contactor, US Patent 6,149,817, 2000.
128. Sengupta A, Runkle CJ, Vido TR, and Kitteringham BA, Economy of scale: Large membrane modules for degasification and purification, International Water Conference, Pittsburgh, PA, October 2003.

---

# 3 Membrane Chromatography

*M.E. Avramescu, Z. Borneman, and M. Wessling*

## CONTENTS

3.1	Introduction .....	25
3.2	New Types of Membrane Chromatography Supports .....	26
3.3	Types of Materials Used in Adsorptive Membranes Preparation.....	28
3.4	Adsorptive Membranes Preparation.....	34
3.4.1	Membrane Preparation in Affinity Chromatography .....	34
3.4.1.1	Basic Membrane Preparation .....	34
3.4.1.2	Basic Membrane Modification.....	34
3.4.2	Preparation of Monolithic Stationary Phases.....	35
3.4.2.1	Preparation of Silica Monoliths .....	36
3.4.2.2	Preparation of Organic Polymer Monoliths.....	36
3.4.3	Preparation of Particle-Loaded Membranes.....	38
3.4.4	Membrane Activation and Ligand Coupling .....	40
3.4.5	Affinity Ligands .....	44
3.4.6	Spacer Molecules .....	45
3.5	Advantages of Membrane Chromatography .....	46
3.6	Mass Transfer in Affinity Columns .....	47
3.6.1	Design Parameters.....	48
3.6.2	Axial Dispersed Plug Flow Model .....	48
3.6.3	Dispersion.....	49
3.6.4	Determining the Average Residence Time and the Variance.....	50
3.6.5	Brownian Motion .....	50
3.6.6	Interaction with the Matrix and Active Sites.....	51
3.7	Adsorptive Membrane Geometry and Operation Modes.....	51
3.8	Applications of Membrane Chromatography .....	53
3.9	Conclusions .....	56
	References.....	56

## 3.1 INTRODUCTION

In the pharmaceutical and biotechnological industry, the downstream processing of fermentation broths normally involves numerous steps for biomass removal and product purification. In the early days of biomolecule purification, the only practical method used for protein separation from complex mixtures was based on protein precipitation by water miscible organic solvents [1]. Alteration of the solvent properties by the addition of neutral salts and organic solvents leads to precipitation of the macromolecule due to differences in solubility. Alternative processes including adsorption techniques, gel filtration, liquid phase partitioning, electrophoretic methods, and membrane technologies have been developed recently for protein purification. Adsorption techniques often result in purification steps that give the greatest increase in protein purity. Therefore, they became widely employed especially when adopted in combination with chromatographic and membrane processes.

Column chromatography is a highly developed method used as a final step (in both capturing and polishing) in the purification of biomolecules out of crude mixtures. Despite their large static adsorption capacity, conventional stationary phases involved in chromatographic separations are generally not suitable for operating with high linear velocities of the mobile phase. The first chromatographic columns were realized in packed beds with  $\sim 100 \mu\text{m}$  beads. Their main drawback is the compression and compaction at high velocities [2]. The pressure drop over the column is high even for low flow rates and increases during

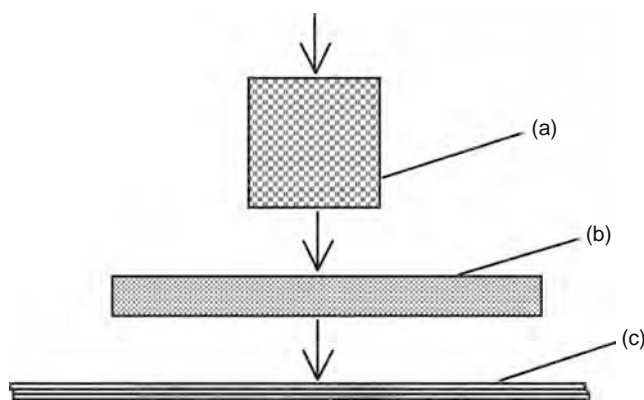


**FIGURE 3.1** Evolution of affinity column bed geometry: (a) packed bed (100  $\mu\text{m}$  beads), (b) short “fat” bed (1  $\mu\text{m}$  beads), and (c) microporous hollow fiber (pore size  $>1 \mu\text{m}$ ).

the process time due to bed consolidation and plugging. For a given pressure drop across the bed, the throughput is inversely proportional to the bed height. For these reasons other column configurations were investigated, which range from stacked configurations (a number of short beds connected in series–parallel combinations) to radial flow arrangements (a short, wide bed curled up end-to-end upon itself).

For an efficient use of the adsorptive sites inside the chromatographic support, a certain residence time dependent on the particle size and porosity is required. Short diffusion distances lead to fast flows of the feed solution. This results in the development of chromatographic columns with smaller diameter particles, with the drawback that smaller particles pack more densely and create higher pressure drops. The pressure drop in conventional chromatographic columns with particles with a diameter of 2  $\mu\text{m}$  is usually high, up to 25 MPa [3]. The use of nonporous, rigid particles as chromatographic media can partially solve this problem. Furthermore, for such supports, the ligands are located on the particle surface and not inside the pores, thus the solute diffusion into the particle pores is no longer a limiting factor allowing for much faster mass transfer. Unfortunately, the use of nonporous supports usually causes lower protein-binding capacities (due to a small binding surface), low reproducibility, and high process costs [4]. Micropellicular stationary phases, prepared by coating a very thin sorbent layer onto the nonporous particle surface, also showed improved chromatographic characteristics [5].

In the last few decades, in parallel with the development of nonporous chromatographic particles, new types of stationary phases including perfusive and super-porous beads were investigated. The particles for perfusion chromatography have large, interconnected canals allowing the solute molecules to pass quickly through the support at lower backpressure. Moreover, the binding capacity for perfusive media is higher than for nonporous supports leading to a more efficient separation process [6,7]. Furthermore, since neither binding capacity nor flow rate is the limiting factor, the scaling up of a perfusive chromatographic column can be relatively easy.

A different approach to lowering the pressure drop present in classical packed beds was the development of chromatographic shallower adsorption columns with larger cross section. In fact, the ideal column has an infinitely short bed height to minimize operating pressure and maximize throughput, and an infinite width so that the ligand loading and binding capacity are maximized. In recent years, hollow fiber membranes have also been proposed as an attractive alternative to porous beads as an affinity substrate in chromatographic separation processes (Figure 3.1).

In this chapter, the latest developments in stationary phases based on membranes (affinity membranes as well as mixed matrix membrane adsorbers) and monolithic separation media (both organic and inorganic) will be discussed. In the following sections, we first give some background information regarding the new types of chromatographic supports, focusing on the membrane materials, their properties, and preparation. Membrane activation and ligand coupling are discussed separately for polymers containing different types of functional groups. Advantages of membrane chromatography, as well as an introduction to the mass transfer in different affinity supports, are then presented. An outlook to possible applications of the chromatographic membranes in various process conditions is finally given.

### 3.2 NEW TYPES OF MEMBRANE CHROMATOGRAPHY SUPPORTS

The chromatographic separation process based on membranes has recently become an attractive and competitive method for purifying proteins and other biomolecules from biological fluids [8–13]. The membrane chromatographic system was originally designed to bypass the fundamental limitations of packed-bed adsorbers. The system consists of one or more microporous membranes as stationary phase, carrying adsorptive moieties based on ion exchange, affinity or hydrophobic interactions. The individual membranes can have different geometries, from disks, flat or layered sheets to full or hollow fibers. Since the

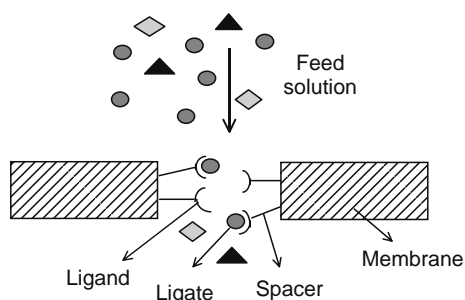


**FIGURE 3.2** Principle of affinity membrane chromatography.

adsorption capacity of a single membrane is limited, multiple membrane layers may be stacked together in series and housed within the filtration modules. Depending on the type of module involved in the separation process, different operation modes (dead-end, cross-flow, or radial flow) may be used.

Based on a literature survey, affinity-based chromatography seems to be the largest segment in membrane chromatography. In affinity membranes, the ligand is immobilized on the membrane surface (Figure 3.2). When the solution containing the compound of interest is filtrated, the desired molecule binds selectively and reversibly to the ligand immobilized on the membrane surface. In case of sterical hindrance the so-called spacer molecule can be introduced between the polymeric support and the ligand. These spacers permit free rotation of the ligand and thus provide more opportunities for the orientations necessary for ligand–ligate complex formation to occur. The conditions of the surrounding milieu determine the stability of the ligand–ligate complex. Changes in the physical or chemical environment conditions can disrupt the biological complexes.

In chromatographic separations using flat sheet membranes, compact porous disks, fibers, tubes, or rods, the interaction between the ligate molecule and the immobilized ligand takes place in the through-pores of the matrix and not in the dead-end pores of the conventional packed-bed particles. This method resembles affinity membrane separation with a very short affinity chromatography column [2].

Solid phase extraction using particle-loaded membranes (mixed matrix membrane adsorbents) and particle-embedded fibers became a widely used laboratory technique to isolate and concentrate selected analytes before chromatographic processes [14,15]. The incorporation into a porous polymeric membrane of functional particles, such as silica and its derivatives (containing, for example, ethyl, butyl, phenyl, octyl, octadecyl, or cyanopropyl functional groups), styrene/divinylbenzene-based ion-exchange resins, or fibrous cellulose derivatives, results in adsorptive structures that can be applied to isolate peptides, proteins, nucleic acid, or other organic compounds from complex mixtures [16–18]. Most suitable particles display, in combination with the porous matrix morphology, rapid adsorption kinetics, a capacity and selectivity commensurate with the specific application and allow for fast desorption of the targeted molecule. The affinity of suitable adsorptive particles for specific molecules can be defined in terms of hydrophobic, hydrophilic or charged functionalities, molecular (imprinted) recognition, or other specific interactions. However, these materials differ from the classical affinity membranes because the binding process takes place at the small particles embedded in the porous matrix and not at the pore wall itself. Nevertheless they show hydrodynamic advantages similar to those of the adsorptive chromatographic membranes.

Monolithic stationary phases (also called continuous beds) have emerged as an alternative to traditional packed-bed columns since the late 1980s, due to their easy preparation with good reproducibility, versatile surface chemistry, low backpressure, and fast mass transport. Their advantages are similar to membrane chromatography, but differ from the classical membrane media in terms of material, preparation, and morphology [19–21]. The monoliths are prepared mainly by in situ polymerization of organic species or silicon alkoxides and consolidation inside the column. Fusion of the porous packing material inside the column tubing by a sintering process has also been reported. As a result of the polymerization conditions (ratio and concentration of monomer and cross-linker, temperature and presence of porogenic solvents), the bed macroporous structure can be adjusted. If necessary the surface modification of the obtained porous matrix may be performed to improve the chromatographic-binding capacity.

The monoliths usually possess a bimodal pore size distribution consisting of large micrometer-size through-pores (which allow the liquid to pass through the matrix under low pressure even at high flow rates) and much smaller pores in the 10 nm range that contribute significantly to the overall surface area. Due to their well-defined bimodal pore size distribution, the monolithic supports provide high separation power offering good chemical stability and flow characteristics [22]. The continuous beds have a longitudinal dimension usually exceeding their lateral dimension. This brings the monoliths closer to the packed-bed columns than to membrane chromatography. Nevertheless, they were recently successfully used for high-speed separation in reverse-phase, ion exchange, hydrophobic interaction, or affinity modes especially for separation of biomolecules.

### 3.3 TYPES OF MATERIALS USED IN ADSORPTIVE MEMBRANES PREPARATION

Numerous natural and synthetic polymers such as polysaccharides, polyamide, polysulfone (PSf) and its derivatives, polyethylene and polypropylene, acrylic copolymers, polycarbonates, polyvinyl alcohol, have been explored as potential materials in chromatographic processes. The substrates used in successful membrane chromatography applications should fulfill several conditions including: (i) high macroporosity with large internal and external surface areas to maximize interaction of matrix-bound ligands with the ligate during the binding step; (ii) high mechanical stability and resistance to compaction under pressure; (iii) high chemical and physical stability under harsh conditions used for the ligand coupling and ligand–ligate complex formation; (iv) hydrophilic surfaces to minimize the nonspecific adsorption of bioactive species, and to minimize competition for the desired ligates; and (v) high density of reactive groups for subsequent coupling of spacer arms and ligand molecules [8]. Because very few materials fulfill these conflicting requirements, the choice of the support for a particular application is very often a compromise among the above-mentioned conditions. In this section, a number of often-used support materials is described.

Polysaccharides including cellulose and its derivatives, agarose, dextran, starch, chitin, and chitosan (Figure 3.3) have been widely used as a support material in affinity chromatographic separations.

Celulose is a 1,4- $\beta$ -linked D-glucose linear polymer with occasional 1,6-bonds (Figure 3.3a), derived both from plant and bacterial sources. The glucose segments contain three hydroxyl groups that are very susceptible to chemical reaction, forming esters (cellulose acetate, cellulose nitrate) and ethers (ethyl cellulose) and allowing for easy ligand immobilization.

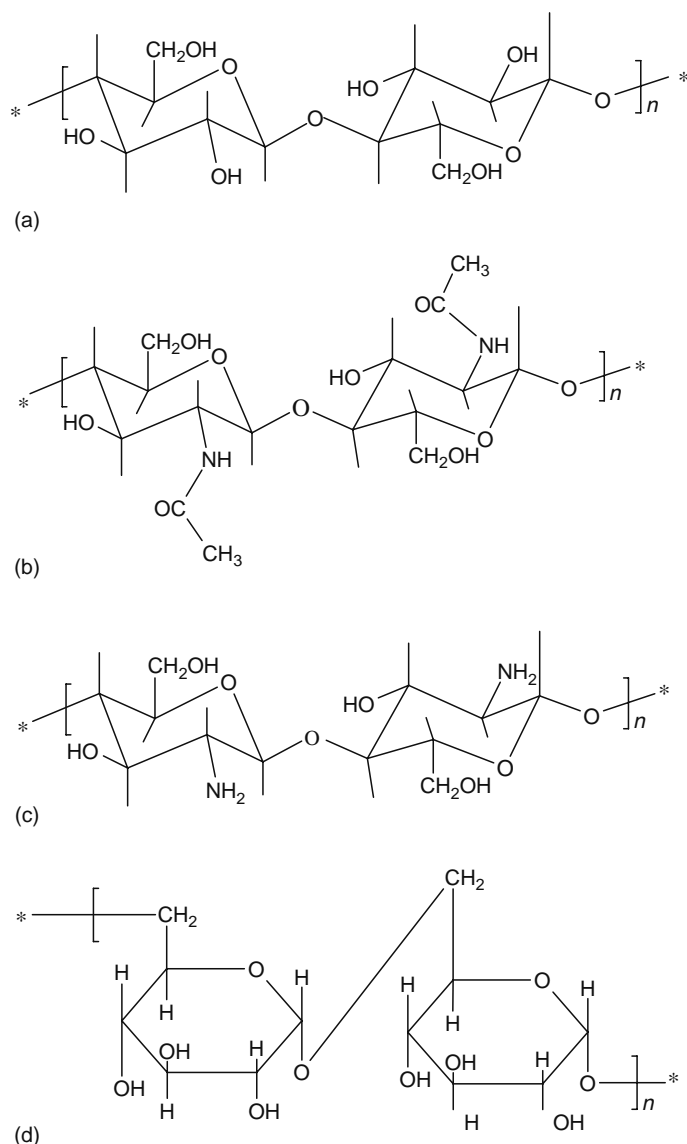


FIGURE 3.3 Structure of polysaccharides (a) cellulose, (b) chitin, (c) chitosan, and (d) dextran.

The commercially available cellulose is generally cross-linked with a bifunctional reagent such as epichlorohydrin and is remarkably stable to chemical attack. The glycosidic linkage is susceptible to acid hydrolysis, which under extreme conditions can yield almost quantitative amounts of pure crystalline D-glucose. Oxidizing agents such as sodium periodate can generate aldehyde groups and carboxyl groups.

Native cellulose imbibes only 30%–40% water compared with agarose that can hold 8–16 times its weight of water. The limited cellulose swelling results in a small available pore surface and unfortunately is associated with relatively small pores. This makes the number of applications of native cellulose in membrane chromatography quite low. Special procedures are necessary to produce cellulose disks, films, or other formats, which permit diffusion of large proteins into the structure. Nevertheless, several methods for the preparation of stable macroporous cellulose membrane as well as composite cellulose membranes were proposed in the literature [23–31]. The new types of cellulose microfiltration membranes (based mainly on regenerated cellulose, hydroxyethyl cellulose [HEC], and cellulose acetate) are characterized by high levels of water imbibition and by much larger pore sizes. Additionally, they present hydrophilic surfaces hence a low nonspecific adsorption and abundant functional groups.

Guo et al. [23] prepared epoxypropane chloride cross-linked macroporous cellulose affinity membranes with triazine dyes ligands. These membranes consist of coarse fibers with high porosity and large pores but with a less uniform morphology. The preparation of diethylaminoethyl-derivatized cellulose membranes with high protein loading was reported by Gerstner et al. [25]. The membranes were used for preparative-scale separation of cytochrome, lysozyme, and  $\alpha$ -chymotrypsinogen. Chen et al. [26] prepared a modified cellulosic microfiltration membrane by blending cellulose acetate with polyethyleneimine followed by cross-linking with polyisocyanate. These membranes were investigated in affinity processes for metal chelating, removal of endotoxins, or ion-exchange separations. Composite membranes of cellulose with grafted acrylic polymers [27,28] or blends of polyethersulfone and polyethylene oxide coated on all surface with a covalently bound layer of HEC were also prepared [29,30]. Yang et al. [31] prepared composite cellulose membranes containing epoxide functional groups via grafting polymerization of glycidyl methacrylate to dispersed cellulosic fibers. The obtained membranes possess high porosity and good flow characteristics and could be further modified for affinity ligand coupling.

Cellulose-based monoliths prepared from cross-linked sponge-like regenerated cellulose with a continuous, interconnected, open pore structure (50–300  $\mu\text{m}$ ) are commercialized by Sepragen under the trade name Seprasorb and are available for ion-exchange chromatography.

Chitin and its deacetylated product Chitosan are good biological materials due to their easy availability, hydrophilicity, biocompatibility, and chemical reactivity. They can be obtained on a large scale from the outer shells of crustaceans and have numerous potential applications in biomedicine, biochemistry as well in pharmaceutical or chemical industries. Both have a structure similar to that of cellulose, possess a large number of reactive groups ( $\text{CH}_2\text{OH}$  in chitin and chitosan, or the more reactive  $\text{NH}_2$  in chitosan, Figure 3.3b and 3.3c), and can be easily modified to meet various needs. Chitin is usually insoluble in acid and basic solutions as well as in common organic solvents. Therefore, preparation of macroporous chitin membranes by the usual phase inversion method is difficult. However, acetylated chitin membranes with good chemical and mechanical properties were prepared by acetylation of chitosan macroporous membranes [32].

Chitosan is, on the other hand, soluble in acidic solutions and has an excellent film-forming ability. Microporous chitosan membranes were prepared by phase inversion method and subsequently coupled with various types of ligands to generate chitosan affinity membranes [32–34]. Zeng et al. [32] prepared macroporous chitosan membranes using silica particles, which in contrast with chitosan, are insoluble in acidic solutions and soluble in basic ones. A dope solution of acidic aqueous chitosan and silica particles was poured on a glass plate after which the water was evaporated. The dried formed films were immersed into an aqueous NaOH solution under heat conditions to dissolve the silica particles. The obtained macroporous membranes were reported to have controlled porosity and pore sizes, and good mechanical strength. To prevent dissolution in acidic media, the chitosan membranes can be cross-linked with epichlorohydrin or ethylene glycoldiglycidyl ether (EGDGE).

Due to its good properties chitosan was also employed in preparing composite membranes. Klein et al. [35] reported the preparation of chitosan-coated sulfonated poly(ethersulfone) membranes as affinity chromatographic supports. Through the use of the charge attraction, the chitosan is localized at the fiber surface and subsequently cross-linked in situ with EGDGE, which also supplies new reactive groups. These coatings are not covalently linked to the supporting fiber, but rely on the insolubility of the cross-linked coating for stability. The hydroxyl and amino glucose repeated units can be further modified to bind the affinity ligand.

Dextran, a linear water-soluble polysaccharide composed of more than 90% 1,6-linked  $\alpha$ -D-glucose (Figure 3.3d), is produced by fermentation of sucrose by microorganisms of the genus *Leuconostoc*.

The soluble linear dextran chains are cross-linked with epichlorohydrin in alkaline solution to yield a three-dimensional gel, which solidifies exothermically. The commercially available dextran gels (Sephadex) are very stable to chemical attack and can be heated up to 110°C in an autoclave for 40 min without impairment of properties. The gels swell to some extent in ethanol, ethylene glycol, formamide, *N,N*-dimethylformamide (DMF), and dimethylsulfoxide (DMSO).

Dextran is mainly used as a coating material on available microfiltration membranes. Breifs and Kula [36] reported the use of dextran-coated nylon membranes as affinity media. The ligand was first coupled with dextran (both by adsorption and

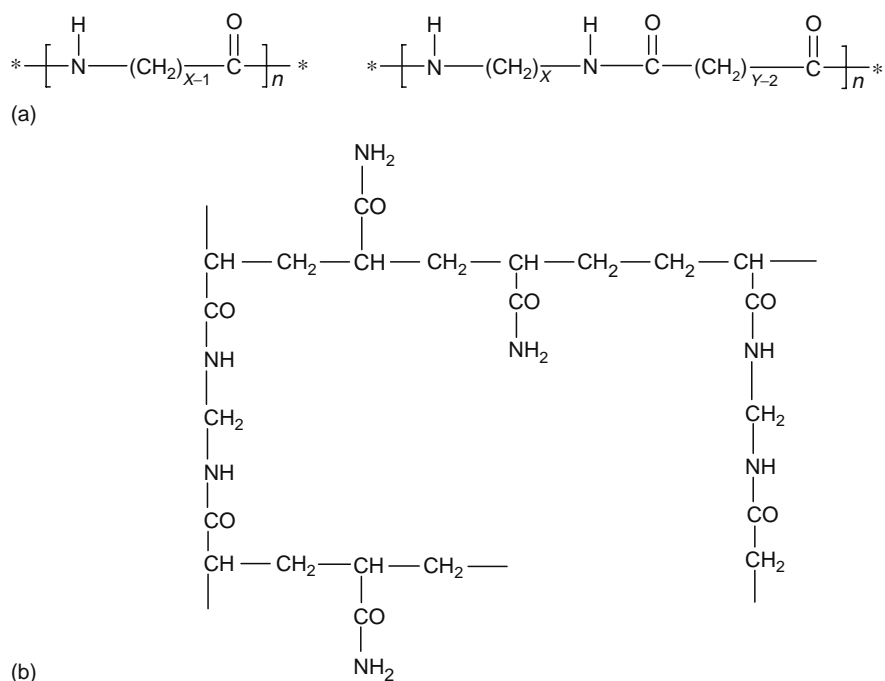


**FIGURE 3.4** Structure of (a) aliphatic polyamides (nylon- $x$  and nylon- $x$ - $y$ ) and (b) polyacrylamide.

covalent reactions), followed by attachment of the ligand-coupled dextran to the inner porous surface of a trichloro-triazine activated nylon membrane. Tang et al. [37] also prepared dextran-coated nylon membranes as glucose-sensitive hydrogel membranes. They used a polymer produced by cross-linking of two dextrans with different molecular weights. The smaller dextran was functionalized with covalently grafted concavaleine A (conA). This material was mixed with a larger, non-functionalized dextran, allowing easy control of the overall amount of grafted conA in the material. The mixture was cast on a porous nylon support, which provides mechanical strength, between two glass plates using spacers to give the required total membrane thickness.

Polyamides are synthetic amides in which recurring amide groups ( $\text{---NHCO---}$ ) are an integral part of the main polymer chain. A large number of polyamide types, both aliphatic and aromatic, with very different properties are commercially available. The schematic structure of the basic aliphatic polyamides referred to as nylons is presented in Figure 3.4a. Aromatic polyamides are good membrane materials because of their outstanding mechanical, thermal, and chemical stability but aliphatic polyamides such as nylon-6, nylon-6-6, or nylon-4-6 are of greater interest as microfiltration membranes.

Nylon is known to be resistant to a large number of organic solvents, partly because of its crystalline nature. It is also highly resistant to aliphatic and aromatic hydrocarbons as well as to some linear alcohols and aprotic liquids such as  $n$ -methylpyrrolidone or dimethylformamide. However, nylon membranes only have a low concentration of terminal amino groups to serve as functional groups for ligands coupling. They also present a high nonspecific adsorption of biomolecules during affinity separation processes. Therefore, hydrolysis of nylon membranes is necessary to both increase the active groups and prevent electrostatic interaction with proteins.

Although the hydrophobic surface of nylon membranes may be improved by hydrolysis or chemical modification, composite polyamide membranes are preferred in chromatographic applications. Klein et al. [38] prepared polyamide microporous membranes by modification of terminal amino groups. The density of activation sites for ligand coupling is increased by covalent binding of a polyhydroxyl-containing material to the polyamide membrane by reaction with the activated terminal groups. Composite nylon membranes prepared by coating of HEC on microfiltration polyamide membranes were also reported by Beeskow et al. [39]. HEC was immobilized on the pre-activated nylon membrane surface via amino end-groups or amide groups in the nylon chain. Subsequently the HEC hydroxyl groups were activated with epichlorhydrin or bioxirane to bind specific ligands suitable for affinity chromatography.

The neutral hydrophilic polyacrylamides are entirely gels formed by copolymerization of acrylamide ( $\text{CH}_2=\text{CH---CONH}_2$ ) with the bifunctional cross-linking agent,  $N,N'$ -methylene-bis-acrylamide ( $\text{CH}_2=\text{CH---CONHCH}_2\text{NHCO---CH}=\text{CH}_2$ ) (Figure 3.4b).

The ratio and concentration of acrylamide to that of the cross-linking agent in the reaction mixture can be varied to give an infinite series of insoluble covalently bonded gel products that differ in their average pore size. The polyacrylamide gels are chemically stable in dilute solutions of salts, detergents, guanidine-HCl, urea, and most organic solvents. They are nevertheless

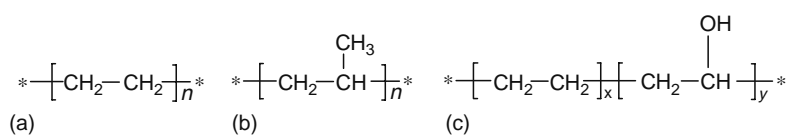


**FIGURE 3.5** Structure of (a) polyethylene, (b) polypropylene, and (c) polyvinyl alcohol-*co*-ethylene (EVAL).

hydrolyzed at extreme pH or by nitrous acid to yield carboxyl functions. The gels are biologically inert and generally are not subject to enzymatic digestion or metabolism by microorganisms.

The principal advantage of polyacrylamide in chromatographic processes is polyacrylamide possesses an abundant supply of modifiable groups, which allows the covalent attachment of a variety of ligands. The use of polyacrylamide carriers for affinity separations has nevertheless been limited. Principally this appears to be the result of the low degree of porosity of the beads currently available and to the shrinkage observed during the chemical modifications required for attachment of the ligand. However, Gupta and Anjum [40] prepared ion-exchange polyethylene-*g*-polyacrylamide membranes via graft polymerization of acrylamide onto polyethylene films using a pre-irradiation method. The alkaline hydrolysis of radiation-grafted polyethylene-*g*-polyacrylamide films transformed the amide groups into carboxyl groups, resulting in membranes with good binding capacity for mercury ions.

Composite membranes of cellulose and acrylamide polymer are also produced by Cuno Life, Meriden, USA. The Zeta Plus H series of filter cartridge employs two layers of graded-density filter media, the upstream layer consisting of a more open structure compared to the downstream layer. This allows the upstream layer to essentially act as prefilter, retaining large particles, yeast, and colloids, while the tighter downstream layer removes remaining microorganisms and haze components.

Hjerten and his research group [41] introduced monolithic columns based on acrylamides as chromatographic separation media in the late 1980s. Xie et al. [42] prepared rigid porous polyacrylamide-*co*-butylmethacrylate-*co*-*N,N'*-methylene-bis-acrylamide monolithic column for hydrophobic interaction chromatography. They also prepared polyacrylamide-*co*-*N,N'*-methylene-bis-acrylamide monolithic rods and studied the effect of polymerization conditions on rods' morphology.

Polypropylene, polyethylene, and its copolymers, including polyvinyl alcohol-*co*-ethylene (EVAL) and polyethylene-*co*-maleic anhydride, are often reported in the literature as affinity supports for different ligand chemistries (Figure 3.5). Bare polyethylene and polypropylene membranes have good thermal, mechanical, and chemical resistance but are inert and show a too high nonspecific adsorption of biomolecules. Therefore, an additional surface modification step is necessary to introduce various functional groups and to decrease the surface hydrophobicity. Microporous polyethylene and polypropylene membranes were grafted with various monomers, containing ion-exchange groups ( $-\text{NH}_2$ ,  $-\text{SO}_3\text{H}$ ,  $-\text{COOH}$ ), such as sodium styrenesulfonates, vinyl acetate, hydroxyethyl methacrylate, or glycidyl methacrylates, to acquire active epoxide groups. The latest membranes can be further modified with ion exchange, metal chelate (iminodiacetate), or hydrophobic groups (butyl, phenyl, phenylalanine, or tryptophan) [43–46]. Kim et al. [43,47] reported the preparation of polyethylene microfiltration hollow fibers grafted with glycidyl-methacrylate, hydroxyethyl-methacrylate, or vinyl acetate followed by coupling of affinity ligands. The nonselective protein adsorption of the obtained membranes was obviously diminished while maintaining water permeability. Using radiation-induced graft polymerization of acrylic acid and glycidyl-methacrylate, Kiyohara et al. [48] carried out surface modification of porous polyethylene membranes to introduce succinimide and epoxy groups into the hollow fibers. The resulting membranes showed higher permeabilities and lower nonspecific protein adsorption.

Poly(vinyl alcohol-*co*-ethylene) is derived from copolymers of vinylacetate and ethylene by hydrolysis of the acetyl function of the ester comonomer. EVAL is a random copolymer carrying hydrophilic (vinyl alcohol) and hydrophobic (ethylene) segments in a single molecule (Figure 3.5c). It is insoluble in water and combines a good wet strength with hydrophilicity. EVAL shows good membrane characteristics for use in various kinds of blood purification devices, including hemodialyzer and plasma separation. The membrane properties are closely associated with the ratio of composition of hydrophilic groups to hydrophobic groups of poly(vinyl alcohol-*co*-ethylene). The polymer whose ethylene content is about 30% (molar) is nowadays involved in medical applications.

Commercial EVAL hollow fiber membranes prepared via the copolymerization of ethylene and vinyl alcohol have been recently explored for protein immobilization. L-histidine has been coupled onto EVAL-fibers activated with epichlorhydrin or butanediol diglycidyl ether to prepare an affinity support for immunoglobulin G (IgG) purification [49]. Furthermore, histidine-immobilized hollow fiber membranes have been employed for endotoxin removal from solutions of snake antivenom serum [50]. Avramescu et al. [51] prepared EVAL microfiltration membranes from the quaternary water/1-octanol/DMSO/EVAL system, using 1-octanol as non-solvent additive in the casting solution. To couple the affinity ligand, surface functionalization reactions in aqueous and organic media (via glutaraldehyde, oxiran, trichloro-*s*-triazine, and sulfonyl chloride reactions) as well as surface activation by a low-pressure glow discharge treatment, were performed. They also prepared EVAL porous membrane adsorbers with various ion-exchange particles incorporated into the matrix by an immersion phase separation process [52]. The prepared particle-loaded EVAL membranes were employed in protein recovery, as a protein concentration medium for the separation of similar-sized proteins with different isoelectric points and as adsorptive devices for endotoxin removal.

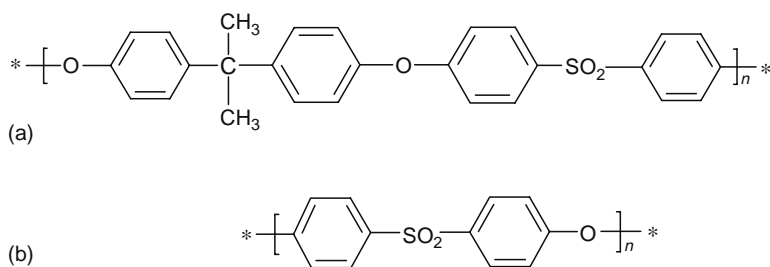


FIGURE 3.6 Structure of (a) polysulfone and (b) polyethersulfone.

Polysulfone and its derivatives mainly polyethersulfone (Figure 3.6) are suitable membrane materials because of their good film-forming properties and high thermal, chemical, and biological resistance. However, their strong hydrophobicity and nonwettability are usually undesirable in membrane chromatography.

Various methods to improve the characteristics of polysulfone membrane include preparation of copolymers with desired functionality, blending with hydrophilic polymers, surface coating, or introduction of hydrophilic groups into the polymer backbone. Klein et al. [29] modified microporous polysulfone membranes by reacting terminal phenol groups with EGDGE to produce terminal epoxy groups. These were used to covalently link HEC polymers to the membrane surface. Further epoxidation of the HEC and reaction with hexanediamine produced amine-terminated leashes on the microporous membrane. Heterogeneous polysulfone affinity flat filter membranes having chelating groups for  $\text{Hg}^{2+}$  were prepared by Wang et al. [53] via phase separation, using blends of chelating resin and polysulfone as membrane materials, *N,N*-dimethylacetamide as solvent, and water as extraction solvent. Higuchi et al. [54,55] modified the PSf fiber surface with propane sulfone and  $\text{SnCl}_4$  as catalyst obtaining membranes with low nonspecific protein adsorption. They also prepared PSf hollow fiber membranes containing hydroxide groups by a single-step reaction with propylene oxide and Friedel–Crafts catalyst.

Other polymeric materials (Figure 3.7) including polystyrene, polyvinylchloride (PVC), polytetrafluoroethylene (PTFE), polyvinylidene difluoride (PVDF), polyacrylonitrile (PAN), polycarbonates, polyacrylates and polymethacrylates, polyetherurethane, as well as various inorganic materials have been used as chromatographic supports.

Polystyrene and its derivatives (mainly chloromethylstyrene) are widely used in chromatography to prepare monolithic rods frequently using divinylbenzene (DVB) as cross-linker [20,21,56]. Polystyrene-*co*-divinylbenzene polymers possess good chemical and biological stability and due to their highly hydrophobic character can be used as reversed phases in chromatographic applications. Hydrophilic monolithic rods based on polystyrene have been also prepared by modification of 4-chloromethylstyrene with ethylenediamine followed by a  $\gamma$ -gluconolactone reaction, which provides the necessary degree of hydrophilicity [57].

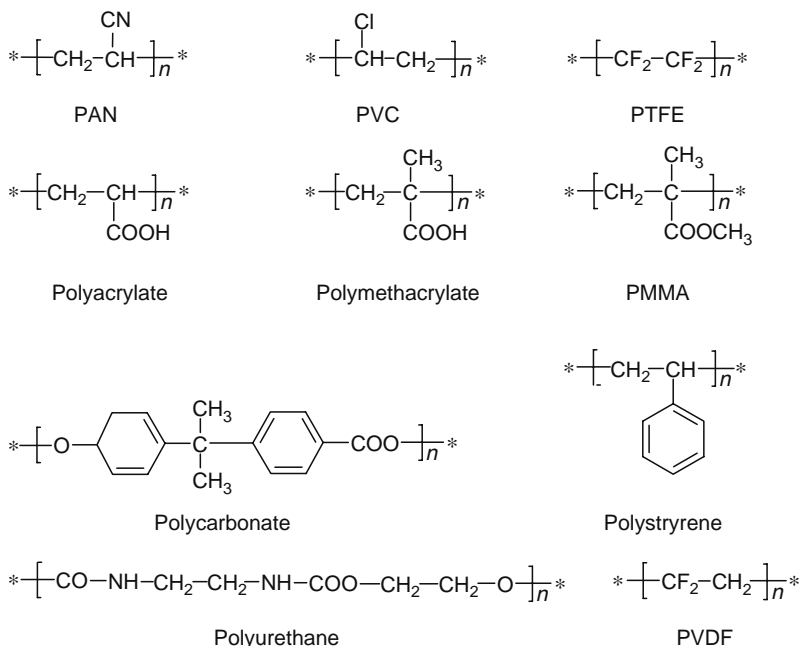


FIGURE 3.7 Structure of other polymers used in membrane preparation.

Acrylate- and methacrylate-based polymers are stable under extreme pH conditions, which cannot be tolerated by typical chromatographic packing materials, and can be easily functionalized using glycidyl methacrylates. Poly(glycidyl methacrylate-*co*-ethylene dimethacrylate) is the most frequently used material in the preparation of monolithic rod. Thin discs of macroporous poly(GMA-*co*-EDMA) have been synthesized by azo-bis-isobutyronitrile-initiated free-radical polymerization of a mixture of monovinyl and divinyl monomers in the presence of a porogenic agent [58–59]. The preparation route leads to controlled porous media with good mechanical strength and high density epoxy active groups, which provide reactive sites for further ligand coupling.

Porous affinity membranes based on hydrolyzed poly(GMA-*co*-EDMA) grafted with glycidyl methacrylates oligomers were also reported [2,60]. Tennikova et al. [2] prepared functionalized macroporous poly(GMA-*co*-EDMA) membranes by reaction with propane sulfone, diethylamine, or water, leading to the formation of corresponding sulfonic acid, diethylamino or diol-derivatized stationary chromatographic phases. Unfortunately, the poly(GMA-*co*-EDMA) membranes are mechanically weak and due to their hydrophobic character may cause nonspecific adsorption of proteins.

Hydrophilic microporous polyvinyl chloride membranes activated with glutaraldehyde or treated with polyvinyl imine (Acti-Disks) are produced by FMC Bioproducts. PVC membranes with embedded fibrous cellulose derivatives or functionalized silica beads were developed by Manganaro et al. [61]. A mixture of PVC powder, cyclohexane (as porogen), particulate materials, and water (as swelling agent) was cast into a sheet form. The solvent was extracted with hot water resulting in membranes with rigid structure, good chemical resistance, and low nonspecific adsorption.

Polytetrafluoroethylene (PTFE) microporous composite membranes were prepared in a similar way [62] using silica derivatives and ion exchange or iminodiacetate-cellulose resins embedded in the PTFE matrix and is used mainly for protein separation and water purification.

Dalven et al. [63] prepared various membranes with pore sizes ranging from 60 to 180 nm, using different copolymers of acrylonitrile and a vinyl comonomer containing arylamine, pyridine, or an aliphatic hydroxyl group. The obtained membranes proved to be suitable for protein immobilization, although various copolymers differed with respect to the weight loading of protein upon a membrane. Maximal protein loading was observed routinely with acrylonitrile-*m* aminostyrene membranes. Godjevargova et al. [64] surface-modified poly(acrylonitrile-methylmethacrylate-sodium vinylsulphonate) membranes with sodium hydroxide and hexamethylenediamine, hydroxylamine, and hydrazine dihydrochloride to introduce amino groups onto the porous surface. The membranes prepared from the modified copolymer possess the same porosity as the membranes of unmodified acrylonitrile copolymer. Glucose oxidase was immobilized on the hydroxylamine modified membranes, combining high activity with good thermal and storage stability.

Microporous polyetherurethane-urea membranes were prepared from DMAc and methylethylketone solutions by electrostatic spinning method [65]. The membranes were functionalized using isocyanate agents and further activated with succinimide, diimidazole, or sulfonyl reactions. Early attempts to prepare monolithic stationary phases involved open-pore polyurethane foams [66,67]. These monoliths possess not only good permeabilities but also high swelling ratios in different solvent classes, which made them inapplicable in large-scale chromatographic processes.

Hydrophilic polyvinylidene difluoride (PVDF) membranes prepared by a strong basic treatment of hydrophobic PVDF supports followed by grafting of glycine molecules onto their surface [68] showed good properties for downstream protein purification and immunoassays [69,70]. Activated acrylate coated microporous PVDF membranes (Immobilon) are also commercially available from Millipore.

Inorganic supports (including glass materials, ceramic, metallic, or zeolitic membranes) offer, when used in chromatographic separation processes, the advantage of high mechanical strength, regenerability, resistance to solvents, and microbial attack. The inorganic materials, such as alumina, bentonite, glass, nickel oxide, silica, and magnetic iron oxide powders, do not change the structure over wide temperature, pH, or pressure. Nevertheless, in operation processes their compressibility and resulting pressure drop increase that is a major obstacle for large-scale applications. Li and Spencer [71] prepared alkali-stable ion-exchange titanium dioxide membranes coated with polyethyleneimine (PEI). PEI ion paired with the oxide support was subsequently cross-linked with glutaraldehyde to form reactive films to which the affinity ligands can be coupled. The preparation of immobilized metal-chelate affinity membranes using glass hollow-fiber membranes as substrate was reported by Serafica et al. [72]. The microporous glass membranes were activated with glycidoxypropyl trimethyl silane to generate epoxide groups, to which iminodiacetate was coupled. The authors compared protein adsorption behavior on the prepared membranes with results from a mathematical model.

Despite the fact that the first silica monolithic supports have been already reported in the late 1970s, the first uniform porous silica rods used for reverse-phase chromatography were introduced in 1996 by Minakuchi et al. [73]. They were produced according to a solgel approach consisting of hydrolytic polycondensation of alkoxy silane in water in the presence of a water-soluble organic polymer and acetic acid as catalyst. The prepared rods possess 1–2  $\mu\text{m}$  size through-pores and 5–25  $\mu\text{m}$  mesopore size and can further be octadecylsilylated to give the  $\text{C}_{18}$  reverse phase. A second method for preparation of silica monoliths, similar to the one used to cast column end frits in fused-silica tubing for HPLC, was reported by Fields [74]. Although the method leads to continuous silica xerogels, the obtained materials possess heterogeneous morphologies.

### 3.4 ADSORPTIVE MEMBRANES PREPARATION

Many publications of the last decades reported the preparation, characterization, and performances of various types of adsorptive membrane. Ion exchange, affinity, reverse phase, or hydrophobic interaction membrane chromatography have been described. In the following, various methods involved in the preparation of different classes of adsorbers will be discussed.

#### 3.4.1 MEMBRANE PREPARATION IN AFFINITY CHROMATOGRAPHY

Since chromatographic membranes consist of a substrate to which the interactive ligand is coupled, three main steps are usually involved in their preparation: (i) basic membrane preparation; (ii) functionalization (activation) of the basic membranes; and (iii) spacer arms and ligand molecules coupling on the activated porous membrane surface [9]. The preparation of basic materials is essential for the performances of the separation process.

##### 3.4.1.1 Basic Membrane Preparation

Most of the available commercial microporous membranes such as polysulfone, polyethersulfone, polyamide, cellulose, polyethylene, polypropylene, and polyvinylidene difluoride are prepared by phase inversion processes. The concept of phase inversion in membrane formation was introduced by Kesting [75] and can be defined as follows: a homogeneous polymer solution is transformed into a two-phase system in which a solidified polymer-rich phase forms the continuous membrane matrix and the polymer lean phase fills the pores. A detailed description of the phase inversion process is beyond the scope of this section as it was widely discussed in Chapters 1 and 2; nevertheless a short introduction of this process will be presented.

A homogenous polymer solution is cast as thin film and subsequently immersed into a non-solvent bath. The diffusional exchange of solvent and non-solvent brings the film solution into an instable state resulting in phase separation, either by liquid-liquid ( $l-l$ ) or by solid-liquid ( $s-l$ ) demixing, depending on the type of polymer and the precipitation conditions employed [76,77]. The following phase inversion processes can be distinguished: (i) precipitation from the vapor phase; (ii) precipitation by controlled evaporation; (iii) thermal precipitation; and (iv) immersion precipitation.

For amorphous polymer systems, liquid-liquid phase separation occurs by nucleation and growth of the polymer-lean phase when the film composition enters locally the metastable region between the binodal and the spinodal (unstable with respect to  $l-l$  demixing). The unstable polymer solution falls apart in a polymer-rich and a polymer-poor phase. The polymer-rich phase will form the matrix where the polymer-lean phase will form the pores. [78]. The (partial) phase inversion process performed can result in a variety of different cellular morphologies including open and closed sponge or finger-like pores. The (cellular) morphology depends strongly on the diffusion kinetics and thus on the rate of transfer of solvent and non-solvent [79,80]. For semicrystalline polymer systems, delayed conditions suppress  $l-l$  demixing and thus favors  $s-l$  demixing by allowing crystallization to take place.

Ternary mass transfer models have been used to calculate the diffusion trajectories and the (polymer) concentration profiles within the film in the first stages of immersion [81–84]. Generally, two types of demixing are distinguished, namely *instantaneous* and *delayed* demixing with respect to  $l-l$  phase separation. Instantaneous  $l-l$  demixing occurs when the composition of the film falls immediately after immersion within the binodal envelope. This is normally the case when a (strong) non-solvent with a high affinity to the solvent is used in the coagulation bath (Figure 3.8a). The corresponding polymer concentration profile shows a steep increase near the film/bath interface leading to asymmetric open cellular membranes (Figure 3.8c) with typically a thin dense top layer (skin) and possibly macrovoids in the porous support layer [77,81].

If the demixing is delayed, compositional changes in the film will not be disrupted by phase separation. Desolvation can thus proceed for a longer time without triggering demixing (Figure 3.8b) resulting mainly in higher polymer concentration throughout the polymeric film. In this case, the polymer concentration profile within the film becomes less steep and more symmetric structures are obtained. Delayed demixing conditions generally suppress macrovoid formation and lead for amorphous polymer systems to the formation of a thick dense top layer (Figure 3.8d). Additional morphological fine-tuning has been performed by adjusting the temperature of the precipitation bath or by addition of a fourth component to the casting solution [82–84]. For microfiltration processes, the resulting membrane morphologies are far more regular and show higher permeabilities while retaining the required retention properties.

##### 3.4.1.2 Basic Membrane Modification

Most commercial microporous membranes are hydrophobic and relatively inert. If the selected basic membrane does not possess the functional groups necessary for spacers arms and ligand coupling, it can be activated to acquire reactive groups such as hydroxyl, carboxyl, halogen, or amine groups using similar methods as for particulate materials. The major methods employed to modify the porous membranes (some of them already mentioned) are based on

- *Coating Technique:* This technique usually deposits a hydrophilic layer such as HEC, polyvinyl alcohol, chitosan, polyacrolein, and polyethylenimine on a hydrophobic one [13,71,85,86]. The coating layers prepared are, however,

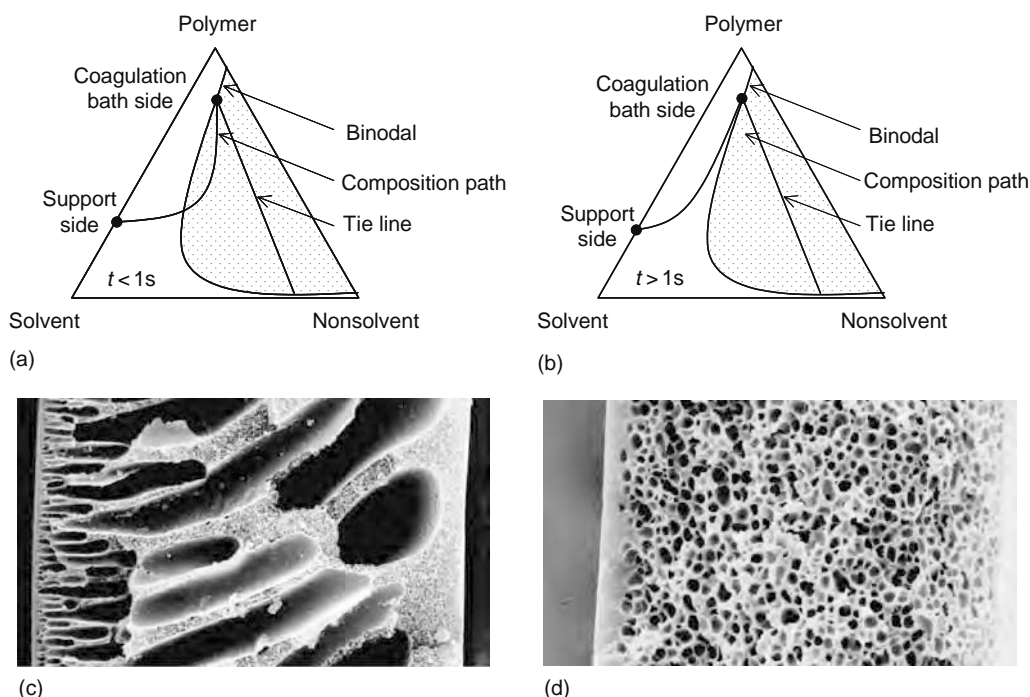


**FIGURE 3.8** Schematic representation of the composition path of the cast film immediately after immersion in the coagulation bath for (a) instantaneous and (b) delayed demixing systems, and the scanning electron microscope (SEM) picture of the resulting membranes (c) and (d).

not durable and stable and can be easily leached out. To overcome this drawback, the membranes (polyvinylidene fluoride, polyethersulfone polytetrafluoroethylene, polycarbonate, nylon, etc.) are coated with a mixture containing a functional monomer (hydroxyalkyl acrylate or methacrylate), a polymerization initiator (ammonium or potassium persulfate), and a cross-linking agent (difunctional acrylates, methacrylates, or acrylamides) and are exposed to radical polymerization initiated by heating UV or  $\gamma$ -radiation [72].

- *Grafting Polymerization*: A technique suitable for hydrophobic and inert microporous membranes such as polyethylene and polypropylene. The membranes can be grafted with monomers like sodium styrenesulfonates, vinyl acetate, 2-hydroxyethyl methacrylate to introduce various ion-exchange groups ( $-\text{NH}_2$ ,  $-\text{SO}_3\text{H}$ ,  $-\text{COOH}$ ) or with glycidyl methacrylate to acquire reactive epoxide groups that can be further modified with ionic-exchange groups, metal chelate groups, or hydrophobic groups (phenyl, butyl, phenylalanine, tryptophan) [45,87,88].
- *In Situ Copolymerization*: In situ copolymerization of two different monomers is often used for single step preparation of mechanical stable microporous membranes with functional groups. One of the monomers, such as vinylpyridine, acrylamide, vinyl alcohol, glycidyl methacrylate, and its derivative, serves as the core support material for functional groups. The second monomer (divinylbenzene, ethylene dimethacrylate, and methylene-bis-acrylamide) functions as a cross-linker and offers mechanical strength. Inorganic salts or organic solvents are usually used as porogen agents.
- *Other Methods*: Examples for other methods include co-casting of a hydrophobic and a hydrophilic polymer that contains amine, imine, hydroxyl, or carboxyl groups [61,89]; surface modification by oxidation with ozone or by exposure to an electron or ion-beam; ultrasonic etching; and UV or laser irradiation [90–92]. A variety of functional groups have been also introduced onto the membrane surfaces by applying the gas discharge techniques (plasma treatment) operated at low or ambient pressure [93,94].

However, the methods applied to obtain membranes with hydrophilic and chemically modifiable surfaces via physical or chemical posttreatment of hydrophobic membranes often result in unwanted and irreproducible inhomogeneities [95]. Thus the main limitation for supports in affinity separation presently encountered lies in the availability of membranes with functional groups suitable for ligand coupling. This imposes an increased need for the development of hydrophilic microfiltration membranes with suitable functionalizable groups.

### 3.4.2 PREPARATION OF MONOLITHIC STATIONARY PHASES

The monoliths are prepared both from organic (mainly based not only on polystyrene, acrylamides, acrylates, or methacrylates but also on imprinted polymers) and inorganic materials (based on silica, zirconia, titania, or aluminium oxide) as continuous

block interlaced with free dead-ends channels. They have similar advantages compared to membrane chromatography but their preparation differs from the classical membrane supports. The preparation of continuous beds can be generally divided in to: polymerization of an organic monomer in the presence of additives, formation of silica-based network via the so-called solgel process, and fusing the porous packing material inside the chromatographic column by a sintering process.

### 3.4.2.1 Preparation of Silica Monoliths

Until now few methods are reported for the preparation of silica monoliths. The extensively used solgel technology was introduced by Minakuchi et al. [73] and produced the first uniform porous silica column for reversed-phase chromatography. The method is based on hydrolytic polycondensation of alkoxy silicon derivatives (e.g., tetraethyl or tetramethyl orthosilicate) in aqueous media followed by phase separation in the presence of water-soluble organic polymers. The reaction occurs as follows: tetramethoxysilane (TMOS) is added to a polyethylene oxide (PEO) aqueous solution, in the presence of 0.01 N acetic acid as reaction catalyst. The resulting mixture is stirred at 0°C for 30 min and then poured into a polycarbonate mould where it is allowed to react at 40°C. Within 2 h of reaction the gelation occurs. The gelation process starts with polymer aggregation, followed by interpenetration of the formed clusters. Finally, the clusters link together to form the network. The gel is subsequently aged at the same temperature for a day to increase the stiffness and the strength of the silica network. The obtained silica rods are washed with water and aqueous ammonium hydroxide to adjust the mesopore structure and then cut to the desired length upon drying. The rods can be derivatized to C<sub>18</sub> phase by applying a toluene solution of octadecyldimethyl-(*N,N*-diethylamino)silane at 60°C, followed by trimethylsilylation with hexamethyldisilazane.

Several groups are nowadays involved in the preparation of silica monoliths using modified versions of the solgel technology proposed in 1996 by the Tanaka group. Research is carried out to improve the polycondensation starting material, different precursors such as TMOS, polyethoxydisiloxane, methyltriethoxysilane, aminopropyltriethoxysilane, 3-2-aminoethylaminopropyltriethoxysilane, or *N*-octyltriethoxysilane were investigated [96–100]. Numerous procedures concerning the reaction parameters are described in literature. It is commonly accepted that linear or randomly branched silica chains are formed under acid catalyses [101,102]. In contrast, under basic catalytic conditions a network of uniform particles with a large pore volume is formed [103,104]. The addition of additives such as polyethylene oxide or polyethylene glycol to the sol leads to the formation of silica monoliths of different morphologies and subsequently different properties [105,106].

Various aging, drying, and cladding steps are also presented in literature. Gel drying is a critical step in silica monoliths preparation, which can cause large gel shrinkage and cracking. Therefore, besides classical drying at room temperature (with or without solvent exchange), many drying methods including the replacement of alcohol by washing with liquid CO<sub>2</sub> and drying above the critical point, replacement of alcohol by water followed by washing with acetone and liquid CO<sub>2</sub>, and supercritical drying at 35°C and 8.5 MPa have been investigated [107,108]. Despite the efforts in finding the most suitable drying methods, gel shrinkage may cause void spaces between the formed silica network and the column wall. A way to avoid these problems is encasing the resulting silica gel into a polytetrafluoroethylene tubing compressed under external pressure. A good review paper on the preparation of silica gel-based monoliths via solgel method has been recently published [109].

Another approach for the preparation of silica-based continuous beds belongs to Fields [74]. He synthesized a porous chromatographic support inside a silica tube by the following procedure: a fused silica column is filled with a 10 wt% solution of formamide in potassium silicate and placed in a 100°C gas chromatograph oven for 1 h. The column is then washed with water, 50/50 water/methanol, methanol, and tetrahydrofuran and purged with dry helium for 24 h at 120°C. Subsequently, the mixture is reacted with 10% dimethyloctadecylchlorosilane (ODS) in dry toluene for 5 h [110,111]. The morphology of the material was clearly inhomogeneous with a distribution of the mean pore diameter ranging from ~0.2 to ~3 μm. Nevertheless the prepared monoliths were used for separation of alkylbenzenes and polypeptides in reverse-phase chromatography with reasonable efficiency.

Embedding particulate material within a porous matrix may decrease the shrinking and cracking of the solgel prepared monoliths resulting in increased separation efficiency. Dulay et al. [112] produced particle-loaded monoliths by heating a tube filled with a mixture of TEOS and ODS particles in ethanol. Preparation of monoliths with entrapped silicate particles (coated with ODS or *L*-dansylphenylalanine imprinted polymers) was reported by Chirica and Remcho [113], resulting in faster and more efficient chromatographic media.

### 3.4.2.2 Preparation of Organic Polymer Monoliths

The preparation of polymeric monoliths is relatively simple compared with those of the silica rods. A polymerization mixture consisting of monomer, cross-linker, initiator, and porogenic solvent is introduced into a sealed tube. The reaction can be temperature or redox initiated and in the case of transparent molds UV light can also be used to trigger the polymerization. At the end of the reaction the seals are removed and the tubes are attached to a pump, which flushes solvent through the monolith to remove the porogens and the unreacted components. The obtained monolith can be radial or axial compressed to prevent the formation of voids and further functionalized for different chromatographic modes. The majority of current monolithic supports

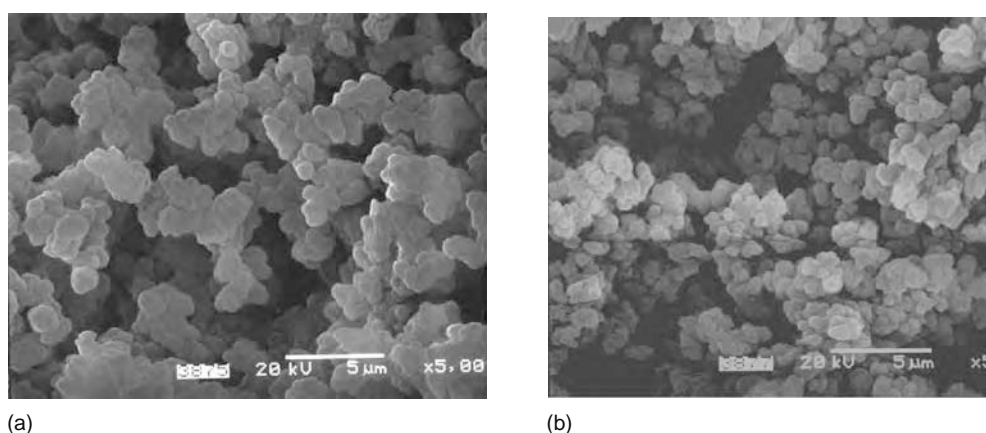


**FIGURE 3.9** SEM picture of monoliths prepared from (a) polystyrene-divinylbenzene and (b) methylmethacrylate. (Courtesy BIA Separations, Ljubljana, Slovenia.)

used in chromatographic processes recently reviewed in Refs. [56,114–116] are based on polystyrene-divinylbenzene, polyacrylamides, polyacrylates, and polymethacrylates (Figure 3.9a). The reader should realize that there is a very large class of monomers with different functionalities, which can be used in the preparation of continuous beds. Multifunctional oligomers or polymers including derivatives of cyclodextrins and proteins (acting simultaneous as cross-linkers and chiral selectors) have recently been used in monoliths preparation [117,118].

#### 3.4.2.2.1 Preparation of Polystyrene-Based Monoliths

The commonly used monomers in the preparation of polystyrene (PS)-based monolithic columns are styrene and 4-chloromethylstyrene while divinylbenzene (DVB) is usually the cross-linker. The PS-DVB continuous beds were introduced by Svec and Fréchet [119] in the early 1990 as protein separation media. They were prepared by free radical polymerization of styrene and divinylbenzene in the presence of dodecylalcohol as pore-forming agent and 2,2'-azo-bis-isobutyronitrile (AIBN) as initiator. The polymerization mixture was reacted inside the mold at 70°C for 24 h. Due to its highly hydrophobic nature, the prepared continuous bed can be directly used in reverse-phase or precipitation-redissolution chromatography [120,121]. To increase chromatographic interactions, the monolithic surface can be modified by including an alkylstyrene monomer in the polymerization mixture. The modification can also be achieved by introducing functional groups onto the polymeric surface after monolith formation using, for example, a strong Friedel–Craft catalyst (aluminium chloride) and an alkyl halide (chlorooctadecane) in nitrobenzene [114].

Hydrophilic polystyrene-based continuous beds bearing a hydrophilic surface on a hydrophobic polymeric support were prepared by a two-step modification of polychloromethylstyrene monolith first with ethylenediamine followed either by a reaction with  $\gamma$ -gluconolactone or with chloroacetic acid [57,122]. Activation could also be performed by grafting 4-vinyl-2,2-dimethylazactone onto the monolith porous surface [123].

#### 3.4.2.2.2 Preparation of Polyacrylamide Monoliths

Hjerten et al. [124] introduced the monolithic stationary phases based on acrylamides in the late 1980s. The cross-linked polyacrylamide can be directly synthesized within the mold by a one step free-radical chain polymerization. Acrylamide, methacrylamide, or piperazine diacrylamide are often employed as monomers, while *N,N'*-methylene-bis-acrylamide is used as a cross-linker. 2-acrylamido-2-methylpropane sulphonic acid, vinylsulphonic acid, butyl methacrylate, or stearyl methacrylate are usually added to the polymerization mixture to provide charge and functional groups [114].

Xie et al. [42] prepared rigid porous polyacrylamide-*co*-butylmethacrylate-*co*-*N,N'*-methylene-bis-acrylamide monolithic columns with controlled hydrophobicity for chromatographic separation of proteins. They also prepared porous hydrophilic polyacrylamide-*co*-*N,N'*-methylene-bis-acrylamide monolithic rods using alcohols with different carbon chain lengths (from methanol to decanol) as pore-forming agents [125].

#### 3.4.2.2.3 Preparation of Polymethacrylate-Based Monoliths

Continuous beds prepared from acrylates and methacrylates were introduced as chromatographic media in the early 1990s by Svec and Fréchet [126]. The polymerization mixture generally consists of a mixture of monomers including glycidyl methacrylate (GMA), diethyleneglycidyl methacrylate (DEGMA), 2-hydroxyethyl methacrylate, ethylene dimethacrylate (EDMA, which can also act as a cross-linker), and other methacrylate-esters, one or more porogenic solvent (such as methanol, propanol, cyclohexanol, isooctane, dodecanol, toluene, dioxane, acetone, or acetonitrile) and a radical initiator (usually AIBN) temperature or UV light activated. The monoliths morphology with well-defined bimodal pore size distribution (Figure 3.9b)

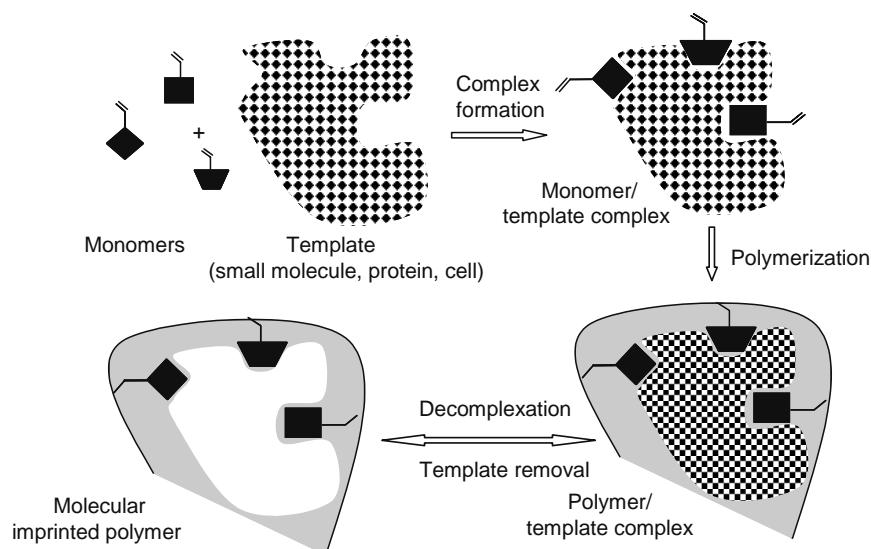


FIGURE 3.10 Principle of molecular imprinting technique.

can be adjusted by varying the percentage of cross-linking monomer, the type and quantity of porogenic agents as well as the ratio between the monomer and the porogen phase.

Poly(glycidyl methacrylate-*co*-ethylene dimethacrylate) is a material most often used in the preparation of monolithic rods, since it possesses reactive groups that allow for easy functionalization. Preparation of poly(GMA-*co*-EDMA)-based monoliths bearing functional amino groups via a diethylamine reaction was reported by Svec et al. [127]. Viklund et al. [128] reported a photo-initiated in situ polymerization method for the preparation of monolithic stationary phases containing sulfonic acid group by grafting poly(2-acrylamido-2-methyl-1-propanesulfonic acid) onto the internal surface of hydrolyzed poly(GMA-*co*-EDMA) monoliths. A  $^{60}\text{Co}$   $\gamma$ -radiation-induced copolymerization of DEGMA and GMA monomers using different porogenic agents (including alcohols, acetone, THF, and dioxane) was recently proposed by Grasselli et al. [129] to prepare monolithic columns with adjustable morphologies.

Although the preparation of continuous beds on a small scale is easy, the preparation of large-size monoliths is quite difficult. The unstirred nature of the polymerization within the mold leads to a low capacity to effectively dissipate the exothermic reaction heat. The appearance of radial temperature gradient across the reaction mixture also results in the formation of inhomogeneities in the pore structure of the obtained monolith. This is the reason why most of the work reported in the last decades focused on the application of small-size monoliths in chromatographic processes.

#### 3.4.2.2.4 Preparation of Monolithic Molecularly Imprinted Polymers

Molecular imprinting technique was recently used to prepare highly selective tailor-made synthetic affinity media used mainly in chromatographic resolution of racemates or artificial antibodies [130–133]. A complex between the template molecule and the functional monomer is first formed in solution by covalent or non-covalent interactions (Figure 3.10). Subsequently, the three-dimensional architecture of these complexes is confined by polymerization with a high concentration of cross-linker. The template molecules are then extracted from the polymer leaving behind complementary sites (both in shape and functionality) to the imprinted molecules. These sites can further rebind other print molecules.

Matsui et al. [134] first reported the preparation of molecularly imprinted monoliths based on functional monomer such as methacrylic acid or 2-trifluoromethyl-acrylic acid via in situ polymerization. The reaction mixture consisting of monomer, cross-linker (ethylene glycol dimethacrylate), porogenic solvents (cyclohexanol and 1-dodecanol), initiator, and template molecule was degassed and poured into a column where the polymerization took place. When the reaction was completed, the template molecule and the porogenic solvents were extracted with methanol and acetic acid resulting in monoliths with molecular recognition in the separation of positional isomers of diamionaphthalene and phenylalanine anilide enantiomers.

### 3.4.3 PREPARATION OF PARTICLE-LOADED MEMBRANES

Nowadays, methods are known for the preparation of porous polymeric supports comprising particulate material from an appropriate mixture of starting components. Such a material prepared by a casting process is limited in its three dimensional size by the housing it is cast into (Zip Tip, Millipore, Figure 3.11a and 3.11b) or is in the form of a sheet (Empore; Acti-Mod, FMC Bioproducts; Biorex, Bio-Rad) [16,17].

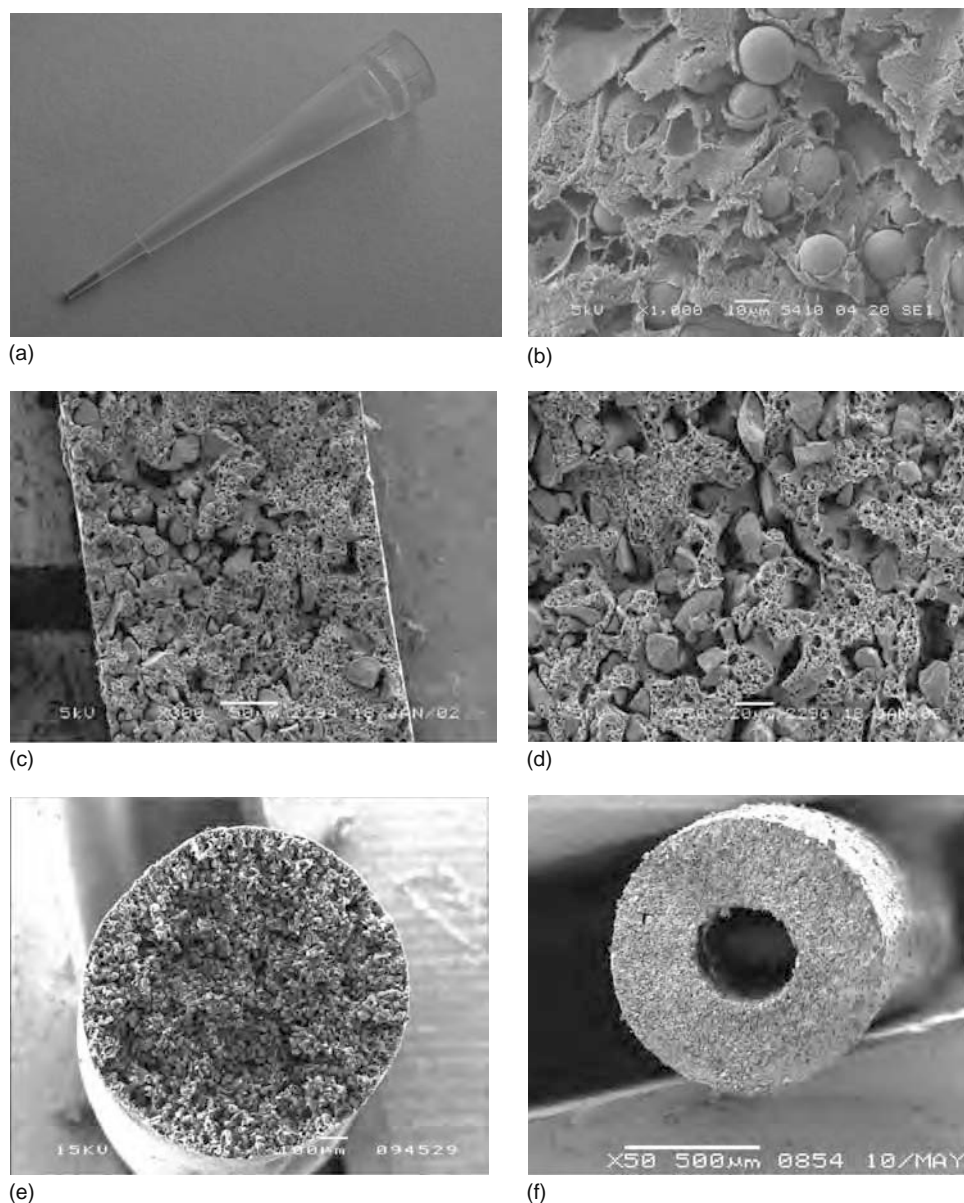


**FIGURE 3.11** Particle-loaded membrane adsorbers in different geometries (a) zip-tip millipore adsorber, (b) zip-tip adsorber, higher magnification, (c) flat membrane, (d) flat membrane, higher magnification, (e) full fiber, and (f) hollow fiber.

The available preparation routes for porous polymeric fibers with particulate material incorporated require an additional process steps to introduce the desired porosity [135]. After the preparation of the matrix comprising particulate material, either the particulate material is removed from the nonporous fiber or the nonporous fiber is stretched resulting in porous fibers. In the latter case, a microporous fiber comprising particles having a certain sorptive function can be obtained. Depending on the actual process steps needed to come to the final product, suitable starting materials with properties that can sustain the conditions of the additional process steps have to be selected. Obviously, such a requirement limits the type of polymeric material that can be used. Furthermore it puts limitations on the type of particulate material that can be comprised in the polymeric matrix. A very high degree of particle loading will reduce the mechanical strength of the mixed matrix and therefore restrict the stretching procedure. The force required to reach sufficient stretching of the matrix material limits the degree of loading. By stretching the particle comprising material the particulate material can drop out of the porous structure to be formed. In processes involving melt extrusion, only particulate material that can sustain temperatures required to melt the matrix polymer, usually above 200°C [18], can be applied.

Disadvantages of the known porous polymeric membrane preparation processes are that they involve additional process steps after the formation of the fiber to come to a final product. It is therefore desirable to have a more efficient preparation process. A new method to prepare structures of any geometry (Figure 3.11c through 3.11f) and large variety of functionality

was recently proposed [52]. The authors proposed to incorporate the functionality by dispersion of particles in a polymeric porous structure formed by phase inversion. A slurry of dissolved polymer and particulate material can be cast as a flat film or spun into a fiber and can then be solidified by a phase inversion process. This concept is nowadays commercialized by Mosaic Systems. The adsorber membranes prepared via this route contain particles tightly held together within a polymeric matrix of different shapes, which can be operated either in stack of microporous flat membranes or as a bundle of solid or hollow fiber membranes.

These membranes may also serve as a platform to which an end-user can couple the specific ligate needed. This has been recently pointed out by Klein [10] as one of the significant opportunities in membrane chromatography. The reader may note that the function of polymer binder is to be highly porous, having a high degree of pore interconnectivity as well as having a low-adsorption tendency toward the desired products. By choosing the particles and the binder one can establish various functions such as ion exchange, adsorption, catalysis, and hybrid such as reactive chromatography.

### 3.4.4 MEMBRANE ACTIVATION AND LIGAND COUPLING

The spacer arms and the affinity ligand molecules may be directly or indirectly linked to residual functional groups of the membrane by any procedure that retains the mechanical and hydraulic membrane properties while substantially retaining the binding activity of the affinity ligand. The monolithic stationary phases used in affinity chromatography are typically prepared by ligand immobilization onto the in situ polymerized support. Nevertheless, methods in which the ligand is attached to one of the comonomers were also reported [136]. In the following section, the reactions widely used for membrane activation and ligand coupling and extensively reviewed in recent literature are discussed separately for different types of functional groups containing polymers (Table 3.1).

1. Polymers containing hydroxyl groups including polysaccharide, polyvinyl alcohol and its copolymers, polyhydroxyethyl methacrylate, silica, and porous glass can be used as material supports not only for direct ligand coupling via, e.g., cyanogen bromide, triazine, or cyclic carbonate reaction, but also for modification reactions leading to other reactive functional groups such as carboxyl, carbonyl, and mercapto groups (Figure 3.12) [137].
  - *Cyanogen Bromide Reaction* (Figure 3.13a): This reaction was introduced by Axen et al. [138] in late 1960s and became one of the most extensively used coupling method. The hydroxyl-containing polymer is activated with cyanogen bromide at pH 10–11.5. Compounds containing free amino groups can be attached covalently to the activated polymer at mild alkaline pH values. The cyanogen bromide activation reaction is considered to proceed via the 2,3-*trans*-imidocarbonate intermediate, leading to the formation of three possible types of bonds with protein amino groups: N-substituted imidocarbonate, N-substituted carbamate, and N-substituted isoureas. The cyanogen bromide method was used for immobilization of different proteins on cellulose, agarose, dextran, and copolymers of hydroxyethyl methacrylate with acrylamide [139–142].
  - *Cyclic trans-2,3-Carbonate Method*: This method was first used for immobilization of different biomolecules on cellulosic materials [143]. The reaction of cellulose with ethyl chloroformate in anhydrous organic solvents gives

**TABLE 3.1**  
**Modification Reactions with Polymers Containing Different Functional Groups**

Functional Groups	Material Type	Modification	References
Hydroxyl	Polysaccharides (cellulose, agarose, dextran, chitin, chitosan), inorganic glass, polyvinylalcohol, polyhydroxyethyl methacrylate	Cyanogen bromide, triazine method, cyclic <i>trans</i> -2,3-carbonate reaction, carbonylation, periodate oxidation, epoxide activation	[137–150]
Carboxyl	Poly(acrylic acid), poly(glutamic acid), CM-cellulose, poly(acryl amide)	Curtis azide rearrangement, coupling reagent method, acid anhydride reaction	[151–154]
Aldehyde and acetal	Polymers reacted with glutaraldehyde, polysaccharides reacted with periodate	Schiff base formation reaction	[137,155,156]
Amide	Polypeptides and polyamides such as nylon	Peptide amide bond cleavage, <i>N</i> -alkylation of the amide bonds, imidoester reaction	[137,151]
Amino	Aminoethylated polysaccharides and silica, arylaminated polysaccharides, poly-( <i>p</i> -aminostyrene), synthetic polymers	Carbamylation and thiocarbamylation method, diazotization, the four-component condensation reaction, glutaraldehyde treatment	[155,157–161]
Mercapto	Glutathione-agarose, thiolated agarose, Enzacryl polythiol	Treatment with dipyridyldisulfide, carbodiimide activation, thiol-disulfide interchange reactions	[137,153,154,162,163]

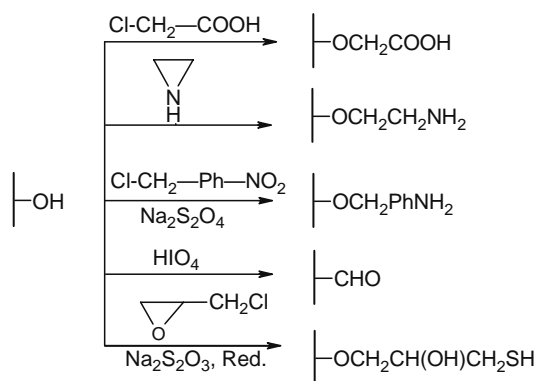


**FIGURE 3.12** Coupling reactions for ligands immobilization on polymers containing hydroxyl groups.

cyclic *trans*-2,3-carbonate derivative of cellulose (Figure 3.13b). The *trans*-2,3-carbonate group is analogous to the cyclic *trans*-2,3-imidocarbonate structure, which is assumed to be the intermediate reactive in cyanogen bromide activation. Nucleophilic attack on the cyclic carbonate by a ligand containing amino group leads to ring opening and the formation of N-substituted carbonates.

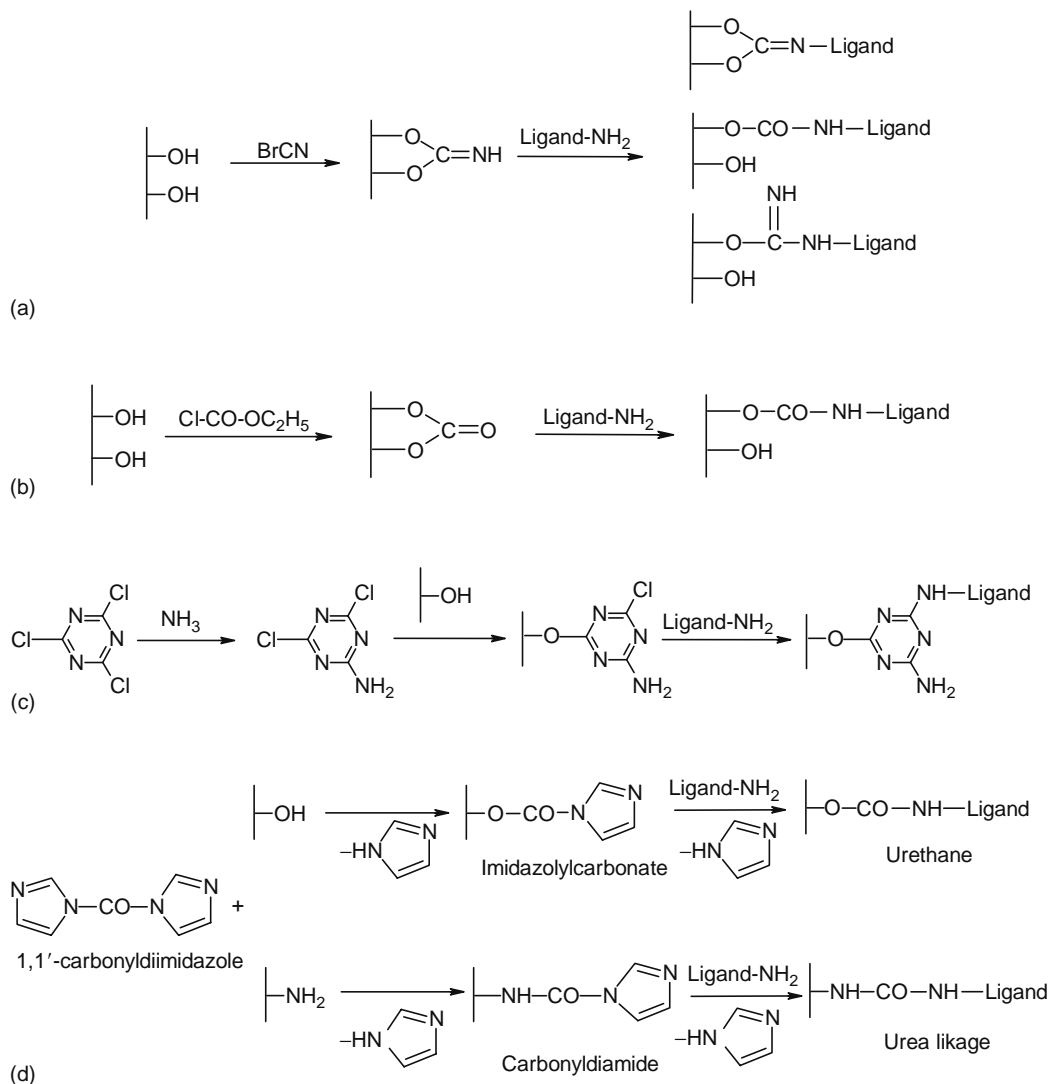


**FIGURE 3.13** Schematic representation of (a) cyanogen bromide reaction, (b) cyclic *trans*-2,3-carbonate activation method, (c) triazine activation method, and (d) carbonylation reaction.

- *Triazine Method* (Figure 3.13c): The method was used mainly for polysaccharides including cellulose, agarose or cross-linked dextran, and vinyl alcohol supports [144,145]. Dichloro-*s*-triazinyl derivatives that react rapidly with protein are prepared by reaction with 2,4,6-trichloro-*s*-triazine (cyanuric chloride) at room temperature. The temperature may be raised to accelerate the reaction. The remaining chlorines may be treated with an amine to prevent further reaction, including polymer cross-linking. As the reaction of the second chlorine with protein is very fast, it is preferable to replace the second chlorine and use the third chlorine for the coupling reaction. Monochloro-*s*-triazinyl derivatives can be prepared by allowing the polymer to react initially with cyanuric chloride followed by a reaction with a low molecular weight amine under controlled conditions to leave the third chlorine unreacted. It is, however, preferable to use 4,6-dichloro-*s*-triazine derivative, 2-amino-4,6-dichloro-*s*-triazine, or the so-called Procion M dyes.
  - *Carbonylation* with carbonyldiimidazoles or carbonylditriazoles to form the corresponding carbonate esters can be easily performed in the presence of sodium alcoholates catalyst on hydroxyl containing polymers [146,147]. The resulting iminocarbonate ester can react further with amines forming stable urethane linkage between the hydroxylic support and the amino containing ligand (Figure 3.13d). If the support material contains amine groups instead of hydroxyl groups, the first intermediate formed is a carbonyldiamide, which can easily react with nucleophilic groups of the ligand [148].
  - *Periodate Oxidation* mainly of polysaccharide supports has become a popular activation technique for protein immobilization [149]. Sodium periodate ( $\text{NaIO}_4$ ) can react with vicinal *cis*-hydroxyl groups on cellulose, dextran, or any other diols to produce aldehyde groups. These aldehyde groups can easily be transformed into secondary amines by reductive oxidation or to hydrazides by reaction with dihydrazine. Further attachment of ligands or spacer molecules can be performed via primary amino groups.
  - *Epoxide Activation* using bioiranes (such as 1,4-butanediol dicyclydyl ether), epichlorhydrine, or epoxy bromopropane is also intensively described in literature [150]. The epoxide groups can react with nucleophilic reagents including  $-\text{OH}$  and  $-\text{NH}_2$  by ring opening. Condensation of the first ring with hydroxyl groups can be catalyzed at pH 11 while coupling amine or thiol groups with the second ring takes place at a lower pH value. Simultaneously hydrogel cross-linking may occur.  $\text{NaBH}_4$  can be added to the reaction mixture to prevent the oxidation of the di-epoxides.
2. Polymers containing carboxyl groups activated as acylazide, acid anhydride, or active ester by condensation reagents and four-centered reaction can be used for ligand immobilization employing various coupling reactions via amino groups of the protein to form an amide bond (Figure 3.14) [151]. Polyacrylic acid and polymethacrylic acid are typical polymers used for these activations. They can be applied as homopolymer or copolymers with acrylamide.
- *Curtis Azide Rearrangement*: The polymer containing carboxyl groups is modified to a methyl ester, which reacts further with hydrazine hydrate to form a hydrazide derivative. The hydrazide subsequently reacts with an aqueous sodium nitrate solution to give an azide derivative, which can react with a ligand amino group under mild alkaline conditions (Figure 3.14a) [152].

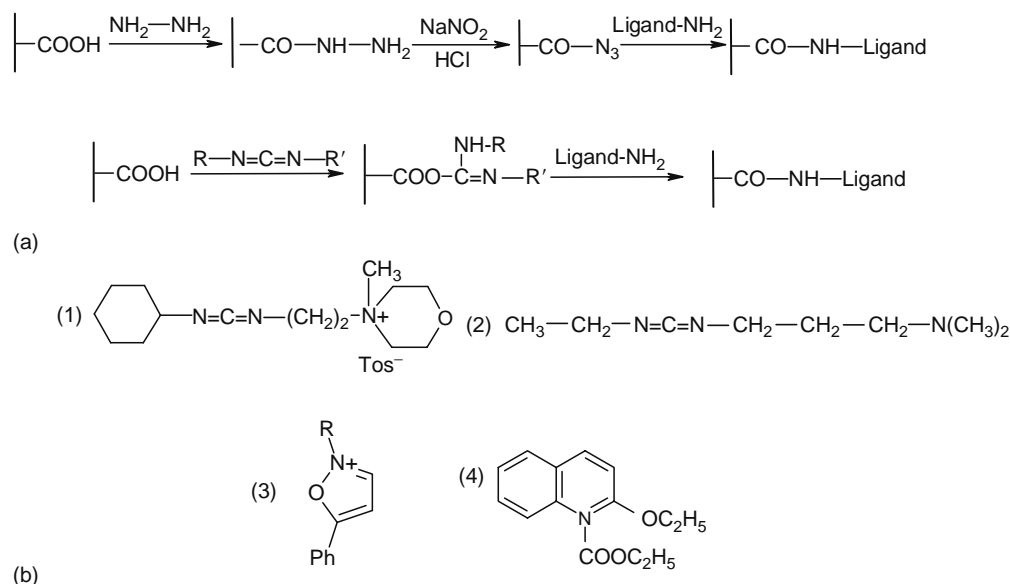


FIGURE 3.14 Schematic representation of (a) Curtis azide activation and (b) coupling reagents activation method.

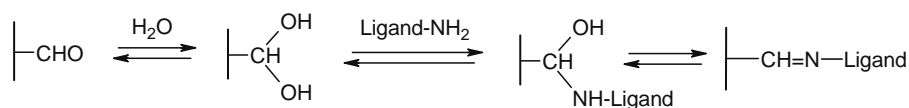


FIGURE 3.15 Coupling reactions for ligands immobilization on polymers containing aldehyde groups.

- Coupling Reagents Method:** This method involves water-soluble carbodiimides and similar coupling reagents that react with carboxyl groups of the polymer at room temperature and slightly acidic pH values (pH 4–5) to give *O*-acyl isourea derivatives. These highly reactive intermediates either condense with amines to yield the corresponding amides or rearrange to an acyl urea. The most widely used water-soluble carbodiimides for the activation of carboxyl groups are 1-cyclohexyl-3,2-(4-*N*-methylmorpholinium) ethyl carbodiimide tosylate (1) and 1-ethyl-3-(3-dimethylaminopropyl) carbodiimide (2). Other coupling reagents *N*-alkyl-5-phenylisoxazolium salt (3) and *N*-ethoxy carbonyl-2-ethoxy-1,2-dihydro-quinoline (4) can be used in a similar manner (Figure 3.14b) [153,154].
- Widely used as polymeric supports for protein immobilization are the polymers containing aldehyde and acetal functional groups (Figure 3.15) [155].

    - Schiff Base Formation Reaction:** This reaction (especially the glutaraldehyde reaction) is an inexpensive and easy to use method extensively used for the immobilization of various ligands (such as proteins, enzymes, and cells), on amine, amide, or hydroxyl-containing support materials [49,156]. At low pH in dilute solution, glutaraldehyde (GA) is present as monomer in its free aldehyde form, as hydrate or hemiacetal, while at higher concentrations it polymerizes into oligomeric hemiacetals. All of these species can react with proteins and lead to immobilization. Activation of the support is often conducted at low pH to catalyze acetal formation, while the coupling of the biomolecule is carried out at elevated pH to promote the nucleophilic attack onto the carbonyl group improving thus the immobilization yield.
  - Polymers containing amino groups are used as support materials in chromatographic separation processes using various coupling methods. The amine groups can be activated using, for example, glutaraldehyde and cyanuric chloride reaction. They can also be modified by phosgene and thiophosgene to isocyanate and thioisocyanate groups, respectively. The newly formed functional groups can react with the ligand amino groups (Figure 3.16). The carboxyl groups of the bioligands can also be directly coupled onto polymers containing amino groups using carbodiimide or similar coupling reactions to form stable amide bonds.

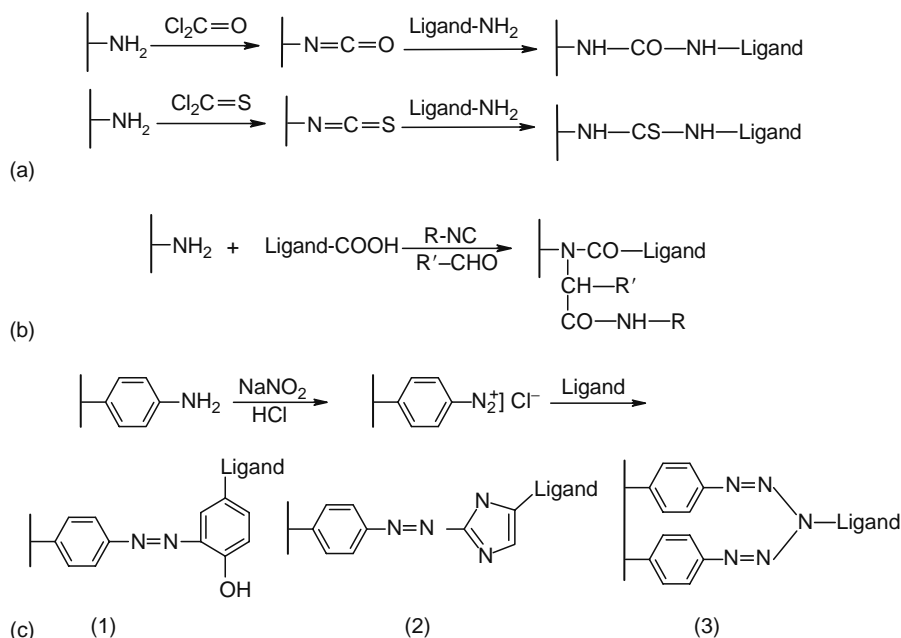


FIGURE 3.16 Schematic representation of (a) carbamylation and thiocarbamylation reactions, (b) four-component condensation reaction, and (c) diazotization activation.

- *Carbamylation and Thiocarbamylation Reactions* (Figure 3.16a): These reactions have been widely used for protein immobilization on many polymers, including polyisocyanate and polyisothiocyanate styrene and on other copolymers containing these styrene units and isocyanate or isothiocyanate groups [157,158].
  - *The Four-Component Condensation Reaction*: The reaction combines the carboxyl and amino groups to form an amide bond in an aqueous medium at neutral pH (Figure 3.16b) and allow for considerable versatility and high selectivity. This reaction can be used for carboxyl and amine-containing polymers [159].
  - *The Diazotization Reaction*: This reaction can be applied for different proteins coupling to polymers containing arylamino functional groups [160,161]. The polymers are reacted with nitrous acid to form aryl diazonium functional groups. The electrophilic aryl diazonium ion mainly attacks activated aromatic rings, such as phenols of tyrosine or imidazole of histidine to form the corresponding azo derivatives. Tyrosine and histidine react at mild alkaline pH values (8–9) at comparable rates to form monoazo derivatives (1, 2) (Figure 3.16c). Amino groups ( $\alpha$ -amines and the  $\epsilon$ -amino groups of lysine) react under similar conditions with 2 moles of diazonium salt to give the disubstituted bis-azo derivatives known as triazenes (3).
5. Polymers with other functional groups including polymers possessing amide bonds, polyacrylamide and polyamides are useful hydrophilic and electrically neutral supports for ligand coupling. Polymers containing mercapto functional groups, such as glutathione-agarose or thiolated-agarose [162,163], were used for specific reversible coupling to protein mercapto groups (cystein) via thiol-disulfide interchanging reactions. Polyacrylamide supports can be chemically modified by reacting with hydrazine or ethylenediamine to obtain the corresponding acyl hydrazide or aminoethyl derivatives. Polymers containing 3-fluoro-4,6-dinitrophenyl groups, such as poly(methacrylic acid-*co*-methacrylic acid 3-fluoro-4,6-dinitroanilide) or poly(methacrylic acid-*co*-methacrylic acid 3-fluoro-4,6-dinitrostyrene), can be used for ligand coupling via arylation with the amino groups of different biomolecules [151].

Very often used in various applications are the monoliths whose preparation routes involve chemical modifications with ethylenediamine, diethylamine or periodate, as well as grafting of monolithic pore surface via attachment of glucose, polyvinyl alcohol, dextran, ethyl cellulose, or 1,3-di-trimethylolpropane [122,128,164–167].

In case of proteins or enzymes as bioligand in the affinity separation processes, all the available information on amino acid composition, effects of specific chemical modifications on activity, or three-dimensional structure of the protein should be considered in selecting appropriate coupling reaction and functionalized polymer. The types of functional groups through which the covalent bond between the ligand and the polymeric support is formed should be nonessential for the biological activity of the biomolecule. Moreover, binding reactions that can be carried out under mild conditions and especially the reactions in aqueous media are preferred.

### 3.4.5 AFFINITY LIGANDS

In general, affinity binding between a ligand and a protein is more complex than protein adsorption on a plain surface. The ligands normally are positioned at a small distance from the solid surface and are able to form a sterical contact with the biomolecule. The ligands may also possess various functional groups that bind with the protein molecules through different types of interaction [168]. Depending on the product to be isolated the ligands can be, for instance a hormone, an inhibitor, an antigen, a specific-binding protein, or a cofactor, specifically chosen for an affinity adsorption process [10]. A brief list of ligands and their corresponding ligates are presented in Table 3.2.

The ligand molecules can be divided into two groups [12]: (i) specific ligands, which show specificity for only one complementary biomolecule; and (ii) group ligands that are based on biological recognition parameters but, which are not targeted to a very specific conformation or sequence of the ligate. A group-specific ligand may be a large macromolecule such as lectin, protein A, or protein G. They may also be small coenzymes such as adenosine monophosphate (AMP) or adenosine triphosphate (ATP), and nicotinamide-adenine dinucleotide (NAD) or nicotinamide-adenine dinucleotide phosphate (NADP). A large number of metabolic toxins such as free fatty acids, endotoxins of gram-negative bacteria, mercaptans as well as medications like nortriptyline, amitriptyline, diazepam, bromazepam bind preferentially to the albumin fraction of blood plasma.

Affinity ligands can also be classified into biospecific and pseudo-biospecific ligands. The biospecific ligands, although possessing high specificity with proteins, have certain deficiencies such as high cost, low stability for potential large-scale application and difficulties in immobilization. Nevertheless, a large number of such substances including various enzymes, protein A and protein G isolated antibodies, receptors or inhibitors have so far been investigated in affinity applications [8,12,169]. Ligands with pseudo-biospecific affinity have been recently employed in membrane chromatography. They can be distinguished by biological (amino acids, specially histidine, lysine, tryptophan) or nonbiological molecules (hydrophobic side chains, triazine dyes, metal ions). Immuno-adsorbers based on polyvinyl alcohol materials containing phenylalanine or tryptophan have been used for rheumatism and myasthenia gravis therapy [170]. Phenylalanine has been used as a ligand

**TABLE 3.2**  
**List of Ligands and Their Corresponding Ligates**

Ligand	Ligate
Dyes (Cibacron blue, red, active red, Procion yellow, Procion blue)	Various enzymes, lysozyme, catalase, phosphatase, malate/formate dehydrogenase, adenylase kinase, pyruvate decarboxylase, alkaline phosphatase, serum albumin, lipoprotein, interferon, growth factor, polypeptide hormone
Amino acids (Trp, Arg, Lys, His, Phe)	DNA, RNA, $\gamma$ -globulin, proteinase, carboxypeptidase, endotoxins, pyrogen, IgG, trypsin inhibitor, transferrin, casein, L-benzoyl arginine ethyl ester, cytochrome C
Peptides (pentadecapeptide, hexadecapeptide, poly-L-lysine)	IgG, heparin
Organic acids (oxaloacetic, citric, isocitric, pirivic)	Enzymes (malate dehydrogenase, lactate dehydrogenase, isocitrate dehydrogenase, citrate lyase)
Protein A/G, protein L, recombinant protein A/G, Concanavalin A, Annexin, Bradykinin	IgA, IgG, IgM, insuline-like growth factor, antibody, $\gamma$ -globulin, recombinant human IgGs, glucose oxidase, glycoproteins
IgG, IgM, IgE	Protein A, protein G, anti-IgE antibody
Metal chelates	Various histidine-, tryptophan-, cysteine-containing proteins, BSA, HSA, $\gamma$ -globuline, liver catalase, IgG, Concanavalin A, ovalbumin, lysozyme, histidine/tryptophan, cytochrom c, ribonuclease A, chymotrypsinogen A
Enzyme cofactor and inhibitors	Enzymes
Antibody/antigen	Antigen/antibody
Hormone	Receptor

for the purification of serum proteins and enzymes [171]. The compact porous separation units with immobilized histidine were applied in immunoglobulin G isolation [172]. Anion exchange membranes with immobilized histidine have also been used for removal of endotoxins from protein mixtures [173].

Affinity chromatography using immobilized metal ions (IMAC) is a highly efficient and flexible method for protein fractionating. The immobilized metal ligand has high affinity for a group of proteins whose exposed surface contains histidine, cysteine, or tryptophan amino acid residues. Iminodiacetic acid (IDA), a widely used metal-chelating ligand, can be bound to membranes or disks including agarose or poly(vinyl alcohol) matrixes, in a way similar to the silicagel or polymeric beads chemistry. The ions most efficiently chelated by the IDA, such as  $\text{Cu}^{2+}$ ,  $\text{Ni}^{2+}$ ,  $\text{Zn}^{2+}$ ,  $\text{Co}^{2+}$ , and  $\text{Fe}^{2+}$ , are able to interact with histidine residues of various proteins. The resulting molecules can be specifically recognized and bound by IMAC allowing fast isolation from complex mixtures [2,174]. Few detailed reviews of these applications have recently been published [175,176].

Immobilized dyes have been found to act as pseudo-affinity ligands for a large number of biological molecules. The dyes are chemically stable, relatively inexpensive and have binding coefficients in the range needed for ready elution of ligates. Triazine-linked dyes have been used to mimic coenzymes that bind a number of dehydrogenases, hexokinases, alkaline phosphatase, ribonuclease, and carboxypeptidase. The Cibacron blue was used for the purification of microbial or plasma proteins and various proteins from yeast extracts [177]. The Procion blue binding of albumin is a well-known method for purifying proteins from contaminating transferrin, or a protein of similar physico/chemical properties that often contaminate albumin. Immobilized Cibacron Blue F3GA has been used for the purification of over 80 enzymes and proteins [8].

Combinatorial synthetic ligands (derived from a combinatorial library) started to be recently investigated in membrane chromatography for purification of valuable therapeutic proteins including human insulin precursor or immunoglobulin G [178,179]. Combinatorial peptides also proved to be suitable for immobilization on monoliths. Amatschek et al. [180] prepared continuous beds bearing newly designed combinatorial octapeptides for affinity separation of FVIII with good performances. Synthetic pentadecapeptides, hexadecapeptides, and nonapeptide hormone bradykinin immobilized on monolithic supports were investigated by Platonova et al. [181] for the purification of nonspecific polyclonal antibodies.

The affinity ligands may be directly or indirectly linked to residual functional groups of the matrix membrane by any procedure that substantially retains the mechanical and hydraulic properties of the membrane while substantially retaining the binding activity of the affinity ligand. The degree of ligand attachment to the activated sites is dependent on the ligand–ligand and ligand–activator interactions, charge and steric effects, the nature of the matrix material, as well as number of activated functional groups available for ligand coupling. An excessive number of ligands coupled to the support surface has to be avoided because this may otherwise lead to crowding and interferes with ligate recovery.

### 3.4.6 SPACER MOLECULES

Ligand–ligate complexes able to form in solution may not be able to form when one of the components is immobilized on a porous support. The interference may derive from the nearby support material itself or from other adsorbed proteins (especially

if the support participates in nonspecific bonding). Complex formation is inhibited because the ligate and ligand must compete with other proteins for the restricted space available adjacent to the immobilizing polymer. Impaired diffusion of the ligate to the ligand site due to the channel size or tortuosity may also cause interferences with the complex formation and the requirements for spatial orientation may not be achievable [8].

The employment of a spacer molecule facilitates molecular interactions between immobilized ligands and the targeted molecules. Relatively short aliphatic chains (4–10 carbon atoms in length) are ineffective for interactions involving one or more macromolecules, but longer aliphatic chains can alter undesirable hydrophobicity of the membrane surface. The length of the spacer molecule is often experimentally determined. Free hydroxyl groups of a polysaccharide or vinyl alcohol copolymer support can be linked to a protein ligand via a bifunctional spacer containing at least one terminal primary amino or hydrazido functional group. The remaining terminal group of the spacer can react with free amino or carboxyl functions of the ligand, or with free hydroxyl groups of a glycoprotein ligand. Convenient spacer molecules for these applications include diamine and dihydrazides such as C<sub>1</sub>–C<sub>6</sub>-alkyldiamines and C<sub>1</sub>–C<sub>6</sub>-dihydrazides, and β-alanine hydrazide, which provide free amino and hydrazido groups for reaction with the ligand. They can also be C<sub>4</sub>–C<sub>6</sub>-alkylamino acids, which provide free carboxyl groups.

The immobilization of different enzymes via a spacer molecule such as 6-aminocaproic acid yielded kinetic and structural characteristics similar to the free enzyme while providing increased stability and reusability. Triazine dyes (Cibacron Blue F3GA or one of the Procions) were coupled using polyethyleneimine (PEI) as a spacer to nylon membranes and their adsorption capacities for lysozyme, bovine serum albumin, malate dehydrogenase, or glucose-6-phosphate dehydrogenase were investigated. The use of long spacer molecules proved to reduce the steric interference allowing for multiple layering of large macromolecules at the membrane surface. Polyethylene glycol with a suitable chain length, generally between 50 and 250 carbon atoms, can be covalently coupled to the membrane surface through its amino groups by a proper immobilization method. The advantages of polyethylene glycol as a spacer molecule are its hydrophilic nature and biological inertness, quite beneficial in a device that contacts blood or plasma.

### 3.5 ADVANTAGES OF MEMBRANE CHROMATOGRAPHY

In chromatographic separations based on membranes, compact porous disks, tubes or rods, the ligate–ligand interaction takes place predominantly in the support through-pores rather than in the stagnant fluid inside the dead-end pores of the adsorbent particle as in the case of packed-bed chromatography. In membrane-based processes the transport of solute molecules to the corresponding binding sites takes place mainly by convection, while diffusion is usually involved in the mass transport within the dead-end pores of particles. This minimizes some of the common limitations of classical chromatographic beds such as process time, channeling, and intra-bed diffusion. Since a typical membrane bed (including single or stacked membranes as well as disks and monolithic columns) has a much larger cross-sectional area relative to the bed length compared with packed-bed columns, the pressure drop is drastically reduced resulting in higher flow rates and thus higher productivities. Short diffusional distances allow optimal utilization of the immobilized ligand situated at the inner surface of the membrane pores. Furthermore, ligand and product are, compared to packed columns, only for a short time exposed to harsh elution conditions, which decreases their possible denaturation. The affinity membranes also offer the possibility to operate sterile, in good conditions of reproducibility [2,13]. An additional advantage in membrane chromatography is their relative low production cost. This allows the development of disposable membrane adsorbers, which can be replaced when the desirable properties (mainly binding capacity, selectivity, or permeability) go below the efficiency value.

Membrane chromatography proved to be a successful tool especially for separation of macromolecules. The large-size proteins cannot enter the small pores of the particles in the packed-bed columns, while in membrane-based processes they have access to a much higher binding surface due to the macroporous nature of the supports. One problem may nevertheless appear for membranes with large pore distribution. Suen [182] reported that a variation of ±12% in porosity can be responsible for a loss of 50% of adsorption capacity at the breakthrough point. For variations in the membrane thickness a three times less-sensitive behavior was found.

Due to the fact that the membrane thickness is in the range of several hundreds up to thousands microns there is often a nonuniformity in the thickness as well as in the porosity within the sheets, which results in a decline of membrane performance. A variance in porosity creates channeling in the membrane, causing a tremendous loss in loading capacity. In this case, the solute molecules preferentially flow through the larger pores and quickly saturate the adsorptive-sites on such large diameter and low-surface area pores. Subsequent flow through the adsorptive saturated large pores does not result in any further capture of solute. Meanwhile, residual capacity for the adsorber located in small pores, which exhibit high resistance to flow, is not completely utilized causing a lower dynamic binding capacity. This is the main drawback of adsorber membranes compared with packed beds.

Another major advantage of membrane chromatography is their relative easy packing and scale-up, which unfortunately was not extensively investigated until now. The reader should also be aware that scaling-up to larger supports diameter could cause inefficient flow distribution across the membrane thus broadening the shape of the breakthrough curve and reducing the

separation efficiency [183]. Proper design of inlet flow distributors recently proved to diminish this problem leading to more uniform flows. However, more investigations need to be performed in the area of process and equipment design if membrane chromatography is to be a competitive separation process.

### 3.6 MASS TRANSFER IN AFFINITY COLUMNS

Mass transfer is the physical process, which involves molecular and convective transport of atoms and molecules within physical systems. The rate of mass transfer is very important because the mass transfer step has to be carried out before the reaction or the adsorption step can take place. A low mass transfer rate slows down the process thereby requiring bigger reactors or purification systems. This means that mass transfer always had to be taken into account when new processes are designed.

By the production of biologics, the manufacturers are facing two critical parameters: capacity and flow uniformity. Chromatography with gel-type particles is nowadays an established and reliable process in biotechnology. The particles are among others applied for capturing and polishing of proteins, enzymes and DNA(-fragments), or for viral and endotoxin removal. The main disadvantages of chromatographic columns, especially when using gel-type resins, are flow irregularity and channeling. This results in simultaneously adsorption and breakthrough behavior, destroying the adsorption power of the chromatographic media.

Membrane chromatography, with functionalized or particle-loaded membranes, eliminates the slow diffusional process step since the feed comprising the target molecules flows in convective mode through the activated matrix. The only conditions the membranes should possess to perform a separation with high specificity and resolution are a low flow resistance, a high density of active groups, and a low nonspecific background sorption. In theory, the adsorptive membrane efficiencies should exceed those of granular beds by a factor of ten or even higher. However, a number of anomalous mass transfer effects such as nonuniform flow, dead spaces, and extra-column dispersion have been observed.

In classical bed chromatography the majority of the active sites are located in the interior of the beads, resulting in long diffusion paths or even to exclusion of the active sites for the bigger target molecules. In contrast, the membrane chromatographic devices are three-dimensional structures with a high surface over volume aspect ratio, offering easy access for the target molecules to the active sites. The ratio of BSA (67 kDa) adsorption within Mustang Q-membranes (Pall) and Q-beads of 90  $\mu\text{m}$  is 9 where as the ratio of adsorption for DNA-plasmid (2.880 kDa) within the previous mentioned adsorbers is close to 30. This shows the exclusion of bigger molecules within the beads due to the limited pores size, whereas the membranes with big convective pores allow for a higher access for large macromolecules [184]. The binding capacity of membrane adsorbers for small proteins is lower than that of the gel-based beads, but it is still significantly higher than the adsorption capacity of nonporous rigid media.

The separation efficiency in adsorptive processes is dependent on the amount and the availability of adsorptive sites during processing. The effectiveness of an adsorber can be visualized by measuring the breakthrough curve (Figure 3.17) where the load is plotted against the eluent concentration. At a certain point, depending on the physical characteristics of the target molecule and on the capacity, the flow rate and the packing of the adsorber, the concentration in the eluent is raising. A breakthrough curve covers two different areas: the area above the curve corresponds to the operational column capacity, which after the breakthrough is the unused capacity and the area under the curve represents the product loss. The lower the breakthrough point is chosen, the smaller is the amount of product waste.

A broadly disperse breakthrough curve causes a decrease in ligand utilization, delay in saturation time, or waste of feed solution [182]. The sharpness of the breakthrough curve depends on the unique relation between the number of transfers for the

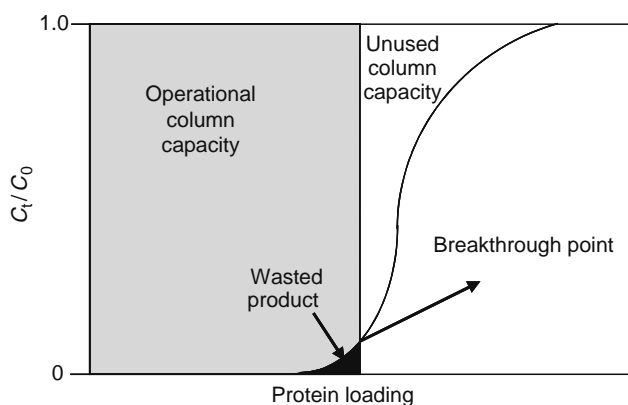


FIGURE 3.17 Visual representation of a breakthrough curve.

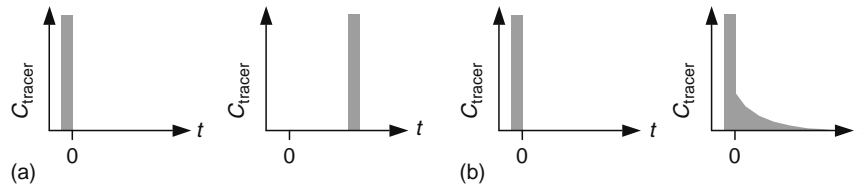


FIGURE 3.18 Tracer profiles in (a) plug flow mode and (b) ideal stirred reactor.

adsorption process ( $n$ ), the separation factor ( $r$ ), and the dimensionless effluent volume ( $V_e$ ) [185,186]. When  $r$  is smaller than 10,  $n$  is increasing quickly, while for a value of  $r$  higher than 500,  $n$  decreases rapidly with a further increase of  $r$ . According to the Thomas model [185], which assumes laminar flow through porous membranes, constant interstitial flow velocity, and neglectable concentration gradient in radial direction, the exit concentration depends only on  $r$ ,  $n$ , and  $V_e$ . The model proposed by Suen [182] is more sophisticated taking also into account the ratio of ligand capacity to feed concentration and the axial Peclet number.

### 3.6.1 DESIGN PARAMETERS

Two flow patterns are imaginable for continuous flow through a column (Figure 3.18):

- Plug flow reactor (PFR) for which defined volume elements flow through a column without mixing with other volume elements. A liquid element will travel from the inlet to the outlet for a period of time equal to the reactor volume ( $V$ ) divided by the flow rate ( $Q$ ).
- Ideal continuously stirred reactor (CSTR) for which a volume element entering the CSTR will become uniform dispersed with all the other volume elements in the reactor. The initial outlet will be equal to the ratio of the tracer volume divided by the reactor volume times the initial tracer concentration, and would then exponential decay in time.

### 3.6.2 AXIAL DISPERSED PLUG FLOW MODEL

The length-based Peclet number ( $Pe_L$ ) is determined with the axial dispersed plug flow model and it is defined as

$$Pe_L = \frac{\langle v \rangle \cdot L}{D_{ax}} = \frac{\text{Transport rate for convection}}{\text{Transport rate by diffusion}}$$

At a small  $Pe_L$  the breakthrough curve is broadened, the time of total saturation is delayed, and the breakthrough point is shifted to the front. When the  $Pe_L$  increases the breakthrough curves become steeper. For  $Pe_L$  values higher than 40 the breakthrough curve is close to the Thomas model, which assumes no axial diffusion [182,186]. Axial diffusion becomes important when using thin membranes. Since  $Pe_L$  decreases with decreasing membrane thickness, the influence of axial diffusion also decreases. When  $Pe_L > 40$  the loss of loading capacity is below 3%. The timescale for axial diffusion is much bigger than that of the radial diffusion indicating mass transfer resistance in the boundary layer. This means that the concentration gradient in radial direction can be neglected when the condition  $d_p^2/4D \leq L/v$  is fulfilled. In general, axial diffusion is neglected when the radial Peclet number ( $Pe_r$ ) is smaller than 0.04.

$$Pe_r = \frac{d_p^2 v}{4DL} < 0.04$$

When individual membranes are stacked into a column, it is advisable to use at least 30 membranes on top of each other to average out the membrane heterogeneities and the channeling effects. The pressure drop over the membrane stack should be as low as possible. Therefore, producers like Sartorius, Millipore, and Pall advise not to apply pressures  $>4$  bar.

$$\text{Fanning equation: } \Delta P = \frac{4 \cdot 24 \cdot v \cdot L}{d^2} \cdot \frac{1}{2} \cdot \rho \cdot u$$

where

$v$  = viscosity ( $m^2/s$ )

$d$  = pore diameter (m)

$\rho$  = density ( $kg/m^3$ )

$u$  = linear velocity in the pore (m/s)

$L$  = thickness of membrane stack (m)

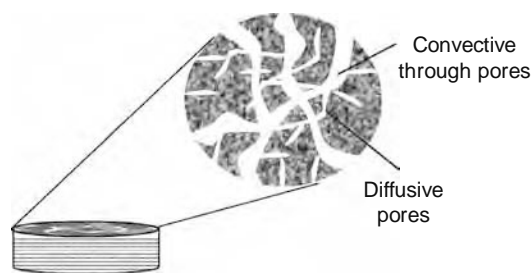


FIGURE 3.19 Visual representation of a stacked column.

For particles under viscous conditions and  $Re \leq 1$  a more simplified form, known as the Kozeny–Carman equation, can be used to calculate the pressure drop within the chromatographic column.

$$\text{Kozeny–Carman equation: } \Delta p = \frac{150 \cdot v \cdot u \cdot L \cdot (1 - \varepsilon)^2}{d_p^2 \cdot \varepsilon^3}$$

where

$d_p$  = equivalent spherical particle diameter (m)

$\varepsilon$  = void fraction of the bed (–)

$L$  = column length (m)

When diffusion inside the adsorbent is the limiting mass transfer step, two different diffusion mechanisms with different driving forces namely pore diffusion and surface diffusion have to be considered [187]. Surface diffusion is often neglectable in case of proteins for which the lumped sum is often described as effective pore diffusivity while it has to be taken into account in case of ions. However, using high surface coverage surface diffusion can really contribute to the mass flux. For high capacity membrane adsorbers the surface diffusion is the dominating factor in the mass transfer thus the shape of the breakthrough curve is strongly dependent on the feed concentration. In membrane chromatography the target solutes are transported by convective bulk flow to the active sites. The solutes experience three different resistances against transport [188].

### 3.6.3 DISPERSION

Membranes act as short wide chromatographic columns with pore sizes up to 3  $\mu\text{m}$  (Figure 3.19) resulting in very low resistance against mass transport and high fluxes of over 1000 cm/h coupled with a low-pressure drop. Longitudinal dispersion and convection of matter by flowing through a packed bed or membrane are coupled. This can be visualized by the maximum when the  $Pe_L$  number is plotted against the Reynolds number [189].

The residence time distribution (RTD), also referred to as the distribution of ages, is based on the assumption that each element traveling through the column takes a different route and will therefore have a different residence time. Different methods are developed to determine the RTD in a module or in a reactor [190]. The RTD of a chromatographic column is defined by a function  $E$  (Figure 3.20), such that  $E dt$  is the fraction of material in the exit stream with an age between  $t$  and  $t + dt$ . The  $E$ -curve lies between the extremes of plug flow and continuously stirred tank reactor. The surface below the curve between  $t = 0$  and  $t = \infty$  has to be equal to unity  $\int_0^\infty E(t) dt = 1$ , because all elements that enter the module must also exit the module.

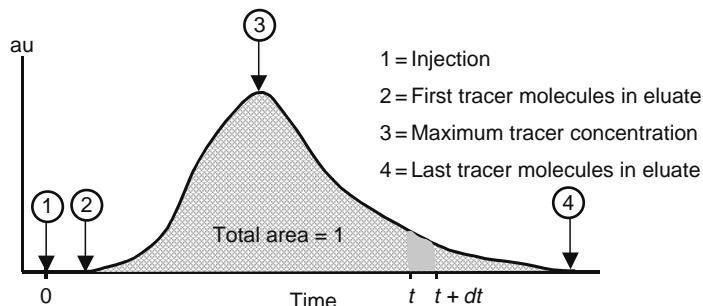


FIGURE 3.20 Example of an  $E$ -curve.

The  $E(t)$  curve is obtained out of the tracer concentrations. The existing relationship between the  $E(t)$  and  $C(t)$  is  $E(t) = \frac{C(t)}{\sum C(t)}$ . The average residence time can be determined by  $\bar{t} = \int_0^{\infty} t \cdot E(t) dt$ . This  $E(t)$  can be obtained by various methods of which the two most common are given below:

- *Tracer Impuls Method*: In this method a certain amount of tracer is injected (very short time interval) into the system and the concentration is measured at the outlet of the column. The concentration followed in time can directly be converted to the  $E(t)$  curve as described above.
- *Heaviside Step Function*: This function implies measurements of the integrated function of the distribution curve, cumulative RTD function  $F(t)$ . This can be established by changing one liquid (usually water) from one steady value to another with a detectable tracer. The equation that relates this measurement to the tracer impulse method is  $F(t) = \int_0^t E(t) dt$ .

### 3.6.4 DETERMINING THE AVERAGE RESIDENCE TIME AND THE VARIANCE

The recorded  $F(t)$  curves can be translated to the  $E(t)$  curve by taking the derivative of the recorded curve. The data were translated with  $E(t_n) = \frac{\partial F(t)}{\partial t} = \frac{F(t_{n+1}) - F(t_{n-1})}{\Delta t}$ .

First, the area under the curve is determined by the zero moment  $MO_0$ . In this way the curve can be normalized if necessary.

$$\begin{aligned} MO_0 &= \int_0^{\infty} E(t) dt = 1 = \sum_{n=0}^{n=x} \frac{1}{2} \{E(t_n) + E(t_{n+1})\} \Delta t_n \\ &= \frac{1}{2} \{E(t_0) + E(t_1)\} (t_1 - t_0) + \cdots + \frac{1}{2} \{E(t_{x-1}) + E(t_x)\} (t_x - t_{x-1}) \end{aligned}$$

Second, the average residence can be determined by calculating the first moment

$$\begin{aligned} MO_1 &= \bar{t} = \int_0^{\infty} t \cdot E(t) dt = \sum_{n=0}^{n=x} \frac{1}{2} \{t_n E(t_n) + t_{n+1} E(t_{n+1})\} \Delta t_n \\ &= \frac{1}{2} \{t_0 E(t_0) + t_1 E(t_1)\} (t_1 - t_0) + \cdots + \frac{1}{2} \{t_{x-1} E(t_{x-1}) + t_x E(t_x)\} (t_x - t_{x-1}) \end{aligned}$$

For the calculations of the variance determined by  $\sigma_t^2 = MO_2 - MO_1^2$ , it is necessary to determine the second moment

$$\begin{aligned} MO_2 &= \int_0^{\infty} t^2 \cdot E(t) dt = \sum_{n=0}^{n=x} \frac{1}{2} \{t_n^2 E(t_n) + t_{n+1}^2 E(t_{n+1})\} \Delta t_n \\ &= \frac{1}{2} \{t_0^2 E(t_0) + t_1^2 E(t_1)\} (t_1 - t_0) + \cdots + \frac{1}{2} \{t_{x-1}^2 E(t_{x-1}) + t_x^2 E(t_x)\} (t_x - t_{x-1}) \end{aligned}$$

The RTD measurement is a dynamic measurement meaning that the volume in the column measured with the experiments ( $V_{\text{flow-through}}$ ) can be determined. Static volume measurements can also be done to determine the column hold up,  $V_{\text{hold up}}$ . The average residence time,  $\tau_{V_{\text{hold up}}}$ , based on the column hold up can be determined by  $\tau_{V_{\text{hold up}}} = \frac{V_{\text{hold up}}}{Q}$ .

The following is possible:

- $\bar{t} > \tau_{V_{\text{hold up}}}$  adsorption of the tracer in the column or transport into the porous structure
- $\bar{t} = \tau_{V_{\text{hold up}}}$  completely utilized column
- $\bar{t} < \tau_{V_{\text{hold up}}}$  presence of dead volume and channeling within the column

When the determined residence time approaches the  $\tau_{V_{\text{hold up}}}$  just external flow is obtained whereas for residence time getting closer to the  $\tau_{V_{\text{accessible}}}$  value, internal flow (due to diffusion or convection) is also obtained. It may be seen that a single parameter  $\sigma_t^2 / (\bar{t})^2$  is sufficient to characterize the sharpness of the peak. The inverse of this parameter is the number of theoretical plate heights of the adsorber, which describes the efficiency of the system.

### 3.6.5 BROWNIAN MOTION

During the convective transport individual target molecules are dispersed by the presence of small eddies. The random walk motion of small particles suspended in a fluid due to bombardment by molecules obeys the Maxwellian velocity distribution. If a number of particles subject to Brownian motion are present in a given medium and there is no preferred direction for

the random oscillations, then over a period of time the particles will tend to be spread evenly throughout the medium. Thus, if two compartments one containing component A and the other containing component B are brought together then component A will move to compartment B. The speed of this transport is dependent on the concentration difference within the two compartments, the particle size, the viscosity of the medium, and the temperature. This process is called diffusion and is the macroscopic manifestation of Brownian motion on the microscopic level.

In a convective fluidum the movement of one component in a certain medium, in a time interval ( $t$ ) and in a certain direction, from its starting point over the distance ( $x$ ) is related to the diffusion coefficient ( $D$ ) of that component.

### 3.6.6 INTERACTION WITH THE MATRIX AND ACTIVE SITES

In membrane chromatography the active sites are immobilized inside the membrane pores. For particle-loaded membranes the active sites are immobilized at the outer surface of the imbedded particles or, to increase the total active surface area, they can also be located inside the porous particles. In the latest case if very small pores are involved, the productivity is low even in spite of a high active surface area. This is because the transport of the target molecules to the active sites is by diffusion alone, which is a much slower process than the convection through the big pores. Therefore, the loading step is much more time-consuming. The interaction between the target molecules and the ligands is often considered instantaneous. Nevertheless, in the case of affinity complex formation the building of the complex can be that slow that the limiting step is not longer the convection or the diffusional transport to the active site but the complex formation.

## 3.7 ADSORPTIVE MEMBRANE GEOMETRY AND OPERATION MODES

Membrane chromatography can be performed on units of various geometry, microporous adsorptive membranes and related systems such as single or staple flat-sheet membranes, hollow-fiber, spiral-wound and cassette devices being already commercially available. An overview of commercially available supports in membrane chromatography is presented in Table 3.3. Few of these systems (Sartobind, Sartorius [Figure 3.21]; MemSep, Millipore; Quik Bind, Sepracor; Biorex, Bio-Rad; Lowprodyne, Pall; AbSorbent, Genex; ActiDisk, FMC Bioproducts; MAC, Amicon) have been already developed for a small number of technical applications [8–10].

Continuous beds including methacrylate-based disks CIM QA from BIA Separations (Figure 3.22) and SWIFT from Isco, acrylamide UNO monoliths from Bio-Rad, Ultimate polystyrene divinylbenzene disks from LC-Packings, cellulose-based Seprisorb monoliths from Sepragen and silica units Conchrom from Conchrom or Chromolith from Merck are also

**TABLE 3.3**  
**Examples of Commercially Available Membrane and Monolithic Products**

Trade Name	Manufactures	Module Type	Material	Separation Principle
Sartobind, Vivapure	Sartorius, Vivascience (Germany)	Flat sheets, disks	Regenerated cross-linked cellulose	IEX, AF, IMAC
Immobilon, Intercept Q, MemSep, Zip Tip	Millipore (USA)	Flat sheets, syringe, disks, pipette tips	PVDF, regenerated cellulose, silica, polypropylene	AF, IEX, RP
ActiDisk	FMC (USA)	Flat sheets	PVC	IEX
ZetaPlus/PolyNet	Cuno Life (USA)	Depth filter	Cellulose, polypropylene	IEX
Biodyne, Mustang (Q, S, and E)	Pall (USA)	Flat sheets, disks	Nylon, PES	IEX, AF
Fractoflow, Chromolith	Merck (Germany)	Hollow fibers, monolithic rods	Polyamide, silica	IEX, RP
Empore	3M	Particle-loaded membranes, disks	PTFE, PS-DVB, silica	IEX, AF
Mosaic Systems	Mosaic Systems (The Netherlands)	Particle-loaded membranes, full/hollow fiber modules	PES	IEX, AF
Seprisorb	Sepragen (California, USA)	Monolithic columns	Regenerated cellulose	IEX
CIM disk	BIA (Slovenia)	Monolithic rods, disks, tubes	Polyglycidyl methacrylate-co-ethylene dimethacrylate	IEX, RP, AF
Swift	Isco (USA)	Monolithic columns	Styrene, methacrylate	IEX, RP
Conchrom	Conchrom (Germany)	Monolithic rodss	Modified silica	IEX, RP
UNO	Biorad (California, USA)	Monolithic rods	Polyacrilamide	IEX

Note: IEX = ion-exchange chromatography; AF = affinity chromatography; IMAC = (metal-)chelate chromatography; RP = reversed-phase chromatography.

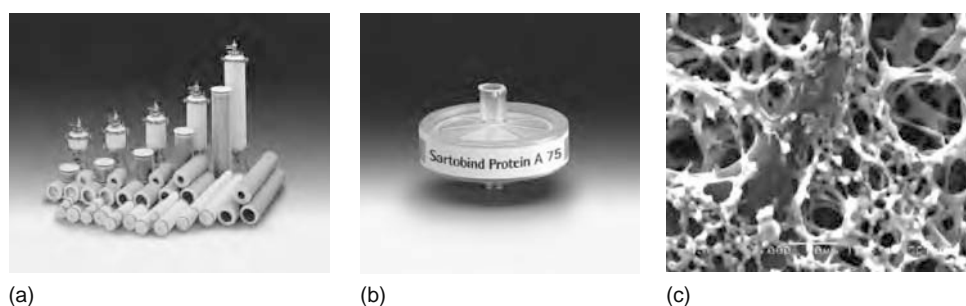


**FIGURE 3.21** (a) Layered membrane adsorbers, (b) lab-scale membrane adsorber, and (c) higher magnification membrane adsorber. (Courtesy Sartorius, Göttingen, Germany.)

manufactured as large scale. The smaller laboratory scale systems often contain various amounts of stacked flat sheet membranes; single sheet adsorbers are rarely used. The bigger process systems consist of radial fed layered or layered and pleated sheets [184]. For an optimal design of the membrane chromatographic systems several parameters have to be taken into account.

Most commercial systems like Mustang from Pall and Sartobind from Sartorius make use of functionalized microporous membranes. The fibrils reinforced membranes are (pleated) layered around a porous core. The feed is forced to permeate through the membranes in radial direction. This approach results in high area to volume ratio. The 3M and Mosaic Systems approach is different. Instead of functionalization of a porous support they make use of already functionalized beads, which are embedded in a porous support. In this approach, the beads are responsible for the capacity and selectivity where the porous matrix controls the hydrodynamics. The 3M modules consist of stacked flat sheet or pleated membranes, while Mosaic Systems makes use of porous fibers in which the active particles are embedded (Figure 3.23).

In processes where large macromolecules with slow associated kinetics are involved, the adsorption kinetics between the ligand and the dissolved molecule in the feed solution is the rate-limiting step. Not often the pressure drop or the membrane mechanical strength is the limiting factor. When thin membranes are applied the axial diffusion also becomes more dominant and requires a lower linear flow rate through the matrix. Besides this in-homogeneities in porosity and thickness affect the performance of the system negatively. To overcome this problem, often a stack of at least 30 membrane sheets are stacked to average out these heterogeneities.

By using hollow fiber membranes the ideal module comprises short fibers with a wide bore to avoid a high pressure drop in the flow direction thereby disturbing the uniform radial flow pattern and creating channeling. The membranes should also possess thick porous walls with small pore size and a high ligand density. The hollow fiber modules can be operated in cross flow mode what makes them especially suitable in the treatment of solutions containing particulate material.

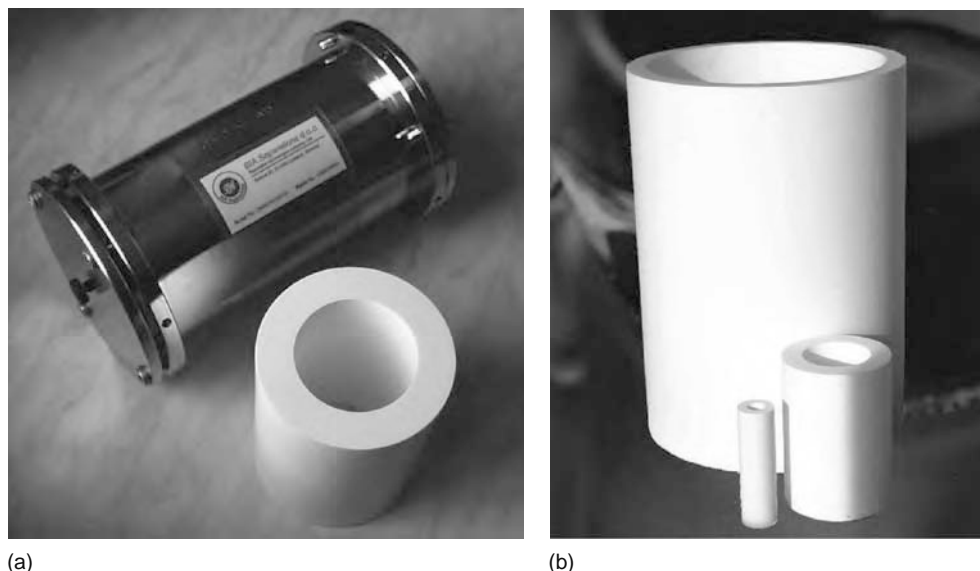


**FIGURE 3.22** (a) A 800 mL continuous bed module and (b) 8, 80, and 800 mL monoliths. (Courtesy BIA Separations, Ljubljana, Slovenia.)

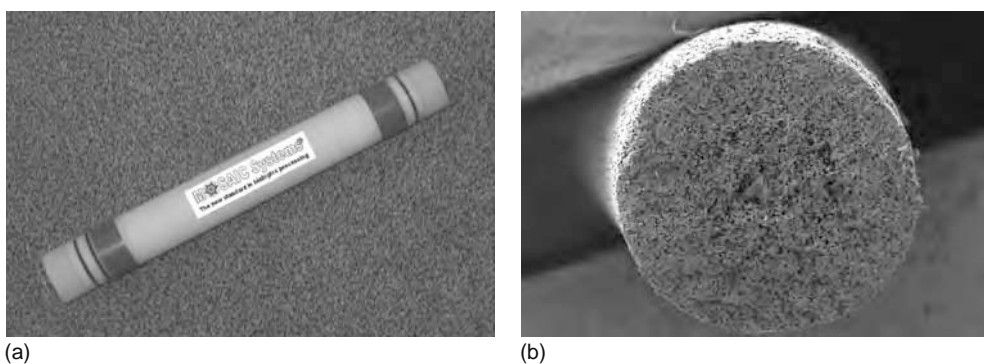


**FIGURE 3.23** (a) Particle-loaded fiber module and (b) SEM picture of a particle loaded fiber. (Courtesy MOSAIC Systems, Breda, The Netherlands.)

### 3.8 APPLICATIONS OF MEMBRANE CHROMATOGRAPHY

The operating interactions within the microporous media involved in chromatographic separation processes are identical to those in the packed columns including affinity interactions, size-exclusion, ion exchange, hydrophobic interactions, and reverse phase (Table 3.4). The functional groups immobilized on the porous membrane surface include, depending on the target application, (i) affinity ligands, e.g., Protein A/G, BSA, biomimetic dyes, immobilized metal, various hydrophobic amino acids; (ii) ion-exchange groups such as carboxylic or sulfonic acid, tertiary or quaternary amines; and (iii) hydrophobic ligands, e.g., octyl and phenyl groups. Several detailed reviews of the various applications of membranes in chromatographic separations have been recently published [8–13]. Therefore, in the following, we will give just a short overview of some of the successful applications of membrane chromatography, classified as a function of the interaction mode involved in the separation process. Readers should also take into account the possible application of membrane chromatography already mentioned in Section 3.3. The different modes of chromatography reports are briefly summarized in Table 3.5. Detailed overview of tables on application in membrane chromatography may be found in Refs. [8,12,13].

The affinity techniques performed on single or stacked membranes, disks, tubes, and rods are based on a biospecific interaction that results in a change of protein properties such that the protein can be separated from other complex biomolecule-containing mixtures. The ligand molecule is immobilized on the porous surface and the mixture containing the protein of interest is passed through the adsorptive membrane. A specific interaction takes place between ligand and ligate and retains the desired protein within the matrix support, while the other components from the feed solution pass freely through the adsorber. Affinity chromatography allows for purification of biopolymers based on biological functions rather than individual physical or chemical properties. Isolation of a protein or a group of proteins such as  $\gamma$ -globulin fractions, human serum albumin, and various clotting factors from body fluids was successfully achieved by using affinity membrane chromatography.

Immunoaffinity techniques were widely employed for the analyses and purification of proteins [191–193]. Immobilized antibodies were used, e.g., for industrial scale production of human interferon- $\alpha$ 2a, interleukin-2, and interleukin-2 receptor, while protein A and protein G were successfully used in therapeutic applications including purification of human immunoglobulin G from plasma and serum [194–196].

Pseudoaffinity ligands such as dyes, lysine, and histidine are now well established in membrane chromatography. Cibacron Blue F3GA dye membranes (having a specific binding for nicotinamide adenine dinucleotide dependent enzymes) and Procion Red HE-3B (with a specific binding for nicotinamide adenine dinucleotide phosphate dependent enzyme) were successfully employed in purification of several enzymes including human serum albumins from plasma, dehydrogenases

**TABLE 3.4**  
**Types of Interactions Involved in Chromatographic Separation Processes**

Type of Chromatography	Separation Mode/Interaction Type
Affinity chromatography	Molecular structure/biospecific adsorption
Ion-exchange chromatography	Surface charge/ionic binding
(Metal-)chelate chromatography	Metals complex formation/coordination complex
Size-exclusion chromatography	Molecular size and shape/size exclusion
Normal/reversed-phase chromatography	Hydrophobicity/hydrophobic complex formation

**TABLE 3.5**  
**Examples of Membrane Chromatographic Applications**

Separation Mode	Ligate Type	Ligand Type	References
Affinity chromatography (immunoaffinity, metal affinity, chiral)	Human interferon- $\alpha$ 2a, interleukin-2 receptor, human IgG, human serum albumin, dehydrogenases glucose-6-phosphate dehydrogenase, formate dehydrogenase, pyruvate decarboxylase, S-oxynitrilase, bovine liver catalase, recombinant protein G, plasmid DNA, human blood coagulation factor VIII, enantiomers of kynurenine, tryptophan, $\beta$ -blockers, practolol, thiopental	Antibodies, protein A and protein G, lysine, histidine, Cibacron Blue F3GA, Procion Red HE-3B, combinatorial peptides, metals	[36,135,191–201, 218–225]
Ion exchange	Serum proteins, microbial proteins and enzymes, membrane proteins, cytokines or nucleic acids, BSA, HSA, $\alpha$ -chymotrypsinogen, lysozyme, trypsin inhibitor, cytochrom c, ovalbumin, $\alpha$ -lactoalbumin, conalbumin, ferritin, myoglobin, chymotrypsin, human recombinant antithrombin, monoclonal and polyclonal antibodies, immunofusion proteins	Quaternary amino, diethylaminoethyl groups	[36,58,202–211, 222–224,226]
Hydrophobic interaction/reverse phase	Recombinant tumor necrosis factor, myoglobin, ovalbumin, lysozyme and chymotrypsinogen, chymotrypsinogen A, ribonuclease, myoglobin, trypsinogen and lysozyme, tricyclic antidepressants, antiarrhythmic drugs, amiodarone, desethylamiodarone, mexiletine, flecainide, alcohols, phenols, aldehydes, ketones, esters, polar pesticides from water	C <sub>4</sub> , C <sub>6</sub> , C <sub>8</sub> , or C <sub>10</sub> linear aliphatic chains	[2,14,205,212–217,226]

glucose-6-phosphate dehydrogenase from a clarified yeast solution, formate dehydrogenase from *Candida bodinii* and pyruvate decarboxylase from *Zymomonas mobilis* homogenates [36,197].

Applications of metal affinity chromatography include separation of S-oxynitrilase from *Sorghum bicolor* on IDA-Cu<sup>2+</sup> ion membranes, purification of human serum albumin with an IDA-Ni<sup>2+</sup> membranes cartridge and purification of bovine liver catalase (both on an analytical and preparative scale) by IDA-Cu<sup>2+</sup> composite cellulose membrane [198,199]. A unique application for affinity purification is the separation of proteins differing by a single histidine molecule in their sequence by immobilized metal affinity chromatography.

Kasper et al. [200] proposed an affinity-chromatographic method for a fast, semipreparative isolation of recombinant protein G from *Escherichia coli*. Rigid, macroporous affinity discs based on a GMA-co-EDMA polymer were used as chromatographic supports. Human immunoglobulin G was immobilized by a single-step reaction. The globular affinity ligands were located directly on the pore wall surface and were therefore freely accessible to target molecules (protein G) passing with the mobile phase through the pores.

Examples of bioaffinity separations using monolithic stationary phases based on antigen-antibody, enzyme-substrate, enzyme-inhibitor, receptor-ligand interactions were reviewed recently [201]. Giovannini et al. [202] prepared poly (GMA-co-EDMA) membranes for the separation of supercoiled plasmid DNA. Gradient and isocratic elution was investigated and high-performance membrane chromatography experiments were compared with similar ones performed on a conventional packed-bed column. Amatschek et al. [135] developed an affinity-chromatographic method in which peptides, derived from a combinatorial library, were used as immobilized ligands for the purification of human blood coagulation factor VIII. Affinity monoliths based on a copolymer of glycidyl methacrylate and ethylene dimethacrylate using rabbit IgG and anti-FITC antibodies as ligands were recently developed for ultrafast immunoextractions [203].

Ion-exchange chromatography is probably the most widely used chromatographic method for protein separation. The principle of protein separation by ion exchange is the electrostatic interaction between the charges of the macromolecule and the adsorber surface. The protein must displace the counter ion of the exchangers and become attached on the sorbent's surface. The amount of macromolecule bound per unit volume of adsorptive membrane can be very high. However, for most exchangers, the binding capacity depends on the molecule size of the protein and adsorption conditions (pH, ionic strength, and protein concentration). Ion-exchange membranes can be produced by modification of commercially available microfiltration membranes.

Anion-exchange chromatography on membranes, disks, and rods bearing mainly quaternary amino groups or diethylaminoethyl groups as ligands has been used for the separation of serum proteins, microbial proteins and enzymes, membrane

proteins, cytokines, or nucleic acids [36,58,204–209]. BSA and HSA,  $\alpha$ -chymotrypsinogen, lysozyme, trypsin inhibitor, cytochrome c, ovalbumin,  $\alpha$ -lactoalbumin, conalbumin, ferritin, myoglobin, and chymotrypsin are just a few of the compounds isolated by anion-exchange membrane chromatography. The implementation of a CIM DEAE (diethylaminoethyl) monolith-based step into a large-scale plasmid DNA purification process was recently performed [210].

Cation-exchange membranes, despite the fact that they are not as widely investigated as that of anion-exchange membranes, allow recovery of human recombinant antithrombin from cell culture supernatants, purification of monoclonal and polyclonal antibodies, and isolation of immunofusion proteins produced extracellularly by *E. coli* [211–213]. The separation of similar size proteins such as serum albumin and hemoglobin using adsorber membranes loaded both with cation or anion-exchange particles was recently reported [214]. Li et al. [215] have used a cation-exchange monolith (prepared by polymerization of aqueous solution of appropriate monomers including the desired ligand directly in a fused-silica tube), as chromatographic supports for separation of four standard proteins (cytochrome c, lysozyme, myoglobin from horse and whale). High adsorption of lysozyme on macroporous chitosan carboxymethyl/cellulose blend membranes was recently reported [216].

The protein separations based on hydrophobic interactions and reverse phase use the interaction between aliphatic chains on the adsorbent and corresponding hydrophobic regions on the protein surface. Typical hydrophobic adsorbents commercially available include C<sub>4</sub>, C<sub>6</sub>, C<sub>8</sub>, or C<sub>10</sub> linear aliphatic chains, eventually with a terminal amino group. The main problems in hydrophobic chromatography are the slow association–dissociation processes and protein–protein interactions. Similar proteins can interact with each other as well as with the adsorbent leading to a large degree of overlapping between the elution components.

Hydrophobic chromatography has not been used in protein separation as intensive as ion exchange or affinity chromatography since sharp separations are not achieved. Nevertheless, chromatographic units with butyl ligand were used for purification of the recombinant tumor necrosis factor [207]. Tennikova et al. [2] reported separation of a protein mixture containing myoglobin, ovalbumin, lysozyme, and chymotrypsinogen on monolithic columns with C<sub>4</sub> or C<sub>8</sub> ligands. Zeng et al. [217] reported intensive studies on the preparation of monolithic stationary phases based on acrylic comonomers including piperazine diacrylamide, methacrylamide, and *N*-isopropylacrylamide for application in hydrophobic interaction chromatography of proteins. Chymotrypsinogen A, ribonuclease, myoglobin, trypsinogen, and lysozyme could be recovered with estimated values ranging from 91% to 99%. PS-*co*-DVB continuous rods were also investigated for the reversed-phase separation of proteins, alkylbenzenes, and peptides [218,219].

Particle-loaded membranes with embedded C<sub>8</sub> hydrophobic adsorbents were intensively investigated for several drug separations. Tricyclic antidepressants, antiarrhythmic drugs, amiodarone and its metabolite desethylamiodarone, and mexiletine and flecainide were extracted from serum using a 11 mm C<sub>8</sub> membrane adsorber with recoveries ranging from 82% to 98% [14,220].

Highly hydrophobic sorbents including porous carbon and copolymers of styrene and divinylbenzene (SDB) were widely investigated for environmental applications. The particle-loaded membranes containing modified SDB particles with surface sulfonic acid groups were successfully used for recovering different alcohols, phenols, aldehydes, ketones, or esters from aqueous samples [221]. Carbon-based PLM were also used for isolation of highly polar pesticides from water [222].

Chiral crown ether bonded on negatively charged polyacrylamide gels was prepared by Koide et al. [223] for enantiomeric separation of primary amino compounds with high efficiency and good reproducibility. Monolithic columns prepared by free radical polymerization of piperazine diacrylamide and methacrylamide in the presence of acetylsalicylic acid and L-tryptophan as additives were recently reported [224]. The monoliths, carrying immobilized human serum albumin as chiral selector, showed improved resolution when used for kynurenine and tryptophan enantiomeric separation. Continuous polymeric beds prepared either by entrapment in and simultaneous covalent linkage of allyl cellulose to the polymeric bed during preparation or by covalent immobilization of cellulose on an epoxy-activated continuous bed were investigated for enantiomers separation by Mohammad et al. [225]. Enantiomers of  $\beta$ -blockers and practolol were rapidly separated with good resolution.

Wang et al. [226] prepared a microfluidic system containing porous PVDF and PDMS membranes impregnated with bovine serum albumin as chiral chromatographic support. On-line BSA adsorption onto the membranes was employed for the preparation of chiral stationary phase allowing separation of racemic tryptophan and thiopental mixtures with high resolution. Chiral separation of racemic tryptophan, phenylglycine, and phenylalanine was also investigated through immobilized DNA membranes [227].

Multistage chromatography combines different types of chromatographic supports to achieve a higher degree of selectivity. A sequence of three membrane-based separation steps (including cation exchanger, dye-ligand, and anion-exchange membranes) enabled the purification of formate dehydrogenase from *C. bovidinii* [228] in micro- and laboratory scale. Using a sequence of ultrafiltration, diafiltration, Cibacron blue, anion exchanger, and heparin-membrane adsorber, pure recombinant human antithrombin III was obtained from hamster cell culture.

Branovic et al. [229] combined affinity and ion-exchange chromatography in a single column used to determine the impurities in immunoglobulin preparation. In their method, a monolithic disk bearing immobilized protein G with the leading role of retaining the immunoglobulins was placed on top of an ion-exchange disk, which could capture the impurities. Using specific elution conditions the immunoglobulins could be separated. A strong ion-exchange membrane adsorber carrying

**TABLE 3.6**  
**Comparison among Conventionally Packed Beds, Membrane and Monoliths Used in Bioseparations**

	Packed Bed		Membrane Adsorber		
	Big Beads	Small Beads	Particle Loaded	Chemical Functionalized	Monolithic Column
Capacity	+	++	+	+-	+-
Flow rate	+	-	++	++	++
Productivity	+	+	++	+	+
Resolution	+-	++	+	+	+
$\Delta P$	++	--	++	++	+
Prepurification	+	--	+	+	+-

sulfonic acid or quaternary ammonium groups and a Cibacron blue immobilized affinity adsorber were also investigated for mixed-mode interactions chromatography of standard protein mixtures as well as for the separation of whey proteins (BSA, IgG,  $\alpha$ -lactalbumin, and  $\beta$ -lactoglobulin) and recombinant human antithrombin III from biotechnological culture supernatants [230]. Using a series of four continuous beds each carrying a different affinity ligand, the one-step fractionation of four different antibodies from biological mixtures was achieved [231].

A mixed particle-loaded membrane consisting of a C<sub>8</sub> or C<sub>18</sub> hydrophobic adsorbents and a strong cation-exchange material can be used for selective extraction of pigments or imiquimod metabolites from urine with up to 95% recovery [232].

### 3.9 CONCLUSIONS

Packed-bed chromatography is still the standard method involved in capturing and polishing of biomolecules despite some major disadvantageous such as sensitivity to fouling and plugging, bed consolidation and compression, and high pressure drop and long cycle times. Membrane chromatography has obvious advantages over packed bed (Table 3.6). It uses microporous membranes that contain biospecific ligand molecules attached to their inner pore surface, as adsorbents. As a result of the convective flow of the feed solution through the porous structures the mass transfer resistance is tremendously reduced and the binding kinetic is usually dominating the adsorption process. This results in rapid processing and improved adsorption, washing, elution and regeneration steps, and minimize the probability of protein denaturation.

The technology is robust, fast and able to process huge volumes containing low concentrations of target molecules. Especially in the area where packed beds have severe shortcomings because of their limited pores size, for example, DNA recovery and virus removal, the membrane chromatography has a good opportunity to expand till market leader. The advantages of membrane chromatography have been confirmed by many successful applications. Nevertheless there is a scope for further improvement of the adsorptive membrane design by increasing the binding capacity, extension of the supplied ligands, and optimization of the hydrodynamics, and to assess the use of membrane chromatography in large-scale processes. In the near future, membrane chromatography may be the synergetic outcome of two mature techniques, chromatography and filtration that are at this moment the standards in biologic processing.

### REFERENCES

- Scopes RK. *Protein Purification: Principle and Practice*, New York: Springer-Verlag, 1995.
- Tennikova TB, Bleha M, Svec F, Almazova TV, and Belenkii BG. High-performance membrane chromatography of proteins: A novel method of protein separation. *J. Chromatogr.* 1991; 555: 97–107.
- Hoffer L, Schwinn H, and Josic D. Production of highly purified clotting factor IX by a combination of different chromatographic methods. *J. Chromatogr. A* 1999; 844: 119–128.
- Gemeiner P, Polakovic M, Mislovicová D, and Stefuca V. Cellulose as a (bio)affinity carrier: Properties, design and applications. *J. Chromatogr. B* 1998; 715: 245–271.
- Huber CG. Micropellicular stationary phases for high-performance liquid chromatography of double-stranded DNA. *J. Chromatogr. A* 1998; 806: 3–30.
- Afeyan NB and Fulton SP. High-throughput chromatography using perfusive supports. *LC-GC* 1991; 9: 824–832.
- Fulton SP and Afeyan NB. Very high speed separation of proteins with a 20- $\mu$ m reversed-phase sorbent. *J. Chromatogr.* 1991; 547: 452–456.
- Charcosset C. Purification of proteins by membrane chromatography. *J. Chem. Technol. Biotechnol.* 1998; 71: 95–110.
- Thommes J and Kula MR. Membrane chromatography—an integrative concept in the downstream processing of proteins. *Biotechnol. Prog.* 1995; 11: 357–367.
- Klein E. Affinity membranes: A 10-year review. *J. Membr. Sci.* 2000; 179: 1–27.

11. Roper DK and Lightfoot EN. Separation of biomolecules using adsorptive membranes. *J. Chromatogr. A* 1995; 702: 3–26.
12. Zou HF, Luo QZ, and Zhou DM. Affinity membrane chromatography for the analysis and purification of proteins. *J. Biochem. Biophys. Methods* 2001; 49: 199–240.
13. Zeng XF and Ruckenstein E. Membrane chromatography: Preparation and applications to protein separation. *Biotechnol. Prog.* 1999; 15: 1003–1019.
14. Lingeman H and Hoekstra-Oussoren SJF. Particle-loaded membranes for sample concentration and/or clean-up in bioanalysis. *J. Chromatogr. B* 1997; 689: 221–237.
15. Lensmeyer GL, Onsager C, Carlson IH, and Wiebe DA. Use of particle-loaded membranes to extract steroids for high-performance liquid chromatographic analyses improved analyte stability and detection. *J. Chromatogr. A* 1995; 691: 239–246.
16. Kopaciewicz W, Sheer DG, Arnold TE, and Goel V. Cast membrane structure for sample preparation, US Patent 6,048,457, 2000.
17. Boggs DR, Sternberg S, Pauley R, and McLarty DL. Composite membranes, methods for making such membranes, WO 00/02638, 2000.
18. Nagou S, Nakamura S, and Nishibayashi T. Microporous shaped article, process for preparation thereof, US Patent 5,238,735, 1993.
19. Josic D, Buchacher A, and Jungbauer A. Monoliths as stationary phases for separation of proteins and polynucleotides and enzymatic conversion. *J. Chromatogr. B* 2001; 752: 191–205.
20. Zou H, Huang X, Ye M, and Luo Q. Monolithic stationary phases for liquid chromatography and capillary electrochromatography. *J. Chromatogr. A* 2002; 954: 5–32.
21. Strancar A, Podgornik A, Barut M, and Necina R. Short monolithic columns as stationary phases for biochromatography. *Adv. Biochem. Eng. Biotechnol.* 2002; 76: 49–85.
22. Leinweber FC, Lubda D, Cabrera K, and Tallarek U. Characterization of silica-based monoliths with bimodal pore size distribution. *Anal. Chem.* 2002; 74: 2470–2477.
23. Guo W, Shang Z, Yu Y, and Zhou L. Membrane affinity chromatography of alkaline phosphatase. *J. Chromatogr. A* 1994; 685: 344–348.
24. Kubota N, Nakagawa Y, and Eguchi Y. Recovery of serum proteins using cellulosic affinity membrane modified by immobilization of  $\text{Cu}^{2+}$  ion. *J. Appl. Polym. Sci.* 1996; 62: 1153–1160.
25. Gerstner JA, Hamilton R, and Cramer SM. Membrane chromatographic systems for high-throughput protein separations. *J. Chromatogr.* 1992; 596: 173–180.
26. Chen ZA, Deng MC, Yong C, He GH, Ming W, and Wang JD. Preparation and performance of cellulose acetate/polyethyleneimine blend microfiltration membranes and their applications. *J. Membr. Sci.* 2004; 235: 73–86.
27. Hou KC and Zaniewski R. Purification of urokinase by combined cation exchanger and affinity chromatographic cartridges. *J. Chromatogr. B* 1990; 525: 297–306.
28. Hou KC, Zaniewski R, and Roy S. Protein A immobilized affinity cartridge for immunoglobulin purification. *Biotechnol. Appl. Biochem.* 1991; 13: 257–268.
29. Klein E, Eichhloz E, and Yeager DH. Affinity membranes prepared from hydrophilic coatings on microporous polysulfone hollow fibers. *J. Membr. Sci.* 1994; 90: 68–80.
30. Charcosset C, Su Z, Karoor S, Daun G, and Colton CK. Protein A immunoaffinity hollow fiber membranes for immunoglobulin G purification: Experimental characterization. *Biotech. Bioeng.* 1995; 48: 415–427.
31. Yang L, Jia L, Zou H, and Zhang Y. Immobilized metal affinity composite membrane based on cellulose for separation of biopolymers. *Sci. China B* 1998; 41: 596–605.
32. Zeng XF and Ruckenstein E. Control of pore sizes in macroporous chitosan and chitin membranes. *Ind. Eng. Chem. Res.* 1996; 35: 4169–4175.
33. Zeng XF and Ruckenstein E. Cross-linked macroporous chitosan anion-exchange membranes for protein separations. *J. Membr. Sci.* 1998; 148: 195–205.
34. Ruckenstein E and Zeng XF. Albumin separation with Cibacron blue carrying macroporous chitosan and chitin affinity membranes. *J. Membr. Sci.* 1998; 142: 13–26.
35. Klein E, Eichhloz E, Theimer F, and Yeager DH. Chitosan modified sulfonated poly(ethersulfone) as a support for affinity separations. *J. Membr. Sci.* 1994; 95: 199–204.
36. Briefs KG and Kula MR. Fast protein chromatography on analytical and preparative scale using modified microporous membranes. *Chem. Eng. Sci.* 1992; 47: 141–149.
37. Tang M, Zhang R, Bowyer A, Eisenthal R, and Hubble J. A reversible hydrogel membrane for controlling the delivery of macromolecules. *Biotech. Bioeng.* 2003; 82: 47.
38. Klein E, Yeager DH, Seshadir R, and Baurmiester U. Affinity adsorption devices prepared from microporous poly(amide) hollow fibers and sheet membranes. *J. Membr. Sci.* 1997; 129: 31–46.
39. Beeskow TC, Kusharyoto W, Anspach FB, and Kroner KH. Surface modification of microporous polyamide membranes with hydroxyethyl cellulose and their application as affinity membranes. *J. Chromatogr. A* 1995; 715: 49–65.
40. Gupta B and Anjum N. Preparation of ion-exchange membranes by hydrolysis of radiation-grafted polyethylene-g-polyacrylamide membranes. *J. Appl. Polym. Sci.* 2003; 90: 149–154.
41. Liao J, Zhang R, and Hjerten S. Continuous beds for standard and micro high-performance liquid chromatography. *J. Chromatogr.* 1991; 586: 21–26.
42. Xie S, Svec F, and Fréchet JMJ. Rigid porous polyacrylamide-based monolithic columns containing butyl methacrylate as a separation medium for the rapid hydrophobic interaction chromatography of proteins. *J. Chromatogr. A* 1997; 775: 65–72.
43. Kim M, Saito K, Furusaki S, Sugo T, and Ishigaki I. Protein adsorption capacity of a porous phenylalanine-containing membrane based on a polyethylene matrix. *J. Chromatogr.* 1991; 586: 27–33.

44. Plessier C, Gupta B, and Chapiro A. Modification of polypropylene fiber by radiation-induced graft copolymerization of acrylonitrile monomer. *J. Appl. Polym. Sci.* 1998; 69: 1343–1348.
45. Iwata H, Saito K, and Furusaki S. Adsorption characteristics of an immobilized metal affinity membrane. *Biotechnol. Prog.* 1991; 7: 412–418.
46. Kubota N, Kounosu M, Saito K, Sugita K, Watanabe K, and Sugo T. Preparation of a hydrophobic porous membrane containing phenyl groups and its protein adsorption performance. *J. Chromatogr.* 1995; 718: 27–34.
47. Kim M, Kojima J, Saito K, and Furusaki S. Reduction of nonselective adsorption of proteins by hydrophilization of microfiltration membranes by radiation-induced grafting. *Biotechnol. Prog.* 1994; 10: 114–120.
48. Kiyohara S, Kim M, Toida Y, Saito K, Sugita K, and Sugo T. Selection of a precursor monomer for the introduction of affinity ligands onto a porous membrane by radiation-induced graft polymerization. *J. Chromatogr. A* 1997; 758: 209–215.
49. Bueno SMA, Haupt K, and Vijayalakshmi MA. Separation of immunoglobulin G from human serum by pseudobioaffinity chromatography using immobilized L-histidine in hollow fibre membranes. *J. Chromatogr. B.* 1995; 667: 57–67.
50. Acconci C, Legallais C, Vijayalakshmi M, and Bueno SMA. Depyrogenation of snake antivenom serum solutions by hollow fiber-based pseudobioaffinity filtration. *J. Membr. Sci.* 2000; 173: 235–245.
51. Avramescu ME, Sager WFC, and Wessling M. Functionalised ethylene vinyl alcohol copolymer membranes for affinity protein separation. *J. Membr. Sci.* 2003; 216: 177–193.
52. Avramescu ME, Gironès M, Borneman Z, and Wessling M. Preparation of mixed matrix adsorber membranes for protein recovery. *J. Membr. Sci.* 2003; 218: 219–233.
53. Wang B, Cui YF, Du QY, and Pei GL. Study on preparation of heterogeneous polysulfone affinity filter membrane and its sorption properties for  $Hg^{2+}$ . *J. Appl. Polym. Sci.* 2003; 87: 908–915.
54. Higuchi A, Iwata N, and Nakagava T. Surface-modified polysulfone hollow fibers. II. Fibers having  $CH_2CH_2CH_2SO_3^-$  segments and immersed in HCl solution. *J. Appl. Polym. Sci.* 1990; 40: 709–717.
55. Higuchi A, Iwata N, and Nakagava T. Electroconducting polyaniline composite films prepared by chemical oxidative polymerization at gas/liquid interface. *J. Appl. Polym. Sci.* 1990; 41: 1073–1086.
56. Buchmeiser MR. New synthetic ways for the preparation of high-performance liquid chromatography supports. *J. Chromatogr. A.* 2001; 918: 233–266.
57. Wang QC, Svec F, and Fréchet JMJ. Hydrophilization of porous polystyrene-based continuous rod column. *Anal. Chem.* 1995; 67: 670–674.
58. Josic D, Reusch J, Loster K, Baum O, and Reutter W. High-performance membrane chromatography of serum and plasma membrane proteins. *J. Chromatogr.* 1992; 590: 59–76.
59. Tennikova TB and Svec H. High-performance membrane chromatography: Highly efficient separation method for proteins in ion-exchange, hydrophobic interaction and reversed-phase modes. *J. Chromatogr.* 1993; 646: 279–288.
60. Abou-Rebyeh H, Korber F, and Schubert-Rehberg K. Carrier membrane as a stationary phase for affinity chromatography and kinetic studies of membrane-bound enzymes. *J. Chromatogr. B* 1991; 566: 341–350.
61. Manganaro JL and Goldberg BS. Protein purification with novel porous sheets containing derivatized cellulose. *Biotechnol. Prog.* 1993; 9: 285–290.
62. Hagen DF, Mary SJA, Errede LA, and Carr PW. Composite chromatographic article. US Patent 4,810,381, 1989.
63. Dalven PI, Hildebrandt JR, Shamir A, Laccetti AJ, Hodgins LT, and Gregorh HP. Acrylonitrile-based copolymers: Synthesis, characterization, and formation of ultrafiltration membranes utilized for the immobilization of proteins. *J. Appl. Polym. Sci.* 1985; 30: 1113–1132.
64. Godjevargova Z, Dimon A, and Petrov S. Chemical modification of dialysis membrane based on poly(acrylonitrile-methylmethacrylate-sodium vinylsulfonate). *J. Appl. Polym. Sci.* 1992; 44: 2139–2143.
65. Bamford CH, Al-Lamee KG, Purbrick MD, and Wear TJ. Studies of a novel membrane for affinity separations. I Functionalisation and protein coupling. *J. Chromatogr.* 1992; 606: 19.
66. Hileman FD, Sievers RE, Hess GG, and Ross WD. In situ preparation and evaluation of open pore polyurethane chromatographic columns. *Anal. Chem.* 1973; 45: 1126–1130.
67. Hansen LC and Sievers RE. Highly permeable open-pore polyurethane columns for liquid chromatography. *J. Chromatogr.* 1974; 99: 123–133.
68. Sternberg S. Process for grafting amino acid molecules onto performed polymer surfaces and products prepared thereby. US Patent 4,340,482, 1982.
69. Blankstein LA and Dohrman L. An advanced affinity membrane for immunodiagnostic tests. *Am. Clin. Prod. Rev.* 1985; 4: 33.
70. Ritter K. Affinity purification of antibodies from sera using polyvinylidenedifluoride (PVDF) membranes as coupling matrices for antigens presented by autoantibodies to triosephosphate isomerase. *J. Immunol. Methods* 1991; 137: 209.
71. Li Y and Spencer HG. *Polymers of Biological and Biomedical Significance*, Washington DC: American Chemistry Society, 1994.
72. Serafica GC, Pimbley J, and Belfort G. Protein fractionation using fast flow immobilized metal chelate affinity membranes. *Biotechnol. Bioeng.* 1994; 43: 21.
73. Minakuchi H, Nakanishi K, Soga N, Ishizuka N, and Tanaka N. Octadecylsilylated porous silica rods as separation media for reversed-phase liquid chromatography. *Anal. Chem.* 1996; 68: 3498–3501.
74. Fields SM. Silica xerogel as a continuous column support for high-performance liquid chromatography. *Anal. Chem.* 1996; 68: 2709–2712.
75. Kesting RE, Fritzsche AK, Murphy MK, Cruse CA, Handermann AC, Malon RF, and Moore MD. The second-generation polysulfone gas-separation membrane. The use of Lewis acid: Base complexes as transient templates to increase free volume. *J. Appl. Pol. Sci.* 1990; 40: 1557–1574.

76. van Witte P, Dijkstra PJ, van Berg JWA, and Feijen J. Phase separation processes in polymer solutions in relation to membrane formation. *J. Membr. Sci.* 1996; 117: 1–31.
77. Bulte AMW, Mulder MHV, Smolders CA, and Strathmann H. Diffusion induced phase separation with crystallizable nylons. Mass transfer processes for nylon 4,6. *J. Membr. Sci.* 1996; 121: 37–49.
78. Mulder MHV. *Basic Principles of Membr. Technology*, Dordrecht, the Netherlands: Kluwer Academic, 1996.
79. Zeeman LJ and Zydney AL. *Microfiltration and Ultrafiltration: Principles and Applications*, New York: Marcel Dekker, 1996.
80. Reuvers AJ and Smolders CA. Formation of membranes by means of immersion precipitation: The mechanism of formation of membranes prepared from the system cellulose acetate–acetone–water. *J. Membr. Sci.* 1987; 34: 67–86.
81. Cheng LP, Dwan AH, and Gryte CC. Wholly aromatic thermotropic liquid crystalline polyesters of 4,4'-biphenol, substituted biphenols, and 1,1'-binaphthyl-4,4'-diol with 3,4'-benzophenone dicarboxylic acid. *J. Polym. Sci. Polym. Phys. B* 1995; 33: 211–225.
82. Reuvers AJ, van den Berg JWA, and Smolders CA. Formation of membranes by means of immersion precipitation: A model to describe mass transfer during immersion precipitation. *J. Membr. Sci.* 1987; 34: 45–65.
83. Tsay CS and McHugh AJ. Mass transfer modeling of asymmetric membrane formation by phase inversion. *J. Polym. Sci. Polym. Phys. B* 1990; 28: 1327–1365.
84. Cheng LP, Soh YS, Dwan AH, and Gryte CC. An improved model for mass transfer during the formation of polymeric membranes by the immersion-precipitation process. *J. Polym. Sci. Polym. Phys. B* 1994; 32: 1413–1425.
85. Klein E and Yeager D. Surface modified affinity separation membrane, WO 96/27614, 1996.
86. Cohen MAS, Flerer GJ, Lyklema J, Norde W, and Scheutjens JMH. Adsorption of ions, polyelectrolytes and proteins. *Adv. Colloid Interface Sci.* 1991; 34: 477–535.
87. Rodemann K and Staude E. Synthesis and characterization of affinity membranes made from polysulfone. *J. Membr. Sci.* 1994; 88: 271–278.
88. Nilsson JL. Fouling of an ultrafiltration membrane by a dissolved whey protein concentrate and some whey proteins. *J. Membr. Sci.* 1988; 36: 147–160.
89. Klein E, Eichholz E, and Yeager D. Affinity membranes prepared from hydrophilic coatings on microporous polysulfone hollow fibers. *J. Membr. Sci.* 1994; 90: 69–80.
90. Golub MA. Concerning apparent similarity of structures of fluoropolymer surfaces exposed to an argon plasma or argon ion beam. *Langmuir* 1996; 12: 3360–3361.
91. Sprang N, Theirich D, and Engemann J. Plasma and ion beam surface treatment of polyethylene. *Surf. Coat. Technol.* 1995; 74–75: 689–695.
92. Fozza A, Roch J, Klemberg-Sapieha JE, Kruse A, Hollander A, and Wertheimer MR. Oxidation and ablation of polymers by vacuum-UV radiation from low pressure plasmas. *Polym. Prepr.* 1997; 38: 1097.
93. Suhr H, Hollahan J, and Bell AT. eds., *Techniques and Applications of Plasma Chemistry*, New York: Wiley, 1974.
94. Olde Riekerink MB, Terlingen JGA, Engbers GHM, and Feijen J. Selective etching of semicrystalline polymers: CF<sub>4</sub> gas plasma treatment of poly(ethylene). *Langmuir* 1999; 15: 4847–4856.
95. Matsuyama H, Berghmans S, and Loyd DR. Formation of hydrophilic microporous membranes via thermally induced phase separation. *J. Membr. Sci.* 1998; 142: 213–224.
96. Wagh PB, Begar R, Pajonk GM, Venkateswara Rao A, and Haranath D. Comparison of some physical properties of silica aerogel monoliths synthesized by different precursors. *Mater. Chem. Phys.* 1999; 57: 214–218.
97. Colon LA, Guo Y, and Fermier A. Fritless packed columns for capillary electrochromatography: Separation of uncharged compounds on hydrophobic hydrogels. *Anal. Chem.* 1996; 68: 2753–2757.
98. Mansur HS, Vasconcellos WL, Lenza RS, Orefice RL, Reis EF, and Lobato ZP. Sol–gel silica based networks with controlled chemical properties. *J. Non-Cryst. Solids* 2000; 273: 109–115.
99. Alie C, Pirard R, Lecloux AJ, and Pirard JP. Preparation of low-density xerogels through additives to TEOS–based alcogels. *J. Non-Cryst. Solids* 1999; 246: 216–228.
100. Rodriguez SA and Colon LA. Investigations of a sol–gel derived stationary phase for open tubular capillary electrochromatography. *Anal. Chim. Acta* 1999; 397: 207–215.
101. Murata H, Meyers D, Kirkbir F, Ray CS, and Sarkar A. Drying and sintering of bulk silica gels. *J. Sol–Gel Sci. Technol.* 1997; 8: 397–402.
102. Murata H, Meyers DE, Kirkbir F, Ray CS, and Sarkar A. Sol–gel optics, Vol. III, In: J.D. Mackenzie (ed.), *SPIE Proceedings—The International Society for Optical Engineering*, Washington, DC: SPIE Vol. 2288, 1994.
103. Dieudonne P, Hafidi Alaoui A, Delord P, and Phalippou J. Transformation of nanostructure of silica gels during drying. *J. Non-Cryst. Solids* 2000; 262: 155–161.
104. Brinker CJ, Keefer KD, Schaefer DW, Assink RA, Kay BD, and Ashley CS. Sol–gel transition in simple silicates II. *J. Non-Cryst. Solids* 1984; 63: 45–59.
105. Nakanishi K, Minakuchi H, Soga N, and Tanaka N. Structure design of double-pore silica and its application to HPLC. *J. Sol–Gel Sci. Technol.* 1998; 13: 163–169.
106. Judenstein P, Titman J, Stamm M, and Schmidt H. Investigation of ion-conducting ormolytes—structure-property relationships. *Chem. Mater.* 1994; 6: 127–134.
107. Einarsrud MA. Light gels by conventional drying. *J. Non-Cryst. Solids* 1998; 225: 1–7.
108. Scherer GW. Effect of drying on properties of silica gel. *J. Non-Cryst. Solids* 1997; 215: 155–168.
109. Siouffi A-M. Silica gel-based monoliths prepared by the sol–gel method: Facts and figures. *J. Chromatogr. A* 2003; 1000: 801–818.

110. Minakuchi H, Nakanishi K, Soga N, Ishizuka N, and Tanaka N. Effect of skeleton size on the performance of octadecylsilylated continuous porous silica columns in reversed-phase liquid chromatography. *J. Chromatogr. A* 1997; 762: 135–146.
111. Minakuchi H, Ishizuka N, Nakanishi K, Soga N, and Tanaka N. Performance of an octadecylsilylated continuous porous silica column in polypeptide separations. *J. Chromatogr. A* 1998; 828: 83–90.
112. Dulay MT, Yan C, Rakestraw DJ, and Zare RN. Automated capillary electrochromatography: Reliability and reproducibility studies. *J. Chromatogr. A* 1996; 725: 361–366.
113. Chirica G and Remcho VT. Silicate entrapped columns—new columns designed for capillary electrochromatography. *Electrophoresis* 1999; 20: 50–56.
114. Legido-Quigley C, Marlin ND, Melin V, Manz A, and Smith NW. Advances in capillary electrochromatography and micro-high performance liquid chromatography monolithic columns for separation science. *Electrophoresis* 2003; 24: 917–944.
115. Zou H, Huang X, Ye M, and Lou Q. Monolithic stationary phases for liquid chromatography and capillary electrochromatography. *J. Chromatogr. A* 2002; 954: 5–32.
116. Maruska A and Kornysova O. Continuous beds (monoliths): Stationary phases for liquid chromatography formed using the hydrophobic interaction-based phase separation mechanism. *J. Biochem. Biophys. Methods* 2004; 59: 1–48.
117. Végvári Á, Földesi A, Hetényi C, Kochegarova O, Schmid MG, and Kudirkaite V. A new easy-to-prepare homogeneous continuous electrochromatographic bed for enantiomer recognition. *Electrophoresis* 2000; 21: 3116.
118. Ljunberg H and Nilsson S. Protein-based capillary affinity gel electrophoresis for chiral separation of  $\beta$ -adrenergic blockers. *J. Liq. Chromatogr.* 1995; 18: 3685.
119. Wang QC, Svec F, and Fréchet JMJ. Macroporous polymeric stationary-phase rod as continuous separation medium for reversed-phase chromatography. *Anal. Chem.* 1993; 65: 2243–2248.
120. Petro M, Svec F, Gitsov I, and Fréchet JMJ. Molded monolithic rod of macroporous poly(styrene-*co*-divinylbenzene) as a separation medium for HPLC of synthetic polymers. *Anal. Chem.* 1996; 68: 315–321.
121. Petro M, Svec F, and Fréchet JMJ. Molded continuous poly(styrene-*co*-divinylbenzene) rod as a separation medium for the very fast separation of polymers. *J. Chromatogr. A* 1996; 752: 59–66.
122. Luo Q, Wei Y, Liu T, Lei G, and Geng X. Poly(chloromethyl) styrene-*co*-divinylbenzene continuous rod column of weak cation exchange chromatography and its applications in the separation of biopolymers. *Chin. Chem. Lett.* 1999; 10: 215–218.
123. Tripp JA, Stein JA, Svec F, and Fréchet JMJ. “Reactive filtration”: Use of functionalized porous polymer monoliths as scavengers in solution-phase synthesis. *Org. Lett.* 2000; 2: 195–198.
124. Hjerten S, Liao JL, and Zhang R. High-performance liquid chromatography on continuous polymer beds. *J. Chromatogr.* 1989; 473: 273–275.
125. Xie SF, Svec F, and Fréchet JMJ. Preparation of porous hydrophilic monoliths: Effect of the polymerization conditions on the porous properties of poly(acrylamide-*co*-*N,N*-methylenebisacrylamide) monolithic rods. *J. Polym. Sci. A* 1997; 35: 1013–1021.
126. Svec F and Fréchet JMJ. Modified poly(glycidyl methacrylate-*co*-ethylene dimethacrylate) continuous rod columns for preparative-scale ion-exchange chromatography of proteins. *J. Chromatogr. A* 1995; 702: 89–95.
127. Svec F and Fréchet JMJ. “Molded” rods of macroporous polymer for preparative separations of biological products. *Biotechnol. Bioeng.* 1995; 48: 476–480.
128. Viklund C, Svec F, Fréchet JMJ, and Irgum K. Fast ion-exchange HPLC of proteins using porous poly(glycidyl methacrylate-*co*-ethylene dimethacrylate) monoliths grafted with poly(2-acrylamido-2-methyl-1-propanesulfonic acid). *Biotechnol. Prog.* 1997; 13: 597.
129. Grasselli M, Smolko E, Hargittai N, and Safrany A. From microspheres to monoliths: Synthesis of porous supports with tailored properties by radiation polymerization. *Nucl. Instrum. Methods Phys. Res. B* 2001; 185: 254–261.
130. Wulff G. Molecular imprinting in cross-linked materials with the aid of molecular templates—a way towards artificial antibodies. *Angew. Chem. Int. Ed. Engl.* 1995; 34: 1812–1832.
131. Mosbach K. Molecular imprinting. *Trends Biochem. Sci.* 1994; 19: 9–14.
132. Ansell RJ, Ramström O, and Mosbach K. Towards artificial antibodies prepared by molecular imprinting. *Clin. Chem.* 1996; 42: 1506–1512.
133. Remcho VT and Tan ZJ. MIPs as chromatographic stationary phases for molecular recognition. *Anal. Chem.* 1999; 71: 248–255A.
134. Matsui J, Kato T, Takeuchi T, Suzuki M, Yokoyama K, Tamiya E, and Karube I. Molecular recognition in continuous polymer rods prepared by a molecular imprinting technique. *Anal. Chem.* 1993; 65: 2223–2224.
135. Parham ME, Duffy RL, and Nicholson DT. Process of making a membrane for high efficiency removal of low density lipoprotein-cholesterol from whole blood. US Patent 5,258,149, 1993.
136. Hahn R, Podgornik A, Merhar M, Schallaun E, and Jungbauer A. Affinity monoliths generated by in situ polymerization of the ligand. *Anal. Chem.* 2001; 73: 5126–5132.
137. Takemoto K, Yoshiaki I, and Ottenbrite R. *Functional Monomers and Polymers*, New York: Marcel Dekker, 1987.
138. Axen R and Porath J. Preparation of cyanogen bromide-activated agarose gels. *Nature* 1966; 210: 367.
139. Patel AB, Stasiw R, Brown HD, and Ghioron C. Water insoluble pronase. *Biotechnol. Bioeng.* 1972; 14: 1031–1034.
140. Porath J, Aspberg K, Drevin H, and Axen R. Preparation of cyanogen bromide-activated agarose gels. *J. Chromatogr.* 1973; 86: 53–56.
141. Johansson AC and Mosbach K. Acrylic copolymers as matrices for the immobilization of enzymes: I. Covalent binding or entrapping of various enzymes to bead-formed acrylic copolymers. *Biochem. Biophys. Acta* 1974; 370: 339–347.
142. Axen R, Myrin P, and Janson J. Chemical fixation of chymotrypsin to water-insoluble crosslinked dextran (Sephadex) and solubilization of the enzyme derivatives by means of dextranase. *Biopolymers* 1970; 9: 401–413.
143. Kennedy JF and Zamir A. The use of cellulose carbonate for the insolubilisation of enzymes. *Carbohydr. Res.* 1973; 29: 497–501.
144. Kennedy JF and Zamir A. Use of cellulose xanthate for immobilization of biological molecules. *Carbohydr. Res.* 1975; 41: 227–233.

145. Kay G and Lilly MD. The chemical attachment of chymotrypsin to water-insoluble polymers using 2-amino-4,6-dichloro-s-triazine. *Biochim. Biophys. Acta* 1970; 198: 276–285.
146. Hearn MTW, Bethell GS, Ayers JS, and Hancock WS. Application of 1,1'-carbonyldiimidazole-activated agarose for the purification of proteins. *J. Chromatogr.* 1979; 185: 463–470.
147. Bethell GS, Ayers JS, Hearn MTW, and Hancock WS. Investigation of the activation of various insoluble polysaccharides with 1,1'-carbonyldiimidazole and of the properties of the activated matrices. *J. Chromatogr.* 1981; 219: 361–371.
148. McConway MG and Chapman RS. Application of solid-phase antibodies to radioimmunoassay evaluation of two polymeric microparticles, dynospheres and nylon, activated by carbonyldiimidazole or tresyl chloride. *J. Immunol. Methods* 1986; 95: 259–266.
149. Turkova J, Vajcner J, Vancurova D, and Stamberg J. Immobilization on cellulose in bead form after periodate oxidation and reductive alkylation. *Collect. Czech. Chem. Commun.* 1979; 44: 3411–3417.
150. Sundberg L and Porath J. Preparation of adsorbents for biospecific affinity chromatography: I. Attachment of group-containing ligand to insoluble polymers by means of bifunctional oxiranes. *J. Chromatogr.* 1974; 90: 87–98.
151. Shtilman MI. *New Concepts in Polymer Science, Immobilization on Polymers*, Utrecht: VSP, 1993.
152. Epstein CJ and Anfinsen CB. The reversible reduction of disulfide bonds in trypsin and ribonuclease coupled to carboxymethyl cellulose. *J. Biol. Chem.* 1962; 237: 2175–2179.
153. Bartling GJ and Brown HD. Protein modification in nonaqueous media. Preparation and properties of matrix-supported lysozyme. *Biotechnol. Bioeng.* 1974; 16: 361–369.
154. Scouten WH. *Affinity Chromatography*, New York: Wiley, 1981.
155. Weakley FB and Mehlretter CL. Binding of papain to dialdehyde starch. *Biotechnol. Bioeng.* 1973; 15: 1189–1192.
156. Walt DR and Agayn VI. The chemistry of enzyme and protein immobilization with glutaraldehyde. *Trends Anal. Chem.* 1994; 13: 425–430.
157. Traher AD and Kittrell JR. Immobilization of catalase on nickel-silica alumina. *Biotechnol. Bioeng.* 1974; 16: 413–417.
158. Van Leemputten E and Horisberger M. Immobilization of enzymes on magnetic particles. *Biotechnol. Bioeng.* 1974; 16: 385–396.
159. Jost R, Miron T, and Wilchek M. The mode of adsorption of proteins to aliphatic and aromatic amines coupled to cyanogen bromide-activated agarose. *Biochim. Biophys. Acta* 1974; 362: 75–82.
160. Manecke G, Gunzel G, and Forster HJ. Enzymes covalently bound to various polymers and effects on properties of these enzymes. *J. Polym. Sci. Polym. Symp.* 1970; 30: 607.
161. Weetall HH and Mason RD. Studies on immobilized papain. *Biotechnol. Bioeng.* 1973; 15: 455–466.
162. Carlsson J, Axen R, Brocklehurst K, and Crook EM. Immobilization of urease by thiol-disulphide interchange with concomitant purification. *Eur. J. Biochem.* 1974; 44: 189–194.
163. Bartling GJ, Brown HD, Forester LJ, Koes MT, Mather AN, and Stasiw RO. A study of the mechanism of cyanogen bromide activation of cellulose. *Biotechnol. Bioeng.* 1972; 14: 1039–1044.
164. Svec F and Fréchet JMJ. Continuous rods of macroporous polymer as high-performance liquid chromatography separation media. *Anal. Chem.* 1992; 64: 820–822.
165. Pan Z, Zou HF, Mo W, Huang X, and Wu R. Protein A immobilized monolithic capillary column for affinity chromatography. *Anal. Chim. Acta* 2002; 466: 141–150.
166. Müller W. New ion exchangers for the chromatography of biopolymers. *J. Chromatogr.* 1990; 510: 133–140.
167. Peters EC, Svec F, and Fréchet JMJ. Thermally responsive rigid polymer monoliths. *Adv. Mater.* 1997; 9: 630–633.
168. Mohr P and Pommerening K. *Affinity Chromatography: Practical and Theoretical Aspects*, New York: Marcel Dekker, 1986.
169. Klein E. *Affinity Membranes. Their Chemistry and Performance in Adsorptive Separation Processes*, New York: Wiley, 1991.
170. Hirata N, Kuriyama T, and Yamawaki N, Immusorba TR and PH. *Therap. Apheresis Dial.* 2003; 7: 85–90.
171. Bayramoglu G, Denizli A, and Arica MY. Membrane with incorporated hydrophobic ligand for hydrophobic interaction with proteins: Application to lipase adsorption. *Polym. Int.* 2002; 51: 966–972.
172. Mandjiny S and Vijayalakshmi MA. Membrane based pseudobioaffinity chromatography of placental IgG using immobilized L-histidine. *Biotechnol. Blood Proteins* 1993; 227: 189–195.
173. Legallais C and Anspach FB. Strategies for the depyrogenation of contaminated immunoglobulin G solutions by histidine-immobilized hollow fiber membrane. *J. Chromatogr. B* 1997; 691: 33–41.
174. Reif OW and Nier V. Immobilized metal affinity membrane adsorbents as stationary phases for metal interaction protein separation. *J. Chromatogr. A* 1994; 664: 13–25.
175. Ueda EKM, Gout PW, and Morganti L. Current and prospective applications of metal ion-protein binding. *J. Chromatogr. A* 2003; 988: 1–23.
176. Chaga GS. Twenty-five years of immobilized metal ion affinity chromatography: Past, present and future. *J. Biochem. Biophys. Methods* 2001; 49: 313–334.
177. Denizli A and Piskin E. Dye-ligand affinity systems. *J. Biochem. Biophys. Methods* 2001; 49: 391–416.
178. Fassina G, Ruvo M, Palombo G, Verdoliva A, and Marino M. Novel ligands for the affinity-chromatographic purification of antibodies. *J. Biochem. Biophys. Methods* 2001; 49: 481–490.
179. Kabir S. Immunoglobulin purification by affinity chromatography using protein A mimetic ligands prepared by combinatorial chemical synthesis. *Immunol. Invest.* 2002; 31: 263–278.
180. Amatschek K, Necina R, Hahn R, Schallaun E, Schwinn H, Josic D, and Jungbauer A. Affinity chromatography of human blood coagulation factor VIII on monoliths with peptides from a combinatorial library. *J. High Resol. Chromatogr.* 2000; 23: 47–58.
181. Platonova GA, Pankova GA, Il'ina IY, Vlasov GP, and Tennikova TB. Quantitative fast fractionation of a pool of polyclonal antibodies by immunoaffinity membrane chromatography. *J. Chromatogr. A* 1999; 852: 129–140.

182. Suen SY and Etzel MR. A mathematical analysis of affinity membrane bioseparations. *Chem. Eng. Sci.* 1992; 47: 1355–1364.
183. Lightfoot EN, Coffman JL, Lode F, Yuan QS, Perkins TW, and Root TW. Refining the description of protein chromatography. *J. Chromatogr. A* 1997; 760: 139–149.
184. Pendlebury D. Life science: New innovations in membrane chromatography. *A2C2 Live Sciences*, May 2003.
185. Thomas HC. Heterogeneous ion exchange in a flowing system. *J. Am. Chem. Soc.* 1944; 66: 1664.
186. Tejada A. Optimal design of affinity membrane chromatographic columns. *J. Chromatogr. A* 1999; 830: 293–300.
187. Athalye AM, Gibbs SJ, and Lightfoot EN. Predictability of chromatographic protein separations: Study of size-exclusion media with narrow particle size distributions. *J. Chromatogr. A* 1992; 589: 71–85.
188. Gebauer KH, Thommes J, and Kula MR. Breakthrough performance of high-capacity membrane adsorbers in protein chromatography. *Chem. Eng. Sci.* 1997; 52: 405–419.
189. Westerterp KR, van Swaaij WPM, and Beenackers AACM. Residence Time Distribution and Mixing in Continuous Flow Reactors, Chapter 4, *Chemical Reactor Design and Operation*, John Wiley & Sons, Chichester, 1984, 160–226.
190. Britannica Encyclopaedia, 1997.
191. Zhou D, Zou H, Ni J, Wang H, Yang L, and Zhang Y. Membrane affinity chromatography for analysis and purification of biopolymers. *Chromatographia* 1999; 50: 23–27.
192. Zhou D, Zou H, Ni J, Yang L, and Jia L. Fast assay and minipurification of proteins by high performance membrane affinity chromatography. *Chin. J. Biotechnol.* 1998; 14: 389–391.
193. Zhou D, Zou H, Ni J, Yang L, Jia L, and Zhang Y. Membrane support as stationary phase in high-performance chromatography. *Anal. Chem.* 1999; 71: 115–118.
194. Nachman M, Azad ARM, and Bailon P. Efficient recovery of recombinant proteins using membrane-based immunoaffinity chromatography (MIC). *Biotech. Bioeng.* 1992; 40: 564–571.
195. Malakian A, Golebiowska M, and Bellefeuille J. Purification of monoclonal and polyclonal IgG with affinity membrane matrix coupled with proteins A and G. *Am. Lab.* 1993; 25: 40P–40V.
196. Bueno SMA, Haupt K, and Vijayalakshmi MA. In vitro removal of human IgG by pseudobiospecific affinity membrane filtration on a large scale. A preliminary report. *Int. J. Artif. Organs* 1995; 18: 392–398.
197. Champluvier B and Kula MR. Dye-ligand membranes as selective adsorbents for rapid purification of enzymes: A case study. *Biotech. Bioeng.* 1992; 40: 33–40.
198. Woker R, Champluvier B, and Kula MR. Purification of *S*-oxynitrilase from *Sorghum bicolor* by immobilized metal ion affinity chromatography on different carrier materials. *J. Chromatogr. B* 1992; 584: 85–92.
199. Yang L, Jia L, Zou H, and Zhang Y. Immobilized iminodiacetic acid (IDA)-type  $\text{Cu}^{2+}$  chelating membrane affinity chromatography for purification of bovine liver catalase. *Biomed. Chromatogr.* 1999; 13: 229–234.
200. Kasper C, Meringova L, Freitag R, and Tennikova TB. Fast isolation of protein receptors from streptococci-G by means of macroporous affinity discs. *J. Chromatogr. A* 1998; 798: 65–72.
201. Platonova GA and Tennikova TB. Affinity processes realized on high-flow-through methacrylate-based macroporous monoliths. *J. Chromatogr. A* 2005; 1065: 19–28.
202. Giovannini R, Freitag R, and Tennikova TB. High-performance membrane chromatography of supercoiled plasmid DNA. *Anal. Chem.* 1998; 70: 3348–3354.
203. Jiang T, Mallik R, and Hage DS. Affinity monoliths for ultrafast immunoextraction. *Anal. Chem.* 2005; 77: 2362–2372.
204. Reif O-W and Freitag R. Characterization and application of strong ion-exchange membrane adsorbents as stationary phases in high-performance liquid chromatography of proteins. *J. Chromatogr. A* 1993; 654: 29–41.
205. Josic D and Lim Y-P. Application of high-performance membrane chromatography for separation of annexins from the plasma membranes of liver and isolation of monospecific polyclonal antibodies. *J. Chromatogr. B* 1994; 662: 217–226.
206. Broverman SA and Prestwich GD. Fast ion-exchange membrane purification of a microsomal protein. *BioTechniques* 1995; 19: 874–875.
207. Luksa J and Menart V. Purification of human tumour necrosis factor by membrane chromatography. *J. Chromatogr. A* 1994; 661: 161–168.
208. Huynh N and Motte JC. Sequential elution of denatured proteins, hydrolyzed RNA and plasmid DNA of bacterial lysates adsorbed onto stacked DEAE-cellulose membranes. *Anal. Biochem.* 1993; 211: 61–65.
209. Krajnc P, Leber N, Štefanec D, Kontrec S, and Podgornik A. Preparation and characterisation of poly(high internal phase emulsion) methacrylate monoliths and their application as separation media. *J. Chromatogr. A* 2005; 1065: 69–73.
210. Urthaler J, Schleg R, Podgornik A, Strancar A, Jungbauer A, and Necina R. Application of monoliths for plasmid DNA purification. Development and transfer to production. *J. Chromatogr. A* 2005; 1065: 93–106.
211. Langlotz P and Kroner KH. Surface-modified membranes as a matrix for protein purification. *J. Chromatogr.* 1992; 591: 107–113.
212. Lütkemeyer D and Siwiora S. Fast antibody purification by ion-exchange based on microporous membranes. *BioEngineering* 1992; 2: 34–44.
213. Wang WK and Lei S-P. Membrane adsorber process development for the isolation of a recombinant immunofusion protein. *BioPharm* 1995; 8: 52–59.
214. Avramescu ME, Sager WFC, Borneman Z, and Wessling M. EVAL-based adsorptive membranes for bilirubin removal. *J. Chromatogr. B* 2004; 803: 215–223.
215. Li Y, Liao J, Nakazato K, Mohammad J, Terenius L, and Hjerten S. Continuous beds for microchromatography: Cation-exchange chromatography. *Anal. Biochem.* 1994; 223: 153–158.

216. Chen X, Liu JH, Feng ZC, and Shao ZZ. Macroporous chitosan/carboxymethylcellulose blend membranes and their application for lysozyme adsorption. *J. Appl. Polym. Sci.* 2005; 96: 1267–1274.
217. Zeng CM, Liao J-L, Nakazato K, and Hjertén S. Hydrophobic-interaction chromatography of proteins on continuous beds derivatized with isopropyl groups. *J. Chromatogr. A* 1996; 753: 227–234.
218. Wang QC, Svec F, and Fréchet MJ. Reversed-phase chromatography of small molecules and peptides on a continuous rod of macroporous poly(styrene-*co*-divinylbenzene). *J. Chromatogr. A* 1994; 669: 230–235.
219. Xie SF, Allington RW, Svec F, and Fréchet MJ. Rapid reversed-phase separation of proteins and peptides using optimized “moulded” monolithic poly(styrene-*co*-divinylbenzene) columns. *J. Chromatogr. A* 1999; 865: 169–174.
220. Wells DA, Lensmeyer GL, and Wiebe DA. Particle-loaded membranes as an alternative to traditional packed-column sorbents for drug extraction—in-depth comparative-study. *J. Chromatogr. Sci.* 1995; 33: 386–392.
221. Johannes I and Tiikma L. Solid-phase disk extraction of resorcinol series phenols by BAKERBOND Speedisk (TM) DVB. *Oil Shale* 2000; 17: 323–333.
222. Bengtsson S, Berglof T, Granat S, and Jonsall G. Solid-phase extraction of pesticides from surface water using discs, bulk sorbents and supercritical fluid extraction (SFE). *Pesticide Sci.* 1994; 41: 55–60.
223. Koide T and Ueno K. Enantiomeric separations of primary amino compounds by capillary electrochromatography with monolithic chiral stationary phases of chiral crown ether-bonded negatively charged polyacrylamide gels. *J. Chromatogr. A* 2001; 909: 305.
224. Machtejevas E and Maruska A. A new approach to human serum albumin chiral stationary phase synthesis and its use in capillary liquid chromatography and capillary electrochromatography. *J. Sep. Sci.* 2002; 25: 1303–1309.
225. Mohammad J, Li YM, El-Ahmad M, Nakazato K, Pettersson G, and Hjerten S. Chiral-recognition chromatography of  $\beta$ -blockers on continuous polymer beds with immobilized cellulase as enantioselective protein. *Chirality* 1993; 5: 464–470.
226. Wang PC, Gao J, and Lee CS. High-resolution chiral separation using microfluidics-based membrane chromatography. *J. Chromatogr. A* 2002; 942: 115–122.
227. Higuchi A, Hayashi A, Kanda N, Sanui K, and Kitamura H. Chiral separation of amino acids in ultrafiltration through DNA-immobilized cellulose membranes. *J. Mol. Struct.* 2005; 739: 145–152.
228. Champluvier B and Kula MR. Sequential membrane based purification of proteins, applying the concept of multidimensional liquid chromatography (MDLC). *Bioseparation* 1992; 2: 343–351.
229. Branovic K, Lattner G, Barut M, Strancar A, Josic D, and Buchacher A. Very fast analysis of impurities in immunoglobulin concentrates using conjoint liquid chromatography on short monolithic disks. *J. Immunol. Methods* 2002; 271: 47–58.
230. Freitag R, Splitt H, and Reif OW. Controlled mixed-mode interaction chromatography on membrane adsorbers. *J. Chromatogr. A* 1996; 728: 129–137.
231. Vlach E, Ostryanina N, Jungbauer A, and Tennikova T. Use of monolithic sorbents modified by directly synthesized peptides for affinity separation of recombinant tissue plasminogen activator (t-PA). *J. Biotechnol.* 2004; 107: 275–284.
232. Asafu-Adjaye EB and Shiu GL. Solid-phase extraction high-performance liquid chromatography determination of verapamil and norverapamil enantiomers in urine. *J. Chromatogr. B* 1998; 707: 161–167.



---

# 4 Membranes in Gas Separation

*May-Britt Hägg*

## CONTENTS

4.1	Introduction .....	66
4.2	Transport Mechanisms for Gas through Membranes .....	68
4.2.1	Solution Diffusion .....	69
4.2.2	Knudsen Diffusion .....	71
4.2.3	Selective Surface Flow .....	71
4.2.4	Molecular Sieving .....	72
4.2.5	Ion-Conductive Transport .....	73
4.2.5.1	Proton-Conducting Membranes .....	73
4.2.5.2	Oxygen-Conducting Membranes .....	73
4.2.6	Facilitated Transport .....	74
4.3	Membrane Materials Used for Gas Separation .....	74
4.3.1	Polymeric Membranes .....	74
4.3.1.1	Polymers Receiving Special Interest .....	78
4.3.1.2	Fixed-Site Carrier Polymers .....	79
4.3.2	Carbon Molecular Sieving Membranes .....	80
4.3.2.1	Separation Properties for CMS Membranes .....	81
4.3.2.2	Regeneration .....	83
4.3.3	Mixed Matrix Membranes/Nanocomposites .....	83
4.3.3.1	MMM: Polymer with Carbon Molecular Sieves .....	84
4.3.3.2	MMM: Polymer with Nonporous Nanoparticles .....	84
4.3.4	Inorganic Membranes .....	84
4.3.4.1	Modified Inorganic Membranes .....	85
4.3.5	Ion-Conducting Membranes .....	86
4.3.5.1	Proton-Conducting Pd Membranes .....	86
4.3.5.2	Proton-Conducting Polymeric Membranes .....	87
4.3.5.3	Oxygen-Conductive Membranes .....	87
4.4	Module Design .....	88
4.4.1	Flat Sheet Plate and Frame/Envelope Type .....	89
4.4.2	Spiral-Wound Membrane .....	89
4.4.3	Hollow Fiber Membranes .....	90
4.4.4	Membrane Contactors .....	90
4.4.5	System Design .....	91
4.5	Current Applications and Novel Developments .....	91
4.5.1	Hydrogen Recovery .....	92
4.5.1.1	Novel Applications for Hydrogen: Fuel Cells .....	93
4.5.2	CO <sub>2</sub> Removal .....	94
4.5.2.1	CO <sub>2</sub> Removal from Natural Gas .....	94
4.5.2.2	CO <sub>2</sub> Removal from Biogas .....	95
4.5.2.3	Novel Applications for CO <sub>2</sub> Capture .....	96
4.5.3	Air Separation .....	98
4.5.3.1	Production of High-Purity Nitrogen .....	98
4.5.3.2	Oxygen-Enriched Air .....	98
4.5.3.3	Novel Developments for High-Purity Oxygen .....	99
4.5.4	Recovery of Volatile Organic Compounds .....	100

4.5.5	Separation of Hydrocarbons—Novel Membrane Developments .....	100
4.5.6	Other Applications .....	101
4.5.6.1	Water Vapor Removal from Air .....	101
4.5.6.2	Dehydration of Natural Gas .....	101
4.5.6.3	Helium Recovery .....	101
4.5.6.4	Recovery of Aggressive Gases: Cl <sub>2</sub> and HCl .....	101
4.6	Summary .....	101
	Acknowledgments .....	101
	References .....	102

## 4.1 INTRODUCTION

The application of membranes for gas separation is a fairly young technology compared to the use of membranes for liquid separation. Although the basic theoretical principles were partly understood and date back to the early nineteenth and twentieth century with Fick's law (1855), osmotic pressure (Van t'Hoff, 1887 and Einstein 1905), and membrane equilibrium (Donnan 1911), it was not until around 1950 that theories for gas transport through a membrane were presented and later further developed (pore model by Schmid in 1950 and Meares in 1956, solution-diffusion model by Lonsdale in 1965) [1]. The breakthrough for industrial membrane applications came with the development of the asymmetric membranes achieved by Loeb and Sourirajan around 1960 [2]. These membranes were developed for reverse osmosis and consisted of a very thin dense top layer (thickness <0.5 μm) supported by a thicker porous sublayer; hence the flux which is inversely proportional to the selective membrane thickness could be dramatically increased. The work of Loeb and Sourirajan resulted in commercialization of the reverse osmosis process for desalting of water, and had also a major impact on the further development of ultrafiltration and microfiltration processes. The development of gas separation membranes is based on their achievement and about 20 years later (~1980) the work of Henis and Tripodi made industrial gas separation economically feasible. They developed further the technique of putting a very thin homogenous layer of a highly gas permeable polymer on top of an asymmetric membrane, ensuring that pores were filled so that a leak-free composite membrane for gas separation was obtained. The first major development was the Monsanto Prism membrane for hydrogen recovery from a gas stream at a petrochemical plant [3]. Within a few years Dow Chemical Company was producing systems to separate nitrogen from air, and Cynara NATCO Group and Separex UOP LLC systems for separation of carbon dioxide from natural gas. These first membranes were all composite membranes where a very thin nonporous layer with high gas permeation rate (usually polysulfone or cellulose acetate (CA)) was placed on a support structure for mechanical strength—later other techniques for membrane formation were developed (i.e., interfacial polymerization, multilayer casting, and coating).

The interest from industry in membrane gas separation has nearly exploded over the last 10–15 years—the potential is enormous. So what are the attractive features to industry of membrane gas separation? The most obvious answer is the simplicity of the separation process. The standard units for gas separation usually involve large towers for absorption towers or stripping, adsorption beds, cryogenic distillation, large compressors, recovery and recycling of chemicals, all resulting in expensive and energy-demanding processes—not always without harmful effects to environment. This does not mean that a membrane process will be more economical nor as efficient as the traditional separation process used. However, as the trend goes, the development of tailor-made membranes for specific gas applications will most likely continue to bring the technology into focus as an attractive, economical, and environmental friendly alternative for gas separation. In theory the limitations are few for membrane applications, but in practice the challenges to succeed are numerous. For each application process, conditions must be taken into account (volume and composition of gas stream, pressures and temperatures, durability of the material), as the membrane separation properties may vary dramatically depending on these variables. This means that focus also must be on utilities and pretreatment of the gas in order to evaluate the economics and performance of the membrane process. Quite often a hybrid process combining membranes and standard unit operations may be the best solution.

As a general rule, the driving force of membrane gas separation is the difference in partial pressures (concentrations) between feed side and permeate side. It is however more correct to say that the driving force is the difference in chemical potential, thereby including the effect of temperature. An additional driving force may be an electric potential or a carrier effect for certain types of membranes. New membrane materials may combine different transport mechanisms, and thereby increase the flux and selectivities. A more detailed discussion on these issues will be given in Section 4.2.

The need for optimized membrane separation properties for specific gas mixtures kicked off an explosive development with respect to tailor-made polymeric membrane materials in the mid-nineties. The approach had until then been to look at existing polymeric materials and try to tailor separation properties by making moderate changes in the material. This could be done by synthesizing families of polymers (for instance polyimides, polycarbonates) with different fractional free volume (FFV) and glass transition temperature ( $T_g$ ), by using various methods for crosslinking or combining polymers like block copolymers.

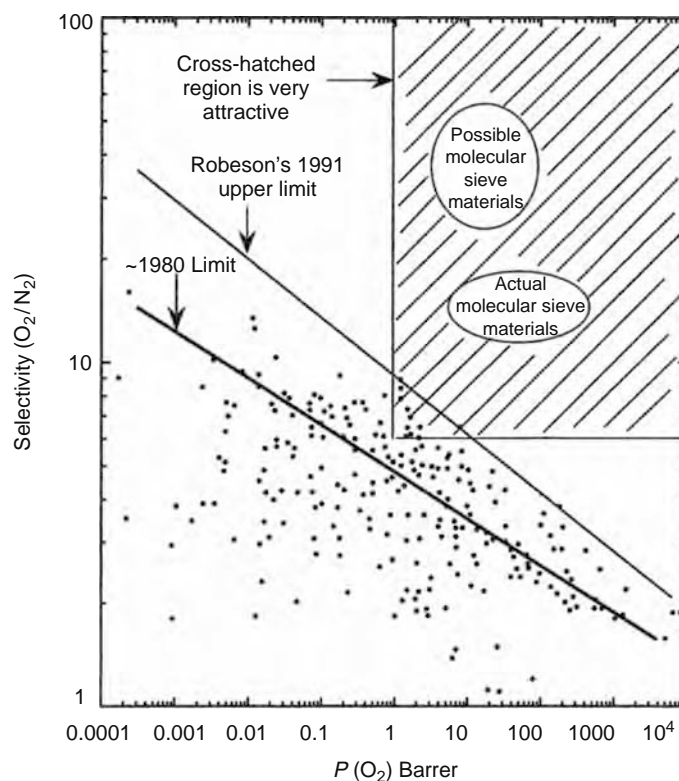


**FIGURE 4.1** Selectivity for the gas pair  $O_2-N_2$  as a function of  $O_2$  permeability. Properties of materials like molecular sieves and mixed matrix are expected to be found in the upper right corner (hatched area; modified Robeson plot). (From Singh A., Koros W.J., *Ind. Eng. Chem. Res.*, 35, 1231, 1996. With permission.)

Then in 1991 the now so well-known Robeson plot for polymeric membranes was published [4], an upper performance limit which has later challenged membrane scientists all over the world. New types of membrane materials started to emerge, challenging the separation properties shown in this plot. A new class of materials for gas separation was brought into focus: the carbon membranes. The concept of carbon membranes was known already around 1970, but it was not until the late 1980s with the published results of Koresh and Soffer that [5] these membranes caught general interest. Several scientists have later reported impressive gas separation properties with carbon molecular sieve (CMS) membranes pyrolyzed from different precursors [6–8]. In 1996, Singh and Koros presented a revised Robeson plot which included the potential of the CMS membranes (see Figure 4.1) [9]. Around the same time a patent for making such membranes on a commercial scale was obtained by Soffer et al. [10]. Later development has shown that despite excellent separation properties, also at high temperatures, these membranes are fairly brittle and expensive to process, so there is a need to find cheap precursors and secure mechanical strength in order to make them an economically good choice. The development following the pyrolyzed carbon membranes was actually one step back, now trying to combine the excellent separation properties of the carbon membranes with the more robust polymers—the mixed matrix membranes (MMM) are today in focus as a group of membranes with very high expectations. And parallel to this development, polymeric functionalized membranes, nanocomposite materials, as well as new block copolymers are being reported with intriguing gas separation properties—this is elaborated on in Section 4.3.

Inorganic materials usually possess superior chemical and thermal stability compared to polymers. However, their use as gas membrane materials has been limited up to now. The only application in the past was the enrichment of uranium hexafluoride ( $^{235}U$ ) by Knudsen flow through a porous ceramic membrane. Today a growing interest is being observed, and new materials are being developed for gas separation. Zeolite membranes have very narrow pore-size distribution, and are usually prepared by sintering or solgel processes. In combination with organic surface treatment for pore tailoring, acceptable gas separation properties have been reported. A good overview on inorganic membranes for gas separation is given by Burggraaf [11].

Last but not least, special membranes being 100% selective for a specific gas component should be mentioned. One of the most interesting materials is the metal palladium-based membranes for transport of hydrogen as proton through the membrane. This is especially interesting for fuel cells where high purity hydrogen is needed. Ceramic oxygen-conducting membranes producing high-purity oxygen have been reported by several investigators [12,13]. All these inorganic membranes are suitable

for high-temperature applications. The separation properties for these materials are excellent, and a significant breakthrough may be in the near future. The challenge will however still be the module making (brittle!) and price of the materials.

Membranes with carrier-facilitated transport for specific gas components have also been in focus for some years, but some of these membranes studied seem to be “dead-end” developments. Of special interest are however those reported for CO<sub>2</sub> capture, either as liquid membranes or as fixed-site carriers (FSC) in polymers [14,15].

All the materials mentioned above are discussed in the current chapter. If possible, SI units are applied for the data—the reader may find a useful table for conversion of units in Ref. [16]. Many good review papers and chapters in books on membranes for gas applications have been published recent years; only a few are referred to here [17–19]. A rich source of information on membrane materials and gas separation may also be found on the Web site of membrane producers and research institutes. One example is MTR [20].

## 4.2 TRANSPORT MECHANISMS FOR GAS THROUGH MEMBRANES

The most common types of membranes for gas separation in use today are still the dense polymeric materials where transport takes place according to a solution-diffusion mechanism with flux based on Fick’s law (Equation 4.1). For the microporous membranes (inorganic or hybrid), the transport mechanisms may be according to one of the following mechanisms or combinations of these: Knudsen diffusion, selective surface flow, or molecular sieving. The average pore size and pore-size distribution is important since it will give an indication of which transport mechanism can be expected to be dominant for a given gas mixture in a defined material and at given process conditions.

Fick’s law gives the mass flux through an area perpendicular to the flow direction:

$$J_i = -D_{ij} \frac{dc_i}{dx} \quad (4.1)$$

where

$J_i$  is the flux of component  $i$  (mol/(m<sup>2</sup> s))

$D_{ij}$  is the diffusion coefficient (m<sup>2</sup>/s)

$dc_i/dx$  is the concentration gradient for component  $i$  over the length  $x$  (mol/(m<sup>3</sup> m))

Fick’s law integrated and applied for a membrane yields  $dx = l$  (membrane thickness), and  $dc_i = \Delta p_i$  (concentration difference (i.e., partial pressures for gases) over the membrane.  $D_{ij}$  will vary according to the dominating transport mechanism.

The permeance  $P/l$  [mol/(m<sup>2</sup> Pa s)] (SI units) for a given gas ( $i$ ) is defined by

$$\frac{P_i}{l} = \frac{J_i}{\Delta p_i} \quad (4.2)$$

$P/l$  is also referred to as permeability flux and expressed as (m<sup>3</sup> (STP)/(m<sup>2</sup> bar h)).  $\Delta p_i$  is the partial pressure difference of “ $i$ ” across the membrane measured in pascals or bars. This equation shows that the flux through the membrane is proportional to the pressure difference across the membrane and inversely proportional to the membrane thickness. For selectivity between gas components the Equations 4.3 and 4.4 are referred to. The “ideal” separation factor,  $\alpha^*$  (Equation 4.3), may be expressed by the ratio of the pure gas permeabilities for the individual components  $i$  and  $j$ .

$$\alpha_{ij}^* = \frac{P_i}{P_j} \quad (4.3)$$

The separation factor for gases in mixture  $\alpha_{ij}$  (Equation 4.4) is expressed by the mole fractions of the components in the feed ( $x$ ) and the permeate ( $y$ ), respectively:

$$\alpha_{ij} = \frac{y_i/y_j}{x_i/x_j} \quad (4.4)$$

The permeability,  $P$ , can be expressed as the product of diffusion ( $D$ ) and solubility ( $S$ ) of the gas through the membrane (Equation 4.5):

$$P = D \cdot S \quad (4.5)$$

Depending on type of gas and type of membrane material, the importance of these two variables,  $D$  and  $S$ , will vary. Both the diffusion and the solubility coefficient for the gas are temperature dependent, while a pressure dependency is only observed for certain gases and materials.

Dense inorganic or metallic membranes for gas separation are usually ion-conducting materials, while membranes with carriers are polymers or supported liquid membranes (SLM). For transport through these materials, different flux equations should be applied. Figure 4.2 sums up and generalizes the various types of transport, which may take place in gas-separation membranes [21].

### 4.2.1 SOLUTION DIFFUSION

The transport of gas (permeability) through a dense, polymeric membrane can be described in terms of a solution-diffusion mechanism with permeability expressed as in Equation 4.5.

Type	Typical features of current primary membrane types
A. Asymmetric polymeric solution diffusion	<p>Thin selective skin layer (0.1 μm) Highly porous support (250 μm OD) (0.1–10 μm) <math>D_i = f_i \lambda_i^2 / 6</math> Diffusion step</p>
B. Molecular sieving (zeolite or carbon)	<p>Reverse selective skin layer (0.1 μm) Highly porous support layer (Wide range of sizes and morphologies)</p>
C. "Reverse selective" surface diffusion	<p>Reverse selective skin layer (1–5 μm) Highly porous ceramic or carbon support (7600 μm)</p>
D. Complexing and reactive	<p>e.g., O<sub>2</sub> carrier facilitated membranes N<sub>2</sub>, O<sub>2</sub>, Air e.g., palladium alloy membranes for H<sub>2</sub> H<sub>2</sub> → H<sub>2</sub> → 2H</p>
E. Proton exchange (PEM) (e.g., Nafion)	<p>750 μm PEM H<sup>+</sup> Load Hydrogen source Fuel cell</p>
F. Solid oxides	<p>1000 μm O<sup>2+</sup> Load Air Fuel cell</p> <p>1000 μm O<sup>2-</sup> 2e<sup>-</sup> Air Oxidative coupling membrane reactor</p>

**FIGURE 4.2** Illustration of transport mechanisms in microporous membranes. (From Koros W.J., *Macromol. Symp.*, 188, 13, 2002. With permission.)

TABLE 4.1

Permeabilities ( $P$ ) and Selectivities ( $\alpha$ ) of Various Gas Pairs in Silicone Rubber (PDMS) and Polycarbonate (PC)

Polymer	$T$ (°C)	$P_{\text{He}}$ (Barrer)	$\alpha_{\text{He}/\text{CH}_4}$	$\alpha_{\text{He}/\text{C}_2\text{H}_4}$	$P_{\text{CO}_2}$ (Barrer)	$\alpha_{\text{CO}_2/\text{CH}_4}$	$\alpha_{\text{CO}_2/\text{C}_2\text{H}_4}$	$P_{\text{O}_2}$ (Barrer)	$\alpha_{\text{O}_2/\text{N}_2}$
PDMS	35	561	0.41	0.15	4550	3.37	1.19	933	2.12
PC	35	14	50	33.7	6.5	23.2	14.6	1.48	5.12

Source: From Table of units, *J. Membr. Sci.*, 2, 237, 2004; Stern S.A., Shah V.M., Hardy B.J., *J. Polym. Sci. Part B Polym. Phys.*, 25, 1263, 1987; Koros W.J., Chan A.H., Paul D.R., *J. Membr. Sci.*, 2, 165, 1977; Jordan S.M., The effects of carbon dioxide exposure on permeability behaviour of silicone rubber and glassy polycarbonates. PhD dissertation, University of Texas at Austin, Austin, TX, 1988.

Note: 1 Barrer =  $7.52 \times 10^{-15} \text{ m}^3 \text{ (STP)/mm}^2 \text{ s kPa}$ .

The thermodynamic parameter,  $S$ , gives the pressure normalized amount of gas sorbed in the membrane under equilibrium conditions. This parameter is usually very low for gases in polymers, but will vary depending on physical properties of the gas (ideal, nonideal) and state of the polymer (glassy or rubbery). The state of the polymer is characterized by the material's glass transition temperature,  $T_g$ . Above  $T_g$  the polymer is in its rubbery state, and below  $T_g$  it is glassy. In glassy polymers the segmental motions of the chains are more restricted, and these materials are therefore able to discriminate more effectively between small differences in molecular dimensions. They exhibit an enhanced mobility selectivity compared to rubbery polymers. Table 4.1 shows a comparison of permeabilities and selectivities for both a rubbery (PDMS) and a glassy (PC) polymer. Crystallinity in a polymer will also restrict the gas transport.

For ideal systems (usually as in elastomers), the solubility will be independent of concentration and the sorption curve will follow Henry's law (Equation 4.6), i.e., gas concentration within the polymer is proportional to the applied pressure. For nonideal systems (usually as in glassy polymers), the sorption isotherm is generally curved and highly nonlinear. Such behavior can be described by free-volume models and Flory–Huggins thermodynamics—comprehensive discussions on this may be found elsewhere [1,25,26].

$$c_i = S_i p \quad (4.6)$$

The diffusivity,  $D$  (see Equation 4.5), is a kinetic parameter, and is dependent on the geometry of the polymer as well as its state (glassy, rubbery, swollen, etc.). A small molecule will more easily diffuse through a polymer than a larger one; however, large (organic or nonideal) molecules may have the ability to swell the polymer, hence large diffusion coefficients result and “reverse selectivity” may be observed. It is quite clear that the interdependency of molecular size, ideal or nonideal gases in mixtures, and structure and state of the polymer must be carefully evaluated in order to fully understand transport through polymers. This fundamental understanding will also govern how a membrane material may be best tailored for a given separation. For illustration of the complexity, Figure 4.3 shows the diffusion and sorption coefficient for some gases through natural rubber [27].

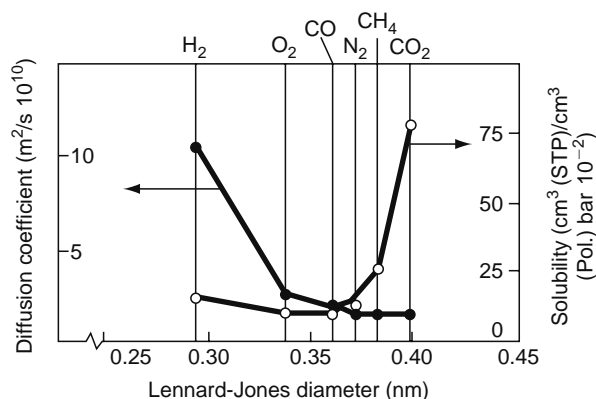


FIGURE 4.3 Solubility and diffusivity of various gases in natural rubber. (From Baker R.W., Blume I., *Chemtech.*, 16, 232, 1986. With permission.)

Transport through a dense polymer may be considered as an activated process, which can be represented by an Arrhenius type of equation. This implies that temperature may have a large effect on the transport rate. Equations 4.7 and 4.8 express the temperature dependence of the diffusion coefficient and solubility coefficient in Equation 4.5:

$$D = D_0 \exp(-E_d/RT) \quad (4.7)$$

$$S = S_0 \exp(-\Delta H_s/RT) \quad (4.8)$$

where

$E_d$  is the activation energy for diffusion

$\Delta H_s$  is the heat of solution

$D_0$  and  $S_0$  are temperature independent constants

By inserting Henry's law (Equation 4.6) into Fick's law (Equation 4.1), integrating across the membrane and remembering the definition of the permeability coefficient (Equation 4.5), Equation 4.2 was developed as the standard equation for transport through a dense polymeric membrane.

For gases in mixture, Equation 4.2 may be detailed out as in Equation 4.9:

$$J_i = \frac{P_i}{l} (p_h x_{i0} - p_l y_p) \quad (4.9)$$

where  $p_h$  and  $p_l$  denote pressure on feed side and permeate side, respectively. The fraction  $x_{i0}$  is the fraction of gas  $i$  on feed side, and depending on the design of the membrane module and flow regime for the gas, different calculation methods are adapted for this variable—details on this may be found elsewhere [1,28]. Parameters influencing the separation efficiency of polymers are elaborated on in Section 4.3.1.

#### 4.2.2 KNUDSEN DIFFUSION

Knudsen diffusion may take place in a microporous inorganic membrane or through pinholes in dense polymeric membranes. It may also take place in a mixed matrix membrane with insufficient adhesion between the phases.

Knudsen flow is characterized by the mean free path ( $\lambda$ ) of the molecules, which is larger than the pore size, and hence collisions between the molecules and the pore walls are more frequent than intermolecular collisions. A lower limit for the significance of the Knudsen mechanism has usually been set at  $d_p > 20 \text{ \AA}$  [28]. The classical Knudsen equation for diffusion of gas is

$$D_{Kn} = \frac{d_p}{3} \bar{v}_A = \frac{d_p}{3} \sqrt{\frac{8RT}{\pi M_A}} = 48.5 d_p \sqrt{\frac{T}{M_A}} \quad (4.10)$$

where

$d_p$  = average pore diameter (m)

$\bar{v}_A$  = average molecular velocity (m/s)

$M_A$  = molecular weight of gas component A (g/mol)

$T$  = temperature (K)

Hence for Knudsen diffusion, the square root of the inverse ratio of the molecular weights will give the separation factor. However, recent findings of Gilron and Soffer [29] indicate that the Knudsen mechanism can be significant for pore sizes as small as  $d_p \sim 5 \text{ \AA}$ . The Knudsen flow in this region takes on a slightly different form as indicated in the following expression derived as transport through a series of constrictions using resistance in series model:

$$D_{act, Kn} = g_d d_p \sqrt{\frac{8RT}{\pi M_A}} \exp\left(-\frac{\Delta E}{RT}\right) \quad (4.11)$$

Here  $g_d$  is the probability that a molecule can make a jump in the right direction given the jump length is  $d_p$  and the velocity is  $\bar{v}_A$ .

#### 4.2.3 SELECTIVE SURFACE FLOW

Selective surface flow is, as Knudsen diffusion, associated with transport through microporous membranes, usually inorganic materials. The mechanism of surface diffusion is disputed and several different approaches have been proposed in the literature.

Theories ranging from viewing the low surface coverage adsorbed gas as a 2D gas through a hopping model and into a more liquid like sliding layer exist. The mechanism dominating the surface diffusion coefficient will be influenced by a number of factors such as homogeneity of the surface, the temperature versus the adsorption enthalpy, and the surface concentration,  $c_s$  [30]. All three regimes can be described by a 2D analogue of Fick's law (Equation 4.1, given for a single component,  $a$ ). The flux,  $J_a$ , is now evaluated as molecules crossing a hypothetical line in the surface perpendicular to the direction  $x$ .  $D_s$  is the surface diffusion coefficient and  $dc_s/dx$  is the surface concentration gradient in the  $x$ -direction. The following expression may be used to determine if the surface transport is dominated by the 2D-gas model [30]:

$$q/RT < 1/a \quad (4.12)$$

where

$q$  is the adsorption enthalpy (J/mol)  
 $a$  is an energy fraction factor

The energy barrier for surface migration,  $E$ , is then defined as

$$E = aq \quad (4.13)$$

The 2D-gas is characterized by a surface mean free path,  $\lambda_s$ , inversely proportional to the surface concentration,  $c_s$ , and this  $\lambda_s$  value can be much larger than the spacing between adjacent surface sites.

If the  $q/RT$  part of Equation 4.12 is increased, then  $\lambda_s$  will no longer be controlled by collisions between adsorbed molecules. As  $q/RT$  increases,  $\lambda_s$  decreases and is approaching the spacing between adjacent sites, and a hopping mechanism is observed.

If the  $c_s$  is low then a random walk diffusion of independent molecules can be expected, and  $D_s$  would be given as

$$D_s = \frac{1}{4}\nu\lambda_s^2 \quad (4.14)$$

where  $\nu$  is the jump frequency factor, a factor which has a temperature dependence according to Arrhenius' law,  $\nu = \nu_0 \cdot \exp(-aq/RT)$  [1/s].

When  $c_s$  is increased, the chance of a molecule hitting another molecule increases and this interaction will bear some similarity to diffusion in liquid. Thus, the region of the sliding layer prevails. A more comprehensive discussion on this theory may also be found in Ref. [31].

Selective surface diffusion is governed by a selective adsorption of the larger (nonideal) components on the pore surface. The critical temperature,  $T_c$ , of a gas will thus indicate which component in a mixture is more easily condensable. The gas with the highest  $T_c$  will most likely be the fastest permeating component where a selective surface flow can take place. For a mixed gas an additional increase in selectivity may be achieved if the adsorbed layer now covering the internal pore walls restricts the free pore entrance so that the smaller nonadsorbed molecules cannot pass through.

#### 4.2.4 MOLECULAR SIEVING

Molecular sieving is the dominating transport mechanism when the pore size is comparable to the molecular dimensions, 3–5 Å; hence the smallest molecule will permeate, and the larger will be retained. The dimensions of a molecule are usually described with either the Lennard-Jones radii or the Van der Waal radii. For separation by molecular sieving, this is not a satisfactory way of stating the molecular size; a shape factor should also be included [9].

The sorption selectivity has little influence on the separation when molecular sieving is considered. An Arrhenius type of equation is still valid for the activated transport, but attention should be drawn to the pre-exponential term,  $D_0$  (see Equation 4.7). From transition state theory this factor may be expressed as shown in Equation 4.15 [32]:

$$D_0 = e\lambda^2 \frac{kT}{h} \exp\left(\frac{S_{a,d}}{R}\right) \quad (4.15)$$

where

$k$  and  $h$  are Boltzmann's and Planck's constants, respectively  
 $S_{a,d}$  is the activation entropy for diffusion  
 $e = g_d d_p$  in Equation 4.11

A change in entropy will thus have a significant effect on the selectivity when molecular sieving is considered. This is thoroughly discussed by Singh and Koros [9]. The flux may be described as in Equation 4.16 where  $E_{a,MS}$  is the activation energy for diffusion in the molecular sieving media.

$$J_a = \frac{\Delta p}{RTl} D_0 \exp\left(\frac{-E_{a,MS}}{RT}\right) \quad (4.16)$$

The selectivity for separation will normally decrease with increasing temperature because of increased diffusion rate for permeating components, and the sorption will be of minor importance.

#### 4.2.5 ION-CONDUCTIVE TRANSPORT

There are two important types of ion-conducting membranes for gas separation: (1) the proton ( $H^+$ )-conducting palladium membranes which are of great interest for combination with fuel cells and (2) the oxygen ion ( $O^{2-}$ )-conducting inorganic membranes, usually perovskite-type of oxides. Both are suitable for high temperature/high pressure applications, and an interesting feature is the 100% selectivity in favor of  $H_2$  and  $O_2$ , respectively.

##### 4.2.5.1 Proton-Conducting Membranes

Palladium and its alloys are recognized as very efficient proton-conducting membranes, which may be used for hydrogen separation and membrane reactor (MR) applications. The alloys are less apt to hydrogen embrittlement than pure Pd, and alloys with silver or copper represent the least expensive alternative of the alloys. These alloys also seem to produce membranes with enhanced chemical resistance (for instance toward  $H_2S$ ), additionally Pd–Ag alloys have a relatively higher  $H_2$  permeability than pure Pd. Efforts to produce economically viable Pd membranes have focused on preparing supported composite membranes with a thin dense Pd or Pd alloy layer. Forming this thin layer from two or more metals is quite challenging. The advantages of palladium membranes are especially the ability to separate out high-purity  $H_2$ , and that it may be used at high temperatures (300°C and above).

Hydrogen is present in many gas streams, being a product from dehydrogenation of hydrocarbons, a component in syngas or byproduct in bioprocesses. The basic flux equation for hydrogen,  $J_{H_2}$  (mol/m<sup>2</sup> s), is given in the following equation [33]. The flux for hydrogen atoms will be twice that of  $J_{H_2}$ :

$$J_{H_2} = -\frac{D_M}{2} \left( \frac{K_S(p_{H_2,ret}^n - p_{H_2,perm}^n)}{l} \right) \quad (4.17)$$

where

$D_M$  is the diffusion coefficient of a hydrogen atom in the metal (m<sup>2</sup>/s)

$K_S$  is the Sievert constant (mol/(m<sup>3</sup> Pa<sup>0.5</sup>))

For bulk transport of hydrogen,  $n = 0.5$  but approaches 1 for transport limited by surface kinetics. The exponent of 0.5 reflects the dissociation of the gaseous hydrogen molecule into two hydrogen atoms (protons) diffusing into the metal where an ideal solution of hydrogen in palladium is formed, then association again as  $H_2$  on the other side of the membrane. The hydrogen permeability of the palladium, here denoted as  $k$ , corresponds to the constants in Equation 4.17, expressed as in the following equation:

$$k = \frac{1}{2} D_M K_S \text{ (mol/m s Pa}^{0.5}\text{)} \quad (4.18)$$

Among the proton-conducting membranes Nafion or Nafion-like sulfonated perfluorinated polymers should also be mentioned. These materials are used for polymer electrolyte membrane (PEM) fuel cells, and in addition to being chemically very stable, they exhibit high proton conductivity at temperatures lower than 100°C. It is believed that permeability and thermal stability may be increased if tailor-made lamellar nanoparticles are added to a proton conducting polymer.

##### 4.2.5.2 Oxygen-Conducting Membranes

The zirconia and perovskite membranes may be considered as solid electrolyte membranes containing an oxygen ion conductor (various oxides). Depending on the type of materials used, the oxygen separation may take place according to direct excitation of the oxygen at several hundred degrees (gas separation controlled by electric current) or a mixed conductor method where the gas separation is proportional to  $\log(p_1/p_2)$ , the ratio of the partial pressures. (The reaction taking place at the electrodes is  $\frac{1}{2} O_2 + 2e^- \leftrightarrow O^{2-}$ , at the positive electrode the reaction is shifted to the left, at the negative electrode it is shifted to the right.) Detailed equations for transport can be found elsewhere [34,35].

### 4.2.6 FACILITATED TRANSPORT

Facilitated transport indicates that a carrier is introduced into the membrane matrix, usually a polymer matrix. This carrier will be selective for a certain gas component and enhance the transport of this component through the membrane.

The use of facilitated transport membranes for gas separation was first introduced by Ward and Robb [36] by impregnating the pores of a microporous support with a carrier solution, and a separation factor of 1500 was reported for CO<sub>2</sub>/O<sub>2</sub>. These membranes or supported liquid membranes (SLM) are discussed by several investigators, and initially very good separation properties are observed [37–40]. They are however known to have serious degradation problems like loss of carrier solution due to evaporation or entrainment with the gas stream, and the complexing agent (carrier) can be deactivated. These problems have restricted further development of SLMs. The use of ion exchange membranes as supports was proposed as an approach to overcome the problems of SLMs, and the application of ion exchange membranes for the facilitated transport of CO<sub>2</sub> and C<sub>2</sub>H<sub>4</sub> was first reported by LeBlanc et al. [41]. Since then a number of papers have been published on this type of membrane. Along with the use of ion exchange membranes as supports, another approach to overcome the above mentioned limitations was developed by introducing carriers directly into solid polymer membranes as illustrated in Refs. [42,43]. The FSC membranes have carriers covalently bonded to the polymer backbone, hence the carriers have restricted mobility, but are favorable when stability is considered. It is obvious that the diffusivity (and thus permeability) in an FSC membrane is lower than that of a mobile carrier membrane. The diffusivity of a swollen FSC-membrane should however show diffusivities between that of a mobile and a fixed carrier. Various ways of enhanced carrier transport have later been suggested [15,44,45]. It is suggested by many that CO<sub>2</sub> will be transported as carbonate or bicarbonate anions in anion-exchange membranes and as anions of various amines in cation-exchange membranes.

The characteristic of a facilitated or carrier-mediated transport is the occurrence of a reversible chemical reaction or complexation process in combination with a diffusion process. This implies that either the diffusion or the reaction is rate limiting: The total flux of a permeant A will thus be the sum of both the Fickian diffusion and the carrier-mediated diffusion as illustrated in Equation 4.19 [46]:

$$J_A = \frac{D_A}{l} (c_{A,0} - c_{A,l}) + \frac{D_{AC}}{l} (c_{AC,0} - c_{AC,l}) \quad (4.19)$$

where the first term on the right hand side of the Equation 4.19 is the Fickian diffusion ( $D_A$ ), and the second term represents the carrier-mediated diffusion ( $D_{AC}$ ).  $l$  is the thickness of the membrane, while  $c$  (as defined by Henry's law, Equation 4.6) is the concentration of the component A and its complex AC at the interfaces of the membrane, and 0 and  $l$  indicate feed side and permeate side, respectively. The concentration difference of the complex AC in Equation 4.19 must be further expressed by an equilibrium constant of the complexing reaction and a distribution coefficient. This is given in detail by Cussler [46]. Nonpolar gases in a gas mixture will exclusively be transported through the membrane by Fickian diffusion, while by using partial pressures ( $p_A$ ) instead of concentration  $c_A$  (inserting Equation 4.6 into Equation 4.19), it can easily be seen that the driving force through the membrane will be the difference in partial pressures for the Fickian diffusion, and that transport also will depend on the solubility coefficient,  $S_A$ , for the gas in the polymer. For carrier-mediated transport (second term in Equation 4.19), the driving force will be the concentration difference of the complex AC through the membrane. The permeation of the nonpolar gases may additionally be hindered by polar sites introduced into the membrane matrix [15,44,45]. This should then lead to an increased permeance of the carrier-transported gas compared to ideal gases in the mixture (like CH<sub>4</sub>, N<sub>2</sub>, and O<sub>2</sub>), giving high selectivities in favor of the complexed gas (like for instance CO<sub>2</sub>). A proposed mechanism for facilitated transport for CO<sub>2</sub> in an FSC membrane is illustrated in Figure 4.4 [15].

## 4.3 MEMBRANE MATERIALS USED FOR GAS SEPARATION

To select the right membrane for a given gas separation is very challenging as the criteria are quite complex. The first choice is usually based on favorable flux and selectivity for a given gas mixture. Membrane performance will however have to be evaluated with respect to operating conditions as well as mechanical strength and durability. Finally, separation efficiency will have to be balanced against cost for each case evaluated. Choice of "the right membrane" may therefore have more than one answer. In this section properties for various materials available for gas separation membranes are discussed.

### 4.3.1 POLYMERIC MEMBRANES

Polymeric materials are still the most widely used membranes for gas separation, and for specific applications the separation technology is well established (see Section 4.6). Producing the membranes either as composites with a selective skin layer on flat sheets or as asymmetric hollow fibers are well-known techniques. Figure 4.5 shows an SEM picture of a typical composite polymeric membrane with a selective, thin skin layer of poly(dimethyl)siloxane (PDMS) on a support structure of polypropylene (PP). The polymeric membrane development today is clearly into more carefully tailored membranes for specific

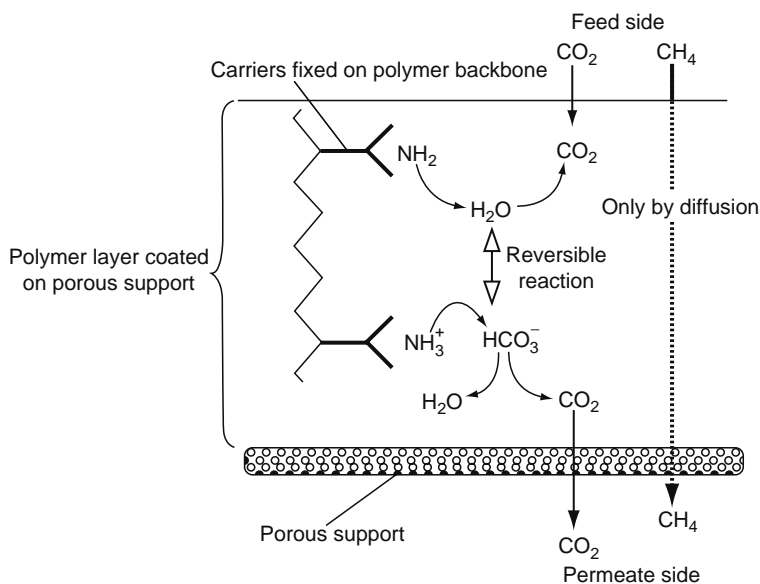


**FIGURE 4.4** A proposed mechanism of facilitated transport of CO<sub>2</sub> in an FSC membrane. (From Kim T.J., Hägg M.B., *J. Pol. Sci. Part B Polym. Phys.*, 42, 4326, 2004. With permission.)

applications. The important material properties defining the separation performance are molecular structure, glass transition temperature ( $T_g$ ), crystallinity, degree of crosslinking, and as a function of these variables, durability with respect to possible degradation or loss of performance.

The basic transport mechanism through a polymeric membrane is the solution diffusion as explained in Section 4.2.1. As noted, there is a fundamental difference in the sorption process of a rubbery polymer and a glassy polymer. Whereas sorption in a rubbery polymer follows Henry’s law and is similar to penetrant sorption in low molecular weight liquids, the sorption in glassy polymers may be described by complex sorption isotherms related to unrelaxed volume locked into these materials when they are quenched below the glass transition temperature,  $T_g$ . The various sorption isotherms are illustrated in Figure 4.6 [47].

The solubility in glassy polymers is usually described by the so-called dual-mode model, which implies that there is a need for a more detailed definition of the sorption,  $c$ , in the flux Equation 4.1. Equations 4.20 and 4.21 illustrate this and can relate to

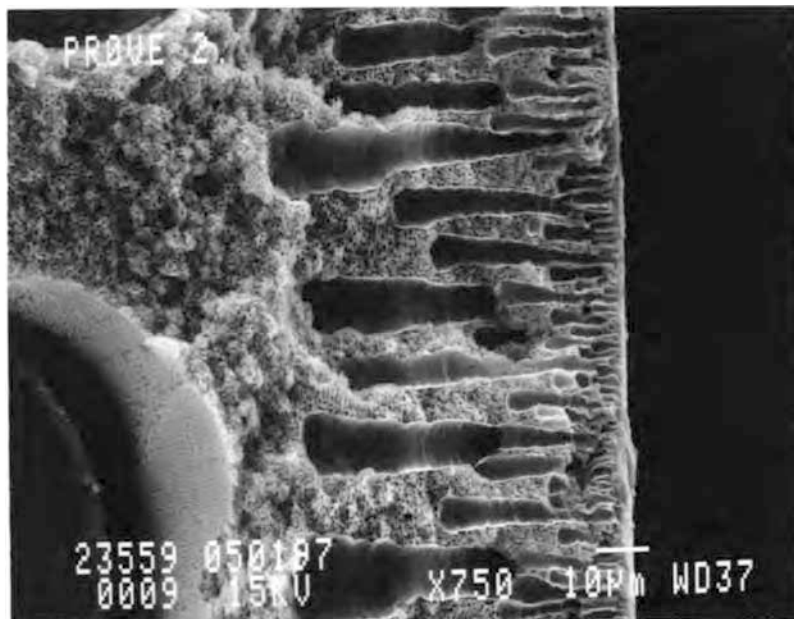


**FIGURE 4.5** SEM-picture of a typical composite membrane comprising of support structure of PP and a selective skin layer of PDMS.

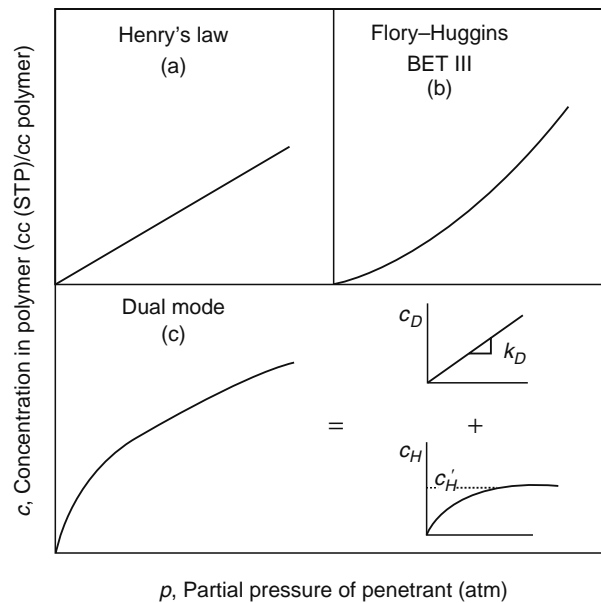


**FIGURE 4.6** Typical gas sorption isotherms for polymers: (a) Henry's law illustrating ideal sorption as in a rubbery polymer where solubility is independent of concentration, (b) illustrating a highly nonlinear behavior according to Flory-Huggins; as can be expected for interactions between organic liquids or liquids with polymers (swelling results), and (c) illustrating the dual mode sorption (Langmuir) typical for a glassy polymer. (From Koros W.J., Chern R.T., *Separation of gaseous mixtures using polymer membranes*. In: Rousseau R.W., ed. *Handbook of Separation Process Technology*. John Wiley & Sons, New York, 862, 1987. With permission.)

Figure 4.6. The term  $c_D$  accounts for Henry's law, while  $c_H$  is the Langmuir term with  $b$  being the hole affinity constant ( $\text{bar}^{-1}$ ) and  $c'_H b$  is the saturation constant ( $\text{cm}^3 (\text{STP})/\text{cm}^3$ ):

$$c = c_D + c_H \quad (4.20)$$

$$c = k_D p + \frac{c'_H b p}{1 + b p} \quad (4.21)$$

The dual-mode model has been extensively covered by several authors [25,47–49].

Figure 4.7 illustrates how the available free volume for transport increases with increasing temperature ( $V_f = V_T - V_l$ ), and the remarkable change when passing the  $T_g$  of a polymer [50]. According to the free volume diffusion model, the diffusion of molecules depends on the available free volume as well as sufficient energy to overcome polymer–polymer attractive forces. The specific volume at a particular temperature can be obtained from the polymer density, whereas the volume occupied at 0 K can be estimated from group contributions. Details on this theory may be found in relevant handbooks, textbooks, and numerous publications [25,48–52].

Nonideal gases dissolve more easily in polymers, and hence the separation factor may easily be in favor of a larger, nonideal gas component, compared to a small ideal gas. At the same time the nonideal component may swell the membrane, hence the net result is a decrease in selectivity. For a polymeric membrane, flux and selectivity are inversely related, hence a high flux usually means low selectivity. Elastomers have higher flux and lower selectivity for a given gas pair than a glassy material. This problem can be addressed by various methods: controlled crosslinking, opening the matrix by inserting carefully designed side groups to the main polymer chain, or functionalizing the polymer. Tables 4.2 and 4.3 illustrate how separation properties may be changed within two families of polymers by the change of side groups: polycarbonates [25,53] and polyimides [54].

Glassy polymers may swell in the presence of plasticizing agents, hence selectivities will be reduced and flux will be increased—the membrane loses performance. One way of avoiding this problem may be to incorporate cross-linkable functional groups in the polymer backbone. The crosslinking will be performed in the posttreatment process, and will hinder uncontrolled swelling. Regions of crystallinity and chemical crosslinking have somewhat similar effects on the transport properties of a rubber by causing restrictions of swelling and suppression of long-chain segmental motion. Transport in semicrystalline polymers is more complex due to tortuosity caused by the presence of the typically impermeable crystalline regions. Studies of gas sorption and transport strongly support the notion of the impenetrability of crystalline domains by even tiny gas molecules. The sorption coefficient seems to be essentially proportional to the volume fraction of amorphous material, while the effect on diffusion is more complex [25].

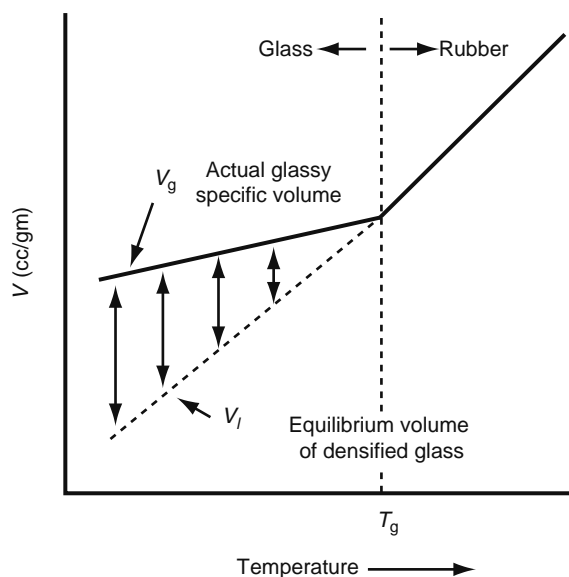
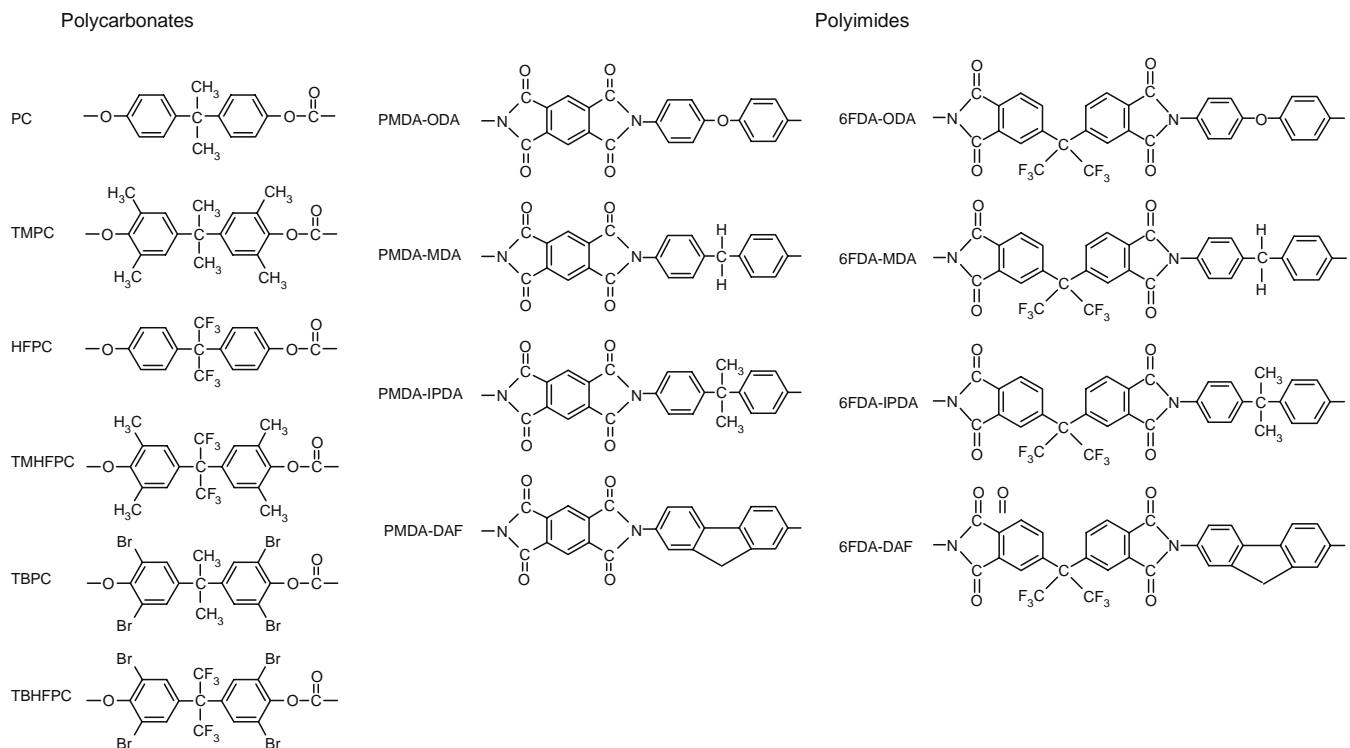


**FIGURE 4.7** Polymeric specific volume as a function of temperature. (From Chern R.T., Koros W.J., Sanders E.S., Chen S.H., Hopfenberg H.B. In: Whyte T., Yon C.M., Wagener E.H., eds. *ACS Symposium Series 223 on Industrial Gas Separations*. American Chemical Society, Washington DC, 47, 1983. With permission.)

**TABLE 4.2**  
**Structures of Characterized Families of Polycarbonates and Polyimides**



Source: From Koros W.J., Hellums M.W., Transport properties. In: Kroschwitz, J.I., ed. *Encyclopedia of Polymer Science*. 2nd ed. Wiley-Interscience Publishers, New York, 1989: Supplement vol. 724–802; Koros W.J., Hellums M.W., *Fluid Phase Equilibria*, 53, 339, 1989; Kim T.H., Koros W.J., Husk G.R., O'Brien K.C., *J. Membr. Sci.*, 37, 45, 1988.

Note: See Table 4.3 for properties.

**TABLE 4.3**  
**Permeabilities and Selectivities of Polycarbonates and Polyimides**

Polymer	Permeabilities at 35°C (Barrer)			Ideal Selectivities at 35°C		
	He 10 atm	O <sub>2</sub> 2 atm	CO <sub>2</sub> 10 atm	He/CH <sub>4</sub> 10 atm	O <sub>2</sub> /N <sub>2</sub> 2 atm	CO <sub>2</sub> /CH <sub>4</sub> 10 atm
<b>Polycarbonates</b>						
PC	13	1.6	6.8	35	4.8	19
TMPC	46	5.6	18.6	50	5.1	21
HFPC	60	6.9	24	57	4.1	23
TMHFPC	206	32	111	44	4.1	24
TBPC	18	1.4	4.2	140	7.5	34
TBHFPC	100	9.7	32	112	5.4	36
TB/TBHF-co-PC	49	4.9	16	110	6.2	34
<b>Polyimides</b>						
PMDA-ODA	8.0	0.61	2.71	134.9	6.1	45.9
PMDA-MDA	9.4	0.98	4.03	94	4.9	42.9
PMDA-IPDA	37.1	7.1	26.8	41.1	4.7	29.7
PMDA-DAF	1.9	—	0.15	921	—	71.6
6FDA-ODA	51.5	4.34	23	135.4	5.2	60.5
6FDA-MDA	50	4.6	19.3	117.1	5.7	44.9
6FDA-IPDA	71.2	7.53	30	102.1	5.6	42.9
6FDA-DAF	98.5	7.85	32.2	156.3	6.2	51.1

*Source:* From Table of units, *J. Membr. Sci.*, 2, 237, 2004; Koros W.J., Hellums M.W., Transport properties. In: Kroschwitz, J.I., ed. *Encyclopedia of Polymer Science*. 2nd ed. Wiley-Interscience Publishers, New York, Supplement vol. 1989, 724–802; Koros W.J., Hellums M.W., *Fluid Phase Equilibria*, 53, 339, 1989; Kim T.H., Koros W.J., Husk G.R., O'Brien K.C., *J. Membr. Sci.*, 37, 45, 1988.

*Note:* 1 Barrer =  $7.52 \times 10^{-15}$  m<sup>3</sup> (STP)/mm<sup>2</sup> s kPa.

#### 4.3.1.1 Polymers Receiving Special Interest

The block copolymers form an interesting group of materials with promising separation properties for selected gas mixtures. These membranes usually combine the flexible phase of an elastomer with a dispersed phase of a glassy or crystalline polymer. The hard domains will act as physical crosslinks, and the temperature should not be raised above the  $T_g$  of the glassy polymer. Morphology and properties of the block copolymers are mainly determined by the  $A/B$  ratio and the size of the blocks. The separation mechanism in these membranes is typically based on sorption diffusion, but if correctly tailored, the sorption selectivity will be governing the separation. Examples that can be mentioned are copolymers of ethylene and vinyl alcohol. These two components are able to co-crystallize in the same crystal lattice, and the material can be tailored by varying the amount of the highly polar, diffusion-inhibiting vinyl alcohol component without strongly affecting the crystallinity [25]. Another example reported is block copolymers composed of polyamide (PA) and polyethylene glycol (PEG). In this material, the semicrystalline PA blocks will ensure the structural integrity while high molecular weight PEG will control the separation [55]. The permselectivity will typically be reverse, and these membranes may have a great potential for CO<sub>2</sub> capture or VOC removal from gas streams. Interesting results for CO<sub>2</sub>-H<sub>2</sub> separation (reverse selective) have been published by several authors [56,57].

The perfluorinated polymers are materials of special interest due to their exceptionally good chemical and thermal stability compared to other polymers. The challenge has however for many years been to prepare these materials with suitable gas separation properties. They used to be either very crystalline or too porous, hence selectivities were low. They may however be prepared as high flux—low selectivity membranes, which is acceptable for certain applications. Materials prepared from tetrafluoroethylene (TFE)

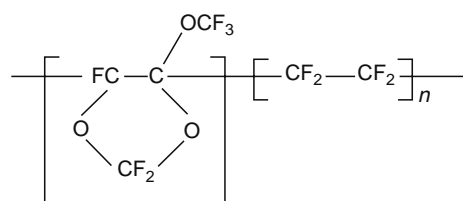


**FIGURE 4.8** Structure of Hyflon AD.

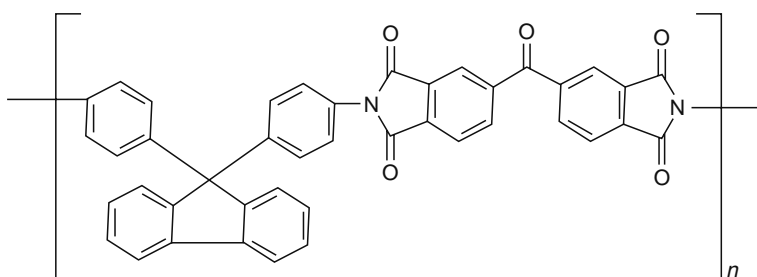


FIGURE 4.9 Example of structure of a cardopolymer based on polyimide.

and cyclic dioxole (TTD) are highly hydrophobic and have good potential for use in gas–liquid membrane contactors. The copolymer known commercially as Hyflon AD is made from TFE and TTD, and is an amorphous perfluoropolymer with glass transition temperature ( $T_g$ ) higher than room temperature. Hyflon AD 60 shows values of permeability and selectivity for gases that make the material interesting for separation—this was documented by Arcella et al. [58].

Kharitonov et al. [59] have shown that direct fluorination of the polyimide Matrimid is possible, hence the resulting membrane should have a nice potential for use in harsh environment. Perfluorinated materials were also studied by Hägg [60] for chlorine gas purification, and were shown to be exceptionally stable in these harsh environments. The selectivity was however too low. In a later publication on chlorine purification [31] it was suggested to use perfluorinated monomers as surface-modifying compounds for pore tailoring of glass membranes for chlorine gas separation.

Hydrophilic perfluoromembranes may be prepared from TFE and copolymerized with perfluorosulfonylfluoridevinylether (SFVE), making a so-called Hyflon ion polymer, which is a rubbery polymer at room temperature. This polymer contains the group  $-\text{SO}_2\text{F}$  where F can be exchanged for a metal or hydrogen atom. This makes the material suitable for a wide variety of fields ranging from electrochemical electrolyzers (chloralkali and HCl), proton exchange fuel cells, energy storage, and electro dialysis to membrane catalytic reactors and many more applications [58].

The cardopolymers are polymers containing very bulky aromatic structure in the main chain. This structure can be coupled to a polyimide, polyamide, or polysulfone. Example of a cardopolymer based on polyimide is shown in Figure 4.9. The polymer may be further modified by substituting methyl groups or halogens into the aromatic rings. The bulky structure gives the polymers high gas permeability and high solubility for nonideal gases (like  $\text{CO}_2$  and hydrocarbons); they can be easily processed and are fairly heat stable. These materials have been extensively studied at Research Institute of Innovative Technology for the Earth (RITE) in Japan, and papers have been published documenting nice separation properties for  $\text{CO}_2/\text{N}_2$  ( $>35$ ) [61,62]. This makes the cardopolymers, especially the polyimide based, interesting for recovery of  $\text{CO}_2$  in flue gas. Takeuchi et al. [63] evaluated the costs of a global process of  $\text{CO}_2$  fixation and utilization using catalytic hydrogenation reaction, and converting  $\text{CO}_2$  to methanol. The recovered  $\text{CO}_2$  was then based on a membrane process using a cardopolymer.

The acetylene-based polymers have received new interest. These glassy polymers are amorphous and characterized by very high glass transition temperature (typically  $>200^\circ\text{C}$ ), high free volume, and very high gas permeabilities. The well-known poly(1-trimethylsilyl-1-propyne) (PTMSP) has the highest gas permeability of all known polymers. This polymer and other acetylene-based polymers show higher permeabilities to large condensable organic vapors than to small permanent gases [64], and PTMSP has the highest  $\text{C}_{2+}/\text{CH}_4$  and  $\text{C}_{2+}/\text{H}_2$  selectivities of any known polymer [65]. The selectivity of these gases is typically reverse compared to what is expected in a polymeric membrane. This can be understood by the large free volume in these polymers, and the high solubility of the hydrocarbons in the material. The transport may be described in the same way as the selective surface flow through a microporous membrane or a mixed matrix material (see Sections 4.3.2 and 4.3.3). Pinnau et al. [66], among others, have investigated the effects of the side-chain structure of substituted polyacetylenes on their gas permeation properties (see Figure 4.10).

#### 4.3.1.2 Fixed-Site Carrier Polymers

As an alternative to conventional polymeric membranes, facilitated transport membranes have attracted attention due to the potential of achieving both high permeabilities and high selectivities. Facilitated transport membranes may for instance selectively permeate  $\text{CO}_2$  by means of a reversible reaction of  $\text{CO}_2$  with incorporated complexing agent (carrier) in the membrane, whereas gases such as  $\text{H}_2$ ,  $\text{N}_2$ , and  $\text{CH}_4$  will permeate exclusively by the solution diffusion mechanism. As pointed out in Section 4.2.6, the ion exchange membranes were introduced as an approach to overcome the problems of SLMs, and the application of ion exchange membranes for the facilitated transport of  $\text{CO}_2$  and  $\text{C}_2\text{H}_4$  was first reported by LeBlanc et al. [41]. Since then a number of papers have been published on this type of membrane [67–70]. Along with the use of ion exchange membranes as supports, yet another approach to overcome the above limitations was developed by introducing carriers directly into polymer membranes [42,71,72]. These FSC membranes have carriers covalently bonded to the polymer backbone, hence the carriers have restricted mobility, but are favorable when stability is considered. It is obvious that the diffusivity (and thus

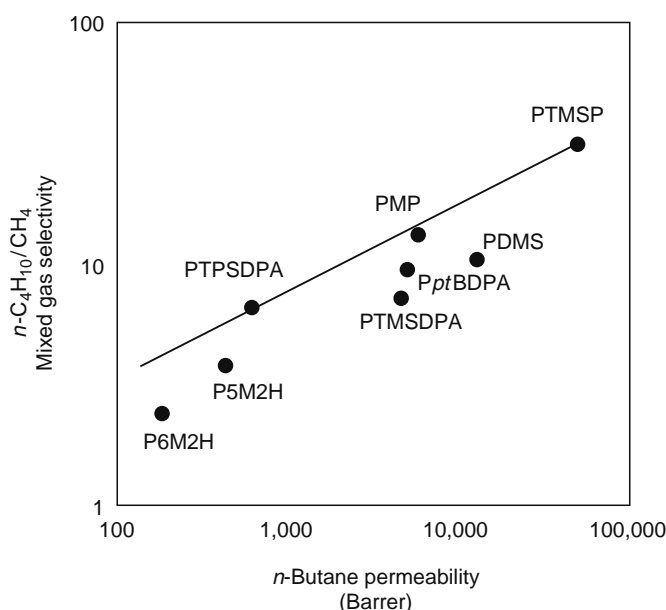


**FIGURE 4.10** Relationship between mixed gas  $n$ -butane permeability and  $n$ -butane/methane selectivity for a series of glassy polyacetylenes and rubbery PDMS. Feed pressure: 10 bar; permeate pressure: 1 bar; temperature: 25°C. (From Pinnau I., He Z., Morisato A., *J. Membr. Sci.*, 241, 363, 2004. With permission.)

permeability) in an FSC membrane is lower than that of a mobile carrier membrane. The diffusivity of a swollen FSC membrane should however show diffusivities between that of a mobile and a fixed carrier.

The aminated polymeric membranes for facilitated transport of CO<sub>2</sub> have been investigated extensively in recent years [69,73–75,15]. The findings of several of these investigators were that the aminated polymeric membranes showed higher permselectivity in water swollen condition than in dry condition—an ideal selectivity as high as 1000 for CO<sub>2</sub>/CH<sub>4</sub> was documented by Kim et al. [15]. Although promising, a mixed gas selectivity is, however, expected to show a significantly lower value. The anticipated mechanism for transport through the membrane is described in Section 4.2.6 and is illustrated in Figure 4.4. There has been a major increase in published papers and patents within the field of facilitated transport membranes during the period between writing and publishing of the current chapter; the author apologize for not having been able to incorporate these references.

The biomimetic membranes represent a special group of carrier membranes. They are artificial membranes based on biomembrane mimicking, i.e., imitation of the essential features biomembranes use for separation. Nitrocellulose filters impregnated with fatty acids, their esters, and other lipid-like substances may be used—in other words, an imitation of many nonspecific barrier properties of biomembranes. The transport of gas through these membranes will essentially be according to facilitated transport (see Section 4.2). Biomimetic membranes for CO<sub>2</sub> capture will transport the gas as HCO<sub>3</sub><sup>-</sup>. Development of these materials may be expected for selected applications.

### 4.3.2 CARBON MOLECULAR SIEVING MEMBRANES

The carbon molecular sieving (CMS) membranes are microporous carbon fibers or flat sheets prepared from carbonization of polymeric precursors under controlled conditions. Depending on the membrane pore size and the process conditions, the separation may take place according to (1) molecular sieving ( $d_p < 5 \text{ \AA}$ ), (2) selective surface flow ( $5 \text{ \AA} < d_p < 12 \text{ \AA}$ ), (3) Knudsen diffusion ( $d_p > 20 \text{ \AA}$ ), or combinations of these [6,29] (see Sections 4.2.2 through 4.2.4). The membranes for gas separation are prepared as hollow fibers or flat sheets. The hollow fibers may have the largest potential for becoming a successful separation unit on an industrial scale due to the possibility of making modules with a high packing density (m<sup>2</sup>/m<sup>3</sup>). The production process of these membrane modules is however challenging and expensive, and costs need to be brought down to be interesting for larger gas volume applications. The use of cheap polymeric precursors is favorable. Properties that should place the carbon membranes among the most promising membrane materials are their high temperature resistance and excellent chemical resistance to acids, hot organic solvents, and alkaline baths. The carbon membranes are fairly easy to produce as much is known about how carbonization conditions affect separation properties [6–11]. A carbon membrane can thus be tailored with a pore size giving excellent separation properties for a given gas mixture (high flux for permeating component and high selectivity for gas pairs).

The most serious disadvantages that have to be overcome or controlled are brittleness and the vulnerability of membranes to oxidizing agents and water vapor resulting in performance loss over time, hence regeneration is needed at intervals. When these effects are detected in the membrane performance, it is important to know how to address the problem (or preferably how to avoid it). It is important to know how to “open” pores which are blocked, how to regenerate the membrane, or how to optimize

separation performance by controlling the process variables. If basic knowledge about these membranes is not known to a user, he or she may very quickly draw the conclusion that CMS membranes are unstable, have too large a decrease in performance over time, and will probably judge them as “not suitable.” This may be very wrong. When used correctly, CMS membranes are promising candidates for gas separation and moderate volume gas streams.

The CMS membranes may be prepared in two different ways, and in both cases the pore tailoring is the focus for the final membrane:

1. By careful control of carbonization conditions; this is done by controlling heating rate, heating temperature, and choice of inert gas or vacuum during the process [76].
2. As explained in the patent of Soffer et al. [10], where microporous cellulose fibers are treated with CVD, and pores are tailored by postoxidation.

CMS membranes may also easily be functionalized, i.e., metals (like  $\text{AgNO}_3$ ,  $\text{MgO}$ ,  $\text{Fe}_2\text{O}_3$  or others) are imbedded in the structure of the precursor, and will enhance the separation for certain gas pairs.

A comprehensive review on carbon membranes has been given by Ismail and David [77].

#### 4.3.2.1 Separation Properties for CMS Membranes

The ability of a microporous carbon fiber to separate gases depends on the pore size of the membrane, the physiochemical properties of the gases, and surface properties of the membrane pore. The pore size of a carbon fiber for gas separation is usually within the range of 3.5–10 Å, depending on the conditions for preparation of the membrane during carbonization or treatment afterward (postoxidation or chemical vapor deposition) [6–11]. With reference to the typical range indicated above for the transport mechanisms, one would expect that the dominating mechanisms will be either molecular sieving or selective surface flow.

Figure 4.11 illustrates a carbon membrane with pores in the range suitable for molecular sieving [78]. As expected, there is a clear and indisputable correlation between flux and molecular size. In Figure 4.12, the carbon membrane is more open (pore size in the range 6–10 Å). The gas pair reported is  $\text{CO}_2$  and  $\text{CH}_4$ , and as can be seen, the selectivity is clearly in favor of  $\text{CO}_2$  indicating selective surface flow. The critical temperatures,  $T_c$ , and Lennard-Jones diameters,  $d_{L-J}$ , for the two gases are

$$\text{CO}_2: d_{L-J} = 3.94 \text{ \AA}, T_c = 304 \text{ K}$$

$$\text{CH}_4: d_{L-J} = 3.74 \text{ \AA}, T_c = 190.4 \text{ K}$$

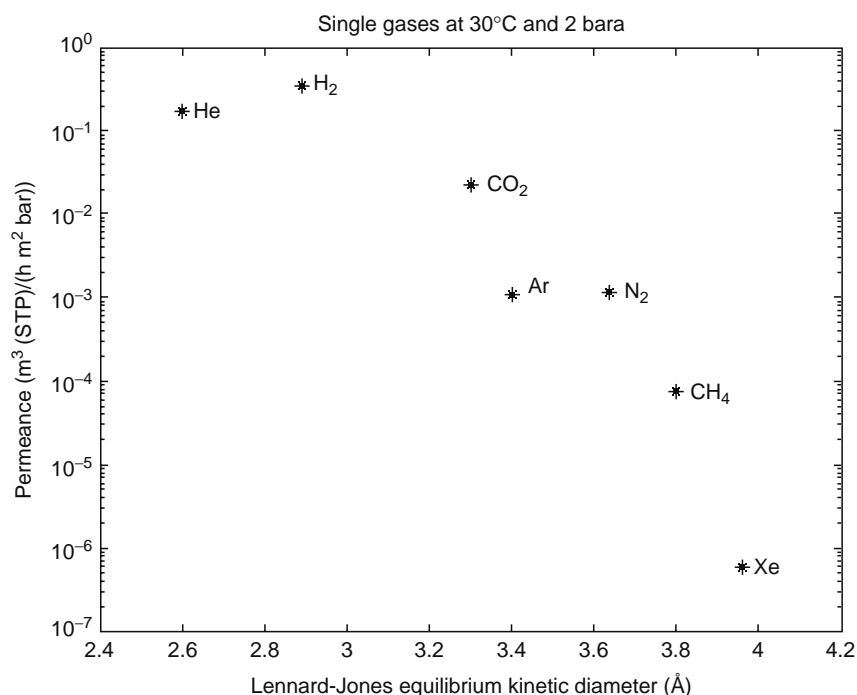


**FIGURE 4.11** Permeance as a function of L–J diameter for a sieving carbon membrane. (From Lie J.A., Synthesis, performance and regeneration of carbon membranes, Doctoral thesis NTNU 2005: 152, Trondheim, Norway, 2005. With permission.) Note: 1 [Å] = Ångstrom = 10<sup>-10</sup> m.

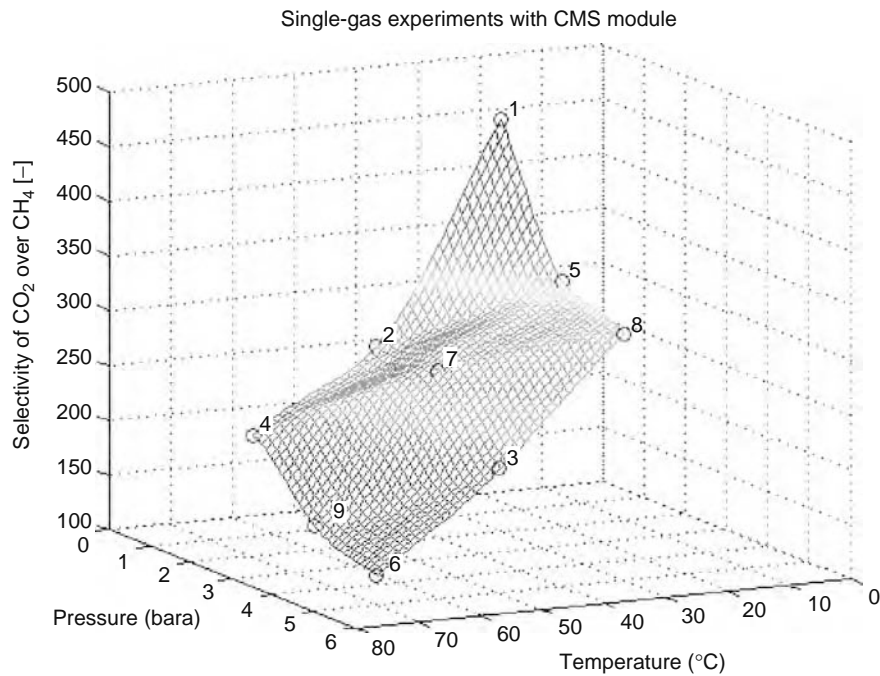


**FIGURE 4.12** Selectivity of  $\text{CO}_2/\text{CH}_4$  as a function of pressure and temperature for a CMS membrane. (From Lie J.A., Hägg M.B., Characterization of carbon membranes. Poster at The European Membrane Society's 20th Summer School, Trondheim, Norway, 2003. With permission.)

The easily condensable  $\text{CO}_2$  molecule will follow an SSF mechanism and seriously hinder  $\text{CH}_4$  to permeate, hence high selectivities are obtained.

Figure 4.13 illustrates the importance of finding the optimum process conditions (temperature, pressure) for the gas mixture to obtain maximum separation effect [79]. The diagram shows how the flux of propane changes with temperature and pressure. At  $\sim 3\text{--}4$  bar and 320 K, the flow changes from SSF to Knudsen diffusion. This “window” will vary for different gases, hence

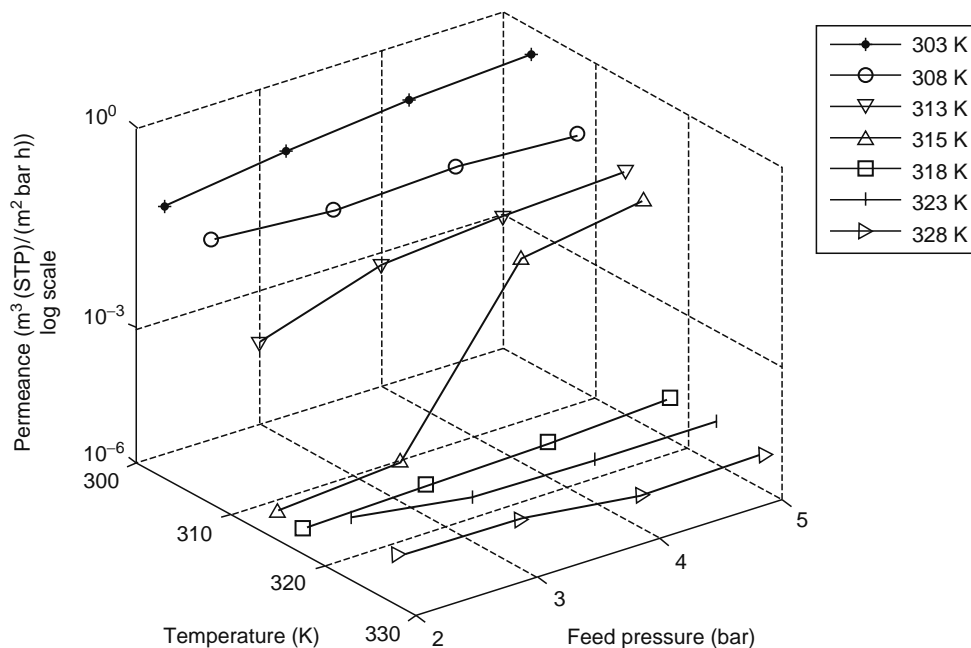


**FIGURE 4.13** Permeance of propane as a function of pressure and temperature through a CMS membrane. (From Lie J.A., Synthesis, performance and regeneration of carbon membranes, Doctoral thesis NTNU 2005: 152, Trondheim, Norway, 2005. With permission.)

the optimum separation conditions can be found where the nonideal component will permeate according to SSF, and more ideal gases in the mixture, according to Knudsen flow.

#### 4.3.2.2 Regeneration

A CMS membrane will typically have a flux decline over time and regeneration will be necessary at intervals. Oxygen is one of the most detrimental species for a CMS membrane. When carbon materials are exposed to air at room temperature, irreversible chemisorption of oxygen may take place and C–O surface groups are formed [80]. These groups also provide sites of adsorption for H<sub>2</sub>O. Both phenomena will slightly reduce the effective size of micropores. The chemically bonded oxygen is only completely removed (as CO and CO<sub>2</sub>) by heating the sample to temperatures as high as 700°C–800°C with an inert gas.

Adsorption of water may result in flux decline as well. At low relative humidity, only active polar sites seem to be involved, and this sorption is so weak that the negative effect can easily be managed. With a high relative humidity (>25%), the negative effect may be substantial, caused by hydrogen bonding by neighboring water molecules forming clusters of adsorbed water [81]. It should be noted though that water uptake from various gases with same humidity level may differ greatly, and will therefore also be more or less easily removed.

Adsorption of organics may cause the same type of flux decline. To recover a decreased membrane flux, three main approaches are reported:

1. The membrane may be treated at elevated temperatures, at least 200°C, under vacuum or inert atmosphere. If the flux is only partially restored after regeneration, this could be the result of incomplete removal of C–O surface groups.
2. If exposed to organics, treatment of the membrane with propene may be a good solution. Jones and Koros [82] found propene to be very effective in removing sorbed organics. In some cases the flux was completely restored—this was also confirmed by Hägg et al. [83].
3. The use of electrothermal regeneration (low voltage direct current) has successfully been tested out online [78].

#### 4.3.3 MIXED MATRIX MEMBRANES/NANOCOMPOSITES

Mixed matrix membranes (MMM) consist of a continuous polymeric phase wherein nanoporous or dense inorganic materials such as silica, zeolite, carbon particles/nanotubes are dispersed. The separation efficiency can be “tuned” by judiciously selecting the constituent materials (and their intrinsic properties), as well as the composition of the resultant nanocomposite. Molecular separation through the polymer occurs according to solution diffusion and is combined with surface diffusion or molecular sieving through the inorganic phase when a microporous filler is added (see Sections 4.2.1, 4.2.3, and 4.2.4). When dense fillers are added (silica, carbon nanoparticles), the membrane may become reverse selective, but still separate according to solution diffusion (see Section 4.3.3.2). The choice of polymer governs the application temperature range, and fabrication requires excellent adhesion between the filler and the polymer to avoid the formation of voids and, consequently, undesirable Knudsen diffusion [84]. Methods under current investigation to improve such adhesion rely on polymer softening (at temperatures near  $T_g$  or through the use of plasticizing agents) or reactive coupling with or without surface treatment of the filler.

The field of polymer nanocomposite membranes is developing rapidly due to the wide range of new properties that can be addressed within this unique class of materials. Resulting properties of these hybrid organic/inorganic materials (which differ significantly in property behavior) rely to a large extent on successful blending. Both enhanced thermomechanical properties and separation properties can be expected. The choice of polymers and inorganic fillers must be based on fundamental knowledge about separation properties as well as miscibility of the materials. For illustration of a mixed matrix membrane with microporous filler, see Figure 4.14 [85].

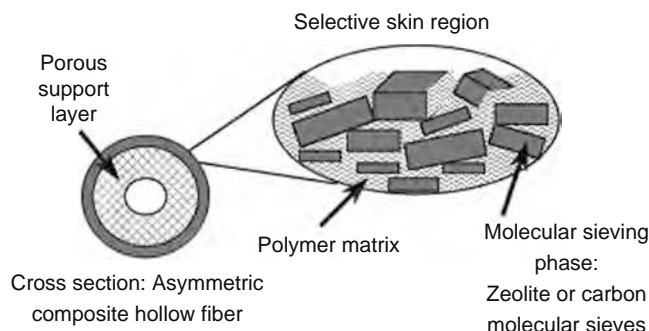


**FIGURE 4.14** Illustration of a mixed matrix membrane. (From Koros W.J., Mahajan R., *J. Membr. Sci.*, 175, 181, 2000. With permission.)

Robeson [4] showed that there exists a “trade-off” relationship between selectivity and permeability for dense polymer membranes. This plot was later updated by Singh and Koros [9] (see Figure 4.1). Molecular transport of light gases in such membranes typically occurs by a solution diffusion mechanism (as discussed in Section 4.2.1). For a polymer membrane to be commercially considered for the removal of CO<sub>2</sub> from H<sub>2</sub>, CH<sub>4</sub>, or air, both the CO<sub>2</sub> permeability and selectivity must be competitively high. Since the gases in the mixture with CO<sub>2</sub> often are smaller (H<sub>2</sub>) or about the same size as CO<sub>2</sub>, they may diffuse more rapidly through the polymers, and it follows that the diffusion selectivity ( $D_{\text{CO}_2}/D_{\text{gasB}}$ ) will be  $\leq 1$ . The only way to increase CO<sub>2</sub> permeability and selectivity simultaneously is thus to increase the solubility of CO<sub>2</sub> in the membrane. Such solubility enhancement is achieved by the introduction of chemical moieties (nanofillers) into the polymer to promote the permeation flux of CO<sub>2</sub> by increasing the free volume, or by using physically modified polymer nanocomposites (molecular sieving materials) suitable for adsorption flow. Both result in a mixed matrix membrane. Examples of porous nanofillers are carbon molecular sieves; examples of nonporous nanofillers are fumed silica and carbon black.

#### 4.3.3.1 MMM: Polymer with Carbon Molecular Sieves

Mixed matrix membranes with molecular sieves incorporated combine the high separation capacity of molecular sieving materials (see Section 4.3.2) with the desirable mechanical properties and economical processing attributes of polymeric materials.

Vu et al. [86] incorporated CMS materials into polymers to form mixed matrix membrane films for selective gas separations. The CMS, formed by pyrolysis of a polyimide precursor and exhibiting an intrinsic CO<sub>2</sub>/CH<sub>4</sub> selectivity of 200, was dispersed into a polymer matrix. Pure-gas permeation tests of such MMMs revealed that CO<sub>2</sub>/CH<sub>4</sub> selectivity enhanced by as much as 40%–45% relative to that of the pure polymer. The effective permeabilities of fast-gas penetrants (e.g., O<sub>2</sub> and CO<sub>2</sub>) through these MMMs are also improved relative to the intrinsic permeabilities of the unmodified polymer matrices. For a CO<sub>2</sub>/H<sub>2</sub> gas mixture, the CO<sub>2</sub> will serve as the fastest permeating component, and H<sub>2</sub> will be retained on the feed side to avoid repressurization, in which case the polymer matrix dictates the minimum membrane performance. Properly selected molecular sieves can only improve membrane performance in the absence of defects. The polymer matrix must be chosen so that comparable permeation occurs in the two phases (to avoid starving the sieves) and so the permeating molecules are directed toward (not around) the dispersed sieve particulates. The molecular sieve must be selected so that its pores can separate the gas molecules of interest according to size. In the case of CMSs, varying the carbonization conditions during fabrication controls the pore size. This is an advantage of CMS membranes over zeolitic molecular sieves, in which the pore size is fixed for a given zeolite type.

#### 4.3.3.2 MMM: Polymer with Nonporous Nanoparticles

Nanoscale inorganic fillers will affect the local chain packing, which affects the local free volume, and hence the molecular transport of permeating species. The polymer may be a rigid-chain polymer or a self-organized block copolymer. If the dispersed filler in MMMs consists of a nonporous material (e.g., carbon nanotubes, fumed or colloidal silica), the nanoscale particulates may disrupt the packing of the polymer chains, if they are rigid, and consequently increase the accessible free volume in the polymer matrix. This increased free volume augments molecular diffusion and weakens the size-sieving nature of the polymer, thereby increasing both permeability and reverses the selectivity. Since permeability depends on diffusivity and solubility, these MMMs will favor permeation of the larger (and more soluble) components through the membrane. The introduced nanoparticles may also alter the mechanism by which a copolymer self-organizes, hence influencing the equilibrium morphology and polymer thermodynamics (and then properties).

Merkel et al. [87] mixed a substituted polyacetylene, poly(4-methyl-2-pentyne) (PMP), with fumed silica particles possessing hydrophobic trimethylsilyl surface groups. Dispersion of the particles was achieved by matching the polarity of the polymer and the particle surface groups, as well as by controlling film-drying conditions. Addition of fumed silica (up to 30 vol %) (size ~10 nm) promoted a considerable increase in the permeability of CH<sub>4</sub> relative to that of pure PMP. In Figure 4.15 various forms of carbon molecules are illustrated [88]. Fullerenes generally refer to the entire class of closed spheroidal aromatic molecules consisting of only carbon atoms, up to 600 atoms.

#### 4.3.4 INORGANIC MEMBRANES

The inorganic membranes had until the late nineties received fairly little attention for applications in gas separation. This has mainly been due to their porous structure, and therefore lack of ability to separate gas molecules. Within the group of inorganic membranes there are however the dense metallic membranes and the solid oxide electrolytes; these are discussed separately in Section 4.3.5. With reference to Section 4.2, the possible transport mechanisms taking place in a porous membrane may be summarized as in Table 4.4 below, as well as the ability to separate gases (+) or not (–). Recent findings [29] have however documented that activated Knudsen diffusion may take place also in smaller pores than indicated in the table.

The increasing interest in inorganic membranes for gas applications is undoubtedly due to their excellent high temperature resistance. Inorganic membrane reactors (including carbon membranes) may thus have a very nice potential for industrial

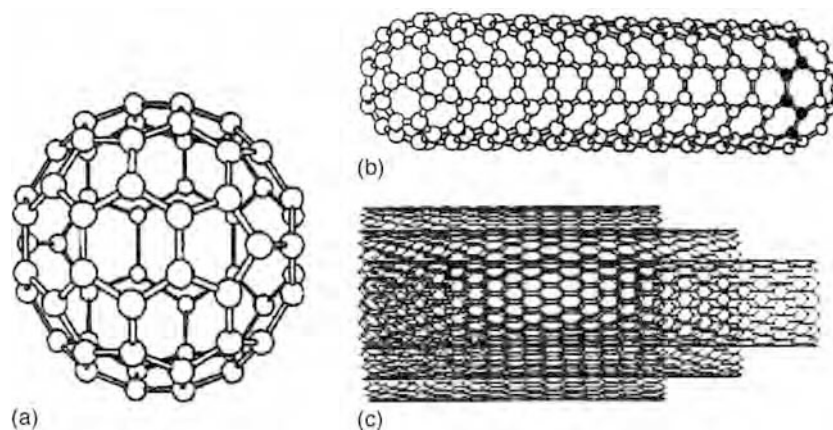


**FIGURE 4.15** Schematic illustration of different nanostructured carbons. (a) A C60 fullerene, (b) A single-wall carbon nanotube, and (c) a multi-wall carbon nanotube. (From Kroto H.W., Heath J.R., O’Brian S.C., Curl R.F., Smalley R.E., *Nature*, 318, 162, 1985. With permission.)

applications. The various configurations of membrane reactors are however not discussed in this chapter. Their separation properties may be understood on the basis of the materials used, kinetics, and process conditions.

Porous materials have very complex structure and morphology, and parameters like porosity, pore size distribution, and pore shape are extremely important variables affecting gas separation properties. A schematic of different pores is given in Figure 4.16 [89]. As can be seen, pore constrictions, dead-end pores, and interconnection between pores will contribute to the characterization of the membrane, hence the tortuosity ( $\tau$ ) plays an important role. The tortuosity will have a value equal to unity ( $= 1$ ) for a cylindrical pore. The inorganic membranes may be symmetric or asymmetric. The symmetric membranes are systems with a homogenous structure throughout the membrane. Capillary glass membranes and anodized alumina membranes are examples within this group. In most cases however the inorganic membranes are asymmetric with a composite structure consisting of several layers with a gradual decrease in pore size to the feed side. Examples are ceramic aluminas synthesized by the solgel technique or carbon–zirconia membranes. For gas separation, surface-modified inorganic membranes have become increasingly important. An introduction to the synthesis and properties of inorganic membranes may be found in comprehensive textbooks [11,90,91].

#### 4.3.4.1 Modified Inorganic Membranes

As illustrated in Table 4.4, the pore size of a microporous inorganic membrane has to be brought down in order to separate gases. Only for pore sizes in the range below Knudsen flow, the separation may be efficient and follow either selective surface flow or capillary condensation. Separation according to configurational diffusion may take place if the pore size is sufficiently small ( $<1$  nm). The surface may also be modified to change its chemical nature and thus separation properties. Several ways of modifying the surface structure of ceramic membranes have been suggested by Burggraaf and Keizer [90], and pore sizes  $<1$  nm have been obtained (see Table 4.5). The main questions related to economy of production and brittleness of these

**TABLE 4.4**  
**Transport Regimes in Porous Membranes**

Type of Transport Mechanism	Pore Diameter	Selectivity
Viscous flow	$>20$ nm	–
Molecular diffusion	$>10$ nm	–
Knudsen diffusion	2–100 nm	$1/\sqrt{M}$
Surface diffusion		+
Capillary condensation		++
Micropore (configuration) diffusion	$<1.5$ nm	+++

*Source:* From Burggraaf A.J., Transport and separation properties of membranes with gases and vapours. In: Bruggraaf A.J., Cot L., eds. *Fundamentals of Inorganic Membrane Science and Technology*. Elsevier, Amsterdam, 1996, 331–427.

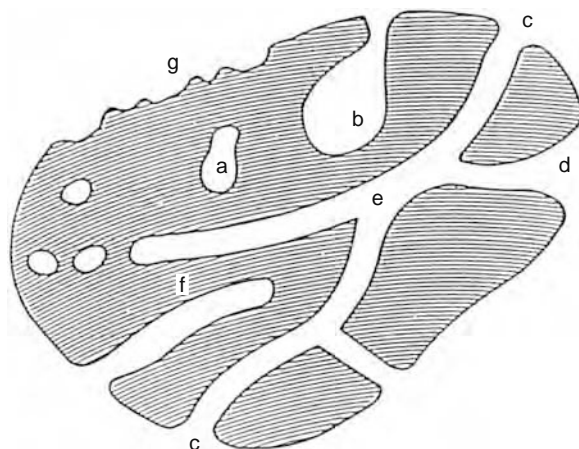


**FIGURE 4.16** Schematic illustration of pore types in porous solid with open pores (c,d), locked-in (a) and dead-end pores (b,e,t). (From Rouquerol J., Avnir D., Fairbridge C.W., Everett D.H., Haynes J.H., Pernicone N., Ramsey J.D.F., Sing K.S.W., Unger K.K., *Pure Appl. Chem.*, 66, 1739, 1994. With permission.)

membranes are still to be solved although the materials may show excellent separation properties for selected gas mixtures, especially in the range of selective surface flow.

Effects of temperature and pressure will play an important role for the resulting separation. This has been discussed for different MFI zeolite membranes by Posthusta et al. [92].

A usually less expensive way for surface modification is using organic compounds. The range for application will then be determined by the decomposition temperature of the organic compound. Several papers have been published reporting promising results for separation [93,94]. The glass membranes (silicate membranes) should be especially mentioned since they have proved to be exceptionally resistant to aggressive gases like chlorine and hydrochloric acid [60,95], and have a nice potential for separation of such gases when membranes are surface modified with chemically resistant perfluoro compounds [31].

### 4.3.5 ION-CONDUCTING MEMBRANES

#### 4.3.5.1 Proton-Conducting Pd Membranes

For the transport of hydrogen through a palladium membrane, please refer to Section 4.2.5.1. The membranes may be prepared as pure palladium membranes, but the trend has moved in the direction of preparing composites and using Pd alloys. There seems to be a number of advantages using composite palladium membranes supported on porous substrates over palladium foils

**TABLE 4.5**  
**Some Modified Nanoscale Ceramic Microstructures within Membranes with Pore Diameters of 3–5 nm**

Membrane Material	Modification by	Modified Structure	Size (nm)	Loading (wt%)
$\gamma$ -Al <sub>2</sub> O <sub>3</sub>	Fe or V-oxide	Monolayer	≈0.3	5–10
$\gamma$ -Al <sub>2</sub> O <sub>3</sub>	MgO/Mg(OH) <sub>2</sub>	Particles		2–20
$\gamma$ -Al <sub>2</sub> O <sub>3</sub>	Al <sub>2</sub> O <sub>3</sub> /Al(OH) <sub>3</sub>	Particles		5–20
$\gamma$ -Al <sub>2</sub> O <sub>3</sub>	Ag	Particles	5–20	5–65
$\gamma$ -Al <sub>2</sub> O <sub>3</sub>	CuCl/KCl	Multilayer	>20	
$\gamma$ -Al <sub>2</sub> O <sub>3</sub>	ZrO <sub>2</sub>	Surface layer	<1	2–25
$\gamma$ -Al <sub>2</sub> O <sub>3</sub>	SiO <sub>2</sub> (amorphous)	20 nm layer + porous plugs	<1.5	5–100
a-TiO <sub>2</sub> <sup>a</sup>	V <sub>2</sub> O <sub>5</sub>	Monolayer	≈0.3	2–10
Al <sub>2</sub> O <sub>3</sub> /TiO <sub>2</sub>	V <sub>2</sub> O <sub>5</sub> or Ag	As for a-TiO <sub>2</sub> or Al <sub>2</sub> O <sub>3</sub>		
θ/α-Al <sub>2</sub> O <sub>3</sub>	ZrO <sub>2</sub> /Y <sub>2</sub> O <sub>3</sub>	Multilayer/porous plugs	Few nm pore size	1–100

Source: From Burggraaf A.J., Keizer K., Synthesis of inorganic membranes. In: Bhawe R.R., ed. *Inorganic Membranes, Synthesis, Characterisation and Applications*, Van Nostrand Reinhold, New York, 1991, 11–63.

<sup>a</sup> a-TiO<sub>2</sub>: anatase titania.

and tubes—one important aspect is the stability of the system as stability problems increase with a reduction in thickness [96]. Stability is also alloy dependent. The porous supports used comprise porous alumina or glass, and porous metals including porous Ni and porous stainless steel. However, from an industrial perspective, alumina supports have disadvantages in terms of insufficient sealing and difficult fabrication of large modules. (This is often a general problem with inorganic membranes for gas separation.)

There are various techniques for the deposition of Pd or its alloys on a support; details on this may be found elsewhere [96,97]. Among these methods, electroless plating is quite attractive due to the possibility of uniform deposition on complex shapes and large substrate areas, hardness of deposited film, and very simple equipment. The main advantage of Pd alloys compared to pure Pd for use in hydrogen separation and MR applications is that Pd alloys have a reduced critical temperature for the  $\alpha$ - $\beta$  transition, and may therefore be operated in the presence of hydrogen at temperatures below 300°C without risking the hydrogen embrittlement observed for pure Pd membranes [98]. The components most used in the Pd alloys are silver (Ag) or copper (Cu) added in a weight percentage up to around 30.

The palladium–silver alloys have attractive enhanced permeability compared to pure Pd while the palladium–copper alloys are more resistant to sulfur. The hydrogen flux through a 20  $\mu\text{m}$  thick palladium membrane was measured by Mardlovich et al. [97] at 350°C to be between 2 and 2.5  $\text{m}^3/\text{m}^2 \text{h}$ , while the performance of palladium–copper alloy membranes over a wide range of temperatures and pressures is presented by Howard et al. [99]. Coexisting hydrocarbons in the gas stream may influence hydrogen permeation through palladium membranes. It has been documented that especially propylene in the gas mixture may seriously affect hydrogen permeation [100]. Propylene decomposes and the carbonaceous matter forming would chemisorb to the membrane surface. Regeneration with pure hydrogen at high temperature (600°C) may however restore the flux. Other components of concern that may cause deactivation and poisoning of a palladium membrane are CO, H<sub>2</sub>O, H<sub>2</sub>S, and Cl<sub>2</sub>.

The very attractive feature of palladium membranes and its alloys is clearly the favorable selectivity for hydrogen permeating at high temperatures. This makes the membranes attractive for use in fuel cells.

#### 4.3.5.2 Proton-Conducting Polymeric Membranes

Many different kinds of fuel cells are presently known, most of them suitable for high-temperature applications—for details see Ref. [101]. The polymeric proton-conducting membranes (polymer electrolyte membranes; PEM) are however suitable for low temperature operations (<100°C) and have the advantage of low weight.

In a fuel cell, electricity is produced by an electrochemical reaction. The proton is produced at the anode by oxidation of the fuel, and will diffuse through the proton-conducting membrane to the cathode where water is formed (see Figure 4.17). The fuel may be hydrogen or hydrogenated molecules. When hydrogen is used as fuel, the PEM fuel cells will use Nafion or Nafion-like sulfonated perfluorinated polymers. These materials have high proton conductivity combined with high stability. For more details on these membrane please see Refs. [101,102].

#### 4.3.5.3 Oxygen-Conductive Membranes

Industry is continuously in search for suitable membrane materials which may produce high purity oxygen at low cost and preferably at low temperature. This type of material is yet to be developed. Presently the zirconia and perovskite membranes

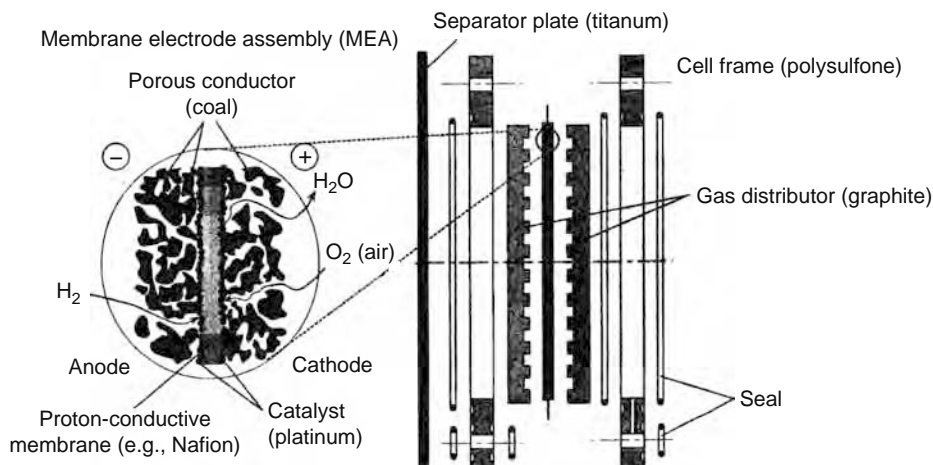


**FIGURE 4.17** Transport through a fuel cell. (From Cappadonia M., Stimming U., Kordesch K.V., de Oliveira J.C.T., Fuel cells. In: *Ullmann's Encyclopedia of Industrial Chemistry*. Vol. 15. 6th ed. Wiley-VCH, Weinheim, Germany, 95, 2003. With permission.)

may be used to produce pure oxygen at high temperatures as these materials (solid electrolytes) contain an oxygen ion conductor. When used as an MR, the permeating oxygen may be used for oxidation of ethane on the permeate side, hence producing syngas [103]. (For details on the transport, see Refs. [34,35].)

Air Products and Chemicals Inc. presented recently a ceramic oxygen-transporting membrane operating at high temperature (transporting  $O_2^-$ ). The material is a mixed-conductor where both oxygen ions and electrons are highly mobile within the solid. The technology makes use of an oxygen partial pressure gradient across the ceramic membrane to drive the oxygen flux [13]. The technology is suited for advanced power generation that requires oxygen for combustion or gasification.

#### 4.4 MODULE DESIGN

Depending on the type of materials to be used for membrane separation, the module may have different configurations. The footprint of the membrane separation unit may be an important issue where it is going to be placed, and packing density of the module ( $m^2/m^3$ ) will then have to be considered. Some modules may be suitable for large-volume applications, some for smaller. In most cases investment cost and lifetime of the membrane will decide which one should be chosen. If specific process conditions are necessary for optimum performance of the membrane (pressure, temperature, filtering, and drying of gas), required utilities must be included in cost estimation.

For calculation of required membrane permeation area, flow patterns for the various module designs must be considered. The cross-flow, counter-current, cocurrent, or complete mixing flow will result in different degrees of purity for the same stage cut,  $\theta$  ( $= q_p/q_f$ ). This is illustrated in Figure 4.18 below [104].

The basic equations for flux and selectivity are given in Section 4.2. Inserting the relevant flux equation for  $J_i$  into Equation 4.22 below, the required membrane permeation area,  $A_m$ , may be calculated:

$$A_m = q_{p,i}/J_i \quad (4.22)$$

where

$q_{p,i}$  is the permeation rate ( $m^3$  (STP)/h) of component  $i$

$J_i$  the flux ( $m^3$  (STP)/ $m^2$  h)

In a real case there are several additional variables to be taken into account: possibility of concentration polarization, pressure drop, heat transfer, and Joule–Thomson effect across the membrane. The J–T effect may be significant when there is a large  $\Delta P$  across the membrane and with nonideal gases permeating. Fugacities should then be used in the calculations. These effects are discussed by several authors [105,106].

The standard module configurations are presented below. With the development of new membrane materials for various applications (as discussed in Section 4.3), new configurations for optimum gas separation may be expected on the market in the future.

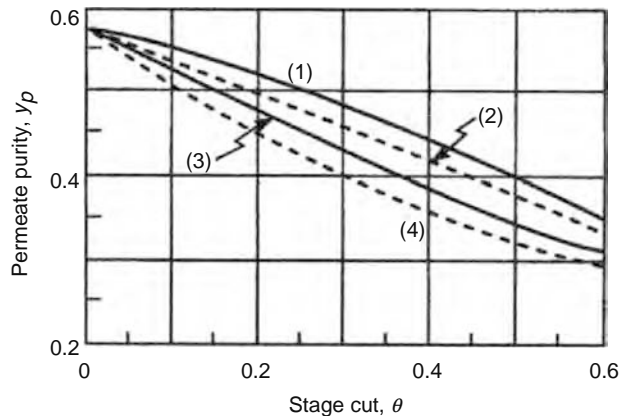


**FIGURE 4.18** Effect of stage cut  $\theta$ , and flow pattern on permeate purity. Operating conditions (air) are as follows:  $x_{f,O_2} = 0.21$ ,  $\alpha^* = 10$ ,  $p_h/p_l = 5$ ,  $P_{O_2} = 500$  Barrer. Line (1) is counter-current flow, line (2) is cross-flow, line (3) is cocurrent flow, and line (4) is complete mixing. (From Walawender W.P., Stern S.A., *Sep. Sci.*, 7, 553, 1972. With permission.)

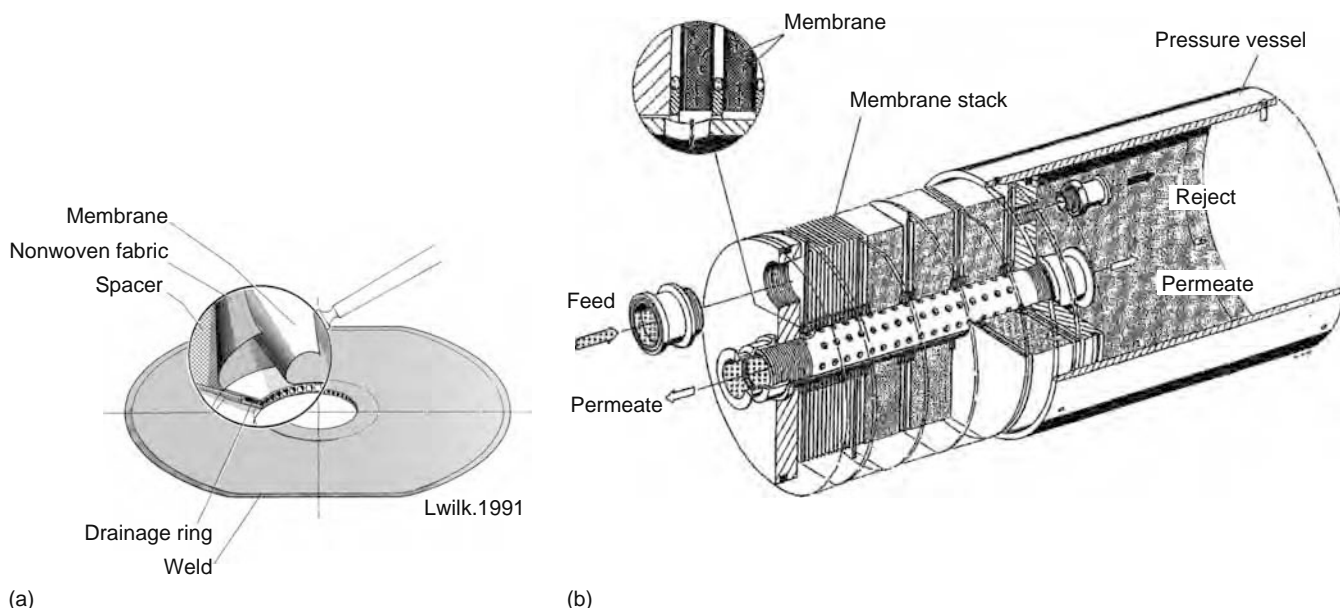


**FIGURE 4.19** The Borsig envelope-type membrane module. (From Ohlrogge K., In: Final Report for EU-project BE97-4589. Dehydration and dewpointing of natural gas by membrane technology. GKSS, Germany, 2002. With permission.)

#### 4.4.1 FLAT SHEET PLATE AND FRAME/Envelope Type

Inorganic or metallic membranes for gas separation are usually prepared as discs or flat sheets. These thin sheets or discs may be quite vulnerable to breakage, and to assemble the membranes in modules is quite challenging. These membranes are usually intended for high-temperature gas applications, and sealing technology may be complicated. Carbon membranes are also facing this challenge at high temperatures.

Polymeric flat sheet membranes are easy to prepare, handle, and mount. For gas separation, the flat sheet membranes are composites with a selective polymer coated on a support. A commercial configuration that has been quite successful for hydrocarbon vapor recovery is the Borsig envelope type module (see Figure 4.19) [107]. Packing densities for flat sheet membranes may be in the range of 100–400 m<sup>3</sup>/m<sup>2</sup> [1].

#### 4.4.2 SPIRAL-WOUND MEMBRANE

The typical spiral-wound membrane, as shown in Figure 4.20, consists of four layers wrapped around a central collection pipe: membrane, spacer (providing a permeate channel), membrane, and a new spacer (providing a feed channel). The feed-side spacer acts as a turbulence promotor, whereas on the permeate side the flow is directed toward the central pipe. The spiral-wound membrane will typically be a polymeric composite material, and is much used also for liquid separation. The packing density of this type of module will depend on the channel height, but is usually within the range of 300–1000 m<sup>2</sup>/m<sup>3</sup> [1]. Several modules may be assembled in one pressure vessel.

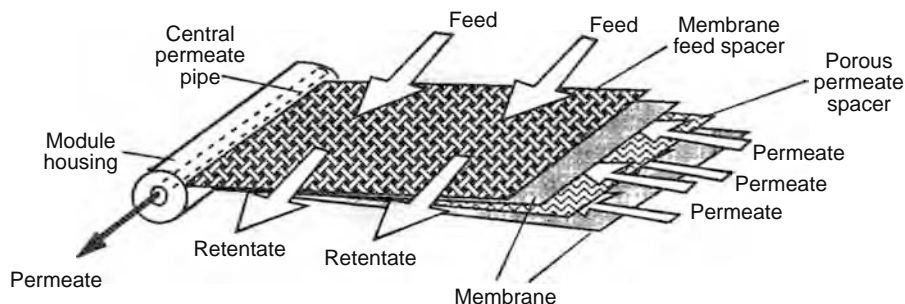


**FIGURE 4.20** A spiral wound membrane module. (From Mulder M., *Basic Principles of Membrane Technology*. 2nd ed. Dordrecht, Kluwer Academic Publishers, 1996. With permission.)

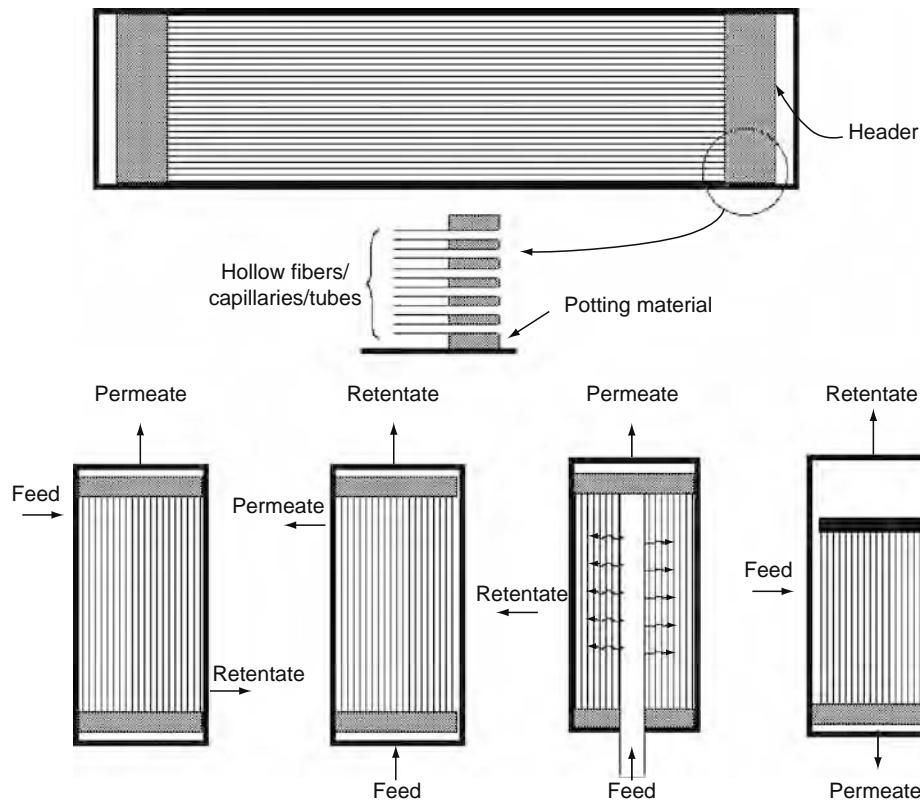


**FIGURE 4.21** Hollow fiber membrane modules with different configurations. (From Pellegrino J., Sikdar S.K., Membrane Technology, Fundamentals of Bioremediation [http://membranes.nist.gov/Bioremediation/fig\\_pages/f5.html](http://membranes.nist.gov/Bioremediation/fig_pages/f5.html) (accessed September 2004). With permission.)

#### 4.4.3 HOLLOW FIBER MEMBRANES

The hollow fiber membranes are the optimum choice for gas separation modules due to their very high packing density (up to  $30,000 \text{ m}^3/\text{m}^2$  may be attained [1]). Figure 4.21 shows alternative configurations for such modules [108]. Modifications of this configuration exist, where possibility for introduction of sweep gas on permeate side is included, or fibers may be arranged transversal to the flow in order to minimize concentration polarization [109,110]. The hollow fiber membranes are usually asymmetric polymers, but composites also exist. Carbon molecular sieve membranes may easily be prepared as hollow fibers by pyrolysis.

#### 4.4.4 MEMBRANE CONTACTORS

A membrane contactor may be considered as a new unit operation where the membrane acts as a barrier between a gas and a liquid phase. The most important advantages of a membrane contactor compared to a traditional absorber are (1) reduction in size and weight (important when used offshore), (2) with the gas and liquid separated by a barrier, the liquid and gas flow rate may be adjusted independently, (3) no entrainment, flooding, or channeling, and (4) reduction in solvent loss. The membrane contactor may have different module configurations, an illustration of the Aker Kvaerner membrane contactor is shown in Figure 4.22 [111]. A different design is presented by Liqui-Cel [112]. Only the component to be removed from the gas mixture will be able to diffuse through the membrane and into the selective liquid absorbent. A typical example is the removal of  $\text{CO}_2$  from a gas stream using an amine absorbent on the liquid side. Factors like pore size, pore size distribution, hydrophobicity, and hydrophilicity of the membrane will play a major role in order not to have breakthrough of gas or liquid across the membrane. Membrane-based absorption and desorption is widely used and studies are reported in several papers [113–117].

The governing equation to avoid breakthrough is the LaPlace equation as shown in the following equation:

$$r_p = \frac{2\gamma}{\Delta P} \cos \Theta \quad (4.23)$$

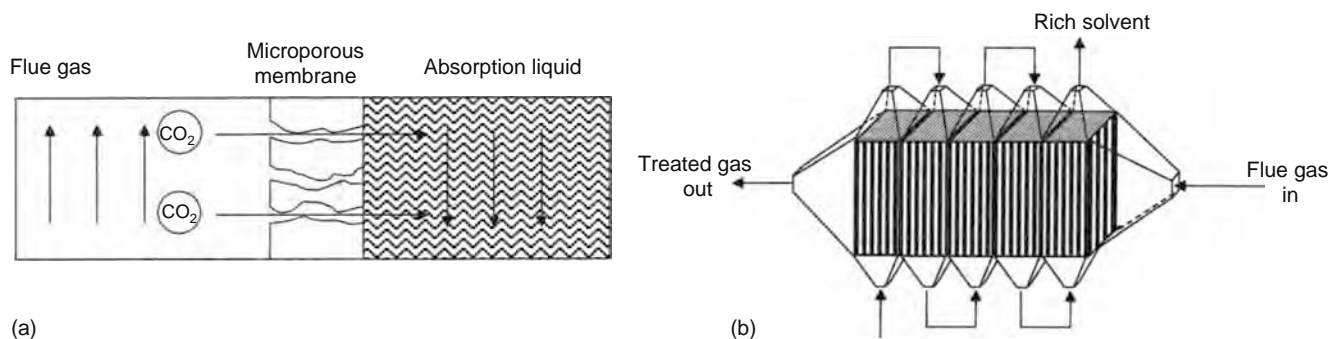


**FIGURE 4.22** Illustration of the principle for removal of CO<sub>2</sub> from a gas stream (left) using a membrane contactor with hollow fibers (right). (From Hoff K.A., Modeling and experimental study of CO<sub>2</sub> absorption in a membrane contactor. Thesis NTNU, Trondheim, 2003. With permission.)

where

- $r_p$  = pore radii
- $\gamma$  = surface tension at liquid/gas interface (N/m)
- $\theta$  = contact angle

#### 4.4.5 SYSTEM DESIGN

Quite often a single stage membrane unit cannot give the desired product quality, and the product may be either the permeate or retentate. A cascade solution may then be a viable option where a fraction of permeate streams are being recompressed and recycled, membrane units are placed in combinations of series or parallel, or permeate streams are being fed to a second stage for further permeation. These calculations will very quickly become quite complicated, and should preferably be performed with an integrated membrane simulation tool hooked up to a standard simulation program (like Hysys, ProII, or Aspen). Relevant papers for design of the gas separation process design may be found in Refs. [28,118,119]. Figure 4.23 illustrates a three stage separation unit typically developed for separation of CO<sub>2</sub> from CH<sub>4</sub> (natural gas) [120].

### 4.5 CURRENT APPLICATIONS AND NOVEL DEVELOPMENTS

As already mentioned, most of the membranes used in gas applications today are still the polymeric solution diffusion materials, and among these, the glassy materials separating according to molecular size are dominating the market. This will probably change when new tailor-made materials (see Section 4.2) are commercialized. For all membrane applications the gas mixture and process conditions (volumes, pressures, temperature, specifications of product for purity) will be governing the choice of membrane material and module design.

The dominating processes for industrial membrane applications are still production of high purity nitrogen, recovery of hydrogen from gas streams, and recovery of carbon dioxide. With respect to both hydrogen and CO<sub>2</sub>, a major increase in membrane applications may be expected with the development of tailor-made materials and with the focus worldwide on renewable energy and emission of greenhouse gases. The removal of volatile organic compounds (VOCs) is also a major potential area for membrane applications due to environmental concern and international agreements on reduction of emissions. There is only a selection of about 8–9 materials used for 90% of the total gas separation membranes today [121]. An overview of commercial-scale membrane suppliers is presented in Table 4.6, adapted and updated after Spillman by Zolands and Fleming in 2001 [122].

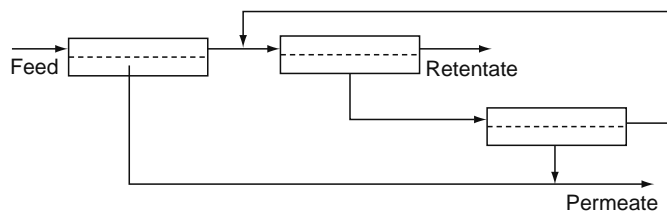


**FIGURE 4.23** A three stage membrane separation process—the recycled gas from stage three need to be recompressed. This configuration could typically be used for removal of CO<sub>2</sub> from gas stream where the retentate is the product. (From Spillman R.W., *Chem. Eng. Progr.*, 85, 41, 1989. With permission.)

**TABLE 4.6**  
**Commercial-Scale Membrane Suppliers for Gas Separation**

Company	CO <sub>2</sub>	H <sub>2</sub>	O <sub>2</sub>	N <sub>2</sub>	Other <sup>a</sup>	Website address
A/G Technology (AVIR)	X		X	X		www.agtech.com
AGA (Linde)			X	X		www.linde-gas.com
Aquilo (Whatman)				X		www.aquilo.nl
Asahi Glass (HISEP)			X	X		www.agc.co.jp
Borsig					X	www.borsig.de
Cynara (Dow)	X				X	www.dow.com
Generon (Dow)			X	X	X	www.generon.com
Grace MS (Aker-Kvaerner)	X	X			X	www.akerkvaerner.com
Medal (Du Pont/Air Liquide)	X	X		X		www.medal.airliquide.com
Membrane Techn. and Research				X	X	www.mtrinc.com
Nitto Denko	X				X	www.nitto.com
Osaka Gas			X		X	www.osakagas.co.jp
Permea (Air Products)	X	X	X	X	X	www.airproducts.com
Praxair			X	X		www.praxair.com
Toyobo			X		X	www.toyobo.co.jp
Ube Industries	X	X	X	X	X	www.ube.com
Union Carbide (Dow)	X	X	X			www.unioncarbide.com
UOP (Separex)	X	X			X	www.uop.com

Source: Partly adapted from Zolands R.R., Fleming G.K., Applications. In: Ho W.S.W., Sirkar W.S., eds. *Membrane Handbook*. Kluwer Academic Publishers, London, 2001, 78–94.

<sup>a</sup> Includes solvent recovery, dehumidification, pervaporation, and helium recovery membranes.

#### 4.5.1 HYDROGEN RECOVERY

Hydrogen is typically being recovered from gas streams at refineries (from hydrocrackers), petrochemical plants (adjustment of syngas ratio, dehydrogenation), and from other streams where hydrogen is present, for example at an ammonia plant. Syngas contains in addition to H<sub>2</sub> and CO impurities like N<sub>2</sub>, CO<sub>2</sub>, CH<sub>4</sub>, and water. It is produced mainly from hydrocarbons by (1) stream reforming and (2) partial oxidation of heavy oils or gasification of coke or coal. There may be a significant variation in the stoichiometric ratio of H<sub>2</sub>/CO for the various chemical syntheses, and the adjustments of syngas ratio may easily be performed by the application of membrane units. The commercial units today are usually either based on polysulfone hollow fibers or spiral-wound CA membranes. Membranes compete with pressure swing adsorption (PSA) and cryogenic systems in hydrogen recovery applications over a wide range of operating conditions. Membrane systems have the advantage of low capital cost and ease of operation. The competing systems however usually deliver the purified hydrogen at almost the same pressure as the feed gas, which results in lower compression costs than those of the membrane system where the hydrogen product always is at a pressure lower than the original feed when using these conventional membranes. Typical performance of membranes for hydrogen recovery in refining applications is shown in Table 4.7 [123].

**TABLE 4.7**  
**Typical Hydrogen Membrane Performance in Refining Applications**

Process Stream	Hydrogen Membrane Recovery			
	Primary Separation	Feed Purity (%)	Permeate Purity (%)	Recovery (%)
Catalytic reformer offgas	H <sub>2</sub> /CH <sub>4</sub>	70–80	90–97	75–95+
Catalytic cracker offgas	H <sub>2</sub> /CH <sub>4</sub>	15–20	80–90	70–80
Hydroprocessing unit purge gas	H <sub>2</sub> /CH <sub>4</sub>	60–80	85–95	80–95
Pressure swing adsorption offgas	H <sub>2</sub> /CH <sub>4</sub>	50–60	80–90	65–85
Butamer process	H <sub>2</sub> /CH <sub>4</sub>	70	90	

Source: From Scott K., *Handbook of Industrial Membranes*. 2nd ed. Elsevier Science Publishers, Oxford, 1998, 297.

**TABLE 4.8**  
**Overview of Fuel Cells: Capacity and Potential Application Areas**

Type of Fuel Cell (FC)	Acronym	Cell Output	Temperature Range (°C)	Field of Application	Special Features
Alkaline FC	AFC	(0.5–5) kW	50–100	Micropower, domestic	Very pure fuel needed
Direct methanol FC	DMFC	Depending on power density	80–100	Domestic, residential	Easily stacked
Proton exchange FC	PEM	(50–250) kW	50–100	Residential, transport	Pure fuel, Pt catalyst
Solid oxide FC	SOFC	100 kW	850–1000	Residential	Large units
Phosphoric acid FC	PAFC	200 kW; 11 MW units	190–210	Power station	1.5% CO tolerance
Melted carbonate FC	MCFC	2 MW; 100 MW units	600–1000	Power station	

Source: Adapted from Nunes S.P., *Review on fuel cells*. Presentation at EMS Summer School, NTNU, Trondheim, Norway, 2003.

#### 4.5.1.1 Novel Applications for Hydrogen: Fuel Cells

With the new scenario of hydrogen as a future energy carrier for use in fuel cells, the hydrogen source will no longer only be fossil fuels but will also be produced from biomass and water electrolysis, and possibly from water splitting by algae. There are two ways of producing hydrogen from biomass: either via bio-oil followed by catalytic steam reforming (as for natural gas) or by carefully controlled anaerobic digestion where biogas is produced in mixtures of  $\text{CH}_4$ ,  $\text{CO}_2$ ,  $\text{N}_2$ , and  $\text{H}_2$ . A production based on algae and bacteria is a potentially large resource, but the hydrogen production rate is slow, and large areas are needed. The most appropriate organisms are not yet found, and this resource is still far into the future. Depending on whether the hydrogen is going to be stored, transported, or fed directly to a fuel cell, the specifications for product purity may vary. There is a wide variety of fuel cells under development, some are already commercial and in operation, especially within the transport sector. Table 4.8 presents an overview of the various types of fuel cells, their capacity, and potential applications [124]. A schematic illustration of how two different fuel cells work is shown in Figure 4.24, with pure hydrogen as fuel (left), and with methanol as fuel (right) [124].

When pure hydrogen is to be used as fuel, the gas must first be recovered from the process stream where it is produced. Membranes may be used for this purpose, and several of the new materials under development may be suitable depending on gas volume to be handled and process conditions like temperature and pressure. Along with the introduction of fuel cells, development of small-scale gas-processing units will follow. Several small, integrated production units with direct conversion of fuel to hydrogen gas combined with a membrane unit for hydrogen recovery are patented [125,126].

With reference to Section 4.3 on materials, the proton-conductive palladium (alloys) and carbon membranes will most likely be among the new suitable membranes for hydrogen recovery. Palladium will be a good choice when the highest purity hydrogen is needed, while for this an adsorption unit may be needed in combination with carbon molecular sieves. Both can operate at high temperatures, palladium at the highest. For low temperature applications MMMs have a very promising potential; these materials will be easier to produce on a large scale, and most likely, at a lower price.

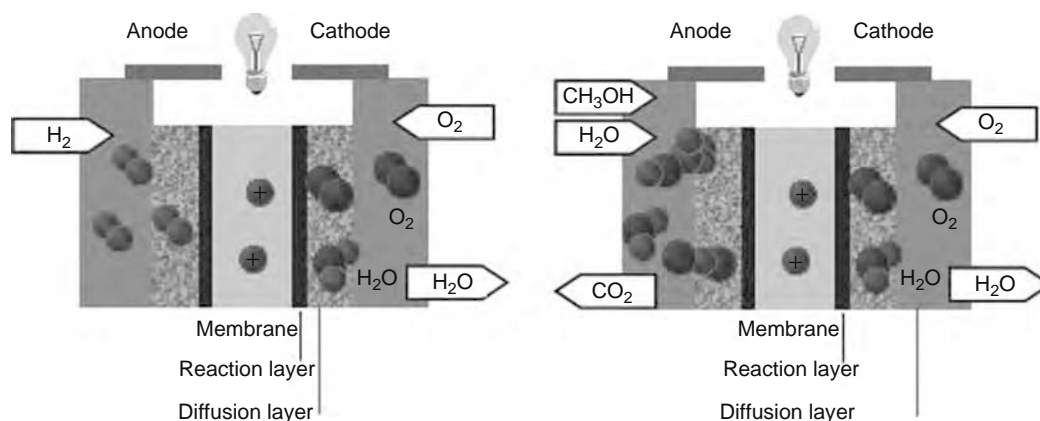


**FIGURE 4.24** Schematic illustration of how two different fuel cells work: with pure hydrogen as fuel (left), and with methanol as fuel (right). (From Nunes S.P., *Review on fuel cells*. Presentation at EMS Summer School, NTNU, Trondheim, Norway, 2003. With permission.)

**TABLE 4.9**  
**Market Predictions for Fuel Cell Systems**

Technology Application	Projected Average Annual Shipment	In Europe	In the United States	In Japan	Rest of the World
Distributed generation; low temperature FC	370 MW (starting 2001)	50 MW	100 MW	200 MW	20 MW
Distributed generation; high temperature FC	1,400 MW (starting 2005)	300 MW	500 MW	500 MW	100 MW
Vehicle FC	200,000 engines (starting 2003)	30,000	100,000	60,000	10,000

Source: From Hagler Baily Consultants. EU brochure. In: Nunes S.P., *Review on fuel cells*. Presentation at EMS Summer School, NTNU, Trondheim, Norway, 2003.

The purified hydrogen needs to be stored as liquid (at  $-253^{\circ}\text{C}$ ) or compressed gas at around 200 bar—this is due to the low energy density of hydrogen (0.003 kWh/l at 1 bar and ambient temperature, and 0.5 kWh/l at 200 bar). When used in the transport sector, thick steel cylinders for the compressed gas are needed, and stacks of the cylinders must be carried under or on the top of the vehicle (bus, truck, ferry). For private cars the “direct methanol fuel cell” (DMFC—see Figure 4.24) is more attractive. For a DMFC, methanol ( $\text{CH}_3\text{OH}$ ) is carried as fuel and converted directly to hydrogen.  $\text{CO}_2$  will however then be produced, and depending on the source for the fuel, may add to the emissions of greenhouse gases. Impurities like CO and  $\text{H}_2\text{S}$  in the feed will poison fuel cells.

Another approach to solve the problem of transport of hydrogen over long distances is to introduce hydrogen gas into the existing domestic natural gas net. This is seriously being looked into also by gas suppliers [127]. At the user end, the gas will be decompressed (to  $\sim 7$  bar), and the hydrogen may be separated from the natural gas and fed to fuel cells where applicable. The ratio of  $\text{H}_2$ /natural gas can also be adjusted by membranes to specified mixtures of natural gas and hydrogen (Hythan; a mixture of hydrogen and methane), mixtures which are currently being tested out as an alternative fuel in the transport sector to reduce emissions while waiting for the fuel cells. The percentage of hydrogen mixed into the transport pipe system must be carefully evaluated for safety reasons, leakage, and material fatigue of the steel pipes. The preferred solution for production of  $\text{H}_2$  in future would be to use renewable energy (solar, wind, waves) for electrolysis of water, or direct production by algae.

The market predictions for fuel cell systems worldwide presented by Hagler Bailey is shown in Table 4.9 [128].

## 4.5.2 $\text{CO}_2$ REMOVAL

Separation of  $\text{CO}_2$  from gas streams is required in four areas: (1) purification of natural gas (gas sweetening), (2) separation of  $\text{CO}_2$  from enhanced oil recovery (EOR) gas streams, (3) removal of  $\text{CO}_2$  from flue gas, and (4) removal of  $\text{CO}_2$  from biogas. A fifth area vital for the space age should be mentioned: removal of  $\text{CO}_2$  from life support systems onboard space ships, and also in submarines. All these applications have different specifications for the purified gas or for the recovered  $\text{CO}_2$ , and future membrane applications will most likely be based on tailor-made materials.

### 4.5.2.1 $\text{CO}_2$ Removal from Natural Gas

The application of membranes today for  $\text{CO}_2$  recovery and natural gas processing is mainly used for moderate-volume gas streams. For large-volume gas streams, membrane separation today cannot yet compete with the standard amine absorption—the flux and selectivity of the membranes are too low for processing large gas volumes. The membrane separation units found at sites today will often be hybrid solutions with membranes combined with traditional technology. The  $\text{CO}_2$  (and  $\text{H}_2\text{S}$ ) must be removed from crude natural gas in order to increase heating value and reduce corrosion during transport and distribution. The amount of  $\text{CO}_2$  in natural gas is typically in the range of 10% by volume or less, and the gas is at very high operating pressures (35–80 bar or even higher). The specifications for removal of sour gases are very strict, and content of  $\text{CO}_2$  should typically be brought down to  $< 2$  vol% for sales gas. The membranes in operation are typically made from polyimides (PI) as hollow fibers, or asymmetric cellulose acetates (CA) as spiral wound modules. The PI membranes have a higher flux and selectivity ( $\sim 20$ ) compared to the CA membranes, and are basically hydrophobic and therefore less vulnerable to water. The CA are, however, more resistant to heavier hydrocarbons. The hollow fiber configurations will be able to handle large gas volumes with relatively few modules due to high packing density ( $\text{m}^2/\text{m}^3$ ).

Recovery of  $\text{CO}_2$  in the oil and gas production is of major importance to promote enhanced oil recovery (EOR) from depleted fields: High pressure  $\text{CO}_2$  is then pumped back into the reservoir at the periphery of the field and diffuses through the formation to drive residual oil toward the wells. The recycled gas generally needs to have a purity of at least 95 vol%  $\text{CO}_2$ .

The main companies producing membranes for  $\text{CO}_2$  removal are listed in Table 4.6.



**FIGURE 4.25** Picture from Qadirpur, Pakistan, the world's largest membrane-based natural gas processing plant. (From Dortmund D., Doshi K., Recent developments in CO<sub>2</sub> removal membrane technology [http://www.uop.com/gasprocessing/TechPapers/CO<sub>2</sub>RemovalMembrane.pdf](http://www.uop.com/gasprocessing/TechPapers/CO2RemovalMembrane.pdf) (accessed March 2004). With permission.)

Some examples of installed membrane units for gas processing are given below:

#### EXAMPLE 1

One of the earliest (and largest) membrane plants for EOR was at the SACROC unit in West Texas, which started up in 1984. (The hollow fiber membrane units are owned and operated by Cynara, a subsidiary of Dow.) In this process, the purified CO<sub>2</sub> stream from the membranes is further treated with hot potassium carbonate before reinjection into the oil field. A single-membrane stage is used followed by multiple banks of membrane permeators in parallel, thus plant performance can be optimized under varying feed conditions by adjusting the number of permeators in operation. (Over the years the CO<sub>2</sub> content increased from 0.5 vol% up to a level of ~60 vol%.) The Cynara membrane system would successfully process 70 million SCFD of gas containing 40–70 vol% CO<sub>2</sub> around 1990 [122].

#### EXAMPLE 2

In Qadirpur, Pakistan, the world's largest membrane-based natural gas processing plant is situated (see picture in Figure 4.25). The plant is processing 265 MMSCFD natural gas at 59 bar, and with plans for expanding the plant to handle 400 MMSCFD [129]. The CO<sub>2</sub> content is reduced from 6.5 mol% to less than 2 mol% using a CA membrane. The plant is also designed for gas dehydration with membranes.

#### EXAMPLE 3

Other operating membrane plants around the world include (1) Kadanwari, Pakistan, where a two-stage unit for treatment of 210 MMSCFD gas at 90 bar is operating, (2) Mexico, where an EOR facility is installed to process 120 MMSCFD of gas containing 70 mol% CO<sub>2</sub>, and (3) Egypt, where a three stage unit is operating at Slalm & Tarek with each unit treating 100 MMSCFD natural gas at 65 bar.

All the plants mentioned are operating with membranes based on hollow fiber polyimides or spiral-wound CA, which is considered proven technology. The environmental aspect related to CO<sub>2</sub> as a green house gas has triggered the development of better membranes for CO<sub>2</sub> removal—this is more closely discussed in Section 5.2.3.

#### 4.5.2.2 CO<sub>2</sub> Removal from Biogas

Biogas will have different compositions depending on the source where it is being produced (see Table 4.10) [130]. If the methane is going to be used for high energy fuel, it must be purified to contain ~95 vol% CH<sub>4</sub>. Processing of biogas may, in some cases, be handled by using the existing CO<sub>2</sub>-selective membranes. However, the presence of nitrogen in biogas is a major challenge, especially when the biogas is produced from a landfill (see Table 4.10). Nitrogen will remain on the feed side with

**TABLE 4.10**  
**Composition of Biogas from Different Sources**

Component	Municipal Wastewater Treatment Plants (vol%)	Dedicated Reactors (Organic Waste) (vol%)	Landfills (vol%)
CH <sub>4</sub>	55–75	50–90	40–55
CO <sub>2</sub>	25–45	10–50	30–40
N <sub>2</sub>	Traces	Traces	2–25
O <sub>2</sub>	Traces	Traces	0–5
H <sub>2</sub>	<1	<1	<1
H <sub>2</sub> S	<1	<1	<1
H <sub>2</sub> O	4–7	4–7	4–7

Source: From Maltesson, H.Å., *Biogas för fordonsdrift*. KFB, Stockholm, 1997 (in Swedish).

the methane, and fuel specifications may be difficult to reach. About 3200 m<sup>3</sup> (STP)/h of biogas can be collected from a medium-size dumpsite, which is equivalent to 1700 L/h of fuel oil [131]. The standard way of utilizing the biogas (if at all considered) is by burning the gas on site in combination with a turbine, thus producing energy. This may be sensible if the energy distribution net is easily available. A more environmental friendly solution is to upgrade the gas to fuel specifications by using membranes. Several pilot plants are in operation both in the United States and in Europe based on existing membrane materials. New CO<sub>2</sub>-selective materials will most likely enhance the development of utilizing this valuable energy resource (see Section 4.5.2.3).

#### 4.5.2.3 Novel Applications for CO<sub>2</sub> Capture

Due to the environmental focus on CO<sub>2</sub> emissions around the world, there are numerous CO<sub>2</sub> selective materials under development—several hundred polymers are reported (articles and patents). The main challenge for bringing these membranes into commercialization is to document durability over time (maintaining separation properties) during real operating conditions.

##### 4.5.2.3.1 Natural Gas Sweetening

New materials for natural gas sweetening are basically based on further developments of existing polymeric materials, which can easily be made into hollow fiber or spiral-wound membrane modules. This is mainly due to the large permeation areas needed. When CO<sub>2</sub> permeates the higher hydrocarbons, C<sub>3+</sub> will co-permeate. It is important that the sales gas specifications can be met when membranes are being used for CO<sub>2</sub> removal and dew point control. Several promising materials are under development and being tested out—the market potential is huge. This development is typically done in cooperation with the oil and gas companies, and little information is being released until the membrane is ready for commercialization. MMMs with high selectivities in favor of CO<sub>2</sub> will still need many years of development to compete with tailor-made polymeric membranes as well for this application. The cardopolymers as well as the facilitated transport polymers may be interesting candidates for natural gas sweetening.

##### 4.5.2.3.2 CO<sub>2</sub> Removal from Flue Gas

Removal of CO<sub>2</sub> from exhaust gas from combustion is a major driver for membrane material development. Also integrated membrane solutions to power cycles (gas turbines) are in focus. In the exhaust gas, CO<sub>2</sub> will be in a mixture with H<sub>2</sub>O, N<sub>2</sub>, NO<sub>x</sub>, O<sub>2</sub>, possibly SO<sub>2</sub>, and some hydrocarbons, and at low pressure and high temperature. In addition, there will also be dust particles in the gas. The membrane separation will, in this case, meet challenges, which are different from those for natural gas sweetening. Integrated membrane solutions are often being considered when combustion/energy production is discussed, both in precombustion and in postcombustion. A solution with integration of H<sub>2</sub>-separating membrane technology in gas turbine processes for CO<sub>2</sub> capture is shown in Figure 4.26 [132].

Membranes do not tolerate particles, so the gas has to be filtered before separation. Then for several membrane materials water vapor may also be a problem, causing plugging (inorganic microporous materials) or swelling (polymeric materials). Hence for these applications, the gas must be dried. Depending on the specifications for the CO<sub>2</sub>, co-permeation of gases (especially remaining HC) may be a problem. What can then be recommended for removal of CO<sub>2</sub> from flue gas? Some alternatives are presented below:

- Securing complete combustion using oxygen-enriched air (will give higher CO<sub>2</sub>% in exhaust gas, hence higher driving force for CO<sub>2</sub> removal)
- Using an integrated solution with a gas turbine so that CO<sub>2</sub> gas is removed at higher pressure (securing higher driving force over the membrane)

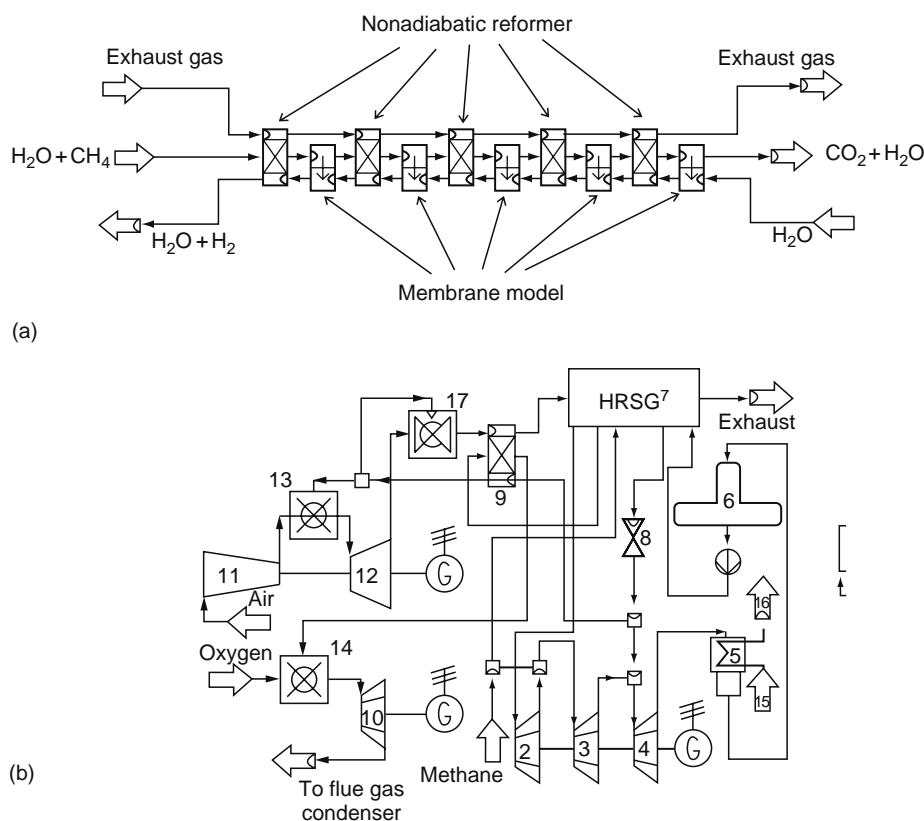


**FIGURE 4.26** A suggested integration of  $H_2$ -separating membrane technology in the gas turbine process for  $CO_2$  capture. (a) Shows a membrane steam reactor model with  $H_2$  separation; this corresponds to unit 9 in (b) showing the flowsheet of a combined cycle with the membrane reactor integrated. (From Jordal K., Bredesen R., Kvamsdal H.M., Bolland O., *Energy*, 29, 1269, 2004. With permission.)

- High temperature in the flue gas ( $>100^\circ C$ ) most likely requires inorganic materials; hence ceramics or carbon membranes could be chosen (see Section 4.3.4)
- If the gas is cooled down, a  $CO_2$ -selective polymeric membrane may be used (cardopolymers and carrier membranes are especially interesting. Problem: compression of exhaust gas may be needed; see Section 4.3.1)
- If the gas is cooled, a  $CO_2$ -selective membrane with facilitated (carrier) transport may be used with vacuum or water vapour sweep on permeate side (no compression needed, only a fan; see Section 4.3.1.2)
- For large gas stream volumes the membrane contactor using amines as absorbent may be the best solution (see Section 4.4.4 and below)

The membrane contactor for  $CO_2$  removal deserves special attention. It can be used for natural gas treatment, dehydration, and removal of  $CO_2$  from flue gas (see Section 4.4.4). A contactor (see Figure 4.22) patented and developed for this purpose by Aker Kvaerner—pilots have been installed and tested both in Norway (at Kårstø) and at a gas terminal in Scotland. This module is based on PTFE membranes. A different commercial contactor based on polyimide membranes was recently installed at Santos Gas Plant in Queensland, Australia (December 2003). Santos is the largest gas producer in Australia.

#### 4.5.2.3.3 $CO_2$ Removal from Biogas

Biogas is a valuable energy resource, which can be processed in small plants all over the world. Biogas has different compositions depending on the source. The gas is easily collected from dumpsites or anaerobic digesters, and may be processed at moderate pressures and ambient temperature. Membrane systems are excellent for this purpose, operating at pressures in the range of 5–7 bar. The choice of membrane materials are therefore also quite flexible, and small-scale processing units are likely to be developed—a few already exist. Highly  $CO_2$ -selective polymeric membranes (cardopolymers, fixed-site carriers), carbon molecular sieves, mixed matrix, or biomimetic materials are potential membrane materials for this application. The purified methane can then be compressed to 300 bar, and stored in tanks for fuel in the transport sector, or for conversion to methanol used for fuel cells.

#### 4.5.2.3.4 CO<sub>2</sub> Removal in Life Support Systems

CO<sub>2</sub> removal in life support systems is becoming increasingly important as man is going into space for longer journeys. The standard way of removing CO<sub>2</sub> from breathing air is to adsorb the gas on molecular sieves, mainly using carbonates. This is a safe way as long as there is enough adsorbent. The preferred way would be to separate CO<sub>2</sub> from the air without using adsorbents but rather highly CO<sub>2</sub>-selective membranes, then dispose of it or bring it back into the life cycle by using water (from urine) and green plants grown artificially in space. Nanostructured materials, fixed-site carriers, or biomimetic membranes would most likely be suitable for this application.

### 4.5.3 AIR SEPARATION

Membranes for air separation have become increasingly important over the years, and the development of continuously better materials has been rapid since Dow and Permea presented their first membrane systems in 1985. The first membranes used for air separation were based on poly(4-methyl-1-pentene) (TPX) and ethyl cellulose and had selectivities for O<sub>2</sub>/N<sub>2</sub> around 4–5 [133]. Today second generation air separation membranes are on the market, usually as hollow fiber modules with very high packing density, and based on polymers such as polysulfones (PS) and poly(phenylene)oxide (PPO). Remembering the very strong inverse relationship between selectivity and permeability for oxygen and nitrogen as illustrated by Robeson in Figure 4.1 [4], it may easily be understood that there is a major difference in producing high-purity nitrogen compared to high-purity oxygen. Air separation using membranes is today considered proven technology, and there are several producers in addition to Dow (now upgraded system Generon II) and Permea (Prism Alpha; now Air Products)—see Table 4.8. Detailed information on membrane solutions for air separation are found in many textbooks, handbooks, and references [1,50,122,133].

#### 4.5.3.1 Production of High-Purity Nitrogen

High-purity nitrogen is used for many applications as blanketing gas in oil and gas industry, as purge and blanketing in chemical industry, in food industry for packaging, and various others. When air is separated by polymeric membranes, oxygen will be the faster permeating component with a selectivity in the range of 2–9 compared to nitrogen. (With carbon membranes selectivity ~15 has been measured.) This means that when compressed air is fed to the membrane, nitrogen is retained at high pressure on the feed side, which is usually an advantage. The competing separation technologies are typically cryogenic distillation and PSA. Figure 4.27 illustrates the recommended production range for applying the different technologies [133]. Even with low selectivity membranes, high-purity nitrogen may be obtained (99.9%), but the cost of the system increases significantly in the range of 95%–99% nitrogen purity. Various process designs may be considered for cost reduction. Figure 4.28 illustrates how a process may be optimized to reduce membrane area and compressor cost for a required product of 99% purity nitrogen. The three-step process will however be limited to large systems where energy and membrane area savings compensate for the extra complexity and higher maintenance cost of a second compressor. A comprehensive discussion of factors affecting the design of nitrogen plants is given by Prasad et al. [134].

#### 4.5.3.2 Oxygen-Enriched Air

Oxygen-enriched air will be produced on the low pressure permeate side of the air-separating membranes. The oxygen-enriched permeate stream is usually vented, but there is an increasing interest in using this gas for combustion. High-purity oxygen

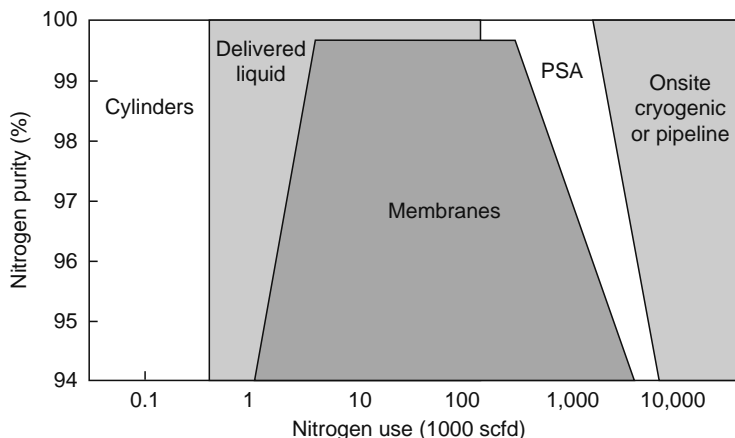


**FIGURE 4.27** Illustration of the approximate competitive range of current membrane nitrogen production systems. Many site-specific factors can affect the actual system selection. (From Baker R., *Membrane Technology and Applications*, McGraw-Hill, New York, 2000. With permission.)

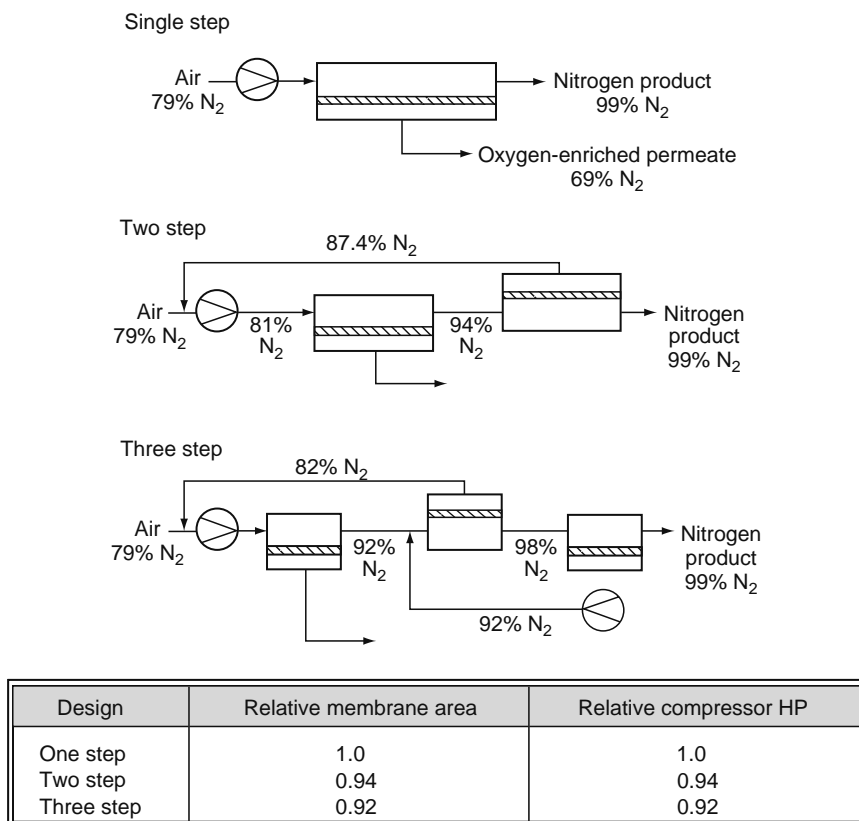


**FIGURE 4.28** Illustrations of single-step, two-step, and three-step designs for nitrogen production from air. The table shows the effect of the different designs on membrane area and energy demand for compressor. (From Baker R., *Membrane Technology and Applications*, McGraw-Hill, New York, 2000. With permission.)

cannot be produced with the polymeric air separation membranes. Calculations will easily show that with a selectivity of 8 for O<sub>2</sub>/N<sub>2</sub>, and with an infinite pressure ratio and zero stage cut, the permeate can only reach as “best case” 68% purity for O<sub>2</sub>. These constraints explain why oxygen-enriched air in these systems usually is in the range of 30%–50% purity for O<sub>2</sub>.

### 4.5.3.3 Novel Developments for High-Purity Oxygen

In Section 4.3.5.3 it was stated that oxygen-conductive membranes are under development. These membranes are suitable for advanced power generation requiring oxygen for combustion or gasification, and are based on zirconia and perovskite where oxygen is transported through the material as O<sub>2</sub><sup>-</sup>. The materials are stable at very high temperatures (>500°C). A schematic illustration of the ion transport membrane (ITM) developed by Air Products is shown in Figure 4.29 [13]. Details on this

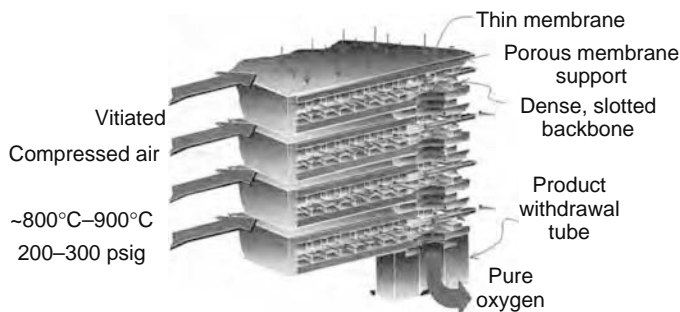


**FIGURE 4.29** A schematic illustration of the ion transport membrane (ITM) device developed and patented by Air Products and Chemicals, Inc. The supported membrane wafers are separated by spacer rings and attached to a common product withdrawal tube. (From Armstrong P.A., Stein V.E.E., Bennet D.I., Foster E.P., *Ceramic Membrane Development for Oxygen Supply to Gasification Applications*, Air Products and Chemicals, Inc., Allentown, PA, 2002. With permission.)

technology can be found in Ref. [135]. The Danish company, Haldor Topsoe A/S, has presented a patented solution with an integrated ion-conducting membrane for autothermal steam reforming [136]—several other patents are being announced.

#### 4.5.4 RECOVERY OF VOLATILE ORGANIC COMPOUNDS

With the increased focus on climate changes and greenhouse gases, the need for reducing VOC emissions has been brought into focus. Major sources for these emissions are evaporation from oil and gas tankers during transport and bulk handling of oil at buoys and terminals, refineries, and petrochemical plants. On the basis of international agreements on Long Range Transboundary Air Pollution (Geneva convention of 1979 with later protocols) and Clean Air Act Amendments of 1990 in the United States, various technologies for VOC recovery have been developed. The main technologies are based on recirculation of the VOC rich stream for absorption in the oil. For large gas volumes this demands a complicated system of cooling and recompressions of the VOC and venting of the purified air. Process units for installation on tankers are developed by several companies (Aker Kvaerner Process Systems, Hamworthy and others). For moderate volume air streams, membrane solutions exist. The GKSS module (see Figure 4.20) was developed for this purpose, and is today considered proven technology. A rubbery membrane allowing the VOCs to permeate and inerts to be retained is used. A hybrid solution with PSA may be necessary to remove the traces of VOC before the gas is vented (see Figure 4.30 [137]). The challenge is still to develop efficient process schemes for filling and unloading of tankers. The volume percent VOC in the inert gas stream may vary between 8% and 60% from start to end of filling operation—this complicates the recovery process. Combinations with membranes for concentrating the VOC before absorption are being looked into.

#### 4.5.5 SEPARATION OF HYDROCARBONS—NOVEL MEMBRANE DEVELOPMENTS

Successful separation of alkanes and alkenes has been documented when microporous membranes have been used [79,138]. The physiochemical properties, size, and shape of the molecules will play an important role for the separation, hence critical temperatures and gas molecule configurations should be carefully evaluated for the gases in mixture. On the basis of gas properties and process conditions, the separation may be performed according to selective surface flow or molecular sieving (refer to Section 4.2 on transport). The transport may also be enhanced by having a Ag compound in the membrane. The  $\text{Ag}^+$  ion will form a reversible complex with the alkene, and facilitated transport results. Selectivities in the range of 200–300 have been reported for separation of ethene–ethane and propene–propane [138]. Successful separation of alkanes and alkenes will be important for the petrochemical industry. Today the surplus hydrocarbons in the purge gas are usually flared. Membranes which should be suitable for this application are the carbon molecular sieves (see Section 4.3.2) and nanostructured materials (Section 4.3.3).

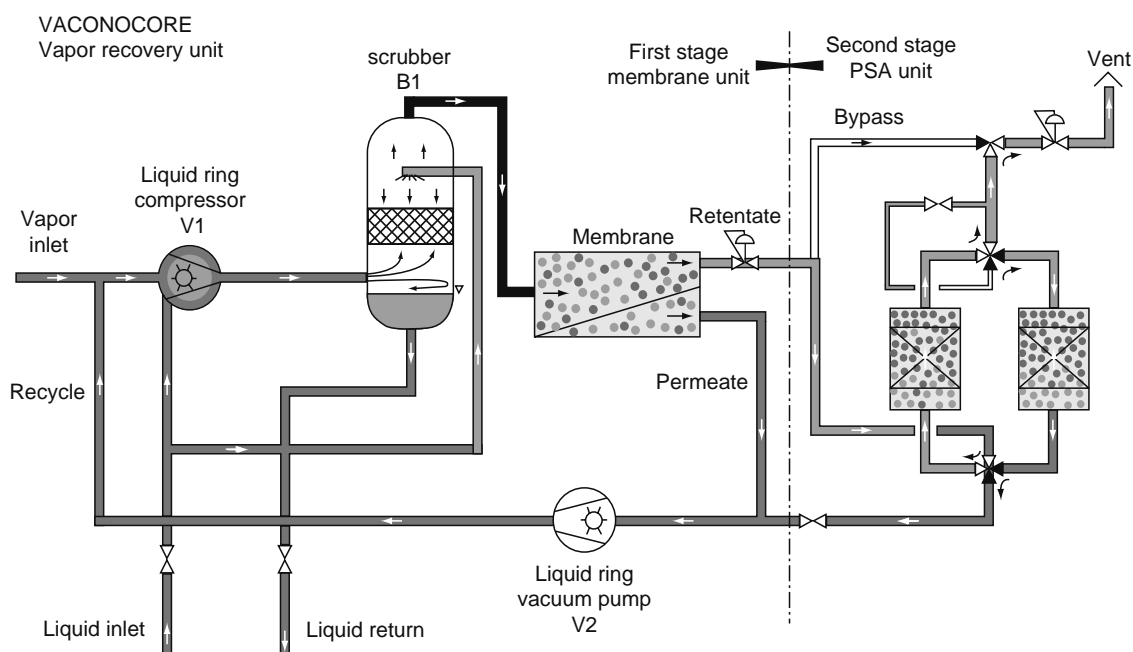


**FIGURE 4.30** Illustration of a hybrid solution for removal of organic vapor from a gas stream, as documented by Vaconocore. (From Ohlrogge K., Wind J., Behling R.D., *Erdoel & Kohle Erdgas Petrochemie*, 46, 326, 1993. With permission.)

## 4.5.6 OTHER APPLICATIONS

### 4.5.6.1 Water Vapor Removal from Air

Membranes are used to dehydrate process air streams as replacement for desiccant dryers or adsorption systems. Such membrane units have been on the market for many years, but they are mainly for small gas streams. The membranes being used have very high water to air selectivity. The dehumidification units are usually connected to a compressed air line, and loss of pressurized air through the membrane may be a major cost.

### 4.5.6.2 Dehydration of Natural Gas

Natural gas has to be dried in order to prevent water from freezing or hydrates to form in pipelines for gas distribution. The potential application of membranes for gas dehydration is very large. There are already numerous polymers available with very high selectivities for water vapor: 500–2000 are beneficial, and a breakthrough for commercialization of a few materials is to be expected. The water permeance should preferably be at least  $30 \text{ m}^3 \text{ (STP)/m}^2 \text{ h bar}$  [139]. The problem is that with increasing selectivity at a given water vapor flux, the necessary permeation area also increases. If the gas on the permeate side could be used for low-pressure fuel at the site, a membrane solution for dehydration would be economical and competitive to glycol dehydration. If the permeate gas has to be recompressed, the costs will probably be too high. Permea Maritime Protection (division of Air Products) is one of the companies having presented a commercial unit, already installed in the North Sea.

Zeolites have been used for many years as an adsorbent in a wide range of industrial applications (also for smaller volumes of natural gas) because of the regular and controllable pore size in their crystalline structure. The highly hydrophilic nature of these materials means that water is always preferentially adsorbed. Regeneration is however necessary when the adsorbent is fully loaded.

### 4.5.6.3 Helium Recovery

Helium is present in low concentrations in natural gas, and is also used as a diluent in breathing gas mixtures for deep-sea divers. Helium is a valuable gas, and is therefore important to recover. As the permeability of helium normally is slightly higher than hydrogen, the recovery of helium from natural gas may be feasible with hydrogen separation membranes. However, when the concentration is very low, a very high selectivity for  $\text{He}/\text{CH}_4$  is needed ( $>500$ ) or a staged system with recompression. For recovery of helium from breathing gas, a selectivity of  $\text{He}/\text{N}_2$  should be in the range 50–100 [140].

### 4.5.6.4 Recovery of Aggressive Gases: $\text{Cl}_2$ and $\text{HCl}$

Membranes for purification or recovery of aggressive gases have been under development for many years, and is expected to be commercialized within a few years. The main challenge for membrane separation of gases like  $\text{Cl}_2$  and  $\text{HCl}$  is the durability of the material—this has been thoroughly documented by several researchers [31,60,141,142]. The only polymers that can withstand the aggressive process environment are the perfluorinated materials. These membranes do not yet have satisfactory separation properties for  $\text{Cl}_2$  or  $\text{HCl}$  in mixtures with more inert gases. There are two ways for membrane development for this application: (1) using perfluorinated compounds to surface modify microporous glass membranes or (2) possibly make a mixed matrix membrane with the perfluorinated polymer as the continuous phase and molecular sieving glass fibers as the sieving phase. The potential for membrane application within this field is very large as chlorine is a widely used chemical in numerous industries worldwide. The competing purification methods today are based on chemical reaction with additives or cryogenic distillation.

## 4.6 SUMMARY

It can be concluded that there is a potential for membrane separation of almost any gas from a mixture of gases if physical and chemical properties are carefully considered as well as material properties and durability, possible transport mechanisms, and optimum process conditions evaluated. Creative reflection and advanced research will be able to develop this environmental friendly separation technique for applications within many areas in the future, and hopefully be able to displace old, energy-consuming (and not so clean) technology or combine with them in hybrid process solutions. The costs of the final solution will always be a major issue for commercialization.

## ACKNOWLEDGMENTS

The author wants to thank colleagues and researchers in the membrane research group, MEMFO at NTNU, for valuable discussions and patience while writing up this chapter. Special thanks to the following members of my research group: Jon Arvid Lie, Arne Lindbrathen, and Taek-Joong Kim for valuable help with references and figures.

## REFERENCES

1. Mulder M. *Basic Principles of Membrane Technology*. 2nd ed. Dordrecht: Kluwer Academic Publishers, 1996.
2. Loeb S and Sourirajan S. Sea water demineralisation by means of an osmotic membrane. *Adv. Chem. Ser.* 1962; 38:117–132.
3. Henis JMS and Tripodi MK. A novel approach to gas separation using composite hollow fiber membranes. *Sep. Sci. Tech.* 1980; 15:1059–1068.
4. Robeson LM. Correlation of separation factor versus permeability for polymeric membranes. *J. Membr. Sci.* 1991; 62:165–185.
5. Koresh JE and Soffer A. The carbon molecular sieve membranes. General properties and the permeability of CH<sub>4</sub>/H<sub>2</sub> mixture. *Sep. Sci. Tech.* 1987; 22:973–982.
6. Rao MB and Sirkar S. Nanoporous carbon membranes for separation of gas mixtures by selective surface flow. *J. Membr. Sci.* 1993; 85:253–264.
7. Jones CW and Koros WJ. Carbon molecular sieve gas separation membranes. Part I: Preparation and characterization based on polyimide precursors. *Carbon* 1994; 32:1419–1425.
8. Fuenes AB. Adsorption-selective carbon membrane for gas separation. *J. Membr. Sci.* 2000; 177:9–16.
9. Singh A and Koros WJ. Significance of entropic selectivity for advanced gas separation membranes. *Ind. Eng. Chem. Res.* 1996; 35:1231–1234.
10. Soffer A, Gilron J, Saguer S, Hed-Ofek R, and Cohen H. Inventors. 1995. European patent 95103272.1, September 13, 1995.
11. Burggraaf AJ. Transport and separation properties of membranes with gases and vapours. In: Bruggaaf AJ and Cot L, eds. *Fundamentals of Inorganic Membrane Science and Technology*. Amsterdam: Elsevier, 1996, pp. 331–427.
12. Bouwmeester HJM and Burggraaf AJ. Dense ceramic membranes for oxygen separation. In: Bruggaaf AJ and Cot L, eds. *Fundamentals of Inorganic Membrane Science and Technology*. Amsterdam: Elsevier, 1996, pp. 435–515.
13. Armstrong PA, Stein VEE, Bennet DI, and Foster EP. *Ceramic Membrane Development for Oxygen Supply to Gasification Applications*. Allentown, PA, Air products and Chemicals, Inc., 2002.
14. Ward WJ and Robb WL. Liquid membranes for use in the separation of gases, U.S. Patent 3,396,510, 1968.
15. Kim T.J. and Hägg MB. Novel fixed-site-carrier polyvinylamine membrane for carbon dioxide capture. *J. Pol. Sci. Part B Polym. Phys.* 2004; 42:4326–4335.
16. Koros WJ (Editor-in-chief). Table of units, *J. Membr. Sci.* all issues since 2004; 2.
17. Noble RD and Stern SA. *Membrane Separation Technology. Principles and Applications*, Amsterdam, Elsevier Science, 1995, p. 718.
18. Nunes SP and Peineman KV (eds.). *Membrane Technology in the Chemical Industry*, Wiley-VCH, 2001, p. 299.
19. Baker RW. *Membrane Technology and Applications*, Chichester: John Wiley, 2004.
20. MTR Inc., www.mtrinc.com, 2004 (date of access: October, 2004).
21. Koros WJ. Gas Separation Membranes: Needs for combined materials science and processing approaches. *Macromol. Symp.* 2002; 188:13–22.
22. Stern SA, Shah VM, and Hardy BJ. Structure–permeability relationships in silicone polymers. *J. Polym. Sci. Part B Polym. Phys.* 1987; 25:1263–1298.
23. Koros WJ, Chan AH, and Paul DR. Sorption and transport of various gases in polycarbonates. *J. Membr. Sci.* 1977; 2:165–190.
24. Jordan SM. The effects of carbon dioxide exposure on permeability behaviour of silicone rubber and glassy polycarbonates. PhD dissertation, Austin, TX: University of Texas at Austin, 1988.
25. Koros WJ and Hellums MW. Transport properties. In: Kroschwitz, JI, ed. *Encyclopedia of Polymer Science*. 2nd ed. New York: Wiley-Interscience Publishers, 1989; Supplement vol. pp. 724–802.
26. Koros WJ and Fleming GK. Membrane-based gas separation. Review. *J. Membr. Sci.* 1993; 83:1–80.
27. Baker RW and Blume I. Permselective membranes separate gases. *Chemtech.* 1986; 16:232–238.
28. Geankoplis CJ. *Transport Processes and Separation Process Principles*. 4th ed. New Jersey, Prentice-Hall International Editions, 2003.
29. Gilron J and Soffer A. Knudsen diffusion in microporous carbon membranes with molecular sieving character. *J. Membr. Sci.* 2002; 209:339–352.
30. Gilliland ER, Baddour RF, Perkinso GP, and Sladek KJ. Diffusion on surfaces. 1. Effect of concentration on the diffusivity of physically adsorbed gases. *Ind. Eng. Chem. Fundam.* 1974; 13:95–100.
31. Lindbråthen A and Hägg MB. Glass membranes for purification of aggressive gases. Part I: Permeability and stability. *J. Membr. Sci.* Accepted for publication January 2005.
32. Glasstone S, Laidler KJ, and Eyring H. *The Theory of Rate Processes*. 1st ed. New York, McGraw-Hill Book Co., Inc., 1941.
33. Buxbaum RE and Marker TL. Hydrogen transport through non-porous membranes of palladium coated niobium, tantalum and vanadium. *J. Membr. Sci.* 1993; 85:29–38.
34. Kondo T. *New Developments in Gas Separation Technology*. Shiga, Japan: Toray Research Center, Inc., Asahi Kousoku Insatsu K.K. 1992.
35. Wang H, Cong Y, and Yang W. Oxygen permeation study in a tubular Ba<sub>0.5</sub>Sr<sub>0.5</sub>Co<sub>0.8</sub>Fe<sub>0.2</sub>O<sub>3-δ</sub> oxygen permeable membrane. *J. Membr. Sci.* 2002; 210:259–271.
36. Ward WJ and Robb WL. Carbon dioxide-oxygen separation: Facilitated transport of carbon dioxide across a liquid film. *Science* 1967; 156:1481–1484.
37. Majumdar S and Sirkar KK. Hollow—fiber contained liquid membrane. In: Ho, WSW and Sirkar, KK, eds. *Membrane Handbook*, New York: Van Nostrand Reinhold, 1992, p. 764.
38. Majumdar S, Sengupta A, Cha JS, and Sirkar KK. Simultaneous SO<sub>2</sub>/NO<sub>x</sub> separation from flue-gas in a contained liquid membrane permeator. *Ind. Eng. Chem. Res.* 1994; 33:667.

39. Sirkar KK. Hollow fiber-contained liquid membranes for separations—an overview, In: Bartsch, RA and Way, JD, eds. *Chemical Separations with Liquid Membranes*, ACS, 1996, p. 222.
40. Jeong SH and Lee KH. Separation of CO<sub>2</sub> from CO<sub>2</sub>/N<sub>2</sub> mixture using supported polymeric liquid membranes at elevated-temperatures. *Sep. Sci. Techn.* 1999; 34:2383.
41. LeBlanc OH, Ward WJ, Matson SL, and Kimura SG. Facilitated transport in ion-exchange membranes, *J. Membr. Sci.* 1980; 6:339–343.
42. Yoshikawa M, Ezaki T, Sanui K, and Ogata N. Selective permeation of carbon dioxide through synthetic polymer membranes having pyridine moiety as a fixed carrier. *J. Appl. Polym. Sci.* 1988; 35:145–154.
43. Noble R. Analysis of facilitated transport with fixed site carrier membranes. *J. Membr. Sci.* 1990; 50:207–214.
44. Quinn R, Appleby JB, and Pez GP. New facilitated transport membraness for the separation of carbon dioxide from hydrogen and methane. *J. Membr. Sci.* 1995; 104:139–146.
45. Quinn R and Laciak DV. Polyelectrolyte membranes for acid gas separations. *J. Membr. Sci.* 1997; 131:49–60.
46. Cussler EL. Facilitated and active transport. In: Paul DR and Yampol'skii YP, eds. *Polymeric Gas Separation Membranes*. Boca Raton, FL: CRC Press, 1994: Chap. 6.
47. Koros WJ and Chern RT. Separation of gaseous mixtures using polymer membranes. In: Rousseau RW, ed. *Handbook of Separation Process Technology*. New York: John Wiley & Sons, 1987, pp. 862–953.
48. Chern RT, Koros WJ, Sanders ES, Chen SH, and Hopfenberg HB. Implications of dual mode sorption and transport for mixed gas permeation. In: Whyte T, Yon CM, and Wagener EH, eds. *ACS Symposium Series 223 on Industrial Gas Separations*. Washington DC: American Chemical Society, 1983, pp. 47–73.
49. Kesting RE and Fritzsche AK. *Polymeric Gas Separation Membranes*. New York: John Wiley & Sons, 1993.
50. Vieth WR. *Diffusion in and through polymers*. Munich: Carl Hanser Verlag, 1991.
51. Vrentas JS and Duda JL. Diffusion in polymer-solvent systems. *J. Polym. Sci. PartB Polym. Phys.* 1977; 15:403–439.
52. Vrentas JS and Duda JL. Solvent and temperature effects on diffusion in polymer solvent systems. *J. Appl. Polym. Sci.* 1977; 21:1715–1728.
53. Koros WJ and Hellums MW. Gas separation membrane material selection criteria: Differences for weakly and strongly interacting feed components. *Fluid Phase Equilibria* 1989; 53:339–354.
54. Kim TH, Koros WJ, Husk GR, and O'Brien KC. Relationship between gas separation properties and chemical-structure in a series of aromatic polyimides. *J. Membr. Sci.* 1988; 37:45–62.
55. Lin H, and Freeman BD. Gas solubility, diffusivity and permeability in poly(ethylene oxide). *J. Membr. Sci.* 2004; 239:105–117.
56. Patel NP, Miller AC, and Spontak RJ. Highly CO<sub>2</sub>-permeable and selective polymer nanocomposite membranes. *Adv. Mater.* 2003; 15:729–733.
57. Hirayama Y, Kase Y, Tanihara N, Sumiyama Y, Kusuki Y, and Haraya K. Permeation properties to CO<sub>2</sub> and N<sub>2</sub> of poly(ethylene oxide)-containing and crosslinked polymer films. *J. Membr. Sci.* 1999; 160:87–99.
58. Arcella V, Ghielmi A, and Tommasi G. High performance perfluoropolymer films and membranes. In: Li NN, Drioli E, Ho WSW, and Lipscomb GG, eds. *Annals of the New York Academy of Sciences vol. 984: Advanced Membrane Technology*. New York: The New York Academy of Sciences, 2003, pp. 226–244.
59. Kharitonov AP, Moskvina YL, Syrtsova DA, Starov VM, and Teplyakov VV. Direct fluorination of the polyimide Matrimid 5218: The formation Kinetics and Physicochemical properties of the Fluorinated layers. *J. Appl. Pol. Sci.* 2004; 92:6–17.
60. Hägg MB. Membrane purification of Cl<sub>2</sub> gas II. Permeabilities as function of temperature for Cl<sub>2</sub>, O<sub>2</sub>, N<sub>2</sub>, H<sub>2</sub>, and HCl in perfluorinated, glass and carbon molecular sieve membranes. *J. Membr. Sci.* 2000; 177:109–128.
61. Hirayama Y et al. Novel membranes for carbon dioxide separation. *Energy Conv. Mgmt.* 1995; 36(6–9):435–438.
62. Haraya K. Possibility of utilization of gas-separation membranes as countmeasure of global warming. *Membr. Techn. Environm.* 1998; 28(5):299–303.
63. Takeuchi M, Sakamoto Y, and Niwa S. Study on RITE CO<sub>2</sub> global recycling system. Proc. of 5th Int. Conf. on CO<sub>2</sub> Utilization (CO<sub>2</sub> ICCDU V) Karlsruhe, Germany September 1999.
64. Schultz J and Peinemann K-V. Membranes for separation of higher hydrocarbons from methane. *J. Membr. Sci.* 1996; 110:37–45.
65. Pinnau I, Casillas CG, Morisato A, and Freeman BD. Long-term permeation properties of poly(1-trimethylsilyl-propyne) membranes in hydrocarbon-vaport environment. *J. Polym. Sci. PartB Polym. Phys.* 1997; 35:1483–1490.
66. Pinnau I, He Z, and Morisato A. Synthesis and gas permeation properties of poly(dialkylacetylenes) containing isopropyl-terminated side-chains. *J. Membr. Sci.* 2004; 241:363–369.
67. Ward WJ and Robb WL. Liquid membranes for use in the separation of gases. U.S. Patent 3,396,510, 1968.
68. Way JD, Noble RD, Reed DL, Ginley GM, and Jarr LA. Facilitated transport of CO<sub>2</sub> in ion exchange membranes. *AIChE J.* 1987; 33:480–487.
69. Pellegrino J, Wang D, Rabago R, Noble RD, and Koval CA. Gas transport properties of solution-cast perfluorosulfonic acid ionomer films containing ionine surfactants. *J. Membr. Sci.* 1993; 84:161–169.
70. Matsuyama H, Teramoto M, and Iwai K. Development of a new functional cation-exchange membrane and its application to facilitated transport of CO<sub>2</sub>. *J. Membr. Sci.* 1994; 93:237–244.
71. Noble RD. Analysis of ion transport with fixed site carrier membranes. *J. Membr. Sci.* 1991; 56:229–234.
72. Noble RD. Facilitated transport mechanism in fixed site carrier membranes. *J. Membr. Sci.* 1991; 60:297–306.
73. Matsuyama H, Masui K, Kitamura Y, Maki T, and Teramoto M. Effect of membrane thickness and membrane preparation condition on facilitated transport of CO<sub>2</sub> through ionomer membrane. *Sep. Purif. Tech.* 1999; 17:235–241.
74. Yamaguchi T, Koval CA, Noble RD, and Bowman CN. Transport mechanism of carbon dioxide through perfluorosulfonic ionomer membranes containing an amine carrier. *Chem. Eng. Sci.* 1996; 51:4781–4789.

75. Matsuyama H, Terada A, Nakadawara T, Kitamura Y, and Teramoto M. Facilitated transport of CO<sub>2</sub> through polyethylenimine/poly(vinyl alcohol) blend membrane. *J. Membr. Sci.* 1999; 163:221–227.
76. Geizler V and Koros WJ. Effects of polyimide pyrolysis conditions on carbon molecular sieve membrane properties. *Ind. Eng. Chem. Res.* 1996; 35:2999–3003.
77. Ismail AF and David LI. A review of the latest development of carbon membranes for gas separation. *J. Membr. Sci.* 2001; 193:1–18.
78. Lie JA. Synthesis, performance and regeneration of carbon membranes. Doctoral thesis 152, NTNU, Trondheim, Norway, 2005.
79. Vennes K. Studies of gas transport through carbon membranes. MSc Thesis (in Norwegian), NTNU, Trondheim, Norway, 2002.
80. Mattson JS and Mark HB. *Activated Carbon*. New York: Marcel Dekker, 1971.
81. Gawrys M, Fastyn P, Gawlowski J, Gierczak T, and Niedzielski J. Prevention of water vapor adsorption by carbon molecular sieves in sampling humid gases. *J. Chrom. A* 2001; 933:107–116.
82. Jones CW and Koros WJ. Carbon molecular sieve gas separation membranes—II. Regeneration following organic exposure. *Carbon* 1994; 32:1427–1432.
83. Hägg MB, Lie JA, and Lindbråthen A. Carbon molecular sieve membranes—a promising alternative for selected industrial applications. In: Li NN, Drioli E, Ho WSW, and Lipscomb GG, eds. *Annals of the New York Academy of Sciences vol. 984: Advanced Membrane Technology*. New York: The New York Academy of Sciences, 2003, pp. 329–345.
84. Mahajan R and Koros WJ. Factors controlling successful formation of mixed matrix gas separation materials. *Ind. Eng. Chem. Res.* 2000; 39:2692–2696.
85. Koros WJ and Mahajan R. Pushing the limits on possibilities for large scale gas separation: which strategies? *J. Membr. Sci.* 2000; 175:181–196.
86. Vu DQ, Koros WJ, and Miller SJ. Mixed matrix membranes using carbon molecular sieves: I. Preparation and experimental results. *J. Membr. Sci.* 2003; 211:311–334.
87. Merkel TC, Freeman BD, Spontak RJ, He Z, Morisato A, Pinnau I, Meakin P, and Hill AJ. Ultrapermeable, reverse-selective nanocomposite membranes. *Science* 2002; 296:519–522.
88. Kroto HW, Heath JR, O'Brian SC, Curl RF, and Smalley RE. C-60-Buckminsterfullerene. *Nature* 1985; 318:162–163.
89. Rouquerol J, Avnir D, Fairbridge CW, Everett DH, Haynes JH, Pernicone N, Ramsey JDF, Sing KSW, and Unger KK. Recommendations for the characterization of porous solids. *Pure Appl. Chem.* 1994; 66:1739–1758.
90. Burggraaf AJ and Keizer K. Synthesis of inorganic membranes. In: Bhave RR, ed. *Inorganic Membranes, Synthesis, Characterisation and Applications*. New York: Van Nostrand Reinhold, 1991, pp. 11–63.
91. Bhave RR. (ed.) *Inorganic Membranes. Synthesis, Characteristics and Applications*. New York: Van Nostrand Reinhold, 1991.
92. Posthusta JC, Noble RD, and Falconer JL. Temperature and pressure effects on CO<sub>2</sub> and CH<sub>4</sub> permeation through MFI zeolite membranes. *J. Membr. Sci.* 1999; 160:115–125.
93. Javaid A and Ford DM. Solubility-based gas separation with oligomer-modified inorganic membranes. Part II: Mixed gas permeation of 5 nm alumina membranes modified with octadecyltrichlorosilane. *J. Membr. Sci.* 2003; 215:157–168.
94. Hwang G-J, Kim J-W, Choi H-S, and Onuki K. Stability of a silica membrane prepared by CVD using  $\gamma$ - and  $\alpha$ -alumina tube as the support tube in the HI-H<sub>2</sub>O gaseous mixture. *J. Membr. Sci.* 2003; 215:293–302.
95. Kuraoka K, Chujo Y, and Yazawa T. Hydrocarbon separation via porous glass membranes surface modified using organosilane compounds. *J. Membr. Sci.* 2001; 182:139–149.
96. Ma YH, Mardilovich IP, and Engwall EE. Thin composite palladium and palladium/alloy membranes for hydrogen separation. In: Li NN, Drioli E, Ho WSW, and Lipscomb GG, eds. *Annals of the New York Academy of Sciences vol. 984: Advanced Membrane Technology*. New York: The New York Academy of Sciences, 2003, pp. 346–360.
97. Mardilovich PP, She Y, Ma YH, and Rei MH. Defect-free palladium membranes on porous stainless steel support. *AICHE J.* 1998; 44:310–322.
98. Lewis FA. *The Palladium Hydrogen System*. London: Academic Press, 1967.
99. Howard BH, Killmeyer RP, Rothenberger KS, Cugini AV, Morreale BD, Enick RM, and Bustamante F. Hydrogen performance of palladium-copper alloy membranes over a wide range of temperatures and pressures. *J. Membr. Sci.* 2004; 241:207–218.
100. Jung SH, Kusakabe K, Morooka S, and Kim S-D. Effects of co-existing hydrocarbons on hydrogen permeation through a palladium membrane. *J. Membr. Sci.* 2000; 170:53–60.
101. Cappadonia M, Stimming U, Kordesch KV, and de Oliveira JCT. Fuel cells. In: *Ullmann's Encyclopedia of Industrial Chemistry*. Vol. 15, 6th ed. Weinheim, Germany: Wiley-VCH, 2003, pp. 95–115.
102. Alberti G, Casciola M, Pica M, and De Cesare G. Preparation of nano-structured polymeric proton conducting membranes for use in fuel cells. In: Li NN, Drioli E, Ho WSW, and Lipscomb GG, eds. *Annals of the New York Academy of Sciences vol. 984: Advanced Membrane Technology*. New York: The New York Academy of Sciences, 2003, pp. 208–225.
103. Wang H, Cong Y, and Yang W. Partial oxidation of ethane to syngas in an oxygen-permeable membrane reactor. *J. Membr. Sci.* 2002; 209:143–152.
104. Walawender WP and Stern SA. Analysis of membrane separation parameters. 2. Countercurrent and cocurrent flow in a single permeation stage. *Sep. Sci.* 1972; 7:553–584.
105. Keil B, Wind J, and Ohlrogge K. In: Pierucci S, ed. *Membrane simulation tools for flowsheeting programmes*. AIDIC Milan: Proceedings IcheaP-5. Vol. 2, 2000.
106. Ohlrogge K and Brinkmann T. Natural gas cleanup by means of membranes. In: Li NN, Drioli E, Ho WSW, and Lipscomb GG, eds. *Annals of the New York Academy of Sciences vol. 984: Advanced Membrane Technology*. New York: The New York Academy of Sciences, 2003, pp. 306–317.

107. Ohlrogge K. in Final Report for EU-project BE97–4589. Dehydration and dewpointing of natural gas by membrane technology. GKSS, Germany, 2002.
108. Pellegrino J and Sikdar SK. Membrane Technology, Fundamentals of Bioremediation [http://membranes.nist.gov/Bioremediation/fig\\_pages/f5.html](http://membranes.nist.gov/Bioremediation/fig_pages/f5.html) (accessed September 2004).
109. Baudet J, Rochet M, Salmon M, and Vogt B. Hollow fiber assembly for use in fluid treatment apparatus. US Patent 3,993,816, Nov 1976.
110. Nichols RW. Hollow fiber separation module and method for the use thereof. US Patent 4,959,152, Sept 1990.
111. Hoff KA. Modeling and experimental study of CO<sub>2</sub> absorption in a membrane contactor. Thesis NTNU, Trondheim, 2003.
112. Liquei-Cel Membrane Contactors, Membrana, <http://www.liquicel.com/>, 2005 (date of access: January 2005).
113. Nishikawa N, Ishibashi M, Ohta H, Akutsu N, Matsumoto H, Kamata T, and Kitamura H. CO<sub>2</sub> removal by hollow-fiber gas-liquid contactor, *Energy Conversion and Management* 1995; 36:415.
114. Lee YT, Noble RD, Yeom BY, Park YI, and Lee KH. Analysis of CO<sub>2</sub> removal by hollow-fiber membrane contactors. *J. Membr. Sci.* 2001; 194:57.
115. Ivory J, Feng XS, and Kovacic G. Development of hollow fiber membrane systems for nitrogen generation from combustion exhaust gas—Part II: Full-scale module test and membrane stability. *J. Membr. Sci.* 2002; 202:195.
116. Klaassen R and Jansen AE. Achieving flue gas desulphurization with membrane gas absorption. *Filtration Separation* 2003; 40:26.
117. Mavroudi M, Kaldis SP, and Sakellaropoulos GP. Reduction of CO<sub>2</sub> emissions by a membrane contacting process. *Fuel* 2003; 82:2153.
118. Sengupta A and Sirkar KK. Analysis and design of membrane permeators for gas separation, In: Noble RD and Stern SA, eds. *Membrane Separation Technology. Principles and Applications*, Amsterdam: Elsevier Science, 1995, p. 498.
119. Rautenbach R. Membranverfahren. *Grundlagen der Modul- und Anlagenauslegung*. Berlin: Springer, 1997, p. 363.
120. Spillman RW. Economics of gas separation membranes. *Chem. Eng. Progr.* 1989; 85:41–62.
121. Baker RW. Future directions of membrane gas separation technology. *Ind. Eng. Chem. Res.* 2002; 41:1393–1411.
122. Zolands RR and Fleming GK. Applications. In: Ho WSW and Sirkar WS, eds. *Membrane Handbook*. London: Kluwer Academic Publishers, 2001, pp. 78–94.
123. Scott K. *Handbook of Industrial Membranes*. 2nd ed. Oxford: Elsevier Science Publishers, 1998, p. 297.
124. Nunes SP. Review on fuel cells. Presentation at EMS Summer School, NTNU, Trondheim, Norway, 2003.
125. Edlund DJ, Pledger WA, and Studebaker T. Hydrogen-selective metal membrane modules and method of forming the same. US Patent 6,458,189, Oct 2002.
126. Franz AJ, Schmidt MA, Jensen KF, and Firebaugh S. Integrated palladium-based micromembranes for hydrogen separation and hydrogenation/dehydrogenation reactions. US Patent 6,541,676, Apr 2003.
127. EU-integrated project 2004–2008 within Sustainable Energy Systems in 6FW-program: Preparing for the hydrogen economy by using existing natural gas system as a catalyst (NATURALHY) <http://www.naturalhy.net> (accessed December 2004).
128. Hagler Baily Consultants. EU brochure. In: Nunes SP. Review on fuel cells. Presentation at EMS Summer School, NTNU, Trondheim, Norway, 2003.
129. Dortmund D and Doshi K. Recent developments in CO<sub>2</sub> removal membrane technology [http://www.uop.com/gasprocessing/TechPapers/CO<sub>2</sub> RemovalMembrane.pdf](http://www.uop.com/gasprocessing/TechPapers/CO2%20RemovalMembrane.pdf) (accessed March 2004).
130. Maltesson, HÅ. *Biogas för fordonsdrift*. Stockholm: KFB, 1997 (in Swedish).
131. Hägg M-B. Membranes in Chemical Processing. *Sep. Purif. Methods* 1998; 27:51–168.
132. Jordal K, Bredesen R, Kvamsdal HM, and Bolland O. Integration of H<sub>2</sub>-separating membrane technology in gas turbine processes for CO<sub>2</sub> capture. *Energy* 2004; 29:1269–1278.
133. Baker R. *Membrane Technology and Applications*. New York: McGraw-Hill, 2000, Chap. 8.
134. Prasad R, Shaner L, and Doshi KJ. Comparison of membranes with other gas separation technologies. In: Paul DR and Yampol'skii YP, eds. *Polymeric Gas Separation Membranes*. Boca Raton, FL: CRC Press, 1994.
135. Dyer PN, Richards RE, Russek SL, and Taylor DM. Ion transport membrane technology for oxygen separation and syngas production. *Solid State Ionics* 2000; 134:21–33.
136. Aasberg-Petersen K. Autothermal steam reforming with modified catalyst. US Patent 6,338,833, Jan 2002.
137. Ohlrogge K, Wind J, and Behling RD. Membrane technique in the chemical and petrochemical industry. *Erdoel & Kohle Erdgas Petrochemie* 1993; 46:326–332.
138. Ryu JH, Lee H, Kim YS, Kang YS, and Kim HS. Facilitated olefin transport by reversible olefin coordination to silver ions in a dry cellulose acetate membrane. *Chem. Eur. J.* 2001; 7(7):1525–1529.
139. Peinemann KV. Membrane technology in industrial processes. In: Proceedings; The ForuM Seminar, Oslo, Norway, 1997.
140. Peinemann KV, Ohlrogge K, and Knauth HD. The recovery of helium from diving gas with membranes. In: Membranes with gas separation and environment. Special Publication No. 62. London: Royal Society of Chemistry, 1986, pp. 329–341.
141. Hägg M-B. Membrane purification of Cl<sub>2</sub> gas I. *J. Membr. Sci.* 2000; 170:173–190.
142. Eikeland MS, Hägg M-B, Brook MA, Ottøy M, and Lindbråthen A. Durability of poly(dimethylsiloxane) when exposed to chlorine gas. *J. Appl. Pol. Sci.* 2002; 85:2458–2470.



---

# 5 Pervaporation: Theory, Practice, and Applications in the Chemical and Allied Industries

*Vishwas G. Pangarkar and Sangita Pal*

## CONTENTS

5.1	Introduction .....	107
5.2	Transport through Membranes .....	109
5.2.1	Transport in Pervaporation .....	109
5.2.1.1	Preferential Sorption–Capillary Flow Model .....	109
5.2.1.2	Solution Diffusion Model .....	110
5.2.2	Concentration Polarization and Permeation .....	114
5.2.3	Selectivity in Pervaporation .....	115
5.3	Membrane Fabrication Methods and Membrane Modules .....	116
5.3.1	Introduction .....	116
5.3.2	Ideal Membrane for Pervaporation .....	116
5.3.3	Composite Membranes .....	117
5.3.3.1	Importance of the Support Layer .....	117
5.3.3.2	Techniques for Fabrication of Composite Membranes .....	118
5.3.4	Pervaporation Modules .....	118
5.3.5	Selection of the Membrane Module .....	119
5.3.6	Some Problems in Industrial Use of Pervaporation .....	119
5.4	Applications of Pervaporation .....	120
5.4.1	Dehydration of Organics .....	120
5.4.2	Removal of Organics from Aqueous Phase .....	123
5.4.3	Organic–Organic Separations .....	128
	Nomenclature .....	131
	Greek Letters .....	132
	Abbreviations .....	132
	Acknowledgment .....	133
	References .....	133

## 5.1 INTRODUCTION

The contributions of separation to human society cannot be underestimated. Different types of chemicals meet various requirements in our daily life. Most of these are synthetics manufactured by different techniques. These chemicals are an essential part of our life and it is impossible to imagine a civilized society devoid of them. These chemicals range from foods, medicinal drugs, and colorful dyes of our clothes to detergents for washing and cleaning of every essential commodity. There is very little doubt that much of these activities involved in the manufacture of the synthetics are causing certain damage to the delicate balance in the ecosystem. Developments in “Green” technologies are not just academic curiosities but are increasingly finding commercial applications. The widespread use of the natural resources has led to depletion of natural, nonrenewable energy sources. There is an ever-increasing awareness about optimum utilization of the nonrenewable sources (NRS). One major mode of consumption of NRS in the chemical process industries (CPI) is the use of fossil fuels as a source of

heating the various process equipments. Separation processes are an integral part of the CPI. Amongst the various separation processes used in the CPI, the major consumption of fuels in the CPI occurs in distillation. It is impossible to build a chemical plant without using distillation at some point in the process. Even isolation of natural products such as essential oils, spices, photochemical, etc. cannot be accomplished without resorting to distillation. Distillation as commonly employed uses a high grade heat in the reboiler and rejects the same as very low-grade heat in the condenser. With the awareness about optimum and efficient utilization of these NR fuels, the CPI is looking at alternatives to this highly energy intensive operation. Thus, membrane separations that either do not involve a phase change or use low-grade heat for the phase change during separation are becoming significantly important as an alternative to distillation. Several new, promising approaches have been made recently. A large number of separation processes are available for separation of components from a mixture. Amongst these the membrane-based separation techniques include microfiltration, ultrafiltration, nanofiltration, reverse osmosis, and pervaporation (PV). Pervaporation in which permeation through a dense membrane is followed by evaporation is the subject of this chapter.

Kobar first used the term “Pervaporation” in 1917 [1] to denote a phenomenon observed during laboratory experiment. In the course of some experiments on dialysis, his assistant, C.W. Eberlein, pointed out the fact that a liquid in a collodion bag, which was suspended in air, evaporated, although the bag was tightly closed. These investigators alluded it to evaporation, presuming that it has taken place through a small aperture at the top of the bag. Further experiments and especially the speed of evaporation soon led them to the conclusion that aqueous vapor is given off through the membrane. This phenomenon was termed pervaporation by Kobar in an article published in the *Journal of American Chemical Society* in 1917 [1].

In 1952, Schwob [2] in his doctoral thesis employed the PV process for dehydration of alcohol using a regenerated cellulose film. Between 1958 and 1962, Binning et al. [3] carried out a series of investigations using hydrophobic membranes such as polyethylene for the separation of hydrocarbon mixtures. Meanwhile, Neel and coworkers had also started systematic PV studies [4–6]. In between, Tusel and his coworkers also started to work on dehydration through PV [7]. Besides these, investigations by Sander [8] and Asada [9] on pervaporative dehydration resulted in establishing PV as a safe and energy efficient process for the separation of components in a homogeneous liquid mixture.

PV as a separation process has potential applications in almost all categories. These include: (i) industrial dehydration applications, such as alcohol–water, organic–water, and chlorinated-hydrocarbon water system [10–15]; (ii) removal of organics from water [16–20]; and (iii) separation of organic–organic mixtures [21–27]. Although the first application category has seen widespread application, the other two are not as commercially successful as the first category. The process is currently best identified with dehydration of ethanol, isopropyl alcohol, and ethylene glycol. Due to its favorable economics, efficiency, and simplicity, PV can be easily integrated with distillation and other rectification processes. In the mid 1970s, the German company GFT first commercialized an economical process for dehydrating ethanol producing anhydrous ethanol at high purities that rival azeotropic distillation. Subsequently, continuing into the early 1980s other integrated distillation/PV plants were built in Europe and Asia. Currently, a number of commercial PV plants exist for recovery of solvents, removal of organics from wastewaters, dealcoholization of wines and liquors, as well as many more for ethanol dehydration. A 150,000 L/day ethanol dehydration plant in Betheniville, France was started up in early 1988 and became the world’s largest PV facility. The groups of Mulder, Rautenbach, Huang, Cabasso, and Pangarkar have also carried out considerable work at various universities.

Pervaporation has the following advantages:

1. Very low capital and operating cost: The separation could be made more economical by using a hybrid membrane process, i.e., a combination of distillation and pervaporation processes. Thus, a part of the total separation employs distillation where it is economical. PV replaces the subsequent separation where distillation becomes expensive. The overall operating cost of such a hybrid process is much lower than that of distillation alone.
2. Azeotropes can be readily broken by using an appropriate membrane.
3. No additive is needed for the final separation.
4. Easy operation and space saving.
5. Reduced energy demand, low-grade heat, and a vacuum pump are required.
6. Freedom from environmental pollution caused by the entrainers.
7. Possibility of multipurpose application and easy scale-up.
8. Membrane properties can be varied and adjusted to suit different applications.
9. Closed loop operations with only a small volume of recycled permeate.

Selective separation of liquids by pervaporation is a result of selective sorption and diffusion of a component through the membrane. PV process differs from other membrane processes in the fact that there is a phase change of the permeating molecules on the downstream face of the membrane. PV mechanism can be described by the solution–diffusion mechanism proposed by Binning et al. [3]. According to this model, selective sorption of the component of a liquid mixture takes place at the upstream face of the membrane followed by diffusion through the membrane and desorption on the permeate side.

Based on the above proposed mechanism pervaporation can be divided into three distinct steps:

1. Sorption: At the membrane–liquid interface, the membrane sorbs the components according to their relative sorption behavior.
2. Diffusion: The sorbed components diffuse across the swollen membrane under a chemical potential gradient.
3. Evaporation: Permeate desorption takes place at the downstream surface of the film.

Selectivity and productivity depend on sorption and diffusion. Sorption is dictated by thermodynamic properties, namely, the solubility parameter of the solute(s)/membrane material system. On the other hand, the size, shape, molecular weight of the solute, and the availability of inter/intra molecular free space of the polymer largely govern the second property, the diffusion coefficient. For an ideal membrane, both the sorption and diffusion processes should favor the chosen solute. If one step becomes unfavorable for a given solute the overall selectivity will be poor [28].

Desorption on the downstream side of the membrane is generally considered to be rapid and nonselective. The gas phase diffusivities in the final step of transport are very high and hence this step offers the least resistance in the overall transport process. As a separation process, pervaporation relies on the difference in membrane permeabilities, which are dependent on the thermodynamics activities of the components to be separated.

This chapter deals with the following:

1. Basic aspects of PV and the related theory with a view to familiarize the reader with the selection of the membrane material for a given application.
2. The membrane modules used industrially and their specific areas of applications.
3. A comprehensive survey of the literature on PV for all the three categories is finally presented to update the reader with the latest research findings.

## 5.2 TRANSPORT THROUGH MEMBRANES

The mode of transport through a membrane may be passive, active, or facilitated type. In passive transport, the membrane acts as a barrier and permeation of the components is determined by their diffusivity and concentration in the membrane or just by their size. In facilitated transport along with the chemical potential gradient, the mass transport is coupled to specific carrier components in the membrane. In active transport driving force for transport is achieved by a chemical reaction in the membrane phase.

### 5.2.1 TRANSPORT IN PERVAPORATION

In PV, the transport of the solutes occurs under a chemical potential gradient. This gradient is maintained by applying a lower pressure at the downstream face of the membrane in the classical PV mode. The low pressure creates a lower activity at the downstream face as compared to the higher activity at the feed face where the solutes are in liquid phase. A different method, which can also maintain an activity gradient, utilizes an inert carrier gas as a sweep gas past the downstream face of the membrane. The inert gas plays the same role as vacuum in creating a driving force for transport through the membrane. The whole transport process is purely physical since no chemical reaction with either a carrier or membrane material occurs. The permeate is passed through a condenser wherein the solutes are condensed. When a sweep gas is used to create the driving force, the presence of noncondensable components calls for much lower temperatures due to the much lower dew point of the mixture. This fact must be considered while designing the condenser and coolant circuit as well calculating the operating cost. Overall the vacuum mode is more popular since no extra cost associated with the sweep gas and its recirculation is involved. Different models have described passive transport through the membrane in PV. Mulder [29] has discussed this subject in detail. The following discussion is therefore limited to the two main models:

#### 5.2.1.1 Preferential Sorption–Capillary Flow Model

The preferential sorption–capillary flow model, proposed by Sourirajan and Shiyao [30], depicts the membrane as a porous barrier. The model is based on a combination of preferential sorption of the rapidly permeating solute followed by flow through the capillaries and finally evaporation at the downstream face of the membrane. The extent of separation is governed by the effective molecular sizes of the permeants, the pore size, and its distribution besides the interactions between the membrane polymer and the solutes, which result in preferential sorption. According to the PSCF model liquid feed flow through the cylindrical pores of the membranes is rate determining. Liquid–vapor transition occurs at the pore outlet in the downstream side and phase equilibrium between liquid–vapor is established. A straight cylindrical pore is assumed at the surface layer of the membrane and cylindrical coordinates ( $r, z$ ) are set in the pore. Diffusion forces working on components A and B (permeants),

the viscous force, and the pressure force are those which have to be balanced at the steady state of the liquid movement in the pore leading to the equation:

$$\frac{D^2U}{dr^2} + \frac{1}{r} \frac{dU}{dr} + \frac{1}{\eta} \frac{(p_2 - p_3)}{\delta p} = 0 \quad (5.1)$$

where

$U$  is the solution velocity

$\eta$  is the solution viscosity in the pore

$\delta$  is the length of the pore

$p_2$  and  $p_3$  are effective pressure (atmospheric pressure/RO pressure) at pore inlet and outlet A and B

To find the concentration of A in the permeate, diffusive force is considered to work only on A, friction force between A and B, and A and pore wall. This leads to the differential equation:

$$-RT \frac{d \ln a_A(r,z)}{dr} / r = r, \quad -(c_{AB} + c_{AM})U(r) \frac{C_{A3}(r)}{C_A(r,z)} + \chi_{AB}U(r) \frac{C_{B3}(r)}{C_B(r,z)} = 0 \quad (5.2)$$

where

$a$  is the activity

$\chi_{AB}$  is the friction constant between A and B

$\chi_{AM}$  is the friction constant between component A and pore well

$C_{i3}(r,o)$  is the molar concentration at the pore outlet, where  $i$  represents solute A or B

$C_i(r,z)$  is the molar concentration in the pore at a position represented by a cylindrical coordinate  $r, z$ , respectively, where  $i$  represents solute A or B

Both Equations 5.1 and 5.2 can be solved with appropriate boundary conditions and interfacial interaction force constants, generated from liquid chromatography experiments.

*Limitations of the Preferential Sorption–Capillary Flow Model:* The PSCF pore flow mechanism has a number of limitations. The assumption of the so-called cylindrical pores in PV membranes and the effect of its size and distribution in the membrane on separation performance of the membrane are not always explainable. In fact the concept of pore size and its distribution in PV membrane is not so important as membrane made by ordinary solution casting method has been found to show reproducible performance. It is not possible to get membranes, always with the same pore size and its distribution by ordinary solution casting coating method and according to PSCF model a slight difference in pore size and its distribution would drastically affect the membrane performance. Similarly, PSCF model cannot explain the simple inverse relation of flux and membrane thickness, membrane swelling, and trade-off relationship between flux and selectivity. According to this model an asymmetric membrane made by phase inversion technique would be the most ideal PV membrane. However, this membrane has not been found to give better performance than the prevailing PV membranes made by ordinary solution casting method [31].

### 5.2.1.2 Solution Diffusion Model

The solution diffusion model is the most widely used model to describe permeation in dense membranes, as is the case for PV [3,32]. This model is based on the following assumptions:

1. Sorption of the feed liquid mixture in the membrane (upstream side) as per the sorption behavior of the solute(s)/polymer system
2. Diffusion of the solutes through the membrane under an activity gradient
3. Desorption of the permeants at the downstream side in the vapor phase

The first two steps, i.e., sorption and diffusion are dominant contributors for separation of the mixture by PV. Desorption of the permeant vapor in the permeate side under low pressure (applying vacuum) is very fast and unlike pore flow mechanism does not offer significant resistance to the transport of the solute.

#### 5.2.1.2.1 Sorption in the Membrane

##### 5.2.1.2.1.1 Sorption Selectivity and Membrane Polymer

Relative sorption of the permeants in the membrane depends on the interactions between the solutes and the membrane polymer. Solubility or miscibility of a component with the membrane polymer depends on their relative solubility parameter values. For mutual solubility of two components their free energy of mixing,  $\Delta G_m$  should be negative.

$\Delta G_m$  is defined as

$$\Delta G_m = \Delta H_m - T\Delta S_m \quad (5.3)$$

Enthalpy of mixing,  $\Delta H_m$ , can be correlated to cohesive energy density, i.e., solubility parameter ( $\delta$ ) as

$$\Delta H_m = n_1 n_2 V_1 (\delta_1 - \delta_2)^2 \quad (5.4)$$

In Equation 5.4, the solubility parameter is that due to only dispersive force between structural units of the concerned solute and polymer since the original Regular solution theory of Scatchard and Hildebrand was restricted to nonpolar, non-hydrogen bonding solutes–polymer systems. However, for many liquid and amorphous polymers, contribution from polar forces and hydrogen bonding [33] need to be considered. Accordingly, Equation 5.4 becomes

$$\Delta H_m = n_1 n_2 V_1 [(\Delta\delta_d)^2 + (\Delta\delta_p)^2 + (\Delta\delta_h)^2] \quad (5.5)$$

From Equations 5.3 and 5.4, it is clear that to make  $\Delta G_m$  negative, the difference between  $\delta_1$  (solvent) and  $\delta_2$  (polymer), i.e.,  $(\Delta\delta)$  for all the three forces of interactions should be as small as possible. It implies that the membrane polymer and the desired component to be separated should be of comparable polarity to achieve similar solubility parameter values. This will result in preferential sorption of the desired component in the membrane.

#### 5.2.1.2.1.2 Sorption and Nature of Membrane Polymer

*Ideal Case:* If sorption process is ideal, the concentration of a component  $i$ ,  $C_{mi}$  in the membrane is linearly proportional to the concentration of this component in the feed mixture,  $C_{bi}$ .

From Henry's law for dilute solutions,

$$C_{mi} = kC_{bi} \quad (5.6)$$

$k$  denotes the sorption coefficient for the solute in the polymer. This relationship holds good for sorption of a component present in trace amounts in a solution (dilute solutions) and when specific interactions between the solute and polymer are absent. However, in most of the cases membrane phase concentration of a component is not a linear function of its bulk concentration. Further, it is also influenced by the presence of the other components.

#### 5.2.1.2.1.3 Sorption Isotherms

Rogers [34] described four different types of sorption isotherms. For very dilute feed solution sorption isotherm is linear obeying Henry's law (Equation 5.6). It is also called type-I sorption isotherm.

For polymeric membranes filled with absorptive fillers, sorption in the filler occurs in accordance with the Langmuir adsorption isotherm while Henry's law governs that in the polymer matrix. This kind of sorption isotherm is designated as type-II isotherm.

For polymers with high degree of crystallinity, and stiff and inflexible chains along with strong cohesive force; type-III sorption isotherm is observed. In this case, the mutual interaction of the sorbed molecules is greater than their interaction with the polymer. Thus, these molecules forms cluster within the polymer matrix.

Type-IV sorption isotherm is a combination of type-II sorption at low concentration and type-III sorption at high concentration. Type-V isotherm as defined here (Figure 5.1) is exhibited by glassy polymers/polymers containing adsorptive fillers. This type of sorption is defined as dual mode sorption, which is a combination of Henry's type and Langmuir type. The former applies to the bulk polymer and the latter to the filler/micro-voids in the polymer. Netke et al. [35] have studied the permeation of acetic acid–water mixtures in silicalite filled PDMS. Equations governing type-V isotherm are

$$C_T = C_M + C_Z \quad (5.7)$$

$C_M$  is given by

$$C_M = H_M C_b \quad (5.8)$$

And  $C_Z$  is given by

$$C_Z = \frac{C^* k_Z C_M}{1 + k_Z C_M} \quad (5.9)$$

Figure 5.1 shows the sorption isotherm data of Netke et al. [35] for acetic acid–water–PDMS containing 20% silicalite SA-5 (UOP) converted to the form given by Equation 5.7.

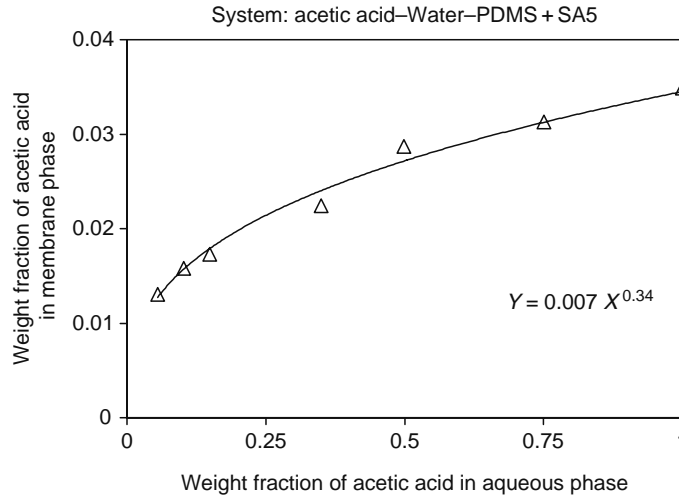


**FIGURE 5.1** Dual mode sorption isotherms. (From Netke, S.A., Sawant, S.B., Joshi, J.B., and Pangarkar, V.G., *J. Mem. Sci.*, 107, 23, 1995.)

#### 5.2.1.2.1.4 Sorption of Single Component in Amorphous Polymers

Sorption of a pure component  $i$  in a membrane of amorphous polymer may be described by the Flory–Huggins [36] equation:

$$\Delta\mu = RT \ln(1 - \Phi_p) + \Phi_p(1 - 1/n_i) + \chi_{ip} \Phi_p^2 = 0 \quad (5.10)$$

where

$n_i$  is the ratio of molar volume of polymer to solute  $i$

$\Phi_p$  is volume fraction of the polymer

The membrane phase concentration of  $i$ , i.e.,  $1 - \Phi_p$  may be calculated from Equation 5.10 provided interaction parameter,  $\chi_{ip}$ , is known.

#### 5.2.1.2.1.5 Sorption of Binary Liquid in Amorphous Polymer

If interaction parameters are concentration independent, in the simplest case [36],

$$\ln(\Phi_1/\Phi_2) - \ln(V_1/V_2) = (1 - 1/n) \ln(\Phi_1/V_2) - \chi_{12}[(V_1 - V_2) + (\Phi_2 + \Phi_1)] - \Phi_3(\chi_{1,3} - \chi_{2,3}) \quad (5.11)$$

#### 5.2.1.2.1.6 Sorption of Pure Component in Cross-Linked Polymer

Cross-links retard swelling and thus decrease concentration of the permeants in the polymer matrix. Effect of cross-linking on the sorption of low-molecular weight components in polymers can be obtained by Flory–Huggins thermodynamics [36]

$$\ln(1 - \Phi_p) + \Phi_p \left(1 - \frac{1}{n_i}\right) + \chi_{ip} \Phi_p^2 + \frac{V_i \rho_p}{M_c} \left(\Phi_p^{1/3} - \frac{\Phi_p}{2}\right) = 0 \quad (5.12)$$

where

$M_c$  is the molecular weight between two cross-links

$\rho_p$  is the polymer density

#### 5.2.1.2.1.7 Sorption of Pure Liquid in Semicrystalline Polymer

The crystallites are impermeable to penetrants leading to a hindered diffusion (tortuosity effect). For a semicrystalline polymer, sorption of pure liquid is given by [36]

$$\ln(1 - \Phi_p) + \Phi_p \left(1 - \frac{1}{n_i}\right) + \chi_{ip} \Phi_p^2 + \frac{V_i \rho_p}{M_v} \left[ \frac{\frac{\Delta H_f}{R} \left(\frac{1}{T} - \frac{1}{T_m}\right)}{\frac{3}{2} \lambda \Phi_p} \right] = 0 \quad (5.13)$$

where

$\lambda$  is the fraction of noncrystalline polymer, i.e., elastically effective

$M_v$  is the molecular weight of the repeating unit of the polymer

$\Delta H_f$  is the heat of fusion of the polymer

$T_m$  is melting temperature of the crystalline phase

The affinity of the solute for the polymer is judged from the value of the interaction parameter. A low value of  $\chi$  indicates greater affinity between the solute and the polymer. It is relatively very easy to measure single component,  $\chi$ , by carrying out sorption experiments and using the experimentally measured sorption data in Equations 5.11 through 5.13 as the case may be. For a binary mixture the values of  $\chi$  so obtained for the two components can be used to ascertain the relative sorption of the two components by the given polymer.

#### 5.2.1.2.2 Diffusion

Similar to sorption, diffusion is also important in determining the separation characteristics of a membrane in that difference in diffusion rate through a membrane gives a permeate rich in one of the component. The diffusion coefficient of a permeant through a polymer is a strong function of the size and shape of the permeant. In a homologous series, molecules with low molecular weight will move faster. When molecular weight and chemical nature are the same, molecules with smaller cross-section diffuse faster. However, sorption has a strong bearing on diffusion. High sorption always results in higher rates of diffusion as explained below:

1. An increase in the concentration of the permeant in the polymer swells it and promotes the free rotation of the polymer segments about the chain axis resulting in lower activation energy for diffusion.
2. In PV, the amorphous region is responsible only for permeation and on sorption, this region in the polymer swells—thus more free volume becomes available for permeation.
3. When the membrane is highly sorbed, a major part of the polymer matrix contains the liquid permeants and diffusion of the incoming permeant through this “liquid zone” of the solid polymer is faster than through the dry solid polymer.

##### 5.2.1.2.2.1 Single-Component Diffusion

The diffusion coefficient is a strong function of concentration. Long [37] expressed it as an exponential function of concentration

$$D_i = D_{i0}e^{(A_i C_i)} \quad (5.14)$$

$A_i$  is the plasticization coefficient to account for interaction of the particular permeant and polymer. It represents the magnitude of the effect of solvent concentration on solvent mobility in the membrane.

Greenlaw et al. [38] proposed another relationship between diffusivity and concentration:

$$D_i = D_{i0}(1 + A_i C_i^n) \quad (5.15)$$

and found that the following simplified expression

$$D_i = kC_i \quad (5.16)$$

fitted the data from Rogers et al. [39] up to a vapor phase activity of 0.5 for diffusion of hexane in polyethylene membranes. In their analysis for single-component permeation, Rautenbach and Albrecht [40,41] used a modified form of Greenlaw and coworker's equation with the exponent  $n$  equal to unity.

$$D_i = D_{i0}(1 + A_i C_i) \quad (5.17)$$

##### 5.2.1.2.2.2 Multicomponent Diffusion

Diffusion in multicomponent system is difficult to analyze. Transport of one component is affected by the presence of the other component due to their mutual interaction. This results in the coupling of fluxes. Thus, single-component diffusion equation cannot be used to predict diffusion in a multicomponent system. Greenlaw et al. [38] proposed a simple relationship in which the diffusion coefficients for components  $i$  and  $j$  are interdependent on both component concentrations:

$$D_i = k_{di}(C_i + B_{ij}C_j) \quad (5.18)$$

and

$$D_j = k_{dj}(C_j + B_{ji}C_i) \quad (5.19)$$

Shelden and Thompson [42] used the following equation while modeling PV of toluene/ethanol mixture with polyethylene membrane, and water/ethanol with both homogeneous and asymmetric PVA membranes.

$$D_i = D_{i0} + k_{di}(C_i + B_{ij}C_j)^{ki} \quad (5.20)$$

and

$$D_j = D_{j0} + k_{dj}(C_j + B_{ji}C_i)^{kj} \quad (5.21)$$

Brun et al. [43] described binary pervaporative transport using an exponential diffusion model that is dependent on individual component concentrations:

$$D_i = D_{i0} \exp(A_{ii}C_i + A_{ij}C_j) \quad (5.22)$$

and

$$D_j = D_{j0} \exp(A_{jj}C_j + A_{ji}C_i) \quad (5.23)$$

This model includes the mutual coupling effect of the permeants. A positive or negative value of  $A_{ii}$  or  $A_{ij}$  indicates a positive or negative effect of the presence of one component on the transport of the other component. Sferrazza et al. [44] have analyzed the behavior of binary systems using an approach similar to that of Brun et al. [43]. They used a similar model to describe diffusion:

$$D_i = D_{i0} \exp[(A_i(C_i + B_{ij}C_j))] \quad (5.24)$$

and

$$D_j = D_{j0} \exp[(A_j(C_j + B_{ji}C_i))] \quad (5.25)$$

The interaction coefficients give an indication of the extent of coupling in the membrane.

#### 5.2.1.2.2.3 Transport Equation through Membrane

The permeation of component  $i$  through the membrane can be described by Ficks' first law as

$$J_i = -D_i \frac{dC_i}{dx} \quad (5.26)$$

As mentioned earlier, the diffusion coefficient is a function of membrane phase concentration of the permeants. Hence Equation 5.26 yields:

$$J_i = -D_{i0} f(C_i) \frac{dC_i}{dx} \quad (5.27)$$

where  $D_{i0}$  is the diffusion coefficient of component  $i$  at infinite dilution. Integrating Equation 5.27 over the entire membrane thickness  $L$  assuming that the variation in  $D$  along the membrane thickness is accounted by the first two terms on the right-hand side of Equation 5.27, the equation reduces to

$$J_i L = -D_{i0} \int_{C_{fi}}^{C_{pi}} f(C_i) C_i dC_i \quad (5.28)$$

Membrane phase concentration of component  $i$  in the feed side,  $C_{fi}$ , can be calculated from its bulk concentration by Henry's equation (Equation 5.8) provided it is present in trace amount in the feed solution. For higher concentration of component  $i$ ,  $C_{fi}$  can be obtained from experimental sorption data. Membrane phase concentration on the permeate side of component  $i$ , i.e.,  $C_{pi}$  may be neglected due to the low pressure the activity of the component in the downstream side is very low. Thus, Equation 5.28 can be readily solved to calculate the theoretical flux and diffusion coefficient of  $i$  or  $j$  component employing any of the above equations relating the diffusion coefficient and concentration, Equations 5.14 through 5.25 depending on its best matching with the experimental data.

## 5.2.2 CONCENTRATION POLARIZATION AND PERMEATION

Concentration polarization (CP) of the permeants and its resistance to permeation through the membrane is encountered in most membrane processes. In an ideal case, in the absence of any CP, the concentration of the permeants should not change from

bulk-feed to membrane-feed interfaces. However, due to fluid viscosity (shearing action between two successive liquid layers opposing their relative velocity) there is a decrease in velocity of the permeants from bulk-feed to the stationary membrane surface where the velocity of the fluid is zero. Thus, the concentration of the permeant at the membrane interface becomes lower than that in bulk-feed. In the case of UF, MF, or RO, the retained solute on the membrane surface may cake out (when its concentration exceeds its solubility product) and thus choke the membrane pores and as it accumulates more and more, a diffusive back flow from membrane phase to bulk liquid is developed. These are accompanied by a decreased flux with time. In the case of pervaporation, CP is not so important due to relatively low permeation rates experienced in these dense membranes. Further, unlike UF, RO, or MF, none of the permeants is retained on the membrane surface. In PV all of the permeants pass through the membrane by a solution–diffusion mechanism. However, in these membrane processes CP becomes significant, when the membrane is very thin and highly selective to one of the permeants present in very low concentration (e.g., removal of traces of volatile organic compound from its aqueous feed). In this case, the rate of permeation of this permeant through the membrane becomes much faster than its rate of supply from bulk-feed to the feed-membrane interfaces resulting in CP for this permeant. However, in the case of PV, on the downstream side no such CP occurs due to very large values of the gas phase diffusion coefficient.

In industrial application, a thin PV membrane on a UF porous support membrane is generally employed. Thus, the concentration gradient on the feed side cannot be ignored. By assuming boundary layer resistance in series with membrane resistance the following equation [29,45] may be derived:

$$\frac{1}{K_o} = \frac{1}{k_L} + \frac{L}{D \cdot S} \quad (5.29)$$

where

$K_o$  is the overall mass transfer coefficient

$k_L$  is the mass transfer coefficient for the boundary layer

$S$  is the sorption coefficient defined as the ratio of the membrane phase concentration and feed phase concentration ( $C_M/C_F$ )

$L$  is the membrane thickness

The product  $D \cdot S$  is the intrinsic permeability that can be obtained from experimentally determined values of  $D$  and  $S$  or through experiments at very high levels of turbulence such that the boundary layer resistance is eliminated ( $K_o = L/D \cdot S$ ). A number of correlations are available in the literature for reliable estimates of  $k_L$  for various geometries of the modules [29,45].

Sufficient turbulence at the membrane surface is required to eliminate CP. In PV fluxes are measured at different turbulence rates in the feed side are determined till a constant flux is achieved. At this turbulence, the rate of mass transfer in the membrane phase boundary layer may be assumed to be eliminated ( $k_L \gg D \cdot S/L$ ). Proper hydraulic management on the feed side generally eliminates CP. However, for very dilute solutions where the driving force for the fluid-membrane mass transfer process is relatively very low, CP cannot be avoided. In addition to CP, temperature polarization may also affect the overall flux. This is due to the fact that the enthalpy of vaporization of the solute in the permeate compartment is supplied by the hot feed. The hot fluid transfers sensible heat to the membrane (by convection) which in turn supplies it by conduction to the permeate side of the membrane. This is also a case of resistances in series and an equation similar to Equation 5.29 can be written. When the supply of sensible heat from the bulk-feed side to the membrane is much less as compared to the heat required to vaporize the solute in the permeate compartment, temperature polarization develops. Thus, there is a drop in temperature from the bulk-feed to the membrane surface. This phenomenon is termed “temperature polarization” similar to its mass transfer counterpart, in concentration polarization Mulder [29] has given detailed description of both these phenomena and methods of tackling them. In particular the loss of sensible heat by the feed stream must be compensated. This is generally achieved by employing interstage heat exchangers.

In the PV mode the feed side is in contact with a liquid, which tends to sorb in the polymer and swell it. As the solute(s) diffuse across the membrane at the permeate side face of the membrane, the solutes are vaporized. Thus, the membrane exhibits different structures from the feed to the permeate side. The former is wet and swollen and hence yields high diffusion rates. The downstream part being fairly dry affords much lower diffusion coefficients than the swollen feed side. The assumption of a diffusion coefficient independent of the distance inside the membrane in Equation 2.38 is therefore not rigorously correct.

### 5.2.3 SELECTIVITY IN PERVAPORATION

The overall selectivity in PV  $\alpha_o$  is determined by (1) sorption and (2) diffusion selectivities.

Sorption selectivity,  $\alpha_s$ , can be defined as the ratio of the sorption coefficient for solutes A and B in a binary mixture:

$$\alpha_s = \frac{S_A}{S_B} \quad (5.30)$$

Diffusion selectivity,  $\alpha_D$ , can also be similarly defined as the ratio of the two diffusion coefficients:

$$\alpha_D = \frac{D_A}{D_B} \quad (5.31)$$

The overall selectivity,  $\alpha_o$ , is given by

$$\alpha_o = \alpha_S \times \alpha_D \quad (5.32)$$

Another parameter used to define the selectivity of a membrane is the separation factor,  $\beta$ :

$$\beta = \frac{C_{Pi}}{C_{Fi}} \quad (5.33)$$

where  $C_P$  and  $C_F$  are the concentrations of the selectively permeating solute  $i$  in the permeate and feed, respectively.

In general, for PV  $\alpha_S$  is the dominating contributor to  $\alpha_o$  and most membranes are designed to achieve high values of  $\alpha_S$  [21,25]. However, in some cases although  $\alpha_S$  is favorable,  $\alpha_D$  is not and in such cases  $\alpha_o$  is poor [28].

The pervaporation separation index (PSI) indicates the overall productivity of PV membrane:

$$\text{PSI} = J_i \times \beta \quad (5.34)$$

## 5.3 MEMBRANE FABRICATION METHODS AND MEMBRANE MODULES

### 5.3.1 INTRODUCTION

The membrane is the heart of any membrane-based separation processes. The initial breakthrough in the membrane technology came from the phase inversion technique, developed by Loeb and Sourirajan [46]. The membrane prepared by adopting the phase inversion technique became the first commercial UF membrane and the membranes prepared by this technique are finding widespread use in industrial separations. A second breakthrough in the membrane development occurred in the early 1970s. That was the thin film composite (TFC) membrane made by interfacial polymerization technique pioneered by Cadotte et al. [47]. It is now a well-established method for preparing defect-free membranes only a fraction of a micron in thickness from a variety of polymeric materials particularly for UF and RO. Development of composite membranes, in 1980s by Brusckie et al. [48], allowed the transformation of PV process from laboratory to industrial scale. The German company GFT reported the first commercial use of membranes in pervaporation. This section covers the various methods used for making PV membranes and corresponding modules.

### 5.3.2 IDEAL MEMBRANE FOR PERVAPORATION

An ideal pervaporation membrane should consist of an ultra thin defect free skin layer (dense layer) supported by a porous support. The skin layer is perm-selective and hence responsible for the selectivity of the membrane. However, the porous support also plays an important role in overall performance of the membrane. The effect of the porous support, of a composite membrane, on the permeation properties of the membrane is discussed in details in the composite membranes section.

Ideal pervaporation membrane should possess the following characteristics:

1. The top layer/skin should be as thin as possible and without any defects.
2. It should exhibit high sorption and diffusion selectivities for the desired solute when contacted with a mixture containing it.
3. It should not swell excessively to maintain the selectivity and structural stability.
4. It should possess good mechanical strength, chemical and heat stability.
5. It should offer high fluxes without compromising selectivity.

Quantitatively the performance of a PV membrane can be described by the PSI defined by Equation 5.34. A higher value of PSI indicates better overall productivity. In view of the various advantages of PV there is considerable research interest in developing suitable membranes for different applications. The efforts in this direction are not limited to the academic sector.

The industrial sector has also made significant contributions with companies, such as Sulzer ChemTech, Membrane Technology and Research (MTR), USA; Mitsui Engineering, Ube (Japan) leading the field. Different factors that have a major impact upon membrane morphology are listed below:

1. Choice of polymer
2. Viscosity of casting solution
3. Curing temperature
4. Glass transition temperature ( $T_g$ ) of the polymer

Amongst these the choice of the polymer is the most important since it decides the sorption selectivity for the solute of interest. The methods adopted to prepare PV membranes can be broadly classified into three types:

1. Phase inversion
2. Coating of the perm-selective polymer skin on a UF support
3. Other types

Amongst these, membranes prepared by phase inversion technique are generally used for UF and RO processes. Theoretically, phase inversion process can be used to prepare a dense top layer (perm-selective layer) on a porous support of the same polymer. This is achieved by proper selection of the polymer-solvent and precipitating bath composition so as to allow a delayed de-mixing process during the phase inversion process. Mulder [29] has discussed the relevant thermodynamic aspects of selection of the polymer-solvent-non-solvent bath compositions in detail. The phase inversion technique is, however, not very popular for making PV membranes. On the other hand, membranes prepared by the phase inversion technique are invariably used as the porous support to prepare composite membrane by the polymer solution coating process. Composite membranes prepared by this coating method are most widely used as PV membranes. The major advantage of this type of membranes is that the perm-selective polymer coating and the polymer for the UF support can be selected independent of each other's physical properties. The only requirement is that the two polymers should form a strong bond to prevent the peeling out of the skin layer from the support membrane. The techniques for making composite membranes are discussed briefly in the following sections.

### 5.3.3 COMPOSITE MEMBRANES

For industrial applications, where the membrane sizes are larger, reinforcement of the thin skin membrane by an appropriate support is required to maintain dimensional stability. This type of membrane consisting of a skin layer (perm-selective layer) supported by a suitable support is called a composite membrane.

#### 5.3.3.1 Importance of the Support Layer

The support membrane has a strong influence on the performance of the perm-selective skin layer. Heinzelmann [49] has given the consequences of the various types of support defects leading to change in permeation properties of the composite membranes. Recently, Trifunovic and Tragardh [50] have studied the role of the support layer of a composite membrane in PV. Although the mass transport of permeants through the active, dense layer is the rate-determining step, the support layer can also be a contributor to the overall mass transport resistance, especially in the case of components which, under the operating conditions employed, can condense/vaporize due to small variations in the pressure. The support layer used for pervaporation membranes is usually an asymmetric ultrafiltration membrane. There is a variation in the pore diameter across the thickness of such an asymmetric membrane. Next to the dense layer the pore diameter in the support is relatively very small. The pores widen as the solute diffuses across the support. At the permeate side face the support has the largest pores. A simple model for the porous support is that of a bundle of straight cylindrical capillaries. The type of flow in a pore depends upon the relative size of the pore and the mean free path of the molecules involved. When the mean free path is much smaller than the pore diameter, viscous flow prevails. In such a case the support layer does not create any serious impediment to mass transport. However, if the pores are smaller than the mean free path, Knudsen diffusion, which has a much lower rate, can cause significant reduction in the overall mass transport. In these pores, the local vapor pressure can exceed the critical condensation pressure resulting in capillary condensation. Rautenbach and Albrecht [51] have indicated that in such a case a part of the pore length contains the solute(s) in liquid form and the remaining part only contributes to the evaporation process. Thus, in case of capillary condensation there is a reduction in membrane selectivity due to the decrease in the driving force for pervaporation. The Kelvin equation can be used to predict the critical (partial) vapor pressure at which condensation occurs in the pore:

$$P_i^C = P_i^0 \exp\left(-\frac{4\sigma_p V_i}{d_{\text{pore}} RT}\right) \quad (5.35)$$

Trifunovic and Tragardh [50] in their study of PV of homologous series, alcohols, and esters using POMS membranes with different supports derived the following general conclusions:

1. Larger molecules with lower Knudsen diffusion coefficients suffer higher loss in selectivity.
2. Solutes with low vapor pressures (easily condensable) suffer greater loss in selectivity due to the pressure build-up in the Knudsen capillaries.
3. The capillary inside surface also affects the composite membrane performance. For alcohols with hydrophilic OH groups it is desirable to have a hydrophobic capillary surface.
4. To avoid the detrimental effects mentioned above the Knudsen capillaries should be as short as possible.

### 5.3.3.2 Techniques for Fabrication of Composite Membranes

Following methods can be adopted to prepare composite membranes used for pervaporation.

#### 5.3.3.2.1 Direct Coating

Heinzlmann [49] and Briston [52] have given details of these methods. The main problem with direct coating is that incompatibility of the porous support with polymer solution can result in the formation of pinholes in the membranes. However, this problem can be overcome if care is taken to ensure sufficient wetting of the support by the polymer solution. Parameters that can be varied in optimizing the process for a defect free membrane are

1. Pretreatment of the support prior to coating
2. Optimization of composition, viscosity, and surface tension of the polymer solution

Choice of appropriate coating method along with drying/curing conditions can yield a stable defect-free membrane.

#### 5.3.3.2.2 Interfacial Polymerization

Interfacial polymerization provides another method for depositing a thin layer upon a porous support [47,49]. In this case polymerization occurs between the two reactive monomers at the interface of the two-immiscible solvents. Heat treatment is often applied to complete the interfacial polymerization, to cross-link water-soluble monomer or prepolymer. The advantage of this technique is that the reaction is inhibited by the passage of a limited supply of reactants through the already formed polymer layer, resulting in extremely thin film of thickness in the range of 1–2 nm. Such membranes are therefore referred to as thin film composites. TFCs of various poly(amides) are very popular in RO applications.

#### 5.3.3.2.3 Radiation-Induced Formation of Composite Membranes

The radiation-initiated grafting of polymer films (i.e., radiation-induced grafting), radiation-initiated curing of thin film coating on porous supports (i.e., radiation cured composite membrane), and coating of porous substrate by plasma polymerization (i.e., plasma chemical processes) are an alternative method to prepare nonporous flat sheet PV membranes. Specific sorption capability for distinct solutes is achieved by introducing different functional groups, which show specific interactions with the solute onto the polymer backbone of supporting substrate [53–55].

#### 5.3.3.2.4 Transfer Coating

Details of this method for transfer coating or lamination of perm-selective skin on a porous support can be found in the literature [49,52]. First, the advantage of this method is that a definite predefined skin layer thickness can be achieved. Second, the problem of insufficient wetting of support by coating solution and incompatibility of the support with solvent can be overcome.

#### 5.3.3.2.5 Other Techniques

In another popular technique the skin layer polymer is independently prepared by means of suitable polymerization techniques, such as formation of copolymers [21], graft [56] and block polymers, polymer blends [57], cross-linked polymer [58], and interpenetrating polymer networks (IPNs) [11] and then coating this polymer solution on the porous support to form a composite membrane for pervaporation application. Membranes prepared by these techniques offer easy tailoring of membrane properties for different applications. As dictated by the sorption diffusion model, a skin layer that has selective but limited sorption should be prepared. Further, membrane strength can be increased by adjusting the crystalline portion (backbone) of the polymer films. Different membranes can be readily prepared according to the application, simply by changing the functional groups of the polymer.

### 5.3.4 PERVAPORATION MODULES

Pervaporation modules have been basically adapted from the module designs already used in other applications, such as RO, NF, and UF. However, the major difference is that in the latter case the applications mainly pertain to treatment of predominantly aqueous solutions. Therefore, the glues, gaskets, etc. to be used do not require any special consideration except

that they should yield a strong bonding. In the case of pervaporation one of the two sides of the module (feed/permeate) is in contact with an organic solvent. This solvent may attack the glue/gasket used. Therefore, selection of the glue/gasket material needs special attention. In the case of dehydration of organics the feed side is in contact with a predominantly organic medium, while for removal of trace organics from water the permeate side has to bear the attack of the organic solvent. Finally, in the case of organic–organic separations both the feed and permeate sides have to be designed properly considering the presence of organics that may have high solvent power. Thus, besides the strength of the bond the solvent resistance of the glue is also important. In view of this the plate and frame module was initially much more popular than the spiral wound module.

Another consideration that is important in pervaporation is the prevention of excessive pressure drop on the permeate side. Too high a pressure drop reduces the flux (also see Section 5.4.3: Importance of support layer). Therefore, to avoid excessive pressure drop, generally the permeate side is kept open directly to the condenser/heat transfer surface.

The economic advantage of pervaporation lies in the fact that particularly for the two extreme applications: dehydration of organics and removal of organics from water, the focus is on the trace quantity. In the case of dehydration of organics a highly water-selective membrane is used. On the other hand, for removal of organic from water an organophilic membrane is used. In both these cases, the solute to be removed is a minor/trace quantity. With this approach the duty of the module (total amount to be removed) is greatly reduced. However, since the solute is present in much smaller quantities in the feed side, concentration polarization can be a serious draw back. To overcome this, the design of the feed side needs some attention. The design to be used should allow rapid mass transfer from bulk liquid to the membrane surface so as to achieve the intrinsic membrane flux. Generally, the flow Reynolds number on the feed side should be sufficiently high so as to overcome concentration polarization. This condition implies a higher power input because of high flow rates on the feed side.

A number of module designs are possible and all are based on the two types of membrane configuration, (i) flat sheet and (ii) tubular. These are plate and frame, spiral wound, tubular, capillary, and hollow fiber.

### 5.3.5 SELECTION OF THE MEMBRANE MODULE

Choice and arrangement of the membrane module in a system is based on economic considerations with the correct engineering parameters being employed to achieve this. Some aspects to be considered are

1. Nature of the separation problem
2. Ease of cleaning
3. Ease of maintenance
4. Compactness of the system
5. Membrane replacement

Depending upon the nature of application and operating conditions the module is selected. Table 5.1 gives a qualitative comparison of the various types of modules available and can be used as a reference guide for module selection.

### 5.3.6 SOME PROBLEMS IN INDUSTRIAL USE OF PERVAPORATION

The major application of PV has been in the dehydration of ethyl and isopropyl alcohols. In both these case severe fouling of the membranes was observed. In the case of ethyl alcohol the fouling was attributed to the rust particles from the mild steel fermenters used. In the case of *i*-propanol the applications were for its recovery from a mixture containing water and dissolved

**TABLE 5.1**  
**Qualitative Comparison of Various Membrane Modules**

Properties	Tubular	Plate and frame	Envelope	Spiral wound	Capillary	Hollow fiber
Packing density	Low	Low	Moderate <sup>a</sup>	Moderate	High	Very high
Investment	High	High	Moderate <sup>a</sup>	Moderate	Moderate	Low
Fouling	Low		Moderate <sup>a</sup>	Moderate	High	Very high
Cleaning	Excellent	Good	Good <sup>a</sup>	Fair	Poor	Very poor
Replacement of individual membrane	Yes/no	Yes	Yes <sup>a</sup>	No	No	No

Source: Adapted from Mulder MHV. *Basic Principles of Membrane Technology*, Dordrecht, The Netherlands: Kluwer Academic, 2000.

<sup>a</sup> Data not available. Estimated from description available in the literature [59].

salts from the washing operations. In this application the membranes developed severe blisters and became useless. These blisters can be traced to the crystallization of the salt in the membrane. Some ingress of the salt cannot be avoided due to the high water sorption in the membrane. The membrane removes water. The water is volatile and is evaporated at the downstream face. The salt, however, cannot do so and is hence trapped in the membrane. As the water is removed the salt introduced in the top layer with the water crystallizes out of the alcohol-rich phase. This is probably the most likely reason for the formation of blisters. Observation of the blisters under a microscope showed presence of solid particles confirming the above postulate. This problem can be overcome by resorting to vapor permeation (VP) rather than PV. Thus, the alcohol stream is boiled to supply a vapor to the membrane module. VP obviously has a higher energy requirement than PV since the liquid needs to be vaporized. Careful design of the reboiler and provision of a mist eliminator prevents any carry over of the salt. Thus a mixture of water and alcohol vapors totally devoid of the salts is supplied to the membrane module. This arrangement has been found to be quite effective in ensuring a longer membrane life.

## 5.4 APPLICATIONS OF PERVAPORATION

As discussed in Section 5.1, PV has applications in all types of separations involving aqueous/organic phases. These are

1. Dehydration of organics
2. Removal of organics from aqueous phase
3. Organic–organic separations

The discussion in Section 5.2 on theory of PV indicates that the membrane polymer to be selected for a given separation should have high sorption affinity for the solute to be removed preferentially. For the first two categories it is relatively easy to choose a polymer. Thus, the following types of polymers are suitable as membranes materials for these two cases: (1) hydrophilic polymers with large contributions due to hydrogen bonding and polar forces to the overall solubility parameter and (2) hydrophobic (organophilic) polymers with major contributions from dispersion forces. These applications are discussed separately in the following sections.

### 5.4.1 DEHYDRATION OF ORGANICS

Most of the commercialization of PV technology occurred in this category for dehydration of ethanol and *i*-propanol. For ethanol, a hybrid system comprising of distillation to remove bulk of the water (enrichment of ethanol from 8 wt% to ~85 wt%) followed by a PV module to reach 99.8 wt% ethanol has been popular. This hybrid system combines the strengths of distillation and PV in their respective areas. In this case generally a small amount of water (<10 wt%) is required to be removed by PV. It is evidently far more economical to focus on the removal of this small water quantity rather than trying to remove the organic. With this logic the membrane polymer selection becomes very easy. Thus, hydrophilic polymers that selectively sorb water are used. Poly(vinyl alcohol), PVA, is a very popular polymer for dehydration of organics. The hydroxyl group in PVA imparts high hydrophilicity to PVA since the OH group has a dominant effect in deciding the properties rather than the relatively small CH<sub>2</sub>=CH alkyl group. However, the high hydrophilicity, which is the strong point in favor of PVA, also turns out to be its weak point. The thin top selective layer made of PVA that is in continuous contact with water-rich solution gradually dissolves and hence the membrane loses its permselectivity. To enhance the active life of such a PVA membrane the polymer is cross-linked by a suitable compound having a functional group that can react with the OH group of PVA. Suitable cross-linkers are carboxylic acids/anhydrides, dialdehydes, etc. Maleic anhydride is reportedly used in the first PVA membrane commercialized by GFT (now Sulzer Chemtech). Cross-linking connects two polymer chains (Figure 5.2) and hinders the dissolution of individual chains that are now bound to other chains through the cross-links. The advantage of extended life gained by the cross-linking is however, offset by the reduced mobility/flexibility of the chains due to the same cross-links. This reduced flexibility of the polymer chains results in a reduction in the diffusion coefficient of the solute and hence the flux decreases (Equation 2.26).

In view of this the cross-linking is moderate. The usual range is about 4%–8% of the total functional groups being cross-linked. This is a case of the classical trade-off between low depreciation due to extended life, and low productivity due to lower flux.

In many cases the organic to be dehydrated (e.g., acetic acid) attacks the ether linkage in the PVA membrane. Indeed, the PVA membrane has very limited life in the presence of most acids. Ray et al. [14] used the concept of copolymer membranes to dehydrate acetic acid over the entire range of concentration from 0% to 100%. These investigators prepared copolymers of acrylonitrile (AN) with different hydrophilic monomers like hydroxy ethyl methacrylate, acrylic acid, methacrylic acid, and itaconic acid. These copolymers have carbon–carbon bonds, which unlike the ether linkage in the cross-linked PVA membrane are stable to the attack by carboxylic acids. The acrylonitrile part is not sufficiently hydrophilic but imparts mechanical strength while the other monomers improve the hydrophilicity. The overall result is an efficient yet stable membrane. Variation of the ratio of AN to (the other) monomer allows freedom of adjusting the hydrophilicity of the membrane to achieve certain

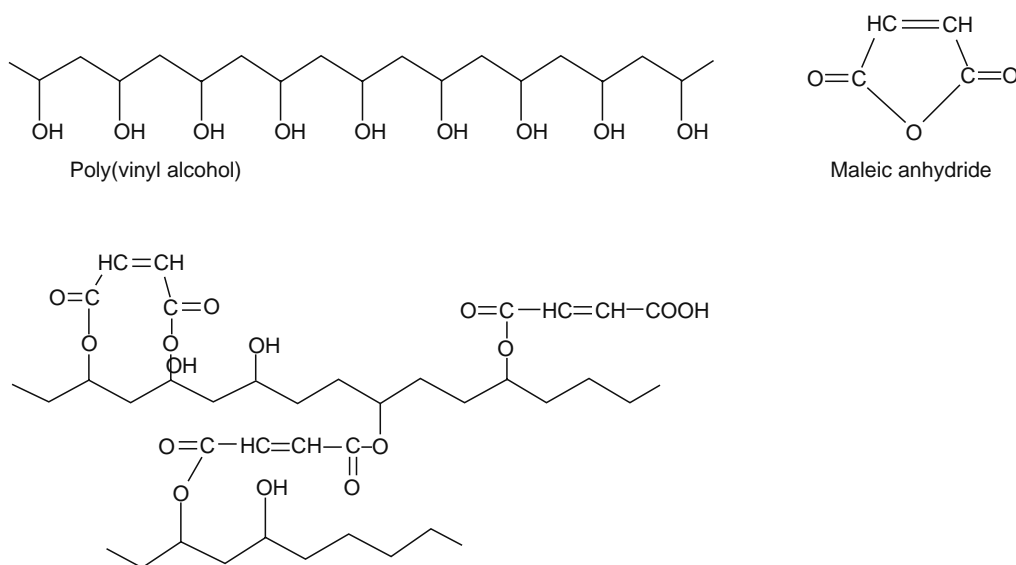


**FIGURE 5.2** Cross-linking of poly(vinyl alcohol) with maleic anhydride.

selectivity and flux. High ratio of the more hydrophilic comonomer to AN increases water sorption and hence flux but results in a concomitant loss in selectivity. Ray et al. [14] showed that this concept of copolymer membrane yields a low-cost alternative to the more expensive hydrophilic polymers like Nafion and polyimide.

Another interesting application of hydrophilic membranes is in esterification reactions. These reactions are generally equilibrium limited. High conversions (low acid numbers) are possible when the equilibrium is displaced by removal of the water formed in the reaction. Distillation has been a popular method for water removal. However, hydrophilic membranes in the PV mode are an attractive alternative because of the high selectivities and low-operating cost. Brusckhe [59] has described the details of the first continuous industrial plant combining PV with an esterification reaction employing a cascade of reactors and PV units. A simple mathematical model described can be used to calculate the optimum membrane area per unit mass of the reaction mixture. The kinetics of the esterification reaction required for use in this model are either available in the existing literature or can be obtained using standard laboratory techniques for measurement of kinetics.

Another very promising application of PV is in dehydrating glycerin. Glycerin is mainly produced as a by-product in the fat splitting process for manufacturing fatty acids. The scale of operation is quite large (~300 t/day of fatty acids). The glycerin is produced as a weak (~10–15 wt%) aqueous solution referred to as sweet water. Conventionally it is converted to anhydrous glycerin using distillation. The low decomposition temperature of glycerin necessitates distillation under high vacuum. Even with this distillation under high vacuum some degradation of glycerin cannot be prevented. PV can be an ideal low energy alternative to distillation [12,60]. It has been shown [60] that PV can yield selectivities 1000 times higher than the corresponding distillation selectivity at temperatures as low as 70°C.

Table 5.2 lists the various hydrophilic polymers used for dehydration applications. Table 5.3 gives a comprehensive coverage of the available literature on dehydration of organics. It is evident from Table 5.3 that this application is the most widely investigated class of PV. Further, as mentioned in Section 5.1 this category has seen the most significant commercial utilization amongst the three categories listed earlier. Further there are other potential large-scale applications yet to be

---

**TABLE 5.2**  
**Hydrophilic Polymers Available for**  
**Selective Water Removal**

Poly(vinyl alcohol) (different cross-linkers)  
 Poly(acrylic acid) (different cross-linkers)  
 Various poly(amide)s (different substituents)  
 Various poly(imide)s (different substituents)  
 Nafion  
 Cellulose acetate (various degrees of hydrolysis)  
 Other cellulose derivatives/forms

---

**TABLE 5.3**  
**Dehydration of Organics**

System	Membrane Used	Remark	Reference
Ethanol (water)	Cross-linked PVA	$\beta = 260$ at 75°C for 50% aqueous ethanol solution	[61]
Phenol (water)	PVA-PAA Cross-linked	$\beta = 3500$ for aqueous phenol solution	[62]
Phenol (water)	Cross-linked PVA (PAA = 80/20)	$\beta = 2580$ at 70°C for 80% aqueous phenol solution	[63]
Ethylene glycol (water)	Partially hydrolyzed polyacrylonitrile/1-poly(acrylic acid) blend layer membrane	An 85:15 (wt%) ethylene glycol:water solution was separated by pervaporation to give 25:25 ethylene glycol:water permeate at 70°C	[64]
Ethanol (water) and propanol (water)	Regenerated cellulose and cross-linked PVA membrane	$\beta = 3500$ for aqueous ethanol solution and $\beta = 6000$ for aqueous IPA solution	[65]
EtOH, MeOH, iso-PrOH, dioxane or EtOAC (water)	PVA membrane	Total flux decreases with increasing permeate pressure	[66]
Methanol (water)	Cross-linked PVA membrane	$\alpha = 2650$ for PVA/PAA = 80/20 and 465 for PVA/PAA = 90/10	[67]
Organic aqueous and organic-organic binary mixture	Silicone grafted polymers, styrene fluoroacrylate copolymers silicate filled silicone films	Pervaporative separation of organic-aqueous and organic-organic liquid mixture with different membranes is studied	[68]
Methanol (water separation)	Hybrid PV + distillation	A review on dehydration of solvents in the fine chemical industry	[69]
Alcohol mixture (water)	Polyelectrolyte multilayer membrane	Best results are obtained when temperature is raised from 25°C-80°C. A membrane with double layers yielded $\beta = 900$	[70]
Dehydration of isopropanol/water	Polymeric (PERVAP 2510, Sulzer Chemtech GmbH) and Ceramic membranes (NaA type zeolite, Mitsui & Co.)	Traditional azeotropic distillation was compared with a hybrid system consisting of distillation followed by pervaporation and a hybrid system consisting of distillation followed by pervaporation followed by a second distillation	[71]
Dehydration of acetic acid, alcohols, and acetone by pervaporation	Acrylonitrile-maleic anhydride copolymer membrane	The membrane exhibits reasonable performance with respect to both separation factor and permeance (11.0 and 279.4 g/m <sup>2</sup> h/bar, respectively, at 92 wt% feed conc. of water) for acetone dehydration	[72]
Dehydration of IPA	Hybrid PV-distillation processes intensification	Hybrid process economics	[73]
1-methoxy propanol-water	Polyimide (PI), cellophane, poly(vinyl alcohol) (PVA), cellulose diacetate (CDA), cellulose triacetate, two separate blends of cellulose acetate and CDA with cellulose acetate propionate, and PVA cross-linked with multifunctional cross-linkers	The effects of different substitution derivatives of cellulosic materials were investigated	[74]
1-methoxy propanol-water	Acrylonitrile-based copolymer membrane	The copolymer properties, in particular, solubility parameter, component group contribution, and interaction parameter values are used to explain perm-behavior (selectivity and flux). Copolymers of AN showed good selectivity with reasonable flux	[15]
Dehydration of organic liquids	Water-selective membrane	Some perm-selective membranes and separation processes are introduced	[75]
Dehydration of organic liquids	Aromatic polyamide membrane	Effect of type of diamine on water selectivity studied (Japanese)	[76]
Separation of water/acetone mixture	Acrylamide-acrylic acid copolymer gel prepared in porous of ceramic thin membrane	Controlled cross-linking gives very high selectivity for water	[77]
Organic-organic and organic compounds/water separation	Acrylonitrile-vinyl compounds copolymer membrane	$\alpha = 1747$ for 80% aqueous acetic acid at 70°C	[78]
H <sub>2</sub> O/organic separations	Copolymers of peptides/proteins having amino groups with acrylonitrile	High permselectivity for water reported	[79]
Dehydration of organic liquids	Hydrophilic polymer membranes	Mass transfer analysis of pervaporation	[80]

**TABLE 5.3 (continued)**  
**Dehydration of Organics**

System	Membrane Used	Remark	Reference
Dehydration of organic solvents	Plasma or electric beam induces graft polymer and cellulose membrane	A review with 25 references on recent progress in the preparation of pervaporation membranes for the H <sub>2</sub> O/organic solvent separation including dehydration, selective separation of EtOH, and solvent removal or recovery from effluents	[81]
Water + methanol, ethanol, <i>n</i> -propanol, isopropanol, <i>n</i> -butanol and isobutanol	PVA cross-linked with a multifunctional cross-linker	The activation energy of diffusion for water was found to vary with water–alcohol systems in the range 20–50 kJ mol <sup>-1</sup>	[10]
Enzymatic esterification of oleic-acid and <i>i</i> -amyl alcohol	Hydrophilic membrane for water removal	Influence of pervaporation process parameters on enzymatic catalyst deactivation is studied. Below a certain level of water concentration, enzymatic catalyst activity is very low. On the other side, high initial concentrations of alcohol deactivate the catalyst	[82]
Lipase-catalyzed enantioselective esterification of racemic ibuprofen coupled with pervaporation	A cross-linked poly(vinyl alcohol) (PVA) membrane and commercially available per fluorinated membranes (Nafion 117 and Nafion NE 450)	Effects of the reaction temperature, the concentration and nature of alcohol on the reaction rate and enantioselectivity were investigated systematically with and without pervaporation. The PVA pervaporation membrane appeared to be more suitable for the enantioselective esterification of ibuprofen than the Nafion membranes	[83]
Pervaporation separation of an aqueous organic mixture	Poly(acrylonitrile- <i>co</i> -vinyl phosphonic acid) membrane	High selectivity toward water. PANVA membrane exhibited 99.8% H <sub>2</sub> O concentration on permeate side in case of pyridine–H <sub>2</sub> O mixture	[84]

explored. This use of hydrophilic membranes to remove water in esterification or similar equilibrium limited reactions can be used conveniently to reach practically 100% conversion to the product. However, in most such cases an acid is used as a catalyst and the conventional PVA-based membranes are easily attacked leading to short lives. The copolymer membranes proposed by [14] can be used in these applications since C–C bond is not prone to attack by acids. Alternatively ion exchange (H<sup>+</sup> form) resins can be used as catalyst if it is decided to employ the PVA-based membranes. This possibility has however, not been tested commercially.

#### 5.4.2 REMOVAL OF ORGANICS FROM AQUEOUS PHASE

These classes of application deals with removal of trace organics from a predominantly aqueous body. Several organic chemicals have solubilities in water sufficient to reckon both in terms of the potential economic loss and pollution. The solubilities are too low to be dealt with by distillation since distillation is expensive. PV is an ideal alternative in this case. In stark contrast to distillation wherein the selectivities are in single digits, PV can yield several orders of magnitude higher selectivities [16,18,20] resulting in very high recovery of the dissolved organics at much lower cost. The selectivities can be further improved albeit at a loss of flux by incorporating hydrophobic fillers in a hydrophobic membrane. Netke et al. [36] developed a comprehensive dual mode model for permeation in membranes containing adsorptive fillers. The model proposed can predict the effects of various parameters like adsorbability of the solute and loading of the filler. The proposed model also correctly describes the asymptotic behavior of such membranes.

The polymers used for this class of application are listed in Table 5.4. Although the other polymers listed in Table 5.4 are easily available and less expensive, the standard for hydrophobic membranes has been set by poly(dimethylsiloxane) a silicone rubber membrane popularly abbreviated as PDMS. This is a room temperature vulcanization (RTV) type rubber. It is generally made from a two-pot mixture consisting of the silicone rubber and a cross-linker. Poly(octyl methyl siloxane), POMS, is a similar silicone rubber. POMS has a higher hydrophobicity than PDMS but is more expensive. Most investigators have used PDMS although some have also used EPDM and other rubbers [16]. PDMS appears to be the optimum membrane polymer for high selectivity, flux, and durability. Table 5.5 gives a summary of the literature investigations on removal/recovery of organics from aqueous solutions.

PV offers an extremely promising technology for treating effluents containing dissolved organics, which is apparent from Figure 5.2. A hydrophobic membrane module is used to recover (almost) completely the dissolved organics from the effluent.

**TABLE 5.4**  
**Hydrophobic/Organophilic Polymers Available**  
**for Selective Removal of Organics from**  
**Aqueous Solutions**

Poly(dimethyl siloxane) (PDMS)  
 Poly(octyl methyl siloxane) (POMS)  
 Ethylene propylene diene rubber (EPDM)  
 Natural rubber (NR)  
 Styrene butadiene rubber (SBR)  
*N*-butyl rubber (NBR)  
 Nitrile rubber  
 Poly(ether block amides) (PEBA)  
 Elastomeric poly(urethanes)

**TABLE 5.5**  
**Removal of Organics from Aqueous Solutions**

System	Membrane Used	Remark	Reference
Recovery of phenol from wastewater streams arising from a phenolic resin production plant	70 wt% PDMS with 30 wt% SiO <sub>2</sub>	Application of membrane aromatic recovery system (MARS). The average phenol recovery was 84%	[88]
Toluene, trichloroethane, and methylene chloride–water	Poly(dimethylsiloxane), polyether-block-polyamides and polyurethane membranes	Module performance and economics: effect of operating condition	[89]
Aniline–water and methylene chloride–water	Polyether-block-polyamides membrane and polybutadiene membrane	Both membranes yielded high selectivity for aniline with fluxes good enough for practical application	[90]
Enrichment of Cl-containing organic hydrocarbons 1,1,2-trichloroethane (1) trichloroethylene (2) tetrachloroethylene (3)	Cross-linked poly(Bu acrylate (I), <i>tert</i> -Bu acrylate (II), lauryl methacrylate (III), benzyl acrylate (IV), cyclohexyl acrylate (V)- <i>co</i> -acrylic acid)	$\beta = 500$ of (1)-water at 25°C for (I)-acrylic acid copolymer membrane	[91]
Removal of organic solvent from wastewater	Organophilic membrane	Study on solvent concentration, operating and capital cost of pervaporation for solvent removal	[92]
Removal of toluene and methylene chloride	Organophilic membranes	Data for removal of toluene and methylene chloride given	[93]
Removal of mixture of organic acid	Membranes having amino group containing polymer surface coating	High $\alpha$ and flux for organic acids reported	[94]
Separation of aqueous phenol	Polyurethane membrane	Polyurethane has high affinity for phenol. The total flux increased up to 930 g/m <sup>2</sup> h with increasing phenol partial flux. Phenol selectivity was based on high solubility in the polyurethane membranes	[95]
Selective removal of phenol from industrial wastewater	Polyurethane urea	About 88% phenol was obtained. Maximum flux of 33.8 g/m <sup>2</sup> h	[96]
Separation of alcohols and aqueous organic liquids	Polymeric membranes	Selective separation of alcohols	[97]
Recovery of VOC from surfactant containing aqueous solutions	Plasma polymerized PDMS on PP support	Recovery of trichloroethylene from sodium dodecyl sulfate–water mixture at high selectivities reported	[98]
Separation of dichloroethane, trichloroethane and toluene–water	PDMS membrane fabricated by the addition cross-linking reaction	Clustering of water results in high separation factor for organics	[99]
Removal of 1,2-dichloroethane from aqueous solutions	PDMS membrane and oligomeric silylstyrene as a cross-linking agent	$\beta = 230$ –1750	[100]

**TABLE 5.5 (continued)**  
**Removal of Organics from Aqueous Solutions**

System	Membrane Used	Remark	Reference
Removal of traces of organics from aqueous solutions	PDMS	3-D solubility parameter approach shown to be useful in predicting $\alpha$	[18]
Separation of organic solvents from aqueous solution	Methacrylate polymer membrane	Review (Japanese)	[101]
Separation of organic solvent from water containing 0.1%–0.2% styrene, PhMe, CHCl <sub>3</sub> , hexane, cyclohexane, AcOBu or Et <sub>2</sub> O	Silicone rubber membrane	High $\alpha$ and flux for organics reported	[102]
Separation methods for environmental technologies	High surface area membrane	Review with 32 references	[103]
Removal of tetrachloroethylene from surfactant-based soil remediation fluid	Hydrophobic membranes	TCE removal averaged 95.8% during peak surfactant levels and exceeded 99.9% in the absence of surfactant	[104]
1-Methoxy propanol and water	PDMS and linear low density poly(ethylene), LLDPE	PDMS gave better results than LLDPE	[74]
Separation of acetic acid from dilute aqueous solution	Supported liquid membrane PV (tri-alkyl amines as reversible reactants)	$\alpha$ for acetic acid as high as 33	[105]
Separation of volatile organic compounds from aqueous solutions	Styrene butadiene block copolymer	$\beta$ for VOC as high as 5000. H <sub>2</sub> O flux increased rapidly with temperature thereby decreasing $\beta$ for VOCs	[106]
Organic/aqueous separations	Liquid crystalline polyphosphazene membrane	Good separation capabilities reported Review (Chinese)	[107]
Ethanol–water	Poly(perfluoroalkylacrylate-g-dimethylsiloxane)	$\beta$ increased with decreasing temperature (Japanese)	[76]
Organic–organic and organic compounds/water separation	Acrylonitrile-vinyl compounds copolymer membrane	$\alpha = 1747$ for 80% aqueous acetic acid at 70°C	[78]
Separation of VOC from surfactant solution	Hydrophobic membrane	This process can be used to remove volatile nonaqueous phase liquids from surfactant-based soil washing and soil flushing solutions for recovery of the volatile compounds and reuse of the surfactant	[108]
Removal of VOCs from water	Silicalite-filled poly(siloxane imide) membranes	The sorption selectivity of the PSI membranes for chloroform/water solutions was investigated. The silicalite-filled membrane with 120 $\mu\text{m}$ thickness exhibit a high total permeation flux of 280 $\text{gm}^2/\text{h}$ with separation factor of 52.2 for 1.2 wt% of the chloroform/water mixture	[109]
Separation of water–acetic acid mixtures	poly(vinyl alcohol) membranes cross-linked with glutaraldehyde	Pervaporative separation of acetic acid–water mixtures was performed over a range of 70–90 wt% acetic acid in the feed at temperatures varying from 35°C to 50°C	[110]
<b>Aroma compound separation, pharmaceutical and flavor-perfume industry</b>			
Extraction of aromatic compounds (1-octene-3-ol and 2–5 dimethylpyrazine)	PDMS and micro-porous PP	PDMS better than porous PP, $\beta$ for PDMS > 600	[111]
Aroma compound recovery from Muscat wine	PDMS	Temperature effects are studied	[112]
Pervaporation of grape fruit aroma	PDMS	Increasing the feed concentration from 20–200 ppm did not affect the flux but decreased the selectivity from 10 to 4	[113]
Organic–water mixture	Membrane made of elastomeric or hydrophobic polymeric material	Modeling studies and application aroma compound recovery	[114]

(continued)

**TABLE 5.5 (continued)**  
**Removal of Organics from Aqueous Solutions**

System	Membrane Used	Remark	Reference
Recovery of aroma compounds from wine-must fermentation	PDMS on polyetherimide	Continuous recovery of very complex and delicate aromatic profiles, produced during microbial fermentation	[115]
Recovery and separation of 1-octene-3-ol from aqueous solution	PDMS membrane	Good selectivity and permeability	[116]
Recovery of aroma compounds (1-octene-3-ol, ethyl acetate/butyrate/hexanoate)	Plain PDMS and PDMS filled with silicalite	Influence of different permeates studied. Filled membrane gives better selectivity than plain PDMS but lower flux	[117]
Recovery of picolines from aqueous solutions	Elastomeric membranes	$\alpha$ as high as 150 reported	[118]
Recovery of aroma compounds	Poly(octyl methyl siloxane) (POMS) and PDMS	The effects of operating conditions on separation performance were studied. POMS membrane was more perm-selective to the aroma compound than PDMS. $\beta$ higher for ETH than for ETB	[119]
Recovery of aroma compounds	Organophilic membranes	Review. Comparison of membrane performance for aroma compounds with different functional groups	[120]
Recovery of apple juice aroma compounds	PDMS	$\beta$ values ranging from 5–10 for ethanol to >100 for esters reported	[121]
Recovery of tea aroma compounds ( <i>trans</i> -hexenal 2-methyl propanal 3-methylbutanal phenyl acetaldehyde benzyl alcohol Linalool <i>cis</i> -3-hexenol-ionone)	Poly(octyl methyl siloxane) and poly(dimethylsiloxane)	Wider range of $\beta$ (20 to 1100) depending upon the functional group. PDMS found to be better than POMS	[20]
Removal of various organic compounds from industrial effluent; recovery of apple aroma	Composite MTR 100	Selectivities vary with the nature of the organic compound ranging from >100 for highly hydrophobic to ~5 for highly hydrophilic compounds	[122]
Scale-up of pervaporation for the recovery of natural aroma compounds in the food industry. Part 2: Optimization and integration	Hydrophobic membranes	Economic analysis of PV shows high potential for aroma recovery	[123]
Scale-up of pervaporation for the recovery of natural aroma compounds in the food industry. Part 1: Simulation and performance	Hydrophobic membranes	Importance of simulation in recovery from multicomponent mixtures revealed	[124]
Pervaporation for aroma isolation	Organophilic membrane	Recent developments in this field and the economic implications of the technology for producing natural aroma extracts are studied	[125]
Aroma compounds recovery of tropical fruit juice by pervaporation	Composite membranes (flat or hollow fiber),	The water permeability and the overall mass transfer coefficient for each organic solute was determined	[126]
<b>Bioproduction</b>			
Ethanol production	Silicone composite on polysulfone	Productivity of 20–30 g/L h	[127]
Acetone, butanol, ethanol fermentation	SBR,EPDM,PDMS plain and filled with silicalite	Highest $\alpha$ obtained for filled PDMS and lowest for EPDM. SBR yielded highest PSI	[87]
Recovery of acetone and butanediol from fermentation broth	PDMS and PEBAX	PEBAX better than PDMS. Fermentation coupled with PV at $\beta > 2$ can eliminate product inhibition	[128]

**TABLE 5.5 (continued)**  
**Removal of Organics from Aqueous Solutions**

System	Membrane Used	Remark	Reference
Recovery of volatile organic flavor compounds (ethyl acetate, EA; ethyl propionate, EP; ethyl butyrate, EB)	Surface modified tube-type alumina membrane	$\beta$ for EA, EP, and EB at 40°C were in the range of 66.9–78.9, 106.5–97.3, and 120.5–122.8, respectively. Phase separation in permeate allows facile recovery of the aroma compounds	[129]
Product recovery from biomass fermentation processes	Hydrophobic/hydrophilic membranes for recovery of biofuel and dehydration, respectively	Several issues and research priorities which will impact the ability of pervaporation to be competitive for biofuel recovery from fermentation systems are identified and discussed	[130]
Ethanol recovery from fermentation broth by pervaporation	Composite polydimethylsiloxane membrane	Ethanol concentration in fermentation broth decreased to a relatively low level when pervaporation was coupled with fermentation. More active cells appeared accompanied by better membrane performance	[131]

The selectivities of a typical organophilic membrane [16,18] are such that the permeate is enriched in terms of the organic well above its solubility limit. At these concentrations phase splitting occurs. In the liquid–liquid separator (Figure 5.3), two separate layers (1) organic rich with minute quantity of dissolved water and (2) water rich but saturated with the organics are obtained. The second small stream containing water saturated with the organics is returned to the feed side of the module. Figure 5.3 shows a closed loop operation with only the untreated (mainly aqueous) stream going to the effluent treatment plant. An idea of importance of the process shown in Figure 5.3 can be obtained from the following example. Although benzene has a low solubility (~1000 ppm) in water each mole of benzene requires 7.5 moles of oxygen for complete conversion to CO<sub>2</sub> and H<sub>2</sub>O. Removal of more than 90% of the benzene is possible by employing the process in Figure 5.3. This implies a significant decrease in the chemical oxygen demand (COD) load on the effluent treatment plant. At the same time the recovered organic is an added value to the organization.

Another very important application of PV in this class is recovery of high value aroma compounds. Baudot and Marin [85] have presented an excellent review on recovery of aroma compounds by PV. A comparison with recovery by stripping is also made. A recent paper [20] covers the subsequent literature. From the available literature, it is clear that PV is a far better option than stripping for aroma recovery. The major advantages of PV are (1) high selectivities and (2) mild operating conditions, which prevent the thermal degradation of the relatively sensitive aroma compounds. However, as pointed out by Kanani et al. [20] the sensory profile of the recovered aroma mixture can be significantly different because of the different selectivities offered by the membrane for the various aroma compounds present in the original mixture. In their study on recovery of tea aroma compounds by PV the following observations were made.

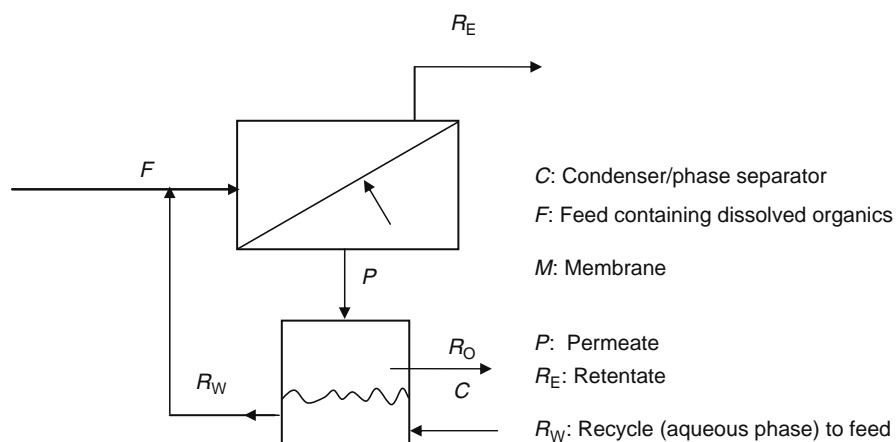


**FIGURE 5.3** Schematic of recovery of dissolved organics using pervaporation.

Generally, alcohols showed higher separation factors when present in model multicomponent solutions than in binary systems with water. On the other hand, aldehydes showed an opposite trend. The actual tea aroma mixture showed a rather different behavior from the model aroma mixture, probably because of the presence of very large numbers of unknown compounds. Overall, the PDMS membrane with vinyl end groups used by Kanani et al. [20] showed higher separation factors and fluxes for most of the aroma compounds. Pervaporation was found to be an attractive technology. However, as mentioned above the varying selectivities for the different aroma compounds alter the sensory profile and therefore application of PV for recovery of such mixtures needs careful consideration on a case-by-case basis.

PV has another potential application in the biotechnology industry, which may expand rapidly [86]. There is a clearly perceptible trend of use of biotechnology for the manufacture of specialty flavor materials. The product of the process inhibits most fermentation. If this product is continuously removed from the broth much higher productivities can be obtained. Liquid extraction, which was studied in the 1960s and 1970s, for removal of the fermentation products has the drawback that the solvent used may be toxic to the microorganisms. Inert gas stripping/vacuum stripping offer much lower separation factors. In view of the capability of PV to efficiently separate organic compounds under mild conditions, it is a far better substitute to these competing methods particularly if the product is volatile enough to be amenable to removal by PV. Kawedia et al. [87] have studied the pervaporative removal of the products in acetone–butanol–ethanol (ABE) fermentation using various organophilic membranes. These investigators studied both binary (organic–water) and quaternary (A/B/E/H<sub>2</sub>O) systems. In this fermentation butanol has the most detrimental effect on the activity of the microorganisms. Amongst the various polymers studied styrene butadiene rubber was found to be best for removal of the toxic products from the quaternary mixture. Similar applications in the manufacture of other aroma/flavor compounds such as *cis*-3-hexenol (leaf alcohol), pyrazines, etc. need urgent attention. Table 5.5 lists the available literature investigations on removal of organics from predominantly aqueous systems.

### 5.4.3 ORGANIC–ORGANIC SEPARATIONS

In the applications of PV discussed in Sections 5.5.1 and 5.5.2, there are clear and substantial differences in the properties of the solutes to be separated. The major distinguishing features relate to the polarity/hydrogen bonding properties of the solutes. Thus, the selection of the membrane polymer is relatively easy. In the case of organic–organic systems only in the case when one of the solutes contains strong hydrogen bonding (OH) or polar groups while the other is entirely nonpolar, the selection of the polymer can be done by the thumb rule of hydrophilicity/hydrophobicity of the polymer. Examples of such systems are: methanol–toluene, methanol–benzene, *i*-propanol–toluene/benzene, etc. [25–28]. On the other hand, when both the solutes have similar properties the selection of the membrane polymer requires careful consideration. However, in this case also small differences in the polarity of the solutes can be exploited to effect relatively good separation. Ray et al. [23,24] developed several methanol-selective copolymer membranes for separating methanol from MTBE and ethylene glycol. These investigators used the concept of three-dimensional (3-D) solubility parameter and prepared several copolymers of AN with other hydrophilic monomers like HEMA, vinyl pyrrolidone, etc. By properly tuning the copolymer composition membranes with relatively high selectivities for methanol were obtained. These membranes have good stability because the hydrophilic group, which is bonded to the AN backbone, is not easily plasticized by methanol. Similar approach was successfully applied by Ray et al. [22] to effect the much more difficult separation of benzene and cyclohexane. These two compounds have substantially the same properties except that due to the continuous shifting of the double bonds in benzene there is a small contribution from polar and hydrogen bonding forces to the overall solubility parameter of benzene. In this case copolymers of AN with relatively hydrophobic compounds like methyl methacrylate, vinyl acetate, and styrene were employed for obtaining benzene-selective membranes. The choice of the comonomers was dictated by the fact that their homopolymers are soluble in benzene and thus their inclusion in the copolymers would enhance benzene sorption. The extent of the comonomer in the copolymer was varied to obtain an optimum composition. All the membranes were found to yield benzene selectivities much higher than those reported earlier. The selectivities depended upon the copolymer type and its composition, and varied from 5 to 80. This work clearly proves the utility of the copolymer concept combined with the 3-D solubility parameter theory to design suitable membranes for relatively difficult separations. Further, because of the presence of the relatively tough and insoluble AN backbone these membranes are very stable.

Table 5.6 gives a summary of the literature investigations on organic–organic separations. The early enthusiasm for PV was a result of its various advantages vis-à-vis distillation. This was evident from the fact that most majors like Exxon, Standard Oil, British Petroleum, Texaco established research groups devoted to PV. The group at Exxon made a concerted effort at developing membranes for separating close boiling aromatic/aliphatic compounds. However, the selectivities obtained with the optimized membranes were still not good enough to encourage a change over from distillation. Indeed, these rather unsuccessful efforts eventually resulted in closure of many groups. Currently, only a small number of companies (Sulzer Chemtech, Ube and Mitsui, Japan and MTR, USA) are active in this area. Thus, despite the advantages of PV and its potential applicability to a wide range of organic–organic separations of great industrial interest, there are very few known actual examples of industrial use. Steinhauser et al. [132] have described the separation of an azeotropic mixture of trimethyl borate

**TABLE 5.6**  
**Organic–Organic Separation**

System	Membrane Used	Remark	Reference
Butadiene is separated from its mixture with <i>trans</i> -2-butene	Polybenzimidazole membrane	$\beta = 4.9$	[134]
1,3-butadiene is separated from its mixture with <i>trans</i> -2-butene	PVC membrane	Separation of dienes from mono-olefins	[135]
Removal of methanol from organic mixture	Membrane prepared by plasma polymerization	High $\alpha$ and flux for methanol reported	[136]
Separation of organic–organic mixture	Various organic and inorganic membranes	Review on current scientific and technological factors governing separation of organic mixtures	[137]
Toluene/heptane	Polyacrylonitrile composite membrane	High selectivity and high permeate fluxes were obtained	[138]
Separation of MeOH-hydrocarbon and EtOH-ETBE mixtures	Plasma polymerized PERVAP 1137	High methanol/MTBE and ethanol/ETBE selectivities. PV + distillation more economical	[139]
Separation of alcohol toluene mixture	<i>N</i> -acetylated chitosan membrane	Additional acetyl groups in the membrane decreased the flux but increased $\alpha$	[140]
<i>N</i> -butyl acetate- <i>n</i> -butanol-methyl acetate-methanol	Sulzer Pervap-2255 membrane	Combination of reactive distillation and pervaporation allowed 100% conversion	[141]
Pervaporation of methanol-methyl acetate binary mixtures	Cuprophane membranes	Experimental fluxes and selectivities of the permeating components were determined and evaluated on the basis of the feed mixtures and membranes. The effect of vacuum/pressure on total flux and selectivity is discussed	[142]
Separation of organic–organic mixture	Hydrophilic polymer membrane	Review: Mass transfer analysis of pervaporation	[80]
MeOH-cyclohexane, EtOH-cyclohexane, Me-pentane, and MeOH-MTBE	Membrane from a 5% NA cellulose sulfate solution and 20%–40% solutions of cationic surfactants e.g., <i>N</i> -dodecylpyridinium chloride or hexadecylpyridinium chloride	In all cases high fluxes and good selectivities at 50°C were found	[143]
Separation of azeotropic mixtures like water, MeOH, and EtOH from organic solvents	Hybrid PV + distillation systems	Applications and flow sheets for hybrid processes	[144]
Separation of azeotropic organic liquid mixtures	PFSA polymer composite membrane	The composite membrane gave 4–5 times larger flux than commercial membrane without appreciable loss in selectivity. Downstream pressure of ~6.67 KPa had little effect on the total flux	[145]
Methanol-benzene and methanol-toluene	Regenerated cellulose (cellophane), poly(vinyl alcohol) (PVA), cellulose acetate (CA), cellulose triacetate (CTA), two blends of CTA (B1 and B2) with acrylic acid, poly(dimethylsiloxane) (PDMS), and linear low density polyethylene (LLDPE) membrane	Methanol selectivity PVA > CA > CTA > B1 > B2. The influence of the membrane material with varying solubility parameter is investigated	[24]
1-Methoxy propanol and water	Polyimide (PI), cellophane, poly(vinyl alcohol) (PVA), cellulose diacetate (CDA), cellulose triacetate, two separate blends of cellulose acetate and CDA with cellulose acetate propionate, and PVA cross-linked with multifunctional cross-linkers	The effects of different substitution derivatives of cellulosic materials were investigated	[74]
1-Methoxy propanol and water	Acrylonitrile-based copolymer membrane	3-D solubility parameter and interaction parameter values used to explain behavior (selectivity and flux). Copolymers of AN showed good selectivity with reasonable flux	[15]

(continued)

**TABLE 5.6 (continued)**  
**Organic–Organic Separation**

System	Membrane Used	Remark	Reference
IPA/benzene, IPA/toluene	Regenerated cellulose (cellophane), poly(vinyl alcohol) (PVA), cellulose acetate (CA), cellulose triacetate (CTA), two blends of CTA (B1 and B2) with acrylic acid, poly(dimethylsiloxane) (PDMS), and linear low density polyethylene (LLDPE) membrane	The IPA selectivity performance was: cellophane > PVA > CA > CDA > CTA	[26]
Methanol-toluene	Acrylonitrile-based copolymer membrane	The permeation, selectivity, and flux variation with methanol concentration has been explained using the solubility parameter approach	[15]
Benzene and cyclohexane mixtures	Copolymers of acrylonitrile with styrene, methyl methacrylate, and vinyl acetate	Copolymers of acrylonitrile with methyl methacrylate and vinyl acetate showed good selectivity and moderate flux	[146]
Methanol removal from mixtures with toluene, MTBE, IPA, and acetonitrile	Polypyrrole membrane doped with hexafluorophosphate (I) and p-toluenesulfonate (II)	Membrane (I) gave high selectivity and acceptable flux	[147]
Separation of organic liquid mixtures	Liquid crystalline polymer networks	Change in selectivity from H <sub>2</sub> O selective to ethanol selective at the nematic-isotropic transition temperature	[148]
Separation of the benzene/cyclohexane mixtures	Poly(methyl methacrylate) (PMMA) and poly(ethyl methacrylate) (PEMA) cross-linked with ethylene glycol dimethacrylate (EGDM)	The depression of swelling of membranes with the increase of the cross-linker content in the benzene/cyclohexane mixtures enhanced benzene permselectivity	[149]

### Special Applications

#### *Petroleum Industries*

System	Membrane Used	Remark	Reference
Design and analysis of combined distillation and pervaporation processes for methanol/DMC, methanol/MTBE, and IPA/water	Cross-linked PVA (PERVAP 1510) and plasma polymerized PERVAP 1137	Hybrid PV + distillation has better economics particularly in terms of low premium energy requirement	[150]
Sulfur removal from gasoline	Copolymers of AN with HEMA/MMA	$\beta = 1.5\text{--}15$	[151]

#### *General and Review Articles*

System	Membrane Used	Remark	Reference
Development in membrane technology	Polymeric and ceramic membranes	Review (German)	[152]
PV and other membrane separations	Polymer grafted membrane	An overview of selected membrane techniques for environmental applications	[153]
Production of desalinated water from highly contaminated water	Polyetherimide-based polymer film of 40 $\mu\text{m}$ thickness	Measured fluxes are independent of severe fouling and virtually independent of concentration up to 100 g/L total solids	[154]
Separation of ethanol from a real yeast solution	PDMS composite membrane	With the increase of glucose concentration from 0 to 100 g/L, the total flux decreases by 25% but the separation factor for ethanol increases from 7.7 to 10	[155]
Solvent recovery	Polymeric membrane	Review (Chinese)	[156]
Separation of organic mixtures	Facilitated transport supported liquid membrane (FTSLM)	Some examples of separation of organic compounds from mixtures ( <i>p</i> -xylenes/ <i>m</i> -xylenes, benzene/cyclohexane) were discussed, including separation of organic gases, wastewater, and organic solutions	[157]
Organic–water	Dehydration of organics and organic removal from aqueous streams	Review (Chinese)	[158]

**TABLE 5.6 (continued)**  
**Organic–Organic Separation**

*General and Review Articles*

System	Membrane Used	Remark	Reference
Separation of liquid mixture	Application of PV and VP	General review, examples of polymers for membrane preparation, as well as performance parameters of pervaporation and vapor permeation membranes, are described	[159]
Esterification/alkylation, deNO <sub>x</sub> reaction, hydrogenation, and dehydrogenation studied	Zeolite molecular sieve membrane	It is found that zeolite membranes, disk, and coating show high performance or potential as catalysts compared with conventional catalysts	[160]

and methanol using vapor permeation unit. VP is the analog of PV wherein the feed is vapor instead of liquid. Another documented application is in the manufacture of MTBE and ETBE. Both these ethers form an azeotrope with the alcohol. In a detailed engineering study Hommerich [133] has shown that PV can be advantageously used in a large-scale plant with significant savings in operating costs.

With the rising cost of crude oil and hence that of fuel, distillation may be placed at a greater disadvantage because of its energy intensive nature. PV, with its low-operating costs is most likely to receive a revived interest. Particularly important applications of interest will be separation of organic azeotropes and close boiling mixtures. A concerted effort is needed to develop membranes with higher selectivities than the currently available one to ensure that PV does not remain a small-scale application [59].

## NOMENCLATURE

$a_i$	activity of component $i$
$A_{ii}, A_{ij}, A_{jj}, A_{ji}, B_{ij}, B_{ji}$	diffusional interaction parameters in Section 5.2
$A_i$	plasticization coefficient ( $\text{m}^3/\text{mol}$ ) <sup><math>n</math></sup> in Equations 5.15 and 5.17
$C_3(r, \phi)$	molar concentration at the pore outlet ( $\text{mol}/\text{m}^3$ )
$C_3(r, z)$	molar concentration in the cylindrical pore at a point ( $\text{mol}/\text{m}^3$ )
$C_{bi}$	concentration of component $i$ in the bulk in Equation 5.6 ( $\text{mol}/\text{m}^3$ )
$C_{fi}$	concentration of selectively permeating solute $i$ in the feed in Equation 5.28 ( $\text{mol}/\text{m}^3$ )
$C_{pi}$	membrane phase concentration of 'i' in the permeate side in Equation 5.28 ( $\text{mol}/\text{m}^3$ )
$C_{mi}$	concentration of a component $i$ in the membrane in Equation 5.6 ( $\text{mol}/\text{m}^3$ )
$C_m$	membrane phase concentration of the solute in Equations 5.7 and 5.8 (wt. fraction)
$C_b$	bulk liquid phase concentration of the solute in Equation 5.8 (wt. fraction)
$C_T$	total concentration of the solute in the membrane in Equation 5.7 ( $\text{mol}/\text{m}^3$ ) (wt. fraction)
$C_z$	weight fraction of solute in zeolite phase
$D$	diffusion coefficient ( $\text{m}^2/\text{s}$ )
$D_i$	diffusion coefficient of component $i$ ( $\text{m}^2/\text{s}$ )
$D_{io}$	diffusion coefficient of component $i$ at infinite dilution ( $\text{m}^2/\text{s}$ )
$D_{jo}$	diffusion coefficient of component $j$ at infinite dilution ( $\text{m}^2/\text{s}$ )
$d_{\text{pore}}$	pore diameter (m)
$\Delta H_f$	heat of fusion of polymer in Equation 5.13 (kJ/kmol)
$H_M$	Henry's constant in Equation 5.8 (—)
$J_i$	flux of component $i$ ( $\text{kg}/\text{m}^2\text{s}$ ) ( $\text{mol}/\text{m}^2\text{s}$ )
$K$	sorption coefficient for the solute in the polymer in Equation 5.6 (—)
$k_o$	overall mass transfer ( $\text{m}/\text{s}$ )
$K_o$	overall mass transfer coefficient in Equation 5.29 ( $\text{m}/\text{s}$ )
$k_L$	fluid to membrane mass transfer coefficient in Equation 5.29 ( $\text{m}/\text{s}$ )
$k_{di}, k_{dj}$	constants in Equations 5.18 through 5.21
$L$	thickness of membrane in Equation 5.28
$M_c$	molecular weight between two cross-links
$M_V$	molecular weight of repeating unit of polymer ( $\text{kg}/\text{mol}$ )
$n$	constant in Equation 5.15

$n_1, n_2$	number of moles of component 1 and 2, respectively, in Equation 5.4
$n_i$	ratio of molar volume of polymer to solute in Section 5.2
$P_i^C$	critical (partial) vapor pressure of component $i$ in Equation 5.35
$P_i^o$	partial pressure of component $i$ at equilibrium state in Equation 5.35
$p_2$	effective pressure (atmospheric pressure/RO pressure) of A and B at the pore inlet in Equation 5.1 (—)
$p_3$	effective pressure (atmospheric pressure/RO pressure) of A and B at the pore outlet in Equation 5.1 (—)
$R, z$	cylindrical coordinates (m)
$R$	universal gas constant (8.314 kJ/kmol K)
$S$	sorption coefficient in Equation 5.29 (—)
$S_A$	sorption coefficient for A (—)
$S_B$	sorption coefficient for B
$T$	temperature (K)
$T_m$	melting temperature of the crystalline phase (K)
$U$	solution velocity in pore (m/s)
$V_i$	molar volume of component $i$ (cm <sup>3</sup> /mol)
$V_1, V_2$	molar volumes of components 1 and 2, respectively, in equations in Section 5.2 (m <sup>3</sup> /mol)

### GREEK LETTERS

$\alpha_S$	sorption selectivity (—)
$\alpha_D$	diffusional selectivity (—)
$\alpha_o$	overall selectivity (—)
$\beta$	separation factor defined by Equation 5.33 (—)
$\chi_{AB}, \chi_{AM}$	friction constants between A
$\chi_{ip}$	interaction parameter for component $i$ (—)
$\delta$	overall solubility parameter (MPa) <sup>1/2</sup>
$\delta_p$	length of the pore (m) in Equation 5.1
$\delta_d$	contribution of dispersive force toward solubility parameter (MPa) <sup>1/2</sup>
$\delta_h$	contribution of hydrogen bonding toward solubility parameter (MPa) <sup>1/2</sup>
$\delta_p$	contribution of polar forces toward solubility parameter (MPa) <sup>1/2</sup>
$\Phi_p$	volume fraction of the polymer (—)
$\eta$	solution viscosity in the pore (Pa s)
$\lambda$	fraction of noncrystalline polymer in Equation 5.13 (—)
$\Delta\mu$	chemical potential difference between the two phases in Equation 5.10
$\rho_p$	polymer density (kg/m <sup>3</sup> )
$\sigma_p$	surface tension of liquid in pore (N/m) in Equation 5.35

### ABBREVIATIONS

A	solute, A
ABE	acetone–butanol–ethanol
AN	acrylonitrile
B	solute, B
CA	cellulose acetate
CDA	cellulose diacetate
COD	chemical oxygen demand
CP	concentration polarization
CPI	chemical process industries
CTA	cellulose triacetate
EA	ethyl acetate
EB	ethyl butyrate
EGDM	ethylene glycol dimethacrylate
EP	ethyl propionate
EPDM	ethylene propylene diene
ETBE	ethyl <i>tert</i> -butyl ether
FTSM	facilitated transport supported liquid membrane

HEMA	hydroxyethyl methacrylate
IPN	interpenetrating polymer networks
LDPE	low density polyethylene
MARS	membrane aromatic recovery system
MF	microfiltration
MMA	methyl methacrylate
MS	mild steel
MTBE	methyl <i>tert</i> -butyl ether
NBR	<i>N</i> -butyl rubber
NR	natural rubber
NRS	nonrenewable resources
PAA	poly(acrylic acid)
PCE	perchloroethylene
PDMS	poly(dimethylsiloxane)
PEBA	poly(etherimide block polymer)
PEMA	poly(ethyl methacrylate)
PFSA	perfluoro sulfonic acid
PMMA	poly(methyl methacrylate)
POMS	poly(octyl methyl siloxane)
PP	poly(propylene)
PSCF	preferential sorption–capillary flow
PSI	pervaporation separation index
PV	pervaporation
PVA	poly(vinyl alcohol)
PVC	poly(vinyl chloride)
RO	reverse osmosis
RTV	room temperature vulcanization
SBR	styrene butadiene rubber
Δ	signifies difference in two properties

## ACKNOWLEDGMENT

VGP wishes to gratefully acknowledge the Herculean efforts of Mr. Rajendra Prasad and Ms. C. Sona in editing the manuscript as per CRC format.

## REFERENCES

1. Kobar PA. Pervaporation, perstillation and percrystallization. *J. Am. Chem. Soc.* 1917;39:944–950.
2. Schwob Y. Sur l'hémi-perméabilité à l'eau membranes de cellulose régénérée. These de doctorat s Sciences Toulouse (France), 1949.
3. Binning RC, Lee RJ, Jenning JF, and Martin EC. Separation of liquid mixtures by permeation. *Ind. Engg. Chem.* 1961;53:45–50.
4. Neel J, Nguyen QT, Clement R, and Le Blanc L. Fractionation of a binary liquid mixture by continuous pervaporation. *J. Memb. Sci.* 1983;15:43–62.
5. Neel J. Fundamental and general engineering aspects of pervaporation. In: Drioli E and Nakagaki M, eds., *Proceedings of the Europe–Japan Congress on Membranes and Membrane processes*. STRESA, Italy, June 18–22, 1984; New York, Plenum Press, 1986; 595–607.
6. Neel J, Aptel P, and Clement R. Basic aspects of pervaporation. *Desalination.* 1985;53:297–326.
7. Tusel GF and Ballweg A. Method and apparatus for dehydrating mixtures of organic liquids and water, US Patent 4405409, September 20, 1983.
8. Sander U and Soukup P. Design and operation of a pervaporation plant for ethanol dehydration, *J. Memb. Sci.* 1988;36:463–475.
9. Asada T. Dehydration of organic solvents. Some actual results of pervaporation plants in Japan. In: Backish R. ed., *Proceedings of the Third International Conference on Pervaporation Processes in Chemical Industry*. Nancy, France, September 1988; Englewood, NJ: Bakish Materials Corporation, 1988; 379–386.
10. Burshe MC, Sawant SB, Joshi JB, and Pangarkar VG. Sorption and permeation of binary water–alcohol systems through PVA membranes crosslinked with multi-functional crosslinking agents. *Sep. Purific. Tech.* 1997;12(2):145–156.
11. Burshe MC, Sawant SB, and Pangarkar VG. Dehydration of ethylene glycol by pervaporation using hydrophilic ipns of PVA, PAA and PAAM membranes. *Sep. Purific. Tech.* 1998;13(1):47–56.
12. Burshe MC, Sawant SB, and Pangarkar VG. Dehydration of glycerine–water mixtures by pervaporation. *J. Am. Oil. Chem. Soc.* 1999;76(2):209–214.

13. Burshe MC, Netke SA, Sawant SB, Joshi JB, and Pangarkar VG. Pervaporative dehydration of organic solvents. *Sep. Sci. Tech.* 1997;32(8):1335–1349.
14. Ray SK, Sawant SB, Joshi JB, and Pangarkar VG. Dehydration of acetic acid by pervaporation. *J. Memb. Sci.* 1998;138(1):1–17.
15. Mandal S and Pangarkar VG. Pervaporative dehydration of 1-methoxy-2-propanol with acrylonitrile based copolymer membranes prepared through emulsion polymerization: A solubility parameter approach and study of structural impact. *J. Memb. Sci.* 2002;209(1):53–66.
16. Netke SA, Sawant SB, Joshi JB, and Pangarkar VG. Comparative study of membranes for pervaporation of trace organics from aqueous solutions. In: Bowen WR, Field RW, and Howell JA, eds., *Proceedings of the Euro-Membrane-95 Conference*. Bath, UK, September 18–20, 1995; *Europ. Soc. Memb. Sci. Technol.* 1995;2:116–121.
17. Netke SA, Sawant SB, Joshi JB, and Pangarkar VG. Sorption and permeation of aqueous picolines in elastomeric membranes. *J. Memb. Sci.* 1994;91(1–2):163–171.
18. Samdani AR, Mandal S, and Pangarkar VG. Role of and criterion for sorption selectivity in pervaporative removal of trace organics from aqueous solutions. *Sep. Sci. Tech.* 2003;38(5):1069–1092.
19. Kabra MM, Netke SA, Sawant SB, Joshi JB, and Pangarkar VG. Pervaporative separation of carboxylic acid–water mixtures. *Sep. Tech.* 1995;5(4):259–264.
20. Kanani DM, Nikhade BP, Balakrishnan P, Singh G, and Pangarkar VG. Recovery of valuable tea aroma components from steam distillation condensate by pervaporation. *Ind. Eng. Chem. Res.* 2003;42(26):6924–6932.
21. Ray SK, Sawant SB, Joshi JB, and Pangarkar VG. Development of new synthetic membranes for separation of benzene-cyclohexane mixtures by pervaporation: A solubility parameter approach. *Ind. Eng. Chem. Res.* 1997;36(12):5265–5276.
22. Ray SK, Sawant SB, Joshi JB, and Pangarkar VG. Development of methanol selective membranes for separation of methanol-MTBE mixtures by pervaporation. *J. App. Poly. Sci.* 1999;74(11):2645–2559.
23. Ray SK, Sawant SB, Joshi JB, and Pangarkar VG. Methanol selective membranes for separation of methanol–ethylene glycol mixtures by pervaporation. *J. Memb. Sci.* 1999;154(1):1–13.
24. Mandal S and Pangarkar VG. Separation of methanol-benzene and methanol–toluene mixtures by pervaporation: Effects of thermodynamics and structural phenomenon. *J. Memb. Sci.* 2002;201:175–190.
25. Mandal S and Pangarkar VG. Development of copolymer membranes for pervaporative separation of methanol from methanol–benzene mixtures—a solubility parameter approach. *Sep. Purif. Tech.* 2003;30(2):147–168.
26. Mandal S and Pangarkar VG. Effect of membrane morphology in pervaporative separation of isopropyl alcohol–aromatic mixtures—a thermodynamic approach to membrane selection. *J. App. Poly. Sci.* 2003;90(4):3912–3921.
27. Mandal S and Pangarkar VG. Acrylonitrile based copolymer membranes for the separation of methanol from methanol–toluene mixtures through pervaporation. *J. App. Poly. Sci.* 2005;96:243–252.
28. Dagaonkar MV, Sawant SB, Joshi JB, and Pangarkar VG. Sorption and permeation of aqueous alkyl piperazine in hydrophillic and organophillic membranes: A transport analysis. *Sep. Sci. Tech.* 1998;33(3):311–331.
29. Mulder MHV. *Basic Principles of Membrane Technology Dordrecht*. The Netherlands: Kluwer Academic, 2000.
30. Sourirajan S and Shiyao Y. An approach to membrane separations by pervaporation. In: Bakish R. ed., *Proceedings of Second International Conference on Pervaporation Processes in the Chemical Industries*. Englewood, NJ: Bakish Materials Corporation, 1987;1–10.
31. Rautenbach R and Albrecht R. On the behaviour of asymmetric membranes in pervaporation. *J. Memb. Sci.* 1984;19(1):1–22.
32. Bining RC and James FE. Permeation: New way to separate mixtures. *Petrol. Refiner.* 1958;37(5):214–215.
33. Hansen CM. The three-dimensional solubility parameter—key to paint component affinities. *J. Paint Tech.* 1967;39(505):104–117.
34. Rogers CE. Permeation of gases and vapors in Polymers. In: Comyn J. ed., *Polymer Permeability*. New York: Elsevier Applied Sciences, 1985;11–73.
35. Netke SA, Sawant SB, Joshi JB, and Pangarkar VG. Sorption and permeation of acetic acid in zeolite filled membranes. *J. Mem. Sci.* 1995;107(1–2):23–33.
36. Flory PJ. *Principles of Polymer Chemistry*. Ithaca, NY: Cornell University Press, 1953;495–540.
37. Long RB. Liquid permeation through plastic films. *Ind. Eng. Chem. Fund.* 1965;4:445–451.
38. Greenlaw FW, Sheldon RA, and Thompson EV. Dependence of diffusive permeation rates on upstream and downstream pressures: V. Experimental results for the hexane/heptane (ideal) and toluene/ethanol (non-ideal) systems. *J. Memb. Sci.* 1977;2(4):333–348.
39. Rogers CE, Stannett V, and Swarc M. The sorption, diffusion and permeation of organic vapors in polyethylene. *J. Poly. Sci.* 1960;845:61–82.
40. Rautenbach R and Albrecht R. The separation potential of pervaporation: I Discussion of transport equations and comparison with reverse osmosis. *J. Memb. Sci.* 1985;25:1–23.
41. Rautenbach R and Albrecht R. The separation potential of pervaporation: II Discussion of transport equations and comparison with reverse osmosis. *J. Memb. Sci.* 1985;25:25–54.
42. Sheldon RA and Thompson EV. Dependence of diffusive permeation rates on upstream and downstream pressures. III—Membrane selectivity and implications for separation processes. *J. Membr. Sci.* 1978;4:115–127.
43. Brun JP, Larchet C, Melet R, and Bulvestre G. Modelling of the pervaporation of binary mixture through moderately swelling, non-reacting membranes. *J. Memb. Sci.* 1985;23(3):257–283.
44. Sferrazza RA, Escobosa R, and Gooding CH. Estimation of parameters in a sorption–diffusion model of pervaporation. *J. Memb. Sci.* 1988;35(2):125–136.
45. Raghunath B and Hwang ST. General treatment of liquid-phase boundary layer resistance in the pervaporation of dilute aqueous organics through tubular membranes. *J. Memb. Sci.* 1992;75(1–2):29–46.

46. Loeb S and Sourirajan S. Sea water demineralization by means of an osmotic membrane In: Saline water conversion II, *Adv. Chem. Ser. Am. Chem. Soc.*, Washington DC: 1963;38:117–132.
47. Cadotte JE, King RS, Majerle RJ, and Merten U. Interfacial synthesis in the preparation of reverse osmosis membranes. *J. Macromol. Sci. Chem. A.* 1981;A15(5):727–755.
48. Brusckhe HEA. State of art of pervaporation. In: Bakish R. ed., *Proceedings of the Third International Conference on Pervaporation Processes in the Chemical Industry*. Nancy, France, September 19–22; Englewood, NJ: Bakish Materials Corporation, 1988;2–11.
49. Heinzelmann W. Fabrication methods for pervaporation membranes. In: Bakish R. ed., *Proceedings of the Fifth International Conference on Pervaporation Processes in the Chemical Industry*. Nancy, France, September 19–22; Englewood, NJ: Bakish Materials Corporation, 1991;22–30.
50. Trifunovic O and Tragardh G. The influence of support layer on mass transport of homologous series of alcohols and esters through composite pervaporation membranes. *J. Memb. Sci.* 2005;259:122–134.
51. Rautenbach R and Albrecht R. On behavior of asymmetric membranes in pervaporation. *J. Memb. Sci.* 1984;19:1–22.
52. Briston JH. *Plastic Films*, 2nd ed. New York: Longman, 1983;282–300.
53. Aptel P, Cuny J, Jozefowicz J, Morel G, and Neel J. Liquid transport membranes prepared by grafting polar monomers onto poly(tetra fluoro ethylene) films: I. Some fractions of liquid mixtures by pervaporation. *J. App. Poly. Sci.* 1972;16:1061–1076.
54. Ellinghorst G, Niemolar N, Scholz M, and Steinhauser H. Membranes for pervaporation by radiation grafting and curing by plasma processing. In: Bakish R. ed., *Proceedings of the Second International Conference on Pervaporation Processes in the Chemical Industries*. Englewood, NJ: Bakish Materials Corporation, 1987;33–42.
55. Yamamoto M, Sakata J, and Hirai M. Plasma polymerized membranes and gas permeabilities. *J. App. Poly. Sci.* 1984;29:2981–2987.
56. Blanc LL, Clement R, Nguyen QT, and Neel J. Fractionation of a binary liquid mixture by continuous pervaporation. *J. Memb. Sci.* 1983;5:43–62.
57. Nguyen QT, Blanc LL, and Neel J. Pervaporation membranes from poly(acrylonitrile)-poly(vinyl pyrrolidone) blends and the study of their behavior in the pervaporation of water–organic liquid mixtures. *J. Memb. Sci.* 1985;22:245–255.
58. Huang RYM and Yeom CK. Pervaporation separation of aqueous alcohol mixtures using cross-linked poly(vinyl alcohol) membranes: III: Permeation of acetic acid–water mixtures. *J. Memb. Sci.* 1991;58:33–47.
59. Brusckhe HEA. State-of-art of pervaporation processes in the chemical industry. In: Nunes SP and Peinemann KV, eds., *Membrane Technology in the Chemical Industry*. Weinheim, Germany: Wiley-VCH, 2001;127–172.
60. Khairnar DB and Pangarkar VG. Dehydration of glycerin/water mixtures by pervaporation using homo and copolymer membranes. *J. Am. Oil Chem. Soc.* 2004;81(5):505–510.
61. Lee KH, Kim HK, and Rhim JW. Pervaporation separation of binary organic–aqueous liquids mixtures using crosslinked PVA membranes III ethanol–water mixture. *J. App. Poly. Sci.* 1995;58(10):1707–1712.
62. Rhim JW, Sohn MY, and Lee KH. Pervaporation of binary organic–aqueous liquid mixture using PVA–PAA crosslinked membrane. In: Bakish R. ed., *Proceedings of the Sixth International Conference on Pervaporation Processes in the Chemical Industries*. Englewood, NJ: Bakish Materials Corporation, 1992;242–251.
63. Rhim JW, Sohn MY, and Lee KH. Pervaporation separation of binary organic–aqueous liquids mixtures using crosslinked PVA membranes II phenol–water mixture. *J. App. Poly. Sci.* 1994;52(9):1217–1222.
64. Chou KJ and Hellmuth KM. Membrane separation process. US Patent 5143620, 1992.
65. Fujita M, Watanabe N, Sakota N, Suematsu H, Harada K, Inoue S, and Isozaki C. Membranes for separation of water soluble organic compounds. Japanese Patent 04090833, 1992.
66. Wesslein M, Heintz A, and Lichtenthaler RN. Pervaporation of binary and multicomponent mixture using poly(vinyl alcohol) (PVA) membrane. *J. Memb. Sci.* 1990;51(1–2):169–179.
67. Rhim JW, Kim HK, and Lee KH. Pervaporation separation of binary organic–aqueous liquids mixtures using crosslinked PVA membranes IV methanol–water mixture. *J. App. Poly. Sci.* 1996;61(10):1767–1771.
68. Aminabhavi TM, Khinnavar RS, Harogopall SB, Aithal US, Nguyen QT, and Hansen KC. Pervaporation separation of organic aqueous and organic–organic binary mixtures. *Rev. Macromol. Chem. Phys. C.* 1994;34(2):139–204.
69. Sterauch P and Martin N. Combined distillation—pervaporation systems for separation of water and methanol in fine chemistry. *Recent Progres en Genie des Procedes.* 2003;89:259–266.
70. Lenk W and Meier-Haack J. Polyelectrolyte multilayer membranes for pervaporation separation of aqueous–organic mixtures. *Desalination.* 2002;148(1–3):11–16.
71. Van HV, Vanden AL, Buekenhoudt A, Dotremont C, and Leysen R. Economic comparison between azeotropic distillation and different hybrid systems combining distillation with pervaporation for the dehydration of isopropanol. *Sep. Purific. Tech.* 2004;37(1):33–49.
72. Ray S and Ray SK. Dehydration of acetic-acid, alcohols and acetone by pervaporation using acrylonitrile-maleic anhydride copolymer membrane. *Sep. Sci. Tech.* 2005;40(8):1583–1596.
73. Sommer S and Melin T. Design and optimization of hybrid separation processes for the dehydration of 2-propanol and other organics. *Ind. Eng. Chem. Res.* 2004;43(17):5248–5259.
74. Mandal S and Pangarkar VG. Pervaporative separation of 1-methoxy propanol and water mixture. *J. App. Poly. Sci.* 2002;86:2194–2210.
75. Jean N and Ping Z. Present trend in pervaporation. *Gaofenzi Tongbao.* 1995;4:193–204.
76. Takegami S, Tujii S, and Yamada H. Pervaporation of ethanol–water mixtures using novel hydrophobic membranes containing polydimethylsiloxane. *Jpn. J. Poly. Sci. Tech.* 1992;49(12):981–991.
77. Sakohara S, Sakata T, and Asaeda M. Separation of water–acetone mixtures by acrylamide-acrylic acid copolymer gel prepared in pores of ceramic thin membrane. *Kobunshi Ronbunshu.* 1989;46(10):635–638.

78. Maeda Y, Magara K, and Tsugaya H. Pervaporation of aqueous acetic acid mixture through poly(acrylic acid-co-acrylonitrile) membranes. *PCT Int. Appl.* 1993 JP 19910903.
79. Yamada H and Fuwa Y. Manufacture of pervaporation membranes. Japanese Patent 05345118, 1993.
80. Neel J. Pervaporation: Fundamental and practice. *34th International Symposium on Macromolecules* 1993;70–71.
81. Yamaguchi T, Nakao S, and Kimura S. Design of pervaporation membrane for organic-liquid separation based on solubility control by plasma-graft filling polymerization technique. *Ind. Eng. Chem. Res.* 1993;32(5):848–853.
82. Koszorz Z, Nemestothy N, Ziobrowski Z, Belafi BK, and Krupiczka R. Influence of pervaporation process parameters on enzymatic catalyst deactivation. *Desalination.* 2004;162(1–3):307–313.
83. Won K, Hong JK, Kim KJ, and Moon SJ. Lipase catalyzed enantioselective esterification of racemic ibuprofen coupled with pervaporation. *Proc. Biochem.* 2006;41(2):264–269.
84. Park CH, Nam SY, and Lee YM. Pervaporation separation of an aqueous organic mixture through a poly(acrylonitrile-co-vinylphosphonic acid) membrane. *J. App. Poly. Sci.* 1999;74(1):83–89.
85. Baudot A and Marin M. Pervaporation of aroma compounds: Comparison of membrane performances with vapor liquid equilibria and engineering aspects of process improvement. *Trans. Inst. Chem. Eng. C.* 1997;75:117–142.
86. Baker R, Nunes SP, and Peinemann KV. *Membrane Technology in the Chemical Industry: Future trends.* Weinheim, Germany: Wiley-VCH, 2001;268–295.
87. Kawedia JD, Pangarkar VG, and Niranjana K. Pervaporative stripping of acetone, butanol and ethanol. *Bioseparation.* 2000;9(3):145–154.
88. Frederico CF, Ludmila PA, Boam SZ, and Andrew L. Pilot scale application of the membrane aromatic recovery system (MARS) for recovery of phenol from resin production condensates. *J. Memb. Sci.* 2005;257:120–133.
89. Ji W, Hilaly A, Sikdar SK, and Hwang ST. Optimization of multicomponent pervaporation for removal of volatile organic compounds from water. *J. Memb. Sci.* 1994;97:109–125.
90. Meckl K and Lichenthaler RN. Hybrid processes including pervaporation for the removal of organic compounds from process and waste water. In: Bakish R. ed., *Proceedings of the Sixth International Conference on Pervaporation Processes in the Chemical Industries.* Englewood, NJ: Bakish Materials Corporation, 1992;476–483.
91. Hoshi M, Saito T, Higuchi A, and Nakagawa T. Separation of aqueous organic solvents through crosslinked poly(acrylate-co-acrylic acid) membranes by pervaporation. *Sen'i Gakkaishi.* 1991;47(12):644–649.
92. Baker R, Kaschmekat J, Wijmans H, and Simmons V. Separation of organic solvents from aqueous streams by pervaporation. *Adv. Filtr. Sep. Technol.* 1990;1:330–335.
93. Cox G and Baker R. Pervaporation. *Ind. Waste Water.* 1998;6(1):35–37.
94. Amakawa M and Ishisaki C. Membranes for separation of organic acids from wastewater and manufacture of the membranes. Japanese Patent 19940411, 1995.
95. Hoshi M, Kogure M, Saitoh T, and Nakagawa T. Separation of aqueous phenol through polyurethane membranes by pervaporation. *J. App. Poly. Sci.* 1998;65(3):469–479.
96. Gupta T, Pradhan NC, and Adhikari B. Synthesis and performance of a novel polyurethaneurea as pervaporation membrane for the selective removal of phenols from industrial waste water. *Bull. Mater. Sci.* 2002;25(6):533–536.
97. Nagase Y, Naruse A, and Matsui K. Chemical modification of polysulphone. 2. Gas and liquid permeability of polysulphone/polydimethylsiloxane graft copolymer membranes cf: *Polymer.* 1990;31(1):121–125.
98. Abou-Nemeh I, Das A, Saraf A, and Sirkar KK. A composite hollow fiber membrane-based pervaporation process for separation of VOCs from aqueous surfactant solutions. *J. Memb. Sci.* 1999;158(1–2):187–209.
99. Rhim JW and Kwon YM. Pervaporation separation of trace vocs from water through PDMS membrane. *Korean Memb. J.* 1999;1(1):73–80.
100. Yeom CK, Dickson JM, and Brook MA. A characterization of PDMS pervaporation membranes for the removal of trace organic from water. *Korean J. Chem. Engg.* 1996;13(5):482–488.
101. Hoshi M. Present status and application of the organic solvent permselective membrane. *Kagaku to Kogyo.* 1996;70(4):151–159.
102. Eustache H, Foucreas J, and Histi G. Separation of liquid mixtures. Patent FR 19780518, 1979.
103. Sikdar SK, Burckle J, and Rogurt J. Separation methods for environmental technologies. *Environ. Progr.* 2001;20(1):1–11.
104. Vane LM, Hitchens L, Alvarez FR, and Giroux EL. Field demonstration of pervaporation for the separation of volatile organic compounds from a surfactant-based soil remediation fluid. *J. Hazard. Mater.* 2001;81(1–2):141–166.
105. Qin Y, Sheth JP, and Sirkar KK. Pervaporation membranes that are highly selective for acetic acid over water. *Ind. Engg. Chem. Res.* 2003;42(3):582–595.
106. Dutta BK and Sikdar SK. Separation of volatile organic compounds from aqueous solutions by pervaporation using S-B-S block copolymer membranes. *Env. Sci. Tech.* 1999;33(10):1709–1716.
107. Li X and Huang M. Liquid crystalline polyphosphazene and its separation membrane. *Jianzhu Cailiao Xuebao.* 1998;1(4):348–353.
108. Vane LM, Giroux EL, Alvarez FR, and Hitchens L. Separation of VOC from surfactant solution by pervaporation. *ACS Symp. Series.* 2000;740:57–75.
109. Liu QL and Xiao J. Silicalite-filled poly(siloxane imide) membranes for removal of VOCs from water by pervaporation. *J. Memb. Sci.* 2004;230(1–2):121–129.
110. Yeom CK and Lee KH. Pervaporation separation of water-acetic acid mixtures through poly(vinyl alcohol) membranes crosslinked with glutaraldehyde. *J. Memb. Sci.* 1996; 109(2):257–265.

111. Voilley A, Schmidt B, Simatos D, and Baudron S. Extraction of aromatic compounds by pervaporation technique. In Bakish. R., ed., *Proceedings of the 3rd International Conference: Pervaporation Process in the Chemical Industry*. Englewood, NJ: Bakish Material Corporation, 1998;429.
112. Karlsson HOE, Loureiro S, and Tragardh G. Aroma compound recovery with pervaporation–temperature effects during pervaporation of Muscat wine. *J. Food Eng.* 1995;26:177.
113. Rajagopalan N and Cheryan M. Pervaporation of grape fruit aroma. *J. Memb. Sci.* 1995;104(3):243.
114. Karlsson HOE and Tragardh G. Pervaporation dilute organic–water mixtures: A literature review on modeling studies and application to aroma compound recovery. *J. Memb. Sci.* 1993;76:121.
115. Schafer T, Bengston G, Pingel H, Boddeker KW, and Crespo JPSG. Recovery of aroma compounds from wine-must fermentation by organophilic pervaporation. *Biotechnol. Bioeng.* 1999;62(4):412.
116. Voilley A, Charbit G, and Gobert F. Recovery and separation of 1-octene-3-ol from aqueous solutions by pervaporation through silicone membrane. *J. Food Sci.* 1990;55:1399.
117. Lamer T and Voilley A. Influence of different parameters on the pervaporation of aroma compounds. In: Bakish. R., ed., *Proceedings of the 5th International Conference. Pervaporation Process in the Chemical Industry*. Englewood, NJ: Bakish Material Corporation, 1991;110.
118. Netke SA, Sawant SB, Joshi JB, and Pangarkar VG. Sorption and permeation of aqueous picolines in elastomeric membranes. *J. Memb. Sci.* 1994;91:163–171.
119. Samparanpiboon P, Jiratananon R, Uttapap D, Feng X, and Huang RYM. Separation of aroma compounds from aqueous solution by pervaporation using poly-octylmethylsiloxane (POMS) and poly-dimethylsiloxane (PDMS) membranes. *J. Memb. Sci.* 2000;71:55.
120. Boudot A and Marin M. Pervaporation of aroma compounds: Comparison of membrane performance with vapor-liquid equilibria and engineering aspects of process intensification. *Trans I Chem E.* 1997;75:177.
121. Bengsten E, Tragardh G, and Hallstrom B. Recovery and concentration of apple juice. *J. Food Engg.* 1989;10:65.
122. Kaschemekat J, Wijmans JG, and Baker RW. Removal of organic solvent contaminants from industrial effluent stream by pervaporation. In: Bakish R., ed., *Proceedings of the 4th International Conference Pervaporation Process in the Chemical Industry*. Englewood, NJ: Bakish Material Corporation, 1989;321.
123. Lipnizki F, Olsson J, and Trägardh G. Scale-up of pervaporation for the recovery of natural aroma compounds in the food industry. Part 1: Simulation and performance. *J. Food Engg.* 2002;54:183–195.
124. Lipnizki F, Olsson J, and Trägardh G. Scale-up of pervaporation for the recovery of natural aroma compounds in the food industry. Part 2: Optimization and integration. *J. Food Engg.* 2002;54:197–205.
125. Willemsen JHA, Dijkink BH, and Togtema A. Organophilic pervaporation for aroma isolation—industrial and commercial prospects. *Memb. Tech.* 2004;2:5–10.
126. Pereira CC, Rufino JRM, Habert AC, Nobrega R, Cabral LMC, and Borges CP. Aroma compounds recovery of tropical fruit juice by pervaporation: Membrane material selection and process evaluation. *J. Food Engg.* 2005;66(1):77–87.
127. Shabtai Y, Chaimonitz S, Freeman A, Katchalski KE, Linder C, Nemas M, Perry M, and Kedem O. Continuous ethanol production by immobilized yeast reactor with membrane pervaporation unit. *Biotech. Bioengg.* 1991;38:869–876.
128. Dettwiller B, Dunn IJ, and Prenosil JE. Bioproduction of acetoin and butanediol: Product recovery by pervaporation. In: Bakish. R., ed., *Proceedings of the 5th International Conference. Pervaporation Process in the Chemical Industry*. Englewood, NJ: Bakish Material Corporation, 1991;308–318.
129. Song KH, Lee KR, Rim JM, and Lim JH. Recovery of volatile organic flavor compounds by pervaporation. *J. Chem. Engg. Jpn.* 2004;37(1):82–88.
130. Vane LM. A review of pervaporation for product recovery from biomass fermentation processes. *J. Chem. Tech. Biotech.* 2005;80:603–629.
131. Wu Y, Huang W, Xiao Z, and Zhang Y. Ethanol recovery from fermentation broth by pervaporation using a composite polydimethylsiloxane membrane. *Chinese J. Chem. Engg.* 2004;12(4):586–589.
132. Steinhauser H, Bruschke HEA, and Ellinghorst G. Verfahren zur Abtrennung von C1–C3 Alkoholen aus Gemischen dieser Alkohole mit anderen organischen Flüssigkeiten, European Patent EP 0 593 011 cf. [59].
133. Hommerich U. Integration der Pervaporation in den MTBE-Herstellungsprozess, IVT Information der RWTH Aachen, 26:Nr.2 1996 cf. [59].
134. Perry E and Strazik WF. Separation of dienes from organic mixtures. US Patent 3789073, 1974.
135. Monsanto Company. Separation of dienes from organic mixtures Japanese Patent 50095205, 1975.
136. Steinhauser H. Pervaporation: Removal of methanol from organic mixtures. *Chemie Technik.* 1994;23(2):50–53.
137. Smitha B, Suhanya D, Sridhar S, and Ramakrishna M. Separation of organic–organic mixture by pervaporation—a review. *J. Membr. Separ.* 2004;241(1):1–21.
138. Frahn J, Malsch G, and Schwarz HH. Photoinitiated generation of a selective layer on polyacrylonitrile composite membrane. *J. Mater. Process. Technol.* 2003;143–144:277–280.
139. Streicher C, Kermer P, Tomas V, Hubner A, and Ellinghorst G. Development of new pervaporation membrane, system and processes to separate alcohols/ethers/hydrocarbone mixture. In: Bakish. R., ed. *Proceedings of the 7th International Conference on Pervaporation Process in the Chemical Industry*. Englewood, NJ: Bakish Material Corporation, 1995;297–309.
140. Huang RYM, Moon GY, and Pal R. N-acetylated chitosan membranes for the pervaporation separation of alcohol/toluene mixtures. *J. Memb. Sci.* 2000;176(2):223–231.

141. Steinigeweg S and Gmehling J. Transesterification processes by combination of reactive distillation and pervaporation. *Chem. Engg. Proc.* 2004;43(3):447–456.
142. Sain S, Dinçer S, and Savascyi OT. Pervaporation of methanol–methyl acetate binary mixtures. *Chem. Engg. Proc.* 1998;37(2):203–206.
143. Schwarz HH, Apostel R, and Paul D. Membranes from surfactants for separation of polar organic liquids. In: Bakish. R., ed., *Proceedings of the 7th International Conference on Pervaporation Process in the Chemical Industry*. Englewood, NJ: Bakish Material Corporation, 1995;374–382.
144. Martin N. Separating azeotropic mixtures. *Tech. Rev.* 1998;80(3):12–15.
145. Dutta BK and Sirkar SK. Separation of azeotropic organic liquid mixture by pervaporation. *AIChE J.* 1991;37(4):581.
146. Ray SK, Sawant SB, Joshi JB, and Pangarkar VG. Development of new synthetic membranes for separation of benzene-cyclohexane mixtures by pervaporation: A solubility parameter approach. *Ind. Eng. Chem. Res.* 1997;36(12):5265–5276.
147. Zhou M, Persin M, and Sarrazin J. Methanol removal from organic mixtures by pervaporation using polypyrrol membranes. *J. Memb. Sci.* 1996;117(1–2):303–309.
148. Inui K, Miyata T, and Uragami Ti. Angewandte makromolekularre. *Chemie.* 1996;240:241–250.
149. Inui K, Okumura H, Miyata T, and Puragami T. Permeation and separation of benzene/cyclohexane mixtures through cross-linked poly(alkyl methacrylate) membranes. *J. Membr. Sci.* 1997;132(2):193–202.
150. Rautenbach R and Vier J. Design and analysis of combined distillation/pervaporation process. In: Bakish. R., ed., *Proceedings of the 7th International Conference on Pervaporation Process in the Chemical Industry*. Englewood, NJ: Bakish Material Corporation, 1995; 70–85.
151. Pore AS. Studies in membrane separations. M. Chem. Engg. Thesis, University of Mumbai, Mumbai, India, 2005.
152. Bittermann HJ. Developments and novelty with regard to membrane technology. *Process.* 2004;11(1–2):54–56.
153. Ritchie SMC. Polymer grafted membranes. *Membrane Science and Technology Series.* 2003;8:299–327.
154. Zwijnenberg HJ, Koops GH, and Wessling N. Solar driven membrane pervaporation for desalination processes. *J. Memb. Sci.* 2005;250 (1–2):235–246.
155. Shi E, Huang WX, Xiao ZY, Wu Y, and Xu RQ. Separation performances of PDMS membrane in an ethanol fermentation–pervaporation coupled process. *J. Sichuan Univ.* 2004;36(2):41–45.
156. Chen C, Yu L, Qi X, and Jiang W. Development of pervaporation membrane separation technology and its application in petrochemical industry. *Mo Kexue Yu Jishu.* 1997;17(3):14–18.
157. Wang M, Wang B, Zhao H, and Gao CA. Review on the separation of organic mixtures based on facilitated transport supported liquid membrane. *Petrochem. Technol.* 2004;3(2):177–183.
158. Jiang XJ, Shi YQ, and Chen GW. Permselective pervaporation membrane for the separation of organic solutions. *Gongneng Gaofenzi Xuebao.* 2000;13(2):233–239.
159. Kujawski W. Application of pervaporation and vapor permeation in environmental protection. *J. Env. Stud.* 2000;9(1):13–26.
160. Mizukami F. Application of zeolite membranes, films and coatings. *Stud. Surf. Sci. Catal.* 1999;125:1–12.

---

# 6 Current Status and Prospects for Ceramic Membrane Applications

*Christian Guizard and Pierre Amblard*

## CONTENTS

6.1	Introduction .....	140
6.2	Ceramic Membrane Technologies .....	140
6.2.1	Description of Ceramic Membranes .....	140
6.2.1.1	Membrane Elements .....	140
6.2.1.2	Porous Membrane Structure .....	142
6.2.1.3	Dense Membrane Structure.....	145
6.2.2	Mass Transfer and Separation Properties.....	146
6.2.2.1	Liquid Filtration .....	147
6.2.2.2	Gas and Vapor Transport across Porous Membranes.....	151
6.2.2.3	Ion-Conducting Membranes .....	152
6.2.3	Commercially Available Ceramic Membranes and Implementation in Devices.....	153
6.2.3.1	Membrane Modules .....	153
6.2.3.2	Modules Arrangement.....	154
6.2.3.3	Competitiveness of Ceramic Membranes .....	156
6.3	Current Applications of Ceramic Membranes .....	158
6.3.1	Treatment of Waste Liquids and Gases .....	158
6.3.1.1	Cross-Flow Filtration .....	158
6.3.1.2	Membrane Bioreactors .....	159
6.3.1.3	Air Purification and Hot Gas Filtration .....	160
6.3.2	Liquid Processing.....	160
6.3.2.1	Drinking and Domestic Water .....	160
6.3.2.2	Food and Beverage Processing .....	161
6.3.3	Product Recovery .....	162
6.3.3.1	Purification of Pharmaceuticals and Bioproducts.....	162
6.3.3.2	Products Manufacturing and Recycling in Various Industries.....	163
6.4	Recent Developments and Prospects .....	164
6.4.1	Filtration and Separation in Liquid Media.....	164
6.4.1.1	Nanofiltration with Ceramic Membranes.....	164
6.4.1.2	Membrane Contactors and Distributors .....	165
6.4.2	Gas and Vapor Separation .....	166
6.4.2.1	Gas Separation .....	166
6.4.2.2	Pervaporation and Vapor Permeation .....	167
6.4.3	Catalytic Membrane Reactors .....	169
6.4.3.1	Chemical Reactors Based on Gas–Liquid–Solid Membrane Contactors .....	170
6.4.3.2	Biocatalytic Membrane Reactors .....	171
6.4.3.3	High-Temperature Catalytic Membrane Reactors .....	172
6.5	Conclusion.....	173
	References.....	174

## 6.1 INTRODUCTION

Ceramic membranes offer significant advantages of polymeric membranes in many applications where the last ones cannot withstand operating conditions (pH, temperature, chemicals, etc.). Indeed polymeric membranes are still cheaper to produce than ceramic membranes and are commercially available in a large range of polymeric materials and module geometry. Nevertheless, a technical and economical comparison between different membrane processes must take into account both investment and maintenance costs. Investment involves the cost of equipments for pretreatment and posttreatment of fluids in addition to the cost of the membrane plant. Maintenance includes replacement of membranes, electricity consumption, cleaning products, and labor costs. Accordingly, a comparison of overall costs, including membrane lifetime, cleaning procedures, and pretreatment requirements, may be in favor of inorganic membranes in a number of applications. Moreover, the technical progress made in the fabrication of ceramic membranes with production costs getting closer to those of many polymeric membranes explains why they are entering markets much broader than those accessible to the first generation of ceramic membranes.

Porous ceramic membranes are now widely applied in microfiltration and ultrafiltration, and they are getting to enter the nanofiltration domain. In fact, the structure of ceramic membranes readily changed since their first development. Membrane elements have gained higher compaction and are now produced with pore sizes down to the microporous range referring to IUPAC classification. Actual ceramic membrane elements are composed of a macroporous inorganic material (with a flat, tubular, multichannel, or monolithic geometry) supporting a multilayer porous ceramic structure exhibiting a non-deformable porosity with pore sizes ranging from macropores to micropores. Ceramic membrane elements are the basic units in which mass transfer and separation obey different transport mechanisms relating first to membrane physical characteristics (pore size, porosity, and membrane thickness), then to physicochemical interactions between feed liquid and membrane surfaces, and finally to hydrodynamics in the element. Most often, commercial ceramic membrane modules are made of a stainless steel housing containing one or several membrane elements. Beyond the current porous ceramic membranes devoted to liquid filtration, new generations of microporous or dense ceramic membranes are likely to develop for gas and vapor separation or biological and chemical catalytic reactors. In particular, much attention has been paid recently to dense ceramic membranes exhibiting high oxygen or hydrogen separation selectivity in view of applications in new technologies for power generation. Transport mechanisms in these dense ceramic membranes are based on ion conduction in the solid at high temperature.

This chapter is divided in three main parts. A current status of ceramic membrane technology is presented in the first part dealing with the description of commercially available ceramic membrane elements and modules as well as a brief overview of basic transport and separation mechanisms of these membranes. The second part looks through the current applications of ceramic membranes that have been classified into three domains: treatment of wastes, processing of liquids, and recovery of products. The third and last part of this chapter presents recent developments and prospects in the segment of ceramic membrane technologies. Part of these new developments anticipate the emergence of new ceramic membranes exhibiting a higher selectivity and able to withstand much severe working conditions than currently available ceramic membranes.

## 6.2 CERAMIC MEMBRANE TECHNOLOGIES

### 6.2.1 DESCRIPTION OF CERAMIC MEMBRANES

Currently available ceramic membranes are generally made up of a macroporous support, one or several macroporous intermediate layers, and a meso- or microporous top-layer. A comprehensive description of ceramic membrane top-layers can be found in a number of papers, reviews, and books [1–7]. In these publications, data are mainly devoted to the membrane top-layer, but less information is available on ceramic membrane elements. These elements may differ in structural shape and in chemical composition. The production of membrane elements combines the utilization of processing technologies such as ceramic paste extrusion for supports, slip-casting of powder suspensions for microfiltration layers [2], or solgel processing [8] of colloidal suspensions for ultra- or nanofiltration layers. The latest developments of ceramic membranes also include dense ion-conducting materials used for gas separation at high temperature. At the commercial level, ceramic membranes are available as modules made up of a rigid casing that contains one or several membrane elements.

#### 6.2.1.1 Membrane Elements

Although some ceramic membrane elements are proposed with a flat geometry, most of them exhibit a cylindrical shape for a multichannel element (Figure 6.1). The reason for that is the much better mechanical properties obtained for cylindrical-shaped ceramics and the easier sealing of the elements compared to flat shapes.

Since their early development, the geometrical and structural characteristics of ceramic membrane elements have readily changed (Figure 6.2). Originally, they were prepared as single tubes with an inside diameter ranging from ~6 to 15 mm and a wall thickness of about 2 mm. These ceramic tubes are still available from some suppliers, but the main handicaps with such

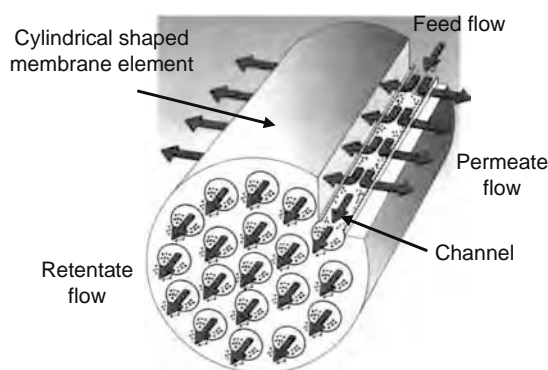


**FIGURE 6.1** Schematic representation of the multichannel structure of a ceramic membrane element.

tubular geometry are the high element volume to membrane surface ratio and the high liquid flow required for module feeding. The problem was solved rapidly by developing multichannel geometries as shown in Figure 6.2a. Actually, channels of a few millimeters in diameter minimize both the volume to membrane surface ratio and the feed flow inside the modules. Later on, the volume to membrane surface ratio was still increased by changing the cylindrical shape of the channels for non-cylindrical flower-like geometries, optimizing both space occupancy of the membrane and channel wall thickness in the element (Figure 6.2b). Recently, monolithic structures (Figure 6.2c) with a high density of cells and thin walls led to much larger hydraulic section and high membrane surface per element. Such an evolution of element geometry has resulted in a significant improvement of the filtration capability of ceramic membranes. All these ceramic membrane elements are currently available on the market. A number of relevant examples showing the evolution of these products are discussed hereafter [9].

Originally, multichannel ceramic membranes have been produced at the industrial scale by SCT-Exekia and Orelis in France with commercial elements registered, respectively, as Membralox and Kerasep. The membrane filtration area in this case can reach  $0.35 \text{ m}^2/\text{element}$  depending on channel diameter and the number of channels per element. FILTANIUM elements, representative of flower-like geometries, have been produced more recently by TAMI industries in France (Figure 6.3). These elements with a cross-section diameter of either 10 or 25 mm exhibit a number of channels that vary from 3 to 39 and a membrane filtration area of  $0.5 \text{ m}^2$  for the largest elements. The increase in membrane surface compared to equivalent cylindrical-shaped channels can be estimated at 30%.

The more recent monolithic structure (Figure 6.2c) results in a significant increase in surface to element volume ratio compared to the previous geometries. A typical monolith membrane element has multiple square-shaped parallel passage ways separated by porous walls through which permeate is drained at the exterior of the element. The tight arrangement of cells with a small cross-section area generates an efficient turbulent flow in the channels, a reduced pumping energy for feed flow, and a high filtration surface per element. Manufacturing of these large monoliths, up to 200 mm in diameter and 1.50 m long, has been successfully achieved by a number of companies mentioned in Table 6.1. The image of such full-size  $10.7 \text{ m}^2$  membrane element from CeraMem (Waltham, Massachusetts) is displayed in Figure 6.4.

However, there is a limitation in increasing the diameter of monolith membrane elements. The upper limit is when the hydraulic resistance of the porous walls becomes higher than the hydraulic resistance of the membrane top-layer developing in the element. A solution to this problem was found by introducing permeate conduits within the monolith. An example of such monolith design, patented by CeraMem, is given in Figure 6.5. Permeate conduits are obtained by cutting slots on both ends of the monolith, and sealing the ends of these slots. Then the cells at the opposite end of the monolith, opening into the slots are sealed. After sealing the slots/cell opening at both ends of the monolith, it is coated with membrane.

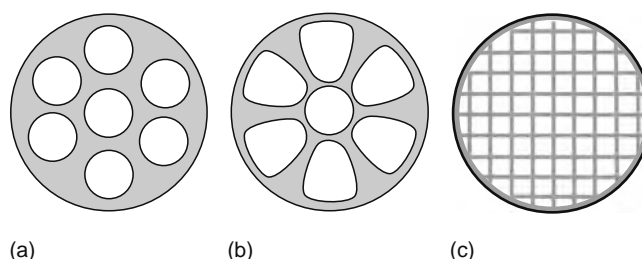


**FIGURE 6.2** Evolution of the geometry of ceramic membrane elements. (a) Conventional cylindrical-shaped channels; (b) flower-like designed channels; and (c) honeycomb-type structure.



**FIGURE 6.3** Ceramic membrane elements with a flower-like geometry, from TAMI industries.

Hollow fiber (outer diameter  $<0.5$  mm) and capillary (outer diameter  $>0.5$  mm) ceramic membranes constitute the very last development in the field of inorganic membranes. As for polymer hollow fiber membranes, a large surface/volume ratio is expected for the modules as well as the possibility of keeping uppermost properties of ceramics, i.e., high mechanical, chemical, and temperature resistance. Interestingly, ceramic hollow fibers or capillaries with an asymmetric structure (Figure 6.6a) have been obtained in single-stage process and used as support for coating of microporous membrane top-layers [10]. CEPARation, newcomer on the ceramic membrane market, has developed compact and low-cost ceramic filters based on hollow fiber and capillary ceramic membranes. The modules ranging from  $0.05$  to  $1$  m<sup>2</sup> are claimed to be suitable for micro-, ultra-, and nanofiltration. Certain modules can be specially designed for gas separation and high-temperature applications up to  $700^{\circ}\text{C}$ . Polymeric resin or ceramic potted inserts of such ceramic hollow fibers or capillaries, suitable for plastic or stainless steel housing, are shown in Figure 6.6b and 6.6c.

### 6.2.1.2 Porous Membrane Structure

Homogeneous ceramic porous structures with pore diameter larger than  $1$   $\mu\text{m}$  can be used directly for microfiltration, however, most of ceramic membrane elements are constructed from supported multiple ceramic layers constituting an asymmetric porous structure. Scanning electronic microscopy (SEM) images are shown in Figure 6.7 of asymmetric or homogeneous porous structures encountered in glass, carbon, or ceramic membrane materials. The most common ceramic materials used for ceramic membranes and support fabrication have been alumina, titania, and zirconia. Cordierite, silicon carbide, and silicon nitride have been used more recently, in particular for membrane monoliths. Glass as a homogeneous porous material may also be included in the category of available inorganic membrane materials. To a less extent, metallic or carbon macroporous materials may be mentioned as other types of support elements used for ceramic membrane deposition.

The porous structure of ceramic supports and membranes can be first described using the IUPAC classification on porous materials. Thus, macroporous ceramic membranes (pore diameter  $>50$  nm) deposited on ceramic, carbon, or metallic porous supports are used for cross-flow microfiltration. These membranes are obtained by two successive ceramic processing techniques: extrusion of ceramic pastes to produce cylindrical-shaped macroporous supports and slip-casting of ceramic powder slurries to obtain the supported microfiltration layer [2]. For ultrafiltration membranes, an additional mesoporous ceramic layer ( $2$  nm  $<$  pore diameter  $<50$  nm) is deposited, most often by the solgel process [11]. Ceramic nanofilters are produced in the same way by depositing a very thin microporous membrane (pore diameter  $<2$  nm) on the ultrafiltration layer [4]. Two categories of micropores are distinguished: the supermicropores  $>0.7$  nm and the ultramicropores  $<0.7$  nm.

**TABLE 6.1**  
**Characteristics of Inorganic Membrane Products Currently Available on the Market**

Manufacturer	Trade Name	Membrane Material	Pore Size	Shape
Asahi Glass		Glass	0.1–1.4 $\mu\text{m}$	Tube
Atech		SiC/SiC	0.05–1.0 $\mu\text{m}$	Tube
		$\text{Al}_2\text{O}_3$		Multichannel
Bekaert		SS fiber media	Macroporous	Tube
CEPARation		$\text{Al}_2\text{O}_3$	0.3–40 nm	Hollow fiber
CeraMem		Cordierite/SiC		Monolith
CERASIV		$\text{Al}_2\text{O}_3$ , $\text{TiO}_2$ , $\text{ZrO}_2$	5 nm to 1.4 $\mu\text{m}$	Tube
				Multichannel
ECO Ceramics	Sephi-Matic	$\text{Al}_2\text{O}_3$	6 nm to 0.2 $\mu\text{m}$	Tube, disc
Fairey		$\text{Al}_2\text{O}_3$	0.2–0.35 $\mu\text{m}$	Multichannel
Fuji Filters		Glass	4–90 nm	Tube
LiqTech	CrystaMem	SiC	0.5–0.5 $\mu\text{m}$	Monolith
MAST Carbon	Novacarb	Carbon	4–20 $\mu\text{m}$	Tube
			Microporous	Multichannel
				Monolith
Mitsui		Zeolite	Ultramicropous	Tube
				Multichannel
NGK		$\text{Al}_2\text{O}_3$	Macroporous	Monolith
NOK		$\text{Al}_2\text{O}_3$	0.2–6 $\mu\text{m}$	Tube
Pall Exekia	MEMBRALOX	$\text{Al}_2\text{O}_3/\text{ZrO}_2$	20–100 nm	Multichannel
		$\text{Al}_2\text{O}_3/\text{Al}_2\text{O}_3$	0.1–5 $\mu\text{m}$	
Pall	PMF	SS fiber media	Macroporous	Pleatable media
	AccuSep	$\text{TiO}_2$ , $\text{ZrO}_2$ , Ag	1–300 kDa	Disk
Novasep Orelis	CARBOSEP	Carbon/ $\text{ZrO}_2$	1.5 kDa to 0.14 $\mu\text{m}$	Tube
	KERASEP	$\text{Al}_2\text{O}_3/\text{TiO}_2/\text{ZrO}_2$	0.5 kDa to 0.8 $\mu\text{m}$	Multichannel
Sterlitech		ATZ	0.14–14 $\mu\text{m}$	Disk
		$\text{TiO}_2$ , $\text{ZrO}_2$ , Ag	1–300 kDa	
			0.2–5 $\mu\text{m}$	
Sulzer		$\text{SiO}_2$	Micropous	Tube
		Zeolite	Ultramicropous	Multichannel
Sumitomo	Poreceram	$\text{Si}_3\text{N}_4$	50–200 nm	Monolith
Synkera Tech		$\text{Al}_2\text{O}_3$ (anodic)	18–80 nm	Disk
TAMI	FILTANIUM	$\text{TiO}_2$	0.14–1.4 $\mu\text{m}$	Tube
			1–300 kDa	Multichannel
Whatman	ANOPORE	$\text{Al}_2\text{O}_3$	20 nm to 0.2 $\mu\text{m}$	Disk

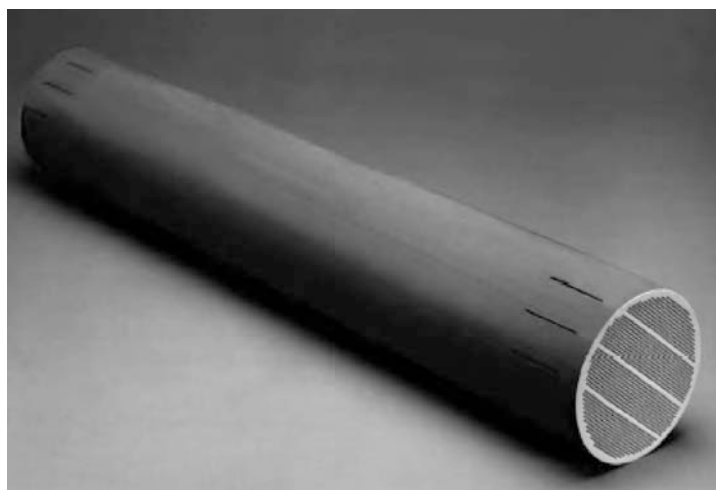


**FIGURE 6.4** Image of a monolith membrane element, 150 mm in diameter and 1.5 m long, produced by CeraMem.

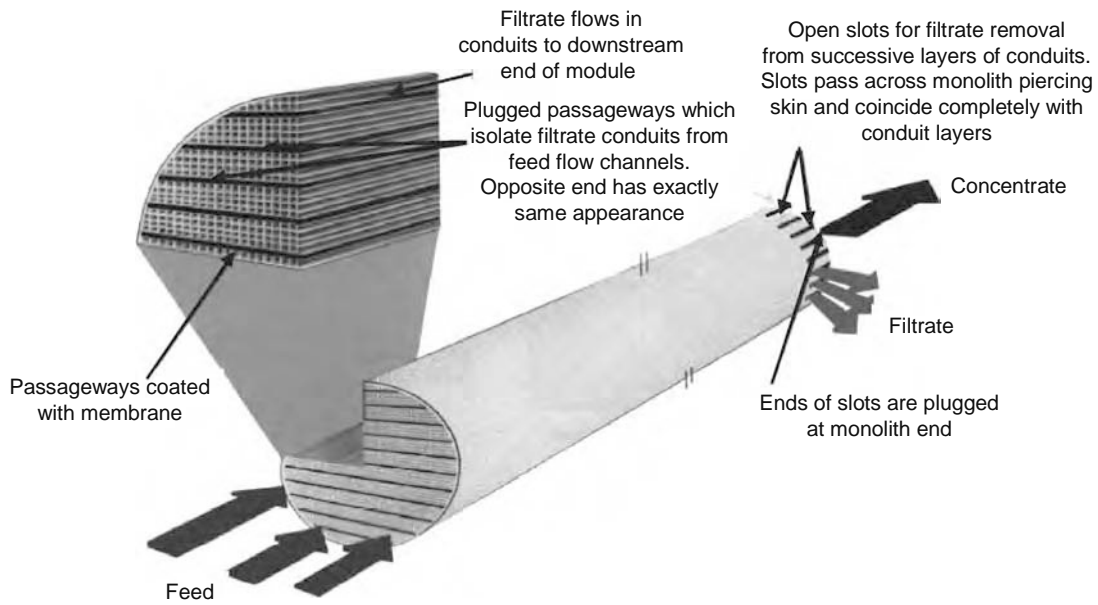


**FIGURE 6.5** Details of the structure of a monolithic ceramic membrane element with filtrate conduits, from CeraMem.

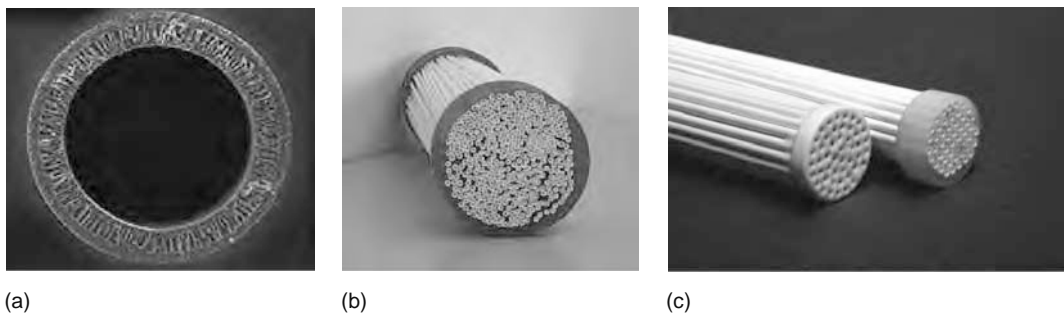


**FIGURE 6.6** Asymmetric structure of a ceramic hollow fiber (a) from the Fraunhofer IGB (Stuttgart). Ceramic hollow fiber (b) and capillary (c) membrane inserts from CEPAration.

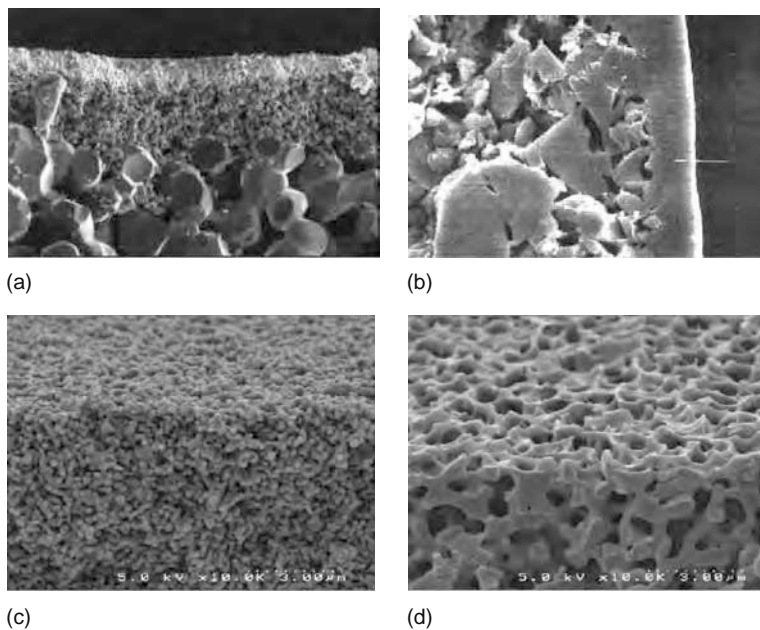


**FIGURE 6.7** Scanning electronic microscopy images of inorganic membrane porous structures: (a) asymmetric alumina structure; (b) asymmetric carbon structure; (c) homogeneous alumina structure; and (d) homogeneous glass structure.

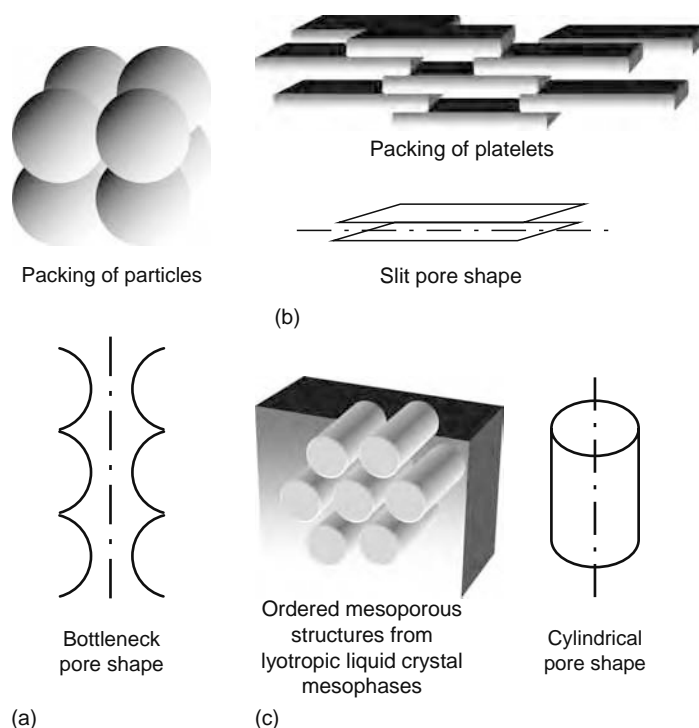


**FIGURE 6.8** Geometry of pores resulting from different particle shapes and processing methods. (a) Bottleneck pore shape; (b) slit pore shape; and (c) ordered porosity.

Ultrafiltration with ceramic membranes is based on mesoporous top-layers. Mesoporosity usually results from residual spaces created between ceramic particles during sintering. Pore sizes are determined by particle size and sintering procedure, while pore geometry depends on particle shape or template effect. A bottleneck geometry (Figure 6.8a) is representative of pores resulting from sintering of almost spherical particles, for example, this is the case of porous structures obtained with titania, zirconia, or  $\alpha$ -alumina particles. When membrane top-layers are produced from platelets suspensions, like clays or  $\gamma$ -alumina particles, slit pore shapes are obtained (Figure 6.8b). More recently, defined pore geometry and regular porous structures have been formed by templates in solgel templated processing methods [12,13]. For example, a cylindrical pore shape may be obtained with lyotropic liquid crystal phases or block copolymer templates (Figure 6.8c).

Presently, plenty of works on microporous inorganic membrane materials are intended to the development of nanofiltration, gas and vapor separation membranes [7]. Two categories of pores are distinguished in microporous inorganic membranes, those resulting from the arrangement and sintering of ceramic oxide nanoparticles and those created during the formation of the intrinsic structure of materials. The ceramic oxide nanoparticles are typically obtained by the solgel process from colloidal suspensions in which particle sizes do not exceed 10 nm [4] or by CVD infiltration techniques [14,15] (Figure 6.9a). One specific feature of these nanograined microporous structures is the presence of a large proportion of surface atoms, 30%–60% for individual grains smaller than 10 nm. Such elevated proportion of surface atoms in the microporous structure of ceramic nanofilters will have a strong influence on mass transport. The second category of micropores is an integral part of the structure of membrane materials such as in zeolite [16] (Figure 6.9b), or carbon materials [17]. For zeolite membranes, top layers are prepared by growth and interpenetration of zeolite crystals under hydrothermal conditions. These layers are supported on/in macroporous ceramic or metal elements. In carbon membranes, the microporous top-layer is generally obtained from graphitization at high temperature of an organic resin. These different microporous structures can be divided in two categories of pore: the supermicropores from 2 to 0.7 nm and the ultramicropores for pores <0.7 nm. Due to the very small size of the pores, surface interaction forces in liquid media or surface adsorption phenomena in gas and vapor media will have a strong effect on mass transfer with these membranes.

### 6.2.1.3 Dense Membrane Structure

Mixed ion and electron conducting (MIEC) or purely ion-conducting ceramics are emerging as an important class of dense inorganic membranes with many potential applications, particularly in the petrochemical and energy sectors [18]. Actually, these membranes are investigated as a potentially economical, clean, and efficient means of producing oxygen by separation from air, and in the future may be for producing pure hydrogen and syngas from industrial processed gases. Membrane design for MIEC ceramic membranes has followed a parallel way to the development of solid oxide fuel cells exhibiting a flat or

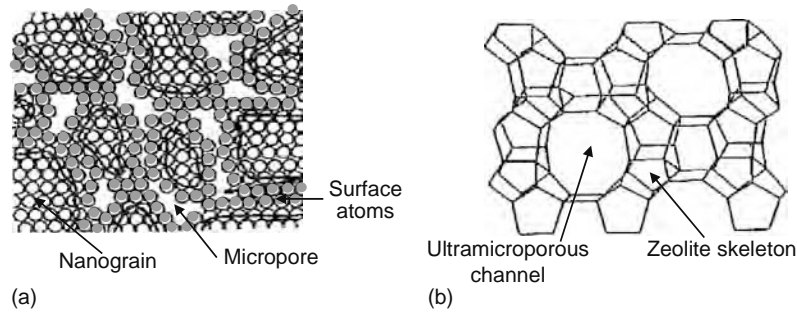


**FIGURE 6.9** Microporous membrane structures: (a) resulting from packing and sintering of ceramic nanoparticles and (b) ultramicroporous channels in the crystalline structure of a zeolite.

tubular geometry. Up to now these membranes have been studied mainly on the laboratory scale, however, recent achievements in pilot plants development have been mentioned in relation to hydrogen and syngas production. Air Products & Chemicals and partners have produced planar membranes while Praxair showed tubular membranes up to 2 m in length [19]. Tubular membranes have potential advantage of simpler membrane design based on ceramic membranes currently produced for liquid filtration. This could allow faster ceramic fabrication scale-up and development. However, the special microchannel geometry designed by Air Products & Chemicals for planar membranes brings the advantages of superior heat and mass transfer, and higher membrane surface area to system volume ratio leading to more compact system design.

The different membrane concepts currently investigated for selective oxygen transport are shown in Figure 6.10. In the conventional membrane concept, the membrane element consists of a self-supported thick (tubular) material or can be supported as a thin top-layer on a porous support (Figure 6.10a). In advanced designs, the structure of the membrane is made of a dense core material with two porous interfaces made of the same material (mixed ionic–electronic conducting ceramic) in contact with gas phases (Figure 6.10b). The porous interface exhibits a graded porosity and its role is to increase, on one side, the conversion of oxygen molecules from air to ionic species, which are selectively transported in the membrane and converted to oxygen molecules or oxidative species on the other side. A second case is when the two porous interfaces, acting as mixed ionic–electronic conducting electrodes, are made of materials different from the membrane (purely ion-conducting electrolyte), as shown in Figure 6.10c for the oxygen pump application.

### 6.2.2 MASS TRANSFER AND SEPARATION PROPERTIES

This brief overview of mass transfer and separation mechanisms involved in ceramic membrane processes will be useful not only for a better understanding of actual operating conditions of ceramic membranes, but also for anticipating future applications. For example, a same microporous membrane can serve theoretically as liquid or gas separation membrane. However, transport mechanisms and operating conditions being totally different, a good membrane permeability and selectivity in the former case cannot be systematically transposed to the second case.

In liquid filtration using micro-, ultra-, and nanofiltration porous membranes, the driving force for transport is a pressure gradient. Solvent permeability and separation selectivity are the two main factors characterizing membrane performance. Convective flux is predominant with macroporous and mesoporous membrane structures, the selectivity being controlled by a

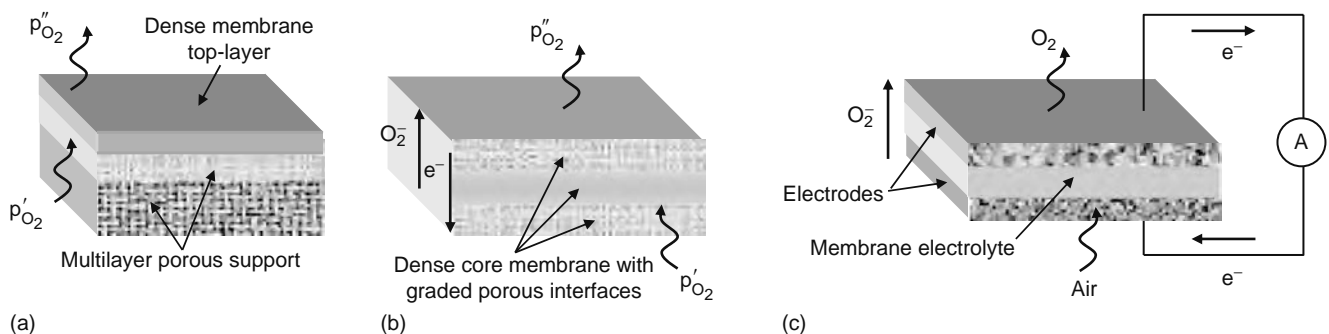


**FIGURE 6.10** Different membrane concepts for oxygen-ion conducting membranes. (a) Dense mixed conducting membrane top-layer supported on an asymmetric macroporous support; (b) dense self-supported mixed conducting membrane with graded porous interfaces; and (c) solid electrolyte cell (oxygen pump).

sieving effect. In the case of microporous membranes, additional contributions to solute transport and separation must be introduced accounting for diffusive flux and charges exclusion when the solutes and the membrane are carrying electrical charges. Basically, the intrinsic membrane characteristics (pore size, porous volume, thickness, etc.) and operating conditions (transmembrane pressure, cross-flow velocity, concentration polarization, etc.) are the as many parameters influencing permeability and selectivity. Moreover, when real fluids are processed, fouling phenomena due to the accumulation of filtered matter on/in the membrane results in an additional resistance to permeate flux and even in a modification of selectivity. Fouling is a reversible effect as far as effective cleaning procedures can be applied to recover initial permeate flux (see Section 6.2.3.3).

In gas and vapor separation with microporous ceramic membranes, the driving force is still the pressure gradient across the membrane, but this parameter is not a determinant for mass transfer as in liquid filtration. Depending on pore size, viscous flow, Knudsen flow, or configurational diffusion are the main mechanisms involved in gas transport. For condensable gases and vapors, adsorption phenomena, surface diffusion, and capillary condensation are other factors influencing molecular separation. In other respects, gas separation with dense ceramic membranes is a totally different mechanism based on ionic transport through a dense ceramic structure. The chemical potential or the electrical field gradient across the dense membrane material determines the selective transport of ionic species. The chemical and crystalline structure stability as well as the mechanical resistance under operating conditions are the major parameters quantifying the performance of dense inorganic membranes.

### 6.2.2.1 Liquid Filtration

Microfiltration and ultrafiltration are the two main filtration techniques for which ceramic membranes have been widely used to date. As described in Section 6.2.1.2, MF and UF ceramic membranes exhibit macro- and mesoporous structure, respectively, which result from packing and sintering of ceramic particles. Liquid flow in such porous media is convective in nature and the simplest description of permeation flux,  $J$ , is given by the Darcy's equation [20]:

$$J = -L_p \, dP/dx \quad (6.1)$$

where

$L_p$  ( $\text{m}^3/\text{m}^2 \text{ Pa s}$ ) is the permeability coefficient

$dP/dx$  is the driving force expressed as the pressure gradient across the membrane

In fact  $L_p$  contains information about the porous structure (porosity, pore size, and tortuosity) of the membrane as well as the viscosity of the filtrated liquid varying nonlinearly with the temperature. For the sake of comparison between membranes exhibiting different thicknesses, the membrane thickness  $\Delta x$  can be introduced in the permeability coefficient whose dimension becomes ( $\text{m}^3 \text{ m}/\text{m}^2 \text{ Pa s}$ ).

In the case where pore can be considered as cylinders with the same radius, the volume flux through the pore may be described by the following Hagen–Poiseuille equation, for example, when the porous structure is obtained by a templating method, as shown in Figure 6.8c:

$$J = \frac{\varepsilon^* r^2}{8\eta\tau} \frac{\Delta P}{\Delta x} \quad (6.2)$$

where

$\varepsilon^*$  is the surface porosity

$r$  is the pore radius

$\eta$  is the viscosity of the filtrated liquid

$\tau$  is the pore tortuosity

$\Delta P$  is the pressure gradient across the membrane

$\Delta x$  is the membrane thickness

The surface porosity is equal to the ratio of the pore area to membrane area multiplied by the number of pores. In most cases volume flux through ceramic membranes can be best described by the Kozeny–Carman relationship, which corresponds to a system of close packed spheres (see Figure 6.8a):

$$J = \frac{\varepsilon^3}{K\eta S^2(1-\varepsilon)^2} \frac{\Delta P}{\Delta x} \quad (6.3)$$

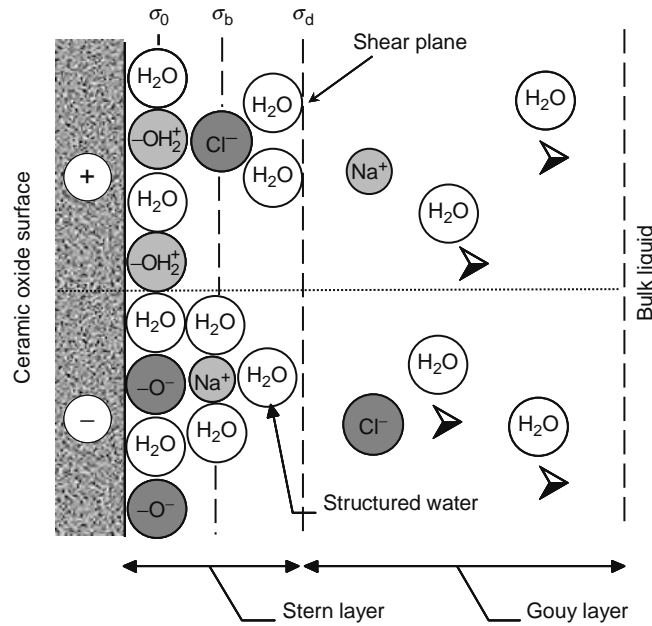


**FIGURE 6.11** Schematic representation of positively or negatively charged double layer forming in aqueous media on ceramic oxide surface in presence of electrolytes.

where

$\varepsilon$  is the volume fraction of the pores

$S$  is the internal surface area

$K$  is the Kozeny–Carman constant, which depends on the shape of the pores and the tortuosity

Equations 6.1 through 6.3 are no more applicable for low UF and NF ceramic membranes, typically when pore sizes are close or in the nanometer range. In this case, surface energy and electrostatic interactions influence mass transfer and retention in a non-negligible manner. In aqueous media, ceramic oxide surface exhibits an amphoteric behavior leading to a negatively or positively charged surface double layer (Figure 6.11) depending on the pH of the feed liquid and the isoelectric point of the ceramic in contact with this liquid. Accordingly, an electrical potential, also called zeta potential, establishes between the charged double layer and the solution, whose barrier intensity depends on the ionic strength of the solution. When pore radius is in the same order of magnitude than the zeta potential barrier, transport of ionic species is affected by the fixed charge of the membrane. Ions with the same charge as the fixed ions in the membrane are excluded and cannot pass through the membrane. This effect is known as the Donnan exclusion and can be described by equilibrium thermodynamics from which the chemical potential of the ionic species can be calculated in the membrane and in the solution, and then the concentration of the different species. If the concentration in the feed is low and the concentration of the fixed charge is high, the Donnan exclusion is very effective.

When a driving force (transmembrane pressure) is applied to these low UF and NF membranes, a basic irreversible thermodynamics approach is most often used to describe the solvent flux, which can be calculated by using Equation 6.4:

$$J_V = \frac{L_p}{\Delta x} (\Delta P - \sigma \Delta \Pi) \quad (6.4)$$

In this equation compared to Equation 6.1, the osmotic pressure,  $\Delta \Pi$ , of the feed solution and a reflection coefficient,  $\sigma$ , have been introduced to account for the counter flux due to the difference in concentration of small solutes (molecule or ion) between the feed phase and the permeate phase.

Concerning the transport of solute, a first equation can be written for neutral species that accounts for the diffusion and the convective transport of species through the membrane:

$$J_S = \omega(C_m - C_p) + (1 - \sigma)J_V \bar{C} \quad (6.5)$$

where

$\omega$  is the permeability coefficient

$(C_m - C_p)$  is the concentration gradient across the membrane

$\bar{C}$  is the mean concentration in the membrane for the solute

For electrically charged membranes and when ionic solutes are present in the feed liquid, transport for each species should be appropriately described by the general Nernst–Planck equation:

$$j_i = -D_{i,p} \frac{dc_i}{dx} - \frac{z_i c_i D_{i,p}}{RT} F \frac{d\psi}{dx} + K_{i,c} c_i j_v \quad (6.6)$$

where

$D_{i,p}$  is the diffusion coefficient of species  $i$  in membrane pores

$c_i$  is the concentration of this species in the membrane and  $z_i$  its charge number

$F$  is the Faraday constant

$\psi$  is the electrical field

$K_{i,c}$  is the friction coefficient due to convective transport of species by the volume flux  $j_v$

Actually, as schematized in Figure 6.12, species will be retained by the membrane according to their size (sieving effect) or to their electrical charge (Donnan exclusion). Accordingly, ionized small molecules can be retained even if they are smaller than pore size. For a mixture of multivalent and monovalent co-ions in the feed, multivalent co-ions are retained due to their higher electrical charge, while a part of monovalent co-ions pass through the membrane with counterions to fulfill charge equilibrium criterion on both sides of the membrane. This may lead to a negative retention of monovalent co-ions.

Retention of ionic species modifies ionic concentrations in the feed and permeate liquids in such a way that osmotic pressure or electroosmotic phenomena cannot be neglected in mass transfer mechanisms. The reflexion coefficient,  $\sigma$ , in Equations 6.4 and 6.5 represents, respectively, the part of osmotic pressure force in the solvent flux and the diffusive part in solute transport through the membrane. One can see that when  $\sigma$  is close or equal to zero the convective flux in the pores is dominant and mostly participates to solute transport in the membrane. On the contrary when  $\sigma$  is close or equal to 1, mainly diffusion phenomena are involved in species transport through the membrane, which means that the transmembrane pressure is exerted across an almost dense structure. Low UF and NF ceramic membranes stand in the former case due to their relatively high porous volume and pore sizes in the nanometer range. Recently, relevant results have been published concerning the use of a computer simulation program able to predict solute retention and flux for ceramic and polymer nanofiltration membranes [21].

Furthermore, as ceramic membranes offer specific advantages for organic solvents filtration, it is worthwhile considering the involved liquid/solid interaction phenomena when organic solvents are flowing through porous ceramic oxide structures made of small mesopores or micropores. The porous structure of ceramic oxide membranes can be considered as a high-energetic surface medium and the interaction force per interfacial area may be quantified using different surface energy concepts as the disjoining pressure or the density variation resulting from molecular ordering of solvent molecules at the

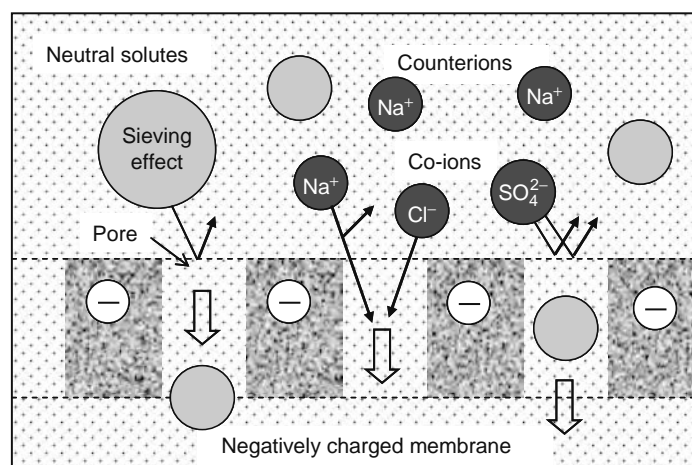


FIGURE 6.12 Schematic representation of retention mechanisms involved in aqueous medium for low UF and NF ceramic membranes.

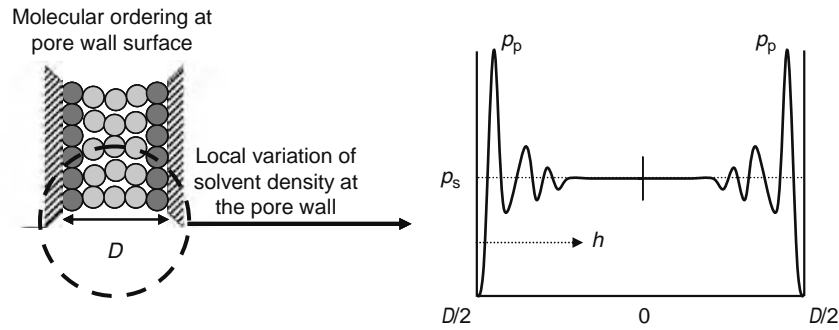


FIGURE 6.13 Local variation of solvent density near pore walls due to solvation and structural forces.

solid interface [22]. Accordingly, it is useful to compare solvation forces for aqueous systems and for nonaqueous systems. In the former case, repulsive hydration forces arise from strongly H-bonding surface groups ( $-\text{OH}$  for ceramic oxides) and they are affected by the presence of electrolytes. In the case of nonaqueous liquids in contact with high-energetic surfaces, the magnitude of attractive (adhesive) or repulsive forces are affected by molecular ordering which in turn depends on the shape and nature (polar or nonpolar) of molecules. With nonpolar, roughly spherical and rigid molecules like  $\text{CCl}_4$ , benzene, toluene, or cyclohexane, beyond the adhesive force at the solid interface there is the possibility of a long-range molecular ordering with a characteristic length of several molecular dimensions. On the contrary, nonpolar, small flexible molecules such as alkanes may be considered as being internally liquid-like and they have no need to reorder resulting in short-range structure not exceeding two or three molecular packing dimensions. For polar solvents like alcohols the repulsive solvation forces are predominant at short distances near the solid interface, while the DLVO theory applies at large distances. Considering now the change in liquid density profile near the solid interface due to solvation or structural forces (Figure 6.13), it is likely that solvent flux may be affected when pore sizes are in the same order of magnitude that the characteristic length for molecular ordering at pore wall surface.

Basically, for nonpolar liquids on more polar substrates, as it is the case for most of organic solvents in contact with a ceramic oxide surface, substrate-wetting films are stable. From consideration of the surface energies involved in the wetting processes of solid substrates, it can be readily shown that they can be related to the liquid–vapor surface tension ( $\gamma_{\text{lv}}$ ) and contact angle ( $\theta$ ). Thus, a liquid will stick to a solid if  $\theta < \pi$  corresponding to a work of adhesion,  $W_a = \gamma_{\text{lv}} (\cos \theta + 1)$ , and then for total wetting,  $\theta = 0$  and  $W_a = 2\gamma_{\text{lv}}$ . In general, the enhanced attractive interaction between a liquid and a solid substrate improves wetting. In the case of a porous substrate, a useful parameter accounting for liquid penetration in the pores is the capillary pressure that must be passed for observing liquid flowing through a membrane:

$$P_c = 2\gamma_{\text{lv}} \cos \theta / r_p \quad (6.7)$$

In summary, for ceramic membranes exhibiting low pore dimensions, penetration of liquids including organic solvents in the membrane pores is governed first by the capillary pressure. This may be the reason why zero flux may be observed at too low transmembrane pressure with ceramic nanofilters. Moreover, when the characteristic length for molecular ordering at the pore wall is on the same order as the pore size, the disjoining pressure of wetting films cannot be neglected. It results in repulsive forces with aqueous or polar solvents having a positive contribution to the driving force, while attractive (adhesive) forces encountered with nonpolar solvents will have a negative contribution with an additional resistance to permeate flux. Presently, the few results available in the literature confirm that organic solvent filtration with ceramic nanofilters does not obey the Hagen–Poiseuille or Kozeny–Carman equations [23]. Actually, finding a reliable relationship, able to describe organic solvent permeation through low UF and NF ceramic membranes, would require further experimental results.

For all the aforementioned liquid filtration technologies, membrane selectivity is most often expressed as the membrane retention,  $R$ , toward the species to be separated.

$$R = \frac{C_f - C_p}{C_f} = 1 - \frac{C_p}{C_f} \quad (6.8)$$

where

$C_f$  is the concentration of the species in the feed

$C_p$  is the species concentration in the permeate

$R$  is the dimensionless parameter that varies from 100% for an ideal semipermeable membrane to 0% when the species and the solvent pass freely through the membrane

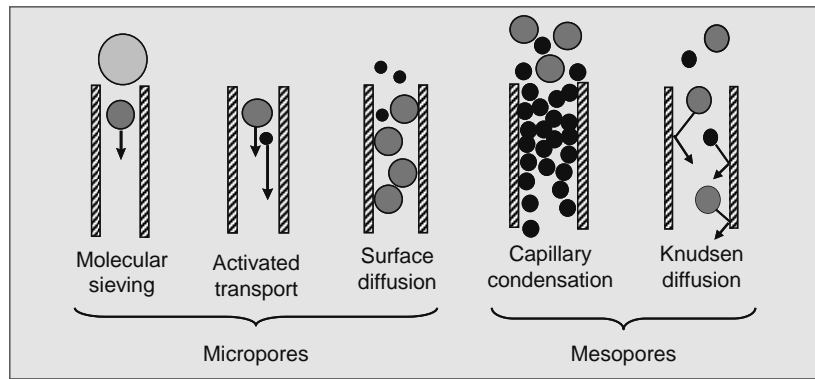


FIGURE 6.14 Different mechanisms involved in gas and vapor transport through meso- and microporous ceramic membranes.

### 6.2.2.2 Gas and Vapor Transport across Porous Membranes

Basic mechanisms involved in gas and vapor separation using ceramic membranes are schematized in Figure 6.14. In general, single gas permeation mechanisms in a porous ceramic membrane of thickness  $\ell$  depend on the ratio of the number of molecule–molecule collisions to that of the molecule–wall collisions. In membranes with large mesopores and macropores the separation selectivity is weak. The number of intermolecular collisions is strongly dominant and gas transport in the porosity is described as a viscous flow that can be quantified by a Hagen–Poiseuille type law:

$$j_v = \frac{\varepsilon}{8\eta\tau} \frac{r^2 P}{RT\ell} \Delta P \quad (6.9)$$

where

$R$  is the gas constant

$T$  is the temperature

$P$  the mean pressure in the membrane has been introduced to account for specific gas phase behavior in the porosity,  $\varepsilon$  (Equation 6.9 is similar to Equation 6.2 for liquids)

On the contrary, when the number of molecule to wall collisions is strongly dominant (mesopores), gas transport is described by the Knudsen flow. According to the Equation 6.10

$$j_K = \frac{2\varepsilon r}{3\tau\theta_k\ell} \sqrt{\frac{8}{\pi RTM}} \Delta P \quad (6.10)$$

where

$M$  is the molecular weight of the gas molecule

$\theta_k$  accounts for the wall roughness

In this case the permeation is proportional to the average pore radius  $r$  and inversely proportional to  $M^{0.5}$ , but is independent of the mean pressure  $P$  that is an important difference from viscous flow. The separation selectivity between two gases will be proportional to  $(M_2/M_1)^{0.5}$ . In the case of vapor transport in mesopores, another mechanism that may occur is the capillary condensation leading to selective filling of pores by a molecule and preferential transport of this molecule.

In comparison with the two previous cases, a much more complex description should be necessary for configurational diffusion of gases through microporous membranes. Here the driving force must be described in terms of a chemical potential gradient, which is coupled to partial pressure via adsorption isotherms. In fact, several mechanisms can operate simultaneously requiring simplifying assumptions. Surface diffusion at low temperature and activated transport at high temperature are the two main mechanisms exploited for gas and vapor separation with ultramicroporous membranes, such as zeolite membranes. At low occupancy of molecules in the pores (Henry regime) the gas flux through the membrane can be described by the general equation (Equation 6.11):

$$j_g = k \frac{D_0 K_0 q_{\text{sat}}}{\ell} \exp\left(-\frac{E_d - Q_a}{RT}\right) \Delta P \quad (6.11)$$

where

$k$  is the geometric correction factor

$D_0$  is the intrinsic diffusion coefficient of gas molecules

$K_0$  is the Langmuir constant

$q_{\text{sat}}$  is the amount of adsorbed gas

$E_d$  is the activation energy (Arrhenius relation for the diffusion coefficient  $D$ )

$Q_a$  is the heat of adsorption (van't Hoff relation for Langmuir constant  $K$ )

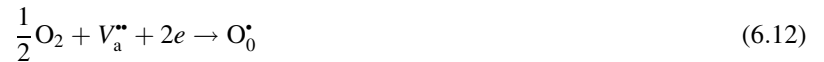
When kinetic diameters of molecules are almost similar to pore sizes, a molecular sieve effect is observed. In molecular sieve membranes, such as microporous carbons, the pore opening is sufficiently small relative to the size of the diffusing molecule, so that repulsive forces dominate and the molecules require activation energy to pass through the constrictions. In this region of activated diffusion, molecules with only slight differences in size can be effectively separated through molecular sieving.

In summary, one can see that separation selectivity for gas and vapor molecules depends on the category of pores (mesopores, supermicropores, and ultramicropores) and on the related transport mechanisms. Either size effect or preferential adsorption effect (irrespective of molecular dimension) is involved in selective separation of multicomponent mixtures. The membrane separation selectivity for two gases is usually expressed either as the ratio between the two pure gas permeation fluxes (ideal selectivity) or between each gas permeation flux measured from the mixture of the two gases (real selectivity). More detailed information on gas and vapor transport in porous ceramic membranes can be found in Ref. [24].

### 6.2.2.3 Ion-Conducting Membranes

Dense ceramic ion-conducting membranes (CICMs) are emerging as an important class of inorganic membranes based on fluorite- or perovskite-derived crystalline structures [18]. Most of the ion-conducting ceramics discovered to date exhibit a selective ionic oxygen transport at high temperatures  $>700^\circ\text{C}$ . Ionic transport in these membranes is based on the following successive mechanisms [25]:

1. Conversion of molecular oxygen in ionic species on the membrane feed side



2. Migration of vacancies,  $V_a^{\bullet\bullet}$ , in the dense material and transfer of electronic species,  $e$ , either in the dense material or in an external circuitry, depending on the conduction mode (mixed ionic–electronic or purely ionic).
3. Recombination of ionic oxygen species on the permeate side with production of molecular oxygen



The oxygen flux can be pressure or electrically driven as shown in Figure 6.10. For a mixed ionic–electronic conduction, both ions and electron are transferred in the ceramic under an oxygen pressure gradient. On the contrary, for a purely ionic conducting material, an external electrical circuitry is used for electron transport. These membranes are very selective and able to produce pure oxygen ( $>99\%$ ) from air. More recently proton–conducting ceramics at high temperature have been described in Ref. [26]. Although performances of these membranes need to be improved, a very high selectivity is expected in hydrogen separation. The flux of oxygen or hydrogen in these membranes is expressed in Equations 6.14 and 6.15:

$$J_{\text{O}_2} = -\frac{RT}{16F^2L} \int_{p_{\text{O}_2}^I}^{p_{\text{O}_2}^{II}} t_i t_{el} \sigma_t d \ln p_{\text{O}_2} \quad (6.14)$$

$$J_{\text{H}_2} = -\frac{RT}{4F^2L} \int_{p_{\text{H}_2}^I}^{p_{\text{H}_2}^{II}} t_i t_{el} \sigma_t d \ln p_{\text{H}_2} \quad (6.15)$$

where

$L$  is the membrane thickness

$p^I$  and  $p^{II}$  are the partial pressures of oxygen or hydrogen at the two sides of the membrane

$\sigma_t$  is the total conductivity

$t_i$  and  $t_{el}$  are the ionic and electronic transport numbers

### 6.2.3 COMMERCIALY AVAILABLE CERAMIC MEMBRANES AND IMPLEMENTATION IN DEVICES

The number of commercially available inorganic membranes has considerably increased over the past 20 years. Although ceramic membranes are presently the most widespread on an industrial scale, metallic, glass, or carbon membranes are also for sale from membrane suppliers. A non-exhaustive list of major inorganic membrane suppliers are given in Table 6.1. Beyond these inorganic membrane core industries whose activity is focused on membrane and module design, there are a lot of companies involved in membrane and filtration activities, offering among others inorganic membrane-based technologies.

#### 6.2.3.1 Membrane Modules

As previously mentioned, most of ceramic membrane elements are produced under cylindrical shapes, i.e., tube, multichannel, and monolith elements. Membrane modules are composed of one or more of these filtration elements, inserted in stainless steel housing (Figure 6.15). Plastic housings are also used, but stainless steel is often preferred to fully exploit specific properties of inorganic membranes, in particular, their ability to work in tough chemical and temperature conditions. Sealing of filtration elements in modules is a critical point so far as it must suit operating conditions of ceramic membranes, i.e., long durability in use under high temperature, aggressive chemicals, organic solvent environment, sterilization, and cleaning procedures. Membrane suppliers have their own technology for sealing the membrane elements in modules, which can be more or less sophisticated depending on the element geometry and the size of the modules.

Compared to modules based on cylindrical elements, flat ceramic membrane modules are not developed in a large extent and are limited to date to small liquid volume treatment [27]. Flat ceramic membranes are generally implemented as disks in laboratory scaled cells, offering a limited filtration surface area. Indeed a diameter of 90 mm that is one of the largest available dimensions for these membrane disks results in a filtration surface of  $\sim 56 \text{ cm}^2$ . Anopore alumina membranes supplied by Whatman or ATZ ceramic membrane disks with zirconia or titania top-layers from Sterlitech are typical examples of these commercially available flat ceramic membranes. Sterlitech ATZ ceramic membrane disks and the corresponding membrane holder are shown in Figure 6.16.

Interestingly, an innovative design has been described recently by the Fraunhofer IGB, Germany [27], allowing the production of flat membrane modules with an effective filtration area of  $1 \text{ m}^2$  (Figure 6.17a). This concept is based on novel flat ceramic supports specially processed to produce corrugated channels and able to receive micro- and ultrafiltration membranes (Figure 6.17b).

In a general way, most of ceramic membrane modules operate in a cross-flow filtration mode [28] as shown in Figure 6.18. However, as discussed hereafter, a dead-end filtration mode may be used in some specific applications. Membrane modules constitute basic units from which all sorts of filtration plants can be designed not only for current liquid applications but also for gas and vapor separation, membrane reactors, and contactors, which represent the future applications of ceramic membranes. In liquid filtration, hydrodynamics in each module can be described as one incoming flow on the feed side  $Q_f$ , which results in two

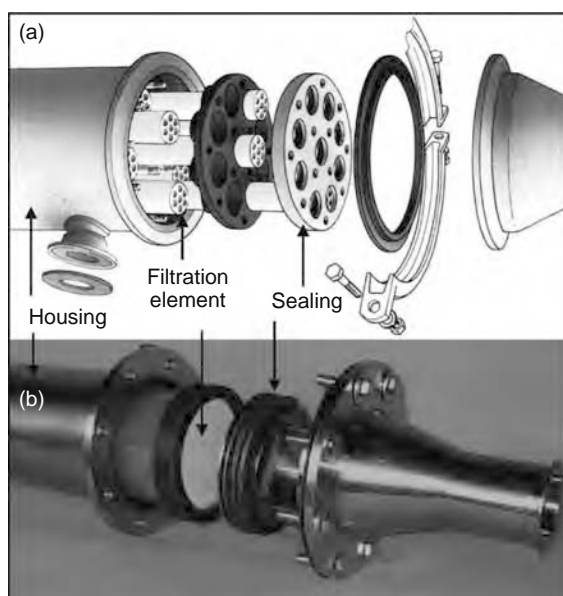


**FIGURE 6.15** Examples of ceramic membrane modules. (a) Multi-elements module from Orelis and (b) single-element module from CeraMem.



**FIGURE 6.16** Ceramic membrane disks and membrane holder from Sterlitech.

outgoing flows related to retentate  $Q_r$  and permeate  $Q_p$  sides, respectively. The permeation flux  $J$  per membrane surface unit is directly calculated from  $Q_p$ . Two important parameters account for hydrodynamic working conditions of a module, one is the flow velocity,  $\nu$ , in the module calculated as the ratio of the incoming flow  $Q_f$  ( $\text{m}^3/\text{s}$ ) by the hydraulic section of the module  $\Omega$  ( $\text{m}^2$ ), the other is the transmembrane pressure,  $P_{tm}$ :

$$P_{tm} = \frac{P_i + P_r}{2} - P_p \quad (6.16)$$

where

- $P_i$  is the incoming pressure of the liquid in the module
- $P_r$  the pressure of the outgoing liquid
- $P_p$  the pressure in the permeate compartment

### 6.2.3.2 Modules Arrangement

In industrial plants, ceramic membrane modules are arranged in different ways based on the general principles used for the design of membrane processes. The simplest module implementation is the dead-end operation mode. Here, the feed is forced through the membrane, which implies that the concentration of rejected components on the feed side of the membrane increases continuously and consequently the quality and the flux of permeate decrease with time. The main advantage of the dead-end

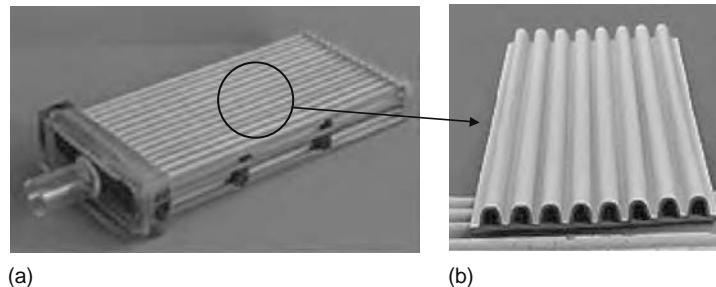


**FIGURE 6.17** Flat membrane module with an effective membrane area of  $1 \text{ m}^2$  (a), obtained by assembling channel corrugated porous ceramic supports (b), from (IGB, 26).

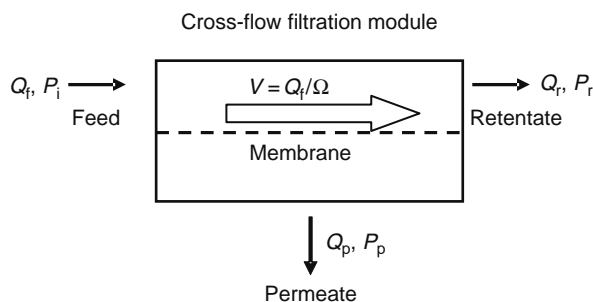


FIGURE 6.18 Schematic drawing of a module.

filtration mode is weak energy consumption. An example of a submerged module working in the dead-end filtration mode is shown in Figure 6.19. Usually, a cross-flow operation for the modules is preferable because of a lower fouling tendency relative to the dead-end mode and because it results in much higher permeate fluxes. In fact the choice between the two modes is related to the mass transfer coefficient that strongly depends on the bulk diffusion coefficient of the species retained by the membrane and the system hydrodynamics, in particular the cross-flow velocity. The logarithmic linear relationship (Equation 6.17) between measured permeate flux,  $J$ , in real conditions and Reynolds number,  $Re$ , may be helpful for choosing between the two operating conditions, dead-end or cross-flow filtration mode.

$$\ln J = a \ln Re, \quad \text{with} \left( Re = \frac{\rho \nu d_h}{\eta} \right) \quad (6.17)$$

The  $Re$  number accounts for both hydrodynamics and fluid characteristics, i.e., on the one hand cross-flow velocity,  $\nu$ , and hydraulic diameter,  $d_h$ , in the module; on the other hand dynamic viscosity,  $\eta$ , and mass density,  $\rho$ , of the fluid. Normally,  $Re > 2100$  guarantees a turbulent flow in the module and a minimum thickness for the concentration polarization layer. A small value of coefficient  $a$  means that  $\nu$  has a weak influence on  $J$ , so that a weak fluid velocity or even a dead-end filtration mode can be used. On the contrary, when the value of  $a$  is high ( $>0.5$ ), a cross-flow filtration mode with a high-fluid velocity is necessary.

Different module assembling and working conditions exist in the cross-flow filtration mode. For small- and medium-scale applications, the batch configuration is often followed with the possibility to perform diafiltration and concentration operations. As shown in Figure 6.20, retentate can be either concentrated in a recirculation loop or recycled continuously in the feed tank. An intermediate operating mode consists of recycling only a part of the retentate in the feed tank. Moreover, the possibility of adding water in the feed tank to compensate permeate flux results in a diafiltration process used for the elimination of unwanted species from the retentate. Another advantage of this configuration is that permeate or retentate can be easily recovered as the desired product. In short, batch filtration is a very versatile system able to adapt to many operating conditions and is widely used in many applications where the volume of liquid to be treated does not exceed a few tens of cubic meters per day.

Often a single-stage process does not result in the desired product quality and for this reason, permeate or retentate stream must be treated in a second stage. Then a combination of stages, called a cascade operation, with a more or less complex design can be imagined depending on whether the final permeate or retentate is the desired product. A simple multistage process consists of assembling a number of same modules in successive stages operating in a simple-pass mode (Figure 6.21). Hence

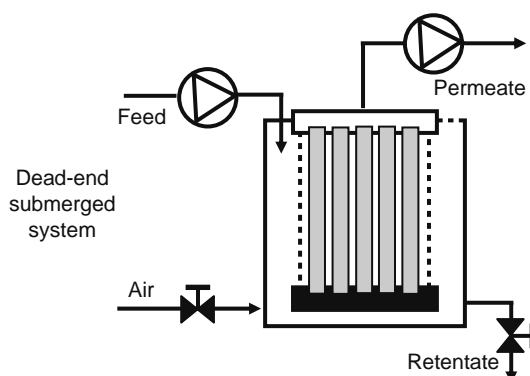


FIGURE 6.19 Schematic representation of a submerged module working in the dead-end filtration mode.

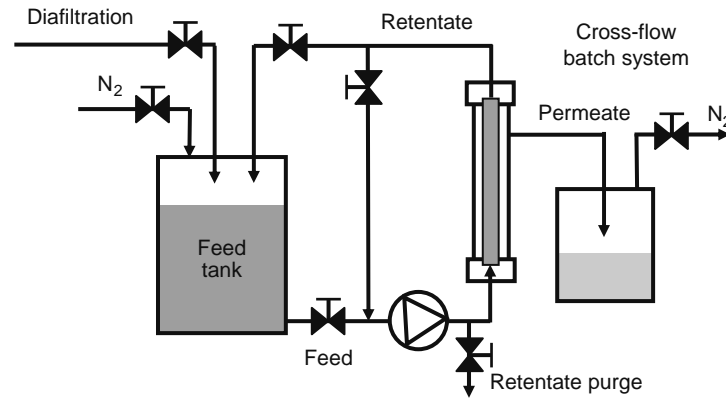


FIGURE 6.20 Schematic representation of a batch filtration system.

the volume of the feed decreases with the number of stages and logically the number of modules per stage is adapted to the loss of feed volume. In this arrangement the cross-flow velocity through the system remains virtually constant, but the pressure drop is important. This kind of system is usually implemented for the treatment of large quantities of liquid when permeate is the desired product.

A more complex and costly multistage system is when the feed flow is recycled several times on each stage. Two kinds of pumps are required in this case, one or more for plant feeding and a recirculation pump on each stage (Figure 6.22). Several advantages arise from this system compared to the simple-pass filtration mode. The flow velocity and pressure can be adjusted in every stage. Membranes with different characteristics can be implemented in two successive stages. The feed recycle system is more flexible than the single-pass system and is to be preferred in cases where severe fouling and concentration polarization occur as in microfiltration and ultrafiltration. With regard to the common applications of ceramic membranes (food and beverage industry, wastewater treatment, very turbid fluid pretreatment), the feed recirculation system is more often used than the simple-pass system.

### 6.2.3.3 Competitiveness of Ceramic Membranes

The design and implementation of a membrane process, whatever the nature of the membrane (polymer or ceramic), is a long procedure starting from membrane testing on a laboratory scale and ending in implementation of an industrial plant. It includes both technical and economical evaluation, which makes the membrane process viable or not compared to alternative separation processes. The overall costs are distributed in investment costs and running costs. As already mentioned ceramic membranes are more expensive than their polymeric counterpart and will result in higher investment costs, at least for the membrane system alone. However, the high investment cost can be balanced by a lower running cost when using ceramic membranes (i.e., less pretreatment, longer membrane lifetime, and more efficient cleaning and sanitizing conditions).

Indeed, in many cases the membrane system cannot be used directly and often pretreatment is necessary to facilitate the membrane process. Pretreatment is important and necessary in micro-, ultra-, and nanofiltration, while it is not that important for pervaporation (PV), vapor permeation (VP), or gas separation for which feed streams are usually much cleaner and do not contain many impurities. The cost of pretreatments can contribute appreciably to the overall costs. However, due to the intrinsic

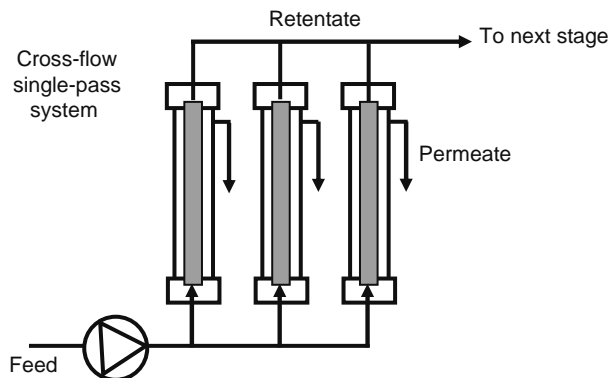


FIGURE 6.21 Schematic representation of a simple-pass modules stage.

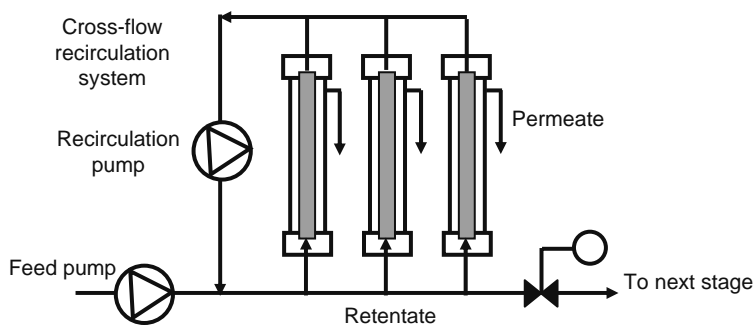


FIGURE 6.22 Schematic representation of a feed recirculation modules stage.

characteristics of modules and membrane material, ceramic membranes require less feed stream pretreatment and authorize very efficient cleaning and sanitizing procedures.

Two phenomena are responsible for flux decline during membrane operation with real fluids [20]. One is related to polarization phenomena (concentration and temperature polarization), which normally are reversible processes. Thus, at a finite time, when steady-state conditions have been attained, the flux stabilizes at a value always less than the original one. Membrane fouling is the second phenomenon responsible for flux decline. It consists of the deposition of retained particles, colloids, emulsions, suspensions, macromolecules, salts, etc. on/in the membrane. Fouling always results in a continuous (ir)reversible decrease of membrane flux with time and constitutes one of the major problem to be managed during filtration plant operation. This is a very complex phenomenon and the methods for reducing fouling must be adapted to the different used membranes and treated fluids. Several aspects such as pretreatment of feed solution, membrane and module characteristics, and operating parameters have to be anticipated during the process design, otherwise heavy cleaning procedures should be carried out on the membrane plant in operation.

The utmost advantage of ceramic membranes is to allow in-place chemical cleaning at high temperature, while using caustic, chlorine, hydrogen peroxide, ozone, and strong inorganic acids. Moreover steam sterilization can be used for sanitizing membrane plants. Another specific advantage of ceramic membranes is the possibility to be back-pulsed which is basically a permeate flow reversal technique to reduce fouling and to increase filtration efficiency. As shown in Figure 6.23, back-pulsing consists of periodically reversing the permeate flow by applying pressure to the permeate side of the modules. In this manner, the accumulated matter on the feed side of the membrane is periodically removed from the surface and carried away by the circulating fluid. Other physical methods recently investigated utilize gas bubbling [29] or ultrasound [30] to prevent fouling or for cleaning fouled membranes.

One can see that ceramic membranes differ from their polymeric counterparts by intrinsic properties (rigid porous structure, high-temperature resistance, high-chemical resistance to aggressive aqueous and organic media, insensitiveness to biological attack) which are based on the inorganic nature of the membrane material. In current applications mainly devoted to the treatment of liquids, general principles of membrane processes apply equally to ceramic and polymeric membranes. For both membrane categories, the modules are implemented in industrial plants, following the same hydrodynamic laws and mass transfer mechanisms. Most often, the choice of ceramic membranes is driven by economical considerations and despite its inherent qualities ceramic membranes are considered as expensive compared to polymeric ones. Nevertheless, a large number of applications are described in Section 6.3, showing that in many cases ceramic membranes have been considered as competitive compared to alternative processes.

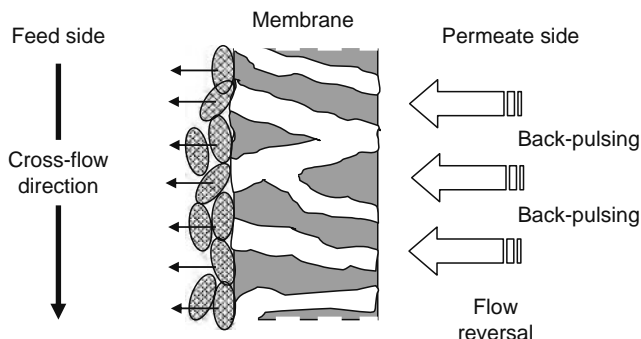


FIGURE 6.23 Schematic representation of permeate back-pulsing allowing in-place removal of accumulated matter on membrane surface.

## 6.3 CURRENT APPLICATIONS OF CERAMIC MEMBRANES

The number of applications of ceramic membranes has continuously been increased over the past 20 years. Even if data on the extent of installed plants are not directly available, the sales in inorganic membranes are estimated between €250 and €350 million in 2005 with a potential growth of 10%–15% a year. Many references on the use of ceramic membranes can be found in the proceedings of the successive International Conferences on Inorganic Membranes as well as in the books of Bhave [1], and Burggraaf & Cot [3]. The aim of this part is not to provide an exhaustive overview of all possible applications but to focus on relevant examples of current ceramic membrane processes. These applications have been classified into three main groups: (i) the treatment of waste liquids and gases; (ii) liquid processing including drinking water, domestic water, and food beverages; (iii) product recovery in various industries. Due to its robustness, ceramic membranes are developing faster in the treatment of liquid wastes than in other sectors. Actually, the demands of efficient liquid waste treatment are being pushed up both by regulatory and cost pressures to reduce environmental impact of human activity [31,32]. In a general way, there are many water shortage problems currently in the world so that the recycling of wastewater streams is an urgent necessity. In liquid processing, the sector of food beverages is the first one where ceramic membranes have been developed at the industrial scale, in particular in the dairy industry. Actually the demand for more secure membranes is increasing in the food industries as an alternative to polymer membranes that are less amenable to sanitary requirements. Finally ceramic membranes can be used in many industries, directly for the recovery of various products, not only from micrometer-sized species (mineral particles, microorganisms, macromolecules, etc.) down to nanometer-sized species (viruses, colloids, molecules, ions), but also as a filtration pretreatment before other separation techniques including polymer membranes.

### 6.3.1 TREATMENT OF WASTE LIQUIDS AND GASES

#### 6.3.1.1 Cross-Flow Filtration

The demand for industrial water in developed countries is increasing continuously in comparison with the limited natural resources. In recent years, recovery and reuse of industrial wastewater has arose as one of the important economical and ecological issues for a sustainable economy, the challenge in the modern technology being to allow industry to move toward the “zero discharge” concept. Membrane technology can afford viable solutions to the problem of water recycling in numerous industrial processes. Beyond the large availability and versatility of polymer membrane processes, the performance of ceramic membranes has considerably improved during the last 10 years. They are now able to provide long and reliable service life in many processes where polymer membranes cannot withstand operating conditions including the cleaning procedures, in terms of mechanical, chemical, and temperatures resistances. Moreover, the presence of abrasive particles, extreme pH conditions, organic solvents, and an elevated temperature in certain industrial wastewater effluents renders compulsory the use of inorganic membranes in the implementation of membrane processes.

A number of application areas have been identified in which cross-flow filtration with ceramic membranes revealed competitive compared to other separation processes [33]. Several cases can be mentioned: for example, removal of heavy metals from metal-finishing shop wastewater and treatment of spent chemical baths; heavy metal removal from acid mining drainage; recycling of laundry water by removing dirt, oil, and metals from wash water; treatment of wastewater chemical planarization of semiconducting; treatment and recycling of lubricating liquids used for cutting tools in mechanical industry; and in a general way all sorts of cleaning and rinsing waters from food and beverage processing industries. The following examples are representative of the current developments in the treatment of industrial waste liquid streams with ceramic membranes. Textile printing is a water-consuming industry where membranes and, in particular, ceramic membranes are well-adapted techniques for process intensification [34–36]. Ceramic membranes are also used for recycling process water in basic domestic activities like laundries [37] as well as in advanced industrial processes like polishing and washing stages of lens [38]. Ceramic membranes participate also to water and chemicals recovery in the automotive industry [39]. For example, a mean volume of 500 L of water per car body is used in pretreatment before electrophoretic painting. In this process, ceramic nanofilters have been chosen for water recycling due to the capacity of enduring working environment with long-service lifetime. New applications are also arising thank to the tight cut-off characteristics of ceramic nanofilters. Enormous volumes of bleach pulp effluent and black liquor are produced in kraft pulp mills. The bleaching process is highly water-consuming, while black liquor is regarded as a bottleneck by-product, which is usually burned in a recovery boiler after concentration by evaporation. Nano- and ultrafiltration techniques using ceramic membranes appear as efficient methods for water recycling in the bleach pulp process and lignin recovery from black liquor [40,41].

Another domain in which membrane separation technologies can afford viable solutions in the near future is the treatment of domestic wastewater [42]. Here, membranes are considered as too expensive and the technology is too sophisticated for sewage treatment. Nevertheless recent works by the European Space Agency [43] have shown that membrane technology including a ceramic membrane stage can cope with the life-support needs and isolation constraints during long-duration missions in space or in isolated scientific bases like in Antarctica. These space-related technologies including membranes used

for the treatment of wastewater should benefit to our daily lives by providing innovative and efficient solutions for domestic wastewater treatment.

### 6.3.1.2 Membrane Bioreactors

The membrane bioreactor (MBR) technology is a real alternative to pure filtration processes for the treatment of wastewater and industrial effluents. An MBR is the combination of an activated-sludge process with a membrane filtration. MBRs are composed of two primary parts: the biological unit responsible for the biodegradation of the waste compounds and the membrane module responsible for the physical separation of the treated water from mixed liquor. These systems are implemented based on two main configurations (Figure 6.24). The first (integrated) configuration consists of outer skin membranes that are internal to the bioreactor (Figure 6.24a). The driving force across the membrane is achieved by pressurizing the bioreactor or creating negative pressure on the permeate side. In the second (external) configuration, the mixed liquor is recirculated through a membrane module that is outside the bioreactor. In this case, the driving force is the pressure created by the high cross-flow velocity along the membrane surface (Figure 6.24b). Current available ceramic membranes having internal membrane top-layers are more adapted to the second MBR configuration.

There are a large number of potential applications of the MBR technology for the treatment of wastewater from agricultural and agri-industry sources [44]. Manure and wastewater from livestock can be treated by a technique coupling anaerobic digestion with an aerobic/anoxic membrane bioreactor, producing water for direct reuse or safe discharge. Wastewater generated from food processing industries such as slaughterhouses, meat, dairy, egg, and potato processing could potentially be treated with MRBs resulting in compact systems producing high-quality reusable water. Also effective removal of nitrates,

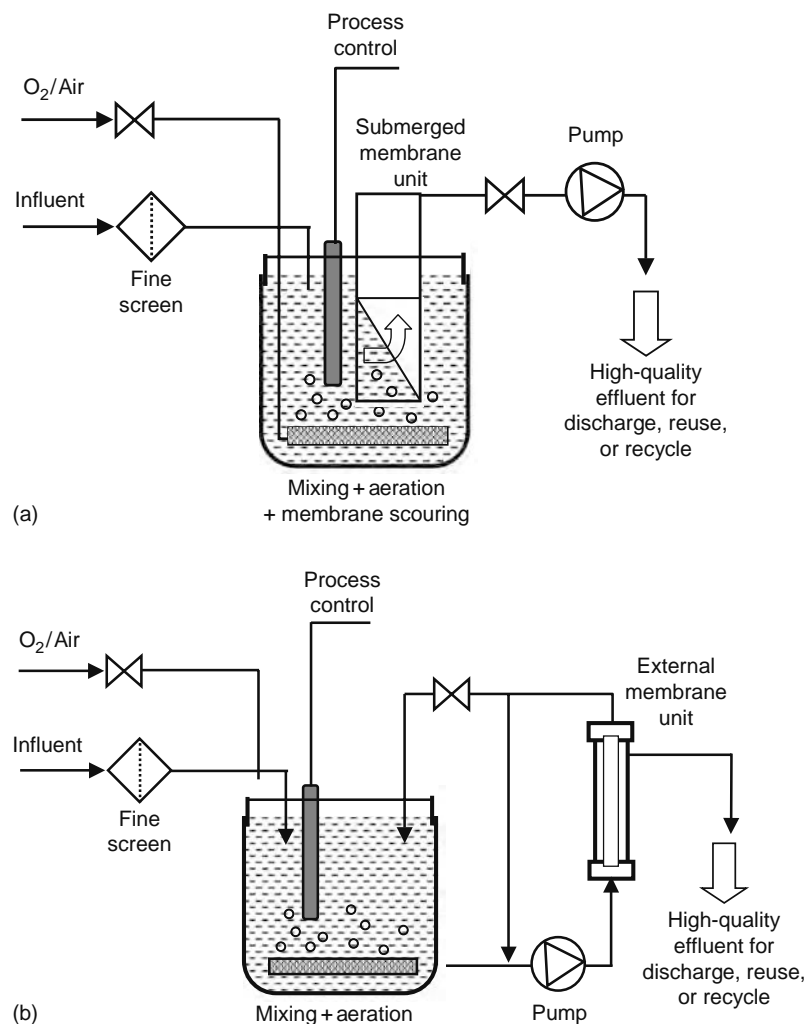


FIGURE 6.24 Membrane bioreactors configurations. (a) Internal outer-skin membranes and (b) outside membrane module.

herbicides, pesticides, and endocrine disrupting compounds may be achieved by MBRs. In drinking water treatment, either biological (bio-denitrification) or physicochemical (reverse osmosis, ion exchange, electrodialysis) techniques can be used for removal of nitrates. The advantage of coupling biodegradation and membrane separation in the MBR concept is to allow the removal of organic matter and the complete conversion of nitrates into nitrogen gas in a one-step relative easy operation. Another example of MBR utilization is the treatment of acid mine drainage. These drainages typically contain dissolved metals at high concentration and more than 3 g/L sulphate. The use of sulphate reducing bacteria (SRB) has been proposed as an alternative to hydroxide precipitation. Generally, MBRs can afford viable solutions to the treatment of industrial waste streams containing high organic loading, and very specific and difficult to treat compounds.

MBR are implemented with MF or UF membranes. Several types and configuration of membranes are used, including tubular, plate and frames, rotary disk, hollow fiber, organic, metallic and ceramic membranes [45]. However, ceramic membranes offer inherent advantages over polymeric membranes (possible high-sludge concentration, very efficient cleaning procedures, resistant to microorganisms) for this technology [46]. Although they have suffered from their high prices in the past, low-cost ceramic cross-flow membrane modules were successfully tested, able to promote a low-cost ceramic air lift MBR [47]. Large (200 mm hydraulic diameter by 1500 mm long), high surface area (15–28 m<sup>2</sup> depending on cell size) silicon carbide monolith membranes are envisioned in this application with projected membrane price in the range of €200/m<sup>2</sup>. The modules could be used in either a submerged MBR or an external airlift configuration. Sewage treatment [48] should be an attractive market for MBRs based on this new generation of ceramic membranes exhibiting low fouling behavior, high cleaning ability, and long durability.

### 6.3.1.3 Air Purification and Hot Gas Filtration

At the boarder line with ceramic membrane filtration, air purification and hot gas filtration using ceramic filters are technologies attracting significant attention in a wide variety of domestic applications and industrial processes [49–53]. The main difference with membrane technologies is that ceramic gas filters operate in a dead-end filtration mode and often as particle traps. Conversely, a major concern with ceramic membrane and filter technologies is the increasing demand for ceramic porous elements with a high efficiency in the retention of very small species (molecules with membranes or nanoparticles with filters). Ordinarily, ceramic filters for gas application exhibit low-density structure with high porous volume and pore size of several micrometer. Particulate structures, fabric, or fibrous media and more recently foams are commonly used as in-line filters to remove particulate contaminants from process gases. Today, new designs are considered for gas ceramic filters based on ceramic porous structures already developed for cross-filtration with ceramic membranes. The major evolution of these new filters compared to other available filters is the submicronic pore size adapted to the treatment of nanoparticulate aerosols, which will be a big issue in the development of nanoparticle production and its utilization in nanotechnologies. The difficulties involved in operating these new filters include the high pressure drop due the tight porous structure of the filter and the evaluation of filter efficiency by measuring low nanoparticle number concentrations downstream. For fabrication and utilization reasons, decreasing filter media thickness to lower pressure drop is not ever practical, hence an alternative approach is the application of new concepts based on hierarchical asymmetric filters [54]. The development of characterization setup and methodology to evaluate the filtration performance are also important aspects to deal with for the future utilization of these new filters [55].

## 6.3.2 LIQUID PROCESSING

### 6.3.2.1 Drinking and Domestic Water

Water purification for producing drinking and domestic waters is a quite complicated process, which must be adapted to the multiple water resources available as surface or ground water. Due to considerable pollution of natural waters, more and more stringent requirements are applied to natural water treatment. Contamination cases where traditional technological systems are ineffective are increasing continuously. High selectivity of membrane processes and no pollution charged to the environment make these methods very attractive as alternative or complementary processes. Membrane are effective for the removal of suspended particles, precipitates caused by water hardness or salts, organic compounds, and microorganisms (bacteria, spores, even viruses). The basic problem involving the application membrane processes in the treatment of natural water is the decrease of yield with time due to concentration polarization layer and reversible or irreversible fouling phenomena. Periodical renewal of the membranes and cleaning of the filtration plants considerably increase the price of produced water so that a number of methods have been proposed to prevent fouling or at least to make longer the time between two cleaning operations by removing continuously accumulated matter on membrane surface. For example, to maintain high permeate fluxes over long periods of time, adsorbents or coagulants can be used in conjunction with filtration [56]. In general, current commercial ceramic membranes (MF, UF, and NF) are able to treat turbidity and to remove biocontaminants from natural water [57,58]. The modules accept highly turbid waters, stringent cleaning conditions and can take advantage of in-place back-pulsing.

Utilization of ceramic membranes for water purification started in the 1980s [59] with the implementation of small size membrane plants (5–100 m<sup>3</sup>/h). Imeca in France was one of the first membrane suppliers entering this market with inorganic membranes. This membrane technology is now developing at a larger industrial scale with, for example, the ceramic-membrane water-purification systems designed by NGK in Japan. This company trusts systems based on ceramic membranes, because they are producing water that is safer to use than polymer membrane-based systems. Effectively, the elements have superior mechanical strength, which prevents them from being easily damaged, and they have lower running costs. However, the relatively high initial cost for these systems is a major concern in applications where large volume of purified water a day must be delivered. Estimated prices for polymer membranes currently in operation for drinking water treatment are about 30–50 €/m<sup>2</sup> for micro- and ultrafiltration, and 15–30 €/m<sup>2</sup> for nanofiltration and reverse osmosis. In order to render ceramic membrane elements more cost-effective compared to those based on polymer materials, a number of membrane manufacturers develop large ceramic membrane monoliths offering a large filtration surface per element (see Section 6.2.1.1). Thus a long membrane lifetime, a high membrane surface to volume achieved in the modules as well as a high permeate flow are expected to reduce significantly both investment and running costs of ceramic membrane plants. Several tens of cubic meters per hour of purified water are expected for the larger planned elements, which will render this technology competitive in a near future for large water purification systems.

### 6.3.2.2 Food and Beverage Processing

Contrary to water treatment, general principles cannot be stated for food and beverage processing with membranes. Each sort of food and beverage is a very complex system with specific components interacting with each other so that membrane processes must be specifically adapted to each case. Accordingly, a more detailed description of membrane processes is provided hereafter for the current major applications, i.e., milk, to some extent beer and wine, and a number of other applications showing the continuous expansion of ceramic membrane technologies in food industries.

#### 6.3.2.2.1 Fractionation of Valuable Milk Components

Milk is of the utmost importance for human feeding. It contains about 2000 components, which have been thoroughly studied not only for their nutritional properties, but also for the potential utilization of some of them in pharmaceuticals. The milk industry has been the first food sector in which membrane processes have been implemented at an industrial scale. The earliest development dates back to the end of the 1960s with ultrafiltration plants devoted to whey concentration. Since this period, almost all the membrane processes ordinarily used in liquid treatment (micro-, ultra-, and nanofiltration, diafiltration, reverse osmosis, electro dialysis) have been applied to the treatment of milk and its derivatives. Both ceramic and polymer membranes are used in milk industry; however, the ceramic membranes offer specific advantages in terms of cleaning procedure and sanitary conditions [60]. Compared to polymer membranes, they are able to withstand better harsh cleaning conditions used in the milk industry. Indeed, in-place chemical cleaning at high temperatures, while using caustic, strong inorganic acids, chlorine, hydrogen peroxide, ozone, and steam sterilization, are as many procedures used at different stages of milk transformation and conditioning.

In some cases, ceramic membranes are an integral part of new processes in milk transformation. One example is the fractionation of globular milk fat by membrane microfiltration [61]. Separation of milk fat in small globules (SG) (diameter lesser than 2 μm) and in large globules (LG) (diameter greater than 2 μm) was realized by a patented process using special ceramic microfiltration membranes. Transformation in drinking milks, yoghourts, sour cream, camembert, Swiss cheese, and butters was realized from milks of which the fat content was adjusted from the SG or the LG fractions. These products exhibit significant differences in texture and organoleptic properties compared to traditionally manufactured products, which make them more attractive for consumers. Ceramic membranes with pore diameters of about 2 μm have been identified as very suitable for this application. Permeate fluxes in this case vary from 200 to 700 L/h m<sup>2</sup>, which make the process economically viable. In a more general way, milk fractionation will lead to a more efficient and diverse use of milk and membrane separation seems a logical choice for that [62]. In addition to the aforementioned separation and fractionation of milk fat from whole milk, removal of bacteria and spores from skim milk (cold pasteurization), concentration of casein micelles from skim milk, and recovery of serum proteins from cheese whey are as many operations that can be currently carried out with membranes. Thanks to the availability of new ceramic membranes with smaller cut-off and narrow pore size distribution, new milk component-based products are under development such as edible coatings, bioactive peptides, or dairy and nutritious beverages. However, fouling is still considered as the limiting factor in milk filtration requiring further work on new membranes, module design, fouling control, and modeling to achieve rational design of milk fractionation processes.

#### 6.3.2.2.2 Beer and Wine Cross-Flow Microfiltration

Filtration is an important step in beer production that is traditionally done with filter aids, usually Kieselguhr. The use of Kieselguhr, diatomeaceous earth in a form of silica, is, however, getting more unfavorable in several aspects because the filter aids have to be disposed of or regenerated. Disposal is not environmental friendly and is getting more and more expensive. Moreover dusty atmosphere resulting from Kieselguhr handling is hazardous for the workers. The filterability of beer is an

important parameter and poor filterability can lead to an increase in production cost and also be a big bottleneck concerning the production volume with a significant quantity of wasted beer and spent yeast. Ceramic cross-flow filtration processes have been proposed as a solution with systems able to recover more than half of previously wasted beer, to eliminate disposal costs and to minimize environmental impact. In addition they have the potential to create new revenue streams, as yeast is concentrated to make it more viable for use as a base in animal feed, human food supplements, or as an additive for pharmaceuticals.

Wine manufacturing is still a very traditional process in which filtering is a very tricky subject, especially for prestigious wines. However, one can say that nowadays fining and filtering have been accepted by winemakers as useful tools in building a better wine. The challenge in fining and filtering wines is elimination of unwanted flavors and particles, and preserving of all the components that will create the personality of a good wine [63]. Concerning filtration, winemaking consultants agree to say that wines should be filtered to the minimum necessary. As for beer, filtration of wine has been achieved for years by diatomaceous earth filters with the same pending problems. In the 1990s, cross-flow microfiltration emerged as a very promising technology for this purpose because of its ability to perform wine clarification/filtration/hygienization in one single step. At that time, microfiltration with ceramic membranes offered real advantages over classical filters. Indeed, ceramic membranes function better under pressure, handling 35%–50% throughput. They can be cleaned by a “cleaning in-place” procedure based on an automatic reverse permeate flush. They can work in a continuous mode 18–20 h/day. Finally they last two or three times longer than organic filters.

Most of ceramic membrane equipment suppliers have entered the beer and wine filtration market with membrane products adapted to the specificity of these products [64–66]. The pore diameter of available membranes ranges between 0.1 and 1.5  $\mu\text{m}$ , but the choice of pore size cannot be systematically categorized for each family of products, in particular for wines. In fact filtration requirements are not the same for red wines and white wines. Even, in each of these categories the quality properties of the final product are not exactly predictable and render the choice of the membrane pore size very uncertain. Adsorption of wine compounds on membrane surface also influence filtration effectiveness. Polysaccharides with polyphenols are usually the main responsible compounds of the fouling in wine clarification with membranes [67]. Moreover the retention of these compounds will affect the organoleptic characteristics of the filtrated wine so that their retention and their fouling effect must be reduced. Up to now, filtration tests have shown that 0.1  $\mu\text{m}$  for white wines and 0.2–0.4  $\mu\text{m}$  for red wines are the most recommended pore sizes. The choice of pore size about 0.4  $\mu\text{m}$  for beer filtration looks easier but fouling phenomena are still present [68]. The  $\beta$ -glucans contained in the beer seem to be the major factor for membrane fouling. When they are subjected to high shear stress, high pressure, and rapid cooling, they elongate and form hydrogen bonds resulting in a gel-layer formation on the membrane. In order to improve the filterability many breweries add flocculants before filtration and let them sediment to remove big particles. This flocculation/sedimentation step can impact membrane filtration negatively or positively depending on if membrane modules are sensitive or not to residual particles in the feed stream.

#### 6.3.2.2.3 Other Food Components

Many other applications for ceramic membranes exist in the food industry [1,69]. First, a wide range of fruit juices (apple, pear, peach, orange, grape fruit, pineapple, kiwi fruit, strawberry, cranberry, carrot, date, etc.) are now processed using ceramic membrane technologies, in particular, for clarification and pasteurization. However, flux decline due to membrane fouling is a major concern as it has been shown for apple juice [70]. Membrane technology has also shown high promise in starch processing industry for reducing evaporation costs, improving product recovery, and removing solids before wastewater treatment [71]. Effectively, membranes can be used in many operations of corn, potato, and wheat starch processing. For example, one of the most common applications for membranes in corn wet milling is the removal of residual lipids, proteins, and colorants from corn syrup [72]. It was reported [71] that in 1997 approximately 75% of the US-produced corn syrup was clarified using membrane filtration instead of conventional vacuum filtration. Moreover, the use of MF or UF with nominal pore sizes 0.01–0.1  $\mu\text{m}$  can provide pasteurization without use of heat, as most microorganisms are larger than this pore size. Here also, clarification and pasteurization are typical operations for which UF and MF ceramic membranes are of great interest [72]. Another interest in membrane filtration is in the sugar industry for which it has been shown that the conventional purification can be partially or completely replaced by UF and NF [73]. Indeed, ceramic membranes are well adapted to the treatment of highly viscous sugar syrups for which separation of colored matter from a green syrup is a crucial step in sucrose crystallization [74,75]. In other respects, it has been reported that the pretreatment of molasses with MF ceramic membranes can be beneficial to ethanol fermentation [76].

### 6.3.3 PRODUCT RECOVERY

#### 6.3.3.1 Purification of Pharmaceuticals and Bioproducts

Membrane filtration technologies are finding applications in pharmaceuticals industry for genomics, proteomics, drugs discovery, and generally for laboratory applications in life science, with additionally the possible production of ultra pure process water. In the bioindustry, recovery and purification of products also involve membrane technologies. Although polymer membranes are

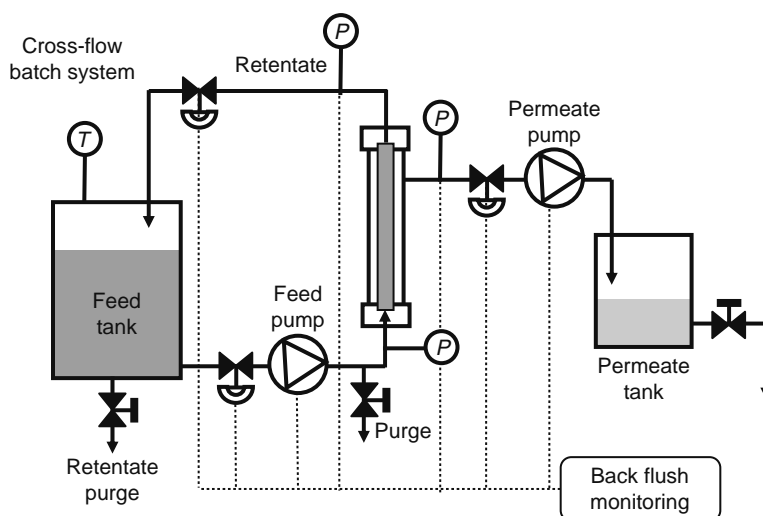


**FIGURE 6.25** Configuration of a batch system membrane plant designed for microfiltration of fermentation broth.

largely used in these sectors, the place of ceramic membranes is increasing due to a better capability to be efficiently cleaned and sterilized. In particular, the new generation of microporous ceramic membranes able to work in the nanofiltration domain (see Section 6.4.1.1) is of great interest to extend current applications. The use of ceramic membranes in biotechnology was reviewed some years ago [69] showing that this sector was primarily interested by the microfiltration of fermentation broth to separate the yeast cells or cell fragments. Today the separation of microorganisms is still of interest and microfiltration is becoming more common compared to centrifugation, especially when it is used as cell separator in continuous fermentation or biological wastewater treatment. One problem is that during the filtration of cells a filter cake is formed on the membrane surface that reduces permeate flow. This is an example where back flushing has been successfully used to push the filter cake off the membrane surface back into the feed stream [77]. More recently an original idea was proposed for the same application, consisting of the implementation of a pump to withdraw permeate at a constant rate [78]. The advantage of a permeate pump compared with using a valve on the permeate side is the easiness to control the permeate flux and by the way the connective transport of material toward the membrane, and thus preventing filter cake formation. Process monitoring can be made by controlling the increase in transmembrane pressure, which can be used in turn as an indication of filter cake formation (i.e., the occurrence of critical flux for the membrane) showing when the membrane has to be cleaned [79]. A schematic representation of what could be a batch system process combining controlled permeate flux with sequential back flushing for membrane cleaning is shown in Figure 6.25.

Next to microfiltration, the commercial availability of ultrafiltration ceramic membranes with well-defined cut-off characteristics allowed the development of membrane processes dedicated to the separation of proteins and enzymes, not only in biotechnology but also in more established industries like dairy [62], fish meal transformation [80], etc. The central problem to protein separation is the adsorption of proteins on the membrane surface and even inside the porosity for molecular weight fractions smaller than pore sizes. This adsorption phenomenon results in most cases in a significant flux decline responsible for intensive cleaning operations impeding the economical feasibility of such processes. The chemical modification of membrane surface has been studied as a way of improving the separation of proteins either by generating specific interaction between the surface and proteins to be recovered or by preventing adsorption to promote a purely size separation effect [81]. An other way is to select membrane materials with a weak tendency to protein adsorption. For example, silicon carbide membrane could be very promising for protein filtration so far as a very low protein adsorption has been evidenced for this membrane material [82]. For the future, interesting developments are expected from the utilization of hybrid organic–inorganic membranes for the separation of molecules of biological or pharmaceutical interest. Chiral-selective membranes [83] or supramolecular chemistry-based membranes for biomimetic transport [84] are studied on the laboratory scale with the aim to separate a number of valuable molecules from reaction mixtures or natural extracts. These studies are attendant to the research on filtration and separation microdevices, which have high development potential in pharmaceuticals and bio-industry.

### 6.3.3.2 Products Manufacturing and Recycling in Various Industries

Separation of manufactured solids from process liquids and recycling of these liquids (water or organic solvents) is an interesting way to valorize by-products and to minimize the production of liquid effluents in a number of industries. Microfiltration ceramic membranes have been already used for the recovery of particles in the ceramic industry and in drilling operations, of pigments in paint and ink industries, and have potential applications in a wide variety of liquid–solid separation

processes. Due to the high inlet cross-flow velocity used in microfiltration, most of these particle suspensions have a strong abrasive effect on the membrane that justifies the use of ceramic membranes with good hardness properties, e.g.,  $\alpha$ -alumina or silicon carbide. The rheological behavior of particle suspensions under shear stress and the formation of a filtration cake are the two main problems, which must be addressed in these applications [85,86]. Cake formation depends not only on applied hydrodynamics in the module, in particular, the shear rate, but also on the interaction between particles depending on several parameters (pH, zeta potential, presence of surfactants or coagulants, etc.). According to Ref. [85], it is likely that cakes formed under cross-flow conditions are more compact than those formed under dead-end or stagnant conditions. This may explain the low permeate flow encountered in microfiltration of particulate suspensions when the chemistry of these suspensions as well as the applied hydrodynamics are not correctly monitored. Coupling with techniques like flotation can help the microfiltration process in solid-liquid separation [87].

Another important application domain for ceramic microfiltration membranes is the recovery of waste oils from industrial wastewater streams or the cleaning of used mineral oils. For example, to prevent formation of higher soot and ash accrument compared to the utilization of original fuel oil, the cleaning of waste oils used as a substitute for fuel oil can be upgraded using microfiltration [88]. In regard to mineral oil regeneration, successful regeneration treatments have been achieved with ceramic ultrafiltration membranes. Moreover, it has been shown that mixing of supercritical CO<sub>2</sub> with oil before the filtration process allows for a significant improvement of permeate flux by reducing oil viscosity [89,90]. Microfiltration can also extend the lifetime of cleaning baths in metal surface treatment or of lubricating fluids in machining industry. These fluids contain dirt particles as well as oil and detergents that must be separated and recycled, while the concentration must be adjusted at the correct level in order to be directly reused in the cleaning or machining process. Here also ceramic membranes offer better durability compared with their polymeric counterpart, because of the presence of abrasive particles and aggressive components. Separation of oil/water suspension using cross-flow filtration is another domain of application for ceramic membranes [91]. Ordinarily, ceramic microfiltration membranes with pore sizes close to 0.2  $\mu\text{m}$  are used for demulsification [92] and product recovery [93]. As for the other applications, there is a flux decline with time and backflushing is necessary to reduce the formation of the gel polarization layer and membrane fouling. The use of hydrophilic membranes is preferred to hydrophobic membranes for which oil is easily wetted on the hydrophobic membrane surface and induces more fouling of the membrane. Moreover, the operating pressure must be lower than capillary pressure to avoid the contamination of permeate with oil.

As a conclusion to the aforementioned current applications of ceramic membranes, a considerable change is under way for the utilization of these technologies in industry, in particular, for waste treatment and product recovery. In order to adapt to environmental regulation and to look for a sustainable economy, the tendency is to develop long-lasting solutions for clean and efficient industrial production processes. Actually, splitting between manufacturing and treatment of end-of-pipe effluents before disposal or simple discharge in the rivers or in the sea, even if these effluents are reputed to be non toxic, is expensive and not totally satisfactory on an environmental point of view. The reclamation of by-products and process fluids is one of the ways being currently explored to improve the productivity and to lower the environmental impact of industrial activities. Membrane processes have been identified as one of the suitable technologies for the development of sustainable processes in which product manufacturing and recycling are combined, thus avoiding the discharge of large quantity of wastes. Section 6.4 describes a number of new membrane processes that modify the current status of ceramic membrane technologies. Most often, they are based on new ceramic membrane prototypes not totally tested out at an industrial scale.

## 6.4 RECENT DEVELOPMENTS AND PROSPECTS

A number of new applications are likely to come in the near future for ceramic membranes, in particular the expected short-term developments for ceramic nanofilters and ceramic membrane contactors applied to liquid treatment, including biological membrane reactors. Gas and vapor separations with ceramic membranes seem to be more distant applications, although microporous silica and zeolite membrane modules are currently in operation in pervaporation or vapor separation processes. High-temperature catalytic membrane reactors (CMRs) constitute a more prospective field of investigation with high potential applications in the chemical and petrochemical industry, in particular, for producing hydrogen from fossil fuels. Most of these developments should be based on new membrane materials exhibiting either carefully controlled pore sizes down to the nanoporous range or dense crystalline structures with ion-conducting properties. Moreover, in most of these new applications, the membranes should have to withstand harsh working environment like corrosive chemical fluids and high process temperatures.

### 6.4.1 FILTRATION AND SEPARATION IN LIQUID MEDIA

#### 6.4.1.1 Nanofiltration with Ceramic Membranes

As the newest development of the liquid filtration family, nanofiltration (NF) is capable of retaining small molecules from 200 to 1000 Da, and multivalent ions. The main current applications of NF polymeric membranes are dealing with the production of drinking and process water, the sulphate removal of seawater or the desalination of cheese whey. Ceramic nanofilters were

commercialized recently and operate in a cut-off domain 500–2000 Da, higher than for polymeric NF membranes [94]. Up to now, several application areas have been identified in which the utilization of ceramic NF membranes is highly suitable, for example, when liquid media contain organic solvents. However, depending on solvent polarity and due to ceramic hydrophilicity, filtration and separation of organic solvents with ceramic nanofilters is not an easy operation. Works from the literature have shown that membrane flux is drastically decreased with apolar solvents compared to water or alcohols in the case of ceramic oxide nanofilters [23]. On the basis of these results, surface-modified ceramic membranes have been recently described, in which the wet ability was changed from hydrophilic to hydrophobic with the aim to develop membranes well adapted to apolar organic solvents [95].

Other relevant examples of application for ceramic nanofilters were recently reported [96]. The first separation problem in which ceramic NF membranes are likely to compete with polymeric membranes is the concentration of pharmaceutical components in their reaction solvents. Ceramic nanofilters are also of interest in the agro-food industry for separation processes working at relatively high temperature and or in the presence of organic solvents. Another potential application is in the production of chemically modified sugars in which the *N*-methyl-pyrrolidone (NMP), used as the solvent for the reaction, needs to be removed from the product (minimum molecular weight about 1000 Da) down to 0.1%. In this case, diafiltration with a ceramic NF membrane has shown to be an efficient way of decreasing the NMP content down to the intended low NMP residual concentration. Also in the sugar industry, where micro- and ultrafiltration are already used for pretreatment of sugar juices, a potential application of ceramic nanofilters is the purification of clarified or pre-evaporated juices as an alternative to ion exchange resins. Typical fluid parameters (sugar concentration from 7 to 25 Brix, feed temperature of 90°C–100°C) justify the use of ceramic membranes instead of polymer membranes. Ceramic nanofilters have also been tested for the treatment of textile wastewater, of alkaline solution from bottle washing machines, or of pickling bath solutions from the metal-working industry [97]. For the future, new applications are expected in the chemical industry. A typical problem for which ceramic NF membranes could afford a viable solution is the recovery of homogeneous catalysts from nonaqueous solvents, in particular the recuperation of transition metal complexes [95].

#### 6.4.1.2 Membrane Contactors and Distributors

There are many operations in chemistry, biotechnology, or agro-industry in which membranes can serve as contactors and distributors between two phases: liquid/liquid or gas/liquid. The high contact surface displayed by the porosity of a membrane allows highly efficient exchanges between hydrophilic phases and gaseous or lyophobic phases. Moreover a narrow distribution of pore sizes allows very sharp process control in a number of applications like emulsification, micromixing, osmotic distillation, perstraction, ozonation, or oxygenation [98–101]. All these technologies can be equally developed with polymer or ceramic membranes, although the very well-defined porosity and the extended range of operating conditions for ceramic porous materials are of specific interest in many applications of membrane contactors and distributors.

Membrane emulsification is a relatively new technique with specific advantages (simplicity, potentially less energy demands, less surfactant, and narrow droplet-size distributions) compared to conventional emulsification techniques [102]. Depending on the membrane hydrophilicity/hydrophobicity and the composition of the two liquid phases, O/W, W/O, or MW emulsions may be produced. Most often used, O/W membrane emulsification consists of the pressurization of oil (dispersed phase) through membrane pores at high pressure (Figure 6.26). The oil jet flows formed in the circulating continuous phase are

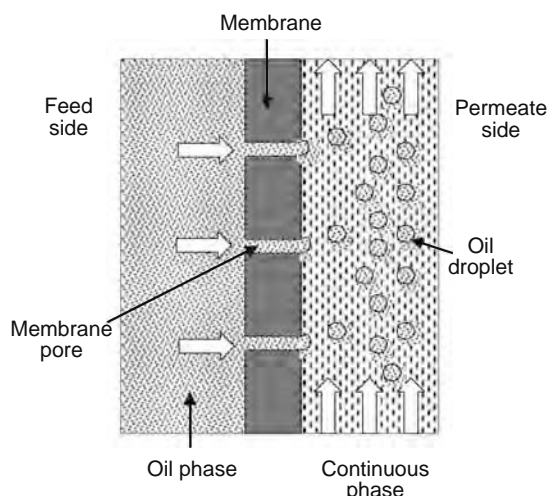


FIGURE 6.26 Schematic representation of cross-flow membrane emulsification.

ruptured to calibrated droplets by action of shearing force. The pore size of membrane and pressure determine the droplet size of the emulsion at the same time. It has been established that for producing O/W emulsions with droplet sizes of about 1  $\mu\text{m}$ , membranes must exhibit a nominal pore size in the range 0.2–0.8  $\mu\text{m}$  with a limitation on applied transmembrane pressure. Therefore there is a strong economical limitation because of the low membrane fluxes (a few liters per hour and square meter) expected for such operating conditions. Recently, a two-stage ceramic membrane jet flow emulsification process has been proposed able to solve the paradox between the flux and droplet size [103]. In this process, a coarse emulsion of oil droplets (size  $\sim 50 \mu\text{m}$ ) is prepared on the first membrane stage at a pressure allowing a high membrane flux ( $J > 100 \text{ L/m}^2 \text{ h}$ ). Droplets result from thin streamlines of oil formed under jet flow, which are then ruptured by action of shearing force along the membrane. Then the coarse emulsion is pressurized on the second membrane stage (pore size  $> 1 \mu\text{m}$ ). Normally, at low pressure when oil droplets are larger than pore size, the oil phase is separated from water (see Section 6.3.3.2). In the present case, due to the combination of high pressure (250 kPa) and high membrane flux ( $J \gg 100 \text{ L/m}^2 \text{ h}$ ), the droplets are pressured through the membrane pores resulting in the formation of a monodispersed emulsion with micron size droplets. In fact, the second stage looks like a multiple emulsification process.

A wide range of application areas of membrane emulsification have been developed from simple food spreads to the manufacture of complex colloidal assemblies [99]. This method affords the production of a variety of structured particulate materials by means of sequential secondary reactions/processes in the emulsified droplets, such as polymerization, gelation, evaporation, freeze-drying, solidification, crystallization, and droplet swelling. For example, nonaqueous droplets containing a monomer mixture can be converted to polymer microspheres by heat-induced polymerization. Besides, the oil droplets can be made up of a high melting-point oil and can be transformed into solid particles by cooling. Similarly the hot droplets of a metal solder can be solidified to produce fine solder powder. Derived from membrane emulsification, membrane micro-mixing and dispersion/precipitation have been described as an innovative method to produce unagglomerated inorganic spherical nanoparticles with a narrow size distribution [104]. In this last example, barium sulphate particles (widely used in pigment, printing ink and medicine) with diameters in the range of sub-200 nm have been produced using a low-energy consumption method developed from the combination of direct precipitation method with an inorganic membrane dispersion technology.

Another important application area for membrane contactors consists of gas–liquid absorption or liquid–liquid extraction (LLE) processes. For example, ozonation is applied in several environmental engineering processes, such as disinfection of drinking water, oxidation of micropollutants, or removal of odor, color, and particles. Operational disadvantages of conventional ozonation processes are an inefficient control of mass transfer because of independent contact between gas and liquid phases resulting in flooding, uploading, emulsion, and foaming. The utilization of membranes for ozonation of liquids affords decisive advantages over conventional processes: (1) much higher interfacial area per volume; (2) higher mass transfer coefficient; (3) easy recycling of  $\text{O}_2/\text{O}_3$  gas mixture back to ozone generator; (4) easily control of ozone gas concentration at liquid–gas interface [105]. Ceramic membranes are superior to polymer ones in this application because of the much better resistance of ceramic material to ozone, a strong oxidant agent. However, to be competitive, ceramic membranes that are hydrophilic by nature, should exhibit a stable hydrophobic surface in this case, to provide high gas transfer rates [106]. Membrane contactors can be also proposed as an alternative to conventional LLE, with the implementation of techniques such as membrane extraction and in a less extent membrane pertraction. These techniques can avoid specific problems of LLE, e.g., solvent loss, emulsion formation, and complex phenomena resulting from the physicochemical instability of the organic–aqueous phase interface [107]. Two other techniques based on a membrane contactor design should be mentioned: (i) osmotic evaporation, which is based on a water vapor pressure difference induced by the difference in the water activity of two aqueous solutions, separated by a porous hydrophobic membrane [108], (ii) membrane distillation in which transport depends upon the vapor pressure gradient caused by the difference in temperature across an hydrophobic membrane [109]. Nevertheless, the utilization of ceramic membranes as contactors for all these applications will require the development of ceramic membranes with a stable hydrophobic surface and a narrow pore size distribution [110].

## 6.4.2 GAS AND VAPOR SEPARATION

### 6.4.2.1 Gas Separation

In most of the literature, gas separation using ceramic membranes, including carbon membranes, is considered to be very promising. However, there are still economical and technical limitations to the industrial development of gas separation processes based on inorganic membranes. Most often, the synthesis of ceramic gas separation membranes is a tricky and not reproducible process with the presence of residual defects and pinholes in the membrane top-layers, which induces high production costs. Accordingly, most of R&D projects in this area are still focused on the membrane as a material and much less on the membrane process, so that insufficient data are available on the real possibility of developing large-scale applications. Anyway, the last decade has seen significant progress in microporous and dense ceramic membranes exhibiting fascinating gas permeation and separation properties [7]. These inorganic membranes able to carry out gas separation at elevated temperatures are potentially useful in emerging areas such as catalytic reactors for gas oxidation and hydrogenation reactions, natural gas or

biogas processing, power generation using fuel cells, and hydrogen production from different fuel sources. There are three main categories of porous inorganic membranes currently investigated for gas molecular separation [111], e.g., silica-based, zeolite, and carbon membranes, while dense gas separation membranes refer to polycrystalline materials in which gas molecules permeate as ionic species [25]. Hybrid organic–inorganic membranes have also been mentioned to having potential application in gas processing, in particular, for natural gas processing and the production of high-density hydrogen without any impurities [112].

Since the very early publications dealing with gas separation using inorganic membranes, a large part of the studies have been based on silica and its derived materials. Silica microporous membranes have been extensively studied and most often synthesized by the solgel process [113–115]. These membranes are quite stable when used in dry atmosphere, but gas permeance decreases drastically in humid conditions due to silica network rearrangement and subsequent formation of a more tight structure. Silica-based inorganic membranes selectively separate hydrogen from other gases, but permselectivity between similar sized molecules, such as oxygen and nitrogen, is not sufficient [116]. Different ways have been explored for increasing performance of silica membranes, for example, by improving the quality of support (smaller pores and smoother surface) as well as coating of silica films under clean-room conditions [116,117], by the templating solgel approach [118–122], or by CVD-based preparation methods [14,15]. The hydrophobic modification of pore surface has also been used to prevent interaction with water [123].

In other respects, we can consider zeolite membranes as pertaining to the ceramic material category. Indeed zeolites are classified for the most part as microporous, crystalline silico–aluminate structures with different aluminum/silicon ratios. Thus, the chemical compositions are close to those of ceramic oxide membranes, in particular of microporous silica and alumina membranes. On the other hand, zeolites are crystalline materials and they have a structural porosity very different from microporous amorphous silica [124]. Zeolite membranes are well adapted to the separation of gases, in particular  $H_2$  from hydrocarbons, but these membranes are not very selective for the separation of mixtures of noncondensable gases.

Besides the aforementioned crystalline or amorphous microporous ceramic membranes, molecular sieve carbon (MSC) membranes have been identified as very promising candidates for gas separations [125,126]. Ordinarily these membranes are prepared by pyrolyzing thermosetting polymers and exhibit pore diameters of 3–5 Å. They have ideal separation factors for various combinations of gases ranging from 4 to greater than 1000. Carbon membranes can be prepared as supported and unsupported membranes. They have been produced under different membrane geometries: flat or tube for the former, and flat, hollow fiber, or capillary for the latter. Carbon membranes have strong application potential for hydrogen recovering from waste gases or for alkenes/alkanes separation. However, MSC membranes are very brittle and fragile, requiring careful handling. When they are operated with non-purified gases, they require a pre-purifier step for removing traces of strongly adsorbing vapors, which can clog up the pores. This problem may be avoided by operating at high temperature, but carbon membranes are not stable at an elevated temperature under oxygen or steam atmospheres.

The last category of inorganic membranes used for gas separation is constituted of dense materials including metals and ceramics [127].

Metallic membranes are not considered as belonging to ceramic membranes so that its related applications will not be discussed in detail. Ordinarily these membranes are mainly made up of Pd-based alloys and are used for hydrogen separation and hydrogenation or dehydrogenation reaction control [128–130]. Metallic membranes exhibit high hydrogen separation selectivity but most of the used metal alloys suffer from instability and must be used in controlled atmosphere and temperature range. Many basic research projects on this topic are still in progress [131,132]. However, metallic membranes have been already used at an industrial scale, for example, in semiconductor industry to produce ultra-high purity hydrogen [133].

The second class of dense membranes thoroughly investigated for gas separation involves ceramic oxide materials exhibiting high solid-state diffusion rates of oxygen ions and protons at high temperature [25,134]. At this time, the development of inorganic proton-conductive membranes able to work at intermediate and high temperatures, in absence of water, is very challenging in many industrial sectors such as hydrogen separation in gas processing, hydrogen or direct methanol fuel cells, electrochemical treatment of aqueous solutions, electrosynthesis, or advanced ceramic membrane electrolyzers for hydrogen production [135,136].

For comparison, the characteristics, permeation, and selectivity of these different categories of gas separation membranes are summarized in Table 6.2. By nature, mesoporous membranes exhibit high permeation flux, but low selectivity based on the Knudsen diffusion mechanism. On the contrary, permeate flux for microporous membranes is at one order of magnitude lower with higher separation selectivity than for the mesoporous membranes, but which strongly depends on temperature [137]. In other respects, for defect-free dense ion-conducting membranes the selectivity is infinite as only oxygen ions or protons can migrate through the crystalline structure [25].

#### 6.4.2.2 Pervaporation and Vapor Permeation

Pervaporation and vapor permeation are typical membrane processes with high application potential in chemical industry due to their high efficiency in the separation or the dehydration of organic solvents. Developed initially with organo-polymeric

**TABLE 6.2**  
**Gas Separation Characteristics of Inorganic Membranes**

Membrane Type	Pore Size Range	Membrane Thickness Range	Permeation Range (mol/m <sup>2</sup> s Pa)	Separation Mechanism (Gas/Gas Selectivity <sup>a</sup> )
Mesoporous ceramics	~4 nm	1–5 μm	10 <sup>-5</sup> to 10 <sup>-6</sup>	Knudsen diffusion (<10)
Mesoporous glass	~4 nm	5–300 μm	10 <sup>-6</sup> to 10 <sup>-9</sup>	Knudsen diffusion (<10)
Microporous oxides	<1 nm	0.1–1 μm	10 <sup>-7</sup> to 10 <sup>-8</sup>	Temperature activated transport (<200)
Microporous carbons	~0.5 nm	1–10 μm	10 <sup>-7</sup> to 10 <sup>-8</sup>	Microsieving <200
Zeolites	~0.5 nm	1–5 μm	10 <sup>-6</sup> to 10 <sup>-7</sup>	Surface diffusion + temperature activated transport (<100)
Ion conductive ceramics	Dense	10 μm to 5 mm	10 <sup>-9</sup>	Ionic transport (infinite)

<sup>a</sup> In the case of H<sub>2</sub>, the separation selectivity is one to two order of magnitude larger than the figures listed in this column due to the high diffusivity of this gas compared to other gases.

membranes, the main limitation to industrial application is still the lack of membranes being selective and chemically resistant in an organic solvent environment. In comparison, the high thermal and mechanical stability as well as the excellent chemical resistance of inorganic membranes make them well adapted to working conditions of chemical processes. The general principle of PV or VP separation is shown in Figure 6.27. In PV processes the feed is a liquid, while vapor exits the membrane on permeate side. VP has certain similarities with PV but uses gaseous components on the feed side of the membrane. However, some differences between these two processes have to be mentioned with respect to operating conditions [138]. First, vapor permeation fluxes depend strongly on feed pressure whereas pervaporation fluxes are independent. Then, heat transfer within the membrane is more a consideration for pervaporation because of vaporization phenomenon. Finally, concentration polarization in the feed is more likely to occur during pervaporation because of slower diffusion in the liquid phase than in the vapor phase. PV and VP inorganic membranes are implemented most often as tubular modules. Microporous silica and zeolites have been identified as suitable membrane materials for PV and VP applications.

Currently, pervaporation with zeolite membranes is the most advanced technology at an industrial scale [138]. The growing interest for zeolite-based pervaporation process lies not only in the excellent chemical resistance of these membranes, but also in the high separation selectivity and high permeate fluxes compared to organo-polymeric membranes. The current large-scale commercial application of zeolite membranes is dehydrating alcohols and other organic compounds for solvent recovery. A typical example is the zeolite membrane pervaporation plant built by Mitsui Engineering & Shipbuilding Company, Japan [139]. It produces 530 L/h of dehydrated alcohol (0.2% residual water content) from feed alcohol containing 10% water, with separation factors as high as 10,000. Recently this company has implemented in Europe, 6 large module vapor permeation plant for dehydration of biomass ethanol at 135°C [140]. Each module is composed of 550 zeolite NaA membrane elements and is able to produce 5000 L of dehydrated ethanol per day. The NaA zeolite membrane has been demonstrated to be very effective for the separation of water/organic liquid mixtures, while the NaY zeolite membrane is more adapted to the separation of organic binary mixtures [141]. The permeation and selectivity characteristics of these membranes are reported on Table 6.3. One can see that membrane performance may be very different depending on

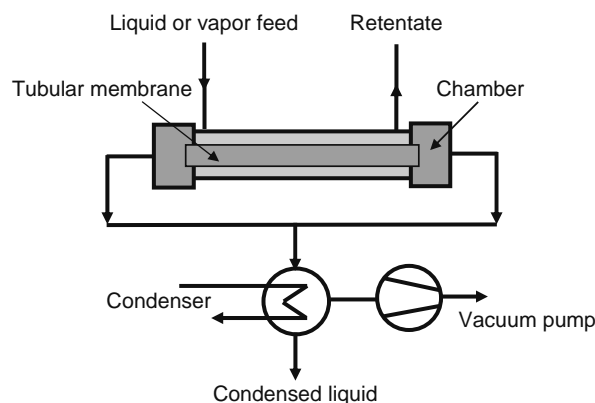


**FIGURE 6.27** General working principle of a pervaporation or vapor permeation module equipped with tubular ceramic membrane elements.

**TABLE 6.3**  
**Performance of NaA and NaY Zeolite Membranes for Component Separation in Respective Water/Organic and Binary Organic Mixtures**

Zeolite	Feed Solution (A/B) (wt% of A)	Temperature (°C)	Separation Factor (A/B)	Flux (kg/m <sup>2</sup> h)
NaA	Water/methanol [10]	50	2,100	0.57
		105	5,700	3.50
	Water/ethanol [10]	75	10,000	2.15
		105	30,000	4.53
	Water/2.propanol [10]	75	10,000	1.76
	Water/acetone [10]	50	5,600	0.91
	Water/dioxane [10]	60	9,300	1.87
		105	8,900	7.80
	Water/DMF [10]	60	8,700	0.95
	NaY	Water/ethanol [10]	75	130
Methanol/benzene [10]		60	3,800	0.93
		60	5,300	1.70
Methanol/MTBE [10]		105	6,400	2.13
		150	600	2.59
		60	930	0.22
Ethanol/benzene [10]		60	1,000	0.27
Ethanol/cyclohexane [10]		50	1,200	0.21
Benzene/ <i>n</i> -hexane [50]		65	7	0.02
		105	29	0.05
Benzene/cyclohexane [50]		150	18	0.21
		105	45	0.007
		150	41	0.01

the nature of the binary organic mixtures. In fact each zeolite membrane is revealed to be efficient, only in a limited number of applications. This explains the ongoing important research works devoted to zeolite membranes to cover all potential applications. Small-, medium-, and large-pore zeolites such as Mordenite, ZSM5, Silicalite-1, or SAPO-34, with an hydrophilic or hydrophobic behavior, are currently investigated as pervaporation or vapor permeation membranes. Today more than 14 zeolite structures have been prepared as membranes [138].

Microporous membranes based on hydrophilic silica have also been developed [142] in view of industrial application for the dewatering of organic solvents. Silica membranes are less selective than zeolite membranes but they exhibit higher permeate fluxes. For example, in the case of ethanol dewatering at 80°C, the required membrane area for a silica membrane can be 10 times lower than for the equivalent polymeric membrane. As for zeolite membranes, the price of silica membranes dominates the investment cost and dampens industrial developments. A recent study on PV silica membranes pointed out the possibility of substantial cost savings by designing new modules and optimizing module arrangements [143]. It has been shown that conventional modules need up to 50% more membrane surface than a new isothermal module design [144] developed by Sulzer Chemtech. In the same way operating costs are reduced by 20% with optimized working conditions for module setup. Other materials are currently investigated on the laboratory scale to extend the categories of available PV or VP membranes. For that purpose, a better thermochemical stability is expected from binary oxide systems [145,146]. Hydrophobic PV membranes have been also studied for separating organic compounds from organic/water mixtures having low organic concentration [147].

### 6.4.3 CATALYTIC MEMBRANE REACTORS

Many research efforts have been devoted to the application of inorganic membranes in catalytic reactors on the basis that all types of homogeneous or heterogeneous catalytic reactions can be in principle assisted by membranes. The concept of combining reaction and separation is being explored in various configurations, which can be classified into three groups related to the role of the membrane in the process [148]. In a chemical reaction involving two reactants A and B, yielding one or two products C and D, the three different roles of the membrane for improving selectivity and conversion are schematized in Figure 6.28. Note that for extractors and distributors, inert membranes are used, while membranes are catalytically active for contactors. These designs are common to the three main types of membrane reactors investigated to date and involving ceramic membranes, i.e., gas-liquid-solid, biocatalytic, or high-temperature reactors. In the future, it is likely that new reactor concepts

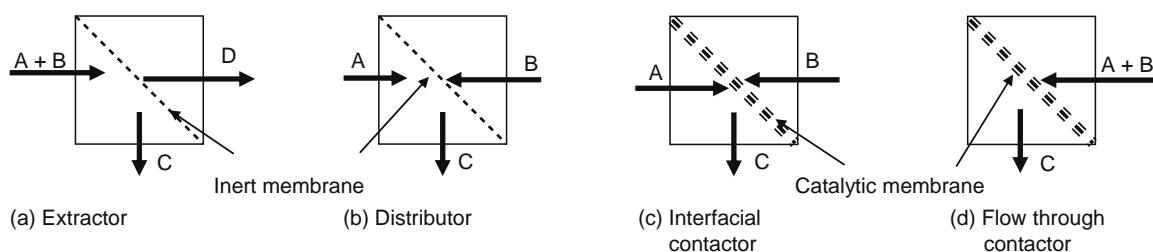


**FIGURE 6.28** Roles of the membrane in membrane reactors. (a) Extractor: the removal of product(s) increases the reaction conversion by shifting the reaction equilibrium; (b) distributor: the controlled addition of reactant(s) limits side reactions; (c) and (d) active contactors: the controlled diffusion of reactant(s) to the catalytic membrane can lead to an engineered catalytic zone.

will extend the list of membrane reactor concepts such as membrane-mediated reactions in supercritical fluids [149] or photocatalytic assisted membranes for the treatment of water and wastewater [150].

### 6.4.3.1 Chemical Reactors Based on Gas–Liquid–Solid Membrane Contactors

Ceramic catalytically active membranes have high potential for supporting gas–liquid reactions [151–153]. This non-separative prospective application does not require a permselectiveness of the membrane. In fact the role of the porous ceramic membrane is to provide a well-defined contact region among the gas phase, the liquid phase, and the catalytic active phase deposited on the membrane. In this configuration the membrane material itself may exhibit intrinsic catalytic activity. As for simple membrane contactors, an additional benefit of using such reactor configuration is the high interfacial area per volume due the high specific surface area developed in the porous structure of the membrane.

Two reactor concepts may be distinguished [153], which are schematized on Figure 6.29. One consists of the gas phase and the liquid phase flowing, respectively, on each side of the membrane (Figure 6.29a). In this case one reactant is dissolved in the liquid phase, which is sucked by capillary forces into the catalytic membrane layer, getting the reactant in contact with the catalytic sites. The gaseous reactant is fed on the other side through the porous support of the membrane. As a result, a gas–liquid phase boundary establishes, which is determined by the pressure difference between the gas and the liquid side. The pressure must be controlled in order to have the phase boundary in the membrane layer where catalytic active sites are located so that the contact between the liquid reactant, the gas reactant, and the solid catalyst are optimum, enhancing overall reaction rate. The second type of reactor configuration is based on a through flow concept (Figure 6.29b). This configuration may be useful when the reaction is very fast. Contrary to the first configuration in which the limiting step was mass transport due to reactant diffusion in the liquid phase, in the second case, instead of establishing a phase boundary in the membrane, the gas reactant and the liquid phase reactant are mixed prior to be forced through the catalytic active membrane layer. Accordingly, avoiding the problem of reactant diffusion in the pores, the contact time at the catalytic sites can be varied by changing the flow rate through the membrane, so that very short contact times can be achieved.

These two concepts have been proved on a laboratory scale, mainly for hydrogenation reactions but can be transposed to many gas–liquid catalyzed reactions. Interesting potential applications have been mentioned, such as asphaltene hydrocracking or nitrate and nitrites removal from drinking water by catalytic nitrate reduction. However, the characteristics of ceramic

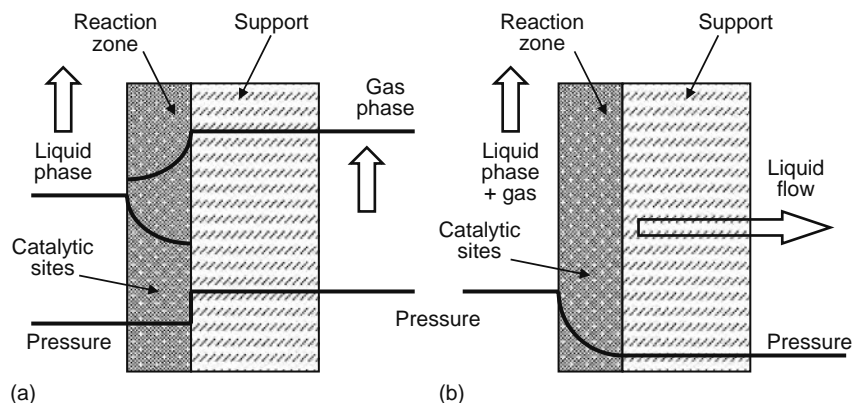


**FIGURE 6.29** Concepts of membrane reactor based on gas–liquid–solid ceramic membrane contactors.

membrane devoted to this application have still to be improved to significantly increase mass transfer and efficiency of these systems. For the first concept in which a gas–liquid boundary is established in the membrane, thinner ceramic membrane layers with a narrow pore size distribution should be produced, ensuring shorter diffusion paths and efficient mass transfer [152]. For the flow through concept, a homogeneous distribution and a good accessibility of catalytic sites in the membrane porosity are the main conditions for a successful process.

### 6.4.3.2 Biocatalytic Membrane Reactors

These reactors constitute a complementary and more prospective aspect to membrane bioreactors described in Section 6.3.1.2. The aim of developing such reactors is to use the catalytic action of enzymes for large-scale production in agro-food or pharmaceutical industries [154]. Possible applications in biomedical or environmental sectors have also been mentioned [155]. The interest of using the catalytic action of enzymes is that they are extremely efficient and selective. In general enzymes demonstrate higher reaction rates, milder reaction conditions, and greater stereospecificity compared to chemical catalysts. Thus, this category of membrane reactors offers the advantage of environmental-friendly technologies.

Here also ceramic membranes may have a number of specific advantages over polymeric membranes. Porous ceramics exhibit a non-deformable porous structure, which resists to microbiological attacks and can withstand different reaction media (aqueous, organic, and supercritical fluids). Moreover ceramic porous media can be reused after elimination of aged biological catalysts followed by a thorough reactor cleaning and sterilization with chemicals and steam. Different configurations have been proposed for these enzymatic membrane reactors. Two ways have been effectively tested for coupling enzymatic activity with membranes: the one in which the biocatalytic medium is flushed along the membrane module (Figure 6.30a) and the other with enzymes fixed or entrapped in the porous medium (Figure 6.30b). In the former case, the membrane is used to retain the enzymes and the substrate(s), while allowing the products to pass through. In other respects, when the enzymes are immobilized in the porosity of the membrane, pores containing the enzymes can be considered as many of microreactors in which much higher conversion and selectivity can be achieved than in a batch reactor [154]. Actually in the microreactor concept, an outstanding property is the extremely large surface-to-volume ratio inducing a minimization of mass transfer path and a substantial increase of transfer rate.

The use of enzymatic membrane reactors on an industrial scale is not yet fully established, however, some interesting reactor designs have been proposed in the literature. One of them combines a ceramic membrane as the support for enzymes with supercritical CO<sub>2</sub> as the reaction solvent [156]. The objective of this work was to obtain high-value products in the food and health industry from enzymatic modification of fats and oils. For that, an enzyme (a lipase) is chemically immobilized in a proteinic membrane top-layer supported on a macroporous ceramic element. The enzymatic reactor works according to the flow through concept, the role of supercritical CO<sub>2</sub> being the fluidization of a viscous mixture of substrates (castor oil and methyl oleate) to facilitate mass transfer across the membrane top-layer and diffusion path to enzymatic catalytic sites. This reactor concept is very promising as it showed a good stability for enzyme activity with pressure, temperature, and time under supercritical condition as well as an enhanced conversion rate due to the supercritical medium. More generally biocatalytic membrane reactors are studied for agro-food, pharmaceutical, biomedical industries, and even for wastewater treatment [155]. Except for biomedical applications dealing with artificial organs, all the other sectors could benefit from enzymatic reactors equipped with ceramic membrane elements. In the agro-food sector enzymatic membrane reactors could be used for: reducing

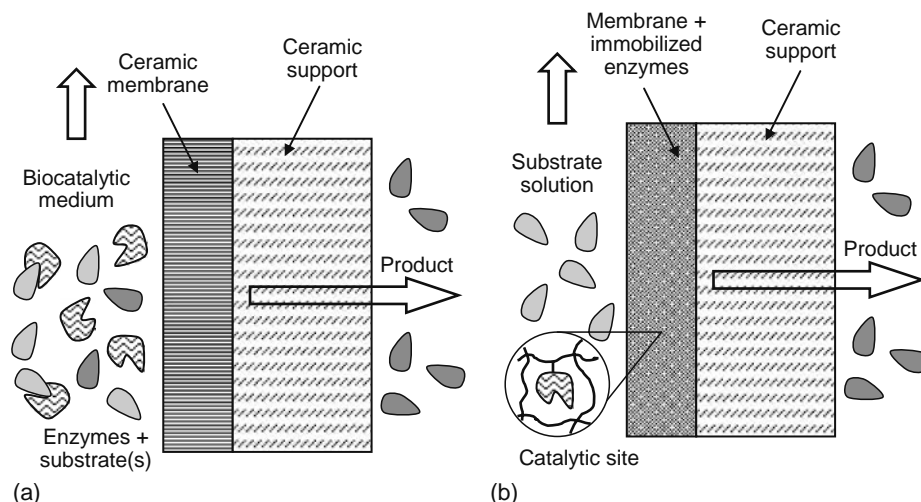


FIGURE 6.30 Concepts of biocatalytic membrane reactors with (a) non-immobilized or (b) immobilized enzymes.

the viscosity of juices by hydrolyzing pectins, reducing the lactose content in milk and whey by its conversion into digestible sugar, the treatment of musts and wines by the conversion of polyphenolic compounds and anthocyanes, and the removal of peroxides from dairy products. In the pharmaceuticals sector, these reactors could be implemented for the production of amino acids, antibiotics, anti-inflammatories, anti-cancer drugs, vitamins, etc. For water and wastewater treatment, biocatalytic membrane reactors are of interest for converting highly hazardous contaminants, which cannot be destroyed or removed by conventional treatments.

### 6.4.3.3 High-Temperature Catalytic Membrane Reactors

Catalytic membrane reactors working at high temperature are certainly the most innovative and challenging developments expected for ceramic membranes in the near future [157,158]. These reactors offer the possibility of combining reaction and separation at high temperature to overcome the equilibrium limitations experienced in conventional reactor configurations. A number of industrial applications have been identified in chemical industries, which include hydrogenation, dehydrogenation, oxidation, and catalytic decomposition processes. Many examples of the potential utilization of the different categories of inorganic membranes in CMRs can be found in the literature [159–171]. More recently, the new power generation technologies based on hydrogen or syngas production arose as a very promising industrial activity in which ceramic membrane reactors can be considered as a key technology. However, few of these processes have passed the laboratory scale, although some important R&D projects, carried out by industrial consortia, were mentioned recently [19].

In fact there has been a shift of interest for CMRs during the last decade [172]. In the early 1990s, dehydrogenation of styrene and butane with the shift reaction equilibrium was a major concern in the studies. From 1994–2000 interest was mainly focused on methane processing with the aim of gas-to-liquid fuel transformation or hydrogen production. At the moment, industrials involved in new hydrogen or syngas-based power technologies are seeking to develop reliable CMRs for the partial oxidation or direct coupling of methane, natural gas, or biogas. Many research efforts are devoted to these technologies including the investigation of new membrane materials, the design of innovative reactor systems, and the coupling with other technologies like solid oxide fuel cells or energy cogeneration systems. Actually the development of CMRs working at high temperature is still constrained at the one hand by the cost of these systems, which should be less than 1000 €/m<sup>2</sup> for installed membranes, on the other hand by the need for more selective and reliable ceramic membranes, able to withstand high temperature and harsh operating conditions. Three main designs (Figure 6.31) have been proposed for these membrane-reaction systems, going from a simple and reliable implementation configuration to more sophisticated, but risky configurations. These three configurations consist of (i) separate membrane and catalyst; (ii) catalyst dispersed in the membrane; and (iii) inherently catalytic membrane material. It is apparent that the failure of the membrane in the second and third categories will necessitate complete replacement of the entire membrane reactor system, while catalyst or membrane failure may be treated independently in the first category.

Inorganic membranes exhibiting either dense structures or macro-, meso-, and microporous structures can be implemented in CMR devices. At this time, the former category includes dense metal membranes for hydrogen extraction as well as ion and mixed ion-electron conducting ceramic membranes active in the selective transport of oxygen ions and protons at high temperature. Originally dense metal membranes based on Pd and Pd-alloys have been developed for shifting equilibrium in dehydrogenation reactions. In the case of oxygen-ion conducting ceramic membranes, the partial oxidation of methane has been the most studied reaction involving two types of membrane reactors: pressure driven devices using mixed ions-electrons conducting membranes [160] or electrically driven devices using membrane electrolytes made of purely ion-conducting metal oxides [165,166]. Oxygen transport membranes are also envisioned as a part of Integrated Gasification Combined Cycle (IGCC) systems [173] or as a way of mitigating CO<sub>2</sub> emission by enabling the recycling of a O<sub>2</sub>/CO<sub>2</sub> mixture in fuel combustion plants [174]. Proton-conductive ceramic membranes have been studied recently. This kind of membrane is designed for the transport of protons and electrons at high temperature, producing a stream of pure hydrogen suitable for use in hydrogen technologies [175]. An interesting process concept has been proposed by Praxair, Inc. and Argonne National

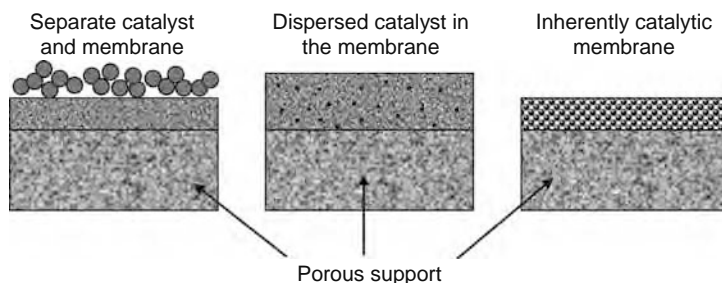
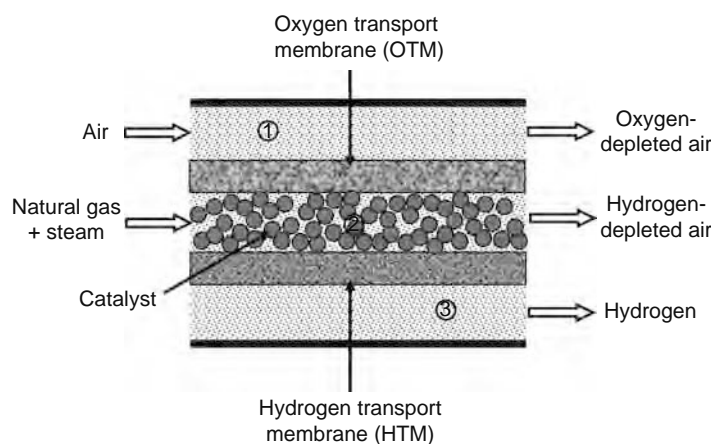


FIGURE 6.31 Different catalyst-membrane designs for implementation in catalytic membrane reactors (CMRs).



**FIGURE 6.32** Schematic diagram of an integrated distributor/extractor membrane reactor based on the combination of dense ceramic oxygen and hydrogen transport membrane for syngas production.

Laboratory combining both dense ceramic oxygen (OTM) and hydrogen (HTM) transport membranes to produce syngas and purified hydrogen from natural gas [176]. This process concept integrates various processing steps in a single distributor/extractor membrane reactor. The reactor is divided in three compartments separated by the OTM and HTM membranes (Figure 6.32). Natural gas and steam are introduced in the central reactor compartment containing a catalyst, where partial oxidation, steam reforming, and water gas shift reactions take place. Simultaneously, oxygen is distributed from the air compartment to the reactor compartment through the OTM membrane whereas the hydrogen is extracted from the reactor compartment through the HTM membrane. The development of reliable and cost-effective OTM and HTM membranes able to be implemented in this kind of reactor is very challenging for future hydrogen-based energy production.

In other respects, the role of porous ceramic membranes in CMRs must be regarded in close relation with the mode of gas transport through the membrane porous structure (see Section 6.2.2.2). The viscous flow controlled by the transmembrane pressure in macroporous ceramic membranes is well adapted to the distribution of reactive gases in a reactor. A very innovative concept has been proposed recently for oxygen distribution in partial oxidation membrane reactors [177,178], based on an infiltrated membrane system. Mesoporous ceramic membranes are more suitable for catalytic membrane contactors because of the Knudsen diffusion that promotes the contact between gas molecules and catalytic sites present on pore walls [179,180]. Finally molecular sieving, surface diffusion, or temperature-activated transport in microporous ceramic membranes can be advantageously used for selective gas extraction in reactors. These membranes can be an alternative to dense metallic membranes that do not withstand extreme operating conditions, for example, in the case of hydrogen extraction from the reaction zone in a fluidized-bed reactor specially designed for oxo-alcohol synthesis gas production [181].

## 6.5 CONCLUSION

As mentioned in this chapter, the field of membrane technology is broad and continuously expanding in many industrial sectors. It involves different aspects starting with the production of membranes with well-defined characteristics and ending with the implementation of various processes dealing with a large number of operations such as simple filtration, selective separation, solutes or solid matter concentration, fluid distribution, and even catalytic conversion or reaction control. The potential growth for worldwide membrane markets is 10%–15% a year. Even if the share of ceramic membrane-based processes is quite small compared to polymeric membranes, the continuous increase in ceramic membrane equipment sales during the last decade, estimated at €300 million in 2005, holds high promise for the future.

Since the first industrial developments in cross-flow microfiltration in early 1980s, significant progress was achieved with ceramic membranes presently, affording new products with improved permeate flux, separation selectivity, and system compactness. Effectively, monolithic and hollow fiber elements have resulted in a significant increase in membrane surface to volume ratio, closer to the compactness of polymeric membrane systems. Ceramic nanofilters are able to carry out separation on the molecular scale in liquid, gas, or vapor media. The commercial availability of inorganic membrane materials now includes nonoxide ceramics (silicon carbide or silicon nitride), zeolites, and will extend to nanophase and hybrid materials in the near future. CICMs are under development for high-temperature membrane processes that will be central to new power generation technologies (hydrogen and syngas production, solid oxide fuel cells).

The actual interest for ceramic membranes in many applications dealing with the treatment of liquids results from an increasing demand for secure and reliable membrane processes. In the food and pharmaceutical industries for which sanitary requirements are of the utmost importance, ceramic membranes afford a very good reliability in terms of cleaning and

sanitization procedures. For the treatment of liquid wastes and the regeneration of process fluids, the high resistance and the long durability of ceramic membranes are a great asset to the development of clean and efficient processes in many industries. In a general way, ceramic membranes should actively participate to the implementation of modern technologies and should be able to adapt to environmental regulation by avoiding the discharge of large quantities of wastes.

For the future, ceramic membrane technologies will extend to the treatment and the separation of gases and vapors up to elevated temperatures (800°C–900°C). Moreover, membranes and modules with new designs will diversify the role of the membranes as extractor, distributor, or contactor in biological or chemical processes. On this basis, new generation of membranes, ceramic membrane reactors arise as an innovative and challenging technology combining separation and reaction, able to overcome the equilibrium limitations experienced in conventional reactor configurations. Ceramic membranes afford specific advantages in these applications, in particular the biological inertness, the high chemical and mechanical resistance, and the ability to work at elevated temperature. Nevertheless, two difficulties have to be surpassed to allow the industrial development of these new technologies, still experienced on the laboratory scale. One is technical with the expected development of large scale and reliable membrane fabrication processes and the other is economical with the necessity to significantly decrease the production cost of these membranes.

## REFERENCES

1. Bhavé RR. *Inorganic Membranes: Synthesis, Characteristics and Applications*. New York: Van Nostrand Reinhold, 1991.
2. Guizard C, Julbe A, Larbot A, and Cot L. Ceramic Membrane Processing. In: Pope EJA and Lee BI (eds.), *Chemical Processing of Ceramics*. New York: Marcel-Dekker, 1994:501–553.
3. Burggraaf AJ and Cot L. *Fundamentals of Inorganic Membrane Science and Technology*. Amsterdam: Elsevier, 1996.
4. Guizard C, Julbe A, and Ayrál A. Design of nanosized structures in sol–gel derived porous solids. Application in catalyst and inorganic membranes preparation. *J. Mater. Chem.* 1999;9:55–65.
5. Cot L, Ayrál A, Durand J, Guizard C, Hovnanian N, Julbe A, and Larbot A. Inorganic membranes and solid state sciences. *Solid State Sci.* 2000;2:313–334.
6. Tsuru T. Inorganic porous membranes for liquid phase separation. *Sep. Purif. Method.* 2001;30(2):191–220.
7. Lin YS. Microporous and dense inorganic membranes: Current status and prospective. *Sep. Purif. Technol.* 2001;25:39–55.
8. Guizard C, Ayrál A, Barboiu M, and Julbe A. Sol–Gel processed membranes. In: Sakka S (ed.), *Sol–Gel Technology*, Vol. 3: Kozuka H (ed.), *Application of Sol-Gel Technology*. New York: Kluwer, 2004:141–180.
9. <http://www.exekia.fr>; <http://www.orelis.com>; <http://www.tami-industries.com>; <http://www.ceramem.com>; <http://www.ceparation.com>. (Accessed 23/02/2005).
10. Xu X, Yang W, Liu J, Lin L, Stroh N, and Brunner H. Synthesis of NaA zeolite membrane on a ceramic hollow fiber. *J. Membr. Sci.* 2004;229:81–85.
11. Guizard C. Sol–gel chemistry and its application to porous membrane processing. In: Burggraaf AJ and Cot L (eds.), *Fundamentals of Inorganic Membrane Science and Technology*. Amsterdam: Elsevier, 1996:227–258.
12. Klotz M, Ayrál A, Guizard C, and Cot L. Synthesis and characterization of silica membranes exhibiting an ordered mesoporosity. Control of the porous texture and effect on membrane permeability. *Sep. Purif. Technol.* 2001;25(1–3):71–78.
13. Bosc FA, Ayrál AP-A, Albouy P-A, and Guizard C. A simple route for low-temperature synthesis of mesoporous and nanocrystalline thin films. *Chem. Mater.* 2003;15:2463–2468.
14. Kuruoka K, Shugen Z, Okita K, Kakitani T, and Yazawa T. Permeation of methanol vapour through silica membranes prepared by the CVD method with aid of evacuation. *J. Membr. Sci.* 1999;160:31–39.
15. Prabhu AK and Oyama TS. Highly hydrogen selective ceramic membranes: Application to the transformation of greenhouse gases. *J. Membr. Sci.* 2000;176:233–248.
16. Jansen JC, Koegler JH, van Bekkum H, Calis HPA, van den Bleek CM, Kapteijn F, Moulijn JA, Geus ER, and van der Puil N. Zeoliting coatings and their potential use in catalysis. *Micropor. Mesopor. Mat.* 1998;21:213–226.
17. Ismail AF and David LIB. A review on the latest development of carbon membranes for gas separation. *J. Membr. Sci.* 2001;193:1–18.
18. Kilner JA, Benson S, Lane J, and Waller D. Ceramic ion conductive membranes for oxygen separation. *Chem. Ind.* 1997;17 November:907–911.
19. Carolan MF. Hydrogen and syngas production using ion transport membranes. Proceedings of the Eight International Conference on Inorganic Membranes, Cincinnati, OH, July 18–22, 2004:1–8.
20. Mulder M. *Basic Principles of Membrane Technology*. Dordrecht: Kluwer Academic, 1991.
21. Lefebvre X, Palmeri J, Sandeaux J, Sandeaux R, David P, Maleyre B, Guizard C, Amblard P, Diaz J-F, and Lamaze B. Nanofiltration modelling: A comparative study of the salt filtration performance of a charged ceramic membrane and an organic nanofilter using the computer simulation program NANOFILUX. *Sep. Purif. Technol.* 2003;32(1–3):117–126.
22. Israelachvili JN. *Intermolecular and Surface Forces*. London: Academic Press, 1991.
23. Guizard C, Ayrál A, and Julbe A. Potentiality of organic solvents filtration with ceramic membranes. A comparison with polymer membranes. *Desalination* 2002;147:275–280.
24. Burggraaf AJ. Transport and separation properties of membranes with gases and vapour. In: Burggraaf AJ and Cot L (eds.), *Fundamentals of Inorganic Membrane Science and Technology*. Amsterdam: Elsevier, 1996:331–433.
25. Bouwmeester HJM and Burggraaf AJ. Dense ceramic membranes for oxygen separation. In: Burggraaf AJ and Cot L (eds.), *Fundamentals of Inorganic Membrane Science and Technology*. Amsterdam: Elsevier, 1996:435–515.
26. Norby T. Solid-state protonic conductors: principles, properties, progress and prospects. *Solid State Ionics* 1999;125:1–11.

27. <http://www.whatman.com>; <http://www.sterlitech.com>; <http://www.igb.fhg.de/WWW/GF/GrenzflMem/Membranen> (accessed 17/09/2004).
28. Ripperger S and Altmann J. Cross-flow microfiltration—state of the art. *Sep. Purif. Technol.* 2002;26:19–31.
29. Cui ZF, Chang S, and Fane AG. The use of gas bubbling to enhance membrane processes. *J. Membr. Sci.* 2003;221:1–35.
30. Lamminen MO, Walker HW, and Weavers LK. Mechanisms and factors influencing the ultrasonic cleaning of particle-fouled ceramic membranes. *J. Membr. Sci.* 2004;237:213–223.
31. Howell JA. Future of membranes and membrane reactors in green technologies and for water reuse. *Desalination* 2004;162:1–11.
32. Kentish SE and Stevens GW. Innovations in separations technology for the recycling and re-use of liquid waste streams. *Chem. Eng. J.* 2001;84:149–159.
33. Sondhi R, Bhave R, and Jung G. Applications and benefits of ceramic membranes. *J. Membr. Technol.* 2003; November:5–8.
34. Xu L, Li W, Lu S, Wang Z, Zhu Q, and Ling Y. Treating dyeing wastewater by ceramic membrane in cross-flow microfiltration. *Desalination* 2002;149(1–3):199–203.
35. Van der Bruggen B, Curcio E, and Drioli E. Process intensification in the textile industry: the role of membrane technology. *J. Environ. Manage.* 2004;73:267–274.
36. Šostar-Turk S, Simonič M, and Petrić I. Laundry wastewater treatment using coagulation and membrane filtration. *Res. Conserv. Recycling* 2005;44:185–196.
37. Šostar-Turk S, Simonič M, and Petrić I. Wastewater treatment after reactive printing. *Dyes Pigments* 2005;64:147–152.
38. [http://www.canon.com/environmental/technology/close\\_system.html](http://www.canon.com/environmental/technology/close_system.html) (accessed Juillet 2004).
39. Holmes D. Waters and chemicals recovery in the German automotive industry. *Membr. Technol.* 2002;October:6–10.
40. De Pinho MN, Geraldés VM, Rosa MJ, Afonso MD, Figueira H, Taborda F, Almeida G, Ganho R, Creusen R, Hanemaaijer J, Gaeta S, Amblard P, Gavach C, and Guizard C. Water recovery from bleached pulp effluents. *Tappi J.* 1996;79(12):117–124.
41. Keyoumu A, Sjö Dahl R, Henriksson G, Ek M, Gellerstedt G, and Lindström ME. Continuous nano- and ultrafiltration of kraft pulping blackliquor with ceramic filters. A method for lowering the load on the recovery boiler while generating valuable side-products. *Ind. Crop. Prod.* 2004;20:143–150.
42. Ahn K-H, Song J-H, and Cha H-Y. Application of tubular ceramic membranes for reuse of wastewater from buildings. *Water Sci. Technol.* 1998;38(4–5):373–382.
43. Battrick B and Perel J. *Water Recycling Systems for the Antarctic Concordia Station*. ISBN 92-9092-695-3, ESA Publication Division, Noordwijk, The Netherlands, 2004.
44. Cicek N. A review of membrane bioreactors and their potential application in the treatment of agricultural wastewater. *Can. Biosyst. Eng.* 2003;45:1–13.
45. Visvanathan C, Ben AR, and Parameshwaran K. Membrane separation bioreactors for wastewater treatment. *Crit. Rev. Environ. Sci. Technol.* 2000;30(1):1–48.
46. Nomura T, Fujii T, and Suzuki M. Application of the ceramic membrane with hydrophobic skin layer to separation of activated sludge. *Water Sci. Technol.* 1997;35(8):137–144.
47. Bishop B, Judd S, Cardin J, Alvarez Vazquez H, Jefferson B, and Goldsmith R. Use of ceramic membranes in airlift membrane bioreactors. Proceedings of the Eight International Conference on Inorganic Membranes, Cincinnati, OH, July 18–22, 2004:142–145.
48. Zhang S, van Houten R, Eikelboom DH, Doddema H, Jiang Z, Fan Y, and Wang J. Sewage treatment by a low energy membrane bioreactor. *Bioresour. Technol.* 2003;90(2):185–192.
49. Miller BG, Wincek RT, Glick DC, Scaroni AW, Makris P, Kreckler J, Jung G, and Stubblefield J. Ceramic membrane filters and conventional fabric filters for fine particulate removal from a coal-fired industrial boiler. Proceedings of the 23rd International Conference on Coal Utilization and Fuel Systems, Clearwater, FL, March 9–13, 1998:807–818.
50. Startin A and Elliot G. Treating industrial hot gases with ceramic filters. *Filtr. Sep.* 2001; November:38–40.
51. Heidenreich S and Scheibner B. Hot gas filtration with ceramic filters: Experiences and new developments. *Filtr. Sep.* 2002;May:22–25.
52. Heidenreich S and Wolters C. Hot gas filter contributes to IGCC power plant's reliable operation. *Filtr. Sep.* 2004; June:22–25.
53. Larbot A, Bertrand M, Marre S, and Prouzet E. Performances of ceramic filters for air purification. *Sep. Purif. Technol.* 2003;32:81–85.
54. DeFriend KA and Barron AR. A simple approach to hierarchical ceramic ultrafiltration membranes. *J. Membr. Sci.* 2003;212:29–38.
55. Endo Y, Chen D-R, and Pui DYH. Collection efficiency of sintered ceramic filters made of submicron spheres. *Filtr. Sep.* 2002; March:43–47.
56. Sakol D and Konieczny K. Application of coagulation and conventional filtration in raw water pre-treatment before microfiltration membranes. *Desalination* 2004;162:61–73.
57. Sui X and Huang X. The characterization and water purification behaviour of gradient ceramic membranes. *Sep. Purif. Technol.* 2003;32:73–79.
58. Lee S and Cho J. Comparison of ceramic and polymeric membranes for natural organic matter (NOM) removal. *Desalination* 2004;160:223–232.
59. Pouët MF, Persin F, Gros M, and Rumeau M. Etude du couplage électrocoagulation-flottation pour limiter le colmatage des membranes en traitement des eaux. Proceedings of the 2nd International Conference on Inorganic Membranes, Montpellier, France, 1–4 July 1991, Trans Tech Publications, Zurich, 1991:237–242.
60. Bird MR and Bartlett M. Measuring and modelling flux recovery during the chemical cleaning of MF membranes for the processing of whey protein concentrate. *J. Food Eng.* 2002;53:143–152.
61. Goudéranche H, Fauquant J, and Maubois J-L. Fractionation of globular milk fat by membrane microfiltration. *Lait* 2000;80:93–98.
62. Brans G, Schroën CGPH, van der Sman RGM, and Boom RM. Membrane fractionation of milk: state of the art and challenges. *J. Membr. Sci.* 2004;243:263–272.
63. Gergely S, Bekassy-Molnar E, and Vatai G. The use of multiobjective optimization to improve wine filtration. *J. Food Eng.* 2003;58:311–316.

64. Burrell K, McKechnie M, and Murray J. Advances in separation technology for the brewer: ceramic crossflow filtration of rough beer. *Tech. Q. Master Brew Assoc. Am.* 1994;31(2):42–50.
65. Reed R. Current and future roles of membranes in brewing. *Membr. Technol.* 1998;101:5–8.
66. Manninger K, Gergely S, Bekassy-Molnar E, Vatai G, and Kallay M. Pretreatment effect of the quality of white and red wines using cross-flow ceramic membrane filtration. *Acta Aliment.* 1998;27(4):377–387.
67. Vernhet A, Pellerin MP, Belleville J, Planque J, and Moutounet M. Relative impact of major wine polysaccharides on the performances of an organic microfiltration membrane. *Am. J. Enol. Vitic.* 1999;50(1):51–56.
68. Fillaudeau L and Carrère H. Yeast cells, beer composition and mean pore diameter impact on fouling and retention during cross-flow filtration of beer with ceramic membranes. *J. Membr. Sci.* 2002;196:39–57.
69. Siskens CAM. Applications of ceramic membranes in liquid filtration. In: Burggraaf AJ and Cot L (eds.), *Fundamentals of Inorganic Membrane Science and Technology*. Amsterdam: Elsevier, 1996;619–639.
70. Vladislavljević GT, Vukuosavljević P, and Bukvić B. Permeate flux and fouling resistance in ultrafiltration of depectinized apple juice using ceramic membranes. *J. Food Eng.* 2003;60(3):241–247.
71. Rausch KD. Front end to backpipe: Membrane technology in the starch processing industry. *Starch/Stärke* 2002;54:273–284.
72. Singh N and Cheryan M. Process design and economic analysis of a ceramic membrane system for microfiltration of corn starch hydrolysate. *J. Food Eng.* 1998;38:57–67.
73. Gyura J, Šereš Z, and Eszterle M. Influence of operating parameters on separation of green syrup colored matter from sugar beet by ultra- and nanofiltration. *J. Food Eng.* 2005;66:89–96.
74. Kishihara S, Wakiuchi N, Hosokawa T, Fujii S, and Tamaki H. Clarification of sugar solution by ultrafiltration. Effect on crystallization of sucrose. *Proceedings of the Research Society Japan Sugar Refineries Technologist*, 1997;45:1–14.
75. Kishihara S, Tamaki H, Fujii S, and Komoto M. Clarification of technical sugar solution through a dynamic membrane formed on a porous ceramic tube. *J. Membr. Sci.* 1989;41:103–108.
76. Kokugan K and Kokugan T. The effect of molasses pretreatment by ceramic microfiltration membrane on ethanol fermentation. *J. Ferment. Bioeng.* 1997;83(6):577–582.
77. Kamoshita Y, Ohashi R, and Suuzuki T. Improvement of filtration performance of stirred ceramic membrane reactor and its application to rapid fermentation of lactic acid by dense cell culture of *Lactococcus lactis*. *J. Ferment. Bioeng.* 1998;85(4):422–427.
78. Persson A, Jönsson A-S, and Zacchi G. Separation of lactic acid-producing bacteria from fermentation broth using a ceramic microfiltration membrane with constant permeate flow. *Biotechnol. Bioeng.* 2001;72(3):269–277.
79. Chen V, Fane AG, Madaeni S, and Wenten IG. Particle deposition during membrane filtration of colloids: transition between concentration polarization and cake formation. *J. Membr. Sci.* 1997;125:109–122.
80. Afonso MD, Ferrer J, and Bórquez R. An economic assessment of proteins recovery from fish meal effluents by ultrafiltration. *Trends Food Sci. Tech.* 2004;15:506–512.
81. Chan R and Chen V. Characterization of protein fouling on membranes: opportunities and challenges. *J. Membr. Sci.* 2004;242:169–188.
82. Rosenbloom AJ, Sipe DM, Shishkin Y, Ke Y, Devaty RP, and Choyke WJ. Nanoporous SiC: a candidate semi-permeable material for biomedical applications. *Biomed. Microdev.* 2004;6(4):261–267.
83. Krieg HM, Breytenbach JC, and Keizer K. Chiral resolution by  $\beta$ -cyclodextrin polymer impregnated ceramic membranes. *J. Membr. Sci.* 2000;164:177–185.
84. Barboiu M. Hybrid supramolecular membranes as selective biomimetic transport devices. Proceedings of the Eight International Conference on Inorganic Membranes, Cincinnati, OH, July 18–22, 2004:159–162.
85. Mikulášek P, Doleček P, Šmidová D, and Pospíšil P. Crossflow microfiltration of mineral dispersions using ceramic membranes. *Desalination* 2004;163:333–343.
86. Zaho Y, Xing W, Xu N, and Shi J. Hydraulic resistance in microfiltration of titanium white waste acid through ceramic membranes. *Sep. Purif. Technol.* 2003;32:99–104.
87. Matis KA, Peleka EN, Zamboulis D, Erwe T, and Mavrov V. Air spargling during the solid/liquid separation by microfiltration: application of flotation. *Sep. Purif. Technol.* 2004;40:1–7.
88. Psoch C, Wendler B, Goers B, Wozny G, and Ruschel B. Waste oil conditioning via microfiltration with ceramic membranes in cross flow. *J. Membr. Sci.* 2004;245:113–121.
89. Gourguillon D, Schrive L, Sarrade S, and Rios G. An environmentally friendly process for the regeneration of used oil. *Environ. Sci. Technol.* 2000;34:3469–3473.
90. Rodriguez C, Sarrade S, Schrive L, Dresh-Bazile M, Paolucci D, and Rios GM. Membrane fouling in cross-flow ultrafiltration of mineral oil assisted by pressurized CO<sub>2</sub>. *Desalination* 2002;144:173–178.
91. Ohya H, Kim JJ, Chinen A, Aihara M, Semenova SI, Negishi Y, Mori O, and Yasuda M. Effects of pore size on separation mechanisms of microfiltration of oily water, using porous glass tubular membrane. *J. Membr. Sci.* 1998;145:1–14.
92. Srijaroonrat P, Julien E, and Aurelle Y. Unstable secondary oil/water emulsion treatment using ultrafiltration: fouling control by backflushing. *J. Membr. Sci.* 1999;159:11–20.
93. Novalic S, Heisler G, and Lahnsteiner J. Cross-flow filtration of latex emulsion on a pilot scale using organic and inorganic membranes with different cut-off values. *J. Membr. Sci.* 1997;130:1–5.
94. Guizard C. *Nanofiltration Guide*. Montpellier, France: CFM Booklet N ISBN 2.9516158-0-9, 2000.
95. Voigt I, Puhlfuß P, Dudziak G, and Mutter M. Ceramic nanofiltration membranes for the retention of homogeneous catalysts. Proceedings of the Eight International Conference on Inorganic Membranes, Cincinnati, OH, July 18–22, 2004:67–71.
96. Buekenhoudt A, Dotremont C, Aerts S, Vanckelecom I, and Jacobs PA. Successful applications of ceramic nanofiltration in non-aqueous solvents. Proceedings of the Eight International Conference on Inorganic Membranes, Cincinnati, OH, July 18–22, 2004:278–281.

97. Weber R, Chmiel H, and Mavrov V. Characteristics and application of new ceramic nanofiltration membranes. *Desalination* 2003;157:113–125.
98. Stanojević M, Lazarević B, and Radić D. Review of membrane contactors designs and applications of different modules in industry. *FME Trans.* 2003;31:91–98.
99. Vladisavljević GT and Williams RA. Recent developments in manufacturing emulsions and particulate products using membranes. *Adv. Colloid Interfac.* 2005;113:1–20.
100. Jiao B, Cassano A, and Drioli E. Recent advances on membrane processes for the concentration of fruit juices: a review. *J. Food Eng.* 2004;63:303–324.
101. Schlosser Š, Kertész R, and Marták J. Recovery of organic acids by membrane-based solvent extraction and pertraction. An overview with a case study on recovery of MPCAs. *Sep. Purif. Technol.* 2005;41:237–266.
102. Gijsbertsen-Abrahamse AJ, van der Padt A, and Boom RM. Status of cross-flow membrane emulsification and outlook for industrial application. *J. Membr. Sci.* 2004;230:149–159.
103. Jing W, Xing W, Jin W, and Xu N. Preparation of monodispersed o/w emulsion by ceramic membrane jet-flow emulsification. Proceedings of the Eight International Conference on Inorganic Membranes, Cincinnati, OH, July 18–22, 2004:76–80.
104. Chen GG, Luo GS, Xu JH, and Wang JD. Membrane dispersion precipitation method to prepare nanoparticals. *Powder Technol.* 2004;139:180–185.
105. Phattaranawik J, Leiknes T, and Pronk W. Mass transfer studies in flat sheet membrane contactor with ozonation. *J. Membr. Sci.* 2005;247:153–167.
106. Janknecht P, Wilderer PA, Picard C, and Larbot A. Ozone-water contacting by ceramic membranes. *Sep. Purif. Technol.* 2001;25:341–346.
107. Wódski R and Szczepański P. Integrated hybrid membrane systems—membrane extraction and pertraction coupled to a pervaporation process. *J. Membr. Sci.* 2002;197:297–308.
108. Kunz W, Benhabiles A, and Ben-Aim R. Osmotic evaporation through macroporous hydrophobic membranes: a survey of current research and applications. *J. Membr. Sci.* 1996;121:25–36.
109. Lawson KW and Lloyd DR. Review: Membrane distillation. *J. Membr. Sci.* 1997;124:1–25.
110. Larbot A, Gazagnes L, Krajewski S, Bukowska M, and Kujawski W. Water desalination using ceramic membranes distillation. *Desalination* 2004;168:367–372.
111. Morooka S and Kusakabe K. Microporous inorganic membranes for gas separation. *MRS Bulletin* March 1999;25–28.
112. Olsen S, Tripathi B, Mill H, and Gobina E. Hybrid inorganic membrane technology shows promise in gas processing. *Membrane Technol.* 2002;6:6–11.
113. Nair BN, Yamagushi T, Okubo T, Suematsu H, Keizer K, and Nakao S-I. Sol–gel synthesis of molecular sieving silica membranes. *J. Membr. Sci.* 1997;135:237–243.
114. Asaeda M and Yamasaki S. Separation of inorganic/organic gas mixtures by porous silica membranes. *Sep. Purif. Technol.* 2001;25:151–159.
115. Dinis da Costa JC, Lu GQ, Rudolph V, and Lin YS. Novel molecular sieve silica (MSS) membranes: characterisation and permeation of single-step and two-step sol–gel membranes. *J. Membr. Sci.* 2002;198:9–21.
116. De Vos RM and Verweij H. Improved performance of silica membranes for gas separation. *J. Membr. Sci.* 1998;143:37–51.
117. Tsai CY, Tam SY, Lu YF, and Brinker CJ. Dual-layer asymmetric microporous silica membranes. *J. Membr. Sci.* 2000;169:255–268.
118. Kusakabe K, Sakamoto S, Saie T, and Morooka S. Pore structure of silica membranes formed by a sol–gel technique using tetraethoxysilane and alkyltriethoxysilanes. *Sep. Purif. Technol.* 1999;16:139–146.
119. Kusakabe K, Shibao F, Zhao G, Sotowa K-I, Watanabe K, and Saito T. Surface modification of silica membranes in a tubular type module. *J. Membr. Sci.* 2003;215:321–326.
120. Lu Y, Cao G, Kale RP, Prabakar S, Lopez GP, and Brinker CJ. Microporous silica prepared by organic templating: relationship between the molecular template and pore structure. *Chem. Mater.* 1999;11:1223–1229.
121. West GD, Diamond GG, Holland D, Smith ME, and Lewis MH. Gas transport mechanisms through sol–gel derived templated membranes. *J. Membr. Sci.* 2002;203:53–69.
122. Xomeritakis G, Naik S, Braunbarth CM, Cornelius CJ, Pardey R, and Brinker CJ Organic-templated silica membranes: I. Gas and vapour transport properties. *J. Membr. Sci.* 2003;215:225–233.
123. De Vos RM, Maier WF, and Verweij H. Hydrophobic silica membranes for gas separation. *J. Membr. Sci.* 1998;158:277–288.
124. Tavolaro A, and Drioli E. Zeolite membranes. *Adv. Mater.* 1999;11:975–996.
125. Ismail AF and David LIB. Future direction of R&D in carbon membranes for gas separation. *Membrane Technol.* 2003;4:4–8.
126. Saufi SM and Ismail AF. Fabrication of carbon membranes for gas separation—a review. *Carbon* 2004;42:241–259.
127. Ma YH. Dense palladium and perovskite membranes and membrane reactors. *MRS Bulletin* March 1999;46–49.
128. Bryden KJ and Ying JY. Nanostructured palladium-iron membranes for hydrogen separation and membrane hydrogenation reaction. *J. Membr. Sci.* 2002;203:29–42.
129. Tosti S. Supported and laminated Pd-based metallic membranes. *Int. J. Hydrogen Energy* 2003;28:1445–1454.
130. Yamakawa K, Ege M, Hirscher M, Ludescher B, and Kronmüller H. Hydrogen permeation through Pd/Fe and Pd/Ni multilayer systems. *J. Alloys Compd.* 2005;393:5–10.
131. Ryi S-K, Park J-S, Choi S-H, Cho S-H, and Kim S-H. Fabrication and characterization of metal porous membrane made of Ni powder for hydrogen separation. *Sep. Purif. Technol.* 2006;47:148–155.
132. Zhang Y, Maeda R, Komaki M, and Nishimura C. Hydrogen permeation and diffusion of metallic composite membranes. *J. Membr. Sci.* 2006;269:60–65.

133. Lin YS and Buxbaum RE. Metal membranes: membranes separation. In: Wilson ID, Adlard TR, Poole CF, and Cooke M (eds.), *Encyclopedia of Separation Science*. SanDiego: Academic Press, 2000:3365–3374.
134. Guizard C and Julbe A. Nanophase ceramic ion transport membranes for oxygen separation and gas stream enrichment. In Kanellouopoulos NK (ed.), *Recent Advances in Gas Separation by Microporous Ceramic Membranes*. Amsterdam: Elsevier 2000:435–471.
135. Linkov V. New inorganic proton-conducting membranes for hydrogen separation and electro-catalysis. *Membr. Technol.* 2001;132:4–8.
136. Bredesen R, Jordal K, and Bolland O. High-temperature membranes in power generation with CO<sub>2</sub> capture. *Chem. Eng. Process.* 2004;43:1129–1158.
137. Fain DE. Mixed gas separation technology using inorganic membranes. *Membr. Technol.* 2000;120:9–13.
138. Bowen CT, Noble RD, and Falconer JL. Fundamentals and applications of pervaporation through zeolite membranes. *J. Membr. Sci.* 2004;245:1–33.
139. Morigami Y, Kondo M, Abe J, Kita H, and Okamoto K. The first large-scale pervaporation plant using tubular-type module with zeolite NaA membrane. *Sep. Purif. Technol.* 2001;25:251–260.
140. Yamamura T, Kondo M, Abe J, Kita H, and Okamoto K. The vapor permeation module using zeolite NaA membrane for producing absolute ethanol from biomass ethanol. Proceedings of the Eight International Conference on Inorganic Membranes, Cincinnati, OH, July 18–22, 2004:599–603.
141. Kita H. Pervaporation using zeolite membranes. Proceedings of International Workshop on Zeolitic Membranes and Films; Post Conference of ICIM5, Gifu, Japan, June 28–30, 1998:43–46.
142. Van Veen HM, van Delft YC, Engelen CWR, and Pex PPAC. Dewatering of organics by pervaporation with silica membranes. *Sep. Purif. Technol.* 2001;22–23:361–366.
143. Schleger M, Sommer S, and Melin T. Module arrangement for solvent dehydration with silica membranes. *Desalination* 2004;163:281–286.
144. Wynn N. Dehydration with silica pervaporation membranes. *Membr. Technol.* 2001;129:10–11.
145. Sekulic J, Luiten MWJ, ten Elshof JE, Benes NE, and Keizer K. Microporous silica and doped silica membrane for alcohol dehydration. *Desalination* 2002;148:19–23.
146. Yang J and Asaeda M. Permeation mechanism of water through microporous SiO<sub>2</sub>-ZrO<sub>2</sub> membranes for separation of aqueous solutions of organic solvents by pervaporation. *Sep. Purif. Technol.* 2003;32:29–36.
147. Park D-H, Nishiyama N, Egashira Y, and Ueyama K. Separation of organic/water mixtures with silylated MCM-48 silica membranes. *Micropor. Mesopor. Mat.* 2003;66:69–76.
148. Dalmon JA. Catalytic membrane reactors. In *Handbook of Heterogeneous Catalysis*. In: Ertl G, Knözinger H, and Weitkamp J (eds.), VCH Pub. 1997; Chapter 9.3; 1387–1398.
149. Goetheer ELV, Verkerk AW, van den Broeke LJP, de Wolf E, Deelman B-J, van Koten G, and Keurentjes JTF. Membrane reactor for homogeneous catalysis in supercritical carbon dioxide. *J. Catal.* 2003;219:126–133.
150. Bosc F, Ayrat A, and Guizard C. Mesoporous anatase coatings for coupling membrane separation and photocatalysed reactions. Proceedings of the Eight International Conference on Inorganic Membranes, Cincinnati, OH, July 18–22, 2004:114–117.
151. Raeder H, Bredesen R, Crehan G, Miachon S, Dalmon J-A, Pintar A, Levec J, and Torp EG. A wet air oxidation process using a catalytic membrane contactor. *Sep. Purif. Technol.* 2003;32:349–355.
152. Vospernik M, Pintar A, Berčič G, and Levec J. Experimental verification of ceramic membrane potentials for supporting three phase catalytic reactions. *J. Membr. Sci.* 2003;223:157–169.
153. Reif M and Dittmeyer R. Porous, catalytically active ceramic membranes for gas–liquid reactions: a comparison between catalytic diffuser and forced through flow concept. *Catal. Today* 2003;82:3–14.
154. Rios GM, Belleville MP, Paolucci D, and Sanchez J. Progress in enzymatic membrane reactors. *J. Membr. Sci.* 2004;242:189–196.
155. Giorno L and Drioli E. Biocatalytic membrane reactors: applications and perspectives. *Tibtech* 2000;18:339–349.
156. Pomier E, Galy J, Paolucci-Jeanjean, Pina M, Sarrade S, and Rios GM. A new reactor design combining enzyme, membrane and SC CO<sub>2</sub>: application to castor oil modification. *J. Membr. Sci.* 2005;249:127–132.
157. Sarraco G, Neomagus WJP, Versteeg GF, and van Swaaij WPM. High temperature membrane reactors: potential and problems. *Chem. Eng. Sci.* 1999;54(13/14):1997–2017.
158. Julbe A, Farrusseng D, and Guizard C. Porous ceramic membranes for catalytic reactors—overview and new ideas. *J. Membr. Sci.* 2001;181:3–20.
159. Harold MP, Lee C, Burggraaf AJ, Keizer K, Zaspalis VT, and De Lange RSA. Catalysis with inorganic membranes. *MRS Bull.* 1994;19(4):34–39.
160. Balachandran U, Dusek JT, Mieville RL, Poeppel RB, Kleefisch MS, Pei S, Kobylinski TPC, Udovich A, and Bose AC. Dense ceramic membranes for partial oxidation of methane to syngas. *Appl. Catal. A Gen.* 1995;133:19–29.
161. Hsieh HP. *Inorganic Membranes for Separation and Reaction, Membrane Science and Technology*, Series 3. Amsterdam: Elsevier 1996.
162. Binkerd CR, Ma YH, Moser WR, and Dixon AG. An experimental study of the oxidative coupling of methane in porous ceramic radial-flow catalytic membrane reactors. Proceedings of ICIM4 (Inorganic Membranes), Gatlinburg, TN: D.E. Fain (ed.), 1996:441–450.
163. Yeung AKL, Sebastian JM, and Varma A. Mesoporous alumina membranes: synthesis, characterization, thermal stability and nonuniform distribution of catalyst. *J. Membr. Sci.* 1997;131:9–28.
164. Lange C, Storck S, Tesche B, and Maier WF. Selective hydrogenation reactions with a microporous membrane catalyst, prepared by sol–gel dip coating. *J. Catal.* 1998;175(2):280–293.
165. Hamakawa S, Hayakawa T, Suzuki K, Murata K, and Takehira K. Methane conversion with an electrochemical membrane reactor. Proceedings of ICIM 5 (Inorganic Membranes), Nagoya, Japan: S. Nakao (ed.), 1998:350–353.

166. Hamakawa S, Shiozaki R, Hayakawa T, Suzuki K, Murata K, Takehira K, Koizumi M, Nakamura J, and Uchijima T. Partial oxidation of methane to synthesis gas using Ni/Ca<sub>0.8</sub>Sr<sub>0.2</sub>TiO<sub>3</sub> anode catalyst. *J. Electrochem. Soc.* 2000;147:839–844.
167. Steele B. Ceramic ion conducting membranes and their technological application. *C.R. Acad. Sci. (Paris)* 1998; Part1, Series IIc:533–43.
168. Gellings PJ and Bouwmeester HJM. Solid state aspects of oxidation catalysis. *Catal. Today* 2000;58:1–53.
169. Maiya PS, Anderson TJ, Mieville RL, Dusek T, Picciolo JL, and Balachandran U. Maximizing H<sub>2</sub> production by combined partial oxidation of CH<sub>4</sub> and water gas shift reaction. *Appl. Catal. A Gen.* 2000;196:65–72.
170. Kikushi E. Membrane reactor application to hydrogen production. *Catal. Today* 2000;56:97–101.
171. Julbe A and Guizard C. Role of membranes and membrane reactors in the hydrogen supply of fuel cells. *Ann. Chim. Sci. Mat.* 2001;26(4):79–92.
172. Tennison S. Current hurdles in the commercial development of inorganic membrane reactors. *Membr. Technol.* 2000;128:4–9.
173. Chen J, Sirman J, lane J, Chen HC, van hassle B, Apte P, and Prasad R. Advances in oxygen transport membranes for gas separation. Proceedings of the Eight International Conference on Inorganic Membranes, Cincinnati, OH, July 18–22, 2004:38–41.
174. Yantovski E, Gorski J, Smyth B, and ten Elshof J. Zero-emission fuel-fired power plants with ion transport membrane. *Energy* 2004;29:2077–2088.
175. Cheng S, Gupta VK, and Lin YS. Synthesis and hydrogen permeation properties of thin proton-conducting ceramic membranes. Proceedings of the Eight International Conference on Inorganic Membranes, Cincinnati, OH, July 18–22, 2004:50–53.
176. Shah M, Drnevich, Balachandran U, Dorris SE, and Lee TH. Technoeconomic feasibility analysis of hydrogen production by integrated ceramic membrane system. Proceedings of the 2001 DOE Hydrogen Program Review: NREL/CP-570–30535.
177. Farrusseng D, Julbe A, and Guizard C. The First redox switchable ceramic membrane. *J. Am. Chem. Soc.* 2000;122(50):12592–12593.
178. Julbe A, Farrusseng D, Cot D, and Guizard C. The chemical valve membrane: a new concept for an auto-regulation of O<sub>2</sub> distribution in membrane reactors. *Catal. Today* 2001;67:139–149.
179. Pina MP, Menéndez M, and Santamaria J. The Knudsen-diffusion catalytic membrane reactor: an efficient contactor for the combustion of volatile organic compounds. *Appl. Catal. B Environ.* 1996;11(1):L19–L27.
180. Olsen S and Gobina E. GTL synthesis gas generation membrane for monetizing stranded gas. *Membr. Technol.* 2004;6:5–10.
181. Gobina E and Gordon R. Inorganic membranes tackle oxo-alcohol synthesis gas production in a fluidised-bed reactor. *Membr. Technol.* 2000;125:4–8.



---

# 7 Membrane Technologies and Supercritical Fluids: Recent Advances

*D. Paolucci-Jeanjean, G.M. Rios, and S. Sarrade*

## CONTENTS

7.1	Introduction .....	181
7.2	Solvent Recovery .....	182
7.2.1	Caffeine/SC CO <sub>2</sub> Separation .....	182
7.2.1.1	Separation through Adsorption Mechanism .....	183
7.2.1.2	Molecular-Sieving Mechanism .....	184
7.2.2	Essential Oils/SC CO <sub>2</sub> Separation .....	185
7.2.3	Organic Compounds/SC CO <sub>2</sub> Separation .....	185
7.3	Coupling SCF Extraction with Nanofiltration for Process Intensification .....	185
7.4	Membrane Reactors with Supercritical Fluids .....	186
7.5	Supercritical Fluid Membrane Contactors .....	187
7.6	SC CO <sub>2</sub> -Assisted Ultrafiltration .....	188
7.7	Membrane Preparation .....	188
7.7.1	Inorganic Materials .....	189
7.7.2	Polymeric Materials .....	189
7.8	Conclusions .....	190
	References .....	190

## 7.1 INTRODUCTION

Worldwide, billions of pounds of organic solvents are used as processing tools, cleaning agents, and dispersants. Due to their specific properties, which overcome the disadvantage of costly high-pressure conditions, supercritical fluids can be proposed as alternative solvents. Supercritical carbon dioxide (SC CO<sub>2</sub>) which is low cost and nontoxic, and presents intermediate thermodynamic (density, solvent power) and transport (viscosity, diffusivity) properties between gases and liquids easily tuneable with temperature and pressure, is certainly one of the most attractive. Because of its high potentials in the fields of solid and liquid extraction, chromatography, particle formation, dyeing of yarns, and reactions, SC CO<sub>2</sub> has been largely used already in food and pharmaceutical areas. Large-scale applications incorporating other kind of compounds can also be found (such as compressed gases like propane and butane in petrol refining).

Among processes involving supercritical fluids, high-pressure reactions or separation applications with membranes have recently attracted interest. It was notably the case for operations involving barriers robust enough to support high-pressure conditions required in this field. Both kinds of membranes (i.e., organic and inorganic) are supposed to be used. In other works (presented in Section 7.7), authors have also considered supercritical fluids as attractive media for the preparation of the membranes themselves.

Inorganic membranes are very resistant and quite stable at hard-operating conditions. Several materials are available. Different membranes have been successfully tested for separations involving supercritical fluids such as tubular carbon membranes [1], tubular silica membranes [2–5], silica hollow fiber membranes [6], zeolite membranes [7–10], titanate–nafion membranes [11], polycarbonate membrane [12], nanofilter having a thin layer of ZrO<sub>2</sub>–TiO<sub>2</sub> [12], and silicalite membranes [4].

Transfer mechanisms involved in SC CO<sub>2</sub> permeation through such porous membranes can be convection (Poiseuille law), diffusion (Knudsen flow), and surface membrane interaction by adsorption, capillary condensation, etc. [11]. Mechanisms have been specifically investigated for nanofiltration and zeolite membranes. With a nanofilter presenting a pore diameter of about 1 nm, Sarrade [11] mentioned a Poiseuille flow associated with an irreversible CO<sub>2</sub> adsorption on the micropore wall. Transfer

of SC CO<sub>2</sub> through a zeolite membrane (pore diameter 0.55 nm) was based on the combination of surface diffusion (adsorption) and Knudsen diffusion [8].

Organic membranes have also been used for supercritical fluids applications in specific equipments. In that view, Damle and Koros [13] proposed a permeation equipment for high-pressure gas separation able to work with polyimide organic membrane as an example. The membrane was placed in a commercial membrane testing cell (initially dedicated to high-pressure mixed gas testing), which was previously modified to allow SC fluids permeation. In addition, Spricigo et al. [14] succeeded to perform SC CO<sub>2</sub> permeation in a dead end flow regime through a cellulose acetate reverse osmosis membrane, which was placed over a perforated metallic support; sealing was made with poly(tetrafluoroethylene) rings. Other membranes like polyamide [15] or cellulose triacetate/diacetate [16] membranes were also tested using the same apparatus.

A particular phenomenon can occur when organic membranes are in contact with SC CO<sub>2</sub>. Under high pressure, most membrane materials tend to plasticize. Specifically, the presence of the adsorbed CO<sub>2</sub> at high pressure tends to soften and dilate the membrane material [13]. This phenomenon can constitute a great limitation with the use of polymeric membranes because it induces a strong swelling of the membrane and often leads to a lack in stability of the system on the medium-long range. In what follows the different applications are examined successively.

## 7.2 SOLVENT RECOVERY

Due to its unique characteristics and physicochemical properties such as being less toxic, nonflammable, and having the extraction power tuned by temperature and pressure, SC CO<sub>2</sub> can be used as a green solvent for extraction of substances especially from solid or liquid substrates. Such extraction has been carried out on commercial scale for more than two decades and applications like decaffeination of coffee beans and black tea leaves and hops extraction are involved in large-scale processes [17]. Other extractions such as extraction of flavors, spices, and essential oils from plant materials are under investigation. An overview of published data for different materials is given in the review of Marr and Gamse [18].

As the solubility of solutes is generally low and as high pressures are often required to enhance it, large amounts of CO<sub>2</sub> are required for the extraction process. Thus, CO<sub>2</sub> regeneration for recycling use is essential to make the process economically viable.

As supercritical fluids solvent power depends on pressure and temperature, solute and supercritical solvent can be separated by acting on these parameters. In addition to the extraction step, a complete process typically includes an expansion step at subcritical pressure (corresponding to solute/solvent separation), a cooling step until a liquid phase, and a pressurization-heating system to recover extraction conditions [19]. To replace this supercritical fluid cycle, which is characterized by a high-energy requirement, it is possible to regenerate solute and solvent while maintaining supercritical conditions for the solvent. In those cases, an additional mass-separating agent inducing small changes in conditions of state is added. On the one hand, a substance can be added to reduce the solvent power: For example, addition of nitrogen decreases remarkably the solubility of caffeine in carbon dioxide. On the other hand, solute can be removed from the solvent thanks to an absorbent or adsorbent for which the solute has more affinity than for the supercritical fluid. These possibilities can be preferred to the supercritical fluid cycle only if the following separations (i.e., reducing solvent power additive from supercritical fluid in the first case, or solute from the absorbent/adsorbent in the second case) are feasible with less effort than for the compression [17].

To make supercritical extraction processes more economic, separation of solute and solvent can be performed thanks to a membrane system. Sartorelli and Brunner [19] demonstrated that a membrane separation process can be proposed instead of the typical supercritical fluid cycle in the case of supercritical extraction to drastically reduce the energy losses. In fact, a stream of low volatile compounds (LVC) extracted by SC CO<sub>2</sub> can be discharged of 80%–90% of LVC using a nanofiltration membrane with a drop of pressure equal to 2 MPa instead of about 20 MPa in the typical supercritical fluid cycle.

### 7.2.1 CAFFEINE/SC CO<sub>2</sub> SEPARATION

Because caffeine extraction is an important industrial application of SC CO<sub>2</sub> technology, different studies have been recently conducted on solvent recovery by membrane separation. As the molecular weight (MW) (194 g mol<sup>-1</sup>) of caffeine is higher than CO<sub>2</sub> (44 g mol<sup>-1</sup>), classical suitable membrane for this application needs to reject caffeine while letting CO<sub>2</sub> cross through the membrane. Thus, pure CO<sub>2</sub> can be obtained on permeate side and recycled.

All published experiments on caffeine/SC CO<sub>2</sub> membrane separation are made according to the same principle. A schematic diagram presenting roughly the process is given in Figure 7.1. Carbon dioxide (1) is first liquefied in the cooler (2), pressurized in the pump (3), and heated until its working temperature in the heat exchanger (4). SC CO<sub>2</sub> is then passed through the extractor (5) to recover caffeine. This binary solution flows into the membrane module (6) where separation takes place. The operating pressure and transmembrane pressure are controlled with backpressure regulators (7) on the permeation and retention sides of the membrane. The pressure of SC CO<sub>2</sub> solution is released down to atmospheric pressure at the outlet of backpressure regulators, and the solute may be easily separated from CO<sub>2</sub> in gas/liquid separators (8).

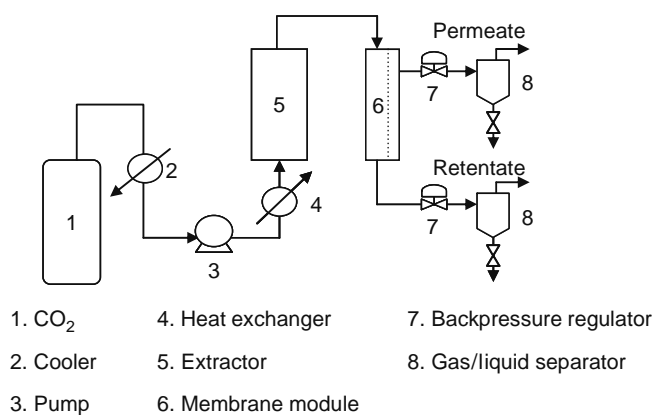


**FIGURE 7.1** Schematic diagram of the caffeine/CO<sub>2</sub> membrane separation process.

Two main criteria are used to describe performance of separation process. The solute (caffeine) rejection rate,  $R$ , which characterizes the selectivity of the membrane, can be calculated by the following equation:

$$R = 1 - \left( \frac{C_p}{C_f} \right)$$

where  $C_p$  and  $C_f$  are solute concentrations on permeate and feed sides, respectively.

As to membrane flow properties, they can be estimated through permeability constant value  $P_c$ :

$$P_c = \frac{J}{\Delta P}$$

where  $J$  is the permeate flux of SC CO<sub>2</sub> and  $\Delta P$  the transmembrane pressure.

Values of  $R$  and  $P_c$  already published for caffeine/SC CO<sub>2</sub> membrane separation are reported in Table 7.1 and will be discussed further.

Two mechanisms can act on transport phenomena, either alone or simultaneously: adsorption and molecular sieving.

### 7.2.1.1 Separation through Adsorption Mechanism

Various authors accounted for this mechanism. Adsorption properties of caffeine, compared to *n*-octanoic acid (which presents a molecular size nearly equal to that of caffeine), on a thin porous silica membrane prepared by a sol-gel method were investigated by Fujii et al. [5]. As shown in Table 7.1, the rejection value of caffeine was positive and equal to 0.65 whereas for *n*-octanoic acid it was negative (about  $-2$ : this means that concentration in the permeate was higher than in the retentate). This quite surprising result was explained while proposing the idea of differentiated adsorption/desorption properties of solutes on the membrane surface. Both solutes are strongly adsorbed (even if adsorption rate is slightly higher for *n*-octanoic acid); but contrarily to *n*-octanoic acid, caffeine is slowly desorbed. In such a case, a permanent adsorption layer is formed, making the

**TABLE 7.1**

**Comparison of the Use of Different Types of Membranes for Caffeine/Supercritical Carbon Dioxide Membrane Separation**

Type of Membrane	Pore Diameter (nm)	Pressure (MPa)	Temperature (°C)	Rejection, $R$	Permeability Constant, $P_c$ (mol m <sup>-2</sup> s <sup>-1</sup> Pa <sup>-1</sup> )	References
Thin silica porous membrane	3.3	20	40	0.65	$2.3 \times 10^{-8}$	[5]
Hydrophilic thin silica membrane	2.5	14	35	0.98	$4.4 \times 10^{-7}$	[4]
Zeolite membrane	1.1 <sup>a</sup>	20	40	0.98	$1.1 \times 10^{-8}$	[10]
Thin layer ZrO <sub>2</sub> -TiO <sub>2</sub> nanofilter	3	8	35	1.00	$1.2 \times 10^{-7}$	[12]

<sup>a</sup> Membrane pore diameter estimated from the Dubinin–Astakhov analysis [20].

pore narrower and causing a molecular-sieving effect which is responsible for the positive observed rejection. On the contrary, *n*-octanoic acid preferentially passed within the membrane pores under the effect of partition adsorption coefficient; but it is then taken away by solvent flow and solute rejection would be negative. Fujii et al. [5] observed caffeine rejection rates equal to 0.65, which are not satisfactory for practical purpose.

Tan et al. [4] proposed to use a thin silica membrane (prepared by them), which presents hydrophilic properties. They obtained very interesting results, i.e., a rejection rate and a permeability of  $0.98$  and  $4.4 \times 10^{-7} \text{ mol m}^{-2} \text{ s}^{-1} \text{ Pa}^{-1}$ , respectively (see Table 7.1). To underline the effects of adsorption, the same membrane was turned hydrophobic by chemical vapor deposition (CVD) treatment and tested. A very low rejection was obtained and no significant selectivity was given by this membrane. On the basis of the fact that caffeine has more affinity with hydrophilic surfaces, these results gave evidence that adsorption was the major mechanism. Therefore, adsorption phenomenon should be taken into account for membrane choice to control solute/membrane interactions.

### 7.2.1.2 Molecular-Sieving Mechanism

Even if Tan et al. [4] could obtain very interesting results based on adsorption effects, it is worth mentioning that getting steady-state working conditions with this technology is hard to achieve: caffeine rejection rate would drop when adsorption equilibrium is approached. This constitutes a strong limitation for industrial applications.

That is the reason why lower pore size membranes working by molecular-sieving mechanism have been tested with a view to perform continuous operations. The use of a zeolite membrane (pore diameter estimated from the Dubinin–Astakhov analysis [20]: 1.1 nm) provided an interesting rejection of 0.98 [10] (see Table 7.1). In that case, caffeine adsorption was weak and zeolite membrane could not be easily fouled with the solute. Transport was mainly controlled by molecular sieving, as indicated by the good rejection rate also obtained with other molecules (e.g., lauric acid) having molecular weight close to caffeine.

Due to low membrane pore size, permeability was strongly reduced ( $1.1 \times 10^{-8} \text{ mol m}^{-1} \text{ s}^{-1} \text{ Pa}^{-1}$  as presented in Table 7.1). The challenge will consist in obtaining good separation properties with a membrane having larger pores. An idea was to try to take advantages of the formation of clusters in the near critical region [21]. Built from approximately 100  $\text{CO}_2$  molecules surrounding a solute molecule, these clusters would present a global size largely higher than the isolated solute and could lead to a high solute rejection even with larger pore membranes. In that view, Chiu and Tan [12] tested caffeine/ $\text{CO}_2$  separation under different conditions (subcritical, critical, and supercritical states) through a thin layer  $\text{ZrO}_2\text{-TiO}_2$  nanofilter (pore diameter 3 nm). Results obtained in terms of rejection rate and permeability constant are reported in Figure 7.2. It appears that there is a maximum of caffeine rejection rate (equal to 100% as reported in Table 7.1) and permeability constant around 8 MPa, which is nearly the pressure at  $\text{CO}_2$  critical point. Cluster sizes as calculated by Chiu and Tan [12] are also indicated in Figure 7.2; it is worth noting that the biggest clusters, corresponding to a total amount of 135  $\text{CO}_2$  molecules around caffeine, are formed at the same pressure. Thus, for a pressure equal to 8 MPa, the size of caffeine clusters is so high that the solute is completely rejected by the membrane through molecular-sieving effect. For  $\text{CO}_2$  molecules whose diameter is less than 0.4 nm, it becomes easier to pass through the pores inducing an optimal  $\text{CO}_2$  permeability constant. When the pressure is larger than 8 MPa, clusters are smaller and some of them can enter into membrane pores. As a consequence,  $\text{CO}_2$  permeation is hindered.

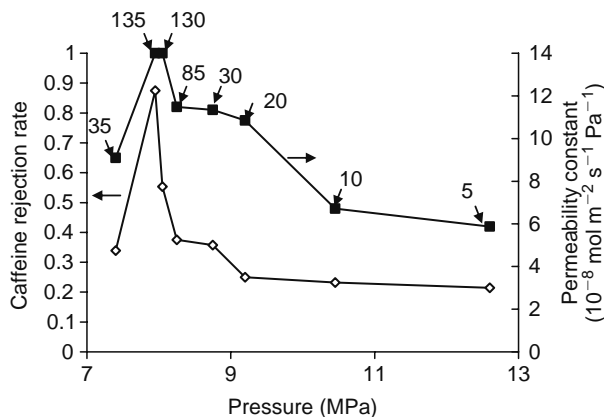


**FIGURE 7.2** Caffeine rejection rate (◇) and permeability constant (■) obtained during caffeine/ $\text{SC CO}_2$  separation on a nanofilter having a thin layer of  $\text{ZrO}_2\text{-TiO}_2$  ( $t = 308 \text{ K}$ , transmembrane pressure = 0.2 MPa). Values of estimated cluster size for each experimental point are indicated. (Adapted from Chiu, Y.-W. and Tan, C.-S., *J. Supercrit. Fluids*, 21, 81, 2001.)

This example clearly presents the importance of operating conditions such as pressure or even temperature on process performance.

However, there is a drawback with this way of doing when considering the entire extraction process. Indeed, it is worth recalling that solute extraction is generally conducted at pressure higher than the critical point; to continue after that separation of solvent by membrane at a lower pressure will need in its turn to increase again pressure before recycling pure SC CO<sub>2</sub>. These changes in pressure will be energy consuming. Nevertheless, the idea of performing separation at near critical pressure with relatively large pores still has its applicability based on the fact that high CO<sub>2</sub> permeation fluxes are obtained in addition to high solute rejection.

### 7.2.2 ESSENTIAL OILS/SC CO<sub>2</sub> SEPARATION

Essential oils are high value products mainly composed of terpene-like compounds. Their extraction with SC CO<sub>2</sub> was largely investigated and is now on the market as reported in the review of Reverchon [22].

Different studies were performed on the possibility of separating essential oils and SC CO<sub>2</sub> through a reverse osmosis membrane in a dead end flow regime. First, a cellulose acetate membrane was tested for nutmeg essential oil separation [14], which led to interesting results as retention was equal to about 0.96 and attractive CO<sub>2</sub> fluxes were obtained (permeability constant from 2.0 to  $1.1 \times 10^{-7}$  mol m<sup>-2</sup> s<sup>-1</sup> Pa<sup>-1</sup> depending on essential oil concentration in the feed). In addition, rejection rate remained stable over a period of 180 h indicating a good resistance of the membrane to the supercritical environment. These experimental results were discussed in the sense of study of transport phenomena and modeled through the irreversible thermodynamics approach [23]. Results proved a linear relationship between the CO<sub>2</sub> flux with the transmembrane pressure and the insensibility of the flux to tested temperatures (corresponding to different density values), which would indicate a predominant convective behavior during the CO<sub>2</sub> permeation through the membrane. Transmembrane pressure is thus the driving force. This was explained by the fact that CO<sub>2</sub> is able to plasticize cellulose acetate membranes. In that specific case, the swelling of the polymer chains does not induce disadvantages but facilitates the transport of the solvent.

The possibility of using commercial reverse osmosis membranes for solute/CO<sub>2</sub> separation was then extended to other essential oils such as lemongrass and orange ones [16] or to D-limonene [15].

### 7.2.3 ORGANIC COMPOUNDS/SC CO<sub>2</sub> SEPARATION

Some specific studies were performed for separation of organic compounds from SC CO<sub>2</sub> through an asymmetric polyimide membrane. Different solutes were investigated: ethanol [24], isooctane [25], and some petroleum components [26]. Results were expressed as separation factor  $\alpha_{\text{sol}/\text{CO}_2}$ :

$$\alpha_{\text{sol}/\text{CO}_2} = \frac{y_{\text{sol}}/y_{\text{CO}_2}}{x_{\text{sol}}/x_{\text{CO}_2}}$$

where  $y_i$  and  $x_i$  are the mole fractions of the component  $i$  ( $i = \text{sol}$  [for the solute] or CO<sub>2</sub>) in the permeate and in the feed, respectively.

Separation factor was from 4 to 7 for petroleum components and the best values obtained for ethanol and isooctane were 87 and 12.8, respectively.

## 7.3 COUPLING SCF EXTRACTION WITH NANOFILTRATION FOR PROCESS INTENSIFICATION

Considering that nanofiltration and supercritical fluid extraction processes are intended to act on the same chemical species (i.e., low-molecular weight compounds up to 1500 Da), Sarrade et al. proposed the idea of a hybrid process coupling the two functions, using one single pumping device and developing synergistic effects. This new process enables to conduct in one single apparatus solutes extraction and purification or fractionation of the extracted mixture. A pilot plant similar to the one presented in Figure 7.1 may be used; simply CO<sub>2</sub> obtained in the retentate stream is recycled. The role of the membrane is not here to separate solvent from solutes, but to extract selectively some kind of solutes.

The first awaited advantage of the process is to be able to work with a high permeate flux because of the low viscosity of SC CO<sub>2</sub> (10 times lower than for water). Indeed the membrane used in the process is a hybrid nanofiltration element, constituted from an inorganic substrate (TiO<sub>2</sub> with a mean pore diameter of about 10 nm) on which a nafion layer had been deposited, the prevailing mass transfer mechanism of which is convection. This fact could be checked through experiments conducted successively with water and SC CO<sub>2</sub>, flows obtained being in the opposite ratio of fluid viscosities within less than 10%.

Another expected advantage of the technique is a good control of the whole extraction/separation process. It is worth recalling that, with the classical supercritical fluid extraction process, the choice of optimal extraction conditions is often

blocked by a preoccupation with a good final fractionating of extracts. Thermodynamic conditions that make it possible to obtain a maximum extraction of compounds on one side, and an optimal selectivity during further separation of extracted species on the other side, are seldom identical; this makes it necessary to choose intermediate working conditions or expensive equipment involving several pressure release steps. Because with the new process the two functions are clearly independent; they may be optimized separately.

Finally, a reduced energy consumption may be expected because only permeate flux, and not the entire fluid stream as in classical supercritical fluid extraction process, must endure rising and falling pressure cycles.

All these advantages have been checked. First, experiments were carried out with model solutions constituted from small polyethyleneglycols—mixtures of EG/PEG400 or PEG200/PEG400—dissolved in SC CO<sub>2</sub> at temperatures and pressures between 300 and 450 K, and 10 and 30 MPa, respectively [11,27]. Then extraction/separation of natural products was investigated [28]: recovery and fractionation of unsaturated fatty acids from fish oil such as EPA (eicosapentaenoic acid) and DHA (docosahexaenoic acid), today used in human medicine for reduction of lipid absorption and prevention for heart disease; extraction and purification of  $\beta$ -carotene (provitamin A), an antioxidant supposed to prevent some cancers and also a well-known yellow-orange natural colorant of agro-food industries. For these applications, the new technique provides an original and effective way to get good quality extracts in safeguarding environmental conditions.

#### 7.4 MEMBRANE REACTORS WITH SUPERCRITICAL FLUIDS

SC CO<sub>2</sub> has some clear advantages over organic solvents for reaction purposes [29–32]. These advantages fall into different categories: environmental benefits, health and safety benefits, and process and chemical benefits. It is worth recalling that small changes in pressure or temperature cause large changes in density, enabling the fine tuning of the physical properties of the fluid, which facilitates optimization of reaction rate and selectivity. Moreover, the high diffusivity in SC CO<sub>2</sub> (one or two orders of magnitude higher than in common solvents) enhanced the mass transfer in the system, thus increasing reaction rate especially when mass transfer is limiting [33].

Catalytic reactions can be successfully performed in SC CO<sub>2</sub> as reviewed by Jessop et al. [29] and Hyde et al. [31]. Different reactions were studied in the field of homogeneous catalysis [29]—isomerization, hydrogenation, hydrosilylation, olefin metathesis, cyclization, and other C–C bond forming reactions, oxidation- or heterogeneous catalysis [31]—hydrogenation and dehydrogenation, hydroformylation, Friedel–Crafts acylation and alkylation, etherification, oxidation. It could be particularly attractive to use membrane reactors to conduct such reactions, thus pooling the advantages of supercritical fluid solvents and membrane reactors (principally the possibility of reusing and recycling the catalyst: see Chapter 36 of this book).

As shown in Figure 7.3, two membrane reactor configurations can be proposed: one with free catalyst and the other one with catalyst fixed on the membrane. In the first case, the membrane insures rejection of catalyst and keeps it in a restricted part of the system where reaction takes place. In the second case, the catalyst is fixed on the surface or in the pores of the membrane and reaction takes place at crossing.

In spite of the potential advantages of the use of a catalytic membrane reactor to perform chemical reactions in SC CO<sub>2</sub>, very few references are available on this topic. The concept was however demonstrated for the hydrogenation of 1-butene using a fluoros derivative of Wilkinson's catalyst [32]. The reaction was successfully performed in a free catalyst membrane reactor equipped with a silica membrane.

In addition to chemicals, biological catalysts such as enzymes can be used to catalyze reactions in SC CO<sub>2</sub>. Since the first attempt to operate reactions in supercritical fluids published by Randolph et al. [34], various type of enzymes were studied: lipase, oxidase, decarboxylase, dehydrogenase, proteinase, etc. [33,35–37]. The effect of different parameters was extensively reported by Ballesteros et al. [35]. Enzyme activity and stability in supercritical conditions as well as the benefits of using supercritical fluids for enzymatic reactions (improved reaction rates, control of selectivity, etc.) have been demonstrated [36].

Enzymatic reactions were then performed in both free and immobilized catalyst reactors. Knez and Habulin [38] studied sunflower oil hydrolysis in a continuous stirred tank reactor acting as a free catalyst reactor. Enzyme was retained in the reactor

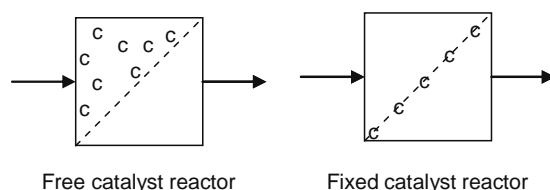


FIGURE 7.3 Schematic diagram of free and fixed catalyst reactors (c, catalyst; ---, membrane).

thanks to a polysulfon membrane placed between two sintered plates and fitted in the reactor: a conversion close to 20% was obtained in the permeate. It is also conceivable to perform biocatalyzed reactions in a fixed catalyst reactor either with permeate flow or not. Such an enzymatic membrane reactor was studied for butyl butyrate synthesis by immobilized lipase on an active membrane [39]. As permeate exit was closed, the reactor worked on a batch mode. The synthetic activity of the enzymatic membrane in SC CO<sub>2</sub> was 33-fold higher than that in most hydrophobic solvent (hexane) thus showing the suitability of this reaction media for this model reaction. In addition, by carrying on the synthesis of L-tyrosine methyl ester catalyzed by a protease in the same reactor, Lozano et al. [37] obtained a productivity 1.5-fold higher than with a fixed bed reactor constituted of celite on which enzymes were previously adsorbed. Thus the interests of the membrane reactor and of the supercritical media were proved. Finally, by working in a flow through mode (i.e., with a permeate stream) a 3-fold increase was observed in productivity which enhances the attraction of the process.

## 7.5 SUPERCRITICAL FLUID MEMBRANE CONTACTORS

Recently, a new kind of membrane processes has emerged—the so-called membrane contactors [40] in which the membrane mainly acts as a physical barrier between two phases without significant direct effect on selectivity. In such devices, the membrane acts as packing material in traditional columns but with considerably enhanced performance: it insures a well-controlled contact between the two fluids, and improved solute extraction from one side to the other. A schematic diagram of a membrane contactor (with only one membrane in this example) performing gas/liquid or liquid/liquid mass transfer is given in Figure 7.4. One fluid is flowing on one side of the membrane while the other phase circulates in counter current on the other side of the wall. Most of the time, hydrophobic porous membranes are involved, and by tight control of transmembrane pressure, the interfacial area may be maintained inside the pores [41].

Membrane contactor represents an attractive alternative process over conventional dispersed phase contactors as regards its numerous advantages: absence of emulsions, absence of flooding at high flow rates, absence of unloading at low flow rates, etc. In addition, as this process do not require density difference between fluids, it is possible to carry on extraction with an enhanced number of couples of fluids. Moreover, membrane contactors offer a very high interfacial area: 30 times higher than what is achievable in gas absorbers, and 500 times higher than what is obtainable in liquid/liquid extraction columns, leading to remarkably low height of a transfer unit (HTU) values [41].

Carrying on membrane contactors with supercritical fluids as extracting solvent can lead to very attractive extraction results due to the specific properties of supercritical fluids. Advantages of membrane contactors and supercritical fluid extraction were thus coupled in an integrated process which was patented by Robinson and Sims [42] and commercialized as the PoroCrit process. The principle is the same as presented in Figure 7.4 where one of the fluids is constituted of a subcritical or supercritical fluid. The process is conducted with high pressures on both sides of the membrane, and the solute is extracted across the membrane as driven by a concentration gradient. Any pumpable fluids including suspensions can be treated, thus inducing a wide range of applications [43]. CO<sub>2</sub>-soluble components can be stripped from aqueous stream such as fruit juices, fermentation broth, enzyme reaction mixture, wastewater, or oils. As examples, polypropylene membranes with a pore size equal to 0.2 μm and configured as hollow fiber bundles were used for orange aroma, caffeine, or vanillin extraction by SC CO<sub>2</sub> [43] and organic solvent recovery from water solutions. [44]. Although CO<sub>2</sub> is often the solvent of choice in dense gas extraction, other solvents such as compressed ethane and propane were tested for ethanol and acetone extraction from aqueous mixtures, and compared to SC CO<sub>2</sub> [45]. No significant extraction of ethanol by ethane was observed in the tested conditions while propane allows extraction but at a significantly lower level than SC CO<sub>2</sub>. Thus, SC CO<sub>2</sub> remains the more attractive solvent for this application; in addition it is worth recalling that SC CO<sub>2</sub> presents the great advantage to be nonflammable contrarily to propane.

Mass transfer in such membrane contactors was modeled for different applications involving SC CO<sub>2</sub> or other compressed gas [40,46–48].

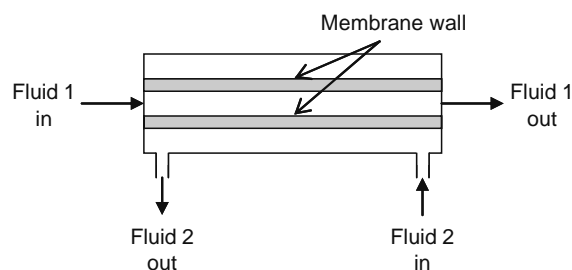


FIGURE 7.4 Schematic diagram of a membrane contactor.

## 7.6 SC CO<sub>2</sub>-ASSISTED ULTRAFILTRATION

Ultrafiltration of highly viscous liquids (particularly oils) is an uneasy and expensive operation mainly characterized by low permeate flux and high energy consumption. To overcome these difficulties, it has been already proposed to decrease viscosity by either increasing the process temperature (up to 350°C) [49] or adding specific chemicals (such as surfactants or organic solvents) [50]. However, increasing the process temperature requires very high temperatures that degrade the temperature-sensitive compounds in the oil and induce additional costs and risks, whereas adding specific chemicals raises the problem of solvent removing after filtration. That is the reason why a new cross-flow ultrafiltration process, taking advantage of the low viscosity, low surface tension, and tuneable solvent power properties of supercritical CO<sub>2</sub> to improve hydrodynamics, has been recently proposed [51,52]. Moreover, the process appears as particularly interesting for safeguarding of product quality and environment. In that alternative process, viscosity reduction is induced by fluidification of the viscous fluids following SC CO<sub>2</sub> injection.

The principle of experimental setup is presented in Figure 7.5. In addition to a loading stage, it mainly consists of a gas-pressurized cross-flow filtration circulation loop where the membrane allows the separation of the feed in two streams: the permeate and the retentate. Each stream is further separated into gas and liquid parts in the separation stage. Membranes are inorganic to ensure hard-operating conditions without failure.

With model solutions constituted of different base oils, it was first proved that, thanks to the viscosity reduction, the permeate flux is enhanced in the presence of SC CO<sub>2</sub> [52].

Then, the process was applied to an used motor oil [51]. It appears clearly that an increase of CO<sub>2</sub> pressure still permits to increase the permeate flux; but the effect is not significant above 15 MPa, which represents the optimum pressure for oil filtration. As a whole, a flux increase higher than 300% may be reached. Finally, from analysis of permeate and retentate, it follows that there is an excellent rejection rate of metals—Fe, Zn, Cu, etc.—which increases with transmembrane pressure up to more than 99% depending on species. For mass concentration factors of about 27, residues with a total metal content less than 4% of the initial load were found: oil regeneration was very effective.

In a more recent work, Rodriguez et al. [53] tried to perform the filtration of mineral oil fluidified by subcritical SC CO<sub>2</sub>. A strong fouling was observed. It was assumed that demixion occurs in the pores because of pressure reduction and shear stress, thus leading to the creation of very small bubbles of CO<sub>2</sub> which would obstruct membrane pores. Therefore, it is better to work at higher pressure to prevent this detrimental effect.

Combining this idea with the concept of membrane reactor leads to a new way for performing reaction on viscous solutions. In this view, a new process combining enzyme (as catalyst), membrane, and SC CO<sub>2</sub> has been proposed recently [54]. By replacing the classical barrier by a catalytic membrane with immobilized enzymes, the filtration system presented in Figure 7.5 may act as a catalytic membrane reactor. This new concept has been justified using as model system the interesterification of castor oil and methyl oleate catalyzed by a lipase from *Candida antarctica*. A conversion of about 30% was obtained and stability was verified on a 25 h experiment. In that case, SC CO<sub>2</sub> acts as a fluidifying agent that would enable on the one hand an interesting flux across the membrane due to viscosity reduction, and on the other hand an increase in conversion rate thanks to improved mass transfer properties.

## 7.7 MEMBRANE PREPARATION

Supercritical fluids offer new possibilities for the preparation of membranes, either inorganic or organic. Particularly, SC CO<sub>2</sub> can be usefully used instead of main classical organic solvents. Although SC CO<sub>2</sub> is a nonpolar solvent, which limits solubility of polar reactants, its combination of liquid-like density and gas-like viscosity/diffusivity leads to high reaction rate and easy recovery of products. Commonly used in organic chemistry, CO<sub>2</sub> is now proposed to be used in inorganic synthesis.

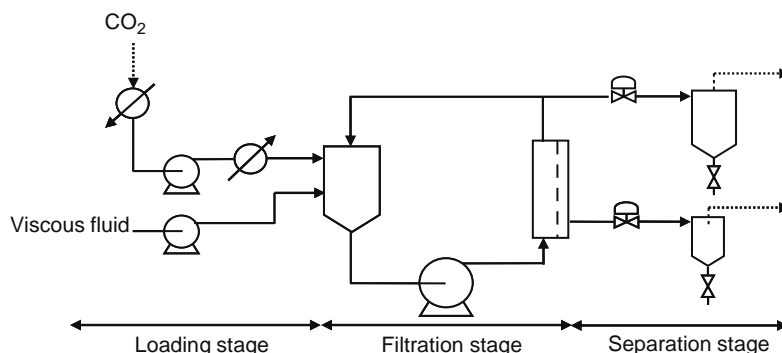


FIGURE 7.5 Experimental setup of the supercritical fluid-assisted ultrafiltration.

### 7.7.1 INORGANIC MATERIALS

A number of very interesting applications namely chromatographic stationary phase, adsorbent, catalytic support, or mineral membrane can be achieved using ultrafine metal-oxide particles. Supercritical fluids have been investigated as suitable and novel reaction media for the synthesis of such particles starting from titanium alkoxide precursors [55].

In 1999, Brasseur-Tilmant [56] presented a work dealing with modification of macroporous alumina media by  $\text{TiO}_2$  particles deposition using supercritical isopropanol. The aim was to prepare inorganic membranes for cross-flow filtration. Anatase particles were deposited on plane alumina support after thermal decomposition of titanium alkoxide precursors. A slight infiltrated zone was observed and a pore size reduction was achieved from 110 to 5 nm, leading to obtain fine ultrafiltration membranes. The main problem was to control the reaction at the membrane interface and not in the porosity, and moreover, this process was suitable for tubular membrane preparation.

Papet et al. [57] described the preparation of titanium hydroxide particles in a high-pressure stirred vessel using SC  $\text{CO}_2$  followed by particle recovery. Because of the high reactivity of the titanium alkoxide for hydrolysis, highly volatile amorphous fine powders of titanium hydroxide were formed at the pressure vessel surfaces. Scanning electron microscopy (SEM) observations of this powder (Figure 7.6) revealed a relatively homogeneous size distribution of microsized spherical particles depending on the reaction parameters.

Later, Papet [58] presented an alternative process for preparing tubular ceramic cross-flow filtration membranes. Papet's method consists of the casting of tubular mineral microfiltration membranes with titanium dioxide suspensions. The deposited particles on the porous support were then compressed and finally, the layer was consolidated by firing.

One issue to control the final pore size of the consolidated layer is to control the size of the deposited particles. Actually, using the submicronic titanium dioxide particles previously described, the preparation process allowed the authors to control the particle size (i.e., the layer pore diameter) by tuning the operating parameters during the process (temperature, pressure, contact time). The influence of the synthesis parameters on morphology and texture of titanium dioxide particles and the preliminary results concerning membrane preparation using the layer compression process show that the obtained membranes were still in the ultrafiltration range, due to shrinkage during sintering related to the low primary particles size and high specific surface area.

Further work in progress concerns other precursors for the production of ceramic oxide materials ( $\text{Ce}_{1-x}\text{Gd}_x\text{O}_{2-x/2}$  or doped  $\text{ZrO}_2$  and  $\text{LaGaO}_3$ ), which are oxides of interest as oxygen ion conductors [55].

### 7.7.2 POLYMERIC MATERIALS

Today the majority of polymeric porous flat membranes used in microfiltration, ultrafiltration, and dialysis are prepared from a homogenous polymer solution by the wet-phase inversion method [59–66]. This method involves casting of a polymer solution onto an inert support followed by immersion of the support with the cast film into a bath filled with a non-solvent for the polymer. The contact between the solvent and the non-solvent causes the solution to be phase separated. This process involves the use of organic solvents that must be expensively removed from the membrane with posttreatments, since residual solvents can cause potential problems for use in biomedical applications (i.e., dialysis). Moreover, long formation times and a limited versatility (reduced possibility to modulate cell size and membrane structure) characterize this process.

The difficulty in analyzing the phase inversion process is due to the interactions between the three components involved, and to the complex diffusion and convective processes that play an important role during the membrane formation. However, many researchers agree that there are two dominating factors controlling the formation of phase inversion membranes: thermodynamics and kinetics, correlated to each other during the solidification of casting solutions.

A new technique in which SC  $\text{CO}_2$  is used to induce the phase separation of the polymer solution has been recently proposed by different authors. Kho et al. [67] used compressed  $\text{CO}_2$  for the formation of Nylon 6 membranes. The process was

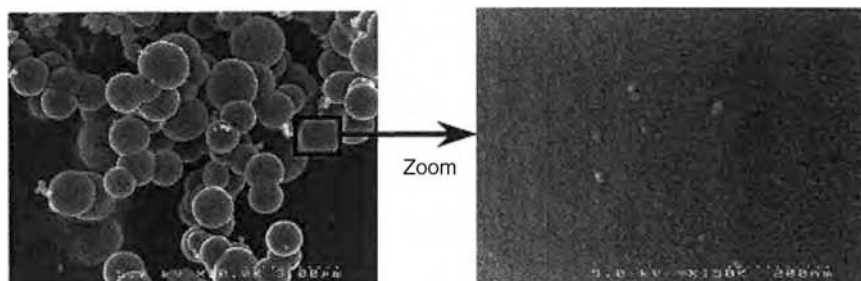


**FIGURE 7.6** Spherical nanophased titanium hydroxide particles obtained in SC  $\text{CO}_2$  from hydrolysis and condensation of tetraisopropyl-orthotitanate at 323 K and 30 MPa.

performed at 35°C with the final pressure up to 174 bar for 30 min. Thin films (thickness ranging from 150 to 250  $\mu\text{m}$ ) were obtained with uniform structures and cellular pores of 0.4  $\mu\text{m}$  in diameter. Matsuyama et al. on their side studied the formation of thin polystyrene membranes [68] and analyzed the effect of several process conditions (temperature, pressure, polymer concentration) on the pore size. They also investigated [69] the influence of different solvents during the formation of cellulose acetate membranes. Finally, Reverchon and Cardea [70] looked at the formation of cellulose acetate membranes from acetone using the supercritical  $\text{CO}_2$ -assisted phase inversion method. They reported the effect of an increase/decrease in affinity between supercritical  $\text{CO}_2$  and acetone (i.e., increasing/decreasing the supercritical  $\text{CO}_2$  solvent power). They also observed that polymer concentration influences the mean diameter of the cells that ranges from 2 to 50  $\mu\text{m}$  by varying the polymer concentration from 40% to 5% (w/w). A membrane formation mechanism was postulated. Yet more recently, these authors have investigated [71] the possibility of obtaining polysulfone membranes with a flexible and solvent-reduced supercritical  $\text{CO}_2$ -assisted technique. Polysulfone is a “green material,” biodegradable and biocompatible, which could be particularly interesting for medical applications.

Compared with the liquid-phase inversion method, this phase separation process has several advantages [59]:

- SC  $\text{CO}_2$  can dry the polymer membrane rapidly and totally without the collapse of the structure due to the absence of a liquid–vapor interface. The membrane can be obtained without additional posttreatments because there are no solvent residues.
- It is easy to recover the liquid solvent; it is dissolved in SC  $\text{CO}_2$  and can be removed from gaseous  $\text{CO}_2$  in a separator located downstream the membrane formation vessel.
- SC  $\text{CO}_2$  versatility allows modulation of the membrane morphology, cells, and pore size by simply changing the operative conditions.
- $\text{CO}_2$  is nontoxic, nonflammable, and cheap.

## 7.8 CONCLUSIONS

The review here proposed shows clearly that the use of a membrane in the presence of a supercritical fluid makes it possible the design of very attractive and powerful processes to improve transfer or reaction, to set in contact different phases, to fluidify highly viscous liquids, etc. or for the preparation of new generations of membranes. This is to be connected to the specific thermodynamic and transport properties of supercritical fluids and the particular environment that is created for all these operations.

For industrial applications, specific constraints flow from particular conditions of pressure and temperature. But there is no real impediment, which could obstruct practical implementation of these processes. Overall, the major interest of all these processes is that they are safeguarding for environment and product quality (which is essential in particular when working with biological compounds).

## REFERENCES

1. Katsaros FK, Steriotis TA, Stubos AK, Mitropoulos A, Kanellopoulos NK, and Tennison S. High pressure gas permeability of microporous carbon membranes. *Microporous Mater.* 1997; 8(3–4):171–176.
2. Koukou MK, Papayannakos N, Markatos NC, Bracht M, Van Veen HM, and Roskam A. Performance of ceramic membranes at elevated pressure and temperature: Effect of non-ideal flow conditions in a pilot scale membrane separator. *J. Membr. Sci.* 1999; 155(2):241–259.
3. Verkerk AW, Goetheer ELV, Van den Broeke LJP, and Keurentjes JTF. Permeation of carbon dioxide through a microporous silica membrane at subcritical and supercritical conditions. *Langmuir* 2002; 18:6807–6812.
4. Tan C-S, Lien H-C, Lin S-R, Cheng H-L, and Chao K-J. Separation of supercritical carbon dioxide and caffeine with mesoporous silica and microporous silicalite membranes. *J. Supercrit. Fluids* 2003; 26(1):55–62.
5. Fujii T, Tokunaga Y, and Nakamura K. Effect of solute adsorption properties on its separation from supercritical carbon dioxide with a thin porous silica membrane. *Biosci. Biotech. Biochem.* 1996; 60(12):1945–1996.
6. Hassan MH, Way DJ, Thoen PM, and Dillon AC. Single component and mixed gas transport in a silica hollow fiber membrane. *J. Membr. Sci.* 1995; 104(1–2):27–42.
7. Romero J, Gijiu C, Sanchez J, and Rios GM. A unified approach of gas, liquid and supercritical solvent transport through microporous membranes. *Chem. Eng. Sci.* 2004; 59(7):1569–1576.
8. Romero J, Le Cam S, Sanchez J, Saavedra A, and Rios GM. Permeation of supercritical fluids through a MFI zeolite membrane. *Chem. Eng. Sci.* 2001; 56(10):3139–3148.
9. Poshusta JC, Noble RD, and Falconer JL. Temperature and pressure effects on  $\text{CO}_2$  and  $\text{CH}_4$  permeation through MFI zeolite membranes. *J. Membr. Sci.* 1999; 160(1):115–125.
10. Tokunaga Y, Fujii T, and Nakamura K. Separation of caffeine from supercritical carbon dioxide with a zeolite membrane. *Biosci. Biotech. Biochem.* 1997; 61(6):1024–1026.
11. Sarrade S, Rios GM, and Carles M. Nanofiltration membrane behavior in a supercritical medium. *J. Membr. Sci.* 1996; 114(1):81–91.

12. Chiu Y-W and Tan C-S. Regeneration of supercritical carbon dioxide by membrane at near critical conditions. *J. Supercrit. Fluids* 2001; 21(1):81–89.
13. Damle S and Koros WJ. Permeation equipment for high pressure gas separation membranes. *Ind. Eng. Chem. Res.* 2003; 42:6389–6395.
14. Spricigo CB, Bolzan A, Machado RAF, Carlson LHC, and Petrus JCC. Separation of nutmeg essential oil and dense CO<sub>2</sub> with a cellulose acetate reverse osmosis membrane. *J. Membr. Sci.* 2001; 188(2):173–179.
15. Carlson LHC, Bolzan A, and Machado RAF. Separation of D-limonene from supercritical CO<sub>2</sub> by means of membranes. *J. Supercrit. Fluids* 2005; 34(2):143–147.
16. Sarmento LAV, Spricigo CB, Petrus JCC, Carlson LHC, and Machado RAF. Performance of reverse osmosis membranes in the separation of supercritical CO<sub>2</sub> and essential oils. *J. Membr. Sci.* 2004; 237(1–2):71–76.
17. Brunner G. *Gas Extraction*. New York: Springer, 1994, pp. 165–179.
18. Marr R and Gamse T. Use of supercritical fluids for different processes including new developments—a review. *Chem. Eng. Process* 2000; 39(1):19–28.
19. Sartorelli L and Brunner G. Separation of extracts from supercritical carbon dioxide by means of membranes. International Symposium on Supercritical Fluids, Atlanta, GA, April 8–12, 2000.
20. Dubinin MM and Astakhov VA. Description of adsorption equilibria of vapors on zeolites over wide ranges of temperature and pressure. *Adv. Chem. Series.* 1971; 102:69–85.
21. Debenedetti P. Clustering in dilute, binary supercritical mixtures: A fluctuation analysis. *Chem. Eng. Sci.* 1987; 42(9):2203–2212.
22. Reverchon E. Supercritical fluid extraction and fractionation of essential oils and related products. *J. Supercrit. Fluids* 1997; 10(1):1–37.
23. Spricigo CB, Bolzan A, Machado RAF, and Petrus JCC. Mathematical modeling of the membrane separation of nutmeg essential oil and dense CO<sub>2</sub>. *J. Membr. Sci.* 2004; 237(1–2):87–95.
24. Semenova SI, Ohya H, Higashijima T, and Negishi Y. Separation of supercritical CO<sub>2</sub> and ethanol mixtures with an asymmetric polyimide membrane. *J. Membr. Sci.* 1992; 74(1–2):131–139.
25. Ohya H, Higashijima T, Tsuchiya Y, Tokunaga H, and Negishi Y. Separation of supercritical CO<sub>2</sub> and iso-octane mixtures with an asymmetric polyimide membrane. *J. Membr. Sci.* 1993; 84(1–2):185–189.
26. Higashijima T, Ohya H, Tsuchiya Y, Tokunaga H, Aihara M, and Negishi Y. Separation of supercritical fluid mixtures of CO<sub>2</sub> and petroleum components with an asymmetric polyimide membrane. *J. Membr. Sci.* 1994; 93(2):165–173.
27. Sarrade S, Rios GM, and Carles M. Dynamic characterization and transport mechanisms of two inorganic membranes for nanofiltration. *J. Membr. Sci.* 1994; 97:155–166.
28. Sarrade SJ, Rios GM, and Carles M. Supercritical CO<sub>2</sub> extraction coupled with nanofiltration separation: Applications to natural products. *Sep. Purif. Technol.* 1998; 14(1–3):19–25.
29. Jessop PG, Ikariya T, and Noyori R. Homogeneous catalysis in supercritical fluids. *Chem. Rev.* 1999; 99:475–493.
30. Krmelj V, Habulin M, Vasic-Racki D, and Knez Z. Polymeric membranes for the use in high pressure membrane reactors. International Symposium on Supercritical Fluids, Atlanta, GA, April 8–12, 2000.
31. Hyde JR, Licence P, Carter D, and Poliakov M. Continuous catalytic reactions in supercritical fluids. *Appl. Catal. A Gen.* 2001; 222(1–2):119–131.
32. Goetheer ELV, Verkerk AW, van den Broeke LJP, de Wolf E, Deelman B-J, van Koten G, and Keurentjes JTF. Membrane reactor for homogeneous catalysis in supercritical carbon dioxide. *J. Catal.* 2003; 219(1):126–133.
33. Krieger N, Bhatnagar T, Baratti JC, Baron AM, De Lima VM, and Mitchell D. Non-aqueous biocatalysis in heterogeneous solvent systems. *Food Technol. Biotechnol.* 2004; 42(4):279–286.
34. Randolph TW, Blanch HW, Prausnitz JM, and Wilke CR. Enzymatic catalysis in a supercritical fluid. *Biotechnol. Lett.* 1985; 7(5):325–328.
35. Ballesteros A, Bornscheuer U, Capewell A, Combes D, Condoret JS, Koenig K, Kolisis FN, Marty A, Menge U, Scheper T, Stamatis H, and Xenakis A. Review article: Enzymes in non-conventional phases. *Biocatal. Biotransform.* 1995; 13:1–42.
36. Matsuda T, Watanabe K, Harada T, and Nakamura K. Enzymatic reactions in supercritical CO<sub>2</sub>: Carboxylation, asymmetric reduction and esterification. *Catal. Today* 2004; 96(3):103–111.
37. Lozano P, Belleville MP, Rios GM, and Iborra, JL. Transesterification enzymatic process with a dynamic membrane reactor in supercritical media. Seventh Meeting on Supercritical Fluids, Antibes, France, 2000.
38. Knez Z and Habulin M. Compressed gases as alternative enzymatic-reaction solvents: A short review. *J. Supercrit. Fluids* 2002; 23(1):29–42.
39. Lozano P, Villora G, Gomez D, Gayo AB, Sanchez-Conesa JA, Rubio M, and Iborra JL. Membrane reactor with immobilized *Candida antarctica* lipase B for ester synthesis in supercritical carbon dioxide. *J. Supercrit. Fluids* 2004; 29(1–2):121–128.
40. Bocquet S, Torres A, Sanchez J, Rios GM, and Romero J. Modeling the mass transfer in solvent-extraction processes with hollow-fiber membranes. *AIChE J.* 2005; 51(4):1067–1079.
41. Gabelman A and Hwang S-T. Hollow fiber membrane contactors. *J. Membr. Sci.* 1999; 159(1–2):61–106.
42. Robinson JR and Sims MJ. Method and system for extracting a solute from a fluid using dense gas and a porous membrane. US Patent 5,490,884, 1996.
43. Sims M, McGovern WE, and Robinson JR. Porocritical fluid extraction from liquids using near-critical fluids. *Membr. Technol.* 1998; 97:11–12.
44. Towsley RW, Turpin J, Sims MJ, Robinson J, and McGovern W. Porocritical fluid extraction using CO<sub>2</sub> for industrial organic solvent recovery and recycle. 6th Meeting on Supercritical Fluids, Nottingham, England, April 10–13, 1999.
45. Bothun GD, Knutson BL, Strobel HJ, Nokes SE, Brignole EA, and Diaz S. Compressed solvents for the extraction of fermentation products within a hollow fiber membrane contactor. *J. Supercrit. Fluids* 2003; 25(2):119–134.

46. Bothun GD, Knutson BL, Strobel HJ, and Nokes SE. Mass transfer in hollow fiber membrane contactor extraction using compressed solvents. *J. Membr. Sci.* 2003; 227(1–2):183–196.
47. Gabelman A, Hwang S-T, and Krantz WB. Dense gas extraction using a hollow fiber membrane contactor: Experimental results versus model predictions. *J. Membr. Sci.* 2005; 257(1–2):11–36.
48. Gabelman A and Hwang S-T. Experimental results versus model predictions for dense gas extraction using a hollow fiber membrane contactor. *J. Supercrit. Fluids* 2005; 35(1):26–39.
49. Arod J, Bartoli B, Biedermann JM, Caminade P, Martinet JM, Maurin J, and Rossarie J. Procédé de traitement par ultrafiltration à température élevée d'une charge hydrocarbonée. EC Patent 0,041,013, 1985.
50. Rambault D. Procédé de désasphaltage d'un résidu pétrolier par ultrafiltration sur membranes inorganiques: Etude des paramètres de filtration et des mécanismes de séparation. PhD dissertation, University of Montpellier, France, 1993.
51. Gourgouillon D, Schrive L, Sarrade S, and Rios GM. An environmentally friendly process for the regeneration of used oils. *Environ. Sci. Technol.* 2000; 34:3469–3473.
52. Sarrade S, Schrive L, Gourgouillon D, and Rios GM. Enhanced filtration of organic viscous liquids by supercritical CO<sub>2</sub> addition and fluidification. Application to used oil regeneration. *Sep. Purif. Technol.* 2001; 25(1–3):315–321.
53. Rodriguez C, Sarrade S, Schrive L, Dresch-Bazile M, Paolucci D, and Rios GM. Membrane fouling in cross-flow ultrafiltration of mineral oil assisted by pressurised CO<sub>2</sub>. *Desalination* 2002; 144(1–3):173–178.
54. Pomier E, Galy J, Paolucci-Jeanjean D, Pina M, Sarrade S, and Rios GM. A new reactor design combining enzyme, membrane and supercritical CO<sub>2</sub>: Application to castor oil modification. *J. Membr. Sci.* 2005; 249(1–2):127–132.
55. Sarrade S, Guizard C, and Rios GM. New applications of supercritical fluids and supercritical fluids processes in separation. *Sep. Purif. Technol.* 2003; 32(1–3):57–63.
56. Brasseur-Tilmant J. Elaboration de membranes inorganiques. Modification d'un support macroporeux en alumine par dépôt de particules de TiO<sub>2</sub> en milieu supercritique. PhD dissertation, University of Paris XIII, France, 1999.
57. Papet S, Sarrade S, Julbe A, and Guizard C. Titanium hydroxide synthesis in supercritical solvent. Sixth Meeting on Supercritical Fluids, Nottingham, England, 1999.
58. Papet S. Etude de la synthèse de matériaux inorganiques en milieu CO<sub>2</sub> supercritique. Application à l'élaboration de membranes minérales de filtration tangentielle. PhD dissertation, University of Montpellier, France, 2000.
59. Reverchon E and Cardea S. Formation of polysulfone membranes by supercritical CO<sub>2</sub>. *J. Supercrit. Fluids* 2005; 35(2):140–146.
60. Van de Witte P, Dijkstra PJ, van den Berg JWA, and Feijen J. Phase separation processes in polymer solutions in relation to membrane formation. *J. Membr. Sci.* 1996; 117(1–2):1–31.
61. Bulte AMW, Folkers B, Mulder MHV, and Smolders CA. Membranes of semicrystalline aliphatic polyamide nylon 4,6: Formation by diffusion-induced phase separation. *J. Appl. Polym. Sci.* 1993; 50(1):13–26.
62. Young T-H and Chen L-W. Pore formation mechanism of membranes from phase inversion process. *Desalination* 1995; 103(3):233–247.
63. Han M-J and Nam S-T. Thermodynamic and rheological variation in polysulfone solution by PVP and its effect in the preparation of phase inversion membrane. *J. Membr. Sci.* 2002; 202(1–2):55–61.
64. Van de Witte P, Esselbrugge H, Dijkstra PJ, van den Berg JWA, and Feijen J. Phase transitions during membrane formation of polylactides. I. A morphological study of membranes obtained from the system polylactide-chloroform-methanol. *J. Membr. Sci.* 1996; 113(2):223–236.
65. Han M-J. Effect of propionic acid in the casting solution on the characteristics of phase inversion polysulfone membranes. *Desalination* 1999; 121(1):31–39.
66. Lee K-W, Seo B-K, Nam S-T, and Han M-J. Trade-off between thermodynamic enhancement and kinetic hindrance during phase inversion in the preparation of polysulfone membranes. *Desalination* 2003; 159(3):289–296.
67. Kho YW, Kalika DS, and Knutson BL. Precipitation of Nylon 6 membranes using compressed carbon dioxide. *Polymer* 2001; 42(14):6119–6127.
68. Matsuyama H, Yano H, Maki T, Teramoto M, Mishima K, and Matsuyama K. Formation of porous flat membrane by phase separation with supercritical CO<sub>2</sub>. *J. Membr. Sci.* 2001; 194(2):157–163.
69. Matsuyama H, Yamamoto A, Yano H, Maki T, Teramoto M, Mishima K, and Matsuyama K. Effect of organic solvents on membrane formation by phase separation with supercritical CO<sub>2</sub>. *J. Membr. Sci.* 2002; 204(1–2):81–87.
70. Reverchon E and Cardea S. Formation of cellulose acetate membranes using a supercritical fluid assisted process. *J. Membr. Sci.* 2004; 240(1–2):187–195.
71. Reverchon E and Cardea S. Membranes formation by supercritical fluids. Proceedings of the 9th Meeting on Supercritical fluids, Trieste, Italy, 2004.

---

# 8 Techniques to Enhance Performance of Membrane Processes

*A.G. Fane and S. Chang*

## CONTENTS

8.1	Process Limitations and Enhancement .....	194
8.1.1	Limitations due to Concentration Polarization and Fouling .....	194
8.1.2	Critical Flux and Sustainable Flux .....	195
8.1.3	Methods to Control Concentration Polarization and Membrane Fouling .....	197
8.2	Secondary Flows .....	198
8.2.1	Dean Vortices .....	198
8.2.1.1	Characteristics of Dean Flow .....	198
8.2.1.2	Dean Flow-Enhanced Membrane Process .....	199
8.2.2	Taylor Flow .....	201
8.2.2.1	Characteristics of Taylor Flow .....	201
8.2.2.2	Membrane Filtration with Taylor Flow .....	202
8.3	Flow Channel Spacers .....	203
8.3.1	Net-Type Spacers .....	203
8.3.1.1	Geometrical Characteristics of Net-Type Spacers .....	203
8.3.1.2	Effect of Spacer Geometry .....	203
8.3.2	Other Turbulence Promoters .....	206
8.3.2.1	Helical Inserts .....	206
8.3.2.2	Corrugated Membranes .....	208
8.4	Pulsed Flow .....	210
8.4.1	Hydrodynamic Characteristics of Pulsatile Flow .....	210
8.4.2	Pulsatile Flow-Enhanced Membrane Processes .....	212
8.4.3	Transmembrane Pressure Backshock Technique .....	214
8.5	High Shear Devices .....	215
8.5.1	Rotating Systems .....	215
8.5.2	Vibratory Systems .....	216
8.5.2.1	Vibratory Shear-Enhanced Process .....	216
8.5.2.2	Vibratory Hollow Fiber Membranes .....	217
8.6	Two-Phase Flows .....	218
8.6.1	Gas-Liquid Two-Phase Flow .....	218
8.6.1.1	Two-Phase Flow Filtration with Tubular Membranes .....	218
8.6.1.2	Bubbling with Submerged Membrane Systems .....	221
8.6.2	Solid-Liquid Two-Phase Flow—By Particle Addition .....	223
8.7	Other Techniques .....	224
8.7.1	Electrofiltration .....	224
8.7.2	Ultrasound-Enhanced Filtration .....	226
8.8	Conclusions .....	227
Nomenclature .....		227
Greek Letters .....		229
References .....		229

The performance of a membrane process is a function of the intrinsic properties of the membrane, the imposed operating and hydrodynamic conditions, and the nature of the feed. This chapter describes methods available to enhance performance by various techniques, mainly hydrodynamic but also chemical and physical. The focus is on the liquid-based membrane processes where performance is characterized by attainable flux, fouling control, and separation capabilities. The techniques discussed include secondary flows, flow channel spacers, pulsed flow, two-phase flow, high shear devices, electromagnetic effects, and ultrasound.

## 8.1 PROCESS LIMITATIONS AND ENHANCEMENT

Performance is usually compromised by concentration polarization and fouling, which is explained below. This is followed by a discussion of the strategies available to limit their impact.

### 8.1.1 LIMITATIONS DUE TO CONCENTRATION POLARIZATION AND FOULING

A range of membrane processes are used to separate fine particles and colloids, macromolecules such as proteins, low-molecular weight organics, and dissolved salts. These processes include the pressure-driven liquid-phase processes, microfiltration (MF), ultrafiltration (UF), nanofiltration (NF) and reverse osmosis (RO), and the thermal processes, pervaporation (PV) and membrane distillation (MD), all of which operate with solvent (usually water) transmission. Processes which are solute transport are electrodialysis (ED) and dialysis (D), as well as applications of PV where the trace species is transmitted. In all these applications, the conditions in the liquid boundary layer have a strong influence on membrane performance. For example, for the pressure-driven processes, the separation of solutes takes place at the membrane surface where the solvent passes through the membrane and the retained solutes cause the local concentration to increase. The concentration profile of the retained solutes depends on the balance between the convective drag toward and through the membrane (resulting from the permeation flux) and back transport away from the membrane. The properties of this deposited layer could be either reversible or irreversible.

Concentration polarization is the reversible buildup of dissolved or suspended species in the solution phase, as depicted in Figure 8.1. The influence of concentration polarization on performance varies with different membrane processes. For RO and NF, concentration polarization can result in a significant increase in osmotic pressure. As a result, higher delivery pressure is required to provide the driving force to achieve reasonable flux values. For UF, the macromolecular solutes and colloidal species could have modest osmotic pressures and also the concentration at the membrane surface can rise to the point of incipient gel formation which is typically in the range of 20%–60% solute by volume [1]. This can lead to a transition from concentration polarization to membrane fouling. For MF membranes without a fouling layer formed on the surface or in the pores, concentration polarization of macromolecules should be negligible because large pore membranes are essentially not retentive to most macromolecules. However, MF membranes can experience particle polarization due to the retention of colloids and particulates.

Concentration polarization and particle polarization are related to the permeation-induced buildup of the concentration profile on the membrane surface without changing the characteristics of the permeability and selectivity of the membranes. Membrane fouling is related to irreversible changes in membrane permeability due to retained species deposition on the surface or the internals of the membrane. Figure 8.2 shows typical forms of membrane fouling applicable to MF and UF, including pore constriction, pore blocking, and gel/cake formation. This can also apply to NF and RO. Consider a particle with diameter  $d_p$  and a pore with  $d_{\text{pore}}$ , when  $d_p \ll d_{\text{pore}}$ , the particle can enter the membrane pore and pore constriction may occur. When  $d_p = d_{\text{pore}}$ , deposition of the particle onto the membrane surface may cause pore blocking. For  $d_p > d_{\text{pore}}$ , particles will be

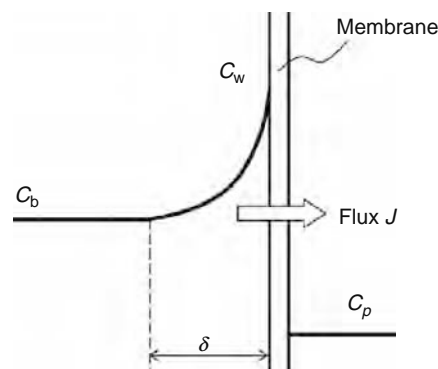
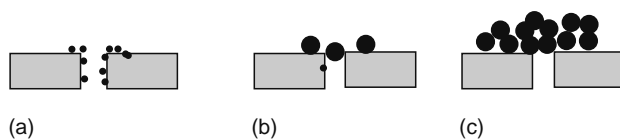


FIGURE 8.1 Schematics of the concentration polarization boundary layer for membrane filtration.



**FIGURE 8.2** Fouling schematics for different mechanisms. (a) Pore construction, (b) pore blocking, and (c) cake formation.

retained in a cake on the membrane surface. In a membrane filtration process, fouling could be a combination of different mechanisms due to the distribution of species sizes in real feeds. Usually, in the initial stages, membrane fouling could be dominated by pore constriction and pore blocking. Once the first cake layer has formed on the membrane surface, gel/cake formation may become the dominant fouling mechanism. The filtration behavior of the cake layer, including compressibility and permeability, is a function of the properties of the colloids deposited. For highly compressible cakes, usually formed by particles with strong interparticle interactions, the cake resistance may be dominated by a very thin layer adjacent to the membrane surface. Analogous phenomena occur with macro solutes and sparingly soluble solutes because concentration polarization frequently leads to fouling.

Membrane fouling may result in a significant increase in filtration resistance, leading to unstable filtration behavior. The pressure-driven membrane processes can be operated either with constant feed pressure or in the constant flux mode. For constant pressure operation where the transmembrane pressure (TMP) is maintained at a constant value during the filtration, the flux will decline with time due to the increased filtration resistance as shown in Figure 8.3a. It is observed that a quasi-steady state can be reached for crossflow membrane filtration when the flux drops to a value called the limiting flux where the particle deposition caused by the flux is balanced by the crossflow-induced particle back transport. The limiting flux is independent of the TMP and the filtration resistance but depends on the hydrodynamically induced back transport and is a function of surface shear, particle size, and the physical characteristics of the solution. The limiting flux can be experimentally determined or estimated based on the mechanisms of back transport, as discussed below. Membrane filtration can also be operated in the constant flux mode by extracting permeate at a constant flow rate, for example by using a suction pump. With fixed flux, the suction pressure and TMP could theoretically be maintained steady if the flux is below a critical flux (see Section 8.1.2). More typically, suction pressure will increase with time due to membrane fouling as depicted in Figure 8.3b. Constant flux operation has the advantage of avoiding rapid development of membrane fouling caused by a high initial flux as typically found with constant pressure filtration. This observation leads to the critical or sustainable flux strategy to enhance the performance of membrane processes.

### 8.1.2 CRITICAL FLUX AND SUSTAINABLE FLUX

For crossflow filtration, the tangential flow tends to sweep the particles away from the membrane surface or promote particle back transport. It can be assumed that the particle will not deposit onto the membrane surface if the permeate flux is controlled below a value such that the drag force exerted on the particle by the permeate flow is smaller than the lift force caused by the crossflow. Based on experimental observation, Field et al. [2] first suggested that there may be a critical flux below which species in the feed have negligible interactions with the membrane and the TMP is similar to that of pure water at the same flux (the strong form of critical flux). If some interaction (such as adsorption) occurs, the flux at which the TMP-flux line becomes nonlinear is the weak form of the critical flux. Using a technique called direct observation through the membrane (DOTM), Li et al. [3] were able to visually confirm that a clean membrane without deposition was attainable during the microfiltration of latex particles if the flux was controlled below a certain critical value that is dependent on the crossflow velocity and particle size.

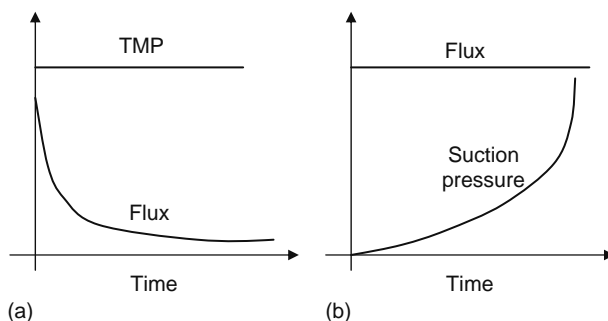


**FIGURE 8.3** TMP and flux profiles for (a) constant pressure and (b) constant flux filtration.

A number of mechanisms have been related to the particle back transport induced by crossflow. Among them, Brownian diffusion, shear-induced diffusion, and initial lift mechanisms are most widely accepted [4]. The Brownian diffusion model suggests that molecular diffusion in the boundary layer is responsible for the particle back transport, implying that the concentration polarization is inevitable in membrane filtration. Shear-induced diffusion arises from multiparticle interactions induced by shear flow. The essential requirement for these mechanisms is that the particle concentration should be sufficiently high to result in a significant particle interaction [5]. Inertial lift was first studied by Segre and Silberberg [6], who identified a “tubular pinch effect” in which lateral migration occurs both from the center and from the tube wall toward an eccentric equilibrium position for a range of particle size and flow conditions. Inertial lift was regarded to arise from nonlinear interactions of a particle with the surrounding flow field under conditions where the Reynolds number ( $Re$ ) based on the particle size is not negligible and so the nonlinear inertial terms in the Navier–Stokes equations play a role. The critical flux for different back transport mechanisms can be expressed in the following general form:

$$J_{cr} = c\gamma^n r_p^m \phi_b^p L_f^q \eta^s \quad (8.1)$$

where

- $\gamma$  is the shear rate at the membrane surface
- $r_p$  is particle radius
- $\phi_b$  is the solid volume fraction in the feed
- $L_f$  is the filter length
- $\eta$  is the viscosity
- $c, n, m, q,$  and  $s$  are coefficients

Equation 8.1 highlights the importance of shear rate in raising critical flux, and illustrates why the majority of performance enhancing techniques involve methods of increasing surface shear phenomena. Table 8.1 shows the coefficients in Equation 8.1 for different back transport mechanisms.

For a given crossflow filtration, the dominant particle back transport mechanism may depend on the shear rate and the particles size [4]. Brownian diffusion is only important for particles smaller than only a few tenths of a micron in diameter with relative low shear, whereas inertial lift is important for particles larger than several tens of microns with higher shear rates. Shear-induced back transport appears to be important for intermediate particle sizes and shear rates. Li et al. [7] reported that the shear-induced mechanism was able to predict fluxes comparable with the critical fluxes identified by the DOTM.

For mixed feed, the limiting critical flux will be that of the component with lowest critical flux; in practice, this may be impractically low and a sustainable flux, requiring infrequent cleaning, may be adopted. For soluble species and fine colloids, the critical flux can be considered as the flux below which the wall concentration does not initiate fouling.

One of the earliest approaches to sustainable operation was the Bactocatch process applied in the dairy industry [8] where in effect the TMP was maintained at a low-controlled value to limit flux and fouling. In this process, the axial feed flow in a ceramic tubular module was matched by the recirculation of permeate in the shell. It is now recognized that constant flux operation applying critical or sustainable flux concepts is attractive. A prime example is the large-scale membrane bioreactor (MBR) used for wastewater treatment where the long-term stable operation with minimum membrane chemical cleaning is desirable. In this application, controlling flux below the sustainable flux has become a common strategy to fight membrane fouling. The critical flux can be experimentally identified through constant flux filtration experiments by incrementing the flux until the TMP (or suction pressure) is no longer steady as depicted in Figure 8.4. For a real feed, the suction pressure may slightly increase even at very low flux. Figure 8.4 shows a typical TMP profile with stepped flux increase at 2 L/m<sup>2</sup> h obtained in filtration of synthetic wastewater [9]. From Figure 8.4, it can be seen that the increase in the rate of TMP became significant when the flux was higher than 10 L/m<sup>2</sup> h. However, closer observation indicates that the TMP started to increase even at a flux

**TABLE 8.1**  
**Coefficient in Equation 8.1 for Different Mechanisms**

Coefficients	Brownian Diffusion	Shear-Induced Diffusion	Inertial Lift
$c$	1.31	0.072	0.036
$m (r_p)$	-0.67	1.33	3
$n (\gamma)$	0.33	1	2
$p (\phi_b)$	-0.33	-0.33	0
$q (L_f)$	-0.33	-0.33	0
$s (\eta)$	-1	-0.33	0

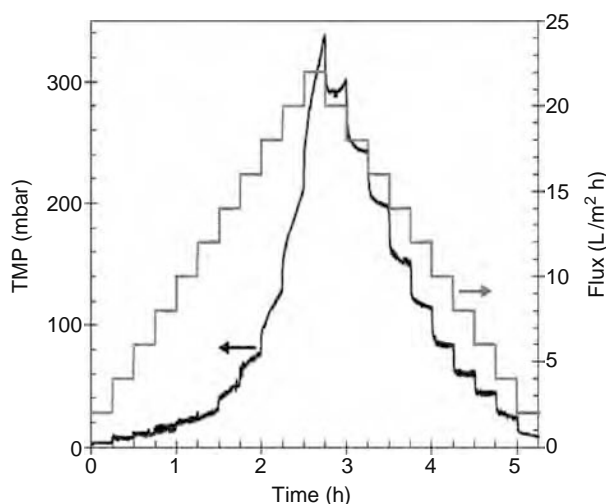


**FIGURE 8.4** Determination of the critical flux by stepped TMP increase protocols. (From Figure 3 in Le-Clech, P., Jefferson, B., Chang, I.S., and Judd, S.J., *J. Memb. Sci.*, 227, 81, 2003. With permission.)

as low as 2 L/m<sup>2</sup> h [9]. For cases like this (i.e., an MBR), a specific rate of increase in TMP (dTMP/dt) can be used for determination of the critical flux or the sustainable flux as discussed by Le-Clech et al. [9].

**8.1.3 METHODS TO CONTROL CONCENTRATION POLARIZATION AND MEMBRANE FOULING**

Figure 8.5 summarizes the range of methods used to control concentration polarization and membrane fouling. These include chemical, hydrodynamic, and physical methods. The most direct chemical approach to control membrane fouling is modification of the surface properties of the membranes, such as surface charge and hydrophilicity. Some methods used to modify membrane properties include heterogeneous chemical modification [10], adsorption of hydrophilic polymers [11], irradiation methods [12], and low temperature plasma activation [13]. The chemical methods also include application of coagulants to change particle size distribution in the treated feeds (note the importance of particle size in Equation 8.1). Addition of inorganic salts and polyelectrolytes as well as pH shifts in the feeds can destabilize colloids and result in formation of larger flocs, reducing the concentration of the colloids in the feeds that are mainly responsible for formation of high resistance. For applications such as macrosolute UF, pH adjustment to the feed can alter solute–membrane interactions and reduce fouling [14].

Most of hydrodynamic methods have focused on increasing the particle back transport from the membrane–liquid interface by increasing the shear rate and the flow instability in the boundary layer. These techniques include secondary flows, spacers and inserts, pulsed flow, high shear rate devices, vibrations, and two-phase flow. The physical methods that are currently been tested to enhance filtration performance of membranes include the application of electric fields and ultrasound.

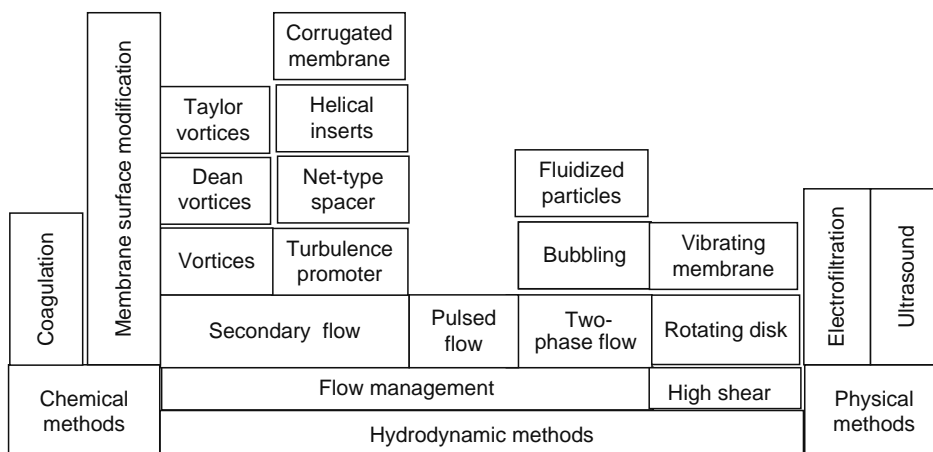


**FIGURE 8.5** Methods used for performance enhancement of membrane filtration.

The performance enhancement by a specific hydrodynamic technique is assessed by comparing the steady flux obtained under the same filtration conditions with and without imposition of the hydrodynamic technique. However, since most of the hydrodynamic techniques used for flux enhancement also result in an increase in the energy consumption, there is a trade-off between capital cost (related to flux enhancement) and operating cost (related to energy consumption). In filtration processes, the energy will be dissipated by crossflow and driving the permeate going through the membrane. Thus the overall power expenditure within the module ( $P_d$ ) can be approximated by

$$P_d = |Q_f \Delta P_L + Q_p P_{tm}| \quad (8.2)$$

where

$Q_f$  is the crossflow flow rate

$Q_p$  is the permeate flow rate

$P_{tm}$  is the TMP

$\Delta P_L$  is the pressure loss in the module (a part of which is used to generate surface shear)

Then the energy expenditure per unit volume of permeate in  $\text{kw h/m}^3$  is

$$E_d = \frac{1}{3.6 \times 10^6} \left( \frac{Q_f \Delta P_L}{Q_p} + P_{tm} \right) \quad (8.3)$$

The costs of the filtration processes include module and energy cost. The module cost depends on the membrane area (inversely related to flux), so the module cost per unit filtrate can be calculated by

$$\text{Module cost } (\$/\text{m}^3) = \left( \frac{1}{J_d} \right) (\text{s/m}) \times C_{\text{mem}} (\$/\text{m}^2\text{s}) \quad (8.4)$$

where

$J_d$  is the design flux of the filtration process

$C_{\text{mem}}$  is the cost of capital related to membrane area per unit time

The critical flux or sustainable flux can be used as the design flux for the processes, which is to be enhanced by the hydrodynamic techniques applied.

The energy cost can be estimated by

$$\text{Energy } (\$/\text{m}^3) = E_d (\text{kW h/m}^3) \times \text{cost } (\$/\text{kW h}) \quad (8.5)$$

Most of hydrodynamic techniques will reduce the module/membrane cost due to enhancement of the design flux but increase the energy cost due to increased pressure drop through the module. The optimal process design should result in a minimum total cost or the sum of the energy and module cost. An example of this trade-off is described in Section 8.3. The important point to note is that the performance enhancing techniques involve a cost that must provide a benefit and return on investment.

## 8.2 SECONDARY FLOWS

### 8.2.1 DEAN VORTICES

#### 8.2.1.1 Characteristics of Dean Flow

Dean vortices are the secondary flows that occur in the cross section of a curved channel or helically coiled tubes. Figure 8.6 shows the secondary flow developed in a helically coiled tube. When fluid flows through the helically curved tube, the faster elements of the fluid in the center of the tube tend to be moved outward by centrifugal force, while the slower elements of the fluid are forced inward to maintain mass balance, resulting in counter rotating vortices in the cross section of the channel as shown in Figure 8.6. The intensity of the secondary flow depends on the fluid flow in the tube and the geometric features of the curved channel, characterizing by the so-called Dean number ( $De$ ):

$$De = Re \sqrt{\frac{d_t}{D_t}} \quad (8.6)$$

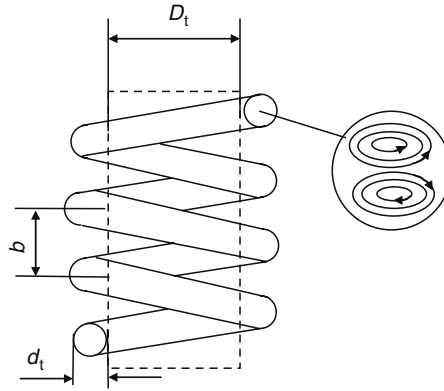


**FIGURE 8.6** Dean flow formed in a coiled helical tube.

where

$D_t$  is the coil diameter

Reynolds number,  $Re = d_t V_m / \nu$

$d_t$  is the tube diameter

$V_m$  is the mean azimuthal velocity

$\nu$  is the kinematic viscosity

A modified curvature diameter  $D'_t$ , which takes into account the torsion effect and varies with the pitch  $b$ , is formulated as below for helically coiled tubes:

$$D'_t = D_t \left[ 1 + \left( \frac{\pi}{b D_t} \right)^2 \right] \quad (8.7)$$

It is suggested that the appearance of the Dean vortices depends on the magnitude of the Dean number. Although it is suggested that the secondary flow can only appear above a critical Dean number [15], flow simulation indicates that a secondary flow field could be developed even at very low Dean number [16]. However, the effect of the secondary flow on mass and heat transfer is difficult to detect experimentally at Dean numbers lower than about 20.

The following empirical correlation from Mishra and Gupta [17] can be used to calculate the friction factor ( $f_c$ ) in a torus, coil, or helical tube under the conditions: Laminar,  $1 < De < 3000$ ;  $3 \times 10^{-3} < d_t/D_t < 0.15$ ;  $0 < (b/D_t) < 25.4$ .

$$f_c = f_s [1 + 0.033(\log De)^4] \quad (8.8)$$

where  $f_s$  is the friction factor in a similar straight tube. For Newtonian laminar flow,  $f_s$  can be calculated by

$$f_s = \frac{64}{Re} \quad (8.9)$$

The axial pressure drop due to friction for a helical coil tube can then be calculated by

$$\Delta P_L = f_c \frac{L_f}{d} \frac{1}{2} \rho V_m^2 \quad (8.10)$$

### 8.2.1.2 Dean Flow-Enhanced Membrane Process

Experimental evidence has demonstrated that Dean vortices can be effective for enhancement of membrane performance under laminar conditions [18]. As flow conditions approach the transition and turbulent flow regimes, straight membranes have a better mass transfer and higher wall shear rate than in flows with curved membrane channels. The effects of Dean vortices on the performance of membrane filtration have been studied experimentally and theoretically by Belfort and coworkers [19–22]. Mallubhotla and Belfort [21] assessed the filtration of suspensions of polydispersed polystyrene particles (mean diameter 25  $\mu\text{m}$ ) and silica particles (mean diameter 20  $\mu\text{m}$ ) with and without the presence of Dean flow using an 180° U-bend channel

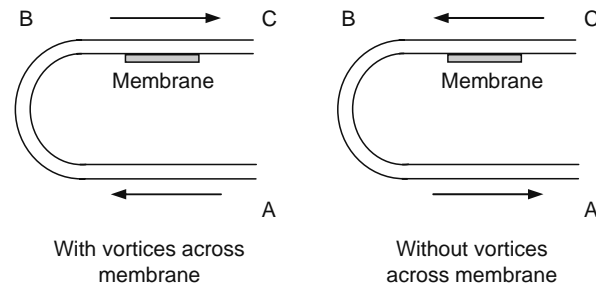


**FIGURE 8.7** Configuration of Dean generator test cell. (Adapted from Figure 1 of Brewster, M.E., Chung, K.Y., and Belfort, G., *J. Membr. Sci.*, 81, 127, 1993.)

with a membrane attached on the lower surface of the upper linear part of the U channel after the curve. With such a test cell, the filtration can be conducted with and without the appearance of the Dean vortices in the crossflow over the membrane by using the flow setting shown in Figure 8.7. Figure 8.8 shows the permeation flux-time profiles for filtration of the polydispersed polystyrene particles with and without the Dean vortices. It can be seen from this figure that a significantly higher pseudo-steady state can be reached at an earlier stage in the filtration with Dean vortices than that without Dean vortices, indicating an improvement in filtration performance.

Although some of the earlier work on Dean flow-enhanced membrane filtration was conducted with modules designed by placing a half spiral tube onto a flat sheet membrane [19], most recent studies have been carried out with helical hollow fiber membrane modules. Moulin et al. [23] compared the ultrafiltration of colloidal bentonite and dextran solution with a coiled and a straight hollow fiber membrane, with hollow fiber configuration of  $d_{fi} = 0.93$  and  $0.7$  mm in the laminar flow region. It was reported that the secondary flow induced by the coiled geometry could enhance the limiting flux by up to a factor of 2 or 3 for the colloidal suspension and the macromolecular solution, respectively. The flux enhancement increased when the coil diameter was reduced from 11 to 4.1 cm, implying increased enhancement with increase in Dean number (Equation 8.6). Mallubhotla et al. [22] studied the effect of Dean vortices on nanofiltration of inorganic and amino acid solutions using helical hollow fiber membrane modules that were made by wrapping a 0.27 mm fiber (inner diameter) around a steel rod of 3.18 mm diameter. The results showed the flux of the helical module was about 16% higher for 0.02 mol KCl and  $K_2SO_4$  solution and about 32% higher for  $K_3PO_4$  than those with the straight module. For filtration of different amino acid solutions, the flux enhancement by Dean flow was found to be a strong function of the pH of the solution, ranging from less than 5% to 35% in the pH range of 3–10 with an increased enhancement at high pH. Although helically coiled hollow fibers have proved to be effective for flux enhancement, no large-scale commercial hollow fiber membrane module has adopted the design to date, probably due to the difficulty of fabrication.

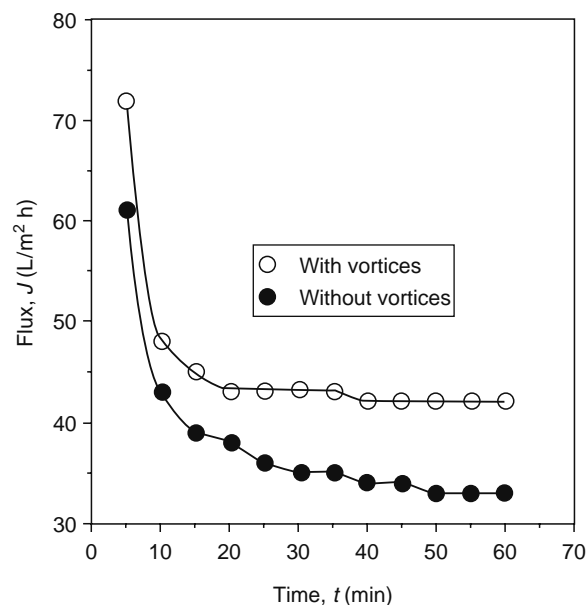


**FIGURE 8.8** Flux-time profile with and without Dean flow for filtration of S/DVB particles. (From Figure 3 in Mallubhotla, H. and Belfort, G., *J. Membr. Sci.*, 125, 75, 1997. With permission.)

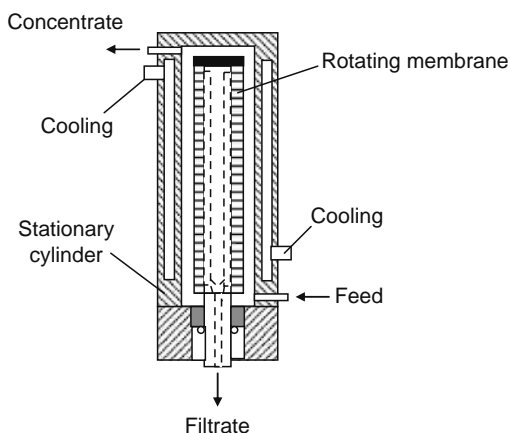


FIGURE 8.9 Schematics of axial rotatory membrane module.

## 8.2.2 TAYLOR FLOW

### 8.2.2.1 Characteristics of Taylor Flow

Another method that has been used to promote secondary flow is the generation of Taylor vortices in the annulus of two concentric cylinders with a rotating cylindrical filter. Figure 8.9 shows a typical rotatory membrane module that consists of two coaxial cylinders with the inner cylinder driven by an electric motor and the outer fixed. The membrane is usually attached to the inner rotating cylinder. The feed flows along the  $z$ -axis in the annular gap between the two concentric cylinders with the permeate were collected by a duct along the axis of rotation. When the inner cylinder rotates, a hydrodynamic regime is generated with annual counter rotating vortices (Taylor vortices) as shown in Figure 8.10. The Taylor flow can be characterized by the Taylor number:

$$Ta = \frac{\omega R_1 \Delta R}{\nu} \left( \frac{\Delta R}{R_1} \right)^{0.5} \quad (8.11)$$

where

$\omega$  is angular velocity

$R_1$  is radius of the rotating cylinder

$R_2$  is the inner radius of the fixed cylinder

$\Delta R = (R_2 - R_1)$ , i.e., the width of the annular gap

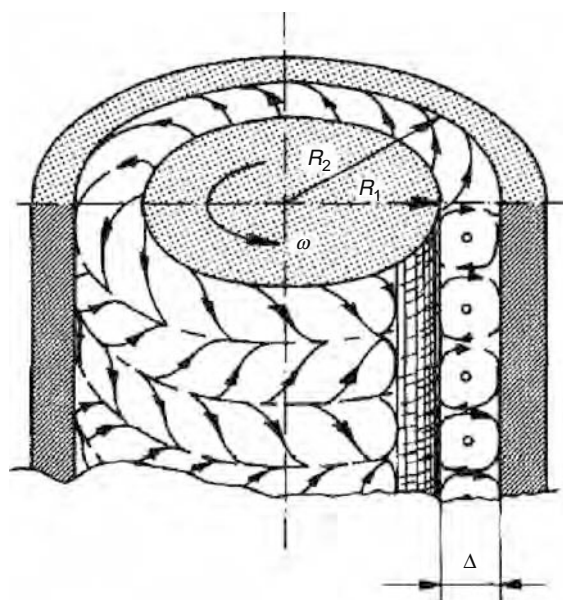


FIGURE 8.10 Schematic illustration of the Taylor vortices in the annulus of an axial rotating dynamic membrane filter. (From Figure 3 in Kroner, K.H. and Nissinen, V., *J. Membr. Sci.*, 36, 85, 1988. With permission.)

When the Taylor number exceeds a critical value ( $Ta_c$ ), a transition from stable Couette flow to vortical Taylor–Couette flow occurs. The critical Taylor number can be calculated by [24]:

$$Ta_c = 20.1 + 13.6 \left( \frac{\Delta R}{R_i} \right) + 1.4 \left( \frac{\Delta R}{R_i} \right)^2 \quad (8.12)$$

### 8.2.2.2 Membrane Filtration with Taylor Flow

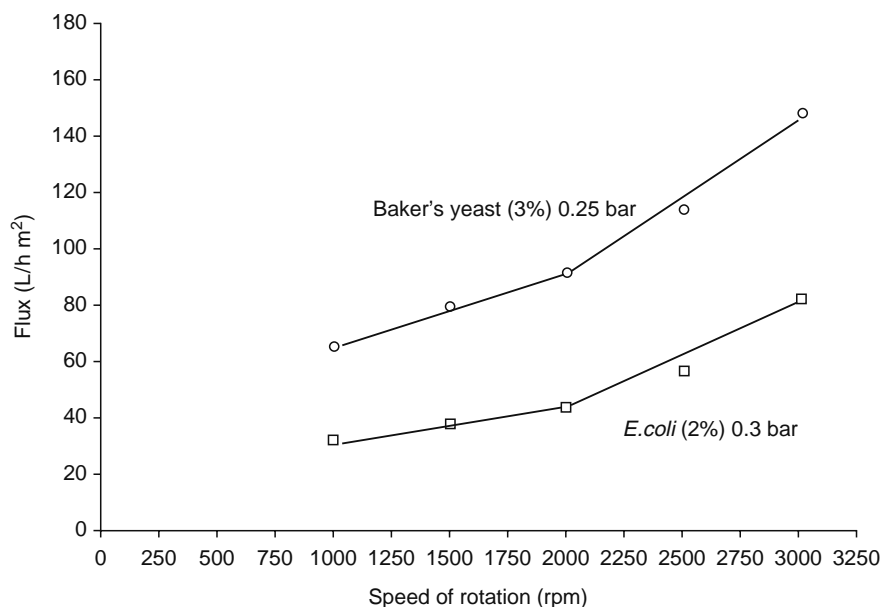
The rotating filter has been tested for a wide range of applications, including concentration of biological suspensions [25], skim milk separation [26], separating plasma from whole blood [27], and oil–water separation [28]. The flux obtained with a rotating filter will depend on the rotating speed, operating pressure, and the structure of the filter such as the gap size and the roughness of the rotating surface. It was reported that a flux from 50 to 150 L/m<sup>2</sup> h has been achieved for UF of 20% cutting oil emulsion under conditions of 300 kPa and rotating speeds from 210 to 2550 rpm [28]. Kroner and Nissinen [25] reported fluxes of 60–140 L/m<sup>2</sup> h for MF of 3% Baker’s yeast suspensions at 25 kPa and a flux range 30–75 L/m<sup>2</sup> h for MF of 2% *Escherichia coli* broth at 30 kPa in the rotating speed range 1000–3000 rpm. For cell concentration, a final batch concentration of 30%–70% for baker’s yeast and 9%–53% for bacterial suspensions, accompanied by a high protein transmission, was reported with the application of the rotating filter [25].

Figure 8.11 shows the effect of rotation speed for filtration of baker’s yeast suspension and *E. coli* fermentation broth [25]. In both cases, the increase in rotation speed in the range of 1000–3000 rpm, which corresponds to a range of  $Ta$  from about 2000–6000 for the test device, resulted in a substantial increase in flux with a transition point observed at a rotation speed of 2000 rpm—this corresponds approximately to a Taylor number of 3500, where turbulent Couette flow can be assumed.

An empirical correlation which expresses the Sherwood number ( $Sh$ ) as a function of the Taylor number was proposed by Holeschovsky and Cooney [29] as

$$Sh = 1.26Ta^{0.5} \left( \frac{2d}{R} \right)^{0.17} Sc^{0.33} \quad (8.13)$$

The main limitation of the axially rotating filter is difficulty of scale-up. Most of the reported experiments have been carried out with lab-scale units with the radius of the rotating cylinder <50 mm and the total filtration area <0.05 m<sup>2</sup>.



**FIGURE 8.11** Effect of rotating speed on permeate flux for filtration of baker’s yeast and *E. coli* suspensions. (From Figure 8 in Kroner, K.H. and Nissinen, V., *J. Membr. Sci.*, 36, 85, 1988. With permission.)

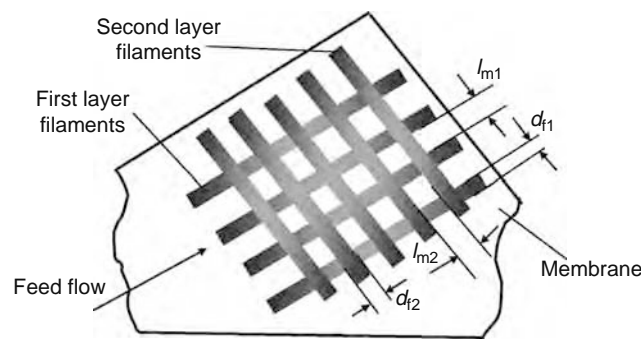


FIGURE 8.12 Schematics of net-type spacers.

## 8.3 FLOW CHANNEL SPACERS

### 8.3.1 NET-TYPE SPACERS

#### 8.3.1.1 Geometrical Characteristics of Net-Type Spacers

The net-type spacer is a key feature in the spiral wound module (SWM) widely used in RO (desalination), NF (water treatment), and some large-scale applications of UF (dairy and food). The spacers in the SWM have the dual function of keeping adjacent membranes apart to form a feed channel and of promoting turbulence in the feed channel. As shown in Figure 8.12, the net-type spacer usually consists of two layers of cylindrical filaments joined together to form a screen-like mesh. The typical mesh geometries include square, rhomboid, and parallelogram, with cell sizes of the order 4 mm and mesh heights of 1–2 mm. The diameter of the filaments in the top and the bottom layers could be identical (symmetric spacers) or different (asymmetric spacer). The main characteristic parameters of the spacers include filament diameter, mesh size, and the angle between the filaments (Figure 8.12). Other defined spacer parameters include the specific area,  $S_{vsp}$  [30], and spacer voidage  $\varepsilon$  [31].

#### 8.3.1.2 Effect of Spacer Geometry

In the SWM flow through the spacer-filled channel induces unsteady flows and increases local shear rates and local mixing, which reduce the boundary layer thickness and the concentration polarization. The mass transfer and pressure drop in a spacer-filled channel can be significantly affected by the geometric characteristics of the spacer. Figure 8.13 shows some typical commercial net-type spacers studied by Da Costa et al. [32]. Table 8.2 shows their characteristic parameters. Figure 8.14 shows the steady flux at different TMPs for filtration 1 g/L dextran (average molecular weight 500,000 Da) using a Koch Systems HFK-131 polysulphone 5 KDa UF membrane in a test cell with channel dimensions of 25 mm width and 285 mm long. Comparing the flux obtained with and without spacers, the flux was significantly higher (three to fivefold) for the filtration with

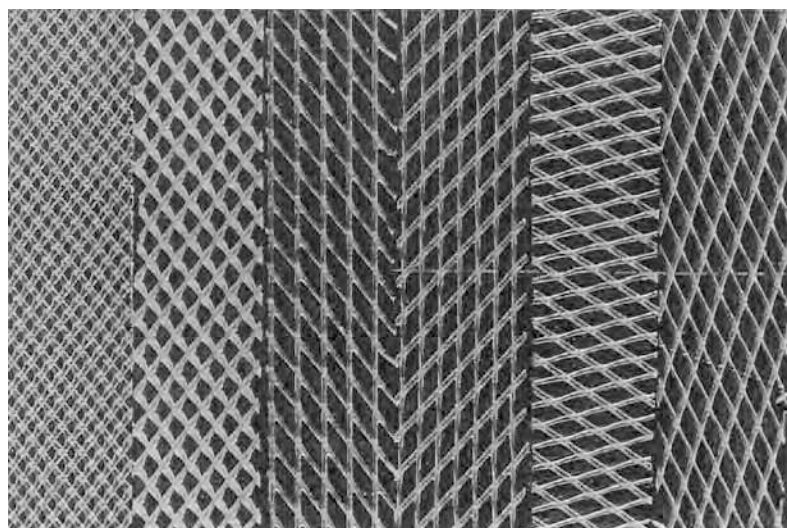


FIGURE 8.13 Typical commercial net-type spacers. (From Figure 2 in Da Costa, A.R. and Fane, A.G., *Ind. Eng. Chem. Res.*, 33, 1845, 1994. With permission.)

**TABLE 8.2**  
**Geometrical Characteristics of Spacers**

Spacer	$h_{sp}$ (mm)	$d_f$ (mm)	$l_m^*$	Angle (Degree) <sup>a</sup>	Flow Angle (Degree) <sup>b</sup>
80 MIL-1	2.1	1.15	1.85	80	40
80 MIL-2	2.1	1.15	1.85	80	50
80 MIL-1E	2.1	1.15	4.85	80	40
80 MIL-2E	2.1	1.15	4.85	80	50
UF3	1.7	0.76 (1.07) <sup>c</sup>	4.06 (5.3) <sup>d</sup>	45	60
UF4	1.7	0.76 (1.07) <sup>c</sup>	4.06 (5.3) <sup>d</sup>	45	20

<sup>a</sup> Angle between the filaments facing the main flow direction.

<sup>b</sup> Angle between the filament and channel axis (main flow direction).

<sup>c</sup> Thin and thick filaments.

<sup>d</sup> Short and long filaments.

spacers. Inspection of Figure 8.14 shows that the flux enhancement was significantly influenced by the spacer geometry. The spacers also increased the channel pressure loss from about 1 kPa (empty channel) to as high as 167 kPa.

Da Costa et al. [32] showed that the mass transfer coefficient for various net-type spacers can be represented by a Sherwood correlation:

$$Sh = cRe^m Sc^p \left( \frac{d_h}{L_s} \right)^q \quad (8.14)$$

where

$L_s$  is channel length

$d_h$  is the hydraulic diameter

The hydraulic diameter can be calculated by

$$d_h = \frac{4 \times \text{cross section}}{\text{wetted perimeter}} = \frac{4\varepsilon}{2/h_{sp} + (1 - \varepsilon)S_{vsp}} \quad (8.15)$$

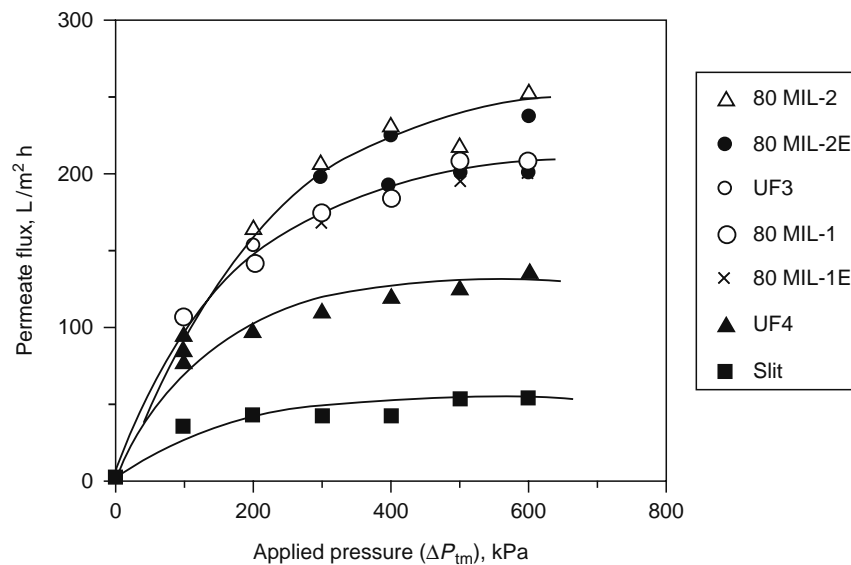


**FIGURE 8.14** Flux versus transmembrane pressure for different spacers. (From Figure 4 in Da Costa, A.R. and Fane, A.G., *Ind. Eng. Chem. Res.*, 33, 1845, 1994. With permission.)

where  $h_{sp}$  is the thickness of the spacer. This is equal to the height of the spacer-filled channel, but it is less than  $(d_{f1} + d_{f2})$  because the filaments are slightly embedded in each other. The other dimensionless numbers in Equation 8.14 can be calculated as

$$Sh = \frac{kd_h}{D} \quad (8.16)$$

$$Re = \frac{Vd_h}{\nu} \quad (8.17)$$

$$Sc = \frac{\nu}{D} \quad (8.18)$$

where  $V$  is the superficial channel axial velocity.

The friction factor for channel pressure loss can be related to the Reynolds number by the following empirical correlation:

$$f = \frac{A}{Re^n} \quad (8.19)$$

According to Da Costa and Fane [31], a lower value of  $n$  is indicative of a higher degree of turbulence in the fluid flow.

Table 8.3 shows the experimentally determined coefficients for the mass transfer and the friction coefficient correlations for the spacers shown in Figure 8.13 [32]. The coefficients in Equations 8.14 and 8.19 are highly spacer geometry dependent and different for various arrangements of the spacer in the channel. Da Costa et al. [32] also carried out an illustrative economic analysis on membrane (capital) and energy (operating) costs for the spacers tested based on hypothetical cost parameters. Table 8.3 shows the total costs of different spacer options under conditions of flow rate 3 L/min. Under such a flow condition, it seems that the UF4 was the most efficient spacer compared with the others. However, the total cost of the membrane process would be a function of the crossflow rate. A high crossflow rate can result in a high energy cost but a reduced membrane area because an increased flux should be achieved under high crossflow conditions. This implies that there may be an optimal crossflow rate at which the minimum total cost (i.e., the sum of the operating and capital costs) can be achieved. Figure 8.15 shows the estimated costs versus crossflow for the spacers tested by Da Costa et al. [32]. Given that typical spiral wound elements are usually operated with a crossflow velocity less than 0.6 m/s due to the limitation of the maximum pressure drop across the elements to avoid telescoping, the 80 MIL design could be the optimal spacer in this set of spacer designs for a practical crossflow range.

While the average mass transfer in a space-filled channel can be experimentally related to the spacer configuration and the average flow conditions, computational fluid dynamics (CFD) can be used to analyze the details of the local hydrodynamic characteristics and the wakes formed behind the filaments. Figure 8.16 shows the results of CFD simulations of the local flow patterns in a spacer-filled channel with the cavity, zigzag, and submerged spacer arrangements [33]. The simulations indicate that large recirculation regions may be formed behind the filaments and the shed vortices can scour the channel wall and enhance the shear stress at the membrane surface. For the cavity geometry spacer, the recirculation regions between sequential filaments influence each other and merge to form one large recirculation region between sequential filaments above a critical Reynolds number or below a critical mesh length. In contrast, the zigzag spacers forced the channel flow into an up-and-down zigzag pattern, which caused the recirculation region to reattach to the wall.

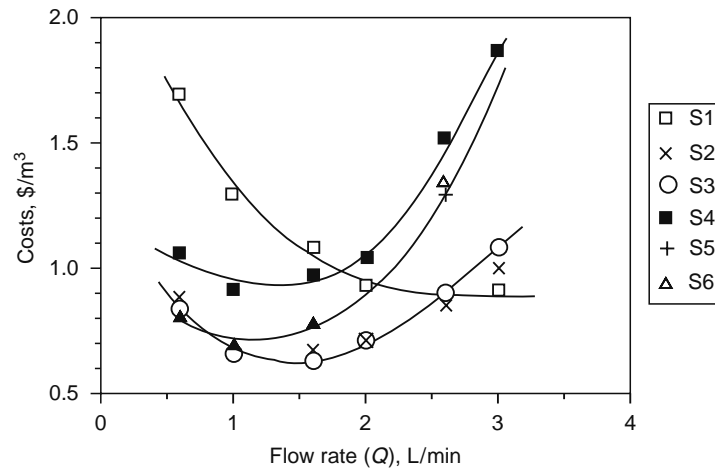
**TABLE 8.3**

**Summary of Mass Transfer Coefficients, Coefficients in Equations 8.18 and 8.23, and Cost Estimation for Filtration with Spacers Tested in Figure 8.13**

Spacer	$K (\times 10^6) \text{ m/s}$	$c$ (Equation 8.18)	$m$ (Equation 8.18)	$p$ (Equation 8.18)	$q$ (Equation 8.18)	$A$ (Equation 8.23)	$n$ (Equation 8.23)	Total Cost $\$/\text{m}^3$
Slit	1.0 (0.24 <sup>a</sup> )	1.86	0.43	0.32	0.33	—	—	1.98
80 MIL-1	6.0 (0.44)	0.0096	0.62	0.58	—	0.54	0.26	1.09
80 MIL-2	6.0 (0.44)	0.0096	0.66	0.58	—	0.91	0.23	1.73
80 MIL-1E	6.0 (0.25)	—	—	—	—	2.16	0.17	1.02
80 MIL-2E	6.0 (0.25)	—	—	—	—	4.51	0.15	1.71
UF3	5.0 (0.27)	0.0096	0.59	0.60	—	3.3	0.17	1.87
UF4	3.0 (0.27)	0.0096	0.50	0.59	—	0.61	0.30	0.80

Source: From Da Costa, A.R., Fane, A.G., Fell, C.J., and Franken, D., *J. Membr. Sci.*, 62, 275, 1991.

<sup>a</sup> Flow rate (L/min).



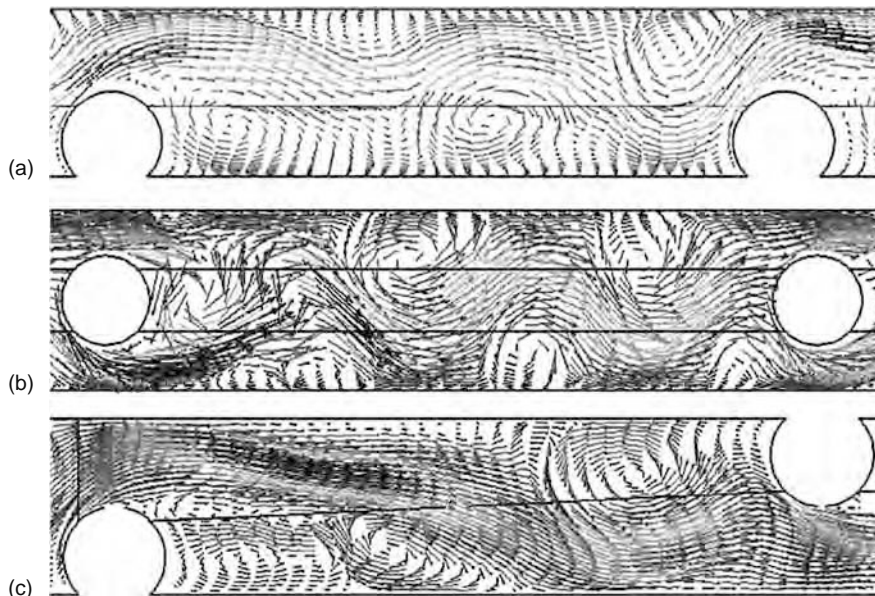
**FIGURE 8.15** Unit processing costs for different spacers. (From Figure 11 in Da Costa, A.R. and Fane, A.G., *Ind. Eng. Chem. Res.*, 33, 1845, 1994. With permission.)

Figure 8.17 shows experimental data for the typical particle deposition pattern in a spacer mesh with one filament orientated perpendicular to the main flow direction and the other filament parallel with the main flow. The deposition was recorded using a technique called DOTM [33]. The observation shows that there is a clear area with negligible deposition on the membrane behind and in front of the transverse filaments due to the effect of the inertial force and the scouring of the eddies. The clear area was observed to increase with increase in the crossflow velocity. Using the DOTM technique, Neal et al. [34] measured the effect of spacers on the critical flux of small particles and found that critical fluxes were enhanced by up to twice that of an empty channel. In summary, the flow channel spacers used in the popular SWM significantly enhance flux and performance for feeds with both dissolved solutes and particulates. The penalty is increased pressure loss. This leads to an optimal design and operating range that minimizes the processing costs.

### 8.3.2 OTHER TURBULENCE PROMOTERS

#### 8.3.2.1 Helical Inserts

Figure 8.18 shows a typical design of a winding helical insert that is centrally located in a tubular membrane. This type of insert can be easily fabricated by winding a metal or plastic wire onto a rod. The main structural parameters of this insert include



**FIGURE 8.16** CFD simulation for unsteady flow for  $Re = 1200$  for the (a) cavity, (b) submerged, and (c) zigzag spacer at a fixed mesh length and filament diameter. (From Figure 16 in Schwinge, J., Neal, P.R., Wiley, D.E., Fletcher, D.E., and Fane, A.G., *J. Membr. Sci.*, 242, 129, 2004. With permission.)

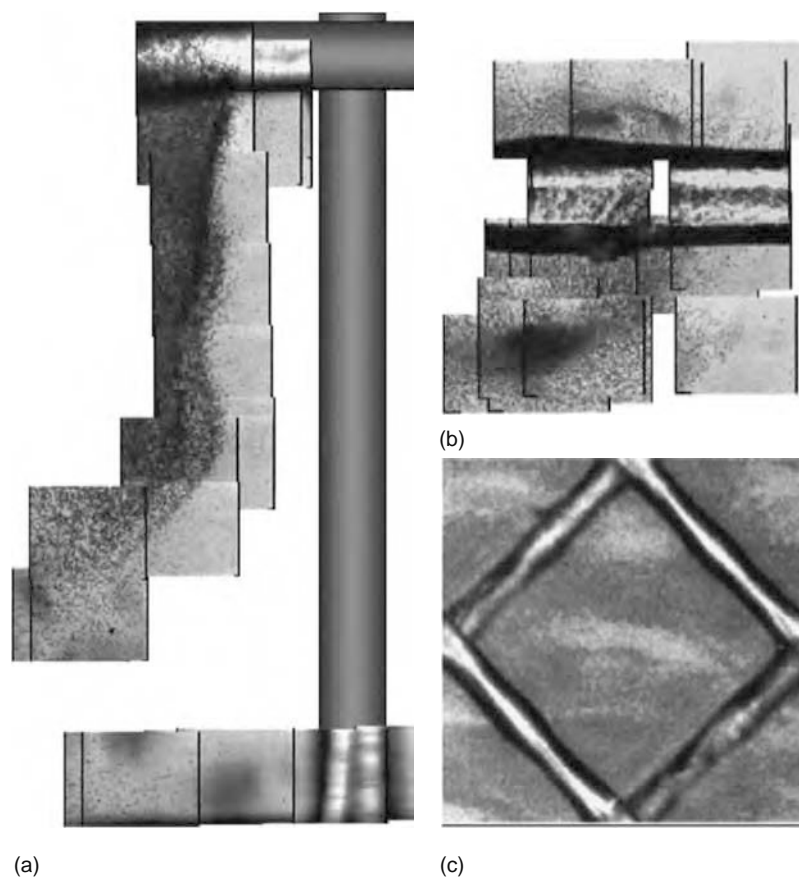


**FIGURE 8.17** DOTM revealed particle deposition pattern for different spacer orientations (a–c). (From Figure 13 in Schwinge, J., Neal, P.R., Wiley, D.E., Fletcher, D.E., and Fane, A.G., *J. Membr. Sci.*, 242, 129, 2004. With permission.)

the rod diameter, pitch, and the clearance distance between the tubular membrane and the insert. Flow visualization shows that the presence of the helical baffle in the tubular membrane induces a rotational flow within the baffle and the angle of rotation depends on the pitch or the number of turns over the length of the baffle. Three flow components were identified, which are the tangential flow in the clearance between the membrane and the insert, the rotational helical flow following the shape of the helical, and a reverse flow generated by the secondary flows on the cylindrical rod surface [35]. The flow near the membrane surface is dominated by tangential and rotational flows. It was reported that no obvious vortices were observed in the tube with helical inserts even at relatively high flow rate.

Figure 8.19 shows the flux-time profiles obtained in filtration of 5% yeast cell suspension using a tubular membrane of 6 mm i.d. (inside diameter) and 0.14  $\mu\text{m}$  pore size with a helical baffle (HB), a rod baffle (RB), and the tubular membrane without baffle (NB) [35]. The comparison has been made at the same hydraulic-dissipated power, which is defined as the product of the flow rate and the pressure drop along the tubular membrane, or the energy consumed to generate the crossflow through the tubular membrane. Using the hydraulic-dissipated power rather than the crossflow rate as a control parameter for the comparison of the tubular membrane with and without inserts eliminates the effect of the reduced crossflow section by



Main types of flow

- Perimeter component
- Helical component
- Reverse flow

**FIGURE 8.18** Schematics of a helical baffle. (From Figure 2 in Gupta, B.B., Howell, J.A., Wu, D., and Field, R.W., *J. Membr. Sci.*, 102, 31, 1995. With permission.)

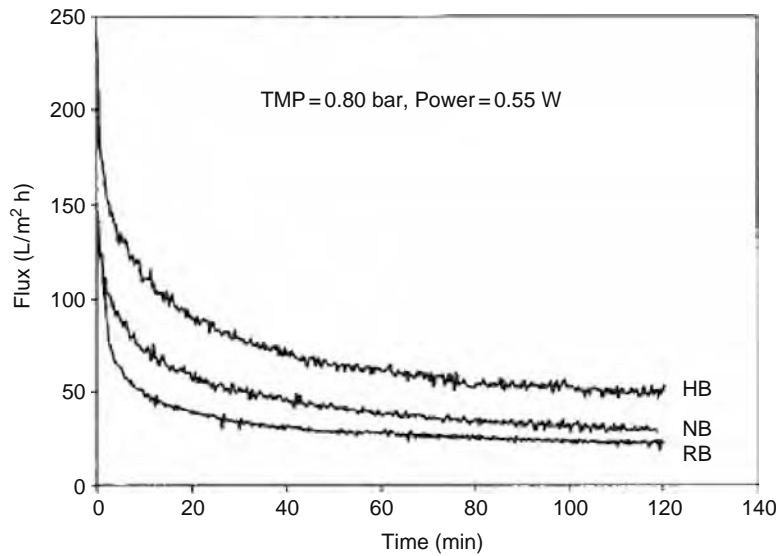


**FIGURE 8.19** Flux-time profiles for filtration with HB, RB, and NB modes. (From Figure 4 in Gupta, B.B., Howell, J.A., Wu, D., and Field, R.W., *J. Membr. Sci.*, 102, 31, 1995. With permission.)

introduction of the inserts. From Figure 8.19, it can be seen that the presence of the helical baffle resulted in a higher flux, but the flux with the RB mode was slightly lower than the NB mode. The rod-type baffle (RB mode) has a similar parallel flow pattern to the NB mode but the value of the tangential velocity is lower than that with the NB mode for a given hydraulic-dissipated power. This explains the slightly lower flux with the RB mode. The enhancement of filtration performance by helical baffles was also reported in the filtration of different difficult feeds using tubular membranes, including crude oil emulsions and mixtures of crude oil with biological solids from activated sludge processes [36], dextran T500 [37], and municipal wastewater [38].

One of the important characteristic parameters of the helical inserts is the pitch, or the turns per unit length. A large pitch means fewer turns of the helices over a certain length of the baffle. However, the limit of indefinitely increasing the number of turns or reducing the pitch will be a geometry approaching a rod-type baffle with negligible rotational flow. Thus there should be an optimal number of helices for flux enhancement. Gupta et al. [35] experimentally determined that a helical baffle made up of four turns per 25 mm length was optimal, which is similar to the optimal 5 mm pitch determined by Xu et al. [38]. Gupta et al. [35] also suggested that a gap of about 1 mm between the membrane inner surface and the baffle height is appropriate for good filtration performance using this type of baffle.

### 8.3.2.2 Corrugated Membranes

Corrugated membranes have been tested and were formed by spreading flat sheet membranes over a corrugated supported plate. The corrugated structure of the plate was made by half-cylindrical bars attached to or grooves machined into the plate [39,40]. The depth of the semicircular bar or groove could be from less than 1 mm to several millimeters. van der Waal and Racz [39] studied the effect of corrugations on filtration with 3 mm circular bars glued onto the support plate. Flow visualization revealed that the membrane corrugations resulted in a transition from laminar to turbulent flow at a lower velocity than with a flat membrane. Circulation eddies formed behind the corrugation over a downstream distance up to about 10–15 mm. The filtration experiments indicated that corrugations can result in an enhancement in mass transfer coefficient, provided the separation distance between corrugations was in the range 15–40 mm. However, no significant effects were observed with larger or smaller mutual distances, such as 80 and 10 mm, respectively.

Stairmand and Bellhouse [40] tested the combined effect of corrugated membranes and pulsated flow on mass transfer in a blood oxygenator. Figure 8.20 shows the schematics of the device used in their experiments. The corrugated structure tested by them was formed by semicircular grooves of 0.75 mm depth and 1.25 mm separation, much shallower and more closely spaced than that tested by van der Waal and Racz [39]. The pulsated flow was produced by a rotating 0.5 in. ball that intermittently closed the line and a section of flexible tube, which could be clamped to varying degrees to alter the stroke of the pulsations. During the experiments, the oxygen was convectively transferred from the high pressure chamber (1 bar) to the low pressure chamber (0 bar) through the liquid flowing through the channel between these two chambers. The rate of convective transfer across the channel would depend on the intensity of mixing of the fluid flowing through the channel. Figure 8.21 [40] shows the effect of pulsations on oxygen transfer between the two corrugated membranes with water and milk-filled channels under conditions of different Reynolds number. The experimental data indicate that for nonfouling liquid medium (distilled water)

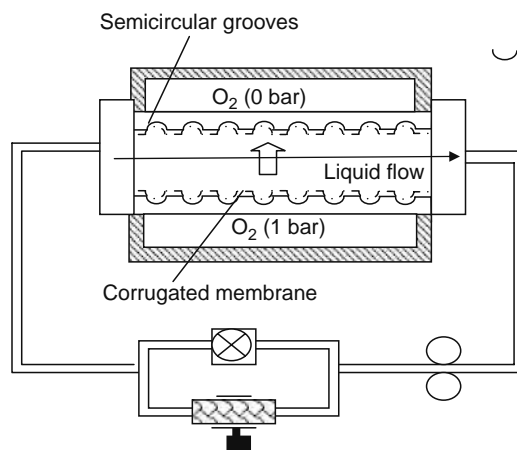


**FIGURE 8.20** Schematics of simulated oxygenator employed with corrugated membrane and pulsatile flow. (Adapted from Figures 1 and 2 of Bertram, C.D., Hoogland, M.R., Li, H., Odell, R.A., and Fane, A.G., *J. Membr. Sci.*, 84, 279, 1993.)

where the Reynolds number exerted a dominant effect on oxygen transfer rate applying an 8 Hz pulsation to the water-filled channel could enhance the Sherwood number by about 20%. For fouling medium (milk-filled channel), the effect of Reynolds number on oxygen transfer could be considerably limited by membrane fouling. However, this phenomenon was found to be partially reversed by the application of pulsations. For Reynolds numbers larger than 10,000, the Sherwood number was enhanced by a factor of about 2 by imposition of pulsations, confirming the effect of pulsations on reducing concentration polarization with corrugated membranes.

Instead of using a furrowed or dimpled membrane support plate, Sobey [41] observed that a single flow deflector in a flat membrane channel could produce many vortices under oscillatory flow conditions, an effect named the “vortex wave.” An important feature of the vortex wave is that it could occur under low crossflow velocity conditions or with laminar flow so that it can be used for shear-sensitive fluids. Millward et al. [42] tested the effect of vortex waves on plasma filtration with waves produced by flow deflectors with cross-sectional area of  $1 \times 1 \text{ mm}^2$  in a 2.25 mm high channel as shown in Figure 8.22. The aim was to improve membrane applications for the separation of plasma from cellular blood components for both donor

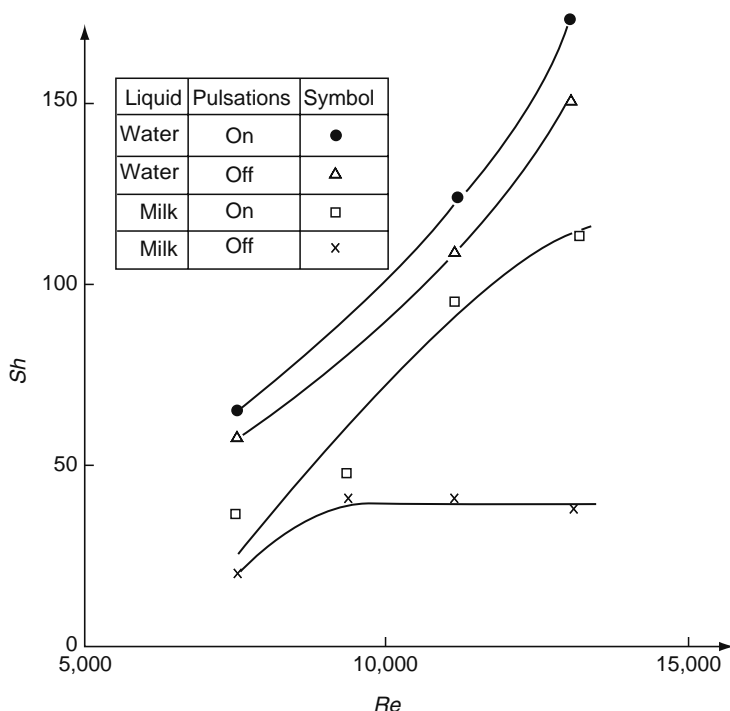


**FIGURE 8.21** Effect of pulsatile flow on oxygen transfer with water and milk medium. (From Figure 3 in Stairmand, J.W. and Bellhouse, B.J., *Int. J. Heat Mass Transfer*, 27, 1405, 1985. With permission.)

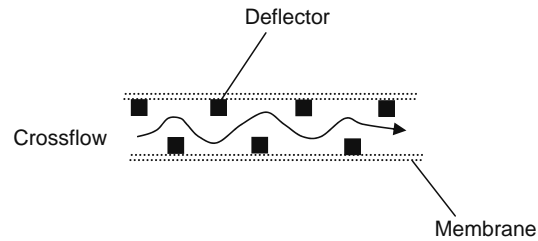


**FIGURE 8.22** Schematics of membrane flow channel equipped flow deflector.

plasmapheresis and the treatment of autoimmune disease. For this application, it is important to achieve a high-plasma filtration rate with negligible damage to the blood components under limited blood flow rate conditions so there would be a need to employ secondary flows to control concentration polarization and membrane fouling. Figure 8.23 shows the plasma flux obtained with different spacings of flow deflector under relatively low Reynolds numbers, in the range of 50–200, using 0.2  $\mu\text{m}$  flat sheet membranes. The results indicate that the addition of narrowly spaced (4 mm) flow deflectors to the membrane channel enhanced the flux significantly by a factor of 3.5 compared to an empty channel at a Reynolds number  $Re = 123$ . More importantly, it was found that the deflectors did not increase the channel pressure drop significantly in such a low Reynolds range. Millward et al. [42] also demonstrated that the oscillatory flow component was an essential feature of the vortex wave design. They found that the plasma flux dropped from 0.1 to 0.01 cm/min by removing the oscillations during the filtration with a channel with 4 mm spaced deflectors. These results demonstrate that significant flux enhancement could be obtained by combining a turbulence promoter and pulsation design even with laminar flow conditions.

## 8.4 PULSED FLOW

### 8.4.1 HYDRODYNAMIC CHARACTERISTICS OF PULSATILE FLOW

Pulsatile flow can be defined as flow with a periodic pressure fluctuation wave travelling along the flow path. As in a steady Poiseuille's flow, it is the pressure gradient along the flow path that determines the instantaneous pulsatile flow rate. For the flow path shown in Figure 8.24, the pressure gradient is determined by the pressure difference between the pressure recorded at upstream point A and that recorded at the downstream point B. Owing to the pressure pulse transfer from the original source of the pulsation down along the flow path, the crest of the wave reaches point A short time before it reaches the downstream

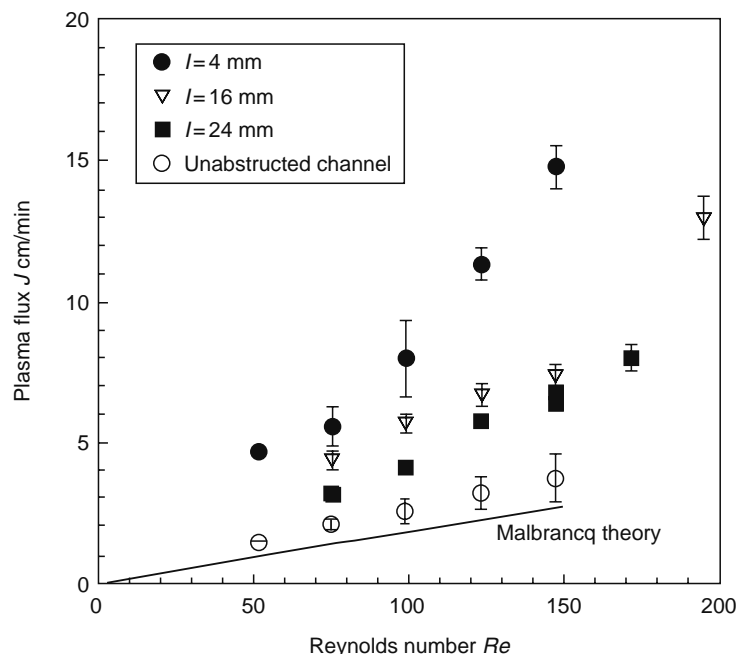


**FIGURE 8.23** Plasma flux obtained with flow deflector-equipped channel with and without pulsation. (From Figure 3 in Millward, H.R., Bellhouse, B.J., Sobey, I.J., and Lewis, R.W.H., *J. Membr. Sci.*, 100, 121, 1995. With permission.)



**FIGURE 8.24** Pulsed flow between two points a short distance apart along a channel.

point B, at this time the pressure at point A is higher than that at point B. A short time later, as the crest reaches at the point B, the pressure at the point B will be higher than that at the point A. Thus, the pressure pulsation will cause a rapid forward-and-reverse pressure gradient oscillation over the flow path AB. Figure 8.25 shows how a travelling sinusoidal pressure waveform creates an oscillatory pressure difference. Figure 8.25a shows two simulated waveforms recorded at two points over a short distance of a flow path with a  $10^\circ$  interval and Figure 8.25b shows the instantaneous pressure gradient between the upstream and the down stream points. From this figure it can be seen, during one period of the pressure fluctuation the pressure gradient over the short flow path also experiences change from a negative to positive value. The motion of the fluid that is driven by an oscillating pressure gradient is complicated. The following momentum equation has been developed for an incompressible laminar pulsatile flow in a circular rigid tube:

$$\frac{\partial^2 w}{\partial r^2} + \frac{1}{r} \frac{\partial w}{\partial r} + \frac{1}{\eta} \frac{\partial P}{\partial z} = \frac{\rho}{\eta} \frac{\partial w}{\partial t} \quad (8.20)$$

where

$P$  is the pressure

$w$  is the velocity in the axial direction

For steady flow the velocity does not vary with time, so that  $\partial w / \partial t = 0$ . The pressure gradient  $\partial P / \partial z$  can be measured over a finite distance and written as

$$\frac{\partial P}{\partial z} = \frac{P_1 - P_2}{L} \quad (8.21)$$

When the pressure gradient is in the form of single harmonic with complex components

$$-\frac{\partial P}{\partial z} = A^* e^{i\omega t} \quad (8.22)$$

where

$A^*$  is the amplitude of pressure gradient in complex form

$\omega$  is the angular velocity

For symmetric flow with nonslip conditions applied, the solution of equation is [43]

$$w = \frac{A^* R^2}{i\eta\alpha^2} \left\{ 1 - \frac{J_0(\alpha y l^{3/2})}{J_0(\alpha l^{3/2})} \right\} e^{i\omega t} \quad (8.23)$$

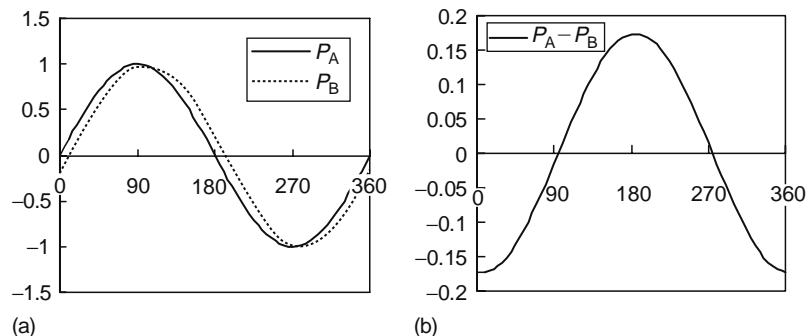


**FIGURE 8.25** Waveform of pressure difference. (a) Two simulated waveforms recorded at two points over a short distance of a flow path with a  $10^\circ$  interval and (b) instantaneous pressure gradient between the upstream and the down stream points.

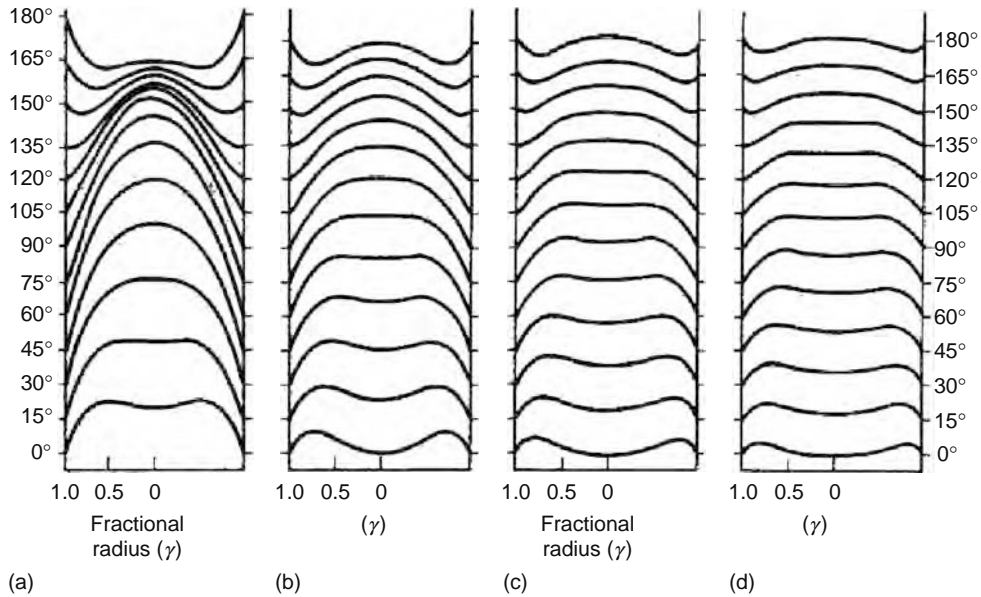


**FIGURE 8.26** The velocity profiles of the flow resulting from a sinusoidal pressure gradient ( $\cos \omega t$ ) in a tube. (a)  $\alpha = 3.34$ , (b)  $\alpha = 4.72$ , (c)  $\alpha = 5.78$ , and (d)  $\alpha = 6.67$ . (From Hale, J.F., McDonald, D.A., and Womersley, J.R., *J. Physiol.*, 128, 629, 1955. With permission.)

where  $J_0(\alpha i^{3/2})$  is a Bessel function of the first kind of order zero and complex argument,  $y = r/R$ . The parameter  $\alpha$  is a dimensionless number that characterizes the kinematic similarities in the liquid motion, known as the Womersley number. It is written as

$$\alpha = R(\omega/\nu)^{1/2} \quad (8.24)$$

The volume flow can be obtained by integrating the velocity across the lumen of the tube:

$$Q = \frac{\pi A^* R^2}{i\omega\rho} \left\{ 1 - \frac{2J_1(\alpha i^{3/2})}{\alpha i^{3/2} J_0(\alpha i^{3/2})} \right\} e^{i\omega t} \quad (8.25)$$

where  $J_1$  is Bessel function of order one.

The velocity profile across the tube lumen with pulsatile flow is not of the same parabolic form as that found in a steady laminar flow. The velocity profiles oscillate sinusoidally as discussed in detail by Hale et al. [44]. For example, Figure 8.26 shows the velocity profiles, at intervals of  $15^\circ$ , resulting from a simple sinusoidal pressure gradient ( $\cos[\omega t]$ ) during the half cycle ( $0^\circ$ – $180^\circ$ ); as for a simple harmonic motion, the second half is the same.

It can be seen from Figure 8.26, for a pulsed pressure gradient, the characteristic parabolic velocity profile observed in steady laminar flow does not appear at any time during the cycle. There is a phase lag between the pressure gradient and the liquid movement, and being a cosine function, the maximum amplitude of the pressure gradient occurs at  $0^\circ$ , while the maximum for the total flow is at  $60^\circ$  in Figure 8.26a and at about  $70^\circ$  in Figure 8.26b. Significant shear is found only in the region near the wall with the liquid in the central portion of the tube virtually unshered. Thus, the liquid behavior for pulsatile flow is rather like a solid mass sliding inside a thin layer of viscous liquid surrounding it. The higher the Womersley number (the higher the frequency or the larger the tube diameter), the flatter is the velocity profile, implying a thinner boundary layer at higher Womersley number.

#### 8.4.2 PULSATILE FLOW-ENHANCED MEMBRANE PROCESSES

Two mechanisms, shear-related and oscillated backflushing, have been suggested for pulsatile flow-enhanced membrane processes by Li et al. [45]. The shear-related mechanisms contribute to the filtration enhancement by a reduced boundary layer and enhanced particle back transport. Since the shear scouring effect is not direction dependent, the maximum absolute value of the shear may be used to estimate the limiting or critical flux for filtration under certain conditions. For laminar flow, the wall shear can be calculated based on the Womersley equation (Equation 8.24). For turbulent flow, there is no simple solution for the wall shear next to the membrane surface. Li [46] suggested estimating the wall shear based on the measured pressure gradient with the assumption that the same pressure gradient should also apply to the boundary layer.

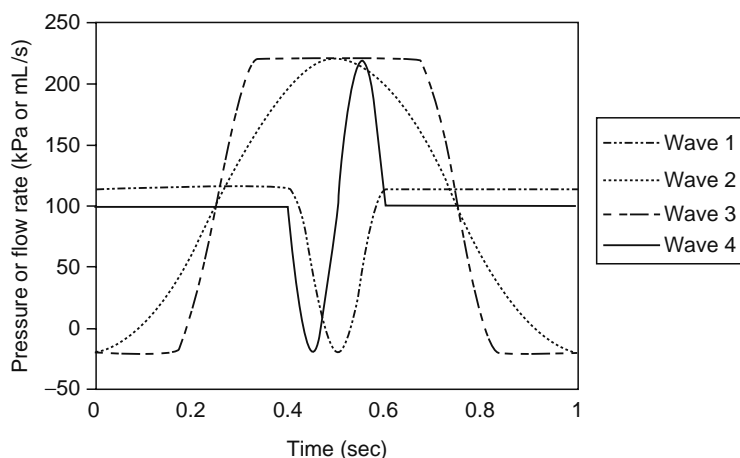


**FIGURE 8.27** Design waveform for pressure and flow rate. (From Figure 2 in Li, H. and Bertram, C.D., *AIChE J.*, 44, 1950, 1998. With permission.)

Thus, the maximum shear can be regarded as being proportional to the maximum absolute pressure gradient along the membrane module [46].

The oscillated backflushing mechanism accounts for the effect of the pressure waveform on TMP. When the minimum pressure of the pulsatile pressure waveform results in a negative TMP, a reverse permeate flow may occur that acts as a backwash flow that drives particles deposited on or near the membrane surface back to the bulk flow. In this way, concentration polarization and cake formation caused by the filtration operation could be limited, depending on the properties of the particles and the magnitude of the reverse pressure.

To obtain oscillated backflushing and enhanced membrane performance, the design of the pressure waveform is crucial. The pressure waveform can be characterized by the minimum and maximum pressure, the duration of the negative pressure and the positive pressure, and the pulsation frequency. Figure 8.27 shows four typical pressure waveforms studied by Li [46]. Wave-type 1 has a long steady-pressure phase and a short negative pulsation. Wave-type 2 has an approximate sinusoidal form with smooth variation of the pressure. Wave-type 3 is approximately square shaped and wave-type 4 had a shortened sinusoidal disturbance. Figure 8.28 shows the cake-resistance reduction results as a function of the minimum TMP obtained by Li et al. [45] for pulsatile flow filtration with the four pressure waveforms shown in Figure 8.27 for two amplitudes. It can be seen from Figure 8.28 that a significant reduction in cake resistance in filtration of 0.5 g/L silica suspension using a ceramic membrane of 0.2  $\mu\text{m}$  was obtained by using waveform-type 1 and 3 with relatively large negative TMPs. Waveform-type 1 had a long steady-pressure phase and a short, negative low pressure pulse which may result in a short period backflushing. For this waveform-type about 80% reduction in cake resistance was achieved when the minimum TMP was reduced to about  $-60$  kPa.

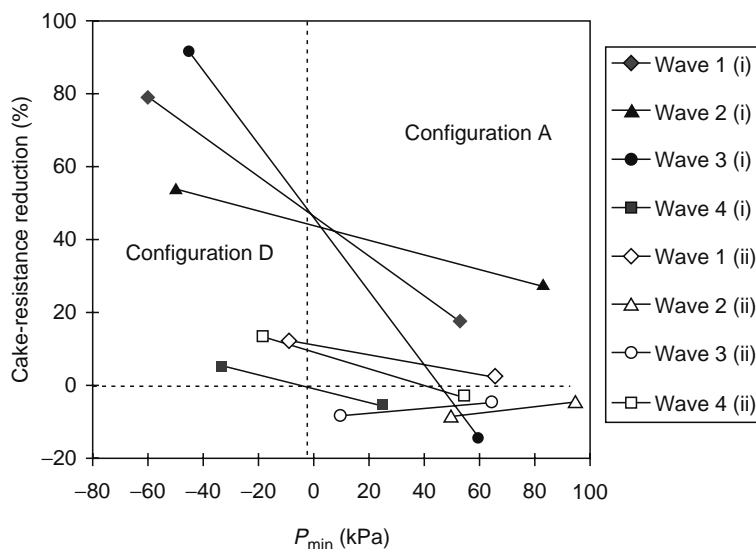


**FIGURE 8.28** Cake-resistance reduction with different waveform-type designs. (From Figure 9 in Li, H. and Bertram, C.D., *AIChE J.*, 44, 1950, 1998. With permission.)

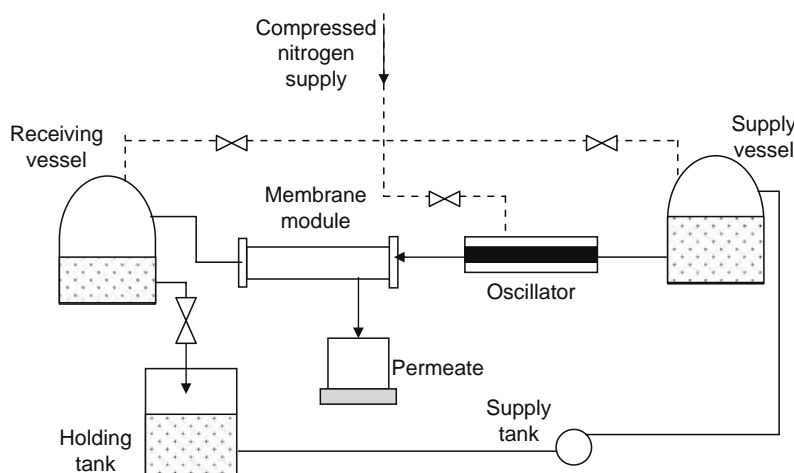


**FIGURE 8.29** Schematics of the filtration setup with collapse-tube pulsation generator. (Adapted from Figure 1 of Bertram, C.D., Hoogland, M.R., Li, H., Odell, R.A., and Fane, A.G., *J. Membr. Sci.*, 84, 279, 1993.)

The waveform-type 3, which had a longer negative pressure period than waveform-type 1, resulted in more than 90% reduction in filtration resistance with a minimum TMP of about  $-40$  kPa, implying the effect of duration of the backflushing. Waveform-types 3 and 4 were long and short sinusoidal forms, providing a continuous variation of pressure. There seemed to be less effective reduction in cake resistance with the shorter negative pressure period (waveform-type 4).

Pulsated flow can be achieved by various flow control methods. Figure 8.29 shows a lab-scale membrane filtration setup with the so-called collapsible-tube oscillator used by Bertram et al. [47] for producing pulsated flow in membrane filtration. This system included a supply vessel, a membrane module, a receiving tank, a holding tank, and the collapsible-tube oscillator. The collapsible-tube oscillator consisted of a horizontally mounted 365 mm length of silicone rubber tube with unstressed inside diameter 13.2 mm and wall thickness 3.2 mm, clamped at each end by stainless steel fittings. The pulsations with this device are produced by periodic collapse and reopening of the tube induced by pressure applied to the chamber surrounding the tube. With this arrangement the frequency of the pulse flow can be controlled in a range of 7–12 Hz, depending on the volume of fluid downstream being oscillated, tube parameters, and pressure manipulation.

Many researchers have assessed the effect of pulsatile flow on different membrane processes with wide range of feeds. One of the first studies was by Kennedy et al. [48] who showed that flux in the RO of sucrose solution could increase by 70% by pulsatile flow at 1 Hz. Gupta et al. [49] reported a 45% enhancement of flux in MF of raw apple juice with a pressure waveform provided by a fast piston return followed by a fast forward stroke at 1 Hz. Jaffrin [50], using hollow fiber filters, demonstrated a 45% enhancement in flux in plasma filtration. Using the collapsible-tube oscillation generator described above, Bertram et al. [47] demonstrated that pulsation resulted in a 60% increase in permeate flux in the filtration of silica suspensions.

### 8.4.3 TRANSMEMBRANE PRESSURE BACKSHOCK TECHNIQUE

Instead of exerting pressure pulsing on the feed side, Rodgers and Sparks [51] tested periodic pressurization of the filtrate from 5 to 30 kPa above the respective operating pressure to obtain pulsatile negative TMBs. With a short period of negative pressure or backshock (0.01–0.38 s) presented at a frequency of 0–5 Hz, their experiments showed average increase in permeate flux of 62%–174% for ultrafiltration of 1% bovine serum albumin (BSA) solutions with laminar crossflow. However, no improvement in flux was observed with turbulent flow as a result of TMP pulsing. Guerra et al. [52] assessed the effect of backshock on the filtration of skim milk using so-called normal and reverse asymmetric membranes. The normal asymmetric membrane refers to the asymmetric membrane with the tight skin of the membrane facing the feed (as is usual practice). The reverse asymmetric membrane was with the porous support layer facing the feed. Guerra et al. [52] reported that for filtration with the normal asymmetric membrane, the permeate flux could be increased by 100% by applying a backshock of 0.022 s at a frequency 0.33 Hz for the filtration of skim milk. For filtration with the reverse asymmetric membrane without backshock, it was found that concentration polarization formed within the porous support layer and it was impossible to filter skim milk with such a flow arrangement. However, with backshock, the imposed flux in filtration of skim milk with reverse asymmetric membrane was able to be stepped up to higher than  $350 \text{ L/m}^2 \text{ h}$  without resulting in a significant increase in TMP at a crossflow velocity of 1 m/s; an immediate decrease was observed after the backshock was stopped [52]. This combination of reverse asymmetric membranes and backshock has been patented [53].

Another reported application of backshock is in filtration using membranes called microsieves, which are very thin and smooth membranes with uniform pores made by silicon micromachining [54]. The thinness (ca.  $1.2 \mu\text{m}$ ) and high porosity of

microsieves can result in a high flux in the order of  $10^4 \text{ L/m}^2 \text{ h}$  even under very low TMP conditions. However, such a high flux could result in the rapid formation of a cake layer on the membrane surface within a fraction of a second. To control the cake formation caused by high flux, TMP pulsation is usually applied in filtration by microsieves. Kuiper et al. [55] reported that the cake layer formed by yeast particles in microsieving filtration of lager beer could be largely prevented by applying a backflush of  $-0.05 \text{ bar}$  with a pulse duration  $0.05 \text{ s}$  at a frequency of the order of seconds. Moreover, direct observation revealed that the backpulse could lift particles that stayed on the membrane surface after backflushing off the surface. These loosely attached particles or flocs were found to be eventually removed by a sudden increase in the crossflow velocity for a short period.

The efficiency of backshock can be assessed based on the ratio of the filtrate volume obtained during the filtration period to the volume of permeate lost during the backshock period in a working cycle. The ratio of gained and lost filtrate volume is a function of backflush frequency, the period of backflushing, the operation conditions, and the properties of the foulant materials. A high-operational flux usually needs a strong backflush, which may correspond to an increased loss of permeate volume, to maintain stable performance. Therefore, the backflush conditions need to be optimized to maximize the productivity of the process.

## 8.5 HIGH SHEAR DEVICES

In conventional crossflow filtration, the shear on the membrane surface is usually produced by the feed flow driven by a pump. The shear rate can get up to the order of  $10^4 \text{ s}^{-1}$ . High liquid flow results in high pressure drop along the membrane module, leading to considerable energy consumption and nonuniform distribution of TMP over the flow path of the feed channel. Such a close dependence between high crossflow velocity and pressure drop limits the use of high crossflow in various commercial membrane modules. However, in high shear membrane filtration devices, the relative movement between the liquid and the membrane surface is induced by an independent device rather than a liquid transport pump. With shear rate independent of the feed bulk flow, the high shear membrane filtration devices can be operated at a relatively homogeneous and controllable TMP. The typical high shear membrane filtration devices include rotating disks and vibrating dynamic membrane filtration systems, as described below.

### 8.5.1 ROTATING SYSTEMS

Figure 8.30 shows the typical structure of a rotating dynamic membrane system which consists of a stationary flat membrane, a rotating disk, a hollow shaft, and a cylindrical housing with feed inlet and permeate outlet. During filtration, the feed is pumped into the closed housing, flowing through the membrane and evacuating through the hollow shaft. The permeate flow comes out of the system from the permeate outlet. Driven by an electric motor, the rotating disk rotates at high speed ( $100\text{--}1000 \text{ s/rpm}$ ) to produce shear on the membrane surface. The TMP can be controlled by a valve in the retentate outlet line.

The centrifugal forces generated by the disk induce an outward radial flow near the rotating disk and inward radial flow toward the axis near the membrane surface. If there is a relative large gap (several millimeters) between the membrane and the rotating disk, the flow in the gap can be approximately treated as a flow core that rotates at an angular velocity of  $k\omega$  between two boundary layers on the membrane and the rotating disk surface, where  $\omega$  is the rotating velocity of the disk and  $k$  is a coefficient between 0.3 and 0.44 [56]. The azimuthal Reynolds number can be defined as  $Re = k\omega R/\nu$ . The shear on the membrane surface at radius  $r$  can be calculated based on the expressions for different flow regimes [57].

Laminar boundary layer regime,  $Re < 2.5 \times 10^5$ ,  $e/R > 0.05$  (where  $e = \text{gap height}$  and  $R = \text{radius}$ )

$$\gamma = \frac{0.77(k\omega)^{3/2}r}{\nu^{1/2}} \quad (8.26)$$

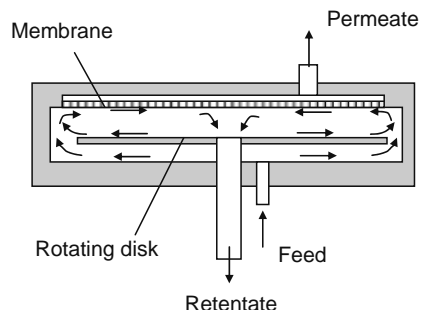


FIGURE 8.30 Schematic diagram of rotating disk dynamic membrane filter.

In the turbulent regimes ( $Re > 2.5 \times 10^5$ ,  $e/R > 0.05$ ),

$$\gamma = \frac{0.0296(k\omega)^{9/5}r^{8/5}}{\nu^{4/5}} \quad (8.27)$$

Typically, for a disk with diameter 150 mm rotating at speeds of 500 or 2000 rpm, the calculated shear rates at the edge of the disk based on Equation 8.27 with  $k=3.7$  are  $6.4 \times 10^3$  and  $7.7 \times 10^4 \text{ s}^{-1}$ , respectively.

The pressure in the gap is also a function of the radius distance. The radial gradient in the boundary layer is equal to that in the inviscid core as given by [56]

$$\frac{\partial P}{\partial r} = \rho r(k\omega)^2 \quad (8.28)$$

The pressure distribution can be obtained by integrating Equation 8.28 from  $r=0$  to  $r$ , assuming  $k$  is independent of  $r$ .

$$P = \frac{1}{2}\rho(k\omega r)^2 + p_0 \quad (8.29)$$

For a rotating disk dynamic membrane filter, the TMP and the shear rate on the membrane surface vary radially as indicated by the above equations. Bouzera et al. [56] studied the averaged filtration resistance at different radial zones for different rotating speeds using calcium carbonate particle (mean diameter 4.7  $\mu\text{m}$ ) suspension as the model fluid. In the experiments, several Nylon membranes were partially sealed with epoxy to obtain membranes with different centric permeable zones:  $r < 3$ ,  $3 < r < 4.5$ ,  $4.5 < r < 6$ , and  $6 < r < 7.5$  cm. The results indicated that for the filtration zones  $r > 3$  cm, the resistance is equal to the membrane resistance for all the rotating speeds  $\geq 200$  rpm, implying that the particle deposition can be effectively arrested by a rotating speed as low as 200 rpm in this membrane zone. For the center filtration zone ( $r < 3$  cm), the filtration resistance was a strong function of the rotating speed, and the filtration resistance became equal to the membrane resistance only at 2100 rpm, at lower rpm the filtration resistance was greater. Jaffrin et al. [57] reported that the permeate flux of the rotating disk can be significantly enhanced by equipping the rotating disk with radial vanes of a certain height, which can increase the shear rate on the membrane surface considerably.

The following empirical relationship has been suggested to correlate the filtration flux to the shear rate for filtration with a rotating disk dynamic membrane filter:

$$J = A\gamma_m^n \quad (8.30)$$

$A = 1$ ,  $n = 0.5$ , and  $A = 0.30$ ,  $n = 0.55$  were suggested for filtration of silica suspension [58] and skim milk [59], respectively.

Several commercially available rotating disk dynamic membrane systems have been tested for different applications. The CR (cross-rotational) system (Radisio-Flootek, Finland, Northern Europe) is multistage with 50 cm diameter disks, providing a total membrane area up to 20  $\text{m}^2$ . It has been tested by Nuortula-Jokinen and Nyström [60] for concentrating paper-mill effluents at a rotor-tip azimuthal velocity of 13 m/s. The SpinTek ST II module (SpinTek, Huntington Beach, California), which can reach an azimuthal velocity of 20 m/s at the tip, has been tested for filtration of oil-water microemulsions with a 500  $\text{cm}^2$  membrane area module [61]. The DMF module (Pall Corp., New York) consists of several disks mounted on the same shaft, such that each can rotate between two annular membranes with maximum rotation speed of 3450 rpm, corresponding to an azimuthal velocity of 20 m/s at the disk tip. Pall's lab-scale system has been tested for protein separation [62] and filtration of recombinant yeast cells [63]. The reported studies of the application of the rotating disk dynamic membrane indicate that high shear-induced filtration is much less sensitive to the solids concentration. High concentration factors achieved at significantly higher fluxes than the conventional processes have been reported with quite a range of feeds, including ferric hydroxide, yeast suspension, and skim milk, etc. [56,59,64].

## 8.5.2 VIBRATORY SYSTEMS

### 8.5.2.1 Vibratory Shear-Enhanced Process

The concept of the vibratory shear-enhanced process (VSEP) (New Logic International, Emeryville, California), proposed by Armando et al. [65], came with the idea to combat concentration polarization and membrane fouling by directly moving the membranes rather than by moving the liquid. The VSEP system consists of a stack of parallel circular membranes mounted in a cylindrical housing which is spun in torsional oscillation at a resonant frequency of about 60 Hz as shown in Figure 8.31.

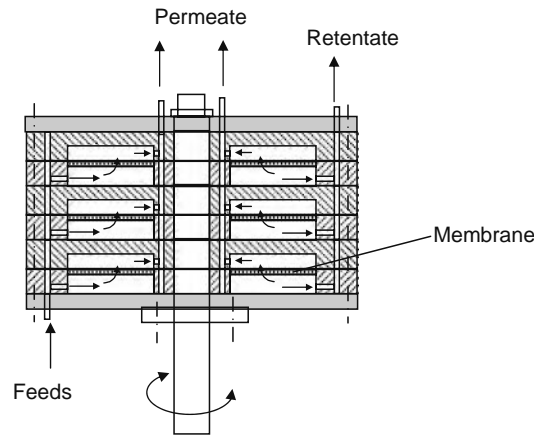


**FIGURE 8.31** Schematic diagram of vibrating flat sheet membrane module.

The shear rate at the VSEP membrane is created by the inertial-induced relative motion of the fluid, and can be of the order  $10^5 \text{ s}^{-1}$ . The shear rate varies sinusoidally and increases proportionally with local membrane azimuthal displacement to radius. The maximum shear rate at the periphery can be related to the vibrating frequency ( $F$ ) and the membrane displacement at the periphery ( $d$ ) by the following equation [66]:

$$\gamma_{\max} = 1.414d(\pi F)^{3/2} \nu^{-1/2} \quad (8.31)$$

In VSEP,  $F = 60.75 \text{ Hz}$ ,  $d = 3 \text{ cm}$ , so for water-like liquids the value of  $\gamma_{\max}$  is about  $1.1 \times 10^5 \text{ s}^{-1}$ .

The mean shear rate obtained by averaging the absolute value of shear rate over a period and over the membrane area which, for VSEP, is an annular region with radii  $R_1$  and  $R_2$ , can be formulated as

$$\bar{\gamma} = \frac{2.828(R_2^3 - R_1^3)}{3\pi R_2(R_2^2 - R_1^2)} \gamma_{\max} \quad (8.32)$$

Jaffrin et al. [57] have made a hydrodynamic comparison between the rotating disk and the VSEP system based on the flux achieved under similar maximum shear rates for baker's yeast microfiltration with an  $0.2 \mu\text{m}$  MF and skim milk UF at 50 kDa. They found that the flux variation with time in these two modules was nearly identical when they were operated at the same maximum shear rate, suggesting the dominant effect of shear rate on the filtration performance.

### 8.5.2.2 Vibratory Hollow Fiber Membranes

While VSEP demonstrated that vibrations can be applied to flat sheet membrane to enhance membrane filtration, the effect of vibrations on the performance of hollow fibers has also been investigated by a number of researchers for different separation processes. Krantz et al. [67] designed the system shown in Figure 8.32a to assess the effect of axial membrane vibrations on mass transfer in a hollow fiber oxygenator. In this system, a shell and tube silicon fiber module was mounted vertically and connected to the liquid flow inlet and outlet lines via flexible bellows couplings. The membrane module was rigidly attached to the plate of an electromechanical shaker, which could axially vibrate the hollow fiber module over a frequency range from 6 to 18 Hz with an amplitude range of 0.05–1.2 cm. Surge tanks were employed on the liquid inlet and outlet lines to eliminate liquid pressure pulsation in the fiber lumen. The experimental results showed that a maximum enhancement of 1.58 in the Sherwood number ratio was achieved for oxygen transfer to water when the surge tanks were employed to suppress liquid pulsations in the fiber lumen. Without the surge tanks, the vibrations were even more effective and caused a secondary flow in the fiber lumen so that the combined effect of the vibrations and secondary was to increase the enhancement factor to 2.65.

Figure 8.32b shows a vibrating submerged hollow fiber membrane system for filtration applications [68]. In this system, the submerged membrane is vibrated by a mechanical device, which converts the rotating motion of the electric motor to vertical oscillations of the vertical fiber bundles. The system can be operated in a frequency range of 1–10 Hz with a maximum displacement of 4 cm. Figure 8.33 shows the experimentally determined relationship between critical flux and the vibration frequency for filtration of 5 g/L baker's yeast suspensions, indicating a nearly monotonic increase in critical flux with increase in the vibration frequency over the frequency range tested.

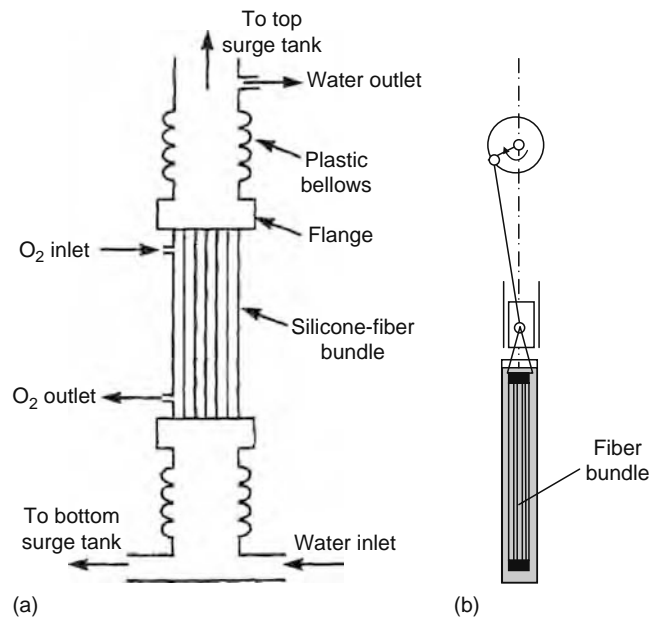


**FIGURE 8.32** Schematic diagram of (a) vibrating hollow fiber membrane. (From Figure 5a in Krantz, W.B., Bilodeau, R.R., Voorhees, M.E., and Elgas, R.J., *J. Membr. Sci.*, 124, 283, 1997. With permission.) and (b) vibrating submerged hollow fiber membrane. (From Genkin, G., Waite, T.D., Fane, A.G., and Chang, S., *J. Membr. Sci.* 281, 726, 2006.)

## 8.6 TWO-PHASE FLOWS

Another strategy to provide additional shear or flow instability in the boundary layer is the use of two-phase flow. Two approaches have been applied to membrane processes: bubble addition for gas–liquid two-phase flow and particle addition for solid–liquid two-phase flow.

### 8.6.1 GAS–LIQUID TWO-PHASE FLOW

Over the past decade, there has been an upsurge of interest in the use of gas bubbles to enhance membrane processes. The typical applications include two-phase flow filtration with tubular membranes and submerged membrane systems. A major stimulus for the latter has been the development of MBRs.

#### 8.6.1.1 Two-Phase Flow Filtration with Tubular Membranes

As depicted in Figure 8.34, the flow patterns formed in a vertical tube follow a trend with increasing gas flow of bubble flow, slug flow, churn flow, and annular flow. These regimes are described briefly below.

- **Bubble Flow:** the gas phase is approximately uniformly distributed in the form of discrete bubbles in a continuous liquid phase.
- **Slug Flow:** most of the gas is located in large bullet-shaped bubbles, which have diameters almost equal to the tube diameter and are sometimes designated as Taylor bubbles. They move uniformly upward and are separated by liquid

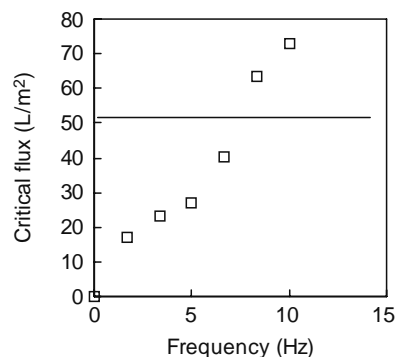


**FIGURE 8.33** Experimentally determined critical flux for filtration of 5 g/L yeast using vibrating hollow fiber membrane.

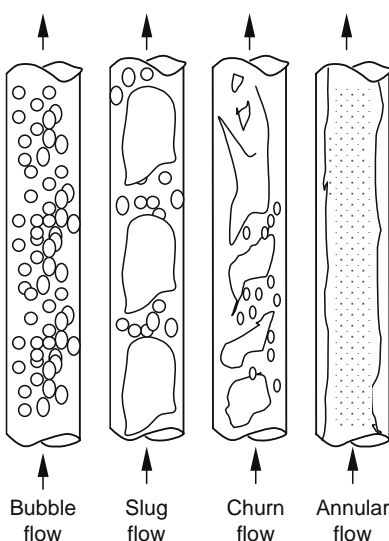


FIGURE 8.34 Flow pattern of gas–liquid two-phase flow in a tubular duct.

slugs which may contain small gas bubbles. Around the Taylor bubbles, there is a thin liquid falling film which causes turbulence in the wake of the Taylor bubble.

- Churn Flow: is somewhat similar to slug flow but is more chaotic, frothy, and disordered.
- Annular Flow: is characterized by the continuity of the gas phase along the core of the tube. The liquid phase moves upward partly as wavy liquid film and partially in the form of drops entrained in the gas flow.

The flow pattern depends on the gas and liquid flow rate as well as the diameter of the duct [69]. For two-phase flow filtration, the flow path for the gas–liquid mixture is relatively narrow and the liquid velocity is usually set at a low value, so the prevalent flow pattern for two-phase flow filtration would be slug flow. When the bubble size reaches about 60% of the tube diameter, the bubble can be categorized as a slug with its characteristic bullet-shaped nose. The rising velocity of the slug depends on the tube size. For tubes of above 10 mm diameter ( $d_b$ ) with a slug length  $1.5d_b$  or above, the rising velocity of bubble can be calculated by

$$U_b = 0.35(gd_b)^{1/2} \quad (8.33)$$

If the tube diameter is less than 10 mm, the liquid surface tension will affect the slug velocity and simulation predicts that for diameters less than about 5 mm with water the surface tension can stop the upward motion of the slug causing an air lock, implying careful assessment is required before applying bubbling to the lumen of hollow fiber membranes.

Many studies have been carried out to evaluate the effect of injection of air into the lumen of tubular and hollow fiber membranes on the performance of membrane filtration. Figure 8.35 shows the filtration results obtained by Cui et al. [70] using a vertically installed tubular membrane module (12.7 mm i.d., PVDF, MWCO: 100 kDa) with dextran solution (MW: 87 kDa) as the test media. As can be seen, injecting gas bubbles, even at quite low gas flow rates caused significant flux increase. The flux improvement was about  $\times 2.0$  for the minimum gas rate and only increased to  $\times 2.4$  for the maximum gas rate. Cabassud et al. [71] and Mercier et al. [72] studied the effect of slug flow on particle fouling in the ultrafiltration of bentonite suspensions with organic hollow fibers (0.01  $\mu\text{m}$ ,  $d_i = 0.93$  mm,  $L = 1.2$  m) and a mineral tubular membrane (0.02  $\mu\text{m}$ ,  $d_i = 15$  mm, 0.75 m). Although an initial flux decline also occurred for filtration with air injection, an enhancement of steady-state flux of 110% for hollow fibers and of 300% for tubular membranes was observed in the experiments. Gas sparging inside the tubes has also been shown to be efficient for improvement of performance of filtration of biomass. Mercier et al. [73] combined two-phase flow ultrafiltration (tubular: 50 kDa,  $d_i = 6$  mm,  $L = 1.2$  m) with a continuous alcohol fermentation process to investigate the feasibility of its long-term application in an MBR. Their results indicated that with air injection, a stable flux of 58  $\text{L}/\text{m}^2 \text{ h}$  was maintained over 100 h of fermentation until a final biomass concentration of 150 g (dry)/L was achieved, while the filtration without bubbling was prematurely stopped at about 30 h with a final concentration of 50 g (dry)/L due to membrane fouling. Performance enhancement for biomass filtration by gas injection was also reported by Imasaka et al. [74] for filtration of methane fermentation broth and by Vera et al. [75] for activated sludge.

Two-phase gas–liquid flow clearly reduces concentration polarization, and this can improve membrane separation. For example, Ghosh et al. [76] assessed the effect of gas sparging on protein fraction with BSA (MW 67,000) and lysozyme (MW 14,100) as model solutes. They reported that a nearly complete separation of these two model proteins was achieved with

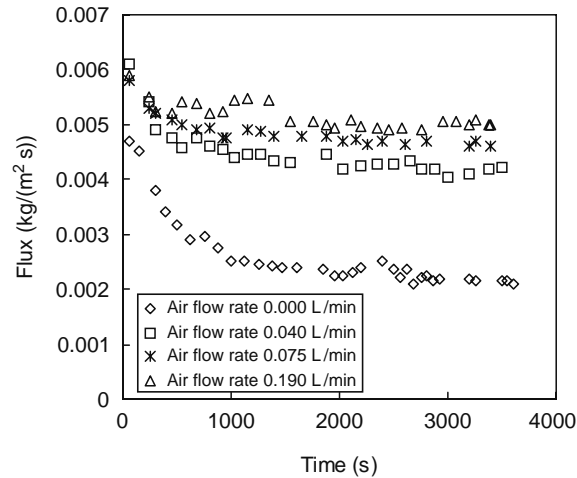


**FIGURE 8.35** Bubbling enhanced flux for filtration of dextran solution. (Adapted from Cui, Z.F., Experimental investigation on enhancement of crossflow ultrafiltration with air sparging, in: Aterson, R.P. (Ed.), *Effective Membrane Processes-New Perspective*, Mechanical Engineering Publications, London, 1993, 237–245.)

two-phase flow ultrafiltration (MWCO 100 kDa), indicating an 18-fold increase in selectivity compared to that without air injection. The enhancement in selectivity was believed to be caused by the disruption of the concentration polarization so that solute retentions were closer to the intrinsic values. Although the depolarization decreased transmission for both BSA and lysozyme, the theoretical analysis suggested that air injection affected more the transmission of the more rejected component (BSA) so that high-separation efficiency was achieved.

An assessment of the literature over a wide range of operating conditions and feeds indicates that flux enhancement for tubular membrane filtration can be affected by module configuration and operation conditions such as feed concentration, liquid velocity, bubble size, and TMP. The trends have been summarized by Cui et al. [77], as follows:

1. Benefit of bubbling becomes more significant when polarization is more severe, for example, at high TMP (or flux), a low liquid velocity, and a high feed concentration, due to the disruption effect of bubbling on concentration polarization.
2. Orientation of the tubular membrane is important. Cui et al. [78,79] indicated that greater flux enhancement can be obtained with vertical tubular membranes with rising bubbling coupled with a moderate downward liquid flow than with a horizontal tube. Cheng et al. [80,81] suggested that there is an optimal mounting angle for tubular membranes and they concluded that around 50° inclination gave the maximum enhancement because gas slugs on an angle move faster than in a vertical tube.
3. Flux enhancement by bubbling is significant in the laminar regime of liquid flow and becomes insignificant as the liquid flow Reynolds number approaches 2500–3000. The enhancement is relatively insensitive to the actual liquid flow over much of the laminar region. This is because the filtration is dominant by the secondary flows induced by the bubbles.

For bubbling-enhanced tubular membrane filtration, Cui et al. [77] have attributed the main mechanisms to

1. Bubble induced secondary flow: Moving bubbles generate secondary flows and wakes which promote local mixing near the membrane surface. Slug flow also results in an annular falling film as displaced liquid flows downward between the slug and the tube wall.
2. Physical displacement of the concentration polarization layer: Gas slugs can penetrate into the concentration polarization layer and displace the upper part of it.
3. Pressure pulsing caused by passing slugs: A moving slug causes pressure pulsing in the liquid around it, with a higher pressure at its nose and lower pressure at its tail. This is similar to imparting a local pulsatile flow during the filtration. In addition, injection of bubble may also result in an increase in mean TMP. Both of these factors could contribute to an increased flux.

Al-Akoum et al. [82] compared the bubbling, Dean flow, and vibrating-enhanced membrane processes in terms of the shear stress and the permeate fluxes obtained in filtration of yeast suspension. The filtration with two-phase flow was carried out using 15 mm ceramic mono tubular UF (permeability 250 L/m<sup>2</sup> h bar) and MF (permeability 1500 L/m<sup>2</sup> h bar) membranes with TMPs of 100 and 25 kPa for UF and MF, respectively. The yeast concentrations used in the two-phase experiments were 1

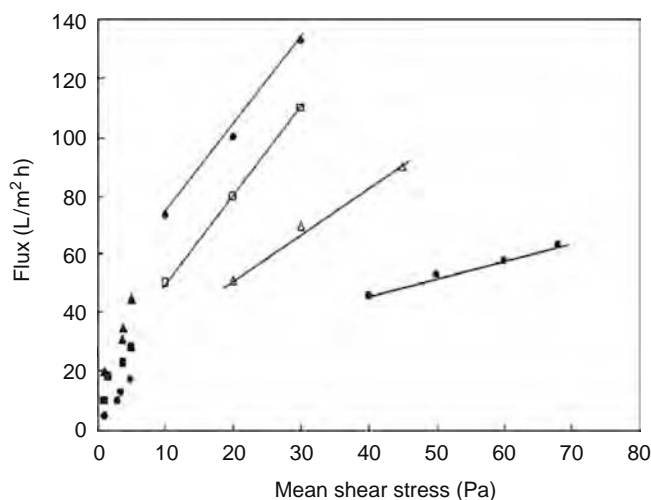


**FIGURE 8.36** Comparison of variation of permeate flux with mean wall shear stress two-phase flow, Dean, and vibratory shear-enhanced process (VSEP) system. (From Figure 6 in Al-Akroum, O., Mercier-Bonin, M., Ding, L., Fonade, C., Aptel, P., and Jaffrin, M.Y., *Desalination*, 147, 31, 2000. With permission.)

and 20 g/L and different ratios of gas flow rate to liquid flow rate were tested with a superficial liquid velocity of 0.45 and 0.38 m/s for UF and MF, respectively. The Dean flow experiments were conducted using yeast concentrations of 0.5–60 g/L with 0.93 mm (inside diameter) cellulose hollow fiber membranes (permeability 270 L/m<sup>2</sup> h bar) in helical form under a TMP of 110 kPa over a liquid velocity range of 0.81–1.64 m/s. A VSEP device was used for the vibrating-enhanced process and the yeast concentration used in the experiments was 20 g/L. Figure 8.36 shows the permeate flux and mean shear stress relationship for the three systems. The shear stress range for the three systems was determined as <10 Pa for two-phase flow, 10–40 Pa for the Dean flow system, and >40 Pa for the VSEP systems. For these shear ranges, it was observed that the flux with the three systems tested obeyed the empirical law:  $J = A\tau_{wm}^n$ , where  $\tau_{wm}$  is the averaged wall shear stress, with different coefficients shown in Figure 8.36. However, although the shear stress with the VSEP system was higher than those with the other two systems, a lower flux with VSEP was observed, indicating that other factors, such as membrane properties (materials, pore size, and surface morphology) and hydrodynamic instability behavior of the fluid, may affect membrane fouling and performance.

### 8.6.1.2 Bubbling with Submerged Membrane Systems

Bubbling seems to be an obvious strategy to induce flow and produce shear at the membrane surface in submerged systems to control concentration polarization and fouling. This is particularly attractive in MBRs for wastewater treatment where bubbling is already required as an oxygen supply. Figure 8.37a and 8.37b shows two different submerged membrane filtration modules:

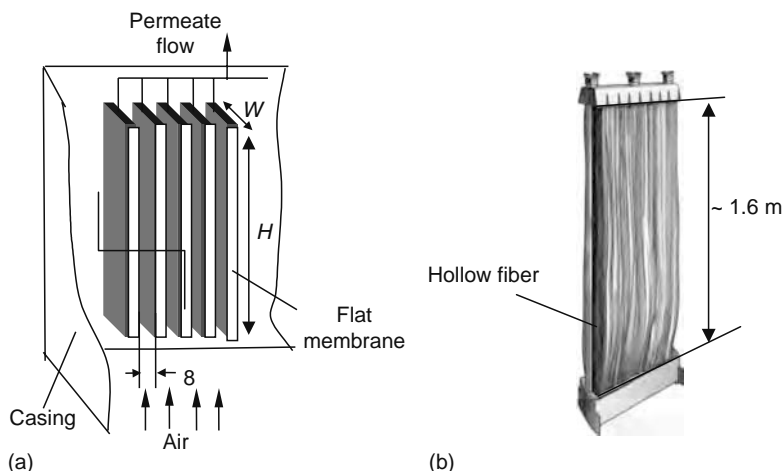


**FIGURE 8.37** Submerged hollow fiber membrane module. (a) Flat sheet and (b) hollow fiber. (From Figures 19a and 21b in Cui, Z.F., Chang, S., and Fane, A.G., *J. Membr. Sci.*, 221, 1, 2003. With permission.)

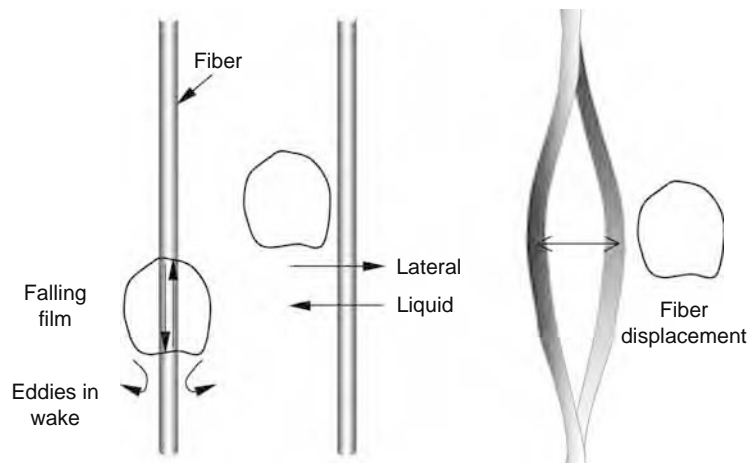
the submerged flat sheet system and the submerged hollow fiber membrane system. The flat sheet concept has been developed successfully by Kubota as a feature of their MBR system. As shown in Figure 8.37a, the Kubota flat sheet-submerged membrane unit may consist of multiple independent module panels that are arranged vertically at a distance of about 5–8 mm from each other. Each panel has its own support plate, membranes, and permeate collector. Air is injected from a distributor below the plates generating a well-defined flow in the channel. A potential advantage of the flat sheet arrangement is that the membranes are precisely located and more accessible to well-directed bubbles. The disadvantages are that membrane packing density is relatively low and vigorous backwashing is not feasible.

The submerged hollow fiber membrane was introduced in Japan in the mid-1980s. A patent by Tajima and Yamamoto [83] described a filter for nuclear power plants which incorporates U-shaped hollow fibers ( $0.1 \mu\text{m}$ ) in a vessel with intermittent air bubbling around the fibers to “vibrating the hollow fibers to remove solid particles trapped thereby.” Yamamoto et al. [84] are believed to be the first to report the use of submerged hollow fibers in a wastewater MBR; the role of the gas was described as for aeration, mixing, and inducing liquid flow. They also emphasized the importance of low-imposed flux and the use of intermittent suction for long-term stable operation of the submerged hollow fibers. This concept has become the generally accepted approach for submerged membranes in MBRs. In the early 1990s, Zenon developed their commercial submerged hollow fiber system with bubbling for wastewater and water treatment. Figure 8.37b shows the Zenon concept of the submerged hollow fiber membrane module, which involves use of a vertical loose fiber curtain supported at top and bottom and a gas bubble distribution system along the edge of the fiber bundle. Vigorous intermittent coarse bubble flow is applied to prevent particle deposition on the fiber surface.

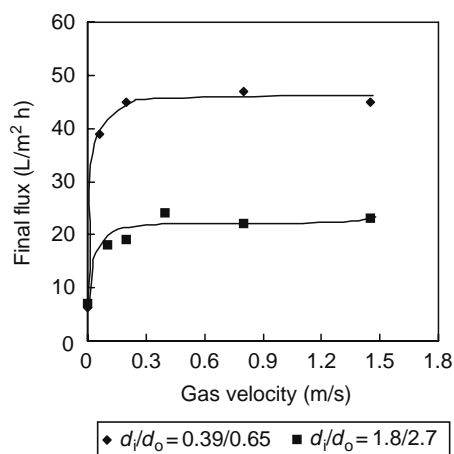
Figure 8.38 [77] depicts the likely mechanisms of depolarization and flux enhancement with vertical hollow fibers. For bubble flow outside hollow fibers, the vertical flow channels are less distinct and comprise the outer edge of fibers rather than randomly positioned. Surface shear on the hollow fiber membrane could be produced by large-scale liquid circulation induced by bubble flow. The local bubble behavior as bubbles or slugs move upward, including eddies in the wake and falling film around the slug, will enhance the mixing of the local liquid. In addition, the bubbles induce fluctuating liquid flow that transverses the fibers and causes lateral fiber movement, depending on the looseness of the fiber.

Figure 8.39 shows the results of tests at fixed TMP and plots ‘the steady-state flux’ versus gas flow rate using a test system with fibers vertically immersed in the stagnant feed with well-controlled spacing [85]. This study shows that bubbling could significantly enhance the performance of the filtration with a moderate gas rate but the enhancement did not increase much with further increase in the gas flow rate. The experimental results also indicate that the effect of bubbling on filtration could be affected by fiber size. From Figure 8.39 it can be seen that the final flux obtained in the filtration with the  $d_i/d_o = 0.39/0.65$  fiber was significantly higher than that with the  $d_i/d_o = 1.8/2.7$  mm fiber. Flux decline, defined as  $[100(\text{initial flux} - \text{final flux})/(\text{initial flux})]$ , is shown in Figure 8.40 for a wide range of fiber diameters; a clear advantage for the smaller diameter fiber is evident [85]. An explanation for the better response of the smaller fiber is that they are more flexible and able to move laterally as bubbles pass. This explanation is supported by the observation that the benefit of the small fiber increased with higher crossflow velocity or the injection of air. However, it should be noted that there is a practical constrain on using very small fiber diameters due to the increased pressure drop on the lumen side that causes a significant flux distribution along the fiber and adds to the energy cost.

The flexibility of the submerged hollow fibers under bubbling conditions can be promoted by having the fibers held loosely rather than tightly. Chang and Fane [86] indicated that there are significant differences in suction pressure profiles for filtration



**FIGURE 8.38** Mechanisms of cake depolarization—bubbles outside fibers. (From Figure 24 in Cui, Z.F., Chang, S., and Fane, A.G., *J. Membr. Sci.*, 221, 1, 2003. With permission.)



**FIGURE 8.39** Effect of gas velocity on final flux in filtration with submerged membranes. (From Figure 7 in Chang, S. and Fane, A.G., *J. Membr. Sci.*, 184, 221, 2001. With permission.)

with tightly and loosely fixed fiber modules. Similarly, Wicaksana et al. [87] showed that the rate of suction pressure rise with a tight fiber was 50% faster than a fiber of 96% tightness, for a 5g/L yeast suspension and the same airflow rate. In addition, the depolarization due to fiber movement was shown to be up to 40% of the overall bubbling effect. Commercial hollow fiber systems have recognized the importance of a certain degree of fiber looseness and flexibility.

### 8.6.2 SOLID-LIQUID TWO-PHASE FLOW—BY PARTICLE ADDITION

An early study by Bixler and Rappe [88] showed that glass beads (up to 100  $\mu\text{m}$  size) added to a stirred cell UF of a macrosolute were able to significantly enhance flux. The mechanism was probably eddy formation and thinning of the concentration boundary layer by particle interaction. Similar effects were reported by Fane [89] who noted that enhancement required significantly supramicron particles and that smaller particles could in fact add to the deposit resistance.

The added-particle effect is also evident in the application of fluidized beds to provide turbulence promotion. Figure 8.41 is a schematic diagram of a combined tubular membrane-fluidized beds system. It consists of a tubular membrane module, fluidized particles, a feed pump, and the feed storage tank. During the operation, the particles are fluidized by the pumped liquid flow. The drag forces on the solid particles are a function of the liquid velocity and the porosity of the bed. Usually the liquid velocity will be adjusted to a value that results in a balance between the gravity and drag forces so that the particle will not be hydraulically transported. The enhanced mass transfer is caused by the irregular flow of the liquid between the particles and the erosive action of the randomly moving particles at the membrane surface.

Noordman et al. [90] assessed the performance enhancement of ultrafiltration of 10 g/L BSA solution by fluidized particles of different materials and size using a polysulfone tubular membrane with inside diameter of 14.4 mm and 1.75 m length and an MWCO of 10 kDa. Table 8.4 summarizes the fluxes and the mass transfer coefficients obtained under different experimental

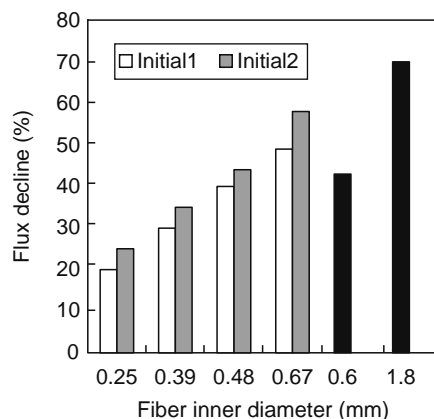


**FIGURE 8.40** Effect of fiber diameter on flux decline in filtration with submerged hollow fiber. (From Figure 8 in Chang, S. and Fane, A.G., *J. Membr. Sci.*, 184, 221, 2001. With permission.)

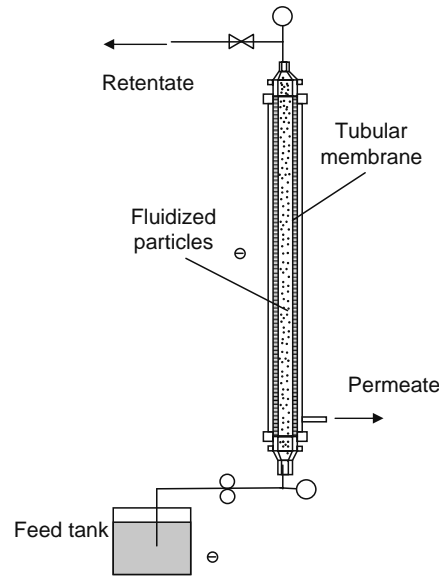


FIGURE 8.41 Schematics of tubular membrane with fluidized particles.

conditions. The mass transfer coefficients have been calculated using the film model based on the experimentally determined fluxes with the assumption of a constant gel concentration of 120 g/L. From Table 8.4 it can be seen the fluidized particles resulted in an enhancement in mass transfer of up to 15. The particle size and density seem to only have a limited effect on the process. Given that increasing the particle size and density may increase the risk of membrane damage by the fluidized particles [91] and require greater energy consumption, Noordman et al. [90] suggested that light and relatively small particle should be used in fluidized particle-enhanced membrane processes.

## 8.7 OTHER TECHNIQUES

### 8.7.1 ELECTROFILTRATION

Electrofiltration is related to application of an electric field to improve the efficiency of pressure-driven membrane filtration [92]. Figure 8.42 shows the basic configuration of electrofiltration, where an electric field is applied across micro or ultrafiltration membranes in flat sheet, tubular, and SWMs. The electrode is installed on either side of the membrane with the cathode on the permeate side and the anode on the feed side. Usually, the membrane support is made of stainless steel or the membrane itself is made of conductive materials to form the cathode. Titanium coated with a thin layer of a noble metal such as platinum could, according to Bowen [93], be one of the best anode materials. Wakeman and Tarleton [94] analyzed the particle trajectory in a combined fluid flow and electric field and suggested that a tubular configuration should be more effective in use of electric power than flat and multitubular module.

**TABLE 8.4**  
Mass Transfer and Flux for Filtration with Different Fluidized Particles

Material	$d_p$ (mm)	$\rho_s$ (kg/m <sup>3</sup> )	$k$ ( $\mu\text{m/s}$ )	Flux (L/m <sup>2</sup> hr)	Flux Enhancement
Empty tube	—	—	0.54	6.26	1
Glass	1	2900	4.3	49.8	8.0
Glass	1	2900	6.4	74.2	11.8
Glass	0.46	2900	5.9	68.4	10.9
Stainless steel	1	7800	7.6	88.1	14.07
Stainless steel	2	7800	8.1	93.9	15

Source: From Noordman, T.R., De Jonge, A., Wesselingh, J.A., Bel, W., Dekke, M., Ter Vorde, E., and Grijpma, S.D., *J. Membr. Sci.*, 208, 157, 2002.

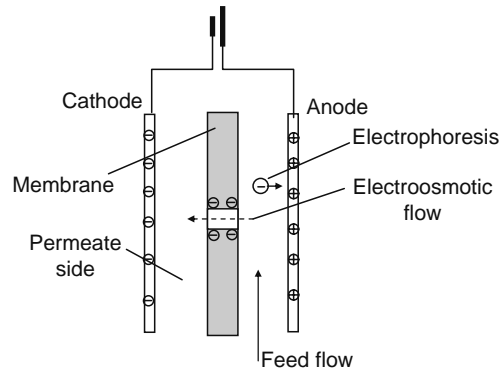


FIGURE 8.42 Schematics of electrofiltration.

Filtration enhancement by an electric field results from the influence of the applied electric field on particle deposition via electrophoresis. Most particles acquire a surface charge when in contact with a polar (e.g., aqueous) medium due to ionization, ion adsorption, and ion dissolution. This surface charge influences the distribution of nearby ions of opposite charge and leads to the formation of an electrical double layer at the interface between the particle and the dispersion medium (water). An imaginary boundary, the surface of shear, separates the double layer into two parts: the bound and mobile parts. If a voltage gradient is applied the charged particle (plus bound ions) tends to move in the appropriate direction, whilst the ions in the mobile part of the double layer show a net migration in the opposite direction carrying solvent along with them. Electrophoresis is the movement of the charged particle relative to stationary liquid under the effect of an applied electric field. This movement depends on the potential at the surface of shear, known as the zeta potential, and the strength of the electric field applied. The electrophoretic mobility ( $u_E$ ), or the electrophoretic velocity ( $v_E$ ) produced by unit electric field strength ( $\mathbf{E}$ ), can be related to the zeta potential by

$$u_E = \frac{v_E}{\mathbf{E}} = \frac{\varepsilon_r \xi}{\eta} \quad (8.34)$$

where

$\varepsilon_r$  is the electrolyte permittivity

$\xi$  is the zeta potential

$\eta$  is the viscosity

Surfaces in contact with the aqueous media are more usually negatively charged (negative zeta potential in a liquid) than positively charged; the effect is pH dependent with negative charge increasing with pH. When an external electric field is applied across the membrane with its anode in the feed side, the electrophoretic movement of negatively charged particles in the feed be away from the membrane and will augment diffusive back transport.

This means that the conventional film model relationship can be modified to show the augmentation due to electrophoretic velocity ( $v_E$ ) [92], so

$$J = \ln\left(\frac{C_w}{C_b}\right) + v_E \quad (8.35)$$

The critical electric field strength at which the net migration of the particles toward the membrane is zero can be calculated by combining Equations 8.34 and 8.35 with  $C_w = C_b$ .

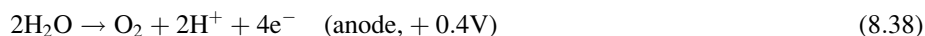
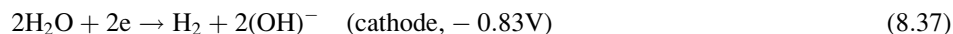
$$\mathbf{E}_{\text{crit}} = \frac{J\eta}{\varepsilon\xi} \quad (8.36)$$

When the electric strength is equal to or larger than the critical value the particle deposition can be arrested by the electrophoretic movement or the particles will even move in the opposite direction to the permeate flow. It should be noted that electrofiltration requires charged particles in the feed, and that the zeta potential will depend on the pH and the ionic environment. This means it will not be effective close to the isoelectric point or with raised levels of salts.

Another electrokinetic phenomenon that may occur during electrofiltration is electroosmosis or the movement of liquid relative to a stationary charged surface. If the membrane itself is charged, the electrical field applied across the membrane will

try to shear off the mobile part of the double layer of the pore wall, leading to an electroosmotic flow in the pores. For a negatively charged membrane, the electroosmosis flow will be in the same direction as the permeate flow if the applied electric field is as shown in Figure 8.42. It has been reported the electroosmosis could result in up to 15% enhancement in permeate flux [95], although the main process enhancement mechanism has been attributed to the electrophoretic movement of the charged particles that limit cake formation. Visvanathan and Ben Aim [96] describe the combined application of electrofiltration and electroosmotic backwashing, which involves polarity reversal to keep both the membrane and the electrode free from deposits.

Apart from electrokinetic phenomena, the electrofiltration process may also be affected by the electrochemical reactions that occur at the electrodes. A typical cathodic process and anodic process in aqueous systems are the formation of hydrogen gas at the cathode and oxygen at the anode:



Electrochemical reactions can be harmful to the filtration processes by causing foaming or pore obstruction due to production of gas. However, anodic oxidation can also be used as a method of removing organic molecules from the effluent. It seems further studies are still needed to justify the role of electrode reactions in electrofiltration.

The flux enhancement by electric field has been reported by many researchers. Huotari et al. [97] reported five time increase in flux by applying 2.4 kV/m external electric field in filtration of oily waste water using a tubular carbon fiber—carbon composite membrane with membrane pore size of 0.05  $\mu\text{m}$  and an inside diameter of 5.7 mm with the membrane itself as the cathode and a stainless steel of 2 mm in diameter located in the central of the tubular membrane as the anode. For this enhancement, the zeta potential of the particle and the membrane was  $-67$  and  $-50$  mV, respectively. Akay and Wakeman [98] obtained 10-fold enhancement of the flux using an electric field strength in the microfiltration of an anionic, hydrophobically modified water-soluble polymer (HMWSP). Rios et al. [99] reported that the flux in filtration of gelatin solution can be increased from 4 to 12  $\text{L}/\text{m}^2 \text{h}$  with an electric field strength of 2.4 kV/m. To achieve this effect, it was necessary to operate at a pH above the isoelectric point of gelatin to give it a net negative charge.

Although it has been reported that an external DC electric field can induce an electrophoretic back transport that can significantly enhance flux in crossflow membrane filtration, its commercial implementation appears to be restricted by several factors. These include lack of suitably inexpensive corrosion-resistant electrode materials, concerns about energy consumption, and the complexity of module manufacture.

The application of an external AC field effect has also been reported to enhance the performance of RO membranes [100]. The electromagnetic field is said to reduce fouling by scale formers and to reduce particulate fouling and biofilm development. The mechanisms involved are still under investigation but could include a change to crystal morphology and aggregation of particles and bacteria, raising their critical flux.

### 8.7.2 ULTRASOUND-ENHANCED FILTRATION

Ultrasound occurs at a frequency above 16 kHz and is typically associated with the frequency range of 20 kHz to 500 MHz. The frequency level is inversely proportional to the power output. The high intensity, low frequency ultrasound can alter the state of the medium chemically or physically and be used for applications such as cleaning, emulsification, crystallization, sonochemistry, etc. [101]. The chemical and physical effects of ultrasound are related to the cavitation phenomenon induced by rarefaction and compression of the sound wave. When ultrasound is irradiated through a liquid medium, an alternating adiabatic compression and rarefaction cycle of the medium occurs. During the rarefaction period, negative pressures occur and microbubbles can be formed and grown at sites where there is some gaseous impurity. The formed bubbles may suddenly collapse during the compression period after a few acoustic cycles with a release of energy. This helps to generate micromixing in the liquid, or form liquid microjets near a solid surface, or cause chemical changes in reactants in the cavitation bubbles. The power dissipated ( $P_{\text{diss}}$ ) in the liquid medium can be determined calorimetrically in terms of the change in temperature of the medium with the assumption that all the energy delivered to the system is dissipated as heat, as shown by

$$P_{\text{diss}} = \left( \frac{\Delta T}{\Delta t} \right) C_p M \quad (8.39)$$

where

$\Delta T$  is the change of temperature during time period  $\Delta t$

$C_p$  is heat capacity of water

$M$  is the water mass

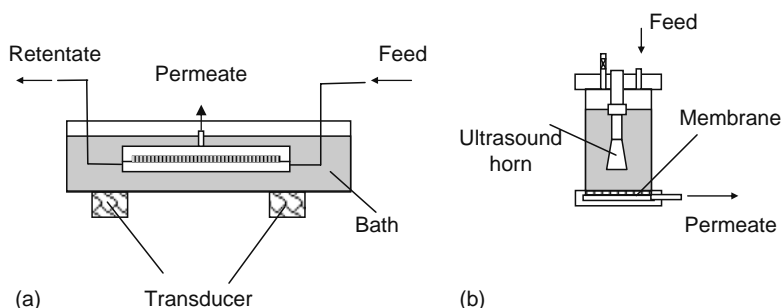


**FIGURE 8.43** Schematics of ultrasound membrane filtration systems. (a) Ultrasound bath and (b) ultrasound horn.

Figure 8.43 depicts two typical configurations used to assess the effect of ultrasound on membrane filtration and cleaning. Figure 8.43a shows a bath configuration where the crossflow cell is immersed in a water bath with ultrasonic transducers attached to the bottom of the bath. Figure 8.43b shows horn configuration where an ultrasonic horn is installed in a conventional cell.

Juang and Lin [102] assessed the effect of ultrasound on flux recovery in the ultrafiltration (YM 10, regenerated cellulose) of  $\text{Cu}^{2+}$ -polyethylenimine (PEI) solution and W/O/W solutions using a filtration cell equipped with an ultrasound horn (Misonix Sonicator 3000 [600 W, 20 kHz], horn type 200). Their results indicated that the ultrasound can even increase the pure water flux due to the cavitation induced TMP increase. For ultrafiltration of  $\text{Cu}^{2+}$ -PEI solution at 69 kPa, a 70%–80% flux recovery was obtained for an ultrasonic power  $>30$  W at the optimal tip height 65 mm. For ultrafiltration of the W/O/W emulsions, a 30%–60% flux recovery was achieved at 145 W, depending on the volume ratio of the water to oil in the emulsions. Analysis, based on the resistances in series model, revealed that the resistances caused by pore blocking and cake compressibility were reduced by increased ultrasound power. They also reported that the structure of the regenerated cellulose and polyethersulfone membranes tested could be affected by ultrasonics at powers greater than 80 W but no obvious change was observed with the polyvinylidene fluoride and polyacrylonitrile membranes. Simon et al. [103] defined an imaginary ultrasonic stirring speed at which the mass transfer coefficient will be similar to that obtained by a traditional stirrer at the same stirring speed. They suggested that the ultrasonic stirring speed is proportional to the ultrasound power by comparing the mass transfer coefficients obtained in ultrafiltration of dextran (500 kDa) using a classical stirred cell and an ultrasound-assisted cell. Kobayashi et al. [104] assessed the effect of ultrasonic frequency on ultrasound membrane cleaning for dextran-fouled ultrafiltration membranes (10 kDa) and milk-fouled cellulose microfiltration membranes using a crossflow cell immersed in an ultrasound bath. For the tested frequencies of 28, 45, and 100 kHz, they reported the cleaning can be significantly affected by the frequency with 28 kHz identified as the optimal. Muthukumaran et al. [105] examined the effect of low power ultrasonics on the UF of dairy whey. They found flux enhancements of  $\times 1.2$ – $\times 1.7$  and that this could be improved when used in combination with flow channel spacers.

All the reported studies indicate that low frequency ultrasound can enhance the filtration process and improve membrane cleaning efficiency to some extent. However, reducing energy losses, increasing the efficiency of the ultrasound and system scale-up are challenges that need to be overcome before serious commercial application can be considered.

## 8.8 CONCLUSIONS

Many strategies are available for the enhancement of performance of membrane processes. All of these techniques aim to limit the effect of concentration polarization at the membrane surface. The majority of techniques is hydrodynamic and therefore involves additional energy input or some extra design feature. To obtain the enhancement in performance, there is an investment that requires a pay back. Thus in each case, there will be a trade-off between operating and capital cost that provides an optimum condition that minimizes total production cost. The most prevalent strategies for enhancement are the flow channel spacers used in the SWM for RO, NF and some UF, and two-phase flow by air sparging used in the increasingly ubiquitous-submerged membranes applied to water and wastewater treatment. High shear devices, with rotations and vibrations, also demonstrate significant ability for enhanced performance, particularly for difficult feed materials in niche applications.

## NOMENCLATURE

$B$	pitch of helical coil tube
$C$	coefficient (Equation 8.1)
CFD	computational fluid dynamics
$d_b$	bubble diameter

$d_f$	filament diameter of spacer
$d_i$	inner diameter
$d_o$	outer diameter
$d_p$	particle diameter
$d_{\text{pore}}$	membrane pore diameter
$d_{\text{ti}}$	tube internal diameter
$d_v$	displacement
$De$	Dean number
$D_t$	coil diameter
$D_t'$	modified coil diameter
$D$	dialysis
DOTM	direct observation through membrane
$E_t$	energy consumed per unit volume of filtrate
ED	electrodialysis
$F$	frequency
$f_c$	friction factor in a coil tube
$f_s$	friction factor in a straight tube
$J_{\text{cr}}$	critical flux
$J_d$	design flux
$l_m$	length of filament of spacer
$L$	length
$L_f$	filter length
$L_s$	length of space channel
$m$	coefficient
MBR	membrane bioreactor
MF	microfiltration
MWCO	molecular weight cut off
$n$	coefficient
NF	nanofiltration
$p$	coefficient
$P$	pressure
$P_d$	overall power expenditure
$\Delta P_L$	pressure drop along the filter
$\Delta P_{\text{tm}}$	transmembrane pressure
PV	pervaporation
$Q$	coefficient
$Q_f$	feed flow rate
$Q_p$	permeate flow rate
$R$	radial coordinate
$r_p$	particle radius
$R$	radius
$Re$	Reynolds number
RO	reverse osmosis
$s$	coefficient
$Sc$	Schmidt number
$Sh$	Sherwood number
$S_{\text{sp}}$	filament surface area of spacer
$S_{\text{vsp}}$	specific surface area of spacer
SWM	spiral wound module
$U_b$	bubble rising velocity
$V_m$	mean azimuthal velocity
$T$	time
TMP	transmembrane pressure
UF	ultrafiltration
$u_E$	electrophoretic mobility
$v_E$	electrophoretic velocity
$V_{\text{sp}}$	filament volume of space filament

$V$	velocity
$V_{\text{total}}$	channel volume of spaced-filled channel
$w$	axial velocity of pulsatile flow
$z$	coordinate

### GREEK LETTERS

$\varepsilon$	voidage of spacer
$\varepsilon_r$	electrolyte permittivity
$\phi_b$	solid volume fraction in the solution
$\gamma$	shear rate
$\eta$	viscosity
$\nu$	kinematical viscosity
$\rho$	liquid density
$\omega$	angular velocity
$\xi$	zeta potential

### REFERENCES

- Porter MC, Membrane filtration, in: Schweitzer, PA (Ed.), *Handbook of Separation Techniques for Chemical Engineers*, McGraw-Hill, 1979, Chapter 2.1.
- Field RW, Wu D, Howell JA, and Gupta BB, Critical flux concept for microfiltration fouling, *J. Membr. Sci.* 1995; 100: 259.
- Li H, Fane AG, Coster HGL, and Vigneswaran S, Direct observation of particle deposition on the membrane surface during crossflow microfiltration, *J. Membr. Sci.* 1998a; 149: 83.
- Belfort G, Davis RH, and Zydney AL, Review: The behavior of suspensions and macromolecular solutions in crossflow microfiltration, *J. Membr. Sci.* 1994; 96: 1–58.
- Eckstein EC, Bailey DG, and Shapiro AH, Self-diffusion of particles in shear flow of a suspension, *J. Fluid Mech.* 1977; 79: 191.
- Segre G and Silberberg A, Behavior of microscopic rigid spheres in Poiseuille flow, Part 1 and 2, *Fluid Mech.* 1962; 14: 115–157.
- Li H, Fane AG, Coster HGL, and Vigneswaran S, An assessment of depolarisation models of crossflow microfiltration by direct observation through the membrane, *J. Membr. Sci.* 2000; 172: 135–147.
- Holm S, Malmberg R, and Svensson K, Method and plant for producing milk with a low bacterial content, Alfa-Laval Food and Dairy Engineering AB, Sweden, Assignee Int., World Patent (WO) 86/01687, 1986.
- Le-Clech P, Jefferson B, Chang IS, and Judd SJ, Critical flux determination by the flux-step method in a submerged membrane bioreactor, *J. Membr. Sci.* 2003; 227: 81–93.
- Steuck MJ and Reading N, Porous membrane having hydrophilic surface and process, US Patent 4,618,533, 1988.
- Kim KJ, Fane AG, and Fell CJD, The performance of ultrafiltration membrane pretreated by polymers, *Desalination.* 1988; 70: 229–249.
- Nyström M and Jarvinen P, Modification of polysulfone ultrafiltration membrane with UV irradiation and hydrophilicity increasing agent, *J. Membr. Sci.* 1991; 60: 275–296.
- Kramer PW, Yeh YS, and Yasuda H, Low temperature plasma for the preparation of separation membranes, *J. Membr. Sci.* 1989; 46: 1–28.
- Fane AG, Ultrafiltration: Factors influencing flux and rejection, in: Wakeman RJ (Ed.), *Progress in Filtration and Separation*, Vol. 4, Elsevier Science, Amsterdam, 1986, pp. 101–179.
- Reid WH, On the stability of viscosity flow in a curved channel, *Proc. Royal Soc. A.* 1928; 121: 402.
- Moulin PH, Veyret D, and Charbit F, Dean vortices: Comparison of numerical simulation of shear stress and improvement of mass transfer in membrane processes at low permeation fluxes, *J. Membr. Sci.* 2001; 183: 148–162.
- Mishra P and Gupta SN, Momentum transfer in curved pipes, 1. Newtonian fluids, *Ind. Eng. Chem. Proc. Des. Dev.* 1979; 18: 130.
- Bubolz M, Wille M, Langer G, and Werner U, The use of Dean vortices for crossflow microfiltration: Basic principles and further investigation, *Sep. Purif. Technol.* 2002; 26: 81–89.
- Winzeler HB and Belfort G, Enhanced performance for pressure-driven membrane processes: The argument for fluid instabilities, *J. Membr. Sci.* 1993; 80: 35–47.
- Brewster ME, Chung KY, and Belfort G, Dean vortices with wall flux in a curved channel membrane system, 1. A new approach to membrane module design, *J. Membr. Sci.* 1993; 81: 127–137.
- Mallubhotla H and Belfort G, Flux enhancement during Dean vortex microfiltration: 8. Further diagnostics, *J. Membr. Sci.* 1997; 125: 75–91.
- Mallubhotla H, Schmidt M, Lee KH, and Belfort G, Flux enhancement during Dean vortex tubular membrane nanofiltration: 13. Effect of concentration and solute type, *J. Membr. Sci.* 1999; 153: 259–269.
- Moulin PH, Manno P, Rouch JC, Serra C, Clifton MJ, and Aptel P, Mass transfer improvement by Dean vortices: Ultrafiltration of colloid suspensions and macromolecular solutions, *J. Membr. Sci.* 1999; 156: 109–130.
- Murase T, Iritani E, Chidphong P, Kano K, Atsumi K, and Shirato M, High-speed microfiltration using a rotating, cylindrical, ceramic membrane, *Int. Chem. Eng.* 1991; 31(2): 370–378.

25. Kroner KH and Nissinen V, Dynamic filtration of microbial suspensions using an axially rotating filter, *J. Membr. Sci.* 1988; 36: 85–100.
26. Hallström B and Lopez-Levia M, Description of a rotating ultrafiltration module, *Desalination.* 1978; 24: 273–279.
27. Ohashi K, Tashiro K, Kushiya F, Matsumoto T, Yoshida S, Endo M, Horio T, Ozawa K, and Sakai K, Rotation-induced Taylor Vortex enhances filtrate flux in plasma separation, *ASAIO Trans.* 1988; 34(3): 300–307.
28. Vigo F and Uliana C, Influence of the velocity at the membrane surface on the performance of the ultrafiltration rotating module, *Sep. Sci. Technol.* 1986; 21(4): 367–381.
29. Holeschovsky UB and Cooney CL, Quantitative description of ultrafiltration in a rotating filtration device, *AIChE J.* 1991; 37(8): 219–227.
30. Shock G and Miquel A, Mass transfer and pressure loss in spiral wound modules, *Desalination.* 1978; 64: 339–352.
31. Da Costa AR and Fane AG, Net-type spacers: Effect of configuration on fluid flow path and ultrafiltration flux, *Ind. Eng. Chem. Res.* 1994; 33: 1845–1851.
32. Da Costa AR, Fane AG, Fell CJ, and Franken D, ACM, Optimal channel spacer design for ultrafiltration, *J. Membr. Sci.* 1991; 62: 275–291.
33. Schwinge J, Neal PR, Wiley DE, Fletcher DE, and Fane AG, Spiral wound modules and spacers: Review and analysis, *J. Membr. Sci.* 2004; 242: 129–153.
34. Neal PR, Li H, Fane AG, and Wiley DE, The effect of filament orientation on critical flux and particle deposition in spacer-filled channels, *J. Membr. Sci.* 2003; 214: 165–178.
35. Gupta BB, Howell JA, Wu D, and Field RW, A helical baffle for cross-flow microfiltration, *J. Membr. Sci.* 1995; 102: 31–42.
36. Elmaleh S and Ghaffor N, Cross-flow ultrafiltration of hydrocarbon and biological solid mixed suspensions, *J. Membr. Sci.* 1996; 118: 111–120.
37. Yeh HM and Chen KT, Improvement of ultrafiltration performance in tubular membrane using a twisted wire-rode assembly, *J. Membr. Sci.* 2000; 178: 43–53.
38. Xu N, Xing W, Xu N, and Shi J, Application of turbulence promoters in ceramic membrane bioreactor used for municipal wastewater reclamation, *J. Membr. Sci.* 2002; 210: 307–313.
39. van der Waal MJ and Racz IG, Mass transfer in corrugated-plate membrane module. 1. Hyperfiltration experiments, *J. Membr. Sci.* 1989; 40: 243–260.
40. Stairmand JW and Bellhouse BJ, Mass transfer in a pulsating turbulent flow with deposition onto furrowed walls, *Int. J. Heat Mass Transfer.* 1985; 27(7): 1405–1408.
41. Sobey IJ, Observation of waves during oscillator channel flow, *J. Fluid Mech.* 1985; 151: 247.
42. Millward HR, Bellhouse BJ, Sobey IJ, and Lewis RWH, Enhancement of plasma filtration using the concept of the vortex wave, *J. Membr. Sci.* 1995; 100: 121–129.
43. Womersley JR, Method for the calculation of velocity, rate of flow and viscous drag in arteries when the pressure gradient is known, *J. Physiol.* 1955; 127: 553–563.
44. Hale JF, McDonald DA, and Womersley JR, Velocity profiles of oscillating arterial flow, with some calculations of viscous drag and the Reynolds number, *J. Physiol.* 1955; 128: 629–640.
45. Li H and Bertram CD, Mechanisms by which pulsatile low affects cross flow microfiltration, *AIChE J.* 1998; 44(9): 1950–1961.
46. Li H, Mechanism study for crossflow microfiltration with pulsatile flow. PhD thesis, The University of New South Wales, Australia, 1995.
47. Bertram CD, Hoogland MR, Li H, Odell RA, and Fane AG, Flux enhancement in crossflow microfiltration using a collapsible-tube pulsation generator, *J. Membr. Sci.* 1993; 84: 279–292.
48. Kennedy TJ, Merson RL, and McCoy BJ, Improving permeation flux by pulsed reverse osmosis, *Chem. Eng. Sci.* 1974; 29: 1927–1931.
49. Gupta BB, Blanpain P, and Jaffrin MY, Permeate flux enhancement by pressure and flow pulsations in microfiltration with mineral membranes, *J. Membr. Sci.* 1992; 70: 257–266.
50. Jaffrin MY, Ding LH, and Gupta BB, Rationale of filtration enhancement in membrane plasmapheresis by pulsatile blood flow, Life Support Systems, *J. Eur. Society Artif. Organs.* 1987; 5: 267–271.
51. Rodgers VGJ and Sparks RE, Effect of transmembrane pressure pulsing on concentration polarization, *J. Membr. Sci.* 1992; 68: 149–168.
52. Jonsson GA, Waagner RA, Nielsen E, and Edelman D, Low cross-flow velocity microfiltration of skim milk for removal of bacterial spores, *Int. Dairy J.* 1997; 7: 849–861.
53. Wenten IG, Koenhen DM, Roesink HDW, Rasmussen A, and Jonsson G, Method for the removal of components causing turbidity, from a fluid, by means of microfiltration, US Patent 5,560,828, October 1996.
54. Kuiper S, van Rijn CJM, Nijdam W, and Elwenspoek MC, Development and applications of very high flux microfiltration membranes, *J. Membr. Sci.* 1998; 150: 1–8.
55. Kuiper S, van Rijn C, Nijdam W, Raspe O, van Wolferen H, and Krijnen G, Elwenspoek M, Filtration of lager beer with microsieves: Flux, permeate haze and inline microscope observations, *J. Membr. Sci.* 2002; 196: 129–170.
56. Bouzerar R, Jaffrin MY, Lefevre A, and Paullier P, Concentration of ferric hydroxide suspensions in saline medium by dynamic cross-flow filtration, *J. Membr. Sci.* 2000; 165: 111–123.
57. Jaffrin MY, Ding LH, Akoum O, and Brou A, A hydrodynamic comparison between rotating disk and vibratory dynamic filtration systems, *J. Membr. Sci.* 2004; 242: 155–167.
58. Chang S, Li H, and Fane AG, Characteristics of operation of a rotating disk membrane filter, in: Schäfer AI, Basson L, and Richards BS (Eds.), *Environmental Engineering Research Event*, Terrigal, New South Wales, 1998, pp. 153–158.

59. Ding LH, Akoum O, Abraham A, and Jaffrin MY, High shear skim ultrafiltration using rotating disk filtration systems, *AIChE J.* 2003; 49(9): 2433–2441.
60. Nuortula-Jokinen J and Nyström M, Comparison of membrane separation processes in the internal purification of paper mill water, *J. Membr. Sci.* 1996; 119: 99.
61. Dal-Cin MM, Lick CN, Kumar A, and Lealess S, Dispersed phase back transport during ultrafiltration of cutting oil emulsions with a spinning disc geometry, *J. Membr. Sci.* 1998; 141: 165.
62. Frenander U and Jönsson AS, Cell harvesting by crossflow microfiltration using a shear-enhanced module, *Biotechnol. Bioeng.* 1996; 52: 397.
63. Lee S, Burt A, Russoti G, and Buckland B, Microfiltration of recombinant yeast cells using a rotating disk dynamic filtration system, *Biotechnol. Bioeng.* 1995; 48: 386.
64. Brou A, Ding L, Boulnois P, and Jaffrin M, Dynamic microfiltration of yeast suspensions using rotating disks equipped with vanes, *J. Membr. Sci.* 2002; 197: 269–282.
65. Armando AD, Culkin B, and Purchas DB, New separation system extends the use of membranes, Proceedings of the Euromembrane'92, Vol. 6, Lavoisier, Paris, 1992, pp. 459–462.
66. Al-Aloum O, Mercier-Bonin M, Ding L, Fonade C, Aptel P, and Jaffrin M, Comparison of three different systems used for flux enhancement: Application to crossflow filtration of yeast suspensions, *Desalination.* 2002; 147: 31–36.
67. Krantz WB, Bilodeau RR, Voorhees ME, and Elgas RJ, Use of axial membrane vibrations to enhance mass transfer in a hollow tube oxygenator, *J. Membr. Sci.* 1997; 124: 283–299.
68. Genkin G, Waite TD, Fane AG, and Chang S, The effect of vibration and coagulation addition on the performance of submerged hollow fibre membranes. *J. Membr. Sci.* 2006; 281: 726–734.
69. Hewitt GF, Multiphase fluid flow and pressure drop: Introduction and fundamentals, in: Hewitt GF (Ed.), *Hemisphere Handbook of Heat Exchanger Design*, Hemisphere Publishing Corporation, New York, 2.3.1-1–2.3.1-10, 1990.
70. Cui ZF, Experimental investigation on enhancement of crossflow ultrafiltration with air sparging, in Aterson RP (Ed.), *Effective Membrane Processes—New Perspective*, Mechanical Engineering Publications, London, pp. 237–245, 1993.
71. Cabassud C, Laborie S, and Lainé JM, How slug flow can improve ultrafiltration flux in organic hollow fibers, *J. Membr. Sci.* 1997; 128: 93.
72. Mercier M, Fonade C, and Lafforgue-Delorme C, How slug flow can enhance the ultrafiltration flux in mineral tubular membranes, *J. Membr. Sci.* 1997; 128: 103–113.
73. Mercier M, Maranges C, Fonade C, and Lafforgue-Delorme C, Flux enhancement using upward gas liquid slug flow: Application to continuous alcoholic fermentation with cell recycle, *Biotech. Bioeng.* 1998; 58: 47.
74. Imasaka T, So H, Matsushita HK, Furukawa T, and Kanekuni N, Application of gas–liquid two-phase crossflow filtration to pilot scale methane fermentation, *Drying Tech.* 1993; 11: 769.
75. Vera L, Delgado S, and Elmaleh S, Gas sparged cross-flow microfiltration of biologically treated wastewater, Proceedings of the Membrane Technology in Environmental Management, Tokyo, 1999, pp. 131–137.
76. Ghosh R, Li Q, and Cui ZF, Fraction of BSA and lysozyme using ultrafiltration: Effect of gas sparging, *AIChE J.* 1998; 44(1): 61–67.
77. Cui ZF, Chang S, and Fane AG, The use of gas bubble to enhance membrane processes, *J. Membr. Sci.* 2003; 221: 1–35.
78. Cui ZF and Wright KIT, Gas–liquid two-phase crossflow ultrafiltration of dextran and BSA solutions, *J. Membr. Sci.* 1993; 90: 183–189.
79. Cui ZF and Wright KIT, Flux enhancement with gas sparging in downwards crossflow ultrafiltration: Performance and mechanisms, *J. Membr. Sci.* 1996; 117: 109–116.
80. Cheng TW, Yeh HMG, and Wu JH, Effects of gas slugs and inclination angle on the ultrafiltration flux in tubular membrane module, *J. Membr. Sci.* 1999; 158: 223–234.
81. Cheng TW, Influence of inclination on gas-sparged cross-flow ultrafiltration through an inorganic tubular membrane, *J. Membr. Sci.* 2002; 196(1): 103–110.
82. Al-Akoum O, Mercier-Bonin M, Ding L, Fonade C, Aptel P, and Jaffrin MY, Comparison of three different systems used for flux enhancement: Application to yeast crossflow filtration of yeast suspensions, *Desalination.* 2000; 147: 31–36.
83. Tajima F and Yamamoto T, Apparatus for filtering water containing radioactive substances in nuclear power plants, Toshiba, US Patent 4,756,875, 1988.
84. Yamamoto K, Hiasa M, Mahmood T, and Matsuo T, Direct solid–liquid separation using hollow fiber membrane in an activated sludge aeration tank, *Water Sci. Technol.* 1989; 21: 43–54.
85. Chang S and Fane AG, The effect of fiber diameter on filtration and flux distribution—relevance to submerged hollow fiber modules, *J. Membr. Sci.* 2001; 184: 221–231.
86. Chang S and Fane AG, Filtration of biomass with lab-scale submerged hollow fiber membrane module: Effect of operational conditions and module configuration, *J. Chem. Technol. Biotechnol.* 2002; 77: 1030–2212.
87. Wicaksana F, Fane AG, and Chen V, Fibre movement induced by bubbling using submerged hollow fibre membranes, *J. Membr. Sci.* 2006; 271: 186–195.
88. Bixler HJ and Rappe GC, Ultrafiltration process, US Patent 3,541,006, November 1970.
89. Fane AG, Ultrafiltration of suspensions, *J. Membr. Sci.* 1984; 20: 249–260.
90. Noordman TR, De Jonge A, Wesselingh JA, Bel W, Dekke M, Ter Vorde E, and Grijpma SD, Application of fluidised particles as turbulence promoters in ultrafiltration improvement of flux and rejection, *J. Membr. Sci.* 2002; 208: 157–169.
91. van der Waal MJ, van der Velden PM, Koning J, Smolders CA, and van Swaay WPM, Use of fluidized beds as turbulence promoters in tubular membrane systems, *Desalination.* 1977; 22: 465–483.

92. Henry JD, Lawler LF, and Kuo CHA, A solid/liquid separation process based on crossflow and electrofiltration, *AIChE J.* 1977; 23(6): 851–859.
93. Bowen WR, Electrochemical aspects of microfiltration and ultrafiltration, in: Howell JA, Sanchez V, and Field RW (Eds.), *Membranes in Bioprocessing*, Chapman & Hall, Cambridge, 1993, pp. 265–292.
94. Wakeman RJ and Tarleton ES, Membrane fouling prevention in crossflow microfiltration, *Chem. Eng. Sci.* 1987; 42(4): 829–842.
95. Radovich JM and Behnam B, Concentration ultrafiltration and diafiltration of albumin with an electric field, *Sep. Sci. Technol.* 1983; 18(3): 215–222.
96. Visvanathan C and Ben Aim R, Enhancing electrofiltration with the aid of an electro-osmotic backwashing arrangement, *Filt. Sep.* 1990; Jan/Feb, pp. 42–44.
97. Huotari HM, Huisman IM, and Trägårdh G, Electrically enhanced crossflow membrane filtration of oily waste water using the membrane as a cathode, *J. Membr. Sci.* 1999; 156: 49–60.
98. Akay G and Wakeman RJ, Electric field enhanced crossflow microfiltration of hydrophobically modified water soluble polymers, *J. Membr. Sci.* 1997; 131: 229–236.
99. Rios GM, Rakotorisoa H, and Tarodo de la Fuente B, Basic transport mechanisms of ultrafiltration in the presence of an electric field, *J. Membr. Sci.* 1988; 38: 147–159.
100. Zhang YP, Chong TH, Fane AG, Law A, Coster HGL, and Winters H, Implications of enhancing critical flux of particulates by AC fields in RO desalination and reclamation, *Desalination*, 2008; 220: 371–379.
101. Thompson LH and Doraiswamy LK, Sonochemistry: Science and engineering, *Ind. Eng. Chem. Res.* 1999; 38: 1215–1249.
102. Juang RS and Lin KH, Flux recovery in the ultrafiltration of suspended solution with ultrasound, *J. Membr. Sci.* 2004; 243: 115–124.
103. Simon A, Penpenic L, Gondrexon N, Taha S, and Dorange G, A comparative study between classical stirred and ultrasonically-assisted dead-end ultrafiltration, *Ultrason. Sonochem.* 2000; 7: 183–186.
104. Kobayashi T, Kobayashi T, Hosaka Y, and Fujii N, Ultrasound-enhanced membrane-cleaning processes applied water treatments: Influence of sonic frequency on filtration treatments, *Ultrasonics* 2003; 41: 185–190.
105. Muthukumar S, Kentish SE, Ashokkumar M, and Stevens GW, Mechanisms for the ultrasonic enhancement of dairy whey ultrafiltration, *J. Membr. Sci.* 2005; 258: 106–114.

---

# 9 Separation and Removal of Hydrocarbons Using Polymer Membranes

*S.I. Semenova\**

## CONTENTS

9.1	Introduction and Background .....	234
9.2	General Considerations: Physicochemical Regularities of Hydrocarbon Permeation in Membranes Based on Glassy and Rubbery Polymers .....	234
9.2.1	Thermodynamic Factor of Permeability .....	234
9.2.2	Kinetic Factor of Permeability .....	237
9.2.2.1	Effective Sizes of Diffusing Molecules .....	237
9.2.2.2	Effect of Cohesion Energy Density of the Polymer on Diffusion of Hydrocarbons in the Polymer .....	239
9.2.2.3	Effect of Free Volume of the Polymer on Diffusion of Hydrocarbons in the Polymer .....	240
9.2.2.4	Concentration Dependencies of Diffusion Coefficients of Hydrocarbons .....	240
9.3	Separation and Removal of Hydrocarbons Using Membranes Based on Rubbery Polymers .....	240
9.3.1	Selective Separation and Removal of Hydrocarbon Vapors from Gas Mixtures .....	240
9.3.1.1	Effect of Chemical Composition of Organosilicon Polymers on Their Gas Separation Properties to Hydrocarbons .....	240
9.3.1.2	Pressure Dependence of Hydrocarbon Permeability in Rubbery Polymers: Effect of Plasticization of the Polymer by the Penetrant .....	243
9.3.1.3	Temperature Dependence of Hydrocarbon Permeability in Rubbery Polymers .....	245
9.3.1.4	Polytrimethylsilylpropyne as a Membrane Material for Hydrocarbons Separation and Removal from Gas Mixtures .....	246
9.3.2	Application of Rubbery Polymers for Pervaporation Removal of Hydrocarbons from Their Aqueous Solutions .....	246
9.4	Separation and Removal of Hydrocarbons Using Membranes Based on Glassy Polymers .....	248
9.4.1	Separation of Olefins and Paraffins .....	248
9.4.1.1	Effect of Unsaturated Bonds on the Size of Olefin Molecules and on the Capability of Olefins to Enter into Specific Interactions with the Membrane Matrix .....	248
9.4.1.2	Effect of Chemical Composition of Glassy Polymers on Their Gas Separation Properties to Hydrocarbons .....	249
9.4.1.3	Pressure Dependence of Hydrocarbon Permeability and Selectivity in Glassy Polymers .....	254
9.4.1.4	Temperature Dependence of Hydrocarbon Permeability and Selectivity in Glassy Polymers .....	255
9.4.1.5	Kinetics of the Permeation Process .....	256
9.4.2	Separation of Aromatic, Alicyclic, and Aliphatic Hydrocarbons .....	257
9.4.2.1	Problem of Separation of Aromatic, Alicyclic, and Aliphatic Hydrocarbons .....	257
9.4.2.2	Diffusion Component of Separation Factor .....	258
9.4.2.3	Sorption Component of Separation Factor .....	260
9.5	Industrial Removal of Hydrocarbons from Their Mixtures with Various Gases and Vapors .....	262
	References .....	264

---

\* The author is deceased.

## 9.1 INTRODUCTION AND BACKGROUND

Separation of hydrocarbons and their removal from various gaseous and liquid mixtures are important objectives of chemical and petrochemical industries. These objectives can be achieved by adsorption, rectification, or cryogenic technology. In the last 20 years this list of traditional methods was supplemented by membrane technology. A significant corpus of patent and literary data accumulated so far requires generalization (about 2000 documents over the last 20 years). The flow of patent and periodic information on the problem of membrane separation of hydrocarbons is steadily growing [1–4]. The flow is dominated by articles in journals whereas the share of patents is only about one third. This indicates that at present researchers are mainly taking a scientific, rather than commercial, interest in the problem [1].

Several areas can be singled out in membrane separation techniques differing by a number of criteria, primarily by the material of construction of the membrane's selective layer. Materials of construction of the membrane's selective layer can be broken down into the following groups: polymers (41% in the total information flow), inorganic materials (37.7%), liquids (4.8%), combined organic/inorganic materials (3.2%), and other materials (13.1%). A noteworthy fact is the growing interest shown by researchers in inorganic membranes [1]. A major breakthrough in the development of inorganic membranes (zeolites, aluminium oxide, ceramics, silica, various metals, metal oxides, etc.) has been on the cards for the last 10 years. However, the use of membranes with inorganic selective layers is now only at the stage of intense investigation and is still a long way from commercial implementation. The share of patents in the information flow on this subject is only 19.9% [1].

Membranes having a polymer-based selective layer make up the most broadly represented segment in the information flow. In terms of the share in this total information flow, polymer materials can be arranged in the following series: polyimides (15.3%), polyolefins (8.2%), polysulfones (7.2%), polyamides (7.2%), fluorine-containing polymers (4.8%), and organosilicon polymers (7.1%). Polyamides are the most widely represented class of polymers in both periodical and patent literature. As years go by, the interest shown by researchers (especially in Japan) in the use of polyimides is not waning. A lot of documents can also be found in the information flow that makes reference to the use of rubbery polymer materials, including polysiloxanes, which in fact indicates that practical use of these materials may hold much promise [1].

The materials of the selective layer of the membranes dominating in the data are polymers. The polymers used can be both glassy and rubbery. It is therefore worthwhile to consider physicochemical regularities of hydrocarbon mass transfer across polymer membranes.

## 9.2 GENERAL CONSIDERATIONS: PHYSICO-CHEMICAL REGULARITIES OF HYDROCARBON PERMEATION IN MEMBRANES BASED ON GLASSY AND RUBBERY POLYMERS

There is no fundamental qualitative difference in mechanisms of low molecular weight (MW) penetrant diffusion in polymers above and below glass transition temperature,  $T_g$ , of the polymers [5,6]. The difference lies only in the fact that the movement of structural units of the macromolecule that are responsible for the transfer of penetrant molecules takes place at different supermolecular levels of the polymer matrix. At  $T > T_g$  the process of diffusion takes place in a medium with equilibrium or near-equilibrium packing of chains, and the fractional free volume,  $\nu_f$ , in the polymer is equal to the fractional free volume in the polymer determined by thermal mobility of structural units of macromolecules  $\nu_{f(T)}$ , i.e.,  $\nu_f = \nu_{f(T)}$ . At  $T < T_g$  the process of diffusion comes about under nonequilibrium packing conditions, although there exists a quasi-equilibrium structural organization of the matrix, where  $\nu_f > \nu_{f(T)}$ . It is assumed that in this case  $\nu_f = \nu_{f(T)} + \nu_{f(v)}$ , where  $\nu_{f(v)}$  is the fractional free volume responsible for nonequilibrium character of the polymer matrix [5].

Permeability of low MW penetrants in polymers is determined by both thermodynamic (sorptive) and kinetic (diffusive) factors.

### 9.2.1 THERMODYNAMIC FACTOR OF PERMEABILITY

In the absence of specific penetrant/polymer interactions, solubility of the penetrant is determined mainly by its chemical nature and depends on condensability, which is represented by boiling temperature ( $T_b$ ), critical temperature ( $T_{cr}$ ), or Lennard–Jones constant ( $\epsilon/k$ ) [7,8]. It is known that in the hydrocarbon series the increase in condensability is accompanied by a parallel increase in the size of molecules (Table 9.1 [9–17]). It is therefore not surprising that in both glassy and rubbery polymers correlations of hydrocarbon solubility in the polymers with condensability and sizes of hydrocarbon molecules are observed (Figures 9.1 through 9.3).

To analyze sorption of penetrants, including hydrocarbons, in glassy polymers, the dual-mode sorption model is most frequently used. For a number of glassy polymers, correlations between the constants of the dual-mode sorption model and the condensability of hydrocarbons have been established (see, e.g., Figure 9.4a through 9.4c and data presented in Refs. [18–20]). Temperature dependence of model constants is described by Vant-Hoff equation, where the exponent contains heat of penetrant sorption  $\Delta H_s$ . This quantity is essentially dependent on the heat of penetrant condensation,  $\Delta H_{\text{cond}}$ :  $\Delta H_s = \Delta H_{\text{cond}} + \Delta H_1$ , where  $\Delta H_1$  is partial molar enthalpy of penetrant dissolution in the polymer,  $\Delta H_1 = [\partial(\Delta G_1/T)/\partial(1/T)]_c$ ,  $\Delta G_1$  is the partial molar free

**TABLE 9.1**  
Physical Properties of Some Gases and Vapors

Penetrant	Condensability		Size of Molecule		
	$T_b$ (K)	$\varepsilon/k$ (K)	$\sigma_{LJ}$ (nm)	$\sigma_{kt}$ (nm)	$a_D$ (nm <sup>2</sup> )
N <sub>2</sub>	77.4	91.5	0.368	0.364	
O <sub>2</sub>	90.2	113	0.343	0.346	
CO	81.7	110	0.359	0.376	
CH <sub>4</sub>	111.7	137	0.382	0.380	
C <sub>2</sub> H <sub>4</sub>	169.5	205	0.423	0.390	
C <sub>2</sub> H <sub>6</sub>	184.5	230	0.442		
C <sub>3</sub> H <sub>6</sub>	225.5	303	0.468	0.450	
C <sub>3</sub> H <sub>8</sub>	231.1	254	0.506	0.430	
C <sub>4</sub> H <sub>6</sub>	281.2			0.440	
C <sub>4</sub> H <sub>8</sub>	266.9	330	0.528	0.560	
<i>n</i> C <sub>4</sub> H <sub>10</sub>	272.7	410	0.534	0.430	
<i>iso</i> C <sub>4</sub> H <sub>10</sub>	261.3	313	0.534		
<i>n</i> C <sub>5</sub> H <sub>12</sub>	309.2	345	0.578		
C <sub>6</sub> H <sub>6</sub>	353.3	412	0.527	0.660	0.21
C <sub>6</sub> H <sub>5</sub> CH <sub>3</sub>	383.8		0.593		0.23
<i>n</i> C <sub>6</sub> H <sub>14</sub>	341.9	413	0.591		0.18
<i>ciclo</i> C <sub>6</sub> H <sub>12</sub>	353.9	324	0.609	0.670	0.33
<i>n</i> C <sub>7</sub> H <sub>14</sub>	371.6				
<i>n</i> C <sub>8</sub> H <sub>18</sub>	398.8	320	0.745		0.18
<i>iso</i> C <sub>8</sub> H <sub>18</sub>	390.8		0.762		0.36

Source: From Semenova, S.I., *J. Membr. Sci.*, 231, 189, 2004. With permission.

Notes:  $\sigma_{LJ}$  = molecular collision diameter calculated from the Lennard–Jones potential;  
 $\sigma_{kt}$  = molecular kinetic diameter determined using zeolites;  $a_D$  = minimum molecular cross-section determined from Stuart's molecular model [9–16].

energy of the penetrant dissolution in the polymer. The sorption of easily condensable hydrocarbons features negative values of sorption heat as a result of high negative values of their condensation heat.

A linear correlation between solubility of various gases in glassy polymers and distance between chains of macromolecules has been established using x-ray structural analysis. The solubility of gases, including lower hydrocarbons, increases with this distance [8,21,22]. Similarly it has been found that the solubility of gases in glassy polymers increases with the molar fraction of free volume of the polymer (see Figure 9.5) [8,23,24]. It was reported that the Langmuir mode saturation constant is

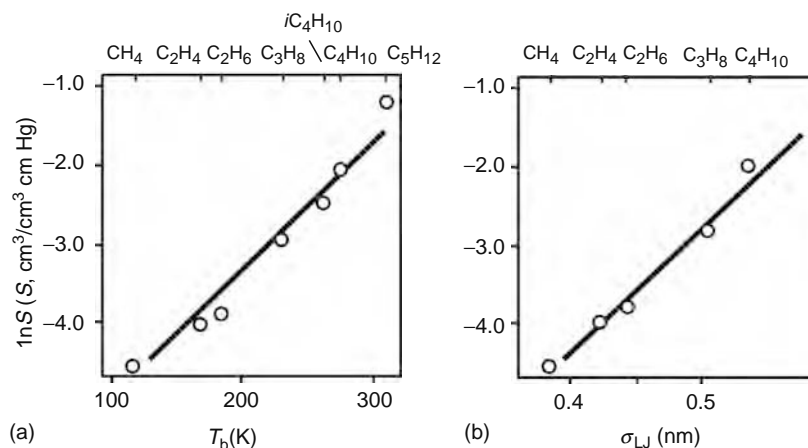


**FIGURE 9.1** Dependence of solubility coefficient of various hydrocarbons in natural rubber on hydrocarbon boiling temperature,  $T_b$  (a) and on diameter of their molecules calculated from Lennard–Jones potential,  $\sigma_{LJ}$  (b). (From Semenova, S.I., *Membranes* (in Russian), 13, 37, 2002.)

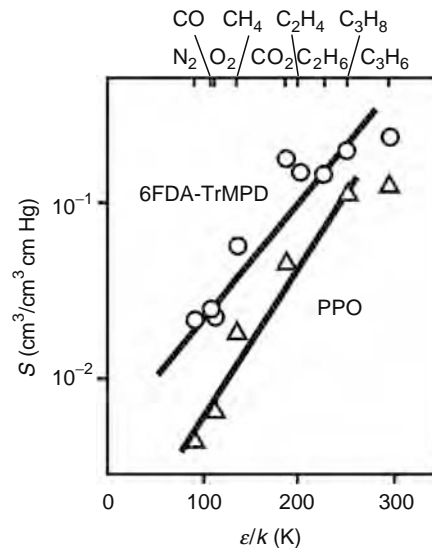


**FIGURE 9.2** Dependence of hydrocarbon solubility coefficient in glassy polymers on hydrocarbon Lennard–Jones force constant,  $\epsilon/k$ , at  $T=323$  K and pressure of 2 atm (6FDA-TrMPD is polyimide based on dianhydride of 4,4'-hexafluoroisopropylidene diphthalic acid and 2,4,6-trimethyl-1,3-phenylenediamine; PPO is polyphenylene oxide). (From Tanaka, K., Taguchi, A., Hao, J., Kita, H., Okamoto, K., *J. Membr. Sci.*, 121, 197, 1996. With permission.)

dependent on the accessible free volume of the polymer, and the accessible free volume of the same polymer decreases with the increase in the size of the penetrant molecule [18].

The solubility of hydrocarbons in rubbery polymers can be described in more detail by several theories of solutions using various criteria of thermodynamic affinity [7,25–28], of which the Flory–Huggins theory is the most popular one. It takes into account the volume content of the penetrant dissolved in the polymer and the change in the length of the polymer's thermodynamic segment as a result of dissolution [7]. However, it should be pointed out that to describe dissolution, a refined dual-mode sorption model can be used, e.g., the model by Pace and Datyner [7,29,30].

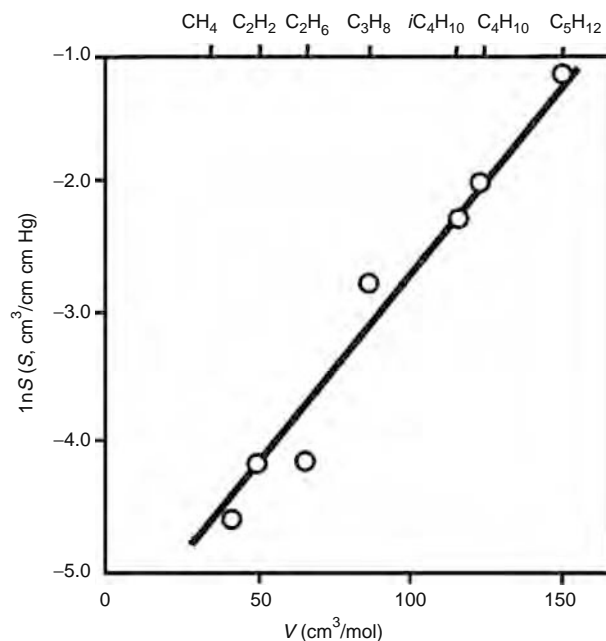


**FIGURE 9.3** Dependence of Henry's solubility coefficient on Van der Waals volume of penetrant molecules for the systems of natural rubber/hydrocarbons. (From Semenova, S.I., *Membranes (in Russian)*, 13, 37, 2002; Baker, R.W. and Wijmans, J.G., Membrane separation of organic vapors from gas streams. In: Paul D, Yampolskii Yu, Eds., *Polymeric Gas Separation Membranes*. CRC Press, 1994: 353–397; Crank, J. and Park, G., Ed., *Diffusion in Polymers*. London, Academic Press, 1968.)

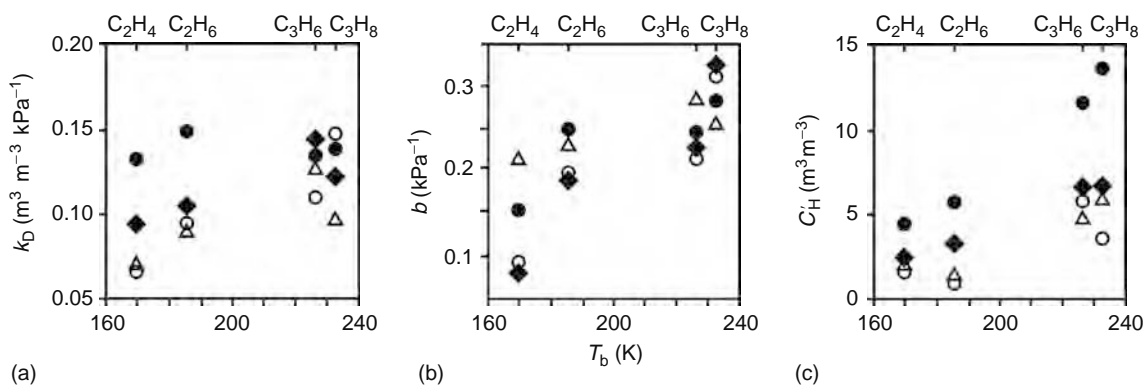


**FIGURE 9.4** Dependence of constants (a, b, and c present Henry constant, sorption affinity constant, and Langmuir sorption capacity respectively) of the model of dual-mode sorption of hydrocarbons by glassy polyphenylene oxides on boiling temperatures of hydrocarbons  $T_b$ : ● is pDMePO, poly-2,6-dimethyl-1,4-phenylene oxide; ○ is pDPhPO, poly-2,6-diphenyl-1,4-phenylene oxide; ◆ is pDMePO/pDPhPO copolymer (97.5/2.5% mol); ▽ is pDMePO/pDPhPO copolymer (75/25% mol). (From analysis of results presented in Lapkin, A.A., Roschupkina, O.P., and Ilinitich, O.M., *J. Membr. Sci.*, 141, 223, 1998.)

## 9.2.2 KINETIC FACTOR OF PERMEABILITY

Diffusion selectivity is based on the ability of the polymer matrix to transmit molecules of a certain shape and size. This ability is determined by the structure of the polymer and the rigidity of the macromolecular ensemble as well as by the properties of the penetrant, the size and shape of its molecules.

### 9.2.2.1 Effective Sizes of Diffusing Molecules

To estimate the molecular size of low MW penetrants permeating through the polymer membrane, the following parameters are used: Van der Waals volume of the molecule,  $V$ ; collision diameter calculated from Lennard-Johns potential,  $\sigma_{LJ}$ ; kinetic diameter of the molecule  $\sigma_{kt}$  determined using molecular sieves; minimum cross-section of the molecule  $a_D$ , determined from Stuart's molecular model [9–16]. Values of these parameters can differ significantly, especially for molecules of oblong shapes (Table 9.1). Comparison of molecules of inorganic gases and methane in terms of collision diameter  $\sigma_{LJ}$  and kinetic diameter  $\sigma_{kt}$  shows that the difference between the two is insignificant and both can be used to estimate the size of diffusing molecules. An exception is the quadrupole molecule of  $\text{CO}_2$ , whose effective diameter is determined on the basis of the correlation between  $\ln D$  and the diameters of molecules of several penetrants in various polymers [8]. The difference between  $\sigma_{LJ}$  and  $\sigma_{kt}$  increases with the increase in the number of carbon atoms in the hydrocarbon molecule.

The effect of the size of hydrocarbon molecules on their diffusion coefficients in glassy and rubbery polymers has been discussed in the literature [17,31–33]. It has been shown that effective cross-sections of diffusing hydrocarbon molecules determined from diffusion of permanent gases, whose molecular cross-section was derived from Stuart's model, have different

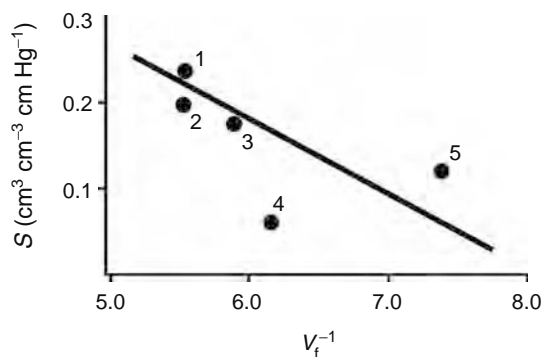


**FIGURE 9.5** Dependence of solubility coefficient of propylene in various polyimides on the content of free volume in polyimide: (1) 6FDA-TrMPD; (2) 6FDA-TeMPD; (3) 6FDA-DDBT; (4) 6FDA-ODA; (5) BPDA-TeMPD (6FDA is dianhydride of 4,4'-hexafluoroisopropylidene diphthalic acid; BPDA is dianhydride of 3,3',4,4'-diphenyltetradiphenyltetracarboxylic acid; TrMPD is 2,4,6-trimethyl-1,3-phenylene diamine; TeMPD is 2,3,5,6-tetramethylphenylene-1,4-diamine; DDBT is dimethyl-3,7-diaminobenzothiophene-5,5'-dioxide; ODA is diaminodiphenyl ether). (From analysis of results presented in Tanaka, K., Taguchi, A., Hao, J., Kita, H., and Okamoto, K., *J. Membr. Sci.*, 121, 197, 1996.)



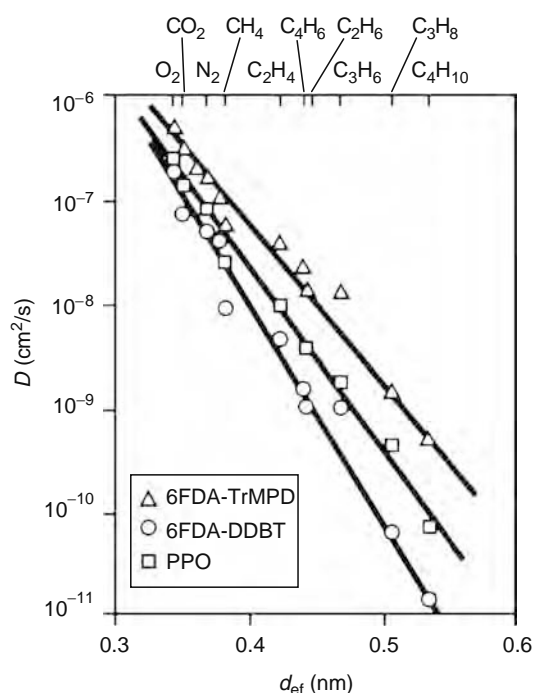


**FIGURE 9.7** Dependence of hydrocarbon diffusion coefficients on the effective diameter of hydrocarbon molecules  $d_{ef}$  at temperature,  $T = 323$  K and pressure of 2 atm (1 atm for  $C_4H_6$  and  $C_4H_{10}$ ) in various glassy polymers: 6FDA-TrMPD and 6FDA-DDBT are polyimides, PPO is polyphenylene oxide (values of effective diameter of molecules were: 0.35 nm for  $CO_2$ , 0.44 nm for  $C_4H_{10}$ , and for other gases  $d_{ef} = \sigma_{LJ}$  was assumed). (From Okamoto, K., Noborio, K., Hao, J., Tanaka, K., and Kita, H., *J. Membr. Sci.*, 134, 171, 1997. With permission.)

its oblong shape. The effective diameter of the  $C_4H_6$  molecule that reflects the diffusion of this vapor was 0.4 nm. This value was obtained using linear correlation between  $\ln D$  and effective diameters of molecules known for other gases and vapors.

### 9.2.2.2 Effect of Cohesion Energy Density of the Polymer on Diffusion of Hydrocarbons in the Polymer

In accordance with the equation for the activation energy of diffusion proposed by Meares [31], cohesion energy density (CED) of the polymer has a significant effect on diffusion coefficients of lower hydrocarbons. This is especially typical of rubbery polymers: an increase in CED results in reduction of diffusion coefficients. Similar dependencies also apply to glassy polymers [9,32]. For example, Figure 9.8a shows the dependence of diffusion coefficient of propylene on CED of both glassy and rubbery polymers.

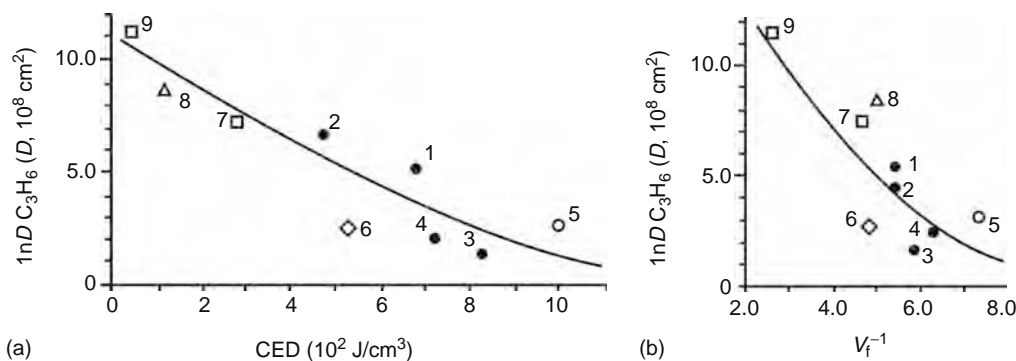


**FIGURE 9.8** Dependence of propylene diffusion coefficients in various polymers on cohesion energy density (CED) of the polymer (a) and on inverse mole fraction of free volume of the polymer (b): ●1, 6FDA-TeMPD polyimide; ●2, 6FDA-TrMPD polyimide; ●3, 6FDA-DDBT polyimide; ●4, 6FDA-ODA polyimide; ○5, BPDA-TeMPD polyimide; ◇6, PPO, polyphenylene oxide; □7, P4MP, polymethylpenetene; △8, 1,2PB, polybutanediene; □9, PDMS, polydimethylsiloxane. (From analysis of results presented in Tanaka, K., Taguchi, A., Hao, J., Kita, H., and Okamoto, K., *J. Membr. Sci.*, 121, 197, 1996; Okamoto, K., Noborio, K., Hao, J., Tanaka, K., and Kita, H., *J. Membr. Sci.*, 134, 171, 1997.)

### 9.2.2.3 Effect of Free Volume of the Polymer on Diffusion of Hydrocarbons in the Polymer

The effect is especially significant in the case of glassy polymers [8,9,32]. It was shown in several studies that diffusion coefficients of penetrants, including hydrocarbons, decrease with the decrease in molar fraction of free volume of the polymer (see, e.g., Figure 9.8b).

### 9.2.2.4 Concentration Dependencies of Diffusion Coefficients of Hydrocarbons

The models most frequently used to describe the concentration dependence of diffusion and permeability coefficients of gases and vapors, including hydrocarbons, are: transport model of dual-mode sorption (which is usually used to describe diffusion and permeation in polymer glasses) as well as its various modifications; molecular models analyzing the relation of diffusion coefficients to the movement of penetrant molecules and the effect of intermolecular forces on these processes; and free volume models describing the relation of diffusion coefficients and fractional free volume of the system. Molecular models and free volume models are commonly used to describe diffusion in rubbery polymers. However, some versions of these models that fall into both classification groups have been used for both rubbery and glassy polymers. These are the models by Pace–Datyner and Duda–Vrentas [7,29,30].

The experimental and theoretical data presented in the literature show that selective permeability of rubbery polymers for hydrocarbons follows the general rule of being dominated by the sorption component. Selective permeability of glassy polymers for hydrocarbons follows the general rule of being dominated by the diffusion component.

Thus, the permeation of hydrocarbons in polymer membranes is governed by the basic regularities typical of permeation of low MW penetrants, modified however by certain peculiarities related to the structure and shape of hydrocarbon molecules. We will now discuss the physicochemical regularities of hydrocarbon separation and removal using polymer membranes, by trying to reveal the relationship between the chemical structure of polymers and their separation properties with respect to mixtures containing hydrocarbons. It follows from literary data that rubbery polymers are mainly used in gas/vapor separation processes for selective separation of hydrocarbon vapors from their mixtures with air as well as in pervaporation processes for the removal of hydrocarbons from their aqueous solutions. In practice, glassy polymers are used for separation of olefins and paraffins as well as for separation of aromatic, alicyclic, and aliphatic hydrocarbons.

## 9.3 SEPARATION AND REMOVAL OF HYDROCARBONS USING MEMBRANES BASED ON RUBBERY POLYMERS

### 9.3.1 SELECTIVE SEPARATION AND REMOVAL OF HYDROCARBON VAPORS FROM GAS MIXTURES

The polymer materials mainly used for the selective separation of hydrocarbon vapors from their mixtures with air are organosilicon polymers.

#### 9.3.1.1 Effect of Chemical Composition of Organosilicon Polymers on Their Gas Separation Properties to Hydrocarbons

This subject was dealt with by several researchers, most comprehensively by Stern [19,20,34–37]. Permeability of several gases and vapors, including hydrocarbons, in various organosilicon polymers has been investigated after modification of chemical composition of the polymers by introducing substituent groups in both side and main chains. The following polymers have been investigated:  $[-(\text{CH}_3)(\text{R}_1)\text{Si}-\text{O}-]_n$ , where  $\text{R}_1 = -\text{CH}_3$ ;  $-\text{C}_2\text{H}_5$ ;  $-\text{C}_3\text{H}_7$ ;  $-\text{C}_8\text{H}_{17}$ ;  $-\text{CH}_2\text{CH}_2\text{CF}_3$ ;  $-\text{C}_6\text{H}_5$ ; and  $[-(\text{CH}_3)_2\text{Si}-\text{R}_2-\text{Si}(\text{CH}_3)_2-\text{O}-]_n$ , where  $\text{R}_2 = -(\text{CH}_2)_2-$ ;  $-(\text{CH}_2)_6-$ ;  $-(\text{CH}_2)_8-$ ;  $-m\text{C}_6\text{H}_4-$ ;  $-p\text{C}_6\text{H}_4-$ . Results of the research are presented in Tables 9.2 and 9.3, and Figure 9.9.

It follows from analysis of these results that the increase in the volume of the substituent group results in higher rigidity and density of the polymer. This manifests itself in higher glass transition temperatures and densities of the polymers. Introduction of substituent groups into the side chain has a significantly greater effect on these parameters as compared to substitutions in the main chain. Variation in flexibility of the polymer chain also has a significant effect on permeability. In this connection it makes sense to compare polymers  $[-(\text{CH}_3)_2\text{Si}-\text{CH}_2-]_n$  and  $[-(\text{CH}_3)_2\text{Si}-(\text{CH}_2)_8-\text{Si}(\text{CH}_3)_2-\text{O}-]_n$ . The relatively low permeability of the first polymer is due to the lack of flexible siloxane  $-\text{Si}-\text{O}-$  bonds in the main chain. The presence of only one siloxane bond per eight recurrent  $-\text{CH}_2-$  groups in the second polymer makes the chains much more flexible and results in a more than twofold increase in permeability as compared with the first polymer (see Table 9.2).

The permeability of polymers decreases with the increase in their glass transition temperature. This dependence becomes more pronounced with increasing kinetic diameter of penetrant molecules (Figure 9.9).

It can be seen from the data presented in Table 9.2 that the parallelism of the decrease in permeability with the increase in glass transition temperature of the polymer is somewhat disrupted for He and  $\text{CO}_2$ . Helium has the lowest solubility among the penetrants under study. However, the permeability of organosilicon polymers for helium is higher than could be expected from

**TABLE 9.2**  
**Effect of Chemical Structure of Organosilicon Polymers on Their Physical Properties and Mass Transfer Properties**  
**with respect to Individual Gases and Vapors**

Polymer	$T_g$ (°C)	$\rho$ (g/cm <sup>3</sup> )	He	O <sub>2</sub>	CH <sub>4</sub>	CO <sub>2</sub>	Permeability Coefficient, $P$ (10 <sup>-2</sup> Barrer)												
							C <sub>2</sub> H <sub>6</sub> , p/p <sup>o</sup>			C <sub>3</sub> H <sub>8</sub> , p/p <sup>o</sup>									
							0.1	0.2	0.3	0.1	0.2	0.3							
—(CH <sub>3</sub> )(R <sub>1</sub> )Si—O—, where R <sub>1</sub> =																			
—CH <sub>3</sub>	-123	0.971	5.6	9.3	13.5	45	45	50	100	130	170								
—C <sub>2</sub> H <sub>5</sub>	-135	0.978	2.3	3.1	4.7	15	16	18	38	52	70								
—C <sub>3</sub> H <sub>7</sub>	-120	0.916	2.5	3.8	5.7	23	17	20	42	56	76								
—C <sub>8</sub> H <sub>17</sub>	-92	—	1.3	1.9	3.1	9.3	11	13	23	34	48								
—CH <sub>2</sub> CH <sub>2</sub> CF <sub>3</sub>	-70	1.292	2.5	2.2	2.0	14	3.1	3.6	4.5	6.5	8.5								
—C <sub>6</sub> H <sub>5</sub>	-28	1.138	0.34	0.32	0.36	2.4	1.1	1.3	1.7	2.7	4.0								
—(CH <sub>3</sub> ) <sub>2</sub> Si—CH <sub>2</sub> —	-92	0.917	0.98	1.0	1.3	5.5	4.3	5.0	10	17	26								
—(CH <sub>3</sub> ) <sub>2</sub> Si—R <sub>2</sub> —Si(CH <sub>3</sub> ) <sub>2</sub> —O—, where R <sub>2</sub> =	-88	0.890	2.7	3.9	6.0	19	20	22	42	62	83								
—(CH <sub>2</sub> ) <sub>6</sub> —	-90	—	1.9	2.7	4.0	13	13	16	34	50	70								
—(CH <sub>2</sub> ) <sub>8</sub> —	-88	0.889	1.7	2.4	3.6	12	12	14	28	38	54								
— <i>m</i> C <sub>6</sub> H <sub>4</sub>	-48	1.025	0.84	0.74	1.1	5.2	3.4	4.2	8	13	22								
— <i>p</i> C <sub>6</sub> H <sub>4</sub>	-18	—	0.33	0.11	0.12	0.64	0.22	0.33	0.4	0.7	1.3								

*Source:* The data are given at different values of their activities from the analysis of results presented in Stern, S.A., Shah, V.M., and Hardy, B.J., *J. Polym. Sci.*, B25, 1263, 1987.

*Notes:*  $T = 308$  K, for He, O<sub>2</sub>, CH<sub>4</sub> and CO<sub>2</sub>; pressure,  $p = 6.8 \times 10^5$  Pa, for C<sub>2</sub>H<sub>6</sub> and C<sub>3</sub>H<sub>8</sub>.

**TABLE 9.3**  
**Mass Transfer Properties of Various Organosilicon Polymers with respect to Methane and Propane**

Polymer	$T_g$ (°C)	$D$ ( $10^6$ cm <sup>2</sup> /c)		$S$ ( $10^{-2}$ cm <sup>3</sup> /cm <sup>3</sup> cm Hg)		$P$ ( $10^{-2}$ Barrer)		$\alpha_P^{id}$	$\alpha_D^{id}$	$\alpha_S^{id}$
		CH <sub>4</sub>	C <sub>3</sub> H <sub>8</sub>	CH <sub>4</sub>	C <sub>3</sub> H <sub>8</sub>	CH <sub>4</sub>	C <sub>3</sub> H <sub>8</sub>			
—(CH <sub>3</sub> ) <sub>2</sub> Si—O—	-123	24.5	10.1	0.59	8.49	14.5	85.8	5.9	0.41	14.4
—(CH <sub>3</sub> )(C <sub>3</sub> H <sub>7</sub> )Si—O—	-120	7.59	2.72	0.70	9.10	5.34	29.6	5.6	0.36	13.0
—(CH <sub>3</sub> )(C <sub>8</sub> H <sub>17</sub> )Si—O—	-92	6.54	2.60	0.48	7.81	3.14	20.3	6.4	0.40	16.3
—(CF <sub>3</sub> CH <sub>2</sub> CH <sub>2</sub> )(CH <sub>3</sub> )Si—O—	-70	5.58	1.55	0.36	3.78	2.01	5.84	2.9	0.28	10.5
—(C <sub>6</sub> H <sub>5</sub> )(CH <sub>3</sub> )Si—O—	-28	1.2	0.29	0.30	4.87	0.36	1.39	3.9	0.24	16.2
—(CH <sub>3</sub> ) <sub>2</sub> Si— <i>p</i> C <sub>6</sub> H <sub>4</sub> —Si(CH <sub>3</sub> ) <sub>2</sub> —	-18	0.44	0.07	0.23	3.69	0.10	0.27	2.6	0.16	15.8

Source: The data are given at different values of their activities from the analysis of results presented in Stern, S.A., Shah, V.M., and Hardy, B.J., *J. Polym. Sci.*, B25, 1263, 1987; Semenova, S.I., *J. Membr. Sci.*, 231, 189, 2004.

Notes:  $T = 308$  K; pressure,  $p = 0$  Pa.

its solubility. Thus, polymers with  $R_1 = -CH_3$ ;  $-C_2H_5$ ;  $-C_3H_7$ ;  $-C_8H_{17}$ ;  $R_2 = -(CH_2)_{2-8}-$ ;  $-m,p$  C<sub>6</sub>H<sub>4</sub>— are more permeable for helium than for nitrogen, although the solubility of nitrogen in them is considerably higher than that of helium. A similar regularity exists for polymers with  $R_1 = -CH_2-CH_2-CF_3$ ;  $-C_6H_5$ ;  $R_2 = -mC_6H_4-$ ;  $-pC_6H_4-$ . Introduction of bulky substituent groups into the side or main chain of the polymer changes the diffusion of all penetrants; however, the diffusion of helium decreases to a smaller degree than that of other penetrants. These regularities are probably due to fast diffusion of helium in polymers, as a result of the small kinetic diameter of its molecules compared to those of other gases and vapors. A number of polymers, e.g., polymers with  $R_1 = -CH_2-CH_2CF_3$ ;  $R_2 = -m(p)C_6H_4-$  have higher permeability for CO<sub>2</sub> than for other gases. This is explained by the ability of the CO<sub>2</sub> quadrupole to have specific interactions with polar groups and aromatic nuclei. Thus, in the case of polymers having  $-CH_2-CH_2-CF_3$  side groups, the high solubility of CO<sub>2</sub> results from dipole-dipole interaction of CO<sub>2</sub> molecules with the electronegative atom of fluorine.

Variation in the structure of the organosilicon polymer has a much stronger effect on the diffusion component of permeability than on the sorption component (see Table 9.3). For example, the increase in glass transition temperature from  $T_g = -123^\circ\text{C}$  in the case of polydimethylsiloxane (PDMS), to  $T_g = -28^\circ\text{C}$ , in the case of polymethylphenylsiloxane, results in reduction of the diffusion coefficient of propane from  $10.1 \times 10^{-6}$  to  $0.29 \times 10^{-6}$  cm<sup>2</sup>/s, i.e., by a factor of more than 30, whereas the sorption coefficient of propane changes from  $8.49 \times 10^{-2}$  to  $4.87 \times 10^{-2}$  cm<sup>3</sup>/cm<sup>3</sup> cm Hg, i.e., by a factor of  $<2$ .

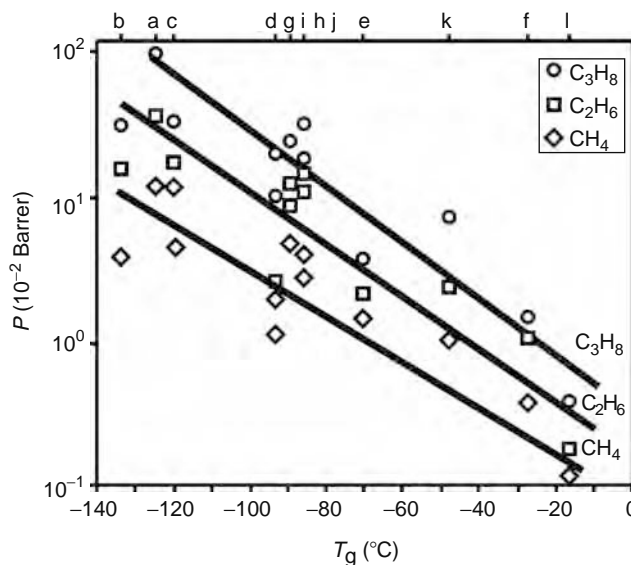


**FIGURE 9.9** Dependence of permeability coefficients of methane, ethane, and propane in various organosilicon polymers on the glass transition temperature of the polymer: (a) —(CH<sub>3</sub>)<sub>2</sub>Si—O—; (b) —(CH<sub>3</sub>)(C<sub>2</sub>H<sub>5</sub>)Si—O—; (c) —(CH<sub>3</sub>)(C<sub>3</sub>H<sub>7</sub>)Si—O—; (d) —(CH<sub>3</sub>)(C<sub>8</sub>H<sub>17</sub>)Si—O—; (e) —(CH<sub>3</sub>)(CF<sub>3</sub>CH<sub>2</sub>CH<sub>2</sub>)Si—O—; (f) —(CH<sub>3</sub>)(C<sub>6</sub>H<sub>5</sub>)Si—O—; (g) —(CH<sub>3</sub>)<sub>2</sub>Si—CH<sub>2</sub>—; (h) —(CH<sub>3</sub>)<sub>2</sub>Si—(CH<sub>2</sub>)<sub>2</sub>—(CH<sub>3</sub>)<sub>2</sub>Si—O—; (i) —(CH<sub>3</sub>)<sub>2</sub>Si—(CH<sub>2</sub>)<sub>6</sub>—(CH<sub>3</sub>)<sub>2</sub>Si—O—; (j) —(CH<sub>3</sub>)<sub>2</sub>Si—(CH<sub>2</sub>)<sub>8</sub>—(CH<sub>3</sub>)<sub>2</sub>Si—O—; (k) —(CH<sub>3</sub>)<sub>2</sub>Si—*m*C<sub>6</sub>H<sub>4</sub>—(CH<sub>3</sub>)<sub>2</sub>Si—O—; and (l) —(CH<sub>3</sub>)<sub>2</sub>Si—*p*C<sub>6</sub>H<sub>4</sub>—(CH<sub>3</sub>)<sub>2</sub>Si—O—. (From analysis of results presented in Semenova, S.I. *J. Membr. Sci.*, 231, 189, 2004. With permission.)

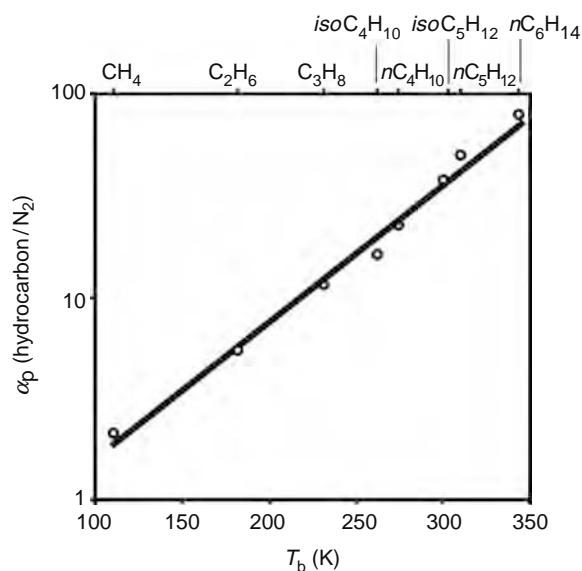


**FIGURE 9.10** Dependence of ideal hydrocarbon/nitrogen permselectivity on the boiling temperature of the hydrocarbons for a polyorganosilicon membrane produced by GKSS [39–43]. (From Semenova, S.I., *J. Membr. Sci.*, 231, 189, 2004. With permission.)

The permselectivity of hydrocarbon vapors,  $\alpha_p$ , is dominated by the sorption component, and sorption of hydrocarbon vapors by rubbery polymers is determined by the condensability of their vapors. It can be seen from Table 9.3, that in organosilicon polymers the propane/methane sorption selectivity,  $\alpha_s$ , is 10.5–16.2, whereas diffusion selectivity,  $\alpha_D$ , is only 0.16–0.41. Refs. [39–43] report values of permselectivity of hydrocarbon mixtures with nitrogen for organosilicon membranes produced by GKSS (see Figure 9.10). It can be seen that separation selectivity increases with rising boiling temperature of the hydrocarbon, which points to domination of the sorption component of selectivity.

### 9.3.1.2 Pressure Dependence of Hydrocarbon Permeability in Rubbery Polymers: Effect of Plasticization of the Polymer by the Penetrant

With the increase in relative pressure of hydrocarbon vapor, i.e., with the increase in its activity, the plasticizing effect on the polymer becomes stronger, resulting in the increase in permeability (see Figures 9.11 and 9.12; Table 9.2).

Investigation of a wide range of block copolymers, consisting of various flexible (polydimethylsiloxane, polybutadiene) and rigid (polycarbonate, polysulphone, polyarylate) phases [44], shows that irrespective of the chemical nature of copolymer, content and molecular weight of blocks as well as pressure and composition of the hydrocarbon mixture, sorption, and mass transfer of alkanes take place primarily in the rubbery phase. The phenomenon of plasticization of polymers by hydrocarbons was demonstrated by baromechanical methods [7,45–48]. Figure 9.13 shows baromechanical curves for the block copolymer

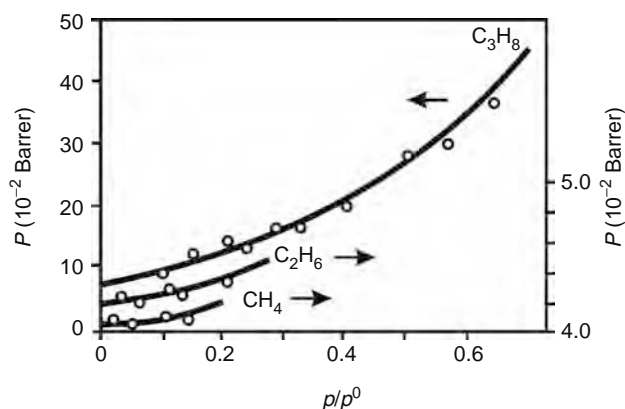


**FIGURE 9.11** Dependence of permeability coefficients of methane, ethane, and propane in polydimethylsiloxane on the corresponding hydrocarbon activity. (From analysis of results presented in Semenova, S.I., *J. Membr. Sci.*, 231, 189, 2004. With permission.)

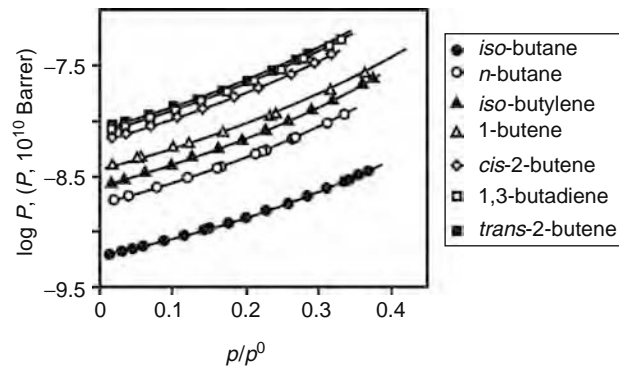


**FIGURE 9.12** Dependence of permeability coefficients of individual hydrocarbons in polybutadiene on the corresponding hydrocarbon activity. (From Kamiya, Y., Terada, K., Naito, Y., and Wang, J.S., *J. Polym. Sci.*, B33, 1663, 1995.)

Sulfosil (polysulfone/polydimethylsiloxane) in pentane vapor for various levels of polydimethylsiloxane content. By analyzing these curves, the effect of the flexible/rigid phase ratio on mechanical properties of the block copolymer in the plasticizing vapor environment can be considered. Block copolymers having PDMS content <50 wt% display a minor increase in elastic compliance (which is the reciprocal value of elasticity modulus,  $E$ ). If the flexible phase content is more than 50%, elastic compliance smoothly increases with pentane activity. Analysis of the dependence of the block copolymer's elasticity modulus in vacuum on the composition of the block copolymer shows that phase inversion is completed around 55 wt% PDMS. Specifically, the rigid phase is continuous if PDMS content is below 50 wt%, and the flexible phase is continuous if PDMS content is above 50 wt%. It is therefore clear that block copolymer plasticization is mainly caused by PDMS phase plasticization. Increased elastic compliance of block copolymer is particularly noticeable if flexible phase content exceeds 50 wt%. It has been established that the nature of the rigid phase has a negligible effect on the elasticity modulus of block copolymers in saturated hydrocarbon environment [44]. Elastic compliance of block copolymers in the region of low values of the volume fraction  $\varphi$  of the hydrocarbon, dissolved in the block copolymer (with  $\varphi < 0.3$ , which corresponds to hydrocarbon vapor activity  $\sim 0.8$ ) can be described by the equation:  $1/E = k\varphi$ , where  $k$  is the coefficient of proportionality for the sorbed hydrocarbon. Thus, elastic compliance is directly proportional to the volume fraction of the sorbate, coefficient  $k$  increasing with thermodynamic affinity of the system. Values of ideal selectivity  $\alpha_p^{\text{id}} = P_{\text{Ci}}/P_{\text{C1}}$  were calculated from data of transfer of individual alkanes. With increasing

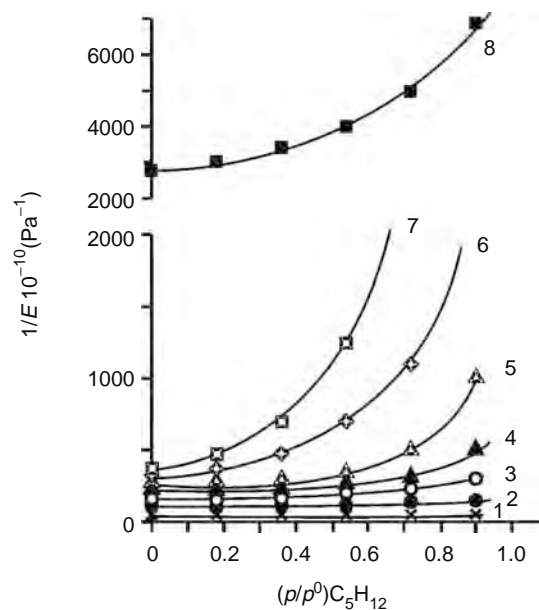


**FIGURE 9.13** Elastic compliance vs  $n$ -pentane relative pressure curves (baromechanical curves) for block-copolymer sulfosil (polysulfone/polydimethylsiloxane) for various polydimethylsiloxane contents (wt%): (1) 0; (2) 16; (3) 22; (4) 42; (5) 50; (6) 55; (7) 63; (8) 80.  $T = 293$  K. (From Sidorenko, V.M., *Membrane Separation of Hydrocarbons of Oil and Natural Gases*. PhD dissertation. Vladimir, NPO "Polimersintez", 1991, in Russian.)

molecular weight of the hydrocarbon, the concentration dependence of  $\alpha_p^{\text{id}}$  becomes more pronounced. High values of selectivity of *n*-alkanes, which noticeably rise in the sequence C<sub>2</sub>–C<sub>4</sub> and achieve the order of magnitude of 10<sup>2</sup> in the case of *n*-butane, point to the possibility of using siloxane-containing block copolymers to separate vapor–gas mixtures of saturated hydrocarbons.

### 9.3.1.3 Temperature Dependence of Hydrocarbon Permeability in Rubbery Polymers

Semenova et al. [7,49–52] show that for gases and vapors strongly sorbed by polymers, non-monotonic temperature dependences of mass transfer coefficients are observed. This results from negative heat of penetrant sorption and plasticization of the polymer by the penetrant in the course of sorption. Negative heat of penetrant sorption can be caused by its specific interaction with the polymer as well as high values of condensation heat, which is typical of easily condensable hydrocarbons. The possibility of existence of non-monotonic temperature dependencies of mass transfer coefficients is demonstrated and corroborating experimental data are presented for penetrants interacting with polymer membranes in a specific way. It has been demonstrated, among other things, that in the case of variation of temperature, at constant concentration (pressure) of a strongly sorbable penetrant in the polymer, the condition for existence of a temperature corresponding to the minimum value of diffusion coefficient,  $T_{\text{min}}(D)$ , is a negative value of sorption heat  $\Delta H_s$ , and for emergence of a temperature corresponding to the minimum value of permeability  $T_{\text{min}}(P)$ , an additional condition should be met:  $|E_D| > |\Delta H_s|$ , where  $E_D$  is diffusion activation energy. It has been established that since at  $\Delta H_s < 0$   $E_D > E_D + \Delta H_s$  (because the diffusion activation energy is an essentially positive quantity),  $T_{\text{min}}(D) < T_{\text{min}}(P)$  is observed, i.e., the minimum point in the permeability curve  $P(1/T)$  is shifted with respect to the minimum point in the diffusion curve  $D(1/T)$  toward higher temperatures. In the curves showing the dependence of selectivity on temperature at constant penetrant pressure  $\alpha_p(T)_p$  as well as in curves showing the dependence of selectivity on penetrant pressure at constant temperature  $\alpha_p(p)_T$ , emergence of maxima is possible. These conclusions are quite important for selection of an optimum mode of using the membranes. Theoretical findings of Refs. [7,52] experimentally corroborated for interacting polymer–penetrant systems can certainly be applied to systems consisting of a polymer and an easily condensable hydrocarbon. Unfortunately, sufficient experimental data corroborating this conclusion are not yet available in the literature.

As reported in studies by Stern et al. [20,34–37], permeation coefficients of hydrocarbons in organosilicon polymers, including PDMS, change monotonically (decreasing in the case of propane and increasing in the case of methane) with rising temperature from 10°C to 55°C. For methane penetrating through PDMS,  $E_D \sim 12$  kJ/mol,  $\Delta H_s \sim -8$  kJ/mol whereas for propane  $E_D \sim 12$  kJ/mol,  $\Delta H_s \sim -18$  kJ/mol. That is, the condition  $|E_D| > |\Delta H_s|$  holds for methane and an extreme temperature dependence of permeability can be discovered for methane. Figure 9.14 shows the dependence of the values of diffusion activation energies for several polymers on the kinetic diameter of the penetrant molecule. It can be seen that diffusion activation energy increases with the kinetic diameter of the penetrant molecule and the more rigid is the polymer (i.e., the higher is its glass transition temperature), the stronger is this dependence. Analysis of the data reported in Refs. [34–37] shows that propane permeability is observed in organosilicon polymers with different glass transition temperatures, while the condition  $|E_D| > |\Delta H_s|$  holds for organosilicon polymers with glass temperature  $T_g > 185$  K. Extreme temperature dependence of propane permeability can be found for these polymers.

Gas permeabilities of isotropic PDMS films were determined over a temperature range of 35°C to –20°C for pure gases and a series of binary *n*-butane/methane and multicomponent hydrocarbons/hydrogen mixtures [38]. Pure-gas permeabilities in PDMS as a function of reciprocal temperature are presented in Figure 9.15. It can be seen that the decrease in temperature

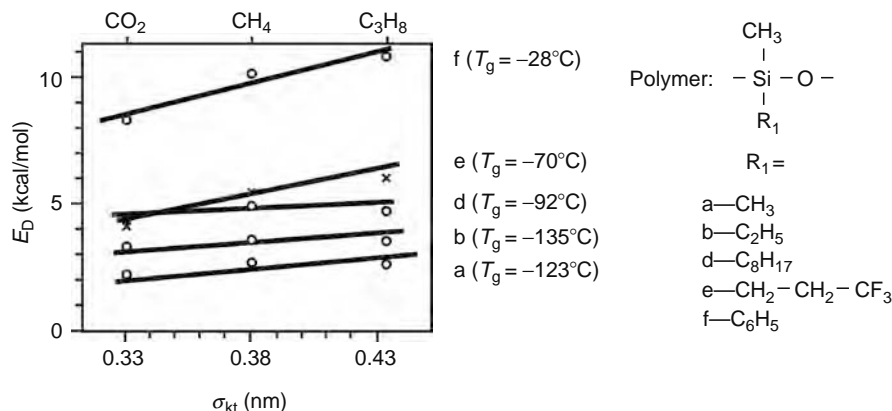


**FIGURE 9.14** Dependence of the diffusion activation energy of carbon dioxide, methane, and propane in organosilicon polymers on the kinetic diameter of the penetrant molecules (designations of polymers are the same as in Figure 9.9). (From analysis of results presented in Semenova, S.I., *J. Membr. Sci.*, 231, 189, 2004. With permission.)

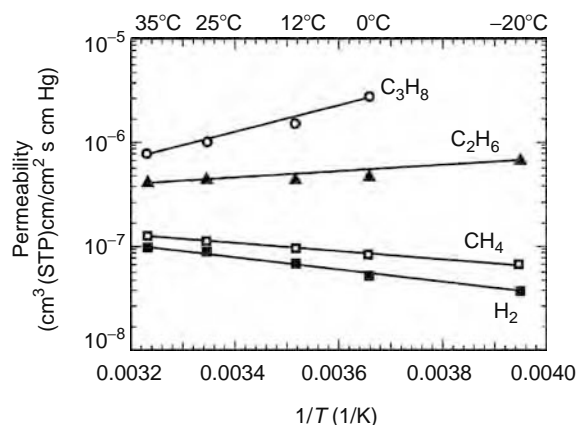


**FIGURE 9.15** Pure-gas permeabilities of an isotropic PDMS film as a function of reciprocal temperature. Feed pressure: 4.4 atm; permeate pressure: 1 atm. (From Pinnau, I. and He, Z., *J. Membr. Sci.*, 244, 227, 2004. With permission.)

results in a monotonic increase in permeability of ethane and propane and a decrease in permeability of methane and hydrogen. There is no turning point in Figure 9.15, but for methane it can be below  $-20^{\circ}\text{C}$ , i.e., beyond the considered temperature range. The permeabilities of all gas mixture components depend strongly on feed gas composition and temperature. An increase in organic vapor concentration, at constant feed pressure and temperature, leads to increased chain mobility in PDMS, and, consequently, higher diffusivity and permeability. The relative increase in permeability is higher for large, condensable vapors, such as *n*-butane, than for small, permanent gases, such as hydrogen or methane. As a result, selectivities for mixed gas hydrocarbon/methane and hydrocarbon/hydrogen increase with the increase in feed vapor concentration. A decrease in feed temperature also results in higher organic vapor permeability and vapor/permanent-gas selectivity. The mixed gas *n*-butane/methane selectivity of PDMS film increased from 9°C at  $35^{\circ}\text{C}$ , to 25°C at  $-20^{\circ}\text{C}$  using a binary feed mixture containing 2 vol% *n*-butane in methane.

#### 9.3.1.4 Polytrimethylsilylpropyne as a Membrane Material for Hydrocarbons Separation and Removal from Gas Mixtures

PTMSP is a unique glassy polymer with glass transition temperature  $T_g$  of  $>250^{\circ}\text{C}$ . Because of its stiff backbone, in combination with the bulky  $-\text{Si}(\text{CH}_3)_3$  side group, PTMSP is known to have a fairly high fractional free volume of  $\geq 25\%$ . The gas permeability coefficients of PTMSP are one order of magnitude higher than those of PDMS. Butane/methane selectivity of PTMSP is higher in mixed gas measurements (at 10 atm,  $35^{\circ}\text{C}$ , 3% butane) than the ideal selectivity measured with single gases  $\alpha^{\text{mix}} = 27$ ,  $\alpha^{\text{id}} = 3.5$ . For PDMS the values are  $\alpha^{\text{mix}} = 5$ ,  $\alpha^{\text{id}} = 16.5$  [53]. It has been shown that butane condenses in the pores of PTMSP. Surface diffusion and diffusion of methane through pores filled with condensate are hindered. Condensed butane, however, does not inhibit significantly the transport of butane molecules. Consequently, only the flux of methane is reduced by the presence of butane while the flux of butane remains almost unaffected.

Unfortunately there is an aging problem for PTMSP, resulting in deterioration of its transport properties with time. As shown in Figure 9.16, permeability decreased by one order of magnitude during the first 3 months, whereupon permeability stabilized. Selectivity remained stable during this period. But even the aged PTMSP is still a viable alternative to rubbery polymers for heavy hydrocarbon removal.

#### 9.3.2 APPLICATION OF RUBBERY POLYMERS FOR PERVAPORATION REMOVAL OF HYDROCARBONS FROM THEIR AQUEOUS SOLUTIONS

The need for removal of hydrocarbons from their aqueous solutions and emulsions generated in a large number of processes is accounted for by both economical and environment protection considerations. One possible way of solving this problem is pervaporation separation of water–organic mixtures. The materials used to make membranes for these applications are rubbery polymers. Nijhuis et al. [54] investigated pervaporation properties of several rubbery polymers with respect to the saturated toluene/water mixture. It has been established that with the increase in the glass transition temperature of the polymer, i.e., with the increase in its rigidity, a decrease in permeability is observed. The separation factor also decreases, although the latter dependence is not very strict, probably due to the swelling of the membrane (see Figure 9.17). With an increase in the content of nitrile groups in nitrile butadiene rubber, a decrease in permeability is also observed, because rigidity of the polymer increases with the increase in the content of polar groups (see Figure 9.18). Effectiveness of pervaporation removal of organic substances, including hydrocarbons, from water–organic mixtures is determined by both sorption and diffusion components of the separation factor. With an increase in the sorption component, affinity of the polymer for the organic component increases,

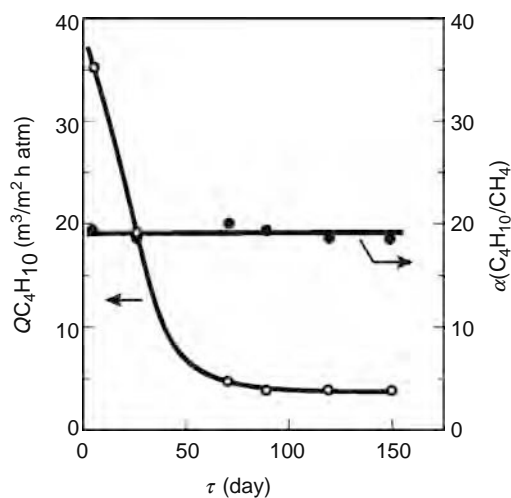


**FIGURE 9.16** Aging effects of PTMSP during storage at ambient conditions:  $\circ$  butane flux and  $\bullet$  selectivity (measurements were made at 10 atm, 35°C, for methane/butane mixture with 3% butane; composite membrane had the selective layers 3–5  $\mu\text{m}$ ). (From Schultz, J. and Peinemann, K.V., *J. Membr. Sci.*, 110, 37, 1996. With permission.)

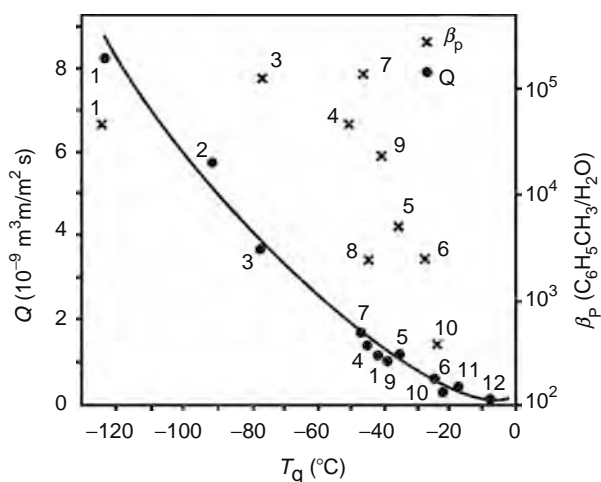


**FIGURE 9.17** Dependence of productivity and separation factor  $\beta_P$   $\text{C}_6\text{H}_5\text{CH}_3/\text{H}_2\text{O}$  of membranes based on various rubbery polymers on the glass transition temperature of the polymer (pervaporation separation of saturated toluene/water mixture,  $T = 308$  K): (1) polydimethyl siloxane; (2) polybutadiene; (3) polyoctylmethyl siloxane; (4) nitrile butadiene rubber with 18% mol of nitrile groups; (5) the same, 28% mol of nitrile groups; (6) the same, 38% mol of nitrile groups; (7) ethylene/propylene copolymer; (8) polyepichlorohydrin; (9) polychloroprene; (10) polyurethane; (11) polyacrylate rubber; (12) fluorocarbon elastomer. (From analysis of data presented in Semenova, S.I., *J. Membr. Sci.*, 231, 189, 2004. With permission.)

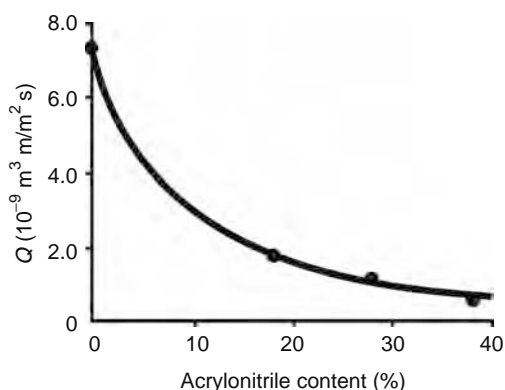


**FIGURE 9.18** Dependence of productivity of membranes based on nitrile butadiene rubber on content of nitrile groups (pervaporation separation of saturated toluene/water mixture,  $T = 308$  K). (From Semenova, S.I., *J. Membr. Sci.*, 231, 189, 2004. With permission.)

as a result the swelling of the polymer is enhanced, which can result in reduction of the diffusion component of the separation factor. This issue is quite complicated and deserves separate consideration [55].

In selective separation of hydrocarbons from their mixtures with air or from their aqueous solutions, it makes sense to use membranes based on rubbery polymers, whose permeability increases with the decrease in glass transition point. Permselectivity of rubbery polymers is dominated by the sorption component, which increases with condensability of the hydrocarbon penetrant. Higher activity of the component being separated in the feed mixture results in plasticization of the membrane and can make it swell. This can produce a non-monotonic dependence of selective properties of the membrane on activity of the component being separated. As a rule, permselectivity for mixtures of penetrants is significantly lower than their ideal values. Negative values of sorption heat of easily condensable hydrocarbons can result in existence of non-monotonic temperature dependencies of mass transfer coefficients.

## 9.4 SEPARATION AND REMOVAL OF HYDROCARBONS USING MEMBRANES BASED ON GLASSY POLYMERS

### 9.4.1 SEPARATION OF OLEFINS AND PARAFFINS

Ethylene is found in coke-oven gas (3–5 vol%), gases resulting from oil processing, e.g., cracking (up to 20 vol%). It is produced by pyrolysis of liquid distillates of oil or lower paraffin hydrocarbons (ethane, propane, and butane), or by dehydration of ethanol. Ethylene is used to produce polyethylene and its copolymers, oxides of ethylene, ethanol, ethyl benzene, acetaldehyde, vinyl chloride, and vinyl acetate. Propylene is used as feedstock in the production of polypropylene, acrylonitrile, propylene oxide, allyl chloride, acrolein, acrylic acid and its ethers/esters, cumene, butanols. Propylene is one of the products of catalytic cracking of liquid hydrocarbon waste products. It is also produced by dehydrogenation of propane. 1,3-butadiene is produced by catalytic dehydration of butane and *n*-butylenes present in natural gas and gas resulting from oil processing, as a side product of ethylene production by pyrolysis of oil stock or by catalytic decomposition of ethanol. Propylene is used in the production of rubbers and plastics.

It is very difficult to separate the mixtures of olefins and paraffins produced in the above processes because of similar physical properties of the vapors. To solve this problem, the membrane method holds much promise. When using this method the correct choice of the membrane material is very important.

#### 9.4.1.1 Effect of Unsaturated Bonds on the Size of Olefin Molecules and on the Capability of Olefins to Enter into Specific Interactions with the Membrane Matrix

In membrane separation of the olefin/paraffin mixture, the predominant selective separation of the olefin is evident. First, the olefin molecule is smaller in size compared to the respective paraffin. Specifically, C—C distance in paraffins is 0.1534 nm, whereas the C=C distance in olefins is 0.1337 nm. Atoms of carbon in paraffins feature  $sp^3$  hybridization and free rotation around C—C bonds. Atoms of olefins feature  $sp^2$  hybridization. The rigid C=C bond impedes internal rotation in the olefin molecule and makes it flat. It is therefore clear why olefin molecules are smaller in size compared to paraffin and why the diffusion coefficients of olefins in polymers would be higher than those of paraffins. Second, the presence of unsaturated bonds in olefin molecules makes them capable of specific interactions with the membrane matrix. Efforts to take advantage of these capabilities resulted in the development of an important field of research: facilitated transport.

Several studies are concerned with the problem of separating olefins and paraffins using membrane technology, including facilitated transport using liquid membranes or ion-exchange charged membranes containing ions of transition metals as complexing agents [56–65]. It is known that olefins are capable of reversible complexing with transition metals, containing d-orbitals. The nature of this interaction was first explained by Dewar in 1951 in terms of molecular orbital theory. Dewar postulated that the interaction with the atomic orbitals of the olefin determines the stability of the complex formed. In the course of complexing, metal and olefin act as electron donor and electron acceptor, respectively.  $\sigma$  is the bond component in the complex that is formed as a result of overlapping between external s-orbitals of the metal and the bonding  $\pi$ -molecular orbital of the olefin (in the case of positively charged metal ions the absent valent s-electrons can be regarded as a vacant s-orbital).  $\pi$  is the bond component in the complex that is formed as a result of transfer of electrons from the completely filled d-atomic metal orbital to the vacant antibonding  $\pi^*$  molecular orbital of the olefin. In assessing the possible use of complexing agents for selective separation of olefins from gaseous mixtures, the price of the complexing agent and the strength of the complex formed should be considered. Such transition metals as Pt (II) and Pd (II) are expensive and form too strong complexes with olefins, whereas Cu (I) and Ag (I) are relatively cheap and form reversible complexes. Such membranes have very high olefin/paraffin selectivity (up to 200–300) and relatively high permeability to olefin. However, processes based on facilitated transport have several limitations, e.g., they should be carried out in saturated water vapor. In addition, there exists the serious problem of carrier aging. The use of membranes operating on the basis of facilitated transport for separation of olefins and paraffins is beyond the scope of this chapter and has been already considered in the literature [56–65] in sufficient detail. However, the

**TABLE 9.4**  
**Permeability Coefficients of Propylene, C<sub>3</sub>H<sub>6</sub> and Propane, C<sub>3</sub>H<sub>8</sub>,  
 as well as Selectivity C<sub>3</sub>H<sub>6</sub>/C<sub>3</sub>H<sub>8</sub> for Some Glassy Polymers**

Polymer	P (Barrer)		
	C <sub>3</sub> H <sub>6</sub>	C <sub>3</sub> H <sub>8</sub>	$\alpha_P$ C <sub>3</sub> H <sub>6</sub> /C <sub>3</sub> H <sub>8</sub>
PPO	9	2.1	4.3
EC	52	16	3.3
CA	15.2	5.8	2.6
PSF	25	17.8	1.4

Source: From Sridhar, S. and Khan, A., *J. Membr. Sci.*, 159, 209, 1999.

Notes: PPO = polyphenylene oxide; EC = ethyl cellulose; CA = cellulose acetate; PSF, polysulfone for mixed vapors of C<sub>3</sub>H<sub>6</sub>/C<sub>3</sub>H<sub>8</sub> composition 55/45 mol%,  $p = 3-4 \times 10^5$  Pa,  $T = 303$  K.

example of facilitated transfer shows that it is possible to achieve high values of permselectivity by exploiting specific interactions of olefins with the membrane matrix.

#### 9.4.1.2 Effect of Chemical Composition of Glassy Polymers on Their Gas Separation Properties to Hydrocarbons

Separation of olefins and paraffins using polymer membranes without carrier is dealt with in several reports [66–76]. Henley and Santos [66] investigated the permeability of polyethylene films and found that olefin flux and olefin/paraffin selectivity are very low. Ito and Hwang [67] as well as Sridhar and Khan [68] investigated permeability of derivatives of cellulose and established that ethyl cellulose is a good material for selective removal of olefins from its mixtures with saturated hydrocarbons. The use of polysulfone as a membrane material for separation of olefins and paraffins is also reported [67]. Table 9.4 presents transport properties of some glassy polymers with respect to propylene/propane mixtures, C<sub>3</sub>H<sub>6</sub>/C<sub>3</sub>H<sub>8</sub> [68]. It can be seen that among polymers listed in Table 9.4, polyphenylene oxide is the most selective whereas ethyl cellulose and polysulfone yield the highest flux. However, analysis of literature data shows that for the above purposes polyimides offer the highest fluxes and selectivities, closely followed by polyphenylene oxides. The properties of these polymers are discussed below. Ideal olefin/paraffin selectivity is three times higher in polyimides than in cellulose derivatives and polysulfone [69]. Permeability of various polymers to olefins rises with increasing free volume of the polymer; the process is accompanied by parallel reduction of ideal olefin/paraffin selectivity (see, e.g., the data in Figure 9.19). Let us consider these effects in more detail for the best known and promising polymer materials: polyimides and polyphenylene oxides.

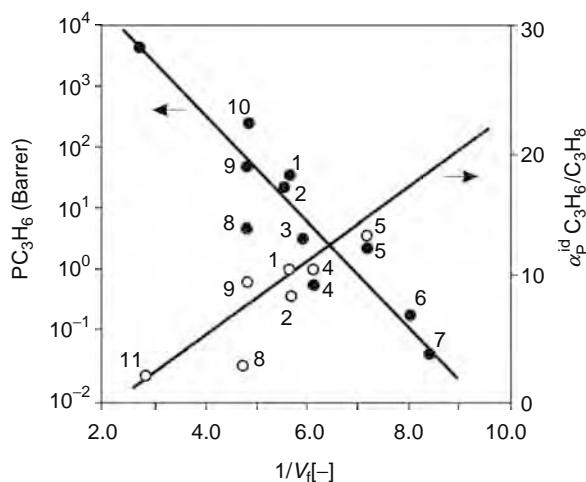


**FIGURE 9.19** Dependence of permeability coefficient of propylene C<sub>3</sub>H<sub>6</sub> (●) and ideal selectivity propylene/propane  $\alpha_P^{\text{id}}$  (C<sub>3</sub>H<sub>6</sub>/C<sub>3</sub>H<sub>8</sub>) (○) in various polymers on the inverse molar fraction of free volume of the polymer: polyimides (1) 6FDA-TeMPD; (2) 6FDA-TrMPD; (3) 6FDA-DDBT; (4) 6FDA-ODA; (5) BPDA-TeMPD; (6) BPDA-TeMPD; (7) BPDA-ODA; (8) PPO—polyphenylene oxide; (9) P4MP—poly-4-methylpentene-1; (10) 1,2PB—polybutadiene; (11) PDMS—polydimethylsiloxane. (Experimental temperature 323 K, pressure 2 atm. From analysis of results presented in Semenova, S.I., *J. Membr. Sci.*, 231, 189, 2004. With permission.)

**TABLE 9.5**  
**Permeability, Diffusion and Sorption Coefficients, as well as Their**  
**Ideal Ratios, for Vapors of C<sub>2</sub>H<sub>4</sub> and C<sub>2</sub>H<sub>6</sub>**

Polymer	$P_{C_2H_4}$	$D_{C_2H_4}$	$S_{C_2H_4}$	C <sub>2</sub> H <sub>4</sub> /C <sub>2</sub> H <sub>6</sub>		
				$\alpha_p^{id}$	$\alpha_D^{id}$	$\alpha_s^{id}$
6FDA-TrMPD	58	390	1.5	2.9	2.9	1.0
BPDA-TeMPD	5.8			4.3		

Source: From Okamoto, K., Noborio, K., Hao, J., Tanaka, K., and Kita, H., *J. Membr. Sci.*, 134, 171, 1997. With permission.

Notes:  $T = 323$  K, pressure =  $2 \times 10^5$  Pa;  $P$  (Barrer),  $D$  ( $10^{-10}$  cm<sup>2</sup> s<sup>-1</sup>),  $S$  ( $10^{-1}$  cm<sup>3</sup>cm<sup>-3</sup>cm Hg<sup>-1</sup>).

#### 9.4.1.2.1 Polyimides as Membrane Materials for Separation of Olefins and Paraffins

Semenova [8] contains a detailed analysis of the relationship between chemical composition of polyimides and their separation properties. It is shown that the molar fraction of free volume of the polymer increases after introduction of bulky substituents into the elementary unit. It is therefore not surprising that the attention of researchers is focused on polyimides with bulky substituents, e.g., polyimides produced on the basis of such dianhydride as 6FDA-dianhydride 4,4'-hexafluoroisopropylidene of diphthalic acid (containing two bulky CF<sub>3</sub>-groups in the acid fragment) and such diamines as TrMPD-2,4,6-trimethyl-1,3-phenylenediamine (containing three CH<sub>3</sub>-groups in the amine fragment), TeMPD-2,3,5,6-tetramethyl-1,4-phenyldiamine (containing four CH<sub>3</sub>-groups in the amine fragment), 4APF-4,4'-hexafluoroisopropylidene dianiline (containing two bulky CF<sub>3</sub>-groups in the amine fragment), DDBT-dimethyl-3,7-diaminodiphenyl-thiophene-5,5'-dioxide (industrial product of Ube: a mixture of isomers having two methyl groups located differently in the phenyl nucleus, e.g., 63% in the 2,8-position, 33% in the 2,6-position, and 4% in the 4,6-position).

Molecules of olefin have  $\pi$ -electrons, and in an aromatic polyimide, charge transfer complexes can be formed.  $\pi$ -electrons of aromatic rings can interact with  $\pi$ -electrons of olefin. Intrinsic gas permeabilities, diffusivities, and solubilities of the olefin and paraffins in aromatic 6FDA-1,5NDA/TeMPD copolyimide (where 1,5NDA is 1,5-naphthalene diamine) were reported in Ref. [76]. Copolymers with higher 6FDA-1,5NDA compositions show a better packing density, which is most probably due to the enhanced interchain interactions resulting from the charge transfer complexes. The two benzene rings fused together in the naphthalene diamine moiety of the polyimide may actively promote electron transfer between electron-rich donor molecule and electron-deficient acceptor molecule. The four methyl groups in the TeMPD diamine moiety successfully inhibit dense chain packing and promote gas diffusivity and solubility.

*Permeability to Vapors of Ethylene and Ethane:* Table 9.5 shows values of mass transfer parameters of ethylene and ethane for 6FDA-TrMPD and BPDA-TeMPD polyimides (where BPDA is 3,3',4,4'-diphenyltetracarboxylic dianhydride), and Table 9.6, those for 6FDA-*m*PDA, 6FDA-*i*PDA, and 6FDA-4APF polyimides (*m*PDA—*meta*-phenylenediamine; *i*PDA-2,2'-bis(4-amino-phenyl) isopropane). It can be seen that the permeability of ethylene is higher compared with that of ethane. The ideal permselectivity in these polymers is  $\alpha_p^{id} C_2H_4/C_2H_6 = 2.9$ –4.4. The main contribution to the permeation selectivity is made by the diffusion selectivity. Thus, for 6FDA-TrMPD polyimide  $\alpha_D^{id} C_2H_4/C_2H_6 = 2.9$ , while the sorption selectivity is only  $\alpha_s^{id} C_2H_4/C_2H_6 = 1.0$ .

*Permeability to Vapors of Propylene and Propane:* It can be seen from the data shown in Figure 9.19 as well as Tables 9.6 and 9.7 that sufficiently high permeability to propylene and the highest values of ideal selectivity  $\alpha_p^{id} C_3H_6/C_3H_8$  are found in

**TABLE 9.6**  
**Permeability Coefficients of Ethylene and Propylene, as well as Values**  
**of Olefin/Paraffin Ideal Selectivity for Several Polyimides**

Polyimide	$P_{C_2H_4}$ (Barrer)	$\alpha_p^{id} C_2H_4/C_2H_6$	$P_{C_3H_6}$ (Barrer)	$\alpha_p^{id} C_3H_6/C_3H_8$
6FDA- <i>m</i> PDA	0.3	3.3	0.13	10
6FDA- <i>i</i> PDA	1.4	3.8	0.58	15
6FDA-4APF	2.1	4.4	0.89	16

Source: From Staudt-Bickel, C. and Koros, W.J., *J. Membr. Sci.*, 170, 205, 2000. With permission.

Notes:  $T = 308$  K; pressure =  $3.8 \times 10^5$  Pa.

**TABLE 9.7**  
**Permeability, Diffusion and Sorption Coefficients as well as Their Ideal Ratios**  
**for Vapors of C<sub>3</sub>H<sub>6</sub>, C<sub>3</sub>H<sub>8</sub>**

Polymer	$v_f$	$P_{C_3H_6}$	$D_{C_3H_6}$	$S_{C_3H_6}$	C <sub>3</sub> H <sub>6</sub> /C <sub>3</sub> H <sub>8</sub>		
					$\alpha_P^{id}$	$\alpha_D^{id}$	$\alpha_S^{id}$
6FDA-TeMPD	0.182	37	190	2.0	8.6	7.0	1.3
6FDA-TrMPD	0.182	30	130	2.3	11	8.8	1.2
6FDA-DDBT	0.169	0.76	4.2	1.8	27	27	1.0
6FDA-ODA <sup>a</sup>	0.165	0.48	8.7	0.54	11	8.9	1.3
BPDA-TeMPD	0.136	3.2	21	1.5	13	11	1.2
BPDA-DDBT <sup>a</sup>	0.125	0.12					
BPDA-ODA <sup>a</sup>	0.121	<0.05					
PPO	0.206	2.3	18	1.3	9.1	8.2	1.1
P4MP	0.209	54	2,100	0.26	2.0	2.3	0.9
1,2PB	0.200	260	4,600	0.57	1.7	1.7	1.0
PDMS	0.362	6,600	90,000	0.73	1.1	1.3	0.9

Source: From Semenova, S.I., *J. Membr. Sci.*, 231, 189, 2004. With permission.

Notes:  $T = 323$  K, pressure =  $2 \times 10^5$  Pa [9,32];  $P$ , Barrer;  $D$ ,  $10^{-10}$  cm<sup>2</sup> s<sup>-1</sup>;  $S$ ,  $10^{-1}$  cm<sup>3</sup> cm<sup>-3</sup> cm Hg<sup>-1</sup>.

<sup>a</sup>  $T = 373$  K.

polyimides of the composition 6FDA-TeMPD, 6FDA-TrMPD, 6FDA-DDBT, 6FDA-ODA, and BPDA-TeMPD (ODA, oxide aniline). Among polyimides, the highest flux to propylene is found in 6FDA-TeMPD polyimide ( $P_{C_3H_6} = 37$  Barrer at 323 K and propylene pressure  $P_{C_3H_6} = 2 \times 10^5$  Pa), and the highest selectivity to the propylene/propane system is found in 6FDA-DDBT polyimide ( $\alpha_P^{id} C_3H_6/C_3H_8 = 30$  at 323 K and pressure of individual components of  $2 \times 10^5$  Pa). Diffusion selectivity of polyimides is  $\alpha_D^{id} C_3H_6/C_3H_8 = 7-27$ , whereas sorption selectivity is much lower, only  $\alpha_S^{id} C_3H_6/C_3H_8 = 1.0-1.3$ .

*Permeability to Vapors of 1,3-Butadiene, C<sub>4</sub>H<sub>6</sub>, n-Butane, C<sub>4</sub>H<sub>10</sub>, and 1-Butene, C<sub>4</sub>H<sub>8</sub>*: Okamoto et al. [32] investigated the permeability of individual vapors of 1,3-butadiene and *n*-butane in some glassy polymers: in 6FDA-TrMPD, 6FDA-DDBT polyimides, and in polyphenylene oxide (see data presented in Table 9.8). The investigated polyimides had high permeability to 1,3-butadiene  $P_{C_4H_6} = 6.5-110$  Barrer, as well as high values of ideal permselectivity  $\alpha_P^{id} C_4H_6/C_4H_{10} = 67-190$  (at pressure  $1 \times 10^5$  Pa and 323 K). Diffusion selectivity was  $\alpha_D^{id} C_4H_6/C_4H_{10} = 45-110$ , whereas sorption selectivity is much lower and corresponds to only  $\alpha_S^{id} C_4H_6/C_4H_{10} = 1.5-1.7$ .

Shimazu et al. [70] investigated the permeability of 1,3-butadiene, *n*-butane, 1-butene in various glassy polymers, including polyimides based on 6FDA anhydride, notably 6FDA-*p*ODA and 6FDA-4APF polyimides. Figure 9.20 shows the dependence of ideal selectivity  $\alpha_P^{id} C_4H_6/C_4H_{10}$  and ideal selectivity  $\alpha_P^{id} C_4H_6/C_4H_8$  on the permeability of 1,3-butadiene. It can be seen that polymers having the highest permeability ( $P_{C_4H_6} = 10^2-10^3$  Barrer) and the highest selectivity ( $\alpha_P^{id} C_4H_6/C_4H_{10} = 10^4-10^5$  and  $\alpha_P^{id} C_4H_6/C_4H_8 = 10^3-10^4$ ) are polyimides based on 6FDA-dianhydride.

*Comparative Permeability of C<sub>2</sub>, C<sub>3</sub>, and C<sub>4</sub> olefins*: It is interesting to compare permeability, diffusion, and solubility coefficients of various olefins, as well as ideal olefin/paraffin selectivity in a glassy polymer. Such comparison can be made,

**TABLE 9.8**  
**Permeability, Diffusion and Sorption Coefficients, Their Ideal Ratios**  
**for Vapors of C<sub>4</sub>H<sub>6</sub> and C<sub>4</sub>H<sub>10</sub>**

Polymer	$P_{C_4H_6}$	$D_{C_4H_6}$	$S_{C_4H_6}$	C <sub>4</sub> H <sub>6</sub> /C <sub>4</sub> H <sub>10</sub>		
				$\alpha_P^{id}$	$\alpha_D^{id}$	$\alpha_S^{id}$
6FDA-TrMPD	111	225	4.1	67	45	1.5
6FDA-DDBT	6.5	14	4.4	190	110	1.7
PPO	4.2	15	2.7	33	22	1.5

Source: From Okamoto, K., Noborio, K., Hao, J., Tanaka, K., and Kita, H., *J. Membr. Sci.*, 134, 171, 1997. With permission.

Notes:  $T = 323$  K, pressure  $1 \times 10^5$  Pa;  $P$ , Barrer;  $D$ ,  $10^{-10}$  cm<sup>2</sup> s<sup>-1</sup>;  $S$ ,  $10^{-1}$  cm<sup>3</sup> cm<sup>-3</sup> cm Hg<sup>-1</sup>.

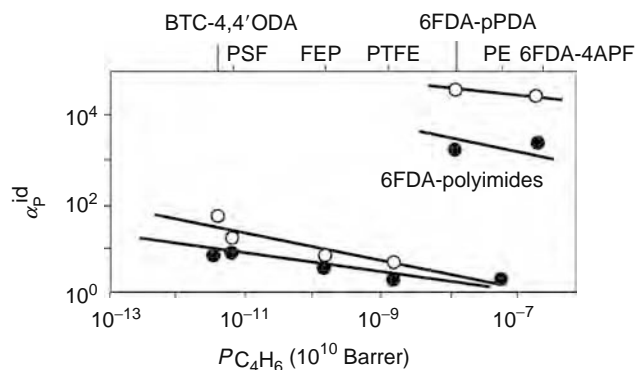


**FIGURE 9.20** Dependence of 1,3-butadiene/*n*-butane ideal selectivity,  $\alpha_P^{\text{id}} \text{C}_4\text{H}_6/\text{C}_4\text{H}_{10}$ , (O) and 1,3-butadiene/1-butene ideal selectivity,  $\alpha_P^{\text{id}} \text{C}_4\text{H}_6/\text{C}_4\text{H}_8$ , (●) on the permeability of 1,3-butadiene,  $P_{\text{C}_4\text{H}_6}$ , for various polymers: polyimides 6FDA-pODA and 6FDA-4APF. (PSF, polysulfone; FEP, Teflon; PTFE, polytetrafluoroethylene; PE, polyethylene; BTC, 4,4'ODA-polycarbonate). (From Semenova, S.I., *J. Membr. Sci.*, 231, 189, 2004. With permission.)

e.g., for 6FDA-TrMPD polyimide, by analyzing its properties with respect to individual components, such as ethylene, propylene, and 1,3-butadiene (see Tables 9.5–9.8 as well as data presented in Refs. [9,32]).

The diffusion coefficients of olefins can be arranged in a series that is the reverse of the series of effective molecular diameters:  $d_{\text{ef,C}_2\text{H}_4} = 0.423 < d_{\text{ef,C}_4\text{H}_6} = 0.440 < d_{\text{ef,C}_3\text{H}_6} = 0.468 \text{ nm}$ ;  $D_{\text{C}_2\text{H}_4} = 390 > D_{\text{C}_4\text{H}_6} = 225 > D_{\text{C}_3\text{H}_6} = 130, 10^{-10} \text{ cm}^2/\text{s}$ . The boiling temperatures of olefins, reflecting condensability of olefins, can be arranged in a series that corresponds to the series of their solubility coefficients:  $T_{\text{b,C}_2\text{H}_4} = 169.5 < T_{\text{b,C}_3\text{H}_6} = 225.5 < T_{\text{b,C}_4\text{H}_6} = 282.2 \text{ K}$ ;  $S_{\text{C}_2\text{H}_4} = 0.15 < S_{\text{C}_3\text{H}_6} = 0.23 < S_{\text{C}_4\text{H}_6} = 0.41 \text{ cm}^3/\text{cm}^3 \text{ cm Hg}$ . On the basis of sequences reflecting the correspondence between diffusion and solubility coefficients, the series of permeability coefficients of olefins is quite explicable:  $P_{\text{C}_3\text{H}_6} = 30 < P_{\text{C}_2\text{H}_4} = 58 < P_{\text{C}_4\text{H}_6} = 92 \text{ Barrer}$ . The values of ideal olefin/paraffin selectivity can be arranged in the following series:  $\alpha_P^{\text{id}} (\text{C}_2\text{H}_4/\text{C}_2\text{H}_6) = 2.9 < \alpha_P^{\text{id}} (\text{C}_3\text{H}_6/\text{C}_3\text{H}_8) = 11 < \alpha_P^{\text{id}} (\text{C}_4\text{H}_6/\text{C}_4\text{H}_{10}) = 67$ .

#### 9.4.1.2.2 Polyphenylene Oxides as Membrane Materials for Separation of Olefins and Paraffins

Polyphenylene oxides are quite promising materials for separation and removal of olefins and paraffins. In terms of their properties these polymers are only inferior to polyimides (see Tables 9.7–9.9; Figures 9.19, 9.21, and 9.22).

Separation properties of poly-2,6-dimethyl-1,4-phenylene oxide (p-DMePO) and poly-2,6-diphenyl-1,4-phenylene oxide (p-DPhPO), as well as chemically modified p-DMePO have been studied by a number of researchers for the purpose of using these polymers in gas separation and pervaporation processes [18,68,71]. p-DMePO/p-DPhPO copolymers offer a number of advantages compared to homopolymers: better mechanical properties, higher resistance to oxidants and radiation, which is why these copolymers have also been studied rather closely [18,71]. Investigation of p-DMePO and p-DPhPO homopolymers has

**TABLE 9.9**  
**Comparison of Permeability and Separation Properties of the  $\text{C}_3\text{H}_6/\text{C}_3\text{H}_8$  System for Individual Penetrants, as well as for Their Equimolar Mixture, in Various Polyimides and in Polyphenylene Oxide PPO**

Polymer	Penetrant	$P_{\text{C}_3\text{H}_6}$ (Barrer)	$P_{\text{C}_3\text{H}_8}$ (Barrer)	$\alpha_P^{\text{id}}$ or $\alpha_P$
6FDA-TrMPD	Individual	27	2.7	10.0
	Mixture	20	3.3	6.0
BPDA-TeMPD	Individual	4.0	0.3	13.0
	Mixture	3.4	0.42	8.0
PPO	Individual	2.9	0.32	9.0
	Mixture	2.7	0.50	5.4
6FDA-DDBT(373 K)	Individual	2.6	0.17	15.0
	Mixture	2.0	0.20	10.0

Source: From Tanaka, K., Taguchi, A., Hao, J., Kita, H., and Okamoto, K., *J. Membr. Sci.*, 121, 197, 1996. With permission.

Notes: Partial pressure of penetrants  $2 \times 10^5 \text{ Pa}$ ;  $T = 323 \text{ K}$ .

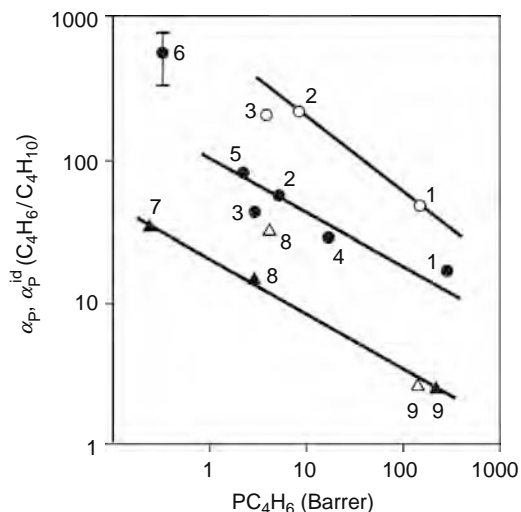


**FIGURE 9.21** Permeability and selectivity of polyimides (O, ●), as well as of some other polymers (▽, ▼) with respect to individual vapors of  $C_4H_6$ ,  $C_4H_{10}$ , and their mixtures. (Properties to individual penetrants were determined at  $1 \times 10^5$  Pa, 323 K and are designated with open symbols (O, ▽); properties with respect to equimolar mixtures of penetrants were determined at total pressure of  $1.5 \times 10^5$  Pa, 323 K and are designated with closed symbols (●, ▼).) Polyimides: (1) 6FDA-TrMPD, (2) 6FDA-DDBT, (3) 6FDA-4APF, (4) BPDA-TrMPD, (5) BTDA-TrMPD, (6) DSDA-DDBT; other polymers: (7) PSF—polysulfone, (8) PPO—polyphenylene oxide, and (9) P4MP—polymethylpentene. (From Okamoto, K., Noborio, K., Hao, J., Tanaka, K., and Kita, H., *J. Membr. Sci.*, 134, 171, 1997. With permission.)

shown that side groups have a significant effect on free volume of the polymer and its transport properties. It has been established that the molar fraction of free volume of p-DPhPO having phenyl side groups is smaller than the molar fraction of free volume of p-DMePO having methyl side groups. Therefore permeability and diffusion coefficients of hydrocarbons in the p-DPhPO polymer are smaller compared to the p-DMePO polymer (see Figure 9.23). It is also not surprising that permeability and diffusion coefficients of hydrocarbons decrease with the increase in the content of the diphenyl-substituted component in the copolymer.

Thus, it follows from the above data that glassy polymers are promising materials for selective separation of olefins from their mixtures with paraffins. The main contribution to the high values of permselectivity is made by the diffusion component  $\alpha_D$ . However, unsaturated bonds in olefin molecules make them capable of specific interactions with  $\pi$ -conjugated polar

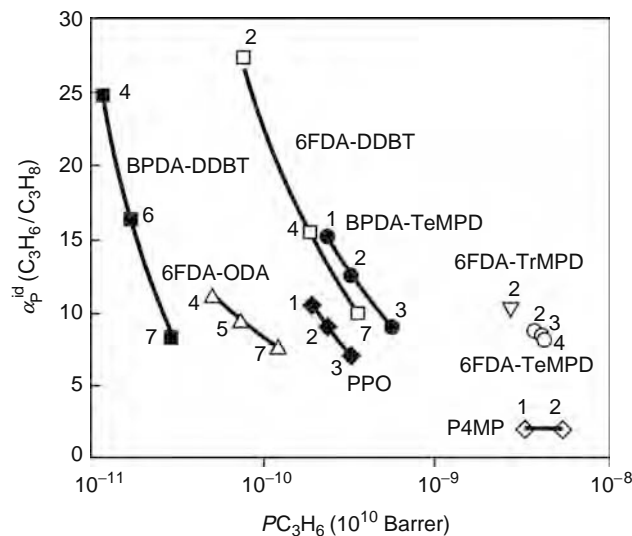


**FIGURE 9.22** Dependence of ideal selectivity  $\alpha_P^{\text{id}} C_3H_6/C_3H_8$  on permeability coefficient of propylene in polyimides at various temperatures: (1) 308 K; (2) 323 K; (3) 353 K; (4) 373 K; (5) 393 K; (6) 398 K; (7) 423 K (pressure  $2 \times 10^5$  Pa). (From Tanaka, K., Taguchi, A., Hao, J., Kita, H., and Okamoto, K., *J. Membr. Sci.*, 121, 197, 1996. With permission.)

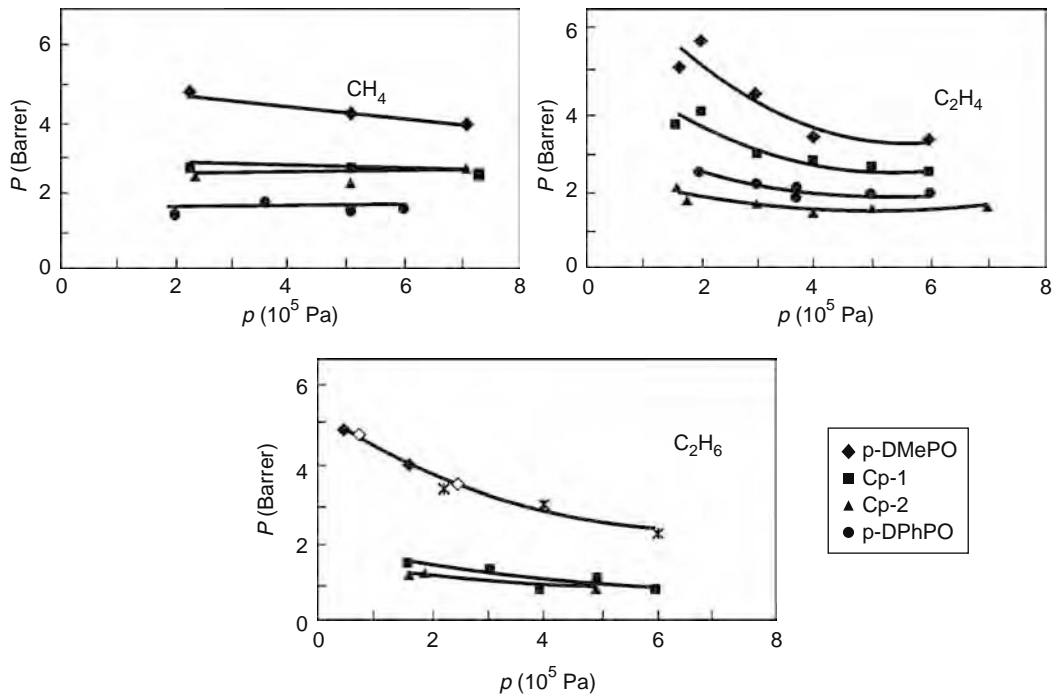


**FIGURE 9.23** Dependence of permeability coefficients of polyphenylene oxides with respect to individual penetrants  $\text{CH}_4$  and  $\text{C}_2\text{H}_4$  on pressure of  $\text{CH}_4$  and  $\text{C}_2\text{H}_4$ , respectively ( $T = 298 \text{ K}$ ). Dependence of permeability coefficient of polyphenylene oxides to  $\text{C}_2\text{H}_6$  on partial pressure  $\text{C}_2\text{H}_6$ :  $\blacklozenge$   $\text{C}_2\text{H}_6/\text{He}$  20%/80% mol. mixture;  $\blacksquare$   $\text{C}_2\text{H}_6/\text{He}$  35%/65% mol. mixture;  $\times$  pure  $\text{C}_2\text{H}_6$  (pDMePO, polydimethylphenylene oxide; pDPhPO, polydiphenylphenylene oxide; CP1, pDMePO/pDPhPO 97.5/2.5% mol. copolymer; CP2, pDMePO/pDPhPO 75/25% mol. copolymer). (From Lapkin, A.A., Roschupkina, O.P., and Ilinitich, O.M., *J. Membr. Sci.*, 141, 223, 1998. With permission.)

groups. Introduction of such groups into the polymer membrane would make it possible to significantly raise sorption selectivity  $\alpha_S$ . Unfortunately, research activity in this field is not sufficiently extensive.

#### 9.4.1.3 Pressure Dependence of Hydrocarbon Permeability and Selectivity in Glassy Polymers

Permeability coefficients of olefins and paraffins and olefin/paraffin selectivity coefficients in polymers are essentially dependent on partial pressure of the penetrants. Figure 9.24 shows the dependence of the permeability of 6FDA-TrMPD

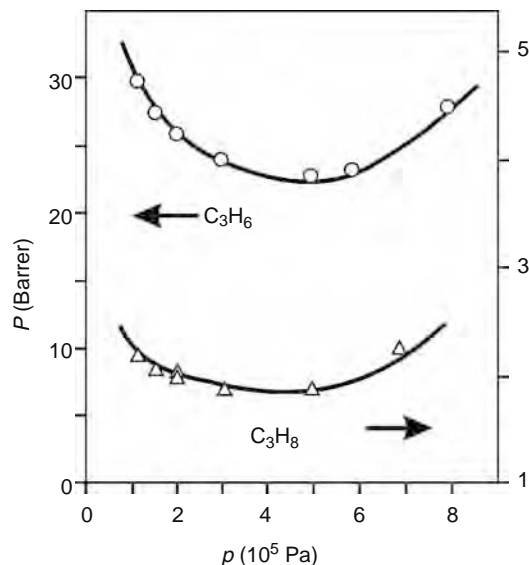


**FIGURE 9.24** Dependence on pressure of permeability coefficients of propylene and propane for 6FDA-TrMPD polyimide ( $T = 323 \text{ K}$ ). (From Tanaka, K., Taguchi, A., Hao, J., Kita, H., and Okamoto, K., *J. Membr. Sci.*, 121, 197, 1996. With permission.)

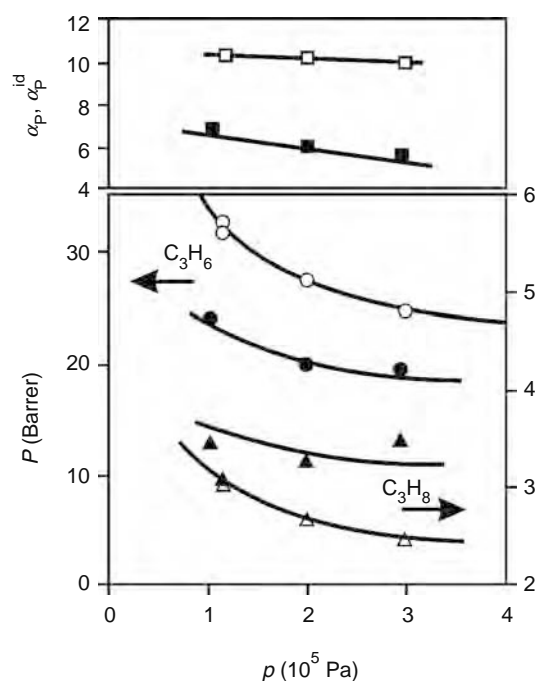


**FIGURE 9.25** Dependence of permeability coefficients of propylene  $P_{C_3H_6}$ , propane  $P_{C_3H_8}$ , and selectivity on partial pressure for the equimolar gas mixture in 6FDA-TrMPD polyimide (total pressure  $3.1 \times 10^5$  Pa,  $T = 323$  K). For comparison, the corresponding data for individual components designated with open symbols. (From Tanaka, K., Taguchi, A., Hao, J., Kita, H., and Okamoto, K., *J. Membr. Sci.*, 121, 197, 1996. With permission.)

polyimide to such individual components as propane and propylene on their partial pressure. It can be seen from the figure that the permeability decreases until pressure reaches  $5 \times 10^5$  Pa, and then begins to rise. The reduction of permeability is explained by the dual-mode sorption model and is related to sorption sites of the polymer being filled by the penetrant. The increase in permeability at pressures above  $5 \times 10^5$  Pa is accounted for by plasticization of the polymer by the penetrant [9,32].

No  $C_2H_6$  and  $C_2H_4$  plasticization was detected for 6FDA-1,5NDA/TeMPD copolyimides even up to 16 atm [76]. However, plasticization was observed for  $C_3H_8$  and  $C_3H_6$  because of their high condensability and strong polymer-penetrant interactions. 6FDA-TeMPD has a lower plasticization pressure than 6FDA-1,5NDA for  $C_3H_8$  and  $C_3H_6$ . The plasticization pressures for the copolymers fall between the ranges of their parent homopolymer. The plasticization pressure is higher with an increase in 6FDA-1,5NDA content in these copolymers.

Permeability and diffusion coefficients of hydrocarbons in polyphenylene oxides are also essentially dependent on pressure (see Figure 9.23). It can be seen that in the case of ethylene, with the increase in pressure, the permeability coefficients first decrease, and then begin to rise. Ref. [18] quotes constants of the dual-mode sorption model for a number of hydrocarbons permeation through polyphenylene oxide.

Table 9.9 compares the separation properties of various polyimide to individual penetrants, propane and propylene, as well as their mixtures. Figure 9.25 shows dependencies of the permeability coefficients  $P_{C_3H_6}$  and  $P_{C_3H_8}$  and of the selectivity coefficient  $\alpha_P C_3H_6/C_3H_8$  for gaseous mixtures, as well as for individual penetrants, in 6FDA-TrMPD polyimide on partial pressure. Comparison of permeabilities of penetrants in the case of individual transport to those in the case of transport of an equimolar mixture (at equal partial pressure) shows that the permeability coefficient of propylene  $P_{C_3H_6}$  for mixtures is lower by 20%–30%, and the permeability coefficient of propane  $P_{C_3H_8}$  is higher by 10%–40% than those for individual penetrants. As a result, the selectivity in the mixture is much lower than the ideal selectivity [9]. Similarly, in the case of permeation of the  $C_4H_6/C_4H_{10}$  mixture through polyimides, the permeation selectivity is much lower than the ideal value which is also accounted for by the plasticization effect.

#### 9.4.1.4 Temperature Dependence of Hydrocarbon Permeability and Selectivity in Glassy Polymers

Theoretical findings of Refs. [7,52] experimentally corroborated for interacting polymer-penetrant systems can certainly be applied to systems consisting of a glassy polymer and an easily condensable hydrocarbon. Unfortunately, sufficient experimental data corroborating this conclusion are not yet available in the literature, although some regularities of variation of mass exchange properties as a function of temperature are considered in several reports [9,32]. Figure 9.22 shows dependencies of ideal selectivity  $\alpha_P^{id} C_3H_6/C_3H_8$  on permeability coefficient  $P_{C_3H_8}$  for polyimides and polyphenylene oxide at various

**TABLE 9.10**  
**Activation Energies of Permeability  $\Delta E_P$ , diffusion  $\Delta E_D$ , as well as Heat of Penetrant Sorption  $\Delta H_S$  for  $C_3H_6$  and  $C_3H_8$  in Polyimides**

Polymer	$C_3H_6$			$C_3H_8$		
	$\Delta E_P$	$\Delta E_D$	$\Delta H_S$	$\Delta E_P$	$\Delta E_D$	$\Delta H_S$
6FDA-TeMPD	2	16	-14	4	17	-13
6FDA-TrMPD	4	15	-11	9	20	-11
6FDA-DDBT	18	30	-13	29	44	-15
6FDA-ODA	24	43	-19	34	56	-22
BPDA-TeMPD	18			28		
BPDA-DDBT	23			52		
PPO	11			19		

Source: From Tanaka, K., Taguchi, A., Hao, J., Kita, H., and Okamoto, K., *J. Membr. Sci.*, 121, 197, 1996.  
 With permission.

Notes: Pressure  $2 \times 10^5$  Pa;  $\Delta E_P$ ,  $\Delta E_D$ ,  $\Delta H_S$  (kJ/mol).

temperatures, and Table 9.10 lists values of permeability and diffusion activation energies, as well as heat of hydrocarbon sorption. It can be seen that the increase in temperature in the range 308–423 K is accompanied by an increase in the permeability and a decrease in the selectivity coefficient of the polymers. However, the existence of turning points is possible in a different range of temperatures and concentrations (see Section 9.3.1.3).

#### 9.4.1.5 Kinetics of the Permeation Process

Investigation of permeation of three-component hydrocarbon mixtures through polyphenylene oxides revealed a more complicated pattern compared to what is found by comparing permeabilities of individual gases. In a three-component mixture, the component having the highest penetration rate occupies free voids of the polymer ahead of other components, and is then gradually replaced by a more sorbable component from the occupied sorption sites [18]. It is known that sorption of an individual gas by a glassy polymer is higher than sorption of the same gas mixed with other gases. This effect results from competitive sorption [72,73]. Similarly, permeability of an individual gas through a glassy polymer is higher than that of the same gas penetrating in mixture with other gas. It has been established however that this applies only to the steady state. In the unsteady state the ratio of the diffusion coefficients of the penetrants plays an important role. Methane is the fastest and least sorbable component of the mixture. It occupies the microvoids of the polymer's free volume ahead of other components, as is clear from the kinetic permeability curves shown in Figure 9.26. This effect can be used to set up a pulse mode in the process of hydrocarbon separation.

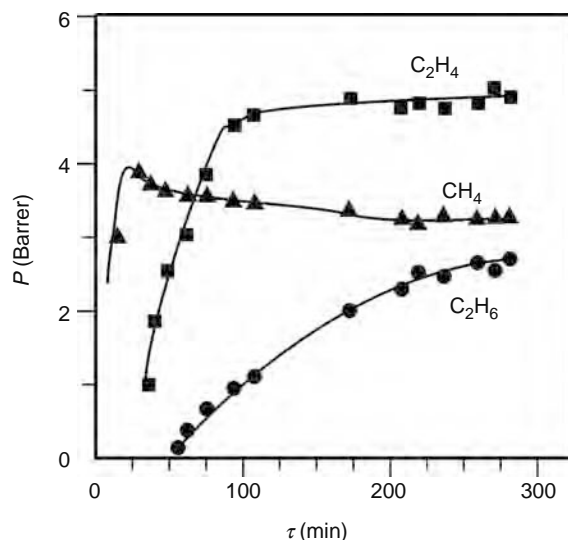


**FIGURE 9.26** Time dependence of permeability coefficients for the mixture of gases  $CH_4/C_2H_4/C_2H_6$  (71%/19%/10% mol) for the membrane based on poly-2,6-dimethyl-1,4-phenylene oxide (pressure of the mixture  $5 \times 10^5$  Pa,  $T = 298$  K). (From Lapkin, A.A., Roschupkina, O.P., and Ilinitich, O.M., *J. Membr. Sci.*, 141, 223, 1998.)

## 9.4.2 SEPARATION OF AROMATIC, ALICYCLIC, AND ALIPHATIC HYDROCARBONS

### 9.4.2.1 Problem of Separation of Aromatic, Alicyclic, and Aliphatic Hydrocarbons

The separation of mixtures of aromatic, alicyclic, and aliphatic hydrocarbons, as well as their isomers, e.g., benzene and cyclohexane, toluene and iso-octane, and isomers of xylene has been actively developing in recent years. At present such separations are performed by fractional distillation, which is very energy expensive. In addition, this method cannot be used for separation of organic mixtures having similar boiling temperatures. Pervaporation is a good alternative in this case. Research in this area is mainly focused on development of membranes offering high-separation properties and good stability to the feed mixture [10,11,77–137].

#### 9.4.2.1.1 Aromatic–Alicyclic Hydrocarbons

Separation of benzene/cyclohexane mixture is investigated most extensively. This is not surprising because separation of this mixture is very important in practical terms. Benzene is used to produce a broad range of valuable chemical products: styrene (polystyrene plastics and synthetic rubber), phenol (phenolic resins), cyclohexane (nylon), aniline, maleic anhydride (polyester resins), alkylbenzenes and chlorobenzenes, drugs, dyes, plastics, and as a solvent. Cyclohexane is used as a solvent in the plastics industry and in the conversion of the intermediate cyclohexanone, a feedstock for nylon precursors such as adipic acid,  $\epsilon$ -caprolactam, and hexamethylenediamine. Cyclohexane is produced mainly by catalytic hydrogenation of benzene. The unreacted benzene is present in the reactor's effluent stream and must be removed for pure cyclohexane recovery.

A significant number of works are concerned with the development of new membranes for the separation of mixtures of aromatic/alicyclic hydrocarbons [10,11,77–109]. For example, the following works can be mentioned. A mixture of cellulose ester and polyphosphonate ester (50 wt%) was used for benzene/cyclohexane separation [113]. High values of the separation factor and flux were achieved (up to 2 kg/m<sup>2</sup> h). In order to achieve better fluxes and separation factors the attention was shifted to the modification of polymers by grafting technique. Grafted membranes were made of polyvinylidene fluoride with 4-vinyl pyridine or acrylic acid by irradiation [83]. 2-Hydroxy-3-(diethyl-amino) propyl methacrylate-styrene copolymer membranes with cyanuric chloride were prepared, which exhibited a superior separation factor  $\beta_P = 190$  for a feed aromatic component concentration of 20 wt%. Graft copolymer membranes based on 2-hydroxyethyl methacrylate-methylacrylate with thickness 10  $\mu\text{m}$  were prepared [85]. The membranes yielded a flux of 0.7 kg/m<sup>2</sup> h (for feed with 50 wt% of benzene) and excellent selectivity. Benzene concentration in permeate was about 100 wt%. A membrane based on polyvinyl alcohol and polyallyl amine was prepared [87]. For a feed containing 10 wt% of benzene the blend membrane yielded a flux of 1–3 kg/m<sup>2</sup> h and a separation factor of 62.

#### 9.4.2.1.2 Aromatic/Aliphatic-Aromatic Hydrocarbons

According to literary data, the following mixtures of aromatic/aliphatic-aromatic hydrocarbons were separated: toluene/*n*-hexane, toluene/*n*-heptane, toluene/*n*-octane, toluene/*i*-octane, benzene/*n*-hexane, benzene/*n*-heptane, benzene/toluene, and styrene/ethylbenzene [10,82,83,109–129]. As membrane media, various polymers were used: polyetherurethane, polyesterurethane, polyetherimide, sulfonyl-containing polyimide, ionically cross-linked copolymers of methyl, ethyl, *n*-butyl acrylate with acrylic acid. For example, when a composite polyetherimide-based membrane was used to separate a toluene (50 wt%)/*n*-octane mixture, the flux  $Q$  of 10 kg  $\mu\text{m}/\text{m}^2$  h and the separation factor of 70 were achieved [121]. When a composite membrane based on sulfonyl-containing polyimide was used to separate a toluene (1 wt%)/*n*-octane mixture, the flux  $Q$  of 1.1 kg  $\mu\text{m}/\text{m}^2$  h and the separation factor of 155 were achieved [10]. When a composite membrane based on ionically cross-linked copolymers of methyl, ethyl, *n*-butyl acrylate with acrylic acid was used to separate toluene (50 wt%)/*i*-octane mixture, the flux  $Q$  of 20–1000 kg  $\mu\text{m}/\text{m}^2$  h and the separation factor of 2.5–13 were achieved [126,127].

#### 9.4.2.1.3 Isomers

In oil processing, separation of aromatic isomers C<sub>8</sub> (ethylbenzene  $T_b = 136^\circ\text{C}$ , *p*-xylene  $T_b = 138.3^\circ\text{C}$ , *m*-xylene  $T_b = 139.1^\circ\text{C}$ , *o*-xylene  $T_b = 144.4^\circ\text{C}$ ) is required. According to the literary data, the following isomers of hydrocarbons are separated: *p*-xylene/*m*-xylene, *p*-xylene/*o*-xylene, *n*-hexane/2,2-dimethylbutane, *n*-hexane/3-methylpentane, and *n*-butane/*i*-butane [8,83,130–137]. Pervaporation method is the most effective for this purpose. To separate the isomers, membranes based on various polymers were used. Good separation for all isomer mixtures was attained by the polyimide Kapton film ( $\beta_P = 1.43$ –2.18) but parylene films and cellulose acetate also exhibited a relatively high separation factor ( $\beta_P = 1.22$ –1.56 and  $\beta_P = 1.23$ –1.56, respectively). Temperatures  $>200^\circ\text{C}$  were required to obtain a reasonable flux through the polyimide film and a pressure of about 20 atm was necessary to keep the feed stream liquid [8].

Thin films based on cellulose esters treated with an organic solvent were used for separation of isomeric xylenes, however, low values of factor  $\beta_P$  were achieved [130]. Modifications of hydrophylic membranes were used for separation of C<sub>8</sub>-aromatic isomers. Separation factor for *p*- to *m*-xylene was 1.69 [131]. Commercial polyvinyl alcohol membrane in the presence of CBr<sub>4</sub> as a selective feed complexing agent was used to separate *p*- to *m*-xylene [133]. Dense homogenous polyethylene membranes were used for separation of aromatic C<sub>8</sub>-isomers [132]. The rate of mass transport across the membrane increased

for the isomers in the order: *o*-xylene < ethylbenzene < *m*-xylene < *p*-xylene. The very small separation factors obtained restricted the use of polyvinyl alcohol membranes for purification of mixed xylenes on an industrial level. However, when a membrane based on polyvinyl alcohol filled with  $\beta$ -cyclodextrin was used to separate xylene isomers, the separation factor  $\beta_P$  of 2.96 was achieved [135].

The polymer materials mainly used for the membranes are glassy polymers, the first and foremost polyimides. The use of glassy polymers having a rigid ensemble of macromolecules results in high separation effectiveness. Separation effectiveness in pervaporation processes is characterized by the separation factor,  $\beta_P$ , which is determined by the diffusion component,  $\beta_D$ , and the sorption component,  $\beta_S$  [8,55]. Let us consider the effect of chemical composition of polymer membranes on their transport properties with respect to aromatic, alicyclic, aliphatic hydrocarbons and analyze ways to improve these properties.

#### 9.4.2.2 Diffusion Component of Separation Factor

This parameter is determined by the ratio of molecular sizes of the penetrants being separated and by rigidity and packing density of macromolecules. The greater the difference between molecular sizes of penetrants and the more dense and rigid the polymer matrix, the larger is the diffusion component of the separation factor [8,55].

##### 9.4.2.2.1 Dependence of Diffusion Component of Separation Factor on the Size of Penetrant Molecule

Section 9.2.2 deals with the issue of values of effective diameters of hydrocarbons penetrating through rubbery and glassy polymers (see Table 9.1). As shown in Refs. [10,11], when comparing sizes of differently shaped molecules it would be more correct to use as a criterion the minimum cross-section of the diffusing molecule  $a_D$  determined from Stuart's molecular model. This is especially important for oblong molecules, e.g., *n*-hexane and *n*-octane. It can be seen from the data presented in Table 9.1 that molecules of hydrocarbons can be arranged by the size of minimum cross-section in the following series: *n*-hexane  $\leq$  *n*-octane < benzene < toluene < cyclohexane < *iso*-octane. It is clear that the diffusion coefficients of these penetrants should vary in reverse order. This conclusion has been confirmed in Ref. [10] where the possibility of pervaporation separation of hydrocarbon mixtures using membranes based on DSDA-DDBT polyimide (DSDA, dianhydride of 3,3',4,4'-diphenylsulfonetetracarboxylic acid; DDBT, dimethyl-3,7-diaminobenzothiophene-5,5'-dioxide) has been investigated. Diffusion coefficients of the investigated hydrocarbons are indeed arranged in the series that is reverse to the series of minimum cross-sections of penetrant molecules. The membranes had preferential permeability for aromatic over aliphatic compounds. The strongest dependence of the separation factor and the permeability on the composition of the mixture being separated has been found in mixtures whose components display the greatest difference in molecular size.

Ref. [77] deals with the pervaporation separation of benzene/cyclohexane, toluene/*iso*-octane mixtures using DSDA-TrMPD/2,2'-diethynylbenzidine (DEB) copolyimide. The dominant role of the diffusion component  $\beta_D$  in the separation process has been established. It can be seen from the data in Table 9.11 that the increase in the difference between ratios of minimum cross-sections of penetrant molecules results in an increase of the separation factor  $\beta_P$  which is determined mainly by the diffusion component  $\beta_D$ .

##### 9.4.2.2.2 Factors Determining Rigidity of the Ensemble of Macromolecules

An important factor that determines diffusion selectivity of the membrane is the rigidity and regularity of the polymer structure and stability of the membrane to the mixture being separated. The rigidity of the polymer structure is determined

**TABLE 9.11**  
**Pervaporation Properties of the Membrane Based on DSDA-TrMPD/DEB Polyimide**

Composition of the mixture	$(\alpha_D)_{\text{arom}}/(\alpha_D)_{\text{al}}^a$ (nm/nm)	$Q_w$ (kg $\mu\text{m}/\text{m}^2\text{h}$ )	$\beta_P$ (Arom./Al.) <sup>b</sup>
Benzene/ <i>n</i> -hexane	0.21/0.18	2.8	9.1
Toluene/ <i>n</i> -octane	0.23/0.18	2.1	13
Benzene/cyclohexane	0.21/0.33	0.44	48
Toluene/ <i>iso</i> -octane	0.23/0.36	1.1	330

Source: From Semenova, S.I., *J. Membr. Sci.*, 231, 189, 2004. With permission.

Notes: Content of aromatic component in mixtures being separated 40–50 wt%,  $T = 343$  K, membrane thickness 21  $\mu\text{m}$  [10,11,77].

<sup>a</sup>  $(\alpha_D)_{\text{arom}}/(\alpha_D)_{\text{al}}$ , minimum cross-section of diffusing molecule determined from Stuart's molecular model, for aromatic and alicyclic (or aliphatic) component of the mixture being separated.

<sup>b</sup>  $\beta_P(\text{arom./al.})$ , separation factor of aromatic component with respect to alicyclic (or aliphatic) component.

**TABLE 9.12**  
**Effect of Polyimide DSDA-TrMPD/ODA/DEB Chemical Composition (the Content of Amine Coreagents), Cross-Linking of Polyimide and Addition of Tetracyanoethylene (TCNE) to the Polymer on the Membrane Pervaporation Properties**

Amine Coreagent Content (mol%)			Cross-Linking (Yes/No)	Addition of TCNE (wt%)	Q (kg $\mu\text{m}^2/\text{h}$ )	Separation Factor Benzene/Cyclohexane		
TrMPD	ODA	DEB				$\beta_P$	$\beta_D$	$\beta_S$
100	0	0	Yes	—	10.6	7.3		
90	0	10	Yes	—	4.1	14.0	5.2	2.7
			No	—		7.0	2.9	2.4
75	0	25	Yes	—		11.1	3.7	3.0
			Yes	10		30.0	6.9	4.4
75	12.5	12.5	Yes	—	3.4	13.3		
50	25	25	Yes	—	1.5	21.0		

Source: From analysis of data presented in Fang, J., Tanaka, K., Kita, H., and Okamoto, K., *Polymer*, 40, 3051, 1999.

Note: Composition of the mixture to be separated is benzene/cyclohexane with 50–60 wt% of benzene,  $T = 343$  K.

by the make-up of individual macromolecules (primarily by potential barriers to rotation around intramolecular bonds) as well as the rigidity of the ensemble of macromolecules (primarily, strength of intra- and intermolecular interactions in the polymer). Intra- and intermolecular interactions in the polymer and between polymers produce a network of bonds, cross-links. Intermolecular interactions can be of various types, including dipole–dipole, dispersion interactions, hydrogen bonds, ion–ion interactions, as well as chemical and radiation cross-linking. In all cases cross-link density and strength of bonds in the cross-links, and, consequently, of the diameters of the diffusion channels in the polymer, are ultimately governed by the chemical structure of the polymer [8,55].

**9.4.2.2.3 Effect of the Increase in Rigidity of the Polymer System on the Diffusion Component of Separation Factor Thermal Cross-Linking of Unsaturated Bonds of Macromolecules:** Fang et al. [77] are concerned with the pervaporation properties, with respect to benzene/cyclohexane mixture being separated, of several ethynyl-containing copolyimides (the original composition for preparation of polyimides contained 2,2'-diethynylbenzidine) that were thermally cross-linked through unsaturated bonds. It can be seen from the data presented in Table 9.12 that the increase in the content of diethynylbenzidine (i.e., in the content of unsaturated bonds used for cross-linking) enhances the separation factor  $\beta_P$  (benzene/hexane). Table 9.12 also shows pervaporation properties of cross-linked and non-cross-linked DSDA-TrMPD/DEB polyimides. It can be seen that thermal cross-linking results in a nearly twofold increase in the diffusion component of the separation factor  $\beta_D$  with an insignificant change of the sorption component  $\beta_S$ .

**Increasing Cohesion Energy of the Polymer by Introducing Active Additives:** To increase the sorption component of the separation factor for the benzene/cyclohexane mixture, the matrix of DSDA-TrMPD/DEB polyimide was filled with a homogeneously distributed TCNE an electron acceptor having high affinity for ethynyl-containing fragments (DEB component in polyimide) and aromatic substances [77]. As a result, there was an increase not only in the sorption component (which will be discussed in Section 9.4.2.3) but also in the diffusion component of the separation factor  $\beta_D$  (see Table 9.12). This effect can be explained by the increase in rigidity of the polymer system as a result of the rise in cohesion energy after introduction of the additive, whose active groups display  $\pi$ -electron acceptor properties and can form charge transfer complexes with unsaturated fragments of macromolecules.

**Increasing Cohesion Energy of the Polymer by Introducing Polar Groups:** Introducing a polymer of polar groups with  $\pi$ -electron acceptor properties (such as ethynyl, phosphorylate, sulfone, acrylate, and phenyl groups) increases the cohesion energy of the polymer, which enhances the rigidity of the polymer ensemble, inhibits swelling, and thus increases the diffusion component of the separation factor [10,79–82]. For example, a series of copoly(methacrylates) with pendant phosphate and carboxylphosphonate groups were synthesized [109]. The copolymer membranes were cross-linked by the chemical reaction of either ethylene glycol diglycidyl ether or toluene diisocyanate with hydroxyl or secondary amine groups in copolymer segments. Although being in the rubbery state, the membranes displayed the behavior of low diffusion coefficient and positive aromatic/aliphatic diffusion separation factor ( $\beta_D$  up to 1.4 for benzene/*n*-hexane) and large activation energy of pervaporation, which has been observed in typical glassy polymers. This diffusion behavior can be explained by dense polymer-chain packing due to the hydrogen bonding between carbonyl and hydroxyl groups of polymer side-chain as well as relatively high cross-linking density. Pervaporation separation of toluene/*i*-octane mixtures using 6FDA-TrMPD/DABA copolyimide membranes

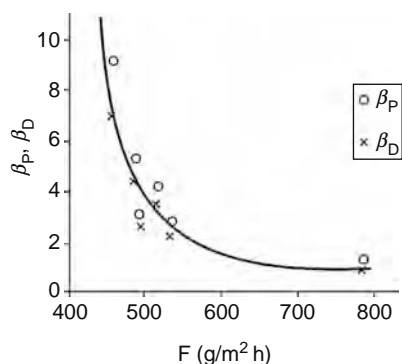


**FIGURE 9.27** Dependence of separation factor  $\beta_P$  (benzene/cyclohexane), as well as its diffusion component  $\beta_D$  based on styrene/butadienestyrene/acrylic acid copolymers on permeation flux (benzene/cyclohexane 50/50 wt% mixture,  $T = 293$  K). (From analysis of data presented in Semenova, S.I., *J. Membr. Sci.*, 231, 189, 2004. With permission.)

containing 3,5-diaminobenzoic acid (DABA) was investigated in Ref. [128]. It was found that incorporation of the diamino-benzoic acid units promotes segmental packing, reduces membrane swelling, and improves the separation factor and durability of the membrane. The improvement in separation factor, with respect to the polymer without diaminobenzoic acid, is mainly due to the increase in the diffusion component  $\beta_D$ . It was established that the diffusion separation factor is exponentially correlated with the reciprocal of neat polyimide fractional free volume.

In addition, the polar groups enhance the affinity of the membrane for the aromatic component, as will be discussed below in Section 9.4.2.3.

*Increase in the Content of the Rigid Component of Copolymers:* Sun and Ruckenstein [78] deal with copolymers of styrene/butadiene and styrene/acrylic acid. Rigidity of the copolymer was regulated by changing the ratio of components. Rigidity of the copolymer is enhanced by the increase in cohesion energy, which is achieved by increasing the content of polar groups. This is accompanied by reduced permeability and enhanced benzene/cyclohexane separation factor, due to the increase in the diffusion component of separation factor up to  $\beta_D \approx 10$  (see Figure 9.27), while the sorption component of separation factor changes insignificantly:  $\beta_S \approx 1$ –1.3.

Tsubouchi and Yoshikawa [79] are concerned with pervaporation separation of benzene/cyclohexane mixtures using membranes based on polyamide/polyether block copolymers. It has been established that the separation factor increases with the increase in the polyamide component containing polar amide groups capable of forming hydrogen bonds: e.g., the 1:1 block copolymer of polyamide 12 and polyoxyethylene has the benzene/cyclohexane separation factor  $\beta_P = 2.8$  and the flux  $Q = 300$  g/m<sup>2</sup> h; a more rigid 3:1 polyamide 12/polyoxyethylene block copolymer has a much higher separation factor:  $\beta_P = 5.0$  and  $Q = 80$  g/m<sup>2</sup> h.

### 9.4.2.3 Sorption Component of Separation Factor

In the absence of specific penetrant/polymer interactions, the sorption component  $\beta_S$  is mainly determined by the ratio of boiling temperatures of the components being separated [8]. However, aromatic penetrants, as  $\pi$ -electron systems, can have specific interactions with active groups or fragments of the polymer. If such interactions are realized, the sorption component of the separation factor is increased. For selective removal of aromatic compounds from their mixtures with aliphatic and alicyclic compounds, the parameter  $\beta_S$  can be increased by introducing active groups or fragments having  $\pi$ -electron acceptor properties into the polymer. These groups or fragments have  $\pi$ -electron affinity for aromatic compounds (a charge transfer complex can be formed). These effects have been much investigated in polyimides.

#### 9.4.2.3.1 Increasing the Sorption Component of the Separation Factor by Introducing a Homogeneously Distributed Electron Acceptor into the Polyimide Matrix

To increase the sorption component of the separation factor, homogeneously distributed tetracyanoethylene, a strong electron acceptor having high affinity for electron donors, was added to the polyimide matrix [77]. It can be seen from data presented in Table 9.12 that this is accompanied by an increase in the sorption component  $\beta_S$  (benzene/cyclohexane) by a factor of 1.5 probably as a result of selective sorption of aromatic compounds by tetracyanoethylene with a simultaneous increase in the diffusion component  $\beta_D$ . The prepared membranes showed good pervaporation properties with respect to benzene/cyclohexane, toluene/isooctane mixtures. For example, for a two-component 50/50 wt% benzene/cyclohexane mixture at 343 K, the flux was  $Q = 0.44$  kg  $\mu\text{m}^2$  h, and  $\beta_P$  (benzene/cyclohexane) = 48; and for a two-component toluene/isooctane mixture, 45/55 wt%, at 343 K the flux was  $Q = 1.1$  kg  $\mu\text{m}^2$  h, and  $\beta_P$  (toluene/*iso*-octane) = 330.

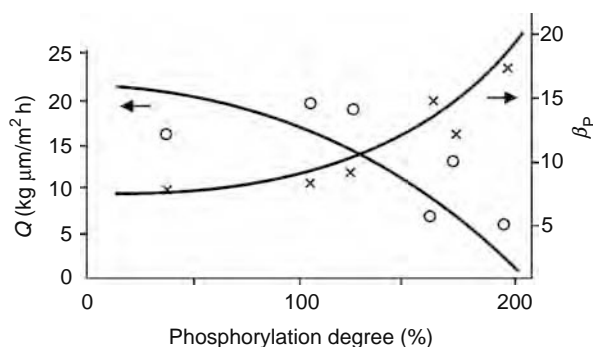


**FIGURE 9.28** Dependence of productivity for the mixture (O) and separation factor of benzene/cyclohexane  $\beta_P(x)$  on degree of phosphorylation for phosphorylated and thermally cross-linked BPDA-TrMPD polyimides: benzene/cyclohexane, 50/50 wt% mixture,  $T = 343$  K, membrane thickness 30–40  $\mu\text{m}$ . (From analysis of data presented in Semenova, S.I., *J. Membr. Sci.*, 231, 189, 2004. With permission.)

#### 9.4.2.3.2 Increasing the Sorption Component of the Separation Factor by Introducing $\pi$ -Electron Acceptor Groups into the Polymer

**Ethynyl Groups:** According to Ref. [77], acetylene fragments introduced into polyimides, e.g., 2,2'-diethynylbenzidine, DEB, have  $\pi$ -electron affinity for aromatic compounds. It can be seen from the data presented in Table 9.12 that the increase in the content of DEB component results in an increase in the separation factor of the benzene/cyclohexane mixture. This is probably caused not only by the growth of the diffusion component  $\beta_D$  (resulting from thermal cross-linking through the unsaturated bonds) but also by enhancement of the sorption component  $\beta_S$ .

**Phosphorylate Groups:** Phosphorylate (phosphonate ester)- $\text{P}(\text{OC}_2\text{H}_5)_2 = \text{O}$  groups have high affinity for aromatic compounds [11,80,81,109]. It is known, e.g., that polymers with such groups are soluble in aromatic, but insoluble in aliphatic, hydrocarbons. Cabasso [80] reported good separation properties of polystyrene diethylphosphate for mixtures of aromatic, alicyclic, and aliphatic hydrocarbons. The separation factor of such membranes was  $\beta_P$  (benzene/cyclohexane) = 12–40 (50/50 wt% mixture, 351 K), and dependence of  $\beta_P$  on the degree of phosphorylation was observed. Ref. [11] deals with membranes based on glassy polymers such as BPDA-TrMPD polyimide, polystyrene, polyphenylene oxide, into whose molecules pendant phosphorylate groups were introduced by chemical modification (treatment with methylbromide followed by phosphorylation resulting from reaction with triethylphosphite). The degree of phosphorylation was up to 200%, i.e., up to two phosphorylate groups per recurrent unit of the polymer. Phosphorylated polyimide membranes were cross-linked thermally and then chemically with diamine. Sorption properties of the prepared polymers, as well as their pervaporation properties for separation of benzene/cyclohexane, benzene/hexane mixtures, were investigated. It has been established that pervaporation properties of modified polyimides depend on the degree of phosphorylation as well as on their degree of cross-linking. The increase in degree of phosphorylation is accompanied by an increase in the separation factor (see Figure 9.28). Compared to the original polyimide, the modified polyimide offers much better separation properties and higher stability to the feed mixture. High pervaporation selectivity of the modified polyimide is due to the presence of phosphorylate groups having high affinity for benzene. For the modified polyimide the sorption component of the separation factor for the benzene/cyclohexane mixture (at 343 K) was  $\beta_S = 6$ –9, whereas the diffusion component was only  $\beta_D = 2$ –3, and for the benzene/hexane mixture,  $\beta_D \approx 1$ . Pervaporation properties of membranes based on cross-linked phosphorylated polyimide are similar to those of membranes based on phosphorylated polystyrene and cellulose acetate.

Wang et al. [109] deal with pervaporation properties of cross-linked membranes of copoly(methacrylates) with pendant phosphate and carbamoylphosphonate groups with respect to aromatic/nonaromatic hydrocarbon mixtures. These groups have high affinity for aromatic hydrocarbons. The increase in the content of phosphorus in the polymer results in the growth of benzene sorption and of the sorption component of the separation factor (e.g., the content of phosphorus changed in the series  $0 < 8.6 < 9.6 < 10.2$  wt%, and the separation factor  $\beta_S$  changed accordingly:  $5 < 7.5 \approx 7.4 < 8.7$ ).

**Sulfone Groups:** It is known that sulfolanes are used for removal of aromatic components in petrochemical production processes. This prompted Hao et al. [10] to investigate sulphonyl-containing polyimides for pervaporation separation of aromatic and aliphatic hydrocarbons: DSDA-DDBT polyimide whose original acid component and original amine component both contained sulfone groups. DSDA-DDBT polyimide displays preferential sorption for aromatic, rather than aliphatic, penetrants. Thus, the amounts of sorbed benzene and toluene in this polyimide were 11 and 15 g, respectively, per 100 g of dry polymer, while the amount of sorbed aliphatic compounds was much lower. The investigated hydrocarbons can be arranged by increasing boiling temperature  $T_b$  in the series:  $n$ -octane > *iso*-octane > toluene > cyclohexane > benzene >  $n$ -hexane (see Table 9.1). In the absence of specific interactions, the sorption of these hydrocarbons should have been arranged similarly. However, the experimental sorption data follow a different series, beginning with aromatic penetrants: toluene > benzene >

*n*-hexane > *n*-octane > *iso*-octane > cyclohexane. This effect can be attributed to selective sorption of aromatic penetrants by sulfone groups. At 351 K, the content of benzene or toluene in the feed flow of the benzene (toluene)/cyclohexane mixture of 60/40 wt%, membrane flux was  $Q = 0.93 \text{ kg } \mu\text{m}^2/\text{h}$ , and the separation factor was  $\beta_P$  (benzene/cyclohexane) = 32; for toluene/*iso*-octane mixtures  $Q = 2.8 \text{ kg } \mu\text{m}^2/\text{h}$ ,  $\beta_P$  (toluene/*isooctane*) = 113.

*Acrylate Groups*: Wang et al. [82] prepared new membranes for separation of aromatic and aliphatic hydrocarbons mixtures by pervaporation. A porous film based on high-density polyethylene was used as support, onto which glycidinemethacrylate, having high affinity for aromatic penetrants, was grafted using various plasma treatment techniques. The prepared membranes displayed good separation properties: permeation flux was 0.30–0.37  $\text{kg}/\text{m}^2 \text{ h}$  and separation factor  $\beta_P$  (benzene/cyclohexane) was 19–22, for a 70/30 wt% composition of the mixture, at 344 K.

*Phenyl Groups*: Styrene has high affinity for aromatic compounds. However, membranes based on polystyrene cannot be used for separation of aromatic and nonaromatic hydrocarbons in practice; because good sorption of aromatic penetrants (much better than that of aliphatic ones) was accompanied by severe swelling with a consequent decrease in diffusion selectivity. It was proposed in Ref. [78] to use membranes prepared by emulsion polymerization of styrene and acrylic acid for separation of the benzene/cyclohexane mixture. The polymer in the disperse phase of the emulsion (polystyrene) swells well in the component being removed (benzene), whereas the polymer in the dispersion medium (acrylic acid which does not swell in either component) restricts membrane swelling and ensures a high separation factor. The flux through these membranes was  $Q = 450\text{--}800 \text{ g}/\text{m}^2 \text{ h}$ , with separation factor,  $\beta_P = 1.7\text{--}9.6$ , and its sorption component  $\beta_S = 1.10\text{--}1.35$  (50/50 wt% benzene/cyclohexane mixture, at 293 K). Reduction of the content of benzene in the feed mixture results in reduction of the flux through the membrane and a significant increase in  $\beta_S$ . Thus, for the 10/90 wt% composition of the benzene/cyclohexane mixture  $\beta_S$  is 1.5–2.5. With the increase in temperature the permeation flux increases and the separation factor decreases.

*Carboxylic Groups*: Pervaporation separation of toluene/*i*-octane mixtures using copolyimide membranes containing 3,5-diaminobenzoic acid (DABA) was investigated in Ref. [128]. It was established that introduction of diaminobenzoic acid into the 6FDA-TrMPD polyimide improves membrane selectivity. The sorption component of the separation factor  $\beta_S$  is linearly correlated with the membrane solubility parameter and with DABA content in the copolymer ( $\beta_S = 3.2, 3.3, 4.3, 5.2$  for DABA contents 0%, 10%, 33%, 60%, respectively).

*Carbon Graphite-Filled Membranes*: An attempt is made in Ref. [93] to improve pervaporation properties of membranes for selective separation of benzene/cyclohexane mixtures by exploiting  $\pi$ -interaction of the membrane and benzene. Carbon graphite was expected to show affinity for aromatics by using  $\pi$ -electron interaction. Novel membranes for pervaporation were prepared from carbon graphite and nylon. Benzene permeated preferentially over cyclohexane and the separation factor was  $\beta_P = 435$ ,  $\beta_S = 48$ , and  $\beta_D = 9.1$  at the weight fraction of benzene in the feed of 0.1. The sorption experiments made it clear that the introduction of carbon graphite into nylon enhances the solubility selectivity toward benzene and as a result, benzene preferentially permeated through the composite membranes.

The dependence of the aromatics/paraffin (or alicyclic hydrocarbon) separation factor on the activity of the hydrocarbon component being separated is not considered in detail in this chapter. This dependence can be non-monotonic as a result of membrane swelling. This issue deserves separate consideration. It should only be pointed out that such regularities are similar to those observed in hydrophilic membranes in selective separation of water from organics to water mixtures. The separation factor of hydrophilic membranes is strongly dependent on water activity in the feed mixture, and this dependence can be non-monotonic as a result of membrane swelling [55].

Thus, summarizing the above information, the following conclusion can be made. Selective separation of olefins and aromatic compounds from their mixtures with paraffins and alicyclic hydrocarbons can be quite effectively implemented using membranes based on rigid-chain glassy polymers, whose permselectivity is dominated by the diffusion component. Especially promising materials are polyimides with bulky substituents in both acid and amine fragments. Permselectivity of membranes with respect to olefins and aromatic compounds, whose molecules contain  $\pi$ -electron bonds (unsaturated bonds in olefins and delocalized  $\pi$ -bonds in aromatics) can be significantly improved by introduction into the polymer matrix of active groups with  $\pi$ -electron affinity having specific interactions with these bonds.

## 9.5 INDUSTRIAL REMOVAL OF HYDROCARBONS FROM THEIR MIXTURES WITH VARIOUS GASES AND VAPORS

Many industrial processes where hydrocarbons are used generate off gases containing vapors of hydrocarbons such as gasoline, naphtha, fuel, and solvents. If they are separated from the generated mixtures, these products constitute valuable chemical feedstock or fuel. However, if they are not separated, they become a source of environmental contamination.

Industrial separation of hydrocarbons from their mixtures with various gases, including air, is a specific case of a more general objective, separation of organic vapors from various gas/vapor mixtures. Early commercial vapor/gas membrane separation plants installed by Nitto Denko, MTR, GKSS were put into operation in 1988–1990. During the last 20 years, sales

of membrane gas separation equipment have been growing to become a \$150 million per year business. More than 90% of this business involves the separation of noncondensable gases (nitrogen from air, carbon dioxide from methane, hydrogen from nitrogen or methane, etc.). However, a much larger potential market for membrane gas separation is to be found in separating mixtures containing condensable gases such as the  $C_{3+}$  hydrocarbons [17,138,139].

To separate hydrocarbons from their mixtures with air, various process systems involving membranes are used. The choice of a particular setup is governed by its economic sensibility. To implement the technology:

- One- or two-stage process of membrane separation of hydrocarbons is used.
- Feed flow to be processed in the membrane unit is pressurized and vacuum is created downstream (on the permeate side).
- Combination of sorption, condensation, and membrane separation methods is used. Various sequences of these methods in the flowchart can be used according to the specific objective.

For example, the following sequence is typically used to separate gasoline vapors from a gasoline/air mixture [140]. A mixture of air and gasoline vapor, e.g., 40 vol%, is compressed to hundreds of millimeters of water and fed to the membrane unit. The downstream pressure is maintained by a vacuum pump at 60–100 torr. If the retentate contains <5 vol% gasoline, it is discharged into the atmosphere. The enriched permeate is fed to the absorber, where gasoline vapor is absorbed by a solvent, e.g., liquid gasoline, since absorption of gasoline vapor consisting of multicomponent mixtures of  $C_3$ – $C_7$  hydrocarbons by fresh liquid gasoline is quite effective. The resultant solution is reused in the process.

The problem of separating vapors of hydrocarbons with air occurs in treatment and transportation of oil products, in particular during filling gasoline to vehicles' tanks at filling stations, filling oil products to railroad tank cars and sea-going tankers. In all said cases there is huge loss of hydrocarbon vapors. For example, during a vehicle's filling the losses of evaporating gasoline are between 0.1% and 1%.

Losses of oil products during tank filling, storage, and vehicle refueling at gas stations can result from evaporations, spills, and spoilage. At gas stations, large volumes of oil products are typically discharged in small doses generating considerable evaporation losses. Evaporation losses can amount to 75%–80% of the total losses. Evaporation losses are caused by inadequate sealing of the process equipment, tanks and vehicles, as well as negligent handling. Gasoline has the highest evaporation losses compared to any other oil products because of higher vapor activity.

Two gasoline vapor recovery systems have been developed by GKSS to reduce gasoline vapor losses at gas stations: balance and vacuum systems [39–43,141]. The balance system has a mouth piece for gasoline discharge or intake, covered by a flexible hose. As a result, the connection between the fitting and filling pump is securely sealed. When the fuel is discharged to the tank of a vehicle, excess pressure is generated in it, pushing hydrocarbon vapors out. Negative pressure sucks the vapor into the empty area of an underground storage tank wherefrom gasoline is discharged. However, this process is difficult to control and therefore not always easy to implement. Efficiency of vapor recovery is about 70%–80% depending on the vehicle's make. The vacuum system is more efficient. Its efficiency can be as high as 99%. To return the hydrocarbon vapor to the storage tank special fittings are used on the device that fills the vehicle tank and meters the fuel feed. At a certain moment the vacuum pump of the membrane module is actuated. As a result of vacuum build-up the air valve in the return line is opened, producing excess pressure and creating feed flow to the membrane surface in the membrane module. Hydrocarbon vapors penetrate through the membrane and return to the storage tank. Exhausted hydrocarbon flow is discharged into the atmosphere.

The systems designed to reduce emissions during car refueling are commercialized under trade names VACONOVENT (supplier Borsig Membrane Gas Processing, Germany) and Permeator (supplier ARID Technologies, USA). More than 130 units have been installed worldwide. Test runs at a gas station in California showed a reduction of gasoline losses of 1,000 gal per month at monthly sales of 330,000 gal of gasoline (approximately 0.3%). Under more severe conditions at a demonstration unit in Shanghai, reduction of losses was 0.6% [141].

There are lots of gas, gas-condensate, and oil fields where the content of heavy fractions of hydrocarbons is quite high. Separation of heavy fractions of hydrocarbons at these fields not only facilitates their subsequent processing but also reduces the dew point, improving reliability, effectiveness, and safety of natural gas transportation to the consumer. Raw gas is usually almost saturated with respect to the heavy fractions of hydrocarbons and water vapor, which will condense at cold spots in the pipeline. To avoid condensation, the dew point of the gas is usually lowered to about  $-20^{\circ}\text{C}$  before being fed to the pipeline by removing propane, butane, and higher hydrocarbons. After compression and cooling to about  $30^{\circ}\text{C}$  by an air cooler, a portion of the water and  $C_{3+}$  hydrocarbons is condensed and recovered. The off-gas from the condenser is then processed using a silicone rubber membrane that preferentially lets through condensable vapors such as  $C_{3+}$  hydrocarbons and retains methane and ethane. The heavy hydrocarbons and the water-rich gas that permeate through the membrane are recycled to the front of the feed gas compressor. Water and  $C_{3+}$  hydrocarbons are eventually removed as condensed liquids. This process is at an early stage of commercialization [138,139]. The future growth of membrane gas separation technology will be in the refinery, petrochemical, and natural gas industries. Very large, untapped opportunities exist for membranes in all of these industries, and despite past failures, acceptance of membrane technology is increasing.

One of the most potentially successful and promising petrochemical applications is separation of the olefin/nitrogen mixture. In the process of polyolefin production, a mixture of olefin monomer (20%–50%) and nitrogen is formed. The compressed gas mixture is supplied to a condenser, where olefin portion is removed as a liquid. The remaining uncondensed olefin and nitrogen are separated in a membrane unit, which produces an olefin-enriched permeate and purified nitrogen stream (>98% nitrogen). The olefin-enriched permeate is recycled to the front of the compressor. The olefin liquid stream is upgraded in the monomer purification section of the plant and then recycled to the reactor [138,139].

Separation of mixtures of olefin vapors and paraffins should become a very promising market for membrane technologies. Mixtures of olefins and paraffins occur in several large-volume oil refining and organic synthesis processes, including the synthesis of polyethylene and polypropylene. For example, propane enters the process of polypropylene production as an impurity in the feed gas, which typically contains 99% propylene and about 1% propane. Unreacted propane builds up in the reactor to concentrations of 20–30 vol%. Propane build up is controlled by continually removing a fraction of the tank recycle stream as a purge, which is subsequently flared. Propane removal would significantly increase the output capacity of the polymerization process and the yield of the final product, polypropylene. This problem looks quite ripe for solution by membrane methods which would require the development of membranes offering propylene/propane selectivity of 3–5.

The separation of mixtures of aromatic, alicyclic, and aliphatic hydrocarbons, as well as their isomers, e.g., benzene and cyclohexane, toluene and iso-octane, isomers of xylene has an enormous potential market for membrane technologies. Membrane methods can be used, for example, in aromatic and alicyclic hydrocarbon production processes. Benzene is a component of all crude oils, it is present in the light oil recovered from coal carbonization gases. It is well known that benzene can be produced from toluene by transalkylation (toluene disproportionation), a process that also generates mixtures of xylenes. The production of benzene by reforming separation process is associated with the production of toluene and xylene (BTX plants). In the reforming separation process the aromatic fraction of crude oil is reformed catalytically to the BTX compounds being produced. Cyclohexane can be obtained by direct fractionation of crude gasoline cuts, by catalytic hydrogenation of benzene, and by distillation of naphtha. Separation of benzene and cyclohexane is a very important problem in the petrochemical industry. The unreacted benzene is present in the reactor's effluent stream and must be removed for pure cyclohexane recovery. Selective removal of aromatic components and separation of mixtures of hydrocarbons in all the above processes can be implemented by membrane methods.

By 2010, the total gas separation market is expected to be more than double to \$350 million and to double again by 2020 to \$760 million, an average growth rate of 7%–8% per year [138,139]. Much of this growth is to take place in new applications involving hydrocarbon vapors. Polymer membranes will undoubtedly be used to separate some of these gas mixtures, but new membranes ought to be made from new materials. In the last two decades thousands of new polymer materials were developed and their permeability with respect to various hydrocarbons was investigated. However, permeability and selectivity are only two of the criteria that must be met to produce a useful membrane. Others include the ability to form stable, thin, low-cost membranes that can be packaged into high-surface area modules. Successful industrial implementation of the above objectives would require further development of new polymer and hybrid membranes and membrane modules meeting all the above criteria.

## REFERENCES

1. Semenova SI. Membrane methods of hydrocarbon separation and removal: I. Statistical analysis of patent and periodical flows. *Membranes (in Russian)* 2001; 9: 3–19.
2. Semenova SI. Membrane methods of hydrocarbon separation and removal: II. Hydrocarbon separation and removal using glassy and rubbery polymer membranes. *Membranes (in Russian)* 2002; 13: 37–51.
3. Semenova SI. Membrane methods of hydrocarbon separation and removal: III. Hydrocarbon separation with using glassy polymer membranes. *Membranes (in Russian)* 2002; 14: 29–46.
4. Semenova SI. Polymer membranes for hydrocarbon separation and removal. *J Membr Sci* 2004; 231: 189–207.
5. Chalykh AE. *Diffusion in Polymer Systems*. Moscow: Khimiya, 1987 (in Russian).
6. Chalykh AE. A modern view on the diffusion in polymer systems. *Uspekhi khimii (in Russian)* 1988; 57(6): 903–928.
7. Semenova SI. Mass Transfer of Penetrants Specifically Interacting with Polymer Membranes. Dr. Sci. dissertation, Vladimir, Russia, 1997.
8. Semenova SI. Structure–property relationships of polyimides. Separation properties of polyimides. In: Ohya H, Kudryavtsev VV, and Semenova SI. *Polyimide Membranes*. Tokyo: Gordon & Breach Publishers and Kodansha, 1996: 83–241.
9. Tanaka K, Taguchi A, Hao J, Kita H, and Okamoto K. Permeation and separation properties of polyimide membranes to olefins and paraffins. *J Membr Sci* 1996; 121(2): 197–207.
10. Hao J, Tanaka K, Kita H, and Okamoto K. The pervaporation properties of sulfonyl containing membranes for aromatic/aliphatic hydrocarbon mixtures. *J Membr Sci* 1997; 132: 97–108.
11. Okamoto K, Wang H, Ijuin T, Fujiwara S, Tanaka K, and Kita H. Pervaporation of aromatic/non-aromatic hydrocarbon mixtures through crosslinked membranes of polyimide with pendant phosphonate ester groups. *J Membr Sci* 1999; 157: 97–105.

12. Hirschfelder JH, Curtiss CF, and Bird RB. *Molecular Theory of Gases and Liquids*. New York: Wiley, 1964.
13. Breck DW. *Zeolite Molecular Sieves: Structure, Chemistry and Use*. New York: Wiley, 1976.
14. Weast R, Ed., *Handbook of Chemistry and Physics*, 51st edition. The Chemical Rubber Corporation: Cleveland, OH, 1971.
15. Reid RC, Prausnitz JM, and Sherwood T. *The Properties of Gases and Liquids*, 3rd edition. New York: McGraw-Hill, 1977.
16. Dean JA, Ed., *Lange's Handbook of Chemistry*, 11th edition. New York: McGraw-Hill, 1973.
17. Baker RW and Wijmans JG. Membrane separation of organic vapors from gas streams. In: Paul D, Yampolskii Yu, Eds., *Polymeric Gas Separation Membranes*. Boca Raton: CRC Press, 1994; 353–397.
18. Lapkin AA, Roschupkina OP, and Ilinitich OM. Transport of C<sub>1</sub>–C<sub>3</sub> hydrocarbons in poly(phenylene oxides) membranes. *J Membr Sci* 1998; 141(2): 223–229.
19. Stern SA and Shiah SP. Solubility of inhalation anesthetics in various media. *New Correl Mol Pharmacol* 1981; 19(1): 56–61.
20. Shan VM, Hardy BJ, and Stern SA. Solubility of CO<sub>2</sub>, CH<sub>4</sub> and C<sub>3</sub>H<sub>8</sub> in silicon polymers. Effect of polymer side-chains. *J Polym Sci* 1986; B24(9): 2033–2047.
21. Koros WJ, Fleming GK, Jordan SM, Kim TH, and Hoehn HH. Polymeric membrane materials for solution–diffusion based permeation separations. *Prog Polym Sci* 1988; 13: 339–401.
22. Kim TH. *Gas Sorption and Permeation in a Series of Aromatic Polyimides*. PhD dissertation, University of Texas, Austin, 1988.
23. Hirose T, Mi Y, Stern SA, and Clair AK. The solubility of carbon dioxide and methane in polyimides at elevated pressures. *J Pol Sci* 1991; B29: 341–347.
24. Coleman MR and Koros WJ. The transport properties of polyimide isomers containing hexafluoroisopropylidene in the diamine residue. *J Polym Sci* 1994; B32: 1915–1926.
25. Prausnitz JM, Lichtenthaler RN, de Azevedo EG, Eds., *Polymers: solutions, blends, membranes and gels*. In: *Molecular Thermodynamic of Fluid-Phase Equilibria*, 3rd edition. Prentice-Hall, Int. Series in the Phys & Chem Eng Science, 1996; 417–505.
26. Flory PJ. Thermodynamics of high polymer solutions. *J Chem Phys* 1942; 10(1): 51–61.
27. Huggins ML. Theory of solution of high polymers. *J Amer Chem Soc* 1942; 64: 1712–1719.
28. Tager AA. *Physical Chemistry of Polymers*, Chapter 12. Moscow: Khimiya, 1978 (in Russian).
29. Pace RJ and Datyner A. Model of sorption of simple molecules in polymers. *J Polym Sci* 1980; B18(5): 1103–1124.
30. Pace RJ and Datyner A. The temperature dependence of Langmuir capacity factor in glassy polymers. *J Polym Sci* 1981; B19(10): 1657–1658.
31. Crank J and Park G, Ed., *Diffusion in Polymers*. London: Academic Press, 1968.
32. Okamoto K, Noborio K, Hao J, Tanaka K, and Kita H. Permeation and separation properties of polyimide membranes to 1,3-butadiene and *n*-butane. *J Membr Sci* 1997; 134: 171–179.
33. Kamiya Y, Terada K, Naito Y, and Wang JS. Sorption, diffusion, and partial molar volumes of C<sub>4</sub> hydrocarbons in rubbery polymers. *J Polym Sci* 1995; B33: 1663–1671.
34. Stern SA, Shah VM, and Hardy BJ. Structure–permeability relationships in silicone polymers. *J Polym Sci* 1987; B25: 1263–1298.
35. Shah VM, Hardy BJ, and Stern SA. Solubility of carbon dioxide, methane and propane in silicone polymers. Effect of polymer backbone chains. *J Polym Sci* 1993; B31: 313–317.
36. Stern SA and Trohalaki S. Gas diffusion in rubbery and glassy polymers. *ACS Symp Ser* 1990; 423: 22–59.
37. Stern SA. Polymers for gas separation: The next decade. *J Membr Sci* 1994; 94: 1–65.
38. Pinnau I and He Z. Pure- and mixed-gas permeation properties of polydimethylsiloxane for hydrocarbon/methane and hydrocarbon/hydrogen separation. *J Membr Sci* 2004; 244: 227–233.
39. Ohlrogge K, Brockmoeller J, Wind J, and Behling RD. Engineering aspects of the plant design to separate volatile hydrocarbons by vapor permeation. *Sep Sci Technol* 1993; 28(1–3): 227–240.
40. Ohlrogge K, Wind J, and Behling RD. Membrane processes in the chemical and petrochemical industry. *Erdoel Kohle Erdogas Petrochem* 1993; 46(9): 326–332.
41. Ohlrogge K, Peinemann KV, and Wind J. Separation of hydrocarbons from gas streams. Membranes proved successfully in the chemical and petrochemical industry. *Energy* 1993; 45(6): 29–35.
42. Ohlrogge K, Peinemann KV, and Wind J. *Kohlenwasserstoffe aus Gasstransmen abtrennen*. *GKSS Rept* 1994; E16: 1–7.
43. Ohlrogge K, Wind J, and Behling RD. Off-gas purification by means of membrane vapor separation systems. *Sep Sci Technol* 1995; 30(7–9): 1625–1638.
44. Sidorenko VM. Membrane Separation of Hydrocarbons of Oil and Natural Gases. PhD dissertation. Vladimir, NPO “Polimersintez”, 1991 (in Russian).
45. Semenova SI, Ohya H, and Smirnov SI. Physical transitions in polymers plasticized by interacting penetrant. *J Membr Sci* 1997; 136: 1–11.
46. Belyakov VK, Smirnov SI, Karachevtsev VG, Bondar VI, and Semenova SI. Baromechanical method of investigation of the state of polymers. *Vysokomolek Soed* 1980; A.22(9): 2149–2151.
47. Semenova SI, Belyakov VK, Smirnov SI, and Karachevtsev VG. Sorption and mechanical properties of polyamides in ammonia medium. In: *Transactions of the 3rd All-Union Conference on Membrane Methods of Separation of Mixtures*, Cherkassy: VNIIS, NIITEKhim, 1981:77–82 (in Russian).
48. Smirnov SI, Belyakov VK, Semenova SI, Karachevtsev VG, and Bondar VI. Mechanical properties of polymers in sulphur dioxide medium. In: *Transactions of the 3rd All-Union Conference on Membrane Methods of Separation of Mixtures*, Cherkassy: VNIIS, NIITEKhim, 1981: 85–89 (in Russian).
49. Semenova SI. Effect of Chemical Structure of Polyamides on Ammonia Mass Transfer Parameters. PhD dissertation, Vladimir, NPO “Polimersintez”, 1983 (in Russian).

50. Semenova SI, Smirnov SI, and Ohya H. Performances of glassy polymer membranes plasticized by interacting penetrants. *J Membr Sci* 2000; 172: 75–89.
51. Semenova SI, Smirnov SI, and Karachevtsev VG. On extreme dependence of selectivity coefficients on penetrant temperature and pressure. In: *Transactions of the 4th All-Union Conference on Membrane Methods of Separation of Mixtures*, M.: MKhTI, 1987; (3): 40–43 (in Russian).
52. Smirnov SI, Semenova SI, Belyakov VK, and Karachevtsev VG. Extreme and abnormal temperature dependencies of mass transfer coefficients of gases and vapors in polymers. *Vysokomol Soed* 1984; A26(4): 843–848.
53. Schultz J and Peinemann KV. Membranes for separation of higher hydrocarbons from methane. *J Membr Sci* 1996; 110: 37–45.
54. Nijhuis H, Mulder M, and Smolders C. Selection of elastomeric membranes for the removal of volatile organics from water. *J Appl Polym Sci* 1993; 47(12): 2227–2243.
55. Semenova SI, Ohya H, and Soontarapa K. Hydrophilic membranes for pervaporation: An analytical review. *Desalination* 1997; 110: 251–286.
56. Hu W, Adachi K, Matsumoto H, and Tanioka A. Transport and high-selectivity mechanisms of C<sub>4</sub> hydrocarbons through anhydrous Ag<sup>+</sup>-doped perfluorocarbon-type ion-exchange membranes. *J Chem Soc Faraday Trans* 1998; 94(5): 665–671.
57. Goering RM, Bowman CN, Koval CA, and Noble RD. Mechanisms of olefin transport through facilitated transport membranes. *Polym Mater Sci Eng* 1997; 77: 260–261.
58. Smith BD. Facilitated transport of sugars and amino acids through plasticized cellulose triacetate membranes. *Polym Mater Sci Eng* 1997; 77: 269–270.
59. Davis JC, Valus RJ, Eshraghi R, and Vilikoff AE. Facilitated transport membrane hybrid systems for olefin purification. *Separation Science and Technology* 1993; 28(1–3): 463–476.
60. Safarik DJ and Eldridge RB. Olefin/paraffin separation by reactive absorption: a review. *Ind Eng Chem Res* 1998; 37: 2571–2581.
61. Matsumoto H, Tanioka A, and Kawachi S. Effect of fixed charge groups and counter ions on the transport phenomena and paraffin and olefin across anhydrous negatively charged membranes. *J Colloid Interface Sci* 1998; 208: 310–318.
62. Sungpet A, Way JD, Thoen PM, and Dorgan JR. Reactive polymer membranes for ethylene/ethane separation. *J Membr Sci* 1997; 136: 111–120.
63. Goering RM, Bowman CN, Koval CA, Noble RD, and Williamson DL. Role of ion-exchange membrane morphology and sorption properties in facilitated transport di-olefin/mono-olefin separations. *J Membr Sci* 1998; 144: 133–143.
64. Van Zyl AJ and Kerres JA. Development of new ionomer blend membranes, their characterization and their application in the perstractive separation of alkene-alkane mixtures. II. Electrical and facilitated transport properties. *J Appl Pol Sci* 1999; 74: 422–427.
65. Yang JS and Hsiu GH. Swollen polymeric complex membranes for olefin-paraffin separation. *J Membr Sci* 1998; 138: 203–211.
66. Henley E and Santos M. Permeation of vapors through polymers at low temperatures and elevated pressure. *AIChEJ* 1967; 13: 1117–1125.
67. Ito A and Hwang S. Permeation of propene and propylene through cellulosic polymer membranes. *J Appl Polym Sci* 1989; 38: 483–490.
68. Sridhar S and Khan A. Simulation studies for the separation of propylene and propane by ethylcellulose membrane. *J Membr Sci* 1999; 159: 209–219.
69. Staudt-Bickel C and Koros WJ. Olefin/paraffin gas separation with 6FDA-based polyimide membranes. *J Membr Sci* 2000; 170: 205–214.
70. Shimazu A, Hachisuka H, and Ikeda K. Separation, dissolution and diffusion characteristics of olefins and paraffins using fluorine-containing polyimide membranes. *Kagaku Kogaku* 1996; 60(4): 262–263.
71. Ilinitch OM, Semin GL, Chertova MV, and Zamaraev KI. Novel polymeric membranes for separation of hydrocarbons. *J Membr Sci* 1992; 66(1): 1–8.
72. Chern RT, Koros WJ, Sanders ES, and Yui R. “Second component” effect in sorption and permeation of gases in glassy polymers. *J Membr Sci* 1983; 15: 157–169.
73. Raymond PC, Koros WJ, and Paul D. Comparison of mixed and pure gas permeation characteristics for CO<sub>2</sub> and CH<sub>4</sub> in copolymers and blends containing methyl ethacrylate units. *J Membr Sci* 1993; 77: 49–57.
74. Yoshino M, Nakamura S, Kita H, Okamoto K, Tanihara N, and Kusuki Y. Olefin/paraffin separation performance of asymmetric hollow fiber membrane of 6FDA/BPDA-DDBT copolyimide. *J Membr Sci* 2003; 212: 13–27.
75. Burns RL and Koros WJ. Defining the challenges for C<sub>3</sub>H<sub>6</sub>/C<sub>3</sub>H<sub>8</sub> separation using polymeric membranes. *J Membr Sci* 2003; 211: 299–309.
76. Chan SS, Chung TS, Liu Y, and Wang R. Gas and hydrocarbon (C<sub>2</sub> and C<sub>3</sub>) transport properties of copolyimides synthesized from 6FDA and 1,5-NDA (naphthalene)/Durene diamines. *J Membr Sci* 2003; 218: 235–245.
77. Fang J, Tanaka K, Kita H, and Okamoto K. Pervaporation properties of ethynyl-containing copolyimide membranes to aromatic/non-aromatic hydrocarbon mixtures. *Polymer* 1999; 40: 3051–3059.
78. Sun F and Ruckenstein E. Sorption and pervaporation of benzene-cyclohexane mixtures through composite membranes prepared via concentrated emulsion polymerization. *J Membr Sci* 1995; 99: 273–284.
79. Tsubouchi K and Yoshikawa M. Pervaporation separation of benzene/cyclohexane mixtures through polyamide-polyether block copolymer membranes. *Membrane (Maku)* 1998; 23(6): 322–326.
80. Cabasso I. Organic liquid mixtures separation by permselective polymer membranes. 1. Selection and characteristics of dense isotropic membranes employed in the pervaporation process. *Ind Eng Chem Prod Res Dev* 1983; 22: 313–319.
81. Acharya HR, Stern SA, Liu ZZ, and Cabasso I. Separation of liquid benzene/cyclohexane mixtures by perstraction and pervaporation. *J Membr Sci* 1988; 37: 205–212.

82. Wang H, Tanaka K, Kita H, and Okamoto K. Pervaporation of aromatic/non-aromatic hydrocarbon mixtures through plasma-grafted membranes. *J Membr Sci* 1999; 154: 221–228.
83. Smitha B, Suhanya D, Sridhar S, and Ramakrishna M. Separation of organic–organic mixtures by pervaporation. *J Membr Sci* 2004; 241: 1–21.
84. McCandless FP, Alzheimer DP, and Hartman RB. Solvent membrane separation of benzene and cyclohexane. *Ind Eng Chem Process Des Dev* 1974; 13: 310–315.
85. Terada T, Hohjoh T, Yoshimasu S, Ikemi IM, and Shinohara T. Separation of benzene/cyclohexane azeotropic mixture through polymeric membranes with microphase separated structures. *Polym J* 1982; 14(5): 347–353.
86. Suzuki F and Onozata K. Pervaporation of benzene-cyclohexane mixture by poly( $\gamma$ -methyl glutamate) membrane and synergetic effect of their mixture on diffusion rate. *J Appl Polym Sci* 1982; 27: 4229–4238.
87. Park CK, Lee MY, Oh B, and Choi MJ. Separation of benzene/cyclohexane by pervaporation through chelate poly(vinyl alcohol)/poly(allyl amine) blend membrane. *Polym Bull* 1994; 33: 591–595.
88. Ray SK, Sawant SB, Joshi JB, and Pangarkar VG. Development of new synthetic membranes for separation of benzene/cyclohexane mixtures by pervaporation: A solubility parameter approach. *Ind Eng Chem Res* 1997; 36: 5265–5275.
89. Yoshikawa M, Takeuchi S, and Kitao T. Pervaporation separation of benzene/cyclohexane mixtures with nylon-6-graft-poly(oxyethylene) membranes. *Die Angew Macromol Chem* 1997; 245: 193–202.
90. Inui K, Okumura H, Miyata T, and Uragami T. Permeation and separation of benzene/cyclohexane mixtures through cross-linked poly(alkyl methacrylate) membranes. *J Membr Sci* 1997; 132: 193–201.
91. Inui K, Tsukamoto K, Miyata T, and Uragami T. Permeation and separation of benzene/cyclohexane mixture through benzoylchitosan membranes. *J Membr Sci* 1998; 138: 67–77.
92. Kusakabe K, Seiki Y, and Morooka S. Separation of benzene/cyclohexane mixtures using polyurethane-silica hybrid membranes. *J Membr Sci* 1998; 149: 29–37.
93. Wang H, Lin X, Tanaka K, Kita H, and Okamoto K. Pervaporation of plasma-grafted polymer membranes and their morphology and pervaporation properties towards benzene/cyclohexane mixtures. *J Polym Sci* 1998; A36: 2247–2259.
94. Inui K, Noguchi K, Miyata T, and Uragami T. Pervaporation characteristics of methyl methacrylate-methacrylic acid copolymer membranes ionically crosslinked with metal ions for a benzene/cyclohexane mixture. *J Appl Polym Sci* 1999; 71: 233–241.
95. Sun YM, Chen YK, Wu CH, and Lin A. Pervaporation for the mixture of benzene/cyclohexane through poly-bisphenoxy phosphazene membranes. *AIChE J* 1999; 45(3): 523–534.
96. Yoshikawa M, Shimada H, Tsubouchi K, and Kondo Y. Specialty polymeric membranes. 12. Pervaporation of benzene/cyclohexane mixtures through carbon graphite-nylon 6 composite membranes. *J Membr Sci* 2000; 177: 49–53.
97. Wang YC, Li CL, Huang J, Lin C, Lee KR, Liaw DJ, and Lai JY. Pervaporation of benzene/cyclohexane mixtures through aromatic polyimide membranes. *J Membr Sci* 2001; 185: 193–200.
98. Kao ST, Wang FG, and Lue SJ. Sorption, diffusion and pervaporation of benzene/cyclohexane mixtures on silver-Nafion membranes. *Desalination* 2002; 149: 35–40.
99. Sarkhel D, Roy D, Bandyopadhyay M, and Battacharya P. Studies on separation characteristics and pseudo-equilibrium relationship in pervaporation of benzene/cyclohexane through composite polyvinyl alcohol membranes with polyacrylonitrile supports. *Sep Purif Technol* 2003; 30: 89–96.
100. Yamazaki A and Mizoguchi K. Pervaporation of benzene/cyclohexane and benzene/*n*-hexane mixtures through polyvinyl alcohol membranes. *J Appl Polym Sci* 1997; 64: 1061–1065.
101. Villaluenga JPG and Tabe-Mahammadi A. A review on the separation of benzene/cyclohexane mixtures by pervaporation processes. *J Membr Sci* 2000; 169: 159–174.
102. Huang RYM and Lin VJC. Separation of liquid mixtures by using polymer membranes. I. Permeation of binary organic liquid mixtures through polyethylene. *J Appl Polym Sci* 1968; 12: 2615–2623.
103. Inui K, Okumura H, Miyata T, and Uragami T. Characteristics of permeation and separation of dimethyl acrylamide-methyl methacrylate random and graft copolymer membranes for a benzene/cyclohexane mixture. *Polym Bull* 1997; 39: 733–740.
104. Yamasaki A, Shinbo T, and Mizoguchi K. Pervaporation properties of benzene/cyclohexane and benzene/*n*-hexane mixtures through PVA membrane. *J Appl Polym Sci* 1997; 64: 1061–1065.
105. Inui K, Miyata T, and Uragami T. Permeation and separation of benzene/cyclohexane mixtures through liquid crystalline polymer membranes. *J Polym Sci* 1997; B35: 699–705.
106. Sakohara S, Koshi T, and Asaeda M. Separation of benzene/cyclohexane mixtures by dimethylaminoethyl methacrylate gel membranes formed in pores of a thin silica membrane. *Kobunshi Ronbunshu* 1995; 52: 155–162.
107. Ruckenstein E. Emulsion pathways to composite polymeric membranes for separation processes. *Colloid Polym Sci* 1989; 267: 792–797.
108. Park JS and Ruckenstein E. Selective permeation through hydrophobic–hydrophilic membranes. *J Appl Pol Sci* 1989; 38: 453–461.
109. Wang Y, Hirakawa S, Wang H, Tanaka K, Kita H, and Okamoto K. Pervaporation properties to aromatic/non-aromatic hydrocarbon mixtures of cross-linked membranes of copoly(methacrylates) with pendant phosphate and carbamoylphosphonate groups. *J Membr Sci* 2002; 199: 13–27.
110. Cao B, Hinode H, and Kajiuchi T. Permeation and separation of styrene/ethylbenzene mixtures through cross-linked poly(hexamethylene sebacate) membranes. *J Membr Sci* 1999; 156: 43–47.
111. Kucharski M and Stelmazek J. Separation of liquid mixtures by permeation. *Int Chem Eng* 1967; 7: 618–622.
112. McCandless FP. Separation of aromatics and naphthalenes through modified vinylidene fluoride films. *Ind Eng Chem Process Des Dev* 1973; 12: 354–360.
113. Cabasso L, Jagur-Grodzinski L, and Vofsi D. A study of permeation of organic solvents through polymeric membranes based on polymeric alloys of polyphosphonate and acetyl cellulose. II. Separation of benzene. *J Appl Polym Sci* 1974; 18: 2137–2145.

114. Rautenbach R and Albrect R. Separation of organic binary mixtures by pervaporation. *J Membr Sci* 1980; 7: 203–223.
115. Larchet C, Brun JP, Bulvestre G, and Auclair B. Sorption and pervaporation of dilute aqueous solutions of organic compounds through polymer membranes. *J Membr Sci* 1985; 25: 55–100.
116. Yamaguchi T, Nakao S, and Kimura S. Plasma graft filling polymerization: Preparation of a new type of pervaporation membrane for organic liquid mixtures. *Macromolecules* 1991; 24: 5522–5527.
117. Tanihara N, Tanaka K, Kita H, and Okamoto K. Pervaporation of organic liquid mixtures through membranes of polyimides containing methyl-substituted phenylenediamine moieties. *J Membr Sci* 1994; 95: 161–169.
118. Tanihara N, Umeo N, Kawabata T, Tanaka K, Kita H, and Okamoto K. Pervaporation of organic liquid mixtures through poly(ether imide) segmented copolymer membranes. *J Membr Sci* 1995; 104: 181–192.
119. Liaw DJ and Wang KL. Synthesis and characterization of fluorine containing polyamide derivatives from 2,2-bis[4-(aminophenoxy) phenyl] hexafluoropropane by direct polymerization. *J Polym Sci* 1996; A34: 1209–1215.
120. Suzuki F, Onozato K, and Takahashi N. Pervaporation of thermal mixture of benzene/toluene by poly(ethylene terephthalate) membrane and synergetic effect on concentration dependence of diffusion rate. *J Appl Polym Sci* 1982; 27: 2179–2188.
121. Ho WS, Satori G, and Thaler WA. Polyimide/aliphatic polyester copolymers, US Patent 4,944,880, 1990.
122. Bing C, Hirofumi H, and Toshio K. Permeation and separation of styrene/ethylbenzene mixtures through cross-linked poly(hexamethylene sebacate) membranes. *J Membr Sci* 1999; 156: 43–47.
123. Roizard D, Nilly A, and Lochon P. Preparation and study of polyurethane films to fractionate toluene/*n*-heptane mixtures by pervaporation. *Sep Purif Technol* 2001; (22–23): 45–52.
124. Cao B and Henson MA. Modeling of spiral wound pervaporation modules with application to the separation of styrene/ethylbenzene mixtures. *J Membr Sci* 2002; 197: 117–146.
125. Cunha VS, Pareds MLL, Borges CP, Habert AC, and Nobrega R. Removal of aromatics from multicomponent organic mixtures by pervaporation using polyurethane membranes: experimental and modeling. *J Membr Sci* 2002; 206: 277–290.
126. Matsui S and Paul DR. Pervaporation separation of aromatic/aliphatic hydrocarbons by crosslinked poly(methyl acrylate-co-acrylic acid) membranes. *J Membr Sci* 2002; 195: 229–245.
127. Matsui S and Paul DR. Pervaporation separation of aromatic/aliphatic hydrocarbons by a series of ionically crosslinked poly(*n*-alkyl acrylate) membranes. *J Membr Sci* 2003; 213: 67–83.
128. Xu W, Paul DR, and Koros WJ. Carboxylic acid containing polyimides for pervaporation separations of toluene/iso-octane mixtures. *J Membr Sci* 2003; 219: 89–102.
129. Frahn J, Malsch G, Matsuschewski A, Schedler U, and Schwarz HH. Separation of aromatic/aliphatic hydrocarbons by photo-modified poly(acrylonitrile) membranes. *J Membr Sci* 2004; 234: 55–65.
130. Mulder MHV, Kruit F, and Smolders CA. Separation of isomeric xylenes by pervaporation through cellulose ester membranes. *J Membr Sci* 1982; 11: 349–360.
131. McCandless FP and Downs WB. Separation of the C<sub>8</sub> aromatic isomers by pervaporation through commercial polymer films. *J Membr Sci* 1987; 30: 111–120.
132. Wessling M, Werner U, and Huang ST. Pervaporation of C<sub>8</sub> isomers. *J Membr Sci* 1991; 57: 257–270.
133. Wytcherly RW and McCandless FP. The separation of meta- and para-xylene by pervaporation in the presence of CBr<sub>4</sub>, a selective feed-complexing agent. *J Membr Sci* 1992; 67: 67–75.
134. Miyata T, Tooru I, and Uragami T. Characteristics of permeation and separation of propanol isomers through polyvinyl alcohol membranes containing cyclodextrin. *J Appl Polym Sci* 1994; 51: 2007–2014.
135. Chen HL, Wu LG, Tan J, and Zhu CL. Polyvinyl alcohol membrane filled β-cyclodextrin for separation of isomeric xylenes by pervaporation. *Chem Eng J* 2000; 78: 159–164.
136. Schleiffelder M and Claudia SB. Crosslinkable copolyimides for the membrane-based separation of *p*-/*o*-xylene mixtures. *React Funct Polym* 2001; 49: 205–213.
137. Jonquieres A, Clement R, Lochon P, Neel J, Dresch M, and Chretien B. Industrial state-of-the-art of pervaporation and vapor permeation in western countries. *J Membr Sci* 2002; 206: 87–117.
138. Baker RW. Membrane technology: Retrospective view and lessons for future. Plenum lecture on ICOM'2002, Toulouse, July 6–12, 2002.
139. Baker RW. *Membrane Technology and Applications*. New York: McGraw-Hill, 2000.
140. Nakagawa K. Removing of hydrocarbons from air: Industrial application in Japan. In: Paul DR, Yampol'skii Yu, Eds. *Polymeric Gas Separation Membranes*. Boca Raton, FL: CRC Press, 1994: 433–455.
141. <http://www.ARIDtech.com>; <http://www.borsig.de> (accessed November 2004).

---

# 10 Zeolite Membranes: Synthesis, Characterization, Important Applications, and Recent Advances

*M. Arruebo, R. Mallada, and M.P. Pina*

## CONTENTS

10.1	Introduction .....	270
10.2	Membrane Synthesis and Characterization .....	270
10.2.1	Synthesis Methods .....	274
10.2.1.1	In Situ Hydrothermal Synthesis Methods .....	274
10.2.1.2	Ex Situ Hydrothermal Synthesis or Secondary Growth Methods .....	274
10.2.2	Pre- and Posttreatments to Enhance Membrane Quality .....	277
10.2.3	Increasing Membrane Area .....	277
10.3	New Zeolite-Like Microporous and Mesoporous Materials .....	278
10.4	Gas Separation: Fundamentals and Applications .....	278
10.4.1	Separation Mechanisms .....	279
10.4.1.1	Permeation of Individual Gases .....	280
10.4.1.2	Multicomponent Permeation .....	282
10.4.2	Applications .....	283
10.4.2.1	Separations Controlled by Sorption-Diffusion Mechanisms When Size Exclusion Occurs .....	284
10.4.2.2	Separations Based on Competitive Adsorption without Size Exclusion .....	285
10.5	Pervaporation .....	286
10.5.1	Pervaporation Mechanism in Zeolites .....	289
10.5.1.1	Adsorption: Hydrophobicity and Hydrophilicity .....	290
10.5.1.2	Diffusion .....	291
10.5.2	Applications .....	291
10.5.2.1	Alcohol Dehydration: Zeolite A .....	291
10.5.2.2	Alcohol Dehydration: Other Zeolites .....	293
10.5.2.3	Water Removal in Acid Solutions .....	293
10.5.2.4	Organic Dehydration .....	294
10.5.2.5	Removal of Organics from Water .....	294
10.5.2.6	Organic Separations .....	295
10.6	Zeolite-Membrane Reactors .....	295
10.6.1	General Considerations on Inorganic Membrane Reactors .....	296
10.6.2	Traditional Applications of Zeolite-Membrane Reactors .....	297
10.6.2.1	Zeolite-Membrane Reactors for Conversion Enhancement by Product Removal .....	298
10.6.2.2	Zeolite-Membrane Reactors for Conversion Enhancement by Removal of Catalyst Poisons/Inhibitors .....	300
10.6.2.3	Zeolite-Membrane Reactors as Reactant Distributors for Selectivity Enhancement .....	301
10.6.2.4	Zeolite-Membrane Reactors for Selectivity Enhancement by Control of Reactant Traffic: A Not-So-Classic Application .....	301
10.6.3	Catalytic Zeolite-Membrane Reactors .....	303
10.6.3.1	Catalytic Zeolite-Membrane Reactors for Selectivity Enhancement by Control of Residence Time .....	303
10.6.3.2	Catalytic Zeolite-Membrane Reactors in the Fine Chemicals Industry .....	305

10.6.4	Alternative Supports and Configurations for Zeolite-Membrane Reactors.....	306
10.6.5	Industrial Applications of Zeolite-Membrane Reactors .....	308
10.6.6	New Applications of Zeolite-Membrane Reactors: Microchemical Systems .....	309
10.6.6.1	Zeolite-Based Microreactors and Microseparators .....	309
10.6.6.2	Zeolite-Based Microsensors.....	310
10.7	Conclusions.....	312
	Acknowledgments.....	313
	References.....	313

## 10.1 INTRODUCTION

Various improvements have broadened the research in the field of zeolite membranes and films, such as the development of new synthesis procedures, the use of new supports with specific characteristics (monoliths, foams, etc.) or the use of modified supports by means of masking or grafting techniques, the application of new analytical techniques (isotopic-transient experiments, permoporometry, etc.), the control of the orientation of the crystals (by means of covalent linkages, synthesis conditions, etc.) and of the thickness of the membranes, and the preparation of new zeolites as membranes or new zeolite related-materials. In addition, a variety of zeolites can now be prepared as colloidal systems with particle dimensions ranging from tens to a few hundred nanometers.

Hence, their application field is not only restricted to use in gas separation, pervaporation, and membrane reactors but also applicable in microscale devices (microreactors and microseparators) and for the preparation of functional materials (adsorbents for trace removal, controlled release capsules, and chemical sensors).

This chapter gives an overview of the synthesis procedures and applications of zeolite membranes (gas separation, pervaporation, zeolite-membrane reactors), as well as new emerging applications in the micro- and nanotechnology field. Related areas such as new zeolite and zeolite-related materials for membranes, alternative supports, and scale-up issues are also discussed.

## 10.2 MEMBRANE SYNTHESIS AND CHARACTERIZATION

The term *zeolites* designates a variety of crystalline, hydrated aluminosilicates with a framework structure, which have been used for a long time as detergent builders (in view of their ion-exchange properties), adsorbents, and catalysts. However, since the early 1990s, an intensive research effort has been under way, aimed to the synthesis of zeolite membranes and to the development of separation applications, as is evidenced by large number of reviews recently published [1–6]. Among the 161 framework type codes assigned to date, by the International Zeolite Structure Commission, the most studied structures are MFI, LTA, FAU, MOR, and BEA.

Besides polymer-zeolite composites prepared by embedding zeolite crystals into a polymeric matrix (linked by means of interactions van der Waals or hydrogen bonds or by covalent linkages) and free-standing zeolite films (on temporal supports), the most common and industrially developed zeolite membranes are supported. The porous support introduces mechanical strength to the resulting membrane and allows the development of more extensive structures. Despite the clear advantage of supported zeolite membranes, there are three major disadvantages of using supports in the synthesis of zeolite membranes that make synthesis more difficult to reproduce: the support provides nucleation sites that are not present during homogeneous synthesis in the gel; the support itself can partially dissolve in the synthesis gel and change its composition; also, some components of the support can diffuse into the zeolite layer during calcination step at high temperature [7], and finally, the support imposes spatial constraints on crystal growth and adds a restriction to the nutrients diffusion due to its porosity and tortuosity and because, in some cases, the flux of strong adsorbing compounds can be decreased greatly by the support [8]. Therefore, synthesis inside the support pores may take place with a composition different from that of the bulk liquid.

Different supports are used, (see Section 10.6.4) with different geometry (discs or tubes), thickness, porosity, tortuosity, composition (alumina, stainless steel, silicon carbide, mullite, zirconia, titania, etc.), and symmetry or asymmetry in its structure. Tubular supports are preferable compared to flat supports because they are easier to scale-up (implemented as multichannel modules). However, in laboratory-scale synthesis, it is usually found that making good quality zeolite membranes on a tubular support is more difficult than on a porous plate. One obvious reason is the fact that the area is usually smaller in flat supports, which decreases the likelihood of defects. In Figure 10.1, two commercial tubular supports, one made of  $\alpha$ -alumina (left side) and the other of stainless steel (right side) used in zeolite membrane synthesis, are shown. Both ends of the  $\alpha$ -alumina support are glazed and both ends of the stainless steel support are welded with nonporous stainless steel to assure a correct sealing in the membrane module and prevent gas bypass.

Ramsay and Kallus [9], as well as other authors [10,11] pointed out that the distribution of the zeolite within the support, i.e., the zeolite preferentially deposited inside the porous structure of the support or the zeolite material as a thin layer on top of



**FIGURE 10.1** Commercial  $\alpha$ -alumina and stainless steel supports.

the porous support, apart from influencing its mechanical strength and defect properties of the membrane, may also cause differences in gas separation behavior.

Supported zeolite membranes have been prepared using numerous procedures [4] such as alignment of crystals in electrical fields, electroplating, self-assembly, growth on organic molecular layers, covalent linkages, hydrothermal synthesis (in situ and ex situ), hydrothermal method microwave heating assisted, dry gel method (vapor-phase transport method and steam-assisted crystallization), synthesis at the interface between two fluid phases, etc.

Typically, a zeolite membrane is synthesized by heating in an autoclave under autogenous pressure, an alkaline reaction mixture containing the silica or aluminum sources, water, and in some cases, a template or organic additive (structure-directing agent) and optionally, a metal ion. The replacement of  $\text{OH}^-$  for  $\text{F}^-$  as a mineralizer agent makes possible to obtain zeolites at low pH values, and increases the organophilic character of the resulting zeolite membrane. Most of the synthesis gels have a template in their composition; however, it is necessary to remove this structure-directing agent after synthesis to render the microporous framework. The template is trapped within the growing zeolite framework. An oxidation procedure at a high temperature is the most common method used for template removal from zeolites. Though, due to the different expansion thermal coefficient of zeolites and supports and due to the changes in lattice parameters of the zeolite crystals as a result of the removal, cracks and pinholes appear after calcination. Different techniques have been used to minimize that inconvenience such as synthesis without template, calcination with slow heating and cooling rates (there is controversy in this aspect [12]), calcination at low temperatures in ozone atmosphere [13], UV irradiation with ozone [14], removal of the template by means of extraction [15], and so on.

During the hydrothermal synthesis, different variables affect the quality and purity of the resulting membrane, such as support influence (porosity, composition, structural symmetry, roughness, etc.), chemical gel composition of the precursor gel (ratio Si/OH, ratio Si/Al, Si/cation, Si/template, pH of the solution, etc.), ratio volume precursor gel/autoclave volume, synthesis time, synthesis temperature, aging of the precursor synthesis gel, heating procedure (convection, microwave, etc.), and contact configuration between the support and the precursor gel (static, rotatory, centrifuge, semi-continuous, etc.). In Figure 10.2 (right side) a commercial Parr autoclave used in membrane synthesis is shown. In Figure 10.2 (left side), there are shown two possible placements of the supports and the synthesis gel inside the autoclaves used in membrane synthesis. In the setup 1, shown on the left side, the synthesis takes place under continuous rotation to avoid gravitational crystallization effects and to achieve a more homogeneous deposition. The entire autoclave vessel is filled with the synthesis gel, and the membrane is formed on both sides of the support. In setup 2, the synthesis is static and only the inner part of the support is filled with the synthesis gel, hence, the layer is formed in the inner part of the tube. For the same precursor gel and hydrothermal synthesis conditions, each placement renders membranes with different zeolite material distribution and separation behavior [11].

To assess about the quality and purity of the synthesized membranes, several experimental techniques and procedures are available; many of those are commonly employed in catalyst characterization. Thus, XRD (x-ray diffraction) analysis of the supported samples is conventionally used to identify the type of zeolite, the proportion of amorphous material and impurities, and the preferential orientation of the crystals (XRD-pole figure). However, for the vast majority of the synthesis procedures described, the XRD spectra of the scrapped membrane or the resulting powder from the liquid phase is supplied to avoid the support contribution.

Figure 10.3a and 10.3b shows, respectively, the XRD spectra of a supported NaA zeolite membrane and of the resulting powder after filtering and drying of the liquid phase. Scanning electron microscopy (SEM) observations allow the evaluation of membrane thicknesses, shape, and size of the crystals, homogeneity and uniformity of the zeolite layer, and a first impression on the existence of intercrystalline defects. SEM-EDX (energy-dispersive x-ray analysis) can be used to measure qualitatively and quantitatively the atomic compositions of the zeolite membrane at different axial and longitudinal positions to check the

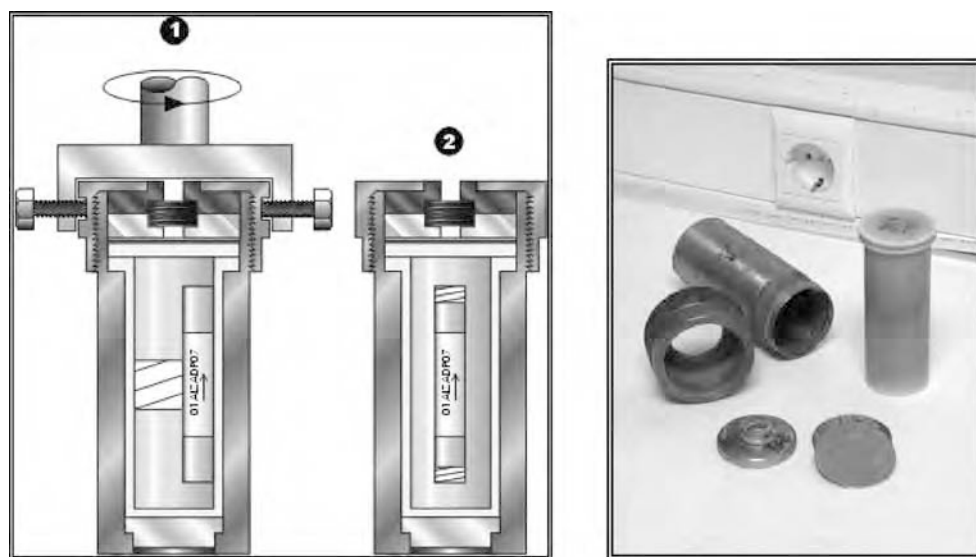


**FIGURE 10.2** Left: two different contact configurations between the support and the synthesis gel during hydrothermal synthesis. Right: Commercial autoclave from Parr Instrument Company (<http://www.parrinst.com/>).

continuity and thickness of the zeolite coating. Figure 10.4 shows the EDX mapping of the cross section of a cordierite ( $\text{Mg}_2\text{Al}_4\text{Si}_5\text{O}_{18}$ ) monolith coated with a mordenite layer ( $\text{Si}/\text{Al} = 10$ ). The different colors are related to the atomic distribution across the sample. The matching between Mg, green colored, inherent to the cordierite, and Si, blue colored, in which MOR is enriched, enables us to distinguish the zeolite distribution. At the same time, it can also be observed that traces of Mg are incorporated in the zeolite layer and to ascertain the penetration of the zeolitic material into the macroporous cordierite support.

XPS (*x*-ray photoelectron spectroscopy) utilizes photoionization and energy-disperse analysis of the emitted photoelectrons to study the composition and electronic state of a region of the surface of a zeolite. However, all these techniques are destructive ones, and for that reason other methods such as isotopic-transient experiments or reflectance [16] and fluorescence [17] imaging can be used to estimate the effective membrane thickness.

The lack of methods for a fast and reliable assessment of membrane quality is still one of the outstanding issues in zeolite membrane development. The usual meaning of the term “quality” relates to the ability of the membrane to carry out a given separation, therefore, is a system-specific property and the universal membrane quality test does not exist. In general, specific permeation measurements at different temperatures, either of single gases (or vapors) or of multicomponent mixtures in the gas or liquid (pervaporation) phase, provide extremely useful information on the effective pore structure of the membrane, on the

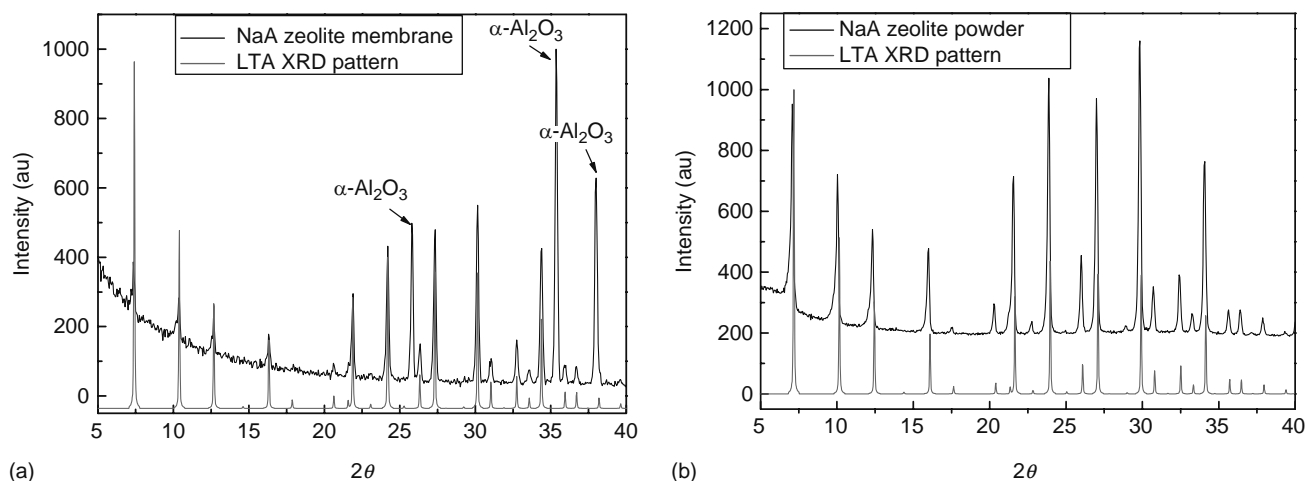


**FIGURE 10.3** (a) XRD spectra of an inner zeolite NaA membrane on  $\alpha$ -alumina support and (b) XRD spectra of the corresponding dry powder collected in the synthesis autoclave.

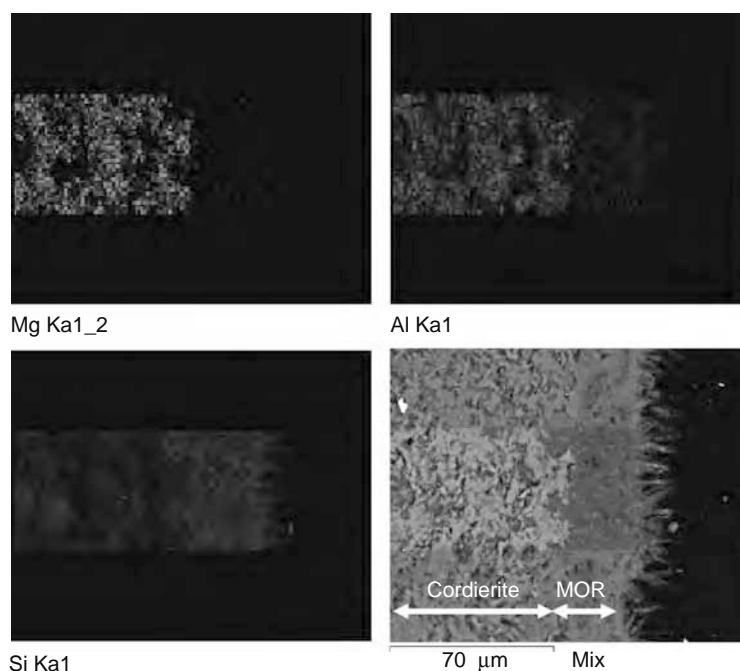


**FIGURE 10.4** (See color insert following page 588.) EDX mapping of the cross section of a cordierite ( $\text{Mg}_2\text{Al}_4\text{Si}_5\text{O}_{18}$ ) monolith coated with a mordenite layer ( $\text{Si}/\text{Al} = 10$ ).

existence of intercrystalline defects, and amorphous material, as well as information about the main transport controlling effect (adsorption or diffusion).

A battery of single-gas permeation experiments using molecules with different kinetic diameters could be used to gauge the effective pore size in defect-free membranes (see Figure 10.5). Usually, the kinetic diameter of the gases is calculated using the critical diameters or the Lennard-Jones kinetic gas theory, and the sizes of the zeolite channel are calculated using XRD data. However, as mentioned earlier, it is important to point out that molecules larger than the zeolite channel windows can absorb and diffuse to some extent, especially at high temperatures, because the zeolite framework is not a rigid structure.

Alternatively, selective blocking of membrane pores by condensing vapors combined with permeation measurements (permporometry) could be used to evaluate defects [18]. However, this method gives only pore sizes and does not consider other specific interactions between the membrane and the permeating molecules. Bernal et al. [19] have developed a fast and simple technique to assess membrane quality taking into account the nature (organophilic vs. hydrophilic) of the zeolite

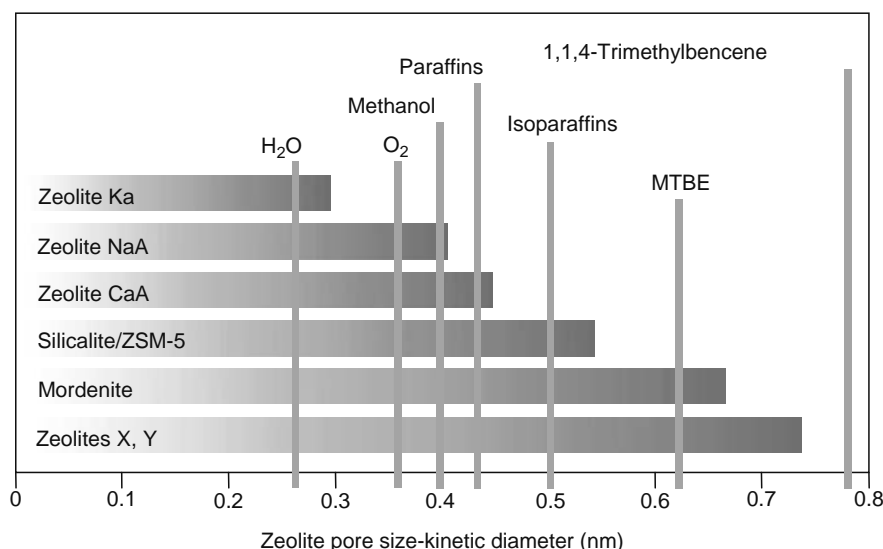


**FIGURE 10.5** Molecules admitted to zeolites according to molecular dimensions and zeolite aperture sizes.

and selecting adsorbate molecules accordingly. The working hypothesis is that specific interactions can be measured by the reduction in flux after exposing the membrane to an appropriate adsorbate or by the time required to reach steady state after exposure of the membrane to quasi-saturation conditions.

Permeation experiments are often complemented by adsorption measurements, which can help to explain the permeation mechanism observed. To this end, temperature-programmed adsorption/desorption experiments are employed, based on weight measurements (thermobalance), or on continuous gas analysis. It is important to ensure that the initial state of the membrane in adsorption experiments is reproducible, i.e., there is no unwanted material previously adsorbed on the membrane.

### 10.2.1 SYNTHESIS METHODS

A survey of recent literature on zeolite membrane preparation reveals that synthesis processes, even for well-known zeolite structures (i.e., MFI, LTA), are still carried out batchwise, using a hydrothermal route to produce a thin layer from hydrogels or sols containing the corresponding nutrients. As a general rule, the reactant mixture in contact with the support changes in composition with time provoking a reduction of the membrane quality.

The so-called dry gel method [20–22] is another alternative for membrane synthesis where vapors containing templates (i.e., amines) and water are employed to crystallize silica or silica–alumina layers previously deposited onto the support (vapor-phase transport method) or where steam is used to crystallize silica and template or silica–alumina and template dry layers previously deposited onto the support (steam-assisted crystallization). Using this approach, the reactant consumption is clearly diminished, an important issue for scale-up purposes; on the other hand, synthesis time is delayed due to transport-controlled phenomena.

Basically, the hydrothermal synthesis procedures used to prepare zeolite membranes can be classified in two general groups: ex situ and in situ methods, that is with and without a previous seeding step, which are briefly discussed below.

#### 10.2.1.1 In Situ Hydrothermal Synthesis Methods

Successful membrane formation in one-step (direct membrane synthesis) requires nucleation and growth of zeolite crystals on the support surface, a process that competes with solution events. Essentially, the as-received porous support is immersed in the liquid precursor gel, and the membrane is heated under autogenous pressure. Using this approach, the crystals grow in all directions, resulting membranes with random orientation in their crystals. However, it is possible, but not common, to obtain oriented membranes using in situ crystallization controlling the temperature, time, and the chemical nature and surface roughness of the substrate. As an example, Wang et al. [23] obtained *b*-oriented MFI zeolite membranes by in situ crystallization.

In situ crystallization shows three disadvantages, first, homogeneous nucleation cannot be avoided within the synthesis gel, second, the obtained membranes show random orientation in their crystals, and therefore, low permeances, and third, an excess of components is used during the synthesis. The great advantages of this synthesis procedure are its simplicity and that it is easy to suppress the defects by growing a thicker zeolite layer, where each new layer of crystals covers the defects in the previous layer. Figure 10.6 represents an H-ZSM-5 membrane obtained using direct in situ hydrothermal synthesis. The random orientation in the crystals is clearly observed.

#### 10.2.1.2 Ex Situ Hydrothermal Synthesis or Secondary Growth Methods

The most successful approach to control membrane formation involves segregation of the processes of crystal nucleation and growth [24]. The so-called ex situ or secondary (seeded) growth methods, unlike the direct synthesis procedures just discussed, include a first step in which a closely packed layer of colloidal zeolite crystals, synthesized homogeneously, is deposited onto

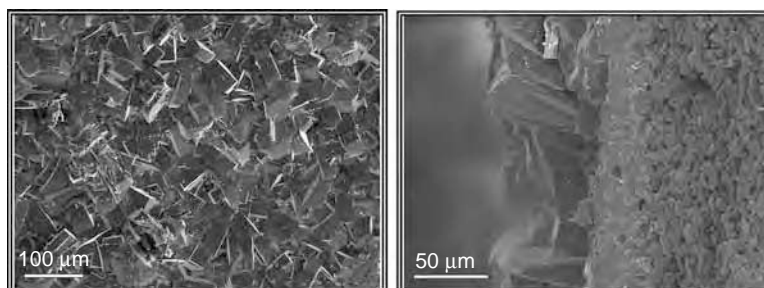


**FIGURE 10.6** Scanning electron photograph of an H-ZSM-5 membrane obtained using in situ crystallization. Left: top view. Right: cross section.

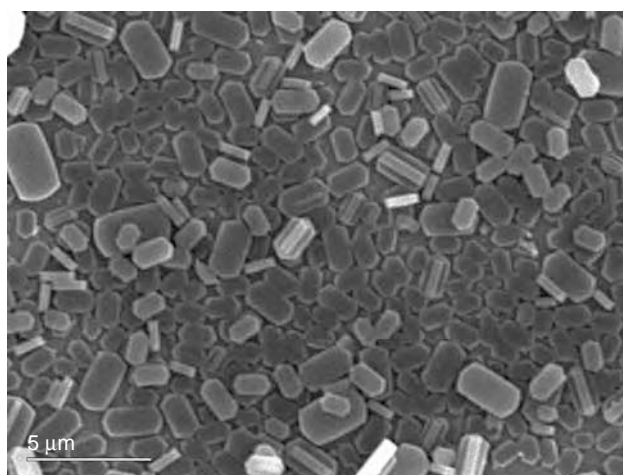


**FIGURE 10.7** Monolayer assembly of SIL-1 microcrystals on a silicon wafer by covalent linkage.

the surface of a support. These seeds act as nuclei for further crystal growth with a secondary gel under hydrothermal synthesis conditions in the second stage.

The coating or seeding methods are dip-coating, slip-casting, rubbing, spraying coating, laser ablation, spin-coating, vacuum seeding, using of electrostatic forces, and covalent linkage. The attachment and bonding properties of the crystals on support depend on the chemical potential of the support to interact or react with the approaching zeolite crystal or crystal growth front. Figure 10.7 shows the monolayer assembly of SIL-1 microcrystals on a silicon wafer by covalent linkage following the procedure described by Lee et al. [25].

Because the concentration needed for secondary growth is lower than that required for nucleation, further nucleation is strongly decreased and almost all of the crystal growth takes place over the existing crystal seeds. By controlling the composition and concentration of the secondary growth solution, the crystallization of undesired zeolite phases and the dissolution of the support can be avoided, and the rate and direction of crystal growth can, to a certain extent, be controlled.

The aim of using *ex situ* techniques is to obtain a better control of the microstructure and a preferential orientation of the crystals in the membrane with a shortened crystallization time. Preferential orientation is needed, not only for separation purposes when high fluxes are required but also for size-selective chemical sensors (see Section 10.6.6.2). Due to the anisotropy in the pore geometry of the zeolite crystals, that orientation which shows the largest channels in the direction of the flux is preferable. For example, on MFI zeolite, the straight and sinusoidal channels run parallel to the *b* and *c* axes, respectively (see Figure 10.8). The membranes prepared by secondary growth have rendered, in general, *c*-oriented membranes [24,26], i.e., sinusoidal channels perpendicular to the support surface. Figure 10.9 shows SEM images of silicalite-1 membranes on nonporous alumina support prepared by secondary growth for which *c* orientation of the crystals is clearly observed. With those zeolites, Lai et al. [27] have obtained *b*-oriented membranes where the fluxes and separation factors are very high using covalent linkages [25,28] to bond the solid crystalline seeds to the support before a secondary synthesis. MFI zeolites show their largest channels in the *b* orientation. For that reason, the membranes of Lai et al. [27] showed a superior performance in

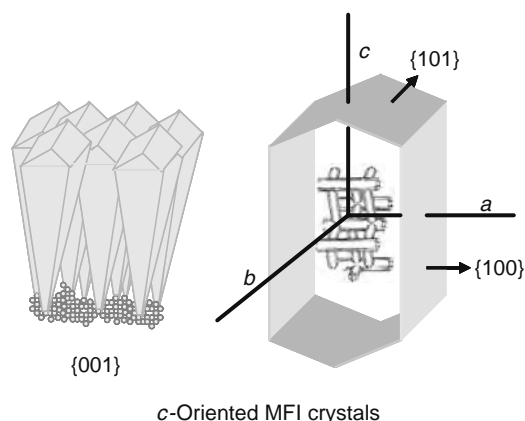


**FIGURE 10.8** (See color insert following page 588.) Schematic representation of a *c*-oriented MFI zeolite crystal.

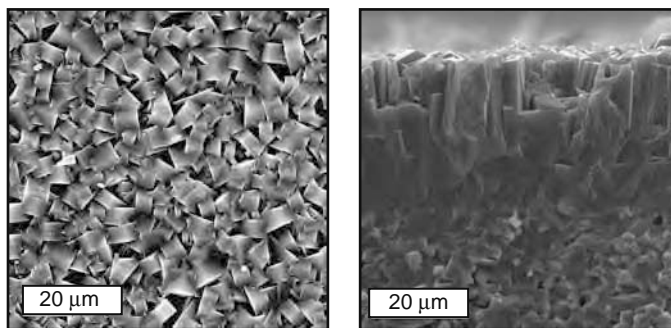


**FIGURE 10.9** Scanning electron microscopy (SEM) analysis of silicalite membranes over nonporous alumina substrates after 20 h of secondary growth synthesis conditions. Left: top view. Right: cross section.

gas separation. In Figure 10.10, top and cross-sectional views of *b*-oriented silicalite-1 layers over silicon wafers are analyzed as a function of synthesis time.

The ability of AFM (atomic force microscopy) to image the surface of nonconducting materials allows the three-dimensional observation of nanometer-size events on the zeolites at a resolution previously unattainable [29]. The complications that can arise have to do with the great surface reactivity of these materials, degrading the image quality. This technique is particularly useful for the study of the crystal growth mechanisms of zeolites, and it has been employed to adjust the synthesis conditions for crystal orientation control. AFM topographic and SEM images from the external surface of silicalite-1 layers over nonporous alumina substrates are shown in Figure 10.11 as a function of synthesis time. It can be observed that at 35 min, nearly secondary growth initiates because the zeolite crystals, circular in shape, correspond to the seeds morphology and size (around 200 nm). Conversely, after 50 min SIL-1 crystals, up to 1  $\mu\text{m}$  in size and mostly *b*-oriented, appear covering the external surface of the alumina substrate.

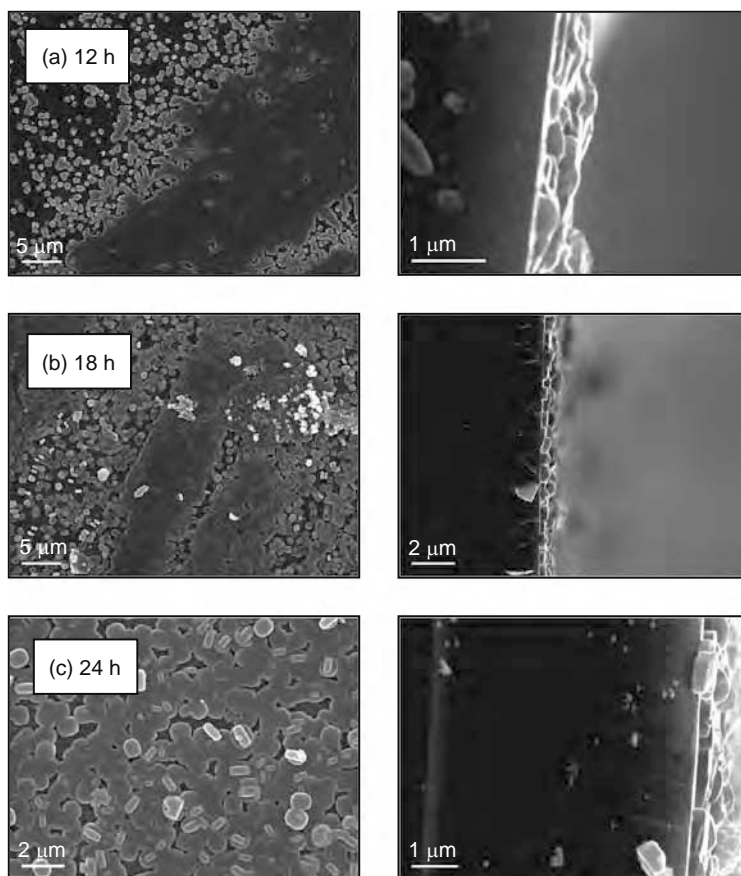


**FIGURE 10.10** A scanning electron microscopy (SEM) analysis of *b*-oriented SIL-1 layers over Si wafers (prepared by secondary growth using dip-coating as seeding technique) as a function of synthesis time.

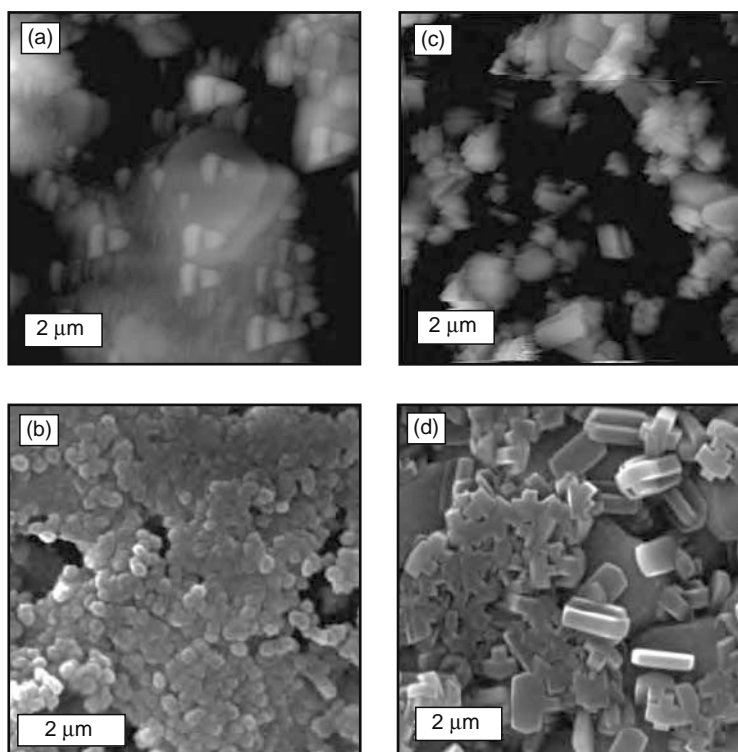


**FIGURE 10.11** AFM topographic and scanning electron microscopy (SEM) images from the external surface of silicalite layers over seeded nonporous alumina substrates after synthesis time of (a, b) 35 min and (c, d) 50 min.

### 10.2.2 PRE- AND POSTTREATMENTS TO ENHANCE MEMBRANE QUALITY

In general, the properties and separation abilities of the resulting membranes depend on the synthesis procedure. The amount of zeolitic material, support composition, penetration and adhesion to the support, orientation of the zeolite crystals, the density and distribution of nonzeolitic pores (i.e., intercrystalline voids), crystal boundaries, and the thickness of the zeolite layer are the main variables which affect the quality of the obtained membrane.

Pretreatment processes, grafting and masking are aimed to improve the adhesion and to prevent the inclusion of the zeolitic material into the support. A grafting step is used when a specific direct interaction between the support and the zeolite seeds is not possible or the attachment opportunities are not available. Using this procedure the surface of the support is previously modified chemically to enhance the attraction between the zeolite seeds and the support. The masking techniques [30] consist of filling all the support pores with wax while leaving the surface free for deposition of the zeolite film, thus protecting the support by this temporary barrier from the synthesis mixture. The zeolite-coated supports are finally calcined to remove the wax from the support and the template molecules from the zeolite. Since the membrane thickness and the width of cracks are notably reduced by support masking, high fluxes and selectivities are obtained [30].

Posttreatment processes have been used to improve the quality of the resulting membranes, such as ion exchange (to provide catalytic properties or change them between hydrophobic and hydrophilic surfaces), liquid or vapor silylation, coke deposition, CVD (chemical vapor deposition), and ALCVD (atomic layer chemical vapor deposition). These techniques are used to reduce the intercrystalline gaps and the pore-mouth size, modify the acid properties of the modified membranes, and remove amorphous material. Some of these modifications have demonstrated very high separation selectivities for the resulting membranes; however, in many cases, they are of limited practical application due to the relatively low fluxes obtained.

### 10.2.3 INCREASING MEMBRANE AREA

Both, direct and secondary synthesis methods may be acceptable for small-scale applications (a few square centimeters of membrane area), but present significant problems of the synthesis of larger structures. Generally speaking, increasing the zeolite membrane area in industrial modules (see Section 10.6.4) involves the use of longer tubular or monolith supports, and reduction of tubular diameters to capillary dimensions to increase the membrane area per unit volume. In addition to the variations of composition with time that necessarily take place during batch processing, the use of longer and narrower supports will likely cause the development of concentration gradients, leading to nonhomogeneous membrane characteristics, and possibly also to the formation of defects and non-desired phases on the membrane. A number of studies have attempted to solve the problems

that prevent the synthesis of large area membranes. Up-to-date, successful membrane formation is typically achieved either by using a suitable excess of reactants or by repeated synthesis cycles. However, new attempts involving the direct heating of the substrate, while the reaction mixture is kept at lower temperature, have been demonstrated at lab-scale by Erdem-Senatarlar et al. [31,32]. In this manner, the reaction is suppressed in the bulk and promoted on the surface, and the phase transformations of metastable materials to other zeolite types thermodynamically favored can be delayed.

Even if the problems of poor crystal intergrowth due to local exhaustion of reactants in the autoclave and synthesis of zeolite material in the bulk of the solution were solved, an important problem remains, related to the fact that several batch synthesis cycles (with their associated heating and cooling processes) are often required to achieve a zeolite membrane of good quality. Thus, a synthesis procedure in which reactants are continuously supplied to the synthesis vessel while this is maintained at a constant temperature would clearly be desirable not only for performance but also for the feasibility of the scale-up. This type of approaches has already been tested for inner MFI and NaA zeolite membranes [33–35], and the results obtained indicate that the formation of concomitant phases and the amount of crystals forming in the liquid phase are greatly reduced. Similarly, the continuous seeding of tubular supports by cross-flow filtration of aqueous suspensions [36–37] has been carried out for zeolite NaA membrane preparation.

Because hydrodynamics and hydrostatics of the synthesis solution have a clear influence in the growth of zeolite films, some authors [38] have attempted to change these parameters using centrifugal forces to drive the crystal nuclei formed in the homogeneous phase toward the support before they reached a size that would be difficult to accommodate into the growing membrane, thus promoting the formation of higher quality zeolite layers.

### 10.3 NEW ZEOLITE-LIKE MICROPOROUS AND MESOPOROUS MATERIALS

In this group we include other ordered microporous structures, different from classical zeolites, containing tetrahedrally coordinated phosphorus, such as  $\text{AlPO}_4$  [39,40], SAPO-34 [41–43], and zeolite membranes containing Ti and V in their structure. These membranes, such as TS-1 [44] and VS-1 [44,45], are potentially very attractive from the catalytic applications point of view. The group of titanosilicates corresponds to framework structures made of  $\text{TiO}_6$  octahedra and  $\text{SiO}_4$  tetrahedra [45]. The ETS-4 structure with a pore size (0.3–0.4 nm) has been synthesized as a layer [46–48], the other titanosilicate with a larger pore size ( $0.49 \times 0.76 \text{ nm}^2$ ) that has been synthesized was ETS-10 [49]. The pure 5  $\mu\text{m}$  thick ETS-10 membrane exhibited a good degree of crystal intergrowth. The microporous titanosilicate ( $\text{K}_2\text{TiSi}_3\text{O}_9 \cdot \text{H}_2\text{O}$ ), with the structure of umbite and a pore size of 0.3 nm, has been reproducibly prepared for the first time as a continuous, ca. 5  $\mu\text{m}$  thick membrane on porous  $\text{TiO}_2$  tubular asymmetric supports [50]. The separation factor reported with this membrane for a  $\text{H}_2/\text{N}_2$  mixture was 48. The development of titanosilicate based membranes is likely to continue on account of some key advantages related to their preparation and properties: (1) in general, a pure phase can be obtained in the absence of costly organic templates, thus, avoiding calcination treatments, which often lead to defects or loss of active surface groups, (2) titanosilicates are usually prepared under relatively mild pH conditions, reducing the chemical attack on the support and synthesis equipment used, (3) mixed octahedral–tetrahedral oxides present novel possibilities of isomorphous framework substitution which allows the fine-tuning of the catalytic and adsorption properties of a given membrane, while preserving its microporous structure, and (4) finally, in general, these materials have a strong basicity, that provides an alternative to the acid properties of classic zeolites and opens up new application possibilities [5].

New materials that expand the microporous region of the zeolite are also interesting. In this group it is possible to find wide pore zeolite such as ITQ-21 which is accessible through six circular 0.74 nm openings [51], and extra-large-pore materials, like the phosphate-based VPI-5 or the more stable silicas UTD-1 and CIT-5 [52] with 0.8–1.2 nm openings.

Other so-called zeolite-related materials, due to their ordered inorganic structure, are the family of mesoporous aluminosilicates MCM discovered by the Mobil group in 1992 [53], with pore size between 2 and 4 nm or materials with even bigger pore sizes such as SBA-15 and SBA-16. The first synthesis of a mesoporous layer was prepared by Yang et al. [54] who deposited a MCM-41 layer on a mica substrate. MCM-41 is a two-dimensional hexagonal-ordered material, and the pores are aligned parallel to the substrate. Some authors tried to align the pores perpendicular to the surface by applying a magnetic field [55] or a pulsed laser deposition method [56]. Another option was the synthesis of the three-dimensional cubic structure with interconnected pores, MCM-48. Nishiyama et al. [57,58] synthesized the MCM-48 structure on flat  $\alpha\text{-Al}_2\text{O}_3$  supports, obtaining high fluxes in the separation of organic mixtures. The silylation of the MCM-48 membranes using trimethylsilane and triethylsilane enhanced the hydrothermal stability and the hydrophobicity reducing the pore size from 2.4 to 1.8 nm [59].

### 10.4 GAS SEPARATION: FUNDAMENTALS AND APPLICATIONS

Zeolite membranes have the potential to selectively separate gas molecules in a mixture operating under steady state, unsteady state, or under cyclic conditions whereas fixed bed adsorbers are typically operated under transient conditions. In addition, because of the inorganic nature of zeolite membranes, they have higher mechanical strength and greater thermal and chemical stability than their polymeric counterparts. Also, their ability to operate under very different conditions (total pressure,

composition, and temperature) on both sides of the zeolite membrane is a great advantage compared to conventional adsorption on discrete zeolite crystals.

Microporous inorganic membranes have pores that can be tuned to the molecular size. This enables zeolite membranes to carry out separations (i.e., the separation of isomer compounds) that are not possible with membranes in which only Knudsen selectivity is possible. Moreover, zeolite microporous membranes can compete with traditional energy costly separation methods, such as distillation of mixtures of close boiling point components, separation of mixtures of low concentration, and azeotropic distillation.

If some molecules in a mixture are too large to enter the pores of the membrane, separation can be obtained by molecular sieving. However, there is a certain degree of flexibility in the molecules and also in the zeolite pores that must be taken into account because the zeolite framework is not a rigid structure [60]. If all the components permeate through the membrane, the separation can be obtained due to differences in polarities of components, adsorption coverages, diffusion rates, and in some circumstances, the ability of one component in the feed to hinder or inhibit others from entering the pores [2]. The permeation flux of a component in a mixture is determined by the adsorption and diffusion characteristics of all the components in that mixture and also the coupling between the diffusing species [61].

### 10.4.1 SEPARATION MECHANISMS

The transport mechanisms through zeolite membranes depend on different variables such as operation conditions (especially temperature and pressure), membrane pore size distribution, characteristics of the pore surface of the zeolitic-channel network (hydrophilicity/hydrophobicity ratio), as well as the characteristics of the crystal boundaries and the characteristics of the permeating molecules (kinetic diameter, molecular weight, vapor pressure, heat of adsorption), and their interactions in the mixture.

Ideally, the zeolite membranes must be continuous with good cross-linking between crystals and free of pinholes and cracks to get high selectivities. However, most of the synthesis procedures render membranes with some intercrystalline gaps and defects. The amount of these membranes and their sizes play an important role in the overall quality of the membrane. Therefore, it has been considered illustrative to explain briefly the transport regimes in porous materials whatever the pore size, after which the mass transport mechanisms through microporous media will be fully described.

Figure 10.12 shows conceptual schemes for the different mechanisms from the nonselective (lower part of the figure) to the most selective one (upper part of the figure). It is important to note that the solution-diffusion mechanism is shown for comparison in the top of the figure, to describe the transport through polymeric membranes. In the bottom part, the nonselective transport through macro- and mesopores due to viscous flow or Poiseuille is shown. Under such regime, there is no possibility of molecular separation. It represents the molecular diffusion, characterized by elastic collisions between molecules, which prevail over molecule-wall collisions. When Knudsen diffusion takes place, i.e., in mesopores, there is possibility of separation. It occurs when the mean free path of the molecules is much larger than the pore radius of the porous media. There are more collisions between the molecules with the pore walls than with other molecules. For a binary mixture, the separation selectivity is expressed as the square root of the molecular weights of the two components. Capillary condensation takes place in mesopores when a condensable vapor is present. This vapor is able to liquefy in the pores even when the saturation partial pressure is not reached,

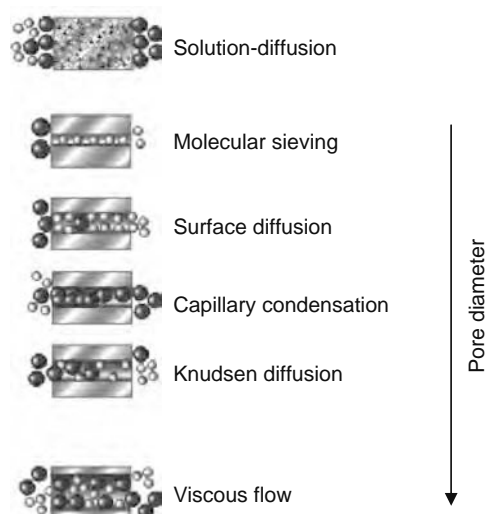


FIGURE 10.12 (See color insert following page 588.) Transport mechanisms in porous materials.

and eventually blocking the permeation of the permanent gases. It is also called liquid diffusion. Surface diffusion takes place in micro- and mesopores when the molecules adsorb on the pore walls and migrate along their surface. The effectiveness of surface diffusion depends on the product of adsorption and mobility of the permeating compounds. Under multilayer diffusion the permeabilities of condensable gases may exceed the permeability for pure gas-phase diffusion. Finally, molecular sieving through micropores represents the exclusion of molecules that are too large to enter the pores.

#### 10.4.1.1 Permeation of Individual Gases

The individual gas permeance that is experimentally measured for a zeolite membrane can be explained as the sum of two phenomena in parallel: the permeation through defects and the permeation through the zeolitic channels. If the diameter of the molecules is larger than the zeolitic channels, the permeation will clearly take place through the existing defects. This permeation can be Knudsen (mesoporous defects) or viscous (macroporous defects), although the balance between both types also depends on the operating pressure and temperature. The permeation through defects can be very substantial for molecules that are weakly or not at all adsorbed on the zeolite. In addition, capillary condensation might occur on mesoporous defects and, therefore, affecting the separation performance of the membrane.

The second contribution, i.e., permeation through the microporous zeolitic-channel network, can be due to activated gaseous diffusion or surface diffusion of adsorbed species. As a general rule, the smaller the pores size the greater the interaction of the adsorbed molecule with the pore walls.

Single-gas permeation of different gases on zeolite membranes is frequently used to estimate the molecular sieving ability of a given membrane. From the absence of a clear cutoff it is possible to conclude that the mass transport is not controlled by the zeolite-pore system.

Generally speaking, the single-gas flux through supported zeolite membranes, for a given temperature, depends on the sorption capacity of the gas on the zeolite pores and its equilibrium adsorption constant (Langmuir isotherm is often used to describe the relationship between the amount adsorbed and the gas-phase pressure), the gas diffusion coefficient, the thickness of the zeolite layer, the porosity of the support, and the pressure at the feed and permeate sides.

Figure 10.13 shows the experimental setup typically used for measuring the single-gas permeances of different gases on tubular zeolite membranes. When measuring single-gas permeances, the membranes are commonly sealed in a stainless steel dead-end module using silicone, Teflon or graphite *o*-rings, and a pressure drop from feed to permeate side is set.

##### 10.4.1.1.1 Qualitative Model of Single-Gas Transport through Microporous Materials

Barrer proposed a qualitative model of single-gas transport through microporous materials [62]. A five-step model can qualitatively describe the transport through a microporous membrane at moderate temperatures (see Figure 10.14):

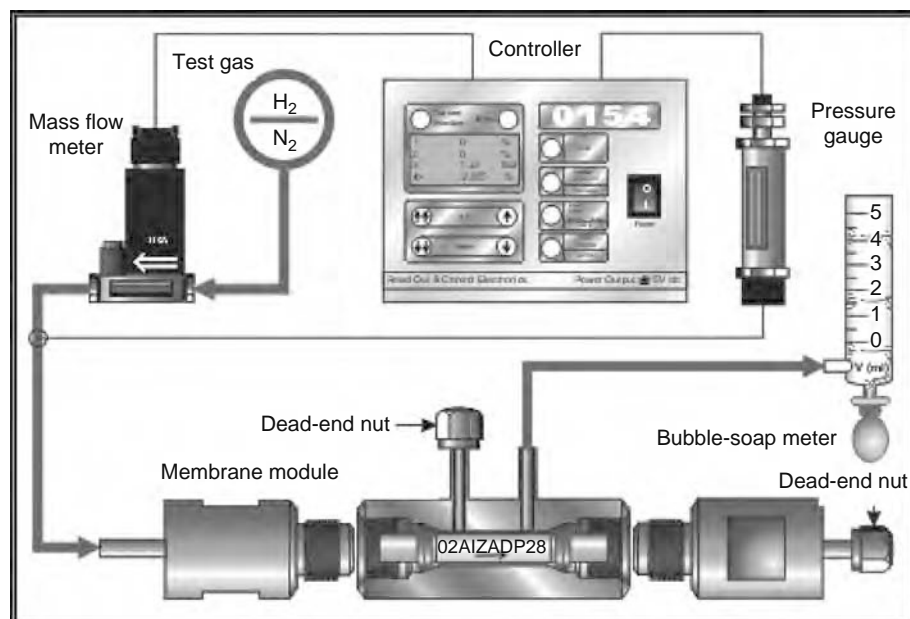


**FIGURE 10.13** (See color insert following page 588.) Experimental system for the calculation of single-gas permeances on zeolite tubular membranes.

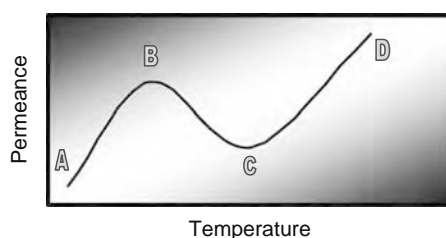


**FIGURE 10.14** Qualitative diagram showing the dependence of single-gas permeance with temperature.

1. Transport from the gas phase to the micropore, which can take place by two parallel streams:
  - (a) Direct entrance in the micropore from the gas phase.
  - (b) Via the external surface. First adsorption of the molecules on the external surface followed by diffusion to the entrance of the micropore across the external surface.
2. Migration in the micropore.
3. Transport from the micropore to the gas phase, which can take place by two parallel streams:
  - (a) Direct exit to the gas phase from the zeolite pore.
  - (b) Via the external surface. First exit from the micropore to the external surface and then desorption of the molecules to the gas phase.

The third step, migration inside the micropore, is also denoted as intracrystalline zeolite diffusion or configurational diffusion.

The relative importance of surface diffusion and activated gaseous diffusion depends strongly on temperature [63–65] because adsorption and diffusion phenomena are molecular processes of opposite temperature dependency. Figure 10.14 is a simplified diagram showing the evolution of permeance as a function of temperature [64].

Initially, ( $A \Rightarrow B$ ), the permeance increases because the increase in temperature enhances the mobility of adsorbed species, even though the amount of physically adsorbed material starts to decrease. Eventually, point B is reached, and from this temperature, the decline in occupancy prevails which gives rise to a decrease in permeance ( $B \Rightarrow C$ ). At a sufficiently high temperature (C) the effect of adsorption becomes negligible, and the permeance is controlled by activated transport (Knudsen-like) through micropores, increasing with temperature ( $C \Rightarrow D$ ) [2]. This transport in the gaseous regime is activated, mainly due to the structural constraints of the lattice upon passage [66]. The total flux through the membrane is then the sum of the surface diffusion and the gaseous diffusion.

As an example, Figure 10.15 compiles the permeance evolution with temperature for single hydrocarbons (from  $C_1$  to  $C_3$ ) over silicalite-1 membranes supported on stainless steel tubes. A specific interaction with linear hydrocarbons appears, as it could be expected due to the organophilic character of SIL-1 membranes. For methane, the temperature used is too high to find

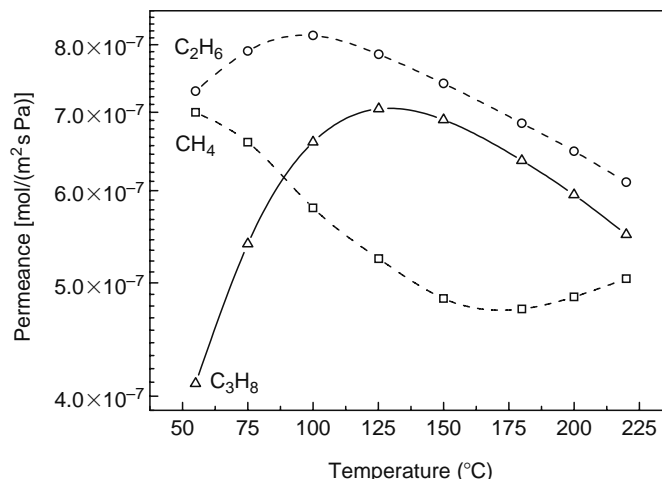


**FIGURE 10.15** Hydrocarbon permeances as a function of temperature for Na-ZSM-5 membranes supported on stainless steel tubes.

a maximum; but in general, the heavier the adsorbate, the stronger the adsorption and coverage degrees. This tendency is in accordance with the temperature-programmed permeance profiles and the point B temperatures (Figure 10.14), which indeed, shift toward higher values with the hydrocarbon chain length (from 100°C for ethane to 130°C for propane). The sequence shown for the permeance maxima is the same as in previous works [64–65], although the individual temperatures slightly change.

#### 10.4.1.1.2 Quantitative Model of Single-Gas Transport through Microporous Materials

Usually the transport of gases is described by Fick's first law:

$$J = -D_F(q) \frac{\delta\mu}{\delta x}$$

where  $D_F(q)$  is the Fickian diffusion constant ( $\text{m}^2/\text{s}$ ) also called transport diffusivity,  $\delta\mu/\delta x$  is the chemical potential gradient, i.e., the driving force for mass transport and might be expressed in terms of the fractional occupancy. The Fickian diffusion coefficient is assumed to be independent of coverage degree.

There are macroscopic (uptake measurements, liquid chromatography, isotopic-transient experiments, and frequency response techniques), and microscopic techniques (nuclear magnetic resonance, NMR and quasielastic neutron spectrometry, QENS) to measure the gas diffusivities through zeolites. The macroscopic methods are characterized by the fact that diffusion occurs as the result of an applied concentration gradient; on the other hand, the microscopic methods render self-diffusion of gases in the absence of a concentration gradient [67].

Conversely, the correct approach to formulate the diffusion of a single component in a zeolite membrane is to use the Maxwell–Stefan (M–S) framework for diffusion in a nonideal binary fluid mixture made up of species 1 and 2; where 1 and 2 stands for the gas and the zeolitic material, respectively. In the M–S theory it is recognized that to effect relative motions between the species 1 and 2 in a fluid mixture, a force must be exerted on each species. This driving force is the chemical potential gradient, determined at constant temperature and pressure conditions [68]. The M–S diffusivity depends on coverage and fugacity, and, therefore, is referred to as the corrected diffusivity because the coefficient is corrected by a thermodynamic correction factor, which can be determined from the sorption isotherm.

#### 10.4.1.2 Multicomponent Permeation

The permeation of mixtures is a more complex phenomenon, and in general, the behavior that is experimentally observed for mixtures cannot be predicted solely from the permeance of the individual components [5]. As will be shown below, it is often the case that in a binary mixture, the component which permeates faster as a single gas (in general the more weakly adsorbed component) is the one giving the lower permeance in the binary mixture.

Although Knudsen diffusion, shape selectivity, and molecular sieving play an important role in the separation of mixtures, the mechanisms which control the majority of the multicomponent separations in zeolite membranes are surface diffusion, and sometimes, capillary condensation. In addition, molecular simulations and modeling of M–S diffusion in zeolites [69,70] show that the slower moving molecules are also sped up in some mixtures [71,72] in the presence of fast-diffusing molecules and other times, slower molecules inhibit diffusion of faster molecules because molecules have difficulty passing one another in zeolite pores [73].

Four groups with different separation-controlling mechanisms can be distinguished: (1) separation of mixtures of non-adsorbing compounds, (2) mixtures of adsorbing organic compounds, (3) permanent gas from vapors, and (4) water or polar molecules from organic compounds.

##### 1. Separation of Mixtures of Nonadsorbing Compounds

In the ideal molecular sieving regime the interaction of the permeating species with the zeolite is minimal, and the separation takes place simply because the size and shape of some of the molecules prevent them from entering the membrane pores or move across them with substantial velocity [2]. In that regime adsorption does not play an important role, and, therefore, separation selectivity (ratio of permeances between species in the mixture) should coincide with ideal selectivity (ratio of single-gas permeances).

##### 2. Separation of Mixtures of Adsorbable Organic Compounds

When all the components in the mixture adsorb onto the zeolite-adsorption sites, the separation can be explained in terms of competitive adsorption between the permeating compounds. In the mixture, the molecules compete for those adsorption sites, and at high coverage degrees, this adsorption depends on the ratio of feed fugacities [74], heats of adsorption, and molecular sizes.

### 3. Separation of Permanent Gas from Vapors

In these mixtures, the vapor or organic compound can either adsorb preferentially on the zeolite pores or undergo capillary condensation in pores of small diameter, therefore blocking the membrane for the other components in the mixture (i.e., permanent gas). The separation selectivity toward the blocking molecule decreases with temperature due to the decrease in adsorption and capillary condensation.

### 4. Separation of Water or Polar Molecules from Organic Compounds

These separations are usually carried out by pervaporation (see Section 10.5) or vapor permeation but they have also been performed using gas-phase feeds on organophilic [75] or hydrophilic membranes [76]. On organophilic membranes the permeation of the organic or less polar compound is favored, while the opposite trend is expected for hydrophilic membranes.

The M–S approach allows the prediction of the mixture diffusion based on the pure component M–S diffusivities, along with the mixture isotherms (i.e., estimated using the ideal adsorbed solution theory [IAST] of Myers and Prausnitz) [68]. Experimentally, the NMR pulse field gradient technique has been used to calculate the mixture diffusion coefficients.

Two experimental setups have been used to calculate transient and steady-state permeation of different gases through zeolite membranes: the Wicke–Kallenbach method [77] and the pressure-drop method. Using the Wicke–Kallenbach method, an inert gas sweeps the permeate side to facilitate the desorption of all the adsorbed compounds and the membrane surface always faces the feed gas. In this way, concentration gradients and an absolute pressure drop can be imposed independently. The major disadvantages are that the counter diffusion of the inert sweep gas can affect the permeation of the feed components and the cost of using a sweep gas reduces its possibilities for industrial applications. Using the pressure-drop method, a pressure gradient is kept in both sides of the membrane; hence, the flux through the membrane is the real one. However, if the membrane has defects, the absolute pressure drop across the membrane might give a considerable contribution of viscous flow to the overall permeation.

## 10.4.2 APPLICATIONS

The actual membrane market for gas separation is being led by polymeric membranes; during the past 20 years, sales of membrane–gas separation equipment have grown to become a \$150 million/year business [78]. However, the future of membrane technology will be in refining, petrochemical, and natural gas industries. Larger opportunities exist for membranes in all these industries, and despite past failures, the acceptance of membrane technology is increasing. These markets will require more robust membranes and modules than those used today due to high-partial pressures of hydrocarbons and the presence of other plasticizing gases are often involved. Currently, several industrial manufacturers prepare a wide variety of organic and inorganic membranes (glass, silica, titania, zirconia, metallic, ceramic, and carbon) [79]. However, commercial applications of zeolite membranes have only been developed for pervaporation and vapor permeation processes. For gas separations, zeolite membranes are still only used on the laboratory scale. The major restriction to the industrial development of zeolite membranes is their high cost. In fact, large-scale separations are unlikely to be implemented industrially unless the price of zeolite membranes undergoes a reduction by a factor of 10 [80].

This cost differential can be tolerated only in applications in which polymeric membranes completely fail in the separation [78]. Demanding separation applications, where zeolite membranes could be justified, due to the high temperatures involved or the added value of the components, and have been tested at laboratory scale, are the following: separation of isomers (i.e., butane isomers, xylene isomers), organic vapor separations, carbon dioxide from methane, LNG (liquefied natural gas) removal, olefines/paraffins and H<sub>2</sub> from mixtures. In most cases, the separation is based on selective diffusion, selective adsorption, pore-blocking effects, molecular sieving, or combinations thereof. The performance or efficiency of a membrane in a mixture is determined by two parameters: the separation selectivity and the permeation flux through the membrane.

In general, when carrying out a new separation, the kinetic diameter and the heat of adsorption of the gases, which compose the mixture, are the main variables used to select the most adequate zeolite. MFI, FAU, LTA, SOD, ANA, DDR, MOR, BEA, CHA, FER, KFI are zeolite structures widely used as membranes for different separations. In gas separation, MFI zeolite membranes (silicalite-1, ZSM-5, and with Al, Fe, B, and Ge isomorphously substituted into their structures) are the most commonly used membranes because their pores (~0.55 nm diameter) are in the size range of many industrial mixtures; furthermore, their synthetic chemistry is well established in the literature.

Table 10.1 summarizes recent results concerning gas separations; for an exhaustive revision up to 1999 the reader is referred to the review of Coronas and Santamaría [2].

We have divided the applications of zeolite membranes for gas separations into two main groups based on and depending on whether there is molecular exclusion or not in one of the components to be separated.

For the separations discussed in the following sections, the separation factor achieved using the same synthesis procedure and experimental setup (Wicke–Kallenbach or pressure drop) strongly depends on temperature and pressure, and to a lesser but still important extent on the orientation of the crystals in the membrane, the effective thickness of the layer, the support (nature

**TABLE 10.1**  
**Gas Separation Results with Zeolite Membranes from 1999**

Zeolitic Structure	Support	Thickness ( $\mu\text{m}$ )	Permeance $10^7$ [ $\text{mol}/(\text{m}^2 \text{ s Pa})$ ]	Mixture Separations	Maximum Separation Factor	Ref.
SAPO-34	$\alpha\text{-Al}_2\text{O}_3$	25	1.6 [ $\text{CO}_2$ at 298 K]	$\text{CO}_2/\text{CH}_4$	67	[43]
DDR	$\alpha\text{-Al}_2\text{O}_3$	5–10	$9^a$ [ $\text{CO}_2$ at 0.25 MPa]	$\text{CO}_2/\text{CH}_4$	220 at 301 K	[81]
MFI	$\alpha\text{-Al}_2\text{O}_3$ , SS	5–80	26 [ $\text{CO}_2$ at 300 K]	$\text{CO}_2/\text{N}_2$	13.7	[82]
FAU	$\alpha\text{-Al}_2\text{O}_3$	3	50 [ $\text{CO}_2$ at 308 K]	$\text{CO}_2/\text{N}_2$	40	[83]
FAU	$\alpha\text{-Al}_2\text{O}_3$	3	10 [ $\text{CO}_2$ at 308 K]	$\text{CO}_2/\text{N}_2$	149	[84]
MFI	$\alpha\text{-Al}_2\text{O}_3$ , SS	10–30	1 [ <i>n</i> -Butane at 393 K]	<i>n</i> / <i>i</i> -Butane	32	[11]
MFI	$\alpha\text{-Al}_2\text{O}_3$ , SS	100	9 [ <i>n</i> -C <sub>4</sub> at 373 K]	<i>n</i> / <i>i</i> -Butane	11.3	[22]
MFI	$\alpha\text{-Al}_2\text{O}_3$	1	3 [ <i>p</i> -Xylene at 423 K]	<i>p</i> / <i>o</i> -Xylene	500	[27]
MFI	Silicon carbide monolith	—	0.33 [ <i>n</i> -C <sub>6</sub> at 430 K]	<i>n</i> -C <sub>6</sub> /2,2DMB	247 at 436 K	[85]
MFI	$\alpha\text{-Al}_2\text{O}_3$	0.5	5.6 [ <i>n</i> -C <sub>6</sub> at 663 K]	<i>n</i> -C <sub>6</sub> /2,2DMB	227	[30]
MFI	$\alpha\text{-Al}_2\text{O}_3$	3	—	Simulated refinery gas	69 at 298 K [ <i>n</i> -C <sub>4</sub> /H <sub>2</sub> ]	[7]
MFI	$\alpha\text{-Al}_2\text{O}_3$ , SS	10–70	2 [ <i>n</i> -C <sub>4</sub> at 298 K]	Synthetic natural gas	15 at 298 K [ <i>n</i> -C <sub>4</sub> /CH <sub>4</sub> ]	[86]
MFI	$\alpha\text{-Al}_2\text{O}_3$	5–6	0.26 [H <sub>2</sub> at 423 K]	H <sub>2</sub> /N <sub>2</sub>	38	[87]
MFI	$\alpha\text{-Al}_2\text{O}_3$	3	0.08 [ <i>n</i> -C <sub>4</sub> at 300 K]	H <sub>2</sub> / <i>n</i> -butane	520	[88]
MFI	$\gamma\text{-Al}_2\text{O}_3$ , SS	—	0.8 [CO at 245 K]	CO/air	3.14	[89]
MFI	$\alpha\text{-Al}_2\text{O}_3$ , SS	—	—	Organic/air	250 at 306 K <i>n</i> -C <sub>6</sub> /air	[90]
FAU	$\alpha\text{-Al}_2\text{O}_3$	30	—	Toluene/heptane	—	[91]
MFI	$\gamma\text{-Al}_2\text{O}_3$ , SS	—	3.9 [water at 304 K]	H <sub>2</sub> O/C <sub>3</sub> H <sub>8</sub>	4.5	[76]
MFI	SS	100	—	H <sub>2</sub> O/He	4.5	
MFI	SS	100	—	CH <sub>4</sub> /CF <sub>4</sub>	0.92 at 298 K	[92]
LTA	$\alpha\text{-Al}_2\text{O}_3$	—	0.007 [H <sub>2</sub> at 473 K]	H <sub>2</sub> / <i>n</i> -C <sub>4</sub>	<sup>b</sup> 5.8 at 473 K	[93]
LTA	$\alpha\text{-Al}_2\text{O}_3$	15	4.8 [H <sub>2</sub> at 323 K]	H <sub>2</sub> /C <sub>3</sub> H <sub>8</sub>	8 at 323 K	[94]

<sup>a</sup> Mol/m<sup>2</sup> s (note that flux is represented not permeance).

<sup>b</sup> Ratio of single-gas permeances.

and resistance), the penetration of the zeolite crystals within the pores of the support, the distribution of non-zeolitic pores, and the grain boundaries.

#### 10.4.2.1 Separations Controlled by Sorption-Diffusion Mechanisms When Size Exclusion Occurs

Separation due to molecular sieving alone can only take place if the membrane is defect free and there is no adsorption of the permeating species on the zeolite crystals (i.e., at high temperatures) or the components in the mixture adsorb with similar heats of adsorption. For those mixtures, the shape and size of the components compared to the zeolite-pore sizes direct the separation toward molecular sieving. For example, the separation of H<sub>2</sub>/SF<sub>6</sub> or N<sub>2</sub>/SF<sub>6</sub> on MFI zeolite membranes at high temperatures where SF<sub>6</sub> does not adsorb significantly. In fact, the latter separation is commonly used to evaluate the membrane quality. Methane/*i*-octane represents another example of this mechanism since *i*-octane cannot fit into the MFI structure and the heat of adsorption of methane is very low in the zeolite [2].

Normally, a combination of molecular sieving and adsorption controls the separation. For separations where the adsorption starts to play an important role, it turns into the controlling separation mechanism, i.e., the separation of *n*-C<sub>6</sub>/2,2 DMB on MFI membranes [30,85]. In this case, not only the exclusion due to the size but also the slight difference in the heats of adsorption of the linear and branched alkanes in the MFI structure can result in a large difference in permeances due to the shape selectivity, because the linear alkanes are located more or less randomly in the zeolitic channels and the branched ones are preferentially adsorbed in the intersections. *n*-Hexane molecules (0.43 nm kinetic diameter) can enter the MFI pore structure and diffuse within MFI channels, whereas the diffusion of 2,2-DMB molecules should be largely restricted by size limitations (0.62 nm kinetic diameter). Although, the flux of 2,2-DMB in MFI membranes may be through defects. Hence, *n*-hexane strongly inhibits 2,2-DMB permeance and molecular sieving plays a secondary role.

Another example where molecular sieving and preferential adsorption control the separation is the separation of CO<sub>2</sub>/CH<sub>4</sub> in CHA and DDR zeolite membranes [43,81]. The separation of CO<sub>2</sub> from natural gas is important during its transport and combustion because of the acidic and corrosive character of CO<sub>2</sub> in the presence of humidity; and moreover, it reduces the methane number (similar to the octane number in gasoline) which is important for getting high efficiency during combustion.

Adsorption isotherms for CO<sub>2</sub> and CH<sub>4</sub> on SAPO-34 crystals reveal that CO<sub>2</sub> is adsorbed more strongly, and thus, preferential adsorption is partially responsible for the selective permeation of CO<sub>2</sub>. Also, SAPO-34 crystals have pores ( $0.38 \times 0.38 \text{ nm}^2$ ) similar in size to CH<sub>4</sub> (0.38 nm), and are bigger than CO<sub>2</sub> (0.34 nm); therefore, CO<sub>2</sub> diffuses faster than CH<sub>4</sub>. Li et al. [43] reported separation selectivities up to 67 with SAPO-34 membranes under conditions (room temperature) where the strongly adsorbing component, CO<sub>2</sub>, hinders methane permeance. Recently, small pore DDR membranes have been used [81] showing CO<sub>2</sub>/CH<sub>4</sub> separation factors as high as 220 at 301 K. Again, DDR membranes have pores ( $0.36 \times 0.44 \text{ nm}^2$ ) that are similar in size to CH<sub>4</sub> and therefore, a configurational impediment to the flux of methane takes place in addition to the preferential adsorption of CO<sub>2</sub>.

The separation of xylene isomers on MFI zeolite membranes can be considered one example of intracrystalline size exclusion and competitive adsorption (strongly dependent on coverage). The difference in their kinetic diameters ( $\approx 0.58 \text{ nm}$  for *p*-xylene and  $0.68 \text{ nm}$  for *o*- and *m*-xylene) indicates the possibility of an effective separation using MFI membranes (see Table 10.1). The kinetic diameter of *p*-xylene is close to one of the MFI channels ( $\approx 0.55 \text{ nm}$ ) whereas *o*- and *m*-xylene might be excluded. Therefore, MFI zeolite channels and crystal grain boundaries determinate the permeation characteristics [27].

#### 10.4.2.2 Separations Based on Competitive Adsorption without Size Exclusion

*n*-C<sub>4</sub>/*i*-C<sub>4</sub> separation on MFI membranes [10,11,21,22] is an example of competitive adsorption, and has been used as a quality-control parameter when adsorption effect is controlling, because *n*-butane strongly adsorbs on the MFI zeolite membrane even at moderate high temperatures. The separation factor *n*-C<sub>4</sub>/*i*-C<sub>4</sub> and permeances for a silicalite membrane are depicted in Figure 10.16a as a function of temperature. A maximum separation factor could be observed at around 55°C, as a result of *n*-butane adsorption and *i*-butane mobility. Figure 10.16b shows the results at different partial pressures of *n*-butane at constant temperature (25°C). As expected, higher the *n*-butane partial pressure higher the coverage degree increasing the blocking effect of *n*-butane and the separation factor.

Nevertheless, even for defective zeolite membranes (i.e., presence of cracks and pinholes), higher *n*-butane/isobutane separation factors [95] could be potentially achieved by intercrystalline adsorption and capillary condensation.

In general, if both components in the mixture strongly adsorb, the separation selectivity increases as the difference in the strength of adsorption of the permeating components increases.

The separation of CO<sub>2</sub>/CH<sub>4</sub>, which was earlier mentioned, can take place with FAU membranes [96], but in this case, only competitive adsorption controls the separation because both CO<sub>2</sub> and CH<sub>4</sub> molecules are much smaller than the FAU channel pores (0.74 nm). Similarly, the separation CO<sub>2</sub>/N<sub>2</sub> on FAU and MFI membranes ( $0.53 \times 0.56 \text{ nm}^2$  and  $0.51 \times 0.55 \text{ nm}^2$ ) [82] is mainly based on the preferential adsorption of the CO<sub>2</sub> that inhibits N<sub>2</sub> permeance. The influence of cation exchanged in FAU was extensively studied by Kusakabe et al. [83,84,97,98]. These authors found out a remarkable increase in the separation factor (from 19 to 39) when the Na-Y zeolite was ion exchanged with K, due to an improvement in the CO<sub>2</sub>/N<sub>2</sub> sorption selectivity [83]. Moreover, the influence of the ion-exchange degree of larger cations such as Rb and Cs and the subsequent washing step after was further analyzed [84]. For the incompletely washed samples, the chloride salts impregnated in the membrane seem to enhance the CO<sub>2</sub> selectivity reaching values of 149 with a CO<sub>2</sub> permeance of  $1 \times 10^{-6} \text{ mol/m}^2 \text{ s Pa}$ .

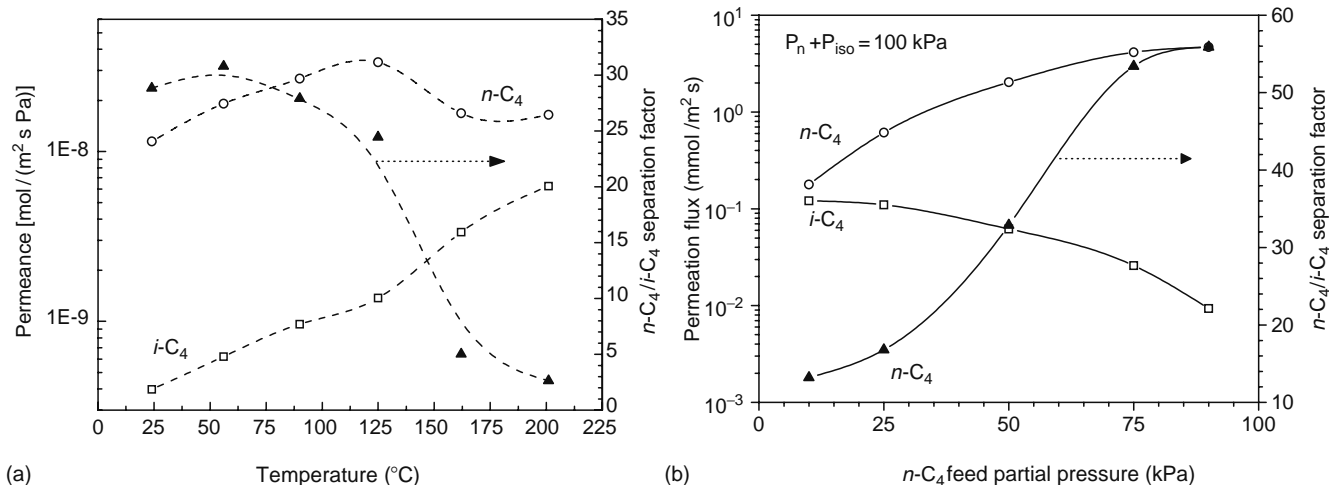


FIGURE 10.16 *n*-C<sub>4</sub>/*i*-C<sub>4</sub> separation performance of a SIL-1 membrane: as a function of (a) temperature and (b) *n*-C<sub>4</sub> feed partial pressure.

The adsorption of gases on zeolites depends on the occluded cations and on the presence of acid sites in the zeolite structure. For instance, alkenes adsorb stronger than alkanes on FAU zeolite membranes because of their higher affinity for the cations [99,100]. In a similar way, on MFI zeolites with acid sites, alkenes adsorb preferentially over alkanes for the same number of carbon atoms [101]. On the other hand, for MFI membranes without acid sites (i.e., silicalite-1) the olefin/paraffin separation principle is just the opposite because the adsorption strength decreases in the following order: alkane > alkene. However, the separation factor could be reversed as a function of the hydrocarbon relative pressure ( $P_{rel}$ ). Thus, in the Henry regime (i.e., at low  $P_{rel}$  values), there is hardly adsorption competition toward zeolite sites, and alkane coverage prevails over alkene one ruled by the adsorption constant value. Near saturation, configurational entropy effects control the separation mechanism rendering in a preferential alkene adsorption [102]. Further efforts need to be concentrated in this field because large opportunities for zeolite membranes in the separation of light hydrocarbon mixtures exist. The separation of propene/propane gas mixtures from various reactor vent streams could open up large new membrane markets. In a recent publication, Giannakopoulos et al. [103] have improved the previously reported results on propene-propane mixtures, achieving maxima values for the separation factor and ideal selectivity of 13.7 and 28 at 100°C and 35°C, respectively.

Zeolite membranes can withstand relatively high temperatures in the presence of oxygen; thus they can compete with polymeric and carbon membranes in the separation of refinery gas streams [7,88,104] and in the removal of heavy hydrocarbons from synthetic natural gas [86]. Those separations are based on competitive adsorption of hydrocarbons on the zeolite, and an increase in the concentration of any of the adsorbing species increases its surface coverage, leading to higher selectivities for that particular specie. In addition, there are some practical limitations for those separations, such as the high pressure of the natural gas in the pipeline, high temperatures in refinery gas streams, and presence of impurities [105], that make the zeolites promising candidates to achieve high selectivities and fluxes. It is worthwhile to emphasize that the capability of zeolite membranes to handle with natural gas separations opens up a remarkable potential market due to the total worldwide production of raw gas is about 50 trillion scf/year. According to the future predictions of Baker [78], over the next 10–20 years, the use of membranes for natural gas processing could easily grow up to become the largest single membrane-gas separation application.

Finally, the separation of vapors or adsorbable organic compounds from nonadsorbing permanent gases, such as alcohol/O<sub>2</sub>, alcohol/H<sub>2</sub>, *n*-C<sub>4</sub>/H<sub>2</sub>/H<sub>2</sub> on MFI membranes when the size of the organic compound does not represent size exclusion; should also be included in this group. In general, the permeance of the nonadsorbing permanent gas is blocked due to the adsorption or capillary condensation of the adsorbable compound within the zeolite channels or onto the intercrystalline defects, respectively. Separation factors as high as 520 have been obtained for an MFI zeolite membrane in the separation of *n*-C<sub>4</sub>H<sub>10</sub>/H<sub>2</sub> with an *n*-butane permeance of  $0.78 \times 10^{-8}$  mol/Pa s m<sup>2</sup> at room temperature [88]. Conversely, separations of H<sub>2</sub> from hydrocarbons on LTA zeolite membranes [93,94] and H<sub>2</sub> from N<sub>2</sub> on MFI membranes (Gavallas ZSM5) represent examples in which diffusion effects play the main role because the molecule with the smaller kinetic diameter permeates preferentially. Although for these cases competitive adsorption does not take place, the authors have considered appropriate to include them within this section to emphasize that the separation factor can be reversed (i.e., *n*-C<sub>4</sub>H<sub>10</sub>/H<sub>2</sub> vs. H<sub>2</sub>/*n*-C<sub>4</sub>H<sub>10</sub>) by choosing the adequate zeolite membrane. However, there are relative few studies found in literature concerning gas separation applications with type-A zeolite membranes ( $0.41 \times 0.41$  nm<sup>2</sup>). With tubular supports, the best results found for gas separation are 8.33 for a H<sub>2</sub>/*n*-butane equimolar mixture with a H<sub>2</sub> permeance value of  $7 \times 10^{-10}$  mol/m<sup>2</sup> s Pa at 473 K [93] and 7.97 for a H<sub>2</sub>/propane equimolar mixture with a H<sub>2</sub> permeance value of  $6.7 \times 10^{-8}$  mol/m<sup>2</sup> s Pa at 323 K [94]. Until now, no highly permselective A-type membranes have been reported; indeed, the permeation tests always revealed that those membranes contain non-zeolitic pores (defects) larger than the zeolitic pores through which large molecules (i.e., *n*-butane with a kinetic diameter of 0.43 nm) were able to diffuse, explaining the selectivities close to the Knudsen values.

Within this group of applications, it is worthwhile to include examples related with separations at trace levels. Recently, Aguado et al. [90] carried out the removal of model pollutants (*n*-hexane, formaldehyde, and benzene) present at very low concentration levels (2–230 ppmv) from indoor air using MFI zeolite membranes achieving separation factors as high as 250 for certain conditions. On the basis of this concept, a novel high-quality air-conditioning system may be envisaged as commercial domestic application for zeolite membranes.

## 10.5 PERVAPORATION

Whenever we are talking about zeolite applications, pervaporation comes to mind, since it is the first industrial application of zeolite membranes that has been successfully operating since May 1999 by Mitsui Engineering & Shipbuilding Co., Ltd. The plant was designed for a feed flow of 600 L/h and a concentration of water in the feed of 10 wt%, using 16 tubular type modules having 125 membranes of zeolite A each [106]. Also, a vapor permeation plant has been operating since September 1999 for a lens cleaning operation process, 24 double-tube type modules having a piece of zeolite membrane each [106,107].

Pervaporation is a separation process where a liquid mixture is fed to one side of the membrane; one component permeates preferentially through the membrane to the other side where it evaporates because the pressure is reduced in this side, either by vacuum or by a sweep gas. After that, the gas is condensed in a cold trap. Figure 10.17 shows a schematic diagram of

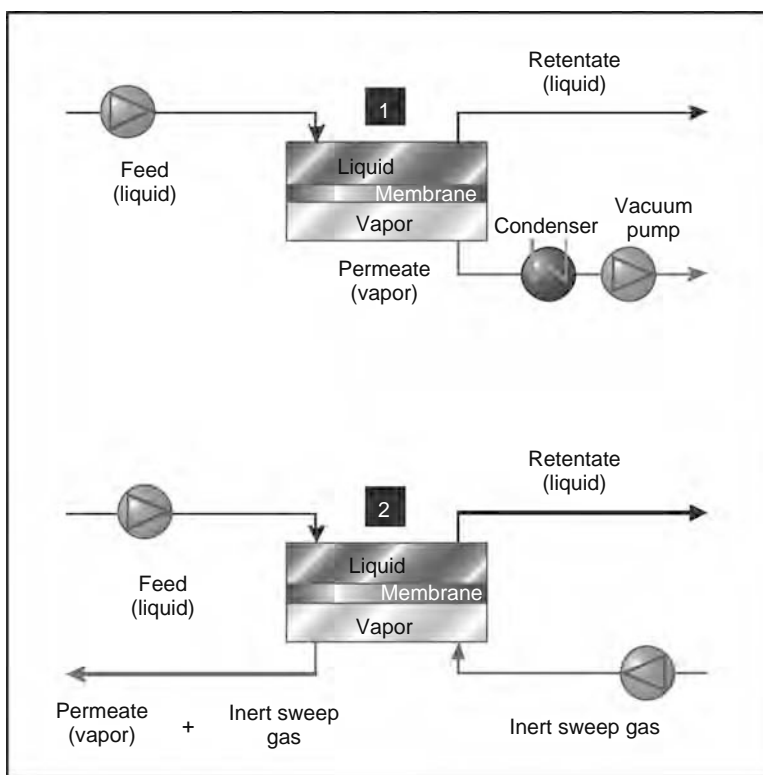


FIGURE 10.17 (See color insert following page 588.) Schematic diagram of pervaporation.

pervaporation. In vapor permeation the feed is a vapor, saturated or not, instead of a liquid. The driving force for pervaporation is the fugacity of the component that permeates through the membrane. Pervaporation occurs in three steps: (1) the liquid feed adsorbs onto the membrane, (2) there is a diffusion process through the membrane, and (3) the component desorbs into the vapor phase at the permeate side. The three steps are illustrated in Figure 10.18.

The performance of a membrane in pervaporation is based on the amount of liquid that permeates, pervaporation flux, which usually is expressed in kilogram per square meter hour, and the ability to separate the components in the mixture, which

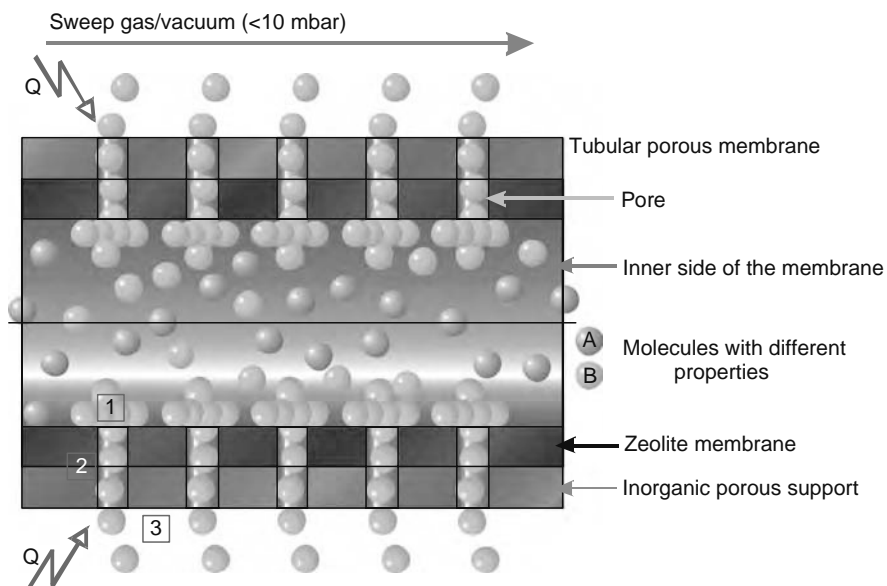


FIGURE 10.18 (See color insert following page 588.) Steps involved in pervaporation: (1) adsorption, (2) diffusion, and (3) desorption.

is given by the separation factor,  $\alpha_{i/j}$ , defined as the ratio of the weight fraction components in the permeate divided by the ratio of the weight fraction of the components in the feed.

$$\alpha_{i/j} = \frac{y_i^p / y_j^p}{x_i^f / x_j^f}$$

Distillation is a unit operation based on the relative volatility of the components in the mixture; this unit operation encounters many problems in the separation of azeotropic mixtures, close boiling point mixtures, isomer separation, and removal of thermally sensitive compounds. Azeotropic distillation is an alternative; however, it adds a third component to break the azeotrope and this solution is not environmental friendly and cost effective. Pervaporation could overcome these drawbacks and it is presented as a solution for the separation of these kinds of mixtures. In this section, we discuss the separation of different azeotropic and close boiling point mixtures.

Zeolite membranes are not the only kind of membranes that have been used in pervaporation, organic and other types of inorganic membranes, different from zeolites, have been employed. Polymeric membranes of PVA (polyvinylalcohol) have been widely employed for dehydration and separation of organic mixtures; however, their main limitations are related to their low thermal and chemical stability. When the water content in the feed mixture is high, polymeric membranes suffer from swelling; moreover, in the separation of organic mixtures they usually present a low selectivity.

Since the pioneering work of Tehennepe et al. [108] in 1987 many efforts have been made filling the polymeric matrix with zeolites to improve their stability. There are several companies, such as Sulzer Chemtech, that offer pervaporation organic membranes and composite membranes [109].

The inorganic silica membranes, also commercial, have solved the problem of thermal and chemical stability; however, these membranes are only used for dehydration purposes, leaving the problem of separation of organic mixtures unsolved. As we have seen previously, due to the versatility and special features of zeolites, new applications in pervaporation that are not possible with other membranes could be developed with zeolite membranes. Gallego-Lizon et al. [110] compared different types of commercial available membranes: zeolite NaA from SMART Chemical Company Ltd., silica (PERVAP SMS) and polymeric (PERVAP 2202 and PERVAP 2510) both from Sulzer Chemtech GmbH, for the pervaporation of water/*t*-butanol mixtures. The highest water flux was obtained with the silica membrane (3.5 kg/m<sup>2</sup> h) while the zeolite membrane exhibited the highest selectivity (16,000).

The main disadvantage of zeolite membranes is their cost; there are several studies related to this subject [80,111]. Meindersma and Haan [80] studied the economical feasibility of pervaporation or vapor permeation processes for the separation of aromatic compounds from a naphtha cracker feed and modeled the separation of benzene from cyclohexane taking into account the separation data presented by Kita et al. [112], with an FAU membrane. The results indicated that the selectivity of the membranes to the aromatics should be at least 40 and preferably 80 to avoid large membrane areas. The conclusion is that the cost of the zeolite membrane, estimated at that time in 2000 £/m<sup>2</sup>, needs to be reduced by a factor of 10 to get an economically feasible application. On the other hand, the recent economic study [111] for the dehydration of isopropyl alcohol comparing azeotropic distillation with pervaporation using either zeolite commercial membrane (NaA type zeolite, Mitsui & Co.) or polymeric (PERVAP 2510, Sulzer Chemtech GmbH) estimated that a hybrid distillation system with zeolite membranes is the most interesting process from an economic point of view. The economic calculations were accompanied by experimental results of both membranes. The zeolite membrane price, including the module obtained from the supplier, was 3400 £/m<sup>2</sup> in this case.

Many publications refer to pervaporation with zeolite membranes and recently the group of Falconer and Noble has presented an excellent review paper [113] about this subject. In a bibliographic search about pervaporation and zeolites for the last 10 years we find that many efforts, 28% of the publications, pertain to composite zeolite-polymer membranes, and the rest correspond to different zeolite structures that are summarized in the pie chart shown in Figure 10.19. The most studied structure

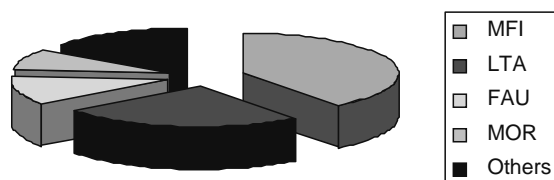


**FIGURE 10.19** (See color insert following page 588.) Distribution of publications about zeolite membranes in pervaporation during the last 10 years. (From ISI Web of Knowledge. Web of Science.)

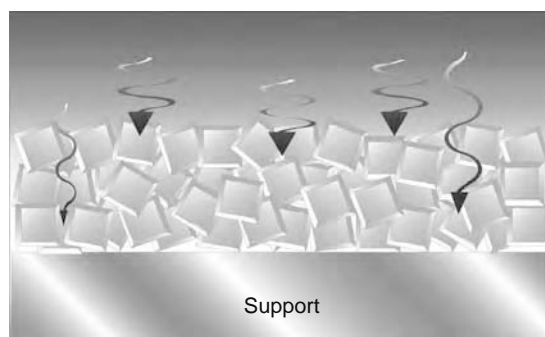


FIGURE 10.20 (See color insert following page 588.) Transport through intercrystalline and intracrystalline pathways.

is the MFI, followed by LTA and a similar number of publications could be found about FAU and MOR. The heading “others” in the pie chart, which represents a 15%, corresponds to FER, BETA, MEL, ZSM-11, and related materials like ETS-10 or ETS-4. The different applications of these zeolites in pervaporation include alcohol dehydration, water removal in acid solutions, organic dehydration separations such as water/tetrahydrofuran, water/dioxane or water/dimethylformamide, removal of organics from water and organic/organic separations such as methanol/MTBE or *p*-xylene/*o*-xylene. In the following sections the mechanism of pervaporation in zeolite membranes are briefly described and the details about the different applications are provided.

### 10.5.1 PERVAPORATION MECHANISM IN ZEOLITES

The different mechanisms that operate in the separation of gases have been previously described in Section 10.4.1. In pervaporation, the transport mechanism can be described by an adsorption–diffusion mechanism [74,114] similar to one for polymeric membranes [115]. However, it is necessary to consider that the specific interactions between the permeating component and the zeolitic material are different in zeolites. Moreover, the diffusion through the ordered zeolite nanopores is different than in the dense organic matrix.

Two important considerations that appear in zeolite membranes should be taken into account for the transport of the molecules through the membrane [113]:

1. Zeolite membranes are formed by a polycrystalline layer, which means that the permeation is not only through the ordered nanopores of the zeolite crystal, intracrystalline pathways, but also through the spaces between the crystals, intercrystalline pathways (see Figure 10.20). Nomura et al. [116] proposed a model taking into account this consideration.
2. Surface of the zeolite crystal is full of siloxane groups, and hydrophilic molecules can take advantage of this and also adsorb into the intracrystalline spaces enhancing the permeance of the hydrophilic molecule. This special feature is an advantage for hydrophilic/hydrophobic separations, and makes the organic/water separations with hydrophobic zeolites more difficult.

These two special features make the modeling issue of pervaporation through zeolite membranes a very challenge topic. It is generally assumed that the diffusion of the species through the zeolite pores can be modeled using the dusty gas model and the M–S equation to correlate the chemical potential with the permeation flux. Considering this model and that there is no counterdiffusion, the adsorption of the species follows Langmuir isotherm, and there is single-file diffusion of molecules through the cages and presence of trace amount of solvent species inside the cages, the flux could be expressed as [114]

$$J_i = \frac{\rho_S \varepsilon D_{i,V}^S(0)}{\delta} (q_{i,f} - q_{i,p})$$

where

$J_i$  is the flux of the component  $i$

$\rho_S$  is the zeolite membrane density

$\varepsilon$  is the porosity of the membrane

$D_{i,V}^S(0)$  is the intracrystalline surface diffusivity

$\delta$  is the thickness of the membrane

$q_{i,f}$  and  $q_{i,p}$  are the adsorbed quantities of component  $i$  on the zeolite membrane at the feed and the permeate side, respectively

A simple model that relates the flux of the component with the driving force, which is the fugacity, has been proposed [74,113,114].

$$J_i = K_i(\hat{f}_i^f - \hat{f}_i^p)$$

In the liquid feed side, the fugacity,  $\hat{f}_i^f$ , could be obtained with the molar fraction,  $x_i$ , the activity coefficient  $\gamma_i$  and the saturated partial pressure of the component at the operating temperature  $P_i^s$ . In the permeate side where the component  $i$  is in the gas phase, fugacity is the result of multiplying  $y_i$  molar fraction of component  $i$  in the permeate by pressure in the permeate side. The following equation is obtained:

$$J_i = K_i(x_i\gamma_iP_i^s - y_iP_p)$$

The constant  $K_i$  is an overall mass transfer coefficient that includes diffusion and adsorption coefficients divided by the membrane thickness.

Finally, it is important to notice the effect of the support in the pervaporation flux, analyzed by Bruijn et al. [117] who proposed a model and evaluated the contribution of the support layer to the overall resistance for mass transfer in the selected literature data. They found that in many cases, the support is limiting the flux; the permeation mechanism through the support corresponds to a Knudsen diffusion mechanism, which makes improvements in the porosity, tortuosity, pore diameter, and thickness necessary for an increase in the pervaporation flux.

### 10.5.1.1 Adsorption: Hydrophobicity and Hydrophilicity

As we have seen previously, the separation mechanism in pervaporation is explained by an adsorption–diffusion process. In this way, the selective adsorption of the components in the zeolite will be responsible for the selectivity in the separation. Adsorption is an exothermic nonactivated process. In general, the isotherm of adsorption on zeolites follows a single site Langmuir-type isotherm [74].

$$q = \frac{q_{\text{sat},i}b_i\hat{f}_i}{1 + b_i\hat{f}_i}$$

where

$q$  is the quantity of gas adsorbed at a given fugacity,  $\hat{f}_i$

$q_{\text{sat},i}$  is the quantity of gas adsorbed when the entire surface is covered with a monomolecular layer

$b_i$  is the Langmuir equilibrium constant

The heat of adsorption is related to the affinity of the component to the surface; a high heat of adsorption means that the zeolite strongly adsorbs this component. The adsorption measurement implies many difficulties as was pointed out by Bowen et al. [113], and the different techniques employed—microcalorimetry, gravimetric, chromatography, and transient permeation—give rise to different values.

Generally speaking, two terms, hydrophobic and hydrophilic, are employed in pervaporation in zeolite membranes, to refer to the affinity of organophilic and water molecules, respectively, toward the zeolite. In this way, a hydrophilic zeolite adsorbs and preferentially permeates water. Gyaya et al. [118] defined a hydrophobicity index (HI), which is the ratio between the amount of organic and the amount of water that a solid adsorbs:

$$\text{HI} = \frac{q_{\text{organic}}}{q_{\text{water}}}$$

The adsorbed amount should be measured at the same conditions that actually are not specified in this definition. However, this hydrophobic index could be very useful for comparison purposes of different zeolites that are later discussed in this chapter.

The hydrophobicity and hydrophilicity character of a zeolite depends on many factors; one of the most important is the Si/Al ratio. The introduction of the trivalent Al in the structure needs to be compensated by adding a cation; the electrostatic forces between the negative charge framework and the cation also attract polar molecules [113]. Moreover, for a given zeolite structure, the Si/Al ratio could also be varied, as in the isomorphs of the MFI structure, ZSM-5, and silicalite-1 [119]. Silicalite-1 with a Si/Al ratio equal to infinity is the most hydrophobic zeolite, and this zeolite will separate organic compounds from water [116,120–126] or organic compounds with different polarity [119,127,128]. On the other hand, zeolite A possesses a ratio of Si/Al=1, which makes this zeolite the most hydrophilic, as a consequence it is employed in the separation of water/organic mixtures (see Section 10.5.2.4). It is important to note that as the Al content increases, the stability of the zeolite in acid medium decreases. This fact moved the researchers to study other zeolites with an intermediate Si/Al ratio that could resist acid medium. Zeolites like mordenite [129], zeolite T [130–132], and ZSM-5 [129] were synthesized and studied in acidic conditions.

**TABLE 10.2**  
**Apparent Diffusivities of MeOH and EtOH as Pure Components**  
**and in Mixtures**

MeOH (%)	EtOH (%)	$D_{\text{MeOH}} \times 10^{13}$ (m <sup>2</sup> /s)	$D_{\text{EtOH}} \times 10^{13}$ (m <sup>2</sup> /s)
100	—	21 ± 2	—
—	100	—	4.4
95	5	19	7.5
5	95	6	5

Source: From Bowen, T.C., Wyss, J.C., Noble, R.D., and Falconer, J.L., *Micropor. Mesopor. Mater.*, 71, 199, 2004.

### 10.5.1.2 Diffusion

Activated surface diffusion or configurational diffusion occurs in molecules with a diameter larger than 60% of the pore diameter, as is the case in pervaporation with zeolite membranes [113]. Diffusion is an activated process and the diffusivity follows an Arrhenius-type equation:

$$D = D_0 \exp\left(-\frac{E_d}{RT}\right)$$

The diffusivity of a molecule gives an idea about its mobility, how fast it is permeating through the membrane, and this value will be very useful for predictions of separations and fluxes. The calculations of diffusivities in pervaporation lead to several difficulties, and arising from those, there are different experimental techniques: pure vapor uptake measurements and liquid chromatography. In the first case, the coverage of the zeolite is smaller than in pervaporation where the liquid is in contact with the membrane, so the liquid chromatography method seems to be more realistic with respect to zeolite coverage. A new isotopic-transient pervaporation method has been employed to measure diffusivities in Ge-ZSM5 membranes [73]. This method also accounts for one of the problems in determining diffusivities which is the measurement in multicomponent mixtures. The results obtained for the MeOH/EtOH mixture are in accordance with the results obtained with the molecular dynamics simulations using the M-S model and the experimental observations. Table 10.2 shows the values of the calculated apparent diffusivities of the pure components and of the components in the mixture; in the pure component the large molecule of ethanol diffuses slower than the small molecule of methanol; however in the mixture, the ethanol speeds up and inhibits the diffusion of methanol (see Section 10.4.1.2).

The third problem associated with the measurement of diffusivities in zeolite membranes is related to the fact that the membrane is a polycrystalline layer that possesses intercrystalline defects and diffusion also takes place through these random defects.

## 10.5.2 APPLICATIONS

### 10.5.2.1 Alcohol Dehydration: Zeolite A

Alcohols and water form azeotropes at different compositions (see Table 10.3) [133] characterized by low-water content. In pervaporation it is important to remove the species present at low concentrations, because heat transfer and the amount of

**TABLE 10.3**  
**Azeotropes of Selected Organic Compounds with Water at 101.33 kPa.**  
**Temperature, Mole Fraction, and wt% of Water**

Compound	Temperature (K)	$y_{\text{H}_2\text{O}}$	wt% of Water
Ethanol	351.25	0.1030	4.30
1-Propanol	360.80	0.5680	28.29
2-Propanol	353.70	0.3260	12.67
Tetrahydrofuran	336.67	0.1828	5.30
1,4-Dioxane	360.65	0.5280	18.62

Source: From Azeotropic data for binary mixtures. In: David R. Lide (Ed.), *CRC Handbook of Chemistry and Physics*, 85th ed. CRC Press 2004–2005: 6-180–6-181.

**TABLE 10.4**  
**Pervaporation Performance for Zeolite NaA in the Separation of Mixtures**  
**H<sub>2</sub>O/EtOH**

Publication Year	Temperature (°C)	% H <sub>2</sub> O	Water Flux (kg/h m <sup>2</sup> )	Separation Factor $\alpha_{\text{H}_2\text{O}/\text{EtOH}}$	Ref.
1995	75	10	2.15	10,000	[134]
	75	5	1.10	16,000	
1997	50	10.09	0.772	46,000	[137]
	75	10.09	2.08	42,000	
	120	10.09	8.37	47,000	
	50	5.02	0.396	4,800	
	75	5.02	1.10	5,900	
	95	5.02	2.35	5,100	
	120	5.02	4.30	5,600	
2000	40	10	0.08	190	[138]
2002	25	10	0.085	1,150	[139]
	50	10	0.14	975	
	75	10	0.18	900	
2003	120	10	8.63	5,730	[107]
2003	93	10	2.5	138	[36]
2003	45	5	0.86	54,000	[136]
2004	125	10	3.8	3,603	[33]
2005	50	10	0.6	500	[35]

energy required for this operation becomes substantial if large quantities are removed [113]. The zeolite most commonly employed for water removal from alcohols is zeolite A. It is a highly hydrophilic zeolite, due to its low Si/Al ratio, and it has a small pore opening of 0.41 nm, bigger than the kinetic diameter of water but smaller than many alcohols [74]; these features make zeolite A the best candidate for the dehydration of alcohols. Since the pioneering work of Kita [134] in 1995, patented by the Mitsui Shipbuilding & Co., Ltd. [135], many authors have attempted to synthesize and test zeolite A membranes for the dehydration of alcohols. Table 10.4 collects the results for the dehydration of ethanol, obtained by several authors. Kita et al. in 1995 patented zeolite A with a 30  $\mu\text{m}$  thickness that clearly outperforms the results obtained up to now, except for the case of Berg et al. [136] using a UV-exposed TiO<sub>2</sub>-coated metal support. They synthesized a well-intergrown thin zeolite layer, 3.5  $\mu\text{m}$ , over a flat support and their flux, obtained with a 5/95 wt% H<sub>2</sub>O/EtOH mixture at 45°C, which was 0.896 kg/m<sup>2</sup> h, was more than twice the flux obtained by Kondo et al. [137] using the same mixture at 50°C, which was 0.396 kg/m<sup>2</sup> h.

Santamaría and coworkers attempted to develop new methods for an easy scale-up of zeolite membranes. Tiscareño-Lechuga et al. [38] synthesized zeolite A membranes under a centrifugal force field. The zeolite layer was synthesized in the lumen of the tubular support, to protect the zeolite layer. A brushing method was employed to seed the support and after two syntheses, the pervaporation results showed a high water flux membrane. Pina et al. [35] used a semicontinuous method to decrease the number of synthesis necessary to achieve a defect-free layer. They obtained very good membranes with high selectivities; however, the fluxes were still lower than those obtained by Kondo [137]. Finally Pera-Titus et al [37], using the centrifugal force field and a controlled seeding method that consisted of a cross-flow filtration of a seed solution, found an optimum for the seeded weight gain of 0.4 mg/cm<sup>2</sup>. The results in pervaporation showed similar fluxes than those of Kondo et al. However, the calculated separation factor of 500 was smaller.

Huang et al. [140] also developed a vacuum seeding method that resulted in a 6  $\mu\text{m}$  zeolite layer that separates a mixture 5/95 = H<sub>2</sub>O/*i*-PrOH at 343 K with a separation factor >10000 and a water flux of 1.67 kg/m<sup>2</sup> h. The optimal conditions corresponded to a solution of a concentration of 7 g/L, with seeds of 3000 nm, and the vacuum applied for the seeding was 0.0150 kPa during 90 s.

Table 10.4 also shows the values obtained by Kondo et al. [137], with varying ethanol concentrations at different temperatures. As the concentration of water in the feed increases, the separation factor increases. The water adsorbs in the inter- and intracrystalline pores of the zeolite A, hindering the permeation of ethanol, which typically occurs up to a value around 10 wt% of H<sub>2</sub>O where there is no more increase, as it was observed by several authors [115,141]. The water flux increases as the water concentration increases, because the driving force for pervaporation increases. The temperature does not affect significantly the separation factor; however, the flux rises markedly since the mobility and diffusion of the molecules increases with temperature, due to surface diffusion is a temperature-activated process.

The separation of other alcohols different from ethanol has also been studied by Okamoto et al. [141] who found out that the separation factor increases in the order *i*-PrOH > *n*-PrOH > EtOH > MeOH as the kinetic diameter decreases. The methanol

**TABLE 10.5**  
**Dehydration of Alcohols Results in Pervaporation for Zeolites Different than Zeolite NaA**

Si/Al	Zeolite	Mixture	Temperature (°C)	Flux (kg/m <sup>2</sup> h)	$\alpha$	Ref.
1.3	X	H <sub>2</sub> O/EtOH (10)	75	0.89	360	[106]
1.9	Y	H <sub>2</sub> O/EtOH (10)	75	1.59	130	[106]
	Y	H <sub>2</sub> O/EtOH (10)	75	3.9	109	[148]
	ZSM-5	H <sub>2</sub> O/ <i>i</i> -PrOH (5)	80	0.14	501	[119]
15.9	ZSM-5	H <sub>2</sub> O/ <i>i</i> -PrOH (10)	75	3.14	690	[142]
	MOR	H <sub>2</sub> O/ <i>i</i> -PrOH (10)	75	0.1	3360	[143]
	MOR	H <sub>2</sub> O/ <i>n</i> -PrOH (10)	75	0.2	1782	[143]
	MOR	H <sub>2</sub> O/EtOH (10)	150	0.33	310	[101]
	MOR	H <sub>2</sub> O/EtOH (15)	70	1.32	5200	[144]
7.3	MOR	H <sub>2</sub> O/ <i>i</i> -PrOH (10)	75	0.255	330	[142]
3.6	T	H <sub>2</sub> O/EtOH (10)	75	0.81	830	[131]
	T	H <sub>2</sub> O/EtOH (10)	75	0.6	4400	[131]
	T	H <sub>2</sub> O/MeOH (10)	75	0.16	37	[130]
		H <sub>2</sub> O/EtOH (10)	75	1.10	900	
		H <sub>2</sub> O/ <i>i</i> -PrOH (10)	75	2.2	8900	
	ETS-4	H <sub>2</sub> O/EtOH (10)	r.t.	0.02	300	[46]
	ETS-10	H <sub>2</sub> O/EtOH (10)	140	1.1	12	[49]

Note: r.t. stands for room temperature.

molecule (0.38 nm) is smaller than the pores of the zeolite A and could enter the pores, decreasing the separation factor and the water flux.

### 10.5.2.2 Alcohol Dehydration: Other Zeolites

Zeolites different from zeolite A have also been employed in the dehydration of alcohols, such as FAU structure with zeolites X and Y [106], ZSM-5 [119,142], MOR [142–147], T [130,131] and also zeolite related materials, ETS-4 [24] and ETS-10 [27]. The published results are shown in Table 10.5. Separation factors and water fluxes are smaller than those in zeolite A. This behavior was expected since zeolite A is the most hydrophilic, which results in higher water fluxes; also, the pore opening in zeolite A is smaller than the alcohol kinetic diameter, which makes it shape selective, and this does not occur in the other zeolites. The Si/Al ratio is higher and makes them more stable under acidic conditions. The highest separation factor could be observed for the zeolite T and the mordenite prepared by Zhang et al. [144]. This result could be explained based on the different structures [113]; FAU structure possesses only 12-membered ring (MR) pores whereas zeolite T (OFF structure) and MOR possesses, in addition, 8-membered ring pores which lay perpendicular to the 12-MR pores. As the zeolite layer is randomly oriented these 8-MR provide an alternative pathway to water, hindering ethanol diffusion and giving rise to higher selectivities for MOR and T.

### 10.5.2.3 Water Removal in Acid Solutions

Although the performance of zeolites different than zeolite A is lower, the acid stability of these zeolites is higher than that of zeolite A and makes them good candidates for the separation of acid mixtures. Both, the separation of water in the esterification reaction for equilibrium displacement in a membrane reactor, and the separation of the water/acetic mixture, required a water permeable acid-resistant membrane. The most promising results concerning separations in acid medium have been obtained with zeolite T [130–132] and MOR [147]. Li et al. [147] synthesized MOR in the outer part of an  $\alpha$ -Al<sub>2</sub>O<sub>3</sub> support, and studied the effect of crystallization time on the separation of water/*i*-propanol mixtures (10/90 wt%). All the membranes showed a high-separation factor around 4000, and as the synthesis time increased the water flux decreased, due to the increase in the membrane thickness. The membrane obtained after 2 h synthesis time was tested in a water/acetic acid mixture (50/50 wt%) at 80°C. A separation factor of 900 and a water flux of 0.67 kg/m<sup>2</sup> h were obtained. The effect of temperature, from 40°C to 90°C, and that of concentration from 50 to 90 wt% of acetic acid in the feed were also studied. The flux of water and acetic acid increased with temperature, due to an increase in the partial vapor pressure, which is the driving force for pervaporation. A linear dependence between the partial vapor pressure and the water and acetic acid fluxes was obtained. At high acetic acid concentration, 90 wt%, the separation factor decreases to almost 50. After the exposure to this mixture, the membrane was cleaned with pure water and tested again in a 50/50 wt% water/acetic acid mixture at 80°C showing a water flux of 0.614 kg/m<sup>2</sup> h, similar to the one obtained previously, and a slight decrease in the separation factor, resulting in a final value of 299. The authors concluded that this decrease was not related to a deterioration of the membrane. The decrease in separation

factor with the acetic acid concentration could be explained by an association of water and acetic acid molecules that lowers the amount of water adsorbed in the zeolite.

For a zeolite T (OFF structure, 0.68 nm XRD pore diameter), Tanaka et al. [131], observed that the separation factor of a water/acetic acid (50/50 wt%) measured at 75°C decreased monotonically after the immersion of the membrane into the acetic acid mixture. Initially, the separation factor and water flux were 182 and 1.46 kg/m<sup>2</sup> h, respectively, and after 32 h these values changed to 86 and 1.77 kg/m<sup>2</sup> h, showing a deterioration of the membrane. Cui et al. [130] also studied the stability of crystals and membranes of zeolite T in acid medium. The powders were immersed in a 50/50 wt% water/acetic acid mixture for 7 days at 75°C and also in HCl solutions 0.5 and 1 M for 1 h at 50°C. The analysis of the samples after the treatment by ICP and XRD indicated that the sample treated in the acetic acid solution maintained its original Si/Al ratio equal to 4; however, the hydrochloridric acid treatment with the 1 M solution destroyed the zeolite structure and the 0.5 M solution dealuminated the zeolite to a Si/Al equal to 8.9 and the XRD analysis corresponded to zeolite T. The membrane performance, after being used for 1 week at different water/acetic acid concentrations, remains almost unchanged and the separation factor of the membrane treated in HCl dramatically decreased as was expected.

The pervaporation of water/acetic acid mixtures was also evaluated with ZSM-5 membranes by the Matsukata group [129]; the initial values of the separation factors in a 50 wt% acetic acid aqueous solution were around 10 to 20 due to the preferential adsorption of acetic acid which decreased the amount of water adsorbed. To increase the amount of water adsorbed, a surface modification that consisted of an alkali treatment with NaOH was carried out. After the treatment, the water flux and separation factor increased markedly, reaching values up to 381 and 0.783 kg/m<sup>2</sup> h, respectively.

Masuda et al. [149] also prepared a hydrophilic acid-proof silicalite-1 membrane by removing the template using a liquid-phase oxidation method with hydrogen peroxide. The selective permeation of water molecules occurred through the silanol groups formed in the micropores of the silicalite and in the intercrystalline defects of the membrane, obtaining very low fluxes of water ( $2 \times 10^{-4}$  kg/m<sup>2</sup> h). Kalipcilar et al. [150] prepared a SSZ-13 membrane able to break the azeotrope of H<sub>2</sub>O/HNO<sub>3</sub>, the permeate concentration was 38.3 wt% HNO<sub>3</sub>, and the total flux was 0.12 kg/m<sup>2</sup> h at 25°C.

#### 10.5.2.4 Organic Dehydration

General-purpose organic solvents used in the chemical industry that are difficult to separate with conventional methods represent a potential area where pervaporation finds applications. The use of polymeric membranes in this case was not very successful due to the low chemical stability of the polymers in the organic solvent. The separations that have been accomplished up-to-date with zeolite membranes include tetrahydrofuran, dimethylformamide, and dioxane.

Tetrahydrofuran, THF, is an important industrial solvent and forms an azeotropic mixture at 5.3 wt% with water (see Table 10.3). To separate water/THF, Li et al. [148] tested the pervaporation performance of different hydrophilic zeolite membranes, zeolite A, zeolite Y, MOR, and ZSM-5. The preliminary test showed that the separation factor increased as the Si/Al ratio of the zeolite decreased, except for the case of zeolite A. This fact is probably due to the lower quality of this membrane with respect to the others; since in the permeation of triisopropylbenzene (TIPB), showed the highest flux, 3.1 g/m<sup>2</sup> h, indicating the presence of nonselective defects. Therefore, the best results were obtained with zeolite Y, rendering a separation factor of 300 with a water flux of 2.24 kg/m<sup>2</sup> h at 60°C. The water flux increased with water concentration in the feed, up to a value of 15 wt%, indicating that the zeolite was saturated, as was the same for the case of water/ethanol mixtures in zeolite A, previously described. At the same time, the separation factor decreases as water concentration decreased. The stability of the membrane was also studied, showing a stable performance after 35 h of operation.

Urtiaga et al. [151] studied the dehydration of industrial solvents, THF and acetone, using a commercial zeolite A membrane (SMART Chemical Company Ltd., United Kingdom). As it was previously pointed out, the separation factor strongly depends on the water concentration in the mixture, achieving a maximum separation factor of 20,000 at 0.8 wt% of water in the feed. In general, separation factors are higher than those obtained by Li et al. [148]. However, water fluxes are smaller despite the water flux increases 2.4 times when the temperature increases from 45°C to 55°C (see Table 10.6). Better results were also attained for a water/THF (10/90) wt% mixture with an inorganic silica–zirconia membrane [152], a separation factor of 2200 and a water flux of 7.2 kg/m<sup>2</sup> h was achieved.

Okamoto et al. [141] studied several water/organic systems that are listed in Table 10.6, and the performance of the zeolite A membrane was excellent for all the separations. These results could be also compared with the ones obtained using microporous silica membranes [153]. Silica membranes, for a water/dioxane (10/90 wt%) mixture at 60°C, showed a separation factor of 125 and a water flux of 2.2 kg/m<sup>2</sup> h. For dimethylformamide, (DMF), the results obtained for a mixture of water/DMF (13.2/86.8 wt%) were 30 and 0.225 kg/m<sup>2</sup> h for the separation factor and water flux, respectively. In both separations, zeolite A outperforms the microporous silica membrane.

#### 10.5.2.5 Removal of Organics from Water

Unlike the others this application demands a hydrophobic membrane; therefore, silicalite-1 with a Si/Al ratio equal to infinity is the most studied for the separation of ethanol from water, although the hydrophobic Ge-ZSM5 [154] and  $\beta$ -type membranes

**TABLE 10.6**  
**Pervaporation Performance in Organic Dehydration of Solvents with Zeolite Membranes**

Zeolite	Solvent (H <sub>2</sub> O wt%)	Temperature (°C)	Flux H <sub>2</sub> O (kg/m <sup>2</sup> h)	$\alpha_{A/B}$	Ref.
A	Dioxane (10)	60	1.87	>9000	[141]
A	DMF (10)	60	0.95	>9000	[141]
A	Acetone (10)	50	0.91	5600	[141]
A	Acetone (5)	50	0.83	6800	[141]
A	THF (6.7)	60	0.49	50	[148]
Y	THF (5)	60	2.1	360	[148]
Y	THF (6.7)	60	2.4	200	[148]
MOR	THF (6.7)	60	0.42	15	[148]
A	Acetone (10)	48	0.314	50	[151]
A	THF (7)	55	0.98	1240	[151]

have been also studied. The separation factors for the ethanol/water mixtures, with values from 10 to 125, and ethanol fluxes, with values from 0.1 to 0.3 kg/m<sup>2</sup> h, obtained with these membranes are far from the values obtained with the hydrophilic membranes for organic dehydration. The presence of silanol groups on the surface of the crystals and in between them (i.e., in the intercrystalline defects) contributes to the permeation of water, decreasing the organic/water selectivity and permeation flux of the organic component [113].

Bowen et al. [74] studied the separation of a wide variety of organic compounds in organic/water mixtures (5 wt %) using a Ge-ZSM-5 membrane. Different organic functional groups were studied: alcohols, aldehydes, carboxylic acids, esters, ethers, and ketones. The separation factor and flux linearly correlated with the fugacity of the organic component in the mixture, which is the driving force for pervaporation.

#### 10.5.2.6 Organic Separations

The synthesis of methyl-*tert*-butyl ether, MTBE, attracted much interest in the past years due to its use as an additive in gasoline; however, after the presence of MTBE in groundwater was observed, as the result of leaks in storage tanks, the Environmental Protection Agency [155] investigated and labeled MTBE as a “potential human carcinogen.” Since January 2004 some states in the United States, including New York and California, banned its use; although this is still a controversial issue since no carcinogenic effects have been demonstrated yet. The separation of MeOH from MTBE was first accomplished by Sano et al. [127] using a silicalite-1 membrane. Their results in pervaporation were above the vapor–liquid equilibrium curve, but the separation factors (4–10) and methanol flux (0.08–0.12 kg/m<sup>2</sup> h) were very low. The results obtained by Kita et al. [112] with zeolites Y and X improved markedly, showing methanol fluxes of 1.70 and 0.46 kg/m<sup>2</sup> h, respectively, and separation factors higher than 5300.

The separation of *n*-hexane/2,2-dimethylbutane, (DMB), another separation where size exclusion takes place, has been accomplished by Flanders et al. [156], using pervaporation and vapor permeation. Both, the *n*-C<sub>6</sub> and DMB fluxes are higher in the former case due to the higher driving force in pervaporation, leading to a lower selectivity compared to vapor permeation. The separation of xylene isomers on MFI membranes has been described in Section 10.4.2.1 as a separation where size exclusion takes place. The results of the separation of these isomers using pervaporation with FER membranes [20] and MFI [21] were not successful, and very low fluxes of 10<sup>-9</sup> and 10<sup>-7</sup> mol/m<sup>2</sup> s, accompanied by separation factors not greater than 16, respectively, were obtained. The best results for the pervaporation of xylenes were obtained by Yuan et al. [129] who prepared a template free silicalite-1 membrane, the separation factor for a 50/50 wt% mixture of *p*-xylene/*o*-xylene at 50°C was 60, and the flux of *p*-xylene was 13.7 × 10<sup>-2</sup> kg/m<sup>2</sup> h.

## 10.6 ZEOLITE-MEMBRANE REACTORS

Zeolite-membrane reactors belong to the area of inorganic membrane reactors, a field that started in the 1980s and has witnessed intense research activity during the last decade as is evident in several reviews [157–164]. Many catalytic processes of industrial importance involve the combination of high temperature and chemically harsh conditions, two factors that strongly favor inorganic membranes over their polymeric counterparts even though there is a large cost differential (ceramic membranes, which are generally used as supports for zeolite layers, are 10–100 times more expensive than polymeric ones [78]).

More specifically in the area of this overview, zeolite materials constitute the main group of microporous membranes with regard to their potential membrane-reactor applications. The wide variety of existing zeolite structures, together with the possibility of modifying their adsorption and catalytic properties, provides us with a working material of high flexibility. As a

**TABLE 10.7**  
**Classification of Inorganic Membrane Reactors**

Inert membrane reactors (IMRs)	The catalyst is located apart from the membrane structure
Catalytic membrane reactors (CMRs)	The membrane material itself is catalytic or becomes catalytically active during preparation by the addition of active precursors
Combined	There is a catalytic material both inside and outside the membrane

matter of fact, zeolite-membrane reactors have undergone an impressive expansion, thanks to the availability of procedures to prepare zeolite membranes and layers with sufficient quality and reliability.

Nevertheless, the development of zeolite-membrane reactors still requires improvements in the fluxes and separation factors attained to date, an objective to which many efforts have been devoted in recent years with the aim of materializing an industrial application of zeolite-membrane reactors. Several reviews have been published in the last 5 years dealing completely or partially with zeolite membranes [2,3,5,161,162,165–167]. Particularly, noteworthy have been the advances regarding the use of supports of different natures and characteristics (see Section 10.6.4), the control of the orientation and thickness of zeolite layers (see Section 10.2.1.2), and the preparation of new zeolite materials such as membranes (see Section 10.3). In spite of these advances, before zeolite-membrane reactors are used in industry (see Section 10.6.5), significant progress must be achieved in more prosaic issues such as scale-up and control of the synthesis process to increase membrane reproducibility.

After a rapid revision of the general working principles of inorganic membrane reactors, comprehensively discussed in the previously quoted reviews; the present overview is focused on applications for already proposed inorganic membrane-reactor types as well as new reactor concepts involving zeolite membranes and coatings [5,6]. Starting from the general basis, we have selected recent developments (mainly over the last 5 years), from authors' point of view, to represent suitable illustrations of reactor concepts, interesting applications, or emerging ideas.

### 10.6.1 GENERAL CONSIDERATIONS ON INORGANIC MEMBRANE REACTORS

The concept of combining membranes and reactors is being explored in various configurations, which can be classified according to the role played by the membrane (see Table 10.7). Different membrane shapes can be used: flat discs, tubes (dead end or not), hollow fibers, metal gauze, foils, or monolith multichannel elements; but for simplification purposes all the reactor schemes shown here are for a tubular geometry. When an inert membrane reactor (IMR) is used, the catalytic material does not form part of the membrane. A typical configuration is a tubular membrane enclosing a fixed bed of catalyst. In this case, the membrane does not participate in the reaction directly, but it is used to add (reactant distribution) or remove (product removal) certain species from the reactor. The most widely used application involves equilibrium displacement by the removal of at least one reaction product, which preferentially (mesoporous membranes) or selectively (dense membranes) permeates through the membrane (see Figure 10.21a). The equilibrium constant does not change, but the product is removed from further contact with the catalyst so that a reverse reaction cannot occur. Most often, the removal of  $H_2$  in dehydrogenation reactions has been the process of choice, although other processes such as decomposition or syngas production have also been studied. Equilibrium displacement can be enhanced through reaction coupling (see Figure 10.21b) on both sides of the membrane where complementary processes are carried out. The reactions often use different catalysts, which are packed on opposite sides of the membrane.

A second application of IMRs consists of using the membrane to distribute a reactant to a fixed bed of catalyst packed on the opposite side (see Figure 10.21c). The most frequent case corresponds to a series-parallel reaction network where there is a favorable kinetic effect regarding the partial pressure of the distributed reactant. Thus, IMRs have been used successfully as oxygen distributors in many oxidations; where not only greater selectivity with respect to conventional arrangements is obtained but also a safer operation where a reduced formation of hot spots, lower probability of runaway, and catalyst life enhancement are achieved.

For catalytic membrane reactors (CMRs), the catalytically active membrane often acts as a contactor in which the diffusion of reactants through a finite catalytic layer inside the porous structure takes place. The concept can be used with an opposing reactant mode or with a forced flow mode. In the former case (see Figure 10.22a), the catalytic membrane is used to keep reactants segregated on its either side providing a safer operation which is really important for oxidation processes. Suitable operation conditions provide us with a catalytic-engineered reaction zone where reactants are in a stoichiometric ratio preventing their slip to the opposite side and minimizing further reaction to undesired by-products by controlling the residence time of the products. This configuration has been applied to both equilibrium (alkenes hydrogenation) and irreversible reactions (partial oxidations, wet air oxidation of organic contaminants). In particular, triphasic (gas/solid/liquid) reactions (see Figure 10.22b), which are limited by the diffusion of the gaseous reactant into the liquid phase up to the catalytic surface, are significantly improved by using this concept [168–173].

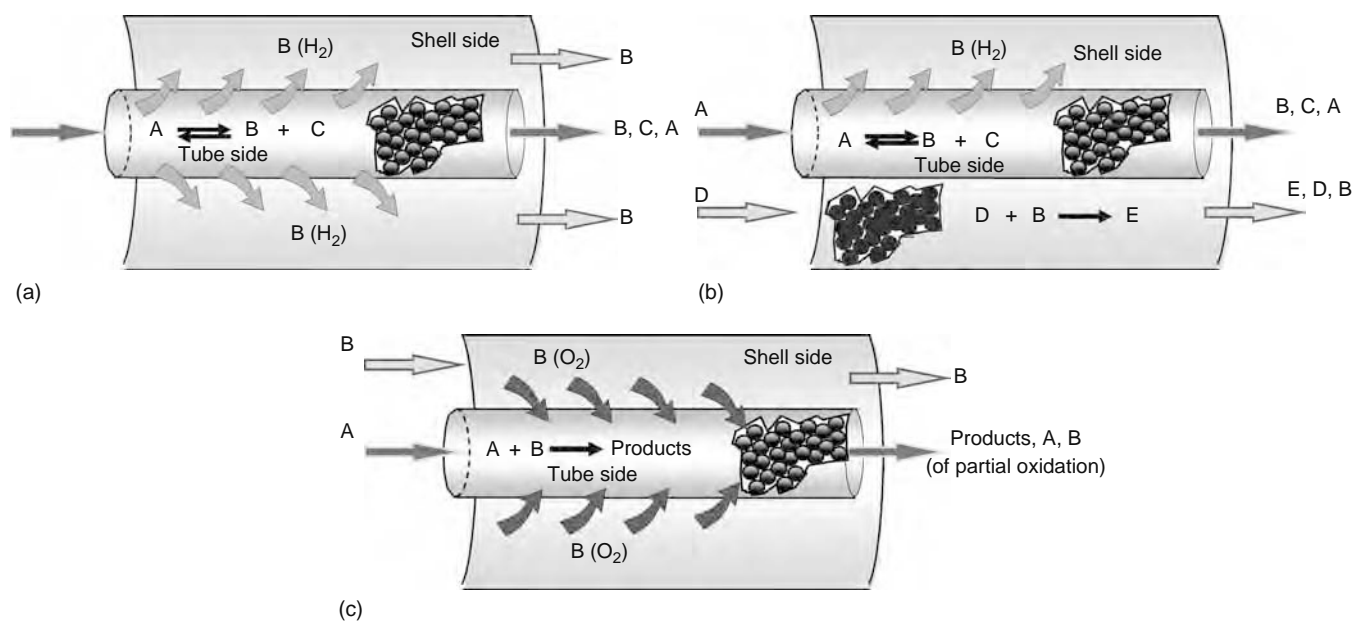


**FIGURE 10.21** (See color insert following page 588.) Traditional applications of inorganic membrane reactors for (a) conversion enhancement by product removal, (b) permeation of products and reaction coupling, and (c) selectivity enhancement by reactant distribution.

Finally, in catalytic membrane reactors operating in flow-through configuration (see Figure 10.22c), largely investigated for enzyme-catalyzed reactions, a premixed feedstream is forced to permeate through the catalytic membrane with the objective of attaining higher conversions by decreasing mass transfer resistances at the expense of a significant pressure drop.

### 10.6.2 TRADITIONAL APPLICATIONS OF ZEOLITE-MEMBRANE REACTORS

It has been considered traditional applications of zeolite-membrane reactors those based on reactor concepts already demonstrated using mesoporous or dense membranes. These include conversion enhancement by equilibrium displacement or by the removal of inhibitors, and selectivity enhancement by reactant distribution. For such cases, the zeolite membrane is usually catalytically inert and is coupled with a conventional fixed bed of catalyst placed on one of the membrane sides.

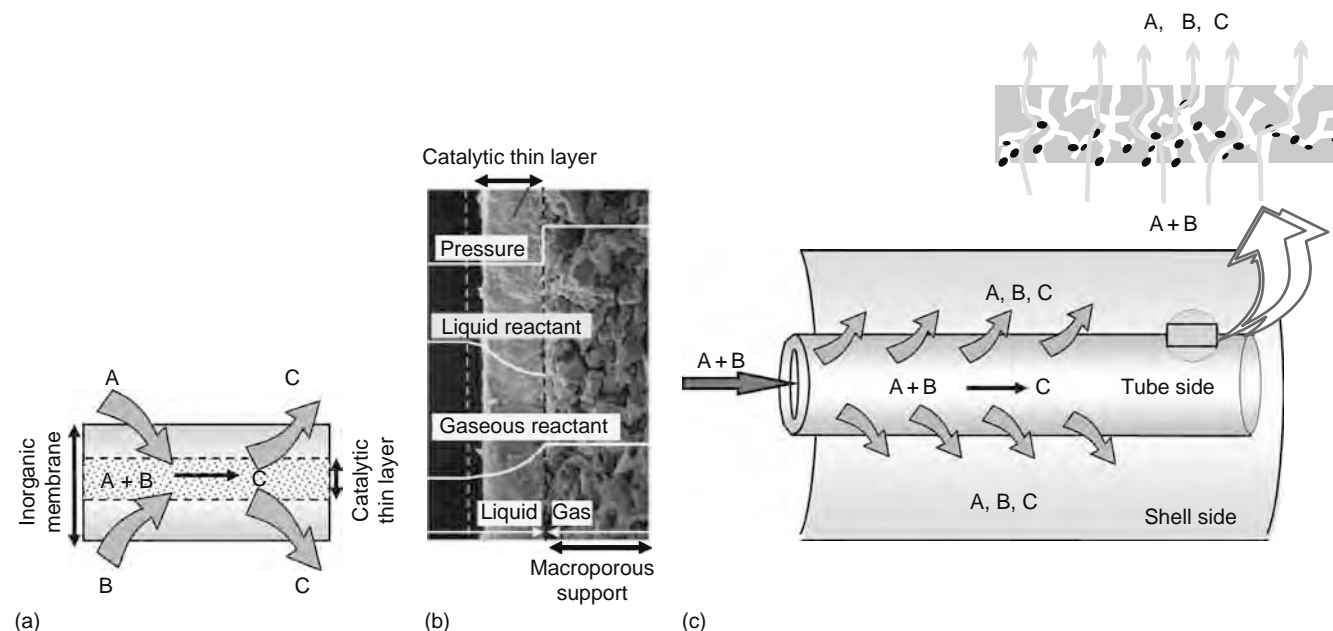


**FIGURE 10.22** (See color insert following page 588.) Applications of catalytic membrane reactors as (a) contactors using opposing reactant mode, (b) interfacial contactors for triphasic reactions, and (c) efficient gas–solid contactor using forced flow mode.

### 10.6.2.1 Zeolite-Membrane Reactors for Conversion Enhancement by Product Removal

The removal of products to increase conversion in equilibrium-limited reactions is indeed one of the first applications that comes to mind when considering membranes in a reaction environment. To make beneficial the use of the membrane reactor, the membrane employed must be able to separate preferentially at least one of the products from the reaction mixture, at a reasonable rate and selectivity. If the selectivity of the membrane is insufficient, reactant loss will become significant and the overall conversion in the membrane reactor will be lower than in a conventional packed bed reactor. If the permeation rate is insufficient, the ratio between the membrane surface area required and the volume of the catalyst bed will become unrealistic.

With the development of zeolite membranes, the field of possible applications has become much broader. Successful reaction-product separation by zeolite membranes is governed by differences in the affinity of the components with the zeolite framework or by differences in the mobility of the components in the zeolite framework; i.e., besides molecular sieving and differences in diffusivities, differences in adsorption appear to be a key factor in separation selectivity [61,174].

The membrane group at IRC (Institute on Research of Catalysis, Lyon, France) has studied intensively isobutane dehydrogenation in a fixed catalytic bed using MFI membranes to permeate hydrogen [175–177]. Silicalite-1 membranes were synthesized hydrothermally [178,179] in the macroporosity of  $\alpha$ -alumina tubular supports to minimize long-range stresses during thermal cycling and to limit the maximum size of defects to the pore of the host. One of the interesting results of these studies was the realization of the need to develop specifically very active catalysts able to keep up with the high extraction ability of the membrane. Thus, catalysts designed for fixed bed operation may not be suitable for use in membrane reactors, where the reactive environment is different (deactivation phenomena may arise) and where there is a clear need to tailor the catalytic activity to match the permeation capabilities of the membrane. The need of an adapted catalyst for use in membrane reactors may be a general requirement of membrane reactors, which perhaps has received less attention than that dedicated to membranes. These authors also stressed the negative effect of reactant (isobutane) loss when the membrane is not selective enough to avoid it.

The catalytic dehydrogenation of cyclohexane in an FAU-type zeolite-membrane reactor packed with a 1 wt% Pt/ $\text{Al}_2\text{O}_3$  catalyst has been studied by Jeong et al. [180,181]. The conversion of cyclohexane in the membrane reactor is increased beyond the equilibrium value (32.2% vs. 72.1% at 473 K) due to the simultaneous and rapid removal of benzene and hydrogen from the reaction-site side by a sweep flow rate, although the separation factors for benzene over cyclohexane were not high enough at reaction temperatures (around 10). Furthermore, the results of the simulation for the membrane reactor in which  $\text{H}_2$  is co feed with cyclohexane demonstrate the coke inhibition by its relatively high-partial pressures in the reaction side. This is probably the most useful feature of zeolite-membrane reactors in comparison with their counterparts based on Pd dense membranes.

Zeolite membranes have also been used for hydrogen separation in syngas production. The study of  $\text{CO}_2$  reforming of methane over a catalytic membrane reactor at 700°C–750°C has been reported by Liu et al. [182,183] who used composite  $\text{La}_2\text{NiO}_4$ -NaY and  $\text{La}_2\text{NiO}_4$ -NaA catalytic membranes, respectively, with an enclosed packed bed of catalyst in the tube side. The randomly oriented zeolite membranes were prepared by in situ crystallization procedures over the internal asymmetric  $\alpha$ -alumina tubular supports, and subsequently were catalytically activated by impregnation of a La-Ni gel. For the as prepared NaY and NaA zeolite membranes, ideal  $\text{H}_2/\text{CH}_4$  separation factors at room temperature were 9.8 and 4.2, respectively; i.e., higher than the value 2.8 governed by Knudsen diffusion. However, separation factors for binary mixtures were not significantly high, not only CO and  $\text{H}_2$  but also  $\text{CH}_4$  and  $\text{CO}_2$ , diffused toward the outer tube of the zeolite membrane. To overcome this problem, the authors adopted a  $\text{La}_2\text{NiO}_4$ -composite zeolite membrane, so that there was methane conversion to syngas before permeation which led to conversion values higher (up to 21.4 mol%) than that of conventional fixed bed reactors. Moreover, the problem of catalyst deactivation due to whisker carbon formation (hard to avoid in a  $\text{CO}_2$  atmosphere) is partly resolved by adopting a membrane reactor in which the surface coking comes to an equilibrium and the performance of the catalytic membrane remains at a high level.

Ostrowski et al. [184] analyze the catalytic partial oxidation of methane at 700°C–750°C in a Ni/ $\alpha$ - $\text{Al}_2\text{O}_3$  catalyst enclosed as fixed bed or fluidized bed in a membrane reactor. The silicalite-1 membranes employed exhibited over more than 100 h of operation high thermal and mechanical stability. In both cases, the separation selectivity was low, mainly controlled by Knudsen diffusion, i.e., large amounts of methane were removed from the catalytic bed through the membrane and therefore, could not be consumed in the reforming steps. However, the stainless steel silicalite-1 immersed in a fluidized bed reactor rendered better separation selectivities to  $\text{H}_2$  but the permeation flux was not sufficient to shift significantly the equilibrium toward syngas. To estimate the permeation rates that are necessary for achieving a marked improvement of the syngas yield, these authors have developed a mathematical model [184] to simulate the membrane reactor performance under conditions relevant for industrial applications (5–30 bar and 750°C–800°C). The Peclet number, which is given by the ratio of the molar flow rates at the reactor inlet and the permeation side, necessary for  $\text{CH}_4$  conversion enhancement is also calculated.

The previous discussion illustrates the difficulties in attaining high gas-phase separation factors with zeolite membranes, even when good quality membranes are employed. In spite of these difficulties, van de Graaf et al. [185,186] managed to obtain a considerable increase in conversion (13% higher than the thermodynamic value under optimal operation conditions) and a very significant shift in product selectivity (a 34% increase in the ratio *trans*-2-butene/*cis*-2-butene) in the metathesis of

propene by using a silicalite-1 membrane supported on a flat stainless steel sheet and 16.4 wt%  $\text{Re}_2\text{O}_7/\gamma\text{-Al}_2\text{O}_3$  as a catalyst. This can be attributed to adsorption selectivity for *trans*-2-butene which is the strongest adsorbing component in the mixture able to block the pores of the zeolite for the permeation of propene (with selectivity in binary mixtures close to 5). These authors also compare the conversion in the membrane reactor with and without the presence of a pre-reactor to equilibrate the feed, making it clear that reactant loss is significantly suppressed by feeding the reactor with an equilibrated mixture.

In general, most of the high-separation factors reported for zeolite membranes are associated with pervaporation processes (see Section 10.5) or with vapor-separation applications where the permeated component is preferentially adsorbed. This has given rise to a variety of works in which the membranes have been used for equilibrium displacement by selective product permeation. The largest group probably corresponds to esterification processes, where hydrophilic zeolite membranes are employed to remove the product, water, replacing the extensively studied polymer membranes [187–192].

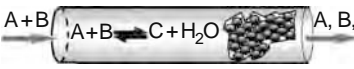
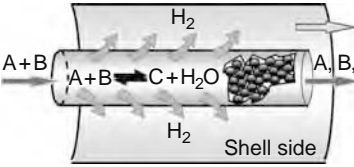
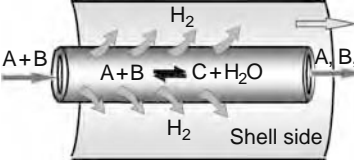
Among the publications related to this subject, Jafar et al. [139] used a tubular NaA zeolite membrane prepared on a carbon–zirconia support in the vapor space of an esterification reactor to remove the product, water, formed in the reaction of lactic acid with ethanol catalyzed by *p*-toluenesulfonic acid. This protected the sensitive zeolite A membrane from acid attack, and still allowed high-permeation fluxes responsible for the enhanced yields of ethyl lactate. Recently, Budd et al. [193] have applied a NaA/polyelectrolyte multilayer-pervaporation membrane showing a greater stability under acidic conditions in comparison with a pure zeolite A membrane and maintaining a high selectivity for water over alcohols. For the same purpose, Tanaka et al. [131,132] proposed a zeolite T membrane, prepared by *ex situ* crystallization [130], for the pervaporation-aided or vapor permeation-aided esterification of acetic acid with ethanol. This membrane has a higher acid resistance and can be directly immersed in the liquid-phase reaction mixture. The conversions achieved exceed the equilibrium limit and reached to almost 100% after a stabilization period of 8 h. Another acid-resistant zeolite with a high-potential applicability in acid–environment reactions is mordenite, which has recently been prepared as a membrane on tubular supports [142–147].

The use of zeolite membranes in esterification reactions was taken a step further by Bernal et al. [194], who used a catalytically active H-ZSM-5 zeolite membrane to carry out the esterification of acetic acid with ethanol. In this work, a closer integration of reaction and separation was sought to minimize the transport resistances present in fixed bed reactors enclosed in inert membranes. In this more traditional type of membrane reactor the products formed on the catalyst must desorb, diffuse to the membrane surface, and transport to the permeate side. Conversely, when a catalytic membrane is used, the products can be removed as soon as they are formed, displacing the local equilibrium and achieving a higher turnover rate. As an example, Figure 10.23 summarizes the results of the study. It can be seen that the conversion obtained at the same feed rate and catalyst loading was greater in noncatalytic membrane reactors (H-ZSM-5 powder catalyst + Na-ZSM-5 membrane) compared to conventional fixed bed reactors (H-ZSM-5 powder catalyst). However, the conversion was further increased with the catalytic zeolite membrane (H-ZSM-5 membrane), which clearly outperformed the catalyst + inert membrane configuration.

Water was also the targeted species in two other reacting systems that will be discussed next. Both correspond to the synthesis of tertiary ethers, i.e., typical examples of equilibrium-limited reactions where the conversion is generally low due to the limits imposed by thermodynamic equilibrium and where the presence of water has a strong inhibiting effect on the catalytic activity [194,195]. Therefore, these examples could be also included in the next section of conversion enhancement by inhibitors removal [196].

Aiouache and Goto [197] coupled a zeolite NaA membrane and a reactive distillation column during *tert*-amyl alcohol etherification with ethanol. The reacting system is complex with several azeotropes and two important side reactions. The study of residue curve maps showed that the azeotropes, where water as a component could be broken by pervaporation, while at the same time displacing the reaction equilibrium. As expected, the experimental study demonstrated significant gains in *tert*-amyl ethyl ether (TAEE) yield when the zeolite membrane tube was placed inside the distillation column. Salomón et al. [198] used Amberlyst enclosed in the annular space of hydrophilic zeolite membranes (mordenite and zeolite NaA) for the gas-phase production of methyl-*tert*-butyl ether (MTBE) from *tert*-butyl alcohol and methanol. In experiments where mixtures of the main components were present in the reactor, it was shown that water, being the most polar component, was adsorbed preferentially, and the separation selectivity obtained with respect to the other components depended inversely on the polarity of the permeating species. The selective permeation of water increased conversion beyond that attainable in a fixed bed reactor. At the same time, in the experiments with mordenite membranes, the permeance of MTBE was between 30% and 50% higher than that of isobutene (an undesired product in this system), leading to a significant enhancement in MTBE selectivity. The increase in conversion and selectivity gave rise to MTBE yields which were 6.7% points above the equilibrium predictions.

$\text{CO}_2$  hydrogenation into methanol is considered today as one of the promising methods to mitigate the greenhouse effect [199]. Barbieri [200] and Galluci [201] have studied theoretically and experimentally  $\text{CO}_2$  conversion into methanol under industrial conditions (200°C–263°C, 20–24 bar) using a fixed bed of  $\text{CuO-ZnO/Al}_2\text{O}_3$  catalyst enclosed in a zeolite-membrane reactor. The use of A-type zeolite-membrane reactors as substitution for traditional reactors is aimed at increasing  $\text{CO}_2$  conversion since, in principle, in a gas–vapor mixture ( $\text{CO}_2$ ,  $\text{H}_2$ ,  $\text{CO}$ ,  $\text{CH}_3\text{OH}$ ,  $\text{H}_2\text{O}$ ) vapors can preferentially permeate through zeolite membranes. They concluded that the selective removal of methanol was effective in reducing the rate of the reverse reaction and also in increasing the turnover rate, via accelerated desorption of methanol and water. An increase of selectivity was also expected by reducing the incidence of the competing reaction producing carbon monoxide. Particularly,

Reactor Type	Reactor Configuration	Reactant Conversion <sup>a</sup> (%)	Equilibrium Displacement <sup>b</sup> (%)
Fixed bed reactor		49.4	—
Inert zeolite membrane reactor		56.9	2.4
Catalytic zeolite membrane reactor		63.1	5.6

<sup>a</sup> Equimolar feed (ethanol/acetic acid) at 359 K

<sup>b</sup> Quaternary feed in equilibrium at 338 K

**FIGURE 10.23** (See color insert following page 588.) Ethanol esterification with acetic acid: comparison performances of different reactor types.

with regard to the methanol yield, the experimental results showed that the zeolite-membrane reactor gives the highest value, 8.7%, compared to a corresponding value of 2.4% for traditional reactor and 2.5% of the lithiated Nafion membrane reactor studied by Struis [202,203].

### 10.6.2.2 Zeolite-Membrane Reactors for Conversion Enhancement by Removal of Catalyst Poisons/Inhibitors

Applications in this field are, as could be expected, system-specific and take advantage of the particular features and operating conditions of the reaction environment. Espinoza et al. [204] used different zeolite membranes for in situ water removal under typical conditions of Fischer–Tropsch synthesis. In this system, water, a reaction product, is able to oxidize cobalt and iron-based catalysts, causing deactivation. In addition, water has an inhibiting effect on the rate of reaction over iron-based catalysts. Selective water removal with hydrophilic zeolite membranes in this system presented significant challenges due to the high temperatures involved (200°C–350°C), as the interaction between the zeolite and the adsorbed water weakens as temperature increases. However, high-partial pressures of water are also present, which help to compensate for the effect of temperature. As a result, satisfactory water/H<sub>2</sub> and water/hydrocarbon separation factors could be obtained, even at temperatures of 250°C and above.

Xiongfufu et al. [205] used Fe-MFI and MFI membranes supported on alumina tubes to carry out the dehydrogenation of ethylbenzene to styrene. The Fe-MFI membranes were prepared by in situ insertion of ferrum species during the hydrothermal treatment to combine catalysis with separation. The H<sub>2</sub>/propane separation factor quoted for the as prepared substrates at 25°C was moderately high (25.8), showing a good molecular sieving effect improved by the incorporation of ferrum species into the zeolite framework. When the Fe-MFI zeolite membrane was applied to ethylbenzene dehydrogenation at 600°C, a 15% and 5% increase in conversion and selectivity, compared with the fixed bed reactor, was observed, respectively, under certain experimental conditions. As such, this work would belong to the previous section on equilibrium enhancement. The reason discussed here is that, according to the findings of this work, the amount of styrene adsorbed on the Fe-MFI membrane was much lower than on its MFI counterpart, leading to a faster removal of the product. The authors concluded that this helped to achieve a higher conversion by preventing carbon deposition on the Fe-MFI membrane. XRD analysis of the used and fresh

membranes showed no change in the overall structure of the membrane, although minor changes have been observed for H<sub>2</sub>/N<sub>2</sub> separation factors, probably due to the pore growth in the presence of water steam at the reaction temperature.

Finally, Nomura et al. [120] used an organophilic silicalite-1 membrane supported on a porous stainless steel disk for the selective pervaporation of ethanol from a fermentation reactor at 303 K. Glucose medium with dry baker's yeast was used for the fermentation broth. In this case, the advantage of using the zeolite membrane was twofold: on the one hand, continuous removal of ethanol enabled the system to operate continuously, avoiding ethanol inhibition by keeping it at a low concentration. On the other, it produced a highly concentrated outlet stream (81%–98%, depending on the ethanol concentration of the broth), which cannot be obtained in conventional fermentation reactors as a result of the relatively high ethanol–water separation factors achieved (from 85.9 to 218).

### 10.6.2.3 Zeolite-Membrane Reactors as Reactant Distributors for Selectivity Enhancement

The concept of reactant distribution was intensely investigated with mesoporous membranes (see Refs. [162,163]), mainly for applications in selective oxidations in instances where low-partial pressures of oxygen would favor the selective oxidation vs. total oxidation. Under these conditions, distributing oxygen was beneficial and the possibility of increasing selectivity by oxygen distribution has been demonstrated for many reactions and for both inert and catalytically active membranes.

There have been a few attempts to achieve the same objective using zeolite membranes. Pantazidis et al. [206] have evaluated and compared the catalytic performances of catalytic V–Mg–O and Ni membrane reactors in the oxidative dehydrogenation of propane between 300°C and 600°C, using macroporous and mesoporous structures, and a silicalite-1 membrane reactor enclosing a fixed bed of V–Mg–O catalyst. When two reactor configurations—separate feed configuration (oxygen distributor) and co-feed configuration (flow-through contactor)—were tested, a selectivity value four times higher for the former mode was observed. Nevertheless, the best performance was achieved with the inert zeolite-membrane reactor when a separate feeding configuration at high oxygen partial pressures was used (yield to propene 14.6 at 480°C). In a second approach to the same reaction, Julbe et al. [207] used MFI and V-MFI membranes [208] between 550°C and 650°C. The direct addition of a very low vanadium content during the formation of the silica-rich zeolite framework led to stable V-MFI/ $\alpha$ -Al<sub>2</sub>O<sub>3</sub> composite membranes free of macrodefects (>50 nm). The observed activity of the MFI membrane, which should be theoretically inactive, may be related to acidic sites created after aluminum dissolution from the support during the hydrothermal synthesis (high pH) and leading to a H-ZSM-5 membrane. The propene yields were only moderate, but they were better for the V-MFI membrane. In spite of this, the performance of the membrane, in terms of selectivity and yield, when used as an oxygen distributor, was no better than in the flow-through configuration, which the authors attributed to back-mixing and residence time effects. In a later work from the same laboratory [209], several tubular inert membranes (microporous MFI zeolite, mesoporous SiO<sub>2</sub>, and meso-macroporous AlPO<sub>4</sub>) were evaluated in view of their ability to control the O<sub>2</sub> partial pressure in the catalyst side and to limit the back-diffusion of C<sub>3</sub>H<sub>8</sub> and derived products to the O<sub>2</sub>-rich side by application of a transmembrane pressure gradient. The best results were obtained with the low porosity meso-macroporous membrane, in which the viscous flow contribution to permeation provided an increased barrier effect.

Similarly, Mota et al. [210] carried out the selective oxidation of butane to maleic anhydride over VPO mixed oxides-based catalysts enclosed in an MFI membrane. Different feed configurations of the zeolite-membrane reactor were tested to outperform the conventional co-feed configuration. The results achieved were rather similar; however, the authors pointed out the possibility to take advantage of the O<sub>2</sub> distribution, which limits the flammability problems and allows operation with higher butane concentrations than those used in conventional processes.

It seems that zeolite membranes may not be the best choice as catalytic contactors and oxygen distributors to enhance selectivity in oxidative dehydrogenation of propane. This may be due in part to the intrinsic catalytic activity of the zeolite material for this reaction, which probably exerts a nonselective contribution. Therefore, this specific application operates at conditions that do not make use of the most important properties, which are characteristic of zeolite membranes. More efficient approaches for selectivity enhancement can be obtained with zeolite membranes, as shown in the next section.

### 10.6.2.4 Zeolite-Membrane Reactors for Selectivity Enhancement by Control of Reactant Traffic: A Not-So-Classic Application

As shown before, secondary reactions represent a common problem in the production of bulk and fine chemicals involving reactions such as oxidation, hydrogenation, alkylation, and halogenation. The well-known kinetic consequences of such successive reactions often require low conversion, reaction control (no transport limitation), and short residence time to achieve acceptable selectivities. Regarding the last issue, in the next section devoted to catalytic zeolite-membrane reactors, the potentiality of this technology for such purposes is demonstrated. However, a more elegant way to overcome this problem is by preventing the product from secondary reactions by taking advantage of the separation properties of microporous membranes. In this section, we are proposing a not-so-classic application for these kinds of membranes that has been scarcely explored up-to-date.

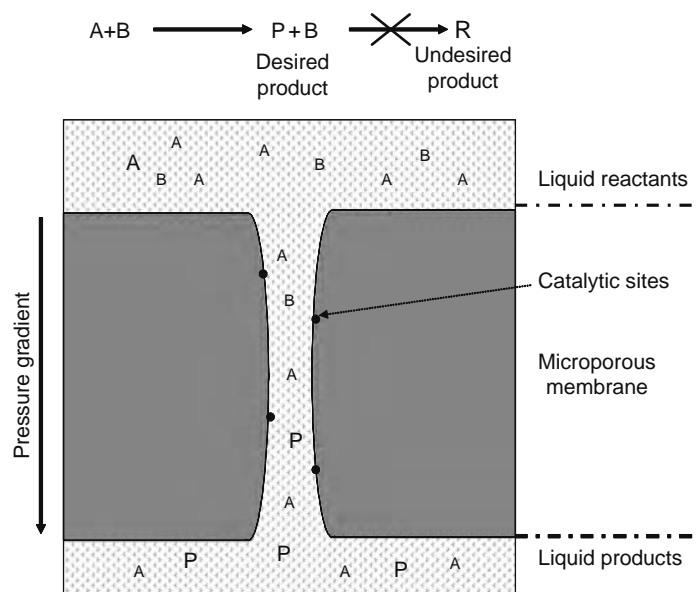


**FIGURE 10.24** Model of the prevention of secondary reactions by single-file diffusion in microporous membranes. (Adapted from Lange, C., Storck, S., Tesche, B., and Maier, W.F., *J. Catal.*, 175, 280, 1998.)

Microporous membranes in general (pore diameter  $<2$  nm) and zeolite membranes in particular have pores whose dimensions are similar to those of many molecules. This means that often molecules cannot pass each other in a restrictive pore medium, and single-file diffusion occurs. Such a molecular queuing (see Figure 10.24) may provide a new scenario for avoiding secondary reactions, i.e., to increase selectivity in consecutive reaction networks with a valuable intermediate product, as demonstrated by Lange et al. [211]. These authors used a non-zeolitic microporous Pt/TiO<sub>2</sub> catalytic membrane supported on an alumina disc to carry out the selective hydrogenation of 2-hexyne and hexadiene at 60°C–120°C. In this case, the hydrocarbon reactant (liquid phase) and the dissolved hydrogen were fed to one side of the catalytic membrane, and forced to permeate through it by using an excess of pressure (0.05–1.5 bar). If the reactants are fed in adequate proportions, under single-file diffusion transport the probability of a new collision of hydrogen with an already semihydrogenated molecule is much lower due to the one-dimensional movement through the membrane brought about by a pressure gradient across the membrane, increasing the yield to selective hydrogenation products. Under these specific conditions, the microporous membranes exhibited hydrogenation activity and selectivity significantly higher than those of comparable batch catalysts. In a mixture of possible reactants, one can also increase the selectivity by opting for the reactant that actually arrives to the catalyst. This was clearly demonstrated some years ago by van der Puil et al. [212,213], who deposited a 0.8–1.3 μm silicalite-1 layer on top of a Pt/TiO<sub>2</sub> catalyst for the competitive hydrogenation of heptene and 3,3-dimethylbut-1-ene at 100°C. Both compounds gave similar conversions when uncoated Pt/TiO<sub>2</sub> catalyst particles were used. However, on the silicalite-1 coated catalyst the conversion of heptane was 37 times faster compared to dimethylbutene due to the selective permeation of the linear compound. A second effect of the silicalite-1 layer was to limit the amount of hydrogen reaching the active layer due to blockage of the hydrogen passage by adsorbed hydrocarbons. This led to an increase in the reaction selectivity toward isomerization products. Similarly, Nishiyama et al. [214] have synthesized a 40 μm silicalite-1 layer on spherical Pt/TiO<sub>2</sub> particles (0.5 mm in diameter) to carry out the hydrogenation of a mixture of 1-hexene and dibranched 3,3-dimethylbut-1-ene. The obtained results indicate the feasibility of the application of catalyst particles coated with a permselective membrane to achieve linear reactant selectivities at molecular level.

This type of approach (reactant filtering) has a tremendous potential in fields such as reactive semiconductor sensors, where the main problem is the lack of selectivity. Figure 10.25a illustrates a typical sensor scheme. The measuring electrodes and the heating resistance are printed on either side of a suitable substrate (i.e., alumina plate). Then, the active layer is screen-printed on top of the electrodes (seen as the obscure area on the front view of the sensor in Figure 10.25b), and after a stabilizing heat treatment, the device is ready for sensing. The sensor material usually contains SnO<sub>2</sub> as the active layer, often doped with Pd, although other base metal oxides and dopants have also been employed. The conductivity of the sensor material changes after exposure to reducing gases, which react with chemisorbed oxygen. With n-type semiconductors such as SnO<sub>2</sub>, adsorbed oxygen immobilizes electrons near the surface of the SnO<sub>2</sub> particles. If a gas, such as a hydrocarbon, reacts with adsorbed oxygen, electrons are released, and the resulting increase in electrical conductivity can be related to the gas-phase concentration of the hydrocarbon. The main problem with existing semiconductor-gas sensors is that they react similarly to a variety of substances. Therefore, they are subject to interference from many other molecules that contribute to the sensor

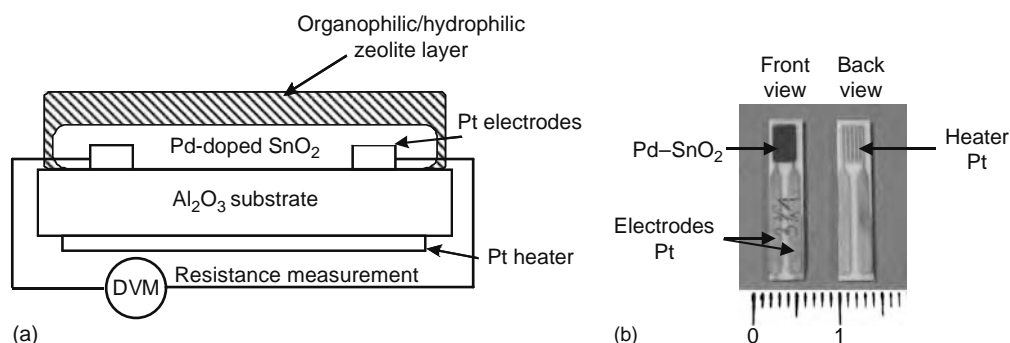


**FIGURE 10.25** SnO<sub>2</sub> sensors modified with zeolitic filters: (a) schematic representation of the zeolite-coated sensor and (b) (See color insert following page 588.) front and back view of the as-received SnO<sub>2</sub> sensors.

response. As shown in Section 10.6.6.2, Vilaseca et al. [215] were able to strongly increase the selectivity of a SnO<sub>2</sub> sensor by using zeolite films grown on top of the SnO<sub>2</sub> layer to discriminate between the molecules reaching the sensing area.

Recently, Gora et al. [216,217] have proposed the use of zeolite-membrane reactors for hydroisomerization of alkanes. Hydroisomerization of light alkanes is becoming extremely important as an alternative for octane upgrading, and consequently the integration of reaction and separation into one unit by a membrane reactor could offer new and promising industrial possibilities, densifying the process and reducing substantially operating costs. Explorative experiments with C<sub>6</sub> were carried out in a reactor in which linear molecules were separated from monobranched ones on a silicalite-1 membrane before conversion on a Pt-loaded chlorinated alumina catalyst. In this way, the equilibrium was shifted toward the product side, and by feeding only reactants to the catalyst bed, the extent of cracking and coking on the catalyst could be limited. Results of the *n*-hexane hydroisomerization experiments performed showed hexane-2-methyl pentane separation selectivity higher than 20, high hexane conversion (up to 72%), and product selectivity toward dibranched isomers (up to 36%). Hence, the inert zeolite-membrane reactor has an enormous potential in upgrading low octane value hydroisomerization feed streams.

### 10.6.3 CATALYTIC ZEOLITE-MEMBRANE REACTORS

The vast majority of the examples discussed up to now, with some exceptions [182,183,194,207], deal with membrane-assisted reactors in which zeolite membranes do not play any direct role in the catalytic reaction because the catalyst is physically separate from the inert support. However, if the membrane acts as an active contactor, the controlled diffusion of reactants to the catalyst can lead to an engineered catalytic reaction zone. Two main configurations of catalytic membrane reactors can be considered here: (1) the catalyst dispersed or immobilized in an inert zeolite membrane, and (2) an inherently catalytic zeolite membrane. In the former approach, the catalytic and separation functions are engineered in a very compact fashion, whereas for the latter, the zeolite membrane serves as both separator and catalyst. Regardless, the concept can be used in flow-through configuration or with an opposing reactant mode (see Figure 10.22) to improve the access of reactants to the catalyst. In general, the flow-through configuration contactor has been traditionally applied for enzyme-catalyzed reactions, whereas the opposing reactant mode is normally used when the reaction is considerably fast compared to transport resistance.

Relatively, few examples have been found in literature about catalytic zeolite-membrane reactors, and most of them are related with the fine chemicals industry as is shown in the following sections.

#### 10.6.3.1 Catalytic Zeolite-Membrane Reactors for Selectivity Enhancement by Control of Residence Time

A high quality zeolite membrane ideally constitutes a controlled thickness interphase with homogeneous properties. When the membrane has catalytic activity it should be possible, theoretically, to tailor the operating conditions in such a way as to obtain an optimum contact time of the reactants, which render in higher yields to the desired product. This concept has been demonstrated for *i*-butene oligomerization in gas phase [218] and methanol reaction into olefins [219]. In the former work, *i*-butene oligomerization was carried out at 323–423 K in a flow-through  $\beta$ -zeolite film prepared on a porous  $\alpha$ -alumina tubular support. The process gives not only *i*-octene from *i*-butene but also unwanted C<sub>12</sub> and C<sub>16</sub> products. By controlling the residence time of the reactants in the membrane pores, the authors not only increased the *i*-octene selectivity and yield with respect to the homologous catalytic fixed bed reactor but also reduced the deactivation of the catalytic membrane. As a result, while deactivation of a fixed bed reactor (containing the same zeolite as a catalyst) occurred in 4 h, the authors were able to operate their membrane reactor for nearly 170 h without loss of activity. This suggests that the same mechanism that minimized the formation of C<sub>12</sub> and C<sub>16</sub> products also prevented the oligomerization processes giving rise to coke precursors.

Using a similar approach, Masuda et al. [219] employed a ZSM-5 zeolite membrane in a flow-through configuration for the methanol-to-olefins process. As in the previous work, permeating molecules would ideally have a uniform residence time

within the catalytic zeolite layer, while a wide distribution of residence times would exist in fixed bed and fluidized bed reactors. In this reacting system, methanol is first converted to dimethylether, then to olefins. However, further reaction produced paraffins and aromatics, which in this case are the unwanted final products. By optimizing the match between diffusion rate and chemical reaction rate, the authors were able to produce olefins with high selectivity (about 80%–90%) from methanol at high conversions (60%–98%).

Another way to control the residence time of valuable intermediate products within the reactor is to use a selective membrane to remove them from the reaction environment as they are produced before they can react further in consecutive reactions. Therefore, it is a classical example of an IMR in which a considerable increase in the yield to the desired product can be obtained, provided that the membrane is sufficiently selective to the intermediate product under reaction conditions. Regarding this approach, Piera et al. [220] solved the selectivity problem already discussed in the oligomerization of *i*-butene by removing selectively the *i*-octene formed using an MFI zeolite membrane surrounding a fixed bed of acid resin catalyst. In liquid-phase experiments (3–25 bar and 20°C–80°C) with different mixtures it was shown that the membrane was able to selectively separate *i*-octene from the other components present in the mixture. This reaction system is not equilibrium limited under the conditions used. However, the simulations carried out showed that the use of a zeolite-membrane reactor could result, not only in higher reaction selectivity but also in a higher conversion, due to the increase of the residence time of *i*-butene in the reactor as products are selectively removed. The experiments confirmed these predictions, and the zeolite-membrane reactor gave *i*-octene yields that were up to 27% higher than those found in a fixed bed reactor under comparable conditions.

Degradation of volatile organic compounds (VOCs) has also been tested on catalytic zeolite-membrane reactors. Maira et al. [221] have studied the photocatalytic oxidation (PCO) of an airborne VOC pollutants such as trichloroethylene. These authors prepared a hybrid membrane-catalyst by secondary growth of silicalite-1 onto a porous stainless steel plate followed by coating with a nanostructured anatase TiO<sub>2</sub> suspension. The reactor could be operated in a flow-through or in a parallel flow configuration, and it was found that both the trichloroethylene conversion and the selectivity to CO<sub>2</sub> were significantly higher in the flow-through configuration. The authors explained the higher selectivity toward deep oxidation products as a result of the molecular sieving function of the membrane toward the smaller products from total mineralization. In this way, the permeation of larger pollutant molecules would be delayed, allowing for longer residence times and higher conversion. In a recent publication, Aguado et al. [222] proposed the use of a Pt-ZSM-5 membrane reactor for the combustion of *n*-hexane, present at low concentrations in air (1000 ppmv), using an opposing reactant mode configuration. The role of the zeolite is to adsorb and concentrate the VOC on the retentate side, thereby facilitating reaction; whereas the presence of air as sweep gas (which in this case is also a reactant) facilitates diffusion toward the permeate side where the catalyst is preferentially located. The investigation deals mainly with the relationship between the permeation properties of the zeolite membrane and its performance as a reactor. Unlike the previous cases, here, the control of the residence time is modulated by the concentration of intercrystalline defects within the zeolite layer. Thus, while it could be expected that membrane reactor performance would increase with membrane quality, this does not seem to be the case. Apparently, in membranes with a moderately high value of the SF<sub>6</sub> permeance, the presence of intercrystalline voids facilitates the penetration of reactant molecules into the membrane and their contact with the catalyst. As a result, nearly complete combustion of *n*-hexane is achieved at 210°C. On the other hand, for membranes with a low SF<sub>6</sub> permeance, diffusion takes place essentially through the zeolite-pore network. This is a slower process in comparison with the reaction kinetics, and given the residence time of the molecules in the retentate side, only a fraction of the molecules actually have the chance to come into contact with the catalyst.

Finally, Hasegawa et al., in a series of works [223–226] dealing with the oxidation of CO when it is present at low concentrations in a hydrogen atmosphere (a very important subject for the practical implementation of fuel cells), have demonstrated the benefits of a zeolite-membrane reactor working in an opposing reactant mode configuration. In the first of these works [223], the authors used Pt-loaded Y-type zeolite membranes, prepared by secondary growth over tubular supports followed by ion exchange, as interphase contactor for a H<sub>2</sub> stream containing 10<sup>4</sup> ppm of CO at temperatures of 200°C–250°C. The residence time of H<sub>2</sub> crossing the membrane was too short to react with O<sub>2</sub>, and the residence time of CO was in the range of values used for selective CO oxidation in a conventional packed bed reactor; thus the reaction of CO was favored. In this way, 1000 ppm of CO in the feed could be reduced to less than 8 ppm at the permeate side. Other metals (Ru, Rh, Ni, Cu, Ag) were also exchanged on zeolite Y [188], but the best results were obtained with the Pt/zeolite Y membrane.

Apart from this, it is worthwhile to emphasize the potential application of zeolite-based membranes as electrolytes for direct methanol fuel cells (DMFCs) due to their proton conduction properties (4227). Existing Nafion-based proton exchange membrane (PEM) fuel cells still face significant challenges related to CO poisoning of the catalyst at the anode, water management, and slow kinetics. Increasing the operating temperature significantly above 100°C would help to solve these problems but would decrease the hydration needed for proton conduction. Zeolite particles seem to be ideal candidates as polymer fillers on account of their hydrophilicity and proton-transport capabilities [228–231]. Although the proton transport across the zeolite membranes tested thus far is still low compared to PEMs employed in fuel cells, transport in zeolites can be optimized by increasing the number of proton exchange sites on the zeolite, an area where work is still lacking. DMFCs add a further constraint: methanol crossover must be avoided as it reduces both the cell efficiency as well as the efficiency of fuel utilization. Methanol leaking is a serious problem for current Nafion membranes, which are good conductors but poor methanol

barriers. Two main alternatives seem possible at this point. On the one hand, Nafion-zeolite membranes could be prepared [230,232], with the aim of maintaining the good proton-conducting properties of Nafion, and at the same time, increasing methanol rejection as the proportion of zeolite filler increases. On the other hand, composite polymer-zeolite membranes could be prepared, where the polymer material is chosen to achieve low methanol diffusion [228]. Libby et al. [231] added a further possibility related to tailoring the properties of the polymer by thermal treatment. After treating their membrane at 150°C for 27 h, the permeability of the PVA phase has decreased enough so that their PVA/mordenite membrane showed a 20-fold improvement in selectivity (defined as the ratio between proton conductivity and methanol permeability) over Nafion. Recent results in high temperature methanol fuel cells 130°C–150°C, published by Baglio et al. [232] over composite Nafion membranes containing mordenite, show improved electrochemical behavior at 140°C over the recast Nafion membrane. The power density achieved (390 mW/cm<sup>2</sup>) is interpreted in light of surface acid–base properties of the zeolitic filler in the composite membrane.

### 10.6.3.2 Catalytic Zeolite-Membrane Reactors in the Fine Chemicals Industry

Membrane technology is a well-established technology for the immobilization of enzymes [233] since Degussa [234] introduced a continuous acylase process employing an enzyme-membrane reactor for the enantiomeric production of pure L-amino acids in 1981. Polymer membranes configured into hollow-fiber modules are, by far, the most widely used membrane where the enzyme is held back by the low cutoff of the membrane.

Matsui et al. [235,236] have recently used zeolites with a higher Si/Al ratio (i.e., Na–BEA) for the purification of nucleic acids and proteins due to the electrostatic and hydrophobic interactions between biopolymers and zeolites. In addition, the activity and structure of the proteins are preserved even under denaturing conditions, thus emerging as promising materials for biochemical and biotechnological applications.

Based on these observations, Wang and Caruso [237] have described an effective method for the fabrication of robust zeolitic membranes with three-dimensional interconnected macroporous (1.2 μm in diameter) structures from mesoporous silica spheres previously seeded with silicalite-1 nanoparticles subjected to a conventional hydrothermal treatment. Subsequently, the zeolite membrane modification via the layer-by-layer electrostatic assembly of polyelectrolytes and catalase on the 3D macroporous structure results in a biomacromolecule-functionalized macroporous zeolitic membrane bioreactor suitable for biocatalysts investigations. The enzyme-modified membranes exhibit enhanced reaction stability and also display enzyme activities (for H<sub>2</sub>O<sub>2</sub> decomposition) three orders of magnitude higher than their nonporous planar film counterparts assembled on silica substrates. Therefore, the potential of such structures as bioreactors is enormous.

Zeolite membranes are amenable by surface modification with a variety of chemical functional groups using simple silane chemistry, which may provide alternative surface chemistry pathways for enzyme immobilization. In this context, Shukla et al. [238] have recently used a chemically modified zeolite–clay composite membrane for the immobilization of porcine lipase using glutaraldehyde to provide a chemical linkage between the enzyme and the membrane. The effects of pH, temperature, and solvent on the performance of such biphasic zeolite-membrane reactors have been evaluated in the hydrolysis of olive oil to fatty acids.

Membrane technology developed for enzymatic reactions is now being introduced to homogeneous organic catalysis with the aim of minimizing the amount of catalyst required per kilogram of product produced. For a large number of reactions, homogenous catalysts show better activity and (enantio) selectivity compared to heterogeneous catalysts. There are, however, two main disadvantages: one caused by the organic solvent used for the reaction medium and the difficult separation of the catalyst from the products. With respect to the first shortcoming, it is generally thought that the use of supercritical solvents (SCFs) [239] could eliminate environmental concerns pertaining to VOC dissemination and at the same time obtain high concentrations of reactants, products, and catalyst due to the solvent properties of SCFs. Regarding the second drawback, one of the most common techniques for catalyst separation is running the reaction mixture through a fixed bed reactor, with the catalyst covalently bounded via a suitable functional linker or tether to an insoluble polymer as support [240].

In particular, for the synthesis of optically pure chemicals, several immobilization techniques have been shown to give stable and active chiral heterogeneous catalysts. A further step has been carried out by Choi et al. [241] who immobilized chiral Co(III) complexes on ZSM-5/Anodisc membranes for the hydrolytic kinetic resolution of terminal epoxides. The salen catalyst, loaded into the macroporous matrix of Anodisc by impregnation under vacuum, must exit near the interface of ZSM-5 film to contact with both biphasic reactants such as epoxides and water. Furthermore, the loading of chiral catalyst remains constant during reaction because it cannot diffuse into the pore channel of ZSM-5 crystals and is insoluble in water. The catalytic composite zeolite membrane obtained acts as liquid–liquid contactor which combines the chemical reaction with the continuous extraction of products simultaneously (see Figure 10.26): the epoxide remained in the organic phase and the hydrophilic diols could diffuse into the aqueous phase across the ZSM-5 film layer. As a result, high enantioselectivity and recyclability are achieved in the asymmetric hydrolysis of terminal and mesoepoxides at room temperature.

The same concept was proposed by Langhendries et al. [242] for the selective liquid-phase hydrocarbon oxidation. In this reactor configuration, the organic substrate (cyclohexane and *n*-dodecane) and the aqueous oxidant phase

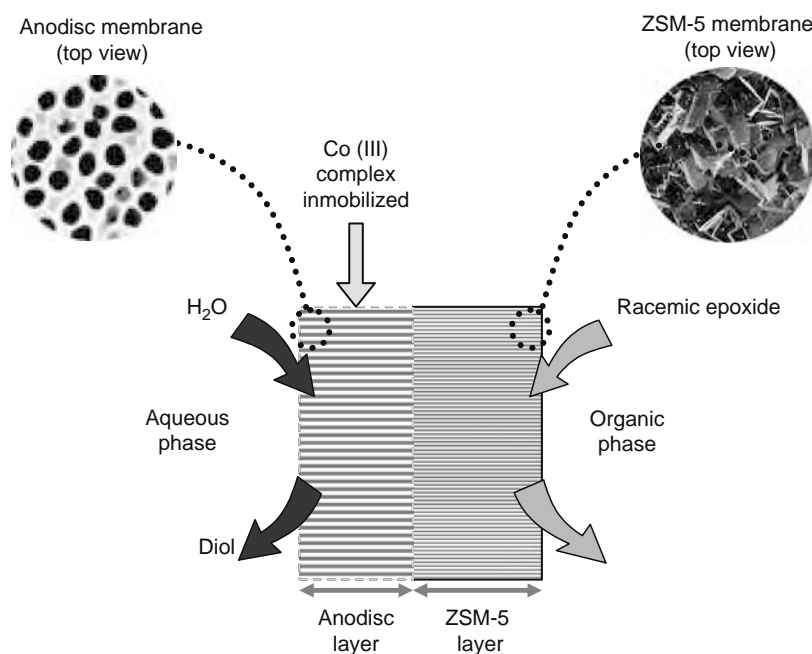


**FIGURE 10.26** (See color insert following page 588.) ZSM-5/Anodisc membrane system used in the enantioselective asymmetric hydrolysis of racemic epoxides. (Adapted from Choi, S.D. and Kim, G.J., *Catal. Lett.*, 92, 35, 2004.)

(*t*-butyl-hydroperoxide) are contacted through a catalytic composite zeolite-membrane; where alcohol and ketone oxidation products are recovered depending on their solubility in both phases. The catalytic composite zeolite-membrane consisted of a NaY-zeolite-encapsulated iron-phtalocyanine complex embedded in a hydrophobic poly(dimethylsiloxane) (PDMS) polymer membrane. In a similar way, Wu et al. [243] have studied the *n*-hexane oxifunctionalization by hydrogen peroxide using a titanium silicalite-1 zeolite/PDMS composite membrane as a liquid-vapor interphase contactor. The value of this approach, is that it eliminates the necessity for a solvent, and, therefore, solves the problem of excess peroxide at the active sites and often increases reaction rates by optimising the substrate/oxidant ratio at the catalyst surface, which has been further demonstrated by different authors [244,245].

Even so, undesirable effects, such as deactivation and loss of selectivity for heterogeneous catalysts, are unavoidable for some specific reactions. Hence, separation of homogeneous chemical catalysts by membrane retention or immobilization is emerging as a new application field, which, in fact, demands supports that combine thermal and mechanical stability with chemical resistance under reactive conditions. As a first approach, zeolite membranes can act as molecular filters able to retain the homogeneous catalyst, i.e., as a simple separator. MFI zeolite membranes have been applied by Turlán et al. [246] in the Heck reaction to allow the permeation of a product (4-cyanomethylcinnamate) while retaining the homogeneous catalyst employed ( $[\text{Pd}(\mu\text{-Cl})(\text{PPh}_3)_2]_2(\text{BF}_4)_2$ ), which has a larger size than the pores of the MFI membranes used. This approach is also being pursued with polymeric membranes that are more flexible in terms of the species that can be targeted, but experience stronger limitations in terms of temperature and solvent resistance. Smet et al. [247] combined nanofiltration with homogeneous catalysis to obtain the best possible reaction rates, chemoselectivities, and enantioselectivities in a continuous operation mode while recycling the catalyst. More recently, silicalite-1 membranes have been successfully employed for catalyst retention ( $[\text{Pd}(\mu\text{-Cl})(\text{Ph}_2\text{P}(\text{CH}_2)_4\text{PPh}_2)](\text{CF}_3\text{SO}_3)_2$ ) from postcatalytic reaction mixtures by the molecular sieving effect in the Diels-Alder reaction [248].

To circumvent simultaneously the two major drawbacks associated with homogeneous catalysis already quoted, Goetheer et al. [249] have proposed a membrane reactor for homogeneous catalysis in supercritical carbon dioxide with in situ catalyst separation. In particular, a membrane reactor working in a flow-through configuration has been tested for the hydrogenation of 1-butene to *n*-butane with a fluorine derivative of Wilkinson's catalyst in  $\text{SCCO}_2$  at 353K and 20 MPa. The microporous silica membrane employed (0.5–0.8 nm as pore diameter) was able to retain completely the catalyst (2–4 nm) under reaction conditions which renders turnover frequencies significantly higher than those obtained using an organic solvent. However, the same concept could be perfectly translated to zeolite membranes with suitable pore diameters and relative low affinity toward carbon dioxide.

#### 10.6.4 ALTERNATIVE SUPPORTS AND CONFIGURATIONS FOR ZEOLITE-MEMBRANE REACTORS

In addition to porous ceramic and stainless steel plates and tubes commonly employed as supports of zeolite membranes and films, a wide variety of alternative supports have been used. Among these are steel [250], ceramic [251,252] monoliths

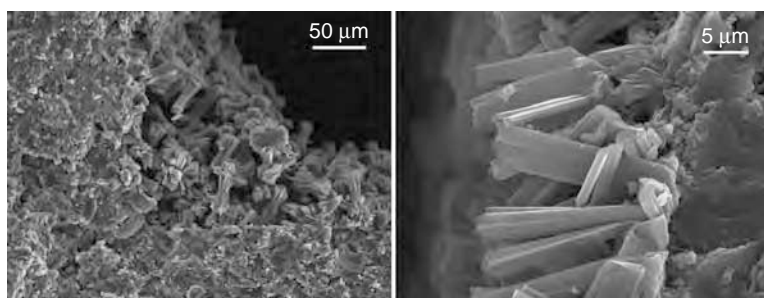


**FIGURE 10.27** Left: cross section of a mordenite film prepared on a cordierite monolith. Right: detail of the film.

(see Figure 10.27) (also shaped as wheels or rotors [253]), stainless steel grids [254,255], wire gauze packings [256], glass fibers [257–258], nonporous ceramic [259], metal [260] plates, and glass and steel beads [261]. Figure 10.28 shows SEM images of ETS-10 and umbite titanosilicate-based membranes supported on commercial carbon Toray paper commonly used as porous electrode for fuel cell applications. The as prepared membrane-electrode assemblies (MEAs) were synthesized by secondary growth following the procedure described by Lin et al. [27].

While, in general, the investigations discussed in this section do not belong to the field of zeolite-membrane reactors, they are mentioned here because they provide interesting clues and ideas for further development of existing systems.

Monoliths have been proposed for different end-of-pipe catalytic processes, on account of their flexibility of operation, good tolerance to the presence of dust, low pressure drop, reasonable commercial costs, and relatively easy scale-up [262]. An additional advantage in zeolite-coated monoliths is the fact that they can be prepared binderless and they do not require a washcoat support layer (an important feature for increasing the catalyst loading over the monolith). Monolithic structures such as ZSM-5 prepared on cordierite by liquid-phase hydrothermal synthesis [251,263,264], or by solid-state in situ crystallization [265,266], are mainly oriented toward automotive applications. Particularly remarkable are the results of Ulla et al. [251,252] where loadings up to about 30% and 50% by weight for ZSM-5 and MOR, respectively, have been reported. After preparation, the zeolite layers can be ion exchanged to modify their activity. Thus, Basaldella et al. [263] prepared Cu-ZSM-5 layers, which are catalytically active for the selective reduction of NO<sub>x</sub>. ZSM-5 coatings have also been prepared on mullite honeycomb supports [267], ceramic slabs [259], and foams [268]. BEA coatings (loadings up to 9 wt%) have been prepared by dipping monolithic and wire gauze packings in a BEA slurry. The resulting structures showed high activity for the acylation of

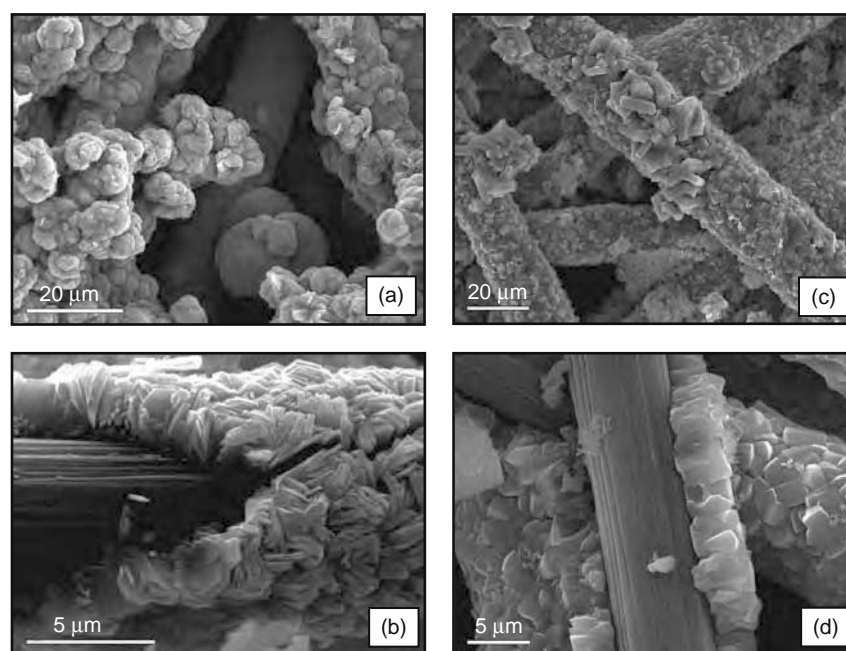


**FIGURE 10.28** Scanning electron microscopy (SEM) images of (a, b) Umbite and (c, d) ETS-10 supported on carbon Toray paper. (From Aused, M.P., Urbiztondo, M.A., Mallada, R., Pina, M.P., and Santamaría, J., Synthesis of proton conducting membranes for direct methanol fuel cells (DMFCs). Books of abstracts of the OSSEP Final Workshop, Tenerife, 2004, pp. 90–91.)

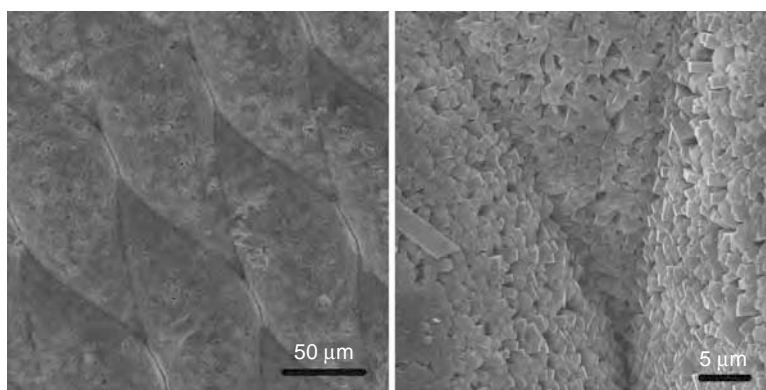


**FIGURE 10.29** Scanning electron microscopy (SEM) images of silicalite membrane on stainless steel grid support.

aromatics [254]. Similarly, a structured catalytic bed made of ZSM-5 coatings grown by hydrothermal synthesis on stainless steel grids has been used for the hydroxylation of benzene [254].

Zeolite monoliths have been useful for such applications as rotatory adsorbers for use as dehumidifiers and desiccant cooling processes [253] or in VOC treatment systems [269]. Alumina-coated silicon carbide monoliths have also been employed as supports for B-ZSM-5 membranes [270] providing a larger surface area per unit volume, compared to traditional membrane supports. With these membranes, these authors have reported *n*/*i*-butane and H<sub>2</sub>/*i*-butane separation selectivities of 35 and 77, respectively [85]. Also, silicalite-1 membranes supported on stainless steel grids (Figure 10.29) have shown a good performance in the separation of *n*/*i*-butane mixtures, with separation factors as high as 53 at 63°C [255].

Finally, zeolite nanoparticles have been used as building blocks to construct hierarchical self-standing porous structures. For example, multilayers of colloidal zeolite crystals have been coated on polystyrene beads with a size of less than 10 μm [271,272]. Also, silicalite-1 membranes with a thickness ranging from 20 to several millimeters and controlled mesoporosity [273] have been synthesized by the self-assembly of zeolite nanocrystals followed by high-pressure compression and controlled secondary crystal growth via microwave heating. These structures could be useful for separation and catalysis applications.

### 10.6.5 INDUSTRIAL APPLICATIONS OF ZEOLITE-MEMBRANE REACTORS

Today, annual market membrane of ca. U.S.  $\$4.5 \times 10^9$  for membranes and membrane modules (mostly polymeric ones) indicates that separation processes seem to be the largest application field, whereas membrane reactors are just on the verge of being considered as a competitive tool [274].

Weisz [275] defined a trade-off range for the operation of catalytic reactors in industry based on the space-time yield (STY) which should be centered around 1–10 mol/s m<sup>3</sup>. This figure is a balance between reactor size and mass and heat transfer limitations. The STY value of catalytic reactors should be compared to the permeability of zeolite membranes to draw conclusions about the feasibility of using zeolite-membrane reactors for industrial applications. Boudart [276] has suggested the use of analysis of orders of magnitude to screen-proposed membrane reactors for practicality under industrial conditions based on the areal time yield (ATY), which is in fact the same as the permeation flux. The feasibility of membrane reactors can be determined by dividing the value for STY by the value for ATY, thus obtaining the area to volume ratio of the catalytic membrane reactor. Realistic values for industrial applications are around 10–100 m<sup>-1</sup>; therefore, based on published permeation data, zeolite-membrane reactors would be a feasible technology for some applications.

Although the enormous potential payoff of this technology has been largely demonstrated at the laboratory scale, the technological gap that still has to be filled to achieve industrial practice is rather clear. Caro et al. [3] pointed out that the challenges for industrial application are in the membrane development and lack of module reliability under extreme temperature cycling. Chiang and Chao [167] noted the need to reduce membrane thickness and to increase the membrane surface to volume ratio, something that could be achieved by the use of alternative supports (monoliths, hollow fibers, metal gauze) as shown in the previous section. A step in this direction is the synthesis of zeolite membrane layers on the inner side of alumina capillaries (1.9 mm inside diameter) recently reported by Richter et al. [277]. Noack et al. [278] stressed the need to develop membranes with larger areas that can be prepared with satisfactory reproducibility. By systematically varying the synthesis conditions, these authors were able to prepare a series of silicalite-1 tubular membranes in which the proportion of high quality membranes was 70%. Recently, Pina et al. [33] have synthesized zeolite NaA membranes on the external surface of  $\alpha$ -alumina tubular supports using a semicontinuous system in which fresh gel is periodically supplied to the synthesis vessel. Compared to traditional batch methods, the procedure developed in this work provides a better control of the synthesis and crystallization conditions and is easier to implement at an industrial scale. Morooka and Kusakabe [279], among others, raised

the issue of durability under elevated pressures and temperatures, stability in steam-containing atmospheres, and membrane regeneration.

In spite of all these hurdles, there are already industrial-scale applications of zeolite membranes for solvent dehydration [106] by pervaporation plants using tubular zeolite A membranes with 0.0275 m<sup>2</sup> of permeation area each (see Section 10.2.3). Li et al. [280] have prepared large area (0.0260 m<sup>2</sup>) ZSM-5 membranes on tubular  $\alpha$ -alumina supports. This work is also interesting from the industrial point of view because the authors used inexpensive *n*-butylamine as template. Indeed, the cost required for industrial modules, on a general basis, is still far from clear. However, it must be noted that most of the costs can be ascribed to the module, and only 10%–20% to the membrane itself [3]. This underlines again the importance of preparation of zeolite membranes on cheaper, alternative supports that can also pack more area per unit volume.

### 10.6.6 NEW APPLICATIONS OF ZEOLITE-MEMBRANE REACTORS: MICROCHEMICAL SYSTEMS

The specificity, adsorption, and catalytic properties, besides the possibility of zeolite pores to host different ions, atoms, molecules, and clusters, have opened up numerous opportunities as advanced nanomaterials [227,281].

The last few years have seen the proposal of new applications for zeolite membranes and coatings involving microchemical systems (microreactors, membrane microseparators, and sensors) in which the characteristic length is measured in microns [6]. Commercial applications of zeolite membranes do not necessarily imply dimensions of many square meters of permeation area in a single unit. Actually, scaling-down should allow preparing defect-free zeolite membranes (eventually single-crystal membranes) over an endless variety of supports, and combinations with other materials at the microscale that would have a higher chance of tolerating the inherent thermal and mechanical stresses produced during thermal cycling (a very important subject for industrial implementation of this technology see Section 10.6.5).

Ideally, microscale systems will be made of smart nanostructured materials capable of very specific interactions with molecules, ions, and atoms. Indeed, the advances in microstructured devices for chemical reactions and the benefits already demonstrated have been impressive [282,283]. Some of these microdevices could integrate what Gavriilidis et al. [284] called novel microengineered structures, capable of performing many of the standard operations of interest to chemical systems. Thus, for instance, the *lab-on-a-chip* represents an increasingly familiar concept to express the miniaturization of chemical, biological, and biomechanical analyses [285], and can be envisaged as a scaled-down analog of a chemical processing plant in which a drastic reduction of reactants and energy consumption is achieved.

One of the keys to the success of such microdevices is the selectivity of the reaction and separation steps and their integration for a given process. Regarding the former requirement, nanoporous interfaces of zeolites and related materials emerge as excellent candidates for these kinds of devices. Tsapatsis [286] has highlighted some of the potential contributions of molecular sieving technology to the nanotechnology field, and remarked the need for fundamental advances in understanding and controlling the preparation of these materials and predicting their properties. These advances are necessary to achieve a degree of structural perfection that is not required by their current technological use but will be needed in micro- and nano-device applications.

#### 10.6.6.1 Zeolite-Based Microreactors and Microseparators

The combination of microreactor and zeolite growth concepts rapidly led to zeolite coatings on microreactors. Thus, Rebrow et al. [287] coated 500  $\mu\text{m}$  channels on a stainless steel plate with ZSM-5 crystals and used the resulting microreactor in the selective catalytic reduction of NO with ammonia, attaining higher reaction rates in comparison with the conventional pelletized catalyst. Wan et al. [288] also deposited zeolite coatings in silicon–glass microchannels fabricated by the patterning and etching of a Si wafer. In this case 5  $\mu\text{m}$  thick TS-1 zeolite films, made up of intergrown 3  $\mu\text{m}$  zeolite crystal grains, were supported on 500  $\mu\text{m}$  wide and 250  $\mu\text{m}$  deep microchannel reactors. The authors tested these microreactors in the epoxidation of 1-pentene with hydrogen peroxide at 298 K in a continuous flow, even though irreversible deactivation was observed due to leaching of framework titanium.

Zeolite micromembranes also would be able to perform the separation and reaction operations of standard zeolite membranes, while providing the following advantages: (1) easy integration, at the microscopic level, of reaction and separation, (2) excellent temperature control, (3) possible higher selectivity and conversion compared to conventional reactor, (4) intrinsic safety, and (5) easier scale-up in a highly compact format. Miniaturization also benefits membrane separation by improving mass and heat transfer rates and by providing a large surface/volume ratio (i.e., 3000 m<sup>2</sup>/m<sup>3</sup>) leading to a more efficient and compact separation unit.

The benefits of the use of micromembranes for the selective removal of one or more products during reaction have been demonstrated for equilibrium-limited reactions [289]. For example, the performance of hydrophilic ZSM-5 and NaA membranes over multichannel microreactors prepared from electro-discharge micromachining of commercial porous stainless steel plates was studied by Yeung et al. in the Knoevenagel condensation [290,291] and aniline oxidation to azoxybenzene [292]. For such kind of reactions, the zeolite micromembrane role consists of the selective removal of water, which indeed yields higher conversions, better product purity, and a reduction in catalyst deactivation in comparison to the traditional packed bed reactor.

A different approach to fabricate a zeolite-based microreactor has been recently proposed by Mateo et al. [293]. These authors fabricated an array of free-standing micromembranes involving laser perforation of a thin stainless steel plate to create microholes (30–70  $\mu\text{m}$  in diameter and 75  $\mu\text{m}$  depth) that were subsequently covered by silicalite-1 layers using hydrothermal synthesis by secondary growth. Patterned structures can also be created by covalent bonding to a previously printed structure, as demonstrated by Ha et al. [294]. These authors have extensively investigated the organization of nano- and microcrystalline zeolite particles into uniformly aligned two- (2D) and three-dimensional (3D) multicrystal arrays on various substrates (platinum, gold, glass plates and fibers, silica, alumina, and vegetable fibers) by inducing large numbers of molecular linkages between organic functional groups tethered to the surfaces of both zeolites and substrates. The scope of application of such monolayers assemblies is particularly attractive for applications of zeolites as advanced nanomaterials [281].

The methods for manufacturing of zeolite-based microreactors and microseparators also use traditional semiconductor fabrication procedures. Jansen and van Rosmalen [295] were among the first to describe the growth of continuous zeolite film on silicon wafer. Some years ago den Exter et al. [296] reported the preparation of silicalite-1 oriented monolayers on silicon wafers subsequently transformed, by selective etching procedures, into unsupported thin zeolite layers. Also, Schoeman et al. [297] studied the optimal conditions for the growth of silicalite-1 films on silicon wafers with thicknesses in the range of 180 nm to 1  $\mu\text{m}$ . Today, semiconductor fabrication technology can be considered an established technique, which allows the manufacturing of a range of microelectromechanical systems (MEMS). Yeung and coworkers have described several strategies for incorporating zeolites within the architectural design of microreactors and microseparators. These authors have demonstrated that microelectronic fabrication technology could readily be adapted to synthesize miniature membrane microseparators containing MFI-type zeolite films prepared by secondary growth [298,299].

#### 10.6.6.2 Zeolite-Based Microsensors

The development of stand-alone devices for monitoring the concentration of selected chemical species in complex samples (or in different environments) has been a major goal in analytical science for several decades. Indeed, chemical microsensors play an increasing role in the areas of environmental monitoring and industrial processing. With the aim of increasing sensitivity and selectivity, zeolites have been used on a variety of chemical sensors, both reactive and nonreactive. Moreover, as a sensing layer, zeolites are very favorable due to their additional high thermal stability and chemical resistance. Thus, zeolites have been employed to improve the surface of conventional chemical electrodes to increase their electroanalytical performance [300], or to conform different types of zeolite-based chemical sensors, as shown below.

Chemical microsensors, having combined molecular sieving effects and selective surface interactions and consisting of zeolite-composite thin films located on the active areas of piezoelectric sensor devices (quartz crystal microbalances, QCMs), have been developed by several authors. The regular micropores of the zeolitic material were found to effectively control molecular access to the device allowing it to sense ethanol (using zeolite MFI, [301]), humidity (using zeolite LTA and BEA, [302]), and NO, SO<sub>2</sub>, and water (using zeolite A, silicalite-1, and sodalite [303,304]). These works demonstrate how the response of zeolite-based piezoelectric sensors can be controlled by the zeolite structure and composition.

Surface acoustic wave (SAW) devices, consisting of a single-crystal quartz substrate with interdigital transducers, can also operate as highly sensitive piezoelectric balances that respond to small fractions of gas adsorption on a single-crystal monolayer via frequency changes of an oscillator circuit. The application of zeolite coatings (H-ZSM-5, zeolite Y, chabazite, and zeolite A) on SAW devices was first applied by Bein et al. [305,306] for humidity and vapor sensing (methanol, ethanol, propanol, isooctane, pyridine, and perfluorotributylamine). These authors found out that selectivity can be enhanced by tailoring the surface and by means of interfacial interactions of zeolite coatings with molecular layers of silane coupling agents [307].

Cantilevers used as nanoscale sensors for AFM have recently been extended beyond those of surface-imaging tools. Similar to QCMs, cantilever-based sensors can also be configured to work as a tiny microbalance in which a resonance frequency analysis can be used to determine mass loading. Standard cantilevers are theoretically capable of detecting a minimum mass loading of 50 fg enabling short response time (milliseconds). Although cantilever exhibits high sensitivity, but, to recognize different specific materials, the improvement of the sensor selectivity becomes a critical factor. For this purpose, attaching zeolite crystals to them further increases their detection sensitivity toward the adsorbed compound while maintaining their micron scale. On the basis of this concept, ZSM-5 crystals (around 500 ng) have been chemically anchored for humidity [307,308] and freon-12 [309] sensing purposes, achieving a satisfactory performance in determining mass loadings at the nanogram scale. Moreover, an array of such devices has been fabricated [308] to conduct complex analysis of vapors by using various microporous materials attached to the sensors.

Optical sensors are among the most important types of chemical sensors that have been produced in the recent past for the continuous and real-time monitoring of diverse analytes [310]. A wide variety of favorable properties for chromophores embedded in inorganic molecular sieves can be expected based on their peculiar host–guest interactions, although they are still at the beginning of their development. Indeed, molecular-sieve encapsulated dye molecules are currently attracting increasing attention with respect to new photonic devices and optical sensor applications [311,312] due to an increased light

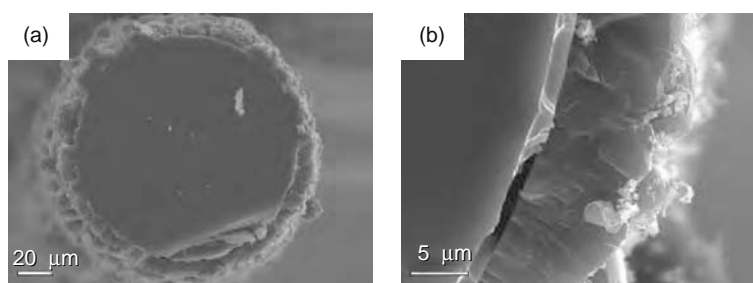


**FIGURE 10.30** Scanning electron microscopy (SEM) images of cross section of a commercial optical fiber coated with a NaA zeolite thick layer: (a) total cross section and (b) magnification view of the NaA zeolite layer. (From López, J., Pina, M.P., Coronas, J., Pelayo, J., and Santamaría, J., A novel optical device for gas sensor applications based on zeolitic materials. Books of abstracts of the 1st NanoSpain Workshop, San Sebastian, 2004.)

durability, migration stability, and photodegradation resistance (up to 2 orders of magnitude) with respect to their organic counterparts.

Brühwiler and Calzaferri [313] have recently reviewed the different organization stages for dye-zeolite systems ranging from the arrangement of the dyes in the zeolite channels to the specific adsorption of molecules at the channel entrances, and subsequently, to the coupling of the dye-zeolite crystals to an external device. However, the majority of publications up-to-date in the field of optical gas sensors deal with the first level of molecular assembling. For instance, the encapsulation of the solvatochromic dye Nile red inside the pores of dealuminated zeolite Y by “ship in a bottle” synthesis has been investigated by Meinershagen et al. [314] for optical sensing of acetone and ethanol using spectral absorbance in the UV–VIS range. Taking advantages of the luminescence properties of rhodamine dyes, covalently anchored at the walls of mesoporous Si-MCM-41, Ganschow et al. [315] have developed a SO<sub>2</sub> optical sensor using a glass carrier to overcome the disadvantages of the powdered state. Many research efforts are focused on integrated optical sensors development, in particular toward optical fiber sensors operating at standard telecommunication wavelengths [316]. Many papers have recently been published concerning NaY, LiY, and BaY zeolite crystals coating quartz fibers using TEOS as a binding agent [285,286] for asymmetric photoreactions and also for sensing aromatic molecules (naphthalene) by means of their phosphorescence. As an example, Figure 10.30 shows SEM micrographs of zeolite NaA films, 7 μm thick, prepared by secondary growth [35] over the external surface of commercial optical fibers previously activated for being used as fiber optic evanescent-field gas sensors using absorption in the near infrared.

Since the adsorption of a gas is able to modify the dielectric constant of zeolites, chemical sensors based on interdigital capacitors (IDCs) using zeolites layers as sensitive coatings offer a wide field of applications depending on the type, modification, and working temperature of the coated IDC sensor.

Thus, zeolite-coated IDCs have been tested for sensing *n*-butane [317] and also, NH<sub>3</sub>, NO, and CO [318,319] on Na–Y and NaPtY zeolite-based sensors at temperatures high enough to where chemical reactions may also occur (above 200°C). The response time is of the order of seconds and the cross-sensitivity to water is small at high temperatures, at which no water condensation occurs in the zeolite-pore system. Under certain conditions, selectivity of these reactive chemical sensors is remarkable. Thus, the detection of 10 ppm of *n*-butane with a NaPtY interdigitated capacitor with no response to CO and H<sub>2</sub> has been reported [318]. Similarly, Moos et al. [320] described a ZSM-5 based capacitor sensor with on-chip heating for temperatures up to 450°C capable of detecting NH<sub>3</sub> with no cross-sensitivity to CO, hydrocarbons, and O<sub>2</sub>.

Reactive chemical sensors and their problems with selectivity have been described above (see Section 10.6.2.4 about control of reactant traffic). The deployment of zeolite barriers has been advocated as a means of increasing the selectivity of optical [291] and semiconductor–gas sensors [321–323]. These latter works, however, used catalyst bed-type filters (up to 250 mg), with a relatively large mass which leads to a slow sensor response. A more sophisticated approach was used by Fukui and Nishida [324], who used commercial crystals of FAU and FER zeolites with colloidal silica as a binder to cover the sensing layer of La<sub>2</sub>O<sub>3</sub>–Au/SnO<sub>2</sub> sensors, and obtained ethanol filtering effects that increased the CO selectivity. Different zeolite masks, also made of commercial crystals, were used to minimize the interference of O<sub>2</sub> in yttria-stabilized zirconia sensors used to analyze nitric oxide [325]. It has also been reported that the modification of semiconductor sensors by mechanically mixing MCM-41 with powdered SnO<sub>2</sub> gave rise to enhanced sensitivity to H<sub>2</sub> [326].

As it was mentioned above (see Section 10.6.2.4), Vilaseca et al. [215] have synthesized MFI and LTA films directly on a Pd-doped SnO<sub>2</sub> layer (see Figure 10.31). These molecular filters hindered the passage of undesired molecules and increased the concentration of the targeted species in the vicinity of the sensitive layer depending on their interactions with the zeolite pores and on the operating conditions. The results showed that a suitable zeolite film can strongly reduce, and in some cases suppress, the response of the sensor to certain species, and thereby increase the sensing selectivity (see Figure 10.32).

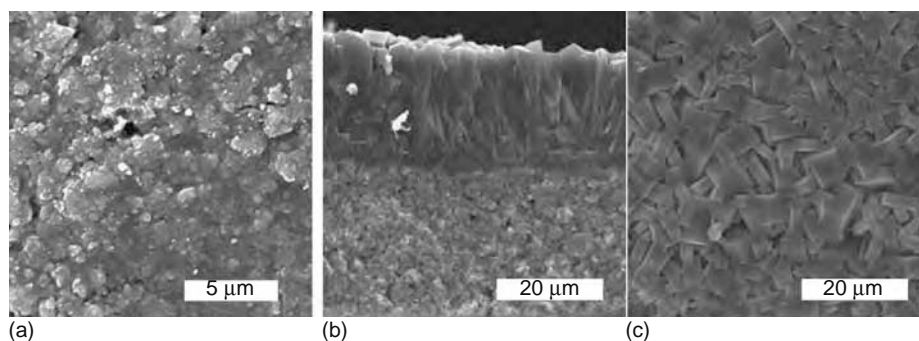


**FIGURE 10.31** (a) Top view of a Pd-SnO<sub>2</sub> layer, (b) cross section of a SIL-1 film on a Pd-SnO<sub>2</sub> layer, and (c) top view of a SIL-1 film onto a Pd-SnO<sub>2</sub> layer.

## 10.7 CONCLUSIONS

The efforts and advances during the last 15 years in zeolite membrane and coating research have made it possible to synthesize many zeolitic and related-type materials on a wide variety of supports of different composition, geometry, and structure and also to predict their transport properties. Additionally, the widely exploited adsorption and catalytic properties of zeolites have undoubtedly opened up their scope of application beyond traditional separation and pervaporation processes. As a matter-of-fact, zeolite membranes have already been used in the field of membrane reactors (chemical specialties and commodities) and microchemical systems (microreactors, microseparators, and microsensors).

Nevertheless, the availability of procedures allows the preparation of zeolite membranes and layers with sufficient quality, reproducibility, and reliability only up to a few hundred square centimeters in surface, delaying the industrial implementation of zeolite membrane-based technology. To be realistic, the lack of module reliability under extreme temperature cycling or harsh environment and the necessary raw material cost reductions (supports and chemicals) are two of the main challenges toward which strong efforts must be targeted.

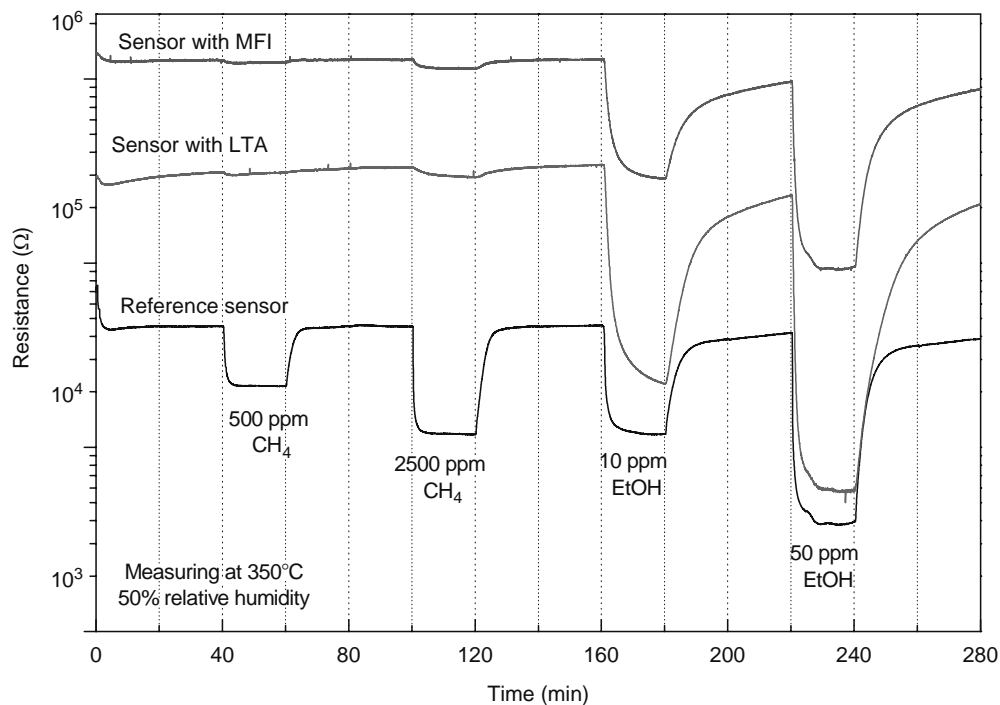


**FIGURE 10.32** Response of Pd/SnO<sub>2</sub> sensors as measured resistance under different concentrations of CH<sub>4</sub> and EtOH.

## ACKNOWLEDGMENTS

We acknowledge the contribution to this chapter of all the current and former members of the Catalysis, Molecular Separations and Reactor Engineering Group at the University of Zaragoza. Particular thanks to Pilar Bernal, Daniel Picaeo, Miguel Urbiztondo, and Montse Vilaseca for their figures and SEM analysis. We would also like to thank the DGA (Aragon), MCYT (Spain), and UE for financial support. Finally, we are really grateful to Professor Santamaría and Dr. Coronas who encouraged us to write this chapter.

## REFERENCES

1. Matsukata M and Kikuchi E. Zeolitic membranes: Synthesis, properties, and prospects. *Bull Chem Soc Jp* 1997; 70(10):2341–2356.
2. Coronas J and Santamaría J. Separations using zeolite membranes. *Sep Purif Method* 1999; 28:127–177.
3. Caro J, Noack M, Kölsch P, and Schäfer R. Zeolite membranes-state of their development and perspective. *Micropor Mesopor Mater* 2000; 38:3–24.
4. Nair S and Tsapatsis M. Synthesis and properties of zeolitic membranes. In: Auerbach SM, Carrado KA, and Dutta PK (Eds.), *Handbook of Zeolite Science and Technology*. New York: Marcel Dekker, 2003; 867–919.
5. Coronas J and Santamaría J. State-of-the-art in zeolite membrane reactors. *Topics Catal* 2004; 29(1–2):29–44.
6. Coronas J and Santamaría J. The use of zeolite films in small-scale and micro-scale applications. *Chem Eng Sci* 2004; 59:4879–4885.
7. Pan M and Lin YS. Template-free secondary growth synthesis of MFI type zeolite membranes. *Micropor Mesopor Mater* 2001; 43:319–327.
8. Vroon ZAEP. Synthesis and transport studies of thin ceramic supported zeolite (MFI) membranes. PhD dissertation, Delft University, Delft, The Netherlands, 2000.
9. Ramsay JDF and Kallus S. Zeolite membranes. *Membrane Science and Technology Series 6* 2000; 373–395.
10. Coronas J, Falconer JL, and Noble RD. Characterization and permeation properties of ZSM-5 tubular membranes. *AIChE J* 1997; 43:1797–1812.
11. Bernal MP, Coronas J, Menéndez M, and Santamaría J. On the effect of morphological features on the properties of MFI zeolite membranes. *Micropor Mesopor Mater* 2003; 60:99–110.
12. Jareman F, Andersson C, and Hedlund J. The influence of the calcination rate on silicalite-1 membranes. *Micropor Mesopor Mater* 2005; 79:1–5.
13. Heng S, Lau PPS, Yeung KL, Djafer M, and Schrotter JC. Low-temperature ozone treatment for organic template removal from zeolite membrane. *J Membr Sci* 2004; 243:69–78.
14. Parikh AN, Navrotsky A, Li Q, Yee CK, Amweg ML, and Corma A. Non-thermal calcination by ultraviolet irradiation in the synthesis of microporous materials. *Micropor Mesopor Mater* 2004; 76:17–22.
15. Christopher JCW, Tsuji K, Takewaki T, Beck LW, and Davis ME. Tailoring molecular sieve properties during SDA removal via solvent extraction. *Micropor Mesopor Mater* 2001; 48:57–64.
16. Nair S and Tsapatsis M. Infrared reflectance measurements of zeolite film thickness, refractive index and other characteristics. *Micropor Mesopor Mater* 2003; 58:81–89.
17. Snyder MA, Lai Z, Tsapatsis M, and Vlachos DG. Combining simultaneous reflectance and fluorescence imaging with SEM for conclusive identification of polycrystalline features of MFI membranes. *Micropor Mesopor Mater* 2004; 76:29–33.
18. Tsuru T, Tomoya H, Tomohisa Y, and Masashi A. Permporometry characterization of microporous ceramic membranes. *J Membr Sci* 2001; 186:257–265.
19. Bernal MP, Coronas J, Menéndez M, and Santamaría J. Characterization of zeolite membranes by measurement of permeation fluxes in the presence of adsorbable species. *Ind Eng Chem Res* 2004; 41:5071–5078.
20. Matsufuji T, Nakagawa S, Nishiyama N, Matsukata M, and Ueyama K. Synthesis and permeation studies of ferrierite/alumina composite membranes. *Micropor Mesopor Mater* 2000; 38:43–50.
21. Matsufuji T, Nishiyama N, Matsukata M, and Uyama K. Separation of butane and xylene isomers with MFI-type zeolitic membrane synthesized by a vapor-phase transport method. *J Membr Sci* 2000; 178:25–34.
22. Alfaro S, Arruebo M, Coronas J, Menéndez M, and Santamaría J. Preparation of MFI type tubular membranes by steam-assisted crystallization. *Micropor Mesopor Mater* 2002; 50:195–200.
23. Wang Z and Yan Y. Oriented zeolite MFI monolayer films on metal substrates by in situ crystallization. *Micropor Mesopor Mater* 2001; 48:229–238.
24. Lovallo MC and Tsapatsis M. Preferentially oriented submicron silicalite membranes. *AIChE J* 1996; 42(11):3020–3029.
25. Lee JS, Ha K, Lee YJ, and Yoon KB. Ultrasound-aided remarkably fast assembly of monolayers of zeolite crystals on glass with very high degree of lateral close packing. *Adv Mater* 2005; 17:837–841.
26. Xomeritakis G, Nair S, and Tsapatsis M. Transport properties of alumina-supported MFI membranes made by secondary (seeded) growth. *Micropor Mesopor Mater* 2000; 38:61–73.
27. Lai ZP, Bonilla G, Díaz I, Nery JG, Sujaoti K, Amat MA, Kokkoli E, Terasaki O, Thompson RW, Tsapatsis M, and Vlachos DG. Microstructural optimization of a zeolite membrane for organic vapor separation. *Science* 2003; 300:456–460.

28. Ha K, Lee YJ, Lee HJ, and Yoon KB. Facile assembly of zeolite monolayers on glass, silica, alumina, and other zeolites using 3-halopropylsilyl reagents as covalent linkers. *Adv Mater* 2000; 12:1114–1117.
29. Vilaseca M, Mateo E, Palacio L, Prádanos P, Hernández A, Paniagua A, Coronas J, and Santamaría J. AFM characterization of the growth of MFI-type zeolite films on alumina substrates. *Micropor Mesopor Mater* 2004; 71:33–37.
30. Hedlund J, Sterte J, Anthonis M, Bons AJ, Carstensen B, Corcoran N, Cox D, Deckman H, de Gijst W, de Moor PP, Lai F, McHenry J, Mortier W, and Reinoso J. High-flux MFI membranes. *Micropor Mesopor Mater* 2002; 52:179–189.
31. Erdem-Senatarlar A, Tatlier M, and Ürgen M. Preparation of zeolite coatings by direct heating of the substrates. *Micropor Mesopor Mater* 1999; 32:331–343.
32. Cetin T, Tatlier M, Erdem-Senatarlar A, Demirler U, and Ürgen M. Lower temperatures for the preparation of thinner zeolite A coatings. *Micropor Mesopor Mater* 2001; 47:1–14.
33. Yamazaki S and Tsutsumi K. Synthesis of A-type zeolite membrane using a plate heater and its formation mechanism. *Micropor Mesopor Mater* 2000; 37:67–80.
34. Richter H, Voight I, Fischer P, and Puhlfür BP. Preparation of zeolite membranes on the inner surface of ceramic tubes and capillaries. *Sep Purif Technol* 2003; 32:133–138.
35. Pina MP, Arruebo A, Felipe A, Fleta F, Bernal MP, Coronas J, Menendez M, and Santamaría J. A semi-continuous method for the synthesis of NaA zeolite membranes on tubular supports. *J Membr Sci* 2004; 244:141–150.
36. Kumakiri I. Preparation and permeation mechanism of zeolite membranes. PhD Dissertation, The University of Tokyo, Japan, 2000.
37. Pera-Titus M, Llorens J, Cunill F, Mallada R, and Santamaría J. Preparation of zeolite NaA membranes on the inner side of tubular supports by means of a controlled seeding technique. *Catal Today*, 2005, 104:281–287.
38. Tiscareño-Lechuga F, Téllez C, Menéndez M, and Santamaría J. A novel device for preparing zeolite—membranes under a centrifugal force field. *J Membr Sci* 2003; 212(1–2):135–146.
39. Guan G, Tanaka T, Kusakabe K, Sotowa K, and Morooka S. Characterization of AlPO<sub>4</sub>-type molecular sieving membranes formed on a porous  $\alpha$ -alumina tube. *J Membr Sci* 2003; 214:191–198.
40. Vilaseca M, Mintova S, Valtchev V, Metzger TH, and Bein TJ. Synthesis of colloidal AlPO<sub>4</sub>-18 crystals and their use for supported film growth. *Mater Chem* 2003; 13:1526–1528.
41. Zhang LX, Jia MD, and Min EZ. Synthesis of SAPO-34/ceramic composite membranes. *Stud Surf Sci Catal* 1997; 105:2211–2216.
42. Poshusta JC, Noble RD, and Falconer JL. Characterization of SAPO-34 membranes by water adsorption. *J Membr Sci* 2001; 186:25–40.
43. Li SG, Falconer JL, and Noble RD. SAPO-34 membranes for CO<sub>2</sub>/CH<sub>4</sub> separation. *J Membr Sci* 2004; 241:121–135.
44. Tavolaro A. VS-1 composite membrane: Preparation and characterization. *Desalination* 2002; 147:333–338.
45. Rocha J and Anderson MW. Microporous titanosilicates and other novel mixed octahedral–tetrahedral framework oxides. *Eur J Inorg Chem* 2000; 5:801–818.
46. Braunbarth CM, Boudreau LC, and Tsapatsis M. Synthesis of ETS-4/TiO<sub>2</sub> composite membranes and their pervaporation performance. *J Membr Sci* 2000; 174:31–42.
47. Guan GQ, Kusakabe K, and Morooka S. Synthesis and permeation properties of ion-exchanged ETS-4 tubular membranes. *Micropor Mesopor Mater* 2001; 50:109–120.
48. Guan G, Kusakabe K, and Morooka S. Separation of nitrogen from oxygen using a titanosilicate membrane prepared on a porous  $\alpha$ -alumina support tube. *Sep Sci Technol* 2002; 37(5):1031–1039.
49. Lin Z, Rocha J, Navajas A, Tellez C, Coronas JQ, and Santamaría J. Synthesis and characterization of titanosilicate ETS-10 membranes. *Micropor Mesopor Mater* 2004; 67:79–86.
50. Sebastián V, Lin Z, Rocha J, Tellez C, Santamaría J, and Coronas J. A new titanosilicate umbite membrane for the separation of H<sub>2</sub>. *Chem Commun* 2005, 24:3036–3037.
51. Corma A, Díaz-Cabañas MJ, Martínez-Triguero J, Rey F, and Rius J. A large-cavity zeolite with wide pore windows and potential as an oil refining catalyst. *Nature* 2002; 418:514–517.
52. Davis ME. Ordered porous materials for emerging applications. *Nature* 2002; 417:813–821.
53. Beck JS, Vartulli JC, and Roth WJ. A new family of mesoporous molecular-sieves prepared with liquid-crystal templates. *J Am Chem Soc* 1992; 114:10834–10836.
54. Yang H, Kuperman A, Coombs N, Mamiche-Afara S, and Ozin GA. Synthesis of oriented films of mesoporous silica on mica. *Nature* 1996; 379:703–705.
55. Tolbert SH, Firouzi A, and Stucky GD. Magnetic field alignment of ordered silicate-surfactant composites and mesoporous silica. *Science* 1997; 278:264–268.
56. Balkus KJ Jr, Scout AS, Gimón-Kinsel ME, and Blanco JH. Oriented films of mesoporous MCM-41 macroporous tubules via pulsed laser deposition. *Micropor Mesopor Mater* 2000; 38:97–105.
57. Nishiyama N, Koide A, and Egashira Y. Mesoporous MCM-48 membrane synthesized on a porous stainless steel support. *Chem Commun* 1998; 19:2147–2148.
58. Nishiyama N, Park DH, Koide A, Egashira Y, and Ueyama K. A Mesoporous silica (MCM-48) membrane: Preparation and characterization. *J Membr Sci* 2001; 182:235–244.
59. Park DH, Nishiyama N, Egashira Y, and Ueyama K. Separation of organic/water mixtures with silylated MCM-48 silica membranes. *Micropor Mesopor Mater* 2003; 66:69–76.
60. van Bekkum H, Flanigan EM, and Jansen JC (Eds.), *Introduction in Zeolite Science and Practice*. Amsterdam: Elsevier, 1991.
61. Krishna R. Diffusion of binary mixtures across zeolite membranes: Entropy effects on permeation selectivity. *Int Commun Heat Mass Transfer* 2001; 28:337–346.
62. Barrer RM. Porous crystal membranes. *J Chem Soc Faraday Trans* 1990; 86:1123–1130.

63. van den Broeke LJP, Bakker WJW, Kapteijn F, and Moulijn JA. Transport and separation properties of a silicalite-1 membrane-I. Operating conditions. *Chem Eng Sci* 1999; 54:245–258.
64. Bernal MP, Coronas J, Menéndez M, and Santamaría J. Characterization of zeolite membranes by temperature programmed permeation and step desorption. *J Membr Sci* 2002; 195:125–138.
65. Bakker WJW, van den Broeke LJP, Kapteijn F, and Moulijn JA. Temperature dependence of one-component permeation through a silicalite-1 membrane. *AIChE J* 1997; 43:2203–2214.
66. Xiao J and Wei J. Diffusion mechanism of hydrocarbons in zeolites 2. Analysis of experimental-observations. *Chem Eng Sci* 1992; 47:1143–1159.
67. van de Graaf JM, Kapteijn F, and Moulijn JA. Diffusivities of light alkanes in a silicalite-1 membrane layer. *Micropor Mesopor Mater* 2000; 35–36:267–281.
68. Krishna R and Baur R. Modelling issues in zeolite based separation processes. *Sep Purif Technol* 2003; 33:213–254.
69. Jost S, Bar NK, Fritzsche S, Haberlandt R, and Karger J. Diffusion of a mixture of methane and xenon in silicalite: A molecular dynamics study and pulsed field gradient nuclear magnetic resonance experiments. *J Phys Chem B* 1998; 102:6375–6381.
70. Krishna R and Paschek D. Self-diffusivities in multicomponent mixtures in zeolites. *Phys Chem Chem Phys* 2002; 4:1891–1898.
71. Snurr RQ and Karger J. Molecular simulations and NMR measurements of binary diffusion in zeolites. *J Phys Chem B* 1997; 101:6469–6473.
72. Paschek D and Krishna R. Diffusion of binary mixtures in zeolites: Kinetic Monte Carlo versus molecular dynamics simulations. *Langmuir* 2001; 17:247–254.
73. Bowen TC, Wyss JC, Noble RD, and Falconer JL. Measurements of diffusion through a zeolite membrane using isotopic-transient pervaporation. *Micropor Mesopor Mater* 2004; 71:199–210.
74. Bowen TC, Li S, Noble RD, and Falconer JL. Driving force for pervaporation through zeolite membranes. *J Membr Sci* 2003; 225:165–176.
75. Piera E, Giroir-Fendler A, Moueddeb H, Dalmon JA, Coronas J, Menéndez M, and Santamaría J. Separation of alcohols and alcohols/O<sub>2</sub> mixtures using zeolite MFI membranes. *J Membr Sci* 1998; 142:97–109.
76. Bernal MP, Piera E, Coronas J, Menéndez M, and Santamaría J. Mordenite and ZSM-5 hydrophilic tubular membranes for the separation of gas phase-mixtures. *Catal Today* 2000; 56:221–227.
77. Wicke E and Kallenbach R. Surface diffusion of carbon dioxide in activated charcoals (English translation of the German title). *Kolloid Z* 1941; 97:135–151.
78. Baker RW. Future directions of membrane gas separation technology. *Ind Eng Chem Res* 2002; 41:1393–1411.
79. <http://www.tcn.zaq.ne.jp/membrane/english/ManufactE.htm> (Accessed March 2008).
80. Meindersma GW and de Haan AB. Economical feasibility of zeolite membranes for industrial scale separations of aromatic hydrocarbons. *Desalination* 2002; 149:29–34.
81. Tomita T, Nakayama K, and Sakai H. Gas separation characteristics of DDR type zeolite membrane. *Micropor Mesopor Mater* 2004; 68:71–75.
82. Bernal MP, Coronas J, Menéndez M, and Santamaría J. Separation of CO<sub>2</sub>/N<sub>2</sub> mixtures using MFI-type zeolite membranes. *AIChE J* 2004; 50(1):127–135.
83. Hasegawa Y, Watanabe K, Kusakabe K, and Morooka S. The separation of CO<sub>2</sub> using Y-type zeolite membranes ion-exchanged with alkali metal cations. *Sep Purif Technol* 2001; 22–3(1–3):319–325.
84. Hasegawa Y, Watanabe K, Kusakabe K, and Morooka S. Influence of alkali cations on permeation properties of Y-type zeolite membranes. *J Membr Sci* 2002; 208(1–2):415–418.
85. Kalipcilar H, Gade SK, Falconer JL, and Noble RD. Synthesis and separation properties of B-ZSM-5 zeolite membranes on monolith supports. *J Membr Sci* 2002; 210(1):113–127.
86. Arruebo M, Coronas J, Menéndez M, and Santamaría J. Separation of hydrocarbons from natural gas using silicalite membranes. *Sep Purif Technol* 2001; 25(1–3):275–286.
87. Lai R and Gavalas GR. ZSM-5 membrane synthesis with organic free mixtures. *Micropor Mesopor Mater* 2000; 38(2–3):239–245.
88. Dong JH, Lin YS, Hu MZC, Peascoe RA, and Payzant EA. Template-removal-associated microstructural development of porous-ceramic-supported MFI zeolite membranes. *Micropor Mesopor Mater* 2000; 34(3):241–253.
89. Piera E, Brenninkmeijer CAM, Santamaría J, and Coronas J. Separation of traces of CO from air using MFI-type zeolite membranes. *J Membr Sci* 2002; 201(1–2):229–232.
90. Aguado S, Polo AC, Bernal MP, Coronas J, and Santamaría J. Removal of pollutants from indoor air using zeolite membranes. *J Membr Sci* 2004; 240(1–2):159–166.
91. Nair S, Lai ZP, Nikolakis V, Xomeritakis G, Bonilla G, and Tsapatsis M. Separation of close-boiling hydrocarbon mixtures by MFI and FAU membranes made by secondary growth. *Micropor Mesopor Mater* 2001; 48:219–228.
92. Skoulidas AI, Bowen TC, Doelling CM, Falconer JL, Noble RD, and Sholl DS. Comparing atomistic simulations and experimental measurements for CH<sub>4</sub>/CF<sub>4</sub> mixture permeation through silicalite membranes. *J Membr Sci* 2003; 127(1–2):123–136.
93. Aoki K, Kusakabe K, and Morooka S. Separation of gases with an A-type zeolite membrane. *Ind Eng Chem Res* 2000; 39(7):2245–2251.
94. Morón F, Pina MP, Urriolabeitia E, Menéndez M, and Santamaría J. Preparation and characterization of Pd-zeolite composite membranes for hydrogen separation. *Desalination* 2002; 147(1–3):425–431.
95. Piera E, Coronas M, Menéndez M, and Santamaría J. Gas separation selectivity with imperfect zeolite membranes. *Chem Commun* 1999; 14:1309–1310.

96. Kusakabe K, Kuroda T, Murata A, and Morooka S. Formation of a Y-type zeolite membrane on a porous alpha-alumina tube for gas separation. *Ind Eng Chem Res* 1997; 36(3):649–655.
97. Kusakabe K, Kuroda T, Uchino K, Hasegawa Y, and Morooka S. Gas permeation properties of ion-exchanged faujasite-type zeolite membranes *AIChE J* 1999; 45(6):1220–1226.
98. Kusakabe K, Kuroda T, and Morooka S. Separation of carbon dioxide from nitrogen using ion-exchanged faujasite-type zeolite membranes formed on porous support tubes. *J Membr Sci* 1998; 148(1):13–23.
99. Nikolakis V, Xomeritakis G, Abibi A, Dickson M, Tsapatsis M, and Vlachos DG. Growth of a faujasite-type zeolite membrane and its application in the separation of saturated/unsaturated hydrocarbon mixtures. *J Membr Sci* 2001; 184:209–219.
100. Bakker WJ, Kapteijn F, Poppe J, and Moulijn JA. Permeation characteristics of a metal-supported silicalite-1 zeolite membrane. *J Membr Sci* 1996; 117:57–78.
101. Masuda T, Okubo Y, Mukai SR, Kawase M, Hashimoto K, Shichi A, Satsuma A, Hattori T, and Kiyozumi Y. Effective diffusivities of lighter hydrocarbons in Cu- and Co-MFI-type zeolite catalysts. *Chem Eng Sci* 2001; 56:889–896.
102. Pascual P, Ungerer P, Tavitian B, and Boutin A. Development of a transferable guest–host force field for adsorption of hydrocarbons in zeolites. II. Prediction of alkenes adsorption and alkane/alkene selectivity in silicalite. *J Phys Chem B* 2004; 108:393–398.
103. Giannakopoulos IG and Nikolakis V. Separation of propylene/propane mixtures using faujasite membranes. *Ind Eng Chem Res* 2005; 44(1):226–230.
104. Dong J, Lin YS, and Liu W. Multicomponent hydrogen/hydrocarbon separation by MFI-type zeolite membranes. *AIChE J* 2000; 46(10):1957–1966.
105. Li S, Alvarado G, Noble RD, and Falconer JL. Effects of impurities on CO<sub>2</sub>/CH<sub>4</sub> separations through SAPO-34 membranes. *J Membr Sci* 2005; 251(1–2):59–66.
106. Morigami Y, Kondo M, Abe J, Kita H, and Okamoto K. The first large-scale pervaporation plant using tubular-type module with zeolite NaA membrane. *Sep Purif Technol* 2001; 25:251–260.
107. Kondo M, Yamamura T, Yuki take T, Matsuo Y, Kita H, and Okamoto K. IPA purification for lens cleaning by vapor permeation using zeolite membrane. *Sep Purif Technol* 2003; 32:191–198.
108. Tehennepe HJC, Bargeman D, Mulder MHV, and Smolders CA. Zeolite-filled silicone-rubber membranes. I. Membrane preparation and pervaporation results. *J Membr Sci* 1987; 35:39–55.
109. <http://www.sulzerchemtech.com/> (Accessed March 2008).
110. Gallego-Lizon T, Edwards E, Lobiundo G, and dos Santos LF. Dehydration of water/*t*-butanol mixtures by pervaporation: Comparative study of commercially available polymeric, microporous silica and zeolite membranes. *J Membr Sci* 2002; 197:309–319.
111. Van Hoof V, Van den Abeele L, Buekenhoudt A, Dotremont C, and Leysen R. Economic comparison between azeotropic distillation and different hybrid systems combining distillation with pervaporation for the dehydration of isopropanol. *Sep Purif Technol* 2004; 37:33–49.
112. Kita H, Fuchida K, Horita T, Asamura H, and Okamoto K. Preparation of Faujasite membranes and their permeation properties. *Sep Purif Technol* 2001; 25:261–268.
113. Bowen TC, Noble RD, and Falconer JL. Fundamentals and applications of pervaporation through zeolite membranes. *J Membr Sci* 2004; 245:1–33.
114. Shah D, Kissick K, Ghorpade A, Hannah R, and Bhattacharyya D. Pervaporation of alcohol–water and dimethylformamide–water mixtures using hydrophilic zeolite NaA membranes: Mechanisms and experimental results. *J Membr Sci* 2000; 179:185–205.
115. Wijmans JG and Baker RW. A simple predictive treatment of the permeation process in pervaporation. *J Membr Sci* 1993; 79:101–106.
116. Nomura M, Yamaguchi T, and Nakao S. Transport phenomena through intercrystalline and intracrystalline pathways of silicalite zeolite membranes. *J Membr Sci* 2001; 187:203–212.
117. de Bruijn FT, Sun L, Olujic Z, Jansens PJ, and Kapteijn F. Influence of the support layer on the flux limitation in pervaporation. *J Membr Sci* 2003; 223:141–156.
118. Arjan Giaya A, Thompson RW, and Denkwicz R. Liquid and vapor phase adsorption of chlorinated volatile organic compounds on hydrophobic molecular sieves. *Micropor Mesopor Mater* 2000; 40:205–218.
119. Noack M, Kolsch P, Caro J, Schneider M, Toussaint P, and Sieber I. MFI membranes of different Si/Al ratios for pervaporation and steam permeation. *Micropor Mesopor Mater* 2000; 35–36:253–265.
120. Nomura M, Bin T, and Nakao S. Selective ethanol extraction from fermentation broth using a silicalite membrane. *Sep Purif Technol* 2002; 27:59–66.
121. Lin X, Chen XS, Kita H, and Okamoto K. Synthesis of silicalite tubular membranes by in situ crystallization. *AIChE J* 2003; 49:237–247.
122. Lin X, Kita H, and Okamoto K. A novel method for the synthesis of high performance silicalite membranes. *Chem Commun* 2000; 19:1889–1890.
123. Sano T, Yanagishita H, Kiyozumi Y, Mizukami F, and Haraya K. Separation of ethanol–water mixture by silicalite membrane on pervaporation. *J Membr Sci* 1994; 95:221–228.
124. Smetana JF, Falconer JL, and Noble RD. Separation of methyl ethyl ketone from water by pervaporation using a silicalite membrane. *J Membr Sci* 1996; 114:127–130.
125. Liu Q, Noble RD, Falconer JL, and Funke HH. Organics/water separation by pervaporation with a zeolite membrane. *J Membr Sci* 1996; 117:163–174.
126. Sano T, Ejiri S, Yamada K, Kawakami Y, and Yanagishita H. Separation of acetic acid–water mixtures by pervaporation through silicalite membrane. *J Membr Sci* 1997; 123:225–233.

127. Sano T, Hasegawa M, Kawakami Y, and Yanagishita H. separation of methanol/methyl-*tert*-butyl ether mixture by pervaporation using silicalite membrane. *J Membr Sci* 1995; 107:193–196.
128. Yuan WH, Lin YS, and Yang WS. Molecular sieving MFI-type zeolite membranes for pervaporation separation of xylene isomers. *J Am Chem Soc* 2004; 126:4776–4777.
129. Li G, Kikuchi E, and Matsukata M. A study on the pervaporation of water–acetic acid mixtures through ZSM-5 zeolite membranes. *J Membr Sci* 2003; 218:185–194.
130. Cui Y, Kita H, and Okamoto KI. Zeolite T membrane: Preparation, characterization, pervaporation of water/organic liquid mixtures and acid stability. *J Membr Sci* 2004; 236:17–27.
131. Tanaka K, Yoshikawa R, Ying C, Kita H, and Okamoto K. Application of zeolite membranes to esterification reactions. *Catal Today* 2001; 67:121–125.
132. Tanaka K, Yoshikawa R, Ying V, Kita H, and Okamoto K. Application of zeolite T membrane to vapor-permeation-aided esterification of lactic acid with ethanol. *Chem Eng Sci* 2002; 57:1577–1584.
133. Lide DR and Kehiaian HV. Azeotropic data for binary mixtures. In: David R. Lide (Ed.), *CRC Handbook of Chemistry and Physics*, 85th ed. CRC Press 2004–2005: 6-180–6-181.
134. Kita H, Horii K, Ohtoshi Y, Tanaka K, and Okamoto KI. Synthesis of a zeolite NaA membrane for pervaporation of water–organic liquid–mixtures. *J Mater Sci Lett* 1995; 14:206–208.
135. Okamoto K, Kita H, Kondo M, Miyake N, and Matsuo Y. Membrane for liquid mixture separation. US Patent 5,554,286. 1996.
136. van den Berg AWC, Gora L, Jansen JC, Makkee M, and Maschmeyer T. Zeolite A membranes synthesized on a UV-irradiated TiO<sub>2</sub> coated metal support: The high pervaporation performance. *J Membr Sci* 2003; 224:29–37.
137. Kondo M, Komori M, Kita H, and Okamoto K. Tubular-type pervaporation module with zeolite NaA membrane. *J Membr Sci* 1997; 133:133–141.
138. Holmes SM, Schmitt M, Markert C, Plaisted RJ, Forrest JO, Sharratt PN, Garforth AA, Cundy CS, and Dwyer J. Zeolite A membranes for use in alcohol/water separations—Part I: Experimental investigation. *Chem Eng Res Des* 2000; 78(A8):1084–1088.
139. Jafar JJ, Budd PM, and Hughes R. Enhancement of esterification reaction yield using zeolite-A vapour permeation membrane. *J Membr Sci* 2002; 199:117–123.
140. Huang AS, Lin YS, and Yang WS. Synthesis and properties of A-type zeolite membranes by secondary growth method with vacuum seeding. *J Membr Sci* 2004; 245:41–51.
141. Okamoto K, Kita H, Horii K, Tanaka K, and Kondo M. Zeolite NaA membrane: Preparation, single-gas permeation, and pervaporation and vapor permeation of water/organic liquid mixtures. *Ind Eng Chem Res* 2001; 40:163–175.
142. Li G, Kikuchi E, and Matsukata M. The control of phase and orientation in zeolite membranes by the secondary growth method. *Micropor Mesopor Mater* 2003; 62:211–220.
143. Lin X, Kikuchi E, and Matsukata M. Preparation of mordenite membranes on alpha-alumina tubular supports for pervaporation of water–isopropyl alcohol mixtures. *Chem Commun* 2000; 11:957–958.
144. Zhang YF, Xu ZQ, and Chen QL. Synthesis of small crystal polycrystalline mordenite membrane. *J Membr Sci* 2002; 210:361–368.
145. Casado L, Mallada R, Téllez C, Coronas J, Menéndez M, and Santamaría J. Preparation, characterization and pervaporation performance of mordenite membranes. *J Membr Sci* 2003; 216(1–2):135–147.
146. Navajas A, Mallada R, Tellez C, Coronas J, Menendez M, and Santamaría J. Preparation of mordenite membranes for pervaporation of water–ethanol mixtures. *Desalination* 2002; 148:25–29.
147. Li G, Kikuchi E, and Matsukata M. Separation of water–acetic acid mixtures by pervaporation using a thin mordenite membrane. *Sep Purif Technol* 2003; 32:199–206.
148. Li SG, Tuan VA, Noble RD, and Falconer JL. Pervaporation of water/THF mixtures using zeolite membranes. *Ind Eng Chem Res* 2001; 40:4577–4585.
149. Masuda T, Otani S, Tsuji T, Kitamura M, and Mukai SR. Preparation of hydrophilic and acid-proof silicalite-1 zeolite membrane and its application to selective separation of water from water solutions of concentrated acetic acid by pervaporation. *Sep Purif Technol* 2003; 32(1–3):181–189.
150. Kalipcilar H, Bowen TC, Noble RD, and Falconer JL. Synthesis and separation performance of SSZ-13 zeolite membranes on tubular supports. *Chem Mat* 2002; 14:3458–3464.
151. Urtiaga A, Gorri ED, Casado C, and Ortiz I. Pervaporative dehydration of industrial solvents using a zeolite NaA commercial membrane. *Sep Purif Technol* 2003; 32(1–3):207–213.
152. Asaeda M, Sakou Y, Yang J, and Shimasaki K. Stability and performance of porous silica–zirconia composite membranes for pervaporation of aqueous organic solutions. *J Membr Sci* 2002; 209:163–175.
153. ten Elshof JE, Rubio Abadal C, Sekuli J, Chowdhury SR, and Blank DHA. Transport mechanisms of water and organic solvents through microporous silica in the pervaporation of binary liquids. *Micropor Mesopor Mater* 2003; 65:197–208.
154. Li SG, Tuan VA, Noble RD, and Falconer JL. A Ge-substituted ZSM-5 zeolite membrane for the separation of acetic acid from water. *Ind Eng Chem Res* 2001; 40(26):6165–6171.
155. <http://www.epa.gov/mtbe/> (Accessed March 2008).
156. Flanders CL, Tuan VA, Noble RD, and Falconer JL. Separation of C-6 isomers by vapor permeation and pervaporation through ZSM-5 membranes. *J Membr Sci* 2000; 176:43–53.
157. Saracco G and Specchia V. Catalytic inorganic-membrane reactors: Present experience and future opportunities. *Catal Rev Sci Eng* 1994; 36(2):305–384.
158. Zaman J and Chakma A. Inorganic membrane reactors. *J Membr Sci* 1994; 92:1–28.

159. Falconer JL, Noble RD, and Sperry DP. In: R.D. Noble and S.A. Stern (Eds.), *Membrane Separation Technology, Principles and Applications*. Amsterdam: Elsevier Science BV, 1995.
160. Hsieh HP. *Inorganic Membranes for Separation and Reaction*. Amsterdam: Elsevier Science BV, 1996.
161. Dixon AG. Innovations in catalytic inorganic membrane reactors, *Specialist Periodical Reports: Catalysis* Vol. 14, pp. 40–92, Royal Society of Chemistry, North Yorkshire, 1999.
162. Coronas J and Santamaría J. Catalytic reactors based on porous ceramic membranes. *Catal Today* 1999; 51:377–389.
163. Saracco G, Neomagus HWJP, Versteeg GF, and van Swaaj WPM. High-temperature membrane reactors: Potential and problems. *Chem Eng Sci* 1999; 54:1997–2017.
164. Julbe A, Farrusseng D, and Guizard C. Porous ceramic membranes for catalytic reactors—overview and new ideas. *J Membr Sci* 2001; 181:3–20.
165. Cot L, Ayrat A, Durand J, Guizard C, Hovnanian N, Julbe A, and Larbot A. Inorganic membranes and solid state sciences. *Solid State Sci* 2000; 2:313–334.
166. Lin YS. Microporous and dense inorganic membranes: Current status and prospective. *Sep Purif Technol* 2001; 25:39–55.
167. Chiang AST and Chao K-J. Membranes and films of zeolite and zeolite-like materials. *J Phys Chem Solid* 2001; 62:1899–1910.
168. Reif M and Dittmeyer R. Porous, catalytically active ceramic membranes for gas–liquid reactions: A comparison between catalytic diffuser and forced through flow concept. *Catal Today* 2003; 82:3–14.
169. Vospernik M, Pintar A, Bercic G, and Levec J. Experimental verification of ceramic membrane potentials for supporting three-phase catalytic reactions. *J Membr Sci* 2003; 223:157–169.
170. Vospernik M, Pintar A, Bercic G, and Levec J. Mass transfer studies in gas–liquid–solid membrane contactors. *Catal Today* 2003; 79–80:169–179.
171. Vospernik M, Pintar A, Bercic G, Levec J, Walmsley J, Raeder H, Iojoiu EE, Miachon S, and Dalmon JA. Performance of catalytic membrane reactor in multiphase reactions. *Chem Eng Sci* 2004; 59:5363–5372.
172. Miachon S, Perez V, Crehan G, Torp EG, Raeder H, Bredesen R, and Dalmon JA. Comparison of a contactor catalytic membrane reactor with a conventional reactor: Example of wet air oxidation. *Catal Today* 2003; 82(1–4):75–81.
173. Raeder H, Bredesen R, Crehan G, Miachon S, Dalmon JA, Pintar A, Levec J, and Torp EG. A wet air oxidation process using a catalytic membrane contactor. *Sep Purif Technol* 2003; 32:349–355.
174. van de Graaf JM, Kapteijn F, and Moulijn J. Methodological and operational aspects of permeation measurements on silicalite-1 membranes. *J Membr Sci* 1998; 144(1–2):87–104.
175. Casanave D, Giroir-Fendler A, Sánchez J, Loutaty R, and Dalmon JA. Control of transport-properties with a microporous membrane reactor to enhance yields in dehydrogenation reactions. *Catal Today* 1995; 25:309–314.
176. Ciavarella P, Casanave D, Moueddeb H, Miachon S, Fiety K, and Dalmon JA. Isobutane dehydrogenation in a membrane reactor— influence of the operating conditions on the performance. *Catal Today* 2001; 67:177–184.
177. van Dyk L, Miachon S, Lorenzen L, Torres M, Fiety K, and Dalmon JA. Comparison of microporous MFI and dense Pd membrane performances in an extractor-type CMR. *Catal Today* 2003; 82:167–177.
178. Giroir-Fendler A, Julbe A, Ramsay JDF, and Dalmon JA. CNRS French Patent, PCT Int Appl. FR 94-5562, 940429. 1994.
179. Giroir-Fendler A, Peureux J, Mozzanega H, and Dalmon JA. Characterization of a zeolite membrane for catalytic membrane reactor application. *Stud Surf Sci Catal A* 1996; 101:127–136.
180. Jeong BH, Sotowa KI, and Kusakabe K. Catalytic dehydrogenation of cyclohexane in an FAU-type zeolite membrane reactor. *J Membr Sci* 2003; 224:151–158.
181. Jeong BH, Sotowa KI, and Kusakabe K. Modeling of an FAU-type zeolite membrane reactor for the catalytic dehydrogenation of cyclohexane. *Chem Eng J* 2004; 103:69–75.
182. Liu BS and Au CT. A La<sub>2</sub>NiO<sub>4</sub>-zeolite membrane reactors for the CO<sub>2</sub> reforming of methane to syngas. *Catal Lett* 2001; 77(1–3):67–74.
183. Liu BS, Gao LZ, and Au CT. Preparation, characterization and application of a catalytic NaA membrane for CH<sub>4</sub>/CO<sub>2</sub> reforming to syngas. *Appl Catal A: Gen* 2002; 235:193–206.
184. Ostrowski T, Giroir-Fendler A, Mirodatos C, and Mleczko L. Comparative study of the partial oxidation of methane to synthesis gas in fixed-bed and fluidized-bed membrane reactors: Part II—development of membranes and catalytic measurements. *Catal Today* 1998; 40(2–3):191–200.
185. van de Graaf JM, Zwiep M, Kapteijn F, and Moulijn JA. Application of a silicalite-1 membrane reactor in metathesis reactions. *Appl Catal A: Gen* 1999; 178:225–241.
186. van de Graaf JM, Zwiep M, Kapteijn F, and Moulijn JA. Application of a zeolite membrane reactor in the metathesis of propene. *Chem Eng Sci* 1999; 54:1441–1445.
187. Okamoto K, Tanihara N, Watanabe H, Tanaka K, Kita H, Nakamura A, Kusuki Y, and Nakagawa K. Vapor permeation and pervaporation separation of water ethanol mixtures through polyimide membranes. *J Membr Sci* 1992; 68(1–2):53–63.
188. Okamoto K, Yamamoto M, Noda S, Semoto T, Otoshi Y, Tanaka K, and Kita H. Vapor-permeation-aided esterification of oleic-acid. *Ind Eng Chem Res* 1994; 33(4):849–853.
189. Zhu Y, Minet RG, and Tsotsis TT. A continuous pervaporation membrane reactor for the study of esterification reactions using a composite polymeric/ceramic membrane. *Chem Eng Sci* 1996; 5(17):4103–4113.
190. Zhu Y and Chen HF. Pervaporation separation and pervaporation-esterification coupling using crosslinked PVA composite catalytic membranes on porous ceramic plate. *J Membr Sci* 1998; 138(1):123–134.

191. Krupiczka R and Koszorz Z. Activity-based model of the hybrid process of an esterification reaction coupled with pervaporation. *Sep Purif Technol* 1999; 16(1):55–59.
192. Koszorz Z, Nemestothy N, Ziobrowski Z, Belafi-Bako K, and Krupiczka R. Influence of pervaporation process parameters on enzymatic catalyst deactivation. *Desalination* 2004; 162:307–313.
193. Budd PM, Ricardo NMP, Jafar JJ, and Hughes R. Zeolite/polyelectrolyte multilayer pervaporation membranes for enhanced reaction. *Ind Eng Chem Res* 2004; 43(8):1863–1867.
194. Bernal MP, Coronas J, Menéndez M, and Santamaría J. Coupling of reaction and separation at the microscopic level: Esterification processes in a H-ZSM-5 membrane reactor. *Chem Eng Sci* 2002; 57:1557–1562.
195. Kiatkittipong W, Assabumrungrat S, Praserttham P, and Goto S. A pervaporation membrane reactor for liquid phase synthesis of ethyl *tert*-butyl ether from *tert*-butyl alcohol and ethanol. *J Chem Eng Jpn* 2002; 35(6):547–556.
196. Assabumrungrat S, Kiatkittipong W, Praserttham P, and Goto S. Simulation of pervaporation membrane reactors for liquid phase synthesis of ethyl *tert*-butyl ether from *tert*-butyl alcohol and ethanol. *Catal Today* 2003; 79–80:249–257.
197. Aiouache F and Goto S. Reactive distillation-pervaporation hybrid column for *tert*-amyl alcohol etherification with ethanol. *Chem Eng Sci* 2003; 58(12):2465–2477.
198. Salomón MA, Coronas J, Menéndez M, and Santamaría J. Synthesis of MTBE in zeolite membrane reactors. *Appl Catal A: Gen* 2000; 200:201–210.
199. Haggin J. New processes target methanol production, off-gas cleaning. *Chem Eng News* 1994; 72(13):29–31.
200. Barbieri G, Marigliano G, Golemme G, and Drioli E. Simulation of CO<sub>2</sub> hydrogenation with CH<sub>3</sub>OH removal in a zeolite membrane reactor. *Chem Eng J* 2002; 85:53–59.
201. Gallucci F, Paturzo L, and Basile A. An experimental study of CO<sub>2</sub> hydrogenation into methanol involving a zeolite membrane reactor. *Chem Eng Proc* 2004; 43:1029–1036.
202. Struis RPWJ, Quintilii M, and Stucki S. Feasibility of Li-Nafion hollow fiber membranes in methanol synthesis: Mechanical and thermal stability at elevated temperature and pressure. *J Membr Sci* 2000; 177(1–2):215–223.
203. Struis RPWJ and Stucki S. Verification of the membrane reactor concept for the methanol synthesis. *Appl Catal A: Gen* 2001; 216(1–2):117–129.
204. Espinoza RL, du Toit E, Santamaría J, Menéndez M, Coronas J, and Irusta S. Use of membranes in Fischer–Tropsch reactors. *Stud Surf Sci Catal* 2000; 130:389–394.
205. Xiongfu Z, Yonsheng L, Jinqu W, Huairong T, and Changhou L. Synthesis and characterization of Fe-MFI zeolite membrane on a porous  $\alpha$ -Al<sub>2</sub>O<sub>3</sub> tube. *Sep Purif Technol* 2001; 25:269–274.
206. Pantazidis A, Dalmon JA, and Mirodatos C. Oxidative dehydrogenation of propane on catalytic membrane reactors. *Catal Today* 1995; 25:403–408.
207. Julbe A, Farrusseng D, Jalibert JC, Mirodatos C, and Guizard C. Characteristics and performance in the oxidative dehydrogenation of propane of MFI and V-MFI zeolite membranes. *Catal Today* 2000; 56:199–209.
208. Giroir-Fendler A, Julbe A, Ramsay JDF, and Dalmon JA. FR Patent 94-5562, PCT Int Appl WO 9529751, 1994.
209. Farrusseng D, Julbe A, and Guizard C. Evaluation of porous ceramic membranes as O<sub>2</sub> distributors for the partial oxidation of alkanes in inert membrane reactors. *Sep Purif Technol* 2001; 25:137–149.
210. Mota S, Micahon S, Volta JC, and Dalmon JA. Membrane reactor for selective oxidation of butane to maleic anhydride. *Catal Today* 2001; 67:169–176.
211. Lange C, Storck S, Tesche B, and Maier WF. Selective hydrogenation reactions with a microporous membrane catalyst, prepared by sol–gel dip coating. *J Catal* 1998; 175(2):280–293.
212. van der Puil N, Creighton EJ, Rodenburg EC, Sie TS, van Bekkum H, and Jansen JC. Catalytic testing of TiO<sub>2</sub>/platinum/silicalite-1 composites. *J Chem Soc Faraday Trans* 1996; 92(22):4609–4615.
213. Jansen JC, Koegler JH, van Bekkum H, Calis HPA, van den Bleek CM, Kapteijn F, Moulijn JA, Geus ER, and van der Puil N. Zeolitic coatings and their potential use in catalysis. *Micropor Mesopor Mater* 1998; 21(4–6):213–226.
214. Nishiyama N, Ichioka K, Park DH, Egashira Y, Ueyama K, Gora L, Zhu WD, Kapteijn F, and Moulijn JA. Reactant-selective hydrogenation over composite silicalite-1-coated Pt/TiO<sub>2</sub> particles. *Ind Eng Chem Res* 2004; 43(5):1211–1215.
215. Vilaseca M, Coronas J, Cirera A, Cornet A, Morante JR, and Santamaría J. Use of zeolite films to improve the selectivity of reactive gas sensors. *Catal Today* 2003; 82(1–4):179–185.
216. Maloney ML, Gora L, McLeary EE, Jansen JC, and Maschmeyer TH. Hydroisomerization of hexane within a reactor composed of a tubular silicalite-1 membrane packed with Pt-loaded chlorided alumina catalyst. *Catal Commun* 2004; 5:297–300.
217. Gora L and Jansen JC. Hydroisomerization of C-6 with a zeolite membrane reactor. *J Catal* 2005; 230(2):269–281.
218. Torres M, López L, Domínguez JM, Mantilla A, Ferrat G, Gutiérrez M, and Maubert M. Olefins catalytic oligomerization on new composites of beta-zeolite films supported on alpha-Al<sub>2</sub>O<sub>3</sub> membranes. *Chem Eng J* 2003; 92:1–6.
219. Masuda T, Asanuma T, Shouji M, Mukai SR, Kawase M, and Hashimoto K. Methanol to olefins using ZSM-5 zeolite catalyst membrane reactor. *Chem Eng Sci* 2003; 58:649–656.
220. Piera E, Téllez C, Coronas J, Menéndez M, and Santamaría J. Use of zeolite membrane reactors for selectivity enhancement: Application to the liquid-phase oligomerization of *i*-butene. *Catal Today* 2001; 67:127–138.
221. Maira AJ, Lau WN, Lee CY, Yue PL, Chan CK, and Yeung KL. Performance of a membrane-catalyst for photocatalytic oxidation of volatile organic compounds. *Chem Eng Sci* 2003; 58:959–962.
222. Aguado S, Coronas J, and Santamaría J. Use of zeolite membrane reactors for the combustion of VOCs present in air at low concentrations *Chem Eng Res Des* 2005; 83(A3):295–301.

223. Hasegawa Y, Kusakabe K, and Morooka S. Selective oxidation of carbon monoxide in hydrogen-rich mixtures by permeation through a platinum-loaded Y-type zeolite membrane. *J Membr Sci* 2001; 190:1–8.
224. Hasegawa Y, Sotowa KI, Kusakabe K, and Morooka S. Selective oxidation of CO in H<sub>2</sub> by permeation through catalytically active zeolite membranes. *J Chem Eng Jpn* 2002; 35(12):1244–1251.
225. Hasegawa Y, Sotowa KI, Kusakabe K, and Morooka S. The influence of feed composition on CO oxidation using zeolite membranes loaded with metal catalysts. *Micropor Mesopor Mater* 2002; 53(1–3):37–43.
226. Hasegawa Y, Sotowa KI, and Kusakabe K. Permeation behavior during the catalytic oxidation of CO in a Pt-loaded Y-type zeolite membrane. *Chem Eng Sci* 2003; 58(13):2797–2803.
227. Simon U and Franke ME. Electrical properties of nanoscaled host/guest compounds. *Micropor Mesopor Mater* 2000; 4:1–36.
228. Rao N, Andersen TP, and Ge P. Tin mordenite membranes for direct methanol fuel-cells. *Solid State Ionics* 1994; 72:334–337.
229. Poltarzewski Z, Wiczorek W, Przyluski J, and Antonucci V. Novel proton conducting composite electrolytes for application in methanol fuel cells. *Solid State Ionics* 1999; 119:301–304.
230. Tricoli V and Nannetti F. Zeolite-Nafion composites as ion conducting membrane materials. *Electrochim Acta* 2003; 48:2625–2633.
231. Libby B, Smyrl WH, and Cussler EL. Polymer-zeolite composite membranes for direct methanol fuel cells. *AIChE J* 2003; 49:991–1001.
232. Baglio V, Arico S, di Blasi A, Antonucci PL, Nannetti F, and Tricoli V. Zeolite-based composite membranes for high temperature direct methanol fuel cells. *J Appl Electrochem* 2005; 35:207–212.
233. Wöltinger J, Drauz K, and Bommarius AS. The membrane reactor in the fine chemicals industry. *Appl Catal A: Gen* 2001; 221:171–185.
234. Wandrey C, Wichmann R, Leuchtenberger W, and Kula MR. US Patent 4,304,858. 1981.
235. Matsui M, Kiyozumi Y, Yamamoto T, Mizushima Y, Mizukami F, and Sakaguchi K. Selective adsorption of biopolymers on zeolites. *Chem Eur J* 2001; 7(7):1555–1560.
236. Chiku H, Matsui M, Murakami S, Kiyozumi Y, Mizukami F, and Sakaguchi K. Zeolites as new chromatographic carriers for proteins—easy recovery of proteins adsorbed on zeolites by polyethylene glycol. *Anal Biochem* 2003; 318:80–85.
237. Wang Y and Caruso F. Macroporous zeolitic membrane bioreactors. *Adv Funct Mater* 2004; 14(10):1012–1018.
238. Shukla A and Kumar A. Experimental studies and mass-transfer analysis of the hydrolysis of olive oil in a biphasic zeolite-membrane reactor using chemically immobilized lipase. *Ind Eng Chem Res* 2004; 43(9):2017–2029.
239. Hyde JR, Licence P, Carter D, and Poliakoff M. Continuous catalytic reactions in supercritical fluids. *Appl Catal A: Gen* 2001; 222(1–2):119–131.
240. Annis DA and Jacobsen EN. Polymer-supported chiral Co(salen) complexes: Synthetic applications and mechanistic investigations in the hydrolytic kinetic resolution of terminal epoxides. *J Am Chem Soc* 1999; 121(17):4147–4154.
241. Choi SD and Kim GJ. Enantioselective hydrolytic kinetic resolution of epoxides catalyzed by chiral Co(III) salen complexes immobilised in the membrane reactor. *Catal Lett* 2004; 92(1–2):35–40.
242. Langhendries G, Baron GV, Vankelecom IFJ, Parto RF, and Jacobs PA. Selective hydrocarbon oxidation using a liquid-phase catalytic membrane reactor. *Catal Today* 2000; 56(1–3):131–135.
243. Wu S, Gallot JE, Bousmina M, Bouchard C, and Kaliaguine S. Zeolite containing catalytic membranes as interphase contactors. *Catal Today* 2000; 56:113–129.
244. Yawalkar AA, Pangarkar VG, and Baron GV. Alkene epoxidation with peroxide in a catalytic membrane reactor: A theoretical study. *J Membr Sci* 2001; 182:129–137.
245. Vankelecom IFJ and Jacobs PA. Dense organic catalytic membranes for fine chemical synthesis. *Catal Today* 2000; 56:147–157.
246. Turlán D, Urriolabeitia EP, Navarro R, Royo C, Menéndez M, and Santamaría J. Separation of Pd complexes from a homogeneous solution using zeolite membranes. *Chem Commun* 2001; 24:2608–2609.
247. de Smet K, Aerts S, Ceulemans E, Vankelecom IFJ, and Jacobs PA. Nanofiltration-coupled catalysis to combine the advantages of homogeneous and heterogeneous catalysis. *Chem Commun* 2001; 7:597–598.
248. Gállego I, Mallada R, Urriolabeitia EP, Navarro R, Menéndez M, and Santamaría J. Selective separation of homogeneous catalysts using silicalite membranes. *Inorg Chim Acta* 2004; 357:4577–4581.
249. Goetheer ELV, Verkerk AW, van den Brooke LJP, de Wolf E, Deelman BJ, van Koten G, and Keurentjes JTF. Membrane reactor for homogeneous catalysis in supercritical carbon dioxide. *J Catal* 2003; 219:126–133.
250. Shan Z, van Kooten WEJ, Oudshoorn OL, Jansen JC, van Bekkum H, van den Bleek CM, and Calis HPA. Optimization of the preparation of binderless ZSM-5 coatings on stainless steel monoliths by in situ hydrothermal synthesis. *Micropor Mesopor Mater* 2000; 34:81–91.
251. Ulla MA, Mallada R, Coronas J, Guitérrez L, Miró E, and Santamaría J. Synthesis and characterization of ZSM-5 coatings onto cordierite honeycomb supports. *Appl Catal A: Gen* 2003; 253(1):257–269.
252. Ulla MA, Miro E, Mallada R, Coronas J, and Santamaría J. Preparation of highly accessible mordenite coatings on ceramic monoliths at loadings exceeding 50% by weight. *Chem Commun* 2004; 5:528–529.
253. Kodama A, Hirayama T, Goto M, Hirose T, and Critoph RE. The use of psychrometric charts for the optimisation of a thermal swing desiccant wheel. *Appl Therm Eng* 2001; 21:1657.
254. Louis B, Reuse P, Kiwi-Minsker L, and Renken A. Synthesis of ZSM-5 coatings on stainless steel grids and their catalytic performance for partial oxidation of benzene by N<sub>2</sub>O. *Appl Catal A: Gen* 2001; 210:103–109.
255. López F, Bernal MP, Mallada R, Coronas J, and Santamaría J. Preparation of silicalite membranes on stainless steel grid supports. *Ind Eng Chem Res* 2005; 44:7627–7632.

256. Beers AEW, Nijhuis TA, Aalders N, Kapteijn F, and Moulijn JA. BEA coating of structured supports—performance in acylation. *Appl Catal A: Gen* 2003; 243:237–250.
257. Larlus O, Valtchev V, Patarin J, Faust AC, and Maquin B. Preparation of silicalite-1/glass fiber composites by one- and two-step hydrothermal syntheses. *Micropor Mesopor Mater* 2002; 56:175–184.
258. Deng Z and Balkus Jr KJ. Pulsed laser deposition of zeolite NaX thin films on silica fibers. *Micropor Mesopor Mater* 2002; 56:47–53.
259. Seijger GBF, Oudshoorn OL, Boekhorst A, van Bekkum H, van den Bleek CM, and Calis HPA. Selective catalytic reduction of NO<sub>x</sub> over zeolite-coated structured catalyst packings. *Chem Eng Sci* 2001; 56(3):849–857.
260. Erdem-Senatalar A, Tather M, and Ürgen M. Preparation of zeolite coatings by direct heating of the substrates. *Micropor Mesopor Mater* 1999; 32:331.
261. Balkus KJ and Scott AS. Molecular sieve coatings on spherical substrates via pulsed laser deposition. *Micropor Mesopor Mater* 2000; 34:31–42.
262. Kapteijn F, Nijhuis TA, Heiszwolf JJ, and Moulijn JA. New non-traditional multiphase catalytic reactors based on monolithic structures. *Catal Today* 2001; 66(2–4):133–144.
263. Basaldella EI, Kikot A, Quincoces CE, and González MG. Preparation of supported Cu/ZSM-5 zeolite films for DeNO(x) reaction. *Mater Lett* 2001; 51(4):289–294.
264. Basaldella EI, Kikot A, Bengoa JF, and Tara JC. ZSM-5 zeolite films on cordierite modules. Effect of dilution on the synthesis medium. *Mater Lett* 2002; 52(4–5):350–354.
265. Madhusoodana CD, Das RN, Kameshima Y, Yasumori A, and Okada K. Preparation of ZSM-5 thin film on cordierite honeycomb by solid state in situ crystallization. *Micropor Mesopor Mater* 2001; 46(2–3):249–255.
266. Madhusoodana CD, Das RN, Kameshima Y, Yasumori A, and Okada K. Characterization and adsorption behavior of ZSM-5 zeolite film on cordierite honeycombs prepared by a novel in situ crystallization method. *J Por Mater* 2001; 8(4):265–271.
267. Katsuki H, Furuta S, and Komarneni S. Formation of novel ZSM-5/porous mullite composite from sintered kaolin honeycomb by hydrothermal reaction. *J Am Ceram Soc* 2000; 83(5):1093–1097.
268. Seijger GBF, Oudshoorn OL, van Kooten WEJ, Jansen JC, van Bekkum H, van den Bleek CM, and Calis HPA. In situ synthesis of binderless ZSM-5 zeolitic coatings on ceramic foam supports. *Micropor Mesopor Mater* 2000; 39:195–204.
269. Aused MP, Urbiztondo MA, Mallada R, Pina MP, and Santamaria J. Synthesis of proton conducting membranes for direct methanol fuel cells (DMFCs). Books of abstracts of the OSSEP Final Workshop, Tenerife, 2004, pp. 90–91.
270. Kalipcilar H, Falconer JL, and Noble RD. Preparation of B-ZSM-5 membranes on a monolith support. *J Membr Sci* 2001; 194(1):141–144.
271. Valtchev V and Mintova S. Layer-by-layer preparation of zeolite coatings of nanosized crystals. *Micropor Mesopor Mater* 2001; 43(1):41–49.
272. Kulak A, Lee YJ, Park YS, Kim HS, Lee GS, and Yoon KB. Anionic surfactants as nanotools for the alignment of non-spherical zeolite nanocrystals. *Adv Mater* 2002; 14(7):526–531.
273. Huang L, Wang Z, Wang H, Sun J, Li Q, Zhao D, and Yan Y. Hierarchical porous structures by using zeolite nanocrystals as building blocks. *Micropor Mesopor Mater* 2001; 48(1–3):73–78.
274. Drioli E. An international report on membranes science and technology. Perspectives and needs prepared and discussed at the international conference on membranes ICOM 2002, Toulouse, France, 2002.
275. Weisz PB. The science of the possible. *Chemtech* 1982; 12(7):424–425.
276. Boudart M. Innovation in applied catalysis. *Cattech* 1997; 12:94.
277. Richter H, Voigt I, Fischer G, and Puhlfürb P. Preparation of zeolite membranes on the inner surface of ceramic tubes and capillaries. *Sep Purif Technol* 2003; 32(1–3):133–138.
278. Noack M, Kölsch P, Schäfer R, Toussaint P, Sieber I, and Caro J. Preparation of MFI membranes of enlarged area with high reproducibility. *Micropor Mesopor Mater* 2001; 49(1–3):25–37.
279. Morooka S and Kusakabe K. Microporous inorganic membranes for gas separation. *MRS Bull* 1999; 24(3):25–29.
280. Li Y, Wang J, Shi J, Zhang X, Lu J, Bao Z, and Yan D. Synthesis of ZSM-5 zeolite membranes with large area on porous, tubular alpha-Al<sub>2</sub>O<sub>3</sub> supports. *Sep Purif Technol* 2003; 32(1–3):397–401.
281. Corma A and García H. Supramolecular host–guest systems in zeolites prepared by ship-in-a-bottle synthesis. *Eur J Inorg Chem* 2004; 6:1143–1164.
282. Kolb G and Hessel V. Micro-structured reactors for gas phase reactions. *Chem Eng J* 2004; 98(1–2):1–38.
283. Jensen KF. Microreaction engineering—is small better? *Chem Eng Sci* 2001; 56(2):293–303.
284. Gavriilidis A, Angeli P, Cao E, Yeong KK, and Wan YSS. Technology and applications of microengineered reactors. *Chem Eng Res Des* 2002; 80(A1):3–30.
285. Chow AW. Lab-on-a-chip: Opportunities for chemical engineering. *AIChE J* 2002; 48:1590–1595.
286. Tsapatsis M. Molecular sieves in the nanotechnology era. *AIChE J* 2002; 48:654–660.
287. Rebrov EV, Seijger GBF, Calis HPA, de Croon MHJM, van den Bleek CM, and Shouten JC. The preparation of highly ordered single layer ZSM-5 coating on prefabricated stainless steel microchannels. *Appl Catal A: Gen* 2001; 206(1):125–143.
288. Wan YSS, Chau JLH, Yeung KL, and Gavriilidis A. 1-pentene epoxidation in catalytic microfabricated reactors. *J Catal* 2004; 223(2):241–249.
289. Men Y, Gnaser H, Zapf R, Hessel V, Ziegler C, and Kolb G. Steam reforming of methanol over Cu/CeO<sub>2</sub>/gamma-Al<sub>2</sub>O<sub>3</sub> catalysts in a microchannel reactor. *Appl Catal A: Gen* 2004; 277(1–2):83–90.
290. Lai SM, Ng CP, Martín-Aranda R, and Yeung KL. Knoevenagel condensation reaction in zeolite membrane microreactor. *Micropor Mesopor Mater* 2003; 66(2–3):239–252.

291. Zhang X, Lai ESM, Martín-Aranda R, and Yeung KL. An investigation of Knoevenagel condensation reaction in microreactors using a new zeolite catalyst. *App Catal A: Gen* 2004; 261(1):109–118.
292. Wan YSS, Yeung KL, and Gavriilidis A. TS-1 oxidation of aniline to azoxybenzene in a microstructured reactor. *App Catal A: Gen* 2005; 281(1–2):285–293.
293. Mateo E, Lahoz R, Fuente G, Paniagua A, Coronas J, and Santamaría J. Preparation of silicalite-1 micromembranes on laser-perforated stainless steel sheets. *Chem Mat* 2004; 16(24):4847–4850.
294. Ha K, Park JS, Oh KS, Zhou YS, Chun YS, Lee YJ, and Yoon KB. Aligned monolayer assembly of zeolite crystals on platinum, gold, and indium-tin oxide surfaces with molecular linkages. *Micropor Mesopor Mater* 2004; 72:91–98.
295. Jansen JC and van Rosmalen GM. Oriented growth of silica molecular-sieve crystals as supported films. *J Crystal Growth* 1993; 128(1–4):1150–1156.
296. den Exter MJ, van Bekkum H, Rijn CJM, Kapteijn F, Moulijn JA, Schellevis H, and Beenakker CIN. Stability of oriented silicalite-1 films in view of zeolite membrane preparation. *Zeolites* 1997; 19(1):13–20.
297. Schoeman BJ, Erdem-Senatalar A, Hedlund J, and Sterte J. The growth of sub-micron films of TPA-silicalite-1 on single crystal silicon wafers from low-temperature clear solutions. *Zeolites* 1997; 19(1):21–28.
298. Chau JLH, Wan YSS, Gavriilidis A, and Yeung KL. Incorporating zeolites in microchemical systems *Chem Eng J* 2002; 88(1–3):187–200.
299. Leung YLA and Yeung KL. Microfabricated ZSM-5 zeolite micromembranes. *Chem Eng Sci* 2004; 59:4809–4817.
300. Walcarius A. Zeolite-modified electrodes in electroanalytical chemistry. *Anal Chim Acta* 1999; 384(1):1–16.
301. Yan Y and Bein T. Molecular-sieve sensors for selective ethanol detection. *Chem Mater* 1992; 4(5):975–977.
302. Mintova S and Bein T. Nanosized zeolite films for vapor-sensing applications. *Micropor Mesopor Mater* 2001; 50(2–3):159–166.
303. Osada M, Sasaki I, Nishioka M, Sadakata M, and Okubo T. Synthesis of a faujasite thin layer and its application for SO<sub>2</sub> sensing at elevated temperatures. *Micropor Mesopor Mater* 1998; 23(5–6):287–294.
304. Sasaki I, Tsuchiya H, Nishioka M, Sadakata M, and Okubo T. Gas sensing with zeolite-coated quartz crystal microbalances—principal component analysis approach. *Sens Actuators B* 2002; 86(1):26–33.
305. Bein T, Brown K, Frye GC, and Brinker CJ. Molecular-sieve sensors for selective detection at the nanogram level. *J Am Chem Soc* 1989; 111(19):7640–7641.
306. Yan Y and Bein T. Molecular recognition on acoustic wave devices: Zeolite thin films coated with organosilane gate layers. *Micropor Mesopor Mater* 1993; 1:413–422.
307. Berger R, Gerber CH, Lang HP, and Gimzewski JK. Micromechanics: A toolbox for femtoscale science: ‘Towards a laboratory on a tip.’ *Microelectron Eng* 1997; 35(1–4):373–379.
308. Scandella L, Binder G, Mezzacasa T, Gobrecht J, Berber R, Lang HP, Gerber CH, Gimzewski JK, Koegler JH, and Hansen JC. Combination of single crystal zeolites and microfabrication: Two applications towards zeolite nanodevices. *Micropor Mesopor Mater* 1998; 21(4–6):403–409.
309. Zhou J, Li P, Zhang S, Long Y, Zhou F, Huang Y, Yang P, and Bao M. Zeolite-modified microcantilever gas sensor for indoor air quality. *Sens Actuator B* 2003; 94(3):337–342.
310. Shi J, Zhu Y, Zhang X, Baeyens WRG, and García-Campaña AM. Recent developments in nanomaterial optical sensors. *Trends Anal Chem* 2004; 23(5):351–360.
311. Calzaferri G, Huber S, Maas H, and Minkowski C. Host–guest antenna materials. *Angewandte Chemie* 2003; 42:3732–3758.
312. Schulz-Ekloff G, Wöhrle D, Duffel B, and Schoonheydt RA. Chromophores in porous silicas and minerals: Preparation and optical properties. *Micropor Mesopor Mater* 2002; 51:91–138.
313. López J, Pina MP, Coronas J, Pelayo J, and Santamaria J. A novel optical device for gas sensor applications based on zeolite materials. Books of abstracts of the 1st NanoSpain Workshop, San Sebastian, 2004.
314. Meinershagen JL and Bein T. Optical sensing in nanopores. Encapsulation of the solvatochromic dye Nile red in zeolites. *J Am Chem Soc* 1999; 121(2):448–449.
315. Ganschow M, Wark M, Wöhrle D, and Schulz-Ekloff G. Anchoring of functional dye molecules in MCM-41 by microwave-assisted hydrothermal cocondensation. *Angew Chem Int* 2002; 39:161–166.
316. Barriain C, Matias IR, Fernández-Valdivieso C, Arregui FJ, Rodríguez-Méndez ML, and de Saja JA. Optical fiber sensor based on lutetium bisphthalocyanine for the detection of gases using standard telecommunication wavelengths. *Sens Actuators B* 2003; 93:153–159.
317. Alberti K and Fetting F. Zeolites as sensitive materials for dielectric gas sensors. *Sens Actuators B* 1994; 21:39–50.
318. Plog C, Kurzweil P, and Maunz W. Combustion gas sensitivity of zeolite layers on thin-film capacitors. *Sens Actuators B* 1995; 25(1–3):403–406.
319. Plog C, Maunz W, Kurzweil P, Obermeier E, and Scheibe C. Impedance of zeolite-based gas sensors. *Sens Actuators B* 1995; 25(1–3):653–656.
320. Moos R, Müller R, Plog C, Knezevic A, Leye H, Irion E, Braun T, Marquardt KJ, and Binder K. Selective ammonia exhaust gas sensor for automotive applications. *Sens Actuators B* 2002; 83(1–3):181–189.
321. Hugon O, Sauvan M, Benech P, Pijolat C, and Lefebvre F. Gas separation with a zeolite filter, application to the selectivity enhancement of chemical sensors. *Sens Actuators B* 2000; 67(3):235–243.
322. Kaneyasu K, Otsuka K, Setoguchi Y, Sonoda S, Nakahara T, Aso I, and Nakagaichi N. A carbon dioxide gas sensor based on solid electrolyte for air quality control. *Sens Actuators B* 2000; 66(1–3):56–58.
323. Szabo NF and Dutta PK. Strategies for total NO<sub>x</sub> measurement with minimal CO interference utilizing a microporous zeolitic catalytic filter. *Sens Actuators B* 2003; 88(2):168–177.

324. Fukui K and Nishida S. CO gas sensor based on Au-La<sub>2</sub>O<sub>3</sub> added SnO<sub>2</sub> ceramics with siliceous zeolite coat. *Sens Actuators B* 1997; 45(2):101–106.
325. Szabo NF, Du H, Akbar SA, Soliman A, and Dutta PK. Microporous zeolite modified yttria stabilized zirconia (YSZ) sensors for nitric oxide (NO) determination in harsh environments. *Sens Actuators B* 2002; 82(2–3):142–149.
326. Li G and Kawi S. MCM-41 modified SnO<sub>2</sub> gas sensors: Sensitivity and selectivity properties. *Sens Actuator B* 1999; 59(1):1–8.



---

# 11 Membrane Fouling: Recent Strategies and Methodologies for Its Minimization

*Mattheus F.A. Goosen, S.S. Sablani, and R. Roque-Malherbe*

## CONTENTS

11.1	Introduction .....	325
11.2	Membrane Fouling Phenomena .....	327
11.2.1	Microbiological Fouling.....	327
11.2.2	Effect of Humic Acids on Fouling Layer.....	329
11.2.3	Effect of Inorganics, Proteins, and Colloids.....	330
11.2.4	Transition from Reversible Adsorption to Irreversible Fouling .....	330
11.3	Analytical Strategies.....	331
11.3.1	Measuring Fouling Layer Morphology and Cell Adhesion Kinetics .....	331
11.3.2	Hydrodynamic Studies of Microbial Adhesion and Passage of Bacteria through Membranes .....	331
11.3.3	Analysis of Deposits on Membrane Surface .....	332
11.3.4	Measurement of Concentration Polarization.....	332
11.3.5	Mathematical Models for Flux Decline .....	332
11.3.6	Variation in Gel-Layer Thickness along Flow Channel.....	333
11.3.7	Pore Blockage and Cake Formation .....	334
11.4	Methodologies for Minimization of Membrane Fouling.....	334
11.4.1	Feed Water Pretreatment Using Filtration and Flocculation .....	334
11.4.2	Effects of Spacers on Permeate Flux and Fouling.....	335
11.4.3	Membrane Surface Modification.....	336
11.4.4	Fouling Resistance of Hydrophilic and Hydrophobic Membranes .....	336
11.4.5	Control of Operating Parameters and Critical Flux.....	336
11.4.6	Membrane Cleaning Using Chemical Agents and Back Pulsing .....	337
11.5	Membrane Fouling and Gas Separations .....	338
11.6	Economic Aspects of Membrane Separations .....	339
11.7	Concluding Remarks.....	339
	Acknowledgments.....	340
	Nomenclature.....	340
	Greek Symbols.....	341
	References.....	341

## 11.1 INTRODUCTION

There is a growing awareness by scientists, political leaders, and the general public, that the best way to approach the world's limited water resources problem lies in a coordinated approach involving water management, water purification, and water conservation [1–5]. Thermal and membrane systems are the two most successful commercial water purification techniques. Desalination using reverse osmosis (RO) membranes, in particular, has become very popular for producing freshwater from brackish water and seawater. The technique has low capital and operating costs compared to other alternative processes like multistage flash [6]. Ultrafiltration (UF) may be used before reverse osmosis for feed water pretreatment [7]. Membrane separation processes are also widely used in biochemical processing, in industrial wastewater treatment, in food and beverage production, and in pharmaceutical applications [8].

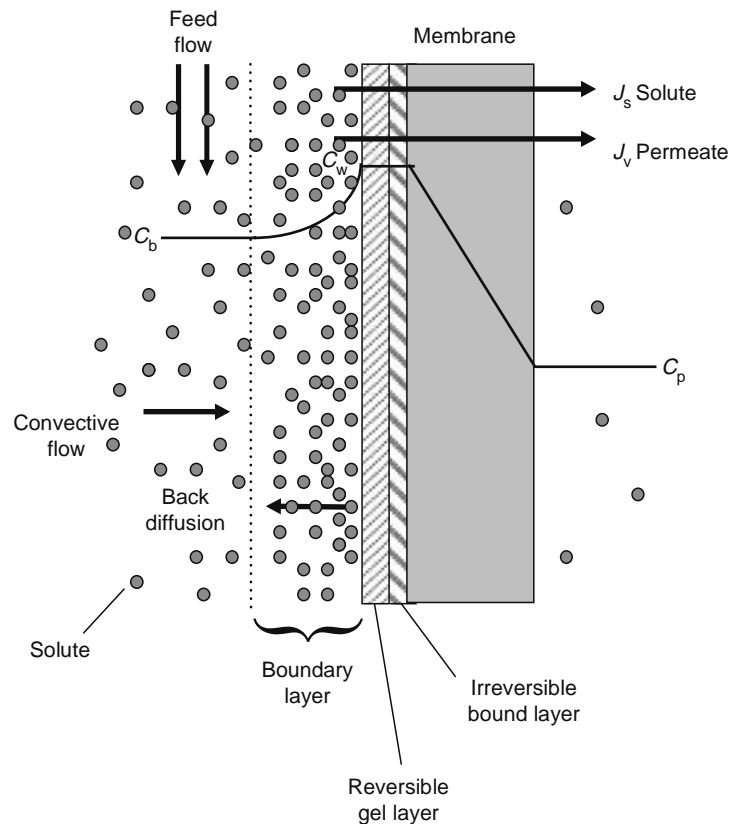


**FIGURE 11.1** A schematic representation of concentration polarization and fouling at the membrane surface. (From Goosen, M.F.A., Sablani, S.S., Al-Hinai, H., Al-Obeidani, S., Al-Belushi, R., and Jackson, D., *Sep. Sci. Technol.*, 39, 2261, 2004.)

Koltuniewicz and Noworyta [9], in a highly recommended paper, summarized the phenomena responsible for limiting the permeate flux during cyclic operation (i.e., permeation followed by cleaning). Membrane lifetime and permeate (i.e., pure water) fluxes are primarily affected by the phenomena of concentration polarization (i.e., solute build-up) and fouling/scaling (e.g., microbial adhesion, gel layer formation, and solute adhesion) at the membrane surface (Figure 11.1) [10]. During the initial period of operation within a cycle, concentration polarization is one of the primary reasons for flux decline,  $J_a$  (Figure 11.2). Large-scale membrane systems operate in a cyclic mode, where clean-in-place operation alternates with the normal run. Figure 11.2 shows a decrease in the flux for pure water from cycle to cycle,  $J_o(t)$ , due to fouling/scaling, the flux decline within a cycle due to concentration polarization,  $J(t_p)$ , and the average flux under steady-state concentration,  $J_a$ . The average flux under steady-state concentration decreasing from cycle-to-cycle suggests irreversible solute adsorption or fouling. Accumulation of the solute retained on a membrane surface leads to increasing permeate flow resistance at the membrane wall region.

One of the most serious forms of membrane fouling is bacterial adhesion and growth [11]. Once they form, biofilms can be very difficult to remove, either through disinfection or chemical cleaning. This wastes energy, degrades salt rejection, and leads to shortened membrane life. This is one area, for example, where further research is required.

A variety of liquids have been treated with reverse osmosis and ultrafiltration membranes ranging from seawater, to wastewater, to milk and yeast suspensions. Each liquid varies in composition and in the type and fraction of the solute(s) to be retained by the membrane. Complicating factors include the presence of substances such as oil in seawater and wastewater [12–15]. The presence of the oil normally necessitates an additional pretreatment step further complicating the fouling process. The presence of humic acids in surface water and wastewater also needs special attention [16,17]. The fouling phenomena, the preventive means (i.e., pretreatment), and the frequency and type of membrane cleaning cycle are all dependent on the type of liquid being treated.

Membrane materials for reverse osmosis and ultrafiltration applications range from polysulfone and polyethersulfone, to cellulose acetate and cellulose diacetate [12,18–23]. Commercially available polyamide composite membranes for desalination of seawater, for example, are available from a variety of companies in the United States, Europe, and Japan [24]. The specific choice of membrane material to use depends on the process (e.g., type of liquid to be treated and operating conditions) and economic factors (e.g., cost of replacement membranes and cost of cleaning chemicals). The exact chemical composition and physical morphology of the membranes may vary from manufacturer to manufacturer. Since the liquids to be treated and

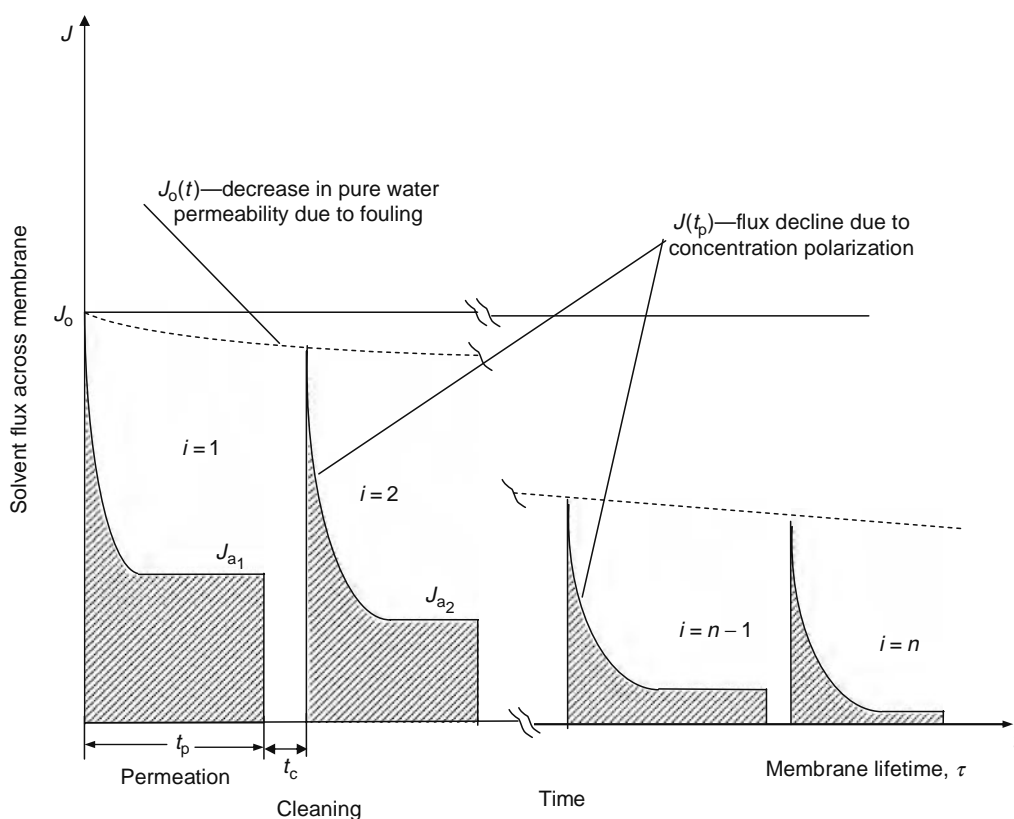


**FIGURE 11.2** Diagram of typical flux–time dependency during cyclic operation in large-scale ultrafiltration systems. (From Koltuniewicz, A. and Noworyta, A., *Indus. Eng. Chem. Res.*, 33, 1771, 1994.)

the operating conditions also vary from application to application, it becomes difficult to conclude which materials are the best to use in order to inhibit membrane fouling.

Concentration polarization is an inherent part of a membrane separation process. Equipment design and operating conditions normally take care of it. Scaling/fouling, which is triggered by concentration polarization, reduces flux that can be minimized using antiscalants. Concentration polarization is not the same as fouling except that by theory it results in flux decline due to higher osmotic pressure and not due to resistance to flow particularly in RO. However, in UF where we deal with high molecular weight solutes, accumulation of large molecules in the boundary layer may cause resistance to flow. In UF, concentration polarization is more often treated as part of fouling but not in RO or nanofiltration (NF).

The primary aim of the chapter is to critically review the literature on the fouling phenomena in reverse osmosis and ultrafiltration membrane systems and methodologies for its minimization (i.e., the analytical techniques employed to quantify fouling, preventive means, and membrane cleaning methods). Fouling of membranes used in gas separation was also briefly reviewed. Specific recommendations were also made on how scientists, engineers, and technical staff can assist in improving the performance of membrane systems through fundamental and applied research.

## 11.2 MEMBRANE FOULING PHENOMENA

The main mechanisms of membrane fouling are adsorption of feed components, clogging of pores, chemical interaction between solutes and membrane material, gel formation and bacterial growth. Let us first consider bacterial growth on membranes. Microbiological fouling of reverse osmosis membranes is one of the main factors in flux decline and loss of salt rejection [25–29] (Table 11.1).

### 11.2.1 MICROBIOLOGICAL FOULING

Bacterial fouling of a surface (i.e., formation of a biofilm) can be divided into three phases: transport of the organisms to the surface, attachment to the substratum, and growth at the surface. Fleming et al. [30] show that bacterial fouling of a surface takes about 3 days to completely cover a reverse osmosis membrane with a biofilm. Ghayeni et al. [25,26] studied initial adhesion of sewage bacteria belonging to the genus *Pseudomonas* to reverse osmosis membranes. It was found that bacteria

**TABLE 11.1**  
**Summary of Membrane Fouling Studies Reported in the Literature**

Fouling Studies	References
<i>Membrane fouling phenomena</i>	
Microbial cell attachment	Fleming et al. [30], Ghayeni et al. [25], Flemming and Schaule [20], Ridgway et al. [28,31] <sup>b</sup> , Ridgway [33]
Humic acids and morphology of fouling layer	Nystrom et al. [16], Schafer et al. [35], Khatib et al. [36], Kabsch-Korbutowicz et al. [17], Tu et al. [37] <sup>a</sup> , Domany et al. [34], Ridgway [31] <sup>b</sup>
Inorganics	Sahachaiyunta et al. [38]
Proteins and colloids	Yiantsios and Karabelas [39], Jarusutthirak et al. [40], Schafer et al. [35], Bacchin et al. [93]
Reversible adsorbed layer	Nikolova and Islam [29] <sup>b</sup> , Koltuniewicz and Noworyta [9] <sup>b</sup>
Transition from reversible to irreversible fouling	Chen et al. [41] <sup>b</sup>
Variation in gel-layer thickness	Denisov [53] <sup>b</sup>
Pore blockage and cake formation	Zydney and Ho [27]
<i>Analytical descriptions</i>	
Fouling layer morphology and growth	Riedl et al. [42], Scott et al. [15]
Adhesion kinetics	Ridgway et al. [18,19]
Hydrodynamics	Altena and Belfort [43], Drew et al. [44] <sup>a</sup> , Cherkasov et al. [32]
Passage of bacteria through membrane	Ghayeni et al. [45] <sup>a</sup>
Analysis of deposits: ATR, FTIR, measuring fouling in real time	Lindau and Jonsson [12], Howe et al. [46], Rabiller-Baudry et al. [22], Chan et al. [47], Bowen et al. [48], Li et al. [23] <sup>b</sup>
Measuring concentration polarization	Gownan and Ethier [49,50] <sup>a</sup> , Pope et al. [14]
Mathematical modeling of flux decline	Dal-Cin et al. [51], Koltuniewicz and Noworyta [9] <sup>b</sup>
<i>Preventive means and cleaning methods</i>	
Feedwater pretreatment microfiltration and ultrafiltration	Wilf and Klinko [55], Glueckstern and Priel [57], Ghayeni et al. [25], Ghayeni et al. [45] <sup>a</sup> , Karakulski et al. [94], Chapman et al. [58], Nguyen and Ripperger [59], Han et al. [60], Choksuchart et al. [61], Park et al. [62], Guigui et al. [63], Lopez-Ramirez et al. [64] <sup>b</sup> , Benito et al. [13], Shaalan [65]
Coagulation and flocculation spacers	Schwinge et al. [67] <sup>b</sup> , Geraldes et al. [66], Sablani et al. [7], Li et al. [23,67], Lipnizki and Johnson [95]
Corrugated membranes	Lindau and Jonsson [12], Scott et al. [15]
Surface chemistry	Jenkins and Tanner [69] <sup>a</sup> , Flemming and Schaule [20], Ridgway et al. [19], Belfer et al. [24]
Hydrophobic and hydrophilic membranes	Kabsch-Korbutowicz et al. [17], Tu et al. [37] <sup>a</sup> , Cherkasov et al. [32]
Control of operating parameters (critical flux)	Song [76] <sup>a</sup> , Chen et al. [41] <sup>b</sup> , Koltuniewicz and Noworyta [9] <sup>b</sup> , Madireddi et al. [71], Mallubhotla and Belfort [74], Avlonitis et al. [72], Goosen et al. [3], Jackson et al. [75]
Rinsing water quality	Tra-Ha and Wiley [77], Lindau and Jonsson [12] <sup>a</sup>
Cleaning agents	Mohammadi et al. [78]
Back pulsing	Mores and Davis [79]
Membrane wear and degradation	Roth et al. [80], Ammerlaan et al. [21] <sup>a</sup> , Ridgway et al. [19]
<i>Economic aspects</i>	Glueckstern et al. [56], Brehant et al. [92]

Source: From Goosen M.F.A., Sablani S.S., Al-Hinai H., Al-Obeidani S., Al-Belushi R., and Jackson D., *Sep. Sci. Technol.*, 39, 2261, 2004.

<sup>a</sup> Recommended papers.

<sup>b</sup> Highly recommended papers.

would sometimes aggregate upon adhering. While minimal bacterial attachment occurred in a very low ionic strength solution, significantly higher numbers of attached microbes occurred when using salt concentrations corresponding to wastewater. Understanding the mechanism of bacterial attachment may assist in the development of antifouling technologies for membrane systems.

Flemming and Schaule [20] also demonstrated that after a few minutes of contact between a membrane and raw water, the first irreversible attachment of cells occurs. Their results suggest that membrane manufacturers should stay away from polyamide and polysulfone materials, at least for wastewater treatment applications. *Pseudomonas* was identified as a fast adhering species out of a tap water microflora. If non-starving cells were used (i.e., sufficient nutrients and dissolved oxygen in the raw water), the adhesion process improved with an increase in the number of cells in suspension. When starving cells were used, incomplete coverage of the surface occurred. This is similar to the surface aggregate formations observed for membranes by Ghayeni et al. [25,26]. Flemming and Schaule [20] also detected a biological affinity of different membrane materials toward bacteria. Polyetherurea, for example, had a significantly lower biological affinity than polyamide, polysulfone, and polyethersulfone.

In a similar but more thorough study than that performed by Ghayeni et al. [25], Ridgway et al. [28,31] in two excellent papers reported on the biofouling of reverse osmosis membranes with wastewater. Cellulose diacetate membranes became uniformly coated with a fouling layer that was primarily organic in composition. Calcium, phosphorous, sulfur, and chlorine were the major inorganic constituents detected. Protein and carbohydrate represented as much as 30% and 17%, respectively, of the dry weight of the biofilm. Electron microscopy revealed that the biofilm on the feed water side surface of the membrane was 10–20  $\mu\text{m}$  thick and was composed of several layers of compacted bacterial cells, many of which were partially or completely autolyzed. The bacteria were firmly attached to the membrane surface by an extensive network of extracellular polymeric fibrils. They showed that mycobacteria adhered to the cellulose acetate membrane surface 25-fold more effectively than a wild-type strain of *Escherichia coli*. In a key finding, the ability of *Mycobacterium* and *E. coli* to adhere to the membrane was correlated with their relative surface hydrophobicities as determined by their affinities for *n*-hexadecane [31]. The results suggested that hydrophobic interaction between bacterial cell surface components and the cellulose membrane surface plays an important role in the initial stages of bacterial adhesion and biofilm formation. A key question that arises is whether the importance of this hydrophobic interaction between the cell and the membrane also holds true for other polymers. This work is similar to that reported by Cherkasov et al. [32] on fouling resistance of hydrophilic and hydrophobic membranes (Figure 11.3). A later research study by Ridgway [33] confirmed these results and conclusions.

### 11.2.2 EFFECT OF HUMIC ACIDS ON FOULING LAYER

The degradation of organic matter, such as plants, in the soil produces a mixture of complex macromolecules called humic acids. These complex molecules have polymeric phenolic structures with the ability to chelate metals especially iron. It is recommended that humic acids be removed from process water before filtration by complexation (i.e., flocculation/coagulation; see Section 11.4.1). Humic acids give surface water a yellowish to brownish color and often cause fouling problems in membrane filtration [16,34]. The fouling tendency of humic acids appears to be due to their ability to bind to multivalent salts. Nystrom et al. [16], for example, showed that humic acids were most harmful in membranes that were positively charged (i.e., containing alumina and silica). Humic acids formed chelates with the metals (i.e., multivalent ions) and could be seen as a gel-like layer on the filter surface.

Schafer et al. [35] studied the role of concentration polarization and solution chemistry on the morphology of the humic acid fouling layer. Irreversible fouling occurred with all membranes at high calcium concentrations. Interestingly, it was found that the hydrophobic fraction of the humic acids was deposited preferentially on the membrane surface. This result is similar to the work of Ridgway et al. [31], who showed that the hydrophobic interaction between a bacterial cell surface and a membrane surface plays a key role in biofilm formation. The formation of two layers, one on top of the other, was also observed by Khatib et al. [36]. The formation of a Fe–Si gel layer directly on the membrane surface was mainly responsible for the fouling.

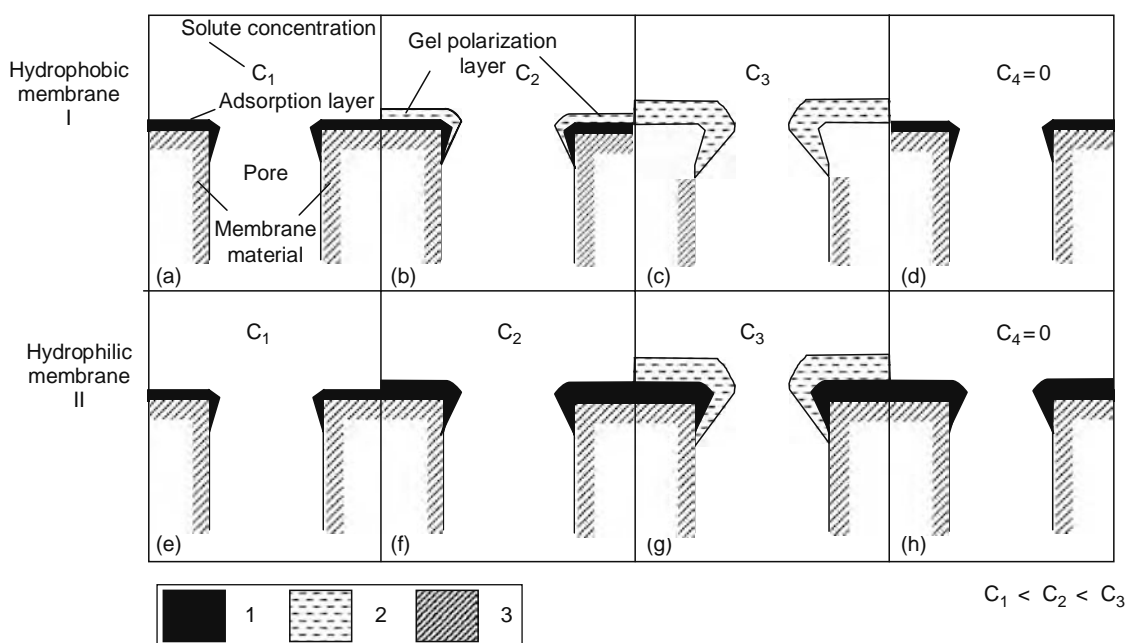


**FIGURE 11.3** Gel-layer formation on surface of an ultrafiltration membrane made from (I) hydrophobic and (II) hydrophilic material.  $C$ , solute concentration;  $C_1 < C_2 < C_3$ , 1 adsorption layer, 2 gel-polarization layer, 3 membrane material. (From Cherkasov, A.N., Tsareva, S.V., and Polotsky, A.E., *J. Membr. Sci.*, 104, 157, 1995.)

Reducing the electrostatic repulsion between the ferric gel and the membrane surface encouraged adhesion. Tu et al. [37] also showed that membranes with a higher negative surface charge and greater hydrophilicity were less prone to fouling due to fewer interactions between the chemical groups in the organic solute and the polar groups on the membrane surface.

What these studies tell us is that in order to reduce fouling due to humic acids, it is best to employ hydrophilic membranes, to have feed water with a low mineral salts content (e.g., calcium), and to work at low pH.

### 11.2.3 EFFECT OF INORGANICS, PROTEINS, AND COLLOIDS

Sahachaiyunta et al. [38] conducted dynamic tests to investigate the effect of silica fouling of reverse osmosis membranes in the presence of minute amounts of various inorganic cations such as iron, manganese, nickel, and barium, which are present in industrial and mineral processing wastewaters. Experimental results showed that the presence of iron greatly affected the scale structure on the membrane surface when compared to the other metal species.

A dual mode fouling process, similar to that observed for humic acids [35], was found for protein (i.e., bovine serum albumin [BSA]) fouling of microfiltration (MF) membranes. Protein aggregates first formed on the membrane surface followed by native (i.e., non-aggregated) protein. The native protein attached to an existing protein via the formation of intermolecular disulfide linkages.

Stable colloidal suspensions can cause less fouling. Yiantsios and Karabelas [39], in a very interesting paper, found that apart from particle size and concentration, colloid stability plays a major role in RO and UF membrane fouling. They demonstrated that standard fouling tests as well as most well-known fouling models are inadequate. A key finding was that the use of acid, which is a common practice to avoid scaling in desalination, might promote colloidal fouling. Lowering the pH reduces the negative charge on particles, causing aggregate formation that deposit on the membrane surface. Wastewater effluent organic matter was isolated into different fractions by Jarusutthirak et al. [40]. Each isolate exhibited different characteristics in fouling of NF and UF membranes. In particular, polysaccharides and amino sugars were found to play an important role in fouling. The colloidal fractions gave a high flux decline due to pore blockage, and hydrophobic interactions were very important for hydrophobic membranes causing a reduction in permeate flux.

### 11.2.4 TRANSITION FROM REVERSIBLE ADSORPTION TO IRREVERSIBLE FOULING

In a key study, Nikolova and Islam [29] reported that the decisive factor in flux decline was the adsorption resistance. With the development of a concentration polarization layer, the adsorbed layer resistance at the membrane wall increased linearly as a function of the solute concentration at the wall. They described the flux by the following relationship:

$$J = \frac{\Delta P - \Delta\pi(w)}{\mu(R_m + kC_w)} \quad (11.1)$$

where

$\Delta P$  is the hydraulic pressure difference across membrane

$C_w$  is the concentration at the membrane surface

$\Delta\pi(w)$  is the corresponding osmotic pressure

$R_m$  is the membrane resistance

$kC_w$  is the adsorbed layer resistance

$\mu$  is the fluid viscosity

In a key finding, they showed that the adsorption resistance was of the same order of magnitude as that of the membrane resistance. Surprisingly, the osmotic pressure was negligible in comparison to the applied transmembrane pressure. The significance of this study is that it showed that the reversible adsorbed solute layer at the membrane surface is the primary cause of flux decline and not the higher osmotic pressure at the membrane surface. This is supported by the work of Koltuniewicz and Noworyta [9] (Figure 11.2).

The transition between the reversible adsorption, described by Nikolova and Islam [29], and irreversible fouling is crucial to determining the strategy for improved membrane performance and for understanding the threshold values for which optimal flux and rejection can be maintained. In a very thorough study, Chen et al. [41] reported on the dynamic transition from concentration polarization to cake (i.e., gel layer) formation for membrane filtration of colloidal silica. Once a critical flux,  $J_{crit}$ , was exceeded, the colloids in the polarized layer formed a consolidated cake structure that was slow to depolarize and which reduced the flux. This paper is a very valuable source of information for membrane plant operators. By operating just below  $J_{crit}$  they can maximize the flux while at the same time reducing the frequency of membrane cleaning. A study by Chen et al. [41] showed that by controlling the flux below  $J_{crit}$ , the polarization layer may form and solute adsorption may occur but it is reversible and responds quickly to any changes in convection.

### 11.3 ANALYTICAL STRATEGIES

#### 11.3.1 MEASURING FOULING LAYER MORPHOLOGY AND CELL ADHESION KINETICS

The smoothness of the membrane surface can influence the morphology of the fouling layer. Riedl et al. [42] employed an atomic force microscopy (AFM) technique to measure membrane surface roughness, and scanning electron microscopy (SEM) to assess the fouling layer. It was shown that smooth membranes produced dense surface fouling layer, whereas this same layer or biofilm on rough membranes was much more open. The primary conclusion of the study was that the fluxes through rough membranes are less affected by fouling formation than fluxes through smooth membranes.

The kinetics of adhesion of *Mycobacterium* sp. to cellulose diacetate reverse osmosis membranes have been described [19]. Adhesion of the cells to the membrane surface occurred within 1–2 h and exhibited saturation-type kinetics, which conformed closely to the Langmuir adsorption isotherm, a mathematical expression describing the partitioning of substances between a solution and a solid–liquid interface. This suggested that cellulose diacetate membrane surfaces may possess a finite number of available binding sites to which the mycobacteria can adhere. Treatment of the attached mycobacteria with different enzymes suggested that cell surface polypeptides, 4- or  $\alpha$ -1.6-linked glucan polymers, and carboxyl ester bond containing substances (possibly peptidylglycolipids) may be involved in the adhesion process. The exact molecular mechanisms of adhesion, however, have not as yet been clearly defined. This is one area where further research is needed.

#### 11.3.2 HYDRODYNAMIC STUDIES OF MICROBIAL ADHESION AND PASSAGE OF BACTERIA THROUGH MEMBRANES

Altena and Belfort [43] and Drew et al. [44] performed fundamental studies of the membrane fouling process based on the movement of rigid neutrally buoyant spherical particles (i.e., a model bacterial foulant) toward a membrane surface. While these researchers did not work directly with microbial cells, their hydrodynamic studies do provide useful information on how the particle size and fluid flow affect microbial adhesion. Their studies were an attempt to give clearer insight into the hydrodynamics behind the mechanism of microbial adhesion in RO systems. Under typical laminar flow conditions, particles with a radius smaller than 1  $\mu\text{m}$  were captured by a porous membrane surface (i.e., the microbial adhesion step) resulting in cake formation. Due to convective flow into the membrane wall, particles moved laterally toward the membrane. The particle concentration near the membrane surface increased significantly over that in the bulk solution and resulted in a fouling layer. In their cross-flow membrane filtration experiments there appeared to be two major causes for lateral migration: a drag force exerted by the fluid on the particle due to the convective flow into the membrane wall (i.e., wall suction effect or permeation drag force) that carried particles toward the membrane, and an inertial lift force that carried particles near the membrane away from the porous wall. For small particles ( $<1 \mu\text{m}$ ) the permeation drag force dominated. An expression was developed from the first principles to predict conditions under which a membrane module exposed to dilute suspensions of spherical particles will not foul.

In a recommended paper, Ghayeni et al. [45] studied the passage of bacteria (0.5  $\mu\text{m}$  diameter) through microfiltration membranes in wastewater applications. Membranes with pore sizes smaller than 0.2  $\mu\text{m}$  still transmitted secondary effluent cells. This is an interesting study, which showed that based on total cell counts (DAPI) up to 1% of the bacteria in the feed can pass to the permeate side. While a significant portion of the cells (e.g., 50%) in the permeate showed biological (CTC) activity, none of the cells were able to reproduce (i.e., culture on agar or in suspension). This is a good quantitative method for measuring cell injury. We can speculate that smaller cells, or membranes with larger pores, would allow for the passage of viable bacteria, which would be able to reproduce. This could occur at some critical cell/pore ratio (Figure 11.4).

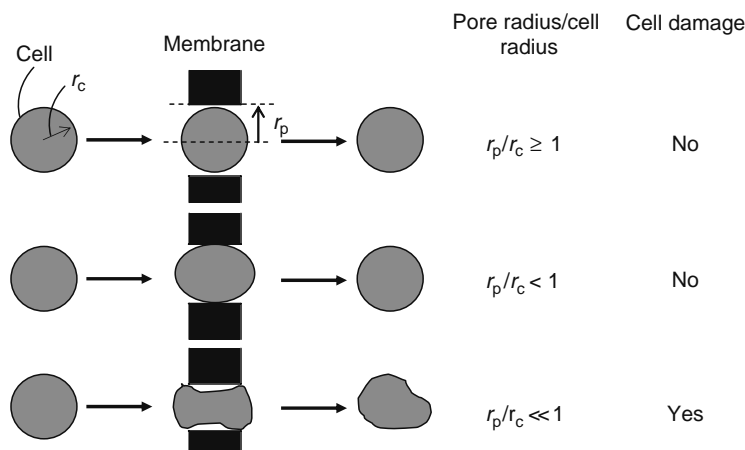


**FIGURE 11.4** Passage of bacterial cells through membrane pores. Cell damage occurs at critical pore radius/cell radius ratio. (From Goosen, M.F.A., Sablani, S.S., Al-Hinai, H., Al-Obeidani, S., Al-Belushi, R., and Jackson, D., *Sep. Sci. Technol.*, 39, 2261, 2004.)

### 11.3.3 ANALYSIS OF DEPOSITS ON MEMBRANE SURFACE

Attenuated total reflection (ATR) Fourier transform infrared (FTIR) spectroscopy can provide insight into the chemical nature of deposits on membranes [46]. The spectra of the foulants can be easily distinguished from the spectra of the membrane material. ATR/FTIR can also indicate the presence of inorganic foulants as well as the ratio of inorganic–organic foulants.

The surface deposits on UF polyethersulfone (PES) membranes fouled by skimmed milk have been studied using ATR-FTIR to detect the functional groups of the fouling species [22]. Some milk components (Lactose and salts) were eliminated by water rinsing, while proteins were only partially removed by chemical cleaning at basic pH. For dynamic conditions, the cleanliness of the membrane was evaluated through two criteria: hydraulic (i.e., recovery of initial flux) and chemical (i.e., no more contaminants detected). The hydraulic cleanliness of the membrane was achieved, while the membrane initial surface state was not restored. ATR-FTIR is also a useful tool for evaluating other fouling species such as oil and humic acids.

Deposits on a membrane surface, before and after cleaning, can also be analyzed using SEM in combination with energy dispersive x-ray (EDX) combined with a microanalysis system permitting quantitative determination of elements [12]. Furthermore, identification of specific species deposited onto membrane surfaces can be carried out using matrix-assisted laser desorption ionization mass spectroscopy (MALDI-MS). Chan et al. [47] employed this technique to differentiate between desorption of proteins from the membrane surface, from the inside pores and from the membrane substrate. It has the potential for quantitative measurement of protein fouling on membrane surfaces. It was shown that the technique is a powerful tool for distinguishing between different proteins in fouling deposits.

Atomic force microscopy has proved to be a rapid method for assessing membrane–solute interactions (fouling) of membranes under process conditions [48]. Given the good agreement between the correlations using AFM and operating performance, it should be possible, in the future, to use these techniques to allow earlier assessment of the fouling propensity of process streams.

Nondestructive, real-time observation techniques to detect and monitor fouling during liquid separation processes are of great importance in the development of strategies to improve operating conditions. In a recommended paper by Li et al. [23], ultrasonic time-domain reflectometry (UTDR) was used to measure organic fouling, in real time, during ultrafiltration with polysulphone (PS) membranes. The feed solution was a paper-mill effluent, which contained breakdown products of lignin or lignosulphonate, from a wastewater treatment plant. Experimental results showed that the ultrasonic signal response can be used to monitor fouling-layer formation and growth on the membrane in real time. The differential signal developed indicated the state and progress of the fouling layer and gave warning of advanced fouling during operation.

### 11.3.4 MEASUREMENT OF CONCENTRATION POLARIZATION

Gowman and Ethier [49,50] developed an automated laser-based refractometric technique to measure the solute concentration gradient during dead-end filtration of a biopolymer solution. This paper attempts to reconcile theory with experimental data. The refractometric technique may be useful to other researchers working on quantification of membrane fouling.

A nuclear magnetic resonance technique was employed by Pope et al. [13] to quantitatively measure the concentration polarization layer thickness during cross-flow filtration of an oil–water emulsion. This method helps to clarify the relative quantitative contributions to flux decline of the adsorbed layer resistance, and the concentration polarization layer gradient and thickness. It helps to explain the flux declines due to different resistances as shown in Figure 11.2. The technique, which measured layer thickness using chemical shift selective microimaging, may be useful in studying other membrane fouling situations that occur in food processing and desalination.

### 11.3.5 MATHEMATICAL MODELS FOR FLUX DECLINE

A series resistance model was developed by Dal-Cin et al. [51] to quantify the relative contributions of adsorption, pore plugging, and concentration polarization to flux decline during UF of a pulp mill effluent. They proposed a relative flux loss ratio as an alternative measure to the conventional resistance model that was found to be a misleading indicator of the flux loss. Using experimental and simulated flux data, the series resistance model was shown to under-predict fouling due to adsorption and to overpredict concentration polarization. This appears to be a disadvantage and would make the model of limited use in its current form. As mentioned in the introduction, Koltuniewicz and Noworyta [9] modeled the flux decline as a result of the development of a concentration polarization layer based on the surface renewal theory developed by Danckwerts [52]. The surface renewal model is more realistic than the commonly used film model since mass transfer at the membrane boundary layer is random in nature due to membrane roughness. Specifically, the membrane is not covered by a uniform concentration polarization layer, as was assumed in the film model, but rather by a mosaic of small surface elements with different ages, and, therefore, different permeate flow resistance. Any element can be swept away randomly by a hydrodynamic impulse, and then a new element starts building up a layer of retained solute at the same place on the membrane surface. They showed that the decrease in flux with respect to time,  $J(t_p)$ , due to the development of the concentration polarization layer is given by the following equation that also takes into account the rate of membrane surface renewal,  $s$  (area/unit time):

$$\bar{J}(t_p) = (J_o - J^*) \frac{s}{s + A} \frac{1 - e^{-(s+A)t_p}}{1 - e^{-st_p}} + J^* \quad (11.2)$$

where

- $A$  is the rate of loss of membrane surface area as a function of time
- $J_o$  is the initial value of the flux
- $J^*$  is the flux observed after infinite time
- $t_p$  is the time of permeation

$$s = A \frac{J_{\text{lim}} - J^*}{J_o - J_{\text{lim}}} \quad (11.3)$$

where  $J_{\text{lim}}$  is the limiting flux that is similar to critical flux,  $J_{\text{crit}}$ . The former can be obtained from literature data. The average flux under steady-state conditions,  $J_a$ , can be calculated directly from Equation 11.6 as a limit:

$$\bar{J}_a = \lim_{t_p \rightarrow \infty} \bar{J}(t_p) = (J_o - J^*) \frac{s}{A + s} + J^* \quad (11.4)$$

In support of this model, calculated values of flux using Equations 11.2 and 11.3 agreed well with experimental data. Equations 11.2 and 11.3 describe a permeation cycle of duration,  $t_p$ , as shown in Figure 11.2. This is a highly recommended paper for those who are operating large-scale continuous ultrafiltration plants, and to a certain extent RO plants. The model developed describes not only the dynamic behavior of a plant, but also allows for optimization of operating conditions (i.e., permeation time, cleaning time, and cleaning strategy).

### 11.3.6 VARIATION IN GEL-LAYER THICKNESS ALONG FLOW CHANNEL

In the case of cross-flow filtration, one can expect that the gel-layer thickness and the surface concentration of the solute will vary with distance from the channel entrance. As a consequence, the local permeate flux will also vary with longitudinal position. In a highly recommended article, Denisov [53] presented a mathematically rigorous theory of concentration polarization in cross-flow ultrafiltration, which takes into account the nonuniformity of the local permeate membrane flux. He derived equations describing the pressure/flux curve.

In the case of the gel-layer model, the theory led to a simple analytical formula for a limiting or critical flux,  $J_{\text{lim}}$ . The flux turned out to be proportional to the cube root of the ratio of the gel concentration to the feed solution concentration, rather than to the logarithm of this ratio, as the simplified Michaels–Blatt theory predicted:

$$J_{\text{lim}} = \left(\frac{3}{2}\right)^{(2/3)} KP_g = 1.31 \left(\frac{C_g}{C_o}\right) \frac{m^{1/3} D^{2/3} U_o^{1/3}}{L^{1/3} h^{1/3}} \quad (11.5)$$

where

$$P_g = \left(\frac{C_g m D^2 U_o}{C_o K^3 L h}\right) \quad (11.6)$$

where

- $K$  is the hydraulic permeability of membrane to pure solvent ( $\text{m}^3/\text{Ns}$ )
- $C_g$  is the gel concentration ( $\text{kmol}/\text{m}^3$ )
- $C_o$  is the solute concentration in feed solution ( $\text{kmol}/\text{m}^3$ )
- $m$  is the channel parameter
- $D$  is the solute diffusion coefficient ( $\text{m}^2/\text{s}$ )
- $U_o$  is the longitudinal component of fluid velocity averaged over the channel cross-section ( $\text{m}/\text{s}$ )
- $L$  is the channel length ( $\text{m}$ )
- $h$  is the transversal dimension of the channel ( $\text{m}$ )

In the case of the osmotic-pressure model, the rigorous theory allowed the conclusion that at high applied transmembrane pressure, the permeate flux increased as a cube root of the pressure, so that the limiting flux was never reached:

$$\bar{J} \approx \left(\frac{3}{2}\right)^{2/3} K \bar{P}^{1/3} P_o^{2/3} \approx 1.31 \left(\frac{\bar{P}}{RTC_o}\right)^{1/3} \frac{m^{1/3} D^{2/3} U_o^{1/3}}{L^{1/3} h^{1/3}} \quad (11.7)$$

where

$$P_o = \left(\frac{mD^2U_o}{RTC_oK^3Lh}\right) \quad (11.8)$$

where

$J$  is the average flux over the channel (m/s)

$P$  is the transmembrane pressure (N/m<sup>2</sup>)

$R$  is the gas constant (J/kmol K)

$T$  is the temperature (K)

However, one minor weakness of the study was that the analysis ignored the concentration dependence of the viscosity and the partial transmission of the solute through the membrane.

### 11.3.7 PORE BLOCKAGE AND CAKE FORMATION

Cake formation, shear forces, and other mathematical aspects and the kinetics of the boundary layer are described in a study by Hermia [54]. To understand the effect of membrane fouling on system capacity the  $V_{\max}$  test is often used to accelerate testing. This test assumes that fouling occurs by uniform constriction of the cylindrical membrane pores. This does not happen in practice. Zydney and Ho [27] examined the validity of the  $V_{\max}$  model and compared the results with predictions from a new model that accounts for fouling due to both pore blockage and cake formation. It was found that the  $V_{\max}$  analysis significantly overestimates the system capacity for proteins that foul primarily by pore blockage, but it underestimates the capacity for compounds that foul primarily by cake formation. In contrast the pore blockage–cake filtration model provides a much better description of membrane fouling, leading to more accurate sizing and scale-up of normal flow filtration devices.

## 11.4 METHODOLOGIES FOR MINIMIZATION OF MEMBRANE FOULING

### 11.4.1 FEED WATER PRETREATMENT USING FILTRATION AND FLOCCULATION

Reverse osmosis seawater systems that operate on surface feed water normally require an extensive pretreatment process to control membrane fouling. Recently new effective water microfiltration technologies have been introduced commercially. Wilf and Klinko [55] and Glueckstern et al. [56] noted that these developments can improve the quality of surface seawater feed to a level comparable to or better than the water quality from well water sources. The utilization of capillary ultrafiltration as a pretreatment step enabled operation of the reverse osmosis system at a high recovery (15%) and permeate flux rate. In a similar study utilizing micro- and ultrafiltration as seawater pretreatment steps for reverse osmosis, Glueckstern and Priel [57] showed that such technology can dramatically improve the quality of the feed water. This is especially important if cooling water from existing power stations is used as feed water for desalination plants.

The reuse of municipal wastewater requires treatment to an acceptable quality level that satisfies regulatory guidelines. Ghayani et al. [25] employed hollow fiber microfiltration as a pretreatment for wastewater for RO in the production of high-quality water. Organisms present in MF-treated secondary effluent were able to attach to RO membranes and proliferate to form a biofilm. Total cell counts in this treated effluent (i.e., permeate from the MF unit) were several orders of magnitude higher than viable cell counts. This was confirmed in a later study [45]. What these results indicate is that microfiltration membranes will not be totally effective in the removal of bacteria from the feed water stream. The result showed that most cells were severely damaged by passage through the membrane (Figure 11.4). However, we can speculate that this damaging effect may be strain-specific and dependent on the cell/pore diameter.

In a study by Chapman et al. [58], a flocculator was used to remove suspended solids (SDI), organics, and phosphorus from wastewater. The flocculator produced uniform microflocs, which were removed by cross-flow microfiltration. Flocculated particles can form a highly porous filtration cake on a membrane surface. This will help inhibit fouling on the membrane by preventing the deposition of particles and therefore reducing the number of membrane cleaning cycles [59]. In practice SDI and modified fouling index are used to reflect the fouling potential.

Arsenic removal from drinking water is a major problem in many parts of the world. Han et al. [60] investigated arsenic removal by flocculation and microfiltration. Ferric chloride and ferric sulfate were used as flocculants. Results showed that flocculation before microfiltration led to significant arsenic removal in the permeate. Furthermore, the addition of small amounts of cationic polymeric flocculants resulted in significantly improved permeate fluxes during microfiltration.

Another commonly used method is coagulation. This technique removes turbidity from water by the addition of cationic compounds. The usefulness of coagulation as a pretreatment to remove microparticles in aqueous suspension before a membrane filtration was shown by Choksuchart et al. [61]. There are several types of coagulation systems. Comparisons were made by Park et al. [62] between coagulation with only rapid mixing in a separate tank (i.e., ordinary coagulation), and coagulation with no mixing tank (i.e., in-line coagulation) before an ultrafiltration process. The ordinary coagulation was superior. An in-line coagulation (without settling) UF process was also employed by Guigui et al. [63]. Floc cake resistance was found to be lower than resistance due to the unsettled floc and the uncoagulated organics. A reduction in coagulant dose induced an increase in the mass transfer resistance.

Combining flocculation and coagulation in a pretreatment process has also been studied. In a key paper by Lopez-Ramirez et al. [64], the secondary effluent from an activated sludge unit was pretreated, before RO, with three levels: intense (coagulation–flocculation with ferric chloride and polyelectrolite and high pH sedimentation), moderate (coagulation–flocculation with ferric chloride and polyelectrolite and sedimentation), and minimum (only sedimentation). The optimum for membrane protection, in terms of calcium, conductivity, and bicarbonates reduction, was the intense treatment. Membrane performance varied with pretreatment but not reclaimed water quality. The study recommended intense pretreatment to protect the membrane.

A modular pilot size plant involving coagulation/flocculation, centrifugation, ultrafiltration, and sorption processes was designed and constructed by Benito et al. [13] for the treatment of oily wastewaters. Empirical equations developed by Shaalan [65] predict the impact of water contaminants on flux decline. These formulae enable decision-making concerning a suitable water pretreatment scheme and also selection of the most appropriate cleaning cycle.

#### 11.4.2 EFFECTS OF SPACERS ON PERMEATE FLUX AND FOULING

The influence of spacer thickness, in spiral-wound membrane units, on permeate flow and its salinity was studied by Sablani et al. [7]. Membrane parameters were also estimated using an analytical osmotic pressure model for high salinity applications. The effects of spacer thickness on permeate flux showed that the observed flux decreases by up to 50% going from a spacer thickness of 0.1168–0.0508 cm. The authors commented that the different geometry/configuration of the spacer-influenced turbulence at the membrane surface and that, in turn, affected concentration polarization. This suggested less turbulence with the smaller spacer thickness and is opposite to what is normally expected. A membrane module with an intermediate spacer thickness of 0.0711 cm was found to be the best economically, since it gave the highest water production rate (L/h).

Geraldes et al. [66] assessed the effect of a ladder-type spacer configuration in NF spiral-wound modules on concentration boundary layer disruption. The results showed that the average concentration polarization for the membrane wall was independent of the distance to the channel inlet, while for the membrane wall without adjacent filaments the average concentration polarization increased with the channel length. This was due to the fact that in the first case the transverse filaments periodically disrupted the concentration boundary layer while in the second case the concentration boundary layer grew continuously along the channel length. The experimental results of the apparent rejection coefficients were compared to model predictions, the agreement being good. Their results clearly established how crucial the spacers configuration is in the optimization of the spiral-wound module efficiency.

The unexpected results of Sablani et al. [7] (i.e., less turbulence with smaller spacer thickness) may be best explained by an excellent paper by Schwinge et al. [67]. The latter employed computational fluid dynamics (CFD) in a study of unsteady flow in narrow spacer-filled channels for spiral-wound membrane modules. The flow patterns were visualized for different filament configurations incorporating variations in mesh length, filament diameter, and for channel Reynolds numbers,  $Re_{ch}$ , up to 1000. The simulated flow patterns revealed the dependence of the formation of recirculation regions on the filament configuration, mesh length, filament diameter, and the Reynolds number. When the channel Reynolds number was increased above 300, the flow became super-critical showing time-dependent movements for a filament located in the center of a narrow channel; and when the channel Reynolds number was increased above 500 the flow became super-critical for a filament adjacent to the membrane wall. For multiple filament configurations, flow transition can occur at channel Reynolds numbers as low as 80 for the submerged spacer at a very small mesh length (mesh length/channel height ( $l_m/h_{ch}$ ) = 1) and at a slightly larger Reynolds number at a larger mesh length ( $l_m/h_{ch}$  = 4). The transition occurred above  $Re_{ch}$  of 300 for a cavity spacer and above  $Re_{ch}$  of 400 for a zigzag spacer. We can speculate that the conclusions of Sablani et al. [7], less turbulence with smaller spacer thickness, were due to fewer recirculating regions as a result of smaller mesh length and filament diameter.

Computational fluid dynamics simulations were used by Li et al. [68] to determine mass transfer coefficients and power consumption in channels filled with nonwoven net spacers. The geometric parameters of a nonwoven spacer were found to have a great influence on the performance of a spacer in terms of mass transfer enhancement and power consumption. The results from the CFD simulations indicated that an optimal spacer geometry exists.

### 11.4.3 MEMBRANE SURFACE MODIFICATION

Belfer [24] described a simple method for surface modification of commercial composite polyamide reverse osmosis membranes. The procedure involved radial grafting with a redox system consisting of potassium persulfate/sodium methabisulfite. ATR-FTIR provided valuable information about the degree of grafting and the microstructure of the grafted chain on the membrane surface. Both acrylic and sulfo-acidic monomers and neutral monomers, such as polyethylene glycol methacrylate, were used to demonstrate the wide possibilities of the method in terms of grafting of different monomers and initiators. It was shown that some of the modified membranes conserved their previous operating characteristics, flux, or rejection, but exhibited a higher resistance to humic acid. Additional work needs to be done to find out what happens to the fouling resistance of such membranes over the long term (i.e., after initial biofilm formation).

A fouling-resistant reverse osmosis membrane that reduces microbial adhesion was reported by Jenkins and Tanner [69]. In this interesting study that confirmed the results of Flemming and Schaule [20], they compared two types of thin-film composite membranes with different chemistries. One type was classified as a polyamide, the other utilized a new chemistry that formed a polyamide-urea barrier (i.e., surface) layer. The latter composite membrane proved superior in reverse osmosis operation similar to that of the polyetherurea membrane of Flemming and Schaule [20], including rejection of certain dissolved species and fouling-resistance. These results suggest that the presence of urea groups in the membrane reduces microbial adhesion, perhaps through charge repulsion. The results of work by Ridgway [19] on the kinetics of adhesion of *Mycobacterium* sp. to cellulose diacetate reverse-osmosis membranes have similar implications. Scientists should therefore be able to minimize microbial adhesion by controlling the surface chemistry of polymer membranes, through, for example, the inclusion of urea groups.

Chemical modification of a membrane surface can be used in combination with spacers and periodic applications of bioacids [70]. The paper by Redondo, however, is short on specifics (e.g., details of chemical modification of aromatic polyamides membrane surface), and therefore not very useful to those looking for insights into membrane fouling.

### 11.4.4 FOULING RESISTANCE OF HYDROPHILIC AND HYDROPHOBIC MEMBRANES

Cherkasov et al. [32] presented an analysis of membrane selectivity from the standpoint of concentration polarization and adsorption phenomena. The results of their study showed that hydrophobic membranes attracted a thicker irreversible adsorption layer than hydrophilic membranes. The layer thickness was determined by the intensity of concentration polarization (Figure 11.3). This may be due to the stronger attraction of water to hydrophilic membranes. Kabsch-Korbutowicz et al. [17] also demonstrated that the most hydrophilic of the membranes tested (i.e., regenerated cellulose) had the lowest proneness to fouling by organic colloids (i.e., humic acids). These conclusions were further supported by the thorough work of Tu et al. [37] who showed that membranes with a higher negative surface charge and greater hydrophilicity was less prone to fouling due to fewer interactions between the chemical groups in the organic solute and the polar groups on the membrane surface.

### 11.4.5 CONTROL OF OPERATING PARAMETERS AND CRITICAL FLUX

A comprehensive difference model was developed by Madireddi et al. [71] to predict membrane fouling in commercial spiral-wound membranes with various spacers. This is a useful paper for experimental studies on the effect of flow channel thickness on flux and fouling. Avlonitis et al. [72] presented an analytical solution for the performance of spiral-wound modules with seawater as the feed. In a key finding they showed that it was necessary to incorporate the concentration and pressure of the feed into the correlation for the mass transfer coefficient. In a similar study, Boudinar et al. [73] developed the following relationship for calculating mass transfer coefficients in channels equipped with a spacer:

$$k = 0.753 \left( \frac{K}{2-K} \right)^{1/2} \frac{D_S}{h_B} Sc^{-1/6} \left( \frac{Pe h_B}{M} \right) \quad (11.9)$$

where

$Pe$  = Peclet number

$K = 0.5$

$M = 0.6$  (cm)

Controlled centrifugal instabilities (called Dean vortices), resulting from flow around a curved channel, were used by Mallubhotla and Belfort [74] to reduce both concentration polarization and the tendency toward membrane fouling. These vortices enhanced back-migration through convective flow away from the membrane-solution interface and allowed for increased membrane permeation rates.

Goosen et al. [3] showed that the polymer membrane can be very sensitive to changes in the feed temperature. There was up to a 100% difference in the permeate flux between feed temperatures of 30°C and 40°C. A more recent study showed that the improved flux was due primarily, though not completely, to viscosity effects on the water. Reversible physical changes in the membrane may also have occurred [75].

The transition from concentration polarization to fouling is a key phase in membrane separation processes that occur at a critical flux. Song [76] indicated that in most theories developed, the limiting or critical flux is based on semiempirical knowledge rather than being predicted from fundamental principles. To overcome this shortcoming, he developed a mechanistic model, based on first principles, for predicting the limiting flux. Similar to the critical flux results of Chen et al. [41] and the limiting flux of Koltuniewicz and Noworyta [9], Song showed that there is a critical pressure for a given suspension. When the applied pressure is below the critical pressure, only a concentration polarization layer exists over the membrane surface. A fouling layer, however, will form between the polarization and the membrane surface when the applied pressure exceeds the critical pressure. The limiting or critical flux values predicted by the mechanistic model compared well with the integral model for a low concentration feed. Operators of RO/UF plants/units should therefore operate their systems just below the critical flux in order to maximize productivity while minimizing membrane fouling.

#### 11.4.6 MEMBRANE CLEANING USING CHEMICAL AGENTS AND BACK PULSING

Membranes used in the food industry for ultrafiltration of milk or whey are cleaned on a regular basis with water and various aqueous solutions to ensure hygienic operation and to maintain membrane performance. Water quality, therefore, is of special importance in the rinsing and cleaning process as impurities present in the water could affect cleaning efficiency, and in the long term, contribute to a reduction in performance and life of the membrane [77]. Membrane manufacturers generally recommend the use of high-quality water such as filtered and demineralized water. Installing and running water purification systems, however, is expensive. Alternatively, water treatment chemicals such as sequestering agents (e.g., EDTA, polyphosphates) can be added to low-quality water to increase the solubility of metal ions such as calcium, magnesium, manganese, and iron. Reverse osmosis permeate may also be of suitable quality for use in cleaning.

In a study by Tran-Ha and Wiley [77], it was shown that impurities such as particulate and dissolved salts present in the water can affect the cleaning efficiency of a polysulphone ultrafiltration membrane. The water used for cleaning was doped with a known amount of specific ions (i.e., calcium, sodium, chloride, nitrate, and sulphate). The presence of calcium in water, at the usual concentrations found in tap water, did not greatly affect cleaning efficiency while chloride was found to reduce it. Sodium, nitrate, and sulphate appeared to improve the flux recovery during membrane cleaning. The cleaning efficiency was also improved at higher ionic strengths. For further reading a similar study by Lindau and Jonsson [12] is recommended. They assessed the influence of different types of cleaning agents on a polysulphone ultrafiltration membrane after treatment of oily wastewater.

The effect of different cleaning agents on the recovery of the fouled membrane was studied by Mohammadi et al. [78]. Results showed that a combination of sodium dodecyl sulfate and sodium hydroxide can be used as a cleaning material to reach the optimum recovery of the polysulfone membranes used in milk concentration industries. Also a mixture of sodium hypochlorite and sodium hydroxide showed acceptable results, where washing with acidic solutions was not effective.

Mores and Davis [79], to view membrane surfaces at different times in cross-flow microfiltration, used direct visual observation (DVO) of yeast suspensions with rapid back pulsing at varied back pulsing duration and pressure. The DVO photos showed that the membranes were more effectively cleaned by longer back pulse durations and higher back-pulse pressures. However, trade-offs existed between longer and stronger back pulses, and permeate loss during the back pulse. Shorter, stronger back pulses resulted in higher net fluxes than longer, weaker back pulses.

Roth et al. [80] proposed a method to determine the state of membrane wear by analyzing sodium chloride stimulus-response experiments. The shape of the distribution of sodium chloride in the permeate flow of the membrane revealed the solute permeation mechanisms for used membranes. For new membranes the distribution of sodium chloride collected in the permeate side as well in the rejection side was unimodal. For fouled membranes they noted the presence of several modes. The existence of a salt leakage peak, as well as an earlier detection of salt for all the fouled membranes, gave evidence of membrane structure modification. The intensive use of the membranes might have created an enlargement of the pore sizes. Salt and solvent permeabilities increased as well. While this is a difficult paper to follow, it may be of use to those who want to develop new methods for measuring membrane degradation.

Ammerlaan et al. [21] reported on membrane degradation resulting in a premature loss of salt rejection by cellulose acetate membranes. Tests were initiated to find a solution to the problem and to gain a better understanding of the mechanisms involved. It was found that removal of all free chlorine solved the problem. This was accomplished by injecting ammonia in the feed water presumably resulting in the formation of ammonium chloride. Membrane damage by chlorine was also reported by Ridgway et al. [18]. They studied membrane fouling at a wastewater treatment plant under low- and high-chlorine conditions. High-chlorine residuals damaged the membrane structure and reduced mineral rejection capacity.

## 11.5 MEMBRANE FOULING AND GAS SEPARATIONS

Many industrial activities, such as gas production [81–83], catalysis [84], and fuel cells [83], require gas separation. Fouling in gas separation processes, however, is less severe than in microfiltration, nanofiltration, and reverse osmosis where it is the main cause of permanent flux decline and loss of product quality [81].

Saracco and Specchia [84] noted that inorganic membranes have great potential in gas separation, catalytic reactors, gasification of coal, water decomposition, and solid electrolyte fuel cells [81–89]. Inorganic membranes are usually made from alumina, silica, carbon, and zeolites [85]. We will only assess porous membranes since fouling is virtually absent in dense membranes [81].

Roque-Malherbe et al. [90] studied the transport of hydrogen and carbon dioxide through porous ceramic membranes (Figure 11.5). The transport mechanism followed the Darcy law [81,82,88,89,91]:

$$J = B \left( \frac{\Delta P}{l} \right) = \Pi \Delta P = \frac{QV_m}{A} \quad (11.10)$$

$$\Pi = \frac{B}{l} \quad (11.11)$$

Darcy law for gaseous laminar flow (Figure 11.5) is described by the following equation [88]:

$$Q = \left( \frac{k}{\mu} \right) * A * \left( \frac{\Delta P}{l} \right) \quad (11.12)$$

where

$$B = \frac{kV_m}{\mu} \quad (11.13)$$

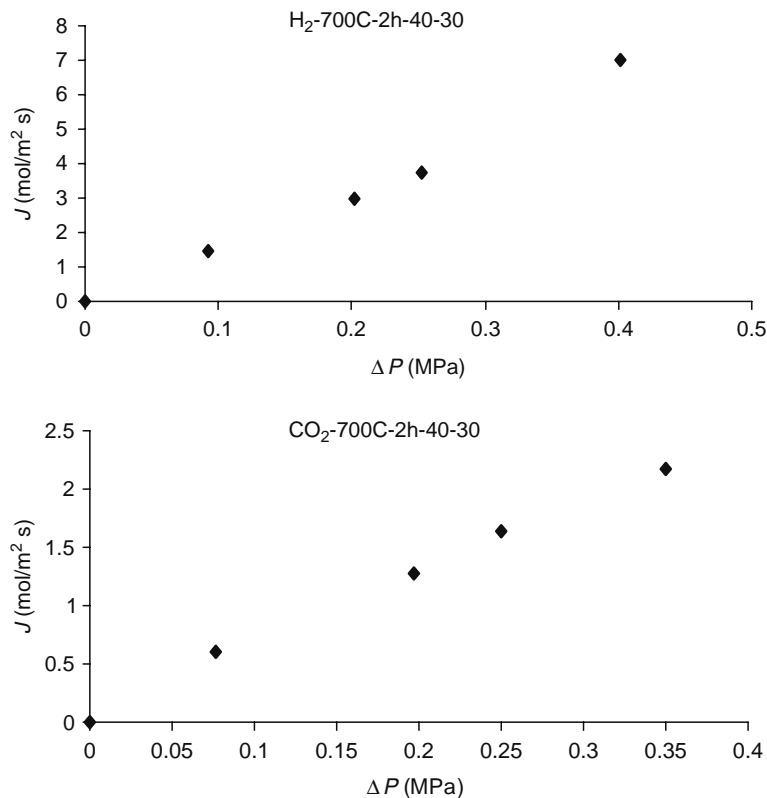


**FIGURE 11.5** Study of the relation between the flux  $J$  and  $\Delta P$ , during the transport of H<sub>2</sub> and CO<sub>2</sub> through a porous ceramic membrane produced by thermal treatment of a natural zeolite. (From Roque-Malherbe, R., Applications of natural zeolites in pollution abatement and industry. In: Nalwa, H.S., ed., *Handbook of Surfaces and Interfaces of Materials*, Vol. 5, Academic Press, New York, 2001.)

The Carman–Kozeny equation for the permeability factor for a membrane formulated with pressed spherical particles is [88]:

$$k = \frac{\varepsilon d_v^2}{16C} \quad (11.14)$$

$$\varepsilon = 1 - \frac{\rho_A}{\rho_R} \quad (11.15)$$

therefore

$$k \approx \frac{\varepsilon d_v^2}{77} \quad (11.16)$$

As the membrane pore dimensions decrease, for example, due to pore blockage, or the mean free path of the molecules increase, the permeating particles tend to collide more with the pore walls than among themselves, then the Knudsen flow regime is established. In this case the expression for the permeation flux across the membrane is given by [83]:

$$J = \left( \frac{G}{(2MRT)^{1/2}} \right) * \left( \frac{\Delta P}{l} \right) \quad (11.17)$$

where  $G$  is the geometrical factor which accounts for membrane porosity and tortuosity.

Flux decline as a result of membrane fouling can be attributed to pore blocking due to the deposition of particles flowing with the gas to be cleaned. In addition, a decrease in the membrane porosity and consequently flux decay, during the gas separation process, could be produced in ceramic membranes because of the sinterization of the particles which constitutes the membrane, if the gas separation process is carried out at high temperatures. This means physical changes in the membrane can occur as a result of the operating parameters. Pore blockage and membrane compaction are two factors that contribute to fouling of membranes during gas separations.

## 11.6 ECONOMIC ASPECTS OF MEMBRANE SEPARATIONS

New separation techniques must, at minimum, be comparable in overall cost, and preferably be lower in cost than traditional technology. Scientists often forget that successful commercialization of a new technology is dependent on economic factors. Just because a novel separation technique works in the laboratory, for example, does not mean that it will replace current methods.

The competitiveness of UF pretreatment in comparison to conventional pretreatment (i.e., coagulation and media filtration) was assessed by Brehant et al. [92] by looking at the impact on RO hydraulic performances. The study showed that ultrafiltration provided permeate water with high and constant quality resulting in a higher reliability of the RO process than with a conventional pretreatment. The combination of UF with a pre-coagulation at low dose helped in controlling UF membrane fouling. The authors concluded that the combined effect of a higher recovery and a higher flux rate promised to significantly reduce the RO plant costs. The conclusions reached were opposite of those reported in the paper by Glueckstern et al. [56] above, and demonstrate the complexity of the overall economics of a membrane separation process.

Field evaluation of a hybrid membrane system consisting of an UF membrane pretreatment unit and an RO seawater unit was conducted by Glueckstern et al. [56]. For comparison a second pilot system consisting of conventional pretreatment and an RO unit was operated in parallel. The conventional pretreatment unit included in-line flocculation followed by media filtration. The study showed that UF provided a very reliable pretreatment for the RO system independent of the raw water quality fluctuations. However, the cost of membrane pretreatment was higher than conventional pretreatment. This suggested that membrane pretreatment for RO desalting systems is only economic for sites that require extensive conventional pretreatment or where wide fluctuations in the raw water quality are expected.

## 11.7 CONCLUDING REMARKS

Membrane fouling is a complex process where the physicochemical properties of the membrane, the type of cells, the quality of the feed water, the type of solute molecules, and the operating conditions all play a role. The end result of most membrane separations is a fouled surface that the operator will not be able to clean to its original state. To reduce the tendency to irreversible fouling it is essential to operate the plant/unit below the critical flux. This must go hand-in-hand with reliable feed water pretreatment schemes.

Studies are required on effective removal of biofilms without damaging the membrane. Additional work needs to be done to find out what happens to the fouling resistance of chemically modified membranes over the long term (i.e., after initial biofilm formation). Membrane resistance to humic acids is another area for further study. Furthermore, the molecular tools needed for exploring the biochemical details of the microbial adhesion process to membranes are now available.

Various aspects of the water problem need to be considered not only by developing nations but also by developed countries. Water is required for urban development, industrialization, and agriculture. An increase in the world population results in an increase in water usage. We can stipulate that in the future, serious conflicts will arise not because of a lack of oil, but due to water shortages. As scientists and engineers continue to improve the technical and economic efficiency of membrane desalination systems, it is imperative that we do not lose sight of the bigger water resources picture. A three-pronged approach therefore needs to be taken by society; water needs to be effectively managed, it needs to be economically purified and it needs to be conserved.

## ACKNOWLEDGMENTS

We gratefully acknowledge the financial assistance of the Middle East Desalination Research Center (MEDRC), and Sultan Qaboos University through grant number IG/AGR/BIOR/02/04 to Mattheus F.A. Goosen. Dr. Roque-Malherbe gratefully recognizes the financial support provided by NASA through the Grant Cooperative Agreement Number NAG10-335. He would also like to acknowledge his colleagues Dr. Clyde Parrish and Mr. William del Valle for the collaboration in the permeation study.

## NOMENCLATURE

$A$	rate of loss of membrane surface area as function of time ( $\text{m}^2/\text{s}$ )
$A$	effective membrane area ( $\text{m}^2$ )
AFM	atomic force microscopy
ATR	attenuated total reflection
$B$	permeability ( $\text{mol}/\text{m s Pa}$ )
$C = 4.8 \pm 0.3$	Carman-Kozeny constant
$C_b$	bulk solute concentration ( $\text{mol}/\text{cm}^3$ )
$C_g$	gel concentration ( $\text{kmol}/\text{m}^3$ )
$C_o$	solute concentration in feed solution ( $\text{kmol}/\text{m}^3$ )
$C_p$	permeate solute concentration ( $\text{mol}/\text{cm}^3$ )
$C_w$	concentration at membrane surface ( $\text{mol}/\text{cm}^3$ )
$d_p$	average grain diameter (mm)
$d_v$	membrane pore diameter
$D$	solute diffusion coefficient ( $\text{m}^2/\text{s}$ )
FTIR	Fourier transform infrared
$G$	geometrical factor (m)
$H$	transversal dimension of channel (m)
$i$	cycle number
$J$	solvent flux across membrane ( $\text{m}^3/\text{m}^2 \text{ s}$ )
$J^*$	flux at infinite time ( $\text{m}^3/\text{m}^2 \text{ s}$ )
$J_a$	average flux under steady-state conditions ( $\text{m}^3/\text{m}^2 \text{ s}$ )
$J_{ai}$	solvent flux at time $a$ and in cycle $i$ ( $\text{m}^3/\text{m}^2 \text{ s}$ )
$J_{\text{crit}}$	limiting or critical flux ( $\text{m}^3/\text{m}^2 \text{ s}$ )
$J_{\text{lim}}$	limiting or critical flux ( $\text{m}^3/\text{m}^2 \text{ s}$ )
$J_o$	solvent flux at beginning of cycle ( $\text{m}^3/\text{m}^2 \text{ s}$ )
$J_s$	solute flux ( $\text{mol}/\text{cm}^2 \text{ s}$ )
$J(t_p)$	solvent flux as function of permeation time ( $\text{m}^3/\text{m}^2 \text{ s}$ )
$J_v$	permeate flux ( $\text{mol}/\text{cm}^2 \text{ s}$ )
$J$	molar gas flow ( $\text{mol}/\text{m}^2 \text{ s}$ )
$K$	hydraulic permeability of membrane to pure solvent ( $\text{m}^3/\text{N s}$ )
$k$	mass transfer coefficient
$kC_w$	adsorbed layer resistance
$L$	channel length (m)
$l$	membrane thickness (m)

$M$	molecular weight of the gaseous permeating species (kg/mol)
$m$	channel parameter
$\Delta P$	hydraulic pressure difference across membrane (cm/s)
$P$	transmembrane pressure (N/m <sup>2</sup> )
Pe	Peclet number
$\Delta P$	= $P_1 - P_2$ trans-membrane pressure (Pa)
$Q$	gas filtrate flux (m <sup>3</sup> /s)
RO	reverse osmosis
$R_m$	membrane resistance
$R$	gas constant (J/kmol K)
$Sc$	Schmidt number
$T$	temperature (K)
$t_p$	permeation time (h)
$t_c$	cleaning time (h)
UF	ultrafiltration
UTDR	ultrasonic time-domain reflectometry
$U_o$	longitudinal component of fluid velocity averaged over channel cross-section (m/s)
$V_m$	molar volume of the flowing gas

### GREEK SYMBOLS

$\varepsilon$	membrane porosity
$\Pi$	gas permeance (mol/m <sup>2</sup> s Pa)
$\rho_A$	apparent membrane density (g/cm <sup>3</sup> )
$\rho_R$	Real membrane density (g/cm <sup>3</sup> )
$\mu$	dynamic viscosity of the gas (Pa s)
$\Delta\pi(w)$	osmotic pressure at membrane surface (cm/s)
$M$	fluid viscosity
$T$	membrane lifetime (year)

### REFERENCES

- Goosen M.F.A., Al-Hinai H., and Sablani S., Capacity-building strategies for desalination: Activities, facilities and educational programs in Oman. *Desalination* 141 2001 181–189.
- Goosen M.F.A., Sablani S.S., Al-Hinai H., Al-Obeidani S., Al-Belushi R., and Jackson D., Fouling of reverse osmosis and ultrafiltration membranes: A critical review. *Separation Science and Technology* 39(10) 2004 2261–2298.
- Goosen M.F.A., Sablani S.S., Al-Maskari S.S., Al-Belushi R.H., and Wilf M., Effect of feed temperature on permeate flux and mass transfer coefficient in spiral-wound reverse osmosis systems. *Desalination* 144 2002 367–372.
- Ahmed M., Arakel A., Hoey D., Thumarukudy M.R., Goosen M.F.A., Al-Haddabi M., and Al-Belushi A., Feasibility of salt production from inland RO desalination plant reject brine: A case study. *Desalination* 158 2003 109–117.
- Goosen M.F.A. and Shayya W.H., eds. *Water Management, Purification and Conservation in Arid Climates; Vol. 1, Water Management*, Technomic Publishing, Lancaster, PA, 1999, pp. 1–6.
- Voros N.G., Maroulis Z.B., and Marinou-Kouris D., Salt and water permeability in reverse osmosis membranes. *Desalination* 104 1996 141–154.
- Sablani S.S., Goosen M.F.A., Al-Belushi R., and Gerardos V., Influence of spacer thickness on permeate flux in spiral-wound seawater reverse osmosis systems. *Desalination* 146 2002 225–230.
- Singh R. and Tembrock J., Effectively controlled reverse osmosis systems. *Chemical Engineering Progress* 95 1999 57–66.
- Koltuniewicz A. and Noworyta A., Dynamic properties of ultrafiltration systems in light of the surface renewal theory. *Industrial Engineering and Chemical Research* 33 1994 1771–1779.
- Sablani S.S., Goosen M.F.A., Al-Belushi R., and Wilf M., Concentration polarization in ultrafiltration and reverse osmosis: A critical review. *Desalination* 141 2001 269–289.
- Upen J., Barwada S.J.M., Coker S.D., and Terry A.R., Winning the battle against biofouling of reverse osmosis membranes. *Desalination and Water Reuse* 10(2) 2000 53–58.
- Lindau J. and Jonsson A.-S., Cleaning of ultrafiltration membranes after treatment of oily wastewater. *Journal of Membrane Science* 87 1994 71–78.
- Benito J.M., Rios G., Ortea E., Fernandez E., Cambiella A., Pazos C., and Coca J., Design and construction of a modular pilot plant for the treatment of oil-containing waste-waters. *Desalination* 147 2002 5–10.

14. Pope J.M., Yao S., and Fane A.G., Quantitative measurements of the concentration polarization layer thickness in membrane filtration of oil-water emulsions using NMR micro-imaging. *Journal of Membrane Science* 118 1996 247–257.
15. Scott K., Mahood A.J., Jachuck R.J., and Hu B., Intensified membrane filtration with corrugated membranes. *Journal of Membrane Science* 173 2000 1–16.
16. Nystrom M., Ruohomaki K., and Kaipa L., Humic acid as a fouling agent in filtration. *Desalination* 106 1996 78–86.
17. Kabsch-Korbutowicz M., Majewska-Nowak K., and Winnicki T., Analysis of membrane fouling in the treatment of water solutions containing humic acids and mineral salts. *Desalination* 126 1999 179–185.
18. Ridgway H.F., Justice C.A., Whittaker C., Argo D.G., and Olson B.H., Biofilm fouling of RO membranes—its nature and effect on treatment of water for reuse. *Journal of American Water Works Association* 76 1984 94–102.
19. Ridgway H.F., Rigby M.G., and Argo D.G., Adhesion of a *Mycobacterium* sp. to cellulose diacetate membranes used in reverse osmosis. *Applied and Environmental Microbiology* 47(1) 1984 61–67.
20. Flemming H.-C. and Schaule G., Biofouling of membranes—a microbiological approach. *Desalination* 70 1988 95–119.
21. Ammerlaan A.C.F., Franklin J.C., and Moody C.D., Yuma desalting plant. Membrane degradation during test operations. *Desalination* 88 1992 33–49.
22. Rabiller-Baudry M., Le Maux M., Chaufer B., and Begoin L., Characterisation of cleaned and fouled membranes by ATR-FTIR and EDX analysis coupled with SEM: Application to UF of skimmed milk with a PES membrane. *Desalination* 146 2002 123–128.
23. Li J., Sanderson R.D., Hallbauer D.K., and Hallbauer-Zadorozhnaya V.Y., Measurement and modeling of organic deposition in ultrafiltration by ultrasonic transfers signals and reflections. *Desalination* 146 2002 177–185.
24. Belfer S., Purinson Y., and Kedem O., Reducing fouling of RO membranes by redox-initiated graft polymerization. *Desalination* 119 1998 189–195.
25. Ghayeni S.B.S., Beatson P.J., Schneider R.P., and Fane A.G., Adhesion of wastewater bacteria to reverse osmosis membranes. *Journal of Membrane Science* 138 1998 29–42.
26. Ghayeni S.B.S., Beatson P.J., Schneider R.P., and Fane A.G., Water reclamation from municipal wastewater using combined micro filtration-reverse osmosis (ME-RO): Preliminary performance data and microbiological aspects of system operation. *Desalination* 116 1998 65–80.
27. Zydney A.L. and Ho C.C., Scale-up of microfiltration systems: Fouling phenomena and  $V_{max}$  analysis. *Desalination* 146 2002 75–81.
28. Ridgway H.F., Kelly A., Justice C., and Olson B.H., Microbial fouling of reverse osmosis membranes used in advanced wastewater treatment technology: Chemical bacteriological and ultrastructural analyses. *Applied and Environmental Microbiology* 46 1983 1066–1084.
29. Nikolova, J.D. and Islam, M.A., Contribution of adsorbed layer resistance to the flux-decline in an ultrafiltration process, *Journal of Membrane Science* 146 1998 105–111.
30. Flemming H.-C., Schaule G., and McDonough R., How do performance parameters respond to initial biofouling on separation membranes? *Vom Wasser* 80 1993 177–186.
31. Ridgway H.F., Rigby M.G., and Argo D.G., Bacterial adhesion and fouling of reverse osmosis membranes. *Journal AWWA* 1985 97–106.
32. Cherkasov A.N., Tsareva S.V., and Polotsky A.E., Selective properties of ultrafiltration membranes from the standpoint of concentration polarization and adsorption phenomena. *Journal Membrane Science* 104 1995 157–165.
33. Ridgway H.F., Bacteria and membranes: Ending a bad relationship. *Desalination* 83 1991 53.
34. Domany Z., Galambos I., Vatai G., and Bekassy-Molnar E., Humic substances removal from drinking water by membrane filtration. *Desalination* 145 2002 333–337.
35. Schafer A.I., Martrup M., and Jensen R.L. Particle interactions and removal of trace contaminants from water and wastewaters. *Desalination* 147 2002 243–250.
36. Khatib K., Rose J., Barres O., Stone W., Bottero J.-Y., and Anselme C., Physico-chemical study of fouling mechanisms of ultrafiltration membrane on Biwa Lake (Japan), *Journal of Membrane Science* 130 1997 53–62.
37. Tu S.-C., Ravindran V., Den W., and Pirbazari M., Predictive membrane transport model for nanofiltration processes in water treatment, *AIChE Journal* 47(6) 2001 1346–1362.
38. Sahachaiyunta P., Koo T., and Sheikholeslami R., Effect of several inorganic species on silica fouling in RO membranes. *Desalination* 144 2002 373–378.
39. Yiantsios S.G. and Karabelas S., The effect of colloid stability on membrane fouling. *Desalination* 118 1998 143–152.
40. Jarusutthirak C., Amy G., and Croue J.-P., Fouling characteristics of wastewater effluent organic matter (EfOM) isolates on NF and UF membranes. *Desalination* 145 2002 247–255.
41. Chen V., Fane A.G., Madaeni S., and Wenten I.G., Particle deposition during membrane filtration of colloids: Transition between concentration polarization and cake formation. *Journal of Membrane Science* 125 1997 109–122.
42. Riedl K., Girard B., and Lencki W., Influence of membrane structure on fouling layer morphology during apple juice clarification, *Journal of Membrane Science* 139 1998 155–166.
43. Altena F.W. and Belfort G., Lateral migration of spherical particles in porous flow channels: Application to membrane filtration. *Chemical Engineering Science* 19(2) 1984 343–355.
44. Drew D.A., Schonberg J.A., and Belfort G., Lateral inertial migration of small sphere in fast laminar flow through a membrane duct. *Chemical Engineering Sciences* 46(12) 1991 3219–3224.
45. Ghayeni S.B.S., Beatson P.J., Fane A.G., and Schneider R.P., Bacterial passage through micro filtration membranes in wastewater applications. *Journal of Membrane Science* 153 1999 71–82.

46. Howe K.J., Ishida K.P., and Clark M.M., Use of ATR/FTIR spectrometry to study fouling of microfiltration membranes by natural waters. *Desalination* 147 2002 251–255.
47. Chan R., Chen V., and Bucknall M.P., Ultrafiltration of protein mixtures: Measurement of apparent critical flux, rejection performance, and identification of protein deposition. *Desalination* 146 2002 83–90.
48. Bowen W.R., Doneva T.A., and Yin H.B., Atomic force microscopy studies of membrane–solute interactions (fouling). *Desalination* 146 2002 97–102.
49. Gowman, L.M. and Ethier, C.R., Concentration and concentration gradient measurements in an ultrafiltration concentration polarization layer. Part I: A laser-based refractometric experimental technique. *Journal of Membrane Science* 131 1997 95–105.
50. Gowman, L.M. and Ethier, C.R., Concentration and concentration gradient measurements in an ultrafiltration concentration polarization layer. Part II: Application to hyaluronan. *Journal of Membrane Science* 131 1997 107–123.
51. Dal-Cin M.M., McLellan F., Striez C.N., Tam C.M., Tweddle T.A., and Kumar A., Membrane performance with a pulp mill effluent: Relative contributions of fouling mechanisms. *Journal of Membrane Science* 120 1996 273–285.
52. Danckwerts P.V., Significance of liquid film coefficients in gas absorption. *Industrial Engineering and Chemistry* 43 1951 460–470.
53. Denisov G.A., Theory of concentration polarization in cross-flow ultrafiltration: Gel-layer model and osmotic-pressure model. *Journal of Membrane Science* 91 1994 173–187.
54. Hermia J., Constant pressure blocking filtration laws: Application to power-law non-newtonian fluids. *Transactions of the Institution of Chemical Engineers* 60(3) 1982 183–187.
55. Wilf M. and Klinko K., Effective new pretreatment for seawater reverse osmosis systems. *Desalination* 117 1998 323–331.
56. Glueckstern P., Priel M., and Wilf M., Field evaluation of capillary UF technology as a pretreatment for large seawater RO systems. *Desalination* 147 2002 55–62.
57. Glueckstern P. and Priel M., Advanced concept of large seawater desalination systems for Israel. *Desalination* 119 1998 33–45.
58. Chapman H., Vigneswaran S., Ngo H.H., Dyer S., and Ben A.R., Pre-flocculation of secondary treated wastewater in enhancing the performance of microfiltration. *Desalination* 146 2002 367–372.
59. Nguyen M.T. and Ripperger S., Investigation on the effect of flocculants on the filtration behavior in microfiltration of fine particles. *Desalination* 147 2002 37–42.
60. Han B., Runnels T., Zimbron J., and Wickramasinghe R., Arsenic removal from drinking water by flocculation and microfiltration. *Desalination* 145 2002 293–298.
61. Choksuchart P., Heran M., and Grasmick A., Ultrafiltration enhanced by coagulation in an immersed membrane system. *Desalination* 145 2002 265–272.
62. Park P.K., Lee C.H., Choi S.J., Choo K.H., Kim S.H., and Yoon C.H., Effect of the removal of DOMs on the performance of a coagulation—UF membrane system for drinking water production. *Desalination* 145 2002 237–245.
63. Guigui C., Rouch J.C., Durand-Bourlier L., Bonnelye V., and Aptel P., Impact of coagulation conditions on the in-line coagulation/UF process for drinking water production. *Desalination* 147 2002 95–100.
64. Lopez-Ramirez J.A., Marquez D.S., and Alonso J.M.Q., Comparison studies of feedwater pre-treatment in reverse osmosis pilot plant. *Desalination* 144 2002 347–352.
65. Shaalan H.F., Development of fouling control strategies pertinent to nanofiltration membranes. *Euromed* May 2002.
66. Geraldés V., Semiao V., and de Pinho M.N., The effect of the ladder-type spacers configuration in NF spiral wound modules on the concentration boundary layers disruption. *Desalination* 146 2002 187–194.
67. Schwinge J., Wiley D.E., and Fletcher D.F., A CFD study of unsteady flow in narrow spacer-filled channels for spiral-wound membrane modules. *Desalination* 146 2002 195–201.
68. Li F., Meindersma G.W., de Haan A.B., and Reith T., Optimization of non-woven spacers by CFD and validation by experiments. *Desalination* 146 2002a 209–212.
69. Jenkins M. and Tanner M.B., Operational experience with a new fouling resistant reverse osmosis membrane. *Desalination* 119 1998 243–250.
70. Redondo J.A., Improve RO system performance and reduce operating cost with FILMTEC fouling resistant (FR) elements. *Desalination* 126 1999 249–259.
71. Madireddi K., Babcock R.B., Levine B., Kim J.H., and Stenstrom M.K. An unsteady-state model to predict concentration polarization. *Journal Membrane Science* 157 1999 13–34.
72. Avlonitis S., Hanbury W.T., and Boudinar M.B., Spiral wound modules performance: An analytical solution Part II. *Desalination* 89 1993 227–246.
73. Boudinar M.B., Hanbury W.T., and Avlonitis S., Numerical simulation and optimization of spiral-wound modules. *Desalination* 86 1992 273–290.
74. Mallubhotla H. and Belfort G., Flux enhancement during Dean vortex micro filtration. 8. Further diagnostics. *Journal of Membrane Science* 125 1988 75–91.
75. Goosen M.F.A., Sablani S., Dal Cin M., Wilf M., Jackson D., Al-Belushki R., and Al Maskri S., Effect of high temperature and pressure on permeation properties of composite polyamide seawater reverse osmosis and brackish water nanofiltration membranes. *Journal of Membrane Science* (Submitted 2008).
76. Song, L., A new model for the calculation of the limiting flux in ultrafiltration. *Journal of Membrane Science* 144 1998 173–185.
77. Tran-Ha M.H. and Wiley D.E., The relationship between membrane cleaning efficiency and water quality. *Journal of Membrane Science* 145 1998 99–110.
78. Mohammadi T., Madaeni S.S., and Moghadam M.K., Investigation of membrane fouling. *Euromed 2002 Conference Proceedings*, Sharm El-Sheikh, Egypt, 1(1) 4–6 May 2002, p. 1.

79. Mores W.D. and Davis R.H., Direct observation of membrane cleaning via rapid backpulsing. *Desalination* 146 2002 135–140.
80. Roth E.M., Kessler, F.B., and Accary A., Sodium chloride stimulus-response experiments in spiral wound reverse osmosis membranes: A new method to detect fouling. *Desalination* 121 1999 183–193.
81. Mulder M., *Basic Principles of Membrane Technology*, Kluwer Academic, Dordrecht, The Netherlands, 1996.
82. Baker R.W., *Membrane Technology and Applications*, John Wiley & Sons, New York, 2004.
83. Ogden J.M., Hydrogen: The fuel of the future. *Physics Today* April 2002 69–75.
84. Saracco G. and Specchia V., Catalytic inorganic-membrane-reactors: Present experience and future opportunities. *Catalysis Reviews—Science and Engineering* 36 1994 305–384.
85. Morooka S. and Kusakabe K., Microporous inorganic membranes for gas separation, *MRS Bulletin* March 1999 25–29.
86. Saracco G., Neomagus H.W.J.P., Versteeg G.F., and Swaij W.P.M., High-temperature membrane reactors: Potential and problems. *Chemical Engineering Science* 54 1999 1997–2017.
87. Lai Z., Bonilla G., Diaz I., Nery J.G., Sujaoti K., Amat M., Kokkoki E., Terakasi O., Thompson R.W., Tsapatis M., and Vlachos D.G., Microstructural optimization of a zeolite membrane for organic vapor separation. *Science* 300 2003 456–460.
88. Mauran S., Rigaud L., and Coudeville O., Application of the Carman–Kozeny correlation to a high-porosity anisotropic consolidated medium: The compressed expanded natural graphite. *Transport in Porous Media* 43 2001 355–376.
89. Burggraaf A.J., Single gas permeation of thin zeolite (MFI) membranes: Theory and analysis of experimental observations. *Journal of Membrane Science* 155 1999 45–65.
90. Roque-Malherbe R., del Valle W., Marquez F., Ducongé J., and Goosen M.F.A., Synthesis and characterization of zeolite-based porous ceramic membranes. *Separation Science and Technology* 41 2006 73–96.
91. Roque-Malherbe R., Applications of natural zeolites in pollution abatement and industry. In: Nalwa, H.S., ed., *Handbook of Surfaces and Interfaces of Materials*, Vol. 5, Academic Press, New York, 2001, Chapter 12, pp. 495–522.
92. Brehant A., Bonnelye V., and Perez M., Comparison of MF/UF pretreatment with conventional filtration prior to RO membranes for surface seawater desalination. *Desalination* 144 2002 353–360.
93. Bacchin P., Aimar P., and Sanches V., Model of colloidal fouling of membranes. *AIChE Journal* 41(2) 1995 368–376.
94. Karakulski K., Gryta M., and Morawski A., Membrane processes used for potable water quality improvement. *Desalination* 145 2002 315–319.
95. Lipnizki J. and Jonsson G., Flow dynamics and concentration polarization in spacer-filled channels. *Desalination* 146 2002 213–217.

---

# 12 Membrane Extraction in Preconcentration, Sampling, and Trace Analysis

*Jan Åke Jönsson*

## CONTENTS

12.1	Introduction .....	346
12.1.1	Sample Preparation for Analysis and Sampling .....	346
12.1.2	Membrane Extraction Systems.....	346
12.1.3	Membrane Devices for Sample Preparation .....	347
12.1.3.1	Flat-Sheet Devices .....	347
12.1.3.2	Hollow Fiber Devices .....	347
12.1.4	Equilibrium and Trapping.....	347
12.2	Variants of Membrane Extraction.....	349
12.2.1	Liquid Membrane Extraction Techniques.....	349
12.2.1.1	Three-Phase Liquid Membrane Extraction.....	349
12.2.1.2	Two-Phase Liquid Membrane Extraction Systems.....	350
12.2.2	Solid (Polymeric) Membrane Extraction Techniques.....	350
12.3	Theory and Principles of Membrane Extraction.....	351
12.3.1	Principles of SLM .....	351
12.3.2	Chemistry of SLM Extraction.....	351
12.3.2.1	Simple Permeation—Acids and Bases.....	352
12.3.2.2	Carrier-Mediated Transport—Metals and Organic Ions.....	353
12.3.3	Analyte Trapping in SLM.....	353
12.3.3.1	Direct Trapping.....	354
12.3.3.2	Indirect Trapping.....	354
12.3.3.3	Immunological Trapping.....	354
12.3.4	Mass Transfer in MMLLE.....	354
12.3.5	Differences between MMLLE and SLM .....	355
12.3.6	Concentration Enrichment.....	355
12.3.7	Selectivity .....	356
12.3.8	Equilibrium Extraction .....	357
12.4	Apparatus for Membrane Extraction.....	357
12.4.1	Stand-Alone Equipment .....	357
12.4.2	Online Connection to Chromatography .....	357
12.4.3	Continuous Flow Liquid Membrane Extraction .....	360
12.4.4	Membrane Extraction with a Sorbent Interface .....	360
12.4.5	Field Sampling Apparatus.....	361
12.5	Applications .....	361
	Acknowledgments.....	363
	References .....	363

## 12.1 INTRODUCTION

The use of membranes for extraction in analytical chemistry has been increasing during recent years. The main intention is to selectively extract and enrich compounds to be determined (analytes) from chemically more or less complex samples. In contrast to many technical uses of membranes, in analytical applications it is imperative to recover as efficiently as possible the extracted analytes so they can be transferred to suitable analytical instruments for the final determination in a quantitative way. Another difference from technical uses is that the volume scale is small; extracts are seldom larger than a milliliter, often only several microliters.

Membrane techniques have a number of clear advantages over other extraction techniques used in analytical chemistry. These advantages especially concern not only selectivity, enrichment power, and automation potential but also economy and occupational health aspects [1–8].

### 12.1.1 SAMPLE PREPARATION FOR ANALYSIS AND SAMPLING

In most cases of chemical analysis, some kind of sample preparation is necessary. One intention could be to bring the sample into a physical form, which is suitable for the further application of an instrumental technique for the final determination. This could be made by, for example, grinding, dissolution, combustion, filtration, etc. In many cases, for example, as a preparation for gas chromatographic analysis, analytes need to be transferred from the original matrix (e.g., water) to a solution in an organic solvent, often even involving a chemical reaction (derivatization) to improve detectability and solubility. For the determination of analytes in very low concentrations (trace analysis) it will be necessary to enrich or preconcentrate the analyte, i.e., increase its concentration to measurable levels. For analysis of complicated samples (e.g., biological or environmental origin) it is additionally crucial to perform cleanup procedures, whereby the concentrations of the analytes are increased relative to the matrix, i.e., a selective enrichment of the analytes [9–12].

Several types of sampling tasks could involve various types of extraction at the sampling site. This would be the case in integrating sampling, where the mean concentration over a period or over an area is sought, or when a speciation sampling is attempted, i.e., where the aim is to determine not only total concentrations but also equilibria (dissolved-bound, different dissociation conditions, different redox conditions, etc.).

For many of these sample preparation tasks, various types of extraction (phase-transfer) procedures are used, such as classical liquid–liquid extraction (LLE) [13–15] in different physical formats, solid-phase extraction (SPE) [16–18], solid-phase microextraction (SPME) [19,20], and other, when studying aqueous and other liquid samples. For solid samples, the classical technique is Soxhlet extraction, and there are a number of modern alternatives [21].

The conventional extraction techniques have a number of drawbacks. The most obvious one is that relatively large volumes of organic (often chlorinated) solvents are used. This aspect is easily illustrated by comparing the relevant EPA (US Environmental Protection Agency) sample preparation protocols. For example, in a generic EPA SPE procedure (Method 3535) [22], 85 mL of organic solvent is needed for extraction of 1 L of water sample (30 mL for elution, 55 mL for washings and conditioning). Method 3510, which is the corresponding LLE method, is applicable to many more analytes. It requires 180 mL of organic solvent, which is more, but not dramatically so. In both methods, the volume of the extract is reduced to 1–10 mL before analysis by evaporation. This applies to each sample, and an environmental laboratory handles thousands of samples. The use of large volumes of solvents leads to a significant expense, especially as high purity solvents are demanded, and also to concerns for occupational safety and for general environmental pollution. These techniques are also quite labor intensive and difficult to automate, why an important area of current research in analytical chemistry aims to the development of alternative extraction techniques meeting some of the disadvantages mentioned. These activities are somewhat moderated by the fact that the area of chemical analysis (especially regarding environmental and pharmaceutical applications, and also in other areas) is heavily regulated by various international and local rules, leading to that the acceptance of new technology is very slow and costly.

### 12.1.2 MEMBRANE EXTRACTION SYSTEMS

In all types of membrane extraction, the membrane separates the sample phase (often called donor or feed solution) from the acceptor or strip phase and the analyte molecules pass through the membrane from the donor to the acceptor. This process is often called pertraction (permeation–extraction). The membrane extraction techniques can be divided into porous and nonporous membrane techniques. Another distinction is between one-, two-, or three-phase membrane extraction techniques.

Typical examples of one-phase techniques are filtration and dialysis. The membrane is porous, so there is a liquid (or gas) contact through the pores between the donor and acceptor phases, which are of similar chemical composition (i.e., both are either aqueous, organic, or gaseous). There is no phase boundary, and therefore, no partition between phases. Thus, physical and not chemical properties govern the process. This review will not consider one-phase systems further. For information on dialysis, especially its analytically interesting version microdialysis, see Refs. [23,24].

Nonporous membrane techniques involve two or three phases separated by distinct phase boundaries. In three-phase membrane systems, a separate membrane phase is surrounded by two different liquid phases (donor and acceptor) forming a system with two phase-boundaries and thus two different extraction (partition) steps. These can be tailored to different types of chemical reactions, leading to a high degree of selectivity. The membrane phase can be a liquid, a polymer, or a gas, and the donor and acceptor phases can be either gas or liquid (aqueous or organic). Liquid membrane phases are often arranged in the pores of a porous hydrophobic membrane support material, which leads to a convenient experimental system, termed supported liquid membrane (SLM). There are several other ways to arrange a liquid membrane phase between two aqueous phases as described below.

In two-phase membrane systems, one of the surrounding phases is the same as the membrane phase, so there could be, for example, an organic solvent both in the membrane pores and in the acceptor, while the donor is aqueous or gaseous. There is only one phase boundary, and consequently, only one partition equilibrium. This technique is chemically analogous to LLE in separation funnels.

### 12.1.3 MEMBRANE DEVICES FOR SAMPLE PREPARATION

#### 12.1.3.1 Flat-Sheet Devices

Classically, flat-sheet porous PTFE or polypropylene membranes are used as support for the membrane liquid and mounted in holders (cells, contactors) permitting one flow channel on each side of the membrane [1,3,6,8,25]. See Figure 12.1. Such membrane units are typically operated in flow systems and in principle applicable to all versions of membrane extraction for analytical sample preparation or sampling. Such a setup can be easily interfaced with different analytical instruments, such as HPLC and various spectrometric instruments, and thereby provides good possibilities for automated operation. Drawbacks of this type of devices are relatively large costs and limited availability, as well as some carryover and memory problems as the membrane units are utilized many times, necessitating cleaning between each extraction.

#### 12.1.3.2 Hollow Fiber Devices

In another type of membrane extraction devices, porous polypropylene hollow fibers are used, often in a disposable way, which minimizes carryover problems and reduces costs [26–33]. On the other hand, manual manipulations are needed, limiting the possibility for automation. With these devices, the extraction can be carried out in a static mode, either in large sample volumes, where the extraction is not intended to be complete, or in small volumes aiming for complete extraction. Usually, stirring is applied to increase the speed of mass transfer. Some typical practical arrangements are shown in Figure 12.2. This type of SLM extraction is often called hollow fiber liquid phase microextraction, or three-phase liquid phase microextraction or two-phase liquid phase microextraction but the terminology in this active field of research has not been settled. Also hollow fibers can be connected in flow systems [34,35].

### 12.1.4 EQUILIBRIUM AND TRAPPING

After an extraction system has been left for enough long time, equilibrium between the phases is reached and mass transfer from the donor to the acceptor has stopped. This is the natural end point for the extraction in many cases. In the majority of

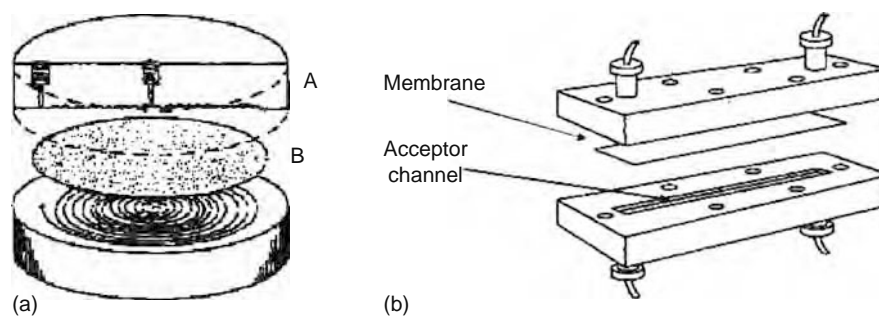


**FIGURE 12.1** Flat-membrane modules for membrane extraction in flow systems. (a) Spiral-channel membrane module with 1 mL channel volume (A, blocks of inert material; B, membrane). (From Jönsson, J.Å. and Mathiasson, L., *Trends Anal. Chem.*, 11, 106, 1992. With permission from Elsevier Science.) (b) Straight-channel membrane module with 10  $\mu\text{L}$  channel volume. (From Lindegård, B., Björk, H., Jönsson, J.Å., Mathiasson, L., and Olsson, A.-M., *Anal. Chem.*, 66, 4490, 1994. With permission.)

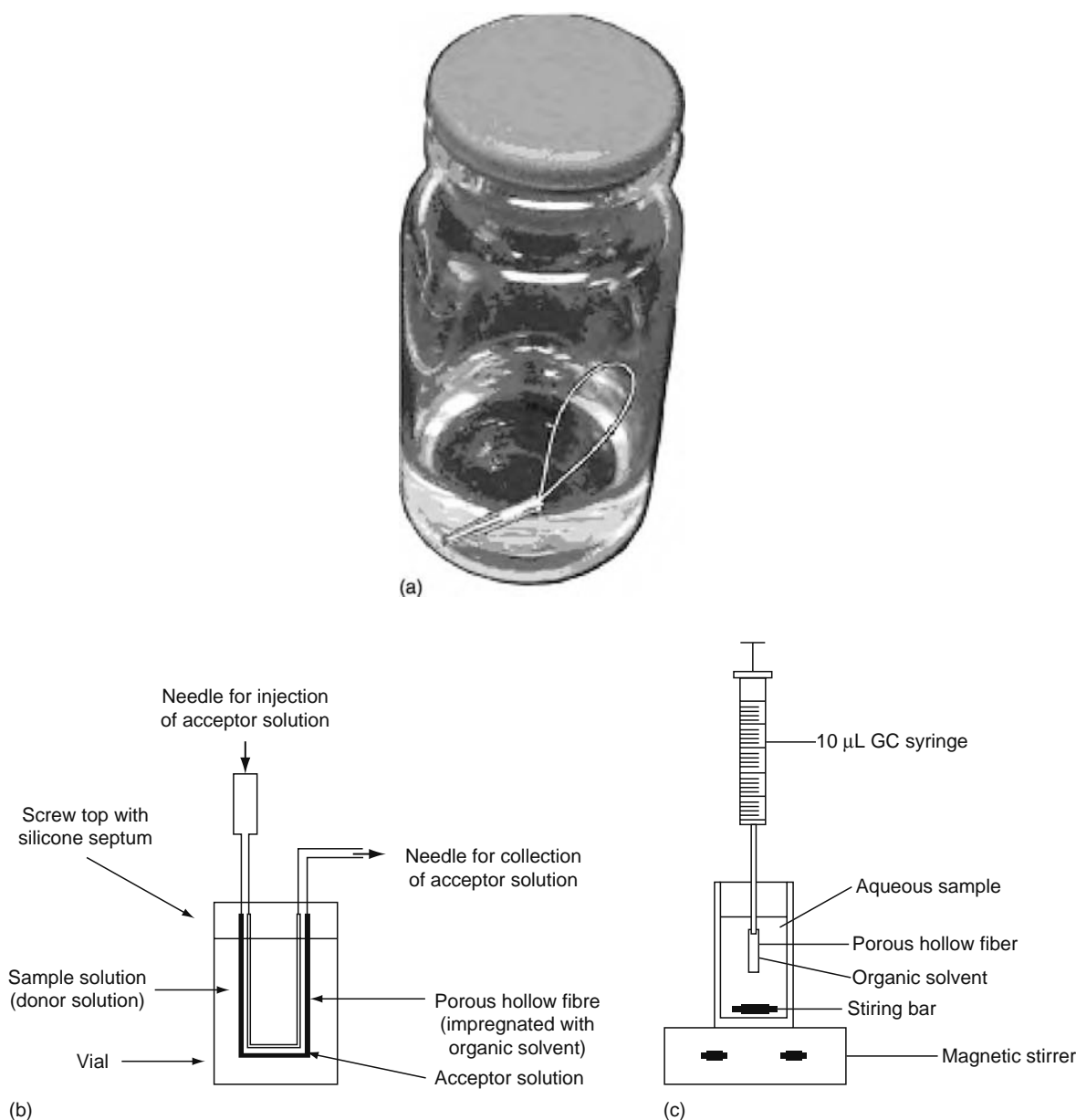


**FIGURE 12.2** Hollow-fiber devices for membrane extraction. (a) Hollow-fiber loops for equilibrium extraction redrawn after Liu et al. (From Liu, J.-F., Jönsson, J.Å., and Mayer, P., *Anal. Chem.*, 77, 4800, 2005.) (b) Liquid-phase microextraction after Pedersen-Bjergaard and Rasmussen. (From Grønhaug Halvorsen, T., Pedersen-Bjergaard, S., Reubsaet, J.L.E., and Rasmussen, K.E., *J. Sep. Sci.*, 24, 615, 2001. With permission.) (c) Syringe-based hollow fiber LPME. (From Zhao, L. and Lee, H.K., *Anal. Chem.*, 74, 2486, 2002. Copyright 2002 American Chemical Society. With permission.)

applications, however, the extraction is stopped well before the equilibrium is attained, as this often results in procedures that are more efficient in terms of time and convenience. In analytical chemistry, a usual aim of the sample preparation is to transfer (recover) as much of the analyte as possible from the donor to the acceptor to maximize sensitivity and minimize detection limits. This recovery can be improved in principally two ways: the acceptor can be continuously changed, or continuously flow past the membrane, so extracted molecules are removed from the membrane surface by convection. This typically leads to a dilution of the analyte. Alternatively, and more efficiently, the analyte molecules can be trapped in a static acceptor by a chemical reaction (e.g., dissociation) or by exploiting a high distribution coefficient. This usually leads to enrichment, and with an efficient trapping reaction there is a potential of obtaining very high enrichment factors.

To improve the overall amount of analyte that is extracted, a flowing donor is often used; i.e., the sample is pumped past the donor side of the membrane in a dynamic flow system. Also static systems with a stagnant donor are common, often with convective mixing by stirring.

This chapter mainly covers extraction systems with liquid membrane phases and trapping in the acceptor. Two- and three-phase systems are compared, as well as dynamic and static systems and flat versus hollow-fiber membrane materials. These types of systems have been successfully applied to a number of analyte and sample types and can be important alternatives to more orthodox approaches to sample preparation.

## 12.2 VARIANTS OF MEMBRANE EXTRACTION

A number of nonporous membrane techniques with different phase systems have been suggested for sample preparation in analytical chemistry. The main versions are summarized in Table 12.1 and described in the following sections.

### 12.2.1 LIQUID MEMBRANE EXTRACTION TECHNIQUES

In all liquid membrane extraction techniques, the membrane is an organic liquid, which is in contact with the aqueous sample. Analytes are extracted either by simple partitioning of uncharged species into the organic phase or by the action of some extractant, a compound present in the membrane liquid which can form complexes with the analyte, thereby facilitating its transport into the membrane liquid. So far, this is in principle the same as classical LLE. The difference between the various liquid membrane extraction techniques refers mainly to the acceptor side of the membrane.

#### 12.2.1.1 Three-Phase Liquid Membrane Extraction

With three-phase liquid membrane extraction techniques, there is a stagnant aqueous acceptor phase, constantly in contact with the liquid membrane, and the analytes are, after travelling through the membrane, transferred to the aqueous acceptor phase. The composition of the acceptor phase is such that the analyte molecules, after entering the acceptor phase become non-extractable, for example by pH changes (for acids or bases) or by some complexation reactions. This is referred to as trapping and it results in a transport of analyte molecules from the donor to the acceptor phase, which after the extraction can be transferred to an analytical instrument, either manually or online by a flow system. Trapping is crucial for the success of the three-phase liquid membrane extraction. By means of suitably selected acceptor conditions, it is possible to tune the mass transfer process and to obtain the desired selectivity and degree of enrichment for a number of useful applications.

##### 12.2.1.1.1 Supported Liquid Membrane Extraction

In SLM extraction, the most widely applied type of three-phase membrane extraction, the membrane consists of an organic solvent, which is held by capillary forces in the pores of a hydrophobic porous membrane supporting the membrane liquid. Such membrane support can be either flat porous PTFE or polypropylene membrane sheet or porous polypropylene hollow fibers. Typical solvents are long-chain hydrocarbons like *n*-undecane or kerosene and more polar compounds like dihexyl ether, dioctyl phosphate, and others. Various additives can increase the efficiency of extraction considerably. The stability of the membrane depends on the solubility and volatility of the organic liquids, and it is generally possible to obtain membrane preparations that are stable up to several weeks.

**TABLE 12.1**  
**Different Types of Membrane Extraction**

Generic Name	Names Used	Abbreviation	References <sup>a</sup>
Three-phase liquid membrane extraction aq/org/aq	Supported liquid membrane extraction	SLM	[6,85]
	Three-phase liquid phase microextraction	LPME3	
	Continuous-flow liquid membrane extraction	CFLME	[79]
Two-phase liquid membrane extraction aq/org/org (org/org/aq)	Microporous membrane liquid-liquid extraction	MMLLE	[6,86]
	Two-phase liquid phase microextraction	LPME2	
Three-phase solid membrane extraction	Polymeric membrane extraction	PME	[41]
	Aq/polymer/aq or org/polymer/aq or aq/polymer/org		
	Membrane extraction with a sorbent interface gas/polymer/gas or liquid/polymer/gas	MESI	[81,87]

<sup>a</sup> First reference for analytical sample preparation, recent review.

### 12.2.1.1.2 *Nonsupported Liquid Membrane Extraction*

In addition to SLM, which is the most commonly used three-phase extraction principle, at least in analytical chemistry, also other ways of placing an organic phase between two aqueous phases are known. In the classical bulk liquid membrane (BLM) setups, U-tubes or similar devices are used to confine bulk volumes of organic liquids between two aqueous phases. This type of devices is very little used for sample preparation in analytical chemistry, as the extraction process becomes slow and the enrichment factors possible are very limited.

Some devices, which permit the stacking of an aqueous acceptor phase above an organic liquid above an aqueous donor phase, have been described [36–38]. Such systems are of course inherently physically unstable, especially when stirring, but some success with such principles has been shown.

A liquid membrane configuration, which is much used for technical applications, is the emulsion liquid membrane (ELM) systems where the acceptor phase is dispersed as a colloid phase, each colloid drop surrounded by a thin organic, surface active phase. This principle does not seem to have been used for analytical sample preparation, probably due to the difficulty of quantitatively recovering the dispersed acceptor phase.

### 12.2.1.2 **Two-Phase Liquid Membrane Extraction Systems**

Two-phase liquid membrane extraction systems can be seen as a variant of SLM, where both the membrane (located in the pores of a hydrophobic porous membrane support) and the acceptor phases consist of an organic solvent. This is mainly suitable for hydrophobic analytes that are non-dissociable and non-charged. These compounds are easily extracted from water to an organic solvent, but they cannot be back-extracted into a second aqueous phase as required by the SLM approach.

This is chemically the same principle as for conventional LLE, but can be performed in a flow system, which permits easy automation and interfacing to analytical instruments. The technique is most easily interfaced to gas chromatography (GC) or to normal-phase high performance liquid chromatography (NP-HPLC), as the extract ends up in an organic phase. In principle, the membrane could also be hydrophilic, which would lead to an aqueous phase in the membrane pores. This seems not yet to have been tried for analytical purposes.

LLE in a flow system (in the form of flow injection analysis) has been described many times as reviewed by Valcárcel and Luque de Casto [39], but then the organic and aqueous phases are mixed in the same flow channel and later separated. The practical problems with the phase separation seem to have prevented this technique to be widely used. Applying a membrane, the phases are never mixed and all mass transfer between the phases takes place at the membrane surface.

As with three-phase membrane extraction, it is also possible here to work either with flat membranes, or with hollow-fiber membranes. In the first case, the technique is usually called microporous membrane liquid–liquid extraction (MMLLE), a name originating from Cussler [40]. With hollow fibers, it can be called two-phase liquid phase microextraction.

With two-phase liquid membrane extraction as with classical LLE, the extraction efficiency is limited by the partition coefficient. If this is very high, it is possible to work with a stagnant acceptor and still obtain a considerable enrichment into a small extract volume. With smaller partition coefficients, it might be necessary to arrange the acceptor phase to move with a slow flow rate to successively remove the extracted analyte and maintain the diffusion through the membrane. This will then lead to a lower degree of enrichment. The situation is similar to that for dialysis, and various focusing approaches can be applied to improve it, such as an SPE column or a retention gap.

## 12.2.2 **SOLID (POLYMERIC) MEMBRANE EXTRACTION TECHNIQUES**

A number of applications with polymeric membranes have been described. The most commonly used membrane material is silicon rubber or polyethylene. The possibility for both aq/polymer/aq extraction (including trapping in the acceptor, very similar to SLM extraction) and also, e.g., aq/polymer/org extraction (similar to MMLLE) has been demonstrated.

Melcher [41–43] first described both these principles in cylindrical configurations, utilizing thin silicone tubes in flow systems. More recently, Hauser et al [44] introduced the principle of MASE (membrane-assisted solvent extraction), which comprises a polypropylene bag in an autosampler vial with an organic solvent inside the bag. This device is commercialized by Gerstel (Mülheim an der Ruhr, Germany).

In the aq/polymer/org situation, the organic solvent typically penetrates the polymer causing it to swell considerably, and the situation is very similar to that of MMLLE. With a fixed composition of the membrane, the possibilities for chemical tuning (such as application of carriers) of the separation process are greatly reduced compared to SLM extraction or MMLLE. Also, as diffusion coefficients in polymers are lower than in liquids, the mass transfer is slower, leading to slower extractions. On the other hand, as the membrane is virtually insoluble, any combination of aqueous and organic liquids can be used, and the entire system becomes very stable.

## 12.3 THEORY AND PRINCIPLES OF MEMBRANE EXTRACTION

### 12.3.1 PRINCIPLES OF SLM

An SLM extraction can be seen as a combination of extraction into an organic solvent followed by a back-extraction into a second aqueous phase. However, as these two extraction steps occur simultaneously, the mass transfer kinetics will be different, and generally more efficient, compared to the situation when the steps are performed in sequence in separation funnels. The general mass transfer theory for SLM extraction in flow systems has been described in detail [45], with some additional aspects described more recently [46].

The rate of mass transfer from donor to acceptor (in any membrane extraction system) is proportional to the concentration difference,  $\Delta C$ , of the diffusing species over the membrane, which can be written

$$\Delta C = C_D - \frac{1}{D} C_A \quad (12.1)$$

where

$C_D$  and  $C_A$  are the total concentrations in the donor and acceptor phase, respectively  
 $D$  is the distribution constant between the acceptor and the donor phases

In SLM,  $D$  is given by the following expression:

$$D = \frac{C_A}{C_D} = \frac{\alpha_D K_D}{\alpha_A K_A} \quad (12.2)$$

where

$\alpha_D$  and  $\alpha_A$  are the fractions of the analytes that are in extractable (usually uncharged) form in the indicated phase  
 $K_A$  and  $K_D$  are the acceptor/membrane and donor/membrane partition coefficients (i.e., pertaining to the uncharged form only), respectively

Note that in many cases it will be a good approximation that  $K_A = K_D$  as both the donor and acceptor phases are aqueous, and deviations from this equality will be mainly due to ionic strength effects. Thus, the main influence in determining the value of  $D$  will be shown by the  $\alpha$ -values, which, for example, for acids or bases can easily be varied over many orders of magnitude by selecting suitable pH values. Often, the extraction conditions are setup so that  $\alpha_D$  is close to 1 and  $\alpha_A$  is a very small value.  $C_A$  is zero from the beginning of the extraction and increases successively, usually to values well over  $C_D$ . The maximum enrichment factor, which is reached when there is a thermodynamic equilibrium between all phases, is equal to  $D$  as in Equation 12.2. In contrast to the conditions for classical LLE and also MMLLE, high partition coefficients are not essential for high enrichment factors in SLM extraction.

The rate at which the equilibrium conditions are approached depends on many parameters, as detailed elsewhere [45] for systems with flowing donor and stagnant acceptor. Briefly, two situations can be distinguished: membrane-controlled extraction and donor-controlled extraction. In the first case, the rate-limiting step is the diffusion of the analyte compound through the membrane. The mass transfer coefficient  $k_M$  is then proportional to  $K_D \cdot D_M/h_M$ , where  $D_M$  is the diffusion coefficient in the membrane and  $h_M$  is the thickness of the membrane.

With donor-controlled conditions, typically, a considerably higher mass transfer rate can be obtained. It is then limited by the diffusion in the donor phase and thus depends on the diffusion coefficient in the donor phase,  $D_D$ , and on the donor convection (flow, stirring, etc.) conditions. As a rule of thumb, the donor-controlled extraction conditions prevail when  $K_D$  is larger than about 10, while the mass transfer is mainly membrane-controlled when  $K_D < 1$ . It is found that the value of the partition coefficient has no large influence on the efficiency of extraction or the enrichment factors that can be obtained, as long as it is reasonably large. On the other hand, the rate at which equilibrium is reached will be influenced by the partition coefficients. Further, there are observations that too large partition coefficients are not favorable, as the transfer of analyte out of the membrane into the acceptor phase in those cases may become less efficient.

### 12.3.2 CHEMISTRY OF SLM EXTRACTION

For SLM extraction a number of chemical principles can be used, which can be summarized according to Table 12.2 and detailed below.

**TABLE 12.2**  
**Schematic Overview of Different Chemical Principles for Extraction and Trapping Used for SLM Extraction**

Analytes	Donor	Membrane	Acceptor	Transported Species	Trapping	References
<i>Simple permeation</i>						
Acids	Acidic	Org (+TOPO)	Basic	Neutral	Anions	[6,88]
Bases	Basic	Org	Acidic	Neutral	Cations	[6]
<i>Carrier-mediated transport</i>						
Metal ions	8-Hydroxy-quinoline	Org	DTPA	Complexes	Charged complexes	[50]
Metal ions, amino acids	Acidic, pH = 3	DEHPA	Acidic, pH = 0	Complexes	Counter transport of H+	[57]
Amino acids, amino phosphonates	Basic	Triocylmethyl ammonium	Acidic, chloride	Ion pairs	Cations	[52,89–91]
Amino acids	Basic	Pd-complex	Acid	Complexes	Cations	[92,93]
Sugars, diol-containing compounds	Neutral	Boronic acid carrier	Acid	Covalently bound complexes	Protonation of carrier	[94,95]
Anionic surfactants	Acidic + amine	Org	Basic	Ion pairs	Deprotonation of amine carrier	[59]
<i>Immunological trapping</i>						
Triazine herbicides	Neutral	Org	Atrazine antibodies	Permeation	Immunological as antigen–antibody complex	[60]

Note: Abbreviations: TOPO, trioctylphosphine oxide; DTPA, diethylenetriaminepentaacetic acid; DEHPA, diethylhexylphosphoric acid.

### 12.3.2.1 Simple Permeation—Acids and Bases

Many applications of SLM extraction in analytical chemistry concern the extraction of acids or bases. Here, the basic principle is that uncharged species can be extracted from an aqueous phase into an organic solvent phase, while the charged species stay in the aqueous phase. This principle is well known from classical LLE, where it is a common practice to extract acids from acidic samples, and back-extract the acids into a second alkaline aqueous phase, using solvents like hexane, diethyl ether, etc.

For an acidic analyte HA, the alpha-factors mentioned above will take the following form:

$$\alpha = \frac{[\text{AH}]}{[\text{A}^-][\text{AH}]} = \frac{1}{1 + 10^{(\text{pH} - \text{p}K_a)}} \quad (12.3)$$

and for a basic analyte B

$$\alpha = \frac{[\text{B}]}{[\text{B}][\text{BH}^+]} = \frac{1}{1 + 10^{-(\text{pH} - \text{p}K_a)}} \quad (12.4)$$

where

$\text{p}K_a$  refers to the dissociation constant

$\text{pH}$  refers to either the donor or acceptor phase

From Equations 12.2 through 12.4, the expression for the overall distribution constant at equilibrium for the extraction from the donor to the acceptor is obtained:

$$D = \frac{C_A}{C_D} = \frac{\alpha_D K_D}{\alpha_A K_A} = \frac{(1 + 10^{s(\text{pH}_A - \text{p}K_a)})}{1 + 10^{s(\text{pH}_D - \text{p}K_a)}} \frac{K_D}{K_A} \quad (12.5)$$

where  $s = 1$  for acids and  $s = -1$  for bases, and as mentioned above, usually  $K_A \approx K_D$ .

Knowing the  $\text{p}K_a$  and the  $\text{pH}$  of the phases, it is easy to calculate the overall distribution constant and thus the maximum enrichment factor possible for SLM extraction of acids or bases with simple permeation.

### 12.3.2.2 Carrier-Mediated Transport—Metals and Organic Ions

Ion-pairing or chelating reagents can be added to the donor phase, which permits SLM extraction of various metal ions. Different carrier molecules or ions can be incorporated in the membrane phase to enhance selectivity and mass transfer. Various trapping reagents in the acceptor phase prevent analytes to be extracted back into the membrane. There are several reviews in this field [47–49].

As an analytical example of an addition of a reagent to the donor phase, extraction of metals from solutions containing a complex former as 8-hydroxyquinoline can be mentioned. This reagent forms extractable complexes with many metals [50]. See Figure 12.3a. The complex will be transported through the membrane and the extracted analyte is trapped in the acceptor by another ligand, in this case DTPA (diethylenetriaminepentaacetic acid), which forms a stronger complex which is charged and therefore non-extractable.

A carrier can be added to the membrane phase in several ways. A common compound is Aliquat-336 (methyltriocetyl-ammonium chloride). This is a tertiary ammonium ion, i.e., permanently positively charged in ion pair with chloride and can thus be added to a suitable membrane solvent. After addition of thiocyanate ions to the donor, a negatively charged metal-thiocyanate complex is formed in the donor and can be extracted as ion pair with the Aliquat-336 cation. It was used for extraction of Cu, Cd, Co, Zn [49] and for chromate [51]. The metal ion is subsequently trapped in the acceptor using DTPA as described above and shown in Figure 12.3b.

Analogous principles have been used to extract organic compounds, for example, amino acids [52] and peptides [53,54]. In a basic donor, the extracted compounds are anionic, and thus easily transported through the membrane by the cationic carrier to the acidic acceptor, where the analytes become cationic, and thus non-extractable.

Another commonly used extraction reagent for metal ions is diethylhexyl phosphoric acid (DEHPA) [55,56]. See Figure 12.3c. In this case a pH gradient must exist over the membrane, so the acceptor is kept more acidic than the donor (typically  $\text{pH} \approx 1$  and  $\text{pH} \approx 3$ , respectively). Speciation of different chromium species (chromate and chromium ion) has been performed by the combination of two membrane extraction systems, one working with DEHPA for extraction of  $\text{Cr}^{3+}$  and the other with Aliquat-336 for extraction of the chromate anions [51]. Using the same principles, also organic compounds, such as amino acids [57] and polyamines [58], can be extracted.

### 12.3.3 ANALYTE TRAPPING IN SLM

To reach a concentration enrichment using SLM for the purpose of sample pre-treatment for chemical analysis, the concept of trapping is imperative. It is necessary that the analyte, which has reached the acceptor phase, is in one way or the other

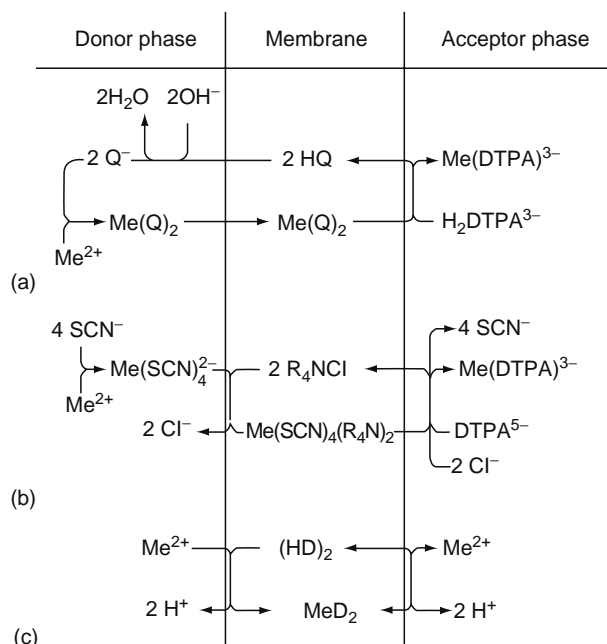


**FIGURE 12.3** Membrane extraction schemes of metal ions (Me). HQ, 8-hydroxyquinoline;  $\text{DTPA}^{5-}$ , diethylenetriaminepentaacetic acid anion;  $\text{R}_4\text{N}^+$ , methyltriocetyl ammonium cation; HD, diethylhexyl phosphoric acid. For a, b, and c, see the text.

prevented from diffusing back into the donor, so that a steady mass transfer of analyte, against a gradient of total analyte concentration, is maintained for sufficient time to permit a substantial concentration enrichment factor.

### 12.3.3.1 Direct Trapping

The simplest principle for analyte trapping was described above in Section 12.3.3. To perform enrichment of an acidic compound, the pH of the acceptor is held enough alkaline, so the main fraction of the acidic analyte becomes charged, and thus non-extractable in the acceptor. This is analogous with the principle of back-extraction in LLE, where an organic extract of an acidified sample is extracted with a second aqueous phase, to isolate acidic compounds. The principle of this type of direct trapping is described by Equations 12.3 through 12.5, showing the influence of pH on the extractability of acidic (or basic) compounds. If the donor pH is selected less than or equal to the  $pK_a$  and the acceptor  $pH > pK_a + 3.3$ , the distribution coefficient between acceptor and donor at equilibrium (Equation 12.5) will be about 2000, promising potentially very high concentration enrichment factors. This is termed “complete trapping.”

Extracting an acid from an acidic donor to a basic acceptor brings about a cotransport of protons through the membrane, eventually neutralizing the pH gradient, why it is imperative for good success that the buffer capacity of the acceptor is sufficient. Conversely, the extraction of a basic compound from a basic donor to an acidic acceptor will transport protons in the opposite direction.

Other variations of the principle to render the analyte non-extractable in the acceptor involve the use of complexing agents. These form charged complexes in the acceptor, preventing back-extraction. The use of DTPA for trapping of metal ions, as described above in Section 12.3.3, is a good example on this.

### 12.3.3.2 Indirect Trapping

In systems employing carrier-mediated transport of the analyte through the membrane, the analyte trapping can be made in a somewhat different way, where the transporting properties of the carrier are influenced, so it can transport the analyte from the donor to the acceptor, but not the other way. An example is the use of DEHPA, for metal extraction, where the carrier is anionic at donor conditions, permitting transport to the strongly acidic acceptor where the carrier is neutralized, preventing back-extraction of the analyte. Here is a counter-transport of protons because the pH gradient drives the extraction, while the analyte is in the same form both in the donor and in the acceptor.

There are other versions of a similar principle. For the extraction of anionic surfactants [59], which are permanently charged, trihexyl amine was used as a carrier. The carrier is added to the sample in the donor. In the acidic donor this amine is charged, and can form ion-pair with the analytes, while in the alkaline acceptor, the amine is neutralized, thus killing the ion-pair.

### 12.3.3.3 Immunological Trapping

To utilize the high degree of selectivity possible with biological recognition in sample preparation, SLM extraction was combined with immunologic recognition, both by using antibodies as trapping reagent in the acceptor, and exploiting the antibody–antigen complex in a flow immunoassay, both for successful determination of nitrophenol [60] and atrazine [61]. In a recent development utilizing magnetic beads with antibodies, simazine was determined in low concentrations [62].

## 12.3.4 MASS TRANSFER IN MMLLE

For two-phase liquid membrane extraction, (MMLLE), the basic principles are more simple than those for SLM, as there is only one phase boundary involved in the extraction, usually from an aqueous to an organic phase, which is chemically equivalent to LLE in a separatory funnel, etc. The extraction is driven by the difference in chemical potential of the analytes in organic solvent and in aqueous solution, which is described as a partition coefficient. In many cases, the octanol–water partition coefficient ( $\log K_{OW}$ ) is considered as estimates for the partition coefficient in MMLLE and LLE, even if the organic solvents used usually are other than octanol. The techniques work best for relatively nonpolar compounds, having values of  $\log K_{OW} > 3$ .

With obvious modifications, Equation 12.1 is valid also for MMLLE. The definition of the relevant distribution coefficient is different. For MMLLE it is

$$D = \frac{C_A}{C_D} = \alpha_D K_D \quad (12.6)$$

Here,  $K_D$  is the partition coefficient between the organic acceptor phase and the aqueous donor (sample) phase. For acidic or basic compounds  $\alpha_D$  is given by Equation 12.3 or 12.4, while for non-chargeable compounds  $\alpha_D = 1$ . Thus in MMLLE, the organic/aqueous partition coefficient directly governs the extraction.

### 12.3.5 DIFFERENCES BETWEEN MMLLE AND SLM

The MMLLE technique can be seen as a complement to the SLM extraction, permitting membrane-based extraction to be extended to further classes of compounds. Compared with SLM, MMLLE has the following characteristics:

- It is applicable to hydrophobic, preferably uncharged compounds, i.e., those that cannot be extracted with SLM.
- Maximum concentration enrichment possible is limited by the partition coefficient (Equation 12.11), whereas in SLM it is dependent on the degree of trapping (Equation 12.2), which can be influenced by controlling the pH of the different phases. Therefore, SLM provides more degrees of freedom by which the conditions of extraction can be tuned.
- Extract ends up in the organic solvent, not in water. Thus MMLLE is more easily interfaced to gas chromatography and NP-HPLC than to SLM, which is most compatible with reversed-phase HPLC.
- Hardware is identical or similar, so the possibilities for automation should be similar, considering the point above.

### 12.3.6 CONCENTRATION ENRICHMENT

One of the main purposes of membrane extraction in sample preparation is to enrich the analyte, i.e., to increase the concentration of the analyte to permit determination of low concentrations. Plotting the concentration of analyte in the acceptor ( $C_A$ ) either directly as determined by analysis of the acceptor phase or as a concentration enrichment factor  $E_e$  ( $C_A/C_S$ —where  $C_S$  is the initial concentration in the sample) versus time will typically produce a curve which initially raises approximately linearly and asymptotically eventually reaches a steady equilibrium value. See Figure 12.4 [46].

Assuming that the rate of mass transfer is proportional to the concentration difference over the membrane according to Equation 12.1 and noting that in static extraction, the concentration in the donor phase  $C_D$  decreases as analyte is transferred over the membrane. We get the following differential equation:

$$\frac{\partial C_A}{\partial t} = k \left( C_S - \left( \frac{V_A}{V_S} \frac{1}{D} \right) C_A \right) \quad (12.7)$$

where

$V_A$  and  $V_S$  are the volumes of the acceptor (strip) phase and the extracted sample, respectively

$C_S$  is the initial concentration in the sample ( $C_S V_S = C_D V_S + C_A V_A$ )

$D$  is the equilibrium distribution coefficient (see Equations 12.2, 12.5, and 12.6)

$k$  is a rate constant

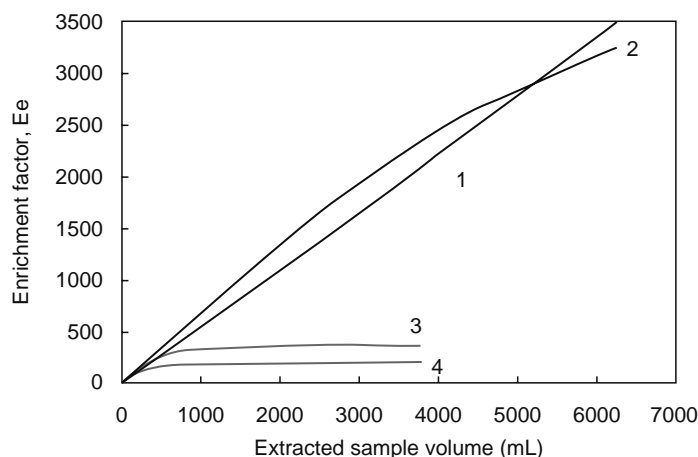


**FIGURE 12.4** Enrichment factors for various aniline compounds with different  $pK_a$  values and  $pH_A = 0$  ( $\alpha_D = 1$ ). (From Chimuka, L., Megersa, N., Norberg, J., Mathiasson, L., and Jönsson, J.Å., *Anal. Chem.*, 70, 3906, 1998. With permission.)

S.No.	Compound	$pK_a$	$\alpha_A$	$D$
1	Aniline	4.6	0.000025	40,000
2	3-Cl-4-Me-aniline	4.0	0.0001	10,000
3	3,5-di Cl-aniline	2.5	0.003	330
4	3-Me-5-nitroaniline	2.3	0.005	200

The general solution expressed as a concentration enrichment factor  $E_e$  is

$$E_e = \frac{C_A}{C_S} = \frac{1}{\left(\frac{V_A}{V_S} + \frac{1}{D}\right)} \left(1 - \exp\left[-k\left(\frac{V_A}{V_S} + \frac{1}{D}\right)t\right]\right) \quad (12.8)$$

The rate of mass transfer through the membrane is proportional to the gradient of this curve, and thus decreases from an initial value to practically zero. The concentration enrichment factor value at equilibrium will be

$$E_{e_{eq}} = \frac{1}{\left(\frac{V_A}{V_S} + \frac{1}{D}\right)} \quad (12.9)$$

Equations 12.7 through 12.9 are basically valid for static extraction. For extraction in a flow system with flowing donor and stagnant acceptor, the phase ratio ( $V_A/V_S$ ) is zero, as depletion of the sample is not possible.

There are several limiting cases for Equations 12.8 and 12.9.

1. With a large equilibrium distribution coefficient  $D$  (complete trapping) and a large phase ratio,  $E_e$  will increase linearly up to large values. In Figure 12.4, which refers to an SLM flow system experiment,  $D$  in curve 1 is approximately 10,000 and the enrichment factor is linear at least up to at least 3000 times. In many cases, especially in flow systems, the extraction is not allowed to go to equilibrium, and an extraction efficiency  $E$  is defined as the fraction of the total amount of analyte that is transferred to the acceptor. Thus

$$E = \frac{C_A}{C_S} \frac{V_A}{V_S}; \quad E_e = E \frac{V_S}{V_A} \quad (12.10)$$

The extraction efficiency is related to the slope of the extraction curve, so if the extraction is linear,  $E$  is constant and less than 100%. By careful calibration and keeping the experimental parameters constant so that the system is kinetically stable, repeatable values for  $E_e$  and  $E$  can be obtained. This will give reproducible quantitative results and most of the applications of membrane extraction to practical analyses are in fact based on this principle.

2. With a finite sample volume in static extraction mode under complete trapping conditions, the sample will eventually be depleted with regard to analyte, so a decrease of mass transfer is due to decrease of analyte concentration and the equilibrium occurs after virtually all analyte has been transferred to the acceptor. Equation 12.9 then leads to

$$E_{e_{eq}} \frac{V_S}{V_A}; \quad C_A = C_S \frac{V_S}{V_A}, \quad (12.11)$$

i.e., the enrichment factor is determined by the phase ratio.

Thus, if the extraction is continued until equilibrium so that the sample is totally depleted with analyte, very simple and straightforward calculations of the enrichment factor are possible, according to Equation 12.11, which contains no other parameters than the phase volumes. This can be the basis for accurate quantitative determinations.

3. The third limiting case of Equation 12.9 is the situation where equilibrium is attained without depletion of the analyte in the sample. It is treated below in Section 12.3.8.

### 12.3.7 SELECTIVITY

To obtain a high selectivity, i.e., discrimination between the analytes and various unwanted matrix compounds, membrane extraction has a clear advantage over other sample preparation techniques, as all compounds that reach the analytical instrument must travel through the membrane. There is no direct connection and possibility for transferring compounds into the analytical instrument in other ways. This is not the case with other extraction techniques. With SPE, SPME, etc., there is a definite possibility that matrix components are adsorbed on the sorbing phase and subsequently being eluted into the extract. With LLE, such a transfer is less probable and it is generally considered that extracts after LLE are cleaner. The possible and common problem of the formation of emulsions at the phase interface with LLE, which is avoided with all types of membrane extraction, is a source of contamination across the phase border.

Further, with SLM extraction, the pH of the donor solution and the acceptor phase can easily be fine-tuned to obtain extraction which is selective for certain groups of compounds, as described above. Alternatively, a carrier can be added in the membrane to increase the selectivity and mass transfer of the compounds of interest. When the primary aim of adding a carrier is to increase the mass transfer of the analytes by analyte-carrier interactions in the membrane, it is important to choose other conditions carefully so that selectivity is still retained.

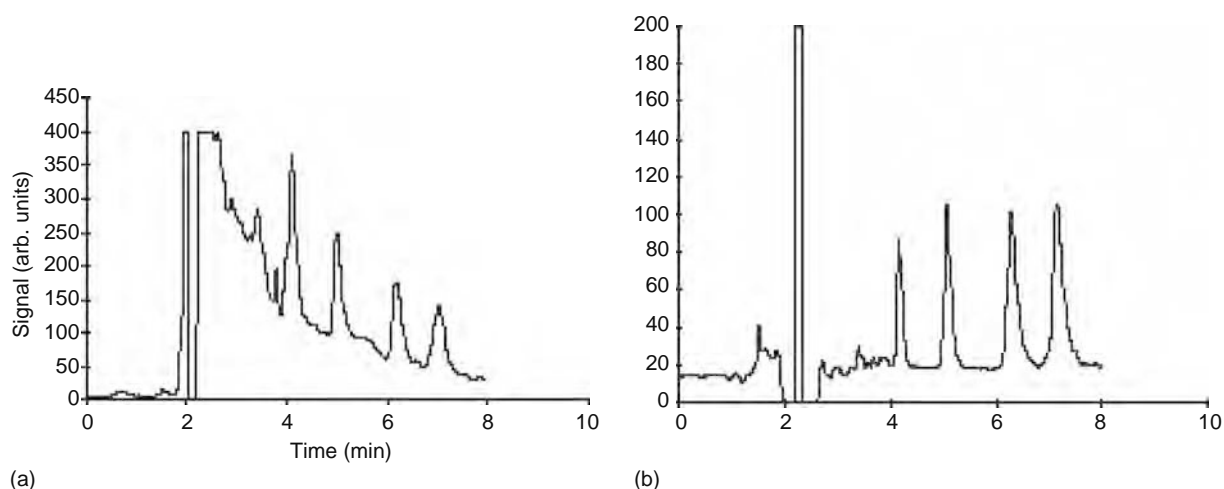


**FIGURE 12.5** Chromatograms (LC-UV) of methoxy-*s*-triazine herbicides (a) SPE of spiked river water (1.0 mg/L of each analyte) (b) SLM extraction of spiked river water (0.5 mg/L of each analyte). Peaks: 1 simetone; 2 atratone; 3 secbumetone; 4 terbumetone. (From Megersa, N., Solomon, T., and Jönsson, J.Å., *J. Chromatogr. A*, 830, 203, 1999. With permission.)

Membrane extraction is especially effective in discriminating toward macromolecules. In environmental analysis, macromolecular humic acids are ubiquitous and usually very efficiently removed. Megersa et al. [63] compared SLM and SPE of some triazine herbicides spiked in river water. As is seen from Figure 12.5, the difference is dramatic. Also, there are many examples of how various drugs can be determined in blood plasma and also urine without matrix interferences [25,64].

### 12.3.8 EQUILIBRIUM EXTRACTION

A somewhat different approach to analytical extraction involves selection of a relatively low value of  $D$  and a virtually infinite phase ratio ( $V_S \gg V_A$ ). With these conditions Equation 12.9 reduces to

$$Ee_{eq} = D \quad (12.12)$$

This is essentially the same as Equation 12.2. Curves 3 and 4 (and to some extent curve 2) in Figure 12.4 are illustrations to this. Experimentally, enrichment factors at equilibrium agree reasonably with calculated (Equation 12.5) values of  $D$  [32,46]. The concentration of analyte in the sample will not be influenced by the extraction, and this permits extraction and sampling without influencing speciation conditions in the sample. This is the basis for a novel sampling technique, called ESTM (equilibrium sampling through membranes) which is currently developed for the measurement of freely dissolved fractions of environmental pollutants (as distinguished from total concentrations). This parameter is of environmental interest, as it describes transport processes and biological activities better than total concentrations [65]. The ESTM principle is especially suitable for polar compounds and metals, in contrast to SPME-based methods [65], which are more suitable for nonpolar compounds. ESTM has been evaluated both with phenolic pollutants [32] and metal ions [66,67]. An analogous problem in pharmacology is the measurement of drug-protein binding, to which ESTM has been successfully applied [33,68].

## 12.4 APPARATUS FOR MEMBRANE EXTRACTION

### 12.4.1 STAND-ALONE EQUIPMENT

Simple and cheap membrane extraction flow systems for relatively large sample volumes can be built up around a peristaltic pump. An example of such a system is seen in Figure 12.6a. Here, the sample is pumped through the donor channel and the acceptor phase is manually removed by the use of a syringe after each extraction. Such systems have been used both for laboratory work [69,70] and for sampling in natural waters [71]. An tutorial for the operation of this type of devices has been published [8].

Hollow fiber devices working in flow systems are also known [34]. In those cases, either single fibers or bundles of fibers, perhaps in commercial cartridges, are employed and used in flow system configurations.

### 12.4.2 ONLINE CONNECTION TO CHROMATOGRAPHY

For online connection to HPLC, SLM is the preferred extraction technique, as the extract obtained is aqueous and therefore in principle compatible with HPLC. With large membrane units (channel volumes around 1 mL), direct transfer of the entire volume

of the acceptor phase to an HPLC can be arranged by a precolumn [72,73] to inject as much as possible of the extracted analyte. See Figure 12.6b. Such systems can be automated with pneumatically or electrically actuated valves controlled by timers or by computer systems. Smaller membrane channels can also be used. Then a heart-cut, which contains a major part of the extract, can be accommodated in the injection loop for direct injection into the HPLC column without a precolumn [41,74,75].

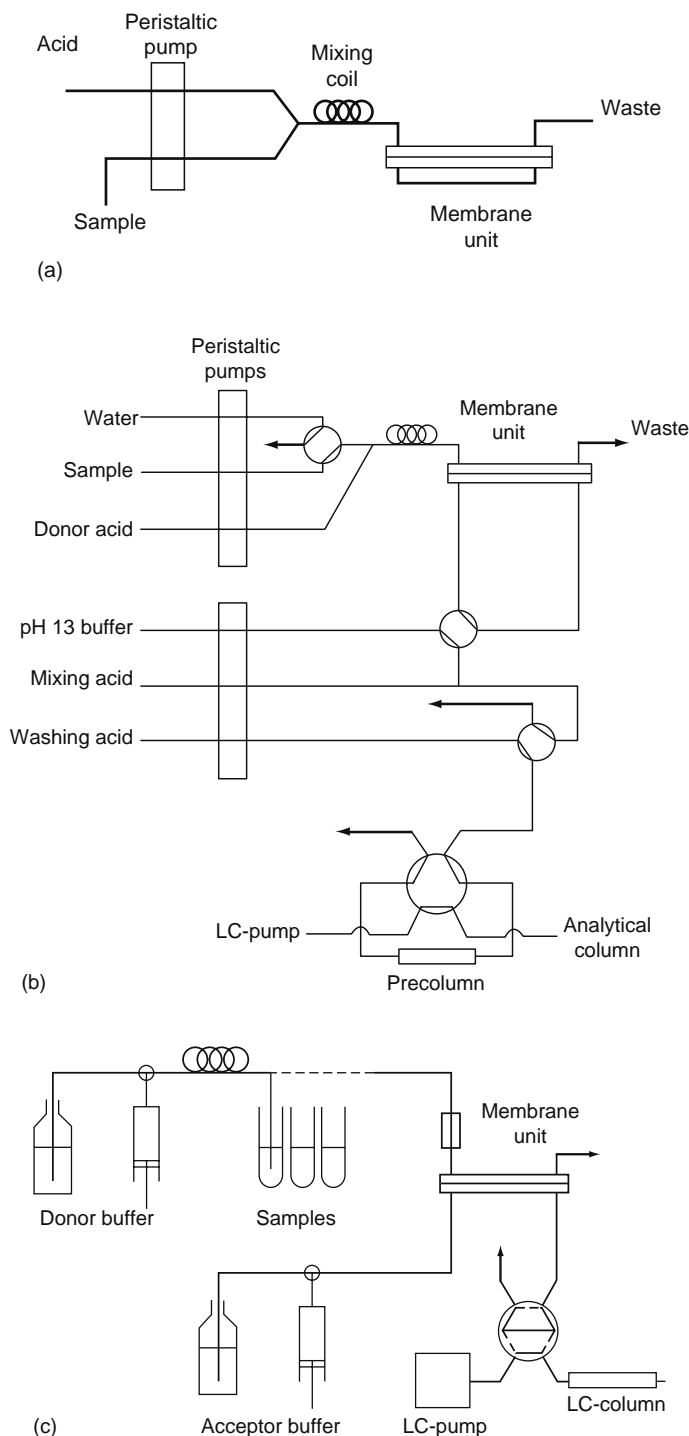


**FIGURE 12.6** Technical setups for membrane extraction. (a) Manual system, utilizing a peristaltic pump. (From Knutsson, M., Nilvé, G., Mathiasson, L., and Jönsson, J.Å., *J. Agric. Food Chem.*, 40, 2413, 1992. With permission.) (b) Automated setup with peristaltic pump and large (1 mL) channel volumes, connected on-line to HPLC. (From Nilvé, G., Knutsson, M., and Jönsson, J.Å., *J. Chromatogr. A*, 668, 75, 1994. With permission.) (c) Automated setup with syringe pumps and small (10  $\mu$ L) channel volumes connected on-line to HPLC. (From Lindegård, B., Björk, H., Jönsson, J.Å., Mathiasson, L., and Olsson, A.-M., *Anal. Chem.*, 66, 4490, 1994. With permission.)

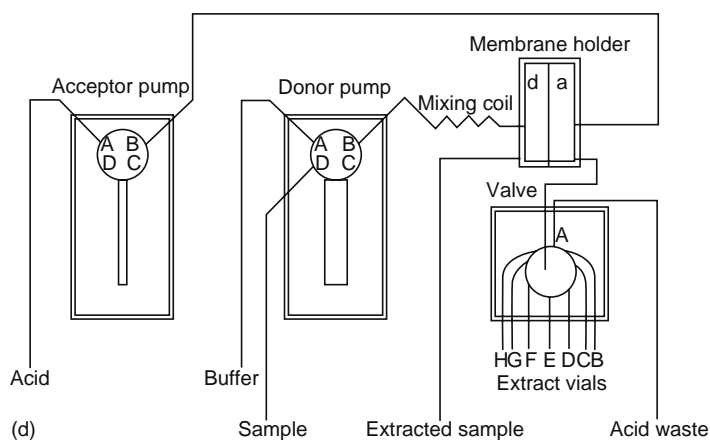


**FIGURE 12.6 (continued)** (d) Portable field sampler, based on syringe pumps. (From Larsson, N., Jönsson, J.Å., Megersa, N., and Berhanu, T., Portable and time integrating field sampling for continuous membrane extraction of *s*-triazine pesticides and their metabolites in a lake in agricultural region of Southern Ethiopia. Manuscript in preparation.)

For small samples (<1 mL) and small channel volumes, the liquid delivery precision of peristaltic pumps is not adequate and membrane extraction equipment based on syringe pumps connected to robotic liquid handlers can be applied [25,64]. A typical example is shown in Figure 12.6c. Here, a robotic needle connected to a syringe pump submits reagent to adjust the pH of samples in the vials, picks up an aliquot and passes it through the donor channel of a small membrane unit (channel volume around 10  $\mu\text{L}$ ). The entire extract collected in the acceptor channel is then transferred to an injection loop injector connected to the HPLC system in the usual manner. Thus, the entire extract from for example 1 mL sample ends up in one chromatographic injection. Typically, while one sample is chromatographed, the next sample is extracted, so the cycle time of the system is determined by the chromatogram time.

For gas chromatography, the most suitable membrane extraction technique is MMLLE. The organic acceptor is better compatible with GC than with HPLC, as are the analytes that are best extracted in such a system, i.e., relatively hydrophobic compounds. A new development is the ESy instrument (ESyTech AB, Lund, Sweden) [76–78] where an MMLLE extraction in microscale (1 mL extracted into a volume ca 1  $\mu\text{L}$ ) is automatically performed and the organic extract is directly injected into the GC by an injection needle, directly connected to the extraction cell. See Figure 12.7.

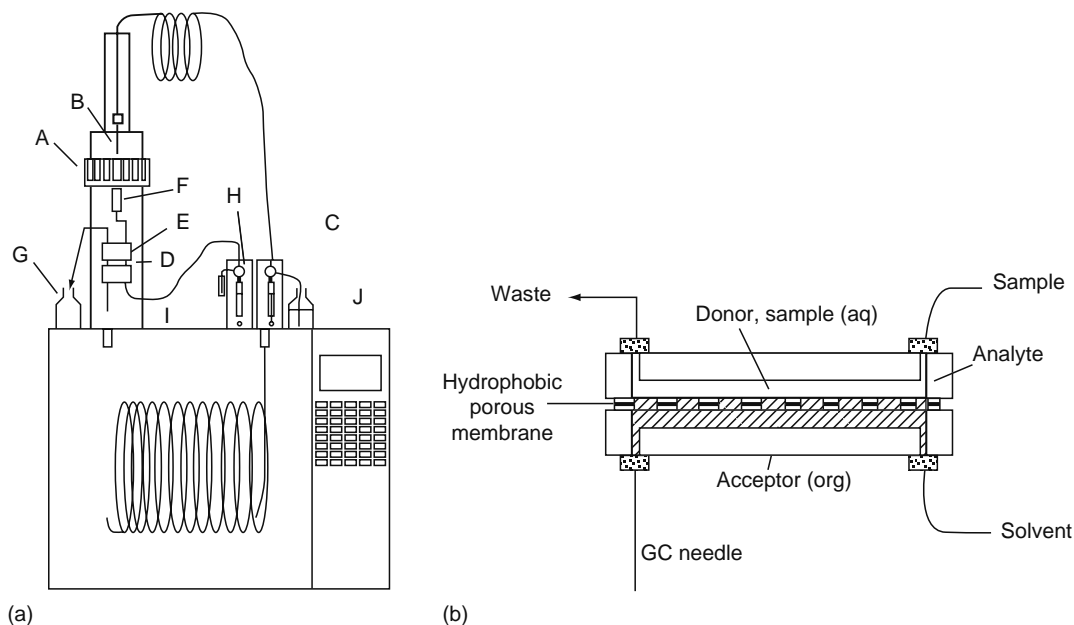


**FIGURE 12.7** Experimental setup for the ESy system. (From Barri, T., Bergström, S., Norberg, J., and Jönsson, J.Å., *Anal. Chem.*, 76, 1928, 2004. With permission.) (a) General setup (A, sample tray; B pipette; C, sample pump; D, membrane; E, extraction card; F, pipette port; G, waste; H, solvent pump; I, needle; J, washing solution) and (b) ESy extraction card with 1.65  $\mu\text{L}$  acceptor and donor channels.

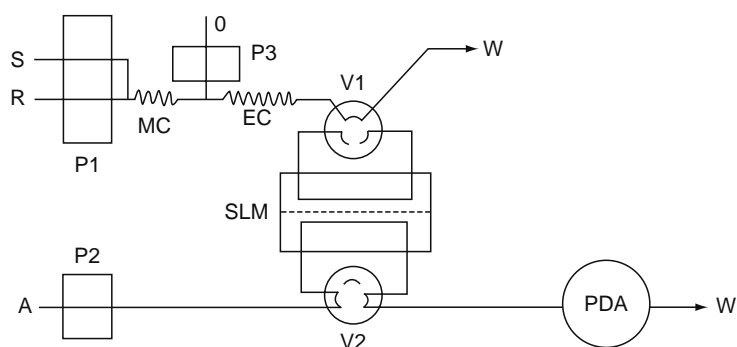


**FIGURE 12.8** Schematic diagram of the CFLME system. (From Liu, J.-F., Chao, J.-B., and Jiang, G.-B., *Anal. Chim. Acta*, 455, 93, 2002. With permission.) S, sample solution; R, 0.5 M sulfuric acid; O, organic solvent; A, acceptor; W, waste; P1, P2, peristaltic pumps; P3, piston pump; MC, mixing coil; EC, extraction coil; V1, V2, 6-port valves; SLM, SLM device; PDA, detector, 240 nm.

### 12.4.3 CONTINUOUS FLOW LIQUID MEMBRANE EXTRACTION

By combining continuous flow LLE and SLM extraction, a novel aqueous–aqueous extraction technique termed continuous flow liquid membrane extraction (CFLME) was developed for trace-enrichment [79]. The setup is shown in Figure 12.8. The aqueous sample is mixed with an organic solvent in a flow system, and the analyte is extracted into the organic phase. This is then transported to the liquid membrane formed in the microporous membrane of the SLM equipment. Finally, it is transferred through the liquid membrane and is trapped by the acceptor. Chemically, this is a three-phase extraction system, analogous to SLM, but it overcomes a disadvantage of SLM, as it is possible to use also relatively volatile and also polar solvents with this principle. On the other hand, it involves a more technically complex arrangement, and it typically requires more solvent (although still very little) than SLM.

### 12.4.4 MEMBRANE EXTRACTION WITH A SORBENT INTERFACE

The techniques mentioned above are all characterized by liquid donor and acceptor phases. However, a gaseous acceptor phase is also possible, and that would be the most convenient and compatible arrangement for direct connection with gas chromatography. This is realized with the membrane extraction with a sorbent interface (MESI) technique [80–82]. MESI can be used for either gaseous or aqueous samples and the equipment employs a membrane module with a (usually) silicone rubber hollow fiber, into which the analytes are extracted from the surrounding liquid or gaseous sample. The carrier gas of a gas chromatograph flows inside the fiber and transports the analyte molecules as they are extracted from the membrane into a cooled sorbent trap where they are trapped. The analytes are subsequently desorbed from the sorbent trap by heating and are transferred to GC analysis.

In Figure 12.9, a typical MESI setup is shown. Sampling can also be made off-line with the extraction module and sorbent trap in, for example, field sampling and the sorbent trap can later be connected to the GC and desorbed in a separate step. Matz [83] recently presented and compared this and a few other variants.

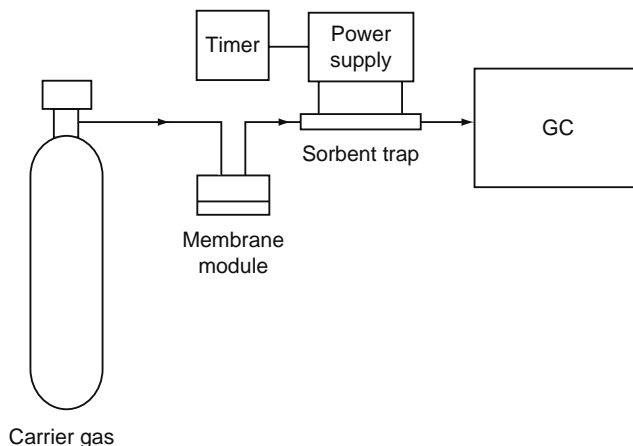


**FIGURE 12.9** Schematic of the MESI system. (From Segal, A., Górecki, T., Mussche, P., Lips, J., and Pawliszyn, J., *J. Chromatogr. A*, 873, 13, 2000. With permission.)

### 12.4.5 FIELD SAMPLING APPARATUS

Simple flow systems comprising flat membrane devices and a peristaltic pump were used for field sampling in natural waters [71] and also for sampling of nutrient solutions for soil-free (hydroponics) growing in greenhouses [70].

A portable sampler (Figure 12.6d) based on syringe pumps and powered by batteries and solar power was recently constructed and used for sampling of triazine herbicides in Ethiopian lakes [84].

## 12.5 APPLICATIONS

Over the last decade, a large number of applications to membrane extraction have been presented. In Tables 12.3 through 12.5, incomplete listings of such applications are presented, divided into environmental, biomedical, and other (mainly industrial) applications. The wide variety of analytes and sample types shows that membrane extraction is very versatile and is an useful tool for the analytical chemist.

**TABLE 12.3**  
**Environmental Applications of Membrane Extraction**

Analytes	Matrices	Membrane Technique	Analytical Technique	References
Metals	Water	SLM	AAS, electrochem	[50,51,55,66,96–106] [101]
Metals	Water	SLM (ESTM)	AAS, Spek	[66,67]
Phenoxy acids	Water	SLM	HPLC	[71,107]
Sulfonylurea herbicides	Water	SLM	HPLC	[73]
Phenolics	Water, nutrient solutions	SLM; LPME3	HPLC	[69,70,72] [108]
Phenolics	Water	LPME3 (ESTM)	HPLC	[32]
Carboxylic acids	Soil liquid, Air	SLM	IC	[74,109,110]
Anilines	Water	SLM	HPLC	[111]
Anionic surfactants	Water	SLM	HPLC	[59]
Glyphosate	Water	SLM	CE	[90,112]
Triazine herbicides	Water	SLM	HPLC	[63,113–116] [117]
Herbicides	Water	SLM	HPLC	[118]
Aliphatic amines	Air (impinger samples)	SLM (gas)	GC	[119,120]
Carboxylic acids	Air (impinger samples)	SLM	IC	[121]
Fungicides	Water	SLM, MMLLE	HPLC	[122,123]
PAH	Soil	MMLLE	GC	[124,125]
PCB	Water	MMLLE (ESy)	GC	[77]
Amines	Water	MMLLE	CE	[126]
Nonylphenol, etc.	Water	MMLLE	HPLC	[127]
Triazine herbicides	Water	MMLLE	FIA	[128]
Cationic surfactants	Water	MMLLE	HPLC	[129]
Semi-volatile organics	Water	PME	HPLC	[130–132] [42]
Organics	Water	PME (MASE)	GC/MS	[44,133–135]
Volatile organics	Water, air	MESI	GC	[82,136–140]
Phenols, sulfonylureas	Water	CFLME	HPLC, CE	[141–146]
Amines	Water	LPME3	HPLC	[147]
Drugs	Water	LPME3	CE, LC/MS	[148–150]
Phenoxy acid herbicides	Milk	LPME3	HPLC	[151]
Triazine herbicides	Water	LPME2	GC/MS	[152]
Phthalate esters	Water	LPME2	GC/MS	[153]
Pesticides	Water	LPME2	GC/MS	[154–156]
Drugs	Water	LPME2	GC/MS	[157]
Vinclozoline	Water, soil	LPME2	GC	[158]
PAH	Soil	LPME2	GC	[159]
Explosives	Water	LPME2	GC	[160]

*Note:* SLM, supported liquid membrane (aq/org/aq); MMLLE, microporous membrane liquid–liquid extraction (aq/org); PME, polymer membrane extraction (aq/polymer/org); MESI, membrane extraction with sorbent interface (aq (or gas)/polymer/gas/sorbent); CFLME, continuous flow liquid membrane extraction (aq/org (in flow)/aq); LPME2, two-phase liquid phase microextraction in hollow fibers (aq/org); LPME3, three-phase liquid phase microextraction in hollow fibers (aq/org/aq).

**TABLE 12.4**  
**Applications of Membrane Extraction to Biological Samples**

Analytes	Matrices	Membrane Technique	Analytical Technique	References
Aliphatic amines	Urine	SLM	GC	[161]
Aliphatic acids	Manure	SLM	GC	[162]
Aliphatic amines	Blood plasma	SLM	GC	[163]
Amperozide	Blood plasma	SLM	HPLC	[25]
Bambuterol	Blood plasma	SLM	CE	[164–166]
Bambuterol	Blood plasma	SLM	LC-CE	[167]
Diprivan (Propofol)	Urine	SLM	HPLC	[168]
Phenols	Blood plasma	SLM	HPLC-biosensor	[169]
Peptides	Blood plasma	SLM	HPLC	[54]
Drugs	Blood plasma	SLM (ESTM) LPME3 (ESTM)	HPLC	[33,68]
Lead	Urine	SLM	AAS	[56]
Lead	Urine	SLM	PSA	[170]
Local anesthetics	Blood plasma	SLM	GC	[86]
Local anesthetics	Blood plasma	MMLLE	GC	[171]
Amphetamine	Blood plasma, urine	LPME3 (LLLME)	CE	[26]
Amphetamines, benzodiazepines, naproxen, citalopram	Blood plasma, urine	LPME2, LPME3	HPLC, GC, CE	[172]
Benzodiazepines	Blood plasma, urine	LPME2	GC	[173]
Ibuprofen, naproxen, ketoprofen	Urine	LPME3	CE	[174]
Metabolites of Ropivacaine	Urine	SLM	HPLC	[64]
Citalopram and metabolites	Blood plasma	LPME3	CE	[175]
Amphetamines	Blood, urine	LPME3	FIA-MS/MS	[27]
Organophosphate esters	Blood plasma	MMLLE	GC-MS	[176]
Sulfonylurea drugs	Blood plasma	PME (off-line)	LC-MS/MS	[177]
Amphetamine	Urine	SLM	HPLC	[178]
Benimidazole anthelmintics	Urine, tissue, milk	SLM	HPLC, LC-MS	[179]

*Note:* Abbreviations as in Table 12.3.

**TABLE 12.5**  
**Various Applications of Membrane Extraction in Chemical Analysis of Industrial and Food Samples**

Analytes	Matrices	Membrane Techniques	Analytical Techniques	References
Phenols	Kerosene, naphtha	PME	FIA	[180]
Triazine herbicides	Cooking oil	MMLLE	FIA, HPLC	[181]
Phenols	Crude oil	PME	HPLC	[182]
Phenols	Gasoline, kerosene	PME	HPLC	[183]
Phenols	Crude oil, fuels	PME	HPLC	[184]
Vitamin E	Butter	PME	HPLC	[75]
Nicotine	Snuff	SLM (solid sample)	UV	[185]
Caffeine	Coffee, tea	SLM (solid sample)	UV	[186]
Pesticides	Eggs	PME	HPLC	[187]
Vanillin	Various food	SLM (solid sample)	Amperometric	[188]
Anionic surfactants	Detergents	MMLLE	FIA	[189]
Phenols	Pyrolysis oil	MMLLE	LC-LC	[190]
Biogenic amines	Wine	SLM	HPLC	[58]

*Note:* Abbreviations as in Table 12.3.

## ACKNOWLEDGMENTS

During recent years, the membrane extraction work at Lund University was supported by grants from the Swedish Science Research Council (VR), the Foundation for Strategic Environmental Research (Mistra), the Swedish Institute (SI), the Swedish International Development Co-operation Agency (SIDA), the Crafoord Foundation, and the Wenner-Gren Foundation. The work would not have been possible without a number of colleagues, especially Professor Lennart Mathiasson, several graduate and undergraduate students, as well as postdoctoral fellows and other guest researchers.

## REFERENCES

1. Jönsson JÅ and Mathiasson L. Supported liquid membrane technique for sample preparation and enrichment in environmental and biological analysis. *Trends Anal. Chem.* 1992; 11:106–114.
2. Jönsson JÅ and Mathiasson L. Liquid membrane extraction in analytical sample preparation. I. Principles. *Trends Anal. Chem.* 1999; 18:318–325.
3. Jönsson JÅ and Mathiasson L. Liquid membrane extraction in analytical sample preparation. II. Applications. *Trends Anal. Chem.* 1999; 18:325–334.
4. Garcia Pinto C, Fernández Laespada E, Pérez Pavón JL, and Moreno Cordero B. Review. Analytical applications of separation techniques through membranes. *Lab. Autom. Inform. Managem.* 1999; 34:115–130.
5. Moreno Cordero B, Pérez Pavón JL, García Pinto C, Fernández Laespada E, Carabias Martínez R, and Rodríguez Gonzalo E. Analytical applications of membrane extraction in chromatography and electrophoresis. *J. Chromatogr. A* 2000; 902:195–204.
6. Jönsson JÅ and Mathiasson L. Membrane extraction in analytical chemistry. *J. Sep. Sci.* 2001; 24:495–507.
7. Jönsson JÅ. Liquid membrane extraction. In: Pawliszyn J, Ed. *Sampling and Sample Preparation for Field and Laboratory*. Amsterdam, The Netherlands: Elsevier Science, 2002: pp. 503–530.
8. Jönsson JÅ. Membrane extraction for sample preparation—a practical guide. *Chromatogr. Suppl.* 2003; 57:S-317–S-324.
9. Mehta AC. Sample pretreatment in the trace determination of drugs in biological fluids. *Talanta* 1986; 33:67–73.
10. Poole SK, Dean TA, Oudsema JW, and Poole CF. Sample preparation for chromatographic separations: An overview. *Anal. Chim. Acta* 1990; 236:3–42.
11. Poole SK and Poole CF. Trends in extraction of semivolatile compounds from water for environmental analysis. *Anal. Commun.* 1996; 33:15H–17H.
12. Lopez-Avila V. Sample preparation for environmental analysis. *Crit. Rev. Anal. Chem.* 1999; 29:195–230.
13. Dean JR. *Extraction Methods for Environmental Analysis*. Chichester, West Sussex, England: John Wiley & Sons, 1998.
14. Holden AJ. Solvent and membrane extraction in organic analysis. In: Handley AJ, Ed. *Extraction Methods in Organic Analysis*. Sheffield, South Yorkshire, England: Sheffield Academic Press, 1999:5–53.
15. Cantwell FF and Losier M. Liquid–liquid extraction. In: Pawliszyn J, Ed. *Sampling and Sample Preparation for Field and Laboratory*. Amsterdam, The Netherlands: Elsevier Science, 2002: pp. 297–340.
16. Thurman EM. *Mills MS. Solid-Phase Extraction, Principles and Practice*. New York: John Wiley & Sons, 1998:384.
17. Fritz JS. *Analytical Solid-Phase Extraction*. New York: John Wiley & Sons, 1999.
18. Poole CF. Principles and practice of solid-phase extraction. In: Pawliszyn J, Ed. *Sampling and Sample Preparation for Field and Laboratory*. Amsterdam, The Netherlands: Elsevier Science, 2002: pp. 341–387.
19. Pawliszyn J. *Solid-Phase Microextraction, Theory and Practice*. New York: John Wiley & Sons, 1997: p. 264.
20. Pawliszyn J. Solid phase microextraction. In: Pawliszyn J, Ed. *Sampling and Sample Preparation for Field and Laboratory*. Amsterdam, The Netherlands: Elsevier Science, 2002: pp. 389–477.
21. Dean JR and Xiong G. Extraction of organic pollutants from environmental matrices: Selection of extraction technique. *Trends Anal. Chem.* 2000; 19:553–564.
22. SW-846, Test Methods for Evaluating Solid Waste: Physical/Chemical Methods 3rd ed. (Updates 1992, 1993, 1995), Washington, DC: US GPO, 1986.
23. Lunte SM and Lunte CE. Microdialysis sampling for pharmacological studies: HPLC and CE analysis. In: Brown P and Grushka E, Eds. *Advances in Chromatography*. Vol. 36. New York: Marcel Dekker, 1995: pp. 383–432.
24. Davies MI. A review of microdialysis sampling for pharmacokinetic applications. *Anal. Chim. Acta* 1999; 379:227–249.
25. Lindegård B, Björk H, Jönsson JÅ, Mathiasson L, and Olsson A-M. Automatic column liquid chromatographic determination of a basic drug in blood plasma using the supported liquid membrane technique for sample pretreatment. *Anal. Chem.* 1994; 66:4490–4497.
26. Pedersen-Bjergaard S and Rasmussen KE. Liquid–liquid–liquid microextraction for sample preparation of biological fluids prior to capillary electrophoresis. *Anal. Chem.* 1999; 71:2650–2656.
27. Grønhaug Halvorsen T, Pedersen-Bjergaard S, Reubsaet JLE, and Rasmussen KE. Liquid-phase microextraction combined with flow-injection thermospray tandem mass spectrometry. Rapid screening of amphetamines in biological matrices. *J. Sep. Sci.* 2001; 24:615–622.
28. Rasmussen KE and Pedersen-Bjergaard S. Developments in hollow fibre-based, liquid-phase microextraction. *Trends Anal. Chem.* 2004; 23:1–10.
29. Pedersen-Bjergaard S and Rasmussen KE. Bioanalysis of drugs by liquid-phase microextraction coupled to separation techniques. *J. Chromatogr. B* 2005; 817:3–12.
30. Cukrowska E, Chimuka L, Nsengimana H, and Kwaramba V. Application of supported liquid membrane probe for extraction and preconcentration of organotin compounds from environmental water samples. *Anal. Chim. Acta* 2004; 523:141–147.

31. Zhao L and Lee HK. Liquid-phase microextraction combined with hollow fiber as a sample preparation technique prior to gas chromatography/mass spectrometry. *Anal. Chem.* 2002; 74:2486–2492.
32. Liu J-F, Jönsson JÅ, and Mayer P. Equilibrium sampling of freely dissolved chlorophenols in water samples with hollow fiber supported liquid membrane. *Anal. Chem.* 2005; 77:4800–4809.
33. Trtic-Petrovic T, Liu J-F, and Jönsson JÅ. Application of equilibrium sampling through membrane in a single hollow fiber for the determination of drug-protein binding and free drug concentration in plasma. *J. Chromatogr. B* 2005; 826:169–176.
34. Jonsson OB, Nordlöf U, and Nilsson UL. The XT-tube extractor: A hollow fiber-based supported liquid membrane extractor for bioanalytical sample preparation. *Anal. Chem.* 2003; 75:3506–3511.
35. Thordarson E, Palmarsdottir S, Mathiasson L, and Jönsson JÅ. Sample preparation using a miniaturized supported liquid membrane device connected on-line to packed capillary liquid chromatography. *Anal. Chem.* 1996; 68:2559–2563.
36. Ma M and Cantwell FF. Solvent microextraction with simultaneous back-extraction for sample cleanup and preconcentration: Quantitative extraction. *Anal. Chem.* 1998; 70:3912–3919.
37. Ma M and Cantwell FF. Solvent microextraction with simultaneous back-extraction for sample cleanup and preconcentration: Preconcentration into a single microdrop. *Anal. Chem.* 1999; 71:388–393.
38. Sarafraz-Yazdi A and Es'haghi Z. Liquid-liquid-liquid phase microextraction of aromatic amines using crown ethers by high-performance liquid chromatography with monolithic column. *Talanta* 2005; 66:664–669.
39. Valcárcel M and Luque de Castro MD. *Non-chromatographic continuous separation techniques*. Cambridge: The Royal Society of Chemistry, 1991.
40. Cussler EL, Callahan RW, and Alexander Jr PR. *Liquid/Liquid Extraction with Microporous Membranes*. Charlotte, North Carolina: Celanese Corp., US Patent 4,966,707, 1990.
41. Melcher RG and Bouyoucos SA. Membrane interface for automatic extraction and liquid chromatographic determination of trace organics in aqueous streams. *Process Control Qual.* 1990; 1:63–74.
42. Melcher RG and Morabito PL. Membrane/gas chromatographic system for automated extraction and determination of trace organics in aqueous samples. *Anal. Chem.* 1990; 62:2183–2188.
43. Melcher RG, O'Connor PJ, and Beach MW. Automated determination of trace organics in aqueous process and wastewater streams using a reversed permeation membrane. *Process Control Qual.* 1994; 6:167–185.
44. Hauser B, Schellin M, and Popp P. Membrane-assisted solvent extraction of triazines, organochlorine, and organophosphorus compounds in complex samples combined with large-volume injection-gas chromatography/mass spectrometric detection. *Anal. Chem.* 2004; 76:6029–6038.
45. Jönsson JÅ, Lökvist P, Audunsson G, and Nilvé G. Mass transfer kinetics for analytical enrichment and sample preparation using supported liquid membranes in a flow system with stagnant acceptor liquid. *Anal. Chim. Acta* 1993; 227:9–24.
46. Chimuka L, Megersa N, Norberg J, Mathiasson L, and Jönsson JÅ. Incomplete trapping in supported liquid membrane extraction with a stagnant acceptor for weak bases. *Anal. Chem.* 1998; 70:3906–3911.
47. Sastre AM, Kumar A, Shukla JP, and Singh RK. Improved techniques in liquid membrane separations: An overview. *Sep. Purific. Meth.* 1998; 27:213–298.
48. de Gyves J and Rodrigues de San Miguel E. Metal ion separations by supported liquid membranes. *Ind. Eng. Chem. Res.* 1999; 38:2182–2202.
49. Buffle J, Parthasarathy N, Djane N-K, and Mathiasson L. Permeation liquid membranes for field analysis and speciation of trace compounds in water. In: Buffle J and Horvai G, Eds. *In Situ Monitoring of Aquatic Systems: Chemical Analysis and Speciation*. Chichester, West Sussex, England: John Wiley & Sons, 2000: pp. 407–493.
50. Papantoni M, Djane N-K, Ndung'u K, Jönsson JÅ, and Mathiasson L. Trace enrichment of metals using a supported liquid membrane technique. *Analyst* 1995; 120:1471–1477.
51. Djane N-K, Ndung'u K, Johnson C, Sartz H, Törnström T, and Mathiasson L. Chromium speciation in natural waters using serially connected supported liquid membranes. *Talanta* 1999; 48:1121–1132.
52. Dzygiel P, Wieczorek P, Mathiasson L, and Jönsson JÅ. Enrichment of amino acids by supported liquid membrane extraction using Aliquat 336 as a carrier. *Anal. Lett.* 1998; 31:1261–1274.
53. Drapala A, Dzygiel P, Jönsson JÅ, and Wieczorek P. Supported liquid membrane extraction of peptides. *Acta Biochim. Pol.* 2001; 48:1113–1116.
54. Drapala A, Jönsson JÅ, and Wieczorek P. Peptides analysis in blood plasma using on-line system of SLM and HPLC. *Anal. Chim. Acta* 2005; 553:9–14.
55. Djane N-K, Ndung'u K, Malcus F, Johansson G, and Mathiasson L. Supported liquid membrane enrichment using an organophosphorus extractant for analytical trace metal determinations in river waters. *Fresenius J. Anal. Chem.* 1997; 358:822–827.
56. Djane N-K, Bergdahl IA, Ndung'u K, Schütz A, Johansson G, and Mathiasson L. Supported liquid membrane enrichment combined with atomic absorption spectrometry for the determination of lead in urine. *Analyst* 1997; 122:1073–1077.
57. Wieczorek P, Jönsson JÅ, and Mathiasson L. Concentration of amino acids using supported liquid membranes with di-2-ethylhexyl phosphoric acid as a carrier. *Anal. Chim. Acta* 1997; 346:191–197.
58. Romero R, Jönsson JÅ, Gázquez D, Bagur MG, and Sánchez-Viñas M. Multivariate optimization of supported liquid membrane extraction of biogenic amines prior to liquid chromatography determination as dabsyl derivatives. *J. Sep. Sci.* 2002; 25:584–592.
59. Miliotis T, Knutsson M, Jönsson JÅ, and Mathiasson L. Determination of aromatic anionic surfactants using supported liquid membrane technique. *Int. J. Environ. Anal. Chem.* 1996; 64:35–45.

60. Thordarson E, Emnéus J, and Jönsson JÅ. Immunological trapping in supported liquid membrane extraction. *Anal. Chem.* 2000; 72:5280–5284.
61. Tudorache M, Rak M, Wiczorek P, Jönsson JÅ, and Emnéus J. Immuno-SLM—a combined sample handling and analysis technique. *J. Immunol. Meth.* 2004; 284:107–118.
62. Tudorache M, Co M, Lifgren H, and Emnéus J. Ultrasensitive magnetic particle-based immunosupported liquid membrane assay. *Anal. Chem.* 2005; 77:7156–7162.
63. Megersa N, Solomon T, and Jönsson JÅ. Supported liquid membrane extraction for sample work-up and preconcentration of methoxy-s-triazine herbicides in a flow system. *J. Chromatogr. A* 1999; 830:203–210.
64. Jönsson JÅ, Andersson M, Melander C, Norberg J, Thordarson E, and Mathiasson L. Automated liquid membrane extraction for HPLC determination of ropivacaine metabolites in urine. *J. Chromatogr. A* 2000; 870:151–157.
65. Mayer P, Tolls J, Hermens JLM, and Mackay D. Equilibrium sampling devices. *Environ. Sci. Technol.* 2003; 37:184A–191A.
66. Romero R and Jönsson JÅ. Determination of free copper concentration in natural waters based on a supported liquid membrane extraction system. *Anal. Bioanal. Chem.* 2005; 381:1452–1459.
67. Romero R, Liu J-F, Mayer P, and Jönsson JÅ. Equilibrium sampling through membranes (ESTM) of freely dissolved copper concentrations with selective hollow fiber membranes and the spectrophotometric detection of a metal stripping agent. *Anal. Chem.* 2005; 77:7605–7611.
68. Trtic-Petrovic T and Jönsson JÅ. Determination of drug-protein binding using supported liquid membrane extraction under equilibrium conditions. *J. Chromatogr. B* 2005; 814:375–384.
69. Knutsson M, Lundh J, Mathiasson L, Jönsson JÅ, and Sundin P. Supported liquid membranes for the extraction of phenolic acids from circulating nutrient solutions. *Anal. Lett.* 1996; 29:1619–1635.
70. Jung V, Chimuka L, Jönsson JÅ, Niedack N, Bowens P, and Alsanus B. Supported liquid membrane extraction for identification of phenolic compounds in the nutrient solution of closed hydroponic growing systems for tomato. *Anal. Chim. Acta* 2002; 474:49–57.
71. Knutsson M, Nilvé G, Mathiasson L, and Jönsson JÅ. Supported liquid membrane technique for time-integrating field sampling of acid herbicides at sub part per billion level in natural waters. *J. Agric. Food Chem.* 1992; 40:2413–2417.
72. Knutsson M, Mathiasson L, and Jönsson JÅ. Supported liquid membrane work-up in combination with liquid chromatography and electrochemical detection for the determination of chlorinated phenols in natural water samples. *Chromatographia* 1996; 42:165–170.
73. Nilvé G, Knutsson M, and Jönsson JÅ. Liquid chromatographic determination of sulfonylurea herbicides in natural waters after automated sample pretreatment using supported liquid membranes. *J. Chromatogr. A* 1994; 668:75–82.
74. Shen Y, Obuseng V, Grönberg L, and Jönsson JÅ. Liquid membrane enrichment for the ion chromatographic determination of carboxylic acids in soil samples. *J. Chromatogr. A* 1996; 725:189–197.
75. Delgado Zamarrero MM, Sánchez Pérez A, Bustamante Rangel M, and Hernández Méndez J. Automated analysis for vitamin E in butter by coupling sample treatment-continuous membrane extraction—liquid chromatography with electrochemical detection. *Anal. Chim. Acta* 1999; 386:99–106.
76. Norberg J and Thordarson E. Extracting syringe-connecting sample preparation and gas chromatography. *Analyst* 2000; 125:673–676.
77. Barri T, Bergström S, Norberg J, and Jönsson JÅ. Miniaturized and automated sample pretreatment for determination of PCBs in environmental aqueous samples using an on-line microporous membrane liquid-liquid extraction-gas chromatography system. *Anal. Chem.* 2004; 76:1928–1934.
78. Barri T, Bergström S, Hussen A, Norberg J, and Jönsson JÅ. Extracting syringe for determination of OCPs in leachate water and water-soil slurry: An environmentally friendly technology in environmental analysis. *J. Chromatogr. A* 2006; 1111:11–20.
79. Liu J-F, Chao J-B, and Jiang G-B. Continuous flow liquid membrane extraction: A novel automatic trace-enrichment technique based on continuous flow liquid-liquid extraction combined with supported liquid membrane. *Anal. Chim. Acta* 2002; 455:93–101.
80. Pratt KF and Pawliszyn J. Gas extraction kinetics of volatile organic species from water with a hollow fiber membrane. *Anal. Chem.* 1992; 64:2101–2106.
81. Luo Y and Pawliszyn J. Solid phase microextraction (SPME) and membrane extraction with a sorbent interface (MESI) in organic analysis. In: Handley AJ, Ed. *Extraction Methods in Organic Analysis*. Sheffield, South Yorkshire, England: Sheffield Academic press, 1999; pp. 75–99.
82. Segal A, Górecki T, Mussche P, Lips J, and Pawliszyn J. Development of membrane extraction with a sorbent interface-micro gas chromatography system for field analysis. *J. Chromatogr. A* 2000; 873:13–27.
83. Matz G, Kibelka G, Dahl J, and Lenneman F. Experimental study on solvent-less sample preparation methods. Membrane extraction with a sorbent interface, thermal membrane application and purge-and-trap. *J. Chromatogr. A* 1999; 830:365–376.
84. Larsson N, Berhanu T, Megersa N, and Jönsson JÅ. Portable and time-integrating field sampling for continuous membrane extraction of s-triazine herbicides and their metabolites in a lake in the agricultural region of Southern Ethiopia. Submitted 2008 to *Anal. Chim. Acta*.
85. Audunsson GA. Aqueous/aqueous extraction by means of a liquid membrane for sample clean-up and preconcentration of amines in a flow system. *Anal. Chem.* 1986; 58:2714–2723.
86. Shen Y, Jönsson JÅ, and Mathiasson L. On-line microporous membrane liquid-liquid extraction for sample pretreatment combined with capillary gas chromatography applied to local anesthetics in blood plasma. *Anal. Chem.* 1998; 70:946–953.
87. Pratt KF and Pawliszyn J. Water monitoring system based on gas extraction with a single hollow fiber membrane and gas chromatographic cryotrapping. *Anal. Chem.* 1992; 64:2107–2110.

88. Shen Y, Grönberg L, and Jönsson JÅ. Experimental studies on the enrichment of carboxylic acids with tri-*n*-octylphosphine oxide as extractant in a supported liquid membrane. *Anal. Chim. Acta* 1994; 292:31–39.
89. Dzygiel P and Wieczorek P. Extraction of glyphosate by supported liquid membrane technique. *J. Chromatogr. A* 2000; 889:93–98.
90. Dzygiel P and Wieczorek P. Supported liquid membrane extraction of glyphosate metabolites. *J. Sep. Sci.* 2001; 24:561–566.
91. Rak M, Dzygiel P, and Wieczorek P. Supported liquid membrane extraction of aromatic aminophosphonates. *Anal. Chim. Acta* 2001; 433:227–236.
92. Calzado JA, Palet C, Jönsson JÅ, and Valiente M. Metal affinity liquid membrane. II. Facilitated transport of tryptophan. *Anal. Chim. Acta* 2000; 417:159–167.
93. Calzado JA, Palet C, and Valiente M. Metal affinity liquid membrane, III. Characterization of transport selectivity. *J. Sep. Sci.* 2001; 24:533–543.
94. Smith BD. Liquid membrane transport using boronic acid carriers. *Supramol. Chem.* 1996; 7:55–60.
95. Di Luccio M, Smith BD, Kida T, Borges CP, and Alves TLM. Separation of fructose from a mixture of sugars using supported liquid membranes. *J. Membr. Sci.* 2000; 174:217–224.
96. Parthasarathy N, Pelletier M, and Buffle J. Hollow fiber based supported liquid membrane: A novel analytical system for trace metal analysis. *Anal. Chim. Acta* 1997; 350:183–195.
97. Rosell A, Palet C, and Valiente M. Solvent impregnated hollow fibre for a selective preconcentration of Pb(II) in an on-line determination by flame atomic absorption spectrometry. *Anal. Chim. Acta* 1998; 370:141–149.
98. Ndung'u K, Djane N-K, and Mathiasson L. Determination of trace metal ions in river water by ion-pair chromatography after enrichment using supported liquid membrane. *J. Chromatogr. A* 1998; 826:103–108.
99. Armalis S, Kriksciuniene I, Kubilene E, Djane N-K, Ndung'u K, and Mathiasson L. Stripping analysis of trace metals at a flow-through reticulated vitreous carbon electrode after the preconcentration by supported liquid membrane technique. *Intern. J. Environ. Anal. Chem.* 1999; 74:233–242.
100. Ndung'u K and Mathiasson L. Microporous membrane liquid–liquid extraction technique combined with gas chromatography mass spectrometry for the determination of organotin compounds. *Anal. Chim. Acta* 2000; 404:319–328.
101. Trtic-Petrovic T and Jönsson JÅ. Application of SLM extraction for investigation of metal-humic acid bindings. *Desalination* 2002; 148:247–251.
102. Chimuka L, Cukrowska E, Soko L, and Naicker K. Supported-liquid membrane extraction as a selective sample preparation technique for monitoring uranium in complex matrix samples. *J. Sep. Sci.* 2003; 26:601–608.
103. Parthasarathy N, Buffle J, and Cuenod F. Speciation of trace metals in waters: Direct selective separation and preconcentration of free metal ion by supported liquid membrane. *Chem. Anal. (Warsaw)* 1999; 44:455–470.
104. Parthasarathy N, Pelletier M, and Buffle J. Permeation liquid membrane for trace metal speciation in natural waters transport of liposoluble Cu(II) complexes. *J. Chromatogr. A* 2004; 1025:33–40.
105. Slaveykova VI, Parthasarathy N, Buffle J, and Wilkinson KJ. Permeation liquid membrane as a tool for monitoring bioavailable Pb in natural waters. *Sci. Total Environ.* 2004; 328:55–68.
106. Brumbaugh WG, Petty JD, Huckins JN, and Manahan SE. Stabilized liquid membrane device (SLMD) for the passive, integrative sampling of labile metals in water. *Water Air Soil Pollut.* 2002; 133:109–119.
107. Nilvé G, Audunsson G, and Jönsson JÅ. Sample preparation by means of a supported liquid membrane for the determination of chlorophenoxyalkanoic acids. *J. Chromatogr.* 1989; 471:151–160.
108. Berhanu T, Liu J-F, Romero R, Megersa N, and Jönsson JÅ. Determination of trace levels of dinitrophenolic compounds in environmental water samples using hollow fiber supported liquid membrane extraction and high performance liquid chromatography. *J. Chromatogr. A* 2006; 1103:1–8.
109. Shen Y, Ström L, Jönsson JÅ, and Tyler G. Low-molecular organic acids in the rhizosphere soil solution of beech forest (*Fagus sylvatica* L.) cambisols determined by ion chromatography using supported liquid membrane enrichment technique. *Soil Biol. Biochem.* 1996; 28:1163–1169.
110. Mårtensson L, Magnusson M, Shen Y, and Jönsson JÅ. Air concentrations of volatile organic acids in confined animal buildings—determination with ion chromatography. *Agric. Ecosyst. Environ.* 1999; 75:101–108.
111. Norberg J, Zander Å, and Jönsson JÅ. Fully automated on-line supported liquid membrane-liquid chromatographic determination of aniline in environmental waters. *Chromatographia* 1997; 46:483–488.
112. Dzygiel P and Wieczorek P. Extraction of glyphosate by a supported liquid membrane technique. *J. Chromatogr. A* 2000; 889:93–98.
113. Chimuka L, Nindi MM, and Jönsson JÅ. Supported liquid membrane enrichment studies of natural water samples applied to liquid chromatographic determination of triazine herbicides. *Int. J. Environ. Anal. Chem.* 1997; 68:429–445.
114. Megersa N and Jönsson JÅ. Trace enrichment and sample preparation of alkylthio-*s*-triazine herbicides in environmental waters using supported liquid membrane technique in combination with high performance liquid chromatography. *Analyst* 1998; 123:225–231.
115. Megersa N, Solomon T, Chandravanshi BS, and Jönsson JÅ. Sample clean-up, enrichment and determination of *s*-triazine herbicides from southern Ethiopian lakes using supported liquid membrane extraction. *Bull. Chem. Soc. Ethiopia* 2000; 14:9–24.
116. Megersa N, Chimuka L, Solomon T, and Jönsson JÅ. Liquid membrane extraction and trace enrichment of triazine herbicides and their metabolites in environmental and biological samples. *J. Sep. Sci.* 2001; 24:567–576.
117. Trocewicz J. Determination of herbicides in surface water by means of a supported liquid membrane technique and high-performance liquid chromatography. *J. Chromatogr. A* 1996; 725:121–127.
118. Mulugeta M and Megersa N. Carrier-mediated extraction of bipyrindilium herbicides across the hydrophobic liquid membrane. *Talanta* 2004; 64:101–108.

119. Grönberg L, Lövkvist P, and Jönsson JÅ. Measurement of aliphatic amines in ambient air and rainwater. *Chemosphere* 1992; 24:1533–1540.
120. Grönberg L, Lövkvist P, and Jönsson JÅ. Determination of aliphatic amines in air by membrane enrichment in a flow system directly coupled to a gas chromatograph. *Chromatographia* 1992; 33:77–82.
121. Grönberg L, Shen Y, and Jönsson JÅ. Ion chromatographic determination of organic acids in air with on-line liquid membrane pretreatment. *J. Chromatogr.* 1993; 655:207–215.
122. Sandahl M, Mathiasson L, and Jönsson JÅ. Determination of thiophanate-methyl and its metabolites at trace level in spiked natural water using the supported liquid membrane extraction and the microporous membrane liquid–liquid extraction techniques combined on-line with HPLC. *J. Chromatogr. A* 2000; 893:123–131.
123. Sandahl M, Mathiasson L, and Jönsson JÅ. On-line automated sample preparation for HPLC using parallel supported liquid membrane extraction and microporous membrane liquid–liquid extraction. *J. Chromatogr. A* 2002; 975:177–183.
124. Kuosmanen K, Hyötyläinen T, Hartonen K, Jönsson JÅ, and Riekkola M-L. Analysis of PAH compounds in soil with on-line coupled pressurised hot water extraction-microporous membrane liquid–liquid extraction—gas chromatography. *Anal. Bioanal. Chem.* 2003; 375:389–399.
125. Kuosmanen K, Hyötyläinen T, Hartonen K, and Riekkola M-L. Analysis of polycyclic aromatic hydrocarbons in soil and sediment with on-line coupled pressurised hot water extraction, hollow fibre microporous membrane liquid–liquid extraction and gas chromatography. *Analyst* 2003; 128:434–439.
126. Zhou Q-X, Jiang G-B, Liu J-F, and Cai Y-Q. Combination of microporous membrane liquid–liquid extraction and capillary electrophoresis for the analysis of aromatic amines in water samples. *Anal. Chim. Acta* 2004; 509:55–62.
127. Liu J-F, Liang X, Jiang G-B, Cai Y-Q, Zhou Q-X, and Liu G-G. High performance liquid chromatography determination of 4-nonylphenol, 4-*tert*-octylphenol, and their short ethoxyl chain polyethoxylates in water samples using a microporous membrane liquid–liquid extraction sample pretreatment technique. *J. Sep. Sci.* 2003; 26:823–828.
128. Carabias Martínez R, Rodríguez Gonzalo E, Santiago Toribio MP, and Hernández Méndez J. Determination of triazines in surface waters by membrane separation coupled on-line to a flow-injection system and partial least squares regression. *Anal. Chim. Acta* 1996; 321:147–155.
129. Norberg J, Thordarson E, Mathiasson L, and Jönsson JÅ. Microporous membrane liquid–liquid extraction coupled on-line with normal-phase liquid chromatography for the determination of cationic surfactants in river and wastewater. *J. Chromatogr. A* 2000; 869:523–529.
130. Guo X and Mitra S. On-line membrane extraction liquid chromatography for monitoring semi-volatile organics in aqueous matrices. *J. Chromatogr. A* 2000; 904:189–196.
131. Morabito PL and Melcher RG. Automated membrane/gas chromatography system for extraction and determination of trace organics in aqueous samples using large volume injection. *Process Control and Quality* 1992; 3:35–42.
132. Kou D and Mitra S. Simultaneous extraction and concentration by on-line hollow fiber membrane extraction. *Anal. Chem.* 2003; 75:6355–6360.
133. Schellin M, Hauser B, and Popp P. Determination of organophosphorus pesticides using membrane-assisted solvent extraction combined with large volume injection-gas chromatography–mass spectrometric detection. *J. Chromatogr. A* 2004; 1040:251–258.
134. Schellin M and Popp P. Membrane-assisted solvent extraction of polychlorinated biphenyls in river water and other matrices combined with large volume injection-gas chromatography–mass spectrometric detection. *J. Chromatogr. A* 2003; 1020:153–160.
135. Schellin M and Popp P. Membrane-assisted solvent extraction of seven phenols combined with large volume injection–gas chromatography–mass spectrometric detection. *J. Chromatogr. A* 2005; 1072:37–43.
136. San Juan A, Guo X, and Mitra S. On-site, and on-line analysis of chlorinated solvents in ground water using pulse introduction membrane extraction gas chromatography (PIME-GC). *J. Sep. Sci.* 2001; 24:599–605.
137. Ciucanu I and Chiriac A. Membrane and trap system for continuous monitoring of volatile organic compounds using a portable gas chromatograph with thermal conductivity detector. *J. Sep. Sci.* 2002; 25:447–452.
138. Hauser B and Popp P. Membrane extraction combined with thermodesorption/gas chromatography and mass selective detection for the analysis of volatile organic compounds in water. *J. High Resol. Chromatogr.* 1999; 22:205–212.
139. Hauser B and Popp P. Combining membrane extraction with mobile gas chromatography for the field analysis of volatile organic compounds in contaminated waters. *J. Chromatogr. A* 2001; 909:3–12.
140. Hauser B, Popp P, and Paschke A. Membrane extraction of volatile organic compounds in combination with mobile gas chromatographic analysis. *Intern. J. Environ. Anal. Chem.* 1999; 74:107–121.
141. Zhu L, Zhu L, and Lee HK. Liquid–liquid–liquid microextraction of nitrophenols with a hollow-fiber membrane prior to capillary liquid chromatography. *J. Chromatogr. A* 2001; 924:407–414.
142. Liu J-F, Chao J-B, Wen M-J, and Jiang G-B. Automatic trace-enrichment of bisphenol A by a novel continuous flow liquid membrane extraction technique. *J. Sep. Sci.* 2001; 24:874–878.
143. Chao J-B, Liu J-F, Wen M-J, Liu J-M, Cai Y-Q, and Jiang G-B. Determination of sulfonyleurea herbicides by continuous-flow liquid membrane extraction on-line coupled with high-performance liquid chromatography. *J. Chromatogr. A* 2002; 955:188–189.
144. Liu J-F, Chao J-B, Jiang G-B, Cai Y-Q, and Liu J-M. Trace analysis of sulfonyleurea herbicides in water by on-line continuous flow liquid membrane extraction-C18 precolumn liquid chromatography with ultraviolet absorbance detection. *J. Chromatogr. A* 2003; 995:21–28.
145. Liu J-F, Liang X, Chi Y-G, et al. High performance liquid chromatography determination of chlorophenols in water samples after preconcentration by continuous flow liquid membrane extraction on-line coupled with a precolumn. *Anal. Chim. Acta* 2003; 487:129–135.

146. Zhou Q-X, Liu J-F, Jiang G-B, Liu G-G, and Cai Y-Q. Sensitivity enhancement of chlorinated phenols by continuous flow liquid membrane extraction followed by capillary electrophoresis. *J. Sep. Sci.* 2004; 27:576–580.
147. Zhao L, Zhu L, and Lee HK. Analysis of aromatic amines in water samples by means of liquid–liquid–liquid microextraction with hollow-fibers and high performance liquid chromatography. *J. Chromatogr. A* 2002; 963:239–248.
148. Hou L, Wen X, Tu C, and Lee HK. Combination of liquid-phase microextraction and on-column stacking for trace analysis of amino alcohols by capillary electrophoresis. *J. Chromatogr. A* 2002; 979:163–169.
149. Quintana JB, Rodil R, and Reemtsma T. Suitability of hollow fibre liquid-phase microextraction for the determination of acidic pharmaceuticals in wastewater by liquid chromatography–electrospray tandem mass spectrometry without matrix effects. *J. Chromatogr. A* 2004; 1061:19–26.
150. Wen X, Tu C, and Lee HK. Two-step liquid–liquid–liquid microextraction of nonsteroidal antiinflammatory drugs in wastewater. *Anal. Chem.* 2004; 76:228–232.
151. Zhu L, Ee KH, Zhao L, and Lee HK. Analysis of phenoxy herbicides in bovine milk by means of liquid–liquid–liquid microextraction with a hollow-fiber membrane. *J. Chromatogr. A* 2002; 963:335–343.
152. Shen G and Lee HK. Hollow fiber-protected liquid phase microextraction of triazine herbicides. *Anal. Chem.* 2002; 74:648–654.
153. Psillakis E and Kalogerakis N. Hollow-fibre liquid-phase microextraction of phthalate esters from water. *J. Chromatogr. A* 2003; 999:145–153.
154. Basheer C, Lee HK, and Obbard JP. Determination of organochlorine pesticides in seawater using liquid-phase hollow fibre membrane microextraction and gas chromatography–mass spectrometry. *J. Chromatogr. A* 2002; 968:191–199.
155. Basheer C, Balasubramanian R, and Lee HK. Determination of organic micropollutants in rainwater using hollow fiber membrane/liquid-phase microextraction combined with gas chromatography–mass spectrometry. *J. Chromatogr. A* 2003; 1016:11–20.
156. Hou L, Shen G, and Lee HK. Automated hollow fiber-protected dynamic liquid-phase microextraction of pesticides for gas chromatography–mass spectrometric analysis. *J. Chromatogr. A* 2003; 985:107–116.
157. Müller S, Möder M, Schrader S, and Popp P. Semi-automated hollow-fiber membrane extraction, a novel enrichment technique for the determination of biologically active compounds in water samples. *J. Chromatogr. A* 2003; 985:99–106.
158. Lambropoulou DA and Albanis TA. Sensitive trace enrichment of environmental antiandrogen vinclozolin from natural waters and sediment samples using hollow-fiber liquid-phase microextraction. *J. Chromatogr. A* 2004; 1061:11–18.
159. King S, Meyer JS, and Andrews ARJ. Screening method for polycyclic aromatic hydrocarbons in soil using hollow fiber membrane solvent microextraction. *J. Chromatogr. A* 2002; 982:201–208.
160. Psillakis E, Mantzavinos D, and Kalogerakis N. Development of a hollow fibre liquid phase microextraction method to monitor the sonochemical degradation of explosives in water. *Anal. Chim. Acta* 2004; 501:3–10.
161. Audunsson GA. Determination of low parts per billion levels of amines in urine by liquid membrane sample cleanup directly coupled to a gas-liquid chromatograph. *Anal. Chem.* 1988; 60:1340–1347.
162. Mathiasson L, Knutsson M, Bremle G, and Mårtensson L. Chemical environment in animal buildings. Determination of organic acids in manure. *Swed. J. Agric. Res.* 1991; 21:147–155.
163. Lindegård B, Jönsson JÅ, and Mathiasson L. Liquid membrane work-up of blood plasma samples applied to gas chromatographic determination of aliphatic amines. *J. Chromatogr.* 1992; 573:191–200.
164. Palmarsdóttir S, Lindegård B, Deiningner P, Edholm L-E, Mathiasson L, and Jönsson JÅ. Supported liquid membrane technique for selective sample work-up of basic drugs in plasma prior to capillary zone electrophoresis. *J. Capill. Electrophor.* 1995; 2:185–189.
165. Palmarsdóttir S, Mathiasson L, Jönsson JÅ, and Edholm L-E. Determination of a basic drug, bambuterol, in human plasma by capillary electrophoresis using double stacking for large volume injection and supported liquid membranes for sample pretreatment. *J. Chromatogr. B* 1997; 688:127–134.
166. Palmarsdóttir S, Thordarson E, Edholm L-E, Jönsson JÅ, and Mathiasson L. Miniaturized supported liquid membrane device for selective on-line enrichment of basic drugs in plasma combined with capillary zone electrophoresis. *Anal. Chem.* 1997; 69:1732–1737.
167. Palmarsdóttir S, Mathiasson L, Jönsson JÅ, and Edholm L-E. Micro-CLC as an interface between SLM extraction and CZE for enhancement of sensitivity and selectivity in bioanalysis of drugs. *J. Capill. Electrophor.* 1996; 3:255–260.
168. Trocewicz J, Suprynowicz Z, and Markowicz J. Determination of diprivan in urine by a supported liquid membrane technique and liquid chromatography–electrochemical detection. *J. Chromatogr. B.* 1996; 685:129–134.
169. Norberg J, Emnéus J, Jönsson JÅ, et al. On-line supported liquid membrane-liquid chromatography with a phenol oxidase-based biosensor as selective detection unit for the determination of phenols in blood plasma. *J. Chromatogr. B.* 1997; 701:39–46.
170. Djane N-K, Armalis S, Ndung'u K, Johansson G, and Mathiasson L. Supported liquid membrane coupled on-line to potentiometric stripping analysis at a mercury-coated reticulated vitreous carbon electrode for trace metal determinations in urine. *Analyst* 1998; 123:393–396.
171. Shen Y, Mathiasson L, and Jönsson JÅ. Automated capillary GC determination of local anaesthetics in plasma samples with supported liquid membranes for sample preparation. *J. Microcol. Sep.* 1998; 10:107–113.
172. Rasmussen KE, Pedersen-Bjergaard S, Krogh M, Ugland HG, and Grønhaug T. Development of a simple in-vial liquid-phase microextraction device for drug analysis compatible with capillary gas chromatography, capillary electrophoresis and high-performance liquid chromatography. *J. Chromatogr. A* 2000; 873:3–11.
173. Ugland HG, Krogh M, and Rasmussen KE. Liquid-phase microextraction as a sample preparation technique prior to capillary gas chromatographic-determination of benzodiazepines in biological matrices. *J. Chromatogr. B* 2000; 749:85–92.
174. Pedersen-Bjergaard S and Rasmussen KE. Liquid-phase microextraction and capillary electrophoresis of acidic drugs. *Electrophoresis* 2000; 21:579–585.

175. Grønhaug Halvorsen T, Pedersen-Bjergaard S, and Rasmussen KE. Liquid-phase microextraction and capillary electrophoresis of citalopram, and antidepressant drug. *J. Chromatogr. A* 2001; 909:87–93.
176. Jonsson OB, Dyremark E, and Nilsson UL. Development of a microporous membrane liquid–liquid extractor for organophosphate esters in human blood plasma: Identification of triphenyl phosphate and octyl diphenyl phosphate in donor plasma. *J. Chromatogr. B* 2001; 755:157–164.
177. Mullins F. Evaluation of a novel non-porous membrane extraction probe to determine sulphonylureas in plasma with analysis by LC–MS/MS. *J. Sep. Sci.* 2001; 24:593–598.
178. Trocewicz J. Sample preparation of amphetamine and methamphetamine by means of supported liquid membrane technique for HPLC analysis. *J. Sep. Sci.* 2001; 24:587–592.
179. Msagati T and Nindi MN. Determination of benzimidazole anthelmintics compounds by supported liquid membrane extraction and liquid chromatography. *J. Sep. Sci.* 2001; 24:606–614.
180. Rodríguez Gonzalo E, Pérez Pavón JL, Ruzicka J, Christian GD, and Olson DC. Flow-injection analysis determination of phenols in kerosene and naphtha by membrane extraction-preconcentration. *Anal. Chim. Acta* 1992; 259:37–44.
181. Carabias Martínez R, Rodríguez Gonzalo E, Hernández Fernández E, and Hernández Méndez J. Membrane extraction - preconcentration cell coupled on-line to flow-injection and liquid chromatographic systems. Determination of triazines in oil. *Anal. Chim. Acta* 1995; 304:323–332.
182. García Sanchez T, Pérez Pavón JL, and Moreno Cordero B. Continuous membrane extraction of phenols from crude oils followed by high-performance liquid chromatographic determination with electrochemical detection. *J. Chromatogr. A* 1997; 766:61–69.
183. Fernández Laespada E, Pérez Pavón JL, and Moreno Cordero B. Continuous membrane extraction coupled with chromatographic analysis for the determination of phenols in fuels. *J. Chromatogr. A* 1998; 823:537–548.
184. Fernández Laespada E, Pérez Pavón JL, and Moreno Cordero B. Automated on-line membrane liquid chromatographic determination of phenols in crude oils, gasolines and diesel fuels. *J. Chromatogr. A* 1999; 852:395–406.
185. Luque-Pérez E, Ríos A, Valcárcel M, Danielsson L-G, and Ingman F. Analysis of solid samples using supported liquid membranes: A method for the evaluation of the release of nicotine from Swedish snuff. *Anal. Chim. Acta* 1999; 387:155–164.
186. Luque-Pérez E, Ríos A, Valcárcel M, Danielsson L-G, and Ingman F. Spectrophotometric flow injection determination of caffeine in solid and slurry coffee and tea samples using supported liquid membranes. *Lab. Autom. Inform. Managem.* 1999; 34:131–142.
187. Carabias Martínez R, Rodríguez Gonzalo E, Paniagua Marcos PH, and Hernández Méndez J. Analysis of pesticides residues in matrices with high lipid contents by membrane separation coupled on-line to a high-performance liquid chromatography system. *J. Chromatogr. A* 2000; 869:427–439.
188. Luque M, Luque-Pérez E, Ríos A, and Valcárcel M. Supported liquid membranes for the determination of vanillin in food samples with amperometric detection. *Anal. Chim. Acta* 2000; 410:127–134.
189. Liu J-F and Jiang G-B. Determination of anionic surfactants in detergents by microporous membrane liquid–liquid extraction and flow-injection spectrophotometry. *Microchem. J* 2001; 68:29–33.
190. Hyötyläinen T, Andersson T, Jussila M, Wiedmer SK, Rautiainen M, and Riekkola M-L. Determination of phenols in pyrolysis oil by on-line coupled microporous membrane liquid-liquid extraction and multidimensional liquid chromatography. *J. Sep. Sci.* 2001; 24:544–550.



---

# 13 Hybrid Liquid Membrane Processes with Organic Water-Immiscible Carriers (OHLM): Application in Chemical and Biochemical Separations

*Vladimir S. Kislik*

## CONTENTS

13.1	Introduction and Definitions .....	371
13.2	Theory: Mass Transfer Mechanisms and Kinetics .....	372
13.2.1	Model for the HLM System .....	374
13.2.1.1	Mass Transfer Mechanisms and Kinetics .....	374
13.2.1.2	Driving Forces .....	378
13.2.2	Numerical Model of Competitive $M^{2+}/H^+$ Counter-Transport .....	379
13.2.3	Theory of Hollow-Fiber Liquid Membrane Transport .....	385
13.3	Module Design for Separation Systems .....	387
13.3.1	Layered Bulk Liquid Membrane Modules .....	387
13.3.2	Rotating Disc Modules .....	387
13.3.3	Creeping Film Modules .....	387
13.3.4	Hybrid Liquid Membrane Modules .....	388
13.3.5	Multimembrane Hybrid Systems .....	388
13.3.6	Flowing Liquid Membrane Modules .....	389
13.3.7	Hollow-Fiber Liquid Membrane Modules .....	390
13.3.8	Capillary Liquid Membrane Systems .....	391
13.3.9	Membrane Types Used .....	392
13.4	Selected Applications .....	393
13.4.1	Metal Separation-Concentration .....	393
13.4.2	Biotechnological Products Recovery-Separation .....	394
13.4.3	Pharmaceutical Products Recovery-Separation .....	394
13.4.4	Organic Compounds Separation, Organic Pollutants Recovery from Wastewaters .....	394
13.4.5	Gas Separations .....	396
13.4.6	Fermentation or Enzymatic Conversion-Recovery-Separation (Bioreactors) .....	397
13.4.7	Analytical Applications .....	397
13.5	Concluding Remarks .....	398
	Nomenclature .....	398
	References .....	399

## 13.1 INTRODUCTION AND DEFINITIONS

Permeation is a general term for the concentration-driven membrane-based mass transport process. Application of a pressure difference, an electric field, or temperature considerably intensifies the process, but these special methods are beyond the scope of this overview. Three groups of liquid membranes are usually considered: bulk liquid membrane (BLM), supported liquid

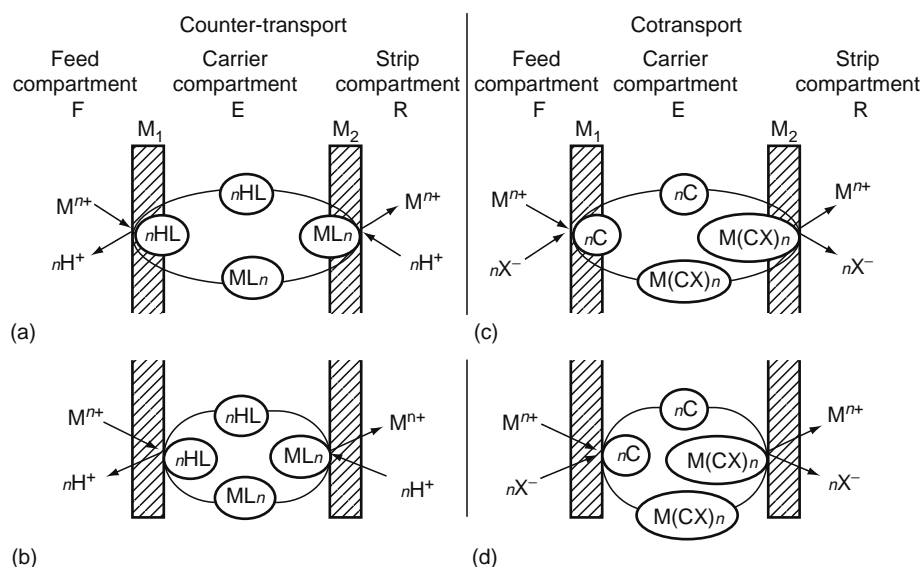


**FIGURE 13.1** Schematic transport models of an OHLM system with a, c: hydrophobic membranes; b, d: hydrophilic or ion-exchange membranes. (From Kislik, V. and Eyal, A., *J. Mem. Sci.*, 111, 273, 1996. With permission.)

membrane (SLM), or immobilized liquid membrane (ILM), and emulsion liquid membrane (ELM). The scope of this chapter is BLM processes.

The term organic hybrid liquid membrane (OHLM) includes all BLM processes incorporating liquid–liquid extraction (LLX) and membrane separation in one continuously working module. OHLM utilizes an extracting reagent (carrier) solution, immiscible with water, circulating or flowing between membranes as barriers. The concept of the OHLM transport is quite simple: a solution of an extracting reagent (carrier phase, E), flows between two membranes, which separate the carrier phase from the feed (F) and receiving (R) phases (see Figure 13.1). A specific solute or solutes diffuse to the F/E interface is extracted from feed phase by an LM extracting reagent as a result of the thermodynamic conditions at the F/E interface, the solute–carrier complex diffuses to the E/R interface and is simultaneously stripped by the receiving phase due to the different thermodynamic conditions at the E/R interface. The membranes are permeable to solutes, but block transfer of the carrier solution to the feed or to the strip solutions. Blocking the carrier is accomplished through membrane hydrophilic/hydrophobic or ion-exchange properties, or through their pore size.

The OHLM term includes several similar LM systems, developed by different research groups, such as hybrid liquid membrane (HLM) by Kislik et al. [1–3], hollow-fiber liquid membrane (HFLM) by Sirkar et al. (HFCLM) [4–8], Schlosser et al. (HFLM) [9–11], pertraction by Boyadzhiev et al. [12–22], Schlosser et al. [23–26], Wodzki et al. [27–29], flowing liquid membranes (FLM) by Teramoto et al. [30–37], membrane-based extraction and stripping by Schlosser et al. [38–40], Kedem et al. [41–43], Eyal et al. [44,45], multimembrane hybrid system (MHS) by Wodzki et al. [46–51]. All these systems are based on the membrane-based nondispersive (as the means for blocking the organic reagent from mixing with the aqueous feed and strip solutions) selective LLX coupled to permselective diffusion of solute–extractant complexes and selective stripping of the solute in one continuous dynamic process. A great number of terms for similar BLM processes confuse the readers. Some of these terms vary by membrane type used (hollow-fiber, flat neutral, ion-exchange sheets) [4–14]; some are by module design [4–8,12–14,23–25,38–40,46–50]. The term pertraction, or perstraction [52] spread over the supported liquid membrane (SLM) and emulsion liquid membrane (ELM) [20,53], what is not so correct, because the SLM (or ILM) and ELM are steady-state processes. Therefore, all above-mentioned BLM processes may be unified under the term OHLM systems.

In this chapter, the basic principles of the OHLM such as interaction mechanisms and theories of transport, design considerations will be analyzed by comparison of modifications of different research groups. Application in the last decade of different modifications of the OHLM systems in solutes separation is presented.

Recently developed aqueous hybrid liquid membrane (AHLM) separation process is similar to the OHLM except the liquid membrane phase is an aqueous solution as are the feed and strip solutions [70,119]. But these systems are not included in this chapter.

### 13.2 THEORY: MASS TRANSFER MECHANISMS AND KINETICS

General properties of liquid membrane systems have been a subject of extensive theoretical studies. Six basic mechanisms of transport are schematically shown in Figure 13.2. In a simple transport (Figure 13.2a), solute passes through due to its solubility

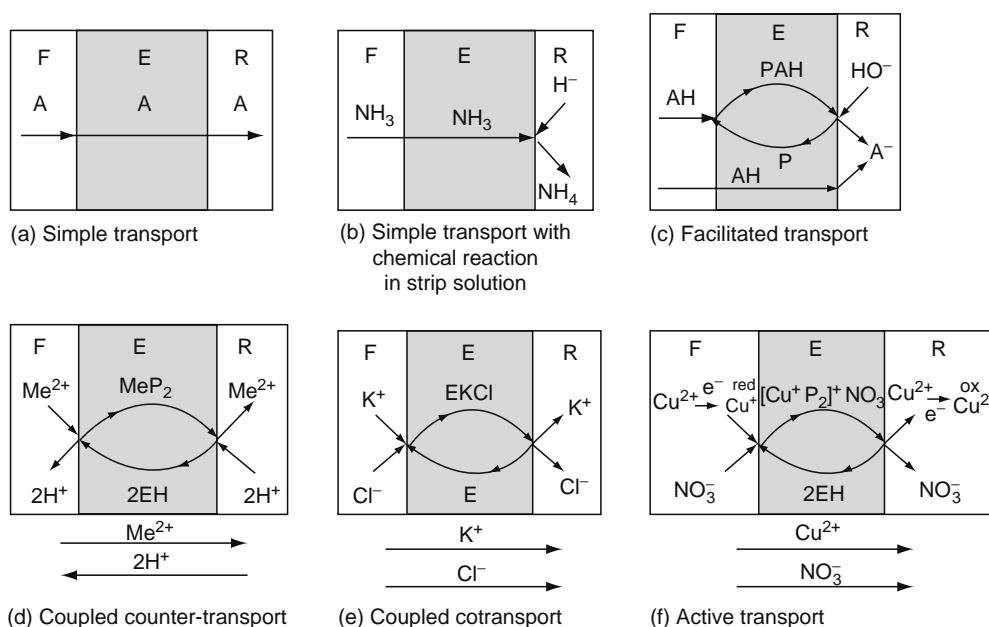


**FIGURE 13.2** Schematic mechanisms of solute transport through the BLMs. A, Me, K, Cu,  $\text{NH}_3$ —solutes, E—carrier, F—feed solution, R—stripping solution. (From Schlosser, S. Pertraction through liquid and polymeric membranes. In: Belafi-Bako, K., Gubicza, L., and Mulder, M. Eds. *Integration of Membrane Processes into Bioconversions*. Proceedings of the 16th European Membrane Society Annual Summer School. Veszprem, Hungary, August 1999. Kluwer Academic/Plenum Publishers, New York, 2000, 73–100. With permission.)

in LM. Permeation stops when concentration equilibrium is reached. The solute is in the same form R in the feed (F), LM (E), and strip (receiving, R) phases. As an example, some carboxylic and amino acids [54,55], phenol transport through xylene, decanol LM [8] may be presented. Uphill transport and selectivity can be achieved at reaction of the solute with components of the stripping solution (see Figure 13.2b).

Facilitated transport takes place when a carrier reacts with a solute on a feed side-LM interface to form complex. This complex reverse reacts on the LM-strip side interface releasing the solute to the strip phase (see Figure 13.2c). Facilitated transport accelerates the transport. For example, trialkylphosphine sulfide increases the rate of phenol transport [11]. At the same time, the simple transport can also take place.

As examples of coupled counter-transport (see Figure 13.2d) and coupled cotransport (see Figure 13.2e) the transport of titanium(IV) from low acidity ( $\text{pH} = 1$ ) and high acidity ( $[\text{H}^+] = 7 \text{ M}$ ) feed solutions, respectively using the HLM system [1,2] may be presented. The di-(2-ethylhexyl) phosphoric acid (DEHPA) carrier reacts with Ti(IV) ion to form complexes on the feed side (see Equations 13.25 and 13.26) and reversible reactions take place on the strip side (see Equations 13.27 and 13.28). Energy for the titanium uphill transport is gained from the coupled transport of protons in the direction opposite to titanium transport from the strip to the feed solutions. In the second case (high-feed acidity), Cl anion cotransported with Ti(IV) cation in the same direction. In both cases fluxes of titanium, protons, and chlorine anion are stoichiometrically coupled.

Active transport (see Figure 13.2f) is driven by oxidation–reduction reactions on the membrane interfaces. No other species are transported in this type of transport. As examples, copper transport by thioether [56] and picrate anions by ferrocene [57,58] as carriers may be presented.

Any universal model for all these types of transport does not exist, and the available knowledge concerning the specific interfacial processes should be taken into account in the description of a real membrane process. There are two general approaches to modeling liquid membrane transport mechanisms: the differential and the integral approach. According to the differential approach [16–22,33–37,59], all phenomena taking place in the feed or in the strip phase, such as diffusion, chemical reactions, etc., are totally ignored. The measured transfer fluxes are dependent on phenomena occurring in the BLM or at the surface of the membrane only. The integral approach [1–12,23–29,40,46–60] considers the three liquid phase system to be a closed\* multiphase system and, therefore, takes into consideration the processes and changes in all three liquids. Most models are very sophisticated because they assume many possible types of control, nonlinear equilibria, phase interactions, etc. The integral approach has been formulated in Ref. [4]:

\* “A closed system is one with boundaries across it, through which no matter may pass, either in or out, but one in which other changes may occur, including expansion, contraction, internal diffusion, chemical reaction, heating, and cooling. An open system is one which undergoes all the changes allowed for a closed system and in addition it can lose and gain matter across its boundaries” [78].

1. Overall mass transfer rate can be controlled by any of the diffusion resistances in the three liquid phases.
2. Aqueous and organic film resistances may be combined with membrane pore diffusion resistance in one-dimensional series of diffusion resistances.

However, the assumption of the steady-state mass transfer through the bulk membrane phase, has been made by some authors [43,61], is oversimplified in many cases, and the assumption of equality of solute distribution coefficients of extraction and back extraction [18,46], is incorrect for most separation systems.

A number of reviews and theoretical articles have appeared on related subjects. Theoretical aspects of the HFLM selective separation processes have been covered in the reviews and articles by Sirkar et al. [4–7,62,63], and in new modifications by Schlosser et al. [9–11,25]. Theory for separations by the FLM is presented in the articles by Teramoto M et al. [31,34–37]; theoretical considerations for rotating film pertraction systems have been described by Boyadzhiev [18,64–68], and theoretical considerations for the MHSs have been described by Wodzki et al. [27,29,46,47,49,51].

Examples of the model considerations, presented below, can be regarded as simplified examples only. The processes have been studied using analytical [1] and numerical [27] solutions for both the local steady-state [1,2,69,70] and dynamic nonstationary [27,71,72] conditions, respectively. Both models, HLM [1] and MHS [27], with some modifications may be used for theoretical analysis of all OHLM systems. Considerations for hollow-fiber systems are presented also in a short.

### 13.2.1 MODEL FOR THE HLM SYSTEM [1–3]

#### 13.2.1.1 Mass Transfer Mechanisms and Kinetics

The theory for HLM was developed for flat thin uncharged symmetric membranes without variation in porosity and pore sizes across the membrane thickness.

To develop three-phase, HLM system model [1,2], the transport model simplification analysis, developed by Shagxu Hu [73] for the two-phase system, is used.

Titanium, as an example for the transport model verification, was chosen because of the extensive experimental data available on LLX and membrane separation [1,2,74–76] and of its extraction double-maximum acidity dependence phenomenon [74]. This behavior was observed for most extractant families: basic (anion exchangers), neutral (complexants), and acidic (cation exchangers). So, it is possible to study both counter- and cotransport mechanisms at  $\text{pH} \geq 0.5$  and  $[\text{H}]^+ \geq 7 \text{ mol/kg}$  feed solution acidities, respectively, using neutral (hydrophobic, hydrophilic) and ion-exchange membranes.

In general, the mass transfer rate (or flux) of any solute passing through the barrier (membrane) is a function of distance and time:  $J = f(x, t)$ . First, let us consider the flux as a function of distance.

Three liquids, having bulk solute *i* concentration  $[C_i]_F$ ,  $[C_i]_E$ , and  $[C_i]_R$ , constant volumes  $V_F$ ,  $V_E$ , and  $V_R$ , respectively, are separated by two membranes with the same working area *S*. Stirring of bulk liquids is effective in such a way that the aqueous ( $h_{fe}$ ,  $h_{re}$ ) and the organic ( $h_{ef}$ ,  $h_{er}$ ) boundary layers become sufficiently thin and constant. Concentration profiles in the HLM system with hydrophobic membranes are demonstrated in Figure 13.3, while those containing hydrophilic or ion-exchange membranes are demonstrated in Figure 13.4.

Using the concept of the one-dimensional series of diffusion resistances, and regarding the principle of resistance additivity [1–40,46–53], the overall mass transfer coefficients or permeability coefficients [58,77]  $K_F$  on the feed side and  $K_R$  on the strip side are related to the individual films (including membrane barrier) mass transfer coefficients, *k*:

For hydrophobic membranes, for hydrophilic or ion-exchange membranes

For hydrophobic membranes

$$K_F = \frac{k_{fe}k_{mf}k_{ef}E_F}{k_{fe}k_{ef} + k_{fe}k_{mf} + k_{mf}k_{ef}E_F} \quad (13.1a)$$

$$K_R = \frac{k_{re}k_{mr}k_{er}}{k_{mr}k_{er}E_R + k_{mr}k_{re} + k_{re}k_{er}} \quad (13.2a)$$

For hydrophilic or ion-exchange membranes

$$K_F = \frac{k_{fe}k_{mf}k_{ef}E_F}{k_{fe}k_{mf} + k_{fe}k_{ef}E_F + k_{mf}k_{ef}E_F} \quad (13.1b)$$

$$K_R = \frac{k_{re}k_{mr}k_{er}}{k_{mr}k_{er}E_R + k_{re}k_{er}E_R + k_{mr}k_{re}} \quad (13.2b)$$

where  $E_F$  and  $E_R$  are distribution coefficients of solutes between membrane and aqueous feed, and strip phases, respectively at local equilibrium.

Individual film mass transfer coefficients may be determined by the following considerations. According to postulates of nonequilibrium thermodynamics [78], the general equation that relates the flux, *J*, of the solute to its concentration, *C*, and its derivative, is [79]

$$J = UC - D \frac{dC}{dx} \quad (13.3)$$

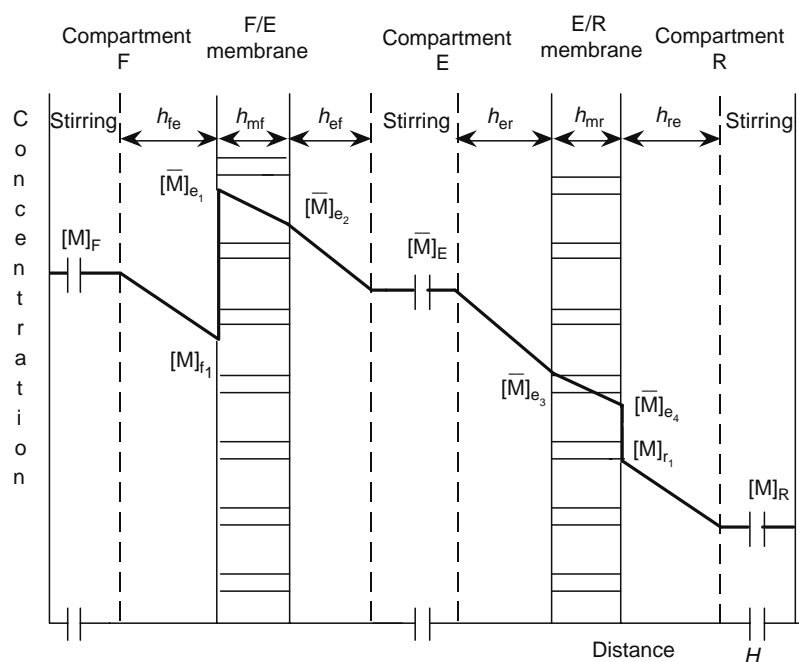


**FIGURE 13.3** Schematic concentration profile of each Ti(IV) chemical species, transported through the HLM system with hydrophobic membranes. Layers controlling the permeation rate are  $h_{fe}$ , feed-side aqueous boundary layer;  $h_{mf}$ , feed-side microporous membrane, immobilized by membrane solution;  $h_{ef}$ , feed-side boundary layer of the membrane solution;  $h_{er}$ , strip-side boundary layer of the membrane solution;  $h_{mr}$ , strip-side microporous membrane, immobilized by membrane solution;  $h_{re}$ , strip-side aqueous boundary layer. (From Kislik, V. and Eyal, A., *J. Mem. Sci.*, 111, 259, 1996. With permission.)

where

$U$  is the flow rate

$D$  is the sum [80] of all effective diffusion coefficients

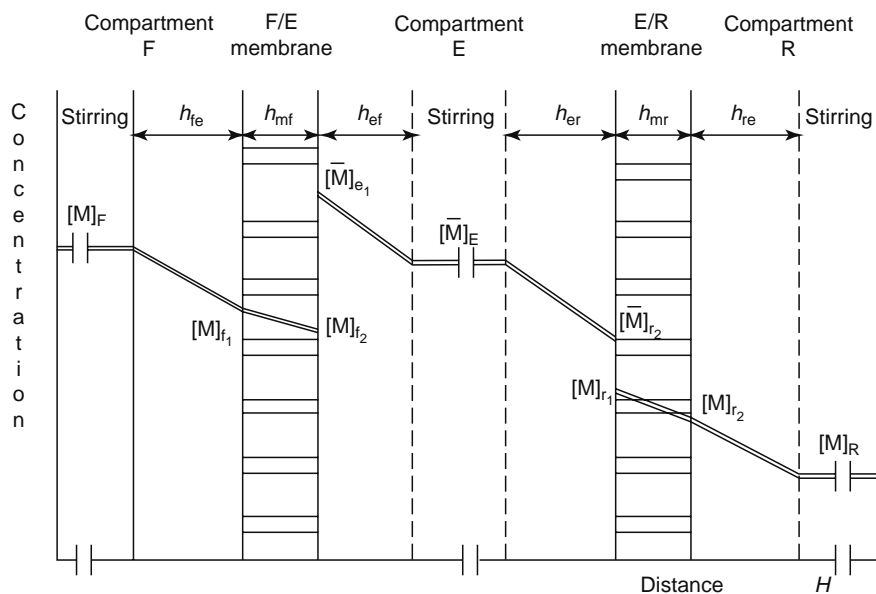


**FIGURE 13.4** Schematic concentration profile of each Ti(IV) chemical species, transported through the OHLM with hydrophilic or ion-exchange membranes. Layers controlling the permeation rate are the same as those in Figure 13.3, except for  $h_{mf}$ , feed-side microporous membrane is immobilized by feed aqueous solution;  $h_{mr}$ , strip-side microporous membrane is immobilized by strip aqueous solution. (From Kislik, V. and Eyal, A., *J. Mem. Sci.*, 111, 259, 1996. With permission.)

Referring to the equation of continuity, as  $x$  approaches zero, the steady-state zones or layers are formed next to the phase's interface (but not for the bulk phases, where  $x \gg 0$ ). Separation then occurs by differential displacement permeation through the interface. Efficiency of the separation hinges directly on the distribution of solute in the steady-state layers.

Using Giddings' analysis [81] of such a system we obtain

$$\ln \left[ \left( C - \frac{J_o}{U} \right) / \left( C_o - \frac{J_o}{U} \right) \right] = U \frac{h}{D} \quad (13.4)$$

According to [4-40,46-53,67,72,82,83] the mass transfer coefficient of every layer,  $k_i$ , is

$$k_i = \frac{D_i}{h_i} \quad (13.5)$$

where

$D_i$  is the free diffusion coefficient of the solute in the layer

$h_i$  is the thickness of the layer [72]

Replacing Equations 13.4 with 13.5 we obtain

$$k_i = U \left\{ \ln \left[ \left( C_i - \frac{J_{ss}}{U} \right) / \left( C_{i-1} - \frac{J_{ss}}{U} \right) \right] \right\}^{-1} \quad (13.6)$$

where

$C_i$  is the concentration of the solute in the bulk solution at time of sampling  $t_i$

$C_{i-1}$  is the concentration of the solute in the same solution at time of previous sampling  $t_{i-1}$

According to Sirkar's assumption [84], diffusion mass transfer rate through a membrane having a solvent-filled pore (hydrophobic), or an aqueous solution-filled pore (hydrophilic or ion exchange) may be expressed through the diffusion coefficients of the solute in the respective interface layers:

For hydrophobic membranes

$$k_{mf} = \frac{D_{ef} \varepsilon_m}{h_{mf} \tau_m} \quad (13.7a)$$

$$k_{mr} = \frac{D_{er} \varepsilon_m}{h_{mr} \tau_m} \quad (13.8a)$$

For hydrophilic or ion-exchange membranes

$$k_{mf} = \frac{D_{fe} \varepsilon_m}{h_{mf} \tau_m} \quad (13.7b)$$

$$k_{mr} = \frac{D_{re} \varepsilon_m}{h_{mr} \tau_m} \quad (13.8b)$$

where

$\varepsilon_m$  is the membrane porosity

$\tau_m$  is the membrane tortuosity

These expressions are valid when the following assumptions are held:

- There is unhindered diffusion of the solute (solute dimensions  $10^2 \leq$  pore dimensions).
- Membrane is symmetric and completely wetted by the designated phase.
- No two-dimensional effects occur.

Applicability of these expressions for charged membranes is doubtful because of hindered diffusion of solute in their pores, but it may be evaluated experimentally. One more serious simplification is that the influence of the flow velocities extends inside the membrane pores.

Another way of evaluating mass transfer coefficients through the membranes may be proposed, providing the membranes possess the same properties (diffusion resistance, porosity, tortuosity, etc.). They may, however, be of different thicknesses. It is clear from Equation 13.4 that diffusion coefficient (exactly  $U/D$ , where  $U$  is known) of the solute through the feed-side and strip-side membranes may be evaluated as a slope of the plots:

$$-\ln\left(\frac{C}{C_0}\right)F = f(h_{mf}) \quad (13.9)$$

$$\ln\left(\frac{C}{C_0}\right)R = f(h_{mr}) \quad (13.10)$$

Individual mass transfer coefficients of the solute (for example, titanium compound) can be experimentally determined in every layer and membrane. Thus, overall mass transfer coefficients of the feed ( $K_{cF}$ ) and strip ( $K_{cR}$ ) sides of the OHLM system may be calculated from Equations 13.1a, 13.1b, 13.2a, and 13.2b.

Now the concentration profiles in the system, as a function of time, can be analyzing.

Introducing the assumptions as

- Linear concentration gradients
- Concentration of the solute permeating species is lower than that of the carrier in the membrane phase
- Instantaneous interfacial chemical reactions and local reaction equilibria at the interfaces [1,4–8,30–37,46–51, 61,77,84]

we can derive the transport rate and distribution relation equations for any solute  $[M]$  permeating species:

$$V_F \left( \frac{d[M]_F}{dt} \right) = -SK_F([M]_F V_F - [\bar{M}]_E V_E) \quad (13.11)$$

$$V_E \left( \frac{d[\bar{M}]_E}{dt} \right) = SK_F([M]_F V_F - [\bar{M}]_E V_E) - SK_R([\bar{M}]_E V_E - [M]_R V_R) \quad (13.12)$$

From overall material balance of the system

$$[M]_R = \frac{Q^0}{V_R} - \frac{V_F}{V_R} [M]_F - \frac{V_E}{V_R} [\bar{M}]_E \quad (13.13)$$

where

$[M]_F^0$ ,  $[\bar{M}]_E^0$ , and  $[M]_R^0$  are initial concentrations of a solute specie in the feed, membrane, and strip phases, respectively  
 $Q^0$  is the overall initial quantity of the solute in the OHLM system

The system described in Equations 13.11 through 13.13 results in an analytical solution under the assumption that the mass transfer coefficients are constant\* (at flow or stirring rates constant). Following are complete set of the model equations:

$$[M]_F = \frac{\gamma}{\beta} + C_1 e^{\gamma t} + C_2 e^{\alpha t} \quad (13.14)$$

$$[\bar{M}]_E = \left[ \frac{\gamma}{\beta} + C_1 e^{\gamma t} \left( 1 + \frac{\gamma_1}{k_F S} \right) + C_2 e^{\alpha t} \left( 1 + \frac{\gamma_2}{k_F S} \right) \right] \frac{V_F}{V_E} \quad (13.15)$$

$$[M]_R = \frac{Q^0}{V_R} - [M]_F \frac{V_F}{V_R} - [\bar{M}]_E \frac{V_E}{V_R} \quad (13.16)$$

$$\alpha = 2S(K_F + K_R) \quad (13.17)$$

$$\beta = 3S^2 K_F K_R \quad (13.18)$$

$$\gamma = K_F K_R \frac{S^2}{V_F} Q^0 \quad (13.19)$$

$$\frac{\gamma}{\beta} = \frac{Q^0}{3V_F} = \frac{[M]_F^0 V_F + [\bar{M}]_E^0 V_E + [M]_R^0 V_R}{3V_F} \quad (13.20)$$

\* In the real continuous OHLM system, mass transfer coefficients  $K_F$  and  $K_R$  may be close to constant at the stabilized conditions of the process (acidity or pH, temperature, flow rates, etc.).

$$y_1 = -\frac{\alpha}{2} + \sqrt{\frac{\alpha^2}{4} - \beta} \quad (13.21)$$

$$y_2 = -\frac{\alpha}{2} - \sqrt{\frac{\alpha^2}{4} - \beta} \quad (13.22)$$

$$C_1 = \frac{y_2 \left( [M]_F^0 - \frac{\gamma}{\beta} \right) - SK_F \left( [\overline{M}]_E^0 \frac{V_E}{V_F} - [M]_F^0 \right)}{y_2 - y_1} \quad (13.23)$$

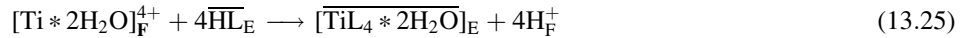
$$C_2 = -\frac{y_1 \left( [M]_F^0 - \frac{\gamma}{\beta} \right) - SK_F \left( [\overline{M}]_E^0 \frac{V_E}{V_F} - [M]_F^0 \right)}{y_2 - y_1} \quad (13.24)$$

### 13.2.1.2 Driving Forces

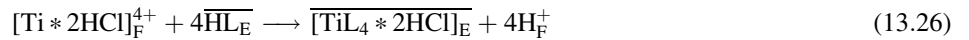
The transport of titanium(IV) species through HLM can be formally described as a simultaneous combination of diffusion, extraction, and stripping operations occurring in nonequilibrium conditions. These systems are very complicated to analyze and therefore, some assumptions are needed for simplification. Extraction kinetics and stripping processes are much faster for most metal ions than their diffusion, and many researchers have adopted the local extraction equilibrium of feed-extractant and extractant-strip phases at the membrane interfaces. So, the chemistry of the OHLM system at equilibrium conditions has to be analyzed.

The chemical reactions responsible for the transport can be schematized [74–76].

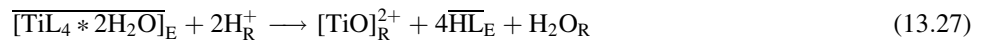
At the feed solution–membrane (carrier) solution interface, for feed at low acidity (pH region)



at high (>7 mol/kg) acidity



At the membrane solution–strip solution interface, at low acidity (pH region)



at high acidity



These reactions are characterized by equilibrium constants:

$$K_{F/E} = \frac{\overline{[\text{TiL}_4 * 2\text{H}_2\text{O}]_E} * [\text{H}]_F^4}{[\overline{\text{HL}}_E]^4 * [\text{Ti} * 2\text{H}_2\text{O}]_F} = E_F * \left( \frac{[\text{H}]_F}{[\overline{\text{HL}}_E]} \right)^4 \quad (13.29)$$

or

$$K'_{F/E'} = \frac{\overline{[\text{TiL}_4 * 2\text{HCl}]_E} * [\text{H}]_F^4}{[\overline{\text{HL}}_E]^4 * [\text{Ti} * 2\text{HCl}]_F} = E_{F'} * \left( \frac{[\text{H}]_F}{[\overline{\text{HL}}_E]} \right)^4 \quad (13.29a)$$

$$K_{E/R} = \frac{[\text{TiO}]_R * [\overline{\text{HL}}_E]^4 * [\text{H}_2\text{O}]}{\overline{[\text{TiL}_4 * 2\text{H}_2\text{O}]_E} * [\text{H}]_R^2} = \frac{[\overline{\text{HL}}_E]^4}{[\text{H}]_R^2} * E_R \quad (13.30)$$

or

$$K'_{E/R'} = \frac{[\text{TiO}]_R * [\overline{\text{HL}}]_E^4 * [\text{CL}]_R^2}{[\text{TiL}_4 * 2\text{HCl}] * [\text{H}_2\text{O}]} = \frac{[\overline{\text{HL}}]_E^4 * [\text{Cl}]_R^2}{E_R} \quad (13.30a)$$

where  $E_F$  and  $E_R$  are distribution coefficients of titanium ions between membrane and aqueous feed, and strip phases, respectively and concentration of  $\text{H}_2\text{O}$  is neglected.

$$K = K_{F/E} * K_{E/R} = \left(\frac{E_F}{E_R}\right) \left(\frac{[\text{H}]_F^4}{[\text{H}]_R^2}\right) \quad (13.31)$$

or

$$K' = K'_{F/E} * K'_{E/R} = \left(\frac{E'_F}{E'_R}\right) ([\text{H}]_F^4 * [\text{Cl}]_R^2) \quad (13.31a)$$

$K$  (or  $K'$ ) is denoted as a driving force coefficient of the HLM system. Consider

$$K = K_c * K_d \quad \text{where } K_c = \frac{E_F}{E_R} \quad \text{and } K_d = \frac{[\text{H}]_F^4}{[\text{H}]_R^2} \quad (13.32)$$

or

$$K' = K'_c * K'_d \quad \text{where } K'_c = \frac{E'_F}{E'_R} \quad \text{and } K'_d = [\text{H}]_F^4 * [\text{Cl}]_R^2 \quad (13.32a)$$

$K_c$  is denoted as an internal [83] (carrier) driving force coefficient, derived from extraction distribution ratio between liquid membrane phase and feed, and receiving phases.  $K_d$  (or  $K'_d$ ) is denoted as an external driving force coefficient, derived from the coupling effect of the HLM system.

These initial parameters are easily accessible experimentally by equilibrium extraction experiments [75]. For example, extraction of titanium(IV) from 0.1 mol/kg Ti(IV) hydrochloric acid solutions at 0.45 mol/kg (pH = 0.65), 2 mol/kg and at 7 mol/kg HCl by 1 mol/kg DEHPA in benzene, at aqueous phase/organic phase = 5/1, have shown the initial distribution coefficients (for details, refer to [75]):

$$\begin{aligned} E_{F1} &= 20-25 \text{ for the aqueous phase at pH} = 0.65, \\ E_{F2} &= 200-220 \text{ for the aqueous phase at } 7.0 \text{ mol/kg HCl}, \\ E_R &= 1.5-2.0 \text{ for the aqueous phase at } 2.0 \text{ mol/kg HCl}. \end{aligned}$$

The initial distribution ratios  $K_c = E_F/E_R$  (internal or liquid membrane driving force coefficients) are

$$K_c = 10-15 \quad K'_c = 100-150$$

Of course, during the transport process in the closed HLM system, the distribution ratio will change in accordance with changing feed and strip phase conditions (acidities, titanium concentration, etc.). At  $K_c = 1$  ( $E_F = E_R$ ), concentration of titanium (IV) in the carrier solution should be  $[\text{Ti}]_R E_R$  (the system at equilibrium). Therefore,  $E_R$  may be denoted as an irreversible coefficient of the HLM for both, closed and open [78] systems (flowing feed, strip streams, buffered acidities, etc.).  $K_c$  is an “uphill pumping” border of the HLM system.

### 13.2.2 NUMERICAL MODEL OF COMPETITIVE $\text{M}^{2+}/\text{H}^+$ COUNTER-TRANSPORT [27,86–89]

A mathematical model to be solved numerically has been developed and used to predict the separation effects caused by nonstationary conditions for a liquid membrane transport. Numerical calculations were made to compute pertraction\* characteristics such as input and output membrane selectivity (ratio of respective fluxes), concentration profiles for cations bound by a carrier in a liquid membrane phase, and the overall separation factors. These quantities are discussed as dependent

\* The term “pertraction,” used by the authors [27,86] has not been changed in the following text (for explanations see Section 13.1).

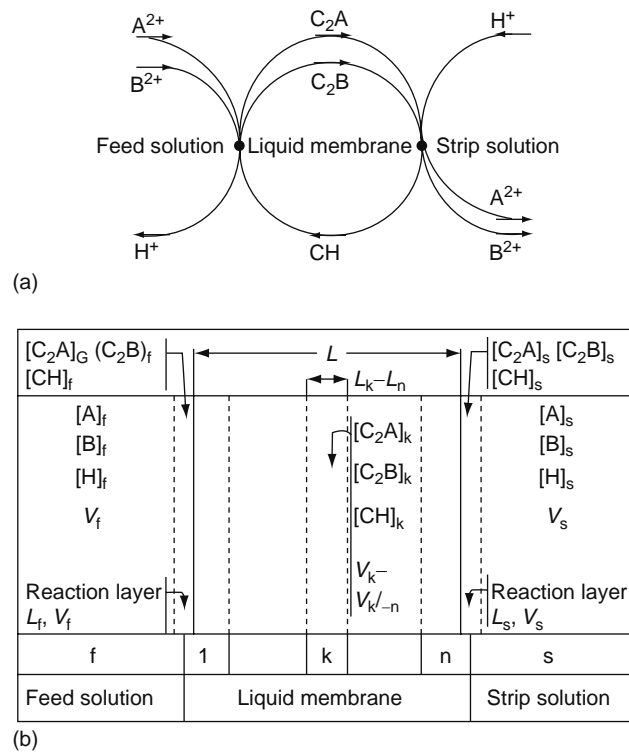


**FIGURE 13.5** (a) Scheme of  $A^{2+}$ ,  $B^{2+}/H^+$  competitive counter-transport mediated by an ionic carrier CH; (b) Compartmental model of pertraction system. (From Wodzki, R., Szczepanska, G., and Szczepanski, P., *Sep. Purif. Technol.*, 36, 1, 2004. With permission.)

on time, the kinetic constants of interfacial reversible reactions, and diffusion coefficients of carrier species in a liquid membrane phase. The computations of fluxes and separation factors as dependent on time have revealed high separation efficiency of unsteady-state pertraction as compared with steady or near-steady-state process (with reactions near equilibrium state).

The mechanism of competitive pertraction system (CPS) is presented schematically in Figure 13.5 together with the compartmental model necessary for constructing the reaction–diffusion network. The overall pertraction process consists of a set of diffusion steps and reactions leading to the uptake or release of cations at two formally independent and possibly different interfaces. The simple flat-layered BLM of the thickness  $L_m$  and interface area  $S$  separates the two reservoirs (f, feed; and s, stripping) containing transported divalent cations  $A^{2+}$  and  $B^{2+}$  (most frequently  $Zn^{2+}$  and  $Cu^{2+}$  or  $Ca^{2+}$  and  $Mg^{2+}$ ) or antiported univalent cations  $H^+$ . At any time of pertraction  $t$ , their concentrations are  $[A]_f$ ,  $[B]_f$ ,  $[H]_f$ , and  $[A]_s$ ,  $[B]_s$ , and  $[H]_s$ , for the feed and stripping solution, respectively. The hydrophobic liquid membrane contains a carrier (C) of the total concentration  $[C]$ . The carrier is confined to the membrane phase and cannot dissolve at the adjacent aqueous solutions. Its main property is the ability to react reversibly with cations at respective reaction zone and to diffuse throughout the liquid membrane phase in its salt ( $C_2A$ ,  $C_2B$ ) or acid (CH) form. It is also assumed that ionic species or their ionic pairs cannot diffuse in membrane phase without the carrier intervention. The membrane is formally divided into  $n$  homogeneous compartments, which contains the carrier in the form  $C_2A$ ,  $C_2B$ , and CH the local concentration of which are equal to  $[C_2A]_k$ ,  $[C_2B]_k$ , and  $[CH]_k$ , with  $k = 1, 2, \dots, n$ . In the case of bulk agitated or flowing liquid membranes, the model should be modified by adding a large central compartment (layer) acting as an additional capacitor enabling convective flow of the membrane liquid.

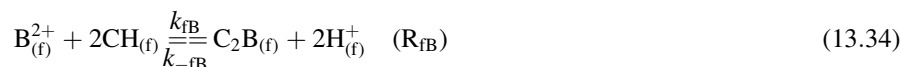
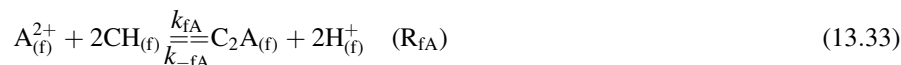
The following are the assumptions of the model:

1. Concentrations of ionic species within interfacial reaction layers of thickness  $L_f$  and  $L_s$  are the same as in the feed or stripping solution, respectively.
2. Concentrations of cations bound by the carrier at respective interfacial layer, i.e.,  $[C_2A]_i$ ,  $[C_2B]_i$ , and  $[CH]_i$  with  $i = f$  or  $s$ , are the same as the concentrations in the membrane compartments indexed by  $k = 1$  or  $n$ .
3. Interfacial carrier molecules are presented by their hydrophilic fragments in adjacent aqueous solutions and by their hydrophobic parts in an organic phase of a liquid membrane. Thus, the reaction can be treated as a homogeneous type occurring in an adjacent reaction zone instead of a heterogeneous adsorption-type reaction process.
4. Initial concentration of the carrier is the same as in a bulk liquid membrane phase.
5. Concentration of free cations is the same as in the bulk aqueous phase.
6. Thermodynamic couplings between transported species are negligible.

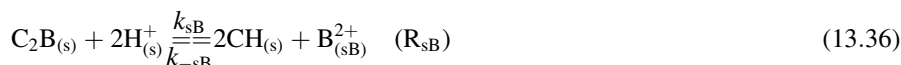
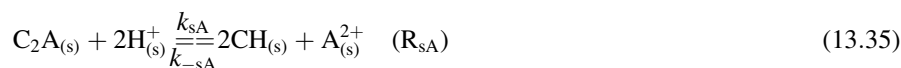
At these assumptions and simplifications the thermodynamic network analysis (TNA) [90] can be applied to analyze LM transport. Certainly in the case of a real specific system, the detailed mechanism of reaction–diffusion interfacial phenomena should be taken into account as far as possible. The above assumptions allow maintaining a concept of a homogeneous reaction. Any universal model does not exist, and in the description of a real membrane process the accessible knowledge concerning the specific interfacial processes should be taken into account. The model presented can be regarded as a simplified example only.

According to the scheme presented in Figure 13.4, two competitive cation-exchange processes occur at each of the interfaces:

At the feed interface



At the strip interface



The reactions between the carrier and the two cations cannot be considered as parallel because  $A^{2+}$  and  $B^{2+}$  compete toward the same carrier or the respective carrier forms compete in the reaction with a stripping agent. Thus, the respective reaction rates are represented by coupled differential equations resulting from networks in Figure 13.6.

The symbols  $k_{i,M}$  and  $k_{-i,M}$  ( $i = f, s, M = A, B$ ) denote the kinetic constants for the rates of reversible reactions given by Equations 13.37 through 13.40:

$$J_{f,A} = k_{f,A}[A]_f[CH]_f^2 - k_{-f,A}[C_2A]_f[H]_f^2 \quad (13.37)$$

$$J_{f,B} = k_{f,B}[B]_f[CH]_f^2 - k_{-f,B}[C_2B]_f[H]_f^2 \quad (13.38)$$

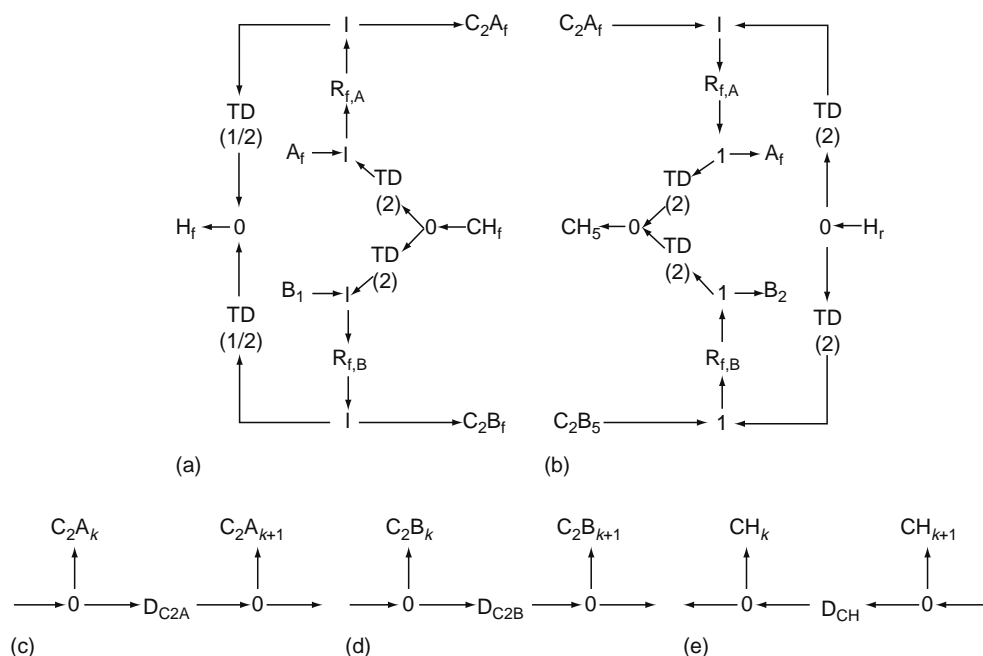


**FIGURE 13.6** Network for feed (a) strip, (b) competitive cation-exchange reactions, and local diffusion processes: (c)  $C_2A$ , (d)  $C_2B$ , and (e)  $CH$  species. (From Wodzki, R., Szczepanska, G., and Szczepanski, P., *Sep. Purif. Technol.*, 36, 1, 2004. With permission.)

$$J_{s,A} = k_{s,A}[C_2A]_s[H]_s^2 - k_{-s,A}[CH]_s^2[A]_s \quad (13.39)$$

$$J_{s,B} = k_{s,B}[C_2B]_s[H]_s^2 - k_{-s,B}[CH]_s^2[B]_s \quad (13.40)$$

According to the scheme of the compartments in the liquid membrane system in Figure 13.5b, all local diffusion fluxes of M species from  $k$  to  $k + 1$  compartment can be defined by a phenomenological Equation 13.41 corresponding with the first Fick's law for diffusion:

$$N_{j(k,k+1)} = P_j \Delta[X]_{j(k,k+1)} \quad (13.41)$$

where  $P_j$  denotes the permeability coefficient of species (e.g., carrier in different forms) between  $k$  and  $k + 1$  compartment:

$$P_j = D_j S / (L_m / n) \quad (13.42)$$

In Equations 13.37 through 13.41  $\Delta[X]_{j(k,k+1)}$  denotes the concentration difference, between the compartment  $k$  and  $k + 1$ , for the carrier transporting cation  $j$  ( $j = A^{2+}, B^{2+}, H^+$ ) with the diffusion coefficient  $D_j$ . Consequently, the diffusion coefficients of a carrier transporting different cations are different but constant throughout the liquid membrane (independent of their local concentration).

To construct the pertraction network, the particular reaction networks should be added via "0" junctions to three linear networks corresponding with the processes of diffusion of  $C_2A$ ,  $C_2B$ , and  $CH$  carrier species. The resulting reaction-diffusion network, as presented in Figure 13.6, consists of four coupled loops representing the pertraction of  $A^{2+}$ ,  $B^{2+}$ , and  $H^+$  cations. The loops are coupled by common capacitances  $A_i$ ,  $B_i$ , and  $H_i$  ( $i = f, s$ ) and by the capacitances  $CH_i$  and  $CH_k$  for a reacting or diffusing acidic form of the carrier. From the network in Figure 13.6, all the model equations used further in numerical calculations can be deduced with the help of Kirchhoff's law for a 0 junction (KCL):

$$\sum_k v_k N_k = 0 \quad (13.43)$$

where

$k$  is the index of the flux entering or leaving a given 0 junction

$v$  is  $\pm 1$  valued depending on the bond direction

Note that all the reactions and diffusion rates should be expressed in moles per second to maintain the compatibility of units.

The mathematical model derived from the network in Figure 13.6 together with the specification of all the local fluxes, time-dependent variables, and parameters is presented in Table 13.1. The model consists of ordinary differential equations (ODE) describing the evolution of all capacitances (local concentrations) characteristic for a membrane and external solutions.

A step-by-step simulation of the system can be carried out by numerical calculations when the initial values of capacitances and the values of parameters (constants) are assigned. The calculations have been performed using the model from Table 13.1 after assuming  $n = 4$ . This value is sufficient [86] to achieve reliable simulation data of typical liquid transport processes under study. However, it should be noted that the increase in the number of layers, i.e., increasing in  $n$  will always result in more precise calculations and predictions comparable to those achieved by analytic calculation methods. The  $n$ -value equal to 4 should be treated as the lowest limit required for obtaining quantitative data sufficient for the interpretation of the separation effects. The problem of proper compartmentalization can be especially significant when reactions locally attain quasi-equilibrium conditions.

The Madonna Berkeley (ver.3) solver of ODE, the set of parameters, and initial conditions describing a liquid membrane system (listed in Table 13.2) were applied to numerically investigate the properties of CPS. The main relations resulting from the computations were time-dependent values of (1) the concentration profiles of transported and antipported species in a liquid membrane, (2) the concentration of  $A^{2+}$  and  $B^{2+}$  in the external aqueous solutions, and (3) input and output fluxes of  $A^{2+}$  and  $B^{2+}$ . To characterize the membrane selectivity toward the target  $A^{2+}$  cations, the following quantities are calculated and discussed.

The selectivity ( $S_{N,i}$ ) is calculated as the ratio of  $A^{2+}$  and  $B^{2+}$  fluxes ( $N$ ) for feed (f) and strip (s) interface, henceforth it is called as input or output flux selectivity:

$$S_i = N_{A,i} / N_{B,i}, \quad i = f \text{ or } s \quad (13.44)$$

TABLE 13.1

### Mathematical Description of Competitive Pertraction of $A^{2+}$ , $B^{2+}$ Cation Mediated by an Ionic Carrier CH

Time-dependent variables—concentrations,  $\text{mol cm}^{-3}$

Feed (f) and strip (s) phase

Interfaces

Membrane

Feed solution

$[A]_i [B]_i [H]_i$   $i = f$  or  $s$

$[C_2A]_i [C_2B]_i [CH]_i$   $i = f$  or  $s$

$[C_2A]_k [C_2B]_k [CH]_k$   $k = 1, 2, \dots, n$

Stripping solution

Capacitance fluxes ( $\text{mol cm}^{-3} \text{ s}^{-1}$ )

$D[A]_f/dt = -(V_{f,r}/V_f)J_{f,A}$

$d[B]_f/dt = -(V_{f,r}/V_f)J_{f,B}$

$d[H]_f/dt = 2(V_{f,r}/V_f)(J_{f,A} + J_{f,B})$

Accumulation of  $A^{2+}$

$d[A]_s/dt = -(V_{s,r}/V_s)J_{s,A}$

$d[B]_s/dt = -(V_{s,r}/V_s)J_{s,B}$

$d[H]_s/dt = 2(V_{s,r}/V_s)(J_{s,A} + J_{s,B})$

Accumulation of  $B^{2+}$

Membrane and interfaces

$d[C_2A]_{f,r}/dt = J_{f,A} - N_{C_2A(f,1)}/V_{f,r}$

$d[C_2A]_1/dt = [N_{C_2A(f,1)} - N_{C_2A(1,2)}]/V_2$

$d[C_2A]_k/dt = [N_{C_2A(k-1,k)} - N_{C_2A(k,k+1)}]/V_k$

$d[C_2A]_n/dt = [N_{C_2A(n-1,n)} - N_{C_2A(n-2,n)}]/V_n$

$d[C_2A]_s/dt = N_{C_2A(n,s)}/V_{s,r} - J_{s,A}$

$d[C_2B]_{f,r}/dt = J_{f,B} - N_{C_2B(f,1)}/V_{f,r}$

$d[C_2B]_1/dt = [N_{C_2B(f,1)} - N_{C_2B(1,2)}]/V_1$

$d[C_2B]_k/dt = [N_{C_2B(k-1,k)} - N_{C_2B(k,k+1)}]/V_k$

$d[C_2B]_n/dt = [N_{C_2B(n-1,n)} - N_{C_2B(n,s)}]/V_n$

$d[C_2B]_s/dt = N_{C_2B(n,s)}/V_{s,r} - J_{s,B}$

Accumulation of  $H^+$

$d[CH]_{f,r}/dt = N_{CH(f,1)}/V_{f,r} - 2J_{f,A}V = SL_r$

$d[CH]_1/dt = [N_{CH(2,1)} - N_{CH(1,2)}]/V_{s,r} = SL_s$

$d[CH]_k/dt = [N_{CH(k+1,k)} - N_{CH(k,k+1)}]/V$

$d[CH]_n/dt = [N_{CH(s,n)} - N_{CH(n-1,n)}]/V_{s,r}$

$d[CH]_{s,r}/dt = 2(J_{A,s} - J_{B,s}) - N_{CH(s,n)}/V_{s,r}$

Reaction rates ( $J/\text{mol cm}^{-3} \text{ s}^{-1}$ ) and local fluxes ( $N \text{ mol s}^{-1}$ )

$J_{f,A} = k_{f,A}[A]_f[CH]_f^2 - k_{-f,A}[C_2A]_f[H]_f^2$

$J_{s,A} = k_{s,A}[C_2A]_s[H]_s^2 - k_{-s,A}[A]_s[CH]_s^2$

$N_{C_2A(f,1)} = 2P_{C_2A}([C_2A]_f - [C_2A]_1)$

$N_{C_2A(k,k+1)} = 2P_{C_2A}([C_2A]_k - [C_2A]_{k+1})$

$N_{C_2A(n,s)} = 2P_{C_2A}([C_2A]_n - [C_2A]_s)$

$N_{CH(1,2)} = 2P_{CH}([CH]_1 - [CH]_2)$

$N_{CH(k,k+1)} = P_{CH}([CH]_{k+1} - [CH]_k)$

$N_{CH(s,n)} = 2P_{CH}([CH]_s - [CH]_n)$

$J_{f,B} = k_{f,B}[B]_f[CH]_f^2 - k_{-f,B}[C_2B]_f[H]_f^2$

$J_{s,B} = k_{s,B}[C_2B]_s[H]_s^2 - k_{-s,B}[CH]_s^2$

$N_{C_2B(f,1)} = 2P_{C_2B}([C_2B]_f - [C_2B]_1)$

$N_{C_2B(k,k+1)} = 2P_{C_2B}([C_2B]_k - [C_2B]_{k+1})$

$N_{C_2B(n,s)} = 2P_{C_2B}([C_2B]_n - [C_2B]_s)$

$P_{C_2A} = nD_{C_2A}S/L_m$

$P_{C_2B} = nD_{C_2B}S/L_m$

$P_{CH} = nD_{CH}S/L_m$

Parameters

Kinetic constants

Diffusion coefficients

Membrane area and thickness

Thickness of reaction compartments

Volume of feed and stripping solutions and membrane

Number of membrane compartments

$k_{f,A}, k_{-f,A}, k_{f,B}, k_{-f,B}, k_{s,A}, k_{-s,A}, k_{s,B}, k_{-s,B}$  ( $\text{mol}^{-2} \text{ s}^{-1} \text{ cm}^3$ )

$D_{C_2A}, D_{C_2B}, D_{CH}$  ( $\text{cm}^2 \text{ s}^{-1}$ )

$S(\text{cm}^2): L_m(\text{cm})$

$L_f, L_s$  (cm)

$V_f, V_s, V_m$  ( $\text{cm}^3$ )

$n$

Source: From Wodzki, R., Szczepanska, G., and Szczepanski, P., *Sep. Purif. Technol.*, 36, 1, 2004. With permission.

The overall concentration of divalent cations bound by the carrier in a liquid membrane phase and reaction zones ( $[A]_m, [B]_m$ ), and their ratio ( $S_m$ ) which characterizes the competitive accumulation of one of the cations in a liquid membrane phase:

$$[A]_m = ([C_2A]_{f,z}V_{f,z} + \sum_{k=1}^n [C_2A]_k V_k + [C_2A]_{s,z}V_{s,z}) / (V_m + V_{f,z} + V_{z,s}) \quad (13.45)$$

$$[B]_m = ([C_2B]_{f,z}V_{f,z} + \sum_{k=1}^n [C_2B]_k V_k + [C_2B]_{s,z}V_{s,z}) / (V_m + V_{f,z} + V_{z,s}) \quad (13.46)$$

$$S_m = [A]_m / [B]_m \quad (13.47)$$

**TABLE 13.2**  
**Parameters and Operational Conditions for Simulation**  
**of Competitive Transport Process**

Parameter Variables	Symbol	Value
<i>Initial concentrations (mol cm<sup>-3</sup>)</i>		
Feed phase	[A] <sub>f,o</sub>	1 × 10 <sup>-5</sup>
	[B] <sub>f,o</sub>	1 × 10 <sup>-5</sup>
	[H] <sub>f,o</sub>	1 × 10 <sup>-10</sup>
Stripping phase	[A] <sub>s,o</sub>	0
	[B] <sub>s,o</sub>	0
	[H] <sub>s,o</sub>	3 × 10 <sup>-3</sup>
Membrane	[C <sub>2</sub> A] <sub>k,o</sub>	0
	[C <sub>2</sub> B] <sub>k,o</sub>	0
	[CH] <sub>k,o</sub>	5 × 10 <sup>-4</sup>
Reaction zones	[C <sub>2</sub> A] <sub>i,o</sub>	0
	[C <sub>2</sub> B] <sub>i,o</sub>	0
	[CH] <sub>i,o</sub>	5 × 10 <sup>-4</sup>
<i>Diffusion coefficients (cm<sup>2</sup> s<sup>-1</sup>)</i>		
	D <sub>C2A</sub>	1 × 10 <sup>-5</sup> to 1 × 10 <sup>-7</sup>
	D <sub>C2B</sub>	1 × 10 <sup>-5</sup> to 1 × 10 <sup>-7</sup>
	D <sub>CH</sub>	1 × 10 <sup>-5</sup> to 1 × 10 <sup>-7</sup>
<i>Kinetic constants (cm<sup>6</sup> mol<sup>-2</sup> s<sup>-1</sup>)</i>		
	k <sub>f,A</sub>	1 × 10 <sup>6</sup> to 1 × 10 <sup>9</sup>
	k <sub>-f,A</sub>	1 × 10 <sup>6</sup> to 1 × 10 <sup>9</sup>
	K <sub>s,A</sub>	1 × 10 <sup>6</sup> to 1 × 10 <sup>9</sup>
	k <sub>-s,A</sub>	1 × 10 <sup>6</sup> to 1 × 10 <sup>9</sup>
	k <sub>f,B</sub>	1 × 10 <sup>6</sup> to 1 × 10 <sup>9</sup>
	k <sub>-f,B</sub>	1 × 10 <sup>6</sup> to 1 × 10 <sup>9</sup>
	K <sub>s,B</sub>	1 × 10 <sup>6</sup> to 1 × 10 <sup>9</sup>
	k <sub>-s,B</sub>	1 × 10 <sup>6</sup> to 1 × 10 <sup>9</sup>
<i>Dimensions</i>		
	V <sub>f</sub> (cm <sup>3</sup> )	100
	V <sub>s</sub> (cm <sup>3</sup> )	10
	L <sub>m</sub> (cm)	2.5 × 10 <sup>-3</sup>
	L <sub>f</sub> (cm)	5 × 10 <sup>-5</sup>
	L <sub>s</sub> (cm)	5 × 10 <sup>-5</sup>
	S <sub>m</sub> (cm <sup>2</sup> )	1

Source: From Wodzki, R., Szczepanska, G., and Szczepanski, P., *Sep. Purif. Technol.*, 36, 1, 2004. With permission.

The overall separation factor ( $\alpha_B^A$ ):

$$\alpha_B^A = \frac{[A]_s[B]_f}{[B]_s[A]_f} \quad (13.48)$$

The above quantities are accessible by standard measurements of liquid membrane transport and are frequently reported in the corresponding literature. To emphasize the kinetic source of separations studied, all computations have been carried out after assuming the same equilibrium constants for cation-exchange reactions appearing in the pertraction system, i.e.,

$$K_{f,A} = K_{f,B} = k_{f,A}/k_{-f,A} = k_{f,B}/k_{-f,B} \quad (13.49)$$

$$K_{s,A} = K_{s,B} = k_{s,A}/k_{-s,A} = k_{s,B}/k_{-s,B} \quad (13.50)$$

The conditions (Equations 13.49 and 13.50) impose no selectivity for the CPS under stationary conditions when the reactions attain their equilibrium state and the diffusion coefficients  $D_{C2A}$  and  $D_{C2B}$  are equal.

The bond-graph network of liquid membrane process can be successfully exploited for modeling the separation and transport ability of complex reaction–diffusion phenomena. However, it should be stated that such models involving appropriate mathematical formulations are especially useful in predicting the system's response to the changes in operating conditions and specific characteristics of the liquid membrane components. In general, such models are not applicable for the assessment of unknown parameters. The idea of network modeling needs as much information as possible to be introduced into a model. Thus, at the initial step no factor can be ignored though it is common in many other phenomenological descriptions assuming diffusion- or reaction-limited conditions. Consequently, the related calculations should be treated as experiments aimed at searching for new quantitative differences in transport and separation systems rather than numerical interpretations of the data that possibly explain the known experimental facts.

### 13.2.3 THEORY OF HOLLOW-FIBER LIQUID MEMBRANE TRANSPORT [5,9–11,38,62,63,91–93]

The theory of a hollow-fiber contained liquid membrane (HFCLM) transport is described in detail by Sirkar et al. in Refs. [58,59,91]. Its modified model, (HFLM), developed by Schlosser et al. [5,9–11,25,38,92] is presented below.

Concentration profiles of a solute in three-phase system transport through LM in a hollow-fiber module are similar to that, presented in Figure 13.3.

Following assumptions are held [11,25]:

1. Steady-state flux.
2. Consider only diffusional resistances,  $R_i$ . Reactions on both interfaces are fast and negligible accumulation in boundary layers is supposed.
3. High stoichiometric excess of reactant in the stripping solution.
4. Fibers are identical and the number of fibers in both bundles (for feed and strip solutions) is the same.

$$S_{wF} = S_{wR} = S_w; \quad \varepsilon_F = \varepsilon_R = \varepsilon; \quad \tau_F = \tau_R = \tau; \quad \text{and } k_{wF} = k_{wR} \quad (13.51)$$

where

- $S_{wF}$ ,  $S_{wR}$ , are surface area (square meters), in the feed and strip
- $\varepsilon$  is porosity of the fiber
- $\tau$  is tortuosity of the pores
- $k_i$  are individual mass transfer coefficients,  $\text{m s}^{-1}$

This results concentration of solute in the feed referring to its concentration in the strip,  $C_{FRM}$ , equal zero:

$$C_{FRM} = C_R * D_R / D_F = 0 \quad (13.52)$$

and

$$R_R = 0 \quad (13.53)$$

where

- $C_i$  are the molar solute concentrations
- $D_i$  are distribution coefficients at equilibrium at feed-membrane and membrane-strip interfaces

Relation for the overall mass transfer resistance can be derived [11,25,91]:

$$\frac{1}{K_p} = \frac{\varepsilon_F}{k_F} + \frac{S_F}{DS_{wF}k_{wF}} + \frac{S_F\varepsilon_F}{DS_Mk_M} + \frac{S_F\varepsilon_F}{DS_{wR}\varepsilon_Rk_{wR}} + \frac{S_F\varepsilon_F}{S_Rk_R} \quad (13.54)$$

$$R = R_F + R_{wF} + R_M + R_{wR} + R_R \quad (13.55)$$

Identification of the individual mass transfer coefficients depends on the construction of the module (material and structure of fibers in both bundles) and on the way of its operation. For the laminar flow inside hollow fibers, the following correlation can be used [93]:

$$\frac{k_F d_i}{D_f} = 1.5 \left( \frac{d_i^2 u_F}{L D_f} \right)^{1/3} \quad (13.56)$$

where

$d_i$  is the fiber diameter (m)

$D_f$  is diffusion coefficient ( $\text{m s}^{-1}$ )

$u_i$  is linear velocities of flow ( $\text{m s}^{-1}$ )

$L$  is the effective length of the fibers (m)

Individual mass transfer coefficients in the pores are estimated by equation

$$k_w = k_{wF} = k_{wR} = \frac{2D_{FM}}{\tau(d_0 - d_i)} \quad (13.57)$$

and

$$R_{wF} = R_{wR} = R_w \quad (13.58)$$

The resistance in the BLM is calculated from equation:

$$R_M = R - (R_F + 2R_w) \quad (13.59)$$

Differential mass balance of solute in the feed stream along the length of the HF contactor for constant volumetric flow rates of the solutions is

$$-V_F \frac{dC_F}{dz} = K_{ploc} (\pi * d_{iF} N_F \varepsilon_F) (C_F - C_{FRM}) \quad (13.60)$$

where

$V_i$  are volumes of the solution passed

$K_{ploc}$  is defined for effective surface area of the feed/LM interface

In cases when concentration  $C_{FRM}$  is close to zero, after rearranging of Equation 13.60:

$$K_{ploc} dz = - \frac{V_F}{\pi d_{iF} N_F \varepsilon_F} \frac{dC_F}{C_F} \quad (13.61)$$

Integrating Equation 13.60 for initial and boundary conditions,  $z=0$ ,  $C_F = C_{F1} = C_{F0}$ , and for  $z=L$ ,  $C_F = C_{F2}$  the following relation is obtained:

$$L = \frac{V_{F0}}{K_p \pi d_{iF} N_F \varepsilon_F} \ln \frac{C_{F0}}{C_{F2}} \quad (13.62)$$

and the concentration of the solute in the strip,  $C_{F2}$  can be calculated by equation:

$$\frac{C_{F2}}{C_{F0}} = \exp [-(\pi d_i N_F / V_F) (K_p L)] \quad (13.63)$$

where  $K_p$  is the integral value of the overall mass transfer coefficient of the module.

These considerations and the set of equations for transport of the solute through the HF modules are modified and simplified in comparison to the HFCLM [91] theoretical considerations. The models presented in Sections 13.2.1 and 13.2.2 consider more detailed diffusion parameters at the F/LM and LM/R interfaces, more detailed kinetics of chemical reactions. So, they are more identical to the real transport processes, therefore, these models, modified for a hollow-fiber permeator, may be used for the hollow-fiber transport also.

### 13.3 MODULE DESIGN FOR SEPARATION SYSTEMS

Technological complexity of ELM and problems with the stability of SLM has led researchers in the recent years to look for alternative BLM or organic (water-immiscible) LM. A big number of OHLM (or BLM) separation systems are described in the literature. They can be divided according to type of membrane walls (barriers) used: planar, spiral wound and hollow fiber, and to hydrophobic/hydrophilic properties of the membrane. The hydrophobic membranes are immobilized by LM organic solutions and hydrophilic or ion-exchange membranes are immobilized by aqueous feed and strip solutions.

Hydrophilic (or ion-exchange) membranes were used for designing rotating disc, creeping film, HLM, and MHSs, HFLM modules. Hydrophobic membranes were used for designing HLM, MHS, FLM, HFCLM, and capillary liquid membrane modules. Below, some of these systems are referenced and described shortly.

#### 13.3.1 LAYERED BULK LIQUID MEMBRANE MODULES [55,94]

The simplest U- or H-shaped layered BLM modules, without membrane walls, are used mainly in transport studies [55,94]. Examples of BLM-layered module with mixing all three solutions are presented in Figure 13.7.

#### 13.3.2 ROTATING DISC MODULES [12,14,16,18,20,95–103]

As seen in Figure 13.8, hydrophilic membrane discs are fixed on a horizontal shaft and their lower parts are immersed to compartments, which are filled with the feed and strip solutions. The remaining parts of the discs, in which aqueous phases (feed or strip) are immersed, due to rotation, are in contact with the LM phase. Mass transfer of the solute from the feed into the strip solutions occurs through the BLM phase.

Contactors with two parallel shafts with discs, one for the feed and one for the strip solutions are presented in the Ref. [96].

#### 13.3.3 CREEPING FILM MODULES [19,21,22,58,104–107]

Creeping film process (CFP) is a liquid membrane technique for simultaneous removal and concentration of dissolved species from their diluted aqueous solutions. CFP contactor is presented schematically in Figure 13.9. Feed and strip solutions flow down the vertical hydrophilic porous membrane sheets. A mobile organic LM is interposed between two creeping aqueous films. CFP is a continuous mass transfer process in which eddy diffusion controls the mass fluxes in all three liquid films.

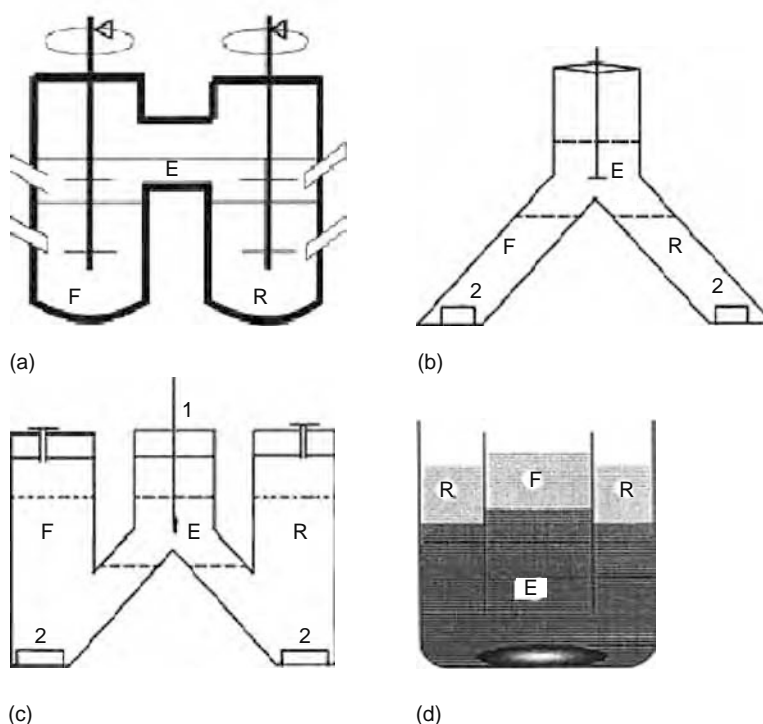
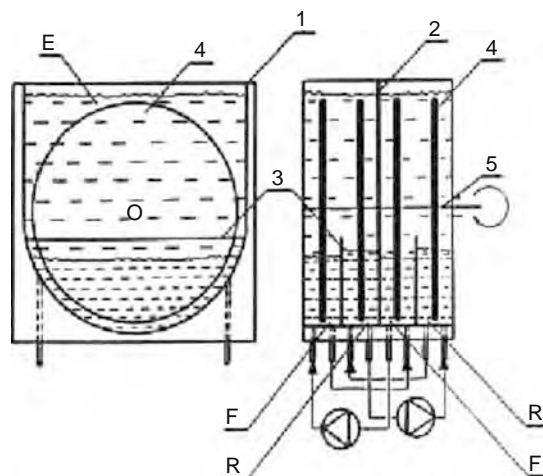


FIGURE 13.7 Examples of layered BLM modules.



**FIGURE 13.8** Scheme of a rotating film contactor: (1) body; (2) stage wall; (3) feed/stripping solution separating walls; (4) rotating discs; (5) common shaft. (From Zhivkova, S., Dimitrov, K., Kyuchoukov, G., and Boyadzhiev, L., *Sep. Purif. Technol.*, 37, 9, 2004. With permission.)

### 13.3.4 HYBRID LIQUID MEMBRANE MODULES [1–3,40,43,44]

Figure 13.1 represents schematically different types of HLM contactors. A liquid membrane solution flows (or circulates) between two membranes, which separate the LM phase (E) from the feed (F) and receiving (R) phases. A solute (or solutes) diffuses to the F/E interface and is extracted from feed phase by a carrier as a result of the thermodynamic conditions at the F/E interface. The solute–carrier complex diffuses to the E/R interface and is simultaneously stripped by the receiving phase due to the different thermodynamic conditions at the E/R interface. The membranes may be hydrophobic, immersed by LM, or hydrophilic (or ion exchange), immersed by feed and strip aqueous phases.

### 13.3.5 MULTIMEMBRANE HYBRID SYSTEMS [29,47,51,56,108]

MHS with pervaporation of water from LM (MHS-PV) is presented in Figure 13.10. Contrary to the simple MHS with an agitated BLM, separated from the feed and strip solutions by flat hydrophobic or hydrophilic or ion-exchange membranes, the MHS-PV system exploits an FLM continuously flowing between the two flat cation-exchange and two pervaporation membranes. To couple the separation and pervaporation processes, the LM is simultaneously pumped through the MHS and

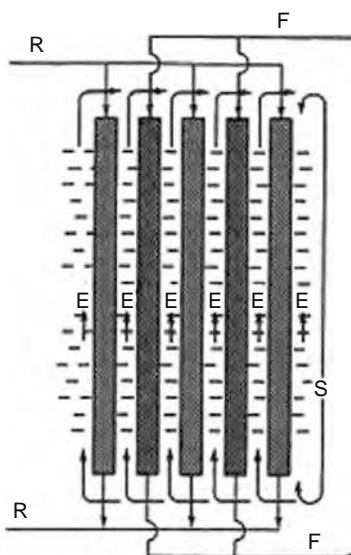


**FIGURE 13.9** Scheme of a creeping film contactor: F, R—inlet and outlet of the feed and receiving solutions, respectively; E—FLM organic solution. (From Boyadzhiev, L. and Lazarova, Z., *Chem. Eng. Sci.*, 42, 1131, 1987. With permission.)

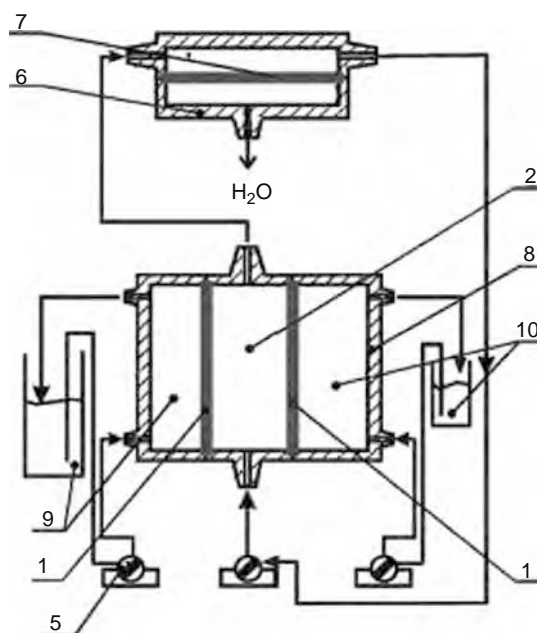


**FIGURE 13.10** Scheme of the MHS[FLM-PV] multimembrane hybrid system: (1) cation-exchange membranes, (2) FLM, (5) vacuum system, (6) pervaporation unit, (7) pervaporation membranes, (8) contactor, (9) feed solution, (10) stripping solution. (From Wodzki, R. and Szczepanski, P., *J. Mem. Sci.*, 197, 297, 2002. With permission.)

PV modules. The pervaporation membranes are placed on a stainless steel porous supports. Aqueous feed and strip solutions are intensively agitated. The MHS (without pervaporation section) and HLM are very similar systems.

### 13.3.6 FLOWING LIQUID MEMBRANE MODULES [19,30,33–36,109]

In FLM, the LM organic solution flows in a thin channel between two hydrophobic microporous membranes separating the LM phase from an aqueous feed and strip solutions. The FLM differs from the HLM and MHS modules with hydrophobic membranes by application of a spiral-type module. A schematic diagram of the spiral-type FLM module is shown in Figure 13.11.

The microporous membrane films (see Table 13.3) and one mesh spacers were spirally wound around acrylic resin pipes through which the feed, strip, and organic LM solutions were supplied to the module [34,36]. The outer surface and the top and bottom ends of the module were sealed with an adhesive.

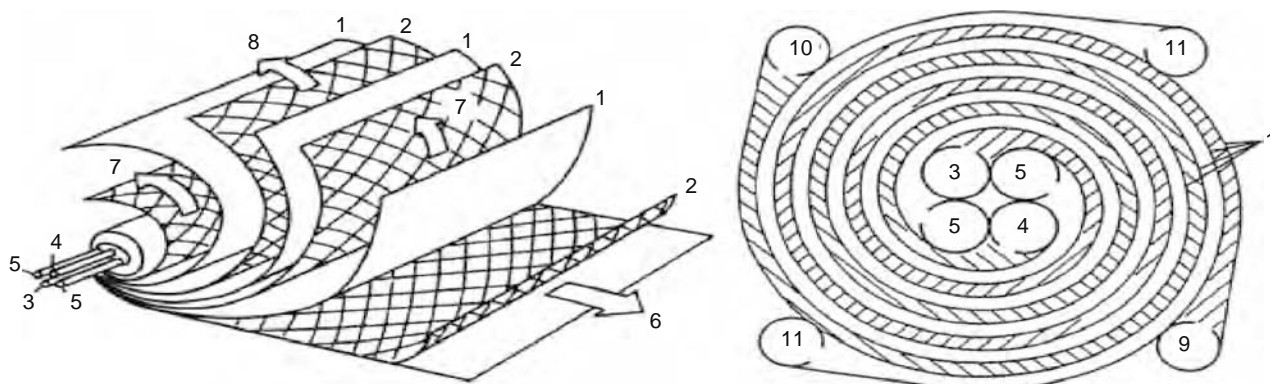


**FIGURE 13.11** Schematic diagram of a spiral-type flowing liquid membrane module: (1) microporous hydrophobic membrane, (2) mesh spacer, (3) inlet and (9) outlet pipe of feed, (4) inlet and (10) outlet pipe of strip, (5) inlet and (11) outlet tube of organic membrane solution, (6) feed solution, (7) organic LM solution, and (8) strip solution. (From Teramoto, M., Matsuyama, H., and Ohnishi, N., *Sep. Sci. Technol.*, 24, 981, 1989. With permission.)

**TABLE 13.3**  
**Examples of Flat Sheet Polymer Membranes Used in the Referenced Works and Their Properties**

Trademark	Supplier	Type	Porosity, %	Pore Size, $\mu\text{m}$	Thickness, $\mu\text{m}$
Celgard 2400	Hoechst-Celanese Co., Charlotte, North Carolina	Hydrophobic	38	0.05–0.125	25
Celgard 2402			38		50
Celgard 4400			38		175
Celgard 3400		Hydrophilic	38		25
Celgard 5401		38	175		
Duragard 2500	Polyplastics Co. Ltd., Tokyo, Japan	Hydrophobic	47	$0.04 \times 0.4$	25
Duragard 2502			45	$0.04 \times 0.4$	50
Fluoropore FP-010	Sumitomo Co. Ltd., Japan		67	0.1	60
Mesh Spacer	Dainippon Plastics Co. Ltd., Osaka, Japan		87	NA <sup>a</sup>	800
KDJ-6			73	NA <sup>a</sup>	900
KDN-4			70	NA <sup>a</sup>	800–1000
Hydrophilic Spacer			70	NA <sup>a</sup>	800–1000
Nylon 6 (polyamide 6)	ENKA America Inc. Ltd.,	Hydrophilic	70	0.2	110
Cuprophane 150 PM (polyamide 150)	Asheville, North Carolina		59	NA <sup>a</sup>	22

Note: Celgard 3400 is made hydrophilic by coating a surfactant onto Celgard 2400.

<sup>a</sup> Pore size not available in manufacturer's catalog.

### 13.3.7 HOLLOW-FIBER LIQUID MEMBRANE MODULES [4–6,9–11,38,104]

Several types of three-phase hollow-fiber (HF) modules have been described. They can be classified into two groups. The first one with parallel phase flow was developed by Sirkar group, termed as a “hollow-fiber contained liquid membrane” (HFCLM) and described in detail in Ref. [4]. The HFCLM module was used for separation of solutes in liquids and gases. Another type of HF modules, developed by Schlosser group, “hollow fibers in tube pertractor” with parallel flow [10,11,23–26,55,104] consists of one or two intermixed U-shaped bundles of microporous polypropylene fibers, inserted into polysulfon (or glass) tubes (see Figure 13.12). For a better mixing, pulsation of the LM phase along the fibers is used. It increases the transport rate by 35%–60%.

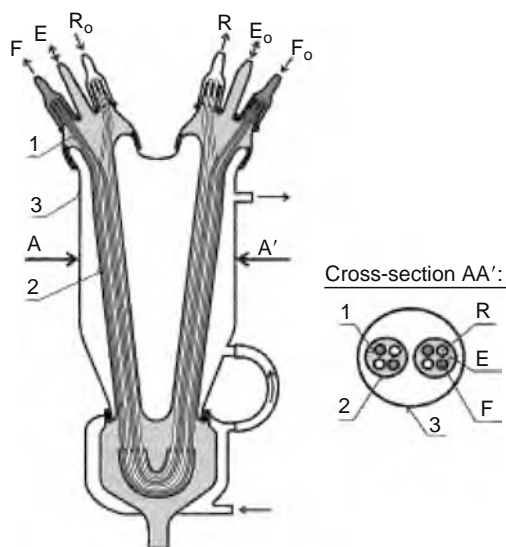


**FIGURE 13.12** Scheme of the hollow-fiber contactor with parallel flow of phases, distributed U-shaped bundles of fibers and with separated inlet and outlet end chambers. F: feed (donor phase), E: liquid membrane phase, R: stripping solution, (1) hollow fiber for the feed, (2) glass tubulet, (3) glass tempering jacket of the contactor. (From Schlosser, S. and Sabolova, E., *J. Mem. Sci.*, 210, 331, 2002. With permission.)

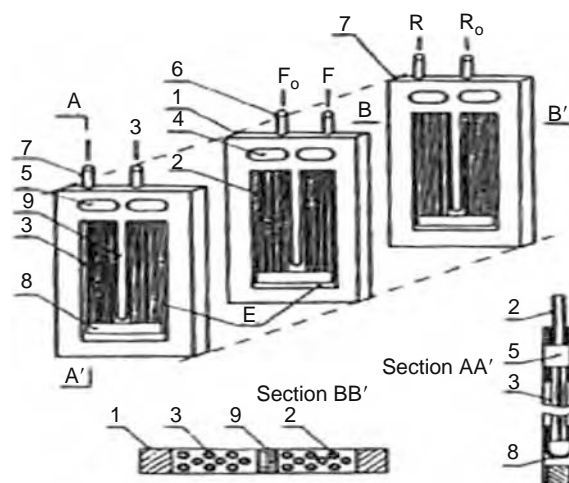


**FIGURE 13.13** Scheme of the hollow-fiber contactor of three phases with cross flow of LM phase: (1) body of element, (2,3) hollow fiber in downstream and upstream part, (4,5) inlet and outlet chamber, (6,7) inlet and outlet tube, (8) flowing head, and (9) central baffle, F: feed, E: LM phase, R: strip solution. (From Schlosser, S., Pertraction through liquid and polymeric membranes. In: Belafi-Bako, K., Gubicza, L., and Mulder, M. Eds. *Integration of Membrane Processes into Bioconversions*. Proceedings of the 16th European Membrane Society Annual Summer School. Veszprem, Hungary, August 1999. Kluwer Academic/Plenum Publishers, New York, 2000, 73–100. With permission.)

The second type of the HF modules has also been developed by Schlosser group [25,38–40,92,104]. This module enables a cross flow of the liquid membrane phase or its pulsation perpendicular to fibers, as shown in Figure 13.13. The planar HF elements can be assembled for contacting four or more phases.

Some modified plate and frame HF modules [110–112] were proposed. Both ends of fibers were potted on opposite sides of the frame-forming elements of the stack. The transversal flow of one phase was possible. The module with “fiber in fiber” units and cross flow of one phase is described in Ref. [9].

### 13.3.8 CAPILLARY LIQUID MEMBRANE SYSTEMS [113–115]

Facilitated transport for gas separation using a capillary membrane module was developed by Teramoto group [113,114]. Concept of capillary membrane apparatus is shown in Figure 13.14. Both an feed gas and an LM solution are supplied to the

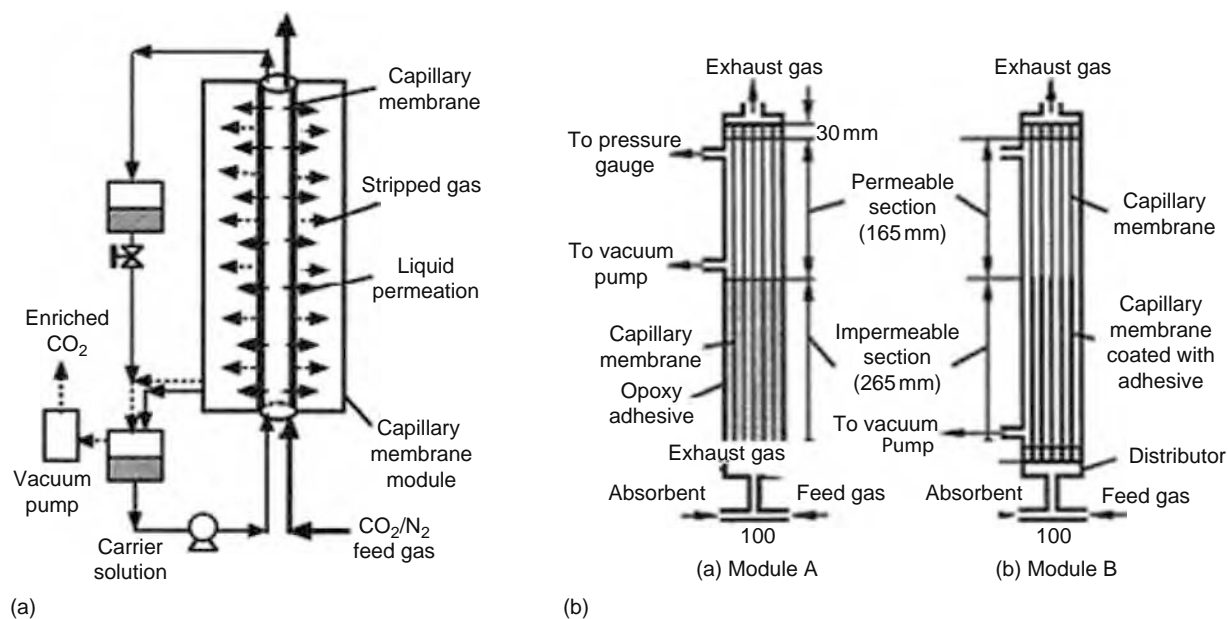


**FIGURE 13.14** Schematic diagrams of facilitated transport of gas using capillary membrane module for removal and enrichment of carbon dioxide. (a) Experimental capillary membrane apparatus and (b) capillary membrane modules with permeation of carrier solution. (From Teramoto, M., Ohnishi, N., Takeuchi, N., et al., *Sep. Purif. Technol.*, 30, 215, 2003. With permission.)

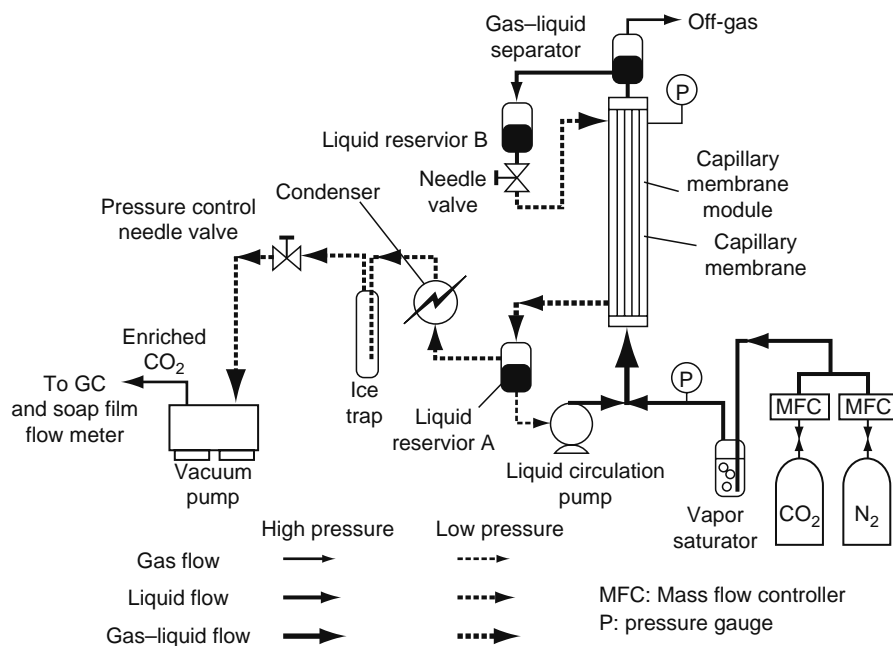


**FIGURE 13.15** Schematic diagram of experimental setup with capillary membrane for simultaneous removal and enrichment of CO<sub>2</sub>. (From Teramoto, M., Kitada, S., Ohnishi, N., et al., *J. Mem. Sci.*, 234, 83, 2004. With permission.)

lumen side (high-pressure feed side) of the capillary ultrafiltration membrane module and flow upward. The LM solution, which contains dissolved solute gas (CO<sub>2</sub> in the present case), flows to the permeate side (low pressure, shell side), where the solution liberates dissolved gas to become a lean solution. The lean solution is returned to the lumen of the capillary module by a pump. In the shell side, dissolved gas is stripped from the liquid flowing down the outer surface of the capillary, and discharged from a vacuum pump through a liquid reservoir. Schematic diagram of experimental setup is shown in Figure 13.15.

Mixtures of CO<sub>2</sub> (5%–15%) and N<sub>2</sub> were used as model feed gas, and monoethanolamine (MEA), diethanolamine (DEA), and 2-amino-2-methyl-1-propanol (AMP) were used as the carriers of CO<sub>2</sub>. The polyethersulfone capillary ultrafiltration membranes (see Table 13.4) were used in the module. The membrane was very stable over a discontinuous 4-month testing period. The energy consumption was found to be much smaller than those of conventional chemical absorption and membrane separation processes.

### 13.3.9 MEMBRANE TYPES USED

Most membranes, used as a wall between phases in the OHLM systems, are polymeric although inorganic membranes have also become available. Membranes can be classified according to structure as homogeneous, asymmetric, or composite, according to geometry as flat sheet, hollow fiber, or tubular, according to pore surface as neutral hydrophobic or hydrophilic and surface

**TABLE 13.4**

**Examples of Hollow-Fiber Membranes, Used in the Referenced Works, and Their Properties**

Trademark	Supplier	Type	ID, $\mu\text{m}$	CD, $\mu\text{m}$	Pore Size, $\mu\text{m}$	Porosity, %
Celgard X-10	Hoechst-Celanese Corporation,	Hydrophobic	100	150	0.03	20
Celgard X-20	Charlotte, North Carolina		240	290	0.03	40
Cuprophan C1	AKZO, Asheville, North Carolina	Hydrophilic	140	200	NA <sup>a</sup>	55
Cuprophan D4			220	270	NA <sup>a</sup>	60
Nylon 6			600	1,000	0.2	75
Capillary ultrafiltration membranes	Daicel Chemical Industries, Ltd., Osaka, Japan	Hydrophobic	800	1,300	1,50,000 <sup>b</sup>	NA <sup>a</sup>

Notes: ID = internal diameter; CD = external diameter.

<sup>a</sup> Data not available in manufacturer's catalog.

<sup>b</sup> Molecular weight cut-off.

**TABLE 13.5**  
**Examples of Ion-Exchange Membranes Used in the Referenced Works and Their Properties**

Supplier	Trademark	Type	Gel water, %	Thickness, mm	Permselectivity, %	Capacity, meq/g
Tokuyama Soda Co, Tokyo, Japan	Neosepta, CMX	Cation-exchange, low-electric resist	24	0.13–0.16	90	2.0–2.5
	Neosepta, AFN-7	Anion-exchange antifouling	45	0.16	NA <sup>a</sup>	3.2
	Neosepta, BP-1	Cation–anion exchange	20	0.3	85	2.0
DuPont De Nemours, Fayetteville, North Carolina	Nafion 117	Cation exchange	18.5	0.22	90	3.9
	Nafion 120		44	0.26	96	4.3
FumaTech GmbH, Germany	FKS	Cation exchange	40	0.6	79	1.8

<sup>a</sup> Not available in manufacturer's catalog.

charged (ion exchange). Hydrophobic membranes, flat sheet, or hollow fibers, (see Tables 13.3 and 13.4) are readily moistenable by most organic solvents, but water does not moisten it. An organic solvent, brought on one side of the membrane, immediately wets the membrane and appears on the other side, or immobilizes the interface. Aqueous solution to be contacted with the organic solution of a carrier is brought at a pressure higher than that of organic solution to prevent the latter from coming through the membrane, but not so high to be able to displace organic phase from inside the pores completely. The two phases contact each other at a mouth of the pores or inside the membrane (see Figures 13.1a, 13.1d, and 13.3).

On the contrary, hydrophilic and ion-exchange membranes (see Tables 13.3 through 13.5) are readily wettable by aqueous solutions, but immiscible by organic phases. So, contact between aqueous and organic phases takes place on the other side to the bulk aqueous phase interface of the membrane (see Figures 13.1b, 13.1e, and 13.4).

Although several inorganic ion-exchange materials (zeolites, bentonites) are now available, most membranes used are polymeric. The properties of ion-exchange membranes are closely related to those of ion-exchange resins. The properties, important for the separation reasons, are permselectivity, long-term electrical (resistance) and chemical stability, and ion-exchange capacity (see Table 13.5). Flat sheet, hollow fiber, and tubular ion-exchange membranes are available.

The limits of pore dimensions in OHLMs are purposely chosen to minimize convective transport. Two solutes can be separated if their diffusion coefficients differ by at least an order of magnitude. This diffusivity is modified by the matrix structure and pore size of the membrane. Knowledge of the relative solute diffusivities in the membrane gives us the knowledge of retention abilities of the membrane. The sieving properties of the membranes allow them to retain some macromolecules while selectively removing solutes of middle molecular weight and less selective removal of solutes with small molecular weight.

The knowledge of the difference between solute diffusivities in the membrane, immobilized by organic phase (hydrophobic), vis-à-vis the membrane, immobilized by aqueous phase (hydrophilic, ion exchange), would aid in the choice of membrane type. In all cases, the membrane material would have to be completely long-term resistant to the solvents of either phase.

The first choice would be to use a membrane as thin as possible, with high porosity, and small pore size, while still providing the mechanical stability for potting and pumping pressure.

## 13.4 SELECTED APPLICATIONS

Applications of the OHLM processes are tested mainly in metal separation, wastewater treatment, biotechnologies, drugs recovery-separation, organic compounds, and gas separation. In the recent years, integrated hybrid systems incorporating two or more functions in one module, for example biotransformation and separation, become systems of great interest to researchers. The recent applications of different types of the OHLM systems are summarized below.

### 13.4.1 METAL SEPARATION-CONCENTRATION

Metal ions separation for hydrometallurgical applications has attracted considerable interest. Selective separations of alkali, alkali earth, heavy metal ions, rare earth, precious metals, etc. are studied by many authors using all the above-described techniques. Referenced works in metal separations classified according to the OHLM techniques with types of membrane walls and carriers used are listed in Table 13.6.

**TABLE 13.6**  
**Selected References on Metal-Ion Separations by OHLM Techniques**

Metal Ions	Liquid Membrane	Polymer Membrane Walls	References
<i>HLM technique</i>			
Ti(IV)	DEHPA	Celgard 2400, 2402, 3400. Neosepta CM-1, ACH-45	[1,2]
Cu(II), Cd(II), Zn(II)	MEHPA, DEHPA Cyanex 302	Neosepta CM-1, CM-2 Celgard 2400, 2402, 3400	[70,85,116–120]
<i>MHS with (or without) pervaporation (PV) technique</i>			
K(I), Na(I), Mg(II), Ca(II), Cu(II), Zn(II)	Star-shaped polymers, PEG	Nafion 117, Neosepta CMX, AFN-7, Pervap 1000, 2201	[28,121,123,125–127]
K(I), Na(I), Zn(II), Cu(II), Mg(II), Ca(II) Zn(II), Mn(II), Cu(II), Co(II), Ni(II), Cr(III), Fe(III)	DEHPA, Acorga P-50, Cyanex 302 DEHPA, Acorga P-50	Nafion 120, FKS Pervap 1000 Nafion-117, 120, Neosepta CMX, BP-1	[29,47,75,87–89,106,124] [49–51,86,122]
<i>Rotating film module</i>			
Cu(II), Zn(II), Fe(II), Ni(II)	Kelex 100, TOA, LIX 54, 65, 65N, 860, Hydroxy-oximes, Acorga P-5100	Hydrophilic coating with viscose Hydrophilic support	[12,14,16,17]
Ag(I)	TIBPS	Hydrophilic support	[21,97–99]
<i>Creeping film module</i>			
Cu(II)	Acorga P-5100, 5300	Hydrophilic support of viscose	[19,22,57]
Jodine	DB18C6	Hydrophilic support	[103]
<i>Hollow-fiber module</i>			
Cu(II), Cr(III), Cr(VI), Hg(II) Nd, Ho	LIX-84, TOA DEHPA	Celgard X-10 Celgard X-10	[8,128,129] [9,24,39,130,131]
<i>Spiral-type flowing module</i>			
Cr(VI), Zn Co, Ni, Zn	TOA, TOMAC, EHPNA DEHPA Cyanex 302	Duragard 2500, 2502 Duragard 2500, 2502, Mesh spacer KDJ-6	[34] [35–37]
<i>Layered (without polymer membrane walls) BLM module</i>			
Li, Ag, Na, K, Sr	Crown 18 C6		[133,139,141,149,154,159,161]
Zn, Co	DEHPA Cyanex 471X		[25,42,53,132]
Cd, Cu, Zn	Calixcrown oligomers, Janus Green, LIX-860		[134–138,141,142,145,148, 150,151,157]
Pd, Au	Crowns 18C6		[140,152,153,155]
Bi	Cyanex 301		[141]
Hg	Crown 18 C6		[143,147,156]
Er, Nd	HEH(EHP)		146,158]
U	TBP, calixarenes		[144,160]

### 13.4.2 BIOTECHNOLOGICAL PRODUCTS RECOVERY-SEPARATION

Recovery from fermentation broth and separation of carboxylic acids, amino acids were tested by many authors using layered BLM, rotating, creeping, spiral-type FLM, HFLM, HLM, and MHS-PV techniques of the OHLM processes. The research works for the last 15 years in this field classified according to the OHLM techniques with types of membrane walls and carriers used are provided in Table 13.7.

### 13.4.3 PHARMACEUTICAL PRODUCTS RECOVERY-SEPARATION

Selected papers for the last 15 years, presenting results of separation of drugs, antibiotics, enantiomers by layered BLM, HFLM, rotating film techniques are listed in Table 13.8. Hollow-fiber contactors, developed modular elements with optimum-configured stacks for individual applications may be an interesting direction in research.

### 13.4.4 ORGANIC COMPOUNDS SEPARATION, ORGANIC POLLUTANTS RECOVERY FROM WASTEWATERS

Separation of ethylene, benzene, propanol, olefin, aromatic amines from organic liquid mixtures, of volatile organic compounds (VOC), and phenol from wastewater, were investigated by the authors (Table 13.9), using rotating film module,

**TABLE 13.7**  
**Selected References on Carboxylic and Amino Acids Separations by OHLM Techniques**

Acids	Liquid Membrane	Polymer Membrane Walls	References
<i>HLM technique</i>			
Lactic, acetic	Alamine 336	Celgard 2400, 3400	[85,162]
Citric, propionic	Alamine 304	Neosepta AM-3, AMX	
<i>MHS with (or without) PV technique</i>			
Acetic, formic, lactic, propionic, oxalic, citric, tartaric	TOPO, TBP, MIBK, TOA, octanol, hydrocarbons C <sub>6</sub> –C <sub>10</sub>	Neosepta AFN-7 Nafion-120	[29,46,48,163–166]
<i>Rotating film module</i>			
Phenol, L-lysine, butyric	DEHPA	Hydrophilic support	[21,23,54,103,106]
<i>Hollow-fiber module</i>			
Phenol, acetic, oxalic, succinic, citric acids	TOA, MIBK, Hostarex A327, Decanol, xylene	Celgard X-10, X-20, Nylon 6, Cuprophan	[6,11,26,40,104,167–169]
Butyric acid, DMCCA, 5-methyl-2-pyrazine carboxylic acid, heterocyclic carboxylic acid, PAA, MAs 6-APA	TOA, Hostarex A327, Cyanex 471, lipase in octanol	Celgard X-10, X-20, Cuprophan	[38,170]
<i>Spiral-type flowing module</i>			
Fatty acids	DEHPA, silver nitrate	Duragard 2500, 2502 Mesh spacer KDJ-6	[32,171]
Eicosapentaenoic acid	Silver nitrate	Fluoropore FP-010	[172]
Docosahexaenoic acid	DEHPA	Mesh spacer KDN-4	
<i>Layered (without polymer membrane walls) BLM module</i>			
Butyric acid 5-methyl-2-pyrazine carboxylic acid	TOA, Hostarex A327, THP		[43,44,170]
Amino acids, L-isoleucine, 7-ACA	DEHPA, DB18C6, Aliquat-336		[173–175]
Aminocephalosporanic, <i>p</i> -amino benzoic acid, phenylalanine	Carboxylated poly (styrene), octanoic, lauric, decanoic acids		[176–178]
Dihydrogenphosphate anion	Oxomolybdenum (V) tetraphenylporphyrin complex		[179]
$\alpha$ -Amino acids	Chiral lipophilic ligand		[180]

**TABLE 13.8**  
**Selected References on Pharmaceutical Compounds Separations by OHLM Techniques**

Separated Compounds	Liquid Membrane	Polymer Membrane Walls	References
<i>Rotating film module</i>			
Erythromycin, tylosin, L-lysin	DEHPA	Hydrophilic coating, hydrophilic support	[15,181]
Phenylalanine	DEHPA	Hydrophilic support	[182]
<i>Hollow-fiber module</i>			
Diltiazem, drugs	Octanol, decanol	Celgard X-10, X-20	[183–188]
Fructose	Alcohols		[189]
Antibiotics	1-Decanol, <i>n</i> -decanol, <i>n</i> -octanol	Cuprophan	[190–192]
<i>Layered (without polymer membrane walls)</i>			
Indole alkaloid vincamine	BLM module Trichloroethylene		[193]
Tryptophan, Serotonin	M <sup>-1</sup> Bu <sub>4</sub> -salphen-3 <i>n</i> -cr- <i>n</i> complexes (M = Mn, Fe)		[194]
Proteins	Reversed micellar solution		[97,195]
Enantiomers	Aerosol-reversed micelles with Ba <sup>2+</sup> , $\beta$ -cyclodextrin		[196–199]
Cephalosporin-C, cephalixin	Aliquat-336		[176,200,201]

**TABLE 13.9**  
**Selected References on Organic Compounds Separations by OHLM Techniques**

Organic Compounds	Liquid Membrane	Polymer Membrane Walls	References
<i>Rotating film module</i>			
Aromatic amines	C11–C13 normal paraffins	Disk with hydrophilic support	[13,21,202]
<i>Spiral-type flowing module</i>			
Ethylene/ethane	Silver nitrate	Duragard 2500, 2502, Mesh spacer KDN-4	[30,203]
Benzene	Silver nitrate	Fluoropore FP-010, Mesh spacer KDN-4	[33]
<i>Hollow-fiber module</i>			
VOC	1-Octanol, vacuum	Silicone-coated HF	[204–208]
2-propanol/ <i>n</i> -heptane	Water, sulfolane	Silicone-coated HF	[209,212]
<i>Layered (without polymer membrane walls) BLM module</i>			
Olefin/paraffin	Silver nitrate		[210,211]
Phenol	Dialkylamine, trioctylamine, Cyanex 923		[23]

spiral-type FLM, hollow fiber and layered LM techniques. High separation factors (>1000) in pilot and industrial scale experiments were found.

#### 13.4.5 GAS SEPARATIONS

Oxygen transport via a hemoglobin carrier was one of the first LM transport systems [53]. It was noted that the rates of complex formation and reversal were very important.

Carbon dioxide separation from the air, mixtures with CH<sub>4</sub>, N<sub>2</sub>, O<sub>2</sub>, has been studied from both biological and engineering applications. Spiral-type FLM, HFLM, and capillary membrane techniques were tested for these purposes.

Hydrogen sulfide and sulfur dioxide removal were studied using HFLM technique for coal gasification applications.

References of the works carried out in the field of gas separations are presented in Table 13.10.

Schematic diagram of experimental setup for gas separation and enrichments is shown in Figure 13.16.

**TABLE 13.10**  
**Selected References on Gas Separations by OHLM Techniques**

Gases	Liquid Membrane	Polymer Membrane Walls	References
<i>Spiral-type FLM module</i>			
CO <sub>2</sub> (mixture with CH <sub>4</sub> )	Water, Solution of K <sub>2</sub> CO <sub>3</sub> /	Duragard 2500, 2502	[213]
CO <sub>2</sub> (mixture with O <sub>2</sub> , N <sub>2</sub> )	KHCO <sub>3</sub> , DEA	Fluoropore FP-010 Spacers: KDJ-6, KDN-4	
<i>Capillary ultrafiltration membrane module</i>			
CO <sub>2</sub> (mixture with N <sub>2</sub> )	Aqueous solution of 2-(butylamino)ethanol, 2-methylamino-1-propanol (AMP) MEA, DEA	Polyethersulfone capillary ultrafiltration membranes	[31,113–115,214]
<i>Hollow-fiber module</i>			
VOC	Inert, nontoxic solvent, silicone oil	Perfluorodimethyldioxole- tetrafluoroethylene (PDD-TFE) hollow fibers	[205–207,215,216]
H <sub>2</sub> S	Aqueous solution of alkali carbonate, MDEA	Hydrophobic or hydrophilic microporous membranes	[222–224]
CO <sub>2</sub> , O <sub>2</sub>	Vacuum	PDD-TFE hollow fibers	[7,221,227]
SO <sub>2</sub> from SO <sub>2</sub> , NO, CO <sub>2</sub> , O mixture	Fe <sup>2+</sup> EDTA or Fe <sup>3+</sup> EDTA aqueous solution	Polypropylene Celgard X-10, X-30	[217]
CO <sub>2</sub> –N <sub>2</sub> mixtures	Water, DEA	Polypropylene Celgard X-10, X-30	[218–220,225,226,228–230]
CO <sub>2</sub> –CH <sub>4</sub> mixture			

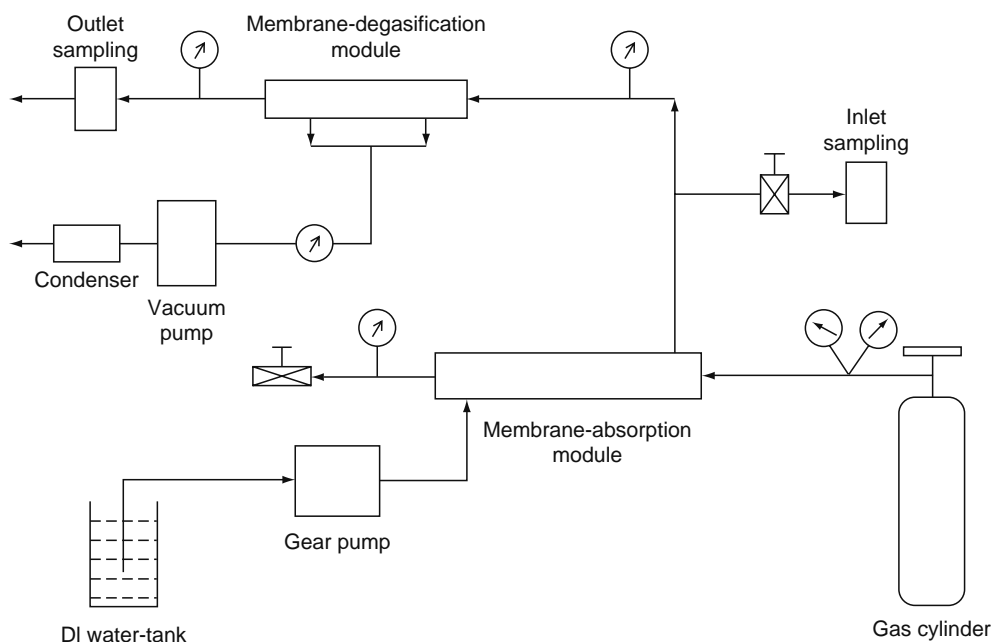


**FIGURE 13.16** Experimental setup; gas absorption and subsequent degasification using membrane modules. (From Bhaumik, D., Majumdar, S., Fan, O., and Sirkar, K.K., *J. Mem. Sci.*, 235, 31, 2004. With permission.)

### 13.4.6 FERMENTATION OR ENZYMIC CONVERSION-RECOVERY-SEPARATION (BIOREACTORS)

The OHLM systems, integrating reaction, separation, and concentration functions in one equipment (bioreactor), find a great interest of researchers in the last few years. A bioreactor combines the use of specific biocatalyst for the desired chemical reactions, and repeatedly or continuously application of it under very specific conditions. Such techniques were termed as hybrid membrane reactors. In biotechnology and pharmacology, these applications are termed as hybrid membrane bioreactors or simply bioreactors (see Table 13.11). Experimental setup of the bioreactor system is shown schematically in Figure 13.17.

### 13.4.7 ANALYTICAL APPLICATIONS

OHLM techniques were used in analytical methods for separation and preconcentration of metals [252–254], organic acids [255,256], and organic and pharmaceutical compounds [257–261]. Preparation of the samples for analytical purposes seems to be one of the perspective directions in application of the OHLM processes.

**TABLE 13.11**  
Selected References on Reactor Conversion-Separations by OHLM Techniques

Solutions Treated	Solutes Treated	Liquid Membrane	Polymer Membrane Walls	References
Wastewater treatment	Reviews	Enzymes, fermentors, biocatalysts, catalysts	UF membranes	[231–234]
	Metals, hydrogen		UF flat sheet (spiral bound), HF, and capillary membrane	[235–237]
	Anions			[238–242]
	Organic compounds			[243–245]
Enzymatic conversion	Organic compounds, hydrolysis	Catalysts	UF flat sheet (spiral bound), HF, and capillary membrane	[246–250]
Electrokinetic conversion	Lactic acid	Fermentors	Ultrafiltration HF membranes	[251]

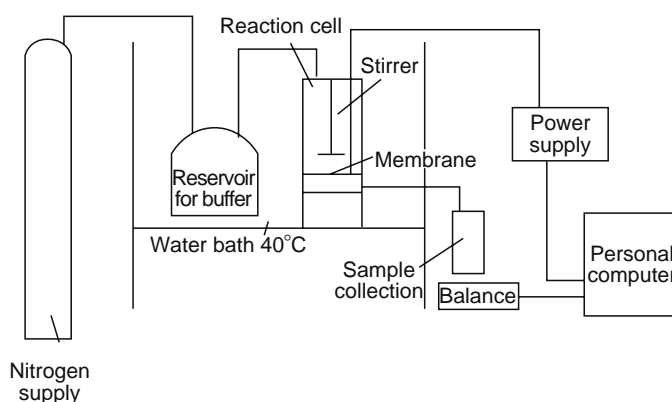


**FIGURE 13.17** Schematic flow diagram of the integrated membrane reactor system. (From Gan, Q., Allen, S.J., and Taylor, G., *Biochem. Eng. J.*, 12, 223, 2002. With permission.)

### 13.5 CONCLUDING REMARKS

In comparison with LLX, SLM, and ELM, the OHLM has the potential of providing many economic and operational advantages such as low-carrier losses, long membrane lifetime, “once through” continuous operation, compact equipment, application of different driving forces (chemical potential, pressure, temperature gradients between different compartments, electric field, etc.), no need of surface formation, impregnation, gravity gradients, high membrane capacity, etc. Commercially available membrane modules and equipment may be used in the OHLM.

Currently, only commercial application of the LM technologies is wastewater treatment (water and degasification), where low concentration solutes are removed from large volume of effluents. Solvent extraction and ion exchange are often not economically convenient at these cases. Due to the complexation reaction and low quantity of complexing agent-carrier required, the OHLM technologies are suited for high recoveries of dilute solutes. LMs are used commercially in production of ion-selective electrodes and gas sensors selective for organic vapors.

Despite promising technological performance, few OHLM techniques have been commercialized. This fact stems from many economic and technical factors. The main drawbacks of the OHLM systems observed are the poisoning of the carrier by irreversible reactions, low-diffusion rate of the large organic molecules, losses of the LM and contamination of the treated and product aqueous solutions by the LM organic components due to the leakage, the membrane walls blinding or fouling due to the emulsion, and gel formation on their surfaces. Long-term stability of complexing agent-carriers in the LM, stability of membrane walls, and their long-term permeability are the problems that limit the commercialization of the OHLM technologies.

It is necessary to develop complexation chemistry and new selective carriers or to improve existing ones for improving separation and transport properties, required to optimize the OHLM processes.

Improving and reducing the price of membrane film or hollow-fiber production will definitely speed industrial application of the OHLM technologies, especially in gas, pharmaceutical, and bioreactor applications.

### NOMENCLATURE

7-ACA	7-aminocephalosporanic
AMP	2-amino-2-methyl-1-propanol
6-APA	6-aminopenicillanic acid
Cyanex 302	di-(2,4,4-trimethyl-pentyl) monothiophosphinic acid, a product of CYTEX Canada Inc. (nowadays Cognis)
Cyanex 471x or TIBPS	triisobutylphosphine sulfide
DB18C6	dibenzo-18-crown-6
DEA	diethanolamine
DEHPA	di-(2-ethylhexyl) phosphate
DMCCA	dimethyl(cyclopropane)carboxylic acid
EHPNA	2-ethylhexyl phosphonic acid, mono-2-ethylhexyl ester (PC-88A), Daihachi Chemical Industry Co., Ltd. Japan
Hostarex A 327	<i>n</i> -octyl( <i>n</i> -decyl)amine
MDEA	methyl-di-ethanol-amine
MEA	monoethanolamine

MEHPA	(2-ethylhexyl) phosphate ( $C_8H_{19}O_4P$ ), containing 45% of mono-(2-ethylhexyl) phosphate on molar basis
MAs	mandelic acids
PAA	phenylacetic acid
PABA	<i>p</i> -aminobenzoic acid
Star-shaped polymer	$[CH_3O(CH_2CH_2O)_n]_x$ -[DGEEG]- $[(CH_2CH_2O)mP(O)(ONa)_2]_x$ , (MPOE-[DGEEG]-POEP), (DGEEG is ethylene glycol diglycidyl ether)
PPOPP	poly[poly(oxypropylene) phosphate]s, ( $M_n = 5,800, 8,100, 10,400$ ), with different POP units (400, 1,200, 2,000)
PEG 4000 and 6000	poly(ethylene glycol)
PPG, PPO	poly(propylene glycol)
MPOEP	methoxy-poly(oxyethylene) phosphate (1)
POEBP	poly(oxyethylene) bisphosphate 2, poly(oxyethylene) bis(di-Me phosphate), 3
POEBMP	poly(oxyethylene) Me ether phosphate
POEP	poly(oxyethylene) phosphate
PEGP	poly(ethylene glycol) phosphate
TBP	tri- <i>n</i> -butylphosphate
THP	tri-hexylphosphate
TOA	tri- <i>n</i> -octylamine
TOMAC	tri-(octylmethyl) ammonium chloride
TOPO	tri- <i>n</i> -octylphosphinic oxide

## REFERENCES

- Kislik V and Eyal A. Hybrid liquid membrane (HLM) system in separation technologies. *J Mem Sci*, 1996; 111: 259–272.
- Kislik V and Eyal A. Hybrid liquid membrane (HLM) and supported liquid membrane (SLM) based transport of titanium(IV). *J Mem Sci*, 1996; 111: 273–281.
- Gega J, Walkowiak W, and Gajda B. Separation of Co(II) and Ni(II) ions by supported and hybrid liquid membranes. *Sep Purif Tech*, 2001; 22–23: 551–558.
- Majumdar S and Sirkar KK. Hollow-fiber contained liquid membrane. In: Ho WSW and Sirkar KK Eds. *Membrane Handbook*. Van Nostrand Reinhold, New York 1992: pp. 764–808.
- Qin Y and Cabral J. Theoretical analysis on design of hollow fiber modules and modules cascades for the separation of diluted species. *J Mem Sci*, 1998; 143(1–2): 197–205.
- Dai XP, Yang ZF, Luo RG, and Sirkar KK. Lipase-facilitated separation of organic acids in a hollow fiber contained liquid membrane module. *J Mem Sci*, 2000; 171(2): 183–196.
- Bhaumik D, Majumdar S, Fan O, and Sirkar KK. Hollow fiber membrane degassing in ultrapure water and microbiococontamination. *J Mem Sci*, 2004; 235(1–2): 31–41.
- Sengupta A, Basu R, and Sirkar KK. Separation of solutes from aqueous solutions by contained liquid membranes. *AIChE J*, 1988; 34(2): 1698–1713.
- Schlosser S and Sabolova E. Three-phase contactor with distributed U-shaped bundles of hollow-fibers for pertraction. *J Mem Sci*, 2002; 210(2): 331–347.
- Schlosser S and Rothova I. A new type of hollow-fiber pertractor. *Sep Sci Technol*, 1994; 29(6): 765–780.
- Schlosser S, Rothova I, and Frianova H. Hollow-fiber pertractor with bulk liquid membrane. *J Mem Sci*, 1993; 80: 99–106.
- Zhivkova S, Dimitrov K, Kyuchoukov G, and Boyadzhiev L. Separation of zinc and iron by pertraction in rotating film contactor with Kelex 100 as a carrier. *Sep Purif Technol*, 2004; 37(1): 9–16.
- Boyadzhiev L, Alexandrova S, Kirilova N, and Saboni A. Pertraction continue de tylosine dans un contacteur a films tournants. *Chem Eng J*, 2003; 95(1–3): 137–141.
- Dimitrov K, Alexandrova S, Saboni A, Debray E, and Boyadzhiev L. Recovery of zinc from chloride media by batch pertraction in a rotating film contactor. *J Mem Sci*, 2002; 207(1): 119–127.
- Kawasaki J, Egashira R, Kawai T, Hara H, and Boyadzhiev L. Recovery of erythromycin by a liquid membrane. *J Mem Sci*, 1996; 112(2): 209–217.
- Boyadzhiev L and Dimitrov K. Recovery of silver from nitrate solution by means of rotating film pertraction. *J Mem Sci*, 1994; 86(1–2): 137–143.
- Lazarova Z and Boyadzhiev L. Kinetic aspects of copper(II) transport across liquid membrane containing LIX-860 as a carrier. *J Mem Sci*, 1993; 78(3): 239–245.
- Lazarova Z and Boyadzhiev L. Liquid film pertraction—a liquid membrane preconcentration technique. *Talanta*, 1992; 39(8): 931–935.
- Boyadzhiev L and Lazarova Z. Study on creeping film pertraction. Recovery of copper from diluted aqueous solutions. *Chem Eng Sci*, 1987; 42(5): 1131–1139.
- Boyadzhiev L. Liquid pertraction or liquid membranes-state of the art. *Sep Sci Technol*, 1990; 25(3): 187–190.

21. Boyadzhiev L and Alexandrova S. Dephenolation of phenol-containing waters by rotating film pertraction. *Sep Sci Technol*, 1992; 27(10): 1307–1312.
22. Boyadzhiev L. Recovery of valuable metals from diluted aqueous solutions by creeping film pertraction. In: Devis GA Ed. *Separation Processes in Hydrometallurgy*. London 1987; Pt. 3, Ch. 26: 259–287.
23. Cichy W, Schlosser S, and Szymanowski J. Transport of phenol through bulk liquid membranes. In: Cox M, Hidalgo M, and Valiente M Eds. *Solvent Extraction for the 21st Century*. Proceedings of ISEC '99, Barcelona, Spain, July 1999. Publisher: Society of Chemical Industry, London, UK 2001; 2: 1065–1070.
24. Cara G, Schlosser S, Munoz M, and Valiente M. Pertraction of neodymium and holmium in a hollow fiber contactor. In: Cox M, Hidalgo M, and Valiente M Eds. *Solvent Extraction for the 21st Century*. Proceedings of ISEC '99, Barcelona, Spain, July 1999. Publisher: Society of Chemical Industry, London, UK 2001; 2: 1023–1028.
25. Schlosser S. Pertraction through liquid and polymeric membranes. In: Belafi-Bako K, Gubicza L, and Mulder M Eds. *Integration of Membrane Processes into Bioconversions*. Proceedings of the 16th European Membrane Society Annual Summer School. Veszprem, Hungary, August 1999. Publisher: Kluwer Academic/Plenum Publishers, New York, 2000: pp. 73–100.
26. Schlosser S, Sabolova E, and Martak J. Pertraction and membrane based extraction of carboxylic acids in hollow fibre contactors. In: Cox M, Hidalgo M, and Valiente M Eds. *Solvent Extraction for the 21st Century*. Proceedings of ISEC '99, Barcelona, Spain, July 1999. Publisher: Society of Chemical Industry, London, UK 2001; 2: 1041–1046.
27. Wodzki R, Szczepanska G, and Szczepanski P. Unsteady state pertraction and separation of cations in a liquid membrane system: Simple network and numerical model of competitive  $M^{2+}/H^+$  counter-transport. *Sep Purif Technol*, 2004; 36(1): 1–16.
28. Wodzki R, Swiatkowski M, and Lapienis G. Properties of star-shaped polymer with poly(oxyethylene) branches and monoesters of phosphoric acid end groups in pertraction of alkali, alkaline earth, and transient metal cations. *React Funct Polym*, 2002; 52(3): 9–161.
29. Wodzki R and Szczepanski P. Integrated hybrid liquid membrane systems—membrane extraction and pertraction coupled to a pervaporation process. *J Mem Sci*, 2002; 197(1–2): 297–308.
30. Teramoto M, Takeuchi N, Maki T, and Matsuyama H. Ethylene/ethane separation by facilitated transport membrane accompanied by permeation of aqueous silver nitrate solution. *Sep Purif Technol*, 2002; 28(2): 117–124.
31. Teramoto M, Takeuchi N, Maki T, and Matsuyama H. Gas separation by liquid membrane accompanied by permeation of membrane liquid through membrane physical transport. *Sep Purif Technol*, 2001; 24(1–2): 101–112.
32. Teramoto M, Matsuyama H, Nakai K, Uesaka T, and Ohnishi N. Facilitated uphill transport of eicosapentaenoic acid ethyl ester through bulk and supported liquid membranes containing silver nitrate as carrier: A new type of uphill transport. *J Mem Sci*, 1994; 91(1–2): 209–213.
33. Teramoto M, Matsuyama H, and Ohnishi N. Selective facilitated transport of benzene across supported and flowing liquid membranes containing silver nitrate as a carrier. *J Mem Sci*, 1990; 50: 269–278.
34. Teramoto M, Matsuyama H, and Ohnishi N. Development of a spiral-type flowing liquid membrane module with high stability and its application to the recovery of chromium and zinc. *Sep Sci Technol*, 1989; 24(12–13): 981–999.
35. Teramoto M et al. Development of spiral-type supported liquid membrane module for separation and concentration of metal ions. *Sep Sci Technol*, 1987; 22(11): 2175–2201.
36. Matsuyama H, Teramoto M et al. Separation and concentration of heavy metal ions by spiral type flowing liquid membrane module. *Water Treat*, 1990; 5: 237–252.
37. Teramoto M et al. Selectivity in the extraction of metals by liquid membranes. In: Proceedings of ISEC-86, Munich 11–16 September, 1986; DECHEMA, Munich, 1986, FRG, Vol. 1: pp. 545–560.
38. Kubisova L, Sabolova E, Schlosser S, Martak J, and Kertesz R. Mass-transfer in membrane based solvent extraction and stripping of 5-methyl-2-pyrazinecarboxylic acid and co-transport of sulphuric acid in HF contactors. *Desalination*, 2004; 163(1–3): 27–38.
39. Vajda M, Kosuthova A, and Schlosser S. Membrane-based extraction joined with membrane-based stripping in a circulating arrangement III. Extraction of zinc. *Chem Pap*, 2004; 58(1): 1–8.
40. Vajda M, Sabolova E, Schlosser S, and Mikulova E. Membrane-based extraction joined with membrane-based stripping in a circulating arrangement II. Extraction of organic acids. *Chem Pap*, 2003; 57(1): 3–10.
41. Kedem O and Bromberg L. Ion-exchange membranes in extraction processes. *J Mem Sci*, 1993; 78: 255–261.
42. Bromberg L, Levin G, Libman J, and Shanzer A. A novel tetradentate hydroxamate as ion carrier in liquid membranes. *J Mem Sci*, 1992; 69(1–2): 143–153.
43. Kedem O, Eyal A, Bromberg L, and Bressler E. Membrane extraction in the fermentation of carboxylic acids. Israeli Patent, 1992; Appl. No. 101905.
44. Eyal A and Bressler EJ. Industrial separation of carboxylic and amino acids by liquid membranes: Applicability, process considerations, and potential advantages. *Biotechnol Bioeng*, 1993; 41: 287–293.
45. Baniel A, Eyal A, and Bressler E. Extraction of electrolytes from aqueous solutions. Israeli Patent, 1992; Appl. No 101906.
46. Wodzki R and Nowaczyk J. Propionic and acetic acid pertraction through a multimembrane hybrid system containing TOPO or TBP. *Sep Purif Technol*, 2002; 26(2–3): 207–220.
47. Wodzki R and Szczepanski P. Integrated process of Donnan dialysis and pertraction in a multimembrane hybrid system. *Sep Purif Technol*, 2001; 22–23: 697–706.
48. Wodzki R, Nowaczyk J, and Kujawski M. Separation of propionic and acetic acid by pertraction in a multimembrane hybrid system. *Sep Purif Technol*, 2000; 21(1–2): 39–54.
49. Wodzki R, Sionkowski G, and Pozniak G. Recovery and concentration of metal ions. IV. Up-hill transport of Zn(II) in a multimembrane hybrid system. *Sep Sci Technol*, 1999; 34: 627–649.
50. Wodzki R and Sionkowski G. Recovery and concentration of metal ions. III. Temperature and concentration effects in multimembrane hybrid system. *Sep Sci Technol*, 1996; 31: 1541–1553.

51. Wodzki R and Sionkowski G. Recovery and concentration of metal ions. II. Multimembrane hybrid system. *Sep Sci Technol*, 1995; 30: 2763–2778.
52. Sirkar KK. Other new membrane processes. In: Ho WSW and Sirkar KK Eds. *Membrane Handbook*. Van Nostrand Reinhold New York 1992: pp. 904–908.
53. Noble RD and Way JD Eds. *Liquid Membranes. Theory and Applications*. ACS symposium series 347, ACS, Washington DC 1987.
54. Strzelbicki J and Schlosser S. Influence of surface-active substances on pertraction of cobalt(II) cations through bulk and emulsion liquid membranes. *Hydrometallurgy*, 1989; 23(1): 67–75.
55. Schlosser S and Sabolova E. Transport of butyric acid through layered bulk liquid membranes. *Chem Pap*, 1999; 53(6): 403–411.
56. Ohki A, Takagi M, Takeda T, and Ueno K. Thioether-mediated copper transport through liquid membranes with the aid of redox reaction. *J Mem Sci*, 1983; 15(3): 231–244.
57. Shinbo T, Kurihara K, Kobatake Y, and Kamo N. Active transport of picrate anion through organic liquid membrane. *Nature*, London, UK 1977; 270: 277–278.
58. Shinbo T, Sugiura M, Kamo N, and Kobatake Y. Coupling between a redox reaction and ion transport in an artificial membrane system. *J Mem Sci*, 1981; 9(1–2): 1–11.
59. Baker R and Blume I. Coupled transport membranes. In: Porter MC, Ed. *Handbook of Industrial Membrane Technology*. Noyes Publications: Park Ridge, NJ 1990: pp. 511–558.
60. Leiber JP, Noble RD, Way JD, and Bateman BR. Mathematical modeling of facilitated liquid membrane transport systems containing ionically charged species. *Sep Sci Technol*, 1985; 20(4): 231–256.
61. Danesi P. Separation of metal species by supported liquid membranes. *Sep Sci Technol*, 1984–1985; 19(11–12): 857–864.
62. Sirkar KK. Membrane separation technologies. Current developments. *Chem Eng Commun*, 1997; 157: 145–184.
63. Sirkar KK. Hollow fiber-contained liquid membranes for separations: An overview. Chemical separations with liquid membranes, ACS Symposium Series 642, ACS, Washington DC 1996; pp. 222–238.
64. Boyadzhiev L and Lazarova Z. Liquid membranes (liquid pertraction). *Mem Sci Technol Series*, 1995; 2: 283–352.
65. Lazarova Z and Boyadzhiev L. Modeling of copper transfer in a three-phase liquid pertraction system. *Dokladi na Bulgarskata Akademiya na Naukite*, 1991; 44(12): 29–32.
66. Lazarova Z, Sapundzhiev T, and Boyadzhiev L. Kinetics and mechanism of copper transfer by hydroxy-oximes in three-phase liquid systems. *Sep Sci Technol*, 1992; 27(4): 493–508.
67. Boyadzhiev L. Extraction of heavy metals from waste waters by liquid membrane techniques. *J Environ Prot Ecol*, 2000; 1(1): 72–80.
68. Alexandrova S, Saboni A, Boyadzhiev L, Mouhab N, and Estel L. Recovery of substances by rotating-film pertraction. *Chem Eng J (Lausanne)*, 2000; 79(2): 155–163.
69. Dindi A, Noble RD, and Koval CA. An analytical solution for competitive facilitated membrane transport. *J Mem Sci*, 1992; 65(1–2): 39–45.
70. Kislik V and Eyal A. Heavy metals removal from wastewaters of phosphoric acid production. A comparison of hybrid liquid membrane (HLM) and aqueous hybrid liquid membrane (AHLM) technologies. In: Proceedings of the Conference on Membrane in Drinking and Industrial Water Production, 2000; 1: 503–514.
71. Davis S, Wydeven T, Yum A, and Neukom C. A computational and experimental study of unsteady facilitated transport. *J Mem Sci*, 1992; 69(1–2): 99–108.
72. Dindi AK and Noble RD. Experimental and modeling studies of a parasitic binding mechanism in facilitated membrane transport. *J Mem Sci*, 1992; 66(1): 55–68.
73. Hu Shangxu. Selective Removal of Metals from Wastewater Using Affinity Dialysis. In: Emerging Technologies in Hazardous Waste Management. *Am Chem Soc*, 1990; 12: 187–198.
74. Kislik V and Eyal A. Acidity dependence of Ti(IV) extraction: A critical analysis. *Solv Extr Ion Exch*, 1993; 11(2): 259–272.
75. Kislik V and Eyal A. Extraction of titanium(IV) by mixtures of mono- and di-(2- ethylhexyl) phosphoric acid esters. *Solv Extr Ion Exch*, 1993; 11(2): 273–281.
76. Kislik V and Eyal A. Mechanisms of titanium(IV) and some other transition metals extraction by organophosphoric acids. In: Logsdail DH and Slater MJ Eds. Proceedings of ISEC'93, London, July 1993. Elsevier Applied Science for SCI 1993; 3: 1353–1361.
77. Danesi P and Reichley-Yinger L. Origin and significance of the deviations from a pseudo first order rate law in the coupled transport of metal species through supported liquid membranes. *J Mem Sci*, 1986; 29: 195–211.
78. Giddings JC. *Unified Separation Science*. John Wiley & Sons, New York, 1991: pp. 17–19, 38.
79. Giddings JC. *Unified Separation Science*. John Wiley & Sons, New York, 1991: pp. 45–48.
80. Giddings JC. *Unified Separation Science*. John Wiley & Sons, New York, 1991: p. 94.
81. Giddings JC. *Unified Separation Science*. John Wiley & Sons, New York, 1991: pp. 112–114.
82. Giddings JC. *Unified Separation Science*. John Wiley & Sons, New York, 1991: pp. 55–71.
83. Giddings JC. *Unified Separation Science*. John Wiley & Sons, New York, 1991: p. 33.
84. Prasad R and Sirkar KK. Membrane-based solvent extraction. In: Ho WSW and Sirkar KK Eds. *Membrane Handbook*. Van Nostrand Reinhold, New York 1992: pp. 727–763.
85. Kislik V. Application of organic and aqueous liquid membranes in separation of metals and acids: Comparative analysis. In: Proceedings of Abstracts on International Conference: Advanced Membrane Technology, October 2001. Italy, p. 214.
86. Wódzki R and Sionkowski G. Exchange diffusion transport of ions in liquid membranes. Part IV. Thermodynamic network analysis of nonstationary transport of divalent ions. *Pol J Chem*, 1995; 69: 407–422.
87. Wodzki R and Sionkowski G. Exchange diffusion transport of ions through liquid membranes. Part III. Competitive transport of divalent cations. *Pol J Chem*, 1992; 66(2): 351–361.

88. Wodzki R. Exchange diffusion transport of ions through liquid membranes. Part II. Stationary process mediated by a multisided carrier. *Pol J Chem*, 1991; 65(9–10): 1715–1729.
89. Wodzki R. Exchange diffusion transport of ions through liquid membranes. Part I. Numerical studies of univalent ions transport limited by diffusion. *Pol J Chem*, 1989; 63(4–12): 557–568.
90. Schnakenberg J. *Thermodynamic Network Analysis of Biological Systems*, Springer, Berlin, Heidelberg, New York: 1977.
91. Majumdar S and Sirkar KK. Hollow-fiber contained liquid membrane. In: Ho WSW and Sirkar KK Eds. *Membrane Handbook*. Van Nostrand Reinhold, New York: 1992: pp. 777–796.
92. Schlosser S, Sabolova E, Kertesz R, and Kubisova L. Factors influencing transport through liquid membranes and membrane based solvent extraction. *J Sep Sci*, 2001; 24(7): 509–518.
93. Dahuron L and Cussler EL. Protein extractions with hollow fibers. *AIChE J*, 1988; 34(1): 130–136.
94. Kubisova L, Martak J, and Schlosser S. Transport of 5-methyl-2-pyrazinecarboxylic acid through a layered bulk liquid membrane. *Chem Pap*, 2002; 56(6): 418–425.
95. Lu HJ, Fan YT, Wu YJ, and Yin MC. Tripodal lipophilic ionophores: Synthesis, cation binding and transport through liquid membranes. *Polyhedron*, 2001; 20(28): 3281–3286.
96. Safavi A and Shams E. Selective transport of silver ions through bulk liquid membrane using Victoria blue as carrier. *Talanta*, 1999; 48(5): 1167–1172.
97. Nishii Y, Kinugasa T, Nii S, and Takahashi K. Transport behavior of protein in bulk liquid membrane using reversed micelles. *J Mem Sci*, 2002; 195(1): 11–21.
98. Bobok D, Schlosser S, and Kossaczky E. Method of solution separation by means of pertraction and equipment for application of this method. Czech 1987. Patent No. CS 235362 Kind B1 Date 19850515.
99. Boyadzhiev L and Dimitrov K. Silver recovery by rotating film pertraction. Process modeling. *Solv Extr Ion Exch*, 1996; 14(1): 105–118.
100. Alexandrova S, Dimitrov K, Saboni A, and Boyadzhiev L. Selective recovery of silver from dilute polymetal solutions by rotating film pertraction. *Sep Purif Technol*, 2001; 22–23(1–3): 567–570.
101. Dimitrov K, Alexandrova S, Boyadzhiev L, Ruellan S, and Burgard M. Recovery of copper from solutions by rotating film pertraction. *Sep Purif Technol*, 1997; 12(2): 165–173.
102. Boyadzhiev L and Alexandrova S. Recovery of copper from ammoniacal solutions by rotating film pertraction. *Hydrometallurgy*, 1994; 35(1): 109–121.
103. Boyadzhiev L and Atanassova I. Extraction of L-lysine from its dilute aqueous solutions by rotating film pertraction. *Appl Biochem Biotechnol*, 1992; 37(1): 89–95.
104. Schlosser S. Separation method of carboxylic acids from aqueous and non-aqueous solutions. Patent No. SK 282775 Kind B6 Date 20021203.
105. Boyadzhiev L and Bezenshek E. Liquid film pertraction. Recovery of iodine from iodine-containing aqueous solutions. *J Mem Sci*, 1988; 37(3): 277–285.
106. Boyadzhiev L and Atanasova I. Recovery of L-lysine from dilute water solutions by liquid pertraction. *Biotechnol Bioeng*, 1991; 38(9): 1059–1064.
107. Boyadzhiev L, Bezenshek E, and Lazarova Z. Removal of phenol from waste water by double emulsion membranes and creeping film pertraction. *J Mem Sci*, 1984; 21(2): 137–144.
108. Wodzki R and Szczepanska G. Design of integrated membrane system with liquid and polymer membranes. *Zeszyty Naukowe Politechniki Slaskiej (Chemia in English)*, 2001; 146: 231–234.
109. Teramoto M, Matsuyama H, and Yonehara T. Selective facilitated transport of benzene across supported and flowing liquid membranes containing silver nitrate as a carrier. *J Mem Sci*, 1990; 50: 269–284.
110. Vladislavjevic G, Pavasovic V, Mitrovic M, and Vulieevic I. *Rev Res Work Fac Agricut* (in Chech), 1995; 40: 147–156.
111. Vladislavjevic G, Eokesa DM, Mitrovic M, and Rajkovic MB. Better transverse flow hollow fiber modules. In: 12th International Congress of Chemical and Process Engineering, CHISA'96, Praha, 25–30 August 1996, Cheh. Rep. pp. 5501–5509.
112. Stevanovic S, Onjia A, and Mitrovic M. Comparative study of arsenic removal from drinking water (precipitation, sorption and membrane extraction treatments). *Zh Prikl Khim* (Sankt-Peterburg, Russia), 1994; 67(10): 1743–1744.
113. Teramoto M, Kitada S, Ohnishi N, Matsuyama H, and Yonehara N. Separation and concentration of CO<sub>2</sub> by capillary-type facilitated transport membrane module with permeation of carrier solution. *J Mem Sci*, 2004; 234(1–2): 83–94.
114. Teramoto M, Ohnishi N, Takeuchi N, Kitada S, Matsuyama H, Matsumiya N, and Mano H. Separation and enrichment of carbon dioxide by capillary membrane module with permeation of carrier solution. *Separ Purif Technol*, 2003; 30(3): 215–227.
115. Teramoto M, Takeuchi N, Maki T, and Matsuyama H. Facilitated transport of CO<sub>2</sub> through liquid membrane accompanied by permeation of carrier solution. *Separ Purif Technol*, 2002; 27(1): 25–31.
116. Eyal AM and Kislik VS. Membrane Recovery of Metal Pollutants from Waste Waters of the fertilizers Industry (MERMEP). Preliminary report of Joint Research Project. Avicenne 1994.
117. Eyal AM and Kislik VS. Hybrid liquid membrane (HLM) process for metal recovery. In: Membrane Recovery of Metal Pollutants from Waste Waters of the fertilizers Industry (MERMEP). First year Report of Joint Research Project, Avicenne 1995.
118. Eyal AM and Kislik VS. Hybrid liquid membrane (HLM) and aqueous hybrid liquid membrane (AHLM) processes for metal recovery. In: Membrane Recovery of Metal Pollutants from Waste Waters of the fertilizers Industry (MERMEP). Second year Report of Joint Research Project, Avicenne 1996.
119. Kislik VS and Eyal AM. Comparison of hybrid liquid membrane (HLM) and aqueous hybrid liquid membrane (AHLM) technologies in separation of heavy metals from wastewaters. In: Proceedings of Abstracts EURO-MEMBRANE-2000, Israel: pp. 237–238.

120. Kislik V and Eyal A. Heavy metals removal from wastewaters of phosphoric acid production. A comparison of hybrid liquid membrane (HLM) and aqueous hybrid liquid membrane (AHLM) Technologies. *Water Sci Water Technol: Water Supply*, 2001; 1(5/6): 119–129.
121. Wodzki R, Swiatkowski M, Pretula J, and Kaluzynski K. Poly[poly(oxypropylene) phosphate] macroionophores for transport and separation of cations in a hybrid: Cation-exchange polymer and liquid membrane system. *J. Appl Polym Sci*, 2004; 93(3): 1436–1445.
122. Wodzki R and Szczepanski P. Treatment of electroplating rinse solution by continuous membrane extraction and diffusion dialysis. *Pol J Environ Stud*, 2001; 10(2): 101–111.
123. Wodzki R, Swiatkowski M, and Lapienis G. Mobile macromolecular carriers of ionic substances, 2 transport rates and separation of some divalent cations by poly(oxyethylene) phosphates. *Macromol Chem Phys*, 2001; 202(1): 145–154.
124. Wodzki R, Szczepanski P, and Pawlowski M. Recovery of metals from electroplating waste solutions and sludge. Comparison of Donnan dialysis and pertraction technique. *Pol J Environ Stud*, 1999; 8(2): 111–124.
125. Wodzki R, Kaluzynski K, and Klosinski P. Mobile macromolecular carriers of ionic substances. Part 1. Transport of heavy metal ions by polymer analogs of teichoic acids. *Macromol Chem Phys*, 1997; 198(6): 1809–1821.
126. Wodzki R and Klosinski P. Magnesium and calcium ions transport by synthetic analogs of teichoic acids with 1,2- and 1,3-linked phosphodiester units. *Makromol Chem*, 1990; 191(4): 921–931.
127. Narebska A, Wodzki R, and Wyszynska AL. Liquid membranes with organic polyphosphates as ionic carriers. *Makromol Chem*, 1989; 190(6): 1501–1506.
128. Yang ZF, Guha AK, and Sirkar KK. Simultaneous and synergistic extraction of cationic and anionic heavy metallic species by a mixed solvent extraction system and a novel contained liquid membrane device. *Indust Eng Chem Res*, 1996; 35(11): 4214–4220.
129. Guha AK, Yun CH, Basu R, and Sirkar KK. Heavy metal removal and recovery by contained liquid membrane permeator. *AIChE J*, 1994; 40(7): 1223–1237.
130. Kertesz R, Schlosser S, and Teixidor F. Pertraction of silver with octylphenylsulfide as carrier in a hollow fiber contactor. *Desalination*, 2002; 148(1–3): 263–265.
131. Marchese J and Campderros M. Mass transfer of cadmium ions in a hollow-fiber module by pertraction. *Desalination*, 2004; 164(2): 141–149.
132. Vajda M, Schlosser S, and Kovacova K. Pertraction of silver through bulk liquid membranes. *Chem Pap*, 2000; 54(6b): 423–429.
133. El Bachiri A, Hagège A, and Burgard M. Recovery of silver nitrate by transport across a liquid membrane containing dicyclohexano 18 crown 6 as a carrier. *J Mem Sci*, 1996; 121(2): 159–168.
134. Granado-Castro MD, Galindo-Riaño MD, and García-Vargas M. Separation and preconcentration of cadmium ions in natural water using a liquid membrane system with 2-acetylpyridine benzoylhydrazine as carrier by flame atomic absorption spectrometry. *Spectrochim Acta Part B: Atomic Spectrosc*, 2004; 59(4): 577–583.
135. Granado-Castro MD, Galindo-Riaño MD, and García-Vargas M. Model experiments to test the use of a liquid membrane for separation and preconcentration of copper from natural water. *Anal Chim Acta*, 2004; 506(1): 81–86.
136. León G and Guzmán MA. Facilitated transport of cobalt through bulk liquid membranes containing diethylhexyl phosphoric acid. *Desalination*, 2004; 162: 211–215.
137. Kontrec J, Kralj D, and Brechevich L. Cadmium removal from calcium sulphate suspension by liquid membrane extraction during recrystallization of calcium sulphate anhydrite. *Colloids Surf A: Physicochem Eng Aspects*, 2003; 223(1–3): 239–249.
138. Al-Marzouqi MH, Hogendoorn KJA, and Versteeg GF. Analytical solution for facilitated transport across a membrane. *Chem Eng Sci*, 2002; 57(22–23): 4817–4829.
139. Kocherginsky NM, Zhang YK, and Stucki JW. D2EHPA based strontium removal from strongly alkaline nuclear waste. *Desalination*, 2002; 144(1–3): 267–272.
140. Alizadeh N, Salimi S, and Jabbari A. Transport study of palladium through a bulk liquid membrane using hexadecylpyridinium as carrier. *Sep Purif Technol*, 2002; 28(3): 173–180.
141. Yamini Y, Chalooosi M, and Ebrahimzadeh H. Highly selective and efficient transport of bismuth in bulk liquid membranes containing Cyanex 301. *Sep Purif Technol*, 2002; 28(1): 43–51.
142. Gong S-L, Zhong Z-L, and Chen Y-Y. Calixcrown oligomers as cation carriers in a bulk liquid membrane. *React Funct Polym*, 2002; 51(2–3): 111–116.
143. Shamsipur M, Mashhadizadeh MH, and Azimi G. Highly selective and efficient transport of mercury(II) ions across a bulk liquid membrane containing tetrathia-12-crown-4 as a specific ion carrier. *Sep Purif Technol*, 2002; 27(2): 155–161.
144. Mishra D and Sharma U. Extraction and bulk liquid membrane transport of some main group metal ions facilitated by triethylene glycol monomethyl ether. *Sep Purif Technol*, 2002; 27(1): 51–57.
145. Safavi A, Peiravian F, and Shams E. A selective uphill transport of copper through bulk liquid membrane using Janus Green as an anion carrier. *Sep Purif Technol*, 2002; 26(2–3): 221–226.
146. Ma M, He D, Wang Q, and Xie Q. Kinetics of europium(III) transport through a liquid membrane containing HEH(EHP) in kerosene. *Talanta*, 2001; 55(6): 1109–1117.
147. Jabbari A, Esmaeili M, and Shamsipur M. Selective transport of mercury as  $\text{HgCl}_4^{2-}$  through a bulk liquid membrane transport using  $\text{K}^+$ -dicyclohexyl-18-crown-6 as carrier. *Sep Purif Technol*, 2001; 24(1–2): 139–145.
148. Gholivand MB and Khorsandipoor S. Selective and efficient uphill transport of Cu(II) through bulk liquid membrane using *N*-ethyl-2-aminocyclopentene-1-dithiocarboxylic acid as carrier. *J Mem Sci*, 2000; 180(1): 115–120.
149. Shamsipur M and Mashhadizadeh MH. Highly efficient and selective membrane transport of silver(I) using hexathia-18-crown-6 as a specific ion carrier. *Sep Purif Technol*, 2000; 20(2–3): 147–153.

150. He D, Ma M, and Zhao Z. Transport of cadmium ions through a liquid membrane containing amine extractants as carriers. *J Mem Sci*, 2000; 169(1): 53–59.
151. Szpakowska M and Nagy OB. Influence of physico-chemical control and of membrane composition on the coupled transport of copper (II) ions through bulk liquid membrane. *J Mem Sci*, 2000; 168(1–2): 183–186.
152. Jabbari A, Mohammadi J, and Shamsipur M. Selective liquid membrane transport of Pd(II) as  $\text{PdCl}_4^{2-}$  ion using potassium-dicyclohexyl-18-crown-6 as carrier. *Microchem J*, 1999; 63(2): 218–225.
153. Khayatian G and Shamsipur M. Highly selective and efficient membrane transport of palladium as  $\text{PdCl}_4^{2-}$  ion using  $\text{NH}_4^+$ -dibenzyl-diaza-18-crown-6 as carrier. *Sep Purif Technol*, 1999; 16(3): 235–241.
154. Bartsch RA, Jeon Eok-Giu, Walkowiak W, and Apostoluk W. Effect of solvent in competitive alkali metal cation transport across bulk liquid membrane by a lipophilic lariat ether carboxylic acid carrier. *J Mem Sci*, 1999; 159(1–2): 123–131.
155. Safavi A and Shams E. Selective and efficient liquid membrane transport of gold as gold cyanide using an anion carrier. *J Mem Sci*, 1999; 157(2): 171–176.
156. Safavi A and Shams E. Selective and efficient transport of Hg(II) through bulk liquid membrane using methyl red as carrier. *J Mem Sci*, 1998; 144(1–2): 37–43.
157. Szpakowska M. Coupled transport of copper through different types of liquid membrane containing Acorga P-50 as carrier. *J Mem Sci*, 1996; 109(1): 77–86.
158. Gaikwad AG, Chitra KR, Surender GD, and Damodaran AD. Studies on kinetics of forward and backward extraction of neodymium by using phosphonic acid monoester as an acidic extractant. *Chem Eng J Biochem Eng J*, 1995; 60(1–3): 63–73.
159. Nakatsuji Y, Inoue M, Matsumoto M, Masuyama A, and Kida T. Selective transport of lithium ion using noncyclic proton-ionizable ionophores through bulk and emulsion liquid membranes. *J Mem Sci*, 1995; 104(1–2): 165–172.
160. Shukla JP and Misra SK. Carrier-mediated transport of uranyl ions across tributyl phosphate—dodecane liquid membranes. *J Mem Sci*, 1991; 64(1–2): 93–102.
161. Wakita R, Matsumoto M, Nakatsuji Y, and Okahara M. Selective transport of lithium ions by an acyclic carboxylic ionophore with a quinaldate moiety through a bulk liquid membrane. *J Mem Sci*, 1991; 57(2–3): 297–306.
162. Kislik V and Eyal A. Application of hydrophobic (water-immiscible) and hydrophilic (water-soluble) liquid membranes in the carboxylic acids separation technologies: Comparative analysis. In: Proceedings of Abstracts of 41st Microsymposium Polymer Membranes Prague 2001: pp. 86–87.
163. Solichien MS, O'Brien D, Hammond EG, and Glatz CE. Membrane-based extractive fermentation to produce propionic and acetic acids: Toxicity and mass transfer considerations. *Enzyme Microbial Technol*, 1995; 17(1): 23–31.
164. Wodzki R and Nowaczyk J. Membrane transport of organics. III. Permeation of some carboxylic acids through bipolar polymer membrane. *J Appl Polym Sci*, 2001; 80(14): 2705–2717.
165. Wodzki R and Nowaczyk J. Membrane transport of organics. II. Permeation of some carboxylic acids through strongly basic polymer membrane. *J Appl Polym Sci*, 1999; 71(13): 2179–2190.
166. Wodzki R and Nowaczyk J. Extraction and separation of propionic and acetic acid by permeation in a hybrid membrane system composed of liquid and ion-exchange polymer membranes. *Solv Extr Ion Exch*, 1997; 15(6): 1085–1106.
167. Basu R and Sirkar KK. Citric acid extraction with microporous hollow fibers. *Solv Extr Ion Exch*, 1992; 10(1): 119–143.
168. Basu R and Sirkar KK. Hollow fiber contained liquid membrane separation of citric acid. *AIChE J*, 1991; 37(3): 383–393.
169. Cichy W, Schlosser S, and Szymanowski J. Recovery of phenol with CYANEX 923 in membrane extraction-stripping systems. *Solv Extr Ion Exch*, 2001; 19(5): 905–923.
170. Zigova J, Sturdik E, Vandak D, and Schlosser S. Butyric acid production by clostridium butyricum with integrated extraction and pertraction. *Process Biochem* (Oxford), 1999; 34(8): 835–843.
171. Teramoto M, Matsuyama H, and Ohnishi N. Uphill transport of polyunsaturated fatty acid ethyl esters through liquid membranes containing silver nitrate as a carrier. In: Shallcross DC, Paimin R, and Prvcic LM Eds. Proceedings of the ISEC'96: Value Adding through Solvent Extraction. Publisher: University of Melbourne, Melbourne, Australia 1996; 2: 917–922.
172. Teramoto M, Matsuyama H, and Nakai K. Separation of ethyl esters of eicosapentaenoic acid and docosahexaenoic acid by circulating liquid membranes using silver nitrate as a carrier. Uphill transport by use of temperature and solvent dependencies of distribution ratio. *Sep Sci Technol*, 1996; 31(14): 1953–1969.
173. Ma M, Chen B, Luo X, Tan H, He D, Xie Q, and Yao S. Study on the transport selectivity and kinetics of amino acids through di(2-ethylhexyl) phosphoric acid-kerosene bulk liquid membrane. *J Mem Sci*, 2004; 234(1–2): 101–109.
174. Ma M, He D, Liao S, Zeng Y, Xie Q, and Yao S. Kinetic study of L-isoleucine transport through a liquid membrane containing di(2-ethylhexyl) phosphoric acid in kerosene. *Anal Chim Acta*, 2002; 456(1): 157–165.
175. Uglea CV and Croitoru M. Transport of amino acids through liquid membranes. III. The alkaline ion role. *J Mem Sci*, 1997; 133(1): 127–131.
176. Sahoo GC, Ghosh AC, Dutta NN, and Mathur RK. Facilitated transport of 7-aminocephalosporanic acid in a bulk liquid membrane. *J Mem Sci*, 1996; 112(2): 147–154.
177. Ersoz M, Vura US, Okdan A, Pehlivan E, and Yildiz S. Transport studies of amino acids through a liquid membrane system containing carboxylated poly (styrene) carrier. *J Mem Sci*, 1995; 104(3): 263–269.
178. Uglea CV and Zanoag CV. Transport of amino acids through organic liquid membranes. II. Aspects of the mechanism. *J Mem Sci*, 1992; 65(1–2): 47–50.
179. Kukufuta E and Nobusawa M. Uphill transport of phosphate ion through an oxomolybdenum(v)-tetraphenylporphyrin-complex-containing bulk liquid membrane: Effect of halogen ions on phosphate ion flux. *J Mem Sci*, 1990; 48(2–3): 141–154.
180. Scrimin P, Tonellato U, and Zanta N. Cu(II) mediated selective transport of  $\alpha$ -amino acids across a bulk liquid membrane using a chiral lipophilic ligand as a carrier. *Tetrahedron Lett*, 1988; 29(39): 4967–4970.

181. Boyadzhiev L and Kirilova N. Extraction of tylosin from its aqueous solutions by rotating film-pertraction. *Bioprocess Eng*, 2000; 22(5): 373–378.
182. Boyadzhiev L and Atanassova I. Extraction of phenylalanine from dilute solutions by rotating film pertraction. *Process Biochem* (Oxford, United Kingdom) 1994; 29(4): 237–243.
183. Sirkar KK. Application of membrane technologies in the pharmaceutical industry. *Curr Opin Drug Discov Devel*, 2000; 3(6): 714–722.
184. Basu R and Sirkar KK. Pharmaceutical product recovery using a hollow fiber contained liquid membrane: A case study. *J Mem Sci*, 1992; 75(1–2): 131–149.
185. Dai XP, Luo RG, and Sirkar KK. A membrane-based integrated bioseparation process. *Adv Filtration Sep Technol*, 1999; 13A: 545–549.
186. Prasad R and Sirkar KK. Hollow fiber solvent extraction: Performances and design. *J Mem Sci*, 1990; 50(2): 153–175.
187. Prasad R and Sirkar KK. Hollow fiber solvent extraction of pharmaceutical products: A case study. *J Mem Sci*, 1989; 47(3): 235–259.
188. Lopez JL and Matson SL. A multiphase/extractive enzyme membrane reactor for production of diltiazem chiral intermediate. *J Mem Sci*, 1997; 125(1): 189–211.
189. Di Luccio M, Smith BD, Kida T, Alves TLM, and Borges CP. Evaluation of flat sheet and hollow fiber supported liquid membranes for fructose pertraction from a mixture of sugars. *Desalination*, 2002; 148(1–3): 213–220.
190. Yang ZF, Rindfleisch D, Scheper T, and Schugerl K. Separation of penicillin G with hollow fiber contained liquid membrane system. In: Paterson R Ed. *Proceedings of 3rd International Conference on Effective Membrane Processes – New Perspectives*. BHR group, Cranfield, Berth, 1993, pp. 49–57.
191. Rindfleisch D, Syska B, Lazarova Z, and Schugerl K. Integrated membrane extraction, enzymic conversion and electro dialysis for the synthesis of ampicillin from penicillin G. *Process Biochem*, 1997; 32(7): 605–616.
192. Miesiac I and Szymanowski J. Pertraction of penicillin G in hollow fiber contained liquid membranes. *J Radioanalyt Nucl Chem*, 1998; 228(1–2): 77–81.
193. Boyadzhiev L and Yordanov B. Pertraction of Indole Alkaloids from Vinca minor L. *Sep Sci Tech*, 2004; 39(6): 1321–1329.
194. Coucouvanis D, Dell Rosa and Jay Pike recognition and transport of amphiphilic molecules by a new class of inorganic ditopic receptors. The synthesis of  $M^{-f} Bu_4$ -salphen-3*n*-cr-*n* complexes and their use ( $M = Mn, Fe, n = 6$ ) in the transport of tryptophan and serotonin across bulk liquid membranes. *Comptes Rendus Chimie*, 2003; 6(3): 317–327.
195. Kinugasa T, Tanahashi S, Takahashi S, and Takeuchi H. Transport of proteins through reversed micellar solution layer as a liquid membrane. In: Proceedings of ISEC'90, 16–21 July 1990; Kyoto, Japan, Vol. 13: pp. 1839–1846.
196. Pietraszkiewicz M, Kozbial M, and Pietraszkiewicz O. Transport studies of inorganic and organic cations across liquid membranes containing Mannich-base calix[4]resorcinarenes. *Pol J Chem*, 1998; 72(5): 886–892.
197. Pietraszkiewicz O, Kozbial M, and Pietraszkiewicz M. Transport studies of inorganic and organic cations across liquid membranes containing Mannich-base calix[4]resorcinarenes. Molecular recognition and inclusion. In: Proceedings of the 9th International Symposium on Molecular Recognition and Inclusion, France 1998: pp. 459–462.
198. Hebrant M, Mettelin P, Tondre C, Joly JP, Larpent C, and Chasseray X. AOT reversed micelles as carriers of amino acids across liquid membranes. Search for selectivity and chirality effect. *Colloids Surf A Physicochem Eng Aspects*, 1993; 75: 257–267.
199. Krieg HM, Lotter J, Keizer K, and Breytenbach JC. Enrichment of chlorthalidone enantiomers by an aqueous bulk liquid membrane containing  $\beta$ -cyclodextrin. *J Mem Sci*, 2000; 167(1): 33–45.
200. Sahoo GC, Dutta NN, and Dass NN. Liquid membrane extraction of cephalosporin-C from fermentation broth. *J Mem Sci*, 1999; 157(2): 251–261.
201. Sahoo GC, Ghosh AC, and Dutta NN. Recovery of cephalixin from dilute solution in a bulk liquid membrane. *Process Biochem*, 1997; 32(4): 265–272.
202. Lazarova Z and Boyadzhiev L. Liquid film pertraction—a liquid membrane method for recovery and preconcentration of aromatic amines from their dilute aqueous solutions. *Int J Environ Anal Chem*, 1992; 46(4): 233–244.
203. Teramoto M, Matsuyama H, Yamashiro T, and Okamoto S. Separation of ethylene from ethane by a flowing liquid membrane using silver nitrate as a carrier. *J Mem Sci*, 1989; 45(1–2): 115–136.
204. Poddar TK, Majumdar S, and Sirkar KK. Removal of VOCs from air by membrane-based absorption and stripping. *J Mem Sci*, 1996; 120(2): 221–237.
205. Yang D, Majumdar S, Kovenklioglu S, and Sirkar KK. Hollow fiber contained liquid membrane pervaporation system for the removal of toxic volatile organics from wastewater. *J Mem Sci*, 1995; 103(3): 195–210.
206. Yun CH, Guha AK, Prasad R, and Sirkar KK. Novel microporous membrane-based separation processes for pollution control and waste minimization. In: Sawyer DT and Martell AE Eds. *Industrial Environmental Chemistry Waste Minimization in Industrial Processes and Remediation of Hazardous Waste*. Proceedings of the Texas A&M University, IUCCP 10th Annual Symposium on Industrial Environmental Chemistry: Waste Minimization in Industrial Processes and Remediation of Hazardous Waste, March 24–26, Plenum, New York 1992: pp. 135–146.
207. Sirkar KK, Yang D, Majumdar S, Kovenklioglu S, and Sengupta A. Hollow fiber-containing liquid membrane pervaporation for removal of volatile organic compounds from aqueous solution. Patent No. US 5637224 Kind A Date 19970610.
208. Shanbhag PV, Guha AK, and Sirkar KK. Membrane-based integrated absorption-oxidation reactor for destroying VOCs in air. *Environ Sci Technol*, 1996; 30(12): 3435–3440.
209. Papadopoulos T and Sirkar KK. Separation of a 2-propanol/*n*-heptane mixture by liquid membrane pertraction. *Indust Eng Chem Res*, 1993; 32(4): 663–673.
210. Bessarabov DG, Theron JP, and Sanderson RD. Novel application of membrane contactors: Solubility measurements of 1-hexene in solvents containing silver ions for liquid olefin/paraffin separations. *Desalination*, 1998; 115(3): 279–284.

211. Ray R, Wytcherley RW, Newbold D, McCray S, Friesen D, and Brose D. Synergistic, membrane-based hybrid separation systems. *J Mem Sci*, 1991; 62(3): 347–369.
212. Bothun GD, Knutson BL, Strobel HJ, and Nokes SE. Mass transfer in hollow fiber membrane contactor extraction using compressed solvents. *J Mem Sci*, 2003; 227(1–2): 183–196.
213. Teramoto M, Ito N, and Matsumoto H. Selective separation and concentration of carbon dioxide by flowing liquid membranes. *Kagaku Kogaku Ronbunshu*, 1990; 16(6): 1234–1240.
214. Teramoto M, Ohnishi N, Kitada S, Matsuyama H, Matsumiya N, and Mano H. Simultaneous recovery and enrichment of CO<sub>2</sub> by novel capillary membrane module with permeation of carrier solution. Abstracts of Papers, 225th ACS National Meeting, New Orleans, LA.: American Chemical Society, Washington, DC 2003; IEC-009.
215. Majumdar S, Bhaumik D, Sirkar KK, and Simes G. A pilot-scale demonstration of a membrane-based absorption-stripping process for removal and recovery of volatile organic compounds. *Environ Progress*, 2001; 20(1): 27–35.
216. Sirkar KK. Gas separation using hollow fiber contained liquid membrane. Patent No. US 6156096 Kind A Date 20001205.
217. Papadopoulos T and Sirkar KK. A modified hollow fiber contained liquid membrane technique for gas separation at high pressures. *J Mem Sci*, 1994; 94(1–3): 163–181.
218. Majumdar S, Sengupta A, Cha JS, and Sirkar KK. Simultaneous SO<sub>2</sub>/NO separation from flue gas in a contained liquid membrane permeator. *Indust Eng Chem Res*, 1994; 33(3): 667–675.
219. Guha AK, Majumdar S, and Sirkar KK. Gas separation modes in a hollow fiber contained liquid membrane permeator. *Indust Eng Chem Res*, 1992; 31(2): 593–604.
220. Guha AK, Majumdar S, and Sirkar KK. A larger-scale study of gas separation by hollow-fiber-contained liquid membrane permeator. *J Mem Sci*, 1991; 62(3): 293–307.
221. Bhaumik D, Majumdar S, and Sirkar KK. Absorption of CO<sub>2</sub> in a transverse flow hollow fiber membrane module having a few wraps of the fiber mat. *J Mem Sci*, 1998; 138(1): 77–82.
222. Kreulen H, Versteeg GF, Smolders CA, and Van Swaaij WPM. Selective removal of H<sub>2</sub>S from sour gas with microporous membranes. Part I. Application in a gas-liquid system. *J Mem Sci*, 1992; 73(2–3): 293–304.
223. Kreulen H, Smolders CA, Versteeg GF, and Swaaij WPM. Selective removal of H<sub>2</sub>S from sour gases with microporous membranes. Part II. A liquid membrane of water-free tertiary amines. *J Mem Sci*, 1993; 82(1–2): 185–197.
224. Meldon JH and Dutta A. Analysis of ultimate permselectivity for H<sub>2</sub>S over CO<sub>2</sub> in alkaline solutions. *Chem Eng Sci*, 1994; 49(5): 689–697.
225. Saha S and Chakma A. Selective CO<sub>2</sub> separation from CO<sub>2</sub>/C<sub>2</sub>H<sub>6</sub> mixtures by immobilized diethanolamine/PEG membranes. *J Mem Sci*, 1995; 98(1–2): 157–171.
226. Kumar PS, Hogendoorn JA, Feron PHM, and Versteeg GF. New absorption liquids for the removal of CO<sub>2</sub> from dilute gas streams using membrane contactors. *Chem Eng Sci*, 2002; 57(9): 1639–1651.
227. Figoli A, Sager WFC, and Mulder MHV. Facilitated oxygen transport in liquid membranes: Review and new concepts. *J Mem Sci*, 2001; 181(1): 97–110.
228. Yongtaek L, Noble RD, Yeom Bong-Yeol, Park Y-I, and Lee K-H. Analysis of CO<sub>2</sub> removal by hollow fiber membrane contactors. *J Mem Sci*, 2001; 194(1): 57–67.
229. Rangwala HA. Absorption of carbon dioxide into aqueous solutions using hollow fiber membrane contactors. *J Mem Sci*, 1996; 112(2): 229–240.
230. Quinn R, Appleby JB, and Pez GP. New facilitated transport membranes for the separation of carbon dioxide from hydrogen and methane. *J Mem Sci*, 1995; 104(1–2): 139–146.
231. Yoon SH, Lee HS, and Kim CG. Comparison of pilot scale performances between membrane bioreactor and hybrid conventional wastewater treatment systems. *J Mem Sci*, 2004; 242(1–2): 5–12.
232. Lesjean B, Rosenberger S, Schrotter J-C, and Recherche A. Membrane-aided biological wastewater treatment—an overview of applied systems. *Membr Technol*, 2004; 2004(8): 5–10.
233. Drioli E, Iorio G, and Catapano G. Enzyme membrane reactors and membrane fermentors. In: Porter MC Ed. *Handbook of Industrial Membrane Technology*. Noyes publications, Park Ridge, NJ 1990: pp. 401–481.
234. Iorio G. Membrane in biotechnology: State of the art and prospects. In: Mika AM and Winnicki TZ Eds. *Advances in Membrane Phenomena and Processes*. Wroclaw Technical University Press, Wroclaw, Poland 1989: pp. 231–248.
235. Pagnanelli F, Beolchini F, Di Biase A, and Vegliò F. Effect of equilibrium models in the simulation of heavy metal biosorption in single and two-stage UF/MF membrane reactor systems. *Biochem Eng J*, 2003; 15(1): 27–35.
236. Konovalova VV, Dmytrenko GM, Nigmatullin RR, Bryk MT, and Gvozdyak PI. Chromium(VI) reduction in a membrane bioreactor with immobilized *Pseudomonas* cells. *Enzyme Microbial Technol*, 2003; 33(7): 899–907.
237. Teplyakov VV, Gassanova LG, Sostina EG, Slepova EV, Modigell M, and Netrusov AI. Lab-scale bioreactor integrated with active membrane system for hydrogen production: Experience and prospects. *Int J Hydrogen Energy*, 2002; 27(11–12): 1149–1155.
238. Hsieh Y-L, Tseng S-K, and Chang Y-J. Nitrogen removal from wastewater using a double-biofilm reactor with a continuous-flow method. *Bioresour Technol*, 2003; 88(2): 107–113.
239. Crespo JG, Velizarov S, and Reis MA. Membrane bioreactors for the removal of anionic micropollutants from drinking water. *Curr Opin Biotechnol*, 2004; 15(5): 463–468.
240. Bae T-H, Han S-S, and Tak T-M. Membrane sequencing batch reactor system for the treatment of dairy industry wastewater. *Process Biochem*, 2003; 39(2): 221–231.
241. Howell JA. Future of membranes and membrane reactors in green technologies and for water reuse. *Desalination*, 2004; 162(10): 1–11.
242. Noronha M, Britz T, Mavrov V, Janke HD, and Chmiel H. Treatment of spent process water from a fruit juice company for purposes of reuse: Hybrid process concept and on-site test operation of a pilot plant. *Desalination*, 2002; 143(2): 183–196.

243. Visvanathan C, Boonthanon N, Sathasivan A, and Jegatheesan V. Pretreatment of seawater for biodegradable organic content removal using membrane bioreactor. *Desalination*, 2003; 153(1–3): 133–140.
244. Tazi-Pain A, Schrotter JC, Bord G, Payreaudeau M, and Buisson H. Recent improvement of the BIOSEP process for industrial and municipal wastewater treatment. *Desalination*, 2002; 146(1–3): 439–443.
245. Liu W, Howell JA, Arnot TC, and Scott JA. A novel extractive membrane bioreactor for treating biorefractory organic pollutants in the presence of high concentrations of inorganics: Application to a synthetic acidic effluent containing high concentrations of chlorophenol and salt. *J Mem Sci*, 2001; 181(1): 127–140.
246. Sun X, Shi Y, Yu H, and Shen Z. Bioconversion of acrylonitrile to acrylamide using hollow-fiber membrane bioreactor system. *Biochem Eng J*, 2004; 18(3): 239–243.
247. Noworyta A and Trusek-Holownia A. Modeling of enzymatic conversion in the catalytic gel layer located on a membrane surface. *Desalination*, 2004; 162(10): 327–334.
248. Jurado E, Camacho F, Luzón G, and Vicaria JM. Kinetic model for lactose hydrolysis in a recirculation hollow-fibre bioreactor. *Chem Eng Sci*, 2004; 59(2): 397–405.
249. Gan Q, Allen SJ, and Taylor G. Design and operation of an integrated membrane reactor for enzymatic cellulose hydrolysis. *Biochem Eng J*, 2002; 12(3): 223–229.
250. Slominska L, Szostek A, and Grzeskowiak A. Studies on enzymatic continuous production of cyclodextrins in an ultrafiltration membrane bioreactor. *Carbohydr Polym*, 2002; 50(4): 423–428.
251. Li H, Mustacchi R, Knowles CJ, Skibar W, Sunderland G, Dalrymple I, and Jackman SA. An electrokinetic bioreactor: Using direct electric current for enhanced lactic acid fermentation and product recovery. *Tetrahedron*, 2004; 60(3): 655–661.
252. Mendiguchía C, Moreno C, and García-Vargas M. Separation of heavy metals in seawater by liquid membranes: Preconcentration of copper. *Sep.Sci Technol*, 2002; 46(1): 35–40.
253. Mendiguchía C, Moreno C, and García-Vargas M. Determination of copper in seawater based on a liquid membrane preconcentration system. *Anal Chim Acta*, 2002; 460(1): 35–40.
254. Djane NK, Malcus F, Martins E, Sawula G, and Johansson G. Hollow fiber cartridges for removal of particulate matter from natural waters prior to matrix isolation and trace metal enrichment using an 8-quinolinol chelating ion exchanger in a flow system. *Anal Chim Acta*, 1995; 316(3): 305–311.
255. Jonsson JA. Membrane extraction for sample preparation—a practical guide. *Chromatographia*, 2003; 57(Suppl.): S/317–S/324.
256. Jonsson JA and Mathiasson L. Membrane-based techniques for sample enrichment. *J Chromatogr A*, 2000; 902(1): 205–225.
257. Jonsson JA and Mathiasson L. Membrane extraction techniques in bioanalysis. *Chromatographia* supplement, 2000; 52: S8–S11.
258. Bazylak G and Nagels LJ. Simultaneous high-throughput determination of clenbuterol, ambroxol and bromhexine in pharmaceutical formulations by HPLC with potentiometric detection. *J Pharm Biomed Anal*, 2003; 32(4–5): 887–903.
259. Jonsson JA, Andersson M, Melander C, Norberg J, Thordarson E, and Mathiasson L. Automated liquid membrane extraction for high-performance liquid chromatography of ropivacaine metabolites in urine. *J Chromatogr A*, 2000; 870(1–2): 151–157.
260. Megersa N, Chimuka L, Solomon T, and Jonsson JA. Automated liquid membrane extraction and trace enrichment of triazine herbicides and their metabolites in environmental and biological samples. *J Sep Sci*, 2001; 24(7): 567–576.
261. Norberg J, Zander A, and Jonsson JA. Microporous membrane liquid–liquid extraction technique combined with gas chromatography mass spectrometry for the determination of organotin compounds. *Anal Chim Acta*, 2000; 404(2): 319–328.



---

# 14 Advancements in Membrane Processes for Pharmaceutical Applications

*Ralf Kuriyel, Masatake Fushijima, and Gary W. Jung*

## CONTENTS

14.1	Membrane Technologies .....	409
14.1.1	Direct Flow Filtration .....	410
14.1.1.1	General Principles .....	410
14.1.1.2	Sterile Filtration .....	410
14.1.1.3	Virus Filtration .....	411
14.1.1.4	Membrane Adsorbers .....	411
14.1.1.5	Depth Filtration .....	411
14.1.2	Tangential Flow Filtration .....	411
14.1.2.1	Fundamentals .....	411
14.1.2.2	Effect of Polarization on Flux .....	412
14.1.2.3	Processing Modes .....	412
14.1.2.4	Membrane Module Configuration .....	413
14.2	Membrane Applications .....	415
14.2.1	Plasma Fractionation .....	415
14.2.1.1	Factor VIII .....	417
14.2.1.2	Immunoglobulins .....	417
14.2.1.3	Albumin .....	417
14.2.1.4	$\alpha$ -1-Protease Inhibitor .....	417
14.2.1.5	Prothrombin Complex .....	417
14.2.1.6	Membrane Operations during Plasma Fractionation .....	417
14.2.2	Enzymes and Antibiotics .....	419
14.2.2.1	Upstream Processing .....	421
14.2.2.2	Downstream Processing .....	422
14.2.3	Active Pharmaceutical Ingredients .....	423
14.2.4	Parenterals .....	424
14.3	Future Trends .....	425
14.4	Conclusion .....	425
	References .....	425

## 14.1 MEMBRANE TECHNOLOGIES

Filtration- and membrane-based separation operations are used in the manufacture of many pharmaceutical products. These operations range, for example, from the clarification of fermentation broths used in the production of antibiotics, to virus clearance for plasma-derived protein therapeutics, to sterile filtration of heat-labile products, and beyond. Innovations in membrane materials and module design allow membranes to be used in an increasingly wider range of manufacturing steps. This chapter describes different membrane technologies and their applications during the manufacture of pharmaceutical products such as antibiotics, plasma-derived proteins, active pharmaceutical ingredients, and parenterals (small and large volume).

Membranes are selective barriers that allow for the transmission of certain feed components while retaining other components. The mechanism behind the selectivity is generally the size of the component—particles or molecules larger

than the membrane pores are retained while the smaller ones pass through. Membrane operations cover a broad range of pore sizes. Microfiltration (MF) membranes have pore sizes ranging from 0.1 to 5  $\mu\text{m}$ , and are used for the separation of particles from dissolved species. Ultrafiltration (UF) membranes have pore sizes ranging from 1 to 100 nm, and are used in applications where the retention of large molecules such as proteins is important. Reverse osmosis (RO) membranes retain practically all solutes other than the solvent. Nanofiltration (NF) membranes have pores, which are between RO and UF. Pore size is used to characterize the retentive properties of MF membranes, while the size of the molecules that would be retained by the membrane, sometimes called nominal molecular weight cutoff (MWCO), is used to characterize UF, NF, and RO membranes.

Membrane operations are conducted either in a direct flow filtration (also called dead end) mode or in a tangential flow filtration (TFF) mode. Direct flow filtration is simple and easy to implement but has limited capacity for applications with high-solid mass. TFF is capable of processing large-solid masses but is more complex and capital intensive.

## 14.1.1 DIRECT FLOW FILTRATION

### 14.1.1.1 General Principles

In the pharmaceutical industry, most of the critical membrane filtration operations, such as sterile and virus filtration, are performed in the direct flow filtration mode where a feed solution passes directly through a membrane. As the solution passes through the membrane, particles are retained by size exclusion or adsorption. Direct flow filtration can be operated under constant flow or constant pressure modes.

The performance of direct flow filters can be characterized in terms of three parameters: flux, throughput, and retention. Flux is the filtration flow rate per unit area and follows D'Arcy's law [1]. It is proportional to the pressure driving force and inversely proportional to the hydraulic resistance of the porous media and the viscosity of the solution.

Throughput characterizes how much filtration can be conducted before the operation needs to be stopped due to fouling. As the membrane fouls there is a decrease in the flux or an increase in transmembrane pressure (TMP) depending on the operation mode, and the operation is stopped when either the flux is too low or the TMP is too high. The amount of filtrate that is processed per unit membrane area is called throughput.

Filter plugging can be caused by different dynamics [2–4]. Particles that are larger than the largest membrane pore are retained on the surface and form a cake. Particles of similar size to the size of the pores can completely block pores and reduce the effective surface area of the membrane. Particles that are smaller adsorb to the internal surface of the pores, reducing their effective diameter and increasing the hydraulic resistance of the media. In an actual filtration operation all these dynamics can work together in fouling the membrane [5]. The amount and type of fouling is strongly dependent on solution properties and operating parameters. The composition, particle size distribution, temperature, pH, and ionic strength of the feed solution can play an important role on the rate of fouling. Operating parameters such as the mode of the filtration operation, i.e., constant flow or constant pressure, and the selected pressure or flow rate are important as well.

Retention is a function of the pore size distribution of the membrane, solution properties, and operating conditions. For critical applications such as sterile or virus filtration, retention should be tested with the actual solution under different operating conditions. Typically, membrane filters are tested for integrity before use to ensure the required retention is obtained during operation. Integrity tests are based on bubble point or diffusion [6].

Direct flow filters are available typically in cartridge format, such as 10–40 in. (25–100 cm) lengths. Cartridges contain membranes that are pleated to provide the maximum amount of surface area within a single cartridge. Direct flow filters are also available as self-contained disposable capsules that do not require the use of housings. The ease of use associated with capsules has increased their use.

There are several categories of direct flow filtration; however, this chapter covers the three major ones—sterile filtration, virus filtration, and membrane adsorbers—as well as depth filtration.

### 14.1.1.2 Sterile Filtration

Sterile filtration is used in the biopharmaceutical industry to sterilize heat-labile products and to keep the bioburden low by filtering process intermediates and buffers. A sterilizing grade filter is defined as a filter that will produce a sterile filtrate when challenged with  $10^7$  colony-forming units of *Brevundimonas diminuta* [7]. The membranes used for sterile filtration can be based on various polymers such as nylon, PVDF, PES, and polypropylene. They can also have different structures such as isotropic or asymmetric. Asymmetric membranes have a graded pore structure that provides for high permeability while maintaining the required mechanical strength. These structures can also result in higher throughput due to particles being retained throughout the depth of the filter.

For sterile filtration, filterability and validation experiments are typically conducted at the laboratory scale to determine the size of the large-scale system and verify the absolute retention of bacteria with the actual process solution and operating conditions.

In a typical application, the filters are sterilized by autoclaving or steaming in place and flushed with water for injection or buffer before filtering the actual process solution. A postuse integrity test is performed after the product solution has been filtered to ensure that the required retention performance was obtained during the filtration process.

#### 14.1.1.3 Virus Filtration

Virus filtration allows for the transmission of the product molecule while retaining virus particles. The extent of virus removal depends on both the pore size distribution of the membrane and the size of the virus. As viruses differ in size, virus filters have been developed accordingly with different pore size ratings. Large virus filters are designed to remove larger viruses typically having lipid envelopes such as retroviruses. They have been labeled as 50 or 70 nm filters. Small virus filters target non-enveloped viruses such as human parvovirus B19 or *Hepatitis A virus*. They are typically rated as 20 or 15 nm.

Virus filtration membranes are made of various polymers such as hydrophilized PVDF, hydrophilized PES, and cellulose. They are available in pleated cartridge and hollow-fiber formats. At present almost all virus filtration applications are performed in the direct filtration mode.

#### 14.1.1.4 Membrane Adsorbers

Membrane adsorbers are made of microfiltration membranes with modified surfaces to attach an appropriate ligand such as ion exchange, affinity, and hydrophobic interaction [8,9]. They are not limited by the mass-transfer resistance associated with conventional chromatography, where large molecules need to diffuse within pores to reach the binding site and adsorb. The slow rate of diffusion within the pores limits the flow rates that can be used in standard chromatography. In membrane chromatography, the separation media has large convective pores that allow for the fast transport of the solute to the binding sites. This results in high-binding capacities at high-flow rates, enabling membrane adsorbers to be operated at high throughputs.

Membrane adsorbers are mostly used in flow-through applications where the contaminants bind to the membrane while the product molecule flows through. In applications where the product molecule is large, membrane chromatography presents significant advantages over beads in the bind-elute mode because the large size of these molecules results in low-binding capacities for beads. Membrane adsorbers with different base membranes such as 0.8  $\mu\text{m}$  hydrophilic PES or 3  $\mu\text{m}$  cross-linked cellulose are available.

#### 14.1.1.5 Depth Filtration

A major alternative to direct flow membrane filtration is depth filtration, in which particles are removed throughout the filtration matrix rather than just at the membrane surface, by various mechanisms such as size exclusion, electrostatic, and hydrophobic interactions. Depth filters are typically composed of a bed of cellulose or polypropylene fibers together with an inorganic filter aid such as diatomaceous earth and a binder to form a filter sheet. The filter aid imparts the matrix very high surface areas and plays an important role in increasing both retention and the capacity. Depth filters can also have an electrostatic charge usually associated with the binder polymer.

### 14.1.2 TANGENTIAL FLOW FILTRATION

#### 14.1.2.1 Fundamentals

Direct flow filtration has certain limitations. The flux (filtration flow rate per unit membrane area) decreases over time as the process continues because the filtering media is loaded with more contaminant particles, as illustrated in Figure 14.1. Moreover, when the concentration of the contaminant in the feed stream is high, the filtering media must be replaced very frequently, which can be economically impractical. Also when the contaminant matter to be separated is small in size, requiring ultrafiltration or reverse osmosis membranes with much smaller pores, then direct filtration is less feasible as the flux declines very rapidly over time, again requiring frequent filter replacement.

Tangential flow filtration technology, also known as crossflow filtration, overcomes these direct flow filtration limitations. TFF is a continuous process in which the feed stream flows parallel (tangential) to the membrane filtration surface, generating two ongoing streams. A part of the feed stream, which gets separated by passing through the membrane is called permeate or filtrate. The remaining portion of the feed stream, called retentate or concentrate, contains the components retained by the membrane [10].

TFF membranes can be cleaned or regenerated using chemicals (sodium hydroxide, acid, sodium hypochlorite, etc.) and mechanical methods (backwash, backpulse, reverse flow, etc.). Regenerated membranes can be used repeatedly, with effective lifetimes ranging from months to years. TFF module configurations and operating modes differ from direct filtration. Table 14.1 shows how TFF products are categorized according to membrane pore size or rating, membrane material, compatibility, shear generating method, etc. As a quick rule of thumb, TFF can be the optimal processing choice for those pharmaceutical

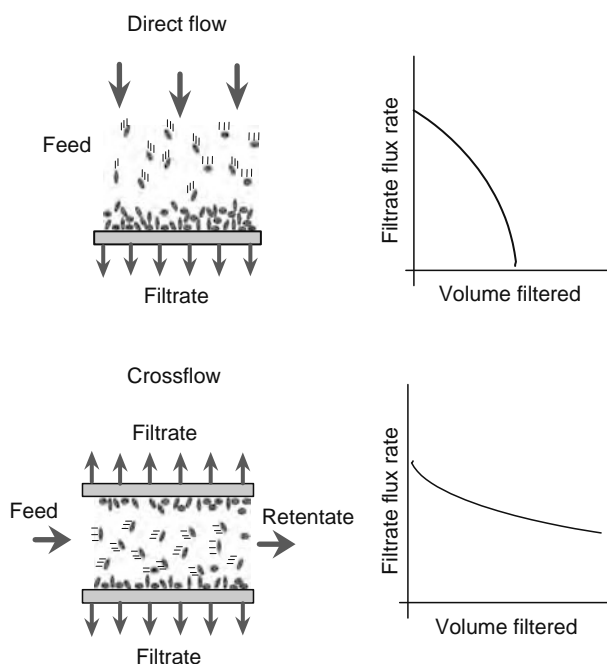


FIGURE 14.1 Direct flow and crossflow.

applications where (1) concentration of retained components is too high for direct flow; (2) concentrated material (retained by membrane) is a desired end product; and (3) diafiltration is required for desalting or buffer exchange or increased recovery.

#### 14.1.2.2 Effect of Polarization on Flux

During TFF, species retained by the membrane form a concentrated boundary layer, called concentration polarization layer, on the surface of the membrane that creates a resistance to the filtrate flow and reduces flux [11]. The effect of polarization is a flux—usually called limiting flux—that does not change with TMP above a critical pressure as shown in Figure 14.2.

#### 14.1.2.3 Processing Modes

TFF is widely applied in biopharmaceutical downstream processes including concentration, clarification, fractionation, and diafiltration.

1. Concentration is probably the most frequently used crossflow processing mode, in which molecules smaller than the membrane pore size rating pass through the membrane as permeate, with a net effect of increasing the concentration of retained components in the feed stream. During a concentration run, the flux decreases with increasing bulk concentration as illustrated in Figure 14.3. Typically, a pharmaceutical feed stream that starts out with a protein content of 1% can be concentrated up to 20% or more.
2. Clarification is another crossflow processing mode, often used as a preliminary step before the concentration operation, in those cases where the feed stream contains excess suspended solids or unwanted microorganisms, usually employing microfiltration membranes.

TABLE 14.1  
TFF Product Categories

Rating	MF/UF/NF/RO
Membrane material	Polymeric (PES, PS, R-CA, PVDF, etc.), inorganic (ceramic, stainless steel)
Configuration	Flat sheet (cassette, P&F, spiral), hollow fiber, tubular, monolith
Operating feature	Backwashable, backpulsable, steamable, autoclavable
Shear generation	Pump, mechanical
Pressure generation	Pressurize feed, vacuum filtrate

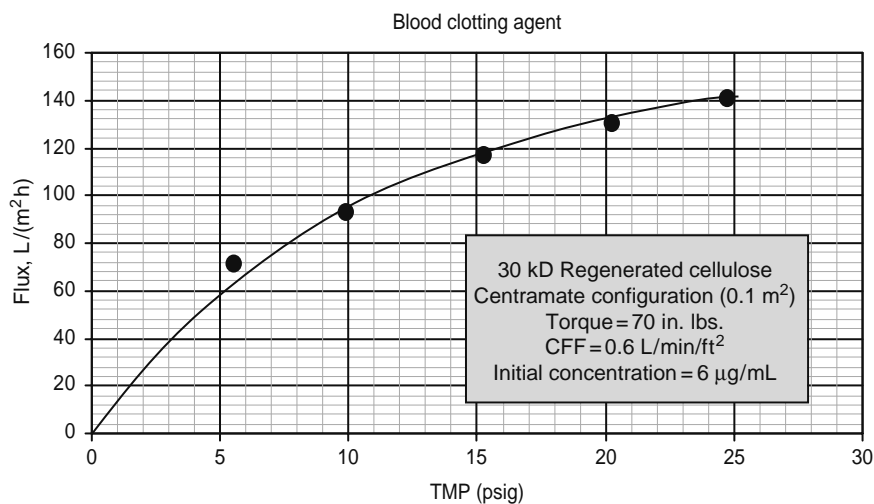


FIGURE 14.2 Flux versus TMP (transmembrane pressure) for a blood clotting agent.

3. Fractionation commonly refers to a process when both the concentrate and the permeate are valuable end products in their own right. The filtration of conjugated vaccine to separate oligosaccharides is a good example of fractionation by TFF in the biopharmaceutical industry.
4. Diafiltration (DF) is conducted by adding fresh solvent or buffer to the feed tank. The removal of salt from a feed solution by diafiltration is illustrated in Figure 14.4. There are several possible diafiltration modes depending upon system configuration and DF solvent/buffer flow direction, but continuous DF (also called constant volume diafiltration) mode is very typical and most often used.

#### 14.1.2.4 Membrane Module Configuration

Crossflow filtration membranes can be produced in flat sheet, hollow fiber, tubular formats when using polymeric materials, and in monolith and tubular configurations when using inorganic membrane materials. Table 14.2 summarizes the various module configurations.

*Cassette:* Cassette products are widely used in the biopharmaceutical industry and specifically dominate the protein concentration purification market due to their compactness, which provides excellent product recovery capability. Cassette modules contain presealed flat sheet membranes separated by feed and filtrate spacers. This is an improved design compared to earlier “plate and frame” configurations, making installation and replacement much easier and more reliable for the end user (shown in Figure 14.5).

Cassettes use a short feed channel path length to reduce the feed channel pressure drop. Flat sheet membranes used in cassettes allow for a wide ranging selection of MWCO in UF membranes, as well as various micrometer ratings in MF

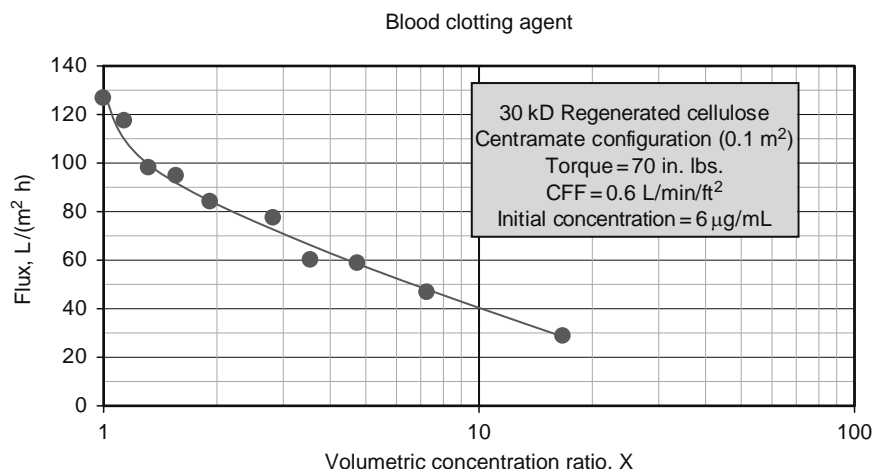


FIGURE 14.3 Flux versus feed concentration for a blood clotting agent.

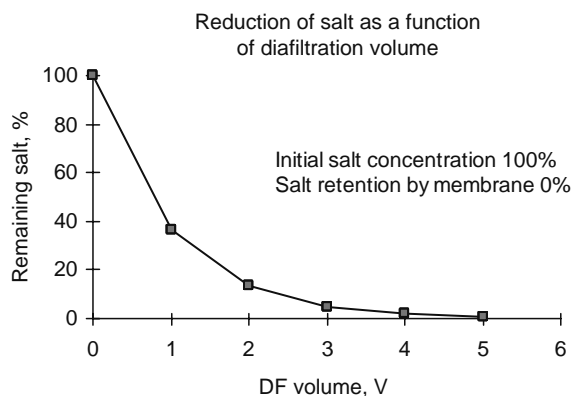


FIGURE 14.4 Salt reduction by diafiltration.

**TABLE 14.2**  
**Membrane/Module Configuration**

Membrane	Module	Feature	Major Application
Flat sheet	Cassette	Compact, high product recovery	Biotechnology, biopharmaceutical
	Spiral wound	Inexpensive	Food and beverage, industrial
	Plate and frame	Open channel	Food and beverage, industrial
Hollow fiber	Hollow fiber	No spacer, easy to replace	Biotechnology, biopharmaceutical, pharmaceutical water, makeup water
Tubular	Tubular	High solids	Food and beverage, industrial

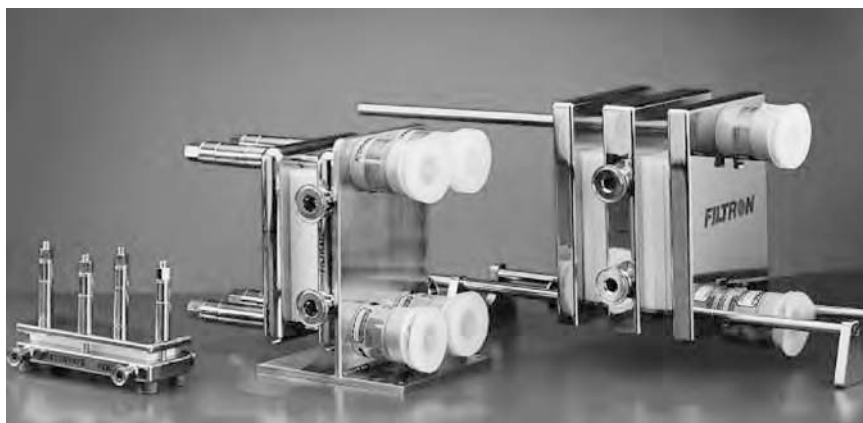
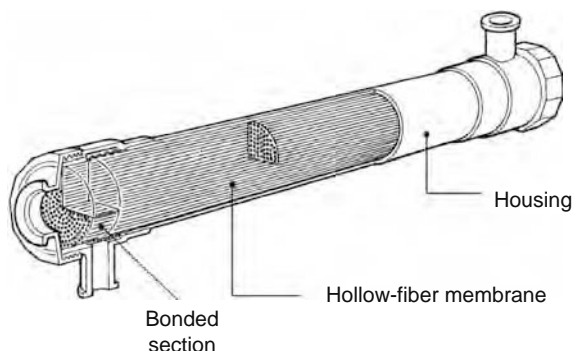
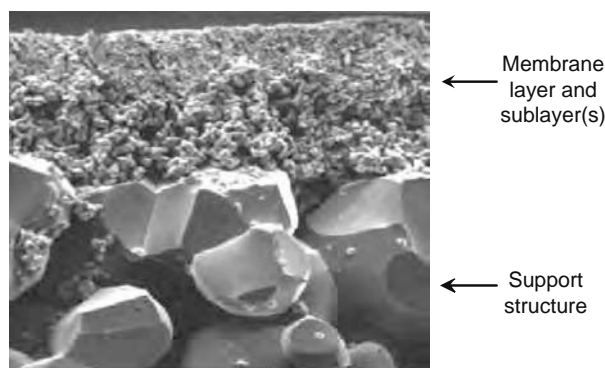


FIGURE 14.5 Cassette modules used in biotechnology applications.



Microza is a tradename of Asahi Kasei Corporation

FIGURE 14.6 Configuration of Microza hollow-fiber module.



**FIGURE 14.7** Structure of ceramic membrane.

membranes. This broad selection is critical for the successful processing of different protein sizes required in the pharmaceutical industry.

*Hollow Fiber:* Hollow-fibers are open channel products; however, due to their small fiber diameters, they do not require the high-energy consumption of tubular membrane products. Hollow fibers are self-supported; they do not require additional support substrates like flat sheet membranes do. Figure 14.6 shows a schematic of a hollow-fiber module.

Hollow fibers can be steamed, autoclaved, and are easy to replace, making them a frequent choice for continuous fermentation applications. They are frequently used for clarifying fermentation broths. Hollow fibers, typically with a 6000 Da MWCO, are also used in producing pharmaceutical grade (WFI) water.

*Ceramics:* Ceramic membranes are manufactured by processes, which are completely different from polymeric membranes. Polymeric membranes are typically formed by the phase inversion process where the polymer dissolved in solvent precipitates upon exposure to nonsolvent. In contrast, ceramic membranes consist of ceramic particles that have been sintered at very high temperatures into one solid shape. It is the gaps or voids between the solid-state ceramic particles that determine the membrane pore size (Figure 14.7).

Ceramic membranes are cast within feed channels, contained in support structures that are then inserted in housings. To reduce energy/flow requirements, up to two to four membrane housings can be connected in series.

Ceramic membranes are robust, easy to clean, and are available with large diameter feed channels, making them a strong technology for clarifying fermentation broths.

*Spiral Wound:* Spiral-wound membrane products are similar to cassettes since they combine flat sheet membranes and feed/permeate spacers, but the flat sheet membrane and the spacer pack are rolled or wound into a spiral form. Spiral-wound modules have much longer feed path lengths than cassettes.

*Vibrating Membrane:* The previously described TFF products require a pump to produce crossflow along the membrane surface to generate the shear rate necessary to reduce polarization and fouling. In contrast, in this configuration the membrane vibrates creating shear at its surface. This vibrating membrane arrangement, suitable for high concentration and viscosity processing, is used in antibiotics and enzyme applications.

## 14.2 MEMBRANE APPLICATIONS

### 14.2.1 PLASMA FRACTIONATION

Human plasma provides the starting material for a large number of proteins (700 or more) that are of therapeutic relevance. These include albumin, immunoglobulins, blood clotting factors such as Factor VIII and Factor IX, and protease inhibitors. Under physiological conditions, plasma proteins have a broad range of concentrations, from 40 g/L for albumin to less than 1  $\mu\text{g}/\text{mL}$  for some clotting factors, and molecular weights (MWs). Some of the important plasma derivatives, their therapeutic use, and concentrations in the plasma are listed in Table 14.3.

The first purification process for plasma-derived products was specifically developed for the supply of albumin by Edwin Cohn during World War II. This process was based on a cold ethanol fractionation relying on the solubility of proteins changing as a function of ethanol concentration, pH, temperature, ionic strength, and protein concentration [12]. During fractionation, the ethanol concentration is raised from 0% to 40% and the pH decreased from neutral to 4.8 through different stages of sequential differential precipitation. A block diagram depicting the stages of Cohn fractionation is shown in Figure 14.8.

**TABLE 14.3**  
**Molecular Weights and Plasma Concentrations of Some Important Plasma Proteins**

Protein	Molecular Weight (Da)	Concentration in Plasma (mg/L)	Indication
Albumin	66,000	40,000	Volume replacement
Immunoglobulin G	160,000	12,500	Replacement therapy in immune deficiency
Von Willebrand factor	220,000	10	Von Willebrand's disease
Factor VIII	330,000	0.3	Hemophilia A
Factor II	72,000	150	Factor II deficiency
Factor VII	50,000	0.5	Factor VII deficiency
Factor IX	57,000	5	Hemophilia B
Factor X	59,000	10	Factor X deficiency
$\alpha$ -1-Protease inhibitor	54,000	1,500	Hereditary emphysema

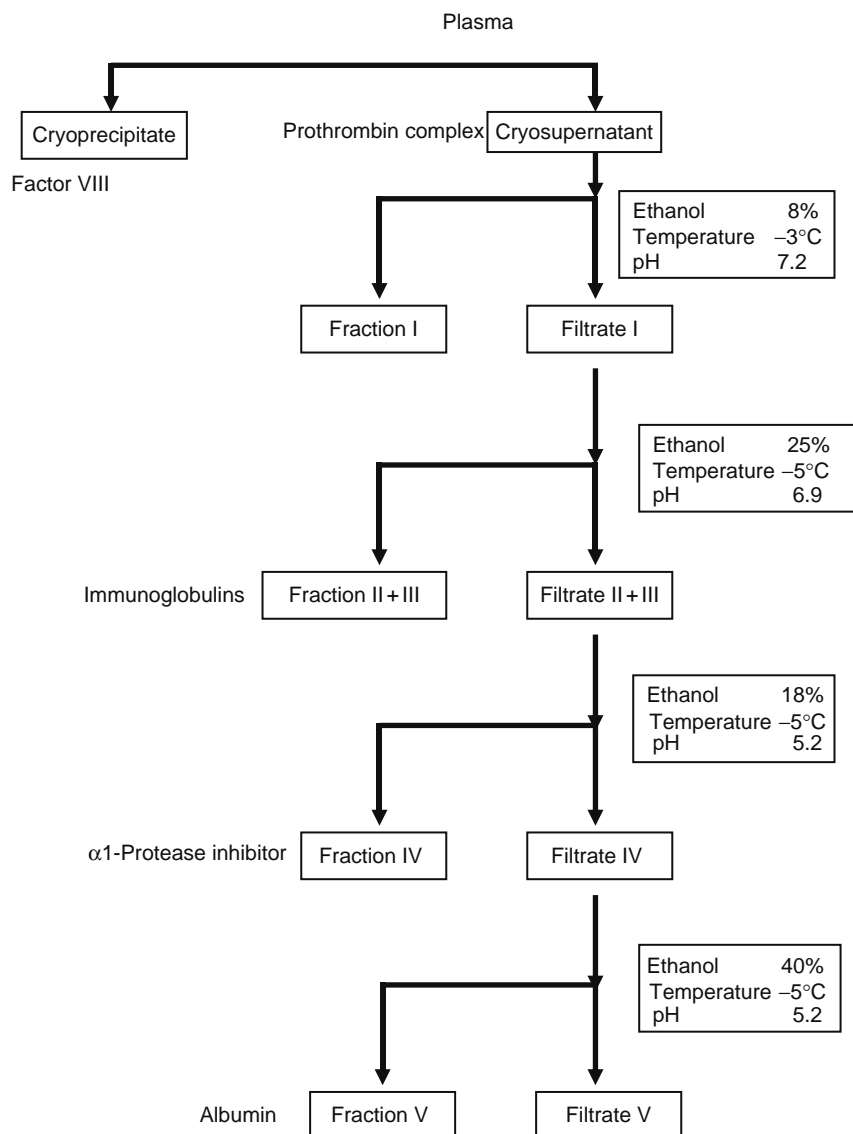


**FIGURE 14.8** Cohn fractionation process (simplified illustration).

### 14.2.1.1 Factor VIII

Factor VIII is a high-molecular-weight protein (approximately 330 kDa) that is involved in blood coagulation cascades. The most important impurities that need to be removed during its purification process are fibrinogen and prothrombin complex (composed of Factors II, VII, IX, and X). The starting point for Factor VIII purification in most production processes is the cryoprecipitate that forms upon thawing frozen plasma at temperatures between 0°C and 4°C. Typically the cryoprecipitate is harvested by centrifugation, suspended in appropriate buffer, and filtered for the removal of fines. In addition, steps such as precipitation and chromatography are used to remove impurities. Virus inactivation/removal is obtained through multiple operations such as solvent/detergent treatment, dry heat treatment, and filtration. Ultrafiltration and diafiltration are performed at the downstream end of the process to concentrate Factor VIII to levels required for the final formulation, remove small-molecular-weight contaminants, and to obtain the desired buffer formulation. Sterile filtration is generally the last step before lyophilization. One of the important challenges in Factor VIII purification is the stability of the protein—it can lose its activity and precipitate easily.

### 14.2.1.2 Immunoglobulins

IgG is a 160 kDa protein that is administered intravenously or intramuscularly. The concentration of IgG for most intravenous formulations is 10% while it can go up to 18% for intramuscular formulations. The source material for IgG in most production processes is Cohn fraction II + III [13,14]. The paste is generally collected by centrifugation and suspended in water for injection. The solution is then clarified through depth filtration and purified by a series of precipitation steps where ethanol, caprylic acid or PEG are used as precipitating agents. Virus inactivation/removal is conducted through solvent/detergent treatment, heat treatment, and membrane filtration. One or more ion-exchange chromatography steps are used to further remove protein impurities and reagents used during solvent/detergent treatment. Ultrafiltration is used to remove precipitating agents and virus-inactivating reagents and to concentrate IgG to the levels desired for the final formulation. The last step in the purification process is sterile filtration.

### 14.2.1.3 Albumin

Albumin is a single-chain protein of 66 kDa molecular weight. It is supplied in concentrations of 5%, 20%, and 25%. The starting material for a typical production process is fraction V [15]. The paste is suspended in water and further purified through precipitation with ethanol. Depth filtration is performed to clarify the supernatant resulting from the precipitation steps. The purity of albumin is increased through polishing ion-exchange chromatography step. Ultrafiltration is used to concentrate albumin, remove ethanol, and provide the final formulation. The last step of the purification process is sterile filtration.

### 14.2.1.4 $\alpha$ -1-Protease Inhibitor

$\alpha$ -1-Protease inhibitor is a 52 kDa protein that protects lungs against proteolytic damage caused by elastase. The source for  $\alpha$ -1-protease inhibitor is Cohn fraction IV-1 [16]. The paste is dissolved in appropriate buffer and subjected to precipitation and chromatography operations for purification. Virus inactivation is provided by solvent/detergent and heat treatments. Ultrafiltration and diafiltration are performed in between chromatography steps to obtain the buffer environment necessary for the subsequent chromatography step. The last step of the purification process is sterile filtration.

### 14.2.1.5 Prothrombin Complex

Prothrombin complex is the combination of Factors II, VII, IX, and X. It is indicated for individuals with hemophilia B. In a typical production process, the supernatant resulting from the separation of cryoprecipitate is filtered to remove particles and applied to an anion-exchange column. The coagulation factors are eluted, ultrafiltered, and exposed to 60°C for 10 h for virus inactivation. This is followed by diafiltration, ultrafiltration, and sterile filtration.

### 14.2.1.6 Membrane Operations during Plasma Fractionation

Filtration plays an essential role during plasma fractionation. Practically all plasma derivatives are processed with sterile filtration at the end of the purification train. Virus filtration is becoming a very important part of viral safety management and it is being incorporated to most processes. Ultrafiltration and diafiltration are used in all processes to remove reagents such as ethanol and salt, concentrate the protein to the desired level, and exchange the buffer to the appropriate conditions before a chromatography operation. Finally, each precipitation step is accompanied with clarification filtration to remove residual precipitates. Below is a more detailed discussion of the various filtration operations.

#### 14.2.1.6.1 Sterile Filtration

Sterile filtration during the production of plasma derivatives is performed to sterilize product intermediates, final product, and buffers. Typically filtration fluxes of 200–1000 Lmh are obtained depending on the solution. Typical operating pressures are within the range of 5–20 psi. In cases of solutions with high protein concentrations or containing aggregates, sterile filtration

can be challenging. For example for IgG and albumin processing where the concentration of the proteins is high (up to 25% for albumin and to 12% for IgG) and the processing temperatures are low, the solutions can be viscous and difficult to filter. Generally, immunoglobulins and Factor VIII are slower to filter than albumin [17].

The presence of colloids in the solutions necessitates pre-filtration to increase the capacity of sterile filters. Usually a filter train of increasingly tighter filters such as 1, 0.45, and 0.22  $\mu\text{m}$  (or 0.65, 0.45, and 0.22  $\mu\text{m}$ ) is used to limit clogging. The sequence of filters and their surface areas in the filter train should be optimized by experiments. In certain cases, depth filters are used to protect sterile filters.

Some large proteins such as fibrinogen or Factor VIII can demonstrate retention by the sterilizing grade filters. The effect of solution properties such as pH, ionic strength, temperature, and operation parameters such as TMP on retention should be understood to minimize the loss of the product protein.

Sterilizing grade filters are available from various suppliers such as Pall Corporation (East Hills, New York), Sartorius AG (Göttingen, Germany), and Millipore Corporation (Billerica, Massachusetts). A typical filtration operation consists of the sterilization of the filters by autoclaving or SIP, flushing the filter with WFI, preuse integrity testing, buffer conditioning, filtering the protein solution, and postuse integrity testing. The filtration of the solution is usually conducted under constant TMP of 5–20 psi. TMP can be increased as the filtration rates decline due to fouling.

#### 14.2.1.6.2 Clarification/Prefiltration

Depth filters are typically used to clarify the paste suspended in WFI or the supernatant from the precipitation step. In many cases, the filtrate from the depth filter is further clarified with a 0.45  $\mu\text{m}$  membrane.

The capacity of expensive sterile and virus filters is usually increased through prefiltration. Typically 0.1  $\mu\text{m}$ -rated membranes are used for prefiltration before virus filtration. Sterile filters are protected by depth filters or 0.45  $\mu\text{m}$  membranes. Some virus inactivation operations such as solvent detergent exposure also require prefiltration for the removal of particulates that can shield viruses from the inactivating effects of solvent detergent agents.

#### 14.2.1.6.3 Virus Filtration

Virus filtration is one of the critical steps in the production of plasma derivatives as outbreaks of hepatitis A, hepatitis C, and HIV in hemophiliac populations have underlined the importance of virus inactivation/clearance during these processes [18]. The concerns about the safety of plasma derivatives are managed by a multilayer approach. As a first step, donors are screened through blood tests, interviews, and review of their medical history. In addition to that the collected plasma is tested for infectious agents, and manufacturing processes have multiple virus inactivation/removal steps with sufficient viral clearance. It is recommended that production processes have at least two virus removal/inactivation steps complementary in their mode of actions. Viral inactivation methods that are commonly used are precipitation, solvent/detergent treatment, pasteurization at 60°C for 10 h, caprylate treatment, and low-pH treatment. Among these methods, solvent/detergent, low-pH, and caprylate treatments are not effective against nonenveloped viruses.

Viruses that contaminate human plasma range from 20 to 200 nm in size, with a majority containing lipid envelopes and a few, such as HAV and B19, being nonenveloped. The difficulties associated with the inactivation of nonenveloped viruses with methods such as solvent/detergent or low-pH exposure makes the clearance of such viruses with filtration important. Virus filters with mean pore sizes of 20 or 15 nm are used for such applications. While this type of filtration is relatively easy for cases where the product protein is small, such as Factor IX, when the size of the product protein is large, the process becomes much more difficult due to the relatively small size difference between the virus and the protein. In these cases the filtration conditions need to be optimized to obtain acceptable viral clearances without compromising from the protein yield. Virus filtration for Factor VIII has mostly been conducted with 35 or 50 nm filters because of the large size of Factor VIII. Certain manufacturers have been successful in using smaller diameter filters without losing significant yield, by dissociating Factor VIII from Von Willebrand Factor. In other cases, the optimization of the filtration conditions has resulted in the acceptable use of 20 nm virus filters for processing Factor VIII [19]. Virus filtration for IgG products has in general been conducted with 35 to 50 nm filters. There have recently been reports of success with the use of 15–18 nm filters for processing IgG [20].

Virus filtration operations typically need prefiltration due to the presence of aggregates that shorten the capacity of the filter. Prefilters with pore sizes of 0.1  $\mu\text{m}$  or 75 nm have been used. In certain cases, the fouling of the filter and the accompanying flux decline result in the degradation of viral retention.

Virus filters are available from various suppliers such as Pall Corporation (East Hills, New York), Sartorius AG (Göttingen, Germany), Asahi Kasei Pharma Corporation (Tokyo, Japan), and Millipore Corporation (Billerica, Massachusetts). A typical virus filtration operation consists of sanitizing or sterilizing the filter, flushing the filter with WFI, preuse integrity testing, filtering the solution, and postuse integrity testing. In most applications the filtration is conducted in the constant TMP mode, at a typical TMP of 10–30 psi. Typical fluxes are in the range of 10–50 L m h.

#### 14.2.1.6.4 Ultrafiltration

Ultrafiltration is conducted to remove precipitating agents such as ethanol, PEG, and caprylic acid through diafiltration and to concentrate the protein to the desired level. It has replaced lyophilization for ethanol removal from albumin and immunoglobulins and size exclusion chromatography for buffer exchange.

The processing of plasma derivatives with ultrafiltration is usually conducted in cold rooms. For albumin processing, cassettes and spirals with 10 kDa polysulfone and polyethersulfone membranes have been used to remove the 40% ethanol as quickly as possible and for concentrating the protein to the final concentration of 25%. Typically, 4–5 diafiltration volumes are used to remove ethanol. For high concentration HSA formulations (25%), the protein is first concentrated to 12%, diafiltration conducted under constant volume conditions at that concentration and the protein subsequently concentrated to 25% [21,22]. Typical fluxes for albumin range between 50 and 100 Lmh with operating TMPs ranging between 30 and 50 psi.

Typically 30 or 50 kDa membranes are used for concentrating and diafiltering immunoglobulins. Diafiltration is generally conducted at IgG concentrations of 7%–8%. Typical fluxes are 25–70 L m h with typical operating TMPs ranging between 20 and 40 psi. For high concentration formulations, the viscosity of the solution increases as IgG is concentrated resulting in high-pressure drops in the feed channel. The user may need to reduce the crossflow rate to keep the pressure drop within specifications. The formation of IgG aggregates during the ultrafiltration operation needs to be minimized by determining the effect of operating and solution conditions on aggregate formation [23].

The processing of Factor VIII is usually conducted under low crossflow rates to avoid any loss in activity.

Ultrafiltration modules are available from various suppliers such as Pall Corporation (East Hills, New York), Sartorius AG (Göttingen, Germany), GE Healthcare (Buckinghamshire, England), and Millipore Corporation (Billerica, Massachusetts). A typical operation consists of WFI flush, water permeability testing, integrity testing, buffer conditioning, protein processing, buffer flush, water permeability testing, and cleaning.

### 14.2.2 ENZYMES AND ANTIBIOTICS

Today, many therapeutics including antibiotics, pharmaceutical enzymes, vaccines, and recombinant proteins are produced through fermentation or cell culture. Table 14.4 lists examples for some of these pharmaceuticals. While the use of fermentation can be traced back over 1000 years, it was following the discovery of penicillin in 1928 and its mass production by fermentation in the 1940s, that a wide range of antibiotics and other pharmaceuticals have come to be produced using large-scale fermentation processes [24]. Today, cephalosporin and penicillin V and G are among the antibiotics with the largest scale production. For some of the so-called semisynthetic antibiotics, fermentation is used to produce an intermediate product, which is then subjected to chemical reactions to produce the final product. Penicillin G and V (especially G) are more likely to be used as a raw material to produce an intermediate product such as 6-APA and 7-ADCA rather than as a final product. 6-APA is made by enzyme modification using penicillin acylase. The intermediate products are then converted to final products such as amoxicillin, ampicillin, and carbenicillin. Fermentation, plus a synthetic modification method, is also used in the manufacture of semisynthetic cephalosporin products.

Enzymes are typically produced using fermentation. They cover a wide variety of applications (see Table 14.5) including their use in the production of antibiotics (as noted above with the use of penicillin acylases to produce 6-APA from penicillin).

Pharmaceutical production processes based on fermentation can be separated into two segments. Upstream processing consists of all the operations that are involved in producing the desired amount of target molecule in fermenters. Downstream processing encompasses all the separation and purification operations that are needed to obtain the required purity for the target molecule. In general, upstream processing consists of media preparation, and fermentation; while downstream processing includes cell separation, clarification, primary isolation, purification, depyrogenation, and final isolation. The objectives and technologies that are used are summarized in Figure 14.9 (although the exact steps will vary for each specific product). We provide more detail on upstream and downstream processing in the sections that follow.

---

**TABLE 14.4**  
**Pharmaceutical Products by Fermentation and Cell Culture**

Antibiotics	Penicillin, erythromycin, cephalosporin, streptomycin, vancomycin, bacitracin, etc.
Enzymes	Amylase, protease, penicillinase, asparaginase, etc.
Recombinant proteins	TPA, protein A, hemoglobin, BMP, human growth hormone, IL2, antibodies
Vaccines	Influenza, hepatitis, DPT, cholera, <i>Streptococcus pneumonia</i>
Vitamins	B <sub>2</sub> (riboflavin), B <sub>6</sub> , B <sub>12</sub> (cyanocobalamin), C (L-ascorbic acid), β-carotene (provitamin A)
Steroids hormones	Cortisone, cortisol, prednisone
Nucleic acids	ATP, IMP, GMP, cAMP, adenine, inosine, etc.

---

**TABLE 14.5**  
**Enzymes for Pharmaceutical Application**

Enzyme	Producing Organism	Application
Amylase	<i>Aspergillus</i> , <i>Rhizopus</i> (mold), <i>Bacillus subtilis</i> (bacteria)	Digestive agent
Asparaginase	<i>Escherichia coli</i> , <i>Serratia marcescens</i>	Leukemia
Lactase	<i>Saccharomyces fragilis</i> (yeast)	Digestive agent
Lipase	<i>Aspergillus niger</i>	Digestive agent
Penicillinase	<i>Bacillus cereus</i> , <i>B. subtilis</i>	Benzyloxyphenylacetic acid production
Penicillin acylase	<i>E. coli</i> , <i>Kluyvera citrophila</i>	6-APA production
Protease	<i>Bacillus subtilis</i> , <i>Clostridium</i> , <i>Lactobacillus</i> (bacteria), <i>Streptomyces griseus</i> (mold)	Digestive agent, blood clotting effect
Urokinase	<i>E. coli</i> , animal cell	Thrombolytic agent, plasminogen activation
Streptokinase		Thrombolytic agent
Lysozyme		Anti-inflammation
Elastase		High-blood pressure, diabetes, arteriosclerosis
Cytochrome		Improves oxygen consumption for strokes, etc.
<b>Diagnosis</b>		
Uricase	<i>Candida utilis</i> , <i>E. coli</i>	Uric acid
Glucose oxidase	<i>A. niger</i> , <i>Penicillium chrysogenum</i>	Glucose
Cholesterol oxidase	<i>Brevibacterium sterolicum</i>	Cholesterol
Lipase	<i>A. niger</i>	Triglyceride

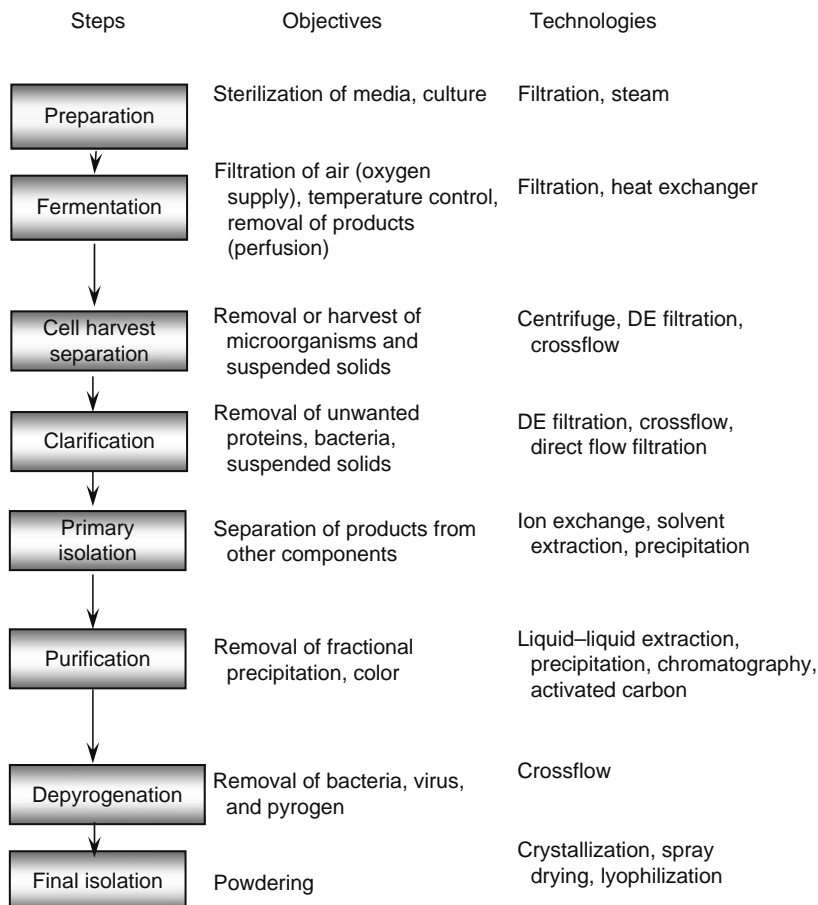


**FIGURE 14.9** Fermentation process.

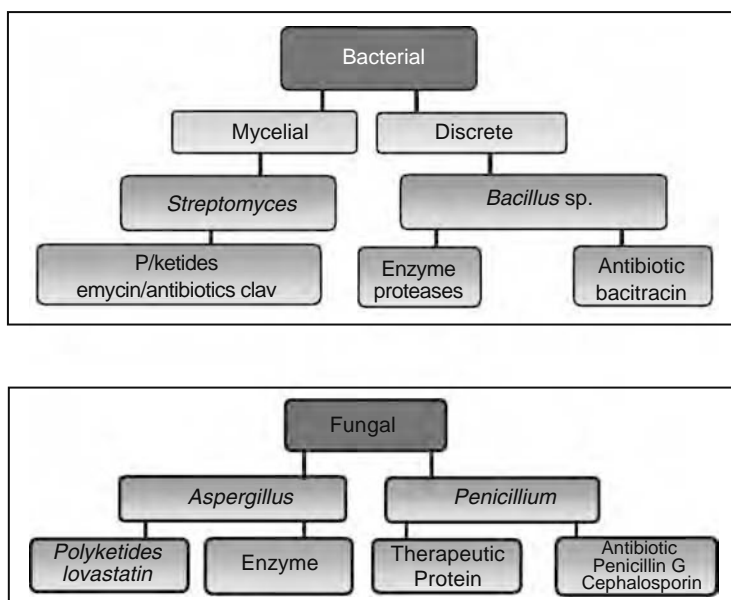


FIGURE 14.10 Large-scale fermentation for antibiotics etc.

### 14.2.2.1 Upstream Processing

Fermentation has been used to produce beer, wine, and other products for thousands of years. At the core of these processes lies the conversion of one component into another by microorganisms; for example the transformation of sugar into alcohol by yeast. For recombinant processes, the transforming microorganisms are modified using plasmids to insert gene sequences coding for the product of interest, along with promoters, etc.

The most commonly used microorganisms for fermentation are bacteria, fungi (mold), and yeasts whereas animal (mammalian and insect) cells and plant cells are used for cell culture (Figure 14.10). If the desired product is contained within the microorganism, it is referred to as intracellular, if outside it is extracellular. Bacteria, which typically produce intracellular products, are 0.2–2  $\mu\text{m}$  in size and can grow to more than  $10^9$  cells/mL. Yeasts are larger (3–4  $\mu\text{m}$ ) and grow to concentrations of over  $10^8$  cells/mL. They generally produce extracellular products. The generation times of bacteria, yeasts, and mammalian cells are 20–30 min, 3–4 h, and 1 day, respectively. In the case of optimized *E. coli* processes, for example 1 cell/mL can grow to  $10^9$  cells/mL after only 10 h.

Most of fermentation and cell culture operations are done in the batch mode where a volume of sterile medium in a vessel is inoculated, the broth is fermented for a period, and the contents of the tank are removed and filtered. Semi-batch or fed-batch modes can also be used during large-scale production processes. Continuous fermentation, where sterile medium is continuously added to the fermentation system with a balancing withdrawal of broth for the extraction of the target molecule, has only been applied to a limited number of products such as those produced with yeast. Such limited application is due to difficulties of maintaining sterility for a long period. However, the implementation of continuous fermentation in the production of antibiotics, amino acids, and nucleic acids is anticipated soon.

Fermentation processes need several components as starting materials: an inoculum, growth medium (carbon source such as carbohydrates and sugars, and nitrogen source such as ammonium salts), air/gas, and water. To have a successful fermentation, all these components have to be maintained as sterile to avoid contamination.

The culture media used in fermentation processes contains a variety of unwanted cells and spores which need to be inactivated or removed before fermentation. The most commonly used inactivation method is heat sterilization. Most cells and some spores can be destroyed at 60°C–80°C, while some heat-resistant spores such as bacterial spores require more than 120°C. Heat-based methods, however, cannot be used when the product molecules, such as vitamins and antibiotics, are heat sensitive, because the application of high temperatures changes their properties. In these cases, sterile filtration with membrane filters or depth filters is used.

During aerobic fermentation, used in the majority of pharmaceutical processes, air has to be supplied as the oxygen source. This leads to processing requirements since air contains as many as  $10^5$  particles/ $\text{m}^3$  and  $10^4$  cells/ $\text{m}^3$  of microorganisms, such as spores and bacteria. Traditional technologies used include heat, glass-packed towers, HEPA filters, and UV. However, these have now been replaced by much more reliable sterile filtration using 0.2 or 0.1  $\mu\text{m}$  filters. Air/gas has to be filtered not only when incoming into the fermenter but also outgoing from the fermenter to avoid any microbial contamination. In many cases, enriched oxygen air or pure oxygen is used to increase the mass transfer of oxygen and to allow for higher cell density and

productivity. Higher oxygen concentration poses a challenge when selecting the material for filter media and its components. PTFE membranes, antioxidant components, and special configurations are used to deal with the corrosion problem as well as the issue of fire hazards.

### 14.2.2.2 Downstream Processing

#### 14.2.2.2.1 Clarification

The first step following fermentation is the separation of solids from the liquid growth media, a step generally referred to as cell separation. More specifically, when the desired products are contained within the cells (intracellular) this step is called cell harvesting and when the products are extracellular it is known as broth clarification. The list of antibiotics with their producer organisms, molecular weight, and whether they are extracellular or intracellular is shown in Table 14.6.

To accomplish this separation step, centrifugation has traditionally been used and is still used for many applications. However, centrifugation has some limitations. Most importantly, it does not achieve the required clarity and therefore, typically leads to further downstream clarification requirements—depth filtration is the most common operation applied to centrate in such cases.

As an alternative to centrifugation, a vibrating membrane filter is used in some applications such as yeast processes (*Pichia pastoris*) and vaccine processes. Diatomaceous earth (DE) filtration is another potential alternative. Figure 14.11 illustrates DE embedded within a filter module structure.

Ceramic membrane systems are achieving widespread application in the place of centrifuges. These systems do not require filter aid media or a separate follow-on clarification step. Hollow-fiber crossflow modules are preferred for the separation of mammalian cells, which require particularly gentle handling. They can also be used as disposable filters for perfusion and vaccine processes.

When clarifying antibiotics there are some specific considerations to keep in mind; most important is whether or not the product is intra or extracellular. Penicillin V, G, and many others are extracellular products. In such cases, the target antibiotics are excreted into the broth. For clarification, a crossflow system with ceramic membranes or hollow fibers is therefore widely used. The permeate (filtrate) contains the desired product. Diafiltration can also be used to improve upon the yield.

If the desired product is intracellular, cells are first concentrated and then lysed to release the product. Extraction by solvent or pH change is used alone or in conjunction with the mechanical disruption. The resulting lysate is then clarified to remove cell debris leaving only the clarified products. With the introduction of ceramic membrane systems, concentration, extraction, and clarification can be done using a single system. One example of an intracellular process, i.e., vitamin B<sub>12</sub> production (185 m<sup>3</sup> broth) is shown in Figure 14.12.

#### 14.2.2.2.2 Purification

The most common operations used for the purification of antibiotics and enzymes are extraction, crystallization, carbon adsorption, chromatography, and filtration. Antibiotics pose some particular challenges because they are small and likely to be purified using solvents. Therefore, purification is often undertaken using solvent extraction as in the case of Penicillin. Cephalosporin uses an ion-exchange resin as the primary isolation method. Enzymes processes use similar technologies but pose some distinct requirements because they are typically large and are produced in aqueous environments. They are therefore more likely to be purified using precipitation, chromatography, and ultrafiltration.

**TABLE 14.6**  
**Typical Antibiotics and Organisms**

Antibiotic	Producer Organism	Molecular Weight	Extra or Intracellular	
Bacitracin	<i>Bacillus subtilis</i>	1391	Extracellular	Intracellular
Cephalosporin	<i>Cephalosporium acremonium</i>	415	Extracellular	
Erythromycin	<i>Streptomyces erythreus</i>	734	Extracellular	
Griseofulvin	<i>Penicillium griseofulvum</i>	353		Intracellular
Neomycin	<i>Streptomyces fradiae</i>	322	Extracellular	
Penicillin	<i>Penicillium chrysogenum</i>	334, 350	Extracellular	
Semduramycin		895		Intracellular
Streptomycin	<i>Streptomyces griseus</i>	582	Extracellular	
Tetracycline	<i>Streptomyces rimosus</i>	444	Extracellular	Intracellular
Vancomycin	<i>Streptomyces orientalis</i>	407	Extracellular	

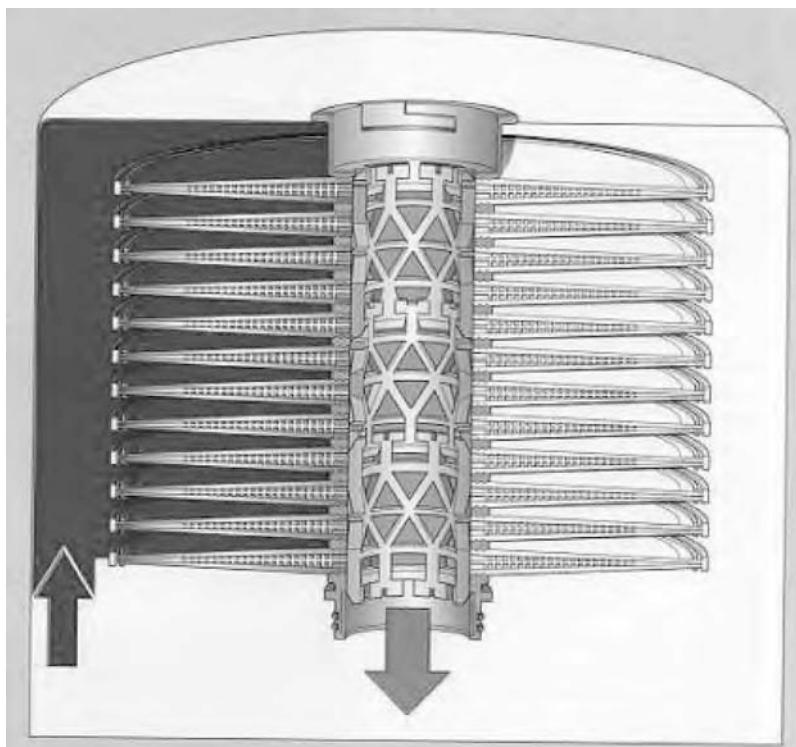


FIGURE 14.11 Diatomaceous earth filtration (SURPRA disc by Pall).

### 14.2.3 ACTIVE PHARMACEUTICAL INGREDIENTS

Most active pharmaceutical ingredients are produced by synthesis through a series of chemical reactions where different functional groups are attached to the starting raw material. In some cases, the production involves a semisynthetic process where the starting material originates from the extraction of a substance from a botanical or animal source or from fermentation.

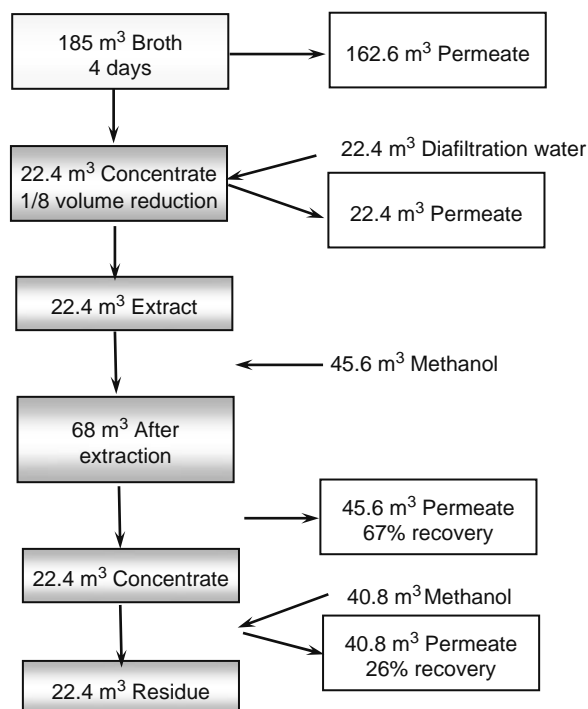


FIGURE 14.12 Clarification/extracton process for vitamin B<sub>12</sub> production.

The products formed after each stage of reaction are termed as intermediates. Some type of isolation operation such as extraction, filtration, or distillation is usually conducted on the reaction mixture at each intermediate step. The final reaction mixture goes through a series of purification operations such as precipitation, distillation, chromatography, filtration, and crystallization where impurities are removed. These impurities can include residual-unreacted starting materials, by-products of reactions, catalysts, residual solvents, and enantiomeric forms of a chiral drug. The last step of the process is usually crystallization where the active product is recovered in the desired morphological form. The crystallized product is typically recovered by filtering, washing, and drying.

Various types of reactions including halogenation, alkylation, arylation, oxidation, reduction, sulfonation, esterification, and amination are used in the production of active pharmaceutical ingredients. These reactions typically take place at high temperatures in stainless steel or glass reactors of various sizes ranging from 50 gal at the pilot scale to 3000 gal at the manufacturing scale and require the use of catalysts and large volumes of solvents. As solvents are pumped from tank farms to the reactors, they need to be filtered to remove any particulate that could interfere with the reaction. For solvents with low solid concentrations polymeric cartridge filters are typically used.

The most important consideration in the selection of the filter is the compatibility of the filter materials of construction with the solvent. The solvents used in pharmaceutical processes can be very aggressive. They include acetone, methanol, ethanol, isopropyl alcohol (IPA), acetonitrile, dimethyl acetamide, dimethyl formamide (DMF), ethyl acetate, tetrahydrofuran (THF), methyl isobutyl ketone (MIBK), and methyl ethyl ketone (MEK). Filters with PTFE membranes and polypropylene supports are used in most applications.

Heterogeneous catalysts made of transition metals on various supports such as carbon are used in many reactions. At the completion of the reaction, the catalyst needs to be removed from the product mixture and recycled. The recovery of the catalysts can be conducted by centrifugal discharge or by using Nutsche-type filters. These types of filters retain large masses of solids and have the capability of washing and drying them. The filtrate is usually filtered through a solvent compatible cartridge to remove any fines that may still be in the liquid. The removal of homogeneous catalysts from the active pharmaceutical ingredient is more difficult. Distillation, adsorption, and extraction have been used. Recently, solvent-resistant nanofiltration devices have been targeted for this application. The filtrate containing the intermediate product can be further purified by activated carbon for clarification. The use of sheets impregnated with carbon simplifies the operation over the batch process by eliminating the carbon removal step.

The gasses going to the reactors, such as nitrogen that is used to blanket the reactor and hydrogen that is used as a reactant, are filtered with gas filters typically made out of PTFE membranes. Since the filters can be exposed to the solvents used in the reactors the materials used in their construction need to be compatible with the solvents.

Usually the type of solvent that is optimum for a particular reaction or purification step is different from what would be optimum for a different step. Therefore, solvents are changed several times during the process. This exchange can be conducted by precipitation and evaporation followed by dissolution in the new solvent. Solvent-resistant nanofiltration can also be used for solvent exchange during the process. Typically the used solvent is purified by distillation and recycled. The product mixture from the last reaction step is typically purified by crystallization, washing, and drying.

#### 14.2.4 PARENTERALS

Parenteral solutions are typically administered intravenously. They are packaged as large volume parenteral (LVP) and small volume parenteral (SVP) solutions. LVP solutions are bags or bottles containing from 100 mL to 1 L solutions. They are usually administered for electrolyte and fluid balance disturbances, nutrition and as a vehicle to administer other drugs. The most common examples of LVPs are sodium chloride, Ringer's, sodium bicarbonate, dextrose, amino acids, dextrans, and other plasma expanders. Due to the large volumes involved, LVPs should not contain bacteriostatic agents, or other additives and excipients. SVPs are 100 mL or less and their primary use is the delivery of a medicine. They can be packaged as 50–100 mL bags, ampules, vials, and prefilled syringes. SVPs can have antibacterial preservatives, solubilizers, antioxidants, and other excipients.

Parenterals are prepared under a controlled environment by dissolving the drug and excipients in water for injection, and sterilizing the bulk solution by passing it through a sterilizing grade filter, filling individual sterile containers. The air to the production facility is filtered by HEPA filters.

The water used for preparing parenteral solutions needs to meet USP requirements for water for injection. These requirements include bacterial endotoxins no greater than 0.25 eu/mL, total organic content less than 500 ppb, and a conductivity of 1.3  $\mu\text{S}/\text{cm}$ . Water for injection is prepared by distillation or a two-stage reverse osmosis process. A typical process to produce water for injection consists of multimedia filtration, softener, activated carbon, 1–5  $\mu\text{m}$  prefiltration, UV treatment, two-stage reverse osmosis, mixed DI, UV, and sterile filtration.

### 14.3 FUTURE TRENDS

Membrane separation applications with higher selectivity, capacity, and flow rates are driven by the need for more economical and robust manufacturing processes providing higher purity products. In the area of virus and sterile filtration, membrane providers are developing high capacity and high-flux membranes by the use of multilayer structures. New module designs are packing more membrane material within the same module volume. Advances in processing are yielding membranes with lower levels of extractables. For TFF, better fluid management technologies will result in processes more resistant to fouling [25]. Advances in module design, membrane chemistry, and application knowledge are resulting in membrane applications with high-purification factors [26]. Disposable TFF devices will eliminate the complexity of TFF systems and eliminate cleaning validation. The use of membrane adsorbers will simplify the purification operations in plasma and enzyme processing. Finally, solvent-resistant nanofiltration will make solvent exchange and catalyst recovery more economical and robust [27].

### 14.4 CONCLUSION

Membranes play an ever growing essential role in the economic manufacture of a multitude of pharmaceutical products. The membranes range from microfiltration and ultrafiltration to reverse osmosis and nanofiltration. Direct flow and crossflow membrane systems are used not only to concentrate, clarify, and diafilter the products themselves but also to pretreat the water needed during the manufacturing process, as well as to post-treat ensuing wastewaters. As membrane technology advances and as materials of construction improve, the process of applying membranes in the pharmaceutical world will expand. Benefits will include new products, lower manufacturing costs, improvements in purity, and rendering the production processes more environmentally friendly.

### REFERENCES

1. D'Arcy, H., Determination of the laws of flow of water through sand. Appendix to *Histoire des Fontaines Publiques de Dijon* pp. 590–595, 1856. Republished on *Fluid/Part. Sep. J.*, 2, 33–35, 1989.
2. van den Berg, G.B. and Smolders, C.A., Flux decline in ultrafiltration processes, *Desalination*, 77, 101–133, 1990.
3. Tarleton, E.S. and Wakeman, R.J., Understanding flux decline in crossflow microfiltration. 1. Effects of particle and pore size, *Chem. Eng. Res. Des.*, 71, 399–410, 1993.
4. Hermia, J., Constant pressure blocking filtration laws—Application to power-law non-newtonian fluids, *Trans. Ind. Chem. Eng.*, 60, 183–187, 1982.
5. Ho, C.-C. and Zydney, A.L., A combined pore blockage and cake filtration model for protein fouling during Microfiltration, *J. Colloid Interface Sci.*, 232, 389, 2000.
6. Emory, S., Principles of integrity testing hydrophilic microporous membranes, *Pharm. Technol.*, 13, 68, 1989.
7. Health Industry Manufacturers Association (HIMA), Microbiological evaluation of filters for sterilizing liquids, HIMA Document No.3, Vol. 4, 34 pp., 1982.
8. Roper, D.K. and Lightfoot, E.N., Separation of biomolecules using adsorptive membranes, *J. Chromatogr. A*, 702(1–2), 3–26, 1995.
9. Ghosh, R., Protein separation using membrane chromatography: opportunities and challenges, *J. Chromatogr. A*, 952(1–2), 13–27, 2002.
10. Cheryan, M., *Ultrafiltration and Microfiltration Handbook*, Lancaster, PA: Technomic Publishing Co., 1997.
11. Blatt, W.F. et al., Solute polarization and cake formation in membrane ultrafiltration. Causes, consequences, and control techniques, in *Membrane Science and Technology*, J.E. Flinn (Ed.), pp. 47–97. Plenum Press, New York, 1970.
12. Cohn, E.J. et al., Preparation and properties of serum and plasma proteins: A system for the separation into fractions of the protein and lipoprotein components of biological tissues and fluids, *J. Am. Chem. Soc.*, 68, 459, 1946.
13. Teschner, W. et al., A new liquid, intravenous immunoglobulin product (IgIV 10%) highly purified by a state-of-the-art process, *Vox Sang.*, 92, 42–45, 2007.
14. Parkkinen, J. et al., A modified caprylic acid method for manufacturing immunoglobulin G from human plasma with high yield and efficient virus clearance, *Vox Sang.*, 90, 97–104, 2006.
15. Matejtschuk, P. et al., Production of human albumin solution: a continually developing colloid, *Br. J. Anesth.*, 85, 887–895, 2000.
16. Mattes, E. et al., Preparation and properties of an alpha-1-protease inhibitor concentrate with high specific activity, *Vox Sang.*, 81, 29–36, 2001.
17. Reti, A.R., The design and use of filtration systems, in *Methods of Plasma Protein Fractionation*, J.M. Curling, (Ed.), Academic Press, London, 1980.
18. Blemchet, V.S. et al., Hepatitis C infection in children with hemophilia A and B, *Blood*, 78, 285–289, 1991.
19. Furuya, K. et al., Implementation of a 20 nm pore size filter in the plasma derived Factor VIII manufacturing process, *Vox Sang.*, 91, 119–125, 2006.
20. Terpstra, F.G. et al., Viral safety of Nanogam, a new 15 nm filtered liquid immunoglobulin product, *Vox Sang.*, 90, 21–32, 2006.

21. Jaffrin, M.Y. and Charrier, J.P., Optimisation of ultrafiltration and diafiltration processes for albumin production, *J. Membr. Sci.*, 97, 71–78, 1994.
22. Jaffrin, M.Y. et al., Effect of ethanol on ultrafiltration of bovine albumin solutions with organic membranes, *J. Membr. Sci.*, 124, 233–241, 1997.
23. Ahrer, K. et al., Effects of ultra/diafiltration conditions on present aggregates in human immunoglobulin G preparations, *J. Membr. Sci.*, 274, 108–115, 2006.
24. Wainright, M., *Miracle Cure: The Story of Penicillin and the Golden Age of Antibiotics*, Oxford: Basis Blackwell, 1990.
25. Luque, S. et al., A new coiled hollow-fiber module design for enhanced microfiltration performance in biotechnology, *Biotech. Bioeng.*, 63, 247, 1999.
26. Zydney, A.L. and van Reis, R., High performance tangential flow filtration, in *Membrane Separations in Biotechnology*, 2nd edn., W.K. Wang, (Ed.), Marcel Dekker, New York, 2001, pp. 277–298.
27. Sheth, J.P. et al., Nanofiltration based diafiltration process for solvent exchange in pharmaceutical manufacturing, *J. Membr. Sci.*, 211, 251–261, 2003.

---

# 15 Membranes in Drug Delivery

*Mario Grassi*

## CONTENTS

15.1	Introduction .....	427
15.2	Mass Transport.....	431
15.2.1	Factors Affecting Drug Permeation.....	431
15.2.2	Continuity Equation.....	432
15.2.3	Diffusion Coefficient .....	433
15.2.4	Modeling Examples: Swellable and Not Swellable Membranes .....	435
15.2.5	Osmotic Systems .....	437
15.2.6	Electrotransport.....	438
15.3	Membranes: Useful Device for Drug Diffusion Coefficient Measurement.....	438
15.3.1	Not Swellable Membranes Modeling: Effect of Stagnant Layers and Drug Dissolution.....	439
15.3.2	Examples: Theophylline Permeation through Calcium Alginate Membranes .....	444
15.4	Oral Delivery Systems .....	446
15.4.1	Membranes for Physically Coated Systems .....	448
15.4.2	Membranes for Physicochemically Coated Systems.....	449
15.4.3	Asymmetric Membranes.....	450
15.4.4	Membranes for Colon Delivery.....	452
15.5	Transdermal Delivery Systems .....	454
15.5.1	Membranes for Passive Delivery Systems .....	456
15.5.2	Membranes for Physically Enhanced Delivery Systems.....	456
15.6	Implantable Delivery Systems .....	459
15.6.1	Membranes for Passive Implants.....	460
15.6.2	Membranes for Active Implants.....	461
15.7	Future Trends .....	461
15.7.1	Molecularly Imprinted Membranes .....	462
15.7.2	Membranes in Micro/Nanotechnologies .....	464
15.8	Conclusions .....	464
	References.....	464

## 15.1 INTRODUCTION

A membrane can be defined as a sheet of solid or semisolid material, insoluble in its surrounding medium, which separates phases that are usually (but not necessarily) fluid [ 1]. A transport system is realized when there is a passage of solute across the membrane.

Based on mechanisms ruling mass transport, typically, membranes can be divided into two main classes: biological and synthetic membranes. Indeed, in synthetic membranes mass transport is usually only due to a chemical potential gradient, while in biological membranes mass transport can also be due to other special mechanisms. Facilitated diffusion implies solute binding to a protein embedded in the biological membrane and, then, protein–solute complex permeation through the membrane (this mechanism does not require energy as solute diffusion takes place according to the chemical potential gradient). Important examples are represented by  $H^+$ /organic cation antiport system and the dipeptide transporter [2]. Active transport denotes carrier transport processes consuming energy since transport often takes place against a chemical potential gradient. The energy required for active transport can be supplied by two different mechanisms: cotransport and ATP pump [3]. In cotransport, the target molecule associates to another compound that crosses the cellular membrane due to the existing

concentration gradient (this is the case of glucose and aminoacids that associate to  $\text{Na}^+$  crossing the cellular membrane according to the concentration gradient). Instead, in the ATP pump case, the energy required for molecules transport is supplied by the hydrolysis of high-energy compounds such as ATP ( $\text{ATP} \Rightarrow \text{ADP} + \text{P} + \text{energy}$ ). A typical example is represented by the  $\text{Na}^+ - \text{K}^+$  pump. Finally, very large molecules are transported by invagination of the membrane and subsequent vesiculation and devesiculation (endocytosis or transcytosis).

While in biological membranes the above-mentioned phenomena can highly influence solute permeability, in synthetic membranes permeability is essentially due to solute chemical-physical properties and membrane microscopic structure. Indeed, synthetic membranes are usually complex structures that can be, in the most general case, composed of three different phases: (a) continuous, (b) shunt, and (c) dispersed [1]. These phase types may be further classified as primary, secondary, and tertiary, the subclassification depending on the spatial relationships of each phase to the other phases present. A primary continuous phase is an uninterrupted phase between membrane surfaces as well as laterally or in the plane perpendicular to the flux vector. Depending on its composition relative to the compositions of associated phases, it may provide an uninterrupted diffusional path for a solute or it represents an un-accessible zone acting as a mere supporting structure. A primary shunt phase completely passes through the membrane but it is laterally discontinuous, i.e., a pore or channel. Of course, this structure may not influence permeability or may affect it by providing parallel diffusional pathways or may be the sole diffusional pathway. Dispersed phases are embedded in continuous or shunt phases. They are discontinuous along the flux vector and do not provide an uninterrupted pathway through the membrane or through any of its subphases. If they are also discontinuous laterally, they are fillers that can be usually adopted to improve mechanical properties such as elasticity and resistance to tear. Netting is sometimes embedded in a membrane structure as a means of reinforcement. Since there can be phases within phases and phases, in turn, within these, it is necessary to designate whether a given identified phase is contributing to the coarsest structural breakdown (primary) or is a subphase of a primary or higher order phase. In this regards, each major phase identified must then be examined for the presence of secondary phases of each type and these, in turn, for tertiary phases, etc., until all distinct regions are accounted. Secondary phasic structure is common in real membranes. Recourse to characterization of tertiary and finer subclassification is generally unnecessary. Indeed, despite this complex frame, in the majority of the situations drug release field deals with polymeric membranes comprised of a continuous phase (usually a liquid phase) trapped in a swollen solid phase (polymeric network) [4]. This structure can be seen as a coherent system, having mechanical characteristics in between those of solids and liquids [5]. The presence of cross-links between polymeric chains hinders polymer dissolution in the liquid phase that can only swell the network. This structure is roughly similar to that of sponge filled by a liquid phase. Nevertheless, this is a particular sponge as, in the case of strong cross-links between polymeric chains (typically chemical covalent bonds), the network does not modify with time. When, on the contrary, weak cross-links prevail (typically physical interactions such as Coulombic, van der Waals, dipole-dipole, hydrophobic, and hydrogen bonding interactions), polymeric chains are not so rigidly connected to each other and the similarity with the sponge is no longer so pertinent. Indeed, while cross-link density (number of cross-links per unit volume) is constant with time (in static conditions), Brownian motion of chains and segment of chains makes the distribution of polymer-polymer junctions (cross-links) time dependent. As a consequence, while average dimensions of network meshes do not modify, each mesh can modify, thus resembling a statistical network. Obviously, this kind of network can easily undergo erosion due to polymer-polymer junction weakness. This physical frame is made more complex by the fact that the whole structure can be constituted by an ensemble of small matrix domains embedded in a continuum, usually represented by a polymer solution as it occurs for Carbopol [6,7]. Finally, the contemporary presence of two networks (interpenetrating structures), originated by two different polymers, can further complicate the scenario. Typically, these systems are produced by an initial swelling of a monomer, reacting to form a second intermeshing network structure [8,9]. Obviously, the choice of the polymer depends on the final administration route (examples include oral, ophthalmic, rectal, vaginal, and subcutaneous) and on different factors such as membrane swelling degree, biodiversity, biocompatibility, and interactions with drug, excipients, and mechanical properties.

Despite the considerable wide application spectrum of membranes, typically, their use in the delivery field falls into drug release modulation based on a diffusive-controlled mechanism [10], isolation of particular structures from the external environment [11], making artificial implants biocompatible [12], allowing drug release (due to membrane dissolution) only when particular environmental conditions take place [13], and simulating the permeation properties of natural tissues [14-23]. At this purpose, it is interesting to consider some typical examples taken from the two most important delivery systems categories: externally regulated and self-regulated delivery systems [24]. For what concerns externally regulated systems, Miyazaki and coworkers [25] use ethylenevinyl alcohol membranes in reservoir-type drug delivery systems for the release of bovine insulin in the presence of ultrasounds. When diabetic rats receiving implants containing insulin are exposed to ultrasound ( $1 \text{ W/cm}^2$  for 30 min), a sharp drop in blood glucose levels is observed after the irradiation. This indicates a rapid rate of release of insulin in the implanted site. The authors attribute this behavior to temperature raising due to the radiating energy supplied. Okahata and coworkers [26,27], working on thermoresponsive delivery systems, use semipermeable nylon capsules prepared by interfacial polymerization (trimesoylchloride as a cross-linking agent) of ethylenediamine and terephthaloylchloride, or 1,10-decanedicarbonylchloride. NaCl-loaded capsules are transferred to dodecane solutions of dialkyl surfactant to introduce an amphiphilic bilayer on the capsule membrane. Remarkable permeability changes induced by

temperature changes are observed at the phase transition temperature, in contrast to the uncoated capsules. Bae and coworkers [28] working on insulin delivery report the use of thermosensitive hydrogel membranes constituted by poly(*N*-acryloylpyrrolidine) and its copolymers with styrene or 2-hydroxyethylmethacrylate cross-linked by ethyleneglycoldimethacrylate. The cross-linked poly(*N*-acryloylpyrrolidine) homopolymer shows thermosensitivity in water swelling, with weak mechanical strength, restricting its practical application to diffusion experiments. The incorporation of a hydrophobic monomer into the polymer improves the mechanical strength and lowers the overall swelling level as well as thermosensitivity. Accordingly, membrane composition and temperature represent two fundamental parameters for the achievement of the desired insulin delivery rate. In particular, insulin permeation through poly(hydroxyethyl methacrylate) increases with an increase in temperature. On the contrary, insulin permeation through poly(*N*-acryloylpyrrolidine) copolymers increases with a decrease in temperature.

Interestingly, membrane permeability can be modified by the action of an electric field. Indeed, electrophoretic migration of a charged macrosolute within a hydrated membrane depends on the effect of electrical forces acting on the solute and its counterions in the adjacent electrolyte solution [29]. It is well known that [30] four distinct electrochemical and electromechanical mechanisms concur in determining transport of proteins and neutral solutes across hydrogel membranes: (a) electrically and chemically induced swelling of a membrane to alter the effective pore size and permeability; (b) electrophoretic augmentation of solute flux within a membrane; (c) electroosmotic augmentation of solute flux within the membrane; and (d) electrostatic partitioning of charged solutes into charged membranes. In other words, the application of an electric field can result in control of solute flux by a combination of the electrophoretic and electroosmotic mechanisms. Pasechnik and coworkers [31] report an increase in the effective pore radius of ultrafiltration membranes due to electrodynamic effects. Burgmeyer and Murray [32] observe changes in the ionic permeability of polypyrrole redox membranes using a voltage-controlled electrochemical reaction. Eisenberg [33] can modify the restricted diffusion of sucrose through collagen membranes via electrodiffusion (this is due to effect of the electric field on concentration profiles within the membrane), obtaining flux changes up to 25%. Nussbaum [34] obtains reversible changes in the uniaxial swelling of poly(methyl methacrylate) (PMMA) membranes via electrodiffusion control of intramembrane ionic strength. Application of an electric field across a hydrated polyelectrolyte membrane, such as PMMA, yields to a net force on the space charge in the fluid phase, which contains an excess of counterions over coions. This force, transferred to the solvent, results in an electroosmotic fluid flow relative to the solid membrane. Grodzinsky [29] observes a volume flux of  $1.2 \times 10^{-6} \text{ m}^3/\text{s}$  at the direction of the current across a  $3.1 \text{ cm}^2$  PMMA membranes, fixing  $\text{pH} = 7$  and current density equal to  $320 \text{ A/cm}^2$ . As soon as the current is cutoff, the flow is stopped.

Mathiowitz [35–40] realizes reservoir-type delivery systems recurring to a photochemical control. Microcapsules, built up by interfacial polymerization of polyamide, also contain azobisisobutyronitrile, a substance that emanates nitrogen due to a photochemical action. Accordingly, after exposition to light, microcapsules' internal pressure increases (as a result of nitrogen release) until membrane rupture and consequent contents release.

Self-regulated delivery systems [41] are closed loop-controlled devices in which the release is modulated by the system, in response to feedback information, excluding any external intervention. For example, it is possible to use pH as an environmental stimulus to deliver a drug in a desired gastrointestinal (GI) zone. Basically, the polymeric membrane ruling drug release rate from the delivery system can be poorly swollen and, thus, scarcely permeable with respect to drug, at a low pH (typical of stomach). On the contrary, if it shows a considerable swelling degree at higher pH, it allows drug release in the intestine where pH is considerable increased. A typical example of self-regulated delivery system using membranes concerns insulin delivery. Some authors suggest the immobilization of glucose oxidase in pH-responsive polymeric hydrogel membranes surrounding a saturated insulin solution (Figure 15.1). As soon as glucose penetrates into the membrane, glucose oxidase catalyses its conversion to gluconic acid. Consequently, pH lowering in the membrane microenvironment takes place. This pH decreases, determining membrane swelling, greatly improves permeability toward insulin that is copiously released. Horbett and coworkers [42], for example, use *N,N*-dimethylaminoethylmethacrylate (DMA), hydroxyethyl methacrylate (HEMA), and tetraethylene glycol dimethacrylate (TEGDMA). Membranes are prepared at  $-70^\circ\text{C}$  by radiation polymerization to preserve enzymatic activity. To get sufficient insulin permeability, HEMA-DMA polymerization is led in order to have a two-phase membrane: the continuous one is the polymer-rich phase, while the dispersed one contains solvent and unreacted monomers. When gelation occurs after the phase separation, the dispersed phase is fixed in the space to form of porous structure. Typically, pores diameter ranges between 1 and  $10 \mu\text{m}$  [43], and the addition of glucose provokes an insulin permeability increase equal to 2.4–5.5 times. Ishihara [44], following a similar approach, uses 2-hydroxyethylacrylate (HEA), *N,N*-dimethylaminoethylmethacrylate (DMA), and 4-trimethylsilylstyrene (TMS) by radical polymerization of the corresponding monomers in DMF. The mole fractions of HEA, DMA, and TMS in the copolymer are 0.6, 0.2, and 0.2, respectively. Membranes are prepared by solvent casting. Capsules containing insulin and glucose oxidase are prepared by an interfacial precipitation method using gelatin as an emulsion stabilizer. The average diameter of the polymer capsules obtained was 1.5 mm. Iwata and coworkers [45] pretreat porous poly(vinylidene fluoride) membranes (average pore size of  $0.22 \mu\text{m}$ ) by air plasma and subsequently acrylamide is graft polymerized on the treated surface. The polyacrylamide is then hydrolyzed to poly(acrylic acid). In the pH range of 5–7, grafted poly(acrylic acid) chains are solvated and dissolved, but cannot diffuse into the solution phase because of grafting to the porous membrane. Accordingly, membrane pores are effectively closed. In the pH range of 1–5, the chains

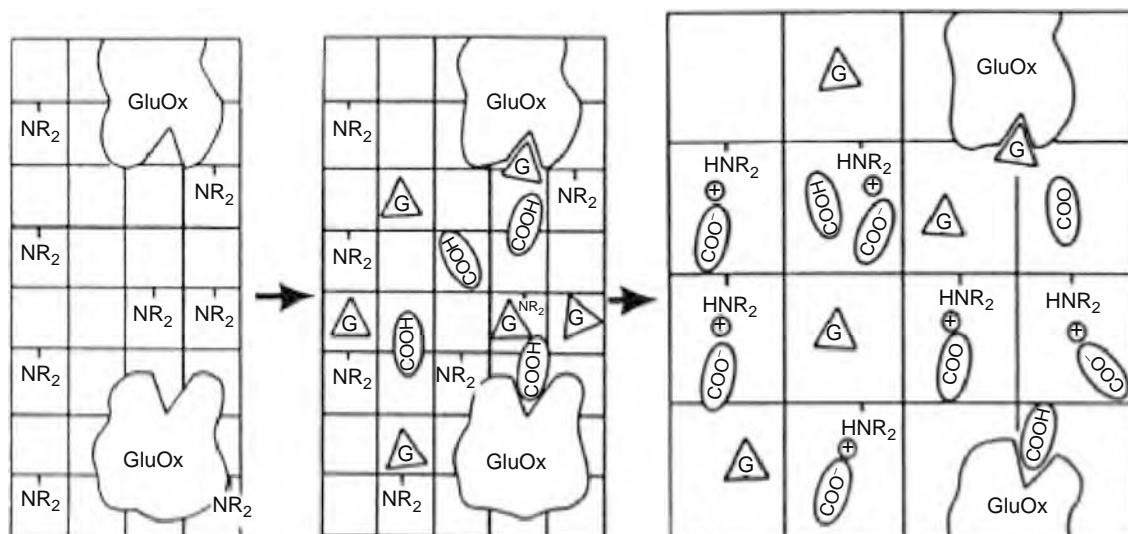


**FIGURE 15.1** Insulin release from glucose-sensitive membranes. (From Kost, J. and Langer, R., *Adv. Drug Deliv. Rev.*, 46, 125, 2001. With permission.)

collapse and the permeability increases. To achieve the sensitivity of the system toward glucose, glucose oxidase was immobilized onto a poly(2-hydroxyethyl methacrylate) gel.

Siegel and coworkers [46] approach insulin delivery by means of an implantable mechanochemical pump converting changes in blood glucose concentration into a mechanical force pumping insulin out of the device. Briefly, this device comprises three chambers (Figure 15.2): Chamber I contains an insulin solution, chamber II contains an aqueous fluid, while chamber III comprises a pH-sensitive polymer membrane that expands as glucose concentration increase. Chamber I is separated from the environment by a one-way valve opening when pressure in the pump exceeds that of the environment. Chamber II communicates with body fluids through a one-way valve opening when the pressure inside the pump

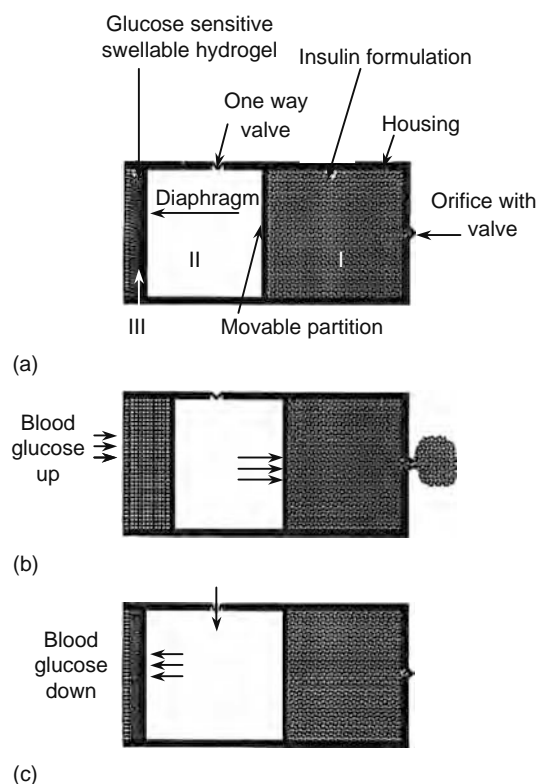


**FIGURE 15.2** Mechanochemical insulin pump. (From Kost, J. and Langer, R., *Adv. Drug Deliv. Rev.*, 46, 125, 2001. With permission.)

is less than that of the external medium. Hydrogel (Chamber III) is maintained in contact with the surrounding environment via a rigid membrane permeable only to small molecules and impermeable to large molecules, such as plasma proteins. Chambers II and III are separated by an elastomeric diaphragm, while chambers I and II are separated by a movable partition.

Of course, insulin release is not the unique target in the delivery field. Indeed, for example, Ishihara [47] matches the problem of urea release using a non-erodible membrane. The system is constituted by a pH-sensitive membrane (copolymerization of 4-carboxyacrylanilide and methacrylate) sandwiched among a membrane containing urease immobilized in free radically cross-linked *N,N*-methylenebisacrylamide. System permeability with respect to a model drug ((1,4-bis-(2-hydroxyethoxy)benzene) varies with urea concentration in the external environment.

Membrane-controlled devices, responsive to the concentration of external amines and amino acids, are prepared by polymerizing 2-hydroxy-dependent ethylmethacrylate and then reacting the polymer with 3,5-dinitrobenzoylchloride to attach 3,5-di-nitrobenzoate groups to the polymer [48]. Upon addition of amine substances to the external solution a charge-transfer complex forms, which increases the permeability of the membrane.

While the above-mentioned examples cannot be considered an exhaustive representation of all the possible uses of membranes in the delivery field, they serve to give an idea of how many and how variegated the applications can be. The aim of this chapter is to first describe the basic principles ruling mass transport through membranes. Then, in the light of the administration route (oral, transdermal, and implantable), some of the most important applications are presented and discussed. Finally, future applications of membranes in the delivery field are briefly treated.

## 15.2 MASS TRANSPORT

### 15.2.1 FACTORS AFFECTING DRUG PERMEATION

As most of the membranes used to modulate drug release kinetics are composed of polymers, this section focuses the attention on the typical mechanisms ruling mass transport through a polymeric network (whose structure has been previously described). At this purpose, it is necessary to first define the concept of membrane porosity as polymeric network can be classified as macroporous, microporous, and nonporous systems [49]. In the first two categories, drug diffusion occurs essentially through pores. For macroporous systems pores range between 0.1 and 1  $\mu\text{m}$ , which are much larger than diffusant molecules size. For microporous systems, pore size ranges between 0.005 and 0.02  $\mu\text{m}$ , which means, approximately, slightly larger than diffusant molecules size. Finally, nonporous systems have no pores and the molecules diffuse through network meshes. In this case, consequently, only the polymeric phase exists and no pore phase is present. While for macro- and microporous networks drug diffusion is mainly affected by pores topology; for nonporous structures, polymer swelling, polymer erosion, network topology, and drug/polymer interaction play the key role in determining drug diffusion. Indeed, it may happen that upon contact with the release environment, polymeric network undergoes a swelling process, particularly important in the case of a dry membrane. This implies molecular rearrangement of polymeric chains that tend to reach a new equilibrium condition as the old one was altered by the presence of the incoming external solvent [50]. The time required for this rearrangement depends on the relaxation time,  $t_r$ , of the given polymer/solvent system which, in turn, is a function of both solvent concentration and temperature. If  $t_r$  is much lower than the characteristic time of diffusion  $t_d$  of the solvent (defined as the ratio of the solvent diffusion coefficient at equilibrium and the square of a characteristic length), then solvent adsorption may be described by means of Fick's law with a concentration-dependent diffusion coefficient. On the contrary, if  $t_r$  is much greater than  $t_d$ , then a Fickian solvent adsorption with constant diffusivity takes place. Despite this complex phenomenology, however, in both cases the diffusion of drug molecules crossing the membrane may be described by Fick's law with a nonconstant diffusion coefficient (this is due to the variations of network meshes) and the macroscopic drug kinetics is defined Fickian. When  $t_r \approx t_d$ , solvent adsorption does not follow Fick's law of diffusion [51–53] and, consequently, also the diffusion of drug molecules crossing the membrane is not Fickian [54,55]. Accordingly, solvent absorption and drug permeation also depend on the polymer/solvent couple viscoelastic properties [56].

Polymer erosion can take place because of chemical and physical reasons. Under particular physiological conditions, the hydrolysis of eventually present water-labile bonds incorporated in the polymer can cause chain breaking. Moreover, erosion can also be due to enzyme attack and chemical reactions on particular polymeric chains sites [49]. On the contrary, in physically cross-linked matrices, erosion is due to chain disentanglement, induced by the matrix swelling fluid and the hydrodynamic conditions imposed in the release environment. Obviously, polymer characteristics play a very important role in erosion kinetics as extensively documented by the review of Miller-Chou and Koenig [57]. Erosion can be of two different types [49,58]: (a) surface or heterogeneous erosion and (b) bulk or homogeneous erosion. While in the first case only the outer parts of the matrix are affected by erosion, in the second case, the phenomenon also affects the polymeric bulk phase. Homogeneous erosion is usually due to a rapid swelling fluid uptake by the matrix system and consequent polymeric network degradation due to chemical reasons discussed above. On the contrary, surface erosion can be caused by both chemical (in this case the swelling fluid uptake is slower) and physical reasons, namely hydrodynamic conditions imposed in the release environment. On the basis of the relative chain cleavage and solvent diffusion rate, a system can be defined “surface eroding” or “bulk eroding.”

In particular, if solvent diffusion is much slower than polymer degradation, we are dealing with a surface eroding system. Surface erosion, also referred to as polymer dissolution in case of physically cross-linked matrices, can be further subdivided into two categories based on the amorphous and semicrystalline nature of the polymer. Indeed, while in the case of amorphous polymers only chain disentanglement is necessary for erosion, in the case of semicrystalline polymers, crystal unfolding precedes chain disentanglement, resulting in slower erosion kinetics [59].

Polymeric network topology heavily reflects on drug diffusion as it concurs in determining the drug diffusion coefficient as discussed later on. Additionally, polymeric network can also be responsible for a non-Fickian diffusion. Indeed, in presence of a very complex topology, deriving from a high internal disorder degree, the network can assume fractal characteristics [60]. If wide network meshes are defined as accessible sites for the diffusing drug and small network meshes (beside, obviously, polymeric chains) as forbidden sites, the entire network can be seen as a percolative network (fractal network), if forbidden sites approach a threshold value [61,62]. It is well known that diffusion on percolative (fractal) networks differs a lot from diffusion in non-fractal networks and release kinetics is different [60,63].

Although drug/polymer interactions can be expected to take place in several cases [64], particular importance is assumed by electrostatic interactions as reported by Singh and coworkers [65,66]. According to these authors, drug binding on polymeric chains follows a Langmuir isotherm mechanism characterized by an adsorption and desorption rates depending on drug free and bound concentration and on adsorption and desorption constants. Consequently, drug permeation through the membrane is the result of two phenomena, namely diffusion and adsorption–desorption.

### 15.2.2 CONTINUITY EQUATION

In the case of diffusion of a substance through a stationary solid or semisolid phase such as the polymeric network of a membrane, it is convenient to view the stationary phase as a fixed reference and to consider only the flux of mobile molecules, namely drug or external solvent. Assuming that the diffusion processes do not imply important variations of membrane density [50] and that no convective flux is present (this is the most common situation met in practice when dealing with membranes), mass conservation law reads [67]:

$$\frac{\partial C_i}{\partial t} = -\nabla \cdot F_i + R_i \quad (15.1)$$

where  $C_i$  and  $F_i$  are, respectively, the  $i$ th species concentration (mass/volume) and flux (mass/surface time),  $t$  is time,  $R_i$  is the  $i$ th component generation rate (mass/volume time), while the scalar product between the operator nabla  $\nabla$  and  $F_i$ , in a cartesian coordinate system, for the  $\nabla$  expression in other coordinate systems [see 67] reads

$$\nabla \cdot F_i = \left( \frac{\partial F_{xi}}{\partial X} + \frac{\partial F_{yi}}{\partial Y} + \frac{\partial F_{zi}}{\partial Z} \right) \quad (15.2)$$

where  $F_{xi}$ ,  $F_{yi}$ , and  $F_{zi}$ , respectively, are the  $x$ ,  $y$ , and  $z$  flux components relative to the  $i$ th species. Typically,  $F_i$  can be expressed according to Fick's law:

$$F_i = -D_i \nabla C_i \quad (15.3)$$

where  $D_i$  is the  $i$ th species diffusion coefficient. Accordingly, in a cartesian coordinate system,  $F_i$  components read

$$F_{xi} = -D_i \frac{\partial C_i}{\partial X}; \quad F_{yi} = -D_i \frac{\partial C_i}{\partial Y}; \quad F_{zi} = -D_i \frac{\partial C_i}{\partial Z} \quad (15.4)$$

As discussed in Section 15.3.1, it may happen that Equation 15.3 does not hold because of polymeric chains relaxation phenomena occurring during diffusion. In this case, indeed, the hypothesis of an instantaneous proportionality between  $F_i$  and  $\nabla C_i$  does not work and a time dependence has to be considered. Several approaches have been proposed to interpret this aspect. For instance, Joshi and Astarita assume a time-dependent composition at the polymer/penetrant interface [68]. In an interesting series of papers, Cohen first generalized Crank's idea [54] of a time-dependent diffusion coefficient [69], and then supposed that flux can be properly described by coupling the concentration and stress gradients, being the stress dependent on concentration and time via a Maxwell-like viscoelastic relationship [70]. Later on, Cohen and coworkers developed and improved the above-mentioned approach by modifying the stress dependence on time and concentration [71–73]. The existence of a stress-related convective contribution to flux is postulated by Frisch [74] and is also taken into consideration by other authors [75,76].

According to Adib and Neogi [77] and Camera-Roda and Sarti [78], the flux may depend on the history of the concentration gradient. The most general theory about diffusion in a viscoelastic polymer matrix was developed by Lustig [79], since he assumes that the flux depends on several driving forces such as temperature gradient, species' inertial and body forces, chemical potentials, and stress gradient. A good compromise between simplicity and theoretical correctness is given by the approach of Camera-Roda and Sarti [80]. Basically they assume that  $F_i$  may be expressed as the sum of two terms:  $F_{if}$ , characterized by a zero relaxation time and representing the Fickian contribution to the global flux, and  $F_{ir}$ , characterized by a nonzero relaxation time and representing the non-Fickian contribution to the global flux.

Accordingly,  $F_i$  can be expressed as

$$F_i = F_{ir} + F_{if}; \quad F_{if} = -D_{if} \nabla C_i; \quad F_{ir} = -D_{ir} \nabla C_i - \tau \frac{\partial F_{ir}}{\partial t} \quad (15.5)$$

where

$\tau$  is the relaxation time of the given polymer/diffusing molecule system

$D_{if}$  is the diffusion coefficient relative to the Fickian flux, while

$D_{ir}$  is the diffusion coefficient relative to the non-Fickian flux

In this approach, the time dependence is considered in the relaxation flux  $F_{ir}$ . Grassi and coworkers [50] improved the Camera-Roda and Sarti model assuming that  $F_{ir}$  is the sum of different contributes, each one characterized by its proper relaxation time. In this manner, the description of membrane viscoelastic properties is more adherent to reality.

While the time-dependent approach applies to describe possible membrane swelling (or deswelling) due to the presence of the external release environment fluid, it is not necessary in the case of drug permeation through a swollen membrane. The same is true when membrane swelling (or deswelling) is very fast or very slow in comparison to the duration of drug permeation through the membrane. A fast membrane swelling (or deswelling) will only reflect on a rapid drug diffusion coefficient variation.

### 15.2.3 DIFFUSION COEFFICIENT

Once an appropriate frame of reference is chosen, a two components (A, B) system may be described in terms of the mutual diffusion coefficient (diffusivity of A in B and vice versa). Unfortunately, however, unless A and B molecules are identical in mass and size, mobility of A molecules is different with respect to that of B molecules. Accordingly, the hydrostatic pressure generated by this fact will be compensated by a bulk flow (convective contribution to species transport) of A and B together, i.e., of the whole solution. Consequently, the mutual diffusion coefficient is the combined result of the bulk flow and the molecules random motion. For this reason, an intrinsic diffusion coefficient ( $D_A$  and  $D_B$ ), accounting only for molecules random motion has been defined. Finally, by using radioactively labeled molecules it is possible to observe the rate of diffusion of one component (let's say A) in a two component system, of uniform chemical composition, comprised of labeled and not labeled A molecules. In this manner, the self-diffusion coefficient ( $D_A^*$ ) can be defined [54]. Interestingly, it can be demonstrated that both  $D_A$  and  $D_A^*$  are concentration dependent. Indeed, the force  $f$  acting on A molecule at point X is [1]

$$f \propto -\nabla \mu_A \quad (15.6)$$

where  $\nabla \mu_A$  is the A chemical potential gradient. Accordingly, the total force  $f_T$  acting on all molecules is

$$f_T \propto -C_A \nabla \mu_A \quad (15.7)$$

where  $C_A$  is concentration. The assumption that the flux  $F_A$  is proportional to the total force yields to

$$F_A = -\frac{C_A}{\sigma_A \eta} \nabla \mu_A \quad (15.8)$$

where  $\sigma_A \eta$  is a resistance coefficient connected with diffusing molecules mobility [1,54]. Remembering the definition of chemical potential [81]:

$$d\mu_A = RT d(\ln(a_A)) \quad (15.9)$$

where

$a_A$  is the activity

$R$  is the universal gas constant

$T$  is temperature

it follows

$$F_A = -\frac{RT}{\sigma_A \eta} \frac{d(\ln(a_A))}{d(\ln(C_A))} \nabla C_A \quad (15.10)$$

Accordingly,  $D_A$  can be expressed by

$$D_A = \frac{RT}{\sigma_A \eta} \frac{d(\ln(a_A))}{d(\ln(C_A))} \quad (15.11)$$

Repeating the same treatment for  $D_A^*$  and remembering that in this case concentration and activity coincide due to obvious solution ideality, it follows that

$$D_A^* = \frac{RT}{\sigma_A \eta'} \quad (15.12)$$

assuming that  $\sigma_A \eta = \sigma_A \eta'$ , it descends that

$$D_A = D_A^* \frac{d(\ln(a_A))}{d(\ln(C_A))} \quad (15.13)$$

In conclusion, thus, the drug diffusion coefficient in a solvent is both concentration and temperature dependent. In the case of drug transport through swollen nonporous membranes, the physical frame is complicated by the presence of polymeric chains. Assuming that only drug molecules are moving due to a chemical potential gradient (in this sense, polymeric chains and the swelling agent molecules are retained immobile), the drug diffusion coefficient will be mainly affected by the presence of polymeric chains. Indeed, polymer chains have been proposed to retard solute movement by reducing the average free volume per molecule available to the solute, by increasing the hydrodynamic drag experienced by the solute, and by acting as physical obstructions thereby increasing the path length of the solute [82]. Basically, drug diffusion estimation can be performed recurring to the free volume theory, the hydrodynamic theory and to the obstruction theory [82]. Free volume theory [83] assumes that solute diffusion in a liquid is due to solute jumping into voids formed in the liquid space due to liquid molecules thermal motion. Solute diffusion is dependent on the jumping distance, the thermal velocity of the solute, and the probability that there is a hole free volume adjacent to the molecule. If, in addition, the presence of a polymeric network is considered, this theory yields, for example, to the model proposed by Peppas and Reinhart [84]:

$$\frac{D_g}{D_0} = k_1 \left( \frac{\overline{M}_c - \overline{M}_c^*}{M_n - \overline{M}_c^*} \right) \exp \left( -k_2 r_s^2 \left( \frac{\varphi}{1 - \varphi} \right) \right) \quad (15.14)$$

where

$D_g$  and  $D_0$  are, respectively, the solute diffusion coefficient in the polymeric network and in the swelling solvent

$k_1$  and  $k_2$  are the two constants

$\overline{M}_c$  is the number-average molecular weight between polymer cross-links

$M_n$  is the number-average molecular weight of the uncross-linked polymer

$\overline{M}_c^*$  is a critical molecular weight between cross-links

$\varphi$  is polymer volume fraction

$r_s$  is solute radius

Hydrodynamic theory [67], based on Stokes–Einstein equation, postulates that solute is represented by a very large sphere in comparison with the surrounding small liquid phase molecules. Solute mobility, and thus its diffusion coefficient, depends on the frictional drag exerted by liquid phase molecules. For heterogeneous gels (rigid polymeric chains), Cukier [85] suggests

$$\frac{D_g}{D_0} = \exp \left( - \left( \frac{3\pi L_c N_A}{M_f \ln(L_c/2r_f)} \right) r_s \varphi^{1/2} \right) \quad (15.15)$$

where

$L_c$  and  $M_f$ , are, respectively, the polymer chains length and molecular weight

$N_A$  is the Avogadro number

$r_f$  is the polymer fiber radius

For homogeneous gels (flexible polymeric chains), the same author proposes

$$\frac{D_g}{D_0} = \exp(-k_c r_s \varphi^{0.75}) \quad (15.16)$$

where  $k_c$  is a parameter depending on the polymer solvent system.

Models based on obstruction theory assume that the presence of impenetrable polymer chains causes an increase in the path length for diffusive transport. The polymer chains act as a sieve, allowing passage of a solute molecule only if it can pass between the polymer chains. Some authors [86], assuming solute molecule of the same size as polymer segments and assuming that solute transport occurs only within the free sites, suggest

$$\frac{D_g}{D_0} = \left( \frac{1 - \varphi}{1 + \varphi} \right)^2 \quad (15.17)$$

On the basis of more refined speculations, Ogston et al. [87] propose

$$\frac{D_g}{D_0} = \exp\left(-\frac{r_s + r_f}{r_f} \varphi^{1/2}\right) \quad (15.18)$$

According to Amsden [82], hydrodynamic approach should be used to deal with homogeneous hydrogels, while, for heterogeneous hydrogels, obstruction are more consistent with experimental data.

In the case of porous membranes, where solute diffusion takes place inside the liquid filling the pores, it is usual defining an effective diffusion coefficient  $D_e$ :

$$D_e = \frac{D_w \varepsilon}{\tau} \quad (15.19)$$

where

$\varepsilon$  is the matrix void fraction (porosity)

$\tau$  is tortuosity

$D_w$  is solute diffusion coefficient in the liquid filling the pores [88]

It is sometimes desirable [89] to incorporate into this expression a partition coefficient,  $K_p$ , for possible solute adsorption on pores walls and a restriction coefficient,  $K_r$ , accounting for hindered diffusion, and defined by

$$K_r = (1 - \lambda)^2 \quad \lambda = \frac{r_s}{r_p} \quad (15.20)$$

where  $r_p$  is the pore radius. Accordingly, Equation 15.19 becomes

$$D_e = D_w \frac{\varepsilon}{\tau} K_p K_r \quad (15.21)$$

#### 15.2.4 MODELING EXAMPLES: SWELLABLE AND NOT SWELLABLE MEMBRANES

Drug diffusion through a not swelling/deswelling/erodible (or through an already swollen) membrane can be described by means of Fick law. Indeed, assuming that drug concentration on one side of the membrane (donor environment) is always constant and equal to  $C_0$ , that drug concentration  $C_r$  on the other side (receiver environment) never sensibly detaches from zero (sink conditions), that drug diffusion takes place only in one dimension ( $X$ ), that membrane thickness is constant, that drug diffusion coefficient  $D_g$  inside the membrane is constant, and that no mass transport resistance exists at the membrane/donor and membrane/receiver interface (this means that, for example, we assume a negligible effect of the unavoidable presence of the stagnant layers sandwiching the membrane), Fick law solution yields (Equation 15.1):

$$C_r = \frac{C_0 K S}{V_r} \left( \frac{D_g}{h_m} t - \frac{h_m}{6} + \frac{2h_m}{\pi^2} \sum_{n=1}^{\infty} \frac{(-1)^n}{n^2} e^{-(n\pi/h_m)^2 D_g t} \right) \quad (15.22)$$

where

$t$  is time

$K$  is the partition coefficient

$S$  is the surface available for diffusion

$h_m$  is membrane thickness

$V_r$  is the receiver volume

For  $t$  approaching infinite, Equation 15.22 coincides with a straight line given by

$$C_r = \frac{C_0 SP}{V_r} (t - t_L); \quad P = \frac{KD}{h_m}; \quad t_L = \frac{h_m^2}{6D} \quad (15.23)$$

where

$P$  is the membrane permeability

$t_L$  is the lag time (intercept of Equation 15.23 on the  $t$  axis)

For thermoreversible gel membranes [90,91], the description of the swelling–shrinking phenomenon (induced by temperature changes) becomes paramount importance for what concerns a correct description of solute permeation. As mentioned in Section 15.3.2, a possible approach is that suggested by Camera-Roda and Sarti [80]. Accordingly, membrane swelling–shrinking can be described by Equation 15.5, provided that the following concentration dependence of  $D_f$ ,  $D_r$ , and  $\tau$  on solvent concentration  $C$  are considered

$$D_f = D_{in} \quad (15.24)$$

$$D_r(C) = D_{eq} \exp[g(C - C_{eq})] - D_{in} \quad (15.25)$$

$$\tau(C) = \tau_{eq} \exp[k(C_{eq} - C)] \quad (15.26)$$

where

$C_{eq}$  is solvent concentration in the swollen membrane ( $C = C_{eq}$ )

$D_{in}$  and  $D_{eq}$  are the diffusion coefficient of the solvent in the membrane at the beginning of the swelling phenomenon and at swelling equilibrium ( $C = C_{eq}$ ), respectively

$g$  and  $k$  are the two adjustable parameters

$\tau_{eq}$  is the membrane relaxation time when  $C = C_{eq}$

Equation 15.5 and Equations 15.24 through 15.26 have to be numerically solved [92] with the following:

Initial conditions

$$J = 0 \quad C = C_{eq}; \quad -L_{in}/2 \leq X \leq L_{in}/2 \quad (15.27)$$

Boundary conditions

$$C = C_{eq}; \quad X = \pm L_b/2 \quad (15.28)$$

where

$L_{in}$  is the initial membrane thickness

$L_b$  is the position of the swelling membrane contours

Of course, membrane thickness can be calculated supposing that its volume is given by the arithmetic addition of solvent and polymer volume. Assuming that the most important effect of matrix swelling/shrinking is to modify the solute diffusion coefficient  $D_g$  (and the Peppas–Reinhart equation [Equation 15.14] can be considered to account for this), permeation can be described by the continuity equation (Equation 15.1) where the generative term  $R_i$  is set to zero and the following initial and boundary conditions hold:

Initial conditions

$$C_d = 0; \quad -L_{in}/2 < X < L_{in}/2 \quad (15.29)$$

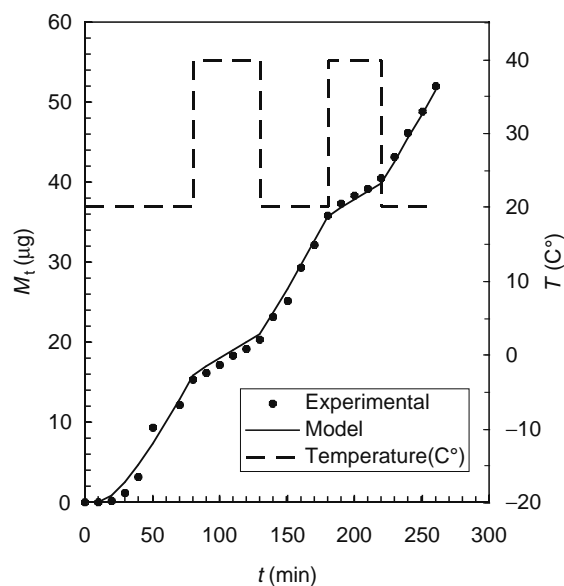


**FIGURE 15.3** Model fitting of the hydrocortisone permeation through a swelling/deswelling copolymer (DMAEMA and AAm (molar ratio: 57% DMAEMA, 33% AAm)) gel undergoing step temperature variations. The permeated amount  $M_t$  is plotted as a function of time  $t$ . The dashed line indicates the temperature profile (From Grassi, M., Yuk, S.H., and Cho, S.H., *J. Membr. Sci.*, 152, 241, 1999. With permission.)

#### Boundary conditions

$$C_d = 0; \quad X = L_b/2 \quad (15.30)$$

$$C_d = C_s; \quad X = -L_b/2 \quad (15.31)$$

where  $C_d$  and  $C_s$  are, respectively, solute concentration and solubility, Equation 15.29 implies that the membrane is solute free at the beginning, Equation 15.30 accounts for sink conditions in the receiver and Equation 15.31 states that solute concentration in the donor is always constant and equal to solubility. Figure 15.3 shows the comparison between model best fitting (solid line) and experimental data relative to hydrocortisone permeation through a copolymer that comprises poly(*N,N*-dimethylaminoethyl methacrylate) (DMAEMA) and acrylamide (AAm) (molar ratio: 57% DMAEMA, 33% AAm). As this copolymer undergoes a sharp deswelling passing from 20°C to 40°C, hydrocortisone permeation is considerably decreased when temperature has risen to 40°C. Model best fitting reveals that hydrocortisone diffusion coefficient in the DMAEMA–AAm copolymer at 40°C is one tenth of that at 20°C.

### 15.2.5 OSMOTIC SYSTEMS

Osmosis is the natural movement of a solvent through a semipermeable membrane into a solution of higher solute concentration, leading to equal solute concentrations on both sides of the membrane [93]. A semipermeable membrane can be crossed by solvent molecules but solute (ionic or high molecular weight compounds) permeation is impeded. Solvent migration from one side of the membrane to the opposite one takes place to render equal solute and solvent chemical potentials across the membrane. Osmotic pressure  $\pi$  can be expressed by

$$\pi = \frac{(\mu_L - \mu_R)}{v} = -\frac{RT}{v} \ln(a) \quad (15.32)$$

where

$v$  is the solvent partial molar volume

$\mu$  is the solvent chemical potential on the left (initially solute-free environment) and on the right of the membrane

$a$  is the solvent activity on the membrane right side environment

When hydrostatic pressure in the right environment (initial solute richer environment) equals the osmotic pressure  $\pi$ , the net solvent flux ends. According to nonequilibrium thermodynamics, the rate of solvent transport  $dV/dt$  through the membrane is given by [94]:

$$\frac{dV}{dt} = \frac{A}{h} L_p (\sigma \Delta\pi - \Delta P) \quad (15.33)$$

where

$A$  is the cross-sectional area for transport

$h$  and  $L_p$  are the membrane thickness and hydraulic permeability, respectively

$\sigma$  is the reflection coefficient while  $\Delta\pi$  and  $\Delta P$  are the osmotic and hydrostatic pressure difference across the membrane

As, typically,  $\Delta P \ll \Delta\pi$ , Equation 15.33 simplifies into

$$\frac{dV}{dt} = \frac{A}{h} k \Delta\pi, \quad k = L_p \sigma \quad (15.34)$$

where  $k$  can be taken as the effective membrane permeability. Equation 15.34 is the basic equation for calculating the amount  $m$  of drug released from an osmotic pump. Indeed, since in an osmotic pump the volume of drug solution pumped out is equal to that ( $V$ ) of the external solvent entered in the pump through the semipermeable membrane, the rate of drug released will be

$$\frac{dm}{dt} = \frac{dV}{dt} c = \frac{A}{h} k \Delta\pi c \quad (15.35)$$

where  $c$  is the drug concentration of the solution contained in the osmotic pump housing.

### 15.2.6 ELECTROTRANSPORT

In order to improve drug permeation through skin, recourse to an electrical field can be made. On this idea, the electrically assisted delivery systems are based. Typically, electrotransport is due to iontophoresis, electroosmosis, and electroporation [95]. Iontophoresis consists in the use of an electric current to drive charged drug molecules into skin by placing them under an electrode of like charge. Accordingly, a positively charged drug should be placed under the anode or positive electrode and the resulting electric repulsion would provide the driving force for drug permeation through skin. Typically, a 0.5 mA/cm<sup>2</sup> current is used (this intensity being unable to cause skin damages) even if drug permeation can be modulated by acting on current intensity. Electroosmosis is the phenomenon according to which a bulk fluid flow rises when a charged porous membrane is subjected to a voltage differences. This fluid flow can be up to microliters per hour per square centimetres of hairless mouse skin [96]. Since skin is a perm-selective membrane with negative charge at physiological pH, the electroosmotic flow occurs from anode to cathode, increasing the flux of positively charged drugs. Unlike iontophoresis adopting a continuous low current, electroporation requires the use of high-voltage pulse for a very short duration to render the skin permeable. Probably, electroporation promotes the formation of new aqueous pathways (open for some microseconds and then closed for a time period ranging from milliseconds to hours) that allow the entry of drug molecules by diffusion and local electrophoresis or electroosmosis.

For iontophoresis, the flux  $F_i$  of an ionic species,  $i$ , is defined by the Nerst–Plank equation:

$$F_i = -D_i \nabla C_i - z_i m f C_i \nabla E \pm C_i V \quad (15.36)$$

where the first right-hand side term accounts for Fickian diffusion, while the second is relative to electrical field  $E$  effect and the third represents the electroosmotic flow. In particular,  $z_i$  is ionic species valence,  $m$  is mobility,  $f$  is Faraday constant, and  $V$  is the velocity of the convective electroosmotic flow. In order to get drug profile concentration, we have to solve the continuity equation (Equation 15.1), provided that Equation 15.36 is considered for the flux expression  $F_i$  and the generative term  $R_i$  is set equal to zero.

### 15.3 MEMBRANES: USEFUL DEVICE FOR DRUG DIFFUSION COEFFICIENT MEASUREMENT

In order to design a controlled release system based on membranes, it is of paramount importance to know the membrane drug diffusion coefficient,  $D$  [97]. Thus, the measure of  $D$  plays a very important role and the necessity of developing proper models able to interpret the experimental data arises. Several methods are available in literature for the experimental determination of  $D$  [98–100]. Among this plethora, I can mention the category of methods derived from nuclear magnetic resonance (NMR) and dynamic light scattering (DLS) experiments, those based on holographic relaxation spectroscopy, those founded on the determination of the drug concentration profile such as the sectioning and inverse sectioning method [101], and the methods based on drug concentration gradient under stationary and nonstationary gradient. This section, in particular, focuses on the  $D$  determination resorting to the analysis of drug permeation through a swollen membrane. At this purpose,

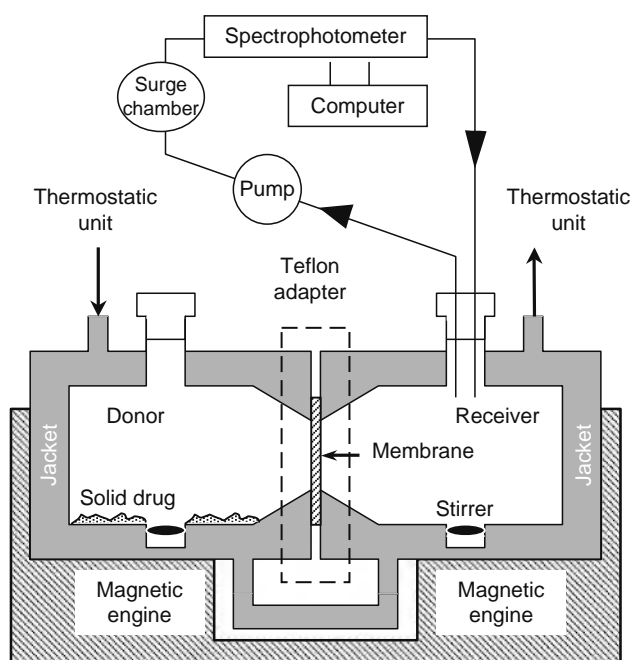


**FIGURE 15.4** Schematic representation of the side-by-side apparatus. The drug moves from the donor to the receiver compartment diffusing through the membrane and the receiver concentration increase is monitored and recorded by means of a personal computer managing an UV spectrophotometer. (From Grassi, M., Colombo, I., and Lapasin, R., *J. Control. Rel.*, 76, 93, 2001. With permission.)

the side-by-side apparatus is considered [102,103]. This device consists (see Figure 15.4) a donor compartment (volume  $V_d = 100 \text{ cm}^3$ ), containing the drug solution, and a receiver compartment (volume  $V_r = 100 \text{ cm}^3$ ) initially filled by pure solvent. Each compartment is equipped with a constant temperature jacket and a magnetic stirrer housed at the bottom of the cell. The membrane (diffusing area  $\approx 10 \text{ cm}^2$ ) is located in the teflon adapter connecting the receiver and the donor compartments. Drug concentration increase is measured and recorded by means of a personal computer managing a UV spectrophotometer connected to the receiver environment as indicated in Figure 15.4. In order to prevent bubble formation in the detecting system, a surge chamber is inserted between the spectrophotometer and the peristaltic pump, which provides for solution recirculation. A more sophisticated configuration permits the substitution of the recirculating system (peristaltic pump, surge chamber, etc.) with an optical fiber apparatus allowing a direct measurement of drug concentration in the receiver environment. The main advantages of this approach lie in the reduction of the receiver environment perturbation and the attainment of an optimal thermal control of the whole system.

### 15.3.1 NOT SWELLABLE MEMBRANES MODELING: EFFECT OF STAGNANT LAYERS AND DRUG DISSOLUTION

One of the most important errors affecting the determination of the drug diffusion coefficient resorting to permeation data through a swollen membrane may be due to the presence of two stagnant layers. Indeed, an insufficient stirring of both the donor and receiver environment gives origin to two stagnant layers sandwiching the membrane. Neglecting these two layers means to determine the value of the diffusion coefficient referred to the whole tri-laminate (comprised of the two stagnant layers and the membrane) instead of that referred to the single membrane. This implies an error depending on the sum of the thickness of the two stagnant layers. Sometimes this error may be not negligible, as the membrane thickness may be not small [104–106].

In order to make the present analysis as general as possible, it is assumed that the donor compartment contains an excess amount of undissolved drug. Indeed, this strategy is usually adopted in the attempt of achieving a constant drug concentration (in this case, drug solubility) in the receiver compartment. Accordingly, the drug dissolution process needs to be taken into account carefully. Nevertheless, it is assumed that Fick's law for diffusion holds inside the tri-laminate, which means that the effects of all possible chemical or electrical interactions between drug molecules and polymer chains or solvent molecules are accounted for by a drug partition coefficient (membrane/release environment medium) different from the value of one. Of course, a more detailed analysis should account for drug/polymer interaction by coupling, for instance, the diffusion with a drug adsorption–desorption phenomenon on polymer chains [107,108]. Anyway, the usual way to proceed [1,54,109,110] is to implicitly incorporate the polymer/drug interactions in the drug partition coefficient this being, in the majority of the situations, more than enough to correct model a permeation experiment. Furthermore, it is supposed that membrane is completely swollen, which means that the solvent concentration has reached its thermodynamic equilibrium value before starting the permeation

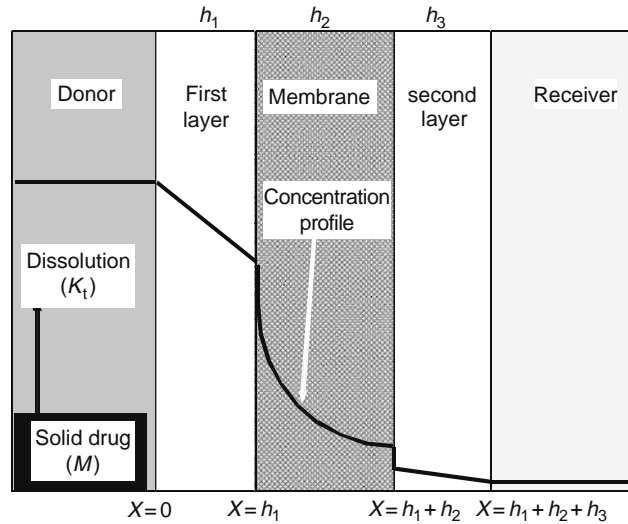


**FIGURE 15.5** Physical setup. A membrane is sandwiched among two layers arising in the donor and receiver compartments due to an insufficient stirring. In the donor volume, a dissolution process may take place. (From Grassi, M. and Colombo, I., *J. Control. Rel.*, 59, 343, 1999. With permission.)

experiments [111]. Indeed, membrane swelling may heavily influence the features of the drug permeation as previously discussed. Figure 15.5 schematically shows the physical setup with which all the following considerations will be referred to. Fick's second law for the first layer, the membrane and the second layer read, respectively:

$$\frac{\partial C_1}{\partial t} = \frac{\partial}{\partial X} \left( D_1 \frac{\partial C_1}{\partial X} \right) \quad (15.37)$$

$$\frac{\partial C_2}{\partial t} = \frac{\partial}{\partial X} \left( D_2 \frac{\partial C_2}{\partial X} \right) \quad (15.38)$$

$$\frac{\partial C_3}{\partial t} = \frac{\partial}{\partial X} \left( D_3 \frac{\partial C_3}{\partial X} \right) \quad (15.39)$$

where

$X$  is the abscissa

$t$  is the time

$C_1, C_2, C_3$  represent drug concentration in the first stagnant layer, in the membrane, and in the second stagnant layer, respectively

$D_1, D_2, D_3$  represent diffusion coefficient in the first stagnant layer, in the membrane, and in the second stagnant layer, respectively

Equations 15.37 through 15.39 must be solved with the following boundary conditions:

$$V_d \frac{dC_d}{dt} = -\frac{dM}{dt} + D_1 S \left. \frac{\partial C_1}{\partial X} \right|_{X=0} \quad (15.40)$$

$$\frac{dM}{dt} = -V_d K_i (C_s - C_d) \quad (15.41)$$

$$D_1 \left. \frac{\partial C_1}{\partial X} \right|_{X=h_1} = D_2 \left. \frac{\partial C_2}{\partial X} \right|_{X=h_1} \quad (15.42)$$

$$D_2 \left. \frac{\partial C_2}{\partial X} \right|_{X=h_1+h_2} = D_3 \left. \frac{\partial C_3}{\partial X} \right|_{X=h_1+h_2} \quad (15.43)$$

$$V_r \frac{dC_r}{dt} = -D_3 S \left. \frac{\partial C_3}{\partial X} \right|_{X=h_1+h_2+h_3} \quad (15.44)$$

$$C_1(X = 0) = K_{1d}C_d \quad (15.45)$$

$$C_2(X = h_1) = K_{21}C_1(X = h_1) \quad (15.46)$$

$$C_2(X = h_1 + h_2) = K_{23}C_3(X = h_1 + h_2) \quad (15.47)$$

$$C_3(X = h_1 + h_2 + h_3) = K_{3r}C_r \quad (15.48)$$

and the following initial conditions:

$$C_d = C_1 = C_{d0}; \quad C_r = C_2 = C_3 = 0; \quad M = M_0 \quad (15.49)$$

where

$C_d$  and  $V_d$  are, respectively, the drug concentration and volume of the donor compartment

$M$  is the time-dependent undissolved (solid) drug amount present in the donor compartment

$S$  is the area available for permeation

$K_t$  is the drug dissolution constant

$C_s$  is the drug solubility

$V_r$  is the receiver compartment volume

$h_1$ ,  $h_2$ , and  $h_3$  are, respectively, the thickness of the first stagnant layer, the membrane, and the second stagnant layer

$C_{d0}$  and  $M_0$  are, respectively, the initial drug concentration and undissolved drug amount in donor compartment, while  $K_{1d}$ ,  $K_{21}$ ,  $K_{23}$ , and  $K_{3r}$  are partition coefficients defined as follows:

$$K_{1d} = \frac{C_1(X = 0)}{C_d} = \frac{C_{1\infty}}{C_{d\infty}} \quad (15.50)$$

$$K_{21} = \frac{C_2(X = h_1)}{C_1(X = h_1)} = \frac{C_{21}}{C_1(X = h_1)} = \frac{C_{2\infty}}{C_{1\infty}} \quad (15.51)$$

$$K_{23} = \frac{C_2(X = h_1 + h_2)}{C_3(X = h_1 + h_2)} = \frac{C_{22}}{C_3(X = h_1 + h_2)} = \frac{C_{2\infty}}{C_{3\infty}} \quad (15.52)$$

$$K_{3r} = \frac{C_3(X = h_1 + h_2 + h_3)}{C_r} = \frac{C_{3\infty}}{C_{r\infty}} \quad (15.53)$$

where

$C_{d\infty}$  and  $C_{r\infty}$  are the drug concentration in the donor and receiver compartments

$C_{1\infty}$ ,  $C_{2\infty}$ , and  $C_{3\infty}$  are the drug concentration in the first layer, the membrane, and the second layer, respectively, after an infinite time

In this way, partition coefficients, defined by Equations 15.50 through 15.53, are thought concentration independent and, thus, time independent. Equation 15.40 represents the drug mass balance made up on the donor compartment: the first right-hand side term takes into account the dissolution, while the second represents the matter flux leaving the donor trough the first stagnant layer. Equation 15.41 takes into account the reduction of the solid drug  $M$  as the dissolution goes on. When  $M$  is zeroed, the first term of the right-hand side of Equation 15.40 vanishes. Equation 15.42 imposes that the matter flux leaving the first stagnant layer is equal to that entering the membrane ( $X = h_1$ ), while Equation 15.43 imposes the equality of the matter flux leaving the membrane and entering the second stagnant layer ( $X = h_2 + h_1$ ). Equation 15.44 represents the drug mass balance made up on the receiver compartment: the right-hand side term is the entering drug flux coming from the second layer. Equations 15.45 through 15.48 indicate the partitioning relation holding at the interface in  $X = 0$ ,  $h_1$ ,  $(h_1 + h_2)$ ,  $(h_1 + h_2 + h_3)$ . Equation 15.49 sets to zero the drug concentration in the membrane, the second layer, and the receiver while it sets to  $C_{d0}$  the drug concentration in the first stagnant layer and in the donor at the beginning of the permeation. An inspection of the above shown set of differential equations makes clear that the simpler situation represented by the absence of undissolved drug present in the donor compartment can be obtained by setting  $M_0 = 0$ .

If drug dissolution takes place from a thin tablet, it is reasonable to assume that  $K_t$  is time independent as dissolution surface is, practically, constant. On the contrary, if we are dealing with the dissolution of a powder, this is no longer true as particle radius and, thus, particle surface (this is the dissolving surface) reduce as dissolution proceeds. Indeed, the dissolution of a solid from a plane and uniform surface may be easily modeled by means of Equation 15.54 [112]:

$$V \frac{dC}{dt} = \frac{D_0 S_p}{h} (C_s - C) \quad (15.54)$$

where

$C$ ,  $C_s$ , and  $V$  are, respectively, the solute concentration, the solute solubility, and the volume of the dissolution medium

$S_p$  is the area of the solid/liquid interface

$D_0$  is the solute diffusion coefficient in the dissolution medium

$h$  is the thickness of the boundary layer arising between the solid surface and the dissolution medium

The thickness of the boundary layer,  $h$ , strongly depends on the stirring conditions of the dissolution medium [113,114]. Remembering that  $K_t$  is equal to

$$K_t = \frac{D_0 S_p}{hV}; \quad K_d = \frac{D_0}{h} \quad (15.55)$$

where  $K_d$  is the drug dissolution rate. Equation 15.54 may be recast in the following form:

$$V \frac{dC}{dt} = K_t (C_s - C)V \quad (15.56)$$

The right-hand side of Equation 15.56 coincides with the dissolution contribute employed in Equation 15.41. Since  $S_p$ , for a plane and uniform surface, does not change as dissolution develops, we may be sure that  $K_t$  is time independent. Unfortunately, this is not the case for a dissolving powder. Indeed, in such hypothesis, the dissolution surface decreases as the time goes on. The initial value of  $S_p$  and  $S_{p0}$  is equal to the powder surface area and, for a monodisperse powder made up of  $N_p$ , all equal, spherical particles, is given by

$$S_{p0} = N_p 4\pi R_0^2 \quad (15.57)$$

where  $R_0$  is the particle radius.

At time  $t$ , the particle radius will be decreased to  $R$  and, as a consequence,  $S_p$  will be equal to

$$S_p = N_p 4\pi R^2 \quad (15.58)$$

Then, the  $K_t$  time dependency will be given by

$$K_t = \frac{K_d}{V} 4\pi R^2 \quad (15.59)$$

Equation 15.59 holds the hypothesis that the whole powder surface is available for dissolution. This is reasonably accomplished when the dissolution medium is highly stirred so that the particles cannot adhere to the vessel walls or each other. Accordingly, the  $K_t$  time dependency, given by Equation 15.59, has to be inserted into Equation 15.40, getting

$$V_d \frac{\partial C_d}{\partial t} = 4\pi N_p R^2 K_d (C_s - C_d) + D_1 S \frac{\partial C_1}{\partial X} \Big|_{X=0} \quad (15.60)$$

Equation 15.60 has to be coupled with the  $R$  time dependency coming out from a mass balance made up on the tri-laminate, donor, and receiver compartments. This mass balance reads

$$M = M_0 + V_d(C_{d0} - C_d) - V_r C_r - \int_0^{h_1} C_1 S dX - \int_{h_1}^{h_1+h_2} C_2 S dX - \int_{h_1+h_2}^{h_1+h_2+h_3} C_3 S dX \quad (15.61)$$

Bearing in mind that

$$M = N_p M_p = N_p \frac{4}{3} \pi \rho R^3 \quad (15.62)$$

it follows

$$R = \sqrt[3]{\frac{3M}{N_p 4\pi\rho}} = R_0 \sqrt[3]{\frac{M}{M_0}} \quad (15.63)$$

where

$$M_0 = N_p \frac{4}{3} \pi R_0^3 \rho; \quad M_0 A = N_p 4\pi R_0^2 \quad (15.64)$$

where  $A$  is the powder surface per unit mass before dissolution. Equation 15.63 is the well-known Hixon–Crowell equation [115]. The effects of the  $K_t$  reduction are more evident when the dissolution phenomenon implies a considerable decreasing of the particle radius. Indeed, in this case, the dissolution surface will be strongly reduced and, as a consequence, the dissolving drug mass going into the donor compartment will be decreased. Obviously, the solution of the above set of equations (Equations 15.61 through 15.64) may be achieved only by means of a numerical method, for example, the control volume method [92] that is an implicit finite differences method suitable to solve such kind of problems.

Interestingly, if the drug concentration profile inside the two stagnant layers and the membrane has always a linear trend,  $K_t$  is time independent and the drug diffusion coefficient is concentration independent (these conditions are usually met for thin membranes and well stirred donor and receiver compartments), the proposed numerical model has the following analytical solution:

$$C_d(t) = A_1 + A_2 e^{(m_1 t)} + A_3 e^{(m_2 t)} \quad (15.65)$$

$$C_r(t) = B_1 + B_2 e^{(m_1 t)} + B_3 e^{(m_2 t)} \quad (15.66)$$

$$M(t) = M_0 + E_1 (e^{(m_1 t)} - 1) + E_2 (e^{(m_2 t)} - 1) \quad (15.67)$$

where  $A_1, A_2, A_3, m_1, m_2, B_1, B_2, B_3, E_1,$  and  $E_2$  are defined by the following equations:

$$m_1 = 0.5 \left( -(Tg - G + xb - Y) + \sqrt{(Tg - G + xb - Y)^2 - 4((xb - Y)(Tg - G) - Tzxa)} \right) \quad (15.68)$$

$$m_2 = 0.5 \left( -(Tg - G + xb - Y) - \sqrt{(Tg - G + xb - Y)^2 - 4((xb - Y)(Tg - G) - Tzxa)} \right) \quad (15.69)$$

$$A_1 = -\frac{(xb - Y)K_t C_s}{m_1 m_2} \quad (15.70)$$

$$A_2 = \frac{K_t C_s - \frac{(xb - Y)K_t C_s}{m_1} - (m_2 - (Tg - G))C_s}{m_1 - m_2} \quad (15.71)$$

$$A_3 = \frac{K_t C_s - \frac{(xb - Y)K_t C_s}{m_2} - (m_1 - (Tg - G))C_s}{m_2 - m_1} \quad (15.72)$$

$$B_1 = -\frac{K_t C_s + (Tg - G)A_2}{Tz} \quad (15.73)$$

$$B_2 = \frac{A_2}{Tz} (m_1 - (Tg - G)); \quad B_3 = \frac{A_3}{Tz} (m_1 - (Tg - G)) \quad (15.74)$$

$$E_1 = \frac{A_2}{m_1}; \quad E_2 = \frac{A_3}{m_2} \quad (15.75)$$

$$G = K_t C_s + \frac{D_1 S K_{1d}}{V_d h_1}; \quad T = \frac{D_1 S}{V_d h_1 K_{21}}; \quad x = \frac{D_3 S}{h_3 V_r K_{23}}; \quad Y = \frac{D_3 S K_{3r}}{h_3 V_r} \quad (15.76)$$

$$a = \frac{\gamma}{\alpha - \delta}; \quad b = \frac{\beta}{\alpha - \delta}; \quad g = \frac{\alpha\gamma}{\alpha - \delta}; \quad z = \frac{\delta\beta}{\alpha - \delta} \quad (15.77)$$

$$\alpha = 1 + \frac{D_3 h_2}{D_2 h_3 K_{23}}; \quad \beta = -\frac{D_3 h_2 K_{3r}}{D_2 h_3}; \quad \gamma = \frac{K_{1d}}{\frac{D_2 h_1}{D_1 h_2} + \frac{1}{K_{21}}}; \quad \delta = \frac{1}{\frac{D_1 h_2}{D_2 h_1 K_{21}} + 1} \quad (15.78)$$

To empirically adapt Equations 15.65 through 15.67 for the description of drug permeation through thick membranes, it is convenient to introduce a lag time  $t_l$  taking in account the time required to get a linear concentration profile in the two stagnant layers and in the membrane. Accordingly, it follows:

$$C_d(t) = A_1 + A_2 e^{(m_1(t-t_l))} + A_3 e^{(m_2(t-t_l))} \quad (15.79)$$

$$C_r(t) = B_1 + B_2 e^{(m_1(t-t_l))} + B_3 e^{(m_2(t-t_l))} \quad (15.80)$$

Equations 15.79 and 15.80 can describe the linear part of the permeation curve [116].

### 15.3.2 EXAMPLES: THEOPHYLLINE PERMEATION THROUGH CALCIUM ALGINATE MEMBRANES

For its large use in the pharmaceutical field, theophylline monohydrated ( $C_7H_8N_4O_2 \cdot H_2O$ ; Carlo Erba, Milano) can be used as model drug to measure the permeability of calcium alginate membranes having different thickness. Membranes are prepared by gradually adding the dry polymer powder (Protanal LF 20/60, Na salt of alginic acid; Protan Biopolymer, Drammen, Norway) into a highly stirred thermostatic (40°C) vessel containing demineralized water. In order to eliminate air bubbles produced by stirring, the solution undergoes a further mixing stage under vacuum for 5 min. The solution is put in a Petri disk, which in turn is immersed for 30 min in an aqueous solution containing 0.05 M  $CaCl_2$  and 0.4 M NaCl.  $CaCl_2$  represents the  $Ca^{++}$  source necessary for the gel formation (based on  $Ca^{++}$  mediated egg-box junctions [5,117]), while NaCl is added to guarantee a better gel homogeneity as suggested by Skiäk-Bræk et al. [117]. The gel membrane is washed for 2 min in demineralized water in order to remove salts from its surfaces and then its thickness is determined as the average of four measurements taken in different membrane points by means of an electronic calibre (Mitutojo, type IDC 112MCB, Japan).

The side-by-side apparatus used (see Figure 15.4) is characterized by donor and receiver compartments having equal volumes ( $V_d = V_r = 100 \text{ cm}^3$ ) and a surface area  $S$  available for permeation of  $\sim 10 \text{ cm}^2$ . While, initially, the donor compartment contains a saturated theophylline solution in presence of not dissolved theophylline, the receiver compartment is initially filled by demineralized water. By means of the surrounding jacket, temperature is kept uniform and constant in the whole system while a magnetic stirrer (600 rpm) ensures good mixing in both the compartments. The drug concentration increase is measured and recorded by means of a personal computer managing an UV spectrophotometer (271 nm, UV (ultra violet)–VIS (visible) Spectrophotometer, Lambda 6, Perkin Elmer) connected to the receiver environment. Permeation experiments, led in duplicate, are performed at 25°C and 37°C, and for three different polymer concentrations (%P): 1, 2, and 4 w/w%. In order to get a reliable determination of the theophylline diffusion coefficient, all other model parameters have to be measured in advance [116]. In particular, theophylline water solubility  $C_s$  ( $6681 \pm 42 \text{ } \mu\text{g}/\text{cm}^3$  at 25°C;  $12495 \pm 104 \text{ } \mu\text{g}/\text{cm}^3$  at 37°C), its water diffusion coefficient  $D_w$  ( $6.1 \pm 0.4 \times 10^{-6} \text{ cm}^2/\text{s}$ , 25°C;  $8.2 \pm 0.6 \times 10^{-6} \text{ cm}^2/\text{s}$ , 37°C), the powder dissolution constant  $K_d$  ( $= 1.57 \times 10^{-3} \text{ cm}/\text{s}$ , 25°C;  $1.52 \times 10^{-3} \text{ cm}/\text{s}$ ,  $T = 37^\circ\text{C}$ ), the partition coefficient  $K_m$  between the membrane (calcium alginate gel) and the donor–receiver fluid (water) and, finally, the thickness  $h_1$  and  $h_3$  of the two stagnant layers (see Table 15.1)

**TABLE 15.1**  
**Theophylline Partition Coefficient ( $K_m$ ), Membrane Thickness ( $h_m$ ), Surface Area ( $A$ ), and Stagnant Layer Thickness ( $h_{ss}$ ) Relative to the Experimental Tests Performed (Calcium Alginate Gels)**

T (°C)	Sl No	%P (–)	$K_m$ (–)	$h_m * 10^4$ (cm)	A (cm <sup>2</sup> )	$h_{ss} * 10^4$ (cm)
25	1	1	0.92 ± 0.02	475	10.8	54.8
	2			425		
	3	2	0.83 ± 0.04	450	10.7	
	4			430		
	5	4	0.88 ± 0.01	870	10.2	
	6			700		
37	7	1	0.83 ± 0.04	280	10.8	60.7
	8			380		
	9	2	0.79 ± 0.001	490	10.7	
	10			480		
	11	4	0.84 ± 0.01	720	10.2	
	12			655		

Source: From Grassi, M., Colombo, I., and Lapasin, R., *J. Control. Rel.*, 76, 93, 2001. With permission.

Notes:  $T$  is the temperature and %P is the polymer percentage in the membrane.

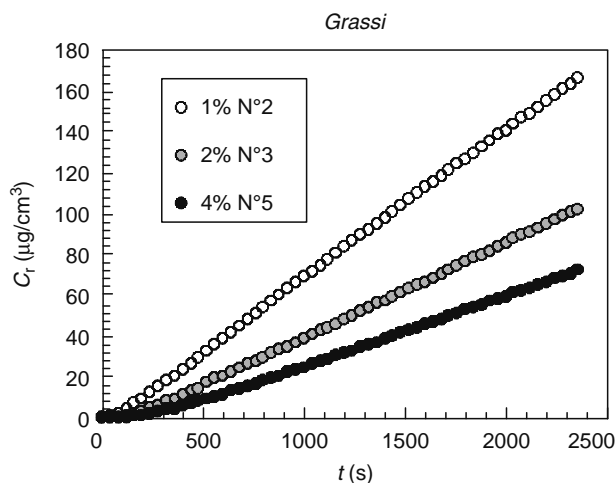


**FIGURE 15.6** Experimental trend of the receiver theophylline concentration  $C_r$  vs. time  $t$  relatively to three different membrane polymer concentrations %P (w/w %): test No. 7%P = 1%, test No. 9%P = 2%, test No. 11%P = 4% ( $T = 37^\circ\text{C}$ ). (From Grassi, M., Colombo, I., and Lapasin, R., *J. Control. Rel.*, 76, 93, 2001. With permission.)

are determined. Figure 15.6 shows the trend of the receiver drug concentration  $C_r$  vs. time  $t$ , for the test performed at  $25^\circ\text{C}$  at three different %P (test N° 2, 3, 5). The difference between the curves obtained from tests 2 and 3 is mainly due to different values of  $D_2$ , since membrane thickness is comparable (see Tables 15.1 and 15.2), while in the case of test 5 membrane thickness is the key parameter governing the difference. Moreover, the nonlinear trend in the beginning part of the curves, regardless the %P value, indicates that the membranes under consideration cannot be defined as thin. Depending on the %P considered, after a sufficiently long time, the permeation curves assume an almost linear trend indicating that, correspondingly, a linear drug concentration profile is attained inside the tri-laminate (two stagnant layers and membrane). Similar considerations can be done for Figure 15.6 where the  $C_r - t$  trend refers to  $T = 37^\circ\text{C}$ . Alginate does not give origin to thermosensitive hydrogels and, hence, an increase in temperature does not lead to appreciable changes in the membrane structure, whereas, the theophylline diffusion coefficient increases with temperature. Accordingly, the permeation kinetics is improved at  $37^\circ\text{C}$  and  $C_r$  increases more rapidly than at  $25^\circ\text{C}$ . An inspection of Table 15.2 reveals that the theophylline diffusion coefficient ( $D_2$ ) does not sensibly vary with %P, regardless temperature. This can be explained with the fact that the %P increase, in the 1%–4% range, does not substantially reflect in an increase of the polymeric network cross-link density, responsible for a reduction of the

**TABLE 15.2**  
Theophylline Diffusion Coefficient Calculated According to the Linear (Equation 15.80) ( $D_{\text{LIN}}$ ) and Numerical ( $D_{\text{NUMERIC}}$ ) Models Data Fitting

T ( $^\circ\text{C}$ )	No.	%P (-)	$D_{\text{LIN}} * 106$ ( $\text{cm}^2/\text{s}$ )	tr (s)	$D_{\text{LIN}} * 106$ ( $\text{cm}^2/\text{s}$ )
25	1	1	$5.6 \pm 0.34$	90.6	$5.6 \pm 0.35$
	2			66.2	
	3	2	$4.3 \pm 0.43$	141.7	$4.2 \pm 0.46$
	4			165.1	
	5	4	$5.0 \pm 0.70$	270.0	$5.1 \pm 0.64$
	6			185.9	
37	7	1	$4.3 \pm 0.59$	38.2	$4.3 \pm 0.22$
	8			51.1	
	9	2	$4.5 \pm 0.21$	154.1	$4.4 \pm 0.22$
	10			133.6	
	11	4	$4.2 \pm 0.11$	167.1	$4.2 \pm 0.12$
	12			194.6	

Source: From Grassi, M., Colombo, I., and Lapasin, R., *J. Control. Rel.*, 76, 93, 2001. With permission.  
Notes:  $t_r$  is the empirical lag time calculated according to the linear model (Equation 15.80) data fitting;  
 $T$  is the temperature and %P is the polymer percentage in the membrane.

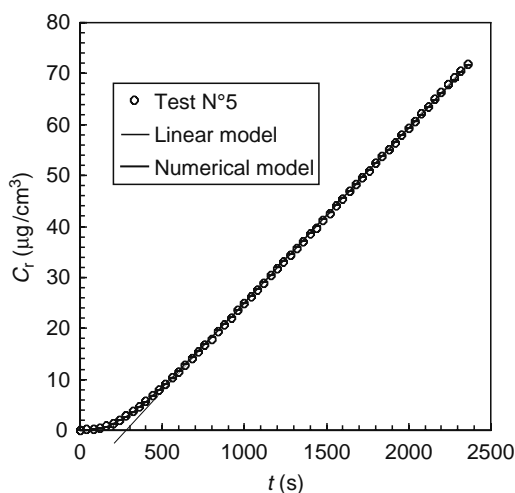


**FIGURE 15.7** Best fitting of the numerical (thick solid line) and linear (thin solid line) models on the experimental data (open circles) referring to test No. 5 (membrane polymer concentrations [w/w %]  $\%P = 4\%$ ,  $T = 25^\circ\text{C}$ ). The two models best fitting practically coincide in the linear part of the curve. (From Grassi, M., Colombo, I., and Lapasin, R., *J. Control. Rel.*, 76, 93, 2001. With permission.)

network mesh size, but it reflects in a higher membrane thickness. Nevertheless, it cannot be also excluded that, due to reduced theophylline dimension ( $\approx 3.8 \text{ \AA}$  [116,118]), polymeric network meshes are always very large even in the case  $\%P = 4$ . Obviously, this result cannot exclude that for higher polymer concentration, typical of some polymeric pharmaceutical membranes,  $\%P$  increase does not reflect in a, reasonable, cross-link density increase.

Finally, it is interesting to note that the results obtained by fitting Equations 15.79 and 15.80 (being  $t_r$  and  $D_2$  the only fitting parameters) on experimental data are, practically, equal to those deducible by fitting the numerical model to the same data (see Table 15.2). Figure 15.7 shows the good agreement between experimental data (open circles) and model best fitting (thick solid line, numerical model; thin solid line Equations 15.79 and 15.80).

## 15.4 ORAL DELIVERY SYSTEMS

Oral administration is the most popular route due to ease of ingestion, pain avoidance, versatility, (to accommodate various types of drug candidates), and, most importantly, patient compliance [119]. In addition, solid oral delivery systems do not require sterile conditions and are, therefore, less expensive to manufacture. Orally delivered pharmacologically active compounds must have favorable absorption and clearance properties, and satisfactory metabolic stability to provide adequate systemic exposure to elicit a pharmacodynamic response. If the compounds possess reasonable physicochemical properties have low to intermediate clearance and reasonable absorption, adequate oral bioavailability may be achieved [120]. Indeed, oral bioavailability, defined as the rate and extent to which the active drug is absorbed from a pharmaceutical form and becomes available at the site of drug action [121], is influenced by several factors including solubility, permeability, intestinal and liver metabolism, rapid biliary and other efflux pump-mediated excretion, and conditions in the gastrointestinal milieu [122,123]. Thus, both absorption and elimination processes determine the oral bioavailability  $F$  of a given drug. Accordingly,  $F$  can be estimated as

$$F = F_a F_g F_h F_l \quad (15.81)$$

where

$F_a$  is the fraction absorbed across the intestinal wall

$F_g$ ,  $F_h$ , and  $F_l$ , are, respectively, the fractions escaping clearance by the gastrointestinal tract, liver, and lung

The product of fraction available after gut and liver extraction ( $F_g F_h$ ) following oral administration primarily determines the oral clearance of the drug, although the contribution of lung clearance should also be considered [124]. It is therefore clear that, due to the complexity of drug absorption, the designing of drug release kinetics is of paramount importance and membranes can play an important role in oral delivery systems that are diffusion and dissolution controlled, as well as in ion exchange resins and osmotic systems. Indeed, apart from the simple taste masking aim (but this aspect becomes very important when dealing, for example, with delivery systems devoted to pediatric applications), typically, membranes are used in oral delivery systems to modulate release kinetics by controlling drug diffusion in the release environment or by controlling external solvent penetration

in the delivery system. Additionally, membrane can be designed to dissolve in particular physiological conditions to ensure drug release in the stomach rather in the intestine or vice versa depending on the drug absorption window. For example, Verapamil (calcium channel blocker, indicated for the hypertension treatment), a water-soluble compound that does not show bioavailability problems, can be administered by means of both reservoir systems (Verelan capsules, Elan Corporation, Gainesville, Georgia) and osmotic pumps (Searle's Covera-HS tablets, Alza Corporation, Palo Alto, California). Verelan contains a mixture of rapid and slow release beads [125] coated by a polymeric film consisting an hydroxypropylmethylcellulose/ethylcellulose blend that is applied in standard coating pan by spraying the coating suspension onto the core beads. The final commercial capsules, containing 20% uncoated beads and 80% coated beads, show a totally pH-independent release kinetics [126]. Covera-HS is designed to be administered at bedtime while active drug release takes place 4–5 h from ingestion as, in general, high blood pressure for many patients with myocardial infarction occurs early in the morning. This device comprises two chambers: the active drug core and the osmotic push compartment. Delayed release is achieved by the presence of an interposed membrane (enteric coating material) between the drug active core and the semipermeable membrane (cellulose acetate, hydroxypropylcellulose, polyethylene glycol). Indeed, the osmotic mechanism does not start until the GI tract water has completely dissolved the enteric coating material.

Nifedipine, another antihypertension drug belonging to the calcium channel blockers, is poorly soluble in water. Accordingly, an effective administration of this drug must be based on erosion or osmotic pressure mechanism. While the osmotic pump (Procardia XL tablets) device adopts the same membranes seen in the Verapamil release (Covera-HS), the erosion driven delivery consists in a compress-coated system. The inner portion (core) contains micronized nifedipine plus various excipients (among which lactose, corn starch, microcrystalline cellulose), while the external membrane is comprised of hydroxypropylcellulose, lactose, and nifedipine. As soon as this delivery system is put in contact with the release environment, the hydroxypropylcellulose hydrates and the soluble lactose erodes allowing nifedipine release at a constant rate. After, approximately 8 h, the external membrane is completely dissolved and the immediate dissolution of the inner core takes place, yielding a very fast release of the remaining nifedipine dose.

Another interesting application of membranes is shown in the work of Järvinen and coworkers [13] who study drug release from pH and ionic strength responsive poly(acrylic acid) (PAA) grafted poly(vinylidene fluoride) (PVDF) membrane bags in vitro. Square-shaped bags ( $2 \times 2$  cm) are formed by placing two PVDF membranes (Millipore; pore size  $0.22 \mu\text{m}$ ) on top of each other and hot-sealing three sides to get a membrane bag. The open side serves to insert model drug inside the bag after grafting. Bags are irradiated with 25 kGy under nitrogen atmosphere and the unsealed side is protected with a copper plate to avoid hot-sealing after grafting. Immediately after irradiation, bags are immersed at room temperature in a graft solution containing AA that is continuously purged with nitrogen to remove oxygen. Then, bags are Soxhlet extracted with water to remove any remaining monomer and dried overnight. Finally, bags are filled manually with model drug (FITC-dextran) and the open side is hot-sealed. The United States Pharmacopeia (USP) 23 rotating basket method (100 rpm,  $37^\circ\text{C}$ ,  $900 \text{ cm}^3$  of dissolution medium: 6 mM phosphate buffer at pH 2.0 or 7.0. The ionic strength is adjusted to 0.15 with NaCl) is used to study release kinetics from bags. Figure 15.8 shows that FITC-dextran release is considerably higher at pH 2.0 than at pH 7.0. Indeed, this is due to changes in the conformation of the grafted PAA chains as a function of pH. As PAA pKa is about 4 [127], at pH 2.0, polymer chains are undissociated resulting in a compact conformation. Accordingly, the pores of the PVDF-PAA membrane are open and the drug can pass through. On the contrary, at pH 7.0, PAA molecules are dissociated and swollen so that pores are partially blocked and drug passage is hindered. On the same principle it is based on the application of Li and

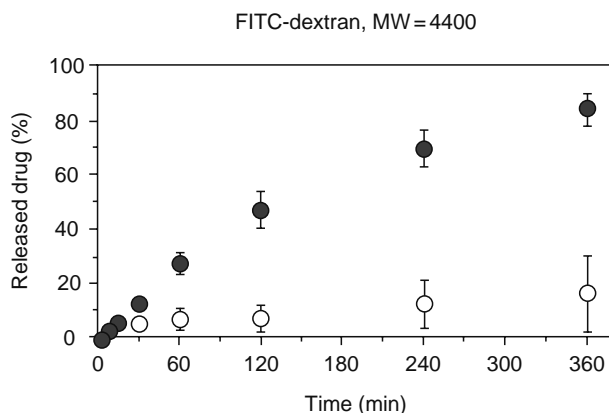


**FIGURE 15.8** Release of FITC-dextran from membrane bags prepared from 50 wt% PAA grafted PVDF membranes into dissolution medium at pH 2.0 (filled circles) and pH 7.0 (open circles). (From Järvinen, K., Åkerman, S., Svarfvar, B., Tarvainen, T., Viinikka, P., and Paronen, P., *Pharm. Res.*, 15, 802, 1998. With permission.)

D'Emanuele [128] who synthesizes cross-linked poly(NIPAAm) hydrogel (thermoresponsive polymer) within the pores of sintered glass filter discs using an in situ free radical polymerization method. At 40°C, poly(NIPAAm) is in the shrunken state so that pores are open and model drug (salicylic acid) permeation is high. On the contrary, at 20°C, poly(NIPAAm) is in the swollen state and pores are filled by the gel that hinders model drug (salicylic acid) permeation. In this manner, the authors can control drug release kinetics acting on temperature.

The aim of this section is to illustrate some coating techniques based on physical and physicochemical principles. In addition, for their potentiality, the attention will be then focussed on asymmetric membranes and on membranes devoted to colon-specific delivery systems.

#### 15.4.1 MEMBRANES FOR PHYSICALLY COATED SYSTEMS

Typically, aqueous and organic techniques can be used to coat solid dosage forms. In general, the choice of aqueous polymer dispersions implies various advantages, such as reduced toxicity and lower processing times, with respect to organic polymer solutions. In addition, aqueous approach, despite much higher polymer concentration, yields to coating formulation characterized by relatively low viscosities compared to those of the respective organic coating solutions. However, aqueous approach suffers for sensitivity to several factors—such as temperature, pH, addition of electrolytes, and other polymers—which, potentially, can lead to dispersion destabilization and coagulation. Obviously, coating properties coming from aqueous or organic techniques are neatly different and this, in turn, is the result of different film formation mechanisms. In the organic solution, macromolecules, highly mobile and interpenetrated (spaghetti like configuration), undergo solgel transition upon solvent evaporation to get film formation. Accordingly, homogeneous and compact films are realized. On the contrary, in the aqueous strategy, polymer particles are dispersed in the liquid and, upon water evaporation, they get well organized on the dosage form solid surface to form close-packed arrays. Capillary forces then drive the particles to coalesce together. Usually, the addition of a plasticizer is required to minimize film formation temperature, making particles softer and facilitating their coalescence. Consequently, film microstructure differs from that of organic-based film and crack formation is, generally, more probable [129].

In both the organic and aqueous approaches, release kinetics from coated systems is not an easy process as many variables, such as water diffusion, polymer swelling and dissolution, drug dissolution, diffusion, and cracks formation through the coating can play a key role [130]. In addition, the use of polymer blends in coating formation, although allowing a broad variety of drug release patterns, makes the release kinetics scenario much more complicated. Indeed, nowadays limited knowledge is yet available on the importance of the coating technique strategy (aqueous or organic) in the case of polymeric blends. Nevertheless, it seems clear that, in blend coatings, the effect of film formation mechanism on film structure and, thus on release kinetics, is more important than in the case of one polymer coating [131].

For example, Lecomte and coworkers [129] study the characteristics of propranolol hydrochloride (Abbot, Ludwigshafen, Germany) loaded pellets (10% w/w loading) coated by a blend of water-insoluble (ethyl cellulose (EC); Ethocel Standard 10 Premium, Dow Chemical Company, Midland, Michigan) and enteric polymers (methacrylic acid–ethyl acrylate copolymer 1:1, Eudragit L100-55, Röhm, Darmstadt, Germany). Triethyl citrate (TEC, Morflex, Greensboro, North Carolina) is used as plasticizer. Drug-loaded pellets are coated with EC and Eudragit L100-55 ethanolic solutions and blends thereof or with the respective aqueous polymer dispersions. EC:Eudragit L blend ratios investigated are 0:100, 25:75, 50:50, and 100:0 w/w, while 0.1 M HCl and phosphate buffer pH 7.4 are the release environments considered in the USP XXV paddle apparatus (37°C). Spraying technique is used to coat the loaded pellets. In virtue of the higher degrees of entanglements, dry films coming from organic solutions show better mechanical properties (energy at break and elongation) for all the blend ratios considered. In addition, dry film mechanical properties do not sensibly depend on plasticizer content. For what concerns release properties, the authors find that release kinetics strongly depends on the coating technique considered (organic or aqueous) and a great variety of release patterns can be obtained by varying blend ratios. In particular, for organic coating, release kinetics increases with Eudragit L content and it is improved by higher pH values. Conversely, in the case of aqueous coating, if pH increase still reflects in improved release kinetics, the effect of Eudragit L content on release kinetics is no longer (increasing) monotone. Finally, wherever low-pH release kinetics from aqueous coating is higher than the organic coating, these differences practically vanishes at high pH where the most important aspect is enteric polymer dissolution.

On the other hand, Siepmann and coworkers [130] focus attention on release kinetics from aqueous coating technique. In particular, theophylline pellets ( $\approx 800 \mu\text{m}$  diameter; Boehringer Ingelheim, Ingelheim, Germany) coated by two different kinds of water-insoluble and enteric polymers: (a) EC (Aquacoat ECD, FMC c/o Interorgana, Köln, Germany) and hydroxypropyl methylcellulose acetate succinate HPMCAS (ShinEtsu c/o Syntapharm, Mühlheim and er Ruhr, Germany); and (b) EC and Eudragit L30D-55 (Röhm, Darmstadt, Germany) are considered. Triethyl citrate (TEC, Morflex, Greensboro, North Carolina) is used as plasticizer. Blend ratios and release apparatus are the same used by Lecomte [129] and Siepmann and coworkers. At low pH, the authors find that release kinetics from EC:Eudragit L and EC:HPMCAS coated pellets is similar and it increases with HPMCAS or Eudragit L content, respectively. At high pH, regardless of the coating type, release kinetics is improved due to the partial dissolution of the enteric polymer. Nevertheless, this is more evident in the EC:Eudragit L coating irrespective of

blend ratio. The authors demonstrate that this is due to the high presence of water-filled cracks in the EC:Eudragit L coating. This affirmation is also supported by mechanical tests on films exposed to high pH release environment (higher energy is required to break EC:HPMCAS films).

It is now interesting to focus the attention on the different techniques used in the coating process. Typically, it involves deposition of uniform polymeric membrane onto the surface of the substrate such as tablets, pellets, or drug particles. Film coating, layering coating, and compressed coating represent the most used techniques [126]. Film coating process is performed in a coating pan, a fluidized bed, or a rotary granulator. Ethylcellulose, methacrylic ester copolymers, methacryl ester copolymers, cellulose acetate, and enteric polymers are widely used either alone or in combination with water-soluble polymers for the preparation of controlled release films. Since the integrity of the film and the absence of flaws or cracks are important factors in controlling the drug release kinetics from such preparation, it is very important that film formulation is optimized. In the light of this, plasticizers are often added to increase flexibility and to reduce the incidence of flaws. Obviously, coating properties also strongly depend on the presence of pigment and solvent, and on process variable such as temperature, spray rate, and so on. Layering coating is often performed in a fluidized bed in a noncontinuous manner. In coating beads, for instance, the seeds may first be coated with one layer of active drug and then with one polymeric layer followed by another active drug layer to get a wafer structure. In some cases, the active drug may be dissolved or dispersed with the coating materials. Compression coating process is performed using a tablet press to make a compress coat surrounding a tablet core (tablet-in-tablet). The compress coat can act as a barrier to drug release or as a part of formulation to provide biphasic release. Initially the process needs to compress the core formulation to get a relatively soft tablet that is then transferred in a larger die for final compression of the compress coat layer. This process can be used to develop a controlled release system with unique release profiles or to formulate two incompatible drugs by incorporating one in the core and the other in the compress coat layer.

Among the novel technologies, electrostatic coating merits to be considered [119]. The interesting advantage of this dry coating process consists in the elimination of blending powders, granulation, drying, lubrication and compression. In addition, it is less operator-dependent, it is continuous and is considerably fast. The principle of electrostatic deposition is based on the fact that opposite charges attract. Material deposition occurs when a pattern of charges is established on the substrate where the deposition is desired, and a supply of material to be deposited is delivered in the form of small, charged particles. The pattern of charges on the substrate will establish an electrical field,  $E$ , that interacts with charges on the material to be deposited according to Coulomb's Law:

$$F = qE \quad (15.82)$$

where

$F$  is the force

$q$  is the charge

The charged particles will be moved by this force, transported to the substrate, and deposited in a pattern determined by the charge on the surface. The key components in the technology may be summarized as four main areas, namely, active pharmaceutical ingredients, substrate, electrostatic chuck, and the controlled field deposition process. For what concerns active ingredients, the technology allows the production of material with controlled size, morphology, uniform flow, and charging properties. Intrinsic surface properties of active ingredients can be modified to enhance charging and handling. The substrate, an insulating film, is defined as the base upon which the drug is deposited. The substrate mechanical properties, such as thickness, modulus, and strength, and the electrical property of bulk resistivity are critical [132]. A chuck is a clamp or a device that holds an object. The role of an electrostatic chuck is to hold the substrate and provide the charged pattern onto the substrate in this technology. The electrostatic chuck can be equipped with an electrode for sensing the number of particles attracted to the chuck, thereby ensuring an accurate amount of particles [133]. Finally, the charging is achieved by using a three layer structure that has a conducting back-plane electrode, an insulating layer, and a patterned conducting top electrode. This controlled field deposition process enables the material to be directly deposited onto a single layer substrate [134]. The electrostatic powder coating process implies electro-charged powder adhesion on a rotating charged cylinder. Then, the powder is put into close proximity to the tablets (to be coated) that are vacuum-held in depressions around another cylinder. An opposite charge is given to the powder by means of a high-tension electrode to transfer it on the exposed tablet surface. Powder fusion to form a film is achieved by brief exposure to a source of long-wave infrared radiation.

#### 15.4.2 MEMBRANES FOR PHYSICOCHEMICALLY COATED SYSTEMS

In contrast to previous paragraph, in this case, coating process can also involve a chemical reaction and this approach can be generally named as microencapsulation. Microencapsulated solid preparations are widely used in pharmaceutical, chemical, and other industries to protect various substances from environmental impact, as well as for extending their action [135]. In the

pharmaceutical field, in particular, these preparations are mainly used to get controlled release drug kinetics, to minimize side effects, to reduce gastric irritations, and to mask the unpleasant taste of the contained drug [135–140]. Indeed, many different active components are microencapsulated: analgesics, antibiotics, antihistamine, cardiovascular agents, iron salts, antipsychotics [141], vitamins, peptides [142], proteins [143], anti-asthma [138,144], broncodilators, diuretics, anticancerogens, tranquilizers, and antihypertensives [135].

Basically, microencapsulation can be performed according to the interfacial polymerization technique and the coacervation/phase separation methods [135,145]. The first approach consists polymerization of a monomer at the interface between two immiscible phases yielding to the formation of a solid film surrounding the dispersed phase (termed microcapsule core or simply core). This technique applies in the case of water-immiscible liquid core, water-miscible liquid core, and solid core. For instance, in the case of a water-miscible liquid core, a hydrophilic polymer aqueous solution is dispersed in an organic phase with the aid of an emulsifier to get a water-in-oil emulsion. The addition of a water-insoluble reactant in the organic phase promotes the polymerization and thus the formation of a solid film around the aqueous dispersed phase. As the penetration of reactants in the polymerization zone is easier in a liquid environment than in a solid one, interfacial polymerization is more suitable for liquid encapsulation. Typically, polyamides, polyesters, and polyurethanes films are realized by using various combinations of water- and oil-soluble monomers and solvents [145]. Microcapsules morphology is characterized by a continuous and smooth external film, while an inner irregular surface is generally encountered. Microcapsules of 20–30  $\mu\text{m}$  diameter (even if smaller 3–6  $\mu\text{m}$  diameter capsules can be produced) characterized by a 20 nm film thickness can be obtained.

The coacervation/phase separation methods can be divided into aqueous and organic groups. In turn, aqueous group can be divided into complex and simple [135]. Simple coacervation, applying only for the microencapsulation of solid and liquid hydrophobic materials, implies the dissolution of a hydrophilic polymer in water where, subsequently, the hydrophobic core is dispersed. Encapsulation occurs due to the deposition of the coacervate (polymeric colloidal phase) on the hydrophobic core following a variation in temperature/pH or the addition of a precipitating agent. While complex coacervation differs from simple coacervation for the presence of more than one colloid, organic coacervation is the inverse of the aqueous one. Indeed, in this case, the core is constituted by a water-soluble material, while the film is an hydrophobic material. Among the many polymers that are used in the coacervation technique, agar, albumin, alginates, chitosan, collagen, pectin, and starch can be remembered for what concerns natural polymers, while acrylic acid, cellulose derivatives, polyurethanes, polyamides, and polyvinylpyrrolidone represent the synthetic part. Typically, microcapsules ranging from 5 up to 5000  $\mu\text{m}$  can be produced while elastic or rigid and fragile or tough films can be obtained.

To achieve maximum efficiency from using microencapsulated particles, it is necessary to know the time needed to extract the solid phase out of the polymeric capsule. The extraction rate of active components through a polymeric coating depends on many factors such as the nature of the polymeric film binder, the conditions under which the coating was applied, its structure, thickness, and porosity [146]. As a consequence, to properly design these particular delivery systems, a deep knowledge of the release mechanism and of the drug–film physical properties is required [147,148]. Indeed, drug release occurs from an ensemble of poly-dispersed spherical particles constituted by an external polymeric film that can undergo both erosion and swelling upon contact with the release environment. In addition, drug dissolution in the inner core (in the case of solid core) and drug diffusion in the film concur to determine the release kinetics. Indeed, as soon as microparticles are put in contact with the release environment, the external fluid crosses the polymeric coating, progressively dissolves the drug core, and fills the inner void space generated by core dissolution. Consequently, the drug present in the inner solution moves through the polymeric film determining the increase of its concentration in the release environment. Thus, drug is distributed among outer solution (release environment), polymeric coating, inner solution, and solid core. Despite the industrial relevance of microencapsulated delivery systems, no many authors matched the mathematical modeling of these systems, probably due its complexity. Nevertheless, some interesting examples can be found in literature [139,146,149,150].

### 15.4.3 ASYMMETRIC MEMBRANES

Asymmetric membranes are composed of a thin, dense skin layer supported by a thicker, porous substructure layer (Figure 15.9). Accordingly, they combine the high selectivity of dense membranes with the good permeability of porous membranes and thin dense membranes [151]. The technique used to produce these particular membranes implies the dissolution of the desired polymer in a solvent mixture composed by at least two solvents. One will be a good solvent for the polymer (more volatile solvent), while the other (less volatile solvent) will be a poor solvent (or non-solvent) for the polymer. Upon evaporation, due to different solvents boiling point, the solution enriches in the less volatile solvent (poor solvent) causing an abrupt precipitation of the polymer [152]. This technique (phase inversion) implies the transformation from a solvent continuous phase to a polymer continuous phase. Indeed, as soon as the drying process develops from the original solvent phase, two inter-dispersed liquid phases grow up. Then, further drying leads to a primary and secondary gel. The initial solvent solution contains also a third solvent (pore former) that has a non-solvent character for the polymer and that is neatly less volatile than the other two solvents. An alternative process implies polymer dissolution in a solvent system, film casting, and subsequently immersion into a quench bath of non-solvent for polymer. The solvent of the first step is extracted from the cast



**FIGURE 15.9** Scanning electron micrograph showing the cross-section of the asymmetric membrane wall. (From Thombre, A.G., Cardinal, J.R., DeNoto, A.R., and Gibbes, D.C., *J. Control. Rel.*, 57, 65, 1999. With permission.)

polymer solution into the quench bath, which leads to the precipitation of the polymer in structured form. In order to infer the desired elasticity and to reduce brittleness to asymmetric membrane, hydrophobic/hydrophilic plasticizers (glycerol, diethyl phthalate) may be added to the coating formulation.

In the delivery field, asymmetric membranes are typically employed as semipermeable membranes in osmotic-controlled delivery systems. Even if the drug release mechanism is mainly governed by the difference in osmotic pressure between the environmental fluid and drug-containing core of the delivery system, the diffusion contribute through the membrane cannot, in principle, be neglected. As soon as the delivery system is put in contact with the external delivery environment, water penetrates the asymmetric membrane, dissolves the inner core-soluble compounds (among which the drug and the osmotic agent), and pumps out drug solution through membranes pores due to increased internal pressure. As asymmetric membrane is not perfectly semipermeable, part of the drug can be delivered also by diffusion. Accordingly, the drug release rate ( $dM/dt$ ) is given by

$$\frac{dM}{dt} = \frac{dM_o}{dt} + \frac{dM_d}{dt} \quad (15.83)$$

where

$t$  is time

$M$  is the total drug amount released until  $t$ ,  $M_o$  and  $M_d$  are the  $M$  contribute due to osmotic pressure difference and diffusion, respectively

According to Equations 15.35 and 15.3, Equation 15.83 becomes:

$$\frac{dM}{dt} = \frac{A}{h} k \Delta \pi c + AD \frac{c}{h} \quad (15.84)$$

where

$A$  and  $h$  are device surface area and membrane thickness, respectively

$k$  is the membrane permeability (with respect to water)

$\Delta \pi$  is the osmotic pressure difference

$c$  is the dissolved drug concentration in the core fluid, while  $D$  is drug diffusion coefficient inside the asymmetric membrane

With respect to other osmotic technologies, asymmetric membranes ensure higher water permeability reflecting in the possibility of greater designing flexibility. Indeed, fast release rate can be achieved and lower solubility drugs can be

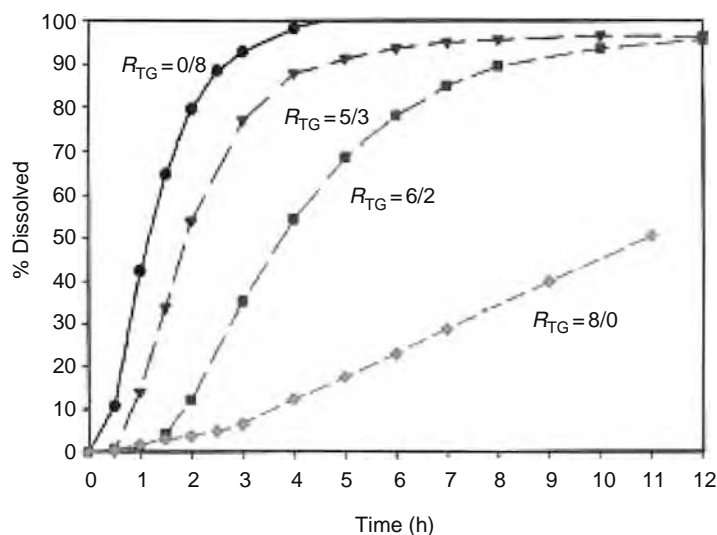


**FIGURE 15.10** Dissolution of glipizide from asymmetric membrane capsules as a function of the wall membrane permeability depending on triethylcitrate (TEC)/glycerol ratio  $R_{TG}$ . (From Thombre, A.G., Cardinal, J.R., DeNoto, A.R., and Gibbes, D.C., *J. Control. Rel.*, 57, 65, 1999. With permission.)

considered. Then, not only membranes porosity can be controlled by choosing the proper pore former, but also asymmetric membranes can be produced by means of conventional pharmaceutical equipment [151]. Typically, polymers such as cellulose derivatives, polysulfones, polyamides, polyurethanes, polypropylene, poly(vinyl chloride), polyvinyl alcohol, poly(vinylidene fluoride), ethylenevinyl acetate, ethylenevinyl alcohol, and PMMA are used to fabricate asymmetric membranes [153]. On the technological side, it has to be remembered that asymmetric membranes can be used to produce capsule shells and tablets by dip-coating process followed by immersion into a quench bath or air drying process [153]. In addition, they can be used to coat beads ( $\approx 1$  mm diameter) by means of the spray-drying and conventional spray-coating technique.

An interesting study about in vitro and in vivo performances of asymmetric membranes is given by Thombre and coworkers [154]. These authors, starting from a standard coating solution (cellulose acetate 15%, acetone 49%, ethyl alcohol 28%, and glycerin 8% [plasticizer, variable: 0%–8%], triethylcitrate [TEC] [variable: 0%–8%]), manufacture capsules, filled by drug, based on a dip-coating process [155]. The in vitro dissolutions are performed using standard USP dissolution methodology (Apparatus 2, rotating paddles, 50 rpm, 37°C, and 900 or 1000 mL of medium). The pharmacokinetic studies are performed in four fasted and fed laboratory beagle dogs using an immediate release tablet as the control. In vitro results clearly evidence how the more soluble the drug the higher the release rate. In addition, the authors observe that membrane permeability decreases with increasing TEC concentration. Indeed, higher amount of TEC reflects in a thicker dense membrane layer. This aspect is well documented by Figure 15.10 showing the percentage of glipizide released from capsules characterized by an increasing TEC concentration. For the in vivo performance of asymmetric membranes (same composition of in vitro test apart from the percentage of glycerin 3% and triethylcitrate 5%) doxazosin (1.5 mg dose) is used as a model drug. Figure 15.11 shows the comparison between mean plasma concentration due to standard immediate release tablets used as the control (Std tablet) and asymmetric membrane capsules (AM Capsules). Four laboratory beagle dogs in fed and fasted conditions are considered. It is clear that AM capsules alter doxazosin pharmacokinetics by reducing the concentration peak and prolonging absorption ( $T_{max} = 59.0$  h fasted and 7.0 h fed).

#### 15.4.4 MEMBRANES FOR COLON DELIVERY

Membranes play a fundamental role also in the colon-specific drug delivery systems. This administration route, whose advantages have been well recognized and documented [156], provides more effective therapy of colon-related diseases such as irritable bowel syndrome, inflammatory bowel disease (IBD) including Crohn's disease and ulcerative colitis. Colon-specific delivery has the potential to address important unmet therapeutic needs including oral delivery of macromolecular drugs. The colon is also viewed as the preferred absorption site for oral administration of protein and peptide drugs, because of the relatively low proteolytic enzyme activities in the colon. For example, insulin, calcitonin and vasopressin can be absorbed in that region [157]. Because of the distal location of colon in the GI tract, a colon-specific drug delivery system should prevent drug release in the stomach and small intestine, and effect an abrupt onset of drug release upon entry into the colon. This necessitates a triggering element in the system that can respond to physiological changes in the colon. Basically, the traditional

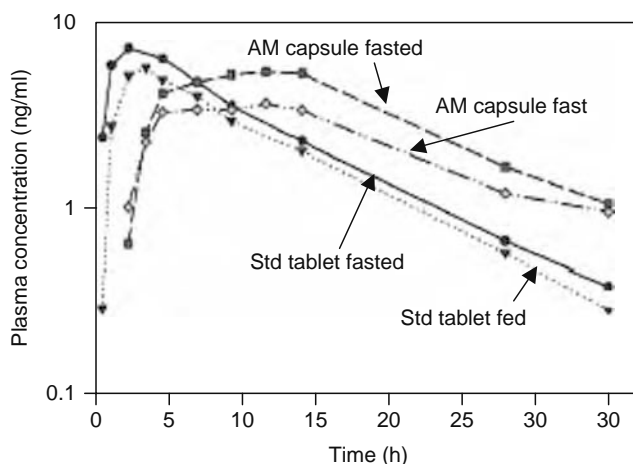


**FIGURE 15.11** Comparison between mean plasma doxazosin concentrations relative to –1 mg standard tablet (Std tablet) and 2 mg asymmetric membrane capsules (AM Capsules). Four laboratory beagle dogs in fed and fasted conditions are considered. (From Thombre, A.G., Cardinal, J.R., DeNoto, A.R., and Gibbes, D.C., *J. Control. Rel.*, 57, 65, 1999. With permission.)

four approaches to colon delivery are pro-drugs, pH-dependent systems, time-dependent systems, and microflora-activated systems [156]. Membranes, typically, are involved in the last three situations. For example, LiuXing [158] studies the delivery of bee venom peptide loaded on liposomes contained in an Eudragit S100 coated calcium alginate beads. Drug release studies are carried out using a USP Dissolution Rate Test Apparatus (Apparatus 1, 100 rpm, 37°C). The coated calcium alginate gel beads are tested for drug release for 2 h in 0.1 M HCl (250 mL), as the average gastric emptying time is about 2 h. Then, the dissolution medium is replaced with pH 6.8 phosphate buffer (250 mL) and tested for drug release for 3 h, as the average small intestinal transit time is about 3 h. Next, pH 7.4 phosphate buffer (250 mL) is used to test drug release for 3 h. As Eudragit S100 dissolves at  $\text{pH} \geq 6.8$ , it is expected that peptide release takes place only after 2 h. Indeed, after coating dissolution, gel beads are exposed to the aqueous environment that promotes polymer matrix swelling and erosion, leading to the liposome-loaded peptide release. Figure 15.12 shows that while the initial release of bee venom from the coated gel beads is very low, it considerably increases later on. Bee venom release in the first 2 h is negligible ( $\text{pH} 1.2$ ), while the fractional drug amount released rises to 5.5% after 3 h and 16% after 4 h. After 8 h, about 90% is released. Siew and coworkers [159] study 5-aminosalicylic acid release from amylose–ethylcellulose coated pellets in batch culture fermentation systems containing amylase enzymes or fecal bacteria. The pellets (100 g batch size) are coated in a fluidized bed coater (GPCG-1 Uni Glatt, Glatt GmbH, Binzen, Germany) using an amylose–ethylcellulose mixture containing 50% amylose to a total weight gain of 15%. The mixture is sprayed at a rate of 0.3 g/min through a 1.1 mm nozzle under a pressure of 2 bars. The bed temperature is maintained at 40°C. These authors find that the rate of release of 5-aminosalicylic acid is slightly faster in the fecal fermentation system than in the enzyme system, although release in both systems is substantially faster than in the control. This proves that the amylose coating can be destroyed by the presence of proper enzymes that can be produced by fecal bacteria. These findings are substantially confirmed both in vitro and in vivo (four healthy volunteers) also by Macleod and coworkers [160] who work

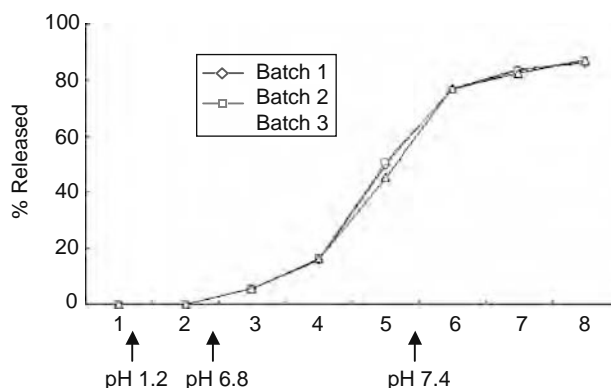


**FIGURE 15.12** Bee venom release profiles from three batch of calcium alginate gel beads coated with Eudragit S 100 in simulated GI pH condition. (From Liu Xing, L., Dawei, C., Liping, X., and Rongqing, Z., *J. Control. Rel.*, 93, 293, 2003. With permission.)

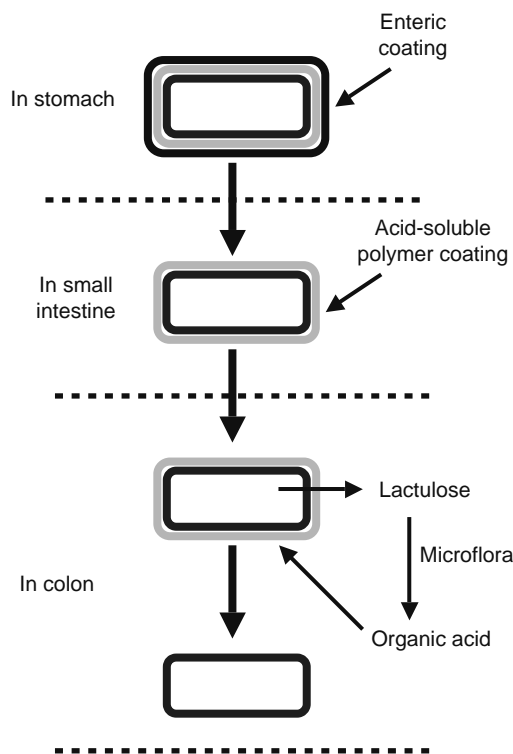


**FIGURE 15.13** CODES approach mechanism of action. (From Yang, L., Chu, J.S., and Fix, J.A., *Int. J. Pharm.*, 235, 1, 2002. With permission.)

on pectin-chitosan-hydroxypropyl methylcellulose (3:1:1) film coated radiolabelled ( $^{99m}\text{Tc}$ ) tablets. For both in vitro and in vivo tests, tablets are provided by an outer enteric coating (hydroxypropyl methylcellulose phthalate). The gastrointestinal transit of the tablets is assessed by gamma scintigraphy while a Caleva dissolution apparatus is used for in vitro release (pectinolytic enzyme is added to Sorensen's phosphate buffer to mimic colon environment). The experimental results show that tablet breakup starts once tablets are in the colon, due to degradation of the coat by colonic bacteria. Basically, this example falls in the so-called CODES approach [156] that couples the action of outer pH-sensitive coatings and an inner bacteria degradable coating as illustrated in Figure 15.13. Three polymeric layers surround the tablet core. The first coating (next to the core tablet) is an acid-soluble polymer (for example, Eudragit E) and outer coating is enteric with a HPMC barrier layer in between to prevent any possible interactions between the oppositely charged polymers. The core tablet is comprised of the active, one or more polysaccharides and other desirable excipients. The polysaccharides, degradable by enterobacteria to generate organic acid, include mannitol, maltose, stachyose, lactulose, fructooligosaccharides, etc. During its transit through the GI tract, CODES remains intact in the stomach due to the enteric protection, but the enteric and barrier coating will dissolve in the small intestine, where the pH is above 6. Because Eudragit E starts to dissolve at  $\text{pH} \leq 5$ , the inner Eudragit E coating is only slightly permeable and swellable in small intestine. Upon entry into the colon, the polysaccharide inside the core tablet will dissolve and diffuse through the coating. The bacteria will enzymatically degrade the polysaccharide into organic acid. The consequent pH lowering is sufficient to affect the dissolution of the acid-soluble coating and the following drug release.

Among newly developed colon-specific drug delivery systems, pressure-controlled delivery capsules (PCDCs) [161] can be mentioned. Their mechanism of action is based on the relatively strong peristaltic waves taking place in the colon and leading to an increased luminal pressure. They consist of a capsular-shaped suppositories coated with a water-insoluble polymer (ethyl cellulose). Once taken orally, PCDCs behave like an ethyl cellulose balloon, because the suppository base liquefies at body temperature. In the upper GI tract, PCDCs are not directly subjected to the luminal pressures since sufficient fluid is present in the stomach and small intestine. The reabsorption of water in the colon provokes an increase of the luminal content viscosity. As a result, increased intestinal pressures directly affect the system via colonic peristalsis. Consequently, PCDCs rupture and drug release in the colon take place.

## 15.5 TRANSDERMAL DELIVERY SYSTEMS

As skin is one of the most readily accessible organs of the body, topical application of drugs for treatment of skin diseases or pathology has been studied for a long time [162]. Indeed, skin separates the vital organs from the outside environment and

**TABLE 15.3**  
**Characteristics of Transdermal Patches**

Drug	Product Name	Dose and Patch Size	Dose Delivered	Clinical Indication
Clonidine	Catapres-TTS	2.5–7.5 mg in 3.5–10.5 cm <sup>2</sup>	0.7–2.1 mg in 7 days	Hypertension
Ethinylloestradiol(EO) norelgestromin (N)	Ortho-Evra	0.75 mg EO and 6 mg N in 20 cm <sup>2</sup>	0.14 mg EO and 1.05 mg N in 7 days	Birth control
Fentanyl	Duragesic	2.5–10 mg	1.8–7.2 mg in 3 days	Analgesia
Lidocaine	Lidodem	700 mg in 140 cm <sup>2</sup>	10–32 mg in 12 h	Post-herpetic neuralgia
Lidocaine (L) epinephrine (E)	Iontocaine	20–50 mg/L and 10–25 µg E in 5.7–11.1 cm <sup>2</sup>	40 mAmin iontophoresis	Dermal anesthesia
Nicotine	Habitrol Nicoderm-CQ Nicotrol Prostep	8.3–114 mg in 3.5–30 cm <sup>2</sup>	5–22 mg in 16–24 h	Smoking cessation
Nitroglycerin	Nitro-Dur Transderm- Nitro	12.5–160 mg in 5–40 cm <sup>2</sup>	1.2–11.2 mg in 12–14 h	Angina
17β-oestradiol	Alora, Climara Esclim, Estradem FemPatch, Vivelle, Vivelle-DOT	0.39–20 mg in 2.5–44 cm <sup>2</sup>	0.075–0.7 mg in 3–7 days	Hormone replacement
Oestradiol (O) norethindrone (N)	CombiPatch	0.51–0.62 mg O and 2.7–4.8 mg N in 9–16 cm <sup>2</sup>	0.15–0.20 mg O and 0.42–1.0 mg N in 3–4 days	Hormone replacement
Oxybutynin	Oxytrol	36 mg in 39 cm <sup>2</sup>	11.7–15.6 mg in 3–4 days	Overactive bladder
Scopolamine	Transderm Scop	1.5 mg in 2.5 cm <sup>2</sup>	1.0 mg in 3 days	Motion sickness
Testosterone	Androderm Testoderm TTS Testoderm	10–328 mg in 37–60 cm <sup>2</sup>	2.5 mg in 1 day	Hypogonadism

Source: From Prausnitz, M.R., Mitragotri, S., and Langer, R., *Nat. Rev. Drug Discovery*, 3, 115, 2004. With permission.

serves as a protective barrier against physical, chemical, and microbial attacks. Though these good protective properties, often topical applications represent a successful drug delivery strategy. Indeed, for many drugs, the transdermal route has the potential to be an extremely efficient delivery site [163]. Topical application avoids the effects of both gastric degradation and hepatic first-pass metabolism, and it presents a large surface area for absorption (~2 m<sup>2</sup>) and has relatively low proteolytic activity [163]. Accordingly, today there exist a number of patches for drugs such as clonidine, fentanyl, lidocaine, nicotine, nitroglycerin, oestradiol, oxybutynin, scopolamine, and testosterone [164,165]. There are also combination patches for contraception, as well as hormone replacement (see Table 15.3). In addition, transdermal administration can represent an opportunity to avoid side effects as it happens in the case of oestradiol patches (used by more than a million patients annually) that, in contrast to oral formulations, do not cause liver damage [166]. Similarly, transdermal clonidine, nitroglycerin, and fentanyl patches exhibit few adverse effects than conventional oral dosage forms. Despite this encouraging frame, however, some problems connected with the transdermal route still remain. Indeed, only low molecular weight (MW < 500), high lipophilicity (oil soluble), and small required dose (up to milligrams) drugs can be successfully administered. The smallest drug presently formulated in a patch is nicotine (MW = 162) and the largest is oxybutynin (MW = 359). Opening the transdermal route to large hydrophilic drugs is one of the major challenges in the field of transdermal drug delivery. Indeed, the possibility of releasing drugs such as proteins and peptides would lead to considerable advantages in terms, for example, of patient's health and compliance. In the light of this, the most clinically significant protein is, of course, insulin. Due to the chronic nature and multiple daily-dosing requirement of its administration schedule and the population of diabetics in the world, providing a noninvasive delivery mechanism for this compound would represent a considerable improvement from both the patient and the manufacturer viewpoint. However, other macromolecules such as cyclosporin, luteinizing hormone-releasing hormone (gonadotrophin-releasing hormone), and thyrotropin-releasing hormone could take advantage of a transdermal administration. Finally, also vaccines could be administered by means of the transdermal route and this assumes a very important aspect if we remember that the World Health Organisation currently recommends that children be immunized with approximately 12–13 different vaccines before 1 year of age which, in addition to the discomfort associated with needle injections, also raises issues about the potential risk of transfer of blood-borne pathogens [163]. Accordingly, the possibility of delivering such large molecules through the skin in a painless way, and yet still achieve sufficient cellular response to elicit immune protection, would be very important. Fortunately, large molecule release through skin may now be possible with some of the physical enhancement technologies. Consequently, the target of this section is to illustrate some examples of transdermal drug delivery focussing on passive diffusion-regulated delivery systems and systems aided by physical enhancing methods.

### 15.5.1 MEMBRANES FOR PASSIVE DELIVERY SYSTEMS

As skin has evolved to impede the flux of toxins into the body and minimize water loss, it shows very low permeability to the penetration of foreign molecules [167]. A unique hierarchical structure of lipid-rich matrix with embedded corneocyte in the upper strata (15  $\mu\text{m}$ ) of skin—the stratum corneum—is essentially responsible for this barrier. The corneocytes, comprising cross-linked keratin fibers, are  $\sim 0.2\text{--}0.4$   $\mu\text{m}$  thick and  $\sim 40$   $\mu\text{m}$  wide [168]. They are held together by corneodesmosomes, which confer structural stability to the stratum corneum. The stratum corneum lipids are composed primarily of ceramides, cholesterol, and fatty acids that are assembled into multi-lamellar bilayers. This unusual extracellular matrix of lipid bilayers serves the primary barrier function of the stratum corneum. The layer of lipids immediately adjacent to each corneocyte is covalently bound to the corneocyte and is important in maintaining barrier function. The stratum corneum is continuously desquamated, with a renewal period of 2–3 weeks. It is actively repaired by cellular secretion of lamellar bodies following the disruption of its barrier properties or other environmental insults [169]. Due to its structural heterogeneity, solute transport in stratum corneum lipid bilayers is highly anisotropic and size dependent, and that is why spatial variations in solute partition and diffusion coefficients are often observed [170].

Just below stratum corneum, we can find the epidermis, a viable tissue devoid of blood vessels 50–100  $\mu\text{m}$  thick. The inner skin layer is represented by the dermis (1–2 mm thick) containing capillary loops able to take up transdermally administered drugs for systemic distribution [164]. On the basis of its morphology, in principle, drug penetration through skin can take place through sweat glands, hair follicles, and transepidermally [171,172]. However, the contribution of follicles is hard to be quantified (in human skin, their contribution is negligible [172]) as their number per unit area is not equal for the different body parts both in humans and animals). Undoubtedly, based on the surface area available to permeation, the diffusion mechanism through stratum corneum is the most relevant one and that is why stratum corneum characteristics, often, discriminate between drugs that can take or cannot take advantage from a purely diffusive transdermal strategy.

The release of a therapeutic agent from a formulation applied to the skin surface and its transport to the systemic circulation is a multistep process involving (a) dissolution within and release from the formulation, (b) partitioning into the stratum corneum (SC), (c) diffusion through the SC, principally via a lipidic intercellular pathway (i.e., the rate-limiting step for most compounds), (d) partitioning from the SC into the aqueous viable epidermis, (e) diffusion through the viable epidermis and into the upper dermis, and (f) uptake into the local capillary network and eventually the systemic circulation [173]. Therefore, an ideal drug candidate would have sufficient lipophilicity to partition into the SC, but also sufficient hydrophilicity to enable the second partitioning step into the viable epidermis and eventually the systemic circulation.

Transdermal patches can be classified into two categories on the basis of their design: reservoir-type and matrix-type patches [164]. A reservoir-type patch consists of four major components: the reservoir, where drug is hosted in a solution or in a gel, the rate-controlling membrane, the adhesive layer, and the backing. Drug release occurs due to drug permeation through the membrane and the adhesive layer to get skin surface. Typically, the reservoir contains also an enhancer, a chemical compound that diffuses through the membrane and the adhesive layer penetrates into skin improving its permeability to drug. A little variation of the reservoir-type patch is represented by the multi-laminate design, where drug is dispersed/dissolved in a solid polymer matrix [174]. By contrast, matrix-type patches, which were introduced after reservoir-type patches, combine drug, adhesive and patch backing into a simpler design that does not involve a rate-controlling membrane. Accordingly, skin permeability usually governs the rate of drug delivery. Although these patches are easier to fabricate, they have limited flexibility in their design compared with reservoir-type patches that also offer the advantage of higher formulation flexibility and tighter control over delivery rates. Obviously, reservoir-type patches usually involve greater design complexity. While reservoir-type patches can provide a constancy of drug release rate, which means that the device can supply a constant amount of drug per unit time, which is not achievable in matrix-type patches. On the contrary, however, reservoir-type patches can have an initial burst of drug release. As membrane plays a fundamental role in reservoir-type patches, it must satisfy some requirements. In particular, a drug diffusion coefficient ranging from about  $10^{-7}$  to  $10^{-9}$   $\text{cm}^2/\text{s}$ , the possibility of being fabricated in form of thin film, a low solubility for the drug, the property of being soft well above shipping temperatures and an elastic modulus about 1000–1 MPa constitute fundamental prerequisites. For example, polyethylene, ethylene vinyl acetate, and polypropylene films match the above-mentioned requirements [174]. In general, however, ethylene vinyl acetate films represent the best candidates for these applications as vinyl acetate content can be modified to tune membrane permeability in relation to drug. In addition, membrane thickness, ethylene components crystallinity, and domain structure are other important variables to properly design release rate characteristics. For what concerns adhesives, they must be very permeable to both drug and enhancers as drug release rate is demanded only to membrane.

### 15.5.2 MEMBRANES FOR PHYSICALLY ENHANCED DELIVERY SYSTEMS

While chemical enhancers can be a successful tool for the improvement of small drug permeability through skin, for big molecules other strategies have to be undertaken. Indeed, proteins and peptides transdermal administration requires the use of

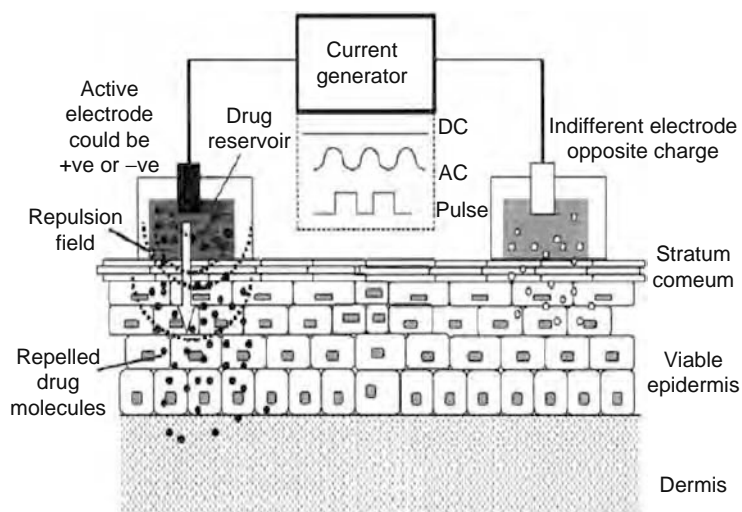


**FIGURE 15.14** Iontophoretic delivery devices basic design. Drug is placed on the skin under the active electrode, with the indifferent electrode positioned elsewhere on the body, and a current ( $<0.5$  mA) passed between the two electrodes effectively repelling drug away from the active electrode and into the skin. (From Cross, S.E. and Roberts, M.S., *Curr. Drug Deliv.*, 1, 81, 2004. With permission.)

physical methods to enhance permeability. Basically, these methods comprehend electrically based techniques (iontophoresis, electroporation, ultrasound, and photomechanical wave), structure-based techniques (microneedles), and velocity-based techniques (jet-propulsion) [163]. Although a detailed description of all these techniques is out of the scope of this section, some details on electrically based systems can be useful in the light of membrane applications in the delivery field.

Iontophoresis was initially developed to facilitate the delivery of ionized solutes, with inherently low partition coefficients due to their charged state, across tissue membranes. The technique involves the application of a small electric current (usually  $0.5 \text{ mA/cm}^2$ ) to a drug reservoir on the surface of the skin, with the same charged electrode as the solute of interest placed together to produce a repulsion effect that effectively drives solute molecules away from the electrode and into the skin [175] (Figure 15.14). The effect of simple electrorepulsion is known to be one of the main mechanisms by which iontophoresis produces its enhancement effects, although other factors such as a permeability increase of the stratum corneum due to an electric current flow, and electroosmosis of uncharged and larger water-soluble molecules can play an important role [176]. If iontophoresis proved to be successful for small molecular weight drugs ( $\text{MW} < 500$ ) [163,175], encouraging results can also be achieved for macromolecules and proteins. At this purpose, we can mention calcitonin (salmon) [177], corticotrophin-releasing hormone [178], delta sleep-inducing peptide [179], dextran sulphate [180], insulin [181], growth hormone-releasing factor [182], leuprolide acetate [183], leutenizing hormone-releasing hormone [184], neutral thyrotrophin-releasing hormone [185], oligonucleotides [186], parathyroid hormone [187], and vasopressin [188].

Electroporation is a technique that was initially developed for transmembrane delivery of macromolecules in isolated cells in culture systems and then expanded to intracellular delivery *in vivo* [189]. The process involves the application of large transmembrane voltages caused by electrical pulses ( $10 \mu\text{s}$  to  $100 \text{ ms}$ ), which probably cause the formation of transient pores (Figure 15.15) in the membrane that subsequently allow the passage of macromolecules from the outside of the cell to the intracellular space via a combination of possible processes including diffusion, local electrophoresis, and electroosmosis [190]. The application of electroporation to skin descends from the theory that the intercellular lipid bilayers of the skin should behave like those of cell membranes and be susceptible to pore formation following high-voltage electrical pulsing [191] (Figure 15.15). The work of Prausnitz and coworkers demonstrates the effectiveness of electroporation in transdermal drug delivery [164]. While the electrical resistance of the skin is reported to decrease as much as three orders of magnitude within microseconds of administration of an electrical pulse [192], skin permeability to drugs is also reported to increase by several orders of magnitude. This is mainly attributed to electrophoretic movement and diffusion through the newly created aqueous pathways [193] (Figure 15.15). *In vitro* experiments proved the increase in transdermal penetration up to  $10^4$ -fold not only for small molecular weight drugs, but also for bigger drugs such as leutenizing hormone-releasing hormone [194], insulin [195], and oligonucleotides [196].

Ultrasound (or sonophoresis) is a technology more traditionally associated with the fields of physiotherapy, sports medicine, and medical imaging rather than transdermal drug delivery. Compared to physiotherapy, where high-frequency energy (1 MHz) is used, in transdermal drug delivery low-frequency energy (20 kHz region) is applied across the skin. Cavitation, the acoustically induced formation and oscillation of gas bubbles formed because of the mechanical energy supplied, is the most probable

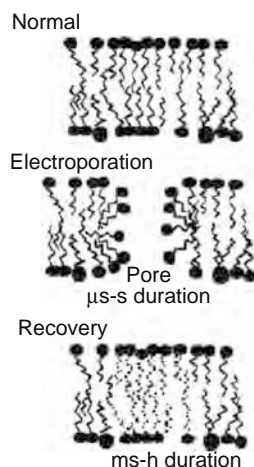


**FIGURE 15.15** Hypothetical bilayer poration model. Pores are hypothesized to form in the intercellular bilayers via momentary realignment of lipids that recover their original position at various times after the electrical pulse. (From Cross, S.E. and Roberts, M.S., *Curr. Drug Deliv.*, 1, 81, 2004. With permission.)

explanation for skin permeability increase [197]. Indeed, bubbles presence and movement produce defects large enough to facilitate the passage of macromolecules through the stratum corneum bilayers. Recent studies demonstrate an increase of 2.6–15-fold of the estradiol, naphthol, aldosterone, lidocaine, and testosterone diffusion coefficient due to ultrasound.

Photomechanical waves (PWs) (also known as laser-generated stress waves) are the pressure pulses produced by ablation of a material target (polystyrene) by Q-switched or mode-locked lasers (Figure 15.16). Although the mechanisms by which PWs increase the permeability of the stratum corneum are not entirely clear, microscopic studies have indicated that the energy supplied promotes to the formation of transient channels through the stratum corneum. The PW delivery of insulin through the skin of diabetic rats was shown to cause reductions in blood glucose of around  $80\% \pm 3\%$ , and was maintained below 200 mg/dL for more than 3 h. The largest molecule that has been reported to be delivered through rat skin to date has been 40 kDa [163].

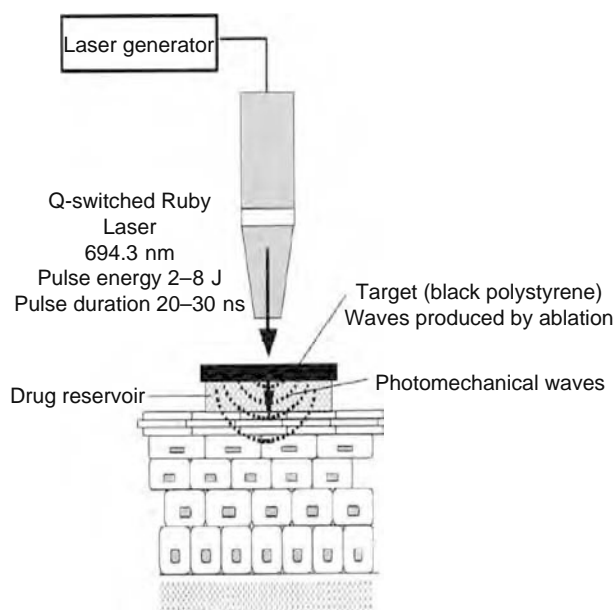


**FIGURE 15.16** Photomechanical wave delivery devices. A drug reservoir backed with a laser target material (e.g., black polystyrene) is placed on the skin. Laser-induced photomechanical waves are supposed to increase the permeability of the stratum corneum allowing the facilitated passage of drug molecules from the reservoir into the skin. (From Cross, S.E. and Roberts, M.S., *Curr. Drug Deliv.*, 1, 81, 2004. With permission.)

## 15.6 IMPLANTABLE DELIVERY SYSTEMS

Implants represent an important witnessing of the fruitful and necessary interaction among different competences typical of engineers, chemists, biologists, and medical doctors. Indeed, if on one hand human mind likes to subdivide and classify knowledge into different sectors (probably in the attempt of getting a simpler management of the complexity of the whole frame) and this gives origin to different professional figures, on the other hand the need for solving more and more complex problems requires the inverse process consisting knowledge sector merging. Accordingly, today, for example, chemical engineers cooperate with chemists and medical doctors to improve therapeutic reliability and the effectiveness of many delivery systems among which implants [198]. This delivery strategy, indeed, preliminary requires careful evaluation of the biocompatibility, defined as the property of a defined substance not to produce any toxic, injurious, or immunological response in living tissue [199]. Only on this basis it is possible to design a successful implantable delivery device that is able to work properly in the long-term period also. Accordingly, it is evident that the importance of the implant coating membrane assumes the role of mediator between the surrounding living tissues and the implants itself. A good implant performance implies a negligible foreign body response, i.e., a good biocompatibility.

Basically, immune response acts by two complementary pathways known as innate and specific immunity. Innate immunity comprises a set of defences not requiring recognition of foreign substances such as defensins, natural antibiotic proteins expressed in the gut and providing nonspecific protection from pathogens. Innate response can represent a serious problem for what concerns biomaterial implantation [199]. Specific immunity, on the contrary, is expressed by humoral and cell-mediated actions. Humoral immunity, devoted to destroy extracellular foreign substances, implies the recognition of a foreign substance (antigen) by antigen-specific B-lymphocytes and the following production of antigen-specific antibodies that coat the antigen (phagocytosis). Cell-mediated immunity, aimed to eliminate intracellular foreign substances (e.g., viruses), consists in the infected cell lysis by cytotoxic T-lymphocytes or in the elimination of intracellular microbes from infected macrophage because of cytokines produced by helper T-lymphocytes. Also cell-mediated immunity can cause problems for what concerns chronic response to implant [199].

In addition to a deep knowledge of immune response mechanisms, a reliable designing of implants needs to consider also timescale of the immune response. Indeed, there are three major timescales of the immune response: hyperacute, acute, and chronic. While hyperacute response, typically connected to innate immunity, develops on the timescale of seconds to minutes, acute response is humoral mediated and occurs on the order of weeks, its intensity and appearance being highly dependent on whether exposure to antigen is the first exposure or a repeated exposure. Finally, chronic response is cell mediated and occurs in the order of months to years.

As soon as an implant is put in its working site, the surrounding living tissue reacts (acute phase). If a consistent chemical or physical irritation takes place (as in the case of moving implants), a chronic inflammatory response occurs [200]. In the opposite case, on the contrary, a normal foreign body response develops and the implant is surrounded by a three-layer membrane [201]. The first stratum comprises macrophages and foreign body giant cell formations whose secretions give origin to the second layer, a dense and fibrous tissue 30–100  $\mu\text{m}$  thick. Finally, the third stratum is composed by highly vascularized tissue (granulation tissue). As this coating tends to be very stable and poorly permeable with respect to most chemical species, it is clear that its formation, de facto, prevents any kind of delivery from the implant to the surrounding living tissues.

Leoni [12,202], leading an interesting study on in vivo biocompatibility, observes different body responses in relation to the materials used and the site of implantation (rats). Silicon membrane (control) and PEG-modified silicon membrane were implanted in rat subcutis for 17 days and was then retrieved for analysis of body response. At gross examination, the tissue surrounding the samples differs mainly in the degree of vascularization. Indeed, very few blood vessels surround the control, while a rich network is present in the proximity of PEG-modified implants. In addition, histologic examination clearly reveals that PEG-modified samples have no sign of infiltration and the tissue has the characteristic structure and composition of the tissue found at the site of implantation. In another experiment, biocapsules were implanted in the rat abdominal wall and the omentum, and they were retrieved after 15 days of implantation. Different host response develops at the two sites of implantation. In the first case, a dense fibrotic tissue, consisting of collagen fibers, with parallel orientation and very poor vascularization is detected. On the contrary, no gross abnormalities of color or consistency are observed in the tissue surrounding omental pouch implants. The membrane surface appears to be free of tissue, while blood vessels are in its proximity. Microscopic analysis of the tissue reveals a nonuniform structure, with prevalence of large round cells typical of adipose tissue and loose connective tissue matrix, characterized by short collagen fibers randomly oriented. In both cases, no signs of infiltration are present.

A possible technique adopted to prevent fibrous capsule formation around the implant is the addition of a tissue intermediary [203,204]. Indeed, if this material has a continuous, interconnected, porous structure (pore diameter  $\geq 8$ –10  $\mu\text{m}$ ), macrophages are capable of invading structure voids. Consequently, vascularized tissue can grow in the implant and the foreign body response is avoided as this porous structure is able to mimic extracellular matrix. The first example of intermediary tissue use concerns the coating of an implanted catheter by means of a silicone rubber cage [205]. Typically,

swollen hydrogels, for their rheological properties and water content resembling those of soft tissues, are good candidate to act as intermediary membranes [198]. In particular, poly(2-hydroxyethyl methacrylate) (HEMA) hydrogels can be easily synthesized into macroporous sponge-like materials.

### 15.6.1 MEMBRANES FOR PASSIVE IMPLANTS

Implantable delivery systems can be classified as passive, biodegradable (bioerodable), and active [198]. In passive implants, drug release kinetics is controlled by drug diffusion through a nondegradable membrane that is usually constituted by silicone and poly(ethylene-co-vinyl acetate), polyacrylates. Indeed, membrane coats an active core represented by solid drug, drug solution, or dispersion. By properly choosing membrane thickness and permeability, release kinetics can be controlled and properly designed for a specific therapeutic target. For example, Norplant, an implantable 5 year contraceptive (developed by the International Committee for Contraception Research of Population Council), is based on this passive strategy for the long-term release of levonorgesterol (LNG) [174]. The first version of Norplant is a capsule system constituted by an LNG crystals core encapsulated by Silastic polymer (polydimethylsiloxane). An updated version consists in a Silastic matrix (containing LNG microcrystals) coated by an external membrane. Both the configurations yield an approximately constant release rate for about 15 months even if the first approach yields an initial nonconstant rate because of the nature of the drug present in the capsule. Indeed, if at the beginning drug transport is mainly ruled by LNG diffusion through membrane, for longer time, LNG dissolution is the rate determining step as slow water penetration transform the solid drug core into drug dispersion.

Alzet pumps (laboratory animal applications) and Duros (human applications) implants represent interesting examples of passive implants based on osmotic pressure [206]. Alzet device is a cylindrical structure composed by three main concentric parts: drug reservoir (the innermost part), osmotic agent, and semipermeable membrane (the outermost part). Drug reservoir is moulded from a flexible synthetic hydrocarbon elastomeric membrane carrying, in the upper part, an orifice for drug delivery. Obviously, the elastomeric wall is impermeable to water and drug to impede drug migration into the osmotic agent and vice versa. Sodium chloride is the osmotic agent filling the osmotic sector surrounding the drug reservoir. A cellulose ester blend constitutes the rigid semipermeable external membrane. The orifice end is equipped by a flow moderator (21 ga stainless steel tube) to reduce passive diffusion and convective losses. As soon as the device is put in contact with an aqueous external environment, the osmotic sector imbibes water, expands, and causes the shrinking of the flexible drug reservoir. Consequently, the release rate of Alzet pump depends on the water flux crossing the semipermeable membrane as predicted by Equation 15.35. It, therefore, clears the paramount importance of the semipermeable membrane that is, ultimately, the real heart of the whole system. On the contrary, except for very viscous or nonhomogeneous suspensions, the characteristics of the drug formulation do not affect the delivery profile. Typically, Alzet pumps deliver at fixed rate between 0.25 and 10  $\mu\text{L}/\text{h}$  for 1 day to 4 weeks. They are commonly implanted subcutaneously or intraperitoneally, although intracerebral, intravenous, and intra-arterial delivery has been used. Anesthetics, antibiotics, growth factors, hormones, and neurotransmitters are some examples of drugs that can be released by means of Alzet pumps. Duros implant is made up of a titanium alloy cylinder capped on one end by a rate-controlling, semipermeable membrane and on the other end by a diffusion moderator (orifice) for drug delivery [206]. Internally, this implant is equipped by a polymeric piston separating the osmotic chamber from drug reservoir. Semipermeable membrane can be made up of cellulose esters, polyamides, or polyurethane materials, which remain chemically stable under physiological conditions. The osmotic chamber contains sodium chloride (>50% wt) (although other solutes can be used) and gelling polymers, such as polyvinylpyrrolidone and sodium carboxymethylcellulose. Upon contact with an aqueous environment, water diffuses through semipermeable membrane, fills the osmotic chamber, and provokes forward piston movement that leads to drug delivery from orifice. Depending on semipermeable membrane characteristics, Duros implant can ensure drug release from 1 month (release rate 4.5  $\mu\text{L}/\text{day}$ ) to 1 year (release rate 0.25  $\mu\text{L}/\text{day}$ ). Due to its metallic nature, this system requires anesthesia to be implanted. Subcutaneous implantation is the preferred strategy, even though it is also adaptable to other sites of administration. Duros has been used to deliver leuprolide (palliative treatment of advanced prostate cancer), salmon calcitonin (osteoporosis treatment), and  $\alpha$ -interferon (antiviral and antiproliferative activity).

A particular kind of passive implants is represented by stents, rigid scaffolds that contribute to prevent artery re-occlusion after the mechanical removal of an atherosclerotic plaque by percutaneous trans-luminal angioplasty [207]. Although they can efficiently prevent early artery elastic recoil and late constrictive remodeling, two known events underlying restenosis [208], in 10%–30% of the cases, induce a pronounced intimal hyperplasia [209] characterized by exuberant proliferation of vascular smooth muscle cells (VSMCs), which contribute to occlude the treated vessel (restenosis) [210]. The pathobiologic events leading to artery restenosis start a few days after treatment [211] and are characterized by the proliferation of VSMC, normally present in a quiescent state in the media layer of arteries, in response to a variety of growth factors released at the site of artery treatment [212]. The process is completed by the migration of VSMC from the media to the intimal layer, followed by a further proliferation step and deposition of extracellular matrix proteins in the subendothelial space (intimal layer) giving origin to the so-called neo-intima [213–215]. In the light of this, membranes (stent coatings) can play a double important task as they can reduce foreign body response at the stent/tissue [216] interface and they can represent a mean for the release of antiproliferative substances at the site of stent implantation [210]. While nylon [217] and silicon [218] gave interesting

results for what concerns the insulation of the stent from surrounding tissues, many other materials have been considered for the in situ release of antiproliferative drugs [216]. Indeed, the choice of the coating material depends also on the drug to be incorporated. Both conventional (synthetic antiproliferative agents) and nonconventional (nucleic acid-based drugs) drugs can be considered [210]. While sirolimus [219] and paclitaxel [207] have been considered as conventional drugs, ribozymes, antisense oligonucleotides, DNA enzymes, and siRNAs, which represent the nonconventional approach [210]. Typically, polyurethane, polyglycol, silicon, polyvinylpyrrolidone-*co*-cellulose ester, and polyethylenglycol can be used for the drug eluting stent technology [220]. In addition, in the frame of ribozymes delivery, the use of thermoreversible gels (such as Pluronic) seems to be promising [221–223].

Apart from the possibility of an abrupt drug release due to membrane disruption when the reservoir-type implant is on site, the main disadvantage of passive implants consists surgical procedure required for their removal. Biodegradable/bioerodable polymers represent a possibility to overcome this problem as they are characterized by bonds that can be hydrolyzed or cloven by enzymes. Moreover, drug release is not only ruled by diffusion but also by polymer degradation kinetics. Finally, this strategy also allows to deliver high-molecular weight drugs, such as proteins whose diffusion in usual membranes is very low. Polyesters are typical biodegradable polymers and poly(lactic acid-*co*-glycolic acid) (PLGA) is one of the most used [198]. Indeed, PLGA hydrolysis leads to lactic acid and glycolic acid, which are natural cellular metabolites and, thus, are easily eliminated by the body. As the hydrolysis of lactic acid monomers is much faster than glycolic monomers, the rate of PLGA degradation can be controlled by simply playing on the copolymer ratio. While PLGA undergoes bulk degradation, poly-anhydrides are subject to surface erosion [57,224], an important advantage in implant designing. Indeed, in the case of surface erosion, system integrity is maintained for the lifetime of the device and drug release kinetics is more uniform. For example, poly(bis(p-carboxyphenoxy)propane-*co*-sebacic acid) is used for implants in local taxol delivery after an excised brain tumor [225]. As surface-eroding polymers exhibit a bigger tendency to degrade with respect to bulk-eroding polymers, drug release duration can represent a drawback for surface eroding polymers. This problem can be overcome by creating a composite release system of polyanhydride coated by a polylactic acid shell as demonstrated by Goeperich [224].

### 15.6.2 MEMBRANES FOR ACTIVE IMPLANTS

While passive and biodegradable implants fit very well a zero-order release demand, they cannot satisfy more complex release rate behaviors. Indeed, as in the case of diabetic patients, insulin release must be ruled by blood glucose concentration and it is well known that it can vary consistently during the circadian loop. Accordingly, an active implant needs to be able to adapt the release rate on the basis of an external, and physiological stimulus, and in this consists its “active” characteristic. Although no completely automated active implants have been yet reported [226], some interesting examples exist. Indeed, microfabrication technology allows developing active implantable microfluidic devices that incorporate micropumps, valves, and flow channels to deliver liquid solutions [226]. One of the key components in those devices is the miniature fluid-dispensing system (micropump). Various pumping methods are available, including electroosmotic pumping for ionic fluids, positive displacement pumps that use piezoelectric components, and pneumatic, bubble, or surface-tension pumps that rely on moving gas-liquid interfaces to displace fluids [227]. Another possibility is represented by the drug array implant, a solid-state silicon microchip for controlled release of single or multiple chemical substances on demand [228]. The release mechanism relies on the electrochemical dissolution of thin anode gold membranes covering microreservoirs containing chemicals in solid, liquid, or gel form. A sequential microfabrication process including photolithography, chemical vapor deposition, electron beam evaporation and reactive ion etching has been used to create 34 microreservoirs on the chip, each covered by a thin gold membrane functioning as the anodes. The gold membrane is dissolved upon application of a desired voltage and this leads to drug release into the surrounding fluid. The possibility of individually controlling each reservoir allows the achievement of many complex release patterns.

## 15.7 FUTURE TRENDS

Previous sections illustrate some different applications of membranes in the delivery field with particular attention to oral, transdermal, and implantable delivery systems. It reports that, basically, membranes are required to modulate mass transport or insulate the delivery system from the surrounding tissues to prevent foreign body response. In most situations, both these tasks take place only on a passive basis in the sense that the delivery system behavior is not influenced by external, physiological stimuli. Nevertheless, it is clear that the new generation of delivery systems (regardless the administration route) will be based on an active basis so that the system is able to autonomously react to external stimuli, such as the concentration of a fixed analyte [229]. This is the reason why smart and biomimetic materials are becoming more and more attractive for the delivery field. Indeed, while the term “smart” is attributed to materials having property of shape memory (these materials, e.g., expand or constrict to external stimuli such as pH, light, or pressure), “biomimetic” refers to materials able to mimic or elicit biological function [198]. The synergic effect of these materials and nano-microtechnologies will determine the characteristics and properties of the future delivery systems [230,231] where membranes will surely play a fundamental role.

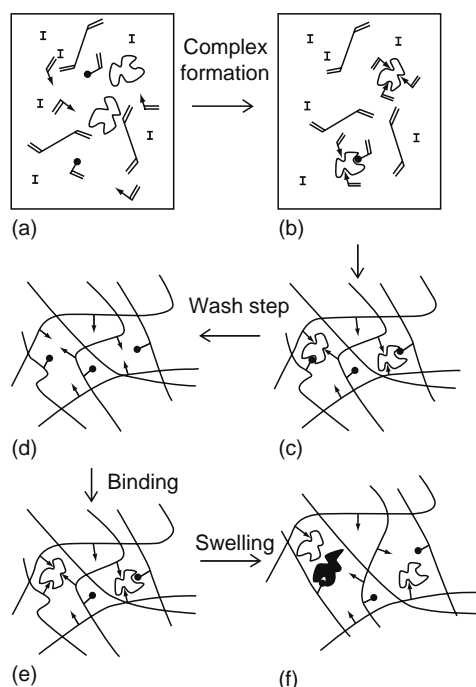


**FIGURE 15.17** Imprinting process scheme. (a) Solution mixture of template, functional monomer(s) (ending with triangles and circles), cross-linking monomer, solvent, and initiator (I). (b) The pre-polymerization complex is formed by means of covalent or non-covalent bonds. (c) Cross-linking yields the network formation. (d) Removal of the original template by a proper washing. (e) Rebinding of template. (f) In weakly cross-linked systems, macromolecular chain movements yield areas of differing affinity and specificity (filled molecule is isomer of template). (From Byrne, M.E., Park, K., and Peppas, N.A., *Adv. Drug Deliv. Rev.*, 54, 149, 2002. With permission.)

### 15.7.1 MOLECULARLY IMPRINTED MEMBRANES

Many of the future drug delivery systems will be based on intelligent gels able to autonomously react to external stimuli to modulate drug release in response to pH, temperature, ionic strength, electric field, or specific analyte concentration differences. Accordingly, the realization of a precise macromolecular chemical network able to recognize target molecules from an ensemble of closely related molecules is of paramount importance. Molecular imprinting is a possible strategy allowing the achievement of the above-mentioned task [231]. This technique (Figure 15.17) implies the formation of a pre-polymerization complex between the template molecule and functional monomers or functional oligomers (or polymers) [233] with specific chemical structures designed to interact with the template either by covalent [234], non-covalent chemistry (self-assembly), or both [235,236]. Once the pre-polymerization complex is formed, the polymerization reaction occurs in the presence of a cross-linking monomer or chemical cross-linking methods and an appropriate solvent controls the overall polymer morphology and network structure. Template removal leads to a heteropolymer matrix able to specifically recognize template molecules. In the light of this, molecular imprinting can be seen as a technique allowing the stabilization of a particular arrangement of chemical groups (triangle and circle ending chains in Figure 15.17) by means of a polymer network. Obviously, the properties of molecular imprinted network (MIP) depend on monomer chemistry (anionic, cationic, neutral, and amphiphilic), on the association interactions between monomers and pendant group, on solvent and on the amount of comonomers present in the mixture from which the structure is formed. In addition, MIP recognizing behavior results from the synergism between shape-specific cavities matching the template molecule and chemical groups orientated to get multiple complexation points (binding sites) with the template molecule. Finally, MIP are characterized by a bimodal distribution of binding sites, meaning that a small number of high-affinity sites correspond a large number of low-affinity sites. In particular, non-covalent MIP will be characterized by a heterogeneous population of binding sites with changing affinity and selectivity [237]. One major problem of MIP depends on the possibility that phenomena such as polymer swelling and macromolecular chains relaxation induce a distortion of the shape-specific cavities leading to an incorrect three-dimensional orientation of complexation points facing in the cavities. This, in turn, reflects in reduced MIP selectivity and specificity. This problem, particularly important for structures undergoing considerable swelling such as gels, can be matched by increasing cross-linking agent in order to get a reduction of the average molecular weight between cross-links this reflecting into a more rigid structure. In particular, Peppas and coworkers [232] suggest to realize a network structure characterized by an inhomogeneous spatial distribution of cross-links so that higher cross-linked regions are embedded in lower cross-linked continuum matrix. Only higher cross-linked zones contain

an effective imprinting structure and a proper rigidity to produce adequate specificity (areas or patches of recognition). In addition, the structure of these two regions allows a better template diffusion, reflecting into higher rebinding percentage with respect to more traditional, one-phase (fully cross-linked) gels. On the other hand, of course, this approach suffers a reduced number of recognizing sites per gel unit mass of volume. An alternative to this strategy is represented by a post cross-linking reaction after gel and imprint formation. Excess functional monomers on opposite macromolecular chains or monomers subsequently added allow the post cross-linking process. In low cross-linked gels, the idea of increasing the molecular mass (linear size) of functional monomers should reduce the loss of active binding sites due to network size fluctuations induced, for instance, by swelling. Indeed, short functional monomers cannot conserve their correct spatial disposition upon mesh enlarging. Irrespective of the low or high cross-linking degree, depending on the template size, there is an optimal value for the network cross-link density.

For biological applications, non-covalent interactions with template molecules are preferred to get an easy binding/nonbinding process. Indeed, in this field, the need for strong template removal conditions would make molecular imprinting useless. Nevertheless, due to the weak nature of non-covalent bond, stable binding and recognition require an increased number of interactions with respect to the case of covalent bond (typically, a covalent bond is 1–3 order of magnitude stronger than a non-covalent one) [237]. The quality of the receptor mechanism of imprinted polymers can be evaluated by means of different parameters. Binding affinity, a measure of how well the template molecule is attracted to the binding site, selectivity, the ability to differentiate between the template and other molecules, and the binding capacity, the maximum amount of template bound per mass or volume of polymer, represent the most important. Less important parameters are binding or imprinting ratios representing the ratio of recognitive network template bound compared to control network. Binding affinity can be quantified by means of the receptor–template dissociation constant  $K_d$ , that can be defined starting from the typical macromolecular–template complex  $[MT]$  reaction [237]:



where

$[M]$  is the macromolecular binding sites concentration

$[T]$  is the template concentration

$k_f$  and  $k_r$  represent the forward and reverse rate constants, respectively

The equilibrium binding constant or association constant,  $K_a$ , and the equilibrium dissociation constant,  $K_d$ , are expressed by

$$K_a = \frac{k_f}{k_r} = \frac{1}{K_d} = \frac{[MT]}{[M][T]} \quad (15.86)$$

Equation 15.86 simply descends from the equilibrium condition requiring that the forward reaction rate ( $R_f$ )

$$R_f = k_f[M][T] \quad (15.87)$$

equates the reverse one,  $R_r$ :

$$R_r = k_r[MT] \quad (15.88)$$

While low  $K_d$ , or high  $K_a$ , indicate a strong interaction between macromolecular binding sites and template molecules, high  $K_d$ , or low  $K_a$ , indicate the opposite situation. The ratio between the association ( $K_a$ ) (or dissociation,  $K_d$ ) constants characterizing templates differing in chemical functionality, orientation of chemical functionality, or physical size, defines the selectivity ( $\alpha$ ) of an imprinted network. Typically, for non-covalent imprinted polymers,  $\alpha$  ranges between 1.1 and 8 [234], and imprinted polymers with high association constants usually display high  $\alpha$  values.

On the basis of the above considerations, the applications of imprinted polymers in the pharmaceutical field are straightforward. Indeed, they can be profitably used both in responsive delivery systems and as biosensors. For example, HEMA-based polymers were imprinted to recognize hydrocortisone as template molecule [238]. Once the template was removed, the imprinted network was loaded with testosterone, a molecule structurally similar to hydrocortisone. The release of testosterone performed in the presence or absence of hydrocortisone in solution was different showing a higher release rate when hydrocortisone was present. Indeed, the high-imprinted network binding affinity for hydrocortisone promoted testosterone detachment from binding sites and this reflected into an increased testosterone release rate. In addition, methacrylic acid (MAA) was used as functional monomer for the controlled release of propranolol ( $\beta$ -blocker), tetracycline, and sulfasalazine (prodrug) [237]. Interestingly, MAA also proved to be effective in the enantioselective-controlled release, minimizing the

transport of a diastomer, the undesirable isomer, while allowing the transport of a eutomer, the isomer of interest [239]. Imprinted polymers have also shown to be profitably employed as biosensors in the detection of nandrolone [240], okadaic acid [241], caffeine [242] and paracetamol [243]. Another interesting application of imprinted polymers is about the optical sensors platform. Indeed, a recent nanoscale-fabricated optical sensor is based on the variation of quantum dots photoluminescence due to template binding on an imprinted polymer membrane coating quantum dots [244].

### 15.7.2 MEMBRANES IN MICRO/NANOTECHNOLOGIES

It is well established that future delivery systems will be completely automated to provide a closed loop therapy [198,229,237,245]. This means that they will (i) monitor the physiological conditions inside the patient body and convert it to electronic signals by means of physical and chemical transducers; (ii) receive the electronic signals, analyze them, and make proper control regulations by means of microcontrollers; (iii) release the appropriate amount of drugs by means of micro-actuators. For this reason, they can be defined as lab-on-a-chip [226,237]. To achieve this target, different components (microactuators, micropumps, microvalves, flow regulators, microsensors, and control electronics) have to be integrated, characterized and assembled on a very small surface. A possible assembling example should not differ too much from an array of microreservoirs etched into a silicon matrix [227,246]. Each reservoir, covered with an individual gold membrane, can be filled with solid or liquid drug. Drug release occurs by gold membrane electrochemically dissolution. ChipRx Company, in Ohio, is developing an integrated, self-regulating responsive therapeutic device of cylindrical shape devoted to release various drugs, e.g., insulin [247]. An external biocompatible permeable membrane surrounds an artificial muscle membrane inside which batteries, control circuit, biosensor, and drug reservoir are housed. When the sensor reveals a variation of the physiological levels of metabolites (i.e., glucose), a signal is sent from the sensor to the batteries, which emit an electrical charge causing the opening of a responsive material that allows the release of the desired therapeutic agent (e.g., insulin) from a reservoir. Once metabolites levels return to normal, the sensor stops the release of electrical charge from the battery, closing the reservoir and preventing the release of more drug. Interestingly, Langer and coworkers proposed a resorbable polymeric microchip device for multipulse drug delivery [248].

Due to a wide variety of possible applications, it is now not easy to predict the exact effect of micro- and nanotechnologies on membranes. However, it is reasonable to suppose that these technologies, for example, will allow producing membranes characterized by an extremely controlled porosity regardless the constituting material. Indeed, it will be possible to drill the membrane getting cylindrical holes characterized by very small diameters and with the desired diameter distribution (mono-dispersed, for example) and spatial collocation. In addition, very thin membranes with very small tolerance on thickness could be produced and this will allow the stratification of many thin layers each one characterized by different properties. Accordingly, the resulting wafer could be very versatile its characteristics resulting from the combination of each layer properties. In turn, this could confer very peculiar behavior for what concerns, for example, mass transport, mechanical, and electrical properties.

## 15.8 CONCLUSIONS

The aim of the chapter is to illustrate and discuss membrane applications in the delivery field devoting particular care to the mechanisms ruling mass transport, make clear that membranes often play a key role as they are very versatile. Indeed, while they can be used to modulate drug mass flux to guarantee the desired release kinetics, they can also act as barriers separating an external environment from an internal environment as explained. Obviously, due to the great variety of applications, it was not possible to consider all of them, but I believe that the most significant have been shown. In addition, some of them, for the sake of brevity, could not be discussed. In particular, I am referring to the wide field of living cells encapsulation techniques used in tissue engineering [12,249]. In this case, interestingly, membranes are called to contemporaneously act as barrier and mass transport modulators. Indeed, they must protect living cells hosted in the microcapsule from the immune response of the hosting body where they are implanted to perform their action (e.g., insulin release in diabetic patients). Accordingly, membrane must be impermeable to immunoglobulins, big molecules devoted to the destruction of foreign bodies. Contemporarily, however, they must allow nutrients ( $\text{Na}^+$ ,  $\text{K}^+$ , oxygen, and glucose) permeation to feed encapsulated cells. Clearly, this is just a further example of the complexity of membrane actions and it underlines that a proper membrane designing is needed. A possible tool to match this goal is represented by mathematical modeling and this is the reason why the initial part of this chapter is devoted to describe release mechanisms, fundamental bases for getting a reliable mathematical model.

## REFERENCES

1. Flynn GL, Yalkowsky SH, and Roseman TJ. Mass transport phenomena and models: theoretical concepts. *J. Pharm. Sci.* 1975;63(4):479–510.
2. Naasani I, Sugawara M, Kobayashi M, Iseki K, and Miyazaki K. Transport mechanism of ceftibuten, a dianionic cepherm, in rat renal brush-border Membrane. *Pharm. Res.* 1995;12:605–608.

3. Rubino A, Field M, and Shwachman H. Intestinal transport of amino acid residues of dipeptides. *J. Biol. Chem.* 1971;246:3542–3555.
4. Grassi M and Grassi G. Mathematical modelling and controlled drug delivery: Matrix systems. *Curr. Drug Deliv.* 2005;2(1):97–116.
5. Lapasin R and Pricl S. *Rheology of Industrial Polysaccharides, Theory and Applications*, London: Chapman & Hall, 1995.
6. Barry BW and Meyer MC. The rheological properties of carbopol gels I. Continuous shear and creep properties of carbopol gels. *Int. J. Pharm.* 1979;2:1–25.
7. Ketz RJ, Prud'homme RK, and Graessley WW. Rheology of concentrated microgel solutions. *Rheol. Acta* 1988;27:531–539.
8. Husseini GA, Christensen DA, Rapoport NY, and Pitt GW. Ultrasonic release of doxorubicin from Pluronic P105 micelles stabilized with an interpenetrating network of *N,N*-diethylacrylamide. *J. Control. Rel.* 2002;83:303–305.
9. Kurisawa M and Yui N. Dual-stimuli-responsive drug release from interpenetrating polymer network-structured hydrogels of gelatin and dextran. *J. Control. Rel.* 1998;54:191–200.
10. Robinson JR and Lee VHL, eds. *Controlled Drug Delivery*. New York: Marcel Dekker, 1987.
11. Desai TA, Chu WH, Tu JK, Beattie GM, Hayek A, and Ferrari M. Microfabricated immunisolating biocapsules. *Biotechnol. Bioeng.* 1998;57:118–120.
12. Leoni L and Desai TA. Micromachined biocapsules for cell-based sensing and delivery. *Adv. Drug Deliv. Rev.* 2004;56:211–229.
13. Järvinen K, Åkerman S, Svarfvar B, Tarvainen T, Viinikka P, and Paronen P. Drug release from pH and ionic strength responsive poly(acrylic acid) grafted poly(vinylidene fluoride) membrane bags in vitro. *Pharm. Res.* 1998;15(5):802–805.
14. Iyer M, Mishra R, Han Y, and Hopfinger AJ. Prediction blood-brain barrier partitioning of organic molecules using membrane-interaction QSAR analysis. *Pharm. Res.* 2002;19(11):1611–1621.
15. Geinoz S, Rey S, Boss G, Bunge AL, Guy RH, Carrupt PA, Reist M, and Testa B. Quantitative structure-permeation relationship for solute transport across silicone membranes. *Pharm. Res.* 2002;19(11):1622–1629.
16. Taillardt-Bertschinger A, Martinet CAM, Carrupt PA, Reist M, Caron G, Fruttero R, and Testa B. Molecular factors influencing retention on immobilised artificial membranes (IAM) compared to partitioning in liposomes and *n*-octanol. *Pharm. Res.* 2002;19(6):729–737.
17. Loidl-Stahlhofen A, Hartmann T, Schöttner M, Röhring C, Brodowsky H, Schmidt J, and Keldenich J. Multilamellar liposomes and solid-supported lipid membranes (TRANSIL): Screening of lipid–water partitioning toward a high-throughput scale. *Pharm. Res.* 2001;18(12):1782–1788.
18. Cross SE, John Pugh WJ, Hadgraft J, and Roberts MS. Probing the effect of vehicles on topical delivery: Understanding the basic relationship between solvent and solute penetration using silicone membranes. *Pharm. Res.* 2001;18(7):999–1005.
19. Sun YM, Hsu SC, and Lai JY. Transport properties of ionic drugs in the ammonio methacrylate copolymer membranes. *Pharm. Res.* 2001;18(3):304–310.
20. Kulkarni AS and Hopfinger AJ. Membrane-interaction QSAR analysis: Application to the estimation of eye irritation by organic compounds. *Pharm. Res.* 1999;16(8):1245–1253.
21. Schwarf FP, Imanidis G, Smith EW, Haigh JM, and Surber C. Effect of concentration and degree of saturation of topical fluocinonide formulations on in vitro membrane transport and in vivo availability on human skin. *Pharm. Res.* 1999;16(6):909–915.
22. Jiang R, Benson HAE, Cross SE, and Roberts MS. In vitro human epidermal and polyethylene membrane penetration and retention of the sunscreen benzophenone-3 from a range of solvents. *Pharm. Res.* 1998;15(12):1863–1868.
23. Reichel A and Begley DJ. Potential of immobilized artificial membranes for predicting drug penetration across the blood-brain barrier. *Pharm. Res.* 1998;15(8):1270–1274.
24. Kost J and Langer R. Responsive polymeric delivery systems. *Adv. Drug Deliv. Rev.* 2001;46:125–148.
25. Miyazaki S, Yokouchi C, and Takada M. External control of drug release: Controlled release of insulin from a hydrophilic polymer implant by ultrasound irradiation in diabetic rats. *J. Pharm. Pharmacol.* 1988;40:716–717.
26. Okahata Y, Lim HJ, Nakamura G, and Hachiya S. A large nylon capsule coated with a synthetic bilayer membrane. Permeability control of NaCl by phase transition of the dialkylammonium bilayer coating. *J. Am. Chem. Soc.* 1983;105:4855.
27. Okahata Y, Noguchi H, and Seki T. Thermoselective permeation from a polymer-grafted capsules membrane. *Macromolecules* 1986;19:493–494.
28. Bae YH, Okano T, and Kim SW. Insulin permeation through sensitive hydrogels. *J. Control. Rel.* 1989;9:271–279.
29. Grodzinsky AJ and Grimshaw PE. Electrically and chemically controlled hydrogels for drug delivery. In: Kost I., ed. *Pulsed and Self-Regulated Drug Delivery*. Boca Raton, FL: CRC Press, 1990, pp. 47–64.
30. Grimshaw PE, Grodzinsky AJ, Yarmush ML, and Yarmush DM. Dynamic membranes for protein transport: Chemical and electrical control. *Chem. Eng. Sci.* 1989;44(4):827–840.
31. Pasechnik VA, Cherkosov AN, Zhemko VP, Chechina VV, and Alimardinov RS. Effect of direct current on the permeability of ultrafiltration membranes. *Kolloid. Zh.* 1979;41(3):586–590.
32. Burgmeyer P and Murray RW. An ion gate membrane: Electrochemical control of ion permeability through a membrane with an embedded electrode. *J. Am. Chem. Soc.* 1982;104:6139–6140.
33. Eisenberg SR and Grodzinsky AJ. The kinetics of chemically induced nonequilibrium swelling of articular cartilage and corneal stroma. *J. Biomech. Eng.* 1987;109:79–89.
34. Nussbaum JH and Grodzinsky AJ. Proton diffusion-reaction in a protein polyelectrolyte membrane and the kinetics of electromechanical forces. *J. Membr. Sci.* 1981;8:193–219.
35. Mathiowitz E, Razieli A, Cohen MD, and Fisher E. Photochemically rupture of capsules. I. A model system. *J. Appl. Polym. Sci.* 1981;26:809–822.
36. Mathiowitz E and Cohen MD. Polyamide microcapsules for controlled release. I. Characterization of the membranes. *J. Membr. Sci.* 1989;40:1–26.

37. Mathiowitz E and Cohen MD. Polyamide microcapsules for controlled release. II. Release characteristics of the microcapsules. *J. Membr. Sci.* 1989;40:27–41.
38. Mathiowitz E and Cohen MD. Polyamide microcapsules for controlled release. III. Spontaneous release of azobenzene. *J. Membr. Sci.* 1989;40:43–54.
39. Mathiowitz E and Cohen MD. Polyamide microcapsules for controlled release. 4. Effect of swelling. *J. Membr. Sci.* 1989;40:55–65.
40. Mathiowitz E and Cohen MD. Polyamide microcapsules for controlled release. 5. Photochemical release. *J. Membr. Sci.* 1989;40:67–86.
41. Kost J, ed. *Pulsed and Self-Regulated Drug Delivery*. Boca Raton, FL: CRC Press, 1990.
42. Albin G, Horbett TA, and Ratner BD. Glucose-sensitive membranes for controlled release of insulin. In: Kost J., ed. *Pulsed and Self-Regulated Drug Delivery*. Boca Raton, FL: CRC Press, 1990, pp. 159–185.
43. Albin G, Horbett TA, Miller SR, and Ricker NL. Theoretical and experimental studies of glucose sensitive membranes. *J. Control. Rel.* 1987;6:267–291.
44. Ishihara K. Glucose-responsive polymers for controlled insulin release. *Proc. Int. Symp. Control. Release Bioact. Mater.* 1988;15:168–169.
45. Iwata H and Matsuda T. Preparation and properties of novel environment-sensitive membranes prepared by graft polymerization onto a porous membrane. *J. Membr. Sci.* 1988;38:185–199.
46. Siegel RA. pH-sensitive gels: Swelling equilibria, kinetics and applications for drug delivery. In: Kost J., ed. *Pulsed and Self-Regulated Drug Delivery*. Boca Raton, FL: CRC Press, 1990, pp. 129–157.
47. Ishihara K, Muramoto N, Fuji H, and Shinohara I. pH induced reversible permeability control of the 4-carboxy acrylanilide-methyl methacrylate copolymer membrane. *J. Polym. Sci., Polym. Chem. Ed.* 1985;23:2841–2850.
48. Ishihara K, Muramoto N, and Shinohara I. Controlled release of organic substances using polymer membrane with responsive functions for amino compounds. *J. Appl. Polym.* 1984;29:211–217.
49. Kuu WY, Wood RW, and Roseman TJ. Factors influencing the kinetics of solute release. In: Kydonieus A, ed. *Treatise on Controlled Drug Delivery*. New York: Marcel Dekker, 1992, pp. 37–154.
50. Grassi M, Lapasin R, and Pricl S. Modeling of drug release from a swellable matrix. *Chem. Eng. Comm.* 1998;169:79–109.
51. Lee PI. Kinetics of drug release from hydrogel matrices. *J. Control. Rel.* 1985;2:277–285.
52. Vrentas JS, Jarzebski CM, and Duda JL. A Deborah number for diffusion in polymer-solvent systems. *AIChE J.* 1975;21(5):894–901.
53. Vrentas JS and Duda JL. Molecular diffusion in polymer solutions. *AIChE J.* 1979;25(1):1–24.
54. Crank J. *The Mathematics of Diffusion*, 2nd edition. Oxford: Clarendon Press, 1975.
55. Edwards DA. Non-Fickian diffusion in thin polymer films. *J. Polym. Sci., B Polym. Phys.* 1996;34:981–997.
56. Grassi M. Diffusione di principi attivi in matrici gel polimeriche di impiego farmaceutico. PhD Thesis, University of Trieste, Department of Chemical Engineering (DICAMP), 1996, VIII ciclo.
57. Miller-Chou BA, Jack L, and Koenig JL. A review of polymer dissolution. *Prog. Polym. Sci.* 2003;28:1223–1270.
58. Siepmann J and Göpferich A. Mathematical modeling of bioerodible, polymeric drug delivery systems. *Adv. Drug Del. Rev.* 2001;48:229–247.
59. Mallapragada SK and Peppas NA. Crystal unfolding and chain disentanglement during semicrystalline polymer dissolution. *AIChE J.* 1997;43:870–876.
60. Adrover A, Giona M, and Grassi M. Analysis of controlled release in disordered structures: A percolation model. *J. Membr. Sci.* 1996;113:21–30.
61. Bunde A and Havlin S. *Fractals and Disordered Systems*. Berlin: Springer-Verlag, 1992.
62. Stauffer D and Aharony A. *Introduction to Percolation Theory*. London: Taylor & Francis, 1992.
63. Giona M. Statistical analysis of anomalous transport phenomena in complex media. *AIChE J.* 1991;37:1249–1254.
64. Vožeh S, Schmidlin O, and Taeschner W. Pharmacokinetic drug data. *Clin. Pharmacokinet.* 1988;254–282.
65. Singh MP, Lumpkin JA, and Rosenblatt J. Effect of electrostatic interactions on polylysine release rates from collagen matrices and comparison with model predictions. *J. Control. Rel.* 1995;35:165–179.
66. Singh MP, Stefko J, Lumpkin JA, and Rosenblatt J. The effect of electrostatic charge interactions on release rates of gentamicin from collagen matrices. *Pharm. Res.* 1995;12(8):1205–1210.
67. Bird RB, Stewart WE, and Lightfoot EN. *Transport Phenomena*. Toronto: John Wiley & Sons, 1960.
68. Joshi S and Astarita G. Diffusion-relaxation coupling in polymers which show two-stage sorption phenomena. *Polymer* 1979;20:455–458.
69. Cohen DS. Theoretical models for diffusion in glassy polymers. *J. Polym. Sci. B Polym. Phys.* 1983;21:2057–2065.
70. Cohen DS. Sharp fronts due to diffusion and stress at the glass transition in polymers. *J. Polym. Sci. B Polym. Phys.* 1989;27:1731–1747.
71. Cox RW and Cohen DS. A mathematical model for stress-driven diffusion in polymers. *J. Polym. Sci. B Polym. Phys.* 1989;27:589–602.
72. Hayes CK and Cohen DS. The evolution of steep fronts in non-Fickian polymer-penetrant systems. *J. Polym. Sci. B Polym. Phys.* 1992;30:145–161.
73. Edwards DA and Cohen DS. A mathematical model for a dissolving polymer. *AIChE J.* 1995;41(11):2345–2355.
74. Frisch HL, Wang TT, and Kwei TK. Diffusion in glassy polymers II. *J. Polym. Sci.* 1969;A2(7):879–887.
75. Peppas NA and Sinclair JL. Anomalous transport of penetrants in glassy polymers. *Coll. Polym. Sci.* 1983;261:404–409.
76. Hariharan D and Peppas NA. Modelling of water transport and solute release in physiologically sensitive gels. *J. Control. Rel.* 1993;23:123–135.
77. Adib F and Neogi P. Sorption with oscillations in solid polymers. *AIChE J.* 1987;33:164–166.

78. Camera-Roda G and Sarti GC. Non-Fickian mass transport through polymers: A viscoelastic theory. *Transp. Theory Statist. Phys.* 1986;15:1023–1031.
79. Lustig SR, Caruthers JM, and Peppas NA. Continuum thermodynamics and transport theory for polymer–fluid mixtures. *Chem. Eng. Sci.* 1992;47(12):3037–3057.
80. Camera-Roda G and Sarti GC. Mass transport with relaxation in polymers. *AIChE J.* 1990;36(6):851–860.
81. Tassios DP. *Applied Chemical Engineering Thermodynamics*. Berlin/New York: Springer-Verlag, 1993.
82. Amsden B. Solute diffusion within hydrogels. Mechanisms and models. *Macromolecules* 1998;31:8382–8395.
83. Vrentas JS, Duda JL, Ju ST, and Liu HT. Prediction of diffusion coefficients for polymer–solvent systems. *AIChE J.* 1982;28(2):279–285.
84. Peppas NA and Reinhart CT. Solute diffusion in swollen membranes. Part I: A new theory. *J. Membr. Sci.* 1983;15:275–287.
85. Cukier RI. Diffusion of Brownian spheres in semidilute polymer solutions. *Macromolecules* 1984;17:252–255.
86. Muhr AH and Blanshard JMV. Diffusion in gels. *Polymer* 1982;23:1012–1026.
87. Ogston AG, Preston BN, and Wells JD. On the transport of compact particles through solutions of chain-polymers. *Proc. R. Soc. London A* 1973;333:297–316.
88. Peppas N. Mathematical models for controlled release kinetics. In: Langer RS and Wise DL, eds. *Medical Application of Controlled Release*, Vol. I. Boca Raton, FL: CRC Press, 1984, p. 169.
89. Narasimhan B. Accurate models in controlled drug delivery systems. In: Wise DL, ed. *Handbook of Pharmaceutical Controlled Release Technology*. New York, Basel: Marcel Dekker, 2000, pp. 155–209.
90. Grassi G, Farra R, Caliceti P, Carezza M, and Grassi M. Temperature-sensitive hydrogels: Potential therapeutic applications. *Am. J. Drug Delivery* 2005;3(4):239–251.
91. Grassi M, Yuk SH, and Cho SH. Modelling of solute transport across a temperature-sensitive polymer membrane. *J. Membr. Sci.* 1999;152:241–249.
92. Patankar SV. *Numerical Heat Transfer and Fluid Flow*. New York: Hemisphere Publishing, 1990.
93. Stevenson CL, Theeuwes F, and Wright JC. Osmotic implantable delivery systems. In: Wise DL, ed. *Handbook of Pharmaceutical Controlled Release Technology*. New York, Basel: Marcel Dekker, 2000, pp. 225–253.
94. Theeuwes F. Elementary osmotic pump. *J. Pharm. Sci.* 1975;64:1987–1991.
95. Banga AK. Electrically assisted transdermal delivery of drugs. In: Wise DL, ed. *Handbook of Pharmaceutical Controlled Release Technology*. New York, Basel: Marcel Dekker, 2000, pp. 567–581.
96. Pikal MJ and Shah S. Transport mechanisms in iontophoresis. II. Electroosmotic flow and transference number measurements for hairless mouse skin. *Pharm. Res.* 1990;7:213–221.
97. Grassi M and Colombo I. Mathematical modelling of drug permeation through a swollen membrane. *J. Control. Rel.* 1999;59:343–359.
98. Westrin BA, Axelsson A, and Zacchi G. Diffusion measurement in gels. *J. Control. Rel.* 1994;30:189–199.
99. Johansson L and Löfroth JE. Diffusion and interactions in gels and solution. I. Method. *J. Colloid Interface Sci.* 1991;142:116–120.
100. Inoue SK, Guenther RB, and Hoag SW. Algorithm to determine diffusion and mass transfer coefficients. Proceedings of the Conference on Advances in Controlled Delivery, Baltimore (USA), August 19–20, 1996, pp. 145–146.
101. Colombo I, Grassi M, Lapasin R, and Priel S. Determination of the drug diffusion coefficient in swollen hydrogel polymeric matrices by means of the inverse sectioning method. *J. Control. Rel.* 1997;47:305–314.
102. Harland RS and Peppas NA. On the accurate experimental determination of drug diffusion coefficients in polymers. *S.T.P. Pharm. Sci.* 1993;3(5):357–361.
103. Tojo K, Sun Y, Ghannam MM, and Chien YW. Characterization of a membrane permeation system for controlled delivery studies. *AIChE J.* 1985;31(5):741–746.
104. Maiatami Y, Sato H, and Nagai T. New method of calculating the diffusion coefficient of drugs from permeability through a membrane using diclofenac and its sodium salt in ethanol aqueous solution. Proceedings of the International Symposium on Controlling Release of Bioactive Materials, Nice, France, June 27–30, 1994;21:1234–1235.
105. Imanidis G, Helbing-Strausak S, Imboden R, and Leuengberger H. Vehicle-dependent in situ modification of membrane-controlled drug release. *J. Control. Rel.* 1998;51:23–34.
106. Nixon JR and Wong KT. Evaluation of drug permeation through polymeric membrane as a model for release (II) ethylcellulose-walled microcapsules. *Int. J. Pharm.* 1990;58:31–40.
107. Singh M, Lumpkin JA, and Rosenblatt J. Mathematical modeling of drug release from hydrogel matrices via a diffusion coupled with desorption mechanism. *J. Control. Rel.* 1994;32:17–25.
108. Adrover A, Giona M, and Grassi M. Controlled release of theophylline from water-swollen scleroglucan matrices. *J. Membr. Sci.* 1996;113:7–20.
109. Peppas N. Mathematical models for controlled release kinetics. In: Langer RS and Wise DL, eds. *Medical Application of Controlled Release*. Boca Raton, FL: CRC Press, Vol. II, 1984.
110. Barrie JA, Levine JD, Michaels AS, and Wong P. Diffusion and solution of gases in composite rubber membranes. *Trans. Faraday Soc.* 1962;59:869–878.
111. Coviello T, Alhaique F, Parisi C, Matricardi P, Bocchinfuso G, and Grassi M. A new polysaccharidic gel matrix for drug delivery: Preparation and mechanical properties. *J. Control. Rel.* 2005;102:643–656.
112. Nogami H, Nagai T, Fukoka E, and Yotsuyanagi T. Dissolution kinetics of barbital polymorphs. *Chem. Pharm. Bull.* 1969;17(1):23–31.
113. Levich VG. *Physicochemical Hydrodynamics*. Englewood Cliffs, NJ: Prentice-Hall, 1962, pp. 39–73.
114. Banakar UV. *Pharmaceutical Dissolution Testing*. New York, Basel, Hong Kong: Marcel Dekker, 1992, pp. 27–36.

115. Banakar UV. *Pharmaceutical Dissolution Testing*. New York, Basel, Hong Kong: Marcel Dekker, 1992, p. 10.
116. Grassi M, Colombo I, and Lapasin R. Experimental determination of the theophylline diffusion coefficient in swollen sodium-alginate membranes. *J. Control. Rel.* 2001;76(1–2):93–105.
117. Skiåk-Bræk G, Grasdalen H, and Smidsrød O. Inhomogeneous polysaccharide ionic gels. *Carbohydr. Polym.* 1989;10:31–54.
118. Coviello T, Coluzzi G, Palleschi A, Grassi M, Santucci E, and Alhaique F. Structural and rheological characterization of scleroglucan/borax hydrogel for drug delivery. *Int. J. Biol. Macromolecules* 2003;32:83–92.
119. Sastry SV, Nyshadham JR, and Fix JA. Recent technological advances in oral drug delivery—a review. *PSTT.* 2000;3(4):138–145.
120. Chaturvedi PR, Decker CJ, and Odinecs A. Prediction of pharmacokinetic properties using experimental approaches during early drug discovery. *Curr. Op. Chem. Biol.* 2001;5:452–463.
121. Pharmacos 4. Medicinal Products for Human Use: Guide-lines; directive 65/65/EEC, 75/318/EEC, 1991. Eudralex Collection; Vol. 3C, p 234 (<http://pharmacos.eudra.org/F2/eudralex/vol-3/home.htm>).
122. van de Waterbeemd H. Intestinal permeability: Prediction from theory. In: Dressman JB and Lennernas, eds. *Oral Drug Absorption: Prediction and Assessment*. New York: Marcel Dekker, 2000, pp. 31–49.
123. Gan LSL and Thakker DR. Applications of the Caco-2 model in the design and development of orally active drugs: Elucidation of biochemical and physical barriers posed by the intestinal epithelium. *Adv. Drug Deliv. Rev.* 1997;23:77–98.
124. Gibaldi M and Perrier D. *Pharmacokinetics*, 2nd edition. New York: Marcel Dekker, 1982.
125. Panoz DE and Geoghegan EJ. Controlled absorption pharmaceutical composition. US Patent 4,863,742, 1989.
126. Qiu Y and Zhang G. Research and development aspects of oral controlled-release dosage forms. In: Wise DL, ed. *Handbook of Pharmaceutical Controlled Release Technology*. New York, Basel: Marcel Dekker, 2000, pp. 465–504.
127. Harada J, Chen RT, and Stannet VT. Polyelectrolyte gels. In: Polyelectrolyte Gels Properties, Preparation and Applications. Harland RS and Prundhomme RK, eds. Washington DC: ACS Symposium Series 480,480, ACS, 1992, ch. 5.
128. Li SK and D’Emanuele A. On-off transport through a thermoresponsive hydrogel composite membrane. *J. Control. Rel.* 2001;75:55–67.
129. Lecomte F, Siepmann J, Walther M, MacRae RJ, and Bodmeier R. Polymers blends used for coating of multiparticulates: Comparison of aqueous and organic coating techniques. *Pharm. Res.* 2004;21(5):882–890.
130. Siepmann F, Siepmann J, Walther M, MacRae RJ, and Bodmeier R. Blends of aqueous polymer dispersions used for pellet coating: Importance of particle size. *J. Control. Rel.* 2005;105:226–239.
131. Zhao CL, Wang Y, Hruska Z, and Winnink MA. Molecular aspects of latex film formation: An energy-transfer study. *Macromolecules* 1990;23:4082–4087.
132. Sun HCS. Method of making pharmaceutical using electrostatic chuck. US Patent 5,846,595, 1998.
133. Sun HCS. Electrostatic chuck and particle deposition apparatus there for. US Patent 5,858,09, 1999.
134. Chrai SS. Electrostatic dry deposition technology. *Pharm. Tech.* 1998;4:106–112.
135. Kas, HS and Öner L. Microencapsulation using coacervation/phase separation. In: Wise DL, ed. *Handbook of Pharmaceutical Controlled Release Technology*. New York, Basel: Marcel Dekker, 2000, pp. 301–328.
136. Laghoueg N, Paulet J, Taverdet JL, and Vergnaud JM. Oral polymer-drug devices with a core and an erodible shell for constant drug delivery. *Int. J. Pharm.* 1998;50:133–139.
137. Gazzaniga A, Sangalli ME, Conte U, Caramella C, Colombo P, and La Manna A. On the release mechanism from coated swellable minimatrices. *Int. J. Pharm.* 1993;91:167–171.
138. Lavasanifar A, Ghalandari R, Ataei Z, Zolfaghari ME, and Mortazavi SA. 1997, Microencapsulation of theophylline using ethylcellulose: In vitro drug release and kinetic modelling. *J. Microencapsulation* 1997;14:91–100.
139. Liu H, Magron P, Bouzon J, and Vergnaud JM. Spherical dosage form with a core and shell. Experiments and modelling. *Int. J. Pharm.* 1998;45:217–227.
140. Lorenzo-Lamosa ML, Remuñán-López C, Vila-Jato JL, and Alonso MJ. Design of microencapsulated chitosan microspheres for colonic drug delivery. *J. Control. Rel.* 1998;52:109–118.
141. Borgquist P, Zackrisson G, and Axelsson A. 2001, Simulation and parametric study of single pellet release. *Proc. Inter. Symp. Control. Release Bioact. Mater.* 2001;28:736–737.
142. Cuña M, Gómez G, Rodríguez M, and Torres D. Microencapsulated lipid cores for peptide colonic delivery. *Proc. Inter. Symp. Control. Release Bioact. Mater.* 2000;27:500–501.
143. Ransone CM, Eyman IV, Litzinger D, Colloton M, and Shah SS. 1999, A novel microencapsulation process for sustained delivery of proteins. *Proc. Inter. Symp. Control. Release Bioact. Mater.* 1999;26:603–604.
144. Lee SJ and Rosenberg M. Preparation and properties of glutaraldehyde cross-linked whey protein-based microcapsules containing theophylline. *J. Control. Rel.* 1999;61:123–136.
145. Atilla A and Kas, HS. Microencapsulation technology: Interfacial polymerization method. In: Wise DL, ed. *Handbook of Pharmaceutical Controlled Release Technology*. New York, Basel: Marcel Dekker, 2000, pp. 271–285.
146. Demchuk IA, Nagurskii OA, and Gumnitskii YM. Mass transfer from a solid spherical particle coated with an insoluble polymeric capsule. *Theor. Found. Chem. Eng.* 1997;31:339–342.
147. Lu SM and Chen SR. 1993, Mathematical analysis of drug release from a coated particle. *J. Control. Rel.* 1993;23:105–121.
148. Narasimhan B and Langer R. Zero-order release of micro- and macromolecules from polymeric devices: The role of the burst effect. *J. Control. Rel.* 1997;47:13–20.
149. Sirotti C, Colombo I, and Grassi M. Modeling of drug release from polydispersed microencapsulated spherical particles. *J. Microencapsulation* 2002;19(5):603–614.

150. Manca D and Rovaglio M. Modeling the controlled release of microencapsulated drugs: Theory and experimental validation. *Chem. Eng. Sci.* 2003;58:1337–1351.
151. am Ende MT, Herbig SM, Korsmeyer RW, and Chidlaw MB. Osmotic drug delivery from asymmetric membrane film-coated dosage forms. In: Wise DL, ed. *Handbook of Pharmaceutical Controlled Release Technology*. New York, Basel: Marcel Dekker, 2000, pp. 751–785.
152. Kestig RE. *Phase-Inversion Membranes in Synthetic Polymeric Membranes: A Structural Perspective*. New York: John Wiley & Sons, 1985, pp. 237–286.
153. Cardinal JR, Herbig SM, Korsmeyer RW, Lo J, Smith KL, and Thombre AG. Use of asymmetric membranes in delivery devices. US Patent 5,612,059, 1997.
154. Thombre AG, Cardinal JR, DeNoto AR, and Gibbes DC. Asymmetric membrane capsules for osmotic drug delivery II. In vitro and in vivo drug release performance. *J. Control. Rel.* 1999;57:65–73.
155. Thombre AG, Cardinal JR, DeNoto AR, Herbig SM, and Smith KL. Asymmetric membrane capsules for osmotic drug delivery I—development of a manufacturing process. *J. Control. Rel.* 1999;57:55–64.
156. Yang L, Chu JS, and Fix JA. Colon-specific drug delivery: New approaches and in vitro/in vivo evaluation. *Int. J. Pharm.* 2002;235:1–15.
157. Saffran M, Field JB, Pena J, Jones RH, and Okuda Y. Oral insulin in diabetic dogs. *J. Endocrinol.* 1991;131:267–278.
158. Liu Xing L, Dawei C, Liping X, and Rongqing Z. Oral colon-specific drug delivery for bee venom peptide: Development of a coated calcium alginate gel beads-entrapped liposome. *J. Control. Rel.* 2003;93:293–300.
159. Siew LF, Man SM, Newton JM, and Basit AW. Amylose formulations for drug delivery to the colon: A comparison of two fermentation models to assess colonic targeting performance in vitro. *Int. J. Pharm.* 2004;273:129–134.
160. Macleod GS, Fell JT, Collett JH, Sharma HL, and Smith AM. Selective drug delivery to the colon using pectin:chitosan:hydroxypropyl methylcellulose film coated tablets. *Int. J. Pharm.* 1999;187:251–257.
161. Shibata N, Obno T, Shimokawa T, Hu Z, Yoshikawa Y, Koga K, Murakami M, and Takada K. Application of pressure-controlled colon delivery capsule to oral administration of glycyrrhizin in dogs. *J. Pharm. Pharmacol.* 2001;53:441–447.
162. Potts RO and Guy RH, eds. *Mechanisms of Transdermal Drug Delivery*. New York: Marcel Dekker, 1997.
163. Cross SE and Roberts MS. Physical enhancement of transdermal drug application: Is delivery technology keeping up with pharmaceutical development? *Curr. Drug Deliv.* 2004;1:81–92.
164. Prausnitz MR, Mitragotri S, and Langer R. Current status and future potential of transdermal drug delivery. *Nat. Rev. Drug Discovery* 2004;3:115–124.
165. Langer R. Transdermal drug delivery: Past progress, current status, and future prospects. *Adv. Drug Deliv. Rev.* 2004;56:557–558.
166. Cramer MP and Saks SR. Translating safety, efficacy and compliance into economic value for controlled release dosage forms. *Pharmacoeconomics* 1994;5:482–504.
167. Hadgraft J and Guy RH, eds. *Transdermal Drug Delivery: Developmental Issues and Research Initiatives*. New York: Marcel Dekker, 1989;1–17.
168. Champion RH, Burton JL, Burns DA, and Breathnach SM, eds. *Textbook of Dermatology*. London: Blackwell Science, 1998.
169. Elias PM and Feingold KR. Coordinate regulation of epidermal differentiation and barrier homeostasis. *Skin Pharmacol. Appl. Skin Physiol.* 2001;14(Suppl. 1):28–34.
170. Marrink SJ and Berendsen JC. Permeation process of small molecules across lipid membranes studied by molecular dynamics simulations. *J. Phys. Chem.* 1996;100:16729–16738.
171. Barry BW. Drug delivery routes in skin: A novel approach. *Adv. Drug Deliv. Rev.* 2002;54(1):S31–S40.
172. Cevc G. Drug delivery across the skin. *Exp. Opin. Invest. Drugs* 1997;6:1887–1937.
173. Kalia YN and Guy RH. Modeling transdermal drug release. *Adv. Drug Deliv. Rev.* 2001;48:159–172.
174. Venkatraman S, Davar N, Chester A, and Kleiner L. An overview of controlled release systems. In: Wise DL, ed. *Handbook of Pharmaceutical Controlled Release Technology*. New York, Basel: Marcel Dekker, 2000:431:463.
175. Roberts MS, Lai PM, Cross SE, and Yoshida NH. Solute structure as a determinant of iontophoretic transport. In: *Mechanisms of Transdermal Drug Delivery*. New York: Marcel Dekker, 1997, pp. 291–349.
176. Barry BW. Novel mechanisms and devices to enable successful transdermal drug delivery. *Eur. J. Pharm. Sci.* 2001;14:101–114.
177. Nakamura K, Katagai K, Mori K, Higo N, Sato S, and Yamamoto K. Transdermal administration of salmon calcitonin by pulse depolarization-iontophoresis in rats. *Int. J. Pharm.* 2001;218:93–102.
178. Clifton VL, Crompton R, Smith R, and Wright IM. Microvascular effects of CRH in human skin vary in relation to gender. *J. Clin. Endocrinol. Metab.* 2002;87:267–270.
179. Chiang CH, Shao CH, and Chen JL. Effects of pH, electric current and enzyme inhibitors on iontophoresis of delta sleep-inducing peptide. *Drug Dev. Ind. Pharm.* 1998;24:431–438.
180. Badkar AV and Banga AK. Electrically enhanced transdermal delivery of a macromolecule. *J. Pharm. Pharmacol.* 2002;54:907–912.
181. Singh P, Anliker M, Smith G, Zavortimk D, and Maibach H. Transdermal iontophoresis and solute penetration across excised human skin. *J. Pharm. Sci.* 1995;84:1342–1346.
182. Kumar S, Char H, Patel S, Piemontese D, Malick AW, Iqbal K, Neuroschel E, and Behl CR. In vivo transdermal iontophoretic delivery of growth hormone releasing factor GRF (1–44) in hairless guinea pigs. *J. Control. Rel.* 1992;18:213–220.
183. Kochhar C and Imanidis G. In vitro transdermal iontophoretic delivery of leuprolide—mechanisms under constant voltage application. *J. Pharm. Sci.* 2003;92:84–96.

184. Smyth HD, Becket G, and Metha S. Effect of permeation enhancer pretreatment on the iontophoresis of luteinizing hormone releasing hormone (LHRH) through human epidermal membrane (HEM). *J. Pharm. Sci.* 2002;91:1296–1307.
185. Burnette RR and Mareo D. Comparison between the iontophoretic and passive transport of thyrotropin releasing hormone across excised nude mouse skin. *J. Pharm. Sci.* 1986;75:738–743.
186. Oldenburg K, Vo KT, Smith GA, and Selick HE. Iontophoretic delivery of oligonucleotides across full thickness hairless mouse skin. *J. Pharm. Sci.* 1995;84:915–921.
187. Suzuki Y, Nagase Y, Iga K, Kawase M, Oka M, Yanai S, Matsumoto Y, Nakagawa S, Fukuda T, Adachi H, Higo N, and Ogawa Y. Prevention of bone loss in ovariectomized rats by pulsatile transdermal iontophoretic administration of human PTH(1–34). *J. Pharm. Sci.* 2002;91:350–361.
188. Chien YW, Lelawongs P, Siddiqui O, and Shi W. Facilitated transdermal delivery of therapeutic peptides and proteins by iontophoretic delivery devices. *J. Control. Rel.* 1990;13:263–278.
189. Weaver JC. Electroporation: A general phenomenon for manipulating cells and tissues. *J. Cell Biochem.* 1993;51(4):426–435.
190. Prausnitz MR. A practical assessment of transdermal drug delivery by skin electroporation. *Adv. Drug Deliv. Rev.* 1999;35:61–76.
191. Edwards DA, Prausnitz MR, Langer R, and Weaver JC. Analysis of enhanced transdermal transport by skin electroporation. *J. Control. Rel.* 1995;34:211–221.
192. Prausnitz MR, Lee CS, Liu CH, Pang JC, Singh TP, Langer R, and Weaver JC. Transdermal transport efficiency during skin electroporation and iontophoresis. *J. Control. Rel.* 1996;38:205–217.
193. Vanbever R and Pr eat V. In vivo efficacy and safety of skin electroporation. *Adv. Drug Deliv. Rev.* 1999;35:77–88.
194. Bommannan D, Tamada J, Leung L, and Potts RO. Effect of electroporation on transdermal iontophoretic delivery of luteinizing hormone releasing hormone (LHRH) in vitro. *Pharm. Res.* 1994;11:1809–1814.
195. Sen A, Daly ME, and Hui SW. Transdermal insulin delivery using lipid enhanced electroporation. *Biochim. Biophys. Acta* 2002;1564:5–8.
196. Regnier V, Le Doan T, and Preat V. Parameters controlling topical delivery of oligonucleotides by electroporation. *J. Drug Target.* 1998;5:275–289.
197. Tang H, Wang CCJ, Blankschtein D, and Langer R. An investigation of the role of cavitation in low-frequency ultrasound-mediated transdermal drug transport. *Pharm. Res.* 2002;19:1160–1169.
198. Dziubla TD, Lowman AM, Torjman MC, and Joseph JI. Implantable drug delivery devices. In: Dillow AK and Lowman AM, eds. *Biomimetic Materials and Design*. New York, Basel: Marcel Dekker, 2002, pp. 507–531.
199. Pals on B and Bhatia SN. *Tissue Engineering*. Upper Saddle River, NJ: Pearson Prentice-Hall, 2004:303–395.
200. Galin JI, Golstein IM, and Snyderman R. *Inflammation: Basic Principles and Clinical Correlates*. New York: Raven Press, 1988.
201. Anderson JM. Inflammatory response to implants. *Trans. Am. Soc. Artif. Intern. Organs* 1988;19:101–107.
202. Leoni L. Biomedical engineering. PhD Thesis, University of Illinois, 2003.
203. Brauker JH, Carr-Brendel VE, Martinson LA, Crudele J, and Johnston WD. Neovascularization of synthetic membranes directed by membrane microarchitecture. *J. Biomed. Mater. Res.* 1995;29:1517–1524.
204. Walton RL and Brown RE. Tissue engineering of biomaterials for composite reconstruction: An experimental approach. *Ann. Plast. Surg.* 1993;30:1441–1452.
205. Thonus IP, De Lange-MacDaniel AV, Otte CJ, and Michel MF. Tissue cage infusion: A technique for the achievement of prolonged steady state in experimental animals. *J. Pharm. Meh.* 1979;2:63–69.
206. Stevenson CL, Theeuwes F, and Wright JC. Osmotic implantable delivery systems. In: Wise DL, ed. *Handbook of Pharmaceutical Controlled Release Technology*. New York/Basel: Marcel Dekker, 2000, pp. 225–253.
207. Bhargava B, Karthikeyan G, and Abizaid AS. New approaches to preventing restenosis. *BMJ* 2003;327(7409):274–279.
208. Labinaz M, Pels K, Hoffert C, Aggarwal S, and O'Brien ER. Time course and importance of neoadventitial formation in arterial remodeling following balloon angioplasty of porcine coronary arteries. *Cardiovasc. Res.* 1999;41:255–266.
209. Kearney M, Pieczek A, and Haley L. Histopathology of in-stent restenosis in patients with peripheral artery disease. *Circulation* 1997;95(8):1998–2002.
210. Grassi G, Dawson P, Guarnieri G, Kandolf R, and Grassi M. Therapeutic potential of hammerhead ribozymes in the treatment of hyperproliferative diseases. *Curr. Pharm. Biothec.* 2004;5(4):369–386.
211. Edelman ER and Rogers C. Pathobiologic responses to stenting. *Am. J. Cardiol.* 1998;81(7A):4E–6E.
212. Kearney M, Pieczek A, Haley L, Losordo DW, Andres V, Schainfeld R, Rosenfield K, and Isner JM. Histopathology of in-stent restenosis in patients with peripheral artery disease. *Circulation* 1997;95(8):1998–2002.
213. Bauriedel G, Schluckebier S, Hutter R, Welsch U, Kandolf R, Luderitz B, and Prescott MF. Apoptosis in restenosis versus stable-angina atherosclerosis: Implications for the pathogenesis of restenosis. *Arterioscler. Thromb. Vasc. Biol.* 1998;18(7):1132–1139.
214. Bennett MR. Apoptosis of vascular smooth muscle cells in vascular remodelling and atherosclerotic plaque rupture. *Cardiovasc. Res.* 1999;41(2):361–368.
215. Ross R. The pathogenesis of atherosclerosis: a perspective for the 1990s. *Nature* 1993;362(6423):801–809.
216. Gunn J and Cumberland D. Stent coatings and drug delivery. *Eur. Heart. J.* 1999;20:1693–1700.
217. Yoshioka T, Mirich D, Wright KC, and Fallace S. Self-expanding endovascular graft: An experimental study in dogs. *Am. J. Radiol.* 1988;15:673–676.
218. Roeren T, Garcia OJ, Rees CR, and Tio FO. Intraarterial compatability of a baloon-expandable tubular graft. *Radiology* 1990;174:1069–1079.
219. Windecker S, Roffi M, and Meier B. Sirolimus eluting stent: A new era in interventional cardiology? *Curr. Pharm. Des.* 2003;9:1077–1094.

220. Al Lamee K and Cook D. Polymer coating techniques for drug eluting stent. Medical device technology 2003; <http://www.medicaldevicessonline.com/mdt/article/detail.js?j=52234>.
221. Crevatin A. Studio reologico di gel a base di Pluronic F127 per la progettazione di stent medicati. Graduate thesis, University of Trieste, Department of Chemical Engineering (DICAMP), 2004.
222. Gu JL, Veerapanane D, Rossi J, Natarajan R, Thomas L, and Nadler J. Ribozyme-mediated inhibition of expression of leukocyte-type 12-lipoxygenase in porcine aortic vascular smooth muscle cells. *Circ. Res.* 1995;77(1):14–20.
223. Lovett DH, Johnson RJ, Marti HP, Martin J, Davies M, and Couser WG. Structural characterization of the mesangial cell type IV collagenase and enhanced expression in a model of immune complex-mediated glomerulonephritis. *Am. J. Pathol.* 1992;141(1):85–98.
224. Goepferich A. Erosion of composite polymer matrices. *Biomaterials* 1997;18:397–403.
225. Hunter WL, Burt HM, and Machan L. Local delivery of chemotherapy: A supplement to existing cancer treatments a case for surgical pastes and coated stents. *Adv. Drug Deliv. Rev.* 1997;26:199–207.
226. Razzacki SZ, Thwar PK, Yang M, Ugaz VM, and Burns MA. Integrated microsystems for controlled drug delivery. *Adv. Drug Deliv. Rev.* 2004;56:185–198.
227. Saltzman W and Olbricht W. Building drug delivery into tissue engineering. *Nat. Rev., Drug Discov.* 2002;1:177–186.
228. Santini J, Cima M, and Langer R. A controlled-release micro-chip. *Nature* 1999;397:335–338.
229. Langer R and Peppas NA. Advances in biomaterials, drug delivery, and bionanotechnology. *AIChE J.* 2003;49(12):2990–3006.
230. Zachary Hilt JZ. Nanotechnology and biomimetic methods in therapeutics: Molecular scale control with some help from nature. *Adv. Drug Deliv. Rev.* 2004;56:1533–1536.
231. Peppas NA. Intelligent therapeutics: Biomimetic systems and nanotechnology in drug delivery. *Adv. Drug Deliv. Rev.* 2004;56:1529–1531.
232. Byrne ME, Park K, and Peppas NA. Molecular imprinting within hydrogels. *Adv. Drug Deliv. Rev.* 2002;54:149–161.
233. Wizeman W and Kofinas P. Molecularly imprinted polymer hydrogels displaying isomerically resolved glucose binding. *Biomaterials* 2001;22:1485–1491.
234. Wulff G. Molecular imprinting in cross-linked materials with the aid of molecular templates—a way towards artificial antibodies. *Angew. Chem. Int. Ed. Engl.* 1995;34:1812–1832.
235. Whitcombe MJ, Rodriguez ME, Villar P, and Vulfson EN. A new method for the introduction of recognition site functionality into polymers prepared by molecular imprinting: Synthesis and characterization of polymeric receptors for cholesterol. *J. Am. Chem. Soc.* 1995;117:7105–7111.
236. Kirsch N, Alexander C, Lubke M, Whitcombe MJ, and Vulfson EN. Enhancement of selectivity of imprinted polymers via post-imprinting modification of recognition sites. *Polymer* 2000;41:5583–5590.
237. Hilt JZ and Byrne ME. Configurational biomimesis in drug delivery: Molecular imprinting of biologically significant molecules. *Adv. Drug Deliv. Rev.* 2004;56:1599–1620.
238. Sreenivasan K. On the applicability of molecularly imprinted poly(HEMA) as a template responsive release system. *J. Appl. Polym. Sci.* 1999;71:1819–1821.
239. Suedee R, Srichana T, and Rattananont T. Enantioselective release of controlled delivery granules based on molecularly imprinted polymers. *Drug Deliv.* 2002;9:19–30.
240. Percival CJ, Stanley S, Braithwaite A, Newton MI, and McHale G. Molecular imprinted polymer coated QCM for the detection of nandrolone. *Analyst* 2002;127:1024–1026.
241. Tang AXJ, Pravda M, Guilbault GG, Piletsky S, and Turner APF. Immunosensor for okadaic acid using quartz crystal microbalance. *Anal. Chim. Acta* 2002;471:33–40.
242. Kobayashi T, Murawaki Y, Reddy PS, Abe M, and Fujii N. Molecular imprinting of caffeine and its recognition assay by quartz-crystal microbalance. *Anal. Chim. Acta* 2001;435:141–149.
243. Tan Y, Zhou Z, Wang P, Nie L, and Yao S. A study of a biomimetic recognition material for the BAW sensor by molecular imprinting and its application for the determination of paracetamol in the human serum and urine. *Talanta* 2001;55:337–347.
244. Lin CI, Joseph AK, Chang CK, and Lee YD. Molecularly imprinted polymeric film on semiconductor nanoparticles analyte detection by quantum dot photoluminescence. *J Chromatogr. A* 2004;1027:259–262.
245. Peppas NA and Langer R. Origins and development of biomedical engineering within chemical engineering. *AIChE J.* 2004;50(3):536–546.
246. <http://www.mchips.com/tech.html>
247. <http://www.chiprx.com/products.html>
248. Grayson AC, Choi IS, Tyler BM, Wang PP, Brem H, Cima MJ, and Langer R. Multi-pulse drug delivery from a resorbable polymeric microchip device. *Nat. Mater.* 2003;2:767–772.
249. Langer R. Biomaterials: Status, challenges and perspectives. *AIChE J.* 2000;46(7):1286–1289.



---

# 16 Bio-Responsive Hydrogel Membranes

*John Hubble and Rongsheng Zhang*

## CONTENTS

16.1	Introduction to Hydrogels .....	473
16.1.1	General Properties .....	473
16.1.2	Materials of Construction .....	474
16.1.3	Synthesis Protocols .....	474
16.1.4	Areas of Application .....	474
16.2	Responsive Hydrogel Membranes .....	476
16.2.1	Reactive Systems .....	476
16.2.2	Binding Systems .....	477
16.3	Membrane Preparation .....	478
16.3.1	Composite Structures .....	478
16.3.2	Direct Casting .....	478
16.3.3	Pore-Filled Systems .....	478
16.4	Theoretical Description .....	478
16.4.1	Equilibrium Swelling Theory .....	479
16.4.1.1	Neutral Gels .....	479
16.4.1.2	Charged Gels .....	480
16.4.1.3	Affinity Cross-Linked Gels .....	483
16.4.2	Prediction of Mesh Size .....	485
16.4.3	Effect of Swelling on Binding Constants .....	486
16.4.4	Prediction of Gel Phase Diffusivity and Performance of Responsive Membranes .....	486
16.4.5	Design Implications of Gel Performance .....	487
16.5	Applications of Responsive Membranes: Insulin Delivery .....	488
16.6	Performance Modeling .....	488
16.7	Outstanding Issues .....	488
	Nomenclature .....	489
	References .....	490

## 16.1 INTRODUCTION TO HYDROGELS

### 16.1.1 GENERAL PROPERTIES

Hydrogels are produced from cross-linked hydrophilic polymers to give three-dimensional mesh structures or networks. By appropriate choice of synthetic conditions, gels can be formed which are either able to hold therapeutic molecules entrapped within the mesh structure or to act as a gating barrier [1]. Immersed in an aqueous solution, these polymeric networks are capable of imbibing large amounts of water or biological fluids [2,3]. However, the internal cross-links prevent complete dissolution and constrain the degree of swelling and hence the release rate of solutes.

Hydrogels have been extensively studied for biomedical applications where their hydrophilic properties and high-water content allow good biocompatibility [4,5], and their soft structure is mechanically similar to that of natural tissue [6]. In addition to a general swelling phenomenon resulting from the balance between the thermodynamic effect of dilution and the opposing retractive force of polymer chain extension, hydrogels may also show swelling changes, which are a function of changes in the chemical composition of their external environment [7].

**TABLE 16.1**  
**Monomers Most Commonly Used in the Synthesis of Synthetic Hydrogels for Pharmaceutical Applications**

Monomer Abbreviation	Monomer
HEMA	Hydroxyethyl methacrylate
HEEMA	Hydroxyethoxyethyl methacrylate
HDEEMA	Hydroxydiethoxyethyl methacrylate
MEMA	Methoxyethyl methacrylate
MEEMA	Methoxyethoxyethyl methacrylate
MDEEMA	Methoxydiethoxyethyl methacrylate
EGDMA	Ethylene glycol dimethacrylate
NVP	<i>N</i> -Vinyl-2-pyrrolidone
NIPAAm	<i>N</i> -Isopropyl AAm
Vac	Vinyl acetate
AA	Acrylic acid
MAA MAA	HPMA <i>N</i> -(2-hydroxypropyl) methacrylamide
EG	Ethylene glycol
PEGA	PEG acrylate
PEGMA	PEG methacrylate
PEGDA	PEG diacrylate
PEGDMA	PEG dimethacrylate

Source: From Peppas, N.A., Buresa, P., Leobandunga, W., and Ichikawab, H., *Eur. J. Pharm. Biopharm.*, 50, 27, 2000. With permission.

### 16.1.2 MATERIALS OF CONSTRUCTION

Hydrogels have been produced using a range of backbone materials. These can be broadly divided into two categories. The first category is based on the cross-linking of preformed polymer chains e.g., dextran [8]; the second category involves building the gel by polymerizing a suitable mixture of monomers [4]. A summary of monomers that have been used for this purpose is given in Table 16.1.

Cross-linking preformed polymers offer potentially simpler coupling chemistry, and the ability to use chains of predefined molecular weights means that final gel properties are easier to predict. Conversely, synthesis of polymer gels directly from their constituent monomers allows considerably more flexibility in terms of the combination of pendant groups incorporated and can be expected to be cheaper. Gels containing charged groups, which show pH-responsive behavior and temperature-responsive gels incorporating poly(*N*-isopropylacrylamide) (PNIPAAm) are often produced in this way [9], although a number of naturally charged polymers, for e.g., alginate and hyaluronic acid can also be used to form pH-sensitive gels [10,11].

### 16.1.3 SYNTHESIS PROTOCOLS

The cross-linking methods used to produce pH-sensitive hydrogels can be either physical or chemical [2]. Physical methods include high-energy radiation and UV-irradiation [12]. Alternatively, emulsification methods [13] and free-radical polymerization [14] have been employed to chemically fabricate pH-sensitive hydrogels. The magnitude of the volume collapse arising from the pH response can easily be detected allowing these hydrogels also to be used for biosensors and permeation switches [15].

Recently, attention has been paid to new syntheses and applications of carbodiimides in hydrogels, allowing bioconjugation based on amide formation under very mild conditions between carboxylic acids and amines in aqueous and organic systems [16]. There are two advantages to using 1-ethyl-(3-(3-dimethylaminopropyl) carbodiimide hydrochloride (EDC) as the cross-linking agent for hydrogel preparation from carboxylated precursor. First, the reaction conditions are mild and easily controlled by the level of COOH group substitution. Second, EDC is not incorporated into the cross-linked structure leaving no potentially cytotoxic groups in the gel [17].

### 16.1.4 AREAS OF APPLICATION

The use of hydrogels has been explored in tissue engineering, drug delivery, biosensors, and biological actuator applications. This results from the ease with which physicochemical properties of the hydrogel can be modified by changing monomer structure, the degree of cross-linking, and the fabrication method [18–21]. In addition, their chemical stability can be varied to give both stable and biodegradable constructs with good biocompatibility [6].

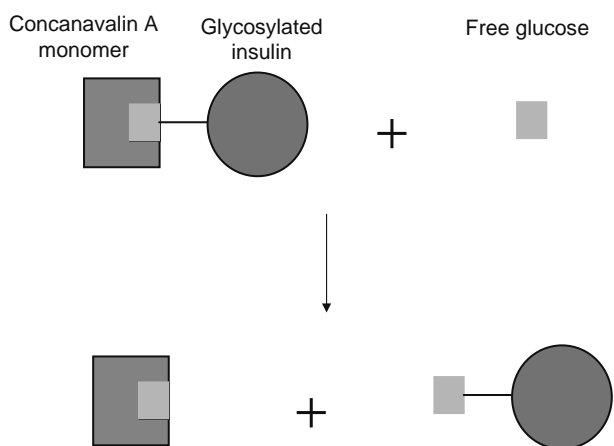


**FIGURE 16.1** (See color insert following page 588.) Displacement of ConA bound glycosylated insulin by free glucose.

In the area of responsive materials pH-sensitive hydrogels have been most frequently studied and have been used to develop a range of controlled release formulations for oral drug administration [22]. The functional mechanism of pH sensitivity is that small changes in pH can result in significant change in the mesh size of the gels' polymeric networks resulting from charge repulsion effects [23].

D-glucose-sensitive hydrogels have been examined for the development of self-regulated insulin delivery systems to act as an artificial pancreas that can administer the necessary amount of insulin in response to the blood glucose concentration [24]. Three approaches have been examined. The earliest reports are based on immobilized glucose oxidase in a pH-responsive hydrogel [25]. The second approach is based on the competitive displacements of affinity cross-links in bio-responsive hydrogels by D-glucose. Here the first systems that were studied used insulin chemically modified to introduce glucose moieties, which bind specifically to the lectin concanavalin A (ConA) [26,27]. In this approach, glycosylated insulin is competitively displaced from immobilized ConA by soluble glucose (Figure 16.1). To avoid problems associated with a derivatized form of insulin, ConA can be used to cause affinity gelation of a polymer containing terminal or pendant glucose moieties to form a responsive hydrogel [28,29].

A nonbiological route to fabricate glucose-sensitive hydrogels has also been developed using polymers having phenylboronic acid groups and polyol polymers, which form a gel through complex formation between the pendant phenylboronic acid and hydroxyl groups of glucose (Figure 16.2). Glucose can compete with polyol polymers for the borate cross-linkages, thus the cross-linking density of the gel decreases and the gel swells or transforms from the gel phase to release more drugs as the glucose concentration increases [30–32].

Owing to their structural similarity to the macromolecular-based components in the body (and their biocompatibility, permeability, and physical characteristics), hydrogels can also serve as a synthetic extracellular matrix (ECM) to organize cultured cells into a three-dimensional architecture and to present stimuli that direct the growth and formation of a desired tissue [33]. The balance between mechanical properties and controlled degradation of hydrogels mainly depends on the original

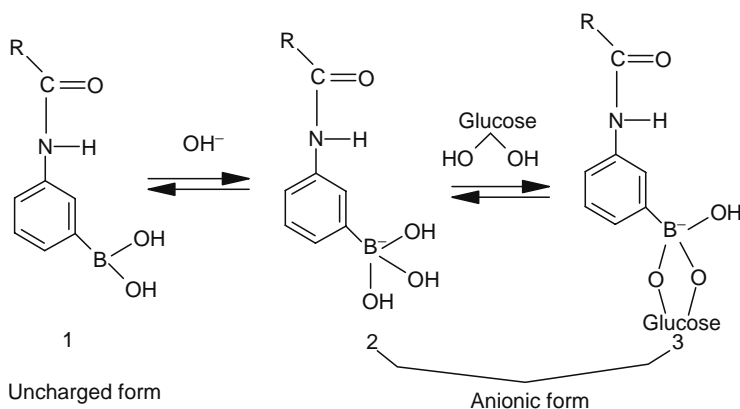


**FIGURE 16.2** Interaction between an immobilized boronic acid group and the vicinal diols of a glucose molecule. (From Kataoka, K., Miyazaki, H., Bunya, M., Okano, T., and Sakurai, Y., *J. Am. Chem. Soc.*, 120, 12694, 1998. With permission.)

rigidity of the polymer chains, the types of cross-linking molecules and the cross-linking density, and swelling as a result of hydrophilic/hydrophobic balance [34]. The ability to cast gels into thin membranes allows fabrication of support matrices with controllable mass-transfer resistances for both drug delivery and cell culture applications.

The development of responsive hydrogels for use in biosensors has been limited by the lack of accurate techniques to gauge their volume change in response to any stimulus. Recently, with the advent of sophisticated micro-fabrication facilities and new material technologies, diffractive and miniaturized optical gratings have been produced using hydrogels for biosensor applications [35]. Using hydrogel membranes in biosensors allow combination of biological receptor compounds (antibody, enzyme, nucleic acid, etc.) with the physical or physicochemical signal transduction required (e.g., optical, mass, electrochemical, or thermal). Ideally, these biosensors permit real-time observation of a specific biological event (e.g., antibody–antigen interaction) and allow the detection of a broad spectrum of analytes in complex sample mixtures. Furthermore, additional applications using immobilizing biocatalysts have been expected to act as biomimetic actuators giving surfaces with switchable hydrophobic–hydrophilic properties [36].

Hydrogels based on dextran have recently received specific attention due to their suitability for a variety of biotechnological and biomedical applications. Owing to their low tissue toxicity and high enzymatic degradability at desired sites, dextran hydrogels are increasingly seen as potential matrix systems for drug delivery [37] and controlled release of bioactive agents [38]. For dextran hydrogels targeted at colon-specific drug delivery, the drug is loaded into the hydrogel, which undergoes no or little release in the stomach and small intestine and is protected against digestion by enzymes [39].

Dextran hydrogels have been successfully applied in biosensors based on surface plasmon resonance. Carboxymethyl-dextran (CM-dextran) hydrogel was the original sensor surface developed for biomolecular interaction analysis and hence the most extensively studied and versatile. It has been used in a very wide range of interaction analyses including those between proteins, nucleic acids, and carbohydrates [40,41].

## 16.2 RESPONSIVE HYDROGEL MEMBRANES

Responsive membranes represent a specific subset of hydrogel applications. Responsive membranes ideally undergo rapid, reversible changes in microstructure. Small changes in the environment trigger changes at the macroscopic level leading to changes in mesh size or swelling ratio. Because these macroscopic changes are reversible, the system returns to its initial state after the triggering agent is removed [42].

Responsive membranes are attractive for drug delivery systems, as the delivery rate, chemical sensing, and triggering can be integrated and precisely controlled. Depending on the chemical composition of the gel, different internal and external stimuli (e.g., changes in pH, changes in specific solute concentration, application of a magnetic or electric field, variations in temperature, or ultrasound irradiation) may be used to trigger the swelling effect [43]. Once triggered, however, the rate of entrapped drug release is determined solely by the cross-linking ratio of the polymer network.

### 16.2.1 REACTIVE SYSTEMS

Reactive or catalytic systems are based on pH-responsive hydrogels where the chosen reaction generates a pH shift, which in turn leads to a swelling change in the hydrogel. This response can either be used to increase the internal mesh size to increase solute diffusivity in the gel phase for a diffusive membrane [44] or alternatively the gel can be used as a mechanical valve within the pores of a microporous membrane such that a convective flux may be turned on or off in response to analyte concentration (Figure 16.3) [45].

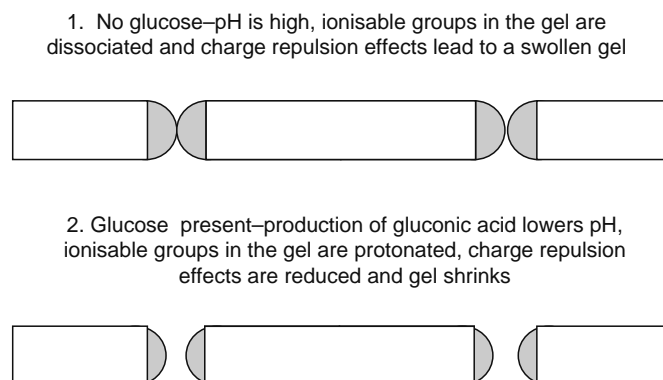


**FIGURE 16.3** Pore opening in a pH-sensitive gel containing glucose oxidase resulting from gel shrinkage.

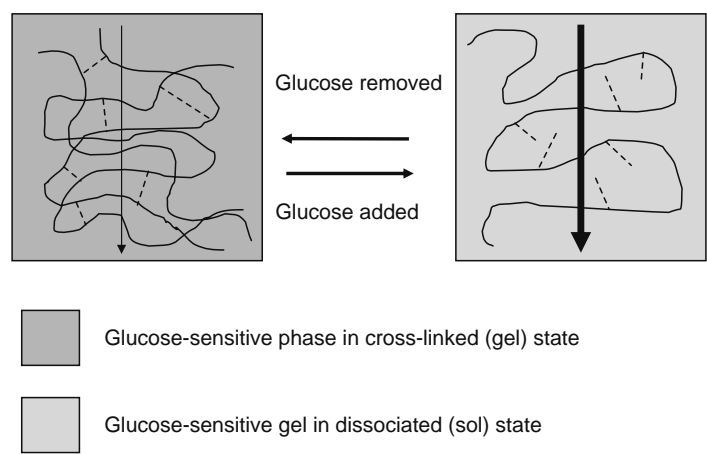


FIGURE 16.4 Schematic diagram showing the effect of competing glucose causing a gel to sol transition and increasing solute diffusion.

### 16.2.2 BINDING SYSTEMS

Cross-linked hydrogels can be formed which contain affinity cross-links between polymer-supported ligands and receptors [46]. Such gels can be based only on these biophysical interactions as described by Taylor et al. [28,29]. In these systems, displacement of affinity cross-links by soluble competitors ultimately leads to a gel/sol transition (Figure 16.4) requiring that the responsive phase be constrained between two diffusive membranes to prevent leakage while in the sol phase (Figure 16.5).

An alternative approach is to augment affinity cross-links with covalent cross-links at a specified density such that the total number of cross-links determines the permeability change and degree of swelling observed in the polymer when exposed to competing diffusible ligands [24,47,48]. In this case, the covalent coupling prevents dissolution of the gel and removes the need for an external diffusive layer (Figure 16.6).

In both types of binding systems competitive reduction of cross-link density will lead to an increased mesh size and hence increase solute diffusion. However, as this will inevitably be accompanied by some degree of gel swelling, these gels cannot be used to switch on convective solute flux as can be done with pH-sensitive gels, where both swelling and contraction effects can be generated.

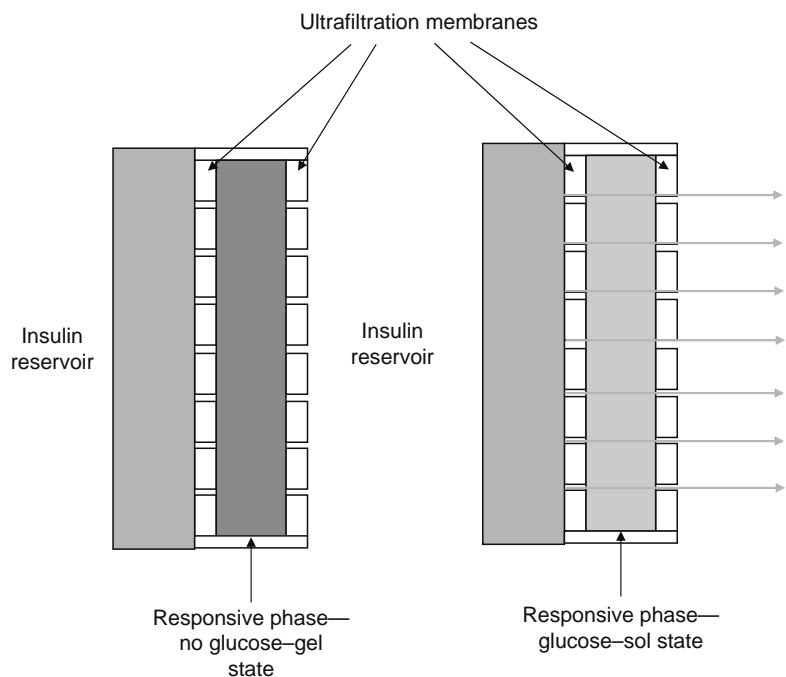
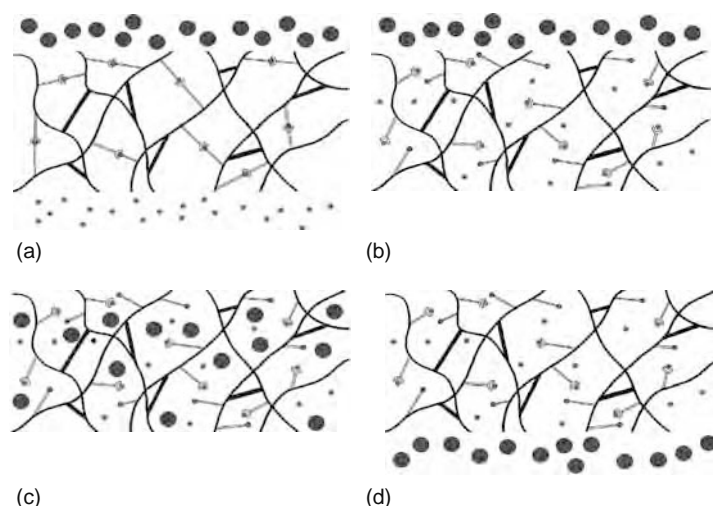


FIGURE 16.5 (See color insert following page 588.) Diagram showing the structural elements of a responsive sol/gel release system.



**FIGURE 16.6** (See color insert following page 588.) Mode of action of a glucose responsive hydrogel based on ligand–receptor interactions (bold lines denote covalent links). (a) Gel porosity reduced by affinity cross-links that exclude large molecules, e.g., insulin (blue), (b) glucose (red) diffuses in and competitively displaces affinity cross-links, (c) insulin is able to diffuse into the more highly porous gel, and (d) insulin diffuses through the gel providing the concentration gradient and glucose concentration is maintained.

## 16.3 MEMBRANE PREPARATION

### 16.3.1 COMPOSITE STRUCTURES

For responsive systems where changes in transport properties result from a sol/gel transition, the active components need to be retained by an ultrafiltration membrane to prevent loss of material while the responsive phase is in a sol state as shown in Figure 16.5. Hydrogels fabricated from ConA with glucose-containing polymer chains can be made to undergo sol–gel phase transformations depending on the glucose concentration in the environment. Because of the non-covalent cross-linking between glucose-containing polymer and ConA, individual free glucose molecules can compete with the polymer-attached glucose molecules and exchange with them as the external glucose molecules diffuse into the hydrogel. It has been shown that diffusion of insulin through the solution (sol) phase is faster than that through the hydrogel (gel) phase, and that insulin release can be controlled as a function of the glucose concentration in the environment [28,29,49–52]. In addition to the use of diffusive membranes to retain the polymer components, leakage can also be reduced by coupling the receptor protein to a larger polymer preparation, e.g., a carbopol [53].

### 16.3.2 DIRECT CASTING

To remove the need for containment membranes, Tang et al. [54] cross-linked ConA with dextran to form a hydrogel which could be cast as a flat sheet membrane. This material was mechanically weak but could be reinforced using internal support gauze. In transport studies, membrane permeability showed a reversible change with the addition and removal of D-glucose and there was no evidence of component leakage from the gel (Figure 16.7). A similar material was developed which changed permeability in response to the coenzyme NAD [48].

### 16.3.3 PORE-FILLED SYSTEMS

To improve the mechanical properties of membranes based on soft gels, a number of groups have developed techniques for casting hydrogels within the pores of preformed microporous membranes (Figure 16.8) [55,56]. These composite membranes have been investigated for a range of applications including water softening [57], synthesis [58], nanofiltration [59], and fuel cells [56,60]. As the transport properties of these membranes will depend on the polymer phase within the pores, transport will still depend on cross-link density [61] and charge effects [62] as discussed below.

## 16.4 THEORETICAL DESCRIPTION

Effective modeling of hydrogel performance requires the effect of environmental changes on both the swelling ratio and mesh size of the gel to be determined. Models have been proposed to describe the effects of environmental changes on both neutral and charged hydrogel matrices where swelling changes result from charge repulsion or hydrophobic effects [4]. Models to

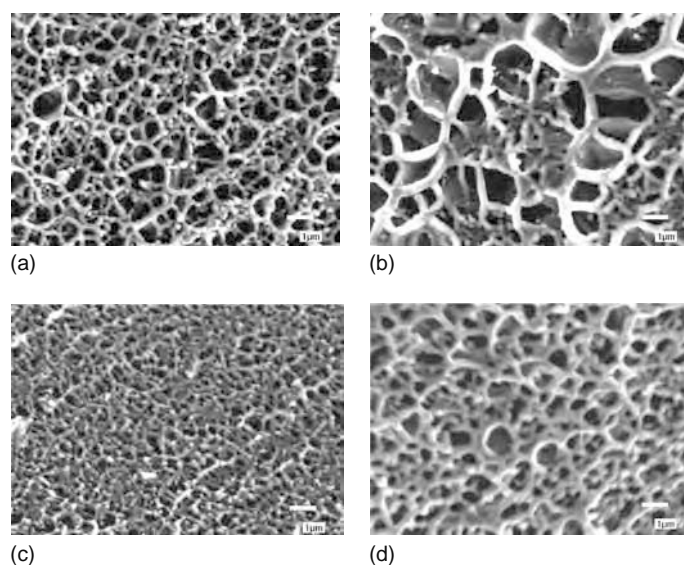


**FIGURE 16.7** SEM pictures showing structural changes in a dextran ConA hydrogel in response to glucose. (a) Buffer, (b) 0.1 M D-glucose, (c) 0.1 M L-glucose, and (d) incubated in 0.1 M D-glucose and then extensively washed. (From Zhang, R., Dextran Hydrogel Preparation and Application in Biomedical Engineering, PhD Thesis, University of Bath, England, 2004. With permission.)

describe the performance of affinity response systems, where swelling results from reversible changes in cross-link density have not previously been described, but can be formulated by combining predictions of affinity cross-link density using quantitative descriptions of binding interactions, with swelling theories developed for use with hydrogel polymers.

## 16.4.1 EQUILIBRIUM SWELLING THEORY

### 16.4.1.1 Neutral Gels

Neutral cross-linked hydrogels are commonly described in terms of the polymer volume fraction in the swollen and unswollen state and the number average molecular weight of the polymer chain between adjacent cross-links. The difference between polymer volume fractions can be determined from the swelling ratio of the gel (Figure 16.9) [63].

The equilibrium swelling theory of Flory and Rehner [64] assumes that the degree of swelling of an uncharged gel results from the effects of just two opposing forces: the thermodynamic effects of mixing tending to dilute the polymer component and the elastic constraints imposed by the force required to stretch the polymer chains. At equilibrium, these two forces are equal.

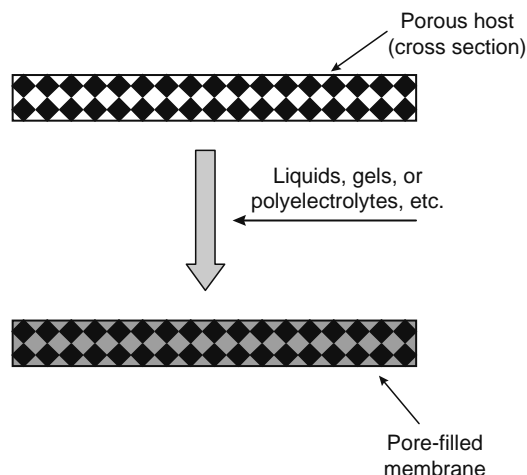


**FIGURE 16.8** Structure of a pore-filled membrane. A responsive hydrogel is incorporated into the pores of the substrate membrane to form a stable composite membrane.

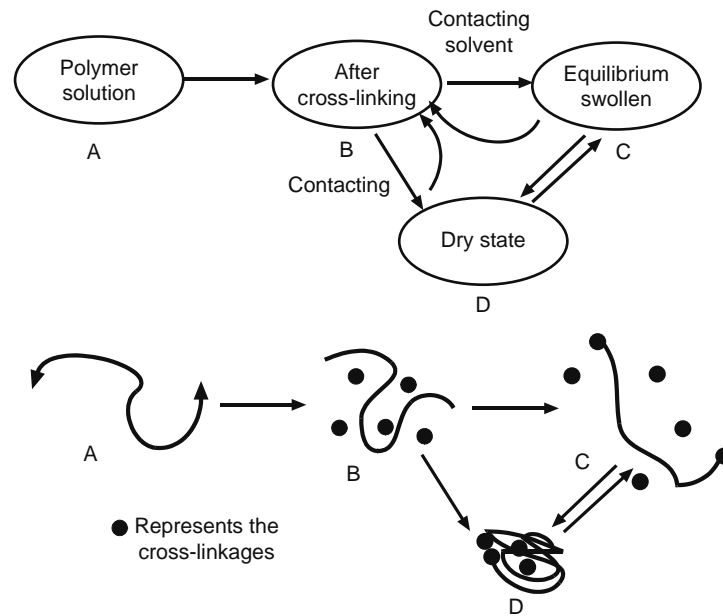


**FIGURE 16.9** Schematic illustration of the different states of gels and their mesh chain conformations: A is the free mesh chain solution, B is the newly formed gel in the relaxed state, C is the equilibrium swollen state after contacting with solvent molecules, and D is the gel in the dried state. (From Huang, Y., Szleifer, I., and Peppas, N.A., *Macromolecules*, 35, 1373, 2002. With permission.)

Peppas and Merrill [65] modified the Flory–Rehner theory to describe the preparation of hydrogels in the presence of water to obtain the following relationship:

$$\frac{1}{\bar{M}_c} = \frac{2}{\bar{M}_n} \frac{\left(\frac{\bar{v}}{V_1}\right) \left[ \ln(1 - v_{2,s}) + V_{2,s} + x_1(v_{2,s})^2 \right]}{v_{2,r} \left[ \left(\frac{v_{2,s}}{v_{2,r}}\right)^{1/3} - 0.5 \left(\frac{v_{2,s}}{v_{2,r}}\right) \right]} \quad (16.1)$$

where

$\bar{M}_c$  is the number average molecular weight of the polymer chain between cross-links

$\bar{M}_n$  is the number average molecular weight of the polymer chain

$\bar{v}$  is the partial specific volume of the polymer

$V_1$  is the molar volume of water

$x_1$  is the Flory polymer-solvent interaction parameter

$v_{2,s}$  is the polymer fraction of the gel at equilibrium swelling

$v_{2,r}$  is the polymer fraction of the gel after gel formation

This relationship is commonly used to determine the cross-link density of a gel from experimentally determined swelling ratios, where the swelling ratio is given by

$$Q = \frac{v_{2,r}}{v_{2,s}} \quad (16.2)$$

However, for membrane applications, where the need to constrain physical dimensions and the mechanical properties required impose limits on the acceptable swelling ratio, Equation 16.1 can be used to predict equilibrium polymer concentration and swelling ratio for a gel with a known cross-link density. Figure 16.10 shows such a prediction for a dextran-based gel with an initial polymer fraction of 0.16 based on a dextran of 500 kDa. Other parameter values are given in Table 16.2.

### 16.4.1.2 Charged Gels

The equilibrium swelling theory assumes that the degree of swelling of a charged gel changes as ions diffuse in and out of the gel (Figure 16.11) [66]. Swelling results from the effects of three forces. In addition to the dynamic effects of mixing and elastic constraints seen with uncharged gels, an additional force will result from the charge effects within the gel [23]. This leads to expressions that also take account of the effects of both pH and ionic strength on gel swelling.

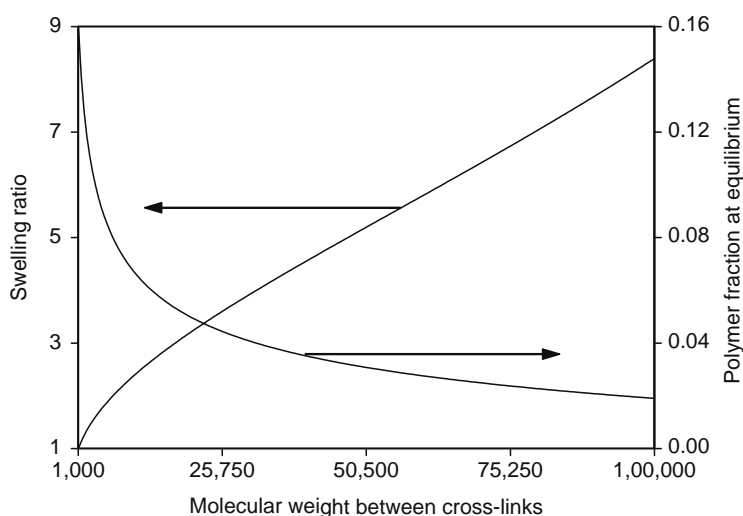


**FIGURE 16.10** Effect of increasing molecular weight between cross-links on swelling ratio and equilibrium polymer fraction of a neutral hydrogel. Simulations conducted for a dextran-based gel using the parameter values in Table 16.2.

#### Anionic gel

$$\frac{V_1}{4l} \left( \frac{v_{2,s}^2}{\bar{v}} \right) \left( \frac{K_a}{10^{-\text{pH}} + K_a} \right)^2 = [\ln(1 - v_{2,s}) + v_{2,s} + x_1 v_{2,s}^2] \left( \frac{V_1}{v\bar{M}_c} \right) \left( 1 - \frac{2\bar{M}_c}{\bar{M}_n} \right) v_{2,r} \left[ \left( \frac{v_{2,s}}{v_{2,r}} \right)^{1/3} - 0.5 \left( \frac{v_{2,s}}{v_{2,r}} \right) \right] \quad (16.3)$$

#### Cationic gel

$$\frac{V_1}{4l} \left( \frac{v_{2,s}^2}{\bar{v}} \right) \left( \frac{K_b}{10^{\text{pH}-14} + K_b} \right)^2 = [\ln(1 - v_{2,s}) + v_{2,s} + x_1 v_{2,s}^2] \left( \frac{V_1}{v\bar{M}_c} \right) \left( 1 - \frac{2\bar{M}_c}{\bar{M}_n} \right) v_{2,r} \left[ \left( \frac{v_{2,s}}{v_{2,r}} \right)^{1/3} - 0.5 \left( \frac{v_{2,s}}{v_{2,r}} \right) \right] \quad (16.4)$$

where

$l$  is the ionic strength

$K_a$  and  $K_b$  are dissociation constants for acid and base, respectively

**TABLE 16.2**  
Parameter Values Used for Simulations (Polymer is Dextran)

Parameter	Definition	Value	Dimensions
$C_n$	Flory characteristic ratio	3.3	—
$fb$	Force per bond	$1.2 \times 10^{-7}$	N
$x_1$	Flory polymer-solvent interaction parameter	0.473	—
$\gamma$	Bond interaction distance	$5 \times 10^{-12}$	m
$v_1$	Partial specific volume of the polymer	0.62	$\text{cm}^3 \text{g}^{-1}$
$D_1$	Diffusate diffusivity in the liquid phase	$1.1 \times 10^{-10}$	$\text{m}^2 \text{s}^{-1}$
$K_c$	Dissociation constant for competitor/ligand	$1 \times 10^{-3}$	M
$V_1$	Molar volume of water	18	$\text{cm}^3 \text{g}^{-1}$
$l$	The unit length along the polymer back bone	$5 \times 10^{-10}$	m
$r$	Hydrodynamic radius of the solute	$1.5 \times 10^{-9}$	m
$v_{2,r}$	Polymer fraction of the gel after gel formation	0.04	—
$\bar{M}_n$	Number average molecular weight of the polymer	$4.8 \times 10^5$	$\text{g mol}^{-1}$
$M_r$	Molecular weight of the monomer (glucose)	180	$\text{g mol}^{-1}$
$K_D$	Dissociation constant for receptor/ligand	$1 \times 10^{-3}$	M

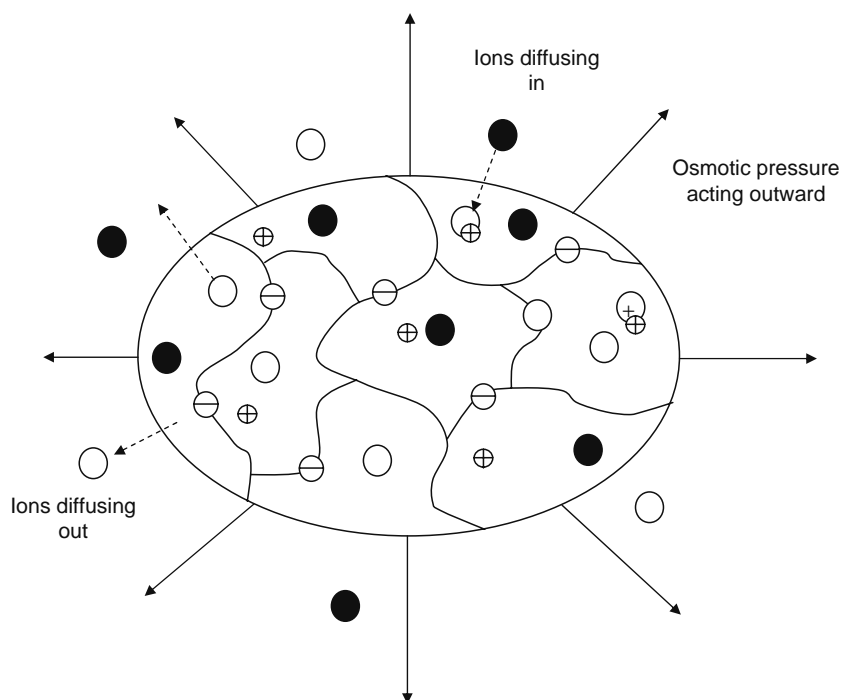


**FIGURE 16.11** Phenomena affecting the swelling of a charged hydrogel in a buffered pH solution. (Redrawn from De, S.K., Aluru, N.R., Johnson, B., Crone, W.C., Beebe, D.J., and Moore, J., *J. Microelectromech. Syst.*, 11, 544, 2002.)

In responsive applications based on these gels the cross-link density does not change, but the gel will swell in response to changes in ionic strength or pH. Figure 16.12 shows simulation results obtained using Equation 16.3 to determine the effect of pH on the equilibrium polymer volume and hence the swelling ratios for a CM-dextran gel. Comparison of the swelling ratios predicted for neutral and charged dextran gels in Figures 16.10 and 16.12 suggests that pH-sensitive gels show much higher swelling ratios even at high cross-link densities. In a range of simulations of swelling effects in carboxylated polyacrylates,

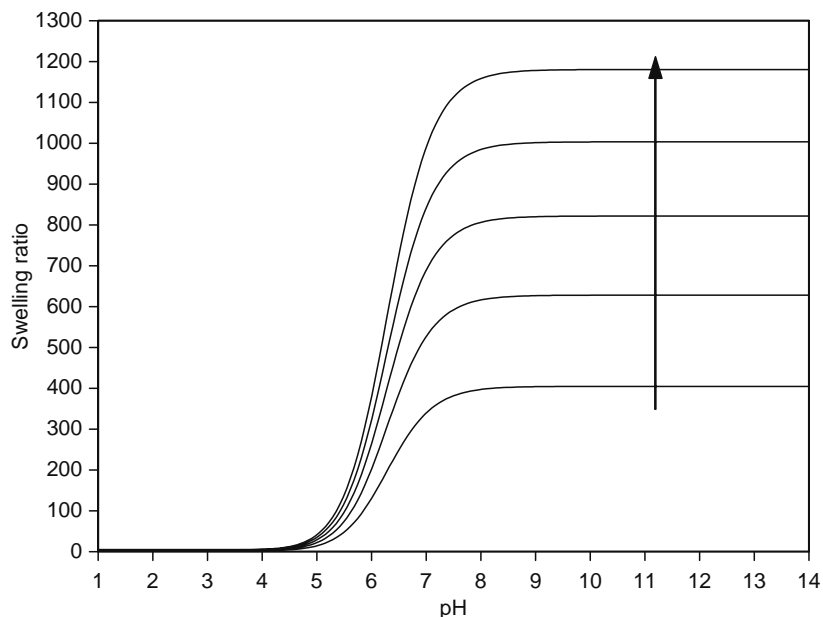


**FIGURE 16.12** Simulation of the effect of pH on the swelling ratio for a carboxymethyl dextran gel. The arrow indicates increasing chain length between cross-links (simulation conditions given in Table 16.2, ionic strength 30 mM).

Brannon Peppas and Peppas [23] found swelling ratios up to 250 for systems where the swelling solution had an ion concentration comparable to the charged groups in the gel. For a preswollen gel, changes in swelling ratio can be computed from  $\nu_{2,s}$  values obtained at appropriate pH values.

These relationships are commonly employed to determine  $\bar{M}_c$  in characterization studies of nonresponsive and responsive hydrogel preparations where the response does not lead to a change in cross-link density.

### 16.4.1.3 Affinity Cross-Linked Gels

In the case of affinity gels, where the response is based on a change in the cross-link density, the effective value of  $\bar{M}_c$  will depend on both covalent and reversible cross-links based on bio-specific or affinity interactions. Here the  $\bar{M}_c$  value resulting from covalent links alone can be determined using Equations 16.1 and 16.2 under conditions where the reversible cross-links are all open, i.e., saturating competitor concentration. Then the effect of a change in competitor concentration ( $C$ ) on the number of affinity cross-links can be predicted together with its effect on gel swelling.

In hydrogel containing fixed concentrations of immobilized ligand and receptor  $L_{\text{tot}}$  and  $R_{\text{tot}}$ , respectively, the mass balance for receptor ( $R$ ) sites within a finite mass of gel can be written as [67]

$$[R_{\text{tot}}] = [R] + [RL] + [RC] \quad (16.5)$$

Assuming mutual depletion of receptor ( $R$ ) and ligand ( $L$ ) populations, but that the competitor ( $C$ ) reservoir is sufficiently large that competitor concentration is unchanged by binding, gives an expression for the dissociation constant for ligand binding:

$$K_L = \frac{([R_{\text{tot}}] - [RL] - [RC])([L_{\text{tot}}] - [RL])}{[RL]} \quad (16.6)$$

The dissociation constant for competitor binding is

$$K_C = \frac{([R_{\text{tot}}] - [RL] - [RC])[C]}{[RC]} \quad (16.7)$$

where  $K_L$  and  $K_C$  are the dissociation constants for the immobilized ligand and competitor interactions, respectively.

Equations 16.6 and 16.7 can be combined to give a quadratic expression in  $[RL]$  which can be used to determine the fraction of receptor, which is bound to immobilized ligand (Figure 16.13). From these equations, the number average molecular weight ( $\bar{M}_c$ ) between affinity cross-links can be determined:

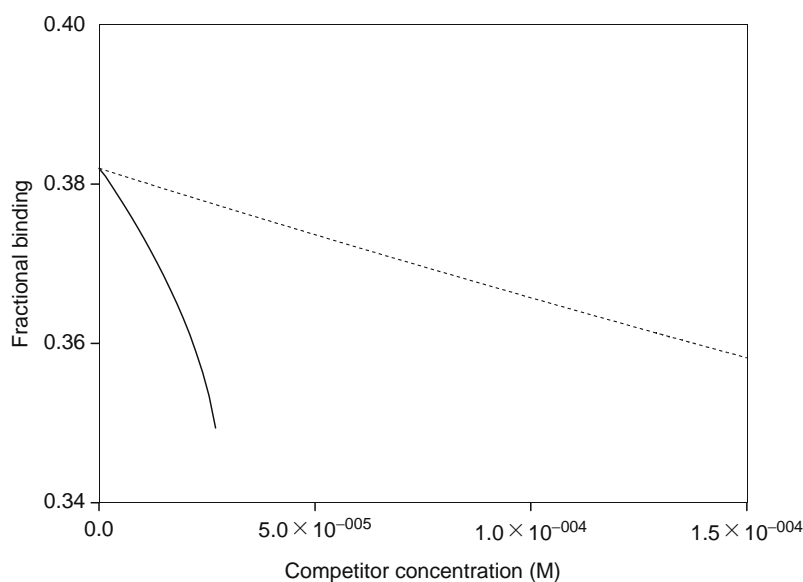


**FIGURE 16.13** Effect of competitor concentration on fractional binding of immobilized receptor to immobilized ligand in a responsive hydrogel. Broken line denotes solution for fixed volume. Solid line accounts for dilution effect of swelling. Both ligand and receptor concentrations 1 mM, other values as per Table 16.2.

$$\overline{M}_c^{\text{aff}} = \frac{[P]\overline{M}_n}{[R_{\text{tot}}]Y} \quad (16.8)$$

where

$[P]$  is the polymer concentration in the gel

$Y$  is the fraction of immobilized ligand bound to receptor ( $[RL]/[R_{\text{tot}}]$ )

The polymer fraction of the gel  $\nu_{2,r}$  after gel formation can be determined from the mixture conditions, as the polymer and total mass of the mixture is known. The effect of changing competitor concentrations can then be expressed in terms of the effect on  $\nu_{2,s}$ . In the case of an affinity response the swelling ratio (sr) of a preswollen gel can be computed from changes in the  $\nu_{2,s}$  resulting from a change in competitor concentration.

$$\text{sr} = \frac{\nu_{2,s}^1}{\nu_{2,s}^2} \quad (16.9)$$

In a chemically cross-linked responsive gel containing both bio-specific or affinity interactions and covalent cross-links at a specified density, the cross-links determining the swelling ratio will represent the sum of both covalent and affinity links ( $\overline{M}_c + \overline{M}_c^{\text{aff}}$ ).

In Equations 16.5 through 16.7,  $R_{\text{tot}}$  and  $L_{\text{tot}}$  are defined relative to the initial gel volume. Therefore, after swelling, these concentrations will be reduced as follows:

$$R_{\text{tot}}^s = \frac{R_{\text{tot}}}{\text{sr}} \quad \text{and} \quad L_{\text{tot}}^s = \frac{L_{\text{tot}}}{\text{sr}} \quad (16.10)$$

This requires iterative solution of Equations 16.2 and 16.5 through 16.10, as changes in ligand and receptor concentrations will change swelling ratio, which will in turn change concentration. Simulations using this approach show that as a soluble competitor for the affinity interaction is introduced, the number of cross-links is reduced and the gel swells (Figure 16.14). In the case of a gel with no covalent cross-links the solution fails when the number of links per polymer chain falls below two, i.e., the minimum theoretical number needed for gel formation.

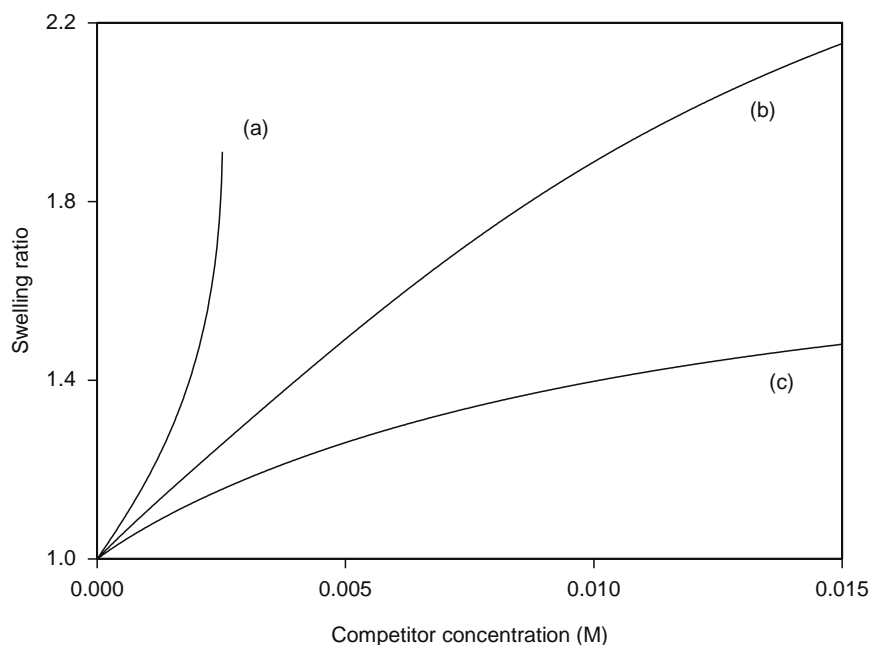


**FIGURE 16.14** Effect of competitor concentration on the swelling of a gel in equilibrium with a solvent at zero competitor concentration.  $R_{\text{tot}}$  and  $L_{\text{tot}}$  5 mM, dissociation constants 1 mM for both ligand and competitor. (a) Zero covalent cross-links per chain—gel/sol transition occurs, (b) 5 covalent cross-links per chain, and (c) 10 cross-links per chain.

### 16.4.2 PREDICTION OF MESH SIZE

Increasing the swelling ratio will have two effects on a gel:

1. For a gel sheet of constrained surface area, the thickness will increase.
2. Mesh size of the gel will increase.

When the gel used as a gating membrane to control the release of solute these will have two competing effects on flux:

1. Increases in mesh size will increase the gel diffusivity tending to increase transmembrane flux.
2. Increases in swelling ratio will increase the membrane thickness tending to decrease transmembrane flux.

The effect of competitor on the thickness of a gel sheet ( $\delta$ ) will be given by

$$\delta^C = sr \delta \quad (16.11)$$

where

$\delta$  denotes membrane thickness

$\delta^C$  denotes membrane thickness in the presence of competitor

The influence of the mesh size will be seen in terms of its effect on diffusivity. Mesh size values for neutral gels have been calculated using the following expression [68]:

$$\xi = v_{2,s}^{-1/3} \left( \frac{C_n \bar{M}_c}{M_r} \right)^{1/2} l \quad (16.12)$$

where

$\xi$  is the gel mesh size

$C_n$  is the Flory characteristic ratio

$l$  is the unit length along the polymer back bone

$M_r$  is the the molecular weight of the repeat unit

Figure 16.15 shows the predicted effect of competitor concentration on mesh size for the conditions reported in Figure 16.14.

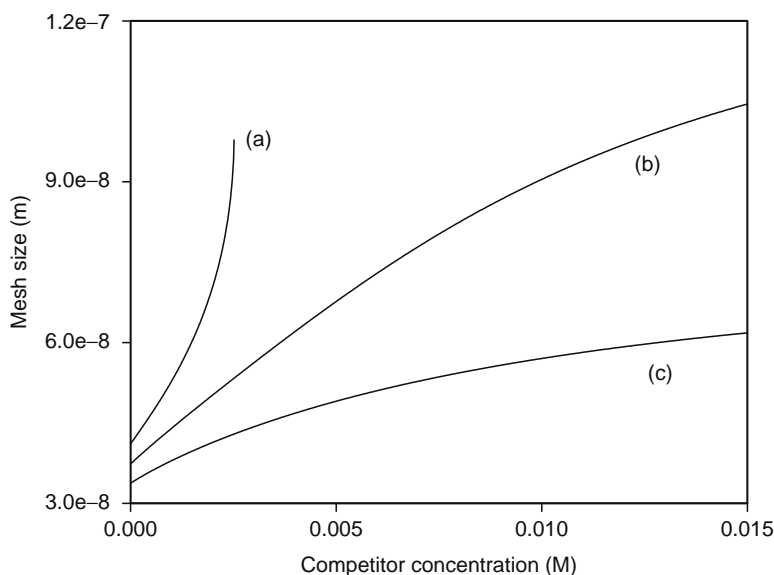


**FIGURE 16.15** Effect of competitor concentration on mesh size, simulation conditions as for Figure 16.14.

### 16.4.3 EFFECT OF SWELLING ON BINDING CONSTANTS

An additional effect, which may be important in affinity gels with high degrees of swelling, is the effect of tensile stress on binding constants. Gel swelling results in a force being applied to the cross-links within the gel [65]. In affinity cross-links, this would be expected to increase the dissociation rate constant. This effect is encountered in studies of affinity-mediated cell-surface interactions and has been described by Bell [69] in terms of the applied force and bond interaction distance.

$$k'_r = k_r \exp\left(\frac{\gamma fb}{k_b T}\right) \quad (16.13)$$

where

- $\gamma$  is the bond interaction distance
- $fb$  is the force acting on the bond
- $k_b$  is the Boltzmann constant

For an apparent dissociation constant expressed as the ratio of reverse to forward rate constants,

$$K'_L = \frac{k'_r}{k'_f} = K_L \exp\left(\frac{\gamma fb}{k_b T}\right) \quad (16.14)$$

These effects can also be incorporated into the iterative prediction swelling but are likely to only be significant at high swelling ratios.

### 16.4.4 PREDICTION OF GEL PHASE DIFFUSIVITY AND PERFORMANCE OF RESPONSIVE MEMBRANES

The ability of a solute to diffuse within a hydrogel has been described in terms of the probability of a solute of characteristic size ( $r$ , defined as the radius of a sphere of equal volume to the solute molecule) passing through an opening equal to the mesh size of the gel ( $\xi$ ). This probability is taken to be a linear function of the ratio of  $r/\xi$ . Therefore, the gel phase diffusivity of a solute can be related to its liquid phase diffusivity, molecular volume, and gel mesh size [70,71].

$$D_{\text{gel}} \cong D_1 \left(1 - \frac{r}{\xi}\right) \exp\left(\frac{-1}{Q-1}\right) \quad (16.15)$$

where

- $D_1$  and  $D_{\text{gel}}$  are liquid and gel phase diffusivities of the solute, respectively
- $r$  is the hydrodynamic radius of the solute

Equation 16.15 shows that, as expected, the gel phase diffusivity approaches zero as the solute radius approaches the mesh size. In a responsive gel, as swelling increases in response to environmental changes gel phase diffusivity increases with increasing mesh size. Figure 16.16 shows the effect of competitor concentration on predicted gel phase diffusivity assuming a solute radius of 1.5 nm. Using this example and a dextran polymer gel, it is not possible to achieve a cross-link density sufficient to give a predicted mesh size sufficiently small to prevent gel phase diffusivity. However, as Equation 16.12 does not consider the steric effects of the immobilized receptor experimentally determined gel phase diffusivities are likely to be lower.

The final step in describing membrane performance is to consider the competing effects of competitor on diffusivity and membrane thickness. Using Fick's first law to describe transport across a thin slab of gel (a membrane)

$$J = \frac{AD_{\text{gel}}}{V\delta^2 C} (C_D - C_R) \quad (16.16)$$

where

- $J$  is the flux (concentration change per unit time)
- $A$  is the membrane area
- $V$  is the volume of receiving compartment
- $C_D$  is the donor compartment concentration
- $C_R$  is the receiving compartment concentration

Simulations of the effect of competitor concentration using Equations 16.11, 16.12, 16.15, and 16.16 are shown in Figure 16.17. This indicates that at low covalent cross-link density where swelling effects are more pronounced, flux passes through a

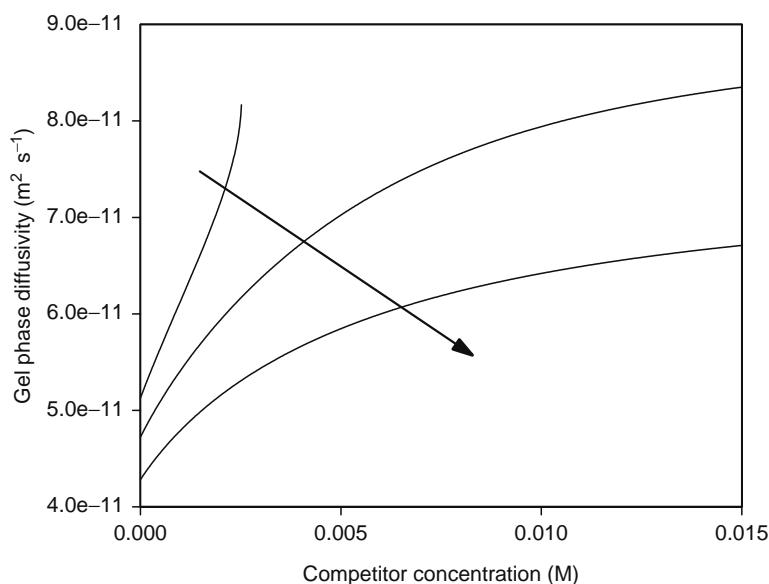


**FIGURE 16.16** Effect of competitor concentration on gel phase diffusivity. Arrow denotes increasing covalent cross-link density from 0 to 10 bonds per chain.

maximum as competitor concentration is increased. Gels which contain a higher covalent cross-link density show less swelling, and flux, although lower across the range, does not decrease at higher competitor concentrations.

#### 16.4.5 DESIGN IMPLICATIONS OF GEL PERFORMANCE

Hydrogel swelling is determined by polymer properties and cross-link density determining the retractive forces which oppose the dissolution effects of mixing and in the case of charged gels—ionic repulsion effects. It is apparent from the simulations and literature data reported above that pH-sensitive gels show much higher swelling ratios than neutral or bio-responsive gels. In membrane applications they will be more suited to a pore gating role in microporous membranes where the gel acts as a valve to control convective flow [45]. While increases in mesh size with swelling will increase gel phase diffusivity, the high swelling ratios seen with many pH-sensitive gels limit their mechanical strength for applications in a diffusive membrane form.

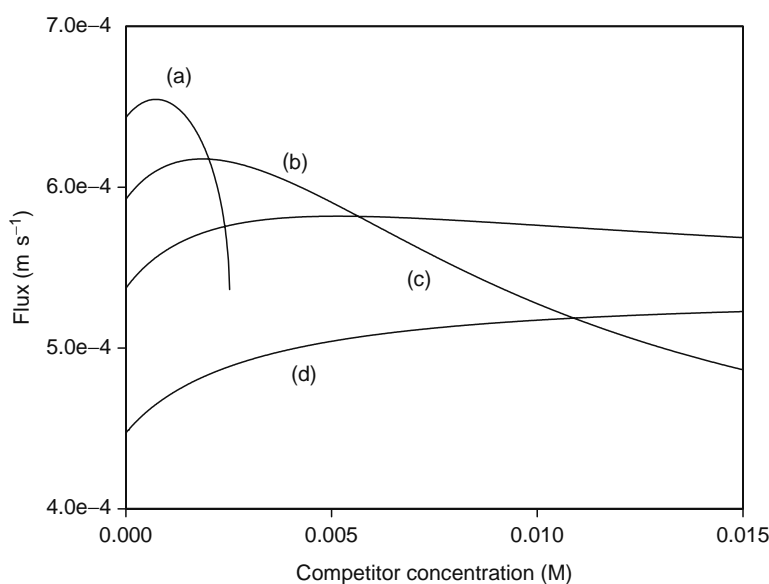


**FIGURE 16.17** Effect of competitor concentration on transmembrane flux showing competing effects of increased mesh size and increased membrane thickness.  $(C_D - C_R) = 1$  M. (a) Zero covalent bonds per chain, (b) 5 covalent bonds per chain, (c) 10 covalent bonds per chain, and (d) 20 covalent bonds per chain.

Conversely, for responsive gels based on ligand–receptor interactions, where swelling and mesh size changes result from changes in cross-link density, changes in swelling ratio are usually much smaller. While this makes them less suitable for pore gating applications, they are potentially more attractive for use in a diffusive membrane construct.

As described above, diffusive systems fall into two categories: (1) diffusive systems that are based on a sol/gel transition [28,29,51,53] and (2) diffusive systems that are based on changes in mesh size [30,46,48,54]. In the sol/gel systems, the gel state results solely from reversible interactions between ligand and receptor; thus increases in competitor concentration will initially lead to increase in transport rate resulting from increases in mesh size, as the gel changes to a sol viscosity effects will predominate (Figure 16.4). In gels which contain both reversible and covalent interactions, gel structure is retained even at saturating competitor concentrations. In both systems, a cross-link density high enough to give a mesh size less than the radius of the solute to be delivered will be required if zero delivery is to be achieved in the absence of competitor (Equation 16.15). This requires a high cross-link density and ideally a polymer with a low molecular weight and short repeat unit (Equation 16.12). Thus when polymers are chosen, the monomer size, covalent cross-link density, and achievable degree of ligand and receptor substitution need to be assessed to ensure that the resulting mesh size is compatible with the molecular weight of the solute to be delivered.

## 16.5 APPLICATIONS OF RESPONSIVE MEMBRANES: INSULIN DELIVERY

In many clinical situations, controlled drug delivery systems, which deliver drugs at a predetermined rate, are replacing conventional drug formulations. However, in diabetes mellitus, there is currently no entirely effectively system for continuous control of blood glucose levels. The treatment of insulin-dependent diabetes requires the provision of insulin in response to increases in blood glucose concentration. Although a conventional oral route would be preferred, this is not practical for the systemic delivery of peptide and protein drugs, including insulin [72]. The consequent required daily injection of insulin may cause discomfort, and can lead to several long-term complications associated with diabetes mellitus such as retinal damage and cardiovascular disease. Therefore, an insulin delivery system capable of mimicking the pancreas and delivering insulin in response to increases in blood glucose would be highly attractive [73]. It is for this reason that many of the responsive hydrogels described above have targeted the controlled release of insulin in response to changes in glucose concentration.

As described previously, the specific interactions between enzymes and lectins with carbohydrates have been evaluated for use in insulin delivery systems based on responses to chemical and biochemical stimuli. These include pH, changes in specific ion concentration, and specific molecular recognition events [15].

An extensively studied approach has been the use of ConA/glucose derivatized polymer mixtures to form reversible sol/gel system, which is sandwiched between two porous membranes [29,51,53]. Gelation is reversible in response to changes in environmental glucose concentration such that the diffusion coefficient for insulin changes with degree of gelation. In earlier studies, the gels were based solely on soluble components. However, leakage of ConA through the membrane during gel–sol transition led to revised systems with ConA coupled to the polymer.

While reducing leakage, coupling of ConA to the polymer still results in a system that is in a soluble form in the presence of glucose [51,52]. Thus, support membranes are still required, leading to increased complexity and slow diffusion rates (Figure 16.5). To address these problems, the covalently cross-linked hydrogels containing glucose moieties and either boronate or lectin-binding groups were developed [30,31,50,54].

## 16.6 PERFORMANCE MODELING

The overall response of the patient to an insulin delivery system can be modeled using compartmental analysis to allow the performance of the release system and its interdependence with factors affecting the physiological response of the patient to be systematically assessed. Several such models have been published [74,75] to describe the response to a bolus input in a glucose tolerance test, but need to be combined with models of responsive gel performance to describe *in vivo* glucose and insulin levels over an extended period in the face of varying levels of input and demand. The ultimate goal is a model that can be used in the validation of control strategies for a gel membrane release system, *i.e.*, the production of a chemical control system analogous to the electronic systems proposed for pump-based closed loop delivery systems [76].

## 16.7 OUTSTANDING ISSUES

Despite considerable research on the development of responsive membranes for drug delivery there are significant hurdles to be overcome before techniques developed in the laboratory are made suitable for *in vivo* use. In insulin delivery, three response mechanisms have been investigated as described above: (1) a catalytically induced pH shift using glucose oxidase, (2) mesh size changes induced by displacement of ConA-mediated gel cross-links, and (3) mesh size changes induced by displacement of boronate-mediated gel cross-links. All three approaches require gel components which are either toxic, immunogenic, or

both. Therefore, these mechanisms pose a significant risk to patient health if membrane components were to leak from a delivery system.

In the glucose oxidase system, dissolved oxygen concentration as well as glucose levels will influence delivery response requiring close control of mass-transfer limitations. For both systems containing a protein component, stability factors may limit operational lifetime. This may be particularly severe in the case of glucose oxidase where the reaction product  $H_2O_2$  will accelerate enzyme denaturation unless it is rapidly removed by diffusion or reaction with a second enzyme (peroxidase or catalase).

In terms of insulin release, catalytic systems offer the advantage of failing safe, i.e., for transport to increase, pH must be actively reduced by the enzyme-catalyzed reaction. Loss of enzyme activity leads to a reduction rather than an increase in release. Conversely, in binding displacement systems protein denaturation will lead to an increase in release as the number of cross-links is reduced.

For extended operation, insulin release systems will need to require many times the lethal dose of insulin. Therefore, in addition to failure of the responsive element, there is a significant risk associated with accidental release resulting from a mechanical failure. This requires careful consideration of the mechanical design of a unit intended to operate as an implant.

Finally, the issue of biocompatibility and location needs to be considered to ensure response is triggered by a local glucose change representative of the wider levels and that release is not compromised by fouling or cell growth over the release surface. For these reasons little work has yet to be carried out in vivo systems. However, Taylor et al. [77] have demonstrated a pharmacological effect using a ConA-based responsive gel to deliver insulin in the rat, highlighting the potential of responsive membrane systems if the technical and safety issues can be resolved.

## NOMENCLATURE

$A$	membrane area ( $m^2$ )
$C$	competitor concentration (M)
$C_D$	Donor compartment concentration (M)
$C_R$	receiving compartment concentration (M)
$C_n$	Flory characteristic ratio
$D_{gel}$	diffusate diffusivity in the gel phase ( $m^2s^{-1}$ )
$D_l$	diffusate diffusivity in the liquid phase ( $m^2s^{-1}$ )
$fb$	force per bond (N)
$I$	ionic strength (M)
$J$	Flux ( $M s^{-1}$ )
$k_r$	dissociation rate constant ( $s^{-1}$ )
$k'_r$	apparent dissociation constant under applied stress ( $s^{-1}$ )
$l$	the unit length along the polymer back bone (m)
$L_{tot}$	immobilized ligand concentration (M)
$k_b$	Boltzmann constant ( $J M^{-1} K^{-1}$ )
$K_a$	dissociation constant for acid (M)
$K_b$	dissociation constant for base (M)
$K_C$	dissociation constant for competitor/ligand (M)
$K_L$	dissociation constant for receptor/ligand (M)
$\bar{M}_c$	number average molecular weight between cross-links ( $kg M^{-1}$ )
$\bar{M}_n$	number average molecular weight of the polymer ( $kg M^{-1}$ )
$nb$	number of bonds
$P$	polymer concentration in the gel (M)
$Q$	ratio of the swollen gel volume to the dry gel volume
$r$	hydrodynamic radius of the solute (m)
$[RC]$	receptor/competitor complex concentration (M)
$[RL]$	receptor/ligand complex concentration (M)
$R_{tot}$	immobilized receptor sites concentration (M)
$sr$	swelling ratio
$v_1$	partial specific volume of the polymer ( $m^3$ )
$v_{2,r}$	polymer fraction of the gel after gel formation
$v_{2,s}$	polymer fraction of the gel at equilibrium swelling
$V$	volume of receiving compartment ( $m^3$ )
$V_1$	molar volume of water ( $m^3 kg^{-1}$ )
$Y$	fraction of immobilized ligand bound to receptor

$\delta$	membrane thickness (m)
$\xi$	mesh size (m)
$x_1$	Flory polymer-solvent interaction parameter
$\gamma$	bond interaction distance (m)

## REFERENCES

- Kost J and Langer R. Responsive polymeric delivery systems. *Advanced Drug Delivery Reviews* 2000; 46:125–148.
- Peppas NA and Mikos AG. Preparation methods and structure of hydrogels. In: Peppas NA Ed. *Hydrogels in Medicine and Pharmacy*, Vol. 1, CRC Press, Boca Raton, FL, 1986: pp. 1–27.
- Brannon-Peppas L. Preparation and characterization of cross-linked hydrophilic networks. In: Brannon-Peppas L, Harland RS Eds. *Absorbent Polymer Technology*, Elsevier: Amsterdam, 1990: pp. 45–66.
- Peppas NA, Buresa P, Leobandunga W, and Ichikawab H. Hydrogels in pharmaceutical formulations. *European Journal of Pharmaceutics and Biopharmaceutics* 2000; 50:27–46.
- Peppas NA, Huang Y, Torres-Lugo M, Ward JH, and Zhang J. Physicochemical foundations and structural design of hydrogels in medicine and biology. *Annual Review of Biomedical Engineering* 2000; 2:9–29.
- Ratner BD and Hoffman AS. Synthetic hydrogels for biomedical applications. In: Andrade JD Ed. *Hydrogels for Medical and Related Applications*, ACS Symposium Series, No. 31, American Chemical Society, Washington, DC, 1976; pp. 1–36.
- Peppas NA. Physiologically responsive gels. *Journal of Bioactive and Compatible Polymers* 1991; 6:241–246.
- Hennink WE, Franssen O, van Dijk-Wolthuis WNE, and Talsma H. Dextran hydrogels for the controlled release of proteins. *Journal of Controlled Release* 1997; 48:107–114.
- Leroux JC, Roux E, Garrec DL, Hong K, and Drummond DC. N-isopropylacrylamide copolymers for the preparation of pH-sensitive liposomes and polymeric micelles. *Journal of Controlled Release* 2001; 72:71–84.
- Rowley JA, Madlambayan G, and Mooney DJ. Alginate hydrogels as synthetic extracellular matrix materials. *Biomaterials* 1999; 20:45–53.
- Tomihata K and Ikada Y. Cross-linking of hyaluronic acid with water-soluble carbodiimide. *Journal of Biomedical Materials Research* 1997; 37:243–251.
- Chen YF and Yi M. Swelling kinetics and stimuli-responsiveness of poly (DMAEMA) hydrogels prepared by UV-irradiation. *Radiation Physics and Chemistry* 2001; 61:65–68.
- Soppimath KS, Kulkarni AR, and Aminabhavi TM. Chemically modified polyacrylamide-g-guar gum-based cross-linked anionic microgels as pH-sensitive drug delivery systems: Preparation and characterization. *Journal of Controlled Release* 2001; 75:331–345.
- Chiu HC, Wu AT, and Lin YF. Synthesis and characterization of acrylic acid-containing dextran hydrogels. *Polymer* 2001; 42:1471–1479.
- Qiu Y and Park K. Environment-sensitive hydrogels for drug delivery. *Advanced Drug Delivery Reviews* 2001; 53:321–339.
- Hennink WE and van Nostrum CF. Novel cross-linking methods to design hydrogels. *Advanced Drug Delivery Reviews* 2002; 54:13–36.
- Benslimane S, Guidoin R, Marceau D, Merhi Y, King MW, and Sigo-Luizard MF. Characteristics of polyester arterial grafts coated with albumin, the role and importance of the cross-linking chemicals. *European Surgical Research* 1988; 20:8–28.
- Gupta P, Vermani K, and Garg S. Hydrogels: From controlled release to pH-responsive drug delivery. *Drug Discovery Today* 2002; 7:569–579.
- Nguyen KT and West JL. Photopolymerizable hydrogels for tissue engineering applications. *Biomaterials* 2002; 23:4307–4314.
- GuÈ vena O, Sena M, Karadag E, and Saray D. A review on the radiation synthesis of copolymeric hydrogels for adsorption and separation purposes. *Radiation Physics and Chemistry* 1999; 56:381–386.
- Byrne ME, Park K, and Peppas NA. Molecular imprinting within hydrogels. *Advanced Drug Delivery Reviews* 2002; 54:149–161.
- Kim B and Peppas NA. Synthesis and characterisation of pH-sensitive glycopolymers for oral drug delivery systems. *Journal of Biomaterials Science, Polymer Edition* 2002; 13:1271–1281.
- Brannon-Peppas L and Peppas NA. Equilibrium swelling behavior of pH-sensitive hydrogels. *Chemical Engineering Science* 1991; 46:715–722.
- Miyata T, Uragami T, and Nakamae K. Biomolecule-sensitive hydrogels. *Advanced Drug Delivery Reviews* 2002; 54:79–98.
- Casolaro M and Barbucci R. An insulin-releasing system responsive to glucose—thermodynamic evaluation of permeability properties. *International Journal of Artificial Organs* 1991; 14:732–738.
- Brownlee M and Cerami A. A glucose-controlled insulin-delivery system: Semisynthetic insulin bound to lectin. *Science* 1979; 206:1190–1191.
- Kim SW and Jacobs HA. Self-regulated insulin delivery—artificial pancreas. *Drug Development and Industrial Pharmacy* 1994; 20:575–580.
- Taylor MJ, Tanna S, Cockshott S, and Vaitha R. A self-regulated delivery system using unmodified solutes in glucose-sensitive gel membranes. *Journal of Pharmacy and Pharmacology* 1994; 46 (Suppl. 2): 1051a.
- Taylor MJ, Tanna S, Taylor PM, and Adams G. Delivery of insulin from aqueous and nonaqueous reservoirs governed by a glucose sensitive gel membrane. *Journal of Drug Targeting* 1995; 3:209–216.

30. Kitano S, Koyama Y, Kataoka K, Okano T, and Sakurai Y. A novel drug delivery system utilizing a glucose responsive polymer complex between poly(vinyl alcohol) and poly(N-vinyl-2-pyrrolidone) with a phenyl boronic acid moiety. *Journal of Controlled Release* 1992; 19:162–170.
31. Kataoka K, Miyazaki H, Okano T, and Sakurai Y. Sensitive glucose-induced change of the lower critical solution temperature of poly[N, N-dimethylacrylamide-co-3-acrylamido[phenylboronic acid]] in physiological saline. *Macromolecules* 1994; 27:1061–1062.
32. Kataoka K, Miyazaki H, Bunya M, Okano T, and Sakurai Y. Totally synthetic polymer gels responding to external glucose concentration: Their preparation and application to on–off regulation of insulin release. *Journal of American Chemical Society* 1998; 120:12694–12695.
33. Yang S, Leong KF, Du Z, and Chua CK. The design of scaffolds for use in tissue engineering. Part I. Traditional factors. *Tissue Engineering* 2001; 7:679–689.
34. Lee KY, Rowley JA, Eiselt P, Moy EM, Bouhadir KH, and Mooney DJ. Controlling mechanical and swelling properties of alginate hydrogels independently by cross-linker type and cross-linking density. *Macromolecules* 2000; 33:4291–4294.
35. Dennis SE, Rosann MK, and Mark LJ. Gel Sensors and Method of use Thereof. 2001 US patent: 6180288B1.
36. Galaev IY and Mattiasson B. ‘Smart’ polymers and what they could do in biotechnology and medicine. *Trends in Biotechnology* 1999; 17:335–340.
37. Hennink WE, Talsma H, Borchet JCH, de Smedt SC, and Demeester J. Controlled release of proteins from dextran hydrogels. *Journal of Controlled Release* 1996; 39:47–55.
38. Vandamme Th F, Lenourry A, Charrueau C, and Chaumeil JC. The use of polysaccharides to target drugs to the colon. *Carbohydrate Polymers* 2002; 48:219–231.
39. Hovgaard L and Brøndsted H. Dextran hydrogels for colon-specific drug delivery. *Journal of Controlled Release* 1995; 36(1–2):159–166.
40. Ballerstadt R and Schultz JS. Kinetics of dissolution of concanavalin A/dextran sols in response to glucose measured by surface plasma response. *Sensors and Actuators B* 1998; 46:50–55.
41. Ehwald R, Ballerstadt R, and Dautzenberg H. Viscosimetric affinity assays. *Analytical Biochemistry* 1996; 234:1–8.
42. Zhang R. Dextran Hydrogel Preparation and Application in Biomedical Engineering. PhD Thesis, University of Bath, England, 2004.
43. Langer R and Peppas NA. Advances in biomaterials, drug delivery, and bionanotechnology. *AIChE Journal* 2003; 49:2990–3006.
44. Podual K, Doyle F, and Peppas NA. Modeling of water transport in and release from glucose-sensitive swelling-controlled release systems based on poly(diethylaminoethyl methacrylate-g-ethylene glycol). *Industrial & engineering chemistry research* 2004; 43:7500–7512.
45. Cartier S, Horbett TA, and Ratner BD. Glucose-sensitive membrane coated porous filters for control of hydraulic permeability and insulin delivery from a pressurized reservoir. *Journal of Membrane Science* 1995; 106:17–24.
46. Miyata T, Asami N, and Uragami T. A reversibly antigen-responsive hydrogel. *Nature* 1999; 399:766–769.
47. Obaidat AA and Park K. Characterization of protein release through glucose-sensitive hydrogel membranes. *Biomaterials* 1997; 18:801–806.
48. Tang M, Zhang R, Bowyer A, Eisenthal R, and Hubble J. An NAD-sensitive hydrogel for the release of macromolecules. *Biotechnology Bioengineering* 2004; 87:791–796.
49. Nakamae K, Miyata T, Jikihara A, and Hoffman AS. Formation of poly(glycosyloxyethyl methacrylate)–concanavalin A complex and its glucose sensitivity. *Journal of Biomaterials Science, Polymer Edition* 1994; 6:79–90.
50. Miyata T, Jikihara A, Nakamae K, and Hoffman AS. Preparation of poly(2-glucosyloxyethyl methacrylate)–concanavalin A complex hydrogel and its glucose-sensitivity. *Macromolecular Chemistry and Physics* 1996; 197:1135–1146.
51. Tanna S, Taylor MJ, and Adams G. Insulin delivery governed by covalently modified lectin-glucogen gels sensitive to glucose. *Journal of Pharmacy and Pharmacology* 1999; 51:1093–1098.
52. Kim JJ and Park K. Glucose-binding property of pegylated concanavalin. *A Pharmaceutical Research* 2001; 18:794–799.
53. Tanna S, Sahota T, Clark J, and Taylor MJ. Covalent coupling of concanavalin A to a Carbolon 934P and 941P carrier in glucose-sensitive gels for delivery of insulin. *Journal of Pharmacy and Pharmacology* 2002; 54:1461–1469.
54. Tang M, Zhang R, Bowyer A, Eisenthal R, and Hubble J. A reversible hydrogel membrane for controlling the delivery of macromolecules. *Biotechnology and Bioengineering* 2003; 82:47–53.
55. Mika AM, Childs RF, Dickson JM, McCarry BE, and Gagnon DR. A new class of polyelectrolyte-filled microfiltration membranes with environmentally controlled porosity. *Journal of Membrane Science* 1995; 108:37–56.
56. Yamaguchi T, Ibe M, Nair BN, and Nakao S. A pore-filling electrolyte membrane-electrode integrated system for a direct methanol fuel cell application. *Journal of the Electrochemical Society* 2002; 149:A1448–A1453.
57. Mika AM, Childs RF, and Dickson JM. Ultra-low pressure water softening: A new approach to membrane construction. *Desalination* 1999; 121:149–158.
58. Winnik FM, Morneau A, Mika AM, Childs RF, Roig A, Molins E, and Ziolo RF. Polyacrylic acid pore-filled microporous membranes and their use in membrane-mediated synthesis of nanocrystalline ferrihydrite. *Canadian Journal of Chemistry-Revue Canadienne de Chimie*. 1998; 76:10–17.
59. Childs RF, Mika AM, Pandey AK, McCrory C, Mouton S, and Dickson JM. Nanofiltration using pore-filled membranes: Effect of polyelectrolyte composition on performance. *Separation and Purification Technology*. 2001; 22:507–517.
60. Yamaguchi T, Miyata F, and Nakao S. Pore-filling type polymer electrolyte membranes for a direct methanol fuel cell. *Journal of Membrane Science* 2003; 214:283–292.
61. Mika AM, Childs RF, Dickson JM, McCarry BE, and Gagnon DR. Porous, polyelectrolyte-filled membranes: Effect of cross-linking on flux and separation. *Journal of Membrane Science* 1997; 135:81–92.

62. Pandey AK, Childs RF, West M, Lott JNA, McCarry BE, and Dickson JM. Formation of pore-filled ion-exchange membranes with in situ cross-linking: Poly(vinylbenzyl ammonium salt)-filled membranes. *Journal of Polymer Science Part A-Polymer Chemistry* 2001; 39:807–820.
63. Huang Y, Szleifer I, and Peppas NA. A molecular theory of polymer gels. *Macromolecules* 2002; 35:1373–1380.
64. Flory PJ and Rehner R Jr. Statistical mechanics of cross-linked polymer networks. I. Rubberlike elasticity. *Journal of Chemical Physics* 1943; 11:512–520.
65. Peppas NA and Merrill EW. Cross-linked poly(vinyl alcohol) hydrogels as swollen elastic networks. *Journal of Applied Polymer Science* 1976; 21:1763–1770.
66. De SK, Aluru NR, Johnson B, Crone WC, Beebe DJ, and Moore J. Equilibrium swelling and kinetics of pH-responsive hydrogels: Models, experiments, and simulations. *Journal of Microelectromechanical Systems* 2002; 11:544–555.
67. Mayes AG, Hubble J, and Eisenthal R. Binding Isotherms for soluble immobilised affinity ligands. *Biotechnology and Bioengineering* 1992; 40:1263–1270.
68. Canal T and Peppas NA. Correlation between mesh size and equilibrium degree of swelling of polymeric networks. *Journal of Biomedical Materials Research* 1989; 23:1183–1193.
69. Bell GI. Models for the specific adhesion of cells to cells. *Science* 1978; 200:618–627.
70. Peppas NA and Reinhaart F. Solute diffusion in swollen membranes Part I. A new theory. *Journal of Membrane Science* 1983; 15:275–287.
71. Lustig SR and Peppas NA. Solute diffusion in swollen membranes IX. Scaling laws for solute diffusion in gels. *Journal of Applied Polymer Science* 1988; 36:735–747.
72. Hinchcliffe M and Illum L. Intranasal insulin delivery and therapy. *Advanced Drug Delivery Reviews* 1999; 35:199–234.
73. Pitt CG. The controlled parenteral delivery of polypeptides and proteins. *International Journal of Pharmaceutics* 1990; 59:173–196.
74. Vicini P, Caumo A, and Cobelli C. Hot IVGTT two-compartment model: Indexes of glucose effectiveness and insulin sensitivity. *American Journal of Physiology* 1997; 273:E1024–E1032.
75. Parker RS, Doyle III FJ, Ward JH, and Peppas NA. Robust  $H_{\infty}$  glucose control in diabetes using a physiological model. *AIChE Journal* 2000; 46:2537–2549.
76. Steil GM, Panteleon AE, and Rebrin K. Closed-loop insulin delivery—the path to physiological glucose control. *Advanced Drug Delivery Reviews* 2004; 56:125–144.
77. Taylor M, Tanna S, and Sahota T. Closed loop insulin delivery in vivo. *Drug Delivery Systems* 2003; 3:11–17.

## *Section II*

---

*Membrane Applications in Biotechnology,  
Food Processing, Life Sciences, and Energy  
Conversion*



---

# 17 Membrane Applications in Biotechnology, Food Processing, Life Sciences, and Energy Conversion: Introduction

*Syed S.H. Rizvi*

## CONTENTS

Reference.....	496
----------------	-----

Biological membranes have long been known to be crucially important in cellular homeostasis and metabolic-energy transduction. They not only control cellular transport processes but also regulate various functional characteristics of multicellular organisms. Recent studies on bipolar membranes have provided a better understanding of the mechanism of ionic transport in cellular systems and have also led to new developments in highly selective membranes with such characteristics as permselectivity for monovalent ions, rectification, and water splitting. These discoveries are indeed harbingers of new heights to be attained in the field of bioseparations.

Developments in synthetic membranes and their utilization are more recent. Industrial applications of membrane-based processes in bioscience and technology have accelerated over the last four decades. The membranes are now used in numerous diverse fields extending from production of potable water and separation of gases, to drug delivery and cold sterilization of beverages and pharmaceuticals. It is often a method of choice for concentration and separation of different components of a macromolecular mixture or solutions, especially if they are sensitive to high temperatures. The physical and chemical make up of these membrane material are exploited to create a selective barrier for separation of species of different size, shape, electrical charge, and related properties. Porous membranes affect separation primarily by discrimination of size and shape, and hydrodynamic sieving; while nonporous membranes depend on sorption and diffusion. There has been tremendous progress in our understanding of how components pass through a membrane; both on the basis of thermodynamics of solubility and kinetics of diffusion that together constitute what is called permeability.

The utility of a membrane system is dictated by the degree of desired separations achieved and the rate of separation. The degree of desired separations is measured in terms of solute selectivity or rejection, while the rate of separation is evaluated by a combination of flux and fouling. The performance of a particular membrane and its replacement frequency will affect operation and maintenance cost, and invariably dictate the process selection. Some of the most attractive features of membranes are already listed in Chapter 1. Among few drawbacks, high initial capital costs, fouling, achievable product purity, and limited durability often pose limitations to their widespread utilization. Nevertheless, numerous industrially significant processes in the food processing and biotechnology industries continue to capitalize on the many products made using membrane-based processes. Some of the current examples include water desalination and purification, and cold sterilization of beverages; recovery and fractionation of proteins from cheese whey; clarification of fruit juice, wines and beer; removal of bacteria from water; effluent treatment for removal of heavy metals and organic materials; separation of oil/water emulsions; removal of VOCs from air; controlled release of drugs; separation of plasma from blood; dewatering of suspended solids such as slurries, among many others.

The statement made by Drioli and Romano in 2001 [1] on performance of various membrane-based installations in France is given as below:\*

It is interesting to mention that statistical analysis carried by Electricité de France on 174 different membrane installation in France using MF, UF, RO, and ED mainly in small- and medium-sized industries found a normal percentage of satisfaction between 70% and 95%, one of the highest positive responses received in this kind of analysis. This result is, in part, surprising because of the high innovative content of the technology and the lack of education still existing on their basic properties. It is, however, consistent with the important contributions that membrane operations can make in terms of cost reduction, quality improvement, pollution control etc.

The potential of membranes to provide nonthermal energy conversion through fuel cells is widely recognized and has received support from governmental agencies. Numerous research teams are working extensively across the world to develop different types of membrane-based fuel cells and a large number of publications have come out in recent years in this area. This clearly indicates that future research will be aimed at commercializing fuel cells as an alternative to current power sources.

The continuous interest and growth of the various new industrial processes related to the life sciences will also require significant contributions from membrane engineering. It is hoped that future research would provide deeper insight on the precise mechanisms involved, which would show new direction for research in membrane science and applications. It is, however, important to recognize that applicability of electroporation has been demonstrated in a variety of bacteria, yeast, and mammalian cells and some applications are ready for exploitation while many new technologies seem potentially possible.

It is indeed impossible to capture all current and future applications, and uses in any one publication. What follows here is a selective presentation from the large number of possible membrane-based processes of relevance to bioprocess industries.

Ultrafiltration-based protein bioseparation is the subject of Chapter 18 and how it can, by judicious choices of operating parameters, significantly reduce the number of purification steps currently in use. Membrane distillation, which is a relatively new and emerging area of application for concentration of dilute aqueous feedstock in which a microporous hydrophobic membrane is used, is covered in Chapter 19. Membrane-based separations in the brewing industry are discussed in Chapter 20 and a variety of uses ranging from beer clarification and cold sterilization to tank bottoms recovery, alcohol removal, as well as water and effluent treatment are detailed. Chapter 21 summarizes the principles of operation of monopolar and bipolar membrane and their applications in food and chemical processing, pollution control, and resource recovery with specific details on electrodialysis. The current state of research and development in the sprawling industrial use of membranes in the dairy industry for various processing purposes is presented in Chapter 22.

Chapter 23 is devoted to one of the most critical medical applications and discusses the principle and design of microporous membrane blood oxygenator that are used to ensure that oxygen-rich blood reaches the cells in the body during cardiopulmonary operations. In Chapter 24, the design, synthesis, characterization, and applications of nanotube membranes in bioextraction and biocatalysis are discussed. The physicochemical properties and modeling of emulsion liquid membranes and their uses in chemical and biotechnological separations are elaborated in Chapter 25. Chapter 26, goes into the mechanics and biophysical aspects of cell membrane and the current understanding of the dynamics involved in electropore formation and molecular transport, which have numerous promising implication to human health. The last chapter of this section, Chapter 27 deals with developments in polymer electrolyte membrane fuel cells, covering the principles, types, transport modeling, and their applications.

It is hoped that the Chapters 18 through 27 would well serve the needs of professionals, both researchers and practitioners, interested in the depth and breadth of membrane-based technologies of utility to them.

## REFERENCE

1. Drioli E and Romano M. Progress and new perspectives on integrated membrane operations for sustainable industrial growth, *Ind. Eng. Chem. Res.*, 40, 1277, 2001.

---

\* From Drioli, E. and Romano, M. *Ind. Eng. Chem. Res.*, 40, 1277, 2001. With permission.

---

# 18 Ultrafiltration-Based Protein Bioseparation

*Raja Ghosh*

## CONTENTS

18.1	Bioseparation .....	497
18.2	Ultrafiltration .....	498
18.3	Membranes .....	499
18.4	Theory of Ultrafiltration .....	502
18.5	Concentration .....	504
18.6	Desalting .....	505
18.7	Clarification .....	509
18.8	Fractionation .....	509
18.9	Conclusions .....	511
	References .....	511

## 18.1 BIOSEPARATION

Bioseparations engineering deals with the large-scale purification of biological products such as proteins that are used as biochemicals, pharmaceuticals, foods, food additives, nutraceuticals, and agrochemicals. Biological products can be categorized in different ways. One way is to classify them based on their applications (see Table 18.1). Developments in the field of bioseparations engineering have largely been fueled by the rapid growth in biotechnology. More and more biological products are now required to be purified in sizable quantities. The separation of biological products from their respective starting material (i.e., biological reaction medium or tissue extract) is technically difficult and expensive and can frequently be the critical limiting factor in biological manufacturing. In many cases, the bioseparation cost is a substantial component of the total cost of production. Manufacturing cost is perhaps a minor issue with newly developed products that enjoy patent protection, since the cost of product bears no correlation with cost of production. This is due to the significantly high markup in product price, which essentially serves to cover the substantial cost of product development. However, for generic biological products, the viability of a manufacturing process depends largely on the cost of production. Table 18.2 lists the bioseparation costs of certain biological products as percentage of total manufacturing cost. For high-value biological products such as generic therapeutic proteins, the purification cost can be very significant, mainly due to the following reasons:

1. Low product yield in bioreactors
2. Product complexity
3. Susceptibility of product degradation
4. Stringent quality requirements
5. Need for multistep separation
6. Need for specialized bioseparation techniques, e.g., affinity chromatography

Conventional bioseparation is based on an RIPP (recovery, isolation, purification, and polishing) scheme [1]. This involves using low-resolution, high-productivity techniques (e.g., precipitation, filtration, centrifugation, and crystallization) first, primarily to reduce the overall volume and concentration of the process stream (this being referred to as recovery and isolation). This is followed by high-resolution, low-productivity techniques (e.g., affinity separations, chromatography, and electrophoresis) for purification and polishing. With the advent of membrane separation processes and other new types of separations, it is now possible to combine high productivity with high resolution, and thus the opportunity exists to potentially

**TABLE 18.1**  
**Classification of Biological Products Based on Their Applications**

Categories	Biological Products
Industrial chemicals	Solvents, organic acids, industrial enzymes
Agrochemicals	Biofertilizers, biopesticides
Biopharmaceuticals	Antibiotics, hormones, monoclonal antibodies, plasma proteins, insulin, vaccines, alkaloids
Food and nutraceuticals	Whey proteins, milk proteins, egg proteins, soy proteins, vitamins, amino acids, protein hydrolysates, yeast cells, yeast extract
Diagnostic products	Glucose oxidase, peroxidase, hormones
Commodity chemicals	Detergent enzymes, insecticides
Laboratory reagents	Bovine serum albumin, ovalbumin, lysozyme
Cosmetic products	Plant extracts, animal tissue extracts

cut down the number of purification steps. Membrane processes such as ultrafiltration inherently give high productivity and can be fine-tuned or optimized to give high selectivity.

## 18.2 ULTRAFILTRATION

Ultrafiltration is a pressure-driven, selective permeability-based separation process in which membranes having pore sizes ranging from 1 to 100 nm are used for processing macromolecules such as proteins. Figure 18.1 shows ultrafiltration relative to other membrane-based separation processes. A common notion about ultrafiltration is that separation is solely based on solute size. However, solute size is only one of the many factors, which influence separation in ultrafiltration. Indeed, a membrane can be made to retain a smaller molecule while allowing a larger molecule to pass through; this phenomenon is referred to as reversed selectivity. One cannot overemphasize the fact that solute separation by ultrafiltration is highly complex in nature, and appreciating this complexity is absolutely essential if ultrafiltration is to be used efficiently. The complexity of ultrafiltration rather than being a weakness is its strength since it makes it possible to carry out separations that would not have been possible had ultrafiltration been a purely size-based separation process [2].

Ultrafiltration has a broad variety of applications ranging from the processing of biological macromolecules to wastewater treatment. Food and biotechnological applications account for nearly 40% of current total usage of ultrafiltration membranes [2]. Processing of biological macromolecules, such as proteins and nucleic acids, has assumed significant importance in the bioprocess industry, where the impact of downstream processing on the overall process economics is now better appreciated. From an operational point of view ultrafiltration is used for

1. Concentration (removal of solvent from protein solutions)
2. Desalting (removal of low-molecular weight compounds from protein solutions)
3. Clarification (i.e., removal of particles from protein solutions)
4. Fractionation (i.e., protein–protein separation)

**TABLE 18.2**  
**Cost of Bioseparation**

Product	Bioseparation Cost (%)
Solvents, e.g., ethanol, acetone	15–20
Cells, e.g., bakers yeast, brewers yeast	20–25
Crude cellular extracts, e.g., yeast extract	20–25
Organic acids, e.g., citric acid, lactic acid	30–40
Vitamins and amino acids, e.g., lysine, ascorbic acid	30–40
Gums and polymers, e.g., xanthan, gellan	40–50
Antibiotics, e.g., penicillins, rifampicin	20–60
Industrial enzymes, e.g., amyloglucosidase, glucose isomerase	40–65
Nonrecombinant therapeutic proteins, e.g., pancreatin, papain, diastase	50–70
r-DNA products, e.g., recombinant insulin, recombinant streptokinase	60–80
Monoclonal antibodies	50–70
Nucleic acid-based products	60–80
Plasma proteins, human albumin, human immunoglobulins	70–80

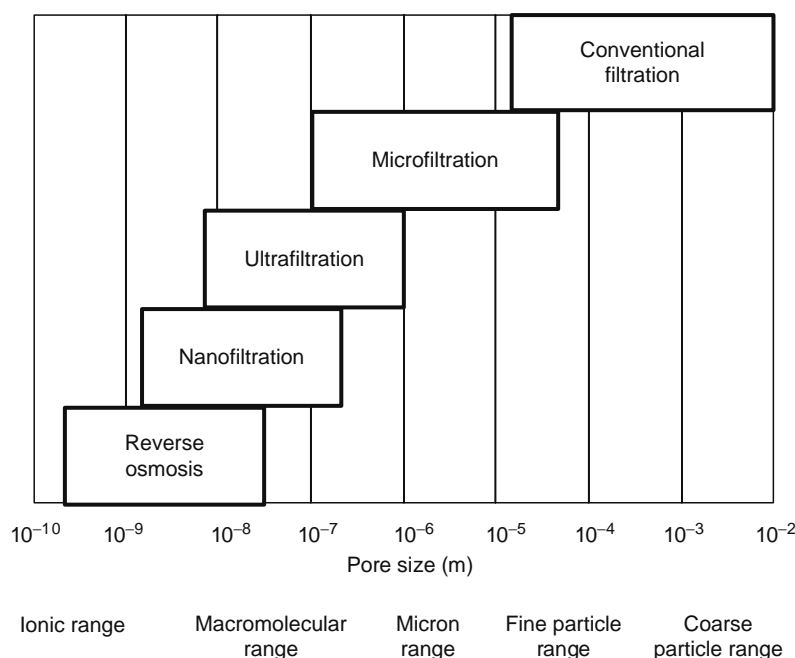


**FIGURE 18.1** Classification of membrane processes.

Concentration, desalting, and clarification processes are well-established operations in the industry for quite some time (since the 1970s). Macromolecular fractionation using ultrafiltration is significantly more challenging and is still a developing field. The major advantages of ultrafiltration over competing separation technologies are high throughput of product, relative ease of scale-up, and ease of equipment cleaning and sanitization.

### 18.3 MEMBRANES

A membrane is the key component of an ultrafiltration process and is defined as a thin barrier through which solutes are selectively transported. Ultrafiltration membranes are prepared from organic polymers, such as cellulose and cellulose derivatives like cellulose acetate (CA), polysulfone (PS), polyethersulfone (PES), polyvinylidene fluoride (PVDF), polyamide (PA), and polyacrylonitrile (PAN). Membranes made from ceramic material are widely used in the water industry but their use in protein processing has been very limited. From a structural point of view polymeric membranes can be broadly divided into two types: symmetric and asymmetric (or anisotropic). A symmetric membrane has similar structural morphology at all positions within it, while an anisotropic membrane is a composite of two or more structural planes of dissimilar morphologies (see Figure 18.2). Most ultrafiltration membranes are anisotropic. The selectivity and hydraulic permeability of an anisotropic membrane are usually due to an ultrathin skin layer, which can be 0.2–1  $\mu\text{m}$  thick. The skin layer is backed up by a microporous-supporting layer, which gives form and mechanical support.

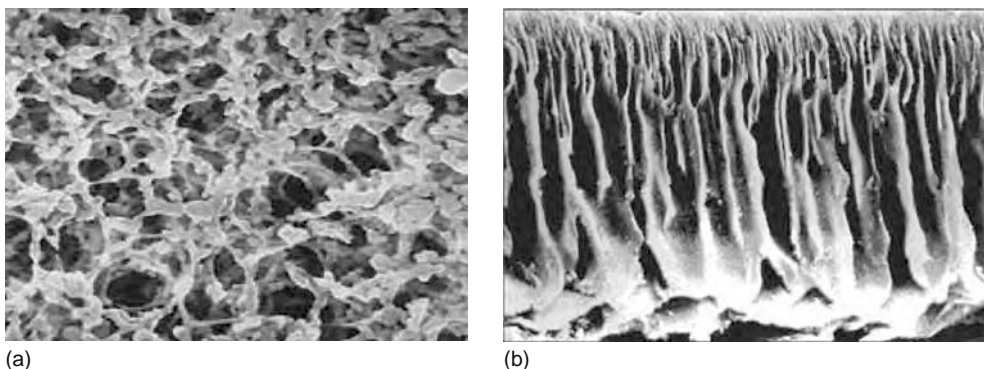


**FIGURE 18.2** (a) Symmetric and (b) asymmetric membranes. (Micrograph of symmetric membrane. Courtesy of Millipore Corporation. With permission.)



**FIGURE 18.3** Stirred cell. (Photo courtesy of Millipore Corporation. With permission.)

The term membrane element refers to the basic form in which a membrane is prepared. There are three types of membrane elements: flat sheets, hollow fibers, and tubular membranes. The device within which the membrane element is housed is referred to as the membrane module. The design of the membrane module largely depends on the type of membrane element, as well as on additional requirements such as the need for cleaning and disassembling, the required transmembrane pressure (TMP), and the required hydrodynamic conditions. Some of the different modules types are (see Figures 18.3 through 18.7):

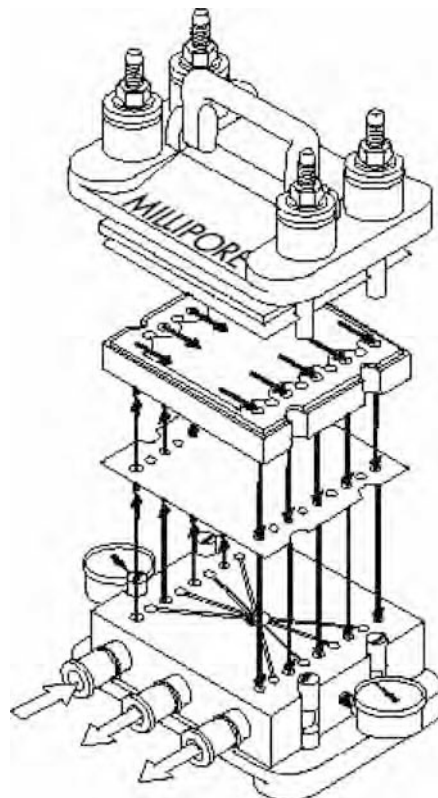


**FIGURE 18.4** Flat sheet TF flow membrane module. (Figure courtesy of Millipore Corporation. With permission.)

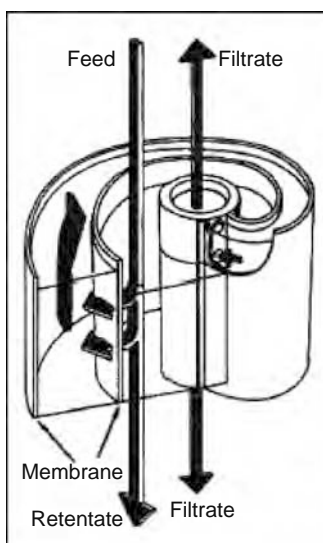


**FIGURE 18.5** Spiral wound membrane module. (Figure courtesy of Millipore Corporation. With permission.)



**FIGURE 18.6** Tubular membrane module. (Photo courtesy of PCI Membranes. With permission.)



**FIGURE 18.7** Hollow fiber membrane module. (Photo courtesy of Millipore Corporation. With permission.)

**TABLE 18.3**  
**Characteristics of Membrane Modules**

Type	Applications	Feed Hold-up	Special Remarks
Stirred cell	Laboratory	High	Sometimes used for dead-end ultrafiltration
Flat sheet TF	Food, pharmaceuticals, biotechnology	Moderate	Easy dismantling and cleaning
Spiral wound	Food, pharmaceutical, water	Low	Uses flat sheet membrane element
Hollow fiber	Pharmaceuticals, water, bioreactors	Low	Susceptible to fiber blocking
Tubular	Water, wastewater, industrial chemicals	High	Easy cleaning

1. Stirred cells (only for laboratory-scale applications)
2. Flat sheet tangential (TF) flow module
3. Spiral wound module
4. Tubular module
5. Hollow fiber module

Table 18.3 lists the relative advantages and disadvantages of the different types of membrane modules.

Membrane modules can be operated in the dead-end or cross-flow modes (see Figure 18.8). Dead-end ultrafiltration is used mostly for laboratory-scale applications and industrial ultrafiltration processes are usually carried out in the cross-flow mode. The main advantage of cross-flow ultrafiltration is the lower extent of concentration polarization. The cross-flow mode also allows recirculation of the retentate stream to the feed tank followed by its mixing with fresh feed that leads to several operational advantages.

#### 18.4 THEORY OF ULTRAFILTRATION

Solvent transport through a membrane is driven by an applied TMP gradient. The TMP used in ultrafiltration ranges from 0 to 500 kPa, though most ultrafiltration processes are carried out at less than 100 kPa TMP. The transport of solvent through an ultrafiltration membrane is quantified in terms of the volumetric permeate flux ( $J_v$ ), which is obtained by dividing the volumetric filtration rate by the membrane area. Solute molecules may be either fully or partially transmitted or indeed totally retained (or rejected) by an ultrafiltration membrane. This depends on a number of factors that include steric, hydrodynamic, thermodynamic, and electrostatic effects. Solute retention leads to its build-up near the membrane surface this being referred to as concentration polarization. Concentration polarization results in generation of an osmotic back pressure, which acts against the TMP. The basic working equation for ultrafiltration processes is the osmotic pressure model [3]

$$J_v = \left( \frac{\Delta P - \Delta \pi}{\mu R_m} \right) \quad (18.1)$$

where

$\Delta P$  is the TMP

$\Delta \pi$  is the osmotic back pressure

$\mu$  is the permeate viscosity

$R_m$  is the resistance offered by the membrane

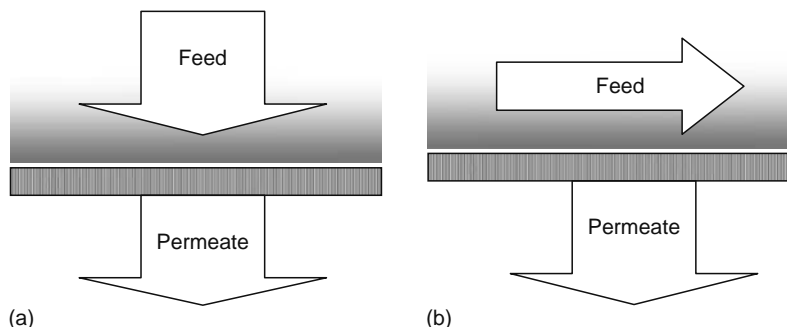


**FIGURE 18.8** Dead-end (a) and cross-flow (b) mode.

In certain cases the accumulated solute may form a gel layer on the membrane leading to an additional gel-layer resistance ( $R_g$ ):

$$J_v = \left( \frac{\Delta P - \Delta \pi}{\mu(R_m + R_g)} \right) \quad (18.2)$$

Concentration polarization is clearly a limiting factor in ultrafiltration. Several methods have been developed to reduce concentration polarization, which includes [4–10]:

1. Creation of pulsatile flow in membrane module
2. TMP pulsing
3. Creation of oscillatory flow
4. Flow obstruction using inserts
5. Generation of Dean vortices in membrane module
6. Generation of Taylor vortices in membrane module
7. Gas-sparging

Ultrafiltration relies on the ability of a membrane to act as a selective barrier. One of the major properties of an ultrafiltration membrane is its ability to act as a sieve for macromolecular substances. The transmission of a particular solute through an ultrafiltration membrane can be expressed in several ways, a commonly used way being in terms of sieving coefficients. The intrinsic or real sieving coefficient ( $S_i$ ) is defined as

$$S_i = \left( \frac{C_p}{C_w} \right) \quad (18.3)$$

where  $C_p$  is the solute concentration in the permeate, while  $C_w$  is that on the membrane surface.  $S_i$  depends on the solute-membrane system, the operating conditions such as pH, ionic strength, temperature, and presence of additives such as surfactants and organic solvents. The intrinsic sieving coefficient of a noninteracting solute can be predicted using the following equation that is based on the diffusive–convective membrane transport theory [11]:

$$S_i = \left( \frac{S_\infty \exp\left(\frac{S_\infty J_v \delta_m}{D_{\text{eff}}}\right)}{S_\infty + \exp\left(\frac{S_\infty J_v \delta_m}{D_{\text{eff}}}\right) - 1} \right) \quad (18.4)$$

where

$S_\infty$  is an asymptotic sieving coefficient

$\delta_m$  is the membrane thickness

$D_{\text{eff}}$  is the effective diffusivity of the solute within the pores

Most proteins would be expected to interact with the membrane to some extent. The intrinsic sieving coefficient of an interacting solute can be determined using Equation 18.5 [12]:

$$S_i^{\text{Interacting}} = S_i \exp\left(-\frac{E}{KT}\right) \quad (18.5)$$

where

$E$  is the activation energy

$K$  is the Boltzmann constant

$T$  is the absolute temperature

Due to concentration polarization, the solute concentration near the membrane surface tends to be higher than that in the bulk feed. Another sieving coefficient term that is commonly used is the apparent or observed sieving coefficient ( $S_a$ ) which is defined as

$$S_a = \left( \frac{C_p}{C_b} \right) \quad (18.6)$$

where  $C_b$  is the solute concentration in the bulk feed. The apparent sieving coefficient of a solute can be predicted using Equation 18.7 [13]:

$$S_a = \left( \frac{S_\infty \left( \frac{S_\infty J_v \delta_m}{D_{\text{eff}}} + \frac{J_v}{k} \right)}{(S_\infty - 1) \left( 1 - \exp\left( \frac{S_\infty J_v \delta_m}{D_{\text{eff}}} \right) \right) + S_\infty \exp\left( \frac{S_\infty J_v \delta_m}{D_{\text{eff}}} + \frac{J_v}{k} \right)} \right) \quad (18.7)$$

where  $k$  is the mass transfer coefficient of the solute and depends on the hydrodynamic conditions within the membrane module. For fully developed laminar flow on the feed side the following correlation could be used to calculate mass transfer coefficient [3].

$$k = 0.816\gamma^{0.33} D^{0.67} l^{-0.33} \quad (18.8)$$

where

$\gamma$  is the wall shear rate

$D$  is the solute diffusivity

$l$  is the length of the membrane module

The different solute concentrations on the feed and permeate sides are linked to the volumetric permeate flux in terms of the concentration polarization model, which is based on the stagnant film theory [14]:

$$J_v = k \ln \left( \frac{C_w - C_p}{C_b - C_p} \right) \quad (18.9)$$

Membrane manufacturers prefer to use a parameter called the nominal molecular weight cut-off (NMWCO) or simply the molecular weight cut-off (MWCO) to specify the sieving properties of their membranes. For a given membrane this is defined as the molecular weight of a solute that has an apparent sieving coefficient of 0.1. Polymers, such as dextran or polyethylene glycol, are usually used to determine MWCO.

Membrane fouling refers to the loss of membrane performance due to adsorption and deposition of material present in the feed on the membrane surface and within the pores. Membrane fouling primarily leads to reduction in volumetric permeate flux and alteration in solute transmission behavior. Membrane fouling usually leads to lowering of the sieving coefficients but in some cases, the sieving coefficients can be increased due to fouling. This is usually due to electrostatic shielding. Fouling can be reversible, i.e., its effects can be reversed by appropriate cleaning methods or irreversible, i.e., membrane properties are permanently altered. Proteins are major foulants and can cause both reversible and irreversible fouling. Fouling is a highly undesirable effect and efforts are necessary to keep it at an acceptably low level. Factors that affect membrane fouling are physicochemical properties of the membrane and the solutes, membrane morphology, operating parameters (TMP, system hydrodynamics), physicochemical properties of the feed solution (pH, salt concentration), and membrane operation history. With certain types of membranes, particularly when operated at high TMP, membrane compaction (i.e., resulting from deformation) may also result in flux decline.

## 18.5 CONCENTRATION

A concentration process involves removal of a solvent, typically water from a macromolecular solution. Ultrafiltration is the method of choice for large-scale concentration. The selectivity issue involving removal of water from a macromolecular solution using ultrafiltration is trivial. The main challenge in a concentration process is maintaining a high productivity on account of the increased macromolecular concentration in the feed solution. Some of the main applications of macromolecular concentration using ultrafiltration are listed below [2]:

1. Concentration of plasma proteins
2. Processing of milk products
3. Concentration of whey proteins
4. Concentration of soy proteins
5. Concentration of enzymes

The type of ultrafiltration membrane to be used for a particular concentration process would depend on the type of protein being concentrated. The membrane should typically give greater than 99% macromolecular retention. Membrane manufacturers frequently provide tabular information to aid membrane selection (see Figure 18.9). Membrane modules used in concentration processes should have low hold-up volume on the feed side, ability to handle viscous feed, and ability to give high mass transfer coefficient of the retained solute. Flag sheet TF flow membrane modules are widely used for concentration-type processes. Where the viscosity of the final concentrated product is low, hollow fiber membrane modules are used. Tubular membrane devices on account of their high hold-up volume are generally not used.

Concentration is commonly operated as a batch process (see Figure 18.10). The liquid to be concentrated is pumped from a feed tank through a cross-flow ultrafiltration membrane module and the retentate is returned to the tank. The ultrafiltration process is generally carried out at a constant TMP, which is generated by throttling the retentate line. The permeate that is free from protein is discarded and hence the feed concentration increases in the feed tank with time. The batch concentration system is conceptually simple and efficient due to the low possible material exposure to the membrane for a given degree of concentration. The main limitation of the batch concentration mode is the need for a large dedicated feed tank. This limitation can be overcome using a fed-batch process (see Figure 18.11) in which a small primary feed tank is fed from a larger secondary feed tank or where relevant, directly from a bioreactor. Batch process is preferred where dedicated equipment is used for a particular product-line. Where the same ultrafiltration equipment is used for multiple product-lines, fed-batch process is preferred since the membrane filtration setup can be mounted on a skid and can be moved around in the manufacturing plant. This provides operational flexibility and versatility. However, the efficiency of membrane usage is lower since the exposure of the membrane to material is greater when compared with the batch mode. Where continuous protein concentration is required, a continuous process can be carried out using the multistep setup shown in Figure 18.12. A single step setup would generally give very low degrees of continuous concentration. A partial recycle process (see Figure 18.13) could achieve reasonable good concentration factors since a certain proportion of the concentrated retentate is directly taken through a recycle line to the feed stream, thus effectively avoiding dilution in the feed tank.

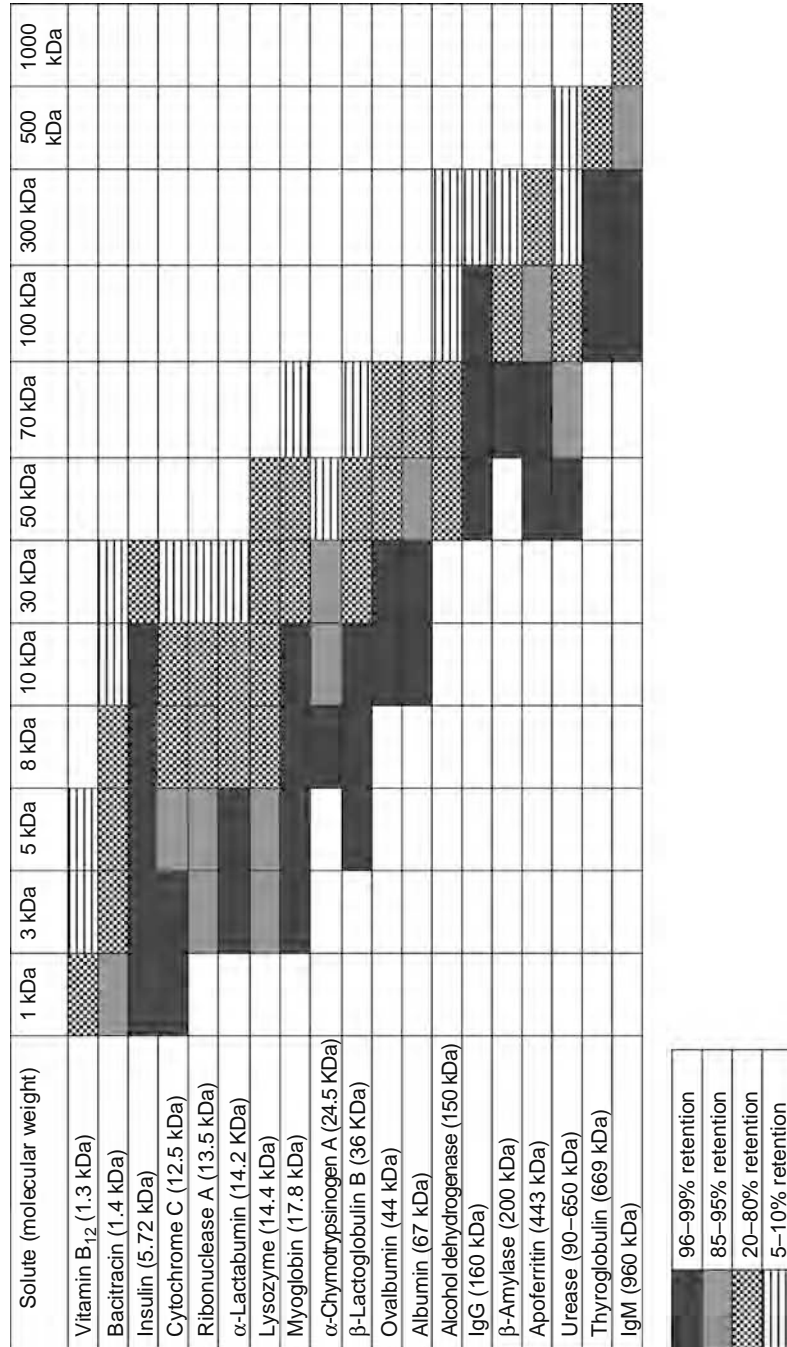
## 18.6 DESALTING

Desalting refers to the removal of low-molecular weight solutes (e.g., salts and peptide fragments) from protein solutions. This is an example of diafiltration and is achieved using an ultrafiltration membrane that retains the protein while allowing the low-molecular weight substance to pass. The macromolecular retention should be in excess of 98%. The principle of desalting is shown in Figure 18.14. Buffer exchange, which is operationally similar to desalting involves the gradual replacement of one buffer by another. Solute selectivity is mostly not a major issue in desalting on account of the significant differences in solute size. However, when low-molecular weight substances interact with proteins, obtaining good selectivity could be challenging. One of the main objectives in a desalting process is to achieve and sustain a high permeate flux. In a desalting process, it might sometimes be desirable to dilute the feed to enhance the permeate flux. Some of the major applications of desalting are listed below [2]:

1. Removal of salts used for precipitation from protein solutions
2. Removal of solvents used for precipitation from protein solutions
3. Removal of peptide fragments from protein solutions
4. Buffer exchange before and after chromatographic separation
5. Removal of toxic metabolites from blood
6. Formulation of therapeutic proteins in solutions
7. Removal of inhibitors from enzyme solutions
8. Protein refolding

Desalting is mostly carried out while keeping the feed volume constant, i.e., by replenishing the liquid lost in the filtrate. Therefore the protein concentration in the feed is also maintained constant. Exceptions are where simultaneous concentration and desalting are carried out.

Industrial-scale desalting processes are carried in the cross-flow mode at constant TMP. A wider variety of membrane modules than in concentration can be used for desalting. This includes flag sheet TF flow, hollow fiber, spiral wound, and tubular modules. A batch process (see Figure 18.15) is most commonly used for desalting. The feed solution is pumped into an ultrafiltration module and the retentate is sent back to the feed tank. The feed volume is usually maintained constant by continuous addition of fresh solvent. In a batch process the concentration of permeable species decreases with time while the concentration of the retained species remains unchanged. This is due to continuous replenishment of liquid by addition into the feed tank. In some separation processes, intermittent replenishment of solvent is preferred to continuous replenishment. Multiple stages are commonly used for continuous desalting (Figure 18.16).



Note: \*Data derived using stirred cells, +0.1%-0.2% buffered solutions at 3.7 bar (55 psig).

FIGURE 18.9 Membrane selection guide. (Data courtesy of Pall Corporation.)

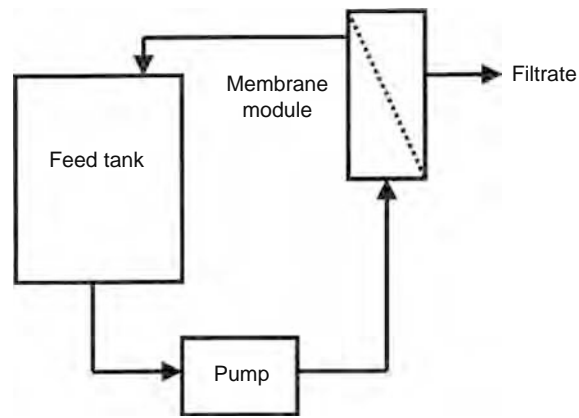


FIGURE 18.10 Batch concentration.

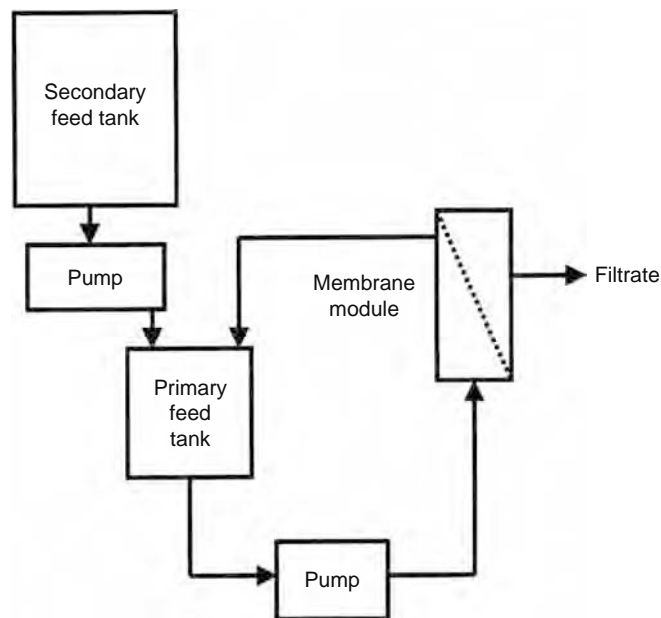


FIGURE 18.11 Fed-batch concentration.

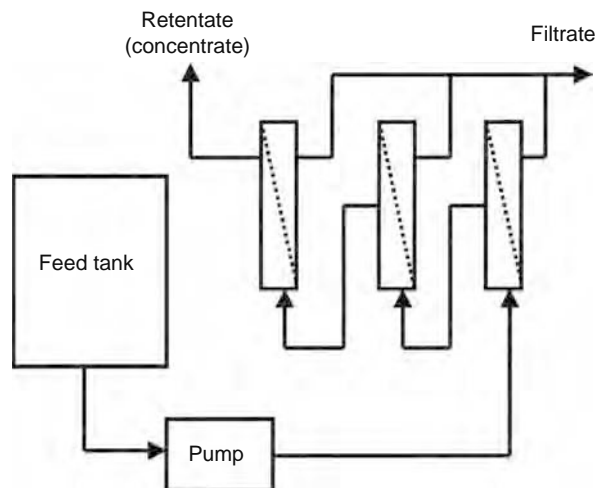


FIGURE 18.12 Continuous concentration.

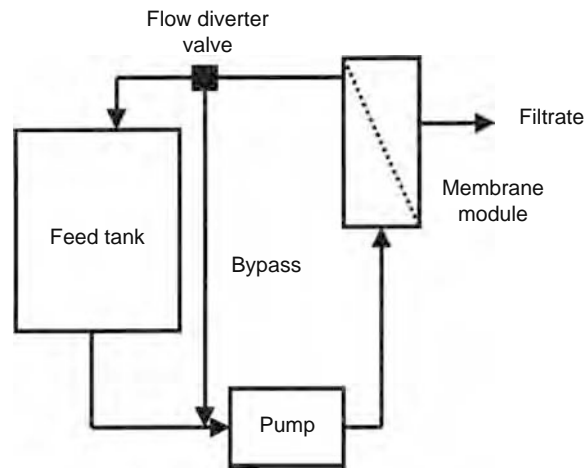


FIGURE 18.13 Concentration with partial recycle.

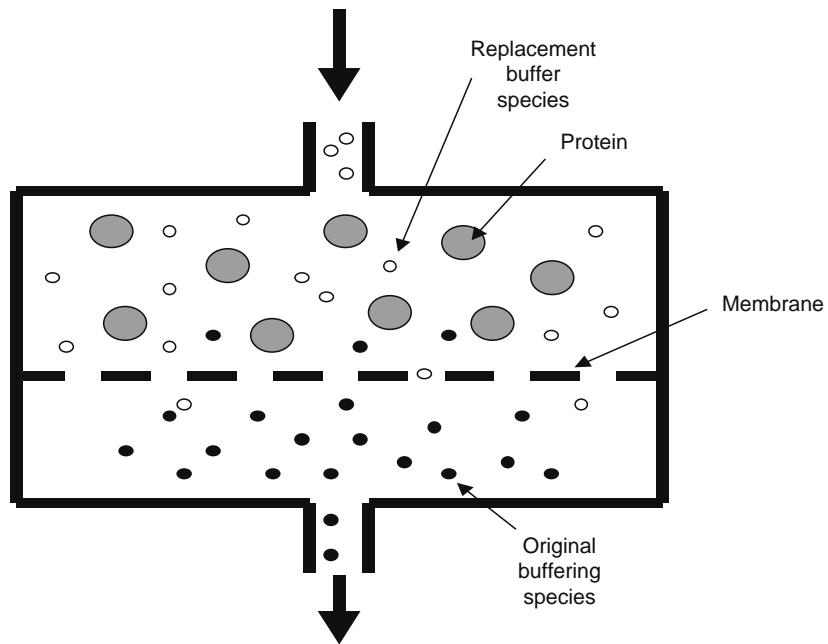


FIGURE 18.14 Desalting.

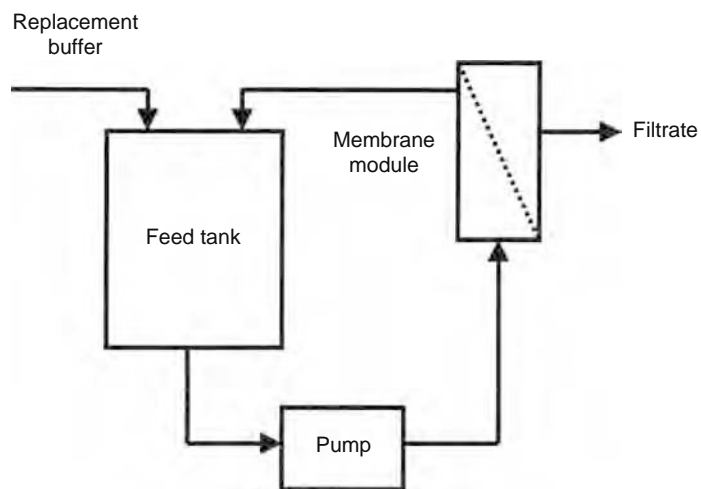


FIGURE 18.15 Batch desalting.

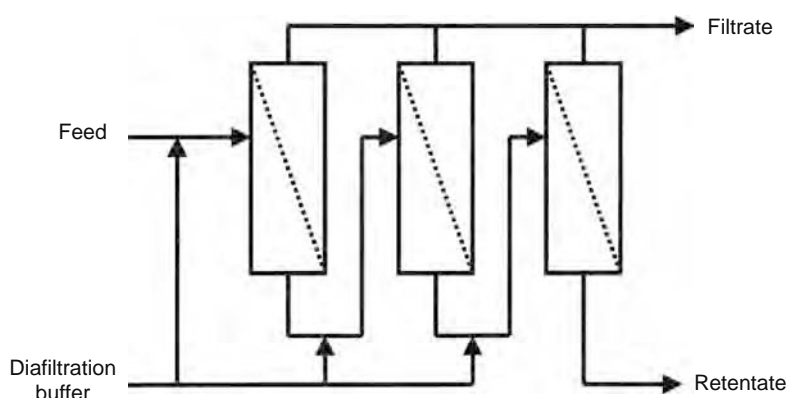


FIGURE 18.16 Continuous desalting.

## 18.7 CLARIFICATION

Clarification refers to the removal of particulate matter from protein solutions. In addition to efficient removal of particulate matter, high-protein transmission through the membrane is desirable. Microfiltration membranes are more widely used for clarification. However, in applications such as virus removal from biopharmaceutical solutions ultrafiltration is increasingly preferred on account of the higher efficiency and reliability of particulate retention. Some of the common applications of clarification are listed below [2]:

1. Sterile filtration of biopharmaceutical solutions
2. Sterile filtration of therapeutic products prior to injection
3. Removal of cell debris
4. Cell harvesting
5. Continuous recovery of products from bioreactor

High-macromolecular transmission through membrane is desirable in clarification. This depends on operating and physico-chemical parameters such as solution pH and ionic strength. These have to be taken into consideration when selecting a membrane and operating conditions for a particular application. Ultrafiltration is mainly used for virus removal from protein solutions. As long as satisfactory virus removal can be ensured, less than 100% protein transmission through the membrane is tolerated as an identified trade-off. Virus particles are removed by geometric exclusion, i.e., by sieving mechanism. The efficiency of virus removal is expressed in terms of the log removal value (LRV):

$$\text{LRV} = \log \left( \frac{N_F}{N_P} \right) \quad (18.10)$$

where

$N_F$  is the number of virus particles per unit volume of feed

$N_P$  is the number of virus particles per unit volume of permeate

Membrane modules suitable for clarification should have low feed hold-up. Stirred cell- and cartridge-type ultrafiltration modules are widely used. These are operated in a dead-end mode. Figure 18.17 shows the setup used for dead-end clarification. If protein is freely transmitted through the membrane, the dead-end mode gives high recovery and is hence preferred. However, if the protein is partially retained, the dead-end mode gives rise to severe concentration polarization and fouling. In such cases tubular and hollow fiber ultrafiltration modules, which are operated in the cross-flow mode are preferred. Figure 18.18 shows a setup used for a cross-flow clarification.

## 18.8 FRACTIONATION

Macromolecular fractionation, which involves high-resolution separation of solutes having comparable molecular weights using ultrafiltration, is challenging primarily due to the broad pore-size distribution of ultrafiltration membranes. This implies that purely size-based fractionation is not feasible using membranes currently available. The development of advanced membranes with narrow pore-size distributions could make fractionation more feasible. With currently available membranes

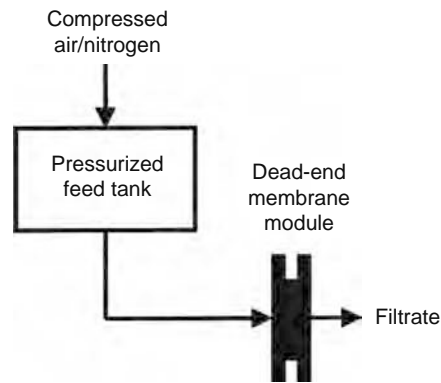


FIGURE 18.17 Dead-end clarification.

other factors such as membrane modification, solute–solute interactions, and solute-membrane interactions have to be utilized for macromolecular fractionation.

The use of ultrafiltration for macromolecular fractionation is not an established operation in the industry. This field is still a domain for fundamental and applied research [15–20]. Some of the projected applications are listed as follows:

1. Fractionation of plasma proteins
2. Purification of monoclonal antibodies
3. Fractionation of whey proteins
4. Fractionation of egg proteins
5. Separation of antivenins

The main challenges that need to be addressed for these applications are

1. Development of better membranes and membrane modification methods
2. Control of concentration polarization
3. Control of membrane fouling
4. Understanding the role of operating and physicochemical parameters on protein transport through ultrafiltration membranes
5. Understanding the role of protein–protein interactions in ultrafiltration
6. Development of processes specifically targeted at macromolecular fractionation

Development of new ultrafiltration membranes is focused on improving permeate, reducing membrane fouling, and increasing selectivity of separation. Increasing permeate flux can be achieved by developing hydrophilic membranes with higher porosities. Hydrophilic membranes inherently foul less. However, for a given membrane fouling increases with increase in permeate flux. Fouling affects both productivity and product quality. Even moderately high permeate fluxes in ultrafiltration give significantly higher productivities than competing separation techniques. Therefore where fouling can become a limiting

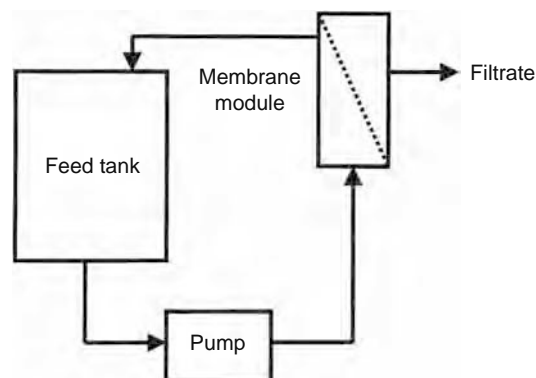


FIGURE 18.18 Cross-flow clarification.

factor a sensible approach is to lower the TMP and hence the flux, thereby reducing membrane fouling. In most ultrafiltration processes, an identifiable flux value exists, below which fouling is negligible, this being referred to as the critical flux [21]. Protein fractionation processes should ideally be carried out at subcritical fluxes. Concentration polarization is recognized as a limiting factor in fractionation processes. Fractionation processes should be carried out under conditions of low concentration polarization. Membrane fouling can also be minimized by reducing concentration polarization.

The transport of proteins is affected by a range of operating and physicochemical parameters such as TMP, feed flow rate, permeate flux, feed solution pH, and ionic strength. These parameters affect the way in which the proteins pass through the membrane, interact with the membrane, and interact among each other. Understanding these intricacies is the key to the development of efficient macromolecular fractionation processes. Development of processes specifically designed for fractionation processes is of equal importance. Currently used membrane processes are focused around concentration and desalting and hence are not suitable for macromolecular fractionation. Development of cascade-type separation processes would lead to more efficient membrane utilization [22].

## 18.9 CONCLUSIONS

The role of bioseparation in biological manufacturing is increasingly becoming important. Ultrafiltration offers an exciting prospect in the area of bioseparations engineering. The main advantages of using ultrafiltration are high productivity, ease of scale-up, and easy device sanitization and cleaning. The use of ultrafiltration in high-productivity, low-resolution operations such as concentration, desalting, and clarification is well established. However, its usage for high-resolution macromolecular fractionation can only be brought about by the development of better membranes, better understanding of membrane transport mechanisms, and better membrane processes.

## REFERENCES

1. Belter, PA, Cussler, CL, and Hu, W-S, *Bioseparations*, John Wiley & Sons, New York, 1988.
2. Ghosh, R, *Protein Bioseparation using Ultrafiltration: Theory Applications and New Developments*, Imperial College Press, London, 2003.
3. Kulkarni, SS, Funk, EW, and Li, NN, Theory and mechanistic concepts, in: Ho, WS and Sirkar, KK, Eds., *Membrane Handbook*, Van Nostrand Reinhold, New York, 1992.
4. Ding, L, Charcosset, C, and Jaffrin, MY, Albumin recovery enhancement in membrane plasma fractionation using pulsatile flow, *Int. J. Artificial Organs*, 14, 61, 1991.
5. Rodgers, VGJ and Sparks, RE, Reduction in membrane fouling in the ultrafiltration of binary protein mixtures, *AIChE J.*, 37, 1517, 1991.
6. Abel, K, Influence of oscillatory flows on protein ultrafiltration, *J. Membr. Sci.*, 133, 39, 1997.
7. Bellhouse, BJ, Costigan, G, Abhinava, K, and Merry, A, The performance of helical screw-thread inserts in tubular membranes, *Sep. Purif. Technol.*, 22, 89, 2001.
8. Brewster, ME, Chung, KY, and Belfort, G, Dean vortices with wall flux in a curved channel membrane system. 1. A new approach to membrane module design, *J. Membr. Sci.*, 81, 127, 1993.
9. Balakrishnan, M, Agarwal, GP, and Cooney, CL, Study of protein transmission through ultrafiltration membranes, *J. Membr. Sci.*, 85, 111, 1993.
10. Cui, ZF and Wright, KIT, Gas-liquid 2-phase cross-flow ultrafiltration of BSA and dextran solutions, *J. Membr. Sci.*, 90, 183, 1994.
11. Opong, WS and Zydny, AL, Diffusive and convective protein-transport through asymmetric membranes, *AIChE J.*, 37, 1497, 1991.
12. Zydny, AL and van Reis, R, High-performance tangential-flow filtration, in: Wang, WK, Ed., *Membrane Separation in Biotechnology*, Marcel Dekker, New York, 2001.
13. Ghosh, R and Cui, ZF, Simulation study of the fractionation of proteins using ultrafiltration, *J. Membr. Sci.*, 180, 29, 2000.
14. Blatt, WF, Principles and practice of ultrafiltration, in: Meares, P, Ed., *Membrane Separation Processes*, Elsevier Science, Amsterdam, 1976.
15. Higuchi, A, Mishima, S, and Nakagawa, T, Separation of proteins by surface modified polysulfone membranes, *J. Membr. Sci.*, 57, 175, 1991.
16. Saksena, S and Zydny, AL, Effect of solution pH and ionic strength on the separation of albumin from immunoglobulins (IgG) by selective filtration, *Biotechnol. Bioengr.*, 43, 960, 1994.
17. Ghosh, R, Li, QL, and Cui, ZF, Fractionation of BSA and lysozyme using ultrafiltration: Effect of gas sparging, *AIChE J.*, 44, 61, 1998.
18. van Reis, R, Gadam, S, Frautschy, LN, Orlando, S, Goodrich, EM, Saksena, S, Kuriyel, R, Simpson, CM, Pearl, S, and Zydny, AL, High performance tangential flow filtration, *Biotechnol. Bioengr.*, 56, 71, 1997.
19. Nystrom, M, Aimar, P, Luque, S, Kulovaara, M, and Metsamuuronen, S, Fractionation of model proteins using their physicochemical properties, *Colloids Surf. A Physicochem. Eng. Aspects*, 138, 185, 1998.
20. Li, QY, Cui, ZF, and Pepper, DS, Fractionation of HSA/IgG by gas sparged ultrafiltration, *J. Membr. Sci.*, 136, 181, 1997.
21. Howell, JA, Sub-critical flux operation, *J. Membr. Sci.*, 107, 165, 1995.
22. Ghosh, R, Novel cascade ultrafiltration configuration for continuous, high-resolution protein-protein fractionation: A simulation study, *J. Membr. Sci.*, 226, 85, 2003.



---

# 19 Membrane Distillation in Food Processing

*Sanjay Nene, Ganapathi Patil, and K.S.M.S. Raghavarao*

## CONTENTS

19.1	Introduction .....	513
19.2	Historical Background .....	514
19.3	Membrane Distillation .....	515
19.3.1	Direct Contact Membrane Distillation .....	515
19.3.1.1	Heat and Mass Transfer .....	516
19.3.1.2	Comparison of the Models .....	525
19.3.1.3	Process Parameters .....	525
19.3.2	Air Gap Membrane Distillation .....	526
19.3.2.1	Heat and Mass Transfer .....	526
19.3.2.2	Process Parameters .....	527
19.3.3	Vacuum Membrane Distillation .....	528
19.3.3.1	Heat and Mass Transfer .....	528
19.3.3.2	Process Parameters .....	529
19.3.4	Sweeping Gas Membrane Distillation .....	529
19.3.4.1	Heat and Mass Transfer .....	530
19.3.4.2	Process Parameters .....	530
19.3.5	Osmotic Membrane Distillation .....	531
19.3.5.1	Heat and Mass Transfer .....	531
19.3.5.2	Mass Transfer through the Membrane .....	532
19.3.5.3	Mass Transfer through Boundary Layers .....	532
19.3.5.4	Process Parameters .....	532
19.4	Membranes .....	533
19.5	Membrane Modules .....	535
19.6	Enhancement of Flux in Membrane Distillation .....	538
19.7	Applications in Food Processing .....	540
19.7.1	Demineralized Water .....	540
19.7.2	Beverages and Fruit Juice .....	541
19.7.3	Integrated Membrane Process .....	542
19.8	Future Directions .....	544
	Glossary .....	544
	Nomenclature .....	545
	Dimensionless Numbers .....	547
	References .....	547

## 19.1 INTRODUCTION

The origin of the term membrane distillation (MD) lies in the essential similarity between the conventional process of distillation and its membrane variant. Both processes depend upon the vapor–liquid equilibrium as a means of phase separation, where the latent heat of evaporation drives the change in phase from liquid to vapor.

Hitherto the commercial use of membranes in food processing was restricted to conventional processes such as micro-filtration, ultrafiltration, nanofiltration, reverse osmosis (RO), gas permeation, and electro dialysis. These unit operations include solid–liquid separation, concentration (dewatering), gassing/degassing, desalting, and deacidification. Membrane distillation (MD) as a concept was first described in a US patent in the early 1960s for making potable water [1]. However, its merits were progressively realized for wide range of application such as desalination of water [2,3]; treatment of oily feeds [4,5], humic acid [6], and solvents [7,8]; concentration of liquid foods [9], sugar solutions [10,11], and beverages [12,13]; and the recovery of products of fermentation [14], mineral acids [15,16], and aromas and fragrances [17].

The advantages of membrane distillation are associated with relatively lower energy costs as compared to competing processes such as distillation, reverse osmosis, and pervaporation (PV); much lower membrane fouling as compared with microfiltration (MF), ultrafiltration, and RO; a quantitative rejection of nonvolatile solutes from the feed stream; lower operating pressure and temperatures, without sacrificing flux as compared with competing processes.

Advances in preparation and modification of membranes used in membrane distillation and their configurations have been covered in a recent review by Curcio and Drioli [18] and it is evident that R&D efforts are largely concentrated on making improvements in these areas.

Concentration and dewatering of liquids are one of the key unit operations encountered in food processing, particularly in the processing of beverages, fruit juice, milk, whey, vegetable extracts, etc. In such unit operations, solid contents are generally increased from an initial value of 10%–12% to a final value of 65%–75% by weight [19]. This concentration step is aimed at lowering storage, packaging, and transport costs. It also helps, to a limited extent, in preventing microbial spoilage of these concentrates.

Today, multistage vacuum evaporation is the predominant method used for liquid food concentration. Its major drawback is that it causes heat-induced deterioration of sensory (color, taste, and aroma) and nutritional (vitamins, etc.) value of the finished product. The food industry has developed alternate methods, such as freeze concentration and thermally accelerated short time evaporation (TASTE) [20] for recovery and blending of such labile constituents for producing concentrates. Though they are currently practiced commercially, the final products in some cases do not satisfy the consumer requirement of their fresh or natural qualities. Some of these processes are energy intensive and therefore unattractive.

Membrane processes, in general, are very attractive for their simplicity and flexibility. They are capable of achieving separations at a molecular level. Membrane modules are often compact and easily scaleable. For clarification and concentration, microfiltration, ultrafiltration, and reverse osmosis are the current methods of choice. RO has been widely used in the food industries as an attractive alternative to classical evaporation; the only limitation being its dependence on osmotic pressure, which practically limits concentration of fluid streams to 25°Bx–30°Bx. Hence, currently it is used more as a preconcentration step. In recent years, membrane processes, notably pervaporation, membrane distillation and osmotic membrane distillation (OMD) [21], have been used either by themselves or in combination with other membrane processes to overcome the problems associated with thermal processes.

## 19.2 HISTORICAL BACKGROUND

Bodell [1] was the first to describe membrane distillation when he was granted a patent on an apparatus and methods for converting nonpotable aqueous fluids to potable water, where vapor and not liquid was permeable through a membrane. He also suggested the use of vacuum for recovery of permeate vapor. However, he did not describe the geometry, the structure of the membrane, and could not quantify his results. In 1967, Weyl [22] employed an air-filled porous hydrophobic membrane for improving the efficiency of desalination. Weyl also proposed a method for placing the hot feed and cold permeate solutions in direct contact with the membrane, thereby eliminating the macroscopic air gap found in other devices of that time. He reported fluxes up to  $1 \text{ kg m}^{-2} \text{ h}^{-1}$  using polytetrafluoroethylene (PTFE) membrane of 3.2 mm thickness with a pore size of 9  $\mu\text{m}$  and porosity of ~42%. In the late 1960s, Findley [23] was the first to publish the basic theory and results of direct contact membrane distillation (DCMD), which were performed using membranes of different materials treated either with silicone or PTFE to achieve the required hydrophobicity. Although, the equipment and experimental procedures used by Findley were rudimentary, he was able to quantify the effects of air trapped in the membrane pores, membrane thickness and porosity, and heat loss by conduction. After the work on desalination of seawater by Findley et al. [24–26] no further development took place till the 1980s. In 1982, Gore proposed a spiral-type module using a Gore-Tex membrane [27], which he called Gore-Tex Membrane Distillation. In 1983, the Swedish Development Co. (Svenska Utvecklings AB) reported similar test results using a plate and frame module. In 1984, Enka AG presented a transmembrane distillation module using hollow fibers, at the Europe–Japan Joint Congress on Membranes and Membrane Processes. At the second world congress on desalination and water reuse in 1985, papers presented on MD [28–31] led to a renewed interest in the subject and facilitated the development of various hydrophobic membranes (polypropylene, polytetrafluoroethylene) with porosities as high as 80% and membrane thickness as low as 50  $\mu\text{m}$ . Subsequently, work by Schofield et al. [32–35] contributed to a better understanding of temperature and concentration polarization, and their effect on membrane distillation.

In the late 1980s, it was observed that the same membranes that had been used in thermal membrane distillation could be used in a concentration-driven process called OMD [36]. Both these processes show great similarity in employing hydrophobic membranes, where a liquid–vapor interface is formed on both sides of the membrane pores. The source for the driving force (vapor pressure difference) is different in both cases. It is a temperature difference in the case of thermal membrane distillation, while it is a concentration difference in the case of OMD [37].

The OMD process can be included in the group of processes under membrane distillation [38], because it meets the terminology for membrane distillation that was decided by the expert committee at the workshop on “membrane distillation in Rome in 1986” [39]. Membranes used in MD need to satisfy certain conditions: For example, the membrane should be porous and should not be wetted by the process liquids; no capillary condensation should take place inside the pores of the membrane; the membrane must not alter the vapor–liquid equilibrium of the different components in the process liquids; at least one side of the membrane should be in direct contact with the process liquid; for each component the driving force of this membrane operation is partial pressure gradient in vapor phase.

Therefore, in this chapter OMD will be considered as a part of membrane distillation. The composition of the gas phase above the liquid surface is often expressed by partial pressure and the difference in partial pressure is therefore accepted as a driving force for the MD process [38–43]. The magnitude of this driving force depends on the solution temperature and composition of the layers adjacent to the membrane surface.

The main advantages of the membrane distillation process over conventional distillation are the configuration of the evaporation surface can be made into various membrane modules with a compact area density, mist can be eliminated, and highly pure water can be obtained as product; corrosion may be less than that with metal surfaces.

Considering these merits, the fundamental characteristics of the membrane distillation process have been studied, and progressively, articles by various researchers [32,33,36–39,41,43,44] have provided insights into various process aspects.

### 19.3 MEMBRANE DISTILLATION

Membrane distillation is a relatively new process in which a microporous hydrophobic membrane separates two aqueous solutions or a solution and gas, either at different temperatures or at different compositions. Because of the vapor pressure difference, water evaporates on one surface of the membrane and passes through the membrane in the form of vapor and gets condensed on the other side of membrane, resulting in the concentration of feed and dilution of permeate solutions. In membrane distillation one side (usually the feed side) of the membrane is always in contact with an aqueous solution. The other side (i.e., the permeate side) may be brought into contact with different phases: For example (1) with an aqueous solution, giving rise to the configuration called DCMD; (2) with a sweeping gas, in which case the process is termed sweeping gas membrane distillation (SGMD); (3) with a stagnant air gap plus a cold plate called air gap membrane distillation (AGMD); (4) with a vacuum and the process is called vacuum membrane distillation (VMD); and (5) with an osmotic solution where the process is termed OMD. While the first four processes are non-isothermal, the last process is isothermal. More details of these processes are discussed in the following sections.

#### 19.3.1 DIRECT CONTACT MEMBRANE DISTILLATION

Direct contact membrane distillation is a form of membrane distillation in which both the heated feed (liquid) and cold permeate (liquid) are kept in contact with porous hydrophobic membrane (Figure 19.1). In the absence of hydrostatic pressure difference, liquid–vapor interfaces are formed at the entrance of each membrane pore, and a vapor pressure difference is maintained on both sides of the membrane by applying a temperature difference. Water molecules evaporate from the hot liquid–vapor interface, diffuses through the membrane in the form of vapor, and get condensed on the permeate liquid–vapor interface kept at

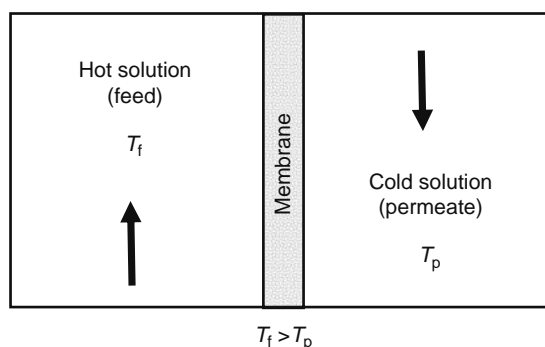


FIGURE 19.1 Schematic representation of DCMD.

lower temperature. Hence the DCMD process takes place at atmospheric pressure and at temperatures much lower than the normal boiling point of the feed solution, thus it can be used for concentration of temperature insensitive liquids, such as liquid foods. Most MD processes are carried out in the form of DCMD, which is easy to operate, consumes relatively low energy, and gives high water permeate flux. It is commonly applied for situations where water is the major fluxing component [39,45,46], such as desalination or the concentration of aqueous solutions. Desalination by DCMD has exhibited fluxes as high as  $75 \text{ kg m}^{-2} \text{ h}^{-1}$  [22], which are comparable with the fluxes typically observed in RO. Additionally, salt rejections of nearly 100% have been observed in DCMD desalination, which cannot be accomplished with RO (at high fluxes) [47].

### 19.3.1.1 Heat and Mass Transfer

Heat and mass transfer takes place simultaneously in DCMD. The mass and heat transport can be described by three steps, namely transport through boundary layer on the feed side, transport through membrane, and transport through boundary layer on the permeate side.

The mass transfer in the boundary layers can be described by a mass transfer coefficient. In the membrane phase, the diffusion of water vapor can be described by either of the four mechanisms, namely molecular/Knudsen diffusion model, or Poiseuille flow, or by the dusty gas model (DGM). Heat transfer coefficients are used to describe the heat transfer in the boundary layer on either side of the membrane. In the membrane heat transfer occurs through the vapor and by conduction. These aspects have been explained in detail in the following sections.

#### 19.3.1.1.1 Heat Transfer

The modes of heat transfer and the possible heat transfer resistances in membrane and the corresponding boundary layers of DCMD are shown in Figure 19.2. The basic equation for the total heat transferred due to the difference in temperatures of the feed ( $T_f$ ) and permeates ( $T_p$ ) is given by

$$Q = H(T_f - T_p) = H\Delta T_f \quad (19.1)$$

where  $H$  is the overall heat transfer coefficient that accounts for all the three resistances for water transport and is given by

$$H = \left[ \frac{1}{h_f} + \frac{1}{\frac{k_m}{\delta} + h_v} + \frac{1}{h_p} \right]^{-1} \quad (19.2)$$

where

$h_f$  and  $h_p$  are the heat transfer coefficients in feed and permeate layers, respectively

$k_m$  is the membrane conductivity

$\delta$  is the membrane thickness

$h_v$  is the vapor heat transfer coefficient

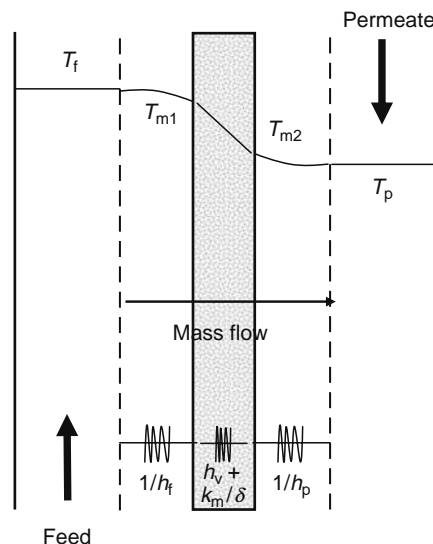


FIGURE 19.2 Heat transfer resistances in DCMD.

### 19.3.1.1.1.1 Heat Transfer through the Membrane

Heat transfer through the membrane occurs by two mechanisms, first, by latent heat through the vapor, and second, by sensible heat conduction across the membrane material.

The latent heat flux for dilute solutions is given by [34]

$$Q_v = J\Delta H_v = h_v\Delta T_m \quad (19.3)$$

The conductive heat flux is given by [32]

$$Q_c = \left(\frac{k_m}{\delta}\right)(T_{m1} - T_{m2}) \quad (19.4)$$

The membrane conductivity  $k_m$  in Equation 19.4 can be estimated using the following three models [48]:

*isostrain or parallel model*

$$k_m = (1 - \varepsilon)k_s + k_g \varepsilon \quad (19.5)$$

*isostress or series model*

$$k_m = \left[\frac{\varepsilon}{k_g} + \frac{(1 - \varepsilon)}{k_s}\right]^{-1} \quad (19.6)$$

and *flux law model*

$$k_m = k_g \left[\frac{1 + (1 - \varepsilon)\beta_{s-g}}{1 - (1 - \varepsilon)\beta_{s-g}}\right] \quad (19.7)$$

where

$$\beta_{s-g} = \frac{\frac{k_s}{k_g} - 1}{\frac{k_s}{k_g} + 2} \quad (19.8)$$

Equation 19.5 is often utilized in MD, while Equations 19.6 and 19.7 are the alternate expressions to calculate the membrane thermal conductivity, where  $\varepsilon$  is the porosity,  $k_s$  and  $k_g$  are thermal conductivities for solid (polymer) and gases in the pores (air and water vapor), respectively. The values of thermal conductivity of polyvinylidenedifluoride (PVDF), Polytetrafluoroethylene (PTFE), and Polypropylene (PP) have been reported in a narrow range 0.17–0.29 W m<sup>-1</sup> K<sup>-1</sup> [48]. The thermal conductivities of air are in the range of 0.026–0.03 W m<sup>-1</sup> K<sup>-1</sup> and that of water vapor in the range 0.020–0.022 W m<sup>-1</sup> K<sup>-1</sup>. Since there is a very small difference between the thermal conductivities of vapor and air, it is possible to assume that the gases in the pores behave as one component.

From Equations 19.3 and 19.4, the total heat transfer across the membrane ( $Q_m$ ) can be written as

$$\begin{aligned} Q_m &= Q_v + Q_c \\ &= \left(h_v + \frac{k_m}{\delta}\right)\Delta T_m \end{aligned} \quad (19.9)$$

Heat transfer through the membrane pores by convection can also be considered. It is the ratio of convective to conductive heat transfer rates within the membrane pores and is given by the Peclet number,  $Pe$  [39]

$$\begin{aligned} Pe &= Re \cdot Pr \\ &= \frac{NC_p}{h_m} \end{aligned} \quad (19.10)$$

where

$N$  is the molar flux

$C_p$  is the molar heat capacity of the vapor

Studies of Schofield [49] and Gostoli [50] showed that, the heat transfer by convection accounts for only 0.6% of the total heat transferred across the membrane and at most 6% of the total heat lost by dissipation in the membrane. So heat transfer by convection is very small as compared to that of conduction and could be neglected.

#### 19.3.1.1.1.2 Heat Transfer through Boundary Layers

Heat transfer across the boundary layers is often the rate-limiting step for mass transfer, because a large quantity of heat must be supplied to the surface of the membrane to vaporize the liquid.

The rate of heat transfer through the feed boundary layer can be given as

$$Q_f = h_f(T_f - T_{m1}) \quad (19.11)$$

The rate of heat transfer through the permeate boundary layer can be calculated using

$$Q_p = h_p(T_{m2} - T_p) \quad (19.12)$$

where  $h_f$  and  $h_p$  are the heat transfer coefficients through the feed and permeate boundary layers, respectively, and can be estimated using empirical equations. Empirical correlations are readily available to estimate the heat transfer coefficients for different geometries and heat transfer mechanisms, and some of these correlations used in the literature are discussed here [51–53].

#### 19.3.1.1.1.3 Heat Transfer Correlations for Turbulent Flow

For fully developed turbulent flow in smooth tubes, Dittus and Boelter have recommended the following relation:

$$\frac{hd}{k_1} = 0.023 \left( \frac{dG}{\mu} \right)^{0.8} \left( \frac{C_p \mu}{k_1} \right)^n \quad (19.13)$$

where

$d$  is the tube diameter

$k_1$  is the thermal conductivity of the liquid

$G$  is the mass velocity

$\mu$  is the bulk liquid viscosity

$C_p$  is the liquid heat capacity

$n$  takes the values of 0.4 and 0.3, for heating and cooling of the fluid

Equation 19.13 is valid for the boundary conditions of  $10^4 < Re < 12 \times 10^4$ ,  $0.7 < Pr < 120$  and  $L/d > 60$  ( $L$  is the tube length). The use of this equation is limited to cases where the difference in tube surface temperature and the bulk fluid temperature is more than 5.5°C for liquids and 55°C for gases. Equations listed in Table 19.1 can be used as an alternative to the Equation 19.13 depending upon hydrodynamic conditions.

**TABLE 19.1**  
**List of Equations Used in MD at Different Hydrodynamic Conditions**

Sl. No	Flow Regime	Equations	Reference
1	Turbulent	$\frac{hd}{k_1} = 0.023 \left( \frac{dG}{\mu} \right)^{0.8} \left( \frac{C_p \mu}{k_1} \right)^n \left( \frac{\mu}{\mu_w} \right)^{0.14}$ (19.14) <sup>a</sup>	[51]
2	Turbulent	$\frac{h}{h_\infty} = 1 + \left( \frac{d}{L} \right)^{0.7}$ or $\frac{h}{h_\infty} = 1.33 \left( \frac{d}{L} \right)^{0.055}$ (19.15) <sup>b</sup>	[51]
3	Laminar	$\left( \frac{hd}{k} \right) = 3.66 + \frac{0.067 G_z}{1 + 0.04 G_z^{2/3}}$ , $G_z = \frac{mC_p}{k_1 L}$ (19.16)	[55,56]
4	Laminar	$h_f = 1.86 K \left( \frac{RePr}{d_h^2 L} \right)^{0.33}$ (19.17)	[58]
5	Transition	$h_f = 0.116 k (Re^{0.66} - 125) Pr^{0.33} \left[ \frac{1 + (d_h/L)^{0.66}}{d_h} \right]$ (19.18)	[58]
6	—	$h_a = 0.206 \left( \frac{k}{d_h} \right) (Re \cos \alpha)^{0.63} Pr^{0.36}$ (19.19) <sup>c</sup>	[58]

<sup>a</sup> Valid at higher Prandtl numbers ( $0.7 < Pr < 16,700$ ) and  $L/d > 60$ .

<sup>b</sup> For short tube  $L/d < 50$ .

<sup>c</sup> To determine the heat transfer coefficient in the permeate side  $h_a$  in Equation 19.58.

These correlations can also be used for noncircular geometry by substituting the equivalent diameter of the flow channel, for example,

$$d_e = 4r_H = 4 \frac{S}{L_p} \quad (19.20)$$

where

$r_H$  is the hydraulic radius

$S$  is the cross-sectional area of the flow channel

$L_p$  is the length of the wetted perimeter of the flow channel

$d_e = d$ , for circular flow channels,  $d_e = 2l$ , for parallel plates separated by a distance  $l$ , and  $d_e = l$ , for a square channel of side  $l$

#### 19.3.1.1.1.4 Heat Transfer Correlations for Laminar Flow

For laminar liquid flow in circular tubes with constant wall temperature, Sieder and Tate have recommended Equation 19.21 [51,53]

$$\frac{hd}{k_1} = 1.86 \left( Re \cdot Pr \cdot \frac{d}{L} \right)^{\frac{1}{3}} \left( \frac{\mu}{\mu_w} \right)^{0.14} \quad (19.21)$$

Knudsen and Katz [54] have shown that it is valid for  $Re \cdot Pr \cdot d/2 > 10$ . Equation 19.21 cannot be used for long tubes, since it would yield zero heat transfer coefficient. Sarti et al. have employed a different Equation 19.16 to estimate the heat transfer coefficient for laminar flow in circular tubes (shown in Table 19.1).

Recently, Phattaranawik et al. [48] have used several equations to estimate the heat transfer coefficient in laminar and turbulent flow regimes. They found that Equation 19.22 is the most suitable for laminar flow, while the Dittus–Boelter equation was most suitable for turbulent conditions.

$$Nu = 4.36 + \frac{0.036 Re Pr \left(\frac{d}{L}\right)}{1 + 0.0011 \left(Re Pr \left(\frac{d}{L}\right)\right)^{0.8}} \quad (19.22)$$

#### 19.3.1.1.2 Mass Transfer

##### 19.3.1.1.2.1 Mass Transfer through the Membrane

Resistance to mass transfer comes both from the membrane structure and the air present within the membrane pores. The resistance by the membrane structure (in the absence of air) can be described by Poiseuille flow. In presence of air within the membrane pores either Knudsen diffusion or molecular diffusion, or a combined Knudsen–molecular diffusion flow model can be used.

The correct choice of model requires some knowledge of the membrane morphology, which is scant in the literature. This problem has been extensively discussed in the literature [32–34,39,57]. A few of these models, which were originally developed for mass transfer through the porous media, have been adopted for MD.

The mass flux may be written as a linear function of the vapor pressure difference across the membrane (Figure 19.3) and is given by

$$J_m = K_m(p_{m1} - p_{m2}) \quad (19.23)$$

where

$J_m$  is the mass flux

$p_{m1}, p_{m2}$  are the partial pressures of vapor (water) at the membrane surfaces on the feed and permeate sides, respectively

$K_m$  is the membrane coefficient that is a function of membrane properties (pore size, thickness, porosity, and tortuosity), properties of the vapor transported across the membrane (molecular weight and diffusivity) and temperature gradient

Any study that relates to the transport of vapor or gas through microporous structure begins with a comparison of the mean free path of the gas ( $\lambda$ ) and the mean pore size of the structure ( $d_p$ ) (shown in Figure 19.4). In general, the Knudsen number ( $Kn$ ) is used to determine the diffusion mechanisms across the pores of the membrane [41], which is defined as

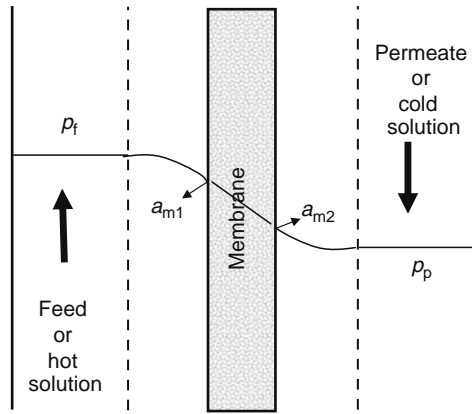


FIGURE 19.3 Water activity profile in MD.

$$Kn = \frac{\lambda}{2r} \tag{19.24}$$

where

$r$  is the pore radius

$\lambda$  is the mean molecular free path defined as the average distance the molecule travels between successive collisions

The value of  $\lambda$  can be calculated using Equation 19.25:

$$\lambda = \frac{k_B T}{P \sqrt{2} \pi \sigma^2} \tag{19.25}$$

where

$k_B$  is the Boltzmann constant

$\sigma$  is the collision diameter of the molecule, for saturated water ( $\sigma = 2.7 \text{ \AA}$ ) at  $60^\circ\text{C}$  and  $20 \text{ kPa}$ , the mean free path is  $0.7 \text{ }\mu\text{m}$  [39] and is a function of temperature ( $T$ ), pressure ( $P$ ), and mean collision diameter of the molecule.

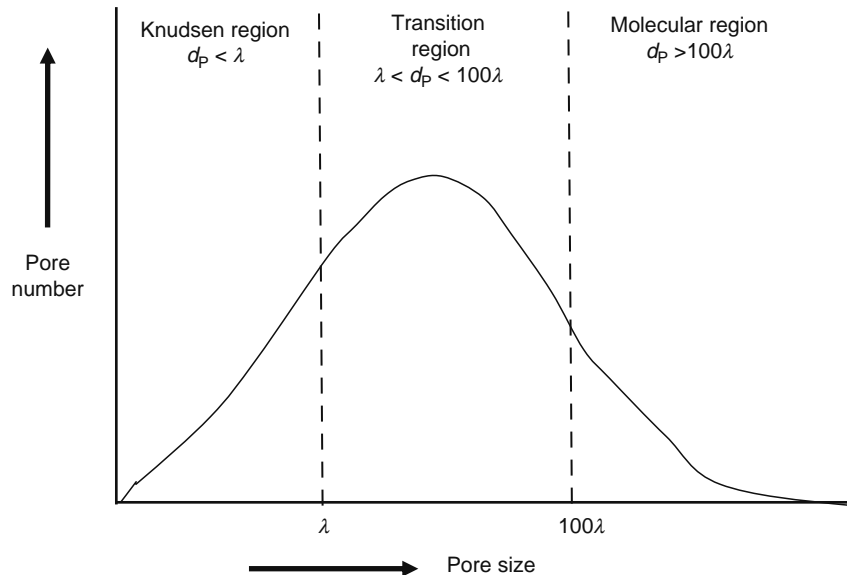


FIGURE 19.4 Regions of gas diffusion.

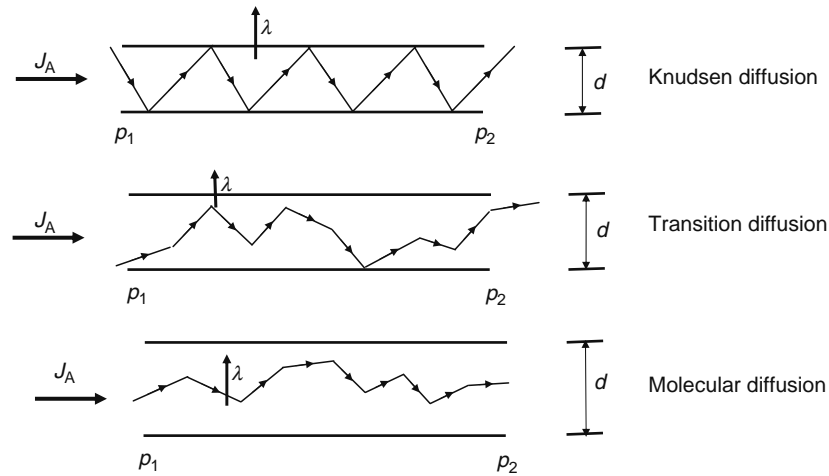


FIGURE 19.5 Types of diffusions of water vapor in a membrane pore.

If the mean free path of the water molecules is much greater than the pore size of the membrane ( $\lambda \gg d_p$ ,  $Kn \geq 10$ ), then the molecules will collide with pore walls and the transport mechanism follows Knudsen diffusion as shown in Figure 19.5. In this case, the membrane coefficient is calculated using Equation 19.26 [32]

$$K_m = 1.064 \frac{r\varepsilon}{\tau\delta} \left( \frac{M}{RT} \right)^{0.5} \quad (19.26)$$

where

- $\varepsilon$  is the fractional void volume
- $\delta$  is the membrane thickness
- $\tau$  is the tortuosity
- $R$  is the gas constant
- $M$  is the molecular mass of water
- $T$  is the absolute temperature

If the resistance caused by the stagnant air is trapped within the membrane pores, for flow of water vapor, the mechanism is called molecular diffusion and the membrane coefficient is expressed as [34]

$$K_m = \frac{1}{Y_{ln}} \frac{D\varepsilon}{\tau\delta} \frac{M}{RT} \quad (19.27)$$

where

- $D$  is the diffusion coefficient
- $Y_{ln}$  is the mole fraction of air (log mean)

It may be noted that in this model the air entrapped in the pore is regarded simply as a motionless medium in which the vapor molecules diffuse. Furthermore, the interaction between the vapor molecules and the membrane pores is not taken into account [57]. However, it is clear that the vapor transport will also be limited by the membrane structure itself that has been indicated in Equation 19.26. If  $Kn$  is between the two limits  $\lambda \ll d_p \ll 100\lambda$ ,  $0.01 \leq Kn \leq 10$ , then both the mechanisms will coexist whereby both molecule–molecule collisions as well as molecule–wall collisions take place. Such a mechanism in this transition region is called the Knudsen molecular diffusion and the following relationship (Equation 19.28) could be used for estimating the membrane coefficient [58].

$$K_m = \frac{M}{RT\delta} \left[ \frac{3\tau}{4\varepsilon r} \left( \frac{\pi M}{2RT} \right)^{0.5} + \frac{\tau PD}{\varepsilon p_a} \right]^{-1} \quad (19.28)$$

If the mean free path of the gas (vapor) is much lower than the pore size ( $\lambda \ll d_p$ ,  $Kn \leq 0.01$ ) then molecules will collide with one another, while permeating through the pore (Figure 19.5), and the mechanism is called viscous or Poiseuille flow. Equation 19.29, which is used for estimating the membrane coefficient is given by

$$K_m = 0.125 \frac{r^2 \varepsilon}{\delta \tau} \frac{MP_{\text{avg}}}{\mu RT} \quad (19.29)$$

where

$\mu$  is the water viscosity

$P_{\text{avg}}$  is the average gas pressure inside the membrane

Similarly, the membrane coefficient to describe the transition region between molecular/Knudsen diffusion and Poiseuille flow can be written as [33]

$$K_m = a\delta[1 + b(P_r - 1)] \quad (19.30)$$

and

$$a = mv(A + BP_{\text{ref}}/L) \frac{1}{\delta} \quad (19.31)$$

$$b = \frac{(BP_{\text{ref}}/L)}{(A + BP_{\text{ref}}/L)} \quad (19.32)$$

where

$a$  is the membrane permeation constant

$b$  is 0 for Knudsen diffusion and 1 for Poiseuille flow

$A = 2r\varepsilon/3\tau RT$ ,  $B = \pi r^2 \varepsilon/32\tau RT$ , and  $v = (8RT/\pi M)^{0.5}$  are the gas mean molecular speed

$L$  is the mean free path at unit pressure

The membrane constant  $a$  is the permeability divided by the membrane thickness evaluated at the reference pressure. The physical significance of  $a$  is that it represents the proportionality constant between flux and pressure drop at the reference pressure. The parameter  $b$  indicates the extent to which Poiseuille flow contributes to the permeability and lies between 0 and 1. Equation 19.30 is known as Knudsen–Poiseuille model, where  $P_r$  is the dimensionless pressure defined as  $P_{\text{avg}}/P_{\text{ref}}$ , the  $P_{\text{ref}}$  is chosen in such a way that  $P_r$  becomes close to unity for the range of application of the equation. If a different pressure is assumed, Equation 19.30 may be modified retaining its original form, but having different values for the parameters  $a^*$  and  $b^*$  with the reference pressure as a new  $P_r^*$  close to unity. In such a case the new parameters  $a^*$  and  $b^*$  can be written as [59]

$$a^* = a \left[ (1 - b) + b \frac{P_{\text{ref}}^*}{P_{\text{ref}}} \right] \quad (19.33)$$

$$b^* = \frac{b(P_{\text{ref}}^*/P_{\text{ref}})}{1 - b + b(P_{\text{ref}}^*/P_{\text{ref}})} \quad (19.34)$$

Equations 19.33 and 19.34 can be employed over a range of pressure using gas permeation data obtained in a different reference pressure.

The mass transport through the membrane can also be described by assuming that the overall membrane resistance is equal to the membrane resistance plus the molecular resistance, where the Knudsen–Poiseuille transition model (Equation 19.30) is coupled with an expression for the resistance due to entrapped air (Equation 19.27), in such case the membrane coefficient can be written as [34,59]

$$K_m = \left[ \frac{1}{a(1 - b) + ab \left( \frac{P_{\text{avg}}}{P_{\text{ref}}} \right)} + \frac{P_{\text{am}} \tau \delta RT}{\varepsilon DPM} \right] \quad (19.35)$$

Equation 19.35 can also be used as general equation for membrane coefficient. When the feed solution is distilled water, Equation 19.35 provides a model that asymptotes to the Knudsen–Poiseuille transition flow Equation 19.30, When the

membrane is deaerated, it asymptotes to molecular diffusion through a stagnant air film Equation 19.27, where the partial pressure of air is high.

The other mechanism that rarely occurs in gas permeation is surface diffusion, where the vapor molecules (solutes) adsorb on to the surface of the pores and diffuse under a pressure gradient. This mechanism is neither likely to be dominant for noncondensable gases at low pressures and ambient temperatures, nor is it expected for water vapor permeation through hydrophobic materials [33].

The models above may be useful for predicting mass fluxes in MD; however, each of these models has its limitations. The Knudsen and Poiseuille model require knowledge of  $r$ ,  $\delta$ , and  $\varepsilon$ , which in general can be estimated by applying the models to experimental gas fluxes through the given membrane. The molecular diffusion model is inadequate at low-partial pressures of air, as it predicts infinite flux since, in totally deaerated membrane  $Y_{in}$  tends to zero.

Most of the general models for describing flux through porous media is given by the DGM. The term DGM, which was first described by Maxwell in 1860 [39], is relatively unfamiliar in the membrane separation field and has only recently been appearing in the membrane literature [33,39,41,60,61]. In this model, the porous medium is visualized as a collection of uniformly distributed dust particles, which are construed to be stationary.

The most general form of DGM applicable to MD is given by Equations 19.36 and 19.37 [39]

$$\frac{N_i^D}{D_{ie}^k} + \sum_{j=1 \neq i}^n \frac{p_j N_i^D - p_i N_j^D}{D_{ije}^o} = \frac{-1}{RT} \nabla p_i \quad (19.36)$$

$$N_i^V = \frac{-p_i B_0}{RT \mu} \nabla P \quad (19.37)$$

where

$N_i$  (total flux) =  $N_i^D + N_i^V$  (diffusive flux + viscous flux)

$P$  is the total pressure

$p_i$  is partial pressure of component  $i$

$\mu$  is the fluid viscosity

Effective diffusivities can be written as

$$D_{ie}^k = K_0 \left( \frac{8RT}{\pi M_i} \right)^{\frac{1}{2}}, \quad D_{ije}^o = K_1 P D_{ij} \quad (19.38)$$

where

$(8RT/\pi M_i)^{0.5} = v_i$  is the mean molecular speed

$D_{ij}$  is the ordinary diffusion coefficient

$M_i$  is the molecular weight of component  $i$

$K_0$ ,  $K_1$ , and  $B_0$  are the constants that are strongly dependent on membrane geometry and the interactions between membrane and molecule

These constants are best determined experimentally as the membrane structure is very complex and difficult to characterize, which makes the direct calculation impossible. However, estimates of the constants can be obtained from the membrane pore radius  $r$ , tortuosity  $\tau$ , and porosity  $\varepsilon$  by assuming that the membrane contains uniform cylindrical pores and can be given as [39,43,59]

$$K_0 = \frac{2\varepsilon r}{3\tau}, \quad K_1 = \frac{\varepsilon}{\tau}, \quad \text{and} \quad B_0 = \frac{\varepsilon r^2}{8\tau} \quad (19.39)$$

Based on the gas permeation experiments, Fernandez et al. [59] concluded that parameters  $K_0$  and  $B_0$  are independent of the gas used, and an average value of the parameters for water vapor:  $K_0 = 3.5 \times 10^{-8}$  m and  $B_0 = 2.1 \times 10^{-15}$  m<sup>2</sup> are used.

When  $\lambda < d_{\text{pore}}$ , the transport mechanism is Poiseuille (viscous) flow and the molar flux  $N_i^V$  from Equations 19.37 and 19.39 can be written as [61]

$$N_i^V = \frac{p_i r^2 \varepsilon}{8RT \mu \tau} \frac{\Delta p_i}{\delta} \quad (19.40)$$

where  $\lambda > d_{\text{pore}}$ , the transport mechanism is Knudsen flow and the molar flux  $N_i^k$  from Equation 19.37 can be given as [39,61]

$$N_i^k = \frac{D_i^k}{RT} \frac{\Delta P_i}{\delta} \quad (19.41)$$

where  $D_i^k$  is the Knudsen diffusion coefficient, which is given by

$$D_i^k = \frac{2r\varepsilon}{3\tau} \left( \frac{8RT}{\pi M_i} \right)^{0.5} \quad (19.42)$$

when  $d_{\text{pore}}$  is much larger than  $\lambda$ , and the stagnant air is trapped within the membrane pores, then the transport of vapor through the membrane is by molecular diffusion. The DGM then gives the well-known diffusion through a stagnant film equation.

$$N_i = \frac{K_1 P D_{w\text{-air}} T^{b-1}}{T^b} \frac{\Delta P_i}{R \delta} \frac{1}{P_{\text{am}}} \quad (19.43)$$

where  $P_{\text{am}}$  is the log mean of air pressures at the feed and permeate vapor–liquid interfaces. The temperature has been separated into two terms  $T^{b-1}$  and  $T^b$  and  $b = 2.334$ .

When the average membrane pore size is comparable to the molecular mean free path length ( $\lambda$ ), that is  $d_p \approx \lambda$ , the surface and molecular diffusion can be neglected and in such case the general form of DGM falls into Knudsen–Poiseuille transition region and can be written as [61]

$$N_i = \frac{1}{RT_{\text{avg}}} \left[ K_0 v \frac{\Delta p_i}{\delta} + B_0 \frac{P_{i\text{avg}}}{\mu} \frac{\Delta P}{\delta} \right] \quad (19.44)$$

where

$P$  is the total pressure

$\Delta p_i$  is the gradient in the partial pressure of  $i$ th species

$T_{\text{avg}}$  is the average temperature

Schofield [49] has shown that in DCMD applications, the net flux of air across the membrane is extremely small relative to the flux of water, and viscous flux can be neglected (unless the process solutions have been degassed). With these assumptions Equations 19.36 and 19.37 reduce to the Knudsen–molecular diffusion transition form and can be written as [43]

$$N_w = \frac{\Delta p_w}{RT\delta} \left( \frac{1}{K_0 v} + \frac{p_a}{K_1 P D_{w\text{-air}}} \right)^{-1} \quad (19.45)$$

where  $D_{w\text{-air}}$  is the ordinary water diffusion coefficient and can be calculated from Equation 19.46 [43,52]

$$P D_{w\text{-air}} = 4.46 \times 10^{-6} T^{2.334} \quad (19.46)$$

From Equations 19.37 and 19.38 another flux Equation 19.47 can be written for water vapor, where the Knudsen and molecular diffusion, and viscous flow are considered, while surface flow was neglected.

$$N = -\frac{M}{\delta} \left[ \frac{K_0 K_1 D_{wa} v}{K_1 D_{wa} + x_a K_0 v} \Delta n_w + \frac{B_0 n_w}{\mu} \left( \frac{\Delta P_T}{1 + (x_a K_0 v / K_1 D_{wa})} \right) \right] \quad (19.47)$$

where

$n_w$  is the mole concentration of water vapor

$\Delta n_w$  is the water vapor mole concentration difference across the membrane

$x_a$  is the mean mole fraction of air, and other parameters as defined earlier

Mass transfer through boundary layer is explained in Section 19.3.5.

### 19.3.1.2 Comparison of the Models

Schofield showed in his model Equation 19.30 (or Equation 19.23) that  $T \propto P\Delta P$  for viscous flux and  $J \propto \Delta P$  for Knudsen flux, and obtained a correlation  $J_m = aP_r^b \Delta P$  that approximates the Knudsen–Poiseuille transition of DGM. However, the Schofield model has the advantage that the exponent  $b$  indicates the extent of Knudsen diffusion and Poiseuille flow contributes to the permeability, while such approximations are not possible from  $K_0$  and  $B_0$  used in the DGM. Schofield tested his model on membranes having different pore sizes ranging from 0.10 to 0.45  $\mu\text{m}$  and estimated the values of  $b$  in a range of 0.1–0.6, which suggest that both the mechanisms (Knudsen and viscous) play an important role in MD flux. On the other hand, Schofield's model has two main disadvantages compared to the DGM model. One is, the components  $a$  and  $b$  are dependent upon the gas used. The other is, reference pressure  $P_{\text{ref}}$  is chosen in such a way that the dimensionless pressure becomes close to unity ( $P_r \approx 1$ ), and  $a$  is evaluated at  $P_{\text{ref}}$ , hence the parameters  $a$  and  $b$  also depend on the reference pressure chosen.

Further, Imdakm and Matsuura [61] have developed a Monte Carlo simulation model to study vapor permeation through membrane pores in association with DCMD, where a three-dimensional network of interconnected cylindrical pores with a pore size distribution represents the porous membrane. The network has 12 nodes (sites) in every direction plus boundary condition sites (feed and permeate). The pore length  $l$  is assumed to be of constant length (1.0  $\mu\text{m}$ ), however, it could have any value evaluated experimentally or theoretically [62].

The mass balance for each node of the entire network, assuming the transport of pure substance (water vapor only) can be written as [61]

$$\sum_j C_{ij} \Delta P_{ij} = 0 \quad (19.48)$$

where  $C_{ij}$  is the mass conductance coefficient in the  $ij$ th pore, for viscous flow transport  $C_{ij}$  is defined as  $C_{ijv}$

$$C_{ijv} = \frac{P_{\text{pavg}} \pi r^4}{8RT_{\text{pavg}} \mu l} \quad (19.49)$$

Similarly for Knudsen transport mechanism  $C_{ijk}$

$$C_{ijk} = \frac{-2r^3}{3l} \left( \frac{8\pi}{RT_{\text{pavg}} M_i} \right)^{0.5} \quad (19.50)$$

where

$\mu$  is the fluid viscosity

$\Delta P_{ij}$  is the pressure drop across the pore

$P_{\text{pavg}}$  and  $T_{\text{pavg}}$  are the average pore pressure and temperature, respectively

Once the pore size and length  $l$  are given to the pore network, one can calculate the effective pressure field (by using iteration method), the temperature field through the network, and its effect on the vapor flux through the membrane. This model takes into account all molecular transport mechanisms based on the kinetic gas theory for a single cylindrical tube and could be applied to all forms of membrane distillation process [61].

### 19.3.1.3 Process Parameters

The effect of parameters such as concentration, operating temperature, and flow rate on permeate flux are generally considered for the optimization of DCMD.

Permeate flux decreases with an increase in feed concentration. This phenomenon can be attributed to the reduction of the driving force due to decrease of the vapor pressure of the feed solution and exponential increase of viscosity of the feed with increasing concentration. The DCMD flux gradually increases with an increase in temperature difference between feed and cooling water. Lagana et al. [63] reported that the viscosity of apple juice at high concentration induces severe temperature polarization. It may be noted that temperature polarization is more important than concentration polarization, which is located mainly on the feed side.

In DCMD, increase in flow rate increases the permeate flux. The shear force generated at high-flow rate reduces concentration polarization. Banat [64] found that the flow rate of cooling water had minimal effect on the permeate flux. Ohta [65] has shown that an increase in coolant velocity from 0.02 to 0.08  $\text{m s}^{-1}$  resulted in 1.5-fold increase in the permeate flux. In the same study, it was found that an increase in velocity of hot feed increased the flux by twofold.

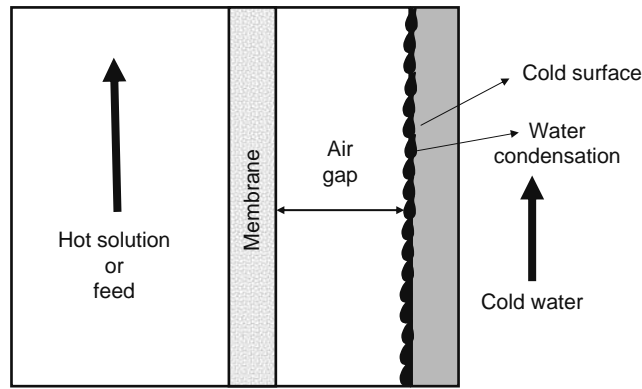


FIGURE 19.6 Schematic representation of AGMD.

### 19.3.2 AIR GAP MEMBRANE DISTILLATION

In air gap membrane distillation (AGMD), an air gap is interposed between the membrane and the condensation surface (Figure 19.6). In this configuration, water evaporates on the feed surface of the membrane, transports through the membrane pores, and condenses on a cold surface, which is separated from the membrane by an air gap. Carlsson [66] was the first to describe the AGMD in 1983, subsequently; more studies were carried out on AGMD and its applications [26,33,67–71]. In AGMD, the presence of air gap acts as a thermal insulation between membrane and condenser wall, and reduces considerably the heat loss caused by conduction and temperature polarization, improving the separation efficiency.

The main advantage of AGMD over DCMD arises from the possibility of condensing the permeate vapors directly in a cold surface rather than in a cold liquid. Additionally, in AGMD the permeate boundary layer is absent thus reducing the overall mass transfer resistance.

#### 19.3.2.1 Heat and Mass Transfer

The stages of heat transfer in AGMD (Figure 19.7) include heat flux from the feed boundary layer to the membrane surface, vapor permeation through the membrane, and the diffusion in air gap, then condensation at the cold surface and finally heat transfer to the cooling water.

Heat flux from the feed boundary layer to the membrane surface can be written similar to Equation 19.11:

$$Q_f = h_1(T_f - T_{s1}) \quad (19.51)$$

where  $h_1$  is the liquid film heat transfer coefficient that can be calculated from Equation 19.21 for laminar flow and Equation 19.13 for turbulent flow.

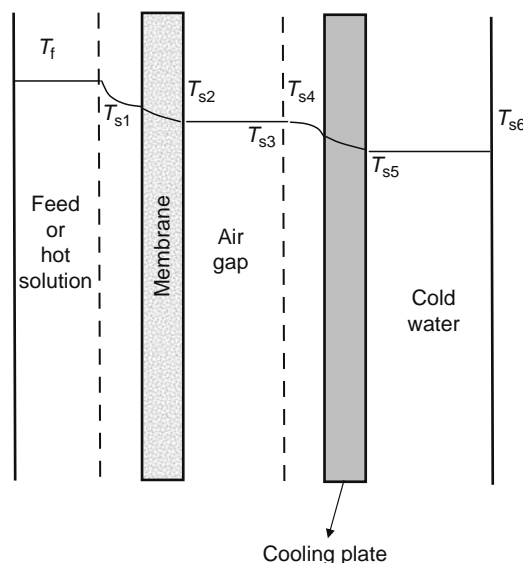


FIGURE 19.7 Temperature profile in AGMD.

The heat transfer through membrane material takes place by conduction and the latent heat transferred by vapor flow through the membrane, which is small and could be neglected. The equation for heat transfer through the membrane can be written as

$$Q_m = \frac{k_m}{\delta} (T_{s1} - T_{s2}) \quad (19.52)$$

The vapors flow from the cold surface of the membrane to the condensation surface through the air gap. Natural convection is very small and could be neglected [72], and only heat transfer ( $Q_a$ ) by conduction across the air gap is considered, which is given by

$$Q_a = \frac{k_g}{(\delta_g - \delta_c)} (T_{s2} - T_{s3}) \quad (19.53)$$

where

$k_g$  is the thermal conductivity of the air

$\delta_g$  and  $\delta_c$  are the air gap and condensate film thickness, respectively

The condensate film thickness can be calculated by [51]

$$\delta_c = \left( \frac{3m\mu_c}{\pi D_t \rho_f^2 g} \right)^{0.33} \quad (19.54)$$

where

$m$  is the flow rate of condensate

$\mu_c$  is the viscosity of condensate film

$D_t$  is the plate thickness

$\rho_f$  is the density of condensate film

The heat transfer by condensation of a pure vapor on a solid surface at constant temperature is given by

$$Q_4 = h_1 (T_{s3} - T_{s4}) \quad (19.55)$$

where  $T_{s3}$  is the dew point temperature of the vapor and  $h_1$  is the film heat transfer coefficient, which can be obtained from Equation 19.56 (for vertical walls) [52]

$$h_1 = 1.333 \left( \frac{k^3 \rho^2 d \pi g}{3 \mu m} \right)^{0.33} \quad (19.56)$$

Heat transferred by conduction through the cooling plate and further by convection to the cooling fluid can be calculated from equations similar to Equations 19.52 and 19.51, respectively.

The mass transfer studies in AGMD suggest that, the transport of vapor through the membrane can be modeled by molecular diffusion mechanism [57], since the pore size of the membrane used is much bigger than the molecular mean free path of water vapor. Equations 19.23 and 19.27 can be used to calculate the mass transfer through the membrane.

### 19.3.2.2 Process Parameters

The process parameters influencing the water vapor flux and energy efficiency are the temperature difference between hot and cold solutions, flow velocities of feed and permeate, air gap pressure, air gap width, and membrane type.

The permeate flux is strongly dependent on the temperature. An increase in inlet temperature of the hot solution from 40°C to 80°C increases the flux by nearly an order of magnitude and the thermal efficiency by 12%, while decreasing the coolant temperature has a lesser effect on the flux increase and even slightly reduces the efficiency [72]. The hot solution temperature has a greater influence because of the exponential increase of the partial pressure of the vapor with the temperature, so the driving force is greater at higher temperature.

The permeate flux increases with increasing feed velocity due to the reduction of the boundary layer thickness. Therefore, the temperature and concentration at the liquid–vapor interface are approaching values close to those in the bulk solution. Garcia et al. [71] have observed that the feed pressure measured at the inlet of the feed cell frame increased with an increase in the feed flow rate consequently increasing the risk of membrane wetting.

The air/vapor gap width is one of the important parameter that plays a major role in AGMD. The major drawback of the air gap is that it creates an extra resistance to mass transfer, which can lower the flux about eight times (for a 5 mm air gap) compared to DCMD under similar conditions [73]. The literature overview of flux obtained so far in flat sheet AGMD [10,50,70,71,73,74] demonstrates that the flux increases considerably by decreasing the air gap width. Alklaibi and Lior [72] and Jönsson et al. [28] observed 2.6-fold increase in the permeate flux as the thickness of the gap is reduced. The increase in permeate flux can be explained by the fact that the air gap conductivity is very low relative to the other regions between the hot and cold solutions. The resultant high temperature and consequent vapor pressure drop across membrane increase flux. Jönsson et al. [28] estimated the optimal air gap width to be 0.2 mm, resulting in large water vapor flux and low-energy loss. However, the practical value of this air gap width has never been tested (because the available space 0.2 mm air gap is quite small for condensed water vapor). Alternative methods to increase the vapor flux, other than reduction of air gap width are reduction in air gap pressure and use of ultrasound technique. Gostoli et al. [50] have showed that decreasing the air gap pressure from 1000 to 400 mbar has increased the flux by 2.4-fold. Reduction of the air gap total pressure from atmospheric to the saturated water vapor pressure of the hot water flow raises the flux by a factor of 2.5–3 in hollow fiber module [75]. Zhu [70] has shown that the permeate flow rate could be increased up to 25% by ultrasonic stimulation.

In practical applications of the membrane distillation processes the most important and crucial issue is heat economy, which is determined by cell design and eventually, the operating parameters. Calculations from the literature [28,69,74] claim theoretical energy efficiencies in the range of 70%–99% for AGMD. In other words 70%–99% of energy drop of the hot water flow is used for evaporation of water and that 1%–30% is lost by heat conduction across the membrane and the air gap. Compared to DCMD, AGMD is expected to be more energy efficient especially at lower feed temperatures. Alklaibi and Lior [72] speculate that air gap width exceeding 2 mm does not raise process efficiency; however, Guijt [75] has shown that the theoretical energy efficiencies of 95%–98% can be achieved in a hollow fiber module of air gap width 3 mm, which could be explained by a small heat loss to the surroundings.

### 19.3.3 VACUUM MEMBRANE DISTILLATION

Vacuum membrane distillation, such as any membrane distillation process, is a thermally driven process in which a feed solution is brought into contact with one side of a microporous membrane and a vacuum is created on the opposite side to create a driving force for transmembrane flux (Figure 19.8). The microporous membrane only acts as a support for a vapor–liquid interface, and does not affect the selectivity associated with the vapor–liquid equilibrium [76].

The experimental procedures are quite similar to and often confused with pervaporation. The main difference between VMD and pervaporation is the nature of the membrane used, which plays an important role in the separations. While VMD uses a porous hydrophobic membrane and the degree of separation is determined by vapor–liquid equilibrium conditions at the membrane–solution interface, pervaporation uses a dense membrane and the separation is based on the relative perm-selectivity and the diffusivity of each component in the membrane material.

#### 19.3.3.1 Heat and Mass Transfer

In VMD, the conductive heat transfer across the membrane is very low, mainly due to the low pressure on the permeate side of the membrane and could be neglected. Thus latent heat of vaporization is the only mode for heat transfer to be considered through the membrane [17,47,77]. Equation 19.3 can be used for calculating the rate of heat transfer across the membrane.

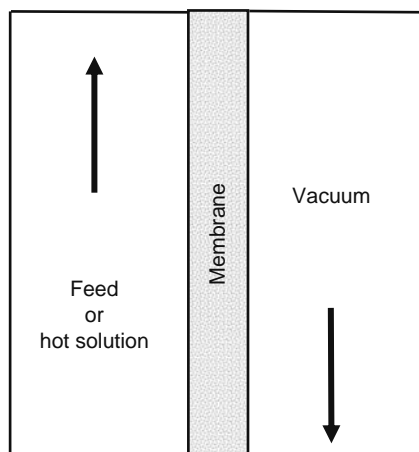


FIGURE 19.8 Schematic representation of VMD.

The heat transfer across the boundary layer present only on feed side (turbulent flow) can be calculated using Equations 19.13 through 19.21, based on the hydrodynamic conditions.

In VMD, the pore size of the membrane falls in the range of 0.1–0.2  $\mu\text{m}$  [17,78]. The mean free path of the diffusing species is usually larger than the pore size of the membrane and under such conditions; Knudsen diffusion is the only mechanism for mass transfer through the membrane and the molecular diffusion resistance can be neglected because the molecular diffusion resistance is proportional to the partial pressure of air in the membrane pores. Since VMD generally operates at total pressures in the order of 10–50 kPa, which is below the vapor pressure of the diffusing species, only trace amounts of air can exist within the membrane pores [77]. Thus, VMD is Knudsen diffusion controlled for the membrane with relatively small pores ( $r \ll \lambda$ ). In this case, the expression is derived based on the kinetic theory of gases or more precisely the DGM Equations 19.26 and 19.23 can be used to estimate the mass transfer across the membrane. However, VMD membranes typically have pores that are comparable to mean free path ( $\lambda$ ), consequently the more complete Knudsen–Poiseuille transition Equation 19.44 is more applicable [77].

### 19.3.3.2 Process Parameters

Feed temperature, flow rate, and solute (nonvolatile) concentrations are some of the parameters commonly studied in VMD.

Mengual et al. have observed an Arrhenius type of dependence of the permeate flux on the feed temperature. An increase in the feed circulation velocity increases the heat transfer coefficient in the liquid boundary layer, which in turn increases the VMD flux due to the reduction in the temperature polarization. Concentration factors increased with a decrease in feed temperature during VMD, and for a decrease of 30°C to 10°C, increase in concentration factors from 7–15.5 to 21–31 were obtained for a highly volatile black currant aroma ester [17].

One of the benefits of VMD relative to the other MD configurations is that conductive heat loss through the membrane is negligible. This enables estimation of the boundary layer heat transfer coefficient. Care must be taken in VMD to prevent membrane wetting, because  $\Delta P_{\text{interface}}$  is typically higher in VMD than in other MD configurations.

### 19.3.4 SWEEPING GAS MEMBRANE DISTILLATION

In this case when the water molecules are collected with the help of a sweeping gas, the process is named SGMD (Figure 19.9). The survey of literature [24,79–82] suggests that very little work has been done with regard to SGMD, although this configuration has the advantages of a relatively low conductive heat loss with a reduced mass transfer resistance. This is probably due to the fact that a very small volume of permeate is vaporized into a large volume of sweep gas and has to be collected in an external condenser, which is not an easy task. Basini et al. [80] were the first to study this configuration for the desalination of water. Later it was employed for the concentration of sucrose solutions and the separation of ethanol–water mixtures [83].

In SGMD, a hot feed solution is circulated on one side of a microporous membrane and cold sweep gas on the other side of the membrane. The temperature difference gives rise to a water vapor pressure difference, and consequently, to a water flux through the membrane.

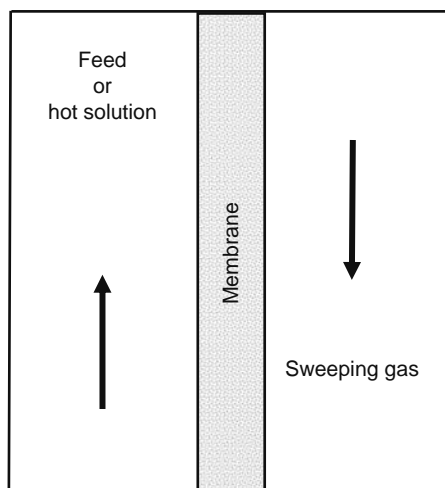


FIGURE 19.9 SGMD configuration of MD.

The SGMD configuration has a great scope for the future due to the advantages mentioned above. SGMD provides much higher permeate fluxes than AGMD while maintaining high temperature polarization coefficient and evaporation efficiency [80–84]. The apparent advantages of SGMD over DCMD are better selectivity, smaller temperature polarization, and higher evaporation efficiency, albeit a low permeate flux [84].

#### 19.3.4.1 Heat and Mass Transfer

The SGMD is a temperature driven process, and it involves: (a) evaporation of water at the hot feed side, (b) transport of water vapor through the pores of hydrophobic membrane, (c) collection of the permeating water vapor into an inert cold sweeping gas, and (d) condensation outside the membrane module. A decrease in driving force has been observed due to polarization effects of both temperature and concentration [80,82]. To calculate both heat and mass transfer through microporous hydrophobic membrane as well as the temperature and concentration polarization layer, the theoretical model suggested by Khayet et al. [58] can be written as

$$N^2 + \left[ (w_{in} + 0.622) \frac{m_a}{A} + B(P - p_v(C_f, T_f)) \right] N + B \frac{m_a}{A} [P w_{in} - p_v(T_a)(w_{in} + 0.622)] = 0 \quad (19.57)$$

where

- $N$  is the mass flux
- $w_{in}$  is the inlet humidity ratio
- $m_a$  is mass flow rate of air
- $A$  is the membrane area
- $P$  is the total pressure
- $p_v$  is the vapor pressure
- $C_f$  is the solute concentration in feed
- $B$  is the net membrane coefficient
- $T_f$  and  $T_a$  are the feed and air temperatures, respectively

In Equation 19.57, the net membrane coefficient  $B$  can be calculated by using Equation 19.45, because the combined Knudsen molecular diffusive flux is responsible for the transport in SGMD [58,81,82], while the temperature of the feed  $T_f$  at the membrane surface can be obtained from

$$T_f = \frac{\frac{\varepsilon k_g + (1-\varepsilon)k_m}{\delta} \left( T_{ba} + \frac{h_f}{h_a} T_{bf} \right) + h_f T_{bf} - N \lambda_L}{\frac{\varepsilon k_f + (1-\varepsilon)k_m}{\delta} + h_f \left[ 1 + \frac{\varepsilon k_g + (1-\varepsilon)k_m}{\delta h_a} \right]} \quad (19.58)$$

where

- $T_{bf}$  is the temperature in the feed (bulk) solution
- $T_f$  is the temperature at the feed membrane surface
- $T_{ba}$  is the temperature in the permeate bulk solutions, respectively
- $\lambda_L$  is the latent heat of vaporization
- $k_g$  and  $k_m$  are the thermal conductivities of the gas in the membrane pores and membrane matrix, respectively

In Equation 19.58, the heat transfer coefficients  $h_f$  and  $h_a$  can be determined using Equations 19.17 and 19.19 (Table 19.1).

#### 19.3.4.2 Process Parameters

In SGMD, the temperature of the liquid feed and the circulation velocity of the sweeping gas are very important parameters. To avoid membrane wetting, it is important that the circulation velocity of the air needs to be varied with caution such that pressure difference between both fluids needs to be lower than the liquid entry pressure of water ( $LEP_w$ ) and the air pressure must be lower than the liquid pressure. The increase in temperature of the feed and the circulation velocity of the sweep gas increases the flux; mainly due to the increase in vapor pressure difference (the driving force). In general, SGMD is the most difficult to describe, since in the downstream compartment, unlike in other MD configurations, none of the variables remain constant along the module. All temperatures, concentrations, as well as heat and mass transfer rates change during passage of gas within the module. Gas entering the cold chamber contains low permeate vapor, with a temperature of cooling water. As it

sweeps the membrane, condensable vapors and heat are accumulated in the gas phase changing its temperature, concentration, and flux. Khayet et al. [79] have observed an increase in the sweep air temperature by 20°C for a module length of 6.5 cm. The heat transferred through the membrane increases the sweep gas temperature along the module length, which results in a progressive increase in partial pressures of the gas. Consequently the driving force decreases rapidly, making the process impracticable at an industrial scale. In order to overcome these problems, Rivier et al. [84] have developed a modified SGMD configuration called thermostatic sweeping gas membrane distillation (TSGMD), in which, a cold wall is added in a downstream compartment to attenuate the increase in sweep gas temperature. Hence the driving force along the module could be enhanced. In TSGMD, an inert gas circulates at more or less constant temperature in the cold chamber and collects the vapors that permeate through the membrane. Part of these permeating vapors condenses inside the module depending on the operating conditions, and the rest in an external condenser.

### 19.3.5 OSMOTIC MEMBRANE DISTILLATION

Osmotic membrane distillation is one of the membrane distillation variants that operate at ambient temperature and atmospheric pressure. In OMD, a microporous hydrophobic membrane separates the two aqueous solutions, namely, feed and osmotic agent (OA) having different solute concentrations (osmotic pressure). The driving force in OMD is vapor pressure difference across the membrane. Water evaporates from the surface of the feed solution having higher vapor pressure, diffuses through the membrane in the form of vapor, and condenses on the surface of a solution with a lower vapor pressure. This results in the concentration of feed and dilution of osmotic agent solution.

Like any other membrane distillation, in OMD the membrane material is also hydrophobic, so that water in liquid form cannot enter the pores unless a hydrostatic pressure exceeds the  $LEP_w$  [37]. In the absence of such pressure difference, a liquid–vapor interface is formed on either side of the membrane pores. In some aspects membrane distillation and OMD can be considered as closely related, although there are some remarkable differences between them. In both cases, it is necessary to maintain a vapor pressure difference across the membrane pores to get a difference in water chemical potential. However, the means of obtaining this vapor pressure difference is different in both the cases. Whereas it is a temperature difference in the case of membrane distillation, it is a concentration difference in the case of OMD.

OMD offers major advantages in comparison with the conventional thermal concentration techniques. The low temperature employed can help avoid chemical or enzymatic reactions associated with heat treatment [85] and prevent degradation of flavor, color, and loss of volatile aroma [38]. The low-operating pressure (atmospheric pressure) results in low investment costs, low risks of fouling, and low limits on compactive strength of the membrane. Since the separation is based on vapor–liquid equilibrium, only volatile compounds which can permeate the membrane and the nonvolatile solutes such as ions, sugars, macromolecules, cells, and colloids are totally retained in the feed. These factors make OMD an attractive alternative to traditional thermal routes currently used for concentration of liquid foods or aqueous solutions of thermally labile pharmaceutical products and biologicals [86].

#### 19.3.5.1 Heat and Mass Transfer

The water transport in OMD is a simultaneous heat and mass transfer process. Evaporation cools the feed and condensation warms the brine solution. This results in a temperature gradient across the membrane, which adversely affects the driving force and in turn the mass flux.

The heat transfer through the membrane can be explained by the convective and the conductive component related to the temperature difference. Thus the expression for rate of heat transfer through the system can be calculated using Equation 19.9. Further, Gostoli [87] attempted to integrate the thermal effect in the mass transfer by introducing an efficiency coefficient,  $\eta$ , which represents the fraction of the driving force really effective for mass transfer through the membrane. This is analogous to MD temperature polarization. The value of  $\eta$  was reported to be 0.85 and the permeability was observed to be 15% lower than the experimental values for NaCl and water system with stirred membrane cell where concentration polarization was neglected. The heat transfer coefficients of the two compartments of the OMD system could be estimated using a friction factor, by combining the experimental pressure loss to the theoretical value that would be obtained in the module having straight shaped circulation channels.

The basic model used to describe the water transport in the system that relates the mass flux ( $J$ ) to the driving force is given by

$$J = K(p_1 - p_2) \quad (19.59)$$

where  $K$  is the overall mass transfer coefficient that accounts for all three resistances (feed, membrane, and OA side) for water transport.

### 19.3.5.2 Mass Transfer through the Membrane

Diffusion is the main mechanism involved in the mass transfer during osmotic distillation and the resistance to mass transfer comes from both membrane structure and presence of air trapped within the membrane pores. While the former resistance can be described by Knudsen diffusion Equation 19.26, the latter is described by molecular diffusion Equation 19.27.

The DGM equations can also be used to find out the mass transfer across the membrane. Since the DGM was derived for isothermal conditions, it would be appropriate to use it for an isothermal membrane process such as OMD. It has been shown that the DGM could be applied to a non-isothermal system also by the inclusion terms for thermal diffusion and thermal transpiration [39,88]. In DCMD, AGMD, VMD, and SGMD these terms are negligible, hence  $T_{\text{avg}}$  has to be used in place of  $T$  in the DGM equations. Since OMD is generally carried out at ambient temperature and atmospheric pressure, using membranes with pore size ranging from 0.1 to 1  $\mu\text{m}$ , so it can be assumed that, the main transport mechanisms present in this case is Knudsen and molecular diffusion, and the Equation 19.45 can be used to calculate the mass transfer through the membrane.

### 19.3.5.3 Mass Transfer through Boundary Layers

Boundary layers of concentrated feed and brine solution are present on either side of the membrane. This results in significant resistance to mass transfer that cannot be neglected.

In order to characterize mass transfer in the boundary layers, it is necessary to determine the respective mass transfer coefficients. These coefficients depend on the properties of the solutions and on the hydrodynamic conditions of the system. Such coefficient can either be obtained by experiments or be estimated with the help of empirical correlations of dimensionless numbers. The majority of the correlations referred to in the literature for various hydrodynamic conditions have the same general form. These include Sherwood number ( $Sh$ ), which contains the mass transfer coefficient, as a function of the Reynolds number ( $Re$ ) and Schmidt number ( $Sc$ ) [89–91]. General mass transfer correlation can be written as

$$Sh = \alpha Re^{\beta} Sc^{\gamma} \quad (19.60)$$

$$Sh = \frac{kb}{D_w}, \quad Re = \frac{\rho Nd^2}{\mu}, \quad Sc = \frac{\mu}{\rho D_w} \quad (19.61)$$

where

$D_w$  is the water diffusion coefficient

$\alpha$ ,  $\beta$ , and  $\gamma$  are constants and are to be selected appropriately for the given hydrodynamic conditions [43,92]

In the case of a noncircular flow channel, for instance a square channel, an equivalent diameter is given by  $d_e = 4S/L_p$  where  $S$  is the cross-sectional area and  $L_p$  the wetted perimeter length of the flow channel [41].

### 19.3.5.4 Process Parameters

Osmotic agent, flow rate, membrane pore size, and feed concentration are some of the key parameters associated with OMD.

The salt chosen as osmotic agent is, in general, NaCl because of its low cost and nontoxicity [57]. Different salts can lead to remarkably different fluxes mainly due to the different osmotic activity of the salts. In general osmotic pressure difference up to 700 bar can be achieved, however, some authors have reported data for pressures as high as 1500 bar [57]. The commonly used OA in OMD other than NaCl are  $\text{CaCl}_2$ ,  $\text{MgCl}_2$ ,  $\text{MgSO}_4$ ,  $\text{K}_2\text{HPO}_4$ , and  $\text{KH}_2\text{PO}_4$ . Potassium salts of ortho- and pyrophosphoric acid offer several advantages, including low-equivalent weight, high water solubility, steep positive temperature coefficients of solubility and safety in foods and pharmaceuticals [93,94].

It has been observed from the literature that transmembrane flux increases with an increase in flow rate. This could be attributed to reduction in the concentration polarization layer. The work carried out by Sheng et al. [95] showed that the transmembrane flux decreased with increase in juice concentration and exhibited a strong dependence on the osmotic pressure difference between the two aqueous solutions. When the difference in osmotic pressure decreased by 33% (from 416 to 280) atmospheric pressure, a fivefold decline in transmembrane flux was observed. As discussed earlier, the pore size plays an important role in influencing the type of diffusion for water transport through membrane. The effect of membrane pore size on transmembrane flux was studied [37,92] and no significant change in flux was observed in the range 0.05–0.2  $\mu\text{m}$  studied. However, from theoretical calculations it was observed that the mode of diffusion (and in turn transmembrane flux) depends on the membrane pore size employed. Naveen et al. [92] have shown the mode of diffusion to be Knudsen when membrane pore size is 0.05  $\mu\text{m}$  and molecular when pore size is 0.2  $\mu\text{m}$ . Brodard et al. [96] who employed ceramic membranes made of alumina having pore sizes of 0.2 and 0.8  $\mu\text{m}$  observed practically no effect of pore size on water flux.

## 19.4 MEMBRANES

Membrane characteristics such as porosity, pore size, tortuosity, and membrane thickness dictate the resistance to mass transfer through microporous membranes used in MD [35,97–99]. Furthermore, studies [100,101] have shown that the relationship between intrinsic membrane properties and operating conditions, e.g., swelling, compaction, and wetting, are important in deciding efficient operations. Therefore, selection of an appropriate membrane that poses the least resistance to mass transfer is crucial. Lefebvre [36] has given some criteria for the choice of membranes.

Both the Poiseuille and Knudsen models show a large dependence of membrane flux on pore radius. Therefore, it is inimical that membranes used in MD should have a high porosity (60%–80%). Since flux is inversely proportional to the membrane thickness, in OMD it needs to be as thin as possible (0.1–1.0  $\mu\text{m}$ ) and should have high heat conductivity to achieve rapid temperature equilibrium near the boundary, while in other variants of MD, such as DCMD, AGMD, SGMD, VMD where temperature gradient is the driving force, membranes should be thicker and should have low thermal conductivity [57]. However, one should not conclude that thick membranes alone are recommended for MD. In fact, with an increase in membrane thickness, the heat resistance increases so also temperature and vapor pressure differences. Similar to OMD, the permeate flux in the DCMD increases with decreasing membrane thickness [102]. The hydrophobic nature of the membrane plays an important role in the performance of MD; a variety of membranes having these characteristics are available. Table 19.2 lists the membranes used by the various researchers till date. This list includes mainly hydrophobic polymers with low surface

**TABLE 19.2**  
**List of Membranes Used by Various Researchers in MD Processes**

MD Configuration	Membrane Module	Membrane Material	Porosity (%)	Nominal Pore Size	$\delta$ (mm)	References
MD	—	PP	80	0.1	60	[103]
		PP	80	0.45	60	
		PP	80	0.2	60	
MD	Tubular	Zirconia	—	50 nm	—	[104]
		Alumina	—	200 nm		
MD	Cross-flow cell	PVDF	75	0.45	110	[105]
MD	Flat membrane	PTFE	80	0.45	60	[106]
DCMD	Flat sheet	PVDF	80	0.2	125	[107]
DCMD	Hollow fibre	PTFE	—	0.45	120	[63]
DCMD	Hollow fibre	PP	40	0.03	31	[108]
DCMD	—	TF-200	80	0.2	178	[109]
		TF-450	80	0.45	178	
		TF-1000	80	1.0	178	
		PTFE	55	0.1	60	
DCMD	Flat sheet	PTFE	57	0.3	60	[46]
		PVDF	70	0.2	60	
		PVDF (GVHP)	62	0.22	126	
		PVDF (GVHZ)	66	0.45	116	
		PTFE	70	0.2	70	
DCMD	—	PTFE	90	0.2	64	[48]
		PVDF	89	0.45	77	
		PP	70	0.22	150	
DCMD	Plate and frame	PTFE	70	0.22	175	[97]
		PTFE	70	0.45	175	
		PVDF	70	1.0	175	
		PTFE	80	0.2	60	
DCMD	Flat sheet	PTFE	80	0.2	60	[110]
DCMD	Sheet membrane	PVDF	75	0.45	110	[34]
DCMD	—	PP	75	0.1	100	[32]
		PP	75	0.2	140	
		PVDF	75	0.45	110	
		PTFE		0.025		
DCMD	Stirred cell	PP	70	0.2	150	[111]
		PP		0.05		

(continued)

**TABLE 19.2 (continued)**  
**List of Membranes Used by Various Researchers in MD Processes**

MD Configuration	Membrane Module	Membrane Material	Porosity (%)	Nominal Pore Size	$\delta$ (mm)	References
DCMD	Flat sheet	TF-200	80	0.2	178	[112]
		GVHP	75	0.22	125	
AGMD	Plate and frame	PVDF	64	0.22 & 0.45	120	[71]
		PTFE	90	0.22 & 0.45	70	
		PTFE	44	0.20	180	
AGMD	Cylindrical (hollow fiber)	PE VA12	77	0.18	90	[75]
		PE FA1	70	0.21	55	
		UPE test	57	0.26	250	
AGMD	—	PTFE	—	0.2–3	80	[44]
AGMD	Flat sheet	PTFE	85	0.1	150	[70]
AGMD	—	PTFE	60	0.2	60	[113]
AGMD	Flat sheet	PVDF	75	0.45	110	[114]
VMD	Tubular	PP	—	0.2	150	[115]
VMD	Shell and Tube C capillary	PP	70	0.2	—	[78]
DCMD		PE	66	0.087	50	
VMD	Hollow fiber	PP	53	0.074	50	[116]
		PP	50	0.044	65	
		PP	47	0.056	42	
SGMD	Plate and frame	TF-200	80	0.2	178	[81]
		TF-450	80	0.45	178	
SGMD	Shell and tube capillary	PP	70	0.2	—	[58]
		GVHP (PVDF)	70	0.2	120	
		FHLP(PTFE)	70	0.2	175	
OMD	Lewis cell	Gelman TF-1000	80	1.0	178	[37]
		Gelman TF-450	80	0.45	178	
		Gelman TF-200	80	0.2	178	
		Gelgard 2400				
		Gelgard 2500	—	0.19	25	
		Accurel IE -PP	—	0.25	25	
OMD	Flat sheet	Accurel 2E -PP	—	0.48	90	
		Durapel VVSP-PP	—	0.54	150	[117]
			—	0.60	120	
		Durapel GVSP-PP	—	0.81	120	
			—	1.08	50	
		Goretex L31189	—	1.10	50	
	Simitomo	—	1.29	50		
	Simitomo					
OMD	Plate and frame	PP	—	0.2	—	[11]
OMD	Stirred cell	PP	55	0.1 mm	90 mm	[91]
OMD	Plate and frame	PTFE	—	0.1	100	[95]
OMD	—	PTFE	80	0.25	175	[118]
OMD	Plate and frame	PTFE	60	0.2	165	[119]
OMD	Hollow fibre	PVDF	75	0.2	125	[120]
		PVDF	64	0.2	125	
OMD	Capillary	PP	70	0.2	—	[121]
		PP/PE	45	0.05	28	
OMD	Cylindrical semicell	PVDF	80	0.2	108	[4]
		UHMWPE	80	0.2	90	
OMD	Flat sheet	TF-200	60	0.20	165	[41]
		TF-450	60	0.45	178	
MD + OD	Lewis cell	PTFE	80	0.25	175	[122]

free energies, i.e., polytetrafluoroethylene (PTFE,  $9.1 \text{ kN m}^{-1}$ ), polyvinylidene fluoride (PVDF,  $30.3 \text{ kN m}^{-1}$ ), polyethylene (PE,  $33.2 \text{ kN m}^{-1}$ ), and polypropylene (PP,  $30.0 \text{ kN m}^{-1}$  surface energy). The survey of literature suggests that the pore size, porosity, and thickness of most of the membranes used in MD fall in the range of  $0.2\text{--}1.0 \text{ }\mu\text{m}$ ,  $65\%\text{--}85\%$ , and  $0.06\text{--}0.25 \text{ mm}$ , respectively. The thermal conductivities of polymers are mainly dependent on temperature and the degree of crystallinity of the polymer, which varies in the range of  $0.15\text{--}0.45 \text{ W m}^{-1} \text{ K}^{-1}$  [123]. Hydrophilic membranes that have been treated to make their surfaces hydrophobic have also been applied successfully to MD [124,125].

The pressure variable can be used in defining wettability in terms of LEP, as represented by the Laplace (Cantor) equation

$$\Delta P_{\text{entry}} = \frac{-2B\gamma_l}{r_{p,\text{max}}} \cos \theta \quad (19.62)$$

where

$\Delta P_{\text{entry}}$  is the entry pressure difference

$\gamma_l$  is the surface tension of the solution

$\theta$  is the angle of contact between the solution and the membrane surface

$B$  is a geometric factor

$r_{p,\text{max}}$  is the largest pore size

Once the pressure drop across the vapor–liquid interface  $\Delta P_{\text{interface}}$  exceeds penetration pressure  $\Delta P_{\text{entry}}$ , the liquid can penetrate the membrane pores and the membrane is termed as wetted. Contact angle measurement and surface tension are the traditional methods to describe the wettability of the membranes. The contact angle comprised of a liquid droplet deposited onto the surface of a smooth solid will have a value higher than  $90^\circ$  if there is low affinity between liquid and solid, and will be less than  $90^\circ$  in the case of high affinity. Wetting occurs at  $0^\circ$ , when the liquid spreads onto the surface. In general the solid–liquid angle of contact for the membrane should be at least  $90^\circ$ , while a value of  $130^\circ$  being the optimal for use in MD [39]. Recently, the use of some copolymers of tetrafluoroethylene (TFE) and 2,2,4-trifluoro-5-trifluoromethoxy-1,3-dioxole (TTD), commercially known as HYFLON AD, for fabricating polymeric membranes have provided an increased reliability to the MD process. They have been used for preparing asymmetric and composite membranes that show a high contact angle ( $120^\circ$ ) for water, demonstrating a highly hydrophobic character [126]. Brodard et al. [96] successfully employed hydrophobic ceramic tubular membranes in the osmotic evaporation process. These ceramic membranes have been obtained by grafting siloxane compounds on alumina porous supports. Ceramic membranes have the advantage of higher physical and chemical stability as compared with polymeric membranes. Barbe et al. [117] have studied nine types of hydrophobic microporous membranes for their influence on the retention of range of volatile organic species. The results of this investigation suggest that membranes having relatively large surface pores have been shown to retain higher organic volatiles per unit water removed than those with smaller surface porosity. However, pores with larger diameters at the membrane surface allow greater intrusion of the feed and OA solutions, leading to an extended boundary layer. This extended layer offers extra resistance for diffusion of volatile components. Further Barbe et al. [127] have studied changes in the surface morphology in hydrophobic membranes. A change in morphology was observed when the membranes were in contact with water as against no change observed when in contact with 30% w/w  $\text{CaCl}_2$ . This was attributed to a lower degree of intrusion of the  $\text{CaCl}_2$  solution, relative to that of water because of the higher surface tension of the former. Their results also suggested that the larger pores become larger while smaller pores showed shrinkage.

Although fouling seems to be of minor importance for MD compared to other membrane techniques, periodic membrane cleaning is necessary. Durham and Nguyen [128] evaluated the effectiveness of several cleaning agents for microporous PTFE and cross-linked acrylic-fluoroethane copolymer membranes. The membranes were cleaned after 2 h of processing of a 21.5% solution of tomato puree, and the change in flux and membrane hydrophobicity measured before and after cleaning. The authors showed that repetitive cleaning and fouling can rapidly destroy certain membranes, an important result in regard to industrial applications.

## 19.5 MEMBRANE MODULES

The choice of membrane module for MD is mainly determined by functional and economic considerations. A large variety of membrane modules, such as plate and frame, spiral wound, tubular, capillary, and hollow fiber have been designed and tested for MD.

In plate and frame modules, the membranes are placed (with or without spacers) between two plates. The packing density of this configuration varies between  $100$  and  $400 \text{ m}^2 \text{ m}^{-3}$ , depending on the number of membranes or cassettes used. Andersson et al. [31] have used a plate and frame configuration for desalination purposes, where various cassettes were stacked together, each consisting of injection molded plastic frames of two membranes. Naveen et al. [92] used a plate and frame membrane

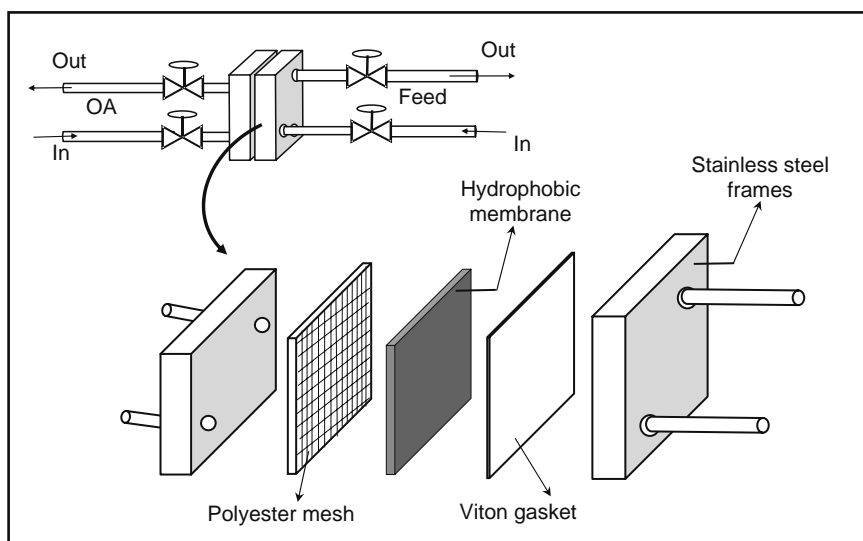


FIGURE 19.10 Plate and frame membrane module.

module having a membrane area of  $0.016 \text{ m}^2$  for the concentration of pineapple and sweet limejuice. The module (Figure 19.10) consists of a polyester mesh, a Viton gasket, and a hydrophobic microporous membrane of pore size ( $0.05\text{--}0.2 \mu\text{m}$ ) supported in between two stainless steel frames. Feed solution and osmotic agent solution were circulated on either side of the membrane in cocurrent mode using peristaltic pumps.

Spiral-wound modules have a packing density of  $300\text{--}1000 \text{ m}^2 \text{ m}^{-3}$ , which is greater than that of the plate and frame module. This packing density depends upon height of the channel spacers. Koschikowski et al. [129] have used a spiral-wound MD module for desalination experiments, which is assembled by spiral winding of PTFE membrane and condenser foils. It has been reported to have a specific thermal energy consumption of  $140\text{--}200 \text{ kW h m}^{-3}$  of distillate and gained output ratio of 4–6. The use of spiral-wound modules has been proposed by Gore [27] for industrial scale desalination units.

Tubular membranes unlike capillaries and hollow fibers are not self-supporting. Hence, such membranes tubes are placed into porous stainless steel, ceramic, or plastic tubes. The diameter of tubular membranes usually varies from 1 to 2.5 cm, with a packing density of about  $300 \text{ m}^2 \text{ m}^{-3}$ . In MD operations, the tubular modules are used either for highly viscous fluids or while operating under high-flow rates. In some cases, tubular modules are used to reduce fouling and concentration polarization phenomena. In order to make SGMD practicable at industrial scale Rivier et al. [84] have used a tubular membrane module (TSGMD) as shown in Figure 19.11. The module is made of glass and has six tubular membranes, each one surrounded by a glass tube of  $13 \times 10^{-3} \text{ m}$  i.d. (inner diameter). The effective membrane surface of the module is  $0.019 \text{ m}^2$ . The feed and sweeping gas are circulated inside and outside the tubular membrane, respectively. Capillary membrane modules consist of a

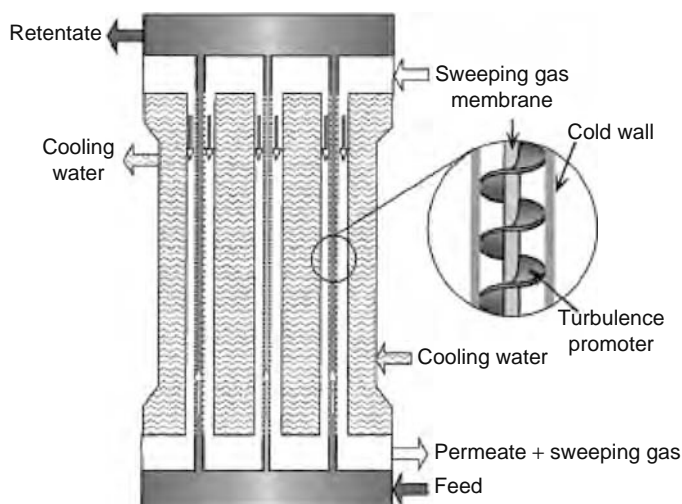


FIGURE 19.11 Schematic representation of TSGMD module.

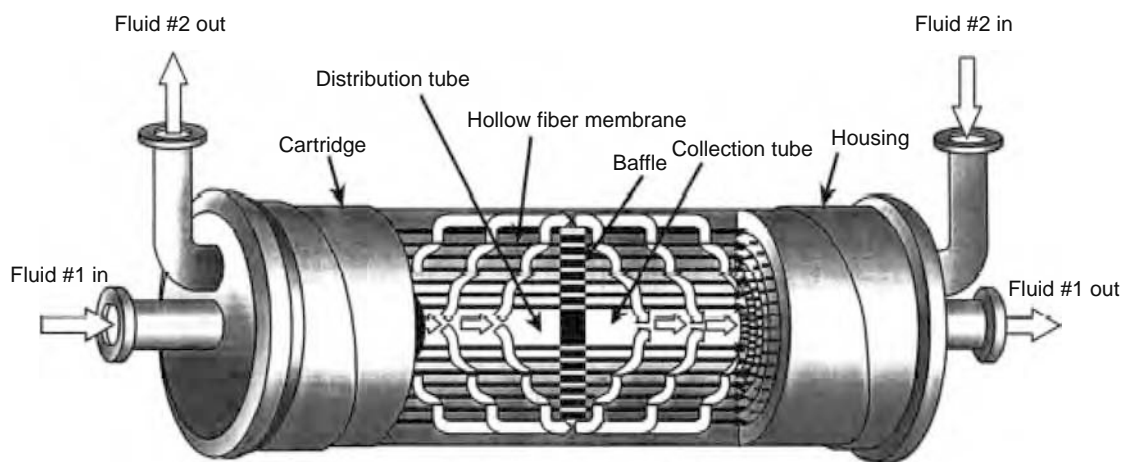


FIGURE 19.12 Liqui-Cel Extra-Flow membrane contractor from CELGARD LLC.

large number of capillaries, which are arranged in parallel as a bundle in a shell and tube configuration. The capillary membranes are self-supporting, and two kinds of module arrangement are possible based on flow of feed or permeate (through the capillary or outside of the capillaries). The packing density is in the order of  $600\text{--}1200\text{ m}^2\text{ m}^{-3}$ , which is between the tubular and hollow fiber modules.

A hollow fiber module is conceptually similar to the capillary module, but differs in dimensions. In this case the diameter of the tubular membrane varies between  $50\text{ and }100\text{ }\mu\text{m}$  and several thousand of fibers can be placed in the vessel. The hollow fiber module is the configuration with the highest packing density (with values up to  $30,000\text{ m}^2\text{ m}^{-3}$ ).

Liqui-Cel Extra-Flow (Figure 19.12) is one of the well studied hollow fiber modules for concentration-driven mass transfer. This module consists of several microporous polypropylene fibers, which are woven into a fabric and wrapped around a central tube feeder that supplies the shell side fluid. The woven fabric allows more uniform fiber spacing, which in turn leads to higher mass transfer coefficients than those obtained with individual fibers. The fiber lumen diameter and wall thickness are  $240\text{ and }30\text{ }\mu\text{m}$ , respectively [93,130]. The smallest Liqui-Cel modules are 2.5 in. in diameter and contain  $1.4\text{ m}^2$  of contact area, while the largest are 10 in. in diameter and offer  $130\text{ m}^2$  of contact area by virtue of 225,000 fibers. The large modules can handle liquid flow rates of several 1000 L/min.

Some more module configurations are reported for use in MD. Lawson and Lloyd [77] have designed a laboratory-scale MD module as shown in Figure 19.13, where the membrane was sandwiched between the two half-cells, and several hose clamps held the module together. The total area available is  $9.7\text{ cm}^2$  and the smooth transitions at the module entrance as well as exit allow achievement of relatively high Reynolds numbers, whereby conventional boundary layer equations are applicable. The module does not require a support in low pressure-drop applications such as DCMD. Wider permeate channels would require a support for VMD experiments. A porous sintered stainless steel material has been used for the gas permeation experiments.

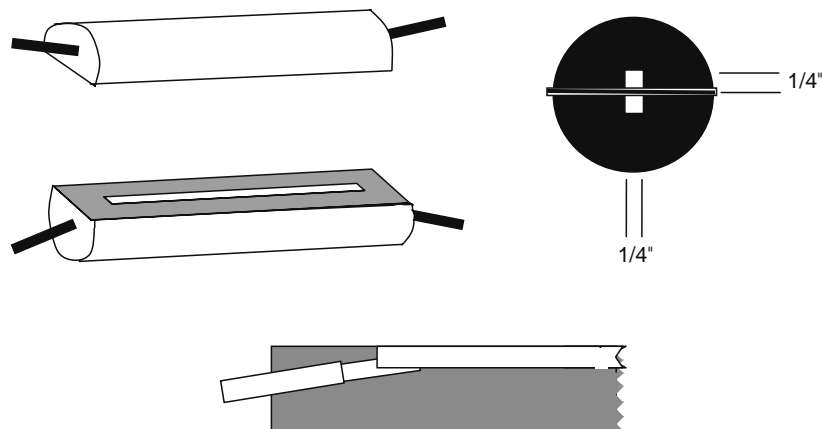
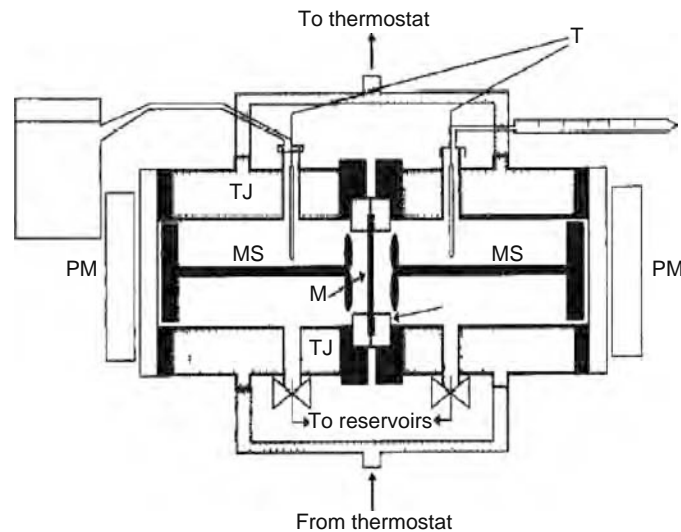


FIGURE 19.13 Schematic diagram of the MD module.



**FIGURE 19.14** Stirred cell. M: membrane, H: membrane holder, MS: magnetic stirrer, PM: propelling magnet, T: thermometer, TJ: thermostated jacket.

Mengual et al. [37] have used Lewis cell (stirred cell) for their experiments on MD (Figure 19.14). This mainly consists of two equal cylindrical chambers made of stainless steel having a length of 20.5 cm. The membrane was fixed between the chambers by means of a PVC holder. Three viton O-rings were employed to eliminate leaks in the assembly. The membrane surface area exposed to the flow was 27.5 cm<sup>2</sup>.

To investigate the role of heat transfer in OMD and measure the asymptotic temperature difference, Celere and Gostoli [86] used the flat sheet membrane module shown in Figure 19.15. This contains a few flat sheet membranes placed 1 mm apart and supported by mesh-type spacers of 2 mm thickness, leaning against polypropylene walls. One stream (feed) flows between the membranes and other (extractant) flows cocurrently through the spacers. The mass transfer zone of each membrane is 80 mm in breadth and 200 mm in length.

## 19.6 ENHANCEMENT OF FLUX IN MEMBRANE DISTILLATION

In spite of their advantage and potential over conventional processes, membrane distillation suffers from the drawback of low transmembrane flux when compared to RO. In the past few years, additional innovations in module design and new strategies have been explored to reduce concentration polarization and to enhance mass transfer. Some of these attempts are discussed here.

Enhancement of transmembrane flux has been shown in OMD of grape juice pretreated by UF [131]. The increase in flux has been attributed to a reduction in the viscosity of the concentrated juice–membrane boundary layer as the result of removal of high-molecular weight biopolymers present in juice. UF is a powerful method for removing natural polymers (polysaccharides, proteins) from fruit and vegetable juices. Lukanin et al. [12] have improved the concept of (UF + OMD), by enzymatic pretreatment of the apple juice prior to the UF step. Introduction of an additional enzymatic deproteinization step with the pectinase/amylase treatment of apple juice followed by UF has yielded minimal biopolymer content. Such a treatment is found to enhance transmembrane flux during concentration of clarified juice by MD. As in the case of grape juice this has been

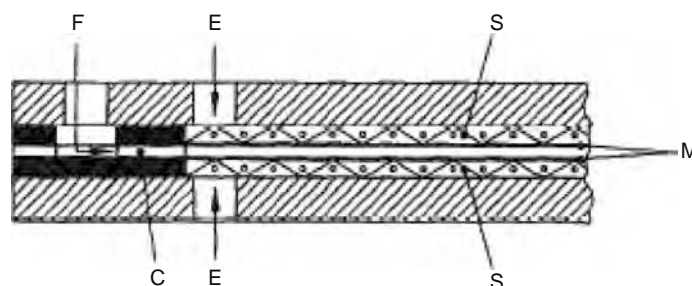


**FIGURE 19.15** Cross section of the MD module. F: feed inlet, C: feed manifold, E: extractant inlet, S: spacers, M: membranes.

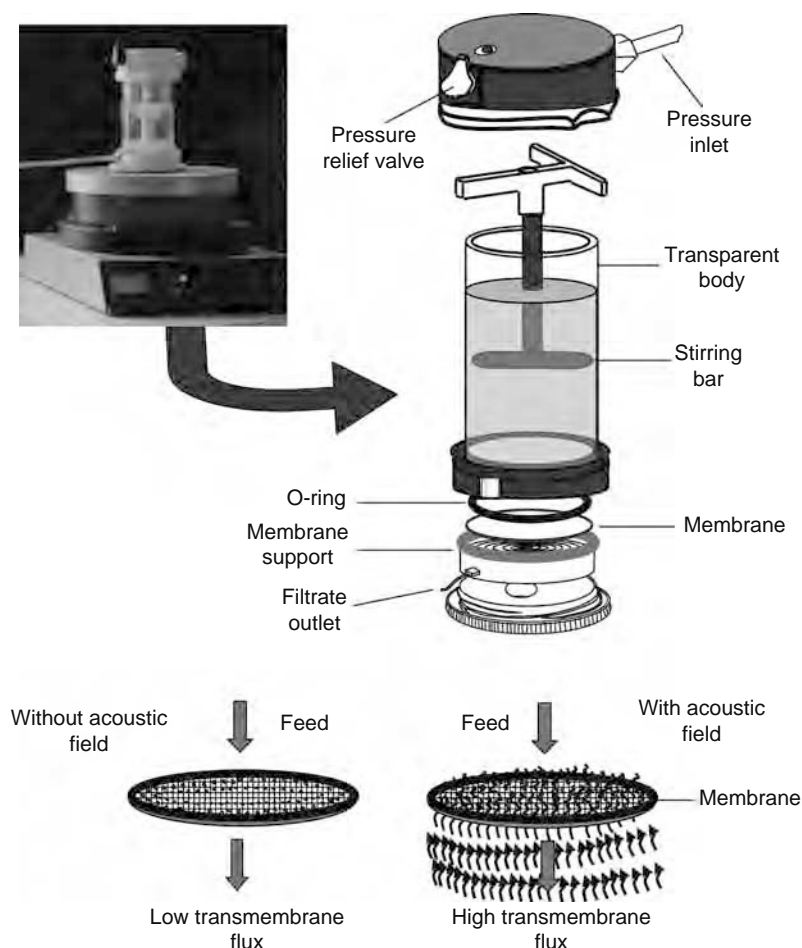


**FIGURE 19.16** Stirred membrane cell with acoustic field.

attributed to reduction in juice viscosity. Lower viscosity improved hydrodynamic conditions in membrane channel thereby decreasing concentration and temperature polarization.

An ultrasonic technique was applied to AGMD to enhance the permeability for the concentration of various aqueous solutions. In this study, an ultrasonic stimulation of resonance frequency of 20 kHz and power up to 90 W was applied to a flat-plate AGMD system of 1  $\mu\text{m}$  PTFE membrane with a temperature difference of 55°C. A 200% improvement in the transmembrane flux was observed with an ultrasonic intensity of 5  $\text{W cm}^{-2}$ . Experimental investigation of the basic mechanism of ultrasonic enhancement of AGMD suggests that, for a continuous ultrasonic stimulation the dominating mechanisms are microstreaming and cavitation [70,130].

Narayan et al. [111] have tried to enhance the transmembrane flux by using an acoustic field (1.2 MHz), by placing the membrane cell over an ultrasonic transducer (Figure 19.16). Their results show an increase in flux by approximately 35% to 98% when compared with control runs (without acoustic field). The increase in flux is due to the fact that acoustic field induces mild circulation currents, which disturbs the hydrodynamic boundary layers of feed and OA solutions, thereby reducing the effect of concentration polarization.

On examining the effect of membrane compaction on the membrane permeability, Lawson et al. [100] concluded that the transmembrane flux in MD could be increased significantly up to 11% with relatively small pressure drops <70 kPa.

Concentration and temperature polarization can be reduced by the presence of spacers that are turbulence promoters, which enhance the mass flux by increasing the film heat transfer coefficient. Spacers also change the flow characteristics and promote regions of turbulence thus improving boundary layer transfer [106]. DCMD in spacer-filled channels have been shown to improve flux by 31%–41% than that without spacers. The temperature polarization coefficients are substantially increased and approach unity when the spacers are used in the channels.

Cath et al. [97] have demonstrated that, careful design of membrane module and configuration of MD processes could simultaneously reduce temperature polarization and permeability obstructions in the DCMD of salt solutions. Results have shown that fluxes almost double those that are observed in the traditional mode of DCMD, can be achieved at relatively low temperatures.

**TABLE 19.3**  
**Comparative Performance of RO and VMD for a Commercial Membrane**

Membrane Process	Energy Consumption (kWh m <sup>-3</sup> )	Flux (L m <sup>-2</sup> h)
RO with energy recovery	4.0	5–10
VMD single pass	3.2	0.7
VMD discontinuous	1.2	0.5–0.7

Source: From Corinne, C. and David, W., *Desalination*, 157, 307, 2003. With permission.

Note: ( $K_m = 3.4 \times 10^{-7} \cdot s \cdot mol^{0.5} \cdot m^{-1} \cdot kg^{-0.5}$  at 20°C)

## 19.7 APPLICATIONS IN FOOD PROCESSING

Most of the applications reported for MD have been carried out at a laboratory scale. Data on pilot scale studies are available for demineralization of water and to a limited extent on beverages and fruit juice, that too for OMD.

### 19.7.1 DEMINERALIZED WATER

This is by far the most promising food-related application of MD. The advantages of MD over traditional methods, such as RO and multiple stage evaporation lie in the quantitative solute rejection achieved and the comparatively low-energy inputs required for MD when feed water has a high salt concentration, as in seawater.

The work carried out by Lawson and Lloyd [47] suggests that, the DCMD is a viable process for seawater desalination, with fluxes of 2 mol m<sup>-2</sup> s<sup>-1</sup>, which is twice that reported for RO. Banat and Simandl [74] have used an AGMD module with PVDF membrane for their desalination experiments. Pure water with less than 5 ppm total dissolved solid was obtained with a reproducibility of ±20%.

Energy consumption for manufacture of demineralized water from seawater is an issue, which has received much attention. Criscuoli and Drioli [132] found the energy costs for RO to be between 4 and 12 kW h m<sup>-3</sup> depending on whether or not an efficient energy recovery system was in place. Cabassud and Wirth [133] have estimated costs for VMD using PVDF hollow fiber membranes for salt concentrations varying between 15 and 300 g L<sup>-1</sup> (Table 19.3).

They proposed that VMD could compete with RO on energy consumption for membranes 100 times more permeable than those used in their experiment at 25°C at the same permeate flux (5–15 L m<sup>-2</sup> h<sup>-1</sup>). However, if coupled to a solar energy-based system, the flux could be enhanced to 40–85 L m<sup>-2</sup> h<sup>-1</sup> and would make it competitive with RO. Reports on using solar energy coupled to MD [134–137] appear to reinforce this belief.

The energy ( $Q_{req}$ ) required increasing inlet feed solution temperature to the hot channel ( $T_{hi}$ ) was expressed by Alklaibi and Lior [123] as follows:

$$Q_{req} = m_h C_{ps} (T_{hi} - T_{sr}) \quad (19.63)$$

where

$T_{sr}$  is the temperature of the feed solution at source

$m_h$  is the mass flow

Drioli et al. [138] suggested an integrated desalination process of MD and RO for decreasing the cost of production. They arrived at the following cost for MD and RO using a fixed membrane area of 116 m<sup>2</sup> (Table 19.4).

**TABLE 19.4**  
**Cost Comparison of Different Processes for Desalination of Seawater**

Process	Cost of Water Produced \$ m <sup>-3</sup>	Production	Recovery Factor (%)
Only RO	1.25	0.391; $F_1$	40.0
Only MD	1.32	0.856; $F_2$	87.6
RO + MD	1.25	0.856; $F_2$	87.6

Source: From Drioli, E., et al., *Desalination*, 122, 141, 1999. With permission.

Note: Fixed cost of \$116 m<sup>-2</sup> membrane area; feed containing  $F_1 = 60.6\%$ ,  $F_2 = 14\%$  salt.

A novel idea for the production of water is by the combination of MD and membrane crystallization [139], where the salt is concentrated on the feed side to a point close to super-saturation, thereby inducing nucleation of crystals. Recently Gryta and Morawski [140] performed experiments using polypropylene capillary membranes with pore diameters ranging between 0.2 and 0.6  $\mu\text{m}$ , and 70% porosity. They found crystallization to occur at the membrane surface, but by increasing the distillate temperature to 328 K, the problem was eliminated and stable flux restored.

A new development reported by Li and Sirkar [141] for MD-based desalination makes use of polypropylene hollow fibers coated with a plasma polymerized silicone-fluoropolymer. This ultrathin coating on the outside of the fiber was water vapor permeable and was instrumental in decreasing the susceptibility of the composite membrane to wetting and fouling. They reported stable water vapor fluxes between 41 and 79  $\text{kg m}^{-2} \text{h}^{-1}$  for runs lasting up to 400 h.

MD holds great promise as a unit operation for water desalination, by itself and in conjunction with other processes such as RO and traditional distillation. Advances in membrane chemistry and module design are expected to close the gap between these processes in the near future.

### 19.7.2 BEVERAGES AND FRUIT JUICE

The concentration of fruit juice and allied beverages is very challenging from the view of retention of natural aroma and flavor, which decides its acceptance by the consumer. The literature indicates membrane processes currently in use, RO for concentration and pervaporation for aroma capture are mature technologies [21,142]. OMD in combination with RO for concentration of juice beyond 25°Bx (when osmotic pressure imposes limits on RO) has greater prospects than as a stand-alone OMD operation [21].

Direct contact membrane distillation was shown by Drioli et al. [143] and Calabro et al. [13] to be very effective in the concentration of orange juice. Drioli et al. report showed that most of the soluble solids in orange juice were rejected by a microporous PVDF membrane, with the exception of vitamin C, which showed passage and oxidation because of the high temperatures employed. While the report of Calabro et al. from the same group using the same membrane indicated that an early UF pretreatment gave steady flux compared with untreated juice. The decay in flux of untreated juice was attributed to pectin fouling of membrane. Bailey et al. [144] observed similar effects for single strength grape juice. This was attributed to increase in viscosity in the juice-membrane boundary layer where the solute concentration is highest. Lukanin et al. [12] in a study carried on apple juice showed that the stability of productivity in MD concentration improved with decreasing viscosity. Lagana et al. [63] were able to concentrate apple juice up to 64°Bx with transmembrane fluxes of 1  $\text{kg m}^{-2} \text{h}^{-1}$ . They too observed that the viscosity of juice at high concentrations induced concentration polarization, thereby causing decline in flux. DCMD offers advantages for processing high-osmotic pressure feeds, extremes of pH solutions, and application in remote systems using solar or waste heat.

Bagger-Jorgensen et al. [17] found VMD to be a promising technique for retaining the aroma compounds in black currant juice. Their observations on the improved retention of aroma compound *cis*-3-hexen-1-ol as a function of increased cross-flow was attributed to reduced temperature and concentration polarization, which in turn increases the aroma concentration at the vapor-liquid interface. The accumulation of aroma compounds at the boundary layer was eventually found to control flux in spite of increase in cross-flow rate.

Sheng et al. [95] reported the concentration of orange, apple, and grape juices using OMD with a plate and frame module having a membrane surface area of 1  $\text{m}^2$ . They quoted typical flux values of 5–10  $\text{L h}^{-1} \text{m}^{-2}$  for a plant installation with spiral-wound membranes and a juice concentration of at least 75% of solid content. In their installation the diluted salt solution is separately concentrated by pervaporation through a hollow fiber membrane at 50°C. Thompson [145] reported a novel application of OMD, for the concentration of grape juice to make wine from reconstituted concentrate. The author mentioned that wine obtained in this way was difficult to be distinguished from wine produced in the conventional way from simple strength grape juice. This was done at a pilot plant scale having a feed rate of approximately 80–100  $\text{L h}^{-1}$ . He mentioned that an OMD plant for processing between 10,000 and 23,000 L of feed grape juice was in operation.

Barbe et al. [117] studied nine different membranes for their retention of aromatic components commonly found in grape and orange. Using GC-MS analysis of the head space of the simulated feed and elaborate scanning electron microscopy, they showed conclusively that membranes with large pore sizes at the surface show higher retention of volatile components than those, which have narrow surface pores. They have proposed a model to explain this phenomenon.

Ali et al. [146] investigated the passage of aroma constituents of fruit juice during OMD on a pilot plant scale. Using headspace analysis of feed and permeate, they concluded that the loss in aroma could be minimized by operating at low temperature and low feed velocity.

In feeds containing oily constituents (limonene in orange juice), there is often the problem of wetting of the pores of hydrophobic membranes. For OMD applications, Mansouri and Fane [4] used polyvinyl alcohol (PVA) and polyhydroxy 2-ethyl methacrylate (PHEMA) hydrogels to coat membranes such that a hydrophilic gel layer was formed near the mouth of pores. This laminate effectively controlled the ingress of oily constituents into the membrane, at the same time the permeability of water vapor through the pore remained unaffected. Recently Xu [147] has reported alginate hydrogel coatings on PTFE

**TABLE 19.5**  
**Comparison of OMD and MD with respect to Aroma**

Process	Feed	$N_{eb}/N_w$ ( $10^{-6}$ )	$N_c/N_w$ ( $10^{-6}$ )
OMD	Only volatiles	2.8	2.3
MD	Only volatiles	7.2	4.5
OMD	Sucrose (45%) + volatiles	2.6	2.4
MD	Sucrose (45%) + volatiles	5.9	5.4

*Source:* From Alves, V.D. and Coelho, I.M., *J. Food Eng.*, 74, 125, 2006. With permission.

*Note:*  $N_{eb}$ ,  $N_c$ , and  $N_w$  are the molar fluxes for ethyl butyrate, citral, and water, respectively.

membrane. They reported a 10-fold increase in the adhesion strength between the hydrophilic alginate and the hydrophobic PTFE, by adjusting the surface tension of the coating material. Resistance to wetting of the composite membrane was tested with feed containing 0.2%–0.8% orange oil over a period of 300 min.

Recently Alves and Coelho [148] have compared the concentration of a simulated orange juice (glucose, citral, and ethyl butyrate) using MD and OMD. Using Accurel PP2E HF (Membrana, GmbH, Waltham, Massachusetts) polypropylene membrane, they concluded that as long as viscosity was low the contribution of the sucrose solution boundary layer (shell side) in OMD was not significant. However, toward the end of the experiment, when kinematic viscosity of sucrose solution increases, this resistance becomes considerable. For MD, using the same feed and similar driving force, the flux was found to be less than half of that for OMD [148]. Transport of aroma compounds (citral and ethyl butyrate) for MD showed greater permeation than in OMD for a normalized water removal rate (Table 19.5).

The results suggest that OMD has a distinct advantage over MD, both in terms of flux and aroma retention.

To summarize some of these observations: The viscosity and colloidal content of juice strongly influenced flux because of concentration polarization; due to passage of vapor through pores, there is a fall in temperature at the vapor–liquid interface causing temperature polarization. An increase in feed velocity would increase this temperature at the interface, thereby maintaining flux; at lower solute concentrations, the water vapor flux is high and therefore aroma compositions at the vapor–liquid interface are high; pores with a wider surface diameter allow greater retention of aroma compounds.

Jiao et al. [21] have compared the overall performance of membrane concentration techniques vis-à-vis conventional evaporation (Table 19.6).

Though MD has provoked intense research activity that has led to numerous publications and patents, it finds relatively fewer commercial applications as a stand-alone process, as compared with other membrane processes.

This could be attributed to some of the disadvantages that continue to plague membrane distillation, namely the lack of selectivity of the pores for permeation of vapor through the membrane; significant energy loss due to conduction across the boundary layers close to the membrane; leakage through the membrane caused by trace constituents of the feed stream that lowers the surface tension at the liquid–membrane interface causing intrusion of liquid into the pores.

### 19.7.3 INTEGRATED MEMBRANE PROCESS

On the one hand, MD and OMD suffer from low flux (compared to RO) and temperature concentration polarization that limits their full commercial application. On the other hand, RO process has the problem of maximum achievable concentration (can

**TABLE 19.6**  
**Salient Features of Evaporation and Membrane Concentration Processes**

Process	Maximum Achievable Concentration (°Bx)	Product Quality	Evaporation Rate (L h <sup>-1</sup> ) or Flux (L m <sup>-2</sup> h <sup>-1</sup> )	Product Flexibility	Operating Costs	Capital Investment	Energy Consumption	Status of Technology
Evaporation	80	Very poor	200–300	No	Moderate	Moderate	Very high	Developed
Reverse osmosis	25–35	Very good	5–10	No	High	High	High	Developed
Direct osmosis	50	Good	1–5	Yes	High	High	Low	Under development
Membrane distillation	60–70	Good	1–10	Yes	High	Moderate	Low	Under development
Osmotic distillation	60–70	Very good	1–3	Yes	High	Moderate	Low	Under development

*Source:* From Jiao, B., Cassano, A., and Drioli, E., *J. Food Eng.*, 63, 303, 2004. With permission.

reach only up to 25°Bx–30°Bx). To overcome these drawbacks and to improve the product quality and process economics integrated process are gaining popularity. They provide an efficient scalable alternative to thermal processes for the concentration of liquid foods, pharmaceuticals, and biologicals.

Johnson et al. [149] have studied the three-stage hybrid membrane process for the concentration of ethanol–water extracts of the *Echinacea* plant, wherein ethanol removal from the extract was achieved by pervaporation in stage 1. This gave an ethanol-free aqueous product containing suspended alkyl amides that were suitable for marketing in tincture form. In stage 2, the precipitated alkyl amides were removed from the product of stage 1 by microfiltration. In stage 3, the MF permeate was concentrated several fold by OMD. This gave a highly concentrated product suitable for marketing in capsule form.

Gryta [150] conducted integration of fermentation process with membrane distillation for the production of ethanol. The removal of by products, which tends to inhibit the yeast productivity, from the fermenting broth by MD process increased the efficiency and productivity of the membrane bioreactor. The ethanol concentration in permeate was 2–6 times higher than that in the fermenting broth. The enrichment coefficient was found to increase with decrease of ethanol concentration in the broth.

The use of an integrated membrane process for the clarification and the concentration of citrus and carrot juices was proposed as an alternative to the traditional techniques of the agro–food industry [151]. The ultrafiltration process was studied on a pilot plant unit to clarify the raw juice. A clear phase was produced in this step and it was used for concentration by successive membrane treatments. The RO process, performed on a laboratory plant unit, was used to preconcentrate the permeate from UF up to 15–20 g TSS/100 g. A final OMD step yielded a concentration of the retentate from the RO up to 60–63 g TSS/100 g.

Shaw [152] has carried out pilot scale experiments for the concentration of orange and passion fruit juices involving microfiltration followed by osmotic evaporation. Both juices were concentrated threefold to 33.5°Bx and 43.5°Bx, respectively.

Cassano et al. [153] proposed an integrated membrane process involving OMD for concentration of kiwifruit juice (Figure 19.17). They passed 10°Bx–11°Bx juice through a UF membrane to separate solids (pulp) from the serum. Solids were passed through a pasteurizer, while serum was preconcentrated using RO to 25°Bx–26°Bx. This was fed to an OMD device, which further concentrated the juice to 63°Bx–65°Bx. The diluted OA (brine) was recycled after concentration using a conventional evaporator. This concentrated juice was reconstituted with the pasteurized pulp. Alvarez et al. [154] conducted an in-depth study on integrated membrane processing of fruit juice, which they found to be comparable if not better than the conventional process. Using an integrated process for treatment of apple juice, they used an enzyme–membrane reactor to clarify the raw juice, reverse osmosis to preconcentrate the juice up to 25°Bx and pervaporation to recover and concentrate aroma compounds. An evaporation step to concentrate apple juice to 72°Bx was followed by an aroma reconstitution step.

These operations were tested in both laboratory and pilot plant units. The product was far superior to apple juice produced by conventional methods. Details on investment cost of conventional and integrated membrane processes are

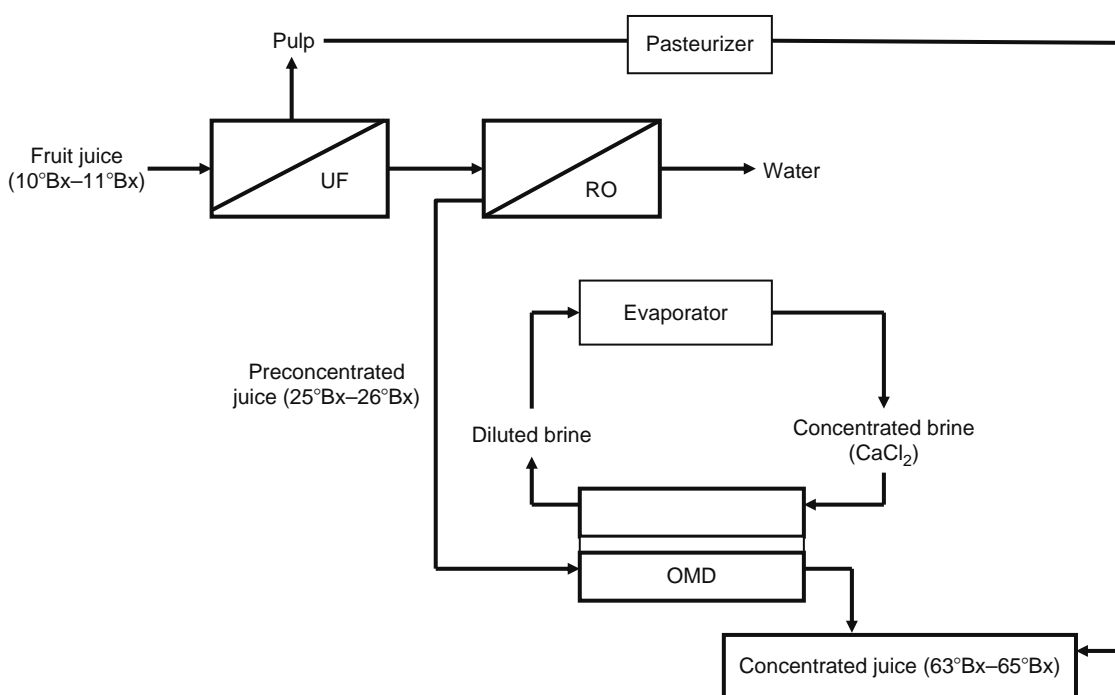


FIGURE 19.17 Integrated membrane process for production of fruit juice concentrates.

**TABLE 19.7**  
**Comparative Investment Cost of Conventional and Integrated Membrane Processes for Processing of Fruit Juice and Beverages**

Investment Head	Cost ECU	
	Conventional Process	Membrane Process
<b>Investment</b>		
Apple storage	$1.7 \times 10^5$	$1.7 \times 10^5$
Washing and inspection of apples	$0.1 \times 10^5$	$0.1 \times 10^5$
Milling of apples	$0.4 \times 10^5$	$0.4 \times 10^5$
Clarification of juice	$6.4 \times 10^5$	$3.9 \times 10^5$
Preconcentration (RO)		$1.3 \times 10^5$
Recovery of aroma compounds and apple juice concentration	$4.2 \times 10^5$	$5.1 \times 10^5$
Total capital investment	$47.72 \times 10^5$	$43.38 \times 10^5$
<b>Operating Cost</b>		
	<b>ECU/ton Concentration</b>	<b>ECU/ton Concentration</b>
Raw materials (apples)	810.0	77.0
Membranes		19.7
Others	99.9	50.2
Total variable cost	909.9	839.9
Labor, maintenance, and other fixed cost	151.9	145.0
Total manufacturing cost	1061.8	984.9

*Source:* From Alvarez, S., et al., *J. Food Eng.*, 46, 109, 2000. With permission.

shown in Table 19.7. The analysis of profitability indicated that return on investment in conventional process and membrane process is 24.6% and 30%, respectively, with corresponding pay back period of 4.1 and 3 years.

## 19.8 FUTURE DIRECTIONS

The MD process has several technical advantages and scope for promoting its industrial application. However, implementation of MD on process scale would require long-term validation on a pilot scale. For achieving these goals more intensive and focused research effort is needed in this field. Research on new membrane materials and composite membranes that enhance transmembrane flux and selectivity is required. Modeling and scale-up studies will form an integral part of this activity.

Studies also need to be undertaken for the enhancement of transmembrane flux in the presence of the acoustic field for applications on a large scale.

Integrated processes encompassing MD and its variants (OMD) are likely to provide solutions to challenging problems like aroma and fragrance retention in food products.

The literature suggests that most of the studies on the application of MD in juice processing have focused on producing highly concentrated juices. However, little attention has been paid to influence juice composition on the mass transfer, membrane properties, and quality of resulting concentrated juices.

In view of the possible industrial applications of MD for concentration of juice, beverages, and aroma compounds, sufficient quantifiable data need to be generated within installations working in continuous mode rather than batch mode.

## GLOSSARY

**Asymmetric membrane**—A composite membrane, consisting of two or more structural planes of nonidentical morphologies.

**Boundary layer**—Fluid layer in contact with membrane surface in which velocity gradient exists unlike the bulk fluid.

**Concentration**—Increasing solute percentage in solution by the removal of solvent.

**Concentration Polarization**—Accumulation of solute rejected by membrane in the vicinity of the membrane surface resulting a gradient in concentration of the solute (higher than the well mixed bulk solution).

**Diffusion**—Process of movement of dissolved solute from higher to lower concentration.

**Fouling**—Deposition or adsorption of particulate or dissolved substances in the openings of the pores.

**Flux**—Amount of fluid passing through the membrane per unit area per unit time.

**Membrane**—A thin barrier or film through which solvents and solutes are selectively transported.

**Membrane Module**—The unit in which the membrane area is packed.

**Osmotic Pressure**—The pressure exerted due to difference in solute concentration between two distinct zones and can be calculated using Vant Hoff equation ( $\pi = CRT/M$ ,  $C$  = concentration of the solution,  $R$  = gas constant,  $T$  = temperature,  $M$  = molecular weight).

**Porosity**—Ratio of void space to total membrane volume (in porous membrane).

**Pore tortuosity**—Ratio of actual pore length to membrane thickness.

**Permeate**—The portion of the feed solution that passes through the membrane.

**Retentate**—The portion of the feed solution that is retained by the membrane.

**Spacers**—A mesh-like material used to separate successive layers of membrane and/or support backing.

**Transmembrane Pressure ( $\Delta P$ )**—Average pressure difference between the upstream and downstream sides of the membrane, which is the driving force.

**Temperature Polarization**—The difference in temperature of the bulk liquid and the membrane surface is called temperature polarization.

**Vapor and Gas**—Any vapor above its critical temperature is called gas.

**Volatile**—A compound is said to be more volatile if it gives more vapor on heating.

**Vapor pressure**—The pressure exerted by the vapor at equilibrium condition where the rate of condensation is equal to the rate of vaporization (all liquids and solids exhibit definite vapor pressure at all temperature).

## NOMENCLATURE

$a$	water activity (–)
$B$	net membrane coefficient ( $s\ m^{-1}$ )
$B_0$	viscous flux coefficient ( $m^2$ )
$b$	stirred cell diameter (m)
$C_p$	molar heat capacity ( $J\ mol^{-1}\ K^{-1}$ )
$C_{ij}$	mass conductance of pore $ij$ (–)
$C_f$	solute concentration in feed ( $mol\ l^{-1}$ )
$D$	diffusion coefficient ( $m^2\ s^{-1}$ )
$D_w$ or $D_{w-air}$	water diffusion coefficient ( $m^2\ s^{-1}$ )
$D_t$	plate thickness (m)
$D^k$	Knudsen diffusion coefficient ( $m^2\ s^{-1}$ )
$D^o$	pressure independent $D$ ( $pa\ m^2\ s^{-1}$ )
$d$	tube diameter (m)
$d_e$ or $d_h$	equivalent diameter (m)
$d_p$	pore diameter (m)
$G$	mass velocity ( $kg\ s^{-1}$ )
$H$	overall heat transfer coefficient ( $W\ m^{-2}\ K^{-1}$ )
$h$	individual heat transfer coefficient ( $W\ m^{-2}\ K^{-1}$ )
$h_1$	film heat transfer coefficient ( $W\ m^{-2}\ K^{-1}$ )
$h_f$	heat transfer coefficient for feed ( $W\ m^{-2}\ K^{-1}$ )
$h_p$	heat transfer coefficient for permeate ( $W\ m^{-2}\ K^{-1}$ )
$h_v$	vapor heat transfer coefficient ( $W\ m^{-2}\ K^{-1}$ )
$h_m$	heat transfer coefficient of the membranes ( $W\ m^{-2}\ K^{-1}$ )
$h_\infty$	heat transfer coefficient for fully developed flow in long pipes ( $W\ m^{-2}\ K^{-1}$ )
$J$	flux ( $l\ m^{-2}\ h^{-1}$ )
$J_m$	mass flux through membrane ( $l\ m^{-2}\ h^{-1}$ )
$K$	overall mass transfer coefficient ( $kg\ m^{-2}\ h^{-1}\ Pa^{-1}$ )
$K_m$	membrane coefficient ( $kg\ m^{-2}\ h^{-1}\ Pa^{-1}$ )
$K_B$	Boltzmann constant ( $J\ K^{-1}$ )
$K_0$	Knudsen diffusion constant (m)
$K_1$	molecular diffusion constant
$k_m$	membrane conductivity ( $W\ m^{-1}\ K^{-1}$ )
$k_s$	thermal conductivity of solid (polymer) ( $W\ m^{-1}\ K^{-1}$ )
$k_g$	thermal conductivity of gases (air and water vapor) ( $W\ m^{-1}\ K^{-1}$ )
$k_l$	thermal conductivity of liquid ( $W\ m^{-1}\ K^{-1}$ )

$k$	mass transfer coefficient through boundary layer ( $\text{m s}^{-1}$ )
$L$	tube length (m)
$L_p$	length of the wetted perimeter (m)
$l$	pore length (m)
$LEP_w$	liquid entry pressure of water (Pa)
$M$	molecular mass ( $\text{kg mol}^{-1}$ )
$m$	mass flow rate ( $\text{kg s}^{-1}$ )
$N$	molar flux ( $\text{mol m}^{-2} \text{sec}^{-1}$ )
$N_i$	total flux ( $\text{mol m}^{-2} \text{sec}^{-1}$ )
$N_i^D$	diffusive flux ( $\text{mol m}^{-2} \text{sec}^{-1}$ )
$N^V$	viscous flux ( $\text{mol m}^{-2} \text{sec}^{-1}$ )
$n_w$	mole concentration of water ( $\text{mol m}^{-3}$ )
$\Delta_{nw}$	water vapor mole concentration difference ( $\text{mol m}^{-3}$ )
$P$	pressure (pa)
$P_{m1}$	partial pressure of vapor at membrane surface on feed side (pa)
$P_{m2}$	partial pressure of vapor at membrane surface on permeate side (pa)
$P_a$	partial pressure of air (pa)
$P_{avg}$	average gas (air) pressure inside the membrane (pa)
$P_{ref}$	reference pressure (pa)
$P_r$	dimensionless pressure ( $P_{avg}/P_{ref}$ )
$P_{am}$	logarithmic mean pressure of air (pa)
$P_w$	partial vapor pressure of water (pa)
$P_{pavg}$	average pore pressure (pa)
$\Delta P$	vapor pressure difference (Pa)
$Q$	heat flux ( $\text{w m}^{-2}$ )
$Q_v$	latent heat flux ( $\text{w m}^{-2}$ )
$Q_c$	conductive heat flux ( $\text{w m}^{-2}$ )
$Q_f$	rate of heat transfer through feed boundary layer ( $\text{w m}^{-2}$ )
$AQ_p$	rate of heat transfer through permeate boundary layer ( $\text{w m}^{-2}$ )
$Q_m$	heat transfer across the membrane ( $\text{w m}^{-2}$ )
$Q_a$	heat transfer across the air gap ( $\text{w m}^{-2}$ )
$R$	gas constant ( $\text{J mol}^{-1} \text{K}^{-1}$ )
$r_H$	hydraulic radius of channel (m)
$r$	pore radius (m)
$S$	cross-sectional area ( $\text{m}^2$ )
$T$	temperature (K)
$T_f$	feed temperature (K)
$T_p$	permeate temperature (K)
$T_{s1}$	hot membrane surface temperature (K)
$T_{s2}$	cold membrane surface temperature (K)
$T_{s3}$	dew point temperature of the vapor (K)
$T_{s4}$	solid surface temperature (K)
$T_{m1}$	feed side membrane temperature (K)
$T_{m2}$	permeate side membrane temperature (K)
$T_a$	air temperature (K)
$T_{avg}$	average temperature (K)
$T_{pavg}$	average pore temperature (K)
$T_{sr}$	temperature of the feed solution at source (K)
$\Delta T_f$	temperature difference (between feed and permeate fluids) (K)
$\Delta T_m$	temperature difference (between membrane surfaces) (K)
$v$	mean molecular speed ( $\text{m s}^{-1}$ )
$w_{in}$	inlet humidity ratio
$x$	liquid mole fraction
$x_a$	mean mole fraction of air
$y$	vapor mole fraction
$Y_{ln}$	mole fraction of air (log mean)
$\mu$	viscosity (Pa s)

$\mu_c$	viscosity of condensate film (Pa s)
$\mu_w$	viscosity at wall temperature (Pa s)
$\lambda$	mean free path (m)
$\lambda_L$	latent heat of vaporization (J kg <sup>-1</sup> )
$\sigma$	collision diameter of the molecule (saturated water $\sigma = 2.7 \text{ \AA}$ )
$\varepsilon$	fractional void volume or porosity (-)
$\tau$	tortuosity factor (-)
$\gamma_l$	liquid surface tension (N m <sup>-1</sup> )
$\delta$ or $\delta_m$	membrane thickness (m)
$\delta_g$	air gap thickness (m)
$\delta_c$	condensate film thickness (m)
$\rho$	density (kg m <sup>-3</sup> )
$\rho_f$	density of condensate film (kg m <sup>-3</sup> )
$\alpha$	yaw angle <sup>o</sup>
$\theta$	contact angle <sup>o</sup>

### DIMENSIONLESS NUMBERS

$Nu$	Nusselt number
$Kn$	Knudsen number
$Pe$	Pecklet number
$Re$	Reynolds number
$Pr$	Prandtl number
$Gz$	Greatz number
$Sh$	Sherwood number
$Sc$	Schmidt number

### REFERENCES

1. Bodell, B.R. Silicon rubber vapor diffusion in saline water distillation. United States Patent Application Serial No: 285,032, 1963.
2. Jian-Mei, L., et al. Microporous polypropylene and polyethylene hollow fiber membranes. Part 3. Experimental studies on membrane distillation for desalination, *Desalination*, 115, 153, 2003.
3. Hanemaaijer, J.H. Memstil—low cost membrane distillation technology for seawater desalination, *Desalination*, 168, 355, 2004.
4. Mansouri, J. and Fane, A.G. Osmotic distillation of oily feeds, *J. Membr. Sci.*, 153, 103, 1999.
5. Gryta, M., Karakulski, K., and Morawski, A.W. Purification of oily wastewater by hybrid of UF/MD, *Water Res.*, 35(15), 3665, 2001.
6. Khayet, M. and Mengual, J.I. Effect of salt concentration during the treatment of humic acid solutions by membrane distillation, *Desalination*, 168(1–3), 373, 2004.
7. Duan, S., Ito, A., and Ohkawa, A. Removal of trichloroethylene from water by aeration, pervaporation and membrane distillation, *J. Chem. Eng. Japan*, 34(8), 1069, 2001.
8. Banat, F.A. and Al-Shannag, M. Recovery of dilute acetone–butanol–ethanol (ABE) solvents from aqueous solutions using membrane distillation, *Bioproc. Eng.*, 23(6), 643, 2000.
9. Konstantinos, B., Petrotos, B., and Lazarides, H.N. Osmotic concentration of liquid foods, *J. Food Eng.*, 49, 201, 2001.
10. Izquierdo-Gil, M.A., García-Payo, M.C., and Fernández-Pineda, C. Air gap membrane distillation of sucrose aqueous solutions, *J. Membr. Sci.*, 155, 291, 1999.
11. Nene, S., et al. Membrane distillation for the concentration of the raw cane-sugar syrup and membrane clarified sugarcane juice, *Desalination*, 147, 157, 2002.
12. Lukanin, O.S., et al. The effect of content of apple juice biopolymers on the concentration by membrane distillation, *J. Food Eng.*, 60, 275, 2003.
13. Calabro, V., Bi Lin, J., and Drioli, E. Theoretical and experimental study on membrane distillation in the concentration of orange juice, *Ind. Eng. Chem. Res.*, 33, 1803, 1994.
14. Gryta, M., Morawski, A.W., and Tomaszewska, M. Ethanol production in a membrane distillation bioreactor, *Catal. Today*, 56, 159, 2000.
15. Tomaszewa, M., Gryta, M., and Morawski, A.W. The influence of salt in solutions on hydrochloric acid recovery by membrane distillation, *Sep. Purif. Technol.*, 14, 183, 1998.
16. Tomaszewa, M., Gryta, M., and Morawski, A.W. Recovery of hydrochloric acid from metal pickling solutions by membrane distillation, *Sep. Purif. Technol.*, 23(1–3), 591, 2001.
17. Bagger-Jorgensen, R., et al. Recovery of volatile aroma compounds from black currant juice by vacuum membrane distillation, *J. Food Eng.*, 64, 23, 2004.
18. Curcio, E. and Drioli, E. Membrane distillation and related operations—a review, *Sep. Purif. Revs.*, 34, 35, 2005.

19. Šulc, D. Fruit juice concentration and aroma separation, *Confructa.*, 28(3), 258, 1984.
20. Rao, M.A. and Vitali, A.A. Fruit juice concentration and preservation. In: Rahman MS. ed. Handbook of Food Preservation. Marcel Dekker, New York, 1999.
21. Jiao, B., Cassano, A., and Drioli, E. Recent advances on membrane processes for the concentration of fruit juices: A review, *J. Food Eng.*, 63, 303, 2004.
22. Weyl, P.K. Recovery of demineralised water from saline waters. United States Patent 3,340,186, 1967.
23. Findley, M.E., Vaporisation through porous membranes, *Ind. Eng. Chem. Proc. Des. Dev.*, 6, 226, 1967.
24. Findley, M.E., et al. Mass and heat transfer relations in evaporation through porous membranes, *AIChEJ*, 15, 483, 1969.
25. Van Haute, A. and Henderyckx, Y. The permeability of membranes to water vapor, *Desalination*, 3, 169, 1967.
26. Henderyckx, Y. Diffusion doublet research, *Desalination*, 3, 237, 1967.
27. Gore, D.W. Gore-Tex membrane distillation. Proceedings of the Tenth Annual Convection of the Water Supply Improvement Association, Honolulu III USA, 1982.
28. Jönsson, A.S., Wimmerstedt, R., and Harrysson, A.C. Membrane distillation—theoretical study of evaporation through microporous membranes, *Desalination*, 56, 237, 1985.
29. Sarti, G.C., Gostoli, C., and Matulli, S. Low energy cost desalination processes using hydrophobic membranes, *Desalination*, 56, 277, 1985.
30. Hanbury, W.T. and Hodgkiess, T. Membrane distillation—an assessment, *Desalination*, 56, 287, 1985.
31. Andersson, S.I., Kjellander, N., and Rodesjo, B. Design and field tests of a new membrane distillation desalination process, *Desalination*, 56, 345, 1985.
32. Schofield, R.W., Fane, A.G., and Fell, C.J.D. Heat and mass transfer in membrane distillation, *J. Membr. Sci.*, 33, 299, 1987.
33. Schofield, R.W., Fane, A.G., and Fell, C.J.D. Gas and vapor transport through microporous membranes I. Knudsen–Poiseuille transition, *J. Membr. Sci.*, 53, 159, 1990.
34. Schofield, R.W., Fane, A.G., and Fell, C.J.D. Gas and vapor transport through microporous membranes II. Membrane distillation, *J. Membr. Sci.*, 53, 173, 1990.
35. Schofield, R.W., et al. Factors affecting flux in membrane distillation, *Desalination*, 77, 279, 1990.
36. Lefebvre, M.S.M. Method of performing osmotic distillation. United States Patent No. 4,781,873, 1988.
37. Mengual, J.I., et al. Osmotic distillation through porous hydrophobic membranes, *J. Membr. Sci.*, 82, 129, 1993.
38. Gryta, M. Osmotic MD and other membrane distillation variants, *J. Membr. Sci.*, 246, 145, 2005.
39. Lawson, K.W. and Lloyd, D.R. Membrane distillation, *J. Membr. Sci.*, 124, 1, 1997.
40. Gryta, M. and Tomaszewska, M. Heat transport in the membrane distillation process, *J. Membr. Sci.*, 144, 211, 1998.
41. Courel, A.M., et al. Modelling of water transport in osmotic distillation using asymmetric membrane, *J. Membr. Sci.*, 173, 107, 2000.
42. Smolders, K. and Franken, A.C.M. Terminology for membrane distillation, *Desalination*, 72, 249, 1989.
43. Alves, V.D. and Coelho, I.M. Effect of membrane characteristics on mass and heat transfer in the osmotic evaporation process, *J. Membr. Sci.*, 228, 159, 2004.
44. Kimura, S. and Shimatani, S.I.N. Transport phenomena in membrane distillation, *J. Membr. Sci.*, 33, 285, 1987.
45. Phattaranawik, J., Jiratananon, R., and Fane, A.G. Effects of net-type spacers on heat and mass transfer in direct contact membrane distillation and comparison with ultrafiltration studies, *J. Membr. Sci.*, 217, 193, 2003.
46. Ding, Z., Runyu, M., and Fane, A.G. A new model for mass transfer in direct contact membrane distillation, *Desalination*, 151, 217, 2002.
47. Lawson, K.V. and Lloyd, D.R. Membrane distillation. II. Direct contact MD, *J. Membr. Sci.*, 120, 123, 1996.
48. Phattaranawik, J., Jiratananon, R., and Fane, A.G. Heat transport and membrane distillation coefficients in direct contact membrane distillation, *J. Membr. Sci.*, 212, 177, 2003.
49. Schofield, R.W. Membrane distillation. Doctor of Philosophy thesis, University of New South Wales, 1989.
50. Gostoli, C., Sarti, G.C., and Matulli, S. Low temperature distillation through hydrophobic membranes, *Sep. Sci. Technol.*, 22, 855, 1987.
51. McCabe, L.W., Smith, J.C., and Harriott, P. Unit operations in chemical engineering, 6th ed., McGraw-Hill, Singapore, 2001.
52. Bird, R.B., Stewart, W.E., and Lightfoot, E.N. *Transport Phenomena*, Wiley International, New York, 1960.
53. Perry, J.H. and Chilton, C.H. *Chemical Engineering Handbook*, 5th ed. McGraw-Hill, New Delhi.
54. Knudsen, J.D. and Katz, D.L. *Fluid Dynamics and Heat Transfer*, McGraw-Hill, New York, 1958.
55. Sarti, G.C., Gostoli, C., and Bandini, S. Extraction of organic components from aqueous streams by vacuum membrane distillation, *J. Membr. Sci.*, 80, 21, 1993.
56. Bandini, S., Gostoli, C., and Sarti, G.C. Separation efficiency in vacuum membrane distillation, *J. Membr. Sci.*, 73, 217, 1992.
57. Kunz, W., Benhabiles, A., and Kim, R.B. Osmotic evaporation through macroporous hydrophobic membranes: A survey of current research and applications, *J. Membr. Sci.*, 121, 25, 1996.
58. Khayet, M., Godino, M.P., and Mengual, J.I. Theoretical and experimental studies on desalination using the sweeping gas membrane distillation method, *Desalination*, 157, 297, 2003.
59. Fernández-Pineda, C., Izquierdo-Gil, M.A., and García-Payo, M.C. Gas permeation and direct contact membrane distillation experiments and their analysis using different models, *J. Membr. Sci.* 198, 33, 2002.
60. Datta, R., et al. Generalized model for the transport of gases in porous, non-porous, and leaky membranes. I. Application to single gases, *J. Membr. Sci.*, 75, 245, 1992.
61. Imdakm, A.O. and Matsuura, T.A. Monte Carlo simulation model for membrane distillation processes: Direct contact (MD), *J. Membr. Sci.*, 237, 51, 2004.

62. Imadakh, A.O. and Sahimi, M. Computer simulation of particles transport processes in flow through porous media, *Chem. Eng. Sci.*, 46, 1977, 1991.
63. Lagana, F., Barbieri, G., and Drioli, E. Direct contact membrane distillation: Modeling and concentration experiments, *J. Membr. Sci.*, 166, 1, 2000.
64. Banat, F.A. Membrane distillation for desalination and removal of volatile organic compounds from water, PhD thesis, McGill University, 1994.
65. Ohta, K. Experiments on seawater desalination by membrane distillation, *Desalination*, 78, 177, 1990.
66. Carlsson, L. The new generation in seawater desalination SU membrane distillation system, *Desalination*, 45, 221, 1983.
67. Kurokawa, H., et al. Vapor permeate characteristics of membrane distillation, *Sep. Sci. Technol.*, 25, 1349, 1990.
68. Udriot, H., Araque, A., and Stokar, U.V. Azeotropic mixture may be broken by membrane distillation, *Chem. Eng. J.*, 54, 87, 1994.
69. Liu, G., et al. Theoretical and experimental studies on air gap membrane distillation, *Heat Mass Trans.*, 34, 329, 1998.
70. Zhu, C. Ultrasonic stimulation on enhancement of air gap membrane distillation, *J. Membr. Sci.*, 161, 85, 1999.
71. García-Payo, M.C., Izquierdo-Gil, M.A., and Fernández-Pineda, C. Air gap membrane distillation of aqueous alcohol solutions, *J. Membr. Sci.*, 169, 61, 2000.
72. Alkhalibi, A.M. and Lior, N. Transport analysis of air gap membrane distillation, *J. Membr. Sci.*, 255(1–2), 239, 2005.
73. Hsu, S.T., Cheng, K.T., and Chiou, J.S. Seawater desalination by direct contact membrane distillation, *Desalination*, 143, 279, 2002.
74. Banat, F.W. and Simandl, J. Desalination by membrane distillation: A parametric study, *Sep. Sci. Technol.*, 33(2), 201, 1998.
75. Guijt, C.M. Air gap membrane distillation 2. Model validation and hollow fibre module performance analysis, *Sep. Purif. Technol.*, 43(3), 245, 2005.
76. Bani-Melhem, K. Using concentration polarization factors to determine the mass transfer resistance in vacuum membrane distillation, *Desalination*, 157, 333, 2003.
77. Lawson, K.W. and Lloyd, D.R. Membrane distillation. I. Module design and performance evaluation using vacuum membrane distillation, *J. Membr. Sci.*, 121, 111, 1996.
78. Mengual, J.I., Khayet, M., and Godino, M.P. Heat and mass transfer in vacuum membrane distillation, *Inter. J. Heat. Mass. Trans.*, 47, 865, 2004.
79. Khayet, M., Godino, P., and Mengual, J.I. Theory and experiments on sweeping gas membrane distillation, *J. Membr. Sci.*, 165, 261, 2000.
80. Basini, L., et al. Desalination process through sweeping gas membrane distillation, *Desalination*, 64, 245, 1987.
81. Khayet, M., Godino, P., and Mengual, J.I. Nature of flow on sweeping gas membrane distillation, *J. Membr. Sci.*, 170, 243, 2000.
82. Khayet, M., Godino, P., and Mengual, J.I. Thermal boundary layers in sweeping gas membrane distillation processes, *AIChEJ*, 48(7), 1488, 2002.
83. Korngold, E. and Korin, E. Air sweep water pervaporation with hollow fibre membranes, *Desalination*, 91, 187, 1993.
84. Rivier, C.A., et al. Separation of binary mixtures by thermostatic sweeping gas membrane distillation. I. Theory and simulations, *J. Membr. Sci.*, 201, 1, 2002.
85. Courel, M. The problem of membrane characterization for the process of osmotic distillation, *Desalination*, 140, 15, 2001.
86. Celere, M. and Gostoli, C. The heat and mass transfer phenomena in osmotic membrane distillation, *Desalination*, 147, 133, 2002.
87. Gostoli, C. Thermal effects in osmotic distillation, *J. Membr. Sci.*, 163, 75, 1999.
88. Jackson, R. In: S.W. Churchill, ed. *Transport in Porous Catalysis*, Elsevier, New York, 1977.
89. Gekas, V. and Hallström, B. Mass transfer in the membrane concentration polarization layer under turbulent cross flow: I. Critical literature review and adaptation of existing Sherwood correlations to membrane operations, *J. Membr. Sci.*, 30, 153, 1987.
90. Cussler, E.L. *Diffusion and Mass Transfer in Fluid Systems*, Cambridge University Press, Cambridge, 1997.
91. Alves, V.D. and Coelho, I.M. Mass transfer in osmotic evaporation: Effect of process parameters, *J. Membr. Sci.*, 208, 171, 2002.
92. Naveen, N., et al. Mass transfer in osmotic membrane distillation, *J. Membr. Sci.*, 268(1), 48, 2006.
93. Hogan, P.A. A new option: Osmotic membrane distillation, *Chem. Eng. Prog.*, 5, 49, 1998.
94. Lefebvre, M.S.M. Osmotic distillation process and semipermeable barriers therefor. United States Patent, 5,098,566, 1998.
95. Sheng, J., Johnson, R.A., and Lefebvre, M.S. Mass and heat transfer mechanisms in the osmotic distillation process, *Desalination*, 80, 113, 1991.
96. Brodard, F., et al. New hydrophobic membranes for osmotic evaporation process, *Sep. Purif. Technol.*, 32, 3, 2003.
97. Cath, T.Y., Adams, V.D., and Childress, A.E. Experimental study of desalination using direct contact membrane distillation: A new approach to flux enhancement, *J. Membr. Sci.*, 228, 5, 2004.
98. Guijt, C.M., et al. Determination of membrane properties for use in the modeling of a membrane distillation module, *Desalination*, 132, 255, 2004.
99. McGuire, K.S., Lawson, K.W., and Lloyd, D.R. Pore size distribution determination from liquid permeation through microporous membranes, *J. Membr. Sci.*, 99, 127, 1995.
100. Lawson, K.W., Hall, M.S., and Lloyd, D.R. Compaction of microporous membranes used in membrane distillation. I. Effect on gas permeability, *J. Membr. Sci.*, 101, 99, 1995.
101. García-Payo, M.C., Izquierdo-Gil, M.A., and Fernández-Pineda, C. Wetting study of hydrophobic membranes via liquid entry pressure measurements with aqueous alcohol solutions, *J. Colloid Interface Sci.*, 230, 420, 2000.
102. Schneider, K., et al. Membranes and modules for transmembrane distillation, *J. Membr. Sci.*, 39, 25, 1988.
103. Martínez, L., et al. Characterisation of three hydrophobic porous membranes used in membrane distillation: Modelling and evaluation of their water vapor permeabilities, *J. Membr. Sci.*, 203, 15, 2002.
104. Larbot, A., et al. Water desalination using ceramic membrane distillation. *Desalination*, 168, 367, 2004.

105. Fawzi, A.B. and Simandl, J. Membrane distillation for dilute ethanol: Separation from aqueous streams, *J. Membr. Sci.*, 163, 333, 1999.
106. Martínez-Díez, L., Vázquez-González, M.I., and Florido-Díaz, F.J. Study of membrane distillation using channel spacers, *J. Membr. Sci.*, 144, 45, 1998.
107. Phattaranawik, J., et al. Mass flux enhancement using spacer filled channels in direct contact membrane distillation, *J. Membr. Sci.*, 187, 193, 2001.
108. Wang, Z., Zheng, F., and Wang, S. Experimental study of membrane distillation with brine circulated in the cold side, *J. Membr. Sci.*, 183, 171, 2001.
109. Rincón, C., Ortiz de Zárate, J.M., and Mengual, J.I. Separation of water and glycols by direct contact membrane distillation, *J. Membr. Sci.*, 158, 155, 1999.
110. Rodríguez-Maroto, J.M. and Martínez, L. Bulk and measured temperatures in direct contact membrane distillation, *J. Membr. Sci.*, 250, 141, 2005.
111. Narayan, A.V., et al. Acoustic field-assisted osmotic membrane distillation, *Desalination*, 147, 149, 2002.
112. Khayet, M., Velázquez, A., and Mengual, J.I. Direct contact membrane distillation of humic acid solutions, *J. Membr. Sci.*, 240, 123, 2004.
113. Gostoli, C. and Sarti, G.C. Separation of liquid mixtures by membrane distillation, *J. Membr. Sci.*, 41, 211, 1989.
114. Banat, F.A. and Simandl, J. Membrane distillation for propanone removal from aqueous streams, *J. Chem. Technol. Biotechnol.*, 75, 168, 2000.
115. Bandini, S. and Sarti, G.C. Concentration of must through vacuum membrane distillation, *Desalination*, 149, 253, 2002.
116. Li, J.M., et al. Microporous polypropylene and polyethylene hollow fiber membranes. Part 3. Experimental studies on membrane distillation for desalination, *Desalination*, 155, 153, 2003.
117. Barbe, A.M., et al. Retention of volatile organic flavor/fragrance components in the concentration of liquid foods by osmotic distillation, *J. Membr. Sci.*, 145, 67, 1998.
118. Bequdy, E.G. and Lampi, K.A. Membrane technology for direct osmosis concentration of fruit juices, *Food Technol.*, 44, 121, 1990.
119. Rodrigues, R.B., et al. Evaluation of reverse osmosis and osmotic evaporation to concentrate camu-camu juice (*Myrciaria dubia*), *J. Food Eng.*, 63, 97, 2004.
120. Bui, V.A., Nguyen, M.H., and Muller, J. A laboratory study on glucose concentration by osmotic distillation in hollow fiber module, *J. Food Eng.*, 63, 237, 2004.
121. Celere, M. and Gostoli, C. Osmotic distillation with propylene glycol, glycerol and glycerol-salt mixtures, *J. Membr. Sci.*, 229, 159, 2004.
122. Godino, M.P., et al. Coupled phenomena membrane distillation and osmotic distillation through a porous hydrophobic membrane, *Sep. Sci. Technol.*, 30(6), 993, 1995.
123. Alklaibi, A.M. and Lior, N. Membrane-distillation desalination: Status and potential, *Desalination*, 171, 111, 2004.
124. Wu, Y., et al. Surface-modified hydrophilic membranes in membrane distillation, *J. Membr. Sci.*, 72, 189, 1992.
125. Kong, Y., et al. Plasma polymerization of octafluorocyclobutane and hydrophobic microporous composite membrane distillation, *J. Appl. Polym. Sci.*, 46, 191, 1992.
126. Arcella, V., et al. A study on a perfluoropolymer purification and its application to membrane formation, *J. Membr. Sci.*, 163, 203, 1999.
127. Barbe, A.M., Hogan, P.A., and Johnson, R.A. Surface morphology changes during initial usage of hydrophobic, microporous polypropylene membranes, *J. Membr. Sci.*, 172, 149, 2000.
128. Durham, R.J. and Nguyen, M.H. Hydrophobic membrane evaluation and cleaning for osmotic distillation of tomato puree, *J. Membr. Sci.*, 87(1-2), 181, 1994.
129. Koschikowski, J., Wieghaus, M., and Rommel, M. Solar thermal-driven desalination plants based on membrane distillation, *Desalination*, 156, 295, 2003.
130. Sirkar, K.K. Membrane separation technologies: Current developments, *Chem. Eng. Commu.*, 157, 145, 1997.
131. Brinck, J., et al. Influence of pH on the adsorptive fouling of ultrafiltration membranes by fatty acid, *J. Membr. Sci.*, 164, 187, 2000.
132. Criscuoli, A. and Drioli, E. Energetic and exergetic analysis of an integrated membrane desalination system, *Desalination*, 124, 243, 1999.
133. Cabassud, C. and Wirth, D. Membrane distillation for water desalination: How to chose an appropriate membrane? *Desalination*, 157, 307, 2003.
134. Morrison, G.L., et al. Solar heated membrane distillation, *Int. Sol. Energy Soc.*, 2(2), 2329, 1991.
135. Chiou, J.S. and Shiu, S.T. Compact device for seawater desalination by solar-energy membrane distillation. Patent No TW 531430 B, 11 May, 2003.
136. Zhang, X., Ren, J., Guo, Z., Liang, X., and Hu, W. Membrane distillation type water treating device by using solar energy or waste heat. Patent No CN 1396120—A, 12 February, 2003.
137. Banat, F., Jumah, R., and Garaibeh, M. Exploitation of solar energy collected by solar stills for desalination by membrane distillation, *Renew. Energy*, 25(2), 293, 2002.
138. Drioli, E., et al. Integrated membrane operation in desalination processes, *Desalination*, 122, 141, 1999.
139. Curcio, E., Criscuoli, A., and Drioli, E. Membrane crystallizers, *Ind. Eng. Chem. Res.*, 40(12), 2679, 2001.
140. Gryta, M., Morawski, A., and Antoni, W. Saline wastewater treatment in membrane distillation crystallizer, *Pol. J. Chem. Tech.*, 4(3), 24, 2002.
141. Li, B. and Sirkar, K.K. Noval membrane and device for direct contact membrane distillation-based desalination processes, *Ind. Eng. Chem. Res.*, 43, 5300, 2004.

142. Girard, B. and Fukumoto, L.R. Membrane processing of fruit juices and beverages—A review, *Crit. Rev. Food Sci. Nutr.*, 40(2), 91, 2000.
143. Drioli, E., Jiao, B.L., and Calabro, V. The preliminary study on the concentration of orange juice by a membrane distillation, *Proc. Int. Soc. Citri. Cult.*, 3, 1140, 1992.
144. Bailey, A.F.G., et al. The effect of ultrafiltration on the subsequent concentration of grape juice by osmotic distillation, *J. Membr. Sci.*, 164, 195, 2000.
145. Thompson, D. The application of osmotic distillation for the wine industries, *Aus. Grape growers. Wine makers*, 11, 11, 1991.
146. Ali, F., et al. Transfer of volatiles through PTFE membrane during osmotic distillation. Proceedings of the ICOM. Toulouse, France, 2002.
147. Xu, J.B. Alginate-coated microporous PTFE membrane for use in osmotic distillation of oily foods, *J. Membr. Sci.*, 240, 81, 2004.
148. Alves, V.D. and Coelho, I.M. Orange juice concentration by osmotic evaporation and membrane distillation: A comparative study, *J. Food Eng.*, 74(1), 125, 2006.
149. Johnson, R.A., Sun, J.C., and Sun, J.A. Pervaporation—microfiltration osmotic distillation hybrid process for the concentration of ethanol and water extracts of the *Enchincea* plant, *J. Membr. Sci.*, 209, 221, 2002.
150. Gryta, M. The fermentation process integrated with membrane distillation, *Sep. Purif. Technol.*, 24, 283, 2001.
151. Cassano, A., et al. Clarification and concentration of citrus and carrot juices by integrated membrane processes, *J. Food Eng.*, 57, 153, 2003.
152. Shaw, P.E. Evaluation of concentrated orange and passion fruit juices prepared by osmotic evaporation, *Lebensmit-wissen. Technol.*, 34(2), 60, 2001.
153. Cassano, A., Jiao, B., and Drioli, E. Integrated membrane process for production of concentrated kiwifruit juice. Proceedings of the 1st workshop Italy–China on state of research and applications of membrane operations for a sustainable growth, Cetraro, Italy, 2002.
154. Alvarez, S., et al. A new integrated membrane process for producing clarified apple juice and apple juice aroma concentrate, *J. Food Eng.*, 46, 109, 2000.



---

# 20 Applications of Membrane Separation in the Brewing Industry

*Carmen I. Moraru and Ernst Ulrich Schrader*

## CONTENTS

20.1	Place and Role of Membrane Separation in the Beer Industry .....	553
20.2	Factors That Influence the Membrane Separation of Beer .....	556
20.2.1	Beer Composition.....	556
20.2.1.1	Haze Formation and Its Impact on Beer Filtration and Stability .....	557
20.2.2	Membrane Characteristics .....	558
20.2.3	Membrane Fouling in Membrane Separation of Beer .....	558
20.2.4	Influence of Process Parameters on Membrane Separation of Beer.....	560
20.3	Solutions for Increasing the Permeate Flux in Membrane Separation of Beer .....	566
20.3.1	Backwashing and Backflushing .....	566
20.3.2	Chemical Cleaning .....	567
20.4	Use of Membrane Systems in Beer Processing .....	568
20.4.1	Beer Filtration .....	568
20.4.1.1	Traditional Methods for Beer Filtration.....	569
20.4.1.2	Use of Membrane Separation .....	569
20.4.2	Final Filtration of Beer.....	570
20.4.2.1	Traditional Methods for Final Filtration .....	572
20.4.2.2	Use of Membranes for Final Filtration .....	572
20.4.3	Recovery of Spent Beer from Yeast and Tank Bottoms .....	573
20.4.3.1	Traditional Techniques Used for Tank Bottoms Recovery .....	573
20.4.3.2	Use of Membrane Separation .....	573
20.4.3.3	Costs of Tank Bottoms Recovery Using Membrane Separation .....	574
20.4.3.4	Examples of Commercial Installations .....	575
20.4.4	Alcohol Removal from Fermented Beer.....	576
20.5	Other Uses of Membrane Separation in the Brewing Industry .....	577
20.5.1	Purification of Brewing Water by Reverse Osmosis .....	577
20.5.2	Utilities Filtration .....	577
20.5.3	Beer Decolorization .....	577
20.5.4	Microbiological Quality Control of Beer.....	577
20.6	An Economical Perspective on the Use of Membrane Separation in Brewing .....	577
	References.....	578

## 20.1 PLACE AND ROLE OF MEMBRANE SEPARATION IN THE BEER INDUSTRY

Beer is the second most consumed beverage in the world after tea [1]. Beer production reached approximately 1.48 billion hL/year\* in 2003 and keeps increasing every year. The world per capita consumption in the same year was 23.6 L, the highest consumption being recorded in the European Union (70 L) and on the American continent (66 L) [2]. The beer industry is continuously challenged to meet the high standards required for producing beer of consistent quality, with unique taste and flavor, while maintaining relatively low production costs and minimizing waste disposal. For the modern, highly demanding consumer, purity and freshness are extremely important characteristics of a good beer, and this is why the beer industry is permanently seeking new technical solutions that will enable it to deliver a product matching its customers' expectation.

---

\* hL = traditional volume unit in brewing. 1 hL = 100L.

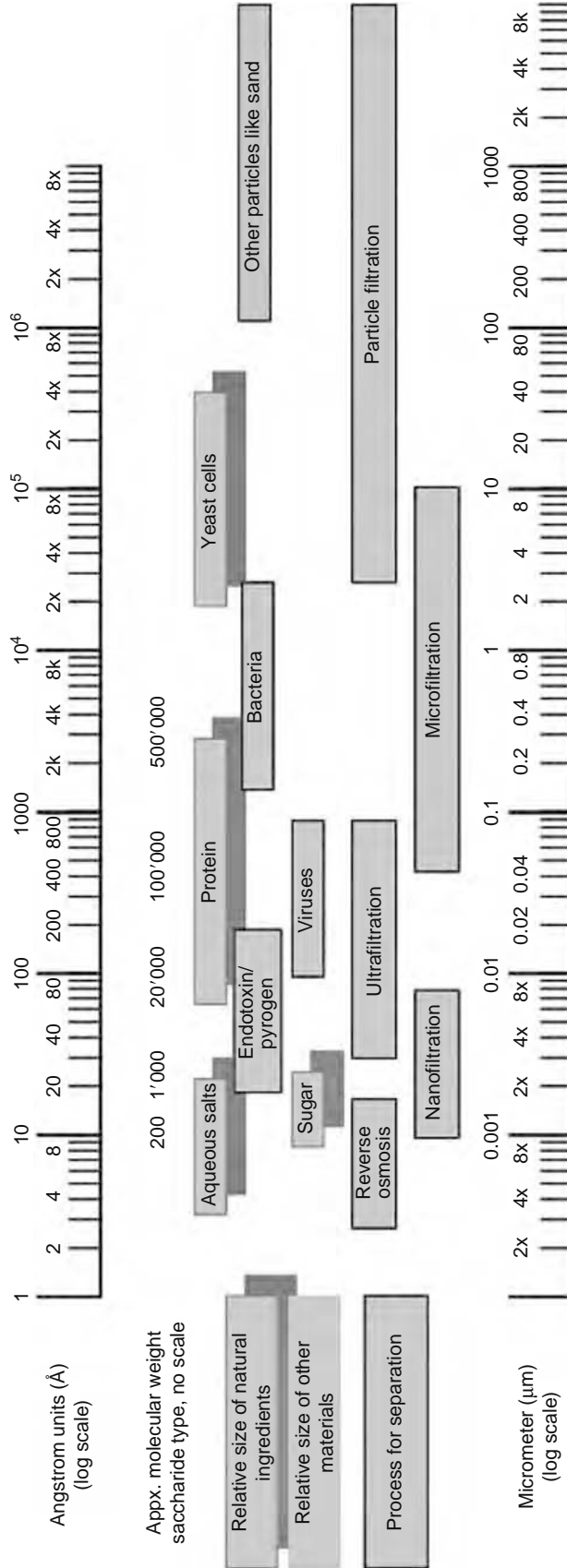


**FIGURE 20.1** Overview of particle sizes and separation processes. The shaded blocks mark the typical range of sizes of some ingredients of beer. 1000 μm = 1 mm. (Courtesy of GE Infrastructure, Water and Process Technologies. With permission.)

Membrane separation is increasingly emerging as an attractive alternative processing method for the brewing industry, with applications ranging from beer clarification and cold sterilization to tank bottoms recovery, alcohol removal, as well as water and effluent treatment. Other applications of membrane separation include the filtration of utilities, such as air filtration for tank venting in yeast storage tanks or the filtration of air used for wort aeration. Another utility that could be filtered is the steam used in the yeast storage and propagation area. Part of this steam or its condensate might come in contact with the yeast, and therefore the steam needs to be filtered to separate any contaminating particles. Figure 20.1 shows an overview of the chemical and biological species that can be found in beer, as well as the membrane processes that can be used to separate these molecules or particles based on their size, from reverse osmosis (RO) to microfiltration (MF). Figure 20.2 provides a simplified process flow diagram of a brewery, indicating the products and processes involving membrane separation reviewed here.

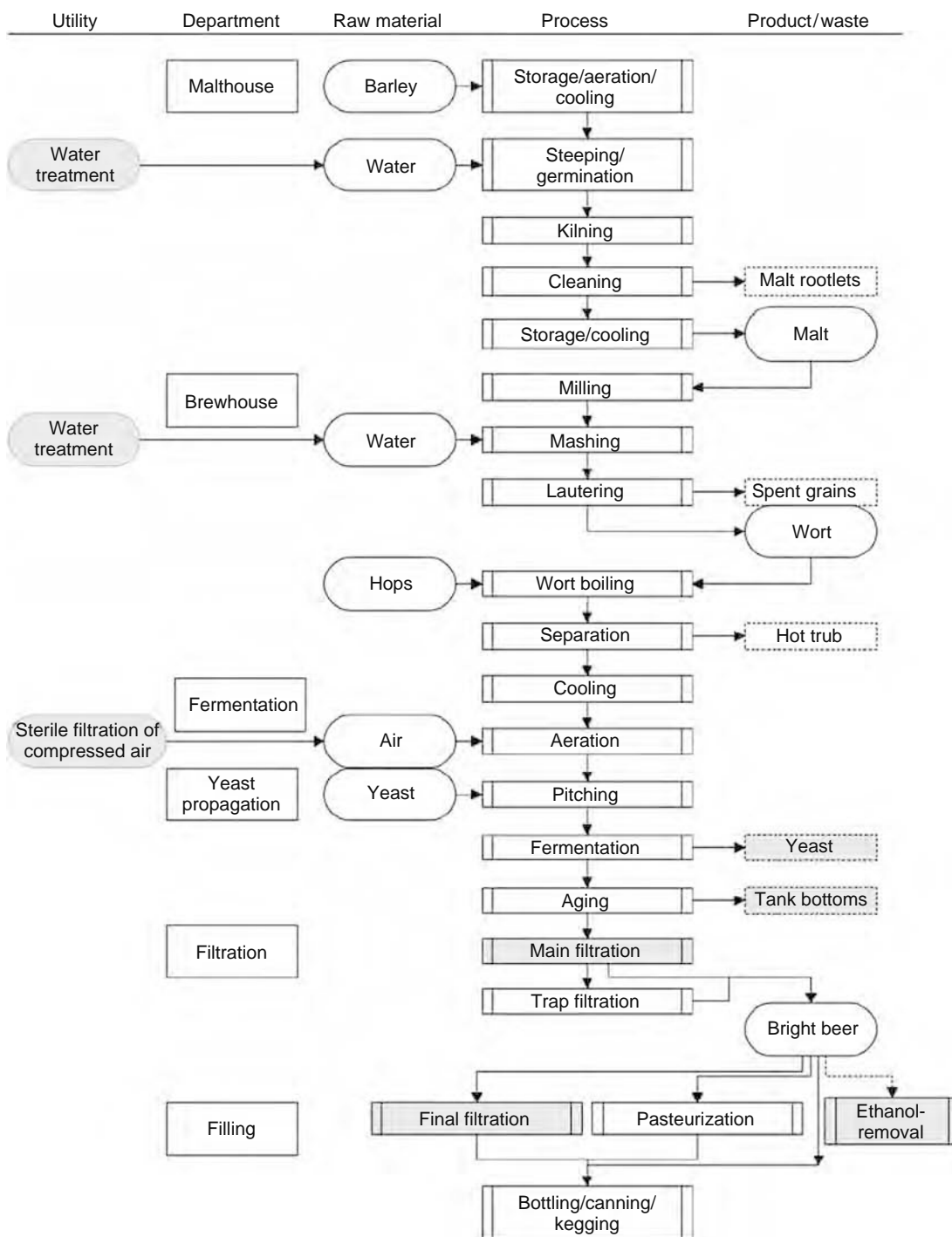


**FIGURE 20.2** Simplified process flow diagram of a brewery. The shaded blocks indicate the products and processes that may use membrane separation.

Laboratory applications for microbiological analyses are another area where membrane separation is used in the brewing industry. Such applications are not described in detail in this chapter, as they are not necessarily specific to brewing.

## 20.2 FACTORS THAT INFLUENCE THE MEMBRANE SEPARATION OF BEER

The main factors that affect the separation efficiency and yield in the membrane separation of beer are beer composition, membrane characteristics, process parameters, and membrane fouling.

### 20.2.1 BEER COMPOSITION

Filtration and storage behavior of beer depend strongly on its chemical composition (Table 20.1). Beer production is based on natural ingredients and therefore beer contains a wide variety of chemical compounds. Most chemical components of beer have an influence on beer filtration in general and membrane filtration in particular. Carbohydrates, such as pentosans and  $\beta$ -glucans, proteins and protein–polyphenol complexes, are of particular importance in membrane filtration of beer, as they are responsible for membrane fouling [3], which has negative consequences on both the flux and quality of the filtered beer, as it will be discussed in detail later on in this chapter.

Among carbohydrates, it is the high mass molecular weight compounds that, under certain conditions, can impede the efficiency of beer filtration. About 80% of these carbohydrates are represented by molecules that contain 4–20 glucose residues, and only about 20% have more than 20 glucose residues. Dextrins ( $\alpha$ -glucans) do not affect beer viscosity and have solely a caloric contribution [4,5].

$\beta$ -glucans are polymers of glucose that are found in the endosperm of barley, primarily in the cell walls. Some  $\beta$ -glucans can have a molecular weight of above  $10^6$  Da. Their presence represents one of the major factors that lead to low filterability of beer, as well as haze formation during storage. Based on their molecular size,  $\beta$ -glucans can be divided into the following categories [6]:

1.  $\beta$ -glucans of molecular size  $>0.2 \mu\text{m}$
2.  $\beta$ -glucans of molecular weight  $>300,000$  Da (which, together with those from the first category, represent about 57% of the total  $\beta$ -glucan amount)
3.  $\beta$ -glucans of molecular weight between 30,000 and 300,000 Da (about 10% of the total)
4.  $\beta$ -glucans of small and medium molecular weight—below 30,000 Da (about 30% of the total)

Despite the fact that the data available in literature is somewhat controversial, the amount of  $\beta$ -glucans in beer is generally considered to range between 300 and 700 mg/L, from which about 10% can be found in gel form [8]. An extensive review and

**TABLE 20.1**  
**Main Nonvolatile Components of Beer**

Category	Compound	Concentration (g/L)	Molecular Weight (Da)
Minerals	Ca, K, Mg, Na, P, and other metals	0.5–2	<100
Carbohydrates	Mono- and oligosaccharides	7–13	200–600
	Dextrins ( $\alpha$ -glucans)	25–35	50,000–200,000
	$\beta$ -glucans	0.07–0.5	50,000–200,000
	Pentosans and others	1.5–3.5	50,000–200,000
	Total	33–44	
Organic Nitrogen	True proteins	Traces	>150,000
	Polypeptides	0.06–0.2	5,000–70,000
	Oligopeptides	0.1–0.5	1,500–5,000
	Amino acids and others	0.02–0.1	<5,000
	Total	0.3–1	
Phenols	Monophenols	0.02–0.06	<200
	Polyphenols (monomers)	0.07–0.1	200–500
	Polyphenols (polymers) and others	0.02–0.1	1,000–5,000
	Total	0.15–0.35	
Lipids		0.01–0.02	200–1,000
Glycerol		1–3	92
Nonvolatile acids	Citric, malic, gluconic, etc.	0.2–1	192, 134, 218, ...
Vitamins	B1, B2, B5, B6, B12	0.005	205–1,355

Source: Adapted from Pollock, J.R.A., ed., *Brewing Science*, Vol. 1. Academic Press, London, 1979.

characterization of barley  $\beta$ -glucans' structure and properties has been published recently by Vaikousia et al. [8]. The flow behavior and gelling properties of barley  $\beta$ -glucans are of special interest in brewing, since an excess of  $\beta$ -glucans can cause problems such as slow filtration of wort and beer, as well as contribute to haze formation during storage [3,9].

The majority of the nitrogen compounds in beer have molecular weights between 5 and 70 kDa. The protein components of this fraction are of particular importance in brewing, as some of them contribute to foam formation (positive effect) while others, in association with polyphenols, lead to haze formation (undesirable effect) [10].

Beer contains a mixture of phenolic compounds, averaging about 150–350 mg/L, out of which about two thirds originate in barley and the remaining in hops [11]. Of these, polyphenols present the greatest interest for beer processing and storage, since they tend to associate with proteins into insoluble complexes, leading to the formation of cold haze in beer.

### 20.2.1.1 Haze Formation and Its Impact on Beer Filtration and Stability

Beer stability, defined as the ability of beer to maintain its properties unchanged from bottling to the end of the estimated shelf life, has three distinct aspects: biological stability, colloidal stability, and sensory stability. The sensory stability of beer is closely related to its biological and colloidal stability, and additionally can be affected by the presence of oxygen, which leads to oxidative processes that can alter the taste of beer.

Biological stability is related to the yeasts and spoilage bacteria, which are possibly present in beer and could trigger undesirable sensory and aspect changes during beer shelf life. In order to ensure its biological stability, microorganisms have to be removed from beer, which for yeast cells is achieved by filtration. The maximum limit allowed for the number of yeast cells accepted for filtered beer is generally 5 cells per 100 mL, but the modern filtration techniques can yield less than 2 cells per 100 mL beer [12].

In colloidal stability the presence of visible haze can significantly limit the shelf life of beer. Haze compounds can also contribute to the fouling of equipment surfaces, forming deposits that are difficult to remove by in-place cleaning [13]. A generic composition of beer haze is given in Table 20.2. Based on their size, the haze-forming particles can be classified into the following categories [14]:

- Coarse dispersions (sizes  $>0.1 \mu\text{m}$ ) represent the macroscopic haze and is formed out of coagulated proteins, yeasts, and bacteria.
- Colloids (size between  $0.01$  and  $0.1 \mu\text{m}$ ), which can be visualized under refracted light, are represented by proteins, gums, and resins from hops.
- Molecular dispersions ( $<0.01 \mu\text{m}$ ) cannot be visualized.

Haze formation is mostly attributed to proteins, polyphenols, and their interactions. It is also possible that there are also other factors that influence haze formation in beer, but their effect has not been yet clearly defined [15]. The amount of haze formed depends both on the concentration of proteins and polyphenols, and on their ratio. Polyphenols can combine with proteins to form colloidal suspensions that scatter light, which creates the cloudy appearance of beer. Beer polyphenols originate partly from barley and partly from hops. The beer polyphenols most closely associated with haze formation are the proanthocyanidins, which are dimers and trimers of catechin, epicatechin, and gallic acid. These have been shown to interact strongly with haze-active proteins [13,15–17] and their concentration in beer was directly related to the rate of haze formation [18]. Ahrenst-Larsen and Erdal [19] have demonstrated that anthocyanogen-free barley produces beer that is extremely resistant to haze formation, without any stabilizing treatment, provided that hops do not contribute polyphenols either. Not all proteins are equally involved in haze formation. It has been shown that haze-active proteins contain significant amounts of proline and that proteins that lack proline form little or no haze in the presence of polyphenols [13,15–17]. In beer, the source of the haze-active protein has been shown to be the barley hordein, an alcohol-soluble protein rich in proline [16].

At least initially, the protein–polyphenol complexes are held together by weak associations and haze can be dispersed by warming, which in brewing is commonly referred to as reversible haze or chill haze. The practical consequence of this phenomenon is that beer should be filtered at the lowest possible temperature. The mechanism of haze formation appears to be

**TABLE 20.2**  
**Main Components of Beer Haze**

Compounds	Concentration (mg/L)
Total nitrogenous substances ( $N \times 6.25$ )	450–650
Polyphenols	200–600
Dextrins plus $\beta$ -glucans	150–200
Glucose	20–40
Minerals	7–35

a non-covalent interaction—a combination of hydrogen and hydrophobic bonding—in which protein molecules are held together by polyphenolic compounds acting as bridges [16]. According to Siebert and Lynn [20], polyphenols bind only to specific sites in haze-active proteins, and the largest amount of haze forms in situations when there are comparable numbers of polyphenol-binding sites in the proteins and binding ends of the polyphenol molecules. Since beer contains a large excess of haze-active proteins as compared to haze-active polyphenols, most of the polyphenols are able to bridge two proteins together, but there are not enough polyphenols to link these protein–polyphenol–protein aggregates, which results in relatively small particles [20].

### 20.2.2 MEMBRANE CHARACTERISTICS

Generally, the operating conditions in a brewing operation involve high flow rates, high pressures, and high production capacity, which is challenging for any type of filtration operation. The filtration media must also withstand the high temperatures, extreme pH conditions, and large temperature differences used during cleaning (i.e., from 0°C during filtration to about 80°C in the cleaning stage). The membranes used in beer processing have to comply with all these conditions. The membrane types typically used in beer filtration applications are flat sheets, hollow fibers, or ceramic. It should be noted that ceramic membranes have better chemical and temperature resistance as compared to polymeric membranes, but typically require higher investment and membrane replacement costs.

Recent research efforts brought about new and exciting developments in membrane technology, some with direct implications for the membrane filtration of beer. For example, Stopka et al. [21] reported flux enhancement in the microfiltration of a beer yeast suspension when using a ceramic membrane with a helically stamped surface. A relatively simple modification of the ceramic membrane surface resulted in modified hydrodynamic conditions and disturbance of the fouling layer. As compared with a regular, smooth ceramic membrane of the same nominal pore size, the stamped membrane leads to higher flux and lower power consumption per unit volume of permeate at the same velocity of the feed.

Kuiper et al., in The Netherlands, developed and fabricated ceramic microsieves with a very small flow resistance and used them for beer clarification [22,23]. They reported fluxes about two orders of magnitude larger than fluxes typically obtained membrane in separation of beer ( $\sim 10^4$  L/(m<sup>2</sup> h)), and a good quality of the filtered beer—a haze value of 0.46 EBC after 9 h of filtration was reported. These membranes allowed for much less fouling as compared to the traditional membranes. Although very promising, the manufacturing of these membranes is still in the experimental stage and scaling up is required.

The development of high-selectivity nanotube membranes might also have some potential for beer membrane filtration. Carbon nanotube membranes can be functionalized and tailored to efficiently separate molecules both on the basis of their molecular size and shape, and on chemical affinity [24]. Newly developed nanotechniques can be used to functionalize supported microfiltration or ultrafiltration polymeric membranes by filling their pores with polymeric or oligomeric liquids that have an affinity for the compound of interest [25]. An Australian–American team of researchers has developed a nanoparticle-enhanced membrane that combines organic polymers with inorganic silica nanoparticles, which enable large molecules to pass through more readily than small molecules [26]. The addition of the silica resulted in over 200% improvement in the flux and increased the permeability of the membrane. The reported use of these membranes is to purify fuel (ethanol and methanol) inexpensively, but food-related applications, including beer filtration, could also become possible. While still too expensive for regular food applications, such technologies might become a feasible technical solution in the future.

### 20.2.3 MEMBRANE FOULING IN MEMBRANE SEPARATION OF BEER

Crossflow microfiltration (CMF) using semipermeable membranes has been evaluated as a potential alternative to conventional processing in the brewing industry since the early 1980s. Yet, the extensive adoption of this technology by the beer industry was hindered by the protein and aroma retention, and the severe flux decline (Figure 20.3) that takes place during this process.

The drastic reduction of the permeate flux to only a fraction of the theoretical capacity of the membrane is rather common in pressure-driven membrane processes, but it is more pronounced for beer as compared to other fluid foods such as milk, wine, or fruit juices. This explains the earlier introduction of membrane technology at a commercial scale in those industries as compared to the beer industry.

Eagles and Wakeman [27] noted that when filtering beer through membranes with pore sizes less than 0.5  $\mu\text{m}$  the filtered beer (permeate) lacks some components that are important for bitterness, fullness, and foam retention characteristic to beer. When filtering beer through a 0.22  $\mu\text{m}$  polysulfone membrane, Ryder and coworkers [28] found decreases in original gravity (12.30–11.73°P)\* alcohol (3.94–3.78 wt%), protein (0.72–0.59 wt%), and bitterness (15.1–13.5 EBU). Both flux reduction and quality effects have been attributed to membrane fouling and concentration polarization.

It is important to distinguish the effects of membrane fouling from those of concentration polarization. At the initial stage of a filtration run, the solids concentration at the membrane level is relatively small, but it builds up progressively as permeate is removed from the system. If a substantial flux decline is observed at low solids concentration, membrane fouling aspects are believed to be important. A flux decrease with an increase in solids concentration is largely due to concentration polarization.

\* °P = Degree Plateau; represent total amount of soluble solids in beer, in kg/100 kg.

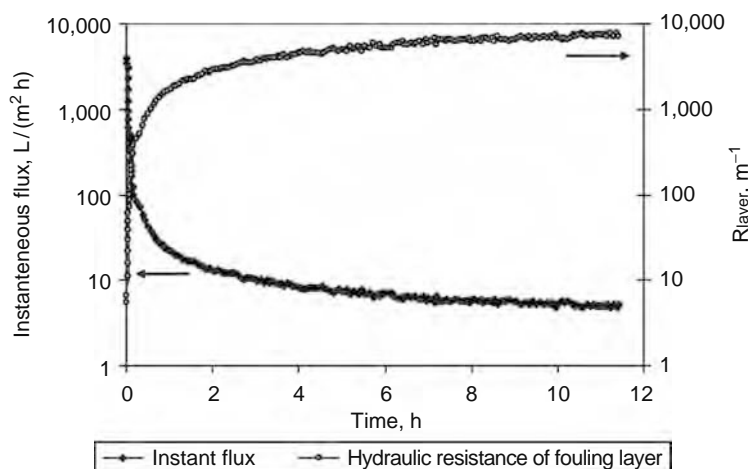


**FIGURE 20.3** Evolution of flux with time in the CMF of rough beer with a cellulose acetate membrane of  $0.45 \mu\text{m}$  pore size. (From Moraru, C.I., Optimization and membrane processes with applications in the food industry: Beer microfiltration. PhD thesis, University “Dunarea de Jos” Galati, Romania, 1999.)

During membrane filtration, some components (dissolved molecular species or particulates) of the feed are rejected by the membrane and are transported back into the bulk by diffusion. If the concentration of the solute(s) at the surface is above the solubility limit, a gel layer is formed.

The occurrence of fouling affects the performance of a membrane either by deposition of a layer onto the membrane surface or by total or partial blockage of the pores, which changes the effective pore size distribution. Blanpain-Avet et al. [29] investigated the fouling mechanisms and protein rejection for the microfiltration of a beer previously clarified by kieselguhr filtration through a  $0.2 \mu\text{m}$  polycarbonate membrane, and concluded that the permeate flux decay was governed by two successive fouling mechanisms. An internal pore fouling took place during the initial stages of filtration, followed by external surface fouling. The change of protein retention level throughout the duration of filtration was found to be closely related to the nature of fouling, with an initial high-protein transmission rate being followed by a sharp decrease. Protein retention remained constant and low ( $<20\%$ ) during the internal pore fouling stage, then increased abruptly (up to  $60\%$ ) and stabilized when a steady fouling gel layer formed over the membrane surface. Figures 20.4 and 20.5 represent a visualization of the fouling layer characteristic for membrane filtration of beer [30].

The analysis of the fouling layer performed by Gans [12] and then by Taylor and coworkers [31] showed that it contains carbohydrates, proteins, and polyphenols, and that the composition is dominated by proteins associated with polyphenols and  $\beta$ -glucans. Gans reported that in the CMF of rough beer with hollow fiber polysulphonic membranes of  $0.45 \mu\text{m}$  pore size the total amount of the fouling layer per unit of membrane area was  $8.6 \text{ g/m}^2$ , and consisted of  $5.5 \text{ g/m}^2$  total nitrogen compounds,  $1.3 \text{ g/m}^2$  polyphenols, and  $1.8 \text{ g/m}^2$   $\beta$ -glucans [12]. Gan noted that, besides the chemical species mentioned in the above

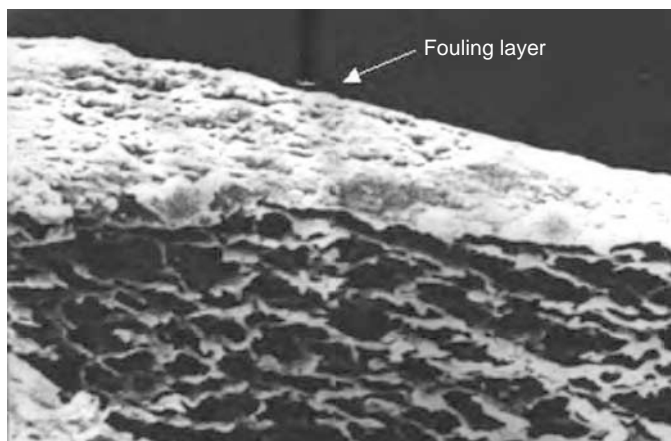


**FIGURE 20.4** Scanning electron micrographs (SEM) micrographs of the cross section of a cellulose acetate membrane of  $0.45 \mu\text{m}$  pore size after being used for beer CMF experiments. A dense fouling layer is observed on the membrane surface. (From Moraru, C.I., Optimization and membrane processes with applications in the food industry: Beer microfiltration. PhD thesis, University “Dunarea de Jos” Galati, Romania, 1999.)

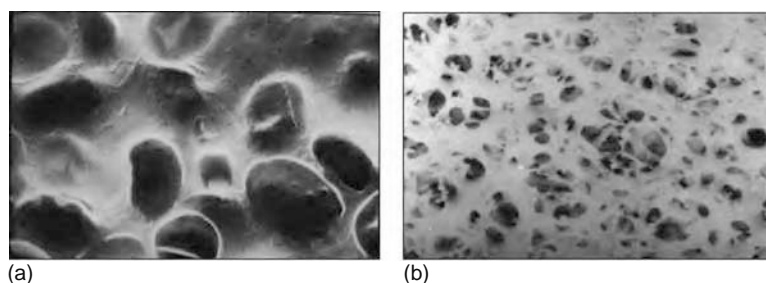


**FIGURE 20.5** SEM micrographs of a cellulose acetate membrane of  $0.45\ \mu\text{m}$  pore size used in beer CMF experiments. (a) New, clean membrane surface; (b) membrane surface after beer CMF. (From Moraru, C.I., Optimization and membrane processes with applications in the food industry: Beer microfiltration. PhD thesis, University “Dunarea de Jos” Galati, Romania, 1999.)

studies, trace minerals such as  $\text{Ca}^{2+}$  and  $\text{Cu}^{2+}$  also play an important role in the surface complexation of the key membrane foulants [32]. The author hypothesized that these ions act as sequestering or chelating agents in the formation of macromolecular complexes, which results in stronger fouling and a tighter structure of the fouling layer. This supports the earlier conclusions of Güell and Davis, who reported that protein fouling of membranes does not depend on the size of individual proteins, but rather on their ability to form aggregates [33].

The presence of  $\beta$ -glucans, and particularly the deposition of a dense  $\beta$ -glucan gel layer at the membrane surface, is considered to be another critical factor in fouling during membrane filtration of beer. The mechanisms of  $\beta$ -glucan gel formation are described in detail by Vaikousia et al. [8]. The  $\beta$ -glucan gel has a thixotropic character [8,34,35], which means that its viscosity becomes smaller at high shear rates. It is also worth mentioning that beer itself has as a Newtonian behavior, and therefore its viscosity is not affected by shear. The enzymatic solubilization of  $\beta$ -glucans could potentially diminish the filtration problems created by the  $\beta$ -glucan gel, but labeling requirements limit this practice in many countries, as the addition of enzymes needs to be specified on the label, which might have a negative impact on traditionalist consumers.

It is generally agreed that yeast cells do not really play a role in membrane fouling [12,30,32]. Gan proved that increasing yeast cell concentration had almost no appreciable effect when the fractional mass concentration of large particles increased from 0.015% to 0.059% [32].

#### 20.2.4 INFLUENCE OF PROCESS PARAMETERS ON MEMBRANE SEPARATION OF BEER

The driving force in CMF is transmembrane pressure (TMP), defined as the pressure differential between the feed side and the permeate side. Given the fact that CMF is a pressure-driven process, it would be expected that the higher the TMP, the larger the permeate flux. Yet, the results of beer CMF studies published in literature demonstrate that the TMP–flux relationship is not necessarily straightforward. Gan reported that changing TMP between 0.3 and 1.15 bar (30–115 kPa) did not produce any significant effect on the 10 h average flux in the CMF of beer with ceramic membranes (Ceramem Corporation, Waltham, Massachusetts) of  $0.5\ \mu\text{m}$  nominal pore diameter [32]. He did, however, observe the beneficial effect of increased TMP when

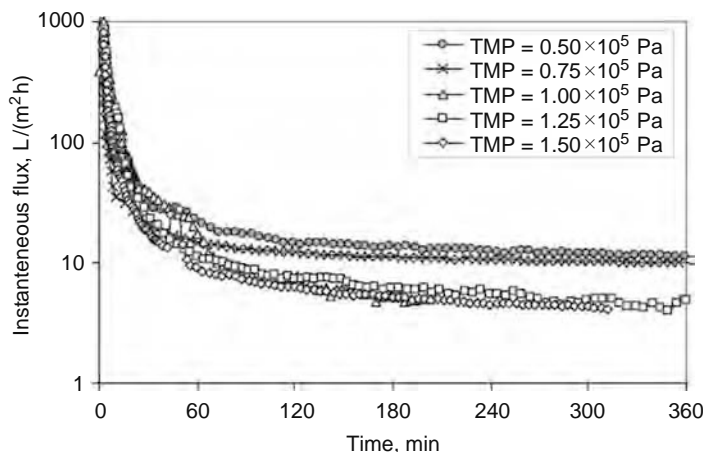


**FIGURE 20.6** Effect of TMP on the permeate flux in beer CMF through a  $0.45\ \mu\text{m}$  cellulose acetate membrane, at  $T = 0^\circ\text{C}$  and  $w = 2\ \text{m/s}$ . (From Moraru, C.I., Optimization and membrane processes with applications in the food industry: Beer microfiltration. PhD thesis, University “Dunarea de Jos” Galati, Romania, 1999.)

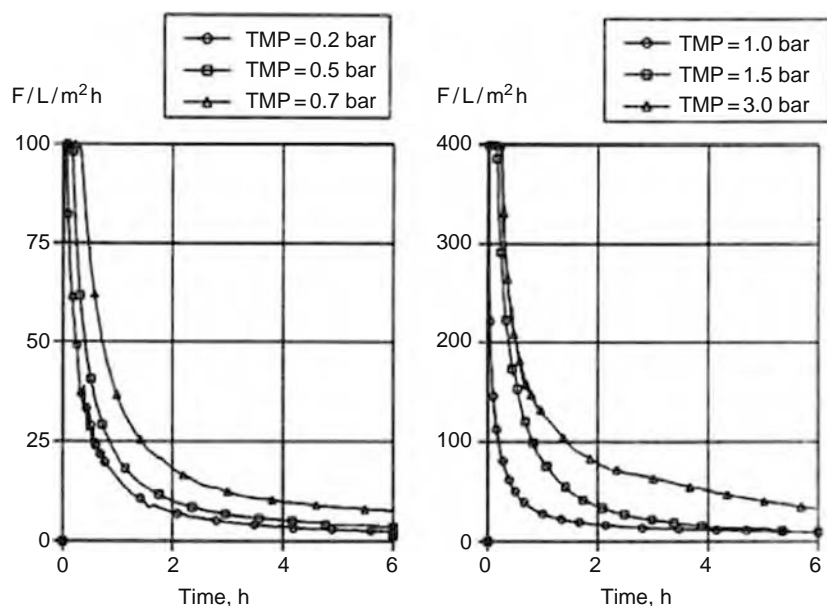


**FIGURE 20.7** Effect of low TMP values on the permeate flux in beer CMF through a  $0.45\ \mu\text{m}$  polysulphonic membrane. (From Gans, U., *Die wirtschaftliche Crossflow-Mikrofiltration von Bier*. Fortschritts-Berichte VDI Reihe 3 Nr. 385. Düsseldorf, Germany: VDI-Verlag, 1995. With permission.)

using a reversed morphology membrane. Details about this technique will be discussed later on in this chapter. On the other hand Moraru [30], who performed beer CMF experiments using single sheet cellulose acetate membranes with  $0.45\ \mu\text{m}$  nominal pore size, observed that generally higher TMP values resulted in higher values of the initial permeate flux, but lower values of the flux after 6 h of microfiltration (Figure 20.6). This is explained by the fast build-up of a fouling layer at high TMP values, which counteracts the faster transport of the filtered beer through the membrane.

These conclusions are similar to those of Gans, who performed beer CMF experiments with a polyethersulphone hollow fiber membrane of  $0.45\ \mu\text{m}$  nominal pore size [12]. He did observe a slight increase of the permeate flux when increasing TMP up to  $\sim 4$  bar (400 kPa) (Figure 20.7), but increasing the TMP to 5–6 bar (500–600 kPa) resulted in a negative effect on the permeate flux (Figure 20.8). The same effect is observed in industrial scale installations.

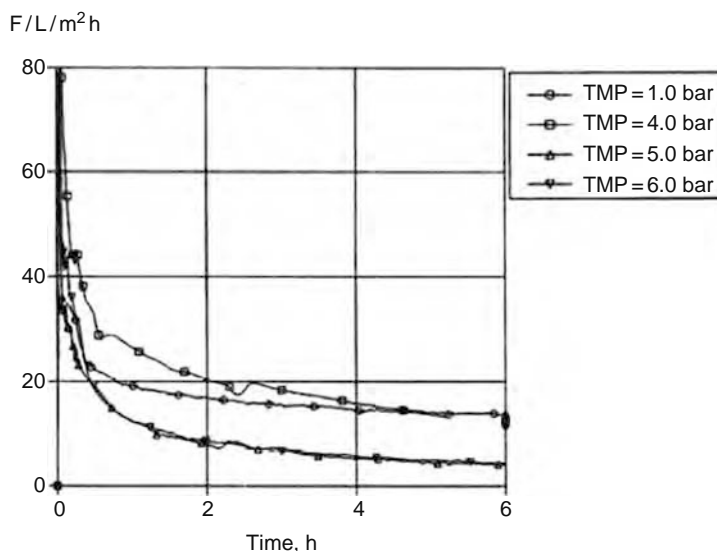


**FIGURE 20.8** Effect of  $\text{TMP} > 1$  bar on the permeate flux in beer CMF through a  $0.45\ \mu\text{m}$  polysulphonic membrane. (From Gans, U., *Die wirtschaftliche Crossflow-Mikrofiltration von Bier*. Fortschritts-Berichte VDI Reihe 3 Nr. 385. Düsseldorf, Germany: VDI-Verlag, 1995. With permission.)

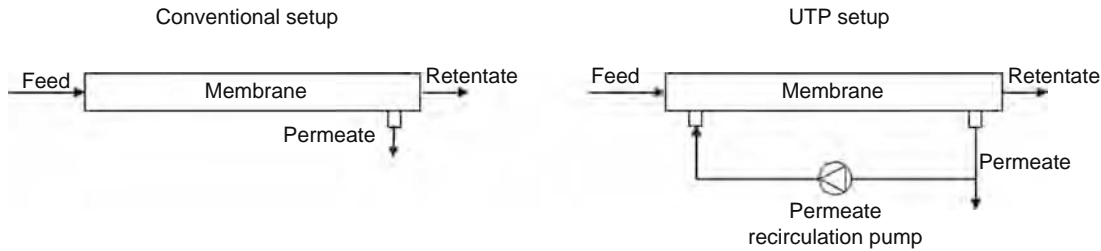


FIGURE 20.9 Conventional vs. UTP configurations in membrane separation.

A direct consequence of the effect of TMP in microfiltration is the unequal distribution of the fouling layer along the membrane. The TMP is the highest next to the feed inlet and decreases toward the end of the flow channel due to the drop in pressure along the membrane, caused by frictional forces. This happens especially when the process is conducted at high crossflow velocities, in which cases it is possible to experience TMP values at the module inlet up to 50% higher than the TMP values at the outlet [36]. The distribution of the fouling layer will closely follow the TMP distribution, with a more pronounced build-up near the entrance in the flow channel, which promotes unequal separation efficiency and yield. A solution that is sometimes used to alleviate this problem is the reversal of flow direction at certain time intervals, which allows the leveling of the fouling layer.

A recent approach to improving the CMF performance involves the concept of uniform transmembrane pressure (UTP). This is achieved by varying the pressure on the permeate side with a recirculation pump, which maintains the TMP at a constant value along the membrane. The schematics of the conventional crossflow and the UTP configurations are shown in Figure 20.9 and the TMP profiles for the two operational modes are shown in Figure 20.10. According to Bhave, flux improvements of up to 500% have been achieved when using UTP systems as compared with the conventional crossflow mode in many practical applications [36]. The membranes used in UTP systems must be able to structurally withstand significant backpressures on the permeate side, and therefore this concept cannot be used with all membrane types.

In beer microfiltration, besides the TMP level—which is chosen to achieve the best possible separation yield and efficiency—there are certain requirements for the value of the absolute pressure. The absolute pressure during this processing step needs to be higher than the saturation pressure of  $\text{CO}_2$  at the process temperature, to ensure that  $\text{CO}_2$  remains solubilized in beer.

It is generally accepted that crossflow velocity has a positive effect on yield in beer CMF, with higher fluxes being recorded at higher flow rates across the membrane surface (Figure 20.11).

In practical applications, one has to keep in mind that the permeate flux will be determined by the combination of crossflow velocity and TMP. As seen in Figure 20.12, the CMF experiments performed by Moraru indicated that the flux enhancement caused by increasing crossflow velocity was particularly pronounced at low values of the TMP ( $<1$  bar), due to the TMP effects discussed above [30]. Thomassen and coworkers studied the effect of varying TMP and crossflow velocity on the microfiltration fouling of a model beer using Carbosep filters of nominal pore size  $0.45 \mu\text{m}$  [37]. Fouling occurred over a range of TMPs and crossflow velocities at a constant temperature of  $20^\circ\text{C}$ . The permeate flux decreased with time during the development of the fouling layer, but once the fouling layer was established, the permeate flux became constant for a given set of experimental conditions. The steady-state flux increased with increasing TMP and with increasing crossflow velocity. For a given crossflow velocity, an increase in TMP resulted in an increase in the fouling layer thickness and density due to higher permeate fluxes. For a given TMP, an increase in crossflow velocity led to increased transmission, due to the inhibition of fouling layer development through the larger wall shear stress and thinner laminar sub-layer. Overall, it is therefore safe to say that moderate TMPs and high flow rates at the membrane surface are conducive of high permeate fluxes in the microfiltration of beer.

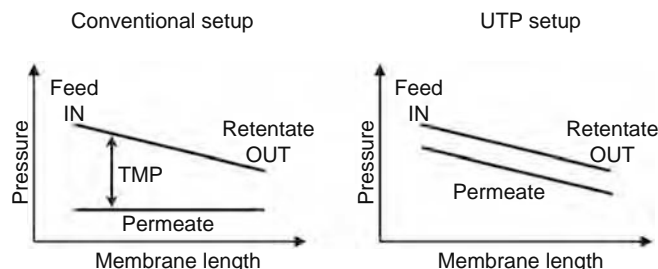
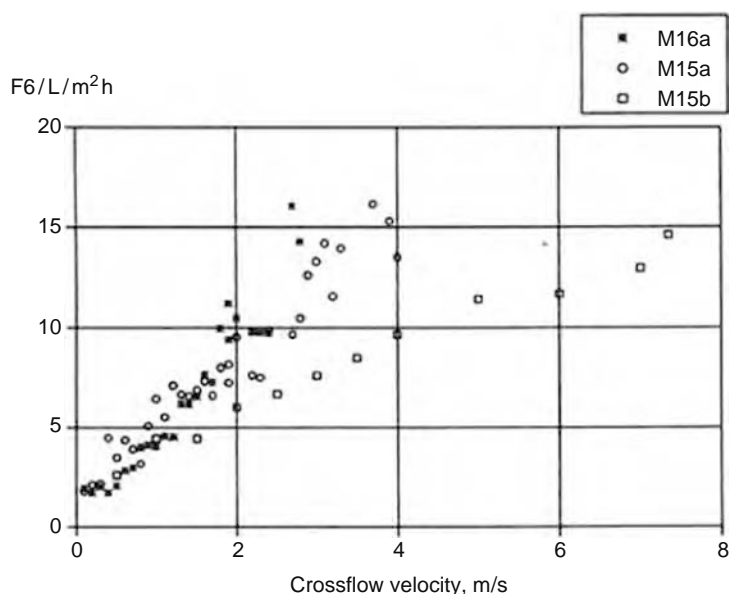


FIGURE 20.10 Pressure profiles in conventional and UTP configurations in membrane separation.



**FIGURE 20.11** Effect of crossflow velocity on the 6 h permeate flux in CMF of beer. Experiments were performed at  $0^{\circ}\text{C}$  and  $\text{TMP} = 1$  bar using  $0.45\ \mu\text{m}$  cellulose acetate membranes. Membranes used: M15a: Cellulose acetate with support,  $d_h = 7.67$  mm; M15b: cellulose acetate with support,  $d_h = 3.92$  mm; M16: cellulose acetate without support,  $d_h = 7.67$  mm ( $d_h =$  hydraulic diameter). (From Gans, U., Die wirtschaftliche Crossflow-Mikrofiltration von Bier. Fortschritts-Berichte VDI Reihe 3 Nr. 385. Düsseldorf, Germany: VDI-Verlag, 1995. With permission.)

The positive effect of velocity on the permeate flux is a result of enhanced hydrodynamic effects at the membrane surface, since high velocities lead to high shear and turbulent flow, which results in the formation of vortices and eddies that minimize the concentration polarization effects and the development of a fouling layer. The bigger the thickness of this layer, the higher its flow resistance and the smaller the permeate flux through the membrane becomes. Under turbulent flow conditions, shear effects induce hydrodynamic diffusion of the particles from the boundary layer back into the bulk, with a positive effect on the permeate flux.

Besides the velocity in the flow channel, the level of turbulence also depends on channel diameter, viscosity, and density of the retentate. The flow hydrodynamics can be characterized by calculating the Reynolds ( $Re$ ) number in the retentate stream.  $Re > 4000$  indicates turbulent flow, while  $Re < 2000$  indicates laminar flow. Gan reported that at  $Re < 2500$  the change of crossflow velocity had little, albeit positive, effect on the overall flux performance. It is important to note that Gan's conclusions are based on only three flow regimes, covering a relatively narrow range of hydrodynamic conditions [32]. A stronger correlation between the permeate flux and  $Re$  was reported both by Moraru [30] and Gans [12], who performed experiments in a much wider range of  $Re$  values. Figure 20.13 shows an overall positive effect of enhanced flow hydrodynamic conditions on the average permeate flux in beer CMF, although in the turbulent regime ( $Re > 4,000$ ) a weaker correlation and more data scattering were observed. In Figure 20.14, the clear correlation between the 6 h flux and  $Re$  in the laminar and transient regime can be observed.

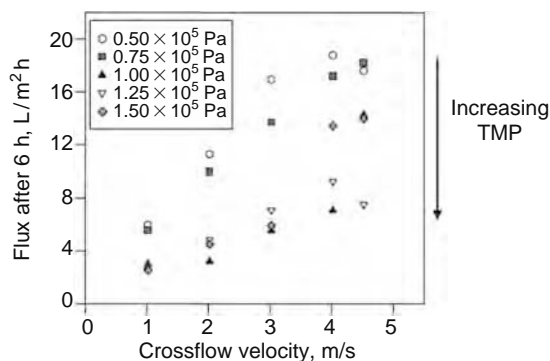


**FIGURE 20.12** Effect of crossflow velocity on the 6 h permeate flux in CMF of beer performed at various TMP values, a process temperature of  $0^{\circ}\text{C}$ , and cellulose acetate membranes of  $0.45\ \mu\text{m}$  pore size. (From Moraru, C.I., Optimization and membrane processes with applications in the food industry: Beer microfiltration. PhD thesis, University "Dunarea de Jos" Galati, Romania, 1999.)

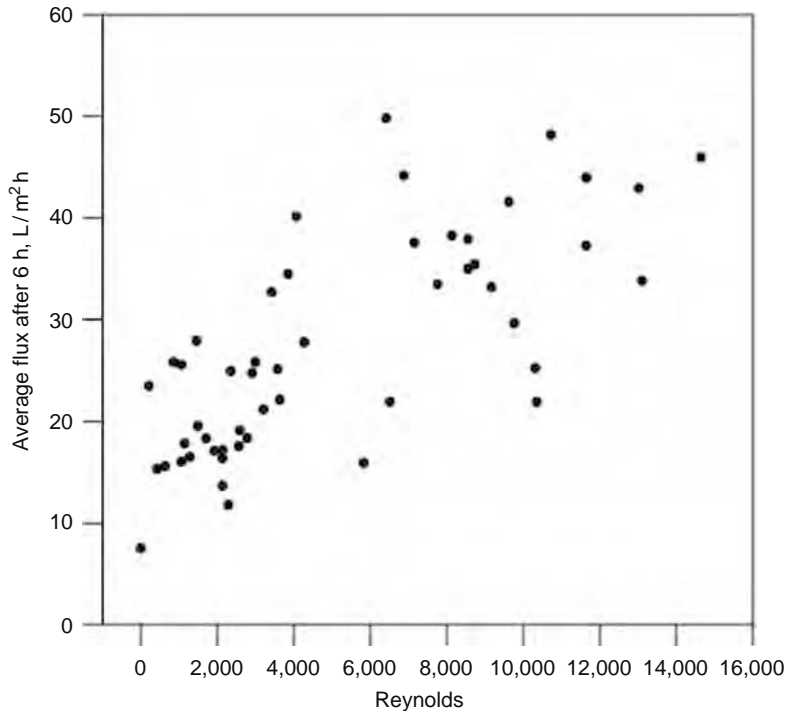


**FIGURE 20.13** The interdependence between average flux and hydrodynamic conditions in a wide range of  $Re$  numbers for beer CMF performed at  $0^{\circ}\text{C}$  and  $\text{TMP} = 1$  bar. (From Moraru, C.I., Optimization and membrane processes with applications in the food industry: Beer microfiltration. PhD thesis, University “Dunarea de Jos” Galati, Romania, 1999.)

The relationship between permeate flux and the flow characteristics in microfiltration processes is often described using the film model, which is based on the concentration polarization concept [38]:

$$J = k \cdot \ln\left(\frac{C_m}{C_s}\right) \quad (20.1)$$

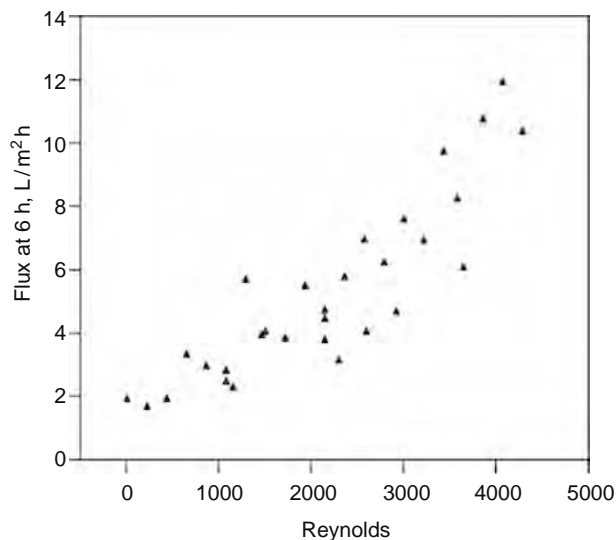


**FIGURE 20.14** Instant flux at 6 h vs.  $Re$  under laminar and transient flow conditions in beer CMF experiments performed at  $0^{\circ}\text{C}$  and  $\text{TMP} = 1$  bar. (From Moraru, C.I., Optimization and membrane processes with applications in the food industry: Beer microfiltration. PhD thesis, University “Dunarea de Jos” Galati, Romania, 1999.)

where

$J$  is the permeate flux (m/s)

$k$  is the mass transfer coefficient (m/s)

$C_m$  is the concentration of the separated species at the membrane level (g/L)

$C_s$  is the concentration of the separated species in the feed (g/L)

The mass transfer coefficient  $k$  in Equation [1] can be estimated using the following correlation [38]:

$$Sh = c \cdot Re^n \cdot Sc^m \quad (20.2)$$

where

$Sh = k \frac{d_h}{D}$  is the Sherwood number

$Sc = \frac{\nu}{D}$  is the Schmidt number

$Re = \frac{w \cdot d_h}{\nu}$  is the Reynolds number

$w$  is the velocity in the flow channel (m/s)

$D$  is the diffusion coefficient (m<sup>2</sup>/s)

$d_h$  is the hydraulic diameter of the flow channel (m)

$\nu$  is the kinematic viscosity of the product in the boundary layer (m<sup>2</sup>/s)

$c$ ,  $m$ ,  $n$  are the numerical coefficients

This leads to the fact that the mass transfer coefficient, and thus the permeate flux, is related to velocity according to the relationship:

$$k \sim w^n \quad (20.3)$$

According to Blatt et al. [39], the value of  $n$  can vary from 0.3 to 0.8 in laminar flow and from 0.8 to 1.3 in turbulent flow, with the lower limit of the range applying to low-particle concentration of the feed, and the upper limit applying to high-particle concentration of the feed. This behavior has been explained by the so-called tubular pinch effect, which enhances the movement of particles away from the boundary layer as turbulence increases, thus reducing the concentration polarization effect [36]. Moraru reported that in CMF of beer  $k \sim w^{0.8}$  for the laminar flow regime, but the dependence of the mass transfer coefficient on crossflow velocity was much weaker in the turbulent range, with  $k \sim w^{0.33}$  [30].

While higher process temperatures do have a positive effect on permeate flux in membrane separation (Figure 20.15), due to lower product viscosity and enhanced hydrodynamics at the membrane surface, in beer microfiltration the value of this parameter is dictated by the technological requirement that beer be filtered cold, typically at temperatures between  $-1.5^\circ\text{C}$  and  $+2^\circ\text{C}$ .

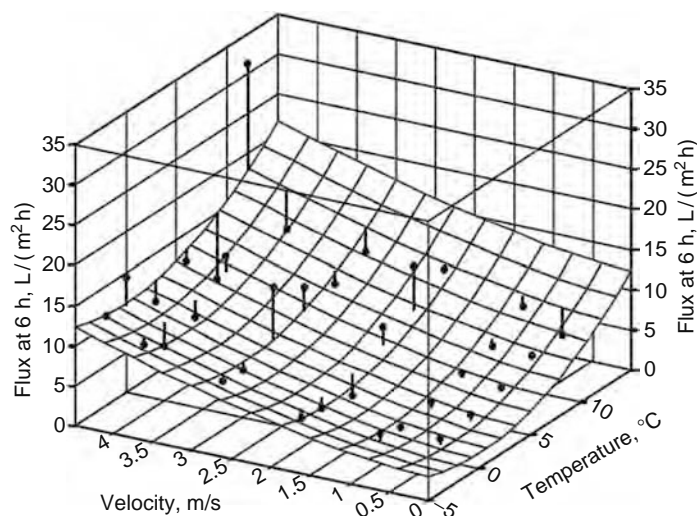


**FIGURE 20.15** Increase of permeate flux as a function of crossflow velocity in beer CMF experiments performed at  $\text{TMP} = 10^5$  Pa. (From Moraru, C.I., Optimization and membrane processes with applications in the food industry: Beer microfiltration. PhD thesis, University “Dunarea de Jos” Galati, Romania, 1999.)

## 20.3 SOLUTIONS FOR INCREASING THE PERMEATE FLUX IN MEMBRANE SEPARATION OF BEER

### 20.3.1 BACKWASHING AND BACKFLUSHING

Prevention or minimization of fouling and concentration polarization represents one of the main challenges that confronts membrane processing in general and membrane filtration of beer in particular. Various approaches have been developed to control membrane fouling and increase the permeate flux in CMF, including membrane selection and modification, boundary layer control, use of turbulence inducers, or pretreatment of the feed. The two main strategies that are currently used in beer CMF are proper membrane selection and boundary layer control.

Membrane fouling is primarily a result of membrane–solute interaction that is generally irreversible and requires chemical cleaning to restore the original separation properties of the membrane. Fouling effects can be accentuated or minimized by proper selection of membrane material properties such as hydrophobicity/hydrophilicity or surface charge, as well as membrane pore size. A discussion on the membranes that are typically used in beer processing was included in Section 20.2.2 of this chapter.

Concentration polarization and membrane fouling are the main factors that limit the commercial application of membrane filtration of beer. Small permeate fluxes increase the capital costs, because larger membrane surface area is necessary to achieve the desired production capacity, and may also result in poor product quality due to the undesirable retention by the membrane of some compounds that are critical for beer quality. The boundary layer can be controlled by backwashing or backpulsing, which consists of applying a negative pressure to the membrane by pushing a certain volume of permeate back through the membrane, with the purpose of reopening the clogged pores and membrane surface. The main difference between these two techniques is the speed and force utilized to dislodge accumulated matter on the membrane surface. In backpulsing, a high permeate backpressure (up to 10 bar) is applied periodically, typically in a fraction of a second, while backwashing uses permeate backpressure values of up to 3 bar for a few seconds. Backwashing is commonly used with polymeric membranes, due to their lower pressure limitation, while backpulsing is mostly used with inorganic membranes [36].

When using these techniques, it is recommended to start the backpulsing/backwashing procedures simultaneously with the filtration process, as they are no longer effective after the boundary layer is fully formed. For maximum economical benefits, it is recommended that backpulsing or backwashing is applied for the shortest duration possible. Since a certain amount of permeate is used by the backpulsing/backwashing programs, minimizing the duration of backpulsing/backwashing minimizes the permeate volume used in this process, thus minimizing the loss of productivity. The permeate volume typically used in such applications is about 1%–3% of the total permeate [36].

Gan reported the development of flux-enhancement techniques by taking into consideration the specific nature of fouling and the synergistic relationship between fouling and flux reduction that occur in beer CMF [32]. He tested a range of techniques, such as (i) enhancing surface hydrodynamics and producing secondary flow vortices through two-way reversing flow pulsation; (ii) superimposition of a helical-flow pattern to the bulk feed flow by installing helically wound baffle inserts within the flow channel; and (iii) an automated multistage backflush facility that generates backpulses of controllable frequency and strength. The author highlighted the predominant in-pore fouling formation in beer CMF and the ineffectiveness of hydrodynamic techniques in tackling this type of fouling. Application of the two-way reversing flow pulsation had little effect except when used in combination with a superimposed helical flow pattern. Backflushing was identified as a more effective technique in reducing the fouling caused by pore-entrance blockage and in-depth particle plugging. Among the multiple backflushing variables, frequency and strength of the backpulse were found to be the two most influential factors in determining the overall effectiveness of the backflush program. The author achieved an even greater flux improvement when applying high-frequency backflushing at reversed membrane morphology, which was achieved by changing port configuration so that the process fluid was fed to the substructure side of the membrane. When coupling backflushing and reversed membrane configuration, a flux increase of more than 870% as compared to the normal CMF was obtained. The author attributed the higher and steadier flux to the progressive interception and holding of particles inside the membrane's open matrix and support sublayer. This particle-holding mechanism was presumably able to prevent particles from directly approaching and blocking membrane pores, thus protecting the pores downstream.

Gans [12] combined the backwashing technique with chemical cleaning in beer CMF experiments performed with polymeric membranes. Such a program involved alternating 60 min filtration cycles with 15 min backflushing cycles (Figure 20.16). The backwashing cycle consisted of a caustic soda (0.05 mol/L) backwash, neutralization with hydrochloric acid, and then rinsing with water. This program was extremely efficient, with the average flux stabilizing at around 80 L/(m<sup>2</sup> h) after 4 h of filtration, which is more than 4 times the permeate flux obtained in the absence of the backwashing program (Figure 20.17). Such a procedure requires extreme caution to avoid the risk of mixing the chemical washing stream with the product stream, and requires special process control measures, preferably automation.

Blanpain-Avet and coworkers [40] reported that the use of oscillatory flow was also capable of permeate flux enhancements in CMF of beer due to disturbing concentration polarization and cake layer formation.

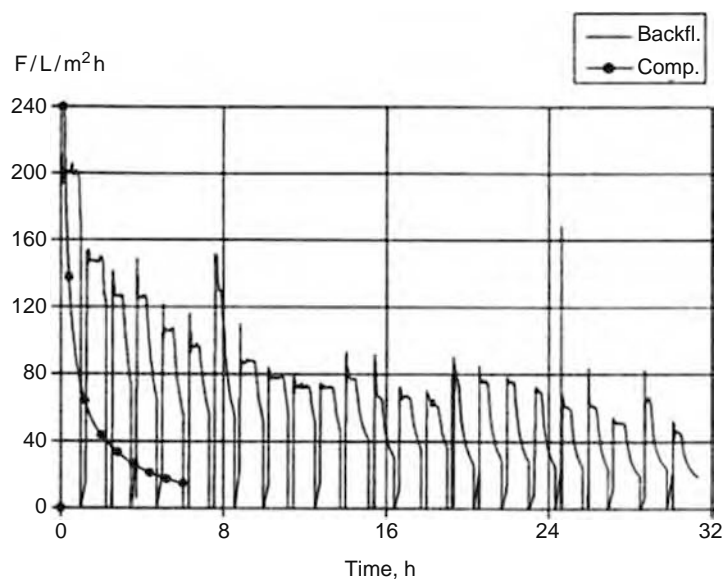


**FIGURE 20.16** Flux recovery using a caustic backwash program in beer CMF experiments performed with a polyethersulphone membrane of  $0.45\ \mu\text{m}$  pore size. Backfl. = CMF using the backwash program; Comp. = comparison experiment without backwashing. (From Gans, U., *Die wirtschaftliche Crossflow-Mikrofiltration von Bier*. Fortschritts-Berichte VDI Reihe 3 Nr. 385. Düsseldorf, Germany: VDI-Verlag, 1995. With permission.)

When such programs become relatively ineffective in preventing the abrupt flux decline, this indicates that irreversible fouling of the membrane has taken place, and this can only be corrected by chemical and thermal cleaning.

### 20.3.2 CHEMICAL CLEANING

The regeneration of membrane properties is key to maintaining its selectivity and yield. Without a safe, practical, reproducible, cost-effective, and efficient cleaning procedure, the viability of crossflow filtration is highly questionable [36]. The use of the mechanical means discussed above can help extend the membrane performance over a limited period of time, but the complete

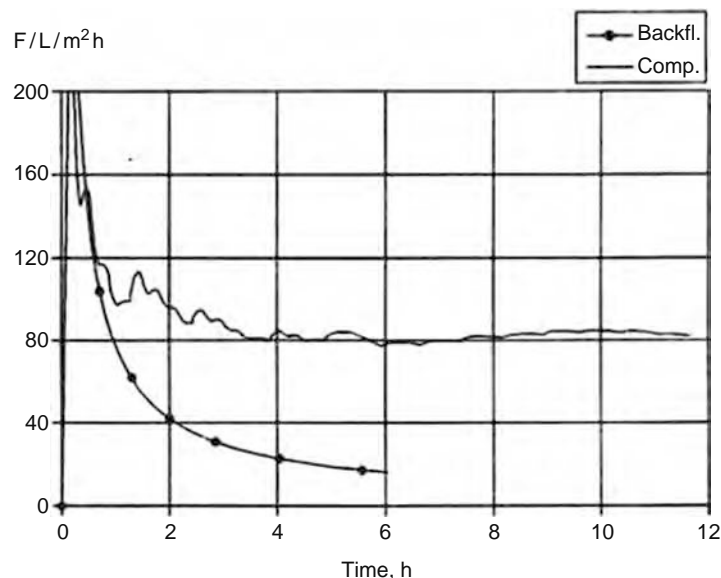


**FIGURE 20.17** Effect of the caustic backwash program on the average flux in beer CMF experiments performed with a polyethersulphone membrane of  $0.45\ \mu\text{m}$  pore size. Backfl. = CMF using the backwash program; Comp. = comparison experiment without backwashing. (From Gans, U., *Die wirtschaftliche Crossflow-Mikrofiltration von Bier*. Fortschritts-Berichte VDI Reihe 3 Nr. 385. Düsseldorf, Germany: VDI-Verlag, 1995. With permission.)

removal of membrane foulants requires the use of chemical cleaning. A flush of warm water or ambient caustic is sometimes performed during the production in the form of an intermediate short-CIP, similar to the procedure designed by Gans [12] and described in Section 20.3.1. The purpose of such a program is not cleaning of the membrane but a mere loosening of the linkages between the gel-like fouling layer and the membrane structure, followed by subsequent flushing and removal with ambient water flush. With this short-CIP most of the membrane characteristics may be regenerated. Even with such programs in place, all membrane-based filtration processes require periodic cleaning that must remove both external and internal deposits.

Gan and coworkers [41] suggest that the most effective cleaning programs for membranes used in beer separations are those that combine the effect of temperature, oxidative agents, and caustic soda. Oxidation proved effective in removing the residual fouling due to the cleavage of covalent and hydrogen bonds by the oxidative attack. The  $\alpha$ -1,4 bonds in polysaccharides and peptide bonds in proteins are also susceptible to oxidative cleavage, and these compounds are degraded down to small molecules such as oxidized di- or monosaccharides, peptide segments, or amino acids. This breaks up the foulants from the membrane surface and opens up the deposit for further attack by the caustic. Such a combination of caustic cleaning and oxidation, when applied at a temperature of 80°C, was able to recover 87% of the original water flux within 8 min [41].

The development of an effective cleaning process has to take into account the nature of the foulants, the thermal and chemical resistance of the membrane material, membrane housing and seals. Typically, membrane manufacturers make specific recommendations regarding the cleaning agents and cleaning procedures that need to be used for different membranes and applications.

Membrane cleaners specifically formulated to remove the organic and inorganic foulants found in food and beverage applications, including beer, include a variety of acid, alkaline, surfactant blend, oxidizer, enzyme, and solvent-based membrane cleaners. Inorganic foulants such as precipitated salts of Ca and Mg can be removed with acidic cleaners, while protein and other biological residues can be removed with alkaline cleaners, with or without bleaching agents or enzyme cleaners. Many acidic and alkaline cleaners also contain small quantities of detergents, which act as complexing or wetting agents to solubilize or remove insoluble particles and colloidal matter. Oxidizing agents such as peroxide or ozone are also sometimes used to remove hardy foulants such as polysaccharides.

For many polymeric MF membranes, material considerations limit the use of high cleaning temperatures and strongly acidic, alkaline, or oxidizing solutions. With time and repeated cleaning, polymeric membranes undergo progressive degradation, which limits their service life to 2–4 years, depending on the polymer. On the other hand, inorganic membranes can be cleaned at high temperatures in strongly alkaline, acidic and oxidizing solutions, and can have a useful service life of 10 years or longer [36].

The useful life of membranes can be significantly extended using suitable cleaning, operating, and maintenance procedures, which will have a major economical impact for the processing plant. Recent developments in improved cleaning of the membrane surface resulted in an increase of the economic efficiency of the membrane separation of beer. The CMF equipment seen in the first industrial installations has been transformed into an integrated combination of filtration and cleaning installations. In some fully automated plants membranes can be switched from production mode to cleaning mode in very short time intervals.

## 20.4 USE OF MEMBRANE SYSTEMS IN BEER PROCESSING

### 20.4.1 BEER FILTRATION

After the fermentation and aging steps the beer is cloudy, despite the fact that after aging the beer is separated from most of the sedimented yeast and tank bottoms. This cloudiness results from the remaining yeast cells—yeast concentrations of approximately 200,000 cells/mL are common for beer after separation from the tank bottoms—and from the haze-forming components of beer.

The size of the haze-forming matter starts at the size of large clusters that are directly visible as particles suspended in the liquid or at the bottom of the bottle, and ends with colloidal haze particles that are not visible as sole particles but at higher concentrations scatter the light and give the beverage a turbid appearance. A certain fraction of the colloidal haze is temperature dependent, meaning that it is fully dissolved in beer at temperatures above +10°C but becomes visible at lower temperatures. To give beer the desired clear appearance, as well as longer stability, a filtration step is typically required. Since the formation of chill haze is temperature dependent, beer filtration is normally performed at low temperatures so that chill haze can be filtered out as large aggregate particles.

The removal of yeast cells and haze-forming colloids without unnecessarily removing other components of beer, especially some of the dissolved proteins, is the task and challenge of the beer filtration step. The efficiency of the main filtration of beer is measured by its removal of the yeast cells and by the remaining turbidity of the filtered beer. A common standard is that

the concentration of yeast cells in the filtered beer should be reduced to <5 yeast cells/100 mL of filtered beer.\* The turbidity of the filtered beer should be less than 1–2 NTU (nephelometric turbidity unit)<sup>†</sup>, depending on the specific beer recipe.

#### 20.4.1.1 Traditional Methods for Beer Filtration

The industry standard method for beer filtration is using diatomaceous earth (DE)<sup>‡</sup>, a sand-like powder with a very high internal surface area and a fine porous structure, as a filter aid in depth- and cake-type filtration. Conventional beer clarification employs filter presses or pressure vessel filters that are pre-coated with porous diatomaceous earth particles as filter aids. In order to minimize clogging of the filtration media and maintain a porous cake, and thus extend the duration of the filtration runs, filter aid is continuously metered into the unfiltered beer as body feed [42].

Nowadays an estimated 95% of the annual volume of beer is clarified using this filter aid. The use of DE in the beer industry has several disadvantages. First of all, this difficult to handle dry powder contains crystalline silica dioxide, a potential health hazard for those who handle it, and therefore it is necessary to prevent its inhalation.<sup>§</sup> Further, the wet filter aid known as DE slurry needs to be disposed after use. In most countries, including the United States, this slurry is simply disposed as landfill. There are, however, some facilities where a thermal recovery of the diatomaceous earth is used to decompose its organic content, and the processed diatomaceous earth can then be reused for filtration purposes. Such a processing facility is Tremonis GmbH in Dortmund, Germany. It is expected that the cost of using filter aids will increase in the future due to more stringent requirements for the disposal of the diatomaceous earth slurry that contains entrapped organic matter.

Sometimes, additional haze removal techniques are used in conjunction with diatomaceous earth filtration to ensure the long-term stability of beer. Based on the knowledge of what causes haze formation, two basic approaches to stabilize beer have been developed: reducing the concentration of haze-active proteins, or reducing haze-active polyphenols, or both. The most common stabilizer used for removing proteins during filtration is amorphous silica gel, while polyvinylpyrrolidone (PVPP) is typically used for removing polyphenols. Since beer has a significant excess of haze-active proteins over haze-active polyphenols, reducing the polyphenol content by adsorption using PVPP is considered an efficient way to haze stabilize beer [43].

The authors of this chapter are unaware of any existing filtration equipment that uses filter aid and is able to completely prevent the bleed of filter-aid particles into the filtered beer in a single filtration step. A small amount of the filter aid dosed into the liquid upstream will always be found in the filtered liquid downstream of the filtration equipment, as clearly shown in a recent paper by Hartmann and coworkers [44]. This bleed is technically inevitable, and a second filtration step is applied normally to remove the filter-aid particles from the filtered beverage.

#### 20.4.1.2 Use of Membrane Separation

Crossflow microfiltration membrane technology represents the best alternative to DE filtration available to date. Among the advantages of CMF as compared to DE filtration one could mention: use of materials (the membrane) that are inert to the product, easy to operate and environmental friendly, regeneration of the filtration media as well as the potential for high final product quality. As compared to DE filtration, membrane filtration does not use any filter aid and, therefore, there are no particles added in the process, rendering the filtered liquid free of foreign particles. Another advantage is that the CMF equipment occupies a much smaller volume than a traditional DE filter. At the initial stage of the process both types of filters are filled with water. The smaller equipment produces a smaller volume of water–beer mix at the outlet. This volume of water–beer mix (called pre- and last-running) is difficult to reuse economically, and therefore the smaller volume produced by a crossflow membrane filtration plant requires less cost to reprocess and reuse.

On the other hand, there are also several challenges associated with the use of CMF for beer clarification: slight variability of permeate quality (either higher turbidity, or protein and aroma retention) between different types of beer filtered with the same equipment and parameters, variability in fluxes due to varying ingredient concentrations in different batches or in different beer brands, and the need for intensive cleaning due to membrane fouling.

Beer clarification by microfiltration requires a fine balance between the retention of large particles and the transmission of soluble macromolecules such as carbohydrates, proteins, as well as flavor and color compounds, which contribute to beer quality. Proteins and carbohydrates are known membrane foulants, but they are also essential for beer quality. Sufficient

---

\* 100 mL equals 0.026 US gal or approximately 3/128 US gal.

<sup>†</sup> In Europe, the use of European brewing convention (EBC) units is more common. 1 NTU = 0.25 EBC.

<sup>‡</sup> Diatomaceous earth is known as kieselguhr, diatomite, or filtration sand. Diatomaceous earth is a nonmetallic mineral composed of the skeletal remains of microscopic single-celled aquatic plants called diatoms. These microorganisms have the unique ability to absorb water-soluble silica present in water and thereby form a skeletal framework of amorphous silica.

<sup>§</sup> IARC monographs on the evaluation of carcinogenic risks to humans. Volume 68 (1997, IARC Press CH-Geneva): Silica, some silicates, coal dust, and para-aramid fibrils. ISBN 92–832–1268–1. The IARC working group decided to classify crystalline silica to class 1 (human carcinogen). This classification has been given only to treated or calcinated diatomaceous earth, which may contain higher levels of crystalline silica. Natural diatomaceous earth, which might contain none or low levels of crystalline silica, has not been considered as a carcinogen to humans (group 3).

transmission of these molecules through the membrane is critical for obtaining a satisfactory quality of the filtered beer. Therefore, the membranes used for the removal of haze, yeast, and bacteria cells from beer require special physical properties to ensure that the separation process is highly selective, and only the desired components in the rough beer pass through the membrane.

One of the main challenges when using membrane filtration at a commercial scale is its limited flexibility, which means the inability of changing the setup or operating conditions according to the properties of the products to be filtered. It is known that the flow of the filtered beer through the membrane (the permeate flux) is influenced by the following main factors:

1. *Applied Transmembrane Pressure and Velocity along the Membrane Surface:* These process parameters may be varied extensively at the laboratory scale to achieve the optimal combination of process parameters for a given beer or application. Variations in industrial installations are normally possible, but limited due to given sizes of the connecting piping, pump capacity etc., which might not allow the process to be conducted under desired process conditions for each individual application.
2. *Interaction between the Product to be Filtered and the Membrane:* The product–membrane interaction plays a dominant role in the membrane filtration of beer. The contribution of the membrane to this interaction is defined by the membrane material, surface structure (i.e., pore size), and the three-dimensional structure of the membrane. Beer is the other major element in this interaction. Since beer is a product made from natural ingredients, its properties can vary significantly, even for the same type of beer. Variations between different types or brands of beer are even larger. Yet, it is expected that the characteristics of the final filtered beer are always the same. When filtration applications are designed, the membrane type and installation are chosen based on given average properties of the beer to be filtered. For economic reasons the membrane elements are only replaced if they are damaged, and cannot be changed according to the varying properties of the rough beer. This might lead to variations in the filtered product throughput and quality, which is obviously undesirable.

The use of membranes for beer filtration was identified as a possible choice some years ago, but the costs have until now been higher than the competitive method of using a filter aid. Intensive research and development efforts have been employed to turn this method from laboratory into industrial scale. Some of the first examples of industrial applications have been recently reviewed by Noordman [45]. These applications have been installed in the Heineken brewery, in Zouterwoude, The Netherlands. Such installations were characterized by a high degree of developmental effort per installation in the brewery. Still, this technique is just becoming available in a repetitive industrial scale. The major membrane manufacturers have reacted to the increasing interest of the brewing sector in membrane technology, and as a result several membrane filtration systems are now commercially available for beer main filtration applications. In the most recent exhibition of brewery equipment held in Munich, Germany (Drinktec 2005) three manufacturers displayed membrane filtration equipment to be used for the main filtration step in breweries: Norit (formerly known as X-Flow, The Netherlands), Pall/GEA, and Alfa Laval/Sartorius.

The crossflow filtration system distributed by Alfa Laval/Sartorius (Figure 20.18) employs a polyethersulphone membrane with an asymmetric pore pattern developed specifically for beer filtration. This system is built on a modular basis, using plate and frame cassettes (Sartocon CFB filtration cassettes) of 0.7 m<sup>2</sup> of filtration area each. Due to its modular design, the system can be sized by combining multiple cassettes into filtration stages to provide the desired filtration area. The systems that are currently being commercialized are capable of handling throughputs of up to 500 hL/h (*Source:* www.alfalaval.com).

To establish a continuous, around the clock operation, an integrated approach to maintain the membrane characteristics using intermediate CIP intervals is applied. The technique consists of reversing the flow and varying the TMP until reaching the point where the membrane surface in one of the filtration stages needs to be cleaned. A possible diagram for this is shown in Figure 20.19. The intermediate CIP can be performed using a cold water rinse, a warm water rinse, or a short-term ambient caustic contact. This intermediate CIP is applied only to one filtration stage of the equipment and consists of displacing the nonfiltered and the filtered product from this stage using carbon dioxide gas or water, then applying the CIP solution (warm water or ambient caustic) to the membranes. After a defined contact time with the membrane, the CIP solution is drained and after intensive rinsing the stage is filled again with product and its status changes to stand-by.\* To perform these steps in the correct and timely manner, automation is required.

#### 20.4.2 FINAL FILTRATION OF BEER

Besides colloidal stability, it is also necessary to ensure the microbiological stability of the bottled product. Even if the primary filtration has been done with utmost care, an additional processing step might be necessary to achieve microbiological safety of

---

\* The described processes may be in part or entirely subject to existing patents held by the equipment manufacturer.



**FIGURE 20.18** Membrane filtration equipment for beer filtration. (Courtesy of Sartorius GmbH, Göttingen, Germany. With permission.)

beer. As illustrated in the overview diagram (Figure 20.2), there are two different techniques that can be used to ensure the microbiological stability of beer: thermal pasteurization or final filtration.

The microorganisms of concern in beer (all of them spoilage microorganisms, as there are no known pathogens in beer) can be inactivated by pasteurization. Two types of pasteurization techniques are typically used by breweries: (i) flash pasteurization, in which bulk beer is continuously pasteurized in a plate heat-exchanger before bottling and (ii) tunnel pasteurization, used for the in-pack treatment of bottles and cans. In flash pasteurization, beer is heated to 71°C–74°C (160°F–165°F) for 15–30 s, while tunnel pasteurization consists typically in applying temperatures of about 60°C (140°F) for a given time interval—typically 10 min. Sometimes, even if short holding times are used, the flavor of the final product is considered to be altered, and beer loses its freshness.

Final filtration has been used as an alternative to pasteurization for many years. It must be noted that sometimes the term “sterile filtration” is used instead of “final filtration,” but this is a misnomer because this processing step achieves only the

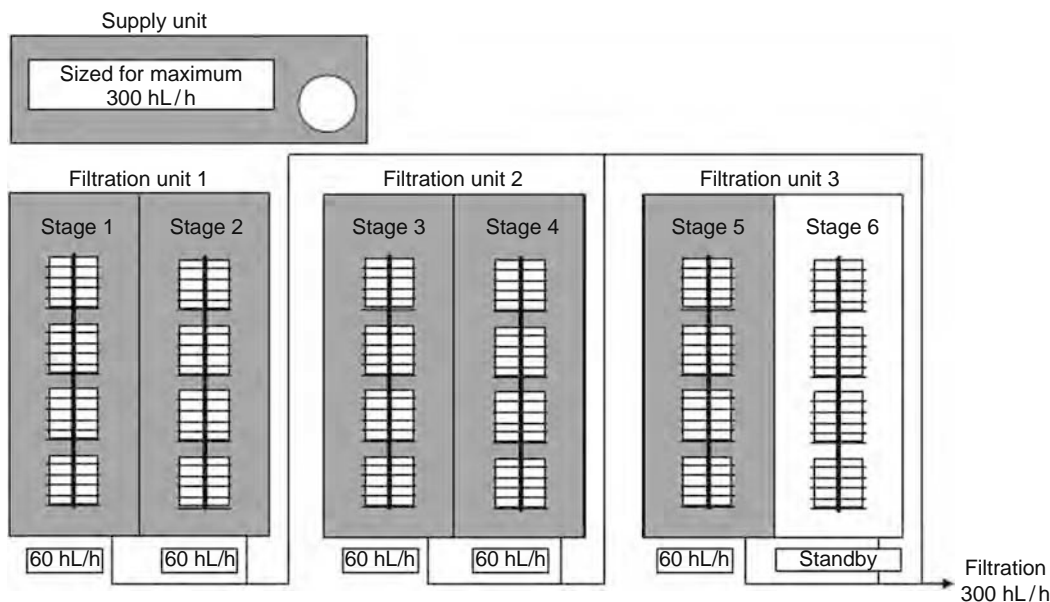


**FIGURE 20.19** A simplified layout/operation scheme of beer filtration equipment using six stages. Stage 6 is in standby mode. As soon as one of the first 5 stages reaches the condition for cleaning, it is switched into cleaning/regeneration mode and stage 6 is switched into filtration mode.

reduction of yeasts and bacteria to levels that do not result in spoilage of the beer during its shelf life, not microbiological sterility. As compared to pasteurization, final filtration has the advantage of eliminating the possible flavor changes caused by the heat treatment. The beers obtained using this technology are marketed and sold as cold filtered or non-pasteurized.

The final filtration step is not meant to remove significant amounts of particles or to reduce turbidity. For economic reasons, there should not be many particles left from the first filtration step when entering into the second (final) filtration step. Only if this condition is maintained the costs for the secondary filtration can be kept low. Also, the filtration should only remove microorganisms, and not retain other useful components of beer, i.e., those proteins that have a role in foam formation and stability. On the other hand, bacteria, which should be separated from beer during final filtration, typically have sizes down to 0.5  $\mu\text{m}$ . This small difference in size between the desirable ingredients and those particles that should be removed, such as bacteria, shows that the selection of the filtration technique and media needs to be done very carefully.

The typical pore size for the membranes used in final filtration of beer is 0.45  $\mu\text{m}$ . The membrane filter systems are installed in the beer processing line between the bright beer tank and the filling machine.

Since final filtration is used to physically remove as many contaminating microorganisms as possible from beer, the membranes have to be checked to be free of defects before and after the filtration process. It should be noted that the integrity of the large surface area of membranes applied in beer filtration applications cannot be tested directly using the bubble-point method, since it is difficult to differentiate between the first bubble of gas passing through the biggest pore in a huge surface area and the diffusion of the same gas through the wet membrane. To monitor the integrity of a large membrane surface, it is either necessary to use special equipment (i.e., particle counters), or to divide the available membrane area into smaller units and test them separately.

To check the ability of various membranes to remove bacteria, they need to be tested in the laboratory. Normally, a sample of the membrane is used to filter a suspension of bacteria of known concentration. *Serratia marcescens* is used as challenge bacteria for such tests. The results of laboratory bacteria challenge tests are commonly reported in the membrane specification sheets. Such tests include detecting the bacteria that pass through the membrane and determining the ratio of cell concentration found on the feed side vs. the concentration on the permeate side of the membrane. This ratio should be high, indicating a high microbial retention. Some membrane manufacturers guarantee a removal rate for bacteria. Typically, the membranes used for beer applications can achieve a reduction greater than 6 log cycles ( $10^6$  CFU\*) for *S. marcescens*.

Back [46] describes a method to check the microbial reduction capability of an installed filtration line. This method employs the use of five different types of microorganisms, which are suspended in water, and consists of inoculating a suspension of about  $10^{12}$  microorganisms the non-filtered beverage with a batch size of 100–500 hL. The ratio of the microbiological count found between the inlet to the first main filtration equipment and the outlet of the final filtration equipment should be higher than  $10^7$ , typically higher than  $10^8$ .

The most common practical method to check the efficiency of filtration or to detect the damage of a membrane filter consists, however, of monitoring the turbidity of the filtered beer using an in-line haze-meter.

#### 20.4.2.1 Traditional Methods for Final Filtration

Two filtration methods can be used for the final filtration of bright beer: depth filtration, which uses filter sheets or pads, and membrane filtration.

Sheet filter media for depth filtration are typically made from cellulose fibers and diatomaceous earths compressed into a thin mat. These sheets are typically mounted in plate and frame filters. There are also some special filters available that consist of filter sheet discs stacked and sealed in modules, which fit in closed filter vessels. The filter sheets can be regenerated several times until they need to be (manually) replaced.

#### 20.4.2.2 Use of Membranes for Final Filtration

The membrane filtration system uses a large number of filter elements that may look like filter cartridges or stacked flat membranes. The filter elements are organized in groups or clusters. Filter clusters are able to handle a significant product flow and can be installed directly upstream of the filling line without any requirement for a buffer plant. Cleaning, sterilization, and integrity testing are done cluster by cluster. A significant advantage of the clustered systems is that the integrity of each cluster is tested separately, which makes it possible to isolate and exclude any “bad” cluster before processing. Figure 20.20 illustrates a final filtration system manufactured by Pall Corporation. Several clusters are installed in one filter vessel using a common product inlet, but each cluster is equipped with its own outlet valve. A membrane cleaning unit (CIP), as well as the integrity testing unit, is connected to the fully automated filtration system. Other systems that can be used for the same purpose are available from Alfa Laval/Sartorius (Göttingen, Germany).

---

\* CFU = colony forming units

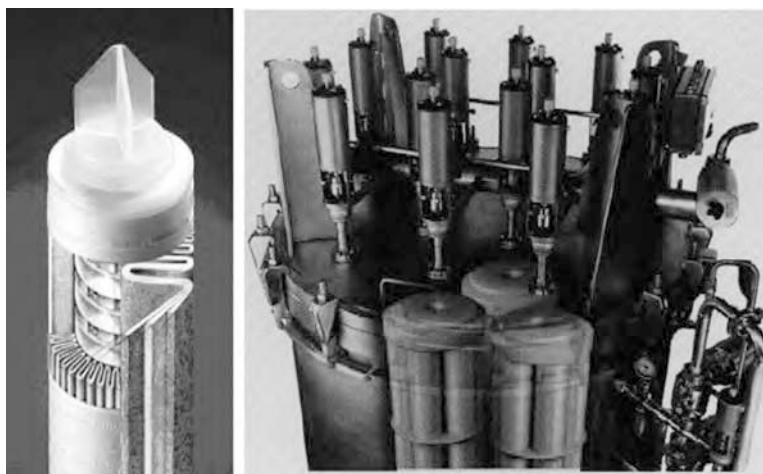


**FIGURE 20.20** Typical filter element showing the membrane in the middle of two supporting layers. Seven of these filter elements are arranged into a cluster. Several of these clusters are incorporated into one pressure vessel. The pressure vessel is equipped to connect or disconnect each of these clusters individually to the filtration outlet. (Courtesy of Pall Corporation. With permission.)

The brewers have the choice to ensure the quality of the finished product using different techniques (e.g., final filtration and pasteurization as mentioned in Figure 20.2). Their choice is mostly driven by economical and marketing considerations. There are breweries, both small and large, known for successfully producing and marketing “cold-filtered” beer in different parts of the world for many years.

### 20.4.3 RECOVERY OF SPENT BEER FROM YEAST AND TANK BOTTOMS

The fermentation of beer is done using different strains of the yeast *Saccharomyces cerevisiae*. At the end of fermentation of lager type beers, the yeast cells sediment at the bottom of the fermentation tanks. At the bottom of the tank the yeast cells are highly concentrated, still suspended in a small amount of beer. This yeast is normally removed from the tanks and sold to other biotechnological industries. For economical reasons, it is necessary to recover as much beer as possible from the tank bottoms, since otherwise a significant amount of beer would be lost with the yeast slurry. The next processing step, aging, is carried out at very low temperatures, typically below 0°C (32°F). During aging, even more yeast settles at the bottom of the tank. The yeast layer formed during aging is smaller than the yeast layer settled after fermentation and this yeast is considered to be less valuable, because the cells are weak after the long and cold treatment.

The volume of yeast slurry harvested from the tanks after fermentation and after aging is estimated to be ~2.5% of the fermented product volume.

#### 20.4.3.1 Traditional Techniques Used for Tank Bottoms Recovery

The most common method to recover the spent beer from the yeast slurry is centrifugation. In this process, beer is separated from the yeast using a centrifuge, based on the difference in specific gravity between beer and yeast. The dry matter content of the centrifugally separated yeast is usually ~22%–25%. An alternative method to recover the beer used by some breweries consists of mechanically pressing the yeast between sheets of cloth.

#### 20.4.3.2 Use of Membrane Separation

The membrane filtration systems are typically completely closed, preventing excessive contact of beer with air or oxygen. Thus, the filtered product is recovered at high quality, which allows it to be used directly in subsequent process steps or in the aging process. In certain instances, a slight change in the quality of the beer recovered from tank bottoms is observed. For example, Eagles and Wakeman [27] reported an increase in the concentration of some yeast metabolic products (ethyl acetate, butyl alcohol, and amyl alcohol) in the permeate obtained by the microfiltration of beer tank bottoms through a 0.45 μm alumina membrane. Such increases were attributed to the leaching of material from the yeast cells and to the secondary fermentation that took place during filtration. Practical experience shows that processing of the tank bottoms should be done as early as possible to minimize the deteriorating effect of storing the harvested yeast slurry over a long period of time.

The typical membranes used for tank bottoms recovery are tubular ceramic membranes. These membranes are available from different equipment suppliers, particularly since they have proven their rigidity against temperature variations, pressure,

and abrasion. Compared to the main beer filtration step, the membranes used for filtration of tank bottoms have larger pore sizes ( $\sim 0.8 \mu\text{m}$ ) and the flow channels have larger diameters.

One important challenge that needs to be taken into account during recovery of beer from tank bottoms is that centrifugal pumps are used, and these pumps can only handle fluids up to a certain viscosity. Additionally, the rheological behavior of the yeast slurry varies with its concentration. The more concentrated in yeast the slurry becomes, its viscosity departs from a Newtonian behavior and gains a shear thinning behavior, which means that its apparent viscosity decreases significantly when the slurry is subjected to higher shear rates (i.e., at high velocities). This effect keeps the concentrated yeast slurry pumpable as long as the pumps keep running. If the pumps stop, for example, due to a power failure, the viscosity of the yeast slurry becomes extremely high and the slurry in the pipe system becomes solid-like. This behavior needs to be taken into consideration, as plants need to have in-place solutions for removing the yeast slurry from the membrane system even after a power failure.

The viscosity of the yeast slurry must be sufficiently low to allow pumping through the recovery membrane equipment, particularly through the narrow membrane channels. At around 30% dry matter the yeast slurry has a consistency comparable to that of the wet sand used to build sand-castles at the beach. In most cases, 18%–20% dry matter is the limit for yeast processing using membranes. In order to increase the recovery yield, the cells can be washed using diafiltration, which consists of replacing the beer suspending the yeast cells with water. Another way to do this is to add water to the concentrated yeast slurry and then filter it again. Figure 20.21 shows the yield of recovered beer as a function of the tank bottom concentration. The diafiltration step enhances the amount of product recovered significantly, but the recovered product is diluted with water. This dilution of the recovered product limits the amount of water to be used during diafiltration.

### 20.4.3.3 Costs of Tank Bottoms Recovery Using Membrane Separation

The main cost factors are represented by equipment depreciation, membrane replacement, and electric power consumption. The other costs (man power and water consumption) are of minor influence. Membrane filtration plants equipped with a low level of automation require only a few hours of attention and direct surveillance by the operator per day. Direct surveillance of membrane filtration equipment is necessary at times when batches need to be changed or during membrane cleaning. The electric power consumption is associated with the use of pumps to move the viscous yeast slurry over the membrane surface, and its estimation is relatively straight forward.

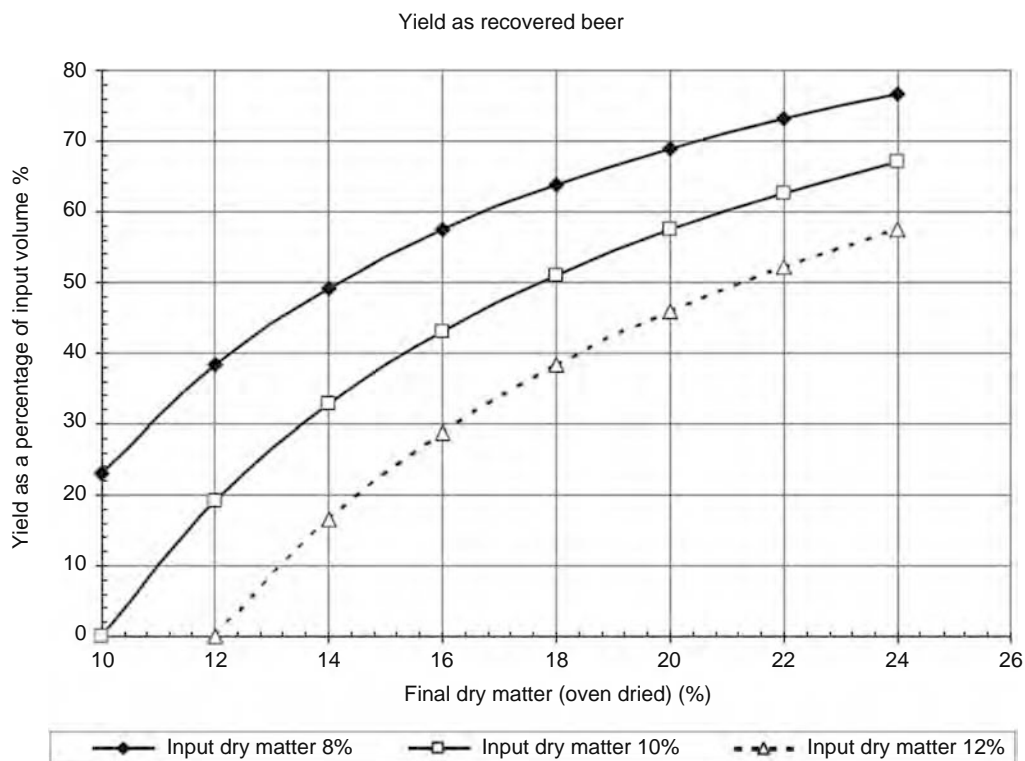


**FIGURE 20.21** Theoretically possible yield as a function of the concentration of the yeast slurry entering and exiting the tank bottoms recovery system, without diafiltration.

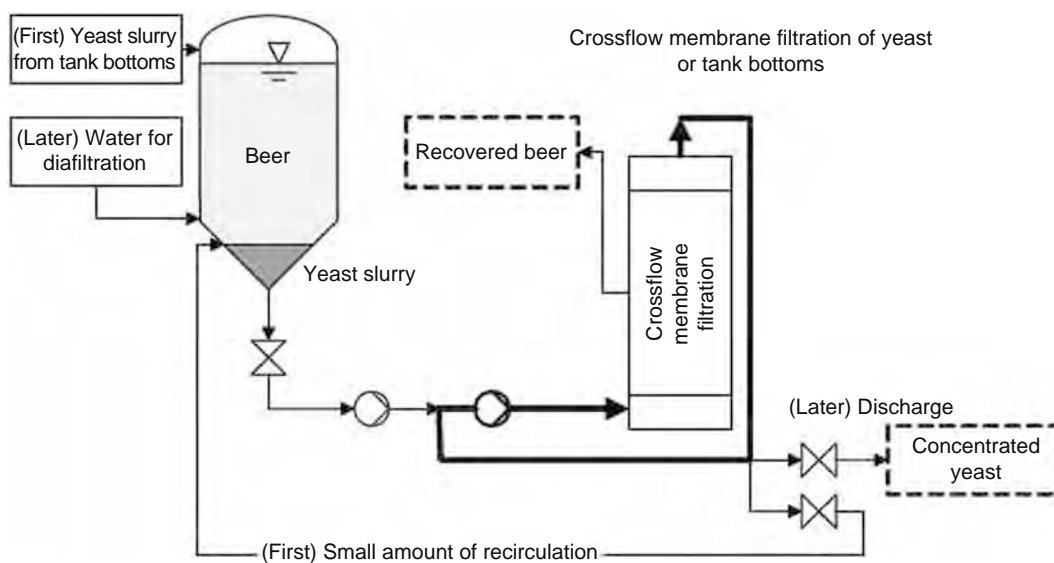


FIGURE 20.22 Process flow diagram of membrane filter plant for tank bottoms or yeast.

The replacement of membranes needs to be done at certain time intervals and membranes are costly. To the knowledge of the authors the ceramic membranes used in one of the oldest tank bottom recovery systems are running for some 10 years now. Sometimes, a membrane replacement in a 5 year time interval is assumed. This long time, which is equivalent to the long-term planning horizon of some companies, and the relatively high membrane prices, makes it difficult to accurately estimate the contribution of this cost factor properly.

#### 20.4.3.4 Examples of Commercial Installations

The general diagram for a tank bottom recovery system that includes a crossflow filtration unit is presented in Figure 20.22. The CMF setup shown in Figure 20.23 is manufactured by Filtrox AG, St. Gallen, Switzerland, and is equipped with 10 vertically mounted membrane units, comprising of ceramic membranes with 90.8 m<sup>2</sup> surface area each. This equipment



FIGURE 20.23 Installation of crossflow membrane filtration for filtration of yeast and tank bottoms in a German brewery. (Courtesy of König-Brauerei GmbH, Duisburg, Germany and Filtrox AG, St. Gallen, Switzerland. With permission.)

is dimensioned for processing 2500 hL yeast slurry per week. When the yeast slurry concentration reaches a final value of 18%–20% dry matter, water is added to increase the total amount of beer recovered (diafiltration). The equipment shown in Figure 20.23 was installed in October 2002 and is running since. A small CIP unit is included in the background for cleaning the membranes.

Another example of CMF equipment used for tank bottom recovery is the Keraflux beer recovery system produced by Pall Corporation. Keraflux systems are available both as a batch version and as a continuous version, the latter being used for larger processing capacities. Other types of membrane systems have also been used for this purpose [47] but the tubular ceramic membrane systems are the current state of the art.

#### 20.4.4 ALCOHOL REMOVAL FROM FERMENTED BEER

Alcohol-reduced beer can be obtained using two different processes. On one hand, it is possible to produce beer with a low ethanol concentration ( $<0.5\%$  v/v) by stopping the fermentation very early, i.e., by keeping the contact time between the wort and the yeast short and the temperatures low, both during fermentation and aging. This can be achieved in a batch process using regular brewing equipment. Some breweries produce alcohol-reduced beer by running a continuous flow of wort through immobilized yeast cells [48].

On the other hand, the ethanol can be removed from the beer after the regular sequence of fermentation, aging, and main filtration steps has been completed. Ethanol removal from fermented beer can be done either by direct heating and ethanol evaporation, or by membrane separation. The use of membranes is meant to avoid the heat treatment of beer, to ensure the desired sensory quality of the final product.

The membrane process used for alcohol removal from beer is dialysis. In dialysis, the driving force for the transport of chemical components through the membrane is the difference in concentration of those components between the two sides of the membrane, unlike the microfiltration processes involved in the applications described so far, which are pressure-driven processes. Dialysis membranes are very tight and allow some of the dissolved ingredients (such as ethanol) and water to pass through, but do not allow the transport of larger molecules. The porous structure of these membranes is similar to ultrafiltration membranes [49]. The dialysis membranes used to process filtered beer are often of the hollow fiber type. Glaser [50] reported the use of a hollow dialysis membrane with an inner diameter of 215  $\mu\text{m}$  and a wall thickness of 16  $\mu\text{m}$  for alcohol removal from beer. A bundle of these hollow fibers (up to 50,000 fibers) are housed in a single membrane module. The static pressure difference across the dialysis membranes is typically kept small, in the range of 3–5 psi (20–35 kPa).

The diagram of a typical installation for the removal of alcohol from finished beer using dialysis is presented in Figure 20.24. The process may be described as follows: the equipment is first filled with water. As soon as the bright beer replaces the water from the product side, alcohol is transported to the intermediate water cycle. The intermediate water–alcohol solution is heated up and then the ethanol is removed in the distillation column using vacuum. Other low molecular ingredients and the dissolved carbon dioxide of the bright beer are partly transported into the recirculated water until the concentration of those ingredients becomes equal on both sides of the dialysis membrane. Since the content in dissolved carbon dioxide gas is

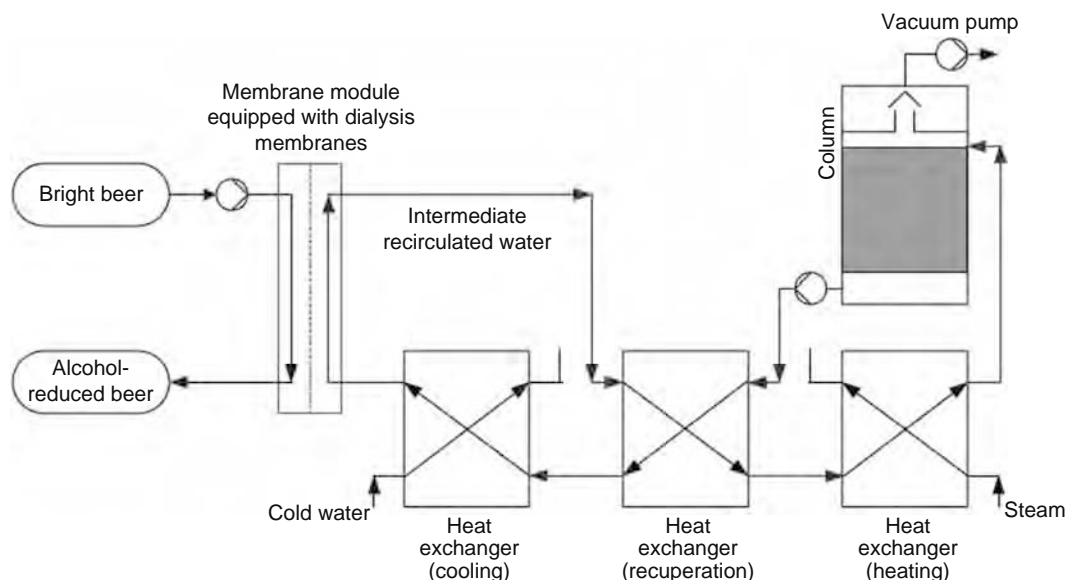


FIGURE 20.24 Schematic of alcohol reduction using dialysis membranes.

constantly reduced in the column due to the higher temperature and lower pressure inside the column, the carbon dioxide content of the low alcohol beer needs to be readjusted downstream of the dialysis process. Such membrane installations are capable of running for about 12 days with a constant throughput until the membranes need to be regenerated using a special CIP procedure.

While very attractive from a product quality point-of-view, it is important to note that alcohol removal by dialysis has to compete economically with thermal evaporation to be adopted by breweries.

## 20.5 OTHER USES OF MEMBRANE SEPARATION IN THE BREWING INDUSTRY

### 20.5.1 PURIFICATION OF BREWING WATER BY REVERSE OSMOSIS

The basic ingredient of beer is water (Figure 20.2), which must meet the highest standards of purity for potable water, and should also have an acceptable taste and odor. In most cases, the water found in natural resources, such as wells or in some countries, rivers does not have the desired composition for direct use in brewing processes. At least a purification step is necessary to remove suspended, colloidal, or dissolved solids from water before processing. The lowering of hardness, which is given by the concentration of calcium bicarbonate, can be done using ion exchange or wet chemistry, i.e., by adding lime to the water, followed by sediment removal.

Reverse osmosis offers the possibility of achieving more than one purification purpose in one step. It simultaneously reduces the hardness and the concentration of other salts, as well as organic molecules, bacteria or viruses. The higher the concentration of undesired ingredients in the well water, the more economic the membrane filtration becomes as compared to the ion exchange treatment. RO for water purification is one of the oldest applications of membrane separation and has been extensively discussed in literature over the years.

### 20.5.2 UTILITIES FILTRATION

Besides its direct use in the final product, water is used in breweries as a utility, for purposes such as cleaning, steam generation, etc. Another common utility in breweries are gases, such as air and carbon dioxide, which sometimes might contain impurities that need to be removed in order to ensure the quality and uniformity of the final product. Besides traditional methods, i.e., activated coal treatment, purification of utilities can also be successfully done by membrane filtration. Some membrane manufacturers (i.e., Pall Corporation, Donaldson Ultrafilter Inc., Sartorius, Millipore, CPM, etc.) offer commercial membrane separation equipment that is specifically designed for the purification of water, steam, air, or carbon dioxide. This enables breweries to produce sterile and particle-free utilities for the brewing processes.

### 20.5.3 BEER DECOLORIZATION

Alcopops and spirit mixed drinks are gaining much popularity in the Western world, reaching impressive growth rates in recent years. Due to its specific color and taste, beer cannot be directly used in such applications. Recently, NORIT process technology (NPT) has developed a method of beer decolorization that enables breweries to produce clear alcohol–water mixtures that can be used in premixes or alcopops (*Source*: <http://www.noritpt.nl>). For beer-based drinks, the NPT membrane-based technology is able to produce a water–alcohol mixture with the taste and smell of beer. For premixes, alcopops, and comparable products, the taste and smell can also be removed in an additional step, using activated carbon.

### 20.5.4 MICROBIOLOGICAL QUALITY CONTROL OF BEER

The microbiological quality of the packaged product is of major concern for beer manufacturers, and therefore needs to be checked before the final product hits the target market. Typically, testing the microbiological quality of beer is done by passing at least 100 mL of beer through a 0.45  $\mu\text{m}$  membrane, followed by plating of the membrane on specific media, incubation, and counting of the microbial colonies that grow on the media. Membranes for microbiological testing are available from companies such as Pall, Millipore, Sartorius, Schleicher & Schuell, and Whatman.

## 20.6 AN ECONOMICAL PERSPECTIVE ON THE USE OF MEMBRANE SEPARATION IN BREWING

These days more and more equipment manufacturers are advertising their membrane filtration equipment for main filtration of beer as a true possibility. This shows that nowadays there are economic circumstances for breweries that facilitate or even induce the switch from the filtration with filter aids to the use of membranes for this purpose. The first installations in small- or medium-sized breweries, as well in a large brewery, are already in successful operation. A higher number of installations is expected.

The global cost for beer filtration is significant, and for the year 2003, it was estimated that a total of  $0.4 \times 10^9$  USD was spent to filter the total volume of  $1.4 \times 10^9$  hL beer produced that year (*Source: www.e-malt.com*). Therefore, the economics of the process will have a decisive role in the expansion of membrane separation as a commercial filtration technique. As all processing methods, CMF will have to cope with the ever-changing economical conditions, such as membrane prices, the cost of electric power, as well as the changing ratio between these costs and the disposal costs of spent diatomaceous earth. Since these costs, as well as the cost of man power, differ at least from country to country, global answers to this are not accurate.

For CMF to be deemed a successful replacement of traditional clarification methods for the main filtration process, a high beer flux is required (generally, a minimum of  $100 \text{ L}/(\text{m}^2 \text{ h})$  is considered necessary), with power costs that do not exceed those associated with the traditional filter aids [37]. Gan [32] considered that an average flux rate of  $40 \text{ kg}/(\text{m}^2 \text{ h})$  over 10 h of continuous filtration is of commercial interest.

Membrane filtration as a technique for final filtration of beer is widely used today, and companies use the term “cold-filtered” and “not pasteurized” for selling their products.

In the area of beer recovery from tank bottoms the use of membranes is a competitive possibility and has been known for some years now. There are numerous breweries using this technique, and the size of the equipment is of a smaller scale than those intended for main filtration.

Briefly, the use of membrane filtration by breweries has been slowed down by the difficulties in filtering this very special beverage made from natural ingredients. To overcome these problems intensive research and resources have been spent, mostly because the market is promising. The bottom line is that membrane filtration produces a high-quality filtered product without the use of filter aids that need to be disposed of, membrane processes are easy to automate, and their operation is more continuous-like as compared to the filter-aid methods.

Membrane separation is becoming increasingly attractive to the beer industry and, as advances that will minimize or even eliminate some of the current challenges associated with membrane separation of beer are made, it is expected that more and more breweries will adopt this technology in the not so distant future.

## REFERENCES

1. Fillaudeau L and Carrere H. Yeast cells, beer composition and mean pore diameter impacts on fouling and retention during crossflow filtration of beer with ceramic membranes. *J. Membr. Sci.*, 2002; 196:39–57.
2. Brauwelt-Brevier. 376 pp. Fachverlag Hans Carl GmbH, Humberg, 2005; p.20.
3. Jin YL, Speers RA, and Paulson AT. Effect of  $\beta$ -glucans and process conditions on the membrane filtration performance of beer. *J. Am. Soc. Brew. Chem.*, 2004; 62(3):117–124.
4. Ragot F, Guinard J-X, Shoemaker CF, and Lewis MJ. The contribution of dextrans to beer sensory properties. Part I. Mouthfeel. *J. Inst. Brew.*, 1989; 95:427–430.
5. Piendl A. The role of beer in present-day nutrition. *Brauwelt Int.*, 1990; III:174–176.
6. Wagner N, Esser KD, and Krüger E. Analytik und Bedeutung hochmolekularer  $\beta$ -Glucan in Bier. *Monatsschrift für Brauwissenschaft*, 1988; 10(41):384–395.
7. Krüger E, Wagner N, and Esser KD. Analytik und rheologisches Verhalten der  $\beta$ -Glucane in Bier, Proceedings of the 22nd Congress of the European Brewing Convention, Zürich, 1989: 425–436.
8. Vaikousia H, Biliaderis CG, and Izydorczyk MS. Solution flow behavior and gelling properties of water-soluble barley (1  $\rightarrow$  3,1  $\rightarrow$  4)- $\beta$ -glucans varying in molecular size. *J. Cereal Sci.*, 2004; 29:119–137.
9. Bamforth CW. Barley  $\beta$ -glucans: Their role in malting and brewing. *Brewers Dig.*, 1982; 35:22–27.
10. Siebert KJ and Knudson EJ. The relationship of beer high molecular weight protein and foam. *Tech. Quart. Master Brew. Assoc. Am.*, 1989; 26:139–146.
11. Pollock JRA, ed., *Brewing Science*, Vol. 1. London: Academic Press, 1979, p. 94.
12. Gans U. Die wirtschaftliche Crossflow-Mikrofiltration von Bier. Fortschritts-Berichte VDI Reihe 3 Nr. 385. Düsseldorf, Germany: VDI-Verlag, 1995. ISBN 3–18–338503–1.
13. Siebert KJ, Troukhanova NV, and Lynn PY. Nature of polyphenol–protein interactions. *J. Agric. Food Chem.*, 1996; 44:80–85.
14. Narziß L. Abriß der Bierbrauerei, 5.Auflage, F.Enke Verlag Stuttgart, 1963.
15. Siebert KJ, Carrasco A, and Lynn PY. Formation of protein-polyphenol haze in beverages. *J. Agric. Food Chem.*, 1996; 44:1997–2005.
16. Asano K, Shinagawa K, and Hashimoto N. Characterization of haze-forming proteins of beer and their roles in chill haze formation. *J. Am. Soc. Brew. Chem.*, 1982; 40:147–154.
17. Outtrup H, Fogh R, and Schaumburg K. The interaction between proanthocyanidins and peptides, Proceedings of the 21st Congress of the European Brewing Convention, Madrid, 1987: 583–590.
18. McMurrrough I, Kelly R, and Byrne J. Effect of the removal of sensitive proteins and proanthocyanidins on the colloidal stability of lager beer. *J. Am. Soc. Brew. Chem.*, 1992; 50:67–76.
19. Ahrenst-Larsen B and Erdal K. Anthocyanogen-free barley—a key to natural prevention of beer haze, Proceedings of the 17th Congress of the European Brewery Convention, Berlin, 1979: 631–644. ISSN: 0367–018X.
20. Siebert KJ and Lynn PY. Mechanisms of adsorbent action in beverage stabilization. *J. Agric. Food Chem.*, 1997; 45:4275–4280.

21. Stopka J, Bugar SG, Broussous L, Schlosser S, and Larbot A. Microfiltration of beer yeast suspensions through stamped ceramic membranes. *Separat. Purif. Technol.*, 2001; 25(1–3):535–543.
22. Kuiper S, van Rijn CJM, Nijdam W, and Elwenspoek MC. Development and applications of very high flux microfiltration membranes. *J. Membr. Sci.*, 1998; 150(1):1–8.
23. Kuiper S, vanRijn C, Nijdam W, Raspe O, van Wolferen H, Krijnen G, and Elwenspoek M. Filtration of lager beer with microsieves: Flux, permeate haze and in-line microscope observations. *J. Membr. Sci.*, 2002; 196:159–170.
24. Moraru CI, Panchapakesan CP, Huang Q, Takhistov P, Liu S, and Kokini JL. Nanotechnology: A new frontier in food science. *Food Technol.*, 2003; 57(12):24–29.
25. Jelinski L. Biologically related aspects of nanoparticles, nanostructured materials and nanodevices. In: *Nanostructure Science and Technology. A Worldwide Study*. Prepared under the Guidance of the National Science and Technology Council and the Interagency Working Group on NanoScience, Engineering and Technology, eds., RW Siegel, E Hu, and MC Roco. 1999. Available online at <http://www.wtec.org> (accessed May 2002).
26. Kingsley D. Membranes show pure promise. ABC Science Online, May 1, 2002. Available online at [www.abc.net.au](http://www.abc.net.au) (retrieved August 22, 2003).
27. Eagles WP and Wakeman RJ. Interactions between dissolved material and the fouling layer during microfiltration of a model beer solution. *J. Membr. Sci.*, 2002; 206(1–2):253–264.
28. Ryder DS, Davis CR, Anderson D, Glancy FM, and Power JN. Brewing experience with crossflow filtration. *Tech. Quart. Master Brew. Assoc. Am.*, 1988; 25:67.
29. Blanpain-Avet P, Fillaudeau L, and Lalande M. Investigation of mechanisms governing membrane fouling and protein rejection in the sterile microfiltration of beer with an organic membrane. *Food Bioprod. Process.*, 1999; 77(C2):75–89.
30. Moraru CI. Optimization and membrane processes with applications in the food industry: Beer microfiltration. PhD thesis, University “Dunarea de Jos” Galati, Romania, 1999.
31. Taylor M, Faraday DBF, O’Shaughnessy CL, Underwood BO, and Reed RJR. Quantitative determination of fouling layer composition in the microfiltration of beer. *Separat. Purif. Technol.*, 2001; 22–23:133–142.
32. Gan Q. Beer clarification by crossflow microfiltration—effect of surface hydrodynamics and reversed membrane morphology. *Chem. Eng. Process.*, 2001; 40(5):413–419.
33. Güell C and Davis RH. Membrane fouling during microfiltration of protein mixtures. *J. Membr. Sci.*, 1996; 119:269–284.
34. Wagner N and Krüger E. Rheologische Eigenschaften der  $\beta$ -Glucane in Bier. Teil 1. *Monatsschrift für Brauwissenschaft*, 1990; 10:328–334.
35. Wagner N and Krüger E. Rheologische Eigenschaften der  $\beta$ -Glucane in Bier. Teil 2. *Monatsschrift für Brauwissenschaft*, 1990; 12:401–406.
36. Bhavé RR. Cross-flow filtration. In: *Fermentation and Biochemical Engineering Handbook—Principles, Process Design, and Equipment*, 2nd edition. eds., Vogel HC and Tadaro CL, William Andrew/Noyes, West Woods, New Jersey, 1997, pp. 271–347.
37. Thomassen JK, Faraday DBF, Underwood BO, and Cleaver JAS. The effect of varying transmembrane pressure and crossflow velocity on the microfiltration fouling of a model beer. *Separat. Purif. Technol.*, 2005; 41(1):91–100.
38. Porter MC. Concentration polarization with membrane ultrafiltration. *Ind. Eng. Chem. Prod. Res. Develop.*, 1972; 3(11):234–248.
39. Blatt WF, Dravid A, Michaels AS, and Nelson L. Solute polarization and cake formation in membrane ultrafiltration: Causes, consequences and control techniques. In: *Membrane Science and Technology*. ed., Flinn JE, Plenum Press, New York, 1970, pp. 47–97.
40. Blanpain-Avet P, Doubrovine N, Lafforgue C, and Lalande M. The effect of oscillatory flow on crossflow microfiltration of beer in a tubular mineral membrane system—membrane fouling resistance decrease and energetic considerations. *J. Membr. Sci.*, 1999; 152(2):151–174.
41. Gan Q, Howell JA, Field RW, England R, Bird MR, and McKechnie MT. Synergetic cleaning procedure for a ceramic membrane fouled by beer microfiltration. *J. Membr. Sci.*, 1999; 155(2):277–289.
42. Goldammer T. *The Brewers’ Handbook—The Complete Book to Brewing Beer*. KVP Publishers, Clifton, Virginia, 2000, 472 pp. ISBN 0967521203.
43. Mikyška A, Hrabák M, Hašková D, and Šrogl J. The role of malt and hop polyphenols in beer quality, flavour and haze stability. *J. Inst. Brew.*, 2002; 108(1):78–85.
44. Hartmann K, Kreis S, Zarnkow M, and Back W. Identifizierung von Filterhilfsmitteln nach den einzelnen Filtrationsschritten. *Der Weihenstephaner* 2004; 72(4):141–143.
45. Noordman TR, van der Noordt M, Hardenbol AFC, Peet CI, Broens L, and Mepschen A. Practical experiences with membrane filtration for the clarification of beer on an industrial scale, Presentation O-15 of World Brewing Congress 2004, San Diego, CA, 2004.
46. Back W. *Farbatlas und Handbuch der Getränkemikrobiologie. Teil 2 Fruchtsaft- und Limonadenbetriebe, Wasser, Betriebshygiene, Milch und Milchprodukte, Begleitorganismen der Getränkeindustrie*. Nürnberg: Hans Carl Fachverlag, 2000. ISBN 3–418–00760–0.
47. Snyder J and Haughney N. Use of a vibrating membrane filter for the recovery of beer from surplus yeast. *MBAA Tech. Quart.*, 1999; 36(2):191–193.
48. Aivasidis A and Wandrey C. Alkoholfreies Bier aus dem Bioreaktor. *Spektrum der Wissenschaft*, 1994; 2:18–20.
49. Kesting RE. *Synthetic Polymeric Membranes. A Structural Perspective*, 2nd edition. John Wiley & Sons, New York, 1985. ISBN 0–471–80717–6.
50. Glaser W. Entalkoholisierung von Bier und Wein mittels Umkehrosmose und Dialyse. In: *Entwicklungsstand der Membrantrennverfahren in der Milch-, Getränke- und allgemeinen Lebensmittelindustrie*, Kessler, HG. Training Seminar at Technical University of Munich, Munich, Germany, 1991.



---

# 21 Developments of Bipolar Membrane Technology in Food and Bio-Industries

*Gerald Pourcelly and Laurent Bazinet*

## CONTENTS

21.1	Introduction .....	582
21.2	Principles of Electromembrane Processes.....	582
21.2.1	Ion-Exchange Membranes.....	582
21.2.1.1	Homopolar Membranes .....	582
21.2.1.2	Bipolar Membranes .....	583
21.2.2	Principle of Conventional Electrodialysis.....	583
21.2.3	Principle of Electrodialysis with Bipolar Membrane.....	584
21.2.3.1	H <sup>+</sup> and OH <sup>-</sup> Generation.....	584
21.2.3.2	Water Dissociation in Bipolar Membrane.....	584
21.2.3.3	Catalysts for Improving Water Dissociation.....	587
21.2.3.4	EDBM Configurations.....	588
21.2.4	Features of EDBM, Difference from the Conventional Electrolysis, Limits .....	589
21.2.5	Cell Equipment and Process Configurations in EDBM.....	589
21.2.6	Scaling-Up and Exploitation Parameters of the BPM Technology .....	591
21.3	Main Applications of the EDBM.....	593
21.4	Applications of EDBM to Food Industries.....	593
21.4.1	Production of Soy Protein Isolate .....	594
21.4.2	Production of Acid Caseinate.....	598
21.4.3	Inhibition of Enzymatic Browning in Cloudy Apple Juice .....	603
21.4.4	Deacidification of Passion Fruit Juice.....	606
21.4.5	Process for Purifying Dairy Wastewater .....	609
21.4.6	Separation of Whey Protein .....	611
21.4.7	Fractionation of Major Soybean Protein Fraction.....	614
21.4.8	Recovery of Protein and Coagulant Agent from Soy Tofu Whey .....	615
21.5	Other Applications: Biotechnology, Nutraceutical, Cosmeceutic, and Biopharmaceutical .....	616
21.5.1	Fermentative Production and Isolation of Lactic Acid.....	617
21.5.2	Production of Phospholipids .....	620
21.6	Successful EDBM Industrial Plants.....	623
21.6.1	History of Electrodialysis with Bipolar Membranes.....	623
21.6.2	EDBM: A Cost-Effective Solution for the Production of Specialty and Fine Chemicals .....	624
21.6.2.1	Criteria for the Application of EDBM.....	624
21.6.2.2	Organic Acid Production in France .....	624
21.6.2.3	Acetic Acid Production in Germany.....	624
21.6.2.4	pH Adjustment of Wine .....	625
21.6.2.5	EDBM Included in Complete Processes.....	625
21.7	Concluding Remarks and Perspectives.....	627
	Abbreviations.....	627
	References.....	627

## 21.1 INTRODUCTION

Membranes may be hastily classified according to the driving force at the origin of the transport process: (1) a pressure differential leads to micro-, ultra-, nanofiltration, and reverse osmosis; (2) a difference of concentration across the membrane leads to diffusion of a species between two solutions (dialysis); and (3) an electric potential difference applied to an ion-exchange membrane (IEM) leads to migration of ions through the membrane (electrodialysis, membrane electrolysis, and electrochemical devices) [1,2].

Today, electrodialysis (ED) is one of a group of membrane-based separation technologies which are finding increasing use in agri-food industries to concentrate, purify, or modify foods. The low-energy consumption, modular design, efficiency, and ease of use as well as the heat sensitivity of many food products are among the reasons for their rapid growth. ED uses an electric field as the driving force and charged membranes to perform the separation: electrodialysis is a combined method of dialysis and electrolysis [3].

Electrodialysis can be performed with two main cell types: multi-membrane cells for dilution–concentration and water dissociation applications, and electrolysis (or electro-electrodialysis [EED]) cells for oxidoreduction reactions. In multi-membrane cells, only the membrane transport phenomena intervene, while electrochemical reactions occurring at the electrodes do not interact with the separation process: the electrodes are simple electrical terminals immersed in electrolytes allowing the current transfer. The electrolysis cell operates with only one membrane that separates two solutions circulating in each electrode compartment. This application is based on electrode redox reactions, which are electrolysis specific properties. The anode induces oxidations, and reductions occur at the cathode [4].

Electrodialysis is a well-proven technology with a multitude of systems operating worldwide. In Europe and Japan, electrodialysis dominates as a desalting process with total plant capacity exceeding that of reverse osmosis and distillation [3]. Electrodialysis with monopolar membranes is applied to different food systems, to demineralization of whey [5–8], organic acids [9], and sugar [10,11], separation of amino acids [12] and blood treatments [13], wine stabilization [14–16], fruit juice deacidification [17–19], and separation of proteins [20–22]. These applications use the sole property of dilution–concentration of monopolar IEMs in a stack of as many as 300 in an electrodialysis cell.

Electrodialysis with bipolar membranes (EDBMs) [23] was applied recently to the production of mineral and organic acids [24–36], inhibition of enzymatic browning [37–39], and separation of protein [40–44]. These applications are based on water dissociation at the interface of a bipolar membrane (BPM) coupled with monopolar membrane action. A recent up-to-date overview gives the possibilities and the economic relevance of BPM technology [45].

In the domain of food industries, EED was used to reduce oxygen in fruit juice [46], to extract cytoplasmic proteins from alfalfa [47,48], to coagulate proteins [49], and to reduce disulfide bonds in proteins [50]. These applications are based on the electrode redox reactions coupled with monopolar membrane action.

This review summarizes the monopolar and BPM principles of operation. Moreover, this review presents shortly the main applications in chemical processing, pollution control, and resource recovery, and details the specific applications of electrodialysis with BPMs to food and bio-industries.

## 21.2 PRINCIPLES OF ELECTROMEMBRANE PROCESSES

### 21.2.1 ION-EXCHANGE MEMBRANES

Two kinds of IEMs are used in electrodialysis (ED): homopolar membranes bearing charges of same sign and BPMs bearing positive and negative charges located separately on each side of a same plane.

#### 21.2.1.1 Homopolar Membranes

These are sheet-shaped materials through which a selective ion transport can be established under a driving force, generally an electric field or a concentration gradient. Most of them are of a polymeric nature. They are constituted by reticulated macromolecular chains forming a tridimensional structure. In this network, ionizable functionalized groups are borne by the polymeric matrix and are at the origin of the membrane selectivity. For example, cation-exchange membranes (CEMs) contain fixed negative charges and mobile cations that can be exchanged with other cations present in an external phase in contact with the membrane. The ions balancing the fixed exchange sites are called counterions. The concentration of counterions within the membrane is relatively high; therefore, counterions carry most of the electric current through the membrane. The fixed charges attached to the polymer matrix repel ions of the same charges (co-ions). This exclusion, which is a result of electrostatic repulsion, is called Donnan exclusion, named for Donnan who first reported the phenomenon in 1911 [51]. However, as the membrane selectivity is never ideal, the membrane material can be penetrated by a non-negligible amount of electrolyte. A schematic structure of such a homopolar IEM (CEM) is depicted in Figure 21.1. Under an applied electric field, the CEM bearing sulfonic exchange groups ( $-\text{SO}_3^-$ ) mainly allows the transport of counterions.

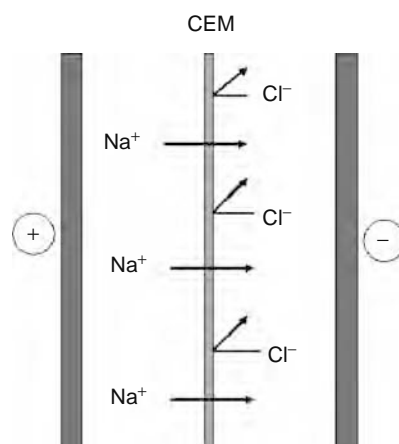


**FIGURE 21.1** Schematic process of transport of counterion ( $\text{Na}^+$ ) through a CEM.

### 21.2.1.2 Bipolar Membranes

Bipolar membranes (BPMs) are composed of two layers of ion exchangers joined by a hydrophilic junction. The diffusion of water from both sides of the BPM allows it dissociation under the electrical field to generate protons and hydroxyl ions, which further migrate from the junction layer through the cation- and anion-exchange layers of the BPM. The principle of this water-splitting phenomenon is depicted in Figure 21.2.

The requirements for suitability of homopolar IEMs for industrial applications are the following:

1. High-ionic conductivity with a concentration of fixed charges
2. High-ionic permselectivity combining simultaneously a high conductivity and a moderate water uptake
3. Chemical stability of the fixed ions and a good mechanical resistance
4. Reasonable cost

In addition, BPM must have an experimental potential to achieve the water-splitting capability as close as possible as the theoretical value equals 0.83 V at 25°C. Nowadays, superior styrene–divinylbenzene copolymer membranes can be easily purchased, perfluorinated membranes with great chemical stability are on the market, and BPM with an industrial-scale lifetime (>10,000 h) is available.

### 21.2.2 PRINCIPLE OF CONVENTIONAL ELECTRODIALYSIS

Electrodialysis can be organized in two, three, or four compartments. Figure 21.3 depicts the schematic configuration of a conventional two-compartment electrodialysis applied to the reconcentration/dilution of NaCl solutions. C and D are the concentrate and diluate, respectively. When an ionic feed solution (e.g., a sodium chloride solution) flows through the channels of the electro dialyzer, the positively charged sodium ions migrate to the cathode and the negatively charged chloride ions

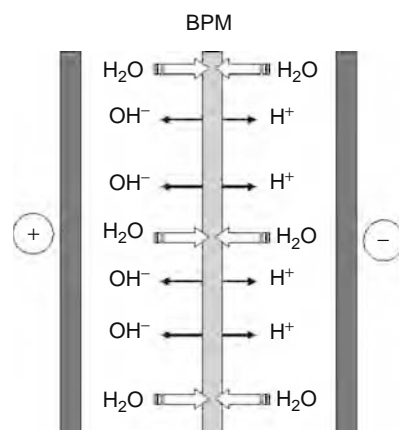


**FIGURE 21.2** Schematic principle of water dissociation by a BPM.

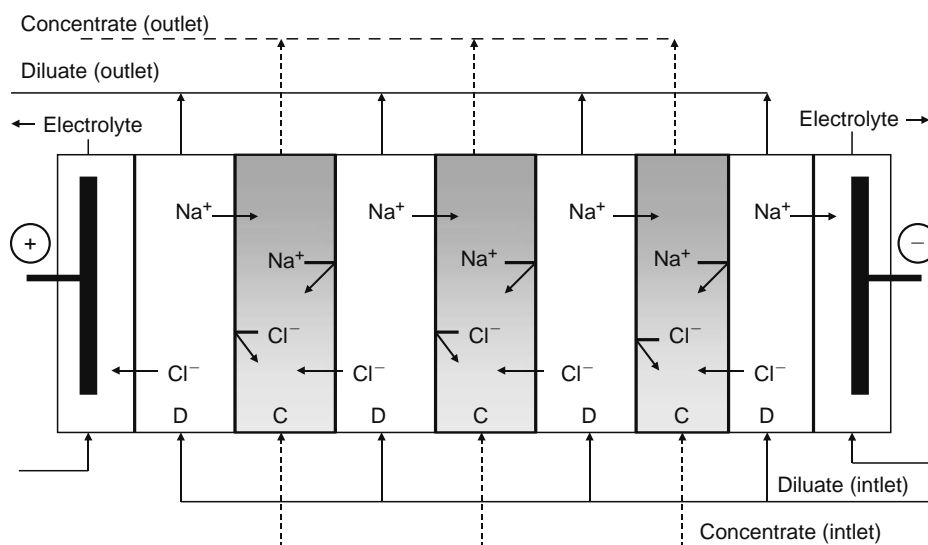


**FIGURE 21.3** Schematic configuration of a conventional two-compartment electrodiagnosis applied to the reconcentration/dilution of NaCl solutions. C and D: concentrate and diluate.

migrate to the anode. As the chloride ions cannot pass the CEM and the sodium ions cannot pass the AEM, the overall effect is a simultaneous ionic concentration increase in alternating compartments and ionic concentration decrease in the other compartments. Consequently, alternate dilute and concentration solutions are formed. A set of two compartments (diluate [D] and concentrate [C]) form a cell pair. In commercial applications, several hundred cell pairs are assembled in a stack.

### 21.2.3 PRINCIPLE OF ELECTRODIAGNOSIS WITH BIPOLAR MEMBRANE

#### 21.2.3.1 $H^+$ and $OH^-$ Generation

The conventional method for generating  $H^+$  and  $OH^-$  ions from water utilizes electrolysis. Electrolysis also generates  $O_2$  and  $H_2$ , and the overvoltage for this generation consumes about half of the electrical energy of the process. Nowadays, special IEMs are available for splitting water directly into  $H^+$  and  $OH^-$  ions without generating gases. Membrane water-splitting technology is a general-purpose unit operation for converting water soluble salts to their corresponding acids and bases. This process uses BPM in conjunction with conventional CEM and AEM, respectively. The separation and rearrangement of ions is effected by a direct current driving force. EDBM is therefore an alternative method to electrolysis for the generation of  $H^+$  and  $OH^-$  ions, which can be used to generate acid and base from salts, without the production of oxygen and hydrogen gases. The application of BPM reduces the energy costs associated with electrode polarization in the more conventional electrolytic approach.

#### 21.2.3.2 Water Dissociation in Bipolar Membrane

The origin of the water-splitting phenomenon in BPM is still a matter of controversy. In fact, ordinary water dissociation cannot explain the magnitude of the electric current and the changes observed in the pH of the solutions in contact with the membrane [52–54]. It is generally believed that the  $H^+$  and  $OH^-$  ions originate in a very thin region at the interface between the two ion-exchange layers [55]. Nevertheless, it is not known exactly which mechanism is responsible for this enhanced dissociation, and up to now three physical models have been proposed: the second Wien effect [56–58], a model based on protonation–deprotonation phenomena [53–58], and recently a more global model [59].

##### 21.2.3.2.1 Second Wien Effect

According to Ohm's law, the conductance of electrolytes in aqueous solutions increases with the applied electric field. However, Wien [56] observed that at high-electric field densities ( $>10^5 \text{ V cm}^{-1}$ ), Ohm's law is no longer valid for electrolyte solutions. In weakly dissociated electrolytes, the ion mobility as well as the degree of dissociation are increasing with increasing field density. This phenomenon is known as the second Wien effect. The deformation of the ion atmosphere and its relaxation time [57] lead to an increase in ion mobility of approximately 20%–30%. The second Wien effect model for BPM considers that water in the space-charge region at the bipolar junction behaves as a weak electrolyte, and uses Onsager's theory

[60] for the increase of the dissociation rate constant of a weak electrolyte in the presence of an external electric field [55,58]. Its application for BPM can be written as

$$k_d^E = \frac{I_1(\sqrt{-b})}{\sqrt{2b}} k_d^0$$

where

$k_d^E$  is the dissociation rate constant of water under the influence of an electric field

$k_d^0$  is the dissociation rate constant of water in the absence of an external electrical field

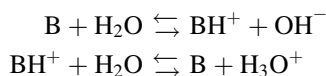
$I_1$  is the first-order Bessel function

$b = 0.09636 E/\varepsilon_r T^2$  with  $E$  the electric field density,  $T$  the temperature, and  $\varepsilon_r$  the relative permittivity

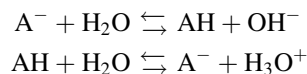
Some limitations of the model should be pointed out. Although the water dissociation rate is increased significantly with increasing electric field density due to the second Wien effect, the calculated values are still at least three orders of magnitude smaller than the experimentally from current densities determined values [57]. In addition, Onsager's theory has been successfully applied only up to  $10^7$ – $10^8$  V m<sup>-1</sup>, and theoretical estimations show that fields as high as  $10^8$ – $10^9$  V m<sup>-1</sup> could exist in the narrow space-charge regions existing in IEMs [53,61]. Hence, some effects not considered in this theory (e.g., the rotation of water molecules) should be included in the model [53]. Furthermore, if the accelerated water dissociation would only be due to the second Wien effect, it should be identical for both anion- and cation-exchange layers forming the BPM while it has been observed that water dissociation is usually larger for AEMs than for CEMs [53,61–63].

#### 21.2.3.2.2 Protonation–Deprotonation Phenomena

Theoretical considerations and experimental evidence strongly support a hypothesis that the accelerated water dissociation is also caused by a reversible proton-transfer reaction between the charged groups and water. In the presence of ionic groups, the water dissociation rate constant may be several orders of magnitude higher than in free solution. The experimental results showing that water dissociation occurs mainly at the surface of the AEMs [53,62,64] indicate that the water splitting does not take place in the solution but in the membrane phase. Furthermore, Simons [52–54,63] showed that (1) water splitting can be eliminated by methylation of the tertiary amines resulting in quaternary amines, (2) degradation of quaternary ammonium groups in strongly basic environment leads to tertiary amines, and (3) water splitting at CEMs can be obtained only when weak acids (proline, phenol) are present in the solution next to the membrane surface, or when the membrane contains weakly acidic groups, such as carboxylic acid [59]. Based on these results, Simons suggested that with AEMs the water dissociation is caused by reversible protonation of weakly basic groups (tertiary amines). For the BPM, both the cation- and anion-exchange groups of the membrane polymer adjacent to the interphase layer can react with the water molecules at the membrane surface by the following mechanisms for water dissociation [59,63]:



and



where

$B$  is a neutral base

$BH^+$  is the catalytic active center (usually the AEM fixed charged group)

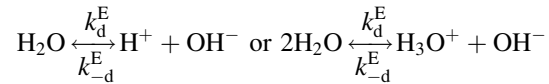
$A^-$  is the CEM fixed charged group

$AH$  is a neutral acid

#### 21.2.3.2.3 Global Model

This water dissociation model developed by Strathmann et al. [59] is described as being a combination of the second Wien effect, the protonation–deprotonation phenomena of functional groups in the membrane, and the reaction zone thickness  $\lambda$ . This model was developed under some assumptions [59]:

- Water dissociation occurs in the transition or depletion layer of the membrane and the dissociated ions removed from this region are replenished by the following water dissociation equilibrium:



- Water dissociation is accelerated by the electric field according to the second Wien effect, which describes the influence of a strong electric field on the water dissociation rate constant  $k_d^E$ , while the recombination rate constant  $k_{-d}^E$  is not affected by the electric field:

$$\frac{k_d^E}{k_d^0} = \left(\frac{2}{\pi}\right)^{1/2} (8b)^{-3/4} \exp\left[(8b)^{1/2}\right]$$

- The generated protons and hydroxyl ions are removed from the transition region by migration and the consumed water can be compensated timely by diffusion from the bulk solution.
- The electric current is calculated from the migration flux of either protons or hydroxyl ions.
- The voltage drop across both anion- and cation-exchange layers of the BPM is neglected, so that voltage across a BPM is equal to that across the transition layer  $U^{tr}$ , and the driving force for the migration of protons and hydroxyl ions is  $U^{tr}/\lambda$ , since the Donnan potential is in equilibrium with the diffusion of ions into the transition region.

Hence, according to Strathmann et al. [59], under the influence of a low-electric field, the salt ions ( $\text{Na}^+$ ,  $\text{K}^+$ ,  $\text{Cl}^- \dots$ ) initially present in the transition layer of the BPM migrate out of the transition region between the two ion-exchange layers. These ions are replaced by salt diffusing and migrating from the bulk solution into the transition region resulting in a steady state with a constant salt concentration in the transition region (Figure 21.4, step 1). When the electric field is increased, the migration from the transition region can no longer be compensated by the diffusive flux into the transition region. In fact, the transition layer becomes completely depleted of salt ions, since all salt ions were removed from the transition region, and a limiting current density is reached (Figure 21.4, step 2). The limiting current density depends on the permselectivity of the BPM as well as on the diffusion

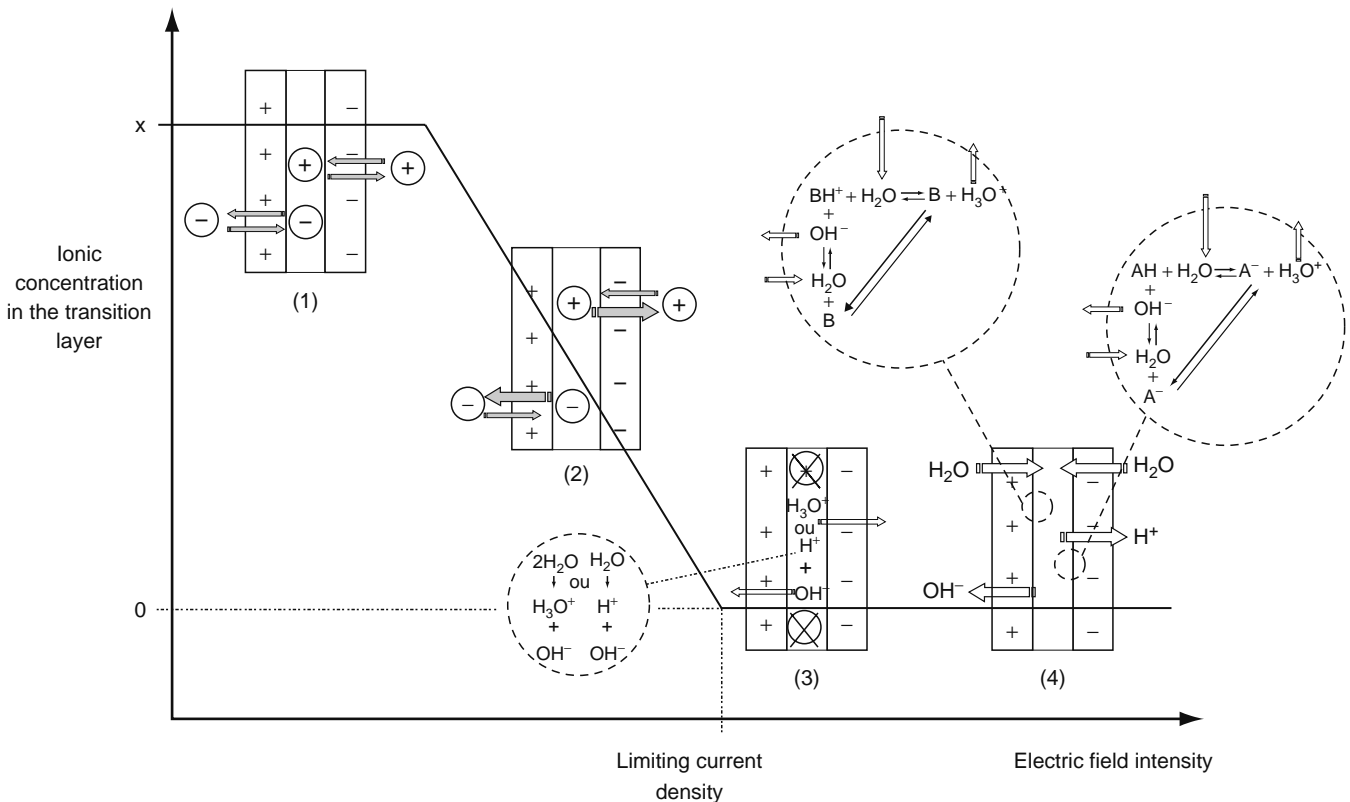


**FIGURE 21.4** Exchange mechanisms leading to water molecule dissociation inside BPM. (Adapted from Bazinet, L., *Industries Alimentaires et Agricoles*, 10, 7, 2003.)

coefficient of the salt in the membrane. When limiting current density is exceeded, water dissociation begins and the current is now carried by protons and hydroxyl ions. These ions are available in very low concentrations ( $10^{-7}$  mol L<sup>-1</sup>) in completely demineralized water. The protons and hydroxyl ions removed from the transition region are replenished by the water dissociation equilibrium (Figure 21.4, step 3). This induces a water concentration gradient between the transition layer and the adjacent compartments, which results in diffusion of water molecules into the hydrophilic layer (Figure 21.4, step 4) [65].

In the BPMs, the water splitting takes place in a very small region of the monopolar ion-exchange layer where uncompensated fixed charges exist [66]. The protonation and deprotonation can take place at basic and acidic groups. According to the global model, the authors demonstrated that for strongly basic groups, the protonation is very fast but the deprotonation is very slow, so that the groups in the membrane remain in the protonated form. For strongly acidic groups, all groups remain in the dissociated, deprotonated form. Consequently, the proton-transfer reactions are capable of explaining the enhanced water dissociation. Because of their higher mobility, the protons will first move faster than the hydroxyl ions. This disturbs the electroneutrality in the transition layer and leads to an additional electric field, which increases the migration of the hydroxyl ions and slows down the protons. The thickness of the transition region between the ion-exchange layers, which includes the reaction zone, is a few nanometers. Due to the roughness of the polymer surfaces, in some cases there might be thin neutral regions (water layer) between the ion-exchange layers. The presence of these regions depends on the production of the BPM.

### 21.2.3.3 Catalysts for Improving Water Dissociation

The theoretical potential to achieve the water-splitting capability is 0.83 V at 25°C. Due to the addition of catalysts, the actual potential drop across a BPM is quite close to this being in the range 0.9–1.1 V for current densities between 50 and 150 mA/cm<sup>2</sup>, which is the general region of practical interest. Examples are the iron(III) as presumably introduced in the cation permeable layer of the Tokuyama Soda membrane [67], and the chromium(III) ion used in the WSI membrane [68,69]. The value of the membrane potential drops equates to theoretical energy consumptions of the order of 600–700 kW h/ton of NaOH. Of course, the actual energy consumptions are significantly higher because of the ohmic resistances in the other cell stack components, in practical operating units.

To enhance water molecule dissociation in BPM, catalysts are required to reduce the electric potential of a BPM. The addition of a catalyst in the contact or transition region increased the water dissociation rate for a fixed electric potential across this region because the activation energy of the overall dissociation reaction is reduced [70]. Catalysts provide alternative reaction paths for the dissociation reaction by forming very reactive, activated complexes [54,69]. The water dissociation is a disproportionation or proton-transfer reaction that is catalyzed by weak acids and bases [45].

It is assumed that the best catalytic effect can be achieved if the  $pK_a$  or  $pK_b$  value of the interphase material is close to 7 [71]. Some weak ion-exchange groups such as tertiary amines, phosphoric acid, carboxylic acids, or pyridine show the required dissociation constant or  $pK_a$ -values. Certain heavy metal ion complexes, such as chromium(III)- or iron(III)-complexes, provide the required catalytic water dissociation effect. In principle, there are many more suitable metal ions available. The metal ions or complexes are immobilized by either including an insoluble salt in the casting solution of the interface layer between the ion permeable layers or by converting a soluble form by a follow-up treatment [45]. An additional requirement for the catalytic material is to be effective and stable for a long period. It must also remain in the interphase, where it is the most active, for the anticipated lifetime of the membrane.

Some metal hydroxides such as chromium(III) and iron(III) hydroxide are suited to be deposited as catalyst in the interphase between the cation- and anion-exchange layers of the BPM. Other catalytic components used in the preparation of BPMs such as tertiary amines or phosphoric acids are generally directly bonded to the polymer matrix of the membrane [45,72]. The most commonly used catalytic components in BPMs are listed in Table 21.1.

**TABLE 21.1**  
**Main Catalysts Used in BPMs**

Material	Remarks	$pK_a$ -Value	References
Cr(OH) <sub>3</sub>	After treatment in OH <sup>-</sup> , and as salt in the cation-exchange layer or the interphase		[69,73]
Fe(OH) <sub>3</sub>	Applied as salt in the cation-exchange layer or interphase		[67]
-NR <sub>2</sub> /-NH <sup>+</sup> R <sub>2</sub> (tertiary amines)	Tertiary amines bond onto the matrix of the anion-exchange layer	≈9–10	[74,75]
Sn or Ru ion			[67,68]
R-PO <sub>2</sub> H <sup>-</sup> /-COO <sup>-</sup>	Bond to the matrix of the cation-exchange layer	≈7	[76]
R-COOH/-COO <sup>-</sup>		4.8	[77]
Pyridine		5.2	[77]

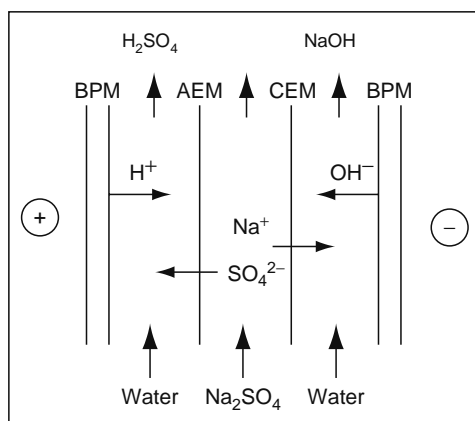


FIGURE 21.5 Generation of acid and base from a salt. The three-compartment configuration.

### 21.2.3.4 EDBM Configurations

The configuration of the EDBM process depends on the application. Typical use of BPM is in the treatment of concentrated salt solutions such as  $\text{Na}_2\text{SO}_4$  from the chemical industry to produce  $\text{H}_2\text{SO}_4$  and  $\text{NaOH}$ . A cell system consists of an anion, a bipolar, and a CEM as a repeating unit. In this case, the configuration is a three-compartment EDBM as illustrated in Figure 21.5. This elementary cell is repeated and placed between two electrodes. The  $\text{Na}_2\text{SO}_4$  solution flows between the CEM and AEM. When direct current is applied, water dissociates in the BPM to form the equivalent amounts of  $\text{H}^+$  and  $\text{OH}^-$  ions. The  $\text{H}^+$  ions flow through the cation-exchange side of the BPM and form  $\text{H}_2\text{SO}_4$  with the sulfate ions provided by the  $\text{Na}_2\text{SO}_4$  solution from the adjacent cell. The  $\text{OH}^-$  ions permeate the anion-exchange side of the BPM and form  $\text{NaOH}$  with the sodium ions permeating into the cell from the  $\text{Na}_2\text{SO}_4$  solution through the adjacent CEM. The final result is the production of  $\text{NaOH}$  and  $\text{H}_2\text{SO}_4$  from  $\text{Na}_2\text{SO}_4$  at a significantly lower cost than by other methods.

There are applications where high purity of both acid and base is not possible to be obtained, or even, may generate problems during the process. For example, in the splitting of a salt from a weak acid (sodium acetate), the pure acid is weakly dissociated, so its conductivity is low. It would not therefore be practical to achieve the splitting of sodium acetate in a three-compartment cell. Instead, a two-compartment cell with the acetate solution flowing between a BPM and a CEM is recommended (Figure 21.6a). When the conversion of the salt stream reaches 95%, the conductivity becomes very low. So, it is not possible to pursue the EDBM more deeply. The EDBM is then stopped and the residual  $\text{Na}^+$  ions are removed using cation-exchange resins. In a similar way, an ammonium or amine salt can be treated in a two-compartment cell with an AEM instead of a CEM (Figure 21.6b).

Moreover, the performance of the two-compartment cell can be enhanced by the introduction of a third chamber. For example, the multichamber cation cell now uses two CEMs [23]. In operation the salt solution is first fed to the chamber between the two CEMs and then passes to the acid compartment. This gives a salt/acid stream with a higher concentration of acid than the standard two-compartment cell. The multichamber anion cell is used in a similar way to that of the cation cell. Clearly, this multicell arrangement incurs a greater electrical energy cost due to the higher cell voltage than that needed in the two-compartment cell.

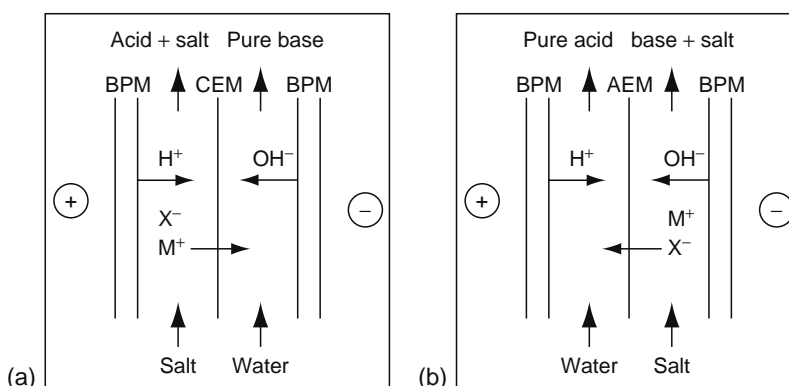


FIGURE 21.6 Two-compartment EDBMs for production of (a) only pure base and (b) only pure acid.

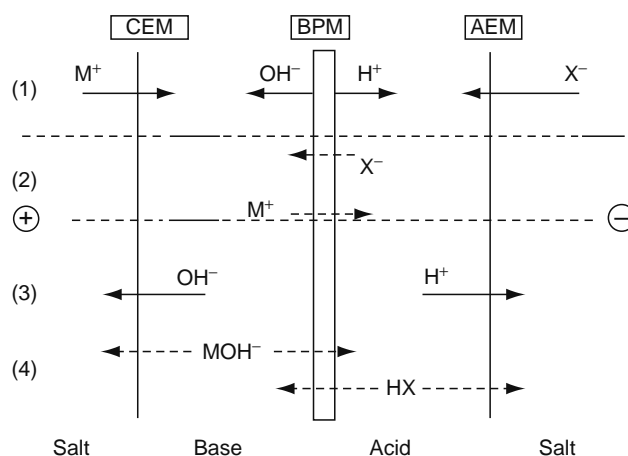


FIGURE 21.7 Processes occurring during EDBM.

### 21.2.4 FEATURES OF EDBM, DIFFERENCE FROM THE CONVENTIONAL ELECTROLYSIS, LIMITS

The main features of EDBM are

- The BPM can dissociate water into  $H^+$  and  $OH^-$  ions.
- Since no gases are generated during water splitting, the energy consumption is very low.
- Since no electrochemical reactions are running, there is no oxidation or reduction, which may generate undesirable products.
- BPM can be used in association with AEM and CEM to produce acids and bases from salts by electrodialysis.

However, and as for all the processes, EDBM presents limits [23]. The performances of a water splitter are controlled by the permselectivities of the individual component membranes and by diffusive transport. Figure 21.7 illustrates the various processes which contribute to the overall current efficiency. Zone 1 concerns the specific process which generates acid and base from salt and water. Competing with this are the undesirable processes, which reduce the current efficiency. Zone 2 represents the loss of permselectivity of each homopolar layers of the BPM. In the three-compartment configuration (Figure 21.5), this factor directly acts on the purity of the acid and base produced. Zone 3 represents the loss of permselectivity of the associated homopolar membranes. Zone 4 concerns the diffusional losses due to the concentration gradients, which significantly occur for poorly ionized small molecules ( $HF$ ,  $NH_3$ ,  $SO_2$ , etc.).

### 21.2.5 CELL EQUIPMENT AND PROCESS CONFIGURATIONS IN EDBM

The principle of the cell design is depicted in Figure 21.8.

The technical requirements of an EDBM module should fulfill the following criteria:

1. Minimal distance between membranes (0.5–1 mm) to reduce the ohmic drop
2. Appropriate hydrodynamic conditions with high superficial velocity for a better control of the concentration polarization
3. High value of the ratio (membrane area/volume of the EDBM module) for a reasonable material flux
4. Avoiding all leakages between the compartments
5. Reducing the short circuits and parasitic currents

From a practical point of view, a filter press module of 30–50 elementary cells with a geometric surface area of 0.3–0.5  $m^2$  seems to be a good configuration [45]. The corrosion stability of the EDBM stack components such as bodies, frame, turbulence promoters, gaskets, and electrodes is of great importance. The corrosion resistance of the electrodes and of course their prices are also decisive elements. Stainless steel is the cheapest choice of material for anode and cathode and is suitable in weakly alkaline or neutral aqueous electrolytes [66]. Nickel electrodes are much more expensive and used when an enhanced passivity is required. Titanium electrodes have excellent stability against acid and slightly basic media. A coating layer of metal oxides (such as  $RuO_2$ ) reduces significantly the overpotential for oxygen or chlorine evolution.

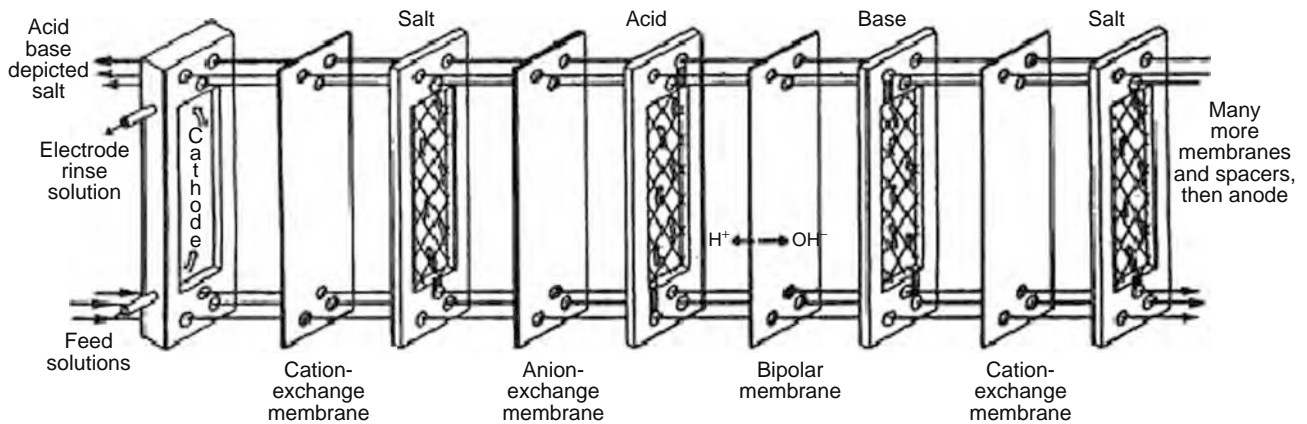


**FIGURE 21.8** EDBM cell assembly. (Reprinted with permission from Kemperman, A.J.B., Ed. *Handbook of Bipolar Membrane Technology*, Twente University Press, Enschede, The Netherlands, 2000. Copyright 2000 Twente University Press, p. 162.)

Three common process configurations are used.

1. The batch mode for small- and medium-scale applications (Figure 21.9). In this case, the process can be easily adjusted to the individual demands with respect to product concentration and mass flow. However, it requires a high expenditure for buffer tanks and tubing and instrumentation.
2. The feed and bleed mode for medium- and large-scale applications (Figure 21.10). In this case, the process can also be easily adjusted to the individual demands with respect to product concentration and mass flow. It is appropriate for a

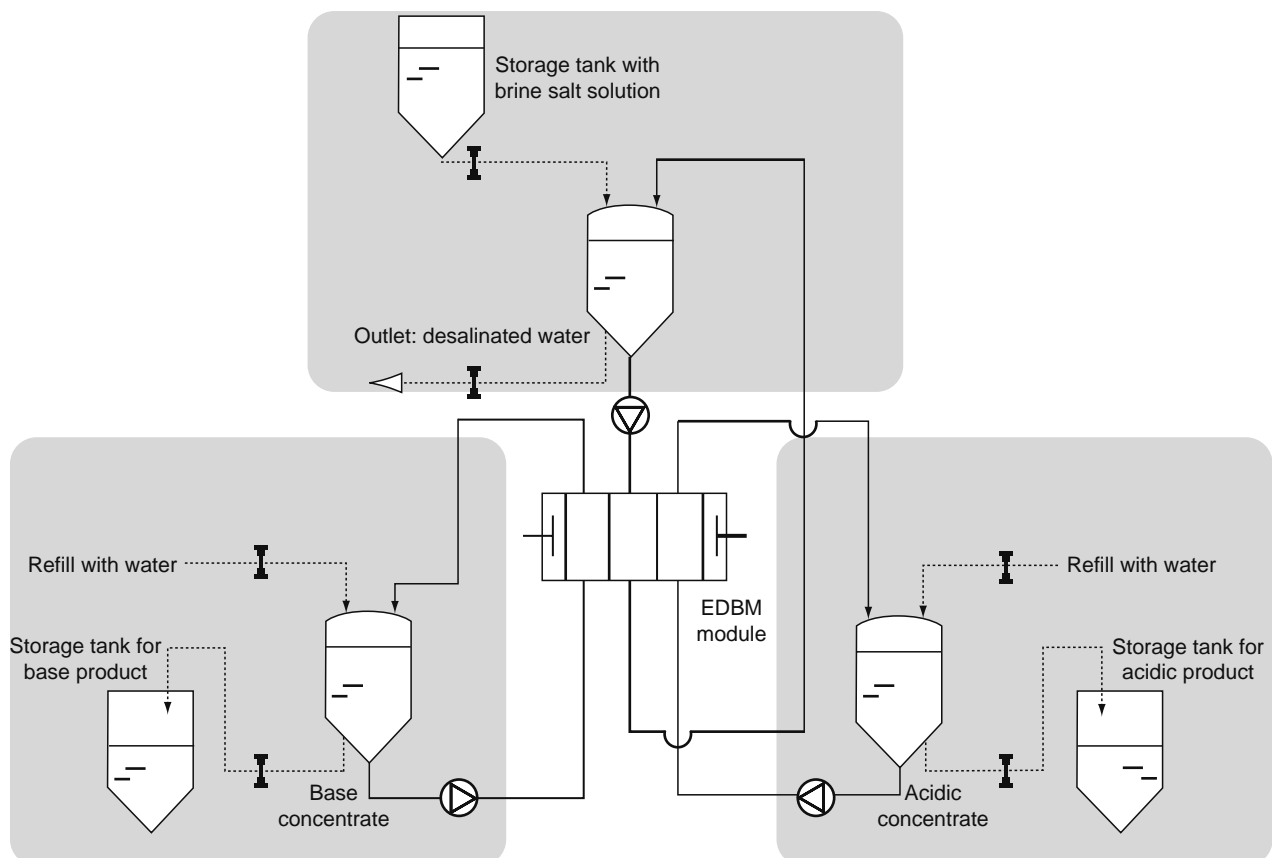


**FIGURE 21.9** EDBM setup for batch mode run. (Reprinted with permission from Kemperman, A.J.B., Ed. *Handbook of Bipolar Membrane Technology*, Twente University Press, Enschede, The Netherlands, 2000. Copyright 2000 Twente University Press, p.182.)

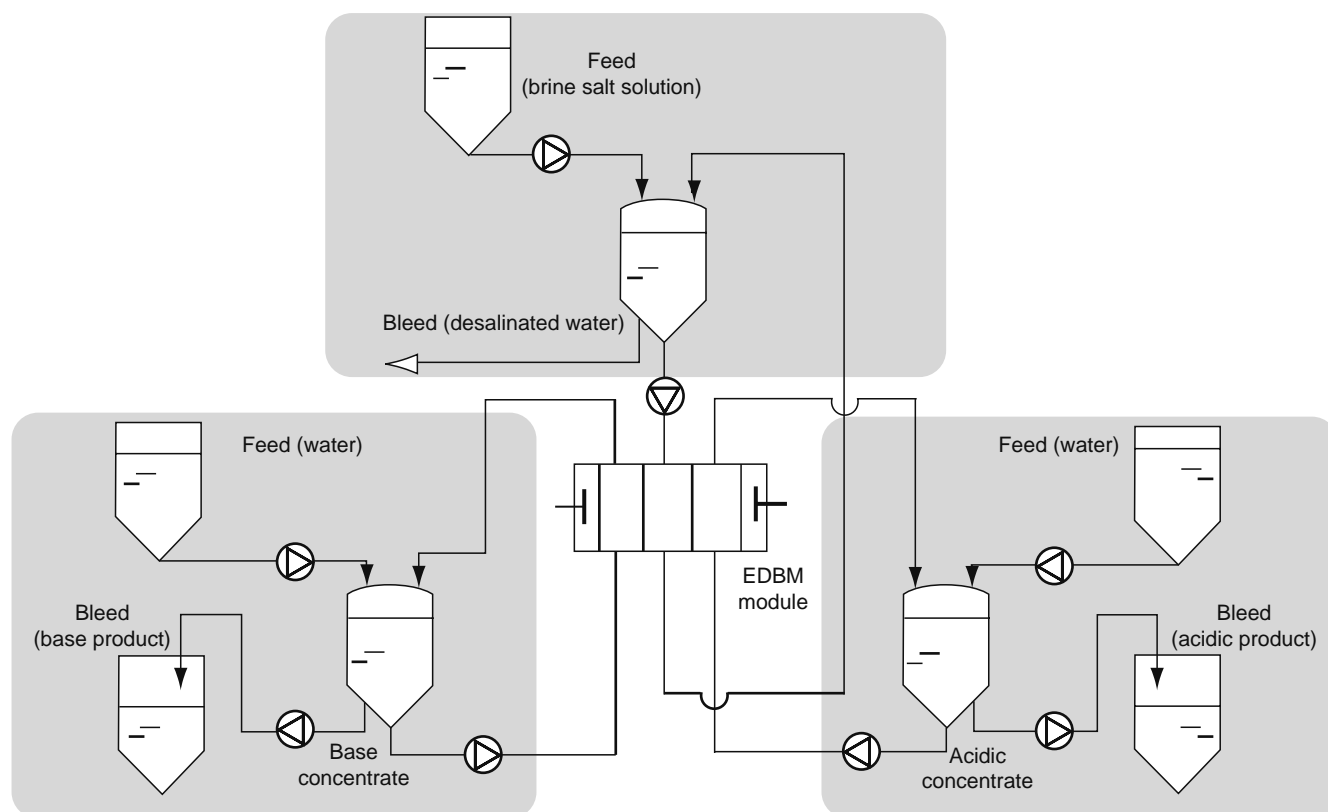


**FIGURE 21.10** EDBM setup for feed and bleed mode run. (Reprinted with permission from Kemperman, A.J.B., Ed. *Handbook of Bipolar Membrane Technology*, Twente University Press, Enschede, The Netherlands, 2000. Copyright 2000 Twente University Press, p. 183.)

continuous production and steady operation conditions. However, it requires also a high expenditure for buffer tanks and tubing and instrumentation.

3. The single-pass continuous flow configuration (Figure 21.11) for medium- and large-scale applications. This mode is suitable for a continuous production and is cheaper than the two previous for buffer tanks, tubing, process control instrumentation, and energy consumption. However, a later adjustment of unit to altered process conditions is not easy.

### 21.2.6 SCALING-UP AND EXPLOITATION PARAMETERS OF THE BPM TECHNOLOGY

To optimize a BPM process, the following parameters have to be respected:

- Purity of the effluent to be treated: organic pollution and multivalent cations must be avoided: (1) IEM and BPM swell in the presence of aromatic compounds and (2) metallic hydroxides precipitate in the membranes when the divalent cation concentrations reach 1 ppm.
- Concentrations of the products: Due to the proton leakage through associated AEMs, the maximum concentration of mineral acid products is 2–3 and 5 N for organic acids. Due to the hydroxide ion leakage through the associated CEM, the maximum concentration of the base produced is 4.5 N.
- The voltage drop per elementary cell has to be maintained in the range 1.5–3 V for 1000 A/m<sup>2</sup>. The applied current density is in the range 50–100 mA/cm<sup>2</sup>.
- The minimal conductivity of the salt loop is 20 mS/cm at 40°C.
- The conversion ratio for organic salts is in the range 95%–98%.

Taking into account the previous recommendations, scale-up of EDBM is really quite simple. In most cases, the operating conditions in a lab-scale EDBM can be reproduced on a commercial scale.

The product concentration (i.e., wt% NaOH resp, HCl) influences the energy demand and throughput. The higher the product concentrations, the lower is the throughput and the higher the energy. The purity of the product is dependent on its

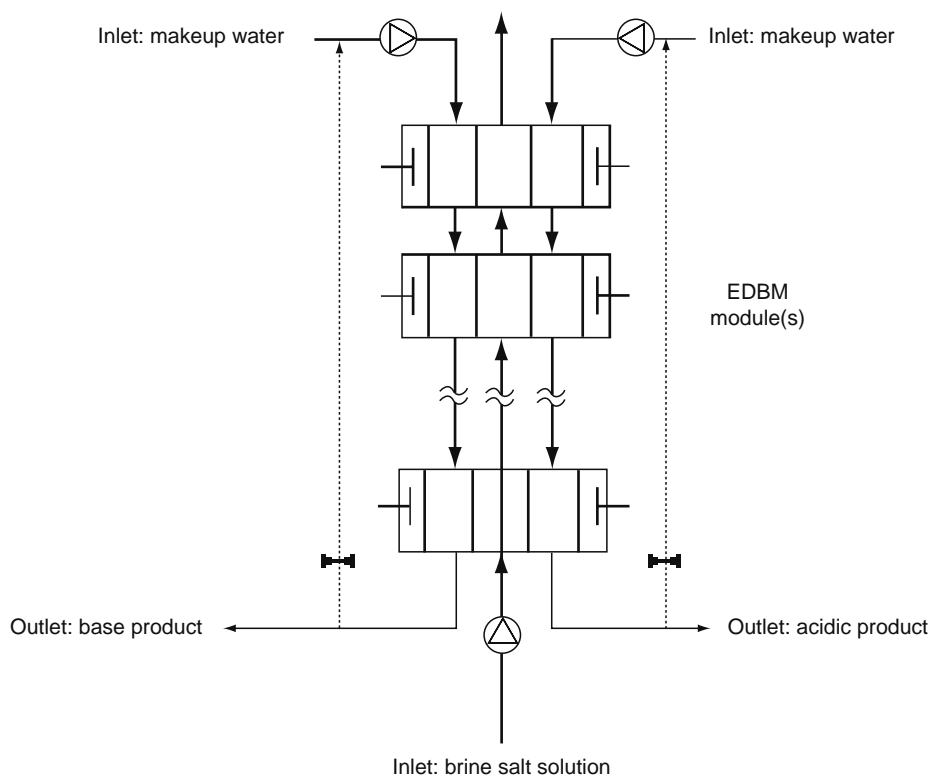


**FIGURE 21.11** EDBM setup for single-pass flow configuration with hydraulic staging. (Reprinted with permission from Kemperman, A.J.B., Ed. *Handbook of Bipolar Membrane Technology*, Twente University Press, Enschede, The Netherlands, 2000. Copyright 2000 Twente University Press, p. 184.)

concentration. The higher the concentration, the higher is the salt contamination of the acid and base. To get high-purity products at a high throughput level, the current density should be as high as possible ( $>100 \text{ mA/cm}^2$ ). Moreover, a well-designed pretreatment is of importance to reduce scaling and fouling.

An example of performance of an EDBM pilot plant is reported in Table 21.2 [79]. It concerns the production of caustic soda from an NaCl waste stream from an amino acid production process. Apart from organic components, this salt stream

**TABLE 21.2**  
**Performance of the EDBM Pilot Plant**

Current density	1000 A/m <sup>2</sup> (100 mA/cm <sup>2</sup> )
Current efficiency (CE) <sup>a</sup>	60%–70% with respect to Na <sup>+</sup>
Total membrane area	1.78 m <sup>2</sup>
Specific energy consumption (SEC) <sup>b</sup>	2.8 kW h/kg NaOH
Throughput	1.5 kg NaCl/(m <sup>2</sup> h)
Potential drop per repeating unit cell	2.7 V
HCl concentration	5.1 wt%
Na <sup>+</sup> contamination in HCl product	1150 ppm
NaOH concentration	10 wt%
Cl <sup>-</sup> contamination in NaOH product	178 ppm

*Source:* Adapted from Engel, D., Lehmann, T.H., Weissland, G., and Picarri, J., Preprints of the Aachener Membrakolloquium, *GVC VDI-Gesellschaft Verfahrenstechnik und Chemieingenieurwesen*, Aachen, 1993.

<sup>a</sup> The CE is defined for each transported ionic species. It is the ratio of the actual molar transport calculated by Faraday's law with the actual current density  $j$  according to  $\text{CE} = F \cdot z_i \cdot n_i / j$  with  $n_i$  the molar flux density (mol/m<sup>2</sup> s) and  $F$  the Faraday's constant.

<sup>b</sup> The SEC is given by the relation  $\text{SEC} = \Delta E \cdot I = \Delta E \cdot j \cdot A = \Delta E \cdot (z_i \cdot F \cdot n_i / \text{CE}) \cdot A$  with  $I$  the current (A),  $A$  the total membrane area (m<sup>2</sup>),  $\Delta E$  the potential difference (V) applied to the EDBM unit.

**TABLE 21.3**  
**Some Applications of EDBM Process**

*Pollution control/resource recovery*

HF/mixed acid recovery	Stainless steel pickle liquor recovery HF/NaOH recovery from spent aluminum potlinings Fluorosilicic acid conversion to HF, SiO <sub>2</sub> Fluoride emission control in chemical processing KF conversion from alkylation process
Sulfate recovery	Battery acid recovery Waste sodium sulfate conversion Sodium sulfate conversion in rayon manufacture
Nitrate recovery	Ammonium nitrate conversion from the uranium processing KNO <sub>3</sub> conversion
Amine recovery	Recovery of a catalyst used to cure epoxy resins in Al coating moulds
Pulp and papers	Sodium alkali recycling in pulping and bleaching operations
Flue gas desulfurization	Soxal process SO <sub>2</sub> recovery Dry sodium scrubbing alkali recovery
<i>Chemical processing</i>	
Organic acid production recovery	Acetic, formic, acetylsalicylic, and organic acids Aminoacids
Ion-exchanger regeneration	Production of highly generated ion-exchange resins
Brine acidification in chlor-alkali industry	
Wastewater treatment from amino acid processing	Salt splitting of NaCl
Potassium and sodium mineral processing	KCl conversion Solution mining of trona and subsequent sodium alkali production Sodium alkali production from natural brines and solid trona
Sodium methoxide production	EDBM in methanolic solutions
Methanesulfonic acid production	EDBM of sodium methanesulfonate
High-purity water production	Continuous electrodeionization for high-purity water production

contains about 500 ppm of Ca<sup>2+</sup>, Mg<sup>2+</sup> ions. A pretreatment including polishing with ion-exchange resins reduces this amount to less than 0.5 ppm. The waste stream is then processed in a three-compartment EDBM unit designed for both batch and feed and bleed mode. The total membrane area is 1.78 m<sup>2</sup> (16 repeating unit cells, each membrane with an area of 0.12 m<sup>2</sup>).

### 21.3 MAIN APPLICATIONS OF THE EDBM

A large number of applications of EDBM have been identified. A classification under two broad categories of pollution control/resource recovery and chemical processing is reported in Table 21.3 [45].

This chapter deals with developments of EDBM technology in food industries and only a short review is devoted to other application domains. The oldest industrial application of EDBM in the pollution control/resource recovery is the recovery of HF and HNO<sub>3</sub> from a stream containing KF and KNO<sub>3</sub> generated from a pickling bath in a steel plant. This first commercial use of BPM began operations in 1987 at Washington Steel in Pennsylvania [80]. This application was stopped in 2000. Among the other examples, one can quote the regeneration of sodium sulfate in a rayon plant [23], a gas absorption process for the conversion of amine in air, the treatment of flue gas for removal of SO<sub>2</sub> [81], the electrodialytic dissociation of alcohols to produce sodium methoxide [82], or the recovery of methanesulfonic acid from sodium methanesulfonate solutions [45]. While the applications of EDBM in the pollution control/resource recovery seem to reach a stage, those concerning chemical processing and food industries are growing [78].

### 21.4 APPLICATIONS OF EDBM TO FOOD INDUSTRIES

In 1990, Hatzidimitriu [83] patented a process for adjusting the pH of aqueous fluids. This process can be used for adjusting the acidity of an edible fluid (specifically sugar syrups, fruit and vegetable juices, wines, sauces, and tomato paste) by electrodialysis in a cell containing membrane pairs comprising a BPM and an ion-selective membrane. More specifically, Dykalo et al. [84] used bipolar membrane ED to control the acidity of dairy products containing an aqueous phase. To control

the pH of dairy products, the solution was circulated on the cationic side of the BPM, where the  $H^+$  ions are generated, to lower the pH and on the anionic side of the BPM, where  $OH^-$  ions are generated, to raise the pH. These applications point the way to new applications for BPMs beyond the production of acids and bases. Recently, EDBM has been applied to protein precipitation and purification, enzymatic browning inhibition, simultaneous recovery of coagulant agent and protein, fruit juice deacidification, and dairy wastewater purification.

### 21.4.1 PRODUCTION OF SOY PROTEIN ISOLATE

A large proportion of the soy protein used in the food industry is in the form of protein isolates (>90% protein). Separation of proteins by isoelectric precipitation at the isoelectric pH range 4.2–4.6 is the recognized industrial process. The isoelectric point is the pH value at which the net global charge of the protein is neutral. At this pH value, the solubility of the protein is minimal and can result in complete precipitation.

The conventional precipitation procedure involves five steps: extraction, precipitation, washing, resolubilization, and drying. The defatted soy flakes are dissolved in water at  $pH\ 9 \pm 2$  in a ratio ranging from 6:1 to 20:1 at  $<80^\circ C$ . The extraction step usually takes ~30 min. Once the extraction is finished, the proteins are precipitated by lowering the pH of the solution to the isoelectric point, ~4.5, using hydrochloric acid. Centrifugation is used to separate the protein-containing curd from the supernatant (or whey) containing the soluble materials and low-molecular-weight compounds. The curd is then washed with water to remove soluble impurities (salts and sugars). After washing, it is neutralized with NaOH to obtain a proteinate, a soluble form of protein. The final product is spray dried, and packaged as a dry material [2].

Most commercial soy protein products have been developed from the acid-precipitated fraction [85]. However, local extremes in pH can cause irreversible denaturation of the proteins [85]. The disadvantages of this method include denaturation of protein on exposure to alkali and acid treatment, high-ash content, and alteration of protein solubility after rehydration [86].

In this context, Bazinet et al. [41] developed a procedure using BPMs to precipitate soy proteins (Figure 21.12a). The protons generated by the BPM come into contact with the protein, bringing them to their isoelectric point resulting in selective separation. Centrifugation can then be used, as in the conventional process for separation of the proteins. To lower the pH of the protein solution, this solution was circulated on the cationic side of the BPM. The pH of the protein solution was lowered from 8.0 to 4.5 in a cell of  $100\text{ cm}^2$  effective electrode surface, at a constant current of  $25\text{ mA/cm}^2$ . Lowering the pH to 4.5 allowed a precipitation of 95% protein. The energy and electroacidification parameters are affected by various factors such as the number of BPMs, the initial concentration of soy protein concentrate (SPC) and KCl in the protein solution, and the temperature.

Electroacidification of soy proteins was related to the generation of  $H^+$  at the surface of BPMs, and increasing the membrane surface accelerated the electrochemical precipitation quasi-linearly: Doubling the number of membranes decreases, by about one-half, the duration of the electroacidification procedure. Increasing the number of BPMs in the electro dialysis cell increases the electrical efficiency of the system while decreasing the time required, but not in a linear fashion. The stacking has no effect on the final protein precipitation rate. The time required to lower the pH to 4.5 is determined primarily by the SPC concentration and the temperature [41]. This is due to the larger quantity of  $H^+$  required from the dissociation of water to overcome the higher buffering capacity associated with a higher protein concentration [87].

When the initial SPC concentration is increased, a change in the percent soluble protein as a function of pH is observed: at 15 g/L a quasi-linear precipitation occurs whereas at 60 g/L the protein precipitation curve takes on a sigmoidal form. From initial pH to 7.0, no real difference is noted; the percent soluble protein was about 100%. A high-protein concentration slows the electroacidification process as a result of the intrinsic buffering capacity of the protein [88,89]. However, the final percent soluble protein is not affected by an increase in the SPC concentration.

Temperature is another factor affecting EDBM. By increasing the temperature, the mobility of the ions is increased and consequently the overall resistance of the system is decreased [90]. The energy required to decrease the pH to 4.4 rises as the SPC concentration is increased, and drops with an increase in the KCl concentration (Table 21.4). With an increase of  $25^\circ C$  in temperature (from  $10^\circ C$  to  $35^\circ C$ ), a 53% decrease in energy consumption was observed. By expressing the energy consumed relative to the production of 1 kg of protein isolate, a drop in energy is observed with an increase in the SPC concentration. In parallel, a drop in energy consumed occurs as the KCl concentration and the temperature rise. This indicates that the SPC concentration and the temperature are the primary factors influencing the energy consumption of the BPM electroacidification cell. At low SPC concentrations, a high level of KCl will improve the overall efficiency of the system. The effect of the SPC concentration is not related to the protein concentration but rather to its intrinsic salt concentration. The proteins have a minor effect on the energy efficiency compared to salts, because the proteins represent a minute proportion of the electrical charges in solution, and possess an extremely limited mobility. In fact, the effect of the SPC concentration is related to a high concentration of minerals, approximately 5% of the dry weight of SPC [91], of which 50% is potassium [91]. Thus, an increase in salt concentration results in a lower resistance of the medium because the added salt supplies the ions necessary to maintain the conductivity of the solution during the production of  $H^+$  by the membrane. The resistance of the solutions depends mainly on the concentration of electrolytes in the medium [92]. Increasing the temperature increases the energy efficiency of the

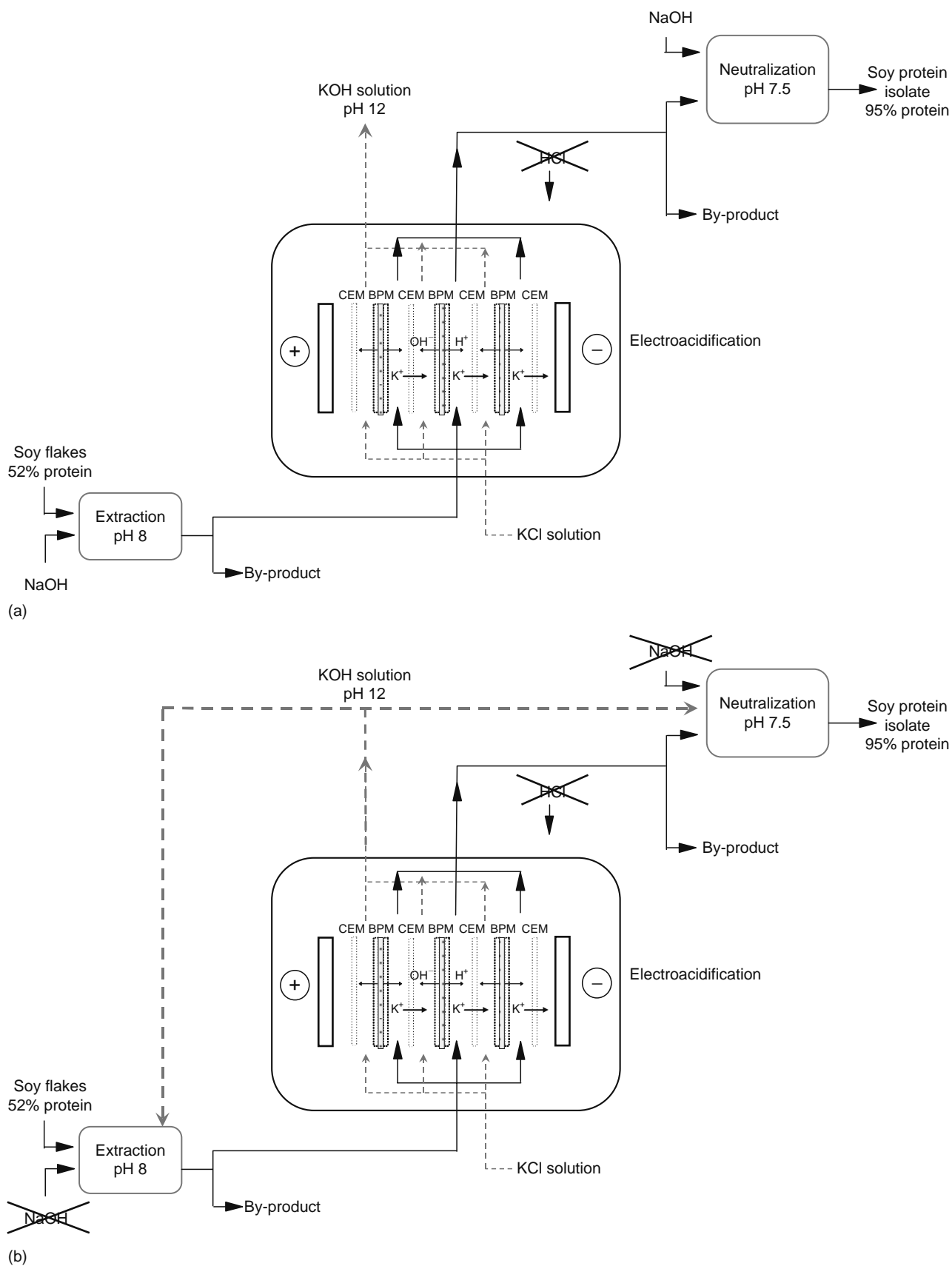


**FIGURE 21.12** BPM electroacidification cell configuration. (a) Process for soy protein isolate production and (b) modified process for production of soy protein isolate. BPM, bipolar membrane; CEM, cation exchange membrane.

**TABLE 21.4**  
**Energy and Relative Energy Consumptions of EDBMs Run with Different Initial Concentrations of SPC and KCl, and at Different Temperatures and Number of BPMs Stacked**

		Duration (min)	Energy (kJ)	Relative Energy (kW h/kg of Isolate)
SPC (g/L)	15	14.7	113	0.610
	30	27.9	187	0.496
	60	54.9	345	0.463
KCl (M)	0.06	32.5	238	0.577
	0.12	32.5	214	0.499
	0.24	32.5	193	0.493
Temperature (°C)	10	30.4	283	0.728
	20	30.2	177	0.455
	35	26.8	133	0.371
Number of BPMs	1	81.3	237	0.639
	2	43.2	192	0.517
	3	27.8	183	0.493
	4	22.1	188	0.507

Source: Adapted from Bazinet, L., Lamarche, F., Labrecque, R., and Ippersiel, D., *J. Agric. Food Chem.*, 45, 2419, 1997; Bazinet, L., Lamarche, F., Labrecque, R., and Ippersiel, D., *J. Agric. Food Chem.*, 45, 3788, 1997.

electroacidification procedure, but in a nonlinear fashion. This increase in efficiency is lower between 20°C and 35°C than between 10°C and 20°C and is related to an increase in ion mobility, the result of a decrease in viscosity brought about by the temperature increase [93]. Viscosity is one of the important parameters for a protein solution undergoing electroacidification, since it affects the hydrodynamics of the system. In an electroacidifier, a high viscosity changes the overall electrical resistance by slowing diffusion and migration of ions in the solution being treated [92].

The authors also compared the chemical and electrochemical acidifications to identify differences between both acidification procedures. During chemical acidification of protein solution, the conductivity increased, while it decreased in electroacidification. In fact, the addition of acid corresponds to an addition of H<sup>+</sup> and Cl<sup>-</sup> ions: their respective conductivities are 349.6 and 76.4 S cm<sup>2</sup> mol<sup>-1</sup> [94]. Consequently, this addition of ionic species contributes to an increase in the overall conductivity of protein solution (Figure 21.13). Electroacidification decreases the conductivity of the solution due to the

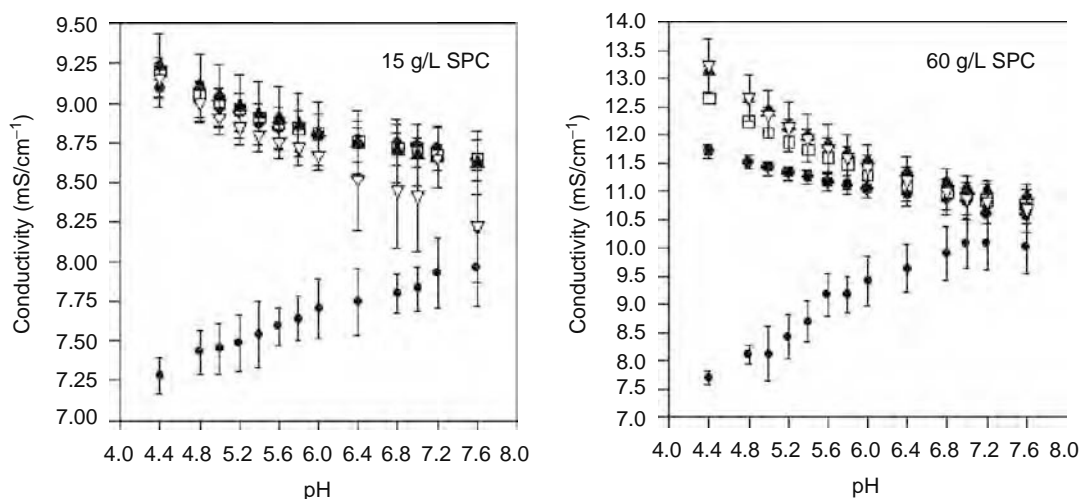


**FIGURE 21.13** Effect of SPC concentration and acidification procedure, 0.25 N HCl (●), 0.5 N HCl (□), 1.0 N HCl (▲), 2.0 N HCl (▽) and electroacidification (◐), on the conductivity measured during the pH decrease of electrochemical and chemical acidifications of soybean protein solutions, with 0.06 M KCl added and maintained at 25°C. (Reprinted with permission from Bazinet, L., Lamarche, F., Labrecque, R., and Ippersiel, D., *J. Agric. Food Chem.*, 45, 2419, 1997. Copyright 1998 American Chemical Society.)

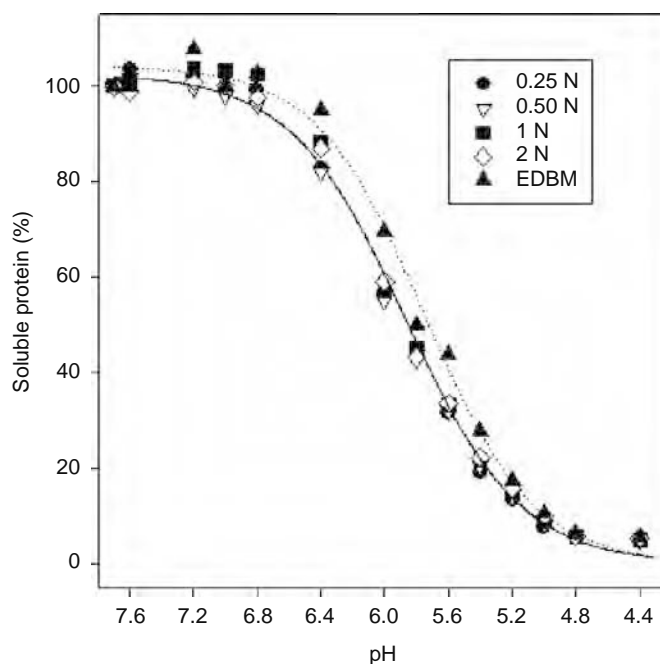


**FIGURE 21.14** Effect of acidification procedure on the percentage of soluble proteins measured during pH decrease of electrochemical and chemical acidification of soybean protein solution, with 0.06 M KCl and maintained at 25°C. (Adapted from Bazinet, L., Lamarche, F., and Ippersiel, D., *J. Agric. Food Chem.*, 46, 2013, 1998.)

desalination phenomenon by electro dialysis [8,95,96]. As the pH decreases, the variation of conductivity depends both on the SPC concentration and the acidification procedure. As the pH is dropped from its initial pH to 4.5, in electroacidification, the variation in conductivity is inversely proportional to the SPC concentration while, in chemical acidification, this variation is proportional (Figure 21.13) [88]. These effects are the results of an increase in buffering capacity of the protein solution coupled, in electroacidification with the migration of cationic species, and in chemical acidification with the addition of ionic species [88].

A comparison of the soluble protein evolution during the pH decrease revealed that there is a difference between the chemical and the electroacidification (Figure 21.14). The protein precipitation curve obtained during electroacidification shows a shift in comparison with those of chemical acidification levels; from initial pH to 6.8, the soluble protein percentage was about 100% for chemical and electrochemical acidification. At pH 6.4, a difference appears between the two procedures of acidification, with 85.1% and 94.9% of soluble protein, respectively, for chemical and electroacidification. This difference increases between pH 6.0 and 5.6 with 57.1% and 32.6%, respectively, of soluble protein for chemical acidification compared to 69.4% and 43.9% for electroacidification. Then, the difference drastically decreases until it disappears; at pH 5.2, 4.8, and 4.4 the soluble protein percentages were 14.5%, 5.7%, and 5.1% compared to 17.4%, 6.4%, and 5.5%, respectively, for chemical and electrochemical acidification. The final precipitation extent of protein is not influenced by the acidification procedure; however, the precipitation is slower during electroacidification. The difference in precipitation of protein between chemical and electrochemical acidification could be related to a lower local excess of acid in electroacidification. In fact, the conventional chemical acidification process to produce protein isolates is known to denature protein by local excesses of acid [85] while electroacidification was demonstrated to precipitate protein with a low extent of protein denaturation [40,92].

The variation of precipitation as a function of pH is related to the different precipitation profiles of the two protein fractions, 7 S and 11 S [97]. According to Thanh and Shibasaki [97], protein concentrations (up to 4%) are favorable for the separation of the two globulin fractions. They noted that the 7 S fraction is not very sensitive to an increase in protein concentration, whereas the 11 S fraction started to precipitate earlier with a higher protein concentration. This correlates with the large change in soluble protein observed for pH 6, a point close to the isoelectric point of the 11 S fraction and the inflection point of the protein solubility curves. The electroacidification process influences the precipitation curve of the 11 S fraction; the electroacidified 11 S fraction precipitation curve presents a slight shift in comparison with the chemical acidification curves (Figure 21.15a and 21.15b). The lower precipitation for the electroacidified proteins is the result of the lower extent of precipitation obtained for the 11 S fraction [88].

Separation of soy protein by EDBM has specific advantages over the conventional isoelectric precipitation used industrially for the production of soybean protein isolates. This technology does not use any added acids or bases during the process to adjust the pH of the protein solution, and the chemical effluents generated during the process could be reused at different stages in the

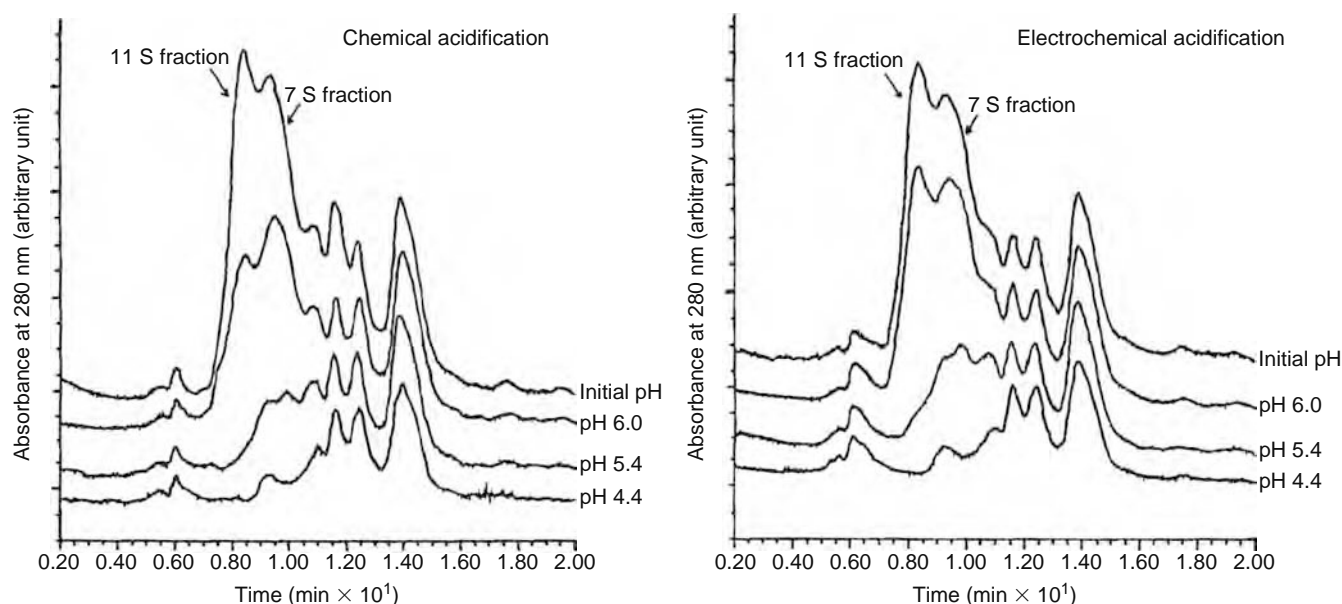


**FIGURE 21.15** Size exclusion HPLC chromatograms of (a) chemically and (b) electrochemically acidified soybean protein solutions, with 0.06 M KCl added and maintained at 25°C, at different pH values. (Reprinted with permission from Bazinet, L., Lamarche, F., and Ippersiel, D., *J. Agric. Food Chem.*, 46, 2013, 1998. Copyright 1998 American Chemical Society.)

process. The water consumption is decreased by reusing the effluents generated, and the cell electrical energy consumption for protein precipitation is low (~0.3–0.7 kW h/kg of isolate). After washing the precipitate, it is possible to resolubilize the proteins by reusing the sodium hydroxide generated on the anionic side of the BPM, or by recirculating the precipitated protein solution on the anionic side during the acidification of another protein solution on the cationic side of the BPM (Figure 21.12b). In addition, the chemical composition of bipolar-membrane electroacidified samples was demonstrated to be superior or equal to that of commercial standards, with functional properties comparable to these standards [40,92].

The application of soybean protein electroacidification at the industrial scale is limited because of gradual protein precipitation in the cell, which results in an increase of the cell resistance (decrease of the system efficiency) and loss of protein (decrease in yield). The blocking which can appear in EDBM of soybean protein is not a form of membrane fouling as in ultrafiltration and nanofiltration, but mainly due to spacer fouling, resulting from a nonoptimized hydrodynamic design of the electro dialysis cell. The fouling is due to the particles in suspension, which agglomerate in the spacers when their concentration is too high. An online centrifugation process has been proposed by Bazinet et al. [2] to allow the recovery of these particles and decreased fouling. More recently, Mondor et al. [98] proposed a combination of electroacidification and ultrafiltration to decrease this fouling.

#### 21.4.2 PRODUCTION OF ACID CASEINATE

Due to its nutritional quality and functional properties, casein is extensively used in the manufacturing of food products. However, pure casein can only be obtained by an insolubilization step followed by a centrifugation for a simple separation of the casein from the whey [99]. Two main types of casein are usually produced in the industry: rennet and acid caseins (Figure 21.16). In rennet casein, the underlying mechanism is identical to that of the production of cheese curd and depends on the unique sensitivity of the Phe<sub>105</sub>-Met<sub>106</sub> bond of  $\kappa$ -casein to hydrolysis by acid proteinases, the active components of rennet. For acid casein production, the three main procedures used are based on isoelectric precipitation of casein by chemical, physicochemical, or fermentation acidification [99–101]. Other techniques have been proposed for the production of acid casein: acidification of milk by ion-exchange plus acid [102] or by ion-exchange alone [103], electro dialysis of skim milk to pH 5.0 followed by acidification to pH 4.6 with acid [104], and acidification by water electrolysis at the surface of monopolar anion or CEMs stacked in an electro dialysis cell [105]. A specific advantage of these methods is the production of acid whey with reduced mineral content. This acid whey is more readily utilized than acid whey produced by the normal acidification process and may increase its value for further processing [101,106].

However, the procedures used in the dairy industry, rennet and acid casein, have the disadvantages to produce large volume of chemical effluents due to the addition of bases and acids during treatments, and to generate inherent risk linked to handling, stocking, and transportation of concentrated bases and acids. In acid casein production, milk pH is decreased to the isoelectric point of the casein by addition of strong acid (hydrochloric, sulfuric, nitric, lactic, etc.). H<sup>+</sup> concentration of milk is increased

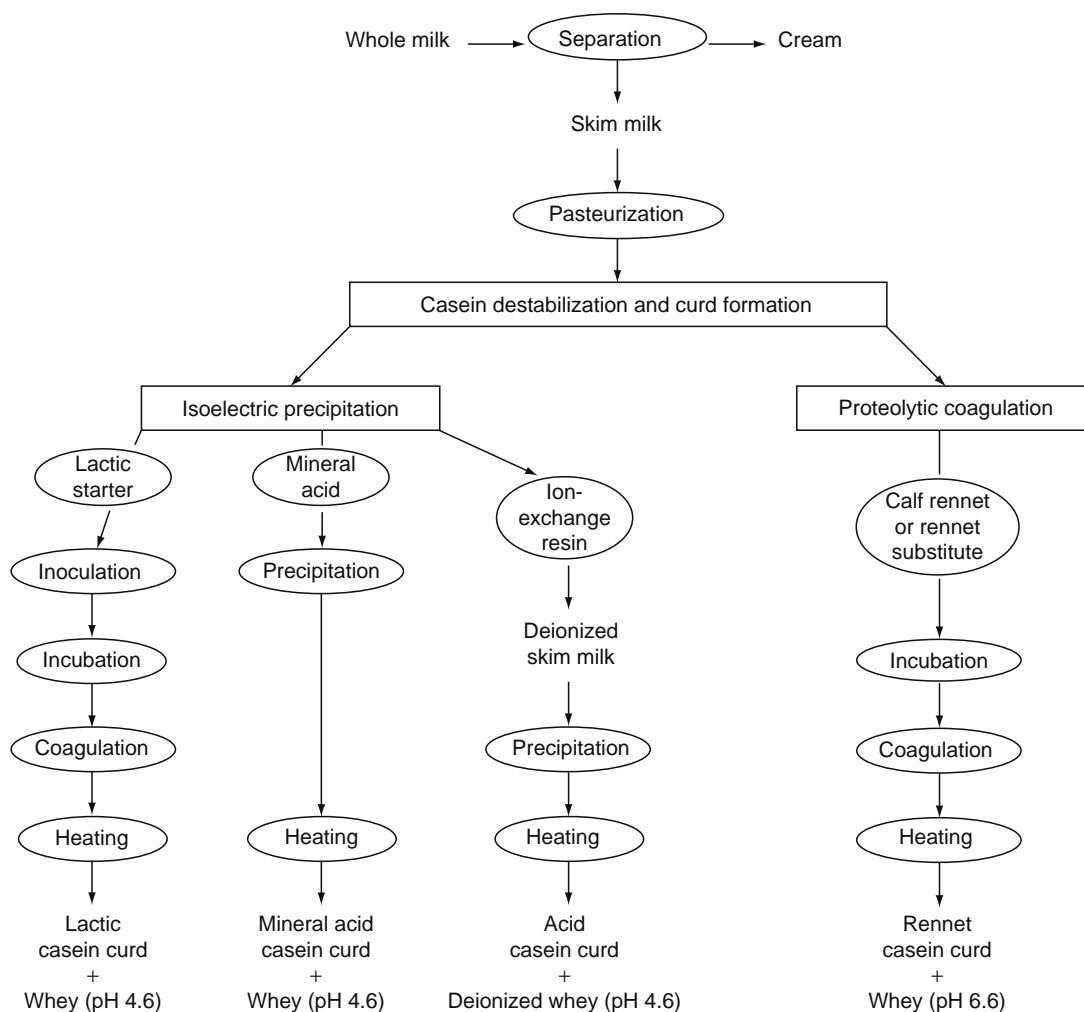


**FIGURE 21.16** Processes for casein and caseinate production. (Adapted from Mulvihill, D.M., Caseins and caseinates: Manufacture. In: Fox, P.F., Ed. *Developments in Dairy Chemistry*, Vol. 4, Elsevier Applied Science Publishers, London, 1989, pp. 97–129.)

with an increase of chloride, sulfate, nitrate, or lactate concentration.  $H^+$  cations are necessary in the process to decrease pH. However, anions are nondesired and contribute in an important manner to the mineral charge. These additional anions are present at the final step in the curd before washing and in the whey. To use whey from hydrochloric casein production it is necessary to demineralize it to decrease the mineral charge. A whey from hydrochloric casein contains 12% to 14% (w/w dry basis) of mineral and approximately 7% to 8% and more chloride. For fermentations, it is necessary to use mixed starter culture and to change them regularly to avoid contaminations by phages. Furthermore, during rennet casein production,  $\kappa$ -casein is denatured by formation of caseinomacropptide and para- $\kappa$ -casein [87,106,107]. In addition in water electrolysis with monopolar membranes, the electrical efficiency is lower than with BPMs [40,92].

In this context, EDBM was used for the precipitation of bovine milk protein, without adding acids, by decreasing the pH through electroacidification [42]. The skim milk was circulated in a three pair cell configuration on the cationic side of the BPM as for soy protein isolate production. The electroacidification was performed in batch process using a current density of  $20 \text{ mA/cm}^2$ . The pH of the solution was lowered from pH 6.6 to 4.4. Lowering the pH to 4.4 allowed a precipitation of 80%–85% of the total protein. The remaining proteins were whey proteins soluble at pH 4.4. This technology allowed the production of bovine milk casein isolates with a similar or higher protein content than those of commercial isolates (97% vs 95% on a dry basis). The protein profiles of the isolates obtained by HPLC showed that caseins represented 98.5% of the total protein precipitated.

As in any electrochemical process, the products to be treated by EDBM must possess a relatively high mineral content to allow a good electrical conductivity to decrease the global resistance of the electroacidification cell. Moreover, Bazinet et al. [108] demonstrated that the electrical efficiency of skim milk electroacidification is decreased, due to a lack of sufficiently mobile ions such as potassium (Figure 21.17). Consequently,  $H^+$  ions have to migrate across the CEM to ensure the electroneutrality.

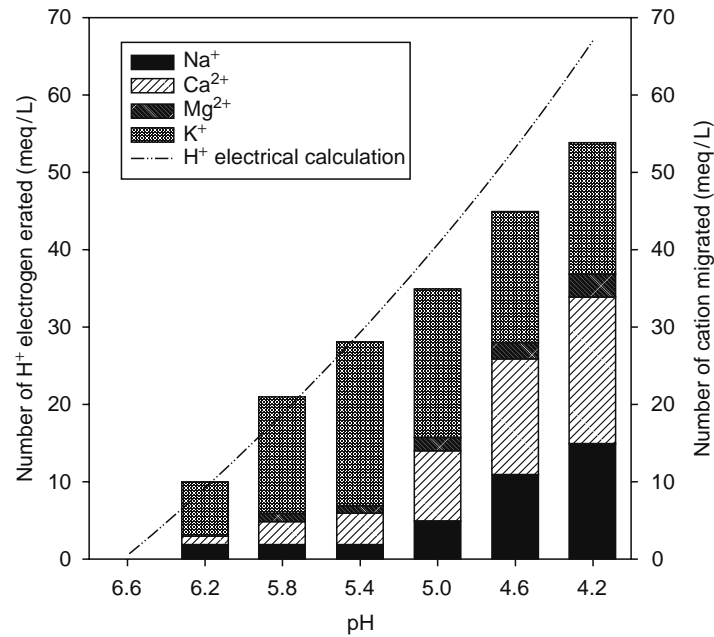


**FIGURE 21.17** Comparison of the amount of electrogenerated  $H^+$  (meq/L) and the amount of cations migrated (meq/L) during electroacidification of skim milk. (Adapted from Bazinet, L., Ippersiel, D., Gendron, C., Beaudry, J., Mahdavi, B., Amiot, J., and Lamarche, F., *J. Membr. Sci.*, 173, 201, 2000.)

These migrated  $H^+$  ions are lost for the process and decrease the electrical efficiency. Bazinet et al. [89] did not observe this phenomenon on soybean protein electroacidification due to the higher concentration in potassium ions in the raw material.

They suggested adding a certain amount of salt to the skim milk to obtain a better electrical efficiency. The performances of EDBM were then evaluated under different conditions of ionic strength added ( $\mu_{\text{added}} = 0, 0.25, 0.5, \text{ and } 1.0 \text{ M}$ ) and added salt ( $\text{CaCl}_2$ ,  $\text{NaCl}$ , and  $\text{KCl}$ ). The evolution of soluble protein during EDBM of skim milk was different according to the salt added and the ionic strength level (Figure 21.18). Moreover, for each added salt, the soluble protein curves had different evolution according to the ionic strength added. For  $\text{NaCl}$ , the soluble protein curves were the same with inflection points close to  $\text{pH } 4.20$  whatever the ionic strength added. In  $\text{CaCl}_2$ , the delay in precipitation increased with an increase in the ionic strength while for the  $\text{KCl}$ , the delay in precipitation was increased with the increase in ionic strength. For  $\mu_{\text{added}}$  ranging from 0.25 to 1.0 M, except for the  $\text{NaCl}$ , the  $\text{pH}_c$  value, at which all the caseins are precipitated, decreased with an increase in ionic strength by salting-in [87]. In  $\text{NaCl}$  addition, the different levels of  $\mu_{\text{added}}$  had no effect on the soluble protein profile;

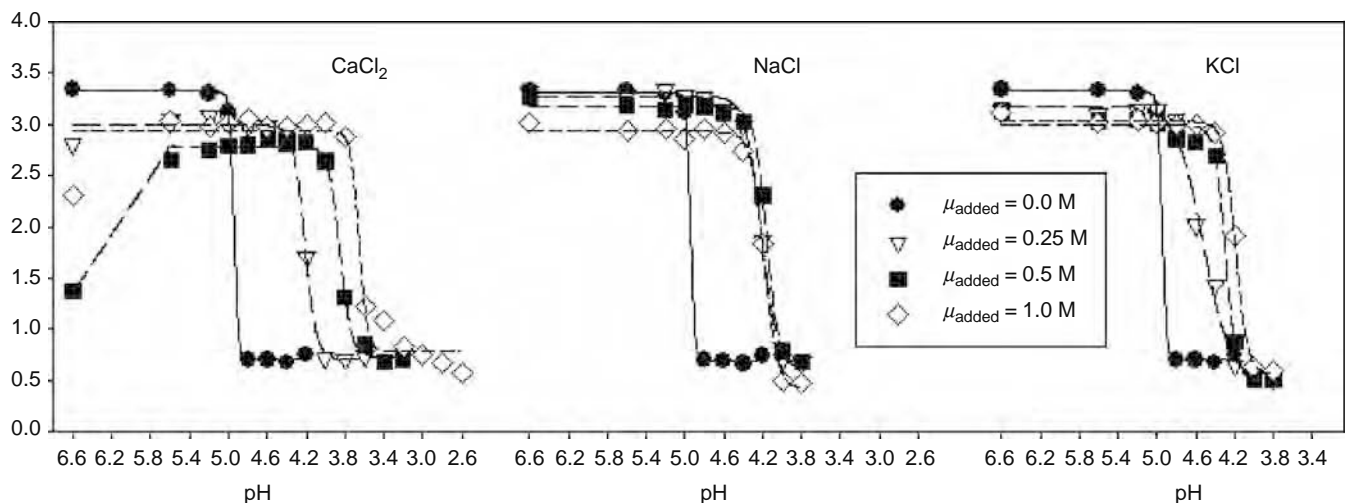


**FIGURE 21.18** Effect of ionic strength (0, 0.25, 0.5, and 1.0 M) and type of salt added ( $\text{CaCl}_2$ ,  $\text{NaCl}$ , and  $\text{KCl}$ ) on soluble protein during BPM electroacidification of reconstituted skim milk, run at a constant current density of  $20 \text{ mA/cm}^2$ . (Adapted from Bazinet, L., Ippersiel, D., Gendron, C., Mahdavi, B., Amiot, J., and Lamarche, F., *J. Dairy Res.*, 68, 237, 2001.)

however, there is an effect of salting-in in comparison with soluble protein of skim milk without NaCl added (Figure 21.18). The results obtained for the KCl are in accordance with the data obtained by Bazinet et al. [41] on soybean protein electroacidification. Repulsive hydration forces between proteins and protein solubility are minimal at the isoelectric pH, unless the net charge on the proteins is controlled in part by highly hydrated cations such as  $Mg^{2+}$ ,  $Ca^{2+}$ , and  $Na^+$  [109]. In the latter situation, coagulation occurs when the  $H^+$  concentration is high enough to replace the hydrated cations. The more  $Ca^{2+}$  present, the higher the  $H^+$  concentration required to cause coagulation. Thus, the highest pH at which casein micelles coagulate decreased from 5.0 to 3.8 as  $CaCl_2$  concentration was increased from 10 to 100 mM [110]. The combination of KCl and  $\mu_{added}=0.5$  M was the best combination with a 45% decrease in energy consumption in comparison with EDBM of skim milk without adding salt. Addition of salt, except for  $CaCl_2$ , resulted in a decrease in energy consumption (Table 21.5) [111,112].

Differences in supernatant composition at pH 4.6 were revealed for  $\alpha_s$ -casein,  $\beta$ -casein, and whey proteins [113]. Thus, the supernatant composition results obtained at pH 4.6 showed that the supernatant of electroacidified milk had a higher whey protein content compared with the supernatants of chemically acidified solutions, with values of 95.0% and 87.2%, respectively. At this pH value, unprecipitated  $\alpha_s$ - and  $\beta$ -casein fractions were observed in the chemical acidification treatments, whereas in electrochemical acidification, there was no trace of these two casein fractions. The difference observed between the protein profiles confirms the results obtained previously for total protein and indicates a slight delay in precipitation of  $\alpha_s$ - and  $\beta$ -caseins during the chemical acidifications. This precipitation difference may be due to a salting-in effect from the addition of salts [114] during chemical acidifications with HCl. By contrast, in electroacidification the impoverishment of salts by electrochemical demineralization, combined with a dilution effect from the system's dead volume, promotes precipitation of the proteins. Indeed, at the isoelectric point (pH 4.5–4.7 for caseins), the proteins have a net charge of zero, and they precipitate due to the effect of hydrophobic interactions. Under these conditions, there are no electrostatic repulsions between the molecules. Hence, if the ionic strength is increased, as in chemical acidifications, the salting-in effect of salts on hydrophobic interactions tends to slow the formation of aggregates and increase their solubility, leading to slower protein precipitation [87,115]. Electroacidification, on the other hand, accelerates the formation of protein aggregates and their precipitation. The salt removal in the milk solution promotes the hydrophobic interactions.

The isolates produced by BPM electroacidification with different type of added salts and ionic strength except at 1 M  $CaCl_2$   $\mu_{added}$  showed similar physicochemical and functional properties than those chemically produced and three commercial sodium caseinates used as references. The chemical composition of the isolates produced by EDBM varied according mainly to the ionic strength of the skim milk solution treated (Table 21.4). At high concentration of added salt, whatever the salt, there was retention of salts and lactose in the isolates decreasing the total protein content of these isolates. For high-salt-concentration isolates, the washing conditions used were not sufficient to allow removal of most of the salts and lactose from the coagulum. Furthermore, the concentration of lactose in the isolates increased with the ionic strength; ionic strength might influence porosity and particle size of coagulum which affect contact with the washing solution, and effectiveness of lactose removal. Many authors have pointed out that processing variables such as heat treatment, number of washes to which the curd is

**TABLE 21.5**  
**Effect of Ionic Strength Added and Type of Salt Added on the Relative Duration**  
**and Energy Consumption of Electroacidification and on Protein, Ash,**  
**and Lactose Contents of EDBM Isolates Produced**

		Duration (min)	Protein (% Dry basis)	Ash (g/100 g Protein)	Lactose (g/100 g Protein)	Energy Consumption (kW h/kg of Isolate)
Control	0.00 M	46.4	86.8	5.3	6.8	0.87
CaCl <sub>2</sub>	0.25 M	97.3	80.8	10.2	9.4	2.11
	0.50 M	106.6	78.5	11.3	14.4	2.36
	1.00 M	134.9	68.0	23.7	19.7	1.64
NaCl	0.25 M	93.6	82.2	8.3	10.0	0.69
	0.50 M	105.7	81.1	10.8	10.7	0.56
	1.00 M	106.9	76.0	16.1	10.0	0.60
KCl	0.25 M	80.2	79.4	9.1	10.6	0.55
	0.50 M	95.1	80.0	9.7	7.9	0.39
	1.00 M	116.9	74.8	20.4	10.9	0.58

Source: Adapted from Bazinet, L., Ippersiel, D., Gendron, C., Mahdavi, B., Amiot, J., and Lamarche, F., *J. Dairy Res.*, 68(2), 237, 2001; Bazinet, L., Gendron, C., Ippersiel, D., René-Paradis, J., Tétreault, C., Beaudry, J., Britten, M., Mahdavi, B., Amiot, J., and Lamarche, F., *J. Agric. Food Chem.*, 50(23), 6875, 2002.

subjected, and the content of iron influence the quality of the rennet casein [116–118]. The type of salt and the ionic strength influenced the functional properties and the structure of the sodium caseinate produced by EDBM. Addition of the KCl and NaCl during EDBM decreased the viscosity of the protein solution but the foaming and emulsifying properties, and also the particle size and the solubility profile, were unchanged [112]. The  $\text{CaCl}_2$  acted in a different way from both previous monovalent salts. It decreased the particle size and the viscosity from 0 to 0.5 M  $\mu_{\text{added}}$  and thereafter increased back both factors. The solubility profile of the isolate produced with addition of  $\text{CaCl}_2$  from 0 to 0.5 M  $\mu_{\text{added}}$  was similar to those from both monovalent salts, while at  $\mu_{\text{added}}$  of 1 M the solubility was decreased. By addition of  $\text{CaCl}_2$ , whatever the ionic strength, the emulsifying and foaming properties were unchanged except for the foaming capacity, which was decreased [112]. As the isolate produced by EDBM with addition of 1 M  $\text{CaCl}_2$  showed a high-calcium content after dialysis, this caseinate could assimilate to a Ca/Na caseinate [119].

These recent results showed that EDBM is a new alternative process for production of high-purity casein bovine milk isolate. At the moment, two main problems limit the application of the EDBM at an industrial level: the fouling of spacers and the fouling of cationic membranes. During EDBM process, the protein curd formed can lead to a fouling of the cell spacers by recirculation and accumulation of protein aggregates in the turbulence promoters of the spacers. However, an online centrifugation at the inlet or outlet of the cell would limit this undesired formation in the system [2]. During long-time process of milk, there is formation of calcium carbonate on the membrane in contact with the base electrogenerated but also inside the membrane and on the surface of the membrane in contact with the milk solution (Figure 21.19) [120]. Calcium carbonate precipitate originated from the skim milk solution. Diffusion of  $\text{H}_2\text{CO}_3$  and migration of  $\text{Ca}^{2+}$  through the CEM toward the basified KCl solution explain the presence of  $\text{CaCO}_3$ , which is practically insoluble in water [121]. In addition, as some  $\text{OH}^-$  leach across the CMX membrane, part of the  $\text{CaCO}_3$  can precipitate inside and on the other side of the membrane [120] (Figure 21.19). This deposit affected the performance of the system and decreased drastically the lifetime of the membrane.

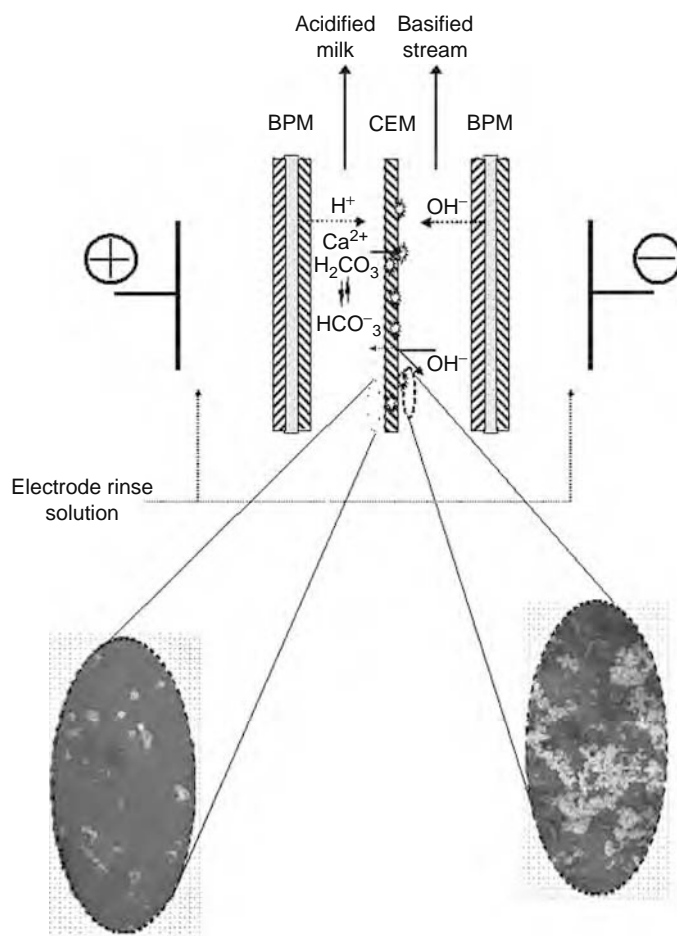


**FIGURE 21.19** Elemental configuration of EDBM cell used for skim milk solution, principles of CEM fouling formation, basified and acidified milk side microscopic photographs (magnitude  $\times 45$ ) of EDBM CMX membrane. (Adapted from Bazinet, L., Montpetit, D., Ippersiel, D., Amiot, J., and Lamarche, F., *J. Interface Colloid Sci.*, 237(1), 62, 2001.)

In this context, the KCl solution was replaced by a 0.25 N HCl solution to neutralize the  $\text{OH}^-$  electrogenerated by the BPM and to evaluate this neutralization effect on the integrity of the cationic and BPMs used [122]. It appeared from these results that the resistance of cationic membranes increased after 27 EDBM of which 13 were carried out with addition of  $\text{CaCl}_2$  at concentrations ranging from 8.9 to 47.3 g/L. This increase was due to an exchange of monovalent counter-cations of the membrane by divalent cations less mobile and to a slight fouling of 0.0103 mm. This fouling was identified as a protein fouling. No mineral fouling was observed on EDBM CEM. In addition, integrity and physical characteristics of EDBMs were preserved. Control of the basified stream compartment pH during EDBM did not result in complete protection of CEM characteristics since a small protein fouling of the membrane occurred during the process. However, when no pH control was applied, after one EDBM of skim milk with addition of 47.3 g/L of  $\text{CaCl}_2$  a mineral fouling thickness measurement of the CEM was up to 0.0431 mm.

### 21.4.3 INHIBITION OF ENZYMIC BROWNING IN CLOUDY APPLE JUICE

Cloudy or unclarified apple juice has increasing customer demand due to its superior sensory and nutritional qualities [123]. This light-colored juice contains a high proportion of pulp in suspension and preserves the flavor of freshly pressed apples [124]. However, production of high quality juice is difficult due to the presence of numerous compounds sensitive to oxidation reactions. In practice, soon after production, apple juice experiences enzymatic changes which modify its taste and color. These enzymatic changes are related to enzymatic browning reactions, which confer a dark color to the juice and have a negative impact on sales [125].

Cloudy apple juice is very sensitive to enzymatic browning since it contains considerable quantities of polyphenols and polyphenol oxidases (E.C.1.14.18.1, PPO) bound to suspended particles. Enzymatic browning reactions are catalyzed by PPO and result in oxidation of phenolic compounds into *o*-quinones which polymerize into complex dark-colored pigments [126]. To limit enzymatic browning and to provide a product with clear and appealing color, cloudy apple juice producers can use treatments such as thermal treatment, flash thermal treatment [127], or add large quantities of antioxidants such as ascorbic acid [128] or its derivatives [129]. In addition, these methods are coupled with an aseptic conditioning to allow the stabilization of the juice. However, such treatment can also alter the sensory and nutritional quality of the juice and induce, during extended storage, nonenzymatic browning reactions that are detrimental to product quality.

Zemel et al. [130] showed that PPO activity could be irreversibly inhibited by temporarily lowering the pH to 2.0 with HCl. According to McCord and Kilara [131], inhibition of PPO activity in acidic media is due to protonation of free carboxyl groups of the enzyme, which neutralize the negative charges of the protein. This change would result in electrostatic repulsion between acids and positively charged amino groups. Such repulsion would greatly affect the tertiary structure of the enzyme. A process solely for acidification of juice has limited commercial applications. To produce a cloudy apple juice preserving its organoleptic properties, it is necessary to readjust the pH to its initial value, pH 3.5. Zemel et al. [130] adjusted the pH to its initial value by adding an NaOH solution. This treatment inhibited enzymatic browning and stabilized the apple juice. However, the dilution effect due to addition of acid and base and the formation of salts rendered the juice flavor unacceptable.

Starting from the observations of Zemel et al. [130], Tronc et al. [37,38] used BPMs to lower the pH of cloudy apple juice. The apple juice was circulated on the cationic side of the BPM where the  $\text{H}^+$  ions are generated (Figure 21.20a). The pH of apple juice was reduced temporarily from 3.5 to 2.0 in 30 min in a small-scale unit at a constant current of 40 mA/cm<sup>2</sup>. However, this level of acidification required the addition of 12.3 mM  $\text{K}^+$  (KCl) every 5 min during the treatment. Exogenous  $\text{K}^+$  compensated for the  $\text{K}^+$  loss from the juice and maintained the electric charge at neutrality, which favored the accumulation of  $\text{H}^+$  in the juice [38]. Reducing the pH of the juice to 2.0 completely inhibited the polyphenol oxidase activity compared with the control. Following acidification, the pH of the juice was returned to its initial value by introducing  $\text{OH}^-$  produced by water splitting; the juice was circulated on the anionic side of the BPM where the  $\text{OH}^-$  ions are generated (Figure 21.20b). The pH readjustment of the juice partially reactivated the PPO, but browning inhibition was complete and irreversible. The treatment enhanced the color of cloudy apple juice during storage without modifying the flavor [38]. However, the ED treatment slightly reduced the malic acid content and substantially reduced the mineral contents.

In these previous studies [37,38], the feasibility of acidifying cloudy apple juice and returning the pH to its initial value without altering flavor was demonstrated by using electrodialysis (ED) with bipolar and cationic membranes. However, the total process was too lengthy, about 90 min, and required the addition of exogenous KCl to the juice to reach pH 2.0. Furthermore, the voltage applied greatly exceeded the 2 V/membrane average and was not compatible with industrial constraints [39].

More recently, Lam Quoc et al. [39] replaced cationic membranes in the stack with anionic membranes and the KCl solution with 0.1 M HCl (Figure 21.21). In this configuration, acidification is still triggered by the introduction of protons generated by the BPMs, but the retention of these protons is more effective owing to the continuous introduction of  $\text{Cl}^-$  counterions from the HCl compartment. The  $\text{Cl}^-$  ions accumulated in the juice will subsequently serve as counterions for the introduction of  $\text{OH}^-$  ions, generated by the anionic side of the BPMs, during the return of the juice pH to its initial value. The accumulated  $\text{Cl}^-$  ions will thus be eliminated from the juice during the acidification period. The impact of this configuration was important on acidification speed. The authors demonstrated that with a 4-membrane stack, the juice pH decreased from 3.35 to 2.0 in 4.7 min. By increasing the number of membranes to 10, the required time dropped

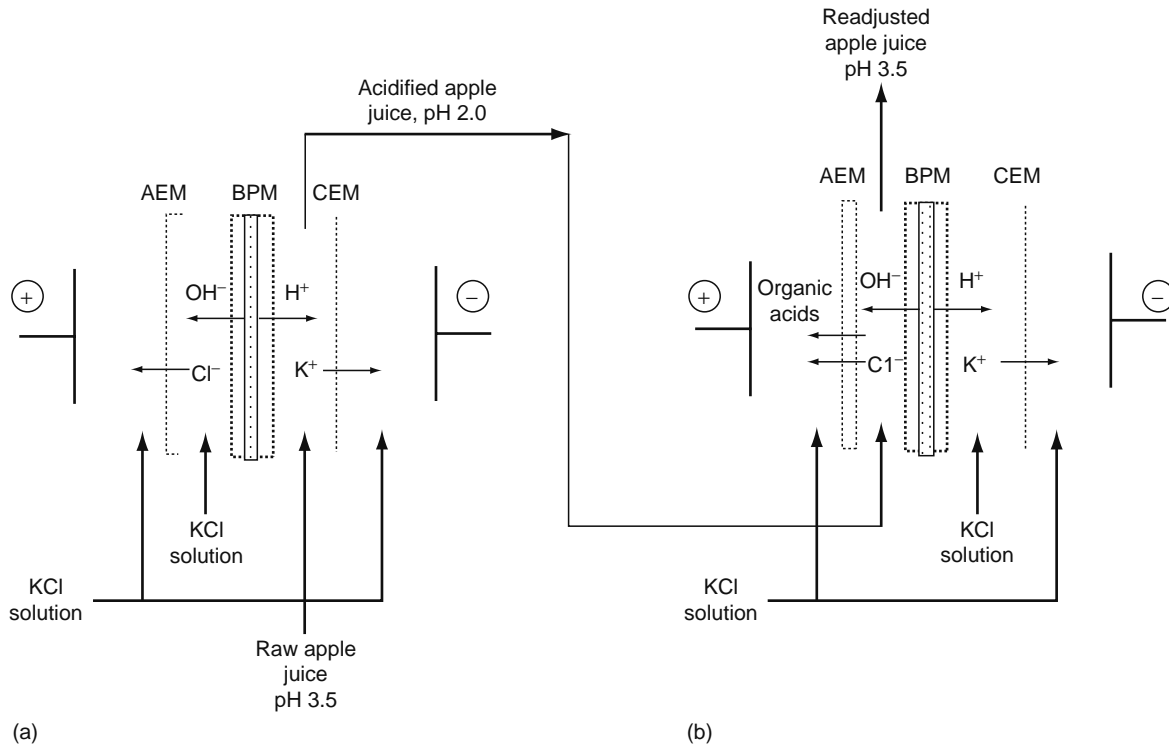


**FIGURE 21.20** Electrodesialysis cells for inhibiting enzymatic browning in cloudy apple juice. (a) Electroacidification step and (b) electroalkalinization step. CEM, cation-exchange membrane; BPM, bipolar membrane; AEM, anion-exchange membrane.

to about 1.5 min. Treatment time is therefore inversely proportional to the number of membranes used, which boosts the introduction of  $\text{Cl}^-$  ions to promote the retention of  $\text{H}^+$ . The HCl solution also serves to neutralize  $\text{OH}^-$  produced by the anionic side of the BPMs by hindering their introduction into the juice. Hence, the juice acidification process is more effective and faster than before. This is confirmed by the conductivity results: conductivity is considerably higher because of the accumulation of ions in the juice. At a pH of 2.0, the  $\text{Cl}^-$  concentration reached 580 mg/L of juice in comparison with 0.7 mg/L in the control juice and 29 mg/L in the adjusted juice (Table 21.6). The increase in conductivity improved EDBM treatment by reducing the applied voltage and energy consumption. The latter was 4–5 kW h/m<sup>3</sup> of juice, which represents very low energy consumption from an industrial standpoint. The yield obtained with a BPM/anionic configuration, independent of the number of membranes used, was three times higher than that of BPM/cationic configuration with the addition of KCl [38].

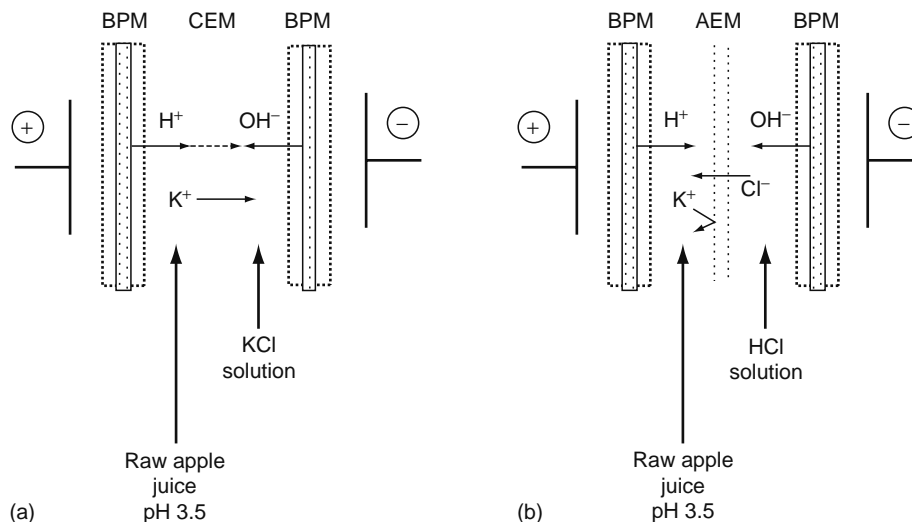


**FIGURE 21.21** Electrodesialysis (ED) configurations used to modify pH of cloudy apple juice. (a) BPM/cationic membrane and (b) BPM/anionic membranes. (Adapted from Lam Quoc, A., Lamarche, F., and Makhoulouf, J., *J. Agric. Food Chem.*, 48, 2160, 2000.)

**TABLE 21.6**  
**Impact of EDBM Treatment on the Chemical Composition**  
**of Cloudy Apple Juice**

Compounds	Control Juice	Acidified Juice	Adjusted Juice
Ash (mg/L)	1730	2010	1750
K <sup>+</sup> (mg/L)	764	774	775
Ca <sup>2+</sup> (mg/L)	27	22	21
Mg <sup>2+</sup> (mg/L)	35	35	32
Cl <sup>-</sup> (mg/L)	0.7	580	29
Malic acid (g/L)	7.8	7.6	6.2
Glucose (g/L)	18.8	18.0	17.3
Fructose (g/L)	84.3	79.4	75.1
Saccharose (g/L)	13.1	11.8	11.7
Anthocyanin (mg/L)	55	55	53
Chlorogenic acid (mg/L)	163	ND	158
(-)-Epicatechin (mg/L)	208	ND	198
Phloridzin (mg/L)	37	ND	36

Source: Adapted from Lam Quoc, A., Lamarche, F., and Makhoulouf, J., *J. Agric. Food Chem.*, 48, 2160, 2000.

Furthermore, by doubling current density to 40 mA/cm<sup>2</sup>, the average applied voltage did not exceed 2 V/compartiment and ranged from 1.5 to 1.8 V. The time required to return juice pH to its initial value with BPM/anionic configuration, where the juice and HCl compartment were reversed, was longer than the time required to reach pH 2 (about 10 min vs 4.7 min) [39]. The difference is because this phase is achieved by replacing the Cl<sup>-</sup> accumulated in the juice with OH<sup>-</sup>. The low conductivity of Cl<sup>-</sup> compared to OH<sup>-</sup> (73.5 cm<sup>2</sup> Ω<sup>-1</sup> equiv<sup>-1</sup> vs 199 cm<sup>2</sup> Ω<sup>-1</sup> equiv<sup>-1</sup>) and the depletion of Cl<sup>-</sup> during treatment caused the low retention of OH<sup>-</sup> in the juice and made it difficult to eliminate Cl<sup>-</sup>. The membrane stacks reduced the time needed to achieve the initial pH of the juice, but the yield remained the same as in the previous study [38], i.e., 2.5 L of juice/m<sup>2</sup> of membrane/min.

The acceleration of acidification by EDBM provides better control over enzymatic browning compared with previous studies [37,38] (Figure 21.22). According to the changes in color of the control juice, enzymatic browning is very active after extraction, and it must be inhibited as fast as possible in the first few minutes following extraction to keep the color of the treated juice essentially like that of freshly pressed juice. The discrepancies observed between the colors of the control and the adjusted juices obtained by Lam Quoc et al. [39] were greater than those obtained by Tronc et al. [38] for the same storage time following extraction. After the acidification and pH adjustments, the color stabilized at about the level for freshly pressed juice, which demonstrates that browning is completely inhibited. However, the acidified juice has a tendency of more red color

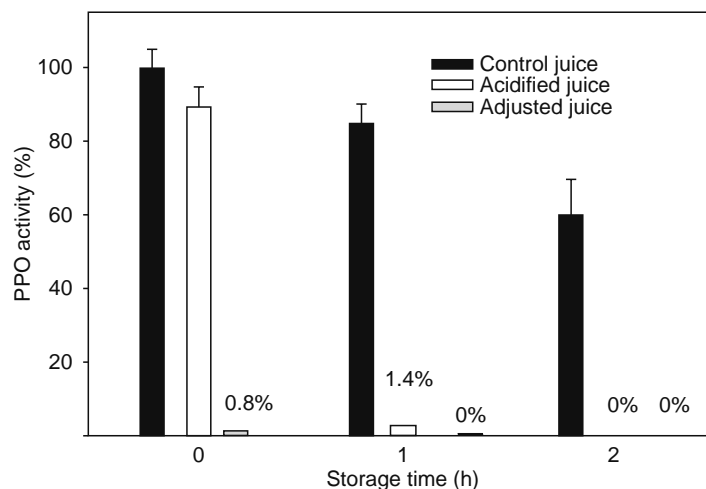


**FIGURE 21.22** Impact of EDBM treatment on PPO activity in apple juice during storage. (Adapted from Lam Quoc, A., Lamarche, F., and Makhoulouf, J., *J. Agric. Food Chem.*, 48, 2160, 2000.)

than the adjusted juice. This is due to the presence of anthocyanins, primarily cyanidin 3-galactoside, whose red color depends on the acidic pH [132], giving acidified juice a red color. The intensity of this coloration, however, lessens when the juice is at a normal pH, as in adjusted juice.

Chemical analyses demonstrated that EDBM treatments have variable effects on the composition of cloudy apple juice (Table 21.6). The percentage of adjusted juice ash remained unchanged by the treatment. A slight increase in ash in acidified juice is because the salts formed after the juice was heated to 600°C are chlorides not carbonates, owing to the accumulation of  $\text{Cl}^-$  ions in the juice during acidification. The main cation in the juice,  $\text{K}^+$ , is preserved owing to the layout of the anionic membranes, which prevent the cations from leaving the juice, representing an advantage from a nutritional standpoint. However, a slight loss in divalent cations ( $\text{Ca}^{2+}$  and  $\text{Mg}^{2+}$ ) was observed, owing to their low solubility. They could be partially precipitated or adsorbed on the surface of the anionic membranes where the pH at the membrane–solution interface is higher [133]. There was no significant change in the concentration of sugars in the juice because the uncharged sugars do not migrate during electro dialysis. Only a major osmotic pressure gradient between two compartments could force them to migrate through membranes [134]. The malic acid concentration of the adjusted juice decreased by about 20%. The loss occurred through the anionic membranes because malic acid is negatively charged.  $\text{Cl}^-$  accumulated in the juice is not totally eliminated after the rise in pH. A residual quantity of 30 mg/L was found in the juice. The use of anionic membranes with greater monovalent anion selectivity would help limit the loss of malic acid and eliminate  $\text{Cl}^-$  more effectively. Sensory evaluation tests revealed that adjusted juice retained the characteristic flavor and color of freshly pressed juice. The presence of a residual quantity of  $\text{Cl}^-$  did not seem to affect the flavor of the EDBM-treated juice. Moreover, the treated juice was slightly fresher, more fruity and sweeter, with a taste of real apple [39].

The configuration with bipolar and anionic membranes provides several advantages over the first configuration. This treatment does not require the addition of exogenous KCl; furthermore, there is no chemical waste since all the electrolytes are reused. It accelerates the treatment and rapidly inhibits enzymatic browning, while preserving freshly pressed taste of cloudy apple juice. However, the concentration of some nutrients such as sugar and malic acid is decreased during the treatment. This pH modification should have other positive consequences on the stability of cloudy apple juice. It is possible that the pectin methyl esterase, responsible for the cloudy precipitate in the juice, can also be affected by the EDBM treatment. The very small loss of divalent ions such as  $\text{Ca}^{2+}$  and  $\text{Mg}^{2+}$  by electromigration should reinforce the stability of the suspended particles [125]. EDBM can be considered as a nonthermal stabilization which is simple, efficient, and applicable to the stabilization of food liquids.

#### 21.4.4 DEACIDIFICATION OF PASSION FRUIT JUICE

The yellow passion fruit, *Passiflora edulis* f. *flavicarpa*, has intense and special aroma and flavor, which make it a desirable ingredient in the formulation of various food products. These fruits are processed and exported as concentrated juice at 50°Brix (500 g/kg of total solids) from several South American countries such as Ecuador, Brazil, Peru, and Colombia. For Ecuador, the principal exporter country [135], in 2000 the passion fruit occupied the second place in exports with 26,000 ton of concentrated juice and is a very important source of income (US\$ 28 millions) [136]. However, due to its high acidity, only limited amounts of juice can be added as an ingredient in the formulation of various preparations such as beverages, ice creams, marmalades, cocktails, pies, etc., which reduces their flavor intensity [137,138]. Addition of sweetening agents or simple neutralization by basic compounds is not a suitable method because they affect the flavor and natural taste of juices, resulting in poor palatability [19]. Therefore, it is important to find a deacidification process having very little effect on the chemical composition and aromatic quality of juice.

Based on these problematics, Vera Calle et al. [19] tested the deacidification of clarified passion fruit juice by EDBM. The stack was equipped with homopolar and BPM, forming two compartments (Figure 21.23). The reduction of acidity was

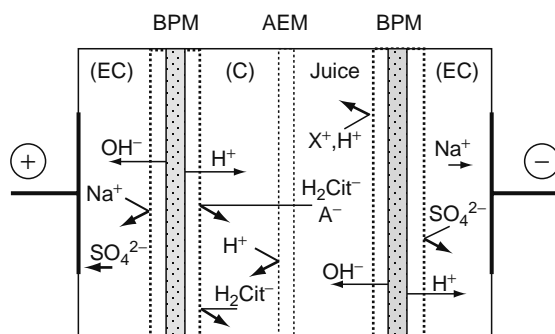


**FIGURE 21.23** Electro dialysis (ED) cell with BPM. (EDBM2C configuration; AEM, anion-exchange membrane; BPM, bipolar membrane.) (Adapted from Vera Calle, E., Dornier, M., Sandeaux, J., and Pourcelly, G., *Desalination*, 149, 357, 2002.)

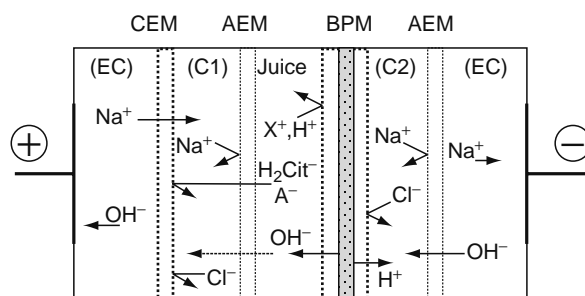


**FIGURE 21.24** Modified configuration of electrodesalination with bipolar and homopolar membranes for juice deacidification. (EDBM3C configuration; BPM, bipolar membrane; AEM, anion-exchange membrane; CEM, cation-exchange membrane.) (Adapted from Vera Calle, E., Ruales, J., Dornier, M., Sandeaux, J., Sandeaux, R., and Pourcelly, G., *J. Chem. Technol. Biotech.*, 78, 918, 2003.)

achieved by increasing the pH from 2.9 to 4.0. This pH limit was chosen to avoid microorganism growth and spoilage [19]. In this EDBM configuration only anions are able to pass through the AEM from the juice to the concentrate (C) compartment. The net effect was the extraction of anions, mainly citrate, and their replacement by hydroxyl ions provided by the BPM. Citric acid was formed in the concentrate (C) compartment by citrate ions extracted from juice and protons provided by the second BPM separating the (C) compartment and electrode compartments. This configuration allowed the production of citric acid with 89% purity and avoids the increase in the sodium concentration in the juice.

In a further study by Vera Calle et al. [136], the previous configuration was compared with a modified one, in which the stack was equipped with homopolar and one BPM constituting three compartments (Figure 21.24). The configurations were compared for their performances in terms of deacidification rate, current efficiency, energy consumption, and characteristics of deacidified juices such as concentration of inorganic and organic ions, color, and flavor. They observed that the deacidification rates and current efficiencies were similar for both processes. However, although the nonmodified configuration induces the greatest energy consumption (0.50 vs 0.38 kW h/L of juice), it offers the advantage of eliminating the consumption of chemicals. The  $K^+$ ,  $Ca^{2+}$ , and  $Mg^{2+}$  concentrations were not modified whereas the  $Na^+$  concentration was markedly increased by using the modified configuration (180 vs 50 mg/L). Both processes did not achieve citrate removal without elimination of other anions. The anions concentration was similar for the two processes. The inorganic ions were almost eliminated, 62% of the citrate ions and 48% of the malate ions were removed from the fresh juice. Nevertheless, the proportion of the anions kept the same value in the fresh and deacidified juices, the citrate ions remaining the major anionic species (about 90%) [136]. The color variations obtained for the configurations, in the  $L, a, b$  space calculated according to  $\Delta E = (\Delta L^2 + \Delta a^2 + \Delta b^2)^{1/2}$  and using the nontreated sample as a reference solution, were 0.5 and 0.2 for the modified EDBM3C and the nonmodified EDBM2C configuration, respectively. Finally, no difference between the untreated and the deacidified juices was observed following the sensory analysis. According to these authors, although the EDBM2C configuration leads to the highest energy consumption, it seems a very interesting option because of the elimination of the soda consumption and the production of citric acid [136], which can be used as a preservative or antioxidant in the food industry.

To assess the feasibility and to verify if the ED operations of the EDBM2C configuration could be expensive because of the NaOH and energy consumption, the authors recently published a work comparing this method with different methods used for deacidification of clarified passion fruit juice [18]. They compared EDBM with other physicochemical technologies, ion-exchange resins, and electrodesalination with homopolar membranes (Figure 21.25), as well as the conventional chemical method based on the precipitation of calcium citrate obtained by addition of calcium hydroxide or carbonate to the clarified juice.

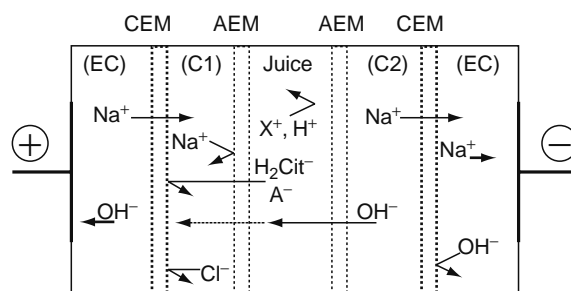


**FIGURE 21.25** Configuration of electrodesalination with homopolar membranes used for juice deacidification. C1 and C2 are separated compartments while the two EC compartments are connected. (ED3C configuration; AEM, anion-exchange membrane; CEM, cation-exchange membrane.) (Adapted from Vera Calle, E., Ruales, J., Dornier, M., Sandeaux, J., Sandeaux, R., and Pourcelly, G., *J. Chem. Technol. Biotech.*, 78, 918, 2003.)

**TABLE 21.7**  
**Comparison of Performances of the Two Electrodialysis Configurations Tested**

	Time to Obtain pH 4.0 (min)	Deacidification Rate (eq/h m <sup>2</sup> )	Current Efficiency for Citric Acid (%)	Energy Consumption (kW h/L of Juice)
ED3C	496	4.9	33	0.38
EDBM2C	549	4.6	31	0.50

Source: Adapted from Vera, E., Ruales, J., Sandeaux, J., Dornier, M., Persin, F., Reynes, M., and Pourcelly, G., *J. Food Eng.*, 59, 361, 2003.

A commercial macroporous weakly basic ion-exchange resin, Amberlite IRA95 from Rohm and Haas, was tested in a column, 1.7 cm in diameter and 60 cm long with a bed volume of 50 mL. The resin matrix consisted of styrene–divinylbenzene. The tertiary amine functional groups were equilibrated in the OH<sup>-</sup> form before use. ED experiments were performed with a laboratory cell of 20 cm<sup>2</sup> of effective area at a constant current density of 400 A/m<sup>2</sup>. The principle of the two electrodialysis configurations used is the extraction of citrate anions from the juice and their replacement by hydroxyl ions provided either by the NaOH solution in the C2 compartment (ED3C configuration, Figure 21.25) or by the BPM sandwiched between the juice and electrode compartments (EDBM2C configuration, Figure 21.23). The performances of the two ED operations were compared (Table 21.7). For the conventional method, the calcium citrate was precipitated by adding calcium hydroxide or carbonate at pH 4.5. Then, the mixture was maintained for 24 h at 4°C, and the precipitated calcium citrate was separated by filtration. After filtration, the pH was adjusted to 4.0 by mixing the filtrate with fresh juice. They determined total soluble solids, acidity and color, as well as inorganic and organic ion concentrations. They completed their analyses by triangular tests to compare the aroma of the fresh juice with the deacidified juices.

The titrable acidity and total soluble solids varied up to 30% according to the deacidification method applied (Table 21.8). Resin treatment induced the greatest change in the total soluble solids and color. In all the deacidified juices, a decrease in the citrate and malate concentrations was obtained. The precipitation of calcium citrate is the most selective technique where citrate ions were preferentially eliminated—the chloride, sulfate, and phosphate concentration remaining unchanged. Nevertheless, a lower elimination of citrate and malate ions was induced by the use of CaCO<sub>3</sub>, 40% and 12.5%, respectively, than with Ca(OH)<sub>2</sub> where it reached 65% and 32%, respectively. The difference between extraction ratios of organic anions was lower for other methods, about 65% and 53% for citrate and malate, respectively. Moreover, the inorganic anions were partially extracted together with organic ions when using resin and electrodialysis. In the electrodialysis method, the elimination of anions is related to their mobility both in the solution and membrane, and consequently the extraction of inorganic anions is easier than that of organic anions. Almost all the chloride ions were eliminated and about 90% of phosphate and 70% of sulfate ions were extracted. Potassium and magnesium concentrations were not affected whatever the method used, while the calcium and sodium concentrations were significantly increased by using the precipitation method and electrodialysis with three compartments (ED3C), respectively [18]. There was no change in the cation concentration while using resins and EDBMs. According to the sensory properties of deacidified juices, the triangular tests did not highlight significant differences between the deacidified juices and the fresh juices. To classify the deacidified juices, a ranking test of degree of preference was done by directly tasting the juices. The juice treated by ion-exchange resin appeared as highly significant as the sample liked least, the precipitation method with calcium hydroxide giving the most liked sample by a narrow margin [18].

**TABLE 21.8**  
**Physicochemical Analysis of the Juices Deacidified by Different Methods and Comparison with Control Clarified Juice**

Deacidification Method	pH	Titrable Acidity (g Citric Acid per kg)	Total Soluble Solids (g/kg)	Color			
				<i>L</i>	<i>a</i>	<i>b</i>	DE
Clarified juice	2.93	43.3	132	30.8	-1.40	5.00	N/A
CaCO <sub>3</sub>	4.00	13.5	130	30.9	-1.50	5.14	0.2
Ca(OH) <sub>2</sub>	4.00	10.4	112	31.0	-1.46	4.94	0.2
IRA95	4.00	10.8	100	31.7	-1.49	4.09	1.5
ED3C	4.00	12.3	111	30.3	-1.26	4.62	0.5
Electrodialysis with bipolar membranes (EDBM)2C	4.00	12.0	111	31.3	-1.30	4.94	0.4

Source: Adapted from Vera, E., Ruales, J., Sandeaux, J., Dornier, M., Persin, F., Reynes, M., and Pourcelly, G., *J. Food Eng.*, 59, 361, 2003.

All the methods tested allowed the deacidification of the clarified fruit juice in which pH was increased from 2.9 to 4.0. Nevertheless, these methods have some different advantages and disadvantages. The deacidification using  $\text{CaCO}_3$  is not recommended due to the liberation of  $\text{CO}_2$ , foam making, and poor pH control during the precipitation phase. The use of  $\text{Ca}(\text{OH})_2$  is easier and gives a good quality product. Besides, citric acid could be recovered by dissolving the precipitated calcium citrate in sulfuric acid, and converting the calcium citrate to calcium sulfate and citric acid [139]. However, the precipitation method has three limitations: the legislation of some countries, the precipitation problems in the final product induced by the increase in the calcium concentration, and the fact that consumers prefer natural product, without chemical addition. The ion-exchange process does not seem to be a good option, since it leads to changes in the organoleptic characteristics of the treated juice, and the large amounts of effluent produced during the regeneration phase of resins. The deacidification by electro dialysis has some advantages over the above methods, especially EDBMs. It is a continuous process without reagents added, giving a high quality juice in terms of physicochemical and sensorial analyses. It was observed that there was no change in the cation concentration, slight color variation, and good flavor. Only organic and inorganic anions were partially eliminated. Nevertheless, electro dialysis is more expensive than the other techniques but the citric acid simultaneously produced during the deacidification could improve the cost of this technique. Therefore, EDBM could be a promising alternative to the conventional calcium precipitation process for the deacidification of the passion fruit juice.

#### 21.4.5 PROCESS FOR PURIFYING DAIRY WASTEWATER

Whey is a by-product of dairy industry with a worldwide annual amount of 96 millions of tons (46 millions of tons in Europe) [140]. One possibility to use the whey is ultrafiltration to produce a protein concentrate for food and feed preparation. The filtrate is whey permeate and its disposal is still a problem because whey permeate contains almost the total lactose and salts derived from milk, resulting in a high chemical oxygen demand (COD) of 50–60 kg  $\text{O}_2$ /metric ton. Consequently, due to its high COD it is not economic and mostly not possible to treat it in communal sewage treatment plants. In addition, in conventional wastewater purification processes, degradable constituents are degraded either anaerobically to form methane and  $\text{CO}_2$  or aerobically to form  $\text{CO}_2$ , water, and biomass. In these processes, a considerable part of the energy contained in the wastewater constituents is lost [141].

In this context, an integrated bioprocess for the dairy sewage treatment, using bipolar membrane ED, was developed recently by Boergardts et al. [141]. They provided a three-stage process for purifying dairy wastewaters obtained from milk-processing enterprises (Figure 21.26). In the first stage, the wastewater was pretreated with base to precipitate out a portion, and

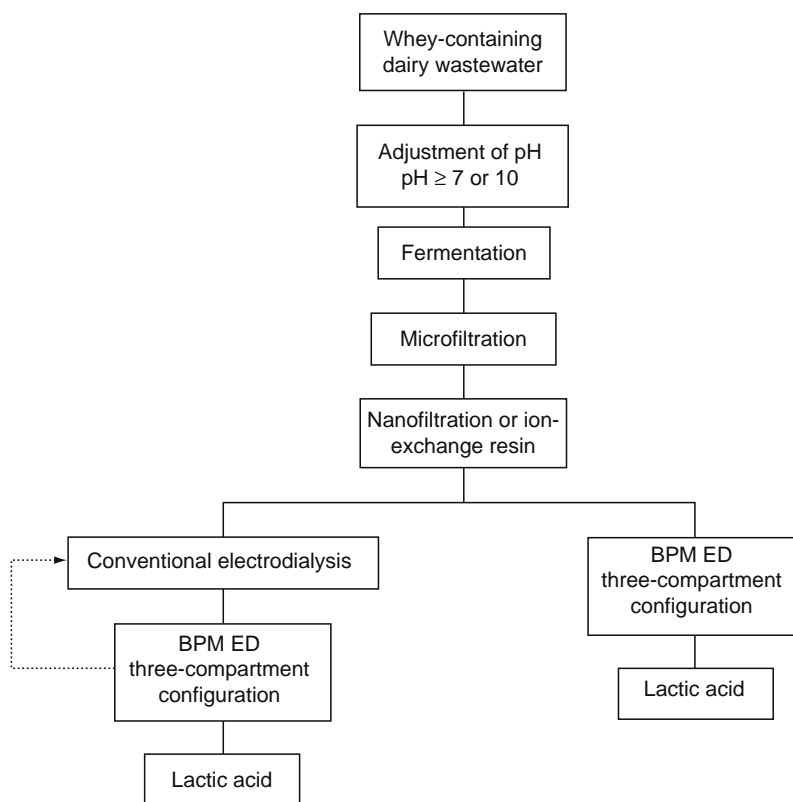
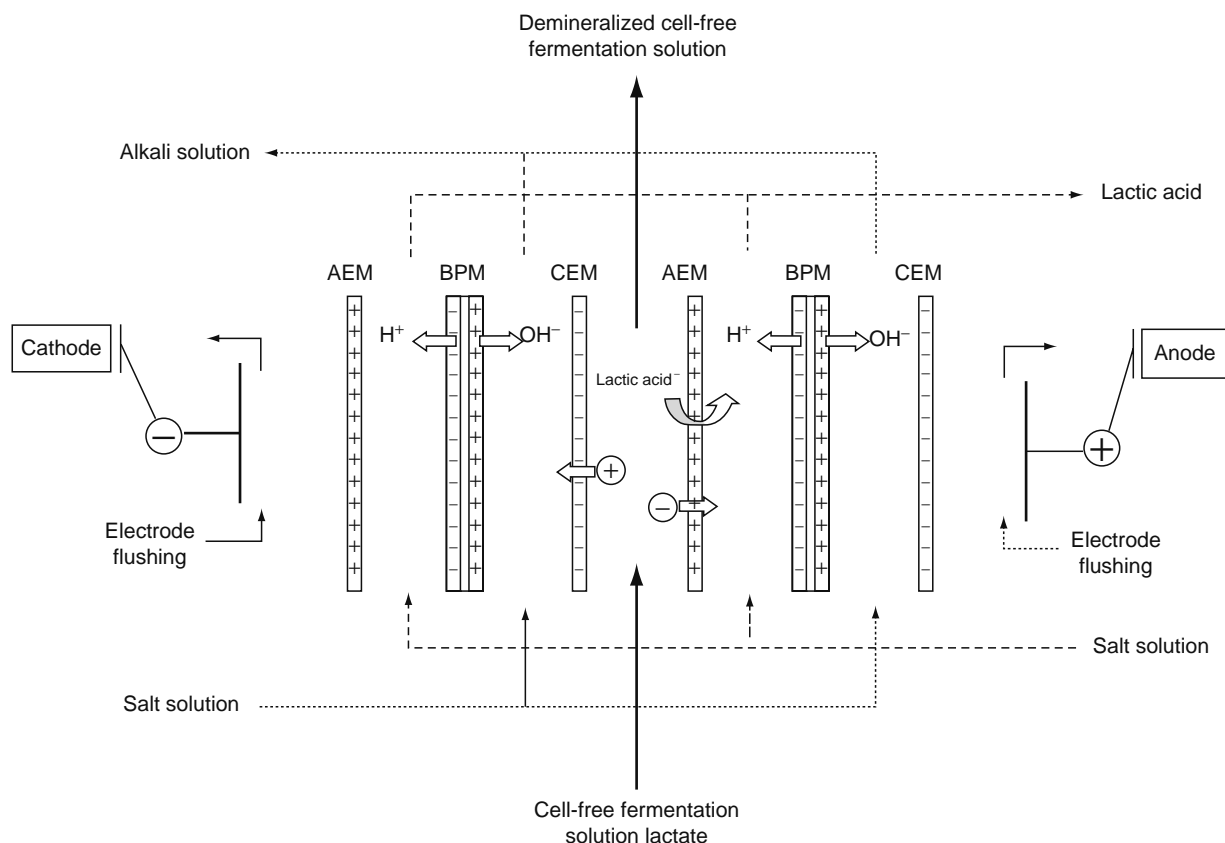


FIGURE 21.26 Process for purifying dairy wastewater. (From Bazinet, L., *Crit. Rev. Food Sci. Nutr.*, 45, 307, 2005.)

to the extent possible, the majority of the  $\text{Ca}^{2+}$  and  $\text{Mg}^{2+}$  ions and  $\text{PO}_4^{3-}$  ions present. In the second stage, the pretreated wastewater was then fed to a fermentation reactor and the fermentation broth formed was given a secondary purification. In the fermenter, the lactose and any other sugars present were converted homofermentatively to lactic acid using lactic acid bacteria. According to the authors, the use of a cell retention system could lead to significantly higher productivities. They used a cell retention system operated by microfiltration membrane unit fed by the circulating stream from the fermenter; complete removal of all components and higher transmembrane fluxes was achieved. However, the cells could be removed by membrane processes or centrifugation. In the third stage, the permeate was fed to the electrodialysis system via a nanofiltration unit or a selective ion exchanger to remove any calcium residues still present. In the third stage, the concentration of lactic acid in the wastewater was reduced and the wastewater produced had a very low COD load. The use of ED with BPMs also had permit isolation of free acid in high concentration and purity directly from the fermentation solution. As a third product in this case, alkali solution was formed which could serve to elevate the pH during pretreatment of the wastewater. Alternately, the alkali solution formed could be used to regulate the pH of the fermenter. The bipolar-electrodialysis configuration was the same as the one used by Van Nispen and Jonker [142] (Figure 21.27), wherein fermentation solution filtrate circulates in the diluate circuit. The pH in each of the two circuits was set by the BPMs. The free lactic acid was taken off from the acidic circuit and the alkali solution formed from the basic circuit. According to the authors, to achieve both low COD and pure lactic acid product with good results in each case, the bipolar ED may be carried out as follows. The fermentation broth is reduced in batchwise concentration to the desired wastewater concentration, and acidic and basic compartments are concentrated up to the maximum product concentration. During this process step, water is continuously transported through the membranes. Therefore, the product streams produced (alkali solution and lactic acid) can be taken off continuously and at constant concentration. Accordingly, the alkali solution produced can be continuously returned to the wastewater during a continuous wastewater pretreatment stage. The lactic acid produced can also be additionally purified in further continuous process steps [143].

In another embodiment of the invention, the authors suggested that the ED could be carried out in two stages. The fermentation broth is subjected in the first stage to bipolar membrane ED in which the broth is continuously reduced in concentration, to about  $10\text{--}15\text{ g L}^{-1}$  diluate concentration. In the second stage, a monopolar ED is carried out in which the concentration is further decreased to the desired wastewater concentration, preferably in a batch procedure. The sodium



**FIGURE 21.27** Operation of BPM ED using a three-compartment configuration for lactate migration. (From Bazinet, L., *Crit. Rev. Food Sci. Nutr.*, 45, 307, 2005.)

lactate produced in the second stage can be returned to the feed stream of the first ED stage to increase the starting concentration of lactate there (Figure 21.26). According to Boergardt et al. [141], the COD value may be decreased by 85%–95% and free lactic acid may be produced at a concentration of approximately 200 g/L. The alkali solution concentration can achieve about 2 mol/L.

#### 21.4.6 SEPARATION OF WHEY PROTEIN

Whey proteins have a high nutritional value and excellent functional properties [107,144]. When concentrated, whey proteins are interesting sources of proteins for young mammal and human nutrition [145]. According to their disponibility, their low cost (in comparison with others sources of proteins), and their characteristics, they are hugely used in the food industry [134]. However, knowledge about the property of the individual fractions of whey proteins commands more research about processes for separation of these fractions to use them separately and to optimize their respective properties in the food industry [146]. The fractionation research aimed at the major protein constituents  $\beta$ -lactoglobulin ( $\beta$ -lg) and  $\alpha$ -lactalbumin ( $\alpha$ -la), and numerous isolation methods for their separation have been proposed. Their fractionation may be performed by ion-exchange chromatography [147,148], metaphosphate complex precipitation [149], heat/acid separation [146,150–152], and ion depletion at low pH [21,22]. Amundson et al. [21] and Slack et al. [22] separated the two major whey protein fractions by demineralizing a concentrated whey solution and adjusting the pH chemically. This process was based on 90% volume reduction of whey by ultrafiltration, partial demineralization of the UF retentate by electrodialysis or diafiltration, pH adjustment of the UF retentate before and after demineralization to pH 4.65, and centrifugation of the retentate. With this method, they produced  $\beta$ -lg-enriched fractions containing 33% of the original acid whey proteins and 17% of the original sweet whey proteins.

Based on these data, Bazinet et al. [44] demonstrated the feasibility of EDBM to fractionate whey proteins from a whey protein isolate (WPI, BiPRO) and studied the effect of protein concentration on its performance in comparison with chemical acidification. The acidification method had a considerable effect on soluble protein as the pH decreased; chemical acidification did not allow precipitation of a large amount of whey protein, while electroacidification succeeded in precipitating up to 54% of the total protein. Effectiveness of electroacidification to precipitate whey protein was improved by increasing protein concentration, but at concentration higher than 10% WPI the conductivity of the solution became the limiting factor. These results were confirmed by protein profiles during acidification since only EDBM allowed a significant precipitation of whey protein (Figure 21.28). In comparison with results for the soluble protein, these results suggest that a part of the other whey proteins were precipitated with  $\beta$ -lg. According to the results of HPLC, the  $\alpha$ -la would be the main protein precipitating with  $\beta$ -lg at high WPI concentration. Since WPI was made from thermal treated milk, a part of the  $\alpha$ -la should have been denatured to form a complex with  $\beta$ -lg or BSA through thiol–disulfur interchange reactions [153–155]. These complexes should have co-precipitated with  $\beta$ -lg during EDBM.

To complete these information, the chemical composition of isolates obtained at pH 4.6 or 5.0 for 20% WPI EDBM was compared (Table 21.9). Isolates produced by EDBM had a lower ash content than isolates produced by chemical acidification (1.61% vs 2.37% dry basis, respectively). The protein content, on a dry basis, of electroacidified isolates was higher than that of chemically produced isolates: 97.2 vs 94.0, respectively. The difference in ash content may explain the difference in percent

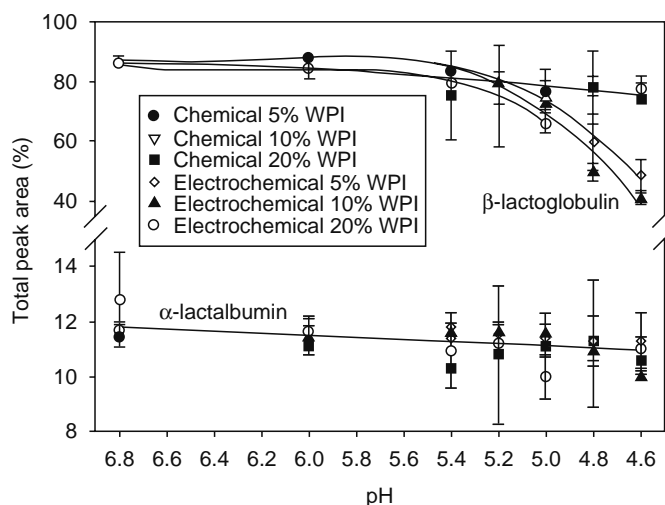


**FIGURE 21.28** Effect of protein concentration on the evolution of protein fraction kinetic during chemical and electrochemical acidification. (Adapted from Bazinet, L., Ippersiel, D., and Mahdavi, B., *Innovative Food Sci. Emerg. Technol.*, 5, 17, 2004.)

**TABLE 21.9**  
**Ash and Protein Composition of the Isolates Produced at 5%, 10%, and 20% WPI**

	Chemical Acidification			Electrochemical Acidification		
	5	10	20	5	10	20
Ash content (% dry basis)	2.3	2.2	2.7	1.5	1.7	1.6
Total protein (% dry basis)	91.7	94.3	96.2	95.3	98.2	98.2
$\alpha$ -lactalbumin ( $\alpha$ -la) (% total peak area)	0.3	2.1	4.7	1.8	2.7	4.8
$\beta$ -lactoglobulin ( $\beta$ -lg) (% total peak area)	99.5	97.7	94.6	98.1	97.3	94.9
BSA (% total peak area)	0.2	0.1	0.7	0.0	0.0	0.4

Source: Adapted from Bazinet, L., Ippersiel, D., and Mahdavi, B., *Innovative Food Sci. Emerg. Technol.*, 5, 17, 2004.

total protein observed for the isolates produced by EDBM vs chemically produced isolates. As expected, the protein content of the isolates increased with an increase in protein concentration. The isolate composition in terms of protein fraction was similar for both acidification methods, but the concentration of  $\alpha$ -la increased while the concentration of  $\beta$ -lg decreased with an increase in total protein concentration.

These results demonstrated the feasibility of EDBM for whey protein separation and the influence of the initial protein concentration on the purity and yield of the separated fraction. At 5% WPI initial concentration, this technology allowed the separation of 98% pure  $\beta$ -lg fraction with a 44% recovery yield, while at 10% WPI initial concentration a  $\beta$ -lg-enriched fraction was produced containing 97.3% of  $\beta$ -lg and 2.7%  $\alpha$ -la, for a 98% total protein purity. The 10% protein concentration seems to be the best level for electrodialytic parameters and protein recovery. Furthermore, EDBM of a 10% WPI solution, by precipitation of 53.4% of the  $\beta$ -lg, allowed the production of an  $\alpha$ -la-enriched fraction in the supernatant. Since the best pH to precipitate  $\beta$ -lg was demonstrated to be pH 4.65 [21], and that the protein yield increases with an increase in initial protein concentration in the solution, it was expected that electroacidification of a 20% WPI solution to pH 4.65 would allow the highest precipitation yield. However, the limiting factor of such a process at 20% was the low conductivity of the protein solution at pH 5.0.

Since the limiting factor of electroacidification by EDBM process at 20% WPI was hypothesized to be the lack of mobile ion inherent to the protein solution at pH 5.0, the authors studied the effect of ionic strength on the precipitation behavior of whey protein [156]. In the first part of this study, electroacidifications of 10% (w/w) WPI solutions were carried out, in batch process using a current density of 20 mA/cm<sup>2</sup>, in different conditions of conductivity control, to evaluate the effect of the conductivity on the precipitation behavior of the whey protein. The highest protein precipitation with 10% WPI solution was obtained at pH 4.6 and at a conductivity level of 200  $\mu$ S/cm maintained with many 0.4 mL-additions of 1.0 M KCl (200  $\mu$ S[+]), with a 46% precipitation of the total protein;  $\beta$ -lg composing the main part of the precipitated protein. One global addition of 1.0 M KCl decreased the protein precipitation yield by resolubilizing protein. The protein fractions showed different trends (Figure 21.29).  $\beta$ -lg composed the main part of the protein-precipitated fraction and the maximum precipitation of  $\beta$ -lg appeared at pH 4.6 and 200  $\mu$ S[+]. The BSA did not seem to be affected during EDBM of 10% BiPRO solution, while a small amount of  $\alpha$ -la was precipitated at pH 4.6 and afterward. These results agreed with the literature [21,157] and previous results obtained for the soluble protein on the optimum precipitation pH of the whey protein at pH 4.65. In a previous work [44], a 40.5% of  $\beta$ -lg at pH 4.6 was obtained with a 25°C normalized conductivity value of 107  $\mu$ S/cm. The difference in  $\beta$ -lg precipitation observed between the present and the previous work may be explained by the different final conductivity levels reached: 200 or 250 vs 107  $\mu$ S/cm. The conductivity appears to influence strongly the extent of protein precipitation.

Since the conductivity control of a 10% WPI solution allowed to reach a lower pH than 4.6, in the second part of their study, Bazinet et al. [156] electroacidified a 20% (w/w) WPI solution with conductivity control: when pH 5.0 or 350  $\mu$ S/cm was reached, conductivity was maintained constant at 350  $\mu$ S/cm. This value was determined as the best combination of protein solubility and system resistance, according to a previous study [44]; at this point the protein insolubility curve was close to its optimum and the system resistance began to increase. With conductivity control at 350  $\mu$ S/cm of the 20% WPI solution, it was possible to reach pH 4.65. A 27% protein precipitation was obtained at pH 4.6. This value was higher than the 21% precipitated protein obtained previously for the same solution at pH 5.0 and at a normalized conductivity value of 161  $\mu$ S/cm [44]. However, this percentage was still low in comparison with the 46% protein recovery obtained with 10% BiPRO solution at 200  $\mu$ S[+]. The apparent viscosity of 10% and 20% BiPRO solution was determined during chemical acidification with 1 N HCl at different shear rates. It appeared that the 10% BiPRO solution should be modeled as a linear surface response regression (Figure 21.30a) while the 20% BiPRO solution should not (Figure 21.30b). Since the viscosity of the 20% whey protein dispersion was very different in comparison with 10% BiPRO and presented a Non-Newtonian profile, the change in viscosity as pH decreases observed at 20% WPI would decrease the precipitation rate of  $\beta$ -lg. Some factors have

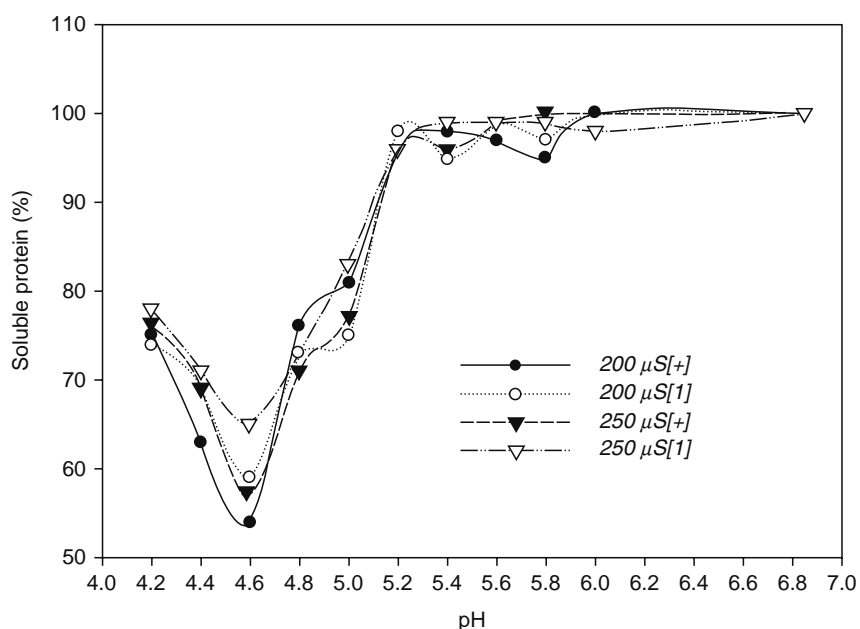


**FIGURE 21.29** Effect of conductivity control on the evolution of the soluble protein during EDBM of 10% BiPRO. (Adapted from Bazinet, L., Ippersiel, D., and Mahdavi, B., *J. Agric. Food Chem.*, 52, 1980, 2004.)

an influence on the viscosity: particle size, polydispersity of diameters, and electroviscous effect in charged particles. Large monodispersed particles tend to give lower relative viscosities than smaller particles at equivalent volume fractions but the differences between them decrease as the mean diameter. This change in viscosity by the means of one or a combination of the three factors would decrease the precipitation yield of  $\beta$ -lg. An increase in the voluminosity of the particles related with an increase in viscosity would slow down the migration or diffusion of the  $\beta$ -lg and consequently its aggregation with other

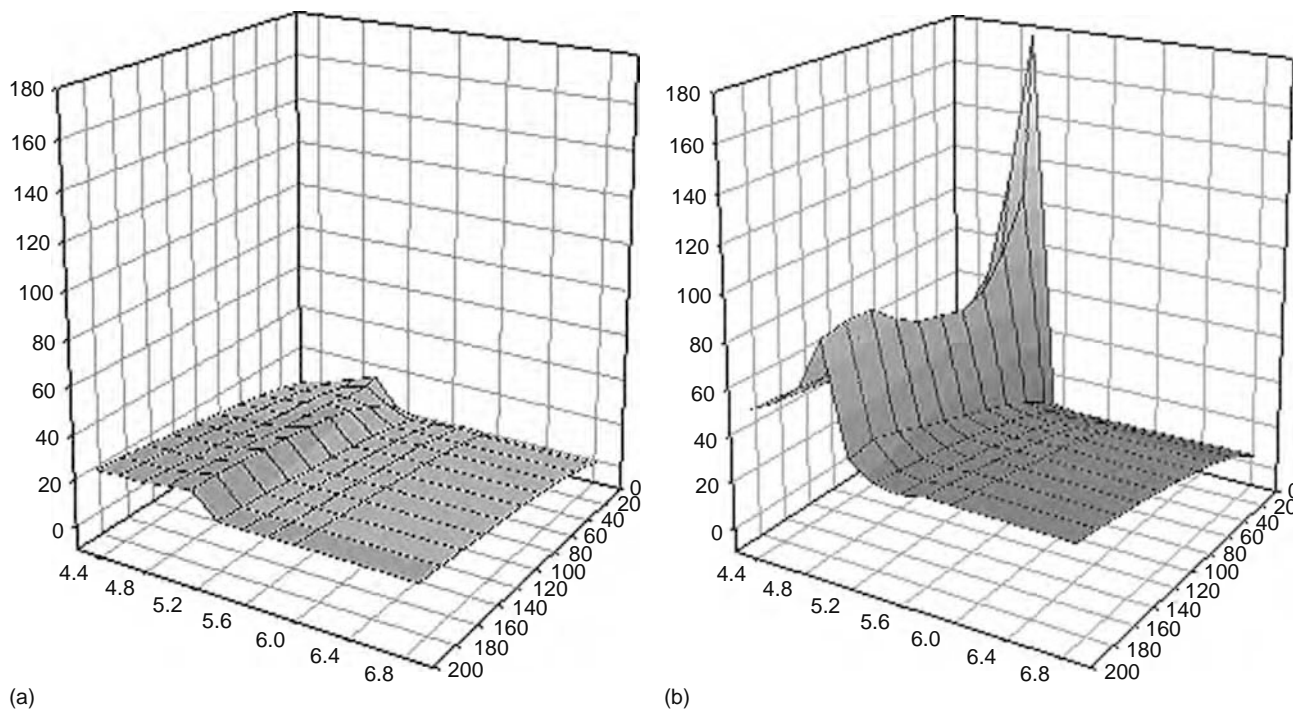


**FIGURE 21.30** Evolution of the apparent viscosity as a function of pH and shear rate of (a) 10% and (b) 20% BiPRO solutions. (Adapted from Bazinet, L., Ippersiel, D., and Mahdavi, B., *J. Agric. Food Chem.*, 52, 1980, 2004.)

monomer or dimer. Moreover, the increase of viscosity should have a direct consequence on the intern hydrodynamic design of the EDBM cell.

EDBM has numerous advantages in comparison with alternative methods for protein fractionation. The process can be precisely controlled, as electroacidification rate is regulated by the effective current density in the cell. The in situ generation and reuse of dangerous chemicals for the environment (acids and bases) suppress the drawbacks and the risks linked to the handling, transportation, use, and elimination of these products. Moreover, by the use of an electroalytic system, which is well known in industry, EDBM technology can easily be transferred to the industrial scale and installation would not need a complete change of the production process, but only some modifications [2]. However, the main advantages of this technology are the high-protein recovery yield, up to 53% in comparison with 33% and 17%, respectively, from acid whey and sweet whey proteins [21,22], and the lower ash content of the isolates.

#### 21.4.7 FRACTIONATION OF MAJOR SOYBEAN PROTEIN FRACTION

Soybean proteins are composed of four protein fractions: 2 S, 7 S, 11 S, and 15 S according to their respective Svedberg units. The two major reserve soybean proteins are the globulins 7 S or  $\beta$ -conglycinin (37% to 39% of total protein) and 11 S or glycinin (31%–44% of total protein). They have different intrinsic properties leading to different functional properties. Saio and Watanabe [158] reported that the 11 S and 7 S have distinct functional properties: 11 S globulin makes much harder tofu gels than 7 S globulin, precipitates faster, and forms larger aggregates relative to 7 S gels. Ning and Villota [159] found that after extrusion the 11 S globulin fraction appeared to favor expansion and water-holding capacity of the finished product. Numerous processes have been patented to separate these proteins based on their different isoelectric points and the capability of the 11 S fraction to precipitate at low temperatures [160].

Adjusting the temperature to 10°C during EDBM allowed a selective fractionation of soybean protein fractions (Figure 21.31a and 21.31b) [43]. In practice, if a sample of precipitated protein was taken at pH 6.2, the protein composition will be composed of 33.8%, 92.9%, 16.2%, and 8.7% of the original content of the 15 S, 11 S, 7 S, and 2 S fractions, respectively. This leads to a solution enriched in the 11 S fraction in the precipitate (71.8% of 11 S and 10.8% of 7 S) and to a solution enriched in the 7 S fraction in the supernatant (46.6% of 7 S and 4.6% of 11 S) [43]. The selective fractionation at low temperature is explained by the fact that proteins which have a high proportion of hydrophobic to polar amino acids, and therefore have structures which depend on hydrophobic interactions, are particularly sensitive to denaturation at the freezing point [87]. According to Chefel et al. [87], soy fractions 11 S and 7 S have relatively high average hydrophobicity values as calculated using Bigelow's equation [161]. Consequently, the combination of the differences in low-temperature sensitivity and in the isoelectric point of both the 11 S and 7 S fractions, the main protein soybean fractions, would allow their selective separation by BPM electroacidification.

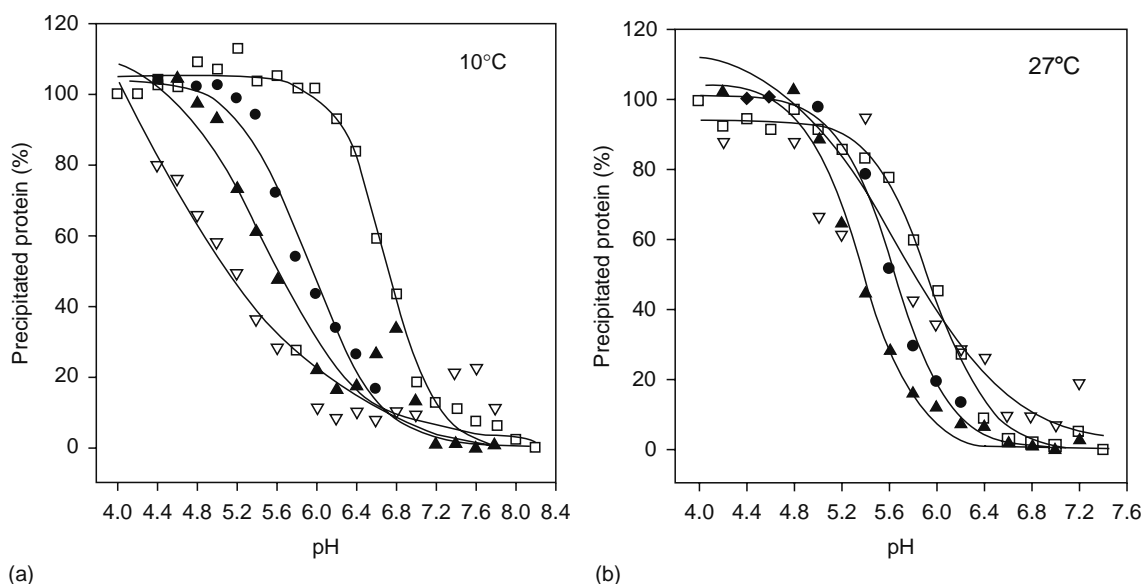


**FIGURE 21.31** Evolution of percent precipitated proteins of the different protein fractions 15 S (●), 11 S (□), 7 S (▲), and 2 S (▽), in a 30 g/L SPC solution with 0.06 M added KCl, during pH decrease by BPM electroacidification at (a) 10°C and (b) 27°C. (Adapted from Bazinet, L., Ippersiel, D., Labrecque, R., and Lamarche, F., *Biotechnol. Prog.*, 16, 292, 2000.)

### 21.4.8 RECOVERY OF PROTEIN AND COAGULANT AGENT FROM SOY TOFU WHEY

In the tofu-making process, coagulant is added to soy milk at a concentration of 2%–4% (w/w) of the soybeans used in the batch [162,163]. The coagulating agent can be calcium sulfate or magnesium chloride. The coagulant causes the protein to aggregate through calcium or magnesium bridging and eventually to precipitate [163]. The combination of coagulant and subsequent heat processing promotes the aggregation and coagulation of the tofu [163], which is then separated from the residual soy tofu whey (STW) and further processed. Disposal of STW, which contains substantial concentrations of pentose and hexose sugars, minerals, proteins, and excess coagulant, is an expensive process that adds significantly to the cost of tofu manufacturing. Now, the whey is discharged to the municipal sewerage system. By rejecting this waste, an important part of the protein (about 20%) and the coagulant is lost; furthermore, these salted effluents pollute the environment. Then, recovering the Mg from STW would decrease the direct cost associated with tofu production while recovering the protein would increase the production yield.

Electrodialysis (ED), EDBM, and a combined configuration of ED followed by EDBM (ED+EDBM) were evaluated for the recovery of magnesium ( $Mg^{2+}$ ) and protein from STW, where magnesium chloride was used as a coagulant [164] (Figure 21.32). ED alone was performed in batch process using a constant current of 1 A for 30 min. EDBM alone was performed in batch process using a constant current of 1 A during the first 40 min, and a constant current of 3 A during the last 20 min of processing, to accelerate the process of electroacidification. In the combined configuration (ED+EDBM), the STW was first treated in the electrodialysis configuration for 60 min, at 1 A constant current, and then in the electroacidification configuration for another 60 min, at 1 A. The configurations were compared on the basis of changes in electrical conductivity,  $Mg^{2+}$  recovery, percent protein precipitation, and energy consumption.

During electrodialysis treatment, total  $Mg^{2+}$  concentration in the STW diminished from 980 to 800 ppm in 30 min: a 18.4% decrease from the initial concentration. This decrease in  $Mg^{2+}$  concentration is due to  $Mg^{2+}$  migration, from the STW solution to the concentrate compartment where its concentration increases proportionally. For cheese whey and skimmed milk, Hiraoka et al. [165] showed that at the early period of demineralization  $K^+$  and  $Cl^-$  are initially removed followed by calcium, magnesium, and phosphorus. However, deashing rate of about 60% and 30% for cheese whey and skimmed milk, respectively, had to be reached before Mg started to migrate. In our case, about 22% of demineralization was reached at the end of the ED configuration.

During EDBM processing, the pH of STW decreased from 5.5 to 3.4 in 60 min. Changing the current from 1 to 3 A allowed a better migration of ions in the solutions and resulted in a faster reduction in pH. The soluble protein concentration decreased

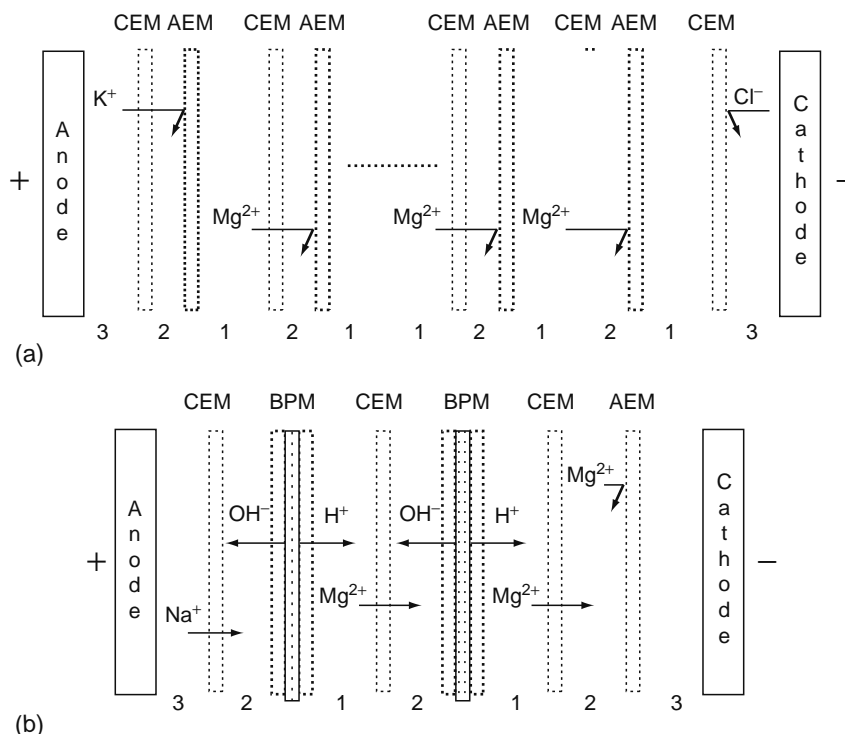


**FIGURE 21.32** (a) Electrodialysis (ED) and (b) electrodialysis with bipolar membrane (EDBM) configurations tested for recovery of magnesium or protein recovery from STW. BPM, bipolar membrane; CEM, cation-exchange membrane; AEM, anion-exchange membrane.

**TABLE 21.10**  
**Energy Efficiency, Recovery Rates of Mg and Protein Obtained**  
**for Three Electrodialytic Configurations**

	Mg <sup>2+</sup> Recovery in 30 min (ppm)	Protein Recovery in 60 min (mg equiv BSA/L)	Energy Consumption (W h)	Relative Energy Consumption (kW h/kg Mg <sup>2+</sup> Recovered)	Relative Energy Consumption (kW h/kg Protein Recovered)
Electrodialysis (ED)	174	0	0.96	0.69	N/A
Electrodialysis with bipolar membranes (EDBM)	35	93	0.34	1.70	0.60
ED +	127	0	0.08	0.08	N/A
EDBM	21	238	0.47	3.76	0.33

Source: Adapted from Bazinet, L., Ippersiel, D., and Lamarche, F., *J. Chem. Technol. Biotechnol.*, 74, 663, 1999.

Note: N/A = not applicable.

from 660 to 510 mg equiv BSA/L: a 22.7% decrease in 60 min. Moreover, this configuration allowed a 14.3% decrease in STW Mg<sup>2+</sup> concentration (decrease from 700 to 600 ppm).

During the ED phase of the combined configuration, the STW pH increased slightly, as previously noted in the ED configuration alone, from 5.6 to 5.9 in 60 min. During the EDBM phase, the pH decreased to 4.0; the pH decreases in the same way in the EDBM configuration and the EDBM step in the combined configuration. The recovery of Mg<sup>2+</sup> from STW was 60.5% during the ED phase in 60 min: the demineralization was performed in a linear fashion during this period (Table 21.10). During the EDBM step, an additional 5% recovery of Mg<sup>2+</sup> was achieved. For the soluble protein concentration, 34.7% of total protein was precipitated during the EDBM configuration step. The combination of the ED and EDBM configurations allowed the recovery of 65% of the Mg<sup>2+</sup> and 34.7% of the proteins from the STW. A demineralization step highly improved the protein precipitation efficiency of EDBM; the efficiency of EDBM increased by a factor of 2 between EDBM configuration and the EDBM step in the combined configuration.

Energy consumption, calculated on a 30 min basis, was about 0.69 kW h/kg Mg<sup>2+</sup> recovered from STW in the ED configuration compared to 0.08 kW h/kg Mg<sup>2+</sup> for the ED step in the combined ED + EDBM configuration (Table 21.10). This could result from the higher temperature of 39°C for the ED+EDBM configuration compared to only 12°C for the ED configuration. Boer and Robbertsen [166] observed that a 10°C change in temperature corresponded to an increase in conductivity and a higher demineralization rate, which had a positive effect on power efficiency. For the EDBM step, values of 1.7 and 3.76 kW h/kg Mg<sup>2+</sup> recovered were obtained, respectively, for the EDBM and the ED + EDBM configurations. The higher initial concentration of Mg<sup>2+</sup> could also be responsible for the higher electrical efficiency for the ED configuration compared to the EDBM configuration [164]. The energy consumption for protein precipitation was lower by a factor of 2 when the STW was partially demineralized by ED before electroacidification by EDBM processing. This confirmed the previous results obtained for protein precipitation slopes.

The combination of demineralization/protein precipitation is an efficient configuration to recover salts and proteins from an STW. Electrodialysis is the most efficient configuration for recovering salts. However for protein recovery, the electroacidification needs a demineralization step to improve its efficiency. Further work is needed to optimize the combined ED + EDBM configuration. Recovery of Mg<sup>2+</sup> and protein from an STW using a two-step process would decrease the cost associated with tofu production. The recovered Mg<sup>2+</sup> could be reused as coagulant thus decreasing the lost of excess coagulant in the effluents. Furthermore, the protein recovered could be reused in the tofu production to increase the protein content of tofu.

## 21.5 OTHER APPLICATIONS: BIOTECHNOLOGY, NUTRACEUTIC, COSMECEUTIC, AND BIOPHARMACEUTIC

BPMs offer a solution to the cation elimination problem accompanying most organic acids: They allow a salt to be split into the corresponding alkali and acid solutions. Consequently, BPMs are used in water-splitting processes and offer possibilities for organic acid recovery from fermentative production. In addition, the decrease in ionic strength induced by cation demineralization coupled with acidification of the solution was also used for the production of phospholipids.

### 21.5.1 FERMENTATIVE PRODUCTION AND ISOLATION OF LACTIC ACID

Lactic acid is one of the organic acids having a wide use in a numerous fields such as food industry, beverage production, pharmaceutical industry, chemical industry, and medicine [167]. Today, more than half of the world production of lactic acid is produced in industrial scale traditionally in simple batch fermentations with low productivities [140]. The conventional fermentation process produces calcium lactate precipitate, which must be concentrated by evaporation and reacidified by a strong acid [168]. The disadvantages of the conventional fermentation processes are a low reaction rate, an elaborate product recovery, a large amount of by-products, and thereby negative impact on the environment. There are other possibilities for lactic acid recovery, but solvent extraction, direct distillation, adsorption, and other relatively simple methods have certain limitations, which obstruct their wider use [169,170]. Electrodialysis is one of the very promising and perspective methods provided by the rapid development of membrane processes.

Bipolar membrane ED was used by Norddahl [171] and Norddahl et al. [172] for fermentative production and isolation of lactic acid (Figure 21.33). A sterilized growth medium as whey permeate from production of whey protein concentrate (WPC) with an admixture of protein-hydrolyzing enzymes was subjected to continuous fermentation in a fermenter by *Lactobacillus* sp. bacteria, which produces lactic acid. The fermentation liquid was ultrafiltered (cutoff 5000 Da, 7.3 m<sup>2</sup> total membrane area) to retain the retentate containing bacteria culture and nonhydrolyzed whey protein, and allowed dissolved matter to pass, including lactic acid formed in the fermentation process. Since ammonia was used to control pH fermentation, the lactic acid was in the form of ammonium lactate. The permeate from the UF process was treated on a chelating resin to bind divalent ions thus preventing precipitation of calcium salts that might otherwise lead to a slow irreversible scaling of the membrane in a subsequent electro dialysis treatment of the permeate. The eluate from the ion-exchange resin was concentrated in a two-step ED process, in which the first step uses conventional ED membranes. In the second step, BPMs separate the salts formed into lactic acid, inorganic acids, and ammonium hydroxide solution (Figure 21.27). Ammonium lactate was thereby converted to ammonium hydroxide and lactic acid in two separate streams. The overall recovery rate of lactic acid was quite high, about 85%–90% based on the amount of sugar added to the fermenter [171].

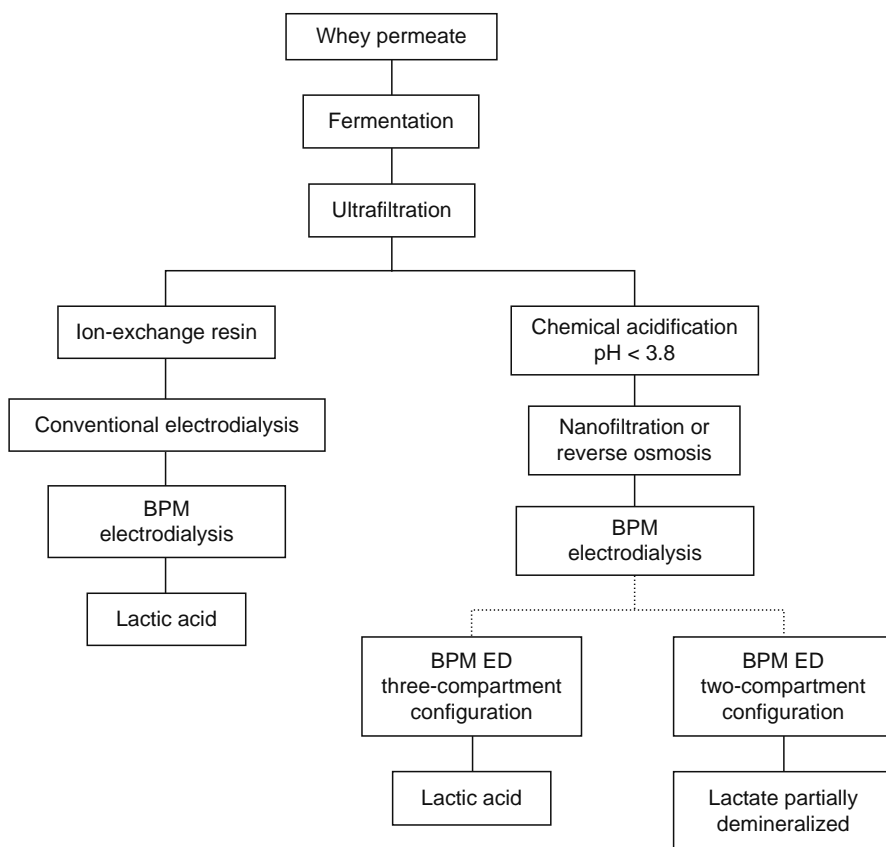
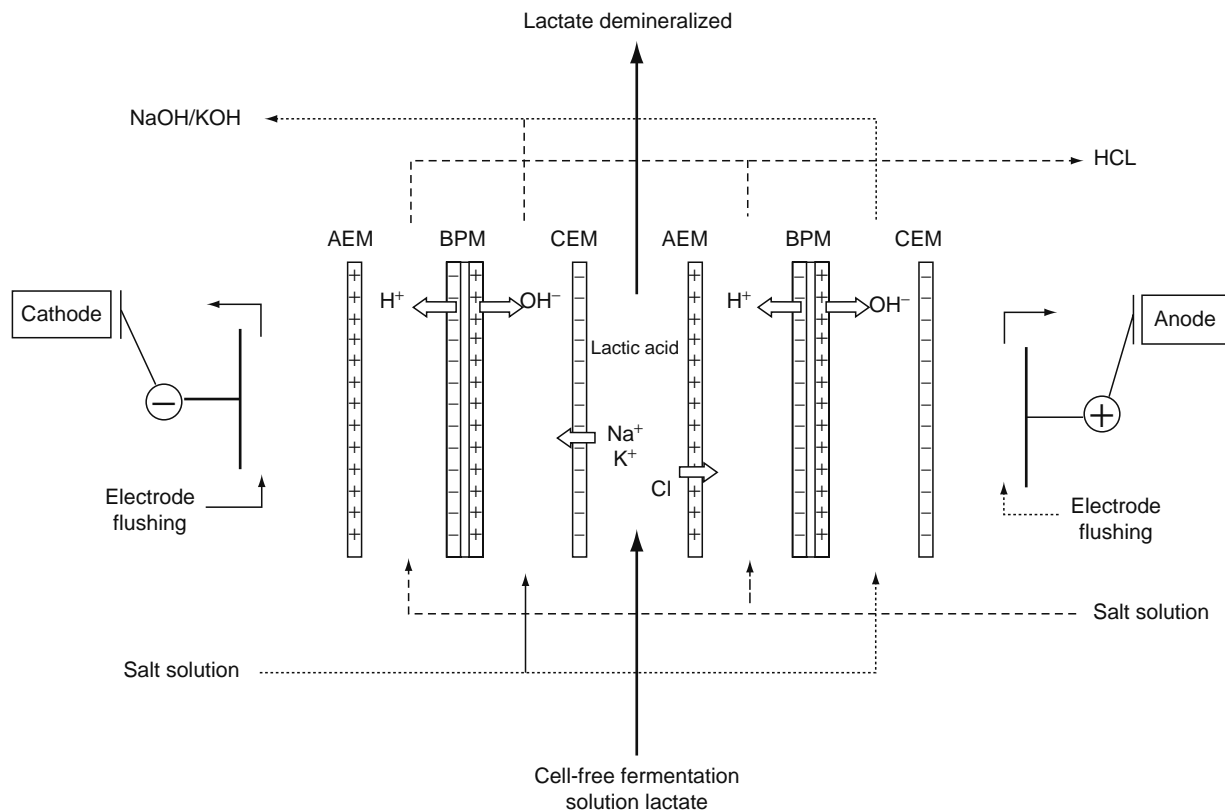


FIGURE 21.33 Process for fermentative and isolation of lactic acid. (From Bazinet, L., *Crit. Rev. Food Sci. Nutr.*, 45, 307, 2005.)

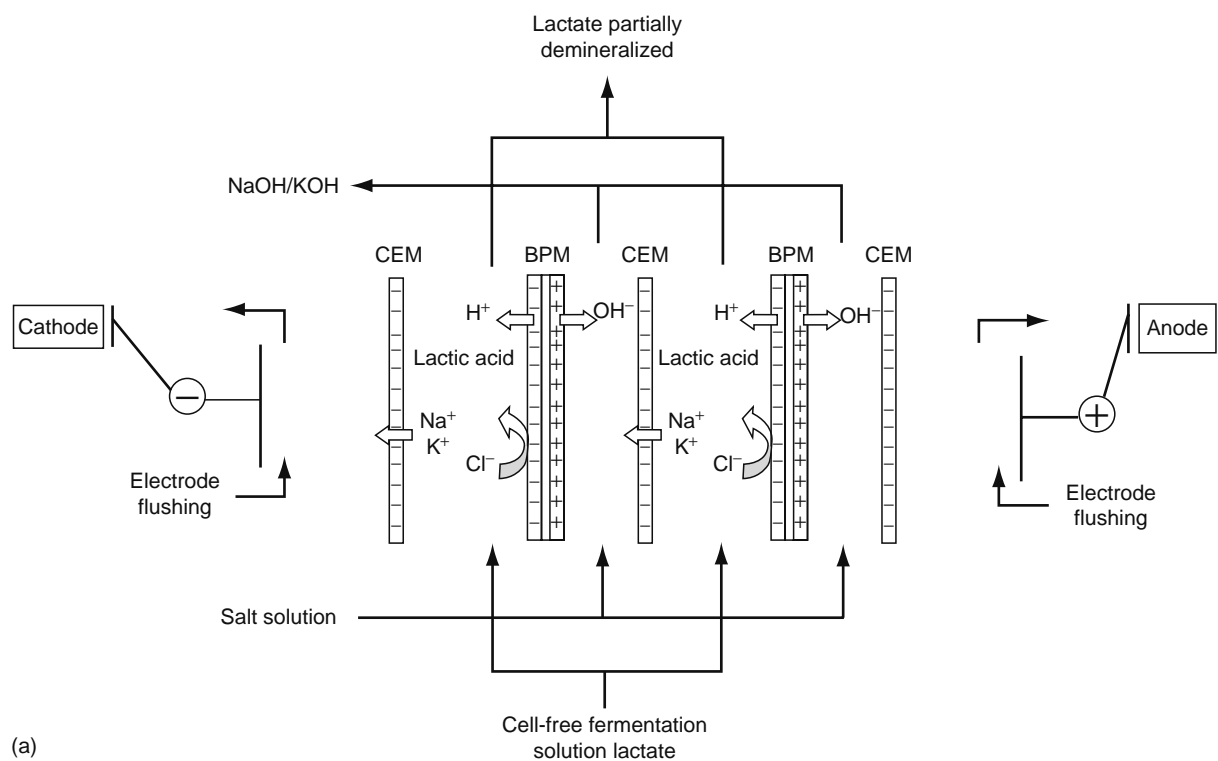
This process was simplified from the general process proposed by Van Nispen and Jonker [142], since the feed stream contained no organic matter that could foul the BPM. Finally, the lactic acid could be purified and concentrated to the desired concentration using a falling film multistage vacuum evaporator or compression evaporator. Recently, a further development based on this process provided a novel purification procedure for isolation [172]. After ultrafiltration of the fermentation liquid, the permeate was acidified (Figure 21.33). The acidification comprises adjustment of the pH to a value of below 3.8, preferably between 2.5 and 3.0, to below the  $pK_a$ -value of lactic acid (3.86). As a result, the free lactate ions combine with hydrogen ions to form lactic acid having no net electrical charge. The resulting acidic solution was then subjected to a nanofiltration or reverse osmosis process to retain divalently charged ions and molecules larger than 180 g/mol. The permeate, free of calcium and magnesium was treated by ED in which ion-selective membrane and BPM separate the inorganic salts from the lactic acid (Figure 21.33). Lactic acid was thus recovered in the feed stream, which was deionized during ED.

Various arrangements are possible for this ED process. Bipolar membrane ED can be operated using a three-compartment configuration, with separate compartments for brine-, base-, and acid-containing streams [142,171,172] (Figure 21.34). The brine compartment, to which the lactate is fed, is passed through the membrane stack in the space between the monopolar and anionic membranes. The base stream is led between the monopolar cationic membrane and the anionic side of the BPM, where the hydroxide ions are generated. The acid stream is led between the monopolar anionic membrane and the cationic side of the BPM, where acid is generated. Thus, the anions (mainly chloride) are transported from the brine compartment, through the monopolar anionic membrane, to the acid compartment, where they combine with protons generated by the BPM to form the corresponding acid. Similarly, cations (Na, K, etc.) are transported from the brine compartment, through the monopolar cationic membrane, to the base compartment, where they combine with hydroxide ions generated by the BPM to form bases. In this way, hydrochloric acid and Na/K hydroxide can be recovered in the acid and base compartments, respectively.

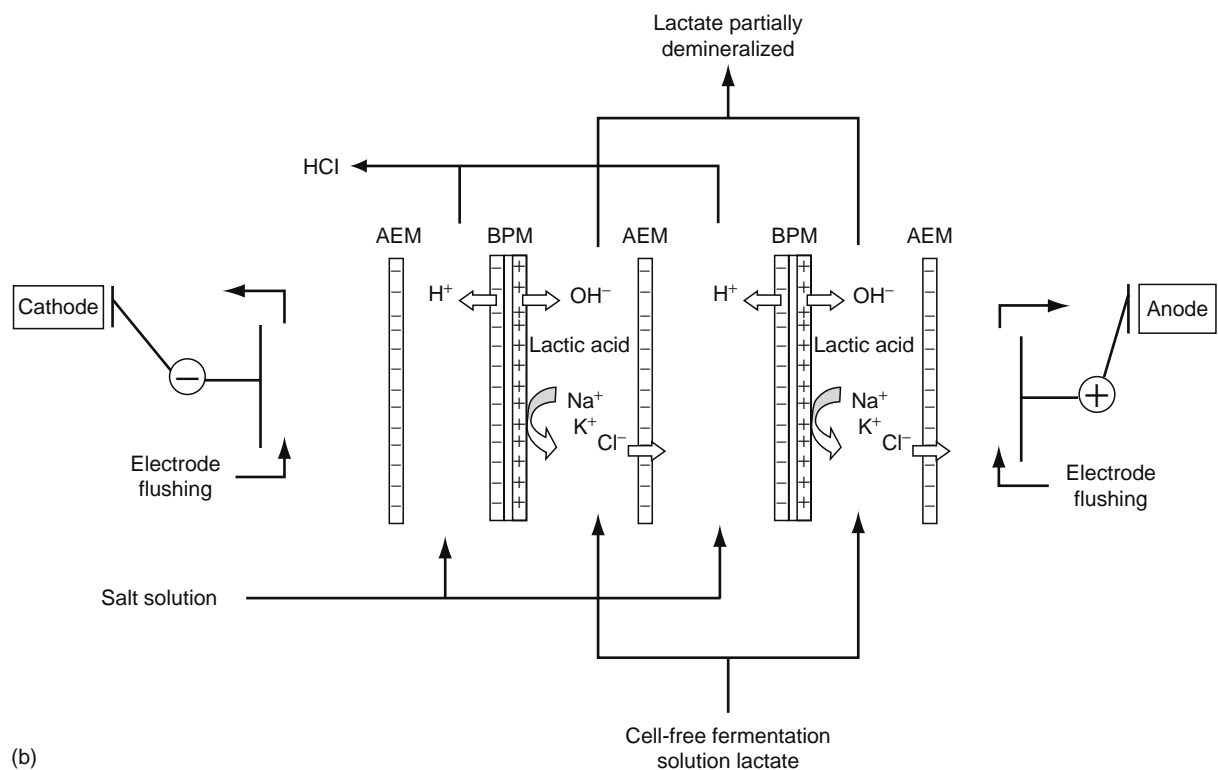
Alternatively, the bipolar membrane ED can be operated using a two-compartment configuration, where either the anionic (Figure 21.35a) or the cationic (Figure 21.35b) monopolar membranes are omitted. In this mode of operation, only cations or anions are removed from the feed compartment and replaced with either protons or hydroxide ions. A brine compartment is



**FIGURE 21.34** Operation of BPM ED using a three-compartment configuration without lactate migration. (From Bazinet, L., *Crit. Rev. Food Sci. Nutr.*, 45, 307, 2005.)



(a)



(b)

**FIGURE 21.35** Operation of BPM ED using a two-compartment configuration coupling. (a) Cation-exchange membrane (CEM) and (b) anion-exchange membrane (AEM). (From Bazinet L., *Crit. Rev. Food Sci. Nutr.*, 45, 307, 2005.)

therefore not present in this configuration. A disadvantage of this configuration, however, is that the lactic acid-containing stream is only partly deionized, since only cations or anions are removed.

This improved process for lactic acid production has the advantage of being simple and inexpensive and resulting in a high-lactic acid recovery rate requiring fewer steps. According to Norddahl et al. [172], it is possible to reach an overall recovery rate of about 90%–95% or more than 98% based on the amount of sugar added to the fermenter. Further, several additional advantages are obtained by the invention, including

1. No need to use chemicals to regenerate ion-exchange materials.
2. Higher operating efficiency, since in contrast to a process using ion exchange, there is no risk of calcium or magnesium ions passing through the ion-exchange resin; therefore, the process is also easier to control.
3. All the effluent streams are recycled, the acids and bases generated in the optional bipolar ED step being returned to the process.
4. A reduction in the amount of waste products, since the only waste generated is in the concentrate from nanofiltration, which contains  $\text{Ca}^{2+}/\text{Mg}^{2+}$  ions and colored compounds.

### 21.5.2 PRODUCTION OF PHOSPHOLIPIDS

Dairy whey is a by-product of cheese and casein manufacture. Cheese whey contains 7–10 g/L of proteins with a high content of  $\beta$ -lactoglobulin (3 g/L) [173] and about 2–8 g/L of lipids [174]. Whey lipids are composed of almost 66% of nonpolar lipids and 33% of polar lipids. Polar lipids are mainly phospholipids with 34% phosphatidylethanolamine, 31% phosphatidylcholine, 15% sphingomyelins, 12% phosphatidylinositol, and 8% phosphatidylserine [175]. In comparison with other sources of phospholipids available in the market (soybean essentially), the dairy phospholipids are original due to the presence of a high concentration in sphingomyelins and a low proportion of polyunsaturated fatty acids [175]. Hence, the presence of a high concentration of sphingomyelins in the lipids of the skin suggests a possible use of whey phospholipids in cosmeceutic. Furthermore, the fact that the fatty acids presented a low rate of polyinsaturation would have a main impact on the susceptibility to oxidation of these lipids.

Whey is generally concentrated by evaporation and spray dried to obtain WPCs. Over the past several years, WPCs have been largely used in the food industry as nutritional and functional ingredients. Typically, conventional WPCs are composed of more than 35% of protein and have a fat content higher than 4% [176]. However, the presence of lipid in these products affects their functional properties [177] and promotes the development of oxidation reactions, which could impart off flavors [178]. For these reasons, methods to decrease fat content in the final product have been developed. Among those methods, the thermocalcic precipitation can be cited. It consisted of the addition of divalent calcium ions to the solution the pH of which was adjusted to 7.3. This solution was then heated to allow aggregation and precipitation of phospholipoprotein complexes [174,179,180]. These complexes were then eliminated by, for example, microfiltration. With this method, it is possible to produce a WPC containing less than 0.5% of lipids [181]. However, this microfiltration process have to be optimized to obtain a satisfactory membrane flow and protein permeation. De Wit and Klarenbeek [182] have found that the decrease of the ionic strength of whey solutions combined with chemical acidification at pH 4.6 allowed the precipitation of lipoproteins, which could be separated by decantation. Ionic strength reduction was carried out by demineralization with ion-exchange resins, electro dialysis, or diafiltration. Another method consisted of an acid precipitation of lipids in a medium with a low-ionic strength. Phillips et al. [183] and Boswell and Hutchinson [176] have proposed a process consisting of a preliminary concentration of the whey by ultrafiltration until a solid value of nearly 23% was reached. This intermediate WPC was then diluted to decrease the ionic strength and was chemically acidified to reach a pH of 4.3. Separation of the fat compounds by flocculation was then obtained. The clarified product was concentrated by ultrafiltration and dried by an atomization process. The final product was then composed of less than 1% of lipids [176]. However, the chemical products used for the WPC acidification present the disadvantage of adding organic or mineral salts which increase the ionic strength of the solution.

Recently, Lin et al. [184] used EDBM technology for acidification and decreasing the ionic strength of a fresh cheddar cheese whey. In this study, EDBM process was carried out with or without preliminary decrease of whey mineral salts content by conventional electro dialysis to obtain precipitates with high level of lipids (Figure 21.36). After centrifugation of the treated whey, composition of flocs and precipitation yields was determined.

Whey centrifugation at 1000 g during 5 min (process 1) allowed a 20.8% recovery of cheddar cheese whey initial lipids (Table 21.10). The other components, proteins and lactose were precipitated at a lower rate (1.1% and 0.6%, respectively). A 32.1% whey lipid precipitation was obtained in process 2 consisting of an electroacidification to reach a pH value of 3.7 before the centrifugation step. This represents a 54% increase of precipitation rate in comparison with process 1, with proteins and lactose precipitation levels quite similar (1.9% and 0.9%, respectively). Demineralization step before electroacidification had only small effect on the precipitation level: Similar precipitation levels for lipids and lactose were obtained in comparison with process 2 values except for proteins. Conventional electro dialysis allowed an increase of protein precipitation from 1.9% to 3.3% (Table 21.11).

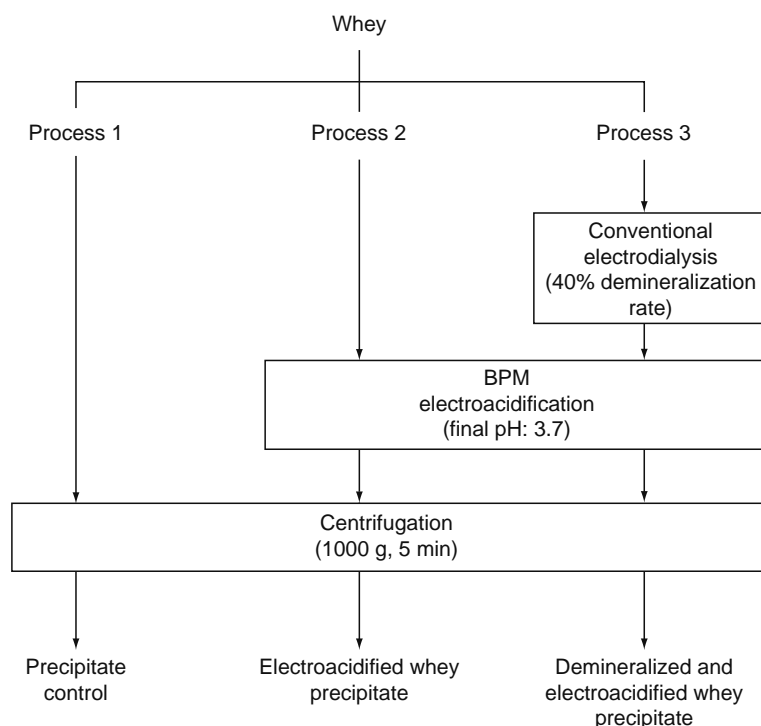


**FIGURE 21.36** Cheddar cheese whey treatment by conventional electro dialysis and EDBM before final centrifugation.

Phosphatidylcholine (PC), phosphatidylethanolamine (PE), and phosphatidylserine (PS) have a nitrogen atom in their structure; then it was possible to estimate the nitrogen content of precipitates from their lipid contents. The calculated nitrogen content from the phospholipids was close to the total nitrogen values detected in the precipitates (except for the process 3), which suggests that precipitates were composed mainly of phospholipids. Other constituents should be proteins, lactose, and mineral salts but at a low level. These latter two compounds could be washed by water.

Lipids recuperation by centrifugation in process 1 was due to residual fat particles. The increase of lipids precipitation levels in processes 2 and 3 may be explained by the formation of lipids/proteins complexes during electroacidification precipitates [182]. The protein–lipid interactions that exist in food systems involve hydrophobic interactions between apolar aliphatic chains of the lipid and the apolar regions of the protein. In model systems, the energy of the protein–lipid interaction reaches a maximum in the neighborhood of the isoelectric point of the protein [87]. The associations between lipids and proteins are probably electrostatic interactions involving the phospholipids. The isoelectric point of the  $\beta$ -lactoglobulin, the main whey protein, is at pH 5.5. So at pH 3.7, the protein carries a positive electric charge [185]. However, some phospholipids have a negative charge at acid pH like the phosphatidylserine which have, at pH 3.7, two negatively charged groups: the phosphoric acid group and the carboxylic acid group [186]. An equation, including calcium ion level that represents the mechanism of protein/lipid complex formation, was reported by Cornell and Patterson [187]:



**TABLE 21.11**  
**Whey Components Precipitation Yields**

	Process 1 (%)	Process 2 (%)	Process 3 (%)
Lipids	20.8 ± 3.5	32.1 ± 4.7	29.7 ± 2.3
Proteins	1.1 ± 0.7	1.9 ± 0.5	3.3 ± 0.4
Lactose	0.6 ± 0.4	0.9 ± 0.2	1.1 ± 0.1
Total solids	1.5 ± 0.6	2.3 ± 0.4	2.6 ± 0.2

where

P denotes protein with a charge  $z$

Ca denotes calcium ion

L denotes phospholipid carrying a negative charge

$n$  denotes number of phospholipids bound per protein group

Lau et al. [188] have shown that calcium ions are linked to phospholipids. The binding of calcium with lipids inhibits the formation of lipid/protein complexes. The decrease in mineral salts, particularly in magnesium and calcium ions, during processes 2 and 3 promotes the lipid/protein complexes formation. This phenomenon was confirmed by higher precipitation levels for lipids and proteins in process 3 in comparison with process 1 (Table 21.11). Equation 21.1 also means that an increase of  $P^{z+}$  components should improve the lipid/protein complexes formation. This increase of  $P^{z+}$  may be obtained by a concentration step of whey solutions by ultrafiltration.

On the basis of these observations, further works were carried out by Bazinet et al. [189] to evaluate the effect of protein concentration on the lipid precipitation. In this second study, a WPC with 55% of protein on dry basis was used. WPC electroacidification was carried out with or without preliminary demineralization by conventional electro dialysis. The effect of the ionic strength on precipitation rates of fats was also evaluated by water dilution of the WPC samples.

Products  $A_1$ ,  $B_1$ , and  $C_1$  which were the supernatants coming from the centrifugation of products A, B, and C (Figure 21.36) presented similar levels of total solids and proteins (Table 21.12). However, the fat contents are significantly lower in products  $B_1$  and  $C_1$ : lipid levels in supernatants  $A_1$ ,  $B_1$ , and  $C_1$  were 0.63%, 0.55%, and 0.47%, respectively. Then, the EDBM process resulted in an increase in the rate of lipid precipitation (35% yield) in comparison with a single-step centrifugation. The demineralization process carried out under the given conditions did not induce a destabilization of the lipids matter which could have resulted in a higher lipid precipitation. However, a more important decrease of the ionic strength can have significant effect on lipids precipitation. This was the object of the second part of this study on the decrease of the ionic strength of solutions by dilution of the acidified WPC.

Hence, in products from D to I, which were the supernatants obtained after dilution, decantation, and centrifugation of previous products, respectively, significant drops in protein and lipid levels were observed in comparison with the initial product composition (Table 21.12). Only samples H and I had a protein level different from the other samples (Table 21.12). The decrease of protein content was of 9% and 8%, respectively, for these products. This suggests that a part of the protein in the supernatants has precipitated. This could be explained by their lower ionic strength (conductivity of 0.4–0.8 mS/cm). Products D, E, F, and G had similar protein contents. In a general manner, the acidification by EDBM followed by a dilution resulted in the preservation of more than 90% of the protein present initially. For the fat content, the more important decrease was observed for products E and F with a respective reduction of their lipid contents of 73% and 66%. In second position are products H and I with 49% and 45% respective reduction of lipids levels (Table 21.12). These different precipitation levels might be explained by the initial fat contents of the products. Effectively, products E and F obtained from samples B and C contained between 0.72% and 0.78% of fat while products H and I obtained from products  $B_1$  and  $C_1$  have fat levels between 0.47% and 0.55%. Samples dilution following the EDBM step resulted in a reduction of lipids from 0.78% to 0.21%, a decrease of nearly 73% of initial content in WPC lipids. It also resulted in clarified supernatants with a low level in lipids and with the majority of the proteins present initially.

This new process would have two advantages, the production of a phospholipid-enriched fraction, which could be used in cosmeceuticals and nutraceuticals and a purified (demineralized and delipided) and more valuable protein fraction after concentration of the whey. EDBM process could be a part of the first step of WPC treatment for the valorization of the whey in the form of lipid fractions of different nature. In comparison with the chemical acidification, EDBM process has the

**TABLE 21.12**  
**Protein and Lipid Contents of Initial Samples (A, B, C,  $A_1$ ,  $B_1$ , and  $C_1$ )**  
**and of the Diluted Samples Supernatants (D to I)**

Products	Protein Content (%)	Fat Content (%)	Products	Protein Content (%) Multiplied by Dilution Factor	Fat content (%) Multiplied by Dilution Factor
A	9.27	0.76	D	9.25	0.54
B	9.72	0.78	E	9.57	0.21
C	8.89	0.72	F	8.04	0.24
$A_1$	9.01	0.63	G	9.00	0.50
$B_1$	9.63	0.55	H	8.80	0.28
$C_1$	8.84	0.47	I	8.17	0.26

advantage of offering continuous acidification without the addition of salt. This could allow, in an industrial process, (1) to maintain a low-ionic strength of the solution, for example, before or after WPC dilution and (2) to produce a purified WPC (with a low ash level).

## 21.6 SUCCESSFUL EDBM INDUSTRIAL PLANTS

Authors are grateful to Eurodia Company (Wissous, France) for its contribution to this part.

### 21.6.1 HISTORY OF ELECTRODIALYSIS WITH BIPOLAR MEMBRANES

Over the past 15 years, more than a dozen known commercial plants totaling about 2500 m<sup>2</sup> of BPMs have been installed throughout the world. These membranes came from two suppliers: Aqualytics Corporation (Warren, New Jersey) and Tokuyama Corporation (Tokyo, Japan) (Neosepta).

Table 21.13 reviews the (known) different plants installed worldwide with above membranes and the corresponding estimated membrane area. The first bipolar system was delivered in 1986 to Washington Steel in Pennsylvania for the recovery of hydrofluoric and nitric acids from stainless steel pickling liquor and the most recent one has been installed in China for the production of an organic acid. In the last few years, some of the plants in operation in the United States have been closed due mainly to overall plant shutdowns, product line changes, or other economical reasons.

Therefore, we know of about 1850 m<sup>2</sup> of BPM currently (or soon) in operation, mainly for the production of specialty and fine chemicals, such as amino and organic acids. The limited number of EDBM plants in operation is the result of many factors, mainly industry concerns over reliability and cost. The relatively high investment of EDBM systems limits its use so far to higher value products. However, improvement in stack and plant design, as well as overall process design, allows its use for the production of a growing number of products. Already, four new plants have been installed in the last 2 years.

**TABLE 21.13**  
**Different Plants Installed Worldwide Operating with Aqualytics and Neosepta BPMs (Tokuyama Corporation)**

Year	EDBM Plants Installed		
	United States	Asia	Europe
1986	Pickling liquor recovery (stainless steel) <sup>a</sup>		
1994	HF recovery (chemical industry) <sup>a</sup>		
1995	Organic acid production (agro industry) <sup>a</sup>		
	Inorganic acid production (chemical industry) <sup>a</sup>		
1996		Organic acid production (specialty chemical industry)	Methane sulfonic acid production (Italy) (specialty chemical industry)
1997	Organic acid recovery (specialty chemical industry)	Organic acid production (specialty chemical industry)	Organic acid production (France) (agro industry)
1998	Inorganic acid production (chemical industry)		Amino acid production (France) Organic acid production (Czech Republic) (agro industry)
1999		Amino acid production (pharmaceutical industry)	
2001	Organic acid production (specialty chemical industry)		
2002	Organic compound production (fine chemical industry)	Organic acid production (China) (agro industry)	Organic acid recovery (Germany) (pharmaceutical industry)
2003	Organic acid production (specialty chemical industry)		
2004	Organic acid production (dairy industry)		
Total installed BPM area (estimated)	1660 m <sup>2</sup>	650 m <sup>2</sup>	700 m <sup>2</sup>

<sup>a</sup> Closed

## 21.6.2 EDBM: A COST-EFFECTIVE SOLUTION FOR THE PRODUCTION OF SPECIALTY AND FINE CHEMICALS

### 21.6.2.1 Criteria for the Application of EDBM

The effective utilization of EDBM requires the following conditions:

- Total multivalent cations content in the treated fluid was in the range less than 1–5 ppm. Indeed, the multivalent cations may precipitate by association with  $\text{OH}^-$  ions in the stack. This precipitation may occur in the CEM during the ionic transfer from the acid to the base compartment, thus destroying this membrane. It is to be noted that the BPM is not affected by this problem.
- Feed concentration in organic acid salt greater than 1 equiv/L: this specification allows a reduction of the membrane area required for the conversion because the current density can remain high enough during most of the conversion. This leads to a decrease of both the investment and operating costs.
- Operating temperature lesser than 40°C.
- No oxidizing compounds. These requirements are related to the materials used to manufacture the membranes.

### 21.6.2.2 Organic Acid Production in France

Eurodia Industry delivered an EDBM plant in 1997 in France for the production of an organic acid from its sodium salt (Figure 21.37). The acid, produced by fermentation, must remain confidential as well as the name of the customer. The plant was initially designed to produce 2600 mton/year of acid (100%) over 8000 h of operation. Two EUR20-240 stacks with 81 m<sup>2</sup> of effective cell area were initially installed in the two-compartment configuration (see Figure 21.37) with Neosepta CMB cation-exchange and BP1 BPM. The acid conversion rate (purity) is 98% with a concentration of 390 g/L: this is equivalent to a final conductivity of 3 mS/cm. The NaOH was initially produced at a concentration of 6 wt% to be reused in the fermentation (most microorganisms do not like acidic conditions). The plant initially operated in a batch mode to consistently meet the customer requirements. The initial battery-limit investment was £1,050,000.

After several years of operation, a membrane life of 20,000 h was reached for the BPMs, while the CEMs have been replaced after 18,000 h. The electrodes have not been changed until now. The customer has increased the capacity in several steps by adding several EUR20 and EUR40 stacks and an additional capacity expansion is being considered. By changing the operation from batch mode to feed and bleed, the base concentration could be increased from 6 to 8 wt% with the same current efficiency (for a new plant, the NaOH could be produced at 10 wt%). The main operating costs are power at 0.88 kW h/kg of produced acid and membrane (electrodes) replacement at 0.077 £/kg.

### 21.6.2.3 Acetic Acid Production in Germany

In 2002, Eurodia has supplied chelating resins and bipolar ED plant for 1700 ton/year acetic acid production, which represents 450 m<sup>2</sup> as total membrane area (Figure 21.38). The purpose of this application is to recover acetic acid from sodium acetate waste effluent and to reuse it in the process. The feed flow of sodium acetate concentration at 210 g/L is 1.5 m<sup>3</sup>/h and 91.5% is converted in acid. Acetic acid is recovered at 3 N and sodium hydroxide at 1.5 N. This plant was built according to pharmaceutical standards.

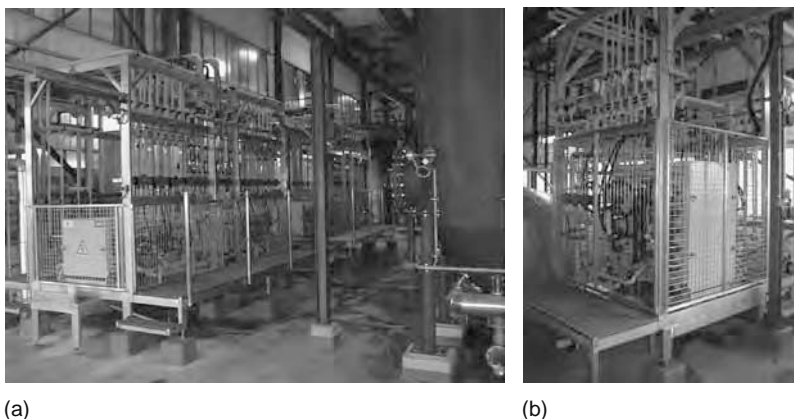


FIGURE 21.37 (See color insert following page 588.) Organic acid production in France. (From Eurodia Co.)



**FIGURE 21.38** (See color insert following page 588.) Acetic acid production in Germany. (From Eurodia Co.)

#### 21.6.2.4 pH Adjustment of Wine

After the development of wine stabilization by conventional ED, INRA Pech-Rouge with Eurodia has developed a new application of EDBM for wine. In many regions, the pH of wine is quite high. To improve the quality, the pH of wine must be increased from 0.3 to 1 pH unit. The EDBP allows this pH decrease in continuous treatment with a high efficiency and without any addition of chemicals (Figure 21.39). The official European Community approval is under progressing for this technology since 2005. This application is allowed in United States after getting Food and Drug Administration approval in 2004.

#### 21.6.2.5 EDBM Included in Complete Processes

As previously mentioned, the efficiency of EDBM, as a single-unit operation, has been demonstrated for the recovery/production of specialty chemicals. However, to propose overall cost-effective solutions, EDBM has frequently to be considered as one step of a complete process. As an example, the process reported in Figure 21.40 could be proposed for the production of an



**FIGURE 21.39** EDBMs for the stabilization of the wine pH. (From Eurodia Co.)

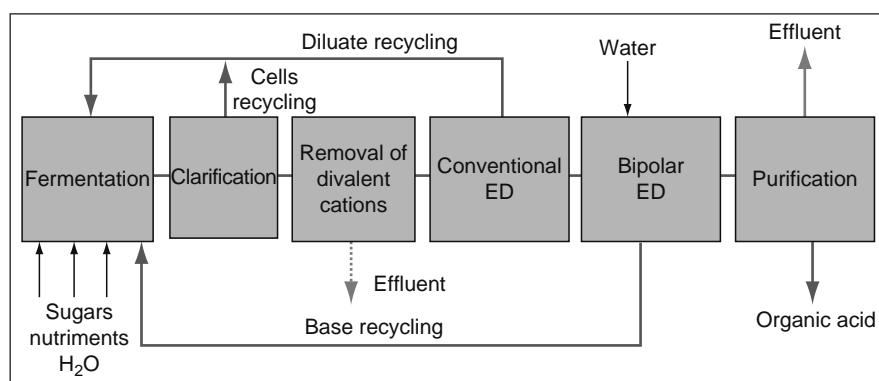


FIGURE 21.40 Organic acid production from a fermentation step. (From Eurodia Co.)

organic acid, such as lactic acid starting from sodium lactate produced by fermentation. The heart of the process is the conversion step performed by EDBM. To meet the feed requirements of EDBM (see above), the fermentation broth is first clarified by microfiltration. Then, the divalent cations content is lowered to a range of 1–5 ppm. The target species, i.e., sodium lactate, are concentrated and purified by conventional electro dialysis. After the conversion of sodium lactate into lactic acid, the product is purified by ion-exchange resins.

It is to be noted that the environmental impact is greatly reduced compared to traditional precipitation processes. Indeed, recycling can be optimized to the extent that the only environmental discharge is due to the use of ion-exchange resins. Furthermore, the effluent generated by the divalent cation removal step can be reduced by coupling both ion-exchange and membrane techniques. In 2002, Eurodia sold an equipment for a 2500 ton/year of lactic acid production in China. It consisted in three conventional ED stacks EUR40 and two EUR40 bipolar stacks, which represent a total membrane area of 2310 m<sup>2</sup> (Figure 21.41). An ultrafiltration skid with organic membranes was installed to clarify the fermentation broth.



FIGURE 21.41 (See color insert following page 588.) Electro dialysis stacks. (a) Aqualyzer EDC (conventional ED) and (b) aqualyzer EDBP (EDBM). (From Eurodia Co.)

## 21.7 CONCLUDING REMARKS AND PERSPECTIVES

EDBM is a recent technology, which appeared only in the 1980s, with the first commercial BPMs. Twenty years later of commercialization, lots of commercial plants are in operation and the demand for this technology grows up due to improved economics resulting from better design for ED stack and operating conditions.

EDBM has numerous advantages. Among others, (1) it uses electricity to generate the desired ionic species to acidify or alkalize the treated solutions, (2) water dissociation at the BPM interface is continuous and the process can be precisely controlled by the effective current density in the cell, (3) the in situ generation and reuse of dangerous chemicals for the environment (acids and bases) suppress the risks linked to their handling, transportation, and elimination, (4) the water consumption is lower by reuse of a part of the effluents generated and a low-energy consumption, and (5) the duration life of BM is more than 10,000 h, and reaches 20,000 h for specific applications.

However, some disadvantages of EDBM still exist: (1) the cost of equipment, which limits its use to high value products, (2) the permselectivity of the associated AEMs, decreasing the effectiveness of the BPM. In addition, presently, the development of EDBM is always limited by the number of applications, which are mainly focused on acid/base production. But, the selectivity and the lifetime of associated homopolar membrane are continuously increasing owing to researches in polymer science, along with the quality of new BPM. Food, nutraceuticals, biotechnology, and pharmaceutical are and will be in the future very interesting fields of application for combining all the advantages of BPM technology in a more competitive market. Promising applications for the production or recovery of organic and amino acids, as well as other specialty/fine chemicals and biomolecules are under study. The development of the technology, and its application in the agri-food and bio-industries, will surely help to minimize the cost of the BPMs equipment. In the future, EDBM would have to be considered as a step of a complete process and not as a single-unit operation, to discover its multiple potential uses not only in the chemical industry.

## ABBREVIATIONS

AEM	anion-exchange membrane
CEM	cation-exchange membrane
IEM	ion-exchange membrane
BPM	Bipolar membrane
EDBM	Electrodialysis with bipolar membrane
COD	chemical oxygen demand
PPO	polyphenols and polyphenol oxidases
SPC	soy protein concentrate
STW	soy tofu whey
WPC	whey protein concentrate
WPI	whey protein isolate

## REFERENCES

1. Davies AT, Genders JD, and Pletcher D. *Ion Permeable Membranes*. The Electrochemical Consultancy, Romsey, England, 1997.
2. Bazinet L, Lamarche F, and Ippersiel D. Bipolar-membrane electrodialysis: An application of electrodialysis for the food industry. *Trends Food Sci. Tech.* 1998; 9: 107–113.
3. Shaposhnik VA and Kesore K. An early history of electrodialysis with permselective membranes. *J. Membr. Sci.* 1997; 136: 35–39.
4. Klein E, Ward RA, and Lacey RE. Membrane processes—dialysis and electrodialysis. In: Rousseau RW, Ed. *Handbook of Separation Process Technology*, John Wiley & Sons, Wiley-Interscience, New York, 1987, pp. 954–981.
5. Glassner D. Ed. Applications in Biotechnology. Proceedings of the 10th Annual Membrane Technology Planning Conference. Business Communications, Norwalk, CA, 1992, pp. 158–165.
6. Houldsworth DW. Demineralization of whey by means of ion exchange and electrodialysis. *J. Soc. Dairy Tech.* 1980; 33: 45–51.
7. Batchelder BT. Electrodialysis applications in whey processing. International Whey Conference, Chicago, IL, October 28, 1986. Paper no TP 343 ST.
8. Pérez A, Andrés LJ, Alvarez R, Coca J, and Hill CG. Electrodialysis of whey permeates and retentates obtained by ultrafiltration. *J. Food Proc. Eng.* 1994; 17: 177–190.
9. Jain SM and Reed PB. Electrodialysis. In: Cooney CL and Humphrey AE, Eds. *Comprehensive Biotechnology, Vol.2: The principles of Biotechnology: Engineering Considerations*, Pergamon, New York, 1985, pp. 575–590.
10. Maigrot E and Sabates J. Apparat zur Läuterung von Zuckersäften mittels Elektrizität. 1890. German Patent no 50 443.
11. Cassel GE and Kempe D. Verfahren: Melasse, Sirup und andere Zuckerlösungen Elektrolytisch zu Reinigen. 1894. German Patent no 78 972.

12. Kikuchi K-I, Gotoh T, Takahashi H, Higashino S, and Dranoff JS. Separation of amino-acids by electro dialysis with ion-exchange membranes. *J. Chem. Eng. Jpn.* 1995; 28: 103–109.
13. Bing DH, DiDonno AC, Regan M, and Strang CJ. Blood plasma processing by electro dialysis. In: McGregor WC, Ed. *Membrane Separations in Biotechnology*, Marcel Dekker Inc., New York/Basel, 1986, pp. 135–160.
14. Guérif G. Electro dialysis applied to tartaric stabilisation of wines. *Revue des Oenologues et des Techniques Viticoles et Œnologiques* 1993; 69: 39–42.
15. Escudier J, Saint-Pierre B, Batlle J, and Moutounet M. Automatically controlled tartaric stabilisation of wine by membrane electro dialysis which reduces its conductivity to the desired level. 1995. World Patent no 9 506 110-A1.
16. Audinos R, Roson JP, and Jouret C. Application de l'électro dialyse à l'élimination de certains composants du jus de raisin et du vin. *Connaissance Vigne Vin* 1979; 13: 229–239.
17. Lamarche F and Boulet M. Électro dialyse et Alimentation: Le Courant Passe! In: *Alimentech*, Agri-Food and Agriculture, Canada, 1992, pp. 14–15.
18. Vera E, Ruales J, Sandeaux J, Dornier M, Persin F, Reynes M, and Pourcelly G. Comparison of different methods for deacidification of clarified passion fruit juice. *J. Food Eng.* 2003; 59: 361–367.
19. Vera Calle E, Dornier M, Sandeaux J, and Pourcelly G. Deacidification of the clarified passion fruit juice using different electro dialysis configurations. *Desalination* 2002; 149: 357–361.
20. Reed PB. Electro dialysis for the purification of protein solutions. *Chem. Eng. Prog.* 1984; 12: 47–50.
21. Amundson CH, Watanawanichakorn S, and Hill CG Jr. Production of enriched protein fractions of  $\beta$ -lactoglobulin and  $\alpha$ -lactalbumin from cheese whey. *J. Food Proc. Pres.* 1982; 6: 55–71.
22. Slack AW, Amundson CH, and Hill CG. Production of enriched  $\beta$ -lactoglobulin and  $\alpha$ -lactalbumin whey protein fractions. *J. Food Proc. Pres.* 1986; 10: 19–30.
23. Mani KN. Electro dialysis water splitting technology. *J. Membr. Sci.* 1991; 58: 117–138.
24. Siebold M, Frieling PV, Joppien R, Rindfleisch D, Schugerl K, and Roper H. Comparison of the production of lactic acid by three different *Lactobacilli* and its recovery by extraction and electro dialysis. *Process Biochem.* 1995; 30: 81–95.
25. Nagasubramanian K, Chandla FP, and Liu KJ. Use of bipolar membranes for generation of acid and base—an engineering and economic analysis. *J. Membr. Sci.* 1977; 2: 109–124.
26. Mani KN, Chlanda FP, and Nagasubramanian K. Aquatech membrane technology for recovery of acid/base values from salt stream. *Desalination* 1988; 68: 149–167.
27. Boyaval P and Corre C. Continuous fermentation of sweet whey permeate for propionic acid production in a CSTR with UF recycle. *Biotech. Lett.* 1987; 9: 801–806.
28. Boyaval P, Terre S, and Corre C. Production d'acide lactique à partir de perméat de lactosérum par fermentation continue en réacteur à membrane. *Le Lait* 1988; 68: 65–84.
29. Boyaval P, Seta J, and Gavach C. Concentrated propionic acid production by electro dialysis. *Enzyme Microb. Technol.* 1993; 15: 683–686.
30. Boyaval P, Corre C, and Terre S. Continuous lactic acid fermentation with concentrated product recovery by ultrafiltration and electro dialysis. *Biotech. Lett.* 1987; 9: 207–212.
31. Alvarez F, Alvarez R, Coca J, Sandeaux J, Sandeaux R, and Gavach C. Salicylic acid production by electro dialysis with bipolar membranes. *J. Membr. Sci.* 1997; 123: 61–69.
32. Xu TW and Yang WH. Effect of cell configurations on the performance of citric acid production by bipolar membrane electro dialysis. *J. Membr. Sci.* 2002; 203: 145–153.
33. Xu TW and Yang WH. Citric acid production by electro dialysis with bipolar membranes. *Chem. Eng. Process.* 2002; 41: 519–524.
34. Xu TW. Effect of asymmetry in a bipolar membrane on water dissociation—a mathematical analysis. *Desalination* 2002; 150: 65–74.
35. Habova V, Melzoch K, Rychtera M, and Sekavova B. Electro dialysis as a useful technique for lactic acid separation from a model solution and a fermentation broth. *Desalination* 2004; 163: 361–372.
36. Person A, Farde A, Jonsson G, and Zacchi G. Conversion of sodium lactate to lactic acid with water-splitting electro dialysis. *Appl. Biochem. Biotechnol.* 2001; 94: 197–211.
37. Tronc J-S, Lamarche F, and Makhoulouf J. Enzymatic browning inhibition in cloudy apple juice by electro dialysis. *J. Food Sci.* 1997; 62: 75–78.
38. Tronc J-S, Lamarche F, and Makhoulouf J. Effect of pH variation by electro dialysis on the inhibition of enzymatic browning in cloudy apple juice. *J. Agric. Food Chem.* 1998; 46: 829–833.
39. Lam Quoc A, Lamarche F, and Makhoulouf J. Acceleration of pH variation in cloudy apple juice using electro dialysis with bipolar membranes. *J. Agric. Food Chem.* 2000; 48: 2160–2166.
40. Bazinet L, Lamarche F, Labrecque R, Toupin R, Boulet M, and Ippersiel D. Systematic study on the preparation of a food grade soyabean protein. Report for the Canadian Electricity Association 9326 U 987, May 1996, Research and Development; Montréal.
41. Bazinet L, Lamarche F, Labrecque R, and Ippersiel D. Effect of KCl and soy protein concentrations on the performance of bipolar membrane electro-acidification. *J. Agric. Food Chem.* 1997; 45: 2419–2425.
42. Bazinet L, Lamarche F, Ippersiel D, and Amiot J. Bipolar membrane electro-acidification to produce bovine milk casein isolate. *J. Agric. Food Chem.* 1999; 47: 5291–5296.
43. Bazinet L, Ippersiel D, Labrecque R, and Lamarche F. Effect of temperature on the separation of soybean 11S and 7S protein fractions during bipolar membrane electroacidification. *Biotechnol. Prog.* 2000; 16: 292–295.

44. Bazinet L, Ippersiel D, and Mahdavi B. Fractionation of whey protein by bipolar membrane electroacidification. *Innovative Food Sci. Emerg. Technol.* 2004; 5: 17–25.
45. Kemperman AJB, Ed. *Handbook of Bipolar Membrane Technology*, Twente University Press, Enschede, The Netherlands, 2000.
46. Hékal IM. Process for the preservation of color and flavor in liquid containing comestibles. 1983. United States Patent no 4 374 714.
47. Labrecque R, Théorêt A, Lamarche F, and Boulet M. Application of electrodialysis for the extraction of cytoplasmic leaf proteins from alfalfa. In: Weinberg N and Genders D, Eds. *Electrochemical Techniques for a Cleaner Environment*, The Electrosynthesis Company Inc., East Amherst, New York, 1990, pp. 221–236.
48. Grebenyuk VD, Koganov MM, Shaparenko LG, Shvaiko LV, Kuznetsov NI, Karnobatskaya TA, and Bogdanova IA. Heat resistant soluble protein electrodialysis fractionation of alfalfa biomass. *Fiziologiya-i-Biokhimiya-Kul'turnykh-Rastenii* 1988; 20: 189–194.
49. Janson HV and Lewis MJ. Electrochemical coagulation of whey protein. *J. Soc. Dairy Tech.* 1994; 47: 87–90.
50. Bazinet L, Lamarche F, Boulet M, and Amiot J. Combined effect of pH and temperature during electroreduction of whey proteins. *J. Agric. Food Chem.* 1997; 45: 101–107.
51. Donnan FG. Theory of membrane equilibrium and membrane potential in the presence of non-dialysing electrolytes: A contribution to physical–chemical physiology. *Z Elektrochem. Angewandte Phys. Chem.* 1911; 17: 572–581.
52. Simons R. The origin and elimination of water splitting in ion-exchange membranes during water demineralisation by electrodialysis. *Desalination* 1979; 28: 41–42.
53. Simons R. Electric field effects on proton transfer between ionizable groups and water in ion exchange membranes. *Electrochim. Acta* 1984; 29: 151–158.
54. Simons R. Water splitting in ion exchange membranes. *Electrochim. Acta* 1985; 30: 275–282.
55. Mafé S and Ramirez P. Electrochemical characterization of polymer ion-exchange bipolar membranes. *Acta Polym.* 1997; 48: 234–250.
56. Wien M. Über die gültigkeit des ohmschen gesetzes für electrolyte bei sehr hohen feldstärken, *Ann. Physik*, 1924; 73: 161–165.
57. Strathmann H, Rapp H-J, Bauer B, and Bell CM. Theoretical and practical aspects of preparing bipolar membranes. *Desalination* 1993; 90: 303–323.
58. Kunst B and Lovreček B. Electrochemical properties of ion-exchange membrane junctions. *Croat. Chem. Acta* 1962; 34: 219–225.
59. Strathmann H, Krol JJ, Rapp H-J, and Eigenberger G. Limiting current density and water dissociation in bipolar membranes. *J. Membr. Sci.* 1997; 125: 123–142.
60. Onsager L. Deviations from Ohm's law in weak electrolytes. *J. Chem. Phys.* 1934; 2: 599–615.
61. Ramirez P, Aguilera VM, Manzanares JA, and Mafé S. Effects of temperature and ion transport on water splitting in bipolar membranes. *J. Membr. Sci.* 1992; 73: 191–201.
62. Rubinstein I, Warshawsky A, Schechtman L, and Kedem O. Elimination of acid–base generation (water-splitting) in electrodialysis. *Desalination* 1984; 51: 55–60.
63. Simons R. Strong electric fields effects on proton transfer between membrane-bound amines and water. *Nature* 1979; 280: 824–826.
64. Kedem O. Reduction of polarization in electrodialysis by ion-conducting spacers. *Desalination* 1975; 16: 105–118.
65. Bazinet L. Application du principe de dissociation électromembranaire des molécules d'eau à la séparation des caséines du lait. *Ind. Alim. Agric.* 2003; 10: 7–13.
66. Simons R and Khanarian G. Water dissociation in bipolar membranes: Experiments and theory. *J. Membr. Biol.* 1978; 38: 11–30.
67. Hanada F, Hiraya K, Ohmura N, and Tanaka S. Bipolar membrane and method for its production. 1991. European Patent no 459 820.
68. Simons R. High performance bipolar membrane. 1989. World Patent no 89/01059 A1.
69. Simons R. Preparation of a high performance bipolar membrane. *J. Membr. Sci.* 1993; 78: 13–23.
70. Mafé S, Ramirez P, and Alcaraz A. Electric field assisted proton transfer and water dissociation at the junction of a fixed-charge bipolar membrane. *Chem. Phys. Lett.* 1998; 294: 406–412.
71. Rapp H-J. Elektrodialyse mit bipolaren Membranen—Theorie und Anwendungen, PhD Thesis, Universität Stuttgart, Institut für Chemische Verfahrenstechnik, Germany, 1994.
72. Strathmann H. In: *Ion-Exchange Membrane Separation Processes*, Membrane Science and Technology Series, 9, Elsevier Scientific, Amsterdam, 2004.
73. Hurwitz H and El Moussaoui R. Bipolar membrane and method for fabricating such bipolar membrane. 1996. World Patent no 96/01286.
74. Gnusin NP, Zabolotskii VI, Shel'deshov NV, and Krikunova ND. Chronopotentiometric examination of MB-1 bipolar membrane in salt solutions. *Elektrokhimiya* 1980; 16: 49–52.
75. Bauer B, Garner F-J, and Strathmann H. Development of bipolar membranes. *Desalination* 1988; 68: 279–292.
76. Shel'deshov NV, Zabolotsky VI, Pis'menskaya ND, and Gnusin NP. Catalysis of water dissociation by the phosphoric acid groups of an MB-3 bipolar membrane. *Elektrokhimiya* 1986; 22: 791–795.
77. Bauer B. Bipolare mehrschichtmembranen (bipolar multilayer membranes). 1992. German Patent no 4 026 154.
78. Pletcher D and Walsh FC. In: *Industrial Electrochemistry*, 2nd ed., Elsevier Scientific, Amsterdam, 1990.
79. Engel D, Lehmann TH, Weissland G, and Picarri J. Preprints of the Aachener Membrakolloquium, *GVC VDI-Gesellschaft Verfahrenstechnik und Chemieingenieurwesen*, Aachen, 1993.
80. Mc Ardle JC, Piccarri JA, and Thornburg CG. Aquatech System's pickle liquor recovery process Washington Steel reduces waste disposal costs and liability. *Iron Steel Eng.* 1991; 68: 39–43.

81. Mani KN and Chandla FP. Electrodialytic water splitter and process for removal of SO<sub>2</sub> from gases containing same and for the recovery of SO<sub>2</sub> and NaOH. 1986. United States Patent no 4 629 545.
82. Sridhar S. Electrodialysis in non-aqueous medium: Production of sodium methoxide. *J. Membr. Sci.* 1996; 73–79.
83. Hatzidimitriu SE. Process for adjusting the pH of an aqueous flowable fluid. 1990. United States Patent no 4 936 962.
84. Dykalo NY, Gavrilov GB, and Kim VV. Controlling acidity of dairy and other products containing aqueous phase by passing product through three-chamber electrodialysis apparatus with alternating anion- or cation-exchange and bipolar membranes. 1996. U.S.S.R. Patent no RU2 052 942-C1.
85. Kilara A and Sharkasi TY. Effects of temperature on food proteins and its implication on functional properties. *CRC Crit. Rev. Food Sci. Nutr.* 1986; 23: 323–395.
86. Nash AM and Wolf WJ. Solubility and ultracentrifugal studies on soybean globulins. *Cereal Chem.* 1967; 44: 183–192.
87. Cheftel JC, Cuq JL, and Lorient D. Amino-acids, peptides and proteins. In: Fenema OR, Ed. *Food Chemistry*: 2nd ed. revised and expanded, Marcel Dekker Inc., New York, 1985.
88. Bazinet L, Lamarche F, and Ippersiel D. Comparison of chemical and bipolar-membrane electrochemical acidification for precipitation of soybean proteins. *J. Agric. Food Chem.* 1998; 46: 2013–2019.
89. Bazinet L, Lamarche F, and Ippersiel D. Ionic balance: A closer look at the K<sup>+</sup> migrated and H<sup>+</sup> generated during bipolar membrane electro-acidification of soybean proteins. *J. Membr. Sci.* 1999; 154: 61–71.
90. Bazinet L, Lamarche F, Labrecque R, and Ippersiel D. Effect of number of bipolar membrane and temperature on the performance of bipolar membrane electro-acidification. *J. Agric. Food Chem.* 1997; 45: 3788–3794.
91. Pearson AM. Soy proteins. In: Hudson BJB, Ed. *Developments in Food Proteins-2*, Elsevier Applied Science Publishers, London, 1983.
92. Bazinet L, Lamarche F, Labrecque R, Toupin R, Boulet M, and Ippersiel D. Electro-acidification of soybean proteins for the production of isolate. *Food Technol.* 1997; 51(9): 52–56, 58, 60.
93. Bourne MC. Viscosity and consistency. In: *Food Texture and Viscosity: Concept and Measurement*. Food Science and Technology, A series of monographs, Academic Press, New York, 1982.
94. Brett CMA and Oliveira- Brett AM. Fundamentals of kinetics and mechanism of electrode reactions. In: *Electrochemistry: Principles, Methods and Applications*. Oxford University: New York, 1993.
95. Lopez Leiva MH. The use of electrodialysis in food processing. Part I: Some theoretical concepts. *Lebensm Wiss Technol.* 1988; 21: 119–125.
96. Lopez leiva MH. The use of electrodialysis in food processing. Part II: Review of practical applications. *Lebensm Wiss Technol.* 1988; 21: 177–182.
97. Thanh VH and Shibasaki K. Major proteins of soybean seeds. A straightforward fractionation and their characterization. *J. Agric. Food Chem.* 1976; 24, 4(6): 1117–1121.
98. Mondor M, Ippersiel D, Lamarche F, and Boye JI. Production of soy protein concentrates using combination of electroacidification and ultrafiltration. *J. Agric. Food Chem.* 2004; 52: 6991–6996.
99. Varnam HA and Sutherland JP. Milk and milk products-technology, chemistry and microbiology. In: *Dairy Protein Products*, Chapman and Hall, London, 1994, Chapter 4, pp. 159–182.
100. Segalen P. Description des différentes techniques de fabrication des caséines et caséinates. In: *Lait et Produits laitiers, Vaches, brebis, chèvres—Vol.2, Les produits laitiers- Transformation et technologies; Techniques et documentation Lavoisier*, APRIA, Paris, France, 1985, pp. 395–405.
101. Southward CR. Utilization of milk components: Casein. In: Robinson RK, Ed. *Modern Dairy Technology, Advances in Milk Processing*, 2nd ed., Vol. 1, Chapman and Hall, London, 1993, Chapter 8, pp. 375–432.
102. Salmon M. Acidulation of milk. 1983. United States Patent no 4 423 081.
103. Rialland JP and Barbier JP. Procédé de traitement du lait sur une résine échangeuse de cations en vue de la fabrication de la caséine et du lactosérum. 1980. French Patent no 2 480 568.
104. Laiteries Triballat, Procédé et installation pour la préparation de la caséine à partir du lait et produits ainsi obtenus. 1979. French Patent no 2 418 627.
105. Bolzer R. Installation and process for the preparation of acid caseinates. 1985. United States Patent no 4 559 119.
106. Mulvihill DM. Caseins and caseinates : Manufacture. In: Fox PF, Ed. *Developments in Dairy Chemistry*, Vol. 4, Elsevier Applied Science Publishers, London, 1989, pp. 97–129.
107. Cayot P and Lorient D. *Structures et technofonctions des protéines du lait, Arilait Recherches*, Technique et Documentation Lavoisier Publishers, Paris, 1998.
108. Bazinet L, Ippersiel D, Gendron C, Beaudry J, Mahdavi B, Amiot J, and Lamarche F. Cationic balance in skim milk during bipolar membrane electroacidification. *J. Membr. Sci.* 2000; 173: 201–209.
109. Pashley RM and Israelachvili JN. DLVO and hydration forces between mica surfaces in Mg<sup>2+</sup>, Ca<sup>2+</sup>, Sr<sup>2+</sup> and Ba<sup>2+</sup> chloride solutions. *J. Colloid Interface Sci.* 1984; 97: 446–455.
110. Bringe NA and Kinsella JE. Forces involved in the enzymatic and acidic coagulation of casein micelles. In: Hudson BJB, Ed. *Developments in Food Proteins*, Vol. 5, Elsevier Applied Science Publishers, London, 1987, pp. 159–194.
111. Bazinet L, Ippersiel D, Gendron C, Mahdavi B, Amiot J, and Lamarche F. Effect of added salt and increase in ionic strength on skim milk electroacidification performances. *J. Dairy Res.* 2001; 68(2): 237–250.
112. Bazinet L, Gendron C, Ippersiel D, René-Paradis J, Tétreault C, Beaudry J, Britten M, Mahdavi B, Amiot J, and Lamarche F. Effect of type of added salt and ionic strength on physicochemical and functional properties of casein isolates produced by electroacidification. *J. Agric. Food Chem.* 2002; 50(23): 6875–6881.

113. Bazinet L, Lamarche F, Ippersiel D, Gendron C, Mahdavi B, and Amiot J. Comparison of chemical and electrochemical acidification of skim milk. *J. Food Sci.* 2000; 65(8): 1303–1307.
114. Ho C and Waugh DF. Interaction of bovine  $\alpha_{s1}$ -casein with small ions. *J. Am. Chem. Soc.* 1965; 87: 110–117.
115. Creighton TE. *Proteins Structure and Molecular Properties*. W.H. Freeman and Co., New York, 1984.
116. Munro PA, Southward CR, and Elston PD. The effect of casein manufacturing variables on the properties of rennet casein plastics. *NZ J. Dairy Sci. Technol.* 1980; 115: 177–190.
117. McDowell AKB, Southward CR, and Elston PD. The effect of ion on the colour of rennet casein plastic. *NZ J. Dairy Sci. Technol.* 1976; 11: 40–45.
118. Weal BC and Southward CR. Recent Developments in Casein Manufacture. I. The production of rennet casein by a “continuous cook” process. *NZ J. Dairy Sci. Technol.* 1974; 9: 2–5.
119. Bastier P, Dumay E, and Cheftel JC. Physico-chemical and functional properties of commercial caseinates. *Lebensm Wiss Technol.* 1993; 26: 529–537.
120. Bazinet L, Montpetit D, Ippersiel D, Amiot J, and Lamarche F. Identification of skim milk electroacidification fouling: A microscopic approach. *J. Interface Colloid Sci.* 2001; 237(1): 62–69.
121. Windholz M, Budavari S, Blumetti RF, and Otterbein ES. In: *The Merck Index: An Encyclopedia of Chemical Drugs, and Biologicals*, 10th ed., p.228. Merck and Co. Inc., Rahway, NJ, 1983.
122. Bazinet L, Montpetit D, Ippersiel D, Mahdavi B, Amiot J, and Lamarche F. Neutralization of hydroxide generated during skim milk electroacidification and its effect on bipolar and cationic membrane integrity. *J. Membr. Sci.* 2003; 26(1–2): 229–239.
123. Guierre G. *Petite Encyclopédie des Fruits*, Le courrier du livre, Paris, 1975: p. 192.
124. Nagel B. Kontinuierliche herstellung von hochwertigen naturtruben apfelsaft unter einbeziehung der zentrifugaltechnik. *Flüssiges Obst.* 1992; 1: 6–8.
125. Tronc J-S. Inhibition des réactions de brunissement enzymatique du jus de pomme frais non clarifié par électrodialyse’ in *Thèse de Maîtrise no14431*, Université Laval: Sainte-Foy, Québec, Canada, 1996.
126. Macheix JJ, Fleuriet A, and Billot J. *Fruit Phenolics*, CRC Press, Boca Raton, FL, 1990, pp. 1–98.
127. Lea AGH. Apple juice. In: Hicks D, Ed. *Production and Packaging of Non-Carbonated Fruit Juices and Fruits Beverages*, Van Nostrand Reinhold, New York, 1990, pp. 182–225.
128. Janovitz-Klapp A, Richard F, Goupy PM, and Nicolas J. Inhibition studies on apple polyphenol-oxidase. *J. Agric. Food Chem.* 1990; 38: 926–931.
129. Saper GM and Ziolkowski MA. Comparison of erythorbic and ascorbic acids as inhibitors of enzymatic browning in apple. *J. Food Sci.* 1987; 52: 1732–1733.
130. Zemel GP, Sims CA, Marshall MR, and Balaban M. Low pH inactivation of polyphenol oxidase in apple. *J. Food Sci.* 1990; 55: 562–565.
131. Mc Cord JD and Kilara A. Control of enzymatic browning in processed mushrooms (*Agaricus bisporus*). *J. Food Sci.* 1984; 48: 1479–1483.
132. Mazza G and Miniati E. Anthocyanins. In: *Fruits, Vegetables and Grains*, CRC Press. Boca Raton, FL 1993; p. 1–38.
133. Brun JP. Électrodialyse. In : *Procédés de séparation par Membrane: Transport, Techniques Membranaires et Applications*. Éditions Masson, Paris, 1989.
134. Audinos R, Lurton L, and Moutounet M. Advantage of electro dialysis to produce sweetening products from grape. *Sciences des Aliments* 1985; 5: 619–637.
135. Loeillet D. Jus de fruit de la passion. *Un modèle d’instabilité. Fruitrop* 1999; 56: 8–15.
136. Vera Calle E, Ruales J, Dormier M, Sandeaux J, Sandeaux R, and Pourcelly G. Deacidification of clarified passion fruit juice using different configuration of electro dialysis. *J. Chem. Technol. Biotech.* 2003; 78: 918–925.
137. Adhikary SK, Harkare WP, Gowindan KP, and Nanjundaswamy AM. Deacidification of fruit juices by electro dialysis. *Indian J. Technol.* 1983; 21: 120–123.
138. Couture R and Rouseff R. Debitting and deacidifying sour orange (*Citrus aurantium*) juice using neutral and anion exchange resins. *J. Food Sci.* 1992; 57: 380–384.
139. Milsom PE and Meers JL. Citric acid. In: Blanch HW, Drew S, and Wang DIC, Eds. *Comprehensive Biotechnology. The Practice of Biotechnology: Current Commodity Products*, Vol. 3, Pergamon, Oxford, 1985, pp. 665–680.
140. Börgardts P, Krischke W, Trösch W, and Brunner H. Integrated bioprocess for the simultaneous production of lactic acid and dairy sewage treatment. *Bioprocess Eng.* 1998; 19: 321–329.
141. Boergardts P, Krischke W, and Troesch W. Process for purifying dairy wastewater. 1998. United States Patent no 5 746 920.
142. Van Nispen JGM and Jonker R. Process for the fermentative preparation of organic acids. 1991. United States Patent no 5 002 881.
143. Bazinet L. Electro dialytic phenomena and their applications in the dairy industry: A review. *Crit. Rev. Food Sci. Nutr.* 2005; 45: 307–326.
144. Hambraeus L. Nutritional aspects of milk proteins. In: Fox PF, Ed. *Development in Dairy Chemistry*. Elsevier Applied Science Publishers, London, 1982, p. 289.
145. Maubois JL. Les protéines du lactosérum extraites par ultrafiltration. In: Bourgeois CM and Le Roux P, Eds. *Protéines Animales, Extraits Concentrés et Isolats en Alimentation Humaine*, Apria-Lavoisier, Paris, 1982, pp. 172–190.
146. Pierre A and Fauquant J. Principes pour un procédé industriel de fractionnement des protéines du lactosérum. *Lait* 1986; 66(4): 405–419.
147. Ayers JS and Petersen MJ. Whey protein recovery using a range of novel ion exchangers. *NZ J. Dairy Sci. Technol.* 1985; 20: 129–142.

148. Skudder PJ. Evaluation of a porous silica-based ion-exchange medium for the production of protein fraction from rennet- and acid-whey. *J. Dairy Res.* 1985; 52: 167–181.
149. Al-Mashikh SA and Nakai S. Reduction of  $\beta$ -lactoglobulin content of cheese whey by polyphosphate precipitation. *J. Food Sci.* 1987; 52: 1237–1240.
150. Pearce RJ. Thermal separation of  $\beta$ -lactoglobulin and  $\alpha$ -lactalbumin in bovine cheddar cheese whey. *Aus. J. Dairy Technol.* 1983; 38: 144–149.
151. Barbier JP and Rialland JP. Selective separation of alpha-lactalbumin from whey proteins. 1987. European Patent no 0 209 414 A1.
152. Bramaud C, Aimar P, and Daufin G. Optimisation of a whey protein fractionation process based on the selective precipitation of  $\alpha$ -lactalbumin. *Lait* 1997; 77: 411–423.
153. Kronman MJ, Andreotti RE, and Vitols R. Inter- and intramolecular interactions of  $\alpha$ -lactalbumin. II. Aggregation reactions at acid pH. *Biochemistry* 1964; 3: 1152–1160.
154. Hines EM and Foegeding EA. Interactions of  $\alpha$ -la and bovine serum albumin with  $\beta$ -lg in thermally induced gelation. *J. Agric. Food Chem.* 1993; 41(3): 341–346.
155. Mulvihill DM and Donovan M. Whey proteins and their thermal denaturation: A review. *Irish J. Food Sci. Technol.* 1987; 11: 43–75.
156. Bazinet L, Ippersiel D, and Mahdavi B. Effect of conductivity control on the separation of whey protein by bipolar membrane electroacidification. *J. Agric. Food Chem.* 2004; 52: 1980–1984.
157. Townend R and Timasheff SN. Molecular interactions in  $\beta$ -lactoglobulin. III. Light scattering investigation of the stoichiometry of the association between pH 3.7 and 5.2. *J. Am. Chem. Soc.* 1960; 82: 3168–3174.
158. Saio K and Watanabe T. Differences in functional properties of 7 S and 11 S soybean proteins. *J. Texture Stud.* 1978; 9: 135–157.
159. Ning L and Villota R. Influence of 7 S and 11 S globulins on the extrusion performance of soy protein concentrates. *J. Food Proc. Technol.* 1994; 18: 421–436.
160. Kolar CW, Richert SH, Decker CD, Steinke FH, and Vander Zanden RJ. Isolated soy protein. In: A.M. Altschul and H.L. Wilcke, Eds. *New Protein Foods*, Vol.5, Academic Press Inc., London, 1985.
161. Bigelow CC. On the average hydrophobicity of proteins and the relation between it and protein structure. *J. Theor. Biol.* 1967; 16: 187–211.
162. Wilson LA. Soy foods. In: Erickson DR, Ed. *Practical Handbook of Soybean Processing and Utilization*. AOCS Press, Champaign, IL, 1995.
163. Valentas KJ, Levine L, and Clark JP. Soy complex. In: *Food Processing Operations and Scale-Up*, Marcel Dekker, New York, 1991.
164. Bazinet L, Ippersiel D, and Lamarche F. Recovery of magnesium and protein from soy tofu whey by electrodialytic configurations. *J. Chem. Technol. Biotechnol.* 1999; 74: 663–668.
165. Hiraoka Y, Itoh K, and Taneya S. Demineralization of cheese whey and skimmed milk by electrodialysis with ion exchange membranes. *Milchwiss* 1979; 34: 397–400.
166. Boer R and Robbertsen T. Electrodialysis and ion exchange processes: The case of milk whey. In: Cantarelli C and Peri C, Eds. *Progress in Food Engineering: Solid Extraction, Isolation and Purification*. Proceedings of a European Symposium of the Food Working Party of the E.F.C.E., Forster Publishing Ltd., Künsnacht, Switzerland, 1981.
167. Vick Roy TB. Lactic acid. In: Young MM, Ed. *Comprehensive Biotechnology*, Pergamon, New York, 1985, pp. 761–775.
168. Buchta K. Lactic acid. In: Dellweg H, Ed. *Biotechnology*, Vol. 3, Verlag Chemie, Weinheim, 1983, pp. 410–417.
169. Lee EG, Moon S-H, Chang YK, Yoo I-K, and Chang HN. Lactic acid recovery using two-stage electrodialysis and its modelling. *J. Membr. Sci.* 1998; 145: 53–66.
170. Heriban V, Škára J, Šturdík E, and Ilavský J. Isolation of free lactic acid using electrodialysis. *Biotech. Tech.* 1993; 7: 63–68.
171. Norddahl B. Fermentative production and isolation of lactic acid. 1998. World Patent no 9 828 433.
172. Norddahl B, Eriksen S, and Pedersen FM. Method for producing lactic acid. 2001. World Patent no 01 92555-A1.
173. Jouan P. Le lactosérum. In: *Lactoprotéines et Lactopeptides, Propriétés Biologiques*. INRA Ed.; Paris, France, 2002, p. 19.
174. Lehmann H and Wasen I. Method of dephospholipidating whey. 1990. United States Patent no 4 897 279.
175. Théodet C and Gandemer G. Devenir des lipides au cours de la clarification du lactosérum. *Lait* 1994; 74: 281–295.
176. Boswell RP and Hutchinson JC. Reduced fat whey protein concentrate and method of manufacture. 2001. International Patent no 0 108 502.
177. Morr CV and Foegeding EA. Composition and functionality of commercial whey and milk protein concentrates and isolates: A status report. *Food Technol.* 1990; 44(4): 100–112.
178. Morr CV and Ha EYW. Off flavors of whey protein concentrates: A literature review. *Int. Dairy J.* 1991; 1: 1–11.
179. Attebery JM. Removing lipid material from whey. 1971. United States Patent no 3 560 219.
180. Fauquant J, Vieco E, Brule G, and Maubois JL. Clarification des lactosérums doux par agrégation thermocalcique de la matière grasse résiduelle. *Le Lait* 1985; 65: 1–20.
181. Karleskind D, Laye I, Mei FI, and Morr CV. Chemical pretreatment and microfiltration for making delipidized whey protein concentrate. *J. Food Sci.* 1995; 60(2): 221–226.
182. De Wit JN and Klarenbeek G. Method for the clarification of liquids containing whey protein. 1978. Great Britain Patent no 1 519 897.
183. Phillips DJ, Allen R, and Khoo JH. Method of producing low-fat proteins. 1987. European Patent no 0 243 544.
184. Lin TSF, Angers P, and Bazinet L. Precipitation of cheddar cheese whey lipids by electrochemical acidification. *J. Agric. Food Chem.* 2005; 53: 5635–5639.

185. Whitney RM, Brunner JR, Ebner KE, Farrell HM, Josephson RV, and Morr CV. Nomenclature of the proteins of cow's milk: Fourth revision. *J. Dairy Sci.* 1976; 59: 795–815.
186. Tatulian SA. Ionization and ion binding. In: Cevc G, Ed. *Phospholipids Handbook*, Marcel Dekker, New York, 1993, p. 511.
187. Cornell DG and Patterson DL. Interaction of phospholipids in monolayers with  $\beta$ -lactoglobulin adsorbed from solution. *J. Agric. Food Chem.* 1989; 37: 1455–1459.
188. Lau A, McLaughlin A, and McLaughlin S. The adsorption of divalent cations to phosphatidylglycerol bilayer membranes. *Biochim. Biophys. Acta* 1981; 645: 279–292.
189. Bazinet L, Ling TSF, and Angers P. Method for extracting lipids and proteins from whey. 1960. United States Patent no 60/562 550.



---

# 22 Applications of Membrane Technology in the Dairy Industry

*Philipina A. Marcelo and Syed S.H. Rizvi*

## CONTENTS

22.1	Introduction .....	636
22.1.1	General Overview .....	636
22.1.2	Current and New Applications .....	636
22.2	Membrane-Based Processes and Their Uses .....	636
22.2.1	Microfiltration .....	636
22.2.2	Ultrafiltration .....	636
22.2.3	Reverse Osmosis .....	637
22.2.4	Nanofiltration .....	637
22.3	Industrial Applications .....	637
22.3.1	Concentration and Fractionation of Whey Proteins by Ultrafiltration .....	637
22.3.2	Pretreatment of Cheese Whey by Microfiltration .....	639
22.3.3	Cheese Manufacturing .....	640
22.3.3.1	Ultrafiltration of Milk .....	640
22.3.3.2	Microfiltration of Milk and Recovery of Native Whey Proteins .....	642
22.3.3.3	Vatless Manufacture of Cheese .....	645
22.3.4	Removal of Microorganisms .....	646
22.3.5	Standardization of Milk and Milk Protein Concentration .....	648
22.3.6	Recovery of Lactose and Minerals .....	649
22.3.7	Fractionation of Milk Fat and Its Components .....	649
22.4	Membrane Performance .....	651
22.4.1	Fouling and Flux Prediction .....	651
22.4.1.1	Mechanistic Models for Flux Decline .....	652
22.4.1.2	Empirical Fouling Models .....	655
22.4.1.3	Limiting Flux versus Critical Flux .....	655
22.4.2	Energy Consumption .....	656
22.5	Cleaning and Sanitation .....	657
22.5.1	Cleaning .....	657
22.5.1.1	Water Rinsing .....	658
22.5.1.2	Chemical Cleaning .....	658
22.5.2	Sanitation .....	660
22.6	Challenges and Emerging Applications of Membranes in the Dairy Industry .....	660
22.6.1	Challenges .....	660
22.6.2	Emerging Applications of Membranes in the Dairy Industry .....	662
	Acknowledgment .....	664
	References .....	664

## 22.1 INTRODUCTION

### 22.1.1 GENERAL OVERVIEW

Microfiltration (MF), ultrafiltration (UF), nanofiltration (NF), and reverse osmosis (RO) are the four major membrane processes that have become standard unit operations in the dairy industry. They often offer cheap capital and utility costs and have displaced conventional separation techniques that require phase change, such as the energy-intensive distillation, evaporation, or freeze concentration. Membrane processes require only small amounts of electrical energy for pumps and small amounts of steam for heating cleaning solutions, so that even RO, which is the most energy intensive of membrane processes, offers economic advantage. Also, unlike most separation processes, which require tall and hence more expensive buildings, membrane systems are relatively compact and they may often be accommodated in existing buildings [1–3].

Since their introduction in the 1960s, membrane technologies have been utilized in food industries because they provide a unique opportunity for accomplishing both the fractionation and the concentration of components in liquid systems without phase change, while retaining desirable physical and chemical characteristics of key food components. Two of such food commodities with various components of desirable functional properties and health-enhancing effects, especially when utilized in purified form, are milk and whey [4–6].

### 22.1.2 CURRENT AND NEW APPLICATIONS

Both retentate and permeate from membrane separation techniques have become important starting materials in producing novel products and ingredients from milk of unique functional properties and organoleptic quality. Henning et al. [7] enumerated the current and new applications of membrane technologies in the dairy industry, which include

- Microfiltration processing for clarification and defatting of cheese whey, for selective separation and concentration of micellar caseins from milk for various purposes, for fractionation of caseins and their peptides, for recovery of native whey proteins from milk, for gentle sterilization of milk to produce extended shelf life liquid milk and cheese milk, for fractionation of globular milk fat and its components, for the reduction of microorganisms in cheese brine, and for the removal of colloidal particles in membrane cleaning solutions.
- Ultrafiltration processing for whey proteins concentration and fractionation, for recovery of lactose from milk and whey, for total milk protein concentration for the production of milk protein concentrate (MPC) or milk protein isolate (MPI), for milk standardization for continuous mechanized manufacture of cheese and other fermented products, and for production of high-solids milk base for dried milk production.
- Application of RO in the partial demineralization or pre-concentration of whey, and the treatment of dairy effluents.
- Application of NF in the simultaneous demineralization and concentration of whey, concentration of lactose from the permeate of the UF whey, and the purification of membrane cleaning solutions.

## 22.2 MEMBRANE-BASED PROCESSES AND THEIR USES

### 22.2.1 MICROFILTRATION

Microfiltration is a technique that allows the differential concentration in the retentate of the feed components that are larger than the average pore diameter of the membrane [8]. Developed as early as 1929 by Sartorius-Werke, in Germany, microfiltration is one of the oldest filtration technologies whose main use was for water and beverage sterilization [9,10]. MF membranes have pore diameter ranging 0.1–10  $\mu\text{m}$ , which can selectively separate particles with molecular weights >200 kDa based on sieve effect [8,11,12].

The advent of ceramic membranes that can withstand pH range from 0.5 to 13.5, or from 0 to 14 for some membranes, such as Membranlox, and temperatures over 100°C provided significant advantages in terms of chemical, thermal, and mechanical stability over the more available polymeric membranes [13]. This and the invention of crossflow microfiltration (CFMF), which is an economic and efficient method for purification of fine particle or proteins, increased the utilization of MF in the dairy industry [14]. Today, CFMF is utilized in the dairy industry in three major applications: (1) removal of bacteria, (2) whey defatting, and (3) micellar casein enrichment of milk for cheesemaking and other applications [10]. A fourth and relatively new application of MF in dairy processing, which is based on the pioneering work of Goudéranche et al. [15], is the recovery and fractionation of native milk fat globule from milk, or even from mixed milk, and whey cream [16,17].

### 22.2.2 ULTRAFILTRATION

Ultrafiltration involves the separation of molecules in solution predominantly according to their sizes and shapes as well as charges and affinity for the membrane [18–20]. It involves the use of membranes with a molecular weight cut-off (MWCO) in

the range of 1–300 kDa and a pore size of  $\sim 0.01 \mu\text{m}$ , which operate at a pressure of  $< 10 \text{ bar}$  (1000 kPa) [11,21]. The nominal MWCO of UF membranes makes them appropriate for processing colloidal suspensions to filter particles or dissolved macromolecules that are  $< 1 \mu\text{m}$  in size [11]. For this reason, crossflow UF is used in a wide range of applications other than those in the food industry, such as biotechnology, pharmaceutical industry, and water and wastewater treatments [21]. When used in milk processing, UF results in a retentate containing proteins, fat, and colloidal minerals at higher proportions than that found in untreated milk, and permeate consisting water, minerals, lactose, nonprotein nitrogen (NPN) compounds, and water-soluble vitamins [11].

The application of UF in the dairy industry started, in the early 1970s, with the separation and concentration of whey proteins from cheese whey to protein-rich retentate and lactose-containing permeate [22–24]. Later, it was introduced as a cheese manufacturing technology, also in the early 1970s, for its potential in increasing cheese yield by the incorporation of whey proteins and other milk constituents in the cheese matrix while allowing a greater degree of control over cheese composition [3,25–28]. Cheesemakers recognize UF technology as more flexible than traditional processing methods and give unique opportunities to meet the demand for large product diversity [29]. The introduction of the thermal and pH resistant polysulfone membranes in the market in the mid 1970s, and the development of ceramic membranes and improved polysulfone membranes in the 1980s contributed to the advancement of UF technology, which was followed by explorations of different applications of UF in the dairy industry [26,29]. Among such applications are the potential of UF as a method for standardizing milk composition and clot-forming properties, and as a technique for developing new cheese varieties with different textural and functional characteristics [27,30–32]. Presently, concentration and purification of milk proteins to produce MPCs and MPis are two of the important applications of UF in milk processing [33].

The purification process for UF retentates is optimized by including a diafiltration (DF) step [3,34]. Compared with conventional processes, UF with DF has the advantage of allowing high product purity and process yield such as the removal of lactose from milk to the desired degree [3,35]. This process commonly includes three basic steps: (1) a pre-concentration stage, (2) a DF stage to purify the retentate and permeate, and (3) a final concentration stage to maximize the concentration of high-molecular weight solute in the retentate [35].

### 22.2.3 REVERSE OSMOSIS

Reverse osmosis membranes are characterized by an MWCO of  $\sim 100 \text{ Da}$ , and the process involves transmembrane pressures (TMP) of 10–50 bar (1000–5000 kPa), which are 5–10 times higher than those used in UF [11,36]. Unlike UF, the separation by RO is achieved not by the size of the solute but due to a pressure-driven solution–diffusion process [36]. Like UF membranes, RO membranes are uniquely structured films from synthetic organic polymers and consist of an ultrathin skin layer superimposed on a coarsely porous matrix [3]. The skin layer of the RO membrane is nonporous, which may be treated as a water-swollen gel, and water is transported across membrane by dissolving in this gel and diffusing to the low-pressure side [3]. In the dairy industry, RO is used to concentrate milk or whey by removal of water and ionized minerals [11].

### 22.2.4 NANOFILTRATION

Nanofiltration separates particles with molecular weights in the range of 100–500 Da and allows the rejection of ions based on their diffusion characteristics and charge [11,24]. NF separation is governed by mass transfer phenomena, which comprises diffusion and flow through pores and involves the use of membranes that are tight enough to retain lactose when utilized for dairy applications [11,24]. Due to the tightness of the membrane, Jelen [37] suggested that the NF process can be considered as an ultratight UF or as a loose RO. Somewhat similar to UF, NF is able to perform simultaneous separation and concentration functions and is commonly used in the dairy industry to process UF and MF permeates [24,36]. NF is often utilized in the concentration and partial demineralization of the UF permeates in whey processing [37].

## 22.3 INDUSTRIAL APPLICATIONS

### 22.3.1 CONCENTRATION AND FRACTIONATION OF WHEY PROTEINS BY ULTRAFILTRATION

To date, the fractionation and concentration of whey proteins from cheese whey remain to be one of the more successful industrial applications of UF [22–24]. Due to flux decline during operation, however, Mulvihill and Ennis [38] reported that the practical limit for whey concentration by UF in modern plants is around 24% total solids, with a protein:total solids ratio limit of  $\sim 0.72:1$ . DF is used to achieve a higher ratio of protein to total solids,  $\sim 0.80:1$ , and a total solids content of about 28% [38].

The efficiency of UF in whey processing is limited by a few factors, the most significant of which are concentration polarization and membrane fouling [6,39–41]. While both factors, which adversely affect permeate flux, may be aggravated by protein–protein and membrane–protein interactions [23,40,42–44], they may also be minimized by choosing suitable membrane material and configuration as well as the appropriate process conditions such as TMP, feed velocity or recirculation rate, temperature, and the chemical environment of whey [42,45,46].

The membrane material and the molecular conformation of the whey proteins are of considerable influence on flux decline [40,41,47]. Opposite charges on the whey proteins and the membrane induce protein–membrane electrostatic attractions that initiate protein adsorption on the membrane surface [23,40,46]. This may result in the undesirable denaturation and aggregation of the adsorbed proteins, especially at high-shear operations [48,49]. To date, the polymeric polysulfone membrane remains to be the most widely used membrane in whey UF primarily because of its low cost, good thermal stability, and mechanical properties [6,50]. It is commonly believed that compared with ceramic membranes and hydrophilic polymeric membranes, the hydrophobic polysulfone membrane gives low fluxes and more severe fouling [40]. However, Doyen et al. [43] showed that in the UF of whey, practically the same flux/concentration factor and whey permeability coefficient are obtained using polysulfone and ceramic membranes. The minimization of the hydrophobic and electrostatically induced interactions between polysulfone membrane and whey proteins, especially denatured whey proteins, which lead to massive fouling is still a challenge to date [40,42,51,52].

While  $\alpha$ -lactalbumin ( $\alpha$ -La) was found to have the greatest gel-forming tendency in UF of whey using polysulfone membranes and is the cause of immediate loss of initial flux,  $\beta$ -lactoglobulin ( $\beta$ -Lg) has great effect on long-term fouling [23,47]. Although whey proteins themselves are the major foulants, calcium and phosphates have been directly implicated with membrane fouling as possible catalysts or bridging agents between the proteins and the membrane or the proteins themselves, and the formation of insoluble calcium salts [23,41,47,53,54]. Rao [41] observed that for both sweet whey and acid whey, flux was controlled by fouling through gradual adsorption of whey proteins to the membrane surface and pore plugging by precipitated calcium phosphate. Hanemaaijer et al. [23] found that the UF membrane characteristics do not influence the deposition of calcium phosphate as strongly as pH and temperature. They observed membrane rejection of Ca at higher pH and temperature because its solubility decreases at these conditions [55]. Their findings were consistent with those of Kuo and Cheryan [45]. Labbé et al. [54] found that phosphates, either calcium phosphate, apatite and hydroxyapatite at pH 6.9, or sodium hydrogen phosphate at pH 5.6, were the main mineral foulants in the UF of raw and clarified whey using ceramic membranes. The same authors suggested the formation and adsorption of calcium–phosphate–protein complexes on the membrane surface at high pH. This explains the gelatin-like and firmly compacted fouling layer at high pH and the loose fouling layer at low pH observed by Kuo and Cheryan [45]. Using sweet whey, data by Hanemaaijer et al. [23] showed that calcium permeates satisfactorily through an acrylic copolymer membrane (30 kDa MWCO) at pH 6.0 and 45°C at a permeate to initial feed calcium content ratio of about 0.9 after 2 h of process time. Marshall and Daufin [56] pointed out that around pH 6, calcium changes to a more soluble form and that phosphate is in the soluble sodium hydrogen phosphate.

Using tubular ceramic membrane, Aimar et al. [19] showed that in the UF of sweet whey at pH 6.3, there was no considerable difference in flux plateau values at crossflow velocities from 1.8 to 4.0 m·s<sup>-1</sup> at 50°C and TMP of 3 bar (300 kPa). This seems to indicate that the critical TMP in UF of whey is ~3 bar (300 kPa), although the absolute flux plateau values might be affected by pH and the membrane material and configuration. Kuo and Cheryan [45] found that the critical TMP in the UF of pre-filtered cottage cheese whey, acidified to pH 3, at 50°C using 20 kDa MWCO polysulfone membrane in spiral wound configuration, was between 3.1 and 3.5 bar (310 and 350 kPa). At higher pressures, these authors pointed out that, even at high flow rates, flux declined rapidly due to extensive fouling and deposit layer compaction, reiterating that higher flow rates are beneficial only at pressures below some critical pressure [40,49]. Brans et al. [6] suggested that concentration of whey should be carried out just above the critical pressure where flux is equal to the limiting flux, to achieve optimal operation. Kuo and Cheryan [45], however, did not observe the critical TMP for hollow fiber module because of the limited pressure rating of the module.

Although flux decline may be minimized through appropriate process variables, energy consumption is a function of these variables [22]. While TMP–flux relationships (for pressure-controlled systems) and fluid velocity–flux relationships (for mass transfer-controlled systems) are relatively independent of module design [22,40,43], the pressure drop–fluid velocity relationship, and thus energy consumption, is a characteristic of the particular module design [22]. Polysulfone membranes are usually in the spiral wound or hollow fiber configurations. The available hollow fiber modules in the industry are limited by their low TMP ratings. The spiral wound modules, which can withstand higher pressures and are able to minimize the occurrence of concentration polarization, involve the lowest in capital and operating cost compared with other configurations [57–59].

Depending on process objective, UF can be carried out below, above, or at the critical TMP in which the flux ceases to increase linearly with increase in TMP, and therefore, referred to as the limiting flux [6,49]. When the feed solute concentration is low, higher TMP is required to achieve the limiting flux [60]. Therefore, using the spiral wound configuration to concentrate large volume of low solute-concentration feed, such as whey, is practical. On the other hand, the hollow fiber configuration has the advantage of giving higher flux than the spiral wound due to higher shear rates developed in the module for the same pressure drop [22,58]. This would be of advantage for high solute-concentration systems, such as pre-concentrated whey, where permeation is more likely to be mass transfer controlled and a high crossflow velocity is needed to maintain reasonable flux [6,22].

In concentrating whey proteins, DF is employed, in which water or buffer is continually added to the retentate while lactose and minerals are simultaneously removed in the filtrate, to increase whey protein purity [4,52,61]. This is commonly done in constant-volume mode where water or buffer is added to the retentate at the same rate as permeation. There is an optimum

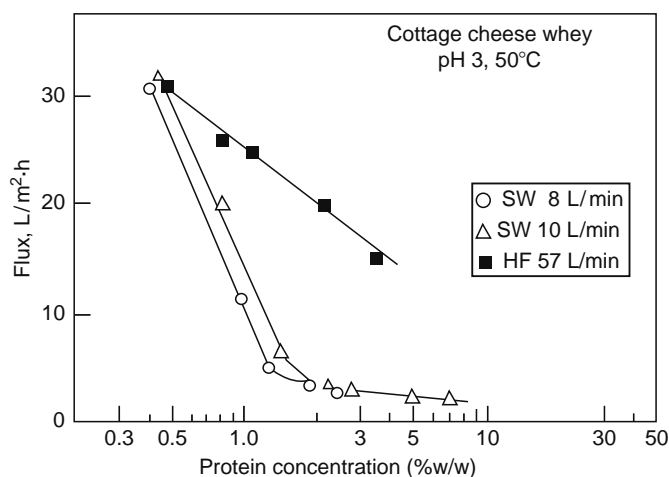


**FIGURE 22.1** Variation of flux with protein concentration during UF of cottage cheese whey. (From Cheryan, M. and Kuo, K.P., *J. Dairy Sci.*, 67, 1406, 1984. With permission.)

protein concentration in the retentate at which DF can be commenced where the trade-off between permeate flux and the number of diaivolutes are balanced, and only the minimum membrane area or process time is necessary [62,63]. Using 20 kDa MWCO polysulfone membrane sheets, Nilsson [18] found that, in the UF of reconstituted WPC-80, the relative flux reduction increased with protein concentration and then plateaued up to about 3.2% protein concentration in the retentate. Above this concentration, the relative flux reduction increased sharply. Cheryan and Kuo [22] showed that at 3.35 bar (335 kPa) TMP and 50°C, the flux approached a minimum when the retentate reached about 3% protein concentration using polysulfone spiral wound membrane while the flux in the polysulfone hollow fiber is four times higher (Figure 22.1). This suggests that DF may be effectively carried out after 3% protein concentration in the retentate has been reached.

### 22.3.2 PRETREATMENT OF CHEESE WHEY BY MICROFILTRATION

Most commercial whey protein concentrate (WPC) and whey protein isolate (WPI) are produced from classic cheese whey. To remove cheesemaking remnants, such as starter culture bacteria, enzymes, glycomacropptide, and fat, the whey is clarified, pasteurized and, in the case of acid whey, decalcified before WPC or WPI manufacture [58,61,64]. Although clarification processes, such as pH adjustment or salt addition followed by gravity settling or centrifugation, are useful in removing colloidal calcium phosphate and protein–mineral complexes, they do not remove phospholipoprotein complexes and the smallest milk fat globules [65]. A number of authors have demonstrated the detrimental effects of fat on the functional and keeping quality of whey concentrates [61,66,67]. Centrifugation reduces the fat content of whey down to only 0.05%, which is predominantly small fat globules between 1 and 2  $\mu\text{m}$  in diameter, and increases up to 3% when whey is concentrated by UF [68].

Pretreatment of cheese whey by MF has emerged as a necessary step in producing WPI and WPC of varying whey protein content [69]. The MF of cheese whey has two specific applications: (1) defatting of whey and (2) removal of bacteria, or cold pasteurization, to produce high-quality WPC or WPI of valuable functional and health or medical properties [70].

Tanny et al. [71] proposed CFMF as a potential solution to the fat removal problem in whey. Using 1.2  $\mu\text{m}$  pore size MF membrane to clarify sweet cheese whey, Merin et al. [68] observed a permeate that was totally free of fat, while containing all the other whey components. Compared to the centrifuge-separated and nontreated whey, Merin et al. [68] reported 30% increase in permeation flux when the MF permeate was used as a feed stream in UF to produce WPC. They explained that this is probably due to the absence of small fat globules and casein fines in the MF permeate, which were suggested as major contributors to permeation resistance in the UF of sweet whey. The same group observed reduction of bacteria in the MF permeate by 1 to 2 orders of magnitude.

Rather than the thermo-calcic aggregation of lipoproteins and subsequent MF, Pearce et al. [72] showed the efficacy of CFMF in the direct removal of residual lipids from separated and pasteurized cheddar cheese whey. Results of their study indicated improvement in the foaming ability of the defatted whey products. Using 0.22  $\mu\text{m}$  cellulosic membrane, Hawks et al. [67] showed that MF is more effective in reducing the fat content of both acid whey and sweet whey compared with centrifugation. However, while MF is effective in removing PLPC, it also partially retains whey proteins, specifically bovine serum albumin (BSA) and immunoglobulin-G (Ig-G) [65]. The extent of retention depends on physicochemical and hydrodynamic conditions during the MF process.

### 22.3.3 CHEESE MANUFACTURING

#### 22.3.3.1 Ultrafiltration of Milk

The French government's dairy research laboratory, the Hungarian Dairy Research Institute, and the Australian Commonwealth Scientific and Industrial Research Organization can be given credit for propelling the UF of milk forward [70]. Since the pioneering work of Professor Maubois and colleagues in France in the 1970s, the concentration of total milk proteins by UF has been utilized extensively in the dairy industry to create a liquid pre-cheese for the production of soft cheese such as feta and Camembert [70,73,74]. In this process, the appropriate amount of water, lactose, and minerals are removed by UF from the milk, to make the pre-cheese, before coagulation and fermentation [25,28,70]. Using the UF pre-cheese, rennet coagulation could take place with the incorporation of whey proteins in the cheese matrix, which substantially increases the yield per liter of milk by 16%–20% while enabling the attainment of a more uniform product [25,28,70].

Ultrafiltration may be integrated into the cheesemaking process either for partial milk concentration or full milk concentration (Table 22.1), in which cutting and whey drainage are entirely eliminated and 100% of the whey proteins of milk are retained in the cheese matrix [28,75,76]. The reduced volume of the liquid pre-cheese and the absence of whey drainage from the curd when UF pre-cheese is used lead to the reduction of rennet requirement by ~80% compared to what is usually needed in conventional manufacture of cheese [25,77].

Pedersen and Ottosen [29] calculated ~13%–14% reduction in skim milk requirement in the German quarg cheese production if UF is employed rather than the conventional thermo-separator technique to recover acid whey after fermentation. They further estimated that the raw material savings for other UF fresh acid cheeses production including cream cheese are in the order of 4%–6% and 0.5%–1.5% fat. In the UF process described by Pedersen and Ottosen [29], the UF is carried out following heat treatment of milk (95°C for 5 min) and fermentation (pH 4.4–4.6), recovering acid whey from the UF step by the end of the process. Schkoda and Kessler [75] suggested the reduction of acid whey drainage by modifying this conventional UF process. They suggested the inclusion of twofold pre-concentration of skim milk by UF before heat treatment (UF–UF process). However, pre-concentration of skim milk by UF was reported to cause bitterness in quarg cheese and other fresh cheeses due to the higher buffering capacity of retentates compared with normal milk, the increased starter growth and possibly the high concentration of calcium in the UF milk [78]. Schkoda and Kessler [75] proposed the use of mesophilic starters of sufficient activity to ensure adequate acid and flavor production in the UF milk and lactose concentration of up to 9% in the retentate. The authors showed that the fresh cheese produced from the UF–UF process had the same quality attributes as those produced from

**TABLE 22.1**  
Composition of UF Raw Milk, Skim Milk, and UF Milk at Different Concentration Factors

Sample	pH <sup>b</sup>	% TS <sup>b</sup>	% Protein	Temperature (°C)	TMP (kPa)	Membrane Module	References
3x concentrate	—	29.71	20.44	60	—	Abcor 22S HFM polystearine, 20 kDa MWCO	[194]
Skim milk	—	8.61	3.22				[133]
5x concentrate	—	20.90	15.16	38	213	Abcor spiral wound UF model 1	[133]
Skim milk	—	—	3.42				[78]
2x concentrate	—	—	6.85	50	121	Amicon H43 PM30; 30 kDa MWCO	[78]
4x concentrate	—	—	13.51	50	121	Amicon H43 PM30; 30 kDa MWCO	[78]
5x concentrate	—	—	17.10	50	121	Amicon H43 PM30; 30 kDa MWCO	[78]
2x concentrate	6.70	13.2	6.80	50	134	Romicon HF15–43-PM50; 50 kDa MWCO	[90]
Skim milk	6.72	9.1	3.10				[80]
2x concentrate	6.71	12.1	6.24	50	200	Protosep III Koch-UF HFM-100; 30 kDa MWCO	[80]
3x concentrate	6.68	14.6	8.90	50	200	Protosep III Koch-UF HFM-100; 30 kDa MWCO	[80]
1.8x concentrate <sup>a</sup>	—	12.85	5.26	50	125	Romicon polysulphone HF; 10 kDa MWCO	[79]
Fresh milk	—	—	3.50				[24]
4x concentration	—	—	13.00	50	404	Zoltek Rt MAVIBRAN FS10; 6–8 kDa MWCO	[24]

<sup>a</sup> From semi-skimmed milk with 1.33% fat content.

<sup>b</sup> — = not reported.

the conventional UF process. They also noted increased firmness and about 50% increase in calcium content in the cheese made from the UF–UF process compared to that made from the conventional UF process, suggesting that high calcium concentration was an unlikely cause of bitterness in fresh acid cheeses from UF milk. They reported at least 50% reduction of acid whey amount from the process compared to the conventional UF process.

Aside from improved yield, the use of UF pre-cheese results in the improvement of product taste and texture compared to cheese produced by conventional methods because of the reduction of lactose content, controlled acidification rate, and increase in the water-holding capacity of the product due to the incorporation of whey, which makes for softer product [25,73,79]. Lucisano et al. [77] noted an enhanced rennet-induced clotting time of UF-concentrated milk as pH is lowered from its natural pH level.

Using hollow fiber membrane with 30 kDa MWCO at 50°C and 0.8 bar (80 kPa) longitudinal pressure drop, Waungana et al. [80] reported that concentration of skim milk by UF to protein levels of ~6% (concentration factor of 2) and ~9% (concentration factor of 3) had no effect on gelation time in rennet coagulation at the natural milk pH. They also noted that an increase in UF milk concentration led to an increase in the curd firming rates and storage modulus, which is a measure of solid-like behavior. This is because reducing the aqueous volume in the retentate decreases the mean path between casein micelles. Since the aggregation rate depends on the number of effective collisions between casein micelles, a gel will form at a lower extent of  $\kappa$ -casein hydrolysis [81–83]. However, Waungana et al. [80] reported that lowering the pH to 6.5 before renneting resulted in shorter gelation time values, which increased with protein concentration, and increased curd firming rates for the UF milk.

Although UF technology has been successfully utilized in the production of soft cheeses, problems were encountered in the production of hard and semi-hard cheeses from UF-concentrated milks. These products tend to be very hard and crumbly in texture, which may be associated with the difference in coagulation properties of UF milk because of high protein and calcium concentration [80]. The coagulation time of UF milk is too short and curd firmness is high which renders cutting of the curd in conventional cheesemaking equipment impossible [82].

Using a UF retentate obtained at low concentration factor [79] is an alternative method for producing hard and semi-hard cheeses with characteristics similar to those produced by the conventional method. Kosikowski [84], for instance, suggested that 1.8x is the limit for making good-quality cheddar cheese. In a related work on raw milk, Hinrichs [76] reported a transition from Newtonian to non-Newtonian flow behavior above a concentration factor of 2 in the UF, which corresponds to more than 8% fat and 3.33% protein in the retentate. Similarly, Erdem [83,85] found that because of concentration by UF to twofold and threefold using 10 kDa MWCO polysulfone membrane, the protein system in skim milk becomes more agglomerated via hydrophobic bonds, which results to reorganization of the protein system into a more compact micellar structure.

Aside from further increasing cheese yield due to enhanced incorporation of whey proteins, heat treatment of UF milk was suggested as appropriate in controlling the rate of curd formation and curd firmness, because the heat-induced interaction between  $\beta$ -Lg and  $\kappa$ -casein prolongs coagulation time and lowers curd firmness [82]. Because rennet-induced gelation of cheese milk is hindered by whey protein denaturation, it has been suggested that high heat treatment (HHT) of milk should be ruled out as a possible application for the production of semi-hard and hard cheeses using normal milk [32]. However, the increase in casein concentration through UF concentration of milk counteracts the reduction in gel strength caused by denatured whey proteins because more caseins for network formation are available [25,86]. Therefore, if UF pre-cheese were used, high heating and denaturation of whey proteins would be permissible to integrate them into the cheese [32].

In 1973, Maubois et al. noted a surprising property of ultrafiltered ultra-high temperature-treated (UHT) milk—its rennet coagulum forming an ability suitable for cheesemaking, which is ordinarily lost as a result of the heat treatment, is restored [87]. Furthermore, Maubois et al. [25] observed that UF retentates containing twice the normal amount of proteins than milk that were easily transformed into cheese, regardless of whether application of UHT treatment was before or after UF. This finding was confirmed by later studies of Sharma et al. [82], who reported that the heat-treated UF milk, concentrated up to 4x, retains its coagulation and curd firming ability despite a slight decrease in the rate of  $\kappa$ -casein hydrolysis. The same group also noted that the initial rate of  $\kappa$ -casein hydrolysis in the heated UF milk was not statistically different from that in unheated milk. Similarly, Guinee et al. [27] observed that concentration of milk by UF helps to restore the gelation properties of HHT milk.

Guinee et al. [27] observed that HHT of skim milk, which brings about whey protein denaturation and reduces cheese curd firming rate, had little influence on the gelation time of high-protein (15%–19%) UF retentates. They reported that the gelation time of HHT milk approached that of normal-pasteurized milk (72°C, 15 s) at protein concentrations greater than ~12%–16%, depending on the level of whey protein denaturation. The authors attributed this whey protein denaturation effect on gelation time to the closer proximity of rennet-altered micelles in the high-protein retentates, which in turn increases the probability of collision and aggregation. Steffl (cited in Ref. [32]) reported that rennet-induced gelation was hindered when more than 60% whey proteins of cheese milk were denatured, prolonging gelation time. Similarly, Waungana et al. [80] reported that gelation time is not affected up to 60% denaturation level of  $\beta$ -Lg in normal skim milk but the storage modulus of rennet gels decreased gradually with increase in the extent in  $\beta$ -Lg denaturation and its association with casein micelles.

When UF milk of 6%–9% protein concentration was heated at 140°C for 4 s, Waungana et al. [80] observed increased gelation time, decreased curd firming rates, and decreased storage modulus values compared with unheated milk of the same protein concentration. The authors noted that these effects were more pronounced when the UHT treatment was done before UF of skim milk. They speculated that the nature of the  $\beta$ -Lg/ $\kappa$ -casein complexes and the way in which these associate with casein micelles upon heating of UF concentrates is different when normal milk is heat treated before UF. In a related study, El-Shibiny et al. [88] reported a reduction of calcium to dry matter ratio during DF of whole milk with distilled water after UF to concentration factor of 5 at 50°C, which they supposed to be the partial dissociation of the colloidal calcium phosphate and its subsequent removal in the permeate during DF. The same group observed an increase in the size and weight of the micelles during DF, which they interpreted as the aggregation of micelles following the partial removal of colloidal calcium. The findings of Pignon et al. [89] are in agreement with these. They found that while the internal structure of globular casein micelles remains significantly unperturbed, they tend to agglomerate when temperature is increased from 20°C to 70°C, or when pH is lowered from 6.6 to 6.0, during UF due to slight loss of calcium phosphate and  $\kappa$ -caseins from the stabilizing layer.

Aside from increased protein concentration, Guinee et al. [27] and Waungana et al. [80] noted that the total effects of heat treatment on rennet coagulation of UF-concentrated skim milk are influenced by changes in mineral equilibria. In relation to this, Hinrichs [76] reported increased resistance from coagulation and gelation during storage of UF-concentrated whole milk compared with NF and RO-concentrated milk. This is due to the UF milk's low ash content and the fact that the initial aggregation reaction in milk is controlled by the salt concentration [76].

Premaratne and Cousin [78] studied the changes in the chemical composition of skim milk during UF (30 kDa MWCO) at 50°C and average TMP of 1.2 bar (120 kPa) to approximate concentration factors of 2, 4, and 5. They noted that milk proteins membrane retention was about 99%. They reported an increase in the protein concentration from an average of 3.42% in skim milk to 6.85%, 13.51%, and 17.10% at concentration factor values of 2, 4, and 5, respectively, while fat was also proportionately concentrated with increase in concentration factor from 0.11% in skim milk to 0.24%, 0.45%, and 0.60%. Because lactose is present in the free state in milk and has a molecular weight lower than the MWCO of the UF membrane used, its concentration decreased progressively during UF from an initial 5.06% to 4.76%, 4.29%, and 4.06% at concentration factor values of 2, 4, and 5, respectively. Bastian et al. [20] reported 100% retention and recovery of fat and rennet clottable N and 1%–3% recovery of lactose in the UF of pasteurized (72.2°C for 16 s) skim milk (pH 6.7) to concentration factor of 5 using spiral wound membrane (10 kDa MWCO) at 54°C and 1.4 bar (140 kPa) TMP.

The concentration of minerals such as  $\text{Ca}^{2+}$  and  $\text{Mg}^{2+}$ , which are associated with milk proteins and fats gradually increased with concentration factor while the free amino acids and the B vitamins (except riboflavin), which are mostly free and not bound to proteins were extensively lost to the permeate in the work of Premaratne and Cousin [78]. The authors commented that the increase in the mineral concentration in the retentate, which increases the buffering capacity of milk, can result in adverse effects such as longer fermentation time and higher than normal final pH of cheese, while the B vitamins could affect the growth of the lactic acid bacteria during cheesemaking. Similarly, Rajagopalan and Cheryan [90] observed that during UF of reconstituted nonfat dry milk (NDM), with composition similar to that of skim milk, the ash decreases initially but becomes constant, indicating that the minerals were being rejected by the membrane. They noted that this led to incomplete removal of the ash components, giving a limiting ash to protein ratio of 0.08, even after exhaustive DF. They surmised that this was because the minerals are insoluble or associated with the proteins. Bastian et al. [20] found that the acidification of milk resulted in loss of Ca, Na, and P from the retentate due to the solubilization of colloidal calcium phosphate. They noted that this result was more pronounced when the retentate was diafiltered.

Cunha et al. [79] noted an increase in the titratable acidity with increasing concentration factor (from 1.2 to 1.8) in the UF of semi-skimmed milk (1.33% fat) using 10 kDa MWCO Romicon polysulfone hollow fiber membrane at 50°C. They explained that this result is mostly due to the protein concentration, which increased the apparent acidity of the retentates and promoted an increase in its buffering capacity. When the UF retentates were made into reduced-fat Minas Frescal cheese, they noted a decrease in yield with increasing concentration factor, due to the decrease in moisture content.

Recently, Atra et al. [24] proposed the integration of two-stage UF in milk and whey proteins concentration for cheesemaking and NF to concentrate lactose from the UF permeate for a cleaner and more economic cheese production (Figure 22.2). The processes incorporate whey proteins into the cheese curd by pre-cheese milk production using first-stage UF to a concentration factor of 4. The whey proteins drained from the curd are recovered and concentrated by a second-stage UF before being added back to the cheese curd. Lactose is recovered from the two UF stages and concentrated by NF.

### 22.3.3.2 Microfiltration of Milk and Recovery of Native Whey Proteins

A major emphasis in the utilization of MF in the dairy industry that is of relevance to cheesemaking is changing the casein to whey protein ratio or the casein to fat ratio in milk fractions [91]. MF of whole or skim milk produces a retentate that is rich in native micellar casein, which improves the cheesemaking process, and a crystal clear and sterile permeate with composition close to that of sweet whey but with greater amount of native whey proteins that is suitable for direct manufacture of whey protein isolate [8,52,92–95]. In processing skim milk using MF membranes of 0.2  $\mu\text{m}$  pore size or smaller, the permeation of

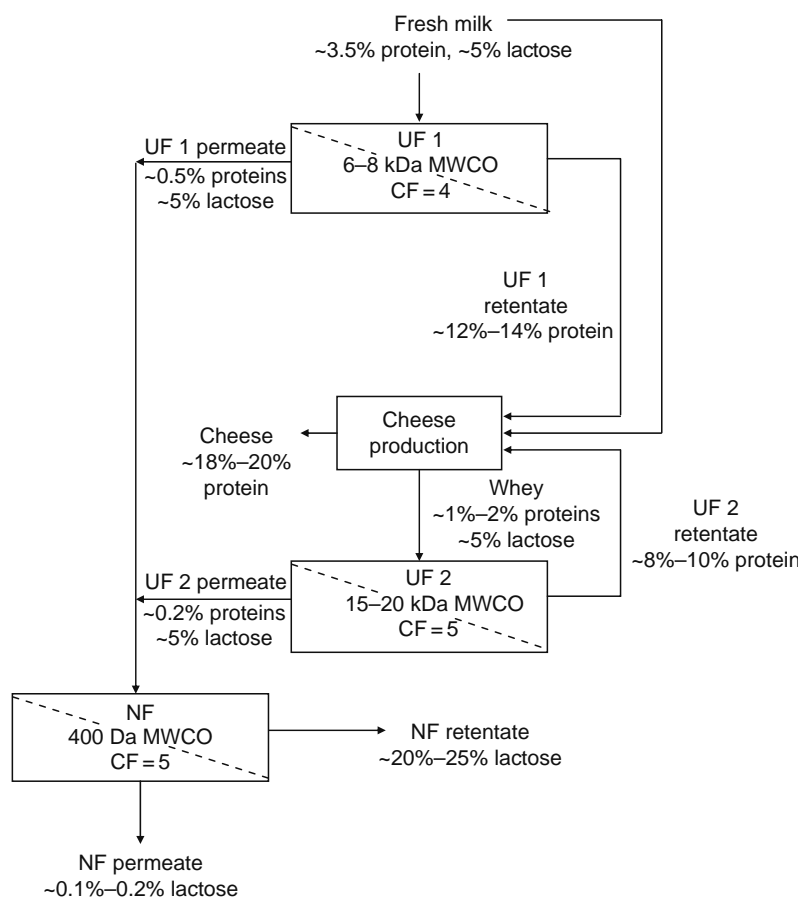


**FIGURE 22.2** Schematic diagram of the proposed combined UF and NF process for more economical cheese production. (From Atra, et al., *J. Food Eng.*, 67, 325, 2005. With permission.)

lactose and minerals is very similar to that observed in the UF of skim milk as the casein to whey protein ratio gradually increases [96].

Le Berre and Daufin [97] reported that >99.6% of casein micelles, 100–300 nm in size, and >30% of whey proteins were retained in the MF of skim milk using 0.1  $\mu\text{m}$  composite membrane consisting of a  $\text{ZrO}_2$  filtering layer on an  $\alpha$ -alumina support at 50°C. The process was carried out at a TMP range of 0.05–0.2 bar (5–20 kPa) until the volume reduction ratio (VRR) of 2 was reached and was then continued in a feed and bleed mode at a TMP of 3.00 bar (300 kPa). On the other hand, Samuelsson et al. [98] reported 12% retention of whey proteins in the MF of skim milk at 55°C, TMP range of 0.1–1.9 bar (10–190 kPa) and 8  $\text{m}\cdot\text{s}^{-1}$  crossflow velocity using 0.14  $\mu\text{m}$   $\text{ZrO}_2$  ceramic membrane in tubular configuration until a VRR of 1.15 was reached. Pierre et al. (cited in Ref. [99]) obtained native phosphocaseinate (PPCN) with casein to total protein ratio of 0.93 by MF of skim milk using 0.14  $\mu\text{m}$  multichannel ceramic membrane under high tangential velocity of  $>6 \text{ m}\cdot\text{s}^{-1}$  and very low uniform TMP along the hydraulic path of 0.1–0.2 bar (10–20 kPa). On the other hand, while flux declined by 50% at concentration factor of 3, Pouliot et al. [99] reported that with conventional CFMF at 50°C, average TMP of 1.9 bar (190 kPa) and 6.9  $\text{m}\cdot\text{s}^{-1}$  crossflow velocity using 0.22  $\mu\text{m}$  pore size membranes, native PPCN may also be produced at a casein to total protein ratio of 0.91. Jost et al. [93] showed that after threefold concentration of milk by MF, the casein-nitrogen (CN) of the retentate increased to 83% of the total nitrogen (TN) in the retentate and after DF using six initial retentate volumes of demineralized water, the casein purity was ~95%.

Casein enrichment of cheese milk significantly improves the rennet coagulability and the productivity of cheese plants, especially those producing hard cheeses [100]. For instance, the rennet coagulation time of a 3% native PPCN solution is reduced by 53% compared to that of raw milk, and the gel firmness after 30 min is increased by more than 50% (Pierre et al., 1992, cited in Ref. [100]).

Milk coagulation depends on a number of factors, such as the kinetics of the enzyme reaction, the concentration, and the state of the proteins, especially casein, the balance of minerals, especially calcium, and pH [101]. Most of these factors are directly influenced by UF or MF processing. Caron et al. [101] compared the rennet coagulation properties of milk enriched with a regular ultrafiltered retentate powder (RUF) to milk enriched with a diafiltered MF (DMF) retentate powder. RUF was prepared by concentrating skim milk to concentration factor of 5 by UF, while DMF was prepared from skim milk concentrated

by MF to concentration factor of 3, diafiltered with deionized water and then concentrated by UF (50 kDa MWCO) to concentration factor of 2 to increase the caseins to whey proteins ratio. They observed that the DMF-enriched milk coagulated faster than the RUF-enriched milk. MF and DF increased the casein content, while reducing whey protein and lactose concentrations in the retentate compared with just UF. Compared with that of control milk (with 3.5% total protein content), they reported an overall improved gel firmness but longer coagulation time for milk enriched to 4.5% and 5.0% total protein, regardless of retentate powder used. The authors reasoned that this may have been due to enzyme diffusion retardation in the casein-enriched milk.

Reduction of microorganisms in milk before cheese production must be achieved in such a way that the functionality of the milk proteins is not affected. Heat-resistant spores, such as *Clostridium tyrobutyricum* and *C. sporogenes* can cause severe spoilage of the cheese by late fermentation that can result in the production of H<sub>2</sub> and CO<sub>2</sub> gases, and unpleasant smelling fermentation products [102]. Although heat sterilization reduces these spores, because of the heat-induced complexation between  $\beta$ -Lg and  $\kappa$ -casein, UHT milk normally does not form a rennet gel and consequently could not be used efficiently for cheesemaking [87].

The partial removal of whey proteins by MF reduces the detrimental effects of heat treatment on the rennet coagulability of milk [100]. The use of MF followed by UF produces micellar casein-rich powder that increases cheese yield. The removal of  $\beta$ -Lg during MF eliminates the heat-induced  $\beta$ -Lg/ $\kappa$ -casein complex typically found in NDM used in cheesemaking [101,103]. The extent of formation of the  $\beta$ -Lg/ $\kappa$ -casein complex decreases and the increase in the electronegativity of casein micelles is not high enough to prevent their aggregation when caseinomacropепptide is cleaved even if the milk is UHT-treated [100]. The MF of raw, pasteurized, UHT, and sterilized whole milks (3.5% fat) using 0.45  $\mu$ m pore size membrane allowed the recovery and quantification of whey proteins and whey protein/ $\kappa$ -casein macroaggregates in the milk, which Carbonaro et al. [104] stressed may lead to finding the mechanisms by which these aggregates are formed during heat treatment of milk. This will be useful for process modeling and in understanding how such aggregates affect the nutritional quality of milk proteins.

To address the adverse effects of heat treatment on the rennet coagulability of milk during cheesemaking, Quiblier et al. (cited in Ref. [105]) developed a process that involves the partial removal of whey proteins, especially  $\beta$ -Lg, from skim milk followed by mild to moderate heat treatment. The process was adapted by Garem et al. [105] to produce milk powder for cheesemaking that is partially depleted of whey proteins to avoid the formation of  $\beta$ -Lg/ $\kappa$ -casein complex during thermal processing. The steps involved in the process are as follows (Figure 22.3): (1) partial or total removal of whey proteins of the milk by 0.1–0.2  $\mu$ m pore size MF membrane, (2) UF of the MF permeate using membranes with MWCO  $\leq$ 20 kDa,

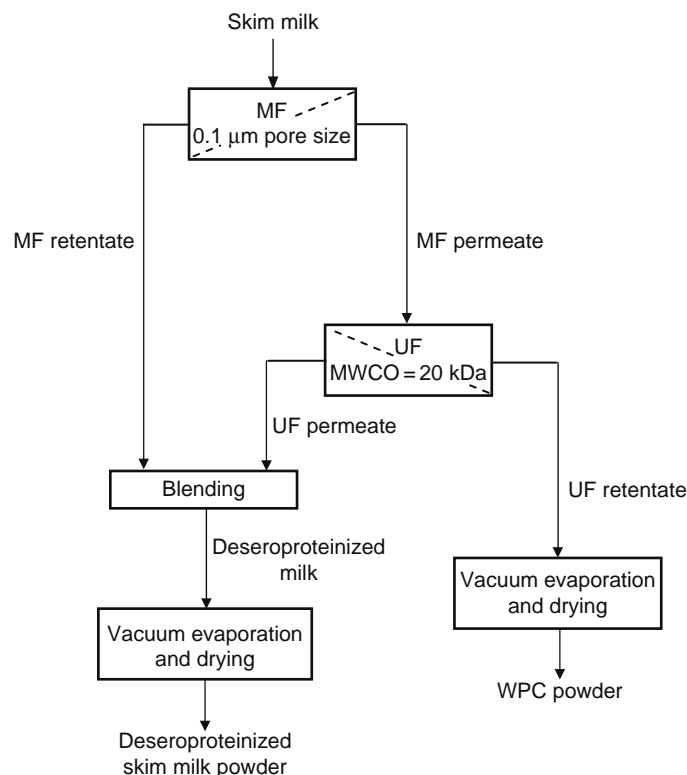


**FIGURE 22.3** Schematic description of the process of preparation of the whey protein-depleted skim milk powder. (From Garem, A., Schuck, P., and Maubois, J.-L., *Lait*, 80, 25, 2000. With permission.)

(3) blending of the MF retentate with the UF permeate, and (4) vacuum evaporation and spray drying of the blend at moderate heat application to produce the recombined milk powder for mozzarella cheese manufacture [105]. They reported about 31% depletion of whey protein from the fresh milk, which resulted in a firmer gel during rennet coagulation and in a significant cheese yield increase of 7.3%. Their data also showed important decrease in stretch water losses without having to modify the cheesemaking process as with common recombined milk. Moreover, since the MF–UF recombined milk does not require the addition of chemical additives, they suggested that its utilization might be of economic advantage over common recombined milk of higher casein to whey protein ratio.

Terré et al. [106] showed that MF membrane of 0.2  $\mu\text{m}$  pore size also allows separation of  $\beta$ -casein when this component, by physicochemical means, is solubilized from the casein micelles [92]. Moreover, at high recirculation velocity of the retentate of at least  $6\text{ m}\cdot\text{s}^{-1}$ , efficiency of separation is strongly related to the maintenance of low temperatures ( $2^\circ\text{C}$ – $6^\circ\text{C}$ ) in the MF equipment and adjustment of ionic strength in the caseinate solution. Products obtained on both sides of the MF membrane are suitable for modifying the  $\beta$ -casein to  $\alpha_s$ -casein ratio of cheese milks and consequently, the texture and flavor of resulting cheeses, which may result to new cheese varieties [92]. van Hekken and Holsinger [91] reported that the cold MF ( $4^\circ\text{C}$ ) of skim milk using either 0.2 or 0.1  $\mu\text{m}$  pore size ceramic membrane gave a permeate, which when ultrafiltered enabled the production of  $\beta$ -casein-enriched retentates with  $\beta$ -casein to  $\alpha_s$ -casein and  $\beta$ -casein to  $\kappa$ -casein ratios that were twofold to fourfold and threefold greater than those of skim milk, respectively. The retentates formed softer gels with greater syneresis and hydration, and lower holding capacities than skim milk gels. They suggested that such gels may be used as starting materials in the production of novel soft cheeses.

### 22.3.3.3 Vatless Manufacture of Cheese

Caron et al. [101] studied the effect of acidification of milk in the MF and UF processes on the rennet coagulability of milk. Diafiltered MF retentate powder from acidified milk (ADMF) was prepared by acidifying milk to pH 6 using lactic acid solution, concentrating the milk by MF 3x with DF, and then concentrating the MF retentate by UF (50 kDa MWCO) 2x. They observed that ADMF contained ~90% protein, while RUF and DMF retentate contained ~69% and ~83%, respectively. They also noted that ADMF had reduced concentrations of mineral, noncasein nitrogen (NCN) and NPN, and whey proteins. This is because acidification of milk increases soluble minerals and during DF of acidified MF milk more lactose and minerals are removed from the retentate while further reducing whey proteins content. This led to decreased gel firmness for milk enriched with ADMF.

In a related study, Brandsma and Rizvi [94] gradually acidified pasteurized skim milk to pH 6.0 using 1.6 g of glucono-delta-lactone (GDL) per kilogram of skim milk to promote solubilization of micelle-bound colloidal minerals into the serum phase of milk. GDL was used in the acidification process for its ability to hydrolyze and form gluconic acid in a temperature-dependent manner that allows highly predictable and controlled method of lowering the MF retentate pH. Using 0.2  $\mu\text{m}$  pore size MF ceramic membrane operated at a TMP of 2.6 bar (260 kPa),  $50^\circ\text{C}$ , and  $7.5\text{ m}\cdot\text{s}^{-1}$  crossflow velocity, they concentrated the acidified skim milk to concentration factor of 8. They observed an effective change in mineral balances, specifically Ca, while maintaining 87.4% nominal whey protein permeation. They reported 20.1% decrease in Ca concentration and 12.6% increase in whey protein concentration in the MF retentate compared to milk at its natural pH of 6.6. The whey protein content of the MF retentate they observed is about 55% lower than typical UF retentates [94].

The process was utilized to produce MF milk for the manufacture of mozzarella cheese using 80–100  $\mu\text{L}$  rennet per kilogram of MF cheese milk at  $32^\circ\text{C}$ – $36^\circ\text{C}$  to give post-coagulation cutting time of 15–20 min. When the same MF retentate and butter oil were utilized in the manufacture of low-moisture part-skim (LMPS) mozzarella cheese, Brandsma and Rizvi [107] observed delay in the rheological and functional development of MF retentate LMPS, which occurred between 30 and 60 days as opposed to 7 and 30 days for commercial LMPS mozzarella. They noted an improvement in rheological and functional behavior in the MF retentate LMPS using starter culture. These indicate that the MF of skim milk with in-process acidification to pH 6 can be potentially developed into a novel cheesemaking process to manufacture cheese of improved textural and functional qualities, along with the recovery of highly functional native whey proteins in the MF permeate, or virgin whey [95].

The virgin whey harvested from the MF, which does not contain cheesemaking remnants, fats, or spores, contained ~5.3% total solids (TS), ~6% of which is whey proteins. Brandsma and Rizvi [94], Punidadas and Rizvi [108], Solanki and Rizvi [109], and Ardisson-Korat and Rizvi [110] showed that the virgin whey's composition is consistent at mass concentration factor of 8. Brandsma and Rizvi [107] suggested uniform transmembrane pressure (UTMP) operation to improve permeate flux and achieve a calcium to total protein ratio in the MF retentate suitable for cheesemaking. Similarly, Vadi and Rizvi [111] suggested that to achieve practical permeate flux values at concentration factor higher than 6 in the MF of skim milk at pH 6 and  $50^\circ\text{C}$  using 0.2  $\mu\text{m}$  pore size membrane, operation in the UTMP mode is necessary. Table 22.2 gives the permeate flux achieved at different concentration factor values in the MF of skim milk.

Using 0.1  $\mu\text{m}$  pore size MF ceramic membranes in a Tetra Alcross M-38 system operated at UTMP of 1 bar (100 kPa),  $50^\circ\text{C}$ , and crossflow velocity of  $5\text{ m}\cdot\text{s}^{-1}$ , Ardisson-Korat and Rizvi [110] showed that at mass concentration factor of 8, the MF retentate contains up to 30% total solids that can be used for semi-continuous vatless manufacture of LMPS mozzarella cheese.

**TABLE 22.2**  
**Permeate Flux Values in the MF of Skim Milk at Different Processing Conditions**  
**under UTMP Mode**

Permeate Flux ( $\text{m}\cdot\text{s}^{-1}$ )	Crossflow Velocity ( $\text{m}\cdot\text{s}^{-1}$ )	Concentration Factor	TMP (kPa)	Membrane	Pore Size ( $\mu\text{m}$ )	References
$2.5 \times 10^{-5}$	6.9	3	190	Ceraflo	0.22	[99]
$1.9 \times 10^{-5}$	7.2	2	193	Membralox	0.2	[111]
$1.3 \times 10^{-5}$	7.2	10	193	Membralox	0.2	[111]
$3.1 \times 10^{-5}$	5.4	2	138	Ceramen	0.05	[108]
$2.8 \times 10^{-6}$	5.0	8	90	Membralox	0.1	[110]

Source: Adapted from Brans et al., *J. Membr. Sci.*, 243, 263, 2004.

They reported 66%–71% whey proteins depletion and calcium to casein ratio in the MF retentate suitable for LMPS mozzarella cheese with properties comparable to those of commercial products.

In a related study, Maubois et al. [112] noted high-protein purity of WPI produced from milk microfiltrate, or ideal whey harvested before cheesemaking, by MF of milk at low concentration factor of 2. The same group suggested the suitability of milk microfiltrate as starting material in obtaining native whey protein fractions. Bacher and K nigsfeldt [113] showed that because of the absence of glycomacropeptide and the relatively large amount of native whey protein in milk microfiltrate WPI (MWPI), it showed vastly improved functionality compared with WPC-80 from cheese whey. However, with the exception of gelation property, MWPI's functionality is similar to cheese whey WPI. They reasoned that this was probably due to a pretreatment that removes denatured WP from the cheese whey before WPI manufacture.

With the objective of increasing calcium and lactose content of MF retentate in addition to micellar casein while maximizing whey protein depletion, Nelson and Barbano [114] developed a multistage MF process that removed ~95% of whey protein from skim milk. They reported that the MF retentate produced from this process contained soluble minerals, NPN, and lactose similar to the original milk. This was accomplished by using the permeate from the UF of the MF permeate to diafilter the MF retentate after achieving a concentration factor of 3 in the MF. Aside from the recovery of native micellar caseins, they showed that the process enabled the production of whey protein stream (UF retentate) with protein content similar to that of commercial WPC.

#### 22.3.4 REMOVAL OF MICROORGANISMS

Since the 1980s, MF has been investigated as an alternative technology to centrifugation for clarification and bacteria removal of milk and whey and is often referred to as a gentle sterilization method [8,68,115,116]. Due to bacterial spoilage, high-temperature, short-time (HTST)-processed milk can last up to 14 days only [117]. Although ultrapasteurization can extend refrigerated fluid milk shelf life to 45 days, it imparts distinct cooked flavor to milk, which may be undesirable to some people [52,118,119]. Unlike UHT pasteurization, MF can reduce the amount of bacteria and spores without affecting the taste of the milk, and provides longer shelf life than pasteurization [6,52,87].

Spore-forming bacteria, which represent the main surviving species after pasteurization, are better retained by MF membrane because of their large cellular volume, giving a decimal reduction of ~4.5 (cited in Ref. [8]). For instance, due to the high retention of *Bacillus cereus* in MF, which is between 99.95% and 99.98%, the shelf life of milk is improved from 6–8 days by conventional pasteurization to 16–21 days by MF [87,120]. Also, decimal reduction factors for MF are higher than that for bactofugation, which is the continuous reduction of bacteria and spores from milk and skim milk by centrifugal force that results to about 98% reduction in spores [6,87].

The work of Holm et al. [121] and that of Piot et al. (cited in Ref. [8]) led to the development of one of the most important applications of MF in the dairy industry, the Bactocatch process with a patent owned by Tetra Pak [8,121]. In this process, cream is removed from whole milk by centrifugation [119]. Skim milk is then passed through 1.4  $\mu\text{m}$  pore size MF membrane where up to 99.99% bacteria reduction at 50°C, UTMP of 0.5 bar, and a high crossflow velocity of 7.2  $\text{m}\cdot\text{s}^{-1}$  is accomplished at a volumetric reduction factor of 20, or 200 in larger membrane modules where the retentate, which represents 5% of the total starting volume, is concentrated 10 times more (Figure 22.4) [6,8,13,87,120]. The MF retentate and cream undergo ultrapasteurization treatment (115°C–130°C for 4–6 s) and are then combined with the nearly bacteria-free MF skim milk [11,119]. Common permeate fluxes obtained in the industry are between 500 and 800  $\text{L}\cdot\text{h}^{-1}\cdot\text{m}^{-2}$ , usually up to 10 h operation, giving average decimal reduction of bacteria above 3.5 while proteins and total solids transmissions are about 99% and 99.5%, respectively [8,52]. Trouv e et al. (cited in Ref. [122]) examined the retention of 7 species of bacteria that typically occur in raw milk using the Bactocatch process and reported 2.6 log reductions during the MF of milk contaminated with initial bacterial levels

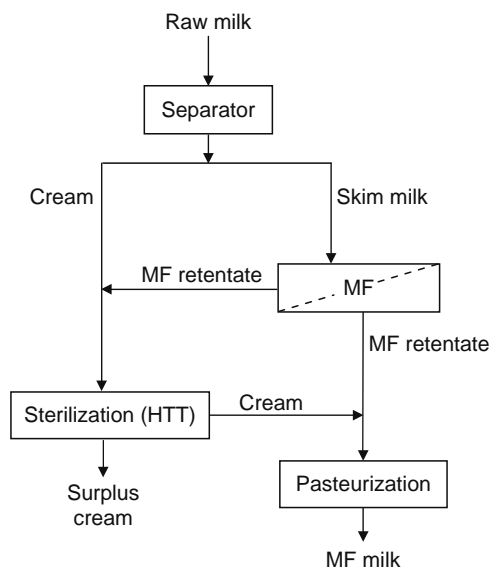


**FIGURE 22.4** MF process used by Olesen and Jensen in collaboration with Alfa-Laval and Ceraver in the integration of CFMF in a milk processing line for the production of milk with low bacteria content. (From Olesen, N. and Jensen, F., *Milchwissenschaft*, 44, 476, 1989. With permission.)

of  $10^2$ – $10^7$  cfu·mL<sup>-1</sup>, where bacterial retention rates were 99.93%–99.99%. While the efficiency of the process in removing bacteria and spores is widely accepted, it does not guarantee the complete removal of pathogenic bacteria in milk as required in milk pasteurization [11].

As the size distribution of bacteria in milk (0.4–2.0  $\mu\text{m}$ ) partly overlaps with that of fat globules (Figure 22.5), MF can be used as a pretreatment of skim milk for the production of raw milk cheeses and reduction of spores in acid cheese milk [6,123]. In 1987, Piot et al. (cited in Ref. [9]) showed that MF process using an inorganic alumina membrane of 1.8  $\mu\text{m}$  pore size could skim 98% of the fat and reduce bacterial counts by 2 orders of magnitude, with no apparent rejection of proteins. Using 1.4  $\mu\text{m}$  ceramic membranes, Pafylas et al. [124] compared the reduction in microbial population in nonfat and 1% fat milk in conventional CFMF operation and UTMP MF operation, which were both run at 50°C, TMP of 1.0 bar, and a crossflow velocity of 5.0 m·s<sup>-1</sup>. They found that, except for fat and bacteria, the distribution of major milk components in the MF milk did not change in either operation modes. While both MF operation modes gave a microfiltered milk with an average fat content of 0.05%, and a bacterial reduction of 4–5 log cycles, the average flux over a concentration factor of 10 was higher with the UTMP mode. The group, however, cautioned that over long-term (8–16 h per day) continuous operation, a gradual increase in fouling or concentration polarization may lead to undesirable changes in milk composition.

Eckner and Zottola (cited in Ref. [124]) reported that sterilizing microfilters, such as the 0.2  $\mu\text{m}$  membranes commonly used in the pharmaceutical industry, would foul too rapidly when operated in the conventional crossflow manner, resulting in low flux and permeates with an undesirable solids profile, making them of little practical value in the dairy industry. Guerra et al. [102] employed the combined benefits of reverse asymmetric 0.87  $\mu\text{m}$  pore size polymeric membranes and backshock technique to control the adverse effects of concentration polarization and fouling in the removal of bacterial spores in skim milk

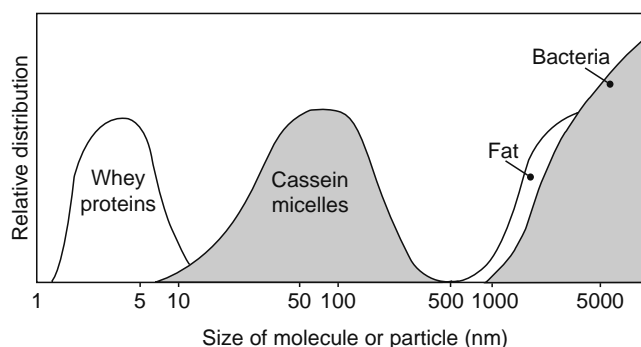


**FIGURE 22.5** Size distribution of major milk components. (From James, B.J., Jing, Y., and Chen, X.D., *J. Food Eng.*, 60, 431, 2003. With permission.)

at low linear velocities and, therefore, low-energy consumption. Reverse asymmetric membranes are those whose porous layer, rather than the skin layer, faces the retentate side, making the fouling layer more loose and consequently result in lower cake resistance as long as the porous layer is not completely filled up [125,126]. The backshock technique involves temporarily forcing the permeate stream backwards through the membrane and into the retentate stream by pressurization of the MF permeate side at short time interval of  $<1$  s at around  $0.2\text{--}1$  s $^{-1}$  frequency to prevent the formation of fouling layer. Guerra et al. [102] reported spores reduction factors of 104–105 at high and stable fluxes of about  $500\%$  L·h $^{-1}$ ·m $^{-2}$  and 100% casein transmission at low-linear velocities of  $0.5\text{--}1.0$  m·s $^{-1}$ .

Elwell and Barbano [119] determined the efficacy of MF, using  $1.4$   $\mu\text{m}$  Membralox ceramic membranes at  $50^\circ\text{C}$  and an average TMP of 39 kPa, followed by pasteurization ( $72^\circ\text{C}$  for 16 s) in reducing the total number of bacteria, spores, and coliforms in skim milk and in extending the shelf life of skim milk at  $0.1^\circ\text{C}$ ,  $2.0^\circ\text{C}$ ,  $4.2^\circ\text{C}$ , and  $6.1^\circ\text{C}$  storage temperatures. They reported an average of 3.79 log reduction in bacterial count by MF and an average of 1.84 log reduction by pasteurization of the MF skim milk, giving an average of 5.6 log reduction from the raw count due to the MF-pasteurization process. They observed that both coliforms and spores in the skim milk were reduced by MF to an undetectable level and that fat was reduced from 0.1% to 0.03%. Bacterial count in the MF pasteurized skim milk did not exceed  $20,000$  cfu·mL $^{-1}$  after 92 days at  $0.1^\circ\text{C}$ – $6.1^\circ\text{C}$  storage temperatures. However, the microbial shelf life is limited by the shelf life due to proteolysis to 78 days for  $2^\circ\text{C}$  storage temperature or 32 days for  $6.1^\circ\text{C}$  storage temperature.

### 22.3.5 STANDARDIZATION OF MILK AND MILK PROTEIN CONCENTRATION

Before the 1990s, there were few options to standardize milk: remove or add fat as cream, add casein as NDM, evaporated milk, or condensed milk [127]. Although to a lesser extent than fat content, the protein content of fluid milk also exhibits considerable natural variability worldwide. This variability is significantly magnified in dairy products that are manufactured by water removal, such as skim milk powder [128]. The International Dairy Federation (IDF) interprets protein standardization to imply relatively small changes in protein content, within the limit of natural variability, that are achieved by the addition or removal of natural milk constituents without altering the natural ratio of whey protein to casein [128].

By UF it is possible to adjust the mass ratios of different milk constituents, including proteins, without adversely affecting their physicochemical properties [11]. The development of more efficient membranes in the 1990s made UF an economically and technologically feasible option to standardize milk proteins and to improve the nutritional uniformity of milk and other dairy products (Figure 22.6) [31,127,128]. Percent total solids as high as 43.3 may be achieved by concentrating whole milk by UF and DF [63], while a volume reduction as high as 85%, with a retentate containing 78% protein (dry basis), may be achieved in the UF of skim milk [129]. This high concentration of solids in the retentate leads to increased viscosity. The viscosity of skim milk UF retentates increases with its dry matter content as follows: 2 cP at 10% dry matter content, 4 cP at 15%, 10 cP at 20%, 33 cP at 25%, and 70 cP at 28% [130], while a drastic increase in the retentate viscosity is observed when the protein concentration exceeds 14% [131].

In the United States, ultrafiltered whole milk is concentrated to approximately 30% total solids and ultrafiltered skim milk to approximately 18% total solids and shipped to cheesemakers for use in standardizing milk or supplementing existing milk supplies to increase manufacturing productivity [127].

Using the appropriate membrane and operating conditions, UF is especially useful in the production of MPI containing low amount of lactose and high amount of native proteins with the same casein to whey proteins ratio as in milk [90]. High milk protein powders (HMPP), or MPC from ultrafiltered milk have become increasingly important over the past years because of their wide range of compositions and hence functionality and applicability [103].

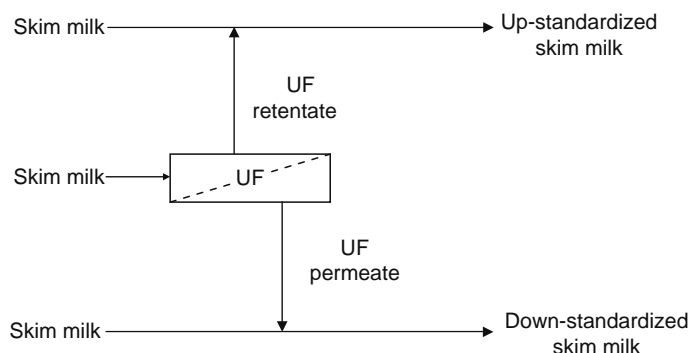


**FIGURE 22.6** Schematic illustration of the use of UF for the production of up-standardized or down-standardized skim milk. (Adapted from Rattray, W. and Jelen, P., *Trends Food Sci. Technol.*, 7, 227, 1996. With permission.)

Alvarez et al. [132] found that UF/DF using polysulfone UF membrane with MWCO of 20 kDa, operated at 5 bar (500 kPa) TMP at recirculation rate of  $6 \text{ m}^3 \cdot \text{h}^{-1}$ , could achieve a protein to lactose ratio ranging from 1.7 to 9.5, 7.9%–12.3% defatted dry matter, 4.7%–8.9% protein, and 2.7%–0.8% lactose. Novák [33] reported a 90% true protein recovery after UF of skim milk and 98.4% recovery after DF using deionized water using spiral wound membrane of 5 kDa MWCO at 50°C and neutral pH. He noted that the process enabled the production of MPC with 90% true protein content after UF, and MPI with maximum total solids of 38% and true protein and lactose contents of 98.4% and 0.7%, respectively, after DF. Using 20 kDa MWCO polysulfone UF membrane operated at 50°C and TMP of 2 bar (200 kPa), El-Shibiny et al. [88] reported 18.5% total solids concentration of MPI with 89.1 total protein to dry matter ratio after UF of whole milk to a concentration factor of 5 and DF using four diavolumes of distilled water. Mistry and Hassan [133] reported 99.7% removal of lactose from pasteurized skim milk after UF to concentration factor of 5 and 3 DF cycles, each time using 4 diavolumes (based on retentate volume at concentration factor of 5) of water, using spiral wound module at 38°C. The final retentate was spray dried to produce delactosed, HMPP, which maintained its white color and bland flavor for 1 year of storage at room temperature. They suggested at least two DF to achieve the lactose reduction they obtained in the UF retentate, which contained total solids of 21.6% and 18.9% protein. The HMPP, which had an average composition of 5.3% moisture, 83.9% total protein, 2.3% fat, 0.7% lactose, and 7.1% ash, was of high-protein content—with caseins to whey proteins ratio similar to skim milk—and low mineral and lactose content [103,133,134]. Mistry [103] reported that because of the low lactose content of HMPP, its microstructure is more similar to that of caseinates but considerably different from NDM. It has a lower foaming capacity compared with commercial protein concentrates because of its relatively high fat content (2.3%) [103].

Milk of UF-standardized protein and total solids content enables the production of fermented dairy products of improved quality and characteristics compared with those produced from milk fortified with milk powder or evaporated milk [11]. Due to the similarity of the protein fractions in HMPP and those of skim milk and the virtual absence of lactose, Mistry and Hassan [134] suggested its utilization for the development of new dairy products and the improvement of existing ones. When these authors used HMPP to produce nonfat yogurt, they found that fortification level up to 5.6% protein can produce acceptable yogurt with smooth texture and firm body that did not exhibit whey separation even without the addition of stabilizers. They noted, however, that  $>5.6\%$  protein concentration, the yogurt becomes excessively firm and has a grainy texture and flat flavor.

Ozer et al. [135] compared the gelation properties of unconcentrated reconstituted milk ( $\sim 16\%$  TS) and milk concentrated by UF, RO, and direct concentration on reconstitution ( $\sim 23\%$  TS) for yogurt making. They found that yogurt from the UF milk contained the highest amount of protein ( $\sim 9\%$ ) and fat ( $\sim 8\%$ ), and the least amount of lactose ( $\sim 0.8\%$ ). They reported that unlike the other milk systems, the complex modulus ( $G^*$ ) of the UF milk did not reach a plateau within the experimental time frame, but continued to increase over the entire period of incubation. Due to the similarity in the loss tangent ( $\tan \delta$ ) values for the UF milk and those of other samples, the authors surmised that although the same interactive forces were involved in the gel formation of the milk samples, the flocculation kinetics for the high-protein UF milk may have changed. The system may have entered into a metastable state, in which the strength of the gel can continue to increase.

Aside from applications to fermented products, UF-standardized milk may also be used for the manufacture of several other dairy products. For instance, Lee and White [136] reported an increase in the protein value of ice cream when UF retentate rather than NDM was used for solids-not-fat (SNF) source in the formulation at substitution levels of 25%–75%. They also reported that because of the high level of casein in the ice cream made from UF retentate, its water-binding capacity increased, which resulted to an improvement in flavor and stability of body and texture.

### 22.3.6 RECOVERY OF LACTOSE AND MINERALS

Vyas and Tong [137] developed a method for calcium fortified reduced lactose skim milk production, which involves two UF steps (Figure 22.7). The process aimed to maximize calcium recovery without adversely affecting the native state of the milk proteins, while effectively removing lactose from the skim milk. In the first UF step (UF1), skim milk was ultrafiltered using a spiral wound module (10 kDa MWCO) at 2 bar (200 kPa) TMP and 10°C to concentration factor of 4. The permeate from UF1 was adjusted to pH 8, heated at 63°C for 30 min, to cause the formation of calcium complex or precipitates, and was then ultrafiltered (UF2) at the same condition as UF1. The retentate from UF2, which contained the concentrated calcium was mixed with the retentate from UF1 to produce the calcium fortified reduced lactose skim milk. They reported 70% recovery of the calcium from UF1 permeate during UF2 while enabling the recovery of high-purity lactose in the UF2 permeate.

### 22.3.7 FRACTIONATION OF MILK FAT AND ITS COMPONENTS

Milk fat globules are composed of triglyceride core and are surrounded by a natural biological membrane, the milk fat globule membrane (MFGM), which contains proteins, glycoproteins, enzymes, phospholipids, triacylglycerols, glycolipids, and other minor compounds, renders them compatible with the aqueous environment [138–140]. Because of its origin and amphiphilic nature, MFGM isolates were found to show good emulsifying properties and nutritional advantages such as modulation of cholesterol uptake, protection against bacterial infections in the gut, and inhibitory effect on colon cancer [141]. Although the

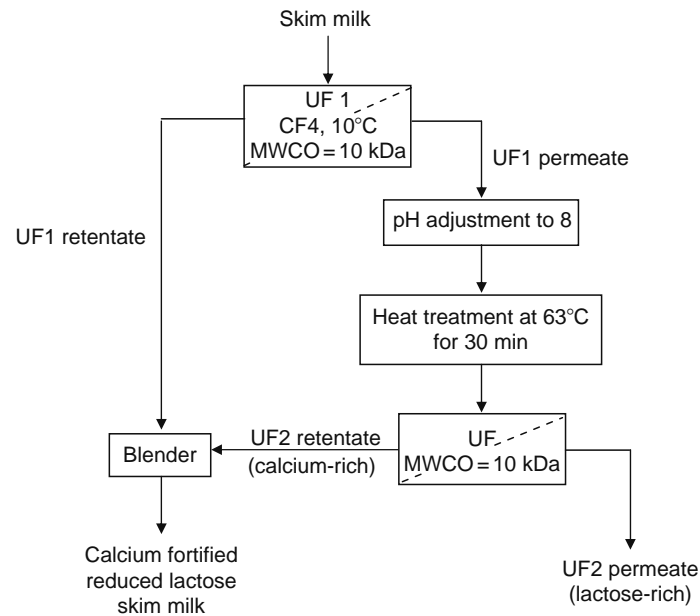


**FIGURE 22.7** Production of calcium fortified reduced lactose skim milk. (From Vyas, H.K. and Tong, P.S., *J. Dairy Sci.*, 86, 2761, 2003. With permission.)

MFGM proteins account for only 0.03%–0.04% of the total proteins in whole milk [139,142], many properties of dairy products are influenced by the responses of the MFGM components to various treatments [139,143]. For instance, it is supposed that a large part of the microstructure and consistency of dairy products, such as cheese, is largely affected by interactions between the casein matrix and fat globule, so that if the number of fat globules in the milk were to be modified without altering its total fat content, it may be possible to manipulate these interactions [144]. Since it is thought that fat globule size, which ranges between 0.2 and 15  $\mu\text{m}$ , could be a much better separation criterion between small and large globules than fat globule density, MF is the preferred technology over centrifugation to separate fat globules according to size rather than density without damaging the MFGM [140,144,145].

Goudéranche et al. [15] developed a CFMF process, which permits the selection of native small fat globules (SFG, 1–3  $\mu\text{m}$ ) and large fat globules (LFG, >5  $\mu\text{m}$ ) in raw milk. Using this process, Goudéranche et al. [144] confirmed that increasing or decreasing the number of native fat globules in milk leads to significant changes in the texture of liquid milk, yogurt, fresh cheese, sour cream, Camembert cheese, and mini Swiss cheese. They reported that products with greater amount of SFG gave creamier, smoother, and finer texture. They suggested the possible differences in triglyceride composition of SFG and LFG to be responsible for their observations. Briard et al. [146] reported that small and large native milk fat globules extracted from the same milk using the MF process developed by Goudéranche et al. [15] exhibited small variations in their total fatty acids. On the other hand, using the same system, Michalski et al. [17] found no major differences in triglyceride structures between native milk SFG and LFG after eliminating thermal history and the influence of cooling rates.

Using the milk fat globule MF fractionation process of Goudéranche et al. [144], Michalski et al. [140] observed pronounced difference in physicochemical and functional properties of Emmental cheeses made using native SFG and LFG. They reported lower flexibility and firmness in SFG cheeses, which had greater moisture and underwent greater proteolysis compared to LFG cheeses, 52 days after manufacture. However, lipolysis was threefold lower in SFG cheeses. Results of these studies confirm that the use of native milk fat globules with different sizes, separated using MF, can lead to a range of new dairy products with different physicochemical and functional properties [140]. Even interactions between milk serum proteins and MFGM proteins at different physicochemical conditions can now be characterized to elucidate their influence on dairy products quality because native milk fat globules can now be recovered by MF [139].

In the manufacture of butter, cream undergoes churning, a mechanical process which involves agitation in the presence of air that disrupts the phospholipid-protein membranes of the fat globules as they aggregate, releasing the water-soluble material, along with most of the proteins, lactose, and minerals, into the aqueous phase, or buttermilk [147–149]. Aside from the proteins in the buttermilk, which are mainly caseins and whey proteins, phospholipids render buttermilk as a potential source of ingredients of functional and nutraceutical applications [147–149]. Although native MFGM have been isolated from cream and purified by repeated washing-off of casein and whey proteins using simulated milk ultrafiltrate (SMUF) for characterization such as those done by Ye et al. [139,143], a commercial isolation and fractionation methods for MFGM components from buttermilk are yet to be developed [147].

Sachedva and Buchheim (cited in Ref. [147]) removed caseins from reconstituted buttermilk by precipitation of the caseins followed by MF of the phospholipids-rich buttermilk serum phase using 0.2  $\mu\text{m}$  pore size ceramic membranes. The authors reported a recovery of 67% of the total phospholipids, giving a final buttermilk extract containing about 1.5% phospholipids and 9% protein (dry basis) but the yields varied depending on coagulation conditions. Corredig et al. [147] observed retention of skim milk-derived peptides, especially caseins, in the UF (250 and 500 kDa MWCO) of reconstituted commercial buttermilk (8% w/v in deionized water) to a concentration factor of 2 and subsequent DF. When a 0.1  $\mu\text{m}$  pore size hydrophilic polysulfone Supor 100 membrane (Pall Gelman, Ann Arbor, Michigan) was used, greater permeation of the whey proteins was observed, although caseins were retained with the MFGM components, allowing the production of buttermilk concentrate. The addition of sodium citrate to buttermilk before MF disrupted the casein micelles, allowing their improved removal from the retentate to produce the MFGM isolate. However, the retention of whey proteins, especially  $\beta$ -Lg, and to a lesser extent,  $\alpha$ -La, by the membrane was still considerable, even at repeated DF. The authors surmised that the retained proteins are probably whey protein aggregates or complexes with caseins or the MFGM components, the amounts of which depend on the heat treatment history of the buttermilk, which is commonly very severe to render the cream sterile before butter manufacture. Nevertheless, the proposed process enabled the production of MFGM isolate with 35% (w/w) lipid and 60% (w/w) protein, which comprised 70% MFGM proteins, 6% caseins, and 24% whey proteins. Roesch et al. [148] showed that emulsions containing MFGM isolates produced from the process, developed by Corredig et al. [147], had small particle distribution with droplets of higher surface coverage showed good stability to creaming compared to buttermilk concentrate.

Morin et al. [149] compared the permeate flux through a 0.45  $\mu\text{m}$  pore size ceramic MF membrane during volumetric concentration to 2x and two-diavolume DF of regular buttermilk and whey buttermilk at 8–10°C and 0.8–0.95 bar (80–95 kPa) TMP. They reported that due to the lower amount of total solids, especially caseins and minerals, in the whey buttermilk, the permeate flux was significantly higher compared with that for regular buttermilk. They suggested that whey buttermilk has the potential of being a suitable starting material in producing MFGM isolate. However, they also recommended the standardization of whey cream before butter making as they noted variability in its lipid and phospholipids content.

## 22.4 MEMBRANE PERFORMANCE

### 22.4.1 FOULING AND FLUX PREDICTION

Concentration polarization and fouling are the main phenomena that limit the practical applications of membrane filtration. Both result in the unfavorable time-dependent flux decline and alteration of the membrane rejection behavior that compromise process efficiency [19,150–153]. Concentration polarization occurs at the beginning of the filtration process when a concentration gradient of the retained components is formed on or near the membrane surface [19]. The underlying mechanism behind this practically reversible phenomenon is the unbalanced transport of dissolved components between the bulk phase and the membrane surface. Fouling, on the other hand, is the largely irreversible deposition of solid materials on the membrane surface or within its pores [154]. Both occurrences limit the permeation rate by increasing hydraulic resistance to permeate flow. The osmotic back-pressure developed due to solids accumulation on the membrane surface also reduces driving force to permeation [49].

The hydrodynamic conditions employed in the process, and the physicochemical properties of the membrane and the feed solution are the main factors that influence the extent of concentration polarization and the occurrence of fouling [150]. For instance, in dairy processing applications where milk proteins are involved, protein–protein interactions can contribute to fouling of membranes in a variety of ways, such as inducing aggregation in solution, adding to the adsorbed protein layer, or altering the effective sieving coefficient of the constituent proteins [155]. Protein–membrane interactions, on the other hand, may lead to pore plugging, pore narrowing, and solids deposition that give rise to cake formation on the membrane surface [46]. On the other hand, the hydrodynamic conditions in crossflow filtration may alleviate fouling because, while the permeate flux drags particles toward the membrane, the crossflow induces particle back transport into the bulk phase [156].

One important finding in membrane fouling during dairy processing is that at a pH equal to the isoelectric point of the proteins, a minimum flux caused by severe fouling is observed. Huisman et al. [150] summarized the possible explanations to this observation that has been put forward by many authors as follows: (1) Hydrophobic interactions between hydrophobic membranes and the proteins are enhanced at the isoelectric point of the proteins where they become hydrophobic. (2) At their isoelectric point, proteins tend to aggregate more readily due to reduced electrostatic repulsion and this causes severe fouling. (3) Aside from enhanced transmission through the membrane, the small sizes of proteins at their isoelectric point cause them to form a densely packed fouling layer of low permeability. (4) Adsorption of more proteins through protein–protein interactions on the protein monolayer, which is usually hindered by electrostatic repulsion at all pH values, is enhanced at the isoelectric point of the proteins. This absence of electrostatic repulsion also leads to increased protein transmission through the membrane.

Mineral precipitation and complexation with proteins also contribute to fouling considerably. Adsorbed minerals may serve as salt bridges between the protein and the membrane, which aggravates fouling. In physicochemical conditions that promote calcium phosphate precipitation or calcium–protein complexation, membrane fouling in the filtration of milk or whey is severe,

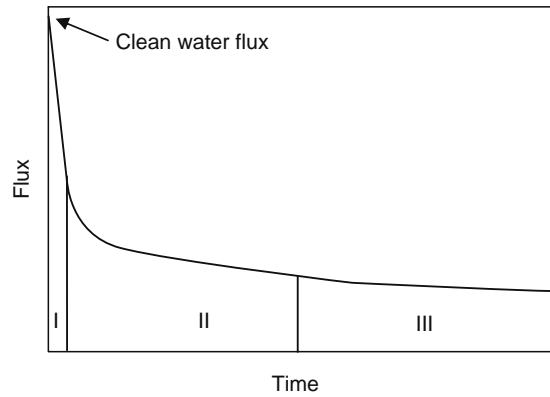


**FIGURE 22.8** Conceptual stages of flux decline in UF at constant-pressure operation: stage I, concentration polarization; stage II, membrane fouling (usually due to protein deposition); stage III, further particle deposition or consolidation of the fouling layer. (Adapted from Marshall, A.D., Munro, P.A., and Trägårdh, G., *Desalination*, 91, 65, 1993. With permission.)

although owing to the stabilizing influence of the casein micelles, the severity of fouling in milk filtration is less compared to that in whey [56]. Away from the isoelectric point of the proteins, added salts that alter the ionic strength tend to reduce the electrostatic repulsion by shielding charges, causing molecular contraction, thereby decreasing permeability [56].

Fat or lipid materials and calcium–lipid complexes also contribute to fouling and flux decline in membrane processing of milk or whey. The transport properties of the feed stream and the changes they undergo as the concentration process proceeds also affect the rate of permeation. At high concentrations, the increased fluid viscosity near the membrane surface limits back-diffusion of solids from the polarized layer to the bulk phase, thereby, depressing flux rate [46].

Huisman et al. [150] observed two fouling regimes in the UF of BSA using flat-sheet module of polysulfone membranes with MWCO of 30, 100, and 300 kDa: (1) the low-fouling regime at the initial stages of filtration and (2) the high-fouling regime at the later stages of filtration. They found that for the more retentive membrane, such as 30 kDa MWCO membranes, the hydrophobic protein–membrane interactions determine the fouling behavior at the low-fouling regime, while in the high-fouling regime, protein–protein interactions determine the overall performance. These were not definitively observed for the less retentive membranes, such as 100 and 300 kDa MWCO membranes, for which they found that the structure of the fouling layer seemed to have a more important influence on the final fouling.

Although permeate flux may decline far below the theoretical capacity of membranes, the typical variation of flux with time is that of an initial rapid decrease followed by a long and gradual flux decline (Figure 22.8) [157]. Modeling this flux decline caused by fouling during filtration provides better understanding of membrane fouling and provides predictive tools for successful scale up or scale down of filtration systems [153].

#### 22.4.1.1 Mechanistic Models for Flux Decline

To understand the flux decline in pressure-driven membrane operations, a number of models were developed. Two of the most widely studied models are the resistance model and the concentration polarization model. The resistance model is the oldest and is based on the cake filtration theory, where it is assumed that a cake layer of rejected particles, which are too large to enter the membrane pores, is formed. The frictional drag due to permeation through these immobile particles leads to additional hydraulic resistance [21]. The cake layer and the membrane are considered as two resistances in series, and the permeate flux is described by Darcy's Law as

$$J \equiv \frac{1}{A_m} \frac{dV}{dt} = \frac{\text{TMP}}{\mu(R_m + R_c)} \quad (22.1)$$

where

$J$  is the permeate flux

$A_m$  is the membrane filtration area

$V$  is the total volume of permeate

$t$  is the filtration time

TMP is the transmembrane pressure

$\mu$  is the viscosity of the permeate

$R_m$  is the intrinsic membrane resistance

$R_c$  is the cake resistance

This model has been successful in describing flux decline during dead-end filtration of particulate suspensions, but is not appropriate for application to crossflow filtration where the feed solution continuously recirculates [158]. Also, neither the occurrence of macromolecules and colloidal particles diffusion nor the influence of solute–solute and solute–membrane interactions on flux decline is considered in this model [42,59,159].

Aimar et al. [19] noted that in the UF of complex liquids, such as cheese whey, which contains proteins, salts and casein fragments, concentration polarization, and adsorption and cake formation play a role in flux behavior during crossflow filtration. They may induce osmotic pressure in the retentate side since the chemical potential of the solute-rich polarized layer is lower than that of the permeate, and therefore at equilibrium, a positive osmotic pressure develops in the retentate to equal that of the permeate. The smaller the solute, the greater is its contribution to the osmotic pressure of the liquid, so that in milk, lactose and the minerals have the biggest contribution to osmotic pressure. In skim milk or whey, the osmotic pressure is around 7 bar (700 kPa) and this must be exceeded in RO to commence permeation; in UF, only the proteins contribute to the osmotic pressure, which increases exponentially with protein concentration [56]. In any case, a TMP greater than the osmotic pressure is required for solvent to flow from the retentate side to the permeate side. This leads to the reduction in the effectiveness of applied TMP as driving force to permeation.

Concentration polarization caused by macromolecules, which may induce a reversible osmotic pressure that disappears after the filtration pressure is released, and the adsorption on the membrane pores of solid materials or inside the membrane pores of solid materials, which are rid of by rinsing the membrane after the filtration process, are occurrences that both contribute to the reversible resistance to permeation,  $R_{rev}$ . On the other hand, the solids that are deposited on the membrane surface or inside the pores, which are removed only by chemical cleaning of the membrane, constitute the irreversible fouling,  $R_{irrev}$ .

When both  $R_{rev}$  and  $R_{irrev}$  are considerable, Equation 22.1 may be written as

$$J = \frac{\text{TMP}_{\text{eff}}}{\mu(R_m + R_{rev} + R_{irrev})} \quad (22.2)$$

where  $\text{TMP}_{\text{eff}}$  is the effective transmembrane pressure which is equal to  $\text{TMP}_{\text{appl}} - \Delta\Pi$ , wherein  $\text{TMP}_{\text{appl}}$  is the applied transmembrane pressure and  $\Delta\Pi$  is the osmotic pressure [19,21].

In systems that involve solutes <100 kDa in size, such as most of the whey proteins, this model is found to be appropriate [56]. In the UF of WPI solutions using dead-end MF with disc-type ceramic membranes of 0.8  $\mu\text{m}$  nominal pore size, Mourouzidis-Mourouzidis and Karabelas [160] observed that irreversible fouling effectively develops during the first cycle. In the UF of sweet whey, Aimar et al. [19] commented that for low levels of  $\text{TMP}_{\text{appl}}$ , the effective pressure is not a function of crossflow velocity while at higher  $\text{TMP}_{\text{appl}}$ , where the extensive occurrence of concentration polarization is more likely, the effective pressure increases with increasing crossflow velocity. On the other hand, the irreversible fouling, which results to the modification of the transport properties of the membrane, is responsible for the variations in time of permeate flux. The rate of tangential flow, which determines the wall shear stress ( $\tau_w$ ), plays a critical role in alleviating this phenomenon in that it helps erode the adsorbed solid materials during the filtration process, limiting the thickness of deposited layer on the membrane surface. In the UF of reconstituted skim milk using tubular polyvinyl difluoride (PVDF) membranes (200 kDa MWCO), Grandison et al. [161] reported that increasing the  $\tau_w$  at constant TMP led to an increase in both the initial flux and subsequent flux decline, and to a decrease in  $R_{irrev}$ .

Where proteins and other dairy components are involved, aside from cake filtration, the occurrence of pore blocking (complete and intermediate pore blockage phenomena) and pore constriction adversely impacts permeation flux [21,112,153,162,163]. For instance, in the MF of skim milk, as the membrane pore size increases, the contribution of irreversible fouling to overall fouling also increases, indicating greater fouling within the membrane structure [151]. The effects of these various fouling occurrences can be estimated using the appropriate equations given in Table 22.3. An alternative approach is to use the general differential equation

$$\frac{d^2t}{dV^2} = k \left( \frac{dt}{dV} \right)^n \quad (22.3)$$

which may also be written as

$$\frac{dJ}{dt} = -kJ(JA_0)^{2-n} \quad (22.4)$$

where the value of the exponent  $n$  specifies the filtration model considered:

$n = 0$  for cake filtration

$n = 1$  for intermediate blocking

$n = 3/2$  for pore constriction

$n = 2$  for complete pore blocking [164]

**TABLE 22.3**  
**Classical Fouling Models**

Model	Governing Equations	Normalized Flow Rate
Complete pore blockage	$\frac{dA_u}{dt} = -\alpha Q_u C_b$	$\frac{Q}{Q_0} = \exp\left(-\alpha \frac{\text{TMP}}{\mu R_m} C_b t\right)$
Intermediate pore blockage	$\frac{dA_u}{dt} = -\alpha' Q_u C_b \frac{A_u}{A_0}$	$\frac{Q}{Q_0} = \left(1 + \alpha' \frac{\text{TMP}}{\mu R_m} C_b t\right)^{-1}$
Cake filtration	$\frac{dR_p}{dt} = f' R' J_b C_b$	$\frac{Q}{Q_0} = \left(1 + f' R' \frac{2\text{TMP}}{\mu R_m^2} C_b t\right)^{-1/2}$
Pore constriction	$\frac{d(N_0 \pi r_p^2 \delta_m)}{dt} = \alpha_{in} Q_u C_b$	$\frac{Q}{Q_0} = \left(1 + \alpha_{in} \frac{Q_0}{\pi r_0^2 \delta_m} C_b t\right)^{-2}$

Source: From Duclos-Orsello et al., *J. Membr. Sci.*, 280, 856, 2006. With permission.

Note:  $A_u$ , area of unblocked membrane ( $\text{m}^2$ );  $A_0$ , initial area of unblocked membrane ( $\text{m}^2$ );  $C_b$ , bulk concentration ( $\text{g}\cdot\text{L}^{-1}$ );  $f'$ , fractional amount of total foulant contributing to deposit growth;  $J_b$ , filtrate flux within the blocked area ( $\text{m}\cdot\text{s}^{-1}$ );  $Q$ , volumetric flow rate ( $\text{m}^3\cdot\text{s}^{-1}$ );  $r_p$ , radius of membrane pore (m);  $R_m$ , resistance of the clean membrane ( $\text{m}^{-1}$ );  $R_p$ , resistance of the deposit ( $\text{m}^{-1}$ );  $R'$ , specific protein layer resistance ( $\text{m}\cdot\text{kg}^{-1}$ );  $t$ , filtration time (s). Greek letters:  $\alpha$ , pore blockage parameter ( $\text{m}^2\cdot\text{kg}^{-1}$ );  $\beta$ , pore constriction parameter (kg);  $\delta_m$ , membrane thickness (m).

The concentration polarization model, which is based on the stagnant film theory, was developed to describe the back-diffusion phenomenon during filtration of macromolecules. In this model, the rejection of particles gives rise to a thin fouling layer on the membrane surface, overlaid by a concentration polarization layer in which particles diffuse away from the membrane surface, where solute concentration is high, to the bulk phase, where the solute concentration is low [158]. At steady state, convection of particles toward the membrane surface is balanced by diffusion away from the membrane. Thus, integrating the one-dimensional convective–diffusion equation across the concentration polarization layer gives

$$J_v = \frac{D}{\delta} \ln \frac{\phi_w}{\phi_b} = k \ln \frac{\phi_w}{\phi_b} \quad (22.5)$$

where

$D$  is the diffusion coefficient

$\delta$  is the thickness of the concentration boundary layer

$\phi_w$  is the solids volume fraction on the wall

$\phi_b$  is the solids volume fraction in the bulk solution

$k$  is the mass transfer coefficient equal to  $D/\delta$

For the UF of proteins, the concentration polarization model has been found to predict the filtration performance reasonably well [56]. However, this model is inherently weak in describing the two-dimensional mass transport mechanism during crossflow filtration and does not take into account the solute–solute interactions on mass transport that occur extensively in colloids, especially during MF [21,44,158,159]. The diffusion coefficient, which is inversely proportional to the particle radius, is low and underestimates the movement of particles away from the membrane [56]. This results to the well-known flux paradox problem where the predicted permeate flux is as much as two orders of magnitude lower than the observed flux during MF of colloidal suspensions [56,58,158]. This problem has then been underlined by the experimental finding of a critical flux for colloids, which demonstrates the specificity of colloidal suspension filtration wherein just a small variation in physico-chemical or hydrodynamic conditions induces important changes in the way the process has to be operated [21].

Modifications of the resistance and the concentration polarization models, which involve inclusion of suitable parameters depending on membrane system and the feed chemistry, were introduced achieving some success in explaining the influence of process conditions on flux decline. Saksena and Zydney [44] extended the stagnant film model to account for the effects of both hydrodynamic and thermodynamic solute–solute interactions on bulk diffusion in binary protein system (BSA-IgG) by making appropriate changes on the diffusion coefficient in the model. The modified model sufficiently explained the flux-pressure dependence during UF of binary protein system in a stirred cell UF. Using the model, the authors deduced that BSA transmission is reduced by the concentration gradient in IgG, which increased BSA's diffusive flux. Bacchin et al. [21] unified the resistance and the concentration polarization models to theoretically describe the crossflow filtration of

colloidal particles and molecules and, by numerical simulations, showed that the unified model can identify the crossover from the occurrence of concentration polarization to irreversible fouling, which is useful in membrane system design. Their findings, however, were not verified by experimental results on real systems.

Using experimental results on ovalbumin, Nyström [165] deduced that the charge on the protein rather than the difference in charge between the membrane and the protein, determines the degree of protein deposition on membrane surface. When the protein is charged, the solubility (protein stability) increases and the affinity for the membrane material decreases. Where the membrane charge is opposite to that of the protein, initial adsorption may result in a thin modified layer of charged proteins on the membrane surface that then repels further deposition as quasi-steady flux is attained [165].

### 22.4.1.2 Empirical Fouling Models

Assuming that the amount of flux decline is a function of cumulative permeate volume, Merin and Cheryan [47] suggested that initial flux decline in the UF of whey be defined by

$$J = J_0 V^{-b} \quad (22.6)$$

where

$J$  is the instantaneous flux at any time,  $t$

$V$  is the volume permeated

$J_0$  is the initial flux at  $t=0$ , which is an indication of the resistance to solvent transport by the membrane as well as the concentration polarization layer formed on the membrane by the proteins

$b$  is the indicator of the rate of fouling during long-term operation, or the true fouling effects, due to specific membrane–solute interactions

Using individual whey and cottage cheese whey as feed streams, the authors used the model to speculate how each protein influences flux decline and how their interactions in whey under certain physicochemical conditions affect flux decline in polysulfone membrane. Although their findings provided useful insights, they were limited to the initial flux decline in the UF. Kuo and Cheryan [45] utilized the same model to investigate long-term fouling of cottage cheese whey on polysulfone membrane in spiral wound configuration. The model proved useful in identifying critical process settings but insufficient in providing basic understanding on membrane–solute interactions, which the authors suggested, have the biggest influence on initial flux decline before attaining quasi-steady flux. The model is limited by its inability to identify the point at which concentration polarization and gel-layer is formed on the membrane surface. Despite this, it is by far, one of the most utilized models in understanding fouling in the UF of whey.

### 22.4.1.3 Limiting Flux versus Critical Flux

In membrane processes, permeate flux generally increases with TMP, although the increase in flux for solutions is lower than that of pure water flux. At high TMP values, the permeate flux is not significantly affected by increases in pressure and it levels off to almost a constant value before dropping at higher TMP values. This constant flux is called the limiting flux, which increases with increasing crossflow velocity. Michaels [166] used the film theory to explain the observed maximum stationary flux when increasing the TMP of a filtration system. Materials deposited on the membrane by mass transport are removed by the wall shear force and diffuse back into the bulk flow. Beyond the limiting flux, operation at sustained permeability and selectivity is not possible due to the accumulation and compaction of the fouling layer on the membrane [167].

Field et al. [157] introduced the concept of critical flux in membrane filtration. They proposed that upon start-up, there exists a flux below which a decline of flux with time does not occur. Although a concentration polarization layer is present, solid deposition on the membrane that gives rise to cake layer formation does not take place, so that a nonfouling or cake-free operation is achieved. This flux is the critical flux and it may either be in “strong” form, in which flux is identical to the clean water flux at the same TMP, or in “weak” form, in which flux varies linearly with TMP but the slope of the line differs from that of clean water [6,157,161].

Figure 22.9 shows the three regimes that are manifested in membrane filtration in accordance to the critical flux theory [6]. Regime I is the subcritical regime where flux varies linearly and reversibly with TMP. Because the operation capacity is small due to low flux values, processing in this regime requires large membrane area otherwise a high crossflow velocity is employed to increase capacity [6]. Due to the effective prevention of fouling or cake formation, the membrane selectivity in this regime is optimal. Processes where high product purity is required, such as the fractionation of whey proteins, are carried out in this regime. The flux in regime II is independent of TMP. It is equal to the limiting flux, which can be described by the cake filtration or back transport model where the transport of particles toward the membrane is balanced by the back-transport toward the bulk flow. Therefore, high crossflow velocity can promote high flux in this regime. For instance, the reduction of

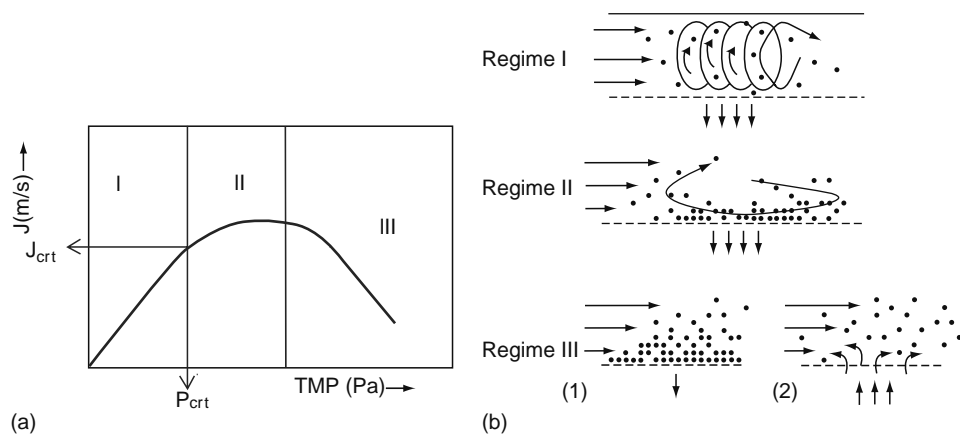


**FIGURE 22.9** (a) Critical flux regimes: (I) Subcritical operation where flux is linear with TMP and no flux-dependent fouling, (II) TMP above the critical pressure and flux is described by gel filtration or back transport model, and (III) TMP is far above critical pressure, time-dependent flux decline occurs. (b) Graphical representation of fouling in the critical flux regimes: (I) Subcritical operation, fouling is prevented by mechanical action such as turbulent mixing, (II) filtration with a dynamic cake layer, showing particle back transport into the crossflow, and (III) time-dependent flux decline with severe cake formation (1), which could be remedied by backpulsing (2). (From Brans et al., *J. Membr. Sci.*, 243, 263, 2004. With permission.)

bacteria and spores, and concentration of casein micelles by MF are carried out just above the critical pressure, or the lower part of regime II, usually utilizing a combination of high crossflow velocity and low UTMP for optimal flux. Although selectivity is not optimal in this regime, it can lead to optimal capacity, which is particularly advantageous when expensive membranes are used. Optimum capacity in the concentration of whey proteins can also be achieved in regime II. The high TMP, which is way above the critical TMP, in regime III results in time-dependent flux decline that is mostly attributed to cake compaction. Therefore, periodic mechanical removal of fouling, such as by backshock or backpulse, is necessary for stable extended operation.

The critical flux value depends largely on the hydrodynamic conditions in the process, the membrane pore size, and the feed physicochemical condition [161,168]. Appropriate manipulation of these parameters, specifically the hydrodynamic condition, may lead to the reduction or even the elimination of both reversible and irreversible fouling of the membrane. Youravong et al. [152] estimated the critical flux in the UF of skimmed milk to lie between 55 and 60  $\text{kg}\cdot\text{h}^{-1}\cdot\text{m}^{-2}$  and that the average critical TMP was 0.22 bar (22 kPa) at 50°C using PVDF membranes with MWCO of 200 kDa. In the UF of WPC and sodium caseinate suspension, Youravong et al. [168] reported that both gave the weak form of critical flux, which increases with increase in crossflow velocity.

Although in many cases, the critical flux is equal to the limiting flux, in other cases operating at the limiting flux causes more fouling [161]. Therefore, it is useful to determine the operating conditions that will sustain satisfactory performance, in terms of selectivity and permeability, around the critical zone especially for an extended period of operation. A pseudo steady-state operation, described by the cake filtration model, is desirable in long-time operations. Since the permeation flux,  $J$ , governs convective mass transport to the membrane and that the efficient wall shear stress,  $\tau_{\text{weff}}$ , governs particle and molecule back-transport from the membrane toward the bulk flow, and that these transport phenomena are necessary for sustained operation, then a critical ratio,  $(J/\tau_{\text{weff}})_{\text{crit}}$ , may also exist for satisfactory long-time membrane operation [96,169]. Le Berre and Daufin [97] as well as Gésan-Guiziou and Daufin [169] determined the value of the critical ratio in the MF of skim milk as 0.95 and 1.00  $\text{L}\cdot\text{h}^{-1}\cdot\text{m}^{-2}$ , respectively. Exceeding these values led to the accumulation of milk components on the membrane surface. This suggests that the critical ratio pertains to the transition to irreversible material deposition on the membrane. Furthermore, the similarity of the critical ratio values that the two groups obtained even when they used different membrane modules and adapted different approach suggests that the critical zone in the MF of skim milk is mainly related to the characteristic of the deposit. These indicate the usefulness of the critical ratio in determining critical operating conditions.

Despite the numerous efforts in understanding the fouling mechanisms and the influence of operating parameters involved that lead to flux decline in filtration systems, there remain significant gaps in the present knowledge on this phenomenon. To date, none of the theoretical models, and their numerous modified forms, and empirical models sufficiently explain the influence of membrane–solute interactions and solute–solute interactions on real dairy systems.

## 22.4.2 ENERGY CONSUMPTION

Aside from mild operating conditions suitable for processing dairy systems, membrane technology involves smaller energy consumption and higher rate of return of investment that punctuates the technology's economic advantages over conventional

**TABLE 22.4**  
**Comparison of Energy Consumption and Average Flux for Various UF Systems Used in Whey Processing**

Module Design	Type of Whey	Membrane Material	Average Flux (L·h <sup>-1</sup> ·m <sup>-2</sup> )	TMP (kPa)	Energy Use (kJ) Per Cubicmeter of Permeate
Spiral wound	Acid whey	Polysulfone	38	480	5.2 × 10 <sup>3</sup>
Spiral wound	Cottage cheese whey	Polysulfone	12	335	3.0 × 10 <sup>3</sup>
Hollow fibers	Cottage cheese whey	Polysulfone	28	155	5.9 × 10 <sup>3</sup>
Plate and frame	Gouda whey	Ceramic	51	300	8.8 × 10 <sup>3</sup>
Tubular	Gouda whey (decalcified)	Ceramic	74	500	1.4 × 10 <sup>4</sup>
Tubular	Cottage cheese whey	Ceramic	24	225	4.5 × 10 <sup>5</sup>

Source: From Cheryan, M. and Kuo, K.P., *J. Dairy Sci.*, 67, 1406, 1984. With permission.

separation techniques [170,171]. For instance, Marshall [1] reported that a single-effect evaporation system and a quadruple-effect evaporation system consume as much as 626 and 126 kWh per ton of water removed, respectively, and that five- to seven-effect evaporation systems and mechanical vapor compression consume 37–53 kWh per ton of water removed. On the other hand, RO system used for water removal of milk consumes only 9–19 kWh per ton of water removed [1]. In the United States, the cost of concentrating skim milk from 8.8% to 45% total solids by plate-and-frame RO plant with a capacity of 9,000 kg·h<sup>-1</sup> was estimated to be 50% cheaper compared to the cost of water removal by evaporation [63,172]. If evaporation and RO were combined to achieve the same total solids concentration, the total energy consumption is less than one-third of that when evaporation alone is employed [63,172].

Although the smaller energy consumption involved in membrane operations is very well known, the membrane type and configuration must be carefully chosen to further optimize energy cost in specific applications. For the same purpose and set of operating parameters, one membrane type or module design might be advantageous over another as far as energy consumption is involved. Cheryan and Kuo [22] compared the amount of energy used in the UF of whey using different membrane types in various configurations (Table 22.4) and found that polysulfone membrane in spiral wound configuration consumed the least amount of energy (kJ) per cubicmeter of permeate collected compared with polysulfone in hollow fiber configuration and ceramic membranes, both in tubular and plate-and-frame configurations.

## 22.5 CLEANING AND SANITATION

Effective cleaning and sanitation are necessary strategies to restore membrane performance after processing and to sustain hygienic operation [170]. It is generally acknowledged that a major cost associated with membrane maintenance in the dairy industry is that incurred from cleaning and sanitizing the membranes after processing. The cost of water and wastewater generated during cleaning alone was estimated to comprise 20% of the total cleaning cost [173]. The fact that cleaning and sanitation protocols affect the membrane lifetime and efficiency is also a concern [55,174]. Therefore, the cleaning process must be optimized to lessen the adverse effects of cleaning agents on membrane life, the cost of purchasing and disposing of cleaning chemicals, as well as the volume of water consumed and wastewater produced [175].

Optimization of membrane cleaning and sanitation processes involves the understanding of: (1) the complex interactions between the foulants and the membrane and (2) the economic impact of the cleaning and sanitation processes [174]. In dairy applications, the usual soil consists of proteins, fat, carbohydrates, and minerals, with fat and protein residues being the most difficult to remove [173]. Interactions between these dairy foulants and the different membrane materials have been the subject of many studies to date.

### 22.5.1 CLEANING

Membrane cleaning involves the removal of a substance that is not an integral part of the membrane material [176]. The process must remove fouling deposits and must restore the normal capacity and separation characteristics of the equipment [175]. The cleaning process is usually divided into two main steps: rinsing and chemical cleaning.

The membrane is rinsed with softened water immediately after processing to remove reversible fouling from the membrane surface by mechanical actions, such as mixing, turbulence, and shear. Marked increase in flux can be achieved by rinsing because of the removal of soluble material or desorption of foulants or additives [175]. In dairy applications, the rinsing water should have a fouling index lower than 1.5 and be of acceptable bacteriological quality [177]. Specifically for MF and UF plants, Krack [173] reiterated that the salt density index of the rinsing water should be <3, otherwise problems may occur.

As a guideline for the water quality, the following may be used: total hardness should be maximum of 3.57 mmol (357 ppm  $\text{CaCO}_3$ ), total amount of bacteria 1000 per mL, total amount of coliform bacteria  $<1$  per mL [173].

After water rinsing, chemical cleaning is carried out to remove tightly bound materials on the membrane surface and pores. Appropriate chemical cleaners are chosen to remove specific foulants, such as nonionic detergents (0.1%) to remove fat deposits, acids to remove inorganic precipitates or oxide films, and alkaline detergents (0.1%–0.5%) to remove protein deposits [3,175]. Nitric and phosphoric acids are the most frequently used acids for cleaning membranes. However, citric acid is also used and favored by some due to its mildness compared with nitric acid [175]. Hydroxide solutions, either sodium hydroxide or a mixture of sodium hydroxide and potassium hydroxide of pH 11–12, added with sodium hypochlorite for improved cleaning and disinfecting power, are usually recommended for the alkali cleaning [175].

Aside from detergent cleaning, enzymatic cleaning is also considered for membranes soiled with dairy foulants. Enzymatic cleaners are usually employed if the membrane pH limitation is at or below 10 or if a high level of contaminants is present [173]. Enzymes are advantageous over traditional chemical cleaners in that they are biodegradable, less aggressive to the membranes, and they can improve cleaning efficiency by reducing energy costs and the amount of chemicals needed [175].

Other than the type and composition of the cleaning agent, the order and duration of the cleaning steps, and the physical operating parameters are key components of an effective cleaning strategy [175]. To obtain good mechanical cleaning effects, it is recommended that the circulation flow rate is to be higher and the pressure lower than those used during the normal operation [178]. Another factor to be considered is the amount of cleaning solution in comparison to the membrane surface, which in process plants today ranges between 4 and 5  $\text{L m}^{-2}$  membrane surface [173].

### 22.5.1.1 Water Rinsing

The first stage of rinsing is usually carried out with the permeate side of the membrane module closed, or TMP values close to zero, to limit convective transport of permeate particles toward the membrane. This prevents adsorbed materials on the membrane surface from migrating to the membrane pores, maximizing the rate of erosion of fouling on the membrane surface. At this stage, the crossflow velocity is a major operation parameter. Later, when permeate convective transport is allowed by opening the permeate side valve, the pore foulants are removed more efficiently [177]. This strategy improves rinsing efficiency, which is measured in terms of hydraulic resistance reduction during rinsing, and helps minimize the consumption of cleaning agents during the chemical cleaning step.

The feeding mode of rinsing water also influences rinsing efficiency. Some membrane modules allow backflushing, where the rinse water is made to flow from the permeate side to the retentate side. This is carried out at the beginning of the rinsing step, or periodically during the rinsing step, to remove internal fouling and to dislodge hard deposits on the membrane surface rather than compressing the fouling layer that renders rinsing inefficient. Whether the rinsing water is recycled or not, especially during the first stage of the rinsing step, also impacts rinsing efficiency. Cabero et al. [177] observed that 15 min rinsing of ceramic membrane, which was previously fouled with whey, without recycling the rinsing water removed larger part of hydraulic resistance compared to when rinsing water was recycled. The same authors also reported that prolonging the rinsing time does not improve the rinsing efficiency when water is recycled.

The temperature at which water rinsing, including intermediate rinsing, is carried out is also a major consideration. Warm water rinsing rather than cold water is preferred to avoid temperature stress on the membrane and to avoid break-up of well-emulsified soil that may lead to redeposition of dairy foulants on the membrane [173]. The duration of rinsing time varies with the size of the membrane plant, and usually ranges between 5 and 20 min.

### 22.5.1.2 Chemical Cleaning

Most chemical cleaning protocols consist of an alkali detergent step followed by an acid step, with appropriate rinses in between. However, for polymeric membranes, it is also common to follow the acid cleaning step with a second alkali cleaning step supplemented with chlorine as this further improves flux [176,179]. In some cases, acid cleaning has been recommended as the first step, especially for whey applications, where mineral fouling maybe more important than protein fouling [176].

Many researchers consider the restoration of clean water flux as a measure of the degree of membrane cleanliness [3,180]. However, it is insufficient to characterize cleaning efficiency by either flux recovery or resistance removal alone because large resistance removal values are often easily obtained even when considerable amounts of foulants are still deposited on the membrane [181]. For instance, Bohner and Bradley [180] utilized a cleaning procedure at 43°C where after processing and flushing with water, acid solution, a 1:1 blend of nitric and phosphoric acids at pH 1.8, was recirculated for 1 h. After another water flush, sodium hydroxide solution with 0.1% surfactant (w/v) at pH 11.8 was then recirculated also for 1 h to clean spiral wound polysulfone UF membranes (10–15 kDa MWCO) soiled with cheddar cheese whey. Results of scanning electron microscopy of the membranes after cleaning indicated that protein deposits and bacteria still contaminated the membrane surface even after reducing the hydraulic resistance and restoring the permeate flux to its value before processing.

To improve the removal of deposits on the membrane surface, Bohner and Bradley [179] modified the cleaning procedure described previously. The modified procedure, which was carried out at 54°C, consisted of a 2 min initial rinsing of the

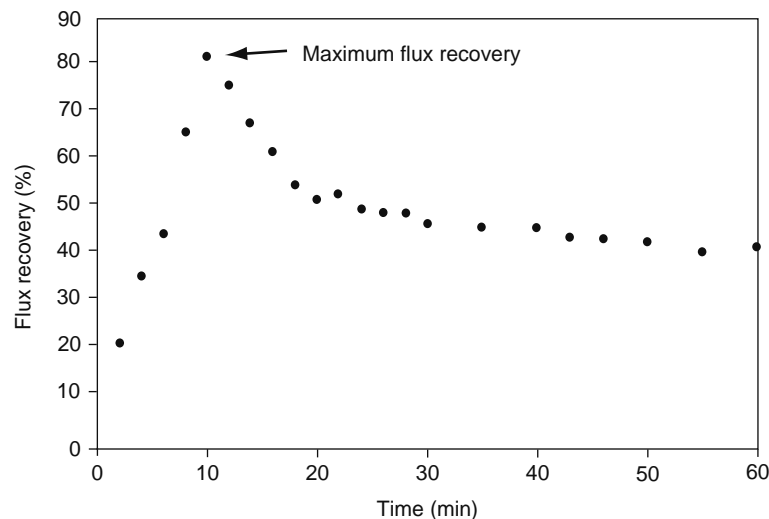


**FIGURE 22.10** Dynamics profile of the flux recovery in cleaning WPC-fouled PVDF MF membranes using NaOH solution at pH 13 and 30°C, and at crossflow velocity of  $0.45 \text{ m}\cdot\text{s}^{-1}$  and 350 kPa TMP. (From Mercadé-Prieto, R. and Chen, X.D., *J. Membr. Sci.*, 254, 157, 2005. With permission.)

membrane system with water. Sodium hydroxide at pH 11.0, with 0.1% of nonionic surfactant added, was circulated for 20 min. After a 2 min rinse with water, a 1:1 mixture of nitric and phosphoric acids at pH 2 was circulated for 20 min before a final water rinsing. With the scanning electron microscopy images of the cleaned membrane, Bohner and Bradley [179] found that the cleaning procedure rid the membrane surface of whey residues. They also noted that the cleaning procedure did not damage the membranes even when it was used continuously for 300 h. However, when the cleaning temperature was increased from 54°C to 63°C, they observed damage on the membrane after 100 h of cleaning.

Although alkali cleaning of membranes soiled with dairy proteins is generally accepted in the dairy industry, its efficacy and optimal cleaning capacity has been the subject of a number of studies. Caustic concentration, operating temperature during alkali cleaning, and the length of cleaning time impact flux recovery (Bird and Bartlett, 2002). An optimal sodium hydroxide concentration where the flux recovery reaches maximum was found to range between 0.075 and 0.5% (w/w) [182]. The typical dynamic flux recovery profile, expressed as the ratio of flux during cleaning to clean water flux, consists of an initial sharp increase followed by an exponential decay to a steady-state value as that shown in Figure 22.10 [182]. The existence of maximum flux recovery has been the subject of a number of investigations.

Using light microscopy, Bird and Bartlett [170] observed that the deposit on sintered stainless steel MF membrane ( $2.0 \mu\text{m}$ ) fouled with whey consists of a loose sheet-like protein-rich structure which is removed during the first few minutes of chemical cleaning (Figure 22.11). Cleaning with sodium hydroxide removes the loose top proteinaceous layer, which results to the sharp

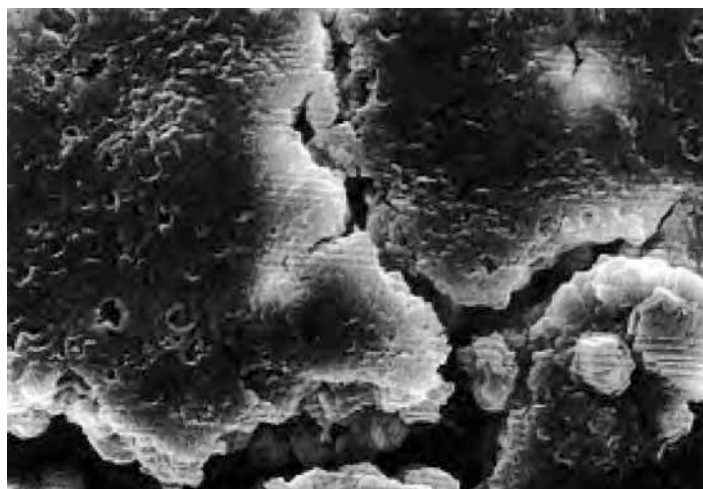


**FIGURE 22.11** Scanning electron microscopy image of sintered membrane surface fouled with WPC deposits. (From Bird, M.R. and Bartlett, M., *J. Food Eng.*, 53, 143, 2002. With permission.)

increase in flux recovery as in Figure 22.10. Bird and Bartlett [170] found that underneath the proteinaceous top layer are aggregates of calcium phosphate imbedded in a protein sheet. Although the protein sheet is eroded with continuous cleaning, the authors found that calcium phosphate remains on the surface of the membrane. They also found that proteinaceous materials are present within the membrane pores. They hypothesized that the flux decline observed during the caustic cleaning of membrane is caused by these proteinaceous in-pore fouling that swells at high pH.

The physicochemical conditions of the foulants and the cleaning agents are important considerations in designing efficient cleaning procedure. Kim et al. [181] studied the cleaning of UF membranes, fouled with BSA, using acid, bases, and anionic and cationic surfactants. They reported that when membranes were fouled at the isoelectric point of BSA (pH 5), hydraulic resistance removal was highest when hydrochloric acid and sodium hydroxide solutions were used. If the membranes were fouled at pH 7, at which BSA has a net negative charge, they found that the cationic surfactant cetyl-trimethyl-ammonium bromide (CTAB) was more effective due to electrostatic interactions between the protein fouling layer and CTAB. Muñoz-Aguado et al. [174] reported that at pH 7, the protein layer on polysulfone UF membrane (30 kDa MWCO), recirculated with BSA solution or reconstituted WPC, was almost three times thicker than that at pH 5. However, the permeate fluxes were lower at pH 5. This was due to the more compact and less permeable protein layer formed on the membranes at pH 5, which is the isoelectric point of BSA and the mean isoelectric point of whey proteins. On the other hand, the significant net negative charge on the proteins at pH 7 causes expansion of the protein fouling layer that results to thicker but more permeable deposit. Such understanding of protein fouling behavior and possible membrane–protein interactions led to the exploration of other cleaning strategies.

Proteases, lipases, or enzyme detergents, which hydrolyze proteins and fats, are sometimes used to supplement or replace alkaline detergent cleaning, particularly when using less alkali-resistant cellulosic membranes [3]. Muñoz-Aguado et al. [174] studied the efficiency of CTAB, the enzyme  $\alpha$ -chymotrypsin ( $\alpha$ -CT), and the complex mixture of detergents and enzymes Terg-A-Zyme (TAZ) in cleaning polysulfone UF membrane fouled with BSA. All the cleaning agents took about 1 h to reach maximum cleaning efficiency at 40°C. The use of CTAB at 0.2% (w/w) concentration resulted to better flux recovery than the use of  $\alpha$ -CT. They reported that, at pH 5 and 7, the efficiency of CTAB is enhanced by the prior cleaning of the membranes with  $\alpha$ -CT, due to the better accessibility of the proteins in the cake layer that has been disrupted by the prior action of  $\alpha$ -CT at 0.01% (w/w) concentration. The inclusion of water rinsing, also at 40°C, in between the  $\alpha$ -CT and CTAB cleaning cycles further improved flux recovery. They also found that excessive treatment with these cleaning agents exacerbates fouling, with  $\alpha$ -CT reinforcing the membrane–protein binding, or acting as a foulant itself. The group reported the highest flux recovery using TAZ at 0.4% (w/w) concentration. They observed similar trends when cleaning membranes fouled with reconstituted WPC. However, because of the more complex fouling layer formed by reconstituted WPC, higher concentration of TAZ, 0.75% (w/w), was necessary to achieve the maximum flux recovery.

Although the effectiveness of multistep cleaning processes using surfactants, enzymes, or surfactant-enzyme system in flux recovery is well-established, the economic impact of these procedures needs to be evaluated for truly optimized membrane cleaning. Physical methods of cleaning membranes simultaneous to processing are also being investigated. One such method is the use of electric field pulse to dislodge membrane fouling and restore initial flux while processing continues [171].

### 22.5.2 SANITATION

Plants are cleaned, sanitized, and rinsed immediately after processing, and right before processing to ensure satisfactory initial process conditions from microbiological standpoint [3]. Because chlorine is freely permeable to most membranes that it is able to sanitize the permeate side of the system as well as the retentate side, using solutions of sodium hypochlorite containing 100–200 ppm of active chlorine is a common sanitation technique for many membranes, except cellulose acetate reverse osmosis membranes, which can only tolerate brief exposure to chlorine at 10–50 ppm level [3].

Bohner and Bradley [180] evaluated the efficiency of a sanitizer whose composition enabled the release of chlorous acid and chlorine dioxide from sodium chlorite at pH 2.7 in destroying bacterial populations in a polysulfone spiral wound UF membranes soiled for 2.5 h by circulating and concentrating cheddar cheese whey and skim milk. Using results from swabbing, they reported that the sanitizer was effective in controlling microbial populations in UF membrane systems. Bohner and Bradley [180] investigated the use of sanitizing cycle at 54°C after cleaning, which consisted of a 15 min recirculation of sodium hypochlorite solution prepared by diluting commercial household bleach solution diluted to contain 100 ppm of active chlorine in warm, softened tap water, and its pH adjusted to 6.5 using nitric acid. The authors commented that an effective cleaning procedure followed by this low-cost sanitizing procedure is able to satisfy industrial concerns.

## 22.6 CHALLENGES AND EMERGING APPLICATIONS OF MEMBRANES IN THE DAIRY INDUSTRY

### 22.6.1 CHALLENGES

A major factor that remains to be the biggest challenge in optimizing the performance of membrane processes in the dairy industry is biofouling, which is caused by specific interactions between the membrane and various proteins, as well as protein–protein interactions that can lead to pore-narrowing or pore-blocking, during the filtration process [40,153,155].

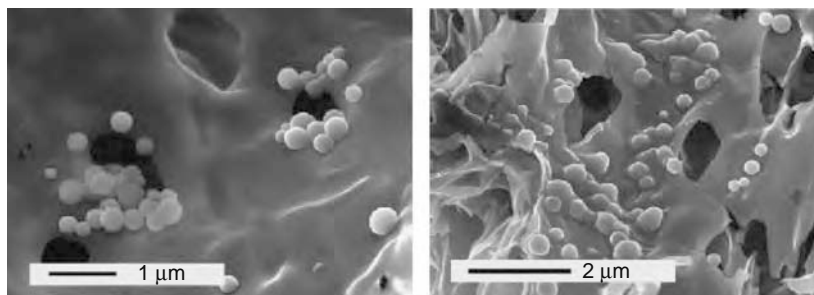


**FIGURE 22.12** Protein fouling of internal pore surfaces of MF membrane following filtration of skimmed milk at 300 psi TMP for 30 min. (From James, B.J., Jing, Y., and Chen, X.D., *J. Food Eng.*, 60, 431, 2003. With permission.)

The irreversible alteration of membrane morphology caused by protein fouling during processing leads to severe flux decline and alteration of membrane rejection properties [153]. Biofouling can adversely impact membrane processing economics because of the loss of filtration efficiency, process down time to clean the membrane, and the decrease in membrane lifespan due to frequent cleaning [183]. Therefore, considerable efforts during the past three decades in the dairy industry were not only concentrated on process innovation, but also in understanding and combating the biofouling phenomenon.

Savello et al. [184] studied the fouling of 0.2  $\mu\text{m}$  pore size MF ceramic membrane by milk proteins in two filtration conditions: (1) static, where the membrane is soaked in skim milk for 5 min to allow the surface adsorption of proteins and (2) dynamic, where the retentate is recirculated continuously until constant permeation rate was achieved. They observed greater reduction in clean water flux under dynamic conditions than static conditions. SEM images of the fouled membrane by static mode showed that the fouling is not only limited to surface deposition of particles, but also by pore-blocking (Figure 22.12). They modified the membrane surface by silanization using glycidoxypolytrimethoxysilane and 3-aminopropyltriethoxysilane to derivatize the membrane surface and block the active sites for protein binding. Washing the surface-modified membrane with protein solvent after static and dynamic fouling tests only partially restored the clean water flux while alkali and acid washes completely restored the flux. This, they deemed, suggests that, aside from milk proteins, minerals play a critical role in the fouling mechanism of ceramic membranes.

James et al. [155] suggested that, in addition to surface chemistry, the surface morphology and internal microstructure of a membrane affect fouling and membrane performance. Klobes et al. [185] suggested the use of capillary pore membranes made from polyester film, which is supported by a nonwoven polypropylene or polyester backing, in the MF of milk systems rather than tortuous path membranes. Such membranes are microporous with cylindrical straight through pores of uniform diameter manufactured by a two-step procedure of heavy ion irradiation and subsequent etching (Figure 22.13). They investigated membranes with pore sizes of 0.4, 0.3, 0.2, and 0.1  $\mu\text{m}$  in fractionating proteins in fresh skim milk at  $48^\circ\text{C} \pm 2^\circ\text{C}$  and flow rates of 3.8, 1.9, and 1.0  $\text{m}\cdot\text{s}^{-1}$ . They reported that the 0.2  $\mu\text{m}$  membrane showed the best skim milk fractionation characteristics where nearly complete retention of caseins at all flow rates considered and whey protein permeation of up to 90% at the lowest flow value investigated were observed. They also noted constant whey protein permeation of around 50% and complete casein retention at all flow rates considered using 0.1  $\mu\text{m}$  membranes.

Aside from membrane morphology, various membrane module geometries were also studied to determine their appropriateness in various dairy processes. Operation of tubular ceramic membranes usually involves high TMP and pressure drop

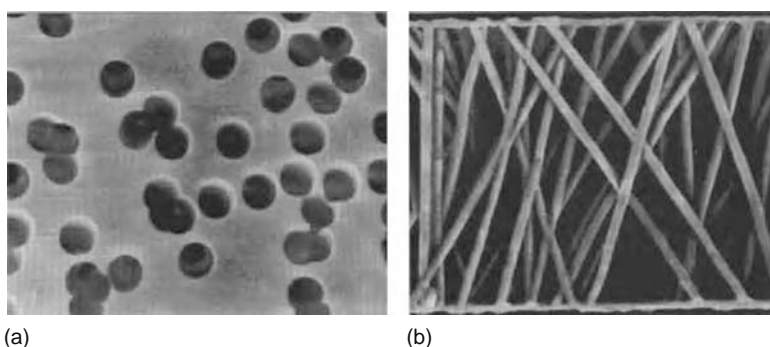


**FIGURE 22.13** Scanning electron micrographs of the surface (a) and the internal structure (b) of a Rotrac capillary pore membrane. (From Klobes et al., *Bull. Int. Dairy Fed.*, 311, 13, 1996. With permission.)

along the filter module, and requires recirculation of permeate to maintain uniform TMP and high permeation throughout the length of the module for a long period of time [9]. The evaluation of flat ceramic membranes for use in the wastewater treatment around 1996, and the reported energy-efficiency and cost-effectiveness of their operations due to small hydraulic diameter prompted studies to use these membranes in milk proteins standardization and whey concentration [186]. To date, however, they have not been utilized commercially in the dairy industry.

A recent development in MF technology is the microsieves, which are MF membranes with uniform narrow pore size distribution and a smooth inert silicon nitride surface, manufactured using micro-machining technology [6,187]. Due to the very low hydrodynamic resistance of microsieves and their open support structure, they enable high fluxes that can be two or three orders of magnitude larger than for conventional membranes even as they are operated at extremely low TMP, which are about two orders of magnitude lower compared to conventional membranes [6,187]. Because permeation in microsieves is faster, the accumulation of particles on the membrane surface may also take place faster compared to conventional MF membranes so that the large-scale MF of milk by microsieves is still in the investigation stage [187].

### 22.6.2 EMERGING APPLICATIONS OF MEMBRANES IN THE DAIRY INDUSTRY

Membranes can be used successfully in several fractionation stages of milk (Figure 22.14) [6,11]. As membrane materials and understanding of processing conditions for efficient operation continue to evolve, new applications of membrane technology in the dairy industry also continue to emerge. The continued development of the state-of-the-art ceramic membrane products that persist to thrive despite the cheaper polymeric membranes and the increasing understanding of fouling that leads to effective flux control contribute to the widespread use of membranes in the dairy industry. Such dynamism results in innovative products of novel applications and unique functionalities.

Microfiltration of milk to separate micellar casein and produce an intermediate for the recovery of individual caseins rather than producing a casein concentrate for cheesemaking alone is a goal of numerous efforts in dairy research. This opened opportunities for more specialized applications of MF in the dairy industry [70]. For instance, recent studies on the biological activities of milk components have propelled interest in recovering IgG in bovine colostrum using MF. Colostrum is a mixture of the lacteal secretions produced by the mammary gland during the three days following parturition [188]. It contains high amount of IgG and was found to have essential physiological action for many species and high efficacy in human clinical applications [188,189].

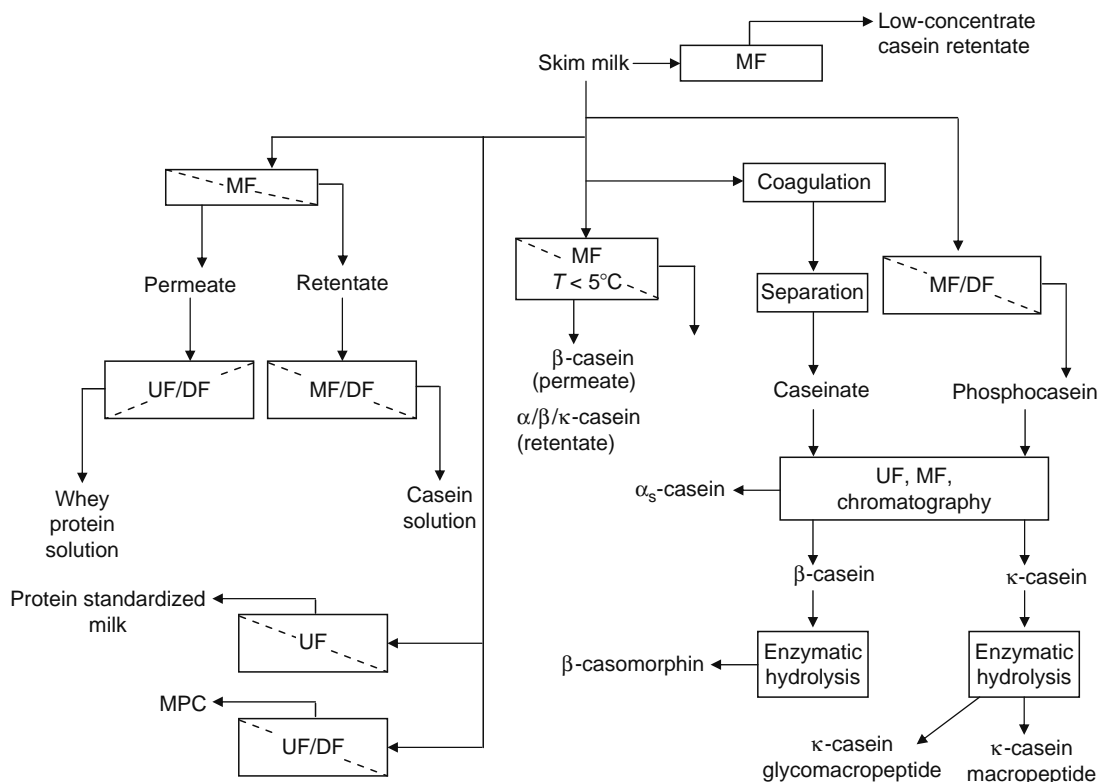


**FIGURE 22.14** Application of MF and UF in milk protein standardization and fractionation. (From Rosenberg, M., *Trends Food Sci. Technol.*, 6, 12, 1995. With permission.)

Using MF ceramic Membralox membranes of 0.1  $\mu\text{m}$  average pore size operated at UTMP of 0.4–0.5 bar (40–50 kPa) and temperature lower than 40°C, Piot et al. [188] employed the patented method developed by Garcin and Paviot [190] to recover “serocolostrum” as permeate, which is crystal clear, free of blood, and somatic cells as well as fat globules and casein micelles, and has high hygienic and bacteriological quality ( $<10 \text{ cfu}\cdot\text{mL}^{-1}$ ), from bovine, caprine, or equine colostrums. The colostrums were skimmed and diluted by 50% of KCl–NaCl saline solution or milk ultrafiltrate before MF. Continuous DF with 8–10 diavolumes of the saline solution followed to recover the whey fraction of colostrums, specifically to maximize the amount of IgG in the permeate. The authors reported about 10% losses of IgG to the cream in the skimmed colostrums and 5.0%–6.7% losses of IgG in the MF retentate. They suggested foregoing the cream separation step and proceeding directly to the MF step with prolonged DF to minimize the losses.

Another recent innovation involves native whey proteins recovery pioneered by Tolkach and Kulozik [191]. They introduced a novel membrane-based approach of separating native whey proteins from caseinomacropptide (CMP) in ultrafiltered and diafiltered sweet whey (Figure 22.15). They used the microbial enzyme transglutaminase (*Tgase*) to cross-link CMP molecules through their glutamine and lysine residues. Although native whey proteins themselves are rich in glutamine and lysine, they are resistant to enzymatic action, especially by *Tgase*, because of their compact globular shape [192,193]. The authors reported that about 92% of the original amount of CMP was cross-linked without affecting native whey proteins quantity and that the remaining CMP that was not cross-linked was mostly the glycosylated variety. The cross-linking of the CMP molecules widened the size difference between CMP and the whey proteins, and rendered effective separation of the two fractions by MF and subsequent DF in 0.1  $\mu\text{m}$  pore size ceramic membrane module operated at 0.4 bar (40 kPa) UTMP and 55°C. The MF permeate, which contained whey proteins, was ultrafiltered using polysulfone (25 kDa MWCO) plate-and-frame module and the UF permeate was used to diafilter the MF retentate, which contained the cross-linked CMP and the remaining fractions of casein fines (about 5%–10% of the total proteins).

A decade ago, Jost and Jelen [96] commented that the success of some of the novel processing applications of MF will depend on unique functionality and specific applications of the final fractions. Today, it is evident that with the use of MF, several advancements have been attained in the dairy industry, such as the dramatic improvement of the hygienic safety of dairy products, nutritional and bioactive properties of milk are kept intact or, at least, very minimally damaged, specific separations of micellar casein and of small and large fat globules. These remarkable developments opened new and diverse avenues in improving current manufacturing processes, product quality, and creating new milk derivatives for novel applications [8].

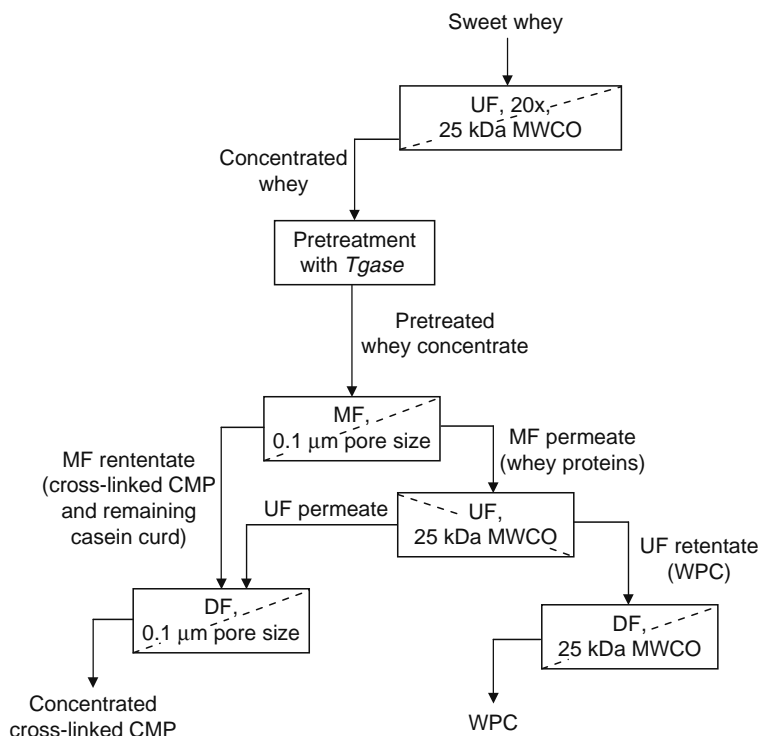


**FIGURE 22.15** Fractionation of whey proteins and CMP by means of enzymatic cross-linking and membrane. (From Tolkach, A. and Kulozik, U., *J. Food Eng.*, 67, 13, 2005. With permission.)

## ACKNOWLEDGMENT

The authors are grateful to Mr Gary W. Jung for his insightful comments and review that were invaluable in writing this chapter.

## REFERENCES

1. Marshall, S.C., Applying membrane processes: The first steps, *Aust. Dairy J.*, 52, 50, 1997.
2. Marriott, J. and Sørensen, E., A general approach to modeling membrane modules, *Chem. Eng. Sci.*, 58, 4975, 2003.
3. Beaton, N.C., Ultrafiltration and reverse osmosis in the dairy industry—an introduction to sanitary considerations, *J. Food Prot.*, 42, 584, 1979.
4. Zydney, A.L., Protein separations using membrane filtration: New opportunities for whey fractionation, *Int. Dairy J.*, 8, 243, 1988.
5. Korhonen, H., Technology options for new nutritional concepts, *Int. J. Dairy Technol.*, 55, 79, 2002.
6. Brans, G., Schroën, C.G.P.H., van der Sman, R.G.M., and Boom, R.M., Membrane fractionation of milk: State of the art and challenges, *J. Membr. Sci.*, 243, 263, 2004.
7. Henning, D.R., Baer, R.J., Hassan, A.N., and Dave, R., Major advances in concentrated and dry milk products, cheese, and milk fat-based spreads, *J. Dairy Sci.*, 89, 1179, 2006.
8. Saboya, L.V. and Maubois, J.L., Current developments of microfiltration technology in the dairy industry, *Lait*, 80, 541, 2000.
9. Merin, U. and Daufin, G., Crossflow microfiltration in the dairy industry: State-of-the-art, *Lait*, 70, 281, 1990.
10. Maubois, J.L., New applications of membrane technology in the dairy industry, *Aust. J. Dairy Technol.*, 46, 91, 1991.
11. Rosenberg, M., Current and future applications for membrane processes in the dairy industry, *Trends Food Sci. Technol.*, 6, 12, 1995.
12. Ripperger, S. and Altmann, J., Crossflow microfiltration—state of the art, *Sep. Purif. Technol.*, 26, 19, 2002.
13. Baruah, G.L., Nayak, A., and Belfort, G., Scale-up from laboratory microfiltration to a ceramic pilot plant: Design and performance, *J. Membr. Sci.*, 274, 56, 2006.
14. Hwang, K.-J., Chou, F.-Y., and Tung, K.-L., Effects of operating conditions on performance of cross-flow microfiltration of fine particle/protein binary suspension, *J. Membr. Sci.*, 274, 183, 2006.
15. Goudéranche, H., Maubois, J.-L., and Fauquant, J., Produits, en particulier laitiers, comprenant des fractions sélectionnées de globules gras, obtention et applications, French Patent FR/2/776/208/A1, 1998.
16. Fauquant, C., Briard, V., Leconte, N., and Michalski, M.-C., Differently sized native milk fat globules separated by microfiltration: Fatty acid composition of the milk fat globule membrane and triglyceride core, *Eur. J. Lipid Sci. Technol.*, 107, 80, 2005.
17. Michalski, M.-C., Ollivon, M., Briard, V., Leconte, N., and Lopez, C., Native fat globules of different sizes selected from raw milk: Thermal and structural, *Chem. Physics Lipid*, 132, 247, 2004.
18. Nilsson, J.L., Fouling of an ultrafiltration membrane by a dissolved whey protein concentrate and some whey proteins, *J. Membr. Sci.*, 36, 147, 1988.
19. Aimar, P., Taddei, C., Lafaille, J.P., and Sanchez, V., Mass transfer limitations during ultrafiltration of cheese whey with inorganic membranes, *J. Membr. Sci.*, 38, 203, 1988.
20. Bastian, E.D., Collinge, S.K., and Ernstrom, C.A., Ultrafiltration: Partitioning of milk constituents into permeate and retentate, *J. Dairy Sci.*, 74, 2423, 1991.
21. Bacchin, P., Si-Hassen, D., Starov, V., Clifton, M.J., and Aimar, P., A unifying model for concentration polarization, gel-layer formation and particle deposition in cross-flow membrane filtration of colloidal suspensions, *Chem. Eng. Sci.*, 57, 77, 2002.
22. Cheryan, M. and Kuo, K.P., Hollow fibers and spiral wound modules for ultrafiltration of whey: Energy consumption and performance, *J. Dairy Sci.*, 67, 1406, 1984.
23. Hanemaaijer, J.H., Robbertsen, T., van den Boomgaard, T., and Gunnink, J.W., Fouling of ultrafiltration membrane: The role of protein adsorption and salt precipitation, *J. Membr. Sci.*, 40, 199, 1989.
24. Atra, R., Vatai, G., Bekassy-Milnar, E., and Balint, A., Investigation of ultra- and nanofiltration for utilization of whey protein and lactose, *J. Food Eng.*, 67, 325, 2005.
25. Maubois, J.L. and Mocquot, G., Application of membrane ultrafiltration to preparation of various types of cheese, *J. Dairy Sci.*, 58, 1001, 1975.
26. Gekas, V., Trägårdh, G., and Aimar, P., Diffusive flows in ultrafiltration and their effect on membrane retention properties, *J. Membr. Sci.*, 80, 73, 1985.
27. Guinee, T.P., O'Callaghan, D.J., Pudja, P.D., and O'Brien, N., Rennet coagulation properties of retentates obtained by ultrafiltration of skim milks heated to different temperatures, *Int. Dairy J.*, 6, 581, 1996.
28. Hinrichs, J., Mediterranean milk and milk products, *Eur. J. Nutr. (Suppl.)*, 43, I/12, 2004.
29. Pedersen, P.J. and Ottosen, N., Manufacture of fresh cheese by ultrafiltration, in New applications of membrane processes, *Int. Dairy Fed.*, Special issue, 9210, 67, 1991.
30. Guinee, T.P., Pudja, P.D., Mulholland, E.O., and Reville, W.J., Ultrafiltration in cheesemaking, in: *3rd Cheese Symposium*, Cogan, T.M., Ed., National Dairy Products Research Center, Moorepark, Fermoy, Co., Cork, Ireland, 1992, p. 21.
31. Puhan, Z., Protein standardization as an international issue, in *Advances in Membrane Technology for Better Dairy Products*, Bulletin International Dairy Federation, 311, 1996, p. 5.
32. Hinrichs, J., Incorporation of whey proteins in cheese, *Int. Dairy J.*, 11, 495, 2001.
33. Novák, Á., Application of membrane filtration in the production of milk protein concentrates, in *Advances in membrane technology for better dairy products*, *Bull. Int. Dairy Fed.*, 311, 26, 1996.

34. Covacevich, H.R. and Kosikowski, F.V., Skim milk concentration for cheesemaking by alternative ultrafiltration procedures, *J. Food Sci.*, 42, 1359, 1977.
35. Lipnizki, F., Industrial applications of ultrafiltration in pharmaceutical biotechnology, *Eng. Life Sci.*, 5, 81, 2005.
36. Kelly, P.M., Horton, B.S., and Burling, H., Partial demineralization of whey by nanofiltration, in *New Applications of Membrane Processes*, Special Issue 9201, International Dairy Federation, Brussels, Belgium, 1991, p. 130.
37. Jelen, P., Pressure-driven membrane processes: Principles and definitions, in *New Applications of Membrane Processes*, Special Issue 9201, International Dairy Federation, Brussels, Belgium, 1991, p. 7.
38. Mulvihill, D.M. and Ennis, M.P., Functional milk proteins: Production and utilization, in: *Advanced Dairy Chemistry, Volume 1: Proteins*, 3rd edn., Fox, P.F. and McSweeney, P.L.H., Eds., New York: Plenum, 2003, 1190.
39. Dejmeek, P. and Nilsson, J.L., Flux-based measures of adsorption to ultrafiltration membranes, *J. Membr. Sci.*, 40, 189, 1989.
40. Marshall, A.D., Munro, P.A., and Trägårdh, G., The effect of protein fouling in microfiltration and ultrafiltration on permeate flux, protein retention and selectivity: A literature review, *Desalination*, 91, 65, 1993.
41. Rao, H.G., Mechanisms of flux decline during ultrafiltration of dairy products and influence of pH on flux rates of whey and buttermilk, *Desalination*, 144, 319, 2002.
42. Palecek, S.P. and Zydney, A.L., Intermolecular electrostatic interactions and their effect on flux and protein deposition during protein filtration, *Biotechnol. Prog.*, 10, 207, 1994.
43. Doyen, W., Andriansens, W., Molenberghs, B., and Leysen, R., A comparison between polysulfone, zirconia and organo-mineral membranes for use in ultrafiltration, *J. Membr. Sci.*, 113, 1996.
44. Saksena, S. and Zydney, A.L., Influence of protein-protein interactions on bulk mass transport during ultrafiltration, *J. Membr. Sci.*, 125, 93, 1997.
45. Kuo, K.P. and Cheryan, M., Ultrafiltration of acid whey in spiral-wound unit: Effect of operating parameters on membrane fouling, *J. Food Sci.*, 48, 1113, 1983.
46. Koehler, J.A., Ulbricht, M., and Belfort, G., Intermolecular forces between a protein and a hydrophilic modified polysulfone film with relevance to filtration, *Langmuir*, 16, 10419, 2000.
47. Merin, U. and Cheryan, M., Factors affecting the mechanism of flux decline during ultrafiltration of cottage cheese whey, *J. Food Proc. Preserv.*, 4, 183, 1980.
48. Sheldon, J.M., Reed, I.M., and Hawes, C.R., The fine-structure of ultrafiltration membranes. II. Protein fouled membranes, *J. Membr. Sci.*, 62, 87, 1991.
49. van Reis, R., Goodrich, E.M., Yson, C.L., Frautschy, L.N., Whiteley, R., and Zydney, A.L., Constant  $C_{wall}$  ultrafiltration process control, *J. Membr. Sci.*, 130, 123, 1997.
50. Qin, J.-J., Wong, F.-S., Li, Y., and Liu, Y.-T., A high flux ultrafiltration membrane spun from PSU/PVP (K90)/DMF/1,2-propanediol, *J. Membr. Sci.*, 211, 139, 2003.
51. Yoo, J.E., Kim, J.H., Kim, Y., and Kim, C.K., Novel ultrafiltration membranes prepared from the new miscible blends of polysulfone with poly(1-vinylpyrrolidone-co-styrene) copolymers, *J. Membr. Sci.*, 216, 95, 2003.
52. Daufin, G., Escudier, J.P., Carrère, H., Bérot, S., Fillaudeau, L., and Decloux, M., Recent and emerging applications of membrane processes in the food and dairy industry, *Trans. IChemE*, 79, 89, 2001.
53. Muller, L.L. and Harper, W.J., Effects of membrane processing of pretreatment of whey, *J. Agric. Food Chem.*, 27, 662, 1979.
54. Labbé, J.-P., Quemeris, A., Michel, F., and Daufin, G., Fouling of inorganic membranes during whey ultrafiltration: Analytical methodology, *J. Membr. Sci.*, 51, 293, 1990.
55. Maubois, J.L., Recent developments of ultrafiltration in the dairy industry, *Polym. Sci. Technol.*, 13, 305, 1980.
56. Marshall, A.D. and Daufin, G., Physico-chemical aspects of membrane fouling by dairy fluids, in *Fouling and Cleaning in Pressure Driven Membrane Processes*, International Dairy Federation, Brussels, Belgium, 1995, p. 8.
57. Mulder, M., *Basic Principles of Membrane Technology*. Dordrecht, The Netherlands: Kluwer, 1991.
58. Cheryan, M., *Ultrafiltration and Microfiltration Handbook*, 2nd ed. Boca Raton, FL: CRC Press, LLC, 1998.
59. Krishna Kumar, N.S., Yea, M.K., and Cheryan, M., Ultrafiltration of soy protein concentrate: Performance and modeling of spiral and tubular polymeric modules, *J. Membr. Sci.*, 244, 235, 2004.
60. Carić, M.D., Milanović, S.D., Krstić, D.M., and Tekić, M.N., Fouling of inorganic membranes by adsorption of whey proteins, *J. Membr. Sci.*, 165, 83, 2000.
61. de Wit, J.N., Klarebeek, G., and Hontelez-Backz, E., Evaluation of functional properties of whey protein concentrates and whey protein isolates. 1. Isolation and characterization, *Neth. Milk Dairy J.*, 37, 37, 1983.
62. Millipore Corporation, Protein concentration and diafiltration by tangential flow filtration. Millipore Technical Brief, Millipore Corporation, Georgia, 2003.
63. Glover, F.A., The processes, in *Ultrafiltration and Reverse Osmosis for the Dairy Industry*, Technical Bulletin 5, The National Institute for Research in Dairying. Reading, England, 1985.
64. Huffman, L.M. and Harper, W.J., Maximizing the value of milk through separation technologies, *J. Dairy Sci.*, 82, 2238, 1999.
65. Morr, C.V. and Ha, E.Y.W., Whey protein concentrates and isolates: Processing and functional properties, *Crit. Rev. Food Sci. Nutr.*, 33, 431, 1993.
66. de Wit, J.N., Functional properties of whey proteins in food systems, *Neth. Milk Dairy J.*, 38, 71, 1984.
67. Hawks, S.E., Phillips, L.G., Rasmussen, R.R., Barbano, D.M., and Kinsella, J.E., Effects of processing treatment and cheesemaking parameters on foaming properties of whey protein isolates, *J. Dairy Sci.* 76, 2468, 1993.
68. Merin, U., Gordin, S., and Tanny, G.B., Microfiltration of sweet cheese whey, *N.Z.J. Dairy Sci. Technol.*, 18, 153, 1983.

69. Gesan, G., Daufin, G., Merin, U., Labbé, J.-P., and Quémerais, A., Fouling during constant flux crossflow microfiltration of pretreated whey. Influence of transmembrane pressure gradient, *J. Membr. Sci.*, 80, 131, 1993.
70. Horton, B.S., Microfiltration—Where is it headed? *Aust. J. Dairy Technol.*, 52, 58, 1997.
71. Tanny, G.B., Hauk, D., and Merin, U., Biotechnical applications of a pleated cross-flow microfiltration module, *Desalination*, 41, 299, 1982.
72. Pearce, R.J., Marshall, S.C., and Dunkerley, J.A., Reduction of lipids in whey protein concentrates by microfiltration—effect on functional properties, in *New Applications of Membrane Processes*, Special Issue 9201, International Dairy Federation, Brussels, Belgium, 1991, 118.
73. McGregor, J.U. and White, C.H., Optimizing ultrafiltration parameters for the development of a low fat cheddar cheese, *J. Dairy Sci.*, 73, 314, 1990.
74. Akoum, O., Jaffrin, M.Y., and Ding, L.-H., Concentration of total milk proteins by high shear ultrafiltration in a vibrating module, *J. Membr. Sci.*, 247, 211, 2005.
75. Schkoda, P. and Kessler, H.G., Manufacture of fresh cheese from ultrafiltered milk with reduced amount of acid whey, in *Advances in membrane technology for better dairy products*, Bulletin International Dairy Federation, 311, 1996, p. 33.
76. Hinrichs, J., UHT processed milk concentrates, *Lait*, 80, 15, 2000.
77. Lucisano, M., Peri, C., and Donati, E., Studies on coagulation of milk ultrafiltration retentates. I. Coagulation kinetics, *Milchwissenschaft*, 40, 600, 1985.
78. Premaratne, R.J. and Cousin, M.A., Changes in the chemical composition during ultrafiltration of skim milk, *J. Dairy Sci.*, 74, 788, 1991.
79. Cunha, C.R., Viotto, L.A., and Viotto, W.H., Use of low concentration factor ultrafiltration retentates in reduced-fat Minas Frescal cheese manufacture: Effect on yield and sensory properties, *Int. J. Dairy Technol.*, 57, 231, 2004.
80. Waungana, A., Singh, H., and Bennett, R.J., Rennet coagulation properties of skim milk concentrated by ultrafiltration: Effects of heat treatment and pH adjustment, *Food Res. Int.*, 31, 645, 1998.
81. Dalgleish, D.G., Effect of milk concentration on the rennet coagulation time, *J. Dairy Res.*, 47, 231, 1981.
82. Sharma, S.K., Hill, A.R., and Goff, H.D., The effect of heat treatment of ultrafiltered milk on its coagulation properties, *Milchwissenschaft*, 45, 432, 1990.
83. Erdem, Y.K., Influence of ultrafiltration on modification of surface hydrophobic sites of the milk protein system in the course of renneting, *J. Food Eng.*, 44, 63, 2000.
84. Kosikowski, F.V., New cheese-making procedures utilizing ultrafiltration, *Food Technol.*, 40, 71, 1986.
85. Erdem, Y.K., Modification of casein micelle structure caused by ultrafiltration and heat treatment: A spectrofluorimetric and kinetic approach, *J. Food Eng.*, 74, 536, 2006.
86. Waungana, A., Singh, H., and Bennett, R.J., Influence of denaturation and aggregation of  $\beta$ -lactoglobulin on rennet coagulation properties of skim milk and ultrafiltered milk, *Food Res. Int.*, 29, 715, 1996.
87. Kosikowski, F.V. and Mistry, V.V., Microfiltration, ultrafiltration, and centrifugation separation and sterilization processes for improving milk and cheese quality, *J. Dairy Sci.*, 73, 1411, 1990.
88. El-Shibiny, S., Shahein, N.M., and El-Sheikh, M., Preparation and functional properties of UF whole milk protein isolates. Advances in membrane technology for better dairy products in: *Bull. Int. Dairy Fed.*, 311, 28, 1996.
89. Pignon, F., Belina, G., Narayanan, T., Paubel, X., Magnin, A., and Gésan-Guiziou, G., Structure and rheological behavior of casein micelle suspensions during ultrafiltration process, *J. Chem. Phys.*, 121, 8138, 2004.
90. Rajagopalan, N. and Cheryan, M., Total protein isolate from milk by ultrafiltration: Factors affecting product composition, *J. Dairy Sci.*, 74, 2435, 1991.
91. van Hekken, D.L. and Holsinger, V.H., Use of cold microfiltration to produce unique  $\beta$ -casein enriched milk gels, *Lait*, 80, 69, 2000.
92. Maubois, J.L. and Ollivier, G., Milk protein fractionation, in *New Applications of Membrane Processes*, Special Issue 9201, International Dairy Federation, Brussels, Belgium, 1991, p. 15.
93. Jost, R., Brandsma, R., and Rizvi, S.S.H., Protein composition of micellar casein obtained by cross-flow micro-filtration of skimmed milk, *Int. Dairy J.*, 9, 389, 1999.
94. Brandsma, R.L. and Rizvi, S.S.H., Depletion of whey proteins and calcium by microfiltration of acidified skim milk prior to cheese making, *J. Dairy Sci.*, 82, 2063, 1999.
95. Brandsma, R.L. and Rizvi, S.S.H., Manufacture of mozzarella cheese from highly-concentrated skim milk microfiltration retentate depleted of whey proteins, *Int. J. Food Sci. Technol.*, 36, 611, 2001.
96. Jost, R. and Jelen, P., Crossflow microfiltration—an extension of membrane processing of milk and whey, *Bull. Int. Dairy Fed.*, 320, 9, 1997.
97. Le Berre, O. and Daufin, G., Skim milk crossflow microfiltration performance versus permeation flux to wall shear stress ratio, *J. Membr. Sci.*, 117, 261, 1996.
98. Samuelsson, G., Dejmek, P., Trägårdh, G., and Paulsson, M., Minimizing whey protein retention in cross-flow microfiltration of skim milk, *Int. Dairy J.*, 7, 237, 1997.
99. Pouliot, M., Pouliot, Y., and Britten, M., On the conventional cross-flow microfiltration of skim milk for the production of native phosphocaseinate, *Int. Dairy J.*, 6, 105, 1996.
100. Maubois, J.L., Current uses and future perspectives of MF technology in the dairy industry, *Bull. Int. Dairy Fed.*, 320, 37, 1997.
101. Caron, A., St. Gelais, D., and Pouliot, Y., Coagulation of milk enriched with ultrafiltered or diafiltered microfiltered milk retentate powders, *Int. Dairy J.*, 7, 445, 1997.

102. Guerra, A., Jonsson, G., Rasmussen, A., Nielsen, E.W., and Edelsten, D., Low cross-flow velocity microfiltration of skim milk for removal of bacterial spores, *Int. Dairy J.*, 7, 849, 1997.
103. Mistry, V.V., Manufacture and application of high milk protein powder, *Lait*, 82, 515, 2002.
104. Carbonaro, M., Bonomi, F., Iametti, S., Cappelloni, M., and Carnovale, E., Aggregation of proteins in whey from raw and heat-processed milk: Formation of soluble macroaggregates and nutritional consequences, *Lebensm. Wiss. Technol.*, 31, 522, 1998.
105. Garem, A., Schuck, P., and Maubois, J.-L., Cheesemaking properties of a new dairy-based powder made by a combination of microfiltration and ultrafiltration, *Lait*, 80, 25, 2000.
106. Terré, E., Maubois, J.L., Brulé, G., and Pierre, A., Manufacture of a composition enriched with  $\beta$ -casein, French Patent No. 2, 592, 769, 1986.
107. Brandsma, R.L. and Rizvi, S.S.H., Effect of manufacturing treatments on the rheological character of mozzarella cheese made from microfiltration retentate depleted of whey proteins, *Int. J. Food Sci. Technol.*, 36, 601, 2001.
108. Punidadas, P. and Rizvi, S.S.H., Separation of milk proteins into fractions rich in caseins or whey proteins by crossflow microfiltration, *Food Res. Int.*, 31, 265, 2001.
109. Solanki, G. and Rizvi, S.S.H., Physico-chemical properties of skim milk retentates from microfiltration, *J. Dairy Sci.*, 84, 2381, 2001.
110. Ardisson-Korat, A.V. and Rizvi, S.S.H., Vatless manufacturing of low-moisture part-skim mozzarella cheese from highly concentrated skim milk microfiltration retentates, *J. Dairy Sci.*, 87, 3601, 2004.
111. Vadi, P.K. and Rizvi, S.S.H., Experimental evaluation of a uniform transmembrane pressure crossflow microfiltration unit for the concentration of micellar casein from skim milk, *J. Membr. Sci.*, 189, 69, 2001.
112. Maubois, J.-L., Fauquant, J., and Famelart, M.-H., Milk microfiltrate, a convenient starting material for fractionation of whey proteins and derivatives, in: *3rd International Symposium of Whey Conference*, Behr's Verlag, Ed., Munich, Germany, 2001, p. 59.
113. Bacher, T. and Königsfeldt, P., WPI by microfiltration of skim milk, *Eur. Dairy Mag.*, 3, 2001.
114. Nelson, B.K. and Barbano, D.M., A microfiltration process to maximize removal of serum proteins from skim milk before cheese making, *J. Dairy Sci.*, 88, 1891, 2005.
115. Merin, U., Bacteriological aspects of microfiltration of cheese whey, *J. Dairy Sci.*, 69, 326, 1986.
116. Rektor, A. and Vatai, G., Membrane filtration of mozzarella whey, *Desalination*, 162, 279, 2004.
117. Boor, K.J., ADSA Foundation Scholar Award, Fluid dairy quality and safety: Looking to the future, *J. Dairy Sci.*, 84, 1, 2001.
118. Chapman, K.W. and Boor, K.J., Acceptance of 2% ultra-pasteurized milk by consumers, 6 to 11 years old, *J. Dairy Sci.*, 84, 951, 2001.
119. Elwell, M.W. and Barbano, D.M., Use of microfiltration to improve fluid milk quality, *J. Dairy Sci.*, 89(E. Suppl.), E10, 2006.
120. Olesen, N. and Jensen, F., Microfiltration: The influence of operation parameters on the process, *Milchwissenschaft*, 44, 476, 1989.
121. Holm, S., Malmberg, R., and Svensson, K., Method and plant for producing milk with a lowered bacterial content, US Patent 4,876,100, 1989.
122. Kelly, P.M. and Tuohy, J.J., The effectiveness of microfiltration for the removal of microorganisms, *Bull. Int. Dairy Fed.*, 320, 26, 1997.
123. Zoon, P. and Hup, G., Process for the preparation of raw milk cheese, European Patent 0546641 A1, 1991.
124. Pafylas, I., Cheryan, M., Mehaia, M.A., and Sagham, N., Microfiltration of milk with ceramic membranes, *Food Res. Int.*, 29, 141, 1996.
125. Jonsson, G., The influence of the porous sublayer on the salt rejection and reflection coefficient of asymmetric CA membranes, *Desalination*, 34, 141, 1980.
126. Jonsson, G. and Wetten, I.G., Control of concentration polarization, fouling and protein transmission of microfiltration processes within the agro-based industry, Proceedings of the ASEAN-EU Workshop on Membrane Technology in Agro-Based Industry, Kuala Lumpur, Malaysia, 1994, p. 157.
127. Johnson, M.E. and Lucey, J.A., Major technological advances and trends in cheese, *J. Dairy Sci.*, 89, 1174, 2006.
128. Rattray, W. and Jelen, P., Protein standardization of milk and dairy products, *Trends Food Sci. Technol.*, 7, 227, 1996.
129. Babella, G., The development and utilization of milk- and whey-protein concentrates in Hungary, *Dev. Food Sci.*, 9, 241, 1984.
130. Prokopek, D., Voss, E., and Thomasow, J., Manufacture of soft cheese without whey separation from ultrafiltered skim milk, *Molkerei-Zeitung Welt. Milch.*, 29, 939, 1975.
131. Abd El-Salam, M.H. and Shahein, N., Ultrafiltration of reconstituted skim milk, *J. Dairy Res.*, 56, 147, 1989.
132. Alvarez, F., Argüello, M., Cabero, M., Riera, F.A., Alvarez, R., Iglesias, J.R., and Granda, J., Fermentation of concentrated skim-milk: Effects of different protein/lactose ratios obtained by ultrafiltration/diafiltration, *J. Sci. Food Agric.*, 76, 10, 1998.
133. Mistry, V.V. and Hassan, H.N., Delactosed, high milk protein powder. 1. Manufacture and composition, *J. Dairy Sci.*, 74, 1163, 1991.
134. Mistry, V.V. and Hassan, H.N., Manufacture of non-fat yogurt from a high milk protein powder, *J. Dairy Sci.*, 74, 1163, 1992.
135. Ozer, B.H., Robinson, R.K., Grandison, A.S., and Bell, A.E., Gelation properties of milk concentrated by different techniques, *Int. Dairy J.*, 8, 793, 1998.
136. Lee, F.Y. and White, C.H., Effect of ultrafiltration retentates and whey protein concentrates on ice cream quality during storage, *J. Dairy Sci.*, 74, 1170, 1991.
137. Vyas, H.K. and Tong, P.S., Process for calcium retention during skim milk ultrafiltration, *J. Dairy Sci.*, 86, 2761, 2003.
138. Mulder, H. and Walstra, P., The milk fat globule, Emulsion science as applied to milk products and comparable foods, Commonwealth Agricultural Bureaux, Farmham Royal, Bucks, UK, 1974.
139. Ye, A., Singh, H., Taylor, M.W., and Anema, S., Interactions of whey proteins with milk fat globule membrane proteins during heat treatment of whole milk, *Lait*, 84, 269, 2004.
140. Michalski, M.-C., Camier, B., Briard, V., Leconte, N., Gassi, J.-Y., Goudéranche, H., Michel, F., and Fauquant, J., The size of native milk fat globules affects physico-chemical and functional properties of Emmental cheese, *Lait*, 84, 343, 2004a.

141. Rombaut, R., Dejonckheere, V., and Dewettinck, K., Microfiltration of butter serum upon casein micelle destabilization, *J. Dairy Sci.*, 89, 1915, 2006.
142. Patton, S. and Huston, G.E., A method for isolation of milk fat globules, *Lipids*, 21, 170, 1986.
143. Ye, A., Singh, H., Taylor, M.W., and Anema, S., Characterization of proteins components of natural and heat-treated milk fat globule membranes, *Int. Dairy J.*, 12, 393, 2002.
144. Goudédranche, H., Fauquant, J., and Maubois, J.-L., Fractionation of globular milk fat by membrane microfiltration, *Lait*, 80, 93, 2000.
145. Rodríguez, J., Requena, T., Fontecha, J., Goudédranche, H., and Juárez, M., Effect of different membrane separation technologies (ultrafiltration and microfiltration) on the texture and microstructure of semihard low-fat cheeses, *J. Agric. Food Chem.*, 47, 558, 1999.
146. Briard, V., Leconte, N., Michel, F., and Michalski, M.C., The fatty acid composition of small and large naturally occurring milk fat globules, *Eur. J. Lipid Sci. Technol.*, 107, 80, 2003.
147. Corredig, M., Roesch, R.R., and Dalgleish, D.G., Production of a novel ingredient from buttermilk, *J. Dairy Sci.*, 86, 2744, 2003.
148. Roesch, R.R., Rincon, A., and Corredig, M., Emulsifying properties of fractions prepared from commercial buttermilk by microfiltration, *J. Dairy Sci.*, 87, 4080, 2004.
149. Morin, P., Poliout, Y., and Jiménez-Flores, R., A comparative study of the fractionation of regular buttermilk and whey buttermilk by microfiltration, *J. Food Eng.*, 77, 521, 2006.
150. Huisman, I.H., Prádanos, P., and Hernández, A., The effect of protein-protein and protein-membrane interactions on membrane fouling in ultrafiltration, *J. Membr. Sci.*, 179, 79, 2000.
151. Krstić, D.M., Tekić, M.N., Carić, M.D., and Milanović, S.D., The effect of turbulence promoter in cross-flow microfiltration of skim milk, *J. Membr. Sci.*, 208, 303, 2002.
152. Youravong, W., Lewis, M.J., and Grandison, A.S., Critical flux in ultrafiltration of skimmed milk, *Trans. IChemE*, 81, 303, 2003.
153. Duclos-Orsello, C., Li, W., and Ho, C.-C., A three-mechanism model to describe fouling of microfiltration membranes, *J. Membr. Sci.*, 280, 856, 2006.
154. Muthukumar, S., Kentish, S.E., Ashokkumar, M., and Stevens, G.W., Mechanisms for the ultrasonic enhancement of dairy whey ultrafiltration, *J. Membr. Sci.*, 258, 106, 2005.
155. James, B.J., Jing, Y., and Chen, X.D., Membrane fouling during filtration of milk—a microstructural study, *J. Food Eng.*, 60, 431, 2003.
156. Huisman, I.H. and Trägårdh, C., Particle transport in crossflow microfiltration—I. Effects of hydrodynamics and diffusion, *Chem. Eng. Sci.*, 54, 271, 1999.
157. Field, R.W., Wu, D., and Howell, J.A., Critical flux for microfiltration fouling, *J. Membr. Sci.*, 100, 259, 1995.
158. Lee, Y. and Clark, M.M., Modeling of flux decline during crossflow ultrafiltration of colloidal suspensions, *J. Membr. Sci.*, 149, 181, 1998.
159. Chen, V., Fane, A.G., Madeini, S., and Wenten, I.G., Particle deposition during membrane filtration of colloids: Transition between concentration polarization and cake formation, *J. Membr. Sci.*, 125, 109, 1997.
160. Mourouzidis-Mourouzidis, S.A. and Karabelas, A.J., Whey protein fouling of microfiltration ceramic membranes—pressure effects, *J. Membr. Sci.*, 282, 124, 2006.
161. Grandison, A., Youravong, W., and Lewis, M.J., Hydrodynamic factors affecting flux and fouling during ultrafiltration of skimmed milk, *Lait*, 80, 165, 2000.
162. Palacio, L., Ho, C.-C., and Zydny, A.L., Application of a pore-blockage—cake-filtration model to protein fouling during microfiltration, *Biotech. Bioeng.*, 79, 260, 2002.
163. De Bruijn, J.P.F., Salazar, F.N., and Bórquez, R., Membrane blocking in ultrafiltration: A new approach to fouling, *Trans. IChemE C. Foods Bioproducts Process.*, 83(C3), 211, 2005.
164. Ho, C.-C. and Zydny, A.L., A combined pore blockage and cake filtration model for protein fouling during microfiltration, *J. Colloid Interface Sci.*, 232, 389, 2000.
165. Nyström, M., Fouling of unmodified and modified polysulfone ultrafiltration membranes by ovalbumin, *J. Membr. Sci.*, 44, 183, 1989.
166. Michaels, A.S., New separation technique for the CPI, *Chem. Eng. Prog.*, 64, 31, 1968.
167. Howell, J.A., Sub-critical flux operation of microfiltration, *J. Membr. Sci.*, 107, 165, 1995.
168. Youravong, W., Grandison, A.G., and Lewis, M.J., Effect of hydrodynamic and physicochemical changes on critical flux of milk protein suspensions, *J. Dairy Res.*, 69, 443, 2002.
169. Gésan-Guiziou, G., Boyaval, E., and Daufin, G., Critical stability conditions in crossflow microfiltration of skimmed milk: Transition to irreversible deposition, *J. Membr. Sci.*, 158, 211, 1999.
170. Bird, M.R. and Bartlett, M., Measuring and modeling flux recovery during the chemical cleaning of MF membranes for the processing of whey protein concentrate, *J. Food Eng.*, 53, 143, 2002.
171. Tarazaga, C.C., Campderrós, M.E., and Padilla, A.P., Physical cleaning by means of electric field in the ultrafiltration of a biological solution, *J. Membr. Sci.*, 278, 219, 2006.
172. Stabile, R.L., Economics of reverse osmosis and multistage evaporation for concentrating skim milk from 8.8% to 45% solids, *J. Dairy Sci.*, 66, 1765, 1983.
173. Krack, R., Chemical cleaning agents and costs in cleaning and disinfection of membrane equipment, in *Fouling and Cleaning in Pressure Driven Membrane Processes*, Special Issue 9504, International Dairy Federation, FIL-IDF, Brussels, 1995, p. 151.
174. Muñoz-Aguado, M.J., Wiley, D.E., and Fane, A.G., Enzymatic and detergent cleaning of a polysulfone ultrafiltration membrane fouled with BSA and whey, *J. Membr. Sci.*, 117, 175, 1996.
175. D'Souza, N.M. and Mawson, A.J., Membrane cleaning in the dairy industry: A review, *Crit. Rev. Food Sci. Nutr.*, 45, 125, 2005.
176. Trägårdh, G., Membrane cleaning, *Desalination*, 71, 325, 1989.

177. Cabero, M.L., Riera, F.A., and Álvarez, R., Rinsing of ultrafiltration ceramic membranes fouled with whey proteins: Effects on cleaning procedures, *J. Membr. Sci.*, 154, 239, 1999.
178. Jönsson, A.-S. and Trägårdh, G., Ultrafiltration applications, *Desalination*, 77, 135, 1990.
179. Bohner, H.F. and Bradley, R.L., Effective cleaning and sanitizing of polysulfone ultrafiltration membrane systems, *J. Dairy Sci.*, 73, 2309, 1992.
180. Bohner, H.F. and Bradley, R.L., Effective control of microbial populations in polysulfone ultrafiltration membrane systems, *J. Dairy Sci.*, 73, 2309, 1990.
181. Kim, K.-J., Sun, P., Chen, V., Wiley, D.E., and Fane, A.G., The cleaning of ultrafiltration membranes fouled by protein, *J. Membr. Sci.*, 80, 241, 1993.
182. Mercadé-Prieto, R. and Chen, X.D., Caustic-induced gelation of whey deposits in the alkali cleaning of membranes, *J. Membr. Sci.*, 254, 157, 2005.
183. Colton, R.H., Pahl, I., Ottaviano, L., Bodeutsch, T., and Meyeroltmanns, F., Study of protein adsorption effects on crossflow filtration using BSA and milk protein, *J. Pharm. Sci. Technol.*, 56, 20, 2002.
184. Savello, P., Caric, M., and Mahmoud, R., Fouling of ceramic membrane by milk proteins during microfiltration, *Aust. J. Dairy Technol.*, 52, 60, 1997.
185. Klobes, H., Nieweg, A., Lück, H.B., and Buccheim, W., Fractionation of skim milk proteins with capillary pore membranes, advances in membrane technology for better dairy products, *Bull. Int. Dairy Fed.*, 311, 13, 1996.
186. Grangeon, A. and Lescoche, P., Flat ceramic membranes for the treatment of dairy products: Comparison with tubular ceramic membranes, *Lait*, 80, 5, 2000.
187. Brans, G., Kromkamp, J., Pek, N., Gielen, J., Heck, J., van Rijn, C.J.N., van der Sman, R.G.M., Schroën, C.G.P.H., and Boom, R.M., Evaluation of microsieve membrane design, *J. Membr. Sci.*, 278, 344, 2006.
188. Piot, M., Fauquant, J., Madec, M.-N., and Maubois, J.L., Preparation of serocolostrum by membrane microfiltration, *Lait*, 84, 333, 2004.
189. Scammell, A.W., Production and uses of colostrums, *Aust. J. Dairy Technol.*, 56, 74, 2001.
190. Garcin, I. and Paviot, G., Composition cosmétique ou pharmaceutique á usage cutané et procédé pour la preparation d'une telle composition, Brevet européen Gattefossé S.A. n° 0334776, 1989.
191. Tolkach, A. and Kulozik, U., Fractionation of whey proteins and caseinomacropéptide by means of enzymatic crosslinking and membrane separation techniques, *J. Food Eng.*, 67, 13, 2005.
192. Aboumahmoud, R. and Savello, P., Crosslinking of whey protein by transglutaminase, *J. Dairy Sci.*, 73, 256, 1990.
193. Traoré, F. and Meunier, J.-C., Crosslinking activity of placental F XIIIa on whey proteins and caseins, *J. Agric. Food Chem.*, 40, 399, 1992.
194. Sood, V.K. and Kosikowski, F.V., Ripening changes and flavor development in microbial enzyme treated cheddar cheese slurry, *J. Food Sci.*, 44, 1690, 1979.



---

# 23 Microporous Membrane Blood Oxygenators

*S.R. Wickramasinghe and B. Han*

## CONTENTS

23.1	Introduction .....	671
23.2	History .....	673
23.2.1	Film and Bubble BOs .....	673
23.2.2	Nonporous Membrane BOs .....	673
23.2.3	Microporous Membrane BOs.....	673
23.2.4	Flat Sheet versus Hollow Fiber.....	674
23.3	Design of BOs.....	676
23.3.1	Oxygenation and Deoxygenation of Water .....	677
23.3.1.1	Flat Sheet BOs .....	678
23.3.1.2	Hollow Fiber BOs.....	679
23.3.2	Effects of Non-Newtonian Blood Rheology.....	682
23.3.3	Effects of Oxygen Binding to Hemoglobin.....	682
23.3.4	Value of Lumped Parameter Approaches .....	685
23.4	CFD Methods in BOs .....	685
23.4.1	CFD Application in BO Studies .....	685
23.4.2	Limitations .....	686
23.5	Future Trends .....	688
	Nomenclature .....	688
	Greek Symbols .....	689
	Dimensionless Group .....	689
	Subscripts .....	689
	References.....	689

## 23.1 INTRODUCTION

Cardiac surgery is generally performed on a motionless heart.\* The heart consists of two separate pumps: right ventricle pump and left ventricle pump. The right ventricle pumps oxygen-depleted blood to the lungs while the left ventricle pumps oxygen-rich blood to the body. Figure 23.1 shows the human circulatory system as well as the relationship between the heart and lungs. Cardiopulmonary bypass therefore must ensure that oxygen-rich blood reaches the cells in the body.

During cardiopulmonary bypass, blood from the vena cava is directed to the external cardiopulmonary bypass circuit, where it is oxygenated and returned to the aorta. Thus it is essential that an external blood oxygenator (BO) should be used to oxygenate the blood. An additional circuit is required to ensure that the heart is provided with oxygenated blood.

Figure 23.2 is a simplified schematic diagram of the cardiopulmonary bypass circuit. During cardiopulmonary bypass, a cannula is inserted into the right atrium to drain venous blood into the main blood reservoir. The cardiotomy reservoir receives blood that has been aspirated from the heart or pericardium. The cardiotomy reservoir usually includes a defoaming chamber. The cardiotomy reservoir also serves as a buffer storage reservoir in case there is a sudden change in blood pressure. Blood from the cardiotomy reservoir flows into the main reservoir. The blood from the blood reservoir is pumped through a BO,

---

\* Recently “beating heart” surgery has increased in popularity for more simple procedures where cardiac surgery is conducted on a beating heart. However cardiopulmonary bypass will be needed for more complicated procedures.

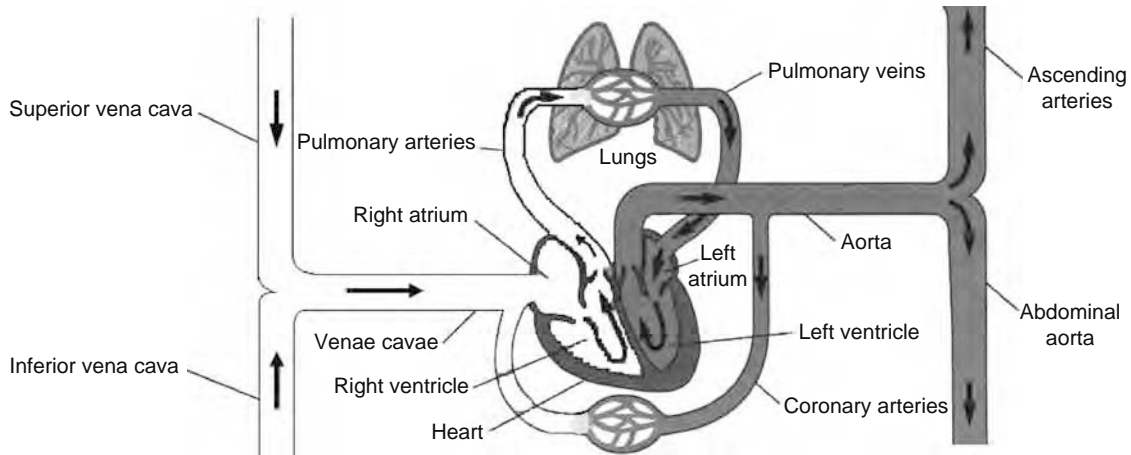


**FIGURE 23.1** Human circulatory system as well as the relationship between the heart and lungs.

which replaces the gas transfer function of the lungs; oxygenation of the blood, and removal of carbon dioxide. A heat exchanger is included with the blood oxygenator. Hot water is pumped through one side of the heat exchanger while the blood flows through the other side, allowing control of the patient's body temperature. A major concern during cardiopulmonary bypass is the entrapment of air in the blood. Antifoaming compounds, e.g., silica A, are usually added to the blood [1,2]. Further, blood filters (e.g., polyester or nylon filters with pore size between 20 and 40  $\mu\text{m}$ ) are used to remove any air bubbles that may be present. The blood returns to the body via a second cannula placed in the aorta.

The presence of an extracorporeal bypass circuit results in large heat losses from the blood. Thus an integral heat exchanger is essential to regulate the patient's body temperature. To decrease the oxygen demand during surgery, the patient's body temperature is often maintained at 5°C–10°C below normal body temperature.

The first cardiopulmonary bypass procedure was conducted on May 6, 1953 using a heart–lung machine invented by John and Mary Gibbon [3]. Today cardiopulmonary bypass procedures are routine. Figure 23.3 shows the increase in cardiopulmonary bypass procedures in United States from 1979 to 2002 [4]. From 1995 to 2002 about 700,000 cardiopulmonary bypass procedures were conducted each year in the United States. Among these, more than 50% of cardiopulmonary bypass procedures were conducted on patients above 65 years, while 40% were conducted on patients between 45 and 64 years of age.

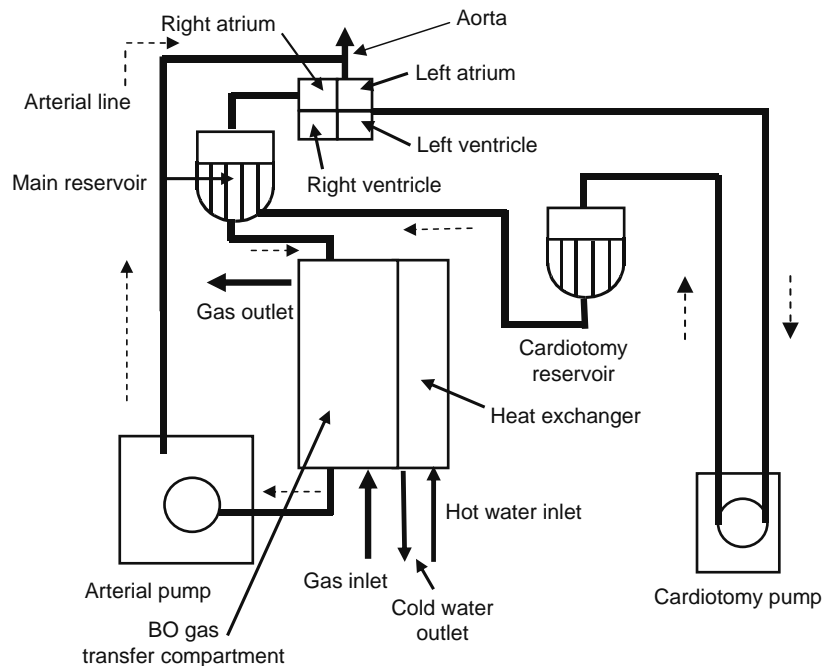


**FIGURE 23.2** Simplified schematic presentation of the cardiopulmonary bypass circuit. Direction of blood flow is shown by the dashed arrows.

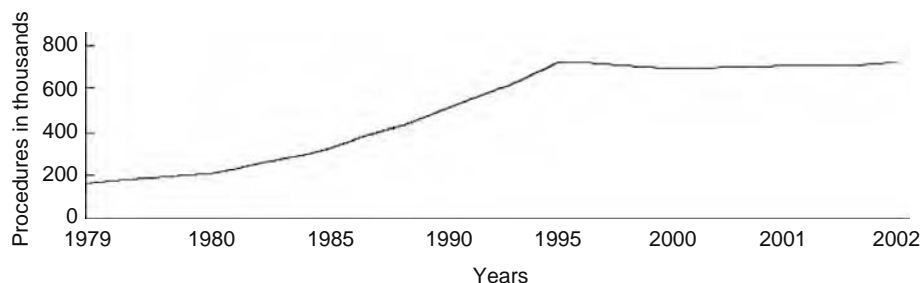


FIGURE 23.3 Cardiopulmonary bypass procedures conducted each year in the United States.

## 23.2 HISTORY

The BO is a major component of the cardiopulmonary bypass circuit. A tremendous amount of research, as evidenced by the numerous research papers and patents, has been devoted to the design of the highly efficient microporous membrane BOs available today. In the following section, the forerunners to today's microporous membrane BOs, the film and bubble BOs are briefly described.

### 23.2.1 FILM AND BUBBLE BOs

The original BOs were the film BOs. These BOs used rotating cylinders to spread blood in a continuously renewed thin film while oxygen flowed over the film of blood. Though there was direct contact between the blood and gas phases, the gas exchange efficiency was low leading to devices that had very large priming volumes. The first film BO was invented by von Frey and Gruber in 1885 [5]. Using the same principle, Gibbon developed his first film BO in 1937 [6]. After more than 10 years of testing, Gibbon performed the first successful open-heart surgery using his film BO in 1953 [3,7].

Next came the bubble BOs. In these devices, the gas exchange efficiency was increased by dispersing bubbles of oxygen in the blood, which resulted in significantly reduced priming volumes compared to the film BOs [8]. Since bubbling gas through blood leads to foam formation, silicone compounds were used as defoaming agents [9]. In 1955, DeWall et al. performed the first successful cardiopulmonary bypass procedure using a bubble BO [10].

Although the benefits of bubble versus film BOs were often debated, both have their own limitations. For film BOs, though the blood surface area is large, the gas transfer efficiency was often compromised by channeling of the blood flow [5,11,12]. Further, a large priming volume was usually required to obtain sufficient gas exchange. On the other hand, bubble BOs caused significant damage to the blood.

### 23.2.2 NONPOROUS MEMBRANE BOs

To improve the hemocompatibility of BOs, and avoid direct contact between the blood and gas phases, a nonporous membrane was placed between the blood and gas phases giving rise to membrane BOs [13–17]. The initial challenge in membrane technology was to produce reliable membranes with high permeabilities for  $O_2$  and  $CO_2$ . The first nonporous membrane materials included polyethylene, polypropylene, and ethylcellulose. The permeability of  $CO_2$  in these membrane materials was only five times greater than the permeability of  $O_2$ . Consequently, given the much lower  $CO_2$  concentrations of  $CO_2$  transfer were membrane limited.

The second generation of nonporous membranes was silicon based which displayed increased  $CO_2$  permeabilities. In 1965, Bramson et al. commercialized the first nonporous membrane BO [18]. Since the diffusion coefficient of oxygen and carbon dioxide in air is about four orders of magnitude higher than in blood, the gas side mass-transfer resistance was negligible. The major resistance to respiratory gas transfer was due to the membrane and the liquid side concentration boundary layer [19]. Though nonporous membrane BOs reduced blood damage, up to  $5.5 \text{ m}^2$  membrane surface area was often required to ensure adequate gas transfer rates.

### 23.2.3 MICROPOROUS MEMBRANE BOs

The next major advance in the development of membrane BOs came with the introduction of hydrophobic microporous membranes. These membranes were made from polypropylene or Teflon. Membrane pore diameters ranged from 0.02 to 0.6  $\mu\text{m}$ . Red blood cells on the other hand consist of biconcave discs with an average diameter of 6–8  $\mu\text{m}$ . Since the membranes are hydrophobic, the pores are gas filled. Even though many plasma proteins are much smaller than the membrane pores, the blood plasma cannot flow through the pores as long as the pressure drop from the blood side to the gas side is lower than the threshold value, called the breakthrough pressure. The respiratory gases pass through the membrane pores rather than the membrane material. Consequently, the major resistance to gas transfer is the blood side concentration boundary layer.

### 23.2.4 FLAT SHEET VERSUS HOLLOW FIBER

In 1980, microporous membrane BOs accounted for only 20% of all BOs sold in the United States [20]. At that time, the gas transfer performance of membrane BOs, such as the Baxter Travenol Modulung-Teflo and Travenol TMO (Baxter Travenol Laboratories, Inc., now Baxter International, Deerfield, Illinois), was not yet comparable with that of bubble BOs. Further the membrane BOs were complex to operate. During the early 1980s, the designers of membrane BOs started to focus on incorporating passive mixing of the blood to reduce the blood side resistance to gas transfer. For example, the Cobe CML (Cobe Cardiovascular, Arvada, Colorado) contained a microporous flat sheet membrane with a screen (spacer) in the blood channels to induce mixing [21]. The membrane surface area was reduced to 2.5 m<sup>2</sup>. The Johnson and Johnson Extracorporeal Maxima (Johnson and Johnson Cardiovascular, Anaheim, California) used cross-wound hollow fibers where the blood flowed outside the fibers [22]. By increasing the gas transfer efficiency of these BOs, the membrane surface area and priming volume were reduced. As a consequence of these improvements, by 1986, membrane BOs accounted for more than 60% of all BOs sold in the United States. This number further increased to 98% in 1992 and then to 99% in 1994. Today nearly 100% of BOs sold in the United States contain microporous membranes. In 1999, the total BO market was worth about \$460 million. In 2001, this number had risen to over \$500 million and is expected to be almost \$650 million in 2006 [23]. Table 23.1 summarizes some of the BO manufacturers today whereas Table 23.2 lists major BO membrane suppliers.

**TABLE 23.1**  
**Main BO Manufactures**

Manufacturer	Contact Information	BO Trade Name	Membrane Material	Membrane Type	Membrane Surface Area (m <sup>2</sup> )	Priming Volume (mL)
COBE Cardiovascular, Inc. (a Sorin Group company)	14401 W. 65th Way Arvada Colorado 80004-3599 Tel: 303 425 5508 800 221 7943 Fax: 303 467 6525 <a href="http://www.cobecv.com">http://www.cobecv.com</a>	Apex	Polypropylene (PP)	Hollow fiber		
		Optima XP	PP	Hollow fiber	1.9	
		Optimin	PP	Hollow fiber	1.0	
		Sorin Monolyth Pro	PP	Hollow fiber	2.2	
		Avant	PP	Hollow fiber	2.0	310
		CML DUO	PP	Flat sheet	2.6	
		Lilliput I	PP	Hollow fiber	0.34	60
		Lilliput II	PP	Hollow fiber	0.6	105
Dideco (a Sorin Group company)	Dideco s.r.l. Via Statale 12 Nord, 86 41037 Mirandola Modena Italy Tel: 39 0535 29811 Fax: 39 0535 25229 <a href="http://www.dideco.com">http://www.dideco.com</a>	ECC.O	PP	Hollow fiber	1.1	380
		D903 Avant	PP	Hollow fiber	1.7	250
		D902 Lilliput 2	PP	Hollow fiber	0.6	105
		D901 Lilliput 1	PP	Hollow fiber	0.34	60
		Compact flo Evo	PP	Hollow fiber	1.7	250
		D905 EOS	PP	Hollow fiber	1.1	160
SORIN BIOMEDICA CARDIO (a Sorin Group company)	Strada Per Crescentino 13040 Saluggia (VC) Via Crescentino, Italy Tel: 39 0161 4871 Fax: 39 0161 487316 <a href="http://www.sorincardio.com">http://www.sorincardio.com</a>	Synthesis	PP	Hollow fiber	2.0	430
		Monolyth	PP	Hollow fiber	2.2	285
		Monolyth C	PP	Hollow fiber	2.2	285
		Monolyth Pro	PP	Hollow fiber	2.2	286
Terumo Corporation	44-1,2-Chrome Hatagaya, Shibuya-Ku Tokyo, 151-0072 Japan Tel: 81 333 74 8111 Fax: 81 333 74 8399 <a href="http://www.terumo.co.jp">http://www.terumo.co.jp</a>	CAPIOX RX05 Baby RX	PP	Hollow fiber	0.5	43
		CAPIOX RX25R	PP	Hollow fiber	2.5	250
		CAPIOX SX10X and SX10RX	PP	Hollow fiber	1.0	135
		CAPIOX SX18X and SX18RX	PP	Hollow fiber	1.8	270
		CAPIOX SX25X and SX25RX	PP	Hollow fiber	2.5	340
Gish Biomedical, Inc.	22942 Arroyo Vista Rancho Santa Margarita California 92688 Tel: 800 938 0531 Fax: 949 635 6296 <a href="http://www.gishbiomedical.com">http://www.gishbiomedical.com</a>	Vision(r)	PP	Hollow fiber	2.45	

**TABLE 23.1 (continued)**  
**Main BO Manufactures**

Manufacturer	Contact Information	BO Trade Name	Membrane Material	Membrane Type	Membrane Surface Area (m <sup>2</sup> )	Priming Volume (mL)	
Medtronic	710 Medtronic Parkway Minneapolis, Minnesota 55432-5604 Tel: 1 763 514 4000 Fax: 1 763 514 4879 <a href="http://www.medtronic.com">http://www.medtronic.com</a>	AFFINITY NT		Hollow fiber			
		TRILLIUM		Hollow fiber			
		AFFINITY NT					
		Carmeda			Hollow fiber		
		AFFINITY NT					
		ECMO	Silicone polymer				
		I-Series	Silicone polymer				
		Minimax Plus		Hollow fiber			
Maquet Cardiopulmonary AG	Hechinger Strasse 38 72145 Hirrlingen Germany Tel: 49 07478 921-0 Fax: 49 07478 921-100 <a href="http://www.maquet-cp.com">http://www.maquet-cp.com</a>	Jostra Quadrox	PP	Hollow fiber	1.8	250	
		Jostra Quadrox D	Polymethyl pentene	Hollow fiber	1.8	250	
NovoSci	2828 N. Crescent Ridge Drive The Woodlands, Texas 77381 Tel: 800 854 0567 Fax: 888 570 4009 <a href="http://www.novosci.us">www.novosci.us</a>	Ready System		Hollow fiber			

Today both flat sheet and hollow fiber BOs are sold though the hollow fiber geometry is more common. BOs with very low membrane surface areas (e.g., Sarns Turbo, 3M Health Care, Ann Arbor, Michigan; and Cobe Optima, Cobe Cardiovascular, have surface areas of 1.9 and 1.7 m<sup>2</sup>, respectively) have been built using carefully spaced mats of woven hollow fibers [24,25]. These woven hollow fibers provide uniform flow channels, which minimizes channeling of the blood. Figures 23.4 and 23.5 are schematic representations of typical flat sheet and hollow fiber BOs. Flat sheet BOs are made from a flat sheet hydrophobic membrane. To introduce passive mixing and provide proper flow distribution, screens are placed between membranes. During operation, gas flows on one side of the membrane, while blood is delivered to the other side, as shown in Figure 23.4. Typical flat sheet BOs include Cobe VPCML Plus and Cobe Duo (Cobe Cardiovascular).

Hollow fiber BOs use hydrophobic membranes. In most designs, the blood flows outside and across the fibers. Consequently, the fibers help disrupt the blood side concentration boundary layer. Hollow fiber and flat sheet BOs have almost equivalent hemocompatibility and gas exchange performance. However, the gross air handling is different due to differences in the packing density (total available membrane surface area per unit volume). For flat sheet BOs, the packing

**TABLE 23.2**  
**Main BO Membrane Suppliers**

Suppliers	Contact Information	Membrane Commercial Name	Membrane Material	Membrane Type
Celgard LLC	13800 South Lakes Drive Charlotte, North California 28273 Tel: 704 588 5310 Fax: 704 587 8585 <a href="http://www.celgard.com">http://www.celgard.com</a>	Celgard	Polypropylene (PP), polyethylene (PE), PP/PE/PP trilayer, surfactant coated PP	Flat sheet
Membrana	Membrana GmbH Öhder Straße 28 42289 Wuppertal Tel: 49 202 6099 -0 Fax: 49 202 6099 -241 <a href="http://www.membrana.com">http://www.membrana.com</a>	OXYPHAN	PP	Hollow fiber
		CELGARD	PP	Hollow fiber

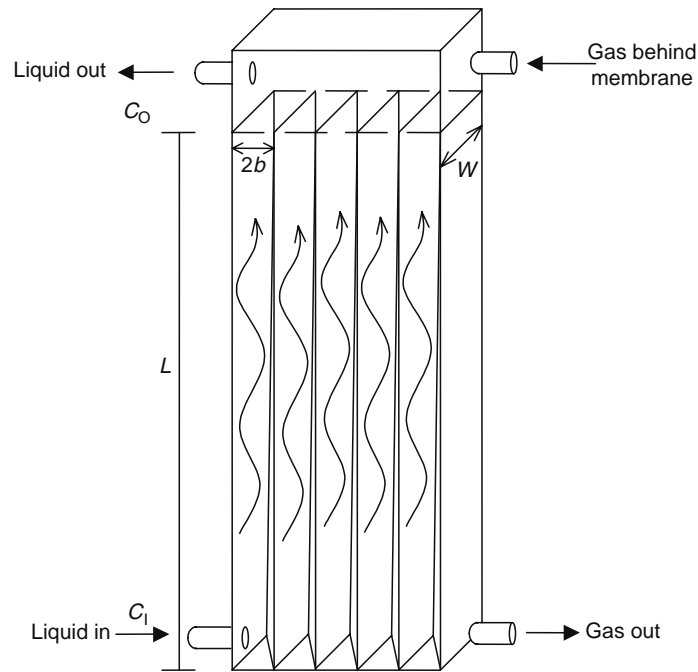


**FIGURE 23.4** Schematic diagram of flat sheet BOs.  $C_1$  and  $C_0$  refer to the inlet and outlet oxygen concentrations in the liquid phase.

density is usually less than  $400 \text{ m}^2 \text{ m}^{-3}$  while for hollow fiber BOs, the packing density can approach  $3000 \text{ m}^2 \text{ m}^{-3}$ . Table 23.3 summarizes some advantages and disadvantages of flat sheet and hollow fiber membrane BOs.

Gu et al. compared flat sheet and hollow fiber BOs in terms of pressure drop, shear stress, and activation of leukocytes or white blood cells [26]. They found that both configurations displayed similar gas transfer performance. However, the pressure drop along the blood flow path of the flat sheet BOs was higher than that for hollow fiber BOs. Moreover, activation of leukocytes in flat sheet BOs was greater.

### 23.3 DESIGN OF BOs

Designing improved BOs is complex, given the interdependence of the important design variables. Increasing the rate of gas transfer per priming volume of the device will minimize the transfusion requirements. This is particularly important, given the risk of contamination of the patients' blood by pathogens associated with the donated blood. Reducing the membrane surface

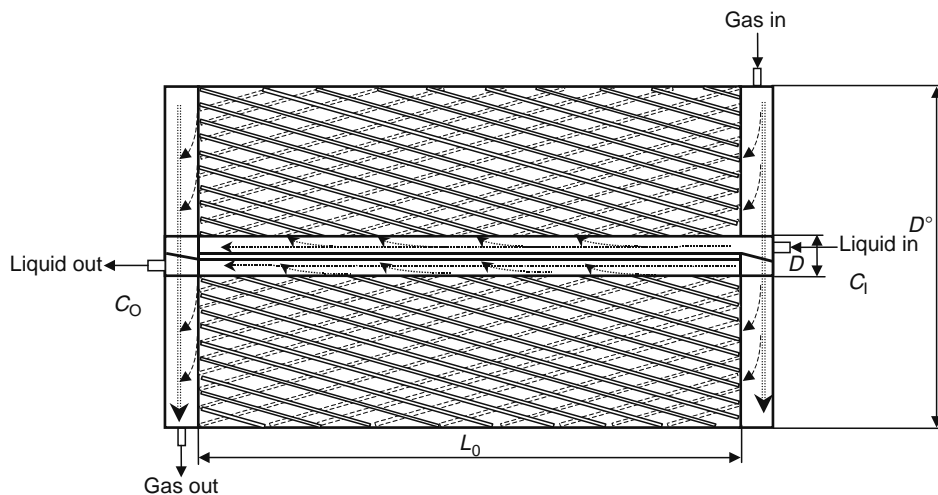


**FIGURE 23.5** Schematic diagram of hollow fiber BOs.  $C_1$  and  $C_0$  refer to the inlet and outlet oxygen concentrations in the liquid phase.

**TABLE 23.3**  
**Comparison between Flat Sheet and Hollow Fiber Membrane BOs**

Membrane Module	Advantages	Disadvantages
Flat sheet	Better consistency Air handling Low gas side pressure Low plasma weepage	Low packing density Poor pulse transmission High priming volume
Hollow fiber	High packing density More efficient Low priming volume	Priming more difficult High gas side pressure

area present will reduce the cost of the device. Finally, ideal designs are ones which disrupt the blood side mass-transfer boundary layer thus enhancing the rate of gas transfer yet minimizing blood damage.

**23.3.1 OXYGENATION AND DEOXYGENATION OF WATER**

Due to the complexity of dealing with human blood, many previous fundamental studies have focused on developing mass-transfer and friction factor correlations for BOs using Newtonian fluids such as water and glycerol water mixtures as a substitute for blood [27–35]. The use of a nonbiological, nonpathogenic blood analogue fluid to test BOs provides a number of advantages. Units of human and animal blood show a great deal of biological variability. Further a number of safety procedures, especially when using human blood, must be followed to minimize the risk of transmission of pathogens from the blood being tested to the operator.

The transfer of oxygen to Newtonian blood analogue fluids may be described by the following equation [36]:

$$N = K\Delta C \tag{23.1}$$

where

- $N$  is the total molar flux
- $\Delta C$  is the overall concentration difference
- $K$  is the overall average mass-transfer coefficient

A mass balance over the liquid phase results in the following expression for the overall average mass-transfer coefficient:

$$K = \frac{Q}{A} \int_{C_1}^{C_0} \frac{dC}{C^* - C} \tag{23.2}$$

where

- $Q$  is the fluid flow rate
- $A$  is the membrane surface area
- $C_1$ ,  $C_0$ , and  $C^*$  are the inlet and outlet oxygen concentrations in the fluid, and the oxygen concentration in the fluid if it were in equilibrium with the gas phase, respectively; see Figures 23.4 and 23.5 [27,37]

Integration of Equation 23.2 results in the following equation, which may be used to calculate the mass-transfer coefficient from the experimentally determined oxygen concentration in the liquid phase:

$$K = \frac{Q}{A} \ln \left( \frac{C_1 - C^*}{C_0 - C^*} \right) \tag{23.3}$$

Since the liquid side concentration boundary layer represents the major resistance to gas transfer, the overall average mass-transfer coefficient may be approximated by the liquid side mass-transfer coefficient [27,38–40]. Experimentally, this means that the overall average mass-transfer coefficient is independent of gas flow rate.

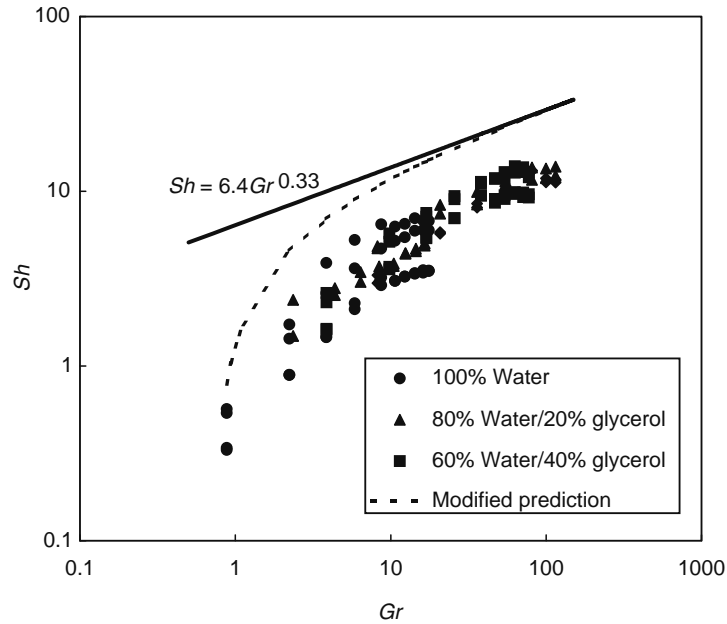


**FIGURE 23.6** Mass transfer results for flat sheet BOs. Two different flat sheet BOs were tested. (From Goerke, A.R., Leung, J., and Wickramasinghe, S.R., *Chem. Eng. Sci.*, 57, 2035, 2002. With permission.)

### 23.3.1.1 Flat Sheet BOs

Goerke et al. [29] determined mass-transfer and friction factor correlations using the Cobe VPCML Plus and Cobe CML Duo (Cobe Cardiovascular). Water and water/glycerol mixtures were used as the liquid phases. Figure 23.6 shows the variation of the Sherwood number with the Graetz number where the Sherwood number and Graetz numbers are defined as [29]

$$sh = \frac{K(4B)}{D} \quad (23.4)$$

$$Gr = \frac{(4B)^2 u}{DL} \quad (23.5)$$

where

- $K$  is the overall mass-transfer coefficient
- $D$  is the diffusion coefficient of oxygen in the liquid fluids
- $B$  is the average half thickness of rectangular blood flow channel
- $L$  is the length of rectangular blood flow channel
- $u$  is the velocity

In Figure 23.6, different symbols are used for different liquids. As can be seen, the Sherwood number increases with increasing Graetz number.

Goerke et al. [29] noted that the correlation

$$Sh = 6.4 Gr^{0.33} \quad (23.6)$$

does not fit the experimental data. Equation 23.6 represents the mass-transfer analogue of the L ev eque solution [41] modified for flow in rectangular ducts. The mass-transfer analogue of the L ev eque solution has been shown to predict the mass-transfer coefficient for flow in circular channels [41]. Goerke et al. used the following equations to describe their experimental data [29]:

$$Sh = 0.5 Gr \quad \text{for } 0.5 < Gr < 10 \quad (23.7)$$

$$Sh = 3.0 Gr^{0.33} \quad \text{for } 10 < Gr < 500 \quad (23.8)$$

At higher Graetz numbers, the experimental data lie parallel to but below the L ev eque solution. This is most likely because the screen, placed in the blood flow channel, touches the membrane. Thus the membrane surface area available for gas transfer is

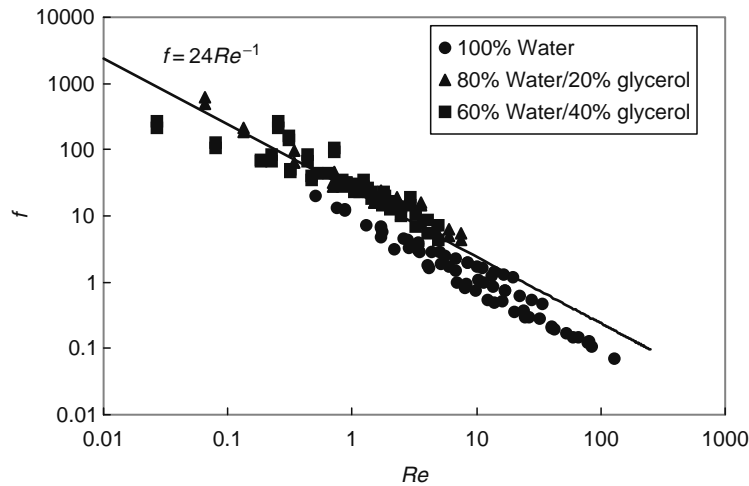


**FIGURE 23.7** Variation of the friction factor with Reynolds number. Two different flat sheet BOs were tested. (From Zhang, Q. and Cussler, E.L., *J. Membr. Sci.*, 23, 333, 1985. With permission.)

less than the actual membrane surface area present in the BO. At lower Graetz numbers, small variations in the thickness of the blood flow channels can lead to compromised gas transfer.

Goerke et al. [29] assumed that the actual thickness of the blood flow channels may be described by a truncated normal distribution. They then derived the following expression for the effective mass-transfer coefficient that incorporates the effects of variations in channel thicknesses

$$\langle K \rangle = K \left[ 1 - \left( \frac{9KA}{Q} - 3 \right) \varepsilon_0^2 + L \right] \tag{23.9}$$

where  $\varepsilon_0$  is the standard deviation of the channel thickness divided by the mean thickness. As can be seen, use of Equation 23.9 gives a better fit to the experimental data at low flow rates (i.e., low Graetz numbers, see Figure 23.6).

The variation of the friction factor with Reynolds number for flat sheet BOs is given in Figure 23.7 [29] where the Reynolds number is defined as

$$Re = \frac{u(4B)}{\nu} \tag{23.10}$$

where  $\nu$  is the kinematic viscosity.  $f$  is the friction factor which can be calculated by

$$f = \frac{B}{L} \frac{\Delta P}{\frac{1}{2} \rho \nu^2} \tag{23.11}$$

where

- $\Delta P$  is the pressure drop for liquid flow through the membrane channel
- $\rho$  is the liquid density

For laminar flow in rectangular ducts [42],

$$f = \frac{16}{Re \left[ \frac{2}{3} + \frac{11}{24} \frac{2B}{W} \left( 2 - \frac{2B}{W} \right) \right]} \approx \frac{24}{Re} \tag{23.12}$$

Equation 23.12, which is shown as a solid line in Figure 23.7, agrees very well with the experimental results [29].

### 23.3.1.2 Hollow Fiber BOs

Today most hollow fiber BOs are designed such that the gas phase flows inside the fibers and the blood flows outside and across the fibers (Figure 23.8). Like flat sheet BOs, several investigators have used a lumped parameter approach to determine mass-transfer and friction factor correlations for BOs. Different investigators have developed slightly different correlations. The differences in the correlations are probably indicative of the level of accuracy of this approach.

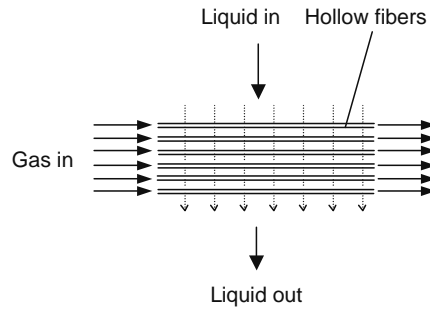


**FIGURE 23.8** Schematic diagram of hollow fiber BO where the blood flows outside and across the fibers.

Wickramasinghe et al. [28] studied various hollow fiber BOs. They found that for oxygen transfer into and out of water, a mass-transfer correlation of the form,

$$Sh = aRe^b Sc^c \quad (23.13)$$

could be used to describe the data. In Equation 23.13  $Sc$  is the Schmidt number defined as

$$Sc = \frac{\nu}{D} \quad (23.14)$$

In Equation 23.13,  $a$ ,  $b$ , and  $c$  are empirical constants. The Sherwood and Reynolds numbers are defined as

$$Sh = \frac{Kd_e}{D} \quad (23.15)$$

$$Re = \frac{ud_e}{\nu} \quad (23.16)$$

where  $d_e$  is the equivalent diameter defined as [30]

$$d_e = \left( \frac{\varepsilon}{1 - \varepsilon} \right) d_0 \quad (23.17)$$

where

$\varepsilon$  is the void fraction defined as the ratio of the empty volume within the mass-transfer chamber to the total volume of the mass-transfer chamber

$d_0$  is the outside diameter of the hollow fibers

They suggested the following correlation [28]:

$$Sh = 0.8Re^{0.47} Sc^{0.33} \quad (23.18)$$

More recently, Goerke et al. [29] studied three commercially available hollow fiber BOs (Cobe Optima, Cobe Optima XP, and Cobe Optimin, Cobe Cardiovascular). They obtained slightly different mass-transfer correlations for BOs with different hollow fiber diameters:

$$Sh = 0.39Re^{0.59} Sc^{0.33} \quad \text{for } 200 \mu\text{m ID fibers} \quad (23.19)$$

$$Sh = 0.20Re^{0.59} Sc^{0.33} \quad \text{for } 280 \mu\text{m ID fibers} \quad (23.20)$$

In a later publication, Wickramasinghe et al. [30] varied the Schmidt number of the liquid phase by conducting experiments with various water/glycerol mixtures. The results are shown in Figure 23.9. They obtained the following mass-transfer correlation [30]:

$$Sh = 0.8Re^{0.59} Sc^{0.33} \quad (23.21)$$

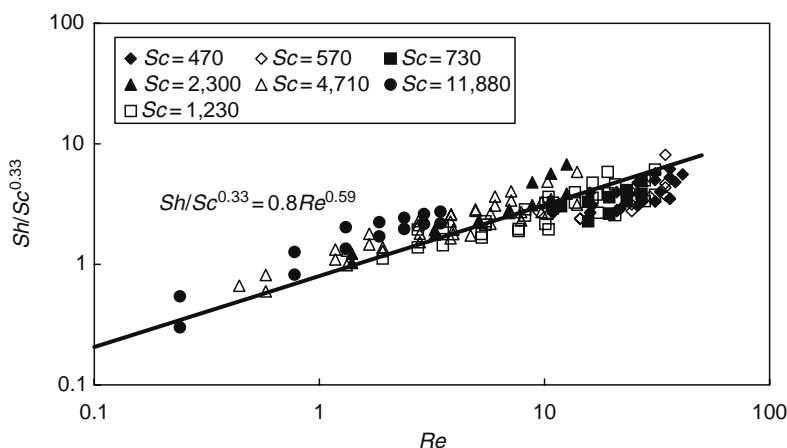


**FIGURE 23.9** Variation of  $Sh/Sc^{0.33}$  with Reynolds number for Newtonian fluids. (From Wickramasinghe, S.R., Garcia, J.D., and Han, B., *J. Membr. Sci.*, 208, 247, 2002. With permission.)

It is likely that the correlations (Equations 23.18 through 23.21) are in fact the same, given the accuracy of the lumped parameter approach.

Wickramasinghe et al. [30] also determined the variation of the friction factor with Reynolds number. The results are given in Figure 23.10. They used the following correlations to describe the friction factor for flow across woven hollow fibers [30]:

$$f = 260Re^{-1.1} \quad 0.1 < Re < 5 \tag{23.22}$$

$$f = 100Re^{-0.5} \quad 5 < Re < 100 \tag{23.23}$$

The range of liquid flow rates used to generate the data in Figure 23.10 is similar to the blood flow rates used in clinical practice. Figure 23.10 shows that for Reynolds numbers between 5 and 10, the slope of the friction factor versus Reynolds number curve changes suggesting the onset of boundary layer separation. Boundary layer separation will lead to mixing of the blood and a decrease in the blood side mass-transfer resistance.

Catapano et al. [35] studied the mass and momentum transport in hollow fiber BOs. Water and oxygen were used as the liquid and gas phases, respectively. They investigated the effect of the shell void fraction ( $\epsilon$ ) and the membrane angle with respect to the main direction of liquid flow ( $\phi$ ). They proposed the following correlations [35]:

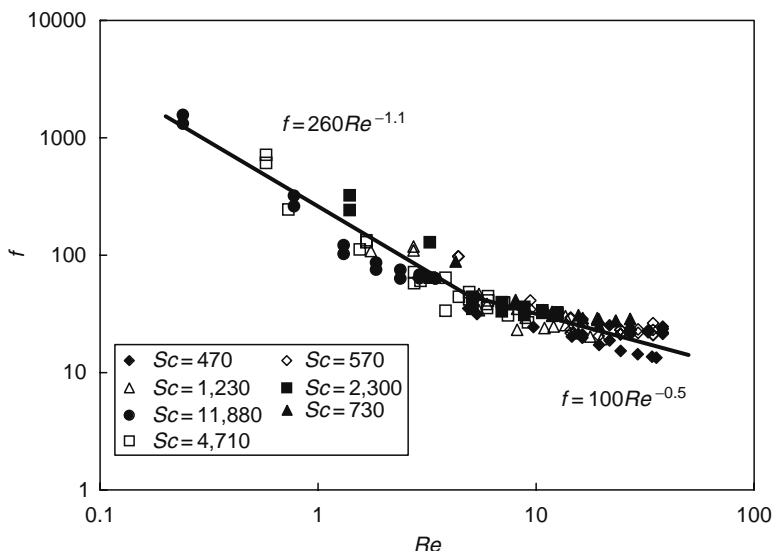


**FIGURE 23.10** Variation of friction factor with Reynolds number for Newtonian fluids. (From Wickramasinghe, S.R., Garcia, J.D., and Han, B., *J. Membr. Sci.*, 208, 247, 2002. With permission.)

$$Sh = \left( Re \frac{d_c}{4L} \right)^{0.15} \left( \frac{\varepsilon}{1 - \varepsilon} \right)^{-0.13} Sc^{0.33} (1.1 + 1.2e^{-0.1\phi}) \quad (23.24)$$

$$f = Re^{-0.43} (1 - \varepsilon)^{-1.22} (1.75 + 0.049\phi) \quad (23.25)$$

Their mass-transfer and friction factor correlations were derived for a range of Reynolds numbers between 20 and 60.

Rajasubramanian et al. [43] investigated oxygen transfer to saline in a commercial available hollow fiber BO (Avecor affinity BO, Avecor Cardiovascular Inc., Minneapolis, Minnesota). They obtained the following mass-transfer correlation:

$$Sh = 0.34Re^{0.18} Sc^{0.33} \quad (23.26)$$

Vaslef et al. [44] determined oxygen transfer rates in water using three commercial available hollow fiber BOs (SMO1 and Sarns Turbo Oxygenator, Sarns/3M, Ann Arbor, Minnesota; Bentley Univox, Bentley Laboratories, Irvine, California). They found that

$$\text{For SMO1: } Sh = 0.136Re^{0.832} Sc^{0.33} \quad (23.27)$$

$$\text{For Turbo: } Sh = 0.159Re^{0.751} Sc^{0.33} \quad (23.28)$$

$$\text{For Univox: } Sh = 0.256Re^{0.779} Sc^{0.33} \quad (23.29)$$

### 23.3.2 EFFECTS OF NON-NEWTONIAN BLOOD RHEOLOGY

The preceding studies used Newtonian fluids, generally water and glycerol water mixtures, to model blood. However, the rheological behavior of blood is complex. Blood is a shear-thinning, viscoelastic fluid. Further, blood also shows thixotropic properties due to its slow recovery from shear degradation and displays an apparent yield stress [45]. Blood rheology is often described in terms of two basic phenomena [46]: red cell deformation and red cell aggregation. Red cell deformation causes the viscosity of blood at high shear rates to be less than that obtained at low shear rates, while red cell aggregation causes a large increase in viscosity at low shear rates. At high cell concentrations, cell–cell interactions are also thought to play a critical role in determining the overall rheological properties of blood [47].

During cardiopulmonary bypass, addition of fluids such as anticoagulants leads to a reduction in the hematocrit or percentage of the total blood volume that is made up of red blood cells. Thus the elastic properties of blood do not affect blood flow in a BO [48]. Further, since the hematocrit of the blood is low, cell–cell interactions are likely to be less important. In modern BOs, the average relative shear stress on the blood is about 5–30 Pa [20]. Under these conditions, blood may be modeled as a shear-thinning fluid. Consequently, a Newtonian blood analogue fluid cannot model the variation of blood viscosity with shear rate.

Wickramasinghe et al. prepared non-Newtonian blood analogue fluids by adding polyacrylamide and xanthan gums to water and glycerol/water mixtures [32]. Mann and Tarbell [49] found that xanthan gum solutions model the viscous and elastic behavior of blood more accurately than polyacrylamide solutions. For shear-thinning fluids, the kinematic viscosity is not constant but varies with the shear stress. By using generalized Reynolds and Schmidt numbers, assuming power law fluid behavior, Wickramasinghe et al. found that the results for non-Newtonian fluids can be described using the same correlations derived for Newtonian fluids [32–34].

### 23.3.3 EFFECTS OF OXYGEN BINDING TO HEMOGLOBIN

In human blood, oxygen not only dissolves in the plasma but also binds to hemoglobin. The reaction between oxygen and hemoglobin leads to an enhanced rate of oxygen transfer compared to nonreactive blood analogue fluids. Thus to predict the performance of a BO, the effect of the oxygen–hemoglobin reaction must be included in the mass-transfer coefficient. Based on film theory [50], Wickramasinghe et al. introduced a mass-transfer enhancement factor to account for the increased rate of oxygen transfer due to the oxygen–hemoglobin reaction [33,34]. Figure 23.11 is a schematic representation of the liquid film that is assumed to exist at the membrane surface.

Hemoglobin is a globular protein composed of four polypeptide chains each containing a heme group. The oxygen-binding curve for hemoglobin (i.e., percentage of saturation of hemoglobin as a function of oxygen partial pressure) may be described empirically assuming the reaction between hemoglobin and oxygen is given by the following expression:



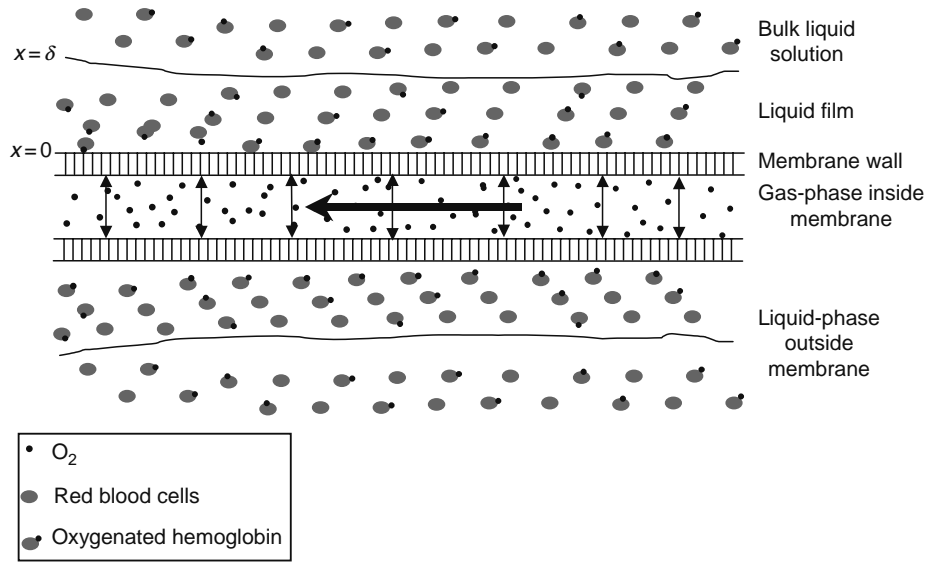


**FIGURE 23.11** (See color insert following page 588.) Schematic representation of liquid film at the surface of a hollow fiber. (From Wickramasinghe, S.R. and Han, B., *Chem. Eng. Res. Des.*, 83(A3), 256, 2005. With permission.)

where

$n$  is a measure of cooperatively between heme units [51]

$k_1$  and  $k_{-1}$  are the forward and backward rate constants

An apparent equilibrium constant,  $K_E$ , based on Equation 23.30 may be defined as

$$K_E = \frac{k_1}{k_{-1}} = \frac{[\text{Hb}(\text{O}_2)_n]}{[\text{Hb}][\text{O}_2]^n} \quad (23.31)$$

where  $[\text{Hb}(\text{O}_2)_n]$ ,  $[\text{Hb}]$ , and  $[\text{O}_2]$  are the concentrations of oxygenated hemoglobin, nonoxygenated hemoglobin, and dissolved oxygen in the plasma, respectively.

Since the gas side resistance to mass transfer is negligible in microporous membrane BOs, only the liquid side film is considered. Mass transfer by convection within the film is negligible. Further there is no mass accumulation at any point within the film. Consequently, steady-state mass balances in the liquid film on  $[\text{O}_2]$ ,  $[\text{Hb}]$ , and  $[\text{Hb}(\text{O}_2)_n]$  lead to Equations 23.32 through 23.34 [36,52]:

$$0 = \frac{\partial[\text{O}_2]}{\partial t} = D_{\text{O}_2} \frac{\partial^2([\text{O}_2])}{\partial x^2} + nk_{-1}[\text{Hb}(\text{O}_2)_n] - nk_1[\text{Hb}][\text{O}_2]^n \quad (23.32)$$

$$0 = \frac{\partial[\text{Hb}]}{\partial t} = D_{\text{Hb}} \frac{\partial^2([\text{Hb}])}{\partial x^2} + k_{-1}[\text{Hb}(\text{O}_2)_n] - k_1[\text{Hb}][\text{O}_2]^n \quad (23.33)$$

$$0 = \frac{\partial[\text{Hb}(\text{O}_2)_n]}{\partial t} = D_{\text{Hb}(\text{O}_2)_n} \frac{\partial^2([\text{Hb}(\text{O}_2)_n])}{\partial x^2} - k_{-1}[\text{Hb}(\text{O}_2)_n] + k_1[\text{Hb}][\text{O}_2]^n \quad (23.34)$$

The general solution for Equations 23.32 through 23.34 is [53]

$$D_{\text{O}_2}[\text{O}_2] + nD_{\text{Hb}(\text{O}_2)_n}[\text{Hb}(\text{O}_2)_n] = a_1x + a_2 \quad (23.35)$$

$$D_{\text{Hb}}[\text{Hb}] + D_{\text{Hb}(\text{O}_2)_n}[\text{Hb}(\text{O}_2)_n] = a_3x + a_4 \quad (23.36)$$

where  $a_1$ ,  $a_2$ ,  $a_3$ , and  $a_4$  are empirical constants. Four boundary conditions are required. At the gas–liquid interface (surface of the membrane on the liquid side),  $x=0$ . Here,

$$[\text{O}_2] = [\text{O}_2]_0 \quad (23.37)$$

where  $[O_2]_0$  is the dissolved oxygen concentration in the liquid phase that is in equilibrium with the gas-phase concentration. At the outer edge of the stagnant film,  $x = \delta$ . Here

$$[O_2] = [O_2]_\delta \quad (23.38)$$

$$[Hb] = [Hb]_\delta \quad (23.39)$$

where  $[O_2]_\delta$  and  $[Hb]_\delta$  are the same as the dissolved oxygen and nonoxygenated hemoglobin concentrations in the bulk liquid.

Neither hemoglobin nor oxygenated hemoglobin can leave the liquid phase. Thus the fourth boundary condition states that the flux of total hemoglobin is zero.

$$D_{Hb} \frac{d[Hb]}{dx} + D_{Hb(O_2)_n} \frac{d[Hb(O_2)_n]}{dx} = 0 \quad (23.40)$$

The rate of oxygen transfer through the stagnant film is equal to the dissolved oxygen flux plus the oxygenated hemoglobin flux. Thus the oxygen flux,  $J$ , is given by

$$J = -D_{O_2} \frac{d[O_2]}{dx} - nD_{Hb(O_2)_n} \frac{d[Hb(O_2)_n]}{dx} = -a_1 \quad (23.41)$$

Substituting Equations 23.31 and 23.35 through 23.40 into Equation 23.41 results in

$$J = \frac{D_{O_2}}{\delta} ([O_2]_0 - [O_2]_\delta) \left\{ 1 + \frac{nD_{Hb(O_2)_n}}{D_{O_2}} \cdot \frac{1}{1 + \frac{D_{Hb(O_2)_n}}{D_{Hb}} K_E [O_2]_0^n} \cdot \frac{[O_2]_0^n - [O_2]_\delta^n}{[O_2]_0 - [O_2]_\delta} K_E [Hb]_\delta \right\} \quad (23.42)$$

In the absence of a chemical reaction between oxygen and hemoglobin, the oxygen flux  $J_0$  is given by

$$J_0 = \frac{D_{O_2}}{\delta} ([O_2]_0 - [O_2]_\delta) = k_0 ([O_2]_0 - [O_2]_\delta) \quad (23.43)$$

where  $k_0$  is the mass-transfer coefficient in the absence of chemical reaction. Comparing Equations 23.42 and 23.43,

$$k = k_0 \left\{ 1 + \frac{nD_{Hb(O_2)_n}}{D_{O_2}} \cdot \frac{1}{1 + \frac{D_{Hb(O_2)_n}}{D_{Hb}} K_E [O_2]_0^n} \cdot \frac{[O_2]_0^n - [O_2]_\delta^n}{[O_2]_0 - [O_2]_\delta} K_E [Hb]_\delta \right\} = k_0 E \quad (23.44)$$

where the term in brackets is the enhancement factor,  $E$ . The enhancement factor is a function of the oxygen partial pressure, as the oxygen partial pressure increases, the enhancement factor decreases.

The enhancement factor given by Equation 23.44 contains the diffusivity of oxygen hemoglobin and oxyhemoglobin. Since the hemoglobin is found within the red blood cells, the diffusivity of hemoglobin and oxyhemoglobin is the same as the diffusivity of the red blood cells. The diffusivity of red blood cells is significantly enhanced by rotation and deformation of the cells, which is a function of shear rate [33]. As the shear rate increases so does the diffusivity of the red blood cells and hence the mass-transfer enhancement factor given by Equation 23.44. Consequently, designs which maximize the diffusivity of red blood cells will display higher rates of gas transfer.

The enhancement factor given in Equation 23.44 assumes film theory. Other enhancement factors have also been described [54–56]. For example, Shimizu and Yoshida proposed the following equation to calculate the enhancement factor [54,56]:

$$E = \left( \frac{95,000}{P_{O_2}} \right)^{1/3} \left\{ 1 + 11.8 \left[ (1-s) \frac{Ht}{100} \right]^{0.8} - 8.9 \left[ (1-s) \frac{Ht}{100} \right] \right\} \quad (23.45)$$

In blood, oxygen is present in both dissolved and chemically reacted forms. Therefore, the oxygen concentration in blood is given by

$$C = C_C + C_P = \beta \left( \frac{Ht}{100} \right) S + \alpha P_{O_2} \quad (23.46)$$

where

$\beta$  is the maximum amount of oxygen that can combine with a unit volume of hemoglobin

$C_C$  and  $C_P$  are the oxygen concentration bound to hemoglobin and dissolved in the plasma, respectively

$S$  is the degree of oxygen saturation (oxyhemoglobin saturation), which is given by the ratio  $[\text{Hb}(\text{O}_2)_n]/[\text{Hb}]_t$ , where  $[\text{Hb}]_t$  is the total hemoglobin concentration (oxygenated and nonoxygenated) present

The degree of oxygen saturation is often described by the Hill equation [57–60]:

$$S = \frac{[\text{Hb}(\text{O}_2)_n]}{[\text{Hb}]_t} = \frac{(P_{\text{O}_2}/P_{50})^n}{1 + (P_{\text{O}_2}/P_{50})^n} \quad (23.47)$$

where  $P_{\text{O}_2}$  and  $P_{50}$  are the oxygen partial pressure and the oxygen partial pressure, respectively, at 50% hemoglobin saturation.

By combining Equation 23.46, Equation 23.2 can be rewritten as

$$K = \frac{Q}{A} \int_{C_{P,I}}^{C_{P,O}} \frac{dC}{(C^* - C_P)} = \frac{Q}{A} \int_{C_{P,I}}^{C_{P,O}} \frac{d[\beta(\text{Ht}/100)S + \alpha P_{\text{O}_2}]}{(C^* - C_P)} \quad (23.48)$$

where  $C_{P,I}$  and  $C_{P,O}$  are the oxygen concentration dissolved in the plasma in the inlet and outlet stream, respectively. By using the oxygen partial pressure to replace the dissolved oxygen concentration,

$$K = \frac{Q}{A} \int_{P_{\text{O}_2,I}}^{P_{\text{O}_2,O}} \frac{\beta(\text{Ht}/100)(dS/dP_{\text{O}_2}) + \alpha}{(P_{\text{O}_2}^* - P_{\text{O}_2})} dP_{\text{O}_2} \quad (23.49)$$

where  $P_{\text{O}_2,I}$ ,  $P_{\text{O}_2,O}$ , and  $P_{\text{O}_2}^*$  are the inlet and outlet oxygen partial pressure that would be in equilibrium with the oxygen in the blood and the oxygen partial pressure in the gas phase, respectively.  $dS/dP_{\text{O}_2}$  can be obtained by differentiating Equation 23.47.

Finally, the overall average mass-transfer coefficient in the absence of the reaction between oxygen and hemoglobin may be calculated from

$$K_0 = \frac{Q}{A} \int_{P_{\text{O}_2,I}}^{P_{\text{O}_2,O}} \frac{\beta(\text{Ht}/100)(dS/dP_{\text{O}_2}) + \alpha}{E(P_{\text{O}_2}^* - P_{\text{O}_2})} dP_{\text{O}_2} \quad (23.50)$$

Wickramasinghe et al. used bovine blood to evaluate the Cobe Duo and Cobe Optima XP BOs (Cobe Cardiovascular) [33,34]. By using  $K_0$  to calculate the Sherwood number, as well as the analogous Reynolds and Schmidt number for power law fluids, Wickramasinghe et al. found that results for bovine blood do collapse onto the same curve as the results for Newtonian and non-Newtonian blood analogue fluids. Their results are shown in Figures 23.12 and 23.13 [33,34].

Matsuda and Sakai proposed the following mass-transfer correlation for hollow fiber BOs [61]:

$$Sh = Sc^{1/3} Re^{2/3} \exp(3.29\varepsilon - 4.27) \quad (23.51)$$

However, the range of Reynolds numbers tested was very small being 2–20.

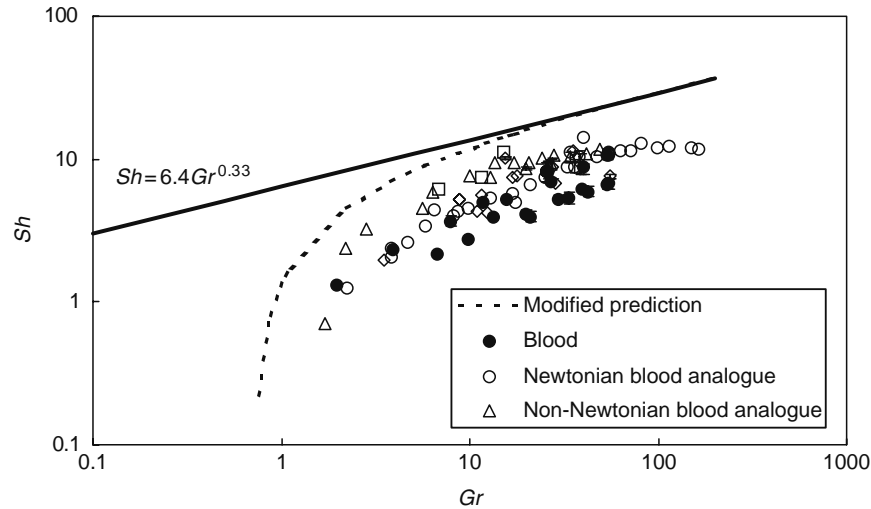
### 23.3.4 VALUE OF LUMPED PARAMETER APPROACHES

Table 23.4 summarizes some of the literature correlations. As can be seen most of these correlations were developed using Newtonian blood analogue fluids such as water and glycerol water solutions. These correlations may be used to help guide better BO designs. Table 23.4 indicates that correlations obtained by different researchers using different modules are not always the same. Thus caution is needed when using these correlations to ensure they are applicable to the operating conditions being considered.

## 23.4 CFD METHODS IN BOs

### 23.4.1 CFD APPLICATION IN BO STUDIES

Recently, computational fluid dynamics (CFD) models have been developed to guide the development of new BO designs [62–67]. Baker et al. developed a two-dimensional finite-difference model to solve the Navier–Stokes equation and to predict



**FIGURE 23.12** Variation of Sherwood number with Graetz number. Results are given for Newtonian and non-Newtonian blood analogue fluids and bovine blood for flat sheet BOs. The solid line depicts Equation 23.6. The dashed line gives the predictions of Equation 23.9. (From Wickramasinghe, S.R., Han, B., Garcia, J.D., and Specht, R., *AIChE J.*, 51, 656, 2005. With permission.)

gas transfer to blood flowing outside hollow fibers [62]. Using this model, Baker et al. calculated the oxygen saturation profile and the velocity profile along the membrane module. They further compared their simulation results to experimental data for bovine and human blood. They obtained reasonable agreement.

Gage et al. developed a three-dimensional CFD model to predict the pressure drop in a membrane BO [63]. They modified a commercial membrane BO to allow pressure measurement along the fiber bundle in all cardinal axes. Close agreement was obtained between experimental and simulated pressure drops at lower flow rates. However, the simulated pressure drops were lower than the experimental results at higher flows.

Funakubo et al. used a CFD model to evaluate 10 artificial implantable lungs [64]. Their research focused on the occurrence of thrombogenesis. They built a prototype to verify their CFD predictions. They found a correlation between predicted areas of low flow and thrombus formation. Further although nearly identical low flow velocity conditions exist at both the inlet and outlet ports, thrombus formation occurs only near the outlet port, which agreed with detailed vectorial analysis. Gartner et al. also used a CFD approach to model flow effects on thrombotic deposition on a membrane BO [67].

### 23.4.2 LIMITATIONS

Although CFD has been widely used to model blood pumps and other membrane processes, its application in membrane BOs is very limited. Development of a CFD model requires simplifying assumptions. In their model, Baker et al. assumed that blood was statistically homogeneous; the reaction between oxygen and hemoglobin was fast; axial diffusion of gas was neglected;

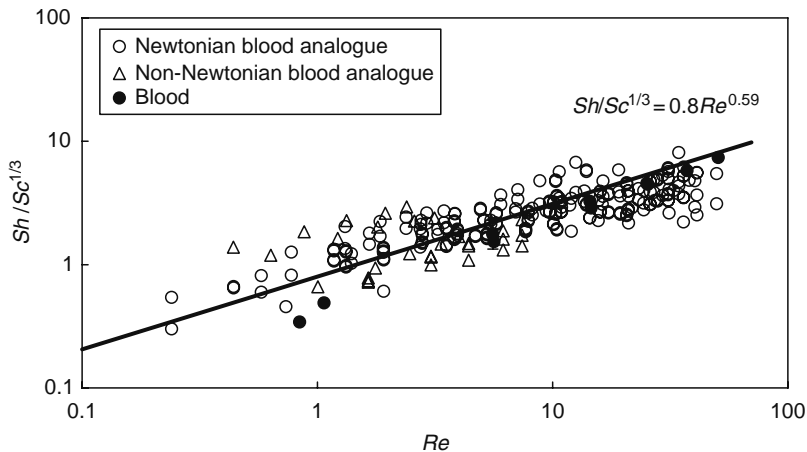


**FIGURE 23.13** Variation of  $Sh/Sc^{1/3}$  with Reynolds number. Results are shown for Newtonian and non-Newtonian blood analogue fluids and bovine blood for hollow fiber BOs. Solid lines depict Equation 23.21. (From Wickramasinghe, S.R., Han, B., Garcia, J.D., and Specht, R., *AIChE J.*, 51, 656, 2005. With permission.)

**TABLE 23.4**  
**Literature Correlations for BOs**

Geometry	Mass Transfer		Friction Factor		Liquid Fluids	References
	Flow Range Investigated	Inferred Correlation	Flow Range Investigated	Inferred Correlation		
Flow in thin channels	$0.5 < Gr < 10$	$Sh = 0.5Gr$	$0.01 < Re < 200$	$f = 24Re^{-1}$	Water, water/glycerol, water/xanthan/glycerol, bovine blood Water	[29]
	$10 < Gr < 500$	$Sh = 3.0Gr^{0.33}$				[27]
	$0.5 < Gr < 11$	$Sh = 1.25Gr$				[27]
	$11 < Gr < 100$	$Sh = 6.0Gr^{0.35}$				
	$4 < Gr < 1000$	$Sh = 1.62Gr^{0.33}$				
	$0.1 < Gr < 4$	$Sh = Sh_0 [1 - (\frac{185Sh_0}{Gr} + 7)e_0^{-2} + L]$				
Flow outside and across fibers	$0.01 < Re < 10$	$Sh = 0.8Re^{0.47} Sc^{0.33}$			Water	[28]
	$0.1 < Re < 100$	$Sh = 0.39Re^{0.59} Sc^{0.33}$ (for 200 $\mu\text{m}$ i.d. fibers)	$0.1 < Re < 100$	$f = 100Re^{-0.9}$	Water	[29]
		$Sh = 0.20Re^{0.59} Sc^{0.33}$ (for 280 $\mu\text{m}$ i.d. fibers)			Water	[27]
	$0.2 < Re < 2.5$	$Sh = 0.12ReSc^{0.33}$				
	$2.5 < Re > 20$	$Sh = 0.15Re^{0.8} Sc^{0.33}$				
	$0.1 < Re < 100$	$Sh = 0.8Re^{0.49} Sc^{0.33}$				
	$20 < Re < 60$	$Sh = (Re \frac{d_f}{L})^{0.15} (\frac{L}{d_f})^{-0.13} Sc^{0.33} (1.1 + 1.2e^{-0.1\phi})$	$0.1 < Re < 5$	$f = 260Re^{-1.1}$	Water, water/glycerol, water/xanthan/glycerol, bovine blood	[30-34]
		$Sh = 0.34Re^{0.18} Sc^{0.33}$	$5 < Re < 100$	$f = 100Re^{-0.5}$	Water	[35]
	$2 < Re < 20$	$Sh = Sc^{1/3} Re^{2/3} \exp(3.29e - 4.27)$	$20 < Re < 60$	$f = Re^{-0.43} (1 - e)^{-1.22} (1.75 + 0.049\phi)$	Saline	[43]
	$10 < Re < 35$	$Sh = 0.136Re^{0.832} Sc^{0.33}$ (SMO1)	$2 < Re < 20$	$f = Re^{-0.496} \exp(7.36e - 3.33)$	Bovine blood	[61]
$8 < Re < 48$	$Sh = 0.159 Re^{0.751} Sc^{0.33}$ (Turbo)			Water	[44]	
$2 < Re < 6$	$Sh = 0.256Re^{0.779} Sc^{0.33}$ (Univox)					

metabolic oxygen consumption by blood was neglected; all flow components were parallel to the fiber axis; fibers were parallel with no fiber crossings; cross-sectional fiber distribution was a uniform triangular array; and the blood and gas flow were fully developed [62]. Other CFD studies use similar assumptions [63–65]. Clearly, the accuracy of the model depends on the validity of the assumptions made.

CFD predictions depend on accurate determination of various parameters. For example, in the CFD model developed by Gage et al. [63], the permeability of the fiber bundle was experimentally determined from pressure drop data obtained from water perfusion testing.

While these CFD models are helpful, a large number of experimental studies are still necessary. The accuracy of a CFD model needs to be verified experimentally. As commercially available CFD software becomes more sophisticated, these simulations will provide a powerful tool to help design better membrane BOs.

### 23.5 FUTURE TRENDS

In 2002, of the 709,000 open-heart surgeries conducted in the United States, 368,000 were for patients over 65 years of age. Another 261,000 were for patients between 45 and 64 while 41,000 for patients between 15 and 44 years of age [4]. Current membrane BOs are very efficient in terms of the rate of gas transfer. The total membrane surface area is around 2 m<sup>2</sup>. During operation, the effective blood film thickness (shown in Figure 23.11) is around 100 μm [20]. By further increasing the gas transfer rate, the total membrane surface may be further decreased. This will further decrease the priming volume as well as the cost of BOs. Since the dominant mass-transfer resistance for BOs is the blood side concentration boundary layer, further increases in gas exchange efficiency will most likely be achieved using newer module designs that involve blood flow augmentation. For example, centrifugal blood flow has been investigated [68]. Although these designs have yet to be commercialized, development of novel auxiliary equipment for these designs may improve their commercial viability.

The primary mode of failure for membrane BOs is due to plasma leakage through the pores of the hydrophobic membrane [69]. This leakage will cause a reduction in the gas transfer efficiency. Most commercial BOs are designed to operate without plasma leakage for at least 6 h. Plasma leakage may be minimized by using smaller membrane pore sizes or coating the membrane pores with a thin film [70]. However, this will lead to an increase in the membrane resistance to gas transfer.

During cardiopulmonary bypass, due to the contact between blood and the membrane surface, the patients' hematological and immune systems may be affected. Thus development of more hemocompatible BO membranes remains an important challenge. Since deposition and activation of platelets, leukocytes, and proteins are thought to be the primary responses that occur when blood contacts a BO membrane surface, the BOs hemocompatibility may be improved by developing materials that suppress adsorption of blood components.

### NOMENCLATURE

$a$	empirical constant
$a_1, a_2, a_3, a_4$	constants
$A$	membrane surface area (m <sup>2</sup> )
$b$	empirical constant
$B$	average half thickness of the rectangular channels (m)
$c$	empirical constant
$C$	concentration (mol L <sup>-1</sup> )
$C^*$	oxygen concentration in the liquid in equilibrium with the gas phase (mol L <sup>-1</sup> )
$C_C$	oxygen bound to hemoglobin (mol L <sup>-1</sup> )
$C_P$	oxygen dissolved in plasma (mol L <sup>-1</sup> )
$C_{P,I}$	physically dissolved oxygen in plasma at the inlet of the BO (mol L <sup>-1</sup> )
$C_{P,O}$	physically dissolved oxygen in plasma at the outlet of the BO (mol L <sup>-1</sup> )
$\Delta C$	overall concentration difference (mol L <sup>-1</sup> )
$D$	diffusion coefficient (m <sup>2</sup> s <sup>-1</sup> )
$d_e$	equivalent diameter (m)
$d_0$	outside diameter of the hollow fibers (m)
$E$	enhancement factor
$f$	friction factor
Ht	hematocrit (%)
$J$	flux (mol m <sup>-2</sup> s <sup>-1</sup> )
$J_0$	oxygen flux in the absence of chemical reaction between oxygen and hemoglobin (mol m <sup>-2</sup> s <sup>-1</sup> )
$K$	overall average mass-transfer coefficient (m s <sup>-1</sup> )
$K_E$	equilibrium constant (units depend on value of $n$ )

$K_0$	overall average mass-transfer coefficient in the absence of chemical reaction in the boundary layer ( $\text{mol m}^{-2} \text{s}^{-1}$ )
$k_1$	forward rate constant (units depend on value of $n$ )
$k_{-1}$	backward rate constant (units depend on value of $n$ )
$\langle K \rangle$	average mass-transfer coefficient for flow in polydisperse channels ( $\text{mol m}^{-2} \text{s}^{-1}$ )
$L$	length of rectangular channel (m)
$n$	measure of cooperativity between heme units
$N$	total molar flux ( $\text{mol m}^{-2} \text{s}^{-1}$ )
$P_{\text{O}_2}$	oxygen partial pressure (Pa)
$P_{\text{O}_2,1}$	inlet oxygen partial pressure in equilibrium with the oxygen in the blood (Pa)
$P_{\text{O}_2,0}$	outlet oxygen partial pressure in equilibrium with the oxygen in the blood (Pa)
$P_{\text{O}_2}^*$	oxygen partial pressure in the gas phase (Pa)
$P_{50}$	oxygen partial pressure at 50% hemoglobin saturation (Pa)
$\Delta P$	pressure drop (Pa)
$Q$	fluid flow rate ( $\text{m}^3 \text{s}^{-1}$ )
$S$	degree of oxygen saturation
$t$	time (s)
$u$	liquid velocity ( $\text{m s}^{-1}$ )
$W$	average width of rectangular blood flow channel (m)
$x$	distance variable (m)

**GREEK SYMBOLS**

$\alpha$	physical solubility of oxygen in blood ( $\text{mol L}^{-1} \text{Pa}^{-1}$ )
$\beta$	maximum amount of oxygen combined with a unit volume of hemoglobin ( $\text{mol L}^{-1}$ )
$\varepsilon$	void fraction of a BO
$\varepsilon_0$	standard deviation divided by the mean of the distribution of channel thickness
$\rho$	liquid density ( $\text{kg m}^{-3}$ )
$\nu$	kinematic viscosity of Newtonian fluids ( $\text{m}^2 \text{s}^{-1}$ )
$\tau$	shear stress (Pa)
$\dot{\gamma}$	shear rate ( $\text{s}^{-1}$ )
$\delta$	thickness of boundary layer (m)
$\phi$	membrane angle with respect to the main direction of liquid flow ( $^\circ$ )

**DIMENSIONLESS GROUP**

$Gr$	Graetz number, $(4B)^2 u / (DL)$
$Re$	Reynolds number, $u(4B) / \nu$ , $u d_c / \nu$
$Sc$	Schmidt number, $\nu / D$
$Sh$	Sherwood number, $K(4B) / D$ , $K d_c / D$

**SUBSCRIPTS**

e	equilibrium; effective
Hb	hemoglobin
$\text{Hb}(\text{O}_2)_n$	oxyhemoglobin
I	inlet
O	outlet
$\text{O}_2$	oxygen
t	total
0	reference point

**REFERENCES**

1. Penry JK, Cordell AR, Johnston FR, and Netsky MG. Cerebral embolism by antifoam A in a bubble oxygenator system: An experimental and clinical study. *Surgery* 1960; 47: 784–794.
2. Cobe Cardiovascular, CML DUO Instructions for use, Catalogue No 050-226-000, 1997, Arvada, CO.
3. Edmunds LH. Cardiopulmonary bypass after 50 years. *N. Engl. J. Med.* 2004; 351: 1603–1606.

4. American Heart Association. Heart Disease and Stroke Statistics—2005 Update. Dallas, TX: American Heart Association, 2005. see: <http://www.americanheart.org/downloadable/heart/1105390918119HDSStats2005Update.pdf> (accessed May 2005).
5. Livesey SA and Lennox SC. Historical aspects. In: Kay PH, Ed. *Techniques in Extracorporeal Circulation*, 3rd ed. Oxford: Butterworth Heinemann, 1992, pp. 1–7.
6. Gibbon JH Jr. Artificial maintenance of circulation during experimental occlusion of pulmonary artery. *Arch. Surg.* 1937; 34: 1105–1131.
7. Gibbon JH Jr. Application of a mechanical heart and lung apparatus to cardiac surgery. *Minn. Med.* 1954; 37: 171–180.
8. Arunachalam VM and Shettigar UR. Bubble blood oxygenator—a design analysis. *Ann. Biomed. Eng.* 1981; 9: 75–87.
9. Clark LC, Gollan F, and Gupta VB. The oxygenation of blood by gas dispersion. *Science* 1950; 111: 85–87.
10. DeWall RA, Warden HE, Read RC, Gott VL, Ziegler NR, Varco RL, and Lillehei CW. A simple, expendable, artificial oxygenator for open heart surgery. *Surg. Clin. N. Am.* 1956; 36(4): 1025–1034.
11. Kirklin JW and Dushane JW. Intracardiac surgery with the aid of a mechanical pump oxygenator system (gibbon type): Report of eight cases. *P. Staff. M. Mayo. Clin.* 1955; 30: 201–206.
12. Wegner JA. Oxygenator anatomy and function. *J. Cardiothorac. Vasc. Anesth.* 1997; 11: 275–281.
13. Kolff WJ and Balzer R. The artificial coil lung. *Trans. Am. Soc. Artif. Intern. Organs* 1956; 1: 39–42.
14. Clowes GHA, Hopkins AL, and Neville WE. An artificial lung dependent upon diffusion of oxygen and carbon dioxide through plastic membranes. *J. Thorac. Surg.* 1956; 32: 630–637.
15. Bodell GR, Head JM, Head LR, Formolo AJ, and Head JR. A capillary membrane oxygenator. *J. Thorac. Cardiovasc. Surg.* 1963; 46(5): 639–650.
16. Dorson WJ, Baker E, and Hull H. A shell and tube oxygenator. *Trans. Am. Soc. Artif. Intern. Organs* 1968; 14: 236–241.
17. Marx TI, Baldwin BR, and Miller DR. Factors influencing oxygen uptake by blood in membrane oxygenators: Report of a study. *Ann. Surg.* 1962; 156(2): 204–213.
18. Bramson ML, Osborn JJ, Main FB, O'Brien MF, Wright JS, and Gerbode F. A new disposable membrane oxygenator with integral heat exchange. *J. Thorac. Cardiovasc. Surg.* 1965; 50(3): 391–400.
19. Weissman MH and Mockros LF. Oxygen and carbon dioxide transfer in membrane oxygenators. *Med. Biol. Eng.* 1969; 7(2): 169–184.
20. Voorhees ME and Brian BF III. Blood gas exchange devices. *Int. Anesthesiol. Clin.* 1996; 34: 29–45.
21. Elgas RJ and Gordon TM. Blood Oxygenator. US Patent 4,451,562, 1984.
22. Iatridis A, Chan T, and Thompson R. Experimental and clinical trials with the extracorporeal hollow fibre lung. *Proc. Am. Acad. Clin. Perf.* 1985; 6: 47–50.
23. Hanft S. *C-208R Key Medical Membrane Devices for the New Millennium*. Connecticut: Business Communications Company Inc., 2002: p. 58.
24. Baurmeister U. Multilayer Hollow Fibre Wound Body. US Patent 4,940,617, 1990.
25. Baurmeister U. Multilayer Hollow Fibre Wound Body, US Patent 5,143,312, 1992.
26. Gu YJ, Boonstra PW, Graaff R, Rijnsburger AA, Mungroop H, and van Oeveren W. Pressure drop, shear stress, and activation of leukocytes during cardiopulmonary bypass: A comparison between hollow fibre and flat sheet membrane oxygenators. *Artif. Organs* 2000; 24(1): 43–48.
27. Wickramasinghe SR, Semmens MJ, and Cussler EL. Mass-transfer in various hollow fibre geometries. *J. Membr. Sci.* 1992; 69(3): 235–250.
28. Wickramasinghe SR, Semmens MJ, and Cussler EL. Hollow-fibre modules made with hollow-fibre fabric. *J. Membr. Sci.* 1993; 84(1): 1–14.
29. Goerke AR, Leung J, and Wickramasinghe SR. Mass and momentum transfer in blood oxygenators. *Chem. Eng. Sci.* 2002; 57: 2035–2046.
30. Wickramasinghe SR, Garcia JD, and Han B. Mass and momentum transfer in hollow fibre blood oxygenators. *J. Membr. Sci.* 2002; 208: 247–256.
31. Wickramasinghe SR and Han B. Mass and momentum transfer in commercial blood oxygenators. *Desalination* 2002; 148: 227–233.
32. Wickramasinghe SR, Kahr CM, and Han B. Mass transfer in blood oxygenators using blood analogue fluids. *Biotechnol. Prog.* 2002; 18(4): 867–873.
33. Wickramasinghe SR, Han B, Garcia JD, and Specht R. Microporous membrane blood oxygenators. *AIChE J.* 2005; 51(2): 656–670.
34. Wickramasinghe SR and Han B. Designing microporous hollow fibre blood oxygenators. *Chem. Eng. Res. Des.* 2005; 83(A3): 256–267.
35. Catapano C, Papenfuss HD, Wodetzki A, and Baurmeister U. Mass and momentum transfer in extra-luminal flow (ELF) membrane blood oxygenation. *J. Membr. Sci.* 2001; 184: 123–135.
36. Cussler EL. *Diffusion: Mass Transfer in Fluid Systems*, 2nd ed. New York: Cambridge University Press, 1997.
37. Sirkar KK. Other new membrane processes. In: Ho WSW and Sirkar KK, Eds. *Membrane Handbook*. New York: van Nostrand Reinhold, 1992, pp. 885–899.
38. Zhang Q and Cussler EL. Microporous hollow fibres for gas-absorption: I. Mass-transfer in the liquid. *J. Membr. Sci.* 1985; 23: 321–332.
39. Zhang Q and Cussler EL. Microporous hollow fibres for gas-absorption: II. Mass-transfer across the membrane. *J. Membr. Sci.* 1985; 23: 333–345.
40. Yang MC and Cussler EL. Designing hollow-fibre contactors. *AIChE J.* 1986; 32: 1910–1916.
41. Shah RK and London AL. Thermal boundary conditions and some solutions for laminar duct flow forced convection. *J. Heat. Transf.* 1974; 96(C2): 159–165.
42. Darby R. *Chemical Engineering Fluid Mechanics*, New York: Marcel Dekker, 1996.
43. Rajasubramanian S, Nelson KD, Shastri P, Constantinescu A, Kulkarni P, Jessen ME, and Eberhart RC. Design of an oxygenator with enhanced gas transfer efficiency. *ASAIO J.* 1997; 43: M710–M714.

44. Vaslef SN, Mockros LF, Anderson RW, and Leonard RJ. Use of a mathematical model to predict oxygen transfer rates in hollow fibre membrane oxygenators. *ASAIO J.* 1994; 40(4): 990–996.
45. Thurston GB. Rheological parameters for the viscosity, viscoelasticity and thixotropy of blood. *Biorheology* 1979; 16: 149–162.
46. Chien S, Usami S, Dellenback RJ, and Gregersen MI. Shear-dependent deformation of erythrocytes in rheology of human blood. *Am. J. Physiol.* 1970; 219: 136–142.
47. Chien S, Usami S, Taylor HM, Lundberg JL, and Gregersen MI. Effects of hematocrit and plasma proteins on human blood rheology at low shear rates. *J. Appl. Physiol.* 1966; 21: 81–87.
48. Brookshier KA and Tarbell JM. Evaluation of transparent blood analogue fluids: Aqueous xanthan gum glycerin. *Biorheology* 1993; 30: 107–116.
49. Mann DE and Tarbell JM. Flow of non-Newtonian blood analogue fluids in rigid curved and straight artery models. *Biorheology* 1990; 27: 711–733.
50. Huang CJ and Huo CH. Mathematical models for mass transfer accompanied by reversible chemical reaction. *AICHE J.* 1965; 11(5): 901–910.
51. Ranney HM and Sharma V. Structure and function of hemoglobin. In: Beutler E, Lichtman MA, Coller BS, Kipps TJ, and Seligsohn U, Eds. *Williams Hematology*, 6th ed. New York: McGraw Hill, 2001, pp. 345–353.
52. Bird RB, Stewart WE, and Lightfoot EN. *Transport Phenomena*, 2nd ed. New York: John Wiley & Sons, 2001.
53. Olander DR. Simultaneous mass transfer and equilibrium chemical reaction. *AICHE J.* 1960; 6: 233–239.
54. Matsuda N, Nakamura M, Sakai K, Kuwana K, and Tahara K. Theoretical and experimental evaluation for blood pressure drop and oxygen transfer rate in outside blood flow membrane oxygenator. *J. Chem. Eng. Jpn.* 1999; 32(6): 752–759.
55. Shimizu S and Yoshida F. New method for evaluation and prediction of oxygen transfer rates in membrane oxygenators. *Jpn. J. Artif. Organs.* 1981; 10: 179–182.
56. Yoshida F. Prediction of oxygen transfer performance of blood oxygenators. *Artif. Organs Today* 1993; 2(4): 237–252.
57. Hill AV. The possible effects of the aggregation of the molecules of hemoglobin on its dissociation curves. *J. Physiol. London* 1910; 40: 4–7.
58. Goldstick TK. Oxygen transport. In: Brown JHU and Gann DS, Eds. *Engineering Principles in Physiology*. Vol. 2. New York: Academic Press, 1973, pp. 257–282.
59. Vaslef SN. *Analysis and Design of an Intravascular Lung Assist Device*. PhD dissertation, Northwestern University, Evanston, IL, 1990.
60. Antonini E and Brunori M. Hemoglobin and methemoglobin. In: Surgenor DM, Ed. *The Red Blood Cell*. Vol. II, 2nd ed. New York: Academic Press, 1975, p. 753.
61. Matsuda N and Sakai K. Blood flow and oxygen transfer rate of an outside blood flow membrane oxygenator. *J. Membr. Sci.* 2000; 170: 153–158.
62. Baker DA, Holte JE, and Patankar SV. Computationally two-dimensional finite-difference model for hollow-fibre blood-gas exchange devices. *Med. Biol. Eng. Comput.* 1991; 29: 482–488.
63. Gage KL, Gartner MJ, Burgreen GW, and Wagner WR. Predicting membrane oxygenator pressure drop using computational fluid dynamics. *Artif. Organs* 2002; 26(7): 600–607.
64. Funakubo A, Taga I, McGillicuddy JW, Fukui Y, Hirschl RB, and Bartlett RH. Flow vectorial analysis in an artificial implantable lung. *ASAIO J.* 2003; 49: 383–387.
65. Goodin MS, Thor EJ, and Haworth WS. Use of computational fluid dynamics in the design of the Avecor affinity oxygenator. *Perfusion* 1994; 9: 217–222.
66. Bludszuweit C. Evaluation and optimization of artificial organs by computational fluid dynamics. *Proceedings of the 1997 ASME Fluids Engineering Division Summer Meeting*, Vancouver, British Columbia, Canada, June 22–26, 1997.
67. Gartner MJ, Wilhelm CR, Gage KL, Fabrizio MC, and Wagner WR. Modeling flow effects on thrombotic deposition in a membrane oxygenator. *Artif. Organs* 2000; 24: 29–36.
68. Krantz WB, Bilodeau RR, Voorhees ME, and Elgas RJ. Use of axial membrane vibrations to enhance mass transfer in a hollow tube oxygenator. *J. Membr. Sci.* 1997; 124: 283–299.
69. Lund LW, Hattler BG, and Federspiel WJ. Is condensation the cause of plasma leakage in microporous hollow fibre membrane oxygenators? *J. Membr. Sci.* 1998; 147: 87–93.
70. Musch G, Verweij M, Bombino M, Banfi G, Fumagalli R, and Pesenti A. Small pore size microporous membrane oxygenator reduces plasma leakage during prolonged extracorporeal circulation: A case report. *Int. J. Artif. Organs* 1996; 19(3): 177–180.



---

# 24 Transporting and Separating Molecules Using Tailored Nanotube Membranes

*Punit Kohli and Charles R. Martin*

## CONTENTS

24.1	Introduction .....	693
24.2	Nomenclature of Nanoparticles.....	694
24.3	Template Synthesis of Nanotubes and Some Recent Advances .....	694
24.4	Silica Nanotubes.....	695
24.4.1	Attaching Different Functional Groups to the Inside vs. Outside Surfaces .....	695
24.4.2	Nanotubes for Chemical and Bioextraction and Biocatalysis: Demonstration of Potential Drug Detoxification Using Nanotubes .....	696
24.5	Nanotube Membranes for Bioseparations.....	698
24.5.1	Antibody-Functionalized Nanotube Membranes for Selective Enantiomeric Separations.....	698
24.5.2	Functionalized Nanotube Membranes with Hairpin-DNA Transporter with Single-Base Mismatch Selectivity.....	699
24.5.3	Enantioseparations of Amino Acids Using Apoenzymes Immobilized in a Porous Polymeric Membrane .....	702
24.6	Conical Nanotubes: Mimicking Artificial Ion Channel.....	704
24.7	Conclusions .....	706
	Acknowledgment .....	707
	References.....	707

## 24.1 INTRODUCTION

The ability to regulate transport across cellular boundaries is essential to the cell's existence as an open system [1]. There is a steady traffic of ions, molecules, polymers, and other species across the plasma membrane. Consider the chemical exchanges between a human muscle cell and the extracellular fluid that surrounds it. For example, sugars, amino acids, and other nutrients enter the cell, and waste products of metabolism leave the cell. The cell takes in oxygen for cellular respiration and expels carbon dioxide. It also regulates its concentrations of inorganic ions, such as  $\text{Na}^+$ ,  $\text{K}^+$ ,  $\text{Ca}^{2+}$ , and  $\text{Cl}^-$ , by shuttling them one way or the other across the plasma membrane. Mother Nature has created natural channels that are highly selective, that is, they allow certain molecules and ions to pass more easily than others (or they reject them). For example, there are highly specialized potassium protein channels that allow potassium cations to pass through with high selectivity than other ions. Other examples include water,  $\text{Na}^+$ ,  $\text{Ca}^{2+}$ ,  $\text{Cl}^-$ , glucose protein channels, nuclear pore, and complexes. The highly selective transportation of molecules and ions is controlled by molecular recognition between transporting species and protein channels present in the cell membranes.

Understanding and mimicking of the cellular transport processes are both challenging and rewarding from scientific and technological point of view. For example in certain inherited diseases (such as cystinuria), specific transport systems are either defective or missing [1]. Cystinuria is a human disease characterized by the absence of a transport system that carries cystine and other amino acids into kidney cells. Kidney cells normally reabsorb these amino acids from the urine and return them to the blood, but a person inflicted with cystinuria develops painful stones from amino acids that accumulate and crystallize in the kidneys. Similarly, there are many technological applications of these transport processes, e.g., bioseparations, bioextractions, and synthetic nano-bioreactors.

We have synthesized highly selective template-synthesized abiotic nanotube membranes that can be used as model systems for mimicking natural ion and protein channels. These nanotubes have diameters of the same order (1–100 nm) as those found

in the natural protein channels. We have designed the nanotube membranes to selectively recognize and transport small molecules and biopolymers by modifying the inner surface of nanotubes with molecular-recognition molecules. These systems are very useful as model systems for better understanding of transport processes of molecules and biopolymers through highly constrained nanotubes. These nanotube membranes have also found many applications in the areas of chemical- and bio-separations, biocatalysis, and drug detoxification.

Here, we will report on the design, synthesis, characterization, and applications of template-synthesized nanotube membranes. Then, we will briefly review the synthesis of the template-synthesized nanotube membranes. Some details of differential-surface chemistry on nanotubes, and nanotubes for bioextraction and biocatalysis are presented. We discuss in detail the drug detoxification using functionalized nanotubes [2], and epoenzyme-, enzyme- and antibody-immobilized nanotubes for enantiomeric separations, biocatalysis, and bioextractions [3–5]. We also describe our recent results on DNA-functionalized nanotube membranes with single-nucleotide mismatch selectivity [6], and the fabrication of artificial ion-channel using single-conical nanotube membrane [7].

## 24.2 NOMENCLATURE OF NANOPARTICLES

In the literature, the tubular structures of interest to this review are called by various names including microtubules, microtubes, nanotubules, and nanotubes. This nomenclature can be simplified by noting that in this context, there is no difference between a tube and tubule; in this review we use only the name tube. Nano vs. micro is a more difficult issue because there is no universally accepted dimension scale above which a particle is micro, and below which it is nano. In our research group we have agreed that if a tube has at least one dimension that is 100 nm or less, it is called a nanotube.

## 24.3 TEMPLATE SYNTHESIS OF NANOTUBES AND SOME RECENT ADVANCES

Spherical nanoparticles are typically used in such applications, but this only reflects the fact that spheres are easier to make than nanoparticles having other shapes. Micro- and nanotubes—structures that resemble tiny drinking straws (Figure 24.1)—are alternatives to spherical nanoparticles. Examples include organosilicon polymer nanotubes [8], self-assembling lipid microtubes [9–13], fullerene carbon nanotubes [14–17], template-synthesized nanotubes [4–6,18–22], and peptide nanotubes [23–26]. Nanotubes offer some interesting advantages relative to spherical nanoparticles for biotechnological applications. For example, nanotubes have large inner volumes (relative to the dimensions of the tube), which can be filled with any desired chemical or biochemical species ranging in size from nucleic acids and proteins to small molecules [4–6]. In addition, nanotubes have distinct inner and outer surfaces, which can be differentially chemically or biochemically functionalized [4]. This creates the possibility, for example, of loading the inside of a nanotube with a particular biochemical payload but imparting chemical features to the outer surface that render it biocompatible. Finally, nanotubes have open mouths, which make the inner surface accessible and incorporation of species within the tubes particularly easy.

The template method is a general approach for preparing nanomaterials that entail synthesis or deposition of the desired material within the cylindrical and monodisperse pores of a nanopore membrane or other solid [20–22]. Cylindrical nanostructures with monodisperse diameters and lengths are obtained, and depending on the membrane and synthetic method used, these may be solid nanowires or hollow nanotubes. This method has been used to prepare nanowires and nanotubes composed

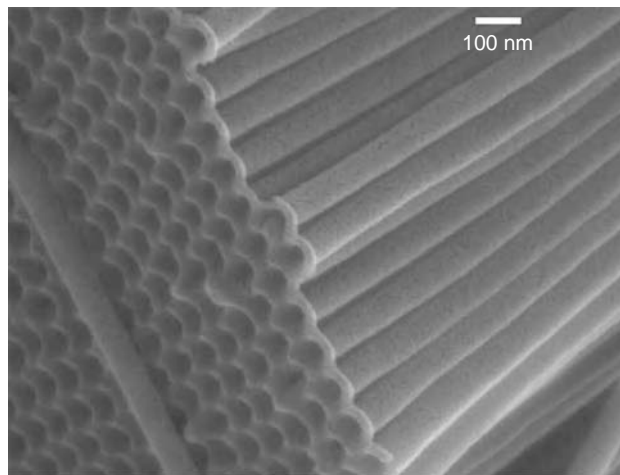


**FIGURE 24.1** Scanning electron micrograph of an array of template-synthesized carbon nanotubes. These nanotubes are composed of disordered graphitic carbon. (From Miller, S.A., Young, V.Y., and Martin, C.R., *J. Am. Chem. Soc.*, 123, 12335, 2001. With permission.)

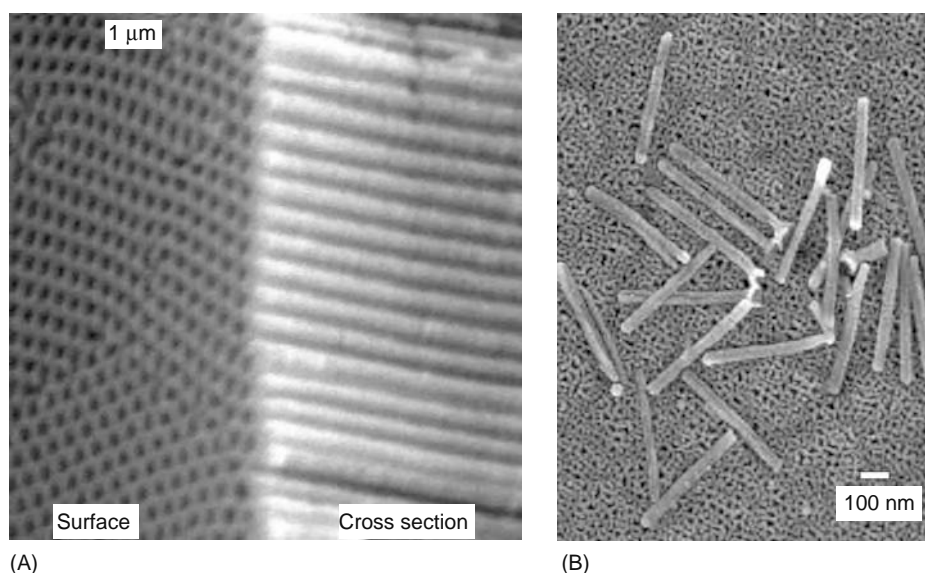


**FIGURE 24.2** Scanning electron micrographs. (A) The surface and cross section of a typical nanopore alumina template membrane prepared in the authors' lab. Pores with monodisperse diameters that run like tunnels through the thickness of the membrane are obtained. (B) Silica nanotubes prepared by solgel template synthesis within the pores of a template like that shown in (A). After solgel synthesis of the nanotubes, the template was dissolved and the nanotubes were collected by filtration. (From Lee, S.B., Mitchell, D.T., Trofin, L., Li, N., Nevanen, T.K., Söderlund, H., and Martin, C.R., *Science*, 296, 2198, 2002. With permission.)

of many different types of materials including metals, polymers, semiconductors, and carbons [20–22]. In addition, the template method can be used to prepare composite nanostructures, both concentric tubular composites [20,27] and segmented composite nanowires [28,29].

How one makes nanotubes within the pores of a template membrane can be illustrated by the carbon nanotubes shown in Figure 24.1 [30]. An alumina template (Figure 24.2A) was heated to 670°C and ethylene gas was passed through the membrane. This causes the ethylene to decompose on the pore walls to yield graphitic carbon nanotubes within the pores. The alumina template membrane can then be dissolved away and the carbon nanotubes are collected by filtration. These tubes have monodisperse outside diameters determined by the diameter of the pores in the template. The inside diameter is determined by the carbon deposition time. Other synthetic methods we have used include in-pore polymerization to make polymeric nanotubes, electroless deposition to make DNA nanotubes, metal nanotubes, and solgel chemistry to make nanotubes comprised of silica and other inorganic materials [20–22,27,30–34]. Templated silica nanotubes (*vide infra*) [4,5] are shown in Figure 24.2B. These nanotubes are of the same length, which is determined by the thickness of the template membrane.

## 24.4 SILICA NANOTUBES

We have used these silica nanotubes as test vehicles to illustrate the power of the template method for preparing nanotubes for biomedical and biotechnological applications [4,5]. Silica nanotubes are ideal for such proof-of-concept experiments because they are easy to make, readily suspendable in aqueous solution, and because silica surfaces can be derivatized with an enormous variety of different chemical functional groups using simple silane chemistry with commercially available reagents [4,5].

### 24.4.1 ATTACHING DIFFERENT FUNCTIONAL GROUPS TO THE INSIDE VS. OUTSIDE SURFACES [4]

As noted above, one of the most important attributes of a nanotube is that it has distinct inner and outer surfaces that can be differentially chemical and biochemically functionalized. The template method provides a particularly easy route to accomplish this differential functionalization. The details of nanotube modifications using differential silane chemistry on nanotubes are available elsewhere [4]. In the following paragraphs, we briefly describe the results of differential-functionalized nanotubes and their applications in highly selective chemical and biochemical extractions [2,4].

To prove this concept, a set of nanotubes were prepared with the green fluorescent silane *N*-(triethoxysilylpropyl)dansylamide attached to their inner surfaces, and the hydrophobic octadecyl silane ( $C_{18}$ ) to their outer surfaces. These nanotubes were added to a vial containing water and the immiscible organic solvent cyclohexane, which were mixed and allowed to separate. Because these nanotubes are hydrophobic on their outer surfaces, they partition into the (upper) cyclohexane phase (Figure 24.3B). This may be in contrast to nanotubes that were labeled on their inner surfaces with the blue fluorescent silane triethoxysilylpropylquinineurethan, but were not labeled with any silane on their outer surfaces. When the same experiment is done on these

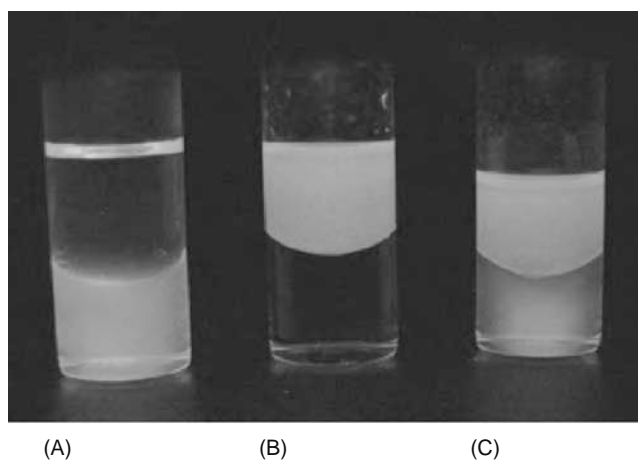


**FIGURE 24.3** (See color insert following page 588.) Photographs of vials containing nanotubes modified with two different fluorophores in two different solvent medium. (A) Cyclohexane (upper) and water (lower) under UV light excitation after addition of 10 mg of nanotubes with dansylamide on inner and  $C_{18}$  on outer surfaces, (B) quinineurethan on inner and no silane on outer surfaces, (C) 10 mg of both (A) and (B) nanotubes. 200 nm diameter nanotubes were used. (From Mitchell, D.T., Lee, S.B., Trofin, L., Li, N., Nevanen, T.K., Söderlund, H., and Martin, C.R., *J. Am. Chem. Soc.*, 124, 11864, 2002. With permission.)

nanotubes, the quinineurethan fluorescence is seen only from the aqueous phase (Figure 24.3A). When both sets of nanotubes are added to the solvent mixture in the same vial, the tubes with the  $C_{18}$  outer surface chemistry go to the cyclohexane and the tubes with the silica outer surface chemistry go to the aqueous phase (Figure 24.3C).

#### 24.4.2 NANOTUBES FOR CHEMICAL AND BIOEXTRACTION AND BIOCATALYSIS: DEMONSTRATION OF POTENTIAL DRUG DETOXIFICATION USING NANOTUBES [2,4]

One application for such differentially functionalized nanotubes is as smart nanophase extractors to remove specific molecules from solution. Nanotubes with hydrophilic chemistry on their outer surfaces and hydrophobic chemistry on their inner surfaces are ideal for extracting lipophilic molecules from an aqueous solution. The hydrophobic molecule 7,8-benzoquinoline (BQ), which has an octanol/water partition coefficient of 10 [3,8] was used as a model compound for such nanophase solvent extraction experiments. Figure 24.4A shows the UV–Vis spectrum of control solution containing  $10^{-5}$  M aqueous BQ. A 5 mg of the silica-outer/ $C_{18}$ -inner nanotubes were suspended into 5 mL of  $1.0 \times 10^{-5}$  M aqueous BQ. The suspension was stirred for

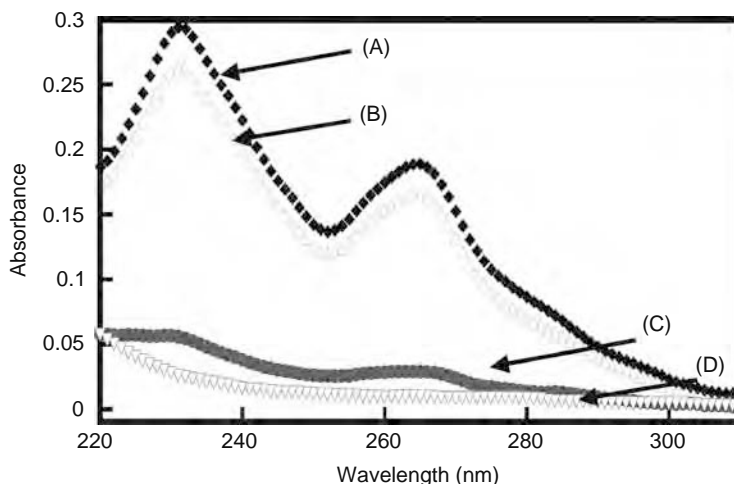


**FIGURE 24.4** UV–Vis spectra showing the extraction of 7,8-benzoquinoline (BQ) from the aqueous solution by nanotubes with  $C_{18}$  silane on their inner surfaces. (A) UV–Vis spectrum of  $10^{-5}$  M aqueous BQ and (B) after extraction with  $SiO_2$  tubes (control experiments). (C) After first extraction with  $C_{18}$   $SiO_2$  tubes. (D) After second extraction with  $C_{18}$   $SiO_2$  tubes. (From Lee, S.B., Mitchell, D.T., Trofin, L., Nevanen, T.K., Soderlund, H., and Martin, C.R. Template-synthesized bionanotubes for separations and biocatalysis. *Carrier-Based Drug Delivery ACS Symposium 879*, ACS, Washington, DC, 2004, pp. 88–117. With permission.)

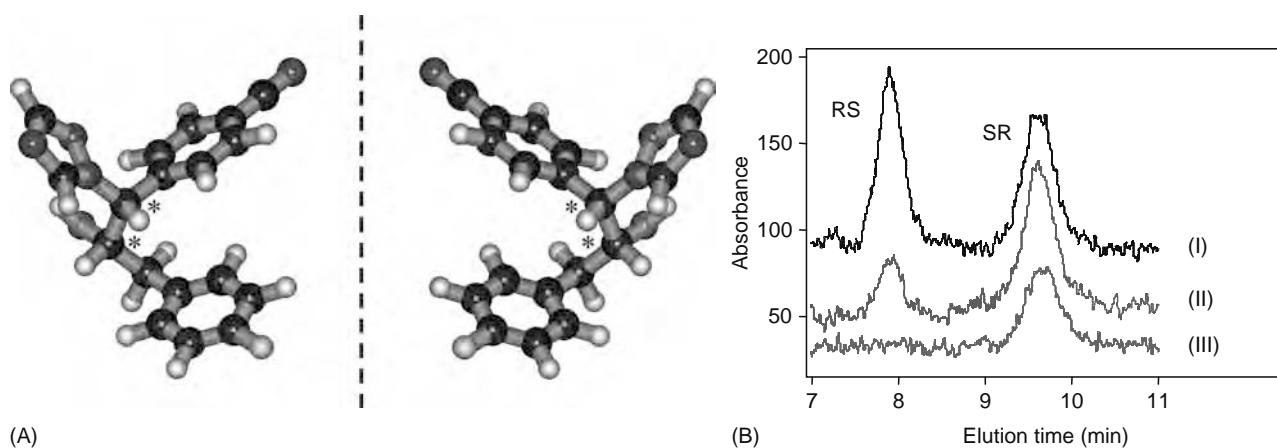


**FIGURE 24.5** (See color insert following page 588.) Enantioseparations. (A) 3-Dimensional structures of the RS enantiomer (left) and the SR enantiomer (right) of the drug FTB. The black, white, blue, red, and yellow balls are carbon, hydrogen, nitrogen, oxygen, and fluorine, respectively, and \* denotes the chiral centers. The geometry optimization was done by ab initio calculation with minimal basis set in HyperChem 6.03. The drug is in clinical trials by Hormos Medical Corp., Turku, Finland. (From Lee, S.B., Mitchell, D.T., Trofin, L., Li, N., Nevanen, T.K., Söderlund, H., and Martin, C.R., *Science*, 296, 2198, 2002. With permission.) (B) Chiral HPLC chromatograms for racemic mixtures of FTB before (I) and after (II, III) extraction with 18 mg/mL of 200-nm Fab-containing nanotubes. Solutions were 5% dimethylsulfoxide in sodium phosphate buffer, pH 8.5. (From Mitchell, D.T., Lee, S.B., Trofin, L., Li, N., Nevanen, T.K., Söderlund, H., and Martin, C.R., *J. Am. Chem. Soc.*, 124, 11864, 2002. With permission.)

5 min and then filtered to remove the nanotubes. UV spectroscopy showed that 82% of the BQ was removed from the solution (Figure 24.4C). When a second 5 mg batch of these nanotubes was added to the filtrate, more than 90% of the original amount of BQ was removed from the solution (Figure 24.4D). Control nanotubes that did not contain the hydrophobic C<sub>18</sub> inner surface chemistry extracted less than 10% of the BQ (Figure 24.4B). This proof of experiment clearly shows that nanotubes are possibly useful in applications involving drug detoxification and other chemical and biochemical extractions.

In principle, nanotubes with the C<sub>18</sub> inside extract any lipophilic molecule. This ability to sequester lipophilic molecules can be viewed as a generic type of extraction selectivity, which might be useful in some applications. However, nanotubes that have molecular-recognition capability and extract only one particular molecule from solution might also be useful. We have shown that antibody-functionalized nanotubes can provide the ultimate in extraction selectivity—the extraction of one enantiomer of a chiral drug molecule.

In collaboration with professor Hans Soderlund of VTT Biotechnology in Finland, we have been investigating an antibody that selectively binds one enantiomer of the drug FTB (Figure 24.5A), an inhibitor of aromatase enzyme activity [35]. This molecule has two chiral centers and thus four stereoisomers, namely, RR, SS, SR, and RS. Professor Soderlund supplied us with the F<sub>ab</sub> fragment [35] of an antibody that selectively binds the RS relative to the SR enantiomer. The antibody was produced against the drug 4-[3-(4-fluorophenyl)-2-hydroxy-1-[1,2,4]triazol-1-yl-propyl]-benzimidazole (FTB, Figure 24.5A). The selectively used antibody binds the RS enantiomer, and F<sub>ab</sub> fragments of this antibody were immobilized to both the inner and outer surfaces of the silica nanotubes. This was accomplished by dissolving the template membrane, collecting the nanotubes, and then dispersing them into a solution of the aldehyde-terminated silane trimethoxysilylbutanal. The nanotubes were then dispersed into a solution of the F<sub>ab</sub> fragments, which resulted in attachment of the F<sub>ab</sub> to the nanotubes via Schiff base reaction between free amino groups on the protein and the surface-bound aldehyde.

The F<sub>ab</sub>-functionalized nanotubes were added to racemic mixtures of the SR and RS enantiomers of FTB. The tubes were then collected by filtration and the filtrate was assayed for the presence of the two enantiomers using a chiral HPLC method (Figure 24.5B). Chromatogram I was obtained from a solution that was 20 μM in both enantiomers, and chromatogram II was obtained for the same solution after exposure to the F<sub>ab</sub>-functionalized nanotubes; 75% of the RS enantiomer and none of the SR enantiomer was removed by the nanotubes. When the concentration of the racemic mixture was dropped to 10 μM, all the RS enantiomers were removed (chromatogram III). Nanotubes containing no F<sub>ab</sub> did not extract measurable quantities of either enantiomer from the 20 μM solution.

We have also developed a chemistry that allows us to attach the F<sub>ab</sub> to only the inner surfaces of the nanotubes. While still within the pores of the template membrane, the inner surfaces were treated with 3-aminopropyltrimethoxysilane. The template membrane was then dissolved and the amino sites on the inner surfaces were coupled to free amino groups on the F<sub>ab</sub> fragment using the well-known glutaraldehyde coupling reaction [4]. When 18 mg of these interior-only F<sub>ab</sub>-modified nanotubes were incubated with 1 mL of a 10 μM racemic mixture of the drug, 80% of the RS (and none of the SR) enantiomer was extracted.

This corresponds to 0.44 nmol RS enantiomer per milligram tubes, whereas almost double that amount, 0.80 nmol/mg, was extracted by the nanotubes with  $F_{ab}$  on both their inner and outer surfaces.

Another example concerns the immobilization of a biocatalyst—the enzyme glucose oxidase (GOD)—to the silica nanotubes [4]. GOD was immobilized, on both the inside and outside surfaces, via the aldehyde silane route. These GOD-nanotubes (60 nm diameter) were dispersed into a solution containing 90 mM glucose and also the components of the standard dianisidine-based assay for GOD activity. A GOD activity of  $0.5 \pm 0.2$  units per milligram of nanotubes was obtained. These studies also showed that protein immobilized via the Schiff base route is not leached from the nanotubes, where GOD activity ceased when the nanotubes were filtered from the solution.

## 24.5 NANOTUBE MEMBRANES FOR BIOSEPARATIONS [3,5,6]

In all the examples cited above, the template membrane was dissolved away and the liberated nanotubes were collected by filtration. The nanotubes may also be left embedded within the pores of the template to yield a freestanding nanotube-containing membrane. We have shown that the nanotubes can act as conduits for highly selective transport of molecules and ions between solutions present on either side of the membrane [5,6,18,19]. For example, membranes containing gold nanotubes with inside diameters of molecular dimensions ( $<1$  nm) clearly separate small molecules based on the molecular size [19]. Gold nanotubes with larger inside diameters (20–45 nm) can be used to separate proteins, and, here again, rendering the nanotubes biocompatible is essential to prevent protein adsorption [36]. Generic chemical transport selectivity (lipophilic vs. hydrophilic) can also be imparted to these gold nanotube membranes [37]. We now present in details of bio-tailored nanotube membranes for separation of enantiomeric amino acids [3] and drug molecules [5], and nucleic acids [6].

### 24.5.1 ANTIBODY-FUNCTIONALIZED NANOTUBE MEMBRANES FOR SELECTIVE ENANTIOMERIC SEPARATIONS [5]

Chiral recognition is a fundamental and very important phenomenon that is observed in all biological systems ranging from single-cell organisms to most complex animals [38]. In fact, specificity and efficacy of many biological reactions depend upon chiral interactions because many biologically molecules and polymers are chiral; they interact more strongly with one enantiomer than another enantiomer. The biological activity of many enzymes depends upon the enantiomeric form of the interacting species, not simply chemical structure. Federal Drug Administration (FDA) requires drug manufacturers to evaluate the effects of individual enantiomers and to verify the enantiomeric purity of chiral drugs that are produced. FDA also mandates that the toxicity and pharmaceutical properties must be established independently for both enantiomers, even if the drug is to be marketed as a single enantiomer.

Enantiomer separation is a challenging problem because two enantiomers have the same physical and chemical properties; the traditional methods of separation (for example, chromatography) generally have relatively low enantiomeric separation selectivity coefficients. We have developed highly selective membrane-based separation methods for enantiomer drug molecules [3,5]. We have shown that membranes containing the silica nanotubes and the enantioselective FTB antibody  $F_{ab}$  fragment (Figure 24.5A) discussed above can be used to make membranes for chiral separations [5]. In this case, the nanotube membrane separates a feed half-cell containing a racemic mixture of the RS and SR enantiomers of FTB and a permeate half-cell that initially contains only buffer solution. The time course of permeation of the two enantiomers across the membrane was determined by periodically assaying the permeate solution. Results for a membrane containing  $\sim 15$  nm diameter silica nanotubes are shown in Figure 24.6 as plots of moles enantiomer transported vs. permeation time. We see that the flux of

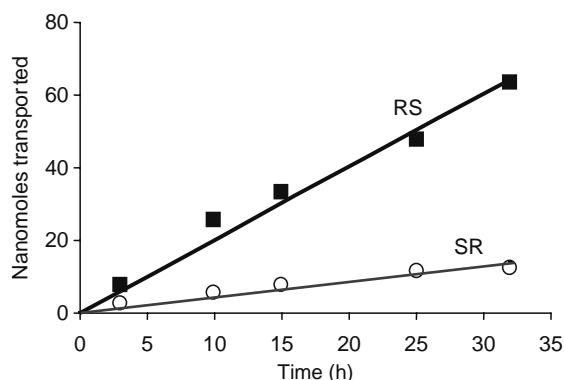


**FIGURE 24.6** Enantioseparations using antibody-immobilized membranes. Plots of moles of each enantiomer transported vs. time for a silica nanotube membrane containing the enantioselective antibody  $F_{ab}$  fragment. The inside diameter of the nanotubes was  $\sim 15$  nm. (From Kohli, P., Harrell, C.C., Cao, Z., Gasparac, R., Tan, W., and Martin, C.R., *Science*, 305, 984, 2004. With permission.)

the RS enantiomer, the one bound by the antibody, is five times higher than the flux of the SR enantiomer. Because in principle, antibodies can be obtained that selectively bind to any desired molecule or enantiomer; this concept might provide a general approach for obtaining selectively permeable membranes for a host of enantio- and bioseparations.

Because it is the RS enantiomer that specifically binds to the immobilized anti-RS, these data suggest that this  $F_{ab}$  fragment facilitating the transport of RS enantiomer. Further evidence that it is the  $F_{ab}$  fragment that is facilitating the transport of RS is obtained from feed concentration of drug vs. flux curve, which showed Langmuirian-type curve.

We have not conducted detailed experiments to elucidate the effect of DMSO concentration on the molecular interactions of binding of  $F_{ab}$  to RS enantiomer drug molecule in PBS. The previous studies, however, have shown that the use of DMSO decreases the binding interactions between drug molecule and  $F_{ab}$ -immobilized silica in chromatography experiments [35]. Qualitatively, our studies agree with these results. We believe that there is an optimum binding affinity between drug and  $F_{ab}$  molecules that is expected to give highest transport selectivity coefficient; and that the addition of DMSO to the solution containing antigen (FTB drug) decreases the binding constant between FTB and  $F_{ab}$  molecules immobilized on inner walls of silica nanotube membranes. In our studies, we have found that there is an optimum concentration of DMSO (~15%) that maximizes the value of selectivity coefficient [5].

We now briefly discuss the possible molecular interactions between  $F_{ab}$  fragment and enantiomeric drug molecules. Our collaborators have produced  $F_{ab}$  fragments that bind only to RS enantiomer of FTB drug molecules, but they do not bind strongly to SR enantiomer [35]. The binding interactions between antibody and antigen depend upon many factors including cumulative interactions between the antibody and antigen as well as entropic factors involved in their binding process. In general, numerous weak electrostatic, hydrogen bonding, van der Waals forces, and hydrophobic interactions give strong and specific binding between antibody and antigen [39]. Although we have not conducted detail studies to elucidate the interaction between  $F_{ab}$  and drug molecules at molecular level, we believe that  $F_{ab}$ -fragments attached to silica nanotubes bind to RS enantiomers through various molecular interactions including hydrogen bonding, van der Waals, and hydrophobic interactions.

Another important factor that is important to consider is the orientation of antibody immobilized on the surface. This factor is very important to maximize the antibody availability for antigen binding because the binding between antigen and antibody requires right orientation of antibody for antigen binding. It is well known that histidine interacts strongly with copper and nickel ions. Therefore, one of the antibody immobilization methods to provide efficient, stable, and right orientation on surfaces for antigen-antibody reaction utilizes histidine-tagged antibodies onto copper- and nickel-containing surfaces [40]. The histidine modification of antibodies can be accomplished using conventional covalent bonding of antibody with a reactive histidine or this can also be accomplished using molecular biology (cloning) techniques. The modification of antibody with histidine should only be carried out only at  $F_c$  fragment of the antibody but not on the  $F_{ab}$  fragment. In principle, the immobilization of histidine tagged at  $F_c$  of antibody should provide surfaces with favorable antibody orientation for antigen-antibody reaction, where antibody-binding fragments ( $F_{ab}$ ) are away from surfaces, and antigens can approach  $F_{ab}$  without significant steric hindrance.

#### 24.5.2 FUNCTIONALIZED NANOTUBE MEMBRANES WITH HAIRPIN-DNA TRANSPORTER WITH SINGLE-BASE MISMATCH SELECTIVITY [6]

There appears to be no previous examples of either biological or synthetic membranes, where nucleic acid hybridization is used as the molecular-recognition event to facilitate DNA/RNA transport through the membrane [41,42]. If such membranes could be developed, they might prove useful for DNA separations and sensors needed, for example, in genomic research.

We now describe synthetic membranes in which the molecular-recognition chemistry used to accomplish selective-permeation is DNA hybridization. These membranes contain template-synthesized gold nanotubes with inside diameter of 12 nm, and a transporter DNA-hairpin molecule is attached to the inside walls of these nanotubes. These DNA-functionalized nanotube membranes selectively recognize and transport the DNA strand that is complementary to the transporter strand relative to DNA strands that are not complementary to the transporter. Under optimal conditions, single-base mismatch transport selectivity is obtained.

The gold nanotube membranes were prepared via the template synthesis [21,22] method by electroless deposition of gold along the pore walls of a polycarbonate template membrane [19,43]. The template was a commercially available filter (Osmonics), 6  $\mu\text{m}$  thick, with cylindrical 30 nm diameter pores and  $6 \times 10^8$  pores per square centimeters of membrane surface area.

The hairpin-DNA transporter (Table 24.1) was 30 bases long (30-mer) and contained a thiol substituent at the 5' end that allowed it to be covalently attached to the inside walls of the Au nanotubes [6]. The first six bases at each end of this molecule are complimentary to each other and form the stem of the hairpin, and the middle 18 bases form the loop (Table 24.1). The permeating DNA molecules were 18-mers that are either perfectly complementary to the bases in the loop, or contain one or more mismatches with the loop (Table 24.1). A second thiol-terminated DNA transporter was investigated (Table 24.1). This DNA transporter was also a 30-mer, and the 18 bases in the middle of the strand were identical to the 18 bases in the loop of the hairpin-DNA transporter. However, this second DNA transporter does not have the complementary stem-forming bases on either end and thus cannot form a hairpin. This linear-DNA transporter was used to test the hypothesis that the hairpin-DNA

**TABLE 24.1**  
**DNA Molecules Used**

Transporter DNAs

Hairpin: 6'HS-(CH<sub>2</sub>)<sub>6</sub>-CGCGAG AAGTTACATGACCTGTAG CTCGCG3'

Linear: 5'HS-(CH<sub>2</sub>)<sub>5</sub>-CGCGAGAAGTTACATGACCTGTAG ACGATC3'

Permeating DNAs

Perfect complement (PC): 3'TTCAATGTACTGGACATC5'

Single base mismatch (3'end): 3'CTCAATGTACTGGACATC5'

Single base mismatch (middle): 3'TTCAATGTAGTGGACATC5'

7-mismatch: 3'AAGTTACATGACCTGTAG5'

FAM-labeled perfect complement: 3'TTCAATGTACTGGACATC-(CH<sub>2</sub>)<sub>6</sub>-FAM 5'

Cy5-labeled single-base mismatch: 3'CTCAATGTACTGGACATC-(CH<sub>2</sub>)<sub>6</sub>-Cy5 5'

*Source:* From Harrell, C.C., Kohli, P., Siwy, Z., and Martin, C.R., *J. Am. Chem. Soc.*, 126, 15646, 2004.

*Note:* For transporter DNAs, the 18 bases that bind to the permeating DNAs are in bold. For permeating DNAs, the mismatched bases are in underlined. FAM is a fluorescein derivative (Applied Biosystems), and Cy5 is a cyanine dye (Amersham Biosciences).

provides better transport selectivity because of its enhanced ability to discriminate the perfect complement-permeating DNA from the permeating DNAs that contain mismatches.

The transport experiments were done in a U-tube permeation cell [43] where the Au nanotube membrane separates the feed half-cell containing one of the permeating DNA molecules (Table 24.1) dissolved in pH 7.2 phosphate buffer (ionic strength ~0.2 M), from the permeate half-cell that was initially only buffer. The rate of transport (flux) of the permeating DNA molecule from the feed half-cell through the Au nanotube membrane and into the permeate half-cell was determined by periodically measuring the ultraviolet absorbance of the permeate half-cell solution, at 260 nm, that arises from the permeating DNA molecule.

Transport plots (Figures 24.7A and 24.8) show the number of nanomoles of the permeating DNA transported through the nanotube membrane vs. permeation time. When the hairpin-DNA is not attached, a straight-line transport plot is obtained for the perfect-complement DNA (PC-DNA, Figure 24.7A), and the slope of this line provides the flux of PC-DNA across the membrane (Table 24.2). The analogous transport plot for the membrane containing the hairpin-DNA transporter is not linear but instead can be approximated by two straight-line segments—a lower-slope segment at short times followed by a higher-slope segment at times longer than a critical transition time,  $\tau$ . This transition is very reproducible; for example, for a feed concentration of 9  $\mu\text{M}$ ,  $\tau = 110 \pm 15$  min (average of three membranes).

Figure 24.7A shows that the flux of the permeating PC-DNA in the membrane containing the hairpin-DNA transporter is at all times higher than the flux for an identical membrane without the transporter (Table 24.2). The hairpin-DNA is acting as a MR agent to facilitate the transport [3,5,44,45] of the PC-DNA. Additional evidence for this conclusion was obtained from

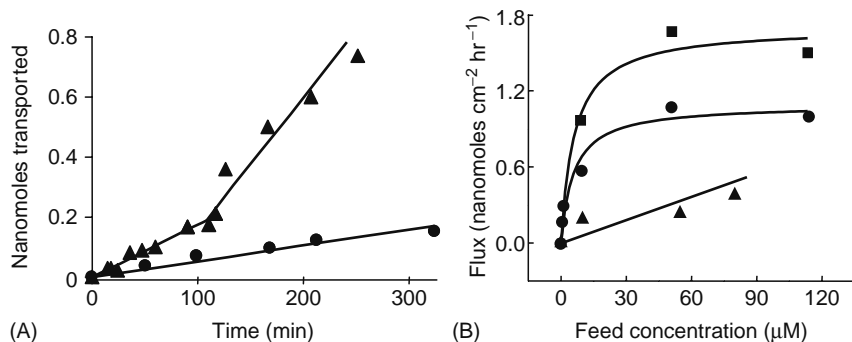


**FIGURE 24.7** (A) Transport plots for PC-DNA through Au nanotube membranes with (▲) and without (●) the immobilized hairpin-DNA transporter. Concentration in feed solution = 9  $\mu\text{M}$ . (B) Flux vs. feed concentration for PC-DNA. The data in squares and circles were obtained for a Au nanotube membrane containing the hairpin-DNA transporter. At feed concentrations of 9  $\mu\text{M}$  and above, the transport plot shows two linear regions. The data in squares were obtained from the high slope at longer times. The data in circles were obtained from the low-slope region at shorter times. The data in triangles were obtained for an analogous nanotube membrane with no DNA-transporter. (From Kohli, P., Harrell, C.C., Cao, Z., Gasparac, R., Tan, W., and Martin, C.R., *Science*, 305, 984, 2004. With permission.)

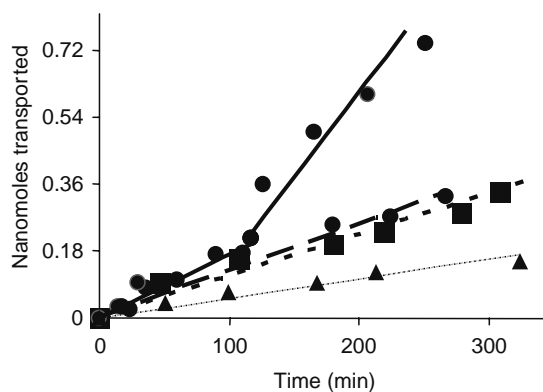


**FIGURE 24.8** Transport plots for a Au nanotube membrane containing the hairpin-DNA transporter. The permeating DNA was (● solid line) PC-DNA. (● dashed line) Single mismatch (end). (▲) Seven mismatch. (■) Single mismatch (middle). Concentration in feed solution = 9  $\mu\text{M}$ . (From Kohli, P., Harrell, C.C., Cao, Z., Gasparac, R., Tan, W., and Martin, C.R., *Science*, 305, 984, 2004. With permission.)

studies of the effect of concentration of the PC-DNA in the feed solution on the PC-DNA flux. If the hairpin-DNA is facilitating the transport of the PC-DNA, this plot should show a characteristic Langmuirian shape [3,5]. Figure 24.7B shows that this is, indeed, the case for transport data both before and after the critical transition time,  $\tau$ . The analogous plot for the identical membrane without the hairpin-DNA transporter is linear (Figure 24.7B), showing that transport is not facilitated but rather described simply by Fick's first law of diffusion. It is interesting to note that the transition to the higher slope segment was not observed, during permeation experiments of total duration 300 min, for feed concentrations below 9  $\mu\text{M}$  (Figure 24.7B).

Analogous permeation data were obtained for the various mismatch-containing permeating DNA molecules (Table 24.2). The transport plots for these mismatch DNAs show only one straight-line segment (Figure 24.8), and their fluxes are always lower than the flux for the PC-DNA obtained from the high slope region of the PC-DNA transport plot (Table 24.2). Note in particular, the membrane containing the hairpin-DNA transporter shows higher flux for PC-DNA than for the two permeating DNAs that contain only a single-base mismatch.

To illustrate this point more clearly, we define a selectivity coefficient  $\alpha_{\text{HP,PC}/1\text{MM}}$ , which is the flux for the PC-DNA divided by the flux for a single-base mismatch DNA in the membrane with the hairpin-DNA transporter. The data in Table 24.2 provide  $\alpha_{\text{HP,PC}/1\text{MM}} = 3$ . The analogous selectivity coefficient for the PC-DNA vs. the DNA with seven mismatches is  $\alpha_{\text{HP,PC}/7\text{MM}} = 7$ . These selectivity coefficients show that nanotube membranes containing the hairpin-DNA transporter selectively transport PC-DNA and that single-base mismatch transport selectivity can be obtained.

The importance of the hairpin structure to membrane selectivity is illustrated by analogous transport data for membranes containing the linear-DNA transporter (Table 24.1). With this transporter, all the transport plots show only a single straight-line segment, and the fluxes for the single-mismatch DNAs are identical to the flux for the PC-DNA (Table 24.2), i.e., the single-base mismatch selectivity coefficient for this linear (LN) DNA transporter is  $\alpha_{\text{LN,PC}/1\text{MM}} = 1$ . The linear-DNA transporter does, however, show some transport selectivity for the PC-DNA vs. the seven-mismatch DNA,  $\alpha_{\text{LN,PC}/7\text{MM}} = 5$ .

We have also investigated the mechanism of transport in these membranes. In such MR-based facilitated-transport membranes, the permeating species is transported by sequential binding and unbinding events with the MR agent [3,5,44].

**TABLE 24.2**  
**Fluxes for Feed Concentration of 9  $\mu\text{M}$**

Transporter DNA	Permeating DNA	Flux ( $\text{nmol cm}^{-2} \text{h}^{-1}$ )
Hairpin	Perfect complement	0.57, 1.14 <sup>a</sup>
Linear	Perfect complement	0.94
None	Perfect complement	0.20
Hairpin	Single mismatch (middle)	0.37
Hairpin	Single mismatch (end)	0.44
Linear	Single mismatch (middle)	0.94
Hairpin	Seven mismatch	0.17
Linear	Seven mismatch	0.20

Source: From Kohli, P., Harrell, C.C., Cao, Z., Gasparac, R., Jan, W., and Martin, C.R., *Science*, 305, 984, 2004.

<sup>a</sup> Two fluxes are obtained because the transport plot shows two slopes (Figure 24.11A).

For these DNA-based membranes, the binding/unbinding events are sequential hybridization/dehybridization reactions between the permeating DNA molecule and the DNA transporter attached to the nanotubes. To show that hybridization occurred in the membrane with the hairpin-DNA transporter, the membrane was exposed to PC-DNA, and then to a restriction enzyme (Sfc I, New England Biolabs) (supplementary materials, [6]). If hybridization between the PC-DNA and the hairpin transporter occurred, this enzyme will cut the resulting double-stranded DNA such that the last five bases of the binding loop, and all the stem-forming regions, at the 3' end of the hairpin are removed. This reaction will substantially damage the binding site, and based on our earlier work [5], we predict that if this membrane is subsequently used in a permeation experiment, a lower PC-DNA flux should be obtained [6].

After exposure to the restriction enzyme, the membrane was extensively rinsed to remove the enzyme and DNA fragments and then used for a transport experiment with PC-DNA as the permeating species. Unlike the data in Figure 24.7A, the transport plot for this damaged-transporter membrane showed only one straight-line segment [6] corresponding to a flux of  $0.2 \text{ nmol cm}^{-2} \text{ h}^{-1}$ . This value is well below what we observe from membranes with undamaged DNA-hairpin transporter (Table 24.2). The damaged DNA transporter was then removed from the nanotubes and fresh DNA-hairpin transporter was applied. A subsequent transport experiment with PC-DNA showed a transport plot identical to that obtained before exposure to the restriction enzyme [6]. These data suggest that hybridization is, indeed, involved in the transport mechanism for the DNA-hairpin-containing membranes.

To show that dehybridization occurs on a reasonable timescale in these membranes, we exposed a hairpin-DNA membrane to a fluorescently labeled version of the PC-DNA (Table 24.1). The membrane was then rinsed with buffer solution and immersed into a solution of either pure buffer or buffer containing unlabeled PC-DNA. If the dehybridization reaction is facile, the fluorescently labeled PC-DNA should be released into the solution. We found that dehybridization does occur, but it is strongly accelerated when unlabeled PC-DNA is present in the solution (Figure 24.9). Hence dehybridization is much faster when it occurs by a cooperative process whereby one PC-DNA molecule displaces another from an extant duplex [46].

We have also investigated transport selectivity for a feed solution containing fluorescently labeled versions (Table 24.1) of both the PC-DNA and the single-mismatch DNA. The fluorescent labels allow for quantification of both these permeating DNAs simultaneously in the permeate solution. In analogy to the single-molecule permeation experiment, the flux of the PC-DNA was five times higher than the flux of the single-mismatch DNA [6]. To assess the practical utility of these membranes, transport studies with more realistic samples (such as cell lysates) will be needed.

Finally, we have not observed a spontaneous transition from a low flux to a high flux state (Figure 24.7A) with our previous MR-based membranes [3,5]. The fact whether this transition is observed depends on the feed concentration suggests that the transition is a transport-related phenomenon. It is possible that this transition relates to the concept of cooperative (high flux) vs. noncooperative (low flux) dehybridization (Figure 24.9), but further studies, both experimental and modeling, will be required before a definitive mechanism for this transition can be proposed.

### 24.5.3 ENANTIOSEPARATIONS OF AMINO ACIDS USING APOENZYMES IMMOBILIZED IN A POROUS POLYMERIC MEMBRANE [3]

Most of amino acids are chiral and as discussed earlier, the chiral separation is a challenging problem. Another possibility to separate amino acids is to use enzymes that can recognize and selectively separate them. As enzymes also catalyze chemical reactions on substrate molecules that they bind to, this creates an unwanted problem because the reaction products must be separated in the following step. This problem can be circumvented by using apoenzymes as molecular-recognition transporter. Apoenzymes are enzymes that lack in their cofactors; they cannot transform substrates into products.

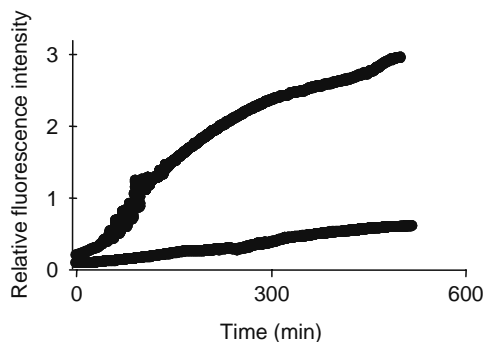


**FIGURE 24.9** Release of fluorescently labeled PC-DNA from a membrane containing the hairpin-DNA transporter. The fluorescently labeled PC-DNA was released into a buffer solution containing no unlabeled PC-DNA (lower curve) or into a buffer containing  $9 \mu\text{M}$  unlabeled PC-DNA (upper curve). (From Kohli, P., Harrell, C.C., Cao, Z., Gasparac, R., Tan, W., and Martin, C.R., *Science*, 305, 984, 2004. With permission.)

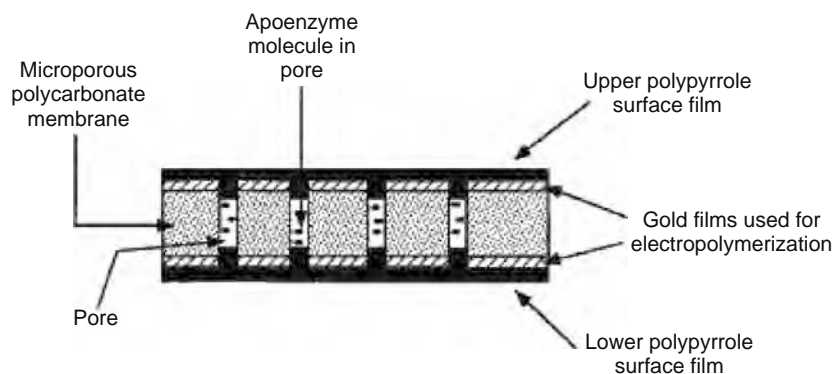


**FIGURE 24.10** Schematic cross section of the polypyrrole/polycarbonate/polypyrrole sandwich membrane with the apoenzyme entrapped in the pores. The membrane is drawn as coming out of the plane of the paper. The various components are not drawn to scale. (From Lakshmi, B.B. and Martin, C.R., *Nature*, 388, 758, 1997. With permission.)

We have used apoenzymes as molecular-recognition transporters for binding and selective transportation of molecules without production of unwanted chemical reactions on reactants. Figure 24.10 shows the design of membrane consisting of microporous polymer membrane sandwiched between two thin films of polypyrrole [3]. The apoenzymes are physically trapped within the pores of the membrane and polypyrrole films. More details regarding the fabrication of the membranes, materials, and experimental setup can be found in the Ref. [3].

The transport flux of ethanol for membranes loaded with alcohol dehydrogenase apoenzyme (apo-ADH) is found to be greater than nine times from those obtained for phenol. The flux vs. feed concentration curves for ethanol showed Langmuir-type isotherm. These observations clearly indicate that apo-ADH acted as molecular-recognition sites for ethanol, and it facilitates the transport of ethanol through the membranes.

To explore the enantioseparation of amino acids which is a more challenging and an interesting problem, D-amino acid oxidase apoenzyme (apo-D-AAO) was trapped in the membrane (containing 400 nm inner pore diameter). The transport fluxes vs. feed concentration of D-phenylalanine and L-phenylalanine through apo-D-AAO-containing membranes were investigated. We found that apo-D-AAO-containing membranes transport D-phenylalanine relative to L-phenylalanine with a selectivity coefficient of 3.3 (Figure 24.11A) [3]. Although the selectivity coefficients obtained using apo-D-AAO-trapped membranes are much higher than those obtained with chromatography-based separation methods, still higher selectivity coefficients are desired. One method to improve selectivity coefficients is to shutdown simple diffusional transport through membrane pores. This can be done by reducing the inner pore diameter of the membranes to reduce the diffusional transport of L-phenylalanine. When apo-D-AAO-trapped within 30 nm inner pore diameter membranes were used, a selectivity coefficient of 4.9 is obtained (Figure 24.11B). As expected the enantiomeric selectivity coefficients were increased, but the transport fluxes were also found to be smaller as compared to those obtained with apo-D-AAO loaded 400 nm pore diameter membranes.

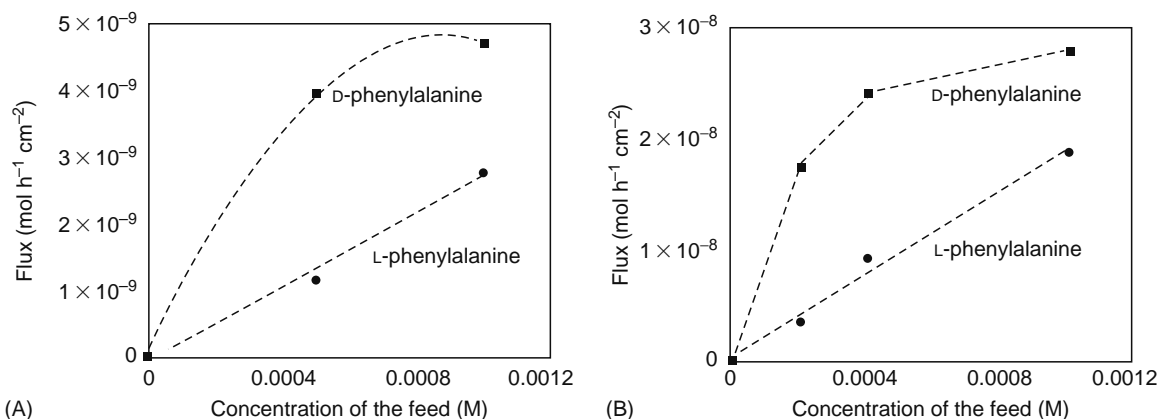


**FIGURE 24.11** (A) Plots of D-phenylalanine and L-phenylalanine flux vs. concentration of these enantiomers in the feed solution for a D-amino acid oxidase apoenzyme (apo-D-AAO)-loaded membrane. The membrane had pores of 400 nm diameter and (B) as (A) but using a membrane with pores of 30 nm diameter (pore density  $6 \times 10^8$  pores  $\text{cm}^{-2}$ ). (From Lakshmi, B.B. and Martin, C.R., *Nature*, 388, 758, 1997. With permission.)

To improve transport rates without sacrificing selectivity, new type of membranes that contain conical pores are being developed. The conical pores containing membranes have much smaller diffusional resistance (higher diffusion coefficients) to molecules for most of the length of the nanotubes except at the narrower tip. We expect conical nanotube membranes to have much higher transport fluxes. The separation selectivity coefficients can be tuned by optimizing the diameter of the narrower tip (pore) in the membranes and by immobilizing molecular-recognition transporters on the inner nanotube walls at optimum concentrations. It is therefore possible to obtain much higher fluxes without sacrificing separation selectivity coefficients.

Recently, we have also conducted experiments with antibody-based nanotube membranes for very high selective protein separations [47]. We found that immobilization of antibodies on the inner walls of the nanotubes selectively bind and transport its antigenic-protein molecules across the membranes. Remarkably, we have routinely observed selectivity coefficients as high as 34 for antibody-based membrane separation. In principle, antibodies can be raised for any molecules, and the antibody-tailored membranes can be used as a general but highly selective separation method.

## 24.6 CONICAL NANOTUBES: MIMICKING ARTIFICIAL ION CHANNEL [7]

There is considerable interest in developing chemical devices that mimic the function of biological ion channels [48]. We recently described such a device, which consisted of a single conically shaped gold nanotube embedded within a polymeric membrane [49]. This device mimicked one of the key functions of voltage-gated ion channels—the ability to strongly rectify the ionic current flowing through it. The data obtained were interpreted using a simple electrostatic model (*vide infra*) [49].

While the details are still being debated [50a–c], it is clear that ion current-rectification in biological ion channels is more complicated and involves physical movement of an ionically charged portion of the channel in response to a change in the transmembrane potential [50d]. We report here the artificial ion channels that rectify the ion current flowing through them via this electromechanical [51] mechanism. These artificial channels are also based on conical gold nanotubes, but with the critical electromechanical response provided by single-stranded DNA molecules attached to the nanotube walls.

Single conically shaped nanopores were etched into 0.07 cm<sup>2</sup> samples of a 12 μm thick polycarbonate membrane [52]. For most of the studies reported here, the large diameter opening of the pore was 5 μm (Figure 24.12A) and the small diameter opening was 60 nm (Figure 24.12B). However, membranes having conical pores with large diameter openings of 5 μm and small diameter openings of 150 and 100 nm were also used. An electroless plating method [18] was used to deposit a correspondingly conical gold nanotube within the pore. This entails coating the pore walls, and membrane faces, with a thin (~10 nm) layer of gold. Because this layer is so thin, the large diameter opening of the conical gold nanotube remained 5 μm. An approximate measure of the diameter of the small opening (here after called the mouth) of the conical nanotube was obtained using a simple electrochemical method [52] (Table 24.3).

In the final step, single-stranded DNA molecules were covalently immobilized to the gold surfaces. The following are the thiol-terminated DNAs: 5'HS-(CH<sub>2</sub>)<sub>6</sub>-CGAGTCCATTCA3' (12-mer), 5'HS-(CH<sub>2</sub>)<sub>6</sub>-GACCGAGTC-CATTCA3' (15-mer), 5'HS-(CH<sub>2</sub>)<sub>6</sub>-CGCGAGAAGTTACAT GACCTGTAGACGATC3' (30-mer), 5'HS-(CH<sub>2</sub>)<sub>6</sub>-A<sub>45</sub>3' (45-mer), and 5'HS-(CH<sub>2</sub>)<sub>6</sub>-CGCGAGAAGTTACATGACCTG-TAGCTCGCG3' (30-mer hairpin) [6,7]. In all the experiments described here, the conically shaped gold nanotube was left embedded within the polycarbonate membrane. However, to prove that this nanotube is, indeed, conical, the membrane can be dissolved away and the liberated nanotube is imaged via electron microscopy (Figure 24.12C).

Current–voltage (I–V) curves for these artificial ion channels were obtained by mounting the membrane sample between the two halves of a U-tube conductivity cell [18]. Each half-cell was filled with ~5 mL of a 10 mM pH 7.0 phosphate buffer that was also 100 mM in KCl. A Ag/AgCl reference electrode was inserted into each half-cell solution, and a Keithley instruments

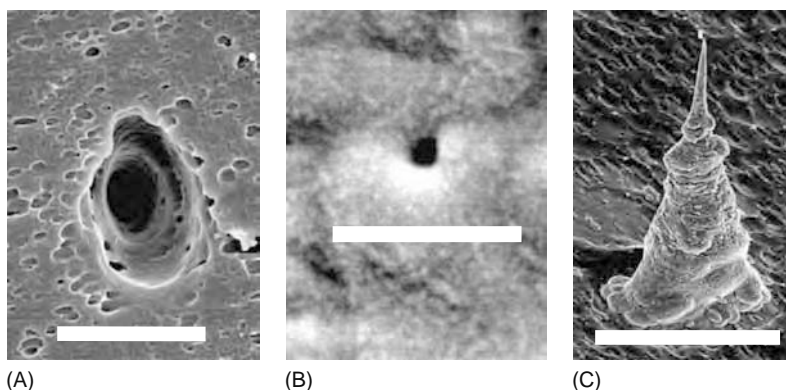


**FIGURE 24.12** Electron micrographs showing (A) large diameter (scale bar 5.0 μm) and (B) small diameter (scale bar 333 nm) opening of a conical nanopore, and (C) a liberated conical Au nanotube (scale bar 5.0 μm). (From Harrell, C.C., Kohli, P., Siwy, Z., and Martin, C.R., *J. Am. Chem. Soc.*, 126, 15646, 2004. With permission.)

**TABLE 24.3**  
**Nanotube Mouth Diameter ( $d$ ), DNA Attached,  $r_{\max}$ , Radius of Gyration ( $r_g$ ), and Extended Chain Length ( $l$ )**

$d$ (nm)	DNA attached	$r_{\max}$	$r_g$ (nm)	$l$ (nm) <sup>a</sup>
41	12-mer	1.5	1.4	5.7
46	15-mer	2.2	1.6	6.9
42	30-mer	3.9	2.9	12.9
38	45-mer	7.1	4.0	18.9
98	30-mer	1.1	2.9	12.9
59	30-mer	2.1	2.9	12.9
39	30-mer	3.9	2.9	12.9
27	30-mer	11.5	2.9	12.9
13	30-mer	4.7	2.9	12.9
39	30-mer hairpin	1.4	n/a	6.9

Source: From Harrell, C.C., Kohli, P., Siwy, Z., and Martin, C.R., *J. Am. Chem. Soc.*, 123, 12335, 2001.

<sup>a</sup> Includes the (CH<sub>2</sub>)<sub>6</sub> spacer.

6487 picoammeter/voltage source was used to apply the desired transmembrane potential and measure the resulting ionic current flowing through the gold nanotube.

In our earlier work, the mouth diameter of the Au nanotubes was 10 nm, and the rectification observed resulted from electrostatic interactions between cations traversing the nanotube and fixed surface charge (due, e.g., to adsorbed Cl<sup>-</sup>) at the nanotube mouth [49]. This mechanism applies only when the mouth diameter is comparable to the thickness of the electrical double layer associated with the fixed surface charge, and this is not the case for the large mouth-diameter nanotubes used here (Table 24.3). This is proven by the fact that without attached DNA molecules, these nanotubes do not rectify, even though there is adsorbed Cl<sup>-</sup> on the nanotube walls (Figure 24.13A). In contrast, the DNA-containing nanotubes rectify the ion current,

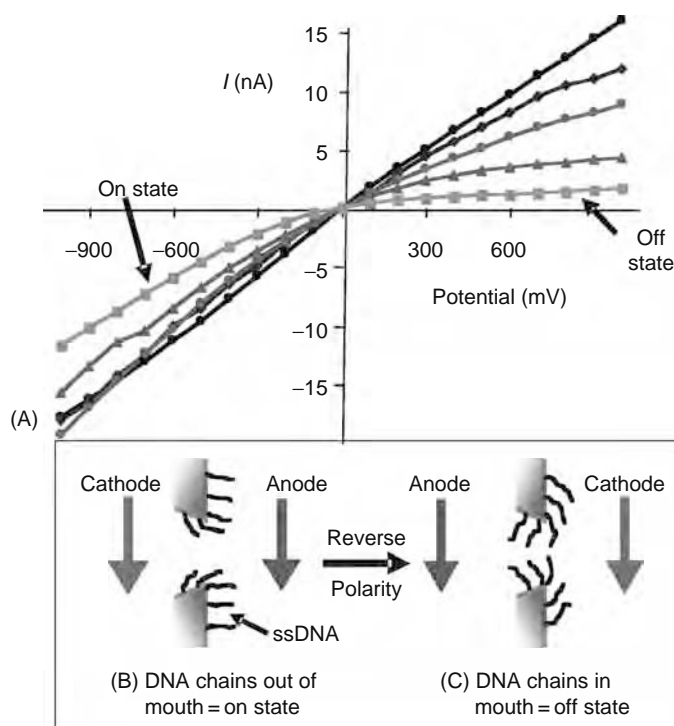


**FIGURE 24.13** (See color insert following page 588.) (A) I-V curves for nanotubes with mouth diameter 40 nm containing no DNA (black) and attached 12-mer (blue), 15-mer (red), 30-mer (green), and 45-mer (orange) DNAs. (B,C) Schematics showing electrode polarity and DNA chain positions for on (B) and off (C) states. (From Harrell, C.C., Kohli, P., Siwy, Z., and Martin, C.R., *J. Am. Chem. Soc.*, 126, 15646, 2004. With permission.)

i.e., they show an on state at negative transmembrane potentials (anode facing the mouth of nanotube, Figure 24.13B) and an off state at positive potentials (Figure 24.13C).

The extent of rectification may be quantified via the ratio,  $r_{\max}$ , which is the absolute value of the current at  $-1$  V (on state) divided by the current at  $+1$  V (off state) (Table 24.3). The first four entries in Table 24.3 correspond to the nanotubes in Figure 24.13A. As is evident from the figure,  $r_{\max}$  increases with DNA chain length. The extent of rectification can also be controlled by holding the chain length constant, and varying the diameter of the nanotube mouth (Table 24.3). With one exception (*vide infra*),  $r_{\max}$  increases with decreasing mouth diameter.

We propose that rectification in these nanotubes entails electrophoretic insertion of the DNA chains into (off state, Figure 24.13C) and out of (on state, Figure 24.13B) the nanotube mouth. The off state is obtained because when inserted into the mouth, the chains partially occlude the pathway for ion-transport, yielding a higher ionic resistance for the nanotube. There is ample evidence in the literature to support this hypothesis. First, because DNA chains are anionic, they can be driven electrophoretically through nanopores, and during translocation, occlusion of the nanopores by the DNA causes a transient increase in the pore's ionic resistance [53]. Furthermore, in complete analogy to our model, if one end of a DNA chain is immobilized in an electrophoresis experiment, the chain extends linearly in the direction of the anode [54]. In addition, simulations of the electric-field strength in conical nanopores, identical to those used here, show that the field in the electrolyte solution in the mouth of the nanopore is  $1 \times 10^6$  V m<sup>-1</sup>, when the total voltage drop across the membrane is only 1 V [55]. This focusing of the electric field strength at the nanotube mouth means that there is ample field to extend the DNA chains toward the anode.

Further support for this model can be garnered from our experimental I–V data. First, the magnitudes of the on state currents in Figure 24.13A decrease with increasing DNA chain length. This is because even in the on state, the DNA chains partially occlude the mouth of the nanotube and increase the nanotube resistance. Second, while the general trend is that  $r_{\max}$  increases with decreasing mouth diameter, one exception was noted; the nanotube with the  $\sim 13$  nm mouth and the 30-base DNA rectifies less than the nanotube with the  $\sim 27$  nm mouth and this same 30-base DNA (Table 24.3). These data suggest that the DNA chain can be too long, relative to the mouth diameter, to allow for efficient rectification. Table 24.3 lists two relevant lengths of the DNA chains: the length if the chains were completely extended [53] and the radius of gyration [56] for the globular form. According to our model to rectify, the chain must have the freedom to extend linearly toward the anode. The nanotube with the 13 nm mouth is the only case where the length of the extended DNA chain is equivalent to the mouth diameter. We suggest that this makes it sterically difficult for the chains to reorient and insert themselves into the mouth, and this is why poor rectification is observed.

Third, according to our model, the DNA chain must have the flexibility to extend in the direction of the anode. This issue was explored by comparing the extent of rectification for a nanotube containing the conventional 30-base DNA and an identical tube containing a hairpin 30-base DNA. The hairpin-DNA [57] folds back on itself because the bases at one end of the chain are complementary to the bases at the other end, making the chain much less flexible. The nanotube containing this 30-base hairpin-DNA is a very poor rectifier, much worse than the same nanotube with the conventional 30-base DNA (Table 24.3).

## 24.7 CONCLUSIONS

We believe that nanotubes offer some important advantages for biotechnological and biomedical applications of nanoparticles. Because of its tremendous versatility in terms of materials that can be used, sizes that can be obtained, and chemistry and biochemistry that can be applied, the template method might prove to be a particularly advantageous approach for preparing nanotubes for such applications. However, this field of nanotube biotechnology is in its infancy, and there is much work to be done before products based on this technology are brought to the market place. For example, in our applications to date, we have incorporated the payload into the nanotubes by either covalent bonding or other chemical interactions. However, in some applications it might be useful to simply fill the nanotube with a payload and then apply caps to the nanotube ends to keep the payload encapsulated. Furthermore, it might be useful to have these caps fall off, thus spilling the payload, when a particular chemical or biochemical signal is detected. We are currently exploring routes for preparing such capped nanotubes. The issues of cost of production and mass production of nanotubes must also be addressed.

Finally, the synthetic nanotubes discussed here can be thought of as mimics of naturally occurring nanotubes–protein channels [7,58]; indeed, the cyclic peptide nanotubes have been used as artificial ion channels [26]. Ion channels open and close in response to chemical and electrical stimuli. We are developing synthetic nanotubes with similar voltage [7,18,49,59] and chemical [60] gating characteristics. These nanotubes can be used in smart membranes whose transport properties change in response to an electrical stimulus [18,59] and in sensing devices where a chemical stimulus turns on a current that can be measured in an external circuit [60]. One of major drawbacks of membrane-based separation method is low transport flux of separating molecules. The use of conical nanotubes-containing membranes can possibly eliminate low transport flux problem because conical pore-containing membranes are expected to have much larger porosity. We have fabricated conical nanotube membranes [7,49]; these membranes have potential of greatly increasing the transport flux without significantly losing the selectivity coefficients. Further, we report on separation of biomolecules and biopolymers using conical-nanotube membranes.

## ACKNOWLEDGMENT

This work was supported by the National Science Foundation (NIRT for Biomedical Nanotube Technology), DARPA, the Office of Naval Research, and the UF Engineering Research Center for Particle Science and Technology. We gratefully acknowledge our collaborator, professor Hans Soderlund, for contributions to the antibody research projects.

## REFERENCES

1. Campbell, N.A. *Biology*. 3rd ed. The Benjamin/Cummings Company: Redwood City, CA, 1993.
2. Lee, S.B., Mitchell, D.T., Trofin, L., Nevanen, T.K., Soderlund, H., and Martin, C.R. Template-synthesized bionanotubes for separations and biocatalysis. *Carrier-Based Drug Delivery ACS Symposium 879*, ACS, Washington, DC, 2004, pp. 98–117.
3. Lakshmi, B.B. and Martin, C.R. Enantioseparation using apoenzymes immobilized in a porous polymeric membrane. *Nature* 388, 758–760, 1997.
4. Mitchell, D.T., Lee, S.B., Trofin, L., Li, N., Nevanen, T.K., Soderlund, H., and Martin, C.R. Smart nanotubes for bioseparations and biocatalysis. *J. Am. Chem. Soc.* 124, 11864–11865, 2002.
5. Lee, S.B., Mitchell, D.T., Trofin, L., Li, N., Nevanen, T.K., Soderlund, H., and Martin, C.R. Antibody-based bio/nanotube membranes for enantiomeric drug separations. *Science* 296, 2198–2200, 2002.
6. Kohli, P., Harrell, C.C., Cao, Z., Gasparac, R., Tan, W., and Martin, C.R. DNA functionalized nanotube membranes with single-base mismatch selectivity. *Science* 305, 984–986, 2004.
7. Harrell, C.C., Kohli, P., Siwy, Z., and Martin, C.R. DNA-nanotube artificial ion channels. *J. Am. Chem. Soc.* 126, 15646–15647, 2004.
8. Linsky, J.P., Paul, T.R., and Kenny, M.E. Planar organosilicon polymers. *J. Polym. Sci. A-29*, 143–160, 1971.
9. Yager, P. and Schoen, P. Formation of tubules by a polymerizable surfactant. *Mol. Cryst. Liq. Cryst.* 106, 371–381, 1984.
10. Schnur, J.M. Lipid tubules: A paradigm for molecularly engineered structures. *Science* 262, 1669–1676, 1993.
11. Selinger, J.V., Spector, M.S., and Schnur, J.M. Theory of self-assembled tubules and helical ribbons. *J. Phys. Chem. B* 105, 7157–7169, 2001.
12. Price, R. and Patchan, M. Controlled release from cylindrical macrostructures. *J. Microencapsul.* 8, 301–306, 1991.
13. Goldstein, A.S., Amory, J.K., Martin, S.M., Vernon, C., Matsumoto, A., and Yager, P. Testosterone delivery using glutamide-based complex high axial ratio microstructures. *Bioorg. Med. Chem.* 9, 2819–2825, 2001.
14. Iijima, S. Helical microtubules of graphitic carbon. *Nature* 354, 56–58, 1991.
15. Ajayan, P.M. *Carbon Nanotubes: Preparation and Properties*, Ebbesen, T.W. Ed. CRC Press: Cleveland, OH, 1997.
16. Ajayan, P.M. Nanotubes from carbon. *Chem. Rev.* 99, 1787–1800, 1999.
17. Dai, H., Kong, J., Zhou, C., Franklin, N., Tomblor, T., Cassell, A., Fan, S., and Chapline, M. Controlled chemical routes to nanotube architectures, physics, and devices. *J. Phys. Chem. B* 103, 11246–11255, 1999.
18. Nishizawa, M., Menon, V.P., and Martin, C.R. Metal nanotubule membranes with electrochemically switchable ion-transport selectivity. *Science* 268, 700–702, 1995.
19. Jirage, K.B., Hulteen, J.C., and Martin, C.R. Nanotubule-based molecular-filtration membranes. *Science* 278, 655–658, 1997.
20. Martin, C.R. and Kohli, P. The emerging field of nanotube biotechnology. *Nature Rev. Drug Discov.* 2, 29–37, 2003.
21. Martin, C.R. Nanomaterials: A membrane-based synthetic approach. *Science* 266, 1961–1966, 1994.
22. Hulteen, J.C. and Martin, C.R. A general template-based method for the preparation of nanomaterials. *J. Mater. Chem.* 7, 1075–1087, 1997.
23. Ghadiri, M.R., Granja, J.R., Milligan, R.A., McRee, D., and Khazanovich, N. Self-assembled organic nanotubes based on a cyclic peptide. *Nature* 366, 324–327, 1993.
24. Khazanovich, N., Granja, J.R., McRee, D.E., Milligan, R.A., and Ghadiri, M.R. Nanoscale tubular ensembles with specified internal diameters. Design of a self-assembled nanotube with a 13 angstrom pore. *J. Am. Chem. Soc.* 116, 6011–6012, 1994.
25. Fernandez-Lopez, S., Kim, H.S., Choi, E.C., Delgado, M., Granja, J.R., Khasanov, A., Kraehenbuehl, K., Long, G., Weinberger, D.A., Wilcoxon, K.M., and Ghadiri, M.R. Antibacterial agents based on the cyclic D,L-alpha-peptide architecture. *Nature* 412, 452–455, 2001.
26. Ghadiri, M.R., Granja, J.R., and Buehler, L.K. Artificial transmembrane ion channels from self-assembling peptide nanotubes. *Nature* 369, 301–304, 1994.
27. Cepak, V.M., Hulteen, J.C., Che, G., Jirage, K.B., Lakshmi, B.B., Fisher, E.R., and Martin, C.R. Fabrication and characterization of concentric tubular composite micro- and nanostructures using the template synthesis method. *J. Mater. Res.* 13, 3070–3080, 1998.
28. Nicewarner-Pena, S.R., Griffith, F.R., Reiss, B.D., He, L., Pena, D.J., Walton, I.D., Cromer, R., Keating, C.D., and Natan, M.J. Submicrometer metallic barcodes. *Science* 294, 137–141, 2001.
29. Nicewarner-Pena, S.R., Carado, A.J., Shale, K.E., and Keating, C.D. Barcoded metal nanowires: Optical reflectivity and patterned fluorescence. *J. Phys. Chem. B*, 107, 7360–7367, 2003.
30. Miller, S.A., Young, V.Y., and Martin, C.R. Electroosmotic flow in template-prepared carbon nanotube membranes. *J. Am. Chem. Soc.* 123, 12335–12342, 2001.
31. Cepak, V.M. and Martin, C.R. Preparation of polymeric micro- and nanostructures using a template-based deposition method. *Chem. Mater.* 11, 1363–1367, 1999.
32. Li, N. and Martin, C.R. A high-rate, high-capacity, nanostructured Sn-based anode prepared using sol-gel template synthesis. *J. Electrochem. Soc.* 148, A164–A170, 2001.
33. Menon, V.P. and Martin, C.R. Fabrication and evaluation of nanoelectrode ensembles. *Anal. Chem.* 67, 1920–1928, 1995.

34. Hou, S., Wang, J., and Martin, C.R. Template-synthesized DNA nanotubes. *J. Am. Chem. Soc.* 67, 8586–8587, 2005.
35. Nevanen, T.K., Soderholm, L., Kukkonen, K., Suortti, T., Teerinen, T., Linder, M., Soderlund, H., and Teeri, T.T. Efficient enantioselective separation of drug enantiomers by immobilized antibody fragments. *J. Chromatogr. A* 925, 89–97, 2001.
36. Yu, S., Lee, S.B., Kang, M., and Martin, C.R. Size-based protein separations in poly(ethylene glycol)-derivatized gold nanotubule membranes. *Nano Lett.* 1, 495–498, 2001.
37. Jirage, K.B., Hulteen, J.C., and Martin, C.R. Effect of thiol chemisorption on the transport properties of gold nanotubule membranes. *Anal. Chem.* 71, 4913–4918, 1999.
38. (a) Stinson, S.C. Counting on chiral drugs, *Chem. Eng. News* 76, 1–136, 1998; (b) Xu, Y. and McCarroll, M.E. Fluorescence anisotropy as a method to examine the thermodynamics of enantioselectivity. *J. Phys. Chem. B*, in press; (c) McCarroll, M.E., Billiot, F.H., and Warner, I.M. Fluorescence anisotropy as a measure of chiral recognition. *JACS* 123, 3173–3174, 2001.
39. Stryer, L. *Biochemistry*, W.H. Freeman and Company: New York, 1995, p. 372.
40. Robinson J.M. Meeting report: Biological labeling and correlative microscopy. *Acta Histochem.* 103, 2001, 261–264.
41. Howorka, S., Cheley, S., and Bayley, H. Sequence-specific detection of individual DNA strands using engineered nanopores. *Nature Biotech.* 19, 636–639, 2001.
42. Fried, H. and Kutay, U. Nucleocytoplasmic transport: Taking an inventory. *Cell. Mol. Life Sci.* 60, 1659–1688, 2003.
43. Martin, C.R., Nishizawa, M., Jirage, K., and Kang, M. Transport properties of gold nanotubule membranes. *J. Phys. Chem. B* 105, 1925–1934, 2001.
44. Mulder, M. *Basic Principles of Membrane Technology*, Kluwer Academic Publishers: Dordrecht, The Netherlands, 1996, pp. 342–351.
45. Osada, Y. and Nakagawa, T., Eds. *Membrane Science and Technology*, Marcel Dekker, New York, 1992, pp. 377–391.
46. Hall, M.C., Wang, H., Erie, D.A., and Kunkel, T.A. *J. Mol. Biol.* 312, 637–647, 2001.
47. Trofin, L., Kohli, P., Mota, M.O., Wang, J., Laukkanen, M.-L., Nevanen, T.K., Soderlund, H., and Martin, C.R. Unpublished results.
48. (a) Siwy, Z. and Fulinski, A. Fabrication of a synthetic nanopore ion-pump. *Phys. Rev. Lett.* 89, 198103, 2002; (b) Synthetic ion channels, special issue of *Bioorg. Med. Chem.* 12, 1265–1569, 2004; (c) Fyles, T.M., Loock, D., and Zhou, X. A voltage-gated ion channel based on a bis-macrocyclic bolaamphiphile. *J. Am. Chem. Soc.* 120, 2997–3003, 1998; (d) Wu, Z., Tang, J., Cheng, Z., Yang, X., and Wang, E. Ion channel behavior of supported bilayer lipid membranes on a glassy carbon electrode. *Anal. Chem.* 72, 6030–6033, 2000.
49. Siwy, Z., Heins, E., Harrell, C.C., Kohli, P., and Martin, C.R. Conical-nanotube ion-current rectifiers: The role of surface charge. *J. Am. Chem. Soc.* 126, 10850–10851, 2004.
50. (a) Yarnell, A. *Chem. Eng. News* 82, 35–36, 2004; (b) Blaustein, R.O. and Miller, C. News and views: Ion channels: Shake, rattle or roll? *Nature* 427, 499–501, 2004; (c) Swartz, K.J. Opening the gate in potassium channels (News and Views). *Nature Struct. Molec. Biol.* 11, 499–500, 2004; (d) Jiang, Y., Lee, A., Chen, J., Ruta, V., Cadene, M., Chait, B.T., and MacKinnon, R. X-ray structure of a voltage-dependent K<sup>+</sup> channel. *Nature* 423, 33–41, 2003.
51. Jiang, Y., Lee, A., Chen, J., Cadene, M., Chait, B.T., and MacKinnon, R. Crystal structure and mechanism of a calcium-gated potassium channel. *Nature* 417, 515–522, 2002.
52. Apel, P., Korchev, Y.E., Siwy, Z., Spohr, R., and Yoshida, M. Diode-like single ion-track membrane prepared by electro-stopping. *Nucl. Instr. Meth. B* 184, 337–346, 2001.
53. Meller, A., Lucas, N., and Branton, D. Voltage-driven DNA translocations through a nanopore. *Phys. Rev. Lett.* 86, 3435–3438, 2001.
54. Maier, B., Seifert, U., and Raedler, J.O. Elastic response of DNA to external electric fields in two dimensions. *Europhys. Lett.* 60, 622–628, 2002.
55. Lee, S., Zhang, Y., White, H.S., Harrell, C.C., and Martin, C.R. Electrophoretic capture and detection of nanoparticles at the opening of a membrane pore using scanning electrochemical microscopy. *Anal. Chem.* accepted.
56. (a) Sorlie, S.S. A dynamic light-scattering study of 4 DNA restriction fragments, *Macromolecules* 23, 487, 1990; (b) Olmstead, M.C., Anderson, C.F., and Record, M.T. Importance of oligoelectrolyte end effects for the thermodynamics of conformational transitions of nucleic acid oligomers: a grand canonical Monte Carlo analysis. *Biopolymers* 31, 1593–1604, 1991.
57. Bonnet, G., Tyagi, S., Libchaber, A., and Kramer, F.R. Thermodynamic basis of the enhanced specificity of structured DNA probes. *Proc. Natl. Acad. Sci. USA*, 96, 6171–6176, 1999.
58. Hille, B. *Ion Channels of Excitable Membranes*, Sinauer: Sunderland, MA, 2001.
59. Kang, M. and Martin, C.R. Investigations of potential-dependent fluxes of ionic permeates in gold nanotubule membranes prepared via the template method. *Langmuir* 17, 2753–2759, 2001.
60. Steinle, E.D., Mitchell, D.T., Witz, M., Lee, S.B., Young, V.Y., and Martin, C.R. Ion-channel mimetic micropore and nanotube membrane sensors. *Anal. Chem.* 74, 2416–2422, 2002.

---

# 25 Use of Emulsion Liquid Membrane Systems in Chemical and Biotechnological Separations

*Jilka M. Perera and Geoff W. Stevens*

## CONTENTS

25.1	Introduction .....	709
25.2	Theory and Mechanism .....	710
25.3	Modeling .....	711
25.3.1	Type 1 Facilitation .....	711
25.3.2	Type 2 Facilitation .....	712
25.3.3	Model Parameters .....	712
25.3.3.1	Internal Droplet Size .....	712
25.3.3.2	Emulsion Globule Size .....	712
25.3.3.3	Biot Number .....	715
25.3.3.4	Damköhler Number .....	718
25.4	Emulsion Liquid Membrane Process .....	718
25.4.1	Emulsification .....	718
25.4.1.1	Surfactants .....	718
25.4.1.2	Diluents .....	718
25.4.1.3	Carriers .....	719
25.4.1.4	Internal Phase .....	719
25.4.2	Permeation and Settling .....	719
25.4.2.1	Composition .....	720
25.4.2.2	Swelling in Emulsion Liquid Membranes .....	721
25.4.2.3	Membrane Leakage .....	722
25.4.3	Demulsification .....	723
25.4.3.1	Chemical Treatment .....	723
25.4.3.2	Physical Treatments .....	723
25.5	Applications .....	724
25.6	Pilot Plant Studies/Commercial Applications .....	727
25.7	Concluding Remarks .....	727
	Symbols .....	733
	Greek Symbols .....	733
	References .....	734

## 25.1 INTRODUCTION

The concept of emulsion liquid membranes (ELM) was first proposed by Li in 1968 [1]. Since their inception in the late 1960s they have been referred to as surfactant liquid membranes, double emulsion membranes or ELM. Regardless of the terminology used, the workings of such systems are as follows: they consist of an emulsion formed by an organic solvent and water, which can be stabilized by the addition of surfactant. This emulsion is then contacted with a continuous phase containing the desired solute, stirred to yield globules, and transported across the extremely thin membrane layer that separates internal phase droplets

inside the emulsion globule. The three phase dispersion can be either a water-in-oil emulsion dispersed in an aqueous phase (W/O/W) or an oil-in-water emulsion dispersed in an oil phase (O/W/O) [2]. According to Ho et al. [3], in general the internal phase droplets are small, with diameters in the order of 1–10  $\mu\text{m}$ . The emulsion globules, however, are much larger usually 0.1–2.0 mm in diameter. On completion of the extraction process, the emulsion needs to be broken/demulsified to recover the internal phase containing the concentrated solute.

Such systems are capable of providing extremely large membrane surface areas and are applicable in situations where the desired solute in the feed stream is in low concentration. Some of the attractive features of ELM systems include simple operation, high efficiency, extraction, and stripping in one stage, large interfacial area and scope for continuous operation [4].

However, these systems are disadvantaged by emulsion swelling, emulsion breakage, lack of stability, and the fact that modeling tends to be complicated and tedious. Despite these disadvantages ELM systems have found applications in numerous situations such as the removal of metal ions, acids and bases from wastewater streams, and the recovery of biochemical products.

The chapter deals with the workings of emulsion liquid membrane systems: the physicochemical properties, modeling of such systems, difficulties associated with these types of membrane systems, and their uses in chemical and biotechnological applications.

## 25.2 THEORY AND MECHANISM

The transfer of the solute from the bulk aqueous phase into the droplets of the internal phase can be via two mechanisms, referred to as type 1 and type 2 facilitations. In type 1 facilitation, the solute species in the continuous phase transfers into the internal phase and reacts with a chemical reagent present in this phase forming a product that is not capable of diffusing back through the membrane. Thus the solute concentration in the internal phase of the ELM is effectively zero. An example of type 1 facilitation is the removal of phenol from wastewaters. The process is illustrated in Figure 25.1.

In this figure, phenol from the continuous phase solubilizes in the membrane oil phase and then diffuses into the internal phase where it reacts with the sodium hydroxide to form sodium phenolate. Being an ionic species, it is not soluble in the oil phase of the membrane and is effectively captured in the internal aqueous phase. The concentration of phenol in the internal phase is effectively zero.

Type 2 facilitation is also known as carrier facilitated transport, since a carrier compound, that is, an extractant or complexing agent, solubilized in the organic phase is used to assist transfer across the membrane. In this situation, the solute of interest reacts with the carrier to form a complex that is only soluble in the membrane phase. The solute is de-complexed by a stripping solution contained in the internal phase. An example of such a process is the removal of a metal ion such as copper or zinc from wastewater by the extractant DEHPA (di-2-ethylhexyl phosphoric acid, represented as HL) as shown in Figure 25.2. In this case, the carrier also enhances the selectivity as most extractants are specifically designed to extract particular metal ions

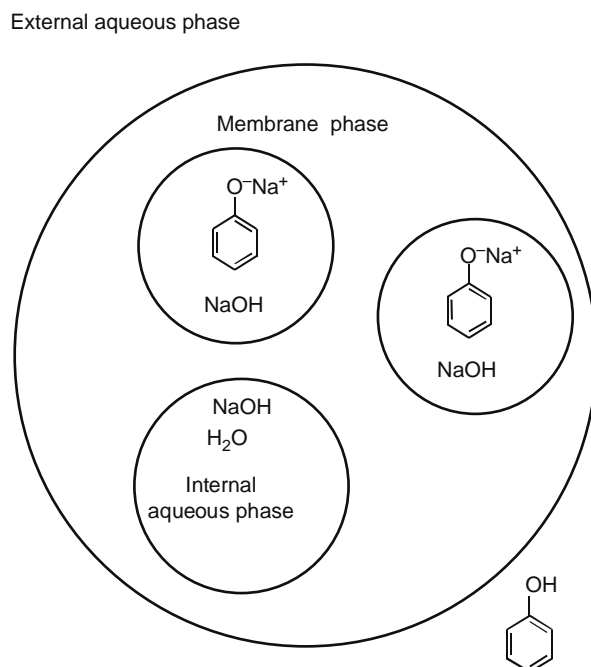
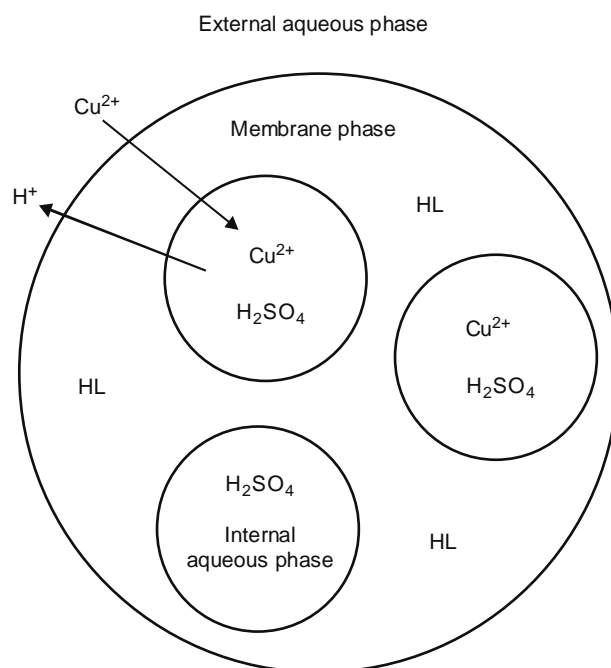


FIGURE 25.1 Schematic diagram of type 1 facilitation in an ELM system.



**FIGURE 25.2** Schematic representation of type 2 facilitated transport in an emulsion liquid system.

under given conditions. The metal ion,  $\text{Cu}^{2+}$  in the continuous phase reacts with the DEHPA in the oil phase to form the oil soluble complex,  $\text{Cu}(\text{HL})_2$ . Concentrated sulphuric acid in the internal aqueous phase strips the metal ion from the oil phase complex and transfers it into the internal phase, exchanging the metal ion for protons.

### 25.3 MODELING

A range of mathematical models were developed to explain solute transfer in ELM systems. Given the nature of these systems, most modeling efforts tend to end up as complicated mathematical structures with too many parameters and are far too tedious to be determined experimentally. The development of these models over the years has been discussed extensively [5–7]. Some of the development highlights are presented in the following sections.

#### 25.3.1 TYPE 1 FACILITATION

Mathematical descriptions of type 1 facilitation began with the pioneering work of Cahn and Li's [8] uniform flat sheet model, which was later adapted with limited success by Kremsec [9], Kremsec and Slattery [10] followed by the hollow sphere model of Matulevicius and Li [11] and later the reaction front concept of Kopp et al. [12].

Models for type 1 facilitation can be divided into two main categories: the state of the art advancing front models and the reversible reaction models.

The advancing front model first proposed by Ho et al. [3] assumes that the solute reacts instantaneously and irreversibly with the internal phase reagent at the reaction surface, which advances into the globule as the reagent is consumed. This model assumes an uniform globule size described by the Sauter mean diameter, no coalescence between emulsion globules, no circulation within the emulsion drop, local equilibrium exists between the internal phase and the membrane phase. The model does not account for mass transfer resistance in the external phase. Fales and Stroeve [13] as well as Stroeve and Varanasi [14] extended the advancing front model to include external phase mass transfer resistance outside the emulsion globules, that is, in the continuous phase.

Teramoto et al. [15] and Bunge and Noble [16] incorporated reaction reversibility in describing the transport process in the emulsion globule. Teramoto et al. [15,17,18] also developed models that accounted for diffusion in the emulsion drops and the drop-size distribution of the W/O emulsion. Kataoka and coworkers [19,20] developed the work of Teramoto et al. [15,17,18] by proposing a model with parameters that could be determined independently or through correlations in the literature.

Teramoto et al. [21] verified that the correlation used in the model of Bunge and Noble [16] was the most accurate of the correlations without adjustment parameters, because of the introduction of the apparent increase of the internal phase diffusivity caused by the diffusion of the reaction product between the solute and the internal stripping reagent (Baird et al. [22]). This effect was not included in the models proposed by Teramoto et al. [17] and Kataoka et al. [20]. Lin and Long [23] tried to

upgrade the model proposed by Bunge and Noble [16] to discard the simplification of considering an average value for the effective diffusivity and its variation with concentration in the model equations, but they ended up developing a slightly different model.

Chan and Lee [24] assumed that a reaction equilibrium existed in both the internal and external continuous phases. They also incorporated the overall mass transfer resistance in their model as well as accounting for leakage of the internal phase into the external phase as did Borwankar et al. [25], Liu and Liu [26], and Boyadzhiev et al. [27]. The reversible model was later extended by Baird et al. [22] to predict the extraction rate for multicomponent systems. A comparison study of the advanced front model and the reversible reaction model for multicomponent systems undertaken by Wang and Bunge [28] found the latter to be significantly better for mixtures of organic acids.

Yan et al. [7] proposed a model based on the model of Ho et al. [3], where the possibility of kinetic control of the stripping reaction is added as well as the mass transfer resistance inside and outside of the emulsion globules. Correia and de Carvalho [29] have presented a comparison between several models for the recovery of 2-chlorophenol from aqueous solutions by ELM, where they proposed the effective upgrade of the Bunge and Noble [16] model. The same authors present an application of the Yan et al. [7] model for the recovery of 4-hydroxybenzoic acid from aqueous solutions by ELM [29,30].

Although most models have been developed for batch extraction, the need to extend to continuous systems has been recognized by researchers (e.g., Rautenbach and Machhammer [31] and Datta et al. [32]).

A selected summary of the various systems, models, and observations for type 1 facilitation is presented in Table 25.1.

### 25.3.2 TYPE 2 FACILITATION

These models take into account the diffusion of the carrier and the metal ion–carrier complex in the emulsion globules. They must also account for the reversible reactions at the external and internal interfaces.

In developing a model for the extraction of copper, Teramoto et al. [34] included external phase mass transfer and also considered leakage. Kataoka et al. [35] included mass transfer resistance in the peripheral thin membrane layer. The results of such models have complicated equations with too many parameters. Lorbach and Marr [36] in what is considered to be the state of the art model, simplified the system by assuming a constant sum of the free and complexed carrier concentration. They also assumed constant pH in the external phase, eliminating mass transfer resistance in the peripheral thin membrane layer. Ortnier et al. [37] extended the model of Lorbach and Marr [36] for countercurrent column separations but found it too complicated.

Yan [38] further simplified the equations for batch extractions by assuming an irreversible, first-order extraction reaction between the solute and the carrier, irreversible first-order stripping reaction between the complex carrier and the internal reagent and constant distribution coefficients. Weiss et al. [39] proposed an empirical model for the extraction of mercury. Recently, Banerjea et al. [40] and Chakraborty et al. [4] presented an unsteady-state mathematical models to explain type 2 facilitation.

A selected summary of the various systems, models, and observations for type 2 facilitation is presented in Table 25.2.

### 25.3.3 MODEL PARAMETERS

Here, some of the physical parameters used in the various models are examined in terms of their contribution to the overall stability and effectiveness of the ELM system.

#### 25.3.3.1 Internal Droplet Size

Extraction and stripping efficiency is greatly enhanced with smaller droplets due to an increased surface area for diffusion. In the study of copper ion extraction, Cahn et al. [45] have shown that the average size of the internal phase droplets significantly influence the extraction rate. They also report that smaller droplets enhance membrane stability and retard leakage. The internal phase and its impact on the ELM process are discussed in Section 25.4.

#### 25.3.3.2 Emulsion Globule Size

According to Gu et al. [46], the size of the emulsion globule, generally characterized by the Sauter mean diameter or radius, is dependent on the viscosity of the emulsion, the type and concentration of the surfactant, and the method of mixing used to form the ELM. The emulsion globule size controls the surface area available for mass transfer between the emulsion and the continuous external phase. In a given volume of an emulsion dispersed in a continuous phase, the smaller the size of the globule, the larger will be the number of globules and therefore the larger the available surface area.

As shown by many studies, the globule size is characterized by the Sauter mean diameter or radius. This diameter/radius must be experimentally determined by photographic and microscopic techniques [34], or be estimated from correlations [47] that are often limited to the system for which they were developed. While the availability of correlations for ELMs is limited,

**TABLE 25.1**  
**Models for Type 1 Facilitated Transport**

Solute	Membrane Phase	Internal Phase	Model Description	Observations	References
Aniline, <i>m</i> -toluidine, <i>p</i> -toluidine	5 vol% SPAN 80, kerosene	0.2–0.4 M HCl	Mass transfer model in which diffusion in the emulsion drop, external mass transfer around the drop, phase, and chemical equilibria are taken into account.	The model satisfactorily predicted the experimental trends observed. A correlation for effective diffusivity in the emulsion globule is presented.	[15]
Phenol, cresol	5 vol% SPAN 80, kerosene	NaOH or LiOH	Modified mass transfer model in which diffusion in the emulsion drop, external mass transfer around the drop, phase, and chemical equilibria and the drop-size distribution of the W/O emulsion are taken into account.	Satisfactory agreement between experimental data and the model.	[17]
Phenol (data of Ho et al. [3])	1 wt% SPAN 80, 3 wt% ENJ 3029, 96 wt% S100N	1.5 wt% NaOH	An extension of previous diffusion models with the incorporation of reaction equilibrium. This model includes the reversibility in the reaction of solute with the reagent present in the internal droplets.	Excellent agreement between experimental data and the model.	[16]
Amines data of Teramoto et al. [15,17]			Mass transfer model that takes into account reversible reactions in both internal and external phases, external continuous phase mass transfer resistance, interfacial resistance, and diffusion within the emulsion globule. The leakage effect of the internal phase due to membrane rupture was also incorporated.	Satisfactory predictions of experimental data obtained for weak acids and bases.	[24]
Acetic acid	8 wt% E644 polyamine, 72 wt% kerosene, 19 wt% paraffin	3 M NaOH	Mass transfer model that accounted for the mass transfer both inside and outside the emulsion globules, the reaction between the diffusing component and the internal reagent in the globules jointly. A perturbation solution to the resulting nonlinear equations contained the parameters <i>Bi</i> and <i>Da</i> .	The model predictions showed that when <i>Da</i> was less than 5 or larger than 200, the overall process was controlled by reaction or diffusion, respectively, and for intermediate values of <i>Da</i> by reaction and diffusion jointly. The model predictions were in good agreement with the experimental data for batch extraction of acetic acid.	[7,33]
500 ppm <i>o</i> -chlorophenol	1–6 wt% ECA 4360 nonionic polyamine, LOPS (Exxon)	2.5 M NaOH	General model for physical transport of solute disregarding any chemical reaction effects. The model accounted for the continuous phase resistance and the interfacial resistance and permeation through a composite emulsion globule. It also quantified the loss in extraction efficiencies by leakage due to membrane breakage.	Satisfactory agreement between experimental and the model predictions with the best fit being achieved with the lowest surfactant concentration.	[25]
Phenol	5 vol% ECA 4306J, kerosene	0.1 M NaOH	General permeation model in which the emulsion drop is composed of the inner core of emulsion phase and the peripheral thin oil layer. The model accounted for chemical reactions, diffusion in the emulsion phase, in the peripheral thin oil layer of the emulsion drop, in the external aqueous film.	All parameters required for simulation can be estimated from the diameters of the emulsion drop and internal water droplet. Experimental results for the batch permeation of phenol were in good agreement with results computed by the model.	[19,20]
<i>m</i> -nitroaniline, <i>m</i> -toluidine	7 wt% SPAN 80, heptane, NaCl	0.1–1.0 M HCl	A new equation for the effective diffusivity of weak bases in the W/O emulsion.	This model is an improvement of the previous model [15,17].	[21]
2-Chlorophenol	2 wt% ECA 4360J, 98 wt% Shellsol T	0.5 M NaOH	Used the advancing front model and three reversible reaction models: Bunge and Noble [16] model, Lin and Long [23] model, modified Bunge and Noble model.	Both sets of models were found to predict the experimental data with reasonable accuracy implying that in the case of 2-chlorophenol the role of reversibility is negligible.	[29]
Aniline	2 vol% SPAN 80, isoparaffin	HCl	Mass transfer within the emulsion globule considered by shrinkage of the unreacted internal zone and the reversible reaction between solute and internal reagent.	Good agreement for the continuous system. Discrepancies at high stirrer speed and residence time.	[31]

**TABLE 25.2**  
**Models for Type 2 Facilitated Transport**

Solute	Extractant	Membrane Phase	Internal Phase	Model	Observations	References
Chromium	0.5 vol% Aliquat 336	1.5 vol% Paranox 106, 5 vol% decanol, kerosene	0.005–0.01 M NaOH	Unsteady-state mathematical model based on the advancing front model of Ho et al. [3] considers a reaction front to exist within the emulsion globule and assumes instantaneous and irreversible reaction between the solute and the internal reagent at the membrane-internal droplet interface.	Simulated curves were found to be in good agreement with the experimental data.	[40]
Citric acid	40 vol% Alamine 336	4 vol% C9232, mineral oil, 8 vol% chloroform	2.5 M NaOH	Modified shrinking core model that accounts for globule aggregation and emulsion break-up.	Model was tested by varying the system parameters. Good agreement between experimental and calculated results.	[43]
Copper Zinc	LIX64N DEHPA	4 vol% SPAN 80, kerosene	0.5 M H <sub>2</sub> SO <sub>4</sub>	General permeation model in which the emulsion drop comprises the inner core of emulsion phase and the peripheral thin oil layer. The model accounted for chemical reactions, diffusion in the emulsion phase, in the peripheral thin oil layer of the emulsion drop, and in the external aqueous film.	All parameters required for simulation can be estimated from the diameters of the emulsion drop and internal water droplet. Experimental results for the batch permeation of copper and zinc were satisfactorily predicted by the model.	[19,20]
Copper, nickel, chromium, iron	10 vol% DEHPA	5 vol% SPAN 80, 80% v/v kerosene + 5% v/v heptane	0.5–1.0 N HCl	Unsteady-state mathematical model based on the advancing front model of Ho et al. [3] neglects external phase mass transfer resistance and the effect of membrane breakage and has no adjustable parameters.	The results obtained from the numerical model were found to be in agreement with the experimental data. A semiempirical correlation between the distribution coefficient and the equilibrium external phase metal ion concentration was developed for use in the modeling.	[3]
Europium	5 vol% 2-ethylhexyl phosphoric acid mono-2-ethylhexyl ester (PC-88A)	4 mol% SPAN 80, kerosene or dodecane	1.5 M HCl	Mass transfer model built on to the immobilized hollow spherical emulsion globule [24].	Model calculations found to agree with experimental data within experimental error limits.	[41]
Gold	1% N503	4% E644, kerosene	0.1 M Na <sub>2</sub> SO <sub>3</sub>	Mass transfer model that accounts for mass transfer and first-order reactions both inside and outside the emulsion globules.	Good agreement between model predictions and the experimental data compared to the advancing front model of Ho et al. [3] and the external boundary layer and membrane diffusion controlled model of Yan [38].	[38]
Nitrate	Tri- <i>n</i> -octyl amine (TOA)	4 vol% SPAN 80, kerosene	Na <sub>2</sub> CO <sub>3</sub>	Modified diffusion model that assumes that the solutes react reversibly with the internal reagents and the effective diffusivity of the solutes in the emulsion globules is dependent upon the local solute concentration in the membrane phase.	Model predictions deviated from experimental data at longer contact times.	[44]

**TABLE 25.2 (continued)**  
**Models for Type 2 Facilitated Transport**

Solute	Extractant	Membrane Phase	Internal Phase	Model	Observations	References
Phenylalanine	4% v/v DEHPA	3% v/v SPAN 80, 93% v/v kerosene	1.5 M HCl	Model accounted for external phase mass transfer resistance, the interfacial reaction resistance, diffusion within the emulsion globule as well as leakage of the internal phase due to membrane breakage.	The model satisfactorily predicted the experimental results, but deviations at low external phase pH and longer contact time were observed. Depending on the experimental conditions, the transport of phenylalanine was governed by mass transfer in the external phase boundary layer, by diffusion within the membrane phase or by a combination of these effects.	[26]
Tellurium	5% DEHPA	3% SPAN 80, kerosene	5.0–6.0 M acid	A diffusion controlled film model that accounts for both the continuous phase and membrane phase resistance in the form of a Biot number.	Good agreement between computed and experimental data. Model capable of predicting the effect of parameters such as Biot number, ratio of emulsion phase volume to continuous phase volume, and membrane thickness on the rate of extraction. The continuous phase resistance was the controlling factor for the extraction of tellurium.	[42]
Zinc	3.5 wt% di(2-ethylhexyl) dithiophosphoric acid (DTPA)	2 wt% ECA 4360, 94.5 wt% Shellsol T	5 N H <sub>2</sub> SO <sub>4</sub>	Mass transfer model based on extraction and stripping reactions that also account for diffusion of the loaded carrier molecules into an emulsion globule.	Good agreement between experimental data and the model predictions. Reaction at the outer interface is important in the transfer process.	[18]

several are reported for oil/water and water/oil systems. A summary of the various correlations for the Sauter mean diameter in oil/water and emulsion systems is presented in Table 25.3.

### 25.3.3.3 Biot Number

Biot number,  $Bi$ , is the ratio of the mass transfer resistance inside the emulsion globules to that of the external phase [5] and is given by Equation 25.1:

$$Bi = kR/\alpha_e D_e \quad (25.1)$$

where

$k$  is the external phase mass transfer coefficient

$R$  is the radius of the emulsion globule (see Section 25.3.3.2 and Table 25.3)

$D_e$  is the effective solute diffusivity in the emulsion mixture and can be estimated from the Jefferson–Witzell–Sibbett equation [3,5–7]

$\alpha_e$  is the distribution coefficient of the solute between the external and membrane phase at equilibrium (dimensionless)

The external phase mass transfer resistance becomes insignificant if the Biot number is  $<20$ . At very high Biot numbers mass transfer resistance in the external phase can be neglected [7]. In general, the Biot number is  $>20$  as a result of good mixing needed to minimize the globule size to obtain a high mass transfer surface area, and therefore the external phase mass transfer resistance is negligible.

If  $k$  is significant, polydispersity of the emulsion globules will need to be considered since the Biot number is dependent on globule size. Correlations for  $k$  are available in the literature [33,41,74–80]. Distribution coefficient data should be experimentally determined for a given system. Data for some systems are available from the literature [21,38,42,81–83].

**TABLE 25.3**  
**Correlations for the Sauter Mean Diameter of the Dispersed Phase Droplets/Globules in Oil/Water and Emulsion Systems**

Correlation	System	Conditions	References	Parameters
$d_{32}/d_s = Bf_\phi W_e^{-0.6}$	Carbon tetrachloride/water, iso-octane/water	$\phi = 0.10-0.40$	[48]	$\Delta\rho$ = density difference between (W/O) emulsion and the continuous phase
$d_{32}/d_s = B(d_s/T)^{-b} W_e^{-0.6}$	Cyclohexane/water	$\phi = 0.50$	[49]	
$d_{32}/d_s = 0.06(1 + 3.75\phi)W_e^{-0.6}$ (4-bladed paddle)	Carbon tetrachloride/water	$\phi = 0.00-0.20$	[50]	$\gamma$ = interfacial tension between the membrane and the external phase
$d_{32}/d_s = 0.06(1 + 9\phi)W_e^{-0.6}$ (6-bladed turbine)	Toluene/water			$\varepsilon = P/V(1 - \phi_{av})\rho_c$
	<i>o</i> -Xylene/water			
	Benzene/water			
	Chlorobenzene/water			
$d_{32}/d_s = BW_e^{-0.6}$	5% shellwax 700/0.1% polyvinyl alcohol, water	$\phi = 0.05$	[51]	$\varepsilon_{av}$ = average energy dissipation rate per unit mass
$d_{32}/d_s = 0.053W_e^{-0.6}$	Xylene/water	$\phi = 0.001-0.005$	[52]	
$d_{32} = 0.0524\gamma^{0.5}\rho_c^{-3/5}\omega^{-6/5}d_s^{-4/5}$	Iso-octane/1% sodium chloride in water	$\phi = 0.00-0.015$	[53]	$\varepsilon_{max}$ = turbulence kinetic energy dissipation rate per unit mass
	25% methyl isobutyl ketone/1% sodium chloride in water	$\phi = 0.25$	[54]	
	Kerosene/water	$\phi = 0.05-0.30$	[55]	$\mu_c$ = dynamic viscosity of the continuous phase
	methylisobutyl ketone/water			
	<i>n</i> -butanol/water			
$d_{32}/d_s = 0.047(1 + 3.14\phi)W_e^{-0.6}$	Benzene/water, Hexane/water	$\phi = 0.04-0.35$	[56]	$\mu_d$ = dynamic viscosity of the dispersed phase
	Octanol/water			
	Styrene/water			
$d_{32}/d_s = 0.047(1 + 2.5\phi)W_e^{-0.6}$	Carbon	$\phi = 0.025-0.34$	[57]	$\nu_c$ = kinematic viscosity of the continuous phase
$d_{32}/d_s = 0.058(1 + 5.4\phi)W_e^{-0.6}$	tetrachloride + iso-octane/polyvinylalcohol + water	$\phi = 0.079-0.593$ batch process	[58]	$\rho_c$ = density of the continuous phase
$d_{32}/d_s = 10(-2.316+0.672\phi_w)\nu_c^{0.0722} \times \varepsilon^{-0.194}(\gamma/\rho_c)^{0.196}$	Cyclohexanone/water octanol/water methylamyl acetate/water isopropyl benzene/water	Continuous process $\phi = 0.05$	[59]	$\phi$ = volume fraction of the dispersed phase
$d_{32}/d_s = 10(-2.066+0.732\phi_w)\nu_c^{0.047} \times \varepsilon^{-0.204}(\gamma/\rho_c)^{0.274}$	Kerosene/water			$\phi_{av}$ = vessel average of $\phi$
$d_{32}/d_s = B(\gamma/\rho_c \varepsilon_{av} t_c)^{0.6}$	methylisobutyl ketone/water			$\omega$ = stirring rate
	<i>n</i> -butanol/water			$B$ = constant
$d_{32}/d_s = 0.08(1 + 4.47\phi)W_e^{-0.6}$	63% kerosene + 37% dichlorobenzene/water	Continuous process $\phi = 0.025-0.15$	[60]	
$d_{32}/d_s = 0.058(1 + 3.6\phi)W_e^{-0.6}$	Kerosene/water	$\phi = 0.05-0.5$	[61]	
	<i>n</i> -octanol/water			
	<i>n</i> -butanol/water			

$d_{32}/d_s = 2.1(\mu_d/\mu_c)^{3/8} Re^{-0.75}$	Silicone oil/water	$\phi = 0.0015$ high $\mu_d$	[62]	$b = \text{constant}$
$d_{32}/d_s = 0.053 W_e^{-0.6} (1 + 0.97 N_{vi}^{0.79})^{0.6}$	Silicone oil/water	$\phi = 0.002$	[63]	$b_1 = \text{constant}$
$d_{32}/d_s = 0.053 W_e^{-0.6} (1 + 0.91 N_{vi}^{0.84})^{0.6}$	Silicone oil/methanol + water	$\phi < 0.005$	[64]	$B_2 = \text{constant}$
$d_{32}/d_s = 0.016 [W_e (\Delta\rho/\rho_c) (\mu_d/\mu_c)]^{-3.75}$	Silicone oil/water	SPAN 80, no carrier, no solute transfer, no swelling	[65]	$B_3 = \text{constant}$
$d_{32}/d_s = 0.012 [W_e (\Delta\rho/\rho_c) (\mu_d/\mu_c)]^{-0.22}$	SPAN 80 or ECA 4360J, kerosene/sodium chloride + water	SPAN 80, carrier, solute transfer, swelling		$d_s = \text{stirrer or impeller diameter}$
$d_{32}/d_s = 0.066 [W_e (\Delta\rho/\rho_c) (\mu_d/\mu_c)]^{-0.75}$		ECA 4360J, carrier, solute transfer, no swelling		$d_{32} = \text{Sauter mean diameter of the dispersed phase droplets/globules}$
$d_{32}/d_s = 0.12 W_e^{-0.5}$	2 wt% SPAN 80, kerosene/water	$\phi = 0.125$	[47]	$f_\phi = \text{ratio of actual mean drop diameter to diameter at } \phi = 0.1$
$d_{32}/d_s = \eta^{0.8} W_e^{-0.5}$	Bee wax/water	$\eta < 0.16 \text{ Ns/m}^2$		$F^{sw} = \text{swelling factor}$
$d_{32}/d_s = 0.95 N_p^{-2/5} (1 + 2.5\phi^{2/3}) (\mu_d/\mu_c)^{1/5} (\mu_d/\mu_c)^{1/8} W_e^{-0.6}$		$\eta > 0.16 \text{ Ns/m}^2$	[66,67]	$P = \text{power input}$
(break up region)		$\phi = 0.0045-0.36$		$N_{vi} = (\rho_c/\rho_d)^{1/2} \mu_d \varepsilon^{-1/3} d_{32}^{1/3} / \gamma$
$d_{32}/d_s = 0.035 N_p^{-1/4} (1 + 3.5\phi^{3/4})$		0.00057-0.001	[68]	$Re = \text{Reynolds number}$
$(\mu_d/\mu_c)^{1/5} (\mu_d/\mu_c)^{1/8} W_e^{-0.6} d_s^{-3/8}$ (coalescence region)	Silicone oil/water			$T = \text{vessel diameter}$
$d_{32}/d_s = 0.49 W_e^{-0.6} (1 + 1.38 N_{vi} (d_{32}/d_s)^{1/3})^{0.6}$	Paraffin oil/water			$t_c = \text{circulation time}$
$d_{32}/d_s = 0.11 (\eta\rho_c/\eta_c\rho)^{0.32} (V_m + V_i/V_e + V_m + V_i)^{0.1} W_e^{-0.2}$	<i>p</i> -Xylene/water	For $Re > 6000$	[31]	$V = \text{volume of the fluids}$
$d_{32}/d_s = 0.024 (\omega d_s^2 \rho_c / \eta_c)^{0.6} W_e^{-1.2}$	4 wt% ECA 4360, Shellsol T/aqueous ammonia, pH 12 internal phase: 20 wt% H <sub>2</sub> SO <sub>4</sub>	$\phi = 0.01-0.03$	[69]	$V_e = \text{total volume of the external phase}$
$d_{32}/d_s = 0.056 (1 + 10.97\phi) W_e^{-0.6}$	Styrene/0.5 g/L polyvinyl alcohol + water	$\phi = 0.025, 0.05$	[70]	$V_i = \text{total volume of the internal phase}$
$d_{32}/d_s = 0.053 (1 + b_1\phi)^{0.5} W_e^{-0.6} (1 + 4.08 N_{vi})^{0.6}$	3 vol% SPAN 80, kerosene/water			$V_m = \text{total volume of the membrane phase}$
$d_{32} = B_2 \gamma^{0.8} / \rho_c^{0.6} / \omega^{1.2} d_s^{0.8}$	solute: 1000 ppm phenol internal phase: 1 wt% NaOH	$\phi = 0.00-0.5$	[71]	$W_e = \text{Weber number} = \omega^2 d_s^3 \rho_c / \gamma$
$d_{32} = 118.6 (\varepsilon_{\max} \omega d_s^2)^{-0.270}$	SPAN 80 or L113B, TBP, kerosene/water			
$d_{32}/d_s = 0.75 W_e^{-0.6} \phi^{0.36} (\mu_c/\mu_d)^{0.11} (1 + F^{sw})^{1/3}$	solute: lactic acid			
	silicone oil/water	—	[72]	
	0.3 M Cyanex 302, 1%-5% v/v Arlancel C, kerosene/water	$\phi = 0.025-0.067$	[73]	
	solute: cadmium sulfate			

Several studies have modeled and attempted to quantify the effect of the Biot number on ELM performance, including Yan et al. [7,33] and Huang et al. [84].

### 25.3.3.4 Damköhler Number

The Damköhler number,  $Da$ , represents the ratio of the reaction rate to the diffusion rate inside the globule [7] and is given by Equation 25.2:

$$Da = \phi_{\text{int}} k_1 R^2 / \alpha_e D_e \quad (25.2)$$

where

$\phi_{\text{int}}$  is the volume fraction of the internal aqueous phase in the emulsion globule

$k_1$  is the reaction rate constant

$\alpha_e$ ,  $R$ , and  $D_e$  are as previously defined

Yan et al. [7] have shown that in the case of batch extraction of acetic acid from dilute solution (using an ELM), when  $Da$  is  $<5$  or  $>200$ , the overall process is controlled by reaction or diffusion, respectively, and by a combination of reaction and diffusion for intermediate values of  $Da$ .

## 25.4 EMULSION LIQUID MEMBRANE PROCESS

Emulsion liquid membrane process can be divided into three stages: 1. emulsification, 2. permeation and settling, and 3. demulsification. Each stage and associated critical parameters are described in the following sections.

### 25.4.1 EMULSIFICATION

The components of an ELM system are the diluent, surfactant, internal aqueous phase, continuous phase, and carrier in the case of type 2 facilitation. Emulsification is usually achieved by high speed or ultrasonic stirrers for batch operations and high-pressure static dispersion or colloid mills for continuous mode [46]. The presence of a surfactant is necessary to ensure adequate stability of the emulsion during the extraction process. However, an ultra stable emulsion is not desirable as it will lead to difficulties in the demulsification stage. For the effective working of an ELM all components must be carefully chosen and each composition is critical. Some of the desirable properties of the various components are listed in the following sections.

#### 25.4.1.1 Surfactants

Surfactant is a key component for the formation of a stable emulsion. Ideal surfactant properties, apart from being relatively cheap and nontoxic include [46]:

1. Virtually no water is carried during operation to prevent/reduce osmotic swelling (see Section 25.4.2.2).
2. No reaction with the extractant in the membrane phase. Any possible reaction should enhance the extraction rather than cause decomposition of the extractant.
3. Low interfacial resistance to mass transfer.
4. Inhibition to demulsification.
5. Solubility in the membrane phase, but not in the internal and external phases.
6. Stability in the presence of acids, bases, and bacteria.

It has been observed that as the hydrophilic lipophilic balance (HLB) value of the surfactant increases, the stability of the emulsion decreases [85]. The contribution of the surfactant to stabilization and swelling is discussed in Sections 25.4.2.1 and 25.4.2.2, respectively.

Stevens et al. [86] proposed the replacement of the surfactant with fluids to modify the rheological properties and stabilize the emulsion. The aim was to slow the drainage of the film between the coalescing drops, thereby increasing the stability of the membrane. Their study on the removal of chromium with Alamine 336 showed that the emulsion stability could be controlled with the addition of small amounts of polymer to the organic phase and that demulsification could be achieved by heating the system.

#### 25.4.1.2 Diluents

The diluent in which the extractant and surfactant are solubilized is a major component of an ELM system. It impacts on the membrane properties such as distribution coefficient and diffusion coefficient and on the effectiveness of the membrane system. Apart from being relatively cheap and readily available, the desired properties of the diluent include [46]:

1. Low solubility in the internal and external aqueous phases.
2. Compatibility with the extractant and surfactant and the inability to form new phases.
3. Moderate viscosity (not too low as to compromise membrane stability).
4. Having a density that is sufficiently different to the aqueous phase.
5. Low toxicity and high flash point.

In general aliphatics are preferred to aromatics as they are more likely to meet most of the listed requirements. To date the most commonly used diluents for ELM systems include kerosene, isoparaffin, cyclohexane, toluene, Shellsol T, heptane, decane, dodecane, nitrobenzene, S100N, and Escaid 110. The pros and cons of specific diluents will be discussed in Section 25.4.2.1.

### 25.4.1.3 Carriers

Carriers tend to be lipophilic and can exhibit quite high interfacial activity [87]. They generally decrease the stability of the ELM due to competitive adsorption (with the surfactant) at the interface [88]. In addition, some carriers have high affinity for water (hydration of their polar groups). Transport of hydrated water can also occur during the metal-carrier complex formation if the metal ion is present as a hydrated complex in the external phase and transports the waters of hydration to the complex formed with the carrier [89]. This effect is more serious in the case of carrier molecules containing many oxygen atoms (such as DEHPA and TOPO) as opposed to those that contain nitrogen (such as LIX64N and Aliquat 336) [89,90]. The interaction of the carrier with the surfactant to form complexes that reduce the free surfactant content of the emulsion has also been reported [90].

Several carriers/extractants/ligands are available commercially for the extraction of acids, bases, elements such as copper, cobalt, nickel, zinc, iron, chromium, precious metals, and the rare earths. The physicochemical properties of the various commercial extractants available for type 2 facilitation have been previously reported by Gu et al. [46] and Cox [91], and the chemical behavior of these extractants can be broadly classified into three categories:

1. Acidic extractants, chelating or non-chelating containing one or more ionizable proton, combine with a metal ion to form a neutral complex. Carriers in this category include hydroxyoximes (P50 (Acorga), LIX 84, LIX 65N, LIX 64N, LIX 860 (Cognis), SME529 (Shell));  $\beta$ -hydroxyquinolines (Kelex 100 (Witco));  $\beta$ -diketones (LIX 54, acetylacetone); carboxylic acids (naphthenic acids, versatic acids); alkyl phosphorous compounds such as organophosphoric acids (DEHPA, DBP); organophosphonic acids (PC 88A, Ionquest 801); organophosphinic acids (Cyanex 272, DTPA); and ionizable crown ethers.
2. Basic or anion exchangers, generally quaternary ammonium compounds and alkylamines, extraction is dependent on the ability of the metal ion to form an anionic species in the aqueous phase and then be extracted as an ion-pair by the amine salt.  
Included in this category are the high-molecular weight primary amines (Primene JMT); secondary amines (Amberlite LA-2); tertiary amines (TOA, TNOA, Alamine 336); and quaternary alkylammonium salts (Aliquat 336).
3. Solvating extractants compete with water for a position in the first solvation shell of the metal ion. The replacement of water molecules by these reagents facilitates the transfer of the metal-ion complex into an organic phase.

Commercial solvating extractants include phosphine oxides (TOPO, Cyanex 923) and phosphorous esters (TBP).

The key criterion in selecting a carrier/extractant is that it and the complex formed must be soluble in the membrane phase, but not soluble in both the internal and continuous phases [46]. Further precipitation within the membrane or at the interfaces must be prevented. To ensure successful stripping, it is necessary to have a solute-complex of moderate stability so as to maximize the effectiveness of the stripping agent [46]. The effect of carrier concentration on the stability of ELM systems is discussed in Section 25.4.2.1.

### 25.4.1.4 Internal Phase

Parameters relating to the internal phase such as volume fraction of the internal aqueous phase, pH, and volume ratio of membrane phase to internal aqueous phase impact on the working of an ELM system. Discussion of the role of the internal phase in terms of swelling, leakage, permeation, and settling is found in Sections 25.4.2.1 through 25.4.2.3.

## 25.4.2 PERMEATION AND SETTLING

Following emulsification, the emulsion is dispersed by mechanical agitation into the external feed phase containing the solute to be extracted. The efficiency of this extraction process is dependent on several parameters as discussed below.

### 25.4.2.1 Composition

A water-in-oil emulsion dispersed in an aqueous phase (W/O/W ELM) is generally stabilized by the addition of a surfactant. In the case of type 2 facilitation, a carrier species is also present. The concentration of these additives together with the composition of the internal aqueous phase, external aqueous phases, and the permeation conditions influence the properties of the ELM system. These effects are summarized as follows:

*Effect of Surfactant Concentration:* Emulsion stability generally increases with increasing surfactant concentration [92,93]. As discussed in Section 25.4.2.3, an increase in surfactant concentration leads to the lowering of leakage due to an increase in the mechanical resistance of the membrane. An increase in this parameter also increases the membrane phase viscosity as well as its resistance to mass transfer including water mass transfer, thus reducing osmosis [89,94].

However, increasing surfactant concentration has the drawback of reducing globule drop size and increasing the interfacial area available for mass transfer of both solute and water. This effect is enhanced in the case where the surfactant molecules themselves have an affinity for water [95,96]. If the surfactant concentration exceeds the critical micelle concentration (cmc), water transport in W/O/W systems by reversed micelles can occur [89,97]. An increase in concentration of some surfactants such as SPAN 80 also leads to an increase in the entrainment of the external phase during permeation promoted by an excess of surfactant molecules [71,98]. Miesiac et al. [99] found that in the case of penicillin G separation, the choice of surfactant could control not only the extraction rate, but also the back transfer rates of the hydrolysis products.

As the surfactant is of key importance in the stability of the ELM much work has been carried out in the area of surfactant development. Wan et al. [100] observed that higher molecular weight surfactants demonstrated much better properties. They have developed a new polymeric-type surfactant: LMA with molecular weights in the range 5,976–56,798 g/mol. Zhang et al. [101] report that LMS-2 is more stable than Span 80 for phenol removal. The anionic, sulfonic-type surfactant EM301 leads to lower swelling than Span 80 and E644 according to Li and Shi [94]. LYF-G2 (sulfonate polybutadiene) showed better emulsion stability than ECA 4360 (polyamine) and EM 301 (surfactant polyisobutylene) for an aqueous HCl feed [102]. Draxler et al. [103] reported that P18 (maleic anhydride/1-octadecene copolymer surfactant) is more compatible with the hydroxyoxime extractant, while Span 80 and polyamine are not. Improved membrane formulation was noted with the addition of 2.5%–5% v/v cyclohexanone [85] as a result of preferential micellization with Span 80, which reduced swelling. Kakoi et al. [104] have developed surfactants that served as both emulsion stabilizer and carrier.

*Volume Fraction of the Internal Phase:* Decreasing the volume fraction of the internal phase will lead to a more stable emulsion in terms of osmosis and leakage due to the increase in the membrane phase layer around the internal droplets [93,105,106]. However, this leads to an increase in surfactant content in the emulsion and a consequent increase in the probability of entrainment [107].

Maximum stability is attained when saturation of the adsorbed surfactant layer is reached. In the case of high-volume fraction at a specific surfactant concentration, if the adsorbed layer is unsaturated, the emulsion stability decreases. In a low-volume fraction case, if the specific surfactant concentration is too high, emulsion stability is also decreased. Therefore, while an increase in surfactant concentration may increase the stability of the internal phase, the absolute stability of the ELM may be decreased [88].

*Carrier Concentration:* Mass transfer rates can be increased by increasing the carrier concentration [41], however, increasing the carrier concentration usually increases swelling and lowers the emulsion stability [33,108]. Other studies have found limits to the carrier concentration where further increases do not lead to an increase in extraction rates as the mobility of the carrier is stifled due to an increase in viscosity [34,41].

*Continuous Phase Composition:* Emulsion liquid membrane properties can be significantly influenced by changing the composition of the external aqueous phase. Emulsion stability can be improved by an increase in the viscosity as a result of the decrease in the rate of fluid drainage between the liquid films [88]. An increase in ionic strength of the external phase has been shown to cause a decrease in entrainment phenomena during permeation. This has been attributed to an alteration of the structure of the interface between the emulsion and the external phase promoted by the presence of electrolytes in the external phase. A reduction in osmosis also occurs due to a reduction in the chemical potential difference between both sides of the membrane [94,98].

*Internal Phase Composition:* As with the continuous phase, the internal phase properties also influence the properties of the ELM. Ionic strength, pH, and the presence of organic species will impact on the stability of the ELM. Emulsion liquid membranes work on the basis that the polar substances (usually high concentrations of acid or base) contained in the internal phase are impermeable to the membrane phase. However, the presence of the surfactant can cause the uptake of these compounds by the formation of reverse micelles [97].

Ma and Shi [109] report on the influence of the internal phase composition on breakage rate in the removal of acetic acid by an ELM system. They found that for a given surfactant concentration and stirring rate, increasing the concentration of NaOH in the internal phase led to an increase in emulsion breakage. These observations have been confirmed by Yan et al. [110] who proposed that high internal reagent concentrations lead to thinning of the electrical double layer, decreasing the stability of the ELM. Bart et al. [89] report on the exponential increase in osmosis with increasing acidity of the internal phase. Care should be taken to ensure that the internal phase reagent concentration is sufficient to effect removal of the solute but not so high as to destabilize the system.

*Internal Phase Droplet Diameter:* Drop size increases with increasing volume [34,41]. However, increasing the drop size will reduce the thickness of the membrane phase and lead to a lower mass transfer resistance. Optimization is a trade-off between interfacial area reduction and the increase in the mass transfer rate because of the reduced membrane thickness and thus small mass transfer resistance [107].

*Diluent and Additives:* There is no doubt that both diluents and any additives have an impact on the efficiency of the ELM system.

Kinugasa et al. [98,111] noted that in the case of aliphatic hydrocarbons, the ELM becomes more stable with increasing number of carbon atoms, while those composed of aromatics, such as toluene, were less stable to mechanical forces. Lin and Long [44] found kerosene to be the more efficient diluent than S100N for nitrate extraction. Kumbasar and Tutkun [112] report that kerosene is a better-performing diluent than STA90 NS for gallium removal by ELM. Lee et al. [41] studied several diluents for europium extraction and report that while *n*-dodecane and kerosene are somewhat similar, xylene demonstrated much lower extraction efficiency. They speculate that the difference may be due to the steric chemistry and polarity effects imposed on the carrier, in this case PC 88A.

Strzelbicki and Schlosser [113] report that the addition of alkylphenol sulphides to ELMs containing ECA 4360 accelerates cobalt ion extraction by DEHPA. Skelland [114] and Skelland and Meng [115] proposed the modification of the rheological properties of the organic phase by the addition of small quantities of polyisobutylene, polybutadiene, or polystyrene. As noted by Shere and Cheung [116], emulsions prepared with high viscosity oils are generally more stable. The effect of such additions includes increases in the membrane viscosity and stability together with a reduction in the amount of surfactant required for stabilization which in turn could lead to a reduction in swelling. Skelland and Meng [115,117] have reported improved performance for the extraction of benzoic acid, phenol, and ammonia with such modifications.

*Permeation Conditions—Stirring Speed, Time, and Temperature:* Turbulent contact of the continuous and emulsion phases can lead to the emulsification of the continuous phase into the emulsion (secondary emulsification) [73]. Swelling also increases with increasing stirring speed [118,119]. Several studies have sought to optimize stirring speed and minimize breakage [41,44]. Gallego-Lizon and Perez de Ortiz [73] state that swelling increases with contact time and may cause emulsion rupture, limiting the operational contact time. Bart et al. [89] report that the degree of osmosis is approximately linear with residence time. The transfer of water across the membrane depends on the temperature that affects the formation of surfactant aggregates, viscosity of the membrane, and the emulsion viscosity.

#### 25.4.2.2 Swelling in Emulsion Liquid Membranes

As mentioned earlier, one of the disadvantages of ELM systems is their tendency to undergo swelling. There are two types of emulsion swelling, namely, osmotic swelling and entrainment swelling. In the case of W/O/W-type systems osmotic swelling occurs as a result of water transfer from the continuous phase into the internal phase due to the large difference in osmotic pressure between the internal and external aqueous phases [120]. Entrainment swelling is caused by the entrainment of the external phase into the internal phase due to the repeated coalescence and re-dispersion of emulsion globules during the dispersion operation thus causing an increase in the volume of the internal phase [33,120].

The disadvantages of swelling are dilution of the separated product in the internal phase, an increase in membrane rupture/breakage, and an increase in agitation power required to disperse the emulsion [121].

Swelling is usually quantified in terms of the swelling ratio, which is defined as the ratio of the diameter of the W/O/W globule at time,  $t$ , to that at time  $t = 0$  [120].

The consequences of swelling according to Yan and Pal [122] are

1. Rapid increase in the internal phase volume
2. Sharp increase in the viscosity of the emulsion
3. Possible breakdown of the globules
4. Retardation of the solute enrichment process
5. Reduced separation efficiency
6. Adverse effects on the final demulsification process

Several mechanisms have been proposed to explain swelling in ELM globules [89,94,122]:

1. Molecular diffusion of water from the external phase to the internal phase [123]
2. Micelle-assisted transport of water from the external phase to the internal phase [124]
3. Water transfer via hydration of the surfactant molecules [123]
4. Entrainment and emulsification of the external aqueous phase due to the presence of excess surfactant; also called entrainment swelling or just entrainment [95,111,117,121]

In most situations, mechanisms (i) and (iii) are the probable reasons for swelling.

Studies on the measurement of swelling in ELM systems have been reported by many, including Li and Shi [94], Wan and Zhang [120], Itoh et al. [121], Yan and Pal [122], and Ramaseder et al. [125]. Yan and Pal [119] proposed an online technique for the measurement of swelling in these systems.

Different methods [120] such as volume variation, internal phase droplet size variation, viscosity variation, density variation, tracer method, Karl-Fischer method, and electrical conductivity have been employed in the measurement of emulsion swelling. The data obtained tends to be as varied as the methods used [120]. One major drawback is that none of the above methods is capable of determining both emulsion swelling and membrane breakage in the same experiment. Further, osmotic swelling cannot be differentiated from entrainment swelling.

Some general observations on swelling in ELM systems suggest that the swelling ratio is dependent on the following four factors [94,119,120,122]:

*Type and Concentration of the Surfactant:* Wan and Zhang [120] observed that both entrainment and osmotic swelling were dependent on the surfactant: in the order of increasing swelling: SPAN 80 > Lan113A > ENJ-3029 > LMA. They note that the low-molecular weight SPAN 80 with a large hydrophilic group mainly comprised oxygen with high electronegativity will have a higher hydration capacity and larger diffusivity compared to the others with high-molecular weight and their hydrophilic group mainly comprised nitrogen with relatively low electronegativity. LMA has the lowest hydration capacity and diffusivity. Li and Shi [94] observed the following order of increasing swelling: SPAN 80 > E644 > EM301, under a given set of conditions. Yan and Pal [119] observed increasing swelling rates with increasing surfactant (EMSORB2500) concentration up to 5 wt% and then a drop with further addition of surfactant.

*Background Electrolyte Concentration:* Since the chemical potential difference between the external and internal phases is the driving force for osmotic swelling [90,120] an increase in the chemical potential difference will result in an increase in osmotic swelling. Wan and Zhang [120] show that electrolyte concentration differences between external and internal phases have no significant effect on entrainment swelling, while this is not the case for osmotic swelling.

*Volume Ratio of the Oil (Membrane) Phase to the Internal Phase:* This parameter can affect the surfactant concentration at the interface of the membrane/aqueous phases and in the bulk membrane phase, affecting emulsion swelling [120]. Both entrainment and osmotic swelling increase with increasing volume ratio of the oil (membrane) phase to the internal phase. The effect of this parameter is also dependent on the surfactant present [120].

*Stirring Speed:* The emulsion is generally dispersed into a large excess of the continuous phase. To maximize mass transfer a large interfacial area is required and this requires a high stirring speed. Increasing the stirring speed not only increases the interfacial area but can also lead to membrane swelling [94] and membrane breakage [120]. Therefore, optimization of the stirring speed is required. This process has been found to be dependent on the surfactant type [94,106,120].

Emulsion swelling is one of the major drawbacks in the use of this technology in industrial situations. For example, the economic advantages of ELM, over conventional solvent extraction for copper processing are lost with a swelling ratio in excess of 30–40 [102]. In terms of processing, an emulsion swelling of about 10% is considered acceptable [45].

### 25.4.2.3 Membrane Leakage

Membrane leakage/rupture/breakdown where the previously extracted solute as well as the stripping reagent are released into the feed stream impacts on the extraction efficiency of the ELM system. It is generally agreed that the properties of the surfactant, diluent, the internal phase, and its volume fraction have significant effects on membrane leakage [46]. Membrane leakage at the rate of ~0.1% is allowable for a practical process [126]. Leakage in ELM systems is well documented: Bunge et al. [93] studied encapsulated phase leakage during ELM extraction of copper ions. They found that the type of surfactant had an impact in that ECA 4360 showed greater encapsulated phase leakage than ECA 5025. The leakage rate decreased with increasing surfactant concentration with a limit at 3 wt%. Leakage is strongly dependent on the volume fraction of the membrane phase with leakage rates increasing greatly when this volume fraction was >0.5. They also noted that the presence of surface active carriers contributed to leakage. Borwanker et al. [25] found that the rate of leakage by membrane rupture is usually a function of surfactant concentration and agitation speed. Okazaki et al. [106] report that the W/O emulsion droplets were not affected by the apparent viscosity of the W/O emulsion but by the organic phase viscosity. They also observed that leakage increased with increasing volume of the internal aqueous phase, leakage was affected by the osmotic pressure difference and that the type of tracer had no effect. In an effort to quantify the effects of such parameters, Okazaki et al. [106] propose two correlations for the leakage rate constant conditional on the osmotic pressure difference between the inner and outer aqueous phases. Shere and Cheung [116] studied the influence of internal phase volume fraction, surfactant concentration, agitation speed, and emulsifying device on leakage. As expected, leakage was significantly dependent on the volume fraction and surfactant concentration. They also found that the use of a high-speed blender rather than an ultrasonic dispenser, for making the emulsion, causes faster leakage and noted that although the viscosity of the emulsion increases if a high-speed blender is used, the stability acquired is offset by the increase in the size of the microdroplets formed with this device. In general, emulsions prepared with a high energy density input such as the ultrasonic method will have smaller

droplets. This will enhance the membrane stability, provided the surfactant concentration is high enough. Smaller droplets also give a large area for interfacial mass transfer [46].

Efforts to compute breakage/leakage in W/O/W include the work of Boyadzhiev et al. [82], Kinugasa et al. [98], Okazaki et al. [106], Martin and Davies [127], and Goto et al. [128]. Nakano et al. [129] report on leakage in O/W/O systems.

### 25.4.3 DEMULSIFICATION

As stated earlier, after extraction the membrane must be broken and the solute recovered. The breaking or demulsification of a loaded emulsion is one of the most important steps in the process as the membrane phase must be available for recycling [46].

The demulsification process can be divided into three stages [130]:

1. Droplet coalescence and growth
2. Droplet settling
3. Coalescence of the large water and oil droplets with their respective continuous phases in the coalescer

To date, chemical or physical treatment is the method used for demulsification.

#### 25.4.3.1 Chemical Treatment

This treatment involves the addition of a demulsifier. For example acetone [85], *n*-butanol [130,131], and 2-propanol [132] have been found to be effective demulsifying agents for particular applications. Although this method is effective, it modifies the properties and prevents reuse because additional separation steps for recovery and recycling are required. Further recovery of the demulsifier by distillation is expensive [101,131].

#### 25.4.3.2 Physical Treatments

Physical treatments include heating, centrifugation, high shear, ultrasonics, solvent dissolution, and the use of high-voltage electrostatic fields [46]. Other nonconventional methods, such as microwave demulsification [134] and the use of porous glass membranes [135], have also been investigated.

##### 25.4.3.2.1 Heat Treatment

The advantages of heat treatment [131] are reduction in the density and viscosity of the oil and an increased solubility of the surfactants in both the oil and water phases. This in turn leads to a weakening of the interfacial film. The main disadvantage is that heat treatment by itself is slow demulsification kinetics.

##### 25.4.3.2.2 High Shear

Emulsion liquid membranes can be effectively demulsified by high shear. A variation on this is to employ centrifugation as a first step, followed by processing in a high shear device [46].

##### 25.4.3.2.3 High-Voltage Electrostatic Fields

By using high-voltage electrostatic fields not only can faster coalescence be achieved, but also the organic phase can be recycled. The mechanisms of electrostatic demulsification are not completely understood. The general belief is that the electric field can polarize and elongate water droplets, neighboring water droplets, after acquiring induced charge from the electric field, will attract each other and coalesce to form a larger drop.

The use of electrostatic fields believed to be the most efficient and economic method of demulsification [46] will be discussed further in terms of equipment used, operating parameters, and proposed models for the process.

*Equipment:* Several types of ac and dc electrostatic coalescers have been developed. Documented equipment for electrostatic demulsification includes the continuous insulated electrode coalescer [130,136], two-phase insulated electrodes in parallel [126], circular coalescer [137], continuous coalescer [138], horizontal insulated electrode [130], box electrostatic demulsifier [139], tubular coalescer [140], and batch cylinder demulsifier [141]. Design criteria for electrostatic demulsifiers have been reported by Draxler and Marr [142] and Draxler et al. [143].

*Operating Conditions:* Parameters such as applied voltage, frequency, waveform, temperature, stirring, and additives have been shown to have an impact on the demulsification process. Kataoka and Nishiki [144] enhanced demulsification with increasing voltage as did Wang et al. [141], Fujinawa et al. [145], and Hauertmann et al. [146]. However, there are limits to maximize voltage that can be applied before formation of a stable sponge emulsion (a high water content water-in-oil emulsion) as noted by Larson et al. [131].

Feng et al. [138] found that coalescence efficiency could be improved with increasing frequency. Draxler et al. [103] demonstrated that for a given degree of demulsification the voltage could be reduced if the frequency was enhanced. It has

been shown that under constant voltage an optimum frequency exists, below which the demulsification rate was enhanced with increasing frequency, but above which the rate decreased with increasing frequency [147–149].

A square waveform has been shown to be more effective than a triangular or sine form [102,148,149]. The proposed explanation of this is that under the same peak voltage, the square waveform offers longer time to act on the water droplets to be coalesced.

Both stirring and temperature elevation have been shown to accelerate demulsification [130,138,150]. Hsu and Li [130] report that insulation material having a dielectric constant  $>4$  offered better demulsification performance. Goto et al. [140] report on the effect of surfactant type on demulsification.

*Modeling:* Many researchers, including Goto et al. [140], Wang et al. [141], Fujinawa et al. [145], and Hano et al. [150], have attempted to quantify the rate of demulsification. In a recent development, Ichikawa et al. [151] and Ichikawa and Nakajima [152] proposed a theory for electrostatic demulsification of O/W emulsions (by low-external electric fields) based on the Poisson–Smoluchowski equation. Their theory revealed that the applied field induced demulsification according to the following mechanisms [152]:

1. Applied field induced a steady-state current of ions in the aqueous phase, which in turn generated an electric field in the aqueous phase.
2. Electric field in the aqueous phase rearranged surface charges on the oil droplets to compensate the field gradient on the surface of each droplet, which caused the polarization of the electrostatic surface potential.
3. Polarization lowered repulsive osmotic pressure in the overlapped diffuse electrical double layers of the droplets and accelerated demulsification.

## 25.5 APPLICATIONS

Documented applications of ELMs include [2,46,153–158]:

1. Wastewater treatment, e.g., removal of zinc, removal of radioactive materials and nuclear wastes, recovery of nickel from plating wastes, and phenol removal.
2. Biochemical processing, e.g., recovery of penicillin and erythromycin.

A summary of a number of systems studied in both categories is presented in Tables 25.4 through 25.8. While the majority of the work to date has been on W/O/W systems, studies on the use of O/W/O systems for the removal of various oils have been reported [1,216,217,129].

**TABLE 25.4**  
**ELM Systems for the Separation of Metal Ions**

Solute	External Feed Phase	Extractant	Surfactant	Diluent	Internal Phase	Efficiency/ Recovery	References
Arsenic	5.5 mg/L As(III) (as As(OH) <sub>3</sub> ) in 0.4 M H <sub>2</sub> SO <sub>4</sub>	10 vol% 2-ethylhexanol	2 vol% ECA 4360 polyamine	88 vol% <i>n</i> -heptane	2 M NaOH	>95%	[159]
Cadmium	Cd(CN) <sub>4</sub> <sup>2-</sup>	Aliquat 336	0.1% SPAN 80, 3% polyamine	86% isoparaffin	EDTA, pH 4–6	99%	[160]
Cadmium	1100 ppm Cd pH 4.45	5 wt% DEHPA	3 wt% ECA 5025	82 wt% tetradecane	6 N H <sub>2</sub> SO <sub>4</sub>	97%	[161]
Cerium	Ce <sup>3+</sup> in 6.0 M NaNO <sub>3</sub> + 0.1 M HNO <sub>3</sub>	0.1 M TOPO	3% SPAN 80/20	Cyclohexane	0.05 M sodium citrate, pH 8	98.5%	[162]
Cesium	0.001 M CsNO <sub>3</sub> in 0.01 M HNO <sub>3</sub>	0.01 M 8,8'-dibromo-bis (1,2-dicarbolly) Co(III) (BR <sub>2</sub> DCC)	4.0% SPAN 80/85	Nitrobenzene	1.0 M KNO <sub>3</sub>	92%	[162]
Chromium	0.1% K <sub>2</sub> Cr <sub>2</sub> O <sub>7</sub>	Alamine 336	0.1% SPAN 80, 3% polyamine	86% isoparaffin	10% NaOH	99.7%	[160]
Chromium	0.06 g/L Cr <sub>2</sub> O <sub>7</sub> <sup>2-</sup>	1% TOA	4% LMS-2	Kerosene	5% NaOH	99.8%	[101]

**TABLE 25.4 (continued)**  
**ELM Systems for the Separation of Metal Ions**

Solute	External Feed Phase	Extractant	Surfactant	Diluent	Internal Phase	Efficiency/Recovery	References
Chromium	$\text{Cr}_2\text{O}_7^{2-}$ in 0.5 N $\text{H}_2\text{SO}_4$	20% tri- <i>n</i> -butyl phosphate (TBP)	4%–5% SPAN 80	<i>n</i> -Hexane	0.1 N NaOH	>99%	[163]
Chromium	0.000962 N $\text{K}_2\text{Cr}_2\text{O}_7$ pH 1.6	0.05 M alamine 336	—	89.8 wt% HYVIS 2, 10 wt% Shellsol 2046, 0.2 wt% polyisobutylene	0.25 M NaOH	80%	[86]
Chromium	75–100 mg/L $\text{K}_2\text{Cr}_2\text{O}_7$ pH 5.1–5.4	0.5 vol% Aliquat 336	1.5 vol% Paranox 106	5 vol% decanol, kerosene	0.005–0.01 M NaOH	—	[40]
Cobalt	$\text{Co}(\text{NO}_3)_2 \cdot 6\text{H}_2\text{O}$ , 0.5 M $\text{KNO}_3$ pH 3.1	6.3% v/v DEHPA	2% v/v SPAN 80	Cyclohexane	2 M $\text{HNO}_3$	~90%	[164]
Cobalt	$\text{Co}(\text{NO}_3)_2 \cdot 6\text{H}_2\text{O}$ , pH 4.5	6.3% v/v DEHPA	5% v/v SPAN 80 or Paranox 100 or ECA 4360	Kerosene	0.5 M $\text{H}_2\text{SO}_4$	~70%–90%	[113]
Cobalt	1.0 g/L $\text{CoSO}_4$ , 0.1 M NaAc, pH 5	DEHPA	ECA 4360	LOPS	50–200 g/L $\text{H}_2\text{SO}_4$	~95%	[165]
Cobalt	$2 \times 10^{-5}$ M $\text{Co}^{2+}$ pH 7.95	0.36% LIX 64 N	2.1% SPAN 80	Toluene	0.005 M EDTA, pH 7.9	99%	[162]
Copper	80–2500 ppm $\text{CuSO}_4$ pH 1.5–7	Shell SME 529	3% wt/wt SPAN 80	Shellsol T	250 g/L $\text{H}_2\text{SO}_4$	90%	[127]
Copper	1000 ppm $\text{CuSO}_4$ pH 6 (buffered with NaAc/HAc)	1.6% w/v benzoylacetone	6.5% v/v Emery DNP-8	65.5% v/v decane	26.4% v/v $\text{H}_2\text{SO}_4$	99%	[166]
Copper	1000 ppm $\text{CuSO}_4$ Unbuffered	10.1% w/w LIX 860	9.98% w/w Emery DNP-8	79.92% w/w Hexadecane	30% w/w $\text{H}_2\text{SO}_4$	~50%	[166]
Europium	$1.3 \times 10^{-3}$ M $\text{Eu}^{3+}$	0.5 vol% DEHPA	2 vol% SPAN 80	87.5 vol% kerosene, 10 vol% polybutadiene	4 N $\text{HNO}_3$	>99%	[167]
Europium	$4.6 \times 10^{-3}$ M $\text{Eu}^{3+}$ pH >2.78	5 vol% 2-ethylhexyl phosphonic acid mono-2-ethylhexyl ester (PC-88A)	4 mol% SPAN 80	Kerosene or dodecane	1.5 M HCl	>99%	[41]
Gold	63.9 ppm Au pH 2.54	1% N503	4% polyamine E644	Kerosene	0.1 M $\text{Na}_2\text{SO}_3/0.5$ M NaOH	99%	[108]
Iron	5 mM $\text{FeCl}_3$	5 mM $\text{CH}_3(\text{C}_8\text{H}_{17})_3\text{NCl}$ (methyltrioctylammonium chloride)	2 wt% SPAN 80	Toluene	1 N HCl	-	[168]
Lead	75–127 $\mu\text{g}/\text{mL}$ $\text{Pb}^{2+}$ ( $\text{PbNO}_3$ ) and in the presence of $\text{LiNO}_3$ or $\text{KNO}_3$	0.1 M dicyclohexano-18-crown-6	1 vol% SPAN 80	70 vol% S-100 N, 30 vol% indopol L-100	0.1 M $\text{Na}_4\text{P}_2\text{O}_7$	>90%	[169]
Lead	1020 ppm Pb pH 4.66	5 wt% DEHPA	3 wt% ECA 5025	82 wt% tetradecane	6N $\text{H}_2\text{SO}_4$	99.95%	[161]
Mercury	2.5–190 ppm $\text{Hg}^{2+}$	2.92 kg/ $\text{m}^3$ 1,1-di- <i>n</i> -butyl-3-benzoyl-thiourea (DBBT)	3.5 vol% Rofetan OM (fatty ester)	Decane	0.1N HCl, 7.6 g/L Thiourea	96%	[39]

(continued)

**TABLE 25.4 (continued)**  
**ELM Systems for the Separation of Metal Ions**

Solute	External Feed Phase	Extractant	Surfactant	Diluent	Internal Phase	Efficiency/ Recovery	References
Mercury	1.1 g/L Hg <sup>2+</sup>	Alamine 336	0.1% SPAN 80, 3% polyamine	86% isoparaffin	2% NaOH	>99%	[160]
Mercury	Mercuric chloride or nitrate	0.35 M oleic acid	3 wt% paramins ECA 5025	95:5 w/w tetradecane: mineral oil	6 N H <sub>2</sub> SO <sub>4</sub>	~80%	[170]
Mercury	Mercury nitrate 0.07–0.35 g/L Hg <sup>2+</sup> pH 2.8–3.0	10% 2:1 mixture of linoleic and oleic acid	2% Arlancel C	Normal paraffins	2 N H <sub>2</sub> SO <sub>4</sub>	>99%	[171]
Molybdenum	1.06 g/L Mo <sub>7</sub> O <sub>24</sub> <sup>6-</sup> , 16 g/L H <sub>2</sub> SO <sub>4</sub>	0.02M TOA	5% SPAN 80	Kerosene	2 M Na <sub>2</sub> CO <sub>3</sub>	99.5%	[172]
Nickel	2.2 g/L Ni <sup>2+</sup>	5% Di(2-ethylhexyl) dithiophosphoric acid (DTPA)	3% ECA 4360, 0.2% SPAN 80	Shellsol T	250 g/L H <sub>2</sub> SO <sub>4</sub>	—	[126]
Nickel	400–6000 mg/L Ni <sup>2+</sup> in H <sub>2</sub> SO <sub>4</sub>	5 wt% DTPA	3 wt% ECA 11522 polyamine	92 wt% Shellsol T (paraffin)	250 g/L H <sub>2</sub> SO <sub>4</sub>	>99.8%	[157]
Nickel	100–500 ppm Ni(II)	6.4 vol% DEHPA	3 vol% SPAN 80	90.6 vol% <i>n</i> -Heptane	1 M H <sub>2</sub> SO <sub>4</sub>	42%	[173]
Nickel	0.2M Ni (NO <sub>3</sub> ) <sub>2</sub> · 6H <sub>2</sub> O pH 2.5–3.5	Di DEHPA + 5,8-dimethyl-7-hydroxydodecane-6-oxime (LIX63) Di-oleylphosphoric acid (DOLPA) + 5,8-dimethyl-7-hydroxydodecane-6-oxime (LIX63)	SPAN 80	Toluene	1 M HNO <sub>3</sub>	>99%	[174]
Palladium	63 ppm Pd <sup>2+</sup> , 25,000 ppm Fe <sup>3+</sup> 1 M HCl	0.1 M MSP-8 (di-2 ethylhexyl monothiophosphoric acid)	0.1 M SPAN 80	<i>n</i> -Heptane	1 M HCl, 0.1 M thiourea	>95%	[175]
Plutonium	50 mg/L Pu <sup>4+</sup> in 3 M HNO <sub>3</sub> /0.05 M NaNO <sub>3</sub>	0.2 M dicyclohexano-18-crown-6 (DC18C6)	3 wt% polyamine or SPAN 80	97 wt% toluene or paraffin	0.5 M Na <sub>2</sub> CO <sub>3</sub>	>90%	[176]
Selenium	1 mg/L Se (IV) or Se (VI) pH 10.5	2% proprietary complexing agent	2% proprietary surfactant	Kerosene + 2% <i>n</i> -decanol	0.5–2.0 M NaCl	>99.9%	[177]
Strontium	100 ppm Sr <sup>2+</sup> pH 5.3	0.2 M DEHPA	3 wt% SPAN 80	97 wt% kerosene	HCl, pH 1.6	92%	[178]
Strontium	5 × 10 <sup>-4</sup> M SrCl <sub>2</sub> in acetate buffer pH 5.5 + 0.025 M CaCl <sub>2</sub>	1.25 × 10 <sup>-2</sup> M DEHPA	2.5% RADIASURF 7155	Dodecane	1 M HNO <sub>3</sub>	99.99%	[162]
Technetium	TcO <sub>4</sub> <sup>-</sup> , 0.1 N HNO <sub>3</sub>	0.5% Aliquat 336	3% SPAN 80	Cyclohexane	1 M NaClO <sub>4</sub>	92%	[162]
Tellurium	TeCl <sub>4</sub> , 4.2–4.5 M HCl	5% DEHPA	3% SPAN 80	Kerosene	5.0–6.0 M acid	~85%	[42]
Uranium	~0.016 g/L UO <sub>2</sub> <sup>2+</sup> , ~6 M H <sub>3</sub> PO <sub>4</sub>	DEHPA/TOPO	Polyamine	LOPS	H <sub>3</sub> PO <sub>4</sub>	>90%	[179]
Uranium	1.15 kg/m <sup>3</sup> UO <sub>2</sub> <sup>2+</sup> , 33 kg/m <sup>3</sup> H <sub>2</sub> SO <sub>4</sub>	0.02 M TOA	5 wt% SPAN 80	Kerosene	1 M Na <sub>2</sub> CO <sub>3</sub>	95%	[180]
Uranium	4.2 × 10 <sup>-3</sup> M UO <sub>2</sub> <sup>2+</sup> , 0.1 M Na <sub>2</sub> SO <sub>4</sub> pH 2	0.075 M DEHPA	0.96% SPAN 80	Cyclohexane	1.30 M H <sub>2</sub> SO <sub>4</sub>	99.7%	[162]

**TABLE 25.4 (continued)**  
**ELM Systems for the Separation of Metal Ions**

Solute	External Feed Phase	Extractant	Surfactant	Diluent	Internal Phase	Efficiency/ Recovery	References
Vanadium	16–604 ppm VO <sup>3-</sup>	2% TOA	4% succinimide derivative	Kerosene	2.5%–5% Na <sub>2</sub> CO <sub>3</sub>	98–99.3%	[181]
Zinc	200 mg/L Zn <sup>2+</sup> in 6 g/L H <sub>2</sub> SO <sub>4</sub>	5 wt% DTPA	3 wt% ECA 11522 polyamine	92 wt% Shellsol T (paraffin)	250 g/L H <sub>2</sub> SO <sub>4</sub>	>99.5%	[126]
Zinc	0.5 g/L Zn <sup>2+</sup>	2–4% DTPA	2% ECA 4360	Shellsol T	250 g/L H <sub>2</sub> SO <sub>4</sub>	99.5%	[103]
Zinc	ZnSO <sub>4</sub> in 50 g/L Na <sub>2</sub> SO <sub>4</sub> pH 1.4	3.5 wt% DTPA	2 wt% ECA 4360	94.5 wt% Shellsol T	5 N H <sub>2</sub> SO <sub>4</sub>	—	[36]
Zinc	0–5 g/L, 0–1 M Na <sub>2</sub> SO <sub>4</sub>	0–10 wt% bis-2-ethylhexyl mono thiophosphoric acid (MTP)	1–20 wt% ECA 4360	C <sub>7</sub> –C <sub>12</sub> <i>n</i> alkane	H <sub>2</sub> SO <sub>4</sub>	—	[89]

## 25.6 PILOT PLANT STUDIES/COMMERCIAL APPLICATIONS

As stated earlier, one of the major advantages of ELM technology is the creation of systems with very high surface area to volume ratios. As noted by Kentish and Stevens [218], with such systems, large interfacial areas can be achieved in units that occupy significantly less floor space and cost much less than traditional solvent extraction columns. This has led to the commercialization of this technology for the extraction of zinc [157,219], phenol [219], and cyanide [219] from wastewater. Pilot plant studies have also been conducted on the use of ELMs for the removal of contaminants such as cadmium [220], copper [221], chromium [160], and zinc [157,219] from wastewaters. Details of some pilot plant and commercial studies are given in Table 25.9. Other plants for the removal of zinc have been noted in the literature [157]: Glanzstoff AG, Austria (7000 L/h), CFK Schwarza, Germany (200 L/h), and AKZO/Ede, the Netherlands (200 L/h).

## 25.7 CONCLUDING REMARKS

Nearly 40 years since the initial reporting of the emulsion liquid membrane concept and the many potential applications discussed in the literature, very few commercial plants are operating successfully. This technology offers a number of distinct advantages including reduction in the volume of organic, the large interfacial area, hence transfer rates are compared with traditional solvent extraction. However, issues of osmotic swelling, the stabilization, and destabilization of the emulsion remain

**TABLE 25.5**  
**ELM Systems for the Separation of Anions**

Solute	External Feed Phase	Extractant	Surfactant	Diluent	Internal Phase	Efficiency/ Recovery	References
Cyanide	130 mg/L CN <sup>-</sup> as in Au(CN) <sub>2</sub> pH 9–9.5	5 wt% extractant M (protonated cation type) (or Alamine)	2 wt% Lan 113-b (or polyamine)	93 wt% kerosene	0.8 wt% NaOH	99.6%	[182]
Nitrate	0.22 g/L NaNO <sub>3</sub>	—	2% SPAN 80	S100 N	50% H <sub>2</sub> SO <sub>4</sub> 20% FeSO <sub>4</sub> 30% H <sub>2</sub> O	84%	[183]
Nitrate	500 ppm HNO <sub>3</sub>	TOA	SPAN 80	Kerosene	Na <sub>2</sub> CO <sub>3</sub>	94%	[44]
Phosphate	0.27%–0.57% PO <sub>4</sub> <sup>3-</sup>	Amines	1–2% SPAN 80, polyamine	Isoparaffin	CaCl <sub>2</sub> NH <sub>4</sub> OH or Ca(OH) <sub>2</sub>	91%–98%	[183]

**TABLE 25.6**  
**ELM Systems for the Separation of Acids and Bases**

Solute	External Feed Phase	Extractant	Surfactant	Diluent	Internal Phase	Efficiency/ Recovery	References
Acetic acid	0.0861 M CH <sub>3</sub> COOH	1 wt% tri- <i>n</i> -butyl phosphate (TBP)	8 wt% E 644 polyamine	72 wt% kerosene, 19 wt% paraffin	3 M NaOH	>95%	[33]
Acetic acid	300 ppm CH <sub>3</sub> COOH	—	10% v/v ethoxylated dinonyl phenol, Emery DNP-8	Decane, dodecane, tetradecane or hexadecane	0.25 M NaOH	Up to 45% depending on the oil phase	[184]
Ammonia	$7.143 \times 10^{-2}$ M NH <sub>3</sub> , pH >12	—	4 wt% SPAN 80	96 wt% paraffin	20 wt% H <sub>2</sub> SO <sub>4</sub>	99.5%	[185]
Aniline	0.5%–1.0% aniline in water	—	SPAN 80	Kerosene	3.0–6.0 M HCl	99.5%	[133]
Aniline	$3.5 \times 10^{-3}$ M aniline pH 8	—	8% SPAN 80	Kerosene and isoalkane fractions	0.1–0.5 N HCl	99%	[186]
<i>o</i> -Chloroaniline	$3.5 \times 10^{-3}$ M chloroaniline pH 8	—	8% SPAN 80	Kerosene and isoalkane fractions	0.1–0.5 N HCl	96.7%	[186]
2-Chlorophenol	7.778 mol/m <sup>3</sup> 2-Chlorophenol	—	2 wt% polyamine ECA 4360	98 wt% Shellsol T	500 mol/m <sup>3</sup> NaOH	>99%	[29]
Citric acid	0.048 M citric acid	40 vol% Alamine 336	4 vol% C9232	Mineral oil, 8 vol% chloroform	2.5 M NaOH	97%	[43]
Ethylaniline	$3.5 \times 10^{-3}$ M ethylaniline pH 8	—	8% SPAN 80	Kerosene and isoalkane fractions	0.1–0.5 N HCl	99%	[186]
Hydroxy benzoic acid	200 mg/L C <sub>7</sub> H <sub>6</sub> O <sub>3</sub> pH 2.3	—	2% ECA 4360J	96% Shellsol T, 2% isodecanol	0.2 M NaOH	99.3%	[30]
<i>m</i> -Nitroaniline	$3.5 \times 10^{-3}$ M nitroaniline pH 8	—	8% SPAN 80	Kerosene and isoalkane fractions	0.1–0.5 N HCl	96%	[186]
Nitrophenol	3000 ppm <i>p</i> -nitrophenol	—	4% v/v SPAN 80	76% v/v kerosene	0.7 M NaOH	95%	[85]
Phenol	1000 mg/L phenol	—	3.5 wt% LMS-2 (anion type)	89.8 wt% kerosene, 6.7 wt% paraffin	5 wt% NaOH	99.95%	[187]
Phenol	200 ppm phenol, pH 7	—	0.1–20 wt% SPAN 80	Dewaxed solvent 100 Neutral	10 wt% NaOH	90%	[8]
Phenol	787 ppm phenols, 3487 ppm formaldehyde pH 4.6	—	2 wt% ECA 4360	98 wt% Shellsol T	500 mol/m <sup>3</sup> NaOH	80–95%	[188]
<i>o</i> -Toluidine	$3.5 \times 10^{-3}$ M <i>o</i> -toluidine pH 8	—	8% SPAN 80	Kerosene and isoalkane fractions	0.1–0.5 N HCl	99.2%	[186]

a problem. Also, the influence of surface active impurities on the stabilization process is an issue during reuse of these systems. These challenges to the industry implementation of this technology remain as barriers to more wide spread application. At present, however, the technology has found some application in the treatment of relatively low-concentration waste streams where other technologies are not economical. Hence experience in these applications will drive further development and confidence in this technology and so find its niche in the available separation technologies.

**TABLE 25.7**  
**ELM Systems for the Separation of Mixtures**

Solute	External Feed Phase	Extractant	Surfactant	Diluent	Internal Phase	Efficiency/ Recovery	References
Americium/ europium	10–6 M Eu(III), Am(III), 1 M lactic acid, $5 \times 10^{-3}$ M diethylenetriamine-N, N',N',N'-pentaacetic acid	0.1 M DEHPA	2% v/v polyethylene glycol dioleate	Cyclohexane	1 M HCl	98%	[189]
Barium	0.01 N BaCl <sub>2</sub> , MgCl <sub>2</sub> , CaCl <sub>2</sub> , SrCl <sub>2</sub> , pH 8.5	0.01 M crown ether carboxylic acid	5 vol% SPAN 80	50 vol% mineral oil/45 vol% toluene	0.2 M HCl	—	[190]
Cobalt/manganese	820 mg/L Co, 1380 mg/L Mn, 3.6 mg/L Ni, 1.4 mg/L Fe, 1.4 mg/L Cr, 410 mg/L Na, pH 3	TBP	3 vol% SPAN 80	Shellsol T	H <sub>2</sub> SO <sub>4</sub>	Co: 64%; Mn: 98.5%	[191]
Cobalt/manganese/ chromium/nickel/ sodium/iron	820 mg/L Co, 1380 mg/L Mn, 3.6 mg/L Ni, 1.4 mg/L Fe, 1.4 mg/L Cr, 410 mg/L Na, pH 3.1	5.5 vol% DEHPA, 0.5 vol% TBP	3 vol% SPAN 80	90% kerosene	2 M H <sub>2</sub> SO <sub>4</sub>	Co: 85%; Mn: 99%	[192]
Cobalt/nickel	0.01 M Co(II), 0.01 M Ni (II) pH 5.5	0.01–0.1 M LIX 65N, LIX 84, LIX 860	0.005–0.05 M cationic L-glutamic acid dioleyl ester quaternary ammonium phosphoric acid (2C <sub>18</sub> Δ <sup>9</sup> GEC <sub>2</sub> QAC <sub>3</sub> PA)	n-Heptane	0.5 M H <sub>2</sub> SO <sub>4</sub>	Cr: 88% Ni: 50%–60% Na: 55% Fe: 60% Co: 99%	[193,194]
Cobalt/nickel	0.16 g/L Co, 0.16 g/L Ni, 0.1 M NaAc-HAc buffer, pH 3.5–5.8	12 mol/m <sup>3</sup> 2-ethylhexyl phosphonic acid mono-2- ethylhexyl ester (PC-88A)	50 mol/m <sup>3</sup> PX-100	n-Heptane	2.0 M H <sub>2</sub> SO <sub>4</sub>	Co: 98% Ni: 13%	[132]
Cobalt/nickel	1.5 g/L Co, 95.0 g/L Ni, 96.0 g/L citric acid buffer	9.5 g/L Cyanex 302	3 vol% ECA 4360	Escaid 110	0.05 M H <sub>2</sub> SO <sub>4</sub>	Co: up to 80%	[195]
Copper	Cu, Mg, Al, Fe, Fe	2.5% LIX 64N	2% polyamine	S100N	20% H <sub>2</sub> SO <sub>4</sub>	99%	[196]
Copper/zinc	8 g/L Cu, 100g/L Zn	5% Acorga PT 5050	2% PA 18	Shellsol T	250 g/L H <sub>2</sub> SO <sub>4</sub>	—	[126] [103]

(continued)

**TABLE 25.7 (continued)**  
**ELM Systems for the Separation of Mixtures**

Solute	External Feed Phase	Extractant	Surfactant	Diluent	Internal Phase	Efficiency/ Recovery	References
Copper, cobalt, nickel	100 ppm Cu, Co, Ni	0.2 mM ammonium thiocyanate	20000 MW PEG	1,2-dichloroethane	1 M KOH	Cu(II): 60% Co(II): 45% Ni(II): 45%	[197]
Copper, cobalt, nickel	1 g/L Cu, Co, Ni	6.3 vol% DEHPA	3 vol% SPAN 80	Kerosene	2 M HNO <sub>3</sub>	Cu(II): 60% Co(II): 60%	[198]
Copper, nickel, chromium, iron	1460 ppm Cu, 900 ppm Ni, 45 ppm Cr, 40 ppm Fe, 0.05 M NaAc-Hac, pH 3.5	10 vol% DEHPA	5 vol% SPAN 80	80% v/v kerosene + 5% v/v heptane	0.5–1.0 N HCl	Ni(II): 50% Cu(II): 90% Ni(II): 46%	[4]
Gallium	100 ppm Ga, 8715 ppm Fe, 60 ppm Co, 80 ppm Ni, 265 ppm Cd, 24,020 ppm Zn, 6592 ppm Pb, 315 ppm Cu, 3100 ppm Al	6% TOPO	8% ECA 4360J	Kerosene	15% w/w HCl	>97%	[112]
Gold	52.8–64.1 ppm Au, Pt, Pd, Ag, Cu, Pb, Fe, pH 3.0	1% N 503	4% polyamine E 644	Kerosene	0.5 M Na <sub>2</sub> SO <sub>3</sub>	>97%	[108]
Lanthanum, europium, lutetium	1 × 10 <sup>-4</sup> M La <sup>3+</sup> , Eu <sup>3+</sup> , Lu <sup>3+</sup> (nitrate), pH 6–7	0.01 M 2-(sym-dibenzo-16-crown-5-oxy)hexanoic acid	5 vol% SPAN 80	45 vol% mineral oil, 50 vol% toluene	HNO <sub>3</sub> , pH 2	Lu <sup>3+</sup> ; >99%	[199]
Lead	Pb <sup>2+</sup> , Na <sup>+</sup> , K <sup>+</sup> , Rb <sup>+</sup> , Cs <sup>+</sup> , Ag <sup>+</sup> , Tl <sup>+</sup> , Mg <sup>2+</sup> , Ca <sup>2+</sup> , Sr <sup>2+</sup> , Ba <sup>2+</sup> , Zn <sup>2+</sup>	0–0.02 M Crown ether dicyclohexano-18-crown-6 (DC18C6)	3% v/v SPAN 80	Toluene	0.05 M Li <sub>4</sub> P <sub>2</sub> O <sub>7</sub>	—	[200]
Nitrophenols	1000 mg/L <i>p</i> -nitrophenol, 1000 mg/L <i>o</i> -nitrophenol, 500 mg/L 2,4-dinitrophenol	—	2 vol% of emulsion SPAN 80	75.5 vol% of emulsion kerosene, 10 vol% of emulsion paraffin, 2.5 vol% of emulsion cyclohexanone	0.7 M NaOH	>98%	[85]

Platinum, palladium Praseodymium, neodymium, lanthanum	100 ppm Pt, 50 ppm Pd 0.0001 M Pr <sup>3+</sup> , 0.00035 M Nd <sup>3+</sup> , 0.0008 M La <sup>3+</sup> , pH 2	— 0.05 M mono(2-ethylhexyl) 2-ethylhexylphosphonate (PC-88A)	0.02 M 2C <sub>18</sub> Δ <sup>9</sup> GEC <sub>2</sub> Q 0.02 M cationic dioleyl L-glutamate quaternary ammonium chloride (2C <sub>18</sub> Δ <sup>9</sup> GEC <sub>2</sub> Q)	<i>n</i> -Heptane <i>n</i> -Heptane	1 M HClO <sub>4</sub> 0.5 M H <sub>2</sub> SO <sub>4</sub>	~95% >99% for Pr <sup>3+</sup> and Nd <sup>3+</sup> (good selectivity vs. La <sup>3+</sup> )	[104] [201]
Silver	Ag <sup>+</sup> Na <sup>+</sup> , K <sup>+</sup> , Rb <sup>+</sup> , Cs <sup>+</sup> , Tl <sup>+</sup> , Mg <sup>2+</sup> , Sr <sup>2+</sup> , Ba <sup>2+</sup> , Pb <sup>2+</sup> , Zn <sup>2+</sup>	0–0.02 M Crown ether dicyclohexano-18-crown-6 (DC18C6)	3% v/v SPAN 80	Toluene	0.05 M Li <sub>2</sub> S <sub>2</sub> O <sub>3</sub>	—	[200]
Sodium	0.01 M NaCl KCl, RbCl, LiCl	0.01 M Crown ether carboxylic acid	5 vol% SPAN 80	50 vol% mineral oil, 45 vol% toluene	0.2 M HCl	—	[190]
Zinc, cadmium, copper	335 ppm Zn 21.6 ppm Cd, 3.9 ppm Cu, 0.3 ppm Co, 73 ppm Mg, 1.7 ppm Fe, 10 g/L Cl, pH 1.4	3–7% monothio or dithio di (2-ethylhexyl) phosphoric acid	2% polyamine ECA 4360	Shellsol T	2.5 M H <sub>2</sub> SO <sub>4</sub>	~97% ~10ppm Zn	[202]
Zinc, cadmium, copper, lead	230 mg/L Zn <sup>2+</sup> 2.7 mg/L Cd <sup>2+</sup> 1.1 mg/L Cu <sup>2+</sup> 0.5 mg/L Pb <sup>2+</sup> pH 3.4	5 wt% di(2-ethylhexyl) thiophosphoric acid (MTPA)	3 wt% ECA 115222 polyamine	92 wt% Shellsol T	250 g/L H <sub>2</sub> SO <sub>4</sub>	~99%, 0.2 mg/L Zn <sup>2+</sup> , 0.02 mg/L Cd <sup>2+</sup> , 0.007 mg/L Cu <sup>2+</sup> , 0.01 mg/L Pb <sup>2+</sup>	[126]
Zinc, calcium, lead	6 g/L Zn, 0.014 g/L Ca, 0.004 g/L Pb	5% DTPA	2% PX100	Shellsol T	250 g/L H <sub>2</sub> SO <sub>4</sub>	—	[103]
Zinc, cadmium, nickel	0.3–1.5 × 10 <sup>-3</sup> M Zn, Cd, Ni, pH 6–8 (acetate or tris buffer), 0.1 M KNO <sub>3</sub>	3.8 × 10 <sup>-3</sup> M 4-acyl-5- pyrazolones	3% ECA 11 523 (Exxon)	Shellsol T or Shellsol AB	0.1 M H <sub>2</sub> SO <sub>4</sub>	—	[203]

**TABLE 25.8**  
**ELM Systems for the Separation of Biochemicals**

Solute	External Feed Phase	Extractant	Surfactant	Diluent	Internal Phase	Efficiency/ Recovery	References
Alanine	6–7 g/L alanine, pH 6	20% v/v DEHPA	1.5% v/v SPAN 80	Kerosene	1.7 M H <sub>2</sub> SO <sub>4</sub>	>60%	[139]
Alkaloid	Berberine or ephedrine	—	2 vol% SPAN 80	Kerosene	0.2 N HCl	~100%	[204]
Barbiturates	50 hexobarbital, amobarbital, or phenobarbital, pH 7.3	—	5–10 vol% mannide monooleate or montanide 80	90–95 vol% paraffin oil	Phosphate buffer pH 7.3 or pH 11 glycine, NaCl, NaOH buffer	Up to 50%	[83]
Cholesterol	Blood	—	SPAN 80	Paraffin	Saponin	80%–85%	[205]
Di and tripeptides	2 M peptide, pH 2.7	15.5 wt% DEHPA	5 wt% SPAN 80	79.5 wt% kerosene	1 M HCl	Up to 80%	[206]
Erythromycin	10 <sup>-3</sup> M erythromycin, pH 8.5–9.5	—	0.05 vol fraction SPAN 80	Heptane or <i>m</i> -xylene	Boric acid-sodium phosphate buffer, pH 5.5–6.5	—	[207,208]
Lactic acid	0.1 M lactic acid	5 wt% Amberlite LA2	5 wt% Paranox 100	90 wt% kerosene	0.6 M Na <sub>2</sub> CO <sub>3</sub>	98%	[209]
Penicillin G	0.02 M penicillin G, 0.408 M citrate buffer, pH 5	0.01 M Amberlite LA2	5 wt% ECA 4360J polyamine	95 wt% kerosene	0.1 M Na <sub>2</sub> CO <sub>3</sub>	80–95%	[210,211]
Penicillin G	0.02 M penicillin G in 0.408 M citrate buffer, pH 5	0.02 M Amberlite LA2 secondary amine	8 wt% ECA 4360J polyamine	Kerosene or kerosene + paraffin oil	0.2 M Na <sub>2</sub> CO <sub>3</sub>	~90% continuous process	[212]
Penicillin G	0.002 M penicillin G, pH 6	0.04 M di- <i>n</i> -octylamine (DOA)	5 wt% Paranox 100	Kerosene + butyl acetate (ratio: 7:3)	0.5 M K <sub>2</sub> CO <sub>3</sub>	85%–90% continuous process	[213]
Phenylalanine	12–35 g/L L-phenylalanine, pH 2.5 (with H <sub>2</sub> SO <sub>4</sub> )	20 wt% DEHPA	5 wt% Paranox 100 polyamine	75 wt% S-60NR (50 vol% Olefins, 49 vol% Paraffins, 1 vol% aromatics)	1.5 M H <sub>2</sub> SO <sub>4</sub>	~80%	[214]
Phenylalanine	0–0.12 M L-phenylalanine, pH 3.0	0.075–0.225 M DEHPA	4% v/v Paranox 100	86% v/v Telura 619	1.6 M HCl	—	[121]
Phenylalanine	<10% w/w phenylalanine	4% v/v DEHPA	3% v/v SPAN 80	93% v/v kerosene	1.5 M HCl	~80%	[26]
Tryptophan	0.4 mM tryptophan, pH 3	15% w/w DEHPA	2% w/w alkylbenzosulfonic acid	Carbon tetra chloride	1.6 M HCl	~80%	[215]
Removal of zinc from a rayon plant waste [219,157]	Lenzing AG, Austria	Pilot plant: 1,000 L/h Commercial plant: 75,000 L/h	450–500 mg/L 350 mg/L	3 wt% DTPA, 2 wt% Exxon PX100 surfactant, 95 wt% Shellsol T 3 wt% DTPA, 3 wt% Exxon PX100 surfactant, 94 wt% Shellsol T	250 g/L H <sub>2</sub> SO <sub>4</sub> 250–300 g/L H <sub>2</sub> SO <sub>4</sub>	20 kV, 50 Hz, 5 kW h/m <sup>3</sup> emulsion	98%

**TABLE 25.9**  
**Pilot Plant and Commercial Applications of ELM Systems**

Application	Company	Plant Size	External Phase	Membrane Composition	Internal Phase	Demulsifier	Efficiency
Removal of copper from mine solutions [221]	Bureau of Mines, United States	Pilot plant: 90–159 L/h	0.12–1.4 g/L Cu(II)	5.0–7.5 wt% Acorga M5640, 1.0 wt% Paradox 100, 91.5–94 wt% 50–50 Isopar	8.5–20 g/L Cu(II), 160–165 g/L H <sub>2</sub> SO <sub>4</sub>	5–8 kV, 60 Hz	>90%
Removal of copper from synthetic mine solutions [45]	Davy McKee Company, United Kingdom	18 L/h	500 ppm Cu(II), pH 2.5	2.5 wt% LIX 64N, 2.0 wt% polyamine, 95.5 wt% S100N	30 g/L Cu(II), 150 g/L H <sub>2</sub> SO <sub>4</sub>	—	95%
Removal of cadmium [220]	Delft University of Technology, the Netherlands	Pilot plant: 90 L/h	100 ppm Cd	0.5%–1.0% Alamine 304 in Shellsol D 70, 0.5–1.0% ECA 4360J	1 M HNO <sub>3</sub> , 10 mM KNO <sub>3</sub>	Electrostatic splitter 3 kV, 4 kHz	95%
Removal of phenol [187,219]	Nanchung Plastic Factory, Guangzhou, PR China	Pilot plant: 200–250 L/h Commercial plant: 400–500 L/h	350–925 mg/L phenol	3.5 wt% LMS-2, 6.7 wt% liquid paraffin, 89.8 wt% kerosene	5 wt% NaOH	Coalescer EC-1 20 kV, 0.6–25 kHz, 50 mA, capacity 20 L, 32–55 L/h	99.6%

## SYMBOLS

$B$	constant
$b$	constant
$b_1$	constant
$B_2$	constant
$B_3$	constant
$Bi$	Biot number
$Da$	Damköhler number
$D_e$	effective solute diffusivity in the emulsion mixture
$d_{32}$	Sauter mean diameter of the dispersed phase droplets/globules
$d_s$	stirrer or impeller diameter
$f_\phi$	ratio of actual mean drop diameter to diameter at $\phi = 0.1$
$F^{sw}$	swelling factor
$k$	external phase mass transfer coefficient
$k_1$	reaction rate constant
$N_{vi}$	$(\rho_c/\rho_e)^{1/2} \mu_d \varepsilon^{-1/3} d_{32}^{1/3} / \gamma$
$R$	radius of the emulsion globule
$Re$	Reynolds number
$P$	power input
$T$	vessel diameter
$t_c$	circulation time
$V$	volume of the fluids
$V_e$	total volume of the external phase
$V_i$	total volume of the internal phase
$V_m$	total volume of the membrane phase
$We$	Weber number = $\omega^2 d_s^3 \rho_c / \gamma$

## Greek Symbols

$\alpha_e$	the distribution coefficient of the solute between the external and membrane phase
$\alpha_i$	the distribution coefficient of the solute between the internal and membrane phase
$\Delta\rho$	density difference between (W/O) emulsion and the continuous phase
$\gamma$	interfacial tension between the membrane and the external phase

$\varepsilon$	$P/V(1 - \phi_{av})\rho_c$
$\varepsilon_{av}$	average energy dissipation rate per unit mass
$\varepsilon_{max}$	turbulence kinetic energy dissipation rate per unit mass
$\mu_c$	dynamic viscosity of the continuous phase
$\mu_d$	dynamic viscosity of the dispersed phase
$\nu_c$	kinematic viscosity of the continuous phase
$\rho_c$	density of the continuous phase
$\phi$	volume fraction of the dispersed phase
$\phi_{av}$	vessel average of $\phi$
$\phi_{int}$	volume fraction of the internal aqueous phase in the emulsion drop
$\omega$	stirring rate

## REFERENCES

- Li NN. Separating hydrocarbons with liquid membranes. US Patent 3,410,794, 1968.
- Ho WS and Li NN. Recent advances in emulsion liquid membranes. In: Bartsch RA, Way JD, eds. *Chemical Separations with Liquid Membranes*. Washington, DC: American Chemical Society, ACS symposium series 1996; 642: 208–221.
- Ho WS, Hatton TA, Lightfoot EN, and Li NN. Batch extraction with liquid surfactant membranes: A diffusion controlled model. *AIChE J* 1982; 28: 662–670.
- Chakraborty M, Bhattacharaya C, and Datta S. Mathematical modelling of simultaneous copper (II) and nickel (II) extraction from wastewater by emulsion liquid membranes. *Sep Sci Technol* 2003; 38: 2081–2106.
- Ho WS and Li NN. Theory. In: Ho WS, Sirkar KK, eds. *Membrane Handbook*. New York: Van Nostrand Reinhold, 1992: 611–655.
- Chan CC and Lee CJ. Mechanistic models of mass transfer across a liquid membrane. *J Membr Sci* 1984; 20: 1–24.
- Yan N, Shi Y, and Su YF. A mass transfer model for type I facilitated transport in liquid membranes. *Chem Eng Sci* 1992; 47: 4365–4371.
- Cahn RP and Li NN. Separation of phenol from waste water by the liquid membrane technique. *Sep Sci Technol* 1974; 9: 505–519.
- Kremsec VJ. Modeling of dispersed-emulsion separation systems. *Sep Purif Methods* 1981; 10: 117–157.
- Kremsec VJ and Slattery JC. Analysis of batch, dispersed-emulsion, separation systems. *AIChE J* 1982; 28: 492–500.
- Matulevicius ES and Li NN. Facilitated transport through liquid membranes. *Sep Purif Methods* 1975; 4: 73–96.
- Kopp AG, Marr RJ, and Moser TF. A new concept for mass transfer in liquid surfactant membranes without carriers and with carriers that pump. *Inst Chem Eng Symp Ser* 1978; 54: 279.
- Fales JL and Stroeve P. A perturbation solution for batch extraction with double emulsions: Role of continuous phase mass transfer resistance. *J Membr Sci* 1984; 21: 35–53.
- Stroeve P and Varanasi PP. Extraction with double emulsions in a batch reactor: Effect of continuous-phase resistance. *AIChE J* 1984; 30: 1007–1009.
- Teramoto M, Takihana H, Shibutani M, Yuasa T, Miyake Y, and Teranishi H. Extraction of amine by W/O/W emulsion system. *J Chem Eng Jpn* 1981; 14: 122–128.
- Bunge AL and Noble RD. A diffusion model for reversible consumption in emulsion liquid membranes. *J Membr Sci* 1984; 21: 55–71.
- Teramoto M, Takihana H, Shibutani M, Yuasa T, and Hara N. Extraction of phenol and cresol by liquid surfactant membrane. *Sep Sci Technol* 1983; 18: 397–419.
- Teramoto M and Matsuyama H. Effect of facilitated diffusion in internal aqueous droplets on effective diffusivity and extraction rate of phenol in emulsion liquid membranes. *J Chem Eng Jpn* 1986; 19: 469–472.
- Kataoka T, Nishiki T, and Kimura S. Phenol permeation through liquid surfactant membrane—permeation model and effective diffusivity. *J Membr Sci* 1989; 41: 197–209.
- Kataoka T, Nishiki T, Kimura S, and Tamioka Y. A model for mass transfer through liquid surfactant membranes. *Water Treat* 1990; 5: 136–149.
- Teramoto M, Matsuyama H, and Izumo Y. Effective diffusivity in W/O emulsion. *J Membr Sci* 1992; 68: 169–181.
- Baird RS, Bunge AL, and Noble RD. Batch extraction of amines using emulsion liquid membranes: Importance of reaction reversibility. *AIChE J* 1987; 33: 43–53.
- Lin CC and Long RL. Phenol removal by emulsion liquid membrane: A modified diffusion model. *Chem Eng Comm* 1996; 156: 45–58.
- Chan CC and Lee CJ. A mass transfer model for the extraction of weak acids/bases in emulsion liquid-membrane systems. *Chem Eng Sci* 1987; 42: 83–95.
- Borwanker RP, Chan CC, Wasan DT, Kurzeja RM, Gu ZM, and Li NN. Analysis of the effect of internal phase leakage on liquid membrane separations. *AIChE J* 1988; 34: 753–762.
- Liu X and Liu D. Modelling of facilitated transport of phenylalanine by emulsion liquid membranes with di(2-ethylhexyl)phosphoric acid as a carrier. *Sep Sci Technol* 1998; 33: 2597–2608.
- Boydazhiev L, Bezenshek E, and Lazarova Z. Removal of phenol from waste water by double emulsion membranes and creeping film pertraction. *J Membr Sci* 1984; 21: 137–144.
- Wang CC and Bunge AL. Multisolute extraction of organic acids by emulsion liquid membranes. I. Batch experiments and models. *J Membr Sci* 1990; 53: 71–103.

29. Correia PFMM and de Carvalho JMR. A comparison of models for 2-chlorophenol recovery from aqueous solutions by emulsion liquid membranes. *Chem Eng Sci* 2001; 56: 5317–5325.
30. Correia PFMM and Carvalho JMR. Recovery of 4-Hydroxybenzoic acid from aqueous solutions by emulsion liquid membranes. In: Cox M, Hidalgo M, Valiente M, eds. *Solvent Extraction for the 21st Century (Proceedings of ISEC'99)*, London: Society of Chemical Industry (SCI), 2001; 2: 977–982.
31. Rautenbach R and Machhammer O. Modeling of liquid membrane separation processes. *J Membr Sci* 1988; 36: 425–444.
32. Datta S, Bhattacharya PK, and Verma N. Removal of aniline from aqueous solution in a mixed flow reactor using emulsion liquid membrane. *J Membr Sci* 2003; 226: 185–201.
33. Yan N, Shi Y, and Su YF. Removal of acetic acid from wastewater with liquid surfactant membranes: An external boundary layer and membrane diffusion controlled model. *Sep Sci Technol* 1987; 22: 801–818.
34. Teramoto M, Sakai T, Yanagawa K, Ohsuga M, and Miyake Y. Modeling of the permeation of copper through liquid surfactant membranes. *Sep Sci Technol* 1983; 18: 735–764.
35. Kataoka T, Nishiki T, Kimura S, and Tomioka Y. Batch permeation of metal ions using liquid surfactant membranes. *J Membr Sci* 1989; 46: 67–80.
36. Lorbach D and Marr R. Emulsion liquid membranes part II: Modelling mass transfer of zinc with bis(2-ethylhexyl)dithiophosphoric acid. *Chem Eng Process* 1987; 21: 83–93.
37. Ortner A, Auzinger D, Wacker HJ, and Bart HJ. Axial and radial simulation of concentration profiles in liquid/liquid dispersions. *Process Technol Proc* 1991; 10: 399–404.
38. Yan N. A mass transfer model for type-II-facilitated transport in liquid membranes. *Chem Eng Sci* 1993; 48: 3835–3843.
39. Weiss S, Grigoriev V, and Muhl P. The liquid membrane process for the separation of mercury from waste water. *J Membr Sci* 1982; 12: 119–129.
40. Banerjee S, Datta S, and Sanyal SK. Mass transfer analysis of the extraction of Cr(VI) by liquid surfactant membrane. *Sep Sci Technol* 2000; 35: 483–501.
41. Lee CJ, Wang SS, and Wang SG. Extraction of trivalent europium via emulsion liquid membrane containing PC-88A as mobile carrier. *Ind Eng Chem Res* 1994; 33: 1556–1564.
42. Chakraborty R and Datta S. Transport of  $\text{Te}^{4+}$  through liquid surfactant membrane using D2EHPA as the carrier. *J Membr Sci* 1994; 96: 233–240.
43. Yordanov B and Boyadzhiev L. Pertraction of citric acid by means of emulsion liquid membranes. *J Membr Sci* 2004; 238: 191–197.
44. Lin CC and Long RL. Removal of nitric acid by emulsion liquid membrane: experimental results and model prediction. *J Membr Sci* 1997; 134: 33–45.
45. Cahn RP, Frankenfeld JW, Li NN, Naden D, and Subramanian KN. Extraction of metal ions by liquid membranes. In: Li NN, ed. *Recent Developments in Separation Science*, Volume VI, Chapter 25.4. Boca Raton, FL: CRC Press, 1981: 51–64.
46. Gu Z, Ho WS, and Li NN. Design considerations. In: Ho WS, Sirkar KK, eds. *Membrane Handbook*. New York: Van Nostrand Reinhold, 1992: 656–700.
47. Ohtake T, Hano T, Takagi K, and Nakashio F. Effects of viscosity on drop diameter of W/O emulsion dispersed in a stirred tank. *J Chem Eng Japan* 1987; 20: 443–447.
48. Vermeulen T, Williams GM, and Langlois GE. Interfacial area in liquid–liquid and gas–liquid agitation. *Chem Eng Prog* 1955; 51: 85F–94F.
49. Roger WA, Trice VG, and Rushton JH. Effect of fluid motion on interfacial area of dispersions. *Chem Eng Prog* 1956; 52: 515–520.
50. Calderbank PH. Physical rate processes in industrial fermentation. Part I: The interfacial area in gas–liquid contacting with mechanical agitation. *Trans Inst Chem Engrs* 1958; 36: 443–463.
51. Shinnar R. On the behaviour of liquid dispersions in mixing vessels. *J Fluid Mech* 1961; 10: 259–275.
52. Chen HT and Middleman S. Drop size distribution in agitated liquid–liquid systems. *AIChE J* 1967; 13: 989–995.
53. Sprow FB. Distribution of drop sizes produced in turbulent liquid–liquid dispersion. *Chem Eng Sci* 1967; 22: 435–442.
54. Sprow FB. Drop size distributions in strongly coalescing agitated liquid–liquid systems. *AIChE J* 1967; 13: 995–998.
55. Brown DE and Pitt K. Drop break-up in a stirred liquid–liquid contactor. In: *Proceedings of CHEMECA 1970*, Melbourne and Sydney, 1970: 83–97.
56. van Heuven JW and Beck WJ. Power input, drop size and minimum stirrer speed for liquid–liquid dispersions in stirred vessels in Proceedings of the International Solvent Extraction Conference (ISEC 1971), Hague, *Soc Chem Ind* 1971; 1:70–81.
57. Mlynek Y and Resnick W. Drop sizes in an agitated liquid–liquid system. *AIChE J* 1972; 18: 122–127.
58. Weinstein B and Treybal TE. Liquid–liquid contacting unbaffled agitated vessels. *AIChE J* 1973; 19: 304–312.
59. Brown DE and Pitt K. Effect of impeller geometry on drop break-up in a stirred liquid–liquid contactor. *Chem Eng Sci* 1974; 29: 345–348.
60. Coualglou CA and Tavlarides LL. Drop size distributions and coalescence frequencies of liquid–liquid dispersions in flow vessels. *AIChE J* 1976; 22:289–297.
61. Godfrey JC and Grilic V. Drop size and drop size distribution for liquid–liquid dispersions in agitated tanks of square cross-section. In: *Proceedings of the 2nd European Conference on Mixing*, Cambridge, UK, 1977: C1–1 to C1–20.
62. Calabrese RV, Chang TPK, and Dang PT. Drop breakup in turbulent stirred-tank contactors. Part I: Effect of dispersed-phase viscosity. *AIChE J* 1986; 32: 657–666.
63. Wang CY and Calabrese RV. Drop breakup in turbulent stirred-tank. Part II: Relative influence of viscosity and interfacial tension. *AIChE J* 1986; 32: 667–676.

64. Calabrese RV, Wang CY, and Bryner NP. Drop breakup in turbulent stirred-tank. Part III: Correlations for mean size and drop size distributions. *AIChE J* 1986; 32: 677–681.
65. Kataoka T and Nishiki T. Dispersed mean drop sizes of (W/O)/W emulsions in a stirred tank. *J Chem Eng Jpn* 1986; 19: 408–412.
66. Nishikawa M, Mori F, and Fujieda S. Average drop size in a liquid–liquid phase mixing vessel. *J Chem Eng Jpn* 1987; 20: 82–88.
67. Nishikawa M, Mori F, Fujieda S, and Kayama T. Scale-up of liquid–liquid phase mixing vessel. *J Chem Eng Jpn* 1987; 20: 454–459.
68. Berkman PD and Calabrese RV. Dispersion of viscous liquids by turbulent flow in a static mixer. *AIChE J* 1988; 34: 602–609.
69. Chatzi EG, Gavrielides AD, and Kiparissides C. Generalized model for prediction of the steady-state drop size distributions in batch stirred vessels. *Ind Eng Chem Res* 1989; 28: 1704–1711.
70. Sharma A, Goswami AN, and Rawart BS. Drop size prediction in liquid membrane systems. *J Membr Sci* 1991; 60: 261–274.
71. Zihao W, Yuanli J, and Jufu F. The entrainment swelling of emulsion during lactic acid extraction by LSMs. *J Membr Sci* 1996; 109: 25–34.
72. Zhou G and Kresta SM. Correlation of mean drop size and minimum drop size with the turbulence energy dissipation and the flow in an agitated tank. *Chem Eng Sci* 1998; 53: 2063–2079.
73. Gallego-Lizon T and Perez de Ortiz ES. Drop sizes in liquid membrane dispersions. *Ind Eng Chem Res* 2000; 39: 5020–5028.
74. Calderbank PH and Moo-Young MB. The continuous phase heat and mass-transfer properties of dispersions. *Chem Eng Sci* 196; 16: 39–54.
75. Rowe PN, Claxton KT, and Lewis JB. Heat and mass transfer from a single sphere in an extensive flowing fluid. *Trans Instn Chem Engrs* 1965; 43: T14–T31.
76. Keey RB and Glen JB. Area-free mass transfer coefficients for liquid extraction in a continuously worked mixer. *AIChE J* 1969; 15: 942–947.
77. Levins DM and Glastonbury JR. Particle-liquid hydrodynamics and mass transfer in a stirred vessel. Part II—Mass transfer. *Trans Instn Chem Engrs* 1972; 50: 132–146.
78. Boon-Long S, Laguerie C, and Couderc JP. Mass transfer from suspended solids to a liquid in agitated vessels. *Chem Eng Sci* 1978; 33: 813–819.
79. Cassamatta G, Chavarie C, and Angelino H. Hydrocarbon separation through a liquid water membrane: Modeling of permeation in an emulsion drop. *AIChE J* 1978; 24: 945–949.
80. Skelland AHP and Lee JM. Drop size and continuous-phase mass transfer in agitated vessels. *AIChE J* 1981; 27: 99–111.
81. Goswami AN, Sharma A, and Sharma SK. A re-appraisal of modelling in a liquid surfactant membrane waste water cleanup process. *J Membr Sci* 1992; 70: 283–288.
82. Boyadzhiev L, Sapundhiev T, and Bezenshek E. Modeling of carrier-mediated extraction. *Sep Sci Technol* 1977; 12: 541–551.
83. Bouboukas G, Colinart P, Renon H, and Trouve G. Transfer of barbiturates through emulsified liquid membranes. In: Li NN, Calo JM, eds. *Recent Developments in Separation Science*, Volume IX, Chapter 25.11. Boca Raton, FL: CRC Press, 1986: 209–226.
84. Huang CR, Wang KC, and Zhou DW. Mathematical modelling of carrier-facilitated transport in emulsion liquid membranes. In: Bartsch RA, Way JD, eds. *Chemical Separations with Liquid Membranes*, Washington, DC: American Chemical Society, ACS symposium series 642, 1996: 115–122.
85. Gadekar PT, Mukkolath AV, and Tiwari KK. Recovery of nitrophenols from aqueous solutions by a liquid emulsion membrane system. *Sep Sci Technol* 1992; 27: 427–455.
86. Stevens GW, Chang C, and Mackay ME. Stabilizing emulsion liquid membranes. *Sep Sci Technol* 1996; 31: 1025–1033.
87. Stevens GW, Perera JM, and Grieser F. Metal ion extraction. *Curr Opin Colloid Interfac Sci* 1997; 6: 629–634.
88. Yurtov EV and Koroleva MY. Emulsions for liquid membrane extraction: Properties and peculiarities. In: Bartsch RA, Way JD, eds. *Chemical Separations with Liquid Membranes*, Washington, DC: American Chemical Society, ACS symposium series 642, 1996: 89–102.
89. Bart HJ, Ramaseder C, Haselgrübler T, and Marr R. The investigation of osmosis in the liquid membrane technique. Influence of key parameters. *Hydrometallurgy* 1992; 28: 253–267.
90. Yan N, Shi Y, and Su Y. A study of swelling behaviour of W/O/W multiple emulsions. *Water Treat* 1992; 7: 67–76.
91. Cox M. Liquid–liquid extraction in hydrometallurgy. In: Thornton JD, ed. *Science and Practice of Liquid–Liquid Extraction*, Volume 2. Oxford, UK: Clarendon Press, 1992: 1–101.
92. Kakoi T, Goto M, and Nakashio F. Development of bi-functional surfactant for extraction of platinum with liquid surfactant membranes. *J Chem Eng Jpn* 1995; 28: 854–856.
93. Bunge AL, Reed DL, and Noble RD. Encapsulated-phase leakage during emulsion liquid membrane extractions. In: *Proceedings of the International Solvent Extraction Conference (ISEC'88)*, Volume 3, Moscow, USSR, 1988: 57–60.
94. Li WX and Shi YJ. Water-permeation swelling of emulsion liquid membrane. *Sep Sci Technol* 1993; 28: 241–254.
95. Ding XC and Xie FQ. Study of the swelling phenomena of liquid surfactant membranes. *J Membr Sci* 1991; 59: 183–188.
96. Mok YS, Lee KH, and Lee WK. Control of swelling in liquid emulsion membranes employed for lactic acid separation. *J Chem Technol Biotechnol* 1996; 65: 309–316.
97. Bart HJ, Jüngling H, Ramaseder N, and Marr R. Water and solute solubilization and transport in emulsion liquid membranes. *J Membr Sci* 1995; 102: 103–112.
98. Kinugasa T, Watanabe K, and Takeuchi H. Stability of (W/O) emulsion drops and permeation through a liquid membranes. *J Chem Eng Jpn* 1992; 25: 128–133.
99. Miesiac I, Schügerl K, Hasler A, and Szymanowski J. Extraction and enzymatic hydrolysis of penicillin G in emulsion liquid membranes. *J Radioanalyt Nuclear Chem* 1996; 208: 133–144.
100. Wan Y, Wang X, Zhu B, and Zhang X. Development of a new series of polymeric-type polymeric surfactants used for emulsion liquid membranes. *J Membr Sci* 2001; 184: 49–57.

101. Zhang XJ, Fan QJ, Zhang XT, and Liu ZF. New surfactant LMS-2 used for industrial application in liquid membrane separation. In: Li NN, Strathmann H, eds. *Separation Technology*, New York: United Engineering Trustees, 1988: 215–226.
102. Liu PY, Chu Y, Wu ZS, Yan Z, and Fang TR. Application of polybutadiene-based polymeric surfactants in liquid membrane separation. *Sep Sci Technol* 1995; 30: 2565–2572.
103. Draxler J, Furst W, and Marr RJ. Separation of metal ion species by emulsion liquid membranes. *J Membr Sci* 1988; 38: 281–293.
104. Kakoi T, Goto M, and Nakashio F. Separation of platinum and palladium by liquid surfactant membranes utilizing a novel bi-functional surfactant. *J Membr Sci* 1996; 120: 77–88.
105. Ma XS and Shi YJ. Study of operating conditions affecting mass transfer rate in liquid surfactant membrane processes. *Sep Sci Technol* 1987; 22: 819–829.
106. Okazaki S, Imai M, and Shimizu M. Leakage suppressing of W/O emulsion using high viscous solvent in Solvent Extraction 1990. In: Sekine T, ed. *Proceedings of the International Solvent Extraction Conference ISEC'90*. New York: Elsevier Science, 1487–1492.
107. Ohtake T, Hano T, Takagi K, and Nakashio F. Analysis of water entrainment into dispersed W/O emulsion drops. *J Chem Eng Jpn* 1988; 21: 272–276.
108. Yan N, Shi Y, and Su Y. A study of gold extraction by liquid membranes. *Water Treat* 1990; 5: 190–201.
109. Ma XS and Shi YJ. Study of operating condition affecting mass transfer rate in liquid surfactant membrane process. *Sep Sci Technol* 1987; 22: 819–829.
110. Yan N, Zhang M, and Ni P. A study of the stability of W/O/W multiple emulsions. *J Microencapsulation* 1992; 9: 143–151.
111. Kinugasa T, Watanabe K, and Takeuchi H. Effect of organic solvents on stability of liquid surfactant membranes. *J Chem Eng Jpn* 1989; 22: 593–597.
112. Kumbasar RA and Tutkun O. Separation and concentration of gallium from acetic acid leach solutions containing various metal ions by emulsion type of liquid membranes using TOPO as mobile carrier. *Hydrometallurgy* 2004; 75: 111–121.
113. Strzelbicki J and Schlosser S. Influence of surface-active substances on pertraction of cobalt (II) cations through bulk and emulsion liquid membranes. *Hydrometallurgy* 1989; 23: 67–75.
114. Skelland AHP. Stabilizing of liquid membranes for separation processes without sacrificing permeability by non-Newtonian conversion of the membrane, US Patent 5,229,004, 1993.
115. Skelland AHP and Meng XM. A new solution to emulsion liquid membrane problems by non-Newtonian conversion. *AIChE J* 1996; 42: 547–561.
116. Shere AJ and Cheung HM. Effect of preparation parameters on leakage in liquid surfactant membrane systems. *Sep Sci Technol* 1988; 23: 687–701.
117. Skelland AHP and Meng XM. Non-Newtonian conversion solves problems of stability, permeability, and swelling in emulsion liquid membranes. *J Membr Sci* 1999; 158: 1–15.
118. Correia PFMM and de Carvalho JMR. Recovery of 2-chlorophenol from aqueous solutions by emulsion liquid membranes: Batch experimental studies and modelling. *J Membr Sci* 2000; 179: 175–183.
119. Yan J and Pal R. Isotonic swelling behaviour of w/o/w emulsion liquid membranes under agitation. *J Membr Sci* 2003; 213: 1–12.
120. Wan T and Zhang X. Swelling determination of w/o/w emulsion liquid membranes. *J Membr Sci* 2002; 196: 185–201.
121. Itoh H, Thien MP, Hatton TA, and Wang DIC. Water transport mechanism in liquid emulsion membrane process for the separation of amino acids. *J Membr Sci* 1990; 51: 309–322.
122. Yan J and Pal R. Osmotic swelling behaviour of globules of w/o/w emulsion liquid membranes. *J Membr Sci* 2001; 190: 79–91.
123. Colinart P, Delepine S, Trouve G, and Renon H. Water transfer in emulsified liquid membrane processes. *J Membr Sci* 1984; 20: 167–187.
124. Garti N, Magdassi S, and Whitehill D. Transfer phenomena across the oil phase in water-oil-water multiple emulsions evaluated by Coulter counter. *J Coll Interf Sci* 1985; 104: 587–591.
125. Ramaseder C, Bart HJ, and Marr R. Phenomenological and mathematical description of the osmotic influence in the liquid membrane technique. *Sep Sci Technol* 1993; 28: 929–945.
126. Draxler J and Marr RJ. Emulsion liquid membranes, part I: Phenomenon and industrial application. *Chem Eng Process* 1986; 20: 319–329.
127. Martin TP and Davies GA. The extraction of copper from dilute aqueous solutions using a liquid membrane process. *Hydrometallurgy* 1977; 2: 315–334.
128. Goto M, Matsumoto M, Kondo K, and Nakashio F. Development of new surfactant for liquid surfactant membrane process. *J Chem Eng Jpn* 1987; 20: 157–164.
129. Nakano K, Kato S, Noritomi H, and Nagahama K. Extraction of polyunsaturated fatty acid ethyl esters from sardine oil using Ag<sup>+</sup>-containing O/W/O emulsion liquid membranes. *J Membr Sci* 1996; 110: 219–227.
130. Hsu EC and Li NN. Membrane recovery in liquid membrane separation processes. *Sep Sci Technol* 1985; 20: 115–130.
131. Larson K, Raghuraman B, and Wiencek J. Electrical and chemical demulsification techniques for microemulsion liquid membranes. *J Membr Sci* 1994; 91: 231–248.
132. Kasaini H, Nakashio F, and Goto M. Application of emulsion liquid membranes to recover cobalt ions from a dual-component sulphate solution containing nickel ions. *J Membr Sci* 1998; 146: 159–168.
133. Devulapalli R and Jones F. Separation of aniline from aqueous solutions using emulsion liquid membranes. *J Haz Mater B* 1999; 70: 157–170.
134. Fang CS, Chang BKL, and Lai PMC. Microwave demulsification. *Chem Eng Sci* 1988; 73: 227–239.
135. Dezhi S, Xiaodong D, Wenxu L, and Ding Z. Demulsification of water-in-oil emulsion by using porous glass membrane. *High Technol Lett* 1999; 5: 98–102.
136. Hsu EC, Li NN, and Hucal T. Electrical coalescence of liquid emulsions. US Patent 4,419,200, 1983.

137. Marr RJ, Bart HJ, and Draxler J. Liquid membrane permeation. *Chem Eng Process* 1990; 27: 59–64.
138. Feng ZL, Wang XD, and Zhang XJ. A new high voltage electrostatic coalescer EC-1 applied to liquid membrane separation. *Water Treat* 1988; 3: 320–328.
139. Shen JQ, Yin WP, Zhao YX, and Yu LJ. Extraction of alanine using emulsion liquid membranes featuring a cationic carrier. *J Membr Sci* 1996; 120: 45–53.
140. Goto M, Irie J, Kondo K, and Nakashio F. Electrical demulsification of W/O emulsion by continuous tubular coalescer. *J Chem Eng Jpn* 1989; 22: 401–406.
141. Wang SS, Lee CJ, and Chan CC. Demulsification of water-in-oil emulsions by use of a high voltage ac field. *Sep Sci Technol* 1994; 29: 159–170.
142. Draxler J and Marr R. Design criteria for electrostatic deemulsifiers. *Int Chem Eng* 1993; 33: 1–7.
143. Draxler J, Weiss C, Marr R, and Rapaumbya GR. Preparation and splitting of emulsions for liquid membranes. In: Bartsch RA, Way JD, eds. *Chemical Separations with Liquid Membranes*, Volume 642. Washington, DC: American Chemical Society, ACS symposium series, 1996: 103–114.
144. Kataoka T and Nishiki T. Development of a continuous electric coalescer of W/O emulsions in liquid surfactant membrane process. *Sep Sci Technol* 1990; 25: 171–185.
145. Fujinawa K, Morishita M, Hozawa M, Imaishi N, and Ino H. Demulsification of W/O emulsion by use of high voltage of AC fields. *J Chem Eng Jpn* 1984; 17: 632–636.
146. Hauertmann HB, Degener W, and Schügerl K. Electrostatic coalescence: reactor, process control and important parameters. *Sep Sci Technol* 1989; 24: 253–273.
147. Bailes PJ and Larkai SKL. Liquid phase separation in pulsed DC fields. *Trans I Chem E* 1982; 60: 115–121.
148. Yan Z, Li SC, Wang LC, and Yang FY. Demulsification of liquid membranes in electric fields. *Water Treat* 1990; 5: 1–6.
149. Yan Z, Li S, Yu Y, and Zheng X. An investigation into the breaking-down of water-in-oil type emulsions by means of pulsed voltage. *Desalination* 1987; 62: 323–328.
150. Hano T, Ohtake T, and Takagi K. Demulsification kinetics of W/O emulsion in an A.C. electric field. *J Chem Eng Jpn* 1988; 21: 345–351.
151. Ichikawa T, Itoh K, Yamamoto S, and Sumita M. Rapid demulsification in dense oil-in-water emulsion by low external electric field. I. Experimental evidence. *Coll Surf A* 2004; 242: 21–26.
152. Ichikawa T and Nakajima Y. Rapid demulsification in dense oil-in-water emulsion by low external electric field. II. Theory. *Coll Surf A* 2004; 242: 27–37.
153. Halwachs W and Schügerl K. The liquid membrane technique—a promising extraction process. *Int Chem Eng* 1980; 20: 519–528.
154. Marr R and Kopp A. Liquid membrane technology—a survey of phenomena, mechanisms, and models. *Int Chem Eng* 1982; 22: 44–60.
155. Ulbrich M and Marr R. Aqueous liquid membranes—state of the art. *Int Chem Eng* 1994; 34: 277–287.
156. Noble RD and Way JD. Liquid membrane technology—an overview. In: Noble RD, Way JD, eds. *Liquid Membranes, Theory and Applications*. American Chemical Society, ACS symposium series 347, 1986: 1–26.
157. Marr RJ and Draxler J. Applications. In: Ho WS, Sirkar KK, eds. *Membrane Handbook*. New York: Van Nostrand Reinhold, 1992; 701–717.
158. Thien MP and Hatton TA. Liquid emulsion membranes and their applications in biochemical processing. *Sep Sci Technol* 1988; 23: 819–853.
159. Huang CR, Zhou DW, Ho WS, and Li NN. Paper No. 89b Presented at AIChE National meeting, Houston, TX, March 19–23, 1995.
160. Kitagawa T, Nishikawa Y, Frankenfeld JW, and Li NN. Wastewater treatment by liquid membrane process. *Environ Sci Technol* 1977; 11: 602–605.
161. Raghuraman BJ, Tirmizi NP, Kim BS, and Wiencek JM. Emulsion liquid membranes for wastewater treatment: Equilibrium models for lead- and cadmium-di-2-ethylhexyl phosphoric acid systems. *Environ Sci Technol* 1995; 29: 979–984.
162. Macasek F, Rajec P, Kopune R, and Mikulaj V. Membrane extraction in preconcentration of some uranium fission products. *Solvent Extr Ion Exch* 1984; 2: 227–252.
163. Vohra DK, Kaur S, and Sharma A. Extraction of Cr(VI) from acid (sulfate) aqueous medium using liquid surfactant membrane emulsions. *Indian J Technol* 1989; 27: 574–576.
164. Strzelbicki J and Charewicz W. Separation of cobalt by liquid surfactant membranes. *Sep Sci Technol* 1978; 13: 141–152.
165. Gu ZM, Wasan DT, and Li NN. Ligand-accelerated liquid membrane extraction of metal ions. *J Membr Sci* 1986; 26: 129–142.
166. Wiencek JM and Qutubuddin S. Microemulsion liquid membranes II. Copper ion removal from buffered and unbuffered aqueous feed. *Sep Sci Technol* 1992; 27: 1407–1422.
167. Yu J, Jiang C, and Zhu Y. Separation of europium with liquid surfactant membranes. In: Li NN, Calo JM, eds. *Recent Developments in Separation Science*, Volume IX, Chapter 25.10. Boca Raton, FL: CRC Press, 1986: 197–208.
168. Ohki A, Hinoshita H, Takagi M, and Ueno K. Transport of iron and cobalt complex ions through liquid membrane mediated methyltriocetylammmonium ion with the aid of redox reaction. *Sep Sci Technol* 1983; 18: 969–983.
169. Biehl MP, Izatt RM, Lamb JD, and Christensen JJ. Use of a macrocyclic crown ether in an emulsion (liquid surfactant) membrane to effect rapid separation of  $Pb^{2+}$  from cation mixtures. *Sep Sci Technol* 1982; 17: 289–294.
170. Larson KA and Wiencek JM. Mercury removal from aqueous streams utilizing microemulsion liquid membranes. *Environ Progress* 1994; 13: 253–262.
171. Boyadzhiev L and Bezenshek E. Carrier mediated extraction: Application of double emulsion technique for mercury removal from waste water. *J Membr Sci* 1983; 14: 13–18.
172. Hirato T, Koyama Y, Awakura Y, and Majima H. Concentration of Mo(VI) from aqueous sulfuric acid solution by an emulsion type liquid membrane process. *Mater Trans JIM* 1990; 31: 213–218.

173. Juang RS and Jiang JD. Recovery of nickel from a simulated electroplating rinse bath solution by solvent extraction and liquid surfactant membrane. *J Membr Sci* 1995; 100: 163–170.
174. Yamashita K, Kakoi T, Kosaka H, Goto M, and Nakashio F. Synergistic extraction of nickel by liquid surfactant membranes. *Sep Sci Technol* 1998; 33: 369–385.
175. Kakoi T, Horinouchi N, Goto M, and Nakashio F. Recovery of palladium from an industrial wastewater using liquid surfactant membranes. *Sep Sci Technol* 1996; 31: 381–399.
176. Shukala JP, Kumar A, and Singh RK. Macrocyclic-mediated selective transport of plutonium (IV) nitrate through bulk liquid and supported liquid membranes using dicyclohexano-18-crown-6 as mobile carrier. *Sep Sci Technol* 1992; 27: 447–465.
177. Gleason KJ, Yu J, Bunge AL, and Wright JD. Removal of selenium from contaminated waters using emulsion liquid membranes. In: Bartsch RA, Way JD, eds. *Chemical Separations with Liquid Membranes*, Washington, DC: American Chemical Society, ACS symposium series 642, 1996: 342–360.
178. Eroglu I, Kalpakici R, and Gunduz G. Extraction of strontium ions with emulsion liquid membrane technique. *J Membr Sci* 1993; 80: 319–325.
179. Hayworth HC, Ho WS, Burns WA, and Li NN. Extraction of uranium from wet process phosphoric acid by liquid membranes. *Sep Sci Technol* 1983; 18: 493–521.
180. Hirato T, Kishigami I, Awakura Y, and Majima H. Concentration of uranyl sulfate solution by an emulsion-type liquid membrane process. *Hydrometallurgy* 1991; 26: 19–33.
181. Zheng XC, Li LX, Guo JJ, and Long FS. Extraction of vanadium from waste water with emulsion liquid membrane. Proceedings of the First International Conference on Hydrometallurgy, Beijing, China, October 12–15, 1988: 508.
182. Jin M and Zhang Y. Study on extraction of gold and cyanide from alkaline cyanide solution by liquid membrane. Proceedings of the International Congress on Membranes and Membrane Processes (ICOM '90), Chicago, IL, August 20–24, 1990; 1: 676–678.
183. Li NN, Cahn RP, and Shrier AL. Liquid membrane process for the separation of aqueous mixtures. US Patent 3,779,907, 1973.
184. Wienczek JM and Qutubuddin S. Microemulsion liquid membranes 1. Application to acetic acid removal from water. *Sep Sci Technol* 1992; 27: 1211–1228.
185. Lee CJ and Chan CC. Extraction of ammonia from a dilute aqueous solution by emulsion liquid membranes. 1. Experimental studies in a batch system. *Ind Eng Chem Res* 1990; 29: 96–100.
186. Stefanut M, Novac A, Amanatidou E, and Csunderlik C. Some aromatic amine transport through emulsion liquid membranes. *Sep Sci Technol* 1996; 31: 2219–2229.
187. Zhang XJ, Liu J, Fan Q, Lian Q, Zhang X, and Lu T. Industrial application of liquid membrane separation for phenolic wastewater treatment. In: Li NN, Strathmann H, eds. *Separation Technology*, New York: United Engineering Trustees, 1988: 190–203.
188. Correia PFMM and Carvalho JMR. Recovery of phenol from phenolic resin plant effluents by emulsion liquid membranes. *J Membr Sci* 2003; 225: 41–49.
189. El-Reefy SA, El-Sourouhy MR, El-Sherif EA, and Aly HF. Europium permeation and separation from americium using liquid emulsion membrane. *Analyt Sci* 1995; 11: 329–331.
190. Bartsch RA, Charewicz WA, and Kang SI. Separation of metals by liquid surfactant membranes containing crown ether carboxylic acids. *J Membr Sci* 1984; 17: 97–107.
191. Abou-Nemeh I and Van Peteghem AP. Extraction of cobalt and manganese from an industrial effluent by liquid emulsion membranes. In: Baird MHL, Vijayan S, eds. *Proceedings of the Second International Conference on Separation Science and Technology*, Volume 2. Ottawa, Ontario: Canadian Society of Chemical Engineering, 1989: 416–423.
192. Abou-Nemeh I and Van Peteghem AP. Extraction of multi-component system of metal from simulated and industrial effluents by liquid surfactant membranes (LSM). *Hydrometallurgy* 1992; 31: 149–162.
193. Kakoi T, Ura T, Kasaini H, Goto M, and Nakashio F. Separation of cobalt and nickel by liquid surfactant membranes containing a synthesized cationic surfactant. *Sep Sci Technol* 1998; 33: 1163–1180.
194. Kakoi T, Goto M, Sugimoto K, Ohto K, and Nakashio F. Separation of cobalt and nickel with phenylphosphonic acid mono-4-tert-octylphenyl ester by liquid surfactant membranes. *Sep Sci Technol* 1995; 30: 637–657.
195. Ribeiro CP, Costa AOS, Lopes IPB, Campos FF, Ferreira AA, and Salum A. Cobalt extraction and cobalt-nickel separation from a simulated industrial leaching liquor by liquid surfactant membranes using Cyanex 302 as carrier. *J Membr Sci* 2004; 241: 45–54.
196. Frankenfeld JW, Cahn RP, and Li NN. Extraction of copper by liquid membranes. *Sep Sci Technol* 1981; 16: 385–402.
197. Uddin MS and Kathiresan M. Extraction of metal ions by emulsion liquid membrane using bi-functional surfactant: equilibrium and kinetic studies. *Sep Purif Technol* 2000; 19: 3–9.
198. Strzelbicki J and Charewicz W. The liquid surfactant membrane separation of copper, cobalt and nickel from multicomponent aqueous solutions. *Hydrometallurgy* 1980; 5: 243–254.
199. Tang J and Wai CM. Transport of trivalent lanthanides through a surfactant membrane containing an ionizable macrocyclic polyether. *J Membr Sci* 1989; 46: 349–356.
200. Christensen JJ, Christensen SP, Biehl MP, Lowe SA, Lamb JD, and Izatt RM. Effect of receiving phase anion on macrocyclic-mediated cation transport rates and selectivities in water-toluene-water emulsion membranes. *Sep Sci Technol* 1983; 18: 363–373.
201. Goto M, Kakoi T, Yoshii N, Kondo K, and Nakashio F. Effect of synthesised surfactants in the separation of rare earth metals by liquid surfactant membranes. *Ind Eng Chem Res* 1993; 32: 1681–1685.
202. Reis MT and Carvalho JMR. Recovery of zinc from an industrial effluent by emulsion liquid membranes. *J Membr Sci* 1993; 84: 201–211.
203. Mickler W, Reich A, Uhlemann E, and Bart HJ. Liquid membrane permeation of zinc, cadmium and nickel with 4-acyl-5-pyrazolones and  $\beta$ -diketones. *J Membr Sci* 1996; 119: 91–97.

204. Tang H, Ma Z, and Liu L. Alkaloid extraction from plants with liquid membranes. *Water Treat* 1990; 5: 214–221.
205. Yagodin GY, Lopukhin Y, Yurtov E, Guseva T, and Sergienko V. Extraction of cholesterol from blood using liquid membranes. Proceedings of the International Solvent Extraction Conference (ISEC'83), Denver, CO, 26 August to 2 September, 1983: 385–386.
206. Hano T, Matsumoto M, Kawazu T, and Ohtake T. Separation of di and tripeptides with solvent extraction and an emulsion liquid membrane. *J Chem Tech Biotechnol* 1995; 62: 60–63.
207. Habaki H, Isobe S, Egashira R, and Kawasaki J. Permeation and concentration of erythromycin by supported and emulsion liquid membranes. *J Chem Eng Jpn* 1998; 31: 47–54.
208. Habaki H, Egashira R, Stevens GW, and Kawasaki J. A novel method of improving low separation performance for w/o/w ELM permeation of erythromycin. *J Membr Sci* 2002; 208: 89–103.
209. Mok YS, Lee SC, and Lee WK. Water transport in water-in-oil-in-water liquid emulsion membrane system for the separation of lactic acid. *Sep Sci Technol* 1994; 29: 743–764.
210. Lee SC and Lee WK. Extraction of penicillin G from simulated media by an emulsion liquid membrane process. *J Chem Tech Biotechnol* 1992; 55: 251–261.
211. Mok YS, Lee SC, and Lee WK. Synergistic effect of surfactant on transport rate of organic acid in liquid emulsion membranes. *Sep Sci Technol* 1995; 30: 399–417.
212. Lee SC, Lee KH, Hyun GH, and Lee WK. Continuous extraction of penicillin G by an emulsion liquid membrane in a countercurrent extraction column. *J Membr Sci* 1997; 124: 43–51.
213. Hano T, Matsumoto M, and Ohtake T. Continuous extraction of penicillin G with liquid surfactant membrane using Vibro Mixer. *J Membr Sci* 1994; 93: 61–68.
214. Hong SA, Choi HJ, and Nam SW. Concentration of amino acids by a liquid emulsion membrane with a cationic extractant. *J Membr Sci* 1992; 70: 225–235.
215. Dzygiel P and Wieczorek P. Extraction of amino acids with emulsion liquid membranes using industrial surfactants and lecithin as stabilisers. *J Membr Sci* 2000; 172: 223–232.
216. Kim SJ, Kim SC, and Kawasaki J. A scale-up of stirred tank contactors for the liquid membrane permeation of hydrocarbons. *Sep Sci Technol* 2001; 36: 3585–3598.
217. Kim SJ and Kim SC. Separation of valuable bicyclic aromatic components from light cycle oil by emulsion liquid membrane. *Sep Sci Technol* 2004; 39: 1093–1109.
218. Kentish SE and Stevens GW. Innovations in separations technology for the recycling and re-use of liquid waste streams. *Chem Eng J* 2001; 84: 149–159.
219. Cahn RP and Li NN. Commercial applications of emulsion liquid membranes. In: Li NN, Calo JM, eds. *Separation and Purification Technology*, New York: Marcel Dekker, 1992: 195–212.
220. Breembroek GRM, Witkamp GJ, and Van Rosmalen GM. Design and testing of an emulsion liquid membrane pilot plant. *Sep Sci Technol* 2000; 35: 1539–1571.
221. Nilsen DN, Hundley GL, Galvan GJ, and Wright JB. Field testing of a liquid-emulsion membrane system for copper recovery from mine solutions. In: Bartsch RA, Way JD, eds. *Chemical separations with liquid membranes*, Washington, DC: American Chemical Society, ACS symposium series 642, 1996: 329–341.

---

# 26 Membrane Electroporation and Emerging Biomedical Applications

*K.P. Mishra*

## CONTENTS

26.1	Introduction .....	742
26.1.1	Cell Plasma Membrane and Biotechnological Potential.....	742
26.1.2	Permeability Barrier and Electroporation Phenomenon.....	742
26.1.3	Scope and Outline .....	743
26.2	Physicochemical Aspects of Cell Membrane.....	743
26.2.1	Phospholipid Bilayer.....	743
26.2.2	Membrane Proteins .....	744
26.2.3	Fluid Mosaic Membrane Structure .....	744
26.2.4	Physical Organization .....	744
26.2.5	Molecular Transport and Permeability Barrier .....	745
26.2.6	Methods to Overcome Bilayer Barrier.....	745
26.3	Cell Membrane Electroporation .....	745
26.3.1	Basic Principle .....	745
26.3.2	Resting and Induced Transmembrane Potential.....	746
26.3.3	Biophysical Basis of Membrane Electroporation .....	746
26.3.4	Electroporation Threshold.....	747
26.3.5	Mechanism of Electroporation .....	747
	26.3.5.1 Pore Model.....	747
	26.3.5.2 Mechanical Breakdown Model .....	747
26.3.6	Resealing of Electroporated Membrane.....	748
26.3.7	Factors That Control Electroporation Outcome.....	748
	26.3.7.1 Electrical Parameters .....	748
	26.3.7.2 Experimental Conditions.....	749
	26.3.7.3 Biological Factors .....	749
26.4	Electroporation Devices .....	749
26.4.1	Electric Pulse Generators .....	749
26.4.2	Cuvettes and Electrodes .....	749
26.5	Some Applications of Electroporation .....	750
26.5.1	Cell Fusion and Hybridoma Technology.....	750
26.5.2	Electrotransfection.....	750
26.5.3	Therapeutic Applications .....	750
26.5.4	Potential for Overcoming Tumor Resistance.....	750
26.5.5	Electro Cell Manipulation.....	751
26.5.6	Electroloading of Cells.....	751
26.5.7	Electrochemotherapy .....	752
26.5.8	Radio-Electrochemotherapy .....	752
26.5.9	In Vivo Applications.....	753
26.5.10	Electroporative Gene Delivery.....	753
26.5.11	Electrodelivery of Proteins.....	753
26.5.12	Incorporation of Radioiodine into Tumor Cells .....	754

26.5.13	Electroporation in Biotechnology .....	754
26.5.13.1	Water Sterilization .....	754
26.5.13.2	Food Sterilization .....	755
26.5.14	Transgenic Plants and Animals .....	755
26.5.15	Transdermal Drug Delivery .....	755
26.5.16	Ex Vivo Applications .....	755
26.6	Single-Cell Electroporation .....	755
26.7	Future Prospects and Challenges .....	756
	Acknowledgments .....	756
	References .....	756

## 26.1 INTRODUCTION

### 26.1.1 CELL PLASMA MEMBRANE AND BIOTECHNOLOGICAL POTENTIAL

Cells are the basic building units of living organisms, which are bounded by intricate plasma membrane guarding the cell interior. Life or death of a cell critically depends on the intactness of outer membrane whose structure and function are intense research curiosity and also, a potential source of developing various technologies for biomedical and industrial applications. Over the years, considerable understanding of cell membrane structure and function has been obtained but much remains to be learned. It is fairly well established that plasma membrane of mammalian cell mainly consists of lipids, proteins, and cholesterol, and a bilayer of lipids forms the core structure separating the cell interior from the exterior surroundings. The recent impetus in biotechnology has propelled membrane research to unravel the molecular design and function of cellular membrane with the hope of developing novel products and processes. A few tools and devices based on membrane have already been developed and employed for practical applications in medicine, industry, and biotechnology. Modeled after cell membrane, liposomes have been prepared in laboratory, which have found numerous biological, medical, and industrial applications. The precision, speed, and sensitivity with which real cell membranes regulate molecular transport, sense tiny concentration of substances, carry out intermolecular communications have much to offer in developing strategic and biocompatible materials, sensor devices, and signal processor technologies. Extensive recent research has provided a few physical and chemical methods to overcome natural transport barrier of membrane, opening many new prospects for cellular engineering and membrane biotechnology. For example, methods have been developed to introduce exogenous molecules into a variety of plant, bacterial, and mammalian cells but some limitations are encountered. Obviously, gaining access to the cell interior without affecting cell viability holds enormous potential to basic research in exploring the tiny internal world of living cells and in providing exciting new opportunities to modify cellular composition in controlled fashion with prospects in nanoscience, biomolecular engineering, cell membrane fusion and intermembrane trafficking and communication, signaling, sensing processes, etc. that are at work in living cell function. To cope with the harsh variable surroundings, cells have evolved antenna network and implanted microswitches on their membrane surface, which allow them to sort specific ligands and deal with the external stresses for maintaining their survival. The precise steps involved in these functions have remained intriguing but they may offer a whole new opportunity for developing devices to recognize and sort out ensemble of molecules required for numerous applications in diagnostic medicine, pollution science, signal processing, and cell biotechnology. The key to success in achieving newer practical applications largely lies in delineation of molecular design of membrane architecture and in accomplishing the controlled permeabilization of plasma membrane. Advanced imaging methods have aided enormously in learning the intricate dynamic structure and function of cellular membrane, which have generated a host of new opportunities for biomolecular engineering, medicine, and structural science.

### 26.1.2 PERMEABILITY BARRIER AND ELECTROPORATION PHENOMENON

Biological cell membrane is composed of phospholipid bilayer core of a few nanometers thickness, which controls molecular transport and separates cellular interior from the surrounding. Cells possess an intrinsic electrical potential across their membrane due to concentration gradient of ions between the cytosol and surroundings, which plays vital role in regulation of a variety of their functions [1,2]. During the late 60s and early 70s, it was observed that application of high intensity, short duration electric field across cells beyond a certain threshold value dramatically increased the permeability of their membrane allowing entry of otherwise impermeant exogenous substances (Figure 26.1). This phenomenon is popularly called electroporation [3] (and references therein). A variety of external bioactive substances, such as, enzymes, drugs, genes, signaling molecules, and DNA constructs, can be incorporated into cells, which has opened many new prospects in cell biology, biotechnology, and medicine. Scientists have long aimed to change natural makeup of plant, bacterial, and animal cells by introducing external DNA with defined traits but efforts were hampered due to tight bilayer membrane barrier. Over the years, a number of bacterial, yeast, plant,

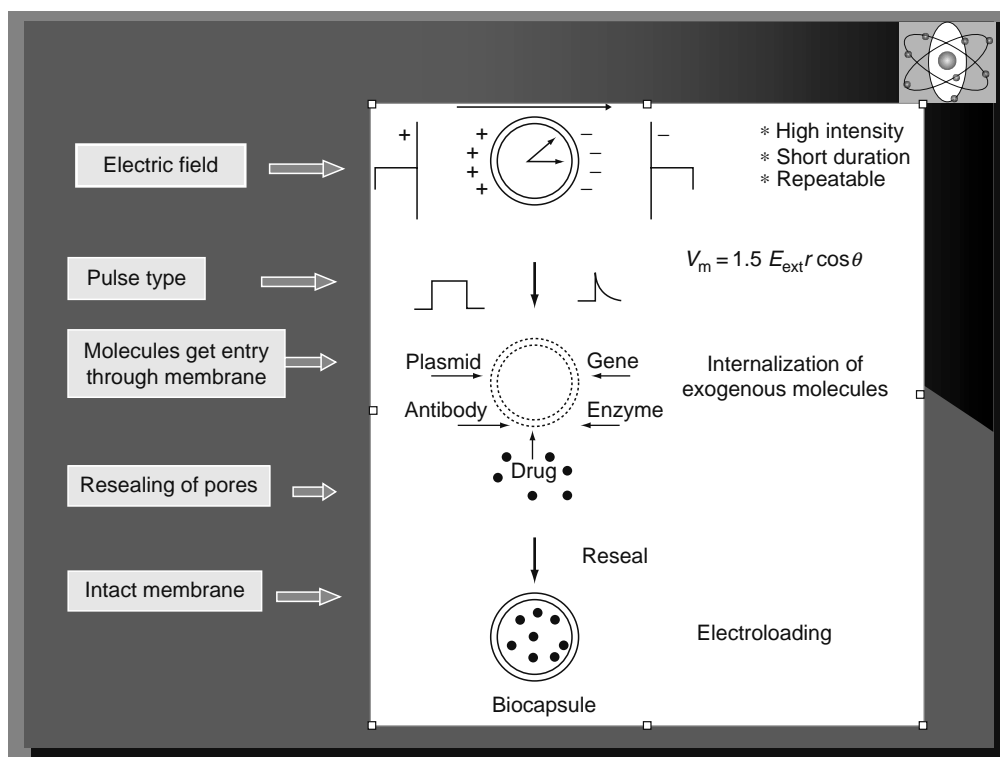


**FIGURE 26.1** Biological cell in electric field and entrapment of exogenous substances.

and mammalian cells have been electroporated for introduction of drugs, genes, enzymes, DNA, and other substances providing a valuable tool and technology for drug loading, cancer treatment, gene therapy, cell fusion, etc. [3].

### 26.1.3 SCOPE AND OUTLINE

The area of membrane science and technology is witnessing rapid progress and several devices and procedures are under development for biomedical and industrial applications. This article is confined to description of cell membrane electroporation/permeabilization with examples of a few biomedical technologies for potential practical applications. The phenomenon of cell electroporation has attracted scientists from both basic science as well as engineering disciplines and, currently, it is viewed as an engineering alternative to biological methods for the genetic engineering of cells.

This chapter presents a brief review of basic and applied aspects of cell membrane electroporation with relevance to cell biology, biotechnology, and medicine. The content material is certainly not intended to be exhaustive. To enable the reader better grasp the phenomenon of electroporation, a brief account of physical–chemical aspects of cell membrane and basic mechanisms of membrane electroporation/permeabilization have been included. The factors that affect the electroporation efficiency of cells have been outlined including a brief mention of technical advances in electroporator instrumentation. Some applications based on membrane electroporation have been described which are relevant to cell biology, health care, and industry. Cell fusion, loading of impermeant exogenous molecules into cells, electroporative drug and gene delivery, and introduction of DNA and proteins have briefly been described. Recent progress on industrial applications, such as, sterilization of water and liquid food and single-cell electroporation, and their future potential applications in biotechnology have been described.

## 26.2 PHYSICOCHEMICAL ASPECTS OF CELL MEMBRANE

### 26.2.1 PHOSPHOLIPID BILAYER

The core structure of cell plasma membrane is made of phospholipids arranged in a bilayer with embedded proteins. The phospholipids are amphipathic in nature having both hydrophilic and hydrophobic moieties. The lipids are packed in the bilayer such that the polar head groups face water and the nonpolar segments form the core, insulating the cell interior from the surroundings (Figure 26.2). The bilayer is a self-organized basic membrane structure (5–10 nm thick). The nature and composition of phospholipids control the physical properties of membrane. Though basic skeleton of the bilayer remains unchanged, the composition of the lipids widely differs in bacteria, plant, and mammalian cells. There are three major membrane lipids, namely, phospholipids, glycolipids, and cholesterol which are prevalent in mammalian cells. Of these, the

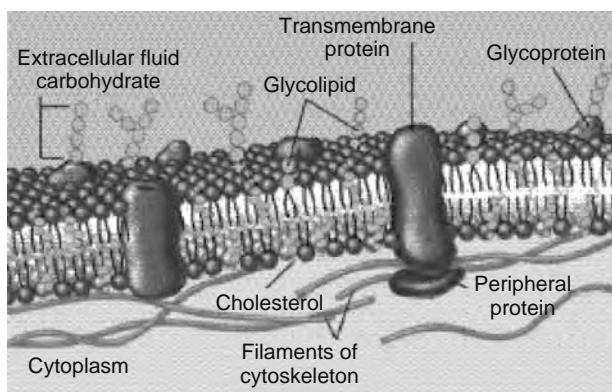


**FIGURE 26.2** Schematic fluid mosaic model of cell membrane structure.

phospholipids are the most abundant. A typical phosphoglyceride molecule consists of a glycerol backbone, a phosphorylated alcohol, and two fatty acid chains (Figure 26.2). The fatty acids consist of long hydrocarbon chains (14–24 carbon atoms) and may be either saturated or have one or more unsaturated chemical bonds in their structure. Glycolipids are the sugar-containing lipids and in animal cells, the glycolipids are derived from sphingosine. Cholesterol forms another important class of lipids, which is mostly present in the eukaryotes and rarely in prokaryotes. Eukaryotic cells have an abundance of the cholesterol in the plasma membrane. The phospholipids and the glycolipids can readily form vesicles (liposomes) with one or multiple concentric spherical bilayers in aqueous medium, which can be easily prepared in laboratory and they serve as model of membrane. Lipid bilayers are the backbone of the biological membrane [1].

### 26.2.2 MEMBRANE PROTEINS

The cell plasma membrane consists of a variety of proteins associated with the lipid bilayer and they perform multitasks in cell function. The control of transport of ions and molecules across membrane is accomplished through specialized function of membrane proteins. These proteins are distributed in membrane on the outer surface, some on the inner surface, and some others are transmembrane proteins with external and cytoplasmic domains. The majority of the transmembrane proteins are the ion channels or signaling proteins. Generally, lipid to protein ratio is 60:40 but this ratio is found variable in different cells and types of membranes. Membrane proteins impart the dynamic structure and selectivity to membrane function. Both proteins and lipids show motional and diffusion properties within the bilayer structure.

### 26.2.3 FLUID MOSAIC MEMBRANE STRUCTURE

Jonathan Singer and Garth Nicolson proposed the fluid mosaic model of the plasma membrane in 1972 based on the available experimental results [1]. The model suggested that essentially, the membranes were two-dimensional solutions of lipids with proteins incorporated into them forming a mosaic structure (Figure 26.2). This model of membrane structure is widely accepted and continues to be the central to our present understanding of membrane structure. The model is based on following salient features: (1) most phospholipids and glycolipids are arranged in bilayer structure, which has a dual role of acting as a solvent for the proteins forming structural assembly and conferring a permeability barrier to membrane, (2) a small proportion of the lipids closely interact and are in intimate contact with the membrane proteins, (3) membrane proteins are free to diffuse laterally in the lipid matrix unless restricted but they are not free to rotate from one side to the other, and (4) lipids are able to diffuse laterally and they also exhibit flip-flop across the bilayer. Major functions of membrane, e.g., selectivity, receptivity, transport, etc., are attributed to proteins present in their structure.

### 26.2.4 PHYSICAL ORGANIZATION

The major physical forces, which help the membrane to maintain their structure, consist of hydrophobic and hydrophilic interactions, electrostatic forces, and van der Waals interactions. The main driving force for formation of the bilayer originates from the hydrophobic interactions and van der Waals interaction forces between hydrocarbon chains of the lipid molecules. The hydrophobic forces control the order and packing of lipids and electrostatic interactions between the polar head groups and their interaction with water molecules contribute to bilayer stabilization. The bilayer is continuous and it exhibits semirigid properties. The fluid nature of the membrane is governed by the lipid composition and the nature of the forces that exist between the constituent lipids and proteins. Due to fluid lipid bilayer, the diffusion constant for a phospholipids is  $\sim 1 \text{ m}^2/\text{s}$ ,

which means a lipid molecule can travel from one end of the cell to the other in  $\sim 1$  s. Nature seems to have chosen the two fatty acid chain phospholipids as basic building block of the membranes because they self-associate in water at very low concentrations and are very hydrophobic, which imparts the internal high lateral tension within the bilayer enabling them exhibit self-healing of structural bilayer alterations including induced transient leaks. Lipids suspended in excess of water tend to form liposomes, which exhibit high degree of stability due the energy minimization principles between the energy needed to bend the bilayer and the energy gained by avoiding the exposure of the hydrophobic regions to water [2]. The self-assembly property of the phospholipids allows formation of liposomes in the laboratory which are magic bags consisting of the bilayer containing an aqueous core, which can be prepared from a variety of lipids and can entrap both hydrophobic and hydrophilic therapeutic drugs with novel prospects in pharmaceutical technology and drug delivery.

### 26.2.5 MOLECULAR TRANSPORT AND PERMEABILITY BARRIER

The plasma membrane carries out the job of specialized and fool-proof security to cell interior with a semipermeable barrier for molecules, allowing some and denying others for entry or exit. The controlled and selective permeability protects cells against unwelcome guest molecules and disallows vital cytosolic molecules to leave and thus maintaining the natural integrity of the cell/organelle. The cellular membranes show high sensitivity and exceptional selective permeability to ions, small solutes, and macromolecules including invading organisms. Channels specific to a particular solute or ion mediate control of the molecular transport across bilayer membrane. Cell membranes are structurally and functionally asymmetric, i.e., the outer and the inner surfaces of biological membranes present different interfaces perhaps an essential component of molecular design for functional sophistication. Mammalian cells have predominance of phosphatidylcholine in the outer layer and phosphatidyl serine in the inner layer. The membrane fluidity is controlled by the nature of the fatty acids of the membrane lipids; the saturated fatty acids tend to make the membrane rigid, whereas the unsaturated acids make them fluid basically due to the bending in the unsaturated hydrocarbon chain.

The transport of the molecules across the membranes takes place in highly regulated fashion for both active, i.e., using metabolically useful energy, and passive, i.e., without any energy requirement. The transport of water seems to occur freely through diffusion process. The transmembrane proteins act as gates or channels for specific ions. The ion channel proteins are called so because they allow only unidirectional passage of ions, e.g.,  $\text{Na}^+$ ,  $\text{K}^+$ , and  $\text{Ca}^{2+}$  channels. There are other proteins that allow the passage of other essential biomolecules. Molecules can be transported across membrane through passive diffusion and facilitated or active transport processes. In addition to plasma membrane, mammalian cells have a several intracellular membranous network in subcellular organelles through which they control molecular trafficking within the cell.

### 26.2.6 METHODS TO OVERCOME BILAYER BARRIER

Extensive research on the attempts to overcome the bilayer membrane barrier has resulted in the emergence of several different methodologies for partial and temporary cell membrane permeabilization. The prominent among them are chemical permeabilizers, liposomal interactions, ultrasonication, ionizing radiation, and electroporation.

The liposome can be made in such a way that they mimic the cellular plasma membrane and drugs/other potential impairment molecules can be loaded in the aqueous core or bilayer milieu of the liposome. Generally, the liposomal membrane fuses with the cell plasma membrane and releases the contents into the cytosol. Thus, liposomes provide an effective tool for overcoming the bilayer barrier and deliver drugs to targets in cells.

A number of chemicals, such as, ammonium chloride, poly(ethylene glycol) (PEG), and calcium salts, have been found to facilitate entry of external molecules into cells, though to a limited extent. Exposure of cells to ionizing radiation, ultrasonic waves, and electric fields has been found to overcome membrane barrier allowing exchange of molecules between cell interior and surroundings. Each method, however, is faced with its own merits and demerits imposing restrictions. In the following sections, the methodology of overcoming the membrane barrier by exposure of cells to external electric field is described with some details.

## 26.3 CELL MEMBRANE ELECTROPORATION

### 26.3.1 BASIC PRINCIPLE

When cells are placed in external applied electric fields, they experience an electric force. Electroporation involves the use of short, high voltage pulses to overcome barrier of the cell membrane. When a cell is submitted to an external electric field of high intensity and short duration ( $\text{kV/cm}$ ,  $\mu\text{s}$ ), transient and dramatic increase in the permeability of the plasma membrane occurs beyond a point. This phenomenon is popularly called electroporation or electroporeabilization, which allows entry of otherwise impermeable exogenous molecules into the cell interior. This phenomenon has been an active area of research in biology and bioelectrochemistry for more than three decades [3,4] and has found many applications in cell biology,

biotechnology, and medicine. The following sections discuss the fundamentals of membrane electroporation and various factors that affect the cell electroporation efficiency.

### 26.3.2 RESTING AND INDUCED TRANSMEMBRANE POTENTIAL

An intrinsic ionic charge gradient across the membrane exists because of semipermeable nature of membrane, which maintains a difference in the concentration of the ions between the cytosol and the extracellular matrix. This difference results in a definite potential across membrane of the normal cells, which is called the resting potential. Normal plant cells, mammalian muscle cells, and neurons have resting potential values of about  $-120$ ,  $-90$ , and  $-70$  mV, respectively. Along with the resistance to the flow of ions, membrane also exhibits a capacitance,  $C_m$ , which is given by

$$C_m = \frac{Q}{V_m} \quad (26.1)$$

where

$Q$  is the net excess positive or negative charge on either side of the membrane

$V_m$  is the potential across the membrane

The typical value of the membrane capacitance is  $\sim 1 \mu\text{F}/\text{cm}^2$  of membrane surface area. A general equation governing the potential difference across the membrane is given by

$$E_k = \frac{RT}{ZF} \ln \frac{P_K[K^+]_O + P_{Na}[Na^+]_O + P_{Cl}[Cl^-]_{IN}}{P_K[K^+]_{IN} + P_{Na}[Na^+]_{IN} + P_{Cl}[Cl^-]_O} \quad (26.2)$$

where

$R$  is the ideal gas constant

$F$  is the Faraday constant

$Z$  is the charge

$T$  is the temperature in Kelvin

$[K^+]_O$  and  $[K^+]_{IN}$  are the concentrations of potassium ions outside and inside the cell, respectively

$[Na^+]_O$  and  $[Na^+]_{IN}$  are the concentrations of sodium ions outside and inside the cell, respectively

$[Cl^-]_O$  and  $[Cl^-]_{IN}$  are the concentrations of chloride ions

The  $P$ 's stand for the partial pressures of the ionic species

A biological cell can be viewed as an electrical entity which can be represented by an equivalent circuit.

### 26.3.3 BIOPHYSICAL BASIS OF MEMBRANE ELECTROPORATION

The cell can be imagined to be a nonconducting sphere with an inner side equipotential. For a spherical cell placed in an externally applied electric field,  $E_e$ , the transmembrane potential at any point on the cell membrane due to the applied field is obtained from Laplace's equation and is given by  $V_m$  or  $\varphi_m$

$$\Phi_m = 1.5r_{\text{cell}}E_e \cos \theta \quad (26.3)$$

where

$r_{\text{cell}}$  is the radius of the cell

$\theta$  is the angle between the radius vector of the point at which the potential is measured in the direction of the electric field

Factor 1.5 represents a constant for the spherical geometry of the cell (Figure 26.1)

At  $\theta = 0$ ,  $\Phi_m = 1.5r_{\text{cell}}E_e$  and at  $\theta = \pi$ ,  $\Phi_m = -1.5r_{\text{cell}}E_e$ . The difference in the transmembrane potential between the two diametrically opposite points of the cell surface is  $3r_{\text{cell}}E_e$ . Thus, rapid application of the electric field results in the membrane polarization changes that can locally deform the membrane leading to formation of leaks or pores. For a cell of radius  $r_{\text{cell}} \sim 10 \mu\text{m}$ , to produce a transmembrane field  $\Phi_m \sim 0.5$  V, the required applied field is  $\sim 300$  V/cm [5–8]. However, this is the effect of the direct field (DC). This equation implies that larger is the radius of a cell, smaller will be the field required to reach threshold value for permeabilization to occur. It is implicit that bacteria will require larger fields than mammalian cells and also, while plasma membrane can be permeabilized at a particular field value, subcellular network of membrane, e.g., mitochondrial, Golgi, lysosomal membranes would largely remain unaffected.

When an alternating field (AC) is applied on the cell, Equation 26.3 is modified as follows:

$$\Phi_{\text{mAC}} = \frac{1.5r_{\text{cell}}E_e \cos \theta}{[(1 + \omega t_{\text{mem}})]} \quad (26.4)$$

where

$t_{\text{mem}}$  is time

$\omega$  is the angular frequency of the AC field

$C_m$  is the membrane capacitance

It may be noted that for  $\omega = 0$ , Equation 26.4 gives rise to Equation 26.3. The changes in the transmembrane potential have been experimentally observed and quantitatively measured.

#### 26.3.4 ELECTROPORATION THRESHOLD

The resting transmembrane potential is important for threshold of membrane permeabilization. The dependence of the transmembrane potential  $\Phi_m$  (Equation 26.1) on the radius and the magnitude of the applied electric field make electroporation a threshold phenomenon. When the field reaches a certain threshold value, a transient reorganization of the phospholipid bilayers takes place, making the membrane temporarily more conducting [4–9]. Evidently, at a constant applied electric field, the electroporation efficiency will depend on the cell size. For a particular cell type, there exists a particular threshold value of the electric field. Thus, electroporation is a threshold process and each type of cell displays its characteristic threshold beyond which membrane permeabilization occurs. The length of the pulse does not seem to alter the threshold voltage for a particular cell. Studies have shown that exposure of cells to multiple pulses of subcritical voltage does not permeabilize membrane [10].

#### 26.3.5 MECHANISM OF ELECTROPORATION

The application of the electric field imposes modulations on the intrinsic membrane potential, which gives in to induced field force beyond a critical stage. This enhanced permeability is believed to be due to a lipid bilayer membrane reorganization [11–13], which can under certain situations convert to structural membrane defect leading to the formation of hydrophilic pores [10]. These induced pores allow the molecules and ions, which are otherwise impermeable to diffuse through membrane [11–15]. However in cellular membrane, the pores are transient and the resealing or reversal begins after withdrawal of the electric fields [16,17]. Contrary to this view, some researchers suggest structural change in membrane state and prefer to call it electropermeabilization [18] and others suggested local electrical breakdown of membrane when cells were exposed to fields beyond critical threshold value [13].

##### 26.3.5.1 Pore Model

Different models have been suggested for observed increase in dramatic membrane permeability under external field. According to one model, permeability increase occurs because of the formation of pore, a hypothetical microstructure of transient nature, in the bilayer portion of a cell membrane. In this model, it has been suggested that rupture of a lipid bilayer underlies the induction of pore formation. As suggested by Chizmadzhev and coworkers [14,15], the initial hydrophobic pores formed can be hypothesized to any size, with radii from zero upward, whereas in contrast, the conversion of hydrophobic pores into hydrophilic pores can take place and they are believed to have a minimum size that is related to the phospholipids head group size and several head groups are needed to involve in formation of hydrophilic pores (Figure 26.3). It is also suggested that possible transient structures for hydrophilic pores may involve a block complex or the cell membranes may involve membrane macromolecules. The concept of pore formation is based on bilayer or planar membrane studies [10–12]. Some scientists believe that electroporation of cellular membrane is peculiar and prefer to call it electropermeabilization and have some reservation about the pore model [18,19]. In actual cell membrane, electroporation process seems to follow complicated mechanism, which is a subject of research and debate.

##### 26.3.5.2 Mechanical Breakdown Model

Another model suggested by researchers consists of the dielectric breakdown of membrane beyond threshold, which largely represents irreversible pores and is believed to be more prevalent in planar bilayer membrane though its occurrence in cells was reported [13]. According to this model, because of action of induced opposite charges across bilayer, thinning of bilayer occurs and at weak locations of bilayer, compression pressure wins resulting in increased thinning of membrane which ruptures beyond a field point due to electromechanical force [8,20]. These concepts are a matter of scientific debate and require

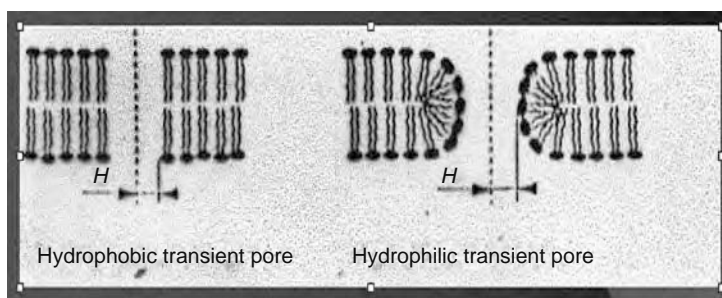


**FIGURE 26.3** Schematic model for hydrophobic and hydrophilic pore formation by electroporation.

clarification from more research but currently most widely accepted model is the formation of micropores in membrane by the action of high voltage external electric field.

### 26.3.6 RESEALING OF ELECTROPORATED MEMBRANE

Resealing characteristics determine the viability as well as nature and size of exogenous molecules for incorporation into electroporated cells [21–24]. The composition of the membrane differs from one cell type to another, and consequently, the obtained electroporation efficiency of cells. In addition, it is evident from Equation 26.3 that the magnitude of induced membrane potential depends on the shape and dimension of the cell.

Exposure of cells to short duration of pulses usually causes reversible micropore formation, which either under certain conditions slip to irreversible hydrophilic pores or may reseal under favorable experimental conditions. The later results in the survival of electroporated cells, which allows several biomedical applications, such as, loading of drug, incorporation of bioactive molecules, gene transfer, etc. However, electric fields causing higher transmembrane potential changes and longer prevailing permeabilization can produce irreversible membrane damage causing cell death [22–25]. The irreversible membrane electroporation is suggested to arise from rupture of a part of the cell membrane creating a permanent hole or due to secondary effects leading to lysis of cells as a result of chemical imbalances caused by the molecular movement across the pores [14,15]. Use of square wave pulse allows control of amplitude and duration separately. In optimized conditions, it is possible to achieve 95% of cells permeabilized with minimum loss of viability in the treated cell population (~5% cells) [26].

### 26.3.7 FACTORS THAT CONTROL ELECTROPORATION OUTCOME

Over the years, extensive research on cell electroporation has revealed that the efficiency of cell poration is governed by several factors, such as, physical, electrical, biological, and suspension medium [22–25,27]. Therefore, optimization of electroporation parameters for each type of cell and for a particular desired application becomes essential for successful outcome. There are several parameters that should be considered for optimization of electroporation outcome especially for in vitro electroporation experiments.

#### 26.3.7.1 Electrical Parameters

##### 26.3.7.1.1 Field Strength and Pulse Shape

External field strength and the shape of electric pulse field play a major role in the electroporation efficiency. The applied electric field is generally DC rectangular or exponentially decaying pulses of variable duration. A rectangular pulse is generated from high voltage power supply, whereas discharging a capacitor through sample containing circuit generates exponential pulse. Research has revealed the dependency of electroporation efficiency on pulse shapes, i.e., shape of the electric pulse being of the type exponential decay, or square wave pulses (Figure 26.1). Use of square wave pulses is suggested preferable over exponential type to eliminate solution conductivity effects on electroporation efficiency. More recently, it has been shown that the electroporation outcome of cells also depends on the type of square wave pulses, namely, monophasic and biphasic [28]. The biphasic square wave pulses have been reported more efficient in causing permeabilization. Although square wave and exponentially decaying pulses were most frequently used, some experiments have used trapezoidal pulses for possible controlled pulse rise and fall time [23]. Fields of a few kilovolts for mammalian cells and pulse durations of microsecond to millisecond ranges have generally been used. When experiments are conducted using population of cells, a trade-off is observed between cell viability and transfection efficiency. Optimization of field strength, pulse length, number of repetitive pulses, and electrode geometry are known to affect the electroporation efficiency.

### 26.3.7.2 Experimental Conditions

#### 26.3.7.2.1 Electrodes and Pulsing Medium

Electroporation efficiency depends on the parameters of electric pulses that are delivered to the treated cells using specially designed electrodes and electronic devices. In vitro experiments usually employ parallel plate types of electrodes made of inert metals like stainless steel or platinum but needle types of electrodes are also used for tissue electroporation [24,25,27,28] as well as for tumor treatment applications [29–32]. There are two types of electroporator devices available: devices with voltage output and those with current output. However, a voltage output device seems to be preferable, which is widely used for diverse applications.

#### 26.3.7.2.2 Pulsing and Incubation Medium

Composition of electroporation buffer is an important factor affecting electroporation yields. Ionic strength of cell suspension medium needs control, which determines resistance of the cell suspension and resultant RC time constant of the field pulse. Medium supplemented with  $\text{Ca}^{2+}$  and  $\text{Mg}^{2+}$  in  $\sim\text{mM}$  concentration range is found to promote efficiency of transformation and cell viability. Erythrocytes electroporated in isotonic buffer in the presence of EDTA or membrane specific drugs showed significant modification in hemolysis response to electroporation [33,34]. Use of square wave pulse removes the medium conductivity mediated effects on cell/tissue electroporation outcome. Generally, cells are pulsed in suspensions of sucrose, mannitol, or sorbitol. Electroporation as well as incubation of pulsed cells can be carried out in medium containing usual cell culture recipes.

#### 26.3.7.2.3 Post Electroporation Incubation Temperature

The temperature of the samples during pulse application and subsequent incubations decisively affects the cell electroporation outcome. Post pulse incubation temperature determines the rate and magnitude of resealing of the electroporated cell membrane: higher the incubation temperature, greater is the percentage cell recovery [35–40]. Results from author's laboratory have shown that the rate and extent of resealing of electroporated human erythrocytes was dependent on the temperature of post pulsing incubation [40]. Higher percentage of hemolysis was found in erythrocytes electroporated and incubated at 4°C. For DNA transfer goals in cells, it has been shown that cooling at the time of permeabilization and subsequent incubation at higher temperature increased transfer efficiency and cell viability [36–40].

### 26.3.7.3 Biological Factors

For the identical experimental conditions, electroporation efficiency depends on the type of cells; the composition of the membrane, shape, and size of cells strongly influences the electroporation efficiency [40–42]. In electroporation of bacteria, the growth phase of cell has significant influence on transformation efficiency, which is higher for cells harvested and electroporated from mid-log phase. However, cells from stationary phase can also be transected with reasonably good efficiency. Mammalian cell can be electroporated at relatively lower fields but pulse length controls the entry of external molecules into cells.

## 26.4 ELECTROPORATION DEVICES

There are many types of electroporation devices capable of delivering electric pulses widely varying in shape, amplitude, and frequency of pulses. Design of sample cuvette and electrode geometry affects the transfection yield. Chambers with parallel electrodes provide uniform fields enabling all cells in the sample exposed to same field. Small sample volumes of 10–100  $\mu\text{L}$  are suitable for parallel plate electrodes. Normally, electrode gap is kept 1–2 mm and field strength across electrode is calculated from voltage divided distance between electrodes ( $V/d$ ). The major components of electroporator consist of the electronic circuit (pulse generator) with discharge switch, electrodes, and cuvette/petri dish.

### 26.4.1 ELECTRIC PULSE GENERATORS

The electric pulse generator (also called electropulsator) is essentially an electronic circuit that is capable of generating steady pulses of defined shapes, voltages, and frequencies. The type and parameters of the electric pulses are characteristics of a particular machine and the output is defined as per the circuit. Most commonly used electroporators provide for exponentially decaying electric pulses. Some of the new generation medical electroporators are capable to produce square wave electric pulses of high voltage. Biorad Gene Pulser, Progenitor Pulse Controller from Hoefer, and BTX Transfecto 100 are designed to produce variable pulses of wide amplitudes and they are most commonly used. More advanced commercial electroporator models (e.g., BTX HT 96-Well Electroporator System, electroporator from Inovio Biomedical Corporation and others) have improved features in terms of field parameters, automation, and larger sample handling capability.

### 26.4.2 CUVETTES AND ELECTRODES

For in vitro studies, specially designed corvettes with parallel plate electrodes are generally employed. The separation between the electrodes ranges (1 to a few millimeters). Electroporation cuvettes are available commercially. Cells suspended in

electroporation buffer are filled in the cuvette and subjected to electric pulses. For *in vivo* studies, parallel plate electrodes with adjustable width are favored. Parallel plates are generally used for application of electric field on solid tumors. For example, solid tumor grown in leg of mice can be easily placed between the electrodes and subjected to electroporation. For the electroporation of deep-rooted tumors, specially designed needle electrodes are used. Sanghvi and Mishra have extensively investigated electroporation of human erythrocytes and have demonstrated the effectiveness of the square wave electroporation over the exponential pulses using the electroporator, which was designed and developed indigenously [28,43] (models: BARC/RB&HSD/01-04, Technology Transfer BARC 2005). Often, vernier caliper types of electrodes have been used for the clinical trials of electrochemotherapy (ECT) in cancer. A variety of sample chambers from spectrophotometer cuvettes to tong type have been used.

## 26.5 SOME APPLICATIONS OF ELECTROPORATION

Electroporation has been demonstrated in a variety of bacteria, yeast, plant, and mammalian cells. Experiments have been carried out using artificial bilayer membranes, cell suspensions, single cells, and biological tissues. A wide range of applications in biotechnology and medicine have been demonstrated using electroporation method, e.g., cell fusion and hybridoma for antibody production, ECT for treatment of cancer, electroloading of drugs for drug delivery, gene transfection for variety of biotechnological goals, gene therapy in treatment of diseases including cancer therapy, food sterilization, etc.

### 26.5.1 CELL FUSION AND HYBRIDOMA TECHNOLOGY

Cell fusion continues to be of great importance in understanding the underlying fundamental processes and for various practical applications through nuclear material transfer in agriculture and medicine because of speed of fusion process, high efficiency of fusion, and possibility of fusing two defined and chosen diverse cells [3,4,35]. Electroporated cell membrane acquires fusogenic state due to surface structural changes, such as, loss of lipid asymmetry, pore formation, etc., and molecular details are under exploration. Usually, cells are brought in contact by dielectrophoresis force using high frequency and low amplitude AC field. Under suitable conditions, pearl chains of cells are formed by application of AC fields and subsequent application of DC pulse causes fusion of permeabilized cells to occur. This technology has been extended to the production of hybrid cells of both plant protoplast and mammalian cells [3,44]. The hybridoma technology involves production of hybrid cells by the fusion of the two or more types of cells into a giant cell. Fusion of lymphocytes with myeloma cell has been used to produce antibodies in therapeutic applications. The phenomenon of electro-cell fusion has been extensively investigated from a fundamental viewpoint and numerous applications such as crop improvement in plant science have been demonstrated. In view of the pharmaceutical and industrial importance, basic and applied aspects of cell fusion technology have been extensively investigated but, for the limitations of space, exhaustive coverage has been avoided in this chapter and readers may refer excellent books and reviews available in this field [3,4,44-48].

### 26.5.2 ELECTROTRANSFECTION

Electroporated cells can be used to transfer DNA in bacterial, plant, and mammalian cells. This method offers rapid and efficient incorporation of plasmid and DNA in cells [49]. The *in vivo* electroporation has been shown to yield enhanced plasmid delivery to a wide range of tissues including muscle, skin, liver, lung, artery, kidney, retina, cornea, spinal cord, brain, synovium, and tumors. The precise mechanisms involved in electroporation applications *in vivo* are uncertain and require further studies, but appear to involve both electropore formation and an electrophoretic movement of the plasmid DNA.

### 26.5.3 THERAPEUTIC APPLICATIONS

Temporary permeabilization of the cells by electric fields provides an opportunity to access the cellular interior in a controlled fashion without seriously compromising the cell viability (Figure 26.4). This technique has the capability to enhance the incorporation of the drug into electroporated cells and has been demonstrated to increase uptake of anticancer drug in cancer cells [42,43,49-52] (ECT). Efforts have also been made by researchers to study the potential of transdermal drug delivery by electroporation. Gene therapy is yet another potential application with considerable promise [42]. Enhanced action of therapeutic drugs after gamma irradiation and electroporation has been demonstrated in normal as well as tumor cells author's laboratory [28,43]. These lines of investigations have generated continued interest and have progressed substantially leading to phase trials for cancer patient treatment in clinics.

### 26.5.4 POTENTIAL FOR OVERCOMING TUMOR RESISTANCE

One of the major problems faced by physicians in clinic is the commonly observed side effects and drug resistance in patients suffering from cancer. The resistance of cancer cells to anticancer drugs, a phenomenon called chemoresistance, is a major

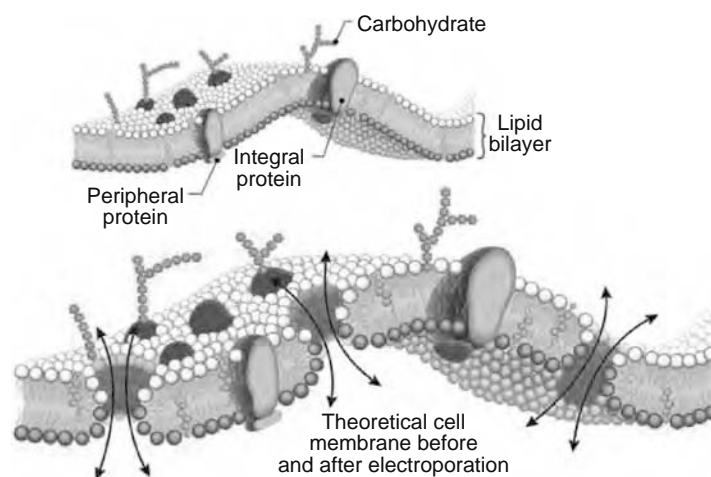


**FIGURE 26.4** Cell electroporation and electrodelivery of therapeutic drug into cells.

hurdle in cancer chemotherapy. The electroporation technique has the potential to overcome the problem of drug toxicity by reducing the dose and making drug-resistant tumor cells to respond. Permeabilization of membrane by electroporation allows incorporation of drugs into cells, which are otherwise impermeant. In vitro studies from our laboratory have shown increased toxicity of resistant tumor cells to doxorubicin when combined with electroporation suggesting possibility of apply this method to treat chemo- and radio-resistance tumors (Table 26.1). Similar results were reported earlier by other investigators using bleomycin and other drugs.

**26.5.5 ELECTRO CELL MANIPULATION**

Fusion of cells by electric pulses is based on electroporation phenomenon and it was first reported by Senda [35]. This technique has become very important in the field of biomedical research. Electroporated membrane acquires fusogenic state due to some structural changes in the membrane surface, which facilitates cell fusion. Usually the cells could be brought in contact with each other by dielectrophoresis using very high frequency and low amplitude AC field. Under suitable conditions, a chain of cells were found to be formed due to the AC field and a subsequent electroporation by DC pulse caused cells to become permeable and fuse. Studies on electric field-induced fusion of fibroblasts and erythrocytes were successfully demonstrated [36]. Using fluorescent probes occurrence of cell fusion involving membranes of participating cells has been reported. Electric field-induced fusion of cells offers advantages in terms of specificity, efficiency, and speed of cell fusion. Author and colleagues have achieved fusion of electroporated human erythrocytes by subsequent centrifugation of cells (unpublished results) [53].

**26.5.6 ELECTROLOADING OF CELLS**

Electroporation methodology offers a novel method to load drugs into cells for controlled release or for targeted delivery of drug. Considerable progress has been made to load enzymes, radioactive molecules, and plasmids in human erythrocytes and

**TABLE 26.1**  
**In Vitro Electroporation of Resistant Ehrlich Ascites Tumor Cells (P 388) in Combination with Doxorubicin Treatment**

Treatment	Cytotoxicity (%)
EP (5 kV/cm)	50
DOX (10 µg/mL)	10
DOX (100 µg/mL)	90
EP (2.5 kV/cm) + DOX (20 µg/mL)	92

Source: From Nanda G.S. PhD Thesis, Mumbai University.  
Notes: P388 EAT cells were in phosphate-buffered saline containing glucose. Exponentially decaying electropulses ( $T_{1/2} = 100 \mu s$ ) were employed.

results have demonstrated the usefulness of loaded drugs in enhancing their lifetime in blood circulation. Among the various systems proposed for delivery of pharmacological substances for improvement of their therapeutic potentials, electroporation has been found to have several merits over other methods. An electroporated cell can be allowed to reseal in the presence of the substance to be loaded into cells. The percentage entrapment can be calculated from the substance remaining in the supernatant to that entrapped in resealed cells. The efficacy of electroporation and membrane resealing was investigated by these investigators by monitoring [ $^{14}$ C]-sucrose (sucrose with radiocarbon) uptake by human erythrocytes [40,53–55]. Dextran and human serum albumin protein (MW 65 kDa) were entrapped in electroporated and resealed erythrocytes (Nanda and Mishra, unpublished results).

### 26.5.7 ELECTROCHEMOTHERAPY

Growing demands in anticancer research and biotechnology necessitates research on developing new modalities of treatment. Significant developments have taken place in using electroporation for increasing cytotoxicity of anticancer drugs, a process called ECT. The methodology involves increasing local potentiation of an anticancer drug by permeabilizing electric pulses. These approaches acquire greater significance in clinical situations where the side effect of chemotherapeutic drug is severe or the cost of drug is prohibitive. This has found enormous potential for developing effective anticancer therapy in recent years. Substantial success of ECT has been demonstrated *in vitro* as well as *in vivo* experiments leading to clinical trials of this approach [43,49–52]. The protocol is mainly focused on three aspects: (1) electroporation of cells in living tissues, (2) potentiation of cytotoxic drugs that are nonpermeant to cells, and (3) intrinsic response of the body systems, i.e., immune response and blood flow patterns of the patient. Undoubtedly, this is a growing field of research with an immense potential for clinical applications. The results of the ECT experiments involving anticancer drugs, doxorubicin, bleomycin, and cisplatin appear close to success.

### 26.5.8 RADIO-ELECTROCHEMOTHERAPY

Research has progressed to suggest that electroporation can enhance the radiation effects on mammalian cells especially tumor cells. It has also been found by author and his coworkers that combined effects of anticancer drug and ionizing radiation can be significantly enhanced by electroporation (Figure 26.5). The results have suggested that radiocytotoxicity of tumor cells *in vitro* as well as *in vivo* was enhanced significantly by electroporation methodology, which may offer a potentially improved treatment of cancer [28,29,43]. The research work author's laboratory has investigated the phenomenon of radio-electrochemotherapy (RECT), which points to enormous potential to effectively kill cancer cells including chemo- and radio-resistant tumors (Table 26.2). It is hoped that optimization of protocols appropriately and clinical evaluation of this approach in radiotherapy settings may offer unique and efficient treatment of patients suffering from cancer [41–43,49–51].

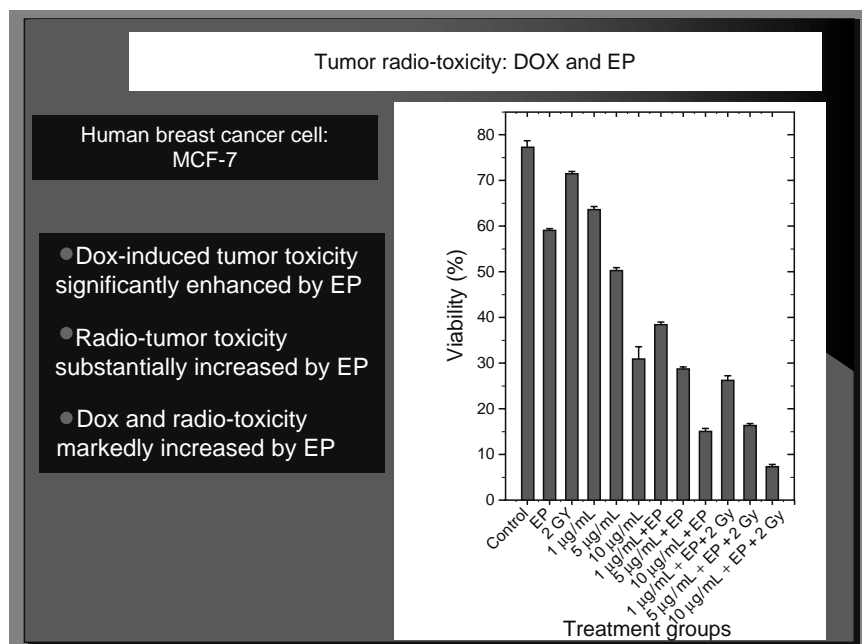


**FIGURE 26.5** Effect of electroporation on radiation and drug-induced tumor cell toxicity, MCF 7. (From Shil, P. et al., *J. Environ. Pathol. Toxicol. Oncol.*, 25, 1, 2006. With permission).

**TABLE 26.2**  
**Effect of Electroporation Combined with Administration**  
**of DOX and  $\gamma$  Irradiation on Growth Delay of Transplanted**  
**Fibrosarcoma Tumor on Hind Leg of Swiss Mouse**

Sample	DT <sup>a</sup> (Days)	TGD <sup>b</sup> (Days)
Control	1.28 ± 0.62	—
Vehicle control	1.30 ± 0.44	—
EP	2.00 ± 0.12	0.72
Radiation	1.82 ± 0.80	0.54
DOX	1.94 ± 0.16	0.66
DOX + radiation	2.48 ± 0.02	1.2
DOX + electroporation	2.5 ± 0.60 <sup>c</sup>	1.22
Radiation + electroporation	2.78 ± 0.22 <sup>c</sup>	1.5
Radiation + DOX + EP	3.00 ± 0.26 <sup>c</sup>	1.5

Source: From Shil, P. et al., *J. Environ. Pathol. Toxicol. Oncol.*, 25, 1, 2006. With permission.

<sup>a</sup> DT: Doubling time (days), mean ± S.D.

<sup>b</sup> TGD: Tumor growth delay (days), mean values.

<sup>c</sup>  $p < 0.001$ , versus control.

## 26.5.9 IN VIVO APPLICATIONS

Recent research in the field of ECT had concentrated on the preclinical experiments in animal models. Many laboratories have developed specially designed parallel plate electrodes to carry out in vivo studies. Murine tumors grown in Swiss mice have been considered as suitable system for such studies. In vitro, it has been established that high percentage of permeabilized cells, with less percentage of cell killing, can be achieved by using eight square wave pulses with individual pulse strength of 1.3 kV/cm, duration 0.1 ms. These pulses were also effective in producing electropermeabilization in vivo in tumor tissues. In a recent study, Satkauskas et al. have successfully studied the effectiveness of the ECT as a function of electric pulse strength and duration on C57B1 mice bearing LLC tumors. Their investigations revealed that the largest antitumor efficiency of ECT was attained for 1.5 kV/cm and duration of 1 ms. These pulse conditions used neither significantly suppressed tumor growth nor induced noticeable side effects [38]. Reports also suggested that both square wave and exponential wave electroporations have helped in overcoming tumor drug resistance to bleomycin and cisplatin. After successful experimentations in mouse models, clinical trials have been initiated [49–51]. Effective delivery of beneficial drugs or genes has the potential of greatly improving vascular therapy. Areas of vascular therapy that may benefit the most from improved local delivery technologies include the prevention and treatment of restenosis following angioplasty.

## 26.5.10 ELECTROPORATIVE GENE DELIVERY

Conventional techniques for the gene transfer include DBA precipitation by Ca<sup>2+</sup> treatment of cells with DEAE, dextran, liposomes, viral vectors protoplast fusion, or direct microinjection into the target cells. Electroporation has been found to be superior to other available methods of gene transfer. It was first demonstrated by Neumann et al. that thymidine kinase (TK) deficient mouse L cells were transformed to TK positive cells by treatment with suitable DC electric pulses in the presence of the plasmid DNA containing TK gene [56]. More recently, short interfering RNA (siRNA) is widely used in vitro to study gene functions or to identify and validate new drug targets. Electroporation-mediated delivery siRNA has been highly efficient method for selective gene suppression with siRNA in various established cell lines and primary cells. High-efficiency gene transfer and eliminated transfection-related toxicity were achieved for a variety of established cell lines as well as primary cell [19,57–59]. This line of research is making rapid progress.

## 26.5.11 ELECTRODELIVERY OF PROTEINS

One of the striking applications of electroporation is incorporation of externally added protein into plasma membrane. Protein molecules with amphipathic nature can be stably entrapped in electroporated membrane when they reseal. This phenomenon called electroinsertion has been demonstrated in a number of investigations. For example, electroinsertion of transmembrane protein CD4 receptors [60] and glycophorin [61] was demonstrated, which may prove valuable in surface engineering and studies on transmembrane proteins. In addition, a number of exogenous peptides and protein enzymes have been introduced

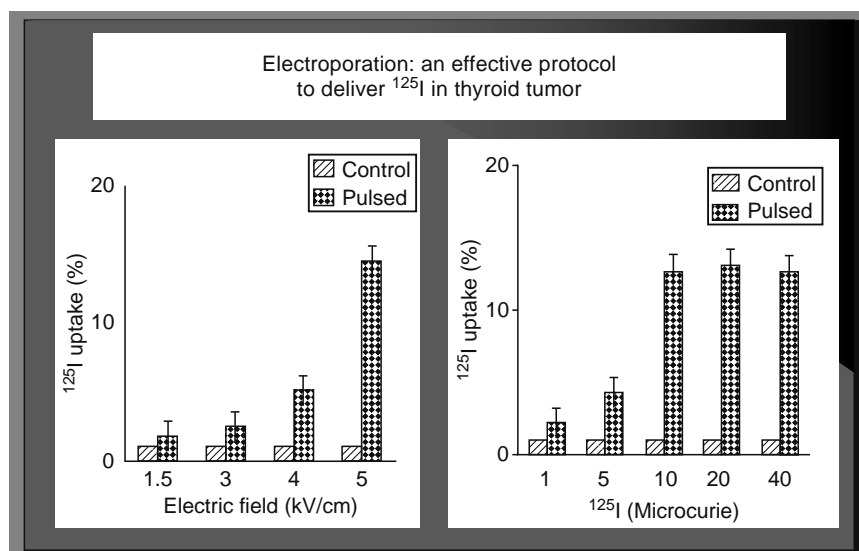


**FIGURE 26.6** Electroporative incorporation and retention of radioiodine in thyroid tumor cell line. (From Gopal, R. et al., *Appl. Radiat. Isot.*, 59, 305, 2003. With permission.)

into cell to study their degradation and therapeutic effects. With the possibility to introduce large proteins, there seems to exist enormous new research in applications of transcriptomics, proteomics, genomics, and nanoscale separation science, which hold promise for future.

### 26.5.12 INCORPORATION OF RADIOIODINE INTO TUMOR CELLS

The efficacy of using the electroporation to cancer has been studied by Gopal et al. [62], who have shown uptake of radioiodine  $^{125}\text{I}$  by human thyroid cancer cells which are otherwise recalcitrant. Electroporator designed and developed indigenously giving exponentially decaying voltage pulse in authors' laboratory was used for this study. It has been inferred that applications of the electroporation-mediated drug delivery may potentially help in overcoming the drug resistance of thyroid tumors. Loss of ability to concentrate iodide makes thyroid cancer cells refractory to radioiodine therapy. In this study, the focus of research was on the effects of post pulse incubation temperature on cell viability, incorporation of  $^{125}\text{I}$ , and its retention in the resealed cells. It was observed that the radioiodine was remarkably retained in the cells for up to 24 h. Effects of pulsing and incubation temperature on  $^{125}\text{I}$  uptake were also investigated. Electroporated cells were found resealing efficiently on incubation at  $37^\circ\text{C}$  (Figure 26.6). Results have shown promise and future validation in in vivo needs to be investigated.

### 26.5.13 ELECTROPORATION IN BIOTECHNOLOGY

#### 26.5.13.1 Water Sterilization

Electroporation-based sterilization of drinking water, wastewater, and seawater has been considered an attractive technology option. An industrial-scale system that utilizes PEF (pulsed electric field) technology results in killing of bacteria in water purification applications surmounting the consumer concern for harmful effects of heat or chemical methods of sterilization.

Microorganisms present in water are retained when it is passed through polarized material and in preparation of injection solutions reinforcing the choice of filtering material to be critical for optimization process. Seawater used in mariculture is the potential carrier of pathogenic bacteria, e.g., *Vibrio parahaemolyticus* and related species. Use of PEF, a nonthermal and nonchemical method, has been demonstrated to overcome the technical problems faced in heat and antibiotic methods of sterilization [63]. Optimization of electric field parameters and other experimental conditions is the main determinant of sterilization outcome. Technologies are also under development to use electroporation for wastewater treatment during filtration of water. Bacteria can be substantially killed by exposure of water to high voltage electric field by irreversible damage to their membrane. It seems interesting that electroporation-based sterilizer of water at lower field strengths can be exploited to increase the efficiency of chemical disinfectants, e.g., chlorine due to transient changes in membrane of the organisms while electroporation at higher field strengths is capable of inactivating/killing bacteria and other pathogens without use of chemicals. Hence, electroporation is at least a partial alternative to chlorination. A prototype of an electroporation system for sterilizing wastewater or drinking water has been developed [45]. Electroporation-based sterilization technology is being developed by Bioelectromagnetics, Inc. (Elm Grove, Wisconsin) in United States to reduce cost and achieve optimum efficiency of water sterilization.

### 26.5.13.2 Food Sterilization

Electroporation technology has been developed to kill spoilage microorganisms, e.g., *E. coli*, fungi, etc. providing scope for the development of nonthermal sterilization of food free from the disadvantages commonly encountered with existing physical, chemical, or radiation sterilization. It is hoped that the application of high amplitude PEFs can make food sterilization economical, compact, energy efficient, and environmentally acceptable. Exposing liquid foods to intense electric fields over short periods effectively inactivates spoilage microorganisms, which results due to cell's membrane damage. The damage is governed by the intensity of the electric field, the treatment time, and on the type of microorganisms. Foods that are free of chemical preservatives and having longer shelf life retaining their natural appearance and flavor would make acceptable technologies. Ionizing radiation-based sterilization liquid food suffers from generation of free-radical and possible undesirable effects on the quality and taste of treated foods. Research results suggest that application of high-field electric pulse technology to kill microorganisms for development of industrial-scale nonthermal sterilization of food seems commercially promising food preservation technique with potential to replace or partially substitute for thermal processes. A recent study has reported that PEFs sterilization technique sterilizes liquid foods effectively while maintaining the food quality and reduced the sterilization cost [46]. The method is claimed to be adaptable to liquid foods, such as, syrup, milk, soup stuff, etc. Electrical sterilization of apple juice by high voltage field pulse has been reported, which overcomes some of the problems faced by sterilization by thermal process [47]. Among others, the pilot plant program on liquid food sterilization of the Ohio State University using high voltage PEF has made considerable progress.

### 26.5.14 TRANSGENIC PLANTS AND ANIMALS

Transgenic technology allows transfer of genes between species and prepared clones. Transgenic organisms carry a foreign gene in their cells, which were introduced by laboratory methods. Genes cloned from microbes, plants, are introduced into plant or animal cells. Transgenic animals and plants (agrobacterium) have been produced by microinjection, embryonic stem cell method, retrovirus but electroporation has been used successfully to produce animal and plant transgenic animals and plants [44,48]. Studies have also shown regeneration of shoot after electrostimulation of hypocotyls of plant [64] and pollen for possible plant transformation [65]. These approaches hold great promise for future applications in plant science.

### 26.5.15 TRANSDERMAL DRUG DELIVERY

Application of external electric field to skin results in large increase in molecular and ionic transport [66]. This method has been applied to several drugs and is called transdermal delivery. The transdermal delivery of biomolecules has several important applications to the practice of dermatology and cosmetics. A prototype for the Inovio's transdermal delivery device has been developed and tested in various applications from drug delivery to cosmetics. Pharmaceutical companies are testing several drugs in the use of transdermal delivery. Transdermal delivery offers a wide range of applications: delivery of classical drugs, such as many different organic chemical compounds, delivery of proteins, peptides, and macromolecules DNA and oligonucleotides for gene therapy-related treatments DNA vaccines. Mammalian skin owes its remarkable barrier function to its outermost and dead layer, the stratum corneum. Transdermal transport through this region occurs predominantly through intercellular lipids, organized largely in bilayers. Electroporation is the creation of aqueous pores in lipid bilayers by the application of a short (microseconds to milliseconds) electric pulse. Flux increases up to four orders of magnitude were observed with human skin in vitro for three polar molecules having charges between  $-1$  and  $-4$  and  $MW > 1000$ . Similar flux increases were observed in vivo with animal skin. These results may have significance for drug delivery and other medical applications.

### 26.5.16 EX VIVO APPLICATIONS

Ex vivo therapy is the transfection of cells outside the body. Typically, a small amount of tissue is removed from the patient and the cells within that tissue are put into the culture, which allows clonal expansion of the cells. The approach simplifies the delivery of the genes and allows for post-transfection manipulation of the cells. The genetically modified cells, typically blood, bone marrow, or others, are then returned back to the patient, usually by blood transfusion or direct engraftment. Ex vivo transfection of cells by electroporation can be done using either a discontinuous or a continuous process.

Due to recent trends in cellular therapy, the pharmaceutical companies have put emphasis on the use of ex vivo electroporation for both DNA and drug delivery. Using the flow thru system, employing a pump that moves the cell suspension through an electroporation chamber where cells are porated. The entire operation is aimed to a closed system to minimize contamination and facilitate commercial scale cell-processing operations.

## 26.6 SINGLE-CELL ELECTROPORATION

Most of electroporation methods have adopted total population cell treatments. Total population methods yield information about average electroporative behavior of cells. Since cells are heterogenic cell population, it is important to examine if average

behavior represents individual cells. Recently, microelectrodes that can produce extremely localized electric fields, such as solid carbon fiber microelectrodes, electrolyte-filled capillaries and micropipettes as well as chip-based microfabricated electrode arrays enabling to electroporate single cells and subcellular structures, have been designed. Single-cell electroporation opens up a new window of opportunities in manipulating the genetic, metabolic, and synthetic contents of single-targeted cells in tissue slices, cell cultures, microfluidic channels or at specific loci on a chip-based device. Automated single-cell methods have been developed allowing to differentially manipulate the genetic, metabolic, synthetic contents of single-targeted adherent cells in a population [67]. In addition, high-throughput and real-time study of single-cell electroporation has been achieved using microfluidics. Recently, nucleofection method has been introduced to much resistant neuron cells by electroporation [68]. Subsequently, an elegant improvement has been introduced to mass 96-well electroporation 96 plasmids in neurons in a single step [69].

## 26.7 FUTURE PROSPECTS AND CHALLENGES

Extensive research during past decades has generated considerable new knowledge on biophysical basis of cell membrane electroporation but our present understanding of the dynamics involved in electropore formation and molecular transport is far from satisfactory. It is hoped that future research would provide deeper insight on the precise mechanisms involved, which would show new direction for research in membrane science and applications. It is, however, important to recognize that applicability of electroporation has been demonstrated in a variety of bacteria, yeast, and mammalian cells and some applications are ready for exploitation while many new technologies seem potentially possible. Notably, some of the biomedical applications have reached close to commercialization (e.g., food sterilization, cancer treatment modality, hybridoma technology for antibody production). Cell electroporation phenomenon would continue to be a frontier area of fundamental and applied research with promise in biomedicine and biotechnology. Electroporation-based tumor killing, gene therapy, cell fusion, drug loading for controlled release, and targeted delivery are some of the attractive developing new technologies with considerable implications to human health such as cancer electrotherapy, RECT, electroporative drug and gene delivery, etc. However, further research is highly warranted to optimize various factors that control the electroporative efficiency of the cells. Current state of development provides enough basis to be optimistic as some of the research progress has reached the pilot plant scale and clinical level evaluations. Combination of electroporation with radiation and anticancer drug is proving an effective way to kill cancer cells *in vitro* as well as *in vivo*. Development of user-friendly clinical electroporator with automation and suitable microelectrode devices are among the greatest challenges for medical biotechnology. Considering the immense potential of electroporation technique in research and applications, greater research efforts are needed to achieve comprehensive understanding of molecular processes involved and to apply the new knowledge in realizing the fruits of electroporation technology for innovative applications in food science, industry, and healthcare.

## ACKNOWLEDGMENTS

Author thanks the coworkers whose work has been cited in this article. The help and cooperation of Dr. B.N. Pandey, Dr. S.H. Sanghvi, Amit Kumar of Baba Atomic Research Center, Mumbai and professor P.B. Vidyasagar and Dr. Pratip Shil of Pune University, Pune are duly acknowledged. Part of this article was prepared when the author was a visiting professor at Research Institute for Radiation Biology and Medicine, Hiroshima University, Hiroshima, Japan. Facilities and encouragements provided by professors H. Hoshi, department of radiation biophysics, and S. Matsuura, department of radiation biology at the institute are deeply acknowledged. The author is also thankful to professor F. Suzuki, Director, RIRBM for his support and patronage. The help extended by Dr. Deborshi Bhattacharjee in organizing some of the content material of this article at final stage of preparation is gratefully appreciated. Lastly, he thanks his family members especially his wife, Usha deserves his deep gratitude for her silent support and exemplary tolerance for the long hours of working during preparation of this chapter.

## REFERENCES

1. Stryer, L., *Biochemistry*, Freeman & Co., New York, 1994.
2. Henrvik, F., Hertz, J., Jensen, M.H., Mouritsen, O.G., and Sneppen, K., *Physics in Biological Systems*, Springer, Heidelberg, 189, 1997.
3. Neumann, E., Sowers, A.E., and Jordon, C.A., *Electroporation and Electrofusion in Cell Biology*, Plenum Press, New York, 1989.
4. Dimitrov, D.S., *Handbook of Biological Physics*, Lipowsky and Sackmann, Eds., 1995, Chapter 18.
5. Kinoshita, K. and Tsong, T.Y., Formation and resealing of pores of controlled sizes in human erythrocyte membrane, *Nature*, 268, 438, 1977.
6. Shil, P., Kumar, A., Vidyasagar, P.B., and Mishra, K.P., Cell electroporation: Biophysical basis and applications to cancer therapy, *Phys. Educ.*, 21, 17, 2004.
7. Neumann, E. and Rosenheck, K., Permeability changes induced by electric impulses in vesicular membrane, *J. Memb. Biol.*, 10, 279, 1972.

8. Coster, H.G. and Zimmermann, U., Mechanisms of electrical breakdown in membrane of *Valonia utricularis*, *J. Memb. Biol.*, 22, 73, 1975.
9. Gabriel, B. and Teissie, J., Time course of mammalian cell electroporation observed by millisecond imaging of membrane property changes during pulse, *Biophys. J.*, 76, 2158, 1999.
10. Coster, H.G. and Zimmermann, U., Dielectric breakdown in the membranes of *Valonia utricularis*. The role of energy dissipation, *Biochim. Biophys. Acta*, 382, 410, 1975.
11. Hibino, M. et al., Time courses of electroporation as revealed by the submicrosecond imaging of transmembrane potential, *Biophys. J.*, 64, 1789, 1993.
12. Kinoshita, K. et al., Electroporation of cell membrane visualized under a pulsed-laser fluorescence microscope, *Biophys. J.*, 53, 1015, 1988.
13. Nanda, G.S. and Mishra, K.P., Electroporation of biological cells: Approaches and emerging applications, *Bull. Electrochem.*, 9, 547, 1993.
14. Chernomordik, L.V., Melikyan, G.B., and Chizmadzhev, Y., Biomembrane fusion: A new concept derived from model studies using two interacting planar lipid bilayers, *Biochem. Biophys. Acta*, 906, 309, 1987.
15. Weaver, J.C., Electroporation of cells and tissues, *IEEE Trans. Plasma Sci.*, 28, 24, 2000.
16. Rols, M.P., Dahhou, F., Mishra, K.P., and Teissie, J., Control of electric field induced cell membrane permeabilization by membrane order, *Biochemistry*, 29, 2961, 1990.
17. Nanda, G.S. and Mishra, K.P., Studies on electroporation of thermally and chemically treated human erythrocytes, *Bioelectrochem. Bioenerg.*, 34, 189, 1994.
18. Rols, M.P. and Teissie, J., Electroporation of mammalian cells. Quantitative analysis of the phenomenon, *Biophys. J.*, 58, 1089, 1990.
19. Walz, D., Teissie, J., and Millazo, G., Eds. *Bioelectrochemistry of Membranes*, Birkhauser, Basel/Boston/Berlin, 2004.
20. Zimmermann, U., Vienken, J., and Oilwat, G., Dielectric breakdown of cell membrane, *Biophys. J.*, 14, 881, 1974.
21. Mishra, K.P. et al., Encapsulation and targeting of drugs in electrically hemolysed red cells, *Bibl. Haemat.*, 51, 115, 1985.
22. Mishra, K.P., Bedekar, V.W., and Singh, B.B., Resealing of electrically hemolysed rat and human erythrocytes, *Ind. J. Expt. Biol.*, 21, 641, 1983.
23. Puc, M. et al., Enhancement of biomolecule transport by electroporation: A review, *Bioelectrochem. Bioenerg.*, 64, 113, 2004.
24. Mir, L.M. and Orłowski, S., Mechanisms of electrochemotherapy, *Adv. Drug Deliv. Rev.*, 35, 107, 1999.
25. Nanda, G.S., Bedekar, V.W., and Mishra, K.P., Biomedical potential of cell membrane electroporation. Proceedings of 2nd Biomedical Symposium, BARC, Mumbai, 1994.
26. Mir, L.M., Therapeutic perspectives of in-vivo cell electroporation, *Bioelectrochemistry*, 53, 1, 2000.
27. Crowley, J.M., Electrical breakdown of bimolecular lipid membranes as an electromechanical instability, *Biophys. J.*, 13, 711, 1973.
28. Shil, P. et al., Enhancement of radiation cytotoxicity in murine cancer cells by electroporation: In vitro and in vivo studies, *J. Environ. Pathol. Toxicol. Oncol.*, 24, 291, 2005.
29. Mir, L.M., Therapeutic perspectives of in vivo cell permeabilization, *Bioelectrochemistry*, 53, 1, 2001.
30. Pliquett, U. and Gusbeth, C., Surface area involved in transdermal transport of charged species due to skin electroporation, *Bioelectrochem. Bioenerg.*, 65, 27, 2004.
31. Sanghvi, S.H., PhD Thesis, Electrical and magnetic field effects on cellular systems to develop instrument for biomedical applications, Mumbai University, 2004.
32. Rols, M.P. et al., In vivo electrically mediated protein and gene transfer in murine melanoma, *Nat. Biotech.*, 16, 168, 1998.
33. Nanda, G.S. and Mishra, K.P., Modification of electroporative response of erythrocytes by EDTA in isotonic solution, *Bioelectrochem. Bioenerg.*, 34, 189, 1994.
34. Mishra, K.P. et al., Effects of dielectric discharge on drug treated mammalian cells, *Ind. J. Exp. Biol.*, 19, 520, 1981.
35. Donald, C.C., Bruce, M.C., James, A.S., and Sowers, A.E., Eds., *Guide to Electroporation and Electrofusion*, Academic Press, San Diego, CA, 1991.
36. Chang, D.C. and Reese, T.S., Changes in membrane structure induced by electroporation as revealed by rapid-freezing electron microscopy, *Biophys. J.*, 58, 641, 1990.
37. Belehradec, J. et al., Electroporation of cells in tissues assessed by the qualitative and quantitative electroloading of bleomycin, *Biochem. Biophys. Acta*, 1190, 15, 1994.
38. Satkauskas, S., Kersiene, R., and Venslauskas, S., Effectiveness of tumor electrochemotherapy as a function of electric pulse strength and duration, *Bioelectrochemistry*, 65, 105, 2005.
39. Sersa, G. et al., Improvement of combined modality therapy with cisplatin and radiation using electroporation of tumors, *Int. J. Rad. Oncol. Biol. Phys.*, 46, 1037, 2000.
40. Mishra, K.P. and Singh, B.B., Temperature effects on resealing of electrically hemolysed rabbit erythrocytes, *Ind. J. Expt. Biol.*, 24, 737, 1986.
41. Gregor, S. et al., Anti-tumor effectiveness of electrochemotherapy with bleomycin is increased by TNF- $\alpha$  on SA-1 tumor in mice, *Cancer Lett.*, 116, 8, 1997.
42. Gehl, J., Electroporation: Theory and methods, perspectives for drug delivery, gene therapy and research, *Acta Physiol. Scand.*, 177, 437, 2003.
43. Shil, P. et al., Radiation cytotoxicity enhancement in murine cancer cells by electroporation, *J. Environ. Pathol. Toxicol. Oncol.*, 25(4), 1, 2006.
44. Schnabl, H., Mahaworasilpa, T.L., Coster, H.G.L., and von Keller, A., Production of hybrid cells from single protoplasts of sunflower hypocotyl and broad bean guard cells by electric fusion, *Plant Cell Tissue Organ Cult.*, 55, 59, 1999.

45. NASA Tech. Briefs, Lyndon B. Johnson Space Center, Houston, TX, 2005.
46. Jayaram, S.H., Optimization of electroporation waveforms for cell sterilization, *J. Am. Sci.*, 2, 39, 2006.
47. Lee, H.K., Electrical sterilization of juice by discharge HV impulse waveform, *Am. J. Appl. Sci.*, 2, 2076, 2006.
48. Nickoloff, J.A., *Animal Cell Electroporation and Electrofusion Protocols: Methods in Molecular Biology*, Vol. 48, Humana Press, Totowa, NJ, 1995.
49. Hui, S.W., The application of electroporation to transfect hematopoietic cells and to deliver drugs and vaccines transcutaneously for cancer treatment, *Technol. Cancer Res. Treat.*, 1, 373, 2002.
50. Dietmar, P. et al., Enhancing the effectiveness of drug-based cancer therapy by electroporation, *Technol. Cancer Res. Treat.*, 1, 71, 2002.
51. Sersa, G. et al., Electrochemotherapy with cisplatin: Clinical experience with malignant melanoma patients, *Clin. Cancer Res.*, 6, 863, 2000.
52. Milkavcic, D. et al., A validated model of in vivo electric field distribution in tissue for electrotherapy and for DNA electrotransfer for gene therapy, *Biochim. Biophys. Acta*, 1523, 73, 2000.
53. Mishra, K.P., Mechanisms of cell electroporation of human erythrocyte for cell fusion by centrifugation. Proceedings of National Symposium on New Methodologies, Indian Institute of Technology, Mumbai, March 7, 1990.
54. Nanda, G.S. and Mishra K.P., Studies on electroporation of thermally and chemically treated human erythrocytes., *Bioelectrochem. Bioenerg.*, 34, 129, 1994.
55. Mishra, K.P., Sarma, H.D., Nanda, G.S., and Singh, B.B., Combined effects of gamma irradiation and electroporation on ascites tumor cells, *Prog. Biophys. Mol. Biol.*, 65, 98, 1996.
56. Neumann, E. et al., Gene transfer into mouse lymphoma cells by electroporation in high electric fields, *EMBO J.*, 1, 841, 1982.
57. Mir, L.M. et al., High efficiency gene transfer into skeletal muscle mediated by electric pulses, *Proc. Natl. Acad. Sci., USA*, 96, 4262, 1999.
58. Dean, D.A. et al., Electroporation as a method for high level nonviral gene transfer to the lung, *Gene Ther.*, 10, 1608, 2003.
59. Kalat, M. et al., In vivo plasmic electroporation induces tumor antigen-specific CD8 + T-cell responses and delays tumor growth in a syngeneic mouse melanoma model, *Cancer Res.*, 62, 5489, 2002.
60. Mouneimne, Y. et al., Electroinsertion of full length recombinant CD4 into red blood cell membrane, *Biochim. Biophys. Acta*, 1027, 53, 1990.
61. Raffy, S. and Teissie, J., Electroinsertion of glycoprotein A in interdigitation-fusion of giant unilamellar lipid vesicles, *J. Biol. Chem.*, 272, 25524, 1997.
62. Gopal, R. et al., Electroporation: A novel approach to enhance the radioiodine uptake in a human thyroid cancer cell line, *Appl. Radiat. Isot.*, 59, 305, 2003.
63. Jong-Chul, P. et al., Inactivation of *Vibrio parahaemolyticus* in effluent seawater by alternating-current treatment, *Appl. Environ. Microbiol.*, 69, 2405, 2003.
64. Gill, R., Mishra, K.P., and Rao, P.S., Stimulation of shoot regeneration of *Vigna aconitifolia* by electrical control, *Ann. Bot. Engl.*, 60, 399, 1987.
65. Mishra, K.P., Joshua, D.C., and Bhatia, C.R., In vitro electroporation of tobacco pollen. *Plant Sci.*, 52, 135, 1987.
66. Prausnitz, M.R., Reversible skin permeabilization for transdermal delivery of macromolecules, *Crit. Rev. Ther. Drug Carrier Syst.*, 14, 455, 1997.
67. Bae, C. and Butler, P.J., Automated single-cell electroporation, *BioTechniques*, 41, 399, 2006.
68. Hamm, A. et al., Efficient transfection method for primary cells, *Tissue Eng.*, 8, 235, 2002.
69. Buchser, W.J. et al., 96-Well electroporation method for transfection of mammalian central neurons, *BioTechniques*, 41, 619, 2006.

---

# 27 Proton-Conducting Membranes for Fuel Cells

*Vineet Rao, K. Andreas Friedrich, and Ulrich Stimming*

## CONTENTS

27.1	Introduction .....	760
27.1.1	Basic Principle of Operation of Polymer Electrolyte Membrane Fuel Cells .....	760
27.2	Physiochemical Requirements for the Membranes in Fuel Cell Applications .....	761
27.2.1	Specific Fuel Cell Applications.....	762
27.2.1.1	Automotive Application.....	762
27.2.1.2	Stationary Application .....	766
27.2.1.3	Portable Applications (H <sub>2</sub> -Fuelled PEMFC) .....	767
27.2.2	Porous Structure and Permeability Requirements.....	768
27.2.3	Catalyst Utilization and Interfacial Aspects.....	770
27.2.4	Membrane Requirements for Direct Methanol Fuel Cells.....	773
27.2.4.1	Methanol Crossover .....	774
27.2.4.2	Water Permeation.....	774
27.3	Mechanistic Aspects of Proton Conductivity (Nafion and Perfluorinated Sulfonic Acids) .....	774
27.3.1	Microscopic Structure .....	775
27.4	Materials: Physiochemical Properties and Fuel Cell Performance .....	776
27.4.1	Perfluorinated Sulfonic Acid Membranes .....	776
27.4.1.1	Properties of Nafion PFSA Membranes .....	777
27.4.1.2	Performance of DuPont Nafion Membranes.....	777
27.4.1.3	Synthesis of PFSA Monomers and Polymers.....	780
27.4.1.4	Short Side Chain Perfluorinated Sulfonic Acid Membranes .....	782
27.4.2	Mechanically Reinforced Perfluorinated Membranes.....	786
27.4.2.1	PFSA Ionomer in Expanded Porous PTFE, Gore-Select Membranes .....	786
27.4.2.2	PFSA Ionomer with PTFE Fibril Reinforcement; Asahi Glass; Flemion .....	789
27.4.2.3	PFSA Ionomer and PTFE Reinforcement at Asahi Kasei; Aciplex Membranes .....	794
27.4.3	Partially Fluorinated Ionomers .....	796
27.4.3.1	FuMA-TECH Membranes .....	796
27.4.3.2	Poly( $\alpha,\beta,\beta$ -Trifluorostyrene) and Copolymers; Ballard Advanced Materials .....	797
27.4.3.3	Radiation-Grafted Membranes .....	799
27.4.4	Inorganic/Organic (Fluorinated) Composite Ionomer Membranes .....	801
27.4.4.1	Hydrophilic Fillers (SiO <sub>2</sub> , TiO <sub>2</sub> , ZrO <sub>2</sub> ) and Ormosil Networks.....	801
27.4.4.2	Properties of Recast Membranes with Inorganic Fillers.....	805
27.4.4.3	Heteropolyacid Additive .....	806
27.4.4.4	Phosphate and Phosphonate Additives .....	807
27.4.4.5	Proton-Conducting Membranes Based on Electrolyte-Filled Microporous Matrices/Composite Membranes .....	809
27.4.4.6	Other Concepts.....	810
27.4.5	Polymer Membranes with Inorganic Acid Impregnation .....	810
27.4.5.1	PEMEAS (Celanese) Membranes .....	811
27.5	Summary .....	814
	References .....	814

## 27.1 INTRODUCTION

Polymer electrolyte-based fuel cells are emerging as attractive energy conversion systems suitable for use in many industrial applications, starting from a few milliwatts for portables to several kilowatts for stationary and automotive applications. The ability of polymer electrolyte fuel cells to offer high chemical to electrical fuel efficiency and almost zero emissions in comparison to today's prevailing technology based on internal combustion engines (ICEs) makes them an indispensable option as environmental concerns rise [1–6].

Although the basic principles of fuel cells have been known for at least a century, the introduction of solid polymer electrolyte membranes (PEMs) a few decades ago revolutionized fuel cell technology. Initially, poly(styrenesulfonic acid) (PSSA) and sulfonated phenol-formaldehyde membranes were used, but the useful service-life of these materials was limited because of their tendency to degrade in fuel cell-operating conditions [7,8]. A critical breakthrough was achieved with the introduction of Nafion, a perfluorinated polymer with side chains terminating in sulfonic acid moieties, which was invented in the 1960s for the chlor-alkali industry at DuPont. This material and its close perfluorosulfonic acid (PFSA) relatives are currently the state of the art in polymer electrolyte membrane fuel cells (PEMFCs). PFSA-based membranes have good proton conductivity, high chemical and mechanical stability, high tear resistance, and very low gas permeability in fuel cell-operating conditions [9,10].

But some problems associated with PFSA-based membranes have precluded large-scale market adoption of fuel cells. Their relatively high cost, limits to the range of temperature over which they can be reliably used (the upper limit is considered to be somewhat above 100°C, because the glass transition temperature  $T_g$  is around 120°C, at higher temperatures >100°C, membranes have low water content and thus low-proton conductivity), faster oxidative degradation and faster deterioration in mechanical properties at elevated temperatures, and a stringent requirement for external humidification of reactant gases under these conditions make the fuel cell balance of a plant (BOP) more complicated. Additionally for liquid-phase direct methanol fuel cells (DMFCs), the PFSA membrane is permeable to methanol and water, whose presence on the cathode side seriously degrades the DMFC performance.

All these drawbacks have led researchers to make more efforts to discover membranes with improved characteristics on all these accounts. Over the past decade, researchers all around the world have reported success in exploring new concepts for improving the properties of proton-conducting membranes. Companies like DuPont, Dow Chemical, W.L. Gore, PolyFuel, Asahi Glass, Asahi Chemical, Ion Power, and Ballard have brought improved membranes onto the market. The main goal of this chapter is to review some of these new ideas in the field of proton-conducting membranes.

### 27.1.1 BASIC PRINCIPLE OF OPERATION OF POLYMER ELECTROLYTE MEMBRANE FUEL CELLS

A fuel cell consists of two electrodes sandwiched around an electrolyte. Air (or oxygen) is supplied to the cathode and hydrogen to the anode, generating electricity, water, and heat. The electrocatalyst used is either platinum or a platinum alloy, usually supported on high-surface area carbon. The hydrogen atom splits into a proton and an electron, which takes different paths to the cathode. The proton passes through the electrolyte, while the electron passes through the external circuit. At the cathode catalyst, oxygen reduction takes place to produce water molecules. The electrons passing through the external load are available for useful work before they return to the cathode, to be reunited with the proton and oxygen in a molecule of water. The theoretical open-circuit potential for a  $H_2/O_2$  fuel cell is 1.23 V at 25°C and unit activity, but because of kinetic losses in the oxygen reduction process at the cathode and ohmic losses in the electrolyte membrane, the workable potential available from this fuel cell is usually around 0.7 V.

The heart of a fuel cell is the membrane electrode assembly (MEA). In the simplest form, the electrode component of the MEA would consist of a thin film containing a highly dispersed nanoparticle platinum catalyst. This catalyst layer is in good contact with the ionomeric membrane, which serves as the reactant gas separator and electrolyte in this cell. The membrane is about 25–100  $\mu\text{m}$  thick. The MEA then consists of an ionomeric membrane with thin catalyst layers bonded on each side. Porous and electrically conducting carbon paper/cloth current collectors act as gas distributors (Figure 27.1). Since ohmic losses occur within the ionomeric membrane, it is important to maximize the proton conductivity of the membrane, without sacrificing the mechanical and chemical stability.

Existing polymer membranes such as PFSA-based membranes operate most effectively within a limited temperature range and require that the membrane must remain constantly hydrated with water, resulting in complex and expensive engineering solutions (see Section 27.2.1.1). More efficient and better performing polymer membranes are needed for continued advancement of PEMFCs. An additional challenge in developing materials for proton-exchange membranes is that these materials need to endure prolonged exposure to the fuel cell environment. Electrolyte membrane materials must resist oxidation, reduction, and hydrolysis. A further challenge is that the material should be affordable. Finally, it is desirable that the material will permit operation at a higher temperature (>120°C).

Carbon monoxide is formed as a by-product when organic fuels are thermally reformed to produce hydrogen ( $H_2$ ), which can then be used in a fuel cell. For such reformat gas-supplied fuel cell systems, high-temperature membranes offer an

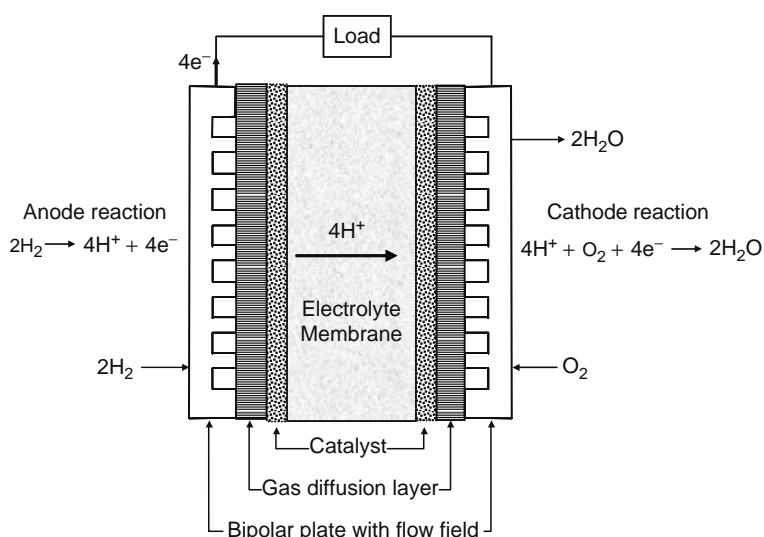


FIGURE 27.1 Diagram of a typical fuel cell.

important advantage because the MEAs based on high-temperature membranes are less susceptible to carbon monoxide (CO) poisoning. Better CO tolerance of high-temperature MEAs results in relatively less stringent demand on purification of the reformat gas to hydrogen. This results in easier and more cost-effective BOP for the fuel cell system. Fuel cells with high-temperature PEMs need smaller and less-expensive cooling systems.

Over the last few years, membrane development has intensified and numerous new developments have been reported [10]. This increase in the interest in novel proton-conducting membranes for fuel cell applications has resulted in several studies and review publications on the overall subject and also on some related topics (e.g., nonfluorinated membranes). The content of these reviews has been used and is cited in the appropriate sections.

Fuel cells, especially PEMFCs, can be used for various applications ranging from portable power supply for use in consumer electronic devices to stationary deployment for combined heat and power generation. Another potential application is transportation, in which fuel cell systems are developed for the propulsion of cars. The performance, operating conditions, costs, and durability requirements differ depending on the application. Transportation applications demand stringent requirements on fuel cell systems. Only the durability requirement in the transportation field is not as rigorous as the stationary application, although cyclic durability is necessary.

## 27.2 PHYSIOCHEMICAL REQUIREMENTS FOR THE MEMBRANES IN FUEL CELL APPLICATIONS

The fuel cell principle is based on the spatial separation of the reaction between hydrogen and oxygen by an electrolyte. An electrolyte needs to conduct either positively charged hydrogen ions (protons) or negatively charged oxygen (or hydroxide or carbonate) ions. For a technical realization, the specific ionic conductivity of the electrolyte has to be in the range of 50–200 mS  $\text{cm}^{-1}$  and the electronic conductivity of the electrolyte should be minimal. It is obvious from the principle of fuel cells that the electrolyte should be mostly gas impermeable to effectively separate the reaction volumes. Furthermore, a high chemical stability is required in oxidizing and reducing atmospheres. Often the MEA made from electrolyte membranes and catalysts has to be pressed against the flowfield/bipolar plates to minimize contact resistance or for sealing purposes. This necessitates good mechanical stability for the membrane. Because of these requirements, only a few systems are suitable for technical applications.

The main requirement—a high specific conductivity of the electrolyte—is illustrated in Figure 27.2, which shows the conductivity of selected electrolytes used in fuel cells. As can be seen in Figure 27.2, suitable materials are available for different operating temperatures and are also quite different ranging from solid-state ceramics to molten salts and aqueous electrolytes. Interestingly, the specific conductivities differ considerably, being higher for the liquids. It should be noted, however, that the important value is the area-specific resistance with a target value of  $<0.15 \Omega \text{ cm}^2$ . Therefore, although the specific conductivity of the oxygen ion conducting yttria-stabilized zirconia (YSZ) is lower compared to the other electrolytes, it can be integrated into a planar fuel cell with a thickness of about 15  $\mu\text{m}$ . To restrict the resistance to  $0.15 \Omega \text{ cm}^2$ , the associated specific ionic conductivity should exceed  $10^{-2} \text{ S cm}^{-1}$ . Figure 27.2 indicates that this value is attained at ca. 700°C for YSZ. The liquid electrolytes generally need a stabilizing matrix and therefore the resulting electrolyte layer is thicker. As a consequence, the specific conductivity has to be higher for these types.

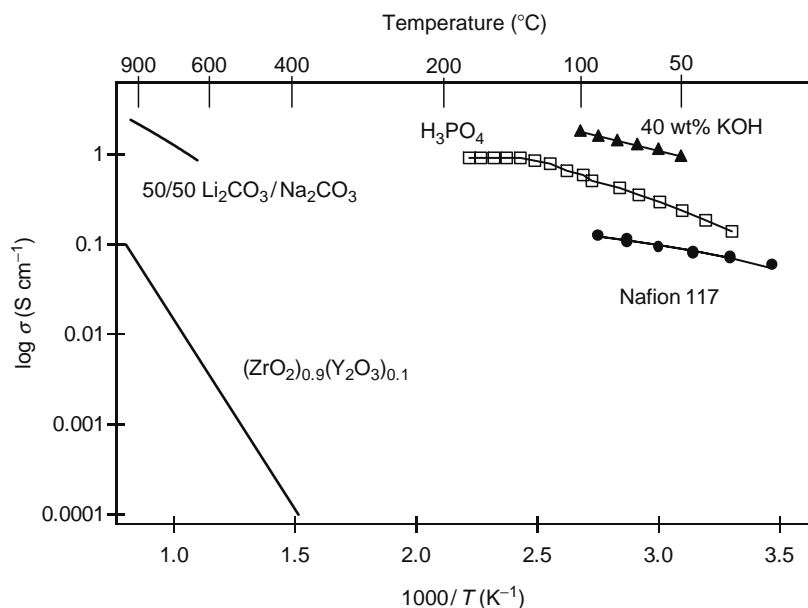


**FIGURE 27.2** Specific conductivities of electrolytes used in fuel cells in different temperature ranges. (Data from Srinivasan, S., *J. Electrochem. Soc.*, 136, C41, 1989; Larminie, J. and Dicks, A., *Fuel Cell Systems Explained*, J. Wiley and Sons, New York, 2000; Carrette, L., Friedrich, K.A., and Stimming, U., *Fuel Cells*, 1, 5, 2001; Metha, V. and Cooper, J.S., *J. Power Sources*, 114, 32, 2003.)

## 27.2.1 SPECIFIC FUEL CELL APPLICATIONS

### 27.2.1.1 Automotive Application

#### 27.2.1.1.1 Cooling Requirements

The main focus in membrane development for automotive applications is the search for membranes, which can operate at higher temperatures and lower relative humidity (RH). The major issues have been published in a series of publications by automotive experts and fuel cell developers [11–13]. The main statements are recapitulated here: assuming the availability of a hydrogen infrastructure, fuel cell-based systems might offer better efficiency than an ICE, which is one of the driving forces behind the development of fuel cells for this application. However, an ICE has the advantage that the waste heat can be removed more efficiently compared to fuel cell stacks. As a rule of thumb, it is stated that in ICEs one-third of the fuel energy is converted into mechanical energy, and two-thirds are converted into heat energy. Half the heat is removed by the coolant and half by the exhaust. Conversely, in a fuel cell system, typically less than 10% of the heat is rejected with the exhaust gases. Although the fuel cell system efficiency of about 50% is higher compared to ICEs, the coolant load is considerably larger. Furthermore, the PEM stack temperature is significantly lower, in the range of 60°C–80°C, as compared to ICE peak coolant temperature of 120°C. Since radiator performance is nearly proportional to the initial temperature difference (ITD) between the coolant and ambient temperatures, an ICE has about 2–4 times the heat rejection capacity during operation at elevated ambient temperatures of 32°C–40°C (an ambient temperature of 38°C is the design value for radiators). The thermal rejection requirements for automotive power trains are shown in Figure 27.3. The necessary radiator face area is plotted versus the ratio of heat power and ITD. The solid line represents the radiator fan's constant electrical power. As can be seen with the present technology, even a modest-sized fuel cell power system in cars requires cooling systems that challenge normal car design. Consequently, stack temperatures coincident with or even higher than normal ICE coolant temperatures would be highly desirable to achieve more efficient cooling. Another aspect is that a well-developed automotive hardware could be used enabling more cost-effective stack sizing and compact packaging.

#### 27.2.1.1.2 Humidification Requirements

The operating temperature ranges of PEMFCs are determined by the humidification requirement of the electrolyte membranes. Also, current membranes have glass transition temperatures in the range of 80°C–120°C and are thus subject to creep and hole formation at temperatures in this range. The implications of operating PEMFCs at higher temperatures and at 100% relative humidity are discussed in detail in the following section.

The membrane and ionomer humidification requirements are of paramount importance for PEMFC operation since the proton conductivity is a fundamental necessity in the membrane as well as in the electrode for the fuel cell to function. The operating conditions of current PEMFCs are dictated by the properties of the membranes/ionomers. Now, the most important membrane type (e.g., Nafion membranes from DuPont) is based on PFSA ionomers that are used in the membrane

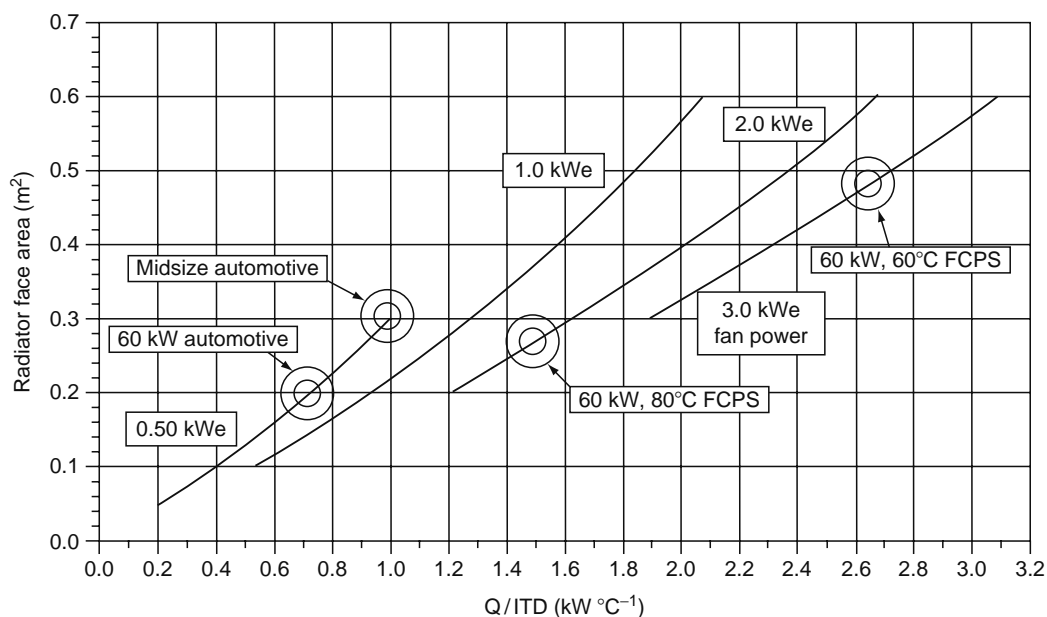


**FIGURE 27.3** Thermal rejection requirements of automotive and fuel cell systems ( $T_{\text{amb}} = 38^{\circ}\text{C}$ ). Solid lines are lines of constant radiator fan power. (Reproduced from Masten, D.A. and Bosco, A.D., in W. Vielstich, H.A. Gasteiger, and A. Lamm (Eds.), *Handbook of Fuel Cells: Fundamentals, Technology and Applications*, Vol. 4, J. Wiley & Sons, Chichester, 2003. With permission.)

and the catalyst layers. Figure 27.4 shows the proton conductivity versus relative humidity for three electrolyte systems, which are either presently available or are being developed for fuel cells. The often used PFSA system is represented by 1100 equivalent weight (EW) Nafion as measured by Alberti et al. [14]. Values at  $80^{\circ}\text{C}$  and  $120^{\circ}\text{C}$  are provided. Further results on sulfonated polyetheretherketone (s-PEEK) membranes are shown; the pure system is compared to an Aerosil-filled membrane. The third system is a high-temperature membrane based on polybenzimidazole (PBI) filled (doped) with phosphoric acid by Ma et al. [15]. The PBI/ $\text{H}_3\text{PO}_4$  conductivity at four temperatures ( $80^{\circ}\text{C}$ ,  $160^{\circ}\text{C}$ ,  $180^{\circ}\text{C}$ , and  $200^{\circ}\text{C}$ ) is given. The minimum

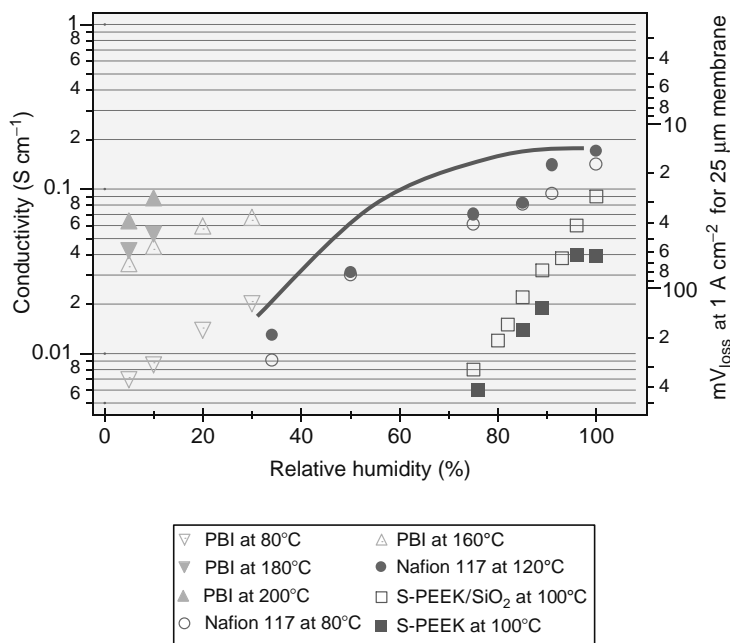
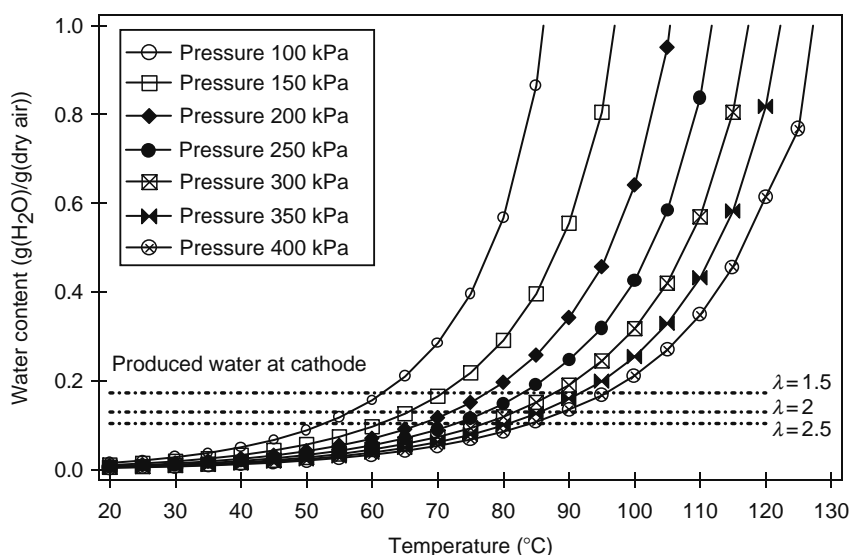


**FIGURE 27.4** (See color insert following page 588.) Conductivity of different membranes as a function of humidity. Requirements for an advanced membrane. (Data from Alberti, G. et al. *Solid State Ionics*, 145, 249, 2001; Ma, Y.L., Wainright, J.S., Litt, M.H., and Savinell, R.F., *J. Electrochem. Soc.*, 151, A8, 2004; Wainright, J.S., Litt, M.H., and Savinell, R.F., in W. Vielstich, H.A. Gasteiger, and A. Lamm (Eds.), *Handbook of Fuel Cells: Fundamentals, Technology and Applications*, J. Wiley & Sons, Chichester, 2003.)

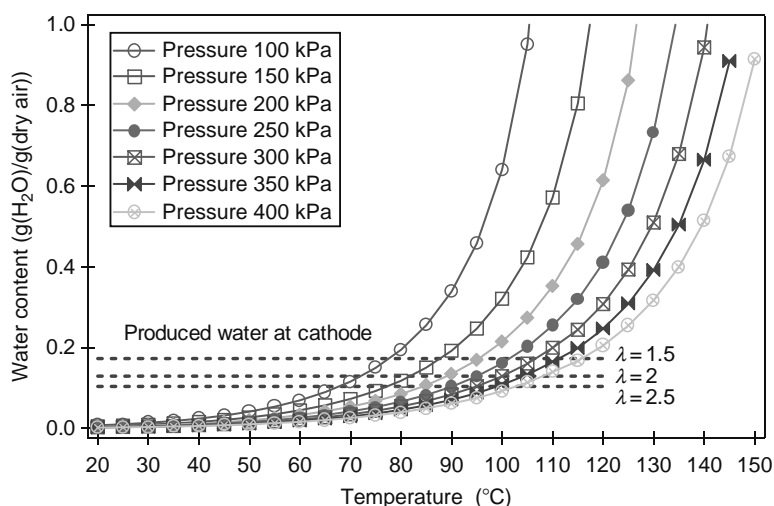
conductivity for fuel cell application was stated earlier in this section as  $50 \text{ mS cm}^{-1}$ . This conductivity is achieved for all membrane systems at different temperatures and different humidification conditions. For Nafion, the conductivity is above  $0.1 \text{ S cm}^{-1}$  for relative humidity (RH) values greater than 90% for both  $80^\circ\text{C}$  and  $120^\circ\text{C}$ , but drops to  $0.01 \text{ S cm}^{-1}$  at 40% RH. Also represented on the right-hand axis of the plot is the ohmic loss for a  $25 \mu\text{m}$  membrane at  $1 \text{ A cm}^{-2}$ . At  $0.1 \text{ S cm}^{-1}$ , the loss is 25 mV, which corresponds to a voltage efficiency loss of about 2%. Although this loss appears relatively small, the overall voltage efficiency is a critical issue and should be kept as high as possible in automotive applications. The problem with the PFSA systems is the need for nearly 100% humidification, which is an important constraint in the system design. An alternative polyarylene membrane system, such as s-PEEK membranes, has the advantage of being potentially more cost effective compared to the fluorinated material but the humidification requirements are similar to or even more stringent than (at least in this example) for the Nafion. A hypothetical-advanced membrane with more suitable properties is represented by the blue line: such an advanced membrane should exhibit conductivity well over  $50 \text{ mS cm}^{-1}$  at relative humidification (RH) of the gases below 50%. A membrane operating in a stable fashion at 50% RH and at  $120^\circ\text{C}$  would be the ideal candidate for a future automotive fuel cell power system. The PBI/ $\text{H}_3\text{PO}_4$  attains appropriate conductivity only above  $160^\circ\text{C}$  at 30% RH. At this high temperature, 30% RH is also critical as discussed below. Furthermore, this membrane system has performance disadvantages in dynamic load and temperature operation as discussed later. As a consequence, this system is better suited to stationary applications.

Figure 27.5 displays the water content of air given as the ratio  $g(\text{H}_2\text{O})/g(\text{dry air})$  for saturation humidity as a function of temperature and pressure. The 100% RH requirement of the membrane means that a low-pressure system is restricted to temperatures below  $100^\circ\text{C}$  since the saturation partial pressure of water increases exponentially with temperature. In addition, it would be highly desirable to have a water neutral situation to obtain a compact and simple system where the water produced at the cathode of the fuel cell as well as the permeated water is collected completely (a condenser would be necessary) to humidify the gases. In this respect, it would be an ideal situation to operate the fuel cell at the intersections of solid and dashed lines, which are the water neutral-operating conditions. The only way to achieve such an operation while maintaining the 100% RH demand at temperatures near  $100^\circ\text{C}$  is to increase the pressure to 400 kPa. However, this means a drastic reduction in system efficiency due to the heavy losses associated with pressurization. These simple relationships exacerbate design complications and have been summarized thus by Masten and Bosco: at higher temperatures and lower pressures, the humidification energy duty and associated condensate water requirements will overwhelm the water and thermal management capabilities of an automotive thermal system. Increased stoichiometry and increased pressure may help in diminishing the water load, but are associated with increased complexity and costs for the compressors and expanders.

Figure 27.6 shows the analogous relationships for 50% RH of the air. If a membrane tolerated such operation conditions over a long time, water neutral operation would be feasible at  $100^\circ\text{C}$  at moderate overpressure of 250 kPa. Ideally, a membrane should operate at 15%–20% RH which would enable water neutral operation at ambient pressure and  $110^\circ\text{C}$ . However, such a membrane would probably be based on a radically different conduction mechanism compared to the present membranes where the proton conductivity is based on the liquid water environment. Such a membrane would be very welcome, but now is far



**FIGURE 27.5** Water content required for membrane saturation versus temperature for different pressures of air. The dashed lines indicate the water produced for different air stoichiometries (ZSW (Zentrum für Sonnenenergie- und Wasserstoff-Forschung) measurements: Internal publication).



**FIGURE 27.6** (See color insert following page 588.) Water content required for 50% RH in air for advanced membranes versus temperature for different air pressures. The dashed lines indicate the water produced for different air stoichiometries (ZSW measurements: Internal publication).

from being realized. Realistically, it has to be assumed that progress in membrane development will consist of gradually improving membrane humidification and temperature stability.

In this respect, however, it is interesting to examine to exactly what degree 100% RH requirement is really necessary for state-of-the-art MEAs in the anode as well as in the cathode compartment under different operating conditions. Figure 27.7 shows single-cell measurements with GORE 5510 MEAs under low humidification conditions. The membranes in these MEAs have a thickness of about 25  $\mu\text{m}$ , which is a low value for PEMFCs. Therefore, it is possible to efficiently humidify the membrane by back-diffusing the liquid product water into the membrane from cathode to anode side. The normal drying-out effect at the anode is diminished in this case because the membrane is thin and does not represent any significant diffusion resistance. With thin membranes, high current densities are also achievable due to their low ionic resistance. These attributes can be seen in Figure 27.7, which shows  $V$ - $I$  curves at a higher temperature of 90°C at the anode with humidification only at the anode as well as at a lower temperature of 60°C with no humidification at all. The  $V$ - $I$  curves exhibit relatively low open-circuit voltages due to a high crossover of the gases and therefore, the temperature difference does not influence the  $V$ - $I$  curve much at lower current densities. At high current densities, humidification is improved and stable operation is observed over about 12 h due to more water formation at the cathode. However, now it is not clear if this performance can be maintained over prolonged operation of more than 1000 h and if the power density is sufficient for transportation applications.

This example shows that efficient management of the liquid water produced at the cathode can be used to attenuate the 100% RH requirement of the membrane. Besides thin membranes, other strategies (described below) involving wicks or water

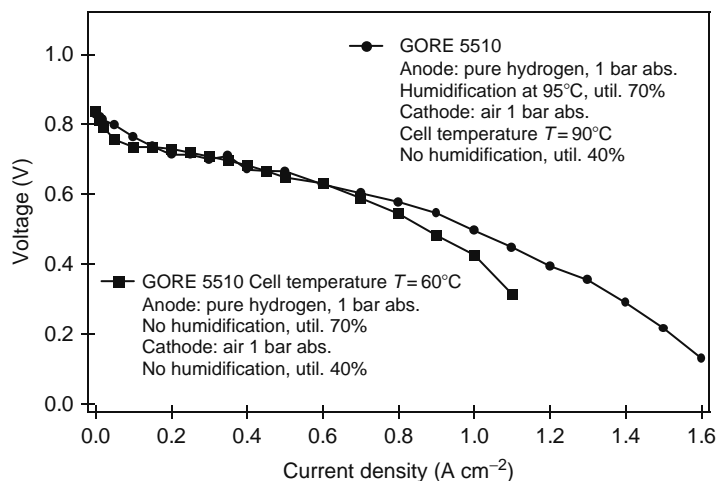


**FIGURE 27.7** Performance of a GORE 5510 MEA in a single cell at a temperature of 60°C as well as of 90°C under reduced humidification conditions (ZSW measurements: Internal publication).

produced by catalysts introduced into the membrane are well known. However, all these strategies involve compromising other properties for water management, e.g., thin membranes are not as durable since the mechanical properties are inferior or the performance of the MEAs is reduced in conjunction with reduced humidification.

The common way of improving the water management is to humidify the gases entering the fuel cell. A less common approach is the direct hydration of the membrane by mounting porous fiber wicks within the membrane itself [16]. Membranes with wicks are developed using twisted threads of porous polyester fibers which are then placed between the membrane and a cast thin film of Nafion ionomer and hot-pressed at 150°C. Such membranes with porous fiber wicks are supplied with water directly through the wicks. The parts of the wicks outside the membrane are kept in contact with a water source such as a humidifier or condenser outside the membrane. Water diffuses through the porous fibers into the membrane, thus keeping it humidified. Similar approaches have also been reported by other authors [17,18].

### 27.2.1.2 Stationary Application

Fuel cells are promising candidates for energy conversion systems used for distributed power generation, which can guarantee uninterrupted power supply and thus cut unnecessary dependence on the grid. Fuel cells are quite efficient at around 60% electrical energy conversion efficiency and the use of waste heat from the fuel cells to houses would make them more efficient. The efficiency of such a CHP fuel cell system depends on the operating temperature of the system, which dictates the amount of recoverable heat. A fuel cell-based system makes very low noise and produces almost zero emissions when direct H<sub>2</sub> from nonfossil fuel sources is used. These are important advantages in comparison to conventional systems based on ICEs. But high costs and problems in long-term durability are major obstacles in the path of wide-scale introduction to the market. PEMs contribute a significant cost factor. The membranes are also primarily responsible for the degradation of the performance of the fuel cell system, being one of the most vulnerable components in the fuel cells. An effective heat removal system and a humidification management system are still very important in stationary fuel cell systems. But stationary applications put the strongest demand on the durability of the PEMs. To understand the durability of the membrane, it is imperative to discuss various modes of its degradation.

#### 27.2.1.2.1 Mechanical Degradation

Mechanical parameters related to preparing an MEA contribute significantly to the overall service-life of the membrane [7]. A high degree of cleanliness and quality control must be maintained to ensure that no foreign particles or fibers are introduced that may perforate the membrane during the MEA fabrication process. Generally, perforation can also take place at the fuel cell reactant inlets where mechanical stress may be highest. Care must be taken to design the fuel cell flow field to avoid local drying due to nonuniform distribution of reactant gases in the cell. Uniform contact pressure should also be maintained between the current collector system and the MEA. Excessive penetration of the catalyst layer into the membrane during MEA fabrication or due to high-localized pressure exertion by the current collector can lead to high local current density and stresses. Excessive-localized pressure close to the edge of the electrode/membrane may also lead to perforation and tearing of the membrane. Care must be taken in designing the fuel cell to avoid unsupported regions in the MEA flow field support structure into which the membrane could extrude and ultimately fail. Generally, when a membrane is perforated, hydrogen and oxygen will cross over to the other sides and react chemically on the catalyst producing only heat. The cell potential will decrease because of this mixing of reactants. The excessive heat produced due to the chemical reaction between hydrogen and oxygen may lead to more holes in the membrane [7].

#### 27.2.1.2.2 Thermal Degradation

PEMFCs generally operate at temperatures <100°C. PFSA-based polymer ionomer membranes like Nafion, Gore, Aciplex, and Flemion are not significantly affected by temperatures up to 150°C where most of the water is lost and membranes may suffer irreversible dry out. Chemical degradation of these membranes in the H<sup>+</sup> form usually starts with the loss of sulfonate groups at over 220°C [7].

#### 27.2.1.2.3 Chemical and Electrochemical Degradation

For properly designed and cleanly operated PEMFCs, polymer electrolyte membrane degradation by electrochemical and chemical mechanisms generally occurs relatively slowly over a period of several hundred hours. PEMs are especially sensitive to metal ions, which may get into the fuel cell via dust particles in the air or even rust. Even the platinum ions ever present in the electrode are not completely benign. Metal ions within the fuel cell would exchange with protons, thereby drastically reducing the proton conductivity of the membrane. It is also known that peroxide radicals are produced at very low levels during fuel cell operation and these radicals are responsible for the chemical and physical deterioration of the membrane after extended use [19,20]. On the basis of these findings, methods have been developed to perform accelerated chemical tests to simulate this type of polymer electrolyte membrane (PEM) degradation. Peroxide radical-assisted degradation has been extensively studied for early PSSA membranes [21]. It was shown that oxygen crossing over to the hydrogen side may lead to the formation of peroxide and hydroperoxide radicals, which can slowly deteriorate the membrane. The PFSA membranes are, relatively

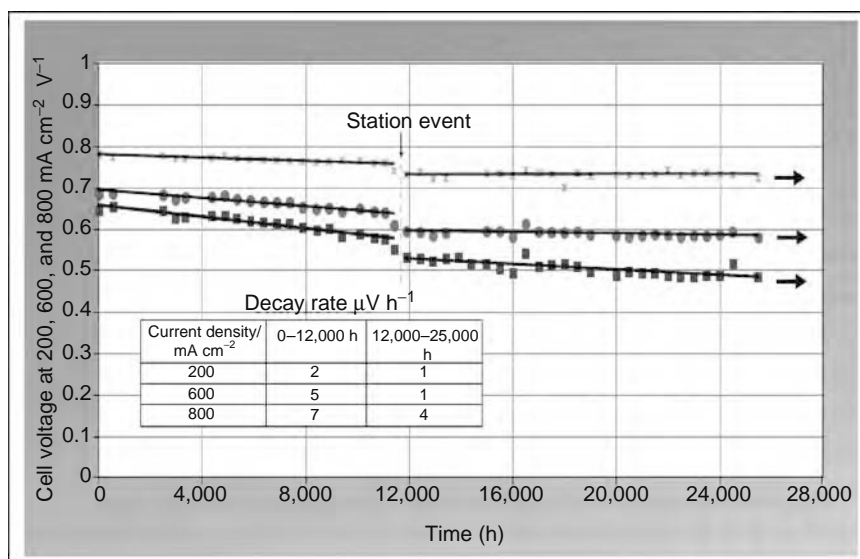


FIGURE 27.8 (See color insert following page 588.) Long-term tests. (From W.L. Gore & Associates, Elkton, Maryland.)

speaking, much better in terms of performance and service-life. But peroxide radicals can still degrade the membrane, albeit to a smaller extent, as the basic backbone  $-\text{CF}_2$  is less susceptible to peroxide attack. The susceptibility to peroxide attack has been attributed to traces of groups such as  $-\text{CHF}_2$ , which are inadvertently introduced into the perfluorocarbon sulfonyl structure during synthesis and can be converted into a carboxyl group by peroxo insertion [22,23].

The sum effect of mechanical, thermal, and chemical degradation of the membrane along with the degradation of catalysts will take its toll on the long-term performance of the fuel cell. A lot of effort is being put into improving membrane service-life as well as MEA service-life by many players in this field. For example, W.L. Gore has demonstrated service-lives exceeding 28,000 h for MEAs targeted for stationary fuel cell systems (Figure 27.8).

### 27.2.1.3 Portable Applications ( $\text{H}_2$ -Fuelled PEMFC)

Portable applications are one of the most attractive segments in terms of fuel cell commercialization as the number of possible units required for consumer electronic market is high and cost limitations are much easier to meet than automotive or stationary applications. Fuel cells in the low power range can be used either as a complete substitute for batteries or in fuel cell/battery hybrid power supply systems. Fuel cells for portable applications usually operate under ambient conditions. For portable power supply applications based on hydrogen-fuelled PEMFC, the most important issue is the power to volume/weight ratio, as more and more miniaturized power sources are needed for consumer electronic devices, like laptops, mobile phones, palmtops, video cameras, and a host of military applications. To a large extent, the power to volume/weight ratio depends on the energy density of the fuel from which  $\text{H}_2$  is extracted. Possible options for hydrogen sources could be metal hydride, chemical hydride, or a thermal reformer, e.g., methanol reformer. But the basic size of a fuel cell system also has a fair share in determining the overall energy density of portable fuel cell-based power supply. Thus to meet these miniaturization challenges, passive thermal and water management and also suitable components for hydrogen/air feeding and pressure control must be realized. In meeting these requirements the polymer electrolyte membrane (PEM) has a big role to play, at least in water management. Water management requires the synergetic action of the gas diffusion layer (GDL) and the PEM. To meet the requirement of complete passive water management, the fuel cell should run on dry  $\text{H}_2$  and dry air and retain just enough water in the membrane.

#### 27.2.1.3.1 Membrane Humidification by Cathode Back Diffusion

One such approach employs a microporous layer (MPL) with an average pore size of around  $1 \mu\text{m}$  between the GDL (with an average pore size of  $10 \mu\text{m}$ ) and the catalyst layer. The MPL is made up of conducting carbon and is hydrophobized with a small amount of Teflon. MPLs do not allow the water to escape as liquid drops because of surface tension in small pores. This builds up hydrostatic pressure on the cathode side. This hydrostatic pressure buildup allows back diffusion to the anode side. The positive role of microporous layers in water management in PEMFCs has been investigated theoretically and experimentally [24–28]. For the back diffusion to humidify, the whole membrane requires a thin and obviously stable membrane. With pure PFSA-based membranes, it has not been possible to reduce the thickness without compromising mechanical strength. To achieve this goal, several new ideas have been pursued which are discussed later in this chapter. One such approach is to reinforce the membranes with polytetrafluoroethylene (PTFE) fibers, a technique pioneered

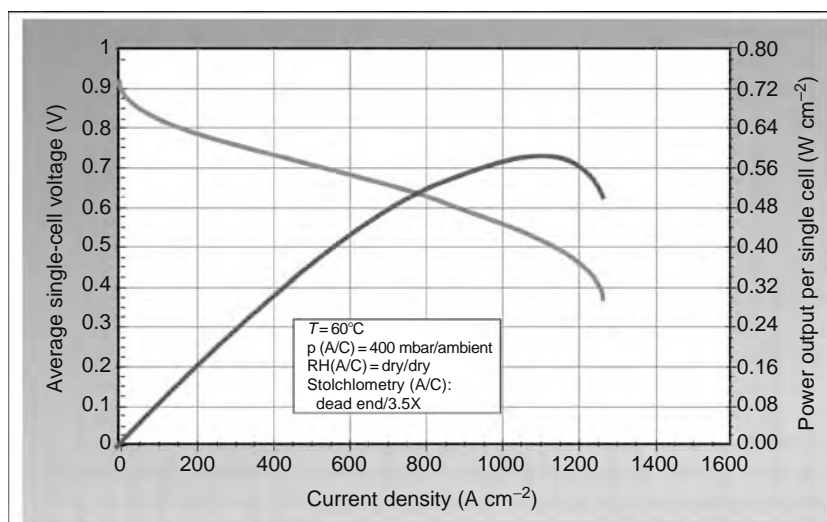


**FIGURE 27.9** (See color insert following page 588.) Performance of the Gore 58 series in completely dry conditions. (From W.L. Gore & Associates, Elkton, Maryland.)

by W.L. Gore, which can reduce membrane thickness to only a few micrometers. Figure 27.9 shows the  $I$ - $U$  (current-voltage) characteristics of a fuel cell using Gore membranes, under completely dry conditions.

### 27.2.2 POROUS STRUCTURE AND PERMEABILITY REQUIREMENTS

The important chemical reactions take place at the interface between an electrode and an electrolyte. Since reactants in fuel cells are mostly gaseous and poorly soluble in the electrolyte, a third phase, the gaseous one, has to be in contact with the interface, leading to a three-phase boundary. Furthermore, a certain solubility and diffusivity of the reactant within the ionomer material in the electrode is needed to achieve greater utilization of the catalyst. This permeability in the ionomer helps to extend the electrochemically active surface area of the catalyst that belongs to the three-phase boundary. A diagram of this zone in a PEMFC is shown in Figure 27.10. Presently, differing opinions exist on the structure of the active layer: It is unclear if the ionomer is present at the interface as a third bulk phase or as a thin film of about 20–50 nm covering the catalyst. Such differences would have considerable implications for the optimization of this interfacial region.

To optimize the kinetics in this area, the following features are required:

- High, electrochemically active surface area of the catalyst
- Good access for the reactants to the electrode-electrolyte interface and sufficient permeability in the ionomer
- Effective water removal from the three-phase zone
- Good electric and ionic contact at the reaction sites

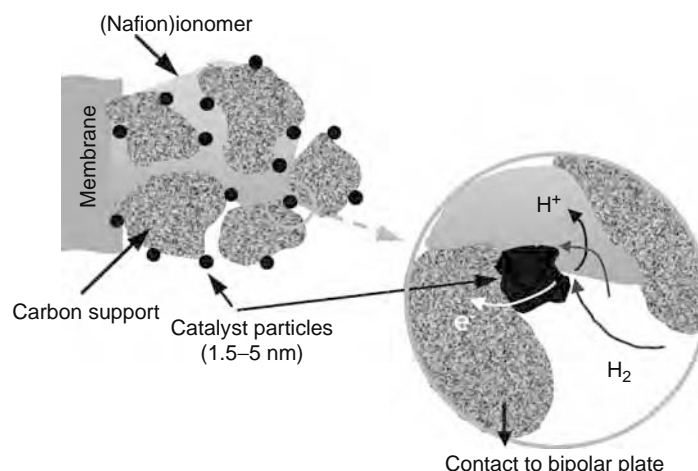


**FIGURE 27.10** Diagram of the active layer of a gas diffusion electrode in a PEMFC.

These requirements can be achieved best with a porous structure, but the realization depends strongly on operating temperature. Since costly precious metals (Pt and Pt alloys) are used as a catalyst, high dispersion of these metals is necessary to optimize the surface to mass ratio. Starting from metal salts, various chemical routes are usually used to achieve very small metal catalyst particles and thus high dispersion. The metal particle sizes are of the order of a few nanometers (platinum surface areas in the range of 20–60 m<sup>2</sup> g<sup>-1</sup> are common). In supported catalysts, the metal clusters are supported on larger electron-conducting and porous carbon particles (usually about 50–100 nm in diameter) to achieve better dispersion of the metal catalyst, higher active surface area and to prevent agglomeration of metal catalyst nanoparticles. The catalyst is introduced into the electrocatalyst layer along with the proton-conducting ionomer component. The ionomer content increases the metal catalyst utilization in the catalyst layer, but normally an optimum content is found and further increase in ionomer content leads to lower catalyst surface utilization. Largely varying utilizations of catalyst surfaces (varying between 50% and 90%) in PEMFC electrodes have been reported [29]. Usually, the catalyst layer has a thickness in the range of about 5–30 μm.

Gasteiger and Mathias have analyzed the requirements of membranes for automotive applications and have stressed that in addition to proton conductivity, other critical ionomer properties include the H<sub>2</sub> and O<sub>2</sub> permeability [12]. Of course, the membrane material must not be too permeable to the reactive gases to avoid excessive gas crossover and resulting fuel efficiency loss. In the other extreme, the ionomer in the electrode must have sufficient gas permeability so that the reactant transport through it occurs without significant concentration gradients and associated mass-transfer losses. Standard perfluorinated membranes allow permeation of gases at a rate proportional to the product of a permeability coefficient (dependent on temperature and RH, normalized by membrane thickness) multiplied by a partial pressure driving force and divided by the membrane thickness. This permeation leads to fuel efficiency loss with two components: direct reaction at the anode determined by the O<sub>2</sub> crossover rate and direct reaction at the cathode determined by the H<sub>2</sub> crossover rate. This fuel loss can be expressed in terms of an equivalent current that would be observed externally, if the H<sub>2</sub> consumed by crossover had reacted electrochemically. A tolerable fuel efficiency loss due to crossover was set at <10% for a low load and <1% for a high load of the MEA. Gasteiger and Mathias assumed a thin-film structure of the ionomer of 0.5–2 nm covering the entire solid catalyst surface. Experimental support for this electrode structure comes from double-layer capacitance measurements using cyclic voltammetry and AC impedance techniques. Gasteiger and Mathias observed values that are typical of Pt and carbon interfaces with electrolyte and imply that the entire solid surface was in contact with electrolyte for these electrodes. Under several assumptions regarding structure, diffusion, and reactivity, a minimum permeability was derived for a maximum of 20 mV loss.

These considerations regarding the membrane permeation properties have been summarized by Gasteiger and Mathias in Figures 27.11 and 27.12, with literature data of gas permeation measurements of Nafion membranes. Following their evaluation, the present membranes are close to the upper limit of gas permeation, which is acceptable, but a further increase in these properties at higher temperatures cannot be tolerated.

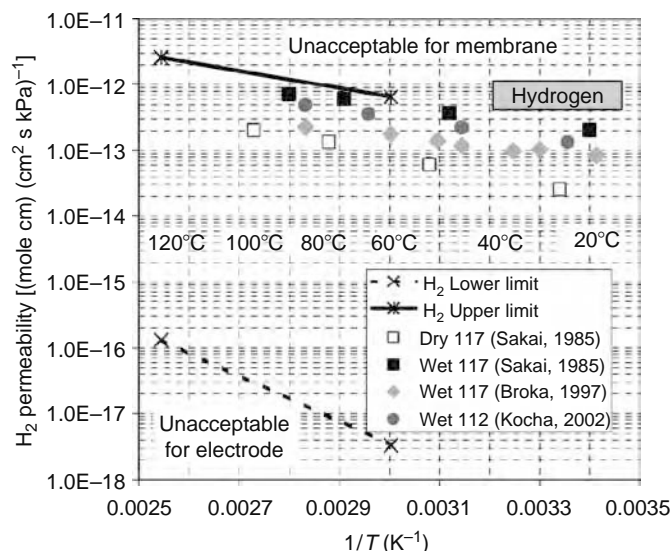


**FIGURE 27.11** (See color insert following page 588.) H<sub>2</sub> permeability as a function of temperature and RH. Upper limit (solid line) defined by crossover losses (assuming no contribution from O<sub>2</sub> crossover), lower limit (dotted line) defined by electrode ionomer film-transport requirements, and data are for wet and dry Nafion 1100 EW-based membranes. (Reproduced from Gasteiger, H.A. and Mathias, M. F., in *Proceedings of the Symposium on Proton Conducting Membrane Fuel Cells III*, 2003. The Electrochemical Society of America. With permission from The Electrochemical Society, Inc.)

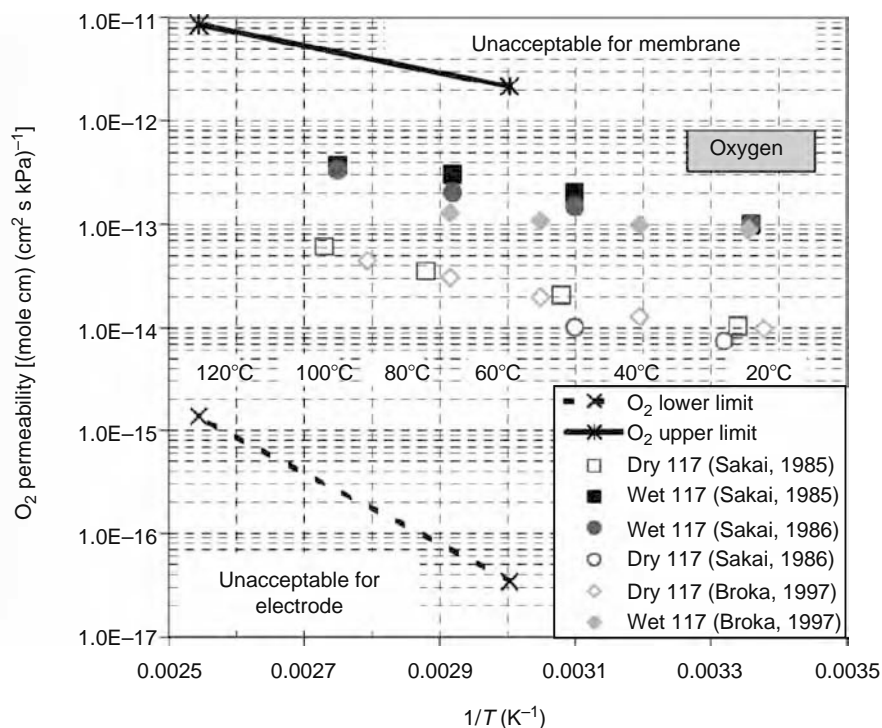


**FIGURE 27.12** (See color insert following page 588.)  $O_2$  Permeability as a function of temperature and RH. Upper limit (solid line) defined by crossover losses (assuming no contribution from  $H_2$  crossover), lower limit (dotted line) defined by electrode ionomer film transport requirements, and data are for wet and dry Nafion 1100 EW-based membranes. (Reproduced from Gasteiger, H.A. and Mathias, M.F., in *Proceedings of the Symposium on Proton Conducting Membrane Fuel Cells III*, 2003. The Electrochemical Society of America. With permission from The Electrochemical Society, Inc.)

Besides the traditional methods of measuring gas permeation by way of gas analysis (a volumetric method or gas chromatography), an electrochemical methodology to determine the gas permeability and solubility of membranes is also used, which seems to have become more popular recently. Using microelectrodes, which are pressed onto a membrane in a solid-state electrochemical cell, electrochemical reactions are investigated by chronoamperometry (recording of current transients) of the diffusion-limited potential ranges. From the transients, gas concentrations (solubility) and diffusion coefficients in various proton-exchange membranes can be measured and diffusion-limited current densities can be determined [30–36]. This is an interesting and simple way of measuring permeabilities since it may enable in situ measurement in a running fuel cell and also a local resolution. However, in contrast to the permeation measurement by gas analysis, no driving force in the form of a partial pressure gradient is applied to the membrane. The comparison of both techniques is therefore not straightforward. Under diffusion-limited conditions, the concentration at the microelectrode interface is zero and therefore, a partial pressure gradient corresponding to the pressure in the cell (e.g., 100 kPa for ambient conditions) is assumed. Under this assumption, the results from both measurements should be comparable and a comparison of selected measurements is shown in Figure 27.13.

As can be seen from Figure 27.13, the permeability measurements of Nafion-like membranes do vary considerably, probably because the state of the membranes is difficult to control (e.g., the dryness of the membrane). There is a pronounced difference in the permeabilities for wet and dry membranes, but the method of measurement does not yield consistent variation in the measured values. It can therefore be concluded that the electrochemical method is equivalent to the gas analysis method, even though the measurement conditions are different from those in fuel cell applications.

### 27.2.3 CATALYST UTILIZATION AND INTERFACIAL ASPECTS

The importance of the ionomer in the electrode for the performance of the PEMFC has been well known since the pioneering work of Raistrick et al. [37]. In the PEMFC, the electroosmotic drag of water due to the proton transport from the anode to the cathode leads to the membrane drying out from the anode side (back diffusion of water from cathode to anode compensates partly for the water loss from the anode side of the membrane). Therefore, the loss of conductivity of the ionomer at the anode is also an additional important issue related to the membrane topic, since the ionomer in the electrode needs to connect ionically and chemically to the membrane. In an investigation of the transverse water profile in Nafion in PEMFCs with a

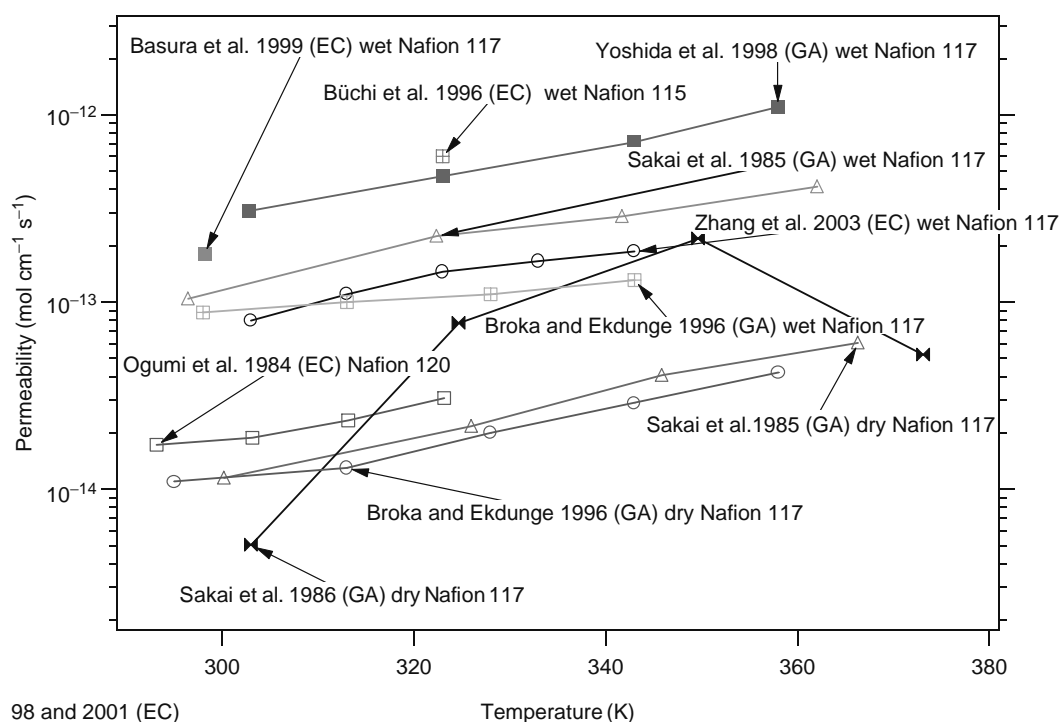


**FIGURE 27.13** (See color insert following page 588.) O<sub>2</sub> permeability as a function of temperature measured using an electrochemical method (microelectrodes, EC) and a gas permeation (gas analysis, GA) method. Permeability calculated for a partial pressure gradient of 100 kPa. (From Vielstich, W., Gasteiger, H.A., and Lamm, A. (Eds.), *Handbook of Fuel Cells: Fundamentals, Technology and Applications*, J. Wiley & Sons, Chichester, 2003; Masten, D.A. and Bosco, A.D., in Vielstich, W., Gasteiger, H.A., and Lamm, A. (Eds.), *Handbook of Fuel Cells: Fundamentals, Technology and Applications*, J. Wiley & Sons, Chichester, 2003; Gasteiger, H.A. and Mathias, M.F., in *Proceedings of the Symposium on Proton Conducting Membrane Fuel Cells III*, The Electrochemical Society of America, 2003; Gasteiger, H.A., Panels, J.E., and Yan, S.G., *J. Power Sources*, 127, 162, 2004; Alberti, G., Casciola, M., Massinelli, L., and Bauer, B., *J. Membr. Sci.*, 185, 73, 2001; Ma, Y.L., Wainright, J.S., Litt, M.H., and Savinell, R.F., *J. Electrochem. Soc.*, 151, A8, 2004; Watanabe, M., Satoh, Y., and Shimura, C., *J. Electrochem. Soc.*, 140, 3190, 1993; Ge, S.H., Li, X.G., and Hsing, I.M., *J. Electrochem. Soc.*, 151, B523, 2004; Ge, S.H., Li, X.G., and Hsing, I.M., *Electrochim. Acta*, 50, 1909, 2005.)

sheet-partitioned membrane, Büchi and Scherer found that the increase in resistance is always confined to the membrane sheet contacting the anode [38]. It cannot be excluded that the main contribution to increased resistance of the MEA at high temperatures is from the ionomer in the electrode. To obtain clarification, cyclic voltammograms (CVs) of a commercial MEA with about 25  $\mu\text{m}$  thick membranes were performed as a function of temperature at 100% RH to detect the influence of these interfacial structures on the performance of PEMFCs. Figure 27.14 shows the CVs of the anode as a working electrode (catalyst loading of 0.3  $\text{mg cm}^{-2}$ ) under nitrogen purging. The cathode was used as a combined counter and reference electrode and purged with hydrogen. Due to the small thickness of the membrane, hydrogen permeates the anode leading to an almost linear slope in the CVs. This current was subtracted to obtain more information regarding the interfacial properties of the MEA. The humidification of nitrogen/hydrogen was achieved by gas bubblers, which were invariably kept at 5°C higher than the cell. Condensation of water was avoided by choosing adequate temperatures for the gas distribution system. Interestingly, the features due to hydrogen adsorption/desorption decrease with increasing temperature, indicating a loss of active catalyst surface area.

From these CVs, the reduction of Pt oxide in the negative going scan can also be used to estimate the contacted catalyst surface area. The integration of the respective areas is not highly accurate and an integration error of  $\pm 15$  mC is displayed in the charges plotted against temperature in Figure 27.15.

As can be seen from Figures 27.14 and 27.15, the hydrogen desorption charge decreases almost monotonically with increasing temperature, indicating a loss of active surface with increasing temperature. At variance with the linear decrease, the charges from Pt oxide first increase up to 60°C and then a strong decrease is observed at higher temperatures of 90°C. The charges from hydrogen desorption are considered to be of higher significance for the active surface determination, since the Pt oxide reduction may be influenced by kinetic and mass-transport properties of the interface, which are strongly affected by the temperature increase. The form of the CV in the oxide region indicates mass-transport limitations due to diffusion in a polymer film. Especially there is a strong decrease in active catalytic area when the pressure is increased, e.g., at the same temperature. This is demonstrated in Figure 27.16 for the temperature of 90°C where the pressure was increased from 1 to 2 bar(abs).

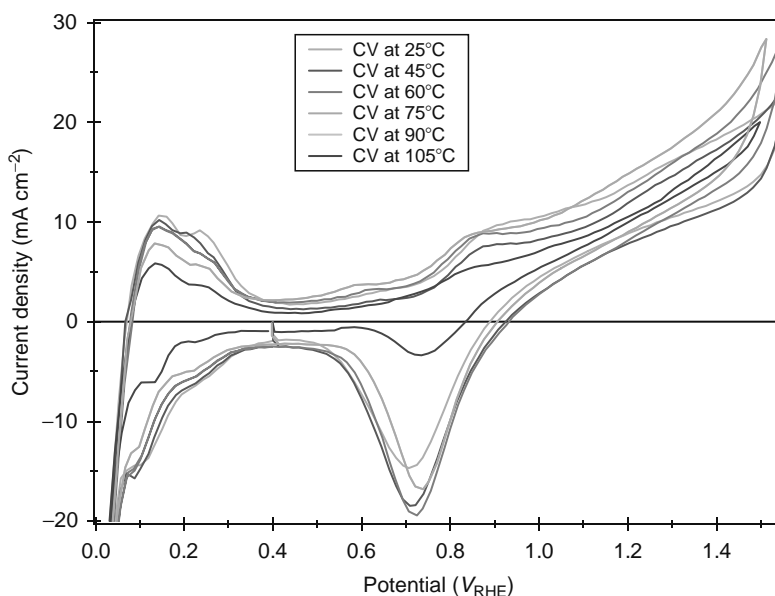


**FIGURE 27.14** (See color insert following page 588.) CVs of a commercial MEA with a 25  $\mu\text{m}$  thick membrane as a function of temperature. Scan rate  $50 \text{ mV s}^{-1}$  (ZSW measurements: Internal publication).

The loss of surface area when increasing the pressure is probably associated with the water content depicted in Figures 27.15 and 27.16. With increasing pressure, the water content decreases and may lead to the ionomer in the electrode drying out. Since the membrane swells considerably with the water content, the higher pressure conversely leads to the ionomer in the electrode shrinking and thereby to reduced catalyst utilization. But then the question remains why the catalyst surface utilization decreases with increasing temperature, although the water content of air/nitrogen increases considerably with temperature. It is well known that the water uptake of Nafion membranes is lower in the gaseous phase compared to the liquid phase (16 versus 22 water molecules per sulfonic acid group). This is an effect that has been discussed for numerous membranes and is termed Schroeder's paradox [39]. Furthermore, Nafion has also been reported by Broka and Ekdunge to adsorb less water with increasing temperature even at constant humidity [40]. The reasons are not yet completely understood, but are associated with the nanoporous structure and the phase-separated hydrous and anhydrous regions of Nafion. This effect is shown in Figure 27.17 for the temperature range of  $20^\circ\text{C}$ – $70^\circ\text{C}$ . If such dependence also exists in the ionomer present in the electrode, it is understandable why, with increasing temperature, the catalyst surface utilization also decreases.

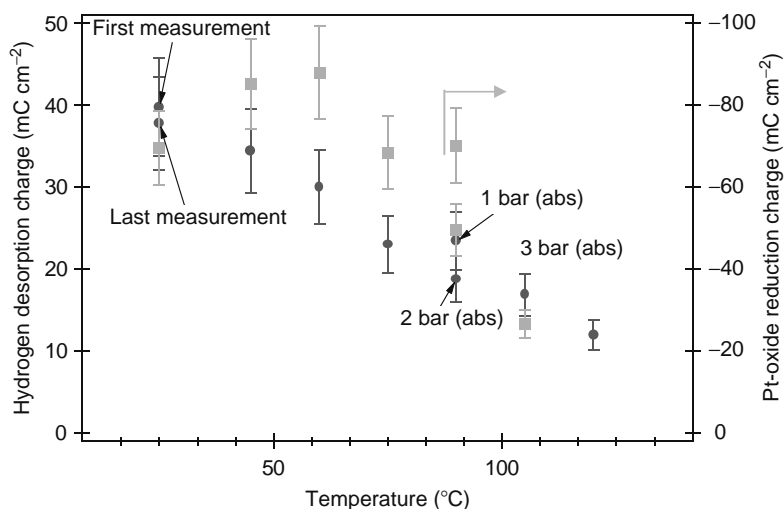


**FIGURE 27.15** Hydrogen desorption charge (left-hand side, circles) and Pt oxide reduction charge (right-hand side, squares) as a function of temperature and pressure (ZSW measurements: Internal publication).

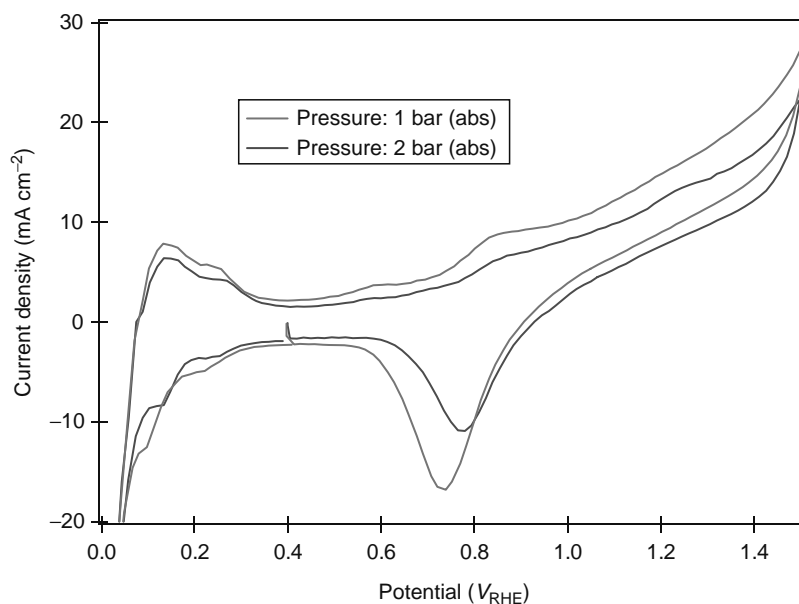


**FIGURE 27.16** (See color insert following page 588.) CVs of a commercial MEA at 90°C for 1 and 2 bar (abs) pressure. Scan rate 50 mV s<sup>-1</sup> (ZSW measurements: Internal publication).

It can be concluded that there are various problems associated with the standard PFSA membranes with increasing temperature:

- Loss of conductivity of membrane
- Loss of conductivity of ionomer in the electrode
- Loss of active catalyst surface area

#### 27.2.4 MEMBRANE REQUIREMENTS FOR DIRECT METHANOL FUEL CELLS

DMFCs have potential near-term applications mainly in the portable power source market, as they are smaller, lighter, simpler, and cleaner than conventional batteries. Liquid methanol is consumed directly in a DMFC, which implies a higher energy density of the fuel cell system. But the power densities achievable with state-of-the-art DMFCs are still smaller in comparison

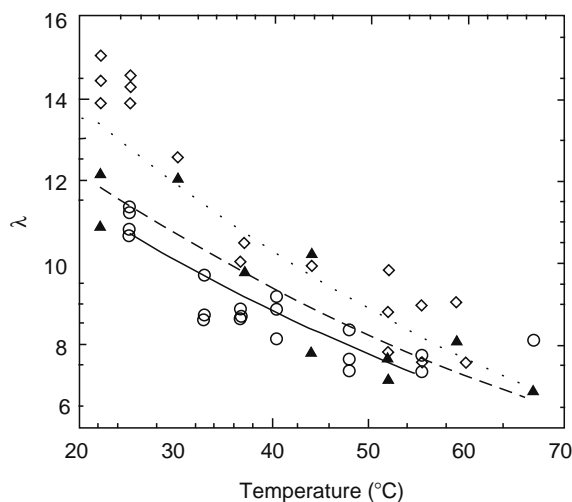


**FIGURE 27.17** Water uptake from vapor phase (100% relative humidity [RH]) by Nafion 117 membrane and recast Nafion film at different equilibration temperatures: (◇) Nafion 117 membrane, (▲) recast Nafion film, (○) heat-treated Nafion 117 membrane. Fitted curves: second order polynomial;  $\lambda$  is the number of water molecules per sulfonate site. (Reproduced from Broka, K. and Ekdunge, P., *J. Appl. Electrochem.*, 27, 117, 1997. With permission from Springer Science and Business Media.)

to hydrogen-fuelled PEMFCs. One of the major problems lies in the use of liquid methanol solution on the anode of the DMFC, which, on the one hand, keeps the ionomeric membrane water saturated (and thus no humidification is needed), but on the other hand, does not keep fuel (methanol or any other organic fuel, e.g., formic acid, ethanol, etc.) and water from permeating to the cathode side, since the basic PFSA membranes are permeable to both methanol and water [41,42]. The fuel and water crossover from anode to cathode hampers the performance of the air cathode.

#### 27.2.4.1 Methanol Crossover

One of the most challenging issues that prevent DMFCs from being used in practical applications is the crossover of methanol fuel through typical PEMs, e.g., Nafion, from the anode to the cathode. It has been found that nearly 30%–40% of methanol can be wasted due to this crossover to the cathode depending on operating conditions like temperature, concentration of methanol in the anode feed, and current density in the cell. The mechanisms responsible for this transport of methanol to the cathode are diffusion due to concentration gradient and electroosmotic drag as moving protons also drag methanol like water, both being polar in nature. Methanol transported through the membrane by diffusion and electroosmotic drag recombines chemically with oxygen at the cathode and therefore, fuel utilization efficiency is lowered. Additionally, methanol present at the cathode depolarizes the oxygen electrode and establishes a mixed potential thus lowering the cathode potential. Methanol competes with the oxygen reduction reaction at the cathode and predominantly reacts with oxygen. This undesired reaction increases the demand for oxygen and therefore requires higher stoichiometric flow rates. To minimize the negative impact of the methanol crossover, fuel cell developers are forced to use thicker membranes which reduce the fuel crossover, but increase the specific cell resistance [8,41,43–46].

#### 27.2.4.2 Water Permeation

Water permeation to the air cathode in liquid methanol solution-fed DMFCs creates a barrier for air diffusion to active sites in the cathode catalyst layer by flooding the electrode. The water transport mechanisms from the aqueous anode to the gaseous cathode are electroosmotic drag and diffusion. The Nafion membrane is saturated with water for DMFCs, which gives rise to high electroosmotic drag coefficients [47] in comparison to partially saturated membranes, as in H<sub>2</sub>/air PEMFCs. At lower current densities, diffusion due to a huge concentration gradient of water between anode and cathode is the dominant water transport mechanism. But with increasing current density, the electroosmotic drag becomes the dominant mechanism as the water transported by electroosmotic drag is proportional to current density. The water transport properties of different types of membranes have been widely investigated by several research groups [45,46,48–54]. The permeated water hampers the performance of the air cathode by flooding the cathode catalyst and GDL and it also makes the self-sustainable high-temperature operation of DMFCs difficult due to excessive heat loss by water vaporization from the air cathode [55,56]. Additionally, it puts a huge demand on the air blower to remove water, making the DMFC's design more complicated and less energy efficient [42,43]. In this vein, DMFCs or any direct liquid oxidation fuel cells using methanol, formic acid, or ethanol, etc. as fuel should have membranes which are more liquid tight and still have sufficient proton conductivity.

### 27.3 MECHANISTIC ASPECTS OF PROTON CONDUCTIVITY (NAFION AND PERFLUORINATED SULFONIC ACIDS)

It is very important that the perfluorinated membrane has sufficient water content to function in fuel cells. The interaction of the perfluorinated membrane with water and the resulting water content of the membrane determine the proton conductivity of the membrane. The mechanistic aspects have been discussed in numerous publications, which cannot be completely recapitulated here [57–67]. When in contact with water vapor or liquid water, Nafion or similar membranes show a pronounced swelling of 20%–50% associated with a considerable water uptake. Due to the ambivalent nature of the polymer, as it has a hydrophobic backbone and hydrophilic head groups, a spontaneous phase separation takes place in the membrane. In a hydrated condition, hydrophilic ionic clusters are formed which are connected through water channels, thereby forming a water network. The hydrophilic clusters contain the solvated SO<sub>3</sub> groups, water, and the cations (normally H<sup>+</sup>, but for cation-exchange membranes Na<sup>+</sup>, K<sup>+</sup>, or Li<sup>+</sup> can naturally also be introduced). This water-filled network in a hydrophobic backbone yields high-proton conductivity, which resembles an aqueous electrolyte (similar conductivities as well as activation energies for the proton conduction are observed). The ambivalent property of the membranes assists their mechanical stability as the strong electrostatic interactions of the ionic clusters are apparently responsible for this stability. Importantly, Nafion can absorb more water from the liquid. For Nafion 117, saturated with liquid water, 22 moles of water are absorbed per mole of sulfonic acid groups. It is detrimental for the applications that Nafion can take up only a maximum of 14 mol of water per mole of sulfonic acid groups from the water in the gaseous phase. As discussed earlier, the conductivity of Nafion membranes is strongly dependent on water content, which is displayed in Figure 27.18 for two different equivalent weights. The membrane with the lower EQ shows the higher conductivity since the concentration of sulfonic acid groups is higher. A dried-out

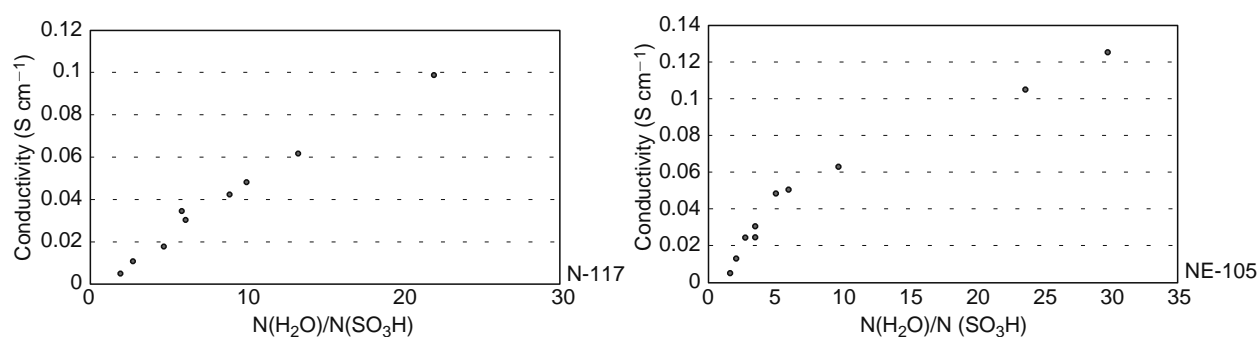


**FIGURE 27.18** Conductivity of Nafion 117 and 105 as a function of water content expressed as the ratio of water molecules per sulfonic acid group. (From Hodgdon, R.B., Boyack, J.R., and Laconti, A.B., The degradation of polystyrene sulfonic acid. *General Electric Company TIS Report 65DE 5 1966*; Laconti, A.B., Fragala, A.R., and Boyack, J.R., in *Proceedings of the Symposium on Electrode Materials and Process for Energy Conversion and Storage*, J.D.E. McIntyre, S. Srinivasan, and F.G. Wills (Eds.), The Electrochemical Society Inc., Princeton, NJ, 1977, p. 354.)

membrane possesses lower proton conductivity. Thus, water management in the membrane is one of the major issues in PEM technology. Processes influencing the water content in the membrane are electroosmotic drag and back diffusion of product water from the cathode into the membrane.

Water in a PEMFC is usually provided by the humidification of the reactant gases or from the cathode reaction. The amount of water fed to a cell by humidifying the reactant gases depends on gas temperature, pressure, and the flow rate. Water production at the cathode is directly proportional to the current density. Water carried to the cathode side by electroosmotic drag combined with the production of water at the cathode results in a gradual accumulation of water at the cathode. The water at the cathode can be carried to the flow channel through the GDL or through the membrane to the anode by back diffusion due to the water concentration gradient between the anode and cathode of the PEMFC. Water transport to the anode by back diffusion, which helps in keeping the membrane humidified, depends strongly on the thickness of the membrane and the properties of the GDL.

### 27.3.1 MICROSCOPIC STRUCTURE

The differences between PFSA membranes and nonfluorinated polyaromatic membranes are discussed on the basis of publications by Kreuer [64]. Perfluorosulfonic polymers naturally combine the extremely high hydrophobicity of the perfluorinated backbone with the extremely high hydrophilicity of the sulfonic acid functional groups in one macromolecule. Especially in the presence of water, this gives rise to some hydrophobic/hydrophilic nanoseparation. The sulfonic acid functional groups aggregate to form a hydrophilic domain. When this is hydrated, protons form within inner space charge layers by dissociation of the acidic functional groups. While the well-connected hydrophilic domain is responsible for the transport of protons and water, the hydrophobic domain provides the polymer with the morphological stability and prevents the polymer from dissolving in water. Kreuer's group found the situation in sulfonated polyetherketones to be distinctly different with respect to both transport properties and morphological stability. In sulfonated polyetherketones, the hydrophilic/hydrophobic difference is less pronounced. This was inferred from the results of small-angle x-ray scattering (SAXS) experiments [64]. For a hydrated sulfonated polyetherketone compared to Nafion, the ionomer peak is broadened and shifted toward higher scattering. This indicates a smaller characteristic separation length with a wider distribution and a larger internal interface between the hydrophobic and hydrophilic domain for the hydrated sulfonated polyetherketone. As schematically illustrated in Figure 27.19, the water-filled channels in s-PEEK are narrower compared to those in Nafion. They are less separated and more branched with more dead-end pockets. These features correspond to the larger hydrophilic/hydrophobic interface and, therefore, also to a larger average separation of neighboring sulfonic acid functional groups. The stronger confinement of the water in the narrow channels of the aromatic polymers leads to a significantly lower dielectric constant of the water of hydration (about 20 compared to almost 64 in fully hydrated Nafion) [59].

The different water interactions of the PEEK membranes are both advantageous and disadvantageous: on the one hand, a disadvantageous swelling behavior and a stronger decrease in water and proton-transport coefficients with decreasing water content are observed; on the other hand, the hydrodynamic flow of the water, i.e., electroosmotic drag and water permeation, is reduced compared to Nafion, which is an essential advantage, especially for DMFC applications [64]. Blending sulfonated polyetherketones with inert or basic polymers (e.g., PBI) significantly improves the swelling behavior without reducing the high-proton conductivity at high water contents. Blending also further reduces the hydrophilic/hydrophobic separation and therefore also hydrodynamic solvent transport (water and methanol permeation). Therefore, polymers based on sulfonated polyarylenes are not only interesting, low-cost, alternative membrane materials for hydrogen PEMFC applications but they may

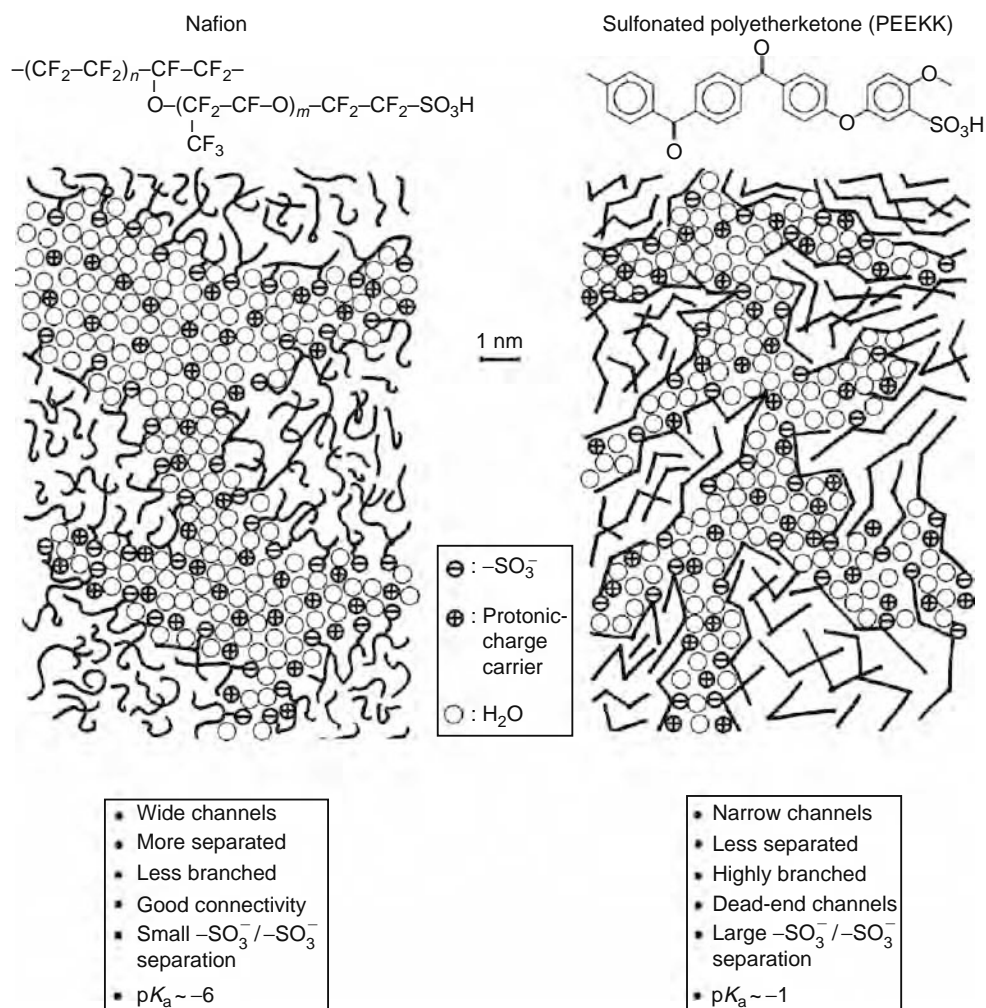


**FIGURE 27.19** Schematic representation of the microstructures of Nafion and a sulfonated polyetheretherketone illustrating the less-pronounced hydrophobic/hydrophilic separation of the latter compared to the former. (Reprinted from Kreuer, K.D., *J. Memb. Sci.*, 185, 29, 2001. With permission from Elsevier.)

also help to reduce the problems associated with high water and methanol crossover in DMFCs using aqueous solutions of methanol as a fuel. An important drawback is their reduced chemical stability, which may well lead to reduced durability of the membranes [68].

## 27.4 MATERIALS: PHYSIOCHEMICAL PROPERTIES AND FUEL CELL PERFORMANCE

The commercial development of single-ion conducting polymer membranes has changed the field of electrochemical devices in a significant way. Traditional systems such as sulfuric acid and potassium hydroxide combine excellent conductivity and cost effectiveness, but the disadvantages are extreme corrosivity and challenging confinement. In this respect, the ion conducting membranes exhibit excellent stability and processability, allowing the flexible design of electrochemical devices.

### 27.4.1 PERFLUORINATED SULFONIC ACID MEMBRANES

PFSA membranes possess high-proton conductivity in the range of  $0.1 \text{ S cm}^{-1}$  at  $80^\circ\text{C}$  and good chemical as well as mechanical stability. The superior stability of Nafion is a consequence of the PTFE-based structure which is chemically inert in reducing and oxidizing environments. The best-known examples of this class of proton-conducting membranes are the Nafion-type membranes from DuPont de Nemours. The most common commercial perfluorinated ionomer membranes used today in various industrial processes are listed in Table 27.1. Asahi, Dow, and DuPont electro dialysis (ED) membranes have similar compositions and structures based on PFSA. The active ionomer component of the Gore-Select membrane is also a PFSA. In their usual form, these polymer membranes require water for conductivity. As long as these proton-exchange

**TABLE 27.1**  
**Commercial Perfluorinated Ionomer Membranes Listed by Trade Name**

Trade Name	Company	Membrane Type
Nafion XR resin	DuPont	Perfluorosulfonic acid (PFSA)
Nafion CR resin	DuPont	Perfluorocarboxylic acid
Flemion XR resin	Asahi Glass	PFSA
Flemion CR resin	Asahi Glass	Perfluorocarboxylic acid
Aciplex XR resin	Asahi Chemical	PFSA
Aciplex CR resin	Asahi Chemical	Perfluorocarboxylic acid

*Source:* From Doyle, M. and Rajendran, G., in W. Vielstich, H.A. Gasteiger, and A. Lamm (Eds.), *Handbook of Fuel Cells: Fundamentals, Technology and Applications*, J. Wiley & Sons, Chichester, 2003, pp. 351–395.)

*Note:* Du Pont de Nemours: Nafion membranes.

membranes (PEMs) are kept hydrated, they function well, but when these membranes dry out, resistance rises sharply. A PTFE backbone is supplemented by regularly spaced perfluorovinyl ether pendant side chains terminated by a sulfonic acid group with the chemical structure shown in Figure 27.20.

Hydrated Nafion 117 (175  $\mu\text{m}$  thick) has conductivities in the range of  $10^{-1} \text{ S cm}^{-1}$  at  $80^\circ\text{C}$ . Nafion has a high electroosmotic drag coefficient that can lead to problems with water management in a PEMFC. Nafion has been extensively studied because of its electrochemical applications such as chlor-alkali production and, more recently, fuel cells. Continued research has sought to explain the high level of the ionomer ionic conductivity. Fuel cell membrane developers are focusing on thinner membranes to decrease resistance and to alleviate the water management problems. Popular Nafion membrane products for fuel cells include NE-112, NE-1135, N-112, N-105, N-115, and N-117. In fuel cell applications, Nafion serves as a solid electrolyte to selectively transport protons across the cell junction. Tables 27.2 through 27.5 summarize the presently available product information provided by DuPont for Nafion PFSA polymers.

#### 27.4.1.1 Properties of Nafion PFSA Membranes

One activity at DuPont's Fuel Cells Business Center is the development of a thinner membrane with sufficient mechanical stability. Thinner membranes translate into higher current density, which in turn means a higher electrical efficiency. The trade-off is a less mechanically robust membrane. Nafion membranes are nonreinforced films based on Nafion resin, a PFSA/PTFE copolymer in the acid ( $\text{H}^+$ ) form. DuPont is especially marketing Nafion PFSA NR-111 and NR-112 membranes as nonreinforced dispersion-cast films for that purpose. These membranes are delivered as a composite with the membrane positioned between a backing film and a coversheet. This composite is wound on a 6 in. i.d plastic core, with the backing film facing out, as shown in Figure 27.21.

The backing film facilitates transporting the membrane into automated MEA fabrication processes, while the coversheet protects the membrane from exposure to the environment during intermediate handling and processing. In addition, the coversheet (in combination with the backing film) eliminates rapid changes in the membrane's moisture content, and stabilizes the dimensions of the membrane as it is removed from the roll. A roll core leader is attached to the membrane, as shown in Figure 27.21, when this option is desired by the customer. The roll core leader material is the same as the backing film. The properties of these thin membranes are specified in Table 27.5.

#### 27.4.1.2 Performance of DuPont Nafion Membranes

It is assumed that DuPont's Nafion membranes are used in about 80% of all publications on PEMFCs. The simple reason is that this was the only commercially available material for long time. Therefore, it is not possible to present here a complete

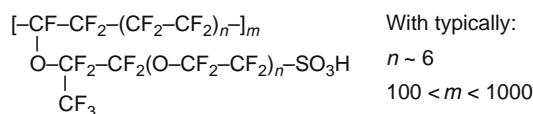


**FIGURE 27.20** Structure of Nafion. The characteristic value of proton-conducting polymer membranes is the EW, which is defined as the weight of polymer that will neutralize one equivalent of base, and is inversely proportional to the IEC. The values  $n$ ,  $m$ ,  $n'$  can be varied to produce materials with different equivalent weights.

**TABLE 27.2**  
**Thickness and Basis Weight Property Measurements Taken with Membrane**  
**Conditioned to 23°C, 50% RH**

Membrane Type	Typical Thickness ( $\mu\text{m}$ )	Basis Weight ( $\text{g m}^{-2}$ )	Equivalent Weight of Polymer That Will Neutralize One Equivalent of Base
N-112	51 (ca. 2 mils)	100	1100
NE-1135	89 (ca. 3.5 mils)	190	1100
N-115	127 (ca. 5 mils)	250	1100
N-117	183 (ca. 7 mils)	360	1100
NE-1110	254 (ca. 10 mils)	500	1100
N-105	127 (ca. 5 mils)	na	1000

**TABLE 27.3**  
**Physical and Other Properties for EW 1100 Membranes. Conditioning State of Membrane**  
**Given. Measurements Taken at 23°C, 50% RH**

Property	Typical Value	Test Method
<b>Physical properties</b>		
<i>Tensile modulus, MPa (kpsi)</i>		
50% RH, 23°C	249 (36)	ASTM D 882
Water soaked, 23°C	114 (16)	ASTM D 882
Water soaked, 100°C	64 (9.4)	ASTM D 882
<i>Tensile strength, maximum, MPa (kpsi)</i>		
50% RH, 23°C	43 (6.2) in MD, 32 (4.6) in TD	ASTM D 882
Water soaked, 23°C	34 (4.9) in MD, 26 (3.8) in TD	ASTM D 882
Water soaked, 100°C	25 (3.6) in MD, 24 (3.5) in TD	ASTM D 882
<i>Elongation at break, %</i>		
50% RH, 23°C	225 in MD, 310 in TD	ASTM D 882
Water soaked, 23°C	200 in MD, 275 in TD	ASTM D 882
Water soaked, 100°C	180 in MD, 240 in TD	ASTM D 882
<i>Tear resistance—initial, <math>\text{g mm}^{-1}</math></i>		
50% RH, 23°C	6000 in MD, TD	ASTM D 1004
Water soaked, 23°C	3500 in MD, TD	ASTM D 1004
Water soaked, 100°C	3000 in MD, TD	ASTM D 1004
		Tear resistance ( $\text{g mm}^{-1}$ ) of dry membrane increases with thickness. Values given are typical for 0.05 mm membrane.
<i>Tear resistance—propagating, <math>\text{g mm}^{-1}</math></i>		
50% RH, 23°C	>100 in MD, >150 in TD	ASTM D 1922
Water soaked, 23°C	92 in MD, 104 in TD	ASTM D 1922
Water soaked, 100°C	74 in MD, 85 in TD	ASTM D 1922
<i>Specific gravity</i>	1.98	
<i>Other properties</i>		
Conductivity, $\text{S cm}^{-1}$	0.083	Conductivity measurement as described by Zawodzinski et al., <i>J. Phys. Chem.</i> , 95 (15), 6040 (1991) [170]. Membrane conditioned in 100°C water for 1 h. Measurement cell submersed in 25°C D.I. water during experiment. Membrane impedance (real) taken at zero imaginary impedance.
Acid capacity, mequiv $\text{g}^{-1}$	0.89	A base titration procedure measures the equivalents of sulfonic acid in the polymer, and uses the measurement to calculate the acid capacity or equivalent weight of the membrane.

*Abbreviations:* MD, machine direction; TD, transverse direction.

**TABLE 27.4**  
**Hydrolytic Properties**

Property	Typical Value	Test Method
Water content, % water	5	ASTM D 570. Water content of membrane conditioned to 23°C, 50% relative humidity (RH), compared to dry weight basis.
Water uptake, % water	38	ASTM D 570. Water uptake from dry membrane to water soaked at 100°C for 1 h (dry weight basis).
<i>Thickness change, % increase</i>		
From 50% relative humidity (RH), 23°C to water soaked, 23°C	10	ASTM D 756
From 50% RH, 23°C to water soaked, 100°C	14	ASTM D 756
<i>Linear expansion, % increase</i>		
From 50% RH, 23°C to water soaked, 23°C	10	Average of MD and TD. MD expansion is slightly less than TD.
From 50% RH, 23°C to water soaked, 100°C	15	ASTM D 756

*Abbreviations:* MD, machine direction; TD, transverse direction.

overview of performance data with Nafion or other membranes. Furthermore, the performance depends strongly on the conditions used as well as MEA preparation (catalyst loading, etc.). As a consequence, only the performance data from the membrane manufacturer itself are reported. Figure 27.22 exhibits performance reports by DuPont in 2002 for a three-layer MEA for neat hydrogen and reformat operation.

According to DuPont, good progress has been made in developing high-temperature operating membranes. Exploratory research membranes in the temperature range of 110°C–140°C have been developed. A further development focus of DuPont membranes is the DMFC application. Beside performance increase, the reduction in methanol permeation is an important aspect of the development. In a presentation, DuPont showed the advantage of using thicker (7 mil) membranes compared to the thinner (2 mil) Nafion 112, which shows good performance for hydrogen/air operation. Figure 27.23 demonstrates this observation.

**TABLE 27.5**  
**Properties of Nafion NR-111 and NR-112 Membranes****Thickness and Basis Weight Properties**

Membrane type	Typical thickness ( $\mu\text{m}$ )		Basis weight ( $\text{g m}^{-2}$ )	
NR-111	25.4		50	
NR-112	50.8		100	

*Physical properties*

Machine direction (MD), transverse direction (TD)	NR-111		NR-112		Test method
	MD	TD	MD	TD	
Property, measured at 50% relative humidity (RH), 23°C					
Tensile strength, maximum, MPa	23	28	32	32	ASTM D 882
Non-std modulus, MPa	288	281	266	251	ASTM D 882
Elongation to break, %	252	311	343	352	ASTM D 882

*Other properties, hydrogen crossover measured at 22°C, 100% RH and 50-psi delta pressure*

Specific gravity (23°C, 50% RH)	1.97	1.97		DuPont
Acid capacity (mequiv $\text{g}^{-1}$ )	$0.95 \pm 0.04$	$0.95 \pm 0.04$		DuPont
Hydrogen crossover ( $\text{mL min}^{-1}\text{-cm}^2$ )	$<0.020$	$<0.010$		DuPont

*Hydrolytic properties, water content of membrane conditioned to 23°C and 50% RH (dry weight basis). Water uptake from dry membrane to conditioned in water at 100°C for 1 h (dry weight basis)*

Water content, % water	$5.0 \pm 3.0\%$		ASTM D 570
Water uptake, % water	$50.0 \pm 5.0\%$		ASTM D 570

*Linear expansion, % increase*

From 50% RH, 23°C to water soaked, 23°C	10	ASTM D 756
From 50% RH, 23°C to water soaked, 100°C	15	ASTM D 756

Source: From DuPont, [www2.dupont.com](http://www2.dupont.com).

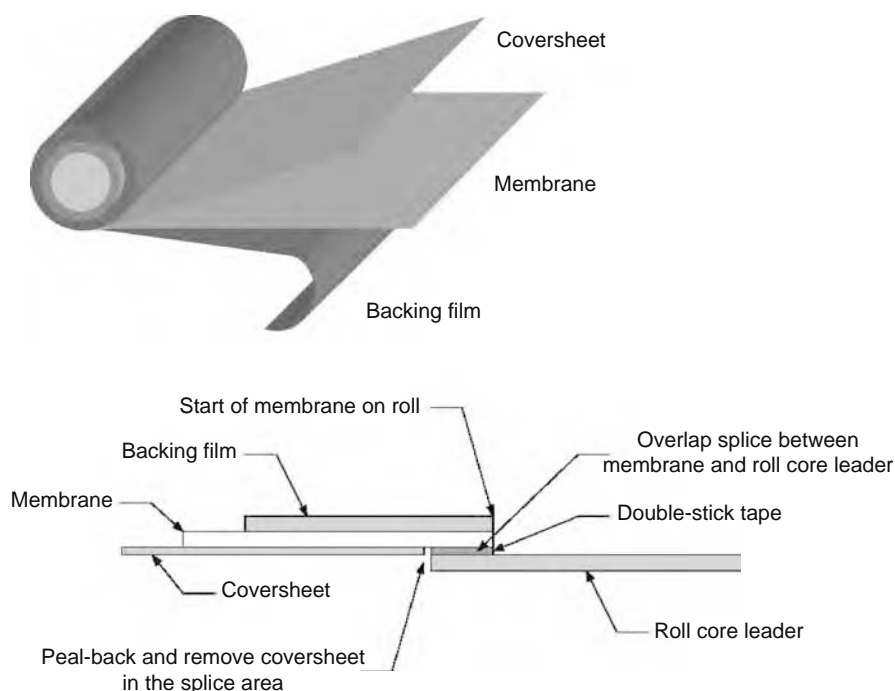


**FIGURE 27.21** Top: diagram of DuPont's Nafion PFSA NR-111 and NR-112 membranes showing roll unwind orientation (backing film facing out). Bottom: splice design for attaching roll core leader to membrane. (From DuPont, www2.dupont.com.)

Another finding reported by DuPont is that the equivalent weight (EW) exhibits a pronounced influence on performance and methanol permeation. Whereas the highest performances were found with low EW membranes, the membranes with high EW had the lowest relative methanol permeation (Figure 27.24). According to DuPont, a 2 mil experimental membrane is in development which exhibits better performance for DMFCs compared to the 7 mil commercial membrane.

### 27.4.1.3 Synthesis of PFSA Monomers and Polymers

The synthesis of the monomers as well as the polymerization of PFSA membranes involve dangerous reactions under conditions of high pressure and temperature. Additionally, the synthesis of the comonomer that is commonly referred to as perfluorosulfonylfluoride ethyl propyl vinyl ether (PSEPVE) involves numerous steps with low yields. These factors contribute to the cost of these materials. The synthesis routes described in detail by Doyle and Rajendran are summarized here. The synthesis of the long-chain PFSA monomers used in commercial systems like Nafion, Flemion, and Aciplex proceeds through

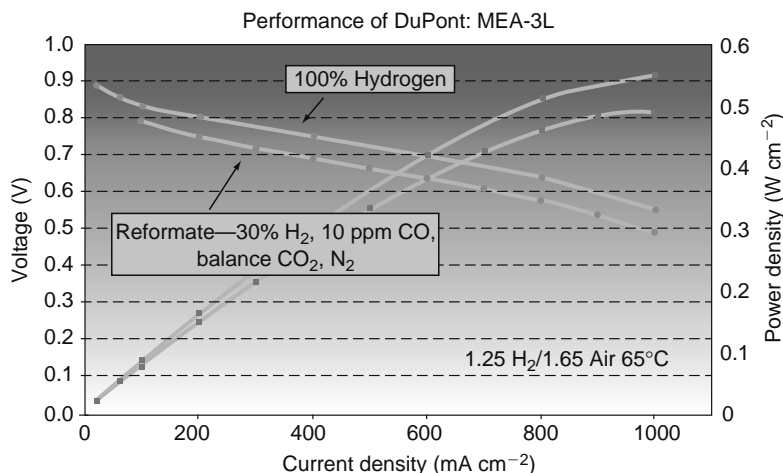


**FIGURE 27.22** Performance for DuPont membrane electrode assembly three-layer (DuPont MEA-3L). (From DuPont 2002, www2.dupont.com.)

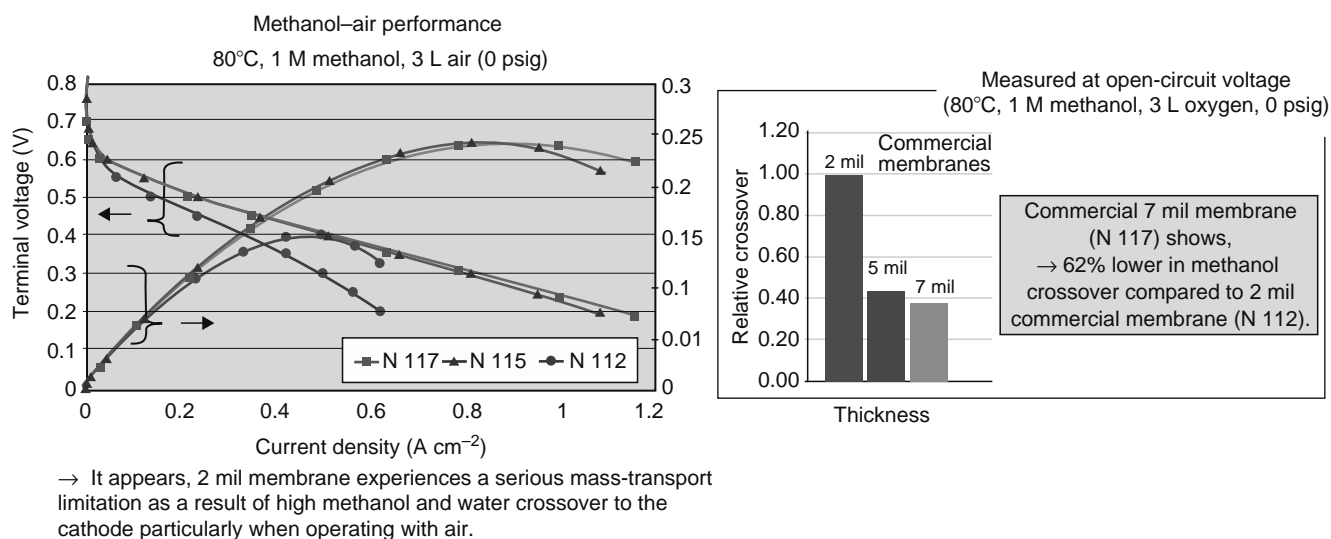


**FIGURE 27.23** (See color insert following page 588.) Comparison of DMFC performance of Nafion 117, Nafion 115, and Nafion 112. (From DuPont 2002, www2.dupont.com.)

the reaction of  $SO_3$  with tetrafluoroethylene (TFE) to form a cyclic sultone. A rearrangement of the cyclic compound yields the so-called rearranged sultone (RSU), which is reacted with hexafluoropropylene oxide (HFPO) to produce sulfonyl fluoride adducts. Heating these compounds in the presence of sodium carbonates yields the comonomer PSEPVE. The synthesis is illustrated in Figure 27.25 from Doyle and Rajendran [8]. Polymerization is typically performed in perfluorocarbon solvents with a perfluorinated free-radical initiator such as perfluoroperoxide.

The short-chain version of the perfluorosulfonyl fluoride vinyl ether monomer is highly desirable for obtaining membranes with improved functionalities. Ionomers with a short chain were intensively developed by Dow Chemical in the early 1990s and almost obtained commercial status. However, the development was abandoned, partly because the synthesis of the short-chain monomer is substantially more challenging. The Dow membrane was based on a copolymer of TFE and  $CF_2=CFOCF_2CF_2SO_2F$ . Since the shorter side chain makes the ionic concentration higher for the same EW, the Dow membrane showed higher conductivity and higher water uptakes under similar conditions. Testing of the Dow polymer in PEMFCs by Ballard in 1987–1988 showed significant improvement in performance compared to Nafion 117 (three times better current density at 0.5 V was reported). The typical functional comonomers of the relevant perfluorinated membranes are given in Figure 27.26 from Doyle and Rajendran.

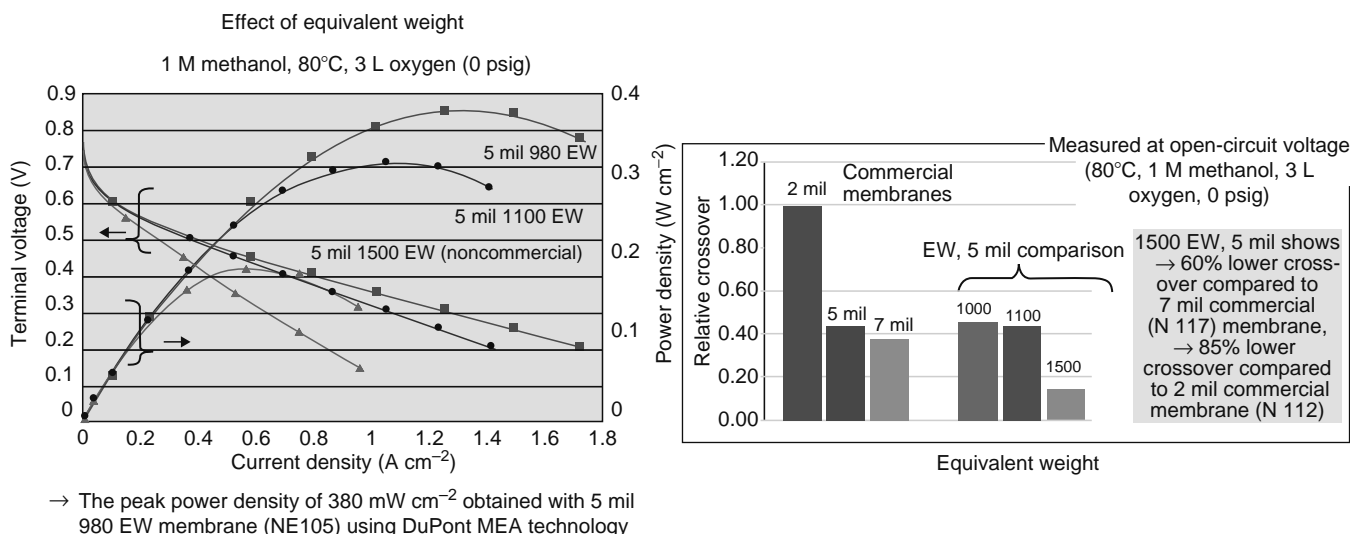


**FIGURE 27.24** (See color insert following page 588.) Comparison of DMFC performance of 5 mil membranes with different EWs. (From DuPont 2002, www2.dupont.com.)

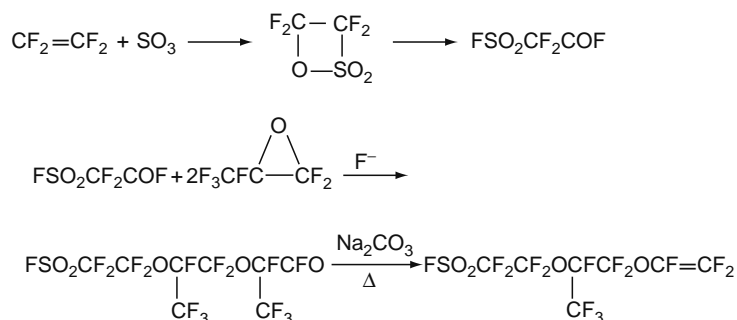


**FIGURE 27.25** Synthesis process for Nafion membrane comonomer PSEPVE. (Reproduced from Doyle, M. and Rajendran, G., in W. Vielstich, H.A. Gasteiger, and A. Lamm (Eds.), *Handbook of Fuel Cells: Fundamentals, Technology and Applications*, Vol. 3, J. Wiley & Sons, Chichester, 2003. With permission.)

Industrial production of perfluorinated ionomers, Nafion membranes, and all perfluorinated membranes is costly due to several factors: first, the monomers used are expensive to manufacture, since the synthesis requires a large number of steps and the monomers are dangerous to handle. The precautions for safe handling are considerable and costly. Secondly, the PSEPVE monomer is not used for other applications, which limits the volume of production. The most significant cost driver is the scale of production. Today, the volume of the Nafion market for chlor-alkali electrolysis ( $150,000 \text{ m}^2 \text{ year}^{-1}$ ) and fuel cells ( $150,000 \text{ m}^2 \text{ year}^{-1}$ ) is about  $300,000 \text{ m}^2 \text{ year}^{-1}$ , resulting in a production capacity of  $65,000 \text{ kg year}^{-1}$ . When compared to large-scale production of polymers like Nylon ( $1.2 \times 10^9 \text{ m}^2 \text{ year}^{-1}$ ), the perfluorinated ionomer membrane is a specialty polymer produced in small volumes.

DuPont predicted in a communication from 1998 that they consider a price of no more than  $\$10 \text{ kW}^{-1}$  realistic in mass production. This prediction was, however, based on optimistic forecasts for transportation applications. The volumes quoted in the press release were 150,000 midsize vehicles (which corresponds to more than 1 million  $\text{m}^2$  worldwide for economics of scale). In 2002, DuPont's expectation for a production volume of 1 million  $\text{m}^2$  was about  $\$25 \text{ kW}^{-1}$  (Figure 27.27). The rule of thumb is to keep the membrane at 5% of the total fuel cell cost. A fairly common figure presently quoted for Nafion is  $\$500 \text{ m}^{-2}$ , although that varies depending on volume and on customer buying power. Several small-scale users have reported much higher costs. DuPont claims that process improvements combined with increasing market volume have yielded, on average, a 50% reduction in the market price of Nafion over the past 3 years. The company has in place a comprehensive, long-term technology and capital investment plan to continue this trend in price reduction. DuPont has reported a market price of Nafion membranes at about  $\$100 \text{ kW}^{-1}$  for the membrane material in a typical reformed hydrogen fuel cell system.

#### 27.4.1.4 Short Side Chain Perfluorinated Sulfonic Acid Membranes

Dow Chemical tested an experimental membrane named XUS 13204.1 in the late 1990s. These Dow experimental membranes are structurally and morphologically similar to the Nafion ionomers, but have shorter side chains and lower equivalent weights in the 800–850 range [69]. The experimental membrane had a reportedly shorter anion–anion distance, which gave it a slight increase in conductivity and greater water retention capability. A thickness of 50–51  $\mu\text{m}$  was considered possible. The patents and related property were reportedly part of the now terminated licensing agreement between Dow and DuPont. The lower equivalent weight ion-selective membranes decrease resistance and therefore lead to power density increase in PEMFCs. According to several sources, an experimental membrane from Dow reportedly exhibited a fourfold increase in power density compared to the Nafion 117 membrane. The disadvantages of lower EW are high swelling in water and

##### XR (sulfonate) comonomer structures

Nafion, Flemion	$\text{CF}_2=\text{CFOCF}_2\text{CF}(\text{CF}_3)\text{OCF}_2\text{CF}_2\text{SO}_2\text{F}$
Aciplex	$\text{CF}_2=\text{CFOCF}_2\text{CF}(\text{CF}_3)\text{OCF}_2\text{CF}_2\text{CF}_2\text{SO}_2\text{F}$
Dow	$\text{CF}_2=\text{CFOCF}_2\text{CF}_2\text{SO}_2\text{F}$

##### CR (carboxylate) monomer structures

Nafion, Aciplex	$\text{CF}_2=\text{CFOCF}_2\text{CF}(\text{CF}_3)\text{OCF}_2\text{CF}_2\text{CO}_2\text{CH}_3$
Flemion	$\text{CF}_2=\text{CFOCF}_2\text{CF}_2\text{CO}_2\text{CH}_3$

**FIGURE 27.26** Typical functional comonomer structures for each ionomer system. (Reproduced from Doyle, M. and Rajendran, G., in W. Vielstich, H.A. Gasteiger, and A. Lamm (Eds.), *Handbook of Fuel Cells: Fundamentals, Technology and Applications*, Vol. 3, J. Wiley & Sons, Chichester, 2003. With permission.)

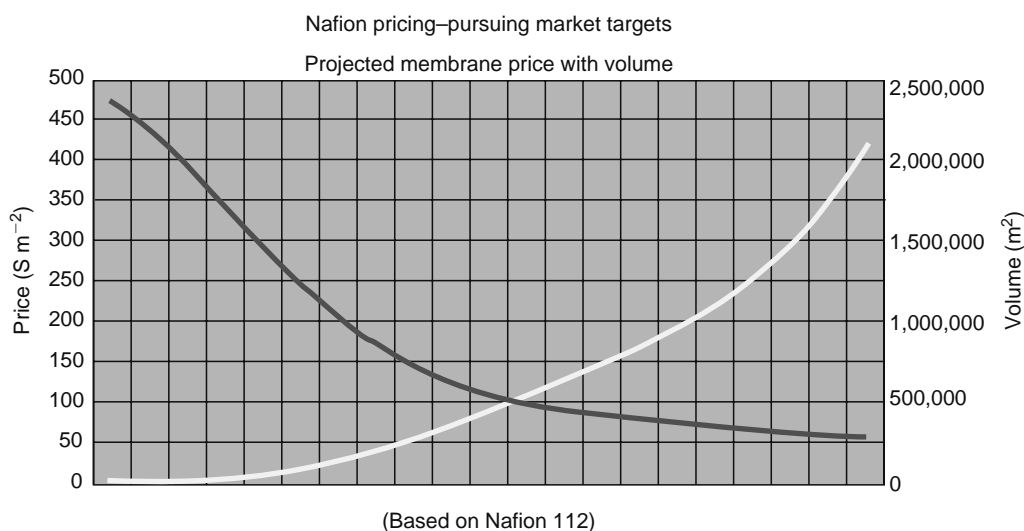


**FIGURE 27.27** DuPont's prediction for cost development in relation to the volume of Nafion produced. (From DuPont 2002, [www2.dupont.com](http://www2.dupont.com). With permission.)

low durability. More recently, similar performances of the experimental Dow membrane and other membranes have been observed [70] (Figure 27.28).

Investigations on Dow membranes can be found in Refs. [70–82]. Solvay Solexis has started a research and development project to create new ionomer membranes for fuel cells and other applications similar to the Dow concept. The development is based on Solexis's capability for producing sulfonylfluorovinylether by a much simpler route than the original Dow synthesis [83]. The Solexis route is schematically represented in Figure 27.29 and the monomer can be produced on an industrial scale. The SSC monomer and TFE are copolymerized by free-radical polymerization to obtain the polymers in Figure 27.30 (named Hyflon Ion).

Starting from the monomers, ionomers are synthesized by taking advantage of a proprietary microemulsion polymerization process. This technology, broadly applied to the polymerization of other fluoropolymers, is able to give very high polymerization kinetics and high-molecular-weight polymers with accurate control of the molecular structure. This fully fluorinated proton-exchange polymer known as Hyflon Ion short side chain polymer obtains results similar to Nafion in fuel cells. This polymer has been used with success in DMFCs up to 130°C within the framework of the EU DREAMCAR program and tested

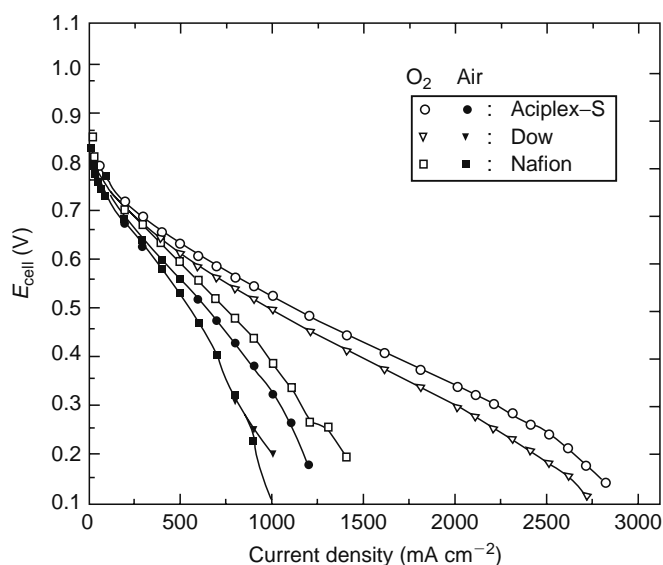


**FIGURE 27.28**  $\text{H}_2/\text{O}_2$ , versus  $\text{H}_2/\text{air}$  performances in PEMFCs with alternate membranes; E-TEK electrodes (20% Pt/C,  $0.4 \text{ mgPt cm}^{-2}$ ), 50°C, 1 atm. Current density versus potential ( $V_{\text{RHE}}$ ). (Reprinted from Wakizoe, M. et al., *Electrochim. Acta*, 40, 335, 1995. With permission from Elsevier.)

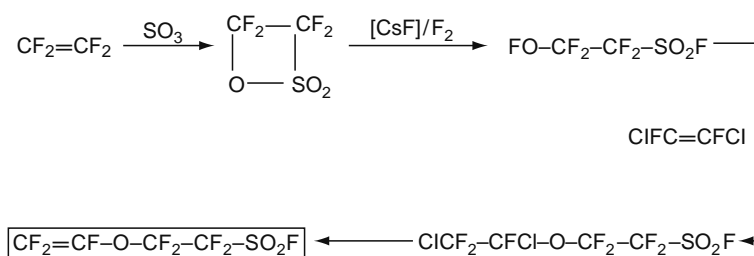


**FIGURE 27.29** Solexis's route for synthesizing the SSC sulfonylfluoridevinylether monomer. (From Arcella, V., Ghielmi, A., and Tommasi, G., *Ann. N.Y. Acad. Sci.*, 984, 226, 2003.)

up to 110°C in hydrogen fuel cells. A solution of Hyflon Ion polymer is also available and will be used as a binder reference polymer in MEAs.

Solvay Solexis has reported composite membranes which have been prepared with EW from 750 to 1100 g mol<sup>-1</sup> and thicknesses from 20 to 80 μm. The ionomer in the acid form, dissolved at ambient or high temperature in water-ethanol mixtures, has been used to impregnate perfluorinated porous supports. These membranes have also shown high conductance as expected considering the low thickness. The casting method, used on a laboratory scale to prepare small membrane samples, was considered by Solexis to be quite complex and is especially susceptible to inconsistency, so not easily industrially viable. Moreover, for the more crystalline higher EW polymers, the limited gain in mechanical stability due to the support is countered by a loss in conductivity due to the presence of a fraction of volume that is occupied by the nonconducting material. Therefore, self-supported semicrystalline membranes have been prepared with an EW higher than 750 g mol<sup>-1</sup> and as slim as 15 μm. These membranes reportedly showed very good conductance and also very good mechanical properties. Furthermore, the ionomer, tuned with the appropriate molecular weight distribution, yielded high-quality and consistent membranes by film extrusion. This last process appeared to be the most viable and low-cost industrial process. Efforts were therefore made to select the ionomer that yielded the best combination of processability, conductance, mechanical properties, and dimensional stability, while also being able to guarantee extremely low membrane thickness and high duration. The reported performance results are presented in Figure 27.31 (no operating conditions were specified). The mechanical properties of Hyflon Ion-FM membranes and other commercial membranes are reported in Table 27.6 and expanding/shrinking characteristics on hydration/dehydration are reported in Table 27.7. Solvay also has access to the polysulfone polymer known under the trade name UDEL. Different grades of this polymer are available and can be supplied to partners on request. Some work on the sulfonation of this polymer in solution has already been carried out within the framework of the EU DREAMCAR project.

Fully assembled five- and seven-layer (include integrated gaskets) MEAs from matched components have been developed by 3M. A further development activity aims at high-speed precision coating technologies and a proprietary, automated MEA production process with online defect inspection. According to 3M, combining manufacture and component integration ensures product uniformity and low defect levels, resulting in high-quality, durable MEAs. A new PFSA-containing membrane has been developed based on a new perfluorinated monomer developed at 3M. This new membrane is designed to have improved thermomechanical properties at higher temperatures compared to currently available PFSA. The characteristics of the new 3M membrane are summarized below, according to statements by 3M [84]:

- Cast 30-μm membrane
- Equivalent weight of 980
- $T_g = 125^\circ\text{C}$  dry
- High modulus over a wide temperature range
- Equivalent or superior conductivity compared to other commercially available membranes
- Equivalent water absorption characteristics to Nafion-based membranes

The properties are summarized in Table 27.8.

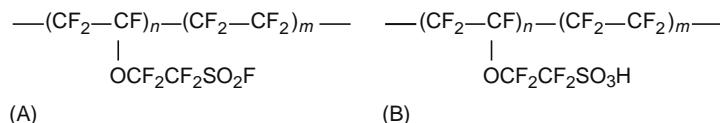


**FIGURE 27.30** Structure of (A) Hyflon Ion and (B) Hyflon Ion H. (From Arcella, V., Ghielmi, A., and Tommasi, G., *Ann. N.Y. Acad. Sci.*, 984, 226, 2003.)

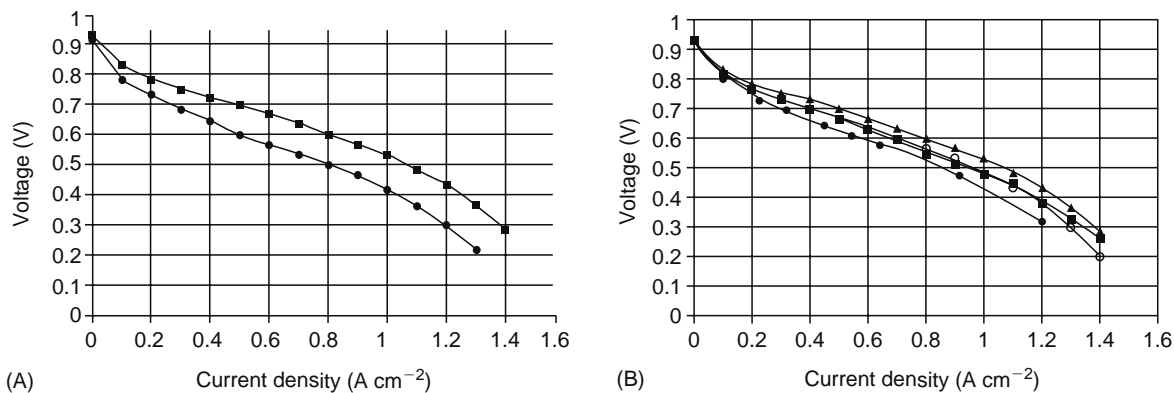


**FIGURE 27.31** (A) Comparison between polarization curves obtained with (■) a self-supported (melt extruded) and (●) supported (on expanded PTFE) membrane. Both membranes have the same thickness (20 μm) and were prepared with the same ionomer (Hyflon Ion, equivalent weight (EW) = 900). (B) Comparison between polarization curves obtained with Hyflon Ion-FM EW = 900 membranes of various thicknesses (● 65 μm, ■ 40 μm, and ▲ 20 μm) and ◊ a Gore-Select membrane. (From Arcella, V., Ghielmi, A., and Tommasi, G., *Ann. N.Y. Acad. Sci.*, 984, 226, 2003.)

**TABLE 27.6**  
**Stress and Strain at Break for Hyflon Ion-FM Membranes and Other Commercial Membranes, Measured at RH = 50% and 23°C**

Membrane	Stress (MPa)		Strain (%)	
	MD	TD	MD	TD
Hyflon Ion-FM EW = 800	14	15	100	125
Hyflon Ion-FM EW = 900	22	17	70	110
Nafion 115	23	18	85	110
Gore-select	32	17	—	—

Source: From Arcella, V., Ghielmi, A., and Tommasi, G., *Ann. N.Y. Acad. Sci.*, 984, 226, 2003.

Note: Membranes pretreated by soaking in water at 100°C for 30 min.

Abbreviations: MD, machine direction; TD, transverse direction.

**TABLE 27.7**  
**Dimensional Increase (%) in the Plane Directions from the Dehydrated to the Hydrated State (Water Soaking at 25°C and 100°C) for Hyflon Ion-FM Membranes and Other Commercial Membranes**

Membrane	25°C		100°C	
	MD	TD	MD	TD
Hyflon Ion-FM EW = 800	7	8	18	20
Hyflon Ion-FM EW = 900	2	5	6	16
Nafion 117	8	10	10	12
Nafion 115	2	10	4	20
Gore-select	—	—	3	3

Source: From Arcella, V., Ghielmi, A., and Tommasi, G., *Ann. N.Y. Acad. Sci.*, 984, 226, 2003.

**TABLE 27.8**  
**Physical Properties of the 3M Membrane and Cast Nafion**

	Tensile Test <sup>a</sup>			Puncture		Notch Tear <sup>a</sup>		Hydration	
	Modulus (Initial) (psi)	Modulus >20% Extension (psi)	Break Stress (psi)	Strain at Break (%)	Puncture Peak Load (g)	Puncture Elongation at Peak Load (mm)	Peak Load (g)	Mass Change (%)	xy Dimensional Change <sup>a</sup>
3M	43,681	1,220	4,345	136	53	1.56	75	40	17
Nafion	35,123	1,138	3,974	184	53	2.22	73	43	21

Source: From Rivard, L., Pierpont, D., Freemyers, H., Thaler, A., and Hamrock, S., *Abstracts of the 2003 Fuel Cell Seminar*, 2003.

<sup>a</sup> Test results are the average of downweb and crossweb film directions.

The performance curves given by 3M are presented in Figure 27.32. 3M has further reported performance reproducibility and durability. Figure 27.33 illustrates cell-to-cell variability in a 60-cell stack with 3M MEAs. For this system, the standard deviation in performance across the 60 cells was less than 5 mV. The MEAs in this stack were 3M seven-layer MEAs in which cell compression was limited by the integrated gasket. Figure 27.34 shows the performance durability of a 3M MEA tested at Osaka Gas in a 25 cm<sup>2</sup> single cell. In this single-cell test, the 3M five-layer MEA achieved more than 17,000 h of continuous operation with approximately 2 mV 1000 h<sup>-1</sup> decay. In addition to the single-cell data shown in Figure 27.34, 3M five-layer MEAs have also been tested in short stacks. Figure 27.35 shows performance in an eight-cell short stack at 70°C under simulated reformat fuel with anode airbled. More than 9000 h of operation were achieved with a decay of approximately 5 mV 1000 h<sup>-1</sup>.

In a recent product bulletin, 3M reported the typical performance data for their seven-layer MEAs (Figure 27.36). The 3M MEA is a seven-layer construction consisting of a proton-exchange membrane, an anode electrode, a cathode electrode, two GDLs, and two integrated seals/gaskets. The 3M MEA is produced using high-speed continuous automated assembly equipment.

## 27.4.2 MECHANICALLY REINFORCED PERFLUORINATED MEMBRANES

### 27.4.2.1 PFSA Ionomer in Expanded Porous PTFE, Gore-Select Membranes

The company W.L. Gore & Associates (Elkton, Maryland) develops membranes under the name Gore-Select consisting of a microporous stretched PTFE (expanded PTFE porous sheet) membrane filled with perfluorinated ionomer. The microporous PTFE matrix provides the mechanical strength and therefore, the thickness of the membrane can be reduced considerably and a thickness of 20–40 μm is commonly used leading to lower ionic resistances. The specific resistance of Gore-Select membranes is relatively high compared with nonreinforced membranes, but this is compensated by the small thickness and by lower equivalent weight ionomers. The membrane is composed of a micronetwork of nodes and fibrils with a continuous internal void volume in which the ionomer is introduced. The expanded PTFE technology has been refined and applied to a variety of

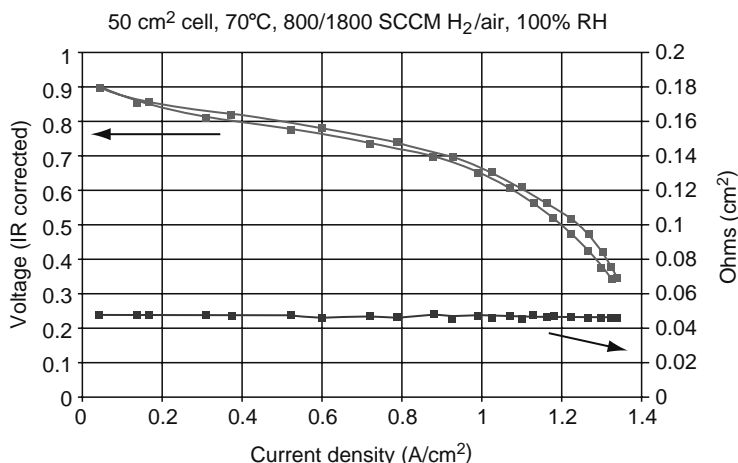


**FIGURE 27.32** Fuel cell polarization curve of a 50 cm<sup>2</sup> MEA made with the new 3M cast membrane (30 μm). (From 3M, www.3m.com.)

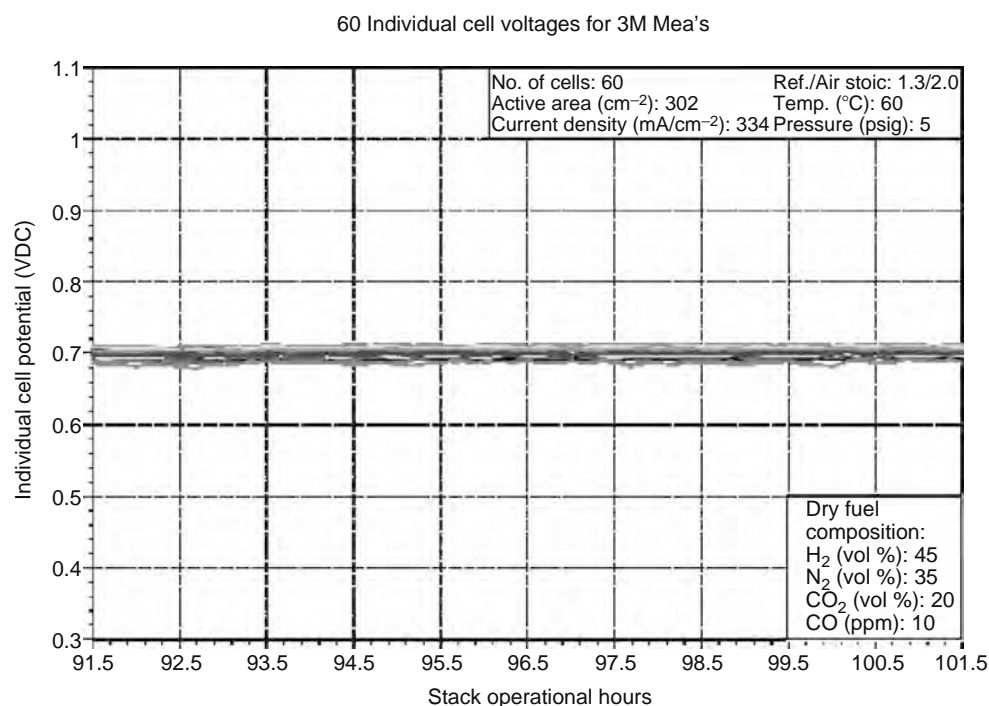


**FIGURE 27.33** Cell to cell uniformity from a 60-cell stack using 3M seven-layer MEA. (From 3M, [www.3m.com](http://www.3m.com).)

applications including use as a PEM in MEAs. In the mid-1990s, Gore began to work on expanded PTFE, which was then applied to PEMFCs. Their MEA is covered in U.S. Patent 5,547,551 issued in 1996 [85]. The fabrication of Gore-Select membranes is described in the patent. The important step is the impregnation with ionomer solution by brush (Figure 27.37). The company does not intend to actively market Gore Select, but will use it in its catalyzed PRIMEA MEA. Gore claims to be the highest MEA volume supplier in the world with a capacity for membrane and MEA fabrication of 100,000 m<sup>2</sup> per year. Gore has demonstrated a current density of 1200 mA cm<sup>-2</sup> at 0.6 V at ambient pressure with hydrogen or reformat fuel. Operating temperatures range from ambient to 60°C–80°C. The company is carrying out research to address activation and mass-transport limitations and advance the performance of the PRIMEA power assemblies. A current goal is to achieve 400 mA cm<sup>-2</sup> at 0.8 V. PRIMEA MEAs have been used in many PEM vehicle demonstrations, including vehicles such as the NJDOT Venturer, which operates on compressed hydrogen, and the NJDOT Genesis, which uses Millennium Cell's sodium borohydride as a hydrogen storage medium. Currently, PEMFC stack technology is being targeted at three major market sectors: portable power, residential, and transportation. Each market is driven by a different combination of features, such as power density, size, and life cycle cost. Gore adapts its MEAs to the specific application by optimizing the ionomer for the requirements. In this respect, specifically developed MEAs with increased performance or with improved durability are reported. The names used by W.L. Gore are the PRIMEA series 56x for the next generation of stationary applications

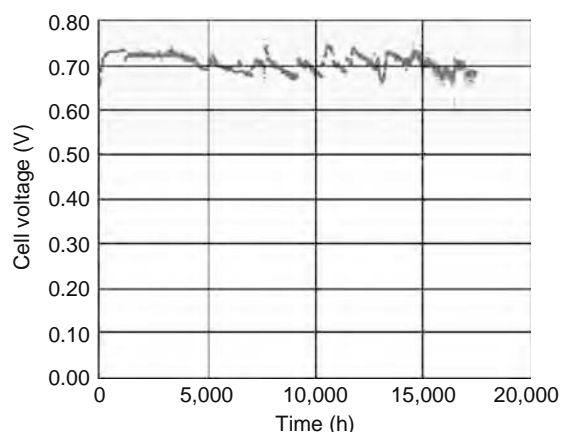


**FIGURE 27.34** Performance stability of a 3M five-layer MEA in single-cell testing at Osaka Gas. (From 3M, [www.3m.com](http://www.3m.com).)

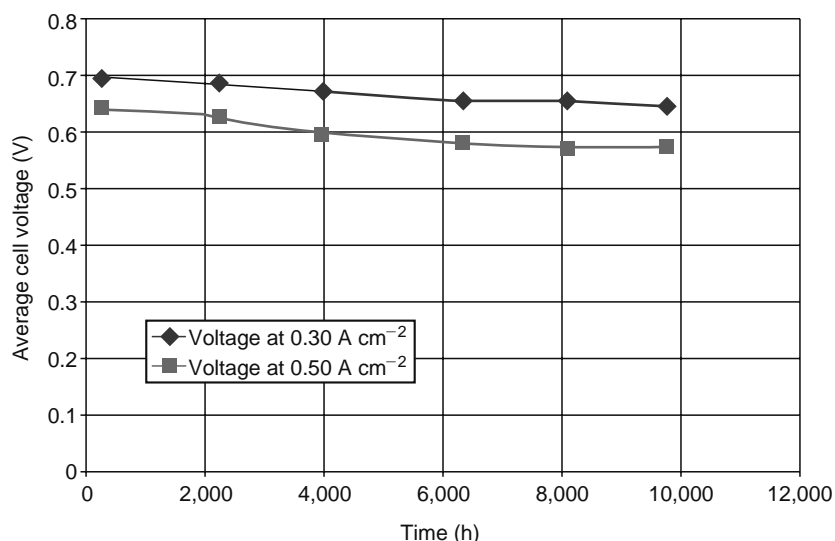


FIGURE 27.35 Short stack durability testing at 70°C with simulated reformat and anode airbled. (From 3M, www.3m.com.)

(presently 5621), the series PRIMEA 57 for transportation systems, and series 58 for portable applications. The reported properties of the MEAs are listed in Table 27.9.

According to Gore, one of the most important criteria in identifying a practical membrane material for MEA manufacturing and membrane service is tear strength or tear resistance. Cleghorn et al. compared reinforced Gore-Select membranes and nonreinforced Nafion 112 and determined the stress required to propagate a membrane tear using (ASTM) test 1922–1994a [86]. The results indicate that both membrane types are anisotropic and have greater tear resistance in the machine direction, and reduced tear resistance when hydrated. However, Gore-Select membranes reportedly show superior tear-resistant properties compared to Nafion 112 membranes. Even the hydrated transverse direction for the Gore-Select membrane is more tear resistant than the dry transverse direction for Nafion 112 membranes (Figure 27.38).

As can be seen in Figure 27.39, the voltage loss at 800 mA cm<sup>-2</sup> of the PRIMEA 56 MEA is in the range of 5 μV h<sup>-1</sup>. The development goal is <1 μV h<sup>-1</sup> to achieve the 40,000 h requirement for stationary applications. In 2003, Gore reported technology status for automotive applications in comparison to their goals (Table 27.10). Surprisingly, a relative humidity below <50% is indicated as already having been achieved in state-of-the-art MEAs with high power density requirements. Gore has reported intensive activity regarding accelerated life test procedures [86,87].

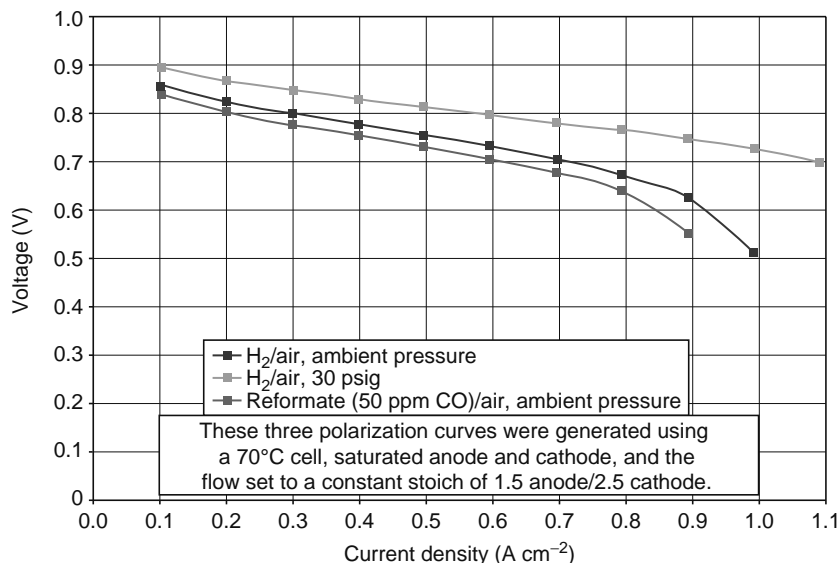
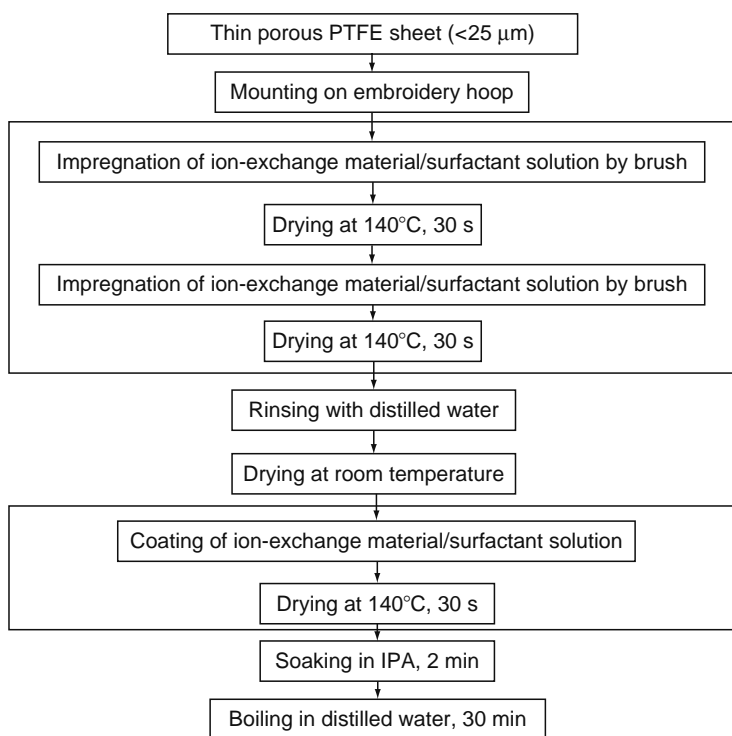


FIGURE 27.36 (See color insert following page 588.) Typical performance data for 3M seven-layer MEAs. (From 3M, www.3m.com.)



**FIGURE 27.37** Fabrication scheme of Gore-Select described in U.S. Patent 5,547,551. (Reproduced from Nakao, M. and Yoshitake, M., in W. Vielstich, H.A. Gasteiger, and A. Lamm (Eds.), *Handbook of Fuel Cells: Fundamentals, Technology and Applications*, Vol. 3, J. Wiley & Sons, Chichester, 2003. With permission.)

Figure 27.40 shows the efforts to reduce noble metal content in MEAs under conditions, suitable for transportation applications. Although a significant reduction in Pt has been achieved in the series 57 MEA, further reduction in platinum is required. Gore's low-loading development still shows good performance, but it is markedly lower compared to the 57 series.

#### 27.4.2.2 PFSA Ionomer with PTFE Fibril Reinforcement; Asahi Glass; Flemion

Asahi Glass Co., Ltd. (AGC) manufactures Flemion, which is based on a PTFE fibril reinforcement which was originally developed for chlor-alkali electrolysis. AGC has participated in the NEDO's PEMFC R&D programs and has developed ion-exchange membrane technologies for PEMFCs since 1992. In the first phase of the NEDO's program, various chemical/physical properties of Flemion membranes were investigated. In the second phase, fundamental properties required for practical use of PEMFCs were evaluated for Flemion membranes that have various thicknesses and ion-exchange capacities, and AGC successfully developed a new technology for membrane reinforcement. In the third phase of program, AGC has been developing some basic technologies for high power density-type MEAs and for high-temperature-type MEAs.

*Reinforcement of Membranes:* AGC's fabrication method consists of dispersing a small amount of PTFE fibers in a polymer matrix consisting of a perfluorosulfonic resin with high-ion-exchange capacity (IEC) (EW 909). In addition (according to Asahi Glass), a novel stretching method is used which leads to an evenly enlarged film with less than  $50 \mu\text{m}$ . The structure of the fibril-reinforcement is shown in Figure 27.41. Nearly 2%–5% of the PTFE microfiber weight is dispersed in the perfluorosulfonic resin. Various mechanical properties are controlled by optimizing the fibril content, length and radii of PTFE fibrils, and other parameters. The trade name for Asahi Glass membranes is Flemion. The Flemion FR30 is  $30 \mu\text{m}$  thick and the SH50 is  $50 \mu\text{m}$  thick [88].

**TABLE 27.9**  
**Properties of W.L. Gore Membrane Development**

Stationary Applications, 56x	Transportation Applications, 57	Portable Applications, 58
Highest durability	Highest power density	Highest power density for dry gas operation
Lowest cost per kilowatt hour	Lowest cost per kilowatt system	Lowest cost per kilowatt system
Commercially available	Highest operational flexibility	Simplified system design

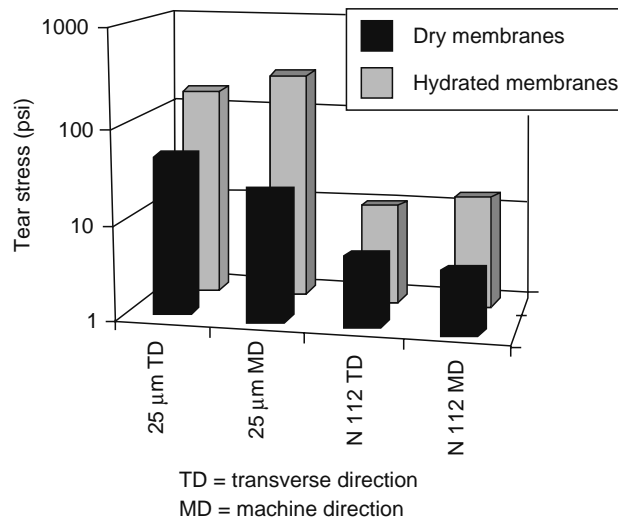


**FIGURE 27.38** Comparison of tear strength for hydrated and dry Gore-Select membranes (25 μm) and Nafion 112 membranes in MD and TD. (Reproduced from Cleghorn, S., Kolde, J., and Liu, W., in W. Vielstich, H.A. Gasteiger, and A. Lamm (Eds.), *Handbook of Fuel Cells: Fundamentals, Technology and Applications*, Vol. 3, J. Wiley & Sons, Chichester, 2003. With permission.)

The key parameter in the preparation of a thin and flat membrane with fibril reinforcement is the uniform dispersion of the fibrils in the matrix. Furthermore, the overall flatness of the membrane is important for coating the electrodes. Asahi Glass's new preparation method is disclosed in European Patent EP1,139,472 [89,90]. A precursor polymer and PTFE powder are kneaded, pelletized, and subsequently extruded to make a thicker base film. This base film is stretched (using a supporting film) to form a thin cationic film. This film then undergoes alkali and acid treatment. The process is schematically illustrated in Figure 27.42. Table 27.11 lists the properties of reinforced and nonreinforced Flemion membranes. The reported durability of the Flemion membranes is also relatively good (Figure 27.43).

Asahi Glass's developments concerning high power density-type MEAs are represented in Figure 27.44, which shows the structure of an MEA at the cathode side, whereby the cathode is fabricated from catalysts and ionomers. Asahi Glass is trying to accommodate all the electrode requirements with improved ionomers and hydrophobic components in the electrode structure.

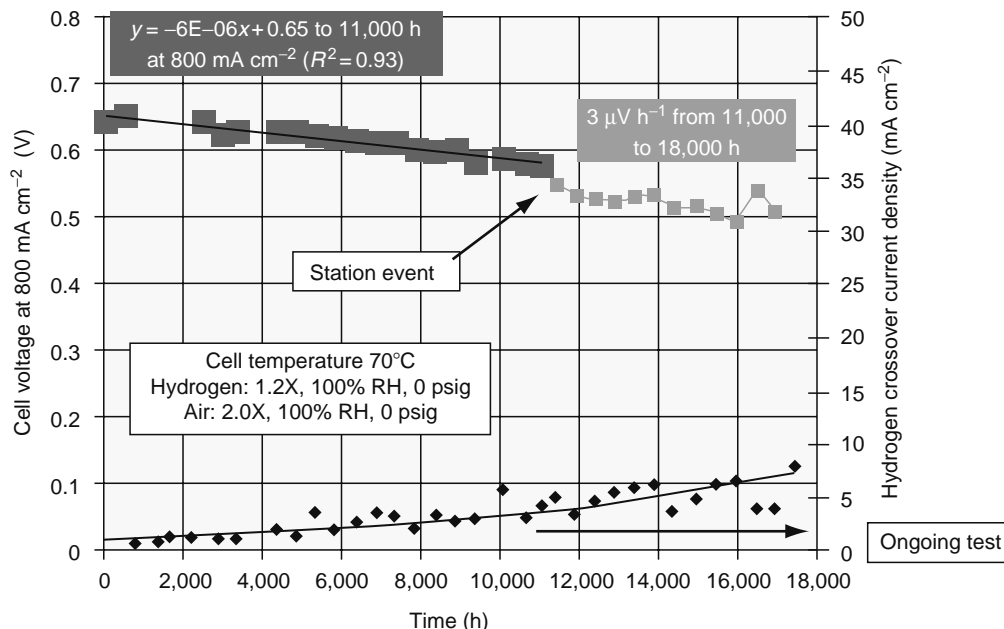


**FIGURE 27.39** (See color insert following page 588.) PRIMEA Series 56 MEA validation life test. Hydrogen fuel—high current density (800 mA cm<sup>-2</sup>). (From W.L. Gore & Associates, Elkton, Maryland.)

**TABLE 27.10**  
**MEA Requirements for Commercial Fuel Cell Vehicles—MEA Technology Development Goals**

	Current Demonstration Vehicles PRIMEA Series 57 MEA	MEA Needs for Commercial Fuel Cell
Vehicle cost (assume dictated by platinum cost)	1 g Pt kW <sup>-1</sup> (at 0.6 V) (75 g for a 75 kW engine)	<0.2 g Pt kW <sup>-1</sup> (>0.6 V) (15 g for a 75 kW engine)
Operating conditions (temperature)	T <sub>cell</sub> 80°C Relative humidity (RH) <50% Pressure <270 kPa	T <sub>cell</sub> 110°C–120°C RH <25% Pressure <150 kPa
Durability (membrane life)	MEA life-accelerated conditions (approximately 1500 h, and <30 μV h <sup>-1</sup> ) (voltage decay rate)	MEA life of 5000 h, consider freeze/thaw, cold start, stop/start, and duty cycle

Source: From Gore, W.L.

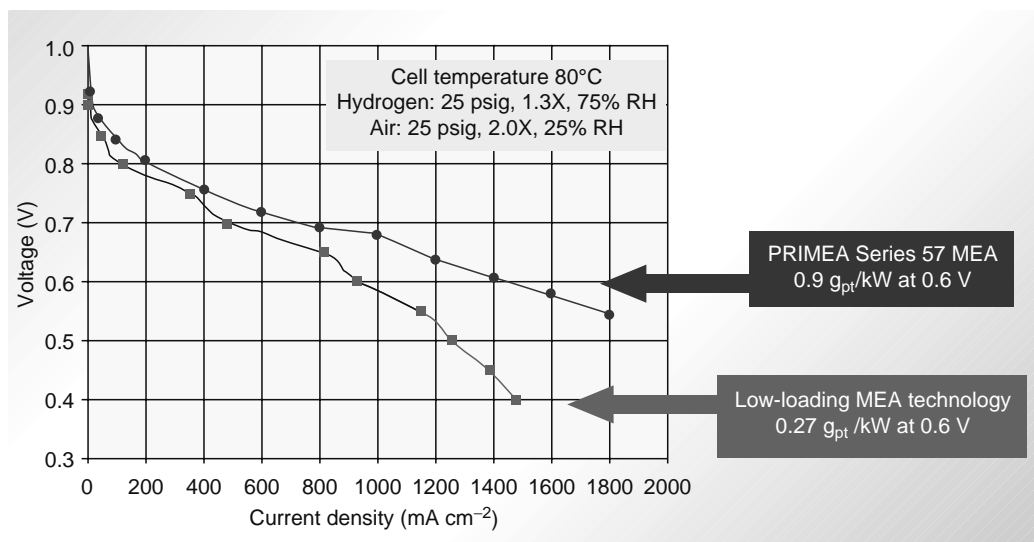


**FIGURE 27.40** (See color insert following page 588.) PRIMEA Series 57 low-loading MEA. (From W.L. Gore & Associates, Elkton, Maryland.)

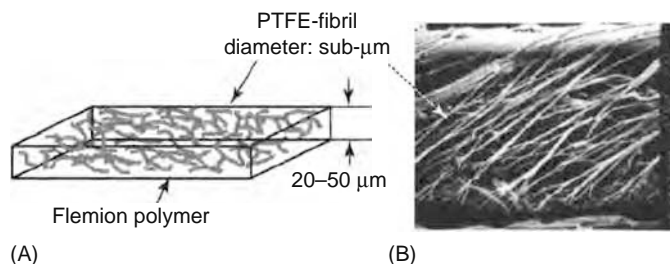


**FIGURE 27.41** (A) Schematic representation of a fibril-reinforced membrane and (B) a cross-sectional image after tearing. (Reproduced from Nakao, M. and Yoshitake, M., in W. Vielstich, H.A. Gasteiger, and A. Lamm (Eds.), *Handbook of Fuel Cells: Fundamentals, Technology and Applications*, Vol. 3, J. Wiley & Sons, Chichester, 2003. With permission.)

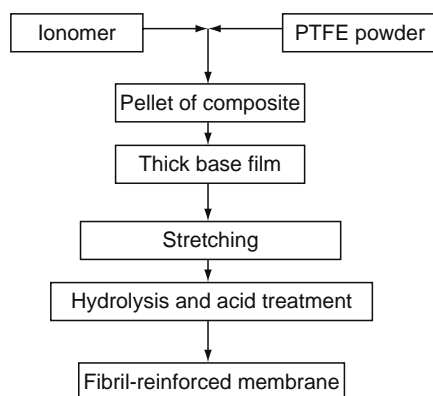


**FIGURE 27.42** Fabrication of PTFE fibril-reinforced Flemion. (Reproduced from Nakao, M. and Yoshitake, M., in W. Vielstich, H.A. Gasteiger, and A. Lamm (Eds.), *Handbook of Fuel Cells: Fundamentals, Technology and Applications*, Vol. 3, J. Wiley & Sons, Chichester, 2003. With permission.)

**TABLE 27.11**  
**Comparison of Reinforced and Nonreinforced Flemion**

Membrane Type	Reinforced 2–3 wt% PTFE Fibril	Nonreinforced
AC resistivity ( $\Omega$ cm) 80°C, 95% relative humidity (RH)	7–8	
H <sub>2</sub> permeability ( $\text{cm}^2 \text{s}^{-1} \text{cm}^{-1} \text{Hg}$ ), 80°C, humidified at 80°C	$10^{-8}$	$8 \times 10^{-9}$
Elastic modulus ( $\text{kg mm}^{-2}$ ), 85°C, 95% RH	9.3	2.8
Tear strength ( $\text{N mm}^{-1}$ ), 25°C, 50% RH	2.7	0.5
Viscoelasticity ( $\text{dyn cm}^{-2}$ ), 25°C, 85% RH	5 to $6 \times 10^{-8}$	1 to $2 \times 10^{-9}$

Source: From Hommura, S., Kunisa, Y., Terada, I., and Yoshitake, M., *J. Fluorine Chem.*, 120, 151, 2003.

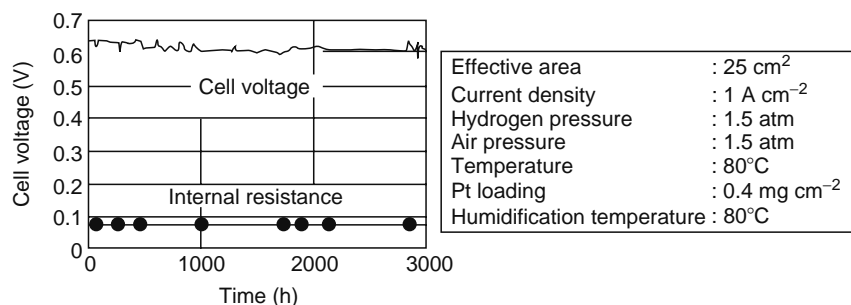


**FIGURE 27.43** Durability of fibril-reinforced Flemion. (Reproduced from Nakao, M. and Yoshitake, M., in W. Vielstich, H.A. Gasteiger, and A. Lamm (Eds.), *Handbook of Fuel Cells: Fundamentals, Technology and Applications*, Vol. 3, J. Wiley & Sons, Chichester, 2003. With permission.)

They are developing high-performance MEAs using candidate materials for improving power density such as high IEC ionomers, new ionomers with high oxygen solubility, and soluble fluoropolymers (Cytop) [91].

Asahi Glass is developing an undisclosed new polymeric ionomer with a superior oxygen solubility and permeability especially for electrodes [91]. Table 27.12 gives the values reported by Asahi Glass. A somewhat better performance is achieved with the new polymer in the electrode (Figure 27.45).

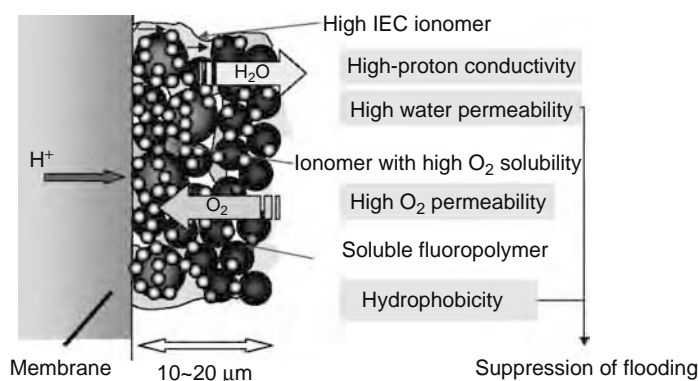


**FIGURE 27.44** (See color insert following page 588.) Pictorial depiction of the development activities of Asahi Glass. (From Yamada, K. et al. *Abstracts of the 2003 Fuel Cell Seminar*. 2003.)

**TABLE 27.12**

**Oxygen Solubility of Flemion, PTFE, and New Polymer**

	$P \times 10^{13}$ $\text{cm}^3(\text{STP}) \cdot \text{cm} \cdot \text{cm}^{-2} \cdot \text{s}^{-1} \cdot \text{Pa}^{-1}$	$D \times 10^6$ $\text{cm}^2 \cdot \text{s}^{-1}$	$S \times 10^6$ $\text{cm}^3(\text{STP}) \cdot \text{cm}^{-3} \cdot \text{Pa}^{-1}$
Flemion (IEC1.1)	0.40	0.026	1.5
PTFE	3.2	0.15	2.1
New polymer	138.6	2.28	6.1

Source: From Yamada, K. et al. *Abstracts of the 2003 Fuel Cell Seminar*, 2003.

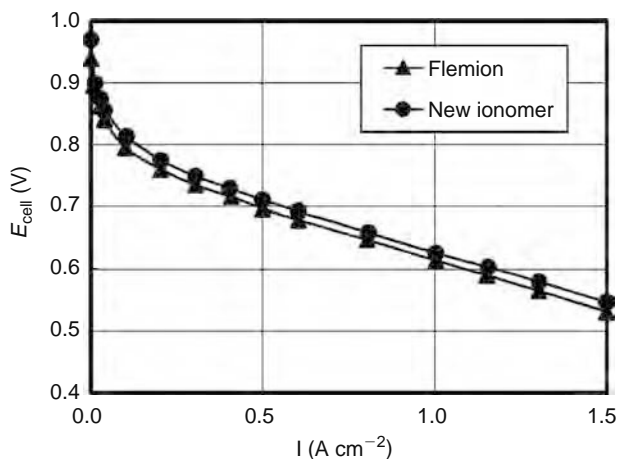


**FIGURE 27.45** Effect of ionomer in the cathode on cell performance. Cell temperature: 80°C. (From Yamada, K. et al. *Abstracts of the 2003 Fuel Cell Seminar*, 2003.)

Hydrogen and oxygen permeabilities of Flemion membranes have been reported in two publications, one from 1998 concerning nonreinforced membranes with different thicknesses and a more recent publication concerning the comparison of nonreinforced and reinforced 50  $\mu\text{m}$  thick membranes [88,92]. The trade names, IECs, and further remarks on the membranes investigated are summarized in Table 27.13. The hydrogen and oxygen permeabilities of these membranes are given in Figure 27.46.

In the development of high-temperature membranes, Asahi is experimenting with different polymer backbones leaving the side chain unchanged. It was found that the softening temperature of the new membrane is 40°C higher than that of conventional Flemion. However, mechanical properties are reported to be insufficient and no performance data with

**TABLE 27.13**  
**IEC and Thickness of Membranes as Reported by Asahi Glass**

	Membrane IEC (mequiv g <sup>-1</sup> )	PTFE-Fibril Content (%)	Thickness (mm)	Remarks
FlemionRf2	1	2.7	50	PTFE-fibril reinforced (2003)
FlemionR	1	—	50	AGC's standard membrane in NEDO's PEMFC program (2003)
Nafion 112	0.91	—	50	Membrane for comparison (2003)
FlemionR	1	—	50	Nonreinforced (1998)
FlemionS	1	—	80	Nonreinforced (1998)
FlemionT	1	—	120	Nonreinforced (1998)
Nafion 117	0.91	—	127	Membrane for comparison (1998)

Sources: From Hommura, S., Kunisa, Y., Terada, I., and Yoshitake, M., *J. Fluorine Chem.*, 120, 151, 2003; Yoshida, N., Ishisaki, T., Watakabe, A., and Yoshitake, M., *Electrochim. Acta*, 43, 3749, 1998.

the new membrane have been reported so far. Figure 27.47 shows the  $I-U$  curves of the MEAs using FlemionRf2 and FlemionR, both having the same membrane thickness. The cell performances are nearly equal to those using a nonreinforced membrane.

### 27.4.2.3 PFSA Ionomer and PTFE Reinforcement at Asahi Kasei; Aciplex Membranes

Asahi Kasei develops membranes mainly for chlor-alkali electrolysis technology with Aciplex F PFSA membranes. The Aciplex F membrane is employed in plants with a total production capacity of over 5 million tons of sodium hydroxide

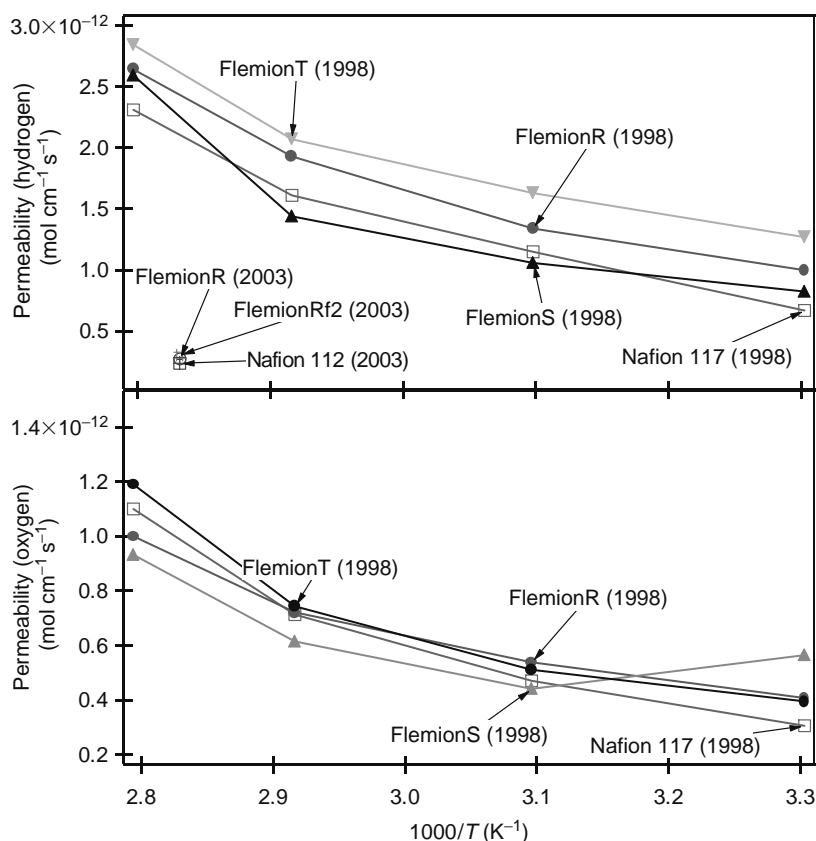


**FIGURE 27.46** (See color insert following page 588.) Oxygen and hydrogen permeabilities of Flemion membranes in comparison with Nafion membranes. (From Pasaogullari, U. and Wang, C.Y., *Electrochim. Acta* 49, 4359, 2004; Stonehart, P., *Berichte der Bunsengesellschaft für Physikalische Chemie* 94, 913, 1990.)

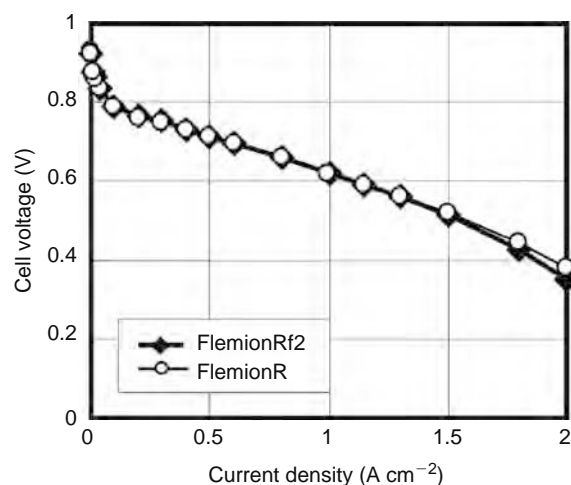


**FIGURE 27.47** Cell performance of an MEA using FlemionRf2 and FlemionR in a single cell (gas: H<sub>2</sub>/air, pressure: 0.15/0.15 MPa, electrode area: 25 cm<sup>2</sup>, cell temperature: 80°C, Pt loading: 0.4/0.4 mg cm<sup>-2</sup>). (Reprinted from S Hommura, S. et al. *J. Fluorine Chem.*, 120, 151, 2003. With permission from Elsevier.)

per year. Since 1996, Asahi Kasei has been developing Aciplex membranes for PEMFCs under a grant from NEDO in view of the rising expectations for the adoption of PEMFCs as an alternative energy source in both transportation and stationary applications and with the specific purpose of identifying the membrane properties required for durable fuel cell stacks. Asahi Kasei is also focusing its activities on reinforced membranes. Reinforced membranes namely Aciplex-S-AH and Aciplex-S-H-EH of 100, 150, and 200 μm thickness have been reported which use reinforcing webs of 150 and 200 denier PTFE, respectively. These membranes have been modified for the conditions of their hydration to increase their water content in comparison to conventional nonreinforced membranes. The dimensional stability of the reinforced membranes, in terms of dimensional change between their wet and dry states, was considerably improved. Shrinkage in drying is reportedly <10% for each of the reinforced membranes, and 14.9%–18.8% for the nonreinforced membranes. As with the previous reinforced membranes, the tensile strength of the reinforced membranes is about twice that of nonreinforced Aciplex-S membranes. The reinforced membranes also show considerably less creep under stress than the other membranes [93].

A new effort by Asahi Kasei involves the development of thermostable membranes for high-temperature cell operation (Table 27.14), based on perfluorocarbon material to satisfy both high performance and high durability by focusing on the design of the polymer structure (Figure 27.48). They are probably modifying the polymer backbone to improve thermal stability. They have achieved a 20°C–30°C higher glass transition temperature  $T_g$  for this new polymer material compared to that of conventional membranes [93]. The performance of the new thermostable membrane as compared to that of Aciplex S1002 (Figure 27.49), is significantly improved [93].

**TABLE 27.14**  
**Overview of Membranes Reported by Asahi Kasei**

Membrane Type	Membrane Equivalent Weight (EW) (g equiv <sup>-1</sup> )	Thickness (mm)	Remarks
Thermostable membrane-1	710	25, 50	New polymer material
Thermostable membrane-2	970	25	New polymer material
Aciplex SF-1001, Aciplex SF-1002	950	25, 50	Highly durable membrane
Aciplex SF-1003	1020	25	Highly durable membrane
Aciplex S1001X	950	25	Conventional membrane, new polymerization, and film formation process
Aciplex S1002	950	50	Conventional membrane, new polymerization, and film formation process

Source: From Wakizoe, M., Kodani, T., and Ota, T., *Abstracts of the 2003 Fuel Cell Seminar*, 2003.

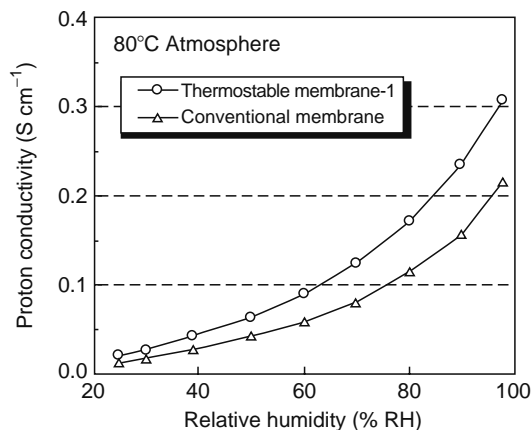


**FIGURE 27.48** Proton conductivity of Asahi Kasei membranes at 80°C. (From Wakizoe, M., Kodani, T., and Ota, T., *Abstracts of the 2003 Fuel Cell Seminar*, 2003.)

An independent study by the Dalian Fuel Cell R&D Center, Dalian Institute of Chemical Physics, China, investigated several perfluorinated membranes, namely Nafion, Flemion, Shanghai (Shanghai Institute of Organic Chemistry), and Aciplex membranes [94]. The performance of Aciplex 1002, 1004, 1104 is presented in Figure 27.50. The conditions for the comparison are as follows: The electrodes were prepared according to a Dalian procedure (20 wt% carbon-supported-platinum [Pt/C] catalyst, carbon paper, PTFE suspension [Teflon T-30, DuPont]), and a Nafion solution (Aldrich, 5 wt% in 15%–20% water/low aliphatic alcohol, 1100 equiv wt) was used for electrode preparation. The catalyst layer (Pt loading of  $0.4 \text{ mg cm}^{-2}$ ) of the electrodes was impregnated with Nafion solution with Nafion loading  $1 \text{ mg cm}^{-2}$ . Two electrodes with an active area of  $5 \text{ cm}^2$  were hot-pressed to one piece of membrane at 135°C to form the MEA, which was then tested in a single cell. Pure hydrogen (99.9%) and pure oxygen (99%) were used for fuel and oxidant with gas pressures 0.30 and 0.50 MPa, respectively. The fuel cells were operated at 80°C.

This chapter also presents a comparison between Nafion 112 and Aciplex 1002 membranes, showing almost indistinguishable performance in the lower current density region (Figure 27.51). At higher current density, the superior behavior of Aciplex was attributed to the lower EW of the Aciplex membranes [94].

### 27.4.3 PARTIALLY FLUORINATED IONOMERS

#### 27.4.3.1 FuMA-TECH Membranes

FuMA-Tech is an established manufacturer of ion-exchange membranes and belongs to the (Best Water Technology) BWT Group based in Austria. With 65 group companies and some 2700 employees, the BWT Group is the leading water

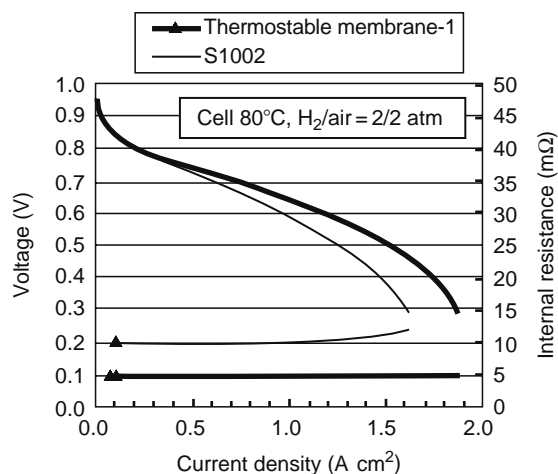


**FIGURE 27.49**  $V$ - $I$  curve of Aciplex membranes. Cell performance was evaluated with a single cell of  $10 \text{ cm}^2$  electrode area. The Pt loadings of anode and cathode were about  $0.1$  and  $0.2 \text{ mg cm}^{-2}$ , respectively. *Source:* Asahi Kasei. (From Wakizoe, M., Kodani, T., and Ota, T., *Abstracts of the 2003 Fuel Cell Seminar*, 2003.)

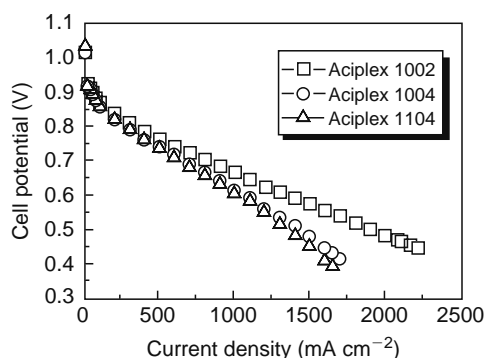


**FIGURE 27.50** Performances of PEM fuel cells with Aciplex according to Du et al. (Reproduced from Du, X.Z., Yu, J.R., Yi, B.L., Han, M., and Bi, K.W., *Phys. Chem. Chem. Phys.*, 3, 3175, 2001. With permission from the PCCP Owner Societies.)

technology company in Europe. FuMA-Tech GmbH develops membranes for PEMFC. FuMA-Tech is the only supplier to offer both fluorinated and nonfluorinated membranes for PEMFCs and DMFCs with application temperatures of up to 130°C. Catalyzed membranes for fuel cells and water electrolysis are manufactured as well. FuMA-Tech offers two membrane families for fuel cell applications. For standard applications in hydrogen/air or oxygen environment, the partially fluorinated (highly conductive and chemically stable) FKH series ranging from 950 to 1500 equiv wt is offered. The membranes are available in two thicknesses and two configurations (not specified). It is stated that membrane electrode processing by way of a standard hot-pressing protocol is possible and that reliable and reproducible results have been obtained. A second class of partially fluorinated membranes consists of glass fiber reinforced FKH/60GF, which was developed to avoid wrinkling and uncontrolled membrane swelling caused by the solvents in most catalyst ink or paste formulations. Besides this feature, the membrane is reported to be insusceptible to mechanical stress. The FKE membranes using polyketone-type sulfonic acids are a completely different type of membrane, being nonfluorinated and intended for medium-temperature applications above 100°C and DMFCs (Table 27.15). According to FuMa-Tech these membranes are offered in standard sheets measuring 30 cm by 30–200 cm. Other dimensions and rollware have to be requested. Curves reported by FuMA-Tech are presented in Figure 27.52.

#### 27.4.3.2 Poly( $\alpha,\beta,\beta$ -Trifluorostyrene) and Copolymers; Ballard Advanced Materials

Ballard Advanced Materials (BAM) ionomers are sulfonated copolymers of trifluorostyrene and substituted trifluorostyrene monomers. BAM, a subsidiary of Ballard Power Systems, investigated the conducting polymers based on polyphenylquinoxaline (PPQ). These can be sulfonated in a wide range and were referred to as BAM1G (Ballard first generation) membranes, but these membranes were found to have short durability. To overcome this problem, BAM developed a second generation of advanced membranes based on two distinct material types. The first material type consisted of a series of sulfonated poly(2,6-diphenyl 1,4-phenylene oxide). The second material type consisted of a series of sulfonated poly(arylether sulfone). But the durability of these membranes was also insufficient. Since the durability of previous membranes was limited, Ballard produced a novel family of sulfonated membranes based on  $\alpha,\beta,\beta$ -trifluorostyrene monomers and a series of substituted trifluoro-comonomers

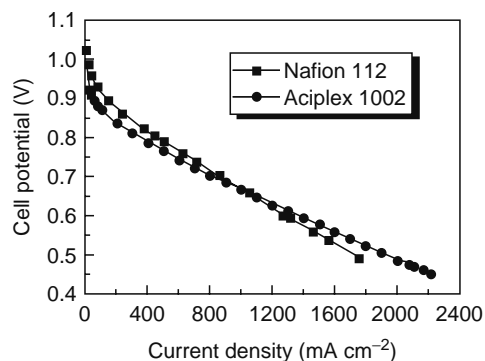


**FIGURE 27.51** Performance comparison between fuel cells with Nafion 112 and Aciplex 1002 membranes according to Du et al. (Reproduced from Du, X.Z., Yu, J.R., Yi, B.L., Han, M., and Bi, K.W., *Phys. Chem. Chem. Phys.*, 3, 3175, 2001. With permission from the PCCP Owner Societies.)

**TABLE 27.15**  
**Overview of FuMA-Tech Membranes**

Membrane	Type	Ion-Exchange Capacity (IEC) (mequiv g <sup>-1</sup> )	Gel-Water (wt%)	Thickness (μm)	Conductance (mS cm <sup>-1</sup> ) at RT Na-Form	Conductance (mS cm <sup>-1</sup> ) at RT H-Form	Conductance (mS cm <sup>-1</sup> ) at 80°C H-Form
<i>Fluorinated types</i>							
FKH950/40	PFSA, plain	1.07	18	42	13.9	>85	>140
FKH950/60 GF	PFSA, fabric	0.60	31	60	3.1	>85	>140
<i>Nonfluorinated types</i>							
FKE-757/45	PK12, plain	1.32	23	45	0.8	>20	>40
FKE-666/20	PK12, plain	1.50	31	20	4.1	>60	>110

Source: From FuMa-Tech, www.fumatech.com.

Abbreviations: PFSA, partially fluorinated sulfonic acid; PK, polyketone-type sulfonic acid.

[95,96]. This family of membranes was named BAM 3G (Figure 27.53). Condensation polymerization techniques were used that did not involve fluoridation technologies. These polymers have low equivalent weights ranging from 375 to 920. Because of this low equivalent weight, these membranes exhibited high water uptake as well as long durability.

Furthermore, in 2001, Ballard entered an alliance with Victrex to produce two new membrane alternatives. One membrane is based on sulfonated poly(arylether) ketone (a variant of PEEK) supplied by Victrex, which may be better suited to PEMFC fabrication applications. In March 2002, U.S. Patent 6,359,019 was issued to Ballard Power for a graft-polymeric membrane in which one or more trifluorovinylaromatic monomers are radiation graft polymerized to a preformed polymeric base. The structures of BAM membranes have been studied by way of small-angle neutron scattering (SANS) [97]. The study of the ionomer peak position suggests the existence of relatively small ionic domains compared to Nafion, despite large water content. Phase separation in the polymer matrix is possibly crucial for the membrane's mechanical and transport properties.

Within the realm of BAM2G membranes, a series of partially fluorinated bisphenol A-type poly(arylether) sulfones were synthesized. As mentioned above, these materials initially exhibited acceptable, useful service-life performance, but were unable to provide more than 500 h of continuous running time. This led to the decision that a perfluorinated backbone would be most beneficial in achieving fuel cell longevity in performance and efficiency. Therefore, the  $\alpha,\beta,\beta$ -trifluorostyrene monomer was chosen as the most suitable platform on which to build BAM3G polymers [98]. The BAM3G has demonstrated over 100,000 h of cumulative performance in a wide variety of Ballard fuel cell hardware. The BAM3G membranes have

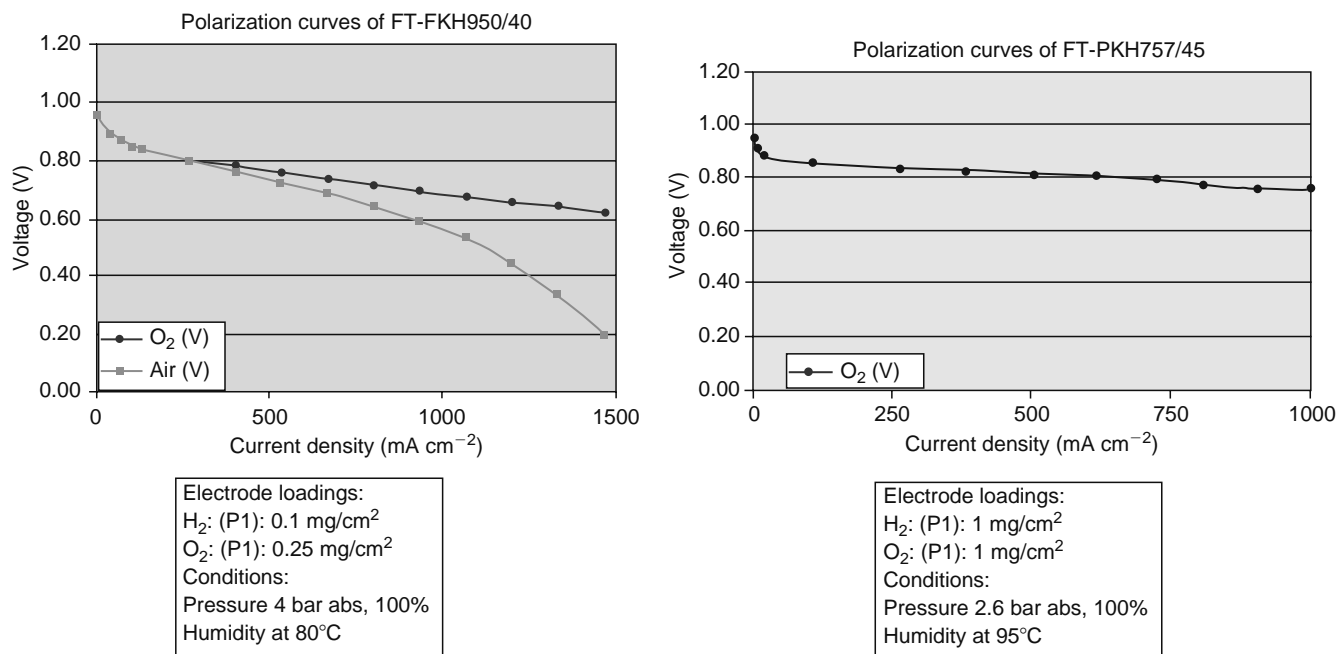


**FIGURE 27.52** Performance curves for FT-PKH950/40 and Ft-PKH/757/45. (From FuMa-Tech, www.fumatech.com.)

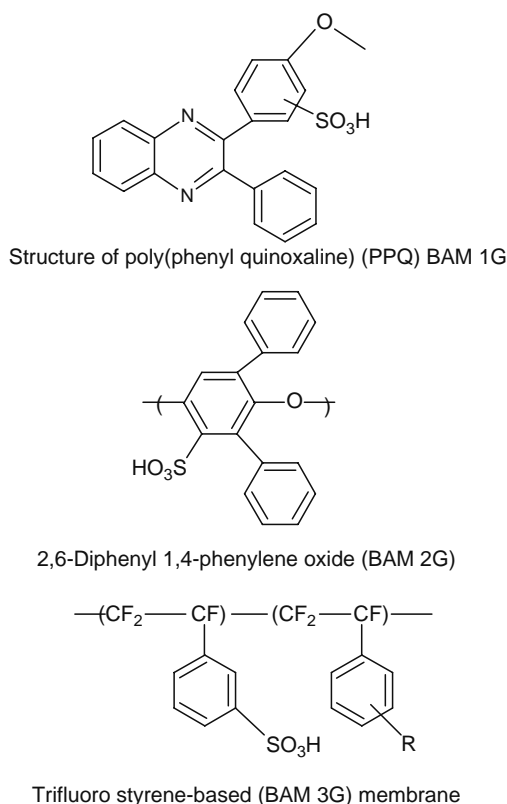


**FIGURE 27.53** Chemical structures monomers of BAM membranes. (From Zhang, L., Ma, C.S., and Mukerjee, S., *Electrochim. Acta*, 48, 1845, 2003; Basura, V.I., Chuy, C., Beattie, P.D., and Holdcroft, S., *J. Electroanal. Chem.*, 501, 77, 2001.)

successfully achieved longevity in various Ballard multistack configurations. BAM reported that a multicell stack has exceeded 3200 h of continuous performance in an ongoing evaluation. Ballard stated that with higher volume production, the BAM3G membranes would meet cost target requirements for automotive PEMFC applications. Ballard Power Systems is developing manufacturing methods for its BAM-grafted proton-exchange membranes for fuel cells. BAM membranes use a commercially available base substrate, to which trifluorovinyl aromatic monomers derivatized via radiation graft polymerization, are added, which are then modified to incorporate ion-exchange groups.

Several publications have investigated mass-transport properties for oxygen in BAM membranes [32,33,99]. These studies have mainly been carried out by the Holdcroft group (Vancouver, British Columbia, Canada) and have determined the permeability, solubility, and diffusion coefficients in BAM membranes by electrochemical chronoamperometric detection with microelectrodes. As an example of the extensive measurements carried out, the dependence of permeability on temperature for different BAM membranes with various equivalent weights is shown in Figure 27.54 [33]. As can be seen and is expected, lower EW membranes exhibit higher permeabilities. Therefore, it is possible to design the ionomer for the electrode to have advantageous permeation properties.

Not many publications report performance data with BAM's membranes. The only publication we are aware of is by Stone et al., which also discusses the possibility of introducing a phosphonic acid functionality [98]. Figure 27.55 shows the performance data from this source.

### 27.4.3.3 Radiation-Grafted Membranes

Partially fluorinated membranes prepared by radiation grafting are under active research, for example, in the groups at the Paul Scherrer Institute (Villigen, Switzerland) and the Helsinki University of Technology (Espoo, Finland) [95,100–113]. The preparation of the membranes involves a  $\gamma$ -irradiation or e-beam step to produce radical sites in perfluorinated polymer membranes, partially fluorinated polymer membranes, and nonfluorinated based membranes [114]. Typically, the membranes are swollen with suitable solutions of polymer network forming compounds (e.g., styrene/divinylbenzene). An interpenetrating polymer grafting network is formed at the radical sites normally by heating up the sample. These membranes are then sulfonated. The preparation process is depicted in Figure 27.56. The advantages of this preparation method are stated as enabling low-cost starting materials, simple chemical reactions, and the possibility to form a cross-linked material directly in its final form. PTFE, poly(tetrafluoroethylene-co-hexafluoropropylene) (FEP), poly(ethylene-tetrafluoroethylene) (ETFE),

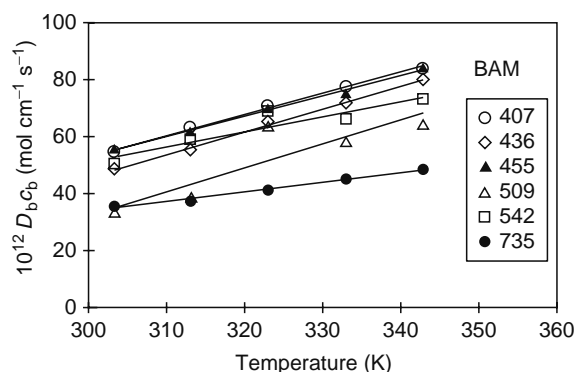


**FIGURE 27.54** The effect of temperature on the permeability  $D_{bc_b}$  for BAM membranes. Conditions: 100% RH and 3 atm oxygen. (Reprinted from Basura, V.I. et al., *J. Electroanal. Chem.*, 501, 77, 2001. With permission from Elsevier.)

poly(vinylidene fluoride) (PVDF), and poly(tetrafluoroethylene-*co*-perfluorovinylether) (PFA) have all been used as host materials for PSSA grafts. Less-investigated alternatives to PSSA include grafting glycidyl methacrylate and methyl styrene with subsequent sulfonation. The exact properties of the membranes may be determined by way of numerous reaction parameters like irradiation dose, thickness of the base polymer film, styrene/divinylbenzene composition, and graft level (determined by ratio of graft material to base material). From the published work it can be derived that there are two main obstacles to realizing technical radiation-grafted membranes. The interface between electrodes and membranes has often shown insufficient bonding and delamination has often been reported. Durability seems to be a critical issue with these membranes [95].

Decent performance curves in short-term operation have been reported for radiation-grafted membranes in DMFC (Figure 27.57). An advantage versus Nafion has been observed by Geiger et al. and Scott et al. (for higher current densities) but so far, all-reported DMFC measurements have been performed for short operating times [115,116].

A publication by the Paul Scherrer Institute reports progress in preparing membrane/electrode assemblies for polymer electrolyte fuel cells based on radiation-grafted FEP PSSA membranes [95]. Hot-pressing with Nafion was used to improve the interfaces. These improved MEAs showed performance data comparable to those of MEAs based on Nafion 112 (Figure 27.58) and an service-life in  $H_2/O_2$  fuel cells of more than 200 h at 60°C and 500 mA cm<sup>-2</sup>.

The long-term performance was found to be stable up to 2000 h (Figure 27.59)—an important improvement on the reported service-lives in the range of 500 h.

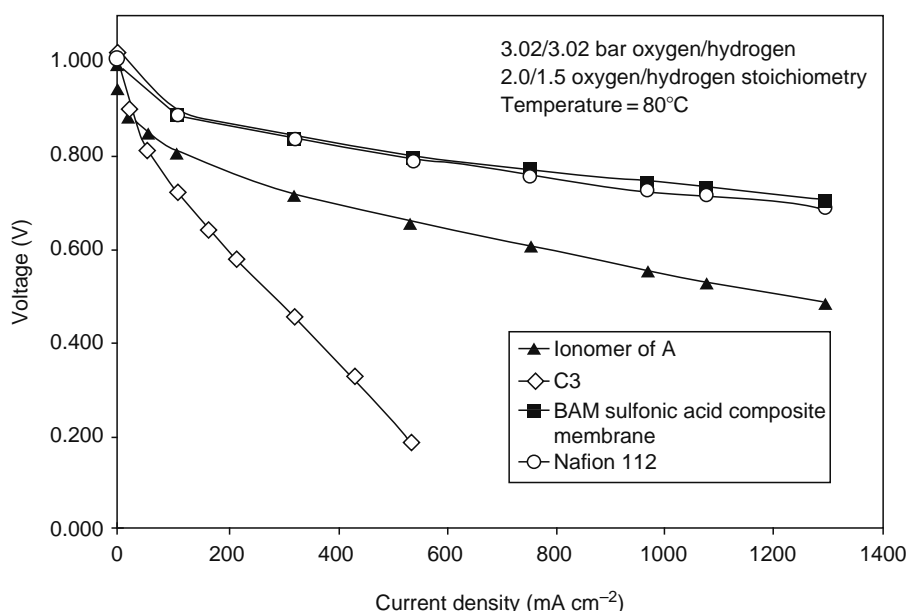


**FIGURE 27.55** Reported  $V-I$  curves for BAM3G membranes in comparison to Nafion. (Reproduced from Stone, C., Daynard, T.S., Hu, L.Q., Mah, C., and Steck, A.E., *J. New Mater. Electrochem. Syst.*, 3, 43, 2000. With permission.)

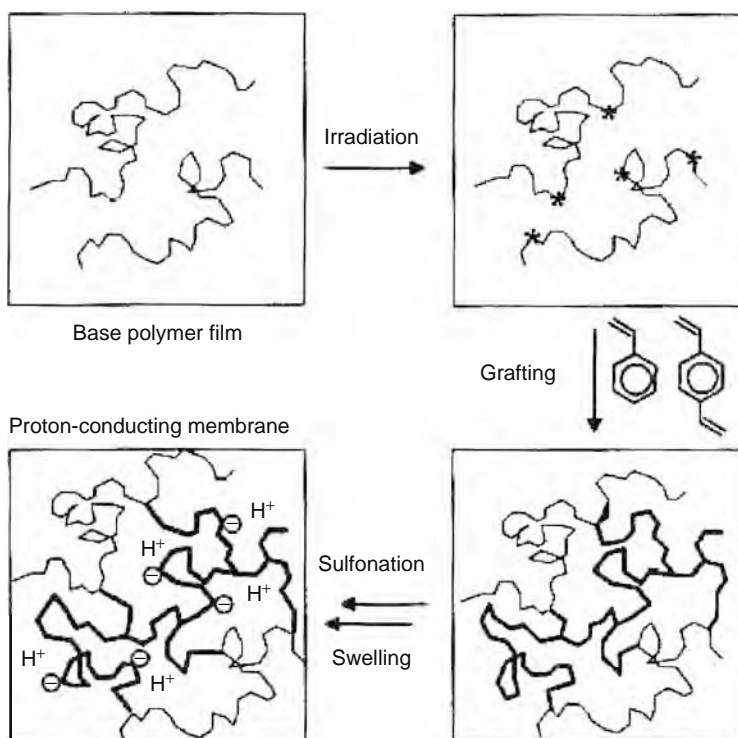


**FIGURE 27.56** Diagram of the preparation process for radiation-grafted membranes. (Reproduced from Geiger, A.B., Rager, T., Matejek, L., Scherer, G.G., and Wokaun, A., in *Proceedings of the 1st European PEFC Forum*, Büchi, F.N., Scherer, G.G., and Wokaun A. (Eds.) 2001. With permission.)

#### 27.4.4 INORGANIC/ORGANIC (FLUORINATED) COMPOSITE IONOMER MEMBRANES

##### 27.4.4.1 Hydrophilic Fillers ( $\text{SiO}_2$ , $\text{TiO}_2$ , $\text{ZrO}_2$ ) and Ormosil Networks

Over the last decade, extensive results have been reported regarding the improvement in the characteristics of known ionomeric membranes by dispersing inside their polymeric matrix, the acids with low solubility (e.g., heteropolyacids) or particles of insoluble solids such as metal oxides, lamellar zirconium phosphates, or phosphonates. A second strategy aims at developing membranes obtained by filling a non-proton-conducting polymeric matrix with ionomers or inorganic particles of high-proton conductivity. The degree of dispersion inside the membrane may vary considerably, leading to nano or microcomposites or even macrocomposites.

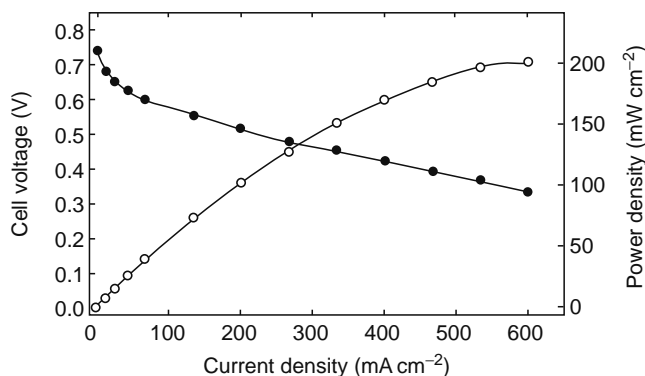


**FIGURE 27.57**  $V$ - $I$  curve of a cross-linked FEP 25 membrane for a 0.5 M aqueous methanol solution at a cell temperature of 110°C. The anodic flow rate was about 37 mL min<sup>-1</sup> and the air stoichiometry was 2. (Reproduced from Geiger, A.B., Rager, T., Matejek, L., Scherer, G.G., and Wokaun, A., in *Proceedings of the 1st European PEFC Forum*, Büchi, F.N., Scherer, G.G., and Wokaun A. (Eds.) 2001. With permission.)

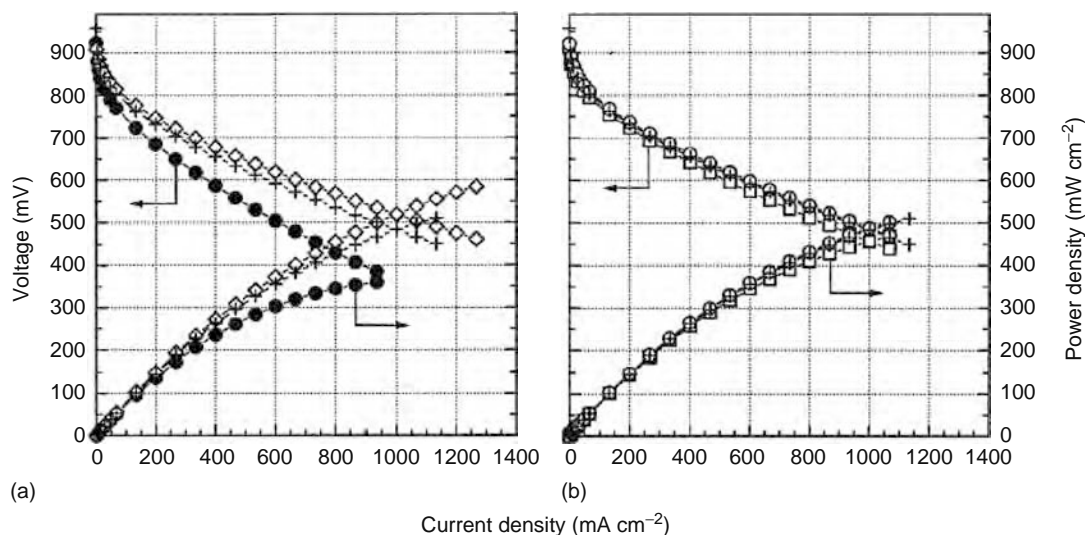


**FIGURE 27.58** Current/voltage and power density curves for MEAs based on Nafion 112 (+: without hot-pressing) and radiation-grafted membranes; influence of hot-pressing on the performance of membrane RG 1 (●, without hot-pressing; ◇, hot-pressed); influence of additional Nafion coating on the performance of membrane RG 2 (□, hot-pressed; ○, Nafion-coated and hot-pressed). ELAT electrodes from E-TEK with  $0.6 \text{ mg cm}^{-2}$  Pt on carbon,  $30 \text{ cm}^2$  graphite cell,  $60^\circ\text{C}$ , 1 atm,  $\lambda(\text{H}_2) = \lambda(\text{O}_2) = 1.5$ ,  $\text{H}_2$  humidified at  $80^\circ\text{C}$ , dry  $\text{O}_2$ . (Reprinted from Huslage, J. et al., *Electrochim. Acta*, 48, 247, 2002. With permission from Elsevier.)

The oldest concept in this respect is Nafion-based membranes, which are prepared by recasting Nafion solution and introducing inorganic hydrophilic additives, quite frequently silica or titania particles. This concept was introduced by Stonehart and Watanabe and is protected and disclosed in U.S. Patent 5,523,181 [117]. Clearly, the silica and titania particles (e.g., nanoporous, highly hydrophilic  $\text{SiO}_2$  from Degussa, Aerosil) are completely nonconductive. However, the composite recast Nafion-based membranes containing hydrophilic  $\text{SiO}_2$  or  $\text{TiO}_2$  particles as well as other inorganic material are expected to increase the water retention and therefore to lead toward increased ionic conductivity at elevated temperatures. The interpretation of improved water retention is backed by the experimental result of a higher water uptake of the membranes. The second concept which is supposed to lead to better distribution of the particles in the membrane is based on producing the particles by hydrolysis in preformed membranes by introducing a precursor (e.g., tetraethoxylane [TEOS]) into the swollen membrane [118–122]. The hydrolysis is catalyzed by the sulfonic groups forming an inorganic network in the membranes. Such structures are named organically modified silicate (ORMOSIL). The Mauritz group has prepared different membranes using this route, namely Nafion with  $\text{SiO}_2/\text{OH}$ , Nafion with  $\text{ZrO}_2/\text{OH}$ , and Surlyn with  $\text{SiO}_2/\text{OH}$ . The disadvantage is that the inorganic content cannot be varied over a large range, but these membranes are nevertheless promising for application at temperatures over  $100^\circ\text{C}$ , and therefore also for DMFCs. However, structural changes in the membrane during preparation have also been observed. Differing results have been reported: whereas the Watanabe group found a significant improvement in

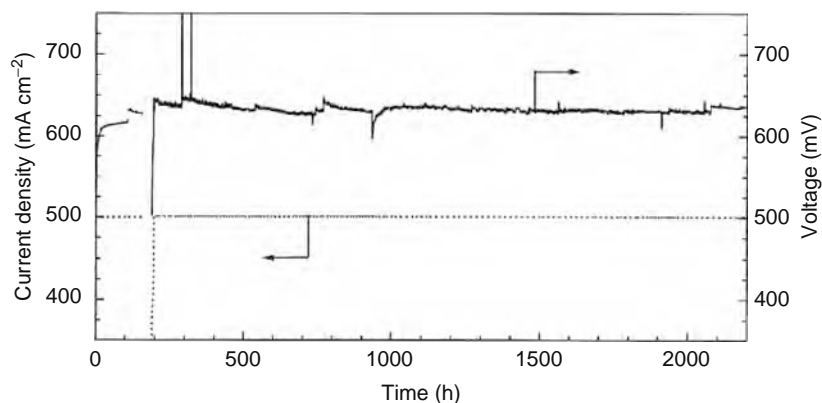


**FIGURE 27.59** Courses of voltage and current during long-term testing of the Nafion-coated and hot-pressed membrane RG 2. Constant current mode. (Reprinted from Huslage, J. et al. *Electrochim. Acta*, 48, 247, 2002. With permission from Elsevier.)

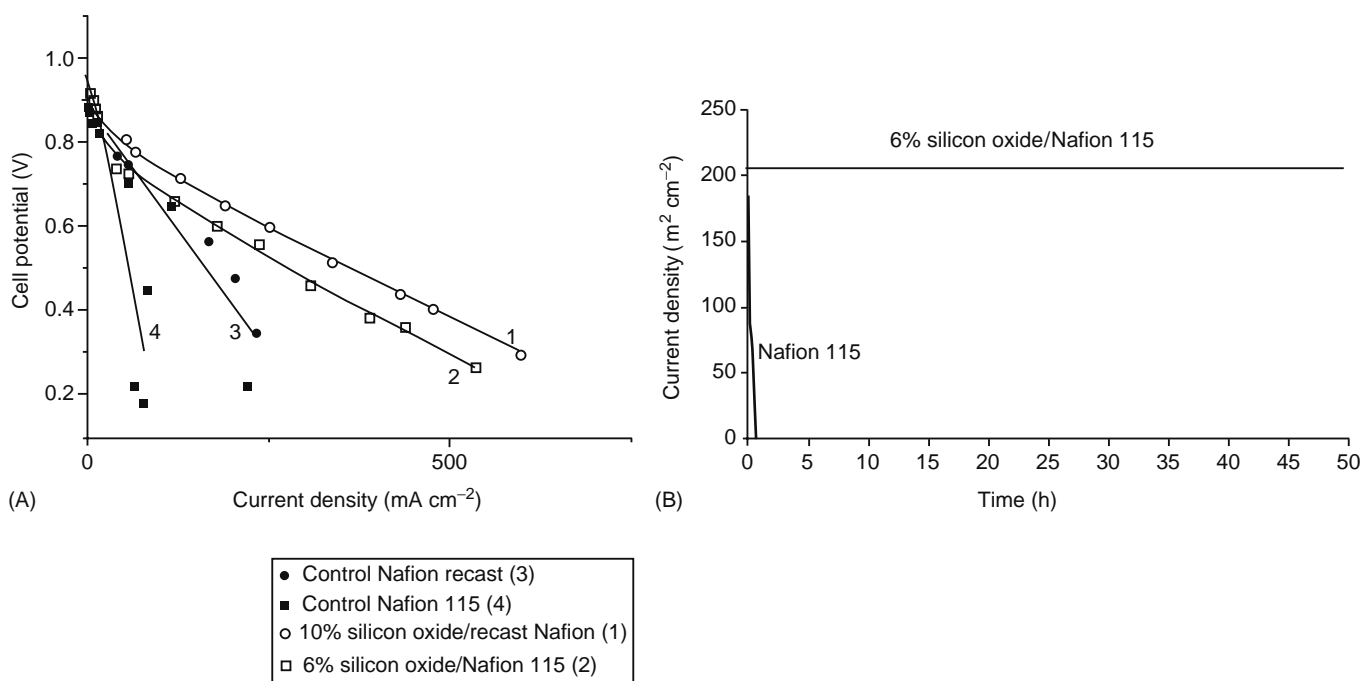


**FIGURE 27.60** (A) Cell potential versus current density of recast Nafion control, Nafion 115 control, 10% silicon oxide/recast Nafion, and ~6% silicon oxide/Nafion 115 membranes at a pressure of 3 atm; H<sub>2</sub> and O<sub>2</sub> humidifier temperature 130°C; cell temperature 140°C. (B) Time performance test of Nafion 115 and Nafion 115/silicon oxide at a pressure of 3 atm H<sub>2</sub> and O<sub>2</sub> humidifier temperature 130°C; cell temperature 130°C. Potential 0.65 V. (Reproduced from Adjemian, K.T., Lee, S.J., Srinivasan, S., Benziger, J., and Bocarsly, A.B., *J. Electrochem. Soc.*, 149, A256, 2002. With permission from The Electrochemical Society, Inc.)

membrane performance without humidification of gases, the Savinell group found no improvement in proton conductivity (although the water content was higher) for nanomodified Nafion prepared following the procedure from Mauritz et al. [123]. Recently, Adjemian et al. reported significant improvement in silicon oxide-modified recast Nafion (Figure 27.60) as well as Nafion 115 [124,125].

Alberti et al. have pointed out that it is unlikely that the improved conductivity of composite ionomer membranes is just due to the improved water absorption and retention properties, because the content of the SiO<sub>2</sub> is in the range of 3–10 wt% [126]. The reported increased water uptakes in the range of 20 wt% if only absorbed in the inorganic particles would lead to a molar ratio nearly equal to 27. Since water is only absorbed on the surface of the nanoparticles, the hydration number of the silanol groups (H<sub>2</sub>O/SiO<sub>2</sub>) would be much higher than 27. This is unrealistic, as it would mean that the hydration of silanol groups is higher than that of the superacid (–SO<sub>3</sub>H) groups. However, as mentioned before, the structure of the membrane is changed upon metal oxide modification leading, for instance, to a large degree in crystallinity of the polymer backbone. Therefore, the increased water content of metal oxide-loaded Nafion is probably associated with structural changes in the polymer matrix induced by the presence of the inorganic nanoparticles.

Several groups have reported increased performances for such membranes in DMFC applications due to a decrease in methanol permeation. A maximum power density of 240 mW cm<sup>-2</sup> at 0.4 V was obtained by Arico et al. and Antonucci et al. [127,128]. The reduced methanol permeation of such membranes is, however, controversial [129]. The Watanabe group proposed a further self-humidifying composite membrane with highly dispersed nanoparticles of Pt and TiO<sub>2</sub> (or other metal oxide particles) [130–133]. The idea is represented in Figure 27.61 and consists of generating water by permeating hydrogen and oxygen with the catalytic active Pt in the membrane and a water storage function of the hydrophilic particles in the membrane.

This concept enables the operation of PEMFCs without any humidification, which should also be interesting for higher temperatures. The corresponding *V–I* characteristics are displayed in Figure 27.62. The disadvantage to this concept, however, is that the cost of the membrane is significantly increased by adding noble metal particles. Composite membranes with nonfluorinated polymer matrices have also been investigated. For instance, high-surface amorphous silica, precipitated from a solution of tetrapropylammonium oligosilicate, was used as a filler of s-PEEK with 1.6 mequiv g<sup>-1</sup> IEC [134]. In this work, microcomposite membranes containing up to 20 wt% silica were prepared by bulk mixing the finely prepared powder with the polymer solution. The membrane containing 10 wt% silica exhibited the best electrical (conductivity rises to 3 × 10<sup>-2</sup> S cm<sup>-1</sup> at 100°C for relative humidity in the range of 75%–100%) and mechanical characteristics.

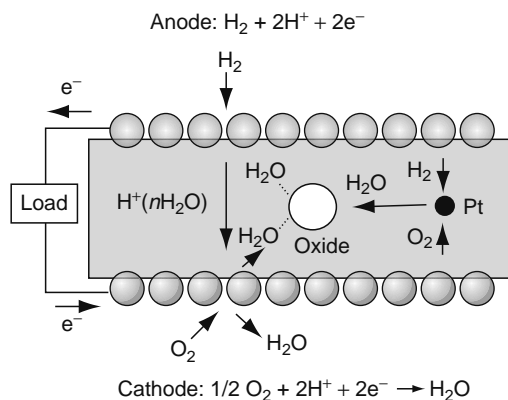


**FIGURE 27.61** Operation concept of a PEMFC using self-humidifying Pt-oxide-PEM. (Reproduced from Uchida, H., Ueno, Y., Hagihara, H., and Watanabe, M., *J. Electrochem. Soc.*, 150, A57, 2003. With permission from The Electrochemical Society, Inc.)

According to a similar synthetic approach reported by Nunes et al., nanocomposite membranes loaded with  $\text{SiO}_2$ ,  $\text{TiO}_2$ , and  $\text{ZrO}_2$  were prepared by way of hydrolysis of silanes and metal alkoxides in solutions of s-PEEK and s-PEK [135]. While homogeneous dispersions of  $\text{TiO}_2$  and  $\text{ZrO}_2$  particles were obtained starting from  $\text{Ti}(\text{OEt})_4$  and  $\text{Zr}(\text{OPr})_4$ , the hydrolysis of  $\text{Si}(\text{OEt})_4$  led to the formation of larger particles and cavities in the polymeric matrix. However, smaller and better-dispersed silica particles (about 100 nm) were formed by using either silanes covalently bonded to the polymer chain or organically modified silanes-bearing imidazole groups. A loading of 14–33 wt% metal oxide resulted in a decrease in the membrane permeability to water and methanol by a factor of 30–60, but also resulted in reduced proton conductivity at 25°C. A good balance of low permeability and high conductivity ( $3.5\text{--}4.5 \times 10^{-3} \text{ S cm}^{-1}$  against  $5 \times 10^{-3} \text{ S cm}^{-1}$  for the unmodified polymer) was achieved by incorporating a mixture of 10–15 wt%  $\text{ZrO}_2$  and 20–14 wt% amorphous ZrP in s-PEEK.

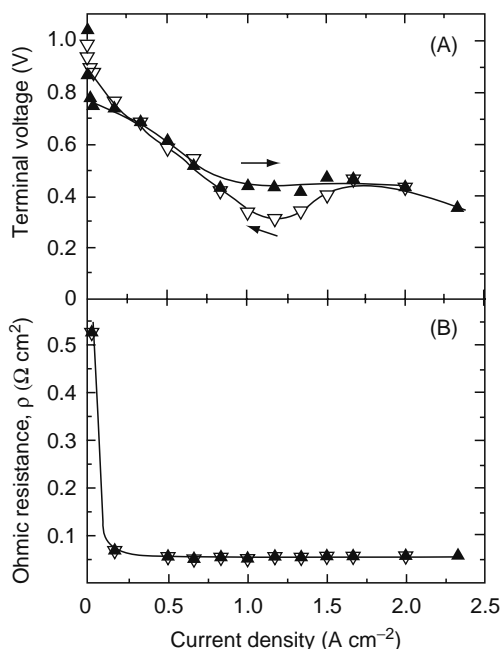


**FIGURE 27.62** (A)  $V$ - $I$  curve and (B) ohmic resistance of a PEMFC using Pt- $\text{TiO}_2$ -PEM operated at 80°C and ambient pressure with no external humidification at the reactant utilization of  $\text{H}_2$  56% and  $\text{O}_2$  54%. An open-circuit voltage (OCV) was measured at a flow rate of  $7 \text{ mL min}^{-1}$  for both dry  $\text{H}_2$  and dry  $\text{O}_2$ . The amount of Pt dispersed in the PEM =  $0.1 \text{ mg cm}^{-2}$ , the amount of  $\text{TiO}_2$  =  $0.42 \text{ mg cm}^{-2}$  (4 wt%). Full symbols measured on increasing current density and open symbols measured on decreasing current density. (Reproduced from Uchida, H., Ueno, Y., Hagihara, H., and Watanabe, M., *J. Electrochem. Soc.*, 150, A57, 2003. With permission from The Electrochemical Society, Inc.)

### 27.4.4.2 Properties of Recast Membranes with Inorganic Fillers

Preparation of membranes using the recast method with inorganic hydrophilic ingredients has proved to be a promising approach to manipulate the membrane properties with respect to liquid permeation (water and methanol), ionic conductivity, and water uptake. This approach was introduced by Stonehart and Watanabe to improve the water management of Nafion membranes in PEMFCs [136]. Several investigations by Antonucci et al. [137] have also reported an advantage to such composite membranes for DMFC applications due to a decrease in methanol permeation induced by a structural change in the polymer associated with a higher crystallinity. Dimitrova et al. [138,139] reported a detailed characterization of a recast ionomer composite membrane with 4.3% Aerosil A380 (silicon dioxide).

#### 27.4.4.2.1 Water Uptake of Composite Membranes

Recast Nafion-based samples with and without fillers absorb more water compared to the commercial Nafion 117, 115, and 112 membranes. It is observed that the water content rises slightly with the thickness of the membranes investigated. Nafion 112 indicates unexpectedly low water content in the swollen state. It is noted that even after many repetitive drying-rehydration treatments, the composite membranes contain more water than the commercial membranes. This finding might be explained by the hydrophilicity of the filler, by the altered physical structure of the ionomer backbone, or possibly by the stronger interactions between the absorbed water and the modified matrix. In particular, the silica nanoparticles retain water even at high temperatures and this property may help to prevent the membrane drying during fuel cell operation. Easier water management during fuel cell operation can be anticipated for the composite membranes.

#### 27.4.4.2.2 Proton Conductivity

Figure 27.63 shows the conductivity as a function of thickness of the commercial membranes and the modified recast Nafion membranes for temperatures of 15°C and 90°C. A proton conductivity for composite recast membranes higher than or comparable to commercial membranes is measured at 15°C. At 90°C, this difference becomes significant. These results manifest that the hydrophilic particles assist in humidifying the membrane, leading to higher proton conductivity. It should be noted that the conductivity is not constant with thickness, but increases in most samples. The increase in conductivity with thickness, which should not occur for homogeneous material, suggests that the properties of the membrane change with the thickness.

#### 27.4.4.2.3 Methanol Permeation Rate

The methanol permeation measurement illustrates the relationship between the methanol permeation rate and the temperature versus the thickness of the membrane. For thinner samples, the permeation rate changes by a factor of 4 or 5 with a temperature change from 25°C to 65°C, while in the thicker membranes this factor is about 3. At lower temperatures, the variation of the methanol flux through the membranes versus thickness is small compared to that at 65°C, where this dependence is pronounced. As anticipated, a strong decrease in permeation with thickness is observed in all cases. For the reciprocal quantity, a linear relationship between permeation rate and thickness can be derived approximately as shown in the inset of Figure 27.64. The comparison between the composite membranes and the commercial Nafion (Nafion 112, 115, and 117) reveals a similar methanol permeation rate at elevated temperature with slightly higher values of the composites.

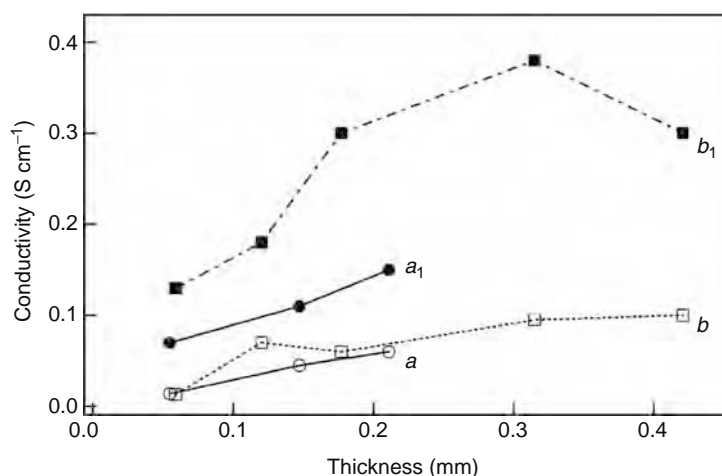


**FIGURE 27.63** Conductivity of the membranes as a function of thickness and at different temperatures: (a, a<sub>1</sub>, ○, ●) commercial samples N 112, N 115, and N 117 (b, b<sub>1</sub>, □, ■) composite membranes. Temperature at 15°C, plots a and b (open symbols) and at 90°C, plots a<sub>1</sub> and b<sub>1</sub> (close symbols). Lines are for guidance.

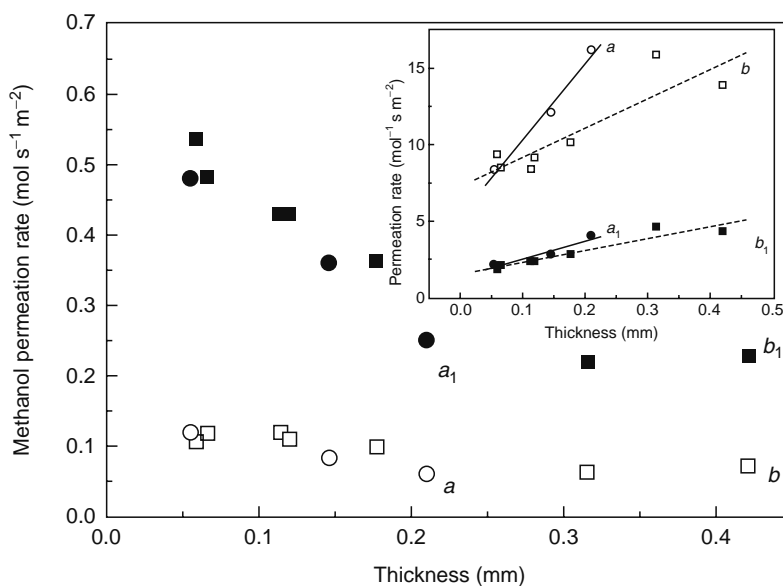


**FIGURE 27.64** Methanol permeation rate of the membranes as a function of thickness and at different temperatures: (*a*, *a*<sub>1</sub>, ○, ●) commercial samples N 112, N 115, and N 117 (*b*, *b*<sub>1</sub>, □, ■) composite membranes. Temperature at 25°C, plots *a* and *b* (open symbols) and at 65°C, plots *a*<sub>1</sub> and *b*<sub>1</sub> (close symbols).

#### 27.4.4.2.4 Water Permeation

It is favorable for fuel cell operation when reduced methanol transport across the membrane is accompanied by proper water management. In particular, a low water crossover from the anode to the cathode is necessary to avoid flooding of the cathode. The dependence of water permeation on the membrane thickness is weak. Only a small decrease in water permeation is observed for the commercial Nafion membranes, whereas the thickness of the recast membranes has no significant influence on the water transport rate. In contrast, the effect of temperature on water permeation is strong. At 65°C, the rates are higher by a factor of 5 compared to those at 25°C.

#### 27.4.4.3 Heteropolyacid Additive

Heteropolyacids possess a relatively high inherent proton conductivity, which increases the overall ionic conductivity of the membrane. Owing to these characteristics, heteropolyacids are suitable membrane fillers for increasing the number of protonic carriers and thus improving the hydrophilic character of the membranes. The major problem with modified membranes is the hydrosolubility of heteropolyacids. Composite Nafion membranes containing heteropolyacids were obtained by simply impregnating preformed membranes with a heteropolyacid solution and mixing a Nafion solution with an appropriate amount of heteropolyacid followed by casting [140,141]. Nafion recast membranes loaded with silicotungstic acid (STA), phosphotungstic acid (PTA), and phosphomolybdic acid (PMA) were investigated regarding ionic conductivity, water uptake, tensile strength, and thermal behavior [140]. In comparison with Nafion 117, all these membranes exhibited higher proton conductivity and greater water uptake, but exhibited a decreased tensile strength. Water uptake, determined by dipping dried membranes in boiling water, increases from 27% for Nafion 117 to a maximum of 95% for the PMA-based membrane. At 80°C, the heteropolyacid-loaded membranes show a better fuel cell performance than unmodified Nafion 117. The current density at 0.600 V increases from 640 mA cm<sup>-2</sup> for Nafion 117 up to a maximum of 940 mA cm<sup>-2</sup> for PMA-Nafion 117. Composite PTA-Nafion 117 membranes, impregnated with PTA solutions in acetic acid or in molten tetra-*n*-butylammonium chloride, were tested in H<sub>2</sub>/O<sub>2</sub> fuel cells working at 1 atm up to 110°C [141]. In comparison with unmodified Nafion 117 (Figure 27.65), these membranes showed a much improved performance that increased with increasing temperature.

Composite membranes with nonfluorinated polymers and heteropolyacid were also prepared. A series of nanocomposite membranes made of s-PEEK and 60 wt% PTA or PMA were prepared by Homna et al. by mixing the heteropolyacid with a polymer solution in dimethylacetamide [142]. In comparison with the pure sulfonated polymers, the composite membranes are characterized by a higher glass transition temperature, probably because of the intermolecular interaction between the sulfonic groups and the heteropolyacids, and by much greater hydration at room temperature (up to five times for PTA-loaded s-PEEK with 80% degree of sulfonation). Conductivity was determined in the range of 20°C–150°C by using an open cell with concomitant water loss (therefore, lower limit of the membrane conductivity). The composite membranes are generally more conductive than the pure polymer, but the conductivity enhancement decreases with an increasing degree of sulfonation. In

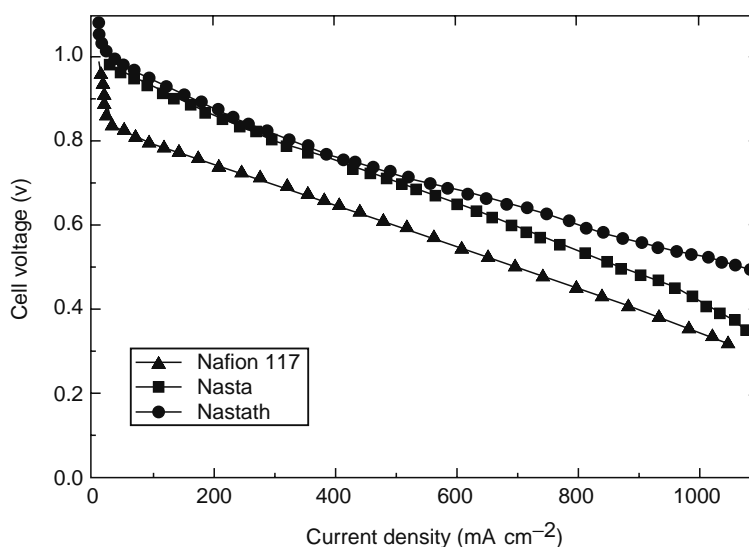


**FIGURE 27.65** Potential–current polarization curves of  $\text{H}_2/\text{O}_2$  fuel cells using Nafion 117 (thickness: 180  $\mu\text{m}$  and 30% water uptake) and STA with and without thiophene (termed NASTATH and NASTA, respectively) (thickness about 175  $\mu\text{m}$  and 60% water uptake). Anode and cathode based on 0.35  $\text{mg cm}^{-2}$  Pt from 20% Pt:C catalyst; pressure ratio  $\text{H}_2/\text{O}_2$  3:5 atm; gas flow rates  $\text{O}_2 = 0.8 \text{ L min}^{-1}$ ;  $\text{H}_2 = 1.2 \text{ L min}^{-1}$ . (Reprinted from Tazi, B. and O. Savadogo, O., *Electrochim. Acta*, 45, 4329, 2000. With permission from Elsevier.)

all cases, the conductivity dependence on temperature shows a maximum around 120°C. In the investigated temperature range, the highest conductivities were found for the PTA-based membranes (at 120°C from  $2 \times 10^{-2}$  to  $0.1 \text{ S cm}^{-1}$  with an increasing degree of sulfonation from 70% to 80%).

#### 27.4.4.4 Phosphate and Phosphonate Additives

This class of composite membranes is strongly favored by the Alberti group [14,126,143–145]. The Alberti group has developed an in situ method for formation of layered metal(IV) phosphonates or phosphate–phosphonates. These compounds can be considered organic derivatives of  $\alpha\text{-ZrP}$  and have the general formula  $\text{M(IV)(O}_3\text{P-G)}_{2-x}(\text{O}_3\text{P-ArX})_x$ , where  $\text{-G}$  may be an inorganic (e.g.,  $\text{-OH}$ ), organic (e.g.,  $\text{-CH}_2\text{OH}$ ) or an inorgano-organic group (e.g.,  $\text{-CF}_2\text{PO}_3\text{H}_2$ ). Ar is an aryl group (e.g., phenyl); X is an acid group (e.g.,  $\text{-SO}_3\text{H}$ ,  $\text{-PO}_3\text{H}_2$ , or  $\text{-COOH}$ );  $x$  is a coefficient that can vary between 0 and 1.5. Important in this respect is that, because of the presence of the electronegative  $\text{O}_3\text{P}$ -group attached to the same ring, the  $\text{-SO}_3\text{H}$  group acquires superacid properties. In Table 27.16, the conductivity of some zirconium phosphonates is reported and compared with that of  $\alpha$  and  $\gamma$ -zirconium phosphates of varying crystallinity. The conductivity of the sulfophenylene derivatives is much higher than that of the best amorphous ZrP and for some compositions, is comparable or even greater than that of Nafion 117. The in situ formation of these insoluble-layered compounds is based on the experimental observation that their soluble precursors can be formed in proton-acceptor solvents commonly used for the solubilization of proton-conducting ionomers

**TABLE 27.16**

**Conductivity of Some Layered Zirconium Phosphates and Phosphonates (100°C, 95% RH)**

	( $\sigma$ ) $\text{S cm}^{-1}$	References
$\alpha\text{-Zr(O}_3\text{P-OH)}_2 \cdot \text{H}_2\text{O}$ (crystalline)	$1.8 \times 10^{-5}$	[171]
$\gamma\text{-ZrPO}_4[\text{O}_2\text{P(OH)}_2] \cdot 2\text{H}_2\text{O}$ (crystal)	$2 \times 10^{-4}$	[172]
$\alpha\text{-Zr(O}_3\text{P-OH)}_2 \cdot \text{H}_2\text{O}$ (semicrystal)	2 to $7 \times 10^{-4}$	[173]
$\text{Zr(O}_3\text{P-OH)}_2 \cdot n\text{H}_2\text{O}$ (amorphous)	1 to $5 \times 10^{-3}$	[174]
$\text{Zr(O}_3\text{P-OH)}1.5(\text{O}_3\text{P-C}_6\text{H}_4\text{SO}_3\text{H})0.5$ (amorphous)	0.9 to $1.1 \times 10^{-2}$	[174]
$\alpha\text{-ZrPO}_4[\text{O}_2\text{P(OH)}_2]0.54[\text{O}_2\text{P(OH)C}_6\text{H}_4\text{SO}_3\text{H}]0.46 \cdot n\text{H}_2\text{O}$ (crystal)	$5 \times 10^{-2}$	[172]
$\text{Zr(O}_3\text{P-OH)}(\text{O}_3\text{P-C}_6\text{H}_4\text{SO}_3\text{H}) n\text{H}_2\text{O}$ (semicrystal)	0.8 to $1.1 \times 10^{-1}$	[174]

Source: From Alberti, G. and Casciola, M., *Annu. Rev. Mater. Res.*, 33, 129, 2003.

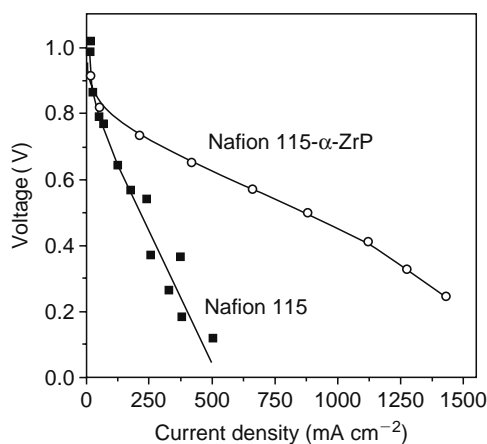


**FIGURE 27.66** Polarization curves of PEMFCs based on Nafion 115 and Nafion 115: 23 wt%  $\alpha$ -ZrP at 130°C and 3 atm with reactants humidified at 130°C. (Reprinted from Costamagna, P. et al., *Electrochim. Acta*, 47, 1023, 2002. With permission from Elsevier.)

(e.g., DMF, NMP, alkanols, etc.). The special property of these compounds is that they can easily be transformed into the final insoluble zirconium phosphonates just by drying at 110°C–130°C.

A composite Nafion 115 and recast Nafion with  $\alpha$ -ZrP nanoparticles were investigated by Costamagna et al. [146]. At 130°C, cell temperature with  $H_2$  and  $O_2$  humidified at 130°C, the nanocomposite membranes displayed much better performance than unmodified Nafion (Figure 27.66). In particular, the polarization curve of a nanocomposite recast membrane at 130°C and 3 atm was equivalent to that of the unmodified recast film at 80°C and 1 atm. Moreover, the composite membranes showed stable behavior over time at 130°C, whereas Nafion was irreversibly degraded under the same conditions. Yang et al. also investigated a Nafion,  $\alpha$ -ZrP nanocomposite membrane in a DMFC which exhibited good performance up to about 150°C, with maximum power densities of 380 and 260  $mW\ cm^{-2}$  under oxygen and air feed, respectively.

Composite polyarylene membranes modified by using organic solutions of zirconium phosphonate precursors were investigated by the Alberti group in combination with FuMA-Tech membranes [126]. Preliminary results from Alberti's group showed that the conductivity of s-PEK membranes of high-molecular weight (FuMA-Tech) is enhanced to a great extent in the presence of nanoparticles of zirconium phosphate sulfophenylphosphonates (Figure 27.67). Taking into account that much lower enhancement was instead obtained with  $\alpha$ -ZrP nanoparticles, these results seem to confirm the importance of the high-proton conductivity and acid strength of the filler. Thus, according to Alberti, superacid zirconium phosphonates deserve further attention as fillers of nanocomposite membranes [126].

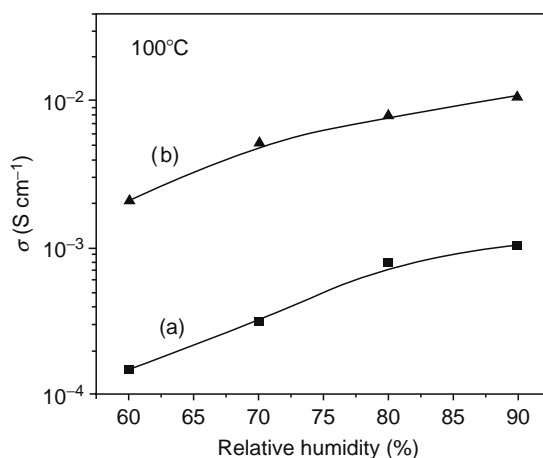


**FIGURE 27.67** Conductivity as a function of relative humidity for (a) a high-molecular-weight s-PEK membrane (FuMA-Tech; thickness 50  $\mu m$ ) and (b) the same membrane filled with 35 wt% of  $Zr(O_3P-OH)(O_3P-C_6H_4SO_3H) \cdot nH_2O$ . (Reprinted from Alberti, G. and Casciola, M., *Annu. Rev. Mater. Res.*, 33, 129, 2003, copyright 2003 by Annual Reviews www.annualreviews.org. With permission.)

#### 27.4.4.4.1 Ammonium Polyphosphate

Ammonium polyphosphate composite-based proton conductors for the intermediate temperature range (200°C–300°C) have been found to possess good proton conductivity ( $0.1 \text{ Scm}^{-1}$  at 300°C) under humidified conditions [147]. This temperature range would not have any kinetics or CO poisoning problem, but improving stability of the proton conductor in fuel cell conditions is still a challenge [148–151].

#### 27.4.4.5 Proton-Conducting Membranes Based on Electrolyte-Filled Microporous Matrices/Composite Membranes

Composites enable the mechanical and electrical properties of the membrane to be separated. In most cases, they consist of a matrix (mechanical support) filled with a protonic electrolyte. Varying the electrolyte and optimizing the structure of its mechanical support enable the working conditions of the cell to be adapted. This implies an improvement in the performance of the cell, along with a possible reduction in the cost of the membrane. Successful efforts have been made by some groups in this direction. Haufe and Stimming [152] prepared and characterized composite membranes made by soaking polysulfone fleece and microglass fiber fleece in 5 M sulfuric acid and ionomer electrolytes.

Figure 27.68 shows the conductivity for the various samples in the form of an Arrhenius plot  $\log(\sigma T)$  versus  $1/T$ . This figure reveals that all samples exhibit similar activation energies (0.10–0.19 eV), which correspond to those commonly measured for acids in the liquid state. Moreover, in the investigated temperature regime, the polysulfone fleece soaked with  $\text{H}_2\text{SO}_4$  had a slightly higher specific conductivity than Nafion 117 membranes. This fact might be considered surprising, since, on the basis of the specific conductivity obtained for the free acids and on the basis of the porosity of the fleece (83%), a much higher conductivity is to be expected. This leads to the conclusion that the pores of the fleeces were not completely filled with  $\text{H}_2\text{SO}_4$ .

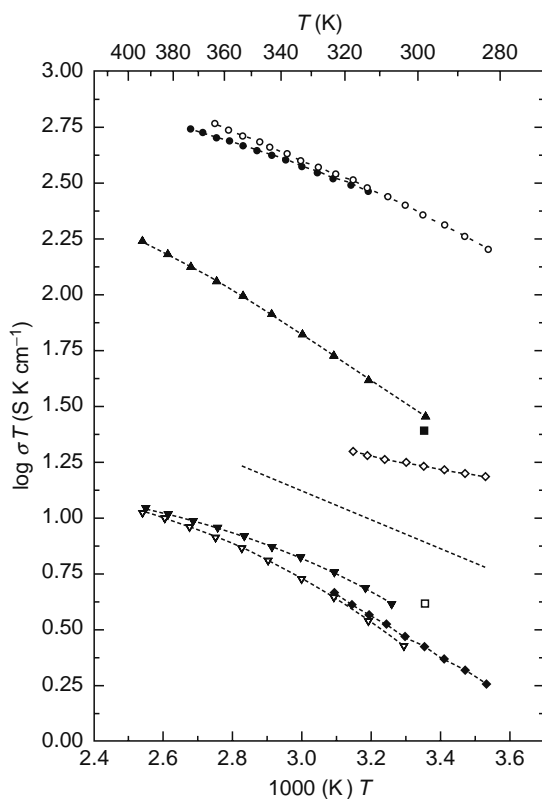


**FIGURE 27.68** Arrhenius plots  $\log(\sigma T)$  versus  $1/T$  of the proton conductivity of  $5 \text{ mol dm}^{-3} \text{ H}_2\text{SO}_4$  (●) according to Ren, X., Springer, T.E., and Gottesfeld, S., *J. Electrochem. Soc.*, 147, 92, 2000, (○); experimental data;  $15 \text{ mol dm}^{-3} \text{ H}_3\text{PO}_4$  (▲); polysulfone fleece filled with  $5 \text{ mol dm}^{-3} \text{ H}_2\text{SO}_4$  (◇); polysulfone fleece filled with  $15 \text{ mol dm}^{-3} \text{ H}_3\text{PO}_4$  (▽) or with  $19 \text{ mol dm}^{-3} \text{ H}_3\text{PO}_4$  (▼); polysulfone fleece filled with Nafion (◆); microglass fiber fleece filled with  $5 \text{ mol dm}^{-3} \text{ H}_2\text{SO}_4$  (■); microglass fiber fleece filled with Nafion (□) and Nafion 117 membrane (dotted line, according to Ren, X.M., Springer, T.E., Zawodzinski, T.A., and Gottesfeld, S., *J. Electrochem. Soc.*, 147, 466, 2000.)

On the basis of a simple geometric consideration, a comparison between the conductivity of the acid and that of the impregnated fleeces results in only 7% of the volume of the polysulfone fleece and 11% of the volume of the microglass fiber fleece contributing to the proton conductivity of the composite. Similarly, the filled volume for  $\text{H}_3\text{PO}_4$  and the fleece impregnated with it amounts to 13%. The difference between the conductivity of Nafion 117 and that measured for the fleeces impregnated with Nafion ionomer is, however, smaller, revealing a filled volume of 34% for the polysulfone fleece and 53% for the microglass fiber fleece. These observations suggest that the surface treatment of the fleece may help in optimally impregnating the matrix.

$\text{H}_2/\text{O}_2$  fuel cell performance using a polysulfone fleece filled with  $\text{H}_2\text{SO}_4$ , microglass fiber fleece filled with Nafion, and a Nafion 117 were found to be comparable. The same kind of composite membranes was also suggested to be a good alternative to Nafion for liquid feed DMFCs. Peled et al. [153,154] reported a family of nanoporous proton-conducting membranes (NP-PCMs). These membranes consisted of electronic nonconductive nanosize ceramic powder ( $\text{SiO}_2/\text{TiO}_2$ ), a polymer binder (PVDF), and an acid. They have the appearance of plastic, good mechanical properties, nanosize pores (typically smaller than 1.5–3 nm) filled with the acid, and room-temperature conductivity of up to  $0.21 \text{ S cm}^{-1}$  (twice that of Nafion) at  $25^\circ\text{C}$ . Their thickness ranges from 40 to 400  $\mu\text{m}$ . Their insensitivity to heavy ion impurities and reduced methanol crossover (by order of magnitude) makes them good low-cost candidates for liquid-feed DMFCs.

#### 27.4.4.6 Other Concepts

Creavis's concept is based on ceramic membrane foils already marketed under the trade name CREAMFILTER. They reportedly combine the characteristics of flexible polymeric membranes and ceramic membranes in a favorable way. The basis of the membrane is a woven or nonwoven support of stainless steel or temperature-tolerant glass fibers. Due to their better chemical stability, stainless steel supports are preferred for filtration applications, whereas nonconducting glass supports are needed for batteries and fuel cells. This support is coated with ceramic materials, e.g., alumina or zirconia, and a flexible membrane with microfiltration (MF) properties is realized. The thickness of the membrane is about 80  $\mu\text{m}$ . This is thin enough for the membrane to retain the flexibility of the support. The pore size of the membrane is in the range of 50–500 nm, depending on the particle size of the ceramic materials. This microfiltration (MF) membrane can be modified by superimposing additional layers with smaller particles or active particles onto the first layer. Coating the MF membranes once results in ultrafiltration (UF) membranes with pore sizes between 5 and 50 nm, while coating them twice produces nanofiltration (NF) membranes with pore sizes smaller than 5 nm. To use the CREAMFILTER membranes in a low-temperature fuel cell, the nonconducting MF membrane has to be transferred into a PEM. This can be achieved in a very similar way to the production process of the filtration membrane described above. The MF membrane is infiltrated with a solution, suspension, or sol of a proton-conducting material. After this impregnation step, the proton-conducting material is immobilized by thermally treating the membrane. From a theoretical point of view, all kinds of proton-conducting materials can be used as active materials for infiltrating CREAMFILTER membranes. Due to the inorganic nature of the support, inorganic compounds are preferably used as active materials. Candidate materials for proton conductors are zirconium phosphates, sulfuric acids based on triethoxy silane compounds, or other Bronsted acids, such as  $\text{H}_3\text{PO}_4$  or  $\text{H}_2\text{SO}_4$ . To immobilize these acids, an inorganic sol is typically prepared which contains the acids. The MF membranes are infiltrated with sols that comprise additional metal oxide compounds. During the thermal treatment, the gelation of the sol occurs and the acids are fixed in the gels. The membranes reportedly do not have pores and are absolutely gas tight. The proton conductivity of the membranes is comparable to Nafion membranes. Due to the inorganic nature of the CREAMFILTER PEMs, these membranes show no swelling and need only a reduced relative humidity to reach high conductivities. Figure 27.69 shows a typical  $V$ - $I$  behavior of the membranes. The CREAMFILTER PEM in Figure 27.69 comprises a  $\text{H}_3\text{PO}_4$ -doped silica gel as the proton-conducting material. Typical working conditions for Nafion are  $80^\circ\text{C}$  and a relative humidity of up to 100%. In contrast, the CREAMFILTER membrane works at temperatures of at least  $90^\circ\text{C}$  and relative humidities of about 30%. With this membrane (Figure 27.69), power densities of more than  $50 \text{ mW cm}^{-2}$  can be achieved (low conductivity of phosphoric acid at  $90^\circ\text{C}$ , slow kinetics). Creavis claims that with other proton-conducting membranes the CREAMFILTER PEM reaches power densities of up to  $200 \text{ mW cm}^{-2}$  under the same conditions.

#### 27.4.5 POLYMER MEMBRANES WITH INORGANIC ACID IMPREGNATION

Aromatic PBIs are highly thermostable, with melting points  $>600^\circ\text{C}$ . The PBI commercially available is poly(2,20-[mphenylene]-5,50-benzimidazole) (PBI) (Figure 27.70). PBI has a tendency to take up water, thus explaining the low-proton conductivity (in the range  $\sim 10^{-7} \text{ S cm}^{-1}$ ) that is observed even for the neat polymer [155]. PBI is basic ( $\text{p}K$  value of  $\approx 5.5$ ), and it readily forms complexes with organic and inorganic bases. It has long been known that PBI can be treated with sulfuric and phosphoric acid, which leads to stabilization as well as to a significant increase in conductivity. The acid uptake reaches 5 mol  $\text{H}_3\text{PO}_4$  per PBI repeat unit. This quantity is much too large to use the term "doped," yet this is the term often inappropriately used to describe PBI-acid complexes. The properties of such impregnated (doped) membranes and their

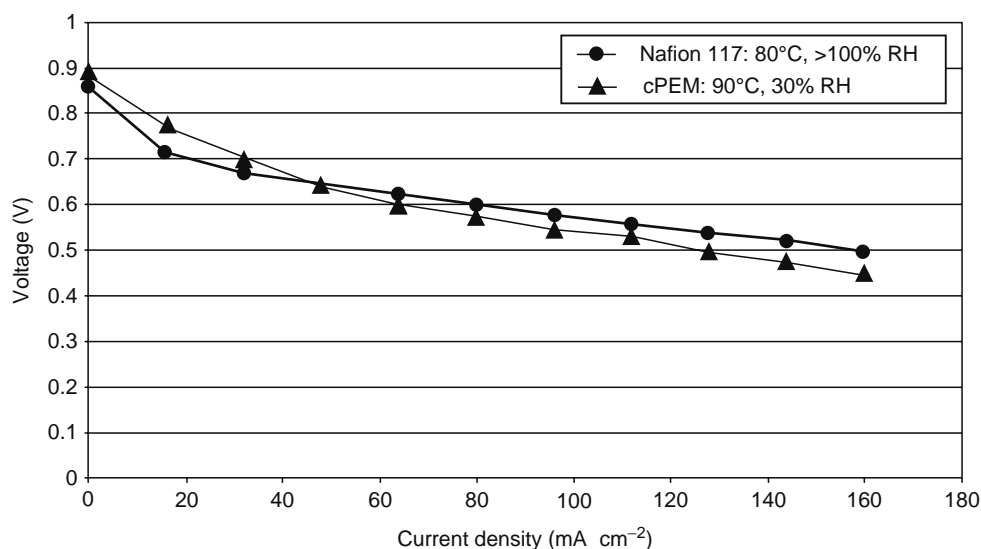


**FIGURE 27.69**  $V$ - $I$  behavior of a CREAMFILTER PEM, compared to Nafion 117. Note the different working conditions of the membranes. (Reprinted from Augustin, S. et al. *Desalination*, 146, 23, 2002. With permission from Elsevier.)

application in PEMFCs and in cells using hydrocarbons and methanol as fuels have been investigated systematically since 1994 by Wainright et al. [15,156–167]. Celanese Ventures is the largest (and for a long time the only) producer of PBI and developed this membrane for fuel cell applications. In 2004, their fuel cell activities were spun off into a new and independent company, PEMEAS, which continues to develop MEAs. These MEAs are based on phosphoric acid-doped PBI. A pilot plant for fuel cell MEAs has been established in Höchst, Frankfurt am Main, Germany. The main advantage of this system is high-temperature operation over 150°C. Doping the membranes with other acids like hydrochloric acid, perchloric acid, or nitric acid leads to high conductivity [163]. Different methods are used to form the PBI/acid complex: immersing a PBI membrane in an acid solution of a given concentration for a given length of time is the most popular method. A second possibility is direct casting from a solution of PBI and phosphoric acid in trifluoroacetic acid. A recent variant of this approach uses polyphosphoric acid as the condensing agent for polymerization and as a membrane casting solvent. Absorption of water after casting leads to in situ hydrolysis of polyphosphoric to phosphoric acid in the membrane [155].

Whether humidification of PBI in fuel cells is necessary remains an open question. Short-term fuel cell tests yielded no or small performance losses when dry fuels were used or humidification was reduced [167,168]. However, membrane conductivity does depend on the water activity: as can be seen in Figure 27.71 taken from a presentation by Savinell, the conductivity of PBI (3 H<sub>3</sub>PO<sub>4</sub>/PBI repeat unit and 6.3 H<sub>3</sub>PO<sub>4</sub>/PBI repeat unit) depends considerably on relative humidity [169]. However, Celanese (PEMEAS) in their publications state that no humidification is required for their PBI systems.

#### 27.4.5.1 PEMEAS (Celanese) Membranes

PEMEAS, a 2004 spin-off from Celanese AG, has developed a membrane made from the heat-resistant polymer PBI. The PBI membrane marketed by PEMEAS under the brand name Celtec enables a fuel cell to operate at temperatures of up to 200°C (392°F), while more conventional technologies allow PEMFC-operating temperatures of up to 100°C (212°F). Due

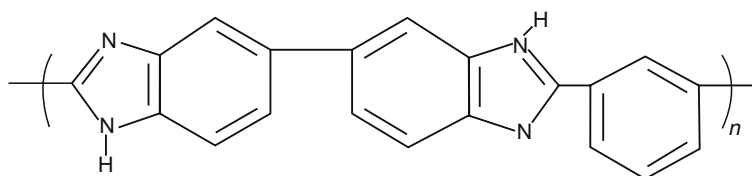


**FIGURE 27.70** Chemical structure of poly[2,20-(*m*-phenylene)-5,50-bibenzimidazole].

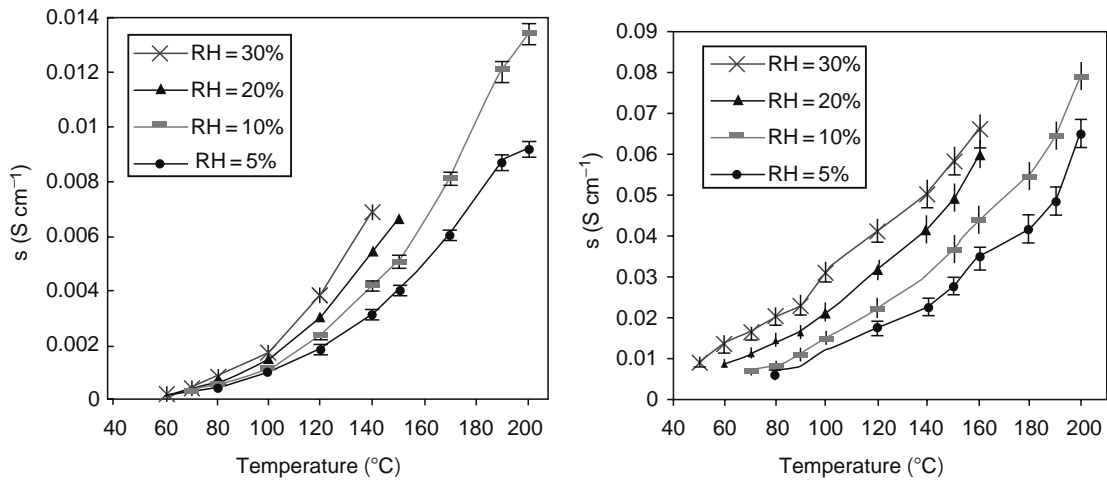


**FIGURE 27.71** Conductivity of PBI versus temperature for various RHs. Left: doping level 300%, right: doping level 630%. (From Ren, X., Zawodzinski, T., and Gottesfeld, S., *Abstr. Pap. Am. Chem. Soc.*, 217, U490–U490, 1999.)

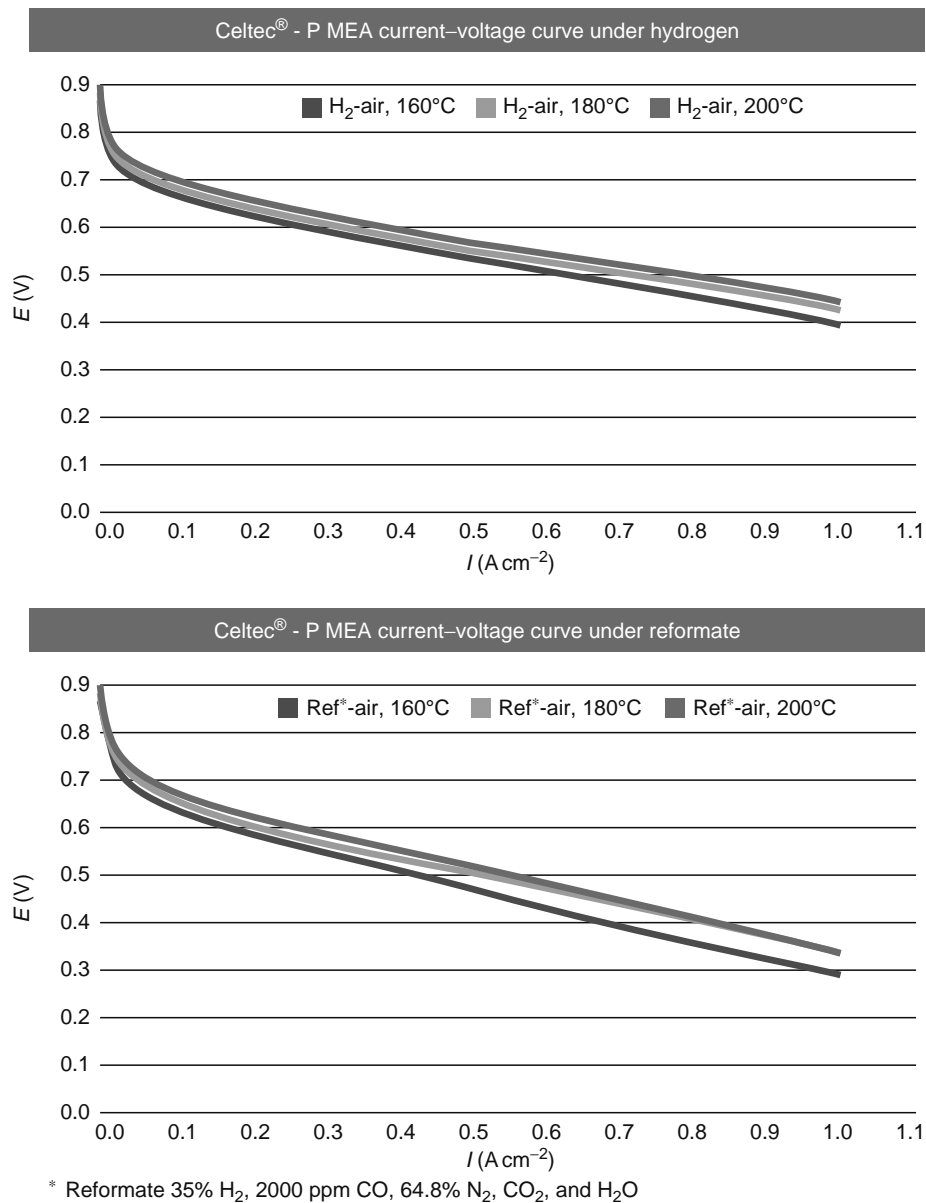


**FIGURE 27.72** (See color insert following page 588.) Celtec P MEA, active cell area:  $45\ cm^2$ , air: $\lambda = 2$ ; 0 bar,  $H_2$ : $\lambda = 1.2$ ; 0 bar, humidification: none. (From Celanese AG, www.celanese.com.)

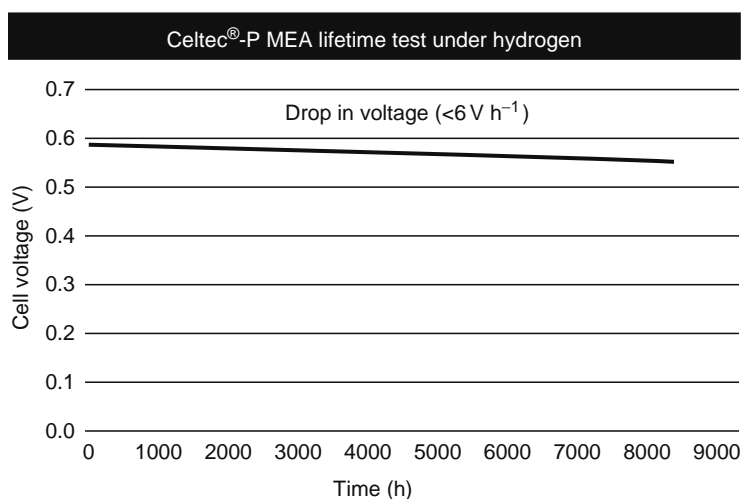


**FIGURE 27.73** Service-life test of Celtec P MEA, active cell area:  $45 \text{ cm}^2$ , cell temperature:  $160^\circ\text{C}$ , current density:  $0.3 \text{ A cm}^{-2}$ , air:  $\lambda = 2.5$ ; 0 bar,  $\text{H}_2$ :  $\lambda = 1.2$ ; 0 bar, humidification: none. (From Celanese AG, www.celanese.com.)

to the operating temperature, PBI is resistant to carbon monoxide (CO) poisoning of the catalyst and at least 100 ppm CO can be tolerated at  $150^\circ\text{C}$ . The need for higher fuel cell-operating temperatures, according to Celanese AG, is outlined below:

- Higher operating temperature PEMFCs operate with smaller cooling elements. This is especially good for automotive applications.
- Higher operating temperature membranes enable more efficient heat recovery for stationary applications of PEMFCs.
- Higher temperature-tolerant membranes are more tolerant to CO poisoning. This reduces the need for ultrapure hydrogen feed.

The performance curves reported by Celanese are shown in Figure 27.72. The interfacial bonding of electrode and membrane is also accomplished using PBI/ $\text{H}_3\text{PO}_4$ .

Celanese AG has reported reasonable long-term durability and operational stability for Celtec P MEAs (Figure 27.73). The properties of Celtec P MEAs, according to Celanese, are given in Table 27.17.

According to Celanese, the MEA and its individual components can be customized in size and shape to meet customer requirements.

Taking the high temperature into account, it is astounding (at least for the authors of this study) that the current densities at high single-cell voltages are comparatively low for PBI. Large losses in the kinetically dominated region of the PBI  $V$ - $I$  curve are observed. This is due to the strong adsorption of phosphoric acid on Pt electrocatalyst and may be difficult to avoid. This effect has been investigated regarding the oxygen reduction reaction by the Savinell group and is summarized in Figure 27.74 for solid Pt electrodes with and without polymer films [165]. PBI and Nafion films do not influence the reactivity appreciably, but in nonadsorbing perchloric acid current density is much higher than in phosphoric acid.

**TABLE 27.17**  
**Celtec P MEA Specifications**

Performance	$0.2 \text{ W cm}^{-2}$ at 0.6 V, $180^\circ\text{C}$ , 0 bar, $\text{H}_2/\text{air}$ $0.13 \text{ W cm}^{-2}$ at 0.6 V, $180^\circ\text{C}$ , 0 bar, Reformate <sup>a</sup> /air
Operational stability (long-term test)	>8000 h
Drop in voltage in a long-term test	< $6 \mu\text{V h}^{-1}$
Operating temperature	$120^\circ\text{C}$ – $200^\circ\text{C}$
CO tolerance	>50,000 ppm
Humidification of reaction gases	Unnecessary

<sup>a</sup> Reformate: 35%  $\text{H}_2$ ; 2000 ppm CO; 64.8%  $\text{N}_2$ ,  $\text{CO}_2$ , and  $\text{H}_2\text{O}$ .

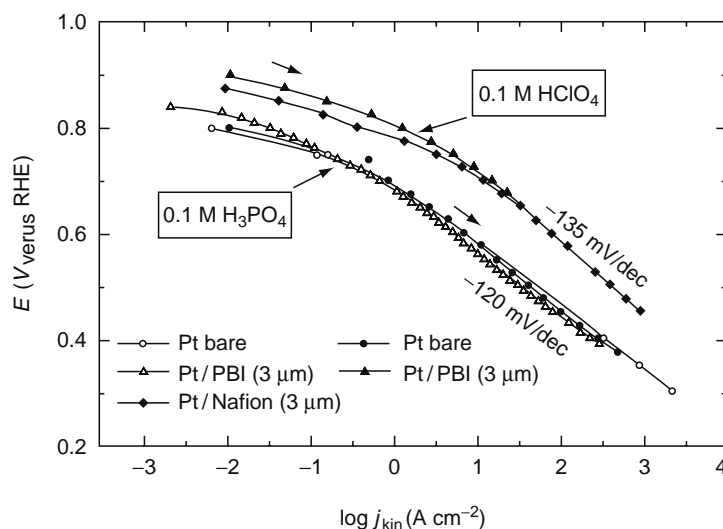


**FIGURE 27.74** Tafel plots for  $O_2$  reduction at  $25^\circ C$  on oxidized Pt bare electrodes and Pt electrodes with PBI or Nafion film in 0.1 M acid solutions as indicated in the diagram. Scan rate  $50\ mV\ s^{-1}$ . Film thickness indicated in the diagram. (From Ren, X., Zawodzinski, T., and Gottesfeld, S., *Abstr. Pap. Am. Chem. Soc.*, 217, U490–U490, 1999.)

## 27.5 SUMMARY

A lot of research has been carried out in past decade to develop membranes for the whole spectrum of applications, namely automotive, stationary, and portable applications. PFSA-based membranes have played the most prominent role until now. Much research has been conducted into the details of proton transport through different polymers and into methods of improving their properties, but a viable and inexpensive substitute to Nafion has yet to be developed. On the other hand, different approaches using PTFE fibril reinforcements have been successfully applied to PFSA-based membranes to make them more mechanically and thermally stable and thus to enhance durability. Such membranes are also reported to have better humidity and heat management characteristics besides lower specific protonic resistance and high power densities. Alternative approaches to modify the properties of PFSA-based membranes by impregnating inorganic fillers have also been reported to produce favorable results. But such membranes still await wide adoption. For liquid-phase operation (as in DMFCs), very inexpensive membranes based on nanoporous inorganic support matrices filled with liquid electrolytes have also shown good potential. PFSA-based membranes cannot be used in the high-temperature range. A good alternative for the high-temperature range critical to automotive applications is the inorganic, acid-doped PBI-based membrane from Celanese AG. In spite of all these improvements, a lot of work is still needed to improve various membrane characteristics which would make designing fuel cell-based systems much simpler and would eliminate the need for several BOP components, which adds to the complexity of the fuel cell systems.

## REFERENCES

1. S. Srinivasan. Fuel cells for extraterrestrial and terrestrial applications. *Journal of the Electrochemical Society* 136, C41–C48 1989.
2. J. Larminie and A. Dicks. *Fuel Cell Systems Explained* J. Wiley & Sons, New York, 2000.
3. L. Carrette, K.A. Friedrich, and U. Stimming. Fuel cells—fundamentals and applications. *Fuel Cells* 1, 5 2001.
4. V. Metha and J.S. Cooper. Review and analysis of PEM fuel cell design and manufacturing. *Journal of Power Sources* 114, 32 2003.
5. K. Kordesch and G. Simader. *Fuel Cells and Their Applications* J. Wiley & Sons, New York, 2000.
6. A.B. Stambouli and E. Traversa. Fuel cells, an alternative to standard sources of energy. *Journal of Power Sources* 86, 23 2000.
7. A.B. LaConti, M. Hamdan, and R.C. McDonald. In *Handbook of Fuel Cells: Fundamentals, Technology and Applications*, H.A. Gasteiger, W. Vielstich, and A. Lamm (Eds.) pp. 647–662, J. Wiley & Sons, Chichester, 2003.
8. M. Doyle and G. Rajendran. In *Handbook of Fuel Cells: Fundamentals, Technology and Applications*, W. Vielstich, H.A. Gasteiger, and A. Lamm (Eds.) pp. 351–395, J. Wiley & Sons, Chichester, 2003.
9. S. Gottesfeld and T.A. Zawodzinski. In *Advances in Electrochemical Science and Engineering*, R.C. Alkire, H. Gerischer, D.M. Kolb, and C.W. Tobias (Eds.) Wiley-VCH, Weinheim, 1997.
10. W. Vielstich, H.A. Gasteiger, and A. Lamm. (Eds) *Handbook of Fuel Cells: Fundamentals, Technology and Applications* J. Wiley & Sons, Chichester, 2003.
11. D.A. Masten and A.D. Bosco. In *Handbook of Fuel Cells: Fundamentals, Technology and Applications*, W. Vielstich, H.A. Gasteiger, and A. Lamm (Eds.) J. Wiley & Sons, Chichester, 2003.

12. H.A. Gasteiger and M.F. Mathias. In *Proceedings of the Symposium on Proton Conducting Membrane Fuel Cells III*, The Electrochemical Society of America, 2003.
13. H.A. Gasteiger, J.E. Panels, and S.G. Yan. Dependence of PEM fuel cell performance on catalyst loading. *Journal of Power Sources* 127, 162–171 2004.
14. G. Alberti, M. Casciola, L. Massinelli, and B. Bauer. Polymeric proton conducting membranes for medium temperature fuel cells (110–160 degrees C). *Journal of Membrane Science* 185, 73–81 2001.
15. Y.L. Ma, J.S. Wainright, M.H. Litt, and R.F. Savinell. Conductivity of PBI membranes for high-temperature polymer electrolyte fuel cells. *Journal of the Electrochemical Society* 151, A8–A16 2004.
16. M. Watanabe, Y. Satoh, and C. Shimura. Management of the water-content in polymer electrolyte membranes with porous fiber wicks. *Journal of the Electrochemical Society* 140, 3190–3193 1993.
17. S.H. Ge, X.G. Li, and I.M. Hsing. Water management in PEMFCs using absorbent wicks. *Journal of the Electrochemical Society* 151, B523–B528 2004.
18. S.H. Ge, X.G. Li, and I.M. Hsing. Internally humidified polymer electrolyte fuel cells using water absorbing sponge. *Electrochimica Acta* 50, 1909–1916 2005.
19. R.B. Hodgdon, J.R. Boyack, and A.B. Laconti. The degradation of polystyrene sulfonic acid. General Electric Company TIS Report 65DE 5 1966.
20. A.B. Laconti, A.R. Fragala, and J.R. Boyack. In *Proceedings of the Symposium on Electrode materials and Process for Energy Conversion and Storage*, J.D.E. McIntyre, S. Srinivasan, and F.G. Wills (Eds.) p. 354, The Electrochemical Society Inc., Princeton, NJ, 1977.
21. A.B. Laconti. *The MIT/Marine Industry Collegium, Power Systems for Small Underwater Vehicles* Cambridge, MA, 1988.
22. G.G. Scherer. Polymer membranes for fuel-cells. *Berichte der Bunsen-Gesellschaft-Physical Chemistry Chemical Physics* 94, 1008 1990.
23. G.G. Scherer. *Berichte der Bunsen-Gesellschaft-Physical Chemistry Chemical Physics* 94, 145 1990.
24. Z.G. Qi and A. Kaufman. Improvement of water management by a microporous sublayer for PEM fuel cells. *Journal of Power Sources* 109, 38–46 2002.
25. U. Pasaogullari, C.Y. Wang, and K.S. Chen. Two-phase transport in polymer electrolyte fuel cells with bilayer cathode gas diffusion media. *Journal of the Electrochemical Society* 152, A1574–A1582 2005.
26. U. Pasaogullari and C.Y. Wang. Liquid water transport in gas diffusion layer of polymer electrolyte fuel cells. *Journal of the Electrochemical Society* 151, A399–A406 2004.
27. U. Pasaogullari and C.Y. Wang. Two-phase transport and the role of micro-porous layer in polymer electrolyte fuel cells. *Electrochimica Acta* 49, 4359–4369 2004.
28. US Patent 6890680. G. Beckmann, X. Ren, P.F. Mutolo, F.W. Kovacs, and S. Gottesfeld. MTI MicroFuel Cells Inc. Albany, NY, 2005.
29. P. Stonehart. Development of advanced noble metal-alloy electrocatalysts for phosphoric-acid fuel-cells (pa-fc). *Berichte der Bunsengesellschaft für Physikalische Chemie* 94, 913–921 1990.
30. P. Gode, G. Lindbergh, and G. Sundholm. In-situ measurements of gas permeability in fuel cell membranes using a cylindrical microelectrode. *Journal of Electroanalytical Chemistry* 518, 115–122 2002.
31. F.N. Büchi, M. Wakizoe, and S. Srinivasan. Microelectrode investigation of oxygen permeation in perfluorinated proton exchange membranes with different equivalent weights. *Journal of the Electrochemical Society* 143, 927–932 1996.
32. L. Zhang, C.S. Ma, and S. Mukerjee. Oxygen permeation studies on alternative proton exchange membranes designed for elevated temperature operation. *Electrochimica Acta* 48, 1845–1859 2003.
33. V.I. Basura, C. Chuy, P.D. Beattie, and S. Holdcroft. Effect of equivalent weight on electrochemical mass transport properties of oxygen in proton exchange membranes based on sulfonated alpha,beta,beta-trifluorostyrene (BAM (R)) and sulfonated styrene-(ethylene-butylene)-styrene triblock (DAIS-analytical) copolymers. *Journal of Electroanalytical Chemistry* 501, 77–88 2001.
34. K. Ota, Y. Inoue, N. Motohira, and N. Kamiya. Hydrogen oxidation and oxygen reduction at Pt microelectrode on polymer electrolytes. *Journal of New Materials for Electrochemical Systems* 3, 193–198 2000.
35. W.J. Liu, B.L. Wu, and C.S. Cha. Surface diffusion and the spillover of H-adatoms and oxygen-containing surface species on the surface of carbon black and Pt/C porous electrodes. *Journal of Electroanalytical Chemistry* 476, 101–108 1999.
36. M. Inaba, T. Kuroe, Z. Ogumi, Z. Takehara, K. Katakura, S. Ichikawa, and Y. Yamamoto. Oxygen permeation through perfluorinated carboxylate ion-exchange membranes. *Electrochimica Acta* 38, 1727–1731 1993.
37. D. Raistrick, J.W. Van Zee, R.E. White, K. Kinoshita, and H.S. Burney. *Symposium on Diaphragms, Separators and Ion Exchange Membranes*. The Electrochemical Society, Pennington, NJ, 1986.
38. F.N. Büchi and G.G. Scherer. Investigation of the transversal water profile in Nafion membranes in polymer electrolyte fuel cells. *Journal of the Electrochemical Society* 148, A183–A188 2001.
39. P. Schroeder. Über Erstarrungs- und Quellung sercheinungen von Gelatine, *Zeitschrift für Physikalische Chemie* 45, 75 1903.
40. K. Broka and P. Ekdunge. Oxygen and hydrogen permeation properties and water uptake of Nafion(R) 117 membrane and recast film for PEM fuel cell. *Journal of Applied Electrochemistry* 27, 117–123 1997.
41. A. Heinzl and V.M. Barragan. A review of the state-of-the-art of the methanol crossover in direct methanol fuel cells. *Journal of Power Sources* 84, 70–74 1999.
42. X. Ren, P. Zelenay, S. Thomas, J. Davey, and S. Gottesfeld. Recent advances in direct methanol fuel cells at Los Alamos National Laboratory. *Journal of Power Sources* 86, 111–116 2000.
43. X. Ren, T.E. Springer, and S. Gottesfeld. Water and methanol uptakes in Nafion membranes and membrane effects on direct methanol cell performance. *Journal of the Electrochemical Society* 147, 92–98 2000.

44. X.M. Ren, T.E. Springer, T.A. Zawodzinski, and S. Gottesfeld. Methanol transport through Nafion membranes—Electro-osmotic drag effects on potential step measurements. *Journal of the Electrochemical Society* 147, 466–474 2000.
45. X. Ren, T.A. Zawodzinski, and S. Gottesfeld. Water and methanol transport in membranes for direct methanol fuel cells. *Abstracts of Papers of the American Chemical Society* 217, U490 1999.
46. X.M. Ren, W. Henderson, and S. Gottesfeld. Electro-osmotic drag of water in ionomeric membranes: New measurements employing a direct methanol fuel cell. *Journal of the Electrochemical Society* 144, L267–L270 1997.
47. T.A. Zawodzinski, J. Davey, J. Valerio, and S. Gottesfeld. The water-content dependence of electroosmotic drag in proton-conducting polymer electrolytes. *Electrochimica Acta* 40, 297–302 1995.
48. S. Gottesfeld. Polymer electrolyte fuel-cells. *Electrochimica Acta* 40, 283 1995.
49. X.M. Ren and S. Gottesfeld. Electro-osmotic drag of water in poly(perfluorosulfonic acid) membranes. *Journal of the Electrochemical Society* 148, A87–A93 2001.
50. T.A. Zawodzinski, T.E. Springer, J. Davey, R. Jestel, C. Lopez, J. Valerio, and S. Gottesfeld. A comparative-study of water-uptake by and transport through ionomeric fuel-cell membranes. *Journal of the Electrochemical Society* 140, 1981–1985 1993.
51. T.A. Zawodzinski, T.E. Springer, F. Uribe, and S. Gottesfeld. Characterization of polymer electrolytes for fuel-cell applications. *Solid State Ionics* 60, 199–211 1993.
52. T.A. Zawodzinski, C. Derouin, S. Radzinski, R.J. Sherman, V.T. Smith, T.E. Springer, and S. Gottesfeld. Water-uptake by and transport through Nafion(R) 117 membranes. *Journal of the Electrochemical Society* 140, 1041–1047 1993.
53. T.A. Zawodzinski, J. Davey, J. Valerio, and S. Gottesfeld. Water transport-properties of various fuel-cell ionomers. *Abstracts of Papers of the American Chemical Society* 205, 75–PMSE 1993.
54. T.A. Zawodzinski, S. Gottesfeld, S. Shoichet, and T.J. McCarthy. The contact-angle between water and the surface of perfluorosulfonic acid membranes. *Journal of Applied Electrochemistry* 23, 86–88 1993.
55. H. Dohle, H. Schmitz, T. Bewer, J. Mergel, and D. Stolten. Development of a compact 500 W class direct methanol fuel cell stack, *Journal of Power Sources* 106, 313–322 2002.
56. H. Dohle, J. Mergel, and D. Stolten. Heat and power management of a direct-methanol-fuel-cell (DMFC) system, *Journal of power sources* 111, 268–282 2002.
57. M. Cappadonia, J.W. Erning, and U. Stimming. Proton conduction of Nafion(R)-117 membrane between 140 K and room-temperature. *Journal of Electroanalytical Chemistry* 376, 189–193 1994.
58. M. Cappadonia, J.W. Erning, S.M.S. Niaki, and U. Stimming. Conductance of Nafion-117 membranes as a function of temperature and water-content. *Solid State Ionics* 77, 65–69 1995.
59. S.J. Paddison, G. Bender, K.D. Kreuer, N. Nicoloso, and T.A. Zawodzinski. The microwave region of the dielectric spectrum of hydrated Nafion (R) and other sulfonated membranes. *Journal of New Materials for Electrochemical Systems* 3, 291–300 2000.
60. T.D. Gierke, G.E. Munn, and F.C. Wilson. The morphology in Nafion perfluorinated membrane products, as determined by wide-angle and small-angle x-ray studies. *Journal of Polymer Science Part B-Polymer Physics* 19, 1687–1704 1981.
61. M. Eikerling, Y.I. Kharkats, A.A. Kornyshev, and Y.M. Volfkovich. Phenomenological theory of electro-osmotic effect and water management in polymer electrolyte proton-conducting membranes. *Journal of the Electrochemical Society* 145, 2684–2699 1998.
62. S.J. Paddison. Proton conduction mechanisms at low degrees of hydration in sulfonic acid-based polymer electrolyte membranes. *Annual Review of Materials Research* 33, 289–319 2003.
63. J.A. Keres. Development of ionomer membranes for fuel cells. *Journal of Membrane Science* 185, 3–27 2001.
64. K.D. Kreuer. On the development of proton conducting polymer membranes for hydrogen and methanol fuel cells. *Journal of Membrane Science* 185, 29–39 2001.
65. M. Elomaa, S. Hietala, M. Paronen, N. Walsby, K. Jokela, R. Serimaa, M. Torkkeli, T. Lehtinen, G. Sundholm and F. Sundholm. The state of water and the nature of ion clusters in crosslinked proton conducting membranes of styrene grafted and sulfonated poly(vinylidene fluoride). *Journal of Materials Chemistry* 10, 2678–2684 2000.
66. M. Kawahara, M. Rikukawa, and K. Sanui. Relationship between absorbed water and proton conductivity in sulfopropylated poly (benzimidazole). *Polymers for Advanced Technologies* 11, 544–547 2000.
67. X. Ren, T.E. Springer, and S. Gottesfeld. Water and methanol uptakes in Nafion membranes and membrane effects on direct methanol cell performance. *Journal of the Electrochemical Society* 147, 92–98 2000.
68. K.D. Kreuer. In *Handbook of Fuel Cells: Fundamentals, Technology and Applications*, H.A. Gasteiger, W. Vielstich, and A. Lamm (Eds.) pp. 420–436, J. Wiley & Sons, Chichester, 2003.
69. D.S. Watkins, K. Dirks, and D. Epp. *33rd International Power Sources Symposium*, The Electrochemical Society. Pennington, NJ, 1988.
70. M. Wakizoe, O.A. Velev, and S. Srinivasan. Analysis of proton-exchange membrane fuel-cell performance with alternate membranes. *Electrochimica Acta* 40, 335–344 1995.
71. K.M. Cable, K.A. Mauritz, and R.B. Moore. Effects of hydrophilic and hydrophobic counterions on the coulombic interactions in perfluorosulfonate ionomers. *Journal of Polymer Science Part B-Polymer Physics* 33, 1065–1072 1995.
72. C. Zaluski and G. Xu. Blends of Nafion and Dow perfluorosulfonated ionomer membranes. *Macromolecules* 27, 6750–6754 1994.
73. G. Xu. High-resolution x-ray-scattering of ionic clusters in perfluorinated ionomers. *Polymer Journal* 26, 840–844 1994.
74. J. Halim, F.N. Buchi, O. Haas, M. Stamm, and G.G. Scherer. Characterization of perfluorosulfonic acid membranes by conductivity measurements and small-angle x-ray-scattering. *Electrochimica Acta* 39, 1303–1307 1994.
75. E.E. Boakye and H.L. Yeager. Water sorption and ionic-diffusion in short side-chain perfluorosulfonate ionomer membranes. *Journal of Membrane Science* 69, 155–167 1992.
76. T.A. Zawodzinski, T.E. Springer, J. Davey, R. Jestel, C. Lopez, J. Valerio, and S. Gottesfeld. A comparative-study of water-uptake by and transport through ionomeric fuel-cell membranes. *Journal of the Electrochemical Society* 140, 1981–1985 1993.

77. J.M. Zen, R. Manoharan, and J.B. Goodenough. Oxygen reduction on Ru-oxide pyrochlores bonded to a proton-exchange membrane. *Journal of Applied Electrochemistry* 22, 140–150 1992.
78. X.M. Ren and S. Gottesfeld. Electro-osmotic drag of water in poly(perfluorosulfonic acid) membranes. *Journal of the Electrochemical Society* 148, A87–A93 2001.
79. S. Srinivasan, D.J. Manko, H. Koch, M.A. Enayetullah, and A.J. Appleby. Recent advances in solid polymer electrolyte fuel-cell technology with low platinum loading electrodes. *Journal of Power Sources* 29, 367–387 1990.
80. S. Srinivasan, M.A. Enayetullah, S. Somasundaram, D.H. Swan, D. Manko, H. Koch and A.J. Appleby. *Proceedings of the 24th Intersociety Energy Conversion Engineering Conference (IECEC)*, 1989.
81. S. Srinivasan, E.A. Ticianelli, C.R. Derouin, and A. Redondo. Advances in solid polymer electrolyte fuel-cell technology with low platinum loading electrodes. *Journal of Power Sources* 22, 359–375 1988.
82. C. Boyer, S. Gamburzev, O. Velev, S. Srinivasan, and A.J. Appleby. Measurements of proton conductivity in the active layer of PEM fuel cell gas diffusion electrodes. *Electrochimica Acta* 43, 3703–3709 1998.
83. V. Arcella, A. Ghielmi, and G. Tommasi. High performance perfluoropolymer films and membranes. *Annals of the New York Academy of Sciences* 984, 226–244 2003.
84. L. Rivard, D. Pierpont, H. Freemyers, A. Thaler, and S. Hamrock. *Abstracts of the 2003 Fuel Cell Seminar* 2003.
85. US Patent 5547551. B. Bahar, A. Hobson, J. Kolde, and D. Zuckerbrod. 1996.
86. S. Cleghorn, J. Kolde, and W. Liu. In *Handbook of Fuel Cells: Fundamentals, Technology and Applications*, W. Vielstich, H.A. Gasteiger, and A. Lamm (Eds.) J. Wiley & Sons, Chichester, 2003.
87. W. Liu, K. Ruth, and G. Rusch. Membrane durability in PEM fuel cells. *Journal of New Materials for Electrochemical Systems* 4, 227–232 2001.
88. S. Hommura, Y. Kunisa, I. Terada, and M. Yoshitake. Characterization of fibril reinforced membranes for fuel cells. *Journal of Fluorine Chemistry* 120, 151–155 2003.
89. EP1139472. Y. Higuchi, I. Terada, H. Shimoda, and S. Hommura. 2001.
90. US Patent 00226883. Y. Higuchi, I. Terada, H. Shimoda, and S. Hommura. 2001.
91. K. Yamada, Y. Kunisa, M. Tsushima, M. Kawamoto, Y. Takimoto, J.-I. Tayanagi, and M. Yoshitake. *Abstracts of the 2003 Fuel Cell Seminar* 2003.
92. N. Yoshida, T. Ishisaki, A. Watakabe, and M. Yoshitake. Characterization of Flemion (R) membranes for PEFC. *Electrochimica Acta* 43, 3749 1998.
93. M. Wakizoe, T. Kodani, and T. Ota. *Abstracts of the 2003 Fuel Cell Seminar*. 2003.
94. X.Z. Du, J.R. Yu, B.L. Yi, M. Han, and K.W. Bi. Performances of proton exchange membrane fuel cells with alternate membranes. *Physical Chemistry Chemical Physics* 3, 3175–3179 2001.
95. J. Huslage, T. Rager, B. Schnyder, and A. Tsukada. Radiation-grafted membrane/electrode assemblies with improved interface. *Electrochimica Acta* 48, 247–254 2002.
96. WO 08581. J. Wei, C. Stone, and A.E. Steck. 1995.
97. G. Gebel, O. Diat, and C. Stone. Microstructure of BAM (R) membranes: A small-angle neutron scattering study. *Journal of New Materials for Electrochemical Systems* 6, 17–23 2003.
98. C. Stone, T.S. Daynard, L.Q. Hu, C. Mah, and A.E. Steck. Phosphonic acid functionalized proton exchange membranes for PEM fuel cells. *Journal of New Materials for Electrochemical Systems* 3, 43–50 2000.
99. P.D. Beattie, F.P. Orfino, V.I. Basura, K. Zychowska, J.F. Ding, C. Chuy, J. Schmeisser and S. Holdcroft: Ionic conductivity of proton exchange membranes. *Journal of Electroanalytical Chemistry* 503, 45–56 2001.
100. H.P. Brack, M. Wyler, G. Peter, and G.G. Scherer. A contact angle investigation of the surface properties of selected proton-conducting radiation-grafted membranes. *Journal of Membrane Science* 214, 1–19 2003.
101. S. Holmberg, P. Holmlund, C.E. Wilen, T. Kallio, G. Sundholm, and F. Sundholm. Synthesis of proton-conducting membranes by the utilization of preirradiation grafting and atom transfer radical polymerization techniques. *Journal of Polymer Science Part A: Polymer Chemistry* 40, 591–600 2002.
102. H.P. Brack, H.G. Buhner, L. Bonorand, and G.G. Scherer. Grafting of pre-irradiated poly(ethylene-alt-tetrafluoroethylene) films with styrene: Influence of base polymer film properties and processing parameters. *Journal of Materials Chemistry* 10, 1795–1803 2000.
103. H.P. Brack, F.N. Buchi, J. Huslage, M. Rota, and G.G. Scherer. *ACS Symposium Series* 744, pp. 174–188 2000.
104. B. Gupta, G.G. Scherer, and J.G. Highfield. Thermal stability of proton exchange membranes prepared by grafting of styrene into pre-irradiated FEP films and the effect of crosslinking. *Angewandte Makromolekulare Chemie* 256, 81–84 1998.
105. G.G. Scherer. Interfacial aspects in the development of polymer electrolyte fuel cells. *Solid State Ionics* 94, 249–257 1997.
106. B. Gupta, F.N. Buchi, G.G. Scherer, and A. Chapiro. Crosslinked ion exchange membranes by radiation grafting of styrene/divinylbenzene into FEP films. *Journal of Membrane Science* 118, 231–238 1996.
107. B. Gupta, F.N. Buchi, M. Staub, D. Grman, and G.G. Scherer. Cation exchange membranes by pre-irradiation crafting of styrene into FEP films. 2. Properties of copolymer membranes. *Journal of Polymer Science Part A: Polymer Chemistry* 34, 1873–1880 1996.
108. F.N. Buchi, B. Gupta, O. Haas, and G.G. Scherer. Performance of differently cross-linked, partially fluorinated proton-exchange membranes in polymer electrolyte fuel-cells. *Journal of the Electrochemical Society* 142, 3044–3048 1995.
109. B. Gupta, O. Haas, and G.G. Scherer. Proton-exchange membranes by radiation grafting of styrene onto FEP films. 4. Evaluation of the states of water. *Journal of Applied Polymer Science* 57, 855–862 1995.
110. B. Gupta, M. Staub, G.G. Scherer, and D. Grman. Surface nonhomogeneity in radiation grafted FEP-g-polystyrenesulfonic acid proton-exchange membranes. *Journal of Polymer Science Part A: Polymer Chemistry* 33, 1545–1549 1995.

111. F.N. Buchi, B. Gupta, O. Haas, and G.G. Scherer. Study of radiation-grafted FEP-g-polystyrene membranes as polymer electrolytes in fuel-cells. *Electrochimica Acta* 40, 345–353 1995.
112. G.G. Scherer, F.N. Buchi, and B. Gupta. Radiation grafted membranes for polymer electrolyte fuel-cells, exsitu and in situ characterization. *Abstracts of Papers of the American Chemical Society*, 205, 74–PMSE 1993.
113. G.G. Scherer, E. Killer, and D. Grman. Radiation grafted membranes—some structural investigations in relation to their behavior in ion-exchange-membrane water electrolysis cells. *International Journal of Hydrogen Energy*, 17, 115–123 1992.
114. N. Walsby. *Faculty of Science of the University of Helsinki*. Helsinki, 2001.
115. A.B. Geiger, T. Rager, L. Matejek, G.G. Scherer, and A. Wokaun. In *Proceedings of the 1st European PEFC Forum 2001*, F.N. Büchi, G.G. Scherer, and A. Wokaun (Eds.) 2001.
116. K. Scott, W.M. Taama, and P. Argyropoulos. Performance of the direct methanol fuel cell with radiation-grafted polymer membranes. *Journal of Membrane Science* 171, 119–130 2000.
117. US Patent 5523181. Stonehart P., Watanabe M., and Associates, S. 1993.
118. S.K. Young, W.L. Jarrett, and K.A. Mauritz. Studies of the aging of Nafion (R)/silicate nanocomposites using Si-29 solid state NMR spectroscopy. *Polymer Engineering and Science* 41, 1529–1539 2001.
119. K.A. Mauritz. Organic–inorganic hybrid materials: Perfluorinated ionomers as sol-gel polymerization templates for inorganic alkoxides. *Materials Science & Engineering C-Biomimetic and Supramolecular Systems* 6, 121–133 1998.
120. M.A.F. Robertson and K.A. Mauritz. Infrared investigation of the silicon oxide phase in [perfluoro-carboxylate/sulfonate (bilayer)]/[silicon oxide] nanocomposite membranes. *Journal of Polymer Science Part B-Polymer Physics* 36, 595–606 1998.
121. P.L. Shao, K.A. Mauritz, and R.B. Moore. [Perfluorosulfonate ionomer] [SiO<sub>2</sub>–TiO<sub>2</sub>] nanocomposites via polymer-in situ sol-gel chemistry: Sequential alkoxide procedure. *Journal of Polymer Science Part B-Polymer Physics* 34, 873–882 1996.
122. P.L. Shao, K.A. Mauritz, and R.B. Moore. [Perfluorosulfonate ionomer] [mixed inorganic oxide] nanocomposites via polymer in-situ sol-gel chemistry. *Chemistry of Materials* 7, 192–200 1995.
123. N. Miyake, J.S. Wainright, and R.F. Savinell. Evaluation of a sol-gel derived Nafion/silica hybrid membrane for polymer electrolyte membrane fuel cell applications. II. Methanol uptake and methanol permeability. *Journal of the Electrochemical Society* 148, A905–A909 2001.
124. K.T. Adjemian, S. Srinivasan, J. Benziger, and A.B. Bocarsly. Investigation of PEMFC operation above 100 degrees C employing perfluorosulfonic acid silicon oxide composite membranes. *Journal of Power Sources* 109, 356–364 2002.
125. K.T. Adjemian, S.J. Lee, S. Srinivasan, J. Benziger, and A.B. Bocarsly. Silicon oxide Nafion composite membranes for proton-exchange membrane fuel cell operation at 80–140 degrees C. *Journal of the Electrochemical Society* 149, A256–A261 2002.
126. G. Alberti and M. Casciola. Composite membranes for medium-temperature PEM fuel cells. *Annual Review of Materials Research* 33, 129–154 2003.
127. A.S. Arico, V. Baglio, V. Di Blasio, A. Di Blasi, E. Modica, P.L. Antonucci and V. Antonucci. Surface properties of inorganic fillers for application in composite membranes-direct methanol fuel cells. *Journal of Power Sources* 128, 113–118 2004.
128. P.L. Antonucci, A.S. Arico, P. Creti, E. Ramunni, and V. Antonucci. Investigation of a direct methanol fuel cell based on a composite Nafion (R)-silica electrolyte for high temperature operation. *Solid State Ionics* 125, 431–437 1999.
129. P. Dimitrova, K.A. Friedrich, U. Stimming, and B. Vogt. Modified Nafion(R)-based membranes for use in direct methanol fuel cells. *Solid State Ionics* 150, 115–122 2002.
130. H. Uchida, Y. Ueno, H. Hagihara, and M. Watanabe. Self-humidifying electrolyte membranes for fuel cells: Preparation of highly dispersed TiO<sub>2</sub> particles in Nafion 112. *Journal of the Electrochemical Society* 150, A57–A62 2003.
131. H. Uchida, Y. Mizuno, and M. Watanabe. Suppression of methanol crossover and distribution of ohmic resistance in Pt-dispersed PEMs under DMFC operation. *Journal of the Electrochemical Society* 149, A682–A687 2002.
132. H. Uchida, Y. Mizuno, and M. Watanabe. Suppression of methanol crossover in Pt-dispersed polymer electrolyte membrane for direct methanol fuel cells. *Chemistry Letters* 11, 1268–1269 2000.
133. M. Watanabe, H. Uchida, and H. Igarashi. Effects of polymer electrolyte membrane's property on fuel cell performances. *Macromolecular Symposia* 156, 223–230 2000.
134. B. Bonnet, D.J. Jones, J. Roziere, L. Tchicaya, G. Alberti, M. Casciola, L. Massinelli, B. Bauer, A. Peraio, and E. Ramunni. Hybrid organic–inorganic membranes for a medium temperature fuel cell. *Journal of New Materials for Electrochemical Systems* 3, 87–92 2000.
135. S.P. Nunes, B. Ruffmann, E. Rikowski, S. Vetter, and K. Richau. Inorganic modification of proton conductive polymer membranes for direct methanol fuel cells. *Journal of Membrane Science* 203, 215–225 2002.
136. M. Watanabe, H. Uchida, Y. Seki, M. Emori, and P. Stonehart. Self-humidifying polymer electrolyte membranes for fuel cells. *Journal of the Electrochemical Society* 143, 3847–3852 1996.
137. P.L. Antonucci, A.S. Arico, P. Creti, E. Ramunni, and V. Antonucci. Investigation of a direct methanol fuel cell based on a composite Nafion (R)-silica electrolyte for high temperature operation. *Solid State Ionics* 125, 431–437 1999.
138. P. Dimitrova, K.A. Friedrich, B. Vogt, and U. Stimming. Transport properties of ionomer composite membranes for direct methanol fuel cells. *Journal of Electroanalytical Chemistry* 532, 75–83 2002.
139. P. Dimitrova, K.A. Friedrich, U. Stimming, and B. Vogt. Modified Nafion(R)-based membranes for use in direct methanol fuel cells. *Solid State Ionics* 150, 115–122 2002.
140. B. Tazi and O. Savadogo. Effect of various heteropolyacids (HPAs) on the characteristics of Nafion(R)—HPAS membranes and their H<sub>2</sub>/O<sub>2</sub> polymer electrolyte fuel cell parameters. *Journal of New Materials for Electrochemical Systems* 4, 187–196 2001.

141. S. Malhotra and R. Datta. Membrane-supported nonvolatile acidic electrolytes allow higher temperature operation of proton-exchange membrane fuel cells. *Journal of the Electrochemical Society* 144, L23–L26 1997.
142. I. Honma, H. Nakajima, and S. Nomura. High temperature proton conducting hybrid polymer electrolyte membranes. *Solid State Ionics* 154, 707–712 2002.
143. G. Alberti, M. Casciola, and R. Palombari. Inorgano-organic proton conducting membranes for fuel cells and sensors at medium temperatures. *Journal of Membrane Science* 172, 233–239 2000.
144. G. Alberti, U. Costantino, M. Casciola, S. Ferroni, L. Massinelli, and P. Staiti. Preparation, characterization and proton conductivity of titanium phosphate sulfophenylphosphonate. *Solid State Ionics* 145, 249–255 2001.
145. G. Alberti and M. Casciola. Solid state protonic conductors, present main applications and future prospects. *Solid State Ionics* 145, 3–16 2001.
146. P. Costamagna, C. Yang, A.B. Bocarsly, and S. Srinivasan. Nafion (R) 115/zirconium phosphate composite membranes for operation of PEMFCs above 100 degrees C. *Electrochimica Acta* 47, 1023–1033 2002.
147. S. Haufe, D. Prochnow, D. Schneider, O. Geier, D. Freude, and U. Stimming. Polyphosphate composite: Conductivity and NMR studies. *Solid State Ionics* 176, 955–963 2005.
148. M. Cappadonia, O. Niemzig, and U. Stimming. Preliminary study on the ionic conductivity of a polyphosphate composite. *Solid State Ionics* 125, 333–337 1999.
149. T. Matsui, S. Takeshita, Y. Iriyama, T. Abe, M. Inaba, and Z. Ogumi. Proton conductivity of  $(\text{NH}_4)_2\text{TiP}_4\text{O}_{13}$ -based material for intermediate temperature fuel cells. *Electrochemistry Communications* 6, 180–182 2004.
150. T. Matsui, S. Takeshita, Y. Iriyama, T. Abe, and Z. Ogumi. Proton-conductive electrolyte consisting of  $\text{NH}_4\text{PO}_3/\text{TiP}_2\text{O}_7$  for intermediate-temperature fuel cells. *Journal of the Electrochemical Society* 152, A167–A170 2005.
151. T. Uma, H.Y. Tu, D. Freude, D. Schneider, and U. Stimming. Characterisation of intermediate temperature polyphosphate composites. *Journal of Materials Science* 40, 227–230 2005.
152. S. Haufe and U. Stimming. *Journal of Membrane Science* 185, 95–103 2001.
153. E. Peled, T. Duvdevani, and A. Melman. A novel proton-conducting membrane. *Electrochemical and Solid-State Letters* 1, 210–211 1998.
154. E. Peled, T. Duvdevani, A. Aharon, and A. Melman. A direct methanol fuel cell based on a novel low-cost nanoporous proton-conducting membrane. *Electrochemical and Solid-State Letters* 3, 525–528 2000.
155. J. Roziere and D.J. Jones. Non-fluorinated polymer materials for proton exchange membrane fuel cells. *Annual Review of Materials Research* 33, 503–555 2003.
156. J.S. Wainright, M.H. Litt, and R.F. Savinell. In *Handbook of Fuel Cells: Fundamentals, Technology and Applications*, W. Vielstich, H.A. Gasteiger, and A. Lamm (Eds.) J. Wiley & Sons, Chichester, 2003.
157. A. Schechter and R.F. Savinell. Imidazole and 1-methyl imidazole in phosphoric acid doped polybenzimidazole, electrolyte for fuel cells. *Solid State Ionics* 147, 181–187 2002.
158. R.H. He, Q.F. Li, G. Xiao, and N.J. Bjerrum. Proton conductivity of phosphoric acid doped polybenzimidazole and its composites with inorganic proton conductors. *Journal of Membrane Science* 226, 169–184 2003.
159. B. Xing and O. Savadogo. Hydrogen/oxygen polymer electrolyte membrane fuel cells (PEMFCs) based on alkaline-doped polybenzimidazole (PBI). *Electrochemistry Communications* 2, 697–702 2000.
160. Q.F. Li, H.A. Hjuler, and N.J. Bjerrum. Oxygen reduction on carbon supported platinum catalysts in high temperature polymer electrolytes. *Electrochimica Acta*, 45, 4219–4226 2000.
161. O. Savadogo and B. Xing. Hydrogen/oxygen polymer electrolyte membrane fuel cell (PEMFC) based on acid-doped polybenzimidazole (PBI). *Journal of New Materials for Electrochemical Systems* 3, 343–347 2000.
162. P. Staiti, M. Minutoli, and S. Hocevar. Membranes based on phosphotungstic acid and polybenzimidazole for fuel cell application. *Journal of Power Sources* 90, 231–235 2000.
163. B.Z. Xing and O. Savadogo. The effect of acid doping on the conductivity of polybenzimidazole (PBI). *Journal of New Materials for Electrochemical Systems* 2, 95–101 1999.
164. M. Kawahara, J. Morita, M. Rikukawa, K. Sanui, and N. Ogata. Synthesis and proton conductivity of thermally stable polymer electrolyte: Poly(benzimidazole) complexes with strong acid molecules. *Electrochimica Acta* 45, 1395–1398 2000.
165. S.K. Zecevic, J.S. Wainright, M.H. Litt, S.L. Gojkovic, and R.F. Savinell. Kinetics of O-2 reduction on a Pt electrode covered with a thin film of solid polymer electrolyte. *Journal of the Electrochemical Society* 144, 2973–2982 1997.
166. S.R. Samms, S. Wasmus, and R.F. Savinell. Thermal stability of proton conducting acid doped polybenzimidazole in simulated fuel cell environments. *Journal of the Electrochemical Society* 143, 1225–1232 1996.
167. J.T. Wang, R.F. Savinell, J. Wainright, M. Litt, and H. Yu. A H-2/O-2 fuel cell using acid doped polybenzimidazole as polymer electrolyte. *Electrochimica Acta* 41, 193–197 1996.
168. Q.F. Li, H.A. Hjuler, and N.J. Bjerrum. Phosphoric acid doped polybenzimidazole membranes: Physicochemical characterization and fuel cell applications. *Journal of Applied Electrochemistry* 31, 773–779 2001.
169. R.F. Savinell, M.H. Litt, and J.S. Wainright. In *Presentation: High Temperature Polymer Electrolyte for PEM Fuel Cells* 2001.
170. T.A. Zawodzinski, M. Neeman, L.O. Sillerud, and S. Gottesfeld. Determination of water diffusion-coefficients in perfluorosulfonate ionomeric membranes. *Journal of Physical Chemistry* 95, 6040–6044 1991.
171. M. Casciola, F. Marmottini, and A. Peraio. AC conductivity of alpha-layered zirconium-phosphate in the presence of water vapour at 100–200°C. *Solid State Ionics* 61, 125–129 1993.

172. G. Alberti, L. Boccali, M. Casciola, L. Massinelli, and E. Montoneri. Protonic conductivity of layered zirconium phosphonates containing  $-SO_3H$  groups. III Preparation and characterization of gamma-zirconium sulfoaryl phosphonates. *Solid State Ionics* 84, 97–104 1996.
173. G. Alberti. Semaine d'étude sur le thème membranes biologiques et artificielles et la desalinisation de l'eau, ed. R. Passino, pp. 629–669. Città del Vaticano: Pontificia Acad. d. Sci. 17, 1975.
174. G. Alberti, unpublished results.

## *Section III*

---

*Membrane Applications in Industrial Waste Management (Including Nuclear), Environmental Engineering, and Future Trends in Membrane Science*



---

# 28 Membrane Applications in Industrial Waste Management (Including Nuclear), Environmental Engineering, and Future Trends in Membrane Science: Introduction

*Ana Maria Sastre and Anil Kumar Pabby*

## CONTENTS

28.1 Industrial Effluent Generated by the Chemical Industry .....	823
28.2 Waste Generated by the Nuclear Industry .....	824
References .....	825

Industrial development in this century will be characterized by technologies that allow not only less consumption of raw materials and energy but also permit recovery and reuse of all process streams with least damage to the environment. Membrane science and technology has a big role to play in this changing industrial environment. Membrane-based separation technology has now reached to full-fledged commercial environmental friendly technology to answer the multifarious demands of industry. The growth of membrane science is largely due to the impressive developments in the field of membrane material science and the evolution of different membrane-related equipment.

This section deals with the application of membranes in the treatment of industrial effluent generated by the chemical industries and waste generated by the nuclear industries. Also, this section focuses on important perspectives on environmental engineering with respect to chemical and nuclear waste processing. Before going into the details of the processes used for this purpose, one should understand the background of these types of waste.

### 28.1 INDUSTRIAL EFFLUENT GENERATED BY THE CHEMICAL INDUSTRY

As a result of the growing world population and rapid industrial development, an increasing amount of wastewater is produced worldwide. Wastewater contaminants may eventually enter the food chain and cause severe health and environmental problems. As a result, many countries have been introducing increasingly stringent wastewater regulations to minimize wastewater-related pollution. Current and impending legislation on wastewater effluent discharge has led to the need for enhanced treatment processes that are capable of removing toxic metal ions, high percentages of BOD, suspended solids, nitrogen, phosphorus, bacteria, and other contaminants.

Many conventional wastewater treatment processes that have long been in use are now considered impractical because they require a large amount of space, a large number of unit operations, and are affected by problems associated with odor and other emissions. Recent years have seen an increasing trend toward process intensification, which has led to the development of advanced membrane processes that are simple to construct and operate, have well-defined flow patterns, better dispersion effects, relatively low power consumption, lower emissions, and high mass-transfer performance, which are compact and recyclable.

The treatment and safe disposal of waste is equally important whether it be waste generated by the pulp and paper industry, by the leather industry or gaseous waste. Recently, in addition to other membrane-based processes, demand has grown in the wastewater treatment industry for a process that uses both a biological stage and a membrane module, known as the membrane bioreactor (MBR) process. The bioreactor and membrane module each have a specific function: (1) the biological degradation

of organic pollution is carried out in the bioreactor by adapted microorganisms and (2) the separation of microorganisms from the treated wastewater is performed by the membrane module. The membranes constitute a physical barrier for all suspended solids and therefore enable not only the recycling of the activated sludge in the bioreactor but also the production of a permeate that does not contain suspended matter, bacteria, or viruses.

## 28.2 WASTE GENERATED BY THE NUCLEAR INDUSTRY

The nuclear industry generates a broad spectrum of low and intermediate level liquid radioactive wastes (LRWs). These liquid wastes may be produced continuously or in batches and may vary considerably in volume, radioactivity, and chemical composition. A wide range of treatment methods have been used throughout the industry to treat these wastes. Treatment methods for LRWs have tended to use the same conventional processes found in industrial and municipal water treatment. These processes typically include chemical treatment, adsorption, filtration, ion exchange, and evaporation. They are limited by either their inability to remove all contaminants or, in evaporation, the high operating costs involved and the large quantities of secondary solid waste produced, which means that satisfactory processing of LRWs is difficult to achieve.

It has been demonstrated that membrane separation processes can be successfully used in the removal of radioactive substances, with some distinct advantages over conventional processes. Following the development of suitable membrane materials and their long-term verification in conventional water purification, membrane processes have been adopted by the nuclear industry as a viable alternative for the treatment of radioactive liquid wastes [1]. In most applications, membrane processes are used as one or more of the treatment steps in complex waste treatment systems, which combine both conventional and membrane treatment technologies. These combined systems have proved more efficient and effective for similar tasks than conventional methods alone.

This section aims to explain the unique features of membrane separation methods, their superior performance in contaminant removal, and their operational sensitivities and limitations. We focus particularly on the factors that need to be carefully assessed when the membrane technology to be used in the treatment of liquid radioactive waste is being considered. These include membrane configuration and arrangement, process application, operational experience, data related to key performance parameters, and plant and organizational impacts.

The use of liquid membranes for the separation of actinides in the nuclear industry is still in its infancy [2]. In the past few decades, exotic reagents such as crown ethers and calixarenes have been used for the selective complexation and removal of actinides from solutions containing complex mixtures of metal ions. However, a recently developed, nondispersive solvent extraction method using a hollow fiber membrane contactor has been used successfully at pilot plant scale with no stability problems. In this method, an organic extractant dissolved in the diluent is passed directly through the shell side of hollow fiber contactors [3]. This technique continuously fills the pores of the membrane with extractant. However, it should be noted that hydrophobic membranes are only impregnated in the liquid membrane technique before the experimental run and the feed and strip solutions are passed through the tube and shell sides, respectively. Another improved technique was to use microporous hollow fiber contactors as an alternative to the direct dispersion of ELMs to minimize membrane swelling and leakage. Hollow fiber contactors do not have the high shear rates that are typical of the agitators used in direct dispersion. This technique has been successfully applied in the removal and recovery of strategic and precious metals from wastewaters and process streams (Chapter 39) and is variously known as supported liquid membrane with strip dispersion (SLMSD), pseudo-emulsion based hollow fiber strip dispersion (PEHFSD), or emulsion pertraction technology (EPP). In this case, the organic (extractant dissolved in diluent) and back-extraction phases are emulsified before injection into the HF module and can be separated at the module outlet. PEHFSD has the following advantages over standard extraction and other membrane processes: (1) extraction and stripping can be carried out in a single operation; (2) there is no possibility of emulsion formation in the water phase; (3) the volume of extractant is relatively small and the process parameters are very flexible; (4) phase separation is not necessary; (5) the hollow fiber membranes and short diffusion paths provide a large specific surface area; and (6) the modular equipment is compact and energy consumption is low.

The membrane separation processes listed are at different stages of development and implementation. While some processes have been widely adopted, others are still under development and some are currently making the transition to industrial use. This section contains chapters that describe the use of various membrane techniques for the treatment of nuclear waste generated by the chemical industry. This chapter gives an introduction to all the chapters in the section. Chapter 29 focuses on the introduction, fundamentals, and scope of membrane processes for the treatment of nuclear waste from various sources. Chapter 30 details advances in membrane processes for nuclear waste processing and describes the current global situation of membrane processes for the treatment of nuclear waste. This chapter also covers the future role of membrane processes in nuclear technology and the advantages and limitations of applied membrane processes. Chapter 31 deals with advances in the field of liquid membranes and their application in the separation of actinides. The present review is a compilation of literature reports on liquid membrane-based separation studies dealing mainly with those actinides that are a long-term environmental hazard. Chapters 32 and 33 present case studies on the treatment of radioactive waste generated in a hospital and in a reprocessing plant, respectively. Chapter 34 presents selective coagulant recovery using the Donnan

membrane process (DMP). A non-pressure-driven DMP, also referred to as Donnan dialysis, is analyzed as a technique for alum recovery. This process is based on the Donnan exclusion principle, according to which negatively charged cation-exchange membranes are impermeable to anions and positively charged anion-exchange membranes are impermeable to cations. Unlike pressure-driven processes such as reverse osmosis, nanofiltration, and ultrafiltration, authors claim that DMP is free from surface fouling by natural organic matter (NOM). The process is able to recover alum that is virtually free of dissolved organic carbon, in which trihalomethane can be formed during the chlorination step in water treatment.

Membrane technology may become essential if zero-discharge mills become a requirement or legislation on water use becomes very restrictive. The type of membrane fractionation required varies according to the use that is to be made of the treated water. This issue is addressed in Chapter 35, which describes the application of membrane processes in the pulp and paper industry for treatment of the effluent generated. Chapter 36 focuses on the application of membrane bioreactors in wastewater treatment. Chapter 37 describes the applications of hollow fiber contactors in membrane-assisted solvent extraction for the recovery of metallic pollutants. The applications of membrane contactors in the treatment of gaseous waste streams are presented in Chapter 38. Chapter 39 deals with an important development in the strip dispersion technique for actinide recovery/metal separation. Chapter 40 focuses on electrically enhanced membrane separation and catalysis. Chapter 41 contains important case studies on the treatment of effluent in the leather industry. The case studies cover the work carried out at pilot plant level with membrane bioreactors and reverse osmosis. Development in nanofiltration and a case study on the recovery of impurity-free sodium thiocyanate in the acrylic industry are described in Chapter 42.

The early membranologists have always been optimistic about the possibilities of membrane operations, but the scientific and technical results reached today are even superior to the expectation. A variety of technical challenges must be overcome to permit the successful industrial application of new membrane solutions. Chapter 43, on the same theme, presents the future scenario of membrane processes covering chemical, biotechnological, pharmaceutical applications, etc., and also focusing future progresses in membrane engineering.

## REFERENCES

1. IAEA Technical Reports Series No. 431. 2005. Application of Membrane Technologies for Liquid Radioactive Waste Processing, pp. 1–145. Consultants: Pabby A.K., Kohout R. (Canada), and Tapsell G. (Australia) [<http://www.iaea.org/Publications/index.html>].
2. Sastre A.M., Pabby A.K., Shukla J.P., and Singh R.K., Improved techniques in liquid membrane separations: An overview. *Sep. Purif. Meth.* 27, 213–298, 1998.
3. Pabby A.K. and Sastre A.M. Developments in non-dispersive membrane extraction–separation processes. In *Ion Exchange and Solvent Extraction*, A.K. Sengupta and Y. Marcus (Eds.), Chapter 8, Vol. 15, Marcel Dekker, New York, 2001, pp. 313–469.



---

# 29 Treatment of Radioactive Effluents: Introduction, Fundamentals, and Scope of Different Membrane Processes

*B.M. Misra and V. Ramachandhran*

## CONTENTS

29.1	Introduction .....	827
29.2	Sources and Characteristics of Radioactive Wastes .....	828
29.3	Processes for Treatment of Radioactive Wastes .....	828
29.3.1	Evaporation .....	828
29.3.2	Chemical Treatment .....	829
29.3.3	Sorption and Ion Exchange .....	829
29.3.4	Membrane Processes .....	829
29.3.5	Reverse Osmosis .....	831
	29.3.5.1 Transport in Reverse Osmosis Process .....	832
29.3.6	Nanofiltration .....	833
29.3.7	Ultrafiltration .....	833
29.3.8	Precipitation Ultrafiltration .....	834
29.3.9	Complexation Ultrafiltration .....	834
29.3.10	Microfiltration .....	836
29.3.11	Osmotic Concentrator .....	836
29.3.12	Electrodialysis .....	836
29.3.13	Electrodeionization .....	838
29.3.14	Diffusion Dialysis and Donnan Dialysis .....	838
29.3.15	Liquid Membranes .....	839
29.3.16	Membrane Electrolyzers for Production of Uranyl Nitrate .....	840
29.3.17	Radiation Effect on Polymeric Membranes .....	840
	References .....	840

## 29.1 INTRODUCTION

Since the breakthrough in synthesis of semipermeable membranes for seawater desalination by reverse osmosis (RO) process in the early 60s, research and development work on membrane technology has been growing steadily. Novel polymeric membrane systems and compact module designs with better performance and newer applications for membrane technology are continuously being reported. The application of membrane technology to the treatment of process streams generated in chemical industries is a subject matter deserving serious attention in the context of rapid industrialization. Nuclear industry covers a wide spectrum of complex chemical operations and hence membrane technology finds several suitable areas of applications, particularly in the field of management of radioactive wastes.

A typical nuclear industry may consist of mining and milling of uranium ore, thorium extraction, fuel fabrication, nuclear reactor operation, and production and application of radioactive isotopes for various industrial medical and research purposes. Almost, in all these steps, waste is generated that needs proper management. Radioactive wastes differ from other industrial wastes due to its radiation exposure and its radiological toxicity to human beings and their environment. Management of radioactive wastes is an important step in a nuclear industry and the objective is to effectively isolate radionuclides from the

**TABLE 29.1**  
**Categorization of Radioactive Wastes**

Category	Solid Surface Dose (mGy/h)	Liquid Activity Level (Bq/m <sup>3</sup> )	Gaseous Activity Level (Bq/m <sup>3</sup> )
I	<2	<3.7 × 10 <sup>4</sup>	<3.7
II	2–20	3.7 × 10 <sup>4</sup> to 3.7 × 10 <sup>7</sup>	3.7 to 3.7 × 10 <sup>4</sup>
III	>20	3.7 × 10 <sup>7</sup> to 3.7 × 10 <sup>9</sup>	>3.7 × 10 <sup>4</sup>
IV	Alpha bearing	3.7 × 10 <sup>9</sup> to 3.7 × 10 <sup>14</sup>	—
V	—	>3.7 × 10 <sup>14</sup>	—

environment to ensure adequate safety and welfare to the public. Since the advent of nuclear power, the search for more effective and efficient technology for the treatment of radioactive wastes has continued.

## 29.2 SOURCES AND CHARACTERISTICS OF RADIOACTIVE WASTES

The main sources of radioactive waste are generated from operation of nuclear reactors and fuel-reprocessing plants. These wastes contain, in varying concentrations, a wide spectrum of fission products, which are beta–gamma active, and actinides possessing alpha activity. Most of the radioactivity is in the form of radioactive cations and complex anions. The liquid wastes from nuclear reactors have high volumes of dilute chemicals with low radioactivity, while reprocessing plants contain almost 99% of the total inventory of radioactivity in the whole fuel cycle that is contained in a relatively small volume. Radioactive wastes are conventionally classified as belonging to various categories depending upon the level of radioactivity. Table 29.1 gives the categories of radioactive wastes [1]. Effluents containing significant quantities of alpha-active isotopes (actinides) in addition to some beta–gamma activity are specified as alpha wastes. Reprocessing plants generate all types of wastes whereas effluents generated in a nuclear reactor have generally low to intermediate level radioactivity with insignificant amount of alpha-active actinides. In both these waste streams, the concentration of two fission product isotopes, namely, <sup>137</sup>Cs and <sup>90</sup>Sr is generally high. With their long half-lives (30 and 28 years, respectively), these elements are important in the treatment of wastes. Actinides have still longer half-lives, of the order of 10<sup>4</sup> to 10<sup>6</sup> years and demand attention because of their sustained radioactivity over much longer period.

## 29.3 PROCESSES FOR TREATMENT OF RADIOACTIVE WASTES

A typical high-level waste contains radioactivity of the order of 3.7 × 10<sup>9</sup> to 3.7 × 10<sup>14</sup> Bq/m<sup>3</sup> in molar concentration of nitric acid. Corrosion products, alloying elements, fission products, actinides, and chemicals introduced during fuel reprocessing are the major constituents of high-level wastes. In addition to the high levels of radioactivity, there is substantial solution heating from radionuclide decay. The combination of heat generation and radioactivity requires quite selective treatment. The treatment of high-level radioactive wastes involves conversion of these wastes into inert matrix such as glass or ceramics with the help of suitable additives. In vitrification, immobilization of radioactivity together with volume reduction is achieved.

For the treatment of low and intermediate level wastes, three processes are generally adopted, namely, chemical precipitation, ion exchange, and evaporation. The efficiency of the treatment scheme is judged by the values of decontamination factor (DF) and volume reduction factors (VRFs), which are defined as follows:

$$\text{Decontamination factor} = \frac{\text{Concentration of radioactivity in the waste before treatment}}{\text{Concentration of radioactivity in the waste after treatment}}$$

$$\text{Volume reduction} = \frac{\text{Initial volume of the waste}}{\text{Final volume of the waste}}$$

### 29.3.1 EVAPORATION

Among the processes mentioned above, evaporation is an efficient process providing very high DFs (10<sup>3</sup>–10<sup>4</sup> typically, with enhancements up to 10<sup>6</sup>) in the distillate, which is suitable for release to the environment. The concentrate exists as a thick liquid of small volume and contains most of the activity together with concentrated salts. The process is nonselective, concentrating all the constituents that are in solution. Evaporation is costly, as it is energy intensive and is used only for the treatment of low volumes of wastes (10–100 L/min) containing moderate levels of radioactivity with low or high concentration of salts.

### 29.3.2 CHEMICAL TREATMENT

Chemical treatment is a well-proven technique and is less expensive. Generally, specific chemical precipitation is carried out in situ in big tanks holding the radioactive waste stream to remove radionuclides while permitting nonradioactive ions to be released in the effluent from the process. The radionuclides present in the waste are precipitated, co-precipitated, carrier precipitated, or adsorbed by insoluble compounds. A clariflocculator is used for flocculation and clarification. This technique is used as a batch or a semibatch process for large volumes of effluents containing only low concentrations of activity. It provides lower DF values (10–100) than evaporation.

### 29.3.3 SORPTION AND ION EXCHANGE

Sorption is a general term commonly used to describe the uptake of radionuclides (ionic or nonionic) by certain materials (sorbents). Ion exchange, specifically, refers to the process of reversible exchange of ions having charges of the same sign between an electrolyte solution and the ion exchanger. Conventional organic ion-exchange resins are not very selective as they remove both radioactive and nonradioactive materials. In many waste streams originating from nuclear installations, the concentrations of nonradioactive constituents are many times ( $>10^6$ ) greater than the radioactive contaminants. Hence, these are normally suitable for decontamination of relatively clean solutions with low salt content. Once resins are loaded with contaminants, they can be regenerated, washing off the collected contaminants into a small volume that may then be immobilized or further volume reduced by evaporation before solidification. The resin can be reused.

Synthetic ion-exchange resins based on phenolic resins have shown promise in radioactive liquid waste treatment containing high inactive concentrations of ions. In alkaline solutions, these resins show very high uptake of cesium due to the ionization of phenolic hydroxyl groups at high pH. Resorcinol-formaldehyde polycondensate resins have also been successfully tested for efficient removal of radioactive cesium from alkaline-reprocessing wastes containing large concentrations of sodium ions. Incorporation of iminodiacetic acid functional groups into the phenolic polymer matrix gives it the additional feature of strontium uptake by chelation. These resins are presently being used on a large scale [2]. Inorganic sorbents/ion exchangers have higher thermal, radiation, chemical stability, and higher selectivity for certain ions and they are more compatible with various immobilization matrices. Vermiculite, a naturally occurring aluminosilicate mineral, is well known for its selective uptake of cesium followed by irreversible trapping due to lattice contraction. Among other promising irreversible sorbents potassium cobalt(II) hexacyanoferrate(II), ammonium molybdophosphate (AMP), resorcinol-formaldehyde polycondensate resin are noteworthy.

### 29.3.4 MEMBRANE PROCESSES

A major deficiency of conventional treatment systems is their inability to make use of a single-process separation for all the dissolved constituents on a molecular or ionic level. Membrane processes operate at ambient temperature and offer one-step separation for all the dissolved constituents on molecular or ionic level without any need for further chemical addition. Table 29.2 gives the application of different membrane processes for diverse contaminants.

Among the disadvantages, the fouling and degradation of membrane surfaces of the polymeric membrane systems under adverse chemical and thermal conditions are often cited. However, these problems may be partly overcome by proper pretreatment of the effluents, optimizing the process variables and selecting suitable membrane materials. The radioactive wastes most suited for membrane separation are characterized by chemically insignificant amounts of radionuclides and small amounts (few hundred parts per million) of inactive ionic species.

In membrane processes, a solute is defined as the chemical species which does not selectively permeate through the membrane barrier and thereby getting enriched on the high-pressure side of the membrane. Permeate refers to the chemical

**TABLE 29.2**  
**Membrane Process for Diverse Contaminants**

Species	Membrane Processes
Particulates	Microfiltration
Colloids	Microfiltration
High-molecular-weight organics	Ultrafiltration (UF)
Middle-molecular-weight organics large ionics	UF/NF
Low-molecular-weight organics ionics	NF/RO
Ionic contaminants	Electrodialysis/RO
Acids	Diffusion dialysis

**TABLE 29.3**  
**Characteristics of Principal Membrane Separation Processes**

Process	Driving Force	Objective
Gas, vapor, and organic liquid permeation	Concentration gradient (pressure, temperature assisted)	Product enriched in a desired component
Dialysis	Concentration gradient	Solution of macromolecules free of microsolutes
Electrodialysis	Electric potential	Solvent free of ionic solutes Concentration of ionic solutes Ion replacement Fractionation of electrolytes
Microfiltration	Pressure	Sterile, particle-free solution
UF	Pressure	Solution of macro solutes free of microsolutes
NF	Effective pressure	Removal of organics, dyes from effluents Fractionation of electrolytes
RO	Effective pressure	Solvent free of all solutes Concentration of solution

species, which selectively permeate through the membrane barrier and thereby getting enriched on the low-pressure side of the membrane. Recovery refers to the quantity of the permeate obtained by the membrane process for a given quantity of feed sent through the system and it is often expressed as either a fraction or in percentage.

The basis design objectives in these systems aim at high VRFs, corresponding to permeate recovery factor of more than 0.9 and a decontamination factor of at least 10 corresponding to solute rejection of more than 90%. Membrane processes are used in radioactive waste treatment primarily to reduce the volume of the waste that is achieved by redistributing the activity in two phases: one depleted of radioactivity having the majority of the original volume and the other concentrated in a lesser volume. The dilute phase depleted in radioactivity (permeate) may be released to the environment if the permeate meets the regulatory guidelines set for its discharge. The concentrated stream (retentate) must be subjected to secondary treatment. Preconcentration by membrane processes is considered desirable from the point of view of generating low volumes of final waste that can be further processed before it is sent for safe disposal. Membrane separation processes offer the possibility of treatment at the point of generation, leading to a much smaller volume of concentrate that has to be transported to a centralized treatment plant.

Membranes are synthetic barriers across which selective permeation of the desired species can be effected by employing appropriate driving force like electric potential, hydrostatic pressure, or concentration gradient. Characteristics of principal membrane processes are given in Table 29.3.

Membrane processes are classified according to the nature of the membrane and the driving force employed. A number of different types of polymeric/inorganic membranes have been developed in recent times in basically four types of modular assemblies, namely, plate and frame, spiral, tubular, and hollow fine fiber. Table 29.4 gives the application of various membrane processes for the separation of different types of contaminants encountered in effluents.

For radioactive effluent treatment, the relevant membrane processes are microfiltration, ultrafiltration (UF), reverse osmosis, electrodialysis, diffusion, and Donnan dialysis and liquid membrane processes and they can be used either alone or in conjunction with any of the conventional processes. The actual process selected would depend on the physical, physico-chemical, and radiochemical nature of the effluents. The basic factors which help in the design of an appropriate system are permeate quality, decontamination, and VRFs, disposal methods available for secondary wastes generated, and the permeate.

**TABLE 29.4**  
**Membrane Applications for Different Contaminants**

Contaminant species	Membrane process
Particulate matter and suspensions	Microfiltration
Colloidal impurities	Microfiltration
High-molecular-weight organics	UF
Middle-molecular-weight organics	UF
Low-molecular-weight organics	NF, RO
Multivalent ionic solutes	NF, RO
Acids	Diffusion dialysis

For example, in fission product effluents where radio-contaminants having longer half-lives are present, the emphasis should be on very high volume reduction with permissible/acceptable decontamination factors so that the permeate could be directly discharged. For effluents contaminated with radionuclides of short half-lives, a good decontamination with reasonable volume reduction may be acceptable because the concentrate could be stored till the activities decay before discharge. The radioactive effluents requiring treatment may vary with respect to the type of radionuclide, its chemical nature, concentration, pH, concentration of inactive solutes, and presence of suspended matter.

### 29.3.5 REVERSE OSMOSIS

Reverse osmosis (RO) involves the passage of solvent through a semipermeable membrane, when a solution is pressurized in excess of its own osmotic pressure. This method uses high pressures (2–4 MPa) to force water through a semipermeable membrane that presents an effective barrier to permeation of ionic species or large molecules. It thus produces a concentrated solution (retentate)-limited to about 0.8 M by osmotic pressure considerations and a dilute (permeate) water stream with a decontamination factor of 10–100 in dissolved salts, for a single-stage process. The lower range is representative of monovalent species, the higher for divalent or trivalent species that are strongly rejected. Still higher values may be expected for alpha emitters owing to their larger atomic/molecular size. The possibility of radioactive effluent treatment by RO was recognized in the early 70s and several studies have been reported on the laboratory scale as well as on the pilot plant scale. Several systems are now in routine use in nuclear installations around the world. A typical flow sheet of a reverse osmosis plant for waste treatment is given in Figure 29.1.

Radioactive waste treatment applications have been reported [3–9] for the laundry wastes from nuclear power plants and mixed laboratory wastes. Another interesting application of reverse osmosis process is in decontamination of boric acid wastes from pressurized heavy water reactors (PHWRs), which allows for the recovery of boric acid, by using the fact that the latter is relatively undissociated and hence will pass with water through the membrane while most of the radioactivity is retained [10]. Reverse osmosis was evaluated for treating fuel storage pool water, and for low-level liquid effluents from reprocessing plants.

A variety of reverse osmosis membrane systems based on cellulose acetate, aromatic polyamides, and other polymers have been tested for their potential applications. Reverse osmosis membrane equipment is available for large-scale operation since the process is widely used for the production of potable water from sea or brackish waters and upstream of ion exchange in the preparation of ultrapure water for steam-generating boilers. In these applications, the feed concentrations may vary from 500 to 40,000 mg/L of dissolved solids. The RO technique can be used at pH values between 3 and 12 and up to 45°C.

In radioactive waste treatment, significant operational aspects include the following. Since the operation requires the use of high pressures, there is a need to ensure control of the activity release from possible leaks. As with evaporation, pretreatment of the feed may be necessary to prevent scaling, and where dirty waters are to be fed directly it would be advisable to consider the use of equipment with larger membrane flow channels, which would permit periodic foam ball cleaning of the membrane surface.

Reverse osmosis is a preconcentration technique and the concentrates, depending on the inactive load, can be sent to evaporation or chemical precipitation step. The permeate, depending on the radioactivity level, may be either discharged directly or released after passing the water through polishing columns. Normally, the decontamination factor achievable varies from a few tens to hundreds, depending on the nature of the input stream, and the membrane. The VRFs depend on the inactive salt load, operating pressure, and the selectivity of the membrane used.

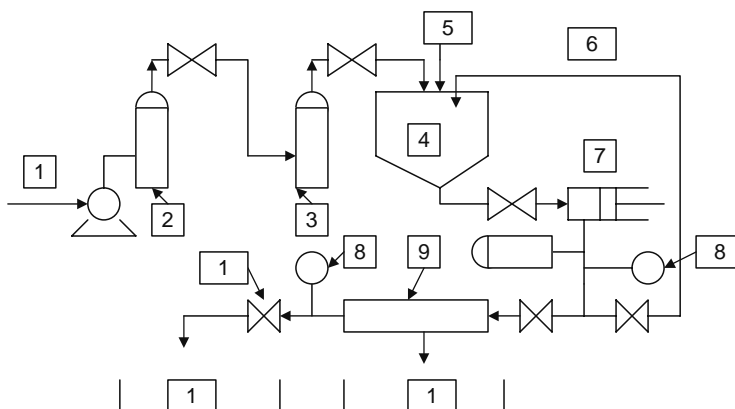


FIGURE 29.1 Flow sheet of RO plant.

Various performance indicators, such as VRF, percent solute rejection (SR), percent permeate recovery ( $R$ ) are computed as follows:

$$\text{VRF} = \frac{\text{initial volume of the feed}}{\text{final volume of the feed}}$$

$$\text{SR} = \left( \frac{\text{feed concentration} - \text{permeate concentration}}{\text{initial feed concentration}} \right) \times 100$$

$$R = \frac{\text{permeate flow rate}}{\text{feed flow rate}}$$

In BARC, a reverse osmosis pilot plant was successfully operated [11] for decontaminating low-level radioactive effluents having total dissolved solids in the range of few hundred parts per million contaminated with radioactive cesium and strontium. The pretreatment section consists of upflow particulate filter and cartridge filter. The upflow filter has been found to be effective in the removal of significant amounts of activity. This indicates that radioactivity is associated with large-sized suspended matter and the decontamination factor associated with upflow filter is directly proportional to the specific radioactivity of the feed introduced to the filter. In large-scale operations, the upflow filter generates significant quantities of secondary aqueous wastes due to the backwashing cycles which increase the waste volume. Also the filter media have to be disposed of periodically due to radioactivity build up that accumulates even with backwashing. On the other hand, only the cartridge filters used can remove the suspended loads, however, with frequent and costly replacement of the cartridges. There is a possibility to incinerate these cartridges, which would reduce the solid waste volume. From our experience, it can be said that there is no need to add any biocides or bio inhibitors as the accumulated radiation sources on the membrane surface themselves can prevent biofouling. Presently a 100 m<sup>3</sup>/day RO plant for decontamination and volume reduction of low-level radioactive effluents is operating at Trombay, India.

Uranium metal processing is one of the important constituents of a nuclear industry where nuclear grade metallic uranium is prepared for use as nuclear fuel. Like all other hydrometallurgical plants, uranium metal-processing plants also produce considerable quantities of metal-bearing liquid effluents, which are radioactive in nature. During the processing of uranium ore to get nuclear grade uranium metal, pure uranyl nitrate solution is obtained which is treated with ammonia-air mixture to precipitate ammonium diuranate.

This ammonium diuranate is filtered. Ammonium diuranate filtrate (ADUF) generated in uranium metal plant contains around 30,000 ppm ammonium nitrate and small amounts of dissolved and suspended uranium and its daughter products. The beta activity levels due to <sup>234</sup>Th and <sup>234</sup>Pa are significant and require processing before disposal of filtrate into the sea. Economic treatment and safe disposal of the filtrate demand a decontamination factor of at least 10 with a VRF of more than 10. This corresponds to a minimum solute rejection of more than 90% at more than 90% permeate recovery under reverse osmosis processing conditions. At first glance, reverse osmosis process with very high permeate recovery and high solute separation at such a high feed solute concentration does not seem reasonable. However, our laboratory studies [12] indicated that both ammonium and nitrate species are poorly rejected by cellulose acetate brackish water desalting reverse osmosis membranes, compared to sodium chloride. The solute rejection of ammonium nitrate decreases with increasing concentration.

### 29.3.5.1 Transport in Reverse Osmosis Process

The transport of solute and the solvent through semipermeable membrane under reverse osmosis conditions are depicted in Figure 29.2. The permeate flux ( $N_B$ ) in reverse osmosis is given by the following equation:

$$N_B = A[P - (\Pi_{X_{A2}} - \Pi_{X_{A3}})]$$

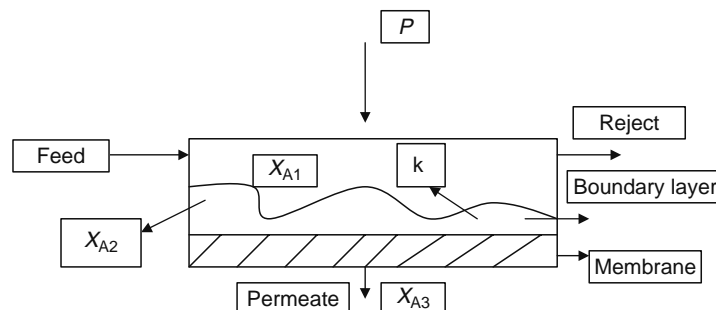


FIGURE 29.2 Membrane-solution interface.

where

$A$  is the membrane constant (m/s bar)

$P$  is the operating pressure (bar)

$\Pi_{X_{A2}}$ ,  $\Pi_{X_{A3}}$  are osmotic pressures of boundary layer and permeate streams with solute mole fractions  $X_{A2}$  and  $X_{A3}$ , respectively

For a solute with high rejection, permeate concentration would tend to zero. Thus,

$$X_{A3} \rightarrow 0 \text{ and } \Pi_{X_{A2}} - \Pi_{X_{A3}} \cong \Pi_{X_{A2}}$$

As recovery increases, the bulk solute concentration and hence  $X_{A2}$  increase. The recovery would then be limited by the value of  $\Pi_{X_{A2}}$  approaching the operating pressure  $P$ .

On the other hand, for poorly rejected solute like ammonium nitrate, the permeate concentration of solute would be significant, and hence

$$\Pi_{X_{A2}} - \Pi_{X_{A3}} < \Pi_{X_{A2}}$$

Since the permeate concentration is considerable, the rise in the bulk concentration of the feed ( $X_{A1}$ ) as well as the boundary layer concentration ( $X_{A2}$ ) with recovery would be less. Moreover, the solute rejection decreases with increasing concentration, thereby always keeping the term  $(\Pi_{X_{A2}} - \Pi_{X_{A3}})$  much less than  $P$ . Under these conditions, one can theoretically go up to a concentration where the osmotic pressure of the feed would approach the operating pressure, subject to the limitations of scaling and fouling. Accordingly, the VRF or recovery would not be a critical design step as long as the permeate quality is maintained within the desired limits. The high solubility of ammonium nitrate and the absence of scaling components make it theoretically feasible to attain high recoveries. However, iron fouling needs to be taken care off. If radioactive contaminants are selectively removed, then it is possible to use this process for decontamination of ADU effluents despite the high concentration of the total dissolved solids.

The treatment of ADUF by reverse osmosis [13] was found to be useful in concentrating activity in small volume while making a larger volume of the decontaminated effluent for direct disposal after required dilution. Porous cellulose acetate membranes were used in plate module configurations. The concentration of ammonium nitrate in the permeate stream is not very different from that of the contaminated retentate. With the addition of flocculating aids, the decontamination factors in the range of 1000 with VRFs in the range of 100 were achieved.

### 29.3.6 NANOFILTRATION

Nanofiltration (NF) membranes have average pore size of 10–30 Å, an intermediate range between reverse osmosis (10 Å) and ultrafiltration (>30 Å). Nanofiltration has the advantage of very low solute rejection for monovalent species, probably due to their very small hydrated radii and higher rejection for multivalent species which are large enough. The decontamination of ADUF was also investigated in a pilot plant study using nanofiltration membranes [12]. Because of the poor separation of ammonium nitrate, NF membranes have the potential to achieve high VRFs with high decontamination factors for radionuclides, which are multivalent. The studies carried out indicate that nanofiltration is better suited for the decontamination of ammonium diuranate filtrate effluents due to their near constant fluxes, high decontamination factors, and low ammonium nitrate solute rejections. Complexation has been used in conjunction with nanofiltration process for selective removal of trace toxic metal ions [14].

### 29.3.7 ULTRAFILTRATION

Ultrafiltration process is basically a physical filtration process on a very fine scale. It can retain large molecules, suspended, and colloidal particles, but can allow dissolved salts to pass through the bulk of the water. To keep the concentrate mostly in a uniform suspension requires high flows of liquid along the membrane surface. The technique uses similar configurations of equipment layouts as are used in reverse osmosis processes.

Ultrafiltration process is used in industries for the treatment of wastes and the associated recovery of useful products in the concentrate. Examples include the fractionation of milk whey and the treatment of cutting oil emulsions. Ultrafiltration process utilizes membranes having pore sizes in the range of 0.01–0.1 μm. The operating pressure is in the range of 3–5 bar. The mechanism of separation is essentially based on the size-based retention of the components. Cellulose esters, polyamide class of polymers, polyacrylonitrile, polyvinylidene difluoride, and polysulfones are largely used as membrane materials. It has application in the concentration of radioactivity, which is or can be converted to a colloidal or suspended state or possible included in large complex molecules. It has the potential advantage over reverse osmosis of being selective in its concentrating

action because soluble salts may pass through the membranes and be discharged with the bulk of the water, provided they are nonradioactive. It also operates at lower pressures (<0.5 MPa) than does reverse osmosis and at higher membrane fluxes. Although in most commercial units the membranes are polymeric materials, they are less sensitive to chemical and temperature conditions than reverse osmosis. Several inorganic membranes are available, permitting treatments which might incur high radiation dose.

Like microfiltration, ultrafiltration process can also be used in conjunction with chemical precipitation techniques to improve decontamination factors. Ultrafiltration processes could be useful for decontaminating alpha wastes from laundry and washing water streams of plutonium-processing plant on a large scale [15,16].

### 29.3.8 PRECIPITATION ULTRAFILTRATION

Removal of  $^{137}\text{Cs}$  by copper ferrocyanide precipitation followed by ultrafiltration is another promising option. This method could give higher DFs (100–1000) under optimum conditions compared to DFs of about 10 obtained in conventional methods of solid–liquid separation like settling or clariflocculation. It also requires lower dosage of chemical thus making it cost effective. Ultrafiltration combined with chemical precipitation or adsorption has been employed for treatment of radioactive effluents to improve the decontamination factors [17,18]. A typical flow sheet of the combined process is represented in Figure 29.3.

### 29.3.9 COMPLEXATION ULTRAFILTRATION

Ultrafiltration membranes work as a molecular size barrier; the pore size is too large to retain metal ions except in the colloidal form. Formation of high-molecular-weight species by complexation with water soluble-chelating agents leads to metal ion capture that permits the concentration of metallic solutions. A schematic of the process is represented in Figure 29.4. Selective metal ion extraction can be achieved if specific chelating groups are anchored on the polymeric chain. This combined process, called complexation ultrafiltration, could provide an alternative to ion-exchange resins.

A solution containing the metal ion to be extracted and a water-soluble polymer is delivered into an ultrafiltration unit (Figure 29.5). The feed stream, upstream of the UF system, is adequately stirred to enhance recovery of the radioactive ions. The metallic macromolecular complex is retained while low-molecular-weight solutes pass through the membrane. The efficiency of the process is mainly characterized by the passage of each species through the membrane. The transfer coefficient of a given solute,  $i$ , is defined by

$$T^i = \frac{C_f^i}{C_0^i}$$

where

$C_f^i$  and  $C_0^i$  are the concentration of species,  $i$ , in the filtrate and the feed solutions, respectively

$T^i$  is usually expressed as an equivalent parameter

$R^i$  is the retention coefficient, given by

$$R^i = 1 - T^i \text{ (when } R^i = 1, i \text{ retention has been completed).}$$

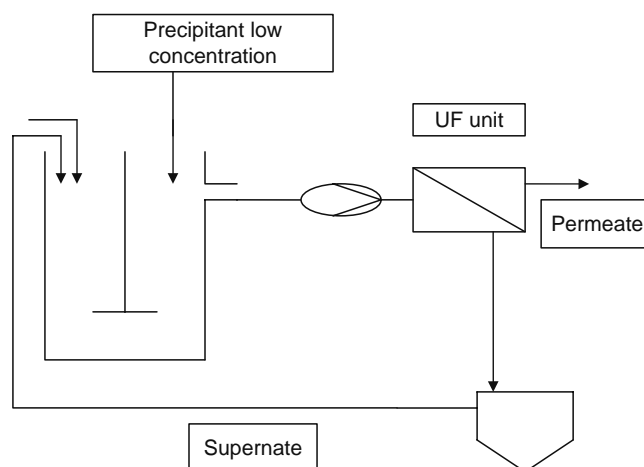


FIGURE 29.3 UF combined with chemical precipitation.

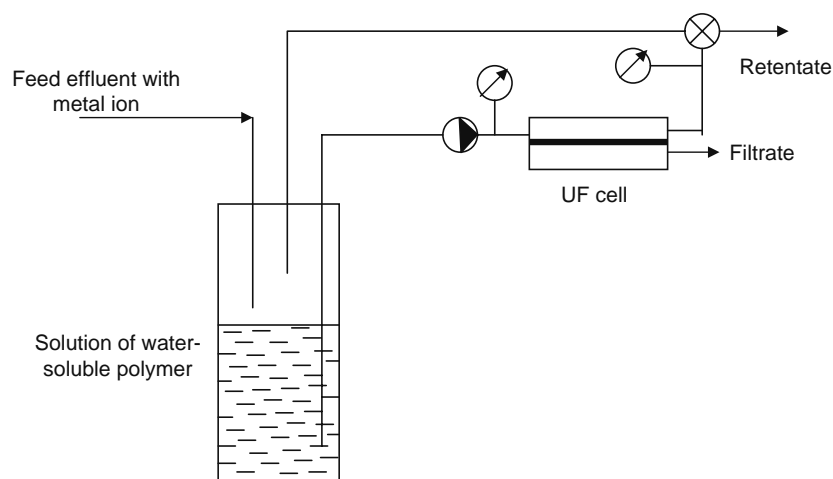


FIGURE 29.4 Schematic diagram of metal removal by means of the diafiltration process.

The filtration rate must be as high as possible so that the required membrane area is minimum. Flux rate ( $J$ ) through the ultrafiltration membrane is related to the applied pressure  $\Delta P$  by Darcy’s law:

$$J = \Delta P(\eta - r_m)$$

where

- $r_m$  represents the hydraulic resistance of the membrane toward the permeate
- $\eta$  is the dynamic viscosity of the solution

The filtration rate increases with increasing molecular weight cut-off (MWCO) by lowering  $r_m$ . MWCO is the molecular weight of the solute retained by the ultrafiltration membrane to the extent of 90% of the initial concentration. The accumulation of the retained solutes on the membrane or in the boundary layer next to the membrane surface, a phenomenon called concentration polarization, is the main cause of limitation of filtration rates. The concentration polarization is usually reduced by stirring the solution in the ultrafiltration unit or by tangential flow to the membrane surface or using higher flows to reduce the boundary layer.

The efficiency of the method is governed by some main requirements, such as complexation ability of the additive polymer and the ability of the membrane to retain the complexed metal ion. The retention of the macromolecular species should be complete to avoid loss of material. This condition entails that the molecular weight distribution of polymers does not overlap the pore size distribution of membranes. MWCO of the membranes should be chosen significantly lower than the average molecular weight of polymers. The treatment of large volumes demands high filtration rates. As can be seen in the above equation describing the flux rate,  $J$  decreases with increasing viscosity of the solution due to the high-molecular weight or to the high concentration of the polymers. Therefore, a compromise has to be found between MWCO and the molecular weight

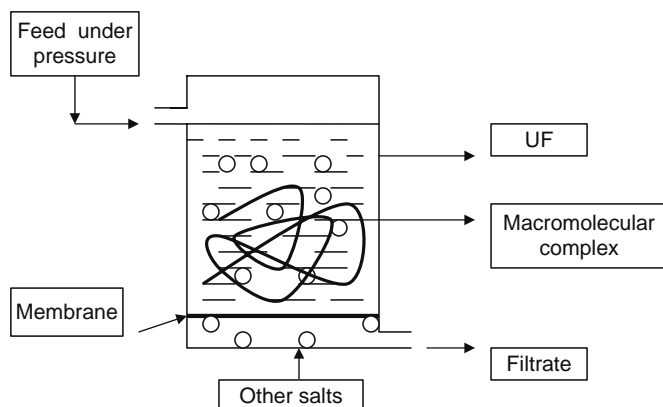


FIGURE 29.5 Principle of complexation UF.

of the polymer macromolecules. On the other hand, fouling of membranes may occur during ultrafiltration by polymer precipitation because of the low water solubility of the polymer. For this reason, polymers with good water solubility and are capable of forming complexes with metal ions should be chosen for use.

A variety of water-soluble macromolecules bearing ion-exchanger groups or chelating functions have been reported for use in complexation ultrafiltration processes [19–21]. Polyethyleneimine (PEI), a polymeric amine, has been used in many studies as a complexing agent as well as a versatile source of chelating derivatives. In addition to its chelating abilities, PEI exhibits good water solubility and chemical stability, yet has a high number of functional groups. However, the range of molecular weights available with PEI complexes does not exceed MW 50,000. This property requires the use of membranes with low MWCO to achieve desirable retention of the PEI.

Ultrafiltration membranes are made of various organic or inorganic polymers. Obviously, the best compatibility has to be found between membranes and solutes to avoid adsorption that will decrease the filtration rate. One of the most commonly used membranes is polyether sulfone—a nonionic hydrophobic polymer having high filtration rate. Unfortunately, this polymer is susceptible to strong interactions with hydrophobic solutes that will lead to irreversible fouling of the membrane surfaces. Hence, cellulosic materials are the preferred choice for these applications because of their low protein-binding properties. Radioactive cerium was separated [22] using polyethyleneimine complexation with indigenously made ultrafiltration membranes. Published results indicate that decontamination factors in the region of 1000 for alpha and 100 for beta–gamma radioactive species can be achieved with overall volume reduction of the order of  $10^4$ .

### 29.3.10 MICROFILTRATION

Microfiltration membranes have pore sizes ranging from 0.1  $\mu\text{m}$  and are suitable for the separation of colloidal impurities and suspended particles of submicron size, present in the raw effluents. The prime separation mechanism is mechanical retention. This process is generally used for the removal of turbidity and microorganisms from drinking water sources. The pressure applied is around 1–2  $\text{kg}/\text{cm}^2$ . In the primary cooling water of a light water reactor (LWR), corrosion products are produced which mainly consist of metal oxides containing radioactive nuclides, usually called cruds. This technique has been used [23] for separation of crud from wastes generated from operational practices in LWRs. While precoat or cartridge-type filters are generally used for removing such crud, these filters when spent produce secondary radioactive wastes. Further, the cartridge filters do not satisfactorily remove submicron-sized crud particles. Microfiltration membrane elements can be used for much longer periods before replacement, while filter-type cartridges may require frequent replacements.

Microfiltration can also be used in conjunction with chemical precipitation methods. Under optimum conditions, an integrated process of chemical precipitation and microfiltration will give a better decontamination and a lower quantity of sludge for disposal than conventional techniques using cartridge filtration and ion exchange [24]. Regenerated cellulose, cellulose acetate, polysulfone, polycarbonate, polypropylene, polytetrafluoroethylene, polyvinylidene difluoride, aromatic polyamide, and polyvinyl chloride are some of the polymeric materials used as microfiltration membrane systems. These membranes have limited radiation resistance and chemical tolerance. Ceramic microfiltration membranes have higher radiation stability and are capable of withstanding severe chemical cleaning to restore fouled membrane surfaces.

### 29.3.11 OSMOTIC CONCENTRATOR

The phenomenon of osmosis which led to the development of reverse osmosis technology has not been adequately exploited for industrial applications. This is primarily because the permeating solvent species is lost in the high concentration saline water stream, which provides the osmotic pressure differential necessary for the osmotic flow. The permeate stream is therefore not recoverable. Direct osmosis (DO) has sufficient potential for concentration of radioactive effluents as this process obviates the requirement of high-pressure support systems with their attendant problems. The driving force for dewatering can be easily realized from the salinity potential of seawater or its concentrates, which are abundant. An osmotic concentrator, fabricated and tested [25], indicated that it is possible to concentrate a radioactive feed solution, containing cesium and strontium isotopes with typically 300 ppm of mixture of inactive cesium and strontium chlorides. A concentration between 10 and 20 times was achieved by utilizing an optimum membrane and osmotic sink concentration. The circulation rates of the feed and sink can also be further controlled to achieve an optimum osmotic flux. The water permeation rate in DO is however less than in RO under comparable osmotic pressure and hydrostatic pressure gradients. A sketch of the osmotic concentration setup is shown in Figure 29.6.

### 29.3.12 ELECTRODIALYSIS

The basic principle of electrodialysis for desalination is to drive the cations and anions from saline water feeds under the influence of an electric potential gradient through cation- and anion-selective membranes. The electric potential prevents diffusion of oppositely charged ions in the other direction. A schematic of the process is shown in Figure 29.7. In a typical electrodialysis cell to deionize a salt solution, anion- and cation-exchange membranes are arranged alternatively in a

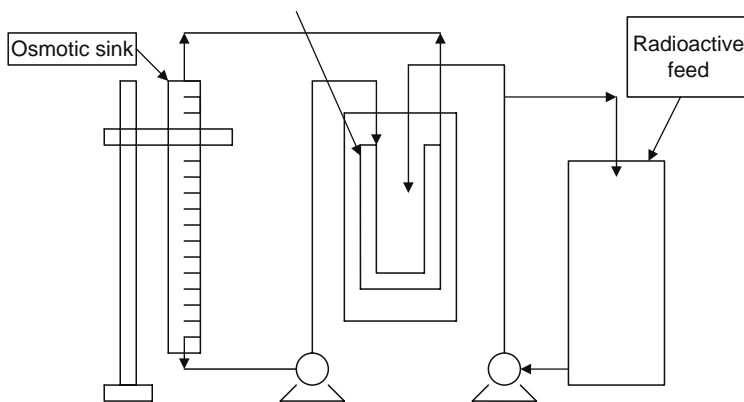


FIGURE 29.6 Bench scale osmotic concentrator.

stack, and a potential difference sufficient to force current through the stack is applied between the two electrodes placed at each end of the stack. For current to pass between the electrodes, ions must be transported through each of the membranes. By arranging the feeds to the various intermembrane compartments, it is possible to force ionic salts to pass from the dilute stream to the concentrated stream. In this way, a salt can also be split into its acid and base components. By combination of several cell pairs that comprise an anion- and a cation-selective membrane sheets in parallel, a stream concentrated in the original salts may be prepared. This configuration is the common method for industrial use, in which electrodialysis gives broadly the same result as reverse osmosis and has found very similar applications to general water treatment.

The energy consumption of an electrodialysis cell is determined effectively by the cell voltage and the current efficiency. The current efficiency is established by the membrane properties. In practice, the cathodic reaction almost always results in hydrogen evolution while the anodic reaction leads to the evolution of oxygen. The cathodic reaction increases the pH of the solution in this compartment, while the anodic reaction decreases the pH.

The cell voltage required depends on the product of current and voltage drop in the dilute streams, particularly toward the end of the process when the total ion concentration is very low. Hence, the cell must be designed to minimize this term, i.e., the gap between the membranes must be as small as possible.

The maximum useful current density through the membrane is normally limited by a phenomenon known as polarization. Concentration polarization is caused due to the depletion of the transported ion at the membrane surface, because of its faster electrolytic transport through membrane phase and its comparatively slower rate of transport through the solution phase. This causes excessive resistance at the stagnant layer near the membrane–solution interface. It is therefore necessary to avoid stagnant layers at the membrane–solution interfaces by operating at high Reynolds number or with turbulence promoters.

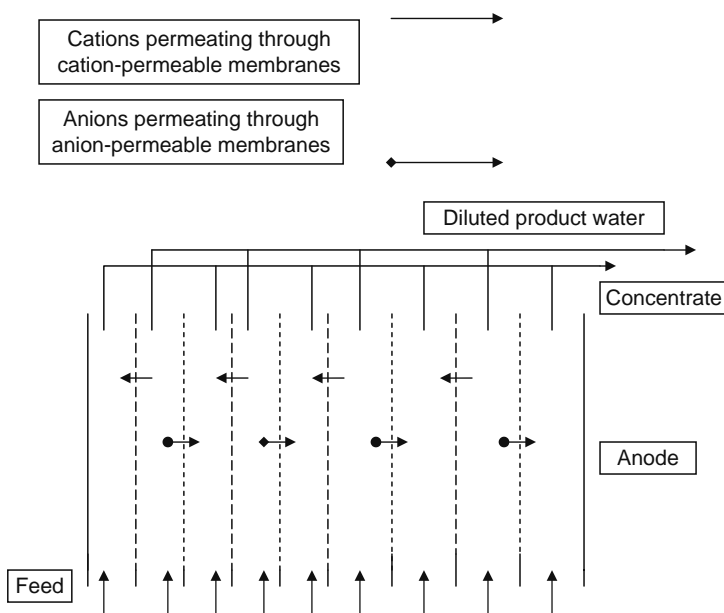


FIGURE 29.7 The principle of electrodialyser operation.

Application of electro dialysis is usually limited by the low electric conductivity of a diluted stream resulting from low concentrations of electrolyte. This limitation may be counteracted by filling the appropriate cells with ion-exchange resins at the expense of complications in construction. Although electro dialysis has the advantage of being a low-pressure process, this advantage is offset by the tendency of the ion-exchange membranes to be fouled by solids deposited on the concentration side of the cell. The construction of electro dialysis cells involves a number of seals around the individual membrane sheets. The assurance of leak-tight joint at all cells adds to the complication of replacement operations under radioactive conditions.

Electro dialysis has been examined [26] at the Japan Atomic Energy Research Institute (JAERI) for the removal of radioactive ions from low- and intermediate-level radioactive liquid waste using inactive coexisting salts as ionic carriers of very small amounts of radioactive ions. It has been found that the nature and the concentration of the existing salt species generally do not influence the decontamination factor obtained for radioactive ions. The efficiency for the decontamination of radioactive ions has been found to be higher for lower valence cations. It has also been observed that addition of inactive coexisting salt ions improves the decontamination factor but lowers the extent of volume reduction achievable.

Another example of electro dialysis applied to the nuclear industry [27] is the recovery of NaOH and H<sub>2</sub>SO<sub>4</sub> from the secondary liquid waste created by the regeneration of ion-exchange columns installed in LWRs. This application has been successfully demonstrated at a plant scale facility using simulated solutions. Long-term life tests on the ion-exchange membranes indicate a shorter life for anionic membranes than cationic membranes.

### 29.3.13 ELECTRODEIONIZATION

Large-scale operation on a radioactive feed stream has been reported [28] from Russia. Rauzen and others described a 100 m<sup>3</sup>/day facility, which was used to purify radioactive effluents. In this plant, two stages of electro dialysis were used in series. The diluate cells in the second stage contained ion-exchange resins and the water produced had a salt content equivalent to distilled water. This arrangement was found to be cheaper than a final ion-exchange cleanup. Another alternative tried was to use electro dialysis to recover acid and alkali from ion-exchange regenerant streams [28].

### 29.3.14 DIFFUSION DIALYSIS AND DONNAN DIALYSIS

Donnan dialysis is a membrane separation process that uses ion-selective membranes to prevent the flow of certain ions from one solution to another. A schematic of the process is presented in Figure 29.8. When a salt solution is separated from its corresponding acid by a cation-exchange membrane, the anions are excluded from the membrane, while the cations are redistributed across the membrane to attain Donnan equilibrium. By changing the salt solution periodically, it would be possible to shift the equilibrium favorably to effect simultaneous neutralization of acid on one side of the membrane (feed compartment) and acid recovery on the other side (receiver compartment). The driving force for ion migration is the chemical potential gradient for the cation across the membranes.

Diffusion dialysis is a special class of Donnan dialysis where anion-exchange membranes are generally used. The membranes do not allow cations to pass through, but anions are free to move across the membrane to equilibrate. However, H<sup>+</sup> ions which are much smaller will diffuse across the membrane to the receiver side. Hence, total acid diffusion is noticed in diffusion dialysis processes. Highly acidic radioactive streams could be deacidified by a diffusion dialysis process where specifically developed ion-exchange membranes are employed in a conventional electro dialysis stack design forming alternate diffusate and dialysate compartments. Free acid selectively diffuses through these anion-exchange membranes. The deacidified radioactive streams could again be treated by a secondary electro dialysis unit. An integrated membrane process consisting of diffusion dialysis followed by electro dialysis was evaluated [29] to deacidify and subsequently decontaminate a high-level radioactive stream by depleting the alpha activity. It was found that a diffusion dialysis process could be used to reduce the

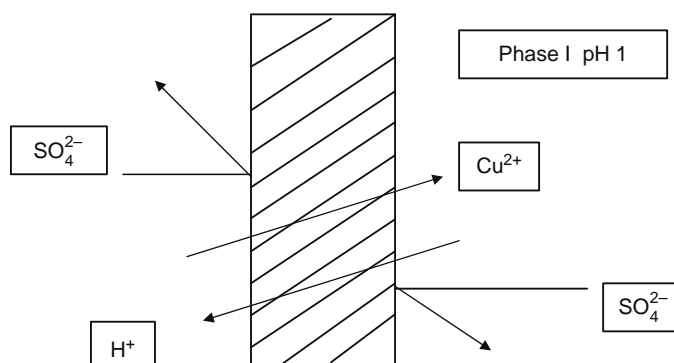


FIGURE 29.8 The principle of Donnan dialysis.

nitric acid concentration in the radioactive effluents from 3 to less than 0.3 M. The decontamination factor obtained with respect to cesium and strontium was in the range of 80–100.

Donnan dialysis and diffusion dialysis techniques are used [30] to deacidify and concentrate actinide bearing acidic solutions. Near complete deacidification could be achieved from 8 M nitric acid solutions with a high decontamination factor for the actinides. With cation-exchange membranes, the deacidification is accomplished by the build up of neutralized salt in the feed. With an anion-exchange membrane, the feed acidic solution is deacidified free of salt buildup. By superimposing direct osmosis with free deacidification, it was simultaneously possible to concentrate the deacidified actinide solution [30].

### 29.3.15 LIQUID MEMBRANES

Liquid membranes are made when a carrier mixed in a suitable solvent is converted to immiscible layer between two aqueous solutions. One of the components in the aqueous solution has preferential permeation into the immiscible membrane layer. The species in the feed can have a neutral, cationic, or anionic charge. Subsequently, these ions are removed by the permeate side solution by decoupling the carrier complex. The success of the liquid membrane process is primarily due to the diffusivity of ionic/nonionic species in liquids being an order of magnitude higher than in polymeric films. Further, the carrier molecules used in liquid membrane systems are very specific to different species and hence result in selective separation. This allows separation against an activity gradient. Various common forms of liquid membranes are bulk, emulsion, and supported liquid membrane (SLM) systems. Schematics of various liquid membrane systems are given in Figure 29.9. SLM systems are extensively investigated where the carrier is held in a porous polymeric membrane [31,32]. Development of liquid membrane process for removal of plutonium, uranium, and americium from dilute acidic solutions has been reported [33]. The removal of uranium and plutonium using SLMs with different carrier agents has been studied in BARC [34]. The recovery of uranium from phosphoric acid by this process has been considered to be an economical and efficient process as compared to solvent extraction.

The removal/recovery of actinides from aqueous reprocessing waste solutions is required to minimize radioactive discharges to the environment. Dihexyl-*N,N*-diethyl carbomoyl methyl phosphonate (DHDECMP) and tributyl phosphate (TBP) supported polypropylene hollow fibers showed promise in transferring americium and plutonium from high nitrate and low acid feeds to dilute oxalic acid-stripping solutions. Hollow fiber membrane supports exhibit the most efficient membrane area to feed volume ratio. Sorption of americium on inorganic exchangers from the strip solutions permits the recovery of americium. High-selective transport of U(VI) and Pu(IV) over several fission product contaminants was achieved employing TBP as the mobile carrier and dodecane as the membrane solvent [35].

For waste management purposes, various solvent extraction processes primarily for the removal of  $^{137}\text{Cs}$  and  $^{90}\text{Sr}$  from alkaline or weak acidic solutions have been developed on bench scale as well as on pilot scale [35,36]. Di-2-ethylhexyl phosphoric acid/kerosene system with Span 80 surfactant showed promise for the pertraction of  $^{90}\text{Sr}$  from aqueous solutions.

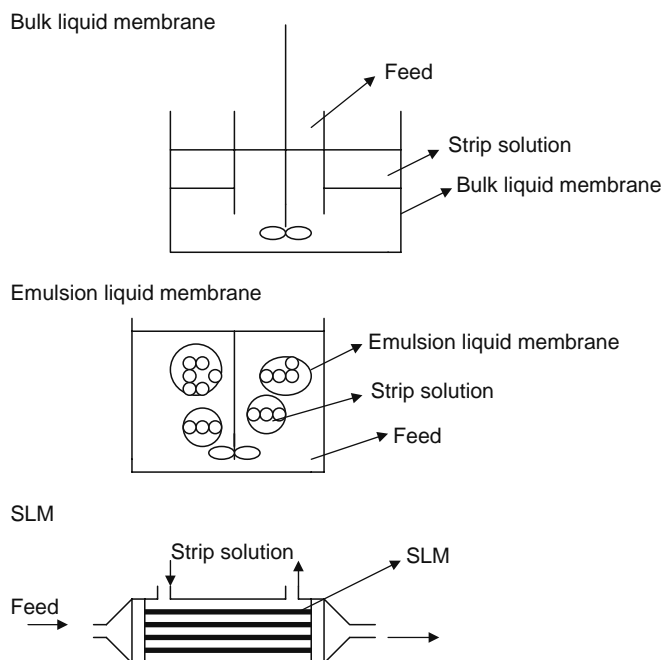


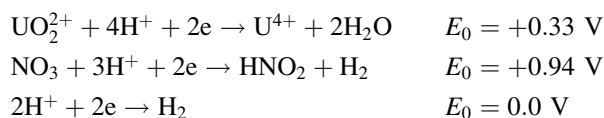
FIGURE 29.9 Schematic of various liquid membrane systems.

Recently, attempts were made to recover inert fission products like palladium from process effluents by SLM with carriers like bis(2-ethylhexyl)sulfoxide and thiocrowns [37].

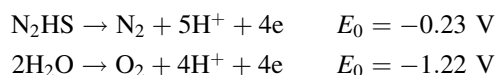
### 29.3.16 MEMBRANE ELECTROLYZERS FOR PRODUCTION OF URANYL NITRATE

The PUREX process is the oldest known and widely adopted for reprocessing of spent nuclear fuel. In this process, uranium and plutonium are co-extracted into an organic phase leaving behind the fission products in the aqueous phase. It is necessary to separate uranium and plutonium from each other for their end use in the manufacture of fuel. Redox reactions can be exploited to change the valency of uranium and plutonium to achieve the objective to separate and produce uranium and plutonium of high purity. Various reducing agents used for this purpose are ferrous sulfamate, hydroxylamine nitrate, hydrogen in presence of a catalyst, and uranyl nitrate. Uranyl nitrate can be produced electrolytically, which is simpler and amenable for large-scale production. Electrochemical reactions involved in this process are given below:

*At the cathode*



*At the anode*



Since oxygen is one of the products of electrolysis, if the electrolytic cell is undivided, reoxidation of  $\text{U}^{4+}$  ion takes place which hampers the production of uranyl with higher concentration. Cation-selective membrane spacers are effective in improving the production of uranyl nitrate solution.

### 29.3.17 RADIATION EFFECT ON POLYMERIC MEMBRANES

Studies on the effect of  $\gamma$  radiations on cellulose acetate reverse osmosis membranes [38] indicate that these membranes undergo degradation beyond a cumulative dose of 500 krad and continue to degrade at higher doses. Beyond a dose of 7 Mrad the membranes become brittle. The degradation is marked by increased water permeation rate and decreased solute separation. The solution viscosity and solubility of the membrane polymer and the tensile strength of the membranes decrease. The presence of dissolved oxygen was found to adversely affect the membranes during irradiation leading to a measurable degree of deacetylation. Ion-exchange membranes have a higher radiation resistance of up to 10 Mrad. At higher doses, loss of exchange capacity and membrane selectivity are noticeable. The electrical resistance of ion-exchange membranes primarily depends on its porosity and charge density as well as on the concentration of the electrolyte solution in which it was in contact. The electrical resistance of ion-exchange membranes decreases at higher radiation doses because of loss of functional groups causing more open channels for the electrolyte solution to freely pass through.

## REFERENCES

1. International Atomic Energy Agency, Standardization of Radioactive Waste Categories, Technical Reports Series No. 101, International Atomic Energy Agency (IAEA), Vienna, 1970.
2. Samanta, S.K., Ramaswamy, M., and Misra, B.M., Studies on cesium uptake by phenolic resins, *Sep. Sci. Technol.* 27, 255, 1992.
3. Beamer, N.V. et. al., Conditioning CANDU reactor wastes for disposal management of radioactive waste from nuclear power plants. In Proceedings of a Seminar, Karlsruhe, 1981, International Atomic Energy Agency, IAEA-TECDOC 276, Vienna, 1983.
4. Basner, C., Hillman, T., and Markind, J., Waste boric reclamation. In Proceedings of Symposium on Waste Management, Tucson, AZ, February 1981, vol. 2, 789, 1981.
5. Andrezej, G. et al., Concentration of low and medium level radioactive wastes with three stage reverse osmosis pilot plant, *Sep. Sci. Technol.* 36, 1117, 2001.
6. Sengupta, S.K., Slade, J.A., and Tulk, W.S., Liquid radioactive waste processing with crossflow microfiltration and spiral wound reverse osmosis, Report AECL-11270, Chalk River, Ontario, February 1995.
7. Advances in Technologies for Treatment of Low and Intermediate Level Radioactive Liquid Wastes, Technical Report Series No. 370, International Atomic Energy Agency (IAEA), Vienna, 1994.
8. Commission of European Community Research and Development on Radioactive Waste Management and Storage, 3rd Annual Progress Report of the European Community Programme 1980–1984, Harwood Academic Publishers, Brussels, 1982.

9. Chmielewski, A.G. et al., Membrane for radioactive waste treatment, *Czech. J. Phys.* 49, 979, 1999.
10. Processing of nuclear power plant waste streams containing boric acid, International Atomic Energy Agency, IAEA-TECDOC 911, Vienna, 1996.
11. Prabhakar, S., Panicker, S.T., and Misra, B.M., Design aspects of reverse osmosis plants for radwaste treatment. Paper presented at the 10th National Conference of Indian Membrane Society, Mumbai, January, 1993.
12. Prabhakar, S., Panicker, S.T., Misra, B.M., and Ramani, M.P.S., Studies on the reverse osmosis treatment of uranyl nitrate solution, *Sep. Sci. Technol.* 27, 349, 1992.
13. Prabhakar, S. et al., Performance evaluation of reverse osmosis (RO) and nanofiltration (NF) membranes for the decontamination of ammonium diuranate effluents. *Sep. Sci. Technol.* 31, 533, 1996.
14. Frederic, C. et al., Caesium/sodium separation by complexation–nanofiltration, *Sep. Sci. Technol.* 36, 1053, 2001.
15. Barnier, R., Caminade, S., Loudenot, L., Maurel, M., and Courtois, F., Ultrafiltration treatment of manual laundry washes from a nuclear research centre, In Conference on Waste Management, Kyoto, Japan, 1989.
16. Astruc, C. et al., Filtration in nuclear power plants, *Euromembrane'99*, Leuven, Belgium, September 19–22, 1999.
17. Harpes, H. and Sellers, P.M., Activity removal from liquid streams by seeded ultrafiltration, In Proceedings of Symposium on Waste Management, University of Arizona, Tucson, AZ, vol. 1, 749, 1991.
18. Roberts, R.C. and Herald, W.R., Progress reports on development of ultrafiltration and inorganic adsorbents, Mound Laboratory, Miamisburg, OH, Report MCM-2684, 1980.
19. Chaufer, B. and Deratini, A., Removal of metal ions by complexation ultrafiltration using water soluble macromolecules: Perspective of application to waste water treatment, *Nucl. Chem. Waste Manag.* 8, 175, 1988.
20. Ru Mean, M. et al., Separation by coupling ultrafiltration and complexation of metallic species with industrial water soluble polymers, *J. Memb. Sci.* 73, 313, 1992.
21. Geckler, K.E. and Volchek, K., Removal of hazardous substances from water using ultrafiltration in conjunction with soluble polymer, *Environ. Sci. Technol.* 36, 725, 1996.
22. Ramachandhran, V., Samanta, S.K., and Misra, B.M., Radiocesium separation behaviour of ultrafiltration membranes, *J. Radioanal. Nucl. Chem.* 237, 121, 1998.
23. Hayashi, K. et al., Membrane filter applications for crud separation from radioactive waste water generated in LWR power plants. In proceedings of Symposium on On-site Management of Power Plant Wastes, Zurich, 1979, OECD/NEA, Paris, 229, 1979.
24. Sengupta, S.K., Slade, J.A., and Tulk, W.S., Liquid radioactive waste processing with crossflow microfiltration and spiral wound reverse osmosis, Report AECL-11270, Chalk River, Ontario, February, 1995.
25. Thomas, K.C., Ramachandhran, V., and Misra, B.M., Studies on osmotic concentration of effluents, *Radiochim. Acta* 40, 217, 1986.
26. Sugimoto, S., Removal of radioactive ions from nuclear waste solutions by electrodialysis, *J. Nucl. Sci. Technol.* 15, 705, 1987.
27. Miyagawa, M., Mizutani, T., Miki, M., and Ohuchi, I., Volume reduction system of radioactive waste by electrodialysis. *Karyaku Karyoku Genshiryoku Hatsuden*, Japan, 30, 351, 1979.
28. Rauzen, F. et al., Use of ion exchange and electrodialysis for purification of liquid radioactive wastes. *Atomnaya Ehnergiya*, 45, 49, 1978, English translation in *Soviet J. Atomic Energy* 45, 705, 1978.
29. Mathur, J.N. et al., Diffusion dialysis aided electrodialysis process for concentration of radionuclides in acid medium, *J. Radioanal. Nucl. Chem.* 232, 237, 1998.
30. Charyulu, M.M. et al., Concentration with selective acid removal from americium solutions using ion exchange membranes, *J. Radioanal. Nucl. Chem.* 243, 697, 2000.
31. Sastre, A.M. et al., Improved techniques in liquid membrane separations, *Sep. Purif. Methods* 27, 213, 1998.
32. Sengupta, A., Basu, R., and Sirkar, K.K., Separation of solutes from aqueous solutions by contained liquid membranes, *AIChE J.* 34, 1698, 1988.
33. Shukla, J.P. et al., Separation of radiotoxic actinides from reprocessing wastes with liquid membranes, *ACS Symposium Series in Chemical Separation with Liquid Membranes*, Bartsch, R.A. and Wey, J.D. (Eds.), American Chemical Society, Washington DC, 1996, chapter 27.
34. Shukla, J.P. and Misra, S.K., Studies on the selective carrier-mediated transport of plutonium (IV) ions through tributyl phosphate/dodecane liquid membranes. *Ind. J. Chem.* 31 A, 323, 1992.
35. Ho, W.S.W. and Li, N.N., Recent advances in emulsion liquid membranes, *ACS Symposium Series 642*, American Chemical Society, Washington DC, 208, 1996, chapter 15.
36. Eroglu, I., Kalpakci, R., and Gunduz, G., Extraction of strontium ions with emulsion liquid membranes, *J. Memb. Sci.* 80, 319, 1993.
37. Kakoi, T. et al., Recovery of palladium from an industrial waste water using surfactant liquid membranes, *Sep. Sci. Technol.* 31, 381, 1996.
38. Ramachandhran, V. and Misra, B.M., Studies on the radiolytic degradation of cellulose acetate membranes, *J. Appl. Polym. Sci.* 30, 35, 1985.



---

# 30 Radioactive Waste Processing: Advancement in Pressure-Driven Processes and Current World Scenario

*Crazyyna Zakrzewska-Trznadel*

## CONTENTS

30.1	Radioactive Waste Treatment by Membrane Methods.....	844
30.1.1	Membrane Selection for Nuclear Applications.....	844
30.1.2	System Design.....	845
30.1.3	Process Operation—Considerations from Radiological Safety Point of View.....	846
30.1.3.1	Process Control.....	846
30.1.3.2	Radiological Protection Requirements.....	847
30.1.3.3	Membrane Control.....	848
30.1.3.4	Decontamination of the Space and Equipment.....	850
30.2	Membrane Processes Employed for Liquid Radioactive Waste Treatment.....	850
30.2.1	Reverse Osmosis.....	850
30.2.1.1	Three-Stage Reverse Osmosis Installation for Low- and Intermediate-Level Radioactive Wastes Processing.....	850
30.2.1.2	Other Applications.....	854
30.2.2	Nanofiltration.....	854
30.2.3	Ultrafiltration.....	854
30.2.3.1	Removal of Radionuclides from Water Solutions by Ultrafiltration/Complexation.....	858
30.2.3.2	Treatment of Original Radioactive Waste.....	860
30.2.3.3	Pilot Plant Experiments.....	863
30.2.4	Microfiltration.....	866
30.2.5	Membrane Distillation.....	866
30.3	Future of Membrane Processes in Nuclear Technology.....	872
30.3.1	Liquid Radioactive Waste Processing by Membrane Processes: Advantages and Limitations.....	872
30.3.2	New Fields of Application of Membrane Processes in Nuclear Industry.....	873
30.3.2.1	Removal of Tritium from Nuclear Waste (Liquid and Gaseous Effluents).....	873
30.3.2.2	Isotope Separation.....	874
30.3.2.3	Gaseous Radioactive Wastes—Noble Gases Separation.....	875
	Nomenclature.....	875
	Abbreviations.....	875
	References.....	876

The fuel cycle, from mining of uranium and preparing the fuel elements for nuclear reactors, through the fuel use for generation of electricity, to management of burnt fuel and decommissioning of nuclear facilities, produces different types of radioactive waste. Radioactive waste is also generated during production and application of radioisotopes, as well as during processing of raw materials containing naturally occurring radioactive isotopes. All those wastes have to be processed and conditioned before safe storage or disposal to protect the human health and natural environment. The management of radioactive waste has to be reached with reasonable cost by implementing appropriate technologies. The treatment requirements depend on the radioactivity level, and chemical and physical properties of the waste streams. Number of methods can be used to treat aqueous

radioactive wastes, including chemical precipitation, evaporation, and ion exchange as well as less-developed solvent extraction, biotechnological processes, and membrane methods. Although membrane processes are still considered as novel technologies in this field, many applications in nuclear centers and laboratories around the world are reported. The chapter deals with some of these applications and research aiming in implementation of membrane techniques in nuclear industry.

### 30.1 RADIOACTIVE WASTE TREATMENT BY MEMBRANE METHODS

Conventional technologies that are used for liquid low- and medium-level radioactive waste processing as precipitation coupled with sedimentation, ion exchange, and evaporation are energy-consuming or introduce the third phase that results in production of secondary wastes (sludge from sedimentation tanks, spent sorbent from ion-exchange columns, or effluents from resin regeneration). These wastes need additional treatment and decontamination. All these disadvantages may be avoided by membrane methods that have already found application in the field of liquid radioactive wastes processing. The most advanced are technologies based on pressure-driven membrane processes: microfiltration (MF), ultrafiltration (UF), and reverse osmosis (RO). The choice of the process depends on waste composition or parameters that have to be reached during processing, e.g., decontamination factors (DFs) in relation to the limits defined in national or international regulations, volume reduction coefficients, or necessity of recycling some components of the solution. Different installations are used for treating the wastes from nuclear power plants or reprocessing plants, and for processing the wastes from production of radiopharmaceuticals and medical diagnostics. Radioactive wastes from production of radioisotopes and medicine are usually classified as low- and medium-level waste. They contained mainly  $\beta$  and  $\gamma$  emitters, while the wastes from the waste processing plants contain  $\alpha$ -bearing elements that can destroy polymeric membrane material. Very often the organic solvents and complexing agents or acids are present in these types of wastes. The wastes coming from nuclear reactor operation contain the fission (e.g.,  $^{89}\text{Sr}$ ,  $^{90}\text{Sr}$ ,  $^{124}\text{Sb}$ ,  $^{132}\text{Te}$ ,  $^{134}\text{Cs}$ ,  $^{136}\text{Cs}$ ,  $^{137}\text{Cs}$ ,  $^{140}\text{Ba}$ ,  $^{141}\text{Ce}$ ) as well as corrosion ( $^{60}\text{Co}$ ,  $^{58}\text{Co}$ ,  $^{51}\text{Cr}$ ,  $^{54}\text{Mn}$ ,  $^{59}\text{Fe}$ ,  $^{65}\text{Zn}$ ,  $^{95}\text{Zr}$ ) products.

Applying the membrane processes, it is possible to achieve the goals:

1. Purification of the effluents to the concentration levels enabling safe discharge to the environment
2. Concentration of the radioactive compounds with volume reduction that is sufficient for solidification
3. Separation and recycling of the valuable components, e.g., boric acid from cooling waters

Reverse osmosis enables complete retention of all dissolved compounds, even small monovalent ions. To avoid the membrane blocking and scaling before reverse osmosis, microfiltration, or ultrafiltration pretreatment can be applied. Apart from preliminary treatment, ultrafiltration can be used for separation of suspensions or colloids, which are often formed by actinides or ions such as  $^{54}\text{Mg}$ ,  $^{55}\text{Fe}$ ,  $^{60}\text{Co}$ , and  $^{125}\text{Sb}$ . Microfiltration found the application for waste dewatering after precipitation. Nanofiltration (NF) that uses lower pressures than reverse osmosis is applied for separation of bivalent from monovalent ions. The most common application of NF process in nuclear industry is boric acid separation from the reactor coolant.

#### 30.1.1 MEMBRANE SELECTION FOR NUCLEAR APPLICATIONS

The membrane is the most important part in separation processes: since its performance controls the efficiency and the selectivity of the process. Both flux and selectivity expressed in terms of separation or retention factors determine the process economics and usability, and finally the costs of the installation.

Radiation resistance of the material used as well as commercial availability of the membrane units and auxiliary equipment, process competitiveness in comparison with conventional methods, its economics and feasibility are important criteria for application of the membranes for radioactive waste processing.

Different membrane materials have found application in nuclear technology; for radioactive waste treatment both polymeric and inorganic membranes are used. The main advantages of polymers are wide spectrum of different types of material, easy formation of membranes, and easy modification for specific applications. The relatively low cost (less than \$1 per squaremeter) is also beneficial, as well as broad commercial availability. The advantages of inorganic membranes come from their extremely good resistance to the temperature, strong chemical environment, and ionizing radiation. Membranes manufactured in some primary processes can be modified for some purposes by regulation of pore size or change of membrane chemical properties. In the process of modification two kinds of material can be combined—organic and inorganic (hybrid membranes), giving tailor-made structure for special applications.

Polymeric membranes are manufactured as flat foils, hollow fibers, or tubular shape. Flat sheets can also be arranged as spiral-wound configuration, or pleated filter cartridges. The module design permits easy connection in any configuration and up-scaling of the installation. Such an arrangement allows gaining high-membrane area to volume ratio, which relatively lowers the cost of apparatus and leads to higher unit capacities. Appropriate selection of membrane configuration has to take into account energy expenditure (pressure drop) per product volume and appropriate hydrodynamic conditions in the apparatus

promoting turbulence and mass transfer, and reducing boundary-layer phenomena, as well as easiness of cleaning. In hollow fiber modules the feed flow in relatively narrow channels is laminar and thus the membrane is particularly susceptible to fouling. The channels in plate-and-frame modules are also small, and membranes are sensitive to fouling, however they are easy to clean. On the contrary, in tubular modules cross-flow velocities are usually larger, giving turbulent flow and large pressure drop. In spiral-wound modules the spacer may act as a turbulence promotor and thus reduces concentration polarization.

The problems with fouling are particularly important for nuclear applications, because frequent cleaning produces the secondary wastes, which are radioactive and need additional processing. The best practice for membrane installation operation is avoiding the fouling and scaling by all available means (antiscalant injection, feedwater pretreatment to remove oxidizing materials, iron, calcium and magnesium salts, particulates and oils, greases, etc.). Proper selection of the module, which can be easily cleaned by back-flushing or washing with cleaning solution, is very important. In tubular modules direct mechanical cleaning by foam balls is also practiced, however it is limited to the small units.

One of crucial parameters of the membranes employed for radioactive waste treatment is their radiation stability and durability. During long-time operation the membrane is exposed to the action of ionizing radiation. This may cause some structural changes in the membrane that affects its permeability and separation characteristics. The variety of the effects in the polymer structure results from ionizing radiation such as cross-linking and formation of a new structure, decrease of molecular weight as a result of breaking of the main chains of macromolecules, change of the character and the number of double bonds, oxidation of the polymer in the presence of oxygen, etc.

The effect of irradiation of polymer membranes was studied by several research groups [1–7]. All studies showed that polymeric membranes exhibit limited resistance to ionizing radiation, however the threshold values of doses are sufficiently high to use the membranes for low and medium radioactive solutions treatment for a period of time. Usually the practical lifetime for most membranes is of the order of 4–5 years that is sufficient to avoid deterioration of filtration and separation abilities. Ceramic membranes are expected to be more resistant to  $\gamma$ ,  $\beta$ , and  $\alpha$  emissions, but systematic studies have not been presented.

### 30.1.2 SYSTEM DESIGN

There are numerous ways in which the membrane modules can be arranged in filtration systems. The factors influencing the choice of the option include the type of the process, the expected concentration in the streams, the volume of the processed wastes, the acceptable dose to the membrane, and desired costs of the plant. The capital costs play an important role in low and medium capacity plants, while the components of operation costs, such as energy consumption, are of less importance. For design of large capacity installations the operation costs are key elements. High investment costs for additional equipments, such as control system, washing installation, or measurement apparatuses, are justified when they cause a decrease of operational costs of the plant. Nuclear installations need special control equipment and security systems and their capital costs are relatively high.

The plant can operate in batch or continuous mode. The simplest design is dead-end operation, frequently used in microfiltration where all the feed is forced through the membrane that results in continuous increase of feed concentration and worsening of permeate quality. This design is used when complete filtration of the feed is necessary. More often used arrangement is cross-flow, which decreases the membrane fouling, and can operate as co-current, countercurrent, cross-flow with perfect permeate mixing. The flow in the module is arranged as a single-pass or flow with recirculation. Batch systems are also employed in small-scale applications when the waste arises discontinuously. Single-pass configuration can be arranged in series arrays, parallel or tapered design. The loss of volume in a single-pass system is compensated by tapered arrangement. The tapered array is rather not considered for ultrafiltration and microfiltration, as the high cross-flow velocities. This result in high pressure drop cause low-permeate flux and small volume reduction, as well as negligible increase in concentration of the retentate. Very frequent arrangement is feed and bleed system that consists of the number of stages each fed with a circulation pump. The feed pump generates the applied pressure, while the circulation pump maintains the cross-flow velocity. All arrangements of the modules are described in various other books on membrane processes [8–10].

When the product from the single stage has no desired quality the cascade system can be employed. The cascade design is frequently used in nuclear industry, especially for isotope separation. The first uranium-235 enrichment as a uranium hexafluoride was conducted in a cascade composed of many stages with porous, metallic membranes. Since the molecular weight ratio of  $UF_6$  isotopomers is about 1.008, the gas diffusion enrichment factor was low ( $\sim 1.0043$ ) and the unit separation effect had to be multiplied in large number of stages to achieve high purity of the product. Stage is an element of separation cascade containing several separation units, connected in series or in parallel and arranged as a tapered or squared off design. A permeate from one stage feeds the next one, however not always permeate is a product of the cascade. The simplest scheme is cascade without reflux (Figure 30.1), which is reasonable when the retentate in enriching section is not a valuable material. The example of such an arrangement is a plant for production of deuterium by water electrolysis operated by Norsk Hydro [8].

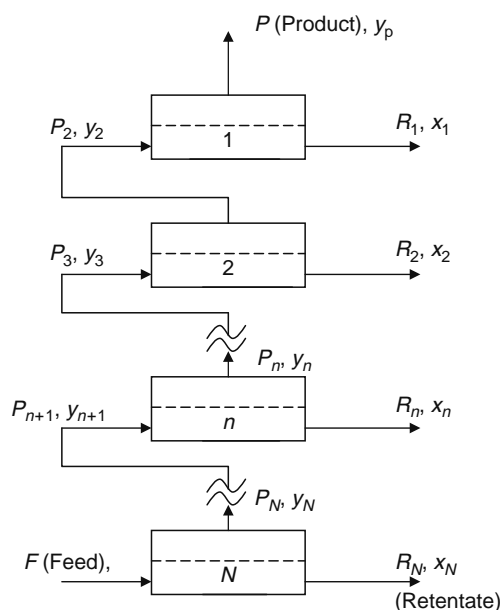


FIGURE 30.1 Cascade without reflux.

To avoid the product losses the recycling cascades are employed (Figure 30.2). The cascades with reflux are more complicated and the capital costs and costs of operation are higher; they are sensible only in the case of expensive raw material. Technical and economic considerations on such systems were performed in basic books for isotope separation [11,12], as well as by Hwang and Kammermeyer [13].

### 30.1.3 PROCESS OPERATION—CONSIDERATIONS FROM RADIOLOGICAL SAFETY POINT OF VIEW

#### 30.1.3.1 Process Control

All installations designed for nuclear industry have to fulfill very strict requirements of safety and reliability in the long run. Control and monitoring systems, automation, and washing installations are considered as essential part of the design.

##### 30.1.3.1.1 Automation

It is common that membrane plants are automated. The automation is used for starting up and shutting the installation, controlling the cleaning cycle, and the process parameters. However, some intervention of the operator in case of emergency has to be foreseen. All valves and remote-controlled devices ought to have the possibility of manual start-up and putting in motion. Membrane installation may be integrated into the central control system in the plant where it is used. However, in case of nuclear industry it is rather recommended to design self-contained units, fully automated by simple ladder logic controller or microprocessor control. All operating parameters such as pressure, temperature, flow, tank level, pH, conductivity, and specific activity are monitored and recorded. Continuous visualization of main parameters' trends is very important and helpful. The control system includes also automatic start-up and shutdown of pressure pumps, dosing pumps, as well as shutdown of the whole installation in the case of unexpected event or emergency. The exceeding of the allowable operating parameters' limits should result in the start-up of appropriate blocs and alarms.

In view of the radiological safety the personal contact with operating installation should be minimized. The location of data acquisition and control systems has to be planned in separate room, away from places of potential contamination. However, the necessity of eventual periodic sampling has to be taken into account, too. The sampling points have to be located in the places with easy operator access and arranged in a way eliminating leaks and contamination.

##### 30.1.3.1.2 Precautions against Uncontrolled Pressure Excess

Membrane installations operated in nuclear industry are pressure-driven systems; majority of them are reverse osmosis plants. Uncontrolled growth of operation pressure may result in module damage and valves' leaks resulted in contamination hazard. The selection of appropriate pumps and security devices can avoid the danger of pressure overgrowth and its detrimental implications. The security valves' outlets have to be connected with existing waste distribution systems to direct the eventual leaks to the waste collecting tanks.

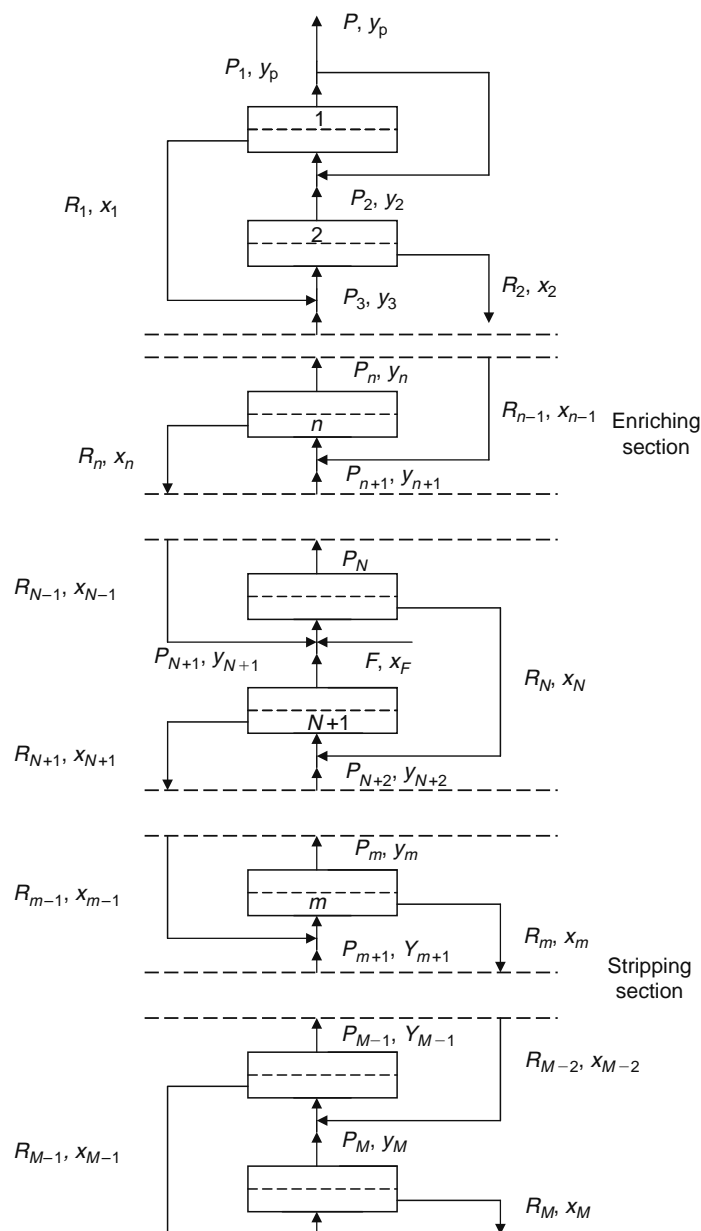


FIGURE 30.2 Recycling cascade with enriching and stripping sections.

#### 30.1.3.1.3 Precautions against Uncontrolled Temperature Excess

All polymeric membranes and modules have admissible temperature of operation. For most of them this temperature is  $40^{\circ}\text{C}$ , only for inorganic materials this temperature is much higher. In case of reverse osmosis there is a possibility of retentate and permeate temperature growth caused by the circulation under high pressure. The continuous temperature control of the streams with upper alarm has to be predicted. The systems collecting the excess heat (radiators, ribbed pipelines) allowing intensive cooling have to be designed.

#### 30.1.3.1.4 Precautions against Uncontrolled Overflow of the Tanks

All the tanks connected with membrane installation have to be equipped with tank level meters with devices and blockades of the pumps secured against overflow. Special collectors in the floor for contaminated solutions in case of unexpected overflow have to be designed.

### 30.1.3.2 Radiological Protection Requirements

Two systems for radiological control are required in case of membrane plant for radioactive waste processing: first, for process control and the second, for securing the staff and for avoiding the spread of contamination. The latter usually exists if the

installation is located in nuclear power plant or some other nuclear center. Some security devices have to be applied in the rooms where membrane plant will be placed. The lead shielding in places where increased radioactivity is expected, should be installed in accordance with precise preliminary measurements and dose estimations.

For process control purposes the radioactivity measurements of feed, permeate, and retentate solutions should be carried out. New batch of waste has to be controlled, and precise characteristics (radioactivity, conductivity, pH) of every new portion of the material should be done. The radioactivity of pure permeate before discharge has to be controlled, as well as periodic radioactivity of retentate before solidification or other stages of processing.

### 30.1.3.3 Membrane Control

#### 30.1.3.3.1 *Fouling in Radioactive Waste Treatment*

Fouling is one of the technical problems of membrane systems operation. The phenomenon occurs mainly in pressure driven membrane processes. There are four types of fouling: precipitation of dissolved solids, sediment of suspended solids, biological fouling and organic nonbiological fouling, caused by carbon-based molecules. The symptoms of fouling are decrease of permeate flow, increase of pressure drop across the module, and increase of total pressure in the unit. Therefore to keep the stable flux, pressure needs to be continuously increased. Usually 10%–15% reduction of the permeate flow should be a reason for immediate membrane cleaning. Otherwise, increase of pressure in the system and crystallization of salts or silica in the pores may result in the irreversible membrane structure change or damage.

Radioactive waste processing is usually a complex process combining often microfiltration and ultrafiltration with some other processes such as precipitation or binding with macromolecular ligands. During filtration of radioactive wastes, especially when suspensions or macromolecular species are separated, some deposit can be formed on membrane surface or inside the pores after several hours of operation. Particles deposited on the membrane surface can form the filter cake, which acts as a secondary membrane. The deposit causes the flux decline, however sometimes separation with secondary membrane can be better. This secondary membrane usually has smaller pores than original one and retains the molecules, which pass through the original membrane. As a result an accumulation of radioactive compounds takes place on the membrane surface. The membrane cleaning is usually done with a small volume of acidic, basic, and water solutions alternately. For polymeric membranes, temperature and chemical resistance of the polymers limit the choice of cleaning solutions. There is no such limitation in the case of inorganic membranes—ceramic or metallic. After washing, high concentration of radioisotopes is obtained in a small volume of cleaning solution. Sometimes the concentration of radioisotopes in secondary membrane can reach 90%. During the removal of radioactive strontium by ultrafiltration combined with precipitation with colloid  $\text{Ti}(\text{OH})_4$  after 2 h of operation 50% reduction of permeate stream was observed but 20-fold volume reduction and 140- to 150-fold decrease of  $^{90}\text{Sr}$  in the permeate were achieved [14]. The strontium balance showed that 94% of  $^{90}\text{Sr}$  was found in the secondary membrane. After washing, the UF membrane recovered its initial permeation properties and over 99.2% of strontium was transferred to the mixture of rinsing solution and retentate, volume of which was 18 times lower than feed solution. Similar effect, but not so intensive, was observed during ultrafiltration enhanced by complexation with polyethyleneimine—in the secondary membrane 7% of  $^{60}\text{Co}$  was retained, but it was hardly removable with rinsing [15]. Radiometric measurements of the membrane sample showed that some part of  $^{60}\text{Co}$  was persistently bound into the membrane. This was disadvantageous; especially for polymeric membranes, as the material of the membranes is permanently exposed to ionizing radiation emitting by bound radioisotopes that can result in the loss of the permeation abilities.

The most common methods of fouling prevention are wastewater pretreatment, the control of hydrodynamic conditions in the apparatus (low flux, high feed flowrates, turbulence promoting, dynamic filtration), or special construction of the module (cross-flow filtration).

#### 30.1.3.3.2 *Scaling Control*

During concentration of radioactive waste by pressure-driven membrane processes, such as reverse osmosis, the solubility limits of some dissolved salts can be exceeded. These salts precipitate on membrane surface or in other parts of the plant causing the damage of the membrane or severe corrosion of the elements of the installation. The most common compounds that precipitate easily causing scaling are calcium salts ( $\text{CaCO}_3$ ,  $\text{CaSO}_4$ ,  $\text{CaF}_2$ ,  $\text{CaHPO}_4$ ), barium and strontium sulfates, and silica and magnesium carbonates. The methods of scale minimization include: proper pretreatment, acid injection to reduce carbonates, water softening by lime or lime soda, ion exchange, removal of bivalent ions with nanofiltration and antiscalant addition. The scale inhibiting compounds are injected into the parts of the installation with the high risk of scale formation. These places have to be specified in the project design of the plant. Antiscalants delay precipitation by formation of microcrystals with low agglomeration abilities that interfere with crystallization of the other salts. The most common scale inhibiting chemicals are polyphosphates, polycarboxilites, polymalonates, and polyacrylates. In Chalk River Laboratories the antiscalant agent effectively preventing scaling in RO plant was Pretreat Plus (King Lee Technologies, San Diego, California) [16–20]. At the Institute of Atomic Energy in Poland in three-stage RO plant the sodium hexametaphosphate (Calgon) was

chosen. To prevent scaling in RO pilot plant designed and operated by ANSTO antiscalants AS-1000 (phosphinocarboxylic acid) and AS-1300 (polycarboxylic acid) were used [21].

One novel method for scale control is magnetic and electrostatic technology suggested by US Department of Energy [22]. This nonchemical technology is recommended for scale and hardness control as a reliable energy saver in certain applications that can be used as a replacement for most water-softening equipment.

#### 30.1.3.3.3 Membrane Cleaning

The periodic cleaning of the membranes exposed to the action of foulants and scalants present in the wastes is necessary. The frequency of the cleaning depends on the composition of the wastes. Its necessity is recognized basing on the pressure drop or rapid flux decrease. If the flux drops by several percent, the membrane has to be restored. The volume of the cleaning solutions should be as small as possible, to minimize the amount of secondary wastes.

The selection of the cleaning agents and their concentration depends on the membrane and on the kind of foulants present in the waste. Manufacturers of the membranes usually recommend some cleaning solutions, acidic or basic and detergents, which have to be tested during pilot plant experiments. The most popular agents are citric acid, sulphuric acid, sodium hydroxide, sodium tripolyphosphate, sodium ethylenediaminetetraacetate, and ethylenediaminetetraacetic acid (EDTA). These compounds are relatively inexpensive and widely applied, however sometimes specially prepared membrane manufacturers' formulations are superior and worthy of consideration. Such reagents, however, are very good centers of nucleation and initialization of fouling and scaling. Therefore, the subsequent fouling can be even more severe after restoration of the membrane. Various cleaning agents are available in the market. They can minimize the production of secondary wastes because they can clean the membranes very effectively. For polymeric RO membranes applied in Chalk River Laboratories, for example, good results were obtained using MEMCLEAN, alkaline detergent containing EDTA [16–20,23]. For cleaning ceramic membranes used at the Institute of Nuclear Chemistry and Technology (INCT), Warsaw, the P3-ultrasil, Henkel EKOLAB, was effective. On the other hand, laboratory preparations (e.g., alkali and acid based solutions) also proved very useful [24].

Apart from chemical cleaning, mechanical or compressed air restoration of the membranes can be possible. Mechanical cleaning is restricted only for some configurations, namely tubular modules, with easy access to the membranes. The foam balls introduced into the tubular membrane lumen can scrape the substances deposited on the surface, however they cannot remove the foulants from the membrane pores. The pores can be cleaned by backflushing with pressurized air or water shock in opposite direction. The method is limited to those membranes which are strong enough to withstand this force, or to the membranes on sufficient support. Some configurations (e.g., spiral wound) are not recommended for this method of cleaning.

A recent approach [25] is a method of direct membrane cleaning (DMC) applied for conductive membranes, such as stainless steel, graphite, and conductive ceramics. By short current pulses (1–5 s at 50–200 mA/cm<sup>2</sup>) electrolytic generation of microscopic gas bubbles takes place, which removes the solid deposit from the membrane surface without interrupting the filtration process. Such a cleaning enables the cross-flow velocities and transmembrane pressures to be reduced that implicates reduced plant wear and low-energy consumption with minimizing the size of the pressure pumps. The process was demonstrated on microfiltration and ultrafiltration membranes of different geometries. DMC was used during the treatment of low-level radioactive waste by microfiltration combined with inorganic sorbents: 44 ppm of nickel hexacyanoferrate for Cs removal, 33 ppm of zirconium phosphate for Sr removal, and 45 ppm hydrous titania for Ru, Ce, and actinides removal. Additionally Fe(OH)<sub>3</sub> was introduced to enhance actinides and Cs retention, and to trap fine particles on precipitated floc. When the mixed sorbents were concentrated to 5% by microfiltration, rinsing with 0.1 mM NaOH, which made the slurry conductive and ready for subsequent electrolytic dewatering up to 30% of solids, reduced the salt content. Finally the concentrate was immobilized with cement powder.

#### 30.1.3.3.4 Secondary Wastes

Membrane installations generate secondary wastes that have to be taken into consideration before plant design. Reverse osmosis produces permeate, which can be discharged after radioactivity control, and retentate that can undergo further processing. Usually the retentate is not suitable for solidification and further volume reduction is necessary.

Secondary wastes are also generated during regular cleaning procedures, because fouled membranes have to be washed or cleaned by cleaning solutions. The concentration of radioisotopes in these solutions is sometimes high and they need treatment by recycling to the feed at the inlet of membrane installation. The additional volume of the waste has to be taken into account in plant design, as well as the influence of extra load on the membrane performance.

The plant itself is a source of secondary solid waste; membranes, and spent filter cartridges and related small parts have to be processed by common methods such as compaction or incineration to reduce their volume or have to be left for decay, if adsorbed radioisotopes have short half-life time.

#### 30.1.3.3.5 Membrane Exchange

For the treatment of conventional, nonradioactive liquid waste the predicted lifetime of membranes is 4–5 years. The effective lifetime depends on the conditions in which the membrane is used; the characteristics of solutions treated, pressure, and temperature. While selecting the membrane for radioactive waste processing, one has to remember about its resistance and

stability under ionizing radiation exposure. The membranes, which are used in the installation, have to be tested before final decision about their application. In spite of that, expected lifetime for polymeric membranes will not be longer than 5 years. After this period membranes have to be exchanged. Depending on membrane type and configuration the whole membrane modules or the cartridges where the membranes are assembled can be exchanged. The necessity of membranes' exchange has to be taken into account on the design stage. Security considerations, easiness of operations, and easiness of decontamination are very important. Sufficient space has to be reserved for work with membrane modules, which have to be exchanged and means of minimization of contamination have to be foreseen.

Spent membranes and membrane cartridges do not undergo regeneration; they are treated as a solid radioactive waste. They can be stored for decay or processed as other solid waste material.

#### 30.1.3.4 Decontamination of the Space and Equipment

All potential points of leaks and other hot spots have to be identified in the stage of design. The decontamination procedures in case of accident have to be elaborated. The specification of the equipment for eventual decontamination and the means of decontamination are defined in laboratory instructions and manuals. All necessary safeguards and security systems are the elements of the project design. In case of emergency all means limiting the decontamination spreading out have to be used.

## 30.2 MEMBRANE PROCESSES EMPLOYED FOR LIQUID RADIOACTIVE WASTE TREATMENT

### 30.2.1 REVERSE OSMOSIS

Reverse osmosis has been employed in full scale in many nuclear centers around the world. Permeate after reverse osmosis can be directly discharged to the environment or recycled as service water within nuclear power plant. There are a number of industrial RO applications and facilities in the stage of pilot plants operating for radioactive waste processing. Some examples of installations are presented in Table 30.1.

#### 30.2.1.1 Three-Stage Reverse Osmosis Installation for Low- and Intermediate-Level Radioactive Wastes Processing

Laboratory and pilot plant experiments carried out at INCT showed that reverse osmosis is very useful for the treatment of liquid low-level radioactive wastes from Polish nuclear laboratories. However, to reach high decontamination the process should be arranged as a multistage operation with microfiltration or ultrafiltration pretreatment [32,33].

The RO process was implemented at the Institute of Atomic Energy, Świerk. The wastes collected there, from all users of nuclear materials in Poland, have to be processed before safe disposal. Until 1990 the wastes were treated by chemical methods that sometimes did not ensure sufficient decontamination. To reach the discharge standards the system of radioactive waste treatment was modernized. A new evaporator integrated with membrane installation replaced old technology based on chemical precipitation with sorption on inorganic sorbents. Two installations, EV and 3RO, can operate simultaneously or separately. The membrane plant is applied for initial concentration of the waste before the evaporator. It may be also used for final cleaning of the distillate, depending on actual needs. The need for additional distillate purification is necessitated due to entrainment of radionuclides with droplets or with the volatile radioactive compounds, which are carried over.

Evaporation is, however, a very efficient cleaning process, although it is highly energy consuming. The application of the membranes at the beginning of cleaning cycle reduced significantly the energy consumption.

Membrane installation, capacity of  $\sim 1 \text{ m}^3/\text{h}$  pure permeate, was composed of three stages of reverse osmosis (Figure 30.3) preceded by pretreatment with polypropylene depth filters. The first two stages were used for purification, and the third one for final concentration. Two types of spiral-wound RO modules were used in the installation: SU-720R and SU-810 (TORAY). Both types of modules worked under a pressure of 20 bar and with high salt rejection, higher than 99%. The membrane was manufactured from cross-linked fully aromatic polyamide composite. Two Model SU-720R modules connected in series placed in a single housing formed the first stage of reverse osmosis. The second stage was the same as the first one: two modules placed in a single housing. The third stage was composed of two housings in parallel, two Model SU-810 (TORAY) modules in each vessel. The view of the plant is shown in Figure 30.4.

Liquid radioactive waste was directed from the waste storage tank to the  $8 \text{ m}^2$  feed reservoir. After pretreatment with PP depth filters and injection of antiscalant, the wastes were directed to the first stage of RO. The retentate from this stage was concentrated in the third RO unit. The concentrated solution could be directly solidified if the concentration of the total solute was appropriate ( $< 250 \text{ g}/\text{dm}^3$ ). The salt concentration is limited by the conditions of concrete solidification. If the concentration was not sufficient, the further concentration took place in the evaporator. Permeate from the first and third stages was directed to the permeate reservoir before the second RO unit. The product from the membrane installation (permeate from the second stage) was of required radiochemical purity and after the control of specific activity and salinity was discharged to the communal sewage.

**TABLE 30.1**  
**Examples of Nuclear Facilities Applying RO for Liquid Radioactive Wastes Processing**

Facility	Type of the Waste	Process and Type of the Membranes Used	Capacity	Results	References
Chalk River Laboratories (Canada)	Mixed aqueous waste	Tubular (TRO) and spiral-wound (SWRO) RO (Filmtec SW30HR) with MF pretreatment	3 m <sup>3</sup> /h	2200 m <sup>3</sup> per year processed wastes VRC = 200–400 Retention: 99.9% ( $\alpha$ ); 99% ( $\beta$ and $\gamma$ ); 99.5%–99.8% solids	[16–19,26]
ANSTO (Australia)	Low-level radioactive wastes from laboratories and radioisotope production	Two passes for permeate purification and two stages of concentration by RO spiral-wound modules (4" Filmtec XLE-4040 and 2.5" Filmtec BW30–2540) with UF pre-treatment (PCI FPA10 modules)	1.2 m <sup>3</sup> /h	High purity effluent was obtained. Flux decline in UF tubular unit was observed, resulting from irreversible fouling of membranes by surfactants coming from radiopharmaceutical production. The additional pretreatment step was recommended	[21,27]
Nine Mile Point nuclear power plant (United States)	BWR floor drains and other wastes from NPP	RO systems based on Thermex	36,300 m <sup>3</sup> /year	11 m <sup>3</sup> /year of solid waste generated; total organic carbon in the effluent <50 ppb, conductivity of 0.058 mS/cm. The plant operates without secondary wastes	[28]
Pilgrim nuclear power plant (United States)	BWR floor drains and various other wastes	RO systems based on Thermex		The waste volume decreased in time of the system operation, personnel exposure associated with radioactive waste operation was reduced	[28]
Wolf Creek nuclear power plant (United States)	Floor drains and other wastes	Spiral-wound RO with tubular UF modules for pretreatment	Processing rate of drum dryer (DD): 4620 L/d	The installation equipped with DD unit and demineralizer system; high-salinity solutions are filtered; VRC = 10–20	[28,29]
Bruce nuclear power plant (Canada)	Wastes from chemical cleaning of steam generator	UF (Zenon ZPF-12 tubular membrane modules) and two-stage RO (Filmtec SW30HR) coupled with wet oxidation technology (WAO)		Permeate meets the criteria for sewer usage; the RO concentrate is returned for further processing (WAO, solidification)	[30]
Comanche Peak nuclear power plant (United States)	Floor drains, resin sluice water, and boron recycling water	UF with RO and NF (RWE NUKEM)	2.28 m <sup>3</sup> /h	The suspended matter is rejected by UF unit, dissolved compounds by RO. NF membranes were used for passage of boron. Membrane technology followed by IEX performed better than existing demineralizer	[28]
Dresden nuclear power plant (United States)	Wastes contaminated by transuranic elements	UF with RO	Two tanks of total volume 1440 m <sup>3</sup> for processing	Permeate from the installation passed deep bed demineralizers; after radioactivity control was discharged from the plant. Volume reduction of tank wastes by factor of 10	[28]
Savannah River site	Reprocessing wastes with high concentration of sodium nitrate	MF (cross-flow filters, 0.2 $\mu$ m) and RO (high salt rejection spirally wound elements)		Plant met the discharge criteria; one of the major problems was biofouling of the MF membranes	[28,31]
IEA, Warsaw, Poland	Wastes from nuclear laboratories and application of radioisotopes	Two passes for permeate purification, two stages of concentration by RO spiral-wound modules (SU-720R, SU-810 [TORAY])	1 m <sup>3</sup> /h	Complete purification of effluent ( $\beta$ and $\gamma$ emitters is lower than 10 kBq/m <sup>3</sup> , $\alpha$ emitters lower than 1 kBq/m <sup>3</sup> , TDS < 0.1 g/dm <sup>3</sup> ), concentrated retentate for solidification	[33]

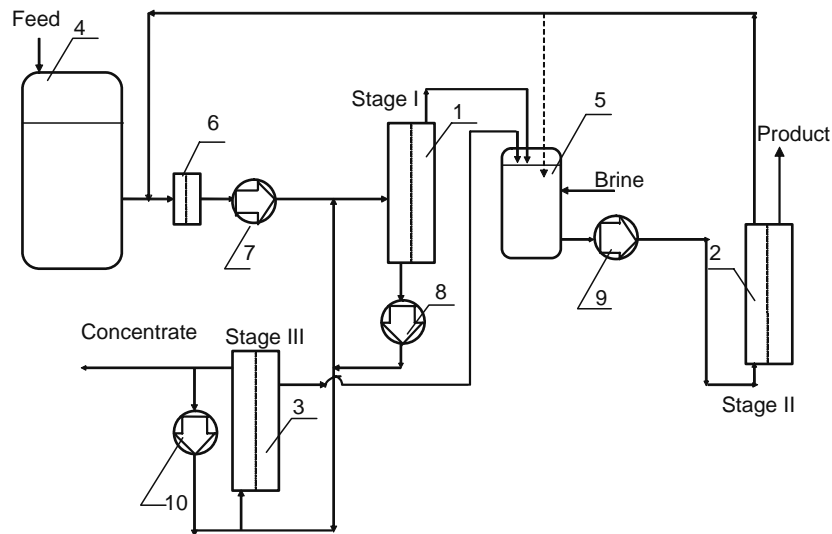


**FIGURE 30.3** A scheme of three-stage RO plant. 1–first stage RO, 2–second stage RO, 3–third stage RO, 4–feed tank, 5–intermediate tank, 6–depth filters, 7,8,9,10–pumps.

The laboratory experiments showed the influence of the total concentration of ballast non-active salts on decontamination factors. As the concentrations of total solute in permeate from the first and third stages were very low a decrease of retention of radionuclides was observed. To improve the efficiency of radioisotopes removal additional salt injection took place before the second stage.

The characteristics of permeate and retentate streams in terms of upper limits at the exit of RO plant were presented in Table 30.2. The concentration of salt in permeate is lower than  $0.1 \text{ g/dm}^3$ . The concentration of some specific elements as heavy metals has to be in conformity with the limits of impurities for wastes discharged to the inland waters. Total specific activity for  $\beta$  and  $\gamma$  emitters is lower than  $10 \text{ kBq/m}^3$ , while for  $\alpha$  emitters it is lower than  $1 \text{ kBq/m}^3$  (the limits for liquid waste). The total salt concentration in retentate is limited by ability of binding the solution with the concrete, the specific radioactivity by nuclear



**FIGURE 30.4** (See color insert following page 588.) Three-stage RO plant for radioactive waste processing at Institute of Atomic Energy in Swierk.

**TABLE 30.2**  
**Characteristics of the Streams After RO Installation**

<i>Retentate</i>	
Total concentration (g/dm <sup>3</sup> )	250
Specific activity	10 <sup>7</sup> kBq/m <sup>3</sup> (0.3 Ci/m <sup>3</sup> )
<i>Permeate</i>	
Total concentration (g/dm <sup>3</sup> )	0.1
Specific activity	0.01 ALI <sub>p</sub> /m <sup>3</sup> or <10 kBq/m <sup>3</sup> (β and γ) and <1 kBq/m <sup>3</sup> (α)

safety regulations. On the basis of parameters defined below the filtration abilities of the membranes to clean radioactive waste and the performance of the installation were assessed. The values calculated from the experimental results are presented in Table 30.3.

$$R = \frac{c_f - c_p}{c_f} \times 100\% \quad (30.1)$$

$$DF = \frac{A_f}{A_p} \quad (30.2)$$

$$K_{TDS} = \frac{c_f}{c_p} \quad (30.3)$$

$$CF = \frac{A_R}{A_f} \quad (30.4)$$

The retention of the dissolved salts by 3RO unit was higher than 99% in each case; decontamination factors were also high. Predominant purification took place in the first stage of reverse osmosis; the second stage played the role of final purification. Permeate in majority of cases was sufficiently pure for discharge. However, when the initial activity of the waste was high (the A feed solution), the radioactivity of the product was too high for discharge and hence permeate was returned to the installation

**TABLE 30.3**  
**Removal of Nonradioactive Substances (Dissolved Salts) and Radionuclides**

	Feed		Permeate		R (%)	K <sub>TDS</sub>	DF	CF
	(ppm)	(Bq/dm <sup>3</sup> )	(ppm)	(Bq/dm <sup>3</sup> )				
<i>Stage I</i>								
A	641.3	1.95 × 10 <sup>4</sup>	3.1	96	99.52	208	203	
B	320.6	280	1.5	1.4	99.60	214	200	
C	769.5	2200	3.9	10.4	99.49	197	211	
<i>Stage II</i>								
A	4.2	136	1.3	44	68	3.14	3.09	
B	2.3	2.3	1.5	1.6	34	1.51	1.44	
C	4.2	12.3	1.2	3.9	71	3.50	3.15	
<i>Stage III</i>								
A	2344.9	7.1 × 10 <sup>4</sup>	8.7	275	99.63	269	258	2.82
B	1265.3	1.1 × 10 <sup>3</sup>	5.6	5.4	99.56	226	204	3.91
C	2455.9	7 × 10 <sup>3</sup>	7.0	23	99.71	322	304	2.39
<i>Entire Plant</i>								
A	641.3	1.95 × 10 <sup>4</sup>	1.3	44	99.79	478	443	10.25
B	320.6	280	1.5	1.6	99.52	209	175	15.36
C	769.5	2200	1.2	3.9	99.84	635	564	7.27

Source: From Chmielewski, A.G. et al., *Sep. Sci. Technol.*, 36, 1117, 2001. Copyright (2001) with permission from Taylor & Francis.

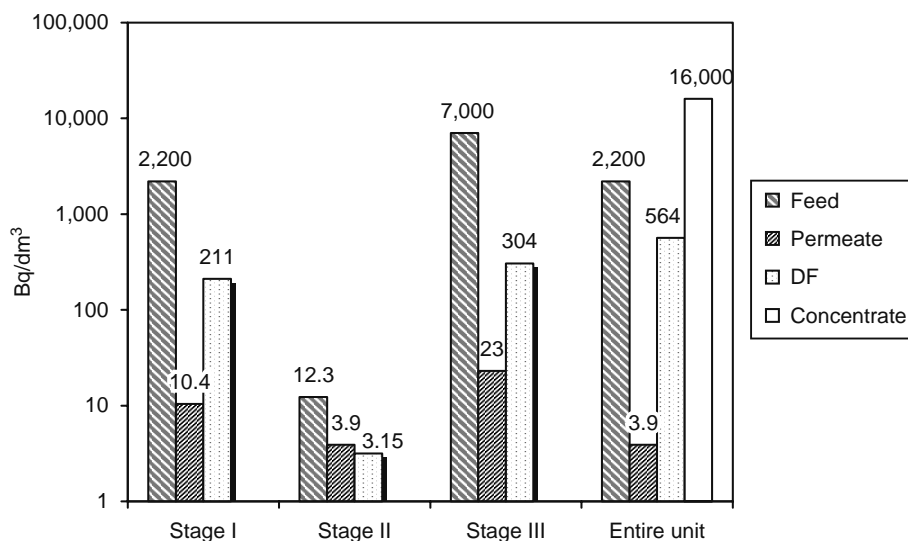


FIGURE 30.5 Removal of radioactive compounds; experiments with three-stage RO plant.

inlet tank. Injection of the salt solution (NaCl) before the second stage increased decontamination factor in that stage from 3.09 to 91 and for entire plant to 13,700 (the numbers obtained for A waste sample).

The results of radioactive waste sample C treatment with 3RO are shown in Figure 30.5. The feed radioactivity is 2,200 Bq/dm<sup>3</sup>. After processing permeate has radioactivity below discharge limits (3.9 Bq/dm<sup>3</sup>) and can be discharged; the concentrate of radioactivity 16,000 Bq/dm<sup>3</sup> can undergo further processing. The average decontamination factor for entire plant is 564.

### 30.2.1.2 Other Applications

Reverse osmosis preceded by microfiltration or ultrafiltration is considered as an option for the treatment of radioactive wastes from Romanian nuclear centers. Effective studies are carried on at Research Center for Macromolecular Materials and Membranes, Bucharest and at Institute of Nuclear Research, Pitesti aiming in employing these pressure-driven techniques for cleaning the wastes from decontamination of nuclear installations and reactor primary circuit [34,35].

There are assessments predicting the use of reverse osmosis for the processing of the wastes from medical application [36,37] and for the removal of caesium-137 from decontamination wastes after accident in the steel production factory [38]. RO is considered as a method for removal of radioactive pollutants from contaminated water (removal of <sup>137</sup>Cs and <sup>90</sup>Sr) in the vicinity of atomic power plants [39], as well as for removal of small quantities of radionuclides (<sup>222</sup>Rn, <sup>234</sup>U, <sup>238</sup>U, <sup>226</sup>Ra) from drinking water [40,41].

## 30.2.2 NANOFILTRATION

Membranes having effective pore sizes between 0.001 and 0.01 μm are used in nanofiltration. NF is placed between reverse osmosis and ultrafiltration, and because of that it is sometimes considered as loose reverse osmosis. Typical operating pressures for NF are 0.3–1.4 MPa. The process allows to separate monovalent ions from multivalent ions, which are retained by NF membrane. The process can be used for separation of organic compounds of moderate molecular weight from the solution of monovalent salts. The very well-known application in nuclear industry is boric acid recovery from contaminated cooling water in nuclear reactor. There are some examples of nanofiltration applications and studies done with the aim of implementation in nuclear centers described in literature. Some of them are listed in the Table 30.4.

## 30.2.3 ULTRAFILTRATION

Ultrafiltration operates at lower pressures (0.2–1 MPa) than reverse osmosis and with higher permeate fluxes. It uses more porous membranes, pore size of 0.001–0.1 μm. In such a case, low-molecular weight dissolved compounds pass through the membrane, while colloid and suspended matters are rejected by UF membrane.

In nuclear industry ultrafiltration was applied in the pretreatment stage before reverse osmosis that needs removal of potential foulants from feed streams. Very often ultrafiltration is combined with precipitation or complexation. Small ions bound by macromolecular chelating agent form complexes, which are retained by UF membrane. Such an enhanced ultrafiltration becomes an efficient separation process with high decontamination factors, sometimes compared with those

**TABLE 30.4**  
**Examples of Application of NF for Liquid Radioactive Wastes Processing and Isotopes Separation**

Facility	Type of the Waste/ Process Stream	Process and Type of the Membranes Used	Results	References
Chalk River Laboratories (AECL, Canada)	Reactor coolant (cleaning and boric acid recovery)	Three-stage installation, NF membranes	The products of the plant are concentrated boric acid, which after purification can be recycled and the concentrate of radioisotopes for immobilization.	[42]
Bugey nuclear power plant (France)	Reactor waters (separation of ionized silica and boric acid)	NF	NF allows the separation with 92% recovery for silica and 16.5% for boron. The corrosion, activated cations ( $\text{Sn}^{2+}$ , $\text{Ag}^+$ , $\text{Co}^{2+}$ ) are retained by the NF membranes.	[43]
ANSTO (Australia)	Uranium mill effluents	NF membranes in cross-flow membrane cell	The rejection for uranium was greater than 75%. Some of the tested membranes showed potential for separation of radium, sulfate and manganese.	[44]
ESWE—Institute for Water Research and Water Technology, Wiesbaden (Germany)	Water with dissolved uranium	NF membranes from Osmonic Desal (Desal 5 DK, Desal 5DL and Desal 51 HL) and Dow (NF 90 and NF 45)	Divalent anion complex $\text{UO}_2(\text{CO}_3)_2^{2-}$ and four- valent anion complex $\text{UO}_2(\text{CO}_3)_3^{4-}$ were rejected between 95% and 98% by four membranes and between 90% and 93% by NF90 membrane.	[40]
Kyungpook National University (Korea)	Simulated nuclear waste containing strontium	NF with complexation with polyacrylic acid, Nitto Denko NTR7410, NTR7250 and NTR729HF membranes	Greater Sr removal at elevated pH was attributed to the formation of $\text{SrCO}_3(\text{s})$ due to dissolution of atmospheric $\text{CO}_2$ . Improvement of Sr removal was achieved with the addition of PAA, an increase of membrane fouling was observed at lower pH.	[45]
CEN de Cadarache	Simulated nuclear waste containing strontium	NF with complexation with polyacrylic acid, Filmtec NF 70 membranes	The effect of complexation was diminished in high concentration of non-active sodium nitrate. 98.2% concentration of strontium was achieved and 70% of sodium nitrate from the waste was eliminated in two-stage process.	[46]
Laboratoire de Catalyse et Synthèse Organique, Université Claude Bernard, Lyon	Separation of lanthanides and actinides, separation of lanthanide isotopes	NF/complexation with EDTA, DTPA and new ligands on the basis of DTPA. Sepa MG-17 NF membrane (Osmonics)	Separation factors $\alpha(^{150}\text{Nd}/^{142}\text{Nd}) =$ $1.0021 \pm 0.0016$ and $\alpha(^{160}\text{Gd}/^{155}\text{Gd}) =$ $1.0028 \pm 0.0014$ were obtained.	[47–50]
Laboratoire de Catalyse et Synthèse Organique, Université Claude Bernard, Lyon	High-salinity wastes containing caesium	NF/complexation with resorcinarens and calixarens	The $\text{Cs}^+/\text{Na}^+$ selectivity from 3 mol/L aqueous $\text{NaNO}_3$ solution was about 90%. With the two- stage process 99% removal of trace quantities of caesium was achieved and sodium retention not higher than 10%.	[51]

obtained by reverse osmosis. Radioactive cations can be removed in precipitation process forming less-soluble particles (carbonates, phosphates, oxalates, or hydroxides) which are later filtered with UF membrane. These hybrid methods are effectively used in many plants processing  $\alpha$ -bearing radioactive waste streams. Number of installations is under operation in nuclear centers and many efforts are done to implement ultrafiltration for radioactive wastes processing. Ultrafiltration installations were tested at nuclear power plants around the United States. These experiments proved usability of UF systems for the treatment of aqueous wastes from floor drains, water from reactor cooling system, as well as for some type of waste from reprocessing plants. In some cases, the pilot plant experiments were followed by construction of full-scale installations. The examples of the full-scale plants operated in some nuclear centers, as well as testing facilities, applying UF for radioactive wastes processing are performed in Table 30.5.

There was a suggestion to treat the wastes from laundries cleaning the contaminated cloths by ultrafiltration [54–56]. These wastes contain surfactants, high alkalinity and high-salt concentration. It is difficult to process them by evaporation where considerable foaming takes place with contaminated droplets carryover. The concept of UF use for this kind of waste is advantageous because of the possibility of detergents recycling and reuse. The detergents are recovered in permeate, while all suspended particles, fibers, and radionuclides are rejected in the retentate.

One of the current researches devoted to membrane treatment of radioactive waste is directed toward seeded ultrafiltration and all methods, which combined with ultrafiltration, give considerable enhancement of separation (Table 30.6).

**TABLE 30.5**  
**Examples of Nuclear Testing Facilities Applying UF for Liquid Radioactive Wastes Processing**

Facility	Type of the Waste	Process and Type of the Membranes Used	Results	References
Enhanced Actinide Removal Plant at Sellafield	Wastes containing actinides after precipitation stage	Two-stage UF	First stage produces a concentrate of a few wt% solid content that is dewatered in a second stage	[25]
Paks nuclear power plant	Contaminated boric acid solutions	Plate and frame UF modules with polysulphone membranes	The volume reduction of about 45 and decontamination factors in the range 10–100 were obtained	[52]
Nukem, Hanau	Low-level wastes from a fuel fabrication plant	UF with co-precipitation pretreatment	DFs of about 100–200; VRC achieved by UF 10–15 times greater than that obtained with precipitation	[53]
River Bend nuclear power plant (United States)	Floor drains from BWR	UF with IEX	Permeate from UF is additionally polished in ion-exchange beds and after that water is recycled in the plant. Feedwater turbidity decreases from 20–150 NTU to <0.1 NTU	[28]
Salem nuclear power plant	Low-level radioactive wastes, which originate from floor drains from PWR, laboratories, sampling points and auxiliary equipment drains	Tubular UF modules and demineralization unit	UF membranes remove particles smaller than 0.05 $\mu\text{m}$ , oil, grease, colloids, and metal complexes protecting IEX beds. The quantity of $^{58/60}\text{Co}$ , $^{54}\text{Mg}$ , and $^{100}\text{Ag}$ , is reduced	[28]
Seabrook nuclear power plant (United States)	Floor drains from PWR and spent resins tank drain-down	UF with cation resin demineralization	Colloidal $^{58}\text{Co}$ removed below discharge limits and more than 90% of TSS was removed by UF system	[28]
Callaway nuclear power plant (United States)	Floor drains and equipment drains tanks, reactor coolant water	UF with IEX	70% of radioactivity and suspended solids were removed from coolant water with UF; 89% of radioactivity and suspended matter from floor drains. The full-scale plant configured in 2001 consisted of UF and ion-exchange units, processed the waste for direct disposal	[28]
Diablo Canyon nuclear power plant (United States)	Spent media transfer liquid containing high concentration of radioactive submicron particles	Two mobile, skid-mounted tubular UF plants	Systems produced the liquid free from particulate activity that can be introduced into the IEX columns without the danger of serious fouling and deterioration of their performance	[28]
Mound Laboratory (United States)	Wastes from a fuel reprocessing plant	4.5 m <sup>3</sup> /h installation composed of 32.3 m long tubular UF elements, of total surface area 6.5 m <sup>2</sup>	80%–99% of $\alpha$ emitters were removed in the test operation and high retention of transuranic elements in full-scale installation was observed ( $^{241}\text{Am}$ —98.9%, $^{238}\text{Pu}$ —98.6%, $^{237}\text{Np}$ —69.1%, $^{233}\text{U}$ —93.7%)	[28]

Extensive studies were done within the International Atomic Energy Agency (IAEA) coordinated research programme on the use of inorganic adsorbents for the treatment of aqueous wastes and backfill of underground repositories [61]. In 1992–1996, IAEA coordinated research programme on waste treatment and immobilization technologies involving inorganic sorbents that resulted in elaboration of new technologies of production of sorbents, which can be applied in nuclear industry. The sorbents can be used in minced form that can be directly introduced into the feed streams treated by ultrafiltration or in more coarse form for ion-exchange columns followed the membrane process [62,63].

The processes of UF and enhanced UF for low and intermediate-level radioactive waste treatment were studied at INCT, Poland. Liquid radioactive wastes originating mainly from application of radioisotopes are collected from all of Poland at Institute of Atomic Energy, in Świerk. They contain various radioactive substances (total specific activity <10<sup>7</sup> kBq/m<sup>3</sup>) and ballast non-active salts (concentration <5 g/dcm<sup>3</sup>), as well. In the solution, small radioactive ions such as  $^{51}\text{Cr}^{3+}$ ,  $\text{H}^{51}\text{CrO}_4^-$ ,  $^{60}\text{Co}^{2+}$ , and  $^{137}\text{Cs}^+$  are present; most of them can easily pass through the membrane for which cutoff value is ~2000 MW. The decontamination factors obtained by using ultrafiltration membranes are low (1.07–1.12). The possibility to improve the removal efficiency and to increase decontamination factors is the application of reverse osmosis or ultrafiltration enhanced by complexation. Ultrafiltration membranes that are permeable to the small ions retain the macromolecules or particles formed in the process of complexation or sorption.

**TABLE 30.6**  
**Examples of Test Facilities Using Enhanced UF for Liquid Radioactive Wastes Processing**

Facility	Type of the Waste/Process Stream	Process and Type of the Membranes	Type of Sorbent/Binding Agent	Results	References
Cadarache Nuclear Research Centre	Synthetic solutions and actual liquid radioactive wastes	UF with sorption	Activated charcoal and nickel hexacyanoferrate, soluble polymers	Good removal of plutonium, strontium, cesium isotopes, moderate of ruthenium and cobalt	[54]
Harwell Laboratory, UK	PWR wastes (wastes containing actinides—colloidal forms of plutonium and americium—in alkaline solutions, laundry wastes)	UF with sorption (seeded UF)	Manganese dioxide, sodium nickel hexacyanoferrate, hydrous titanium oxide, zirconium phosphate, ferric hydroxide, different commercial sorbents	The process is capable of reducing the amount of radioactivity in aqueous effluents to very low levels	[57–60]
University of Colorado, Department of Chemical Engineering	Environmental waters	Polymer-assisted UF	Hyperbranched chelating polymers (glucoheptanamide, polyamidoamine and polyethylenimine derivatives)	Removal of boric acid from water solutions, remediation of water	[64]
Los Alamos National Laboratory	Wastes from decommissioning and decontamination of nuclear facilities	UF/complexation hybrid process	Polymers with functional groups—amine, carboxylic, oxime, pyrrolidone, phosphonic, and sulfonic	Purification of the cellulose materials contaminated with organic substances, toxic and radioactive metals; separation of <sup>241</sup> Am (III) and <sup>238</sup> Pu (IV) from high acidic solutions and real radioactive wastes	[65–67]
Bhabha Atomic Research Centre	Radioactive solutions containing cerium	UF/complexation hybrid process	Polyethylenimine	Radioactive cerium removal	[68]
Institute of Colloid Chemistry and Water Chemistry, Ukrainian Academy of Science	Environmental waters	UF/complexation hybrid process	Polyethylenimine, polyethyleneglycol, carboxymethyl cellulose, and polyacrylamide	Enhancing removal of U(VI) from contaminated environmental waters; 99% removal of uranium was achieved	[69,70]
Institute of Nuclear Chemistry and Technology, Poland	Wastes from nuclear laboratories and application of radioisotopes	UF/complexation hybrid process	Chelating polymers, hexacyanoferrates, manganese dioxide, hydrous titanium oxide	Effective removal of radioactive ions and heavy metals	[24,71–72]

The selection of appropriate complexing agent is very important to remove the radioisotopes with high efficiency. Each ion needs specific ligand, which has to fulfil special requirements:

1. High molecular weight, selected for each UF membrane cutoff
2. Good solubility in water
3. Ability of selective binding the ions and molecules
4. Stability of complexes under the process condition
5. Nontoxic, not causing potential hazard
6. Low price and market availability

Many different complexing agents and adsorbents were examined. As ligands attaching ions of Cr, Co, and Cs, polyethylenimine (PEI), microcrystalline chitosan (MCH), polyacrylic acid (PAA) and its derivatives, polyvinylpyrrolidone (PVD) and suspension of hexacyanoferrates of transient metals were applied [62,71].

The experiments were carried out with laboratory-scale units and with pilot plants. The polymeric (capillary-type UF module Amicon H26P30–43, cutoff =  $3 \times 10^4$  MW, membrane surface area  $2.5 \text{ m}^2$ ) and ceramic UF membranes (Membralox and CeRam Inside) were employed. The solution of selected radionuclides, simulated sewage, and original liquid low-level radioactive wastes was used in filtration tests. Chelating complexing agents were added to the feed solution to bind the radioactive ions. After mixing and seasoning the sample was filtered with UF membrane at fixed pH and ambient temperature.

### 30.2.3.1 Removal of Radionuclides from Water Solutions by Ultrafiltration/Complexation

Membralox tubes, 250 mm long and 7/10 mm diameter with the membrane placed inside the tube and CeRam Inside three-channel tubes, were tested at INCT [24,71,72]. The pore size of ceramic membranes was in 1 kDa to 100 nm range. The tests were performed with non-active and radioactive model solutions. The experiments proved that membranes in UF range were not sufficient to achieve high decontamination factors and the process has to be combined with chemical complexation or sorption. The experiments showed significant increase of retention factors and decontamination factors when macromolecular compounds were added. Example of the results for two membranes: Membralox tube with 50 nm filtering layer and CeRam 15 nm is shown in Figure 30.6. The retention of caesium ions was similar for both membranes. When ultrafiltration was combined with complexation with macromolecular ligands the retention was improved. Retention factors for Membralox 50 nm were higher than for CeRam. An exception was the case when sodium cyanoferrate was added. For both membranes the retention factors were close to 1. For two membranes the application of macromolecules resulted in the increase of retention.

The retention and decontamination factors for cobalt ions were low when UF membranes were applied (Figure 30.7). To intensify effect of separation the complexing agents, polyacrylic acid of different cross-linking, polyacrylic acid salts, polyethylenimine, and Instar AS (complexing agent containing macromolecular acrylamide and sodium acrylate copolymer) were added to the feed solution. The results of ultrafiltration of cobalt ions complexed before filtration by the soluble polymers are presented in Figure 30.7. The experiments showed high influence of the polymer, its chemical form and average molecular weight on retention factors. The best results were obtained when sodium polyacrylate of high-molecular weight or polyethylenimine were employed.

Application of macromolecular chelating polymers allows catching small radioactive ions with good efficiency. Soluble polymers efficiently bound radioactive cobalt and chromium, however the complexation of  $\text{HCrO}_4^-$  ions was difficult. Chromate ions were removed with MCH, which is a good sorbent for all metals, however decontamination factors for radioactive chromium in the form of  $\text{H}^{51}\text{CrO}_4^-$  were moderate. Caesium isotopes were effectively removed with cyanoferrates of transient metals; copper cyanoferrate more effectively binds caesium than cobalt cyanoferrate. The meaningful dependence of retention and decontamination factors on pH was observed (Figure 30.8). Favorable conditions of binding the caesium with cyanoferrates are in alkali environment, under  $\text{pH} > 8$ , while the best complexation abilities of soluble polymers are in neutral conditions. It was found that the best conditions of binding  $^{51}\text{Cr}^{3+}$  and  $^{60}\text{Co}^{2+}$  ions with PEI macromolecules occur at  $\text{pH} = 4-6$ . The most effective adsorption of ions  $^{137}\text{Cs}^+$  by CuFC was found at  $\text{pH} = 9.5-10.5$ .

Binding abilities of the soluble polymers fall down slowly with the concentration of alkali metals. In Figure 30.9, the results of UF/complexation with polyethylenimine (PEI), polyacrylic acid of different cross-linking (PAA1 and PAA2) and polyacrylic acid amide were presented. In each case the decontamination factors for  $^{60}\text{Co}$  decrease when concentration of alkali metals increase from 0.1 to 2.5  $\text{g}/\text{dm}^3$ . The increase of alkali metals causes decline of decontamination factor for radioactive caesium, while cyanoferrates are applied as a sorbents (Figure 30.10).

The concentration of the complexing agent should be selected for each radioisotope–complexing agent pair. Usually the concentration ratio, the ligand to the ion bound by this ligand, is in the range 1–20. Figure 30.11 shows DFs for europium-152 as a function of concentration of NaPAA of MW = 8000, which was selected to remove this radioisotope. The best binding conditions were found at concentration of 8  $\text{g}/\text{dm}^3$ , which corresponds to the concentration ratio of polymer to europium,

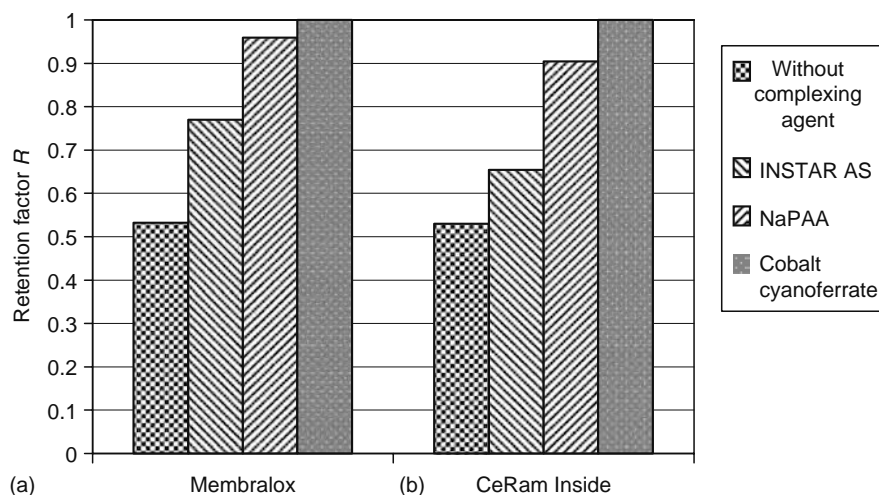


**FIGURE 30.6** The influence of complexing agent on retention factor of  $\text{Cs}^+$  ions. (a) Membralox (50 nm) and (b) CeRam Inside (15 nm). (Reprinted from Zakrzewska-Trznadel, G., *J. Membr. Sci.*, 225, 25, 2003. Copyright [2003] with permission from Elsevier.)

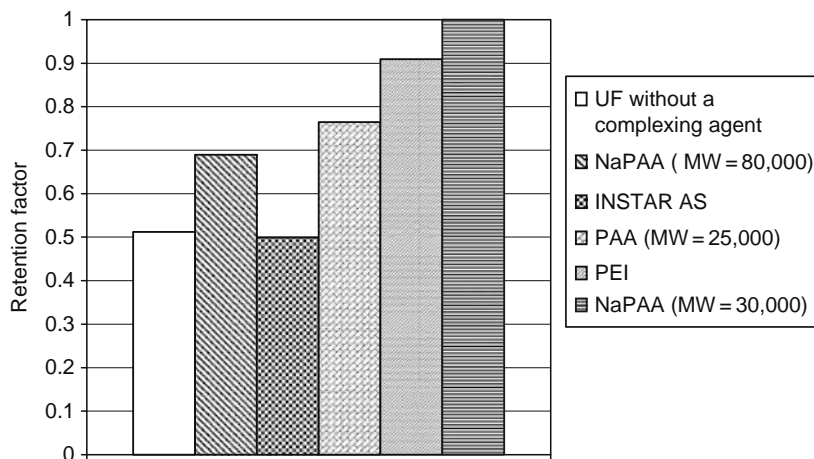


**FIGURE 30.7** The influence of complexing agent on retention of Co<sup>2+</sup> ions, Membralox 50 nm membrane, pH = 6–7. (Reprinted from Zakrzewska-Trznadel, G., *J. Membr. Sci.*, 225, 25, 2003. Copyright [2003] with permission from Elsevier.)

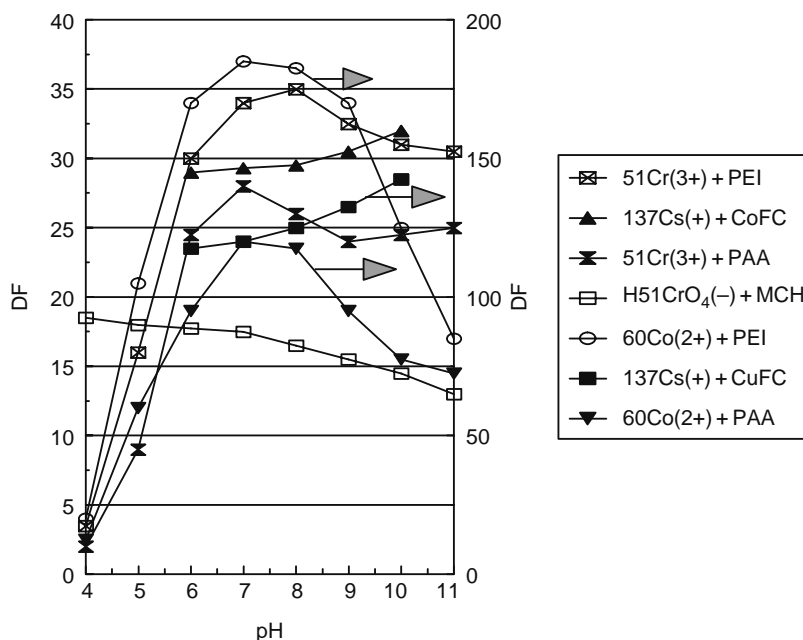


**FIGURE 30.8** DF vs. pH for small ions combined with macromolecules.

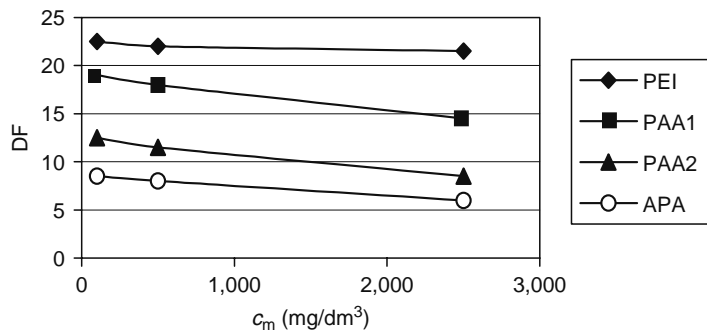


**FIGURE 30.9** <sup>60</sup>Co removal by UF/complexation method; variation of DF on alkali metals concentration;  $c_{Co} = 5$  mg/L,  $c_L / c_{Co} = 10$ , pH = 7,  $T = 20^\circ\text{C}$ . (Reprinted from Zakrzewska-Trznadel, G. and Harasimowicz, M., *Desalination*, 144, 207, 2002. Copyright [2002] with permission from Elsevier.)

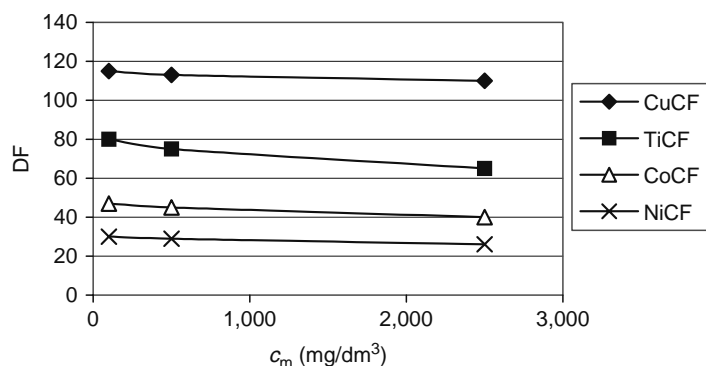


**FIGURE 30.10** <sup>137</sup>Cs removal by UF/complexation method; variation of DF on alkali metals concentration;  $c_{Cs} = 5$  mg/L,  $c_L/c_{Co} = 4$ , pH = 7,  $T = 20^\circ\text{C}$ . (Reprinted from Zakrzewska-Trznadel, G. and Harasimowicz, M., *Desalination*, 144, 207, 2002. Copyright [2002] with permission from Elsevier.)

such as 18.5:1. For this concentration ratio DF was the highest. Further increase of ligand concentration did not result in increase of decontamination factor.

### 30.2.3.2 Treatment of Original Radioactive Waste

When actual radioactive waste is treated by UF/complexation method the decontamination factors for each radioactive component of the sample differ from those obtained for single ion-solutions. The ions interfere and compete in complexation process and the salinity of the wastes influences removal that results in lower decontamination factors. The characteristics of radioactive waste used in ultrafiltration experiments are shown in Table 30.7. The sample had relatively low salinity (<1 g/dm<sup>3</sup>); its specific radioactivity was in medium-level liquid waste range (~150 kBq/dm<sup>3</sup>). The main portion of radioactivity came from cobalt-60 and caesium-137, but some quantities of lanthanides and small amount of actinides (<sup>241</sup>Am) were also present. Decontamination factors obtained for actual waste differed from DFs obtained for solutions of single radioisotopes. As was proved before [71], the concentration of alkaline metals influenced DF markedly. The competition between different ions bound by chelating ligands or adsorbents resulted in increase of retention and decontamination factors for original liquid waste. The results of UF/complexation tests are shown in Table 30.8 and decontamination factors calculated for selected radioisotopes in Figure 30.12.

The hybrid UF/complexation process appeared very effective for removal of americium and europium isotopes; in the majority of permeate samples the concentration of these radioisotopes was below detection limits or very small. Good removal of <sup>60</sup>Co was observed with sodium polyacrylate of MW > 15,000 Da and with polyethyleneimine. The complexation of caesium ions with chelating polymers was rather moderate; good results were obtained with cobalt cyanoferrate and decontamination factors were higher than 100. Average decontamination factors for total waste radioactivity were low, except for the case when two complexing agents were dosed to the effluent simultaneously: PEI and CoCF (Table 30.8). The results obtained in the experiment when cobalt hexacyanoferrate together with soluble polymer (PEI) were applied showed significant

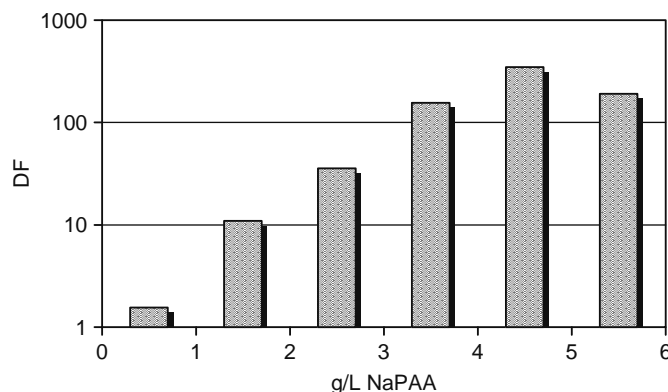


**FIGURE 30.11** DF for europium-152 in function of concentration of NaPAA (MW = 8000), Membralox 5 kDa, 0.5 g/L Eu<sub>2</sub>O<sub>3</sub>, pH = 8. (Reprinted from Zakrzewska-Trznadel, G., *J. Membr. Sci.*, 225, 25, 2003. Copyright [2003] with permission from Elsevier.)

**TABLE 30.7**  
**Characteristics of Radioactive Waste Sample**

Chemical composition <sup>a</sup> (mg/dm <sup>3</sup> )	Na – 274, K – 28, Mn <0.05, Fe –0.60, Cu <0.03, Pb <0.01, Ca <43.35, Mg – 16.18, Cr <0.05, Au <0.1, Cl <sup>-</sup> – 177.5, F <sup>-</sup> – 1.58, NO <sub>3</sub> <sup>-</sup> – 3.83, NO <sub>2</sub> <sup>-</sup> – 1.67, SO <sub>4</sub> <sup>2-</sup> – 195, PO <sub>4</sub> <sup>3-</sup> – 5.37 SiO <sub>2(dissolved)</sub> – 25.7 C <sub>organic</sub> – 120
pH	5.2
Radiochemical composition (kBq/dm <sup>3</sup> )	Co-60 (7.1), Cr-51, Sb-124 (0.01), Sb-125 Cs-137 (139.49), Ce-141, Eu-152 (0.44), Eu-154 (0.065), Am-241 (1.68)

Source: From Zakrzewska-Trznadel, G., *J. Membr. Sci.*, 225, 25, 2003. Copyright (2003) with permission from Elsevier.

<sup>a</sup> Concentration of metals performed as a total concentration of the element in different chemical forms.

increase of <sup>137</sup>Cs removal, however the decontamination factors for other radioisotopes decreased in comparison of the tests when only single chelating polymer was applied as a complexing agent.

One of the major limitations of UF/complexation is that removal of isotopes by this method is efficient when the mixture of the ligands binds the ions effectively under the same conditions (the same pH, concentration of alkali-metals salts, etc.). To overcome this problem the process may be run in multistage system and the complexing agents are dosed in the successive stages to remove some specific ions separately. The above process was divided into two steps to enable high-removal efficiency. At first, CoCF slurry was introduced into the feed solution to bind the caesium ions. After some hours the feed was filtered with UF ceramic membranes up to threefold volume reduction. Sodium polyacrylate, MW 30,000, was added to permeate and after seasoning and pH adjustment the solution was filtered. The DFs for such a process arrangement were performed in Figure 30.13. In the first stage of filtration high removal of Cs-137 was achieved, while other radioisotopes were rejected in moderate rate. In the second stage, where sodium polyacrylate was employed decontamination factors were much higher for most of the radioisotopes present in the waste. Only <sup>137</sup>Cs ultrafiltration gave DFs smaller than 1 that corresponds with higher specific activity in permeate. Low DF < 1 shows that Cs-137 is not bound by NaPAA and passes through the membrane. Additionally, low concentration of this radioisotope and generally low total salinity of the effluent may cause low decontamination for caesium after the treatment in the first stage. This was earlier observed during operation of three-stage RO plant, where decrease of total salinity before the final purification stage caused significant decrease of decontamination factors [33].

For all radioisotopes present in the waste sample DFs, in the case where cyanoferrate and chelating polymer were applied subsequently in two-stage process, were higher than those obtained when the complexing agents were added to the feed solution simultaneously. All decontamination factors were higher than DFs obtained for a single soluble polymer (NaPAA or PEI) (Table 30.9).

**TABLE 30.8**  
**Content of Some Radioisotopes in the Process Streams in UF/Complexation Experiments.**  
**Membrane CeRam Inside 15 kDa**

	Co-60 (kBq/dm <sup>3</sup> )	Cs-137 (kBq/dm <sup>3</sup> )	Eu-152 (kBq/dm <sup>3</sup> )	Eu-154 (kBq/dm <sup>3</sup> )	Am-241 (kBq/dm <sup>3</sup> )	ΣA <sub>pi</sub> (kBq/dm <sup>3</sup> )	DF <sub>total</sub>
Feed solution	7.12	139.49	0.44	0.06	1.68	148.79	
Permeate NaPAA, M <sub>w</sub> = 1,200, c <sub>L</sub> = 4 g/dm <sup>3</sup>	2.48	54.92	0.07	—	—	57.47	2.59
NaPAA, M <sub>w</sub> = 8,000, c <sub>L</sub> = 4 g/dm <sup>3</sup>	1.71	52.64	0.05	—	—	54.40	2.73
NaPAA, M <sub>w</sub> = 15,000, c <sub>L</sub> = 4 g/dm <sup>3</sup>	0.76	48.11	0.05	—	—	48.92	3.04
NaPAA, M <sub>w</sub> = 30,000, c <sub>L</sub> = 4 g/dm <sup>3</sup>	0.33	43.56	0.02	—	—	43.91	3.39
NaPAA, M <sub>w</sub> = 30,000, c <sub>L</sub> = 8 g/dm <sup>3</sup>	0.42	38.74	0.03	—	—	39.19	3.80
PEI c <sub>L</sub> = 4 g/dm <sup>3</sup>	1.07	38.00	0.03	—	—	39.10	3.90
CoFC, c <sub>L</sub> = 4 g/dm <sup>3</sup> PEI, c <sub>L</sub> = 6 g/dm <sup>3</sup>	1.13	1.26	0.11	0.02	0.37	2.89	51.50

Source: From Zakrzewska-Trznadel, G., *J. Membr. Sci.*, 225, 25, 2003. Copyright (2003) with permission from Elsevier.

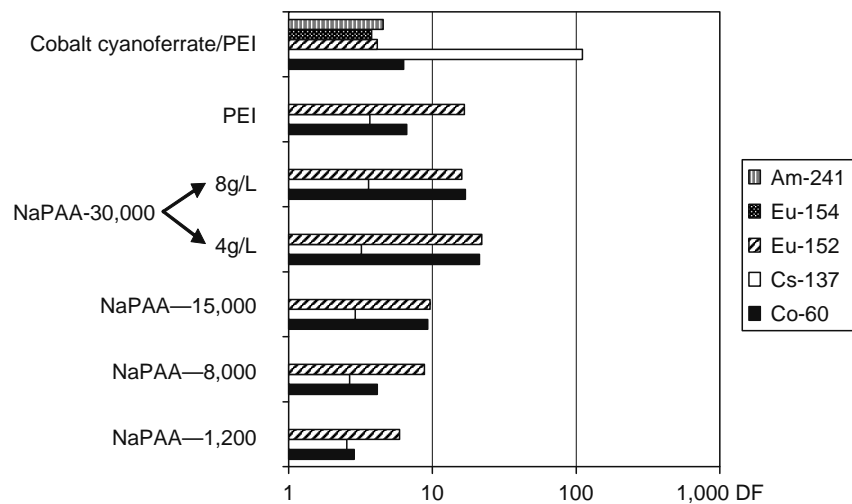


**FIGURE 30.12** Decontamination of the sample of liquid radioactive waste in UF/complexation process with a use of different complexing agents, CeRam Inside membrane, 15 kDa. (Reprinted from Zakrzewska-Trznadel, G., *J. Membr. Sci.*, 225, 25, 2003. Copyright [2003] with permission from Elsevier.)

Apart from radioactive compounds the radioactive wastes may contain non-active but chemically toxic substances. The national standards and regulations describe the discharge limits for these substances, too. Heavy metals are toxic compounds, most often present in liquid radioactive wastes. The experiments showed that most of these metals are removed by UF/complexation method. The method is inefficient for removal of monovalent ions, bivalent cations and anions are retained in 25%–50%, but high retention of the metals like Mn, Fe, Co, Cu, Pb, Cr was observed. The retention factors for those metals in two-stage experiment described above, were as follows:

Mn 94%  
 Fe 99%  
 Cu 99%  
 Pb 87%  
 Cr 75%  
 Co 94%

Advantages of ceramic membranes employed in nuclear industry were found in their extremely high chemical and physical stability (full pH range), resistance to oxidants, solvents, and ionizing radiation. Ceramic materials are advantageous when the solutions composed of organic compounds or high radioactive wastes containing the  $\alpha$  emitters are treated. High

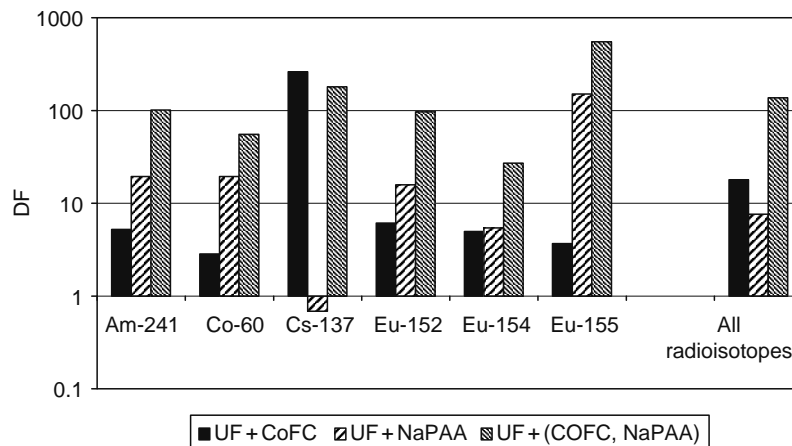


**FIGURE 30.13** Decontamination factors for two-stage process, CeRam Inside 15 kDa. (Reprinted from Zakrzewska-Trznadel, G., *J. Membr. Sci.*, 225, 25, 2003. Copyright [2003] with permission from Elsevier.)

**TABLE 30.9**  
**Decontamination factors in Combined Process UF/Complexation by Use of Different Complexing Agents**

	Am-241	Co-60	Cs-137	Eu-152	Eu-154
Na PAA, 30,000	$\rightarrow \infty$	21.24	3.2	22	$\rightarrow \infty$
PEI, 15,000	$\rightarrow \infty$	6.62	3.67	16.67	$\rightarrow \infty$
CoCF/PEI (simultaneously)	4.54	6.31	110.7	4.14	3.78
CoCF/NaPAA, 30,000 (subsequently)	101.4	55.38	179.5	96.39	26.95

Source: From Zakrzewska-Trznadel, G., *J. Membr. Sci.*, 225, 25, 2003. Copyright (2003) with permission from Elsevier.

temperature resistance allows washing with warm streams and sterilization by steam. This is very important when macro-molecular complexing ligands causing membrane fouling are applied.

### 30.2.3.3 Pilot Plant Experiments

The apparatus equipped with Sunflower CeRam Inside (23–8–1178), characterized in Table 30.10, was used in pilot plant tests. The plant consisted of feed tank (1) equipped with cooler; (2) membrane module housing; (3) pretreatment filters; (4) pressure pump TONKAFLO; (5) circulating pump Grundfos; (6) non-return valve; (7) two needle valves and four ball valves (Figure 30.14).

The filtration experiments were conducted in cross-flow mode at pressure 0.25–0.5 MPa in the system. In that pressure range for filtration of water, permeate flux was 26–85 L/m<sup>2</sup>h. All process parameters were recorded with data acquisition system; periodically the samples of permeate and retentate were collected for chemical analysis.

Original radioactive liquid waste from the storage tank in nuclear center was treated in the process UF/complexation. The main radioactive components of the waste sample were <sup>60</sup>Co, <sup>65</sup>Zn, <sup>133</sup>Ba, <sup>134</sup>Cs, <sup>137</sup>Cs, <sup>152</sup>Eu, and <sup>241</sup>Am. When ultrafiltration was applied solely the rejection of radioactive compounds was very low and the decontamination factors were between 1.02 and 1.05. Therefore ultrafiltration was combined with complexation by soluble polymers. The application of sodium polyacrylate (NaPAA) 15,000 and 30,000 of molecular weight, in concentration range 0.4–3 g/L gave slight increase of decontamination factors to 1.3–2.8. In addition, dosing of INSTAR AS up to concentration 3 g/L resulted in an increase of decontamination factor to 3.1. Since the major portion of total activity came from radioactive isotopes of caesium, the use of cobalt hexacyanoferrate as a binding agent was advisable. The cobalt hexacyanoferrate was introduced as a suspension prepared from 0.02 N solutions of Co(NO<sub>3</sub>)<sub>2</sub> · 6H<sub>2</sub>O and K<sub>4</sub>[Fe(CN)<sub>6</sub>] 3H<sub>2</sub>O. As is shown in Figure 30.15, first portion of the suspension caused an increase of DF to 30 and further increase of complexing agent concentration did not change decontamination factor radically. The results of the radiochemical analysis are shown in Table 30.11, where isotopic composition of the forth samples is performed. The notation of the samples was as follows: S, feed solution composition; P<sub>1</sub>, permeate treated with 1 g/L of NaPAA; P<sub>2</sub>, permeate after complexation with 3 g/L NaPAA; and P<sub>3</sub>, after the treatment with CoCF and INSTAR AS. The calculated decontamination factors for each radioisotope as well as DFs for total activity in processed waste were presented in

**TABLE 30.10**  
**Characteristics of Sunflower CeRam Inside Ceramic Membrane**

Filtration area (m <sup>2</sup> )	0.35
External diameter (mm)	25
Length (mm)	1178
Number of channels	23
Hydraulic channel diameter (mm)	3.6
Flux volume at velocity 1 m/s (m <sup>3</sup> /h)	0.86
Pressure drop at velocity 4 m/s (bar)	1.0
Cutoff (kDa)	8
pH	0–14
Temperature (°C)	Up to 150

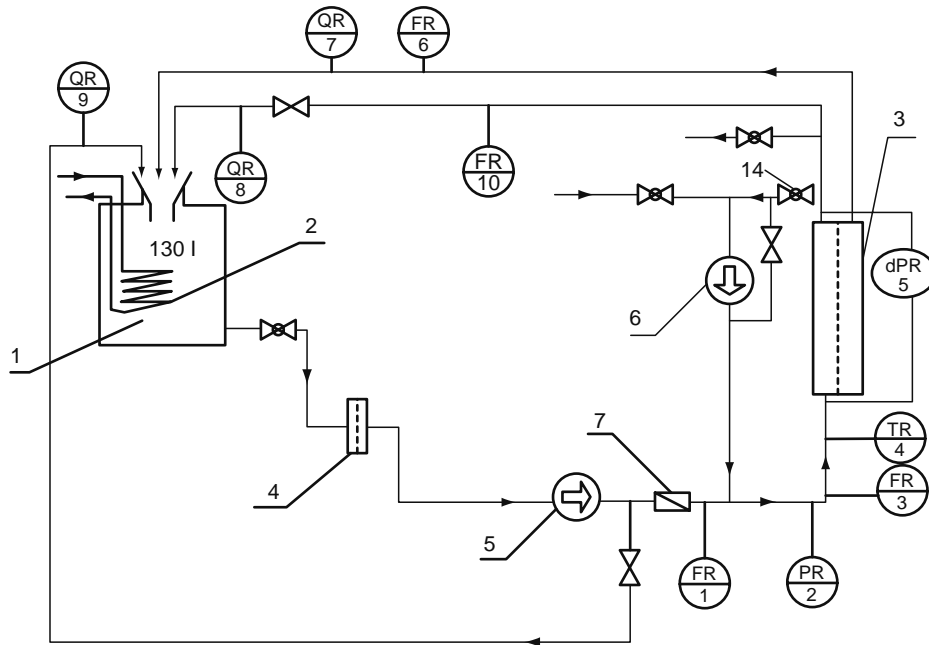


**FIGURE 30.14** Pilot plant for treatment of radioactive wastes by UF/complexation. (Reprinted from Zakrzewska-Trznadel, G. and Harasimowicz, M., *Desalination*, 162, 191, 2004. Copyright (2004) with permission from Elsevier.)

Figure 30.16. The radiochemical analyses of the last sample of permeate showed complete retention of  $^{134}\text{Cs}$ ,  $^{152}\text{Eu}$ , and  $^{241}\text{Am}$  when complexation/UF process was employed. About 1770-fold decrease of concentration of  $^{137}\text{Cs}$  was observed; the decontamination factors for other radioisotopes were high, as well. However, due to high initial  $^{65}\text{Zn}$  content, the concentrations of this radioisotope in permeate ( $P_4$ ) was also high; the radioactive zinc was not removed sufficiently. Therefore, additional cleaning procedure should be applied to reduce  $^{65}\text{Zn}$  concentration and to meet discharge standards. It is likely that the dosage of the polymer was too small to complex all radioisotopes sufficiently (the increase of DF with subsequent dosages of polymer was observed, see Figure 30.16). Further portions of cobalt hexacyanoferrate did not cause the increase of decontamination.

The membrane performance was good, during almost 60-h operation and the permeate flux was stable after initial decline. The biggest flux decrease was observed when macromolecular sodium polyacrylate was introduced: first after dosing 0.4 g/L of NaPAA, then after injection of the next portion (1 g/L NaPAA). In that time, permeate flux declined from 52 L/m<sup>2</sup>h in the beginning (without the complexing agent), to 11 L/m<sup>2</sup>h after injection of 1 g/L of the polymer. Further increase of polymer concentration did not result in the flux decline, as well as addition of CoCF suspension.

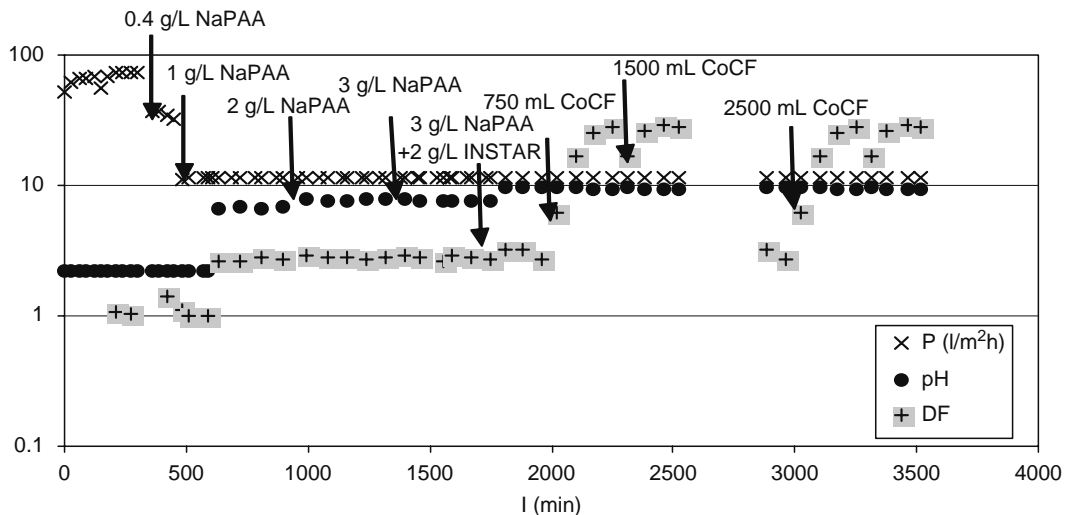


**FIGURE 30.15** Radioactive waste treatment by UF/complexation. (Reprinted from Zakrzewska-Trznadel, G. and Harasimowicz, M., *Desalination*, 162, 191, 2004. Copyright [2004] with permission from Elsevier.)

**TABLE 30.11**  
**Chemical Analysis of the Samples (CeRam Inside, 8 kDa)**

Isotope	S (Bq/L)	P1 (Bq/L)	P2 (Bq/L)	P4 (Bq/L)
Co-60	374	59.5	61.4	70.9
Zn-65	22,038	11,111	2,920	784.6
Ba-133	1,058	113.7	114.3	93.5
Cs-134	22.7	15.2	14.4	0
Cs-137	8,742	6,162	5,823	4.9
Eu-152	27.2	0	0	0
Am-241	1,365	116.8	0	0

Source: From Zakrzewska-Trznadel, G. and Harasimowicz, M., *Desalination*, 162, 191, 2004. Copyright (2004) with permission from Elsevier.

The complexation/ultrafiltration process is efficient for retention of non-active hazardous components of the wastes, e.g., heavy metals, which concentration has to be reduced according to national regulations. In the process described above, the retention of heavy metals was high, and reached 98% for manganese, 98.6% for iron, 92.4% for copper, 91.5% for nickel, and 94.7% for zinc. Some part of bivalent ions was also retained, for instance, Mg in 67%, Ca in 58%,  $\text{SO}_4^{2-}$  in 22.6%.

The enhanced ultrafiltration is effective but hardly controlled process, because of its sensitivity to the process conditions, such as pH, temperature, or concentration of alkaline ions. However, it can be easily applied for the wastes containing the radionuclides that are effectively attached to the macromolecules of the various ligands at the same or similar pH value.

Current development of the hybrid treatment processes is being directed toward searching the new, cheap sorbents, and complexing agents, among them natural polymers such as chitin, lignin, huminates, and lignosulphonate are considered [73]. Using huminates in the ratio 1:25–1:50 with combination of ceramic membranes selectivity higher than 99% for ions such as  $\text{Sr}^{2+}$ ,  $\text{Ni}^{2+}$ ,  $\text{Cu}^{2+}$ ,  $\text{Co}^{3+}$ , and  $\text{Ca}^{2+}$  was obtained. Chitosan and cellulose, mostly abundant biopolymers, are increasingly being used as a coagulant and flocculent in the processes of water and wastewater purification [74,75]. Due to the amine groups present in the polymer chain chitosan is a good sorbent for transient metals [76,77]. It can be formed in granules for fixed beds, as well as a water solution of the acetate [78]. With conjunction of the membrane, chitosan may cause six- to tenfold increase of removal of Cu(II), Co(II), Ni(II), and Zn(II) from water solutions [79]. Apart from other natural sorbents such as biomass, powdered wood bark, nutshell, modified wool or cotton, the use of cheap, inorganic sorbents such as natural zeolites, clays, or fly ash is considered [80].

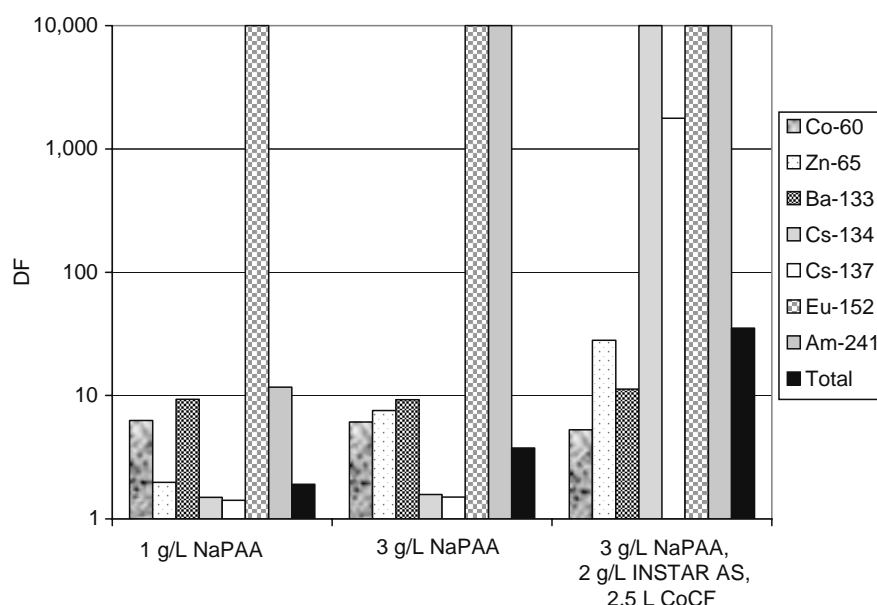


**FIGURE 30.16** Decontamination factors for selected components of radioactive wastes treated in UF/complexation process. (Reprinted from Zakrzewska-Trznadel, G. and Harasimowicz, M., *Desalination*, 162, 191, 2004. Copyright [2004] with permission from Elsevier.)

New potential applications of sorbents in conjunction with a membrane are expected from the development of molecular-imprinted or ionic-imprinted polymers that are capable of metal-ion recognition. This concept based on preparation of matrix in the presence of the molecular or ionic template. After removal of the target molecule/ion the prepared solid can react with the solution of the molecules/ions from which the imprinted molecule/ion should thus be preferentially extracted from the mixture [81–83].

### 30.2.4 MICROFILTRATION

In nuclear technology, microfiltration is used either for pretreatment purposes or for concentration of coarse particles after precipitation process. For high-level radioactive wastes the ceramic filters are used, giving for some types of effluents high decontamination and concentration factors. The MF facilities used in nuclear industry to treat liquid radioactive wastes are summarized in Table 30.12.

### 30.2.5 MEMBRANE DISTILLATION

Membrane distillation (MD) is a separation method that employs porous liophobic membrane, non-wettable by the liquid. Because of liophobicity of the polymer, only vapor is transported through membrane pores. The condensation takes place on the other side of the membrane in air gap, cooling liquid or inert carrier gas. Usually MD is employed to treat water solutions, therefore hydrophobic membranes manufactured from polymers such as polypropylene (PP), polytetrafluoroethylene (PTFE),

**TABLE 30.12**  
**Examples of Nuclear Testing Facilities Applying MF for Liquid Radioactive Wastes Processing**

Facility	Type of the Waste	Process and Type of the Membranes Used	Results	References
AECL Chalk River Laboratory (Canada)	Mixed low-level radioactive wastes	MF was used as a pretreatment step in RO installation	MF hollow fiber membranes remove the suspended solids larger than 0.2 $\mu\text{m}$ . The filtrate from MF forms the feed for the SWRO system, the backwash solution undergo further volume reduction in thin film evaporator	[17,18]
AECL Chalk River Laboratory (Canada)	Groundwater and soils decontamination	Hollow fiber MF system consisted of 40 cross-flow filtration modules, $\sim 6$ cm in diameter, 50 cm long, and 1 $\text{m}^2$ surface area	The system demonstrated the usability of MF for the treatment of soil leachate and removal of radionuclides from ground water. The radioactivity of $^{90}\text{Sr}$ was reduced from 1700–3900 to 2 Bq/L	[28,84–86]
Rocky Flats (United States)	Groundwater containing uranium isotopes, organic toxic compounds, and heavy metals	Tubular MF modules, pore size 0.1 $\mu\text{m}$	The removal efficiency of uranium isotopes by the system was 99.9%	[28]
Idaho National Engineering and Environmental Laboratory (INEEL)	Radioactive wastes from fuel reprocessing	Cross-flow filtration with Mott sintered Hastelloy filter	Good removal of undissolved solids from INEEL radioactive slurries	[87]
Berkeley Nuclear Laboratories	Simulated radioactive wastes	Cross-flow MF; Pall PSS (2.5 $\mu\text{m}$ limit of separation), Fairey Microfiltrex FM4 (1 $\mu\text{m}$ ) and APV Ceraver (1.4 $\mu\text{m}$ ) ceramic and stainless steel membranes	Cross-flow MF was found to be effective dewatering of range of radioactive wastes	[88]
Energy and Environmental Research Center, University of North Dakota	Simulated wastes containing suspended and colloidal solids	SpinTek ST IIL centrifugal membrane filtration technology	Ability to process wastes from decontamination and decommissioning systems within the US DOE; ability to treat hazardous wastewater to a slurry-type level and reduce tank sludge volume	[89]
Los Alamos Nuclear Laboratory (LANL)	Surrogate and real radioactive wastes from LANL	SpinTek ST IIL centrifugal membrane filtration technology	Elaboration of the model for determining the applicability and economics of the system to different DOE waste and process streams	[90]

or poly(vinylidene fluoride) (PVDF) are used in the process. The driving force in the MD process is a gradient of partial pressures of the components of the solution in gaseous phase. The main advantages of membrane distillation applied for radioactive wastes processing are

1. Moderate process conditions, ambient pressure, and moderate temperature
2. High retention and decontamination, higher than that for conventional evaporators
3. Low operational costs for medium-sized installations, the possibility of utilization of waste heat, e.g., from cooling system of nuclear reactor
4. The possibility to achieve high concentrations, close to saturation
5. The possibility of use of plastics as construction materials for apparatus, because of moderate process conditions—minimization of corrosion and capital costs
6. Compact installations (one stage units)

In contrary to other methods, also to reverse osmosis, MD allows complete purification in single stage, not involving additional processes for polishing permeate. It is a simple, economic, and environment friendly method when it is used for radwaste processing.

Membrane distillation was developed at INCT for liquid radioactive waste processing [91]. For many years the process was studied as a method for stable isotopes enrichment. Using porous PTFE membranes, stable isotopes of oxygen and hydrogen were enriched in natural water with relatively high separation factors [92–95]. It was proved that MD distillation is a competitive method for enrichment of oxygen-18, the isotope that finds now a big demand on the market because of high consumption by positron emission tomography [96]. Membrane method in some cases seems useful for heavy water enrichment, as well.

Since membrane distillation exhibits high ability of concentration of aqueous solutions with high retention of acids, salts, and other low-volatile compounds, it can be used for concentration of different radioactive waste streams with high volume reduction and high retention factors [97–99].

The process conducted in batch-type counter-flow apparatus (Figure 30.17) equipped with capillary PP Accurel membranes showed good effectiveness of membrane distillation for purification of radioactive waste. Permeate obtained was pure water. All solutes together with radioactive compounds were rejected by the hydrophobic membrane. At tenfold volume reduction of the initial portion of waste, approximately tenfold concentration of radioactivity in the retentate stream was reached, while radioactivity of permeate retained on the level of natural background (Figure 30.18). As was observed in experiments small sorption in the system took place. However, permeate was free of radioactive substances and other dissolved compounds, the concentration and radioactivity factors sometimes slightly differed from volume reduction factors.

Membrane distillation for concentration of radioactive waste was also tested in pilot plant experiments. The facility used in the tests consisted of spiral-wound module, equipped with PTFE membrane, effective surface area of 4 m<sup>2</sup>. The installation enabled the recovery of the part of heat by two installed heat exchangers (Figure 30.19).

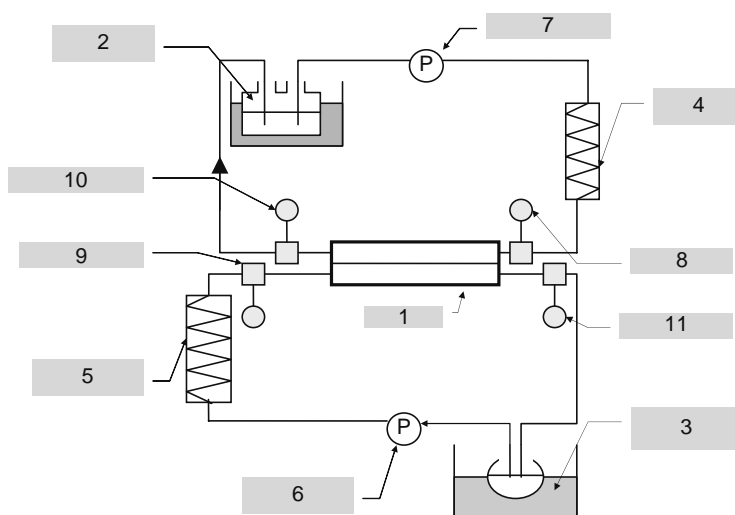


**FIGURE 30.17** Laboratory setup for testing MD process. (1) membrane module, (2) feed reservoir, (3) distillate reservoir, (4,5) heat exchangers, (6,7) peristaltic pumps, (8–11) thermometers.

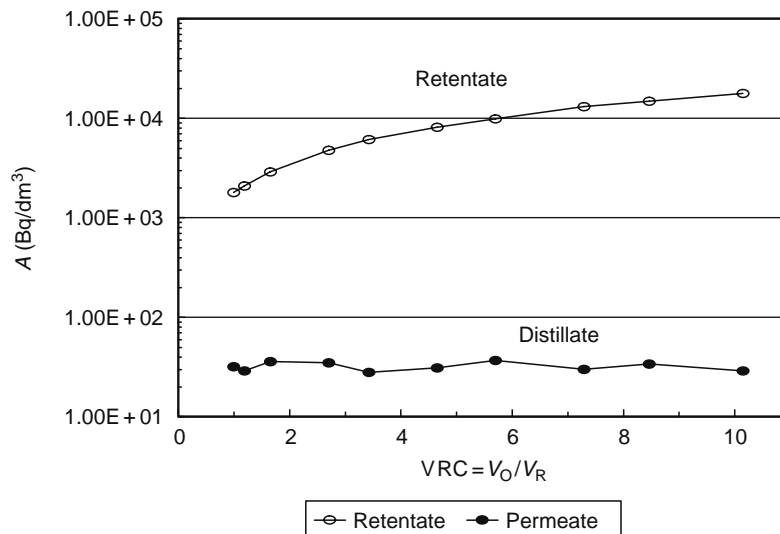


**FIGURE 30.18** Concentration of radioactive waste in batch-type MD apparatus. (From Chmielewski, et al. *Sep. Sci. Technol.*, 32, 709, 1997. Copyright [1997] Reproduced with permission of Taylor & Francis.)

The experiments were conducted in the temperature range 35°C–80°C at feed inlet, and 5°C–30°C at distillate inlet, and with feed and distillate flow rates up to 1500 dm<sup>3</sup>/h. Under these conditions permeate stream was 10–50 dm<sup>3</sup>/h (60–300 dm<sup>3</sup>/m<sup>2</sup> day). During the experiment run the activity of the distillate was stable on the level of natural background radioactivity and the concentrating of radioactive compounds took place in retentate. Retention of radioactive ions in retentate was almost complete (decontamination factors  $\rightarrow \infty$ , Table 30.13). Most of radionuclides were not detected in distillate; only trace amounts of Co-60 and Cs-137 were present. Also retention coefficients of non-active ions were high (Table 30.14).

The experiments have proved that membrane distillation can be applied for radioactive wastewater treatment. In one-stage installation the membrane retained all radionuclides and decontamination factors were higher than those obtained by other membrane methods. The distillate obtained in the process was pure water, which could be recycled or safely discharged into the environment. It seems the process can overcome various problems of evaporation such as corrosion, scaling, or foaming. There is no entrainment of droplets, which cause the contamination of condensate from thin-film evaporator. Operation at low evaporation temperature can decrease the volatility of some volatile nuclides present in the waste, such as tritium or some forms of iodine and ruthenium. The process is especially economic for the plants, which can utilize waste heat, e.g., plants operating in power and nuclear industry.

In membrane distillation, there is a possibility of loss of membrane hydrophobicity during long-time operation. However, during 80-h tests with DM pilot plant the changes in membrane wettability were not observed. The liquid entry pressure for PTFE membrane used in experiments was about 0.23 MPa, which is sufficiently high in comparison with the pressure in the MD installation. According to the manufacturer suggestion the pressure applied in the MD module cannot exceed 0.07 MPa. To reduce the risk of liquid entry into membrane pores the pressure on the distillate side was kept a little higher than pressure on the retentate side.

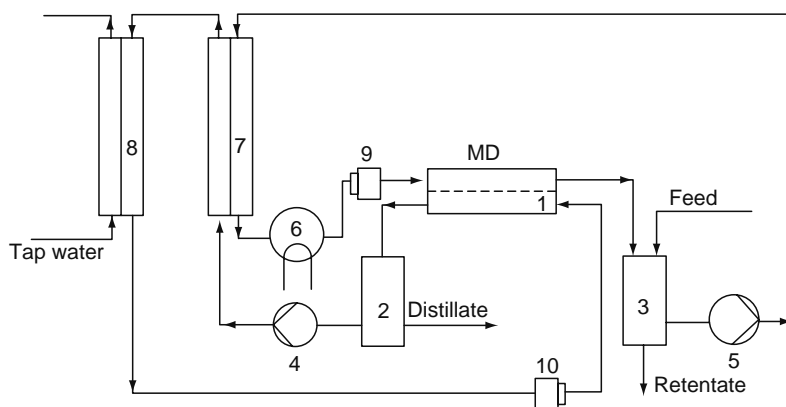


**FIGURE 30.19** A scheme of the pilot plant for radioactive waste concentration. (1) MD module, (2) distillate reservoir, (3) feed tank, (4,5) pumps, (6) heater, (7,8) heat exchangers, (9,10) prefilters. (Reprinted from Zakrzewska-Trznadel, G., Harasimowicz, M., and Chmielewski, A.G., *J. Membr. Sci.*, 163, 257, 1999. Copyright [1999] with permission of Elsevier.)

**TABLE 30.13**  
**Radiochemical Composition of the Waste Sample Used in Experiments and Effluent after MD Plant**

Radionuclide	Activity of the Feed (Bq/dm <sup>3</sup> )	Activity of the Effluent (Bq/dm <sup>3</sup> )	DF
<sup>60</sup> Co	4510	1.04	4336.5
<sup>65</sup> Zn	3390	Not detected	→ ∞
<sup>114m</sup> In	86.2	Not detected	→ ∞
<sup>110m</sup> Ag	10.4	Not detected	→ ∞
<sup>133</sup> Ba	2990	Not detected	→ ∞
<sup>134</sup> Cs	7.84	Not detected	→ ∞
<sup>137</sup> Cs	29.5	0.673	43.8
<sup>140</sup> La	<0.653	Not detected	→ ∞
<sup>170</sup> Tm	526	Not detected	→ ∞
<sup>192</sup> Ir	37.3	Not detected	→ ∞

Source: From Zakrzewska-Trznadel, G., Harasimowicz, M., and Chmielewski, A.G., *J. Membr. Sci.*, 163, 257, 1999. Copyright (1999) with permission from Elsevier.

However, the presence of compounds lowering the surface tension, may result in wetting the hydrophobic membrane. These compounds have to be removed before entering the membrane system by appropriate pretreatment. At small concentration these substances can be removed by sorption, oxidation, or phase separation, whereas at high concentration they can be removed by ultrafiltration. The main nonactive components of the wastes treated in the above experiments, were the inorganic salts such as sulfates, nitrates, or chlorides that increased the surface tension. It was proved that the presence of salts crystallizing in-membrane pores may also result in wetting the membrane during long-time operation of MD installations, especially at low distillate temperatures [100]. Such a situation may take place in the module entrance, when distillate temperature is relatively low. Precipitate deposition, scaling, and pore blocking are the problems of all membrane installations. The appropriate pretreatment or dosing antiscaling additives are the methods of minimization of these phenomena. The problem of scaling is more serious in evaporation installations that are widely used in nuclear industry and operating in higher temperatures than membrane distillation.

The experiments with concentration of inorganic salts showed that 25% concentration of the solute could be achieved by using MD. It is the upper limit for concrete solidification. Usually such a big concentration is not reached, because limit of radiation dose is exceeded for solidified waste, originating from concentrated radionuclides. Distillate is pure water and can be discharged to the sewage or surface waters or can be recycled.

In Table 30.15, decontamination factors for different processes for low- and medium-level radioactive waste treatment are shown. Membrane distillation with its high decontamination factors is a competitive method in this field. However, it has to be mentioned that these high-decontamination factors are achieved from low-volatile solute after adequate pretreatment.

**TABLE 30.14**  
**Chemical Composition of the Waste Sample Used in Experiments and Effluent after MD Plant**

Ion	Concentration in the Feed (mg/dm <sup>3</sup> )	Concentration in the Effluent (mg/dm <sup>3</sup> )	Retention Coefficient (R)
Na <sup>+</sup>	1060.6	3.269	0.9969
NH <sub>4</sub> <sup>+</sup>	207.1	14.584	0.9296
K <sup>+</sup>	21	0.212	0.9899
Mg <sup>2+</sup>	33.7	Not detected	1
Ca <sup>2+</sup>	87.2	2.375	0.9728
F <sup>-</sup>	5.7	0.442	0.9225
Cl <sup>-</sup>	744.2	1.485	0.9980
NO <sub>3</sub> <sup>-</sup>	1832.9	0.065	0.9999
SO <sub>4</sub> <sup>2-</sup>	37.6	0.186	0.9950

Source: From Zakrzewska-Trznadel, G., Harasimowicz, M., and Chmielewski, A.G., *J. Membr. Sci.*, 163, 257, 1999. Copyright (1999) with permission from Elsevier.

**TABLE 30.15**  
**DFs for Most Common Methods of Low- and Medium-Level**  
**Radioactive Wastes Processing**

Process	DF
Chemical precipitation	$10 < DF < 10^2$ ( $\beta, \gamma$ ), $10^3$ ( $\alpha$ )
Organic ion-exchange	$10 < DF < 10^3$
Inorganic ion-exchange	$10 < DF < 10^4$
Evaporation	$10^4 < DF < 10^6$
Bioaccumulation	$DF > 10^3$
Biosorption	$DF < 10^3$
RO	$10 < DF < 10^3$
MD	$DF \rightarrow \infty$

A majority of the methods require multistage systems; even when evaporation does not always yield the product of radiochemical purity. In addition, it is an energy-consuming method and have process barriers described above. The other treatment methods also have some constraints. Ion exchange consumes large volumes of expensive resins that need regeneration and in consequence large quantities of secondary waste are created. Biological processes produce big quantities of sludge with high concentration of radionuclides and intermediate products.

Many years of operation of membrane processing facility in Chalk River Laboratory proved reliability of reverse osmosis. However, reverse osmosis requires involvement of high pressures, cannot avoid membrane fouling and the necessities of frequent cleaning operations resulting in production of secondary wastes. It requires multistage system to achieve sufficient purity of the product and high volume reduction. Thin film composites are less resistant to the radiation and strong chemical environment than PTFE or PP membranes. New possibilities may create the commercialization of inorganic RO membranes.

The opinions on the advantages of membrane distillation are diverse. Low investment costs for small and medium-capacity installations are pointed out on the one hand. For bigger facilities both capital and operation costs can be lower than in conventional processes [101,102]. While on the other hand, more moderate opinions on benefits of membrane distillation are published, as well [103].

One of the main barriers for commercial implementation of membrane distillation is relatively high-permeate fluxes from unit membrane area, along with high-energy consumption in the process. The latter can be overcome when MD installation is used in nuclear power plant, and when waste heat from cooling circuit can be utilized. Another possible way to minimize energy consumption is efficient recovery of heat by appropriate design of the installation or using membrane modules with integrated heat recuperation based on the spiral-wound GORE-TEX principle [101,104]. According to the evaluation of the company these modules consume 150–280 kW h<sub>th</sub>/1 m<sup>3</sup> of distillate, while for modules without integrated heat recovery the energy consumed equals ~600 kW h<sub>th</sub>/m<sup>3</sup>. However, as demonstrated pilot plant experiments performed at INCT, the latter was hardly achieved with the installation described above. In Figure 30.20, energy consumption per unit of the product for various

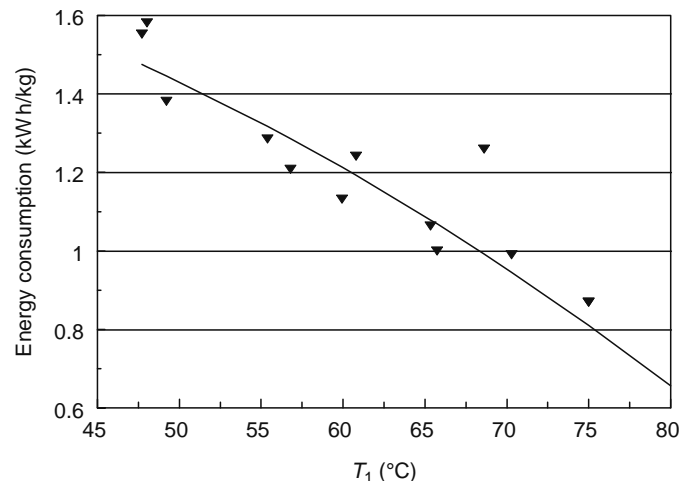


**FIGURE 30.20** Energy consumption per unit of the product in MD process. (Reprinted from Zakrzewska-Trznadel, G., Harasimowicz, M., and Chmielewski, A.G., *J. Membr. Sci.*, 163, 257, 1999. Copyright [1999] with permission from Elsevier.)

**TABLE 30.16**  
**Influence of Process Parameters on Energy Consumption**  
**Per Unit of Permeate**

$T_1$ (°C)	$T_2$ (°C)	$V_R$ (L/h)	$V_D$ (L/h)	$V_{cool}$ (L/h)	$V_P$ (L/h)	$E/V_P$ (kWh/L)
69.6	22.8	720	720	1200	23.60	0.96
65.4	21.7	870	870	1200	18.52	1.06
65.5	16.5	870	870	2700	19.36	1.17
49.3	22.1	1380	1380	840	17.28	1.30
49.3	18.6	1380	1380	1260	18.60	1.38
49.2	22.4	1620	1500	840	24.70	1.31
49.2	20.0	1620	1500	1260	24.95	1.35

feed inlet temperatures ( $T_1$ ), estimated from experimental results, was shown. The favorable are the high process temperatures; at  $T_1$  temperature over 80°C the energy specified by manufacturer of the membrane module can be achieved. The thermal energy consumption in the process depends not only on temperatures, but also on intensity of distillate cooling (to keep the proper temperature gradient across the membrane) and volume flow rates in the apparatus:  $V_R$  and  $V_D$  (Table 30.16), however the influence of these parameters is moderate. The lower cooling water flow implicates decrease of energy consumption. Between flow rate of retentate, distillate, and process temperatures are interactions, therefore optimization of process parameters is necessary to get sufficient permeate fluxes and low-energy consumption per unit of the product.

Membrane distillation modules are at present expensive in comparison with RO elements and their costs influence significantly the capital costs of the MD installations. The market of MD systems is limited; in spite of the many advantages MD method is not widely accepted by the industry. Moderate interest of users influences the production capacities and in consequence reduces the wide implementation of the MD method in different branches of industry. It was proved that advantages of MD decreases with increase of the installation capacity; big installations, of productivity comparable with RO, need large number of modules. Anyway, the comparison of two processes: RO and MD proved technical and economic reasonability of the latter in some cases, such as radioactive waste concentration. The advantages of MD come from

1. Possibility of running the process to high-solute concentrations, sufficient for direct solidification
2. Achieving the high concentration in one stage
3. Elimination of high pressures
4. Reduction of sorption of such radioactive ions, e.g.,  $^{60}\text{Co}^{2+}$ ,  $^{137}\text{Cs}^-$ , and  $^{134}\text{Cs}^-$  inside the pores (the pores are filled with water vapor)
5. Infrequent washing cycles through minimization of fouling and inner sorption, reduction of quantities of secondary wastes

Membrane processes are versatile and flexible; they can be combined with other methods in hybrid processes. Adapted to actual needs they can treat various process streams of different compositions and concentrations. Membrane distillation coupled with evaporation or reverse osmosis may improve the purification efficiency and increase decontamination factors. The flow chart of such hybrid processes is presented in Figure 30.21. In Figure 30.21a, the combination of MD unit with evaporator is shown.

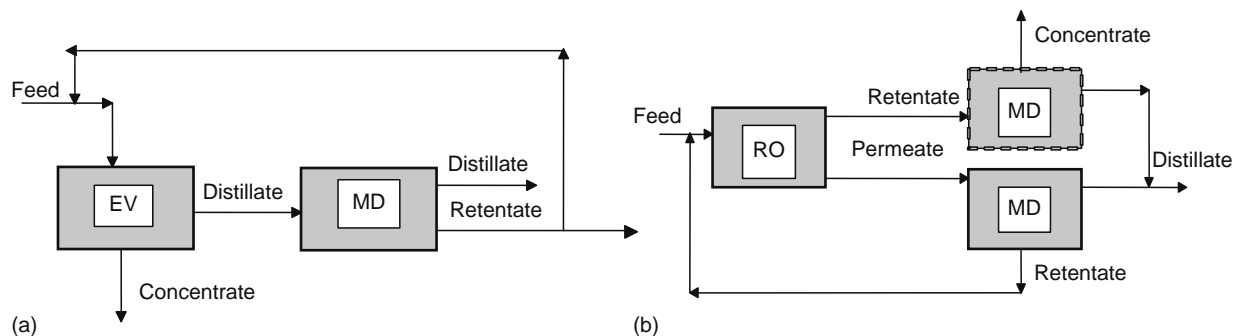


**FIGURE 30.21** (a) Combination of evaporator with MD module. (b) Combination of RO unit with two modules of MD. (Reprinted from Zakrzewska-Trznadel, G., Harasimowicz, M., and Chmielewski, A.G., *Sep. Purif. Technol.*, 22–23, 617, 2001. Copyright [2001] with permission from Elsevier.)

Evaporation is a widely used method for radioactive waste processing. One of disadvantages of the process is radionuclides carry over with small droplets. The contaminated condensate needs additional polishing with ion-exchange resins. The installation of MD module for final cleaning of the condensate can avoid the use of ion exchange. The unit that plays the role of demister can be driven with waste heat from nuclear power plant.

Another possibility of MD use is combination with reverse osmosis that in fact can be the loose RO not involving enormously high pressures. The permeate from RO with reduced amount of multivalent ions is directed to MD module where final polishing takes place (Figure 30.21b). The preliminary volume reduction undergoes in RO module; the retentate is concentrated and volume-reduced in MD module. This solution eliminates the evaporator and ion exchange together replacing these conventional processes with membrane techniques.

The use of hybrid methods gives multiple benefits when it combines the processes which supplement one another or eliminate the drawbacks of the single process. Multistage reverse osmosis results in high-effluent decontamination, however it cannot be run up to high-retentate concentration. High concentration is not the limitation for thin-film evaporators, but the condensate needs final polishing by other method. Membrane distillation combines itself the advantages of both processes, simultaneously avoiding all constraints of RO and EV. In the case of availability of cheap sources of thermal energy, e.g., waste heat, the supplementation of reverse osmosis, or evaporation with membrane distillation seems to be justifiable.

### 30.3 FUTURE OF MEMBRANE PROCESSES IN NUCLEAR TECHNOLOGY

#### 30.3.1 LIQUID RADIOACTIVE WASTE PROCESSING BY MEMBRANE PROCESSES: ADVANTAGES AND LIMITATIONS

Continuous development of membrane processes applied in nuclear technologies is of considerable interest. Implementation of new membrane materials with high chemical and radiation resistance, and new module designs allow spreading applications of membrane processes into different fields of nuclear industry. The main barriers in the use of membrane methods are the following:

1. Necessity of periodical interruption of the process resulting from membrane fouling or blocking and successive cleaning of the installation. It is evaluated that about 1% of secondary wastes come from cleaning the apparatus and membranes [25].
2. Need of pretreatment of the streams before membrane installations.
3. Installations operating under high pressure require sophisticated apparatus and pressure pumps.

The elaboration of proper pretreatment methods, application of antiscalants, and minimization of secondary wastes created during cleaning cycles are of great importance. At present the research work on use of pressure-driven processes for radioactive waste treatment is focused on following issues:

1. Application of ultrafiltration coupled with other processes such as precipitation, sorption, or complexation
2. Combining membrane processes with other methods into integrated processes, such as ultrafiltration–evaporation, reverse osmosis–ion exchange
3. Elaboration of effective methods of fouling control and membrane cleaning, avoiding the membrane blockage and flux decline
4. Use of nanofiltration with pores at the boundary of reverse osmosis and ultrafiltration that allows to separate multivalent ions such  $\text{Ca}^{2+}$ ,  $\text{Al}^{3+}$ ,  $\text{SO}_4^{2-}$  from monovalent. It is possible with nanofiltration to separate multivalent radioactive ions from non-active salts, as sodium nitrate
5. Replacing polymeric membranes by inorganic, more resistant to ionizing radiation and aggressive chemical environment
6. Testing the influence of process conditions on stability and lifetime of particular membrane installation elements—the influence of salts that cause scaling ( $\text{Na}_2\text{SO}_4$ ,  $\text{Na}_2\text{CO}_3$ ,  $\text{NaHCO}_3$ ,  $\text{Ca}_3(\text{PO}_4)_2$ ), the influence of radiation on membrane material

Despite of some technical and process limitations, membrane techniques are very useful methods for the treatment of different types of effluents. They can be applied in nuclear centers processing low- and intermediate-level liquid radioactive wastes or in fuel reprocessing plants. All the methods reported in the chapter have many advantages and can be easily adapted for actual, specific needs. Some of them are good pretreatment methods; the other can be used separately as final cleaning steps, or can be integrated with other processes. Membrane methods can supplement or replace techniques of distillation, extraction, adsorption, ion exchange, etc. Evaluation of membrane processes employed for liquid radioactive waste treatment is presented in Table 30.17.

**TABLE 30.17**  
**Membrane Methods for Liquid Low- and Medium-Level Radioactive Waste Processing**

Process	Advantages	Disadvantages	Abilities and Applications
RO	<ul style="list-style-type: none"> <li>Removes dissolved salts</li> <li>DF 100–1000</li> <li>VRF 100–1000</li> <li>Economical</li> <li>Established for large-scale operation</li> </ul>	<ul style="list-style-type: none"> <li>High-pressure system, limited by osmotic pressure</li> <li>Subject to fouling, non-backwashable</li> </ul>	<ul style="list-style-type: none"> <li>Very well developed technology</li> <li>Ability of rejection of all contaminants</li> <li>Number of industrial applications for treatment of mixed waste, floor drains, waste from reprocessing, from medical applications</li> </ul>
NF	<ul style="list-style-type: none"> <li>Pressures lower than in RO</li> <li>Separate multivalent ions and nonionic organic molecules of MW &gt;300 Da from monovalent ions and non-active salts</li> <li>Inorganic membranes of good radiation and chemical resistance available</li> </ul>	<ul style="list-style-type: none"> <li>Not usable where absolute purification is necessary; monovalent radioactive ions pass through the membrane</li> <li>Membranes subjected to fouling</li> </ul>	<ul style="list-style-type: none"> <li>Ability of separation of monovalent ions from multivalent ions</li> <li>Separation of organic compounds from monovalent salts</li> <li>Application in nuclear industry for boric acid recovery from contaminated cooling water</li> </ul>
UF	<ul style="list-style-type: none"> <li>Separation of dissolved salts from particulate and colloidal material</li> <li>Inorganic membranes available with good chemical and radiation stability can also operate at elevated temperatures</li> <li>Pressure &lt;1 MPa</li> </ul>	<ul style="list-style-type: none"> <li>Fouling-need for chemical cleaning or backflushing</li> <li>Organic membranes subject to radiation damage</li> </ul>	<ul style="list-style-type: none"> <li>Good pretreatment stage for RO</li> <li>Removes colloids (some actinides compounds) and suspensions</li> <li>Many industrial applications and pilot tested installation</li> </ul>
Enhanced UF (UF/complexation, UF/sorption)	<ul style="list-style-type: none"> <li>Possibility to treat wide range of waste streams</li> <li>Removal of small ions without high pressures involved</li> </ul>	<ul style="list-style-type: none"> <li>Strongly dependent on process conditions (temperature, pH)</li> <li>The presence of complexing agents may entail further cleaning</li> <li>Fouling phenomena</li> </ul>	<ul style="list-style-type: none"> <li>Removes small ions with selected ligands</li> <li>Enables recycling of some compounds after break-up of the complexes</li> <li>Pilot plant tests</li> </ul>
MF	<ul style="list-style-type: none"> <li>Low pressure operation (100–150 kPa)</li> <li>Excellent pretreatment stage for RO</li> <li>Inorganic membranes available</li> <li>Low fouling when air backwash is employed</li> </ul>	<ul style="list-style-type: none"> <li>Backwash frequency can be quite high; depends on solid content of waste stream</li> </ul>	<ul style="list-style-type: none"> <li>Very well developed technology</li> <li>Number of implementation in nuclear centers</li> <li>For pretreatment purposes or for concentration of coarse particles after precipitation process</li> </ul>
MD	<ul style="list-style-type: none"> <li>Removes all dissolved salts, very high DF</li> <li>Non-pressure-driven operation</li> <li>Good chemical and radiation resistance of membranes (Teflon)</li> <li>Economical for nuclear industry</li> </ul>	<ul style="list-style-type: none"> <li>High thermal energy consumption comparing with pressure-driven processes unless cheap energy source or waste heat is utilized</li> <li>Cannot be applied for wastes with volatile radioactive compounds</li> </ul>	<ul style="list-style-type: none"> <li>Tested in laboratory and pilot plant</li> <li>Until now no industrial installations in nuclear technology</li> </ul>
Electrodialysis	<ul style="list-style-type: none"> <li>Well-established technology for desalination</li> <li>Separates ionic substances from nonionic, concentrates ionic compounds</li> <li>Minimizes the volume of hazardous wastes and secondary wastes</li> </ul>	<ul style="list-style-type: none"> <li>The necessity of pretreatment and periodical scale removal</li> <li>Process limited by concentration (low conductivity for diluted solutions)</li> <li>Fouling is a problem in higher concentrations</li> </ul>	<ul style="list-style-type: none"> <li>Intensive laboratory and pilot plant studies, small industrial applications</li> <li>For separation of ions from radioactive waste</li> <li>For recovery of acids and alkali from radioactive wastes and salt solutions</li> </ul>

### 30.3.2 NEW FIELDS OF APPLICATION OF MEMBRANE PROCESSES IN NUCLEAR INDUSTRY

#### 30.3.2.1 Removal of Tritium from Nuclear Waste (Liquid and Gaseous Effluents)

Nuclear Energy Agency of the Organisation for Economic Co-operation and Development (OECD/NEA) considers tritium as one of the four volatile, hazardous radionuclides ( $^3\text{H}$ ,  $^{14}\text{C}$ ,  $^{85}\text{Kr}$ , and  $^{129}\text{I}$ ) that are created in nuclear cycle with long-term risk [105]. Tritium, a radioactive isotope of hydrogen, emitting mild  $\beta$  radiation is created in nuclear reactors and in reprocessing plants by neutron activation of isotopes of  $^2\text{H}$ ,  $^3\text{He}$ ,  $^6\text{Li}$ , and  $^{10}\text{B}$ . The largest quantities of tritium are produced in heavy water reactors ( $\sim 5.42 \times 10^7$  GBq/GW<sub>el</sub> per annum) [106]. Less amounts are emitted by fast breeder reactors and high-temperature graphite reactors; the smallest quantities are created in light water reactors ( $\sim 5.55 \times 10^5$  GBq/GW<sub>el</sub> per annum). It was

evaluated that reprocessing plants with a capacity of 1400 t/a, processing fuel from LWR can emit  $(1.85\text{--}3.70) \times 10^7$  GBq per year of radioactive tritium [106], that is commensurate with emission from natural sources.

One of technical problems of removal of tritium is its low concentration in technological and waste streams. In heavy water reactors moderator (PHWR) the ratio DTO:D<sub>2</sub>O is  $10^{-5}$ , and in water streams from fuel reprocessing plants, HTO:H<sub>2</sub>O,  $10^{-7}$  [107]. In this way, great volumes were contaminated with tritium: hundreds and thousands of cubic meters per year need processing. Majority of the treatment methods is based on technologies used for deuterium enrichment such as water distillation, distillation of hydrogen, electrolysis, ion exchange, and some combined methods such as electrolysis–catalytic exchange, the so-called CECE process [108,109].

Among alternative technologies for separation of tritium, membrane methods are considered. *Nafion*, Du Pont membranes, were applied for separation of hydrogen isotopes in installations for tritium removal from heavy reactor water and from nuclear reactor atmosphere. The monitor for HTO and HT control was constructed in Chalk River Laboratories in Canada [110]. At High-Energy Accelerators Research Organization (KEK), Japan, the work on apparatus for measurement of tritium emitted from high-energy accelerators, equipped with hollow-filament membranes for gas separation, is carried on [111].

The studies on separation of water isotopomers (HTO, HDO, H<sub>2</sub>O) with membranes from poly[bis(phenoxy)phosphazene] and carboxylated derivatives were carried on in Pacific Northwest Laboratory [112,113]. Using these membranes tritiated water was extracted from fuel storing pool water of 3  $\mu\text{Ci/L}$  concentration of tritium, and from facilities under supervision of US DOE in Hanford and Savannah River. Separation with 10,800 pCi/L tritiated water obtained by membrane method was not higher than 33% (depletion in the permeate fraction). Water containing 3  $\mu\text{Ci/L}$  of HTO was depleted by 22% in a similar system [113].

The membrane permeation was tested for separation of HTO from water at INCT [114]. Membranes made from regenerated cellulose, polysulphone, and polytetrafluoroethylene were used. Separation factors  $\alpha_{\text{H}_2\text{O}/\text{HTO}}$  obtained in membrane process were not higher than 1.04 for cellulose and 1.02 for polysulphone, while for PTFE membranes were as high as 1.06–1.22.

Number of works published recently concerns application of polymeric gas separation (GS) membranes for separation of hydrogen isotopes, with particular consideration of tritium compounds (HT, HTO) [115–125]. For this purpose, membranes manufactured from glassy and amorphous polymers are applied, mainly polyimide and polycarbonate membranes, as well as polyphenylene oxide membranes assembled in modules of different configuration (e.g., Mc Generon Inc., type B210, Ube Industries, Ltd. Type NM-B05A, Parker, type 2112-NX-1–300 [116]. Super high permeation (SHP) modules—produced by UBE Ltd., which have 10 times higher gas permeability than used at present high-permeable HP modules—seem to be very promising. This allows reducing the space occupied by membrane installation, eliminating the costs of expensive compressors that can be replaced by blower [121]. Conventional methods of tritium removal from atmosphere are limited to catalytic oxidation, followed by adsorption of water on molecular sieves. The method is effective, however has disadvantages resulted from size of apparatus and management of produced water. The method can be used for small glove boxes; in case of large compartment the volumes of installations increase; adsorption system requires large desiccators and high-volume tanks for tritium storage. The advantage of membrane method is the possibility of reduction of processed gas volume to the one tenth of the volume related to conventional method, as well as simultaneous water removal.

### 30.3.2.2 Isotope Separation

The history of separation of isotopes by membrane permeation may be derived from early work of Graham in the middle of nineteenth century on molecular effusion. The most spectacular application of molecular effusion was uranium-235 enrichment for military purpose during the Second World War. In spite of the competitiveness of centrifugal method, up to now gaseous diffusion is an important method of production of fuel based on natural uranium in countries such as United States and France, including EURODIF [126,127], supervised by France, Spain, Italy, and Belgium, which have in their disposal the installations in Tricastin and Pierrelatte, as well as in Russia, China, Great Britain, and Argentina [127]. There is no broad information available on membranes used in gaseous diffusion, however it was known that French technology used sintered and anodic alumina, gold–silver alloys, nickel, Teflon, zirconia, and porcelain [128].

Ceramic and metallic porous membranes are still used for separation of isotopes other than uranium, such as argon and neon [129,130], or hydrogen [131–137]. Polymeric membranes for separation of isotopes of hydrogen were applied at National Institute of Research and Development for Isotopic and Molecular Technologies in Cluj, Romania [138,139]. Polymers such as polyethylene terephthalate (PET), polyethylene (PE), polytetrafluoroethylene (PTFE), cellulose acetate (CA), and polyvinyl chloride (PCV) were used. The selectivity of these membranes was lower than palladium membranes and microporous *Vycor* glass, however number of advantages are expected in low costs of polymeric membranes, the possibility of formation of capillaries with big surface area and avoiding high pressure and temperatures.

Polymeric membranes for separation of hydrogen and oxygen isotopes were studied at INCT, Warsaw [92–95,140–141]. Both hydrophilic barriers, such as regenerated cellulose and hydrophobic PTFE membranes, were tested. The regenerated cellulose appeared to be a very good system to get high separation factors and to consider membrane permeation as possible and competitive method for enrichment deuterium and <sup>18</sup>O in natural water.

Research on separation of hydrogen isotopes is focused on the aspects related to safe operation of nuclear reactors and separation of tritium. Apart from separators based on palladium alloys [142–145], one can find catalytic units with different metallic membranes and various types of integrated systems with catalytic ceramic reactors [146–154].

Using different membranes and various membrane techniques, isotopes of chlorine [155], carbon [156], lithium in aqueous solutions [157,158], and uranium in  $\text{CH}_4$  [158,159] were separated. Isotopes of gadolinium and neodymium were separated in hybrid system of nanofiltration/complexation [50].

### 30.3.2.3 Gaseous Radioactive Wastes—Noble Gases Separation

Apart from radioactive tritium separation from reactor atmosphere or off-gas, polymeric membranes can be applied for separation of noble gases produced by nuclear power plants and fuel reprocessing plants as an alternative to commonly used adsorption or low-temperature distillation methods.

Research on removal of noble gases by permeation method with dimethyl silicon membranes was carried out in Oak Ridge National Laboratory [160]. On the basis of experimental work, the calculations for different industrial cascades separating krypton and xenon from the space of molten salt and sodium cooled breeder reactor or from the off gas from a plant processing spent reactor fuel were performed.

In the process of separation of noble gases, silicon rubber membranes [161,162] and high-resistant siloxane rubbers (polyvinyltrimethylsilane—PVTMS and block-copolymer, composed of polyarylate and polydimethylsiloxane of different weigh ratio, the so-called sylar) [163,164] were employed.

For this purpose the polymer membranes were formed in tubes [165] placed in modules, operating in cascade configuration [166,167]. Preliminary storage of treated gases for decay to prolong the lifetime of membranes were practiced. After 20 day storage of radioactive gases containing  $^{85}\text{Kr}$ —0.004 mol and  $^{133+135}\text{Xe}$ —0.2 mol, at flow rate of  $1\text{ cm}^3/\text{s}$  silicon membranes at the end of the cascade were found to be stable after a number of months. The lifetime could be prolonged to several years by 30 day storing [168]. During separation of mixtures of noble gases the decrease of effective separation factors for particular components was observed. However, the presence of each of them caused plasticizing effect of the polymer enhancing the transport through the membrane [169].

During the last years increasing interest on noble gas separation by membranes is being noticed [170–172]. Hollow fiber membranes from polyimide [171], flat sheet membranes from PET or oriented polypropylene [172] were applied in the tests.

## NOMENCLATURE

$A_f$	specific activity of feed
$A_p$	specific activity of permeate
$A_R$	specific activity of retentate
CF	concentration factor
$c_p$	concentration in permeate
$c_f$	concentration in feed
DF	decontamination factor
$K_{\text{TDS}}$	TDS reduction coefficient
$R$	retention coefficient
$T_1$	feed (warm stream) inlet temperature
$T_2$	cold stream (distillate) inlet temperature
$V_R$	warm stream (retentate) flow rate
$V_D$	cold stream (distillate) flow rate
$V_C$	cooling water flow rate
$E$	energy consumption in MD process
$V_P$	permeate flow rate
VRC	volume reduction coefficient
$x_A, x_B$	A and B components concentration in retentate
$y_A, y_B$	A and B components concentration in permeate
$\alpha_{A/B}$	separation factor for A and B components mixture

## ABBREVIATIONS

AECL	Atomic Energy of Canada Limited
ANSTO	Australian Nuclear Science and Technology Organisation
BWR	boiling water reactor

CA	cellulose acetate
CECE	combined electrolysis-catalytic exchange
DD	drum dryer
DMC	direct membrane cleaning
DSC	differential scanning calorimetry
DTPA	diethylenetriaminepentaacetic acid
EDTA	ethylenediaminetetraacetic acid
EERC	Energy and Environmental Research Center
EV	evaporation
HF	hyperfiltration
IAEA	International Atomic Energy Agency
IEA	Institute of Atomic Energy
IEX	ion exchange
INCT	Institute of Nuclear Chemistry and Technology
INEEL	Idaho National Engineering and Environmental Laboratory
LANL	Los Alamos Nuclear Laboratory
MCH	microcrystalline chitosan
MD	membrane distillation
MF	microfiltration
MWCO	molecular weight cutoff
NF	nanofiltration
OECD/NEA	Organisation for Economic Co-operation and Development/Nuclear Energy Agency
PA	polyamide
PAA	polyacrylic acid
PEI	polyethylenimine
PET	polyethylene terephthalate
PHWR	pressurized heavy water reactor
PLC	programmable logic controller
PP	polypropylene
PS	polysulphone
PSA	polysulphonic acid
PTFE	polytetrafluoroethylene
PU	polyurethane
PVA	polyvinyl amide
PVC	polyvinylchloride
PVD	polyvinylpyrrolidone
PVDF	poly(vinylidene fluoride)
PVTMS	polyvinyltrimethylsilane
PWR	pressurized water reactor
RO	reverse osmosis
SWRO	spiral-wound reverse osmosis
TDS	total dissolved solids
TRO	tubular reverse osmosis
TRU	transuranic elements
TSS	total suspended solids
TUF	tubular ultrafiltration
UF	ultrafiltration
WAO	wet air oxidation

## REFERENCES

1. Dytynierskij, J.I., Puzskow, A.A., and Switcow, A.A., Purification, concentration of liquid wastes with low level of activity by reverse osmosis, *At. Energ.*, 35, 6, 405, 1973.
2. Ramachandhran, V. and Misra, B.M., Studies on the radiolytic degradation of cellulose acetate membranes, *J. Appl. Pol. Sci.*, 30, 35, 1985.
3. Ramachandhran, V. and Misra, B.M., Studies on effect of irradiation on semi-permeable membranes, *J. Appl. Pol. Sci.*, 27, 3427, 1982.

4. Ramachandhran, V. and Misra, B.M., Concentration of radioactive liquid streams by membrane processes, *J. Appl. Pol. Sci.*, 28, 1641, 1983.
5. Ramachandhran, V. and Misra, B.M., Studies on the radiation stability of ion exchange membranes, *J. Appl. Pol. Sci.*, 32, 5743, 1986.
6. Chmielewski, A.G. and Harasimowicz, M., Influence of gamma and electron irradiation on transport properties of ultrafiltration membranes, *Nukleonika*, 37, 4, 61, 1992.
7. Chmielewski, A.G. and Harasimowicz, M., Influence of gamma and electron irradiation on transport properties of nanofiltration and hyperfiltration membranes, *Nukleonika*, 42, 4, 857, 1997.
8. Rautenbach, R. and Albrecht, R., *Membrane Processes*, John Wiley & Sons, Chichester/New York/Brisbane/Toronto/Singapore, 1989.
9. Mulder, M., *Basic Principles of Membrane Technology*, Kluwer Academic, Dordrecht/Boston/London, 1991.
10. Judd, S. and Jefferson, B., eds., *Membranes for Industrial Wastewater Recovery and Re-use*, Elsevier, Oxford/New York/Tokyo, 2003.
11. Cohen, K., *Theory of Isotope Separation as Applied to the Large-Scale Production of  $^{235}\text{U}$* , National Nuclear Energy Series III-1B, McGraw-Hill, New York, 1951.
12. Benedict, M. and Pigford, T.H., *Nuclear Chemical Engineering*, McGraw-Hill, New York, 1957.
13. Hwang, S.-T. and Kammermeyer, K., *Membranes in Separations, Techniques of Chemistry*, Vol. VII, John Wiley & Sons, New York/London/Sydney/Toronto, 1975.
14. Fabiani, C., Strontium separation with ultrafiltration membrane from dilute aqueous solution, *Sep. Sci. Tech.*, 214, 353, 1986.
15. Harasimowicz, M., Application of ultrafiltration and hiperfiltration for concentration of liquid radioactive wastes, PhD thesis, University of Mining and Metallurgy, Krakow, 1995.
16. Gupta, S.K.S., Slade, J.A., and Buckley, L.P., Demonstration of membrane technology for treatment of radioactive liquid waste, *Ultrapure Water J.*, May, 1993.
17. Gupta, S.K.S., Slade, J.A., and Tulk, W.S., *Liquid Radwaste Processing with Crossflow Microfiltration and Spiral Wound Reverse Osmosis*, AECL-11270, Chalk River, Ontario, 1995.
18. Gupta, S.K.S., Buckley, L.P., Rimpelainen, S., and Tremblay, A.Y., Liquid Radwaste Processing with Spiral Wound Reverse Osmosis, WM '96 Conference, Tuscon, Arizona, Feb. 25–29, 1996.
19. Gupta, S.K.S. and Rimpelainen, S., Liquid Radwaste Processing with Spiral-Wound Reverse Osmosis, ULTRAPURE WATER, Knowledgebase, UP140132, 1, 1997.
20. Rimpelainen, S. and Tremblay, A.Y., Effect of Solute Precipitation on RO Elements During Mixed Wastewater Treatment, ULTRAPURE WATER, Knowledgebase, UP160429, 4, 1999.
21. Tan, L. and Tapsell, G., Operation of a membrane pilot plant for ANSTO effluent, WM'04 Conference, Tuscon, AZ, Feb. 29–March 4, 2004.
22. Non-Chemical Technologies for Scale and Hardness Control, Federal Technology Alerts, produced for U.S. DOE by Battelle Columbus Operations, January 1998, <http://www.cisivn.com/fta/>, accessed on 2004-01-10.
23. Rimpelainen, S. and Tremblay, A.Y., Verification of Species Responsible for the Fouling of RO Membranes during Mixed Wastewater Treatment, ULTRAPURE WATER, Knowledgebase, UP170136, 1, 2000.
24. Zakrzewska-Trznadel, G., Radioactive solutions treatment by hybrid complexation—UF/NF process, *J. Membr. Sci.*, 225, 25, 2003.
25. International Atomic Energy Agency, Advances in Technologies for Treatment of Low and Intermediate Level Radioactive Liquid Wastes, Technical Report Series No. 370, IAEA, Vienna, 1994.
26. Bourns, W.T. and Le, V.T., The Reverse Osmosis Plant in CRNL Waste Treatment Centre—Description Design and Operation Principles, Report CRNL-2352, Atomic Energy of Canada Ltd., Chalk River, 1984.
27. Harries, J. et al., Radioactive waste management at ANSTO—managing current and historic wastes, in Book of extended synopses, International Conference on Management of Radioactive Waste from Non-Power Applications—Sharing the Experience, St. Paul's Bay (Malta), 5–9 Nov. 187, 5, 2001.
28. International Atomic Energy Agency, Application of Membrane Technologies for Liquid Radioactive Waste Processing, Technical Report Series No. 431, IAEA, Vienna, 2004.
29. Freeman, J., Wolf Creek's liquid waste processing system improvements, in Proc. EPRI Int. Low-Level Waste Conf. 2000, Electric Power Research Institute, Palo Alto, CA, 2001.
30. Evans, D.W. et al., Treatment of steam generator chemical cleaning wastes: Development and operation of the Bruce spent solvent treatment facility, in Proc. 5th Int. Symp. Nashville, TN, 1995, International Oxidation Application, 1995.
31. McCabe, D.J. et al., Biofouling of microfilters at the Savannah River F/H area effluent treatment facility, W'92 Conference, Tuscon, AZ, 1992, WM Symposia, Inc., Tuscon, AZ, 1992.
32. Chmielewski, A.G., Harasimowicz, M., and Zakrzewska-Trznadel, G., Membrane technologies for liquid radioactive waste treatment, *Czech. J. Phys.*, 49, 979, 1999.
33. Chmielewski, A.G. et al., Concentration of low- and medium-level radioactive wastes with 3-stage reverse osmosis pilot plant, *Sep. Sci. Technol.*, 36, 5–6, 1117, 2001.
34. Dulama, M., Deneanu, N., and Popescu, IV., Liquid radwaste treatment by microfiltration, ultrafiltration and reverse osmosis, in Book of extended synopses, Int. Conf. on management of radioactive waste from non-power applications—sharing the experience St. Paul's Bay (Malta) 5–9 Nov. 2001, IAEA, 187, 168–169, 2001.
35. Roman, G. et al., Removal of some ions from the radioactive liquid wastes by means of membrane techniques, National Physics Conference, Constanta (Romania), 21–23 Sep. 2000, accessed in: Documentation and Publishing Office, Horia Hulubei National Inst. for Phys. and Nucl. Eng., PO Box MG-6, RO-76900 Bucharest-Magurele.

36. Arnal, J.M. et al., Declassification of radioactive waste solutions of iodine ( $I^{125}$ ) from radioimmune analysis (RIA) using membrane techniques, *Desalination*, 129, 101, 2000.
37. Arnal, J.M. et al., Concentration of radioactive waste solutins of iodine ( $I^{125}$ ) from immune analysis (RIA) using membrane techniques, *Desalination*, 119, 185, 1998.
38. Arnal, J.M. et al., Treatment of  $^{137}Cs$  liquid wastes by reverse osmosis. Part I. Preliminary testes, *Desalination*, 154, 27, 2003.
39. Kryvoruchko, A.P. and Kornilovich, B.Yu., Water deactivation by reverse osmosis, *Desalination*, 157, 403, 2003.
40. Raff, O. and Wilken, R.-D., Removal of dissolved uranium by nanofiltration, *Desalination*, 122, 147, 1999.
41. Huikuri, P., Salonen, L., and Raff, O., Removal of natural radionuclides from drinking water by point of entry reverse osmosis, *Desalination*, 119, 235, 1998.
42. Processing of Nuclear Power Plant Waste Streams Containing Boric Acid, IAEA-TECDOC-911, IAEA, Vienna, 1996.
43. Astruc, C. et al., Filtration in Nuclear Power Plants, Euromembrane 99, Sept.19–22, 1999, Leuven, Belgium.
44. Macnaughton, S.J. et al., Application of nanofiltration to the treatment of uranium mill effluents, in Technologies for the treatment of effluents from uranium mines, mills and tailings, IAEA-TECDOC-1296, 55, 2002.
45. Hwang, Eui-Deog et al., Effect of precipitation and complexation on nanofiltration of strontium-containing nuclear wastewater, *Desalination*, 147, 289, 2002.
46. Gaubert, E. et al., Selective strontium removal from a sodium nitrate aqueous medium by nanofiltration–complexation, *Sep. Sci. Technol.*, 32, 1–4, 585, 1997.
47. Chitry, F. et al., Separation of gadolinium (III) and lanthanum (III) by nanofiltration–complexation in aqueous medium, *J. Radioanal. Nucl. Chem.*, 249, 2, 931, 1999.
48. Chitry, F. et al., Lanthanides(III)/actinides(III) separation by nano-filtration-complexation in aqueous medium, in Proceedings of International Conference, Nuclear waste: From Research to Industrial Maturity, Montpellier, Oct. 2–4, 2000.
49. Chitry, F. et al., Separation of lanthanides(III) by nanofiltration–complexation in aqueous medium, *Sep. Sci. Technol.*, 36, 4, 605, 2001.
50. Chitry, F. et al., Nanofiltration–complexation: A new method for isotopic separation of heavy metals, *Chem. Lett.*, 770, 2001.
51. Chitry, F. et al., Cesium/sodium separation by nanofiltration–complexation in aqueous medium, *Sep. Sci. Technol.*, 36, 5–6, 1053, 2001.
52. Vizslay, J. and Toth, S., Operational Experience with Pilot Ultrafiltration Plant, 1st Int. Seminar PWR Water Chemistry, Balatonfüred, Hungary, 1992.
53. Commission of the European Communities, research and development on radioactive Waste management and Storage, 3rd Annual Progress Report 1982 of the European Community Programme 1980–1984, Harwood Academic Publishers, 1982.
54. Barnier, R. et al., Ultrafiltration treatment of laundry liquid wastes from a nuclear research centre, in Proceedings of the Int. Conf. on Waste Management, Kyoto, 1989.
55. Kichik, V.A. et al., Method for complex treatment of laundry liquid radioactive wastes by ultrafiltration, *At. Energ.*, 63, 2, 130, 1987, (in Russian).
56. Karlin, Y. et al., Advantageous technology treatment of laundry waters. Proceedings of the International Symposium on Technologies for the Management of Radioactive Waste for Nuclear Power Plants and Back End of Nuclear Fuel Cycle Activities, Daejeon, 30.08.–03.09.1999. IAEA, Vienna 2001. C&S Papers CD Series no. 6.
57. Cumming, I.W. et al., Development of Combined Precipitation and Ultrafiltration Process and its Application to the Treatment of Low active Wastes, IAEA, 1992, 26 IAEA-SM-303–21P.
58. Hooper, E.W. and Sellers, R.M., Activity Removal from Liquid Streams by Seeded Ultrafiltration, Waste Management '91, Proc. Symp. University of Arizona, Tucson, Vol. 1, 749, 1992.
59. Hooper, E.W., Activity removal from aqueous waste streams by seeded ultrafiltration, in: Use of inorganic sorbents for treatment of liquid radioactive waste and backfill of underground repositories, in Proceedings of Final Research Co-ordination Meeting, Řež, Czechoslovakia, 408 November 1991, IAEA-TECDOC-675, International Atomic Energy Agency, 1992.
60. Hooper, E.W., Inorganic sorbents for removal of radioactivity from aqueous waste streams, in Waste treatment and immobilization technologies involving inorganic sorbents, IAEA-TECDOC-947, Final report of a co-ordinated research programme 1992–1996, International Atomic Energy Agency, 1997.
61. INTERNATIONAL ATOMIC ENERGY AGENCY, Use of Inorganic Sorbents for the Treatment of Liquid Radioactive Waste and Backfill of Underground Repositories, IAEA-TECDOC-675, Vienna (1992).
62. Chmielewski, A. and Harasimowicz, M., Application of ultrafiltration and complexation to the treatment of low-level radioactive effluents, *Sep. Sci. Technol.*, 30, 7–9, 1779, 1995.
63. Kallonen, I., Purification of radioactive liquid wastes at Padliski in Estonia, *Kemia-Kemi*, 23, 7, 550, 1996.
64. Smyth, B.M., Todd, P., and Bowman, N., Hyperbranched chelating polymers for the polymer-assisted ultrafiltration of boric acid, *Sep. Sci. Technol.*, 34, 10, 1925, 1999.
65. Vanderberg, L.A. et al., Treatment of heterogeneous mixed wastes: Enzyme degradation of cellulosic materials contaminated with hazardous organics and toxic and radioactive metals, *Env. Sci. Technol.*, 33, 8, 1256, 1999.
66. Smyth, B.F. et al., Evaluation of synthetic water-soluble metal-binding polymers with ultrafiltration for selective concentration of americium and plutonium, *J. Radioanal. Nucl. Chem.*, 234, 1–2, 219, 1998.
67. Smyth, B.F. et al., Preconcentration of low levels of americium and plutonium from waste waters by synthetic water-soluble metal-binding polymers with ultrafiltration, *J. Radioanal. Nucl. Chem.*, 234, 1–2, 225, 1998.
68. Ramachandhran, V. and Misra, B.M., Radiocerium separation behavior of ultrafiltration membranes, *J. Radioanal. Nucl. Chem.*, 237, 1–2, 121, 1998.
69. Kryvoruchko, A.P. et al., Ultrafiltration removal of U(VI) from contaminated water, *Desalination*, 162, 229, 2004.

70. Kryvoruchko, A.P. and Kornilovich, B.Yu., Baromembrane Decontamination of Uranium-containing Waste Water, in Proceedings of the International Conference. EUROMEMBRANE 99, Leuven, Belgium, V.2, 468, 1999.
71. Zakrzewska-Trznadel, G. and Harasimowicz, M., Removal of radionuclides by membrane permeation combined with complexation, *Desalination*, 144, 207, 2002.
72. Zakrzewska-Trznadel, G. and Harasimowicz, M., Application of ceramic membranes for hazardous wastes processing: Pilot plant experiments with radioactive solutions, *Desalination*, 162, 191, 2004.
73. Mynin, V.N. and Terpigov, G.V., Purification of waste water from heavy metals by using ceramic membranes and natural polyelectrolytes, *Desalination*, 119, 361, 1998.
74. Coughlin, R.W., Deshaies, M.R., and Davis E.M., Chitosan in crab shell wastes purifies electroplating wastewater, *Environ. Prog.*, 9, 35, 1990.
75. Muzzarelli, R.A.A., Chitin and its derivatives: New trends of applied research, *Carbohydr. Polym.*, 3, 53, 1983.
76. Guibal, E. et al., Uranium and vanadium sorption by chitosan and derivatives, *Water Sci. Technol.*, 30, 9, 183, 1994.
77. Onsoyen, E. and Skaugrud, O., Metal recovery using chitosan, *J. Chem. Technol. Biotechnol.*, 49, 395, 1990.
78. Zarzycki, R. et al., The effect of chitosan form on copper adsorption, in *Environmental Engineering Studies*, edited by Pawłowski et al., Kluwer Academic/Plenum Publishers, New York, 2003.
79. Juang, Ruey-Shin and Shiau, Ruey-Chang, Metal removal from aqueous solutions using chitosan-enhanced membrane filtration, *J. Membr. Sci.*, 165, 159, 2000.
80. Bailey, S.E. et al., A Review of potentially low-cost sorbents for heavy metals, *Wat. Res.*, 33, 2, 2469, 1999.
81. Garcia, R., Pinel, C., and Lemaire, M., Ionic Imprinting Effect in Gadolinium/Lanthanum Separation, *Tetrahedron Lett.*, 39, 8651, 1998.
82. Vigneau, O., Pinel, C., and Lemaire, M., Ionic imprinting resins based on EDTA and DTPA derivatives for lanthanides(III) separation, *Anal. Chim. Acta*, 435, 75, 2001.
83. Garcia, R. et al., Solid-liquid lanthanide extraction with ionic-imprinted polymers, *Sep. Sci. Technol.*, 37, 12, 2839, 2002.
84. Bonnema, B.E., Navratil, J.D., and Bloom, R.R., SOIL\*EX process design basic for mixed waste treatment, WM'95 (Proc. Conf. Tuscon, AZ, 1995) WM Symposia, Inc., Tuscon, AZ, 1995.
85. Suzuki, K. et al., A Study of Removal of Hazardous Metals and Radionuclides in Ground Water, WM'97 (Proc. Conf. Tuscon, AZ, 1997) WM Symposia, Inc., Tuscon, AZ, 1997.
86. Buckley, L.P., Vijayan, S., and Wong, C.F., Remediation process technology for ground water, Nuclear Waste Management and Environmental Remediation, in Proc. Int. Conf. Prague, 1993, American Society of Mechanical Engineers, New York, 33, 1993.
87. Mann, N.R. and Todd, T.A., Crossflow filtration testing of INEEL radioactive and non-radioactive waste slurries, *Chem. Eng. J.*, 80, 237, 2000.
88. Brown, R.G. et al., A Comparative Evaluation of Cross-flow Microfiltration Membranes for Radwaste Dewatering, in *Effective Industrial Membrane Processes: Benefits and Opportunities*, M.K. Turner, ed., published by Elsevier Applied Science, London and New York, 1991.
89. Stepan, D.J., Moe, T.A., and Collings, M.E., Task 9 - Centrifugal Membrane Filtration, Semi-Annual Report, April 1-September 30, 1996, DOE/MC/31388-5500, Energy and Environmental Research Center, University of North Dakota, 1996.
90. Green, W.A., Innovative Cross-Flow Membrane System for Volume Reduction of Mixed Waste, in: <http://www.ornl.gov/divisions/ctd/ESP/97tasks/task33.htm>, accessed on 14.08.2002.
91. Chmielewski, A.G. et al., The method of purification of radioactive wastes, PL 179430, 2000.
92. Chmielewski, A.G. et al.,  $^{16}\text{O}/^{18}\text{O}$  and H/D Separation factors for liquid/vapour permeation of water through an hydrophobic membrane, *J. Membr. Sci.*, 60, 319, 1991.
93. Chmielewski, A.G. et al., Cascades for natural water enrichment in deuterium and oxygen-18 using membrane permeation, *Sep. Sci. Technol.*, 28, 1-3, 909, 1993.
94. Chmielewski, A.G. et al., Membrane distillation employed for separation of water isotopic compounds, *Sep. Sci. Technol.*, 30, 7-9, 1653, 1995.
95. Zakrzewska-Trznadel, G., Chmielewski, A.G., and Miljević, N., Separation of protium/deuterium and oxygen-16/oxygen18 by membrane distillation process, *J. Membr. Sci.*, 113, 337, 1996.
96. Chmielewski, A.G. et al., *Stable Isotopes-Some New Fields of Application*, Zarzycki, R., Chmielewski, A.G., and Zakrzewska-Trznadel, G., eds., Polish Academy of Sciences, Lodz Branch, Commission for Environmental Protection, Lodz, 2002.
97. Zakrzewska-Trznadel, G., Harasimowicz, M., and Chmielewski, A.G., Concentration of radioactive components in liquid low-level radioactive waste by membrane distillation, *J. Membr. Sci.*, 163, 257, 1999.
98. Zakrzewska-Trznadel, G., Harasimowicz, M., and Chmielewski, A.G., Membrane processes in nuclear technology—application for liquid radioactive waste treatment, *Sep. Purif. Technol.*, 22-23, 617, 2001.
99. Zakrzewska-Trznadel, G., Membrane distillation for radioactive waste treatment, *Membrane Technology, An International Newsletter*, 103, 9, 1998.
100. Gryta, M., Concentration of NaCl solutions by membrane distillation integrated with crystallization, *Sep. Sci. Technol.*, 37, 15, 3635, 2002.
101. Schneider, K. and Gassel, T.S., Membrane distillation, *Chem. Ing. Tech.*, 56, 7, 514, 1984.
102. Sarti, G.C., Gostoli, C., and Matulli, S., Low energy cost desalination process using hydrophobic membranes, *Desalination*, 56, 277, 1985.
103. Hanbury, W.T. and Hodgkies, T., Membrane distillation—an assessment, *Desalination*, 56, 287, 1985.
104. Schnaider, K. et al., Membranes and modules for transmembrane distillation, *J. Membr. Sci.*, 39, 25, 1989.

105. INTERNATIONAL ATOMIC ENERGY AGENCY, Safe Handling of Tritium, Review of Data and Experience, Technical Reports Series No. 324, IAEA, Vienna, 1991.
106. INTERNATIONAL ATOMIC ENERGY AGENCY, Management of Waste Containing Tritium and Carbon-14, Technical Reports Series No. 421, IAEA, Vienna, 2004.
107. INTERNATIONAL ATOMIC ENERGY AGENCY, Management of Tritium at Nuclear Facilities, Technical Reports Series No. 234, IAEA, Vienna, 1984.
108. Sadhankar, R.R. and Miller, A.I., New heavy water production and processing technologies, 3rd Conference Isotopic and Molecular Processes PIM2003, Sep. 25–27, 2003, Cluj-Napoca, Romania, 2003.
109. Kitamoto, A., Shimizu, M., and Masui, T., The Advanced CECE Process for Enriching Tritium by the Chemical Exchange Method with a Hydrophobic Catalyst, in Proceedings of the International Symposium on Isotope Separation and Chemical Exchange Uranium Enrichment, Oct. 29–Nov. 1, 1990, Tokio, Yasuhiko Fuji, Takanobu Ishida, Kazuo Takeuchi, Editors, 497, 1990.
110. Mc Elroy, R.G.C., Osborne, R.V., and Surette, R.A., A monitor for the separate determination of HT and HTO, *IEEE Trans. Nucl. Soc.*, 29, 1, 1982.
111. Sasaki, Sh. et al., Basic characteristics of hollow-filament polyimide membrane in gas separation and application to tritium monitors, *J. Radioanal. Nucl. Chem.*, 255, 1, 91, 2003.
112. Nelson, D.A. et al., Isotopomeric water separations with supported polyphosphazene membranes, *J. Membr. Sci.*, 112, 105, 1996.
113. Duncan, J.B. and Nelson, D.A., The separation of tritiated water using supported polyphosphazene membranes, *J. Membr. Sci.*, 157, 211, 1999.
114. Zakrzewska-Trznadel, G. et al., Separation of hydrogen and oxygen isotopes by membrane method, *Sudia Universitaties Babes-Bolyai, Physica*, Special Issue 1, XLVIII, 39, 2003.
115. Le Digabel, M. et al., Application of gas separation membranes to detritiation systems, *Desalination*, 148, 297, 2002.
116. Le Digabel, M. et al., Glovebox atmosphere detritiation process using gas separation membranes, *Fus. Eng. Design*, 69, 61, 2003.
117. Labrune, D. et al., Separation of hydrogen isotopes from nitrogen with polyimide membrane, *Fus. Technol.*, 28, 676, 1995.
118. Iwai, Y., Yamanishi, T., and Nishi, M., A steady-state simulation model of gas separation system by hollow fiber type membrane module, *J. Nucl. Sci. Technol.*, 36, 1, 95, 1999.
119. Hayashi, T. et al., Effective tritium processing using polyimide films, *Fus. Eng. Design*, 39–40, 901, 1998.
120. Ishida, T. et al., R&D of compact detritiation system using a gas separation membrane module for the secondary confinement, *Fus. Technol.*, 30, 926, 1996.
121. Ishida, T. et al., Design of a membrane atmosphere detritiation system using super high permeation module, *Fus. Eng. Design*, 49–50, 839, 2000.
122. Hirata, S. et al., experimental and analytical study on membrane detritiation process, *Fus. Technol.*, 28, 1521, 1995.
123. Hayashi, T. et al., Gas separation performance of hollow-filament type polyimide membrane module for a compact tritium removal system, *Fus. Technol.*, 28, 1503, 1995.
124. Ito, H. et al., Separation of tritium using polyimide membranes, *Fus. Technol.*, 21, 993, 1992.
125. Nakagawa, T., Yoshida, M., and Kidokoro, K., Development of rubbery materials with excellent barrier properties to H<sub>2</sub>, D<sub>2</sub> and T<sub>2</sub>, *J. Membr. Sci.*, 52, 263, 1990.
126. Petit, J.F., Technological Aspects of the Historical Development of Eurodif, in Proceedings of the International Symposium on Isotope Separation and Chemical Exchange Uranium Enrichment, Oct. 29–Nov. 1, 1990, Tokio, Yasuhiko Fuji, Takanobu Ishida, Kazuo Takeuchi, Editors, 103, 1990.
127. Douglas, M. ed., *A Kirk-Othmer Encyclopedia of Separation Technology*, Ruthven, John Wiley & Sons, Vol. 1, 1997.
128. Hsieh, H.P., *Inorganic Membranes for Separation and Reaction*, Membrane Science and Technology Series, Vol. 3, Elsevier, Amsterdam–Lausanne–New York–Oxford–Shannon–Tokyo, 1996.
129. Isomura, S. et al., *Nippon Genshiryoku Gakkaishi*, 11, 417, 1969.
130. Fain, D.E. and Brown, W.K., Neon isotope separation by gaseous diffusion transport in the transition flow regime with regular geometries, U.S. Atomic Commission Report, 1974.
131. Latyszew, W.W., Golcow, W.A., and Fiedorow, S.A., Separation of hydrogen isotopes by metal membranes, *Atomnaja Energia*, 53, 1, 7, 32, 1982.
132. Golcow, W.A. et al., Diffusional filter of hydrogen isotopes, *Atomnaja Energia*, 53, 2, 20, 135, 1982.
133. Latyszew, W.W., Gurianow, W.G., and Martynowa, N.A., Dilatation of the B-1 alloy in hydrogen and deuterium atmosphere, *FMM*, 60, 1, 77, 1985.
134. Bieljakow, Yu.I., Permeability of nickel membranes in contact with molecules, atoms and ions of deuterium, *Wiestnik LGU*, 10, 14, 1982.
135. Yoshida, H., Konishi, S., and Naruse, Y., Effects of impurities on hydrogen permeability through palladium alloy membranes at comparatively high pressures and temperatures, *J. Less-Comm. Met.*, 89, 429, 1983.
136. Konishi, S., Yoshida, H., and Naruse, Y., A design study of a palladium diffuser for D-T fusion reactor fuel clean-up system, *J. Less-Comm. Met.*, 89, 457, 1983.
137. Evans, J., Harris, I.R., and Ross, D.K., A proposed method of hydrogen isotope separation using palladium alloy membranes, *J. Less-Comm. Met.*, 89, 407, 1983.
138. Marcea, P., Permeation of H<sub>2</sub> and D<sub>2</sub> through polymers, *Isotopenpraxis*, 19, 5, 153, 1983.
139. Marcea, P. and Tosa, V., Quantum isotope effect in gas transport through polymers, *Isotopenpraxis*, 21, 12, 413, 1985.
140. Chmielewski, A.G. et al., Investigation of the separation factor between light and heavy water in the liquid/vapour membrane Permeation Process, *J. Membr. Sci.*, 55, 257, 1991.

141. Chmielewski, A.G. et al., Multistage process of deuterium and heavy-oxygen enrichment by membrane distillation, *Sep. Sci. Technol.*, 32, 1–4, 527, 1997.
142. Yoshida, H. et al., Preliminary design of fusion reactor fuel clean-up system by the palladium alloy membrane method, *Nucl. Technol./ Fusion*, 3, 471, 1983.
143. Chen, Shaohua, et al., A palladium alloy composite membrane for the purification of hydrogen isotopes, *Sep. Sci. Technol.*, 37, 11, 2701, 2002.
144. Aoki, K. et al., Applicability of palladium membrane for the separation of protium and deuterium, *Int. J. Hydrogen Energy*, 23, 5, 325, 1998.
145. Bridesell, S.A. and Willms, R.S., Tritium recovery from tritiated water with a two-stage palladium membrane reactor, *Fus. Eng. Design*, 39–40, 1041, 1998.
146. Basile, A. et al., Membrane integrated system in the fusion reactor fuel cycle, *Catalysis Today*, 25, 321, 1995.
147. Violante, V. et al., US Patent N. 5366712. 22 Nov. 1994.
148. Drioli, E., Violante, V., and Basile, A., Membrane separation processes in the fusion fuel cycle, in Proceedings of ICOM'90, Chicago, Vol. II, 1040, 1990.
149. Drioli, E., Violante, V., and Basile, A., Membrane separation processes in fusion separation plants, in Proceedings of 5th World Filtration Congress, Nice France, Vol. I, 449, 1990.
150. Violante, V., Basile, A., and Drioli, E., Composite catalytic membrane reactor analysis for water gas shift reaction in the tritium fusion fuel cycle, *Fus. Eng. Design*, 217–223, 30, 1995.
151. Tosti, S. et al., Catalytic membrane reactors for tritium recovery from tritiated water in the ITER fuel cycle, *Fus. Eng. Design*, 49–50, 953, 2000.
152. Konishi, S. et al., Development of electrolytic reactor for processing of gaseous tritiated compounds, *Fus. Eng. Design*, 39, 1033, 1998.
153. Heinze, S., Bussiere, P., and Pelletier, T., French experience in tritiated water management, *Fus. Eng. Design*, 69, 67, 2003.
154. Stolz, T. et al., Self radiolysis of tritiated water, *Fus. Eng. Design*, 69, 57, 2003.
155. Campbell, D.J., Fractionation of stable chlorine isotopes during transport through semipermeable membranes, M.S. Thesis, University of Arizona, 1985.
156. Fritz, S.J., Hinz, D.L., and Grossman, E.L., Hyperfiltration-induced fractionation of carbon isotopes, *Geochim. Cosmochim. Acta*, 51, 1121, 1987.
157. Whitworth, T.M., Mariñas, B.J., and Fritz, S.J., Isotopic fractionation and overall permeation of lithium by a thin-film composite polyamide reverse osmosis membrane, *J. Membr. Sci.*, 88, 231, 1994.
158. Fujii, Y. et al., Separation of isotopes of lithium and uranium by electromigration using cation-exchange membranes, *Isotopenpraxis*, 15, 7, 203, 1979.
159. Okamoto, M. et al., Dependencies of pH and current density on the isotope effect occurred by the electromigration of uranyl ions in a cation exchange membrane, *Isotopenpraxis*, 16, 2, 58, 1980.
160. Rainey, R.H. et al., Separation of radioactive xenon and krypton from other gases by use of permselective membranes, Treatment of Airborne radioactive Wastes, Proceedings of a Symposium, New York, 26–30 August 1968.
161. Kimura, S. et al., Separation of Rare Gases by Membranes, *Radiochem. Radioanal. Lett.*, 13, 56, 349, 1973.
162. Stern, S.A. and Leone, S.M., Separation of Krypton and Xenon by Selective Permeation, *AIChE J.*, 26, 6, 881, 1980.
163. Bożenko, E.I. et al., Primiennienie polimernych membran dla oczystki gazowych wybrosov atomnych elektrostancji, *Plast. Massy*, 2, 51, 1983.
164. Bekman, I.N. et al., Membrannyje metody wydielienija radioaktywnych bĳogorodnych gazow, cz. II, *Radiochimija*, 3, 337, 1984.
165. Nikonow, W.N. et al., Membrannyje metody wydielienija radioaktywnych bĳogorodnych gazow, cz. I, *Radiochimija*, 3, 332, 1984.
166. Ohno, M. et al., Separation of Rare Gases by Membranes, *Radioanal. Lett.*, 27, 5–6, 299, 1976.
167. Ohno, M. et al., Radioactive Rare Gas Separation Using a Separation Cell with Two Kinds of Membrane Differing in Gas Permeability Tendency, *J. Nucl. Sci. Technol.*, 14, 8, 589, 1977.
168. Stern, S.A. and Wang, S.C., Permeation Cascades for the Separation of Krypton and Xenon from Nuclear Reactor Atmospheres, *AIChE J.*, 26, 6, 891, 1980.
169. Jonas, Ch., Zum Einfluss des Plastifizierungseffektes auf den Stofftrennvorgang, *Chem. Techn.*, 35, 2, 77, 1983.
170. Membrane for Separation of Xenon from Oxygen and Nitrogen and method of Using Same, Messer Griesheim GmbH, Germany. WO00/33949. Date of publication: 15 June 2000.
171. Sasaki, Sh. et al., Basic characteristics of hollow-filament polyimide membrane in gas separation and application to tritium monitors, *J. Radioanal. Nucl. Chem.*, 255, 1, 91, 2003.
172. Nörenberg, H. et al., Pressure-dependent permeation of noble gases (He, Ne, Ar, Kr, Xe) through thin membranes of oriented polypropylene (OPP) studied by mass spectrometry, *Polymer*, 42, 10021, 2001.



---

# 31 Liquid Membrane-Based Separations of Actinides

*P.K. Mohapatra and V.K. Manchanda*

## CONTENTS

31.1	Introduction .....	883
31.1.1	Liquid Membranes and Their Classifications .....	885
31.1.2	Mechanism of Metal Ion Transport .....	886
31.1.2.1	Classification of Liquid Membrane Transports.....	887
31.2	Transport of Actinides by Liquid Membranes.....	889
31.2.1	Separation of Actinides by Bulk Liquid Membranes .....	889
31.2.2	Emulsion Liquid Membranes .....	890
31.2.3	Supported Liquid Membranes.....	894
31.2.3.1	Acidic Extractants as Carriers .....	894
31.2.3.2	Neutral Donors as Carrier .....	897
31.2.3.3	Basic Extractants as Carriers.....	902
31.2.4	Hollow Fiber Supported Liquid Membranes .....	903
31.2.5	Track-Etched Membranes.....	904
31.3	Polymer Inclusion Membranes .....	904
31.4	Separation of Radionuclides from Waste Streams.....	906
31.5	Grafted Membranes for Actinide Separation .....	907
31.6	Stability of Liquid Membranes .....	908
31.6.1	Stability of Emulsion Liquid Membrane.....	909
31.6.2	Stability of Supported Liquid Membrane .....	909
31.7	Future Perspectives .....	910
	References.....	910

## 31.1 INTRODUCTION

Separations of long-lived actinides play a pivotal role at different stages of nuclear fuel cycle, namely, (a) recovery and purification of fissile/fertile nuclides from their respective ores, (b) fuel reprocessing using processes such as PUREX/THOREX, (c) minor actinide partitioning, and (d) lanthanide–actinide separations. Their analytical separation is also an important step in chemical quality control of nuclear fuel materials and the estimation of the actinide elements in various waste streams. PUREX process employing tri-*n*-butyl phosphate (TBP) as extractant has been successfully employed for the industrial scale production of Pu from the spent fuels emanating from a variety of thermal and fast reactors. There is, however, only a limited experience in the recovery of  $^{233}\text{U}$  from irradiated Th using the THOREX process. However, separation scientists in nuclear industry are gearing up for the new challenges of reprocessing spent fuels discharged from Pu-based fast reactor fuels as well as Th-based advanced heavy water reactor fuels. Existing processes may have to be further modified to meet the demands of larger Pu content, larger radiation damage to the solvent, larger inventory of fission products, and above all the complex situation of dealing with a Th–Pu–U based ternary system. There is also a growing interest in the areas of partitioning of actinides from high-level waste. In view of its excellent track record, TBP continues to be the prime choice of separation scientists and technologists. However, its poor extractability of trivalent actinides, large secondary waste volumes, and interference of the degradation products in overall Pu recovery and decontamination from fission products are a cause of concern. The actinides, in particular, have a fascinating chemistry in solution (e.g., disproportionation, variable oxidation state, polymerization, etc.), which presents a stimuli as well as a challenge to the separation chemists. Hence, there is a need to develop alternative extractants, which are efficient, versatile, and

environmental friendly. Novel extractants are continuously being designed to carry out selective separation of actinides or fission products from reprocessing/waste streams. Figure 31.1 shows some of the extractants employed for the recovery/purification of actinides in the nuclear fuel cycle or for analytical applications. In view of the high cost of some of these emerging extractants, it is imperative to develop simultaneously novel separation techniques, which employ relatively small inventory of extractants. Liquid membrane (LM)-based separations hold a particular promise toward this end [1–3].

Membrane-based separation methods are popular in chemical industry for effluent treatment, desalination, and gas purification. However, their application for separation of actinides relevant to nuclear industry is still at infancy stage. The past few decades saw the use of exotic reagents such as crown ethers, calixarenes for the selective complexation and removal of actinides

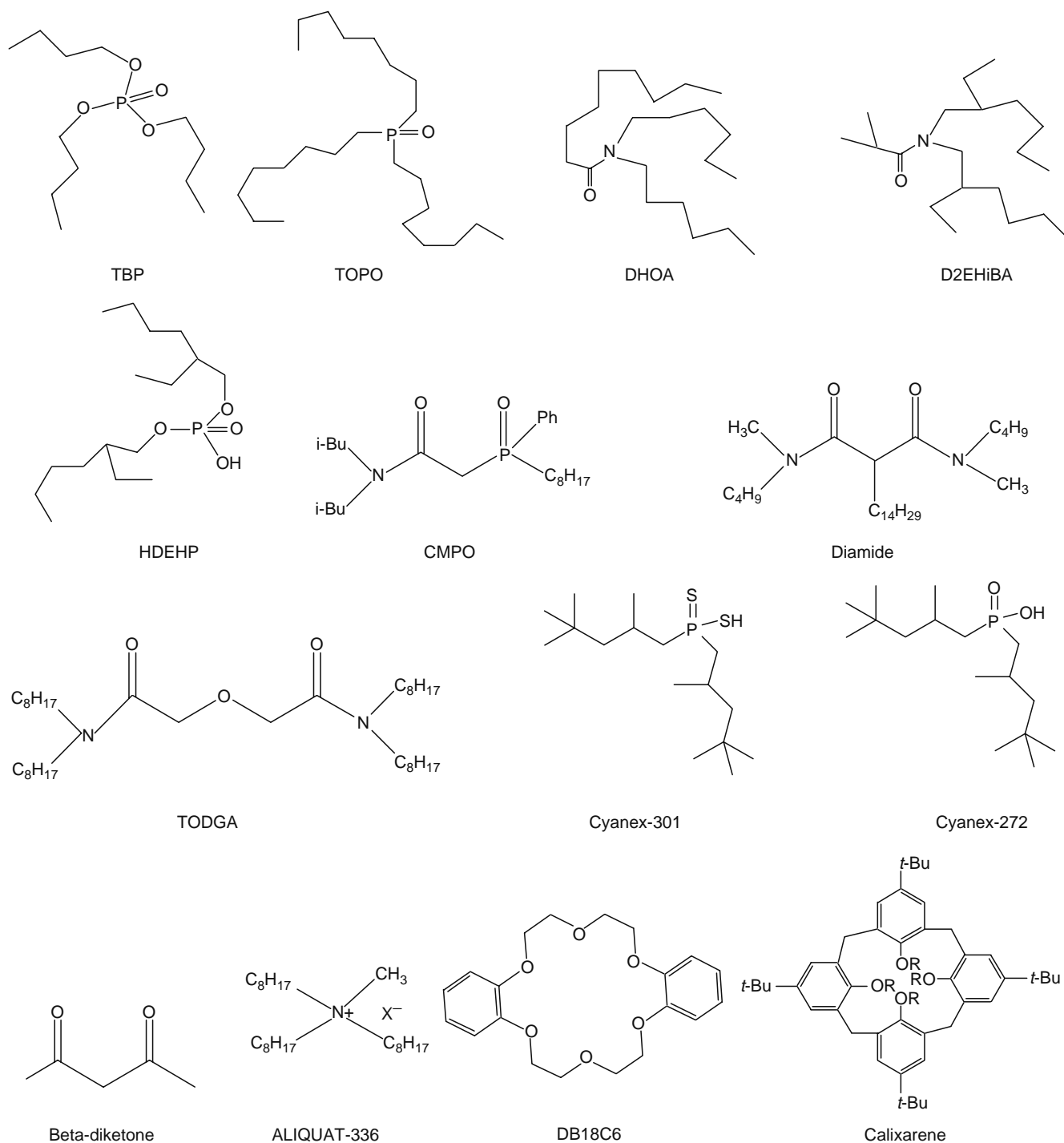


**FIGURE 31.1** Structures of some commonly used extractants for actinide ion extraction. (Reproduced from Mohapatra, P.K. and Manchanda, V.K., *Indian J. Chem.*, 42A, 2925, 2003. With permission.)

**TABLE 31.1**  
**Summary of the Extractants Being Used for Actinide Ions Recovery/Separation by LM-Based Separation Methods**

Extractants	Membrane-Based Separation Methods	Metal Ions Recovered	References
HDEHP	BLM, ELM, SLM, PIM	Am(III), Th(IV), U(VI)	[31,37–44,67–71,73,77,193]
LIX-63	ELM, SLM	U(VI)	[47,84]
Kelex 100 (8-hydroxy quinoline)	ELM, SLM	U(VI)	[44,60,61]
$\beta$ -diketones	SLM, PIM	Am(III), lanthanides	[62,63,191]
Cyanex-301/Cyanex-272	BLM, SLM, PIM	Am(III), U(VI)	[26,82,83,192]
PC-88A	ELM, SLM	Eu(III), U(VI)	[52–54,66]
TBP/TAP/TEHP	BLM, SLM, HFSLM, PIM	Th(IV), Pu(IV), U(VI)	[27,29,85,88,89,92,93,106,107,163,164,189]
TOPO/Cyanex-923/poly phosphine poly oxide	ELM, SLM	Am(III), Pu(III), Th(IV), Np(V), U(VI), Pu(IV)	[44,45,50,55,63,73,77,94–99]
CMP, CMPO	SLM, PIM	Am(III), lanthanides	[104–111,133]
Amides, diamides	SLM, HFSLM, ELM	Am(III), Th(IV), Pu(IV), U(VI)	[48,118–120,121]
TODGA	SLM, PIM	Am(III), lanthanides	[132,133]
Crown ethers	SLM, ELM	Pu(IV), U(VI)	[137–145]
Calixarenes	BLM	U(VI)	[33,146–148]
TOA/TLA/alamine 336/other amines	ELM, SLM	Pu(IV), U(VI)	[44,49,154–156]
Aliquat-336	SLM	U(VI)	[157–160]

*Note:* BLM—Bulk liquid membrane; ELM—Emulsion liquid membrane; SLM—Supported liquid membrane; and HFSLM—Hollow fiber supported liquid membrane.

from solutions containing complex mixture of metal ions [4–7]. Specially designed uranophiles have been synthesized for the recovery of ppb level of uranium from seawater [8,9]. Di-cyclohexano 18 crown 6, a crown ether, was utilized by a French group for the separation of Pu from a synthetic spent fuel solution [10]. The two major drawbacks of the solvent extraction methods, namely, third phase formation and phase disengagement time, can be overcome with the LM-based separation methods as they involve nondispersive mass transfer. Hollow fiber supported liquid membrane (HFSLM) separations are particularly attractive due to large surface to volume ratio, fast mass transfer rates, and continuous flow [11–14].

This chapter deals with the transport of actinide ions across liquid membranes resulting in their recovery/separation from complex matrices. The transport behavior of lanthanides is also discussed in many places, which has chemical similarity with the trivalent actinides and are often used as their homologs. The transport behavior of actinides/lanthanides across other membranes such as ceramic/metallic and grafted membranes is also included. Table 31.1 gives a summary of the extractants discussed in this chapter.

### 31.1.1 LIQUID MEMBRANES AND THEIR CLASSIFICATIONS

Membranes are barriers, which separate two solution phases and allow the selective permeation of solutes from one side of the barrier to the other. Depending on the driving force and dominant mechanism of separation, they are classified into different types. The nonequilibrium membrane processes, such as liquid membranes and diffusion dialysis, are useful in the separation of specific components present in very low concentrations. These techniques have shown good promise in the removal of metal ions, such as uranium and copper, and acids from the effluent streams. Liquid membranes basically comprise of organic carriers with high specificity for a particular species. They usually consist of a water immiscible organic membrane (abbreviated as M) layer separating an aqueous source phase, or feed (abbreviated as s.p. or F), consisting of a mixture of metal ions and receiving aqueous phase where the metal ion of interest gets concentrated (abbreviated as R or r.p.) preferentially. Liquid membranes are also known as liquid pertraction or simply as pertraction and closely resemble solvent extraction, which is pivotal in the metal transport process [15]. In fact, pertraction is a combination of extraction, permeation, and stripping of the desired species and can be treated as a continuous multistage extraction/stripping process. A large number of reviews, appeared during the last few years, underline the importance of this upcoming area [16–20].

Broadly speaking, there are three different types of liquid membranes. Bulk liquid membrane (BLM) is a stirred organic phase of lower density than the aqueous phase positioned under it or vice versa. In emulsion liquid membrane (ELM), the receiver aqueous phase containing oil droplets is dispersed into the feed aqueous phase. The total volume of the receiving phase inside the oil droplets is at least ten times smaller than that of the source phase. The thickness of the membrane (organic film) is very small, while the surface area is enormous resulting in very fast separations. Though the efficiency of mass transfer in the liquid membranes is inversely proportional to the thickness of the membrane phase, too thin a film has poor stability due to low but finite solubility in F and R. It can also be disturbed by pressure differences created by the two aqueous phases.

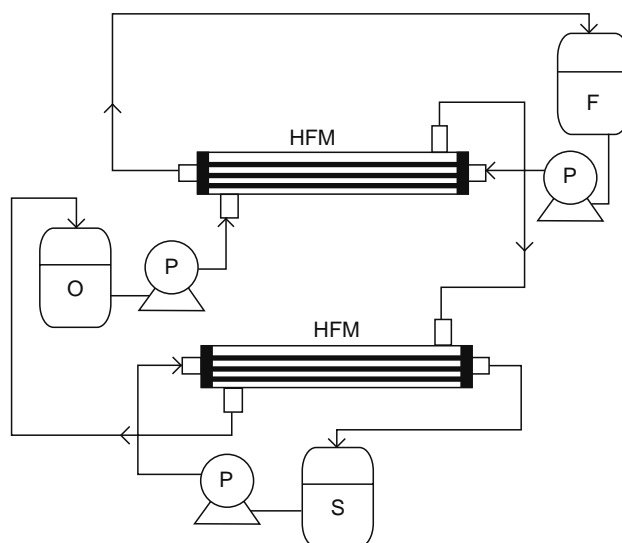


**FIGURE 31.2** Pictorial depiction of a double module hollow fiber liquid membrane set up. HFM—Hollow fiber module; F—Feed; O—Organic extractant; S—Strip or receiver phase; and P—Pump. (Reproduced from Mohapatra, P.K. and Manchanda, V.K., *Indian J. Chem.*, 42A, 2925, 2003. With permission.)

However, ELMs are quite difficult to prepare and after transport, the oil droplets have to be separated and broken up to recover the receiving phase. Compared to the ELM, the BLMs are easier to operate. The supported liquid membranes (SLM) are categorized into two types of supports, namely, a flat-sheet supported liquid membrane (FSSLM) or a hollow fiber supported liquid membrane (HFSLM). Here a polymeric filter with its pores filled with the organic phase acts as membrane. The three different types of liquid membranes have already been schematically represented in Chapter 29. A schematic representation of a hollow fiber setup is shown in Figure 31.2.

### 31.1.2 MECHANISM OF METAL ION TRANSPORT

Due to the favorable thermodynamic conditions created at the F/M interface some components are selectively extracted from the F and transported into the membrane liquid. Simultaneously, at the M/R interface, conditions are such that the back extraction is favored. Various factors that could affect the transport of a metal ion through the LM are (a) the (transport) resistance encountered by the metal ion in the F and R phases, (b) the physicochemical properties of the carrier and diluent, and (c) the nature of membrane support such as its pore size, porosity, tortuosity, hydrophilicity, surface tension, and surface area to volume ratio encountered in the transport process.

In the absence of any external driving force, the simple transport can be expressed by Fick's law of diffusion, where the flux ( $J$ ) is influenced by concentration gradient as follows:

$$J = D_m \{C_{mf} - C_{mr}\} / d_m \quad (31.1)$$

where

$D_m$  is the diffusion coefficient of the complex in the membrane

$d_m$  is membrane thickness

$C_{mf}$  and  $C_{mr}$  are the concentration of metal ion at the membrane–feed interface and membrane–receiver interface, respectively

However, such transport can be limited by concentration gradient and the transport is bound to cease after equalization of the activities of the solute in the source and the receiver phases. In order to effect uphill transport (from nearly half to quantitative transport to the receiver phase), a specific complexing agent for the solute is required. In that case, a finite concentration gradient can always be maintained between the source and the receiver phases, which can effect the uphill transport.

Under efficient stripping condition ( $C_{mf} \gg C_{mr}$ ) and neglecting the aqueous diffusion layer ( $C_{mf} \sim C_f$ ), Equation 31.1 gets simplified to

$$P = J / C_f \quad (31.2)$$

where

$C_f$  is the bulk concentration of metal ion in the feed  
 $P$  is the permeability coefficient [8]

The permeability coefficient,  $P$ , can be obtained using the following equation:

$$\ln(C_{f,t}/C_{f,o}) = -(Q/V)Pt \quad (31.3)$$

where

$C_{f,t}$  and  $C_{f,o}$  are the concentration of metal ion in aqueous feed at time  $t$  and initial metal ion concentration (at  $t=0$ ), respectively  
 $Q$  is  $A\varepsilon$  where  $A$  is the geometrical surface area and  $\varepsilon$  is the porosity  
 $V$  is the aqueous feed volume (mL)

Equation 31.3 is however valid only when carrier is not saturated by the metal ion.

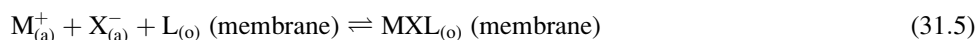
### 31.1.2.1 Classification of Liquid Membrane Transports

In carrier-mediated transport studies, two terms are used, namely, facilitated transport and coupled transport. Facilitated transport is generally referred to as the case where the transport mechanism is independent of any other ion, while in case of coupled transport the transport rate of a particular ion is dependent on the concentration of another ion. The mechanism of facilitated transport is shown in Figure 31.3a, while those of the two different types of coupled transport (cotransport and counter-transport) are schematically explained in Figure 31.3b and 31.3c. In case of cotransport, the metal ion is transferred along with a counter-anion, while simultaneous transport of another ion from receiver phase to source phase occurs in case of counter-transport.

In all the cases described earlier, the LM is interspersed between two aqueous solutions. The distribution ratio ( $D_M$ ) between the organic phase absorbed in the membrane pores and aqueous feed solution (source phase) of metal species permeating the LM is high enough to favor metal extraction into the membrane phase. The distribution ratio of metal ion between the membrane phase and aqueous strip solution (receiving phase) at this stage is made as low as possible to favor complete back extraction of the metal species from the liquid membrane. If the metal carrier is an acidic extractant, HL, the difference in  $D_M$  between the feed and strip sides of the SLM is generally achieved by a pH gradient. In this case, we deal with a counter-transport phenomenon (Figure 31.3c) and the chemical reaction, which is responsible for the coupled transport that can be schematized as



If the metal carrier is a neutral extractant L, the difference in the  $D_M$  between feed and strip is generally obtained by a concentration gradient of the counterion,  $X^-$ , which is accompanying the metal cation into the membrane (Figure 31.3b) and the chemical reaction, which is responsible for the cotransport, can be schematized as



Finally, if the metal carrier is a basic extractant (i.e., a long-chain amine), L, the difference in  $D_M$  between feed and strip is generally obtained by a concentration gradient of the counterion,  $X^-$  as well as  $H^+$  which is accompanying the metal cation into the membrane and the chemical reaction that is responsible for the coupled transport can be schematized as



The aqueous phase pH and counterion concentration gradients are often used as driving forces. However, any other expedient that assures a large chemical potential gradient between the two opposite sides of the membrane can be used as long as coupled transport of metal ions and some other chemical species occur through the SLM.

From this schematic description of coupled transport, it follows that metal species can be transported across the membrane against their concentration gradient. This type of uphill transport will continue until all the metal species, which can permeate the SLM, have been transferred from the feed to the strip side, provided the driving force of the process is maintained. This situation often occurs in practice when very dilute solutions of metal species are involved or when the concentration of the chemicals responsible for the driving force is continuously adjusted to keep it constant. It follows that in an SLM permeation process very high concentration factors can be obtained by using a volume of the strip solution that is much lower than that of

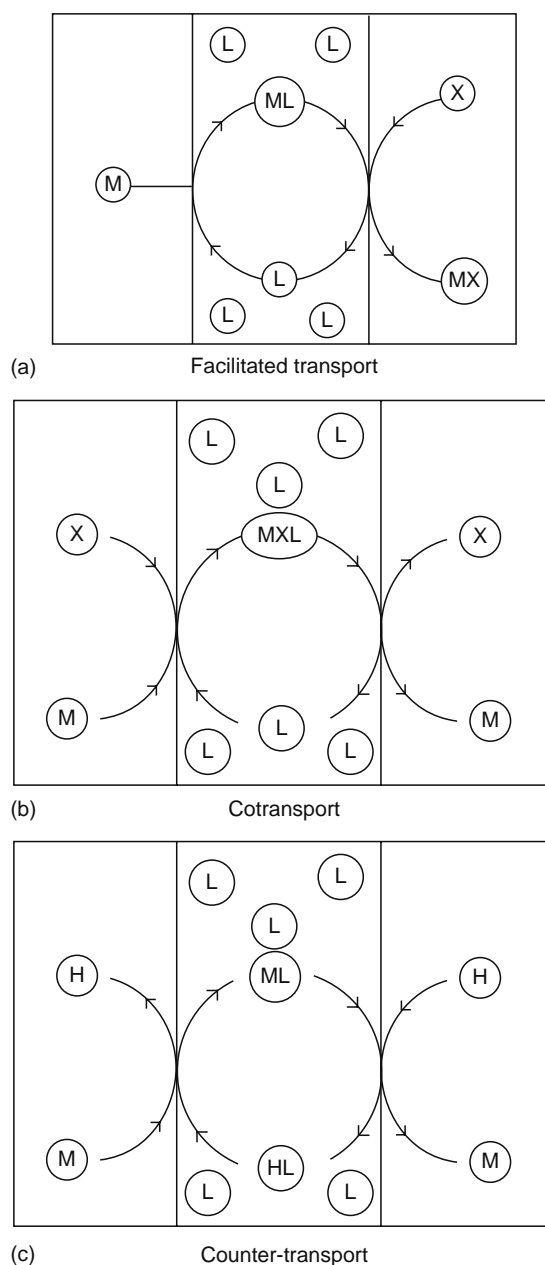


**FIGURE 31.3** Pictorial depiction of metal ion transport in the presence of an organic carrier.

the feed solutions. Moreover, by using a carrier molecule, HL or L, which is very selective for a given metal species, very clean separation processes can be performed. Since, during permeation, the carrier acts as a shuttle moving metal species from the feed to the strip solution and then diffusing back (being continuously regenerated during the process), very small amounts of carrier are used in SLM separation. Other potential advantages of SLM separations over separations performed by traditional solvent extraction technique are the lack of solvent entrainment phenomena, the simplicity of the equipment involved, and the low-energy consumption of the process [21]. Moreover, in comparison to the separation processes performed with solid membranes, SLMs offer the additional advantage of higher fluxes since diffusion in liquids is much faster than that in solids.

The various steps that characterize the transport of metal species through SLMs can be described with the help of Figure 31.4. Step 1: The metal species, after diffusing to the source–membrane interface, react with the metal carrier,  $H^+$  ions are simultaneously released into the feed solution (counter-transport, acidic carrier) or  $X^-$  ions accompany the metal ions into the membrane (cotransport, neutral, or basic carriers), Step 2: The metal–carrier complex diffuses across the membrane because its concentration gradient is negative, Step 3: At the membrane–receiver interface the metal–carrier complex releases metal ions into the aqueous phase,  $H^+$  ions replace  $M^+$  ions into the membrane (counter-transport) or  $X^-$  ions are simultaneously released together with  $M^+$  ions into the strip solution (cotransport), Step 4: The uncomplexed carrier diffuses back across the membrane.

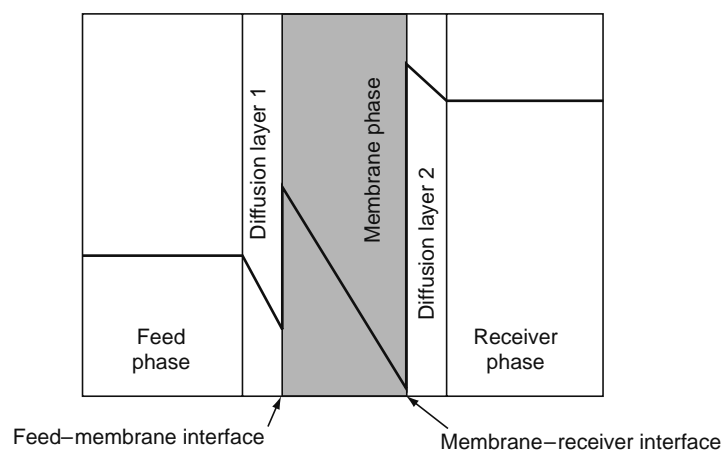


FIGURE 31.4 Mechanism of metal ion transport in the case of an FSSLM. Metal ion concentration is indicated by the thick lines.

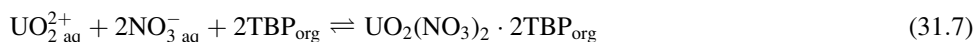
## 31.2 TRANSPORT OF ACTINIDES BY LIQUID MEMBRANES

### 31.2.1 SEPARATION OF ACTINIDES BY BULK LIQUID MEMBRANES

Bulk liquid membrane is a stirred organic phase of lower density than the aqueous phase positioned under it, or vice versa. The two aqueous phases, namely, the feed and the receiver, are separated by an immiscible organic carrier phase. As the driving force in the transport is through the bulk organic phase, it often provides the resistance to the transport of the metal ion of interest. If not stirred properly, the transport rates can be much lower than expected. As the transport rates are diffusion controlled, the membrane thickness or the distance between the feed and receiver phase as well as stirring speed governs the transport behavior of the solutes. Though the Shulman bridge BLM cell is used more often in literature, cells of other designs are also being used. The type of BLM cell is decided by the diluent density. Different types of BLM cell configurations have been used in literature [22–25].

One of the important factors influencing BLM studies is the amount of the organic phase that often decides the transport rates. Effective stirring as well as minimization of the membrane thickness could result in good transport rate. Bhattacharyya et al. have studied the transport of  $\text{Am}^{3+}$  through a toluene solution of Cyanex-301 (bis(2,4,4-trimethylpentyl)di-thio phosphinic acid) as a function of the stirring speed and observed an increase in mass transfer with an increase in the stirring speed [26]. Although >95% Am transport occurred in 5 h, the transport of  $\text{Eu}^{3+}$  was <5% under identical conditions suggesting that their effective separation is feasible on suitable adjustment of feed and strip parameters.

Tri-*n*-butyl phosphate and di-2-ethylhexyl phosphoric acid (HDEHP) have been mainly used as extractants in several hydrometallurgical operations in the nuclear fuel cycle. Shukla and Mishra [27] have studied the extraction as well as transport behavior of uranium through BLM using 40% TBP in dodecane. The transport of  $\text{UO}_2^{2+}$  by TBP at the feed-membrane interphase is represented by the following extraction equilibrium:



Based on Equation 31.1, pertraction rates of uranium were expected to increase with increasing  $\text{HNO}_3$  concentration. A maximum flux ( $J$ ) at 2 M  $\text{HNO}_3$  indicated the formation of  $\text{TBP} \cdot \text{HNO}_3$  complexes at higher nitric acid concentration. Formation of such species is well known in the solvent extraction studies reported earlier [28]. Similarly, the increase in transport rates with increasing TBP concentration was valid up to only 30% TBP beyond which the strong viscosity effects decreased the flux.

Shukla and Mishra have also carried out BLM studies on the transport rates of Pu(IV) from nitric acid medium using 30% TBP in dodecane as the carrier and 0.5 M ascorbic acid as the strippant [29]. The flux is given by the following empirical equation:

$$J_{\text{Pu}} = A(T/\eta)[\text{NO}_3^-]_{\text{a}}^4[\text{TBP}]_{\text{o}}^2 \cdot C_{\text{Pu,feed}} \quad (31.8)$$

where

$A$  is the membrane surface area ( $\text{cm}^2$ )

$T$  is the temperature (K)

$\eta$  is the viscosity (cP)

$C_{\text{Pu,feed}}$  is the concentration of Pu in the feed ( $\text{Mdm}^{-3}$ )

**TABLE 31.2**  
**Effect of Temperature on Kinetic Parameters for the Transport of Eu(III) through a BLM Containing Mono(2-Ethylhexyl)2-Ethylhexyl Phosphonate in Kerosene as the Organic Phase**

Temperature (°C)	$k_1 \times 10^2$ (h <sup>-1</sup> )	$k_{2a} \times 10^2$ (h <sup>-1</sup> ) <sup>a</sup>	$k_{2m} \times 10^2$ (h <sup>-1</sup> ) <sup>b</sup>	Flux $\times 10^2$ (h <sup>-1</sup> )
20	28.7 ± 0.9	7.04 ± 0.2	6.90 ± 0.4	4.46
30	37.0 ± 0.9	16.8 ± 0.4	16.7 ± 0.6	8.72
35	39.2 ± 1.4	23.6 ± 1.0	23.5 ± 1.3	10.9
40	41.3 ± 1.2	32.7 ± 1.5	32.8 ± 1.9	13.5
50	49.7 ± 1.7	53.3 ± 2.6	53.1 ± 2.8	18.9

Source: Data taken from Ma, M., He, D.S., Wang, Q.Y., and Xie, Q.J., *Talanta*, 55, 1109, 2001. With permission.

<sup>a</sup> Rate constant for Eu(III) transport into the strip phase.

<sup>b</sup> Rate constant for Eu(III) transport in the membrane phase.

The species extracted into the BLM phase is  $\text{Pu}(\text{NO}_3)_4 \cdot 2\text{TBP}_{(o)}$  which is similar to that reported in the solvent extraction studies [30]. With increase in carrier concentration in the organic membrane, the increase in the amount of plutonium that could be extracted into the membrane is countered by the increase in the viscosity of the carrier solution. These opposing effects resulted in maximum plutonium permeation with about 30% TBP in dodecane [29]. More than 85% transport was observed in about 5 h when 5 mg/L solution of Pu in 2 M  $\text{HNO}_3$  was used as the feed. Selective transport of Pu(IV) over fission product contaminants, such as Ce-144, Ru-106, and Cs-137, was also observed.

Bulk liquid membrane comprising di-(2-ethylhexyl) phosphoric acid (HDEHP) in chloroform was successfully used as a carrier for the selective and efficient transport of Th. It was observed that 99% of Th selectively permeated across the membrane in <3 h, while the transport of other cations present along with thorium was <3% during the same time [31]. In a study involving Eu(III), coupled transport through a BLM containing mono-2-ethylhexyl 2-ethylhexylphosphonate [HEH(EHP)] in kerosene revealed that there was a counter-transport of protons [32]. Expectedly, increase in the transport rates was observed with increases in the feed pH value and carrier concentration initially. According to the counter-transport mechanism, an increase in the acid concentration in the receiver phase increased the transport rate. There was notable effect of temperature on the transport rates of Eu(III) as indicated in Table 31.2. The activation energy values were calculated to be  $14 \pm 1.0$  and  $54 \pm 3.4$  kJ mol<sup>-1</sup> for the extraction and stripping at the feed–membrane and membrane–strip junctions, respectively [32].

Ramakumar et al. [33] investigated the transport behavior of uranium across the BLM made from several substituted calixarenes (Figure 31.5) in chloroform and 0.1 M nitric acid as the receiver phase. The presence of TOPO and crown ether (18 crown 6) enhanced the transport rate, which was ascribed to synergistic extraction effect.

### 31.2.2 EMULSION LIQUID MEMBRANES

Emulsion liquid membrane is a technique very similar to the solvent extraction process where the separation is achieved by mixing the primary emulsion (strip/organic phase in the emulsion form) with the feed instead of the mixing of aqueous and organic phases as in the solvent extraction processes. Therefore, unlike the solvent extraction processes, ELM studies involve simultaneous extraction and stripping in a single step [34–36]. The emulsification is first done by rapid mixing of the strippant solution and the organic extractant containing the surfactants. The prerequisite is that the primary emulsion must be stable enough so that the mixing of the feed and strip phases is avoided. Precaution must be taken such that the volume reduction of the feed and dilution (due to volume increase) of the strip phases are prevented. Two or more stages are required for a complete separation of the metal ion as the ELM technique is a rate as well as equilibrium-controlled process. The main advantage in the case of ELM is that the use of phase modifier (used in the case of solvent extraction to prevent third-phase formation) is not required. Moreover, the presence of surfactant reduces the loss of the extractant to the aqueous phase significantly. The role of the extractant is extremely important as it helps in getting the metal ion concentrated by active transport against its concentration gradient across the liquid membrane.

Table 31.3 gives a few typical examples on recovery of actinides by ELM. Myriad literature reports exist on the use of HDEHP for metal extraction involve ELMs. Comparative studies between column and batch liquid emulsion membrane techniques based on HDEHP/HCl system were carried out to develop a system for the isolation of <sup>234</sup>Th from natural uranium, which showed that, kinetically, the equilibrium for thorium separation using batch technique is faster than the continuous column system [37]. The effective separation of <sup>234</sup>Th from natural uranium was found to be independent of time. El-Sherif studied

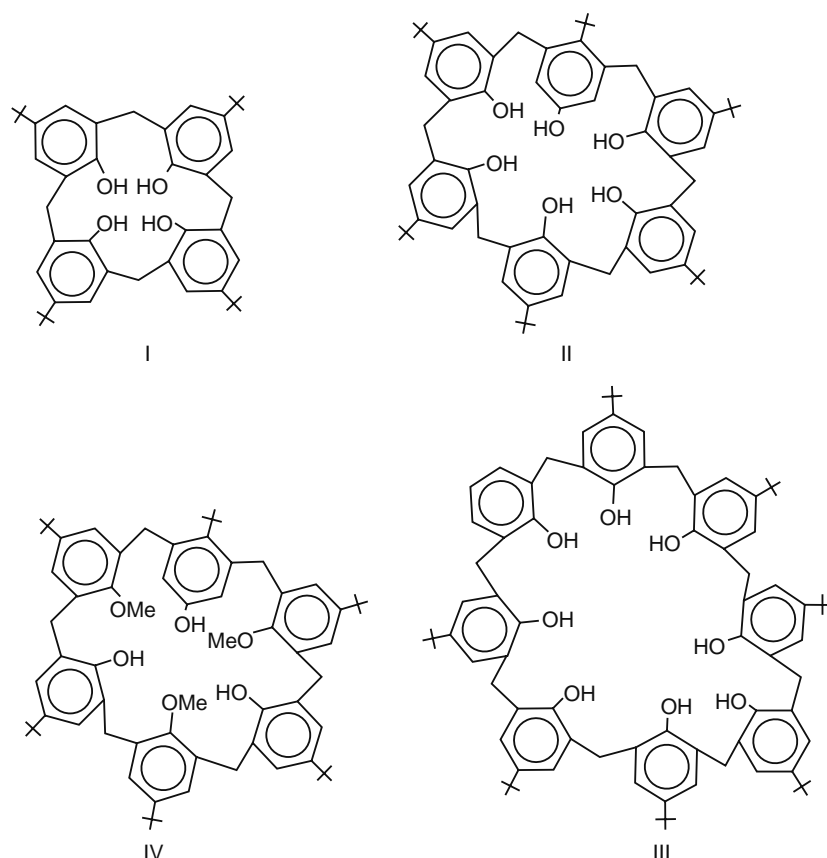


**FIGURE 31.5** Calixarenes used in the BLM experiments for U(IV) transport studies. I: (5,11,17,23-tetra-*tert*-butyl-25,26,27,28-tetrahydroxy calix[4]arene); II: (5,11,17,23,29,35-hexa-*tert*-butyl-37,38,39,40,41,42-hexahydroxy calix[6]arene); III: (5,11,17,23,29,35,41,47-octa-*tert*-butyl-49,50,51,52,53,54,55,56-octahydroxy calix[8]arene); and IV: (5,11,17,23,29,35-hexa-*tert*-butyl-37,39,41-trimethoxy calix[6]arene-38,40,42-triol). (Reproduced from Ramakumar, J., Nayak, S.K., and Maiti, B., *J. Membr. Sci.*, 196, 203, 2002.)

the separation of Th from U and extraction of Am by ELM using HDEHP in cyclohexane as the carrier, polyethylene glycol di-oleate as surfactant, and HCl as a stripping solution [38]. A liquid membrane-based process is used for pilot scale extraction of uranium from wet process phosphoric acid (WPPA) where uranium concentration is up to 100 ppm which in principle makes it

**TABLE 31.3**  
**Comparative Performances of Some ELM Systems Used in Actinide Ion Extraction Studies**

Metal Ion	Organic Phase	Outer Phase	Inner Phase	Comments	References
U(VI)	5% Kelex 100 & SPAN 80 in cyclohexane	Na <sub>2</sub> SO <sub>4</sub>	0.01 M H <sub>2</sub> SO <sub>4</sub>	<50% extraction in 25 min	[44]
U(VI)	LIX 63 & SPAN 80 in kerosene	Dilute acid	H <sub>2</sub> SO <sub>4</sub>	DF of >1000 is achievable	[47]
U(VI)	TOPO & SPAN 80 in cyclohexane	Na <sub>2</sub> SO <sub>4</sub>	Na <sub>2</sub> CO <sub>3</sub> H <sub>2</sub> SO <sub>4</sub> Na-citrate	Breaking of emulsion in case of carbonate as the inner phase due to CO <sub>2</sub> liberation	[45]
U(VI)	HDEHP & SPAN 80 in cyclohexane	Na <sub>2</sub> SO <sub>4</sub>	0.01 M H <sub>2</sub> SO <sub>4</sub>	>99% extraction in 20 min	[43]
U(VI)	TOA & SPAN 80 in kerosene	Dilute H <sub>2</sub> SO <sub>4</sub>	Na <sub>2</sub> CO <sub>3</sub>	>99% extraction in 40 min	[49]
Th(VI)	HDEHP & ethylene glycol dioleate in cyclohexane	0.05 M HCl	1.5 M HCl	>99% permeation in 50 min	[37,38]
Eu(III), Pu(IV)	PC-88A in <i>n</i> -dodecane	HClO <sub>4</sub> /HNO <sub>3</sub>	0.05 M HNO <sub>3</sub> + 0.3 M H <sub>2</sub> C <sub>2</sub> O <sub>4</sub>	>90% recovery of Pu was achieved from HClO <sub>4</sub> medium	[52–54]
Am(III), Eu(III)	HDEHP	DTPA + lactic acid	HCl	Separation of Ln from An is possible	[40]

ideal for treatment with a membrane process [39]. The membrane system studied was based on extraction using HDEHP–TOPO reagents that were contained within the organic phase of water in oil emulsion. El-Reefy et al. have also used HDEHP-based ELM containing aqueous HCl to study the permeation of Eu(III) and Am(III) from aqueous solutions containing lactic acid and diethylenetriamine-*N,N,N',N'',N'''*-pentaacetic acid (DTPA) with a view to separate them [40]. The kinetics of Am permeation was fast under these conditions, <55% permeated within 2 min; while the kinetics of Eu permeation was relatively slower (equilibrium occurred after 8 min). This difference in permeation rates can be used to separate Am(III) from Eu(III).

Uranium extraction by liquid surfactant membranes containing HDEHP as a mobile carrier has been studied by Akiba et al. in connection with the stability of water-in-oil (W/O) emulsion [41]. The apparent rate constant ( $k_{\text{obs}}$ ) increased with increase in carrier concentration and with external pH value, while it varied slightly with internal acid concentrations. The emulsion globules were demulsified by a high-voltage electrostatic method to recover the extracted uranium. The extracted uranium was efficiently recovered leaving little remnants in the liquid membrane phase. The extraction of uranium as uranyl nitrate complex in the nitrate acid solution was also carried out by Suropto et al. [42] using an emulsion that consisted of kerosene as the solvent, sorbitan mono oleate (SPAN 80) as the surfactant, HDEHP as the carrier agent, and phosphoric acids as the internal phase, while 2 M nitric acid was used as the external phase. Within 5 min an extraction efficiency of >94% was obtained though the amount of extracted uranium by the ELM was limited. In a mechanistic study by Zhou et al., the kinetics of extraction of uranium (VI) from sulfuric acid solutions with HDEHP in cyclohexane and liquid surfactant membranes containing HDEHP as a mobile carrier was investigated using Lewis cell technique [43].

Macasek et al. [44] carried out extensive studies on the extraction of U(VI), Ce(III), Tc(VII), Co(III), Sr(II), and Cs(I) using ELM made by various extractants such as TOPO, HDEHP, TOA, dicarbolides, di-picryl amine, etc. in SPAN 80 as the surfactant. When TOPO was used as the extractant, significant extraction of acid was observed. Use of  $\text{Na}_2\text{CO}_3$  as the strippant led to the breaking of the emulsion due to the release of carbon dioxide. On the other hand, the emulsions of diluted sulfuric acid in D2EHFA/cyclohexane solution were very good extractants of uranium as >99% recovery was achieved within 20 min using an emulsion comprising <0.1 M D2EHFA, <1 M SPAN 80, and 1–2 M  $\text{H}_2\text{SO}_4$ . When Kelex 100 (8-hydroxy quinoline) was used as the extractant, the recovery percentage decreased to <50% in about 25 min of agitation. On the other hand, Kulkarni et al. [45] used an ELM comprising TOPO, SPAN 80, and paraffin for the recovery of U from dilute nitric acid medium using 0.05 M  $\text{Na}_2\text{CO}_3$  as the internal phase. Optimization of the mixing time (10 min) was done to achieve maximum pertraction, minimum swelling, and minimum breaking of the emulsion.

The transfer kinetics of uranium (VI) through an ELM with di-1(1-methylheptyl) phosphoric acid (DMHPA) as a mobile carrier was investigated by Han et al. [46]. The experimental results showed that more than 96% of the initial U(VI) is recovered. Extraction of uranium (VI) by a liquid surfactant membrane containing 5,8-diethyl-7-hydroxy-6-dodecanone oxime (LIX 63) was investigated by Akiba et al. [47] and the apparent rate constants were calculated. The feed comprised of tracers ( $10^{-5}$  M) of U in pH 3–4.5, while the strippant used for the water-in-oil emulsion was sulfuric acid (pH 1.5). The apparent rate constants of extraction increased with an increase in carrier concentrations and external pH values, while they were slightly dependent on the stripping phase acidity. Increase in surfactant concentration led to decreased extraction of U and an optimum value was obtained using 2% of SPAN 80. It was important to note that the stripping rate was not the rate-determining step in the mass transfer process.

Han et al. [48] studied the transfer behavior of uranium (VI) through an ELM using *N,N*-di-*n*-butyloctanamide (DBOA) as a mobile carrier and suggested that the liquid membrane process can effectively and rapidly concentrate uranium (VI) from nitric acid medium. Hirato et al. [49] have used tri-*n*-octyl amine (TOA) and SPAN 80 in kerosene as the organic phase and the emulsion was made using 1 M  $\text{Na}_2\text{CO}_3$  solution as the internal phase. The feed comprised of uranium in sulfuric acid medium. More than 99% extraction was achieved using 0.05 M TOA at 3% surfactant concentration. The higher efficiency of the ELM system as compared to the solvent extraction system is clear from the data presented in Table 31.4. Out of the various internal

**TABLE 31.4**  
**Comparison of ELM Extraction and the Conventional SX**  
**for U(VI) Extraction Using TOA**

[TOA], M	[U(VI)], g/L	[ $\text{H}_2\text{SO}_4$ ], g/L	%E (SX)	%E (ELM)
0.05	1.15	33	22	92
0.02	1.15	33	9	90
0.02	0.58	33	16	95
0.02	0.29	33	28	96

Source: Data taken from Hirato, T., Kishigami, I., Awakura, Y., and Majima, H., *Hydrometallurgy*, 26, 19, 1991. With permission.

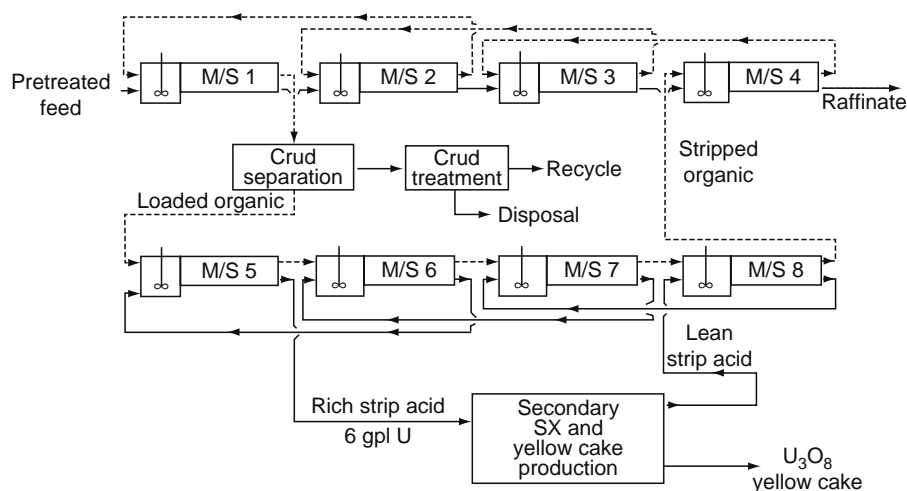


**FIGURE 31.6** Process flow diagram for U recovery by SX method. (Reproduced From Hayworth, H.C., Ho, W.S., Burnes, W.A. Jr., and Li, N.N., *Sep. Sci. Tech.*, 18, 493, 1983. With permission.)

solution used in their study,  $\text{Na}_2\text{CO}_3$  was found to be the most effective. By a two-stage extraction, the U concentration in the outer phase (at a phase ratio of carrier:internal phase:external phase = 1:1:10) could be brought down by a factor of 1000.

Hayworth et al. [50] have investigated the extraction of uranium from WPPA by liquid membranes of the emulsion type containing HDEHP/TOPO as the extractant. They reported that the ELM is economically superior to a system based on solvent extraction. The schematics of U recovery by the solvent extraction and the ELM method are shown in Figures 31.6 and 31.7, respectively. In the ELM process (Figure 31.7), the pretreated feed (or external phase) was contacted with a lean emulsion in a mixer-settler train. The comparison of the current solvent extraction process and proposed ELM process for the recovery of U from wet process phosphoric acid (WPPA) is shown in Figure 31.8. The proposed ELM process is suggested to be more efficient than the solvent extraction process. Bock et al. [51] have also investigated the liquid membrane separation of U from WPPA.

The coupled transport of europium(III) ion and hydrogen ion, via ELM containing PC-88A ((2-ethylhexyl) phosphonic acid mono-2-ethylhexyl ester) as mobile carrier and SPAN 80 as surfactant in diluent *n*-dodecane, was studied by Lee et al. [52]. The extraction behavior of U(VI) by PC-88A was investigated by Nakamura et al. [53] where the extracted species was found to be  $\text{UO}_2(\text{HA})_2$  (where  $\text{HA} = \text{PC-88A}$ ). Uranium was transported from the feed solution to a receiving solution of dilute sulfuric acid and was facilitated by a large concentration gradient of hydrogen ions across two sides of the LM. The addition of 1-decanol to the membrane solution improved the U stripping and contributed further to stabilize the PC-88A membranes

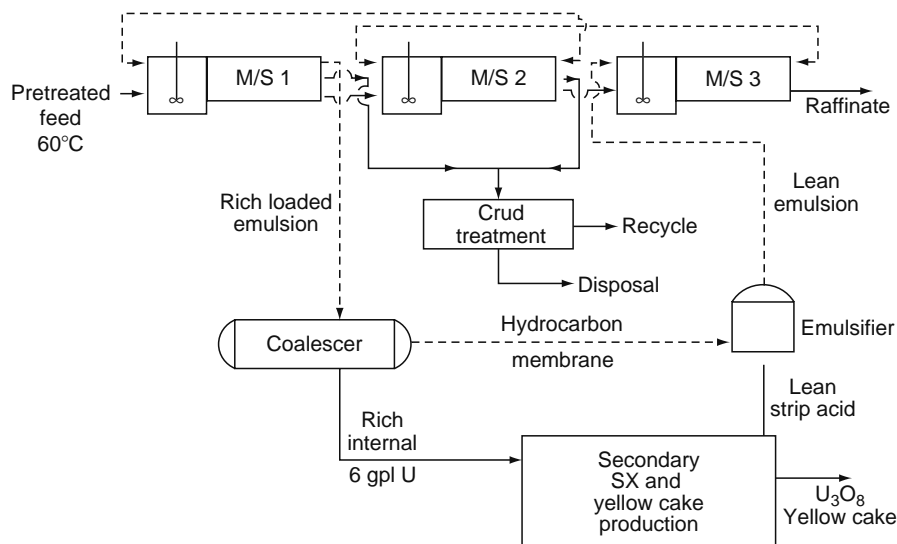


**FIGURE 31.7** Process flow diagram for U recovery by the liquid membrane method. (Reproduced from Hayworth, H.C., Ho, W.S., Burnes, W.A. Jr., and Li, N.N., *Sep. Sci. Tech.*, 18, 493, 1983. With permission.)

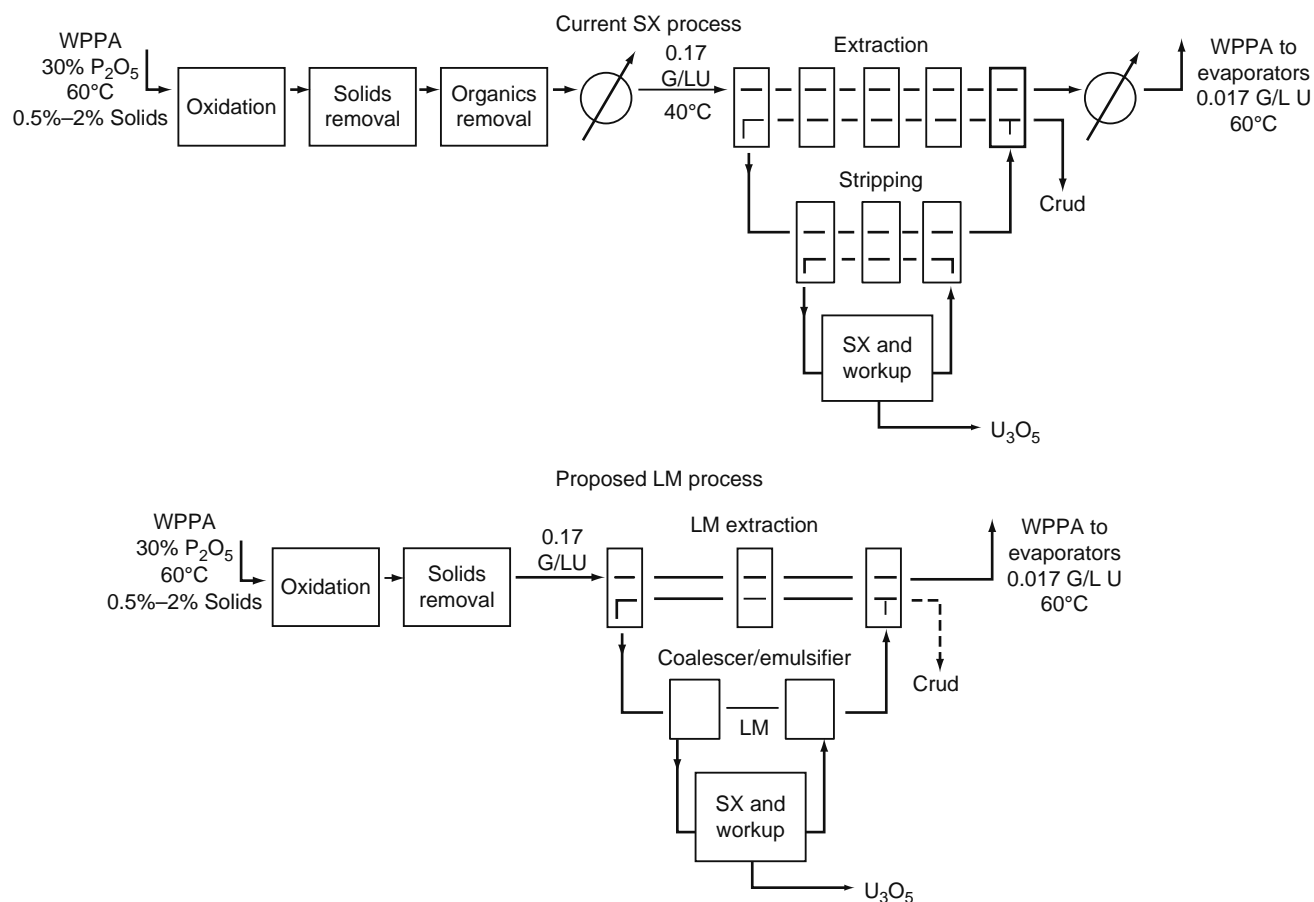


**FIGURE 31.8** Comparison of ELM and SX processes for the recovery of U from WPPA. (Reproduced from Hayworth, H.C., Ho, W.S., Burnes, W.A. Jr., and Li, N.N., *Sep. Sci. Tech.*, 18, 493, 1983. With permission.)

without any leaching into the aqueous phase. ELM recovery of Pu from aqueous nitrate solutions using PC-88A (existing as a dimer) in *n*-dodecane and SPAN 80 as carrier and surfactant, respectively, suggested about 90% recovery/removal of Pu from the waste in perchloric acid medium with the concentration factor of the order of 16 in 20 min of contact time [54]. Larger concentration of Pu (about 20 mg/L in the outer phase) could be extracted from perchloric acid medium using PC-88A in dodecane emulsion in SPAN 80 in about 60 min. Studies from nitric acid medium have shown that a feed comprising 4 M  $\text{HNO}_3$  can be effectively used for Pu separation.

EI-Reefy et al. observed that U(VI), Th(IV), Zr(IV), and Fe(III) were extracted to different extent from 0.1 to 3 M  $\text{HNO}_3$  solution by 0.1 M TOPO in cyclohexane solution using ELM [55]. Among these elements, only U(VI) and Th(IV) were found to be stripped from their organic phase by 0.1 M sodium citrate solution. On the other hand, cerium, copper, and cadmium were not extracted by TOPO under similar conditions. Forward permeation rate of uranyl ion was found to be mainly dependent on TOPO concentration and the concentration of U(VI) and  $\text{HNO}_3$  in the external phase was of little consequence.

### 31.2.3 SUPPORTED LIQUID MEMBRANES

Supported liquid membranes comprised the bulk of the published literature on the transport studies of metal ions across thin polymeric films [16,56–59]. Several literature reports on actinide transport across supported liquid membranes using various types of extractants viz., acidic extractants, neutral extractants and amine extractants are discussed below.

#### 31.2.3.1 Acidic Extractants as Carriers

Acidic extractants are commonly used as carriers for the pertraction of actinide ions across SLMs. Main feature of the acidic extractants is the inverse dependence of transport rates with the feed acidity. The various types of acidic extractants used as carriers for the separation of actinides are summarized in Table 31.5.

**TABLE 31.5**  
**Comparative Performances of Some Acidic Extractants Used as Carriers in SLM Studies**

Metal Ion	Carrier	Feed	Strip	Comments	References
U(VI)	Kelex 100	pH in the near neutral range	0.1 M HNO <sub>3</sub>	Recovery from seawater was possible without pretreatment	[60,61]
U(VI)	Cyanex-272	HNO <sub>3</sub>	HEDPA	Decontamination of Hanford site ground water containing U (>8000 ppb)	[79,80]
U(VI)	HDEHP	pH solutions	5 M H <sub>3</sub> PO <sub>4</sub>	Transport rates controlled by aqueous diffusion layer in Feed side	[67]
U(VI)	LIX 63	pH solution	0.1 M H <sub>2</sub> SO <sub>4</sub>	>99% U recovery was possible with DF exceeding 10 <sup>3</sup>	[84]
U(VI)	HDEHP + TOPO	5–6 M H <sub>3</sub> PO <sub>4</sub>	Fe(II)/H <sub>3</sub> PO <sub>4</sub>	Too low flux for any practical application	[75–77]
Am(III)	HPBI + TOPO	<1 M HNO <sub>3</sub>	1 M oxalic acid	>90% Transport was possible in <4 h	[63]
Am(III)	Cyanex-301	pH solution	0.1 M HNO <sub>3</sub> /0.1 M EDTA (pH 3.4)	Separation of Am(III) from Eu(III) was possible	[82,83]

Akiba et al. investigated the carrier-mediated transport of uranium (VI) by a liquid membrane of 7-dodeceny-8-quinolinol (Kelex 100) [60]. The apparent rate constant of uranium transport was not affected significantly with the increase in the carrier concentration and the pH of the feed solution. They had also reported that uranium can be effectively recovered from seawater through the liquid membranes without any preliminary treatment. Compounds analogous to Kelex 100, with long-chain aliphatic linkages, have been used for this study [61].

Seguira et al. had used 2-thenoyl trifluoroacetone (HTTA) as the carrier for the transport of lanthanide ions [62]. The transport of Am(III) was investigated by Mohapatra et al. employing FSSLM technique using a synergistic mixture of 3-phenyl-4-benzoyl-5-isoxazolone (HPBI) and TOPO in *n*-dodecane as the carrier and 1 M oxalic acid as the strippant [63]. Apart from enhancing the flux due to synergistic extraction, TOPO also helped in the ligand solubility in the membrane phase. It was possible to achieve >90% transport of Am(III) in about 4 h with the feed acidity as 1 M HNO<sub>3</sub> and the carrier concentration as 0.1 M HPBI + 0.2 M TOPO. The major disadvantage was, however, the deterioration of the membrane with increasing acidity due to the formation of TOPO · HNO<sub>3</sub> adducts. This led to the blocking of the membrane pores, thereby decreasing the flux drastically.

Nakamura et al. investigated the permeation of lanthanide ions using an SLM impregnated with Versatic 10 (VA 10) alone in kerosene [64,65]. Separation factors obtained from the transport rates for lighter lanthanoids were larger than those for heavier lanthanoids. The separation factors for heavier lanthanoids were enhanced by the addition of citrate to the feed solution [65]. Several complexing agents have been used in the receiving phase by Chitra et al. [66] during their SLM studies on Eu with PC-88A and VA 10 as immobilized carriers. Under similar experimental conditions, the effect of complexing agents on permeation of europium was found as citric acid > succinic acid > malonic acid. Permeating coefficient of europium was found to be greater with PC-88A in comparison with that of VA 10.

A large number of reports are available in the literature on the pertraction of actinides and lanthanides using dialkyl phosphoric acid as the carrier. Kinetics of the coupled transport of U(VI) across SLM containing bis(2-ethylhexyl)phosphoric acid (HDEHP) in kerosene as a mobile carrier was investigated by Huang and Huang [67]. The transport rates of U(VI) from feed containing  $1.5 \times 10^{-4}$  to  $1.8 \times 10^{-3}$  M uranyl ion and 5 M phosphoric acid as the receiver phase were measured and were found to be controlled by chemical reaction and aqueous film diffusion, both of which occur at the feed–membrane interphase. The transport rate measured was found to be proportional to the concentration of U(VI) in the source phase and increased with the concentration of the HDEHP in the membrane liquid. Mikheeva et al. had investigated the membrane transport of Am under conditions of different redox potentials in aqueous phase using HDEHP as the carrier [68]. The various steps leading to the transport were explained on the basis of physicochemical model of the process including steps of americium oxidation in feed solution, extraction by membrane, partial reduction on membrane surface, transmembrane diffusion, and reextraction to strip solution. In another study, the coupled transport of Eu(III) ions through an SLM consisting of a porous polypropylene film immobilizing HDEHP solution in *n*-dodecane was studied [69]. While modeling the data, it was observed that the deviations from a pseudo-first-order rate law, often observed when measuring the coupled transport of metal species at low concentrations through SLMs, are due to a reasonable value of the distribution ratio at the membrane–strip interphase [70]. The study on tervalent elements in nitrate medium through a flat-sheet membrane comprising HDEHP in dodecane indicated that the transport rates of Ce and Gd decreased with increasing feed acidity. The transport of all the metals increased to some extent with increasing concentration of HDEHP in the feed. Conditions were established for separating the pairs Ce–Tm, Ce–Yb, and Ce–Sc [71].

Separation studies can be performed by a series of composite membranes (using two SLMs in parallel) containing either of the acidic carriers such as HDNNS or HDEHP with a neutral carrier such as a bifunctional neutral organophosphorous

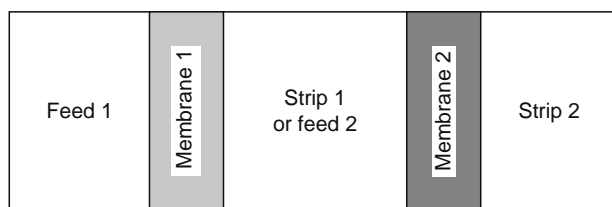


**FIGURE 31.9** Schematic of a composite SLM cell comprising two parallel SLMs for the prevention of counter-transport of acid.

extractant such as CMPO in decalin [72]. The transport behaviors of  $\text{Am}^{3+}$  and  $\text{Eu}^{3+}$  were investigated from feeds containing 0.01 M HCl + 1.0 M NaCl (for HDEHP and CMPO composite membranes) and 0.2 M  $\text{HNO}_3$  + 3.0 M  $\text{NaNO}_3$  (for CMPO and HDNNS composite membranes) where the strip solutions were 0.2 M  $\text{HNO}_3$  + 3.0 M  $\text{NaNO}_3$  and 0.01 M HCl + 1.0 M NaCl, respectively, which on the other hand acted as the feed solution for the second membrane (Figure 31.9). This setup was used to prevent the counter transport of acid from the receiver to the feed side.

Recovery of uranium from WPPA is usually carried out by two extractants: (a) a mixture of HDEHP and TOPO (tri-*n*-octyl phosphine oxide) and (b) octyl-phenyl acid phosphate (OPAP). The first system preferentially extracts U(VI) [73] while the second extracts U(IV) [74]. The application of liquid membrane technology for the recovery of U from WPPA has been discussed in many reports where quantitative recovery is reported [75,76]. Sifniades et al. [77] have attempted to understand the transport behavior of U(VI) from 5 to 6 M phosphoric acid solution through an SLM containing HDEHP and TOPO in kerosene as the organic carrier into a receiver phase containing Fe(II) in  $\text{H}_3\text{PO}_4$ . They developed a model based on the uranium transport through the membranes and through quiescent layers of phosphoric acid and HDEHP/TOPO in kerosene. The average uranium flux from simulated solutions of WPPA at 90% uranium transport was estimated to be  $1.3 \times 10^{-11} \text{ M cm}^{-2} \text{ s}^{-1}$ , which was judged to be too low for SLMs to be competitive with liquid–liquid extraction processes for the recovery of U from WPPA. The SLM method required >10 days for quantitative transport of uranium from 5 to 6 M phosphoric acid solution taken in the feed compartment.

Nakamura and Akiba [78] have investigated the carrier-mediated transport of europium using an FSSLM impregnated with di-*iso*-decyl phosphoric acid (DIDPA) in kerosene as the carrier. Effective pertraction was observed from a feed containing 0.1 M  $\text{HNO}_3$  and a strip phase comprising 5 M  $\text{HNO}_3$ . Interestingly, the efficiency of stripping increased significantly in the presence of 10% 1-octanol added to the carrier phase. The europium flux was found to be proportional to the initial europium concentration at lower concentrations and remained unaffected beyond  $10^{-3}$  M.

Dialkyl phosphinic acids have been used as extractants of lanthanides and actinides. Di(2,4,4-trimethylpentyl)phosphinic acid (DTMPPA or Cyanex-272) has been used for the removal of uranium from contaminated ground water [79] after acidifying the ground water to pH 2. The strip solution contained 1-hydroxyethane-1,1-diphosphonic acid (HEDPA). This separation method was successfully employed for the decontamination of Hanford site ground water containing U concentration >8000 ppb which was brought down to <10 ppb (Table 31.6). This was later scaled up by the HFSLM method to achieve much higher DF values [80]. The transport of Eu(III) at pH 3 across a DTMPPA liquid membrane supported on porous polytetrafluoroethylene to a strip solution (0.1 M nitric acid) was investigated [81]. It was observed that the thio derivative of the ligand has a limited preference of Eu(III).

Separation of lanthanides and actinides is a challenging area of research in separation science. Impetus in this area of research has been provided by the need to develop safer and economically viable methodologies of HLW management. The

**TABLE 31.6**  
**Removal of U(VI), Ca(II), and Fe(III) from Hanford Site Ground Water Containing Known Added Amount of U (Synthetic Samples)**

Time (min)	Uranium Removal (%)	Calcium Removal (%)	Iron Removal (%)
19	50.0	0.004	1.7
63	90.0	0.014	5.5
126	99.0	0.029	10.7
188	99.9	0.043	15.7

Source: Data taken from Chiarizia, R., Horwitz, E.P., Rickert, P.G., and Hodgson, K.M., *Sep. Sci. Tech.*, 25, 1571, 1990. With permission.

Notes: Carrier: 0.1 M Cyanex-272; Strip: 0.1 M HEDPA; Feed linear velocity: 8 cm/s; feed volume: 13 mL.

TRUEX as well as the DIAMEX processes developed during the last decade for actinide partitioning do not distinguish among trivalent lanthanides and trivalent actinides. Either of the two strategies being evolved for the HLW management, namely, vitrification followed by disposal in deep repositories or transmutation of long-lived actinide isotopes to short-lived fission products using high-energy high-flux reactors or accelerator-driven sub-critical systems, require the separation of Ln(III) from An(III). This is necessitated in view of the larger mass of lanthanides (30 times) over that of the minor actinides and high-neutron absorption cross section of some isotopes of lanthanides that may act as neutron poisons thereby rendering the transmutation process inefficient. It is desirable therefore to develop suitable complexing/separating agents, which can recognize trivalent lanthanides from trivalent actinides.

Although literature reports on liquid membrane separation of An(III) and Ln(III) are relatively scarce, some of them are discussed here. Bhattacharyya et al. carried out SLM studies using PP membranes containing 0.1 M bis(2,4,4-trimethylpentyl) dithiophosphinic acid (Cyanex-301) in *n*-dodecane as the carrier, pH 3.4 solution (sulfanilic acid buffer) as the feed, and 0.1 M EDTA as the receiver [82]. Though the quantitative transport (>99% in 20 h) of Am<sup>3+</sup> was observed, transport of Eu<sup>3+</sup> was negligible. Hoshi et al., on the other hand, observed the selective transport of Am<sup>3+</sup> across an SLM by using Cyanex-301 as a mobile carrier [83]. This extractant containing soft donor atoms exhibits strong affinity for actinoids, giving a large separation factor between trivalent Am and Eu. Americium was preferentially transported across the SLM and concentrated in product solution, while most of the Eu remained in the feed solution.

Uranium transport rates were also measured by Akiba and Kanno [84] using an SLM containing LIX 63 (5,8-diethyl-7-hydroxy-dodecan-6-one oxime) in kerosene as the carrier. Uranium transport was facilitated from a feed containing U(VI) at pH 4–5 to the receiver solution containing 0.1 M HNO<sub>3</sub>. The rate of transport was inversely proportional to the feed volume and was independent of U(VI) concentration. More than 99% of U was recovered and the final concentration ratio in the product to the feed exceeded 10<sup>3</sup>.

### 31.2.3.2 Neutral Donors As Carrier

#### 31.2.3.2.1 Alkyl Phosphates and Phosphine Oxides As Carriers

Tri-*n*-butyl phosphate is the work horse of the nuclear industry and is being used at various stages of nuclear fuel cycle. Apart from alkyl phosphates, tri-alkyl phosphine oxides are also used in many plant scale operations as well as in laboratory scale analytical separations. Minimizing their inventory in such separations through SLM methods though professed has not found industrial scale applications. Some of the laboratory scale applications of alkyl phosphates and tri-alkyl phosphine oxides as carriers in SLM will be discussed in this section (Table 31.7).

Similar to the transport behavior in BLM system (Section 31.2.1), several reports are available on the SLM-based transport studies of uranyl ion from feed containing nitric acid using TBP as the carrier. The nature of the species diffusing through the SLM phase is similar to the one given by Equation 31.1. Shukla and Mishra [27] have used 30% TBP in dodecane as the carrier and 1 M (NH<sub>4</sub>)<sub>2</sub>CO<sub>3</sub> as the receiver phase for their transport studies involving uranyl ion from a feed containing 2 M HNO<sub>3</sub>. Uphill transport was observed when both the F and R contained about 35 mg/L of U. In about 7 h, the U concentration in the receiver phase doubled suggesting the feasibility of the use of the SLM system for the preconcentration of the metal ion from dilute solutions. Chaudry et al. [85] have also investigated the transport studies of uranium using TBP in kerosene as the carrier. Permeation of the species of the type UO<sub>2</sub>(NO<sub>3</sub>)<sub>2</sub> · 2TBP<sub>(o)</sub> was confirmed from the log *J*<sub>η</sub> vs. log [TBP], and log *J*<sub>η</sub> vs. log [HNO<sub>3</sub>] plots. The effect of temperature was also studied and was found to have a retarding effect on the metal ion permeation. It was observed that at higher concentration of nitric acid, TBP · *n*HNO<sub>3</sub> complexes (where *n* = 1 or 2) were also transported

TABLE 31.7

Comparative Performances of Some Alkyl Phosphates and Phosphine Oxides Used as Carriers in SLM Studies

Metal Ion	Carrier	Feed	Strip	Comments	References
U(VI)	TBP	1–8 M HNO <sub>3</sub>	1.9 M ammonium carbonate	Quantitative transport (>99%) of uranyl ion is possible as acid transport is found to be insignificant	[27,85]
U(VI)	TBP + D2EHP	HNO <sub>3</sub>		Ion selective electrode	[88,89]
U(VI)	T2EHP	4 M HNO <sub>3</sub>	0.5 M Na <sub>2</sub> CO <sub>3</sub>	>90% transport in a single run	[93]
U(VI)	TOPO	HNO <sub>3</sub>	Carbonate solution	Anionic complexes are stripped	[94]
Pu(IV)	TBP	2 M HNO <sub>3</sub>	0.5 M ascorbic acid	Reduction to Pu(III) helped in quantitative transport	[29]
Pu(IV)	TAP in dodecane	4 M HNO <sub>3</sub>	0.5 M Na <sub>2</sub> CO <sub>3</sub>	>90% transport in a single run	[92]
Pu(IV)	Cyanex-923 in dodecane	Oxalic acid + HNO <sub>3</sub>		>95% Pu recovery	[96,97]
Pu(III)	Bis-(diphenylphosphoryl)-methane	1 M HCl	0.1 M HCl	Ion selective electrode	[98]

along with the  $\text{UO}_2(\text{NO}_3)_2 \cdot 2\text{TBP}_{(o)}$  complex [86]. They have calculated the diffusion coefficient ( $D$ ) for the  $\text{TBP} \cdot n\text{HNO}_3$  complexes from the Stokes–Einstein equation:

$$D = kT/6\pi R\eta \quad (31.9)$$

where

$k$  is the Boltzman constant

$\eta$  is the viscosity of the carrier solution

The diffusion coefficients are listed in Table 31.8. Transport of the  $\text{TBP} \cdot \text{HNO}_3$  complex was also reported in another study on a similar system [87]. However, based on the calculations made using the Stokes–Einstein equation, species of the type  $2\text{TBP} \cdot \text{HNO}_3$  is the more probable species diffusing through the organic layer. The difference between the experimentally observed and predicted values is attributed to the intermolecular interaction and tortuosity factors.

Based on the selective transport properties of TBP and its mixture with di-2-ethylhexyl phosphonate in benzene an uranyl ion selective membrane electrode was developed by Serebrennikova et al. [88]. This membrane electrode possesses higher selectivity as compared to the membrane electrode containing only di-2-ethylhexyl phosphonate in benzene [89]. Transport of  $\text{Pu}^{4+}$  from a feed containing 2 M  $\text{HNO}_3$  to a receiver phase containing 0.5 M ascorbic acid was investigated using Accurel 2E HF-PP flatsheet membrane containing 30% TBP in dodecane as the carrier [29]. Out of various strippants, namely, oxalic acid, ascorbic acid, hydroxyl amine hydrochloride, and sulfamic acid, ascorbic acid was found to be the most promising.

Changing the alkyl groups in TBP had shown interesting selectivities during solvent extraction studies [90,91]. Selective permeation of plutonium from aqueous nitrate medium was investigated using an SLM impregnated with tri-*iso*-amyl phosphate (TAP). More than 90% pertraction of plutonium could be easily accomplished in single run employing a feed solution consisting of about 1 mg/L Pu and 4 M  $\text{HNO}_3$ , at a carrier concentration of 0.8 M TAP/*n*-dodecane while the receiving phase was 0.5 M sodium carbonate or 0.5 M ascorbic acid [92]. Transport of U(VI) from aqueous nitrate solutions across an SLM, impregnated with tris(2-ethylhexyl) phosphate (TEHP), was investigated by Dharmapurikar et al. [93]. The permeability of U(VI) was evaluated as a function of  $\text{HNO}_3$  molarity in the feed phase (F), carrier concentration in the membrane phase, and chemical composition of the receiving phase (R). More than 90% extraction of U can easily be accomplished in single run employing about 0.2 g/L of U in 4 M  $\text{HNO}_3$  as the feed, carrier concentration of 0.6 M TEHP/*n*-dodecane while 0.5 M  $\text{Na}_2\text{CO}_3$  was used as the receiver.

Carrier (TOPO)-mediated transport of uranium(VI) has been studied by Akiba and Hashimoto [94] who have observed that uranium was extracted in the liquid membrane as  $\text{UO}_2(\text{NO}_3)_2 \cdot 2\text{TOPO}$  and stripped into the carbonate solutions as  $\text{UO}_2(\text{CO}_3)_3^{4-}$ . Using TOPO and HDEHP mixture, liquid membrane technique was applied for the recovery of uranium from WPPA [95]. Carrier-facilitated Pu(IV) pertraction through an SLM was standardized for its decontamination from oxalate wastes employing a commercially available Cyanex-923 (TOPO analog) in dodecane as the receptor [96,97]. More than 95% of plutonium could be easily recovered from Pu oxalate wastes solution during Pu reconversion operations.

**TABLE 31.8**  
**Distribution and Diffusion Coefficients of Nitric Acid Complexes of TBP**  
**as a Function of TBP Concentration**

TBP, %	[TBP], M	Distribution Coefficient	Diffusion Coefficients $\times 10^{-12} \text{ m}^2 \text{ s}^{-1}$		
			TBP · HNO <sub>3</sub> Species <sup>a</sup>	2TBP · HNO <sub>3</sub> Species <sup>b</sup>	Experimental Value
10	0.36	0.063	100.5	82.45	53.32
20	0.72	0.135	47.74	39.12	24.97
30	1.08	0.217	26.61	21.84	19.02
40	1.44	0.312	17.23	14.14	13.45
50	1.80	0.424	11.14	9.14	11.42
70	2.51	0.554	9.57	6.12	10.73
100	3.59	1.459	3.99	3.28	5.94

Source: Data reproduced from Chaudry, M.A. and Ahmad, I., *J. Radioanal. Nucl. Chem.*, 148, 15, 1991. With permission.

<sup>a</sup> Assuming  $\text{TBP} \cdot \text{HNO}_3$  is the only species present in the membrane phase.

<sup>b</sup> Assuming  $2\text{TBP} \cdot \text{HNO}_3$  is the only species present in the membrane phase.

**TABLE 31.9**  
**Comparative Performances of Some Substituted CMP, CMPO, and Diamides Used as Carriers**  
**in SLM Studies of Actinides and Lanthanides**

Metal Ion	Carrier	Feed	Strip	Comments	References
Eu(III)	Dihexyl- <i>N,N</i> -diethylcarbamoylmethyl phosphonate (CMP)	HNO <sub>3</sub> /HClO <sub>4</sub>	0.1 M HNO <sub>3</sub>	Concentration of Eu(III) is possible from dilute solutions	[105]
Am(III)	<i>n</i> -Octyl(phenyl)- <i>N,N</i> -diisobutylcarbamoylmethyl phosphine oxide (CMPO) + TBP	HNO <sub>3</sub>	Formic acid (FA) and hydroxylammonium formate (HAF)	Significant amount of acid transport was noticed	[106]
Am(III)	CMPO + TBP	HNO <sub>3</sub>	HCOOH + HAF	Biological sample analysis done using three-compartment cell	[108]
Am(III), Np(IV), Pu(IV)	CMPO	HNO <sub>3</sub>	Citric acid, FA, and hydrazine hydrate	Am(III) was recovered from actual HLW	[109]
Am(III)	Dimethyl dibutyl tetradecyl malonamide	HNO <sub>3</sub>	DTPA + hydrazine + HCOOH	Higher rates of transport were observed compared to pH 2 solution as strippant	[122]
Am(III)	TODGA	HNO <sub>3</sub>	Water	Good membrane stability was observed	[132]

Plutonium(III)-ion selective electrode consisting of phosphine oxides such as bis-(diphenylphosphoryl)-methane as an ionophore was developed by Kitatsuji et al. [98]. The Pu(III)-ISE prepared exhibited Nernstian response to the concentration of Pu<sup>3+</sup> in the sample solution. Interference of UO<sub>2</sub>(VI), U(IV), NpO<sub>2</sub>(V), and Pu(IV) was investigated. Cristau et al. [99] have carried out extraction as well as permeation studies of actinides such as neptunium, plutonium, and americium using polyphosphine polyoxides with (O)PCP(O) linkage, which exhibit very high selectivity.

#### 31.2.3.2.2 CMP and CMPO as Carriers

Current perception of radioactive waste management after operations involving the aqueous processing of the spent nuclear fuel materials involves minor actinide partitioning using exotic reagents as a key step. The recovery of alpha-emitting radioactive materials such as <sup>237</sup>Np, <sup>241</sup>Am, <sup>243</sup>Am, and <sup>245</sup>Cm from the HLW using novel bifunctional organophosphorous extractants such as CMP and CMPO has drawn the attention of many research groups [100–103]. A large number of publications have appeared using these reagents as carriers in the SLM studies. Many of the SLM studies have used lanthanides as surrogates (Table 31.9).

The transport of europium was studied by Nakamura and Akiba [104] through an SLM impregnated with di-*n*-hexyl-*N,N*-diethyl carbamoyl methyl phosphonate (CMP) from the perchlorate solution. The addition of 1-decanol improved the stripping process, and quantitative transport of europium was achieved. By combining the two SLM systems (Figure 31.10), consisting of di-*iso*-decylphosphoric acid and CMP, europium was transported from the feed solution (0.1 M HNO<sub>3</sub>) through the intermediate solution (1 M HClO<sub>4</sub> + 4 M NaClO<sub>4</sub>) to the product solution (0.1 M HNO<sub>3</sub>) and was effectively concentrated by a factor of about 20 [105].

Supported liquid membranes, consisting of an organic solution of *n*-octyl(phenyl)-*N,N*-diisobutylcarbamoylmethylphosphine oxide (CMPO) and tributyl-phosphate (TBP) in decalin, were capable of selective separation and concentration of actinide and lanthanide ions from aqueous nitrate feed solutions and from synthetic nuclear wastes where the strip solution is a mixture of formic acid (FA) and hydroxylammonium formate (HAF) [106,107]. TBP is added to CMPO to improve its solubility in aliphatic diluents. Although low concentration of nitric acid was initially used as the strippant solution, a gradual

Feed 0.1 M HNO <sub>3</sub> 100 mL	SLM (1) 0.2 M (DIDPA) <sub>2</sub> + 10% decanol	Intermediate solution 1 M HClO <sub>4</sub> 4M NaClO <sub>4</sub> 20 mL	SLM (2) 0.1 M CMP + 10% decanol in kerosene	Product 0.1 M HNO <sub>3</sub> 5 mL
---	--	---	---	--

**FIGURE 31.10** Combination of two SLM systems consisting of DIDPA and CMP for the effective transport of Eu(III). (Reproduced from Nakamura, S. and Akiba, K., *Sep. Sci. Tech.*, 24, 1317, 1989. With permission.)

decrease in the transport rates due to the nitric acid transport led to the use of FA + HAF mixture as the strippant. The effectiveness of this strip solution was gradually reduced by the simultaneous transfer of HNO<sub>3</sub> in the strip solution. A possible way to overcome this drawback is to make use of a second SLM consisting of a primary amine that is able to extract only HNO<sub>3</sub> from the strip solution. The use of second liquid membrane in the synthetic nuclear waste/CMPO-TBP membrane/HCOOH-HAF strip solution/primary amine membrane/NaOH solution allowed the quantitative removal of actinide and lanthanide ions from the feed solution. Chiarizia et al. [108] used CMPO loaded membranes for analysis of Am in biological samples after leaching in nitric acid medium. Two membranes were used in the transport studies consisting of 0.25 M octyl(phenyl)-*N,N*-diisobutylcarbamoylmethylphosphine oxide (CMPO)/0.75 M TBP and primary aliphatic amine (PAA) (as a second membrane) for the selective extraction of actinides from nitric acid solutions. In another SLM study using CMPO as the carrier, Ramanujam et al. had used a mixture of citric acid, formic acid, and hydrazine hydrate as the receiving phase for partitioning of actinides from high-level waste of PUREX origin [109]. The studies indicated good transport of actinides such as neptunium, americium, and plutonium across the membrane from nitric acid medium. A high concentration of uranium in the feed retards the transport of americium, suggesting the need for early removal of uranium from the waste. The separation of actinides from uranium-lean simulated samples as well as from actual high-level waste was found to be feasible using the above technique.

Danesi et al. studied the kinetics of transport of Am(III) from aqueous nitrate solutions to formic acid aqueous solutions using an SLM, which consisted of a solution of a new (carbamoylmethyl)phosphine oxide in diethylbenzene (DEB) [110]. In an attempt to treat simulated low-level radioactive wastewater, Teramoto et al. [111] have used an SLM containing CMPO for the uphill transport of Ce(III) from aqueous solution containing a mixture of nitric acid and sodium nitrate. The simulated waste contained Ce(III), Fe(III), Cr(III), and Ca(II), while the strip solution contained water or sodium citrate solution. Though TBP has been used along with CMPO and *n*-dodecane as the carrier solution, it also facilitates the transport of HNO<sub>3</sub> to the strip side. The acid transport was significantly decreased when CMPO alone in 2-nitrophenyl octyl ether was used as the carrier solution.

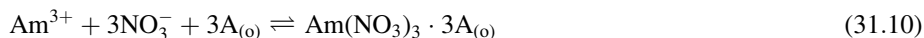
### 31.2.3.2.3 Dialkyl Amides and Diamides As Carriers

With increasing concern for the environment protection, incinerable CHON or the green extractants are becoming more and more popular among chemists involved in separation science and technology. Among these dialkyl amides, pentaalkyl malonamides and tetraalkyl di-glycolamides are the most popular due to their innocuous hydrolytic and radiolytic degradation products and favorable DF values for actinide ions [112–117]. The SLM-related work carried out using amides and diamides as carriers is indicated in Table 31.9.

Di-*n*-hexyl octanamide (DHOA) was used by Patil et al. for effective transport of uranyl ion from 4 M nitric acid to a strip solution containing either 1.0 M Na<sub>2</sub>CO<sub>3</sub> or 0.01 M nitric acid [118]. Several newly synthesized monoamides such as di-butyl octanamide (DBOA), methylbutyldecanamide (MBDA), methyl butyl octanamide (MBOA), di-butyl decanamide (DBDA), di-*n*-octyl ethylhexyl amide (DOEHA), and di-hexyl octanamide (DHOA) were tested by Shukla et al. as carriers across SLMs for selective transport of Pu(IV) [119]. Of them, MBDA and DBOA proved to be quite suitable as ionophores from HNO<sub>3</sub> media providing >95% and >82% transport of Pu(IV) when operated for 7 h. Shailesh et al. [120] have used a sterically modified amide, di-2-ethylhexyl isobutyramide (D2EHIBA) in *n*-dodecane as the carrier for the selective transport of trace U(VI) in the presence of large excess of Th(IV). The decontamination factor obtained in this method is attributed to lower nitric acid transport rates as compared to TBP/*n*-dodecane system, which has much higher permeability coefficient as compared to D2EHIBA/*n*-dodecane system. This work is particularly interesting as it offers an alternative membrane-based separation method to the conventional TBP extraction-based separation methods.

Sriram et al. carried out SLM studies on the transport of Am<sup>3+</sup> from nitric acid medium using dimethyl dibutyl tetradecyl malonamide (DMDBTDMA) in dodecane as the carrier into 0.01 M nitric acid [121]. Significant transport of acid into the strip side resulted in relatively slower transport rate. It was observed that a mixture of 0.1 M DTPA, 0.4 M hydrazine, and 0.4 M formic acid led to highest transport rate (>60% in 8 h) when used as the stripping solution [122].

The effect of organic diluents on the extraction and hence the transport rates of Am<sup>3+</sup> were quantified by an empirical correlation using several diluents, namely, *n*-dodecane, toluene, *n*-hexane, cyclohexane, 1,2-dichloroethane, nitrobenzene, decalin, and diethyl benzene [123]. The extraction equilibria were not affected and the tri-solvate species were transported in all the cases as per the following extraction equilibrium:



The extraction (and hence the transport) efficiency depends on several diluent factors such as Schmidt empirical diluent parameter [124,125], the Swain's acidity and basicity parameters along with the Dimroth and Reichardt polarity indices [126], dielectric constant [127], refractive index [127] and viscosity [127], and the Hildebrand's solubility parameter [128]. The permeability coefficients ( $P_{\text{Am}}$ ) were computed from the Wlke-Chang, Scheibel, and Ratcliff [129,130] equations, which compared reasonably well with the experimentally determined values as shown in Table 31.10. Elhassadi and Do [131] have, on the other hand, taken into account only the viscosity and solubility effect of the diluent and the carrier immobilized in SLM. They have reported that these two factors influenced the transport rates significantly.

**TABLE 31.10**  
**Diluent Effect in the Permeation of Am<sup>3+</sup> through an SLM Containing**  
**DMDBTDMA in *n*-dodecane as the Carrier**

Diluent	Permeability Coefficient ( $P_{Am}$ ) in cm/s ( $\times 10^4$ )			
	$P_{Wilke\text{-}Chang}$	$P_{Scheibel}$	$P_{Ratcliff}$	$P_{Expt}$
<i>n</i> -Dodecane	1.80	1.87	1.75	1.80
Toluene	0.73	0.78	0.84	0.90
<i>n</i> -Hexane	1.80	2.12	2.20	1.63
Cyclohexane	0.54	0.62	0.66	0.76
Dichloroethane	1.99	1.93	2.14	1.80
Nitrobenzene	2.60	2.48	2.62	2.41
Decalin	0.50	0.50	0.50	0.62
di-Ethylbenzene	0.65	0.66	0.66	0.71

Source: Data from Sriram, S. and Manchanda, V.K., *Solv. Extr. Ion Exch.*, 20, 97, 2002. With permission.

Though tetraalkyl di-glycolamides (TODGA) are far superior as extractant as compared to CMPO or diamides, to our knowledge very little work on their use as carrier in SLM studies is reported so far. Ansari et al. [132] have studied the transport of Am<sup>3+</sup> from nitric acid medium into a receiving solution of distilled water using an SLM made from *N,N,N',N'*-tetraoctyl-3-oxapentane diamide (TODGA) in *n*-dodecane as the carrier inside microporous PTFE membranes. The transport of feed acid to the receiver phase was increased with the feed acidity, which influenced the transport rate of the metal ion at higher acidity (>2 M HNO<sub>3</sub>). Maximum transport was observed with a carrier concentration of 0.1 M and a feed acidity of 2 M HNO<sub>3</sub>. The membrane stability was remarkably good when tested for more than 20 days of continuous operation. The use of TODGA as a carrier in the polymer inclusion membrane (PIM) is discussed in Section 31.3 [133].

#### 31.2.3.2.4 Macrocyclic Carriers in Supported Liquid Membrane

Macrocyclic carriers such as crown ethers, cryptands, and calixarenes have been used as carriers for the transport studies involving alkali and alkaline earth metal ions [134–136]. There are a few reports on the use of these ligands as the carriers for the transport of lanthanide/actinides as well. Shukla et al. [137] studied the uranyl ion permeation fluxes, physical stability (loss of carrier), and chemical stability of SLMs using crown ethers in various aromatic and aliphatic diluents. They have concluded that the chlorinated hydrocarbons such as chloroform, 1,2-dichloroethane, dichloromethane afford much poor permeability compared to aromatic diluents such as toluene and *o*-dichlorobenzene. Plutonium transport could be achieved using 0.2 M DC18C6/toluene as carrier and sodium carbonate as strippant. By a combination of both BLM and SLM (using polypropylene filters), >90% transport of Pu was achieved using 0.2 M DC18C6 in toluene as the carrier into dilute sodium carbonate strippant in about 7–8 h without any contamination from fission products such as Ru-106, Cs-137, and Sb-125 [138]. The proven extractability and profound selectivity of dicyclohexano-18-crown-6 (DC18C6) have been exploited by selecting this crown ether as the ionophore in liquid membrane transport studies. Macrocyclic-facilitated transport of Pu(IV) and U(VI) against their concentration gradient from aqueous nitric acid solutions across SLM containing DC18C6 in toluene has also been investigated [139]. In the presence of 0.2 M DC18C6 in toluene as the carrier, uphill transport was observed when both the feed and receiver comprised of 0.8 mg/mL of Pu. The effect of radiation on the transport rates has indicated that the permeation of U(VI) and Pu(IV) was not affected when the membranes containing the carrier were subjected to a total dose of 80 kGy. On the other hand, dry membranes (Accurel HF-PP) became somewhat fragile beyond a total dose of 50 kGy though the transport behavior was not very much affected. The chemical stability of the membrane containing DC18C6 in toluene was satisfactory up to 12 h of continuous operation, beyond which a drop in the permeability coefficient was ascribed to the loss of carrier [140]. In another study involving the transport of Pu(IV), Shukla et al. have investigated the role of polymer support upon the performance and stability of an SLM using several solid supports such as polytetrafluoroethylene (TE-35, TE-36, TE-37), polypropylene (HF-PP), cellulose nitrate (BA-S-83) of different pore sizes and varying thickness, and DC18C6 in toluene as the mobile carrier [141]. Selectivity of plutonium transport from fission product contaminants such as Cs-137, Ru-103, and Ce-144 was found to be poor with large pore size (0.45 μm) support. Polytetrafluoroethylene supports, such as TE-35, TE-36, TE-37, and polypropylene HF-PP membranes, did not show any marked deterioration with nitric acid and organic solvents while cellulose nitrate membrane such as BA-S-83 was attacked by organic solvent. On the other hand, these membranes were found to have good radiolytic stability [142].

Almost no report is available on the membrane transport studies of trivalent actinide ions with macrocyclic carriers. However, there are some literatures available on trivalent lanthanide ions, which can be used as guidelines for any future studies. Brown et al. [143] and Zhu and Izatt [144] have used bis(1-hydroxyheptyl)DC18C6 as the membrane carrier and

attempted separation of Eu from trivalent lanthanide cations by reducing it to the +2 oxidation state. The online reduction was carried out by modifying the transport cell in such a way that the feed compartment contained a mercury pool that acted as the cathode, while a Pt coil worked as the anode. After reduction,  $\text{Eu}^{2+}$  behaved similar to  $\text{Sr}^{2+}$  and selective transport was observed as compared to other lanthanides such as  $\text{Nd}^{3+}$  (4 times lower flux than  $\text{Eu}^{2+}$ ) and  $\text{Gd}^{3+}$  (8 times lower flux than  $\text{Eu}^{2+}$ ). Tang and Wai [145], on the other hand, have studied the transport behavior of trivalent lanthanide ions using a lipophilic crown ether carboxylic acid, 2-(sym-dibenzo-16-crown-5-oxy) hexanoic acid using a surfactant membrane. The activation energies for the transport of lanthanides in the system were determined to be 3–4  $\text{kJ mol}^{-1}$  suggesting that the process is diffusion controlled. This surfactant membrane also shows a selectivity of  $\text{Lu}^{3+}/\text{La}^{3+}$  by 1.25 in the transport process.

Macrocyclic ligands, such as calixarenes, have the flexibility and favorable conformations to form stable complexes with uranyl ion [146–148]. The special structural features of the calixarenes make them selective ionophores for many lanthanide/actinide ions. Uranyl ion, in an aqueous sodium hydrogen carbonate solution of pH 4–8 (source phase), was simultaneously and selectively transported into a dilute sulfuric acid solution (receiving phase) through a membrane (chloroform, BLM) containing a lipophilic ion-associate of methyltrioctylammonium ion and hydroxycalix[*n*]arene-*p*-sulfonate ion,  $2_n$  ( $n = 6, 8$ ),  $\text{MTA}^+ - 2_n$ , as a metal carrier [149]. None of the other metal ions were transported, or obstructed the transport of uranyl ion, while the presence of large amounts of sodium hydrogen carbonate and sodium chloride in the source phase interfered by causing a delay in the start of transport. Ramakumar et al. [33] have used several calixarenes (Figure 31.8) along with neutral donors such as TOPO and 18 crown 6 for the selective transport of uranium from seawater. Calixarene II and IV were found to show very good transport behavior when used as the carrier. Using calixarene II and TOPO mixture in chloroform, they recovered >95% of uranium from seawater while the permeation of ions such as  $\text{Na}^+$ ,  $\text{Mg}^{2+}$ ,  $\text{Ca}^{2+}$ ,  $\text{K}^+$ , and  $\text{Fe}^{3+}$  was negligible. A significant increase in the transport rates of alkali/alkaline earth ions was observed when 18 crown 6 was used as the synergist.

In the minor actinide partitioning by the TRUEX process, CMPO is used as the extractant for the recovery of trivalent actinides from nitric acid medium. A resorcinarene cavitand-based ligand, functionalized with CMPO (carbamoylmethylphosphoryl)-ligating moieties in 2-nitrophenyloctyl ether (NPOE), was utilized for the transport studies of Eu(III) by Boerrigter et al. [150]. The steric pre-organization of four CMPO moieties on the macrocyclic resorcinarene cavitand frame improved the efficiency and selectivity of the metal extraction processes as Eu(III) could be quantitatively removed from acidic solutions using SLM in about 8 h. They had also used the CMPO-functionalized resorcinarene cavitands for the transport studies of  $\text{UO}_2^{2+}$  [151]. Calix-4-arenes mono/bis-crown-6 bound to heteropolysiloxane matrix were used for the selective transport of radionuclides such as Cs-137 from a waste containing Am-241 [152]. Dozol et al. [153] synthesized several grafted membranes containing calixarenes linked to the polypropylene matrix, which were selective for the lanthanides and trivalent actinides. The data with SLM were compared with those obtained with the grafted membranes.

### 31.2.3.3 Basic Extractants as Carriers

Amines have been used as the extractants for the actinide-bearing anionic species. This is usually from high-acidic or high-ionic strength medium, which generally lead to very high decontamination factors. The precondition of their use in SLM-based separation methods is the inertness of the membranes toward high acidic or salt medium. As membranes made from polycarbonate or polyamide may not be very stable toward these medium, most of the reported work in this area is on PTFE or PP membranes.

Chaudry and Mohammad [154] had used tri-*n*-octyl amine (TOA) dissolved in xylene as the SLM in Celgard 2400 polypropylene filter for the transport of uranyl ions from nitric acid solutions to an alkaline aqueous phase. About 10 h were needed for the quantitative transport of uranyl ion from an aqueous feed of 6 M  $\text{HNO}_3$ . Several other tertiary amines along with TOA have been used as carriers in SLM studies by Sonawane et al. [155]. The diffusion-limited and amine-facilitated Pu(IV) cation permeation in nitric acid media across an SLM was investigated to quantify the membrane carrier type effects on its transport using basic extractants, namely, Primene JM-T (JMT) as primary, Amberlite LA-2 (Amb LA-2) as secondary, trilaurylamine (TLA) and triiso-octyl amine (TIOA) as tertiary, and Adogen-464 and Aliquat-336 as quaternary amines. Recovery of Pu steadily increased from primary to quaternary amines as it follows the order quaternary > tertiary > secondary > primary, similar to that generally observed in liquid–liquid distribution experiments. More than 95% pertraction of Pu(IV) was easily accomplished using tertiary or quaternary amine as carrier employing a feed solution containing about 5 mg/L Pu in 4 M nitric acid solution, while the receiving phase was 0.1 M  $\text{NH}_2\text{OH} \cdot \text{HCl}$  (in 0.3 M  $\text{HNO}_3$ ). On the other hand, plutonium permeation was found to plummet to about 49% on employing secondary amine, Amb LA-2, as the carrier [156].

Lakshmi et al. had investigated the transport of uranyl ion from HCl medium using 30% Aliquat-336 in  $\text{CHCl}_3$  as the carrier [157]. Significant amount of acid transport (about 15%) was observed which affected the metal ion transport though >90% transport of U was observed in about 3 h. In another study involving Alamine 336, the same authors had shown that aromatic solvents such as toluene or *t*-butyl benzene effect higher transport rates than solvents such as chloroform or hexane [158]. Subba Rao et al. had investigated the transportation of uranium from HCl medium by an SLM made from Aliquat-336 in xylene as carrier and observed that the flux values for HCl or for uranium were higher at lower carrier concentration, which was

explained based on the aggregation behavior of the carrier molecules in membrane phase [159]. Effect of phase modifier on uranium transportation from hydrochloric acid medium across SLM using Aliquat-336 as the carrier in xylene medium was investigated by them to understand the effect of degree of aggregation of carrier molecules [160]. In this study, reduction of uranium flux was observed at carrier concentration where viscosity effects were not dominant.

### 31.2.4 HOLLOW FIBER SUPPORTED LIQUID MEMBRANE

Several applications are envisaged in nuclear industry for the preconcentration of very lean solution of radioactive material, low- and intermediate-level wastes. There are, of course, reports on the application of HFSLM technique for high-level waste processing. Researchers at the plutonium facility at Los Alamos National Laboratory have studied the separation of actinides from waste solutions [161] using water soluble metal binding polymers (phosphonic acid derivative of polyethyleneimine). Kathios et al. [162] have investigated the use of HFSLM modules for process scale metal separations such as radioactive waste stream clean up and environmental remediation under simulated conditions (Nd was used for Am) using CMPO in di-*iso*-propyl benzene as the carrier. The major challenge in such case is to develop radiation resistant polymers.

Rathore et al. have studied the permeation of U(VI) and Pu(IV) in the presence of fission products from medium active acidic waste employing 30% TBP as a carrier through HFSLM and observed that recovery could be enhanced by using fresh strippant each time [163]. They have also used TBP as the carrier for the quantitative separation and recovery of Pu from nuclear waste solutions [164] using an HFSLM system. In the presence of various fission products, the selective permeation of Pu through the HFSLM was observed to be more than 90% into a stripping phase consisting of 0.1 M  $\text{NH}_2\text{OH} \cdot \text{HCl}$  in 0.3 M  $\text{HNO}_3$ . The membrane radiation stability was found to be good as shown by the scanning electron microscope (SEM) pictures of the irradiated and the nonirradiated membranes (Figure 31.11) even after exposure to 1 M Rad dose. A commercial tri-alkyl phosphine oxide, namely, Cyanex-923 was found to be far superior as the carrier as compared to TBP, as >94% transport was reported in 10 h using 0.1 M concentration of the carrier [97]. The permeation efficiency was found to increase from 75% to 90% by increasing the flow rate from  $3.0 \times 10^{-8}$  to  $1.4 \times 10^{-7} \text{ m}^3 \text{ s}^{-1}$ . Patil et al. have used dihexyl octanamide (DHOA) in normal paraffinic hydrocarbon diluent as the carrier in their HFSLM (operated in the nondispersive extraction mode) study [165,166]. From a feed solution comprising 8 g/L of U in 4 M  $\text{HNO}_3$ , transport was more facile into a strippant solution of 0.01 M  $\text{HNO}_3$  as compared to 1 M sodium carbonate.

Transport of Pu(IV) from 3 M  $\text{HNO}_3$  solutions across Aliquat-336/Solvesso-100 by HFSLM was studied. Permeability of Pu(IV) through a bundle of hollow fibers made up with 20 lumens, of  $67 \text{ cm}^2$  surface area, 9 cm length, and operated at a flow rate of  $10^{-8} \text{ m}^3/\text{s}$  on recycle mode was examined. More than 80% Pu from oxalate bearing wastes generated during reconversion process could be transported through 10% Aliquat-336/Solvesso-100 into hydroxylamine hydrochloride strippant in about three runs [167].

HFSLM studies employing dialkyl phosphinic acid (Cyanex-272) were reported by Chiarizia et al. [80] for the decontamination of the severely contaminated Hanford site ground water. Their HFSLM experiments involved a hollow fiber module containing a total membrane area of  $9.8 \text{ cm}^2$  and the feed contained contaminated Hanford ground water at pH 2 (synthetic samples) circulated through the lumen side, while the strip containing 0.1 M HEDPA was circulated through the shell side. The U(VI) can be concentrated in the strip solution to about  $10^8$  times though significant amount of Fe(III) also gets cotransported.

Lanthanide-actinide separation was also attempted by HFSLM (operated in the nondispersive extraction mode) method using diphenyldithiophosphinic acid derivatives. Geist et al. have employed a synergistic mixture of bis(chlorophenyl)-dithiophosphinic acid and TOPO in a hollow fiber module for the lanthanide-actinide separation [168]. About 99.99% Am

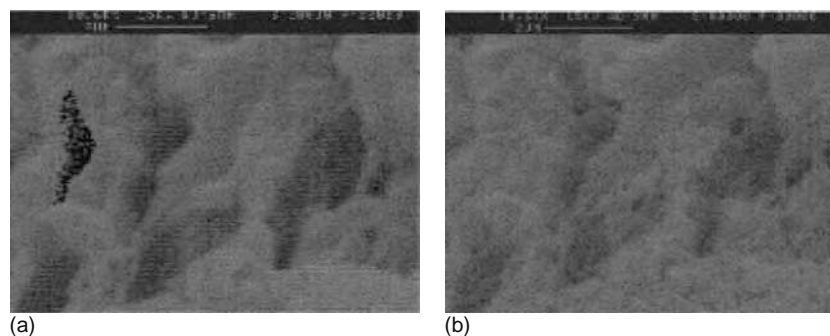


**FIGURE 31.11** SEM pictures of the hollow fiber lumens used in an HFSLM study involving radioactive solutions. (a) Prior to irradiation; (b) after irradiation. (Reproduced from Rathore, N.S., Sonawane, J.V., Gupta, S.K., Pabby, A.K., Venugopalan, A.K., Changrani, R.D., and Dey, P.K., *Sep. Sci. Tech.*, 39, 1295, 2004. With permission.)

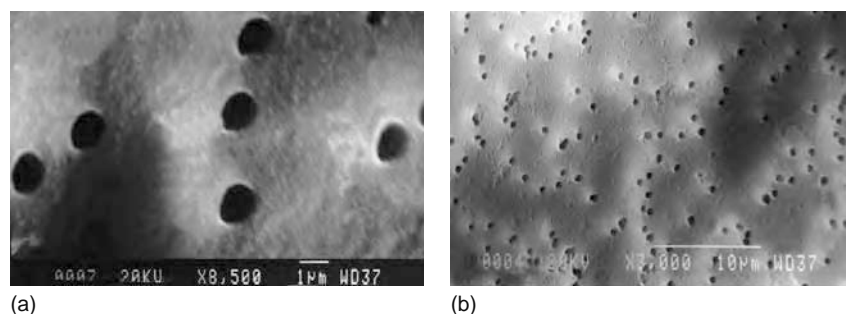


**FIGURE 31.12** Typical representation of the holes formed in a PVDF nuclear track filter after irradiation in accelerator and the subsequent etching with 6 M KOH and 0.1 Fw  $\text{KMnO}_4$ . (Reproduced from Gopalani, D., Kumar, S., Jodha, A.S., Singh, R., Khatri, P.K., and Gopal, R., *J. Membr. Sci.*, 178, 93, 2000. With permission.)

(III) could be extracted by the contactor from 0.5 M nitric acid with about 33% of lanthanides such as Y, La, Ce, Pr, Nd, Sm, Eu, and Gd being extracted.

### 31.2.5 TRACK-ETCHED MEMBRANES

Track-etched membranes (TEM) are, in general, polymeric membranes with artificially made pores made after irradiating with a projectile of heavy ions followed by chemical etching. TEMs, which show a more precise distribution of pores with a known pore size, are used for the transport of ions [169]. Fleischer et al. [170] have used thin sheets of plastics, usually 10–20  $\mu\text{m}$  polycarbonates, perforated with collimated and diffused beams of heavy energetic ions. There is however a limitation on the thickness of the polymeric materials, which can be used for making membranes in view of the limitation of the projectile energy. As a consequence, these thin membranes are not rugged. These membranes with pore sizes in proportion to the energies of the charged particles are used for the investigations involving nonlinear theory in ionic transport [171]. It was reported that track-etched membranes with porosity up to 20% can be prepared using accelerated heavy ions. Pandey et al. [172] had used Makrofol track-etch membranes (after irradiating with 13 MeV Dy-161 ions and etching with 3 M NaOH) for the transport of Am(III) from a feed comprising 1.5 M ammonium nitrate and 0.5 M nitric acid to a strip phase consisting of 1 M oxalic acid using a mixture of 1.2 M TBP and 0.2 M CMPO as the carrier. Both the inner as well as outer diameters of the pores varied linearly with the etching time. The inner pore diameter as well as the porosity were found to govern the metal transport rates. The permeation across the SLM formed by using TEM with 17% porosity was found to be comparable to those SLMs formed by using commercial membranes with much higher porosities. The comparison of  $P$  (permeability coefficient) obtained by using TEMs with 29–30  $\mu\text{m}$  and 10  $\mu\text{m}$  thickness indicated that  $P$  decreased linearly with thickness and hence transport of Am(III) is diffusion controlled, and the extraction and stripping kinetics are fast. Removal of actinide ions from acidic solutions by carrier-mediated facilitated transport across mesoporous substrates with nanoengineered surfaces has been reported very recently [173]. The thiol self-assembled monolayer (SAM) modified with di(*tert*-butyl-phenyl) di(*iso*-butyl)CMPO was used for the selective transport of  $^{239}\text{Pu}$  and  $^{241}\text{Am}$  from a mixture containing fission products such as  $^{137}\text{Cs}$  and  $^{90}\text{Sr}$ , which are not transported to any significant extent.

Nuclear track membranes with other materials, such as mica, oscillating quartz, PVDF, Kapton, and even polyster, have been found to be resistant to chemicals and acid. Figure 31.12 shows a typical representation of the holes formed in a polyster nuclear track filter after irradiation in accelerator and the subsequent etching with 6 M KOH and 0.1 Fw  $\text{KMnO}_4$  [174]. Vater has used track-etched mica filters for collecting the aerosols carrying radioactivity from the environmental air inside a nuclear reactor fuel elements production plant [175]. Ganz et al. [176] have, on the other hand, used Kapton track-etched microfilters (pore size: 3.8–13.4  $\mu\text{m}$  and porosity: 4%–12%) for the separation of  $^{237}\text{Np}$  from a feed containing 2 M  $\text{HNO}_3$ . About 0.5 M HTTA in xylene was used as the extractant, which formed emulsion with the aqueous phase and the Kapton membrane selectively allowed the organic phase to pass through.

## 31.3 POLYMER INCLUSION MEMBRANES

Although FSSLM- and HFSLM-based separation methods are getting increasingly popular, their only disadvantage is the stability, which is primarily due to the irreversible loss of carrier from the pores of the filters/lumens. As an alternative, polymeric films have been prepared along with the ligand and the diluent. These membranes termed as polymer inclusion membranes (PIM) have better membrane stability, although they are not suitable under high concentration of acid or alkali [177,178]. In general, the PIMs have relatively lower transport rates compared to the SLMs. Kim et al. [179] have shown that

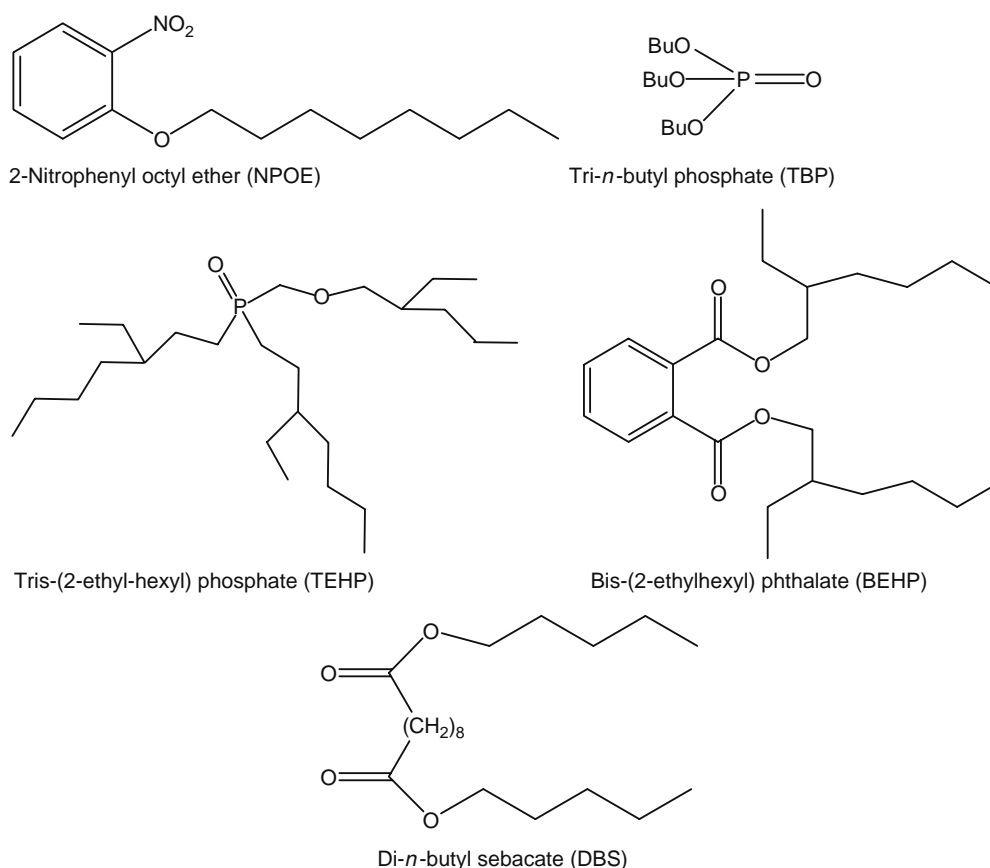
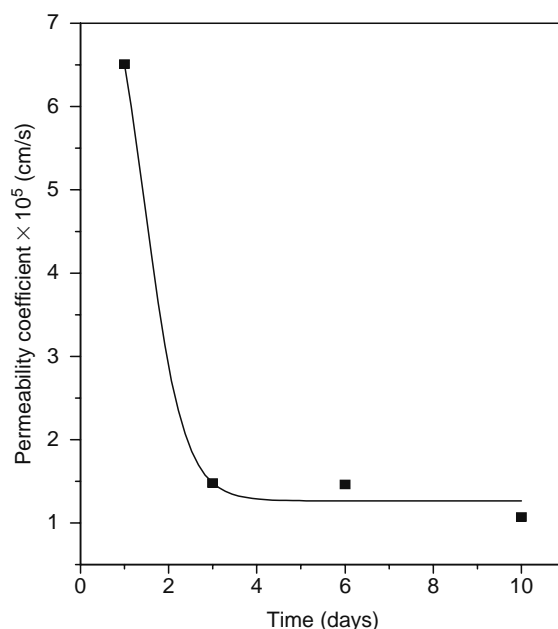


FIGURE 31.13 Structures of some plasticizers being used in the casting of PIM.

the flux in case of PIM is as high as 15 times higher than the corresponding SLM system. The carrier molecules crystallize inside the membrane and no new chemical bonds are formed within the polymer matrix [180]. CTA forms bulk of these types of membranes and is vulnerable to acid/alkali attack due to the possibility of hydrolysis of ester groups. It is understood that by increasing the chain length of the substituents the membranes could be made more acid/alkali resistant. Gardner et al. [181] attempted to vary the type of monomer by using cellulose acetate propionate (CAP), cellulose acetate butyrate (CAB), and cellulose tributyrates (CTB) and concluded that the flux decreases when the membranes were made more hydrophobic. The role of plasticizer is found to be extremely important in deciding the membrane stability and the overall flux of these membranes [182]. Figure 31.13 shows the structures of some of the plasticizers being used conventionally in PIMs. Sugiura [183] has used such membranes made from cellulose triacetate (CTA) with plasticizers such as 2-nitrophenyl octyl ether (NPOE) and tris(2-butoxyethyl) phosphate (TBEP), which enhance the membrane elasticity. He [184] has used  $\beta$ -isopropyl tropolone (HIPT) as the carrier trapped in these membranes for the transportation of lanthanide ions. Though there are many reports available [133,185–188] on the sorption/transport behavior of main group elements, very limited work is reported on the actinides using PIMs. Matsuoka et al. [189] have studied the uphill transport of uranium from nitric acid medium using a PIM containing CTA and TBP. In this case, TBP acted as both the carrier and the plasticizer, while  $\text{Na}_2\text{CO}_3$  was used as the stripping solution. An increase in U permeation (measured as  $D_1 = \Sigma([\text{UO}_2 - \text{X}_i]_{\text{TBP}}/[\text{UO}_2 - \text{X}_i]_{\text{HNO}_3})$ ) was observed with increasing aqueous phase acidity. On the other hand, the U release into the receiver phase (measured as  $D_2 = \Sigma([\text{UO}_2 - \text{X}_i]_{\text{TBP}}/[\text{UO}_2 - \text{X}_i]_{\text{Na}_2\text{CO}_3})$ ) decreased with increasing  $\text{Na}_2\text{CO}_3$  concentration. Significant loss of TBP into the aqueous phase was observed, which was similar to those observed in the case of SLMs. The loss of TBEP was also reported by an energy dispersive x-ray spectroscopic analysis [188]. No such loss of plasticizer is reported in the case of membranes made using NPOE as the plasticizer [190].

There are very limited reports available on the use of PIMs for the uptake/transport studies of trivalent actinides. There are some early reports, by Sugiura [191], on the transport behavior of trivalent lanthanides, which are considered as surrogates of the trivalent actinides. They have used NPOE as the plasticizer and investigated the effect of the alkyl chain length of some of polyoxyethylene *n*-alkyl ether on transport behavior of lanthanide ions and concluded that the flux decreased with an increase in the chain length. Bhattacharyya et al. have used a PIM containing TBP as the plasticizer and Cyanex-301 as the



**FIGURE 31.14** Effect of radiation dose (200 kGy) on the subsequent decrease in the  $\text{Am}^{3+}$  permeability coefficient as a function of time.

carrier for the transport of  $\text{Am}^{3+}$  from an aqueous feed containing 1 M  $\text{NaNO}_3$  [192]. They have observed insignificant transport of  $\text{Eu}^{3+}$  thereby indicating the feasibility of the selective separation of trivalent actinides from lanthanides. However, the major problem of the PIMs is their stability against radiation. The sharp decline in  $\text{Am}^{3+}$  transport rates (Figure 31.14) is a consequence of the significant damaging of the plasticized membranes by gamma radiation (Figure 31.15). Kusumocahyo et al. have demonstrated facile transport of  $\text{Ce}^{3+}$  across a PIM containing TODGA, which was found to be far more superior as a carrier compared to CMPO [133].

Sodaye et al. [193] have developed a scintillating PIM (S-PIM) containing HDEHP as the extractant, and PPO (diphenyl oxazole) and MSB (1,4-bis(2-methylstyryl)benzene) as fluors in plasticized CTA matrix for the assaying of actinide elements from aqueous samples (tap water and seawater). It was observed that the S-PIM could be made selective toward the tetravalent and hexavalent actinides at higher acidity ( $>0.25$  M), while the trivalent actinides could be trapped from pH solutions. The S-PIM could be made alpha-selective by pulse height discrimination. A linear response in a relatively wide range of radioactivity even in the presence of beta-emitting radionuclides such as  $^{154}\text{Eu}$  and  $^{147}\text{Pm}$  (Figure 31.16) underlines the applicability of this analytical method for the assaying of actinides.

### 31.4 SEPARATION OF RADIONUCLIDES FROM WASTE STREAMS

The use of membrane-based separation methods for gas separation is being routinely done in the industry. Reverse osmosis (RO) and ultrafiltration (UF) technologies are also very popular in treatment of industrial wastewater. Nevertheless, ultrafil-

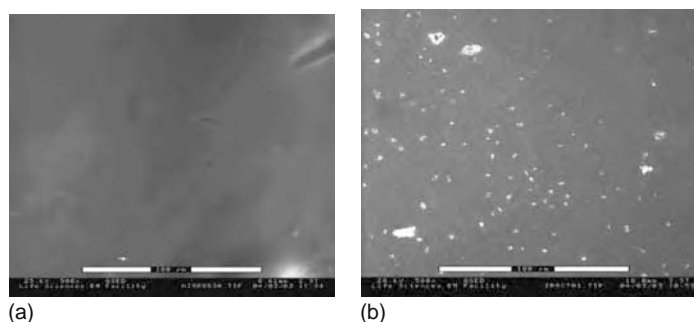


**FIGURE 31.15** Effect of radiation dose (200 kGy) on polymer inclusion membrane stability. (a) SEM pictures of unirradiated PIM; (b) SEM pictures of irradiated PIM.

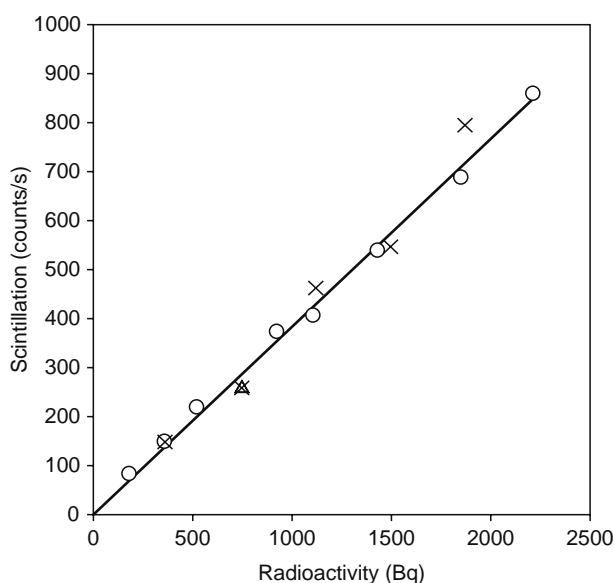


**FIGURE 31.16** Variation of  $\alpha$ -scintillation as a function of  $\alpha$ -activity of  $^{241}\text{Am}$  sorbed in the samples of S-PIM. The symbols ( $\Delta$ ), ( $\times$ ), and ( $\circ$ ) represent the S-PIM samples loaded with  $^{241}\text{Am}$ ,  $^{241}\text{Am}+^{147}\text{Pm}$ , and  $^{241}\text{Am}+^{154}\text{Eu}$ , respectively.  $\beta$ -activity = 1670 Bq; LLD = 4.5 V; amplifier gain = 50. Slope of the fit =  $0.386 \pm 0.013$ ; correlation coefficient = 0.994; S.D. = 29.44; number of data points = 13 (for  $^{241}\text{Am}+^{147}\text{Pm}$  and  $^{241}\text{Am}+^{154}\text{Eu}$ ). (Reproduced from Sodaye, S., Tripathi, R., Pandey, A.K., and Reddy, A.V.R., *Anal. Chim. Acta*, 514, 159, 2004. With permission.)

tration and reverse osmosis membrane technologies for treatment of radioactive liquid effluents are being applied in various nuclear plants [194]. These include the Nine Mile Point nuclear power plant, New York (RO), Comanche Peak nuclear power plant, Glen Rose, Texas (both RO and UF), Dresden nuclear power plant, Morris, Illinois (both RO and UF), Salem nuclear power plant, New Jersey (UF), AECL Chalk River Laboratory, Ontario, Canada (RO), etc. However, the application of liquid membrane-based separation methods for the removal of radionuclides from waste streams is at infancy stage and only a few reports are available. Americium removal from nuclear waste streams has been carried out at the Rocky Flats Plant (RFP) using SLM containing DHDECMP (dihexyl-*N,N*-diethyl carbamoylmethyl phosphonate) supported on Accurel polypropylene hollow fibers [195,196]. The waste from the Pu-purification cycle contained  $\text{HNO}_3$  concentration in the excess of 7 M, which was neutralized partially to yield >7 M nitrate and  $\sim 0.1$  M hydrogen ion concentration. More than 95% transport was observed into a stripping solution containing 0.25 M oxalic acid. The permeability coefficients were maximum up to  $1 \times 10^{-3}$  cm/s. Interference from Fe(III) was minimized by selective complexation.

Teramoto et al. [197] have used octyl(phenyl)-*N,N*-diisobutylcarbamoyl methyl phosphine oxide (CMPO) in diethyl benzene as a carrier and investigated the transport behavior to examine the feasibility of treating low-level radioactive wastewater using a stirred permeation cell. The transport rates were positively influenced by the addition of sodium citrate to the strip solution. For a simulated radioactive waste solution containing  $\sim 550$  ppm of Ce(III), at a treatment rate of  $1 \text{ m}^3$  per day (for >99.9% Ce removal) a membrane of  $3.3 \text{ m}^2$  surface area was recommended. Contaminated reactor pool water was reported to have been treated by SLM method, though the pertraction rates were very low [198]. Chiariasia has used liquid membranes containing three different commercially available long-chain aliphatic amines, namely, Primene JM-T (primary), Amberlite LA-2 (secondary), and triaurylamine (TLA, tertiary) for the treatment of synthetic Hanford site groundwater, where the strip solution was 1 M NaOH and *n*-dodecane was the diluent [199].

### 31.5 GRAFTED MEMBRANES FOR ACTINIDE SEPARATION

Uranium is present in the seawater as an extreme dilute solution. However, the total amount,  $4 \times 10^9$  tons, is ca. 1000-fold of the amount existing in the mines all over the world. Recovery of uranium from seawater is one of the most challenging problems in separation chemistry [200]. The separation methods using chelating resin [201] methods are limited by the low concentration of uranium ( $\sim 3$  ppb) and high concentration of other interfering ions. Kobuke et al. [202] have used a membrane-based separation method using a macrocyclic polycarboxylate ligand as the carrier. In the trial experiment, the feed contained uranyl acetate ( $3.3 \times 10^{-5}$  M) at pH 4–5, while the receiver phase contained 1.0 M  $\text{NaHCO}_3$ . The carrier (Figure 31.17) when modified with tri-*n*-octylmethyl ammonium chloride resulted in a significant enhancement in the transport rates. Selective transport rates of uranyl ion were observed in the presence of  $4.68 \times 10^{-1}$  M Na,  $5.3 \times 10^{-2}$  M Mg,  $1.0 \times 10^{-2}$  M K,

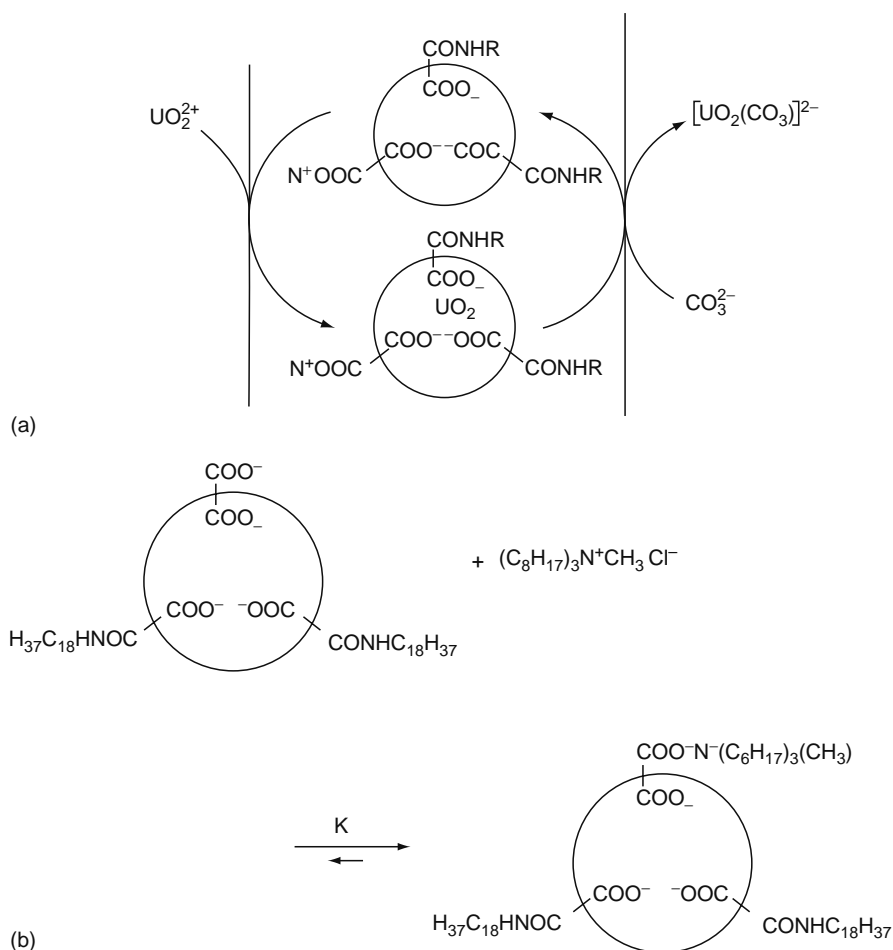


**FIGURE 31.17** Schemes of the highly selective ligand for uranium recovery from seawater. (a) The hexacarboxylate ligand; (b) after reaction with tri-octyl methyl ammonium chloride. (Reproduced from Tabushi, I., Kobuke, Y., Nakayama, N., Aoki, T., and Yashizawa, A., *Ind. Eng. Chem. Prod. Res. Dev.*, 23, 445, 1984. With permission.)

$1.0 \times 10^{-2}$  M Ca along with other ions. Out of these ions,  $\text{Ca}^{2+}$  was found to compete with the uranyl ion. However, due to favorable kinetic factors, a 300-fold increase in  $\text{Ca}^{2+}$  concentration decreased the uranyl ion transport rate only by 2.5 times.

Recently, the use of amidoxime grafted membranes for the recovery of uranium from seawater has shown great promise [203]. A research group at JAERI has proposed a method for the preparation of amidoxime (AO) grafted polyethylene and polypropylene membranes. The schematic of the grafting process is shown in Figure 31.18 wherein methacrylic acid (MAA) and 2-hydroxyethyl methacrylate were cogenerated with acetonitrile onto polyethylene fibers by radiation-induced graft polymerization. The amidoxime group density and water content determined the U sorption onto the membranes. The AN (acrylonitrile)/MAA ratio of 60:40 was found to be optimum and over a period of 20 days contact time showed a maximum uptake of 0.9 g of U/kg. The preconcentration of uranium from dilute solution is extremely slow and is possibly due to kinetic factors, which decide the slow diffusion of uranyl ion into the polymer matrix [204]. Sriram et al. [205] have also investigated the transport of uranyl ion across amidoxime incorporated polypropylene membranes. The feed consisted of 0.5 M  $\text{Na}_2\text{CO}_3$  solution at pH  $\sim 8$ , while the receiver phase was 0.1 M HCl. Using a 38% grafted membrane, they have observed 70% U sorption onto the PP-AN membrane. However, it was relatively difficult to leach out the sorbed U from the membrane ( $\sim 20\%$  with even 10 M HCl). On decreasing the percentage grafting to about 22%, 66% sorption was possible in 6 h and 70% stripping was possible using only 2 M HCl.

### 31.6 STABILITY OF LIQUID MEMBRANES

Despite the many advantages of liquid membranes, which include selectivity and ligand economy, they are not yet applied in industrial scale that is ascribed to their low stability [206]. The common reasons for the instability of liquid membranes are



constant and low solubility in water for the SLMs to be highly stable and permeable. Chiarizia [199] has investigated membrane stability using flat-sheet supports containing long-chain aliphatic amines as the carriers. The following order of stability was measured: tertiary > secondary > primary. This is the reverse order of the interfacial tension lowering at a water-*n*-dodecane interface. The water solubility of the amines also seems to play an important role in determining the membrane stability. This can be improved significantly by presaturating the aqueous phases with organic phase [214]. The performance of the SLM has also been reported to be affected by pore-blocking or fouling. Chiarizia [215] and Mohapatra et al. [63] observed such membrane fouling in their studies using amine and beta-diketone carriers, respectively. Nitrate · trilauryl amine salts and TOPO·HNO<sub>3</sub> complex are the causes for precipitation and subsequent blocking of pores of the membranes in these cases. There are several other mechanisms of membrane degradation and will not be discussed here. In general, the stability of SLM can be increased by increasing the membrane thickness, decreasing the pore size, and enhancing the lipophilicity of the carrier.

Polymer inclusion membranes are reported to have better stability as compared to the SLMs [177]. However, PIMs made from plasticizing agents such as TBP or TBEP (tris-butoxy ethyl phosphate), which have significant solubility in water can degrade with time. Salazar-Alvarez et al. [188] have shown using energy dispersive X-ray scans (EDS) that significant degradation of the membranes containing TBEP as the plasticizer do occur which could be suppressed by the addition of a small quantity of ethanol to the monomer plasticizer mixture prior to the membrane casting.

### 31.7 FUTURE PERSPECTIVES

Membranes have been used extensively for the separation of radionuclides from liquid effluents generated in different nuclear facilities such as fuel fabrication plant, fuel reprocessing plant, and nuclear reactors. These separations, based on size exclusion, are invariably pressure driven and are not useful for the recovery and purification of a specific element present in a mixture where solvent extraction has a distinct advantage. However, liquid membrane techniques offer the advantages of both solvent extraction as well as membrane separations. Liquid membrane separations provide an efficient and excellent opportunity to explore novel and exotic extractants such as calixarenes, crown ethers, thiophosphinic acids, diamides, and carbamoyl methyl phosphine oxides which are of vital interest to the separation scientists engaged in the development of new strategies for the safe management of high-level radioactive waste. Low inventory of the extractants needed for membrane-based techniques makes them attractive not only from cost considerations but also from the ease of disposal of secondary wastes.

Although ELM technique is quite efficient essentially due to the thinness of the membrane, large-scale application of this technique is limited in view of the difficulties encountered in the demulsification step needed for the recovery of the trapped metal ion. On the other hand, promise of the SLM technique has been demonstrated in the lab scale experiments. Large-scale applications of SLM require additional work in the area of stability/reusability of the membranes. Apart from the selective extraction, there is a need to develop the membranes that are compatible with the diluent/solvent mixture with respect to physical properties such as surface tension and viscosity. In addition, chemical/radiation environment of the feed/strip solution to which these membranes are subjected over long duration is an area of particular concern. Additional stability can be obtained by developing chemically grafted membranes.

Recently, emphasis has been shifted to hollow fiber contactors as well as hollow fiber nondispersive solvent extraction technique, which can have surface to volume ratio as high as 10,000 m<sup>2</sup>/m<sup>3</sup>. Hollow fiber modules that offer a continuous means for large-scale separation applications need to be designed and developed keeping in mind the nature of solvent, feed, and strippant. Apart from the design parameters, such as lumen length/diameter, shell length/diameter, and number of lumens, one needs to ensure the compatibility of materials used for making these modules. Nature of adhesives used and microstructures of the polymers used for making lumens also need attention.

### REFERENCES

1. Ho, W.S.W. and Sirkar, K.K., *Membrane Handbook*, Van Nostrand Reinhold, New York, 1992.
2. Boyadzhiev, L. and Lazarova, Z., in: *Membrane Separations Technology. Principles and Applications*. Noble, R.D. and Stern, S.A., Eds., Elsevier Science B.V., Amsterdam, The Netherlands, 1995, pp. 283–300.
3. Zhang, R., *Separation Techniques by Liquid Membranes*, Jiangxi Renmin Publications, Nanchang, 1984.
4. Izatt, R.M., Nilsen, B.L., Christensen, J.J., and Lamb, J.D., Membrane transport of ammonium and alkylammonium cations using macrocyclic carriers. *J. Membr. Sci.*, 1981, 9: 263–271.
5. Mutihac, L., Mutihac, R., Costantinescu, T., and Luca, C., The transport of amino acids by 18-crown-6 through liquid membranes. *J. Incl. Phen. Mol. Recog.*, 1994, 17: 45–51.
6. Mutihac, L., Mutihac, R., and Buschmann, H.-J., Liquid membrane transport of supramolecular complexes of some amines and amino acids with macrocyclic ligands. *J. Incl. Phen. Mol. Recog.*, 1995, 23: 167–174.
7. Duhart, A., Dozol, J.F., Rouquette, H., and Deratani, A., Selective removal of cesium from model nuclear waste solutions using a solid membrane composed of an unsymmetrical calix[4]arenebis-crown-6 bonded to an immobilized polysiloxane backbone. *J. Membr. Sci.*, 2001, 185: 145–155.

8. Ohto, K., Yanu, M., Inoue, K., Yamamoto, T., Goto, M., Nakashio, F., Shinkai, S., and Nagasaki, T., Solvent extraction of trivalent rare earth metal ions with carboxylate derivatives of calixarenes. *Anal. Sci.*, 1995, 11: 893–902.
9. Shinkai, S., Koreishi, H., Ueda, K., Arimura, T., and Manabe, O., Molecular design of calixarene-based uranophiles which exhibit remarkably high stability and selectivity. *J. Am. Chem. Soc.*, 1987, 109: 6371–6376.
10. Lemaire, M., Guy, A., Chomel, R., and Foos, J., Dicyclohexano-18-crown-6 ether: A new selective extractant for nuclear fuel reprocessing. *J. Chem. Soc., Chem. Commun.*, 1991, 1717: 1152–1154.
11. Gabelman, A. and Hwang, S.T., Hollow fiber membrane contactors. *J. Membr. Sci.*, 1999, 159: 61–106.
12. Ortiz, I., Galan, B., and Irabien, A., Membrane mass transport coefficient for the recovery of Cr(VI) in hollow fiber extraction and back-extraction modules. *J. Membr. Sci.*, 1996, 118: 213–221.
13. Yang, Z.F., Guha, A.K., and Sirkar, K.K., Novel membrane-based synergistic metal extraction and recovery processes. *Ind. Eng. Chem. Res.*, 1996, 35: 1383–1394.
14. Geist, A., Weigl, M., Muellich, U., and Gompper, K., Application of novel extractants for actinide (III)/lanthanide (III) separation in hollow-fibre modules. *Membr. Technol.*, 2003, 5: 5–7.
15. Schlosser, S. and Kossaczky, E., *Proceedings of the 5th International Congress CHISA'75, Pertraction through Liquid Membranes*, Prague, Czechoslovakia, 13.15, 1975.
16. Noble, R.D. and Way, J.D., *Liquid membrane: Theory and Applications*, ACS Symposium Series No. 347, American Chemical Society, Washington, DC, 1987.
17. Ruppert, M., Draxler, J., and Marr, R., Liquid-membrane-permeation and its experience in pilot plant and industrial scale. *Sep. Sci. Tech.*, 1988, 23: 1659–1666.
18. Bartsch, R.A., Way, J.D., Chrisstoffels, L.A.J., de Jong, F., and Reinholdt, D.N., in: *Chemical Separations with Liquid Membranes*, Bartsch, R.A. and Way, J.D., Eds., ACS Symposium Series Number 642, ACS, Washington, DC, 1996.
19. Sastre, A.M., Kumar, A., Shukla, J.P., and Singh, R.K., Improved techniques in liquid membrane separations: An overview. *Sep. Pur. Methods*, 1998, 27: 213–298.
20. Mohapatra, P.K. and Manchanda, V.K., Liquid membrane based separations of actinides and fission products. *Indian J. Chem.*, 2003, 42A: 2925–2939.
21. Noble, R.D. and Stern, S.A., *Membrane Separations Technology. Principles and Applications*, Elsevier, Amsterdam, The Netherlands, 1995.
22. Reusch, C.F. and Cussler, E.L., Selective membrane transport. *AIChE J.*, 1973, 19: 736–741.
23. Bacon, E. and Jung, L., Selective extraction and transport of mercury through a liquid membrane by macrocyclic ligands. Improvement in the transport efficiency and an approach to physiological systems. *J. Membr. Sci.*, 1985, 24: 185–199.
24. Melzner, D., Tilkowski, J., Mohrmann, A., Poppe, W., Halwachs, W., and Schuegerl, K., Selective extraction of metals by the liquid membrane technique. *Hydrometallurgy*, 1984, 13: 105–123.
25. Christensen, J.J., Lamb, J.D., Brown, P.R., Oscarson, J.L., and Izatt, R.M., Liquid membrane separation of metal cations using macrocyclic carriers. *Sep. Sci. Tech.*, 1981, 16: 1193–1215.
26. Bhattacharyya, A., Mohapatra, P.K., and Manchanda, V.K., in: *Advances in Nuclear and Radiochemistry*, Qaim, S.M. and Coenen, H.H., Eds., 6th International Conference on Nuclear and Radiochemistry (NRC-6), 29 August to 3 September 2004, Aachen, Germany, 2004, pp. 83–85.
27. Shukla, J.P. and Mishra, S.K., Carrier-mediated transport of uranyl ions across tributyl phosphate–dodecane liquid membranes. *J. Membr. Sci.*, 1991, 64: 93–102.
28. Katz, J.J., Seaborg, G.T., and Morss, L.R., *The Chemistry of the Actinide Elements*, 2nd ed., Chapman & Hall, New York, 1986.
29. Shukla, J.P. and Mishra, S.K., Carrier facilitated transport of plutonium(IV) through tributylphosphate/dodecane liquid membranes. *Ind. J. Chem., Sect. A*, 1995, 34: 778–786.
30. Mohapatra, P.K. and Manchanda, V.K., Role of ligand basicity and stereochemistry in the extraction of plutonium(IV)isoxazonates. *Radiochim. Acta*, 2003, 91: 705–711.
31. Oak, M.S., Nanda, D., and Maiti, B., *INSAC-2001: Proceedings of the Annual conference of Indian Nuclear Society Indore (India) 10–12 Oct 2001*; Venkat Raj, V., Sadasivan, S., Soni, H.C., Bapna, S.C., Rajan, A., Iyengar, T.S., and Pravin Kumar, M., Eds., Nuclear Technology—Challenges in the 21st Century. Vol. 1: Contributed papers Mumbai (India) Indian Nuclear Society, 2001, pp. 18–25.
32. Ma, M., He, D.S., Wang, Q.Y., and Xie, Q.J., Kinetics of europium(III) transport through a liquid membrane containing HEH(EHP) in kerosene. *Talanta*, 2001, 55: 1109–1117.
33. Ramakumar, J., Nayak, S.K., and Maiti, B., Transport of uranyl ion across a bulk liquid membrane using calixarene and synergistic agents as carriers. *J. Membr. Sci.*, 2002, 196: 203–210.
34. Martin, T.P. and Davies, G.A., Extraction of copper from dilute aqueous solutions using a liquid membrane process. *Hydrometallurgy*, 1977, 2: 315–334.
35. Marr, R. and Kopp, A., Liquid membrane technology—a survey of associated phenomena, transport mechanisms, and models. *Chem. Ing. Tech.*, 1980, 52: 399–410.
36. Schuegerl, K., Mohrmann, A., Gutknecht, W., and Hauertmann, H., Application of liquid membrane emulsion for recovery of metals from mining waste waters and zinc liquors. *Desalination*, 1985, 53: 197–215.
37. El-Reefy, S.A., El-Sherif, E.A., and Aly, H.F., Recovery of <sup>234</sup>Th from natural uranium using liquid emulsion membrane based on HDEHP-HCl system. *J. Radioanal. Nucl. Chem.*, 1996, 207: 129–136.
38. El-sherif, E.A.E.E., Studies on the separation of some radioactive elements by liquid membrane. PhD thesis, Ain Shams University, Egypt, 1994.
39. Dickens, N., Davies, G.A., and Rose, M., *Proceedings of the Symposium on Liquid-Liquid Extraction Science*, Extraction '84, 1984: 69–81.

40. El-Reefy, S.A., El-Sourougy, M.R., El-Sherif, E.A., and Aly, H.F., Europium permeation and separation from Americium using liquid emulsion membrane. *Anal. Sci.*, 1995, 11: 329–332.
41. Akiba, K., Kanno, T., and Takahashi, T., Extraction of the uranium to the emulsification type liquid membrane and the collection with deviation from emulsification. *Tohoku Daigaku Senko Seiren Kenkyusho Iho*, 1984, 40: 1–10.
42. Suripto, A., Yuwono, I., Badruzzaman, M., Nasution, H., Kusnowo, A., and Amini, S.S., *Proceedings of the Second Scientific Presentation on Nuclear Fuel Cycle; Nuclear Fuel Element Development Centre*, National Atomic Energy Agency, 1998: 89–94.
43. Zhou, Z., Du, H., Wang, H., and Luo, J., *J. Nucl. Radiochem.*, 1994, 16: 75.
44. Macasek, F., Rajec, P., Kopunec, R., and Mikulaj, V., Membrane extraction in preconcentration of some uranium fission products. *Solv. Extr. Ion Exch.*, 1984, 2: 227–252.
45. Kulkarni, P.S., Mukhopadhyay, S., Bellary, M.P., and Ghosh, S.K., Studies on membrane stability and recovery of uranium (VI) from aqueous solutions using a liquid emulsion membrane process. *Hydrometallurgy*, 2002, 64: 49–58.
46. Han, J., Sun, G., Bao, B., and Sun, S., Study on the structure of *N,N*-dialkyl long chain alkylamides and their extraction performance (2). Extraction of uranium (VI) and thorium(IV) with *N,N*-dibutylalkylamides. *J. Nucl. Radiochem.*, 1999, 21: 119–123.
47. Akiba, K., Takahashi, T., and Kanno, T., Extraction of uranium(VI) by emulsion liquid membrane containing 5,8-diethyl-7-hydroxy-6-dodecanone oxime. *Bull. Chem. Soc. Jpn.*, 1984, 57: 2618–2621.
48. Han, J., Sun, G., Bao, B., and Sun, S., Transfer of uranium (VI) through emulsion liquid membrane with *N,N*-dibutyloctanamide as a carrier. *Nucl. Sci. Tech.*, 1998, 9: 150–152.
49. Hirato, T., Kishigami, I., Awakura, Y., and Majima, H., Concentration of uranyl sulfate solution by an emulsion-type liquid membrane process. *Hydrometallurgy*, 1991, 26: 19–33.
50. Hayworth, H.C., Ho, W.S., Burnes, W.A. Jr., and Li, N.N., Extraction of uranium from wet process phosphoric acid by liquid membrane. *Sep. Sci. Tech.*, 1983, 18: 493–521.
51. Bock, J., Klein, R.R., Valint, P.L., and Ho, W.S., *Sulfuric/Phosphoric Acid Plant Operations*, AIChE, New York, 1982, pp. 175–183.
52. Lee, C.J., Wang, -S.S., and Wang, -S.G., Extraction of trivalent europium via emulsion liquid membrane containing PC-88A as mobile carrier. *Ind. Eng. Chem. Res.*, 1994, 33: 1556–1564.
53. Nakamura, S., Ohashi, S., and Akiba, K., Transport of uranium(VI) through a liquid membrane impregnated with phosphonic acid ester. *Buns. Kagaku Jpn. Anal.*, 1991, 40: 829–834.
54. Kedari, C.S., Pandit, S.S., Misra, S.K., Jambunathan, U., and Ramanujam, A., *Proceedings of the Nuclear and Radiochemistry (NUCAR 2001)*, Ramakumar, K.L., Vaidya, V.N., Kadam, R.M., and Purushotham, D.S.C., Eds., 2001, pp. 206–207.
55. El-Reefy, S.A., Selim, Y.T., and Aly, H.F., Equilibrium and kinetic studies on the separation of uranium and thorium from nitric acid medium by liquid emulsion membrane based on trioctylphosphine oxide extractant. *Anal. Sci.*, 1997, 13: 333–338.
56. Kataoka, T., Nishiki, T., Tamura, Y., and Ueyama, K., Mechanism of chloride ion transport through diaphragm type liquid membrane. *J. Chem. Eng. Jpn.*, 1980, 13: 35–40.
57. Komasaawa, I., Otake, T., and Yamashita, T., Mechanism and kinetics of copper permeation through a supported liquid membrane containing a hydroxyoxime as a mobile carrier. *Ind. Eng. Chem. Fund.*, 1983, 22: 127–131.
58. Gasparini, G.M., Grossi, G.G., Casarci, M., and D'Andrea, A., The recovery of plutonium by means of solid supported liquid membrane. *Proceedings of the ISEC '83*, Denver, Colorado, Solid Supported Liquid Membranes, II, 1983, pp. 395–396.
59. Lee, K.H., Evans, D.F., and Cussler, E.L., Selective copper recovery with two types of liquid membranes. *AIChE J.*, 1978, 24: 860–868.
60. Akiba, K. and Hashimoto, H., Extraction of uranium by a supported liquid membrane containing mobile carrier. *Talanta*, 1985, 32: 824–826.
61. Akiba, K. and Ohashi, K., Concentration of uranium(VI) on long chain 8-quinolinol liquid membrane. *Buns. Kagaku Jpn. Anal.*, 1987, 36: 707–711.
62. Seguiria, M., Kikkawa, M., and Urita, S., Carrier-mediated transport of rare earth ions through cellulose triacetate membranes. *J. Membr. Sci.*, 1989, 42: 47–55.
63. Mohapatra, P.K., Pandey, A.K., and Manchanda, V.K., Facilitated transport of americium(III) from nitric acid media using 3-phenyl-4-benzoyl-5-isoxazolone and tri-*n*-octyl phosphine oxide in dodecane as the carrier. *Radiochim. Acta*, 1999, 84: 147–151.
64. Nakamura, S., Ohashi, S., and Akiba, K., Permeation behaviour of europium through versatic acid liquid membrane. *Sep. Sci. Tech.*, 1992, 27: 741–752.
65. Nakamura, S., Ohashi, S., and Akiba, K., Effects of complexing agents on transport of lanthanoid elements across versatic acid liquid membrane. *Sep. Sci. Tech.*, 1992, 27: 863–873.
66. Chitra, K.R., Gaikwad, A.G., Surender, G.D., and Damodaran, A.D., Permeation of europium through immobilised supported liquid membrane. *Ind. J. Chem. Tech.*, 1996, 3: 77–86.
67. Huang, C.-T. and Huang, T.-C., Kinetics of the coupled transport of uranium(VI) across supported liquid membranes containing bis (2-ethylhexyl)phosphoric acid as a mobile carrier. *Ind. Eng. Chem. Res.*, 1988, 27: 1681–1685.
68. Mikheeva, M.N., Novicov, P., Myasoedov, B.F., and Tikhomirov, S.V., Kinetics of americium(VI) mass transfer through solid supported liquid membrane with HDEHP. *J. Radioanal. Nucl. Chem.*, 1994, 185: 265–271.
69. Danesi, P.R., Horwitz, E.P., and Rickert, P., Transport of  $\text{Eu}^{3+}$  through a bis(2-ethylhexyl)phosphoric acid/*n*-dodecane solid supported liquid membrane. *Sep. Sci. Tech.*, 1982, 17: 1183–1192.
70. Danesi, P.R. and Reichley-Yinger, L., Origin and significance of the deviations from a pseudo first order rate law in the coupled transport of metal species through supported liquid membrane. *J. Membr. Sci.*, 1986, 29: 195–206.
71. Kopunec, R. and Thang, N.M., Carrier-mediated transport of rare earth elements through liquid membranes. III. Transport of Sc, Y, Ce, Eu, Gd, Tm, Yb through supported liquid membrane containing DEHPA. *J. Radioanal. Nucl. Chem.*, 1993, 170: 51–66.

72. Danesi, P.R. and Cianetti, C., Permeation of metal ions through a series of two complementary supported liquid membranes. *J. Membr. Sci.*, 1984, 20: 201–213.
73. Hurst, F.J., Crouse, D.J., and Brown, K.B., Recovery of uranium from wet-process phosphoric acid. *Ind. Eng. Chem. Proc. Des. Dev.*, 1972, 11: 122–128.
74. Hurst, F.J. and Crouse, D.J., Recovery of uranium from wet-process phosphoric acid by extraction with octylphenylphosphoric acid. *Ind. Eng. Chem. Proc. Des. Dev.*, 1974, 13: 286–291.
75. Hayworth, H.C., Advantages of liquid membrane technology for the extraction of uranium from wet process phosphoric acid. 2nd Chemical Congress of the North American Continent, Division of Fertilizer and Soil Chemistry, 1980.
76. Bock, J. and Valint, P.L. Jr., Uranium from wet-process phosphoric acid—a liquid membrane approach. 2nd Chemical Congress of the North American Continent, Division of Fertilizer and Soil Chemistry, 1980.
77. Sifniades, S., Largman, T., Tunick, A.A., and Koff, F.W., Recovery of uranium from phosphoric acid by means of supported liquid membranes. *Hydrometallurgy*, 1981, 7: 201–212.
78. Nakamura, S. and Akiba, K., Transport of europium(III) through supported liquid membrane containing diisodecylphosphoric acid. *Sep. Sci. Tech.*, 1989, 24: 673–683.
79. Chiarizia, R. and Horwitz, E.P., Study of uranium removal from ground water by supported liquid membrane. *Solv. Extr. Ion Exch.*, 1990, 8: 65–98.
80. Chiarizia, R., Horwitz, E.P., Rickert, P.G., and Hodgson, K.M., Application of supported liquid membrane for removal of uranium from ground water. *Sep. Sci. Tech.*, 1990, 25: 1571–1586.
81. Nakamura, S., Sato, A., and Akiba, K., Application of europium(III) extraction with organophosphinic acid to liquid membrane transport. *J. Radioanal. Nucl. Chem.*, 1994, 178: 63–71.
82. Bhattacharyya, A., Mohapatra, P.K., and Manchanda, V.K., Separation of trivalent actinides and lanthanides using a flat sheet supported liquid membrane containing Cyanex-301 as the carrier. *Sep. Purif. Tech.*, 2006, 50: 278–281.
83. Hoshi, H., Tsuyoshi, A., and Akiba, K., Separation of americium from europium using liquid membrane impregnated with organo-dithiophosphinic acid. *J. Radioanal. Nucl. Chem.*, 2000, 243: 621–624.
84. Akiba, K. and Kanno, T., Transport of uranium(VI) through a supported liquid membrane containing LIX63. *Sep. Sci. Tech.*, 1983, 18: 831–841.
85. Chaudry, M.A., Islam, N.U., and Mohammad, D., Uranium(VI) transport through tri-n-butylphosphate kerosene oil liquid membrane supported in polypropylene film. *J. Radioanal. Nucl. Chem.*, 1987, 109: 11–22.
86. Chaudry, M.A. and Ahmad, I., Nitric acid transport across TBP-kerosene oil supported liquid membranes. *J. Radioanal. Nucl. Chem.*, 1991, 148: 15–26.
87. Smit, J.J., Buchalter, E.M., and Craig, W.M., The extraction of uranyl nitrate by the supported liquid membrane method. *S. Afr. J. Sci.*, 1988, 84: 452–455.
88. Serebrennikova, N.V., Kukushkina, I.I., and Plotnikova, N.V., A uranyl-selective membrane electrode based on a mixture of uranyl di-2-ethylhexyl phosphate and tributyl phosphate in benzene. *Zhur. Anal. Khim. USSR*, 1982, 37: 645–649.
89. Mikhajlov, V.A., Osipov, V.V., and Serebrennikova, N.V., Ion-selective electrode based on uranyl di-2-ethylhexylphosphate. *Zhur. Anal. Khim USSR*, 1978, 33: 1154–1158.
90. Pathak, P.N., Kumbhare, L.B., and Manchanda, V.K., Structural effects in *N,N*-dialkyl amides on their extraction behaviour towards uranium and thorium. *Solv. Extr. Ion Exch.*, 2001, 19: 105–126.
91. Suresh, A., Jayanthi, N., Srinivasan, T.G., and Vasudeva Rao, P.R., *Proceedings of Nuclear and Radiochemistry Symposium (NUCAR-95)*, Kulkarni, S.G., Manohar, S.B., and Sood, D.D., Eds., 1995, pp. 124–125.
92. Shukla, J.P., Kedari, C.S., and Dharmapurikar, G.R., Selective permeation of plutonium(IV) through a supported liquid membrane containing tri-*iso*-amyl phosphate as an ionophore. *J. Nucl. Sci. Tech.*, 1998, 35: 419–424.
93. Dharmapurikar, G.R., Kedari, C.S., and Shukla, J.P., *Proceedings of Nuclear and Radiochemistry Symposium (NUCAR 97)*, Ramakumar, K.L., Pujari, P.K., Swarup, R., and Sood, D.D., Eds., 1997, pp. 164–165.
94. Akiba, K. and Hashimoto, H., Uranium(VI) transport through liquid membrane supported with trioctylphosphine oxide. *Anal. Sci.*, 1986, 2: 541–544.
95. Bock, J. and Vallnt, P.L., Uranium extraction from wet process phosphoric acid. A liquid membrane approach. *Ind. Eng. Chem. Fund.*, 1982, 21: 417–422.
96. Sonawane, J.V., Sawant, S.R., Kumar, A., Venugopalan, A.K., Singh, R.K., Bajpai, D.D., and Mathur, J.N., *Proceedings of National Symposium on Nuclear and Radiochemistry (NUCAR 2001)*, Ramakumar, K.L., Vaidya, V.N., Kadam, R.M., and Purushotham, D.S.C., Eds., 2001, pp. 144–145.
97. Sawant, S.R., Sonawane, J.V., Pabby, A.K., Venugopalan, A.K., Dey, P.K., and Venkataramani, B., Transport of Pu(IV) across supported liquid membrane from nitric acid medium using cyanex 923 as the mobile phase. *Ind. J. Chem. Tech.*, 2004, 11: 548–554.
98. Kitatsuji, Y., Aoyagi, H., Yoshida, Z., and Kihara, S., Plutonium(III)-ion selective electrode of liquid membrane type using multidentate phosphine oxide ionophore. *Anal. Chim. Acta*, 1999, 387: 181–187.
99. Cristau, H.J., Virieux, D., Dozol, J.F., and Rouquette, H., Selective extraction of actinides by polyphosphine polyoxides through supported liquid membrane. *J. Radioanal. Nucl. Chem.*, 1999, 241: 543–547.
100. Muscatello, A.C., Horwitz, E.P., Kalina, D.G., and Kaplan, L., The extraction of Am(III) and Eu(III) from aqueous ammonium thiocyanate by dihexyl-*N,N*-diethyl carbamoyl methyl phosphonate and related compounds. *Sep. Sci. Tech.*, 1982, 17: 859–875.
101. Horwitz, E.P. and Kalina, D.G., The extraction of Am(III) from nitric acid by octyl(phenyl)-*N,N*-diisobutyl carbamoyl methyl phosphine oxide (CMPO)—tri butyl phosphate mixtures. *Solv. Extr. Ion Exch.*, 1984, 2: 179–200.

102. Horwitz, E.P., Kalina, D.G., Diamond, H., Vandegrift, G.F., and Schulz, W.W., The TRUEX process—a process for the extraction of the transuranic elements from nitric acid wastes utilizing modified PUREX solvent. *Solv. Extr. Ion Exch.*, 1985, 3: 75–109.
103. Mathur, J.N., Murali, M.S., Ruikar, P.B., Nagar, M.S., Sipahimalani, A.T., Bauri, A.K., and Banerji, A., Degradation, cleanup and reusability of octyl phenyl-*N,N*-diisobutyl carbamoyl methyl phosphine oxide during partitioning of minor actinides from high level waste (HLW) solutions. *Sep. Sci. Tech.*, 1998, 33: 2179–2196.
104. Nakamura, S. and Akiba, K., Transport of europium through supported liquid membrane containing dihexyl-*N,N*-diethyl carbamoyl methyl phosphonate. *Sep. Sci. Tech.*, 1989, 24: 1317–1328.
105. Akiba, K. and Nakamura, S., Transport of metal species through supported liquid membrane containing dihexyl-*N,N*-diethylcarbamoyl methylenephosphonate. in: *Chemical Aspects of Down Stream for Thorium Fuel Cycle*, Suzuki, S., Mitsugashira, T., Hara, M., Satoh, I., and Shiokawa, Y., Eds., Atomic Energy Society of Japan. Tokyo (Japan), 1987, pp. 85–90.
106. Chiarizia, R. and Danesi, P.R., Double liquid membrane system for the removal of actinides and lanthanides from acidic nuclear wastes. *Sep. Sci. Technol.*, 1987, 22: 641–659.
107. Danesi, P.R., Chiarizia, R., Rickert, P., and Horwitz, E.P., Separation of actinides and lanthanides from acidic nuclear wastes by supported liquid membrane. *Solv. Extr. Ion Exch.*, 1985, 3: 111–147.
108. Chiarizia, R., Danesi, P.R., Horwitz, E.P., and Tse, P.K., International Solvent Extraction Conference. ISEC'88. Moscow (USSR), 1988, Vol. 4, pp. 10–13.
109. Ramanujam, A., Dhama, P.S., Gopalakrishnan, V., Dudwadkar, N.L., Chitnis, R.R., and Mathur, J.N., Partitioning of actinides from high level waste of PUREX origin using octylphenyl-*N,N*-diisobutyl carbamoyl methyl phosphine oxide (CMPO) base supported liquid membrane. *Sep. Sci. Tech.*, 1999, 34: 1717–1728.
110. Danesi, P.R., Horwitz, E.P., and Rickert, P.G., Rate and mechanism of facilitated americium(III) transport through a supported liquid membrane containing a bifunctional organophosphorous mobile carrier. *J. Phys. Chem.*, 1983, 87: 4708–4715.
111. Teramoto, M., Fu, S.S., Takatani, K., Ohnishi, N., Maki, T., Fukui, T., and Arai, K., Treatment of simulated low level radioactive wastewater by supported liquid membranes: Uphill transport of Ce(III) using CMPO as carrier. *Sep. Purif. Tech.*, 1999, 18: 57–69.
112. Gupta, K.K., Manchanda, V.K., Sriram, S., Thomas, G., Kulkarni, P.G., and Singh, R.K., Third phase formation in the extraction of uranyl nitrate by *N,N*-dialkyl aliphatic amides. *Solv. Extr. Ion Exch.*, 2000, 18: 421–439.
113. Ruikar, P.B., Physicochemical studies on some actinide complexes. PhD thesis, University of Bombay, 1992.
114. Nigond, L., Musikas, C., and Cuilerdier, C., Extraction by *N,N,N',N'*-tetraalkyl-2-alkylpropane-1,3-diamides II. U(VI) and Pu(IV). *Solv. Extr. Ion Exch.*, 1994, 12: 297–323.
115. Mahajan, G.R., Prabhu, D.R., Manchanda, V.K., and Badheka, L.P., Substituted malonamides as extractants for partitioning of actinides from nuclear waste solutions. *Waste Manag.*, 1998, 18: 125–133.
116. Sasaki, Y., Sugo, Y., Suzuki, S., and Tachimori, S., The novel extractant, diglycolamides, for the extraction of lanthanides and actinides in  $\text{HNO}_3$ -*n*-dodecane system. *Solv. Extr. Ion Exch.*, 2001, 19: 91–103.
117. Ansari, S.A., Pathak, P.N., Manchanda, V.K., Hussain, M., Prasad, A.K., and Parmar, V.S., *N,N,N',N'*-tetraoctyl diglycolamide (TODGA): A promising extractant for actinide-partitioning from high-level waste (HLW). *Solv. Extr. Ion Exch.*, 2005, 23: 463–479.
118. Patil, C.B., Mohapatra, P.K., Lakshmi, D.S., Venugopalan, A.K., Manchanda, V.K., and Mohan, D., Paper presented at the 22nd Annual Conference of the Indian Council of Chemists, IIT Roorkee, Roorkee, India, October 17–19, 2003.
119. Shukla, J.P., Sonawane, J.V., Kumar, A., and Singh, R.K., *Proceedings of the Nuclear and Radiochemistry Symposium (NUCAR 97)*, Ramakumar, K.L., Pujari, P.K., Swarup, R., and Sood, D.D., Eds., 1997, pp. 192–193.
120. Shailesh, S., Pthak, P.N., and Manchanda, V.K., *Proceedings of the Nuclear and Radiochemistry Symposium (NUCAR 05)*, Chander, K., Acharya, R., Tomar, B.S., and Venugopal, V., Eds., Amritsar, India, 2005, pp. 273–274.
121. Sriram, S., Mohapatra, P.K., Pandey, A.K., Manchanda, V.K., and Badheka, L.P., Facilitated transport of americium(III) from nitric acid media using dimethyldibutyltetradecyl-1,3-malonamide. *J. Membr. Sci.*, 2000, 177: 163–175.
122. Sriram, S. and Manchanda, V.K., *Proceedings of Nuclear and Radiochemistry Symposium, (NUCAR-2001)*, Ramakumar, K.L., Kadam, R.M., Vaidya, V.N., and Purushottam, D.S.C., Eds., 2001, pp. 310–311.
123. Sriram, S. and Manchanda, V.K., Transport of metal ions across a supported liquid membrane (SLM) using dimethyldibutyl-tetradecyl-1,3-malonamide (DMDBDMA) as the carrier. *Solv. Extr. Ion Exch.*, 2002, 20: 97–114.
124. Marcus, Y., Diluent effects in solvent extraction. *Solv. Extr. Ion Exch.*, 1989, 7: 567–575.
125. Horwitz, E.P., Martin, K.A., and Diamond, H., The influence of the diluent on the distribution behaviour of octyl(phenyl)-*N,N*-diisobutyl carbamoyl methyl phosphine oxide (CMPO). *Solv. Extr. Ion Exch.*, 1988, 6: 859–888.
126. Marcus, Y., The properties of organic liquids that are relevant to their use as solvating solvents. *Chem. Soc. Rev.*, 1993, 22: 409–416.
127. Lide, D.R., *CRC Handbook of Chemistry and Physics*, CRC Press, Boca Raton, LO, 1999–2000.
128. Barton, A.F.M., *CRC Handbook of Chemistry and Physics*, CRC Press, Boca Raton, LO, 1999–2000.
129. Charpentier, J.C., *Advances in Chemical Engineering*, Vol. 11. Drew, T.B., Coker, G.R., Oopes, J.W. Jr., and Vemeulin, T., Eds., Academic Press, London, 1983, Ch. 1.
130. Kamal, M.R. and Canjar, L.N., Diffusion coefficients. *Chem. Eng. Prog.*, 1966, 62: 82–86.
131. Elhassadi, A.A. and Do, D.D., Effects of a carrier and its diluent on the transport of metals across supported liquid membrane. II. Viscosity effect. *Sep. Sci. Tech.*, 1986, 21: 285–297.
132. Ansari, S.A., Mohapatra, P.K., Prabhu, D.R., and Manchanda, V.K., Transport of americium(III) through a supported liquid membrane containing *N,N,N',N'*-tetraoctyl-3-oxapentane diamide (TODGA) in *n*-dodecane as the carrier. *J. Membr. Sci.*, 2006, 282: 133–141.
133. Kusumocahyo, S.P., Kanamori, T., Sumaru, K., Aomatsu, S., Matsuyama, H., Teramoto, M., and Shinbo, T., Development of polymer inclusion membranes based on cellulose triacetate: Carrier-mediated transport of cerium(III). *J. Membr. Sci.*, 2004, 244: 251–257.

134. Strezelbicki, J. and Bartsch, R.A., Transport of alkali metal cations across liquid membranes by crown ether carboxylic acids. *J. Membr. Sci.*, 1982, 10: 35–47.
135. Christensen, J.J., Lamb, J.D., Brown, P.R., Oscarson, J.L., and Izatt, R.M., Liquid membrane separations of metal cations using macrocyclic carriers. *Sep. Sci. Tech.*, 1981, 16: 1193–1215.
136. Izatt, R.M., McBride, D.W., Brown, P.R., Lamb, J.D., and Christensen, J.J., The influence of halocarbon solvent on macrocycle-mediated cation transport through liquid membranes. *J. Membr. Sci.*, 1986, 28: 69–76.
137. Shukla, J.P., Kumar, A., and Singh, R.K., Effect of solvent type on neutral macrocycle facilitated transport of uranyl ions across supported liquid membranes using dicyclohexano 18-crown-6 as carrier. *Radiochim. Acta*, 1992, 57: 185–194.
138. Shukla, J.P., Kumar, A., and Singh, R.K., Macrocycle mediated selective transport of plutonium(IV) nitrate through bulk liquid and supported liquid membrane using dicyclohexano 18-crown-6 as mobile carrier. *Sep. Sci. Tech.*, 1992, 27: 447–465.
139. Kumar, A., Singh, R.K., Bajpai, D.D., and Shukla, J.P., Some aspects of the extraction-separation of actinides by macrocyclic crown compounds, BARC/1994/E/006.
140. Kumar, A., Singh, R.K., and Shukla, J.P., Macrocycle facilitated transport of uranyl ions across supported liquid membranes using dicyclohexano 18-crown-6 as mobile carrier. *Ind. J. Chem.*, 1992, 31A: 373–375.
141. Kumar, A., Singh, R.K., Bajpai, D.D., and Shukla, J.P., *National Conference of Indian Membrane Society on Recent Trends in Membrane Science and Technology*. Bombay, India, 1993, pp. 75–83.
142. Shukla, J.P., Kumar, A., and Singh, R.K., Influence of gamma-irradiation on extraction and cation transport of uranium(VI) and plutonium(IV) by dicyclohexano 18-crown-6. *J. Nucl. Sci. Tech.*, 1994, 31: 1066–1072.
143. Brown, P.R., Izatt, R.M., Christensen, J.J., and Lamb, J.D., Transport of  $\text{Eu}^{2+}$  in a  $\text{H}_2\text{O}-\text{CHCl}_3-\text{H}_2\text{O}$  liquid membrane system containing the macrocyclic polyether 18-crown-6. *J. Membr. Sci.*, 1983, 13: 85–88.
144. Zhu, C.Y. and Izatt, R.M., Macrocycle-mediated separation of  $\text{Eu}^{2+}$  from trivalent lanthanide cations in a modified thin-sheet-supported liquid membrane system. *J. Membr. Sci.*, 1990, 50: 319–324.
145. Tang, J. and Wai, C.M., Transport of trivalent lanthanides through a surfactant membrane containing an ionizable macrocyclic polyether. *J. Membr. Sci.*, 1989, 46: 349–356.
146. Jung, J., Cho, Y.H., and Hahn, P.S., Scavenging of  $\text{UO}_2^{2+}$  using 4-sulphonic calix[6]arene in the presence of goethite. *J. Radioanal. Nucl. Chem.*, 1999, 241: 635–639.
147. Tabusi, I., Kobuke, Y., Nishiya, T., Kishimoto, M., and Ohara, E., Macrocyclic hexacarboxylic acid. A highly selective host for uranyl ion. *J. Am. Chem. Soc.*, 1980, 102: 5947–5948.
148. Lee, C.W., Cho, Y.H., Lee, M.H., Choi, K.S., Hong, K.H., Sin, H.S., Kim, M.K., and Pak, J.H., Korea Atomic Energy Research Institute, Report KAERI/RR-2037/99.
149. Kondo, H., Nishida, M., and Yoshida, I., Highly selective transport of a uranyl ion through a liquid membrane containing a lipophilic ion-associate of methyltriocetylammmonium and hydroxycalix[n]arene-*p*-sulfonates ( $n = 6, 8$ ) as metal carriers. *Anal. Sci.*, 2002, 18: 113–118.
150. Boerrigter, H., Veltkamp, A.C., Verboom, W., and Reinhoudt, D.N., *Proceedings of the International Conference on Separation of Ionic Solutes (SIS'97)*. Macasek, F. and Kuruc, J., Eds., 1997, 7: 38–39.
151. Boerrigter, H., Verboom, W., and Reinhoudt, D.N., Ligands for  $\text{Eu}^{\text{III}}$ ,  $\text{Fe}^{\text{III}}$ ,  $\text{Sr}^{\text{II}}$ , and  $\text{UO}_2^{\text{II}}$  based on CMPO-functionalized resorcinarene cavitands; synthesis and extraction, *Liebigs Ann./Recueil. Liebigs Ann.*, 1997, 2247–2255.
152. Duhart, A., PhD thesis, Universitaire Montpellier, France, 1998.
153. Dozol, J.F., Rouquette, H., Bohmer, V., Gruttner, G., Jakobi, R.A., Kraft, D., and Vogt, W., FR Patent Document 2729958/A/; FR patent application 9501158.
154. Chaudry, M.A. and Mohammad, D., Uranyl ion transport through tri-*n*-octylamine-xylene based supported liquid membranes. *J. Radioanal. Nucl. Chem.*, 1987, 111: 211–231.
155. Sonawane, J.V., Kumar, A., Sawant, S.R., Singh, R.K., Bajpai, D.D., and Shukla, J.P., Bhabha Atomic Research Centre, Report BARC-1999/E/003.
156. Shukla, J.P., Sonawane, J.V., Kumar, A., and Singh, R.K., Amine facilitated up-hill transport of plutonium(IV) cations across an immobilized liquid membrane. *Ind. J. Chem. Tech.*, 1996, 3: 145–148.
157. Lakshmi, D.S., Mohapatra, P.K., Mohan, D., and Manchanda, V.K., *Proceedings of Nuclear and Radiochemistry Symposium (NUCAR-2003)*. Tomar, B.S., Saxena, M.K., Manchanda, V.K., and Manohar, S.B., Eds., 2003, pp. 209–210.
158. Lakshmi, D.S., Mohapatra, P.K., Mohan, D., and Manchanda, V.K., Uranium transport using a PTFE flat-sheet membrane containing alamine 336 in toluene as the carrier, *Desalination*, 2004, 163: 13–18.
159. Subba Rao, R.V., Natarajan, R., and Vasudeva Rao, P.R., *Proceedings of Nuclear and Radiochemistry Symposium, (NUCAR 99)*, Purushotham, D.S.C., Reddy, A.V.R., Manohar, S.B., and Rama Rao, G.A., Eds., 1999, pp. 189–190.
160. Subba Rao, R.V., Siva Kumar, P., Natarajan, R., and Vasudeva Rao, P.R., *National Symposium on Nuclear and Radiochemistry (NUCAR 2001)*, Ramakumar, K.L., Vaidya, V.N., Kadam, R.M., and Purushotham, D.S.C., Eds., 2001, pp. 266–267.
161. Choppin, G.R. and Morgenstern, A., Radionuclide Separations in Radioactive Waste Disposal. *J. Radioanal. Nucl. Chem.*, 2000, 243: 45–51.
162. Kathios, D.J., Jarvinen, G.D., Yarbrow, S.L., and Smith, B.F., A preliminary evaluation of microporous hollow fiber membrane modules for the liquid–liquid extraction of actinides. *J. Membr. Sci.*, 1994, 97: 251–261.
163. Rathore, N.S., Sonawane, J.V., Gupta, S.K., Pabby, A.K., Venugopalan, A.K., Changrani, R.D., and Dey, P.K., Separation of uranium and plutonium from aqueous acidic wastes using a hollow fiber supported liquid membrane. *Sep. Sci. Tech.*, 2004, 39: 1295–1319.
164. Rathore, N.S., Sonawane, J.V., Kumar, A., Venugopalan, A.K., Singh, R.K., Bajpai, D.D., and Shukla, J.P., Hollow fiber supported liquid membrane: A novel technique for separation and recovery of plutonium from aqueous acidic wastes. *J. Membr. Sci.*, 2001, 189: 119–128.

165. Patil, C.B., Mohapatra, P.K., Venugopalan, A.K., Janardan, P., Changrani, R.D., Dey, P.K., and Manchanda, V.K., *Proceedings of the Nuclear and Radiochemistry Symposium (NUCAR 05)*. Chander, K., Acharya, R., Tomar, B.S., and Venugopal, V., Eds., 2005, pp. 199–200.
166. Patil, C.B., Mohapatra, P.K., Venugopalan, A.K., Janardan, P., Changrani, R.D., Dey, P.K., and Manchanda, V.K., *Proceedings of the Theme Meeting on Emerging Trends in Separation Science and Technology (SESTEC2004)*. Mohapatra, P.K., Vaidya, V.N., and Manchanda, V.K., Eds., 2004, pp. 200–201.
167. Rathore, N.S., Sonawane, J.V., Sawant, S.R., Venugopalan, A.K., Singh, R.K., Bajpai, D.D., and Shukla, J.P., *Proceedings of Nuclear and Radiochemistry Symposium (NUCAR 99)*. Purushotham, D.S.C., Reddy, A.V.R., Manohar, S.B., and Rama Rao, G.A., Eds., 1999, pp. 153–154.
168. Geist, A., Weigl, M., and Gompper, K., Minor actinide partitioning by liquid–liquid extraction using a synergistic mixture of bis (chlorophenyl)dithiophosphinic acid and TOPO in a hollow fibre module for americium(III) and lanthanide(III) separation. *Sep. Sci. Tech.*, 2002, 37: 3369–3390.
169. Fink, D., Apel, P. Yu., and Iyer, R.H., *Transport Processes in Ion-irradiated Polymers*. Fink, D., Ed., Springer-Verlag, Berlin, 2004, p. 269.
170. Fleischer, R.L., Price, P.B., and Walker, R.M., *Nuclear Tracks in Solids: Principle and Applications*, University of California, Berkely, CA, 1975.
171. Grzywna, Z.J., Siwy, Z., and Bashford, C.L., Nonlinear theory for ionic transport through track-etched nuclear membranes. *J. Membr. Sci.*, 1996, 121: 261–269.
172. Pandey, A.K., Gautam, M.M., Shukla, J.P., and Iyer, R.H., Effect of pore characteristics on carrier-facilitated transport of Am(III) across track-etched membranes. *J. Membr. Sci.*, 2001, 190: 9–20.
173. Sportsman, K.S., Bluhm, E.A., and Abney, K.D., Removal of actinides from acidic solution via carrier-mediated facilitated transport across mesoporous substrates with nanoengineered surfaces: Thiol self-assembled monolayers with D(tBu) $\Phi$ D(iBu)CMPO ligands. *Sep. Sci. Tech.*, 2005, 40: 709–723.
174. Gopalani, D., Kumar, S., Jodha, A.S., Singh, R., Khatri, P.K., and Gopal, R., A novel method for production of polyester films-based nuclear track microfilters. *J. Membr. Sci.*, 2000, 178: 93–98.
175. Vater, P., Production and application of nuclear track microfilters. *Nucl. Track Radiat. Meas.*, 1988, 15: 743–749.
176. Ganz, M., Feige, G., Edelstein, N., Bucher, J., Zhu, T.-C., Vater, P., Brandt, R., and Vetter, J., Application of kapton nuclear track microfilters in liquid–liquid extraction of actinoid elements. *Nucl. Track Radiat. Meas.*, 1988, 15: 799–802.
177. Schow, A.J., Peterson, R.T., and Lamb, J.D., Polymer inclusion membranes containing macrocyclic carriers for use in cation separations. *J. Membr. Sci.*, 1996, 111: 291–295.
178. Lamb, J.D. and Nazarenko, A.Y., Selective metal ion sorption and transport using polymer inclusion membrane containing dicyclohexano 18-crown-6. *Sep. Sci. Tech.*, 1997, 32: 2749–2764.
179. Kim, J.S., Kim, S.K., Cho, M.H., Lee, S.H., Kim, J.Y., Kwon, S.-G., and Lee, E.-H., Calix[6]arene bearing carboxylic acid and amide groups in polymeric CTA membrane. *Bull. Korean Chem. Soc.*, 2001, 22: 1085–1089.
180. Gherroue, A., Kerdjoudj, H., Molinari, R., Seta, P., and Drioli, E., Fixed sites plasticized cellulose triacetate membranes containing crown ethers for silver(I), copper(II) and gold(III) ions transport. *J. Membr. Sci.*, 2004, 228: 149–157.
181. Gardner, J.S., Walker, J.O., and Lamb, J.D., Permeability and durability effects of cellulose polymer variation in polymer inclusion membranes. *J. Membr. Sci.*, 2004, 229: 87–93.
182. Mohapatra, P.K., Pathak, P.N., Kelkar, A., and Manchanda, V.K., Selective permeation of radioactive strontium from simulated high level waste solutions using a polymer inclusion filter containing a crown ether carrier. *New J. Chem.*, 2004, 28: 1004–1009.
183. Sugiura, M., Effect of quaternary ammonium salts on carrier mediated transport of lanthanoid ions through cellulose triacetate membranes. *Sep. Sci. Tech.*, 1993, 28: 1453–1463.
184. Sugiura, M., Transport of lanthanide ions through cellulose triacetate membranes containing hinokitiol and flavonol as carriers. *Sep. Sci. Tech.*, 1990, 25: 1189–1199.
185. Sugiura, M., Kikkawa, M., and Urita, S., Carrier-mediated transport of rare earth ions through cellulose triacetate membranes. *J. Membr. Sci.*, 1989, 42: 47–55.
186. Scindia, Y.M., Pandey, A.K., and Reddy, A.V.R., Coupled-diffusion transport of Cr(VI) across anion-exchange membranes prepared by physical and chemical immobilization methods. *J. Membr. Sci.*, 2005, 249: 143–152.
187. Paugam, M.-F. and Buffle, J., Comparison of carrier-facilitated copper(II) ion transport mechanisms in a supported liquid membrane and in a plasticized cellulose triacetate membrane. *J. Membr. Sci.*, 1998, 147: 207–215.
188. Salazar-Alvarez, G., Bautista-Flores, A.N., de San Miguel, E.R., Muhammed, M., and de Gyves, J., Transport characterisation of a PIM system used for the extraction of Pb(II) using d2ehpa as carrier. *J. Membr. Sci.*, 2005, 250: 247–257.
189. Matsuoka, H., Aizawa, M., and Suzuki, S., Uphill transport of uranium across a liquid membrane. *J. Membr. Sci.*, 1980, 7: 11–19.
190. Suvorova, A.I., Denmchik, L.Yu., Peshekhonova, A.L., and Sdobnikova, O.A., Chemical structure of plasticizers, compatibility of components and phase equilibrium in plasticized cellulose diacetate. *Macromol. Chem.*, 1993, 194: 1315–1321.
191. Sugiura, M., Effect of polyoxyethylene-*n*-alkyl ethers on carrier mediated transport of lanthanide ions through cellulose triacetate membranes. *Sep. Sci. Tech.*, 1992, 27: 269–276.
192. Bhattacharyya, A., Mohapatra, P.K., and Manchanda, V.K., Back transport of Am<sup>3+</sup> through a polymer inclusion membrane containing cyanex-301 as the carrier. Paper presented at NUCAR-2005, GND University, Amritsar, India, March 15–18, 2005, CA-78.
193. Sodaye, S., Tripathi, R., Pandey, A.K., and Reddy, A.V.R., Scintillating polymer inclusion membrane for preconcentration and determination of  $\alpha$ -emitting actinides. *Anal. Chim. Acta*, 2004, 514: 159–165.
194. Application of membrane technologies for liquid radioactive waste processing, IAEA Technical Report Series No. 431, Vienna (2004).

195. Muscatello, A.C. and Navratil, J.D., Americium removal from nitric acid waste streams. *J. Radioanal. Nucl. Chem. Letters*, 1988, 128: 449–462.
196. Muscatello, A.C. and Navratil, J.D., *International Conference on Separations Science and Technology*, New York, 15–17 April, 1986, p. 10.
197. Teramoto, M., Fu, S.S., Takatani, K., Ohnishi, N., Maki, T., Fukui, T., and Arai, K., Treatment of simulated low level radioactive wastewater by supported liquid membranes: Uphill transport of Ce(III) using CMPO as carrier. *Sep. Purif. Tech.*, 1999, 18: 57–69.
198. Hofman, D.L., Craig, W.M., Buchalter, E.M., Birkill, R.S., and Smit, J.J., *Proceedings of I. Chem. E. Symposium Series No. 103, Extraction '87: The Recovery of High Value Materials*, 1987, pp. 179–187.
199. Chiarizia, R., Stability of supported liquid membranes containing long chain aliphatic amines as carriers. *J. Membr. Sci.*, 1991, 55: 65–77.
200. Davies, R.V., Kennedy, J., McIlroy, R.W., Spence, R., and Hill, K.M., Extraction of uranium from sea water. *Nature*, 1964, 203: 1110–1115.
201. Tabushi, I., Kobuke, Y., Nakayama, N., Aoki, T., and Yashizawa, A., Chelating resin functionalized with dithiocarbamate for the recovery of uranium from seawater. *Ind. Eng. Chem. Prod. Res. Dev.*, 1984, 23: 445–448.
202. Kobuke, Y., Tabushi, I., Oh, K., and Aoki, T., Transport of uranyl ion through liquid membrane mediated by macrocyclic polycarboxylate in combination with quaternary ammonium cation. *J. Org. Chem.*, 1988, 53: 5933–5940.
203. Kawai, T., Saito, K., Sugita, K., Katakai, A., Seko, N., Sugo, T., Kanno, J., and Kawakami, T., Comparison of amidoxime adsorbents prepared by cografting methacrylic acid and 2-hydroxyethyl methacrylate with acrylonitrile onto polyethylene. *Ind. Eng. Chem. Res.*, 2000, 39: 2910–2915.
204. Zhang, A., Uchiyama, G., and Asakura, T., The adsorption property and kinetics of uranium(VI) with a novel fibrous and polymeric adsorbent containing amidoxime chelating functional group from sea water. *Sep. Sci. Tech.*, 2003, 38: 1829–1849.
205. Sriram, S., Manchanda, V.K., Bharadwaj, Y.K., and Sabharwal, S.C., *Proceedings of Nuclear and Radiochemistry (NUCAR-2001)*. Ramakumar, K.L., Kadam, R.M., Vaidya, V.N., and Purushotham, D.S.C., Eds., Pune, India, 200, pp. 288–289.
206. Kemperman, A.J.B., Bargeman, D., van Den Boomgard, Th., and Strathmann, H., Stability of supported liquid membranes: State of the art. *Sep. Sci. Tech.*, 1996, 31: 2733–2762.
207. Pfeiffer, R.M., Bunge, A.L., and Navidi, W., Leakage and swell in emulsion liquid membrane system: Batch experiments. *Sep. Sci. Tech.*, 2003, 38: 519–539.
208. Takahashi, K., Ohtsubo, F., and Takeuchi, H., Study of the stability of (w/o)w-type emulsions using a tracer technique. *J. Chem. Eng. Jpn.*, 1981, 14: 416–418.
209. Kinugasa, T., Watanabe, K., and Takeuchi, H., Stability of (W/O) emulsion drops and water permeation through a liquid membrane. *J. Chem. Eng. Jpn.*, 1992, 25: 128–133.
210. Danesi, P.R., Reichley-Yinger, L., and Rickert, P.G., Lifetime of supported liquid membranes: The influence of interfacial properties, chemical composition and water transport on the long-term stability of the membranes. *J. Membr. Sci.*, 1987, 31: 117–145.
211. Lamb, J.D., Bruening, R., Izatt, R.M., Hirashima, Y., Tse, P.K., and Christensen, J.J., Characterization of a supported liquid membrane for macrocycle-mediated selective cation transport. *J. Membr. Sci.*, 1988, 37: 13–26.
212. Hill, C., Dozol, J.F., Rouquette, H., Eymard, S., and Tournois, B., Study of the stability of some supported liquid membranes. *J. Membr. Sci.*, 1996, 114: 73–80.
213. Shinbo, T., Yamaguchi, T., Yanagishita, H., Sakaki, K., Kitamoto, D., and Sugiura, M., Supported liquid membranes for enantioselective transport of amino acid mediated by chiral crown ether—effect of membrane solvent on transport rate and membrane stability. *J. Membr. Sci.*, 1993, 84: 241–248.
214. Urtiaga, A., Ortiz, M., Salazar, E., and Irabien, J., Supported liquid membranes for the separation–concentration of phenol. 1. Viability and mass-transfer evaluation. *Ind. Eng. Chem. Res.*, 1992, 31: 877–886.
215. Chiarizia, R., Application of supported liquid membranes for removal of nitrate, technetium (VII) and chromium (VI) from ground-water. *J. Membr. Sci.*, 1991, 55: 39–64.



---

# 32 Reverse Osmosis-Based Treatment of Radioactive Liquid Wastes Generated in Hospital Facility and in Steel Industry: Case Studies

*M. Sancho, J.M. Arnal, G. Verdú, and J. Lora*

## CONTENTS

32.1	Introduction .....	919
32.2	Origin of Radioactive Wastes .....	920
32.2.1	Wastes from the Electric Power Generation Cycle .....	920
32.2.2	Wastes from Medicine, Industry, and Research .....	920
32.2.3	Wastes from the Dismantling of Nuclear and Radioactive Installations .....	920
32.3	Case Studies .....	920
32.3.1	Radiation Influence on Membrane Performance .....	920
32.3.2	Treatment of <sup>125</sup> I Liquid Wastes by Ultrafiltration and Reverse Osmosis .....	924
32.3.2.1	Description of the Problem .....	924
32.3.2.2	Treatment Description .....	924
32.3.2.3	Experimental Test .....	924
32.3.2.4	Radioactivity Removal by Membranes in the Treatment of <sup>125</sup> I Wastes .....	925
32.3.2.5	Treatment Procedure .....	926
32.3.3	Treatment of <sup>137</sup> Cs-Contaminated Water by Reverse Osmosis .....	927
32.3.3.1	Description of the Problem .....	927
32.3.3.2	Treatment Description .....	927
32.3.3.3	Reverse Osmosis Performance in the Treatment of <sup>137</sup> Cs Liquid Wastes .....	927
32.3.4	Radiological Protection in the Treatment of Radioactive Liquid Wastes .....	928
32.4	Future Trends in Radioactive Liquid Waste Disposal .....	931
	Acknowledgments .....	931
	References .....	931

## 32.1 INTRODUCTION

The applications of membrane technology have grown significantly in the last decade. Some advantages of membrane technologies are continuous performance, low energy consumption, modular structure, and easy installation or automation. Due to this, nowadays membrane processes have become an ideal complement or even a suitable replacement of conventional separation processes (evaporation, chemical precipitation, ion exchange, etc.).

Some areas of application are the nuclear industry and the treatment of radioactive liquid wastes, with two main purposes: reduction in the waste volume for further disposal, and reuse of decontaminated water. Pressure-driven membrane processes (microfiltration, ultrafiltration, nanofiltration, and reverse osmosis [RO]) are widely used for the treatment of radioactive waste.

Some research groups worldwide are currently working on the application of membrane technology to the treatment of radioactive liquid wastes with different levels of activity, from low to high activity waste. Research is mainly focused on wastes from the nuclear industry. However, the nuclear industry is not the only source of radioactive wastes; medical and research applications of radioisotopes also generate radioactive wastes.

Since 1995, the Chemical and Nuclear Engineering Department of the Polytechnic University of Valencia in Spain has been working on the application of membrane technology to the treatment of low and medium level radioactive liquid wastes. In this chapter, we describe two practical cases of radioactive liquid waste treatment using membrane processes: the treatment of  $^{137}\text{Cs}$ -contaminated water generated after a radioactive incident in a stainless steel production factory, and the treatment of  $^{125}\text{I}$  liquid wastes from nuclear medicine services at hospitals.

## 32.2 ORIGIN OF RADIOACTIVE WASTES

Radioactive wastes are generated in the following activities: generation of electric power from nuclear fuel; applications of radioisotopes in medicine, industry, and research; and dismantling of nuclear and radioactive installations. With respect to waste volume and specific activity, the activities that generate the highest amounts of waste are those related to electric power generation.

### 32.2.1 WASTES FROM THE ELECTRIC POWER GENERATION CYCLE

This group includes the wastes generated during all the stages of the power production cycle in a nuclear power plant. First, the wastes from uranium mining, concentrate manufacturing, conversion to uranium hexafluoride, uranium enrichment, and fuel manufacturing. Second, the wastes generated during the operation of the nuclear power plant. This includes equipment and devices used for the purification and cleaning of the cooling systems, and other radioactive wastes like tools, working cloths, laundry wastes, papers, etc. Finally, the spent fuel rods that are produced on the completion of the energy production cycle; these elements are temporarily stored in swimming pools or in dry sites in the nuclear power station itself.

### 32.2.2 WASTES FROM MEDICINE, INDUSTRY, AND RESEARCH

In medical installations, the use of radioactive isotopes for diagnosis and therapy has significantly increased in the past years. Nonencapsulated radioactive elements are used for different purposes such as in diagnosis by tracers, treatment of thyroid or blood disorder, and in medical research. These activities produce some solid radioactive wastes like cotton, rubber gloves, syringes, etc., as well as liquid wastes, mainly scintillation liquids. Another type of waste is the encapsulated sources that are used for cancer treatment; these elements must be changed when their activity decays below a certain level.

In industry, radioisotopes are used in encapsulated sources, generally of low activity, for the continuous measurement of level, humidity, density, or thickness. Gamma radiation-encapsulated sources are also used in nondestructive tests in metallic constructions (gammagraphies) and in industrial sterilization.

In the nuclear research centers, the wastes are obtained from research and experimental reactors, hot cells, pilot plants, and decontamination services. These wastes have varying physical, chemical, and radioactive nature due to the great diversity of isotopes used and the wide range of processes in which they are applied.

### 32.2.3 WASTES FROM THE DISMANTLING OF NUCLEAR AND RADIOACTIVE INSTALLATIONS

The dismantling of a nuclear or radioactive installation, when its useful life is finished, generates the following radioactive wastes: reactor vessel and the components inside biological shield, external parts of the biological shield (heat exchangers, circulation pumps, pipes, etc.), activated and contaminated concrete, and auxiliary systems and building structures. Furthermore, some secondary wastes such as decontamination liquids and gas filters are also generated.

## 32.3 CASE STUDIES

This section describes some case studies carried out by the authors, which are related to radioactive liquid waste treatment using membrane processes: a study about the influence of radiation on reverse osmosis membranes, a practical case about concentration of  $^{125}\text{I}$  radioactive liquid wastes by ultrafiltration and reverse osmosis processes, and a practical experience about decontamination of  $^{137}\text{Cs}$  liquid waste by reverse osmosis, including a study of radiological protection during the treatment.

### 32.3.1 RADIATION INFLUENCE ON MEMBRANE PERFORMANCE

The influence of radiation on the transport properties of different reverse osmosis composite membranes was studied by Chmielewski and Harasimowicz [1]. Reverse osmosis membranes were irradiated with a  $^{60}\text{Co}$  source, with a linear accelerator, and were also immersed in a  $^{137}\text{Cs}$  high activity solution, reaching absorbed dose values around 40 kGy. The results of some tests with the irradiated membranes showed that aromatic polyamide composite membranes are highly radiation resistant. This allows these membranes to be used in radioactive solutions with an activity below  $3.7 \times 10^{12} \text{ Bq/m}^3$ , which corresponds to absorbed dose values around 30 kGy.

**TABLE 32.1**  
**Permselective Performance of Gamma-Irradiated Membranes**

Absorbed Dose (Gy)	$J_v$ (L/[m <sup>2</sup> h])	$R$ (%)
0.25	28.0	97.0
0.50	26.7	98.5
1	30.5	98.6
2	31.0	98.7
5	28.5	98.9
10	24.0	98.9
20	20.0	97.7
Nonirradiated	21.6	97.5

Source: Courtesy of M. Balaban, Desalination, Italy. With permission.

Similar studies were carried out by Nakase, who determined the effect of radiation on some mechanical and thermal properties of the polysulphone film of composite membranes. After a complete experimental and microscopic study, the author concluded that polysulphone film almost keeps transport properties and stability up to dose values of 2 MGy [2].

Following these studies, the authors assessed the influence of different kinds of radiation on reverse osmosis composite membranes, applying radiation doses within the range of values that are expected to be absorbed by membranes in the treatment of low and medium radioactive wastes. Samples of reverse osmosis composite membranes were irradiated with gamma radiation using a <sup>60</sup>Co source, in an absorbed dose range between 0.25 and 20 kGy; and with electron radiation using a linear accelerator, in an absorbed dose range between 5 and 25 Gy [3].

The irradiated membranes were then tested in a pilot plant with a plate-and-frame module with capacity for two membranes with an effective area of 90 cm<sup>2</sup> each. Permselective results of irradiated membranes were compared to those of nonirradiated membranes [3]. It was observed that the performance of the samples irradiated with electronic or gamma radiation was very similar to that of the nonirradiated membranes. Tables 32.1 and 32.2 show the results of permeate flux and retention index for gamma- and electron-irradiated membranes, respectively.

The differences in permselective performance between some irradiated and nonirradiated samples cannot be associated with radiation effects, but with membrane structural dispersion. This is because the membrane samples were taken from a spiral wound module; therefore, the differences observed can be due to the lack of homogeneity in the membrane structure and its characteristics along the module. This fact can be illustrated by the dispersion of the experimental results of the nonirradiated samples.

Figure 32.1 shows the permeability obtained for all the nonirradiated samples. The average value of all these samples is  $J_{v,av} = 21.6$  L/m<sup>2</sup>h. The highest value of the statistical dispersion is  $J_{v,av} + 2\sigma = 38.8$  L/m<sup>2</sup>h, and the lowest value is  $J_{v,av} - 2\sigma = 4.4$  L/m<sup>2</sup>h. On the other hand, Figures 32.2 and 32.3 show the permeability of the gamma- and electron-irradiated samples, respectively. As it can be seen, in both cases the dispersion values of permeability are within the limit values of the nonirradiated dispersion, proving that the variability in the results is not the consequence of radiation, but of membrane non-homogeneity.

**TABLE 32.2**  
**Permselective Performance of Electron-Irradiated Membranes**

Absorbed Dose (Gy)	$J_v$ (L/[m <sup>2</sup> h])	$R$ (%)
5	20.0	97.2
10	26.7	97.5
15	18.7	97.4
20	14.0	97.0
25	20.0	97.4
Nonirradiated	21.6	97.5

Source: Courtesy of M. Balaban, Desalination, Italy. With permission.

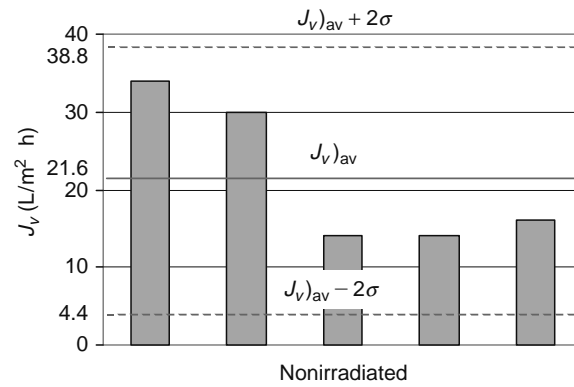


FIGURE 32.1 Permeate flux of nonirradiated membranes.

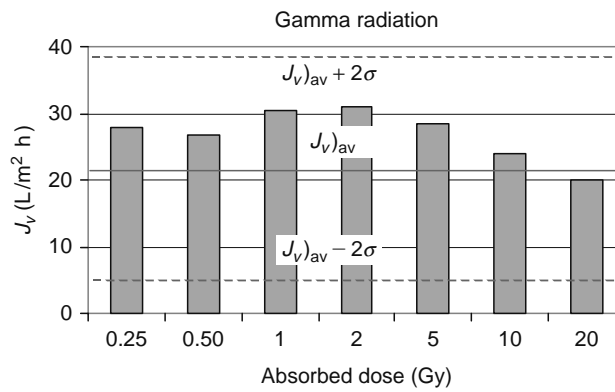


FIGURE 32.2 Permeate flux of gamma-irradiated membranes.

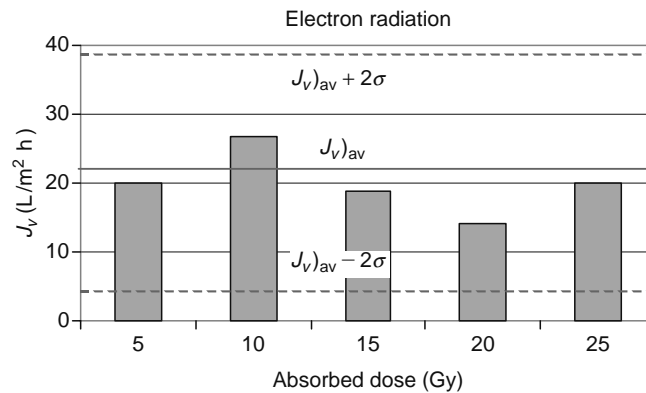


FIGURE 32.3 Permeate flux of electron-irradiated membranes.

With regard to selectivity, Figure 32.4 shows the results of the retention index for all the nonirradiated samples. The average value of all these samples is  $R_{av} = 97.6\%$ . The highest value of the statistical dispersion is  $R_{av} + 2\sigma = 98.1\%$ , and the lowest value is:  $R_{av} - 2\sigma = 97\%$ . On the other hand, Figures 32.5 and 32.6 show the selectivity of the gamma- and electron-irradiated samples, respectively. As it can be seen, the dispersion of selectivity in the electron-irradiated membranes is within the limit values of the nonirradiated dispersion, proving that the variation in the results is not caused by radiation.

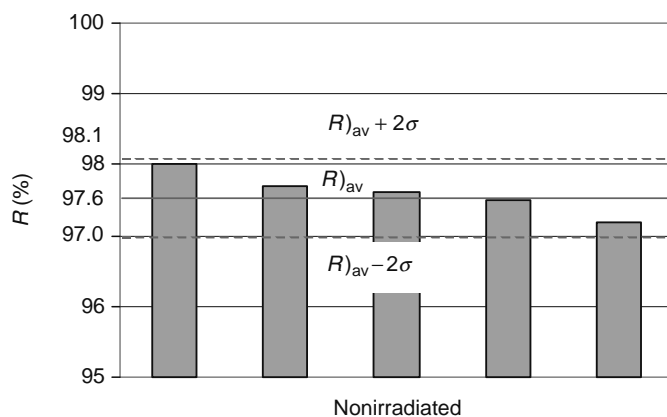


FIGURE 32.4 Retention index of nonirradiated membranes.

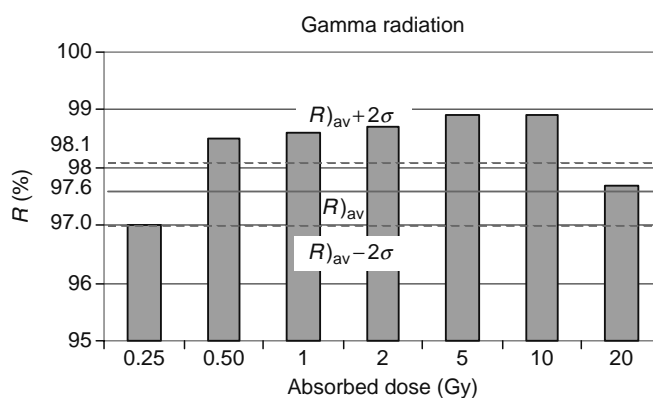


FIGURE 32.5 Retention index of electron-irradiated membranes.

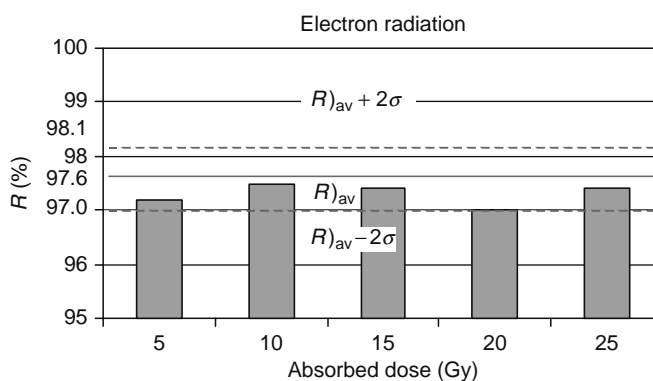


FIGURE 32.6 Retention index of gamma-irradiated membranes.

For gamma-irradiated membranes, the values of experimental selectivity are higher than the upper limit of the nonirradiated dispersion, so it can be said that gamma radiation can even have a beneficial effect on membrane selectivity.

As a conclusion of this study about the influence of electron and gamma radiation on reverse osmosis composite membranes, it can be stated that radiation does not affect membrane performance in a range of absorbed dose values up to 25 Gy, approximately. Therefore, reverse osmosis composite membranes are suitable for use in the treatment of low and medium activity levels, as the values of the radiation absorbed by the membranes will be lower than those assessed in this case study.

### 32.3.2 TREATMENT OF $^{125}\text{I}$ LIQUID WASTES BY ULTRAFILTRATION AND REVERSE OSMOSIS

#### 32.3.2.1 Description of the Problem

Radioimmunoassay (RIA) is used in nuclear medicine for measuring very low levels (concentrations below  $10^{-11}$  g/mL) of some biological compounds in corporal fluids, by means of the combination of radioisotopes and antibodies. The most common radioisotope used in this technique is  $^{125}\text{I}$ , a gamma-emitting radioisotope with a half-life of 60 days, which is used for labelling compounds of interest.

RIA techniques generate great amounts of radioactive liquid wastes whose composition depends on the specific assays that are carried out in each laboratory. Liquid wastes from RIA techniques are usually composed of different types of proteins (some of them radioactively labelled), preservative solutions, several low-molecular-weight organic compounds, and inorganic salts—all in aqueous solutions. These wastes are classified as low and medium radioactive, but they are also potentially infectious since they can contain pathogens from patient's blood [4]. Sometimes, the infectious risks of these wastes can be much more dangerous than the risks associated with radioactivity.

At present, these radioactive wastes are temporarily stored in the sanitary center for partial activity decay. Then, the wastes are disposed of by an officially designated company depending on their radioactivity levels and other biological and chemical risks. Reduction of RIA waste volume would mean an important decrease in waste disposal costs, and would diminish the problems of waste storage in hospitals. Furthermore, an appropriate treatment of RIA liquid wastes would remove pathogens and chemicals that otherwise would remain in the wastes.

#### 32.3.2.2 Treatment Description

Figure 32.7 shows the scheme of the solution proposed by the authors for treating radioactive liquid wastes from RIA laboratories. Since part of the radioisotope is in ionic form [5], reverse osmosis can be used for radioisotope removal. But before the application of reverse osmosis, a pretreatment is required. It consists of the following two stages:

- Filtration in cartridges for removal of suspension solids that could damage the membranes.
- Ultrafiltration membranes are suitable for the treatment of radioactive liquid wastes, especially as reverse osmosis pretreatment [6]. Therefore, ultrafiltration is used for the removal of the radioactivity associated with the proteins and high-molecular-weight organic compounds, as these species can reduce reverse osmosis performance.

The purpose of the treatment is to reduce waste volume for further disposal by an authorized company, and to obtain an organic matter and pathogens-free permeate with an activity level below the legal discharge limit.

#### 32.3.2.3 Experimental Test

Some experiments were carried out with wastes from nuclear medicine services (RIA laboratories). Wastes with different storing periods were used, with activity values between 10 and 1000 kBq/L, depending on their storage time.

The experiments consisted of a first stage of ultrafiltration, after which the UF permeate was treated by reverse osmosis, according to the scheme presented in Figure 32.7. If the RO permeate showed an activity higher than the environmental background level in the treatment area, it was again treated by RO, and so on until reaching an activity level in the permeate close to background levels.

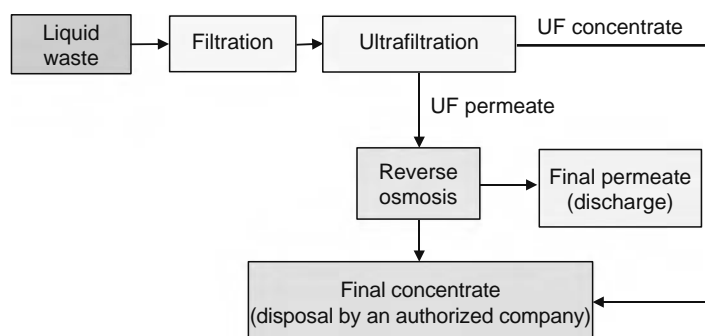


**FIGURE 32.7** Scheme of the RIA liquid waste treatment. (Courtesy of Radiation Protection Dosimetry, Oxford University Press, Oxford. With permission).

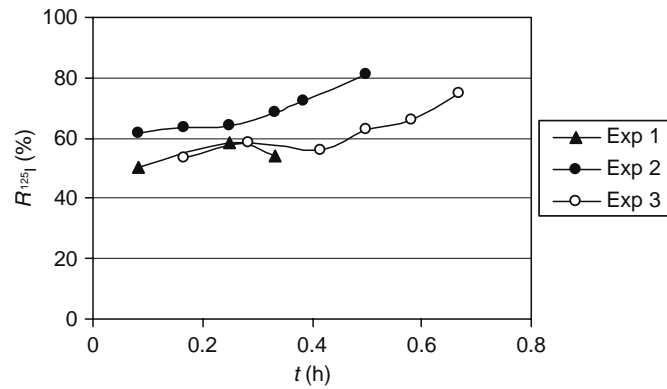


**FIGURE 32.8** Radioactivity removal by UF membranes in the RIA waste treatment. (From Arnal, J.M., Campayo, J.M., Lora, J., Sancho, M., Iborra, I., and Alcaina, I., *Desalination*, 129, 101, 2000.)

During the treatment, periodical measurements of flow and conductivity of the permeate and feed were taken for calculating the permselective parameters of the membranes ( $J_v$ ,  $R$ ). In addition, samples of the feed and permeate were periodically taken for measuring radioactivity. Then, the retention index to  $^{125}\text{I}$  was calculated using the following expression:

$$R_{125\text{I}} (\%) = \frac{A_F - A_P}{A_F} \times 100 \quad (32.1)$$

where  $A_F$  and  $A_P$  are the activities of feed and permeate (Bq/L), respectively.

#### 32.3.2.4 Radioactivity Removal by Membranes in the Treatment of $^{125}\text{I}$ Wastes

In the experiments performed on real wastes, ultrafiltration played an important role in the partial reduction of radioactivity. Figure 32.8 shows the evolution of the retention index to  $^{125}\text{I}$  with time in some of the UF experiments. Most of the time, radioisotope rejection by UF membrane was higher than 50%, even reaching maximum values of about 80%. This fact proves that part of the radioisotope remains labelled to proteins and other organic compounds, most of which are removed in the UF stage [7]. The rest of the radioactivity, associated with low-molecular-weight organic compounds and ionic solutes, will be removed in the RO stages.

In reverse osmosis, radioactivity removal gives two types of results: the results of the first RO application after the UF stage, in which the ultrafiltrate was treated; and the results of the subsequent RO applications, in which an RO permeate of an earlier stage was treated.

Figures 32.9 and 32.10 show the evolution with time of the retention index to  $^{125}\text{I}$  in the first RO application carried out in three experiments, and in the third RO application performed on experiments 2 and 3, respectively. It can be observed that in the first RO application, the retention index to  $^{125}\text{I}$  decreased progressively during the treatment due to an increase of feed activity as a result of concentrate recirculation to the feed tank. Anyway, in this application  $R_{125\text{I}}$  was higher than 90% most of

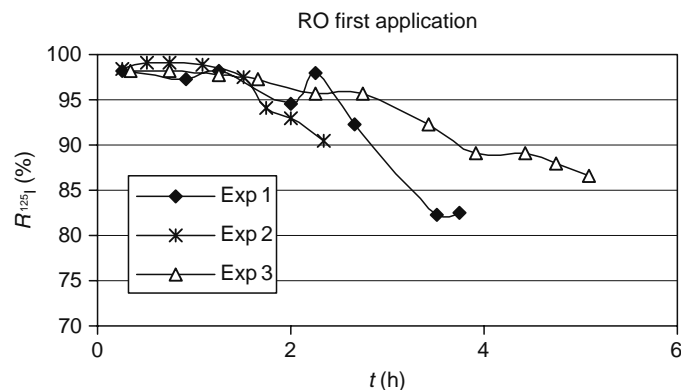


**FIGURE 32.9** Radioactivity removal by RO membranes in the treatment of UF permeate. (From Arnal, J.M., Campayo, J.M., Lora, J., Sancho, M., Iborra, I., and Alcaina, I., *Desalination*, 129, 101, 2000.)

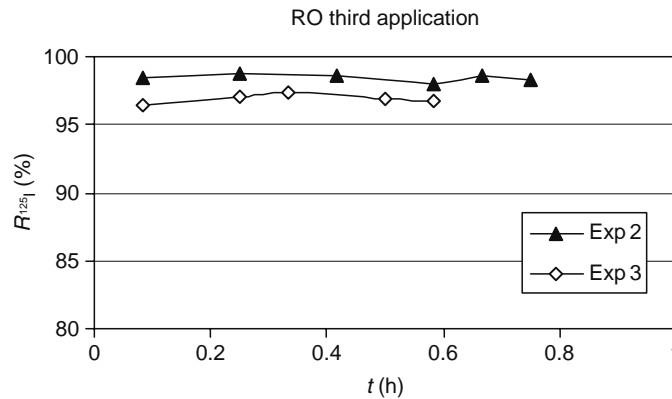


**FIGURE 32.10** Radioactivity removal by RO in the treatment of an earlier RO permeate. (From Arnal, J.M., Campayo, J.M., Lora, J., Sancho, M., Iborra, I., and Alcaina, I., *Desalination*, 129, 101, 2000.)

the time. On the other hand, in the subsequent RO applications (Figure 32.10), the retention index to  $^{125}\text{I}$  remained quite constant with values above 95% in all the experiments. This was due to lower feed activity values and lower feed activity variation.

Table 32.3 shows the values of feed and permeate activity evolution in one of the experiments, representative of a typical treatment process. It can be seen how it is possible to obtain a permeate with a level of activity below the legal discharge limits by means of successive reverse osmosis applications.

### 32.3.2.5 Treatment Procedure

According to the experimental results, the most suitable procedure for RIA waste treatment was defined. This procedure consists of the following stages:

- *Ultrafiltration.* In this stage, high-molecular-weight organic compounds as well as biological contaminants are removed, and the activity is reduced to an average of 50%–60%.
- *First Stage of Reverse Osmosis.* Almost all the organic and biological compounds that were not eliminated previously by ultrafiltration are removed in this stage.
- *Second Stage of Reverse Osmosis.* Salt concentration is reduced below running water levels (lower than 1 g/L).
- *Third Stage of Reverse Osmosis.* After this stage, a permeate with an activity below 100 Bq/L is obtained.

The following options are suitable for the disposal of the final permeate:

- Direct discharge to the sink by dilution, if authorized by the appropriate official institution.
- Temporary storage and further discharge to the sink after checking that the activity is below the legal limit. It must always be authorized by the appropriate entity.

The final concentrate, which includes UF and RO concentrates, should be disposed of by an authorized company, considering not only waste radioactivity levels but also chemical and biological contaminations, specially in the ultrafiltration concentrate since it contains most of the pathogens of the original waste.

**TABLE 32.3**  
**Radioactivity Removal in RO Experiments**

RO Stage	$A_F$ (Bq/L)	$A_P$ (Bq/L)
RO1	117,400	15,360
RO2	15,360	720
RO3	720	70

*Source:* Courtesy of Radiation Protection Dosimetry, Oxford University Press, Oxford. With permission.

### 32.3.3 TREATMENT OF $^{137}\text{Cs}$ -CONTAMINATED WATER BY REVERSE OSMOSIS

#### 32.3.3.1 Description of the Problem

In 1998, a  $^{137}\text{Cs}$  source was accidentally melted in a stainless steel production factory in Spain. As a consequence of this accident, the cooling system of one of the ovens became radioactively contaminated. The decontamination process produced  $40\text{ m}^3$  of  $^{137}\text{Cs}$  contaminated water, with an average activity above  $300\text{ kBq/L}$ .

The authors, in collaboration with LAINSA company, developed the project for decontaminating the radioactive liquids, by means of a reverse osmosis plant. The aim of the treatment was to remove the  $^{137}\text{Cs}$  radioisotope from the treated liquid and to reduce the volume of the solution for further immobilization.

#### 32.3.3.2 Treatment Description

Figure 32.11 shows a scheme of the RO plant for the treatment of the  $^{137}\text{Cs}$ -contaminated liquids. It was equipped with two kinds of spiral wound reverse osmosis membranes: high-pressure (HP) and low-pressure (LP) membranes. Before flowing through the membranes, the feed was pretreated using  $5\text{ }\mu\text{m}$  sleeve filters and  $0.45\text{ }\mu\text{m}$  cartridge filters.

The treatment was divided into two stages. At the first stage, both types of membranes were used, recirculating all the concentrates to the feed tank. The second stage began when the permeate resulting from the first stage was out of the specifications, and then the two reverse osmosis lines were separated. The low-pressure membranes treated the first-stage permeate, while the high-pressure membranes continued treating the concentrate.

The decontamination process by reverse osmosis took about 1 month. After this period,  $36\text{ m}^3$  of liquid was decontaminated from the original  $40\text{ m}^3$ . Later, evaporation was applied to get an additional concentration of the final waste; the volume of concentrate liquid was reduced from  $4$  to  $1\text{ m}^3$ .

#### 32.3.3.3 Reverse Osmosis Performance in the Treatment of $^{137}\text{Cs}$ Liquid Wastes

During the treatment, samples of the permeate, the concentrate, and the feed were taken periodically for measuring radioactivity. The retention index to  $^{137}\text{Cs}$  was calculated by an expression that is analogous to Equation 32.1.

Figure 32.12 shows the results of the retention index to  $^{137}\text{Cs}$  obtained at the two RO treatment stages. From these results, it can be stated that

- At the first RO treatment stage, the retention index to  $^{137}\text{Cs}$  was higher than 98% in most cases.
- At the second RO treatment stage, the retention index values in the high-pressure membranes were slightly lower, but always above 96%.
- At the second RO treatment stage, the retention index to  $^{137}\text{Cs}$  in the low-pressure membranes was always higher than 98%, and above 99.5% in most cases.

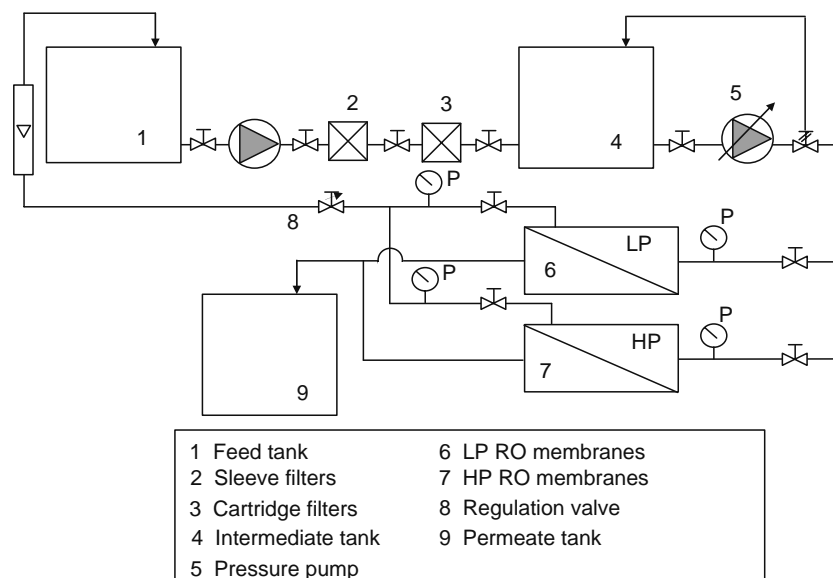


FIGURE 32.11 Scheme of the  $^{137}\text{Cs}$  liquid waste treatment plant.

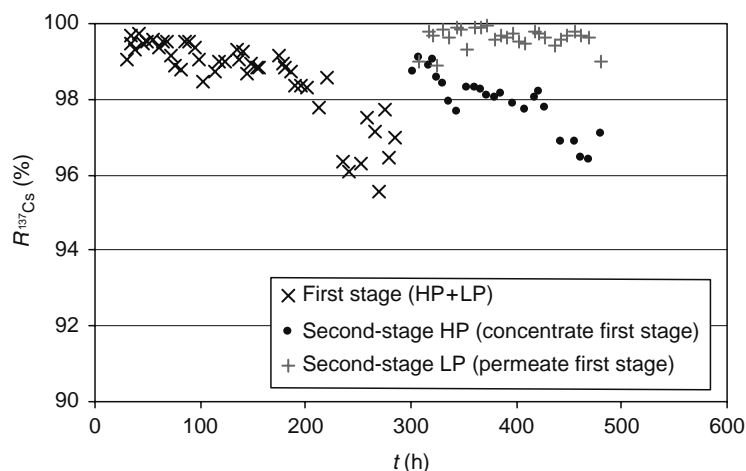


FIGURE 32.12 Retention index to  $^{137}\text{Cs}$  of the RO membranes. (Courtesy of M. Balaban, Desalination, Italy. With permission.)

The progressive decrease of the retention index values at the first stage of the RO treatment and in the high-pressure membranes during the second stage is due to two main factors. On one hand, to the increase in feed concentration as a result of concentrate recirculation, and on the other hand, to the increase in membrane fouling. However, in the low-pressure membranes in the second RO treatment stage high values of retention index were obtained because the permeate of the first stage was treated, so the activity values were much lower (below 100 kBq/L in comparison with values higher than 1500 kBq/L in the other two situations).

In spite of the successful  $^{137}\text{Cs}$  selectivity results, permeability values were not as good as expected; in fact, the low permeability caused the RO treatment to last more than planned. This was mainly due to a lack of knowledge about the characteristics of the solution to be treated; as a result, it was not possible to design a specific pretreatment, and filtration was not enough to avoid severe fouling in the RO membranes.

As a summary, the following conclusions can be drawn from the treatment of  $^{137}\text{Cs}$ -contaminated liquids [8]:

- The application of reverse osmosis was highly successful, decontaminating more than 90% of the original volume.
- The selectivity values confirm the potential of reverse osmosis composite membranes in the treatment of effluents that contain radioactive isotopes.
- The decrease in membrane permeability was caused by membrane fouling. This could have been partially avoided with an appropriate pretreatment design.

### 32.3.4 RADIOLOGICAL PROTECTION IN THE TREATMENT OF RADIOACTIVE LIQUID WASTES

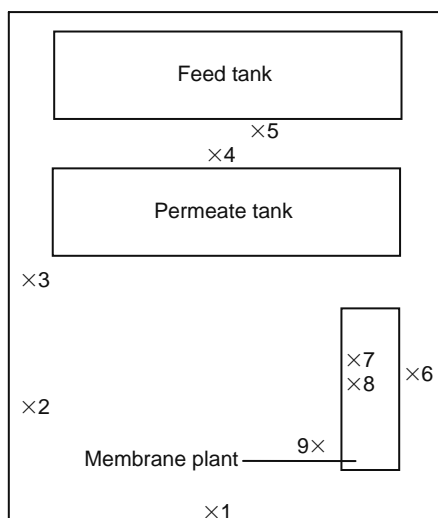
During the RO treatment of  $^{137}\text{Cs}$ -contaminated liquid, dose levels were measured at different sites in the working area with the purpose of following dose evolution and taking the appropriate radiological protection measures [9].

Figure 32.13 shows a scheme of the treatment area, in which the measuring points are indicated by numbers whose description is presented in Table 32.4. Environmental doses were measured at boundary points (1, 2, and 3); in all other points contact, doses were measured. Measures were taken approximately every 12 h in both cases.

The following figures show the dose evolution with time of the points indicated in the scheme shown by Figure 32.13. Figure 32.14 shows radiation evolution at the boundary points. The three points show no significant radiation values, although point 3 has slightly higher values than points 1 and 2 because it is closer to the tanks containing radioactive liquid.

Figure 32.15 shows the radiation evolution in the surroundings of the permeate and feed tanks (points 4 and 5). Near the permeate tank (point 4), dose variation is not very significant since the permeate has a low activity level [10]. However, the radiation evolution near the feed tank (point 5) shows quite high dose values. This is because the liquid inside this tank has much higher activity than the liquid inside the permeate tank. Dose increase around the feed tank is due to progressive concentration of the liquid feed as a result of membrane concentrate recirculation to this tank [11].

Figure 32.16 shows the radiation evolution of the main elements of the membrane treatment plant. Among these elements, the filtration unit showed the highest dose values, particularly the sleeve filters (point 7) with top values around 140  $\mu\text{Sv/h}$ . This high dose is because these filters are the first element through which the feed flows, so they are in contact with a high activity liquid. The dose values at the cartridge filters (point 8) are lower than the values of the sleeve filters, though they are also fairly high, between 10 and 30  $\mu\text{Sv/h}$ , approximately.



**FIGURE 32.13** Diagram of the working area in the treatment of <sup>137</sup>Cs liquid wastes. (From Arnal, J.M. *Tratamiento de Residuos Radiactivos Líquidos y Sólidos Contaminados con Cs-137 Mediante Sistemas Combinados de Separación por Membranas, Lixiviación y Precipitación Química*, 1st ed. Valencia, Spain: Servicio de Publicaciones UPV, 2003.)

**TABLE 32.4**  
**Identification of Dose Measuring Points in the Treatment Area**

Point	Area or Element Represented
1	Boundary
2	Boundary
3	Boundary
4	Permeate tank (treated liquid)
5	Feed tank
6	Intermediate tank and pump
7	Sleeve filter
8	Cartridge filter
9	Membrane modules

Source: From Arnal, J.M. *Tratamiento de Residuos Radiactivos Líquidos y Sólidos Contaminados con Cs-137 Mediante Sistemas Combinados de Separación por Membranas, Lixiviación y Precipitación Química*, 1st ed. Valencia, Spain: Servicio de Publicaciones UPV, 2003.

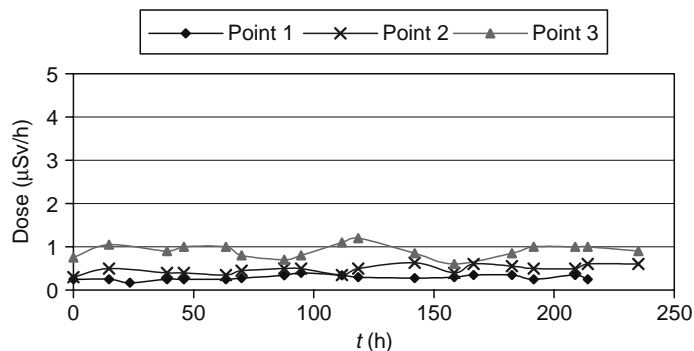


**FIGURE 32.14** Radiation level evolution at the boundary points of the treatment area. (From Arnal, J.M. *Tratamiento de Residuos Radiactivos Líquidos y Sólidos Contaminados con Cs-137 Mediante Sistemas Combinados de Separación por Membranas, Lixiviación y Precipitación Química*, 1st ed. Valencia, Spain: Servicio de Publicaciones UPV, 2003.)

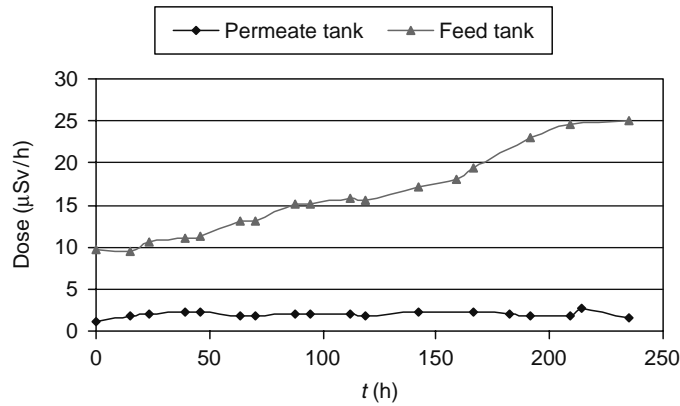


**FIGURE 32.15** Radiation level evolution around the permeate and feed tanks. (From Arnal, J.M. *Tratamiento de Residuos Radiactivos Líquidos y Sólidos Contaminados con Cs-137 Mediante Sistemas Combinados de Separación por Membranas, Lixiviación y Precipitación Química*, 1st ed. Valencia, Spain: Servicio de Publicaciones UPV, 2003.)

Another important point with regard to radiation level at the treatment plant is the intermediate tank in which the liquid is stored after filtering, and the pump placed beside that tank (point 6). The high values at this point, around  $40 \mu\text{Sv/h}$ , are due to the high activity values of the liquid stored in the intermediate tank.

Finally, the point that represents membrane modules (point 9) shows quite significant dose values, which increase progressively as the feed concentrates. From the analysis of radiation evolution in the treatment area, the following conclusions can be stated:

- Most relevant points from the viewpoint of radiological protection are the filtration unit and the intermediate tank, with the highest dose values.
- Filtration unit is a point of necessary and frequent access to change filters. In future treatment plants, it should be isolated to facilitate a safe access to the other elements of the plant.
- Intermediate tank should not be placed in the surroundings of any element that needs frequent access. The pump also has to be placed far from the elements with high dose values, if it requires regular maintenance.
- Membrane modules reach dose values that cannot be ignored. Although they are not as high as the doses reached at the elements mentioned above, membrane modules are points of continuous manipulation, so they have to be considered from the point of view of radiological protection.
- Dose values at the area around the feed tank are fairly high, but it is not an important problem since this tank is not of frequent access.

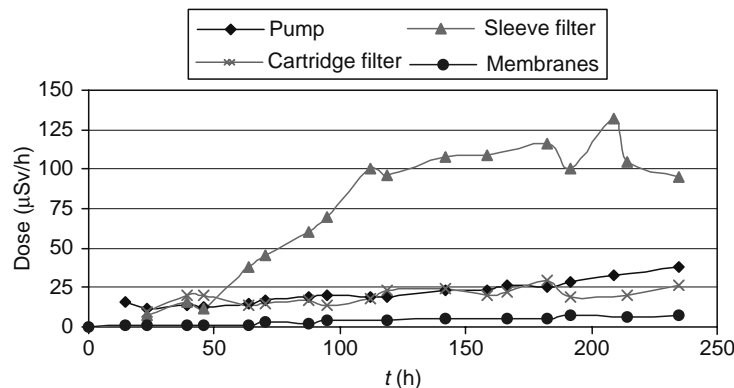


**FIGURE 32.16** Radiation level evolution at the membrane plant. (From Arnal, J.M. *Tratamiento de Residuos Radiactivos Líquidos y Sólidos Contaminados con Cs-137 Mediante Sistemas Combinados de Separación por Membranas, Lixiviación y Precipitación Química*, 1st ed. Valencia, Spain: Servicio de Publicaciones UPV, 2003.)

## 32.4 FUTURE TRENDS IN RADIOACTIVE LIQUID WASTE DISPOSAL

With regard to future trends in the radioactive and nuclear fields, an increasing use of radioisotopes for medical, industrial, and research purposes is expected soon. As a result of this, there will be an increase in the amount of low and medium radioactive wastes.

The benefits of these activities are well known, but design of waste disposal strategies for volume reduction and liquid decontamination is essential, to optimize waste storage installations and reduce waste disposal costs. Among these strategies, the application of an appropriate treatment is essential for suitable waste disposal.

Membrane technologies have a great potential in the treatment of radioactive liquid wastes, as it has been proved throughout this chapter. In this sense, it is expected a growing use of the membrane processes in the radioactive field, with different possibilities: alone, combined between them (microfiltration or ultrafiltration and reverse osmosis) or combined with other conventional processes like evaporation or ion exchange. Furthermore, some special membrane processes, like membrane distillation or liquid membranes, could be applied for the specific treatment of radioactive wastes.

In relation to future trends of the membrane treatments described in this chapter, they are expected to be applied for medical and research wastes of low-medium activity contaminated with  $^{125}\text{I}$ ,  $^{137}\text{Cs}$ , or other radioisotopes with similar characteristics. Furthermore, membrane treatment has been proved as an efficient and quick treatment in an incident that generates low-medium radioactive wastes.

## ACKNOWLEDGMENTS

Authors would like to express their gratitude to the people from La Fe Hospital and LAINSA company of Valencia for their contribution to the research described in this chapter.

We would also like to thank the R & D & I Linguistic Assistance Office at the Universidad Politécnica of Valencia for their help in revising this paper.

## REFERENCES

1. Chmielewski AG and Harasimowicz M. Influence of gamma and electron irradiation on transport properties of nanofiltration and hyperfiltration membranes. *Nukleonika* 1997; 42(4):857–862.
2. Nakase Y. Irradiation effects on properties of reverse osmosis membrane based on crosslinked aromatic polyamide. *J Nucl Sci Technol* 1994; 31:1214–1221.
3. Arnal JM, Sancho M, Verdú G, Campayo JM, and Villaescusa JI, Treatment of  $^{137}\text{Cs}$  liquid wastes by reverse osmosis. Part I. Preliminary tests. *Desalination* 2003; 154:27–33.
4. Peyrin JO. La gestion des déchets radioactifs hospitaliers. *Radioprotection* 1992; 27:47–53.
5. Arnal JM, Campayo JM, Lora J, Sancho M, Iborra I, and Alcaina I. Declassification of radioactive waste solutions of iodine ( $\text{I}^{125}$ ) from radioimmune analysis (RIA) using membrane techniques. *Desalination* 2000; 129(1):101–105.
6. Chmielewski AG and Harasimowicz M. Influence of gamma and electron irradiation on transport properties of ultrafiltration membranes. *Nukleonika* 1992; 37:61–70.
7. Sancho M. *Tratamiento de Residuos Líquidos Hospitalarios Procedentes de RIA (Radioinmunoanálisis) Mediante Técnicas de Membrana*, 1st ed. Valencia, Spain: Servicio de Publicaciones UPV, 2002.
8. Arnal JM, Sancho M, Verdú G, Campayo JM, and Gozávez JM. Treatment of  $^{137}\text{Cs}$  liquid wastes by reverse osmosis. Part II. Real application. *Desalination* 2003; 154:35–42.
9. Arnal JM. *Tratamiento de Residuos Radiactivos Líquidos y Sólidos Contaminados con Cs-137 Mediante Sistemas Combinados de Separación por Membranas, Lixiviación y Precipitación Química*, 1st ed. Valencia, Spain: Servicio de Publicaciones UPV, 2003.
10. Arnal JM, Sancho M, Campayo JM, and Verdú G. Comportamiento de las Membranas Poliméricas en el Tratamiento de Agua Contaminada Con Cs-137. 8th Mediterranean Congress on Chemical Engineering, Barcelona, November 10–12, 1999.
11. Arnal JM, Sancho M, Campayo JM, Villaescusa JI, and Verdú G. Cs-137 Radioactive Liquid Wastes Treatment using Membrane Techniques. 10th International Congress of the International Radiation Protection Association, Hiroshima, May 14–19, 2000.



---

# 33 Evaluation of Membrane-Based Processing of Radioactive Nuclear Plant Waste: Case Studies

*Anil Kumar Pabby, S.K. Gupta, S.R. Sawant, N.S. Rathore, P. Janardan, R.D. Changrani, and P.K. Dey*

## CONTENTS

33.1	Introduction .....	933
33.2	Removal of Activity from Various Waste Streams Using Ultrafiltration and Reverse Osmosis .....	933
33.2.1	Activity Removal from Fuel Pond Water .....	933
33.2.2	Removal of Activity from Delay Tank Solutions Using an RO Unit .....	934
33.3	Electrodialysis for the Decontamination and Concentration of Low-Active Waste .....	937
33.4	Application of a Perfluorinated Membrane in Fuel Reprocessing .....	938
33.5	Nondispersive Solvent Extraction for the Separation, Removal, and Concentration of Actinides .....	939
33.5.1	Separation of Uranium and Plutonium from Oxalate Supernatant .....	940
33.5.2	Extraction of Macro-Quantities of Uranium .....	941
33.5.3	Extraction of Americium from Acidic Media .....	941
	References .....	943

## 33.1 INTRODUCTION

Membrane-based processing of nuclear plant radioactive waste and radioactive liquids in general is rapidly gaining acceptance within the nuclear industry. Whereas early membrane systems were limited by unreliable hardware and inconsistent performance; modern systems have proven to be both cost effective and superior to conventional processing technologies. In specific installations, the conversion to membrane-based processing has produced significantly pure water, with less secondary waste generation and lower operator radiation exposure [1]. The possible applications of membranes in nuclear programmes are (1) treatment of radioactive liquid effluents, (2) separation and concentration of useful radionuclides, and (3) separation of gaseous streams containing radioactive species.

Membrane processes have been introduced on pilot plant scale in the reprocessing plant of the Bhabha Atomic Research Centre (BARC) to treat various low-active streams. The following case studies are discussed in brief.

## 33.2 REMOVAL OF ACTIVITY FROM VARIOUS WASTE STREAMS USING ULTRAFILTRATION AND REVERSE OSMOSIS

### 33.2.1 ACTIVITY REMOVAL FROM FUEL POND WATER

The primary function of ultrafiltration (UF) systems is to remove colloids and other particulate foulants from feed streams. Activity from fuel pond water is currently removed via ion-exchange columns. Among the drawbacks of ion-exchange purification is the production of substantial amounts of secondary waste during regeneration of the ion-exchange bed. Hence, ultrafiltration was thought to be an attractive alternative for treating fuel pond water [2]. We undertook a pilot study at our reprocessing plant. The typical composition of fuel pond and delay tank waters for the plant is shown in Table 33.1. The spiral-wound module used for the UF and reverse osmosis (RO) studies is detailed in Table 33.2, and the basic flow diagram through the spiral-wound membrane is shown in Figure 33.1. The setup of the UF membrane pilot plant is shown in Figure 33.2.

**TABLE 33.1**  
**Composition of Fuel Pond and Delay Tank Solutions**

Fuel Pond Water		Delay Tank Water	
pH	6.8 to 7.8	pH	6 to 8
Total dissolved salts (TDS)	28 ppm	TDS	1700 ppm
Turbidity	0.3 NTU	Gross alpha	$2.8 \times 10^{-5}$ mCi/L
Gross alpha	$4.6 \times 10^{-6}$ mCi/L	Gross beta/gamma activity	$3.5 \times 10^{-4}$ mCi/L
Gross beta/gamma activity	$3.2 \times 10^{-4}$ mCi/L		

*Note:* mCi/L stands for millicuries per liter.

**TABLE 33.2**  
**Details of UF and RO Module**

Details of Membrane Module	UF	RO
Diameter of UF module	2.5 in.	6 in.
Length of module	12 in.	30 in.
Membrane area	0.5 m <sup>2</sup>	3
Centrifugal pump (flow rate)	180 lph	430 lph
Membrane material	Polysulfone	Polyamide TFC (thin-film composite)
Membrane pore size	100 Å	5–10 Å
Operating pressure	1 bar	15 bar

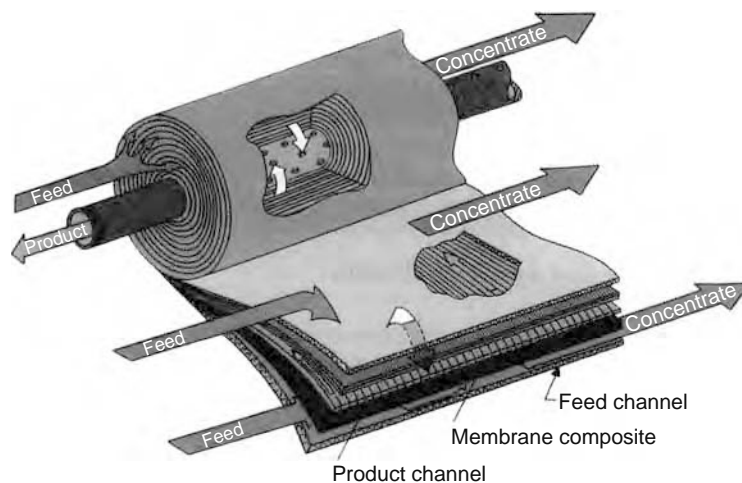


**FIGURE 33.1** Spiral wound module.

The results of the pilot plant study, summarized in Table 33.3, are very positive: 12,000 L of fuel pond water were successfully treated, providing decontamination factor (DF) (Chapter 29) values for alpha and beta of 4 and 5, respectively. The final product obtained from UF had a turbidity of ca. 0.1 NTU (feed turbidity: 0.3 NTU). The flux value was reduced by 15%, which was attributed to possible membrane fouling. The UF module was backflushed with pH 2 solution (HNO<sub>3</sub>), and the original flux value of the permeate was restored. A long-term performance evaluation study was conducted by monitoring the permeate quality (DF value) and radiation dose on the module. No hot spot generation was observed during a pilot run of UF with fuel handling area (FHA) water.

### 33.2.2 REMOVAL OF ACTIVITY FROM DELAY TANK SOLUTIONS USING AN RO UNIT

Adapting RO technology will help to achieve the ALARA concept, which will be beneficial for the environment. In recent years, RO systems have been used to replace or augment existing evaporation or ion-exchange technology due to their lower



FIGURE 33.2 UF membrane setup utilized in fuel handling area.

operating costs [1,3]. The final discharge of low-level active waste (i.e., a mixture of evaporator condensate, ammonium diuranate filtrate, hand washings, etc. from the reprocessing plant) is carried out from the delay tank, which temporarily holds low-active waste. We thus evaluated RO for the removal of alpha activity, beta activity, nitrates, and total dissolved salts (TDS) from delay tank water at the pilot plant.

The specifications of the membrane module, which was supplied by the Desalination Division of the BARC (Mumbai), are listed in Table 33.2. The RO setup installed at the delay tank site is shown in Figure 33.3. The delay tank water composition is given in Table 33.1. The module was operated at a pressure of 15 bar, which was adjusted by a throttle valve placed on the reject line. The experiments were performed both in once-through and recirculation modes. The alpha and beta activities, and nitrate and TDS levels were periodically monitored by sampling the feed, permeate, and reject solutions using standard analytical methods.

The results of the RO studies are summarized in Table 33.4. The DF values for alpha range from 6–10, and for beta, from 6–15. Nitrates and TDS were also strongly rejected by RO. The results from the permeate solution show that after passing 25,000 L, the performance of the pilot plant was quite promising. Furthermore, the same RO setup was used for a delay tank solution containing moderate alpha and beta activity. The DF values (Table 33.4) obtained for alpha are 12–15, which are slightly higher than those obtained for solutions with lower activity. This is because the feed input alpha activity was higher. In recirculation mode, good permeate quality was maintained, whereas alpha and beta activities of the concentrate reached  $10^{-4}$  and  $10^{-3}$  mCi/L, respectively, and TDS levels surpassed 15,000 ppm. The results of the RO studies are summarized in Table 33.5.

**TABLE 33.3**  
Typical Analytical Results of UF Pilot Plant Studies Conducted for Fuel Pond Water

Sample at	Feed Activity (mCi/L)		DF		Permeate NTU	TDS (ppm) <sup>a</sup>	
	Alpha	Beta/Gamma	Alpha	Beta/Gamma		Feed	Permeate
500 L	$2.8 \times 10^{-6}$	$3.5 \times 10^{-4}$	5	4	0.05	28	<10 (45 ppm) <sup>b</sup>
2000 L	$3.8 \times 10^{-6}$	$4.5 \times 10^{-4}$	4	3	0.1	22	<10 (38 ppm)
4000 L	$1.4 \times 10^{-6}$	$5.8 \times 10^{-4}$	4	4	0.1	22	<10 (42 ppm)
8000 L	$2.4 \times 10^{-6}$	$3.9 \times 10^{-4}$	4	4	0.1	35	<10 (54 ppm) <sup>c</sup>
12000 L	$5.2 \times 10^{-6}$	$3.4 \times 10^{-4}$	4	4	0.1	35	<10 (53 ppm) <sup>c</sup>

Note: mCi/L stands for millicuries per liter.

<sup>a</sup> TDS values within the brackets belong to concentrate.

<sup>b</sup> The alpha and beta/gamma activity of concentrate was found to be  $2.2 \times 10^{-5}$  and  $5.5 \times 10^{-3}$  mCi/L, respectively.

<sup>c</sup> The alpha and beta/gamma activity of concentrate was found to be  $3.9 \times 10^{-5}$  and  $3.5 \times 10^{-3}$  mCi/L, respectively.



FIGURE 33.3 RO setup installed at delay tank site in PREFRE plant, Tarapur.

**TABLE 33.4**  
**Typical Analytical Results of RO Pilot Plant Studies Conducted for Delay Tank Solution in Once-through Mode**

Sample at	Feed Activity (mCi/L)		DF		Nitrate (ppm)		TDS (ppm)	
	Alpha	Beta/Gamma	Alpha	Beta/Gamma	Feed	Permeate	Feed	Permeate
400 L	$1.8 \times 10^{-6}$	$2.6 \times 10^{-4}$	10	15	1330	70	2700	150
2800 L	$2.5 \times 10^{-5}$	$2.8 \times 10^{-4}$	8	8	1700	100	3500	300
4000 L	$2.7 \times 10^{-5}$	$3.4 \times 10^{-4}$	7	10	—	—	—	—
8000 L	$1.6 \times 10^{-5}$	$2.2 \times 10^{-4}$	7	8	2200	150	2900	400
15000 L	$2.9 \times 10^{-5}$	$2.4 \times 10^{-4}$	9	8	—	—	—	—
22000 L <sup>a</sup>	$8.0 \times 10^{-5}$	$8.4 \times 10^{-4}$	17	12	1259	278	1875	335
25000 L <sup>a</sup>	$7.0 \times 10^{-5}$	$6.8 \times 10^{-4}$	13	11	—	—	1705	365

Note: mCi/L stands for millicuries per liter.

<sup>a</sup> The delay tank solution contains high alpha and beta activity.

**TABLE 33.5**  
**Typical Analytical Results of RO Pilot Plant Studies Conducted for Delay Tank Liquid in Recirculation Mode**

Sample at	Feed Activity (mCi/L)		DF		Nitrate (ppm)		TDS (ppm)	
	Alpha	Beta/Gamma	Alpha	Beta/Gamma	Feed	Permeate	Feed	Permeate
400 L	$1.7 \times 10^{-6}$	$1.9 \times 10^{-5}$	6	8	1731	294	2080	400
800 L	$2.6 \times 10^{-6}$	$5.0 \times 10^{-5}$	7	8	—	—	—	—
1600 L <sup>b</sup>	$2.2 \times 10^{-6}$	$1.6 \times 10^{-5}$	6	7	1259	278	1875 (15535) <sup>a</sup>	335
2800 L <sup>b</sup>	$1.4 \times 10^{-6}$	$3.6 \times 10^{-5}$	8	8	—	—	—	—
3200 L <sup>b</sup>	$2.6 \times 10^{-6}$	$1.9 \times 10^{-5}$	6	8	—	—	—	—

Note: Initial volume of feed: 400 L; final volume of concentrate: 20 L; volume reduction factor (VRF): 20 m; Ci/L stands for millicuries per liter.

<sup>a</sup> Value given in brackets indicate TDS in reject.

<sup>b</sup> RO in recirculation mode (in the same row, value indicated in bracket shows concentrate TDS).

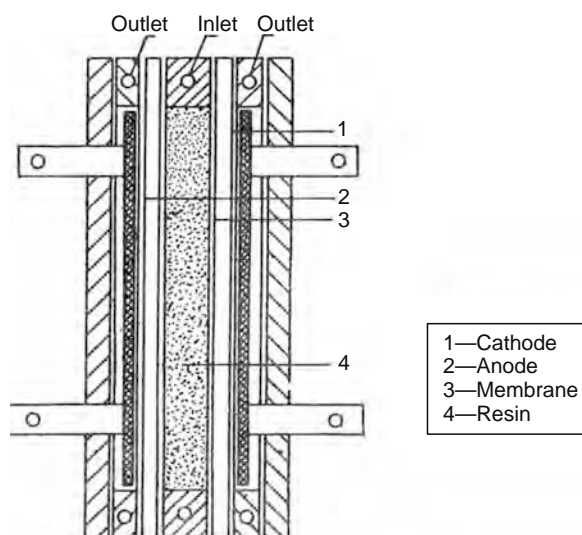


**FIGURE 33.4** Electro-membrane cell for ion concentration. (From Singh, R.K. et al., *Indian J. Chem. Tech.*, 3, 149, 1996. With permission.)

### 33.3 ELECTRODIALYSIS FOR THE DECONTAMINATION AND CONCENTRATION OF LOW-ACTIVE WASTE

Low-active liquid waste (i.e., condensate, regenerant, and detergent) generated in reprocessing plants is subjected to electro dialysis for concentration of radioactive cations into a very small volume, thus rendering a large portion of the waste disposable and environment friendly ( $5 \times 10^{-5}$  mCi/L gross beta activity). For this purpose, an electro-membrane cell containing an ion-exchange membrane in its central compartment was designed and fabricated in the BARC laboratory (Figure 33.4). The electro dialysis (ED) cell was used to further reduce the volume of concentrated stream generated during electro dialysis. The study employed a laboratory model electrolyzer unit (Figure 33.5) that had 41 pairs of vertically alternating cation- and anion-exchange membranes ( $200 \times 80$  mm<sup>2</sup> effective size). The membranes were obtained from M/s. Thermax Ltd. (Pune, India). The interpolymer membranes are composed of high-density polyethylene, polystyrene and divinyl benzene, and functionalized with sulfonic acid, in cation-exchange membranes, and with quaternary ammonium, in anion-exchange membranes [4].

About 5 L each of regenerant and detergent liquid waste were recirculated through the ED cell at the rate of 16 L/h. Samples were collected after each pass and analyzed for fission product activities. Results from a typical test run are given in Tables 33.6 and 33.7. The concentrated stream generated during electrolytic treatment of different waste streams was subjected to electrochemical ion concentration. The electrochemical ion concentrator is composed of three chambers. The central chamber is filled with cation-exchange resin (Zeocarb 225), and is separated from the adjacent cathode and anode chambers by cation-exchange membranes. The electrodes used are made of titanium-expanded sheet metal coated with oxides of precious

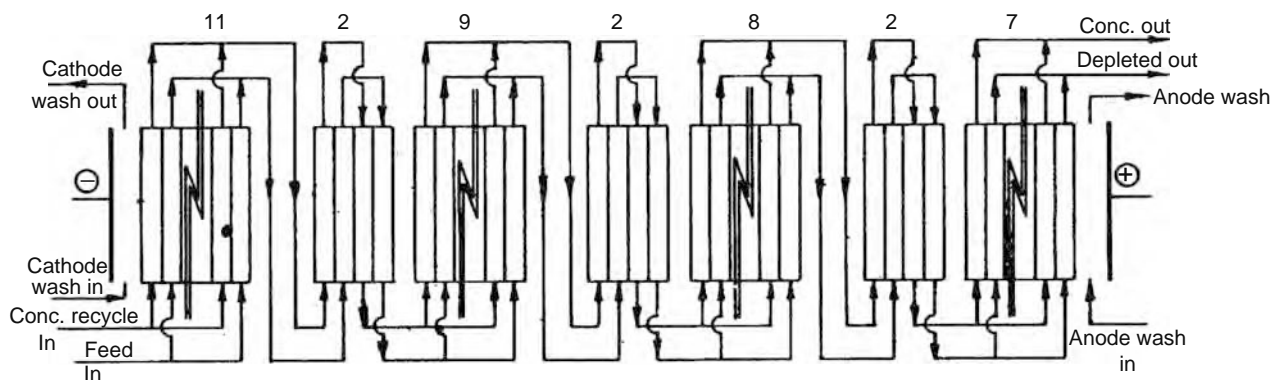


**FIGURE 33.5** Flow diagram of ED cell for concentration of radioactive cations. (From Singh R.K. et al., *Indian J. Chem. Tech.*, 3, 149, 1996. With permission.)

**TABLE 33.6**  
**Electrodialytic Treatment of Regenerant and Detergent Waste**

Radionuclide	Regenerant Waste Activity			Detergent Waste Activity		
	Before ED (mCi/L)	After ED (mCi/L)	DF	Before ED (mCi/L)	After ED (mCi/L)	DF
Cs-134	$3.55 \times 10^{-4}$	$4.36 \times 10^{-5}$	8.1	$7.8 \times 10^{-5}$	$7.09 \times 10^{-6}$	11.0
Cs-137	$4.14 \times 10^{-3}$	$5.57 \times 10^{-5}$	74.3	$1.5 \times 10^{-3}$	$1.36 \times 10^{-4}$	11.0
Ru-106	$6.07 \times 10^{-6}$	$6.96 \times 10^{-7}$	8.7	$8.2 \times 10^{-6}$	$<1.00 \times 10^{-7}$	82.0
Overall DF			45.26			10.73

Source: From Singh, R.K. et al., *Indian J. Chem. Tech.*, 3, 1996. With permission.

Note: Voltage per cell pair: 1–2 V; current density: 20 mA/cm<sup>2</sup>; flow rate: 16 L/h; volume of feed: 5 L; volume of concentrated waste: 0.5 L; VRF: 10; mCi/L stands for millicuries per liter.

metals such as palladium. Inlets and outlets were provided for each chamber. The catholyte and anolyte are fed at the bottom, which overflows from the top. The feed flows into the top of the central chamber and flows out of the bottom. The ions, under the influence of the electric field, move perpendicular to the flow of the solutions. Feed acidity was maintained at 0.01 M HNO<sub>3</sub>. Flow rates for anolyte and catholyte were maintained at about 300–350 bed vol/h. The elutriant in all the experiments was passed at a constant rate of 23 bed vol/h. Samples were drawn at regular intervals and analyzed for Cs-137 activity using a high purity germanium detector coupled with a 4 K multichannel analyzer. Electrochemical ion concentration [5,6] operation involved simultaneous loading and electroelution of cations into the catholyte stream, keeping the effluent activity in the range from  $1 \times 10^{-5}$  to  $1 \times 10^{-4}$  mCi/L. A volume reduction factor (VRF) of ca. 35–40 was easily obtained in this step. An overall VRF of ca. 350–400 was obtained by ED coupled with an ion concentrator.

The main contributors to the radioactivity of the effluent were Cs-137, Cs-134, and Ru-106. Most of the radioactivity from the low-level radioactive effluents could be removed by ED. Greater DF was achieved for cesium than for ruthenium due to the nonionic nature of the latter [12]. The degree of decontamination increased with the number of electrodialysis stages performed. Salt content and radionuclide concentration did not have any marked influence on the decontamination factors of these nuclides [7]. The concentrate streams generated during electrodialysis contained 0.005–0.05 mCi/L of Cs-137, and the VRF achieved in the electrodialysis operation was ca. 10.

### 33.4 APPLICATION OF A PERFLUORINATED MEMBRANE IN FUEL REPROCESSING

Uranous nitrate [U(NO<sub>3</sub>)<sub>4</sub>] solution is used for the quantitative reduction of plutonium from loaded tributyl phosphate (TBP) phase [8]. Membrane cell technology was investigated for the production of 100% uranous nitrate solution [9], which is to be used in the partition cycle of the PUREX process in the fuel reprocessing plant. The membranes used hitherto have suffered from mechanical instability. A study was carried out at the BARC to obtain 100% uranous nitrate solution using a membrane-based electrolytic cell. The membrane used in this study was a thin polymer film reinforced with a Teflon fabric. The film was used as a separator between the anolyte and catholyte chambers, which are made of perfluorinated polymers, thus offering high thermal and chemical stability.

Nafion-perfluorinated membranes are manufactured from copolymers of tetrafluoroethylene and perfluorinated monomers and contain sulfonic groups on one side and carboxylic acid groups on the other. The membranes, originally designed for use in

**TABLE 33.7**  
**Typical Analysis of Concentrate Waste Obtained after ED of Regenerant Waste and Detergent Waste**

Type of Waste	Concentration of Radionuclides (mCi/L)		
	Cs-134	Cs-137	Ru-106
Regenerant	$3.12 \times 10^{-3}$	$4.08 \times 10^{-2}$	$5.35 \times 10^{-5}$
Detergent	$7.11 \times 10^{-4}$	$1.36 \times 10^{-2}$	$<1.00 \times 10^{-5}$

Source: From Singh, R.K. et al., *Indian J. Chem. Tech.*, 3, 1996. With permission.

Note: Volume of concentrated waste: 0.5 L; mCi/L stands for millicuries per liter.

**TABLE 33.8**  
**Details of Electrolytic Membrane Cell**

Material of construction	Perspex, PVC, Neoprene
Capacity of each chamber	100 mL
Total volume of catholyte feed	5 L
Catholyte composition	Uranyl nitrate, 280 gm/L; Hydrazine, 0.5 M; Nitric acid, 3.0 M
Anolyte volume	3 L
Anolyte composition	1.0 M HNO <sub>3</sub>
Membrane	Nafion-900 series
Current density	50 mA/cm <sup>2</sup>

caustic soda production membrane cells, have the extraordinary chemical and thermal stability of Teflon resins but, unlike Teflon, which is among the most hydrophobic substances known, Nafion is among the most hydrophilic. Nafion resins rapidly absorb water at room temperature. The rate of water absorption depends on the number of resin-bound sulfonic and carboxylic groups. We used the cell with different pairs of electrodes to produce a 100% U(NO<sub>3</sub>)<sub>4</sub> solution. Details of the cell are given in Table 33.8, and a schematic of the cell is provided in Figure 33.6. The current efficiency in each case was calculated from measured values (Table 33.9). The membrane was used for over 3 years in nitric acid and hydrazine medium without any apparent damage. It offered high chemical resistance and mechanical strength. In each batch operation, the percentage conversion to uranous nitrate was 100%. The membrane has an established life span of 128 A h/cm<sup>2</sup> with no loss in electrochemical performance. A ca. 10% dilution in product was observed due to electroosmosis. The 100% uranous nitrate solution generated was utilized for the plant process. Several kilograms of uranous nitrate have been produced in the reprocessing plant using this technique.

### 33.5 NONDISPERSIVE SOLVENT EXTRACTION FOR THE SEPARATION, REMOVAL, AND CONCENTRATION OF ACTINIDES

As a part of our comprehensive programme on membrane technology, we evaluated nondispersive solvent extraction (NDSX) with a hydrophobic microporous hollow fiber contactor (HFC) for the separation and removal of actinides [1,10–12]. As the separation and recovery of actinides from different sources is paramount to radiotoxicity, there is a constant need for advances in the field. Among recently developed technologies, membrane extraction using microporous hollow fibers is particularly

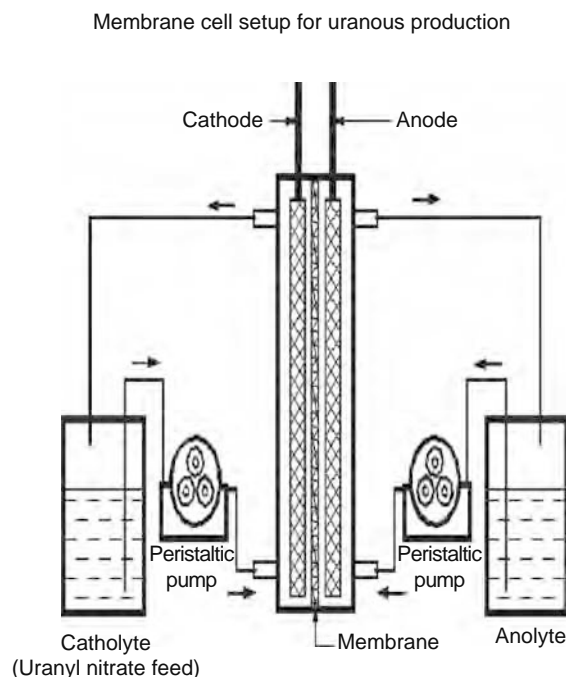


**FIGURE 33.6** Schematic diagram of electrolyzer used for uranous production.

**TABLE 33.9**  
**Electrode Pair versus Current Efficiency**

Sl. No.	Anode	Cathode	Current Efficiency (%)
1	TSIA	TSIA	85
2	Platinized Ti	Platinized Ti	80
3	TSIA <sup>a</sup>	Ti EXP. METAL	100

<sup>a</sup> TSIA stands for titanium substrate insoluble anode.

interesting because of its versatility and the fact that it overcomes problems encountered in conventional liquid–liquid extraction [10,13,14]. NDSX is simply liquid–liquid extraction performed in an HFC, which involves the use of a standard commercial hollow fiber module to bring aqueous and organic phases into contact without dispersion, thereby minimizing the possibility of forming emulsions, third phases, or crud with the extractant. A second module is then used to strip the solute from the loaded organic phase.

### 33.5.1 SEPARATION OF URANIUM AND PLUTONIUM FROM OXALATE SUPERNATANT

Plutonium is recovered by first precipitating out plutonium nitrate as plutonium oxalate, then extracting the oxalate supernatant, which contains milligram levels of plutonium. The typical composition of oxalate supernatant waste is Pu: 25 m/dm<sup>3</sup>, U: 5 gm/dm<sup>3</sup>, Ru<sup>106</sup>: 0.0032 mCi/dm<sup>3</sup>, Cs<sup>137</sup>: 0.003 mCi/dm<sup>3</sup>, HNO<sub>3</sub>: 3M, and H<sub>2</sub>C<sub>2</sub>O<sub>4</sub>: 0.1 M. The separation of uranium and plutonium in presence of fission products from this waste was investigated using 30% TBP/nph. The uranium extraction was quantitative (>99%) from this aqueous waste. Removal of plutonium is more important being a strategic metal and can reduce the load of extraction cycle to achieve high recovery of plutonium. The results from plutonium extractions using acidic, pure plutonium tracer solutions are summarized in Figure 33.7, and were compared to known data for typical plutonium extraction methods. Based on these data, we studied the recovery of U(VI) and Pu(IV) from oxalate supernatant using 30% TBP/*n*-dodecane as extractant, and without addition of nitric acid. The experiments were performed in counter-current recirculation mode with the A/O ratio at 1 using treated (C<sub>2</sub>O<sub>4</sub><sup>2-</sup> ions destroyed by KMnO<sub>4</sub>/H<sub>2</sub>O<sub>2</sub>) and untreated (in presence of C<sub>2</sub>O<sub>4</sub><sup>2-</sup> ions) wastes separately. The results (Figure 33.8) clearly indicate that the recovery of Pu(IV) from untreated waste was >70%, and from treated waste, was >80% whereas uranium recovery was more than 99% from treated oxalate supernatant waste. The same technique was also used to extract and concentrate Pu(IV) from the aqueous phase. We evaluated solutions of uranous nitrate and of hydroxylamine hydrochloride as strippants for the back-extraction of the Pu. The strippants were run through the tube side, and the loaded organic phase was run through the shell side. Extraction of Pu(IV) was not affected by the presence of fission products such as Cs<sup>137</sup>, Ru<sup>106</sup>, and Eu<sup>154</sup>; no Cs, Ru, or Eu was extracted. This may be due to insignificant DF values (partition coefficient for extraction) for such fission products under these conditions [15].

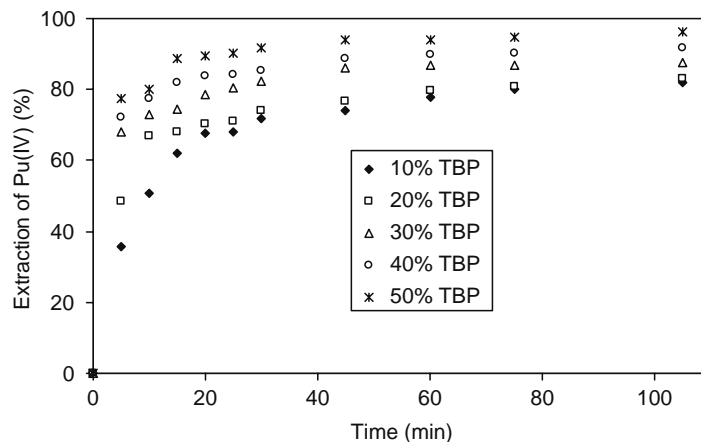


**FIGURE 33.7** Effect of extractant concentration on % Pu(IV) extraction. Feed acidity: 3.0 M HNO<sub>3</sub>; feed concentration:  $1 \times 10^{-5}$  mol/dm<sup>3</sup>; extractant: tributyl phosphate (TBP)/*n*-dodecane; A/O ratio: 1 (200 cm<sup>3</sup> of each). (From Gupta, S.K. et al., *Sep. Sci. Tech.*, 40, 1911, 2005. With permission.)

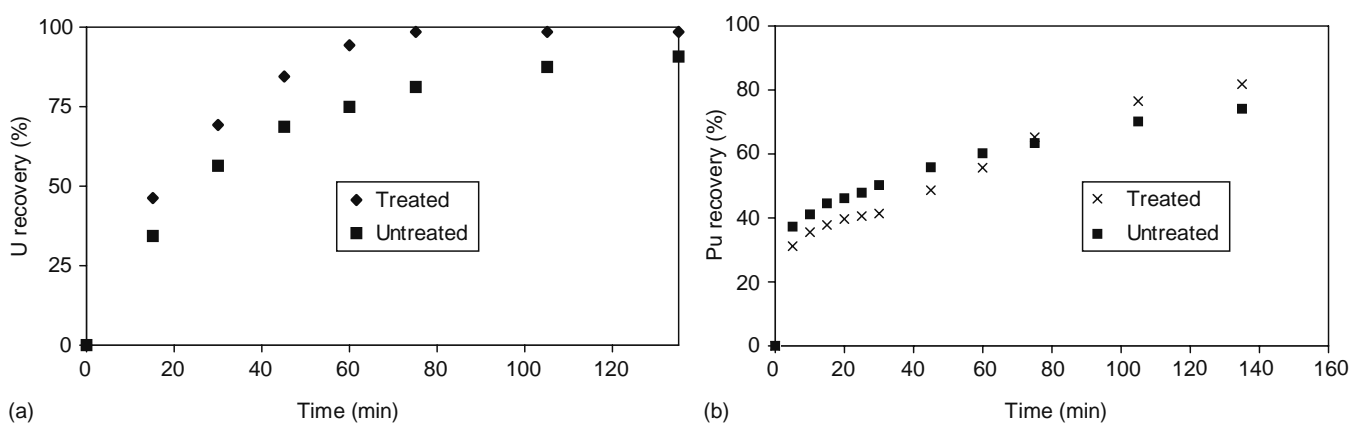


**FIGURE 33.8** Recovery of (a) U and (b) Pu from oxalate supernatant waste (composition of waste given in text). Treated: Waste free from  $C_2O_4^{2-}$  ions; untreated: waste containing  $C_2O_4^{2-}$  ions. (From Gupta, S.K. et al., *Sep. Sci. Tech.*, 40, 1911, 2005. With permission.)

### 33.5.2 EXTRACTION OF MACRO-QUANTITIES OF URANIUM

In the reprocessing plant, macro-quantities of uranium can be separated from several streams. To apply NDSX to the macro-concentration, we first evaluated NDSX for macro-quantities of uranium(VI) using an HFC in recycling mode with tri-*n*-butylphosphate (TBP) in *n*-dodecane as extractant under different chemical and hydrodynamic conditions. A schematic view of the membrane is shown in Figure 33.9. The extraction mechanism of U(VI) through HFC is shown in Figure 33.10. An increase in TBP concentration from 5%–50% led to an increase in U(VI) extraction. However, to ensure economical plant scale operation, we chose 30% TBP as the optimum concentration to evaluate further parameters. A total recovery of >98% was achieved in three consecutive runs using fresh extractant and without adjusting the feed acidity [16]. In studying the effects of U(VI) concentration (ranging 16–116 g/L) on extraction, we observed that for 16 g/dm<sup>3</sup> uranium, 81% extraction was achieved within 135 min (Figure 33.11). However, when the U(VI) concentration was increased to 116 g/dm<sup>3</sup>, the extraction decreased to 51%. This could be due to the limited surface area of the module. U(VI) was stripped from the loaded organic phase using 0.05 M HNO<sub>3</sub> [17].

### 33.5.3 EXTRACTION OF AMERICIUM FROM ACIDIC MEDIA

Since the effluents from nuclear fuel reprocessing plants also contain Am(III), we studied NDSX of Am(III) using the HFC module [17,18], and the acidic extractant PC-88A (2-ethylhexylphosphonic acid mono-2-ethylhexyl ester). The results of the studies are summarized in Figure 33.12. At 30% PC-88A concentration, a maximum extraction of 90% was achieved. Am(III)

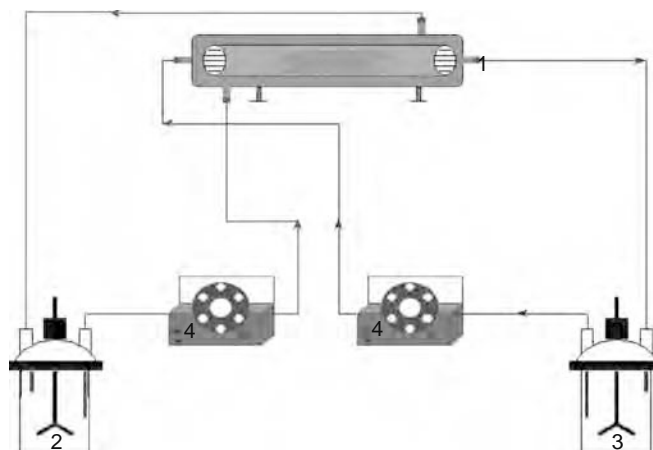


**FIGURE 33.9** Schematic view of hollow fiber membrane contactor operated in recycling mode for U(VI) recovery from aqueous acidic waste: (1) HFC module, (2) feed, (3) extractant, and (4) peristaltic pumps.

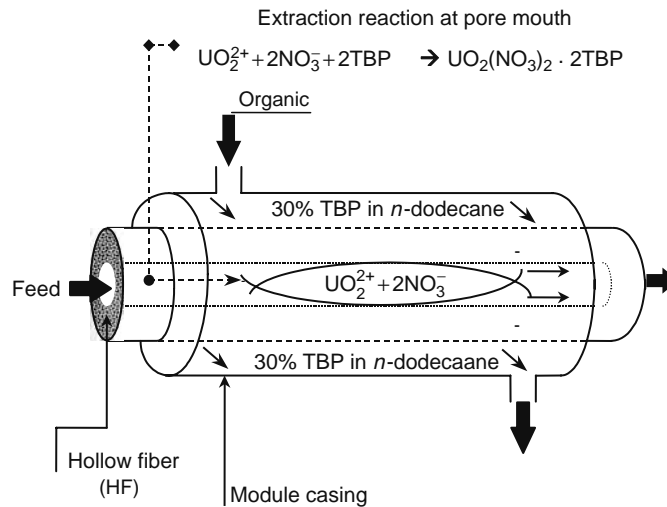


**FIGURE 33.10** Extraction mechanism of U(VI) through HFC. (From Gupta, S.K. et al., *J. Membr. Sci.* 300, 131, 2007. With permission.)

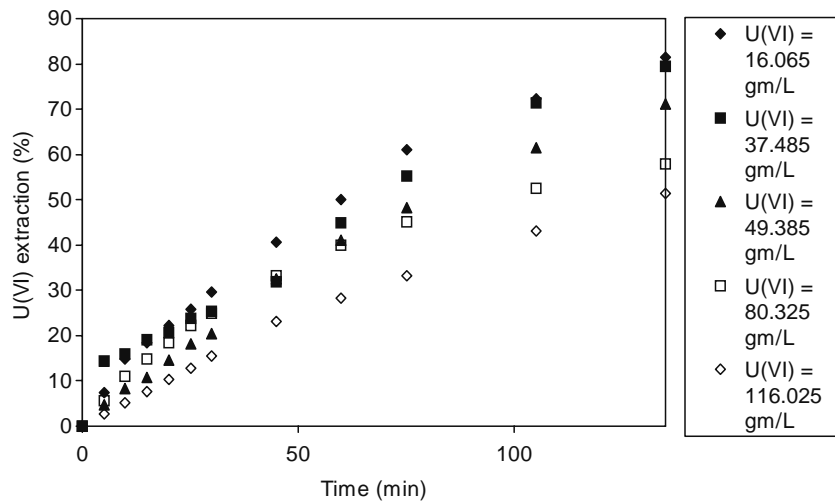


**FIGURE 33.11** Effect of U(VI) concentration on extraction using non-dispersive solvent extraction (NDSX) technique. (From Gupta, S.K. et al., *J. Membr. Sci.* 300, 131, 2007. With permission.)

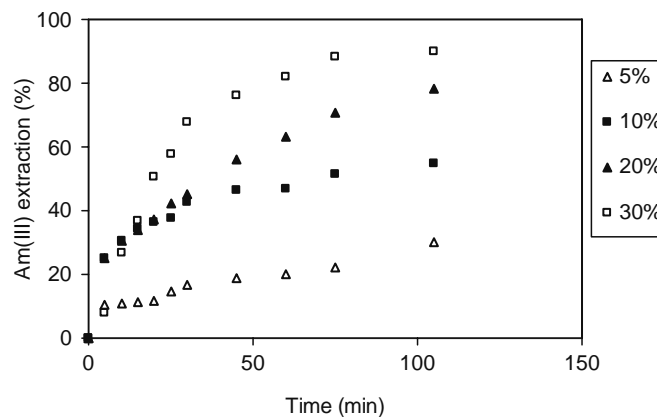


**FIGURE 33.12** Influence of extractant concentration on Am(III) extraction. Extractant: Varying concentration of PC-88A/*n*-dodecane (v/v); feed acidity: 0.001 M HNO<sub>3</sub>; feed Am(III) concentration:  $6 \times 10^{-7}$  M; volume of aqueous/organic: 200 cm<sup>3</sup>; flow rate of aqueous: 5.83 cm<sup>3</sup>/s, flow rate of organic: 1.53 cm<sup>3</sup>/s.

was stripped from the loaded organic using 4.0 M HNO<sub>3</sub>. This technique could be used to pre-concentrate Am(III) from low-active waste using single HFC and maintaining lowest volume of strippant and passing large volume of feed without replacing strippant solution.

## REFERENCES

1. IAEA Technical Reports Series No. 431. 2005. Application of membrane technologies for liquid radioactive waste processing, pp. 1–145. Consultant: Anil K Pabby, Radovan Kohout, and G. Tapsell [<http://www.iaea.org/Publications/index.html>].
2. Pabby AK. et al. Pilot plant experience of ultrafiltration membrane technology for removal of activity from fuel pond water in reprocessing plant at DAE Symposium on Nuclear and Radiochemistry (NUCAR-2005), Guru Nanak Dev University, Amritsar, March 15–18, 2005.
3. Pabby, AK. et al. Role of membrane technology to achieve ALARA concept in reprocessing plant: Utilization of low pressure reverse osmosis for treatment of delay tank solutions at Theme meeting on Trends in Separation Science and Technology-SESTEC 2004 BARC, Mumbai, July 22–23, 2004.
4. (a) Advances in Technologies for Treatment of Low and Intermediate Level Radioactive Liquid Wastes–Technical Report Series No. 370, IAEA, Vienna 1994; (b) Natarajan, R. and Rao, TP. Proceedings of National Workshop on Water Mission, 1988.
5. Helfferich, F. *Ion Exchange*, McGraw Hill, New York, 1962.
6. Singh, RK. Novel method for concentration of low level radioactive waste, *Indian Journal of Chemical Technology*, 3, 149–151, 1996.
7. Sugimoto, S. Removal of radioactive ions from nuclear waste solutions by electrodialysis, *Journal of Nuclear Science and Technology*, 15, 705–709, 1987.
8. Singh, RK. et al. Application of Electrochemical Process in Fuel Reprocessing, BARC Report, BARC/1–1994.
9. Singh, RK. et al. Role of Ion Transfer Membrane in the Production of Uranium Nitrate, BARC Report. BARC/1992/E/002.
10. Pabby, AK. and Sastre, AM. Developments in non-dispersive membrane extraction–separation processes. In *Ion Exchange and Solvent Extraction*, SenGupta, A.K. and Marcus, Y, (Eds.), Chapter 8, Vol. 15, pp. 313–469, Marcel Dekker, New York.
11. Gupta, SK. et al. Application of hollow fiber contactor in non-dispersive solvent extraction of Pu(IV) by TBP, *Separation Science and Technology*, 40, 1911–1926, 2005.
12. Rathore, NS. et al. Hollow fiber supported liquid membrane: A novel technique for separation and recovery of plutonium from aqueous acidic wastes, *Journal of Membrane Science*, 189, 119, 2001.
13. Alexander, PR. and Callahan, RW. Liquid–liquid extraction and stripping of gold with microporous hollow fibers, *Journal of Membrane Science*, 35, 546–49, 1982.
14. Yun, CH. Prasad, R. Guha, AH. and Sirkar, KK. Hollow fiber solvent extraction removal of toxic heavy metals from aqueous waste streams, *Industrial and Engineering Chemistry Research*, 32, 1186–95, 1993.
15. Shukla, JP. and Mishra, SK. Carrier-mediated transport of uranyl ions across tributyl phosphate/dodecane liquid membranes, *Journal of Membrane Science*, 93, 64, 1991.
16. Gupta, SK. et al. Recovery of U(VI) from waste solution using membrane contactor for dispersion-free extraction at Indian Membrane Society Conference, Central Salt and Marine Chemicals Research Institute, Bhavnagar, Gujarat, February 19–20, 2003.
17. Gupta, SK. Actinides Recovery Using Membrane Based Extraction Technique, MSc thesis (Research), University of Mumbai, 2003.
18. Gupta, SK. et al. Non-dispersive extraction of Am(III) using PC-88A as an extractant, at DAE Symposium on Nuclear and Radiochemistry (NUCAR-2003) BARC Trombay, Mumbai, February 10–13, p. 133, 2003.



---

# 34 Application of Donnan Membrane Process for Recovery of Coagulants from Water Treatment Residuals

*Prakhar Prakash and Arup K. SenGupta*

## CONTENTS

34.1	Introduction .....	946
34.1.1	Past Studies on Alum Recovery .....	946
34.1.2	Donnan Membrane Process: New Approach to Alum Recovery .....	947
34.1.3	Scope of This Chapter .....	948
34.2	Donnan Membrane Process: Theory .....	948
34.2.1	Donnan Membrane Process: Basics .....	948
34.2.2	Donnan Membrane Process: Concentration Profile Inside Membranes .....	949
34.2.3	Donnan Equilibrium Condition .....	950
34.2.4	Kinetics of the Donnan Membrane Process .....	951
34.2.5	Transport Equations .....	951
34.2.6	Donnan Membrane Process: Assumptions .....	953
34.2.7	Fundamentals of Alum Recovery .....	953
34.2.8	Solved Example for DMP Application .....	955
34.2.9	Stepwise Modeling Protocol .....	955
34.3	Role of Membrane Structure .....	957
34.4	Diffusion Dialysis: Raising pH of Residual WTR .....	958
34.4.1	Diffusion Dialysis Coefficient .....	959
34.5	Materials and Methods .....	960
34.5.1	Feed and Recovery Solutions .....	960
34.5.2	Donnan Membrane Cell .....	960
34.5.3	Exchange Membrane .....	961
34.5.4	Experimental Procedure and Analytical Techniques .....	961
34.5.5	Jar Tests: Evaluation of Recovered Alum as a Coagulant .....	961
34.5.6	Hydrophilicity of Membranes .....	961
34.5.7	Exchange Capacity ( $Q$ ) of Membranes .....	961
34.5.8	Isotherm Plot Generation .....	962
34.5.9	SEM–XRF Analysis and Analytical Technique .....	962
34.6	Results and Discussion .....	963
34.6.1	Alum Recovery from WTR .....	963
34.6.2	Donnan Exclusion and Fouling .....	963
34.6.3	Fe(III) Recovery .....	963
34.6.4	Relative Carryover .....	965
34.6.5	Recovered Alum as a Coagulant .....	966
34.6.6	Equilibrium Isotherm Plot .....	966
34.6.7	Kinetic Treatment of Alum Recovery in Nafion 117 .....	968
34.6.8	Interdiffusion Coefficient Variation on Membrane Surfaces .....	969
34.6.9	Self-Diffusion Coefficient Comparison in Nafion 117 and Ionac MC 3470 .....	971
34.6.10	Influence of Heterogeneity on Transport Properties of Nafion 117 and Ionac MC 3470 .....	972
34.6.11	Al <sup>3+</sup> Recovery Profile .....	972

34.6.12	Findings from Diffusion Dialysis Experiments .....	974
34.6.13	Influence of Membrane Type on Acid Recovery .....	974
34.6.14	Influence of Acid Type and Concentration on Diffusion Dialysis Recovery .....	975
34.6.15	Aluminum Dissolution Using Diffusion Dialysis .....	975
34.6.16	WTR Dissolution and pH Change .....	975
34.6.17	Fouling of Anion-Exchange Membrane .....	975
34.6.18	Diffusion Dialysis Constant for Acids .....	976
34.7	Conclusions .....	976
34.8	Future Research .....	977
	Acknowledgments .....	978
	References .....	978

## 34.1 INTRODUCTION

There are over 1000 drinking water treatment plants in the United States that use alum,  $\text{Al}_2(\text{SO}_4)_3 \cdot 14\text{H}_2\text{O}$  as a coagulant for the efficient removal of particulate solids and colloids from surface water supplies [1,2]. For alum, the process of coagulation works best in the pH range 4.5–8.0. Similarly, for ferric chloride, another coagulant used in the water treatment plants, the optimum pH range is between 4 and 12. Alum is converted during the process into insoluble aluminum hydroxide, a major component (25%–50%) of solids in water treatment residuals (WTR). Water treatment plants in the United States produce over 2 million tons of aluminum-laden disposable WTR every day [3], which are bulky, gelatinous, and biologically inert slurry composed of suspended inorganic particles, natural organic matter (NOM), trace amounts of heavy metal precipitates, and aluminum hydroxide. The total solids content of the residuals normally ranges from 2% to 10% in mass per unit volume [4,5]. A typical composition of water treatment plant residuals is shown in Table 34.1 [6]. Due to regulatory changes in the recent past, WTR now have to be disposed in landfills or through land application [3,6]. And due to the magnitude and pervasiveness of the problem, the prospect of alum recovery from WTR has received considerable attention in recent years. The toxicity of free and complexed aluminum species toward various aquatic species and benthic organisms has been the focus of several studies [7,8]. Some researchers have linked aluminum ion's contributory influence to occurrence of Alzheimer's disease [9]. It is therefore recognized that the disposal of aluminum-laden solids from water treatment plants will receive a closer scrutiny in the coming years [10]. Ideally, a simple-to-operate process, which can recover alum selectively from the sludge, will significantly reduce the amount of disposable solids. However, the recovered alum has to be sufficiently pure to be reused as a coagulant at the front-end of water treatment. Such a process will truly combine pollution prevention with resource recovery, thus reducing stress on the environment.

### 34.1.1 PAST STUDIES ON ALUM RECOVERY

When WTR are sufficiently acidified with sulfuric acid ( $\text{H}_2\text{SO}_4$ ), insoluble aluminum hydroxide in the solution is converted to aluminum sulfate, which is soluble in the aqueous medium. The stoichiometry of this reaction can be written as follows:

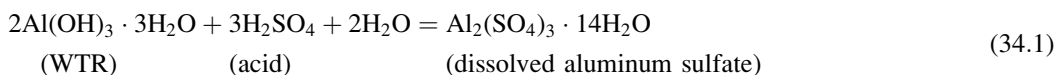


**TABLE 34.1**  
**Typical Composition of WTR**

Substance	Amount (mg/L)
Total suspended solids	100,000–150,000
Total Al(III)	1,000–3,000
Total iron	100–300
Total calcium	<30
Total copper	<10
Total zinc	<20
pH	7.0–7.2
Arsenic	<0.3
Total dissolved organic carbon (DOC)	100–300

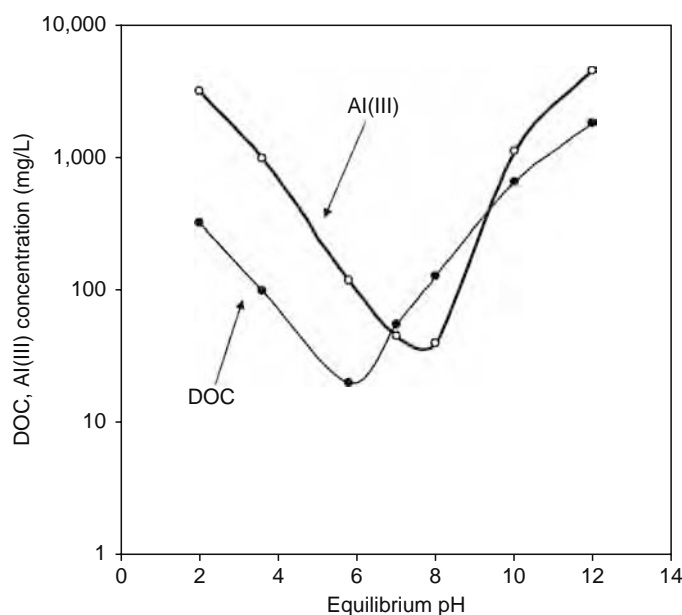


**FIGURE 34.1** Variation of DOC and aluminum ion concentration with pH for WTR from the Allentown Water Treatment Plant (AWTP), Pennsylvania.

Equation 34.1 provides the underlying concept of the *acid digestion process*, which has been tried both at laboratory and at pilot-scale levels [11,12]. The basic concept of the process is simple but the following shortcomings limit the possibility of reusing the recovered liquid alum as a coagulant. The process is nonselective i.e., along with alum it also recovers all other substances that are soluble under highly acidic conditions or that exist as colloids. Thus, naturally occurring organic material (humates and fulvates), which are generally removed quite well by alum coagulation, will be present in the recovered alum. Should this recovered alum be reused as a coagulant, trihalomethane formation potential (THMFP) in the treated water upon chlorination would tend to increase significantly. Trihalomethanes are suspected carcinogens and are regulated by the United States Environmental Protection Agency (USEPA) [13–15].

Since aluminum oxide is amphoteric, alum could theoretically be recovered from the WTR under alkaline conditions as well. Figure 34.1 shows both dissolved organic carbon (DOC) and Al(III) concentration in Allentown, Pennsylvania under water treatment plant conditions. Since a high concentration of dissolved organic matter is very undesirable in recovered alum due to its THMFP, even the *alkali digestion process* is unable to achieve selective alum recovery.

*Liquid ion exchange (LIE)* [16] can concentrate aluminum ions up to 4000 mg/L from an initial 1000 mg/L. But in the stripping stage of LIE, entrainment issues are always a concern, because LIE involves separating aluminum ions from an organic phase into which it is dissolved in the first stage. Since this separation cannot be 100% ideal, one can expect organics being carried over into the alum solution.

*Ultrafiltration* is another technique that can be employed following acid treatment. However, this process suffers from the demerits of fouling, decreased membrane life due to pressure differential, and a decrease in flux with continued deposition [17].

*Two-step composite membrane process* [18] involves selective sorption of aluminum ions from an aqueous phase (containing dissolved aluminum ions in acidified WTR) onto a membrane phase in the first step followed by desorption or regeneration of the composite membrane in a  $H_2SO_4$  solution in the second step with the release of aluminum ions. This patented process was developed in the Department of Civil and Environmental Engineering at Lehigh University. It overcomes many of the shortcomings of the previous processes in that it selectively recovers aluminum ions and prevents passage of natural organic material, heavy metals, and manganese into the recovered alum. However, composite ion-exchange materials are not available in sizes appropriate for large-scale applications.

### 34.1.2 DONNAN MEMBRANE PROCESS: NEW APPROACH TO ALUM RECOVERY

During the last two decades, pressure-driven membrane processes namely reverse osmosis (RO), nanofiltration (NF), and ultrafiltration (UF) have found increased applications in water utilities and chemical industries. Unlike RO, NF, and UF, the Donnan membrane process (DMP) or Donnan dialysis is driven by an electrochemical potential gradient across an ion-exchange membrane. Theoretically, the DMP is not susceptible to fouling because particulate matter or large organic molecules do not concentrate on the membrane surface, as commonly observed with pressure-driven membrane processes. DMP has been used in the past in hydrometallurgical operations [19,20], for concentration of ionic contaminants [21,22] and for separation of

acids from salts [23,24]. Although information on several applications of DMP is available in the open literature, no work is reported on the use of DMP to treat a sludge or slurry with high concentrations of suspended solids or high organic content molecules. It was conceived that a single-step DMP could selectively recover alum, a widely used coagulant, from water treatment plant sludge or WTR.

It is also true that many water treatment plants use ferric chloride as a coagulant in water treatment operations. Ferric ions are trivalent cations, much like aluminum ions. Since the DMP is driven by an electrochemical potential, it is thought that it might be possible to apply it to WTR generated from iron-based coagulants. It was therefore conceived that a single-step DMP could selectively recover ferric ions as well.

### 34.1.3 SCOPE OF THIS CHAPTER

In writing this chapter, the central theme is to detail the readers of the applicability of the DMP for recovering coagulants from WTR. This includes verifying the quality of the recovered alum and studying its usage in coagulation processes. The response of the process to various operating conditions including those of membrane fouling is also discussed. The parameters of study include (1) total coagulant recovery, (2) selectivity of recovered coagulants, (3) effectiveness of recovered coagulants, (4) Donnan exclusion of DOC, (5) feed/sweep solution strength and their volumetric ratio, (6) feed/sweep ion type, (7) membrane area, (8) feed solution turbidity, (9) agitation of solutions, (10) membrane fouling, and (11) settling efficiency of residual WTR. The efficacy of the process for recovery of ferric ions from ferric chloride-based residuals is also discussed briefly.

The other important subject is the comparison of effectiveness of the process in alum recovery for two types of ion-exchange membranes, namely heterogeneous and homogeneous membranes.

In addition, a model has been formulated to predict the self-diffusion coefficient of diffusing species, which are hydrogen and aluminum ions. The interdiffusion coefficient value for the coupled transport of these two ions is also determined for the two types of membranes.

The process of diffusion dialysis is also mentioned briefly, as an attempt to recover spent acid from WTR, after alum recovery. The objective of this process is to estimate the efficacy of the process in (a) raising the pH of the treated WTR and (b) lowering the pH of the fresh WTR before undergoing alum recovery in the DMP.

## 34.2 DONNAN MEMBRANE PROCESS: THEORY

The DMP has been a widely recognized ion-exchange membrane separation process that can be applied to selectively remove ions from a dilute feed solution and to simultaneously enrich them in a sweep solution. The ion of interest (feed ion) in the feed solution is transported to the sweep solution with a counter transport of a driving ion (the sweep ion) from the sweep solution to the feed side. This coupled transport takes place across an ion-exchange membrane until conditions of Donnan equilibrium are achieved. The process utilizes an electrochemical potential gradient that exists between the feed and the sweep solution and requires no external field or pressure gradient to accomplish this transport. The DMP is based on the Donnan co-ion exclusion principle [25], by which negatively charged cation-exchange membranes do not allow anions to pass through the membrane and the positively charged anion-exchange membranes do not allow cations to cross over.

### 34.2.1 DONNAN MEMBRANE PROCESS: BASICS

A fundamental understanding of the DMP requires knowledge of both the ion transport through an ion-exchange membrane and the Donnan equilibrium, the latter indicating the maximum allowable transfer of ions that can take place. The underlying concept can be better explained through an example. This example is also relevant in the context of the objectives of the research, which is alum recovery from water treatment plant residuals [26].

Let us consider aluminum sulfate and sulfuric acid solutions in a Donnan membrane cell divided into two chambers by a cation-exchange membrane that allows only cations to migrate from one side to the other but rejects any passage of anions according to Donnan's co-ion exclusion principle. At equilibrium, the electrochemical potential of aluminum ( $\text{Al}^{3+}$ ) ion ( $\bar{\mu}$ ) in the electrolyte solution on the left hand side (LHS) of the membrane will be the same as that in the electrolyte solution on the right hand side (RHS) i.e.,

$$\bar{\mu}_{\text{Al}}^L = \bar{\mu}_{\text{Al}}^R \quad (34.2a)$$

or

$$\mu_{\text{Al}}^o + RT \ln a_{\text{Al}}^L + zF\phi^L = \mu_{\text{Al}}^o + RT \ln a_{\text{Al}}^R + zF\phi^R \quad (34.2b)$$

where

superscripts “o,” “L,” and “R” refer to standard states of  $\bar{\mu}$ , LHS, and RHS, respectively

$\bar{\mu}$ ,  $a$ ,  $F$ , and  $\phi$  denote electrochemical/chemical potential, chemical potential, activity, Faraday constant, and electrical potential, respectively

$R$  is the universal gas constant

$z$  refers to the charge of the diffusing ion

which is 3 for trivalent aluminum ion  $\text{Al}^{3+}$ . Equation 34.2 gives the following equality for aluminum ions on two sides of the membrane:

$$\frac{F(\phi^L - \phi^R)}{RT} = \ln \left( \frac{a_{\text{Al}}^R}{a_{\text{Al}}^L} \right)^{1/3} \quad (34.3)$$

In a similar way, it can be shown for hydrogen ions that

$$\frac{F(\phi^L - \phi^R)}{RT} = \ln \left( \frac{a_{\text{H}}^R}{a_{\text{H}}^L} \right) \quad (34.4)$$

Since both the feed and the sweep solutions are of similar order of electrolyte strength, it may be assumed that the nonideality effects are about the same on both sides of the membrane, and activities can therefore be replaced by molar concentrations. Equations 34.3 and 34.4 then yield the following:

$$\left( \frac{C_{\text{Al}}^R}{C_{\text{Al}}^L} \right) = \left( \frac{C_{\text{H}}^R}{C_{\text{H}}^L} \right)^3 \quad (34.5)$$

If the ratio  $C_{\text{H}}^R/C_{\text{H}}^L$  is 10, it means  $C_{\text{Al}}^R$  is 1000 times greater than  $C_{\text{Al}}^L$ . Thus, by maintaining high hydrogen ion concentration on the RHS of the membrane, aluminum ions can be driven from the LHS to the RHS even against a positive concentration gradient i.e., from a lower concentration region to a higher concentration one, the impact being more for a higher valent species. For example,  $\text{Al}^{3+}$  will concentrate more than  $\text{Na}^+$ . This example can be extended to any system of coupled transport, a general expression for which would be:

$$\left( \frac{C_i^R}{C_i^L} \right)^{z_i} = \left( \frac{C_j^R}{C_j^L} \right)^{z_j} \quad (34.6)$$

where  $i$  and  $j$  refer to the exchanging ionic species and  $z_i$  and  $z_j$  refer to the valence of these two species.

### 34.2.2 DONNAN MEMBRANE PROCESS: CONCENTRATION PROFILE INSIDE MEMBRANES

A Donnan membrane setup can be divided into two cells by a cation-exchange membrane. Cell I or the feed side solution primarily consists of the feed cation A with a charge  $z_A$  while cell II or the sweep side solution predominantly consists of the sweep cation B, which has a charge  $z_B$ . At the start of the separation process, the concentration of the feed ion A is several folds higher than of sweep ion B in cell I. The cation-exchange membrane has certain selectivity for feed ion A over B. The corresponding selectivity coefficient  $K_B^A$ , described later, relates the preference of the membrane for a particular ion with respect to another ion. A higher selectivity coefficient for A over B in cell I would mean a concentration  $q$  (expressed in moles per cubic millimeter) of cation A on the membrane surface in cell I. In other words,  $q_{A,I}$  will be much higher than  $q_{B,I}$ . The situation is reversed on the sweep side, where there will be a higher concentration of B on membrane surface II, as there is a surplus of sweep ion B in solution. That is to say,  $q_{B,II}$  is much higher than  $q_{A,II}$ . The concentration  $q$  is always less than or equal to the ion-exchange capacity  $Q$  of the membrane. The sum total of the equivalent concentration of the ionic species A and B is equal to the ion-exchange capacity of the membrane, which is defined as the number of ionogenic groups per specified amount of the ion exchanger. For the present case, it is the total number of exchangeable cations per unit volume of the membrane. Exchange capacity determination is discussed in detail, later in this chapter.

The DMP is represented in Figure 34.2a. It can be seen from this figure that the ionic transport is initiated by a concentration gradient across the membrane. It can also be inferred from this figure that the transport process is one of coupled transport, where the movement of feed ion A from the membrane surface in cell I to the membrane surface in cell II is compensated for in the other direction by the sweep ion B. For any amount of ion A transferred to cell II, an equivalent amount of ion B is transferred to cell I, so that the electroneutrality of each solution is maintained. This leads to a change in the fractional concentration of individual species in both cell I and cell II. The resultant change in the membrane phase is a drop in

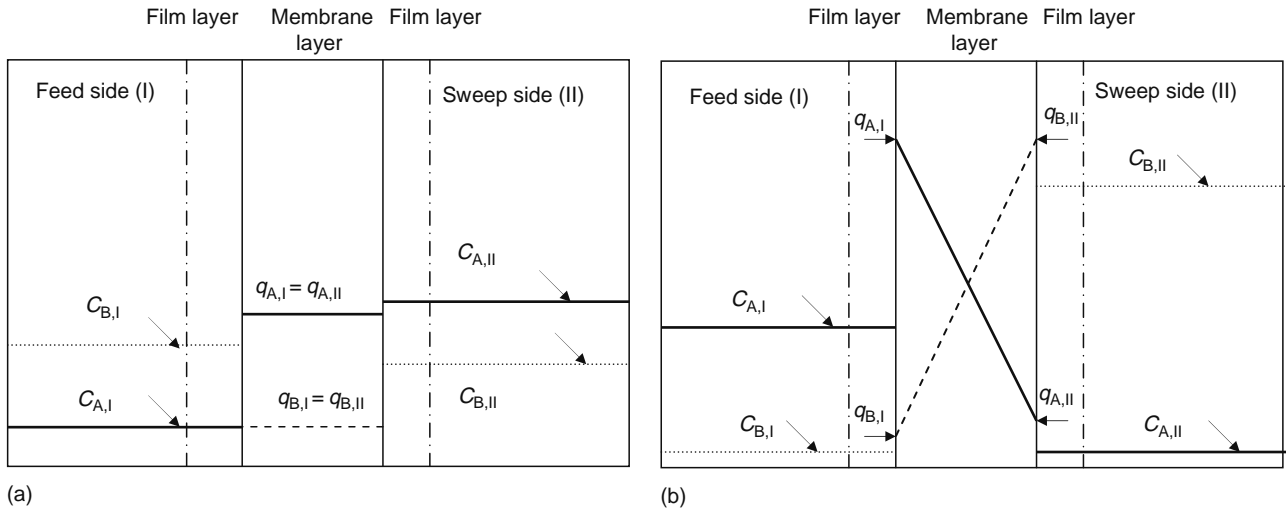


**FIGURE 34.2** (a) Instantaneous ion concentration in the liquid phase and within the membrane under intramembrane transport limited conditions. Note that despite an apparent discontinuity in the concentration of ions at the solution–membrane interface, the chemical potential remains the same in the two phases due to instantaneous equilibrium. (b) Ion concentration at Donnan equilibrium in the liquid phase and within the membrane under intramembrane transport limited conditions. Note that despite an apparent discontinuity in the concentration of ions at the solution–membrane interface, the chemical potential remains the same in the two phases due to instantaneous equilibrium.

$q_{A,I}$  and  $q_{B,II}$  concentration and a simultaneous rise in  $q_{A,II}$  and  $q_{B,I}$  concentration. This leads to a decrease in the gradient. At conditions of Donnan equilibrium,  $q_{A,I} = q_{A,II}$  and  $q_{B,I} = q_{B,II}$ . This situation is represented in Figure 34.2b. The concentration gradient for each ion (A and B) is zero at equilibrium. In addition, species A is concentrated several times over on the sweep side of the Donnan membrane cell at Donnan equilibrium.

### 34.2.3 DONNAN EQUILIBRIUM CONDITION

The conditions of Donnan equilibrium derived in Equation 34.6 can be understood in a slightly different way. For the coupled transport described previously, the heterogeneous exchange of cation A in the aqueous phase and cation B in the membrane phase is represented by the following equation:



The species in the membrane phase have been shown by a bar sign.

The thermodynamic equilibrium  $\hat{K}_B^A$  [27] for this equation can be written as:

$$\hat{K}_B^A = \frac{\bar{a}_A^{z_B} a_B^{z_A}}{a_A^{z_B} \bar{a}_B^{z_A}} \tag{34.8}$$

where  $a$  refers to the activity of the species. For cell I and cell II of the Donnan membrane setup, in contact with the two different surfaces of the membrane, it can be said that

$$\hat{K}_B^A = \frac{\bar{a}_{A,I}^{z_B} a_{B,I}^{z_A}}{a_{A,I}^{z_B} \bar{a}_{B,I}^{z_A}} = \frac{\bar{a}_{A,II}^{z_B} a_{B,II}^{z_A}}{a_{A,II}^{z_B} \bar{a}_{B,II}^{z_A}} \tag{34.9}$$

When the system is in equilibrium, the activity of A and B will be uniform throughout the membrane and there will be no flux. This implies the following:

$$\bar{a}_{A,I} = \bar{a}_{A,II} \tag{34.10}$$

$$\bar{a}_{B,I} = \bar{a}_{B,II} \tag{34.11}$$

Therefore, Equation 34.9 now becomes

$$\frac{a_{B,I}^{z_A}}{a_{A,I}^{z_B}} = \frac{a_{B,II}^{z_A}}{a_{A,II}^{z_B}} \tag{34.12}$$

Since both sides have high electrolyte strength, the activity coefficient term can be assumed identical for a given species in the two solutions, in accordance with the correlation based on modified Debye-Huckel theory proposed by Davies [28]. Therefore, the concentration term can replace the activity coefficient term and the condition for Donnan equilibrium becomes

$$\left(\frac{C_{A,II}}{C_{A,I}}\right)^{z_B} = \left(\frac{C_{B,II}}{C_{B,I}}\right)^{z_A} \quad (34.13)$$

This equation is the same as the one derived in Equation 34.6. It is also worthwhile to point out that for the purpose of our study; the thermodynamic coefficient has been equated to selectivity coefficient, which strictly speaking, takes into account the concentration term of each species and not the activity term. Pellicer et al. [29] have observed in their experimentation that for strong-acid fixed-charge group membranes, the ratio of activity coefficient in the membrane and the aqueous phase approaches unity for strong-acid fixed-charge groups of membranes and for high-ionic strength external solutions. It can therefore be assumed that for the present work, which includes sulfonic acid functional group membranes, the activity coefficient values in both the membrane and the aqueous phase will be close to each other and will cancel out. Therefore, it is assumed that the thermodynamic equilibrium constant can be equated to the selectivity coefficient. Equation 34.8 can therefore be rewritten as

$$K_B^A = \frac{q_A^{z_B} C_B^{z_A}}{C_A^{z_B} q_B^{z_A}} \quad (34.14a)$$

The selectivity coefficient alone will be used throughout this chapter. For the current work, the ions of interest are feed ions ( $Al^{3+}$ ) and sweep ions ( $H^+$ ) and the selectivity of  $Al^{3+}$  with respect to  $H^+$  is defined as

$$K_H^{Al} = \frac{q_{Al}^{z_H} C_H^{z_{Al}}}{C_{Al}^{z_H} q_H^{z_{Al}}} \quad (34.14b)$$

#### 34.2.4 KINETICS OF THE DONNAN MEMBRANE PROCESS

The DMP is an electrochemical-driven process and the driving force is an electrochemical potential gradient that exhibits itself as a passive gradient across the membrane. The coupled transport has been discussed using the Nernst–Planck equation [30]. The DMP involves ion exchange, in which the fluxes of the two species are coupled with one another. The most important feature that distinguishes ion exchange from isotopic exchange is the electric coupling of the ionic fluxes. For conservation of electroneutrality, the fluxes of the exchanging counter ions must be equal in magnitude, since otherwise a net transfer of electric charge would result. The regulating mechanism, which enforces the equality of the fluxes, is the electric field (diffusion potential) set up by the diffusion process. The faster counter ion tends to diffuse at a higher rate. However, any excess charge transfer by the faster ion builds up a space charge, which slows down the faster ion and accelerates the slower ion, and electroneutrality is preserved. These considerations are included in the Nernst–Planck equation. Thus, for any ionic species  $i$ , the flux can be described by the following set of equations:

$$J_{\text{electrical}} = -\left(\frac{\bar{D}_i F}{RT}\right) (z_i) \left(C_i \frac{\partial \phi}{\partial x}\right) \quad (34.15a)$$

$$J_{\text{diffusional}} = -D_i \left(\frac{\partial C_i}{\partial x}\right) \quad (34.15b)$$

$$J_{\text{net}} = J_{\text{electrical}} + J_{\text{diffusional}} \quad (34.15c)$$

The resulting net flux of the species is known as the Nernst–Planck equation, and it holds in ideal systems, for all mobile species present. The set of Nernst–Planck equations must be solved under the appropriate conditions. In derivation of the Nernst–Planck equation, convection and gradients of pressure and activity coefficients are not included.

#### 34.2.5 TRANSPORT EQUATIONS

The fundamental conditions for coupled transport have been discussed in several papers [31,32]. The Nernst–Planck equation can now be applied to the ionic species  $A^{z_A}$  and  $B^{z_B}$ . This flux can be described by a contribution of driving forces:

$$J_A = -\bar{D}_A \left( \frac{\partial q_A}{\partial x} + z_A \right) (q_A) \left( \frac{F}{RT} \right) \left( \frac{\partial \phi}{\partial x} \right) \quad (34.16a)$$

$$J_B = -\bar{D}_B \left( \frac{\partial q_B}{\partial x} + z_B \right) (q_B) \left( \frac{F}{RT} \right) \left( \frac{\partial \phi}{\partial x} \right) \quad (34.16b)$$

where

$J$  and  $q$  are the flux and the concentration of ions in the ion-exchange membrane, respectively  
 $F$ ,  $R$ ,  $T$ , and  $\phi$  are Faraday's constant, gas constant, temperature, and electrical potential, respectively  
 $x$  is the distance in the membrane, perpendicular to the plane of the membrane surface  
 $\bar{D}$  is the self-diffusion coefficient of the diffusing ions

As a special case, when the ions of interest are  $Al^{3+}$  and  $H^+$ , these equations become

$$J_{Al} = -\bar{D}_{Al} \left( \frac{\partial q_{Al}}{\partial x} + z_{Al} \right) (q_{Al}) \left( \frac{F}{RT} \right) \left( \frac{\partial \phi}{\partial x} \right) \quad (34.16c)$$

$$J_H = -\bar{D}_H \left( \frac{\partial q_H}{\partial x} + z_H \right) (q_H) \left( \frac{F}{RT} \right) \left( \frac{\partial \phi}{\partial x} \right) \quad (34.16d)$$

where Al and H refer to  $Al^{3+}$  and  $H^+$  ions.

By the principle of electroneutrality, the concentration of all counter ions is equal to those of fixed ions, namely the exchange capacity ( $Q$ ) throughout the membrane including its two surfaces, as represented by Equation 34.17:

$$z_A q_A + z_B q_B = Q \quad (34.17a)$$

For the case of  $Al^{3+}-H^+$  coupled transport, this translates to

$$z_H q_H + z_{Al} q_{Al} = Q \quad (34.17b)$$

where

$z$  refers to the charge on the ion  
 $Q$  is the exchange capacity of the membrane

Because of the condition of zero current, the sum of the flux of feed ions  $J_A$  and that of the driving ions  $J_B$  is zero:

$$z_A J_A + z_B J_B = 0 \quad (34.18a)$$

For the  $Al^{3+}-H^+$  system, this is represented as

$$z_H J_H + z_{Al} J_{Al} = 0 \quad (34.18b)$$

Using Equations 34.16 through 34.18, the transfer of feed ion A can be described by

$$J_A = -\bar{D}_A \bar{D}_B \left( \frac{z_A^2 q_A + z_B^2 q_B}{z_A^2 q_A \bar{D}_A + z_B^2 q_B \bar{D}_B} \right) \frac{\partial q_A}{\partial x} \quad (34.19a)$$

which for the case of  $Al^{3+}-H^+$  pair is given by

$$J_{Al} = -\bar{D}_H \bar{D}_{Al} \left( \frac{z_H^2 q_H + z_{Al}^2 q_{Al}}{z_H^2 q_H \bar{D}_H + z_{Al}^2 q_{Al} \bar{D}_{Al}} \right) \frac{\partial q_{Al}}{\partial x} \quad (34.19b)$$

Diffusion processes are often described by Fick's first law [33]. For coupled transport, Fick's law can be written as

$$J_A = -\bar{D}_{A,B} \left( \frac{\partial q_A}{\partial x} \right) \quad (34.20a)$$

which describes the coupled interdiffusion of A and B in terms of one diffusion coefficient:

$$\bar{D}_{A,B} = \bar{D}_A \bar{D}_B \left( \frac{z_A^2 q_A + z_B^2 q_B}{z_A^2 q_A \bar{D}_A + z_B^2 q_B \bar{D}_B} \right) \quad (34.20b)$$

This “interdiffusion coefficient” parameter  $\bar{D}_{A,B}$  for the  $Al^{3+}-H^+$  ion pair system can be represented as

$$\bar{D}_{Al,H} = \bar{D}_{Al} \bar{D}_H \left( \frac{z_H^2 q_H + z_{Al}^2 q_{Al}}{z_H^2 q_H \bar{D}_H + z_{Al}^2 q_{Al} \bar{D}_{Al}} \right) \quad (34.20c)$$

Another important point in this mathematical treatment is that the total equivalent strength of the feed and the sweep solution remains conserved in the transfer, as shown

$$z_A C_{A,I} + z_B C_{B,I} = C_{T,I} \quad (34.21a)$$

$$z_A C_{A,II} + z_B C_{B,II} = C_{T,II} \quad (34.21b)$$

where  $C_T$  refers to the total equivalent strength of solution expressed in moles per cubic millimeter.

Once again, the equation can be extended to the  $Al^{3+}-H^+$  ion pair as follows:

$$z_{Al} C_{Al,I} + z_{H,I} C_{H,I} = C_{T,I} \quad (34.21c)$$

$$z_{Al} C_{Al,II} + z_{H,II} C_{H,II} = C_{T,II} \quad (34.21d)$$

Another important term in this discussion is the equivalent ionic fraction of  $Al^{3+}$  which can be written as

$$x_{Al} = \frac{z_{Al} C_{Al}}{C_T} \quad (34.22a)$$

$$y_{Al} = \frac{z_{Al} q_{Al}}{Q} \quad (34.22b)$$

They will be different in cell I and cell II. Equation 34.14b, used to define the selectivity coefficient, can now be rewritten in terms of the equivalent ionic fraction as follows:

$$K_H^{Al} = \left[ \frac{y_{Al}^{z_H}}{(1 - y_{Al})^{z_{Al}}} \right] \left[ \frac{(1 - x_{Al})^{z_{Al}}}{x_{Al}^{z_H}} \right] \left[ \frac{C_T^{(z_{Al} - z_H)}}{Q^{(z_{Al} - z_H)}} \right] \quad (34.23)$$

### 34.2.6 DONNAN MEMBRANE PROCESS: ASSUMPTIONS

The following assumptions have been made in the DMP treatment:

1. Diffusional resistance under experiment conditions lies entirely in the membrane phase i.e., intramembrane solute transport is the rate-limiting step [34].
2. Amount of co-ions (anions) in the membrane is negligibly small compared to its ion-exchange capacity. i.e., Donnan co-ion exclusion principle is valid.
3. Local equilibrium is assumed at the membrane–water interface.
4. Due to equilibrium conditions at the interface, the electrochemical potential of the electrolyte solution is the same as that of the membrane surface contacting it.
5. Amount of ions in the membrane is negligible compared to the amount in the solution.

### 34.2.7 FUNDAMENTALS OF ALUM RECOVERY

The alum recovery process can be conceptualized as in Figure 34.3. Initially, some amount of acid is added to the WTR, to dissolve a portion of the residuals in the aqueous phase and to release  $Al^{3+}$  ions from the solid phase. The resulting solution

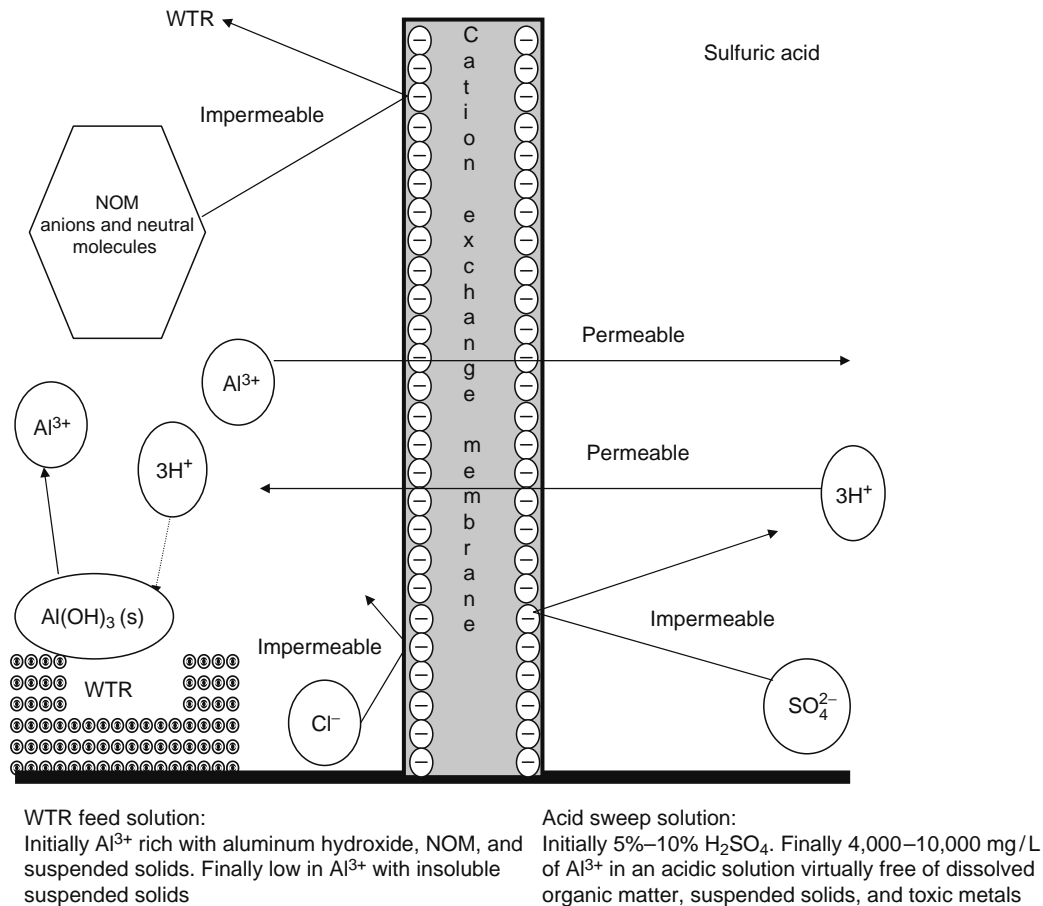


**FIGURE 34.3** Schematic of the DMP illustrating the underlying principles.

constitutes the feed side of the membrane. The sweep side consists of sulfuric or hydrochloric acid (HCl), which supplies hydrogen ions for counter transport. The salient features of the process, as can be seen from this figure are

- $\text{H}_2\text{SO}_4$  or HCl sweep solution allows both dissolution of  $\text{Al}(\text{OH})_3(\text{s})$  and selective  $\text{Al}^{3+}$  recovery through the semipermeable cation-exchange membrane. No pressure differential is required across the membrane.
- Anions (chloride, sulfate, and dissolved organic molecules) cannot permeate through the membrane, and therefore their concentrations on each side remain practically unchanged. The cation-exchange membrane also rejects large-sized neutral organic molecules.
- Process does not have any moving parts and is, therefore, operationally simple. The cation-exchange membranes are chemically stable over the entire range of pH and mechanically strong.
- Since pressure is not the driving force in this process, a high concentration of solids in WTR does not foul the membrane or affect its performance.

The only expendable chemical used in the DMP is  $\text{H}_2\text{SO}_4$  or HCl. It is hypothesized that the application of this process in plants would be beneficial in

- Concentrating aluminum ions in the recovered solution
- Achieving near-complete rejection of NOM or DOC
- Reducing carryover of heavy metals such as copper, zinc, etc., into the recovered alum by offering greater transport to trivalent aluminum ions over these bivalent ions
- Reusing recovered alum as a coagulant in the same plant without the possibility of THM formation upon chlorination
- Reducing the volume of the residuals and the cost of its disposal

A practical application of this process could be in setting up a counter-current flow of acidified water treatment residual feed against an acid sweep solution through a stack of cation-exchange membranes. The process schematic is shown in Figure 34.4 [35].

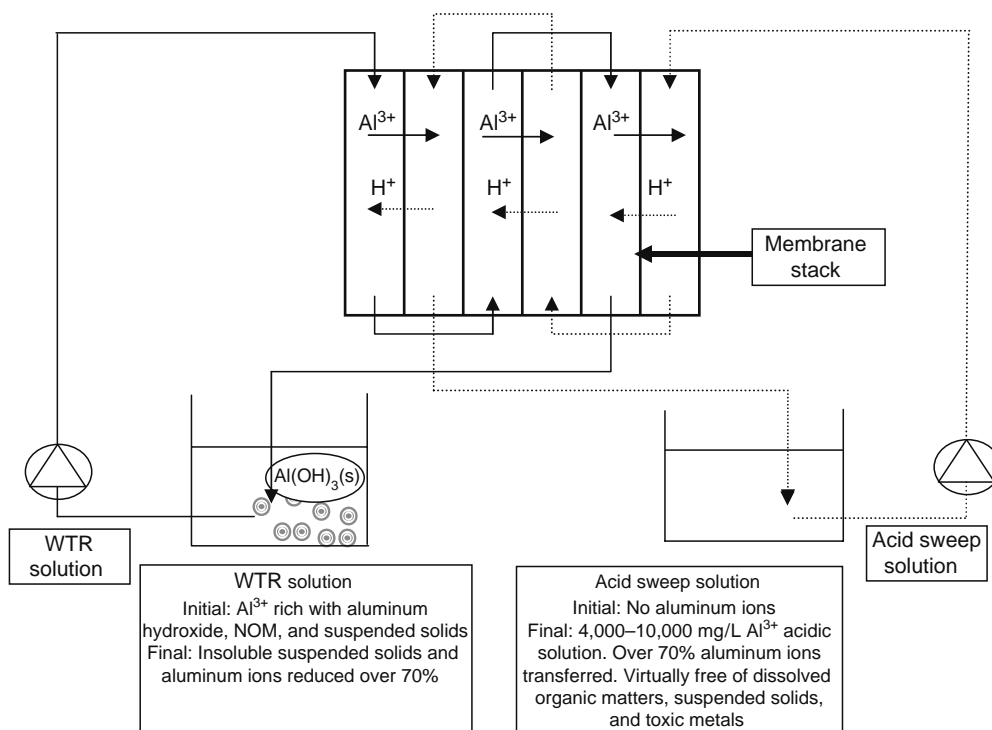


FIGURE 34.4 Process flow diagram for a DMP unit.

### 34.2.8 SOLVED EXAMPLE FOR DMP APPLICATION

Consider a situation with the following initial conditions:

$$\begin{aligned} \text{Cell I volume: } & 6 \text{ L} \\ \text{Cell II volume: } & 2 \text{ L} \\ C_{\text{H},\text{I}}: & 0.001 \text{ M} \\ C_{\text{Al},\text{I}}: & 0.074 \text{ M} \\ C_{\text{H},\text{II}}: & 2.000 \text{ M} \\ C_{\text{Al},\text{II}}: & 0.000 \text{ M} \end{aligned}$$

If  $m$  moles of  $\text{Al}^{3+}$  were transferred from cell I to cell II until Donnan equilibrium was achieved, it would mean that  $3m$  moles of  $\text{H}^+$  would be transferred from cell II to cell I, as the number of equivalents will be preserved in both the cells to maintain zero current conditions. This transfer would satisfy the conditions of Equation 34.5. Substituting for the valence term in this equation,  $m$  can be calculated. It would lead to the following values at equilibrium:

$$\begin{aligned} C_{\text{H},\text{I}}: & 0.221 \text{ M} \\ C_{\text{Al},\text{I}}: & 0.001 \text{ M} \\ C_{\text{H},\text{II}}: & 1.343 \text{ M} \\ C_{\text{Al},\text{II}}: & 0.219 \text{ M} \end{aligned}$$

From this example, it can be concluded that over 98% of  $\text{Al}^{3+}$  ions are recovered in the sweep solution and the sweep-to-feed concentration ratio  $C_{\text{Al},\text{II}}/C_{\text{Al},\text{I}}$  equal to 220 suggests that the recovered ion is also concentrated.

### 34.2.9 STEPWISE MODELING PROTOCOL

Experimental results from our previous studies [26] demonstrated that the diffusional resistance in the liquid phase is negligible under representative experimental conditions and intramembrane transport is the rate-limiting step for the alum recovery process. The following provides a stepwise protocol for the determination of self-diffusion coefficient values and the alum recovery rate for the DMP.

*Step 1: Ion-exchange capacity and  $Al^{3+}/H^+$  isotherm data*

The ion-exchange capacity of the membranes is determined using the standard protocols [36]. Equilibrium data for equivalent ionic fractions of  $Al^{3+}$  and  $H^+$  in the aqueous phase and the corresponding fraction in the membrane phase are then experimentally determined for a given total ionic concentration  $C_T$  expressed in eq/m<sup>3</sup>. Average selectivity value is subsequently generated using Equation 34.14b.

*Step 2: Determination of aluminum flux*

A 24 h experiment (Run 1) is performed for a given feed and sweep solution to generate concentration values of  $Al^{3+}$  in the two solutions at different times. From these concentration values, the average flux data between time  $t_1$  and  $t_2$  can be generated using the following equation:

$$J_{Al} = \frac{(C_{Al,sweep,t_2} - C_{Al,sweep,t_1})V_{sweep}}{(t_2 - t_1)A} \quad (34.24)$$

where

$A$  is the membrane area of exchange

$V_{sweep}$  is the volume of sweep solution

*Step 3: Determination of interdiffusion coefficient*

Once the flux data are available, the average interdiffusion coefficient during that time is given by Equation 34.25 as

$$J_{Al} = -\bar{D}_{Al,H} \left( \frac{q_{Al,I} - q_{Al,II}}{L} \right) \quad (34.25)$$

Local equilibrium is assumed at the membrane–water interface. Thus,  $q_{Al}$  values at both the feed surface ( $q_{Al,I}$ ) and the sweep surface ( $q_{Al,II}$ ) can be computed using the computed average selectivity coefficient value in Step 1 and the known aqueous phase compositions from Step 2. Since  $J_{Al}$ ,  $q_{Al,I}$ ,  $q_{Al,II}$ , and the membrane thickness  $L$  are known, the interdiffusion coefficient  $\bar{D}_{Al,H}$  can be calculated. Note that  $\bar{D}_{Al,H}$  is not constant and it changes with time with the change in membrane composition.

*Step 4: Determination of membrane phase self-diffusion coefficient values*

Equation 34.20c can be arranged as follows:

$$\frac{1}{\bar{D}_{Al,H}} = \frac{1}{\bar{D}_{Al}} + \frac{\bar{D}_{Al} - \bar{D}_H}{\bar{D}_H \bar{D}_{Al}} \left[ \frac{1}{1 + \left( \frac{z_H^2}{z_{Al}^2} \right) \left( \frac{q_H}{q_{Al}} \right)} \right] \quad (34.26)$$

Considering  $z_H = 1$ ,  $z_{Al} = 3$ , and  $y_{Al} + y_H = 1$ , Equation 34.26 becomes

$$\frac{1}{\bar{D}_{Al,H}} = \frac{1}{\bar{D}_{Al}} + \frac{\bar{D}_{Al} - \bar{D}_H}{\bar{D}_H \bar{D}_{Al}} \left[ \frac{1}{1 + \frac{1}{9} \left( \frac{1 - y_{Al}}{y_{Al}} \right)} \right] \quad (34.27)$$

From experimental data, the values of  $\frac{1}{\bar{D}_{Al,H}}$  are plotted against  $\frac{1}{1 + \frac{1}{9} \left( \frac{1 - y_{Al}}{y_{Al}} \right)}$ . Since the membrane has a high selectivity for trivalent

aluminum ion over monovalent hydrogen ion,  $H^+$  ions are essentially the minor species within the membrane phase. The intercept of Equation 34.27 can be used to calculate  $\bar{D}_{Al}$  and it can be substituted in the expression for slope to obtain  $\bar{D}_H$ . This approach can only be applied as a first approximation, as overall interdiffusion coefficient has been used to represent the interdiffusion coefficient value on a membrane surface. This assumption is not true, since interdiffusion coefficient is a function of ionic distribution and is unique at each point across the membrane. It is hypothesized in this model that while the true value of self-diffusion coefficient  $\bar{D}_{Al}$  and  $\bar{D}_H$  needs to be calculated separately from the model, the relative deviation from the true value in the linear regression approach described in Equation 34.27 is the same for both  $Al^{3+}$  and  $H^+$ . Therefore, the ratio  $\bar{D}_{Al}/\bar{D}_H$  determined from the plot for Equation 34.27 is the same as the ratio for the true values obtained from the model.

*Step 5: Aluminum ion concentration profile*

A numerical integration technique is applied to calculate the aluminum ion concentration at intermediate times. The input parameters are (1) initial concentration of the ions in the feed and the sweep solutions,  $C_{Al,feed}$ ,  $C_{Al,sweep}$ ,  $C_{H,feed}$ , and  $C_{H,sweep}$ , (2) volume of the two solutions,  $V_{feed}$  and  $V_{sweep}$ , (3) area of exchange  $A$ , (4) self-diffusion coefficient  $\bar{D}_{Al}$  and  $\bar{D}_{Al}/\bar{D}_H$  determined from Step 4, and (5) wet membrane thickness,  $L$ . Two sets of equations are generated from the isotherm plot for

feed and sweep conditions, relating the ionic fraction of  $\text{Al}^{3+}$  in the membrane phase to that in the aqueous phase. These equations coupled with the Nernst–Planck equations discussed in the theory are applied in a model that uses  $\bar{D}_{\text{Al}}$  as an operating parameter to predict  $\text{Al}^{3+}$  concentration profile in the feed and sweep solutions.

#### Step 6: Osmosis effect

To incorporate dilution effect, a separate experiment is carried out with known concentration of NaCl on the sweep side and deionized water on the feed side of the membrane to determine the osmosis of water. Water flux is related to the difference in electrolyte strength of the two solutions and has been validated in previous studies [37]. For the current work, it can be assumed that the water flux  $\hat{J}_{\text{osmosis}}$  ( $\text{m}^3/\text{m}^2 \text{ h}$ ) is proportional to the difference of ionic concentration in the two solutions.

$$\hat{J}_{\text{osmosis}} = K_{\text{osmosis}} \Delta C \quad (34.28)$$

where

$$\Delta C = C_{\text{sweep}} - C_{\text{feed}}$$

$C$  is the summation of molar concentration of all ionic species in the given solution

$k_{\text{osmosis}}$  is the proportionality constant or the “osmosis parameter”

The value of  $k_{\text{osmosis}}$  was determined from this experiment as  $1.13 \times 10^{-7} \text{ m}^4/\text{mol h}$  and was used in the modeling program.

### 34.3 ROLE OF MEMBRANE STRUCTURE

An investigation into the transport of exchanging ions in the DMP application for alum recovery should consider the structure of the membrane, as the transport of ions is related to the resistance offered in the membrane phase. On the basis of the structure and method of preparation, two different types of ion-exchange membranes have been identified. Homogeneous membranes are coherent ion-exchanger gels. Heterogeneous membranes consist of colloidal ion-exchanger particles embedded in an inert binder. Methods of preparing these membranes are different and are available in the open literature [38].

Several researchers have studied the influence of nonuniformity of ion-exchange membranes on various transport properties of membranes such as electrical conductivity, transport numbers, and diffusion permeability [39–41]. A membrane may be considered to be a system of two or more phases. Timashev [42] proposed a two-phase model with a hydrophobic backbone and a hydrophilic ion-exchange group, including sorbed water. Zabolotsky and Nikonenko [43] suggested that a membrane could be represented as a combination of a conducting phase and a nonconducting phase. The conducting phase or the gel phase comprised a relatively uniform distribution of ionogenic groups, hydrophilic parts of the matrix polymer chains, and an electroneutral solution filling the interstices between these elements in the gel phase. The nonconducting phase or the inert phase formed from the hydrophobic parts of the polymer matrix or from the inert binder introduced during the synthesis stage. It can therefore be stated that the membrane morphology is represented by two constituents or phases:

1. Conducting fraction  $f_{\text{gel}}$  that includes the conducting gel or hydrophilic phase with ionogenic groups
2. Nonconducting fraction  $f_{\text{inert}}$  that includes the nonconducting polymer matrix and inert binding without ionogenic groups

In a homogeneous membrane, the nonconducting fraction  $f_{\text{inert}}$  is much lower than in a heterogeneous membrane. Homogeneous membranes are therefore coherent ion-exchanger gels and heterogeneous membranes consist of colloidal ion-exchanger particles embedded in an inert binder. Conceptually, this information can be represented in Figure 34.5a and 34.5b. Figure 34.5a depicts the distribution of the ionogenic groups within a homogeneous membrane while Figure 34.5b represents the same inside a heterogeneous membrane. It may be noted that the nonconducting inert fraction  $f_{\text{inert}}$  is significantly greater within the heterogeneous membrane. Under nonequilibrium conditions, a diffusing cation hops from one charged site to the next within the membrane and that constitutes the primary ion transport mechanism for homogeneous membranes as illustrated in Figure 34.6a. For heterogeneous membranes, the nonconducting or inert fraction offers resistance to ion transport in the following two ways: first, tortuosity or the path length of ion transfer through the membrane is increased; and second, the stagnant inert phase with minimal or no ionogenic groups is always less conducive to transport of ions. For counter transport of aluminum and hydrogen ions in a heterogeneous membrane, Figure 34.6b illustrates the foregoing effects of the inert phase. In this study, a homogeneous cation-exchange membrane, Nafion 117 from DuPont, Delaware, and a heterogeneous membrane, Ionac MC 3470 from Sybron Chemicals, New Jersey, were used. A series of laboratory experiments were carried out to compare the alum recovery from WTR using these two membranes.

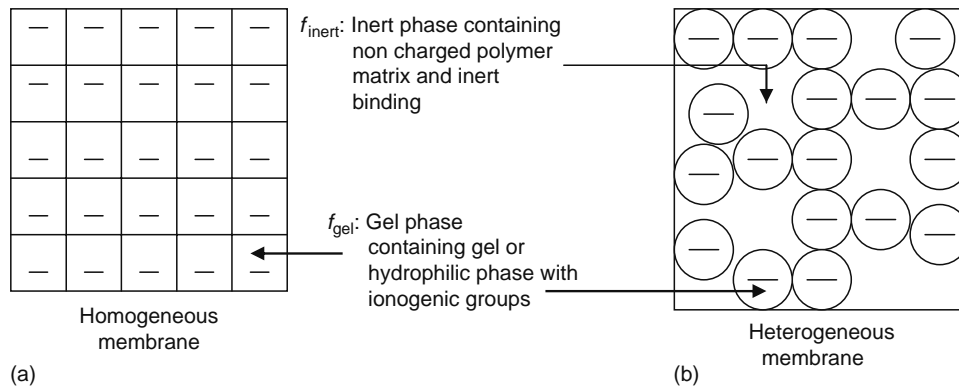


**FIGURE 34.5** Conceptualized distribution of ionogenic groups within cation-exchange membranes for (a) homogeneous membrane and (b) heterogeneous membrane.

#### 34.4 DIFFUSION DIALYSIS: RAISING pH OF RESIDUAL WTR

The residual feed, low in  $\text{Al}^{3+}$  content, has a low pH. Its pH needs to be raised before the residuals are discharged. While an obvious solution is to add lime to raise the pH, in the current research work, a novel application of another membrane process, diffusion dialysis, was tried. Diffusion dialysis has been applied earlier to recover spent acid [23,24]. It was first applied during the 1950–1960s [44–46]. In this process, an anion-exchange membrane separates an acid-rich solution from an acid-deficient solution. The anion-exchange membrane is impermeable to all cations except  $\text{H}^+$  ions. They leak through the membrane as neutral acid molecules under the influence of a chemical potential gradient. It is hypothesized that if diffusion dialysis process is applied in a process in which posttreatment residual feed is separated from fresh WTR solution using anion-exchange membranes, the acid molecules will leak from the residual feed side to the fresh feed side. In the process, the pH of the residual feed will rise and the fresh feed pH will drop, thereby dissolving aluminum ions locked up in the solid phase. Operationally, this process is similar to the DMP shown in Figure 34.5, except that a stack of anion-exchange membranes replaces the cation-exchange membranes and the transport process entails movement of neutral acid molecules from residual feed solution (emerging from a recently completed DMP) to a solution of fresh feed, which is later treated in the DMP. The two processes can be combined together conceptually, as shown in Figure 34.7.

Diffusion dialysis relies on the difference in chemical potential of species on either side of a membrane and external power is only required to circulate the solutions. The separation of acid from its electrolyte solution is achieved by using an anion-exchange membrane. The membrane allows the selective transport of anions across the membrane, while ideally remaining impermeable to cations other than protons. Proton leakage takes place due to its high mobility. This migration takes place by both diffusion and by transfer from a water molecule to another through a mechanism referred to as the Grotthius mechanism [47]. The goal of the diffusion dialysis process is to raise the pH of the residual feed before its disposal and to simultaneously

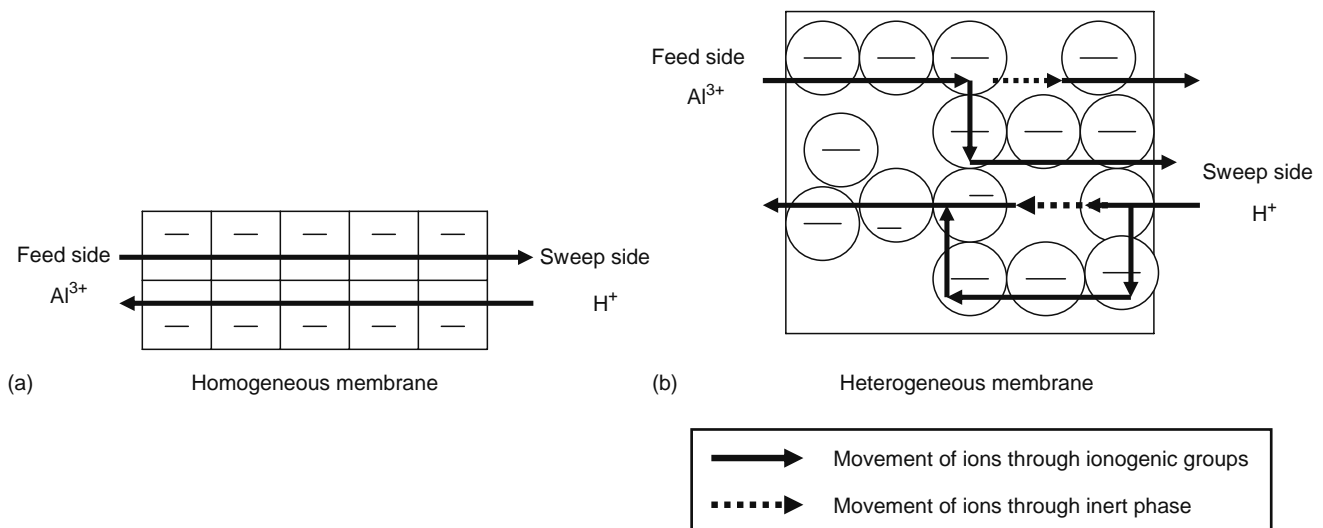


**FIGURE 34.6** Counter transport of (a)  $\text{Al}^{3+}$  and (b)  $\text{H}^+$  through homogeneous and heterogeneous membranes.

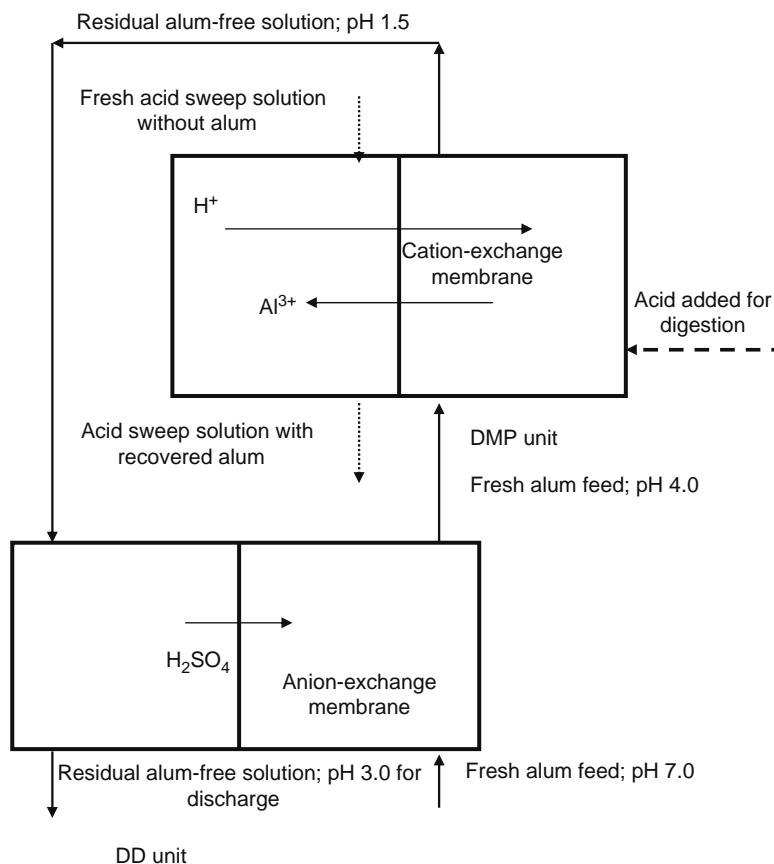


FIGURE 34.7 Integrated process comprising a DMP unit and a diffusion dialysis unit.

dissolve  $Al^{3+}$  ions in the fresh feed. This implies that the acid should diffuse fast enough through the anion-exchange membrane. The kinetics of the process plays an important role. It therefore depends on the choice of the acid used in the diffusion dialysis process and the choice of membrane. Some acids tend to diffuse faster than others and some membranes offer lower resistance to the diffusion process. A parameter often employed to determine the transfer kinetics is the dialysis coefficient,  $U$ .

### 34.4.1 DIFFUSION DIALYSIS COEFFICIENT

The dialysis coefficient  $U$  for a given component in solution in diffusion dialysis cell is given by the amount of the component that is transported per unit active membrane area, per unit time, and per unit concentration difference of the component. This translates into the following equation:

$$U = \frac{W}{(AtM)} \tag{34.29a}$$

where

- $W$  is the amount of the component transported in moles
- $A$  is the active membrane area in square meters
- $t$  is the time in hours

For specific acids, it can be expressed as

$$U_{H_2SO_4} = \frac{W_{H_2SO_4}}{(AtM_{H_2SO_4})} \tag{34.29b}$$

$$U_{\text{HCl}} = \frac{W_{\text{HCl}}}{(AtM_{\text{HCl}})} \quad (34.29c)$$

where  $M$  is the log-mean concentration difference expressed as

$$M = \frac{(C_{f,0} - C_{p,t} - C_{f,t})}{\ln\left(\frac{C_{f,0} - C_{p,t}}{C_{f,t}}\right)} \quad (34.29d)$$

where

$C_{f,0}$  is the concentration of the feed solution at time 0

$C_{p,t}$  is the concentration of the permeate solution at time  $t$

$C_{f,t}$  is the concentration of the feed solution at time  $t$  [48]

The numerator term is not equal to zero because of volume changes that occur in cell chambers caused by water transport across the membrane during the experiment. The selectivity of the membrane for one acid over another can be described as

$$K_{\text{HCl}}^{\text{H}_2\text{SO}_4} = \frac{U_{\text{H}_2\text{SO}_4}}{U_{\text{HCl}}} \quad (34.30)$$

Knowledge of the selectivity and diffusion dialysis coefficient can be used to determine the membrane that offers lower resistance to acid diffusion. It also helps in determining the faster-diffusing acid.

## 34.5 MATERIALS AND METHODS

### 34.5.1 FEED AND RECOVERY SOLUTIONS

The feed consisted of WTR collected from the Allentown Water Treatment Plant (AWTP) (Allentown, Pennsylvania) and the Baxter Plant (Philadelphia, Pennsylvania). The former uses alum as a coagulant and the latter applies ferric chloride in the coagulation process. Total suspended solids content of the WTR obtained from the AWTP varied between 2% and 4% mass per volume. In some experiments, synthetic feed solutions were prepared using aluminum sulfate (Fisher Scientific, Bethlehem, Pennsylvania) and ferric chloride (Sigma Chemicals, Bethlehem, Pennsylvania). The recovery side solution consisted of 10% (2N)  $\text{H}_2\text{SO}_4$  purchased from E M Science, Bethlehem, Pennsylvania. To investigate the effect of turbidity on solute flux and membrane fouling, fine (<200 mesh size) inert glass powder (Potters Industries, Valley Forge, Pennsylvania, Product number: 6000) was used as the source of turbidity.

### 34.5.2 DONNAN MEMBRANE CELL

The Donnan membrane cell was made of Plexiglas, partitioned into two chambers, as shown in Figure 34.8 with dimensions  $L = 30$  cm,  $W = 7$  cm, and  $H = 40$  cm. Fixed volumes of feed (WTR) and recovery (acid) solutions were used for every run;

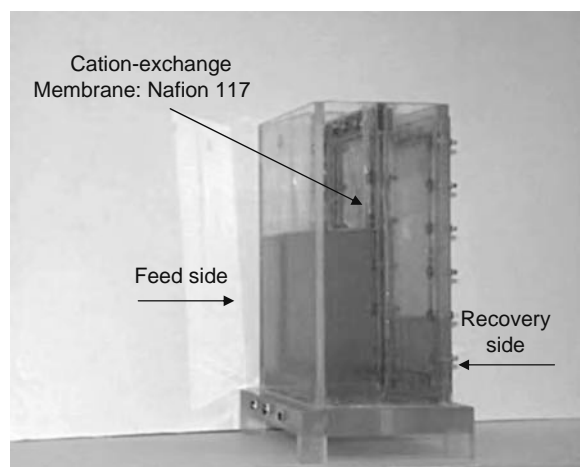


FIGURE 34.8 Laboratory setup for a variable volume Donnan membrane cell.

**TABLE 34.2**  
**Properties of Ionac 3470 and Nafion 117 Membranes**

Type	Heterogeneous <sup>a</sup>	Homogeneous <sup>a</sup>
Ionic form as shipped	Na <sup>+</sup> <sup>a</sup>	H <sup>+</sup> <sup>a</sup>
Exchange capacity (wet basis)	1896 eq/m <sup>3</sup>	1372 eq/m <sup>3</sup>
Membrane thickness (wet basis)	0.466 mm <sup>a</sup>	0.200 mm <sup>a</sup>
Reinforcement	Inert binding <sup>a</sup>	No reinforcement <sup>a</sup>

<sup>a</sup> Information obtained from www.dupont.com and www.sybronchemicals.com.

the ratio of WTR volume to acid volume could be adjusted independently in the test cell. Solutions in both chambers were agitated using instrument quality compressed air at 1 psi g.

### 34.5.3 EXCHANGE MEMBRANE

The cation-exchange membranes used in the experiments were the homogeneous Nafion 117 from Dupont and the heterogeneous Ionac MC 3470. Pertinent details are provided in Table 34.2. The exchange capacity data were determined in the laboratory following standard experimental protocols [31,36].

### 34.5.4 EXPERIMENTAL PROCEDURE AND ANALYTICAL TECHNIQUES

The feed was allowed to exchange aluminum ions with hydrogen ions from the recovery solution for a period of 10–72 h, depending on the objective of each experiment. Samples were collected at regular intervals from both feed and the recovery side. Aluminum was analyzed using UV-VIS spectrophotometer. This analysis involved the eriochrome cyanine R method described in Ref. [49]. Other metals such as iron, copper, magnesium, arsenic, and zinc were analyzed with an atomic absorption spectrometer (Perkin Elmer: Model AA100 and Perkin Elmer: Model SIMAA 6000). The DOC was measured using a TOC Analyzer (Dohrman: Model DC-190) and sulfate ions were analyzed for Donnan exclusion using a dionex ion chromatograph (Model 4500i).

### 34.5.5 JAR TESTS: EVALUATION OF RECOVERED ALUM AS A COAGULANT

Jar tests were conducted to evaluate the coagulation efficiency of the recovered alum. For the purpose of comparison, commercial alum obtained from AWTP and mixed alum (50% recovered alum and 50% commercial alum) were employed as coagulants in jar tests. The water from the Little Lehigh River, which is the primary water source of the AWTP, was used to examine the coagulation efficiency of recovered alum. During the jar tests, predetermined doses (for a typical water treatment plant) were added into beakers, which contained 1.0 L of the AWTP water. After stirring and subsequent settling, samples of water were collected from the top (within 2 in. from the surface) of every beaker and analyzed.

### 34.5.6 HYDROPHILICITY OF MEMBRANES

Experiments were performed to measure the hydrophilicity of the membranes. For this purpose, the two membranes, Nafion 117 and Ionac MC 3470, were dipped in the WTR solution for over 48 h. Samples were viewed under a goniometer (an instrument used to measure contact angles of droplets placed on a substrate surface to indicate surface energies/wetting capabilities), to measure the contact angle of water with the membrane surface. For this purpose, a small sheet of the membrane surface was kept under observation, a drop of water added by a syringe on the surface, and the drop allowed to settle for a few minutes. The contact angle made by the drop with the surface was measured manually. The angle was compared against that for a standard hydrophobic material. For this purpose, PTFE sheet was used. Figure 34.9 shows the different contact angles for the three surfaces. It can be observed that the contact angle for Nafion 117 surface is the lowest at 60°, for Ionac MC 3470 surface it is approximately 70°, and the PTFE surface has a contact angle of approximately 120°. This result is an indication of the hydrophilic nature of the two membranes and it suggests that the cation-exchange membranes may be resistant to membrane fouling by hydrophobic NOM during the DMP.

### 34.5.7 EXCHANGE CAPACITY (Q) OF MEMBRANES

For exchange capacity determination of Nafion membranes, a 10 × 10 cm membrane was completely converted to Na<sup>+</sup> form by allowing it to exchange with 2N NaCl solution for 48 h in two consecutive experimental runs of 24 h each. The membrane was cleaned thoroughly in deionized water, dried with filter paper, and then stripped of Na<sup>+</sup> ions in two batches by exchanging with

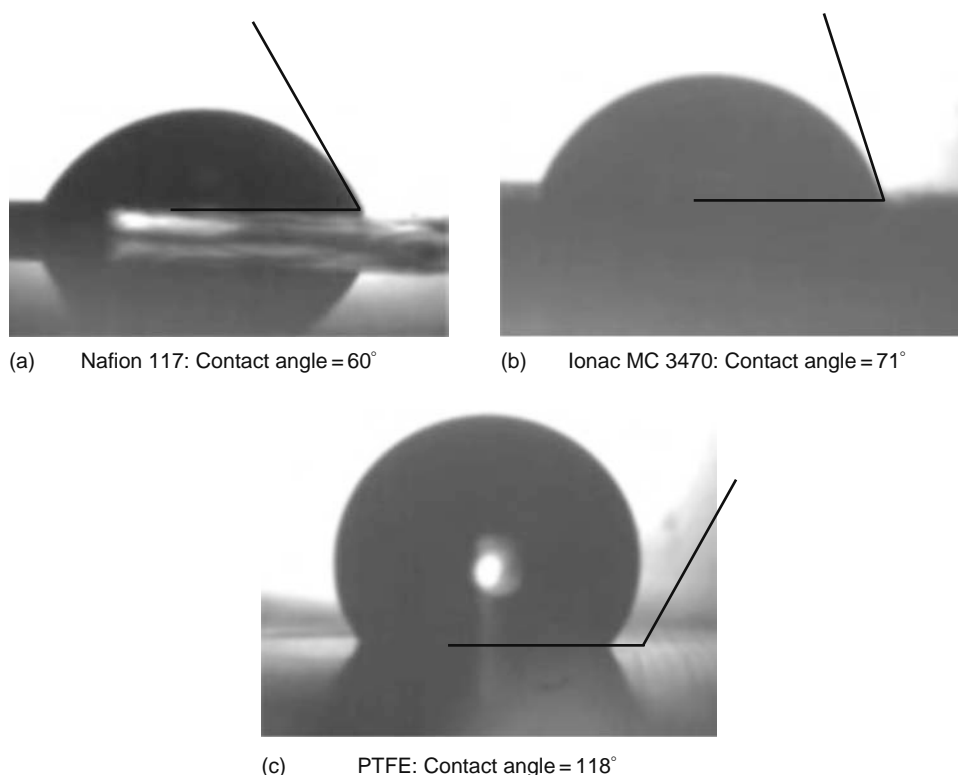


**FIGURE 34.9** Contact angle as a measure of hydrophilicity of (a) Nafion 117, (b) Ionac MC 3470, and (c) PTFE.

$H^+$  ions in a 2N  $H_2SO_4$  solution for 48 h, as before.  $Na^+$  concentration was measured using an atomic absorption spectrometer (Perkin Elmer Model 2380). The expansion of membrane was taken into consideration in calculating the exchange capacity of the wet membrane. For Ionac MC 3470, the exchange capacity was determined the same way, keeping in mind that the membrane was originally in the  $Na^+$  form and that it needed just one stripping step to get the  $Na^+$  ions in solution. The expansion in aqueous phase was taken into account in this case too.

### 34.5.8 ISOTHERM PLOT GENERATION

The membrane was converted to the  $H^+$  form and dipped in an  $Al^{3+}-H^+$  electrolyte solution of known strength  $C_T$  and the solution was stirred for 24 h to attain equilibrium. Aluminum ion uptake by the membrane was determined by mass balance. Several sets of such equilibrium experiments were carried out using different masses/areas of both Nafion 117 and Ionac MC 3470. From these experiments, it was possible to determine  $y_{Al}$ . Four values of  $x_{Al}$  were selected and the experiment was run for different  $C_T$  values such as 50, 1000, and 2000 meq/L (or eq/m<sup>3</sup>) in case of Nafion 117. For Ionac MC 3470, the same was carried out with the  $C_T$  value of 50 meq/L.

### 34.5.9 SEM-XRF ANALYSIS AND ANALYTICAL TECHNIQUE

A  $\frac{1}{2}$ " by  $\frac{1}{2}$ " square piece of the two membranes was taken and converted to the  $Na^+$  form. Since the Sybron membranes are available in the  $Na^+$  form, they were treated "as received". For Nafion 117, the membrane was converted to the  $Na^+$  form. For this purpose, the membrane was dipped in 2% NaOH solution (for 30 min, stir) followed by DI water wash (or soak), and then rinsed. The process was repeated three times with "fresh" NaOH. For each treatment step 200 ml of 2% NaOH was used. Once the membrane was converted to the  $Na^+$  form, it was dried, a cross-section of the sample taken, and mounted for scanning electron microscopy (SEM). A dot-map of  $Na^+$  was performed using x-ray fluorescence (XRF). The sample was taken from the sample's center to eliminate edge effect. The Sybron membrane was also soaked in DI water, and after hydration the membrane was air dried before preparing a cross-section sample for analysis. Aluminum ion was analyzed using UV-VIS spectrometer as before. For pH measurement, Fisher Scientific Accumet pH meter 900 was used. All experiments were conducted at ambient temperature and no significant difference in temperature was noticed between the feed and sweep samples. SEM-XRF analysis was carried out with ThermoNORAN Quest, which is a combination of SEM and XRF.

## 34.6 RESULTS AND DISCUSSION

### 34.6.1 ALUM RECOVERY FROM WTR

In the Donnan membrane cell, the feed side of the membrane contained 6.0 L of the decanted and slightly acidified WTR collected from the AWTP while the recovery side contained 1.5 L of 10% H<sub>2</sub>SO<sub>4</sub> solution. Figure 34.10 shows the results of the process for a period of 24 h; the percentage of aluminum recovery and the concentration of aluminum in the two chambers were plotted against time. It can be seen that over 70% recovery (72%) was attained in 24 h. The noteworthy observation is that the recovered aluminum concentration was 6650 mg/L as Al, and it was significantly greater than the total aluminum concentration (2400 mg/l) present in the parent sludge, as it was recovered in a volume which was four times smaller. Figure 34.11 provides a detailed composition of the recovered alum from the DMP. Besides Al(III) and Fe(III), other contaminants are present only in trace concentrations. It is noteworthy that the recovered alum did not contain any suspended solids while NOM expressed as DOC was consistently less than 5 mg/L. The ratio of individual contaminants to aluminum in the recovered alum was comparable and in some cases lower than in the commercial alum currently being used in AWTP.

### 34.6.2 DONNAN EXCLUSION AND FOULING

One of the primary attributes of the DMP is its ability to exclude anions, NOM, and particulate matter while recovering aluminum from the WTR without being fouled. Figure 34.12a and 34.12b shows the DOC and sulfate (SO<sub>4</sub><sup>2-</sup>) concentrations in the feed side and recovery side of Donnan membrane cell for a run that lasted 72 h. DOC is a measure of NOM in the aqueous phase, and these figures show that both DOC and sulfate remained nearly constant on both sides. DOC concentration in the recovered alum was consistently less than 5 mg/L while the same in the feed side was over 150 mg/L. Likewise, sulfate concentration was close to 2000 meq/L on the recovered solution side and about 200 meq/L on the feed side during the course of the experiment, which implied that the cation-exchange membrane disallowed permeation of NOM and sulfate from one side to the other, validating the premise of the Donnan co-ion exclusion.

Specific experiments were carried out to confirm possible fouling of membranes caused by NOM and particulate matter. During the course of this study, the same Nafion membrane was used repeatedly. The color of the membrane surface turned dark but no noticeable impairment of aluminum flux was observed even after prolonged usage. Figure 34.13 shows the results of two successive runs with a membrane already used in the laboratory for nearly three months. The same feed obtained from AWTP was used for both the runs. Figure 34.13 demonstrates that the rate of increase in aluminum concentration with time in the recovery side was slightly lower during the second run but the overall alum recovery essentially remained the same after 9 h of operation.

To investigate the effect of turbidity independently, two parallel Donnan recovery runs were carried out. During the first run, the synthetic alum feed solution was free of any turbidity while for the second run, 6000 mg/L turbidity was introduced into the feed compartment as fine glass powders with sizes in the vicinity of 1 μm. All other conditions were exactly the same for the two runs. High turbidity in the feed side did not impair the rate of alum recovery, as evidenced from the experimental results in Figure 34.14.

### 34.6.3 FE(III) RECOVERY

Ferric salts (chloride or sulfate) are also used as coagulants in water treatment plants [50], and the resulting ferric hydroxide precipitates constitute a major portion of the clarifier sludge or WTR. In principle, the DMP is capable of selectively recovering

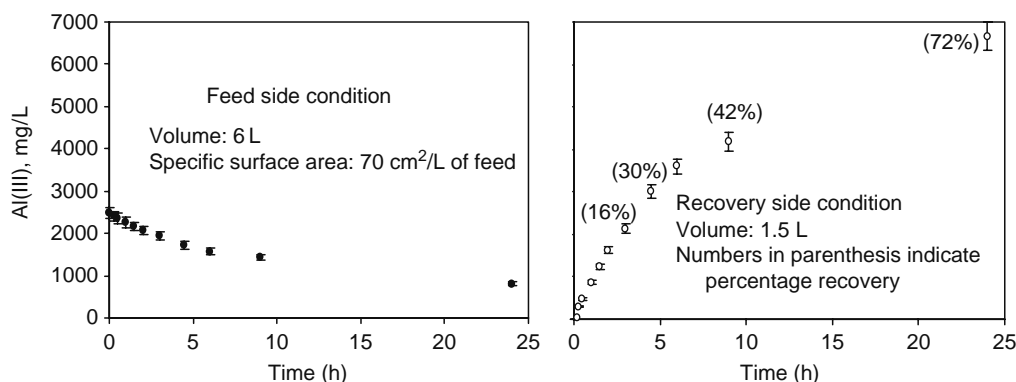


**FIGURE 34.10** Aluminum recovery from the AWTP residuals during the DMP: decrease in Al concentration in feed, percentage recovery, and increase in Al concentration in recovery solution.

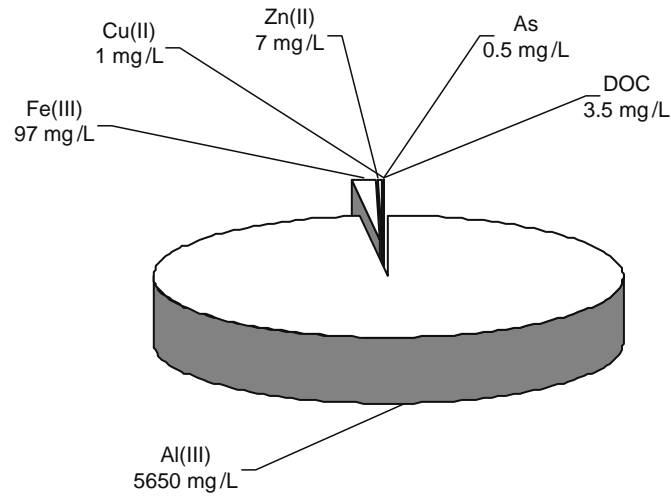


FIGURE 34.11 Composition of alum recovered from the AWTP using the DMP.

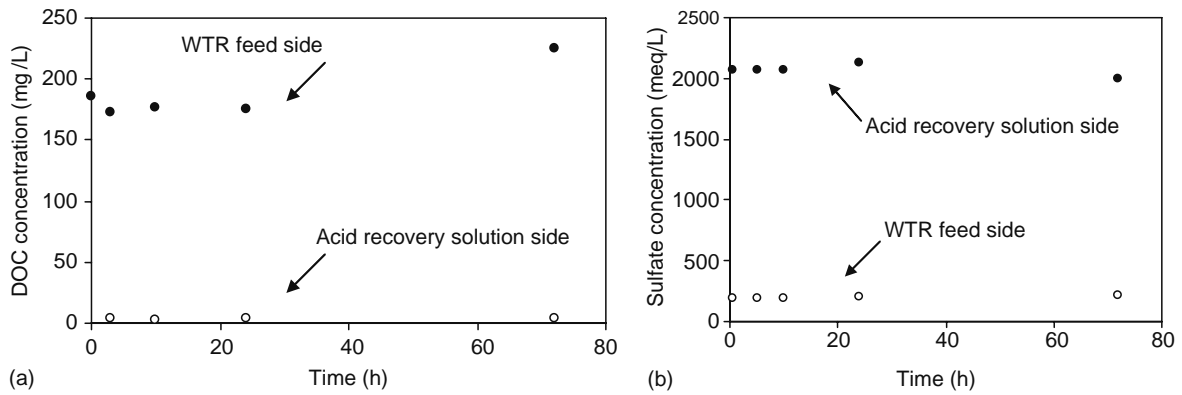


FIGURE 34.12 (a) DOC concentration in feed and recovery solution during an experimental run using the AWTP residuals and (b) sulfate concentration in feed and recovery solution during the same run.

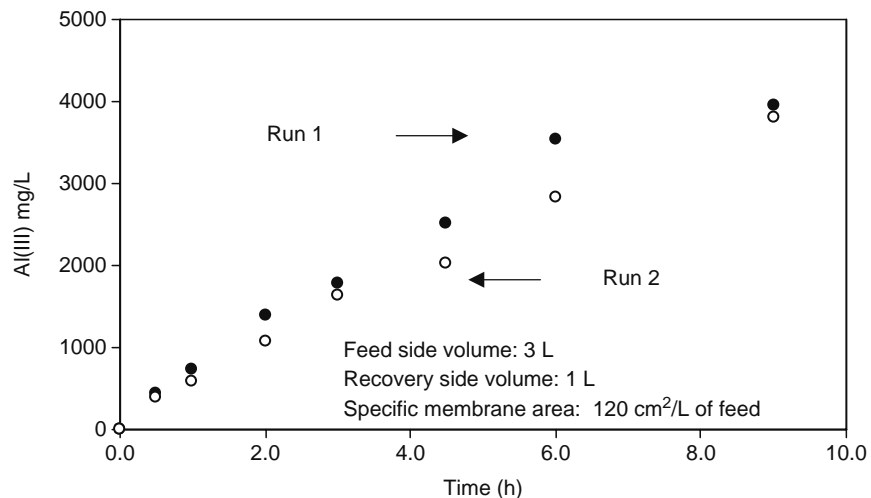


FIGURE 34.13 Aluminum recovery in two consecutive runs with WTR obtained from the AWTP.

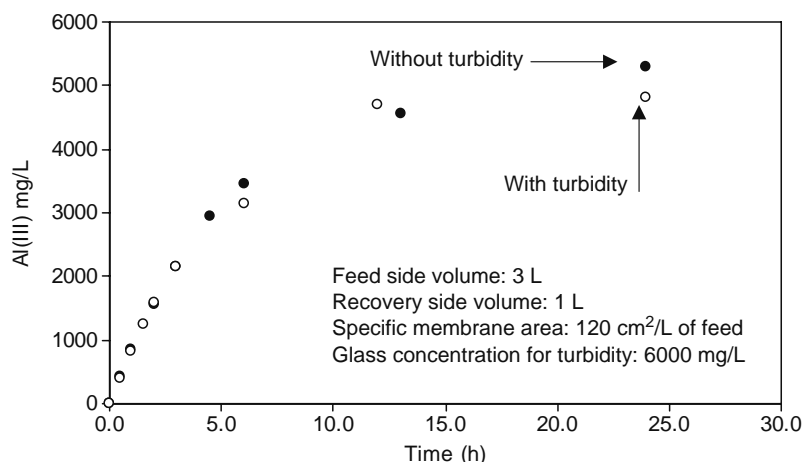


FIGURE 34.14 Influence of turbidity on removal efficiency.

Fe(III) coagulants from these WTR as well. To validate the same, the WTR from the Baxter plant (Philadelphia, Pennsylvania), which utilized FeCl<sub>3</sub> as coagulant, was used in several test runs. Figure 34.15 shows percentage Fe(III) recovery and the concentration of Fe(III) in the feed and recovery side with time. Nearly 75% recovery is attained in 24 h. The resulting Fe(III) is essentially free of NOM, particulate matter, and other impurities.

Figure 34.16a and 34.16b shows the visual comparison of recovered coagulants, both alum and ferric sulfate, between traditional acid digestion process and the DMP. Higher transparency of the coagulants from AWTP and the Baxter Plant, recovered by DMP, is readily noticeable due to the absence of turbidity and NOM. Two separate runs were carried out using synthetic solutions of aluminum sulfate and ferric chloride under otherwise identical conditions. Figure 34.17 shows that the percentage or fractional recovery of Fe(III) or Al(III) remains essentially the same i.e., the process is equally effective for concentrating any trivalent cation.

### 34.6.4 RELATIVE CARRYOVER

Besides Al(III) and Fe(III), undesirable solutes and NOM also get carried over to the recovered solution. Relative carryover ( $\eta_R$ ) of substance *i* with respect to Al is defined as the following dimensionless variable:

$$\eta_R = \left( \frac{C_R^i}{C_R^{Al}} \right) \left( \frac{C_F^{Al}}{C_F^i} \right) 100 \tag{34.31}$$

where

*C* represents concentrations

subscripts R and F denote the recovered solution and the WTR feed, respectively

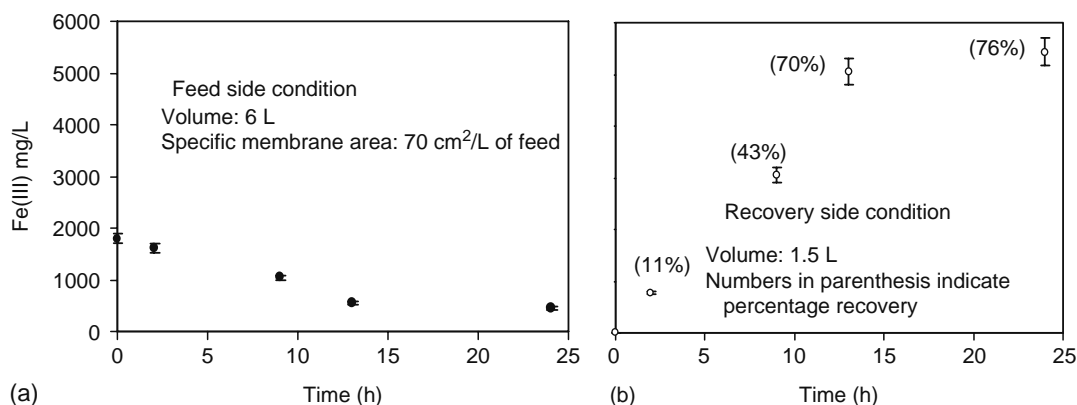


FIGURE 34.15 Ferric(III) recovery from ferric chloride-based WTR from Baxter Water Treatment Plant during DMP. (a) Decrease in Fe concentration in feed and (b) percentage recovery and increase in Fe concentration in recovery solution.

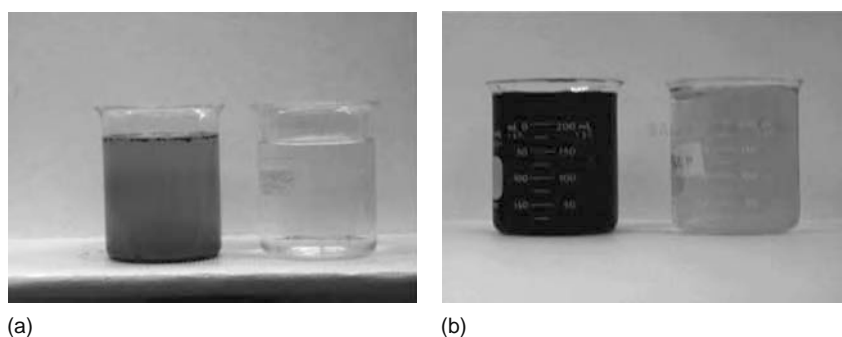


FIGURE 34.16 Visual comparison of recovered alum coagulant from the AWTP residuals by acid digestion process (a) and DMP (b).

Figure 34.18 shows the percentage relative carryover i.e.,  $\eta_R$  values of DOC, Cu(II), Zn(II), and Mg(II). It is noted that  $\eta_R$  values are nearly zero for DOC and significantly less than aluminum for all divalent cations. For conventional acid digestion process, no selective separation is achieved i.e., percentage  $\eta_R$  values of all the contaminants are essentially the same as that of Al(III).

### 34.6.5 RECOVERED ALUM AS A COAGULANT

Jar tests were conducted to evaluate the coagulation efficiency of the recovered alum. For the purpose of comparison, commercial liquid alum that is currently in use at the AWTP and mixed alum (50% recovered alum and 50% commercial alum) were employed as coagulants in the jar tests. Water from the Little Lehigh River, which is the primary raw water source of the AWTP, was used for the test. A conventional jar-test apparatus was employed in the study. Figure 34.19 is a plot of residual turbidity versus alum dosage. For dosages up to 40 mg/L alum, the mixed alum offered higher turbidity removal than commercial alum, all other conditions remaining identical. It is noteworthy that DOC, Zn, As, and Cu were nondetectable in the treated water.

### 34.6.6 EQUILIBRIUM ISOTHERM PLOT

The exchange capacity of Nafion 117 on a wet basis was calculated as 1372 eq/m<sup>3</sup>. The Nafion 117 isotherm plot for Al<sup>3+</sup>-H<sup>+</sup> equilibrium is shown in Figure 34.20a. The experimental data were generated for  $C_T$  values of 50, 1000, and 2000 meq/L. Using these plots and on the basis of selectivity coefficients calculated from Equation 34.14b, a theoretical plot for  $C_T = 222$  meq/L and  $C_T = 2000$  meq/L is obtained. These two  $C_T$  values represent the electrolyte concentration in the experiments performed. These plots were used in the model to predict theoretical concentrations in the feed and sweep solutions. It can be seen from Figure 34.20a that for a low  $C_T$  value of 50 meq/L, the isotherm is close to a rectangular plot. For higher  $C_T$  values of 1000 and 2000 meq/L, the plot approaches linearity. The drop in selectivity with increasing values of  $C_T$  is on predictable lines,

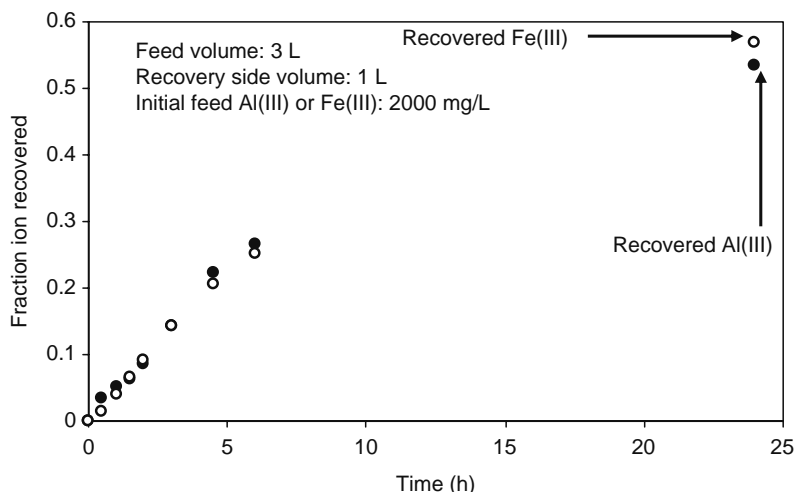


FIGURE 34.17 Fractional recovery of ferric and aluminum ions from synthetic solutions.

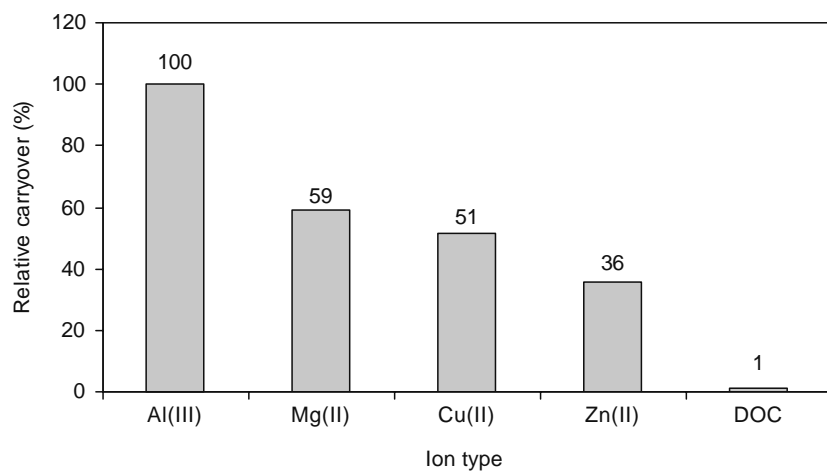


FIGURE 34.18 Relative carryover of undesirable solutes and NOM.

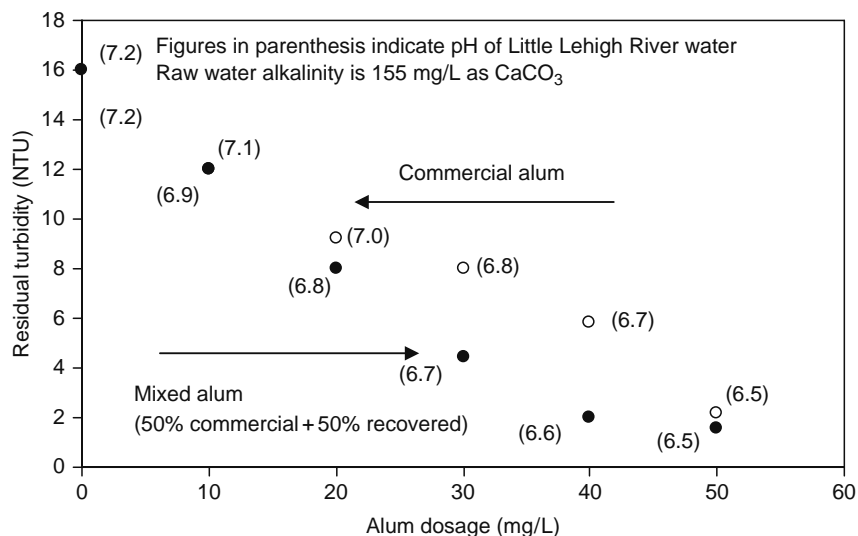


FIGURE 34.19 Residual turbidity versus alum dosage in jar tests using commercial alum and mixed alum.

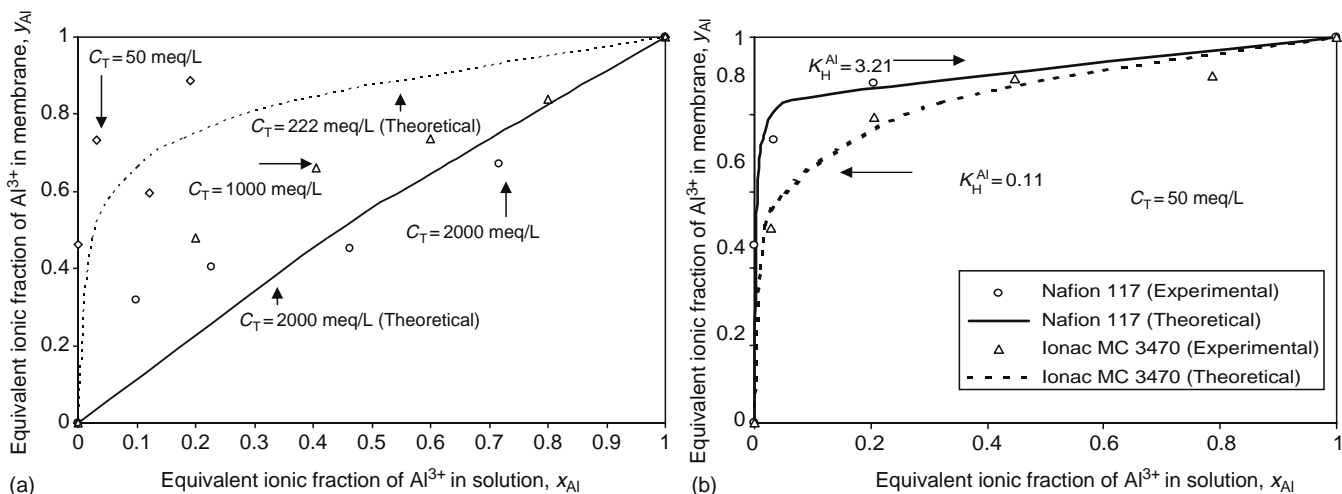


FIGURE 34.20 Al<sup>3+</sup>-H<sup>+</sup> Isotherm plot (a) for Nafion 117 and (b) comparison between Nafion 117 and Ionac MC 3470.

as for a given ionic fraction in solution, the membrane fraction is inversely proportional to the square of  $C_T$ , as observed in Equation 34.23. This implies that with increasing  $C_T$ , the isotherm plot approaches linearity and at a later stage, changes from “convex-up” configuration to “convex-down.”

A study was done to compare the isotherm plots of Nafion 117 and Ionac MC 3470. The comparison in Figure 34.20b shows that Nafion 117 has a more rectangular isotherm than Ionac MC 3470, indicating that the homogeneous membrane has a higher selectivity for  $\text{Al}^{3+}$  ions. In fact, the average selectivity coefficient  $K_H^{\text{Al}}$  was determined to be 3.21 for Nafion 117 and 0.11 (over 30 times lower) for Ionac MC 3470.

### 34.6.7 KINETIC TREATMENT OF ALUM RECOVERY IN NAFION 117

As discussed in Step 1 in the model, the exchange capacity for the membrane and the  $\text{Al}^{3+}\text{-H}^+$  equilibrium isotherm data were generated, as shown in Figure 34.20. Step 2 involved determining the aluminum ion recovery profile using a synthetic solution. The recovery profile for an experiment labeled Run 1 is plotted in Figure 34.21. For this experiment, a feed solution of 6 L ( $C_T = 222$  meq/L) and a sweep solution of 1.5 L ( $C_T = 2000$  meq/L) were used. In the same figure, aluminum flux, calculated from Equation 34.24, is also shown. For a given feed and sweep aluminum ion fraction  $x_{\text{Al}}$  determined from this experimental run, the corresponding fraction  $y_{\text{Al}}$  in the membrane surface exposed to the solution and its concentration was determined using Figure 34.20a. With the aluminum ion transfer, flux data available, and the membrane thickness provided, it was possible to determine the experimental interdiffusion coefficient value  $\bar{D}_{\text{Al,H}}$  with the aid of Fick's law in Equation 34.20a. This plot is shown in Figure 34.22a. It must be noted that this value is only an approximate value of interdiffusion coefficient, as actual values vary across the cross-section of the membrane with varying charge distribution. Using this approximate value of interdiffusion coefficient, the linearization technique described in Step 4 in the modeling section was implemented. The values of  $1/\bar{D}_{\text{Al,H}}$  from Run 1 were plotted against  $\frac{1}{1+\frac{1-y_{\text{Al}}}{y_{\text{Al}}}}$  in Figure 34.22b for surface conditions on feed surface. This plot was

used to determine the initial self-diffusion coefficient values  $\bar{D}_{\text{Al}}$  and  $\bar{D}_{\text{H}}$ . This approach can only be applied as a first approximation, as overall interdiffusion coefficient has been used to represent the interdiffusion coefficient value on feed surface. The ratio  $\bar{D}_{\text{Al}}/\bar{D}_{\text{H}}$  was determined to be 35.0 and was fed into a modeling program. The process was iterated for Run 1 to determine the theoretical recovery. But the recovery was modified to take into account the osmosis effect in solutions. The dilution effect was then imposed on the theoretical recovery plot to determine the sweep side concentration with osmosis. The initial self-diffusion coefficient values,  $\bar{D}_{\text{Al}}$  and  $\bar{D}_{\text{H}}$ , determined from Figure 34.22b underpredicted the experimental findings. So the process was iterated using  $\bar{D}_{\text{Al}}$  as the operating parameter. When the results matched well with the experimental plot for Run 1, the self-diffusion coefficient values obtained were

$$\bar{D}_{\text{Al}}: 6.5 \times 10^{-12} \text{ m}^2/\text{s} \quad \text{and} \quad \bar{D}_{\text{H}}: 2.28 \times 10^{-10} \text{ m}^2/\text{s}$$

Further to this, another experiment was carried out (Run 2). In this experiment, the feed volume was changed to 3 L (from 6 L in Run 1), sweep volume to 1 L (from 1.5 L), and the membrane area to  $370 \text{ cm}^2$  (from  $415 \text{ cm}^2$ ). It was observed that the sweep side concentration profile for these self-diffusion coefficient values matched reasonably well with the experimental findings [51]. The results are shown in Figure 34.22c. The self-diffusion coefficient of  $\text{H}^+$  ions has been investigated earlier

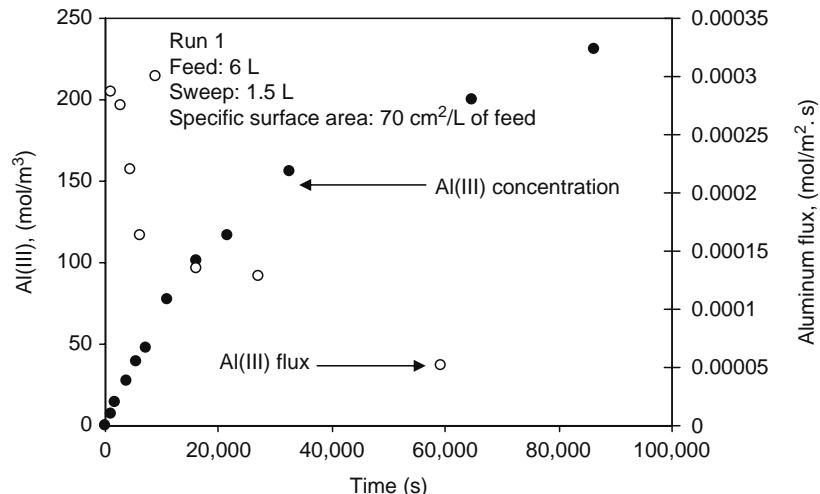
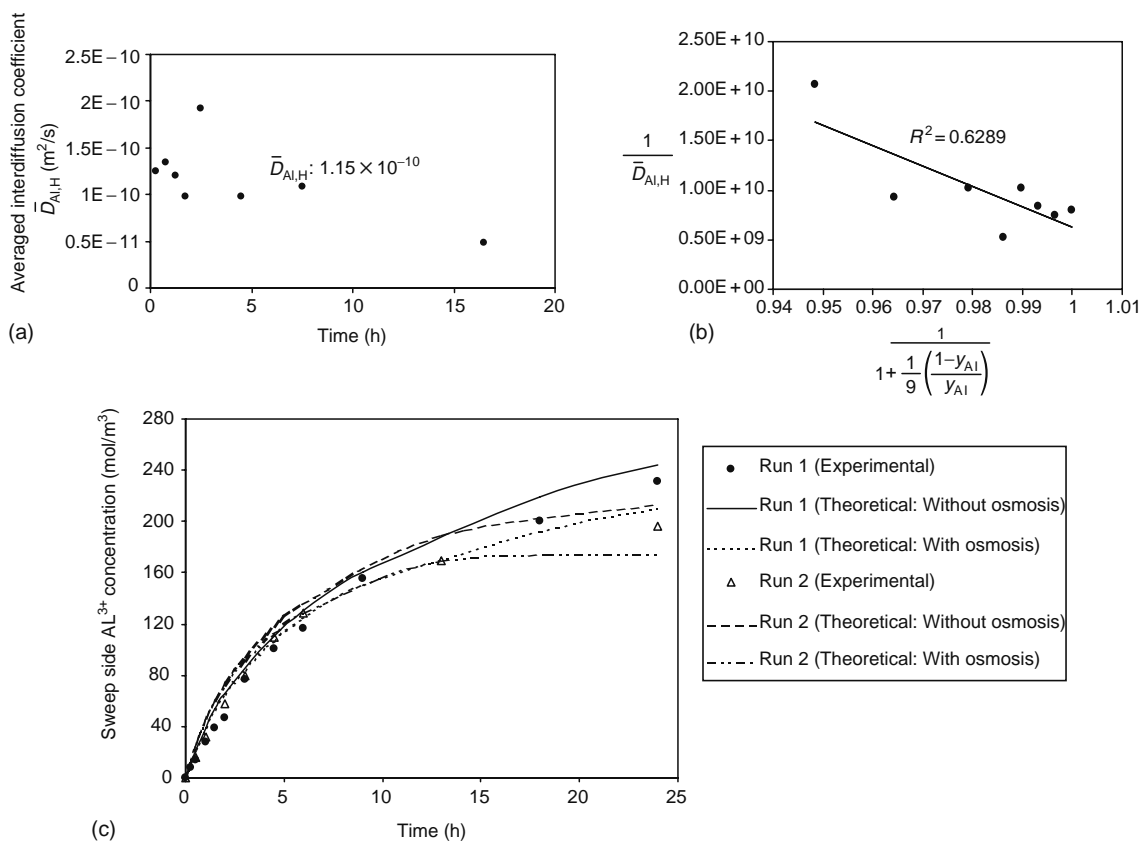


FIGURE 34.21 Sweep side  $\text{Al}^{3+}$  concentration for Run 1 and corresponding aluminum ion flux for Nafion 117 membrane.



**FIGURE 34.22** (a) Average interdiffusion coefficient values based on Run 1, (b) self-diffusion coefficient determination for  $Al^{3+}-H^+$  pair using separation of variables, and (c) recovery profile for  $Al^{3+}$  (theoretical/experimental values) for Run 1 and Run 2: Nafion 117.

[37,52] and the current value is close to the values reported for the case of Neosepta C66-5T membrane by Miyoshi ( $1.33 \times 10^{-10}$  m<sup>2</sup>/s) and Sudoh et al. ( $1.86 \times 10^{-10}$  m<sup>2</sup>/s). When self-diffusion coefficient values for  $H^+$  and  $Al^{3+}$  ions in Nafion 117 were compared with the values in the aqueous phase at infinite dilution [53], the ratio of  $\bar{D}_{Nafion\ 117}/D_{infinite\ dilution}$  was found to be 1/41 and 1/93 for  $H^+$  and  $Al^{3+}$  ions, respectively. Miyoshi [32] had earlier found in their work with  $Na^+$ ,  $K^+$ ,  $Ca^{2+}$ ,  $Cu^{2+}$ , and  $Mg^{2+}$  ions during DMP that the drop in self-diffusion coefficient value in the membrane phase was higher for the bivalent ions than for the monovalent ions. This point can be understood from the fact that in their movement across the membrane, trivalent ions have to link themselves with three negative sites, to maintain electroneutrality, while monovalent ions need to link with only one negative site. Therefore, the efficiency with which a multivalent ion hops within an exchange membrane is significantly reduced in comparison with monovalent ions.

### 34.6.8 INTERDIFFUSION COEFFICIENT VARIATION ON MEMBRANE SURFACES

As mentioned earlier, the interdiffusion coefficient is a variable across the membrane and is dependent on  $Al^{3+}$  and  $H^+$  distribution across the membrane. Using the model,  $q_H$  and  $q_{Al}$  distribution on the two surfaces was determined for Run 1, shown in Figure 34.23a. Data obtained from this finding were further used to calculate the flux variation with time. The results were compared against the flux obtained from the experimental findings. It could be seen, as shown in Figure 34.23b, that the flux values based on the interdiffusion coefficient  $\bar{D}_{Al,H,I}$  for feed surface were very well correlated with the experimental flux in comparison with the results obtained for sweep surface. This finding can be used to conclude that the ion transport for the present case could be well represented by the  $Al^{3+}-H^+$  distribution on feed surface, and that the charge distribution on this surface along with the interdiffusion coefficient values on this surface determined the ion transport.

Another important point that can be noted is that the interdiffusion coefficient values are closer to the self-diffusion coefficient value of  $H^+$  ions and much higher than the values obtained for  $Al^{3+}$  ions, calculations showing that  $\bar{D}_{Al,H,I}/\bar{D}_{Al}$  ranged from 35 (time  $t=0$  h) to 7 (time  $t=24$  h). In fact, the  $\bar{D}_{Al,H}$  values are significantly greater than self-diffusion coefficients of divalent and trivalent cations within a cation exchanger. For instance, the diffusion coefficient values for multivalent ions in cation-exchange resins with 15% crosslinking range between  $10^{-12}$  and  $10^{-14}$  m<sup>2</sup>/s [34]. This observation

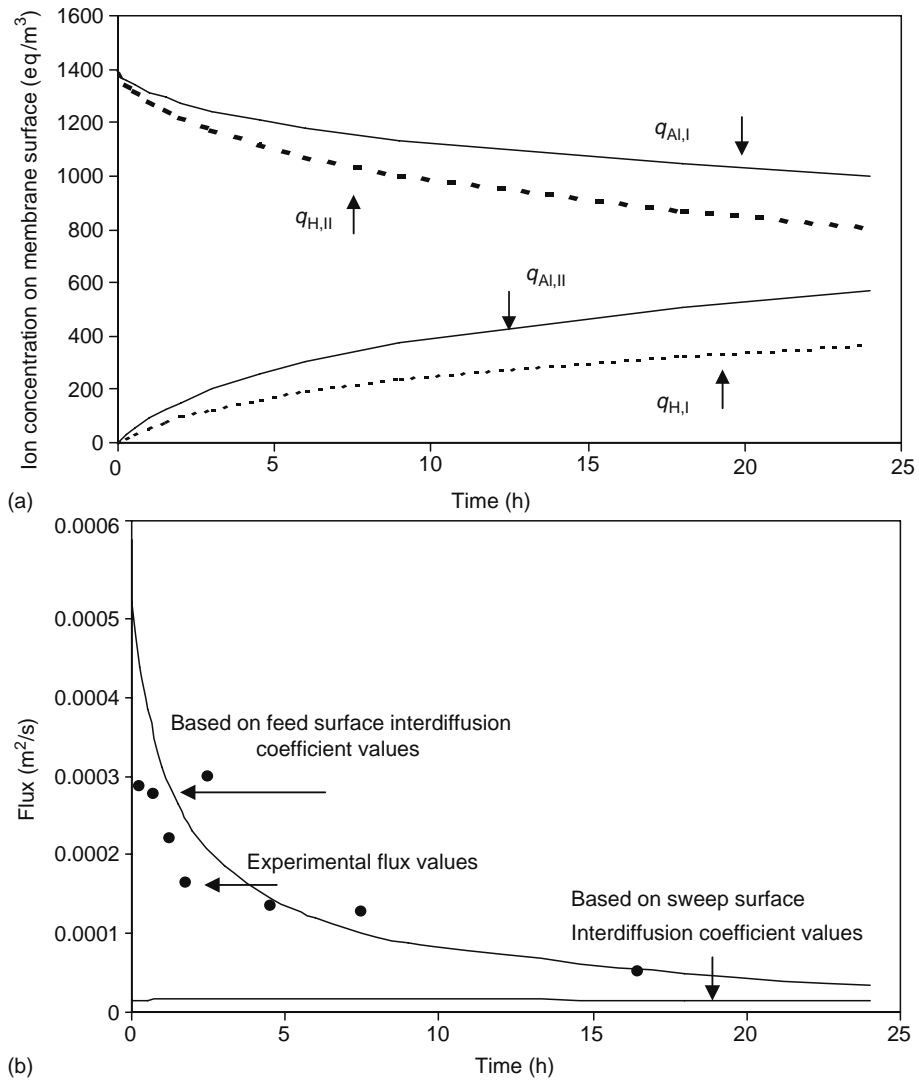


**FIGURE 34.23** (a) Surface concentration of  $Al^{3+}-H^+$  ions: Run 1 and (b) comparison of  $Al^{3+}$  flux based on experiments with flux based on interdiffusion coefficient values on feed surface I and sweep surface II.

of high interdiffusion coefficient ( $\bar{D}_{Al,H}$ ) value in Nafion 117 is counterintuitive and the following provides a scientific explanation for high  $\bar{D}_{Al,H}$  values observed.

The composition of the membrane with respect to  $Al^{3+}$  and  $H^+$  content (i.e.,  $q_{Al}$  and  $q_H$ ) varies across the membrane, influencing the  $Al^{3+}-H^+$  interdiffusion coefficient as discussed earlier in Equation 34.20c and revised as below:

$$\bar{D}_{Al,H} = \bar{D}_H \bar{D}_{Al} \left( \frac{q_H + 9q_{Al}}{q_H \bar{D}_H + 9q_{Al} \bar{D}_{Al}} \right) \tag{34.32}$$

The relative distribution of  $Al^{3+}$  and  $H^+$  in the membrane governs the value of  $\bar{D}_{Al,H}$ . Nafion is a strong-acid cation-exchange membrane and exhibits significantly greater affinity for ions with higher valence. Equilibrium experiments revealed earlier that binary separation factor, which is a measure of relative affinity for two competing ions for an ion exchanger was equal to 70 for  $Al^{3+}$  over  $H^+$  for Nafion 117 at 50 meq/L solution concentration. Thus, at anytime during the process,  $q_{Al}$  is significantly greater than  $q_H$  within the ion-exchange membrane. In fact, the  $q_{Al,I}/Q$  value on feed surface was never below 0.75 during the entire period of the experiment. Considering the extreme case where hydrogen ion is essentially a trace species compared to aluminum ion, i.e.,  $q_{Al} \gg q_H$ , Equation 34.32 reduces to

$$\bar{D}_{Al,H} = \bar{D}_H \tag{34.33}$$

For the alum recovery process, the  $H^+$  ion is a minor species within the membrane. Consequently, the value of interdiffusion coefficient  $\bar{D}_{Al,H}$  approaches that of the faster-diffusing hydrogen ion,  $\bar{D}_H$ . The composition of the membrane changes with the progress of the process, thus altering the  $\bar{D}_{Al,H}$  values, but they always remain significantly greater than the self-diffusion coefficient of aluminum ions. From an application viewpoint, this phenomenon leads to a high mass transfer or alum recovery rate.

### 34.6.9 SELF-DIFFUSION COEFFICIENT COMPARISON IN NAFION 117 AND IONAC MC 3470

Experiments were carried out with Ionac MC 3470 to determine the self-diffusion coefficient values for  $H^+$  and  $Al^{3+}$  in the coupled transport. Data points were used from the experiment involving 2N acid sweep solution in Figure 34.24b, presented later. These values formed the basis for aluminum transport rate or flux ( $J_{Al}$ ) calculation at different time intervals. The equilibrium data generated in Figure 34.20b were used in conjunction with Equation 34.25 to determine the interdiffusion coefficient values. Local equilibrium was assumed at the membrane–water interface. Figure 34.24a shows computed  $\bar{D}_{Al,H}$  values for this membrane. When compared with  $\bar{D}_{Al,H}$  values for Nafion 117, it was noticed that the drop in interdiffusion coefficient values was not so steep, indicative of slow kinetics. The model discussed earlier was applied to determine the self-diffusion coefficient values of aluminum and hydrogen ions in Ionac MC 3470 membrane. A notable point was that the osmosis effect was not taken into account in this case, as no significant osmosis was observed in a separate experiment.

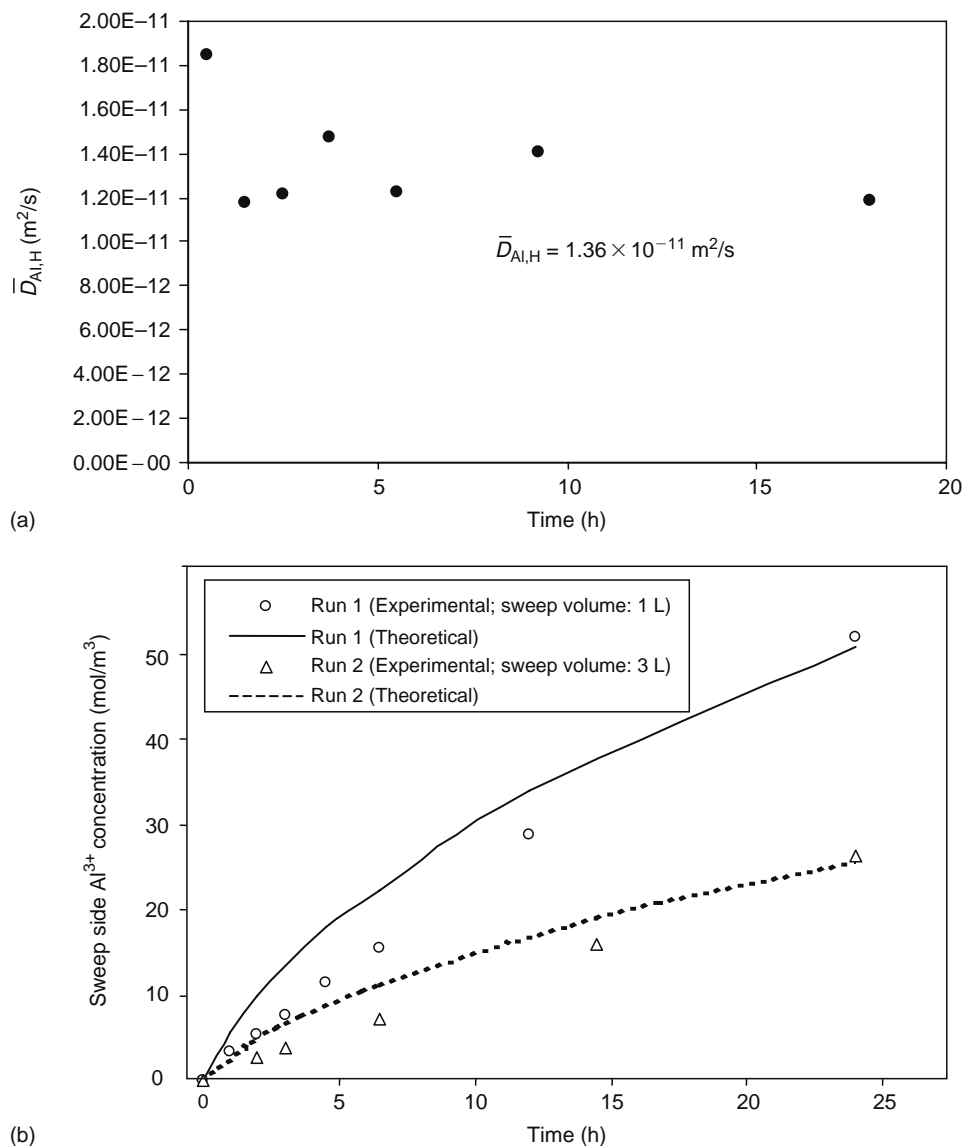


**FIGURE 34.24** (a) Interdiffusion coefficient values for aluminum ion transfer in Ionac MC 3470 and (b) recovery profile for  $Al^{3+}$  (theoretical/experimental values) for Run 1 and Run 2: Ionac MC 3470.

**TABLE 34.3**  
**Diffusion Coefficient Value Comparison in Nafion 117 and Ionac MC 3470**

	$\bar{D}_H$ (m <sup>2</sup> /s)	$\bar{D}_{Al}$ (m <sup>2</sup> /s)	$\bar{D}_{Al,H}$ (m <sup>2</sup> /s)
Nafion 117	$2.28 \times 10^{-10}$ (6.1)	$6.5 \times 10^{-12}$ (13.0)	$1.15 \times 10^{-10}$ (8.45)
Ionac MC 3470	$3.75 \times 10^{-11}$	$5 \times 10^{-13}$	$1.36 \times 10^{-11}$

*Note:* Numbers in brackets indicate ratio of diffusion coefficient in Nafion 117 over Ionac MC 3470.

Two experiments were carried out. Run 1 is the standard run and is the basis for generation of Figure 34.24a. In Run 2, a 2 L sweep solution was used instead of 1 L to verify the findings from Run 1. The findings from the model are presented in Figure 34.24b. The self-diffusion coefficient values were determined to be

$$\begin{aligned}\bar{D}_{Al}: & 5.00 \times 10^{-13} \text{ m}^2/\text{s} \\ \bar{D}_H: & 3.75 \times 10^{-11} \text{ m}^2/\text{s}\end{aligned}$$

Even for Ionac MC 3470, it was the H<sup>+</sup> ion that was the trace species. A comparison of the diffusion coefficient values for the two membranes is presented in Table 34.3. From this table, it can be observed that the self-diffusion coefficient values for aluminum and hydrogen ions are similarly lowered as the experimental interdiffusion coefficient value. This lowering is about one order for both the cases. Explanation for low  $\bar{D}_{Al,H}$  values in the heterogeneous membrane is desired, as it explains the slow transport kinetics in heterogeneous membrane.

#### 34.6.10 INFLUENCE OF HETEROGENEITY ON TRANSPORT PROPERTIES OF NAFION 117 AND IONAC MC 3470

A SEM–XRF analysis was done to verify the hypothesis of conducting and nonconducting sites discussed earlier and by identifying the distribution of charged sites within Nafion 117 and Ionac MC 3470 [54]. A dot-map of Na<sup>+</sup> in Figure 34.25a and 34.25b showed that sodium ions were uniformly distributed in the homogeneous Nafion 117 membrane while they were unevenly distributed in clusters in the Ionac MC 3470. It suggests that there are regions of nonfunctional reinforcement in Ionac MC 3470, which are absent in the unsupported Nafion 117 membrane. This reinforced region is characterized by the absence of ionogenic groups.

#### 34.6.11 AL<sup>3+</sup> RECOVERY PROFILE

To develop an insightful understanding of the effect of the H<sub>2</sub>SO<sub>4</sub> (sweep solution) concentration on aluminum transport, experiments were conducted at two different initial H<sub>2</sub>SO<sub>4</sub> concentrations (C<sub>0</sub>), namely, 1 M and 2 M. Identical synthesized feed solutions of aluminum sulfate (~2000 mg/L as Al) were used in all four experiments that lasted for 24 h. Figure 34.26a and

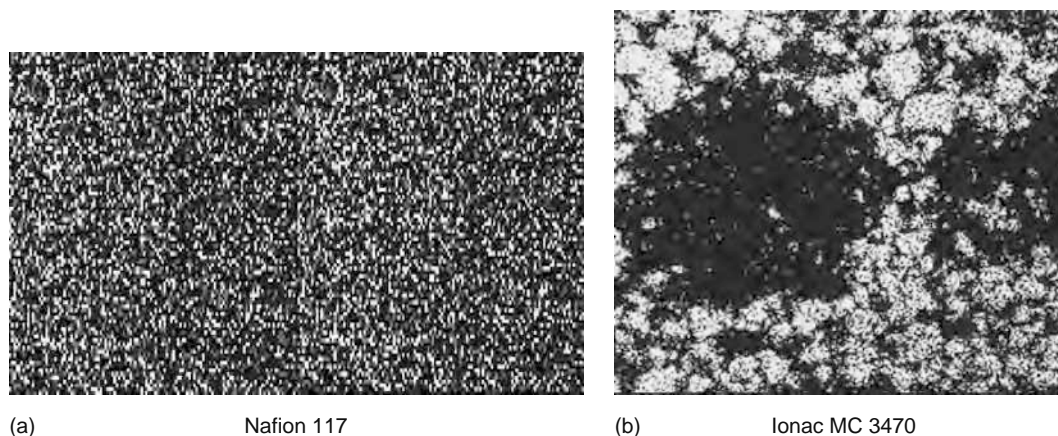


**FIGURE 34.25** SEM–XRF dot-map of Na<sup>+</sup> in a cross-section of (a) Nafion 117 and (b) Ionac MC 3470. It may be noted that the charged sites are more uniformly distributed in the homogeneous membrane Nafion 117, while the heterogeneous membrane Ionac MC 3470 has nonconducting pockets shown by dark space.

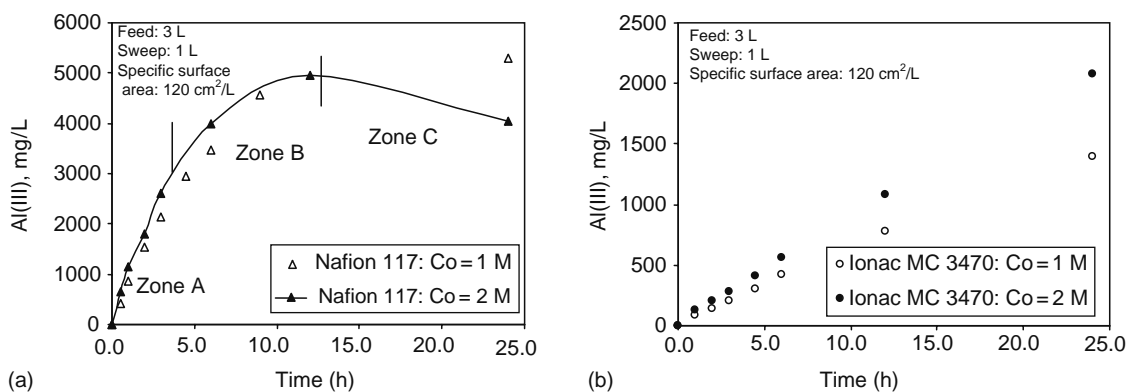


FIGURE 34.26  $\text{Al}^{3+}$  recovery profile for (a) Nafion 117 and (b) Ionac 3470.

34.26b provides plots of aluminum recovery versus time for both Nafion 117 and Ionac 3470. The following observations are noteworthy:

- For Nafion 117, the aluminum recovery profile approached saturation after 12 h but the same was linear after 24 h for Ionac 3470.
- Increasing the initial  $\text{H}_2\text{SO}_4$  concentration,  $C_0$ , from 1 M to 2 M increased aluminum recovery uptake for both membranes but there was a drop in aluminum concentration at the end for Nafion 117. This observation of drop in aluminum concentration beyond saturation is counterintuitive and was reconfirmed through a replicate experiment.

Characteristically, the aluminum recovery plot for Nafion 117 could be identified as a combination of three zones: Zone A (where the plot is linear), Zone B (where the plot reaches a plateau), and Zone C (where it tapers downward). The following provides a scientific explanation leading to the existence of the three zones.

In the beginning of the run, the driving force was characterized by a high electrochemical potential gradient in the membrane phase. The driving force remained nearly constant for the first 5 h, and consequently alum recovery rate was almost linear as shown in Zone A of the recovery plot. Zone A can therefore be termed as “kinetically driven linear zone.” As time progressed, the condition of Donnan equilibrium characterized was approached. Sufficient electrochemical potential gradient was no longer available, thus lowering the aluminum transfer flux. The aluminum recovery rate was thus governed by equilibrium conditions during this period and Zone B can be termed the “equilibrium-driven saturation zone.” In membranes such as Nafion 117, the transfer kinetics is fast enough to exhibit the two zones clearly during a 24 h experiment, as demonstrated in Figure 34.26a. Unlike this, Ionac 3470 is kinetically slower and offers higher resistance to aluminum transport. Therefore, the conditions of equilibrium were delayed and only the linear profile of Zone A was observed with Ionac 3470 during the entire period of experimentation, as shown in Figure 34.26b.

In Figure 34.27a, an interesting and counterintuitive observation was the drop in aluminum concentration with time, when a 2 M acid sweep solution concentration was used. Note that the osmosis of water is an ongoing phenomenon in Nafion 117

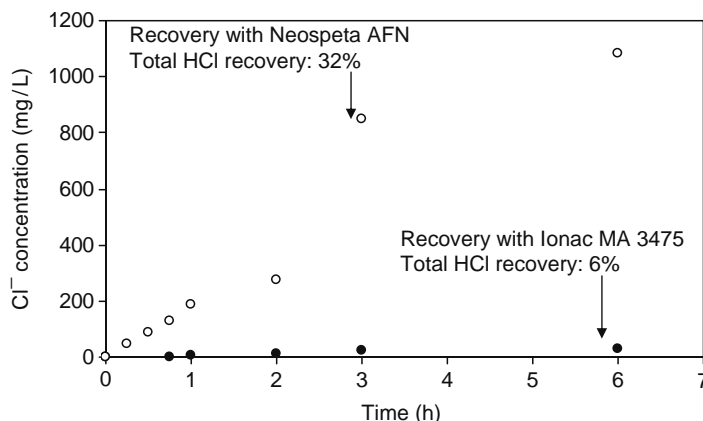


FIGURE 34.27 Influence of membrane type on diffusion dialysis of HCl.

during the DMP. It is noteworthy that osmosis took place independent of the aluminum transfer process. Thus when the aluminum recovery rate became negligible, the water transport due to osmosis still continued leading to a lowering or dilution of aluminum concentration in the recovery side. This situation was identified in Zone C, which is termed “osmosis-driven dilution zone.” Such a tapering was not observed in the experiment involving 1 M sweep solution because the osmosis effect was weaker during the period of experimentation.

Only Zone A was observed in Ionac 3470, primarily due to low aluminum transport flux and partly due to higher resistance offered to solvent osmosis in comparison to Nafion 117. Increasing the sweep side concentration to 2 M led to greater recovery, as shown in Figure 34.26b, because a higher driving force was available in the sweep solution.

### 34.6.12 FINDINGS FROM DIFFUSION DIALYSIS EXPERIMENTS

Diffusion dialysis experiments were not carried out in great detail, but some of the findings of the experiments are worth reporting. They have been discussed in the following paragraphs.

### 34.6.13 INFLUENCE OF MEMBRANE TYPE ON ACID RECOVERY

Two different membranes were used in acid recovery. These are Ionac MA 3475 and Neosepta AFN. Characteristic features of these anion-exchange membranes were discussed earlier. The experimental findings are presented in Figure 34.27. From an initial feed concentration of 5000 mg/L of  $\text{Cl}^-$  ions, only 7% was recovered with Ionac MA 3475, whereas over 30% recovery was made with Neosepta AFN. Clearly, Neosepta AFN was a better membrane for use. The high diffusional resistance to mass transfer in Ionac MA 3475 could be attributed to its membrane thickness, which was over two times more than in Neosepta

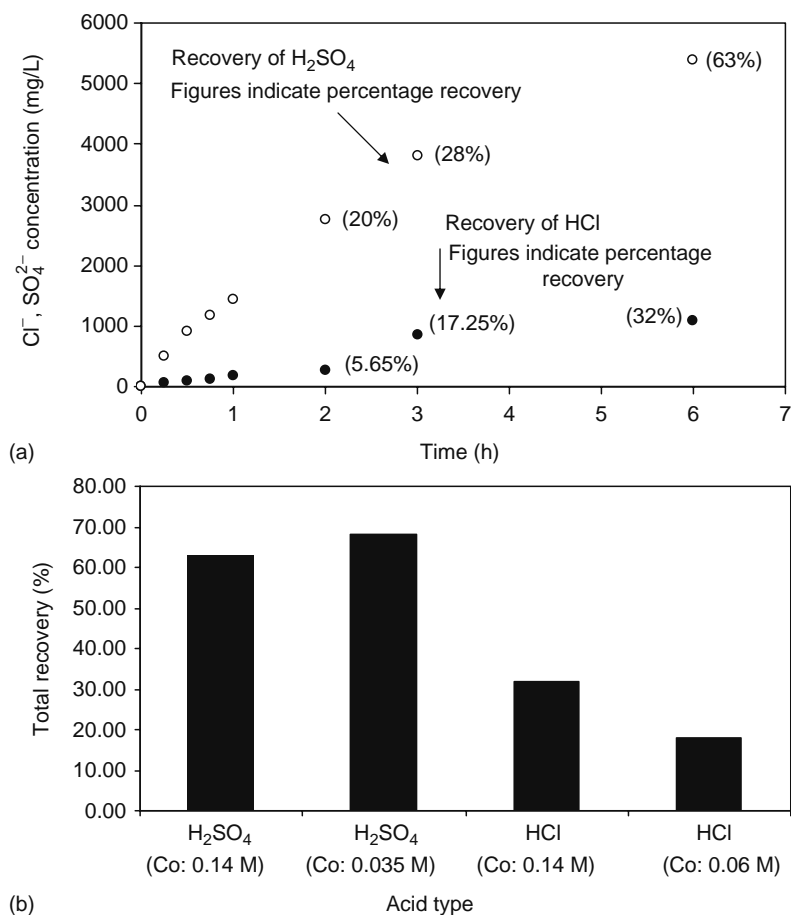


**FIGURE 34.28** (a) Influence of acid type on diffusion dialysis with Neosepta AFN and (b) influence of initial concentration on acid recovery during diffusion dialysis.

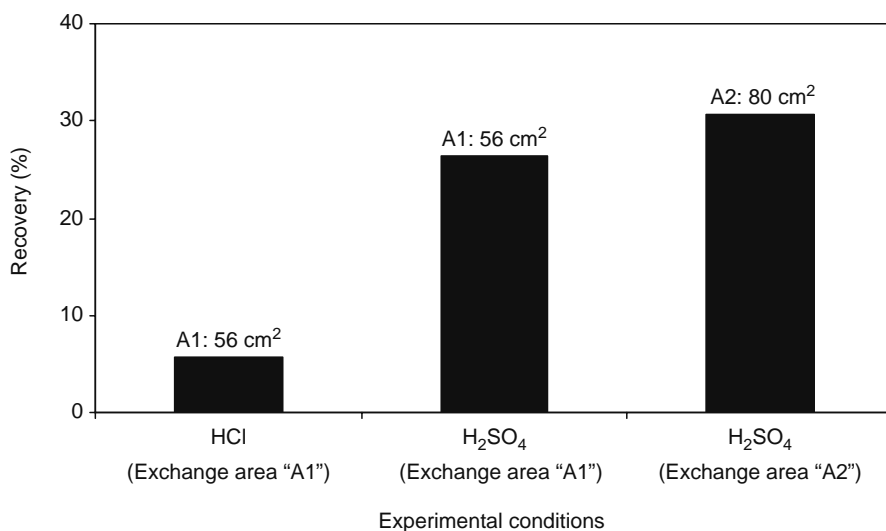


**FIGURE 34.29** Influence of diffusion dialysis on aluminum dissolution.

AFN. There could be other factors too, related to the morphology of the membranes. But these were not investigated in this study.

#### 34.6.14 INFLUENCE OF ACID TYPE AND CONCENTRATION ON DIFFUSION DIALYSIS RECOVERY

For Neosepta AFN, experiments were carried out to find out the diffusion dialysis of HCl and H<sub>2</sub>SO<sub>4</sub>. It could be seen that for a period of 6 h, the total recovery was about 63% for H<sub>2</sub>SO<sub>4</sub>, and for HCl it was around 32%. This finding is represented in Figure 34.28a. In a separate experiment, the initial concentration was changed from 0.14 to 0.06 M for HCl and 0.035 M for H<sub>2</sub>SO<sub>4</sub>. Recovery percentage did not change for H<sub>2</sub>SO<sub>4</sub> but was reduced by half to about 17% with HCl. This result is shown in Figure 34.28b. Two significant inferences drawn from these results were that the Neosepta AFN membrane was better suited for acid recovery from final WTR feed, and H<sub>2</sub>SO<sub>4</sub> could be more readily recovered through the diffusion dialysis process.

#### 34.6.15 ALUMINUM DISSOLUTION USING DIFFUSION DIALYSIS

In this experiment, the sweep side DI water was replaced by a DI water solution containing synthetic samples of aluminum hydroxide. The feed side contained 0.15 M acid solution of HCl or H<sub>2</sub>SO<sub>4</sub>. At the end of 6 h of experimentation, the aluminum concentration in the aqueous phase was higher for the case of H<sub>2</sub>SO<sub>4</sub>. When the area of exchange was increased from 56 to 80 cm<sup>2</sup>, the aluminum concentration went up marginally. Higher area allowed more acid molecules to diffuse through, and thus resulted in more dissolution of aluminum ions. These findings have been summarized in Figure 34.29.

#### 34.6.16 WTR DISSOLUTION AND pH CHANGE

In another experiment, residual WTR after DMP treatment was used as feed, and fresh WTR used as sweep solution for the diffusion dialysis experiment. The total aluminum recovered with time was noted on both the feed and sweep side. The results are shown in Figure 34.30. It can be observed that the pH dropped to a significant value on the sweep side from 6.9 to 3.5. Simultaneously, about 40% of total aluminum was dissolved in the process.

#### 34.6.17 FOULING OF ANION-EXCHANGE MEMBRANE

Two consecutive experiments, Run 1 and Run 2, were performed with the same stock of feed and sweep solutions and the pH changes in both the solutions recorded for each run. The graphs shown in Figure 34.31 show that pH variation with time closely matched for both runs, suggesting that there was no fouling of membranes because of NOM present in solution. But given that anion-exchange membranes are positively charged, their fouling after frequent usage cannot be ruled out. In fact, according to the manufacturer's specifications, fouling of Neosepta AFN may happen if the DOC concentration is greater than 100 mg/L.

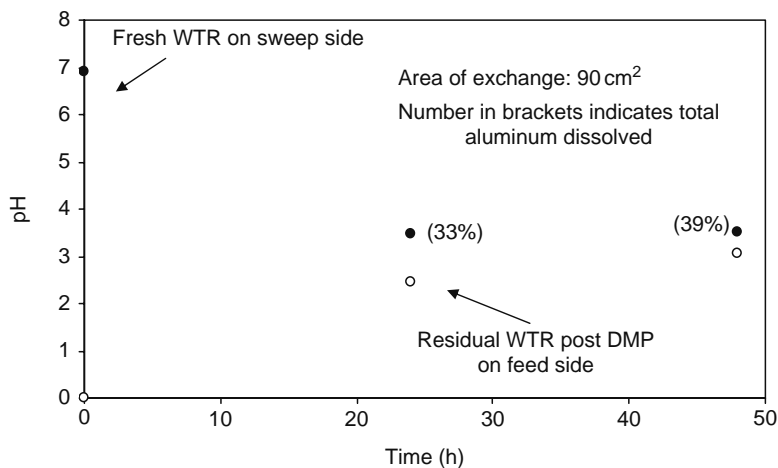


FIGURE 34.30 pH change and aluminum dissolution in fresh WTR feed/residual WTR during diffusion dialysis.

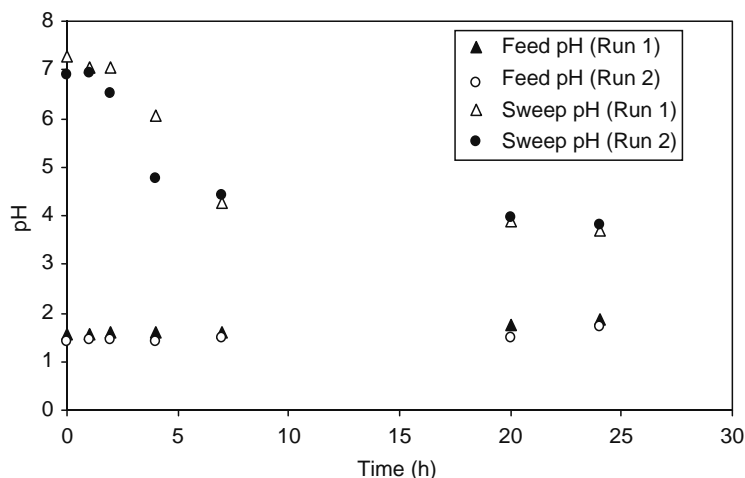


FIGURE 34.31 Study of fouling issues during diffusion dialysis.

### 34.6.18 DIFFUSION DIALYSIS CONSTANT FOR ACIDS

From the findings of the experiment, it was clear that  $\text{H}_2\text{SO}_4$  diffused faster than  $\text{HCl}$  through Neosepta AFN. On the basis of a 2 h experiment, the diffusion dialysis coefficient  $U$  was found as follows:

$$U_{\text{H}_2\text{SO}_4} = 58.6$$

$$U_{\text{HCl}} = 4.6$$

The selectivity of the membrane for one acid ( $\text{H}_2\text{SO}_4$ ) over another ( $\text{HCl}$ ) was found to be 12.7.

## 34.7 CONCLUSIONS

It was hypothesized that as opposed to pressure-driven membrane process applications, namely reverse osmosis (RO), nanofiltration (NF), and ultrafiltration (UF), Donnan membrane process (DMP) or Donnan dialysis was not susceptible to fouling by fine particulates and large organic molecules. It was driven by an electrochemical potential gradient across a semipermeable ion-exchange membrane. In open literature, no work has been reported on the application of DMP to treat slurry or sludge with relatively high concentration of suspended solids or large organic molecules. The current research is therefore novel work in the area of residuals management and it also led to a novel membrane separation application. The key conclusions drawn from this research are

- DMP was successful in recovering alum from WTR based on alum,  $\text{Al}_2(\text{SO}_4)_3 \cdot 14\text{H}_2\text{O}$ , and ferric chloride ( $\text{FeCl}_3$ ) coagulants. A series of laboratory tests confirmed that over 70%  $\text{Al}^{3+}/\text{Fe}^{3+}$  was easily recoverable.
- Alum recovered was essentially free of particulate matter, NOM, and other trace metals. The exclusion of negatively charged DOC was due to the presence of the negatively charged membrane surface through the process of Donnan exclusion.
- Since the DMP is driven by the electrochemical potential gradient, the presence of high turbidity and NOM in the sludge did not influence alum recovery and no noticeable membrane fouling was observed even after multiple runs for long hours of operation.
- DMP process was also selective in preferring trivalent cations over bivalent heavy metal ions.
- Nafion 117 from DuPont Chemical Co. was found to be the most effective membrane in terms of kinetics of ion transfer. The equilibrium isotherm showed that the membrane had a high selectivity for trivalent aluminum ions. This resulted in a rectangular isotherm for the Nafion 117 membrane.
- It was seen that in the experiments performed hydrogen ion was the trace species. Therefore, for coupled  $\text{Al}^{3+}-\text{H}^+$  transport, the interdiffusion coefficient approached the self-diffusion coefficient of the faster-diffusing  $\text{H}^+$  ions. This conclusion appears counterintuitive, but explains the good kinetics of the process.
- It was found that the interdiffusion coefficient values based on membrane surface I (facing the feed solution) concentration represented the actual transport process. The interdiffusion coefficient values were found to be in the range of  $10^{-10} \text{ m}^2/\text{s}$  for the Nafion 117 membrane.
- Another important observation was the osmosis of water from the feed to sweep solution, which resulted in dilution of the sweep solution during the later part of experimentation with Nafion 117. The osmosis effect was not noted for Ionac MC 3470.
- While both the interdiffusion coefficient and concentration gradient are responsible for aluminum ion flux, it was found that the former played a slightly more significant role in aluminum ion flux determination.
- It was also observed that the drop in the self-diffusion coefficient of higher valent ions in the membrane phase in comparison to their self-diffusion coefficient values at infinite dilution in aqueous phase was higher for ions with higher charge. This was attributed to greater difficulty in binding to adjacent sites for a higher valent cation.
- Comparison of a homogeneous membrane (Nafion 117) and a heterogeneous membrane (Ionac MC 3470) with respect to alum recovery showed that the recovered  $\text{Al}^{3+}$  could be concentrated to a high value of over 4500 mg/L (80% recovery) with Nafion 117, but the recovery was relatively low (25% recovery) with Ionac MC 3470. In a comparative study, the interdiffusion coefficient  $\bar{D}_{\text{Al,H}}$  was found to be  $\sim 7.23 \times 10^{-11} \text{ m}^2/\text{s}$  for homogeneous Nafion 117, while it was  $\sim 1.36 \times 10^{-11} \text{ m}^2/\text{s}$  for heterogeneous Ionac 3470.
- Scanning electron microphotograph and x-ray fluorescence showed clusters of nonconducting inert phases within the heterogeneous membrane containing no ionogenic groups. The lower interdiffusion coefficient for Ionac 3470 was attributed to its larger fraction of a nonconducting phase compared to Nafion 117.
- $\text{Al}^{3+}$  recovery profile led to identification of three zones of mass transport, namely a kinetically driven linear zone, an equilibrium-driven saturation zone, and an osmosis-driven dilution zone. All three zones were observed in Nafion 117 during a 24 h experimental run. For Ionac MC 3470, only the linear zone was observed during the period of experimentation.
- Application of diffusion dialysis had a desired effect in transfer of acid molecules from the residual WTR feed to fresh WTR sweep solution. It helped in raising the pH of residual feed from 1–1.5 to approximately 3.0. The simultaneous reduction of pH on the fresh WTR sweep solution helped in dissolving aluminum ions from the solid phase into the aqueous phase up to 40%.
- $\text{H}_2\text{SO}_4$  was found to diffuse faster than HCl. Neosepta AFN membranes were found suited for the current application and responded better than Ionac MA 3475 membranes.

### 34.8 FUTURE RESEARCH

The current research also led to identification of a number of nascent research applications. Further work can be carried out in the following areas [55]:

- Recovered alum can be compared with commercial alum in terms of its application as a coagulant. The possibility of alternative use of recovered alum such as in manufacture of polyaluminum salts and their acceptability as a commercial product must be studied.
- In the current research, a major focus was on alum recovery. A study can be carried out for ferric ion recovery and detailed modeling can be carried out for Fe(III) recovery from ferric chloride-based WTR.
- In the current kinetic modeling, it was assumed that the DMP involved coupling of two ions. A more detailed study can be carried out to study multicomponent systems undergoing DMP. Therefore, the influence of contaminant ions on alum recovery can be better characterized. In this regard, the distribution of aluminum ions in the membrane in presence of other cations may also be evaluated.

- Osmosis of water in charged membranes can be studied as a research subject.
- Diffusion dialysis process was very briefly studied in the current research. A detailed study of acid recovery from water treatment plant residuals can be a subject of research.
- More rigorous treatment of comparison of homogeneous and heterogeneous membranes involving conductivity measurements at different electrolyte strengths can help in characterizing the transport properties of these membranes.

## ACKNOWLEDGMENTS

Industrial ecology fellowship grant from the National Science Foundation and Lucent Technology is gratefully acknowledged. We are also thankful for partial financial support from Pennsylvania Infrastructure and Technology Alliance (PITA). The authors gratefully acknowledge valuable suggestions from Dennis Curtin of Dupont Chemicals.

## REFERENCES

1. James, M. Montgomery Consulting Engineers, Inc. *Water Treatment principles and Design*. John Wiley & Sons: New York, 1985.
2. Technology Transfer Handbook: *Management of Water Treatment Plant Residuals*. ASCE: New York, 1996.
3. Cornwell, D.A. and Westerhoff, G.P. Management of water treatment plant sludges in *Sludge and Its Ultimate Disposal*. J.A. Borchardt (Ed.), Ann Arbor, MI: Ann Arbor Science, 1981.
4. SenGupta, A.K., Li, P., and Cumbal, L. Selective alum recovery from water treatment residuals. AWWA Research Foundation, Denver, CO, ISBN 0-89867-899-4, 140 pp, 1997.
5. Li, P., SenGupta, A.K., and Cumbal, L. Role of morphology and interfacial chemistry of ion exchanger for alum recovery from clarifier sludge. Proceedings of the international conference on ion exchange (IEX'96), Cambridge University, Cambridge, July 1996, Society of Chemical Industry, pp. 104–112, 1996.
6. SenGupta, A.K. and Shi, B. Selective alum recovery from clarifier sludge. *J. AWWA*, 84, 96–103, 1992.
7. Driscoll, C.T. et al. Effects of aluminum speciation in fish in dilute acidified waters. *Nature*, 284, 161–164, 1980.
8. Lamb, D.S. and Bailey, G. Acute and chronic effects of alum to midge larvae. *Bull. Environ. Contam. Toxicol.*, 27, 59–67, 1981.
9. Desroches, S., Dayde, S., and Brethon, G. Aluminum speciation studies in biological fluids. Part 6. Quantitative investigation of aluminum(III)-tartrate complex equilibria and their potential implications for aluminum metabolism and toxicity. *J. Inorg. Biochem.*, 81, 301–312, 2000.
10. American Water Works Association Research Foundation (AWWARF). *Coagulant Recovery: A Critical Assessment*, Denver, CO. AWWA and AWWARF, 1991.
11. Bishop, M.M., Rolan, A.T., Bailey, T.L., and Cornwell, D.A. Testing of alum recovery for solids reduction and reuse. *J. AWWA*, 79, 76–83, 1987.
12. Cornwell, D.A. and Zoltec, J. Recycling of alum used for phosphorous removal in domestic wastewater treatment. *J. WPCF*, 49, 600–612, 1977.
13. Stevens, A.A. and Symons, J.M. Measurement of trihalomethane and precursor concentration changes. *J. AWWA*, 69, 546–554, 1977.
14. Christman, R.F., Norwood, D.L., Millington, J.D.S., Stevens, J.D., and Stevens, A.A. Identity and yields of major halogenated products of aquatic fulvic acid chlorination. *Environ. Sci. Technol.*, 17, 625–628, 1983.
15. Oliver, B.G. and Visser, S.A. Chloroform production from the chlorination of aquatic humic material: The effect of molecular weight, environment and season. *Water Research*, 14, 1137–1141, 1980.
16. Dhage, S.S., Paramsivam, R., Rao, R.R., and Pandey, S. Recovery of alum from water treatment plant sludge by liquid ion exchange technique. *J. IWWA*, XVII, 2, 193–199, 1985.
17. Bregman, J.I. Membrane processes gain favor for water reuse. *Environ. Sci. Technol.*, 4, 296–302, 1970.
18. SenGupta, A.K. Cyclic Process for Selective Coagulant Recovery from Clarifier Sludge. United States Patent 5,304,309, 1994.
19. Wallace, R.M. Concentration and separation of ions by Donnan membrane equilibrium. *Ind. Eng. Chem., Process Des. Dev.*, 6(4), 423–431, 1967.
20. Ersoz, M. and Kara, H. Cobalt(II) and Nickel(II) transfer through charged polysulfonated cation exchange membranes. *J. Colloid Interface Sci.*, 232, 344–349, 2000.
21. Kim, B.M. Donnan dialysis for removal of chromates and cyanides. *AIChE Symp. Ser.*, 76(197), 184–192, 1979.
22. Hichour, M., Persin, F., Molenat, J., Sandeaux, J., and Gavach, C. Fluoride removal from diluted solutions by Donnan dialysis with anion-exchange membranes. *Desalination*, 122, 53–62, 1999.
23. Tongwen, X. and Weihua, Y. Sulfuric acid recovery from titanium white waste liquor using diffusion dialysis with a new series of anion exchange membrane–static runs. *J. Membr. Sci.*, 183, 193–200, 2001.
24. Kobuchi, Y., Motomura, H., Noma, Y., and Hanada, F. Application of ion exchange membranes to the recovery of acids by diffusion dialysis. *J. Membr. Sci.*, 27, 173–179, 1986.
25. Helfferich, F. *Ion Exchange*. Dover Publication Inc: New York, 1995, 134–135.
26. Prakash, P. and SenGupta, A.K. Selective coagulant recovery from water treatment plant residuals using Donnan membrane process. *Environ. Sci. Technol.*, 37, 4468–4474, 2003.
27. Blaedel, W.J. and Hauptert, T.J. Exchange equilibrium through ion-exchange membranes. Analytical applications. *Anal. Chem.*, 38(10), 1305–1308, 1966.
28. Davies, C.W. *Ion Association*. Butterworths, London, 1962.

29. Mafe, S., Ramires, P., and Pellicer, J. Activity coefficients and Donnan coion exclusion in charged membranes with weak-acid fixed charge groups. *J. Membr. Sci.*, 138, 269–277, 1998.
30. Helfferich, F. *Ion Exchange*. Dover Publication Inc: New York, 1995, 267, 385.
31. Sato, K., Yonemoto, T., and Tadaki, T. The determination of diffusion coefficients of counter-ion in the ion-exchange membrane by means of a batchwise Donnan dialytic experiments. *J. Membr. Sci.*, 53, 215–227, 1990.
32. Miyoshi, H. Diffusion coefficients of ions through ion exchange membrane in Donnan dialysis using ions of different valence. *J. Membr. Sci.*, 141, 101–110, 1998.
33. Cussler, E.L. *Diffusion Mass Transfer in Fluid Systems*. Cambridge University Press: Cambridge, 1998, p. 16.
34. Helfferich, F. *Ion Exchange*. Dover Publication Inc: New York, 1995, 348–349.
35. SenGupta, A.K. and Prakash, P. Process for Selective Coagulant Recovery from Water Treatment Plant Sludge. United States Patent 6,495,047, 2002.
36. Miyoshi, H., Yamagami, M., and Katoka, T. Characteristic coefficients of Nafion membranes. *Chem. Express*, 5(10), 717–720, 1990.
37. Sudoh, M., Kamei, H., and Nakamura, S. Donnan dialysis concentration of cupric ions. *J. Chem. Eng. Jpn.*, 20(1), 34–40, 1987.
38. Winston Ho, W.S. and Sirkar, K.K. *Membrane Handbook*. Van Nostrand Reinhold: New York, 1992.
39. Elmidaoui, A., Elattar, A., Pismenskaia, N., Gavach, C., and Porcelli, G. Comparison of transport properties of monovalent anions through anion exchange membranes. *J. Membr. Sci.*, 43, 249–261, 1998.
40. Bouma, R.H.B., Checchetti, A., Chidichimo, G., and Drioli, E. Permeation through a heterogeneous membrane: the effect of dispersed phase. *J. Membr. Sci.*, 128, 141–149, 1997.
41. Moon, S., Kim, S., and Choi, J. Heterogeneity of ion-exchange membranes: The effects of membrane heterogeneity on transport properties. *J. Colloid Interface Sci.*, 241, 120–126, 2001.
42. Timashev, S. *Physical Chemistry of Membrane Processes*. Ellis Horwood: Chichester, West Sussex, England, 1991.
43. Zabolotsky, V.I. and Nikonenko, V.V. Effect of structural membrane inhomogeneity in transport properties. *J. Membr. Sci.*, 79, 181–198, 1993.
44. Chamberlain, N.S. and Vromen, B.H. Make dialysis part of your unit operations with new acid-resistant membranes. *Chem. Eng.*, 4, 117, 1959.
45. Vromen, B.H. Dialysis a sleeper? *Ind. Eng. Chem.*, 54, 20, 1962.
46. Li, N.N., Long, R.B., and Henley, E.J. Membrane separation processes. *Ind. Eng. Chem.*, 57, 18, 1965.
47. Lorrain, Y., Pourcelly, G., and Gavach, C. Influence of cations on the proton leakage through anion-exchange membranes. *J. Membr. Sci.*, 110, 181, 1996.
48. Satchera, D.M., Childs, R.F., Mika, A.M., and Dickson, J.M. Acid recovery using diffusion dialysis with poly(4-vinylpyridine)-filled microporous membranes. *J. Membr. Sci.*, 148, 119–127, 1998.
49. American Public Health Association (APHA), American Water Works Association (AWWA), Water Environment Federation (WEF). *Standard Methods for the Examination of Water and Wastewater*, 18, 3, 44–46, 1992.
50. Johnson, P.N. and Amirtharajah, A. Ferric chloride and alum as single and dual coagulants. *J. AWWA*, 75(5), 232–239, 1983.
51. Prakash, P. and SenGupta, A.K. Coupled transport of trivalent-monovalent ion pair ( $\text{Al}^{3+}$  and  $\text{H}^+$ ) during Donnan membrane process for coagulant recovery. *AIChE J.*, 51(1), 333–344, 2005.
52. Miyoshi, H. Diffusion coefficients of ions through ion-exchange membranes for Donnan dialysis using ions of the same valence. *Chem. Eng. Sci.*, 52(7), 1087–1096, 1997.
53. Weast, R.C. *CRC Handbook of Chemistry and Physics*, chapter 5, Vol. 26, 1989–1990, pp. 95–97.
54. Prakash, P., Hoskins, D., and SenGupta, A.K. Application of homogeneous and heterogeneous cation-exchange membranes in coagulant recovery from water treatment plant residuals using Donnan membrane process. *J. Membr. Sci.*, 237, 131–144, 2004.
55. Prakash, P. Selective coagulant recovery from water treatment plant residuals using the Donnan membrane process, PhD Dissertation, Lehigh University, Bethlehem, PA, 2004.



---

# 35 Utilization of Membrane Processes in Treating Various Effluents Generated in Pulp and Paper Industry

*Mika Mänttari and Marianne Nyström*

## CONTENTS

35.1	Introduction to Membrane Processes in the Pulp and Paper Industry.....	981
35.2	Special Issues Concerning Membranes in the Pulp and Paper Industry .....	982
35.3	Parameters Affecting the Performance of Membrane Separation in the Pulp and Paper Industry .....	983
35.3.1	Characteristics of Membranes .....	983
35.3.2	Solution Properties and Filtration Conditions.....	984
35.4	Pressure-Driven Membrane Processes in the Pulp and Paper Industry.....	985
35.4.1	Microfiltration.....	985
35.4.2	Ultrafiltration .....	986
35.4.3	Nanofiltration and Reverse Osmosis .....	986
35.5	Suitability of Modules and Filters .....	986
35.6	Industrial Applications and Case Studies .....	988
35.6.1	Pulp Mill Applications .....	989
35.6.1.1	Sulfite Pulp Mill Effluents.....	990
35.6.1.2	Sulfate Pulp Mill Effluents.....	991
35.6.1.3	Mechanical Pulp Mill Effluents.....	993
35.6.2	Paper Mill Applications.....	993
35.6.3	Membranes Combined with Biological Treatment .....	995
35.6.3.1	End-of-Pipe Treatment .....	995
35.6.3.2	Membrane Bioreactors .....	996
35.6.4	Board, Recycling Paper, and Deinking Applications .....	998
35.6.5	Freshwater Treatment .....	999
35.6.6	Recovery of Coating Color .....	1000
35.6.7	Medium Density Fiberboard Manufacturing Effluent.....	1000
35.7	Electrodialysis as Post-Treatment .....	1000
35.8	Demands on Membranes Today and in the Future .....	1001
	Acknowledgments.....	1001
	Abbreviations.....	1002
	References.....	1002

## 35.1 INTRODUCTION TO MEMBRANE PROCESSES IN THE PULP AND PAPER INDUSTRY

Membranes are used in the pulp and paper industry in a variety of applications; in particular: for the purification and recovery of water, and for the recovery of raw materials or energy. The pulp and paper manufacturing process requires enormous amount of water; to transport the raw materials, to dissolve impurities, to seal various process equipment, to cool and heat, to wash and clean process equipment, and to generate necessary environment for the formation of the hydrogen bonding network between fibers and fillers, which is the basic mechanism of paper formation. Thus, water and its quality are essential issues in the production of pulp and paper.

A reduction in the volume of water needed at the paper machine is almost impossible because paper formation will be disturbed if the consistency of the pulp suspension becomes too high. Currently, the stock suspension (i.e., pulp and additives) in the head box of a paper machine contains 97%–99.9% water. The constraint of maintaining pulp suspension consistency means a reduction in water intake has to be realized by reusing the process water. Due to the different purposes and applications in which water is used, the water quality demands vary considerably. Membrane processes can be chosen to produce a specific water quality and are attractive alternatives to facilitate the reuse of water, either alone or combined with biological processes or other chemical and physical processes. In addition, membrane processes are an efficient way to recover raw materials, e.g., coating pigments, from effluents.

Membranes have been evaluated for use in the pulp and paper industry since the late 1960s. Initial experiments involved white water (circulation water) from a paper machine, which was purified for reuse, and bleach plant effluents, which were treated for the removal of color. The first reported commercial application of membrane processes was as early as 1972 when Green Bay Packaging (Green Bay, Wisconsin) installed a reverse osmosis (RO) system for the treatment of paper mill circulation water (white water) [1]. At that time, the typical membrane material was cellulose acetate (CA) that had a limited temperature and pH resistance. Generally, the fluxes of the CA membranes were also rather low. Extensive developments in membrane materials as well as in module construction and configurations have occurred since the 1970s. Today, RO and NF (nanofiltration) membranes are mainly thin film composite membranes made mostly from polyamide (PA) or its derivatives. In ultrafiltration (UF) or microfiltration (MF), in addition to materials used in RO, such as polyamide: polysulfone (PSu), polyethersulfone (PES), polyethylene (PE), regenerated cellulose (RC), and polyvinylidene-fluoride (PVDF) are also used as membrane materials in the filtration of pulp and paper industry effluents. Membrane manufacturers may also have chemically modified forms of these base membrane materials, the nature of the modification is generally not disclosed.

During the 1980s, three large-scale ultrafiltration plants started to treat caustic extraction stage effluents in Japan and Sweden to remove color, and reduce chemical oxygen demand (COD) and biological oxygen demand (BOD). In 1988, the first high-shear cross-rotational (CR) filter was started in Sweden (MoDo, Husum, belonging to M-Real since 2000). It was used to remove adsorbable organic halogens (AOX) and COD from the bleach plant effluent. This technology has now been installed in more than forty mills to reuse coating color and process waters, or to purify effluents. During the 1990s two new types of membrane processes, NF and the membrane bioreactor (MBR), were introduced in the pulp and paper industry. The number of studies on MBR increased considerably at the end of the 1990s and, today, some commercial MBRs are in operation in the pulp and paper industry.

Legislation, environmental issues, customer demands, and economic reasons have increased interest in membranes. According to the Paperbase databank, in 1990 the word ultrafiltration was mentioned in more than 100 different papers and reverse osmosis in about 70 papers. In 2005, the corresponding numbers were 500 and 220. However, the seemingly intensive research has not yet created many mill-scale installations.

The chapter will concentrate on membrane processes, in which pressure is the driving force and both the permeate and the concentrate are water solutions. Electrodialysis (ED) will also be reviewed briefly. The idea is to focus on installations and studies of the last 10 years. Readers who are interested in older studies or installations are referred to several review publications [1–3].

## 35.2 SPECIAL ISSUES CONCERNING MEMBRANES IN THE PULP AND PAPER INDUSTRY

In general, the effluent volumes in the pulp and paper industry are huge, even cubic meters per second, and if all the mixed effluent has to be treated by membranes, high fluxes and large membrane areas are needed. By keeping some water streams unmixed the membrane processes could be focussed on the most relevant streams and then only smaller volumes would need to be treated. Obviously, the membrane purification needed differs depending on the demands of the treated waters in the reuse application.

The effluents and process streams in the pulp and paper industry are very complex and comprise heterogeneous combinations of different wood-based compounds and their degradation products, as well as the chemicals used in the processing of the raw materials or additives used in the production of the end products. Thousands of different chemical compounds can be identified from these process streams. Some of them are known to be strongly fouling, limiting the feasibility of membrane processes. Many streams contain fibers or debris, and they can easily plug the flow channels when modules with high packing density (i.e., spiral wound modules) are used. Because the same paper machines are commonly used to manufacture different paper products (i.e., paper grades), which all need tailored process conditions and special raw materials, the concentration and composition of the feed process streams to be filtered vary considerably.

Generally, in the pulp and paper industry the temperature of the process water can vary from 10°C to 90°C, or sometimes even higher. The concentrations vary from less than 100 mg/L dry solids up to 40%–60% (e.g., coating pigments and chemicals) and the pH from <2 to 14 (e.g., in bleaching stages). Generally, in the actual papermaking process the pH is either 5 or 7.

### 35.3 PARAMETERS AFFECTING THE PERFORMANCE OF MEMBRANE SEPARATION IN THE PULP AND PAPER INDUSTRY

The most widely used or tested membrane processes in pulp and paper mill applications are based on pressure-driven membrane processes; MF, UF, NF, and RO. In the following sections, the characteristic properties of the membranes are discussed and their effect on filtration efficiency is summarized. In addition, some common influence of effluent properties and filtration conditions on membrane processes are discussed.

#### 35.3.1 CHARACTERISTICS OF MEMBRANES

Membrane properties have been characterized and their effects on flux, retention, and fouling have been studied extensively by several authors. Some common facts can be concluded from these studies.

Pore size is obviously one of the most important factors affecting flux and retention. However, it has frequently been seen that the membrane with the most open pores does not usually give the highest permeate flux when process waters are filtered. Fouling of the membrane material, particularly pore plugging, can be considerably stronger with microfiltration membranes than with UF or NF membranes [4–7]. Retention is obviously affected by the pore size due to the sieving effect, especially when using microfiltration and ultrafiltration membranes. With tighter (NF and RO) membranes retention will be governed more and more by the electrostatic forces as well as by other interactions between membranes and solutes.

Another factor that has been shown to significantly affect flux and fouling is the hydrophilic character of the membranes [4,8–12]. Water spreads over the surface of a hydrophilic membrane but not on a hydrophobic membrane. The membrane material determines its hydrophilicity, which is typically evaluated by measuring the contact angle at a membrane–water–air interface. Cellulose and hemicelluloses, which form the main part of wood and paper, are extremely hydrophilic. Wood extractives such as fatty and resin acids, on the other hand, have hydrophobic characteristics and, therefore, they are found more on fouled and used hydrophobic membranes than on hydrophilic ones (Figure 35.1) [9,13].

Fatty acids foul membranes more intensive under acidic conditions. When the pH is increased above 5–6, the fatty acids form their corresponding salts, the solubilities of which are up to 100 times higher than that of the neutral acid, and therefore their fouling at high pH due to adsorption is negligible [14]. This is one reason why alkaline filtrates from bleaching or various neutral process waters are usually easier to filter than acidic waters.

Maartens et al. [15] characterized adsorbed foulants calorimetrically and concluded that foulants in pulp and paper mill effluents are phenolic and hydrophobic in nature, a result corroborated by Puro et al. [9]. Maartens et al. also modified their membranes to make them more hydrophilic and achieved less fouling and better cleaning efficiency. Thus, pretreatment or modification of a membrane can improve its fouling resistance, its flux or retention, and can enhance its usability in pulp and paper industry applications [16].

A smooth membrane usually fouls less than a rough membrane, especially, when colloidal solutions, such as waters from the pulp and paper industry, are filtered [17]. Process streams might contain fibers or even some solid particles, which can wear

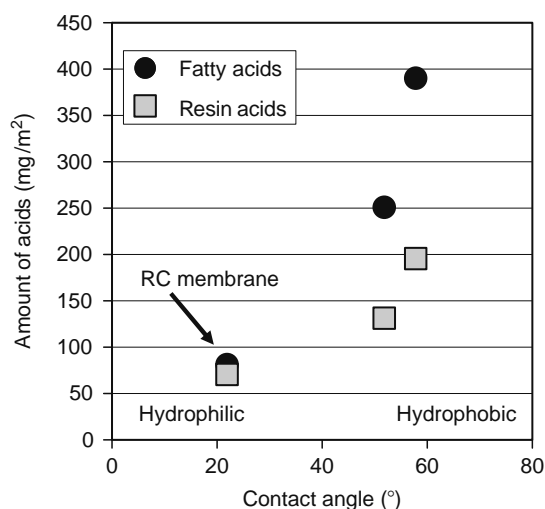


**FIGURE 35.1** The amount of fatty acids and resin acids found in ultrafiltration membranes of varying hydrophilicity after a 30 day test run in an integrated pulp and paper mill at pH 5.3 (the solvent in extraction was an acetone–water solution [9:1]). (Based on data from Puro, L., Tanninen, J., and Nyström, M., *Desalination*, 143, 1, 2002; Huuhilo, T., Väisänen, P., Nuortila-Jokinen, J., and Nyström, M., *Desalination* 141, 245, 2001.)

the membrane surface, particularly under high-shear conditions. A rough membrane contains more mountains (peaks on the membrane surface) where erosion happens easily. In addition, the permeate side support spacer should be smooth, as it could otherwise cause macroscopic roughness on the membrane surface (opposite side) when under pressure. This mechanical erosion of the membrane surface has to be taken into account, when filtering concentrated solutions or solutions containing solids. Fibers have been reported to enhance the flux because of the scouring effect they cause or because of the adsorbed foulants that they carry away [18–20].

Membrane charge [3,8,21] affects membrane efficiency, particularly when low cutoff membranes are used at low salt concentration. Many polymeric membranes are amphoteric, having both negatively and positively charged functional groups in the polymer matrix. Therefore, the membrane might be positively charged at low pH and negatively charged above the isoelectric point (pH where net charge is zero). The isoelectric point of polymeric membranes is often at pH 4–6. When a membrane is charged, it is also more hydrophilic than when uncharged. An increase in the flux of a relatively dense membrane at a high pH may result from an increase in membrane hydrophilicity due to the dissociation of the functional groups in the membrane structure [22,23].

### 35.3.2 SOLUTION PROPERTIES AND FILTRATION CONDITIONS

Pulp and paper industry waters contain thousands of compounds and many of them can be dissociated and charged at the prevailing conditions. When particles are dispersed in water, they usually acquire a certain fixed charge. An increase in pH generally improves the solubility of many dissolved and colloidal substances, and often gives them a negative charge. For instance, carboxylic groups existing in, for example, fatty and resin acids (wood extractives) dissociate (become charged) when a pH of 4–6 is exceeded. Phenolic groups such as those in extractives or lignin are charged above pH 9 when the phenol is dissociated. When the membranes and the compounds have similar charges, they repel each other. The charge effect on retention is very clear as shown in Figure 35.2 [24]. All other measured parameters besides the UV absorption at 280 nm (UVA 280 nm) were retained better at high pH. The compounds absorbing UV light were mostly retained by the sieving effect in nanofiltration and not by charge. Therefore, they were equally well retained in the whole pH range. Unfortunately, the buffering capacity and the volume of the streams in the pulp and paper industry require large amounts of chemicals, making pH adjustment an uneconomical mean when improving filtration performance.

Flux is often less affected by pH than retention, but the common trend is that both are better when electrostatic forces are present. Furthermore, the electrostatic repulsion between dissociated compounds and the membrane prevents them from coming in contact and, therefore, diminishes fouling. However, if some cationic compounds (e.g., retention agents from papermaking) are present in the water stream, because of electrostatic attraction, a negatively charged membrane will most often be fouled more than a membrane, which is more or less uncharged. Regenerated cellulose is a very hydrophilic, fairly uncharged material, thus it is successfully used in the filtration of paper mill process waters.

Pulp and paper industry streams are mostly colloidal, i.e., they contain macromolecules and small particles in the range of 1 nm to 1  $\mu\text{m}$ . Salt and pH affect colloidal stability, rate of precipitation, and colloidal fouling. The higher the surface charge

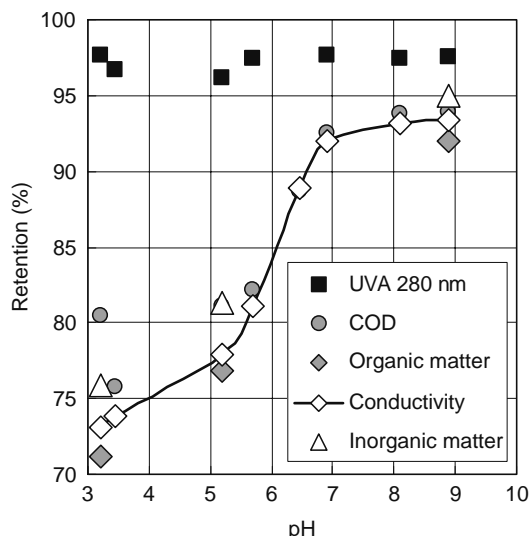


**FIGURE 35.2** Size and charge effects on the retention of various lump parameters when paper mill total effluent was nanofiltered (Desal-5 DK membrane) at different pH. (Adapted from Mänttari, M., Nuortila-Jokinen, J., and Nyström, M., *J. Membr. Sci.*, 137, 187, 1997.)

of the colloidal compounds in the solution, the greater the colloidal stability and the lower the colloidal fouling. Colloidal stability can be improved by softening the water (i.e., removing multivalent ions, e.g., calcium ions, or replacing them with monovalent ions) and by adjusting pH [25,26].

One special property of the process waters discussed is the broad heterogeneity in concentration of the dissolved and dispersed molecules. This is due to different products manufactured using the same machine and also due to shut down and start-up periods. Several authors have shown that the concentrations of organic and inorganic compounds vary even tenfold in process waters [18,27,28]. This means that when using membrane technology the membranes should be resistant to big fluctuations in the feed stream.

A trend in the pulp and paper industry has been toward elevated temperatures. The temperature range of the water circuit in many mills is 50–70°C where higher temperatures yield increased productivity and reduced energy consumption [29]. Occasionally, streams from pulp mills are filtered even at 90°C. Temperature decreases the viscosity of the water stream and, therefore, increases flux. The cleaning efficiency is also usually improved at high temperature. Unfortunately, a high temperature can have a detrimental effect on membrane material properties and filtration efficiency [30]. Too high a temperature may completely destroy the membrane or change its retention properties and flux. Traditional cellulose acetate membranes withstand only 35°C but some PVDF, polysulfone, or polyamide-based membranes can function at temperatures up to 90°C. The synergy of high temperature and high pressure results in compaction of the membrane structure. The compaction irreversibly tightens the membrane structure and as a result the permeability decreases detrimentally. This effect has not been studied thoroughly, but some indications have been reported. Kallioinen et al. showed that a slight compaction of regenerated cellulose ultrafiltration membranes (cutoff 30 kg/mol) occurred already at a pressure of 3 bar [31].

Several researchers have reported significant improvements in flux at high cross-flow velocity or by using other methods to increase shear forces on the membrane surface. Flux is often a trade-off with the energy used to create the shear forces. The effect of the high cross-flow velocity vanishes when the pressure (flux) is decreased. Therefore, it may be advantageous to use a high-turbulence system under medium to high pressure to benefit fully from the high mass transfer coefficient or to use inexpensive low-turbulence filter systems at relatively low-operating pressure, even operating below the critical flux (at subcritical flux) [32–36]. The permeate flux (pressure) has a significant influence on retention especially with tighter membranes (RO, NF, tight UF) [37]. However, too high pressures and fluxes cause polarization of the retained compounds on the membrane surface (concentration polarization) resulting in flux decrease, change of retention, and compact fouling. The critical flux is the highest flux that is obtained without fouling at the applied conditions. Therefore, by controlling the flux, fouling can often be managed [38–40]. In Section 35.5, sophisticated module constructions operating at high shear are presented.

When comparing high-shear and low-shear modules in the filtration of effluents from the pulp and paper industry huge differences have been seen in retention. The colloidal material acts as a secondary layer in the filtration with a low-shear module and increases retention of substances as well as concentration polarization. Approximately a double flux (100–150 L/(m<sup>2</sup> h)) was obtained in a high-shear module compared to a low-shear module, but the retention of conductivity was 10%–15% units lower [41]. The fouling layer was reported also by Woerner et al. to determine retention [42]. Thus, the trade-off between flux and retention depends on both the tightness of the membrane and the flow velocity. Electrical field [34], ultrasonic field [43], and back pulsing with permeate or air and air scouring in hollow fiber modules have also been studied as possible methods to improve flux.

## 35.4 PRESSURE-DRIVEN MEMBRANE PROCESSES IN THE PULP AND PAPER INDUSTRY

### 35.4.1 MICROFILTRATION

Microfiltration membranes can be used as pretreatment for other membrane technologies and to remove microbes and total suspended solids (TSS) including fibers and particles. Retention of salts and dissolved organics is negligible, if they are not bound to the suspended solids. MF can be used for the recovery of coating color pigments. MBRs generally use UF or MF membranes. The materials used in microfiltration are polyvinylidene fluoride (PVDF), polypropylene, polyethylene, polysulfone, polyether sulfone, Teflon, and ceramic materials.

Microfiltration membranes are commonly used in MBRs to separate solids from water. The fluxes are very low, often below critical flux, and at low pressures when hollow fibers are used, backflushing is added to prevent or reduce flux decrease. MBRs are discussed in detail in Section 35.6.3.2, tubular modules with MF membranes have also been tested in the pulp and paper industry.

Pore sizes in MF are typically 0.05–10 μm. Generally, MF membranes suffer from pore plugging because the pulp and paper mill effluents often contain particles of similar sizes as the pores in the membranes. That is why, in many cases, fluxes in ultrafiltration are significantly better than fluxes obtained with microfiltration. Silva et al. [44] studied submerged hollow-fiber microfiltration (a) for the removal of flexographic ink from a deinking plant effluent, (b) for the concentration and recycling of the coating effluent before evaporation in a chemi-thermomechanical pulping plant, and (c) as a separation barrier in MBR for

treating old corrugated cardboard recycled mill effluent. In industrial-scale applications MF is used before other treatment processes, for example, before RO in the zero effluent McKinley mill in Prewitt, New Mexico [45,46].

### 35.4.2 ULTRAFILTRATION

Ultrafiltration is the most widely used membrane process in the pulp and paper industry. UF membranes have been used to remove or reduce suspended solids, color, extractives, turbidity, COD, and AOX from various process streams and effluents, for the recovery of raw materials. The permeate after UF is often good enough to be discharged and can often be reused in many places in the mill. UF of bleaching effluents has been extensively investigated and became established on an industrial scale using tubular (Taio Paper Iyomishima, Japan) and flat sheet (Sanyo-Kokusaku Paper Iwakuni, Japan) membranes in the early 1980s [1]. UF is also used to recover lignosulfonates from spent sulfite liquor. A commonly employed membrane filter in the pulp and paper industry, the CR filter, uses UF membranes. UF of the clear filtrate stream (effluent from the paper machine) is industrially realized in many mills using low pressure and high cross-flow velocities or high-shear rates (Section 35.6.2). Ultrafiltration membranes, in flat sheet, tubular or hollow fiber form, are often the separation barriers in MBRs. In addition, coating color recovery is commonly carried out using UF membranes.

In UF, the separation is mainly based on the difference in the molecular size of the solute compared to the pore size of the membranes. Commercial ultrafiltration membranes are available with cutoff values ranging between 1 and 500 kg/mol. Typically, the membranes used to treat alkaline effluents from pulp bleaching have a cutoff value of 4–8 kg/mol. Membranes used to treat streams from pulp mills are often made of polysulfone, or even ceramic materials such as aluminium oxide and zirconium dioxide. Other materials commonly used in UF membranes are polyamide, polysulfone, and polyethersulfone. Circulation waters of paper machines are purified using polymeric UF membranes having a cutoff around 30–150 kg/mol. Some of the best membranes for process water treatment are manufactured from regenerated cellulose (e.g., C30F from Microdyn/Nadir, cutoff 30 kg/mol). Their extremely high hydrophilicity generates a high flux at low pressure and low fouling (Figure 35.1). Coating colors are recovered using slightly more open membranes (cutoff 30–500 kg/mol). Most industrial-scale pulp and paper mill UF installations are for the recovery of coating colors; however, in process water treatment there are fewer installations but these have larger installed membrane area.

### 35.4.3 NANOFILTRATION AND REVERSE OSMOSIS

Nanofiltration or reverse osmosis treated water is needed in the most demanding places of the mill such as for the high-pressure showers in a paper machine. Surface water used in the mill as intake freshwater may also need NF or RO treatment. Permeation of monovalent ions, in particular chloride ions, is both an advantage and a disadvantage of NF compared to RO. Monovalent salts cause significant osmotic pressure when retained in RO. In NF their permeation keeps the osmotic pressure lower and thus the transmembrane pressure needed to overcome the osmotic pressure is lower. The permeation of chloride ions in NF may restrict the reuse of the permeate because of concerns regarding corrosion caused by chloride. On the other hand, the concentrate then contains less chloride and its reuse or incineration is safer.

Nanofiltration retains 40%–95% of organic compounds and multivalent ions and from –300% (negative retention by the Donnan effect) to +50% chloride ions depending on the concentration of multivalent ions. Retention is greatly affected by electrostatic forces, as discussed in Section 35.3.2, and sulfate ions, in particular, significantly affect the retention of chloride ions [24].

Typical membranes in NF are thin film composite membranes and their surface layers are mostly proprietary and not very easily identified by the user. Some industrial use of sulfonated polyethersulfone membranes has also been seen (see Section 35.6.2. Linpac recycle paper mill in Cowpens, South Carolina). Tubular and spiral wound modules are the dominating module type in NF and RO. Both membrane processes are used in industrial-scale applications in the pulp and paper industry (Table 35.1). When the membranes are installed in spiral wound modules, water pretreatment is often important to prevent plugging of the modules and fouling of the membranes.

## 35.5 SUITABILITY OF MODULES AND FILTERS

The large volumes of effluents or process streams to be treated in the pulp and paper industry require a large membrane surface area. The development of membrane modules has generally been directed to developing equipment with high packing densities, such as hollow fiber and spiral wound modules. Unfortunately, due to their small flow channels these modules tend to plug easily demanding feed streams free of particulate contaminants (e.g., fibers and suspended solids). To reduce the plugging tendency of spiral elements, more open flow channels and special spacer constructions have been developed. A further difficulty with maintaining high-flow rates in a spiral wound module is the fact that the flow rate also increases the pressure loss over the module and this will, when exceeding the upper allowed limit of the modules (typically 0.5–1.5 bar), devastate the module structure. Thus, with these types of modules the boundary layer, i.e., the concentration polarization layer, restricts the

**TABLE 35.1**  
**Reported Existing Membrane Installations Excluding Coating Color Recovery Installations in the Pulp and Paper Industry. The Filters from Burg Plant, Uetersen Plant, and Svanskog Plant Have Recently Been Transferred to Other Mills**

Company and Mill	Place	Application	Membrane Unit	Supplier	Year	Section	Source
UPM-Kymmene Tervasaari	Valkeakoski, Finland	White water (120 m <sup>3</sup> /h)	CR ultrafiltration (560 m <sup>2</sup> )	Metso Paper	2005		[54]
Holmen Paper Madrid	Fuenlabrada, Spain	White water (33 m <sup>3</sup> /h)	CR ultrafiltration (140 m <sup>2</sup> )	Metso Paper	2004		[54]
LINPAC, recycle paper mill	Cowpens, South Carolina	UF concentrate (5 m <sup>3</sup> /h)	VSEP NF (242 m <sup>2</sup> )	New Logic	2004	35.6.4	[50]
Mercel International pulp mill	Stendal, Germany	Raw water (300 m <sup>3</sup> /h)	RO		2004	35.6.5	[55]
LINPAC, recycle paper mill	Cowpens, South Carolina	Mill effluent (50 m <sup>3</sup> /h)	Tubular UF	Koch Membrane	2003	35.6.4	[50]
Papierfabrik Palm	Wörth, Germany	Biotreated effluent (70 m <sup>3</sup> /h)	Tubular UF (2280 m <sup>2</sup> + NF/RO)	Norit	2002	35.6.3.1	[28]
Arctic Paper	Munkedals, Sweden	White water (10 m <sup>3</sup> /h)	Tubular UF (270 m <sup>2</sup> )	Norit	2002	35.6.2	[28]
Propapierfabrik Propapier	Burg, Germany	White water, clear filtrate (108 m <sup>3</sup> /h)	CR-UF (560 m <sup>2</sup> )	Metso Paper	2001		[54]
M-Real Kirkniemi mill	Lohja, Finland	White water (100 m <sup>3</sup> /h)	CR-UF (420 m <sup>2</sup> )	Metso Paper	2001	35.6.2	[53]
Domsjö Fabriker	Örnköldsvik, Sweden	White liquor (45 m <sup>3</sup> /h)	CR-UF (252 m <sup>2</sup> )	Metso Paper	2000	35.6.1.1	[54,56]
Van Houtum & Palm (VHP)	Ughehlen, the Netherlands	Bleaching effluent (10 m <sup>3</sup> /h)	MBR (outside), tubular (83 m <sup>2</sup> )	NORIT membranes	2000	35.6.3.2	[27,28]
Arctic Paper	Munkedals, Sweden	Mill effluent (40 m <sup>3</sup> /h)	Tubular UF (462 m <sup>2</sup> )	Norit	1999	35.6.3.1	[28]
Papeteries du Rhin	France	Board effluent (37.5 m <sup>3</sup> /h)	MBR (inside) (~2500 m <sup>2</sup> )	Biosepe/Zenon	1999	35.6.3.2	[57,58]
Papierfabrik Palm	Eltmann, Germany	Mill biotreated effluent (190 m <sup>3</sup> /h)	Spiral NF (15000 m <sup>2</sup> )	Nadir	1999	35.6.3.1	[59]
M-Real Kirkniemi mill	Lohja, Finland	Ultrafiltered white water (50 m <sup>3</sup> /h)	Spiral NF (900 m <sup>2</sup> )	Metso Paper	1999	35.6.2	[53]
StoraEnso/Fine Paper	Uetersen, Germany	White water (25 m <sup>3</sup> /h)	CR-UF (4 m <sup>2</sup> )	Metso Paper	1999		[53]
Irving Pulp & Paper	Saint John, New Brunswick, Canada	Effluent—no biotreatment (250 m <sup>3</sup> /h)	RO	Zenon	1998	35.6.1.2.3	[60,61]
Mondi sulfite pulp mill	South Africa	Spent liquor (71 m <sup>3</sup> /m)	UF+RO				[62]
Kronospan Ltd, MDF mill	Chirk, North Wales, United Kingdom	Effluent from the MDF panel plant (>5 m <sup>3</sup> /h)	Spiral RO	Esmil/GE Osmonics	1996	35.6.7	[63,64]
Champion International	Arapoti, Parana, Brazil	TMP mill water	MBR+RO	Zenon	1996	35.6.1.3	[65]
M-Real Kirkniemi mill	Lohja, Finland	White water (180 m <sup>3</sup> /h)	CR-UF (756 m <sup>2</sup> )	Metso Paper	1996	35.6.2	[53]
M-Real Kirkniemi mill	Lohja, Finland	White water (40 m <sup>3</sup> /h)	CR-UF (168 m <sup>2</sup> )	Metso Paper	1996	35.6.2	[53]
StoraEnso Nymölla pulp mill	Nymölla, Sweden	Bleach effluent (300 m <sup>3</sup> /h)	Tubular UF (4600 m <sup>2</sup> )	PCI	1995	35.6.1.1	[47,52]
McKinley Paper board mill	Prewitt, New Mexico	Biotreated effluent (MF 69 m <sup>3</sup> /d + RO 28 m <sup>3</sup> /d)	Hollow fiber MF+RO	USF Memcor	1994	35.6.4	[45,46]
M-Real Kirkniemi mill	Lohja, Finland	White water (25 m <sup>3</sup> /h)	CR-UF (84 m <sup>2</sup> )	Metso Paper	1994		[53]
ZPP Czarnkowie	Poland	TDS and TSS separation (3 m <sup>3</sup> /h)	CR-UF (84 m <sup>2</sup> )	Metso Paper	1993		[54]
Bahia Sul Celuloses	Mucuri, Brazil	River water purification (90 m <sup>3</sup> /h)	Spiral RO		1991	35.6.5	[66]
Rottneros Board	Svanskog, Sweden	TDS and TSS separation (12 m <sup>3</sup> /h)	CR-UF (112 m <sup>2</sup> )	Metso Paper	1990		[53]
Borregaard Industries	Norway, Sarpsborg	Ca-sulfite pulp mill spent liquor	Tubular UF (1120 m <sup>2</sup> /spiral RO (400 m <sup>2</sup> ))	PCI, GE Osmonics	1981	35.6.1.1	[47,67]

*Source:* Adapted from Nuortila-Jokinen, J. and Nyström, M., Membrane filtration of coating colour effluent. 8th World Filtration Conference, Brighton, United Kingdom, April 3–7, 2000; Greaves, R., The use of ultrafiltration for COD reduction in pulp mill effluent—a case study from Sweden. International Environmental Conference, Nashville, TN, April 18–21, 1999; Kreuzman, E. and Sutela, T., *Ippta J.*, Conv. Issue, 15, 2004; Membrane filtration in P&P. Reference list, Metso Paper, March 2005; <http://www.watech.de/eng/index.php>; Metso Paper, Domsjö Fabriker AB reference; Webb, L., *Pulp Pap. Int.*, 42, 37, 2000; Brockmann, M. and Praderie, M., Paper production in France. *Zenon bulletin*; Schirm, R., Welt, T., and Ruf, G., Nanofiltration Eine möglichkeit zur kreislaufschließung, Papierfabrik Palm, Werk Eltmann. IMPS Internationales Münchner Papier symposium; FH-München, 23 March 2001, München, Germany; Zenon system achieves zero discharge in pulp and paper plant. *Zenon bulletin*. [http://www.zenon.com/resources/case\\_studies/wastewater/irving.shtml](http://www.zenon.com/resources/case_studies/wastewater/irving.shtml); Webb, L., *Pulp. Pap. Int.*, 44, 28, 2002; Dal-Cin, M.M., Kumar, A., and Brail, J., Membrane technology in the pulp and paper industry. A review of the state of the art, ICPET, Internal Report no PET-1393–97S, May 8, 1997; Anonymous, *Filtr. Sep.*, December, 30, 2002; Finnemore, S. and Hackley, T., *Pap. Techn.*, 41, 29, 2000; Zenon technology treats TMP wastewater for recycle, *Zenon bulletin*; Pohjalainen, T., *Investigation y Tecnica del Papel*, 36, 637, 1999; Durham, B., *Special Publication—Royal Society of Chemistry*, 249, 241, 2000; Merry, A., *Invest. Tec. Pap.*, 36, 568, 1999; Pressurized ozone membrane ultrafiltration/nanofiltration methodology for TDS removal in the paper mill process water for energy saving, production efficiency, and environmental benefits. Available at <http://www.recycle.com/linpacnce3/documents/doctypefinalreport.pdf>; Soalheiro, S.C., *Pulp Pap.*, 74, 63, 2000; Wagner, J., *Special Publication—Royal Society of Chemistry*, 249, 233, 2000.

flux and as a result the flux is often significantly lower than when high-shear modules are utilized. Despite these not so favorable properties of spiral wound modules, their packing density (membrane area/volume) is significantly higher than in tubular or in shear enhanced modules. Spiral wound modules are standardized so that different modules from various manufacturers can be used in the same pressure vessels. Therefore, spiral wound modules are available in a wide variety of membrane materials and the spiral configuration has been the least expensive per unit area of membrane. NF and RO membranes are typically used in spiral wound form and to operate successfully a sophisticated pretreatment is usually needed.

Hollow fibers have the highest packing density of the existing modules but fluxes are low. They are mostly used in MBR in the “outside-in” mode (MF and UF membranes) in the pulp and paper industry at close to subcritical fluxes to avoid fouling. In addition, their cleaning is improved by backflushing techniques. Aeration is used to minimize particle adhesion and concentration polarization.

Tubular modules are not easily plugged and can be used at high cross-flow velocity to minimize the concentration of retained substances on the membrane surface. Cross-flow velocity strongly influences the power consumption because under turbulent conditions the power will vary with the velocity raised to a power of 2.75 [47]. Unfortunately, flux is usually a function of the flow velocity and optimization needs to be done between power consumption (flow velocity  $\rightarrow$  flux) and the installed surface area of the membrane. Tubular modules are relatively easy to clean (even physical cleaning using foam balls is possible) and they can withstand some fibers in the feed water without becoming plugged. The inside diameters of tubular membranes vary from 12 mm (e.g., PCI tubular membranes, see Section 35.6.1.1) to 1.5 mm (e.g., capillary membranes from Norit membrane technology, see Section 35.6.3.1). Ceramic membranes are produced in tubular form such as single tubes or multichannel monoliths.

Because high fluxes and the ability to process streams containing suspended solids and fibers are often wanted in the pulp and paper industry, high-shear modules have been developed. Currently existing high-shear modules, excluding tubular modules, are modified plate and frame constructions. Both a cross-rotational module from Metso Paper and a vibration enhanced module (VSEP) from New Logic Inc. have been industrially used or tested in pulp and paper industry applications [48–51].

In cross-rotational ultrafiltration, the shear rate is generated by a rotating blade near the membrane surface, which forces the feed fluid to move with a high flow velocity across the membrane. The peripheral velocity of the blade can reach 13 m/s. Generally, only a coarse screening of the feed water is needed before the CR filter. Cross-rotational filters are available having membrane areas from 15 to 140 m<sup>2</sup>. The membranes are changed by opening the membrane stack and by simultaneously fitting new membranes to every plate or plates having damaged membranes. The industrial-scale CR filters were designed for ultrafiltration membranes. Some piloting tests have also been made with a modified module and nanofiltration membranes [18]. The principle of a CR filter is presented in Figure 35.3. As Table 35.1 shows, the CR filter is a commonly used membrane filter in the pulp and paper industry.

Another type of high-shear module, known as the vibrating shear enhanced processing (VSEP) filter, was introduced in 1991 by New Logic Inc. The VSEP is a vertical plate and frame-type construction, where membrane leaves are stacked on top of each other. One VSEP module has a membrane area of 14–140 m<sup>2</sup> in a horizontal footprint of only 1.2  $\times$  1.2 m. The CR filters and the VSEP have similar footprints. The maximum operating pressure is 38 bar. In this system, the membrane is moved and not the fluid. The VSEP employs torsional vibration of the membrane stack to generate shear forces at the membrane surface, an order of magnitude higher than those achievable in typical cross-flow modules. This reduces concentration polarization and colloidal fouling significantly and makes filtration possible with minimally pretreated streams. Another advantage of the VSEP filter is naturally a higher flux compared to low-shear filters. The energy consumption is claimed to be as low as 0.073 kW/m<sup>3</sup> of filtrate (tubular modules from 1.5 to 3.9 kW/m<sup>3</sup> [52]). The membranes are not changed individually, but the whole stack is changed when needed [50].

## 35.6 INDUSTRIAL APPLICATIONS AND CASE STUDIES

Industrial-scale applications using membranes in the pulp and paper industry go back to the 1970s and they were mainly concerned with bleach plant effluent treatment and spent sulfite liquor concentration for the recovery of lignosulfonates or energy [1]. In the late 1980s, the high-shear cross-rotational filter entered the market. This heralded probably the most efficient way to use membranes in the paper industry. The recovery of coating pigments using CR ultrafiltration is an economically extremely attractive process. In many cases the payback time of such a membrane plant is <1 year depending on the price of the recovered coating pigments. Either tubular modules or CR filters are mostly used for this application. More than 40 CR filters are recovering coating colors worldwide (Section 35.6.6). In the mid-1990s, two spiral-wound nanofiltration plants were installed for the treatment of total effluent from a paper mill (Section 35.6.3.1). By the end of the 1990s, MBRs were introduced in the pulp and paper industry (Section 35.6.3.2). The first industrial-scale MBR plant was installed in France, in 1999. Table 35.1 summarizes existing membrane filtration plants in the pulp and paper industry. The following sections focus on some recent examples of mill-scale installations as well as on relevant pilot- or laboratory-scale studies. The aim is also to review different types of applications.

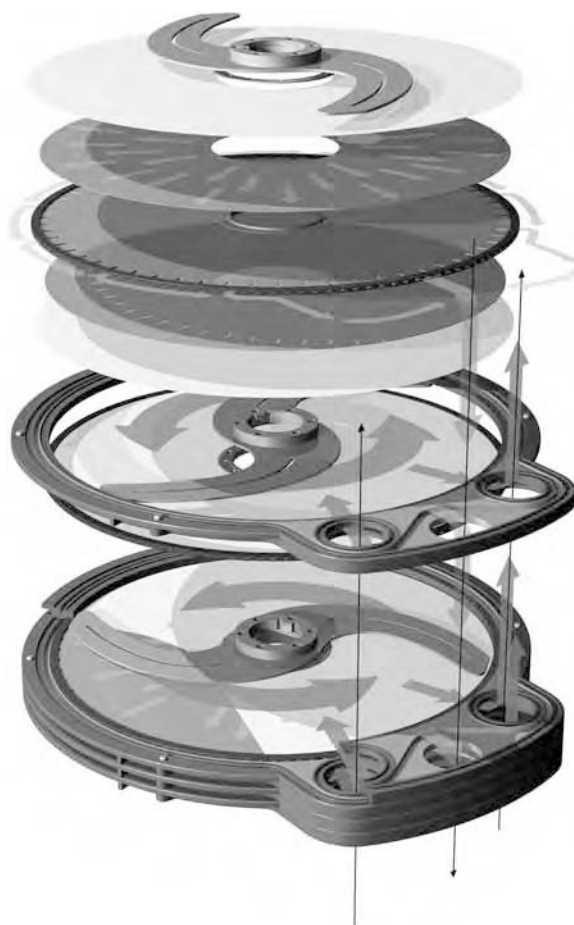


**FIGURE 35.3** (See color insert following page 588.) Principle of the CR filter. (From Kreutzman, E. and Sutela, T., *Ippta J.*, p. 15, 2004; Courtesy of Metso Paper. With permission.)

### 35.6.1 PULP MILL APPLICATIONS

The idea in all pulping processes is to separate the fibers from the wood and to make the fibers suitable for further use, mostly for papermaking. The fibers can be separated from each other if the lignin, and, to a large extent, also the hemicellulose, is either dissolved and removed as in chemical pulping, or more or less softened as in mechanical pulping. There are, in principle, two ways to make chemical pulp, the sulfite and the sulfate (kraft) processes. These processes dissolve the lignin “glue” from the space between the fibers, and also degrade and dissolve some of the polysaccharides. Thus, the rather concentrated spent liquors from the pulping processes contain a large variety of wood-based compounds, their degradation products and also cooking chemicals. These streams represent a considerable pollution problem in the pulp and paper industry.

Bleaching of the pulp removes a large part of the residual lignin improving the color of the pulp. Bleaching chemicals such as chlorine, chlorine dioxide, hypochlorite, peroxide, ozone, and peracetic acid break down the lignin to different degrees and then the lignin is usually extracted in an alkaline stage. The strong color in the alkaline extraction stage effluent is due to the high molar mass lignin molecules. This high molar mass also makes their biodegradation difficult. In addition, the COD and the BOD load of the first alkaline extraction stage (E1) effluent is high. Low-molar mass chlorinated organic compounds (measured as AOX) are formed when chlorine chemicals are used in bleaching. They have mutagenic properties and they bioaccumulate, causing serious problems in the aquatic ecosystem. The E1 effluent represents only approximately 5%–10% of the total effluent load of the mill, but it contains about half of the color discharge of the mill. The bigger sizes of the molecules and their high charge densities due to high pH make the alkaline bleach plant effluent easier to filter than the previous chlorination stage (C-stage) effluents containing smaller molar mass compounds [32]. Therefore, many researchers have filtered the alkaline extraction stage effluents to remove color, to decrease the COD or the BOD load, to decrease the amount of chlorinated organic compounds in the effluents, and to purify the process waters or effluents for reuse [3,37,68–76]. The extraction stage effluents are typically concentrated by UF and the concentrate is burnt in the recovery furnace, where the cooking chemicals are recovered. The resulting filtrate is suitable for washing purposes.

Changes in the pulping and bleaching processes over the last 20 years from elemental chlorine to oxygen delignification and chlorine dioxide bleaching have caused corresponding changes in the composition of the spent liquors and process waters. The use of an increased amount of chlorine dioxide in the bleaching sequence has resulted in a lower discharge of organochlorinated compounds and their molar mass is lower. As a result, the biodegradability of the effluent has increased [77]. However, the introduction of oxygen-based bleaching agents does not seem to have removed the acute toxicity of the process discharges. Toxic compounds such as degradation products of extractives, such as resin acids, do not decompose easily and, therefore, pass into the effluent. To remove these compounds nanofiltration membranes have also been tested with bleaching effluents [3,35,37,68–70,78,80]. Filtration of acidic wastewaters from the chlorine dioxide, ozone, or chelation stages has also been studied but not as intensively as alkaline stage wastewaters [33].

### 35.6.1.1 Sulfite Pulp Mill Effluents

As early as in the 1970s, DDS reverse osmosis plants were installed in the Toten sulfite pulp mill in Norway and the Reed Lignosol mill in Canada. RO membranes were used to concentrate spent sulfite liquor to help the overloaded evaporation systems of the mill [1].

*Borregaard Industries, Sulfite Pulp Mill, Sarpsborg, Norway:* A UF plant with tubular membranes has been in use since 1981 in Norway (Borregaard Industries, Sarpsborg calcium bisulfite pulp mill, Table 35.1) for the fractionation of a lignosulfonate stream (spent sulfite liquor) into two streams, which are further processed into by-products. The composition of the spent sulfite liquor is affected by the type of wood pulped and the digestion process. The liquor typically contains approximately 60% lignin (lignosulfonates), 30% reducing sugars, and 10% inorganic material. The UF concentrate stream contains purified and concentrated lignosulfonates, and it is used for the production of vanillin. Other uses of purified lignosulfonates are, for example, industrial detergents, dispersants, precipitates, binders, and adhesives. By combining ultrafiltration with diafiltration, a purity of over 95% for lignosulfonates can be obtained [67,81].

The lifetime of the tubular membranes in the Borregaard industries' plant (1120 m<sup>2</sup>, PCI) has been about 1 year, when cleaning is made daily with an alkaline detergent. The tubular membranes need only a minimum of pretreatment and can even handle fibers. The 20 kg/mol cutoff polysulfone membrane has mostly been used at high temperature operation (70°C). In addition, a spiral wound RO (polyamide membrane from Osmonics) is used to concentrate the UF permeate from 7% of total solids to 14% before evaporation [47,67].

Generally, most of the sugars and the inorganic matter is found in the UF permeate, especially when diafiltration is used to treat the spent sulfite liquor. The sugars in the permeate stream can be fermented to alcohol (anaerobic process). Using spent liquor, a yeast (torula yeast) can live and multiply synthesizing protein (pekilo) that can be used as animal feed [81]. The sugars in the UF permeate stream or the original spent liquor can also be purified by chromatographic methods or by using nanofiltration. Hardwood hemicellulose, in particular, consists mostly of *O*-acetyl-(4-*O*-methylglucurono)-xylooligosaccharides in acid sulfite pulping to monosaccharides. Therefore, the spent acid sulfite liquor contains 240 kg xylose/t pulp when silver birch (*Betula Pendula*) is used as the raw material in pulping. Nanofiltration can recover the xylose in the permeate to a purity as high as 70% of dry solids [82]. The above-mentioned possibilities to use membranes for the utilization of sugars from spent liquors may become attractive to industries in the near future (e.g., for biofuels).

*Domsjö Fabriker AB, Sulfite Pulp Mill, Örnsköldsvik, Sweden:* The sulfite pulp mill of Domsjö Fabriker produces dissolving and papergrade pulps from spruce. Three CR1000/60-filters (3 × 84 m<sup>2</sup>) were installed in the year 2000 to treat process water after the brown pulp wash (Table 35.1). The filters operate in three stages at a recovery of 80%–90%. The ultrafiltration membranes separate lignin residues and resins and the concentrate is sent to resin recovery. The permeate is re-used in the cooking process and as sealing water. The permeate fluxes decrease with increasing concentration and range from 400 to 200 L/(m<sup>2</sup> h) [56].

*StoraEnso, Sulfite Pulp Mill, Nymölla, Sweden:* A reduction of the COD of the pulp mill effluent was the main goal when StoraEnso Nymölla in Sweden (Table 35.1) started to use tubular UF membranes to purify their oxygen bleach stage effluents [52]. Two production lines in the mill produce pulp from hardwood and softwood using the magnesium bisulfite process and oxygen bleaching (Table 35.2). The mill needed to reduce their COD emissions by 50% to get to an environmentally acceptable level to obtain the “Swan” mark. In addition, the mill wanted the removed COD (50% of the original COD) to be concentrated to 2% of the original liquid volume (a 50 time volumetric concentration) so that it could be incinerated. The dry substance in the concentrate is about 18%. The permeate is discharged to an activated-sludge plant [52].

Even though the ES404 membrane worked reasonably well with the softwood effluent (pH above 11), it fouled significantly with the hardwood effluent even when using a high cross-flow velocity. This forced the manufacturer (PCI) to develop a new more hydrophilic membrane, the EM006 membrane, for the hardwood effluent [52].

The cleaning interval ranges from once a day to twice a week depending on the stages and effluents. The guaranteed membrane lifetime is 15 months. The plant processes >300 m<sup>3</sup>/h of bleach effluents producing a concentrate stream of 6 m<sup>3</sup>/h [52]. The high UF operation temperature (>70°) eliminates the need for rapid cooling before the membrane plant and prevents precipitation of extractives on the membranes. Wallberg et al. [83] found that the presumptive fouling originated mainly from

**TABLE 35.2**  
**Characteristic Data on the Tubular Ultrafiltration Plant**  
**at the StoraEnso Nymölla Pulp Mill**

	Softwood Line	Hardwood Line
Effluent characteristics		
Effluent flow (m <sup>3</sup> /h)	165	135
Temperature (°C)	75	73
Chemical oxygen demand (g/L)	8–12	8–12
TSS (mg/L)	<30	<125
Membrane	ES404	EM006
Cutoff (g/mol)	4000	6000
Surface area (m <sup>2</sup> )	2766	1872
Operating variables		
Pressure (bar)	7	8
Volume reduction	50	50
Power consumption (kW/m <sup>3</sup> )	1.9	3.9 <sup>a</sup>

*Source:* Adapted from Greaves, R. The use of ultrafiltration for COD reduction in pulp mill effluent—a case study from Sweden. International Environmental Conference, Nashville, TN, April 18–21, 1999, 1167–1191; Jönsson, A.S. and Wimmerstedt, R., *Desalination*, 53, 181, 1985.

<sup>a</sup> Higher cross-flow velocity with the hardwood line effluent.

organic compounds, but inorganics, mostly silicon, iron, and magnesium, also caused fouling. They also found that many of the membrane tubes were clogged with a clay-like precipitate consisting of fibers, organic material, and precipitated magnesium hydroxide.

### 35.6.1.2 Sulfate Pulp Mill Effluents

#### 35.6.1.2.1 Black Liquor from Sulfate Pulping

Black liquors from kraft pulping are complex mixtures of inorganic and organic compounds. The organic compounds originate mostly from carbohydrates and lignin degradation reactions. Minor amounts of extractives and cooking chemicals also exist in black liquors. The most common way to treat the black liquor is to burn it in a recovery boiler after it has been concentrated. In that way, the cooking chemicals are recovered and a significant amount of energy is produced.

Fractionation of black liquor using membrane technology has been studied in different groups since the late 1970s, but mill-scale systems have not been introduced. Both polymeric [84–88] and recently ceramic [89–92] membranes have been used to separate lignin from inorganic cooking chemicals. The black liquors are very alkaline, concentrated, and hot solutions and thus their treatment using membranes is challenging.

An increase in pulp production can lead to capacity problems in the recovery boiler. Keyoumu et al. [91] studied filtration of black liquor using ceramic ZrO<sub>2</sub>-coated membranes to lower the load on the recovery boiler in kraft pulping, and simultaneously they generated valuable side-products from the black liquor. The lignin degradation compounds isolated from the permeate of a 1000 g/mol cutoff membrane were highly phenolic in nature and could be polymerized to higher molar mass material from which, by further processing, new products could be made (special polymers).

Wallberg et al. [92] tested tubular ceramic UF membranes (Orelis, Al<sub>2</sub>O<sub>3</sub>-TiO<sub>2</sub>, cutoff 15 kg/mol) to concentrate lignin from kraft black liquor. The overall goal was to decrease the energy surplus of a modern pulp mill by removing lignin and converting it to a usable biofuel. During the UF concentration of very alkaline (pH 13–14) black liquor to a volume reduction of 10, the lignin content increased from 55 to 158 g/L (dry solids increased from 16 to 22 wt%) and at the same time the amount of cooking chemicals in the concentrate was significantly reduced. In addition, more than 50% of multivalent wood-borne elements (magnesium, manganese, and iron) were retained. The average permeate flux at 1 bar was 90 L/(m<sup>2</sup> h) at 90°C during the concentration to a volume reduction of 90% (at the end: 20 L/(m<sup>2</sup> h)).

Cortiñas et al. [89] eliminated colloidal suspended material (pitch) from kraft black liquors and partly recycled the liquor to the digester to reduce the consumption of chemicals. The colloidal pitch is formed by wood extractives. In particular, compounds such as waxes, sterols, and sterol esters that do not form soluble salts or dissolve during cooking form colloidal particles. The concentrated liquors (14%–15% solids) were filtered at high temperature using a 0.2 μm alumina membrane (USF Shumacher, Crailsheim, Germany). The pitch was almost completely retained (>99.9%), but the flux was sensitive to the black liquor composition and sometimes decreased to less than 100 L/(m<sup>2</sup> h).

### 35.6.1.2.2 Bleaching Effluents

Fälth et al. [93] ultrafiltered seven alkaline filtrates from kraft pulp mills. They observed that elemental chlorine free (ECF) and total chlorine free (TCF) filtrates from modern mills contain large fractions of low molar mass substances, which are not as well retained as the first alkaline stage effluent from a traditional mill. The membranes used were tubular polyethersulfone membranes (ES404, cutoff 4 kg/mol and EM006, cutoff 6 kg/mol) from PCI. The flux was mostly observed to depend on the concentration of the feed and slightly on the differences in feed composition. The fluxes varied from 100 to 400 L/(m<sup>2</sup> h) at 7 bar, 65°C and a cross-flow velocity of 4.1 m/s. The COD reduction was approximately 40% (traditional ECF mill 60%). The compounds causing the BOD were retained less than the compounds causing the COD. UF could thus be used before the existing biological treatment to decrease the amount of nonbiodegradable compounds in the effluent before biological treatment. Therefore, the load on the biological treatment plant decreased and the average biodegradability of the remaining substances increased [75,77,93,95].

Several authors have recently reported studies on metal removal from pulp mill wastewaters [95–97]. Tavares et al. [96] treated TCF bleaching wastewater by ultrafiltration and complexation using polymeric ligands (PVA, 60 kg/mol and PEI, 50 kg/mol) with ultrafiltration. The complexation improved the removal of COD and metals significantly, e.g., iron removal increased from 23% to 79%. Lastra et al. [97] used nanofiltration to remove complexed metal from a chelate stage effluent in a totally chlorine-free bleaching plant. The filtrations were made at 80°C using both composite aromatic polyamide membranes (PCI and X-FLOW membranes) and a ceramic membrane (titanium oxide supported on zirconium oxide from Rhodia Orelis). All membranes suffered from a significant flux decrease (cross-flow velocity 3 m/s) at flux values above 170 L/(m<sup>2</sup> h), which indicates that the critical flux was exceeded. The polyamide membranes gave almost complete rejection of the chelates of both iron and manganese ions. These ions are known to catalyze the degradation of hydrogen peroxide and as a result more bleaching chemicals are needed [97].

### 35.6.1.2.3 Evaporation Condensates of Sulfate Pulp Mills

Evaporation condensates are generated in the cooking digesters and in the black liquor evaporation units of kraft pulp mill processes. Evaporator condensates contain hundreds of volatile organic compounds and some extremely odorous compounds. For instance, methanol has been identified as a primary contaminant of concern. In addition, very odorous totally reduced sulfur (TRS) compounds such as hydrogen sulfite, methyl mercaptan, dimethyl sulfite, and dimethyl disulfite have also been identified in condensates. These compounds restrict its reuse without treatment. Foul condensates are typically treated in a biological effluent treatment system before being discharged to the environment [98].

*Irving Pulp and Paper's pulp mill in New Brunswick (Canada)* produces 280,000 t/a bleached kraft pulp without biological wastewater treatment (Table 35.1). In 1997, their discharge of BOD exceeded the regulated limit but the limited land area prohibited the implementation of conventional biological treatment. The mill identified a clean evaporator condensate stream carrying significant amounts of BOD and toxicity. An RO plant was installed in 1998 to purify the condensate. It produces 247.5 m<sup>3</sup>/h permeate that is recycled to the post-oxygen stage washer (and from there to the whole mill wastewater). The recovery, 99%, is extremely high and, thus, only 2.5 m<sup>3</sup>/h concentrate is sent to incineration to provide energy for the facility. The COD and BOD reductions are more than 90% and 80%, respectively, and the acute toxicity in the effluent discharge is virtually eliminated [60,61].

Membrane bioreactors have been tested for the treatment of foul condensates at various temperatures. The temperature of the foul condensates originating from kraft evaporators and digesters is around 50°C–70°C and an interesting option is to treat this stream using MBRs at thermophilic conditions without cooling the stream [98]. Dias et al. [99] used an MBR technique (0.03 µm hollow fiber membrane) to purify foul condensates from a Brazilian kraft mill (Eucalyptus) at different temperatures. They achieved a very high COD removal as shown in Table 35.3.

**TABLE 35.3**  
**Acclimatized Removal Efficiencies for Foul Condensate Treatment**  
**by Membrane Bioreactor (MBR)**

Parameter	MBR Treatment of Foul Condensate Foul Condensate	Removal Efficiency (%)		
		35°C	45°C	55°C
COD (mg/L)	5100	97	94	87
TRS (mg/L)	350	100	99	93
Methanol (mg/L)	3900	99	96	92
BOD <sub>5</sub> (mg/L)	4500	nr	nr	nr

Source: Adapted from Dias, J.C.T., Rezenda, R.T., Silva, C.M., and Linardi, V.R., *Process Biochemistry*, 40, 1125, 2005.

Note: TRS, totally reduced sulphuric compounds; nr, not reported.

### 35.6.1.3 Mechanical Pulp Mill Effluents

*Champion International's pulp mill in Arapoti (Brazil)* tested a ZeeWeed MBR followed by reverse osmosis polishing to recycle thermomechanical pulp mill wastewater within the mill (Table 35.1). Over 4 months of tests showed that the system decreased the COD from 7800 to <20 mg/L. In addition, the total dissolved solids (TDS) content was reduced from 2000 to <300 mg/L in the RO permeate [65].

In Finland, groundwood mill circulation water was treated using an aerobic thermophilic suspended carrier biofilm process and different UF membranes [100]. The biofilm process did not increase the UF flux, which was about 400–500 L/(m<sup>2</sup> h) at 60°C–70°C with the original water using a CR filter and hydrophilic membrane. An 80% reduction in lignans and sugars was achieved in the biofilm process but the color of the water increased and was not reduced by UF. NF also efficiently removed colored compounds and its flux increased after biotreatment and when the pH of the original water (pH 5.3) was adjusted to pH 7 [101]. Nanofiltration also removes color efficiently when thermomechanical pulp (TMP) plant effluent was NF treated using an anaerobic bioreactor at thermophilic conditions as pretreatment [102]. Screw press filtrate from chemi-thermomechanical pulp (CTMP) mills has also been ultrafiltered [4,103].

### 35.6.2 PAPER MILL APPLICATIONS

*M-Real, Paper Mill, Kirkniemi, Finland:* Cross-rotational filtration technology was used in several mills for the purification of paper mill circulation waters, such as white water and clear filtrates [54,104]. M-Real Kirkniemi mill in Lohja (Finland) uses a total of 19 CR units for the treatment of white water from paper machines and for the recovery of coating color (Table 35.1). One paper machine produces 350,000 t/a coated fine paper from aspen-based mechanical and chemical pulps. When the fine paper mill was built, the authorities would not accept an increase in the effluent load. Thus, to lower the use of water, the mill decided to apply ultrafiltration technology. The first filter was installed in 1994. The permeate from the ultrafiltration system is used at the wire section showers and for chemical dilutions. A part of the UF permeate is led to nanofiltration. The permeate from the NF is led to a warm freshwater tank. The ultrafiltration is carried out in three stages (Figure 35.4). High shear on the membrane surface is the key to extremely high fluxes over long filtration periods. Figure 35.5 shows that an average flux over 300 L/(m<sup>2</sup> h) is obtained at a pressure of 0.8 bar and a rotor tip speed of 13 m/s. The UF membrane used (regenerated cellulose, cutoff 30 kg/mol) removes suspended solids, turbidity, and bacteria completely. The reduction of extractives (mainly anionic

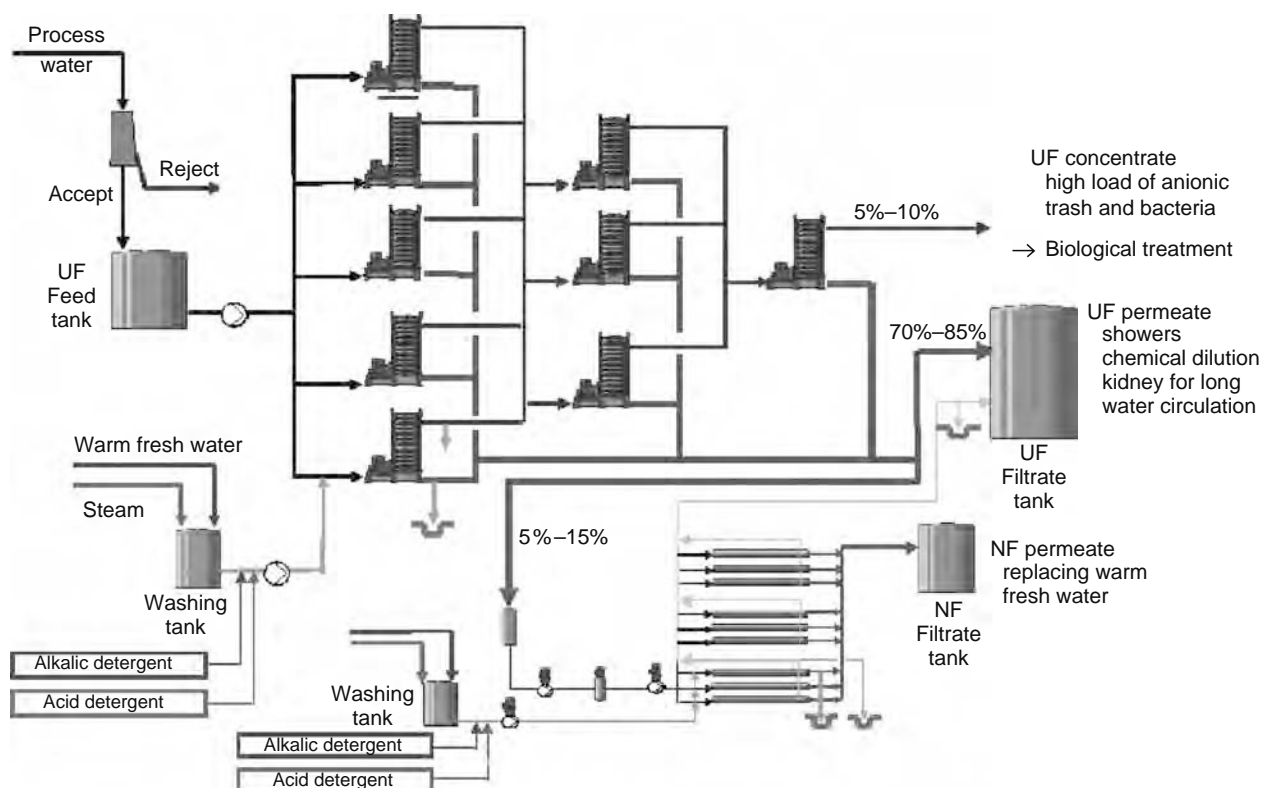


**FIGURE 35.4** Process diagram of CR ultrafiltration and spiral wound nanofiltration systems at M-Real Kirkniemi paper mill. (From Kreutzman, E. and Sutela, T., *Ippita J.*, p. 15, 2004; Courtesy of Metso Paper. With permission.)

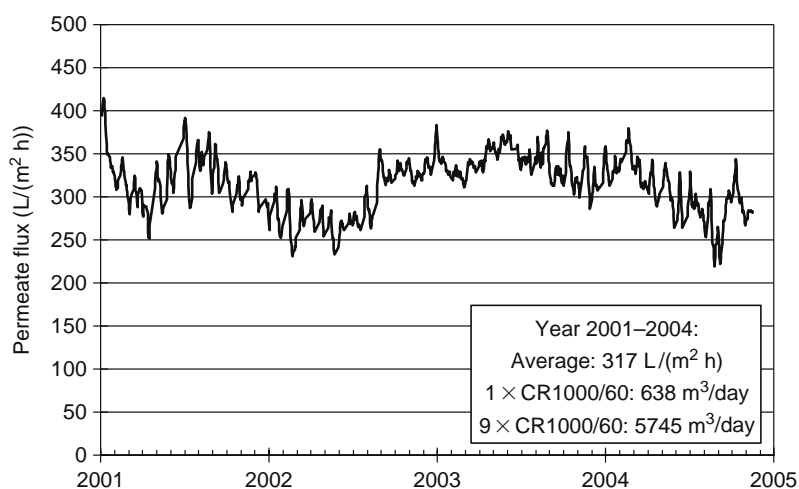


**FIGURE 35.5** Development of permeate flux in white water filtration using CR filters at M-Real Kirkniemi mill. (From Kreutzman, E. and Sutela, T., *Ippita J.*, p. 15, 2004; Courtesy of Metso Paper. With permission.)

trash) and COD is 50% and 10%, respectively. The washing frequency is every fifth day and the membrane lifetime is 15–26 months. The total operating cost for CR ultrafiltration was about 0.12€ per cubicmeter during 2001–2003. The nanofiltration unit operates at flux values of 30–40 L/(m<sup>2</sup> h) and its retention of organics (COD) is 85% and of inorganic matter (conductivity) 75% [53].

*Arctic Paper, Paper Mill, Munkedal, Sweden:* Tubular UF membranes have been used since 2002 in the Arctic Paper Munkedal mill to purify white water (Table 35.4) after sedimentation. UF removes the remaining suspended solids from the water before reuse in spraying applications in the wire section where it replaces fresh water [28]. The data in Table 35.4 are discussed further in Sections 35.6.3.1 and 35.6.3.2.

**TABLE 35.4**  
**Membrane Installations Using Norit Tubular Membranes**

	Arctic Paper (Munkedals, Sweden)	Arctic Paper (Munkedals, Sweden)	VHP Security Paper Mill (Ugchelen, the Netherlands)	Papierfabrik Palm (Wörth, Germany)
Feed stream	Mill effluent	White water	Bleaching effluent, MBR-process	Mill effluent
Module	Tubular	Tubular	Tubular	Tubular
Membrane	NORIT 38GRH/F4125	NORIT 38GRH/B5125	NORIT 33GEF5385	NORIT S225 AQ UFC (1.5 mm)
Membrane area (m <sup>2</sup> )	462	270	83	2280
Capacity (m <sup>3</sup> /h)	40	10	10	70
Feed TSS (mg/L)	1500	20		2
Retention (%)	>95	>95		~100
Feed COD (mg/L)	143	100	3500	
Retention (%)	10–30		>85 (MBR)	
Flux (L/(m <sup>2</sup> h))	50–80	40	160–300	24
Temperature (°C)	40	45	60	30
Transmembrane pressure (bar)	1–4	1–4	4	2
Cross-flow velocity (m/s)	3	3	4–4.5	3
Cleaning	Once a week	Once a week	Twice a year	Acid, alkaline, acid
Lifetime of membranes (months)	35–43	35–43	20	48
Energy consumption (kW h/m <sup>3</sup> )	1.5–2	1.5–2	3	1
Start-up	1999	2002	2000	2002

Source: Adapted from Hepp, B., Joore, L., Schonewille, H., and Futselaar, H., *Pap. Techn.*, 46, 41, 2005; Joore, L., Wortel, N., and Bronold, N., *Pap. Techn.*, 42, 27, 2001.

*Other Reported Studies:* Brady [105] has reported on UF systems (start-up 2000) for mill water recovery and reuse. The Koch tubular HFP-276 (PVDF) membrane used removes 50% of COD, TDS, and total organic carbon (TOC). The UF operating cost is \$1.6 per cubic meter. The plant operates continuously at a recovery rate of 98.7%. The feed stream and the mill are not reported.

Many studies have pointed out that a CR ultrafilter can operate at a flux level of 300–400 L/(m<sup>2</sup> h) when white waters are filtered. The reduction in organic compounds (COD, UV absorption at 280 nm, or sugar) using a UF membrane (cutoff 30–200 kg/mol) has been from 10% to 40% depending on the process water. The reduction of anionic trash is usually better (30%–90%) [48]. A pilot study showed that a high-shear filter (CR-nanofiltration unit) could operate without any pretreatment at a flux level of 50–120 L/(m<sup>2</sup> h) when paper mill clear filtrate was filtered. Mechanical erosion was a problem with some of the NF membranes used [18].

### 35.6.3 MEMBRANES COMBINED WITH BIOLOGICAL TREATMENT

#### 35.6.3.1 End-of-Pipe Treatment

In the mid-1990s, two spiral-wound nanofiltration plants were installed for the treatment of effluent from a paper mill. In both cases, the nanofiltration systems were installed to remove color, organic carbon, and dissolved solids from effluents for reuse or for further processing. Both plants had a very efficient pretreatment before the NF spiral-wound modules to prevent plugging of the filtration elements. For instance, the pretreatment included settling at several stages with chemicals, a sand filter, a back-washable screen filter, and a bag filter (5 μm) [106]. Neither of the plant is in operation today (P. Eriksson, personal communication, 2005).

*Papierfabrik Palm, Newsprint Mill, Eltmann, Germany:* Table 35.1 shows that Eltmann newsprint mill of Papierfabrik Palm has reduced COD, AOX, and color in their effluents using spiral-wound nanofiltration since 1999. Prior to NF, the effluent is biologically treated (activated-sludge plant) and prefiltered using sand filters. The capacity of the NF plant is 190 m<sup>3</sup> permeate per hour. The flux of the Nadir NF-PES-10 membrane has been around 10–30 L/(m<sup>2</sup> h) [107]. The NF-PES-10 membrane was chosen because of its alkaline stability (pH > 12), which was needed when cleaning the membrane. The reported COD removal is 89%, AOX 61%, and color 93% [59].

Table 35.5 compares the process water, freshwater, and NF permeate values for some parameters at the Eltmann. Water hardness measures divalent cations and is well retained in NF but the retention of conductivity is less than 40%. This is due to the negative retention of chloride ions, as often measured for NF membranes, because of the Donnan effect, which is typical for NF membranes. The reuse of NF permeate decreased the need to heat freshwater to the mill process temperature. The concentrate (36 m<sup>3</sup>/h) is recirculated back to the activated-sludge plant after lime precipitation. This precipitation process removes iron nearly completely (99.7%). The removal of color, carbonate, silicate, COD, and AOX are 72%, 66%, 61%, 40%, and 39%, respectively. However, only 10% of the conductivity (28% of sulfate) is removed by lime precipitation [59].

The reviewed mill-scale examples prove NF spiral-wound modules to be useful in the treatment of pulp and paper mill effluents but at the same time it must be concluded that extensive pretreatments are needed when spiral wound modules are utilized. This has also been pointed out in many pilot-scale studies where multilayer filters [108], flotation, and tight cartridge filters have been used before spiral wound modules [109]. Despite efficient pretreatments, the flux has commonly been only 10–40 L/(m<sup>2</sup> h) when NF membranes are used in spiral-wound modules.

*Arctic Paper, Paper Mill, Munkedal, Sweden:* In 1999, a tubular ultrafiltration unit (462 m<sup>2</sup>) was installed to polish 50% of the effluent from the Arctic Paper Munkedal paper mill in Sweden (Tables 35.1 and 35.4). The mill is located next to one of the finest

**TABLE 35.5**  
**Characteristic Properties of Freshwater, Process Water, and NF Permeate**  
**at Eltmann Newsprint Mill of Papierfabrik Palm**

Eltmann Mill of Papierfabrik Palm	Fresh Water	Process Water	NF Permeate
COD (mg/L)	8	587	29
Chloride (mg/L)	35	240	330
Sulfate (mg/L)	92	228	148
Hardness (mg/L)	19	12	7
Anionic trash (mg/L)	5	21	6
Temperature (°C)	18	33	33

*Source:* Adapted; Schirm, R., Welt, T., and Ruf, G. Nanofiltration Eine möglichkeit zur kreislaufschließung, Papierfabrik, Palm, Werk Eltmann. IMPS Internationales Münchner Papiersymposium; FH-München, 23.3.2001, München, Germany; Schirm, R. and Paulitschek, M. Einsatz der membrantechnologie in der papierindustrie, Abwasseraufbereitung mittels membrantechnologie in der papierherstellenden industrie. PTS presentation 12\_2002.

salmon rivers in the country and, therefore, there are high demands for environmentally friendly paper production, for example, by closure of the water circulation. The removal of dissolved organic matter (COD and BOD) varies from 10% to 50%. The permeate is discharged to an external pond and then to the river. About 20% of this water is reused as raw water in the mill [28]. *Papierfabrik Palm, Board Mill, Wörth, Germany*: The company produces corrugating medium and test liner from 100% recovered fiber (Table 35.1). The mill was started in 2002. It has ultrafiltered and NF/RO filtered its biologically treated effluent since start-up [107]. The plant was originally a zero liquid effluent mill (freshwater consumption 1.5 m<sup>3</sup>/t containerboard produced) but has now been allowed to discharge some cubic meters of effluent per ton of paper produced and the RO plant has been shut down (H.-J. Öller, personal communication, 2005). Table 35.4 summarizes some existing membrane applications where Norit tubular membranes are used.

### 35.6.3.2 Membrane Bioreactors

In an MBR two efficient water treatment technologies, namely membranes and biotechnology, are combined into one integrated system. The influent is fed to the aerated bioreactor where the organic compounds are oxidized by microorganisms in the activated-sludge, as in a conventional activated-sludge process. Instead of a clarification tank, micro- or ultrafiltration membranes are used to separate the water from the sludge. Interest in MBR in the pulp and paper industry has increased rapidly during the 1990s and there are currently some full-scale MBR installations in operation to purify selected effluents. In an MBR, the membranes can be installed inside the bioreactor (submerged membranes) or they can be externally installed (side-stream). Generally, hollow fibers (sometimes tubular or flat-sheets) are used inside the reactor. In a reactor with an external membrane unit, all types of modules can be utilized depending on the feed water characteristics. Some of the end-of-pipe membrane systems reviewed in the previous sections could also be counted as side-stream MBR processes [110].

The liquid volume of an MBR is lower than that of a conventional activated-sludge process. Biological processes (i.e., oxidation, nitrification, and denitrification) are exothermic reactions and thus the temperature in the MBR is higher than that in a conventional activated-sludge process. The high temperature and relatively low food to microorganism ratio makes the MBR generate less sludge. Most paper mills operate in a temperature of 50°C–70°C due to the positive effect of high temperature on productivity and energy consumption. Because biological water treatment can be done at the same temperature as the main process, energy is saved since cooling and heating steps are avoided. However, when the temperature increases, the sludge settling properties deteriorate [111–113] and COD removal often decreases in conventional activated-sludge plants. However, the settling problems are avoided in an MBR and some improvement in the COD removal can be achieved. In addition, the effluent from an MBR is free from suspended solids, bacteria, and, often, also from viruses [29].

An MBR operates at a high biomass concentration (up to 30 g/L) making a high volumetric load possible. It is also possible to obtain a long solids retention time or to maintain specifically active organisms to achieve the removal of poorly degradable compounds. This was pointed out when the performance of an MBR and an activated-sludge system for the treatment of a pulping process wastewater were compared. Furthermore, the MBR also adapts well to changes in feed characteristics [40,44,114–116].

*Papeterie du Rhin, Paper Roll Mill, France*: In 1999, Veolia Water STI installed an MBR with Zeeweed ultrafiltration membranes (pore size 0.04 μm) in Papeterie du Rhin's paper roll mill in France (Table 35.1). Recycled (not deinked) paper is used as the raw material. The bioreactor (1500 m<sup>3</sup>) is operated at a mixed liquor suspended solids (MLSS) content of 12–16 g/L. Brockmann and Praderie [58] report an average flux of 15 L/(m<sup>2</sup> h) at a pressure of 0.15 bar over a 1 year filtration period. The wastewater from the mill is first prescreened with drum screens, then sent to an equalization basin, from which it is pumped directly into the bioreactor. Table 35.6 summarizes the performance of the MBR process. The pressure used to draw the water through the membrane is 7–55 kPa. The filtrate is partly recycled as process water [27,57,58].

**TABLE 35.6**  
**Characteristics of the Wastewater and the MBR Treated**  
**Water at the Papeterie du Rhin's Mill in France**

Water Quality Parameter	Wastewater	Permeate of MBR
COD (mg/L)	1500–5400	200
BOD <sub>5</sub> (mg/L)	1700	5
TSS (mg/L)	400	4
Temperature (°C)	35–40	
pH	6	

Source: From Brockmann, M. and Praderie, M., Paper production in France Zenon bulletin.

*Veiligheidspapierfabriek (VHP), Security Paper Mill, Ugchelen, the Netherlands*: Probably the second mill-scale MBR installation in the pulp and paper industry started in November 2000 in the Netherlands. Veiligheidspapierfabriek (VHP) Security Paper mill Ugchelen (Table 35.1) reuses the effluent from the bleaching process, cleaning it by dissolved air flotation (DAF) and an MBR. The installation reduces spring water intake, the costs of heating the spring water and the discharge costs for wastewater. The MBR operates at thermophilic conditions to save heating the water (temperature around 55°C). The membrane unit (82.5 m<sup>2</sup>) is installed outside the bioreactor (volume 250 m<sup>3</sup>) [27,28,57,117].

The mill bleaches raw cotton using sodium hydroxide and hydrogen peroxide. The effluent from the bleaching process has a high temperature (65°C–100°C), high pH (11.5), high oxygen consumption (average COD 3500 mg/L), and fibers. The DAF process is used for the removal of fibers. Instead of air, the DAF process operates with CO<sub>2</sub>-rich waste gas. In that way, the dissolved CO<sub>2</sub> partially neutralizes the effluent to a pH level of 8.2, (feasible for microorganisms) and simultaneously gas bubbles bind and lift the fibers to the surface of the flotation cell [27].

Before mill-scale installation, pilot MBR trials were carried out with pressurized Stork tubular UF membranes (Stork merged with Norit Membrane Technology in 2000) and submerged types of Mitsubishi capillary MF membranes. By increasing the temperature, the COD values of the effluent increased (Dias et al. [99] reported a similar trend, see Table 35.3). The effluent COD was around 1200 mg/L at 68°C and when the temperature was decreased to 50°C the COD in the effluent stabilized to 600 mg/L corresponding to more than 85% removal for COD. The amount of biomass generated was around 0.14 kg TSS per kg of COD. Hydrophilized polysulfone and polyvinylidene fluoride membranes were tested at different transmembrane pressures and flow velocities. Fluxes above 100 L/(m<sup>2</sup> h) were measured for both membranes at a cross-flow velocity of 3.5 m/s. With the submerged membranes the flux was only 15 L/(m<sup>2</sup> h) at a pressure of 0.1–0.3 bar, but the membrane price was lower (\$60 per m<sup>2</sup> against \$200 per m<sup>2</sup> membrane surface), and the submerged membranes did not need pressure tubes and cross-flow pumps. Thus, the total investment costs were more or less equal [27]. The MBR effluents, instead of freshwater, were tested in bleaching experiments and only an additional 10% of chemicals was needed to make the bleaching process as efficient as with ground water [117].

In the mill-scale plant above (Table 35.4), the MBR effluent COD is stabilized to about 500 mg/L (influent 3500 mg/L). By using the MBR to reuse the process water, the mill reduces the freshwater intake to bleaching by 80%, the mill wastewater discharge by 50%, and the gas consumption for heating by about 20% [28].

*Test Cases*: SCA Hygiene Products Suameer BV in the Netherlands has tested a concept where a DAF-unit is placed before a thermophilic MBR and salt is removed by electrodialysis or reverse osmosis. The mill produces tissue, in particular toweling and cleaning tissues. The hygienic paper produced demands for high-quality standards for the process water. Both organic and inorganic compounds need to be removed before reuse of the water. The COD in the feed to the MBR varies depending on the paper grade produced from 350 to 1350 mg/L and the MBR effluent COD stays below 200 mg/L (average 140 mg/L over a 200 day test period). RO and ED were tested and compared in such a way that the permeates after treatment were planned to have equal chloride concentration. The RO permeate had a lower content of COD and conductivity than the permeate from ED [117].

Papierfabrik Niederauer Mühle of Germany specializes in the production of bright white liner. They studied MBR and ED to remove organics and salt from their process water. More than 90% removal of COD and suspended solids was reported with the MBR corresponding to a COD level of 100 mg/L in the permeate [117].

Kimberly Clark's Delyn mill [114] demonstrated the suitability of MBR technology to treat and enable the reuse of water within the papermaking process. Submerged Kubota flat-sheet membrane panels were tested just using the hydrostatic pressure above the membrane pack to provide the driving force for permeate production. The pore size of the membrane was 0.4 μm but during operation the membrane became covered by a dynamic layer of protein and biological cellular material, and the effective pore size was evaluated to be <0.1 μm. Independent of the influent COD load (400–2100 mg/L) the MBR effluent COD remained around 100 mg/L. As observed in many studies, the MBR efficiently balances the variation of incoming water and produces a permeate of a relatively constant quality [58,114,118,119].

Full-scale tests using an internal circulation (IC) reactor from Paques and pilot-scale UF and RO membrane units (hollow fiber and tubular) from KOCH-GLITSCH were carried out at the VPK Oudegem paper mill in Belgium. Thermophilic anaerobic technology was combined with an aeration step and membrane filtration. The anaerobic process converts the organic compounds into methane, which can then be burned as a low cost-fuel for energy recovery. The COD was reduced by 50%–80% and sulfate ions were lowered by 30%–50%. The aeration step subsequent to the anaerobic reactor removes more than 50% of the calcium ions. Pauly and Deschilde [120] concluded that the combined thermophilic anaerobic system and the downstream aeration step were found to be at least as efficient as a mesophilic anaerobic process previously considered to be state-of-the-art in the paper industry. Biological pretreatment was found to increase the retention capability of the membranes from 5%–10% to 30%–40%. Operational stability was tested by long-term trials lasting for more than 1 year in the EU-Brite/Euram project: Paper Kidney. However, only the biological processes are currently implemented in full-scale operation.

Several effluent treatment options were evaluated at the AIPM paper mill in Herada, Israel, (Table 35.7). Stahl et al. [119] studied anaerobic treatment by an upflow anaerobic sludge blanket internal circulation bioreactor (UASB-IC, from Paques) before aerobic treatment. The effluent from the UASB-IC was then further treated by an aerobic activated-sludge-pilot (ASP,

**TABLE 35.7**  
**Effect of Various Biological Treatments and MBR on the Effluent Quality**

	pH	COD (mg/L)	COD (soluble) (mg/L)	BOD (mg/L)	TSS (mg/L)
<i>Aerobic full size ASP</i>					
Influent ± std	6.8 ± 0.6	2363 ± 424		1115 ± 277	223 ± 408
Effluent ± std	7.7 ± 0.2	245 ± 181		21 ± 15	65 ± 122
Average removal		90%		98%	
<i>UASB-IC</i>					
Influent ± std	7 ± 0.3	2365 ± 606	2124 ± 529	1134 ± 353	140 ± 120
Effluent ± std	7 ± 0.2	755 ± 276	461 ± 163	289 ± 136	209 ± 227
Average removal		68%	78%	75%	
<i>Aerobic ASP-pilot</i>					
Influent ± std	7 ± 0.2	743 ± 290	450 ± 173	288 ± 147	214 ± 256
Effluent ± std	7.9 ± 0.2	176 ± 62	141 ± 47	16 ± 8	25 ± 22
Average removal		76%	69%	94%	
<i>Aerobic MBR</i>					
Influent ± std	6.8 ± 0.2	960 ± 764	612 ± 448	363 ± 323	294 ± 407
Effluent ± std	7.8 ± 0.2	129 ± 30		7 ± 7	2.5 ± 2.1
Average removal		86%		98%	>99%

Source: Adapted from Stabl, N., Tenenbaum, A., and Galil, N.I., *Wat. Sci. Techn.*, 50, 245, 2004.

pilot) and aerobic MBR. Significantly lower effluent concentrations of COD, BOD, and TSS were obtained when the MBR was used.

Lombardo et al. [115] and Dufresne et al. [116] have also compared an MBR and an activated-sludge system, both were efficient but the MBR was especially efficient in the removal of COD and acute toxicity.

#### 35.6.4 BOARD, RECYCLING PAPER, AND DEINKING APPLICATIONS

Generally, in board mills lower quality water is needed when higher quality papers, e.g., fine papers, are produced. For that reason many board mills have closed their water circulation systems. However, the more the system is closed, the more the circulated water has to be purified.

*McKinley Paper Company, Board Mill, New Mexico:* Table 35.1 shows that the McKinley Paper Company in New Mexico produces test liner from old corrugated containers (OCC). There is no water recipient near the mill to discharge even a minimal amount of effluent, and raw water availability is restricted because the mill is located in the desert of northwestern New Mexico. Thus, they have minimized their raw water consumption to only 1.5 m<sup>3</sup>/t board product. A waste stream of 3.3 m<sup>3</sup>/t board produced is cleaned and finally concentrated using MF and RO membranes. First, flotation is used to separate fibers, fines, and stickers from the water and then a sequenced batch reactor (SBR) type of activated-sludge treatment is carried out before membrane filtration. The effluent is aerated and clarified in the same basin, in sequence. The COD and the TSS content after biological treatment are 450–500 mg/L (retention 85%–90%) and 40–50 mg/L (retention about 80%), respectively. The efficient pretreatment enables the use of hollow fiber microfiltration (CMF, USF Memcor Ltd.) to remove suspended solids from the effluent to <1 mg/L. In addition, the permeate silt density index (SDI) is <3 and, therefore, the MF permeate is suitable for reverse osmosis treatment. A typical feed pressure in MF is 2.5 bar. During normal operation of the hollow fiber unit, the feed passes the fiber wall from the outside to the inside and an air backpulse is used from the inside to the outside for cleaning of the hollow fibers. The 0.2 μm membrane removes colloidal particles, bacteria, and also to some extent viruses, even metal particles and their hydroxides, algae blooms, yeast cell, etc. are removed [45,46].

The RO treatment removes salts and the concentrate is crystallized by a tube type of falling film evaporator and its condensate is recirculated back to the process. For example, when a stream at McKinley of approximately 660 m<sup>3</sup>/day is RO treated it results in a permeate of about 490 m<sup>3</sup>/day (1–1.3 m<sup>3</sup>/t product). The salt removal is needed because the high conductivity levels disturb the usability of the wet end chemicals [45,46].

*Linpac, Recycle Paper Mill, Cowpens, South Carolina:* The first full-scale commercial pressurized ozone membrane filtration system was tested and installed in the Linpac recycle paper mill in Cowpens, South Carolina (Table 35.1) for TDS removal [50]. The mill produces linerboard and medium for the production of corrugated boxes from an OCC and mixed office waste (MOW) furnish. The mill has no liquid discharge stream.

The principal idea of the pressurized ozone membrane filtration system is to convert total dissolved solids (TDS) to suspended solids, which are then more easily removed by membranes. The installed system consists of two processes. First, the

ozone is injected under pressure to react with the total dissolved solids of the process water, allowing the TDS to coagulate and agglomerate/precipitate as TSS. Second, ultrafiltration/nanofiltration is used to remove the coagulated and precipitated particles [50].

The Linpac linerboard mill has a two-stage tubular ultrafiltration system and VSEP filters as a kidney. The ultrafiltration systems (Koch membrane systems) treat the overflow from DAF clarifiers. TSS removal in the DAF units is improved significantly by pressurized ozone injection before the DAF. To reduce the concentrate (reject) volume from the UF system and to improve the reused water quality, a VSEP nanofiltration system has been installed to further concentrate the two stage UF concentrate [50].

The flux of the NTR-7450 nanofiltration membranes is 33 L/(m<sup>2</sup>h) at a pressure of 17 bar and a recovery of 72% (temperature 68°C–74°C). As Table 35.8 shows, the total solids in the NF concentrate is at a really high level, over 20%. The COD in the NF permeate is 3,100 mg/L, while it is 9,800–12,900 mg/L in the UF permeates. All permeates are returned to the mill [50].

*Deinking Studies:* One particularly dirty effluent is the deinking effluent, which contains printing colors. Deinking is a laundering process where chemicals, heat, and mechanical energy are used to liberate ink particles from the waste paper fiber and disperse them in an aqueous solution and finally remove them from the pulp. No commercial membrane applications exist in the area of deinking as far as the authors know. However, membrane technology has great potential particularly when paper containing water-soluble printing inks are deinked.

Conventional flotation deinking technology, such as flotation and washing processes, is widely used for deinking secondary fiber furnish that has been printed by the letterpress or lithographic (offset) processes. However, water-based inks used in flexographic news printing are ineffectively removed by conventional flotation due to their hydrophilic nature. The ink particles form a stable colloidal suspension of small hydrophilic particles in alkaline repulping conditions and are then too small (<5 μm) and hydrophilic to be removed in flotation cells. Their hydrophilic properties improve the likelihood of them being removed during washing. Washing is an efficient method to remove flexographic pigment dispersion from pulped secondary fiber, but it produces large quantities of filtrate, which can neither be directly recycled to the deinking process without detrimental effects on deinking, operation, and brightness of the deinked pulp nor discharged to the environment. Therefore, the flexographic pigments have to be removed from the wash effluent [121].

Several researchers have investigated the possibilities of membranes for the removal of dispersed water-based ink pigments from wash effluent [121–126]. Generally, membranes, in particular ultrafiltration membranes, have been found to completely remove ink pigments from effluent streams. It has also been observed that the permeate flux and the fouling tendency depend on operational conditions and effluent composition. For instance, coagulation pretreatment [125], feed water acidification [121], and surfactant addition [123] have been found to improve the flux and decrease fouling.

### 35.6.5 FRESHWATER TREATMENT

Purification of incoming water is carried out by membranes at Bahia Sul Celulose in Mucuri, Brazil (Table 35.1). The source of make-up water for the mill is a river that contains high levels of microscopic organisms and total dissolved solids. A reverse osmosis water purification system (capacity 360 m<sup>3</sup>/h, recovery 75%) was installed in 1991 to remove both dissolved solids and microorganisms. Despite various pretreatments before reverse osmosis (chlorination, flocculation, sedimentation, sand filtration, filtration through activated carbon) the membranes have suffered from high levels of biofouling that generates a high pressure drop on the system and demands frequent cleaning. After replacing the standard BW30–365 membrane with the new more fouling resistant BW30–365FR membrane (FilmTec, nowadays DOW) and optimising the operation (maximum flux 22 L/(m<sup>2</sup>h)) and cleaning conditions the fouling has been significantly reduced and the cleaning interval has been doubled to

**TABLE 35.8**  
**VSEP Performance of NTR-7450 Membrane in the Treatment of UF Concentrate at the Linpac Recycle Paper Mill**

	Flow (L/min)	TSS (%)	Calcium (mg/L)	COD (mg/L)
Feed (concentrate from two stage UF)	93	7	1000	
Concentrate from nanofiltration	26	24	2800–3060	
Permeate from nanofiltration	67	0.3	200–300	3100

*Source:* Adapted from Pressurized ozone membrane ultrafiltration/nanofiltration methodology for TDS removal in the paper mill process water for energy saving, production efficiency, and environmental benefits. Available at <http://www.recycle.com/linpac-nice3/documents/doefinalreport.pdf>.

12 days. The standard Platina-cobalt color test is utilized as a criterion to decide when to stop the alkaline cleaning. As a result, the mill saves a significant amount of chemicals. The salt retention is 98% corresponding to a permeate conductivity less than  $6 \mu\text{S}/\text{cm}$  [66]. The Stendal pulp mill in Germany (Table 35.1) also treats their raw water using RO [55].

### 35.6.6 RECOVERY OF COATING COLOR

Probably, the most successful application for membranes in the pulp and paper industry has been the recovery of coating effluents [127]. Although the volumes of coating wastewaters are negligible compared to the overall mill waters, they cause significant color in discharge water because they are not easily treated by conventional treatments. Furthermore, they represent a significant economical loss. Today, more than 40 mill-scale CR filters are recovering coating pigments. Zero effluents from the coating plants, recycling of the concentrated coating color, and reuse of the permeate are the main advantages when coating color is treated by membranes, mostly by UF [7].

The CR technology dominates the installations but tubular modules are also used [104]. Ultrafiltration recovers the color components in the coating color kitchen effluent streams, instead of them being treated with precipitation and used as landfill. The dilute effluents are concentrated with UF membranes to an appropriate total solids content after which the retentate is used in the preparation of fresh coating color. At the same time water is recovered in the permeate and can be used for dilution or washing purposes in the coating color kitchen. The payback time when treating valuable coating color is typically 1–2 years [36,128,129].

*ASSI Frövifors Bruk, Board mill, Frövifors, Sweden:* In 1991, two CR filters were installed at ASSI Frövifors Bruk board mill in Frövifors (Sweden) to concentrate and recover the waste latex coating from an air-knife coater. The 50 kg/mol cutoff polysulfone membrane produces a flux of  $200 \text{ L}/(\text{m}^2 \text{ h})$ . The mill uses  $\text{TiO}_2$  pigment, which makes the recovery process extremely economical. The UF operates at a constant concentrate solids concentration of 20% continuously for 10 days between cleanings [1,130]. When concentrating a standard coating color effluent steady flux of  $120 \text{ L}/(\text{m}^2 \text{ h})$  at a coating color concentration of 10%–15% ( $50 \text{ L}/(\text{m}^2 \text{ h})$  at 40%) is achieved [36].

*M-Real, Art Paper mill, Äänekoski, Finland:* Before their UF installation M-Real Äänekoski Art Paper mill in Finland lost 5.6 t of coating color every day, corresponding to 88% of the solids in the wastewaters. They installed UF in 1997 to recover 80% of the coating colors. A pilot-scale coating test showed that in pre-coating color the portion of recovered coating color could be even 30%, without decreasing the paper quality. However, because UF also concentrates bacteria, the slime level needs to be controlled when recycling coating colors [127].

*M-Real, Fine paper mill, Kirkniemi, Finland:* Alho et al. [127] reported a flux of  $120 \text{ L}/(\text{m}^2 \text{ h})$  in the filtration of coating color at another M-Real paper mill (Kirkniemi fine paper mill). High-shear modules can recover coating color from wastewater to a higher dry solids content than traditional modules. For example, a solids content of 60% has been reached by the CR and the VSEP filters [36,51].

### 35.6.7 MEDIUM DENSITY FIBERBOARD MANUFACTURING EFFLUENT

Several mill-scale RO plants have been installed for the treatment of wood plant effluents in medium density fiberboard (MDF) mills. Traditionally, the effluent is treated in a biological plant, although not very successfully. A very high BOD content and formaldehyde from the glue kitchen makes the effluent difficult to treat. Esmil Process Systems Ltd. has developed a process that recovers all suspended and dissolved solids from the MDF effluent and makes a zero discharge mill possible. The wood plant effluent is first flocculated and filtered in a filter press. The filter cake can be used as a substitute feedstock for the wood fiber board plant or incinerated. After a dual media sand–anthracite filtration, the effluent is treated in a spiral wound reverse osmosis unit. The hybrid process reduces the original effluent COD from 16,000 to 24,000 mg/L to a level of 6,900 mg/L before RO and the RO permeate contains 200–300 mg/L COD. Finally, the permeate is polished with a carbon filter. Water recovery for recycling as general process water, chip-washing, or boiler feed water is 90%–95%. The RO permeate is reused in the factory and the RO concentrate (COD around 200,000 mg/L) is simply sprayed on the fibers before pressing in the manufacturing process. In that way there is no effluent to treat and the sprayed concentrate actually improves the board quality and saves a little glue since the sugars polymerize during heating and form a glue-like material [63,64,67]. Finnemore and Hackley [64] reported the existence of three plants using RO in the year 2000 located in Kronospan's Chirk factory in North Wales (Table 35.1), in Sanem (Luxemburg), and in Poland. In addition, four plants were at that time under construction. The hybrid process used is according to the reports significantly cheaper (£1–£1.5 per cubic meter ultimate disposal) than a biological process (£5 per cubic meter), sewer treatment (£10 per cubic meter) or evaporation (£15 per cubic meter) [64].

## 35.7 ELECTRODIALYSIS AS POST-TREATMENT

Electrodialysis (ED) is a membrane separation process, which exploits an electrical field as the driving force instead of pressure. Charged compounds are separated by ion-exchange membranes. In the pulp and paper industry, ED is being studied for the

removal of chloride ions in the chemical recovery cycle of sulfate pulp mills [37,131]. Nanofiltration typically removes practically all multivalent ions but passes chloride ions even to such an extent that the concentration of chloride ions is higher in the permeate than in the feed (Donnan exclusion). Therefore, polishing of the permeate, e.g., using ED, may be needed. Fouling management of ED membranes is crucially important to avoid an increase in energy consumption. Fouling may also cause a loss in selectivity of the process. Especially, the anion-selective membrane was found to be markedly fouled when an alkaline bleach plant filtrate was processed [132]. Nanofiltration before ED could reduce the fouling in ED. Nanofiltration alone removes about 95% of the color and 90% of the organic compounds from the alkaline extraction stage effluents (E1 stage) and is thus an efficient pretreatment for ED [69]. ED has also been studied for removal of salt from MBR effluents (Section 35.6.3.2).

Geraldes and de Pinho [37] modeled NF permeate using a prepared salt solution to evaluate the feasibility of ED for the removal of chloride ions. The modeled permeates contained chloride ions from 1650 to 2250 mg/L depending on the water recovery. In that study, the quality requirements for the washing waters for pulp bleaching were 350 mg/L of NaCl and 30 PtCo units of color. The NF followed by ED met these requirements and the evaluated costs were \$0.65 per m<sup>3</sup> at 80% water recovery. Rapp et al. [131] reported the electrical power consumption of ED to be 0.97 kW h/kg chloride removed.

### 35.8 DEMANDS ON MEMBRANES TODAY AND IN THE FUTURE

The legislative restrictions (in 2006) are such that most pulp and paper mill wastewaters can be discharged after activated-sludge treatment. Furthermore, there are no restrictions in many countries on the intake of process water. In the future, there will most probably be limitations on the amount of intake water and the limitations for discharge loads will be tightened. The cost of freshwater will not decrease and this will force mills to increase their water reuse.

New regulations on water intake and mill effluent grades will constitute the driving forces for adopting membrane technology in pulp and paper mills. In Europe, the EU Directive on Integrated Pollution Prevention and Control (IPPC) will lead the pulp and paper industry to achieving a high level of protection of the whole environment. The IPPC includes a Best Available Technology (BAT) reference document, BREF, which refers to the pulp and paper industry. The BREF includes, among others, emission levels and flow rates for wastewaters (m<sup>3</sup>/t) and technologies regarding how to obtain these levels. This directive will come into force for existing mills from the year 2007 and will provide further opportunities for membranes in the pulp and paper industry.

One challenge is to find the right membrane and module characteristics for the different streams to be treated combined with the ability to withstand the physical and chemical nature of the streams. The combination of a temperature increase (70°C–90°C) with a high pH during filtration or cleaning makes great demands on the membranes. Furthermore, membranes can sometimes be exposed to oxidizers. High-shear conditions and rigid particles, or even fibers, can cause erosion on the membrane surface. Many applications today operate at high recovery and concentration. This sets limitations for membrane modules but high-shear modules can respond to that challenge.

A challenge will also be the further processing of concentrate or permeate streams. The recovery needs to be high so that the retentate stream can be incinerated, or other ways to treat the concentrate need to be developed. Evaporation or tighter membrane processes can be used to increase the dry solids content of the concentrate. Some mills recirculate the concentrate back to the wastewater treatment process, some sell it to the customer by binding the concentrate to the final product (MDF boards), and some use chemical precipitation to lower the impurities in the concentrate (e.g., Eltmann newsprint mill in Germany). The biodegradability of the concentrate can be enhanced by slight oxidation (e.g., ozone treatment). However, although there are several options to treat the concentrate, its destruction is often problematic.

Membranes should have high flux but at the same time also have the ability to retain small molecules for the permeate to be reused as wash water or make-up water at different places in the process. When membranes are used, fouling management is always crucially important. The development of polymeric membranes has been fast and will probably continue but in the most demanding applications ceramics might be the only solution. Their use has been restricted by the cost of the membrane material but costs will decrease with increased use and new manufacturing processes. However, polymeric membranes will also become cheaper in the future. Ultrafiltration and, in particular, nanofiltration are the membranes of the future when process streams are to be filtered. Ultrafiltration is also the right solution for coating color recovery. As the reviewed membrane installations show, membranes are needed for extremely many different purposes in the pulp and paper industry. This need will increase and more installations will undoubtedly be seen in the future.

### ACKNOWLEDGMENTS

The following persons and organizations are acknowledged for sharing their knowledge on membrane applications in the pulp and paper industry: Lasse Blom (Norske Skog), Peter Eriksson (GeOsmonics), Larry Stowell (New Logic Research, Inc.), Hans-Jürgen Öller (PTS), Peter Ohle (Zenon GmbH), Timo Sutela (Metso PaperChem Oy), Enrico Vonghia (Zenon), Margot Görzel (Microdyn-Nadir), Ryosuke Maekawa (Kubota Membrane Europe Ltd.), PCI, and NanoMemPro network.

## ABBREVIATIONS

AOX	adsorbable organic halogens
BAT	best available technology
BOD	biological oxygen demand
CA	cellulose acetate
COD	chemical oxygen demand
C-stage	chlorination stage
CR	cross-rotational
DAF	dissolved air flotation
E1	alkaline extraction stage
ECF	elemental chlorine free
ED	electrodialysis
IPPC	Integrated Pollution Prevention and Control
MBR	membrane bioreactor
MDF	medium density fiberboard
MF	microfiltration
MLSS	mixed liquor suspended solids
MOW	mixed office waste
NF	nanofiltration
OCC	old corrugated containers
PA	polyamide
PCI	Paterson Candy Int.
PE	polyethylene
PEI	polyethyleneimine
PES	polyethersulfone
PSu	polysulfone
PVA	polyvinyl alcohol
PVDF	polyvinylidene fluoride
RC	regenerated cellulose
RO	reverse osmosis
SBR	sequenced batch reactor
SDI	silt density index
TCF	total chlorine free
TDS	total dissolved solids
TOC	total organic carbon
TRS	totally reduced sulfur
TSS	total suspended solids
UASB-IC	upflow anaerobic sludge blanket internal circulation
UF	ultrafiltration
UVA 280 nm	absorption of UV light at 280 nm
VSEP	vibratory shear enhanced processing

## REFERENCES

1. Jain A and Miner R. Membrane technology applications in the pulp and paper industry, Technical bulletin no 763, NCASI, Research Triangle Park, NC. 1998.
2. Nuortila-Jokinen J, Mänttari M, and Nyström M. The pulp and paper industry. In: *Membranes for Industrial Wastewater Recovery and Reuse*, S. Judd and B. Jefferson, Eds., Elsevier Advanced Technology, United Kingdom, 2003, Chapter 3.2, pp. 102–131.
3. Afonso MD and De Pinho MN. Treatment of bleaching effluents by pressure-driven membrane processes—a review. In: *Membrane Technology: Applications to Industrial Wastewater Treatment*, Cuetano et al., Eds., Kluwer Academic, The Netherlands, 1995.
4. Dal-Cin MM, McLellan F, Striez CN, Tam CM, Tweddle TA, and Kumar A. Membrane performance with a pulp mill effluent: Relative contributions of fouling mechanisms. *J. Membr. Sci.* 1996; 120: 273–285.
5. Mänttari M, Nuortila-Jokinen J, and Nyström M. Evaluation of nanofiltration membranes for filtration of paper mill total effluent. *Filtr. Sep.* 1997; 34(3): 275–280.
6. Choi H, Zhang K, Dionysiou DD, Oerther DB, and Sorial GA. Effect of permeate flux and tangential flow on membrane fouling for wastewater treatment. *Sep. Pur. Techn.* 2005; 45(1): 68–78.

7. Singh S, Matsuura T, and Ramamurthy P. Treatment of coating plant effluent with an ultrafiltration membrane. *Tappi J.* 1999; 82(4): 146–155.
8. Mänttari M., Pihlajamäki A., and Nyström M. Comparison of nanofiltration and tight ultrafiltration membranes in the filtration of paper mill process water. *Desalination* 2002; 149: 131–136.
9. Puro L, Tanninen J, and Nyström M. Analyses of organic foulants in membranes fouled by pulp and paper mill effluent using solid-liquid extraction. *Desalination* 2002; 143: 1–9.
10. Jönsson C and Jönsson AS. Influence of the membrane material on the adsorptive fouling of ultrafiltration membranes. *J. Membr. Sci.* 1995; 108: 79–88.
11. Dal-Cin MM, Striez CN, Tweddle TA, Capes CE, McLellan F, and Buisson H. Effect of adsorptive fouling on membranes performance: Case study with a pulp mill effluent. *Desalination* 1995; 101: 155–167.
12. Mänttari M, Pekuri T, and Nyström M. NF-270, a new membrane having promising characteristics and being suitable for treatment of dilute effluents from the paper industry. *J. Membr. Sci.* 2004; 242: 107–116.
13. Huuhilo T, Väisänen P, Nuortila-Jokinen J, and Nyström M. Influence of shear in membrane filtration of integrated pulp and paper mill circulation water. *Desalination* 2001; 141: 245–258.
14. Brinck J, Jönsson AS, Jönsson B, and Lindau J. Influence of pH on the adsorptive fouling of ultrafiltration membranes by fatty acid. *J. Membr. Sci.* 2000; 164: 187–194.
15. Maartens A, Jacobs EP, and Swart P. UF of pulp and paper effluent: Membrane fouling-prevention and cleaning. *J. Membr. Sci.* 2002; 209: 81–92.
16. Belfer S, Fainshtain R, Purinson Y, Gilron J, Nyström M, and Mänttari M. Modification of NF membrane properties by in-situ redox initiated graft polymerization with hydrophilic monomers. *J. Membr. Sci.* 2004; 239: 55–64.
17. Vrijenhoek EM, Hong S, and Elimelech M. Influence of membrane surface properties on initial rate of colloidal fouling of reverse osmosis and nanofiltration membranes. *J. Membr. Sci.* 2001; 188: 155–128.
18. Mänttari M and Nyström M. Ultrafiltration and nanofiltration in the pulp and paper industry using cross-rotational (CR) filters. *Wat. Sci. Techn.* 2004; 50(3): 229–238.
19. Nyström M, Pihlajamäki A, Liikanen R, and Mänttari M. Influence of process conditions and membrane/particle interactions in NF of wastewaters. *Desalination* 2003; 156: 379–387.
20. Maxinova N, Stenius P, and Salmi J. Lignin uptake by cellulose fibres from aqueous solutions. *Nordic Pulp Pap. Res. J.* 2004; 19(2): 135–145.
21. Lindström M, Nyström M, and Laatikainen M. Interaction between chlorolignin and polysulfone ultrafiltration membranes. *Sep. Sci. Techn.* 1988; 23(6): 703–717.
22. Jönsson AS, Blomberg Y, and Petersson E. Influence of pH and surfactant on ultrafiltration membranes during treatment of bleach plant effluent. *Nordic Pulp Pap. Res. J.* 1988; 3(4): 159–165.
23. Mänttari M, Pihlajamäki A, and Nyström M. Effect of pH on hydrophilicity and charge and their effect on the filtration efficiency of NF membranes at different pH. *J. Membr. Sci.* 2006; 280(1–2): 311–320.
24. Mänttari M, Nuortila-Jokinen J, and Nyström M. Influence of filtration conditions on the efficiency of NF membranes in the filtration of paper mill total effluent. *J. Membr. Sci.* 1997; 137(1–2): 187–199.
25. Jönsson AS and Jönsson B. Colloidal fouling during ultrafiltration. *Sep. Sci. Techn.* 1996; 31(9): 2611–2620.
26. Mänttari M, Daltrophe N, Oren Y, Gilron J, and Nyström M. Treatment of paper mill process water with lime treatment, MF and NF. Proceedings of the Engineering with Membranes, Granada, Spain, June 3–6, 2001, I295–I299.
27. Joore L, Wortel N, and Bronold N. MBR in water loop closure concepts in Dutch recycled paper mills—from pilot towards full-scale installations. *Pap. Techn.* 2001; 42(7): 27–36.
28. Hepp B, Joore L, Schonewille H, and Futselaar H. Membrane filtration: A sustainable water treatment technology within modern papermaking concepts. *Pap. Techn.* 2005; 46(1): 41–48.
29. Lopetegui J and Sancho L. Aerated thermophilic biological treatment with membranes: Alternative to conventional technologies treating paper mill effluents. *Wat. Sci. Techn. Wat. Supply* 2003; 3(5–6): 245–252.
30. Mänttari M, Pihlajamäki A, Kaipainen E, and Nyström M. Effect of temperature and membrane pretreatment by pressure on the filtration properties of nanofiltration membranes. *Desalination* 2002; 145: 81–86.
31. Kallioinen M, Pekkarinen M, Mänttari M, Nyström M, and Nuortila-Jokinen J. Comparison of the performance of two different regenerated cellulose ultrafiltration membranes at high filtration pressure. *J. Membr. Sci.* 2007; 294: 93–102.
32. Jönsson AS. Influence of shear rate on the flux during ultrafiltration of colloidal substances. *J. Membr. Sci.* 1993; 79: 93–99.
33. Zaidi A, Buisson H, Sourirajan S, and Wood H. Ultra- and nano-filtration in advanced effluent treatment schemes for pollution control in the pulp and paper industry. *Wat. Sci. Tech.* 1992; 25(10): 263–276.
34. Ramamurthy P, Poole R, and Dorica JG. Fouling of ultrafiltration membranes during treatment of CTMP screw press filtrates. *J. Pulp Pap. Sci.* 1995; 21(2): J50–J54.
35. Buisson H, Zaidi A, and Koski K. Bench-scale evaluation of ultrafiltration and nanofiltration membranes for the treatment of a kraft-caustic extraction stage effluent from a softwood line. 1992 Environmental Conference, Richmond, VA, April 12–15, 1992, 585–593.
36. Jönsson A-S, Jönsson C, Teppler M, Tomani P, and Wännström S. Treatment of coating colour effluents by membrane filtration. *Desalination* 1996; 105: 263–276.
37. Geraldes V and De Pinho MN. Process water recovery from pulp bleaching effluents by an NF/ED hybrid process. *J. Membr. Sci.* 1995; 102(1): 209–221.
38. Mänttari M. Fouling management and retention in nanofiltration of integrated paper mill effluents. PhD dissertation, Acta Universitatis Lappeenrantaensis 78, Lappeenranta University of technology, Lappeenranta, Finland.

39. Mänttari M and Nyström M. Critical flux in NF of high molar mass polysaccharides and effluents from paper industry. *J. Membr. Sci.* 2000; 170(2): 257–273.
40. Wessberg J. Membrane bioreactors for the treatment of pulp bleaching effluents. Licentiate dissertation, May 2000, Lund University, Sweden, 86 pp.
41. Mänttari M, Viitikko K, and Nyström M. Nanofiltration of biologically treated effluents from the pulp and paper industry. *J. Membr. Sci.* 2005; 272(1–2): 152–160.
42. Woerner P and McCarthy JL. Ultrafiltration of pulp mill liquors. *Tappi J.* 1987; 70(3): 126–130.
43. Kyllönen H, Pirkonen P, Nyström M, Nuortila-Jokinen J, and Grönroos A. Experimental aspects of ultrasonically enhanced cross-flow membrane filtration of industrial wastewater. *Ultrasonics Sonochemistry* 2006; 13(4): 295–302.
44. Silva CM, Reeve DW, Woodhouse KA, Husain H, and Behmann H. Water reuse in the pulp and paper industry: Evaluation of four microfiltration applications. *Can. Pulp Pap.* 1999; 100(5): 38–43.
45. Pohjalainen T. Case study of “closed” board mill and application studies in Finland. *Investigacion y Tecnica del Papel* 1999; 36(142): 637–647.
46. Durham B. Case studies of wastewater re-use for the petrochemical, power and paper industry. *Special Publication—Royal Society of Chemistry* 2000; 249 (Membrane Technology in Water and Wastewater Treatment): 241–247.
47. Merry A. The role of membranes in achieving ZLE. *Invest. Tec. Pap.* 1999; 36(142): 568–574.
48. Nuortila-Jokinen J. Choice of optimal membrane processes for economical treatment of paper machine clear filtrate. PhD dissertation, Research Papers 58, Lappeenranta University of Technology, Lappeenranta, Finland, 1997.
49. Norske Skog Albury, Membrane test report, April 2005.
50. Pressurized ozone membrane ultrafiltration/nanofiltration methodology for TDS removal in the paper mill process water for energy saving, production efficiency, and environmental benefits. Available at <http://www.recycle.com/linpac-nice3/documents/doefinalreport.pdf>.
51. Nuortila-Jokinen J and Nyström M. Membrane filtration of coating colour effluent. 8th World Filtration Conference, Brighton, United Kingdom, April 3–7, 2000, 1007–1010.
52. Greaves R. The use of ultrafiltration for COD reduction in pulp mill effluent—a case study from Sweden. International Environmental Conference, Nashville, TN, April 18–21, 1999, 1167–1191.
53. Kreutzman E and Sutela T. Water management in the European paper industry. *Ippta J.* 2004; (Conv. Issue): 15–22.
54. Membrane filtration in P&P. Reference list, Metso Paper, 03/2005.
55. <http://www.watech.de/eng/index.php>
56. Metso Paper, Domsjö Fabriker AB reference.
57. Webb L. Radical solution in effluent treatment. *Pulp Pap. Int.* 2000; 42(4): 37–43.
58. Brockmann M and Praderie M. Paper production in France. Zenon bulletin.
59. Schirm R, Welt T, and Ruf G. Nanofiltration Eine möglichkeit zur kreislaufschließung, Papierfabrik Palm, Werk Eltmann. IMPS Internationales Münchner Papiersymposium; FH-München, 23.3.2001, München, Germany.
60. Zenon system achieves zero discharge in pulp and paper plant. Zenon bulletin. [http://www.zenon.com/resources/case\\_studies/wastewater/Irving.shtml](http://www.zenon.com/resources/case_studies/wastewater/Irving.shtml)
61. Webb L. Kidney technology brings success. *Pulp Pap. Int.* 2002; 44(4): 28–32.
62. Dal-Cin MM, Kumar A, and Brail J. Membrane technology in the pulp and paper industry, A review of the state of the art, ICPET, Internal report no PET-1393–97S, May 8, 1997.
63. Anonymous, Zero discharge, cost effective MDF effluent treatment plant. *Filtr. Sep.* 2002; December: 30–31.
64. Finnemore S and Hackley T. Zero discharge at Kronospan Mill: Recent advances in wood pulp effluent treatment. *Pap. Techn.* 2000; 41(1): 29–32.
65. Zenon technology treats TMP wastewater for recycle, Zenon bulletin.
66. Soalheiro SC. Membrane technology improves RO system for Bahia Sul celulose. *Pulp Pap.* 2000; 74(10): 63–71.
67. Wagner J. Membrane technology in wood, pulp and paper industries. *Special Publication—Royal Society of Chemistry* 2000; 249 (Membrane Technology in Water and Wastewater Treatment): 233–240.
68. Afonso MD and DePinho MN. Nanofiltration of bleaching pulp and paper effluents in tubular polymeric membranes. *Sep. Sci. Techn.* 1997; 32(16): 2641–2658.
69. De Pinho MN, Geraldés VM, Rosa MJ, Afonso MD, Figueira H, Tabora F, Almeida G, Ganho R, Creuse R, Hanemaaijer J, Gaeta S, Amblard P, Gavach C, and Guizard C. Water recovery from bleached pulp effluents. *Tappi J.* 1996; 79(12): 117–124.
70. Afonso MD, Geraldés V, Rosa MJ, and De Pinho MN. Nanofiltration removal of chlorinated organic compounds from alkaline bleaching effluents in a pulp and paper plant. *Wat. Res.* 1992; 26(12): 1639–1643.
71. Tomani P and Seisto A. Separation methods for closed-loop manufacture of bleached kraft pulp—overview of an EU project. *Desalination* 1999; 124: 217–223.
72. Nyström M and Linsdröm M. Optimal removal of chlorolignin by ultrafiltration achieved by pH control. *Desalination* 1988; 70: 145–156.
73. Jönsson AS. Treatment of effluent from alkaline extraction with ultrafiltration and reverse osmosis. *Nordic Pulp Pap. Res. J.* 1989; 4(1): 33–37.
74. Rosa MJ, De Pinho MN, Figueira H, and Noronha F. Fractionation of organochlorinated compounds by ultrafiltration. Tappi Environmental Conference., Richmond, VA, April 12–15, 1992.
75. Yao KW, Kennedy KJ, Tam CM, and Hazlett JD. Pre-treatment of kraft pulp bleach plant effluent by selected ultrafiltration membranes. *Can. J. Chem. Eng.* 1994; 72(6): 991–999.

76. De Pinho MN, Rosa MJ, Minhalma M, and Taborda F. Integration of flotation/ultrafiltration for treatment of bleached pulp effluent. International Environmental Conference, April 5–8, 1998, 319–327.
77. Sierka RA and Bryant CW. Enhancement of biotreatment effluent quality by illuminated titanium dioxide and membrane pre-treatment of the kraft extraction waste stream and by increased chlorine dioxide substitution. *Wat. Sci. Tech.* 1994; 29(5–6): 209–218.
78. Rosa, MJ and de Pinho MN. The role of ultrafiltration and nanofiltration on the minimisation of the environmental impact of bleached pulp effluents. *J. Membr. Sci.* 1995; 102: 155–161.
79. Ekengren Ö, Filipsson S, and Bjurhem J.-E. Treatment of bleach plant effluents by membrane filtration. Environ. Conf., Boston, MA, March 28–31, 1993, 403–411.
80. Bindoff A, Davies CJ, Kerr CA, and Buckley CA. The nanofiltration and reuse of effluent from caustic extraction stage of wood pulping. *Desalination* 1987; 67: 455–465.
81. Jönsson AS and Wimmerstedt R. The application of membrane technology in the pulp and paper industry. *Desalination* 1985; 53: 181–196.
82. Heikkilä H, Mänttari M, Lindroos, M, and Nyström M. Recovery of xylose, Publication date 11.7.2002, WO02053783.
83. Wallberg O, Jönsson A-S, and Wimmerstedt R. Membrane cleaning—a case study in a sulphite pulp mill bleach plant. *Desalination* 2001; 141: 259–268.
84. Luque S, Rodríguez M, Alvarez JR, and Coca J. Kraft black liquor fractionation by ultrafiltration. 1994 Pulping Conference, San Diego, CA, November 6–10, 1994.
85. De S and Bhattacharya PK. Recovery of water and inorganic chemicals from kraft black liquor using membrane separation processes. *Tappi J.* 1996; 79(1): 103–111.
86. Wallberg O, Jönsson A-S, and Wimmerstedt R. Fractionation and concentration of kraft black liquor lignin with ultrafiltration. *Desalination* 2003; 154: 187–199.
87. Satyanarayana SV, Bhattacharya PK, and De S. Flux decline during ultrafiltration of kraft black liquor using different flow modules: A comparative study. *Sep. Pur. Techn.* 2000; 20: 155–167.
88. Bhattacharjee S, Siddhartha D, and Bhattacharjee C. Performance study during ultrafiltration of kraft black liquor using rotating disk membrane module. *J. Cleaner Production* 2006; 14(5): 497–504.
89. Cortiñas S, Luque S, Alvarez JR, Canaval J, and Romero J. Microfiltration of kraft black liquor for the removal colloidal suspended matter (pitch). *Desalination* 2002; 147: 49–54.
90. Dafinov A, Font J, and Garcia-Valls R. Processing of black liquors by UF/NF ceramic membranas. *Desalination* 2005; 173: 83–90.
91. Keyoumu A, Sjödah R, Henriksson G, Ek M, Gellerstedt G, and Lindström M. Continuous nano- and ultra-filtration of kraft pulping black liquor with ceramic filters. A method for lowering the load on the recovery boiler while generating valuable side-products. *Indust. Crops Products* 2004; 20: 143–150.
92. Wallberg O, Jönsson A-S, and Wimmerstedt R. Ultrafiltration of kraft black liquor with a ceramic membrane. *Desalination* 2003; 156: 145–153.
93. Fälth F, Jönsson A-S, and Wimmerstedt R. Ultrafiltration of effluents from chlorine-free, kraft pulp bleach plant. *Desalination* 2001; 133: 155–165.
94. Svärd SH, Jour P, Bryant PS, Basta J, and Aggarwal P. Increasing the biotreatability of EFC bleaching effluents by ultrafiltration and partial closure of alkaline filtrates. 1998 Pulping Conference, Montreal, Quebec, Canada, Oct 25–29, 1998, 1165–1176.
95. Vieira M, Tavares CR, Bergamasco R, and Petrus JCC. Application of ultrafiltration–complexation process for metal removal from pulp and paper industry wastewater. *J. Membr. Sci.* 2001; 194: 273–276.
96. Tavares CR, Vieira M, Petrus JCC, Bortoletto EC, and Ceravollo F. Ultrafiltration/complexation process for metal removal from pulp and paper industry wastewater. *Desalination* 2002; 144: 261–265.
97. Lastra A, Gómez D, Romero J, Francisco JL, Luque S, and Álvarez JR. Removal of metal complexes by nanofiltration in a TFC pulp mill: Technical and economical feasibility. *J. Membr. Sci.* 2002; 242: 97–105.
98. Bérubé PR, and Hall ER. Treatment of evaporator condensates using a high temperature membrane bioreactor: Determination of maximum operating temperature and system costs. Project report 1999–31, SFM Network Project: Membrane bioreactors for contaminant control in closed pulp and paper mills, 1999.
99. Dias JCT, Rezende RP, Silva CM, and Linardi VR. Biological treatment of kraft pulp mill foul condensates at high temperatures using a membrane bioreactor. *Process Biochemistry* 2005; 40: 1125–1129.
100. Huuhilo T. Fouling, prevention of fouling, and cleaning in filtration. PhD dissertation, Acta Universitatis Lappeenrantaensis, Lappeenranta University of technology, Lappeenranta, Finland.
101. Huuhilo T, Suvilampi J, Puro L, Rintala J, Mänttari M, Nuortila-Jokinen J, and Nyström M. Internal treatment of pulp and paper mill process waters with a high temperature aerobic biofilm process combined with ultrafiltration and/or nanofiltration. *Pap. Timber* 2002; 84(1): 50–53.
102. Nuortila-Jokinen J, Kaipia L, Nyström M, Jahren S, and Rintala J. Internal purification of thermomechanical pulp clear filtrate with a combined biological and membrane filtration method: a preliminary study. *Sep. Sci. Techn.* 1996; 31(7): 941–952.
103. Ramamurthy P, Poole R, and Dorica JG. Fouling of ultrafiltration membranes during treatment of CTMP screw press filtrates. 1993 Environmental Conference, Thunder Bay, Canada, October 26–28, 1993, 67–71.
104. Pauly D. Kidney technology for whitewater treatment. *Pap. Techn.* (Bury, United Kingdom) 2001; 42(8): 29–32.
105. Brady FJ. Industrial wastewater UF and RO treatment for water reclamation and reuse. A survey of commercial membrane system installations. 9th Annual Industrial Wastes Technical and Regulatory Conference, San Antonio, TX, April 13–16, 2003, 443–451.
106. Lien L and Simonis D. Case histories of two large nanofiltration systems reclaiming effluent from pulp and paper mills for reuse, International Environmental Conference, Atlanta, GA, May 7–10, 1995, 1023–1027.

107. Schirm R and Paulitschek M. Einsatz der membrantechnologie in der papierindustrie, Abwasseraufbereitung mittels membrantechnologie in der papierherstellenden industrie. PTS presentation 12\_2002.
108. Mänttari M, Martin H, Nuortila-Jokinen J, and Nyström M. Using a spiral wound nanofiltration element for the filtration of paper mill effluents; pretreatment and fouling. *Adv. Env. Res.* 1999; 3(2): 202–214.
109. Knudsen HH, Wenzel H, Wagner J, Jepsen SE, Kristensen GH, Mortensen AL, and Ringbaek U. Membrane separation processes in recycling paper processing mills. 5th IAWQ Symposium on Forest Industry Wastewaters, Vancouver B.C., Canada, June 10–13, 1996, 83–90.
110. Stephenson T, Judd S, Jefferson B, and Brindle K. *Membrane Bioreactors for Wastewater Treatment*. IWA Publishing, London, 2000.
111. Tripathi CS and Allen DG. Feasibility study of thermophilic aerobic biological treatment of bleached kraft pulp mill effluent. International Environmental Conference and Exhibition, Vancouver, Canada, April 5–8, 1998, 1189–1201.
112. Tripathi CS and Allen DG. Comparison of mesophilic and thermophilic aerobic biological treatment in sequencing batch reactors treating bleached kraft pulp mill effluent. *Wat. Res.* 1999; 33: 836–846.
113. Vogelaar JCT, De Keizer A, Spijker S, and Lettinga G. Bioflocculation of mesophilic and thermophilic activated sludge. *Wat. Res.* 2005; 39(1): 37–46.
114. Kay M, Merritt R, and Capel G. The benefits of MBR: Kimberly-Clark has successfully employed membrane bio-reactor technology at its Welsh mills. *Pulp Pap. Int.* 2004; 46(12): 30–32.
115. Lombardo G, Buisson H, and Paillard H. Membrane bioreactors application in water cycle closure: From concept to full scale installations. PTS-Symposium 1999; 908(Vortragsband—PTS-CTP-Symposium, Umwelttechnik): 19,19E,19/1–19/10.
116. Dufresne R, Lavallee HC, Lebrun RE, and Lo SN. Comparison of performance between membrane bioreactor and activated sludge system for the treatment of pulping process wastewaters. *Tappi J.* 1998; 81(4): 131–135.
117. Ramaekers H, van Dijk L, Lumpe C, Verstraeten E, and Joore L. Thermophilic membrane bioreactors in the paper industry—a successful key to in-mill water treatment. *Pap. Techn.* 2001; February: 32–40.
118. Galil NI. Membrane bioreactor for final treatment of wastewater. *Wat. Sci. Techn.* 2003; 48(8): 103–110.
119. Stahl N, Tenenbaum A, and Galil NI. Advanced treatment by anaerobic process followed by aerobic membrane bioreactor for effluent reuse in paper mill industry. *Wat. Sci. Techn.* 2004; 50(3, Forest Industry Wastewaters VII): 245–252.
120. Pauly D and Deschildre A. New integrated process water treatment concepts for recovery paper mills: KIDNEY-technology. PTS-Symposium 2001; 50 108 (Auf dem Abwasserfreien Papiererzeugung): 8/1–8/18.
121. Chabot B, Krishnagopalan GA, and Abubakr S. Flexographic newspaper deinking: Treatment of wash filtrate effluent by membrane technology. *J. Pulp Pap. Sci* 1999; 25(10): 337–343.
122. Upton BH, Krishnagopalan GA, and Abubakr S. Deinking flexographic newsprint: Using ultrafiltration to close the water loop. *Tappi J.* 1997; 80(2): 155–164.
123. Upton BH, Krishnagopalan GA, and Abubakr S. Ultrafiltrative deinking of flexographic ONP: The role of surfactant. *Tappi J.* 1999; 82(11): 104–114.
124. Chabot B, Krishnagopalan GA, and Abubakr S. Effect of ultrafiltration permeate recycling on deinking efficiency of flexo-printed newspapers. *Progr. Pap. Recycl.* 1998; August: 28–38.
125. Chabot B, Krishnagopalan GA, Abubakr S. Coagulation pretreatment for ultrafiltration of deinking effluents containing flexographic inks. *Progr. Pap. Recycl.* 1999; November: 46–65.
126. Silva CM, Reeve DW, Husain H, Rabie HR, and Woodhouse KA. Model for flux prediction in high-shear microfiltration systems. *J. Membr. Sci.* 2000; 173: 87–98.
127. Alho J, Roitto I, Nygård S, and Hietanen S. A review on coating effluent treatment by ultrafiltration, In Proceedings of 2nd Eco Paper Technical Conference, The Finnish Pulp and Paper Research Institute and The Finnish Paper Engineers' Association, Gummerus, Jyväskylä, Finland, 1998, 219–231.
128. Pichon M, Camatta R, Tardy G, and Woerner D. Ultrafiltration applied to the treatment of effluents to the paper and board coating plants, Tappi 1992 Environmental Conference Book 2, Richmond, VA, April 12–15, 1992.
129. Stuffer P. Ultrafiltration—Ein weg zur reduzierung der umweltbelastung durch die streicherei. *Wochenblatt für Papierfabrikation* 1996; 124(13): 598–603.
130. Jönsson A-S, Jönsson C, Teppler M, Tomani P, and Wännström S. Recovery of dilute paper coating colour effluents by ultrafiltration. *Filtr. Sep.* 1996; June: 453–457.
131. Rapp HJ and Pfromm PH. Electrodialysis for chloride removal from the chemical recovery cycle of a kraft pulp mill. *J. Membr. Sci.* 1998; 146: 249–261.
132. Lindstrand V, Sundström G, and Jönsson AS. Fouling of electro dialysis membranes by organic substances. *Desalination* 2000; 128: 91–102.

---

# 36 Membrane Bioreactors for Wastewater Treatment

*Eoin Casey*

## CONTENTS

36.1	Introduction .....	1007
36.2	Overview of Membrane Bioreactor Operation .....	1008
36.3	Membrane Bioreactor Performance .....	1009
36.3.1	Municipal Wastewater Carbonaceous Removal .....	1009
36.3.2	Nutrient Removal .....	1010
36.3.2.1	Nitrification .....	1010
36.3.2.2	Denitrification.....	1011
36.3.2.3	Phosphorus Removal .....	1011
36.3.3	Benchmarking the MBR against the CAS Process.....	1011
36.3.4	Micropollutant Removal from Municipal Wastewater .....	1011
36.3.5	Carbonaceous Removal from Industrial Wastewater.....	1012
36.3.6	Removal of Specific Organic Pollutants from Industrial Wastewater .....	1012
36.3.7	Energy Consumption.....	1012
36.4	Mechanisms Contributing to MBR Performance .....	1014
36.4.1	Membrane Fouling .....	1014
36.4.2	Biomass Morphology and Rheology .....	1015
36.4.3	Microbial Ecology.....	1016
36.4.4	Microbial Physiology .....	1016
36.4.5	Factors Contributing to Biomass Yield .....	1016
36.4.5.1	Maintenance .....	1017
36.4.5.2	Lysis-Cryptic Growth .....	1017
36.4.5.3	Predation .....	1017
36.4.6	Extracellular Microbial Activity .....	1018
36.5	Process Economics.....	1018
36.6	Novel Membrane Bioreactors: Membrane Attached Biofilms .....	1018
36.7	Conclusions .....	1019
	Abbreviations .....	1020
	References.....	1020

## 36.1 INTRODUCTION

Progressively stringent emission standards have prompted the development of innovative technologies for the treatment of both municipal and industrial wastewater. Perhaps the fastest growing technology in the wastewater treatment sector, the membrane separation bioreactor, generally designated the (MBR), was originally developed as a response to the need to achieve process intensification and the achievement of tighter emission requirements. Recently, the process has been adopted for water recycling applications [1]. Water recycling has become a reality in many countries, for example, 190 million cubicmeter of treated wastewater is reused annually in Japan [2] and the trend is increasing as the demand for water is rising.

The first commercial MBRs, in which an external microfiltration membrane module replaced sedimentation in the activated sludge (AS) process, were introduced in the 1960s by Dorr-Oliver Inc. [3]. Full-scale commercial MBRs entered service in North America in the 1970s, Japan in the 1980s, and Europe in the 1990s [4]. A reputation for excellent effluent quality

together with continuing improvements in process design and a dramatic reduction in membrane cost have seen the number of installations increase substantially in recent years. Several thousand installations now exist worldwide, typically treating effluent quantities of a few hundred cubic meters per day. Indeed, many processes are now operating at several  $1,000 \text{ m}^3 \text{ day}^{-1}$  and plans are advanced for MBR installations that will treat over  $100,000 \text{ m}^3 \text{ day}^{-1}$  [5].

The principal advantages of the MBR process over conventional wastewater technology are

1. Biomass retention is achieved by membrane separation rather than by gravity settling and therefore the process is insensitive to filamentous sludge bulking, and other floc settling and clarification problems commonly encountered in the activated sludge process. Moreover, the biomass concentration in the aeration tank is not dependent on the limitations of the secondary clarifier, thereby permitting typical mixed liquor suspended solids (MLSS) values of  $10,000\text{--}15,000 \text{ mg L}^{-1}$ , a factor four times higher than that in the conventional activated sludge (CAS) process. High volumetric reaction rates in the MBR, therefore, allow high carbonaceous conversion and nitrification rates to be achieved with short hydraulic retention times. Consequently, the size of reactor required is lower than the CAS process.
2. The long solids retention time (SRT) in the MBR is considered to be amenable to specialist slow-growing microorganisms necessary for the biodegradation of specific organic pollutants.
3. Because the membrane acts as a filter, the final effluent (permeate) is generally of a very high quality in terms of turbidity, bacteria, solids, and colloidal material. Rejection of bacteria and viruses is significant with average log reductions of up to 8 for total coliforms [6].
4. A long SRT combined with high MLSS concentrations results in a low-sludge yield. Sludge minimization is particularly an important advantage in the treatment of industrial wastewater, because such sludge is frequently classified as hazardous waste and therefore requires expensive treatment and disposal.

The engineering principles of MBR technology have developed to the extent that the process is reliable at large scale. However, the relatively poor understanding of the biological mechanisms contributing to performance, the inefficiencies associated with amelioration of membrane fouling, and poor oxygen transfer efficiencies are the three issues that need to be addressed if MBR technology is to fully mature. A significant research effort is under way to address these and other MBR performance-related issues, and it is likely that the performance of the process will continue to improve in the years ahead.

The purpose of this chapter is to review the critical factors contributing to MBR process performance and to report recent advancements in key areas. Coverage is directed toward membrane separation bioreactors, although recent developments in membrane biofilm reactors will be briefly discussed. Much of the current MBR research effort is directed toward municipal wastewater applications; however, substantial commonalities exist with respect to industrial wastewater application and where possible, reference is made to the specific aspects of the technology when applied to the treatment of industrial wastewater.

## 36.2 OVERVIEW OF MEMBRANE BIOREACTOR OPERATION

In wastewater treatment systems, the objective is to remove the maximum amount of pollutant at the minimum hydraulic residence time and with minimal production of biomass. Continuous reactors for biological wastewater treatment invariably employ cell recycle to elevate the biomass concentration and thus the productivity. The dominant wastewater treatment process in use today is the activated sludge process and its many variants. The MBR is essentially a variation of the AS process, whereby the sedimentation (secondary clarifier tank) is replaced by a membrane separation step to retain biomass and particulates in the bioreactor. Depending on the nature of the wastewater, the MBR may be configured with a single aeration tank or with separate aerated/unaerated tanks, with appropriate recycle systems. Membrane filtration occurs either within the bioreactor (submerged process) or externally through recirculation (external or sidestream process). Figure 36.1 outlines

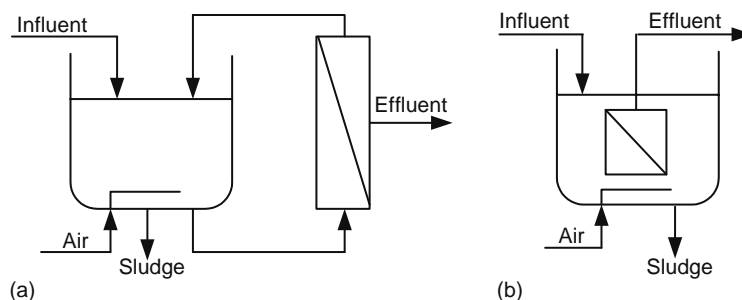


FIGURE 36.1 Schematic layout of (a) external MBR and (b) submerged membrane bioreactor.

schematically the two configurations. The membranes are generally UF or MF, which retain biomass and solids while allowing the water and nondegraded solute species to pass through the membrane. Although inorganic (ceramic) membranes have been used in some applications, capital cost considerations have favored the adoption of polymeric membranes in most MBRs to date.

In the external MBR process, an ultrafiltration or microfiltration membrane module in hollow fiber configuration is employed. In such a system, the driving force for mass transfer is the pressure created by the high cross-flow velocity (typically 2–4 m s<sup>-1</sup>). The membranes are backwashed systematically to remove solids and cleaned chemically at periodic intervals. Although the external MBR is no longer the dominant configuration, principally due to its high energy requirement, the system has some advantages compared to the submerged system, namely, higher permeate fluxes and ease of retrofit to existing biological treatment processes.

The development of the submerged MBR (sometimes known as the integrated MBR) arose out of the need to reduce the energy requirements and is now the dominant configuration in commercial use, particularly for municipal treatment applications. Membranes can be arranged in either hollow fiber (HF) or plate and frame (PF) configuration. In both cases the membranes are mounted in cassettes or modules comprising membranes, support structures, and associated flow connections. Coarse bubble aeration is used to scour the membrane, as a fouling control measure, whilst simultaneously facilitating oxygen mass transfer to the liquid. This system does not offer very high oxygen transfer efficiencies, but the rising bubbles provide a turbulent cross-flow velocity (typically 0.1–0.3 m s<sup>-1</sup>) over the surface of the membrane [7].

A direct comparison between the submerged MBR and external (sidestream) MBR has indicated that submerged MBR has an inherently lower fouling propensity as a result of the slug-flow hydrodynamic regime associated with the coarse bubble aeration [8].

A number of proprietary MBR processes are on the market, the majority of which are based on PF configurations, such as Kubota, or HF membranes, such as Zenon.

The Zenon ZeeWeed MBR process uses a submerged hollow fiber unit mounted vertically. A centrifugal pump is used to create negative pressure on the permeate side and wastewater is drawn into the lumen. For stable operation average fluxes in the region of 20 L m<sup>-2</sup> h<sup>-1</sup> would be typical under a driving transmembrane pressure of 0.2–0.5 bar [9]. Fouling control is provided by coarse bubble aeration, periodic backflushing, and occasional chemical cleaning of the membranes. Fine bubble aerators are required to supply the balance of oxygen. And MLSS concentrations of 10–15 kg m<sup>-3</sup> are typical [10].

The Kubota MBR uses a flat-sheet membrane made of polyolefin with a nonwoven cloth base giving a nominal pore size of 0.4 mm. Each membrane cartridge consists of solid acrylonitrile butadiene styrene support plate with a spacer layer between it and flat-sheet membrane on both sides. Permeate is drawn through the membrane from the bulk fluid by a partial vacuum applied within the membrane plate matrix while retaining the solids in the reactor. The Kubota system operates by gravity, with a head of 1–1.5 m above the membranes sufficient to drive permeate through the membranes. Compressed air is introduced through a distribution manifold at the base of the membrane module. The MLSS is typically maintained within the range of 12–18 kg m<sup>-3</sup> [7].

In addition to the Zenon and Kubota processes, there are several other MBR products on the market from companies such as Mitsubishi Rayon, US Filter, GE Ionics, and Brightwater Engineering. Figure 36.2 shows the MEMBRIGHT process from Brightwater Engineering.

## 36.3 MEMBRANE BIOREACTOR PERFORMANCE

### 36.3.1 MUNICIPAL WASTEWATER CARBONACEOUS REMOVAL

Stephenson et al. [11] conducted a comprehensive review of MBR performance drawing on published data for installations ranging from laboratory scale to full commercial scale, and for a variety of process variants. For the treatment of municipal wastewater, volumetric loading rates ranged between 0.45–3.2 kg COD m<sup>-3</sup> day<sup>-1</sup> and 0.05–0.66 kg BOD m<sup>-3</sup> day<sup>-1</sup> with maximum reported wastewater strengths of 256 BOD<sub>5</sub> mg L<sup>-1</sup> and 900 COD mg L<sup>-1</sup>. Steady-state effluent concentrations were typically <10 BOD<sub>5</sub> mg L<sup>-1</sup> and 40 COD mg L<sup>-1</sup> corresponding to removal efficiencies of 95%–99%. Most MBRs treating municipal wastewater were operated at HRTs between 4 and 8 h. No discernable trend was evident with respect to the effect of HRT on performance. It was noted that the performance was dependent on SRT up to values of 20 days, beyond which no trend was evident. Gander et al. [6] compared the performance of MBRs treating municipal wastewater with the performance of several biological treatment processes. For a given strength of wastewater, organic loading rates in MBR processes are generally higher than that achieved in trickling filters, CAS process and the sequencing batch reactor, this can be attributed to shorter HRT utilized in the MBR. Removal efficiencies for the MBR tend to be higher than the trickling filter (65%–90%), conventional AS process (85%–95%), and sequencing batch reactors (85%–95%). However, to make such quantitative comparisons between effluent quality from the MBR and that from alternative biological treatment processes,

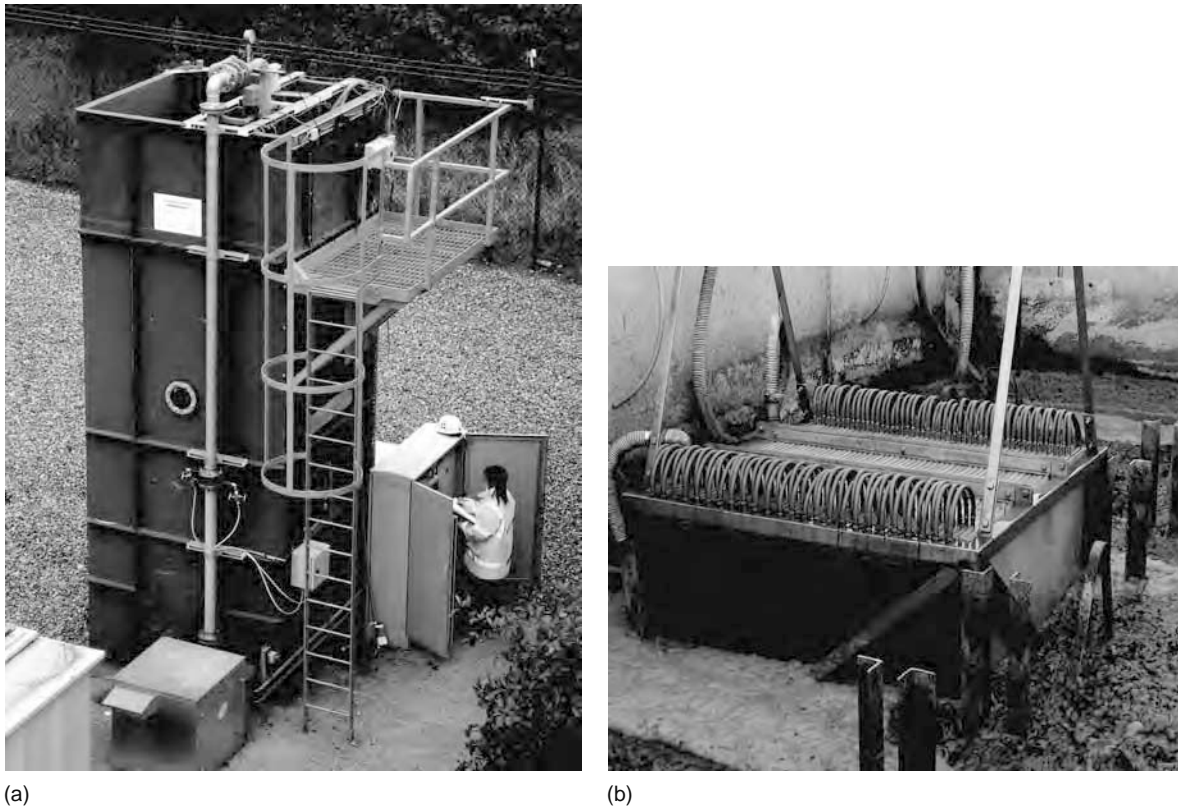


**FIGURE 36.2** (See color insert following page 588.) The MEMBRIGHT process from Brightwater Engineering (United Kingdom) showing (a) a typical plant and (b) the membrane module.

it is important to note that the superior effluent quality produced from MBR processes is as a result of both biological conversion of wastewater constituents combined with particulate retention by the membrane. In fact, the upper limit on permeate flux ultimately limits the loading rate of the MBR and significantly higher organic loading rates are achievable in the complete-mix AS and the BAF [6]. Objective comparisons between MBR and alternative processes are complicated by the sheer variety of reactor designs and size, membrane characteristics, operating conditions, and wastewater characteristics. Notwithstanding this difficulty, it is apparent that effluent quality and removal efficiency in MBRs, at least in terms of chemical oxygen demand and biological oxygen demand (COD/BOD), generally exceed that of all the conventional AS and trickling filter processes.

### 36.3.2 NUTRIENT REMOVAL

#### 36.3.2.1 Nitrification

Nitrification is a microbial process by which reduced nitrogen compounds (primarily ammonia) are sequentially oxidized to nitrite and nitrate. Nitrification is primarily accomplished by aerobic autotrophic bacteria that can build organic molecules using energy obtained from inorganic sources, in this case ammonia or nitrite. Various groups of heterotrophic bacteria and fungi can also carry out nitrification, although at a slower rate than autotrophic organisms. Nitrifying organisms are sensitive to a wide range of organic and inorganic compounds and at concentrations well below those concentrations that would affect aerobic heterotrophic organisms. The specific rate of nitrification in MBRs has been shown to be significantly higher than an equivalent activated sludge process, for example, Zhang et al. [12] achieved an average nitrification rate of  $2.28 \text{ g NH}_4\text{-N kg}^{-1} \text{ MLSS h}^{-1}$  compared to  $0.95 \text{ g NH}_4\text{-N kg}^{-1} \text{ MLSS h}^{-1}$  for CAS. The higher rate believed to be attributable to the enhanced retention of the slow-growing autotrophic bacteria in the MBR and also due to comparatively better mass transfer of nutrients and oxygen into the smaller MBR flocs. However, nitrification rate is sensitive to oxygen limitation and the high biomass concentrations in MBR processes present a challenge to effective and efficient oxygen transfer. Denitrification can be achieved in MBRs either by the use of an anaerobic tank separated from the aerobic tank or the use of intermittent aeration. The denitrifying organisms are predominantly facultative heterotrophs that reduce nitrate ( $\text{NO}_3^-$ ) in the absence of molecular oxygen. The organic content of the wastewater is the energy source for denitrification therefore the anoxic zone should be configured in a manner that ensures adequate carbon sources are available.

### 36.3.2.2 Denitrification

In most conventional WWTPs and MBR plants nitrogen removal is achieved by pre-denitrification [13]. In pre-denitrification systems, the anoxic denitrification tank is typically placed before the aerobic nitrification step. Nitrate is recycled from the aerobic tank to the anoxic zone. Alternative configurations exist but are less common, e.g., intermittent denitrification [13]. The advantages of pre-denitrification are that organic matter available in the anoxic zone improves denitrification rates, hence reducing the required reactor volume. Secondly, the oxidation capacity of nitrate degrades part of the organic matter, hence reducing oxygen demand and achieving savings in aeration requirement. Specific denitrification rates for MBRs are in the region of  $1 \text{ mg NO}_3\text{-N h}^{-1} \text{ g}^{-1} \text{ MLSS}$ .

In post-denitrification systems an anoxic tank is placed downstream of the aeration tank. As most organic matter is removed in the aerated zone, it is necessary to add an external carbon source to the denitrification tank. Kraume et al. [13] have discussed the particular characteristics of the MBR technology that may make post-denitrification a more attractive alternative. Low-denitrification rates in pre-denitrification MBR plants have been attributed to a combination of high-sludge age and a high-oxygen carryover to the anoxic zone from the membrane system. There is some evidence, which reported that overall nitrogen removal rates are higher with post-nitrification MBR processes than with pre-denitrification processes [13]; however, further research is required to confirm this.

### 36.3.2.3 Phosphorus Removal

Phosphorus removal processes can be achieved by two methods: chemical precipitation and biological removal. Current practice with MBR processes favors the precipitation method [14]. Biological phosphorous removal rates of over 99% were reported by Gnriss et al. [14]; however, P concentrations were below  $0.05 \text{ mg L}^{-1}$  (P-total). At higher concentrations ( $4 \text{ mg L}^{-1}$  P-total) removal efficiencies of about 75% are more typical [15]. In a six-stage MBR pilot plant [16], a combination of biological (using an initial anaerobic zone) and chemical (using alum) phosphorous removal was used to consistently achieve total phosphate concentrations of  $<0.1 \text{ mg L}^{-1}$ . The use of alum appeared to enhance the filtration characteristics of the sludge and to reduce membrane fouling. It is believed that the alum enhances the coagulation of the colloidal solids [16].

## 36.3.3 BENCHMARKING THE MBR AGAINST THE CAS PROCESS

A limited number of studies have been reported in which the MBR and AS are compared using the same wastewater. A 40 L MBR was compared to an 11 L AS process over an 80 day operating period using synthetic wastewater [17]. SRT values were 30 and 20 days for the MBR and AS, respectively, and all other conditions were identical, including the HRT which was maintained at 6 h. The MBR consisted of a ceramic tubular external membrane. Removal efficiencies for soluble components in the MBR were higher than the AS, for example, 99.0% vs. 94.5% for COD; 99.2% vs. 98.9% for ammonium; and 96.6% vs. 88.5% for total phosphorous, respectively. Interestingly, the sludge yield was lower in the CAS than the MBR the reason for which was attributed, in part, to the presence of certain types of protozoa, particularly ciliates, detected in the CAS sludge but not the MBR. Ng and Hermanowicz [18] investigated the performance and biomass characteristics of a membrane bioreactor (MBR) and a completely mixed activated sludge (CMAS) treating a synthetic wastewater. Both systems were operated at short SRT ranging from 0.25 to 5 days and hydraulic retention times of 3 and 6 h. Despite SRT values of as low as 0.25 days, the MBR removal efficiencies ranged from 97.3% to 98.4% (TCOD) in the MBR, compared to 77.5%–93.8% (TCOD) and 94.1%–97.0% (SCOD) in the CMAS. The superior performance of the MBR does not appear to be a result of higher biomass concentration. Instead, after analyzing the floc size and structure in both processes, it was speculated that improved mass transfer to the bacteria in the MBR contributed significantly to performance gain. The MBR biomass was composed of small, weak, and uniform-sized flocs with large mass of short filamentous organisms and a significant fraction of dispersed microorganisms. In contrast, the CAS sludge was composed of large flocs with filamentous organisms as a backbone. The yield coefficients for the MBR and CMAS system were  $0.42$  and  $0.35 \text{ g VSS g}^{-1} \text{ COD}$ , respectively. These were close to the theoretical maximum yield because at the relatively short SRT in this study, conditions favored biosynthesis rather than maintenance metabolism. Huang [19] compared variations in the SRT on the performances of the AS and MBR. COD removal remained constant at 90% in MBR but in the AS was 70%–80% with a slight decrease when the SRT was reduced to 5 to 10 days.

## 36.3.4 MICROPOLLUTANT REMOVAL FROM MUNICIPAL WASTEWATER

Micropollutant degrading bacteria generally have a low-specific growth rate and therefore the extended SRT in MBRs should favor the enrichment and growth of specialist bacteria with the ability to assimilate and mineralize specific pollutants. However, when making comparisons between processes, consideration must be given to the possibility that improved removal rates from the MBR may arise from the retention of such pollutants by adsorption on biomass particles rather than by improved biodegradation.

Joss et al. [20] studied the removal of estrogens in three municipal wastewater treatment processes (CAS, MBR, and fixed film). Specific-degradation rates for estrone and estradiol were higher in the MBR sludge than in the CAS sludge by a factor 2–3. It was suggested that the sludge age (30 days compared to 11 days, respectively) and floc size (10–100  $\mu\text{m}$  compared to 100–500  $\mu\text{m}$ , respectively) contributed to the difference in activity between the two processes. Recent study [21] on micropollutant removal was inconclusive on the relative merits of the MBR over CAS. Removal efficiencies ranging from complete (ibuprofen) to virtually zero (carbamazepine). Another recent study examined the potential of the MBR for water reuse applications [2], and showed high removal efficiencies for *Cryptosporidium* and coliphage. With respect to endocrine disruptors, no significant differences were observed between the MBR and the CAS processes [2]. It is evident that further research is needed on the detailed mechanisms of micropollutant removal in MBRs before firm conclusions on performance can be drawn.

### 36.3.5 CARBONACEOUS REMOVAL FROM INDUSTRIAL WASTEWATER

Table 36.1 summarizes the characteristics and performance data from selected published studies of MBRs applied to the treatment of industrial wastewater. Industrial wastewater is typically of a higher strength than municipal wastewater and this is reflected in the higher loading rates, typically in the range 2–16  $\text{kg COD m}^{-3} \text{ day}^{-1}$  for pilot and full-scale installations. COD removal efficiencies are typically greater than 90% and frequently greater than 95% for the reported studies. Corresponding HRT values were in the range of 45–240 h for pilot-scale studies and 36–54 h for the full-scale studies. HRT values are significantly longer than those of municipal applications reflecting the higher organic loading rates and the nature of the wastewater, frequently including oil and grease constituents. Sludge yield are generally quite low, perhaps as a result of the generally high MLSS values and long SRTs.

### 36.3.6 REMOVAL OF SPECIFIC ORGANIC POLLUTANTS FROM INDUSTRIAL WASTEWATER

Reemtsma et al. [27] performed a detailed analysis of the removal efficiencies of a variety of compounds from a tannery wastewater using a commercial scale MBR. The overall removal of aromatic compounds as determined by UV absorbance ( $\text{ABS}_{254}$ ) was 84%, a value significantly higher than that achieved from conventional treatment under similar conditions [28]. However, the removal efficiency of selected polar sulfur-containing aromatic pollutants of borderline biodegradability did not show significantly better results than the CAS process. Naphthalene sulfonates are used as dispersants and are commonly encountered as constituents in industrial wastewater. Reemtsma [27] reported 99% removal of naphthalene monosulfonates and 40% removal of naphthalene disulfonates. Higher removal efficiencies of these compounds have been reported for CAS and despite sufficient time for adaptation in the MBR and a sufficiently low concentration, no explanation for the poor removal of disulfonates was clear. Benzothiazoles are used as fungicides and as vulcanizing agents in rubber production. An average of 87% removal for all compounds in this category was observed in the MBR. However, the removal efficiency varied strongly among compounds in this group. These results indicated comparable, but not significantly better reports for the CAS system. Scholz et al. [23] investigated an oily wastewater-containing surfactant in a laboratory MBR with a typical retention time of 13.5 h. Overall hydrocarbon removal efficiency was >99%; however, this figure refers to the differences between influent and effluent concentrations, and does not take into account significant partitioning of oil and grease into the sludge. Analysis of the biodegradation efficiencies of selected aliphatics (C10–C24) showed that all fractions were degraded at comparable efficiency once sufficient time was allowed for bacterial adaptation. Zaloum et al. [25] reported degradation of an oily wastewater using an external UF MBR. Despite shock loads, excellent removal rates of oil and grease were obtained and total phenol removal was 96%. Morrison et al. [29] studied the removal of methyl tertiary-butyl ether (MTBE) in a 5.9 L MBR equipped with an external ceramic membrane. With a HRT of 1 h and an influent concentration of 5  $\text{mg L}^{-1}$ , removal efficiencies averaged 99.98%. Although it took 150 days to reach steady state, removal efficiencies were 76% within a few days of start-up.

The complex composition of industrial wastewater and the limited number of studies published to date do not allow a definitive conclusion to be drawn on the comparison between the MBR and conventional processes.

### 36.3.7 ENERGY CONSUMPTION

Energy costs account for a significant portion of the life-cycle costs of the MBR, whether sidestream or submerged [10]. Energy is required for pumping feed water, recycling of retentate, aeration and, in certain process variants, permeate suction. Substantial differences in energy consumption exist between submerged and external membrane configurations. External membranes require a high cross-flow velocity (2–4  $\text{m s}^{-1}$ ) and energy requirements in these processes is dominated by the energy associated with pumping. Energy consumption values in the range 0.045–140  $\text{kW h m}^{-3}$  product are reported by Gander et al. [6] for a variety of external processes. Typical values can be expected to be in the midpoint of the range. The wide range in values is a function of several variables including the membrane characteristics, packing density, and recycle flow rate. Aeration requirements contribute about 20% to the overall energy requirements of the external MBR processes. Typically fine bubble aerators are used which have standard oxygen transfer efficiency (SOTE) values of 25%–40% at 5 m depth. In the

**TABLE 36.1**  
**Characteristics and Performance Data from Selected Published Studies of MBRs Applied to the Treatment of Industrial Wastewater**

References	Membrane Type	Wastewater	Volume (m <sup>3</sup> )	HRT (h)	SRT (day)	Organic Loading (kg m <sup>-3</sup> day <sup>-1</sup> )	Influent COD (mg L <sup>-1</sup> )	Effluent COD (mg L <sup>-1</sup> )	Removal Efficiency	MLSS (kg m <sup>-3</sup> )	Sludge Yield (kg kg <sup>-1</sup> COD Removed)	Membrane Flux (L m <sup>-2</sup> h <sup>-1</sup> )
Laboratory scale												
[22]	Submerged HF 0.03 μm pore	Kraft pulp mill	0.004	19	20	6.45	5,120	150	97	3	NA	NA
[23]	External HF with cross-flow of 2.2 m s <sup>-1</sup> , 15 kDa cutoff (UF)	Oil water emulsion containing surfactants	0.011	13.5	NA	8.6–12.9	7,877	243	97	15–25	0.09–0.11	NA
[24]	Tubular UF with cross-flow velocity of 4.5 m s <sup>-1</sup>	Brewery Chemical (di-methyl-terephthalate production) Pharma (production of hormones)	1 1 1	102 140 130	— — —	16 9 3	68,000 52,500 17,000	1,350 6,000 300	98 89 98	38 20 20	<0.1 <0.05 <0.1	>120 >120 >150
[25]	Ultrafiltration, external	Metal mill waste	1.95	240	50	2.5–4.9	2,943	1,395	99.6	5–15	NA	37
[26]	Tubular UF, external	Oily wastewater	3.78	45	100	2.2	5,937	417	93	12.4	0.042	NA
[26]	Tubular UF, external	Oily wastewater	287	54	31	6.3	14,184	799	94	28.7	0.16	63.6
[27]	Tubular UF with cross-flow of 5.6 m s <sup>-1</sup>	Tannery with organic polar micropollutants	680	36	56	2.0	2,990	180	94	1020	NA	130

submerged MBR systems aeration normally contributes  $>70\%$  to the overall energy cost. Coarse bubble aerators provide the dual function of scouring the membrane and providing oxygen to the microorganisms. However, coarse bubble aerators are less efficient than fine bubble aerators with SOTE values of 19%–37% at 5 m depth [6].

### 36.4 MECHANISMS CONTRIBUTING TO MBR PERFORMANCE

Evaluation of MBR process performance is quantified by two principal indicators: (i) effluent quality, incorporating carbonaceous and nutrient removal rate; and (ii) sludge characteristics incorporating yield and treatability. Although each indicator is ultimately determined by a combination of membrane filtration and a broad range of biological reactions, analysis of the process must be built on an integrated framework that incorporates each and every one of the interrelated factors influencing performance. Figure 36.3 schematically outlines the various interrelated factors determining process performance in MBRs. The current understanding of how these interrelated factors impact on MBR performance is discussed in the following sections.

#### 36.4.1 MEMBRANE FOULING

Perhaps the foremost problem that has limited the performance and consequent widespread adoption of the MBR process is membrane fouling. Fouling is a term that encompasses several mechanisms contributing to increased mass transfer resistance across the membrane. It is caused by the accumulation of biomass and particulate matter on the membrane surface, adhesion of macromolecules on the surface, and clogging of the membrane pores. The principal organic foulants in MBR processes are biomass solids, aggregated colloidal material, and extracellular polymeric substances (EPSs). Inorganic foulants include scalants such as calcium carbonate [7]. The relative contribution of different foulants to mass transfer resistance varies widely from study-to-study depending on the characteristics of the wastewater, biomass, and membrane and also the influence of chemical cleaning [30]. A recent study [31] used statistical analysis to investigate the contribution of several biomass characteristics, permeate flux, and the aeration velocity on the fouling rate in a pilot-scale submerged HF MBR. Only the permeate flux, the solid concentration, the carbohydrate concentration in the EPS, and the aeration velocity affected the fouling rate.

The aggregation rate of colloidal and particulate materials is dependent on the permeation rate, hydrodynamics, and surface forces between the membrane and colloid material, therefore fouling rates are system dependent. However, certain broad trends are evident with respect to fouling. Below a certain permeation rate the TMP varies linearly with flux and above this transition flux, a sharp increase in TMP is observed concomitant with a permeate flux decline. A time-dependent flux decline is also

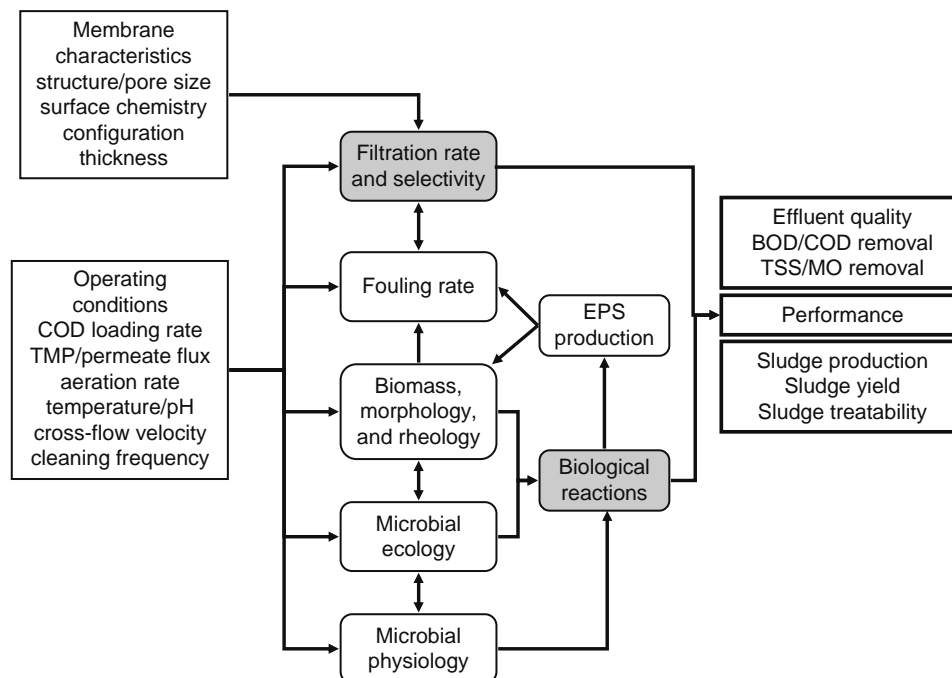


**FIGURE 36.3** Schematic interrelationship between factors that determine process performance in MBRs. Wastewater characteristics are implicit in this outline. The term “biological reactions” includes exogenous and endogenous metabolism, extracellular enzymatic activity, and product formation (EPS).

observed. The critical flux hypothesis is that upon start-up, there exists a flux below which a time-dependent flux decline does not occur, while fouling takes place above this critical value [32]. It is known that the critical flux in MBRs depends on hydrodynamics, particle size, and membrane surface characteristics. Typically MBRs are operated below the critical flux to minimize fouling. However, the validity of the critical flux concept in MBR operation has been questioned recently since after prolonged operation irreversible fouling has been observed at subcritical fluxes [33].

The importance of biopolymer deposition on the membrane has been highlighted by Chu and Li [34] who noted that such material may accelerate bacterial attachment to the membrane in addition to its contribution to fouling resistance. The formation of a slime layer on the membrane, comprising an EPS matrix with embedded bacteria, may be analogous to a biofilm, the significance of which is the difficulty of its removal by nonchemical methods. The question of whether biofilm formation plays a significant role in MBRs is yet to be addressed. Indeed, a comprehensive model of fouling in MBRs is not yet available.

Because fouling rate is highly dependent on the flux, it is essential to optimize the TMP to achieve the best performance without exceeding the critical flux. Clearly the value of the critical flux is dependent on the system design, operating conditions, and wastewater characteristics. Gander et al. [6] report that for many submerged PF MBRs operating at TMP of <0.4 bar, the critical flux is not exceeded. In addition to flux control, several defouling strategies are employed. Coarse bubble aeration promotes the scouring of the membrane to suppress the fouling layer. In some systems (FP) the scouring action is accelerated under zero-flux conditions in an operation known as relaxation. For certain types of membrane (HF) periodic backflushing is employed whereby permeate flow is reversed for a short time, typically for 30–60 s every 15 min. High-frequency backpulsing (typically 0.1–2 Hz) is a very effective defouling approach but, at present, is only suitable for ceramic membranes [30]. Chemical cleaning is necessary in all MBRs after a certain time to remove biopolymers and colloidal residues from the membrane surface. The cleaning frequency can vary from up to 30 days for effluent treatment to every 6 months for water treatment applications [35]. The duration of chemical cleaning is typically in the region of 1–2 h [9]. The intensity or frequency by which these fouling amelioration strategies need to be applied will impact on the economic performance of the process. Inevitably the antifouling strategy will depend on the particular MBR configuration: for example, the Zenon system uses periodic backflushing and coarse bubble aeration scouring, while the Kubota process uses a combination of relaxation and coarse bubble aeration scouring.

### 36.4.2 BIOMASS MORPHOLOGY AND RHEOLOGY

The importance of biomass morphology on process performance relates to its impact on membrane fouling, volumetric reaction rate, adsorption of organic and inorganic particulate matter to flocs, and the treatability of sludge. It is generally acknowledged that biomass morphology in the MBR is markedly different to that of activated sludge in terms of floc size distribution, fraction of dispersed bacteria, and quantity and composition of EPS [36].

The floc, a heterogeneous aggregate of microorganisms and EPS, is the dominant component of the biomass in MBRs, as it is in an activated sludge. EPS is used as a general term for organic macromolecules such as polysaccharides, proteins, nucleic acids, lipids, and other polymeric compounds, which have been found to occur in microbial flocs and biofilms [37]. However, it must be stressed that a significant fraction of the total EPS present exists as soluble components in the bulk liquid. Although the mechanism of flocculation is poorly understood, it is generally accepted that EPSs are central to the aggregation of dispersed bacteria into floc particles. It is also known that hydrodynamic forces including turbulent shear stress contribute to floc size distribution, a mechanism of particular relevance to external MBRs with high cross-flow velocities [17]. Both small floc size distributions and a high fraction of dispersed microorganisms are factors generally regarded as advantageous from the perspective of soluble pollutant degradation. It is believed that mass transfer limitations in larger flocs may limit the reaction rate. This hypothesis was confirmed by Joss et al. [20] who used a mass transfer model to investigate differences between MBR and CAS processes for removal of estrogens from municipal wastewater. CAS floc sizes were in the range of 100–500  $\mu\text{m}$ , while MBR flocs were in the range of 10–100  $\mu\text{m}$ . Activity differences of a factor 3–4, favoring the MBR were found to be attributable to mass transfer limitations in the CAS flocs. It should be noted that mass transfer limitations are dependent not only on floc size but also on the specific reaction rate and on the substrate concentration in the bulk liquid. Nevertheless, high-volumetric removal rates can be expected when the biomass consists of a high fraction of dispersed bacteria and the floc size distribution is small. Indeed, several studies on MBR morphology have reported such a biomass composition. Zhang et al. [12] reported that samples from several MBRs showed the floc size distribution to be in the range of 7–40  $\mu\text{m}$  compared to 70–300  $\mu\text{m}$  from CAS. Witzig et al. [36] analyzed floc size and structures in MBR samples, over a prolonged period of operation. Samples of the sludge taken at regular intervals over the 351 day operation were analyzed and it was confirmed that the relative fraction of flocs to dispersed biomass was low compared to what would be expected in conventional AS.

A widely used parameter in the quantitative analysis of the oxygen transfer rate in wastewater treatment bioreactors is the dimensionless factor,  $\alpha$ , defined by the following equation:

$$\alpha = \frac{k_L a_{\text{sludge}}}{k_L a_{\text{water}}} \quad (36.1)$$

where  $k_1 a$  is the volumetric oxygen transfer coefficient. Several factors contribute to the value of  $\alpha$ ; MLSS concentration, loading rate, surfactant concentrations, and air flow rates, but it is primarily determined by the high apparent sludge viscosity, attributable to flocs, filamentous organisms, and EPS. In a survey of several MBRs, Drews and Kraume [38] reported that  $\alpha$  decreases from about 0.75 to 0.20 as the biomass concentration increases from 5 to 20 kg m<sup>-3</sup>.

The impact of biomass concentration on energy costs is substantial and clearly an optimum biomass concentration exists that maximizes volumetric reaction rate while minimizing the aeration costs. Most full-scale MBR plants aim to operate at a biomass concentration of between 10 and 15 g L<sup>-1</sup> [38]. The average  $\alpha$  value at typical MBR for municipal wastewater with an MLSS concentration of 12 kg m<sup>-3</sup> MLSS for municipal MBRs is about 0.6 [39]. A design value for  $\alpha$  of 0.5 has been recommended [40].

Biomass morphology also impacts on sludge treatability. Ng and Hermanowitz [41] showed that MBR sludge was more difficult to dewater than that from CAS operated under the same conditions. Values of the sludge resistance to filtration (SRF) in the MBR were, in fact, in order of magnitude higher than in the CAS (typically  $1 \times 10^{16}$  m kg<sup>-1</sup>).

### 36.4.3 MICROBIAL ECOLOGY

Microbial ecology in MBRs is an area that has received limited attention until relatively recently and yet, like morphology, substantial differences exist between MBR and AS processes. The poor understanding of microbial ecology in MBRs has limited full exploitation of the biological resource available in MBRs and indeed in biotreatment processes in general. Techniques such as fluorescence in situ hybridization (FISH) with rRNA-targeted oligonucleotide probes and PCR-DGGE have revolutionized microbial ecology research and are only recently being applied to MBRs. Klatt and LaPara [42] analyzed bacterial community dynamics in laboratory scale MBR inoculated with sludge from a conventional AS. It was observed that substantial shift in microbial activity and community structure occurred during the first few days of MBR operation and even after the MBR performance stabilized with respect to pollutant removal, the bacterial community continued to adapt its physiology possibly in a manner that optimized the performance. However, establishment of relationships between community dynamics and process performance requires significant further research. Witzig et al. [36] conducted phylogenetic analysis using FISH and revealed that the subclass  $\beta$ -proteobacteria constitute the dominant group of bacteria within the sludge community of a full-scale MBR. While this result was not unexpected when compared to conventional AS process, it is interesting to note that nitrifying activity in the MBR was not associated with *Nitrosomonas* and *Nitrosospira*, common constituent of conventional AS process. It is clear that microbial ecology differs significantly from the AS process.

### 36.4.4 MICROBIAL PHYSIOLOGY

In any wastewater treatment system, a fraction of the biomass can be categorized as (a) viable cells that assimilate substrate and are capable of division, (b) dormant cells, (c) nonviable cells that can use substrate but cannot grow, and (d) dead cells that have no activity, but still possess a cell wall [43]. Reported biomass concentrations (generally expressed as MLSS) in biotreatment processes may be misleading since they do not indicate the physiological state of the biomass. FISH with rRNA-targeted oligonucleotide probes is now being used to quantitatively investigate the population dynamics and viability of the biomass. Witzig et al. [36] used this approach to determine the overall physiological state of sludge from the MBR. The percentage of FISH detectable cells remained reasonably constant over the entire operating duration of 182–351 days. This is a significant result because it shows the stability of the sludge over long periods despite changes in environmental conditions in the MBR over this period. The percentage of cells with low rRNA molecules remained in excess of 50%. While this indicates domination of cells with low metabolic activity, it does not exclude the possibility that such cells participate in some metabolic transformation processes and contribute to the low observed yield in the MBR process. Hasar et al. [44] estimated the biomass viability in a submerged MBR to be in the region of 50%.

### 36.4.5 FACTORS CONTRIBUTING TO BIOMASS YIELD

Treatment and disposal of sludge from wastewater treatment plants has been estimated to account for about half of the total cost of wastewater treatment [45]. For this reason, the MBR has been receiving significant attention as a viable wastewater treatment technology in which the biomass yield can be expected to be significantly lower than conventional processes if operating conditions are appropriate. Indeed, several studies have demonstrated that zero net sludge production is attainable in MBRs provided the COD loading rate is sufficiently low. For example, Muller et al. [46] operated a full-scale external HF MBR for 300 days with a COD loading rate between 0.9 and 2.0 g COD L<sup>-1</sup> day<sup>-1</sup>. The observed sludge yield is approaching zero; however, this was achieved under such high biomass concentrations (MLSS of 45–50 g L<sup>-1</sup>) that oxygen transfer became limiting. Similarly, Benitez et al. [47] reported a net yield of zero in a laboratory scale external HF MBR over a prolonged period, but again the biomass concentration was relatively high (25 g L<sup>-1</sup>).

The microbial biomass yield coefficient from a carbon energy substrate mixture is defined as the dry weight of microbial biomass produced as a result of the utilization of unit weight of the carbon energy substrate mixture. Yield coefficients vary

remarkably depending on the environmental conditions imposed on the culture system and on the variability of those conditions. In practice, yield coefficient minimization is generally achieved by the exploitation of two separate mechanisms: (a) uncoupling of growth from respiration and (b) enhancement and of the death/lysis/cryptic growth cycle. The ability of the MBR to retain biomass at extended SRTs together with the achievement of relatively high biomass concentrations is advantageous as far as yield coefficient minimization is concerned.

### 36.4.5.1 Maintenance

Anabolic pathways synthesize the molecules (e.g., proteins, nucleic acids, lipids, and carbohydrates) required by the cell with the input of energy. Catabolic pathways break down large organic molecules, with the release of energy, into smaller constituents, which in turn serve as precursors for the biosynthesis via the anabolic reactions. Pirt [48] proposed that a portion of the total carbon energy source is consumed for anabolism and the remaining portion is utilized for maintenance. Maintenance is the collection of cell energetic requirements for survival or for preservation of a certain cell state, which are not directly related to or coupled with the synthesis of more cells. When an exogenous energy supply exists, a portion is diverted intracellularly to meet maintenance requirements and the remainder is used for synthesis. However, if the energy supplied equals the maintenance requirement, the cell mass does not increase, i.e., the observed yield is zero. When the energy supplied is less than the maintenance requirement, the difference will be met by utilization of internal energy supplies, i.e., endogenous metabolism. These concepts are exploited for yield coefficient minimization by operating the MBR in a manner that ensures that pollutant compounds are utilized preferentially for nongrowth cellular functions instead of biosynthesis. If all the substrate was utilized exclusively for anabolism, the net yield would be at its maximum, termed the true growth yield,  $Y_G$ . Substrate utilization for maintenance  $q_M$  is generally assumed to be constant. The relationship between the observed yield ( $Y_S$ ) and the true yield can be described by the following equation [2]:

$$\frac{1}{Y_S} = \frac{q_M}{\mu} + \frac{1}{Y_G} \quad (36.2)$$

Pirt's energy allocation model, in the form of Equation 36.2, is somewhat restricted for application in wastewater treatment. The value of  $\mu$ , the specific growth rate, is difficult to determine due to the variety of physiological states in the biomass, the variety of microbial species, each with different growth rates and substrate affinities.

Pirt's formulation can also be written in terms of the utilization rate of the substrate ( $r_S$ ), being the sum of that utilized by anabolism and that utilized by the biomass for maintenance requirements:

$$-r_S = \frac{-1}{Y_G} r_X - q_M X \quad (36.3)$$

$$r_X = Y_G(r_S - q_M X) \quad (36.4)$$

If it is assumed that  $Y_G$  and  $q_M$  are constant for a given system, it becomes apparent that the rate of biomass synthesis decreases as the biomass concentration increases. It is, therefore, possible to achieve a state in which the amount of substrate provided is diverted entirely to the maintenance demand if the biomass concentration is sufficiently high and consequently a zero sludge yield is achievable. However, high biomass concentrations may not always be desirable from an operational perspective due to difficulties in meeting oxygen demand and the impact on the membrane fouling rate.

### 36.4.5.2 Lysis-Cryptic Growth

Prolonged starvation forces a cell to deplete its endogenous energy supplies until vital functions (e.g., growth, replication, and osmosis) cease. The cell wall ultimately disintegrates with the release of internal components, a process known as lysis. It is important to note that starvation in itself does not initiate lysis [49], but the exact mechanisms for lysis are not yet clear. The products of cell lysis provide a substrate for microbial metabolism, because this autochthonous substrate cannot be distinguished from the growth on the original substrate, it is therefore termed as cryptic growth. Since a portion of the carbon is liberated by respiration, the process of lysis-cryptic growth contributes to overall yield reduction. Indeed, this has been exploited in treatment processes by the use of physical or chemical methods to promote a degree of cell lysis. For example, ozonation has been successfully employed in some processes [50,51].

### 36.4.5.3 Predation

It is becoming apparent that the exploitation of higher organisms such as protozoa, metazoa, and rotifers that predate on the bacteria and particulate organics is a potentially effective method for sludge minimization [45].

Protozoa are motile eukaryotes, the majority of which are aerobic heterotrophs. They are typically an order of magnitude larger than bacteria and often consume bacteria as an energy source. As far as MBRs are concerned it seems that protozoa and metazoa may not be as dominant as in CAS processes. Witzig et al. [36] analyzed samples from an MBR process and found that, with the exception of short periods after changes in operating conditions, protozoa and metazoa were rarely present in the sludge community.

Rotifiers are aerobic heterotrophic animal eukaryotes. They are very effective in consuming both dispersed and flocculating bacteria, and small particles of organic matter. Worms are the largest organisms observed in conventional AS and may have the potential to act as significant contributors to sludge reduction in MBRs. However, the necessary understanding of the connection between worm growth and the operational characteristics of wastewater treatment systems is still lacking [45].

### 36.4.6 EXTRACELLULAR MICROBIAL ACTIVITY

The breakdown and utilization of biopolymeric particulate matter is a common occurrence in wastewater treatment processes. Such material is defined as intact bacterial cell mass, particulate debris resulting from cell lysis and EPS. Bacteria, the major microbial component in most biotreatment processes, are not able to directly assimilate biopolymeric particulate material. The particulates must first be broken down into soluble poly- or monomeric molecules. Cicec et al. [17] conducted a comparison of extracellular enzymatic activity between AS and MBR treating wastewater with identical composition. A comprehensive enzymatic analysis of both soluble and particulate fractions of the mixed liquors in each reactor revealed several informative findings; overall activity was consistently higher in the MBR than in the AS; both systems produced enzymes specific for the degradation of the wastewater constituents only; no enzymes were detected in the MBR effluent, while considerable amounts were detected in the AS effluent; the enzyme concentration in the MBR soluble phase was higher than that in the AS. These findings suggest that the MBR is superior to the AS process in retaining both aqueous phase and particulate phase enzymes, a result that further confirms the performance potential of the MBR.

## 36.5 PROCESS ECONOMICS

Côté et al. [10] undertook a detailed economic analysis to compare the life cycle costs of the MBR to both the conventional activated sludge process and the CAS with tertiary filtration (AS-TF). A range of plant sizes were considered, treating between 3,800 and 76,000 m<sup>3</sup> day<sup>-1</sup> of sewage. The MBR consisted of a Zenon system with an average flux of 20 L m<sup>2</sup> day<sup>-1</sup>. Capital costs included the land costs in addition to the process. For the MBR, capital costs were lower than the CAS options on account of the savings associated with eliminating secondary clarifiers, reduced aeration tank volume, reduced footprint, all of which offset the additional cost of the membrane system and fine screen. Total operation and maintenance (O&M) costs were calculated to include labor, materials (including membrane replacement), energy, and chemicals (e.g., membrane cleaning). The O&M costs for the MBR were 20%–30% higher than the AS plant and slightly higher than the AS-TF process. Total life cycle costs were generated assuming 20 years of operation, 6% interest rate, 2.5% inflation rate, and an energy cost of \$0.10 kW<sup>-1</sup> h<sup>-1</sup>. The MBR had a life cycle cost of 5%–20% higher than CAS increasing with plant size, but was similar to the cost of the CAS-TF. Based on these calculations, it is evident that, at present, MBRs are best suited to small- to medium-size applications. Future developments in MBR technology will rely on methods that reduce the operating cost. Recent innovations have seen improvement in aeration efficiency by methods such as intermittent aeration or stacked membrane modules configurations.

## 36.6 NOVEL MEMBRANE BIOREACTORS: MEMBRANE ATTACHED BIOFILMS

The chapter focuses on membrane bioreactors where a UF or MF membrane is employed for biomass retention and filtration. However, membrane bioreactors where the membrane provides a support for biofilms are an alternative form of membrane bioreactor for wastewater treatment application. Two processes, in particular, the membrane-aerated biofilm reactor (MABR) and the extractive membrane bioreactor (EMB), have seen significant interest in recent years. Figure 36.4 shows these two technologies schematically. The application of biofilms reactors for wastewater treatment systems is advantageous in view of

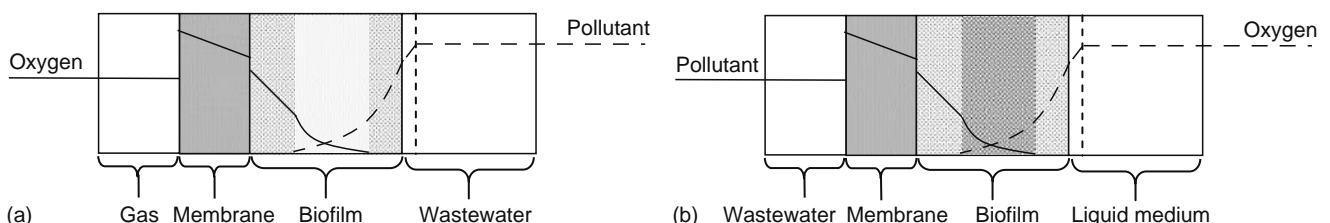


FIGURE 36.4 Schematic diagram of (a) MABR and (b) EMB.

their potentially high volumetric productivity and the ability to completely uncouple SRT from HRT. These reactors are especially useful for slow-growing organisms, which would otherwise be washed out of the system, nitrifying biofilms being a case in point. Biofilm processes are simple, reliable, and stable because natural immobilization allows excellent biomass retention and accumulation without the need for separate solid-separation devices. Conventional biofilm reactors, such as the trickling filter, have traditionally been employed for applications such as nitrification.

In an MABR, first reported in 1978 [52], the biofilm is immobilized on an oxygen permeable membrane, typically in hollow fiber configuration. The membrane lumen is pressurized with oxygen, which diffuses through the membrane into the biofilm where oxidation of pollutants, supplied from the biofilm side of the membrane takes place. In the MABR, the membrane function is solely for oxygen supply as opposed to wastewater filtration. Indeed, dense membranes such as silicone are frequently employed in MABR systems. The MABR has been applied at laboratory scale for the treatment of VOCs [53], and for combined COD removal/nitrification/denitrification [54]. A recent study [55] demonstrated the potential of the concept at pilot scale; however, significant developments are needed, for example, with respect to biofilm thickness control before the commercial potential of the process can be realized [56].

Certain organic constituents in industrial effluents are present in sufficiently high concentrations to inhibit biological growth. The operating principle of the EMB is that organic constituents in the wastewater are selectively transported through a membrane into a compartment in which specialist degrading organism are present. In the EMB wastewater flows in the lumen of hollow fiber membranes and components such as phenol [57], chloronitrobenzene [58], and dichloroaniline [59] are selectively transported through the membranes into biofilms where biodegradation takes place. The EMB process is reviewed by Freitas dos Santos et al. [60].

### 36.7 CONCLUSIONS

There is now a significant body of evidence to demonstrate that the MBR can achieve excellent effluent quality and a reduced sludge yield compared with conventional aerobic biotreatment processes. The MBR has been proven at full commercial scale for both municipal and industrial wastewater applications and has developed a reputation for its high COD, BOD, nitrogen, and pathogen removal efficiencies. Nevertheless, many practitioners are hesitant to adopt MBR technology due to cost, reliability, and operating problems [61]. To address these issues, several engineering and scientific challenges remain to be addressed before the full potential of the process can be fully realized. Poor oxygen transfer efficiencies, particularly at high MLSS concentrations make the life cycle cost of the process uncompetitive against conventional processes. Figure 36.5 illustrates one of the dilemmas in MBR operation; high MLSS values are associated with reduced sludge yield, but there is a corresponding decrease in oxygen transfer efficiency (related to  $\alpha$ ) and therefore an impact on life cycle costs. Most MBRs in commercial operation are currently operated at permeate fluxes and biomass concentrations well below that theoretically possible to

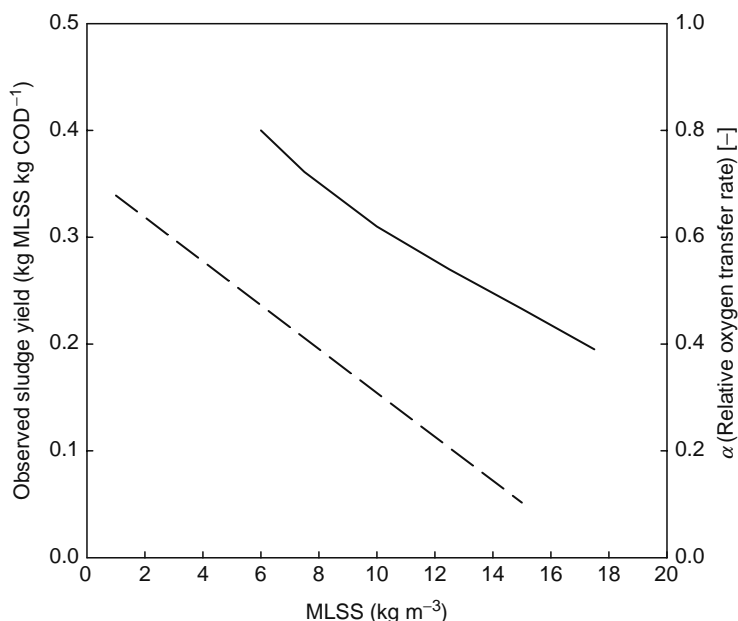


**FIGURE 36.5** Trends in observed sludge yield coefficient (dashed) and dimensionless  $\alpha$ -factor (continuous) as a function of MLSS. Sludge yield calculated according to Equation 36.4, using the values of  $m_s$  and  $Y_G$  suggested by Wiesniwski et al. [62]. (Data for  $\alpha$  is from Cornel, P., Wagner, M., and Krause, S. *Water Sci. Technol.*, 47, 313, 2003.)

minimize fouling and oxygen transfer limitations, respectively. A detailed understanding of the relationship between process variables and microbial physiology, ecology, and morphology is still lacking. Insufficient data currently exists to confirm its superiority in removing micropollutants and organic compounds of borderline biodegradability.

It is likely that over the next decade, the ongoing research effort together with increasing operation experience will bring improvements in the technical and economic viability of the process that will accelerate the uptake of the MBR for both municipal and industrial wastewater treatment.

## ABBREVIATIONS

AS	activated sludge
BAF	biological aerated filter
BOD	biochemical oxygen demand
CAS	conventional activated sludge
CMAS	complete-mix activated sludge
COD	chemical oxygen demand
EMB	extractive membrane bioreactor
EPSs	extracellular polymeric substances
FISH	fluorescent in situ hybridization
HF	hollow fiber
HRT	hydraulic residence time
$k_{La}$	volumetric mass transfer coefficient
MABR	membrane-aerated biofilm reactor
MBR	membrane bioreactor
MF	microfiltration
MLSS	mixed liquor suspended solids
MO	microorganism
MTBE	methyl tertiary-butyl ether
O&M	operation and maintenance
PF	plate and frame
$q_M$	specific substrate utilization rate for maintenance
$r$	reaction rate
$S$	substrate concentration
SCOD	soluble chemical oxygen demand
SOTE	standard oxygen transfer efficiency
SRF	sludge resistance to filtration
SRT	solids retention time
TCOD	total chemical oxygen demand
TF	tertiary filtration
TMP	transmembrane pressure
TSS	total suspended solids
UF	ultrafiltration
$X$	biomass concentration
$Y_G$	true biomass yield coefficient
$Y_S$	observed biomass yield coefficient
$\alpha$	factor indicating effect of biomass on mass transfer coefficient
$\mu$	biomass specific growth rate

## REFERENCES

1. Tao G, Kekre K, Wei Z, Lee TC, Viswanath B, and Seah H. Membrane bioreactors for water reclamation. *Water Sci Technol.* 2005; 51(6–7): 431–440.
2. Oota S, Murakami T, Takemura K, and Noto K. Evaluation of MBR effluent characteristics for reuse purposes. *Water Sci Technol.* 2005; 51(6–7): 441–446.
3. Smith CW, Di Gregorio D, and Taleott RM. The use of ultrafiltration membrane for activated sludge separation. Proceedings of the 24th Annual Purdue Industrial Waste Conference. Purdue University, West Lafayette, Indiana, 1969.
4. Visvanathan C, Ben Aim R, and Parameshwaran K. Membrane separation bioreactors for wastewater treatment. *Crit Rev Environ Sci Technol.* 2000; 30: 1–48.

5. Anonymous. Zenon chosen to supply “world’s largest membrane bioreactor,” *Filtration Separ.* 2005; 42: 14.
6. Gander M, Jefferson B, and Judd S. Aerobic MBRs for domestic wastewater treatment: A review with cost considerations. *Separ Purif Technol.* 2000; 18: 119–130.
7. Judd S. A review of fouling of membrane bioreactors in sewage treatment. *Water Sci Technol.* 2004; 49(2): 229–35.
8. Le-Clech P, Jefferson B, and Judd SJ. A comparison of submerged and sidestream tubular membrane bioreactor configurations. *Desalination* 2005; 173: 113–122.
9. Rosenberger S, Krüger U, Witzig R, Manz W, Szewzyk U, and Kraume M. Performance of a bioreactor with submerged membranes for aerobic treatment of municipal waste water. *Water Res.* 2002; 36: 413–420.
10. Côté P, Masini M, and Mourato D. Comparison of membrane options for water reuse and reclamation. *Desalination* 2004; 167: 1–11.
11. Stephenson T, Judd S, Jefferson B, and Brindle K, Eds. *Membrane Bioreactors for Wastewater Treatment*. IWA Publishing, London, United Kingdom, 2000.
12. Zhang B, Yamamoto K, Ohgaki S, and Kamiko N. Floc size distribution and bacterial activities in membrane separation activated sludge processes for small-scale wastewater treatment/reclamation. *Water Sci Technol.* 1997; 35: 37–44.
13. Kraume M, Bracklow U, Vocks M, and Drews A. Nutrients removal in MBRs for municipal wastewater treatment. *Wat Sci Technol.* 2005; 51(6–7): 391–402.
14. Gnirrs R, Lesjean B, Adam C, and Buisson H. Cost effective and advanced phosphorus removal in membrane bioreactors for a decentralised wastewater technology. *Water Sci Technol.* 2003; 47(12): 133–139.
15. Innocenti L, Bolzonella D, Pavan P, and Cecchi F. Effect of sludge age on the performance of a membrane bioreactor: Influence on nutrient and metals removal, *Desalination* 2002; 146: 467–474.
16. Fleischer EJ, Broderick TA, Daigger GT, Fonseca AD, Holbrook RD, and Murthy SN. Evaluation of membrane bioreactor process capabilities to meet stringent effluent nutrient discharge requirements. *Water Envir Res.* 2005; 77: 162–178.
17. Cicek N, Franco JP, Suidan MT, Urbain V, and Manem J. Characterization and comparison of a membrane bioreactor and a conventional activated-sludge system in the treatment of wastewater containing high-molecular-weight compounds. *Water Environ Res.* 1999; 71: 64–70.
18. Ng HY and Hermanowicz SW. Membrane bioreactor operation at short solids retention times: Performance and biomass characteristics, *Water Res.* 2005; 39: 981–992.
19. Huang H, Gui P, and Qian Y. Effect of sludge retention time on microbial behaviour in a submerged membrane bioreactor. *Proc Biochem.* 2001; 36: 1001–1006.
20. Joss A, Andersen H, Ternes T, Richle PR, and Siegrist H. Removal of estrogens in municipal wastewater treatment under aerobic and anaerobic conditions: Consequences for plant optimization. *Environ Sci Technol.* 2004; 38: 3047–3055.
21. Clara M, Strenn B, Ausserleitner M, and Kreuzinger N. Comparison of the behaviour of selected micropollutants in a membrane bioreactor and a conventional wastewater treatment plant. *Water Sci Technol.* 2004; 50(5): 29–36.
22. Dias JCT, Rezende RP, Silva CM, and Linardi VR. Biological treatment of kraft pulp mill foul condensates at high temperatures using a membrane bioreactor. *Proc Biochem.* 2005; 40: 1125–1129.
23. Scholz W and Fuchs W. Treatment of oil contaminated wastewater in a membrane bioreactor. *Water Res.* 2000; 34: 3621–3629.
24. van Kempen R, Draaijer H, and Postma HJW. A membrane bioreactor for industrial effluents: Compact, versatile and proven. Proceedings of the first international meeting on membrane bioreactors for wastewater treatment, Cranfield, United Kingdom, March 5, 1997.
25. Zaloum R, Lessard S, Mourato D, and Carrière J. Membrane bioreactor treatment of oily wastes from a metal transformation mill. *Water Sci Technol.* 1994; 30(9): 21–27.
26. Knoblock MD, Sutton PM, Mishra PN, Gupta K, and Janson A. Membrane biological reactor system for treatment of oily wastewaters. *Water Environ Res.* 1994; 66: 133–139.
27. Reemtsma T, Zywicki B, Stueber M, Kloepfer A, and Jekel M. Removal of sulfur-organic polar micropollutants in a membrane bioreactor treating industrial wastewater. *Environ Sci Technol.* 2002; 36: 1102–1106.
28. Reemtsma T and Jekel M. Dissolved organics in tannery wastewaters and their alteration by a combined anaerobic and aerobic treatment. *Water Res.* 1997; 31: 1035–1046.
29. Morrison JR, Suidan MT, and Vonosa AD. Use of membrane bioreactor for biodegradation of MTBE in contaminated water. *J Env Eng ASCE.* 2002; 128: 836–841.
30. Marrot B, Barrios-Martinez A, Moulin P, and Roche N. Industrial wastewater treatment in a membrane bioreactor: A review. *Environ Prog.* 2004; 23: 59–68.
31. Germain E, Stephenson T, and Pearce P. Biomass characteristics and membrane aeration: Toward a better understanding of membrane fouling in submerged membrane bioreactors (MBRs). *Biotechnol Bioeng.* 2005; 90: 316–322.
32. Field RW, Wu D, Howell JA, and Gupta BB. Critical flux concept for microfiltration fouling. *J Memb Sci.* 1995; 100: 259–272.
33. Ognier S, Wisniewski C, and Grasmick A. Membrane bioreactor fouling in sub-critical filtration conditions: A local critical flux concept. *J Memb Sci.* 2004; 229: 171–177.
34. Chu HP and Li XY. Membrane fouling in a membrane bioreactor (MBR): Sludge cake formation and fouling characteristics. *Biotechnol Bioeng.* 2005; 90: 323–31.
35. Owen G, Bandi M, Howell JA, and Churchouse SJ. Economic assessment of membrane processes for water and waste water treatment. *J Memb Sci.* 1995; 102: 77–91.
36. Witzig R, Manz W, Rosenberger S, Kruger U, Kraume M, and Szewzyk U. Microbiological aspects of a bioreactor with submerged membranes for aerobic treatment of municipal wastewater. *Water Res.* 2002; 36: 394–402.

37. Flemming H-C and Wingender J. Relevance of microbial extracellular polymeric substances (EPSs). Part II. Technical aspects. *Water Sci Technol.* 2001; 43(6): 9–16.
38. Drews A and Kraume M. Process improvement by application of membrane bioreactors. *Chem Eng Res Design.* 2005; 83(A3): 276–284.
39. Cornel P, Wagner M, and Krause S. Investigation of oxygen transfer rates in full scale membrane bioreactors. *Water Sci Technol.* 2003; 47(11): 313–319.
40. Springer A. Operational problems of a membrane bioreactor. Proceedings of the Third National CIWEM Conference, Leeds, United Kindom, September 2005, pp. 161–175.
41. Ng HY and Hermanowicz SW. Specific resistance to filtration of biomass from membrane bioreactor reactor and activated sludge: Effects of exocellular polymeric substances and dispersed microorganisms. *Water Environ Res.* 2005; 77: 187–192.
42. Klatt CG and LaPara TM. Aerobic biological treatment of synthetic municipal wastewater in membrane-coupled bioreactors. *Biotechnol Bioeng.* 2003; 82: 313–320.
43. Mason CA, Hamer G, and Bryers JD. The death and lysis of microorganisms in environmental processes. *FEMS Microbiol Rev.* 1986; 39: 373–401.
44. Hasar H, Kinaci C, and Unlü A. Viability of microbial mass in a submerged membrane bioreactor. *Desalination.* 2002; 150: 263–268.
45. Wei Y, van Houten RT, Borger AR, Eikelboom DH, and Fan Y. Minimization of excess sludge production for biological wastewater treatment. *Water Res.* 2003; 37: 4453–4467.
46. Muller EB, Stouthamer AH, van Verseveld HW, and Eikelboom DH. Aerobic domestic waste water treatment in a pilot plant with complete sludge retention by cross-flow filtration. *Water Res.* 1995; 29: 1179–1189.
47. Benítez J, Rodríguez A, and Malaver R. Stabilization and dewatering of wastewater using hollow fiber membranes. *Water Res.* 1995; 29: 2281–2286.
48. Pirt, SJ. The maintenance energy of bacteria in growing cultures. *Proc R Soc Lond Biol.* 1965; 163: 224–234.
49. Bryers JD and Mason CA. Bio-polymer particulate turnover in biological waste treatment systems—a review. *Bioproc Eng.* 1987; 2: 95–109.
50. Song K-G, Choung Y-K, Ahn K-H, Cho J, and Yun H. Performance of membrane bioreactor system with sludge ozonation process for minimization of excess sludge production. *Desalination.* 2003; 157: 353–359.
51. Yasui H and Shibata M. An innovative approach to reduce excess sludge production in the activated sludge process. *Water Sci Technol.* 1994; 30: 11–20.
52. Yeh SJ and Jenkins CR. Pure oxygen fixed film reactor. *J Environ Eng (ASCE).* 1978; 14: 611–623.
53. Debus O, Wanner O, and Sekoulov I. Degradation of xylene by a biofilm growing on a gas permeable membrane. *Water Sci Technol.* 1992; 26(3–4): 607–616.
54. Cole AC, Semmens MJ, and LaPara TM. Stratification of activity and bacterial community structure in biofilms grown on membranes transferring oxygen. *Appl Environ Microbiol.* 2004; 70: 1982–1989.
55. Semmens MJ, Dahm K, Shanahan J, and Christianson A. COD and nitrogen removal by biofilms growing on gas permeable membranes. *Water Res.* 2003; 37: 4343–4350.
56. Casey E, Glennon B, and Hamer G. Review of membrane aerated biofilm reactors. *Resour Conserv Recy.* 1999; 27: 203–215.
57. Livingston AG. A novel membrane bioreactor for detoxifying industrial wastewater: I biodegradation of phenol in a synthetically concocted wastewater. *Biotechnol Bioeng.* 1993; 41: 915–926.
58. Livingston AG. A novel membrane bioreactor for detoxifying industrial wastewater: II biodegradation of 3-chloronitrobenzene in an industrial produced wastewater. *Biotechnol Bioeng.* 1993; 41: 927–936.
59. Brooks PR and Livingston AG. Biotreatment of a point-source industrial wastewater arising in 3,4-dichloroaniline manufacture using an extractive membrane bioreactor. *Biotechnol Prog.* 1994; 10: 65–75.
60. dos Santos LMF, Pavasant P, Strachan LF, Pistikopoulos EN, and Livingston AG. Membrane attached biofilms for waste treatment—fundamentals and applications. *Pure Appl Chem.* 1997; 69: 2459–2469.
61. Daigger GT, Rittmann BE, Adham S, and Andreottola G. Are membrane bioreactors ready for widespread application? *Environ Sci Technol A-Page Magazine* 2005; 39(19): 399A–406A.
62. Wisniewski C, Cruz AL, and Grasmick A. Kinetics of organic carbon removal by a mixed culture in a membrane bioreactor. *Biochem Eng J.* 1999; 3: 61–69.

---

# 37 Membrane-Assisted Solvent Extraction for the Recovery of Metallic Pollutants: Process Modeling and Optimization

*Inmaculada Ortiz and J. Angel Irabien*

## CONTENTS

37.1	Introduction .....	1023
37.2	Modeling of Nondispersive Solvent Extraction of Multicomponent Metallic Solutions .....	1024
	37.2.1 Extraction Module .....	1025
	37.2.2 Back-Extraction Module .....	1026
	37.2.3 Stirred Tanks .....	1027
37.3	Modeling and Optimization of Emulsion Pertraction Processes .....	1029
	37.3.1 Optimization of a Pertraction Plant .....	1033
	37.3.1.1 Mathematical Formulation .....	1033
	37.3.1.2 NLP Formulation .....	1034
	37.3.2 Optimization Results .....	1035
37.4	Concluding Remarks and Future Directions .....	1036
	Acknowledgment .....	1037
	References .....	1037

## 37.1 INTRODUCTION

Membrane-assisted solvent extraction processes have known an increasing number of applications in the last decades [1–4]. This technique not only overcomes the limitations of conventional liquid extraction, such as flooding, intimate mixing, limitations on phase flow rate variations, and requirement of density difference but also provides a large surface area of mass transfer per volume of contactor [5]. Excellent reviews of the technology and its applications were presented by Ho and Sirkar in 1992 [6], and by Gabelman and Hwang [7].

Not only the efficient removal of toxic heavy metals like hexavalent chromium (Cr(VI)), cadmium (Cd), zinc (Zn), nickel (Ni), etc., and other contaminants like phenol from industrial wastewaters [8–18] but also the recovery of valuable solutes from aqueous phases, for example, citric acid, carboxylic acids, amino acids, L-phenylalanine, etc. [19,20], are well-demonstrated applications of this technique.

From a practical point of view, it may be important not only to extract the solute but also to concentrate it [21]. For this reason, simultaneous extraction and stripping of the solute has been developed using two hollow-fiber (HF) modules in series, one for the extraction and the other for the back-extraction processes. The modules are connected to each other by an organic extractant in a recirculating line. This configuration guarantees that saturation of the carrier does not occur, as it is continuously regenerated and consequently the carrier concentration can be reduced maintaining the mass transfer rate, and therefore decreasing the associated operating costs of the process. Representative examples of the simultaneous membrane solvent extraction and back extraction of one solute can be found in the literature, for example, removal and concentration of valeric acid [22], sodium lactate [23], Cu [24,25], Cr(VI) [26], etc. Furthermore the technology has also been applied to the separation of the components of metallic mixtures such as the separation of a mixture of Cr(VI) and Cu(II) using LIX84 and H<sub>2</sub>SO<sub>4</sub> in the organic and back-extraction phases, respectively, for the recovery of Cu, and TOA and NaOH for Cr [27], the separation of Zn and Cu [28–30], and more recently the separation of Cd and Ni [30–32].

In addition to the conventional way that needs the use of two HF modules, different efforts have been directed to process design with minimum area requirement. A special configuration of HF modules, i.e., contained liquid membranes (CLMs), was investigated as an alternative trying to maximize the separation driving force in the membrane contactor by incorporating two different bundles of HFs; the aqueous phases flowed through the hollows of the bundles and the organic phase was contained in between them. However, since the first works [33–37], a number of experimental and theoretical analysis have been done on the two fiber membrane contactors, which do not show real advantages if the circulation rate of the organic phase is fast enough.

A somehow larger number of references have been published dealing with applications of supported liquid membranes [38–43]. When HF modules are used as contactors in this technology, the organic phase fills the pores of the HF and the aqueous phases flow along the fibers, through the inner side and through the outer side. The main drawback of the technology is the instability of the supported liquid membrane (SLM) that leads to undesirable results such as quick loss of efficiency and organic pollution of the aqueous phases [41].

More recently HF modules have been used in a different configuration that based on similar fundamentals tries to minimize the required membrane area, that is, emulsion pertraction technology. In this case, the organic and back-extraction phases are emulsified before the entrance to the HF module and they can be separated at the module outlet. Although there are only a few references to this alternative, its viability to the recovery of Cr(VI) and Cu from polluted waters [44–46] as well as to the removal of hydrocarbons [47] has been shown, but much effort is needed on the modeling of this technology before additional successful applications can be developed.

### 37.2 MODELING OF NONDISPERSIVE SOLVENT EXTRACTION OF MULTICOMPONENT METALLIC SOLUTIONS

The design of any process has to be supported by a proper understanding of the system behavior. Next, the kinetics of the simultaneous extraction and back-extraction processes of two metallic ions by membrane-assisted solvent extraction is analyzed theoretically.

Chemical reactions between metallic solutes and organic extractant in the extraction process, and between organic complex species and back-extraction agent, are assumed to take place at the inside wall of the membrane where the aqueous–organic interface is located. The mass transfer process of each solute from the initial phase to the receiving phase is considered to take place through the following steps: (1) diffusion through the feed aqueous layer, (2) interfacial chemical reaction, (3) diffusion through the HF membrane, and (4) diffusion through the organic phase layer. The order of steps is reversed during the back-extraction process.

Considering that the small diameter of the HFs forces the fluid to flow in laminar regime, two different approaches can be followed for the analysis of mass transfer in hollow-fiber modules:

1. The velocity and concentration profiles are developed along the HFs by means of the mass conservation equation and the associated boundary conditions for the solute in the inner fluid. This analysis separates the effects of the operation variables, such as hydrodynamic conditions and the geometry of the system, from the mass transfer properties of the system, described by diffusion coefficients in the aqueous and organic phases and by membrane permeability. The solution of such equations usually involves numerical methods. Different applications can be found in the literature, for example, separation and concentration of phenol, Cr(VI), etc. [48–51].
2. The mass flux of a solute can be related to a mass transfer coefficient which gathers both mass transport properties and hydrodynamic conditions of the system (fluid flow and hydrodynamic characteristics of the membrane module). The total amount transferred of a given solute from the feed to the receiving phase can be assumed to be proportional to the concentration difference between both phases and to the interfacial area, defining the proportionality ratio by a mass transfer coefficient. Several types of mass transfer coefficients can be distinguished as a function of the definition of the concentration differences involved. When local concentration differences at a particular position of the membrane module are considered the local mass transfer coefficient is obtained, in contrast to the average mass transfer coefficient [37].

Although the second approach can be considered a simplification of the first many systems have been satisfactorily described, and it is often preferred due to its mathematical simplicity. Studies on mass transfer through aqueous–organic interfaces immobilized at the pore mouths of a microporous membrane have shown that for a HF device, the overall mass transfer coefficient obtained can be related to the individual phase mass transfer coefficients and the membrane resistance using simple film theory. However, many authors considered that this separation controlling, overall mass transfer resistance was dominated by the resistance of the membrane. This is because the permeability of the membrane is low and because the membrane is thick [4,19,20,23,52,53]. On the other hand, other authors reported for different systems and conditions that the kinetic control of

the whole process could be shared between diffusion in the aqueous phase boundary layer and the kinetics of the chemical reaction [10,54–57].

Next, a mathematical model that allows description of the separation and concentration of the components of a metallic mixture will be detailed; the principal assumptions of the model are (1) convective mass transfer dominates diffusive mass transfer in the fluid flowing inside the HFs, (2) the resistance in the membrane dominates the overall mass transport resistance, therefore the overall mass transfer coefficient was set equal to the mass transfer coefficient across the membrane, and (3) chemical reactions between ionic species are sufficiently fast to ignore the contribution of the chemical reaction rates. Thus, the reacting species are present in equilibrium concentration at the interface everywhere [31,32,58,59]. For systems working under nonsteady state, it is also necessary to describe the change in the solute concentration with time both in the modules and in the reservoir tanks. The reservoir tanks will be modeled as ideal stirred tanks.

With the assumptions mentioned above two main parameters will be necessary in the description of the separation–concentration process of one solute, that is, the membrane mass transport coefficient and the equilibrium parameter of the extraction interfacial reaction.

As a representative example, the model will be applied to the separation of Ni and Cd by nondispersive solvent extraction with the mentioned assumptions; to avoid duplicate equations, the subscript “*i*” has been used, where *i* = 1 represents cadmium and *i* = 2 represents nickel.

### 37.2.1 EXTRACTION MODULE

Differential mass balances of the solutes in the feed and organic solutions in the extraction module are expressed through the following equations:

Aqueous solution extraction (EX):

$$-\frac{1}{v_A} \frac{\partial C_{A_i}}{\partial t} = \frac{\partial C_{A_i}}{\partial z} + \frac{2\pi n_f r_f}{F_A} K_m (C_{O_i} - C_{A_i}) \quad (37.1)$$

with boundary conditions

$$z = 0 \quad C_{A_i} = C_{out_i} \text{ (extraction tank)} \quad (37.2)$$

$$t = 0 \quad C_{A_i} = C_{A_i,initial}, \quad i = 1, 2 \quad (37.3)$$

where  $C_{O_i}$  is the interfacial concentration of the metal in the organic phase that is related to the aqueous metal concentration through the chemical equilibrium equation.

Extraction:



$$K_{\text{EX}} = \frac{(a_{\overline{\text{Me}_i\text{X}_n(\text{HX})_{m-n}}}) (a_{\text{H}^+})^n}{(a_{\text{Me}_i}) (a_{\overline{\text{HX}}_m})^n} \quad (37.5)$$

$$K_{\text{EX}} = \left( \frac{C_{\overline{\text{Me}_i\text{X}_n(\text{HX})_{m-n}}} C_{\text{H}^+}^n}{C_{\text{Me}_i} C_{\overline{\text{HX}}_m}^n} \right) \left( \frac{[\gamma_{\overline{\text{Me}_i\text{X}_n(\text{HX})_{m-n}}}] [\gamma_{\text{H}^+}]^n}{[\gamma_{\text{Me}_i}] [\gamma_{\overline{\text{HX}}_m}]^n} \right) \quad (37.6)$$

In a first approach, it is usually assumed that the ratio of the activity coefficients of the species in the organic phase keeps constant for a range of experimental conditions [60]. If the separation process is carried out at constant value of the pH of the aqueous phases the activity of the hydrogen ions,  $a_{[\text{H}^+]}$ , remains constant in the extraction and back-extraction processes and can be simplified, whereas the activity of the metallic solutes,  $a_{[\text{Me}_i]}$ , varies during the experiment since both the metal concentration and the activity coefficients change significantly with operation conditions. The corresponding values of the activity coefficient of the metal ions in aqueous solutions can be calculated using the Debye–Hückel equation. Also activity changes of complex species in the organic phase may be found, the modeling of the organic phase activity coefficients usually introduces empirical considerations. Therefore, Equations 37.5 and 37.6 can be expressed as follows:

$$K'_{\text{EX}} = K_{\text{EX}} \frac{[\gamma_{\overline{\text{HX}}_m}]^n}{[\gamma_{\overline{\text{Me}_i\text{X}_n(\text{HX})_{m-n}}}]^n} = \left( \frac{C_{\overline{\text{Me}_i\text{X}_n(\text{HX})_{m-n}}} C_{\text{H}^+}^n}{C_{\text{Me}_i} C_{\overline{\text{HX}}_m}^n} \right) \frac{[\gamma_{\text{H}^+}]^n}{[\gamma_{\text{Me}_i}]} \quad (37.7)$$

Organic solution:

$$\frac{1}{v_O} \frac{\partial C_{O_i}}{\partial t} = -\frac{\partial C_{O_i}}{\partial z} + \frac{2\pi n_f r_f}{F_O} K_m (C_{O_i} - C_{O_i}) \quad (37.8)$$

Boundary conditions of the organic phase:

$$Z = 0 \quad C_{O_i} = C_{out_i} \text{ (organic tank)} \quad (37.9)$$

$$t = 0 \quad C_{O_i} = C_{O_i,initial}, \quad i = 1, 2 \quad (37.10)$$

### 37.2.2 BACK-EXTRACTION MODULE

The extraction and back-extraction steps take place consecutively, connected by the concentration of the metal-extractant complex species in the organic phase. The description of the back-extraction process is carried out using similar equations to those used in the extraction process. The equilibrium of the interfacial reaction between the organic complex species and the back-extraction agent is applied in this case.

Aqueous solution back extraction (BEX):

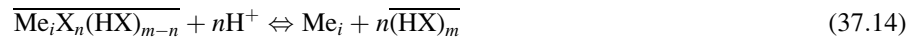
$$\frac{1}{v_S} \frac{\partial C_{S_i}}{\partial t} = -\frac{\partial C_{S_i}}{\partial z} + \frac{2\pi n_f r_f}{F_S} K_m (C_{O_i} - C_{O_i}) \quad (37.11)$$

Boundary conditions for the stripping aqueous phase:

$$z = 0 \quad C_{S_i} = C_{out_i} \text{ (stripping tank)} \quad (37.12)$$

$$t = 0 \quad C_{S_i} = C_{S_i,initial}, \quad i = 1, 2 \quad (37.13)$$

with the equilibrium back-extraction reactions



$$k_{BEX} = \frac{(a_{[Me_i]}) (a_{[(\overline{HX})_m]})^n}{(a_{[Me_i X_n (HX)_{m-n}]} (a_{[H^+]})^n} \quad (37.15)$$

and

$$K_{BEX} = \left( \frac{C_{Me_i} C_{(\overline{HX})_m}^n}{C_{\overline{Me_i X_n (HX)_{m-n}}} C_{H^+}^n} \right) \left( \frac{[\gamma_{Me_i}] [\gamma_{(\overline{HX})_m}]^n}{[\gamma_{\overline{Me_i X_n (HX)_{m-n}}}]} [\gamma_{(H^+)}]^n \right) \quad (37.16)$$

that with similar assumptions to those made in the extraction reactions would transform into

$$K'_{BEX} = K_{BEX} \frac{[\gamma_{\overline{Me_i X_n (HX)_{m-n}}}]^n}{[\gamma_{(\overline{HX})_m}]^n} = \left( \frac{C_{Me_i} C_{(\overline{HX})_m}^n}{C_{\overline{Me_i X_n (HX)_{m-n}}} C_{H^+}^n} \right) \left( \frac{[\gamma_{Me_i}]}{[\gamma_{(H^+)}]^n} \right) \quad (37.17)$$

Organic solution back extraction (BEX):

$$-\frac{1}{v_O} \frac{\partial C_{O_i}}{\partial t} = \frac{\partial C_{O_i}}{\partial z} + \frac{2\pi n_f r_f}{F_O} K_m (C_{O_i} - C_{O_i}) \quad (37.18)$$

Boundary conditions of the organic phase:

$$z = 0 \quad C_{O_i} = C_{O_i} \text{ (outlet extraction module)} \quad (37.19)$$

$$C_{O_i} = C_{O_i,initial}, \quad i = 1, 2 \quad (37.20)$$

### 37.2.3 STIRRED TANKS

In a batch process the dynamic response of the system is determined by simultaneously solving differential Equations 37.1 through 37.20 together with the modeling equations for the three vessels considered as ideal stirred tanks. It is assumed that the solute concentrations at the reservoir and at the module inlet for both phases are identical.

$$V \frac{dC_{out_i}}{dt} = F(C_{in_i} - C_{out_i}) \quad (37.21)$$

$$t = 0 \quad C_{out_i} \text{ (organic tank)} = C_{O_i,initial} \quad (37.22)$$

$$C_{out_i} \text{ (extraction tank)} = C_{A_i,initial} \quad (37.23)$$

$$C_{out_i} \text{ (stripping tank)} = C_{S_i,initial} \quad (37.24)$$

Consequently, the most basic model can be considered to describe the separation of metallic mixtures using HF membranes. It consists of a set of coupled differential equations corresponding to the mass balances of the metallic solutes in the extraction and back-extraction modules, a set of algebraic equations corresponding to the description of the chemical equilibrium reactions, and for batch processes six total differential equations additionally describing the mass balances in the stirred tanks. The use of the mathematical model would require the knowledge of the design parameters, that is, the membrane mass transport coefficient and the parameters of the interfacial chemical equilibria. The model can be generalized and applied to the determination of the response of different systems containing more than one solute.

#### Case study 1: Separation of cadmium and nickel

The case study of multicomponent solvent extraction using HF modules is the separation of Ni and Cd from concentrated solutions that simulated those generated during the leaching step of the recycling process of Ni–Cd batteries. Feed solutions contained the metals in a high concentration range of 0.2–0.4 M, thus an organic phase where the organic extractant has a high concentration value was also needed. Among the commercial extractants available for the separation of Cd and Ni, di(2-ethylhexyl) phosphoric acid has been reported to give excellent results; the extractant was diluted in kerosene that acted as solvent and a third component had to be added to avoid the segregation of a third phase (second organic); tributyl phosphate (TBP) is one of the most common compounds used for this purpose. Finally, a sulfuric acid solution acted as back-extraction phase.

For simultaneous extraction (EX) and back extraction (BEX), two HF modules in series are needed; the organic phase flows from the EX module to the BEX module. In the first module, extraction of solutes is accomplished by the organic phase that contacts the back-extraction solution in the second module, flows to the homogenization tank of the organic phase, and enters again the extraction step (Figure 37.1). Aqueous phases flow through the inner side of the microporous HF membranes whose pores are filled with the organic extractant, and the organic extractant flows concurrently in the shell side in both HF modules.

The mathematical model for the description of the separation kinetics of Cd and Ni in HF modules under non-steady-state conditions has been explained in detail in the previous section. The competition of both components in the complexation reaction with the organic carrier is assumed to be the main difference in the permeation rates of the two components (separation process). This ratio depends on the difference of the individual equilibrium parameters rather than in the different diffusivity of

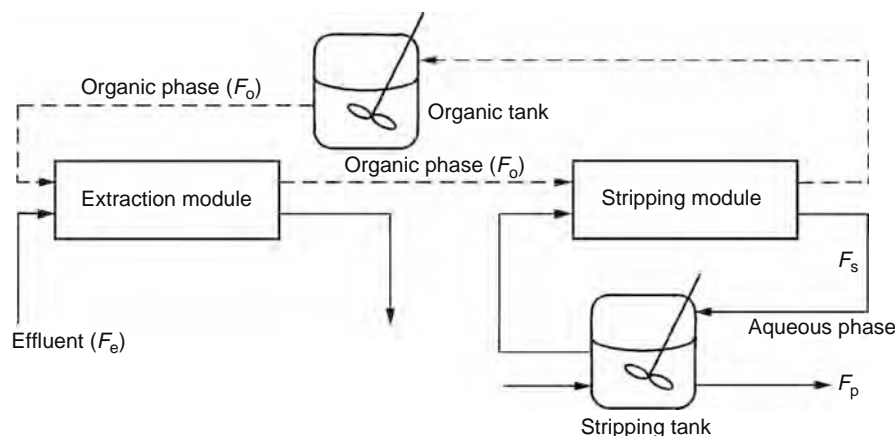


FIGURE 37.1 Flow diagram of a nondispersive solvent extraction process.

the resulting complex species in the organic phase. Thus, the value of the pH of the feed phase can be considered as an optimization variable of the process selectivity.

The determination of the membrane mass transport coefficient can be made by means of the empirical correlation

$$K_m = \frac{D\varepsilon}{\delta\tau} \quad (37.25)$$

after estimation of the corresponding diffusivity of the complex species through the organic membrane from well-known correlations. For simplicity the same value of the membrane mass transport coefficient for both metals can be assumed, equal to  $1.57 \times 10^{-7}$  m/s, the value reported previously [32].

The necessary consideration of equilibrium models of the chemical reactions in the overall mathematical model describing the separation kinetics of both metals involves considerable difficulty since there is no agreement in the literature on the stoichiometry of the ion-exchange reactions of Cd and Ni with the organic carrier D2EHPA, and on what value the equilibrium parameters take. The situation is even more complex when working with highly concentrated solutions since D2EHPA has been reported to exist as a dimer in the organic phase and may form complex species with a metal acting as a dimer. Typical metal ( $\text{Me}^{2+}$ ) complexation with  $n$  dimers,  $\overline{(\text{HX})}_2$ , of D2EHPA could be described by the following equation that represents also the back-extraction reaction:



The equilibrium model and parameters of the reaction of Cd with D2EHPA have been taken from the literature as  $n = 2$  and  $K'_{\text{EX}(\text{Cd})} = 1.82 \times 10^{-5}$  [31].

In the case of Ni, the situation is even more complex since the stoichiometric equations reported in the literature differ widely depending on the diluents used, on the aqueous phase compositions, or on the extractant concentrations employed. A discrimination procedure of the equilibrium models corresponding to the back-extraction reactions has been reported previously by taking into account the expressions given in Table 37.1 and obtaining the best results with the following equation [59]:

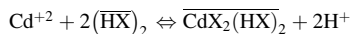
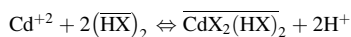
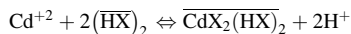
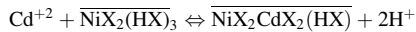
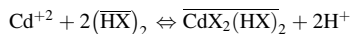


that considers the formation of a mixed complex species in the organic phase between the extractant and both metals and the simultaneous back extraction. After integration of the system of Equations 37.1 through 37.24 and incorporating a model that considers (1) negligible extraction of Ni, (2) the formation of a mixed complex species in the organic phase between the extractant and both metals Cd and Ni, during the initial loading of the organic phase, and (3) the existence of only one reaction responsible for the BEX process of Cd and Ni characterized by the corresponding equilibrium parameter, and simulated data are obtained making use of the set of optimum values of the parameters,  $K'_{\text{EX}(\text{Cd})} = 1.82 \times 10^{-5}$ ,  $K'_{\text{BEX}(\text{NiCd})} = 8.8 \times 10^{-5}$  m<sup>3</sup>/mol, and  $K_m = 1.57 \times 10^{-7}$  m/s. As a representative example, Figure 37.2 shows some comparative results corresponding to an experiment with the following initial concentrations, 0.2 M of nickel and of cadmium in the feed phase and pH equal to 3.5, and 0.2 M of nickel in the back-extraction phase.

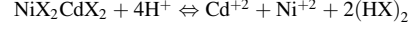
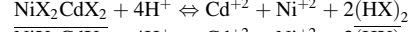
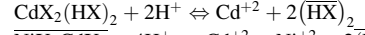
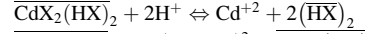
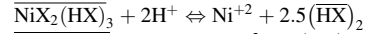
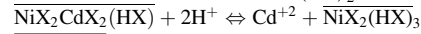
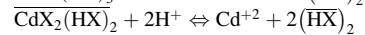
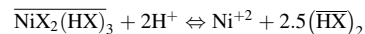
From the curves in Figure 37.2 it is observed that there is a negligible extraction of nickel due to the working value of pH in the feed phase, thus making the process selective toward Cd. Concerning the back-extraction process, both metals are removed from the complex species formed with the organic extractant. Finally, a good agreement between simulated and experimental data is also observed, thus corroborating the validity of the kinetic model for process design and optimization.

**TABLE 37.1**  
**Extraction and Back-Extraction Reactions of Cd and Ni**

**Extraction Reactions**



**Back-Extraction Reactions**



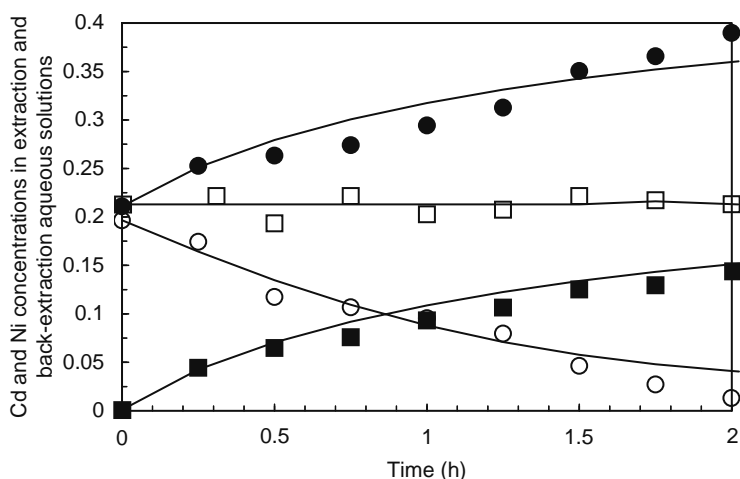


**FIGURE 37.2** Experimental and simulated results of cadmium (Cd) and nickel (Ni) extraction and back extraction; initial concentration of Ni in the back-extraction phase, 0.2 M. (●) Ni in the BEX solution, (■) Cd in BEX, (□) Ni in the extraction, and (○) Cd in the extraction.

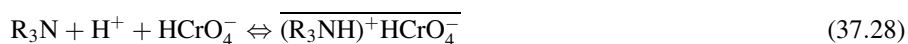
### 37.3 MODELING AND OPTIMIZATION OF EMULSION PERTRACTION PROCESSES

As mentioned in the introduction section, an emerging alternative to achieve the separation of metallic pollutants from aqueous effluents and their concentration in a receiving phase is the emulsion pertraction technology using HF modules.

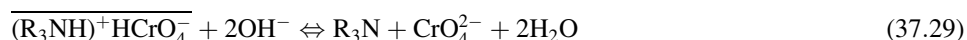
Figure 37.3 shows an enlarged view of the membrane with the aqueous phase in the lumen side and the continuous organic phase and dispersed droplets of the stripping solution (emulsion phase) in the shell side. The hydrophobic microporous membrane is wetted by the organic phase.

The mathematical model needed for process design follows the basis that have been reported for a system with two HF modules but needs to be adapted to describe all the mass transport processes in the same module. As a representative example, it will be applied to the recovery of Cr(VI) from polluted waters that may also contain other competitive anions such as sulfate, chloride, etc.

The extraction reaction of Cr(VI) from acidified solutions using tertiary amines as extractant is represented by the equation



whereas the back-extraction reaction with hydroxyl ions is represented through



In the proposed model, the mass transfer of Cr from the feed to the stripping phase takes place in four steps: (1) diffusion in the feed-phase stagnant layer to the interface with the membrane, (2) interfacial reaction of Cr(VI) with the extractant Alamine 336 to form a complex species (Equation 37.28), (3) diffusion within the supported liquid membrane, and (4) chemical reaction

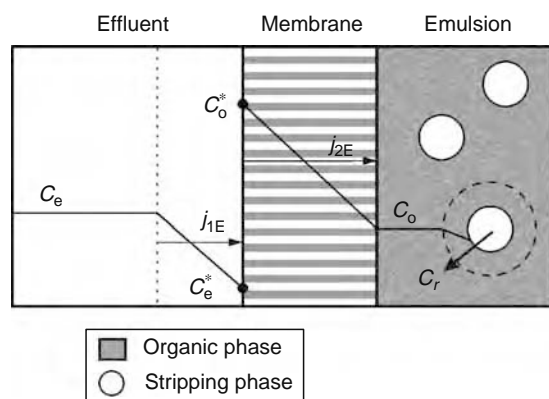


**FIGURE 37.3** Enlarged view of the fiber with the feed aqueous phase in the lumen side and emulsion phase in the shell side.

at the interface of the stripping globules (Equation 37.29). Thus, the main model hypotheses are that the extraction chemical reaction (Equation 37.28) is considered fast enough to reach equilibrium instantaneously and the chromium mass transfer resistance in the stripping phase stagnant film is considered negligible [46]. The diffusion of the other species is assumed to be faster than those corresponding to the Cr compounds.

Then, the mass transfer flux through the feed-phase stagnant layer can be described according to Fick's equation

$$j_1 = k_1 (C_e - C_e^*) \quad (37.30)$$

and in the organic membrane

$$j_2 = k_m (C_o^* - C_o) \quad (37.31)$$

where

$C_e$  is the chromium bulk concentration in the aqueous phase

$C_e^*$  is the aqueous Cr concentration at the membrane interface

$C_o^*$  is the organic Cr concentration at the membrane interface in equilibrium with  $C_e^*$

$C_o$  is the Cr concentration in the organic phase, as shown in Figure 37.3

Interfacial equilibrium concentrations in the extraction side are related through the expression of the chemical equilibrium parameter

$$K_{eq} = \frac{[(R_3NH)^+ HCrO_4^-]^*}{[R_3N]^* [H^+]^* [HCrO_4^-]^*} \quad (37.32)$$

where the superscript (\*) indicates equilibrium concentrations.

Assuming pseudosteady state, then

$$j_1 = j_2 \quad (37.33)$$

For a general case where the hypothesis of chemical equilibrium at the organic–stripping interphase cannot be considered owing to fast consumption of the stripping reagents, the kinetic rates of the involved reactions should be considered [46]. By applying this situation to the back extraction of the chromium–organic complex species, the rates of formation and dissociation of  $CrO_4^{2-}$  in Equation 37.29 are given by  $R_1$  and  $R_{-1}$

$$R_1 = k_1 OH^2 C_o \quad (37.34)$$

$$R_{-1} = k_{-1} C_r \quad (37.35)$$

where  $C_r$  is the chromium concentration at the stripping phase.

Thus, the flux of chromium from the organic phase to the stripping phase through the dispersion bubbles interface is given by

$$j_3 = R_1 - R_{-1} = k_1 \left( OH^2 C_o - \frac{C_r}{K_r} \right) \quad (37.36)$$

The evolution of the  $OH^-$  concentration in the back-extraction phase with time can be considered as an empirical function of the Cr concentration in the same phase of the type

$$OH = C_o - r C_r \quad (37.37)$$

where  $C_o$  is the initial concentration of  $OH^-$  in the stripping phase and  $r$  is a coefficient that would take the value of 2 (stoichiometric coefficient of  $OH^-$  according to Equation 37.29) if there would be no competitive reactions between the extractant Alamine 336 and anions other than that of chromate.

The value of the mass transfer parameter  $k_l$  for fluids flowing through tubes in laminar flow may be calculated from the Levêque equation, neglecting the influence of the concentration changes along the HF [46]

$$\left(\frac{kld}{D_a}\right) = 1.62 \left(\frac{d^2 u_{\text{tube}}}{D_a L}\right)^{\frac{1}{3}} \quad (37.38)$$

where

$d$  is the inside diameter of the HF

$D_a$  is the diffusivity of the chromic anion in the aqueous feed solution

$u_{\text{tube}}$  is the mean velocity of the aqueous feed solution

$L$  is the module length

The membrane mass transport coefficient,  $k_m$ , may be calculated by means of Equation 37.26.

In Equation 37.28, the proton concentration can be expressed according to Cr(VI) concentration in the aqueous phase in the equilibrium

$$H_e^* = H_e - (C_e^{\text{in}} - C_e^*) \quad (37.39)$$

For a system operating at nonsteady state, it is also necessary to describe the change of the solute concentration with time. For simplicity, the concentration of Cr(VI) in the aqueous and organic phases has been described by means of macroscopic mass balances of the permeating solute developed in a certain volume of the fiber at a time interval.

*Module mass balance*

Feed solution:

$$\frac{V_e^M}{L} \frac{dC_e}{dt} = -F_e \frac{dC_e}{dz} - \frac{A}{L} j_1, \quad t = 0, C_e = 0 \quad (37.40)$$

$$z = 0, C_e = C_e^{\text{in}}$$

Organic solution:

$$\frac{V_o^M}{L} \frac{dC_o}{dt} = F_o \frac{dC_o}{dz} + \frac{A}{L} j_1 - \frac{V_r^M}{L} A_v k_l \left( \text{OH}^2 C_o - \frac{C_r}{K_r} \right), \quad t = 0, C_o = C_o^0 \quad (37.41)$$

$$z = L, C_o = C_o^T$$

Stripping solution:

$$\frac{V_r^M}{L} \frac{dC_r}{dt} = F_r \frac{dC_r}{dz} + \frac{V_r^M}{L} A_v k_l \left( \text{OH}^2 C_o - \frac{C_r}{K_r} \right), \quad t = 0, C_r = C_r^0 \quad (37.42)$$

$$z = L, C_r = C_r^T$$

The term on the left-hand side of Equations 37.40 through 37.42 corresponds to the solute accumulation. The first term on the right-hand side represents the convective transport along the tube length, the second term in Equations 37.40 and 37.41 represents the transfer of solute from the aqueous feed phase to the organic phase, and finally the last term in Equations 37.41 and 37.42 shows the flux of Cr(VI) from the organic phase to the stripping phase contained in the emulsion globules where  $A_v$  is the interfacial area of the stripping bubbles by volume of the stripping phase.

For a complete description of the separation process, it is necessary to include the mass balances in the emulsion reservoirs as well as the interfacial equilibrium expression at the feed-membrane side.

*Mass balance of the stripping solution in the stirred tank*

Stripping phase:

$$V_r^T \frac{dC_r^T}{dt} = F_r (C_{r,z=0} - C_r^T) \quad t = 0, C_r^T = C_r^0 \quad (37.43)$$

Organic phase:

$$V_o^T \frac{dC_o^T}{dt} = F_o (C_{o,z=0} - C_o^T) \quad t = 0, C_o^T = C_o^0 \quad (37.44)$$

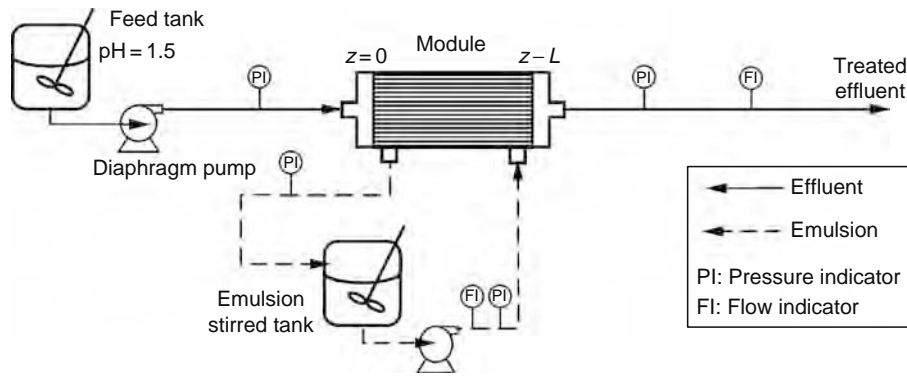


FIGURE 37.4 Flow diagram of an emulsion pertraction process.

where

$F_r$  and  $V_r^T$  are the stripping phase flow rate and stripping volume in the emulsion tank  
 $F_o$  and  $V_o^T$  are the organic phase flow rate and volume in the emulsion tank

*Case study 2: Separation and concentration of hexavalent chromium from waste waters*

The separation and concentration of chromate anions by means of quaternary ammonium salts as extractants and using 2 HF modules deserve attention in the literature [12,13,17,26]. The use of the pertraction emulsion technology allows reduction of the required equipment by achieving the separation and concentration processes in the same module. Figure 37.4 shows a flow diagram of the emulsion pertraction process. Feed phase circulates through the inner side of HFs whereas the emulsion that contains the stripping phase flows through the outer side of the fibers in a recycling mode. Figure 37.5 shows data of a representative run where Cr increases its concentration in the stripping phase whereas it is removed from the feed solution.

To analyze the behavior of the system with the mathematical model proposed in the previous section, three parameters are needed: the chemical equilibrium parameters  $K_{eq}$  and  $K_r$  of the extraction and of the stripping chemical reactions, respectively, and the product,  $A_i k_i$ , of the interfacial area of the emulsion and the kinetic constant of the forward stripping reaction. Estimation of the parameter values needs deep experimental analysis; in the literature the following set of parameter values has been reported:  $K_m = 2.25 \times 10^{-7}$  m/s;  $K_{eq} = 1.041$  mol<sup>-2</sup>/m<sup>6</sup>;  $A_i k_i = 10.62$  m<sup>6</sup> mol<sup>-2</sup> h<sup>-1</sup>; and  $k_r = 10^4$  [46]. The mathematical model and parameters can be used to obtain simulated values at different operation conditions.

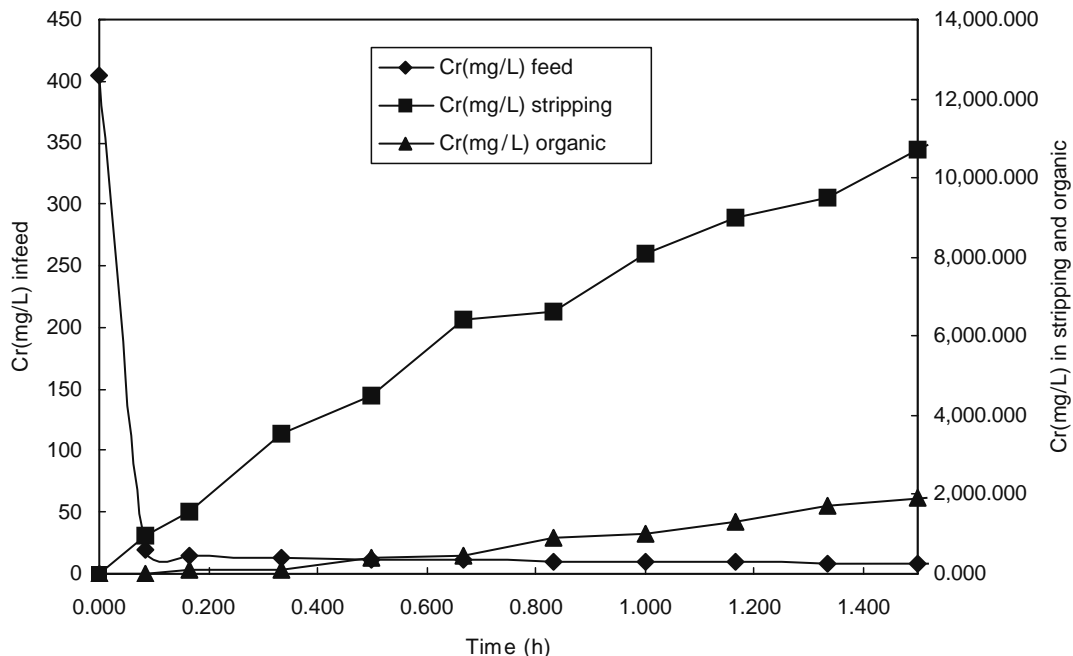


FIGURE 37.5 Experimental results of a representative emulsion pertraction run.

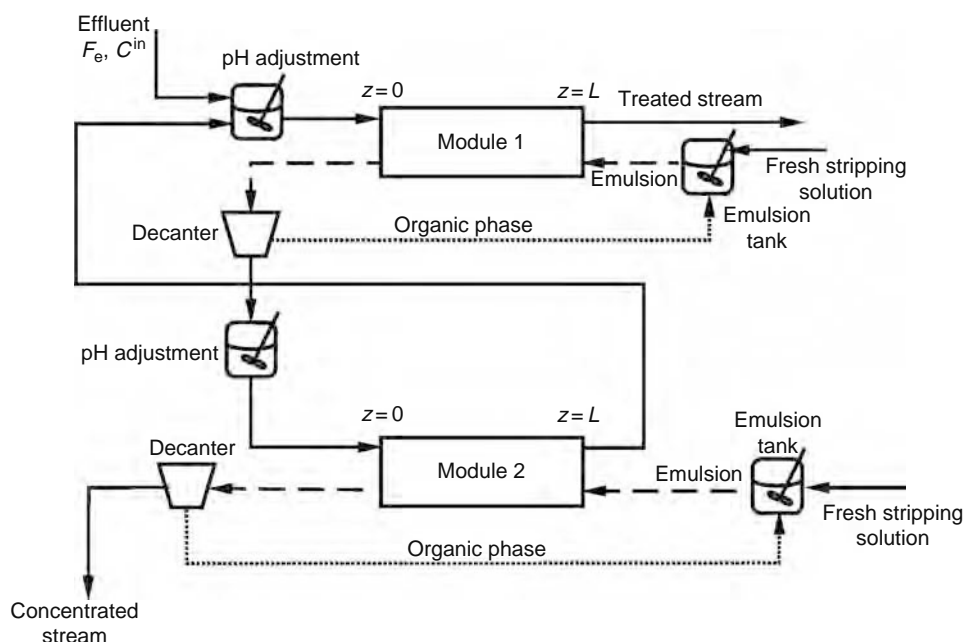


FIGURE 37.6 Proposed configuration for the pertraction plant.

### 37.3.1 OPTIMIZATION OF A PERTRACTION PLANT

In this section, the reported model and the parameters will be used to obtain the optimal operation point that maximizes the amount of Cr treated in an emulsion pertraction plant. It is considered that the plant operates continuously and the reduction target value of Cr(VI) in the effluent as well as the concentration levels are fixed values equal to  $0.00961 \text{ mol/m}^3$  ( $0.5 \text{ mg/L}$ ) and  $384.615 \text{ mol/m}^3$  ( $20,000 \text{ mg/L}$ ), respectively.

For this purpose a cascade-type plant with two membrane modules is proposed, as shown in Figure 37.6. The effluent enters the first module, and leaves it with the imposed output concentration level. In the same module, the emulsion runs in countercurrent mode, and after leaving the module the phases are separated. The organic phase is mixed with fresh back-extraction phase and returns to the first module, while the aqueous phase is acidified to pH 1.5 and then goes to the second module.

In the second module, the aqueous phase transfers the metal to a second emulsion batch, and finally it is mixed with the effluent that enters the first membrane module. The second emulsion concentrates Cr in the back-extraction aqueous phase, and after the phase separation at the output, the organic phase is mixed with fresh back-extraction solution and returned to the same module.

There are two reasons for proposing the previous configuration. The first one is related to the desired Cr levels in the output streams. It is not possible to reach both concentration constraints without a cascade-type configuration in continuous operation. The second reason concerns the undesired presence of other competitive anions such as sulfate in the concentrated stream. The importance of mass transfer of competitive anions is low at high Cr(VI) concentrations but can have a significant influence when the concentration of Cr(VI) is low [44]. Then, in the plant devised, sulfate and other anions are transferred to the stripping phase in the first module, but there is no significant mass transfer from the aqueous stream to the back extraction in the second module, as the aqueous stream has a relatively high Cr concentration.

#### 37.3.1.1 Mathematical Formulation

The model for the pertraction process has been explained in the previous section. A system of partial differential equations describes the behavior of the aqueous and emulsion phases, and ordinary differential equations describe the dynamic behavior of the tanks. There is also a set of algebraic equations for the chemical equilibrium and connections between the equipment.

As the plant to be optimized considers a process operating at steady state, then the variation of the phase concentrations with time is zero. For this reason, the mathematical model that describes the plant is a set of ordinary differential equations, as the phase concentrations depend only on the module axial position. In the tanks, the concentrations are constant. The differential-algebraic nonlinear optimization (DNLP) problem P1 to be solved includes the ordinary differential equations that represent the mass balances for the phases in the membrane module. The objective function to be maximized is the amount of metal processed  $F_e C^{\text{in}}$ , where  $F_e$  is the effluent flow rate whose Cr(VI) concentration after dilution from wastewaters is  $C^{\text{in}}$ . The problem has the following form:

$$\begin{aligned}
& \text{Max}_{\mathbf{v}} F_e C^{\text{in}} \\
& \text{s.t.: } \mathbf{h}(\dot{\mathbf{x}}, \mathbf{x}, \mathbf{w}, \mathbf{v}) = 0 \\
& \quad \mathbf{g}(\dot{\mathbf{x}}, \mathbf{x}, \mathbf{w}, \mathbf{v}) \leq 0 \\
& \quad \mathbf{I}(\mathbf{x}(0), \mathbf{x}(L)) = 0 \\
& \quad \mathbf{x}^{\text{LB}} \leq \mathbf{x} \leq \mathbf{x}^{\text{UB}} \\
& \quad \mathbf{w}^{\text{LB}} \leq \mathbf{w} \leq \mathbf{w}^{\text{UB}} \\
& \quad \mathbf{v}^{\text{LB}} \leq \mathbf{v} \leq \mathbf{v}^{\text{UB}} \\
& \quad \mathbf{x} \in R^n
\end{aligned} \tag{P1}$$

where  $\mathbf{x}$  represents the set of differential distributed variables such as the aqueous, organic, and back-extraction concentration profiles along the modules, and  $\dot{\mathbf{x}}$  is the derivative of  $\mathbf{x}$  with respect to the module axial position  $z$  (with  $z \in [0, L]$ ). The vector  $\mathbf{w}$  is the set of algebraic distributed variables, such as the interface concentration along the modules. The set of nondistributed optimization variables, such as the aqueous or emulsion flow rates in the network, is represented by  $\mathbf{v}$ . For all variables types, upper and lower bounds are imposed.

The mass balances, equilibrium, and interconnection relationships are represented by the set of differential and algebraic equalities  $\mathbf{h}$  for the membrane modules, while the restrictions on the effluent output concentrations and the recovered metal concentration are represented by the inequalities  $\mathbf{g}$ . The initial conditions for the differential equations are given by  $\mathbf{I}$ .

The aim in the optimization problem is to maximize the objective function by selecting the optimum values for the optimization variables  $\mathbf{v}$ . To solve the optimization problem P1, commercial software tools such as GAMS [61] can be used after discretization of the differential equations.

### 37.3.1.2 NLP Formulation

The following is the resulting NLP problem P2, derived from P1 after discretization of the differential equations by using the orthogonal collocation technique:

$$\begin{aligned}
& \text{Max}_{\mathbf{v}} F_e C^{\text{in}} \\
& \text{s.t.: } \mathbf{h}(\mathbf{x}, \mathbf{v}, \mathbf{w}) = 0 \\
& \quad \mathbf{g}(\mathbf{x}) \leq 0 \\
& \quad \mathbf{x}^{\text{LB}} \leq \mathbf{x} \leq \mathbf{x}^{\text{UB}} \\
& \quad \mathbf{w}^{\text{LB}} \leq \mathbf{w} \leq \mathbf{w}^{\text{UB}} \\
& \quad \mathbf{v}^{\text{LB}} \leq \mathbf{v} \leq \mathbf{v}^{\text{UB}} \\
& \quad \mathbf{x} \in R^n
\end{aligned} \tag{P2}$$

The equations included in P2 are described in the next subsections.

#### 37.3.1.2.1 Material Balances for the Membrane Modules

After removing the time derivatives and replacing the differential mass balances given by Equations 37.40 through 37.42 by a set of algebraic equations applying orthogonal collocation, the mass balances for the membrane module  $j$  are as follows:

Aqueous phase:

$$\sum_{q=0}^{N+1} C_{e,q}^j \dot{\phi}_q(z_i) = -k_L \left( C_{e,i}^j - C_{e,i}^{j,*} \right) \frac{A}{L F_e^j}, \quad i = 1, \dots, N+1, \text{ and } j = 1, 2 \tag{37.45}$$

$$C_{e,0}^j = C_e^{j,\text{in}} \tag{37.46}$$

Organic phase:

$$\sum_{q=0}^{N+1} C_{o,q}^j \dot{\phi}_q(z_i) = -k_L \left( C_{e,i}^j - C_{e,i}^{j,*} \right) \frac{A}{L F_o^j} + A_v k_l (\text{OH}_i^j)^2 C_{o,i}^j \frac{V_r^M}{L F_e^j}, \quad i = 0, \dots, N \text{ and } j = 1, 2 \tag{37.47}$$

$$C_{o,N+1}^j = C_{o,0}^j \tag{37.48}$$

Back-extraction phase:

$$\sum_{q=0}^{N+1} C_{r,q}^j \dot{\phi}_q(z_i) = -A_v k_l (\text{OH}_i^j)^2 C_{o,i}^j \frac{V_r^M}{LF_r}, \quad i = 0, \dots, N \text{ and } j = 1, 2 \quad (37.49)$$

$$C_{r,N+1}^j = 0 \quad (37.50)$$

The organic and stripping flow rate that constitutes the emulsion stream are related by

$$4F_r^j = F_o^j, \quad j = 1, 2 \quad (37.51)$$

### 37.3.1.2.2 Chemical Equilibrium and Other Relationships

Equations 37.32 and 37.33 and Equations 37.37 through 37.39 are replaced by the following set of equations:

$$K_{\text{eq}} C_{e,i}^{j*} H_{e,i}^{j*} (CT - C_{o,i}^{j*}) = C_{o,i}^{j*} \quad (37.52)$$

$$k_L (C_{e,i}^j - C_{e,i}^{j*}) = k_m (C_{o,i}^{j*} - C_{o,i}^j) \quad (37.53)$$

$$\text{OH}_i^j = 3000 - r C_{r,i}^j \quad (37.54)$$

$$H_{e,i}^{j*} = H_e^{\text{in}} - (C_e^{\text{in}} - C_{e,i}^{j*}) \quad (37.55)$$

where  $i = 0, \dots, N + 1$  refers to the collocation points along the module axial position, and  $j = 1, 2$  refers to the module number.

### 37.3.1.2.3 Material Balances for Mixers and Tanks

The mass balance for any mixer or a tank of Figure 37.6 is given by

$$F_k^{\text{out}} = \sum_n F_{k,n}^{\text{in}}, \quad k = e, o, r \quad (37.56)$$

where  $k$  represents the organic, stripping, or organic phase, whose inlet streams are represented by  $F_{k,n}^{\text{in}}$  and the output stream by  $F_k^{\text{out}}$ .

The chromium balance for the phases that constitute the emulsion is given by

$$F_k^{\text{out}} C_k^{\text{out}} = \sum_n F_{k,n}^{\text{in}} C_{k,n}^{\text{in}}, \quad k = e, o, r \quad (37.57)$$

## 37.3.2 OPTIMIZATION RESULTS

Let us consider a process that treats an effluent having Cr(VI) using two membrane modules of 19.3 m<sup>2</sup> each. After the optimization procedure that starts with discretization of the differential equations using 10 collocation points in each membrane module, formulation of the NLP problem P2, and solution with the optimization code GAMS using the NLP solver CONOPT2, the solution reported in Table 37.2 was obtained. Both the treated effluent and the concentrated Cr solution for reuse are at their upper and lower bound, respectively. 99.5% of the metal is removed from the wastewater and concentrated for reuse. The Cr concentration profiles along the membrane modules are shown in Figures 37.7 and 37.8. The stripping phase is then concentrated up to nearly 20 mol/m<sup>3</sup> in the first module and then goes to the second one, where its relatively high Cr level allows the mass transfer to the stripping phase at 384.615 mol/m<sup>3</sup>, as shown in Figure 37.8.

It can be seen in Figure 37.7 that almost all the metal is removed from the effluent in the first half of the module. As a consequence, in the second half of Module 1 the effluent concentration remains constant. However, this fact does not imply that the portion of the module is idle, but only that the mass transfer from the effluent to the organic phase is null. In all the modules there is mass transfer from the organic to the stripping phase. This is the reason why the stripping phase increases its concentration as it flows from  $z=L$  to  $z=0$ . The organic phase concentration decreases as it flows from  $z=L$  to a given point located more or less in the middle of the membrane module. This happens as the mass transfer from the effluent to the organic phase is nearly zero, while the mass transfer from the organic to the stripping phase is not null.

**TABLE 37.2**  
**Optimal Operating Conditions of an Emulsion Pertraction Plant for Chromium(VI) Recovery**

	Nonlinear Optimization (NLP) Solution	Lower Bound	Upper Bound
Objective function			
Cr(VI) treated (mol/h)	0.311	0.005	1
Optimization variables			
Effluent flow rate, $F_e$ (m <sup>3</sup> /h)	0.131	0.020	0.200
Effluent input concentration, $C_{in}$ (mol/m <sup>3</sup> )	2.37	1.92	7.77
Emulsion flow rate (Module 1) (mol/m <sup>3</sup> )	0.116	0.020	0.200
Emulsion flow rate (Module 2) (mol/m <sup>3</sup> )	0.004	0.001	0.020
Constraints			
Output stripping concentration (mol/m <sup>3</sup> )	384.615	384.615	500
Output aqueous concentration (mol/m <sup>3</sup> )	0.00961	0.001	0.00961

Mathematically, this occurs because the second term in the right-hand side of Equation 37.47 dominates the first term, which is close to zero.

As the emulsion continues flowing from the middle of the module to  $z=0$ , the mass transfer from the effluent to the organic phase increases and outnumbers the mass transfer from the organic to the stripping phase. In other words, the first term on the right-hand side of Equation 37.47 compensates the second, which has an opposite sign.

As the organic phase is reused after separated from the emulsion in a decanter, the organic concentrations at  $z=0$  and  $z=L$  are the same. The same happens in Module 2, as its organic phase is also separated from the emulsion and reused. The modeling procedure that has been applied to the Cr system allows an understanding of the main phenomena involved in the process and it is recommended to be applied to other systems of practical interest.

### 37.4 CONCLUDING REMARKS AND FUTURE DIRECTIONS

Membrane-assisted solvent extraction processes have known an increasing number of applications in the last decades. The technique not only overcomes the limitations of conventional liquid extraction, such as flooding, intimate mixing, limitations on phase flow rate variations, and requirement of density difference but also provides a large surface area of mass transfer per volume of contactor. Simultaneous extraction and stripping of the solute has been developed using two HF modules in series, one for the extraction and the other for the back-extraction processes.

An important number of references have been published dealing with many applications of supported liquid membranes. Mathematical modeling of the process has been developed and it can be generalized and applied to the determination of the response of different systems containing more than one solute. After evaluation of the parameters, process optimization can be applied using common optimization procedures, as described in the text.

According to previous explanations, the technique is prepared to be managed as more common chemical engineering processes. Previous results indicate that intensification of the processes can be reached leading to new conceptual and practical design of many industrial separations. Special effort should be devoted in the near future to the development of practical applications of the technology.

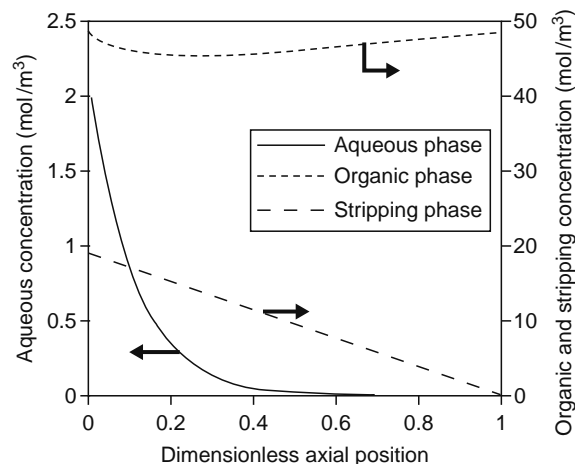


**FIGURE 37.7** Concentration profiles for Module 1 at the optimal point.

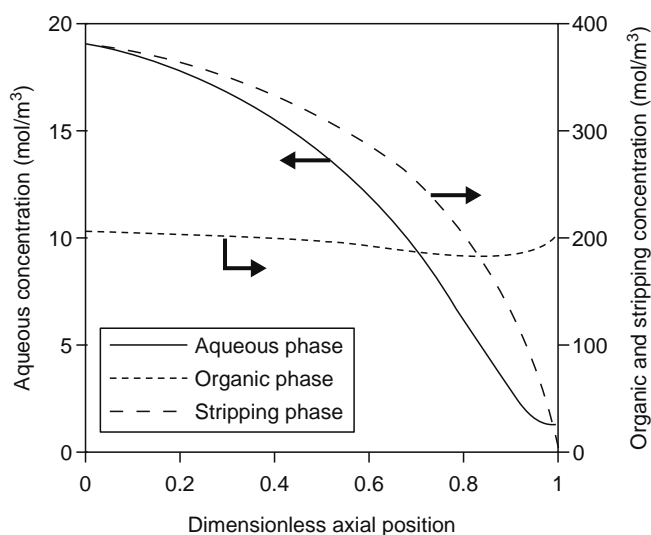


FIGURE 37.8 Concentration profiles for Module 2 at the optimal point.

## ACKNOWLEDGMENT

Financial support to project BQU2002-03357 is gratefully acknowledged.

## REFERENCES

1. D'Elia N.A., Dahuron L., and Cussler E.L., Liquid-liquid extraction with microporous hollow fibers, *J. Membr. Sci.* 29, 309, 1986.
2. Yang M.-C. and Cussler E.L., Designing hollow-fiber contactors, *AIChE J.* 32, 1910, 1986.
3. Prasad R. and Sirkar K.K., Dispersion-free solvent extraction with microporous hollow-fiber modules, 34, 177, 1988.
4. Wickramasinghe S.R., Semmens J., and Cussler E.L., Mass transfer in various hollow fiber geometries, *J. Membr. Sci.* 69, 235, 1992.
5. Yeh H.-M. and Hsu Y.-S., Microporous membrane solvent extraction in multiple-fiber passes and one-shell pass hollow-fiber modules, *Sep. Sci. Technol.* 33, 757, 1998.
6. Ho W.S.W. and Sirkar K.K., Eds. *Membrane Handbook*. Chapman & Hall, New York, 1992.
7. Gabelman A. and Hwang S.-T., Hollow fiber membrane contactors, *J. Membr. Sci.* 159, 61, 1999.
8. Cooney D.O. and Poufos M.G., Liquid-liquid extraction in a hollow-fiber device, *Chem. Eng. Comm.* 61, 159, 1987.
9. Basu R., Prasad P., and Sirkar K.K., Non-dispersive membrane solvent back extraction of phenol, *AIChE J.* 3, 450, 1990.
10. Yun C.H., Prasad R., and Sirkar K., Membrane solvent extraction removal of priority organic pollutants from aqueous waste streams, *Ind. Eng. Chem. Res.* 31, 1709, 1992.
11. Yun C.H., Prasad R., Guha A.K., and Sirkar K.K., Hollow fiber solvent extraction removal of toxic heavy metals from aqueous waste streams, *Ind. Eng. Chem. Res.* 32, 1186, 1993.
12. Alonso A., Urtiaga A.M., Irabien A., and Ortiz M.I., Extraction of Cr(VI) with Aliquat 336 in hollow fiber contactors: Mass transfer analysis, *Chem Eng. Sci.* 49, 901, 1994.
13. Alonso A.I., Galán B., Irabien A., and Ortiz I., Separation of Cr(VI) with Aliquat 336: Chemical equilibrium modelling, *Sep. Sci. Technol.* 32, 1543, 1997.
14. Alonso A.I., Urtiaga A.M., Zamacona S., Irabien A., and Ortiz I., Kinetic modelling of cadmium removal from phosphoric acid by non-dispersive solvent extraction, *J. Membr. Sci.* 130, 193, 1997.
15. Yoshizuka K., Yasukawa R., Koba M., and Inoue K., Diffusion model accompanied with aqueous homogeneous reaction in hollow fiber membrane extractor, 28, 59, 1995.
16. Ortiz I., Galán B., and Irabien A., Membrane mass transport coefficient for the recovery of Cr(VI) in hollow fiber extraction and back-extraction modules, *J. Membr. Sci.* 118, 213, 1996.
17. Ortiz I., Alonso A.I., Urtiaga A.M., Dermircioglu M., Kocacik N., and Kabay N., An integrated process for the removal of Cd and U from wet phosphoric acid. *Ind. Eng. Chem. Res.* 38, 2450-2459, 1999.
18. Breembroek G.R.M., Witkamp G.J., and Van Rosmalen G.M., Extraction of cadmium with tri-laurylamine-kerosine through a flat-sheet-supported liquid membrane. *J. Membr. Sci.* 146, 195, 1998.
19. Basu R. and Sirkar K.K., Citric acid extraction with microporous hollow-fibers. *Solvent. Extr. Ion Exch.* 1, 229, 1992.
20. Escalante H., Alonso A.I., Ortiz I., and Irabien A., Separation of L-phenylalanine by non-dispersive extraction and back-extraction. Equilibrium and kinetic parameters. *Sep. Sci. Technol.* 33, 119, 1998.
21. Basu R., Prasad P., and Sirkar, K., Non-dispersive solvent back-extraction of phenol. *AIChE J.* 36, 450-460, 1990.
22. Rodriguez J., Viegas R.M.C., Luque S., Coelho I.M., Crespo J.P.S.G., and Alvarez J.R., Removal of valeric acid from wastewaters by membrane contactors. *J. Membr. Sci.* 137, 45, 1997.

23. Coelho I.M., Silcivestre P., Viegas R.M.C., Crespo J.P.S.G., and Carrondo M.J.T., Membrane-based solvent extraction and stripping of lactate in hollow-fiber contactors. *J. Membr. Sci.* 134, 19–32, 1997.
24. Lin S.-H. and Juang R.-S., Mass transfer in hollow-fiber modules for extraction and back-extraction of copper (II) with LIX64N carriers. *J. Membr. Sci.* 188, 251–262, 2001.
25. Ortiz I., Urriaga A., Abellan M.J., and San Roman F. Application of hollow fiber membrane contactors for catalyst recovery in the WPO process. *Ann. NY Acad. Sci.* 984, 17–28, 2003.
26. Alonso A., Galán B., González M., and Ortiz M.I., Experimental and theoretical analysis of a non-dispersive solvent extraction pilot plant for the removal of Cr(VI) from a galvanic process wastewater. *Ind. Eng. Chem. Res.* 38, 1666, 1999.
27. Yang Z.-F., Guha A.K., and Sirkar K.K., Simultaneous and synergistic extraction of cationic and anionic heavy metallic species by a mixed solvent extraction system and a novel contained liquid membrane device. *Ind. Eng. Chem. Res.* 35, 4214, 1996.
28. Ilias S., Scimmel K.A., and Yezek P.M., Non-dispersive liquid–liquid extraction of copper and zinc from an aqueous solution by D2EHPA and LIX84 in a hollow fiber membrane module. *Sep. Sci. Technol.* 34, 1007, 1999.
29. Lee J.-C., Jeong J., Park J.T., Youn J., and Chung H.-S., Selective and simultaneous extractions of Zn and Cu Ions by hollow fiber SLM modules containing HEH/EHP and LIX84. *Sep. Sci. Technol.* 34, 1689, 1999.
30. Galán B., San Román F., Irabien A., and Ortiz I., Viability of the separation of Cd from highly concentrated Ni–Cd mixtures by non-dispersive solvent extraction. *Chem. Eng. J.* 70, 237, 1998.
31. Ortiz I., San Román F., and Galán B., Kinetics of the separation of Cd from highly concentrated aqueous solutions by non-dispersive solvent extraction. *Chem. Eng. J.* 81, 129–136, 2001.
32. Ortiz I., Galán B., San Román F., and Ibáñez R., Kinetics of the separation of multicomponent mixtures by non-dispersive solvent extraction. *AIChE J.* 47(4), 895–904, 2001.
33. Sengupta A., Basu R., and Sirkar K., Separation of solutes from aqueous solutions by contained liquid membranes. *AIChE J.* 34, 1698–1708, 1988.
34. Basu R. and Sirkar K., Hollow fiber contained liquid membrane separation of citric acid. *AIChE J.* 37, 383–393, 1999.
35. Dai X.-P., Yang Z.-F., Duo R.G., and Sirkar K.K., Lipase facilitated separation of organic acids in a hollow fiber contained liquid membrane module. *J. Membr. Sci.* 171, 183–196, 2000.
36. Way J.D. and Noble R.D., Facilitated transport. In: Ho W.S.W. and Sirkar K.K., Eds. *Membrane Handbook*. Chapman & Hall, New York, 1992.
37. Cussler E.L., *Diffusion Mass Transfer in Fluid Systems*, 2nd ed. Cambridge University Press, Cambridge, 1997.
38. Lin S.-H. and Juang R.-S., Mass-transfer in hollow-fiber modules for extraction and back-extraction of copper (II) with LIX64N carriers. *J. Membr. Sci.* 188, 251–262, 2001.
39. Yang Z.-F. and Cussler E., Reaction dependent extraction of copper and nickel using hollow fiber. *J. Membr. Sci.* 166, 229–238, 2000.
40. Loiacono O., Drioli E., and Molinari R., Metal ion separation and concentration with supported liquid membranes. *J. Membr. Sci.* 28, 123–138, 1986.
41. Takeuchi H., Takahasi K., and Goto W., Some observations on the stability of supported liquid membranes. *J. Membr. Sci.* 34, 19–31, 1987.
42. Molinari R., De Bartolo L., and Drioli E., Coupled transport of amino acids through a supported liquid membrane. I. Experimental optimisation. *J. Membr. Sci.* 73, 203–215, 1992.
43. Urriaga A.M., Ortiz I., Salazar E., and Irabien A., Supported liquid membranes for the separation–concentration of phenol. 2. Mass transfer evaluation according to fundamental equations. *Ind. Eng. Chem. Res.* 31, 1745–1753, 1992.
44. Ho W.S.W., New membrane technology for removal and recovery of chromium from waste waters. *Environ. Prog.* 20, 44–52, 2001.
45. Hu B.B. and Wiencek J.W., Emulsion liquid membrane extraction of copper using a hollow fiber contactor. *AIChE J.* 44, 570–581, 1998.
46. Ortiz I., San Roman M.F., Corvalan S.M., and Eliceche A.M., Modeling and optimisation of an emulsion pertraction process for removal and concentration of Cr(VI). *Ind. Eng. Chem. Res.* 42, 5891–5899, 2003.
47. Klaassen R., Jansen A.E., Bult B.A., Oesterholt F.I.H.M., and Schneider J., Removal of hydrocarbons from wastewater by pertraction. *Proceedings of the 7th International Symposium on Synthetic Membranes in Science and Industry*, University of Tübingen, Tübingen, Germany, 1994.
48. Urriaga A.M. and Irabien A., Internal mass transfer in hollow fiber supported liquid membranes. *AIChE J.* 39, 521, 1993.
49. Qin Y. and Cabral M.S., Lumen mass transfer in hollow-fiber membrane processes with constant external resistances. *AIChE J.* 43, 1975, 1997.
50. Qin Y. and Cabral M.S., Theoretical analysis on the design of hollow fiber modules and modules cascades for the separation of diluted species. *J. Membr. Sci.* 143, 197, 1998.
51. Alonso A. and Pantelides C.C., Modelling and simulation of integrated membrane process for recovery of Cr(VI) with Aliquat 336. *J. Membr. Sci.* 110, 141, 1996.
52. Juang R.S., Modelling of the competitive permeation of cobalt and nickel in a di(2-ethylhexyl)phosphoric acid supported liquid membrane process. *J. Membr. Sci.* 85, 157, 1993.
53. Juang R.-S. and Huang H.-C., Non-dispersive extraction separation of metals using hydrophilic microporous and cation exchange membranes. *J. Membr. Sci.* 156, 179, 1999.
54. Yoshizuka K., Sakamoto Y., Baba Y., and Inoue K., Solvent extraction of holmium and yttrium with bis(2-ethylhexyl)phosphoric acid. *Ind. Eng. Chem. Res.* 31, 1372, 1992.
55. Kubota F., Goto M., and Nakashio F., Extraction kinetics of rare earth metals by 2-ethylhexyl phosphonic acid mono-2-ethylhexyl ester using a hollow fiber membrane extractor. *Sep. Sci. Technol.* 30, 777, 1995.

56. Mohammed S.A., Inoue K., and Yoshizuka K., Kinetics of palladium extraction with bis(2-ethylhexyl)monothiophosphoric acid in a hollow fiber membrane extractor. *Ind. Eng. Chem. Res.* 34, 3899, 1996.
57. Kondo K., Yamamoto Y., and Matsumoto M., Separation of indium(III) and gallium(III) by a supported liquid membrane containing diisostearylphosphoric acid as a carrier. *J. Membr. Sci.* 137, 9, 1997.
58. Juang R.S., Permeation and separation of zinc and copper by supported liquid membranes using bis(2-ethylhexyl)phosphoric acid as a mobile carrier. *Ind. Eng. Chem.* 32, 911, 1993.
59. Ortiz I., San Román F., and Galán B., Back-extraction of Ni-Cd-D2EHPA compounds. *Sep. Sci. Technol.* 37(3), 607–625, 2002.
60. Galán B., Urtiaga A.M., Alonso A.I., Irabien J.A., and Ortiz I., Extraction of anions with ALIQUAT 336: Chemical equilibrium modelling. *Ind. Eng. Chem. Res.* 33, 1765, 1994.
61. Brooke A., Kendrick D., Meeraus A., and Raman R., *GAMS: A User Guide*. Scientific Press, Palo Alto, CA, 1998.



---

# 38 Membrane Contactors for Gaseous Streams Treatments

*Alessandra Criscuoli and Enrico Drioli*

## CONTENTS

38.1	Introduction .....	1041
38.2	What Is a Membrane Contactor? .....	1041
38.3	Basic Principles of Membrane Contactors for Gas Treatments.....	1042
38.3.1	Mass-Transfer Resistances .....	1042
38.3.2	Membrane Requirements.....	1044
38.3.3	Facilitated Transport.....	1045
38.4	Potentialities of Membrane Contactors in Gas Treatments .....	1047
38.4.1	CO <sub>2</sub> and H <sub>2</sub> S Removal.....	1047
38.4.2	VOCs Removal .....	1049
38.4.3	SO <sub>2</sub> Removal.....	1050
38.4.4	Ammonia Removal.....	1050
38.4.5	Mercury Removal.....	1050
38.4.6	Olefin/Paraffin Separations .....	1050
38.4.7	Air Dehumidification.....	1051
38.4.8	Sparkling Water Production .....	1051
38.5	Module Design.....	1052
38.6	Concluding Remarks .....	1053
	References.....	1053

## 38.1 INTRODUCTION

The process intensification theory, devoted to the development of new systems of production able to work, with respect to conventional operations, with higher efficiency and flexibility, lower energy consumption and waste production, higher capacity/size ratio, is well satisfied by membrane engineering. Beside the well-known membrane operations such as micro/ultra/nanofiltration and reverse osmosis, also membrane contactors (MC) that are gaining particular attention during the past years, as promising alternative systems to be used for the rationalization of industrial cycles, well satisfy the process intensification approach. Membrane contactors are a relatively new class of membrane operations particularly interesting for performing mass transfer between phases. The field of application covers many unit operations such as scrubbing, stripping, extractions, and concentration processes [1]. Membrane contactors are able to efficiently treat diluted streams and this aspect makes them very interesting for the purification of streams containing traces of pollutants that sometimes are difficult to remove up to the desired levels by conventional operations. This contribution would like to point out the potentialities and the drawbacks of membrane contactors, particularly for the treatment of gaseous streams, by presenting and discussing all research efforts made in this field. The role of the membrane properties and of the module design on the membrane contactors performance is underlined.

## 38.2 WHAT IS A MEMBRANE CONTACTOR?

Membrane contactors are membrane systems usually based on microporous membranes that keep two phases in contact. The presence of the membrane and the right choice of the operating pressures avoid the mixing of the phases. This implies that the flow rates of the phases can be varied independently over a wide range without any problem of flooding, loading, channeling,

**TABLE 38.1**  
**Main Advantages and Disadvantages of MC with respect to Conventional Systems**

Advantages	Disadvantages
Higher interfacial area per volume	Operative pressures dependent on breakthrough ones
No dispersion between phases	Additional resistance to mass transfer due to the membrane
Wide range of operative flow rates	Shell side bypassing
No loading or flooding limitations	Membrane fouling
No foaming	Pretreatments to reduce fouling
No separation of phases after the operation	Limited lifetime
Low-pressure drop	
Constant interfacial area between phases	
Flexibility and compactness	
Reduced size and weight	
No moving parts	
Easy scale-up due to a modular design	

or entrainment. Depending on the particular application, membranes can be hydrophobic or hydrophilic, but in both the cases they do not present any selectivity for the species involved in the mass transport: a generic compound  $i$  is transferred through the membrane micropores by only diffusion. The driving force for the permeation is related to a difference of concentration/partial pressure between the phases. Membrane distillation is the only operation that occurs thanks to a difference of temperature across the membrane. Usually the mass-transfer coefficients achievable in these systems are not higher than those related to conventional devices; however, the extremely higher interfacial area available for the mass transport leads to a higher mass transfer. The typical interfacial area per unit of volume of membrane contactors varies between 1500 and 3000 m<sup>2</sup>/m<sup>3</sup>, whereas for conventional contactors this ratio is in the range of 100–800 m<sup>2</sup>/m<sup>3</sup> [2]. Their performance is strongly related to the membrane properties. Important parameters that influence the transport are porosity, pore size, thickness, degree of hydrophobicity, breakthrough pressure, stability, thermal, mechanical, and chemical resistance. The mass transport can be enhanced by also acting on the module design and flow configurations. An uniform and turbulent flow is, in fact, preferred for avoiding fluid bypass or stagnant zones and for reducing the mass-transport resistances. However, pressure drops have to be also carefully controlled. Species that can foul the membrane have to be removed before sending the streams to be processed to the membrane units. The main advantages and disadvantages of membrane contactors are reported in Table 38.1. The following section discusses the basic principles of membrane contactors when applied in gaseous streams treatments.

### 38.3 BASIC PRINCIPLES OF MEMBRANE CONTACTORS FOR GAS TREATMENTS

The removal of species from gaseous streams in membrane contactors is usually accomplished by means of absorbent solutions. The type of absorbent liquid and its temperature, as the concentration of species to be removed in the gas and in the liquid phase, influence the mass transport. The selectivity of separation can be determined by selecting the absorbent solution; making this choice, the eventual production of toxic by-products and the impact on the environment have to be taken into account.

When hydrophobic membranes are used (olefins are preferred because of their low cost), the aqueous absorbent cannot penetrate through the pores and the membrane is gas filled; whereas if hydrophilic membranes are employed, the membrane is liquid filled (Figures 38.1 and 38.2). Latter situation is preferred only if the reaction between the gaseous species and the absorbent solution is fast or instantaneous; if not, it is better to work with a gas-filled membrane, to reduce mass-transfer resistances. The module design and flow configuration also play an important role in defining the membrane contactors efficiency. This aspect is discussed in detail in Section 38.5.

#### 38.3.1 MASS-TRANSFER RESISTANCES

The resistances to the mass transport that a species encounters when is transferred from the gas to the liquid phase are reported in Figure 38.3. Gas and liquid phases contribute to the overall resistance because of the formation of boundary layers close to the membrane surface. This implies that the concentration of a generic species  $i$  in the bulk of the two phases is different from its concentration at the membrane surfaces. The resistance offered by the membrane with gas-filled pores will be different (generally lower) than that with liquid-filled pores, due to the different effective diffusion coefficients. The overall mass-transport coefficient is given by

$$\frac{1}{K_L} = \frac{1}{k_1} + \frac{1}{k_m \cdot H} + \frac{1}{k_g \cdot H} \quad (38.1)$$

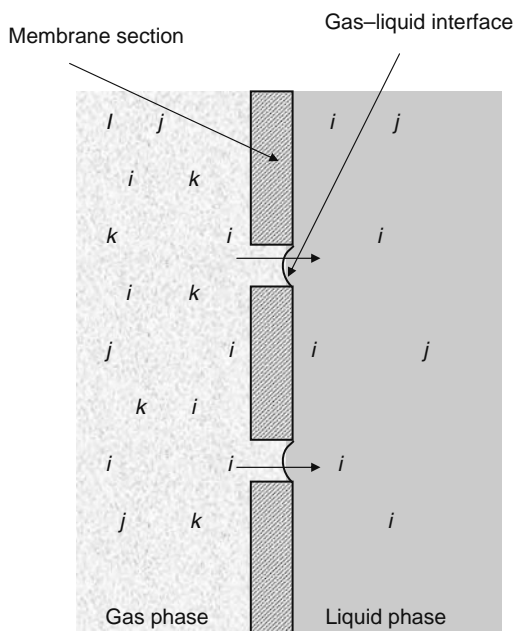


**FIGURE 38.1** Contact between gas and liquid in a hydrophobic membrane contactor. The species *i* diffuses through the membrane gas-filled micropores from the gas phase to the liquid absorbent.

where

- $K_L$  denotes overall mass-transfer coefficient (m/s)
- $k_l$  denotes liquid mass-transfer coefficient (m/s)
- $k_g$  denotes gas mass-transfer coefficient (m/s)
- $k_m$  denotes membrane mass-transfer coefficient (m/s)
- $H$  denotes Henry's constant

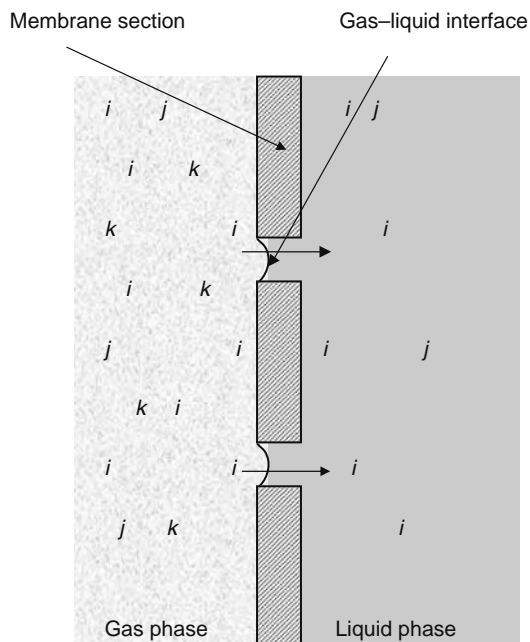


**FIGURE 38.2** Contact between gas and liquid in a hydrophilic membrane contactor. The species *i* diffuses through the membrane absorbent-filled micropores from the gas phase to the liquid absorbent.

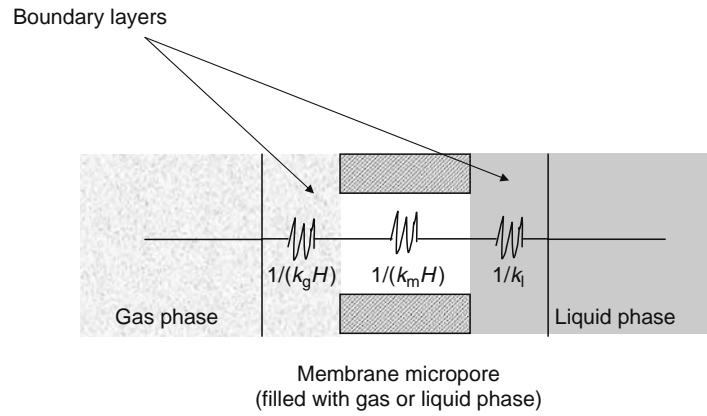


**FIGURE 38.3** Resistances to the mass transport offered by the gas, membrane, and the liquid. The resistance offered by the membrane will depend on the phase presents into the micropores.

$k_g$  and  $k_l$  can be calculated by using correlations that are function of fluid properties and flow rates, such as

$$Sh = aRe^b Sc^c \quad (38.2)$$

where

$Sh$  denotes the Sherwood number

$Re$  denotes the Reynolds number

$Sc$  denotes the Schmidt number

The constants (a, b, and c) that appear in the above expression are available in literature and are specific for the particular system employed for carrying out the experiments [1,3–5].

$k_m$  is usually derived by

$$\frac{1}{k_m \cdot H} = \frac{\delta \tau}{D_{\text{eff}} \varepsilon H} \quad (38.3)$$

where

$\delta$  denotes membrane thickness (m)

$\tau$  denotes membrane tortuosity (dimensionless)

$\varepsilon$  denotes membrane porosity (dimensionless)

$D_{\text{eff}}$  denotes effective diffusion coefficient of  $i$  through the membrane ( $\text{m}^2/\text{s}$ )

For enhancing the removal, it is important to reduce those resistances as much as possible by acting on the fluid dynamic (for  $k_g$  and  $k_l$ ) and on the membrane properties (for  $k_m$ ). Increments of the liquid and gas flow rates, as a module design that promotes turbulent flow, lead to a reduction of gas and liquid boundary layers, with consequent improvements of the mass transport.

The expressions above reported for describing the mass transport are relative to inert membranes; sometimes phenomena of interfacial absorption between the species to be transferred and the membrane material could happen. In these cases, other parameters have to be considered and the equations become more complex.

### 38.3.2 MEMBRANE REQUIREMENTS

From Equation 38.3, it results that the mass-transport coefficient in the membrane increases as the porosity increases and as the thickness and tortuosity decrease. These parameters are related to each other; the tortuosity, for instance, is a function of the porosity of the membrane and the specific porosity–tortuosity relationship depends on the manufacturing method [6].

The two parameters can be correlated by the empirical expression [6]:

$$\tau = \frac{(2 - \varepsilon)^2}{\varepsilon} \quad (38.4)$$

Fractal theories of random walks developed a different expression [6]:

$$\tau = \frac{1}{\varepsilon} \quad (38.5)$$

Iversen et al. [6] found that for a polymer structure similar to the interstices between closely packed spheres (phase inversion membrane), Equation 38.4 is able to well describe the tortuosity–porosity relationship; whereas for a polymer structure similar to random spheres or clusters (stretched membrane), Equation 38.5 has to be used.

Other important properties to consider in membrane manufacturing are the degree of hydrophobicity, the pore size and the pore size distribution, the chemical, thermal, and mechanical stability. The hydrophobicity is fundamental for preventing the presence of liquid through pores. It can be determined by contact angle measurements (CAM). The technique measures the angle formed between the liquid and the membrane pore. The obtained results are dependent on the morphology of the membrane surface, such as the roughness, that strongly influences these types of measures [7]. Higher pore size leads to higher fluxes but also to lower breakthrough pressures (pressures at which liquid starts to penetrate into the pores and the membrane loses its hydrophobic character). The breakthrough pressure for gas/liquid operations is given by the Laplace's equation:

$$\Delta p = \frac{(2\sigma \cos \theta)}{r} \quad (38.6)$$

where

$\sigma$  denotes surface tension

$\theta$  denotes contact angle

$r$  denotes pore radius

The pore size distribution has to be carefully controlled to ensure the same performance along the membrane; moreover, to avoid coalescence of bubbles, a particular distance among adjacent pores is required. The chemical stability of the membrane also plays an important role when using absorbent solutions. Hydrophobic membranes in contact with absorbents can interact with them, changing their structure and morphology and losing hydrophobicity. The resistance to the mass transport increases and also the influence of operating conditions on the system can vary. Malek et al. [8], for example, found that under partially wetted conditions, by increasing the liquid flow rate, there is a maximum for the overall mass-transfer coefficient; whereas for both wetted and nonwetted conditions, the overall mass-transfer coefficient always increased with liquid velocity.

The problem of the interactions between membrane and absorbent solution interests, for instance, the removal of CO<sub>2</sub>. Reactive absorption liquids, such as amines, that are used for this type of removal, usually wet polyolefin membranes. Wettability depends on the surface tension of the liquid, membrane material, contact angle, and pore properties of the membrane. Possible solutions to this problem are to employ more resistant membrane materials, to use different absorbent liquids, and to deposit a nonporous layer on the membrane surface that prevents any passage of the liquid through pores. In order to do not increase too much the resistance to the mass transport, the layer has to be thin and highly permeable to the gaseous species. The dense skin can be useful also for avoiding any possible contamination of the feed gas by the absorbent (Figure 38.4).

Once the absorbent exits from the contactor, it can be regenerated in another membrane contactor unit both by stripping with vacuum or by sweep and by heating. Figure 38.5 reports a simplified scheme for an absorber–desorber flow sheet with the desorber operating under vacuum.

### 38.3.3 FACILITATED TRANSPORT

Beside the systems until now described, facilitated transport membranes can be also used for gas streams treatments [9,10]. Due to the presence of carriers specific for the species to be removed, these types of membrane contactors are characterized by very high selectivity. In supported liquid membranes (or immobilized liquid membranes [ILMs]), a carrier solution is impregnated in the micropores; Figure 38.6 shows the mechanism of these systems. The support properties are certainly important for the overall performance (higher porosity and lower thicknesses, for example, lead to higher fluxes; the substrate structure affects also the minimum thickness needed to maintain the ILM integrity). Membrane instability due to the loss of the carrier solution and the long-term stability of the carrier-self are the main drawbacks of these systems and different solutions have been attempted by researchers to improve their efficiency. Sirkar [11] placed the solution between two porous membranes, but the thickness was too high to guarantee high fluxes. A reduction of the diffusional resistance has been obtained by Teramoto et al. [12] by moving the solution between the two microporous membranes. However, a reduction of selectivity and a wetting of the micropores by the liquid have been registered.

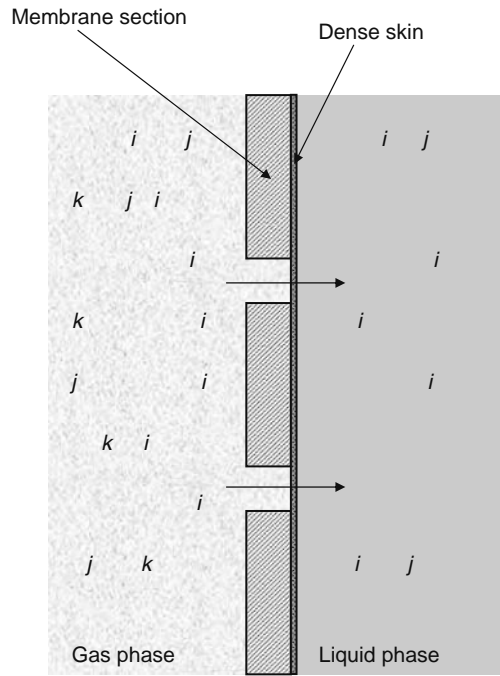


FIGURE 38.4 Composite membrane with a dense skin coated on the microporous surface.

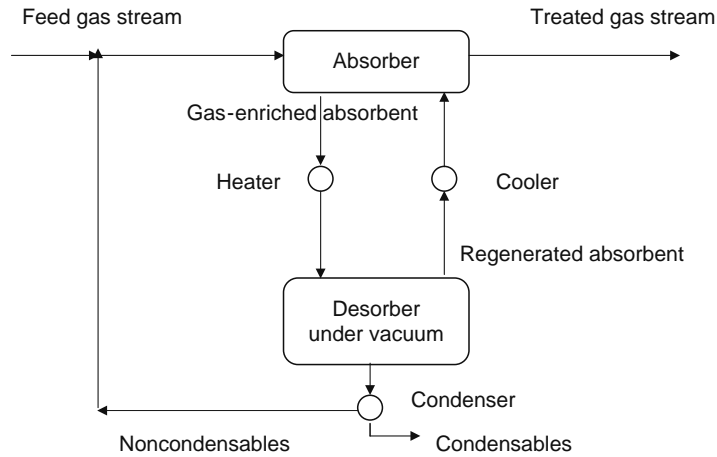


FIGURE 38.5 Schematic absorption-desorption flow sheet with the desorber operating under vacuum.

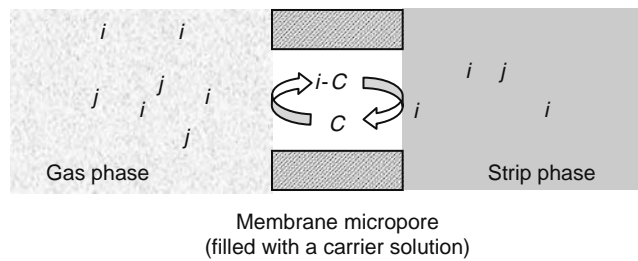


FIGURE 38.6 Example of a supported liquid membrane. The carrier ( $C$ ) contained in the membrane micropore selectively transports the species  $i$  from the gas to the strip phase.

A novel polymeric bicontinuous microemulsion (PBM) membrane, consisting of an interconnecting network of nanometer pore size water channels, was employed as liquid membrane support [13] for the immobilization of new porphyrin carrier [14] for facilitated oxygen transport. Although the membrane resulted to be stable due to the nanoporous structure, a modest (2.3–2.4) O<sub>2</sub>/N<sub>2</sub> selectivity was achieved.

In Section 38.4, studies and results obtained by applying membrane contactors to processes of industrial interest are reported and discussed. In particular, the research efforts made to improve membrane contactors performance are furnished for

- CO<sub>2</sub>, H<sub>2</sub>S, volatile organic compounds (VOCs), SO<sub>x</sub>, NH<sub>3</sub>, and Hg removal
- Olefin/paraffin separation
- Air dehumidification

Results on the use of membrane contactors for the sparkling water production are also presented.

### 38.4 POTENTIALITIES OF MEMBRANE CONTACTORS IN GAS TREATMENTS

Industrial productions lead to substantial emissions of gaseous streams containing pollutants such as acid gases, VOCs, SO<sub>x</sub>, NH<sub>3</sub>, and Hg. Each of them is responsible for severe impact on the environment. CO<sub>2</sub> is the main responsible gas of greenhouse; VOCs are one of the main sources of photochemical reactions in the atmosphere; H<sub>2</sub>S, SO<sub>x</sub>, NH<sub>3</sub>, and Hg are toxic compounds. Traditional techniques more often employed for their recovery are absorption in liquid solvents and adsorption on zeolites or activated carbon. These operations present some drawbacks such as reduced contact area, large-sized equipment, high energy consumption, and regeneration of spent carbon and zeolite beds. Furthermore, on the basis of the more stringent regulations, the desired removals are not easily achieved. When the compounds to be removed are present in the gas stream in ppm, gas separation by membranes can also be not effective because of the low driving force available. On the contrary, membrane contactors in membrane-based absorption process are able to drastically reduce their amount also acting on a very diluted feed.

Results on their performance for the olefin/paraffin separation are also of interest. This type of separation is highly energy intensive because the boiling points are extremely close and conventional cryogenic distillation is difficult and expensive. Another interesting field for membrane contactor applications is the humidity control of air. This process is extremely important in both living and working spaces. The direct-contact systems employed for carrying out this operation suffer from different problems, such as the carryover of solution droplets and the reduced contact area that depends on the relative flow rates.

Membrane contactors can be applied also to the sparkling water production. In beverage industry, the sparkling water is usually produced in two towers of large size (stripper and absorber); on the contrary, membrane contactors are able to carry out the process in the same unit with a substantial reduction in size.

#### 38.4.1 CO<sub>2</sub> AND H<sub>2</sub>S REMOVAL

The removal of CO<sub>2</sub> by membrane contactors has been investigated by several authors. Aqueous solutions of amines are commonly used as absorbers. The complexes that these solutions create with CO<sub>2</sub> are weak and can be easily broken by heating (regeneration step). Mavroudi et al. [15] used a commercial hollow fiber membrane contactor for absorbing CO<sub>2</sub> from a 15% CO<sub>2</sub>–85% N<sub>2</sub> mixture simulating a typical composition of flue gases from a coal combustion power plant. Both water and aqueous DEA were used as absorbents. At low gas flow rates, an increase in the water flow rate led to a higher removal, due to the reduction of the mass-transport resistance, whereas for high gas flow rates, the same removal can be achieved only in a higher volume module that provides more gas–liquid contact area. At low liquid DEA flow rates, the solution is saturated with CO<sub>2</sub> and there is a reduction in the mass transfer; the removal is increased by operating at high flow rates. Higher removals are achieved also at higher DEA concentration, due to the increase in the reaction rate. The removals obtained varied from 75% (water) to 99% (DEA). From a comparison with packed towers, it resulted that membrane contactors have HTU values significantly smaller, representing very compact and efficient systems. The compactness of these systems has been also pointed out by Falk-Pedersen and Dannstrom [16]. Authors studied the separation of CO<sub>2</sub> from offshore gas turbine exhaust by amine absorption. The work was related both to an absorption and a desorption membrane-based unit. The possible wetting of the membrane has been analyzed for different membranes (PP, PES coated with PDMS, PP coated with PDMS, GORE-TEX ePTFE). Among them, only GORE-TEX and PTFE were not wetted. The membranes were chemically stable in both absorber and desorber units. By comparing the conventional absorbers and desorbers and the gas/liquid contactors, for 86% of removal, it resulted in 72% and 78% size reduction for absorber and desorber, respectively and 66% weight reduction for both absorber and desorber. The effect of the

membrane wetting on the mass transfer has been studied also by Rangwala [17] who used water, aqueous NaOH, and DEA for absorbing CO<sub>2</sub> from an air stream in a hollow fiber membrane module equipped with polypropylene fibers. The feed CO<sub>2</sub> concentrations were in the range of 1–10 mol%. Due to the partial wetting of the pores, the mass-transfer resistance offered by the membrane increased significantly. Author calculated that even for less than 2% wetting of pores, the membrane resistance can be the 60% of the total mass-transfer resistance. The effect of DEA on two types of polypropylene microporous membranes (Celgard X40-200 and Celgard X50-215) has been investigated by Wang et al. [18]. The membrane surface morphology and surface tension were monitored with and without CO<sub>2</sub> loading. Both membranes suffered from changes in pore structure and surface roughness and hydrophobicity reduction. However, the Celgard X50-215, due to its thicker microfibrils, presented less morphological and hydrophobic changes. When CO<sub>2</sub> was loaded, carbamate ions were formed from interactions between CO<sub>2</sub> and DEA and the micropores deformation was reduced for both membranes. This result suggests that the use of a membrane with high porosity could lead to an enhancement of the system efficiency, due to the larger contact area between DEA and CO<sub>2</sub>.

CO<sub>2</sub> has been removed from flue gas of thermal power plants by using a PTFE hollow fiber gas–liquid membrane contactor [19]. MEA absorbent (5 mol/L) flowed inside a PTFE hollow fiber membranes while the gas stream (CO<sub>2</sub>, 15%; O<sub>2</sub>, 5%; N<sub>2</sub>, 80%) was fed outside. The membrane was stable for more than 6600 h and the overall volumetric mass-transfer coefficient for the membrane system was more than five times larger than that of the packed bed device. PTFE fibers are usually not available in small diameters and are more expensive than polyolefin membranes. Authors analyzed also the performance of a PE membrane that resulted more susceptible to wetting. By modifying its surface with fluorocarbonic materials, its hydrophobicity was increased. Researches of new absorption liquids for CO<sub>2</sub> have been carried out. TNO, The Netherlands, patented a new absorption aqueous liquid, called CORAL, based on amino acids and alkaline salts. With respect to conventional amines, the new absorber allows to operate for long time with cheaper membranes, such as polyolefins, because it does not wet them, has high oxygen stability, corrosion resistance, and better degradation properties. Furthermore, the vapor pressure of the active component is zero; therefore, its losses due to evaporation are avoided. Kumar et al. [2] reported on the wetting of microporous membranes by different classes of alkanolamines and amino acid salt solutions. The stability of the membrane absorber was tested in a single PP fiber reactor for 72 h. During this period, the CO<sub>2</sub> flux dropped by only 6% in the first 30 min. Feron and Jansen [20] carried out CO<sub>2</sub> absorption and absorber regeneration experiments to verify the feasibility of the process. CO<sub>2</sub> and air were mixed and fed to a prototype transversal-flow membrane absorber equipped with PP fibers. The liquid stream was fed through the membrane lumen and the gas fed outside the fibers. The CO<sub>2</sub> flux increased with the CO<sub>2</sub> partial pressure and the temperature and decreased when the cyclic liquid loading was increased. The CORAL liquid showed a higher mass transfer with respect to other membrane gas absorption systems reported in literature.

Quinn et al. [21] investigated as absorbents for CO<sub>2</sub> melts of salt hydrates such as tetramethylammonium fluoride tetrahydrate [(CH<sub>3</sub>)<sub>4</sub>N]F·4H<sub>2</sub>O and tetraethylammonium acetate tetrahydrate [(CH<sub>3</sub>)<sub>4</sub>N]CH<sub>3</sub>CO<sub>2</sub>·4H<sub>2</sub>O. They found that the CO<sub>2</sub> absorption capacity of salt hydrates is dependent on the water content of the salt, decreasing as the water content increases. The salts showed a large and reversible acid gas absorption capacity and when melts containing CO<sub>2</sub> were cooled to temperatures of solidification, the CO<sub>2</sub> was spontaneously desorbed [22]. This implies that the absorbent can be easily cycled by acting on temperature. Quinn et al. [23] immobilized the melts of salt hydrates in a hydrophilic Celgard 3401 membrane and studied their performance for the separation of CO<sub>2</sub> from H<sub>2</sub> and CH<sub>4</sub> by varying feed and sweep gas (helium) dew point, temperature, and CO<sub>2</sub> partial pressure. For the [(CH<sub>3</sub>)<sub>4</sub>N]F·4H<sub>2</sub>O melt, the CO<sub>2</sub>/CH<sub>4</sub> selectivity ranged between 12 and 120, whereas the CO<sub>2</sub>/H<sub>2</sub> selectivity was extremely low. This result has been attributed to the hydrogen permeability of the Celgard membrane. To reduce the permeation of hydrogen, the liquid melt has been supported on the surface of a film of poly(trimethylsilylpropyne). The new system led to CO<sub>2</sub>/CH<sub>4</sub> and CO<sub>2</sub>/H<sub>2</sub> selectivity ranging between 140–800 and 30–360, respectively, depending on the CO<sub>2</sub> partial pressure. Chen et al. [24] studied the performance of glycerol-based immobilized liquid membranes (ILMs) in the micropores of hydrophilic hollow fibers for the selective separation of CO<sub>2</sub> from N<sub>2</sub> for space suit applications. Two carriers have been considered: sodium carbonate and glycine–Na. The latter carrier is more soluble in glycerol than sodium carbonate, providing more carriers for CO<sub>2</sub> transport and decreasing N<sub>2</sub> permeance. Glycine–Na–glycerol has been immobilized in polysulfone microporous hollow fibers. Due to the low volatility of glycerol, the membranes showed a good stability after 300 h of prolonged runs. Tests have been carried out by feeding the mixture at the tube side and helium at the shell side. CO<sub>2</sub> permeance is increased with the carrier concentration and decreased with an increase of CO<sub>2</sub> partial pressure difference. Feed/sweep relative humidities (RHs) also influenced the performance, by acting on the species solubilities and diffusivities: lower permeance and higher CO<sub>2</sub>/N<sub>2</sub> selectivities were achieved at lower feed stream RHs. The highest obtained selectivity was over 5000. However, to achieve the CO<sub>2</sub> permeances needed for the application, the ILM thickness has to be reduced. The facilitated transport of CO<sub>2</sub> through liquid membranes has been also investigated by Teramoto et al. [25]. To overcome the typical drawbacks of supported liquid membranes, authors propose a system where a carrier solution (liquid membrane) is supplied to the feed side (at high pressure) and permeates through the membrane at the low-pressure side. In these conditions, the membrane is always wetted and its surface is covered with a thin layer of the membrane liquid. A poly(ether sulfone) ultrafiltration membrane and an aqueous solution of DEA as carrier have been chosen for the experiment. The feed mixture was CO<sub>2</sub> and CH<sub>4</sub> and the sweep gas was helium. An interesting result is that by increasing the carrier solution

circulation rate the  $\text{CO}_2$  permeance increases, due to the convective flow. The  $\text{CO}_2/\text{CH}_4$  selectivity was 1970 and the membrane kept its stability for more than 2 months.

As for carbon dioxide, several absorbents can be used for removing hydrogen sulfide from gaseous streams. A comparison among different extractants has been reported by Qi and Cussler [26]. They used a microporous symmetric polypropylene hollow fiber module with the liquid pumped at the tube side and the gas fed outside the fibers. The investigated aqueous solutions were NaOH, MEA, DEA, triethanolamine (TEA), 2-amino-2-methyl-1-propanol (AMP), and 2-(ethylamino)-ethanol (EAE). The mass-transfer coefficients were higher for the strong base (0.0073 m/s), but due to the fast reaction, the main resistance to the transport was located in the membrane. When using amines, the reaction is slower and the mass resistance offered by the liquid becomes more important. This solution is preferred also because amines are cheaper with respect to strong bases. Amine solutions can be effective also for the  $\text{CO}_2$  absorption. Often both gases are present in mixture, and when  $\text{H}_2\text{S}$  is the species to be preferentially absorbed, the  $\text{H}_2\text{S}/\text{CO}_2$  selectivity of the extractants has to be taken into account. Authors studied the simultaneous absorption of the two gases from air (20%  $\text{H}_2\text{S}$ , 17%  $\text{CO}_2$ ). From the experiments, the  $\text{H}_2\text{S}/\text{CO}_2$  selectivity was over 30 for TEA, 11 for AMP, and 5 for EAE. Li et al. [27] used a 10% NaOH solution for the removal of  $\text{H}_2\text{S}$  from a nitrogen stream ( $\text{H}_2\text{S}$  concentration, 16–24 ppm). The solution was fed into the shell side of an asymmetric hollow fiber membrane module, while the gaseous stream flowed countercurrently into the fibers. Two types of asymmetric membranes were prepared: asymmetric polysulfone (microporous) and asymmetric poly(ether sulfone) (dense). The former showed a mass-transport coefficient higher than the one obtained by Qi and Cussler [26] (0.0125–0.025 vs 0.0073 m/s), while the latter showed much lower values ( $5 \times 10^{-4}$  m/s), due to the dense layer formed. However, the membrane resistance controlled the process for both membranes. To improve the removal, it is important to increase the porosity of the layer and to reduce the substrate resistance, keeping the mean pore size of the membrane small to avoid the membrane wetting. Beside these problems, the authors pointed out that the reduction of the mass-transfer rate can be compensated by increasing the driving force (an increase of the feed gas pressure does not lead to bubble formation in the liquid side, due to the presence of the skin layer). Wang et al. [28] reported complete removal of  $\text{H}_2\text{S}$  from a nitrogen stream containing 17.9–1159 ppm  $\text{H}_2\text{S}$ , by using an asymmetric porous PVDF hollow fiber membrane and 2 M  $\text{NaCO}_3$  aqueous solution. The process was strongly influenced by the gas-phase pressure: a small pressure gradient across the membrane resulted in a viscous flow through the membrane that reduced the membrane resistance. Authors compared the results achieved by feeding the gas mixture to the lumen side with those obtained for a feed to the shell side. Due to channeling in the shell side, the gas-film resistance was significant in the latter configuration and the mass-transfer coefficient resulted to be half of that in the lumen side. Furthermore, the resident time is about eight times longer. The absorbent capability for  $\text{H}_2\text{S}$  of  $[(\text{CH}_3)_4\text{N}]\text{F} \cdot 4\text{H}_2\text{O}$  has been investigated by Quinn et al. [29], who immobilized it in a microporous hydrophilic membrane (Celgard 3401).  $\text{H}_2\text{S}$  was preferentially absorbed with respect to  $\text{CH}_4$  (selectivities ranging from 34 to 140) and  $\text{CO}_2$  (selectivities of 6–8). The presence of  $\text{H}_2\text{S}$  in the feed stream strongly reduced the  $\text{CO}_2$  permeation (e.g., from 1300 to 100 Barrer), due to the competition for the same carrier.

### 38.4.2 VOCs REMOVAL

The removal of VOCs from air and gaseous streams can be effectively carried out by membrane contactors. Poddar et al. [30] investigated the performance of a combined absorption-stripping process for removing VOCs from air. The considered VOCs were toluene, dichloromethane, acetone, and methanol. The absorber was a polypropylene microporous hollow fiber where contaminated air was fed at the lumen side and the absorbent was countercurrently sent at the shell side. Two absorbents (silicone oil and Paratherm), water insoluble and nonvolatile, were used. The silicone oil had higher diffusivities but lower stability. The spent absorbent was sent to a desorber, where it was regenerated by applying vacuum and recycled to the absorber unit. The membranes used in the desorber were hydrophobic polypropylene hollow fibers with an ultrathin and highly VOC-permeable plasma-polymerized nonporous silicone skin on the outer surface. The vacuum was applied at the tube side. The VOC concentration in the feed was around 1000 ppmv and the operative temperature was around 22°C. The investigated system resulted to be able to remove VOC. An interesting result achieved was that for dichloromethane, the coupled absorption-desorption system led to a lower removal than the absorption alone with fresh absorbent; whereas for methanol, the performance was almost the same. This difference can be related to the lower Henry's value for methanol that can be desorbed more effectively than dichloromethane. Possible ways for improving the regeneration step are to operate at higher temperatures and/or with a larger membrane area.

VOCs can also be removed by applying vacuum and using composite membranes as, for example, in the VaporSep process commercialized by the MTR, where a porous support is used for a silicone membrane coating in a spiral wound configuration. Hydrophobic polypropylene hollow fibers with an ultrathin and highly VOC-permeable plasma-polymerized nonporous silicone skin on the outer surface can be also effective [31–33].

As the membrane-based absorption process is usually efficient if the VOC concentration in the feed is ranging between 300 and 100 ppmv, whereas the membrane-based vapor permeation process is more effective at higher VOC concentrations, Poddar and Sirkar [34] studied the potentialities of a hybrid system where the two processes are coupled. The vapor permeation

and the desorber operated with the polypropylene having the ultrathin dense layer coating, whereas the absorber employed microporous polypropylene hollow fibers. The hybrid system was effective and led to very high removal of methylene chloride (99.97%).

As for CO<sub>2</sub>, VOCs can also be removed by using immobilized liquid membranes. Obuskovic et al. [35] immobilized a thin layer of silicone oil in the microporous of the hollow fiber polypropylene membrane beneath the dense-coated skin. The performance of the system has been proved for toluene, methanol, and acetone removal from N<sub>2</sub>. With respect to the simple hollow fiber, the presence of the oil layer led to a 2–5 VOC more enriched permeate (due to the reduction of nitrogen flux) with a separation factor of 5–20 times higher (depending on the VOC and the feed gas flowrate). The membrane was stable for 2 years.

### 38.4.3 SO<sub>2</sub> REMOVAL

The removal of SO<sub>2</sub> from gaseous streams can be achieved by absorption in hydrophobic membrane contactors. When strong bases, such as aqueous solutions of NaOH, are used, the main resistance to the mass transport is offered by the membrane [26]. Jansen et al. [36] used Na<sub>2</sub>SO<sub>3</sub> as reactive absorbent and studied its efficiency for removing SO<sub>2</sub> from both nitrogen and real flue gas coming from a coal-fired boiler. In both cases, high recoveries were obtained. The system kept its performance after a period of 500 h, without any problem of fouling or interactions with other flue gas components. On the basis of these results, the TNO group built a pilot plant with a capacity of 100 N m<sup>3</sup>/h in Holland; over 95% of recovery was obtained.

Pilot plant studied have also been performed by Larsen et al. [37], who obtained stable operation and more than 95% SO<sub>2</sub> removal from flue gas streams with a gas-side pressure drop of less than 1000 Pa. The importance of the membrane structure on the SO<sub>2</sub> removal has been studied by Iversen et al. [6], who calculated the influence of the membrane resistance on the estimated membrane area required for 95% SO<sub>2</sub> removal from a coal-fired power plant. Authors performed experiments on different hydrophobic membranes with sodium sulfite as absorbent to measure the SO<sub>2</sub> flux and the overall mass-transfer coefficient. The gas mixture contained 1000 ppm of SO<sub>2</sub> in N<sub>2</sub>. For the same thickness, porosity, and pore size, membranes with a structure similar to random spheres (typical of stretched membranes) showed a better performance than those with a closely packed spheres structure.

### 38.4.4 AMMONIA REMOVAL

Qi and Cussler [26] investigated the removal of ammonia by H<sub>2</sub>SO<sub>4</sub>. H<sub>2</sub>SO<sub>4</sub> being a strong acid, the mass resistance offered by the membrane controlled the process. An industrial membrane gas absorption unit for ammonia recovery from an ammonia containing off-gas stream produced in a dyes intermediates production plant has been installed by TNO. The membrane plant is able to remove 99.9% of ammonia and produces aqueous solutions of 27% ammonia that can be reused in the dyes process [38].

### 38.4.5 MERCURY REMOVAL

Free metallic mercury vapor contained in waste-incineration and soil thermal treatment off-gas, natural gas and the glycol-overhead in a natural gas dryer has been removed by van der Vaart et al. [39] by an oxidative gas absorption. Their study included the selection of the oxidizing agent and the selection of the most suitable membrane material. H<sub>2</sub>O<sub>2</sub> and K<sub>2</sub>S<sub>2</sub>O<sub>8</sub> were chosen for carrying out tests on the basis of their impact on environment and the materials used, the mercury solubility, and the reaction products formed. The stability of several membranes with these oxidizers was also analyzed and the PTFE membrane was selected. The experimental tests were performed in a device patented by TNO, equipped by hollow fibers. At low oxidation potential (H<sub>2</sub>O<sub>2</sub>), the mass-transfer coefficient resulted to be dependent on the liquid flow rate, but at high oxidation potential the mass-transfer coefficient was higher and independent on it. The regeneration of the absorbent liquid was obtained by the precipitation of mercury sulfide. Authors estimated also the membrane area and the costs related to the process for obtaining the target removals of the three streams analyzed and they found that for the glycol-overhead stream, the economy of the process is controlled by the mercury removal step.

### 38.4.6 OLEFIN/PARAFFIN SEPARATIONS

The olefin/paraffin separation has also been studied in membrane contactors, mainly by using as absorbent a solution containing silver nitrate [40,41]. To prevent the wetting of pores by the aqueous solution, efforts have been made for developing a stable composite hollow fiber membrane to be used for ethylene/ethane separation [42]. Polypropylene hollow fibers were used as support material while different top layer materials (ethylene propylene diene terpolymer, EPDM; sulfonated poly(ether ether ketone), SPEEK; polyethylene oxide, PEO; and poly(butylene terephthalate), PBT) were tested and compared in terms of permeability, selectivity, and stability. The experiments included an absorption step coupled to a desorption by stripping gas. The EPDM offered high permeabilities but low selectivities (14.7–72.5), whereas the SPEEK resulted in high selectivities (>2700) and low permeabilities. PEO/PBT top layers gave permeabilities (40–50 Barrer) similar

to EPDM and selectivities of 165. The last system seems to be attractive mainly because it presents the advantage of a constant selectivity even at high liquid flow rates, where the ethylene permeability may exceed the permeability of EPDM.

Tsou et al. [43] removed efficiently ethylene from a mixture of 74/26 ethylene/ethane by using a hydrophilic hollow fiber membrane module with the silver nitrate solution at the tube side.

Selectivities of around 850 for 1-butene/*n*-butene have been achieved by Kovvali et al. [44] by using a glycerol-based immobilized liquid membrane.

### 38.4.7 AIR DEHUMIDIFICATION

Hydrophobic microporous membranes have been applied to the air dehumidification by Isetti et al. [45]. The moisture contained in the air stream was removed by using absorbent solutions such as LiCl and Ca(NO<sub>3</sub>)<sub>2</sub>. Desiccant reactivation can be achieved in a similar device with warm air. In particular, by operating the regeneration step with a thin membrane, the temperature required for obtaining a certain desorbed vapor flux is reduced. With a polyethylene membrane (thickness, 170 μm) vapor fluxes of 200 g/m<sup>2</sup> h are reached at a solution temperature of 323 K, whereas with a PTFE membrane (thickness, 28 μm), the solution temperature can be reduced of 10 K, with a consequent energy saving. Bergero and Chiari [46] used a cross-flow contactor equipped by polypropylene hollow fibers for air humidification with water and air dehumidification with LiCl-saturated solutions. For both cases, high mass-transfer efficiency has been achieved. As important result, they reported that the variation in the specific humidity of the air reduced as the air flow rate increased and was independent on the liquid flow rate; as the air flow rate increased, the contactor reduced its efficiency. GVS SpA (Italy) manufactures and commercializes flat membrane contactors to control air humidity. They are based on microporous hydrophobic materials such as supported (on polyester nonwoven) films in PTFE, PVDF, or PP superficially treated to increase the hydrophobicity. Typical absorbents used are LiCl, TEG, and CaCl<sub>2</sub>. The water vapor exchange achievable in these systems is 1.5 kg/m<sup>2</sup> h. The regeneration step can occur by dry air stripping or by heating the absorbent solution. Among various positive aspects, these membrane contactors have lower capital and operating costs, up to 50% less than traditional dehumidifiers, low-pressure drops, and low noise emissions [47].

### 38.4.8 SPARKLING WATER PRODUCTION

Membrane contactors can be efficiently used also for the sparkling water production. In this case, the water is sent at one side of the hydrophobic membrane and the CO<sub>2</sub> stream is sent at the other side for simultaneously removing the oxygen contained in the water and performing the carbonation. With respect to conventional systems that use two separate columns for the oxygen stripping and the CO<sub>2</sub> injection, membrane contactors are able to carry out the two processes in a single device. Criscuoli et al. [5] analyzed the performance of a commercial hollow fiber module (LiquiCel, Hoechst Celanese), when varying different operating conditions (temperature, pressure, flow rates, oxygen concentration in the water, etc.), in terms of degree of water carbonation, oxygen removal, mass-transport resistances involved. Experimental tests have been coupled to a mathematical model, developed with the aim to establish an appropriate correlation for the calculation of the mass-transfer coefficient at the shell side. In all experimental runs, the system kept its hydrophobicity and the liquid flow rate offered the highest mass-transfer resistance, controlling the transport of both gases between the two phases. Authors applied the model to calculate the membrane area required for treating, with the same efficiency, industrial flow rates. The achieved results were used for determining the costs related to membrane contactors and comparing them with those of traditional devices (Table 38.2). Membrane contactors are more compact, consume less CO<sub>2</sub>, and are less expensive in terms of investment costs, while having higher operating costs related to the membrane replacement voice (about €25,000/year). However, because both capital and operating costs have been calculated on the basis of the unitary cost of a single commercial module, their significant reduction in large-scale applications

**TABLE 38.2**  
**Comparison between Traditional**  
**Systems and MC**

	Traditional/MC
Equipment cost (€)	2.24
CO <sub>2</sub> consumption (kg/h)	1.73
Membrane replacement (€/year)	0
Volume (m <sup>3</sup> )	12

Source: Adapted from Criscuoli, A., Drioli, E., and Moretti, U., *Ann. N.Y. Acad. Sci.*, 984, 1, 2003.

**TABLE 38.3****Summary of the Main Improvements Achieved by MC for Some of the Investigated Applications**

Application	
CO <sub>2</sub> removal	Overall volumetric mass-transfer coefficient more than five times larger than that of the packed bed device [19] 72% reduction in size and 66% reduction in weight for the absorption step, and 78% reduction in size and 66% reduction in weight for the desorption step [16]
H <sub>2</sub> S removal	Complete removal from a nitrogen stream containing 17.9–1159 ppm H <sub>2</sub> S in one stage [28]
VOCs removal	99.97% removal of methylene chloride [34]
NH <sub>3</sub> removal	99.9% removal of ammonia and production of aqueous solutions of 27% of ammonia that can be reused in the dyes process [38]
Olefins/paraffins separations	Lower energy consumption because there is no need to operate at very low temperatures and high pressures
Air dehumidification	Elimination of carryover effects; prevention of any pollution of the hygroscopic solution Lower capital and operating costs, up to 50% less than traditional dehumidifiers; low-pressure drops; low noise emissions [47]
Sparkling water production	Water deoxygenation and carbonation carried out simultaneously in the same device; lower capital cost and CO <sub>2</sub> consumption; over 10 times reduction in size [5]

can be expected. Table 38.3 summarizes the main improvements achieved by membrane contactors for some of the applications described in this contribution.

### 38.5 MODULE DESIGN

The design of membrane contactors is extremely important for improving their efficiency in mass transfer. A long module, for instance, leads to higher membrane area, but implies also an increase of pressure drop. Similarly, higher fibers packing fractions mean higher membrane area, but can result in nonuniform packing with a consequent bad distribution of flow; the difference of fibers diameters (they are not exactly the same) can also deal with an un-uniform flow. Furthermore, the module has to be designed in such a way that the breakthrough pressure is not exceeded.

The most used design for gas–liquid operations is the tube-in-shell configuration with shell side flow parallel (cocurrent or countercurrent) to the lumen side one (Figure 38.7a). However, this type of module suffers from the un-uniform packing and bad flow distribution at the shell side (Figure 38.7b). To guarantee uniform distribution of the flow and to improve the mass-transfer coefficients, alternative geometries and changes in the original parallel configuration have been investigated.

Wickramasinghe et al. [3] studied the performance of different modules for the removal of oxygen from water. The removal of 7% offered by a parallel flow cylindrical module was increased up to 72% with a crimped flat plate, to 82% with a cylindrical bundle, to 86% with a helical bundle, and to 98% with a rectangular bundle; all these configurations operated in cross-flow. The use of woven fibers has been also investigated by Wickramasinghe et al. [48] who claimed the superior performance of this system with respect to the modules built with individual fibers, due to the higher uniformity of fiber spacing.

The strip process has been studied in hollow fiber contactors containing a woven fabric of fibers also by Wang and Cussler [49]. The modules (one rectangular and one cylindrical) contained baffles for increasing the mass transfer, but the rectangular one offered lower mass-transfer coefficients because of stagnant liquid zones between adjacent fibers.

Bhaumik et al. [4] demonstrated the efficiency of transverse flow hollow fiber devices equipped with fibers in a mat wrapped around a central tube (distributor of the liquid) for the absorption of CO<sub>2</sub> in water.

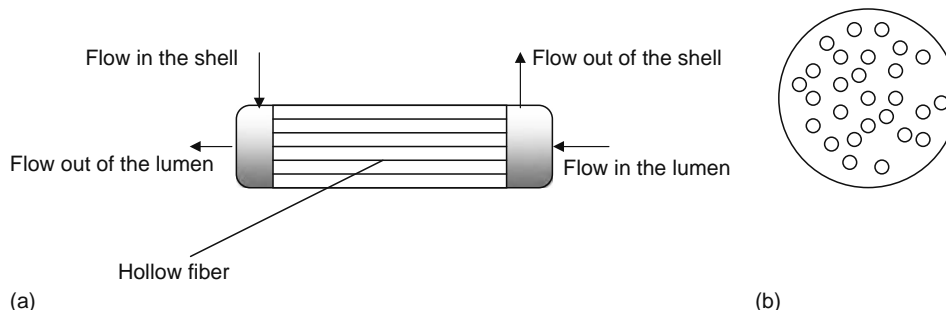


**FIGURE 38.7** Scheme of a tube-in-shell configuration with shell side flow parallel to the lumen side one. (a) Module and (b) un-uniform packing/section view.

Vladisavljevic and Mitrovic [50] developed a three-phase hollow fiber membrane contactor with frame elements. The module consists of stacks of polygonal plates containing internal frames packed with hollow fibers and an external frame where headers for the inlet and outlet of the fluids flowing inside the fibers are provided. Plates can be monoaxial or biaxial, allowing two- and three-phase contact, respectively. Authors calculated, both at tube and shell side, the pressure drops of this system. At the same fluid flow rate, the pressure drop at the shell side was lower than that of the tube side and proportional to the gas flow rate. The pressure drops at the tube side were mainly related to the local obstacles in the module rather than the resistance in the fibers.

The efforts in the research led to the commercialization of different modules. Some of them are described below.

The Liqui-Cel Extra Flow module of the CELGARD LLC (Charlotte, North Carolina) is characterized by a higher mass-transport coefficient than parallel flow configurations because of the presence of a central baffle that forces the liquid stream (sent to the shell side) to flow perpendicular to the hollow fibers. The central baffle also minimizes the shell side bypassing; the system has been designed for avoiding large pressure drops.

Membrane Corporation (Minneapolis, Minnesota) developed a bubble-free gas-liquid mass-transfer module that contains various fiber bundles. To have 100% of gas transfer, the fibers are sealed at one end. The liquid flows outside the fibers that are fluidized. Low-pressure drops, high turbulence, and no plug for suspended solids eventually contained in the liquid stream are ensured by a quite low packing density.

For a bubble-free ozonation of water, W.L. Gore & Associates (Elkton, Maryland) commercializes the DISSO<sub>3</sub>LVE module made of ozone-resistant fibers in PTFE. A helix arrangement of the fibers leads to higher shell side mass-transfer coefficients than the parallel configuration.

TNO (Holland) designed a rectangular module (TNO transversal-flow membrane module) containing hollow fibers. The system performs with high mass-transfer coefficients and low-pressure drops. Furthermore, it shows a good scale-up potential. The module is commercialized by XTO Membrane Technology.

Patents on new module designs have been recently presented. Nitto Denko (Japan) patented a spiral wound design for membrane contactor applications [51]. The system includes a central feed pipe around which one or more membranes are wound. Tests on water ozonation demonstrated that it is possible to achieve a concentration of ozone 10% higher than in hollow fiber.

TNO housed hollow fiber membranes inside a pressure vessel, to be able to operate with gaseous streams at high pressures [52]. This system is useful for treating (by absorbent liquid) natural gas or petrochemical streams containing species such as CO<sub>2</sub> and H<sub>2</sub>S.

### 38.6 CONCLUDING REMARKS

Membrane contactors result to be effective for the treatment of gaseous streams. With respect to conventional operations, they are able to optimize the use of absorbent solutions (it is ensured a constant interfacial area for the all length of the unit and the carryover of droplets is reduced) and to lead to the desired removal (up to 99%) by using modules of reduced size and weight. Sparkling water can be also efficiently produced in modules of reduced size at lower capital costs and CO<sub>2</sub> consumption than conventional operations. Air dehumidification/humidification in membrane contactors is starting to be commercialized; some pilot plants for CO<sub>2</sub>, SO<sub>2</sub>, and NH<sub>3</sub> abatement are also in operation. Efforts made in the research of more stable membrane materials, more efficient module design, and new absorbent solutions deal with a significant improvement of the membrane contactors performance. However, further research needs to be done to overcome some of the drawbacks still present. For example, the mass transport has to be further enhanced by reducing the mass-transfer resistances involved; the relationships among the parameters that determine the membrane performance have to be more deeply studied for improving the membrane preparation techniques; the permeability and selectivity of coated membranes have to be increased; in supported liquid membranes higher permeability, more stable carriers and a reduced loss of the carrier solution have to be obtained; more general correlations for calculating the mass-transfer coefficient in the modules have to be developed, to facilitate the design and scale-up of the membrane units.

All these improvements coupled to further enhancements in the lifetime of the membranes and their compatibility with absorbents, as well as in the mass-transfer design, will allow to extend the use of membrane contactors in industrial productions.

### REFERENCES

1. Gabelman A and Hwang ST. Hollow fiber membrane contactors. *J. Mem. Sci.* 1999; 159:61–106.
2. Kumar PS, Hogendoorn JA, Feron PHM, and Versteeg GF. New absorption liquids for the removal of CO<sub>2</sub> from dilute gas streams using membrane contactors. *Chem. Eng. Sci.* 2002; 57:1639–1651.
3. Wickramasinghe SR, Semmens MJ, and Cussler EL. Mass transfer in various hollow fiber geometries. *J. Mem. Sci.* 1992; 69:235–250.
4. Bhaumik D, Majumdar S, and Sirkar KK. Absorption of CO<sub>2</sub> in a transverse flow hollow fiber membrane module having a few wraps of the fiber mat. *J. Mem. Sci.* 1998; 138:77–82.

5. Criscuoli A, Drioli E, and Moretti U. Membrane contactors in the beverage industry for controlling the water gas composition. *Ann. N.Y. Acad. Sci.* 2003; 984:1–16.
6. Iversen SB, Bhatia VK, Dam-Johansen K, and Jonsson G. Characterization of microporous membranes for use in membrane contactors. *J. Mem. Sci.* 1997; 130:205–217.
7. Taniguchi M and Belfort G. Correcting for surface roughness: Advancing and receding contact angles. *Langmuir* 2002; 18:6465–6467.
8. Malek A, Li K, and Teo WK. Modeling of microporous hollow fiber membrane modules operated under partially wetted conditions. *Ind. Eng. Chem. Res.* 1997; 36:784–793.
9. Noble RD and Way JD. Description of facilitated transport and environmental applications. In: Crespo JG and Boddekar KW, Eds. *Membrane Processes in Separation and Purification*. Dordrecht: Kluwer Academic, 1994; pp. 316–342.
10. Figoli A, Sager WFC, and Mulder M. Facilitated oxygen transport in liquid membranes: Review and new concepts. *J. Memb. Sci.* 2001; 181:97–110.
11. Sirkar KK. Selective-permeation gas-separation process and apparatus, US Patent 4,750,918, 1988.
12. Teramoto M, Matsuyama H, Yamashiro T, and Okamoto S. Separation of ethylene from ethane by a flowing liquid membrane using silver nitrate as a carrier. *J. Mem. Sci.* 1989; 45:115–136.
13. Figoli A. Synthesis of nanostructured mixed matrix membranes for facilitated gas separation. PhD Thesis, University of Twente, The Netherlands, Chapters 5–7, ISBN 90-365-1673-0, 2001.
14. Fiammengo R, Wojciechowski K, Crego-Calama M, Timmerman P, Figoli A, Wessling M, and Reinhoudt DN. Heme-protein active site models via self-assembly in water. *Org. Lett.* 2003; 5:3367–3370.
15. Mavroudi M, Kaldis SP, and Sakellaropoulos GP. Reduction of CO<sub>2</sub> emissions by a membrane contacting process. *Fuel* 2003; 82:2153–2159.
16. Falk-Pedersen O and Dannstrom H. Separation of carbon dioxide from offshore gas turbine exhaust. *Energ. Convers. Manag.* 1997; 38:S81–S86.
17. Rangwala HA. Adsorption of carbon dioxide into aqueous solutions using hollow fiber membrane contactors. *J. Mem. Sci.* 1996; 112:229–240.
18. Wang R, Li DF, Zhou C, Liu M, and Liang DT. Impact of DEA solutions with and without CO<sub>2</sub> loading on porous polypropylene membranes intended for use as contactors. *J. Mem. Sci.* 2004; 229:147–157.
19. Nishikawa N, Ishibashi M, Ohta H, Akutsu N, Matsumoto H, Kamata T, and Kitamura H. CO<sub>2</sub> removal by hollow-fiber gas–liquid contactor. *Chem. Eng. Sci.* 1995; 415–418.
20. Feron PHM and Jansen AE. CO<sub>2</sub> separation with polyolefin membrane contactors and dedicated absorption liquids: Performances and prospects. *Sep. Purif. Technol.* 2002; 27:231–242.
21. Quinn R, Appleby JB, and Pez GP. Salt hydrates: New reversible absorbents for carbon dioxide. *J. Am. Chem. Soc.* 1995; 117:329–335.
22. Quinn R, Appleby JB, Mathias PM, and Pez GP. Liquid salt hydrate acid gas absorbents: An unusual desorption of carbon dioxide and hydrogen sulfide upon solidification. *Sep. Sci. Technol.* 1995; 30:1711–1723.
23. Quinn R, Appleby JB, and Pez GP. New facilitated transport membranes for the separation of carbon dioxide from hydrogen and methane. *J. Mem. Sci.* 1995; 104:139–146.
24. Chen H, Obuskovic G, Majumdar S, and Sirkar KK. Immobilized glycerol-based liquid membranes in hollow fibers for selective CO<sub>2</sub> separation from CO<sub>2</sub>–N<sub>2</sub> mixtures. *J. Mem. Sci.* 2001; 183:75–88.
25. Teramoto M, Takeuchi N, Maki T, and Matsuyama H. Facilitated transport of CO<sub>2</sub> through liquid membrane accompanied by permeation of carrier solution. *Sep. Purif. Technol.* 2002; 27:25–31.
26. Qi Z and Cussler EL. Microporous hollow fibers for gas absorption. II. Mass transfer across the membrane. *J. Mem. Sci.* 1985; 23:333–345.
27. Li K, Wang D, Koe CC, and Teo WK. Use of asymmetric hollow fibre modules for elimination of H<sub>2</sub>S from gas streams via a membrane absorption method. *Chem. Eng. Sci.* 1998; 53:1111–1119.
28. Wang D, Teo WK, and Li K. Removal of H<sub>2</sub>S to ultra-low concentrations using an asymmetric hollow fibre membrane module. *Sep. Purif. Technol.* 2002; 27:33–40.
29. Quinn R, Appleby JB, and Pez GP. Hydrogen sulfide separation from gas streams using salt hydrate chemical absorbents and immobilized liquid membranes. *Sep. Sci. Technol.* 2002; 37:627–638.
30. Poddar TK, Majumdar S, and Sirkar KK. Removal of VOCs from air by membrane-based absorption and stripping. *J. Mem. Sci.* 1996; 120:221–237.
31. Cha JS, Malik V, Bhaumik D, Li R, and Sirkar KK. Removal of VOCs from waste gas streams by permeation in a hollow fiber permeator. *J. Mem. Sci.* 1997; 128:195–211.
32. Bhaumik D, Majumdar S, and Sirkar KK. Pilot-plant and laboratory studies on vapor permeation removal of VOCs from waste gas using silicone-coated hollow fibers. *J. Mem. Sci.* 2000; 167:107–122.
33. Majumdar S, Bhaumik D, and Sirkar KK. Performance of commercial-size plasmopolymerized PDMS-coated hollow fiber modules in removing VOCs from N<sub>2</sub>/air. *J. Mem. Sci.* 2003; 214:323–330.
34. Poddar TK and Sirkar KK. A hybrid of vapor permeation and membrane-based absorption-stripping for VOC removal and recovery from gaseous emissions. *J. Mem. Sci.* 1997; 132:229–233.
35. Obuskovic G, Majumdar S, and Sirkar KK. Highly VOC-selective hollow fiber membranes for separation by vapor permeation. *J. Mem. Sci.* 2003; 217:99–116.
36. Jansen AE, Klaassen R, Feron PHM, Hanemaaijer JA, and ter Meulen BPh. Membrane gas absorption processes in environmental applications. In: Crespo JG and Boddekar KW, Eds. *Membrane Processes in Separation and Purification*. Dordrecht: Kluwer Academic, 1994; pp. 343–356.

37. Larsen T, Bhatia VK, Moller J, Iversen SB, and Felsvang K. Membrane contactors for flue gas cleaning. AICHE Spring National Meeting, Atlanta, GA, March 5–9, 2000.
38. Klaassen R and Jansen AE. The membrane contactor: Practical applications and possibilities. AICHE Spring National Meeting, Atlanta, GA, March 5–9, 2000.
39. van der Vaart R, Akkerhuis J, Feron P, and Jansen B. Removal of mercury from gas streams by oxidative membrane gas absorption. *J. Mem. Sci.* 2001; 187:151–157.
40. Bessarabov DG, Sanderson RD, Jacobs EP, and Beckman IN. High-efficiency separation of an ethylene/ethane mixture by a large-scale liquid-membrane contactor containing flat sheet non-porous polymeric gas-separation membranes and a selective flowing-liquid absorbent. *Ind. Eng. Chem. Res.* 1995; 34:1769–1778.
41. Bessarabov DG. Phenomenological analysis of ethylene transport in a membrane contactor containing solutions of silver nitrate. *Desalination* 1998; 115:265–277.
42. Nymeijer K. Gas–liquid membrane contactors for olefin/paraffin separation. PhD Thesis, University of Twente, The Netherlands, ISBN 90-365-1878-4, 2003.
43. Tsou DT, Blachman MW, and Davis JC. Silver-facilitated olefin/paraffin separation in a liquid membrane contactor system. *Ind. Eng. Chem. Res.* 1994; 33:3209–3216.
44. Kovvali AS, Chen H, and Sirkar KK. Glycerol-based immobilized liquid membranes for olefin–paraffin separation. *Ind. Eng. Chem. Res.* 2002; 41:347–356.
45. Isetti C, Nannei E, and Magrini A. On the application of a membrane air-liquid contactor for air dehumidification. *Energ. Build.* 1997; 25:185–193.
46. Bergero S and Chiari A. Experimental and theoretical analysis of air humidification/dehumidification processes using hydrophobic capillary contactors. *Appl. Ther. Eng.* 2001; 21:1119–1135.
47. Gaeta SN. Membrane contactors: Application to industrial processes. 1st Workshop Italy-Russia, Cetraro (CS), Italy, September 17–20, 2003.
48. Wickramasinghe SR, Semmens MJ, and Cussler EL. Hollow fiber modules made with hollow fiber fabric. *J. Mem. Sci.* 1993; 84:1–14.
49. Wang KL and Cussler EL. Baffled membrane modules made with hollow fiber fabric. *J. Mem. Sci.* 1993; 85:265–278.
50. Vladisavljevic GT and Mitrovic MV. Pressure drops and hydraulic resistances in a three-phase hollow fiber membrane contactor with frame elements. *Chem. Eng. Proc.* 2001; 40:3–11.
51. Nitto Denko, Japan, US Patent 6,168,648, January 2001.
52. TNO, The Netherlands, US Patent 6,355,092, March 2002.



---

# 39 Strip Dispersion Technique: Application for Strategic and Precious Metal Separation and Treatment of Wastewater Streams

*Anil Kumar Pabby, S.C. Roy, J.V. Sonawane, F.J. Alguacil, and Ana Maria Sastre*

## CONTENTS

39.1	Introduction .....	1057
39.2	Why Is a New Strip Dispersion Technique Needed? .....	1057
39.3	Working Function of Pseudo-Emulsion Based Hollow Fiber Strip Dispersion .....	1058
39.4	Application of Pseudo-Emulsion Based Hollow Fiber Strip Dispersion Technology in Metal Separation.....	1059
39.4.1	PEHFSD in Metal Separation .....	1059
39.4.2	PEHFSD in the Separation/Removal/Concentration of Actinides.....	1065
39.4.2.1	U(VI), Pu(IV), and Am(III) Extraction.....	1065
39.4.2.2	U(VI) and Pu(VI) Recovery from Oxalate Supernatant Waste .....	1067
	References .....	1068

## 39.1 INTRODUCTION

Increasingly high demands are being placed on new separation technologies due to stricter product quality requirements, environmental legislation, energy efficiency demands, and the need to reduce costs [1]. To meet these increasing demands, there is a tendency to combine processes into hybrids. In a membrane contactor, separation is fully integrated—with an extraction with stripping or an emulsion liquid membrane (ELM) operation with hollow fiber (HF) contactor or absorption process—into one piece of equipment. This allows the advantages of both processes to be fully exploited [2].

Interestingly, a large number of works have been published that deal with applications of supported liquid membranes [3–7]. When HF modules are used as contactors in this type of technology, the organic phase fills the pores of the HF and the aqueous phases flow along the fibers through the inner side and through the outer side. The main drawback of the technology is the instability of the supported liquid membrane (SLM), which can produce undesirable results [8–10]. Although an SLM process is very effective in reducing trace contaminants to very low levels owing to its ability to circumvent equilibrium limitations [11] and its use has been hampered by a lack of stability. The traditional SLM suffers from a gradual loss of the organic membrane phase to the aqueous feed and strip solutions because of emulsification (e.g., resulting from lateral shear forces) at the membrane–aqueous interfaces, and to the osmotic pressure difference across the membrane [12–13]. The osmotic pressure difference displaces the organic membrane phase from the micropores of the support, which ultimately allows the feed and strip solutions to mix and leads to the complete failure of the separation unit. An improved process is needed that can not only remove metal ions but also recover them.

## 39.2 WHY IS A NEW STRIP DISPERSION TECHNIQUE NEEDED?

Membranes are flexible, modular, energy-efficient devices with a high specific surface area. The extraction or absorption process offers a very high degree of selectivity and a high driving force for transport, even at very low concentrations. As a result, a technique is required that provides all the benefits of the SLM but without stability problems (as discussed in the previous section). HF modules have therefore been used with different process configurations based on similar fundamentals

that aim to minimize the required membrane area by providing better stability and high mass transfer due to a large area per unit volume (advantages of the HF contactor), while incorporating the advantages of highly efficient ELMs. This new technique is known as supported liquid membrane with strip dispersion (SLMSD), pseudo-emulsion based hollow fiber strip dispersion (PEHFSD), or emulsion pertraction technology (EPP). In this case, the organic (extractant dissolved in diluent) and back-extraction phases are emulsified before injection into the HF module and can be separated at the module outlet. Although there are few references to this alternative method in the literature, there are reports on its viability for the recovery of hexavalent chromium and copper from polluted waters [14–17] and for the removal of hydrocarbons [18]. Nevertheless, this technique still needs to be tested in specific applications to evaluate the suitability of the technology for commercial use. Wienczek and his coworkers [19–20] described the use of microporous HF contactors as an alternative method to the direct dispersion of ELMs to minimize membrane swelling and leakage. HF contactors do not have the high shear rates that are typical of the agitators used in direct dispersion. This technique has been successfully demonstrated for the removal and recovery of metals from wastewaters and process streams [21–24]. PEHFSD provides the following advantages over normal extraction and other membrane process:

- Extraction and stripping can be carried out in one operation
- No possibility of emulsion formation in water phase
- Volume of extractant is relatively small
- Process parameters are very flexible
- Phase separation is not necessary
- Large specific surface area is provided by HF membranes
- Diffusion paths are short
- Modular equipment is compact
- Energy consumption is low

### 39.3 WORKING FUNCTION OF PSEUDO-EMULSION BASED HOLLOW FIBER STRIP DISPERSION

The schematic representation of PEHFSD is shown in Figure 39.1. An aqueous strip solution is dispersed in an organic membrane solution containing one or more extractants in a mixer; the water-in-oil dispersion formed is then pumped to contact with one side of a microporous support, which is passed through the shell side of a microporous polypropylene HF module. The aqueous feed solution, which contains a targeted species to be extracted, is on the other side of the support and is passed through the tube side. The continuous organic phase of the dispersion readily wets the pores of a hydrophobic microporous support, and a stable liquid membrane (the organic phase) is formed in the pores of the support. Figure 39.2 shows an enlarged view of the SLM with strip dispersion. A low pressure (less than ~55.1 kPa [8 psi]) is applied to the aqueous feed solution side ( $P_a$ , which is greater than  $P_o$  for the strip dispersion side) to prevent the organic solution of the strip dispersion from passing through the pores into the feed solution side. The dispersed droplets of the aqueous strip solution—with a typical size of 80–800  $\mu\text{m}$ —are orders of magnitude larger than the pores of the microporous polypropylene support employed for the SLM, which range from 0.01 to 0.2  $\mu\text{m}$ . Therefore, these droplets are retained on the strip dispersion side and cannot pass through the pores to the feed solution side. This PEHFSD technique has a constant supply of the organic membrane solution in the pores, which

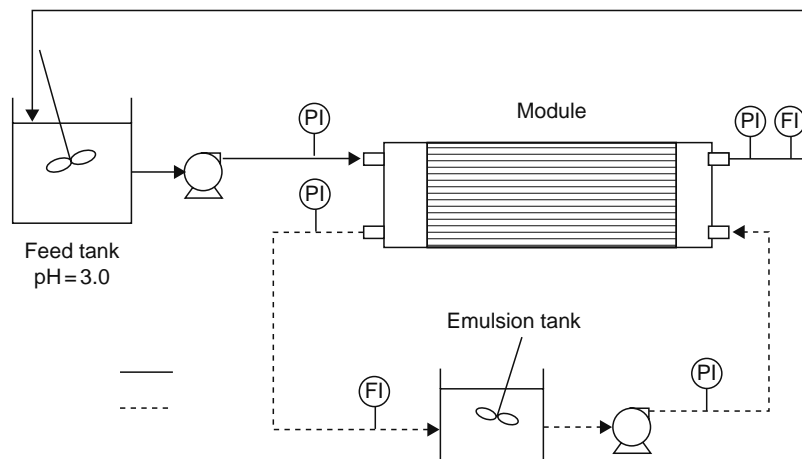


**FIGURE 39.1** PEHFSD setup; continuous line: feed stream; dotted line: emulsion stream. (From Urtiga, A., *J. Membr. Sci.*, 257, 161, 2005. With permission.)

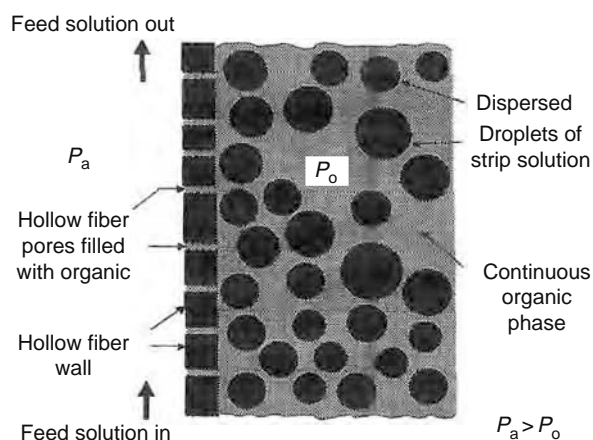


FIGURE 39.2 An enlarged view of the PEHFSD. (From Ho, W.S. and Poddar, T.K., *Environ. Prog.*, 20, 44, 2001. With permission.)

ensures stable and continuous operation. In addition, the direct contact between the organic and strip phases (with high-shear mixing, if necessary) on the strip dispersion side provides an additional area for stripping, which results in very efficient mass transfer. The stripping is more efficient than that achieved with the conventional SLM. As shown in Figure 39.1, PEHFSD combines extraction and stripping, which are normally carried out in two separate steps in conventional processes such as solvent extraction.

### 39.4 APPLICATION OF PSEUDO-EMULSION BASED HOLLOW FIBER STRIP DISPERSION TECHNOLOGY IN METAL SEPARATION

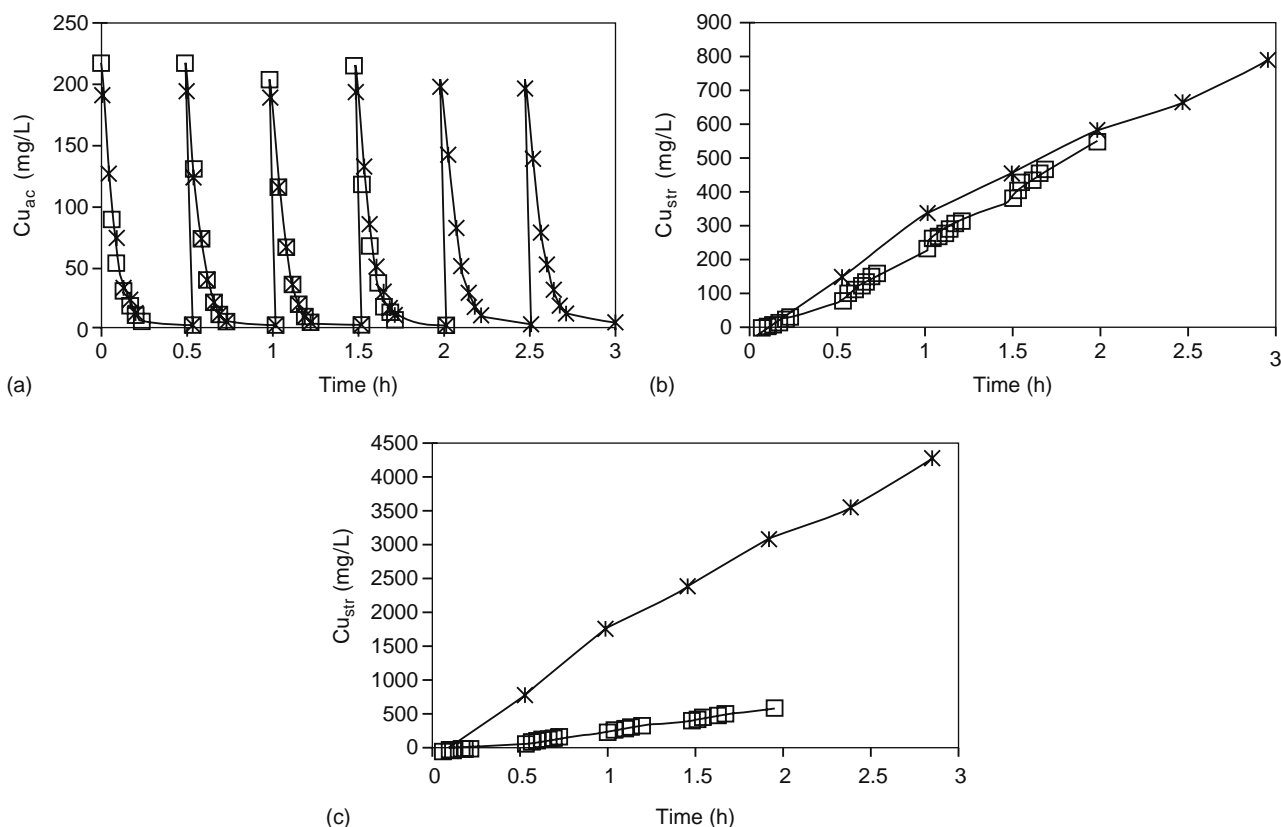
#### 39.4.1 PEHFSD IN METAL SEPARATION

Table 39.1 gives the details of a recently published study that analyzes the use of the pseudo-emulsion based hollow fiber strip dispersion (PEHFSD) technique for different metal ions [25–38]. In another recent study, Urtiaga et al. [39] described a methodology for modeling separation processes based on the use of emulsion pertraction technology. This work gives a comparative analysis of two types of separation process aimed at the recovery of metallic compounds from residual waters using HF modules as membrane contactors: emulsion pertraction (EPP) extraction and nondispersive solvent extraction (NDSX). The recovery of copper, which is the homogeneous catalyst in wet peroxide oxidation (WPO) processes, is analyzed from both an experimental and a theoretical perspective. The separation of the metal was enhanced by using LIX622N as a

TABLE 39.1

#### Details of Recent Published Work on Different Metals Using Strip Dispersion Technique

Metal Ion	Feed Conditions	Extractant	Strippant (Strip Dispersion with Extractant)	References
Cr	[Cr] = 1500 ppm, pH 1.5	10 wt% Amberlite LA2, 1 wt% 1-dodecanol (modifier for the extractant), diluent Isopar L	3 M NaOH and extractant at ratio of 1:2	[25,26]
Cu	[Cu] = 150 ppm, pH 2	15 wt% LIX973N, 2 wt% 1-dodecanol, (modifier for the extractant), diluent <i>n</i> -dodecane	3 M H <sub>2</sub> SO <sub>4</sub> and extractant at ratio of 1:19	[11,27–32]
Zn	[Zn] = 4600 ppm, pH 2	8 wt% Cyanex 301, 2 wt% dodecanol (modifier for the extractant), 90 wt% Isopar L	3 M H <sub>2</sub> SO <sub>4</sub> and extractant at ratio of 1:5.7	[33,34–37]
Sr	Sr-87 and Sr-90	C12 BOPPA (2-butyloctyl phenylphosphonic acid), C16 HDPPA (2-hexyldecyl phenylphosphonic acid), C18 ODPPA/HDPPA (2-octyldecyl phenylphosphonic acid), C20 ODPPA (2-octyldecyl phenylphosphonic acid), 2wt% dodecanol (modifier for the extractant), diluent <i>n</i> -dodecane	1 M HCl and extractant at ratio of 1:3	[33,38]
Co	[Co] = 492 ppm, pH 2	8 wt% Cyanex 301, 2 wt% dodecanol (modifier for the extractant), 90 wt% Isopar L	5 M HCl and extractant at ratio of 13.3	[33,37]



**FIGURE 39.3** Comparison of (×) emulsion pertraction results in one membrane contactor and (□) NDSX results in two membrane contactors. [Cu] feed, initial = 200 mg/L, [LIX622N] = 5% (v/v). (From Urtiga, A., *J. Membr. Sci.*, 257, 161, 2005. With permission.)

selective extractant and the concentration took place in a concentrated sulfuric acid phase. These pertraction results were then compared with the results of the separation-concentration of copper obtained in a previous study [40] performed with NDSX and similar HF membrane contactors. The latter case used two HF modules, with an effective membrane area of 1.4 m<sup>2</sup> each. The first module was used for the extraction operation, in which copper is separated from the feed phase, and the second module was used for the back-extraction operation, in which the organic extractant is regenerated and copper is concentrated in the stripping phase. Comparative results are given in Figure 39.3. It is observed that the evolution of copper concentration in the feed phase (Figure 39.3a) is very similar in both techniques. Figure 39.3b shows the mass of copper in the stripping phase, which follows a similar trend with both techniques. The main difference is observed in Figure 39.3c, which shows that the copper concentration in the stripping phase after four experimental cycles is 5.2 times higher when the pertraction process is used. This value is approximately equal to the ratio of stripping volumes used in both techniques:  $V_{\text{NDSX}}/V_{\text{pertraction}} = 5$ . The small difference was attributed to experimental error and the slight modification of phase volumes produced during the collection of samples. The experimental results therefore demonstrate that, for the present application, emulsion pertraction technology offers significant practical and financial advantages over NDSX technology since the cost of acquiring the membranes—considered to be the most significant cost in membrane contactor operation—is reduced by half.

Similarly, Ho and Poddar [25] developed new SLM technology for the removal and recovery of chromium from wastewaters. The technology not only reduces Cr(VI), ranging from approximately 100 to 1000 ppm, to less than 0.05 ppm in the treated effluent allowable for discharge or recycle but also recovers the chromium product at the high concentration of about 20% Cr(VI) (62.3% Na<sub>2</sub>CrO<sub>4</sub>), which is suitable for resale or reuse. In other words, the authors claimed to have achieved the goals of zero discharge and no sludge. This technology is based on their finding that sulfuric acid flux depends on the Cr(VI) concentration in the feed (at pH 1.5). The sulfuric acid flux decreases significantly as the Cr(VI) concentration in the feed increases. The sulfuric acid flux at a feed Cr(VI) concentration of greater than ~100 ppm is far less than at a lower concentration. The stability of the SLM was ensured by adding the strip dispersion methodology, in which the aqueous strip solution is dispersed in a mixer and the strip dispersion formed is circulated from the mixer to the membrane module so that there is a constant supply of the organic solution in the membrane pores. The chromium flux over its entire range—from low Cr(VI) concentrations in the feed solution to high feed concentrations at which the carrier saturation of the facilitated transport mechanism occurs—showed good agreement with a film model that takes into account mass transfer resistances, both in the

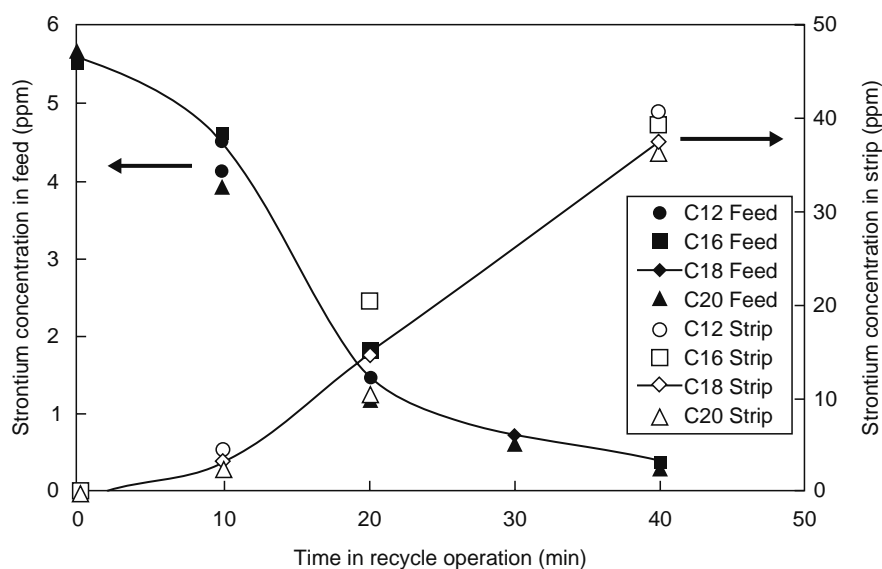


**FIGURE 39.4** Strontium (Sr) concentrations in the feed and strip solutions as a function of time in recycle operation for four extractants (C12 Feed is the concentration in the feed solution or the C12 BOPPA extractant, C12 Strip is the concentration in the strip solution for the C12 BOPPA extractant, and similarly for the C6 HDPPA, C18 ODPPA/HDPPA, and C20 ODPPA extractants; the aqueous feed solutions also contained about 80 ppm of calcium; 20 ppm of magnesium, and 50 ppm of zinc in addition to Sr-87, respectively). (From Ho, W.S. and Wang, B., *Ind. Eng. Chem. Res.*, 41, 381, 2002. With permission.)

feed solution and in the membrane phase. The mass transfer coefficient for the feed solution in the tube side of a HF module was calculated from the well-known Leveque correlation with the estimated diffusivity. The mass transfer coefficient for the membrane phase was governed by the distribution coefficient, the diffusivity, and the thickness, porosity, and tortuosity of the membrane support. The model used the distribution coefficient calculated from a measured equilibrium constant and the diffusivity and tortuosity obtained from the flux data at the carrier saturation. In addition, the distribution coefficient calculated was in very good agreement with that measured for a very wide range of aqueous feed Cr (VI) concentrations from approximately 20–18,000 ppm.

In another study, Ho and Bang [38] proposed a strip dispersion system that removes strontium (nonradioactive Sr-87) to an acceptable level in treated water suitable for discharge or recycling, i.e., 8 pCi/L or lower. For this system, the authors used newly synthesized extractants, branched alkyl phenylphosphonic acids, that proved to be more effective than D2EHPA at low feed pH (e.g., pH 2.5). Figure 39.4 shows the results for all four extractants with 1M HCl as the stripping solution. As can be seen, all four extractants removed strontium from the aqueous feed solutions and recovered it in the aqueous strip solutions. The strontium concentration in the aqueous strip solutions was approximately 40 ppm, which is almost the maximum concentration that can be achieved for a feed-to-strip solution volume ratio of 8. Therefore, the stripping achieved with hydrochloric acid was very satisfactory and nearly quantitative. The aqueous feed solutions also contained approximately 80 ppm of calcium, 20 ppm of magnesium, 50 ppm of zinc, and strontium to simulate ground water. Having tested the performance with nonradioactive Sr-87, experiments were conducted with radioactive Sr-90. Table 39.2 shows the results for Sr-90 removal from aqueous feed solutions at pH 3 with 1 M HCl as the stripping solution. As can be seen, the strip dispersion technique containing C20 ODPPA (2-octyldodecyl phenylphosphonic acid) removed Sr-90 to the target concentration of 8 pCi/L (the drinking water standard) or lower from feed solutions containing 317–1000 pCi/L of Sr-90. This target concentration was also achieved using a feed solution containing 1000 pCi/L of Sr-90 in the presence of approximately 80 ppm of calcium, 20 ppm of magnesium, and 50 ppm of zinc. Figure 39.5 shows a comparison with the results for Sr-87 removal. As can be seen, the C12 BOPPA (2-butyloctyl phenylphosphonic acid) extractant decreased the Sr-87 concentration in the feed solution to lower values (for a given time): that is, it removed Sr-87 more effectively than D2EHPA. For example, C12 BOPPA reduced the Sr-87 concentration in the feed solution by more than a factor of 2 less than D2EHPA at 30 min. Another drawback of D2EHPA is that it typically requires a feed pH of 4.5, which is difficult to maintain because of the proton transfer due to extraction. D2EHPA also requires the removal of zinc before strontium can be removed at a feed pH of 4.5, as the extractant forms a precipitate with zinc in the feed solution.

The same strip dispersion technology was used by Klaassen and Jansen [42] under the new name of “emulsion pertraction.” The authors tested the strip dispersion technique on site at Rogal in Enschede, the Netherlands, to extend the lifetime of their passivating bath (Figure 39.6). The installation was equipped with Celgard Liquid-Cel membrane contactors. Passivating is an operation frequently used in the galvanic industry to improve the corrosion resistance of galvanized objects. The lifetime

**TABLE 39.2**  
**Radioactive (Strontium) Sr-90 Removal Using C20 ODPPA**  
**(2-Octyldodecyl Phenylphosphonic Acid) Extractant**

Run	Sr-90 Concentration in Feed (pCi/L)	Time (min)	Sr-90 Concentration in Treated Feed (pCi/L)
1	317	120	3.3
2	317	120	3.5
3	317	120	3.3
4	317 <sup>a</sup>	240	4.0
5	1,000 <sup>a</sup>	240	5.5
6	1,000 <sup>a</sup>	360	1.0
7	30,000	60	1171
		120	352
8	30,000 <sup>a</sup>	300	84

Source: From Ho, W.S. and Wang, B., *Ind. Eng. Chem. Res.*, 41, 381, 2002. With permission.

<sup>a</sup> The feed solution also contained about 80 ppm calcium, 20 ppm magnesium, and 50 ppm zinc.

of the passivating bath liquid is limited due to the accumulation of zinc and iron. Once the zinc and iron concentrations reach a certain limit, the color and corrosion resistance of the passivated objects no longer meet specifications and the bath liquid has to be replaced. Selective removal of iron and zinc from the passivating bath with an emulsion pertraction installation can extend the lifetime of the bath. Klaassen and Jansen suggested that care must be taken to ensure that neither of the active elements, chromium or cobalt, is removed. On-site tests have shown that the emulsion pertraction installation is easy to operate and that no more than 20 min a week is required. Zinc and iron (III) are removed from the passivating bath with high selectivity. There is a negligible loss of chromium and cobalt. The membranes are resistant to the on-site conditions, and transport rates are sufficiently high that a compact installation can be built. Due to a reduction in the use of raw materials (fresh bath liquid) and in the amount of metal sludge that requires disposal, the installation generates an annual profit of \$10,000, whereas the total annual operation costs is only \$6,000.

In a recent study, Sonawane et al. investigated the strip dispersion technique, with a new name, PEHFSD, for the extraction separation of Au(I) from alkaline cyanide media using LIX79 as an extractant [43–46]. In PEHFSD used for Au(I) extraction from cyanide media, the feed solution containing the target species is circulated through the tube side of a microporous

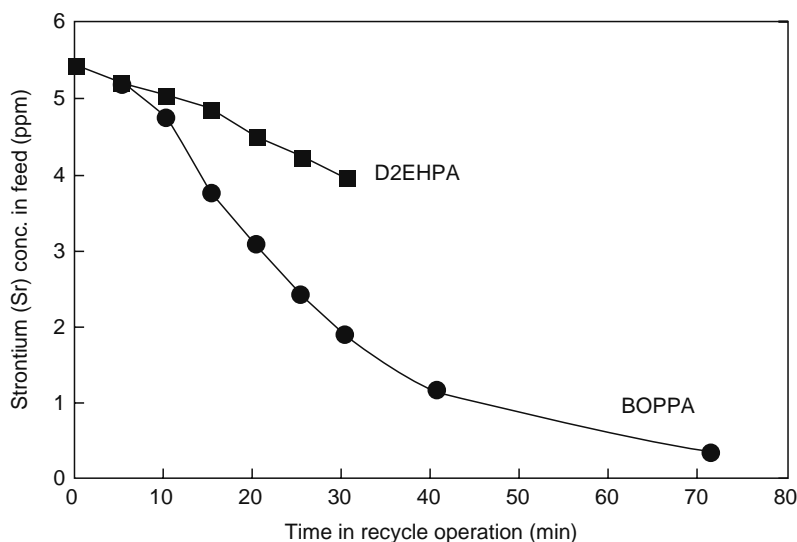


**FIGURE 39.5** Strontium (Sr) concentration in the feed solution as a function of time in recycle operation for the C12 BOPPA and D2EHPA extractants (at feed pH of 2.5 and with 1 M HCl as the stripping solution). (From Ho, W.S. and Wang, B., *Ind. Eng. Chem. Res.*, 41, 381, 2002. With permission.)

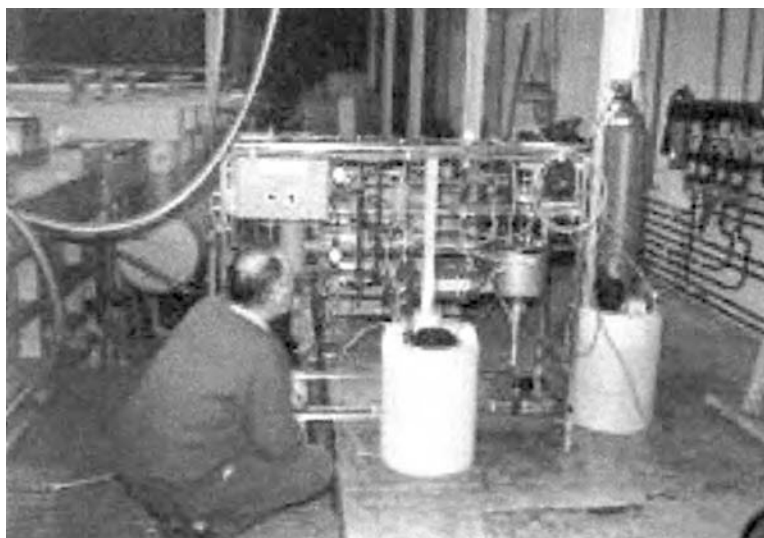


**FIGURE 39.6** Emulsion pertraction installation at Rogal, Enschede, the Netherlands. (From Klaassen R. and Jansen, A.E., *Environ. Prog.*, 20, 37, 2001. With permission.)

hydrophobic polypropylene HF membrane contactor and a dispersion, prepared by continuous stirring of the organic phase and the aqueous stripping phase to form a water-in-oil pseudo-emulsion, is passed continuously through the shell side in counter current mode, using a single HF membrane contactor [43]. Figure 39.7a shows the Liquid-Cel HF contactor used in the present study. As a case study, the extraction of gold cyanide using PEHFSD was carried out using an LIX79/heptane system. The PEHFSD setup (Figure 39.7b) was used for gold recovery and chromium extraction. Figure 39.7c shows the extraction mechanism of Au(I) from alkaline cyanide media with LIX-79/*n*-heptane in a HF membrane module in which a pseudo-emulsion of LIX-79/*n*-heptane and 0.2 M NaOH flows in the shell side, and feed containing gold cyanide flows in the tube side. Experimental results are given in Figure 39.8a and are expressed as the Au(I) concentration in the feed, strip, and organic phase against time obtained in the HF module. Au(I) was almost completely transported from the feed to the organic phase within 100 min, whereas the transfer from the organic phase to the stripping solution took place in 2.5 h (150 min). In this study, the feed was continuously replaced with fresh solution but the stripping solution was recirculated (without replacing with a fresh solution). The extension of this work deals with Au(I) separation from alkaline cyanide media in presence of base metals using a single HF module for both extraction and stripping [44]. The setup described in [43] was used to circulate the feed solution containing  $\text{Au}(\text{CN})_2^-$  with other base metals in a cyanide medium through the tube side. A dispersion was prepared by continuous stirring of the organic phase (12% LIX-79 dissolved in *n*-heptane) and the aqueous stripping phase (0.2 M NaOH) to form a water-in-oil pseudo-emulsion, which was passed continuously through the shell side in countercurrent mode. The influence of different hydrodynamic and chemical parameters was investigated, such as the feed pH, cyanide concentration in the feed, LIX-79 concentration in *n*-heptane, NaOH concentration in the pseudo-emulsion phase, and initial Au(I) concentration in the feed. A detailed evaluation was made of the selectivity of Au(I) against different metal cyanide salts such as Fe(II), Cu(I), Ni(II), Zn(II), and Ag(I) ions. This study is of particular importance as all the chemical parameters were examined using a synthetic hydrometallurgical alkaline solution containing a mixture of gold with other metal cyanide salts and base metals. This was done to optimize the conditions, which are similar to those encountered in the recovery of gold from hydrometallurgical leach solutions containing mixtures of other metal cyanide salts such as Fe(II), Cu(I), Ni(II), Zn(II), and Ag(I). The present study demonstrates that LIX-79/*n*-heptane can be used effectively as a carrier in Au(I) permeation through PEHFSD. This PEHFSD technique was found to be a promising option for the simultaneous separation and concentration of Au(I) from synthetic alkaline cyanide media in the presence of other metal cyanides such as  $\text{Ag}(\text{CN})_2^-$ ,  $\text{Cu}(\text{CN})_4^{3-}$ ,  $\text{Zn}(\text{CN})_4^{2-}$ ,  $\text{Ni}(\text{CN})_4^{2-}$ , and  $\text{Fe}(\text{CN})_6^{4-}$  using LIX-79/*n*-heptane. The use of a stripping solution containing NaOH in the pseudo-emulsion phase provided fast and efficient stripping of Au(I). To achieve a clean separation of Au(I) in the presence of other metals, several experiments were performed with a synthetic hydrometallurgical solution under optimum conditions. A high degree of selectivity was found. The separation of Au(I) based on the experimental results obtained for the cyano ions using 12% LIX-79 (v/v) with 0.2 M NaOH as a stripping agent, a feed pH of 10.3, and a feed linear flow velocity of 1.23 cm/s gave the following order of selectivity:  $\text{Au}(\text{CN})_2^- > \text{Zn}(\text{CN})_4^{2-} > \text{Ag}(\text{CN})_2^- > \text{Ni}(\text{CN})_4^{2-} > \text{Fe}(\text{CN})_6^{4-} > \text{Cu}(\text{CN})_4^{3-}$ . The validity of this model was evaluated using experimental data and the results were found to tie in well with theoretical values. This technique was also applied to chromium extraction from 1 M HCl solution using 0.35 M CYANEX 921/solvesso-100 and 20 g/L hydrazine sulfate as stripping solution [45]. Figure 39.8b shows the performance of PEHFSD expressed as transport of Cr(VI) as a function of varying concentration of HCl in the feed in recycle mode.

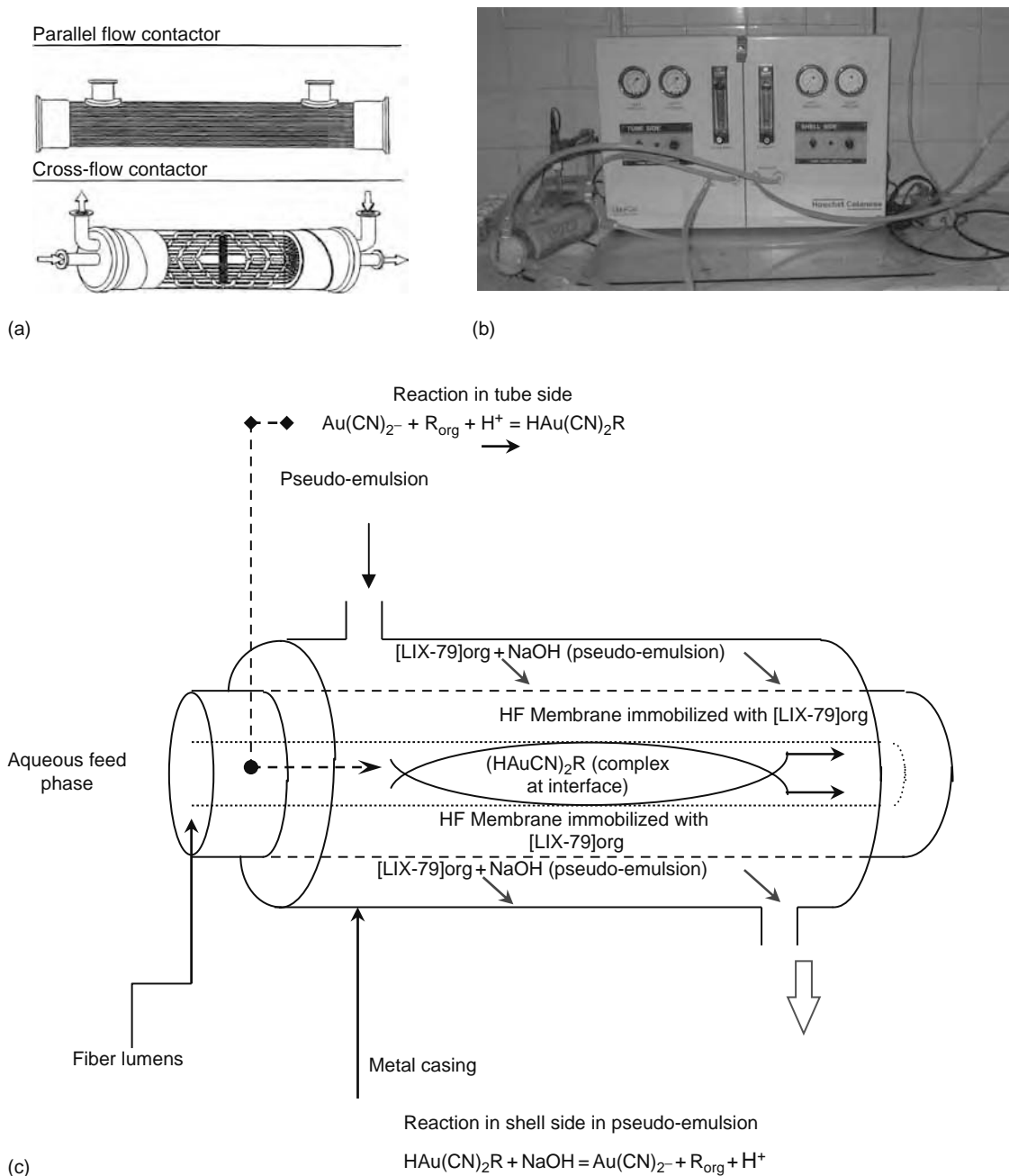


**FIGURE 39.7** (a) Commercial hollow fiber (HF) membrane contactor (Liqui-Cel, Hoechst, Charlotte, New Carolina). (From Cussler, E.L., *Membrane Separation and Technology, Principles and Applications*, Noble, R.D. and Stern, S.A., Elsevier, Amsterdam, 1995. With permission.) (b) NDSX setup used for gold recovery (setup contains two gear pumps, two flow meters, two pressure gauges, and one Liqui-Cel hollow fiber contactor). (From Liqui-Cel, Charlotte, North Carolina. With permission.) (c) Extraction mechanism of Au(I) from alkaline cyanide media with 12% LIX-79/*n*-heptane impregnated in a hollow-fiber membrane module, flowing pseudo-emulsion of 12% LIX-79/*n*-heptane, and 0.2 M NaOH as receiving phase in the shell side and feed containing gold cyanide flowing in the tube side.

In another study, Bringas et al. [46] attempted to separate and recover anionic pollutants using emulsion perttraction technology and advised the remediation of polluted groundwater with C(VI). Polluted groundwater with the following composition (Table 39.3) was treated using emulsion perttraction technology, with Alamine 336 as the extractant and NaOH as the stripping agent, to reduce the concentration of chromate compounds and recover them in a concentrated solution. In the range of studied conditions, the concentration factors achieved were 18,733 for chromium, 29 for sulfate, and 59 for chloride. Kinetic experiments were carried out to analyze the behavior of the separation and concentration process over time. The kinetic model, which consists of a set of coupled differential equations and the solute mass balances of the fluid phases, was solved using the equilibrium expressions of the interfacial chemical reactions between the aqueous solutes and the organic extractants.

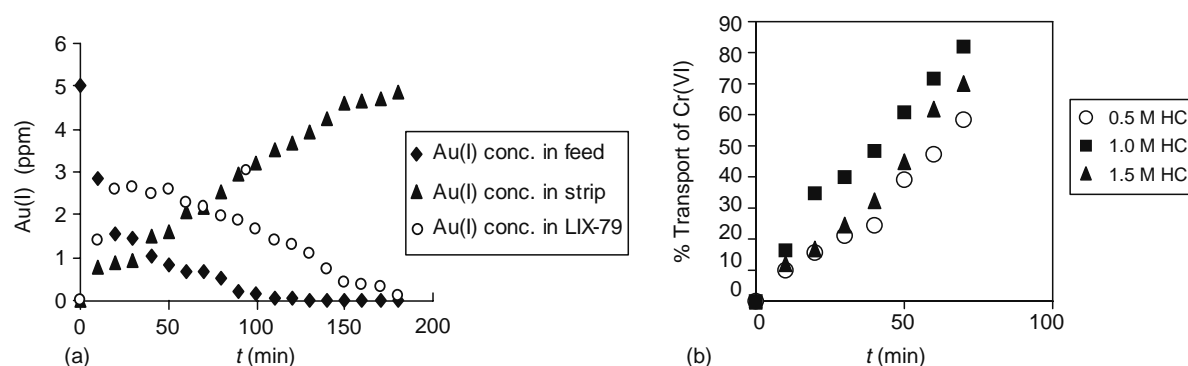


**FIGURE 39.8** (a) Concentration of  $\text{Au}(\text{CN})_2^-$  in the feed, strip, and organic phase as a function of time in recycle mode. (b) % Transport of Cr(VI) with variation of HCl concentration in feed in recycle mode.

Under the experimental conditions, it was concluded that the kinetic control is shared between the feed and the membrane mass transport phenomena, while the resistance associated with the organic phase contained in the emulsion globules can be considered negligible. This situation was found to be consistent with the large interfacial area of the droplets of the stripping phase, which allowed the concentration process to take place at a higher rate than the other separation process. The authors also suggested that the interfacial resistance in the aqueous phase can be reduced by increasing the Reynolds number ( $Re$ ) to values that produce an acceptable pressure drop in the HF's (3.8 bar). The following important findings were made from the analysis of the results obtained: (a) the pseudo-steady state of the system is reached rapidly ( $<0.2$  h), (b) the carrier used, Alamine 336, has a high selectivity for chromium species, and (c) the total chromium concentration decreases from  $9.62 \text{ mol/m}^3$  at the module inlet to  $0.015 \text{ mol/m}^3$  ( $0.8 \text{ mg Cr/L}$ ) at the module outlet in one pass when the residence time in the module is  $0.0014$  h.

### 39.4.2 PEHFSD IN THE SEPARATION/REMOVAL/CONCENTRATION OF ACTINIDES

On the basis of performance of the PEHFSD technique in hydrometallurgy, a comprehensive program was prepared in the laboratory of the author to use PEHFSD with a hydrophobic microporous HF contactor for the recovery of actinides from process effluents. Roy et al. [47–50] carried out a detailed study of actinide transport using PEHFSD. The objective was to evaluate the effect of various chemical and hydrodynamic parameters in optimizing the performance of PEHFSD for the extraction of U(VI), Pu(IV), and Am(III) from nitric acid media. The authors also attempted to apply this technique to the recovery of actinides from the different streams of low-level and medium-level acidic waste. As in hydrometallurgical applications, an organic solution is dispersed in an aqueous strippant and the resulting pseudo-emulsion is then pumped into the shell side of a microporous polypropylene HF module. The aqueous feed solution containing the U(VI), Pu(IV), or Am(III) to be extracted is passed through the tube side of the fibers. The continuous organic phase of the dispersion readily wets the pores of the hydrophobic microporous support and a stable liquid membrane (the organic phase) is formed in the pores of the microporous support. This ensures stable and continuous operation. In addition, the direct contact between the organic and strip phases on the strip dispersion side provides an additional surface area, which results in very efficient stripping.

#### 39.4.2.1 U(VI), Pu(IV), and Am(III) Extraction

The extraction of U(VI) was performed by Roy et al. using the PEHFSD technique with TBP as an extractant [47–48]. A schematic view of the PEHFSD process for U(VI) (as a representative case  $0.01 \text{ M HNO}_3$ ) in recirculation mode (using a

**TABLE 39.3**  
**Composition of Polluted Ground Water**

Component	Concentration	Component	Concentration
Cr(VI)	$26.1 \text{ mol m}^{-3}$	$\text{CO}_3^-$	$1.6 \text{ mol m}^{-3}$
$\text{SO}_4^{2-}$	$33.5 \text{ mol m}^{-3}$	Si	$0.5 \text{ mol m}^{-3}$
$\text{Cl}^-$	$29.1 \text{ mol m}^{-3}$	Al	$2.1 \text{ mol m}^{-3}$
Ca	$13.6 \text{ mol m}^{-3}$	TOC	$4.3 \text{ mol m}^{-3}$
pH	7.3		
Conductivity	$11.8 \text{ mS cm}^{-1}$		

Source: From Bringas, E. et al., *Ind. Eng. Chem. Res.*, 45, 4295, 2006. With permission.

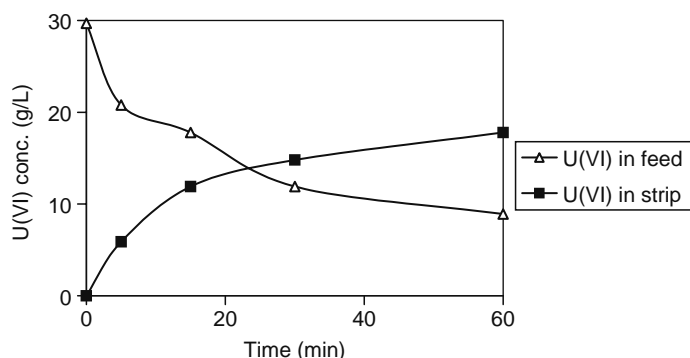


**FIGURE 39.9** Simultaneous extraction and stripping of U(VI) using PEHFSD technique. Feed acidity: 4 M HNO<sub>3</sub>, extractant: 30% TBP in nph, U(VI) ~29.7 g L<sup>-1</sup> (% recovery of U(VI): 68%).

peristaltic pump) is shown in Figure 39.1. In recirculation mode, the feed aqueous phase (300 cm<sup>3</sup>) flowed through the lumen of the fibers at a flow rate of ~12 L/h, and the pseudo-emulsion phase (prepared by stirring [~600 rpm] and the organic phase, TBP + strip solution at a ratio of 1:2) flowed through the shell side at a flow rate of ~5 L/h. In the present setup the pseudo-emulsion phase was 100 cm<sup>3</sup> of TBP diluted in normal paraffin hydrocarbon (nph) plus 200 cm<sup>3</sup> of 0.01 M HNO<sub>3</sub> aqueous stripping solution. By maintaining these conditions, the appearance of the organic phase on the aqueous side of the membrane was prevented as the pressure on the lumen side was higher than on the shell side. Since the emulsion is passed through shell side of HFC, the extraction of metal ions takes place at the pores of the hydrophobic membrane, which is wetted with the organic extractant. Once the pseudo-emulsion is loaded with metal ions, these are recovered instantaneously in the stripping phase (as stripping takes place due to an equilibrium shift caused by 0.01 M HNO<sub>3</sub>). Because of the pseudo nature of the emulsion, the organic and strip phases are separated after the experiment is stopped. This overcomes some of the deficiencies of conventional ELMs, such as the breaking and swelling of the emulsion. In addition, it is difficult to recover metal from the loaded emulsion as the techniques suggested for this purpose (for example, coalescence) are complicated. The transport of U(VI) through the HF membrane contactor was monitored by periodically sampling the feed/strip solution.

The experimental results in Figure 39.9 revealed that when the flow rate of the aqueous phase is higher than that of the organic phase in a hydrophobic membrane and with feed in 4 M HNO<sub>3</sub> and 20% TBP as an extractant, the transport of uranium across the membrane is fast. Therefore, a HF contactor in strip dispersion mode with 20% TBP in nph as an extractant could be successfully used for the separation and concentration of U(VI) from nitric acid media. The feasibility of this technique for the separation of U(VI) from dilute solutions using 0.01 M HNO<sub>3</sub> solution as strippant even in the presence of fission products from waste streams makes it a viable alternative to conventional methods.

The same PEHFSD setup was used for Pu(IV) extraction [49]. The extractant was TBP in nph. The transport proceeds through complexation at the feed phase/membrane interface and the formation of neutral solvated complex species (Pu(NO<sub>3</sub>)<sub>4</sub> · 2TBP), which dissolve in the organic phase. Experiments were performed at concentrations ranging from 5% to 50% of TBP in nph. As can be seen in Figure 39.10, the extraction of Pu increased up to a concentration of 30% and then

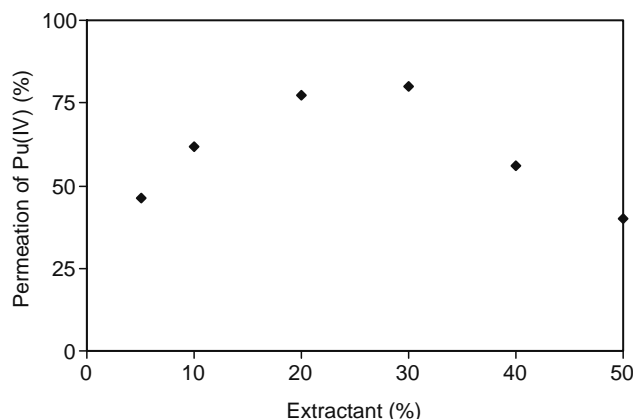


**FIGURE 39.10** Effect of extractant concentration on Pu(IV) transportation. Feed acidity: 4 M HNO<sub>3</sub>, strippant: 0.1 M NH<sub>2</sub>OH · HCl in 0.3 M HNO<sub>3</sub>, Pu(IV) concentration in feed: 1.5 × 10<sup>-5</sup> mol L<sup>-1</sup>.

**TABLE 39.4**  
**Effect of Strippant Concentration**  
**on Am(III) Transport**

S. No.	HNO <sub>3</sub> (M)	% Recovery
1	1.0	39.7
2	2.0	65.4
3	3.0	74.1
4	4.0	75.2
5	5.0	78.5
6	6.0	78.9

*Note:* Final value of transport measured after 90 min.

decreased at concentrations above this value. The diffusion-limited flux increased linearly with the carrier concentration, but at higher carrier concentrations the viscosity of the membrane phase also increased.

Similarly, Am(III) extraction was studied by Roy et al. using the same setup but with a different extractant, i.e., TOPO (trioctylphosphine oxide) in nph [50]. This study analyzed the effect of the concentration of nitric acid, the strippant used, and the variation in the organic–aqueous (O–A) phase ratio on Am(III) transport. The maximum permeation of metal ions was achieved with 6% TOPO in nph as the extractant and 5 M HNO<sub>3</sub> as the strippant. The optimum performance of the TOPO/nph system was attained with an O–A ratio of 0.5. To enable the stripping of metal ions, the nitric acid molarity was varied from 1 to 6 M. The results reveal (Table 39.4) that stripping reaches a maximum at 5 M HNO<sub>3</sub> and then remains steady above this value. Further experiments were carried out with O–A ratios from 0.09 to 0.5 and it was discovered that an O–A ratio of 0.5 gave the maximum permeation of Am(III) (78.5%). Figure 39.11 shows the effect of extractant concentration on Am(III) transport from nitric acid media. When the volume of strippant was decreased, metal recovery also decreased under similar experimental conditions.

### 39.4.2.2 U(VI) and Pu(VI) Recovery from Oxalate Supernatant Waste

During plutonium reconversion in a reprocessing plant, oxalate supernatant is normally generated during plutonium precipitation by oxalic acid as plutonium oxalate. This is further converted into plutonium oxide. This waste solution will have the following composition: uranium (U): 5 gm dm<sup>-3</sup>, plutonium (Pu): 25 mg dm<sup>-3</sup>, ruthenium (Ru<sup>106</sup>): 0.0032 mCi dm<sup>-3</sup>, cesium (Cs<sup>137</sup>): 0.003 mCi dm<sup>-3</sup>, nitric acid: 3 M, and H<sub>2</sub>C<sub>2</sub>O<sub>4</sub>: 0.1 M.

Using the same PEHFSD setup (similar to Figure 39.1), Roy et al. [51] carried out a series of experiments with treated (oxalate ion destroyed by KMnO<sub>4</sub> and H<sub>2</sub>O<sub>2</sub>) and untreated (without oxalate decomposition) waste to recover uranium and plutonium from these acidic solutions using TBP as an extractant in pseudo-emulsion form with nitric acid. The aqueous feed phase flowed through the lumen of the fibers at a flow rate of ~12 L/h and the pseudo-emulsion phase (prepared by stirring [~600 rpm] the organic plus strip solution at a ratio of 1:2) flowed through the shell side at a flow rate of ~5 L/h. The uranium

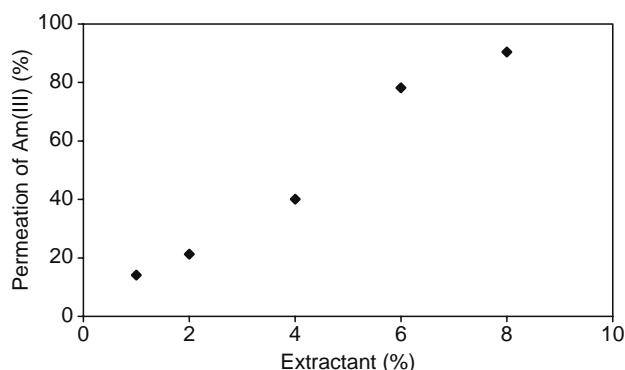


**FIGURE 39.11** Effect of extractant concentration on Am transport. Feed acidity: 0.3 M HNO<sub>3</sub>, extractant: TBP, strippant: 5 M HNO<sub>3</sub>, feed concentration: 10<sup>-6</sup> mol dm<sup>-3</sup> (final value of transport measured after 90 min).

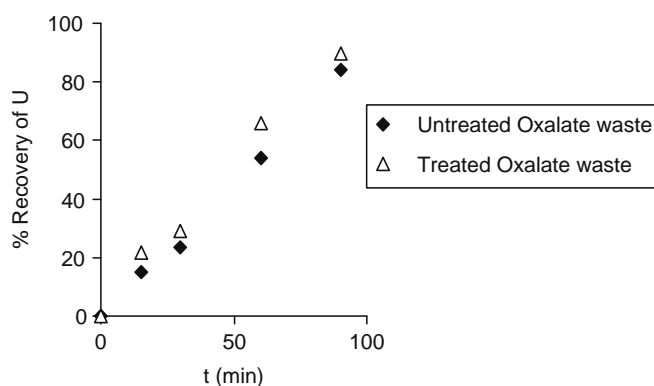


**FIGURE 39.12** % Recovery against elapsed time for U(VI) and Pu(IV) transported for actual untreated and treated oxalate supernatant solution in the feed phase from the experimental results in recycle mode (composition of feed and detail of experiment in text).

and plutonium recovery was well above 80% in the case of untreated waste and over 90% in the case of treated waste (Figure 39.12). The presence of important fission products such as  $^{137}\text{Cs}$  and  $^{106}\text{Ru}$  did not affect the recovery of uranium. This clearly indicates that the present method could be successfully applied to the recovery of both U(VI) and Pu(IV) from oxalate supernatant waste.

## REFERENCES

- Sastre, A.M. et al., Improved techniques in liquid membrane separations: An overview, *Sep. Purif. Meth.*, 27, 213, 1998.
- Kumar, A. and Sastre, A.M., Developments in non-dispersive membrane extraction–separation processes, in *Ion Exchange and Solvent Extraction*, SenGupta, A.K. and Marcus, Y., Eds., Marcel Dekker, New York, 15, 2001, Chapter 8.
- Way, J.D. and Noble, R.D., Facilitated transport, in *Membrane Handbook*, Ho, W.S.W. and Sirkar, K.K., Eds., Chapman & Hall, New York, 1992.
- Cussler, E.L., *Diffusion: Mass Transfer in Fluid Systems*, Cambridge University Press, New York, 1984.
- Molinari, R., de Bartolo, L., and Drioli, E., Coupled transport of amino acids through a supported liquid membrane. Part I: Experimental optimization, *J. Membr. Sci.*, 73, 203, 1992.
- Urtiaga, A.M. et al., Supported liquid membranes for the separation–concentration of phenol. Part 2: Mass transfer evaluation according to fundamental equations, *Ind. Eng. Chem. Res.*, 31, 1745, 1992.
- Urtiaga, A.M. and Irabien, J.A., Internal mass transfer in hollow fiber supported liquid membranes, *AIChE J.*, 39, 521, 1993.
- Alonso, A. et al., Viability and stability study of the recovery of Cr(VI) with hollow fiber contactors, *Latin Am. App. Res.*, 23, 179, 1993.
- Loiacono, O., Drioli, E., and Molinari, R. Metal ion separation and concentration with supported liquid membranes, *J. Membr. Sci.*, 28, 123, 1986.
- Takeuchi, H., Takahashi, K., and Goto, W., Some observations on the stability of supported liquid membranes, *J. Membr. Sci.*, 34, 19, 1987.
- Ho, W.S. and Sirkar, K.K., *Membrane Handbook*, Chapman & Hall, New York, 1992.
- Kemperman, A.J.B. et al., Stability of supported liquid membranes: State of the art, *Sep. Sci. Technol.*, 31, 20, 2733, 1996.
- Dreher, T.M. and Stevens, G.W., Instability mechanisms of supported liquid membranes, *Sep. Sci. Technol.*, 33, 6, 835, 1998.
- Kentish, S. and Stevens, G., Innovations in separations technology for the recycling and reuse of liquid waste streams, *Chem. Eng. J.*, 84, 149, 2001.
- Hu, S.Y.B., Li, J., and Wienczek, J.M., Feasibility of surfactant-free supported emulsion liquid membrane extraction, *J. Colloid Interface Sci.*, 266, 430, 2003.
- Hu, B.B. and Wienczek, J.W., Emulsion liquid membrane extraction of copper using a hollow fiber contactor, *AIChE J.*, 44, 570, 1998.
- Ortiz, I. et al., Modeling and optimisation of an emulsion pertraction process for removal and concentration of Cr(VI), *Ind. Eng. Chem. Res.*, 42, 5891, 2003.
- Klaassen, R. et al., Removal of hydrocarbons from wastewater by pertraction, in Proceedings of the Seventh International Symposium on Synthetic Membranes in Science and Industry, University of Tubingen, Tubingen, Germany, 1994, p. 316.
- Raghuraman, B. and Wienczek, J.M., Extraction with emulsion liquid membranes in a hollow-fiber contactor, *AIChE J.*, 39, 1885, 1993.
- 20a. Hu, S.Y. and Wienczek, J.M., Emulsion-liquid-membrane extraction of copper using a hollow-fiber contactor, *AIChE J.*, 44, 570, 1998.
- 20b. Wienczek, J.M. and Hu, S.Y., Emulsion liquid membrane extraction in a hollow-fiber contactor, *Chem. Eng. Technol.*, 23, 551, 2000.
- Ho, W.S., Supported liquid membrane process for chromium removal and recovery, US Patent No. 6,171,563, 2001.
- Ho, W.S., Combined supported liquid membrane/strip dispersion process for the removal and recovery of penicillin and organic acids, US Patent No. 6,433,163, 2002.
- Ho, W.S. et al., Supported Liquid Membranes for Removal and Recovery of Metals from Waste Waters and Process Streams, Proceedings of the 4th Topical Conference on Separations Science and Technology, AIChE Annual Meeting, Dallas, TX, Paper No. 200d (November 1999); accepted for publication in *Environmental Progress*, 2001.

24. Ho, W.S. and Poddar, T.K., New membrane technology for removal and recovery of metals from wastewaters and process streams, Proceedings of the Topical Conference on Membrane and Extraction Science and Technologies for Environmental Applications, AIChE Spring National Meeting, Atlanta, GA, 2000, p. 38.
25. Ho, W.S. and Poddar, T.K., New membrane technology for removal and recovery of chromium from waste waters, *Environ. Prog.*, 20, 44, 2001.
26. Ho, W.S., Inventor, Commodore Separation Technologies Inc., Assinee. Supported liquid membrane process for chromium removal and recovery, US Patent 6,171,563, 2001.
27. Ho, W.S. and Li, N.N., Definitions and theory for emulsion liquid membranes, in *Membrane Handbook*, Ho, W.S. and Sirkar, K.K., Eds., Chapman & Hall, New York, 1992, p. 595.
28. Gu, Z.M., Ho, W.S., and Li, N.N., Design considerations for emulsion liquid membranes, in *Membrane Handbook*, Ho, W.S. and Sirkar, K.K., Eds., Chapman & Hall, New York, 1992, p. 656.
29. Otto, N.C. and Quinn, J.A., Facilitated transport of carbon dioxide through bicarbonate solutions, *Chem. Eng. Sci.*, 26, 949, 1971.
30. Smith, D.R., Lander, R.J., and Quinn, J.A., Carrier-mediated transport in synthetic membranes. *Recent Dev., Sep. Sci.*, 3(Part B), 225, 1977.
31. Matulevicius, E.S. and Li, N.N., Facilitated transport through liquid membranes, *Sep. Purif. Methods*, 4, 73, 1975.
32. Li, N.N., Facilitated transport through liquid membranes—an extended abstract., *J. Membr. Sci.*, 3, 265, 1978.
33. Ho, W.S., Inventor; Commodore Separation Technologies Inc., Assinee. Combined supported liquid membrane/stripping dispersion process for removal and recovery of radionuclides and metals, US Patent 6,328,782, 2001.
34. Ho, W.S. et al., Supported liquid membranes for removal and recovery of metals from waste waters and process streams, *Environ. Prog.*, 20, 117, 2001.
35. Ho, W.S. and Wang, B., Inventors; Commodore Separation Technologies Inc., Assinee. Combined supported liquid membrane/stripping dispersion process for removal and recovery of metals: Dialkyl monothiophosphoric acids and their use as extractants, US Patent 6,291,705, 2001.
36. Ho, W.S., Poddar, T.K., and Neumuller, T.E., Removal and recovery of copper and zinc by supported liquid membranes with strip dispersion, *J. Chin. Inst. Chem. Engrs.*, 33, 67, 2002.
37. Ho, W.S., Inventor; Commodore Separation Technologies Inc., Assinee, Combined supported liquid membrane/stripping dispersion process for removal and recovery of metals, US Patent 6,350,419, 2002.
38. Ho, W.S. and Wang, B., Strontium removal by new alkyl phenylphosphonic acids in supported liquid membranes with strip dispersion, *Ind. Eng. Chem. Res.*, 41, 381, 2002.
39. Urtiaga, A. et al., Membrane contactors for the recovery of metallic compounds: Modelling of copper recovery from WPO processes, *J. Membr. Sci.*, 257, 161, 2005.
40. Abellán, M.J. et al., Extraction and back-extraction of copper (II) with LIX622N in hollow fiber contactors, in *Chemical Industry and Environment IV, Proceedings of the European Meeting on Chemical Industry and Environment*, A.M. Machín and J. Umbría, Eds., Las Palmas de Gran Canaria, Spain, February 12–14, 2003, pp. 75–84.
41. Klaassen, R. and Jansen A.E., The membrane contactor: Environmental applications and possibilities *Environmental Prog.*, 20, 1, 37, 2001.
42. Sonawane, J.V., Pabby, A.K., and Sastre, A.M., Recovery of gold(I) by supported liquid membrane with strip dispersion using hollow fiber contactors, in 5th European Meeting on Chemical Industry and Environment (EMChIE-2006), Vienna, Austria, 2006.
43. Sonawane, J.V., Pabby, A.K., and Sastre, A.M., Pseudo-emulsion based hollow fiber strip dispersion (PEHFSD) technique: A novel methodology for gold recovery from base metals in cyanide media, *AIChE J.*, 54, 453, 2008.
44. Sonawane, J.V., Pabby, A.K., and Sastre, A.M., Au(I) extraction by LIX-79/n-heptane using the pseudo-emulsion-based hollow-fiber strip dispersion (PEHFSD) technique, *J. Membr. Sci.*, 300, 147, 2007.
45. Sonawane, J.V., Pabby, A.K., and Sastre, A.M., Hexavalent chromium recovery by pseudo-emulsion based hollow fiber strip dispersion with Cyanex-923 from acidic media, *Chemosphere*, 2008 (submitted).
46. Bringas, E., Roman, M.F., and Ortiz, I., Separation and recovery of anionic pollutants by the emulsion pertraction technology. Remediation of polluted groundwaters with Cr(VI), *Ind. Eng. Chem. Res.*, 45, 4295, 2006.
47. Roy, S.C. et al., Pseudo-emulsion based hollow fiber strip dispersion technique: A novel application with U(VI)–TBP system, Theme meeting on Trends in Separation Science and Technology, (SESTEC), BARC, Mumbai, 2004.
48. Roy, S.C. et al., Pseudo-emulsion based hollow fiber strip dispersion technique for U(VI) permeation, *Sep. Sci. Technol.*, 2008 (in press).
49. Roy, S.C. et al., Permeation of Pu(IV) using hollow fiber strip dispersion (PEHFSD) technique at Biennial Symposium on Emerging Trends in Separation Science and Technology (SESTEC), BARC, Mumbai, September 29 to October 1, 2006.
50. Roy, S.C. et al., Simultaneous extraction and stripping of Am(III) using pseudo emulsion based hollow fiber strip dispersion (PEHFSD) technique, DAE Symposium on Nuclear and Radiochemistry (NUCAR-2007), MS University, Baroda, February 14–17, 2007.
51. Roy, S.C., Extraction studies of trans-actinium elements through microporous membrane, PhD thesis, University of Mumbai, Mumbai, 2007 (submitted).



---

# 40 Electrically Enhanced Membrane Separations and Catalysis

*V.M. Linkov, B.J. Bladergroen, and A.M. Maluleke*

## CONTENTS

40.1	Introduction to Water Treatment Technologies Involving Membranes and Electrodes .....	1071
40.2	Electrically Enhanced Membrane Processes for Water Purification .....	1072
40.2.1	Electrochemical Modification of Pollutants .....	1072
40.2.1.1	Electrochemical Oxidation .....	1072
40.2.1.2	Electrochemical Reduction .....	1074
40.2.1.3	Electrochemical Disinfection .....	1074
40.2.2	Electrostatically Driven Pollutants .....	1074
40.2.2.1	Electrofiltration .....	1074
40.2.2.2	Electrodialysis .....	1075
40.2.2.3	Electrosorption .....	1076
40.2.2.4	Electroremediation .....	1077
40.3	Discussion .....	1077
40.3.1	Which Electrically Enhanced Separation Process Treats Which Effluent Most Efficiently? .....	1077
40.3.2	Which New Water Treatment Applications Can Be Identified Specifically for Electrically Enhanced Separation Processes? .....	1078
40.3.3	Future of Electrically Enhanced Separation Processes .....	1078
40.4	Case Study: Electrosorption Membranes for Wastewater Treatment .....	1079
40.4.1	Preparation of the Electrosorption Membrane .....	1079
40.4.2	Methods of Analysis .....	1080
40.4.3	Testing of Electrosorption Materials .....	1080
40.4.4	Conclusion .....	1081
40.5	Case Study: Electrocatalytic Membranes for Decomposition of Organic Pollutants .....	1081
40.5.1	Preparation of Electrocatalytic Membranes .....	1081
40.5.2	Testing of Electrocatalytic Membranes .....	1082
40.5.3	Influence of Chloride Ions on the Electrochemical Oxidation of Phenol .....	1083
40.5.4	Conclusion .....	1083
	Acknowledgments .....	1083
	References .....	1084

## 40.1 INTRODUCTION TO WATER TREATMENT TECHNOLOGIES INVOLVING MEMBRANES AND ELECTRODES

Membranes are employed in various industrial processes because these materials provide an efficient and economical way to separate specific compounds from specific process streams. Membranes and membrane processes are developed and optimized to suit the needs of the separation process where they are to be implemented. The main parameters of membranes are selectivity and permeability toward specific compounds and membrane stability in the process environment. Organic membranes are usually more economical than inorganic membranes unless specific properties of inorganic membranes are required such as chemical inertness, high radiation resistance, or high thermal and mechanical stabilities. Organic and inorganic membranes offer a wide range of applications and occupy an important place in modern process industry, including food, biotechnology, environmental control, and electronics and petrochemical industries [1]. However, membranes have their limitations and many

impurities or pollutants cannot be efficiently or economically removed by the selective properties of ceramic or polymeric membranes only.

Electroseparation is defined as “the use of electricity or electromagnetic fields to produce and enhance chemical or physical separation” [2]. Tsouris and DePaoli [3,4] have presented brief reviews of this topic. Essentially the electrical potential applied between two electrodes is used to promote physical or chemical processes that are not favorable or are too slow under nonelectric process conditions. In the past few decades, scientists have tried to combine the advantages of both electrical and membrane processes. Electrodes with the porosity of a membrane (i.e., electromembranes) offer an advantage in terms of contact: pollutants that are forced through the pores of an electromembrane are more likely to be adsorbed, decomposed, oxidized, or reduced than when passing along the relatively low surface area of a dense electrode.

Electromembranes are commonly made from porous carbon, metals, or metal oxides. Originally, nonconductive ceramic materials such as  $\text{Al}_2\text{O}_3$  and  $\text{TiO}_2$  were modified into electrodes by deposition of electroconductive materials such as (1) carbon by pyrolysis of methane [5] or natural gas [6], (2)  $\text{RuO}_2\text{-TiO}_2$  via solgel techniques [7], (3) metals via electroless plating [6,7], or (4) electromagnetic sputtering [6]. Ebonex ceramic ( $\text{Ti}_4\text{O}_7$ ), the most common of the ceramic-based anode materials, is reported to exhibit electrical conductivity similar to that of graphite ( $6.3 \times 10^{-4} \Omega \text{ cm}$ ) [8]. Ebonex is nonstoichiometric titanium oxide comprised of Magneli phase titanium oxides,  $\text{Ti}_4\text{O}_7$  and  $\text{Ti}_5\text{O}_9$  [9–10]. A significant amount of research has also been conducted on the deposition of platinum onto Ebonex as well as the characterization of platinum-coated Ebonex electrodes [11–13].

This chapter describes water purification processes where an electrode process is combined with a membrane process. Special emphasis is placed on processes where the membrane acts as an electrode. Porous electrodes or electrodes that could potentially be used as membranes are also included in this chapter. The last two sections describe two case studies of electrosorption of ions from wastewater and anodic decomposition of phenol, respectively.

## 40.2 ELECTRICALLY ENHANCED MEMBRANE PROCESSES FOR WATER PURIFICATION

References on electrochemical/electrostatic enhanced water purification processes using ceramic membranes can be divided into two main groups; papers dealing with pollutants that are either

1. electrochemically modified, meaning that the pollutant takes part in an electrochemical reaction, or
2. removed largely by electrostatic attraction/repulsion

Sections 40.2.1 and 40.2.2 highlight the advantages and disadvantages and the role of ceramic membranes in both approaches.

### 40.2.1 ELECTROCHEMICAL MODIFICATION OF POLLUTANTS

Water purification can be achieved by decomposition or destruction of the pollutant on contact with an electrically charged surface. In several cases permeable electrodes are used in a flow-through mode to ensure contact between the pollutant and the electrode. The type of electrode ranges from metal meshes and carbon cloths to ceramic membrane supports coated with a porous layer of electroconductive material.

Ceramic membranes in these kinds of processes are often desirable due to their thermal and chemical stabilities in the oxidative and reducing environment. The types of processes discussed here can be divided into three groups, namely electrochemical oxidation, electrochemical reduction, and electrochemical disinfection and are discussed in Sections 2.1.1, 2.1.2, and 2.1.3, respectively. Jüttner et al. [14] reviewed examples of each group with particular emphasis on anodic oxidation of phenol, aliphatic acids, cyanide, thiocyanide, and sodium dithionite, employing different electrodes, i.e., packed bed and electrodes of graphite, titanium-supported oxides ( $\text{IrO}_2$ ,  $\text{RuO}_2$ ,  $\text{PbO}_2$ , and  $\text{SnO}_2$ ), and Bi- or Fe-doped  $\text{PbO}_2$ .

#### 40.2.1.1 Electrochemical Oxidation

Anodic oxidation was shown to be a useful method for the removal of organic pollutants from aqueous solutions [15]. Partial decomposition of hazardous organic compounds to biodegradable compounds or complete decomposition to  $\text{H}_2\text{O}$  and  $\text{CO}_2$  can be achieved by the electrochemical treatment of waste [14]. Two different categories of electrochemical treatment of wastewater or waste can be distinguished:

- Direct anodic oxidation, whereby organics are oxidized at the electrode surface.
- Indirect oxidation, whereby electrochemically generated oxidants, such as ozone, hydrogen peroxide, hypochlorite, Fenton's reagent, or peroxodisulfate are applied for oxidation [16,17].

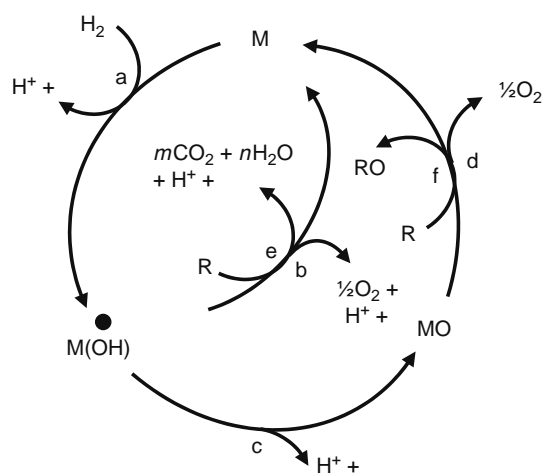


**FIGURE 40.1** Oxidation mechanism on active and non-active anodes. (From Comninellis, CH., *Electrochim. Acta*, 39, 1858, 1994. With permission.)

Mediated electrochemical oxidation (MEO) is a special case of indirect oxidation whereby metal ions with high oxidation potential (e.g., Ag(II), Ce(IV), and Co(III)) are electrochemically generated in a closed cycle [14].

#### 40.2.1.1.1 Direct Oxidation at the Anode

A generalized pathway for anodic oxidation of organics as described by Comninellis [18] is illustrated in Figure 40.1.

The pathway described in Figure 40.1 assumes that six major steps are involved:

1. Electrolysis of water, forming an adsorbed hydroxyl species
2. Electrochemical oxidation of physisorbed hydroxyl radicals ( $\text{H}_2\text{O}/\text{H}_2\text{O}_2$  redox couple)
3. Electrochemical oxidation of the surface (M/MO redox couple)
4. Release of oxygen during chemical decomposition
5. Electrochemical oxidation mediated by physisorbed (\*OH) radicals
6. Heterogeneous catalytic oxidation at electrooxidized active sites

The Ebonex ceramic anode has been used to study the electrolytic oxidation of trichloroethylene to  $\text{CO}_2$ ,  $\text{CO}$ ,  $\text{Cl}^-$ , and  $\text{ClO}_3^-$  [19]. Ebonex and  $\text{PbO}_2$ -coated Ebonex electrodes were used for the electrochemical treatment of phenolic pollutants in water [20].

It was also reported that porous ceramic-based membranes, made from stainless steel supported  $\text{Al}_2\text{O}_3/\text{ZrO}_2$ , were employed as electrodes for the direct oxidation of methanol [21–22]. The electromembranes were prepared by electrodeposition of active materials such as tungsten and molybdenum. Aqueous effluents containing mainly phenol were passed through a flow-through electrochemical reactor equipped with an alumina-based ceramic membrane. The obtained permeate was analyzed and fed back into the reactor for 10 consecutive cycles. During the first three cycles, the phenol concentration was reduced from 100 ppm to 5 ppm. It was clear that *p*-benzoquinone was the most important intermediate product and its concentration increased considerably during the first few cycles. When most of the phenol was converted, a reduction in *p*-benzoquinone concentration could be observed on further cycles. After the tenth cycle the *p*-benzoquinone concentration was 20 ppm [23]. It should be noted that these low concentration could be more harmful than the initial concentration of phenol and full analysis of treated water is therefore recommended.

#### 40.2.1.1.2 Indirect Oxidation

In aqueous waste liquids containing low concentrations of undesired organic compounds (generally less than 100 ppm) only a limited selection of these compounds can be oxidized. Direct electrochemical oxidation at the anode would be an uneconomical option because of the low concentration of the organic compounds to be treated [24]. Hence electrochemically generated oxidants are suitable for these waters.

Chlorine or hypochlorite has been reported as a widely used electrochemically generated oxidant [14]. The  $\text{ClO}^-/\text{Cl}^-$  pair acts as an electron transfer agent that destroys organic pollutants [25]. Electrochemically generated  $\text{ClO}^-$  anions proved to have a positive influence in the fractional conversion of phenol by enhancing degradation over shorter electrolysis periods [26]. Phenol degradation can be carried out near the electrode surface by hypochlorite formed through the oxidation of chloride [27].  $\text{H}_2\text{O}_2$  can also be used as an oxidizing agent and can be electrogenerated via the two electron reduction of  $\text{O}_2$  at the cathode [17]. The oxidative power of the  $\text{H}_2\text{O}_2$  molecules can be enhanced when the reaction conditions favor the Fenton

reaction where the highly reactive one-electron oxidizing agent, the hydroxyl radical ( $\text{OH}^\bullet$ ), can be produced. Wang et al. [17] described how the TOC of a simulated dye waste was reduced to 30% by indirect electro-oxidation using the electro-Fenton reaction. The electrode in this case was an activated carbon.

#### 40.2.1.2 Electrochemical Reduction

Metal ions such as nickel, iron, copper, and zinc are those pollutants most readily treated by an electrochemical reduction method. Metal reduction becomes feasible at concentrations above 0.05 ppm if relatively costly metals can be recovered. In the case of electrochemical reduction the function of the membrane is usually limited to that of a diaphragm and the electrodes used are usually solid.

Another application where the reduction of metallic impurities is possible is in the purification of plating solutions containing negatively charged metal oxides, e.g., chromium plating baths [28]. In this application, negative metal oxide ions migrate away from the cathode where the positive impurities ( $\text{Cu}^+$ ,  $\text{Zn}^{2+}$ ,  $\text{Fe}^{2+}$ ) are reduced.

Bunce et al. [29] employed ion-selective membranes in the reduction of a synthetic acid mine drainage solution containing  $\text{FeSO}_4$  and  $\text{CuSO}_4$ . 50% current efficiencies were reached when the anion-exchange membrane was used as separator between the cathode and the anode compartments. However, as the conductivity of the catholyte solution decreases, increasingly higher potentials are needed to overcome the ohmic losses, and therefore higher energy costs are incurred. This is the case particularly where metal ions are reduced at the cathode and no new source of ion conductivity (such as  $\text{OH}^-$  ions) is generated [29]. A promising application of electrochemical reduction was described by Juang and Lin [30] in which case an electrochemical Cu reduction and citrate recovery system was tested. More than 50% current efficiency and 95% Cu recovery were obtained for concentrations above  $20 \text{ mmol} \cdot \text{L}^{-1}$  at a current density of  $139 \text{ A} \cdot \text{m}^{-2}$ . Patent US4948489 [31] describes an electrochemical cell in which heavy metals can be removed from wastewater in the form of oxides. By applying potentials up to 25 V the oxides of heavy metals (having a standard reduction potential more negative than that of hydrogen) were formed. The oxides can be removed by filtration.

It is not always the direct reduction of metal ions that may lead to their removal. Some metal ions, especially  $\text{Fe}^{2+}$ , are removed by precipitation as a result of an increase in the pH near the cathode [28].

#### 40.2.1.3 Electrochemical Disinfection

Potential applied over granular-activated carbon [32] and compacted activated carbon [33] can be used to kill bacteria, and a potential usually between 0.6–1 V versus the saturated calomel electrode is required. Desorption of dead bacteria from electrode cells can be accomplished via electrostatic repulsion by applying negative potentials. The work of Matsunaga et al. [32] concentrated on the electrochemical oxidation of intracellular coenzyme A and not on the generation of disinfectants by electrochemical oxidation. However, the release of carbon from the electrode was mentioned as one of the drawbacks. In a more recent article, Matsunaga et al. [34] described the application of an alternating positive potential to a titanium nitrate (TiN) mesh electrode that resulted in effective disinfection of water containing several types of bacteria. The TiN films employed exhibited low electrical resistance and good chemical and thermal stabilities. An applied potential of 1.2 V versus the saturated calomel electrode reduced the survival ratio of microorganisms to between 0% and 38% depending on the type of microorganism.

### 40.2.2 ELECTROSTATICALLY DRIVEN POLLUTANTS

Processes whereby purification results by the use of an electrical field, which is not accompanied by decomposition or destruction of the pollutant, can be divided into four different groups: electrodialysis (ED), electrofiltration, electrosorption, and electroremediation. The main electrochemical reaction in these types of processes is decomposition of water.

The process of ED is, by definition, a membrane-based separation process in which ions are driven through an ion-selective membrane under the influence of an electric field [35]. Conversely, in electrofiltration a charged pollutant particle is prevented from moving through a membrane by the influence of an electric field. Electrosorption is an electrically enhanced ion-exchange process and electroremediation is a process developed for the decontamination of polluted soil. Each different process is discussed separately.

#### 40.2.2.1 Electrofiltration

Membrane fouling is an important phenomenon that has a significant effect on the efficiency of a membrane system. This fouling increases the energy consumption of water purification process. The problems associated with fouling are commonly reduced by the following main membrane antifouling strategies: (1) modification of the membrane material, (2) changing of the hydrodynamic conditions in the flow channel, and (3) application of an external force, e.g., electrical field [36]. Most biological colloids in nature possess a small surface charge that will allow small drift velocities when placed in an electrical field [37]. Under the right conditions these drift velocities can help prevent fouling. This principle is schematically

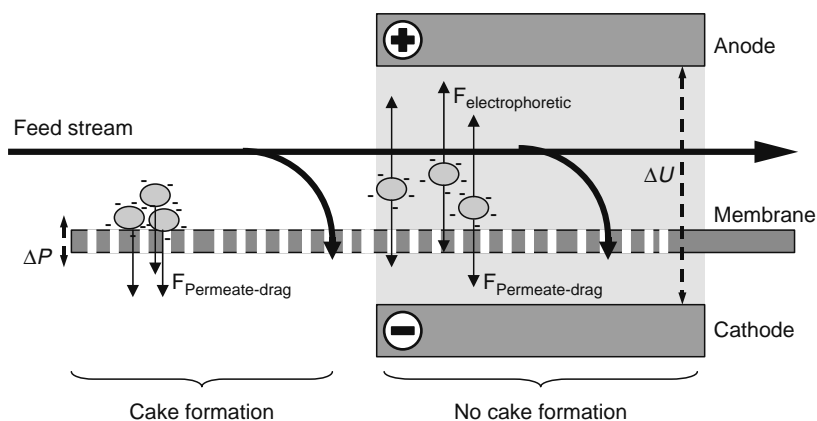


FIGURE 40.2 Schematic representation of the principle of electrofiltration.

represented in Figure 40.2. The force caused by the flow of permeate toward the porous surface accumulates the particles at the pore entrance. With an additional electrophoretic force applied, the net force upon the particle toward the surface decreases and the formation of a “cake layer” (i.e., a layer comprised of rejected particles at the upstream face of the membrane) can be prevented or significantly delayed.

Several researchers have shown that the application of an electrostatic field over the cross section of a membrane leads to a significant reduction in the energy cost per unit of permeate for microfiltration [38–40], ultrafiltration [41–44], and nanofiltration systems [45].

In conventional filtration systems the cake layer adds significantly to the resistance of flow through the membrane, and therefore to the overall operating costs. Several articles [36–40] and some reviews [2,46] describe electrofiltration in more detail. In particular the focus is on specific aspects of electrofiltration for different membranes or pollutant surface charges, and the influence of the magnitude of the imposed field gradient, as well as the role of cross-flow velocity and particle sizes of pollutants. Application of the correct electrical potential can prevent the formation of the cake layer, allowing the steady-state flux to be 10 times higher than the same membrane process without the applied potential [39,41,46]. Electrofiltration becomes especially important for the treatment of effluents with a high total solid content. Such effluent is for example produced during the post-chemical mechanical polishing (CMP) process, an essential step in the production process of integrated circuit (IC) chips. Large volumes of ultrapure water (UPW) are used to remove impurities from wafer surfaces, specifically fine particles from the polishing slurry resulting in wastewaters with a high solid content. Wang and Yang [47] found that this effluent could be treated with electrofiltration very efficiently.

Electrofiltration was investigated using both organic membranes (such as polyamide [41] and polyether sulfone [39]) and inorganic membranes [40]. The main advantage of inorganic membranes when used in electrofiltration is that the membrane can act as the membrane and electrode simultaneously. This not only makes the system simpler but also reduces the distance between electrodes and therefore the necessary potential difference. Robinson et al. [43] investigated the use of alternating current to reach optimum performance of electrofiltration units and argued that direct current is only needed when the particles are uniformly charged (for example, in biological suspensions at relevant pH values). Theoretical models that describe the membrane permeability under the influence of an electrical field are presented in several papers [36,40,46].

#### 40.2.2.2 Electrodialysis

Electrodialysis (ED) is the electrochemical separation process in which an electrical potential difference and ion-selective membranes are used to separate ionic species from an aqueous solute and other uncharged components. A schematic representation of the ED system is given in Figure 40.3. ED systems usually consist of a large number of compartments between two electrodes. The compartments are separated using alternate anion-exchange membranes (AEM) and cation-exchange membranes (CEM), and compartments are filled with polluted water. When a sufficiently large potential difference is applied between the anode and the cathode to start an electrochemical reaction (usually the reduction of water at the cathode and oxidation of water or chloride at the anode), cations are driven through the CEMs into adjacent compartments in the direction of the cathode. Conversely, anions migrate through the AEMs toward the anode. As a result, adjacent compartments will contain either concentrated or diluted solutions, respectively [48]. Note that the rate of the oxidation and reduction reactions on the electrodes is directly coupled to the transport of charges through the ion-exchange membranes to maintain electrical neutrality in each compartment. During the past three decades, a polarity reversal process known as electrodialysis reversal (EDR) has been developed. In this process the polarity is reversed on a regular basis in order that scale is broken up and

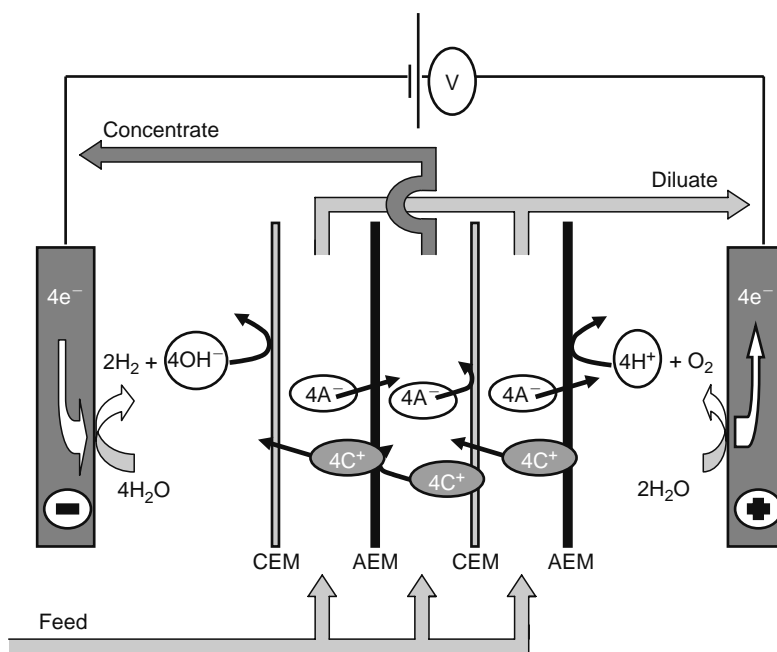


FIGURE 40.3 Schematic representation of the ED process.

flushed out. This makes EDR less sensitive to scaling than ED. However, the complexity of EDR systems leads to relatively high capital and process costs [49].

Major ED/EDR applications include desalination of brackish water, recovery of metals and water from electroplating rinse waters, and demineralization of whey, wine, and sugar process waters [49]. Of all the electroseparation processes, ED has received the most attention and is one of the few electrically assisted membrane technologies to find large-scale industrial applications. Many publications consider different aspects of ED, for example, fouling [50,51], modeling [51,52], use of bipolar membranes [53], ion-selective membranes, and ED-hybrid systems (ion exchange-ED [54], and combined systems such as ED with a bioreactor for denitrification [55,56]). In this chapter, attention will be given to less common, ceramic-based ion-selective membranes. For further information on ED using organic membranes refer to Chapter 12 of Ref. 49.

#### 40.2.2.2.1 Ceramic Ion-Selective Membranes

Sodium super ion-conductors (NaSICON) containing rare earth elements (RE-NaSICON) are commercially available for processes such as the chloro-alkali process. These membranes can also be used in wastewater treatment. Kurath et al. [57] described the electrochemical salt splitting process based on sodium-selective ceramic membranes (i.e., NaSICON containing dysprosium and neodymium). Sodium was removed selectively at  $38 \text{ mA} \cdot \text{cm}^{-2}$  with a current efficiency over 90% from nuclear waste streams to reduce disposal volumes. The ceramic membrane investigated was specifically suitable due to its resistance to radiation damage, superior  $\text{Na}^+$  selectivity, and resistance to fouling owing to its tendency to exclude di- and trivalent cations that can precipitate during salt splitting. Hobbs [58] compared the properties of the NASID inorganic membrane from Ceramtec with the NAFION 324 membrane from DuPont in the recovery of caustic waste from nuclear waste. NASID exhibited superior selectivity toward Na but lower Na conductivity than NAFION 324. One of the drawbacks of the above-mentioned ceramic membranes is their high price. Linkov and Belyakov [59] described a zirconium phosphate based membrane with cation-selective properties suitable for ED. These membranes are much cheaper.

#### 40.2.2.3 Electrosorption

The electrosorption process can be viewed as an ion-exchange bed process in which the resin is regenerated using electrical current. When DC voltage is applied between two electrodes, protons and hydroxyl ions are generated by electrolysis on the surface of the anode and cathode, respectively. As a result of the local change in pH, active sites in the ion-exchange material are produced and may adsorb cations at the cathode and anions at the anode. Subsequent reversal of the voltage enables the adsorbed ions to be eluted so that the working electrode can be regenerated. A schematic representation of electrochemically activated sorption is illustrated in Figure 40.4 [60].

Researchers have described the electrosorption of organics, ions, and bacteria onto carbon [61–65] and polypyrrole composite [66]. Electrosorption electrodes are usually porous since their sorption capacity relates to their surface area; the electrodes do not normally fulfill any separation function. Bladergroen and Linkov described the tubular electrosorption

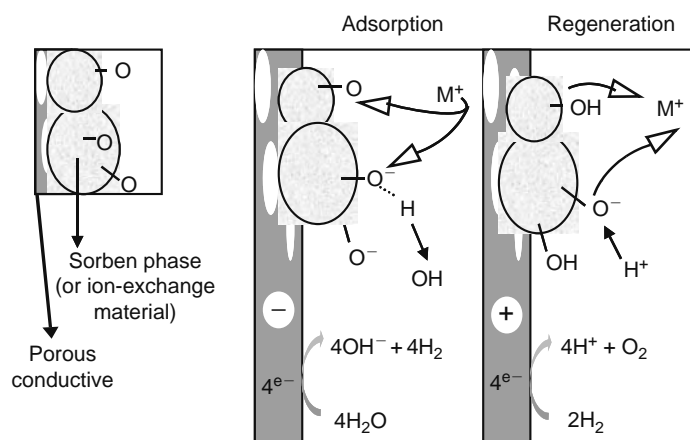


**FIGURE 40.4** Schematic representation of the electrochemically activated sorption process. (From Bladergroen, B.J. and Linkov, V.M., *Sep. Purif. Technol.*, 25, 350, 2001. With permission.)

membrane prepared from a  $ZrO_2/Al_2O_3$  microfiltration membrane, which was first modified with electroconductive carbon coating and subsequently impregnated with inorganic ion-exchange materials ( $ZrO_2$  and  $Zr(HPO_4)_2$ ) to produce electrosorption membranes [60,67]. Activation and regeneration of ion-exchange sites was accomplished by the products of water electrolysis. Synonyms found within the literature for electrosorption include electro-ion-exchange (EIX), electro-deionization (EDI), and capacitive deionization (CDI).

#### 40.2.2.4 Electroremediation

Electroremediation using electrical current is the final purification method discussed in this chapter. Here, an array of anodes are placed in the soil opposite an array of cathodes. When electric potential is applied the following processes occur: electrolysis of water in the soil, dissolution of polluting ions, migration of ions under the influence of the applied potential field, and reduction or pH based precipitation at the cathode [68,69]. This technique, also known as electroreclamation or electrochemical soil decontamination, does not require a membrane; however, improved electroremediation has been reported when ion-exchange membranes were incorporated into the system [70]. The function of the membrane is to retain  $OH^-$  ions produced at the cathode. Migration of these  $OH^-$  ions is prevented to avoid precipitation of the heavy metal ions in the soil.

### 40.3 DISCUSSION

In the previous section examples are presented where the application of an electrical potential difference between two electrodes resulted in a degree of water purification, by a decrease in concentration of organic compounds, pathogens, or ions. These effects are usually more pronounced when the electrode is porous due to its larger surface area compared to that of flat electrodes. When the pollutants are pumped through a membrane electrode the degree of purification may again be increased because of the more intense interaction between the electrode surface and the pollutant. The combination of membrane and electrode processes has been developed into new or advanced purification processes such as electro dialysis and electrofiltration. All separation techniques using a combination of electrodes and membranes have specific advantages dependent upon the specific types of effluent and wastewaters. In this section the following three points are discussed separately:

1. Which electrically enhanced separation process treats which effluent most efficiently?
2. Which new water treatment applications can be identified specifically for electrically enhanced separation processes?
3. Future of electrically enhanced separation processes.

#### 40.3.1 WHICH ELECTRICALLY ENHANCED SEPARATION PROCESS TREATS WHICH EFFLUENT MOST EFFICIENTLY?

In many cases, membrane processes seem to be the most energy efficient separation processes available for industry. However, the costs related to cleaning or replacement of membranes, the need for skilled personnel, and the associated turn down costs determine their economical feasibility. Table 40.1 lists the various electrically assisted membrane processes with the type of effluents that could be treated most efficiently by each process. For most of the electrically assisted membrane processes (1–4), it is expected that the treatment of effluents would be most feasible when ion or particle concentration is high. These are also the effluents where alternative purification processes require a significant part of the process cost to be spent upon membrane

**TABLE 40.1**  
**List of Electrically Assisted Membrane Processes and the Type of Effluents That Will Be Treated Most Efficiently**

Electrically Assisted Membrane Process	Specification of the Most Suitable Effluent to be Treated	Possible Application
Electrofiltration	Effluent with high solid particle content	Effluent from CMP. Chip manufacturing industry
ED	Effluent with high ion content	Potable water production from sea or brackish water
Electro-sorption	Effluents from plating industry with high ion content	Valuable metal recovery and toxic metal removal
Electrochemical reduction	Effluents from plating industry with high ion content	Valuable metal recovery
Electrochemical oxidation	Effluents containing organic pollutants	Decomposition of relatively stable organic compound such as phenol
Electrochemical disinfection	Relative clean surface water containing pathogens	Potable water production

cleaning, fouling prevention, or replacement. Besides, at high levels of impurities the electrical resistance of the effluent and parasitic currents are minimal. Both result in higher energy efficiency of the process.

Electrochemical oxidation becomes a viable option if biological systems cannot utilize a specific organic compound as energy source. Incineration is in most cases the least cost effective option. The process of indirect or direct electrochemical oxidation has to compete with chemical oxidation processes where the purchase cost of oxidizing agents, their transport, storage, and the required dosing systems determine the process cost. If the electrocatalytic system is sufficiently optimized, electrochemical oxidation could become a feasible treatment process for various types of effluents. However, it should be noted that the water should be adequately conducting, and that power consumption is proportional to concentrations of organics to be oxidized.

In contrast with all other electrically enhanced processes, electrochemical disinfection can be employed at low concentration of pollutants (in this case microorganisms). No highly conductive electrolyte is required for effective disinfection. Electrochemical disinfection will have to compete with chemicals normally used for water disinfection, such as chlorine, or ultrafiltration membrane systems. In remote areas (such as rural village water supply) the electrochemical disinfection system, which does not necessarily need a pump, is competitive especially for small-scale processes [71].

#### 40.3.2 WHICH NEW WATER TREATMENT APPLICATIONS CAN BE IDENTIFIED SPECIFICALLY FOR ELECTRICALLY ENHANCED SEPARATION PROCESSES?

Many existing water purification processes not enhanced by an electrical field are potential interesting fields of research. Li et al. described promising results for the adsorption of fluorine on amorphous alumina supported on carbon nanotubes [72]. It is possible that their method can be enhanced by the use of electric field, as other researchers have shown with other electrically enhanced adsorption processes.

The catalytic reduction of nitrates using  $H_2$  or  $NH_4$  as reducing agent was investigated [73–75] using Pd–Cu catalysts supported on  $\gamma$ -alumina. The direct electrochemical reduction of nitrate or indirect reduction by electrochemically produced hydrogen has not received much attention and could be an interesting area of research.

#### 40.3.3 FUTURE OF ELECTRICALLY ENHANCED SEPARATION PROCESSES

With the rapid increase and activities in nanotechnology it may be expected that the volume of effluents containing stabilized nanoparticulates will increase. Electrofiltration processes are specifically suited to treat effluents with nanoparticulates of one specific kind. Because the contaminant particulates will have comparable surface charges, electrical field strength can effectively be optimized to prevent cake formation.

Since the electrical resistance of the effluent and parasitic currents are minimal at high level of impurities, specific interest in electrically assisted membrane processes could increase due to more strict laws and legislation around effluents. The depletion of freshwater resources and the necessity to process brackish or seawater to produce potable water could promote the use of electrically assisted membrane processes in the future. Electrodialysis will have to compete with pressure-driven membrane processes such as reverse osmosis. The growing awareness of the unique cleaning ability of electrically ionized water (EIW) [47], a byproduct of electrodialysis, may be a factor to consider in the choice between ED and RO systems.  $^{17}O$  NMR relaxation measurements were used to determine the water cluster size of electrically ionized water EIW. It is known that the water cluster size of EIW is significantly smaller than that of tap water. The smaller water cluster size is believed to enhance the penetration and extractive properties of EIW. Recently, EIW has been produced and used in several cleaning processes [47] in industry.

The success of indirect electrochemical oxidation and disinfection lies in the production of safe drinking water especially in rural areas where the necessity for skilled maintenance personnel should be avoided. The simplicity, stability, and low power consumption of devices such as the sodium hypochlorite generator described by Bashtan et al. [71] and the TiN reactor described by Matsunaga et al. [34] make these devices most cost effective for small-scale applications in remote locations.

The potential of electrosorption of various ions and anodic decomposition of organic compounds is evident from the results of the case studies in Sections 40.4 and 40.5, respectively.

#### 40.4 CASE STUDY: ELECTROSORPTION MEMBRANES FOR WASTEWATER TREATMENT

The objective of this case study is to show the potential of electrosorption membranes and their application in the treatment of industrial wastewater. A complete report on this study was submitted to the Water Research Commission of South Africa who funded the research (Report number 964/1/02) [76]. A procedure for the preparation and testing of electrosorption material in the form of plates was established by Belyakov, who optimized the following properties of the plate electrosorption membranes [77]:

- Electroconductivity
- Porosity
- Good mechanical properties
- Ability to adsorb cations and anions in an ion-exchange process

##### 40.4.1 PREPARATION OF THE ELECTROSORPTION MEMBRANE

Sorption electrodes in the form of plates were prepared using nonwoven ceramic-based material, Kaowool 700 Grade Paper (Thermal Ceramics, United States), prepared from oxides of multivalent metals. The main characteristics of the ceramic paper are presented in Table 40.2.

To confer electroconductivity upon porous ceramics these materials were coated with a layer of pyrolytic carbon. The deposition of carbon was carried out in the gas phase by pyrolysis of natural gas. The ceramic materials were placed in a quartz reactor under 50 mL/min flow of natural gas. The pyrolysis took place at 900°C for 30 min.

Phosphates of zirconium were selected as additional active sorption components to be introduced into the porous matrices of the sorption electrodes. This choice was justified by the following reasons:

- (a) Phosphates of zirconium are well known inorganic ion exchangers, which possess relatively high ion-exchange capacity.
- (b) Phosphorus-unsaturated materials based on phosphates of zirconium are capable of adsorption of both anions and cations from aqueous solutions.
- (c) Phosphates of zirconium possess high ionic conductivity, which is a very important property for their effective application in the process of electrochemically activated sorption.

The following laboratory method was used for the introduction of zirconium phosphate into ceramic porous structures. The method is based on impregnation of the porous materials with crystalline sol of zirconium dioxide.

For the preparation of sol, 25% solution of NH<sub>3</sub> was added in small portions (2 mL) to 1 L of 1 M solution of ZrOCl<sub>2</sub> while heating under mechanical stirring. The temperature of solution did not exceed 90°C. Each following portion of NH<sub>3</sub> solution was added only after complete dissolution of the zirconium hydroxide precipitate. The addition of the NH<sub>3</sub> solution was terminated once the zirconium hydroxide precipitate did not dissolve within 20 min. The raw sol obtained was boiled using a reflux condenser for 25 h to allow the formation of the crystalline structure. Thereafter the sol was cooled to ambient temperature and filtered. Ceramic materials were immersed in 1 M sol of zirconium dioxide that was prepared as described

**TABLE 40.2**  
Main Characteristics of Kaowool 700 Grade Paper That Was Used for Preparation of Electro-Sorption Membranes

Trade Mark of Ceramic Paper	Chemical Analysis (wt%)		Nominal Density (kg · m <sup>-3</sup> )	Fiber Index (%)
	Al <sub>2</sub> O <sub>3</sub>	SiO <sub>2</sub>		
Kaowool 700 Grade Paper	47	53	175–210	55

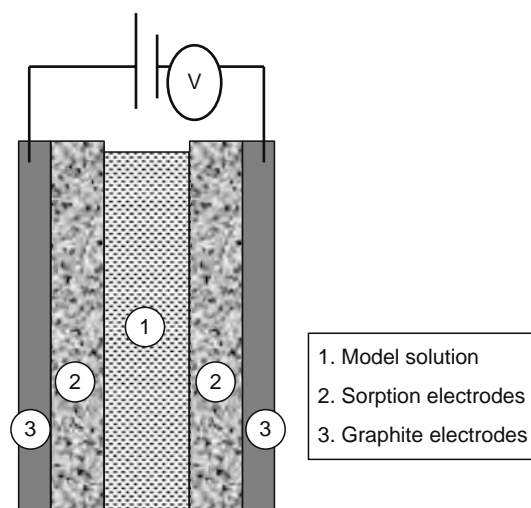


FIGURE 40.5 Schematic representation of the electro-sorption experiment.

above. The immersion time was 12 h. After removal from the sol, the membranes were wiped with filter paper and placed into 15% solution of phosphoric acid for 15 h. This operation was aimed at the transformation of zirconium dioxide into zirconium phosphate.

After phosphoric acid treatment the membranes were washed with distilled water, air-dried for 24 h at room temperature, and then dried for 3 h at 200°C.

To achieve the maximum density of zirconium phosphate deposition inside the membrane porous matrices, the impregnation operations described above were repeated up to three times. A phosphorus–zirconium molar ratio of 1 in the impregnated material was found to be optimal for both cation and anion adsorptions.

#### 40.4.2 METHODS OF ANALYSIS

The concentration of sodium ions was determined by flame photometry. Analysis of nickel, calcium, and magnesium ion concentration was carried out by atomic absorption spectrophotometry (Pye Unicam 8800, United Kingdom). The concentration of sulfate ions was determined by titration with barium chloride ( $\text{BaCl}_2$ ) solution in the presence of rhodizonate as indicator. Chloride ions were determined using ion-selective electrodes (manufactured by Radelkis, Hungary).

#### 40.4.3 TESTING OF ELECTROSORPTION MATERIALS

The sorption electrodes with a total surface area of 315 cm<sup>2</sup> (15 cm × 21 cm) were placed in an electro-sorption cell for sorption capacity measurements. A schematic drawing of this cell is given in Figure 40.5. The design of the electro-sorption cell allowed good contact of the electro-sorption membranes with the graphite current collectors. Working solutions were pumped through the cell at a flow rate of 100 mL · h<sup>-1</sup> using a peristaltic pump. The internal free volume or working volume of the module was 100 cm<sup>3</sup>. The module was sealed with rubber washers.

The polarization of the electro-sorption membranes was carried out at a potential difference of 5 V and 10 V. Electro-sorption tests were carried using a simulated solution of an industrial nickel effluent and a mine water source. The chemical composition of both solutions is given in Table 40.3.

**TABLE 40.3**  
**Chemical Composition of Two Model Effluent Solutions Used in Electro-Sorption Experiments**

Solution	Industrial Nickel Effluent (mg · L <sup>-1</sup> )	Mine Water Effluent (mg · L <sup>-1</sup> )
Sodium	183	1150
Sulfate	1739	1920
Chloride	210	230
Nickel	635	—

**TABLE 40.4**  
**Chemical Composition of Ni Effluent before Electro-Sorption, after Electro-Sorption, and after Desorption Experiment ( $\text{mg} \cdot \text{L}^{-1}$ )**

Constituent	Initial	After Electro-Sorption at		Regenerate
		dU = 5 V	dU = 10 V	
Sodium	183	103	18	1,490
Sulfate	1,739	998	65	17,200
Chloride	210	98	5	220
Nickel	635	424	<1	6,430

Note: dU = The applied potential difference between the electrodes.

The results of the electrosorption experiments with the simulated nickel effluent are summarized in Table 40.4. Nearly 100% of Ni and > 90% of  $\text{Na}^+$ ,  $\text{SO}_4^{2-}$ , and  $\text{Cl}^-$  ions were removed during the electrosorption experiment running at 10 V.

The results of the electrosorption experiments with the simulated mine effluent solution are summarized in Table 40.5. Between 50% and 83% of ion removal was observed depending on the flow rate and the total amount of feed solution.

#### 40.4.4 CONCLUSION

The case study showed a successful method for manufacturing composite sorption materials for ion removal by electro-sorption. The prepared electrosorption membranes that were electrochemically activated at 10 V and removed approximately 100% of Ni and > 90% of  $\text{Na}^+$ ,  $\text{SO}_4^{2-}$ , and  $\text{Cl}^-$  ions from a simulated nickel effluent solution. The energy consumption at  $6.4 \text{ kW} \cdot \text{kg}^{-1}$  removed matter at dU = 5 V and at  $11 \text{ kW} \cdot \text{kg}^{-1}$  removed matter at dU = 10 V. No membrane fouling was observed. For a mine water model solution, 83% of ion removal was observed. At the optimal feed flow rate the energy consumption was  $4 \text{ kW} \cdot \text{kg}^{-1}$  removed matter.

### 40.5 CASE STUDY: ELECTROCATALYTIC MEMBRANES FOR DECOMPOSITION OF ORGANIC POLLUTANTS

In this case study, ceramic-based flexible sheets impregnated with electrocatalysts were used for the treatment of industrial effluents polluted with phenols. The technological objective of this study was to develop a novel purification system in which a feed solution containing organic compounds is passed through an electrochemically charged ceramic-based membrane whereby the organic compounds are decomposed on contact with the electromembrane surface. A simplified explanation of the process is illustrated in Figure 40.6.

The electrocatalytic materials were deposited onto ceramic sheets in the form of nanosized particle-containing inks. The electrocatalytic ink was prepared from carbon black-supported antimony-doped tin oxide. Comparisons were made between the commercially available Sb-doped  $\text{SnO}_2$  as well as the Sb-doped  $\text{SnO}_2$  prepared by a solgel method.

#### 40.5.1 PREPARATION OF ELECTROCATALYTIC MEMBRANES

Commercially available composite ceramic sheets (Lydall, United States), with properties listed in Table 40.6, were used as the catalyst support. The Sb-doped  $\text{SnO}_2$  solutions were prepared from two alkoxides [23] obtained directly from chlorides. 8.37 g of  $\text{SnCl}_2 \cdot 2\text{H}_2\text{O}$  was dissolved in 100 mL of absolute ethanol. The antimony solution was simultaneously prepared from a

**TABLE 40.5**  
**Purification Degree of Mine Effluent Model Solution as a Result of Electro-Sorption Experiment**

Flow Rate ( $\text{mL} \cdot \text{h}^{-1}$ )	Passed Volume (mL)	Purification Degree (%)	Energy Consumption ( $\text{kW} \cdot \text{kg}^{-1}$ )
200	100	83	5.16
400	150	72	4.06
800	200	50	4.38

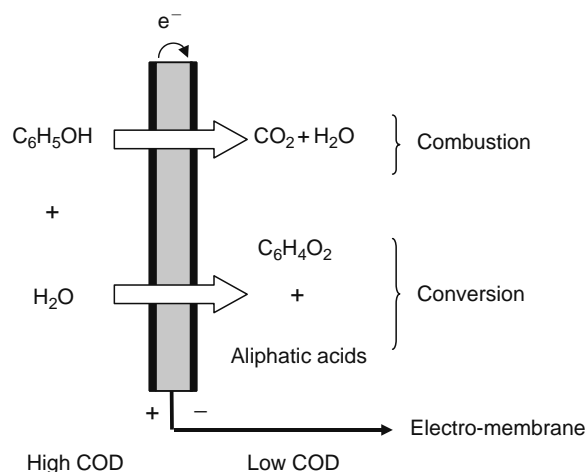


FIGURE 40.6 Schematic of the ceramic-based electromembrane process for the oxidation of phenol.

given amount of  $\text{SbCl}_3$  dissolved in 20 mL of absolute ethanol. Both mixtures were separately stirred and heated in a closed vessel. The vessels were then opened and the solvent completely evaporated to yield two powders. The resulting powders were mixed together in 50 mL of ethanol. The doped mixture was finally stirred and heated at  $50^\circ\text{C}$  for 2 h.

For the preparation of the electrocatalyst or catalytic ink, a predetermined amount of carbon black (VULCAN XC 72) was added to the Sb-doped  $\text{SnO}_2$  sol and stirred at room temperature for several hours. The carbon black was then washed thoroughly with water and dried at  $100^\circ\text{C}$  for 1 h followed by further drying at  $500^\circ\text{C}$  under nitrogen for 30 min.

The ceramic sheets were cut into the correct shape to fit in the electromembrane reactor and then impregnated with the electrocatalyst. A slurry or ink of the carbon black-supported Sb-doped  $\text{SnO}_2$  was prepared in an appropriate solvent followed by ultrasonic treatment for 30–60 min. The resulting ink was sprayed onto the ceramic membrane surface by using commercially available spray guns. The resulting membranes were then dried at room temperature overnight.

#### 40.5.2 TESTING OF ELECTROCATALYTIC MEMBRANES

The electromembrane reactor used in the study was a flow-through undivided electrocatalytic cell. The principal feature of the cell is the ceramic-based sheet, which was coated with the carbon-supported catalyst on one side. The coated side was used as the anode and the cathodic side was not coated with any electroconductive substance or catalyst. Current was supplied to the anode and cathode by means of backing layers, which are connected, to the external power source by means of a conducting wire. The backing layers that were used in this study are carbon cloths 6100–200 purchased from Lydall, United States.

The untreated water was pumped into the electromembrane reactor through the inlet where the feed is guided by means of a stainless steel flow channel. The water came into contact, first, with the carbon cloth on the anodic side and then with the

**TABLE 40.6**  
**Properties of Unmodified Composite Ceramic Sheets Used**  
**for Preparation of Electro-Catalytic Membranes**

Property/Variation	Ceramic Sheet 1P-397-2 (40% Glass)
Basis weight ( $\text{kg} \cdot \text{m}^{-2}$ )	0.267
Caliper at 4 PSF (mils)	64.00
Density ( $\text{kg} \cdot \text{m}^{-3}$ )	164.20
Caliper at 8 PSI (mils)	46.9
MD tensile ( $\text{kg} \cdot \text{m}^{-1}$ )	124.68
CD tensile ( $\text{kg} \cdot \text{m}^{-1}$ )	95.47
Resistance at $32 \text{ L min} \cdot \text{m}^{-2}$ ( $\text{mm} \cdot \text{H}_2\text{O}$ )	284.00
Estimated composition (wt%)	
$\text{Al}_2\text{O}_3$	23.6
$\text{SiO}_2$	51.2
Other metal oxides	25.2

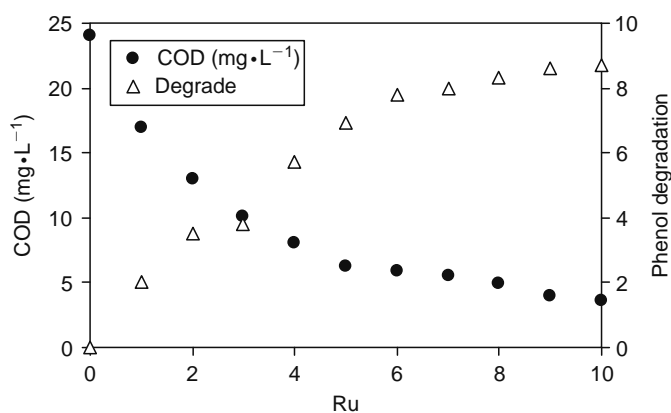


FIGURE 40.7 Degradation of phenol and reduction of COD in the presence of chloride ions.

electrocatalyst on the surface of the ceramic support. The feed was subsequently pumped through the membrane and the oxidized or “treated” water was collected as permeate and analyzed. After collection of the entire batch, the collected water was reintroduced into the reactor and, depending on the nature of the catalyst and experimental conditions, a number of runs were carried out and phenol concentration, oxidation products, and COD were monitored with each run. The geometric surface area of the electrocatalytic membrane in the reactor was 320 cm<sup>2</sup>.

*p*-Benzoquinone was the sole aromatic intermediate detected in the collected samples. The degradation of phenol was improved by applying a higher voltage with phenol completely degraded in nine runs through the electromembrane reactor. The concentration of *p*-benzoquinone increases as the concentration of phenol decreases but since phenol is oxidized simultaneously with its intermediates, *p*-benzoquinone concentration also decreases with time.

Several experiments were conducted to study the influence of feed flux through the electromembrane reactor. The fluxes were varied in the region of 50–200 L · m<sup>-2</sup> · h<sup>-1</sup> and the variation in the flow rate of the feed solution through the electromembrane reactor had a significant effect on the phenol degradation, formation of intermediates, and COD removal. The best results were achieved at fluxes of 150 ± 20 L · m<sup>-2</sup> · h<sup>-1</sup> for phenol degradation (complete degradation) and formation of aromatic intermediates (*p*-benzoquinone < 20.0 mg · L<sup>-1</sup>). COD reduction of 60% was achieved under these conditions.

### 40.5.3 INFLUENCE OF CHLORIDE IONS ON THE ELECTROCHEMICAL OXIDATION OF PHENOL

The need to study the influence of chloride ions on the electrochemical oxidation of phenol was necessitated by the fact that real (industrial) effluents contained chlorides in significantly high concentrations. Chloride ions, in solution, have the ability to produce chlorinated organic products, especially in acidic media. Halocompounds are usually more harmful to the environment than the organic compounds they result from. It has been reported that under certain conditions, electrogenerated chlorine converts to hypochlorite, which is a powerful oxidant but weak chlorinating agent [78].

For the results shown in Figure 40.7, an experiment was conducted using a feed solution of 0.1 g · L<sup>-1</sup> phenol in 0.1 M NaCl electrolyte at flux of 150 L · m<sup>-2</sup> · h<sup>-1</sup> and applied potential of 2.5 V. 87% degradation of phenol was achieved but what is worth noting and of extreme importance is that there were no aromatic intermediates detected in the resulting permeate. This can also be supported by the fact that the initial COD was reduced by 85%.

### 40.5.4 CONCLUSION

The reduction of COD is one of the most challenging tasks for any water treatment process. Electrochemical water treatment is no exception, and even though phenol could be completely degraded, COD as high as 40% can present itself in the form of reaction byproducts. When NaCl was used as electrolyte solution, no aromatic intermediates were detected at the end of the treatment process. The reduction of COD by 87% shows that most of the phenol was degraded to CO<sub>2</sub>. The presence of Cl<sup>-</sup> improved COD reduction, possibly due to the action of hypochlorite formed through oxidation of chloride.

### ACKNOWLEDGMENTS

The authors wish to thank South Africa’s main power utility (ESKOM), the Water Research Commission (WRC) and National Research Foundation (NRF) of South Africa for funding, Professor V.N. Belyakov for close collaboration on various aspects of electromembrane research, and L. Petrik and R. White for their suggestions.

## REFERENCES

1. Hsieh P. *Inorganic Membranes for Separation and Reaction*. Amsterdam: Elsevier, 1996.
2. Byers CH and Amarnath A. Understanding the potential of electroseparations. *Chem Eng Prog* 1995; 91(Suppl. 2):63–69.
3. Tsouris C. Special issue: Electrochemical and reactive separations. *Sep Purif Technol* 1999; 15:193–196.
4. Tsouris C and DePaoli D. Special issue: Electroseparation. *Sep Purif Technol* 1997; 11:143–145.
5. Li Y-Y, Nomura T, Sakoda A, and Suzuki M. Fabrication of carbon coated ceramic membranes by pyrolysis of methane using a modified chemical vapor deposition apparatus. *J Membr Sci* 2002; 197:23–35.
6. Bladergroen BJ, Maluleke MA, and Linkov VM. Electroconductive coatings on porous ceramic supports. *J Appl Electrochem* 2003; 33(Suppl.):475–481.
7. Guizard C, Legault F, Idrissi N, Larbot A, Cot L, and Gavach C. Electronically conductive mineral membranes designed for electro-ultrafiltration. *J Membr Sci* 1989; 41:127–142.
8. Gunnar RD and Langer SH. Comparisons of Ebonex and graphite supports for platinum and nickel electrocatalysts. *Electrochim Acta* 1998; 44:437–444.
9. Clarke RL. *Electrochemical Processing-Innovation and Progress*. Glasgow, Scotland: Moat House International, 1993.
10. Chen G, Betterton EA, and Arnold RG. Electrolytic oxidation of trichloroethylene using a ceramic anode. *J Appl Electrochem* 1999; 29:961–970.
11. Park S-Y, Chi EO, Kwon YU, Park HL, and Mho S-I. Characteristics of Pt thin films on the conducting ceramics TiO and Ebonex (Ti<sub>4</sub>O<sub>7</sub>) as electrode materials. *Thin Solid Films* 1995; 258(Suppl. 1–2):5–9.
12. Farndon EE and Pletcher D. Studies of platinized Ebonex electrodes. *Electrochim Acta* 1997; 42(Suppl. 8):1281–1285.
13. Farndon EE, Pletcher D, and Saraby-Reintjies A. The electrodeposition of platinum onto a conducting ceramic, Ebonex. *Electrochim Acta* 1997; 42(Suppl. 8):1269–1279.
14. Jüttner K, Galla U, and Schmieder H. Electrochemical approaches to environmental problems in the process industry. *Electrochim Acta* 2000; 45(Suppl. 15–16):2575–2594.
15. Comminellis CH and Pulgarin C. Anodic oxidation of phenol for wastewater treatment. *J Appl Electrochem* 1991; 21:703–708.
16. Grimm J, Bessarabov D, and Sanderson R. Review of electro-assisted methods for water purification. *Desalination* 1998; 115(Suppl. 8):285–294.
17. Wang A, Qu J, Ru J, Liu H, and Ge J. Mineralization of an azo dye Acid Red 14 electro-Fenton's reagent using an activated carbon fiber cathode. *Dyes Pigments* 2005; 65:227–233.
18. Comminellis CH. Electrocatalysis in the electrochemical conversion/combustion of organic pollutants for waste water treatment. *Electrochim Acta* 1994; 39(Suppl. 11–12):1857–1862.
19. Dieckmann GR and Langer SH. Comparisons of Ebonex and graphite supports for platinum and nickel electrocatalysts. *Electrochim Acta* 1998; 44(Suppl. 2–3):437–444.
20. Grimm J, Bessarabov D, Maier W, Storck S, and Sanderson RD. Sol-gel film-preparation of novel electrodes for the electrocatalytic oxidation of organic pollutants in water. *Desalination* 1998; 115(Suppl. 8):295–302.
21. Liao S, Linkov V, and Petrik L. Electrooxidation of methanol over a membrane-based electrode and effect of tungsten and molybdenum on the activity. *Appl Catal A: General* 2002; 235:149–155.
22. Linkov V, Petrik L, Vaivars G, Maluleke A, and Gericke G. Ceramic-based materials for electrochemical applications. *Macromol Symp* 2002; 178:153–168.
23. Maluleke MA and Linkov VM. Partial electrochemical oxidation of phenol on ceramic-based flat-sheet type electromembrane reactors. *Sep Purif Technol* 2003; 32:377–385.
24. Jansen LJJ and Koene L. The role of electrochemistry and electrochemical technology in environmental protection. *Chem Eng J* 2002; 85 (Suppl. 2–3):137–146.
25. Almon AC and Buchanan BR. Electrochemical Oxidation of Organic Waste. In: Genders JD and Weinberg NL (Eds.). *Electrochemistry for a Cleaner Environment*. Buffalo, NY: Electrosynthesis Co., 1992.
26. Iniesta J, González-García J, Expósito E, Montiel V, and Aldaz A. Influence of chloride ion on electrochemical degradation of phenol in alkaline medium using bismuth doped and pure PbO<sub>2</sub> anodes. *Water Res* 2001; 35(Suppl. 14):3291–3300.
27. Comminellis C and Nerini A. Anodic oxidation of phenol in the presence of NaCl for wastewater treatment. *J Appl Electrochem* 1995; 25:23–28.
28. Pattanayak J, Mondal K, Wiltowski T, Lalvani SB, and Mandich NV. Recovery of metallic impurities from chromium plating solutions by electromigration. *Met finishing* March 2000; 98(3):39–45.
29. Bunce NJ, Chartrand M, and Keech P. Electrochemical treatment of acidic aqueous ferrous sulfate and copper sulfate as models for acid mine drainage. *Water Res* 2001; 35(Suppl. 18):4410–4416.
30. Juang R-S and Lin L. Electrochemical treatment of copper from aqueous citrate solutions using a cation-selective membrane. *Sep Purif Technol* 2001; 22–23(Suppl. 1):627–635.
31. Greenberg B. Electrolytic treatment apparatus, US Patent no. 4,948,489. August 14, 1990.
32. Matsunaga T, Nakasono N, Takamuku T, Burgess JG, Nakamura N, and Sode K. Disinfection of drinking water by using a novel electrochemical reactor employing carbon cloth electrodes. *Appl Environ Microb* 1992; 58(Suppl. 2):686–689.
33. Okochi M, Lim TK, Nakamura N, and Matsunaga T. Electrochemical disinfection of drinking water using activated carbon reactor capable of monitoring its microbial fouling. *Appl Environ Microb* 1997; 47:18–22.
34. Matsunaga T, Okochi M, Takahashi M, Nakayama T, Wake H, and Nakamura N. TiN Electrode reactor for disinfection of drinking water. *Water Res* 2000; 34(Suppl. 12):3117–3122.

35. Koros WJ, Ma YH, and Shimidzu T. Terminology for membranes and membrane processes. *J Membr Sci* 1996; 120:149–159.
36. Karthik V, DasGupta S, and De S. Modeling and simulation of osmotic pressure controlled electro-ultrafiltration in a cross-flow system. *J Membr Sci* 2002; 199:29–40.
37. Kulkarni P, Dutari G, Weingeist D, Adin A, Haught R, and Biswas P. Capture of water borne colloids in granular beds using external electrical fields: Improving removal of *Cryptosporidium parvum*. *Water Res* 2005; 38:1047–1060.
38. Visvanathan C, Ben Aim R, and Vigneswaran S. Application of cross-flow electro-microfiltration in chromium wastewater treatment. *Desalination* 1989; 71:265–276.
39. Akay G and Wakeman RJ. Electric field enhanced crossflow microfiltration of hydrophobically modified water soluble polymers. *J Membr Sci* 1997; 131:229–236.
40. Huotari HM, Huisman IH, and Trägårdh G. Electrically enhanced crossflow membrane filtration of oily wastewater using the membrane as a cathode. *J Membr Sci* 1999; 156:49–60.
41. Weigert T, Altmann J, and Ripperger S. Crossflow electrofiltration in pilot scale. *J Membr Sci* 1999; 159:253–262.
42. Zumbusch P and Kulcke W. Use of alternating electrical fields as anti fouling strategy in ultrafiltration of biological suspensions: Introduction of new experimental procedure for crossflow filtration. *J Membr Sci* 1998; 142:75–86.
43. Robinson CW, Siegel MH, Condemine A, Fee C, Fahidy TZ, and Glick BR. Pulsed-electric field crossflow ultrafiltration of bovine serum albumin. *J Membr Sci* 1993; 80:209–220.
44. Guizard C, Legault F, Idrissi N, Larbot A, Cot L, and Gavach C. Electronically conductive mineral membranes designed for electro-ultrafiltration. *J Membr Sci* 1989; 41:127–142.
45. Wakeman RJ and Quigley MBC. Membrane filter with electrical and/or acoustic enhancement. WO 9803245, 29 January 1998. (Assigned to Atkins Fulford Ltd).
46. Wakeman RJ and Williams CJ. Additional techniques to improve microfiltration. *Sep Purif Technol* 2002; 26(Suppl. 1):3–18.
47. Wang GCC and Yang TY. Reclamation of high quality water from treating CMP wastewater by a novel crossflow electrofiltration/electrodialysis process. *J. Membr Sci* 2004; 233:151–159.
48. Mulder M. *Basic Principles of Membrane Technology*. 2nd ed., London: Kluwer Academic Publishers, 1996.
49. Mallevalle J, Odendaal PE, and Wiesner MR (Eds). *American Water Works Association Research Foundation, Lyonnaise des Eaux and Water Research Commission of South Africa, Water Treatment Membrane Processes*. New York: McGraw Hill, 1996.
50. Peters S. Surface modification of electro-dialysis membranes to enhance anti-fouling characteristics. PhD dissertation, University of the Western Cape, Cape Town, South Africa, 2000.
51. Mishchuk NA, Koopal LK, and Gonzalez-Caballero F. Intensification of electrodialysis by applying a non-stationary electric field. *Colloids Surfaces A* 2001; 176:195–212.
52. Linnikov OD, Anokhina EA, and Scherbakov VE. Investigation on purification of hydrochloric acid by membrane method. *Desalination* 2000; 132(Suppl. 1–3):299–306.
53. Mavrov V, Chmiel H, Heitele V, and Rögner F. Desalination of surface water to industrial water with lower impact on the environment Part 4: Treatment of effluents from water desalination stages for reuse and balance of the new technological concept for water desalination. *Desalination* 1999; 124(Suppl. 1–3):205–216.
54. Pilat B. Practice of water desalination by electrodialysis. *Desalination* 2001; 139(Suppl. 1–3):385–392.
55. Grebenuyak VD, Cheborateva RD, Linkov NA, and Linkov VM. Electro membrane extraction of Zn from Na-containing solutions using hybrid electrodialysis—ion exchange method. *Desalination* 1998; 115:255–263.
56. Wisniewski C, Persin F, Cherif T, Sandeaux R, Grasmick A, and Gavach C. Denitrification of drinking water by the association of an electrodialysis process and a membrane bioreactor: Feasibility and application. *Desalination* 2001; 139:199–205.
57. Kurath DE, Brooks KP, Hollenberg GW, Sutija DP, Landro T, and Balagopal S. Caustic recycle from high-salt nuclear wastes using a ceramic-membrane salt-splitting process. *Sep Purif Technol* 1997; 11(Suppl. 3):185–198.
58. Hobbs DT. Caustic recovery from alkaline nuclear. *Sep Purif Technol* 1999; 15:239–253.
59. Linkov VM and Belyakov VN. Novel ceramic membranes for electrodialysis. *Sep Purif Technol* 2001; 25(Suppl. 1–3):57–63.
60. Bladergroen BJ and Linkov VM. Electrosorption ceramic based membranes for water treatment. *Sep Purif Technol* 2001; 25(Suppl. 1–3):347–354.
61. Strohl JH and Dunlap KL. Electrosorption and separation of quinones on a column of graphite particles. *Anal Chem* 1972; 44(Suppl. 13):2166–2170.
62. Woodard FE, McMackins DE, and Jansson REW. Electrosorption on organics on three dimensional carbon electrodes. *J Electroanal Chem* 1986; 214:303–330.
63. Gadkaree KP, Mach JF, and Stempin J. Ion-removal from water using activated carbon electrodes. US Patent no. 6,214,204. April 2001.
64. Eisinger RS and Keller GE. Electrosorption: A case study on removal of dilute organics from Water. *Environ Prog* 1990; 9(Suppl. 4):235–244.
65. Salema K, Sandeaux J, Molénata J, Sandeaux R, and Gavacha C. Elimination of nitrate from drinking water by electrochemical membrane processes. *Desalination* 1995; 101(Suppl. 2):123–131.
66. Hepel M. Composite polypyrrole films switchable between the anion and cation-exchanger state. *Electrochim Acta* 1996; 41(Suppl. 1):63–76.
67. Bladergroen BJ and Linkov VM. Electrosorption ceramic based membranes for water treatment. *Sep Purif Technol* 2001; 25(Suppl. 1–3):347–354.
68. Lageman R. Electroreclamation: Applications in the Netherlands. *Environ Sci Technol* 1993; 27(Suppl. 13):2648–2650.

69. Röhrs J, Ludwig G, and Rahner D. Electrochemically induced reactions in soils—a new approach to the in-situ remediation of contaminated soils? Part 2: Remediation experiments with a natural soil containing highly chlorinated hydrocarbons. *Electrochimica Acta* 2002; 47:1405–1414.
70. Puppala SK, Alshawabkeh AN, Acar BY, Gale RJ, and Bricka M. Enhanced electrokinetic remediation of high sorption capacity soil. *J Hazard Mater* 1997; 55:203–220.
71. Bashtan YS, Goncharuk VV, Chebotareva RD, Belakov NV, and Linkov VM. Production of sodium hypochlorite in an electrolyser equipped with a ceramic membrane. *Desalination* 1999; 126:77–82.
72. Li Y, Wang S, Cao A, Zhao D, Zhang X, Xu C, Luan Z, Ruan D, Liang J, Wu D, and Wei B. Adsorption of fluoride from water by amorphous alumina supported on carbon nanotubes. *Chem Phys Lett* 2001; 350:412–416.
73. Prüsse U, Hähnlein M, Daum J, and Vorlop CD. Improving the catalytic nitrate reduction. *Catal Today* 2000; 55:79–90.
74. Ilinitch OM, Cuperus FP, Van Gemert RW, Gribov EN, and Nosova LV. Catalytic membrane in denitrification of water: A means to facilitate intraporous diffusion of reactants. *Sep Purif Technol* 2002; 21(Suppl. 1–2):55–60.
75. Ilinitch OM, Cuperus FP, Ludmila V, Nosova LV, and Gribov EN. Catalytic membrane in reduction of aqueous nitrates: Operational principles and catalytic performance. *Catal Today* 2000; 56(Suppl. 1–3):137–145.
76. Linkov VM. Electromembrane reactors for desalination and disinfection of aqueous solutions, Water Research Commission of South Africa. Report Number: 964/1/02.
77. Belyakov VN and Linkov VM. Electrochemically-stimulated sorption and sorption-membrane methods for removal of ionic impurities from water. In: Omelchenko A, Pivovarov AA, and Swindall WJ. (Eds.). *Modern Tools and Methods of Water Treatment for Improving Living Standards*. The Netherlands: Springer 2005, pp. 115–136.
78. Tremiliosi-Filho G, Gonzalez ER, Motheo AJ, Belgsir EM, Léger J-M, and Lamy C. Electro-oxidation of ethanol on gold: Analysis of the reaction products and mechanism. *J Electroanal Chem* 1998; 444:31–39.

---

# 41 Membrane Processes for Treatment of Industrial Tannery Effluents: A Case Study

*A. Bódalo, E. Gómez, and A.M. Hidalgo*

## CONTENTS

41.1	Introduction .....	1087
41.2	Membrane Bioreactor Pilot Plant .....	1089
41.2.1	Layout .....	1089
41.2.2	Objectives and Working Plan .....	1090
41.2.3	Results and Discussion .....	1090
41.2.3.1	Chemical Oxygen Demand .....	1091
41.2.3.2	Suspended Solids and Volatiles .....	1091
41.2.3.3	Biological Oxygen Demand (BOD <sub>5</sub> ).....	1091
41.2.3.4	Nitrogen .....	1092
41.2.3.5	Chrome and Sulfides .....	1093
41.2.3.6	Phosphorus .....	1094
41.2.3.7	Chlorides and Sodium .....	1094
41.3	Reverse Osmosis Pilot Plant .....	1094
41.3.1	Description of the Plant .....	1094
41.3.2	Objectives and Working Plan .....	1095
41.3.3	Results and Discussion .....	1096
41.3.3.1	Membrane Selection .....	1096
41.3.3.2	Variation of the Recovery Percentage.....	1096
41.4	Brief Description of the Industrial Plant .....	1098
	Acknowledgments .....	1099

## 41.1 INTRODUCTION

Industries dedicated to the treatment of skins are big consumers of water and, as a consequence, big producers of liquid effluents. These effluents are characterized by their high chemical oxygen demand (COD), as well as colors and a high content of salts, oils and fats, and solids, due to the reagents used during the production process. As a result, these effluents have a high pollutant potential and need to be treated before their discharge or elimination.

Effluents from the leather industry of the city of Lorca (Murcia, Spain) have long been a serious problem for this province, because they were commonly discharged into the river Guadalentín, without previous treatment, causing serious environmental problems. The effluents in question contain a great number of polluting products that are impossible to eliminate by standard wastewater treatment processes, which, together with the large volumes involved, increase the difficulty of the purification process.

In an attempt to solve these problems, the Aquagest Levante SA company, belonging to the AGBAR Group (Spain), has constructed a plant in the industrial estate of The Serreta (Lorca) designed to treat the effluents produced by the above mentioned leather industries (5000 m<sup>3</sup>/day) and, in the future, all the effluents from the other industries of the estate.

In the research and development phase, before the design and assembly of the industrial-scale installation, treatment of the effluents of the tanneries concerned was studied in pilot plant units, via collaboration with the Department of Chemical Engineering at the University of Murcia (Spain). The pilot plant was composed of several units: first, a physical–chemical treatment step; then, secondary treatment of the effluent from the first stage in an ultrafiltration tubular membrane bioreactor; followed by a third stage of reverse osmosis basically to eliminate the salts of the ultrafiltration permeate, complying with the specifications concerning the conductivity of wastes; and in the final stage, the brines generated by the concentrate from the reverse osmosis unit were evaporated. The industrial installation was completed with sludge centrifuges and drying tunnel. The data obtained in these pilot plants served as a basis for the design of the industrial plant. A flow diagram of the industrial plant is shown in Figure 41.1.

In this plant, wastewater to be treated is transmitted from the pumping station to the treatment plant. An initial pretreatment eliminates the fats (96%) and the largest solids before the water enters the mixing tank (4000 m<sup>3</sup> capacity), into which oxygen is injected (3500 kg/day) producing a desulfurization process; in this tank the sulfide is converted into sulfate and there is a 30% reduction of the organic matter content. From the tank, the water flows to the settler, where the sludge and the clarified liquid are separated, before the process splits into two differentiated lines: the sludge and the clarified water line.

The sludge passes to the thickeners, where flocculants and coagulants are added to concentrate it. Once thickened, the sludge is treated in the centrifugal system (two centrifuges, with a capacity of 60 m<sup>3</sup>/h) with the objective of separating any remaining fractions of water and to dry the sludge, which, after conditioning, is taken to a secure dump.

The clarified water from the settlers still possesses a high organic load and high conductivity, so that it must be treated before it can be used or disposed of.

The waters in question are pumped to a membrane bioreactor equipped with an air injection system, where part of the feed is recycled, making it move across a membrane ultrafiltration system, to prevent the presence of suspended microelements in the later phase of reverse osmosis. From the ultrafiltration process, two streams are obtained: a concentrated stream of salts and microbial mass, which is recycled to the bioreactor, and a permeate stream that passes to the reverse osmosis plant.

In the reverse osmosis stage of the plant, the water passes through the membranes and is again separated into two streams: one with a high salt concentration destined for the brine evaporation stage and the other clarified, which is directed to a tank of clean water mixture, where other streams of the process meet.

The highly saline stream from the reverse osmosis unit, together with a fraction of the concentrated stream from the ultrafiltration process, undergoes an evaporation stage. Furthermore, this produces two streams: one that goes to the tank containing the clean water and the other, a sludge, which passes to the drying tunnel. Studies carried out in the membrane bioreactor and reverse osmosis pilot plants are described below.

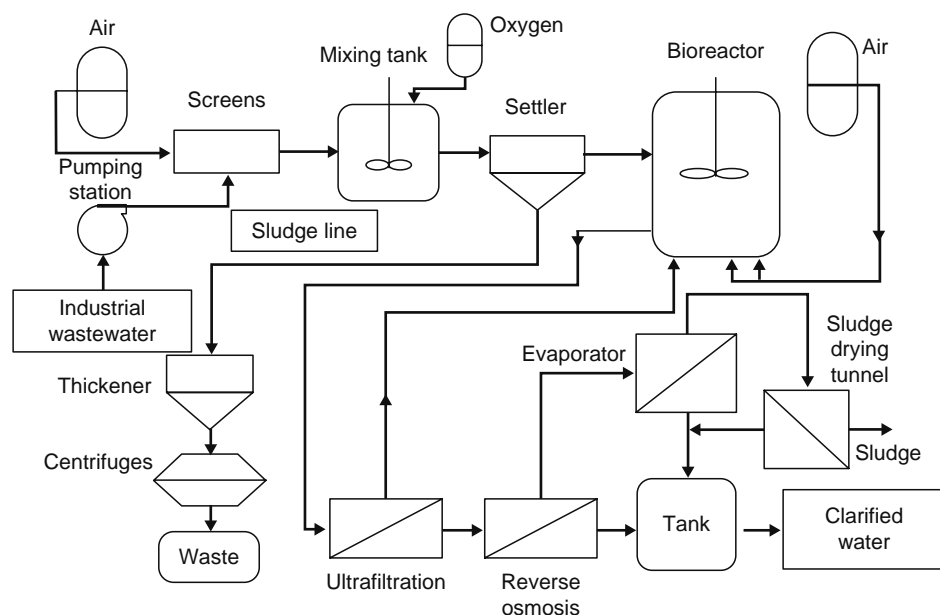


FIGURE 41.1 Flow diagram of the industrial plant.

## 41.2 MEMBRANE BIOREACTOR PILOT PLANT

### 41.2.1 LAYOUT

The principal part of the pilot plant comprises a biological reactor (bioreactor) in whose interior the biomass is placed, and two external modules of ultrafiltration membranes placed in series. Figure 41.2 depicts a flow diagram of this pilot plant, which is described in more detail below.

The reactor of the pilot plant has a volume of 2900 L and it is built of a hard plastic material. The feed enters the biological reactor directly from the settlers used in the physical–chemical process of the industrial plant.

An opening in the top of the reactor allows samples to be obtained from the interior, the corresponding analyses to be carried out and the behavior of the biomass to be followed. The level inside the reactor is controlled by means of a differential controller, while the appropriate oxygen concentration is maintained by means of a blower that blows air into the reactor, although there is also a connection with a pure oxygen supply in case of failure in the blower. The air enters by means of two pipes: one, a venturi and the other linked to four diffusers. Both can be regulated by manual valves.

Oxygen levels were regularly measured in samples taken from the bioreactor by means of a portable oximeter, to maintain the oxygen inside the bioreactor at 2–4 mg O<sub>2</sub>/L. The exit stream of the reactor is impelled to the membranes by a centrifugal pump located at the exit (see Figure 41.2), at a rate of 56 m<sup>3</sup>/h at 4 bar.

The ultrafiltration membranes have the following characteristics:

Length	3 m
Material	Poly(ether sulfone)
N° modules	2
Surface	3 m <sup>2</sup> /module
Transversal flow rate	6 m/s
Pore size	0.1 μm
Maximum working temperature	45°C

The two sequentially connected modules are composed of Berghof tubular membranes, which allow a tangential flow through their interior. Each module is formed of 31 tubes of 10 mm diameter.

The water from the reactor is pumped to these membranes, where two streams are formed: the permeate, which is the water that has passed through the pores and the concentrate, in which biomass remains and which is recycled to the reactor. The entrance pressure at the membranes is 4 bar and the exit pressure is approximately 2 bar.

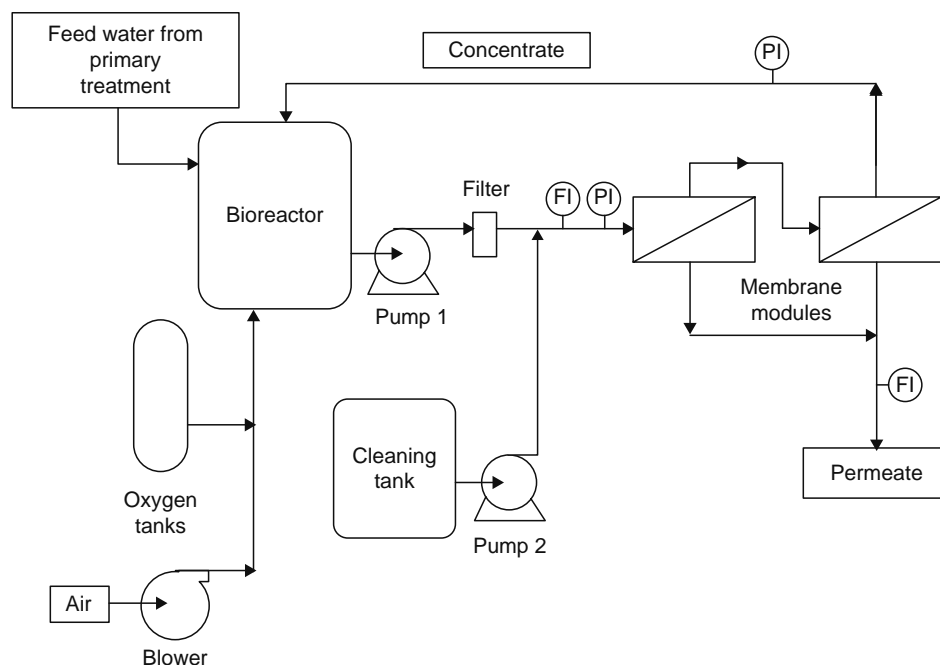


FIGURE 41.2 Flow diagram of the membrane bioreactor pilot plant.

At the exit of the pump that impels the water from the reactor to the membranes, a filter retains the largest solids to prevent obstruction of the membranes.

The main problem arising with the membranes is that they become fouled and it is therefore necessary to flush them daily with water and to occasionally use chemical products. The plant has a 0.5 m<sup>3</sup> cleaning tank of hard plastic that is used for daily cleaning of the membranes with clean water. After stopping the plant, this tank is filled with water several times and the water is pumped through the plant to clean the membranes. The same tank is used for cleaning with chemical products.

The pilot plant is equipped with two gauges: one at the membrane entrance and the other at the exit. The plant is also equipped with two flowmeters: one located at the entrance to the membranes to record the pumped flow and the other in the permeate stream to measure the discharge flow. The plant has a control panel, for starting and stopping the process and for controlling the blower and pump that feeds the bioreactor. The control panel can be set to automatic and the level inside the reactor is kept constant by means of the differential control.

#### 41.2.2 OBJECTIVES AND WORKING PLAN

The objective of the experiments carried out in this pilot plant was to determine the optimal values of some operational parameters, such as biomass concentration, transmembrane pressure, flow rate, and hydraulic retention time, the last defined as the relationship between the volume of the bioreactor and the daily flow discharge of permeate. The working plan was as follows:

The pilot plant was started daily during the 113 days of the experimentation. Samples were taken from the permeate stream, from the bioreactor, and from the water reaching the bioreactor after the physical–chemical treatment. A series of daily, weekly, and monthly analyses were carried out on these samples. The daily analyses included pH, conductivity, temperature, dissolved oxygen in the reactor, COD, and permeate turbidity. The weekly analyses included BOD<sub>5</sub>, suspended solids, volatile solids, ashes, ammonium, nitrates, nitrites, total nitrogen, and total ortho phosphorus. The monthly analyses included sulfides, total chromium, and salts, all referred to as sodium chloride.

Throughout the experiments, the hydraulic retention times varied in light of the values obtained for the different parameters analyzed, which reflected the degree of purification of the wastewaters studied.

#### 41.2.3 RESULTS AND DISCUSSION

As an example of all the results obtained, Table 41.1 summarized the operational data for five working days of the plant, while Table 41.2 shows the results of one of the analyses carried out weekly.

The hydraulic retention time was gradually reduced, with the purpose of acclimatizing the biomass to the bioreactor entrance fluid. The criteria used to reduce this parameter and so increase the discharge flow were mainly based on the reduction in the values of COD, BOD<sub>5</sub>, and concentration of suspended solids in the bioreactor. The retention times for the different periods of operation were the following:

Days 1–13	3 days	Days 55–58	15 h
Days 14–30	2 days	Days 59–70	12 h
Days 31–35	1 day	Days 71–113	19 h
Days 36–54	18 h		

**TABLE 41.1**  
**Operational Data of the Membrane Bioreactor Pilot Plant**

Parameter	Day 1	Day 2	Day 3	Day 4	Day 5
Inlet pressure, bar	4	4	4	4	4
Outlet pressure, bar	2	2	2	2	2
Permeate flow rate, L/h	1113.5	1115.5	1105.2	1098.5	1050
Reactor pH	7.45	8.06	8.27	8.37	8.33
Feed pH	8.16	7.73	7.83	7.97	7.42
Reactor conductivity, $\mu\text{S}/\text{cm}$	—	13,400	13,500	14,000	13,600
Permeate conductivity, $\mu\text{S}/\text{cm}$	9,500	12,600	13,100	13,600	13,100
Feed conductivity, $\mu\text{S}/\text{cm}$	15,000	15,000	16,600	16,000	13,900
Reactor oxygen concentration, mg/L	2.8	3.01	3.5	4.15	4.3
Temperature reactor, °C	16.1	18	19.6	21.2	21
Discharged permeate flow rate, L/day	980	980	980	980	980

*Note:* The transmembrane pressure was optimized at 2 bar (4 bar at the entrance and 2 bar at the exit).

**TABLE 41.2**  
**Weekly Analyses of the Membrane Bioreactor Pilot Plant Streams**

Magnitude	Feed	Permeate	Bioreactor
COD, mg/L	2630	788	844
BOD <sub>5</sub> , mg/L	1600	80	80
Suspended solids, mg/L	207	39	704
Volatile solids, mg/L	180	35	398
Ashes, mg/L	27	4	306
Total nitrogen, mg/L	303	176	—
Ammonium, mg N/L	131.8	122	—
Nitrates, mg N/L	1.9	1.5	—
Nitrites, mg N/L	0.007	0	—
Organic nitrogen, mg/L	169.3	52.5	—
Total phosphorous, mg/L	1.35	40.6	—
Ortho phosphorous, mg/L	0.29	39.4	—
Turbidity, NTU	—	1.1	—

#### 41.2.3.1 Chemical Oxygen Demand

Figure 41.3 shows the COD in the feed, bioreactor, and permeate during the 113 days of experimentation. The results show that, for a hydraulic retention time of 19 h, low levels of COD were obtained in the permeate and in the bioreactor. This time was therefore selected for the operation. The maximum percentage of COD elimination obtained for this period was 91.5%, with a mean value of 86.3%.

#### 41.2.3.2 Suspended Solids and Volatiles

The concentrations of suspended solids and volatiles in the permeate are depicted in Figure 41.4, where it can be seen that levels stabilized with the same hydraulic retention time of 19 h, already considered as suitable. The concentrations reached were approximately 6500 mg/L for the suspended solids and 4600 mg/L for the volatile solids.

#### 41.2.3.3 Biological Oxygen Demand (BOD<sub>5</sub>)

Figure 41.5 represents the evolution of the organic load in the form of BOD<sub>5</sub> in the permeate stream, bioreactor, and feed. As can be seen, the reactor began working with oxygen levels of 400 mg/L, which were decreased in both reactor and permeate to

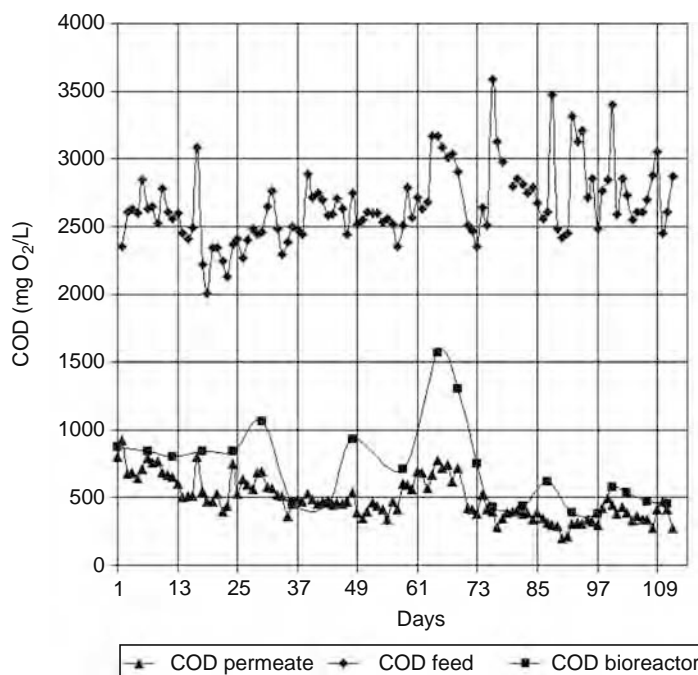


**FIGURE 41.3** COD evolution in the plant streams.

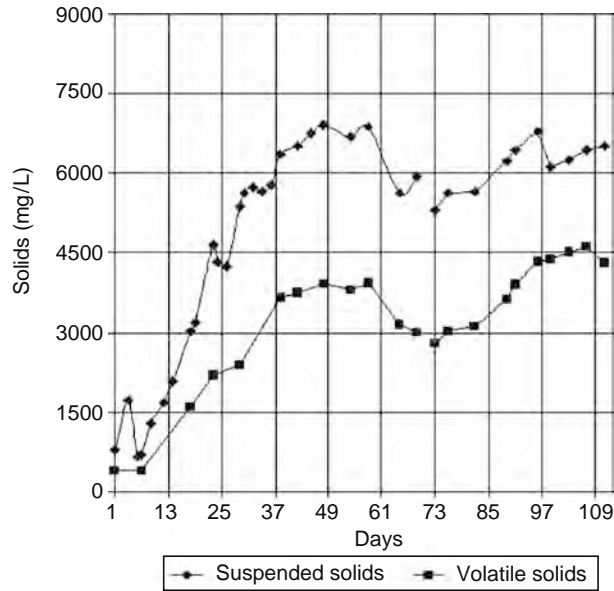


FIGURE 41.4 Evolution of the suspended solids and volatiles in the permeate.

reach minimum values of  $10 \text{ mg O}_2/\text{L}$ . The  $\text{BOD}_5$  values of the feed during the 7 months of experimentation varied between 600 and  $1800 \text{ mg O}_2/\text{L}$ . A maximum  $\text{BOD}_5$  elimination of 99.3% was obtained with the hydraulic retention time of 19 h, the average for this period being 93%.

#### 41.2.3.4 Nitrogen

A beginning to nitrification was achieved after 81 days of operation with a retention time of 19 h. However, nitrification was not complete since the nitrite values remained high, probably due to factors such as temperature, pH, chemical product content of the entrance water, and dissolved oxygen within the reactor, among others. The most appropriate values to achieve nitrification were a pH of between 7 and 7.6 and a temperature of around  $37^\circ\text{C}$ . Figure 41.6 shows the time-course concentrations of total nitrogen, nitrogen in ammonium form, nitrates, nitrites, and organic nitrogen in the permeate stream. As can be seen, nitrification began on day 81 of operation, leading to a decrease in the quantity of  $\text{N}-\text{NH}_4^+$  and organic nitrogen; the quantity of  $\text{N}-\text{NO}_3^-$  and, particularly,  $\text{N}-\text{NO}_2^-$  increased, this last due to the inhibition previously mentioned. Ammonium elimination of around 97% was reached.

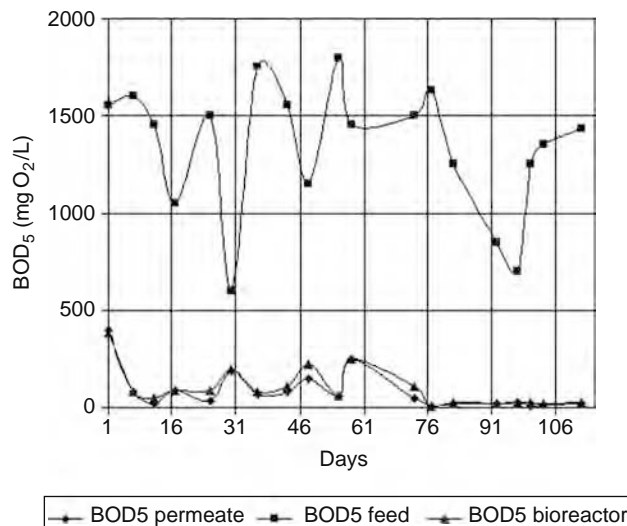


FIGURE 41.5  $\text{BOD}_5$  evolution in the plant streams.

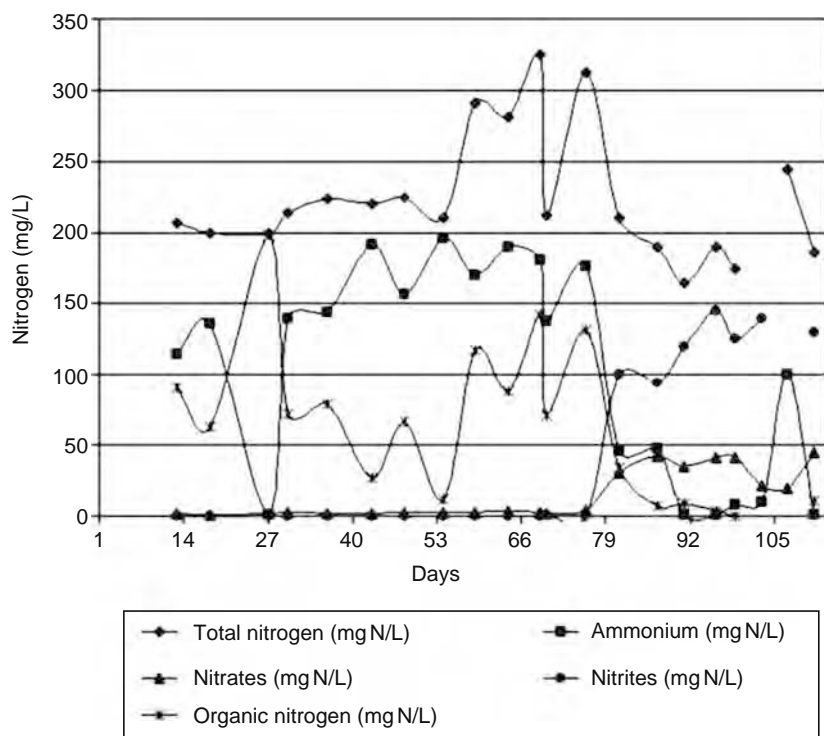


FIGURE 41.6 Nitrogen evolution in the permeate.

#### 41.2.3.5 Chrome and Sulfides

With reference to the monthly monitored parameters, a good degree of chromium and sulfide elimination can be observed in Figures 41.7 and 41.8.

The chromium, Figure 41.7, which showed great variations in the feed stream, was almost totally eliminated from the permeate due to its retention in the sludge, since it is not metabolizable by microorganisms.

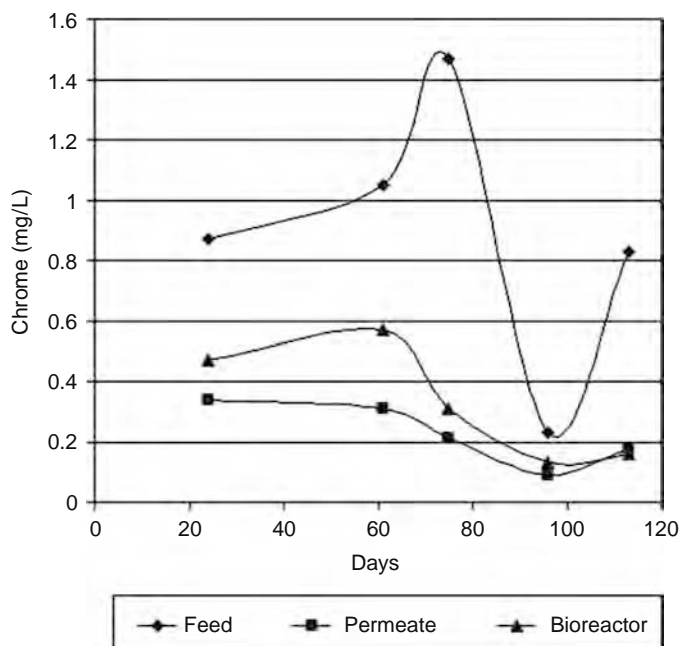
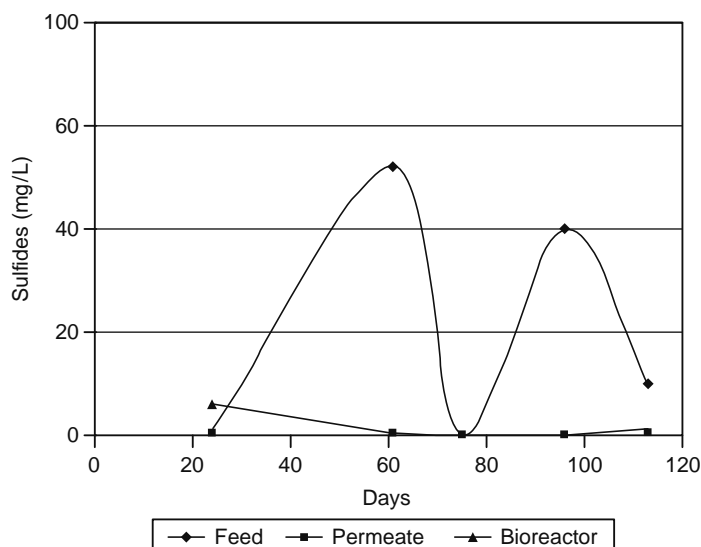


FIGURE 41.7 Monthly analyses evolution of the chrome.



**FIGURE 41.8** Monthly analyses evolution of the sulfides.

The sulfides that may be contained in the feed stream and which have not been eliminated in the previous physical–chemical process become sulfates, as a result of the aerobic-oxidant conditions of the process. Figure 41.8 shows that they disappear in the bioreactor or in permeate.

#### 41.2.3.6 Phosphorus

Phosphorus is a nutrient and therefore influences the elimination of  $BOD_5$ . For biological aerobic processes, BOD/N/P ratio of 100/5/1 can be considered sufficient for the normal development of microorganism's metabolism and growth in wastewater.

The industrial waste from the Lorca tanneries that enters the bioreactor has a low concentration of phosphorus (2–4 mg/L), making it necessary to add a certain quantity of orthophosphoric acid daily, to maintain an appropriate concentration of phosphorus in the bioreactor.

#### 41.2.3.7 Chlorides and Sodium

The chlorides and the sodium, which are responsible for most of the conductivity, together with the sulfates, are not altered in the process, since they are not retained by the biological sludge or by the ultrafiltration membranes, which is why the following reverse osmosis stage is necessary to lower the salinity to levels approved for subsequent dumping.

### 41.3 REVERSE OSMOSIS PILOT PLANT

#### 41.3.1 DESCRIPTION OF THE PLANT

The reverse osmosis plant, Figure 41.9, had a feed tank of 100 L. The feed was impelled by means of a centrifugal pump toward the external part of the cartridge containing the reverse osmosis membrane, passing first through the pressure pumps (modules) to reach a pressure above osmotic pressure. The polyamide membrane had a spiral configuration, and the permeate was collected by the centre of the same before being stored in a 25 L tank, while a similar tank served as cleaning tank.

The pilot plant contained three flowmeters (FI) to measure the permeate, concentrate, and recirculation streams. The flows of the recirculation and concentrate streams could be controlled by means of valves to provide the flows wanted for the experiment, while the permeate stream was a function of the other two. The recirculation flow was fixed at 2.4 m<sup>3</sup>/h and it remained constant in all the experiments.

The centrifugal feed pump provided a flow of 3 m<sup>3</sup>/h at 5 bar. The operating pressure was adjusted with the help of three sequential pressure pumps, each one providing a pressure of 12 bar and able to work in a range of 5–30 bar.

The feed into this plant is the permeate of the ultrafiltration pilot plant, to which antiscalant at a concentration of 16 g/m<sup>3</sup> was added to modify the solubility point of the salts and to prevent their precipitation on the membrane. The ultrafiltration plant effluent has a conductivity of around 14,000  $\mu$ S/cm.

Recovery from the permeate stream is defined as the ratio between the permeate flow and the total flow of permeate plus concentrate.

$$\frac{\text{Permeate flow}}{(\text{Permeate flow} + \text{concentrate flow})}$$

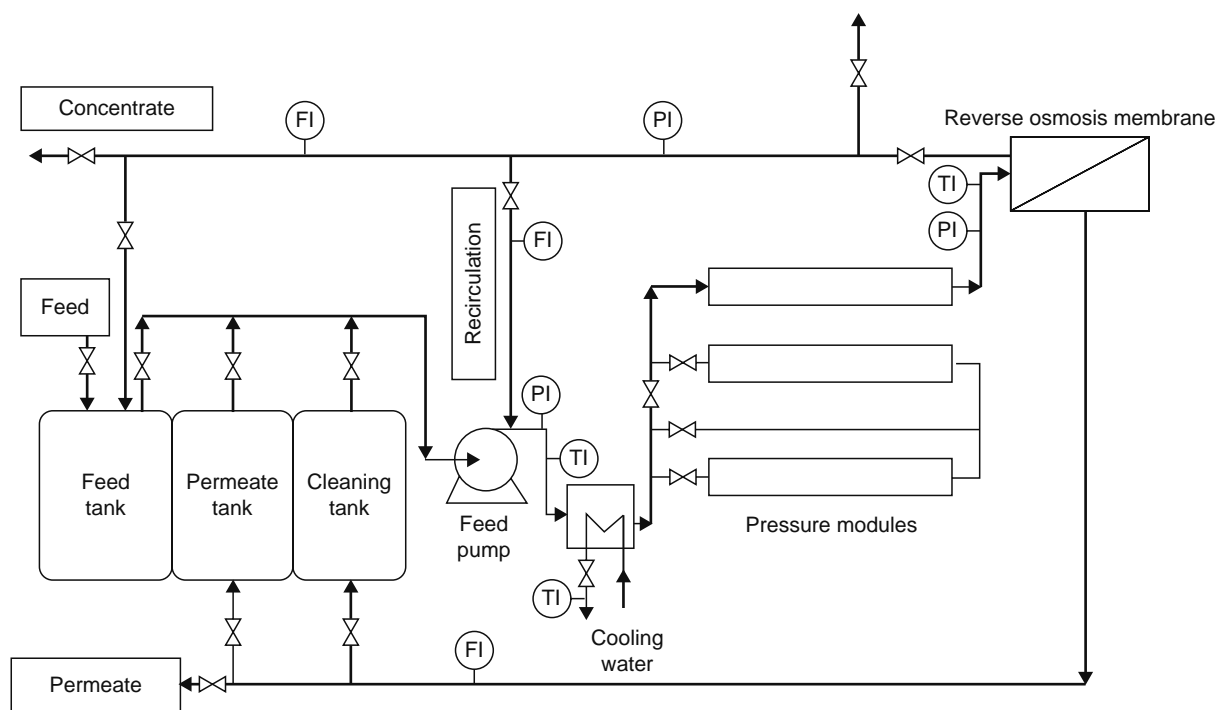


FIGURE 41.9 Flow diagram of the reverse osmosis pilot plant.

The pilot reverse osmosis unit worked with a recovery of 30%–80%, which was obtained by manipulating the valve of the concentrate stream. In this way, the stages that take place in the industrial plant can be simulated. The pilot plant worked 8 h/day, providing continuous streams of permeate and concentrate.

The permeate flow tended to decrease with the operating time due to progressive fouling of the membrane. Depending on the quality of the feed, a film was formed on the surface of the membrane that reduced permeate flow and the quality of the exit water, causing an increase in the pressure difference. To prevent this and the consequent pollution, the membranes were cleaned periodically with acids and alkaline detergents, as well as antiscalant and biocides. Several different membranes from Toray and Osmonics were assayed to choose the most suitable one.

#### 41.3.2 OBJECTIVES AND WORKING PLAN

The objectives of the experiments carried out in this pilot plant were to select a membrane and to simulate industrial operation, varying the percentage of permeate recovery.

According to the foreseen design for the industrial plant of reverse osmosis, this would be formed by three blocks of membranes, each block containing two filtering stages: the first working at a pressure of 15 bar and the second at about 23 bar. Each stage comprises several modules, each of which is formed by six membranes in series. The first unit shows a permeate recovery of 50%, which continues to increase until a value of 80% in the sixth unit.

To attain the above objectives, and bearing in mind the design of the industrial plant, the following experimental steps were followed:

- First, having established a recovery of 80%, long-term experiments were carried out with two membranes, one from Toray and other from Osmonics, to select the most appropriate based, fundamentally, on the permeate and concentrate flows, and on the conductivity of these streams.
- Second, using the selected membrane, a wide sweep of the permeate recovery percentage was made, to simulate the different units of the industrial modules.

In all the experiments, the permeate and concentrate flows leaving the system were measured, as well the conductivities of these streams. Similarly, in the experiments to select the membrane, the following were measured to check whether the permeates complied with dumping specifications: COD, BOD<sub>5</sub>, suspended solids, total solids, total nitrogen, ammonium, nitrates, nitrites, and organic nitrogen, in the feed, permeate, and concentrate streams.

**TABLE 41.3**  
**Technical Characteristics of the Reverse Osmosis Modules**

Characteristics	Toray	Osmonics
Configuration	Spiral	Spiral
Material	Polyamide	Polyamide
Superficial area, m <sup>2</sup>	7	5.5
Molecular weight cut off (MWCO), Da	<100	<100
Operation pressure, bar	18.5–26	18.5–26
Maximum temperature, °C	45	45
pH range	2–11	1.5–10.5
Axial flow rate, m <sup>3</sup> /h	2.4	2.4
Permeate flow, L/m <sup>2</sup> · h	26	23

### 41.3.3 RESULTS AND DISCUSSION

#### 41.3.3.1 Membrane Selection

As mentioned, two membrane modules, Toray and Osmonics, were compared. The technical characteristics of these reverse osmosis modules are detailed in Table 41.3.

Operating conditions for the Toray membrane

Entrance pressure	18.3 bar
Exit pressure	17.5 bar
Temperature	25.2°C
Recovery	80%
Operating time	12 days

The permeate and concentrate flows, and their respective conductivities, are depicted in Figure 41.10 for Toray membrane.

Operating conditions for the Osmonics membrane

Entrance pressure	18.8 bar
Exit pressure	17.8 bar
Temperature	22.2°C
Recovery	80%
Operating time	17 days

Figure 41.11 shows the variation with time of the flows and the conductivities for the permeate and concentrate for Osmonics membrane.

The permeate flow obtained with the Osmonics membrane was lower than that obtained with the Toray membrane. Better separation was observed with the Osmonics membrane, as the conductivity graph indicates, although a bigger decrease of the permeate flow was observed over the whole operating time. It was therefore concluded that the Osmonics membrane presented a bigger risk of fouling.

Table 41.4 presents the analytical results obtained for one of the days of operation, using the Toray and Osmonics membranes. It can be seen that both membranes provided a permeate stream that fulfilled the dumping specifications.

After studying the performance of these two membranes, the Toray membrane was selected to continue the study, since it permitted a bigger permeate flow than the Osmonics membrane. Although its separation performance was worse, its separation potential was considered acceptable and priority was given to obtaining bigger permeate flows.

The permeate flow obtained by these membranes was 20 L/h · m<sup>2</sup> for the Toray membrane, and 16.36 L/h · m<sup>2</sup> for the Osmonics membrane.

#### 41.3.3.2 Variation of the Recovery Percentage

In this study, four experiments were carried out varying the recovery percentage between 30% and 70%. The entrance pressure was set at 18–19 bar, and the exit pressure at 17–18 bar, while the temperatures varied between 32°C and 36°C. The results obtained in these experiments are shown in Table 41.5.

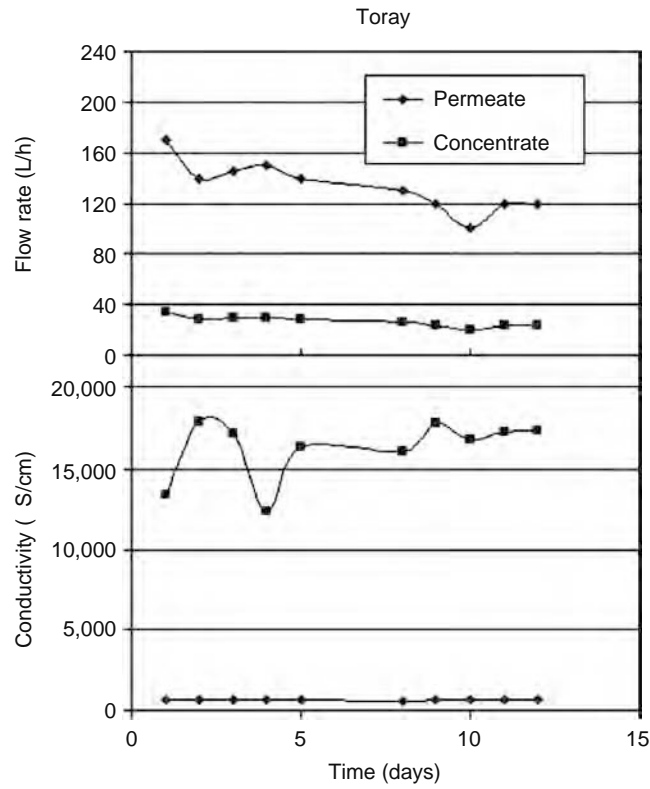


FIGURE 41.10 Flow rate and conductivities obtained with the Toray reverse osmosis membrane.

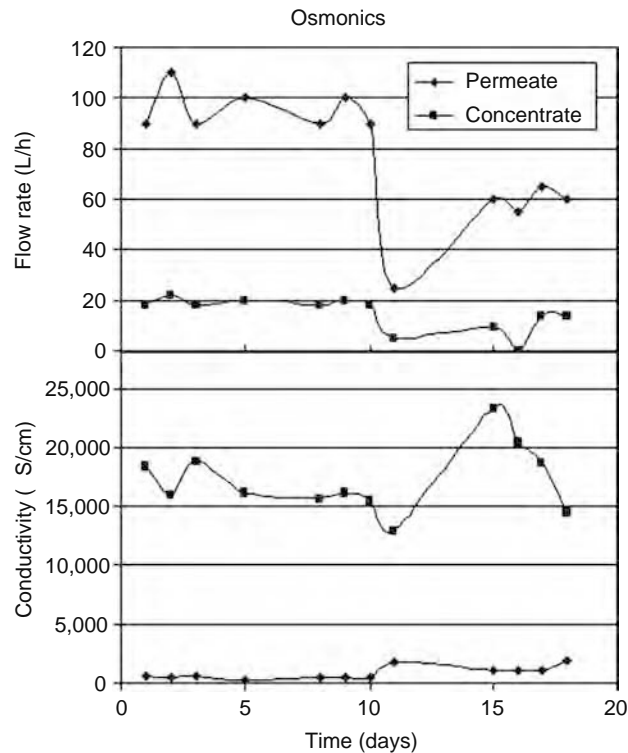


FIGURE 41.11 Flow rate and conductivities obtained with the Osmonics reverse osmosis membrane.

**TABLE 41.4**  
**Analytical Results of an Operation Day in the Reverse Osmosis Pilot Plant**

Membrane	Magnitude	Feed	Permeate	Concentrate
Toray	COD, mg/L	297	60.01	237
	BOD <sub>5</sub> , mg/L	20	5	15
	Suspended solids, mg/L	33.2	6.4	20
	Total solids, mg/L	8096.7	1253.3	7321
	Total nitrogen, mg/L	310	64.1	248.3
	Ammonium, mg · N/L	80	15.21	70.3
	Nitrates, mg · N/L	2.4	0.397	2.336
	Nitrites, mg · N/L	1.21	0.26	1.04
	Organic nitrogen, mg/L	226.39	48.233	174.624
Osmonics	COD, mg/L	241	41.1	149
	BOD <sub>5</sub> , mg/L	50	11	38
	Suspended solids, mg/L	14.4	2	13.8
	Volatile solids, mg/L	9520	2026.7	8840
	Total nitrogen, mg/L	327	63.2	257.8
	Ammonium, mg · N/L	163	10.7	89.2
	Nitrates, mg · N/L	2.64	2.004	0.864
	Nitrites, mg · N/L	0.68	0.16	0.52
	Organic nitrogen, mg/L	160.7	50.336	167.216

In view of the results, it can be concluded that conductivity increases with permeate recovery, that is, the higher the ratio between the permeate and concentrate flows, the lowest the quality of the permeate stream. As a consequence of this, there was a concentration of salts in the concentrate stream, because a higher flow of permeate than of concentrate was being separated from the feed.

#### 41.4 BRIEF DESCRIPTION OF THE INDUSTRIAL PLANT

From the results obtained in the ultrafiltration membrane bioreactor and reverse osmosis pilot studies, the industrial plant was designed with the following general characteristics.

The aerobic bioreactor is a tank measuring 32 m in diameter by 6 m in height, which gives a useful volume of about 5000 m<sup>3</sup>. It has four ABS pumps, each with a power of 45 kW, by means of which the content of the reactor is constantly recirculated at a rate of 1400 m<sup>3</sup>/h per pump, with the objective, obtaining perfect homogenization inside the reactor.

The aeration is produced by diffusion through the pipes that transport the air to four horizontal tubes submerged in the reactor. Three blowers of between 75 and 110 kW inject the air into the sludge or mixture when this is being recycled, just before it returns to the bioreactor. To obtain correct aeration, the bioreactor has an automated system for recording and controlling the quantity of dissolved oxygen that is present in the mixture at each moment. The bioreactor is also equipped with meters to continuously monitor the level and pH.

The ultrafiltration plant is composed of seven blocks of membranes, each with a length of 4.2 m, a width of 3.1 m, and an approximate height of 2.2 m. The length of each module is 3000 mm with a tube diameter of 210 mm and an area of 27 m<sup>2</sup>, the internal diameter of the membranes being 8 mm. The number of modules per block is 14, so that the total membrane surface area installed is 2646 m<sup>2</sup>.

**TABLE 41.5**  
**Results of the Recovery Percentage Variation**

Parameter	Assay 1	Assay 2	Assay 3	Assay 4
Permeate flow rate, L/h	75	105	110	175
Concentrate flow rate, L/h	40	85	105	400
Permeate conductivity, $\mu\text{S}/\text{cm}$	1,331	700	667	400
Concentrate conductivity, $\mu\text{S}/\text{cm}$	25,000	22,000	20,300	18,000
Recovery, %	65.2	55.3	51.1	30.4

The membrane is made of organic, poly(ether sulfone), with a separation limit of approximately 100 kDa, and a transversal flow rate of 1–6 m/s. The entrance pressure to the module is from 6 to 7.5 bar and that of exit is 0.5–1 bar.

The reverse osmosis plant is formed by three blocks of Toray polyamide membranes rolled in spiral, each 7.5 m long, 2.4 m wide, and 2.35 m high. Each block contains two filtering stages: the first composed of eight membrane modules that work at 15 bar and the second composed of five membrane modules at 23 bar. In total, there are 13 pressure tubes, each formed of six membrane units.

In total there are 234 units, providing an average of approximately 75% permeate production, and 99% retention of salts, at 30°C–40°C.

The quality of the effluent obtained by these two treatments can be summarized as follows:

In the membrane bioreactor, there is a reduction of 81% COD, 97.5% BOD<sub>5</sub>, 93% suspended solids, and 80% sulfides. In the reverse osmosis plant, there is a reduction of 96.2% COD, 97% BOD<sub>5</sub>, 80% sulphides, and 93% suspended solids. The conductivity decreased by 98%.

To date, the industrial plant is working satisfactorily, treating the effluent for 30 tanneries at a rate of approximately 5000 m<sup>3</sup>/day. The effluent obtained is suitable for agricultural irrigation purposes.

## ACKNOWLEDGMENTS

We thank Enrique Nicolás, Juan Gozalbo, Philippe Rouge, M. Teresa Pérez, Wolfram Scholz, Manuel Terry, Inmaculada López-Guillén, and Ernesto Sánchez for their contribution in this research and design work. We would also like to thank Aquagest Levante, S.A., Murcia, Spain; AGBAR-Aguas de Barcelona, Barcelona, Spain; and BLC Leather Technology Centre, Northampton, United Kingdom for their support.



---

# 42 New Developments in Nanofiltration Technology: A Case Study on Recovery of Impurity-Free Sodium Thiocyanate for Acrylic Fiber Industry

*S. Sridhar and B. Smitha*

## CONTENTS

42.1	Overview of Nanofiltration .....	1102
42.1.1	Introduction .....	1102
42.1.2	Background .....	1102
42.1.3	Theory .....	1102
42.1.3.1	Sieving Effect due to Steric Hindrance .....	1104
42.1.3.2	Donnan Effect due to Electrostatic Nature .....	1104
42.1.4	Terminology .....	1104
42.1.5	Membranes .....	1106
42.1.5.1	Membrane Materials .....	1106
42.1.5.2	Membrane Modules .....	1107
42.1.5.3	Membrane Synthesis .....	1107
42.1.5.4	Membrane Modification .....	1108
42.1.6	Applications .....	1110
42.1.7	Future Prospects .....	1111
42.2	Case Study .....	1112
42.2.1	Description of the Process .....	1112
42.2.2	Scope and Objectives .....	1113
42.2.2.1	Scope of the Work .....	1113
42.2.2.2	Objectives of the Pilot-Plant Study .....	1113
42.2.3	Experimental Procedures and Protocols .....	1114
42.2.3.1	Materials .....	1114
42.2.3.2	Types of Membranes and Their Preparation .....	1114
42.2.3.3	Description of Pilot-Scale Nanofiltration System .....	1114
42.2.3.4	Nanofiltration Procedure .....	1115
42.2.3.5	Analytical .....	1115
42.2.3.6	Membrane Cleaning and Maintenance .....	1115
42.2.4	Results and Discussion .....	1116
42.2.5	Process Description for Operation of Commercial Nanofiltration Plant .....	1118
42.2.5.1	Cycle 1 .....	1118
42.2.5.2	Cycle 2 .....	1120
42.2.5.3	Membrane Cleaning and Storage .....	1120
42.2.6	Simulation and Design .....	1120
42.2.6.1	Material Balance .....	1121

42.2.7	Economic Estimation .....	1122
42.2.7.1	Capital Investment .....	1122
42.2.7.2	Operating Cost .....	1123
42.2.8	Conclusions .....	1123
	Acknowledgments .....	1124
	References .....	1124

## 42.1 OVERVIEW OF NANOFILTRATION

### 42.1.1 INTRODUCTION

Separation processes as a whole have grown in importance because of increasingly stringent requirements for product purity [1]. Among the different membrane techniques, pressure-driven processes such as microfiltration (MF), ultrafiltration (UF), nanofiltration (NF), and reverse osmosis (RO) were the first to undergo rapid commercialization [2–4]. These processes basically differ in pore size distribution of membranes used and the types of compounds recovered. A typical schematic of the exclusion of various compounds through different membrane processes is illustrated in Figure 42.1.

Nanofiltration is a rapidly advancing membrane separation technique for concentration/separation of important fine chemicals as well as treatment of effluents in pharmaceutical industry due to its unique charge-based repulsion property [5]. Nanofiltration, also termed as loose reverse osmosis, is capable of solving a wide variety of separation problems associated with bulk drug industry. It is a pressure-driven membrane process and indicates a specific domain of membrane technology that lies between ultrafiltration and reverse osmosis [6]. The process uses a membrane that selectively restricts flow of solutes while permitting flow of the solvent. It is closely related to reverse osmosis and is called “loose RO” as the pores in NF are more open than those in RO and compounds with molecular weight 150–300 Da are rejected. NF is a kinetic process and not equilibrium driven [7].

The NF process has the advantage of lower operating pressures compared to RO and higher rejection of organics compared to UF. NF is generally used to separate water from multivalent ions and organic components with relatively low-molecular weights (200–1000 g/mol). It is generally expected to remove between 60% and 80% of hardness, greater than 90% of color, and all the turbidity if applied in a water treatment plant.

### 42.1.2 BACKGROUND

The history of NF dates back to the 1970s when RO membranes with a reasonable water flux operating at relatively low pressures were developed to avoid high pressures traditionally used in RO, which resulted in a considerable energy cost. Thus, membranes with lower rejections of dissolved components, but with higher water permeability, would be a great improvement for separation technology. Such low-pressure RO membranes came to be known as NF membranes [8]. By the second half of the 1980s, NF had become established, and the first applications were reported [9,10]. In the last two decades, considerable effort has been invested in the development of membranes that combine the high retention of RO with the lower pressures of UF. This has resulted in the development of nanofiltration membranes. To date, NF is becoming increasingly important, filling the niche between UF and RO. The pore diameter of NF membranes is ~2 nm or smaller and therefore species in an intermediate range can be retained as a result of their larger size. Additionally, NF materials are charged, and by means of electrostatic effects they can partly retain charged species that are about one order of magnitude smaller than their pore size. By controlling these electrostatic effects, the effective pore size of NF membranes can, to some degree, be regulated and therefore the separation of charged species can be performed without having to resort to smaller pore sizes and, consequently, higher pressures.

### 42.1.3 THEORY

Nanofiltration is a pressure-driven process where the solvent is forced through the membrane by pressure, and other feed constituents randomly pass through the membrane by diffusion. The relative rates of solvent and solute passage determine the quality of the product. Nanofiltration membranes are adept at the separation of small, neutral, and charged solutes in aqueous solutions because they allow the passage of monovalent ions and retain multivalent ions due to their charge. Nanofiltration membranes exhibit two important features in their actual applications. They provide

1. Intermediate molecular weight cutoff (MWCO) [11]
2. Solute rejection caused by the charge effect [12]

In aqueous solutions, NF membranes become charged, allowing separation of specific ionic species. It is believed that sieving (steric hindrance) is the dominant rejection mechanism in NF for colloids and large molecules, while the physico-chemical interactions of solute and membrane become increasingly important for ions and low-molecular-weight organics [13].

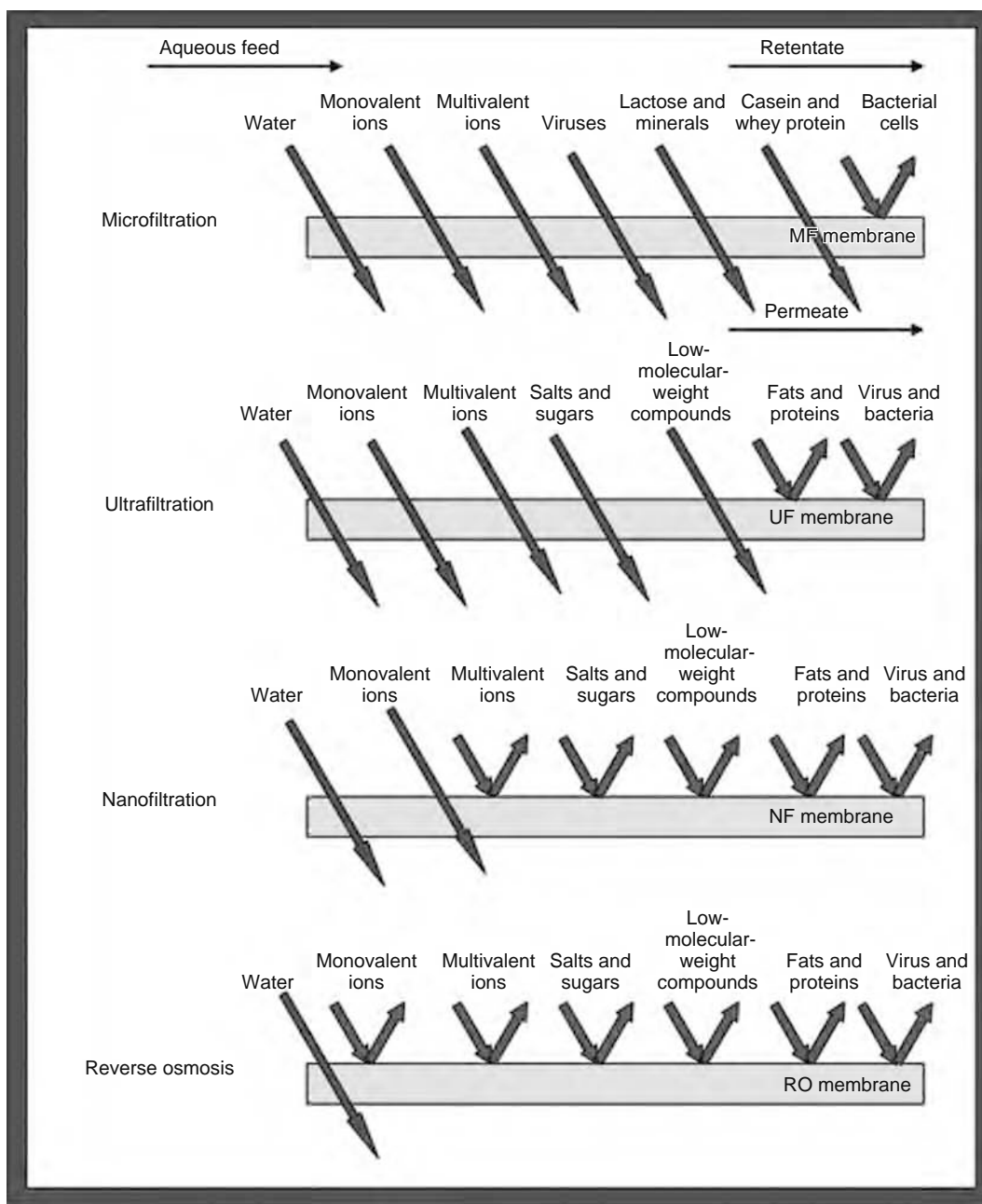


FIGURE 42.1 Exclusion of various compounds through different membrane processes.

Figure 42.2 shows a hypothetical polymeric NF membrane with carboxylic groups attached to the surface of the membrane, which is brought in contact with an aqueous solution of electrolytes. The presence of dissociated carboxylic groups on the membrane surface causes the occurrence of membrane charge.

Based on the above factors separation occurs by the following mechanisms:

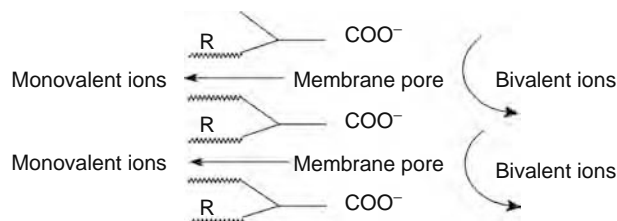


FIGURE 42.2 Principle of nanofiltration. (From Bessarabov, D. and Twardowski, Z., *Membr. Technol.*, 9, 6, September 2002. With permission.)

#### 42.1.3.1 Sieving Effect due to Steric Hindrance

The NF membranes have an intermediate MWCO between reverse osmosis and ultrafiltration membranes, which ranges from 200 to 1000. The solutes having larger molecular weight than the MWCO value of a membrane are almost completely rejected by the membrane and the ones having lower molecular weight will permeate easily through the membrane [14]. This is called sieving effect. Thus, solutes can be separated based on the differences in molecular sizes and shapes.

#### 42.1.3.2 Donnan Effect due to Electrostatic Nature

The Donnan effect of a membrane refers to the electrostatic interactions between the ions and the membrane [15]. The membrane is mostly negatively charged, since the thin film of NF membranes is made of polyelectrolytes. Ions having the same sign of charge as the membrane are excluded and the ions having the opposite sign of charge can be attracted. Separation of ions having different signs and valencies can be manipulated according to the rejection characteristics of the membrane.

#### 42.1.4 TERMINOLOGY

1. *Nanofiltration*: According to the International Union of Pure and Applied Chemistry (IUPAC) recommendations [16] nanofiltration is a “pressure-driven membrane-based separation process in which particles and dissolved molecules smaller than about 2 nm are retained.”
2. *Diafiltration*: Diafiltration [17] is a step in addition to nanofiltration wherein the retentate is further diluted with water and re-nanofiltered to reduce further the soluble components and concentrate further the retained components.
3. *Osmotic pressure*: The osmotic pressure,  $\Pi$ , represents the amount of pressure that can be created between a concentrated solution and pure water separated by a permeable membrane. The equation given below represents the osmotic pressure for a single electrolyte solution [18].

$$\Pi = C_T RT \phi$$

where

- $C_T$  is the total anionic and cationic molar concentration
- $R$  is the ideal gas constant (8,312 Pa/M–K)
- $T$  is the temperature (K)
- $\phi$  is the molar osmotic coefficient

When considering solutions near infinite dilution, the molar osmotic coefficient,  $\Phi$ , reaches unity. The osmotic coefficient will vary for different membrane materials [19].

4. *Transmembrane pressure*: Transmembrane pressure,  $P_{tm}$ , refers to the amount of pressure applied across the membrane filter [20].

$$P_{tm} = \left( \frac{P_i + P_o}{2} \right) - P_p$$

where

- $P_i$  is the element inlet pressure
- $P_o$  is the element outlet pressure
- $P_p$  is the permeate pressure

5. *Transmembrane flux*: At any given temperature or pressure for a given NF module, permeate flow can then be used to determine the amount of water crossing a membrane surface. The transmembrane flux,  $J_t$ , can be defined as [20]

$$J_t = \frac{Q_p}{A_m}$$

where

- $Q_p$  is the permeate flow rate
- $A_m$  is the membrane surface area

6. *Specific flux*: The specific flux,  $J_s$ , allows for the normalization of the transmembrane flux with the transmembrane pressure [20].

$$J_s = \frac{J_t}{P_{tm}}$$

7. *Solute Rejection*: For individual components of the feed solution, the solute rejection,  $X_i$ , is given by

$$X_i = 1 - \frac{C_p}{C_f}$$

where

$C_f$  is the solute concentration in feed

$C_p$  is the solute concentration in permeate

8. *Concentration polarization*: Concentration polarization is important for membrane operation and modeling. It represents increased concentrations of rejected solutes near the membrane surface. The concentration-polarization layer is described with the classic film model [19].

$$\frac{C_w - C_p}{C_f - C_p} = \exp\left(\frac{J_v \delta}{D}\right)$$

where

$D$  is the molecular diffusion coefficient

$C_w$  is the solute concentration at membrane wall

$J_v$  is the water flux

$\delta$  is the thickness of concentration-polarization layer at membrane surface

The performance of membrane operations is diminished by polarization phenomena (concentration and temperature polarization), although the extent to which these phenomena can occur differs considerably.

With all polarization phenomena, the flux at a definite time is always less than the original value. When steady-state conditions have been attained a further decrease in flux will not be observed, i.e., the flux will become constant as a function of time. Polarization phenomena are reversible processes, but in practice, a continuous decline in flux can be observed. Such continuous decline is a result of membrane fouling, which may be defined as the irreversible deposition of retained particles, colloids, emulsions, suspensions, macromolecules, salts, etc. on or in the membrane. This includes adsorption, pore blocking, precipitation, and cake formation.

9. *Membrane fouling*: Fouling is the deposition of solute constituents on the surface of the membrane [21–23]. Membrane fouling is a complicated phenomenon and typically results from multiple causes. In spite of its complexity, electrostatic and hydrophobic/hydrophilic interactions that involve both the membrane and the fouling materials are recognized to have significant bearing, especially for the more-difficult-to-clean membrane fouling dominated by natural organic matter (NOM) and microbial activities. Figure 42.3. shows the influence of concentration polarization and fouling on flux.

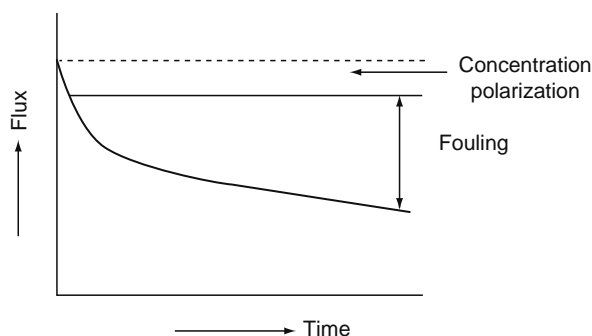


FIGURE 42.3 Pictorial representation of variation of flux with time due to concentration polarization and fouling. (Adapted from Mulder, M., *Basic Principles of Membrane Technology*, Kluwer Academic, Dordrecht, The Netherlands, 1996.)

### 42.1.5 MEMBRANES

In nanofiltration, an array of feed streams must be dealt with for which three relevant areas such as material selection, membrane synthesis, and system configuration must be integrated.

Right from the early 1960s, when work on membrane separations began, a wide range of materials including metals, zeolites, polymers, ceramics, and biological materials are being used for the manufacturing of membranes. However, polymers form the most widely used material for membrane manufacturing at present.

A major consideration in this section will be the selection of polymer materials, membrane synthesis, and modifications, which can be made to such structures that have enabled them in being the most appropriate membranes for nanofiltration. Before exploring the membrane materials used for NF, the preferable membrane morphologies that yield optimum separation must be envisaged. Generally the membranes used for laboratory scale setup for the aqueous mixture filtration by NF are always homogeneous and symmetric, however to attain commercial viability, the membranes successful on the laboratory scale are prepared in asymmetric or composite form [24–26]. These two morphologies offer a possibility of making a barrier with a thin effective separation layer, which enables high flux while maintaining desirable mechanical strength.

#### 42.1.5.1 Membrane Materials

Most MF, UF, RO, and NF membranes are synthetic organic polymers. NF membranes are made from cellulose acetate blends, cellulose triacetate (CTA), or polyamide composites such as the RO membranes, or they could be modified forms of UF membranes such as sulfonated polysulfone [27]. On the other hand, poly(vinyl alcohol) (PVA) is a significant polymer for nonaqueous applications. Chemical structures of a few of the prominent polymers are shown in Figure 42.4.

FILMTEC/Dow has commercialized the NF55, NF70, and NF90 (water flow of NF55 > NF70 > NF90) membranes [28–33], which work in the range of nanofiltration, being able to reject at least 95% magnesium sulfate. The top layer of these membranes is fully cross-linked aromatic polyamide. FilmTec NF50 membranes [28], which were used to replace coagulation, filtration, and ammonia treatment processes in water treatment plants, yielded 96% color removal, besides a reduction of total organic carbon (TOC) by an average of 84% and reducing trihalomethane formation to regulatory levels.

The authors have studied the recovery of sodium thiocyanate, which is used in the manufacture of acrylic fiber, an imperative raw material employed in the textile industry. For this study, the application of the highly advanced hydrophilized polyamide (HPA); a derivative of PA was considered. PA-300 was prepared by interfacial polymerization technique, while the HPA membranes were prepared by coating a novel proprietary copolymer onto a microporous polysulfone substrate followed by cross-linking of the top layer. Thus, the morphology of these membranes was thin-film composite (TFC). Commercial PA and CTA membranes in India were generally available with only one particular MWCO each, 300 and 700, respectively, while the availability of HPA series range has changed the scenario with more widely distributed membranes in the MWCO range of 50–400. Table 42.1 lists the standard nanofiltration membranes available worldwide [1]. The table shows that the maximum extent of rejection of monovalent NaCl through NF membranes is only 50%, while for bivalent salts such as MgSO<sub>4</sub> and Na<sub>2</sub>SO<sub>4</sub> the rejection is as high as 95%–98% on a consistent basis. The table also shows that NF has the potential for concentrating organics such as glucose.

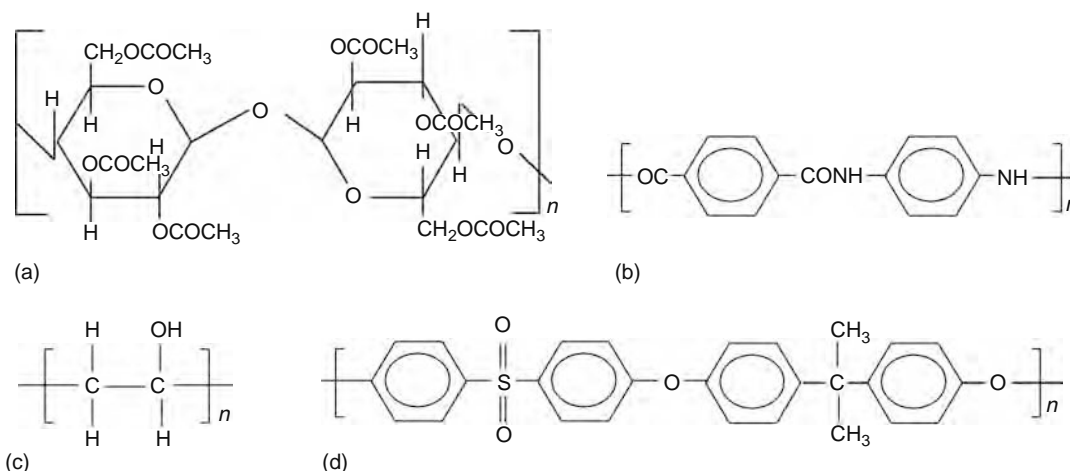


**FIGURE 42.4** Chemical structures of polymers for nanofiltration (a) cellulose triacetate, (b) aromatic polyamide, (c) polyvinyl alcohol, and (d) polysulfone.

**TABLE 42.1**  
**Characteristics of Commercially Available Nanofiltration Membranes**

Commercial Name	Company	Solute	Test Conditions	Flux (L/m <sup>2</sup> h)	Rejection (%)
NF-40	Filmtec, Minneapolis	NaCl	2,000 ppm, 25°C, 16 bar	43	45
NF-70	Filmtec, Minneapolis	MgSO <sub>4</sub>	2,000 ppm 25°C, 5 bar	36	95
NTR-7250	Nitto Denko Co. Ltd., Tokyo, Japan	MgSO <sub>4</sub>	2,000 ppm 25°C, 20 bar	85	98
UTC-20HF	Toray, Japan	NaCl	1,500 ppm 25°C, 15 bar	146	50
MPT-20	Membrane Products, Korntal-Münchingen, Germany	Glucose	10,000 ppm 25°C, 25 bar	70	75
Desal-5	Desalination Systems, Vista, California	NaCl	1,000 ppm 25°C, 10 bar	46	47
DRC-1000	Celfa, Seewen, Switzerland	NaCl	3,500 ppm 25°C, 10 bar	50	10
PERMA-250	Permionics, Vadodara, Gujarat, India	Na <sub>2</sub> SO <sub>4</sub>	2,000 ppm 35°C, 7 bar	60	98
M-N2521A3	Applied Membranes Inc, Vista, California	NaCl	2,000 ppm 25°C, 10 bar	264	30
4040-XN45-TSF	TriSep Corp., Goleta, California	NaCl	500 ppm 25°C, 7 bar	362	20
NE 4040-40	Saehan Industries Inc., Gumi-Si, South Korea	NaCl	2,000 ppm 25°C, 5 bar	200	60

#### 42.1.5.2 Membrane Modules

The central part of any membrane plant is the module, i.e., the technical arrangement of the membranes. Some important aspects to be taken into consideration for the module design include packing density, cost-effective manufacture, easy access for cleaning, and cost-effective membrane replacement. Based on the above, the modules can be distinguished into five major types:

1. *Tubular module*: The membrane here is in hose form [34] on the inside of pressure-tight tubes having 12–24 mm internal diameter (Figure 42.5a). If the material of the support tube is impermeable, then a thin porous tube is fitted between the support tube and the membrane. In many cases, several tubular membranes are assembled in a common support block to increase the packing density. Nanofiltration membranes were developed first in this kind. Though the manufacturing cost of these modules is high, these modules offer excellent resistance to fouling with low-pressure drop, but are not suitable for high-pressure operations.
2. *Hollow fiber module*: Essentially this module consists of a pressure vessel containing a bundle of individual fibers (Figure 42.5b) [34]. The open ends of the fibers are potted into a head plate. The feed solution flows radially or parallel to the hollow fibers. The permeate is collected at the open end of the fibers and hence the parallel flow can be cocurrent or countercurrent depending on the direction of permeate flow with respect to the feed. According to Gill and Bansal [35,36], countercurrent flow is always superior to cocurrent flow in parallel flow conditions. The module lends the membrane higher packing density, enabling production of modules at a lower cost per unit product. These modules offer poor resistance to fouling and are not suitable for high-pressure operations [37].
3. *Plate and frame systems*: Here the feed solution flows through flat, rectangular channels (Figure 42.5c) [34]. Packing densities of about 100–400 m<sup>2</sup>/m<sup>3</sup> are achievable. For NF, plate and frame design has been excluded due to their expensive nature. They are primarily used to treat fouling-prone feed streams and to produce potable water in small-scale applications.
4. *Spiral wound modules*: These are characterized by high packing density (>900 m<sup>2</sup>/m<sup>3</sup>) and a simple design. Essentially, two or more membrane pockets are wound around a centrally located permeate collecting tube with a special mesh used as spacer (Figure 42.5d). The membrane pocket consists of two membrane sheets with a highly porous material in between, which are glued together along three edges. The fourth edge of the pocket is connected to the collecting tube. Several such pockets are spirally wound around the perforated permeate tube with a feed-side spacer placed between the pockets [38]. Usually several such membrane elements are arranged in one pressure vessel. The feed-side flow is strictly axial, while the permeate flows through the porous support inside the pocket, along the spiral pathway to the collecting tube [39]. This module is simple, and is also resistant to fouling at higher pressures.

Most of the commercially available NF membranes are made in spiral wound configuration.

#### 42.1.5.3 Membrane Synthesis

The different procedures for synthesis of NF membranes are listed below:

1. One of the oldest methods in preparing NF membranes is the phase inversion technique involving precipitation of a polymer film from its solution cast film in a nonsolvent bath. The prerequisite for this method is that the solvent of the polymer and the nonsolvent must be thoroughly miscible, while the polymer should not dissolve in the nonsolvent [40–45].

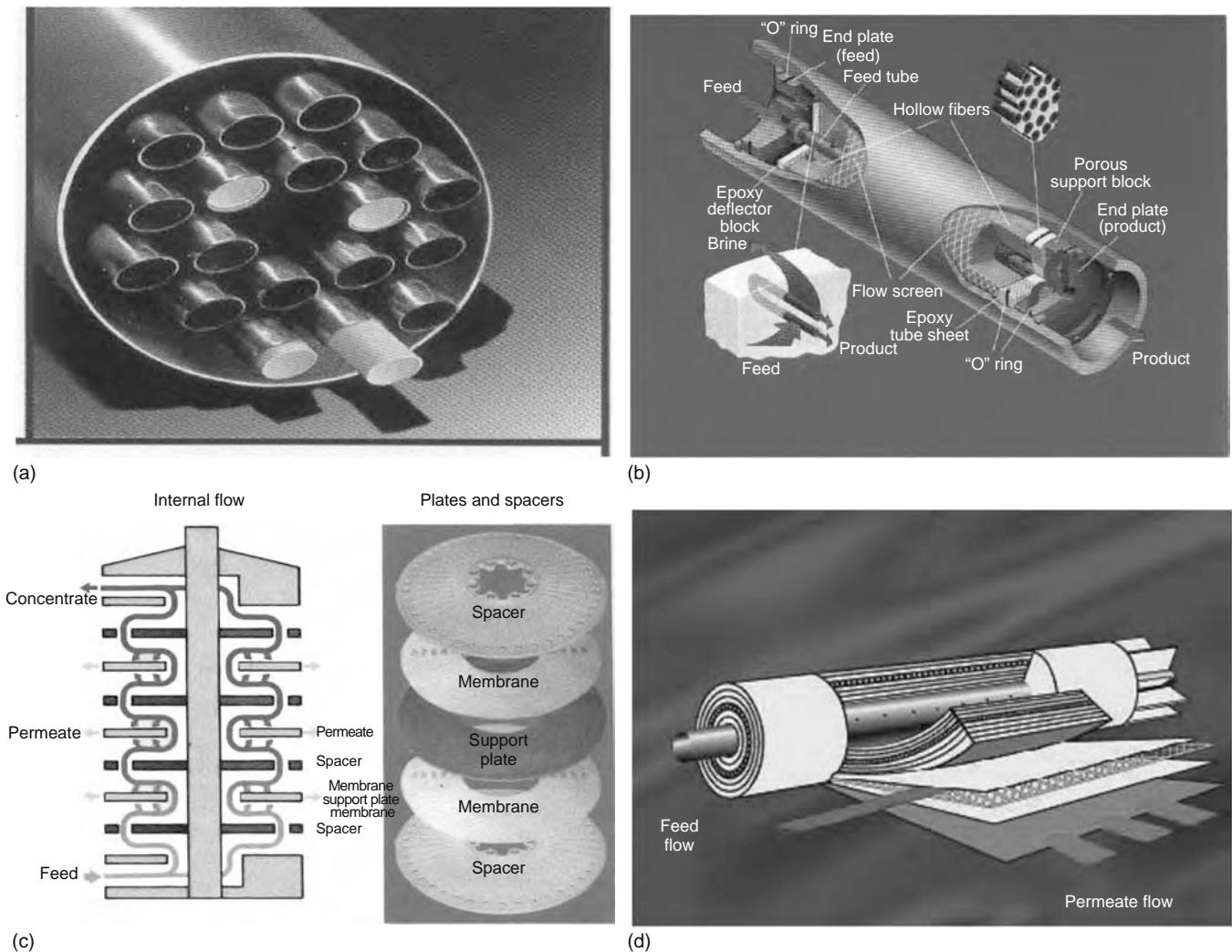


**FIGURE 42.5** Membrane modules. (a) Tubular module, (b) hollow fiber module, (c) plate and frame, and (d) spiral wound module. (Photo courtesy of Genesis Membanes Pvt. Ltd. With permission.)

- Interfacial polymerization between a piperazine, or an amine-substituted piperidine, or cyclohexane, and a polyfunctional acyl halide [46,47].
- Contacting an RO membrane with a strong mineral acid such as phosphoric acid at 100°C–150°C, followed by treatment with a rejection enhancing agent, such as tannic acid, to plug microscopic leaks and defects [48].
- Contacting the cross-linked RO polyamide membrane with ions to form a membrane ion complex, treating the membrane ion complex with an aqueous solution of alkali metal permanganate to form manganese dioxide crystals in the membrane, and finally dissolving the crystals [49].
- Opening the pores of an RO membrane by treatment with triethanol amine. RO cellulose acetate membranes can also be opened by hydrolysis at very high and very low pH [50].
- Coating of ultrafiltration/microfiltration membrane supports such as polyvinylidene fluoride (PVDF) or polysulfone (PSF) with solutions of polymers such as poly(ether-*block*-amide) [51].
- Low-temperature plasma-induced grafting modifications of ultrafiltration membrane to yield hydrophilic nanofiltration membranes. In an investigation by Zhao et al. [52], preparation of hydrophilic nanofiltration membranes has been successfully accomplished using a procedure consisting of plasma irradiation and subsequent grafting in gas of acrylic acid monomers on poly(acrylonitrile) UF membrane.

#### 42.1.5.4 Membrane Modification

From the aforesaid study, it is clear that polyamide membranes have become the main type of membranes used for NF. Despite their excellent performance and superior economics the TFC-based technology is prone to severe organic fouling [53].

The problem seems to have no easy solution and necessitates the use of expensive pretreatment and cleaning systems. The propensity of TFC to undergo fouling arises primarily from the hydrophobicity of the polyamide active layer, onto which many natural organic compounds easily adsorb, eventually leading to irreversible deterioration of the performance. Periodic cleaning does not solve the problem completely and the membranes eventually have to be replaced. Unfortunately, as far as the performance is concerned, no substitute to polyamides has been found so far. A potential way to circumvent the problem is the surface modification. Surface modification is a versatile process to design membranes with tailor-made filtration properties [54]. Nanofiltration membranes can be modified to change their adsorption and solute rejection properties and their susceptibility to fouling.

#### 42.1.5.4.1 Modifications for Improving Performance

*Ion implantation:* This study involves modifying the surface of nanofiltration membranes by ion implantation for increased salt rejection [55].  $F^-$  ions at two different intensities— $1E10$  and  $5E10$  atoms/cm<sup>2</sup>—were implanted on the surface of commercially available nanofiltration membranes to increase the negativity of the membrane surfaces. The objective was to increase the Donnan exclusion effect to improve salt rejection by the modified membranes. It was also noted that this modification did not significantly damage the semipermeable membrane surface.

*Deposition of polyelectrolytes:* Lajimi et al. [56] explored the surface modification of nanofiltration cellulose acetate (CA) membranes by alternating layer-by-layer deposition of acidic chitosan (CHI) and sodium alginate (ALG) as the cationic and anionic polyelectrolyte, respectively. The supporting CA membranes were obtained by a phase separation process from acetone/formamide. The permeation rate of salted solutions was found to be higher than that of pure water. The rejection of monovalent salt was decreased, while that of divalent salt remained constant so that the retention ratio increased. Increasing the concentration of feed solutions enhanced this selectivity effect.

*Polymer grafting:* Surface modification using grafting of a hydrophilic polymer onto the membrane surface is a possible route to improving the fouling properties of polyamide TFC membranes. One way of carrying out this technique would be to graft a hydrophilic polymer onto the polyamide surface making it more hydrophilic and decreasing or weakening the adherence of the organic matter. This approach could be particularly attractive, if one could modify the existing commercial membranes in situ, e.g., inside a module using an inexpensive procedure. It has been shown that the fouling resistance of membranes could be improved without significantly affecting the retentive properties [57–62]. Freger et al. [63] employed grafting of monomers with focus on the acrylic acids. The chemical changes produced an active layer on the membrane surface and they also noted that the effect of modification on the surface roughness was negligible.

*Ultraviolet-photografting:* With this technique [64,65], the chemical bonds in the membrane polymer can be cleaved to form radical sites. In the dip photografting method [66], the monomer to be grafted is present in the superficial liquid film and inside the membrane pores. For a given solution concentration, the quantity of monomer available for grafting depends on the liquid film thickness and on the monomer concentration profile inside the pores. It, therefore, depends on the operating rate and on the contact time in the monomer solution during the dipping. An increase in rate gives an increase in superficial film thickness and a decrease in the amount of monomer in the pores. These phenomena, coupled with the light power of the radiation received and the UV residence time, influence the final permeability.

*Blending:* Ferjani et al. [67] experimented and found that the addition of a small amount of polymethylhydrosiloxane (PMHS) in the dope formulation of CA membranes drastically changed the performance by increasing the NaCl rejection factor and decreasing the permeation rate. This effect can be explained by the morphological changes due to the presence of PMHS. For similar retention values, the blend membranes exhibited better productivity. A thin PMHS top layer coated on the surface of asymmetric CA films produced composite membranes having a similar NaCl rejection factor to that of CA membranes used in RO. This effect stresses out the role played by the hydrophobic nature of PMHS in salt retention. However, the composite membranes were less permeable to the solvent than the corresponding asymmetric membranes.

#### 42.1.5.4.2 Modifications for Improving Fouling Resistance

*Surfactants:* The usage of surfactants for enhancing the fouling resistance of the membranes has also been suggested by Wilbert et al. [68]. Commercial samples of cellulose acetate and polyamide reverse osmosis, and nanofiltration membranes were treated with a homologous series of polyethylene-oxide based surfactants to improve fouling resistance. The fouling solution degraded the untreated cellulose acetate (CA) blend membrane. Triton X100 and Pluronic P84 provided significant protection. Polyamide (PA) membranes treated with surfactant experienced a severe flux decline. A similar decline was caused by fouling of the untreated PA membrane. The treated PA membrane did not have further flux decline with fouling.

*Improvement in hydrophilicity:* A large number of attempts have been made to improve the fouling behavior of available membranes by increasing the hydrophilic character of the membrane surface. The logic behind this approach is clear: for any protein or cell to adsorb (or adhere) to the membrane, it must first displace the water molecules that are chemically associated with the surface groups on the membrane. Several studies have specifically demonstrated that increased hydrophilicity can result in a significant reduction in both protein adsorption and cell adhesion [69,70] and in turn biofouling.

*Introduction of negative charges:* Most proteins and cells are negatively charged in aqueous solution, thus the introduction of negative charges on the membrane surface should (at least in principle) increase the electrostatic repulsion between the membrane and the cells/proteins. Most studies of surfactant-modified membranes provide very clear evidence for this general phenomena, with negatively charged surfactants being much more effective at reducing fouling than the corresponding cationic surfactants [71].

#### 42.1.6 APPLICATIONS

Nanofiltration membranes allow partial permeation of monovalent salts such as sodium chloride, while they completely reject bivalent salts and hardness from aqueous solutions. This has led to the use of NF membranes as water softeners by removal of total hardness and sulfates from seawater and for removal of NaCl from cheese whey. NF membranes have also been successfully utilized for treating textile dye and olive processing wastewaters to recover recyclable water. Another common application is removal of color from effluents and process solutions. One such example is the separation of color causing compounds such as lignin sulfonates from paper pulping wastewater.

*Treatment of groundwater:* The removal of pesticides and some micropollutants from groundwater has been studied by many researchers [72–75]. The NF70 membranes tested on well water in Iowa showed 98% rejections of calcium and magnesium, and 90% and 100% rejections of strontium and barium, respectively. Chloride, alkalinity (CaCO<sub>3</sub>), fluoride, sulfate, iron, silicon, phosphorous, and boron rejections were 45%, 59%, 29%, 98%, 100%, 28%, 60%, and 4%, respectively. The separation of nitrate from well water was another application suggested by Rautenbach and Groschl [31]. Nitrate rejections of the NF40 membrane were low for feed containing sulfate. Sulfate added to well water containing nitrate would result in nitrate passing through the membrane, while sulfate and other highly charged species would be rejected. The permeate could then be treated with ion exchange to remove the nitrate. The NF70 membrane was also used for fluoride removal and for reducing feed levels from 4 to 0.4 mg/L yielding a fluoride rejection of 90%. Kettunen and Keskitalo [76] studied the removal of fluoride and aluminum from groundwater sources in Finland. In addition to the removal of the hardness of nitrates, iron, and strontium, fluoride removal was also mentioned by Pervov et al. [77].

*Treatment of surface water:* The use of NF70 TFC membranes as water softener in removing organics was reported by Cadotte et al. [30]. The low-pressure RO system can lower hardness and TDS, reduce organics that impart color and odor in a single step, thereby replacing multiple processes such as lime softening followed by activated carbon adsorption. Removal of organic micropollutants was also investigated by other researchers [78,79]. Koyuncu and Yazgan [79] had good results in treating salty and polluted water from Kucukcekmece lake in Istanbul using the TFC-S NF membrane. Using a novel NF membrane (NF 200), removal of organics (up to 96%) in a large NF plant in Paris [80] was achieved. NF has also been used to remove both arsenic(V) and arsenic(III) from surface water [81]. These studies showed that (using NF membranes) the rejection of As(V) is relatively high, up to 90%, while As(III) is just around 30%.

*Treatment of wastewater:* Trihalomethanes (THM) such as chloroform, bromodichloromethane, and tribromomethane are carcinogens present in finished drinking water from many treatment plants. The exclusion of these renders them disposable without causing significant harm to environment. High rejections of humic acids (THM precursors) using NF40 membrane were indicated by Bhattacharya and Williams [32]. These membranes gave high rejections even at high water recoveries (80%) with little drop in permeate flux. Hafiarle et al. [82] investigated the removal of chromate from water using a TFC-S NF membrane as a possible alternative to the conventional methods of Cr(VI) removal from an aqueous solution. The results showed that the rejection depended on the ionic strength and pH. Better retention was obtained at basic pH (up to 80% at a pH of 8). Results also showed that NF is a very promising method of treatment for wastewater charged with hexavalent chromium. The same membrane was used by Koyuncu [83] to treat opium alkaloid processing industry effluents. Application of NF in the treatment of textile wastewater has also been conducted by many researchers [84,85].

*Treatment of seawater:* Desalination has been the interest of many researchers [86–89]. The application of NF50, NF70, NF40, and NF40HF for partial water desalination was reported by Eriksson [29]. Studies on surface water treatment in Florida using the NF50 membrane at 0.45 MPa produced a TOC rejection of 94%, color rejection of 96%, 76% alkalinity (as CaCO<sub>3</sub>) rejection of 76%, chloride rejection of 52%, and TDS rejection of 84%. The high rejections rendered this membrane suitable for water softening. Pontie et al. [90] studied the possibility of obtaining a partial demineralization of seawater using two successive NF stages. The treated water (salinity 9 g/L) could be used in the field of human health (i.e., preparation of nasal sprays, medical dietetics, and hot mineral springs).

*Industrial applications:* Nanofiltration has the potential to reduce COD and BOD of industrial effluents, especially those from distilleries and textile industry. Simpson et al. [33] reported the use of nanofiltration for the removal of hardness and organic impurities from a textile mill wastewater. Rejections of the membrane included 29% of conductivity, 33% of sodium, 48% of calcium, 67% of magnesium, and 47% of soluble organic carbon present in the waste stream.

An overview of the possible applications of NF is given in Table 42.2 [72–164]. Except for the removal of solvent from sunflower oil, all applications are in the treatment of aqueous systems. Table 42.2 shows the diversity of opportunities for

**TABLE 42.2**  
**Overview of Possible Applications of Nanofiltration in Industries**

Industry	Application
<i>Water production</i>	
Groundwater	Removal of pesticides [72–75] Hardness removal [76,77]
Surface water	Removal of natural organic matter (acridine orange [ao] color) [78,79] Removal of heavy metals (As, Pb), Fe, Cu, Zn, and Si [80,81]
Wastewater	Removal of trihalomethanes (THM) [82] Removal of degreasing agents from water [83,84]
Seawater	Treatment of brackish water [85] Desalination of water [86–90]
Food	Demineralization of sugar solutions [91] Demineralization of whey [92–95] Recycle of nutrients in fermentation processes [96] Separation of sunflower oil from solvent [97] Recovery of cleaning-in-place solutions [98,99] Recovery of regeneration liquid from decoloring resins in sugar industry [100–103] Effluent treatment [104,105] Purification of organic acids [106–108] Separation of amino acids [109,110] Removal of dyes from wastewater [111]
Textile	
Clothing and leather	Recovery of water and salts from wastewater [112–119] Recovery and reuse of chromium(III) and chromium(II) [120–122]
Paper and graphical	Recovery of wastewater from effluent [123–127]
Chemical	Recovery of bleaching solution [128–130] Sulfate removal preceding chlorine and NaOH production [131–133] CO <sub>2</sub> removal from process gases [134–136] Preparation of bromide [137] Recovery of caustic solutions in cellulose and viscose production [138] CaSO <sub>4</sub> precipitation [139]
Metal plating and product/electronic and optical	Removal of metal sulfates from wastewater [140] Cleaning of machine rinsing solutions [141] Removal of nickel [142] Recovery of Cu <sup>2+</sup> ions from ore extraction liquids [143–145] Al <sup>3+</sup> removal from canning industry wastewater [146]
Landfills agriculture	Removal of phosphate, sulfate, nitrate, and fluoride [147–151] Removal of algal toxins [152,153] Purification of landfill leachate [154–164] Removal of selenium from drainage water [165]

nanofiltration and it can be expected that many are to follow or already exist. However, most of the examples mentioned are developed on a trial-and-error basis and not from basic process knowledge. This means that these processes can run at suboptimal conditions and even membranes with better properties for the application might be available. Improvement of these processes either by finding the optimal conditions or using better membranes will result in economic gain. Additionally, current development times for new pressure-driven membrane processes are typically between 1 and 2 years, which is relatively short and at this moment often results in suboptimal solutions.

#### 42.1.7 FUTURE PROSPECTS

With respect to the aforementioned discussions, it can be noted that even though researchers have attempted to synthesize/use different types of membranes for effective separations, some restrictions for its applications are still encountered. The research direction for NF membranes is mentioned below:

- (i) *Development of high performance NF membranes:* A thorough understanding of the interrelation between membrane chemical characteristics and membrane performance is of paramount importance in membrane research. Improvement of membrane productivity by higher flux membranes has been achieved through the development of TFC with a very thin selective skin layer. In addition, Kurihara and Fusaoka [165] attribute the higher productivity

of current membranes to an increase in surface roughness. Other methods which have been used to improve membrane performance include development of mixed-matrix membrane materials including hybrid organic–inorganic materials and surface modification of membranes [166]. These improvements are not only limited to higher flux at lower operating pressures, but also in terms of less fouling propensity, higher chlorine tolerance, and increased solvent resistance [167]. For NF membranes, in particular, the role of membrane charge in separations of ions has also been studied considerably. Further understanding of the exact nature of charge formation as well as how they contribute toward rejection [168] will definitely lead toward significant improvement on NF membrane performances.

- (ii) *Reduction in fouling*: Fouling refers to the deposition of impermeable substances, present in the feed, on the membrane surface. The suitability of a membrane material for a specific separation problem is also limited by possible interaction with aggressive components in the feed. This can cause reduction in the flux and ultimately renders the membrane useless. Fouling can be prevented by
  - a. Using a highly turbulent flow regime
  - b. Cleaning the membrane semicontinuously
  - c. Using surface modification techniques to change the membrane structure that reduces the interaction between the membrane surface and microorganisms
- (iii) *Development of accurate and practical characterization methods*: The separation mechanisms in NF membranes have been attributed to steric and charge effects as well as the transport mechanisms of diffusion, convection, and electro migration [169,170]. Other factors that may also contribute indirectly include surface roughness, pore size distribution, flow channels, and hindrance mechanisms within the membrane. Identifying and relating the membrane characteristics with all of the above-mentioned effects are not easy to do and, therefore, present NF membranes are normally characterized in terms of pore radius, effective charge, thickness, and porosity. For pore radius, the most common method currently used is fitting solute rejection data of uncharged solute [171]. Several researchers have also attempted to use AFM [172] to determine the pore size distribution. Bubble point method used in UF is not suitable for NF membranes due to the nanometer-range pore sizes [173]. For effective charge, the method used is by measurement of zeta/streaming potential [168,174,175]. Other techniques include fitting of salt rejection data using models such as those based on Nernst–Planck equation [171]. To obtain more accurate characteristics of NF membrane, more innovative and practical approaches should be proposed.
- (iv) *Development of good predictive modeling technique*: A good predictive model will allow users to obtain membrane characteristics, to predict process performance, and to optimize the process. The ability to successfully develop such modeling technique will result in a smaller number of experiments and subsequently save time and money in the developing stage of a process. For NF membranes, the most commonly adapted models have been those based on extended Nernst–Planck equation [169,171]. The Donnan–steric pore model (DSPM) proposed by Bowen and coworkers [171] is one model, which describes rejection in terms of steric and Donnan effects. In addition, the transport of ions through the membrane depends on hindered diffusion and convection as well as electro migration. The model requires the membrane to be characterized in terms of pore radius, effective charge density, and effective membrane thickness over porosity.

From the above descriptions, it is obvious that an understanding of the basic mechanisms underlying the separation is necessary. With this understanding a translation to the development of industrial applications should be made, a step, which is currently not in practice. Keeping in view these research guidelines along with the attempts to enhance membrane life, the application level of NF will definitely rise beyond RO in the near future.

## 42.2 CASE STUDY

### 42.2.1 DESCRIPTION OF THE PROCESS

Acrylic fiber is a vital raw material used in textile industries to manufacture polyester and silk. Several industries worldwide manufacture acrylic fiber by a process where an aqueous solution of 55% sodium thiocyanate (dope) is used for dissolution of polyacrylonitrile (PAN) polymer for spinning the fiber. During the dope-making step, which involves dissolution of the polymer in sodium thiocyanate (NaSCN) solution with addition of a small amount of sodium metabisulfite as oxygen scavenger, the monomer reacts with sodium metabisulfite to form organic impurities such as  $\beta$ -sulpho propionic acid ( $\beta$ -SPA) and  $\beta$ -sulpho propionitrile ( $\beta$ -SPN). During coagulation of the fiber in the spinnerets, NaSCN gets released and is sent for solvent recovery at 20% concentration. This spent NaSCN solution picks up impurities such as color, sodium sulfate,  $\beta$ -SPA,  $\beta$ -SPN, iron, calcium, sodium chloride, low-molecular-weight compounds, and some other unknown impurities.

The conventional techniques applied to recover thiocyanate are solvent extraction, distillation, and gel filtration. These processes suffer disadvantages. The process that resorts to solvent extraction needs a large amount of energy for cooling. The process that utilizes distillation under pressure also needs a huge quantity of energy and gives off toxic thiocyanate gas,

although it yields a pure thiocyanate [176]. The separation of thiocyanate by gel filtration [177] varies from one process to another. One method employed [178] consists of supplying an impure aqueous solution of thiocyanate to a layer of cross-linked dextran, and eluting impurities and then the thiocyanate. Sometimes activated carbon is also employed before gel filtration [179]. The processes that involve gel filtration columns (GFC) are not only expensive (the gel being an imported product), but also slow and inefficient in handling larger feed capacities.

Therefore, the need of the hour was to develop an economical alternate separation technology capable of replacing the GFC system by providing rejection of all impurities in a single step with permeation of NaSCN and water. The membrane-based nanofiltration technique appeared to be a suitable alternative based on some of the aspects discussed in the scope of the work [180–184].

Pilot-scale NF experiments were carried out with intermittent feed dilution using spirally wound membrane modules to extract at least 98% of NaSCN free of most impurities. Among the membrane types tested, PERMA-250 gave optimum results and was chosen for detailed studies. Pilot-plant data were consolidated and fed into a simulation software developed in Microsoft Excel to provide design of a commercial NF plant capable of handling 8 m<sup>3</sup>/day of 10% NaSCN feed solution containing 2%–4% impurities.

## 42.2.2 SCOPE AND OBJECTIVES

### 42.2.2.1 Scope of the Work

The aqueous process stream from acrylic fiber industries generally contains 10% sodium thiocyanate besides 2%–4% of impurities which impart undesired yellow color and cause fiber degradation. The composition of 10% NaSCN process solution is given in Table 42.3. NaSCN needs to be isolated and then concentrated to 60% for spinning of acrylic fiber. Since the impurities present in the aqueous solution are mostly bivalent salts (Na<sub>2</sub>SO<sub>4</sub>, salts of Fe and Ca) or larger compounds ( $\beta$ -SPA,  $\beta$ -SPN, and low-molecular-weight polymer), there is considerable feasibility to extract the monovalent NaSCN using an NF membrane. If successful, NF could offer advantages such as operational flexibility, faster rate of purification (for increased plant capacity), low water consumption, nearly complete removal of color and impurities in a single step, high NaSCN concentration (>3.5%) in purified solution besides low capital and operating costs.

### 42.2.2.2 Objectives of the Pilot-Plant Study

1. Identification of the best polymeric membrane, which not only removes color but also gives maximum rejection of impurities at optimum flux
2. Production of a permeate containing at least 3.5% NaSCN at a flux ranging between 20 and 45 L/m<sup>2</sup> h to minimize membrane fouling
3. Recovery of at least 98% of NaSCN present in the feed and generating a final reject concentration of <0.25% NaSCN for disposal in accordance to environmental regulations
4. Optimization of experimental conditions such as dilution ratios, stage cut, feed pressure, etc. in achieving the above objectives
5. Designing of a commercial membrane system for feed capacity of 8 m<sup>3</sup>/day of 10% NaSCN solution

**TABLE 42.3**  
**Composition of 10% Sodium Thiocyanate Process Solution**

Impurity	Chemical Structure	Negative Impact	Present Concentration	Acceptable Level
$\beta$ -SPA	$\begin{array}{c} \text{CH}_2 - \text{CH}_2 \\   \quad   \\ \text{SO}_3\text{Na} \quad \text{COOH} \end{array}$	Deterioration of solution color	0.3%–0.5%	0.1%
$\beta$ -SPN	$\begin{array}{c} \text{CH}_2 - \text{CH}_2 \\   \quad   \\ \text{SO}_3\text{Na} \quad \text{CN} \end{array}$	Deterioration of solution color	0.8%–1.5%	0.2%
Sodium sulfate	Na <sub>2</sub> SO <sub>4</sub>	Scaling, increased steam consumption	0.4%–2.0%	0.1%
Iron	FeCl <sub>2</sub>	Deterioration of solution color	1–2 ppm	Traces
Calcium	CaCl <sub>2</sub>	Corrosion of evaporator tubes	30–40 ppm	10 ppm
Sodium chloride	NaCl	Corrosion of pipelines	0.3%–0.4%	0.1%
Other impurities	Low-molecular-weight polymer, unreacted monomer	Deterioration of solution color	0.7%–1.0%	0.2
Color	—	Degradation of fiber quality	200–300 APHA	25 APHA
Total impurities			2.0%–4.0%	0.8%

### 42.2.3 EXPERIMENTAL PROCEDURES AND PROTOCOLS

#### 42.2.3.1 Materials

The aqueous process solution containing sodium thiocyanate with impurities was provided by a local industry. All the membrane modules, pressure vessels, and accessories for the nanofiltration pilot plant used in this study were purchased from Permionics Membranes Pvt. Ltd. (Baroda, India) and assembled in the laboratory. Citric acid, tetra sodium salt of ethylene diamine tetraacetic acid (EDTA), trisodium phosphate (TSP), and sodium metabisulfite for cleaning and maintenance of the membranes were procured from Loba Chemie (Mumbai, India).

#### 42.2.3.2 Types of Membranes and Their Preparation

The spiral wound membranes tested for extraction of impurity-free NaSCN from aqueous process solution were polyamide (PA-300), CTA-700, PERMA-400, and PERMA-250. PA-300 was prepared by interfacial polymerization technique, while the PERMA membranes were prepared by coating a novel proprietary copolymer onto a microporous polysulfone substrate followed by cross-linking of the top layer. Thus, the morphology of these membranes was TFC. CTA-700 was asymmetric in nature and was prepared by solution casting and phase inversion method.

#### 42.2.3.3 Description of Pilot-Scale Nanofiltration System

A pilot-scale membrane system (Figure 42.6) was assembled in-house with incorporation of a commercial spiral membrane module of 2.5 m<sup>2</sup> effective area in a stainless steel (SS316L) pressure housing. The system was skid mounted along with a polypropylene feed tank of 100 L capacity and constituted a low-pressure prefiltration pump (2 bar) for continuous transport of the feed through a micron filter cartridge of 0.2 μm pore size, installed upstream of the spiral NF membrane module to prevent entry of suspended particles that could damage the membrane. A high-pressure pump (run by a 1.5 HP single-phase motor) capable of maintaining pressure up to 25 bar and feed flow rate of 17 L/min was installed at the exit end of the micron filter to facilitate the transport of NaSCN feed solution through the membrane module and the entire NF system. A restricting needle valve was provided at the outlet of the concentrate (reject) pipeline to pressurize the feed liquid to a desired value indicated by the pressure gauge installed upstream of the needle valve. A coil-type heat exchanger was introduced in the reject line to minimize the heat generated by the reject stream due to continuous pressurization and recirculation during the batch operation. Though the membranes can withstand temperatures up to 45°C, long-term operation would reduce membrane life, while low temperatures (<15°C) could cause salt precipitation and low flux. The heat exchanger thus enables determination of percentage recovery by continuous removal of water until the flux remains within acceptable limits. Permeate and reject flow rates were measured by means of two glass rotameters containing metal floats. All other connections were made with ½" outer diameter stainless steel 316 piping in the high-pressure region, while the low-pressure lines comprised PVC braided tubing for permeate flow and reject recycle.

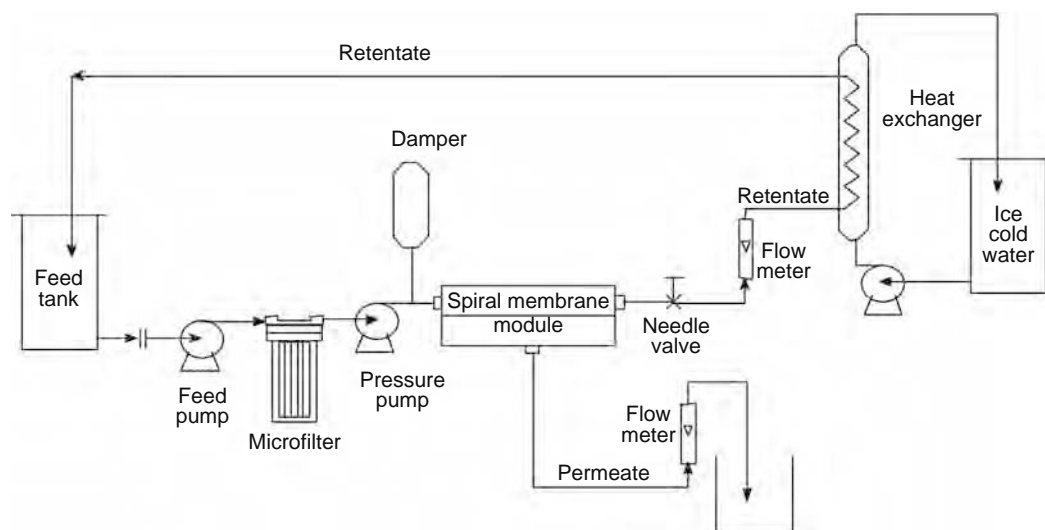


FIGURE 42.6 Schematic view of pilot-scale nanofiltration system.

#### 42.2.3.4 Nanofiltration Procedure

The plant was operated in batch mode with complete recycle of reject at a constant feed rate of 17 L/min. The description here focuses mainly on multistage batch operation with intermittent dilution of the feed (diafiltration) [185]. Initially 50–100 L of the original 10% NaSCN feed mixture containing 2%–4% total impurities was charged into the feed tank and initially pumped with complete recycle of reject and permeate for 5–10 min to ensure homogeneous concentration after which a sample was drawn to note the feed conductivity and temperature. The needle valve in the reject line is throttled to obtain a suitable pressure value in the range of 10–25 bar depending on the type of membrane module used and its MWCO. The initial permeate was recycled until a steady permeate flux was obtained. On the other hand, the reject was continuously circulated back to the feed tank through the heat exchanger. Permeate collection was then begun and conductivities of the feed and permeate were noted for every 5 L of permeate collected. The process was continued until a stage cut of 50%–60% was achieved. The system was stopped and 1 L sample each of the permeate and reject was collected for analysis of NaSCN, color, and other impurities. From the second stage onwards, the reject of the previous stage was diluted with known quantity of demineralized (DM) water and the procedure was repeated.

To obtain better fluxes, lower membrane fouling, and thereby longer membrane life another set of experiments were conducted where the original feed in the first stage (containing 10% NaSCN) was diluted with DM water and the stagewise process was repeated. Permeates for Stages I–III were mixed and the average concentration was noted. Material balance was carried out after thorough analysis to assess percentage recovery of NaSCN.

#### 42.2.3.5 Analytical

The collected feed, permeate, and reject samples were analyzed for sodium thiocyanate, sodium sulfate,  $\beta$ -SPA,  $\beta$ -SPN, Fe, and Ca concentrations and also the total impurity by procedures described in literature [186]. The chemical methods being too lengthy for instantaneous analysis during the course of the experiment, the approximate concentration of sodium thiocyanate especially in the permeate was determined by plotting a graph (Figure 42.7) between known concentrations of NaSCN in DM water and the respective conductivities. The conductivities of the various unknown samples were used to find the corresponding thiocyanate concentrations from the graph.

#### 42.2.3.6 Membrane Cleaning and Maintenance

*General cleaning:* At the end of the operation the membrane was initially washed everyday for 10 min with tap water to displace most of the sodium thiocyanate and impurities present in the pressure housing as well as feed, permeate, and reject lines. The system was operated at a pressure of about 10 bar with total disposal of permeate and reject for 5 min to flush out the dissolved solids present in the pipelines. For the remaining period the exiting streams were recycled back to the feed tank with repeated pressurizing and depressurizing to ensure efficient cleaning.

*Acid/Alkali wash:* To remove mineral scales and metal salt precipitates from the membrane surface, washing with a 1.0% solution of citric acid (or hydrochloric acid) prepared in 25 L of DM water was carried out at a pressure of 10 bar for a 10 min

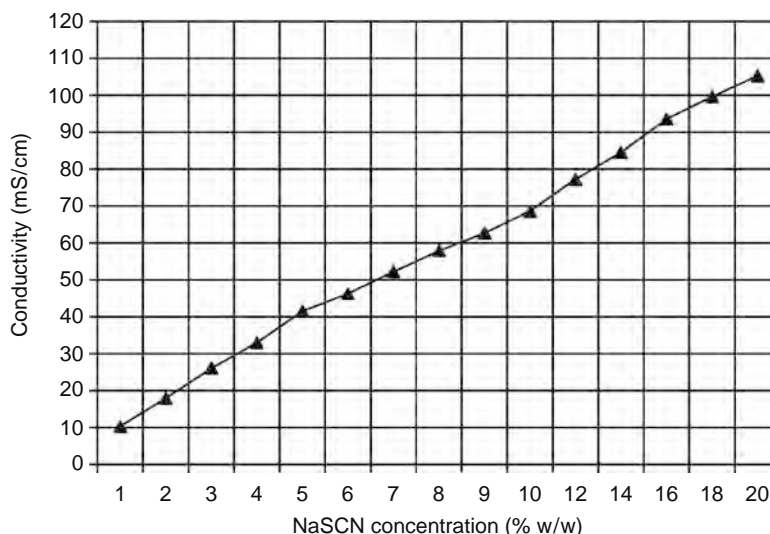


FIGURE 42.7 Concentration versus conductivity plot for sodium thiocyanate.

period everyday with complete recycle of permeate and reject streams after the tap water wash. This was followed by daily washing with a 1.0% solution of TSP for another 10 min at the same operating pressure.

1. *EDTA wash*: To remove organic foulants, a biweekly washing at 20 bar for 15 min with 1.0% aqueous solution of tetra sodium salt of EDTA is recommended. EDTA is a strong chelating agent, which has proven to be capable of flushing out very stubborn organic impurities.
2. *Membrane storage*: Finally at the end of washing, the membrane was stored in 0.5% solution of sodium metabisulfite (SMBS) preservative prepared in DM water. This helps to prevent biological fouling and irreversible destruction of the membrane.

It is worth mentioning that membranes affected by severe chemical fouling can be cleaned using aforementioned reagents but biological fouling causes permanent damage, which on most occasions requires membrane replacement [187]. The membrane is always stored in a horizontal position to prevent it from becoming dry. The above procedures were quite efficient in restoring flux and separation properties of the NF membranes to help them last their stipulated life span.

#### 42.2.4 RESULTS AND DISCUSSION

Table 42.4 exhibits the comparative performance of the four modules (PA-300, CTA-700, PERMA-400, and PERMA-250) in terms of average flux, rejection, NaSCN concentration, and enrichment factor. Operating conditions such as feed pressure, stage cut, and degree of dilution were varied to suit the MWCO of each membrane. From Table 42.4, it can be seen that although the highest pressure followed by initial dilution has been employed for PA-300, the overall flux is still poor, which meant that the commercial viability was quite poor. However, PA-300 gave the highest color and impurity rejections as well as maximum enrichment of NaSCN in permeate. The pore size distribution of CTA-700 was a bit too open for this particular process stream, which consisted of components having molecular weights in the range 50–200, which meant that impurity rejection would be poor in spite of high flux. To strike a balance, the PERMA NF membranes were then tested.

PERMA-400 yielded reasonable results in terms of separation at high flux, even without initial feed dilution. At 18 bar pressure and dilutions of 1:0.5 and 1:0.75 in the second and third stages, PERMA-400 gave high average flux of 43 L/m<sup>2</sup> h, an impurity rejection of 57.5%, and a color rejection of 64.3%, which meant that Fe compounds were rejected to a greater extent. However, the acrylic fiber spun from a concentrated permeate of PERMA-400 still possessed a light yellow tinge, which meant that further improvement in impurity rejection was to be achieved to make NF truly competitive to the conventional purification processes.

PERMA-250 was found to be ideal for this purpose as it gave excellent impurity and color rejections of almost 80% and 90%, respectively, along with a moderate average flux of 27.3 L/m<sup>2</sup> h at 21 bar, even without initial dilution. To further enhance its performance, dilution was introduced in the first stage itself, so that an improvement of the thiocyanate enrichment factor to 1.28 could be obtained. It is thus vivid that PERMA membranes comprised numerous polar moieties in the polymer matrix, which not only improves the water sorption but also its interaction with NaSCN rendering its enhanced transport. The bivalent salts Fe, Ca, and Na and organic impurities such as  $\beta$ -SPA and  $\beta$ -SPN could not penetrate the barrier to a larger extent. On the basis of optimum performance, PERMA-250 was considered as the right candidate for further studies. A five-stage process was employed to achieve the remaining objectives. Table 42.5 summarizes the five-stage process results for HPA-250 membrane. In Stage I, a batch time of 2.3 h was sufficient to obtain 60 L of permeate from a feed of 100 L. The initial flux was 45 L/m<sup>2</sup> h and at a stage cut of 60% the final flux was 7.6 L/m<sup>2</sup> h. High degree of

**TABLE 42.4**  
**Comparative Performance of Four Membranes Studied for Sodium Thiocyanate Extraction in Three Stages**

Membrane Type	Feed Pressure (bar)	Degree of Dilution			Stage Cut (%) I-III			Average Flux (L/m <sup>2</sup> h)	Impurity Rejection (%)	Color Rejection (%)	Average % NaSCN in Permeate	NaSCN Enrichment Factor
PA-300	24	1:0.5	1:1	1:1	60	50	50	5.8	91.3	97.0	4.35	1.38
CTA-700	15	1:0	1:0.5	1:0.75	60	50	60	25.7	42.1	47.6	6.9	1.25
PERMA-400	18	1:0	1:0.5	1:0.75	50	50	60	43.0	57.5	64.3	7.0	1.15
PERMA-250	20	1:0	1:0.5	1:0.75	60	50	60	26.3	78.8	89.4	7.1	1.1
PERMA-250	21	1:0.5	1:0.75	1:0.75	60	60	60	38.6	85.1	98.3	3.6	1.28

Note: Stage cut: 50%–60%.

**TABLE 42.5**  
**Summarized Results for Five-Stage Process without Initial Feed Dilution**

Stage	Dilution Ratio	Volume Recovery (%)	Feed Total Impurity (%)	Permeate Total Impurity (%)	Impurity Rejection (%)	Flux (L/m <sup>2</sup> h)
I	1:0	60	2.43	0.60	75.3	26.3
II	1:0.5	50	3.45	0.65	81.0	27.0
III	1:0.75	60	3.60	0.71	80.2	28.5
IV	1:3	70	2.01	0.17	91.5	30.5
V	1:5	80	1.03	0.05	95.0	54.3

Note: Membrane: PERMA-250, feed pressure 21 bar.

dilutions of 1:3 and 1:5 were applied in the last two stages to counter the effect of increasing impurity build up in the reject. To prevent substantial damage to the membrane, occurring due to fouling, the current five-stage process was made more commercially feasible by employing an initial dilution ratio of 1:0.5 in the first stage. From Table 42.5, it can be seen that the average concentration of NaSCN of 7.1% is achievable in three stages without dilution in Stage I. This reduces the evaporation cost, but leads to increased fouling on the membrane surface due to high TDS concentration in Stage I. Sufficient care was to be taken to avoid excessive dilution of the feeds to prevent a drop in the average concentration of NaSCN below the desirable value of 3.5% to match the conventional technology. Table 42.6 exhibits the performance of PERMA-250 over a five-stage process with initial dilution. Based on the results, a scheme was planned where the permeates of Stages I–III were collected and sent for concentration and spinning, while the permeates from Stage IV to V would be recycled back to the system to obtain 98% NaSCN recovery along with >3.5% NaSCN product concentration and <0.25% NaSCN in final reject (fifth stage) for disposal. It is, therefore, clear from the studies that higher degrees of dilutions produced greater flux as well as higher NaSCN enrichment factors. Figure 42.8 depicts the influence of feed impurity concentration on flux and rejection through PERMA-250 membrane at a constant pressure of 21 bar. Different concentrations of the feed were prepared by dilution with DM water as well as evaporation. As the impurity concentration increased from 0.6% to 3.64%, the flux reduced from 76.7 to 8.4 L/m<sup>2</sup> h for a single stage operation with 60% recovery. The corresponding impurity rejection lowered from 94.2% to 65.7%. Increasing feed concentration results in a rise in the osmotic pressure, which effectively reduces the transmembrane pressure gradient leading to reduced rate of mass transfer. It may be noted that though NaSCN is a permeable component, its presence definitely adds to the osmotic pressure value. The corresponding NaSCN concentration in the feed increased from 2.5% to 15.3%.

The influence of feed pressure on performance of PERMA-250 membrane is depicted in Figure 42.9. Increasing pressure caused enhancement of flux as well as NaSCN enrichment, due to exertion of increasing driving force on the movement of H<sub>2</sub>O and NaSCN molecules, which are preferentially sorbed by the hydrophilic membrane. The permeation rate of the noninteracting impurities remains relatively constant. Figure 42.9 shows that the flux increased from 8.7 to 34.2 L/m<sup>2</sup> h, while the impurity rejection improved from 72.1% to 77.4%. The NaSCN enrichment (not depicted in the figure) increased from 1.23 to 1.30. The effect of feed flow rate was also studied through PERMA-250 and better separation was observed at a feed rate of 17 L/min compared to 2 L/min since greater cross-flow minimizes concentration polarization of solutes near the membrane surface.

**TABLE 42.6**  
**Summarized Results for Five-Stage Process with Initial Dilution**

Stage	Dilution Ratio	Volume Recovery (%)	Feed Total Impurity (%)	Permeate Total Impurity (%)	Impurity Rejection (%)	Flux (L/m <sup>2</sup> h)
I	1:0.5	60	1.62	0.28	82.9	45
II	1:0.75	60	2.10	0.31	85.3	38
III	1:0.75	60	2.73	0.35	87.0	33
IV	1:3	70	1.57	0.18	88.3	52
V	1:5	80	0.80	0.052	93.4	82

Note: Membrane: PERMA-250, feed pressure 21 bar.

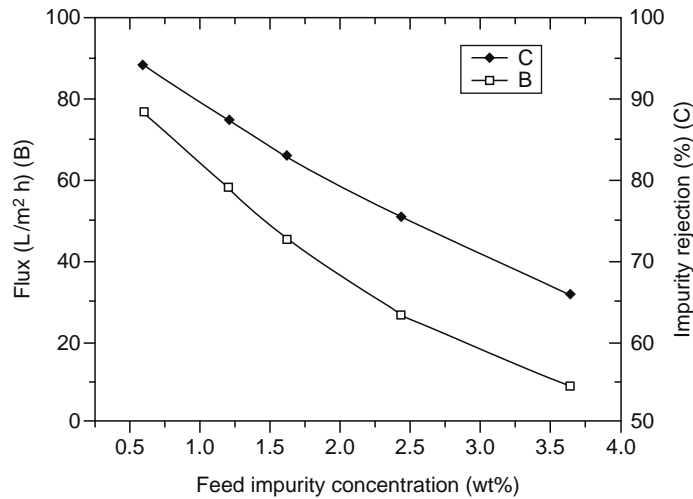


FIGURE 42.8 Effect of impurity concentration on flux and rejection.

#### 42.2.5 PROCESS DESCRIPTION FOR OPERATION OF COMMERCIAL NANOFILTRATION PLANT

Figure 42.10 represents the process flow sheet consisting of membrane module equipment sufficient for one stage. The figure shows the 12 modules arranged in three pressure housings each containing four spiral modules. Two pressure housings are arranged in parallel and the third in series such that the feed is split into two streams while entering the parallel pressure housings and the rejects from these two parallel housings are again combined to form a single stream, which enters as the feed to the third housing. Such an arrangement is self-controlling and leads to constant input and output flow rates making the entire membrane assembly appear as one single membrane module.

The process operation involves five stages in a cycle that is to be completed in a total duration of 12 h; which includes 10 h for the five-stage operation, 1.5 h for reject recycle to feed tank, and 0.5 h for membrane cleaning and storage. The detailed explanation of the process in accordance is given below.

##### 42.2.5.1 Cycle 1

It is assumed that 8 m<sup>3</sup> of 10% sodium thiocyanate feed solution is available in the feed tank and DM water is available at a tapping source at a pressure of 1.5–2 bar. The feed is continuously drawn with the help of a centrifugal pump (feed transfer pump or prefiltration pump) at the rate of 4 m<sup>3</sup>/h, while the DM water for diluting the feed is drawn at a rate of 2 m<sup>3</sup>/h. Both the streams are forced through the static mixer to form a homogeneous solution, which then enters the prefilter assembly consisting

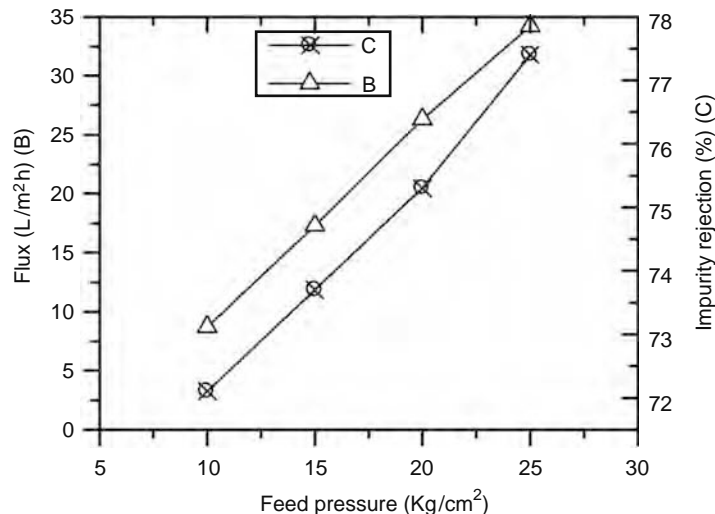


FIGURE 42.9 Influence of feed pressure on flux and rejection.

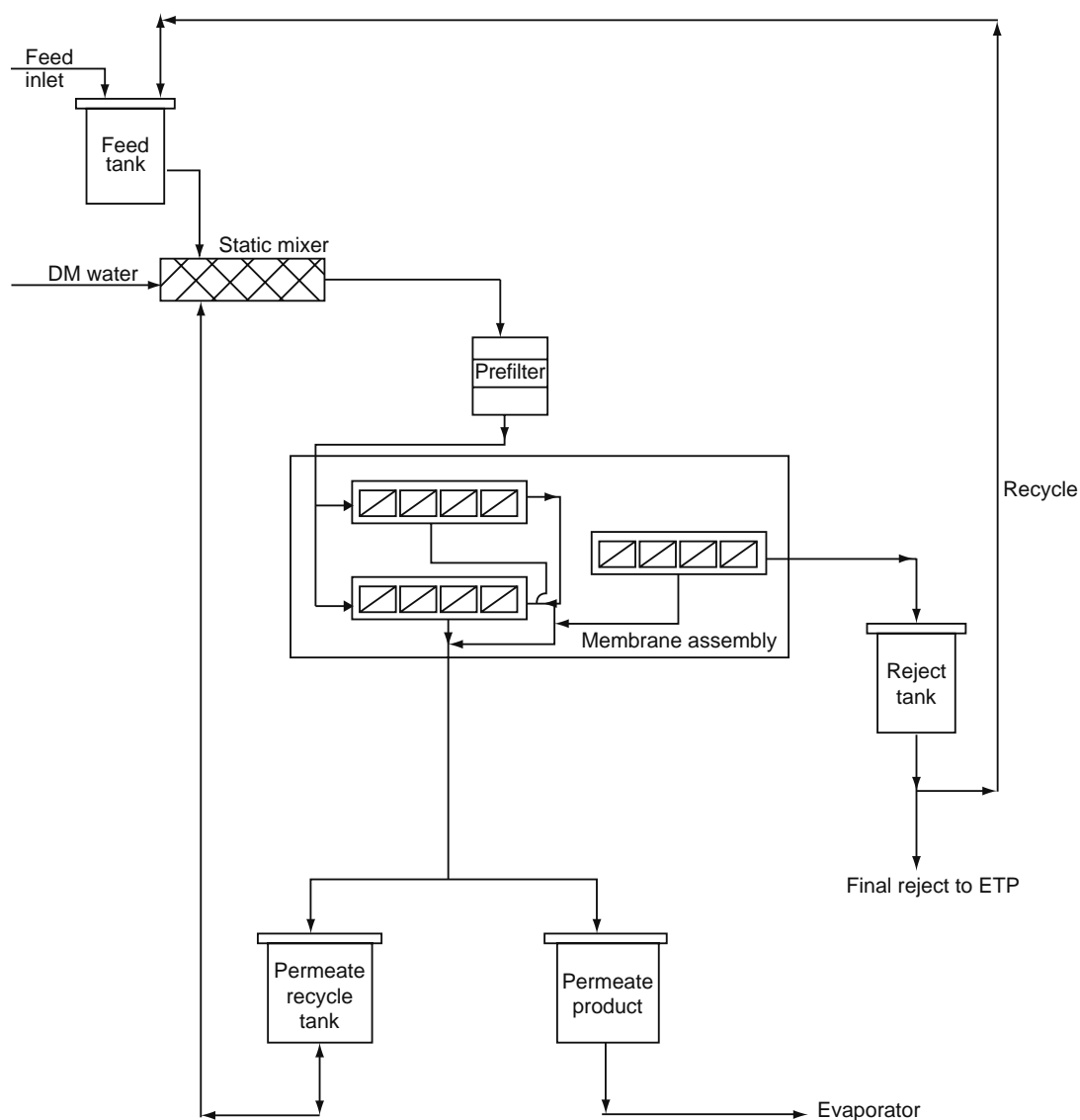


FIGURE 42.10 Process flow diagram for commercial nanofiltration plant of 8 m<sup>3</sup>/day capacity.

of iron filter, bag filter, and micron filter placed in series. The feed is then drawn by the high-pressure pump, and fed into the membrane assembly at 6 m<sup>3</sup>/h. The feed is recirculated for 10 min before the control valve placed on the reject line is throttled to obtain the desired operating pressure (15–25 bar), which signals the beginning of Stage I. The reject is now collected at 2.4 m<sup>3</sup>/h in the reject tank, while the product is collected at the rate of 3.6 m<sup>3</sup>/h in the permeate product tank. Stage I gets terminated in 2 h of operation during which a total feed quantity of 12 m<sup>3</sup> constituting 8 m<sup>3</sup> of original 10% feed is emptied from feed tank and 4 m<sup>3</sup> of DM water is consumed for dilution. A permeate quantity of 7.2 m<sup>3</sup> gets accumulated in product tank and a reject of 4.8 m<sup>3</sup> is separately collected.

Stage II is instantaneously started with 4.8 m<sup>3</sup> of feed (reject of Stage I) being drawn by a centrifugal pump at a decreased rate of 2.4 m<sup>3</sup>/h and DM water drawn at an increased rate of 3.6 m<sup>3</sup>/h. The fluid flow pattern is similar as in Stage I except for the fact that feed and DM water flow rates entering the static mixer are now different. However, the diluted feed flowing into the membrane assembly is once again maintained at 6 m<sup>3</sup>/h. The permeates and rejects are once again collected at rates and quantities similar to Stage I.

Stages III–V follow exactly the same pattern as Stage II. Permeates from Stage I to III constitute a total quantity of 21.6 m<sup>3</sup>, which is the product containing >3.5% sodium thiocyanate. This product is sent to the evaporator for concentration and spinning. However, the permeates for Stages IV and V are collected in the permeate recycle tank for use as diluting liquid from cycle 2 onwards. The reject after Stage V is sent for disposal. It may be noted that the dilution ratio for Stage I is 1:0.5, while it is 1:1.5 for all the subsequent stages. This holds good for all the cycles of operation.

### 42.2.5.2 Cycle 2

The process for cycle 2 is similar to that of cycle 1 except for the fact that initially the 14.4 m<sup>3</sup> of recycle permeate available in the permeate recycle tank is used for feed dilution during a couple of stages. The recycle permeates are used for diluting feeds in Stages II and III, while DM water is tapped for the other stages.

### 42.2.5.3 Membrane Cleaning and Storage

A tank of polypropylene make of 200 L capacity is generally provided along with the membrane system for cleaning in place (CIP). Tap water is collected in the CIP tank and the NaSCN feed present as dead volume in the system is displaced using high-pressure pump. A 200 L of DM water is then filled in the CIP tank to which 2 kg of one of the cleaning agents is added and dissolved. The membrane is thus washed in two or three separate steps using citric acid and TSP on a daily basis and EDTA on a weekly basis for a duration of 10 min each. The membrane is finally stored in 1% sodium metabisulfite (SMBS) aqueous solution prepared in DM water. At the beginning of a fresh cycle of operation the dead volume of 1% w/v SMBS solution present in the membrane and pipeline is removed by displacement with NaSCN feed solution.

### 42.2.6 SIMULATION AND DESIGN

A simulation program was prepared using excel functions based on the results obtained with PERMA-250 membrane in a five-stage process scheme with initial and intermittent dilution. The purpose of simulation [188] was to determine the material balance, membrane area requirement, and compositions of the exiting permeate and reject streams in response to different feed inputs comprising NaSCN concentration, impurity concentration, enrichment factors, quantity of demineralized water required for dilution and permeate percentage recovery in each stage (stage cut). For this study, Table 42.7 describes the base case operating conditions and membrane specifications considered for designing a commercial NF system capable of processing 8 m<sup>3</sup>/day of 10% sodium thiocyanate feed containing 2%–4% of impurities including color, which must be processed to an output product solution containing at least 3.5% NaSCN besides negligible color and other impurities (<0.8%).

**TABLE 42.7**  
**Base Case Operating Conditions for Process Design and Membrane Specifications for Commercial Nanofiltration Plant**

Operating Condition/Parameter	Specification
Feed capacity	8 m <sup>3</sup> /day
Feed concentration	10% NaSCN + 3% total impurity
Feed pressure	21 bar
Feed temperature	Ambient
Number of stages	5
Initial feed dilution ratio	1:0.5
Subsequent dilution ratios	1:1.5
Total feed quantity per stage	12,000 L
Stage cut	60% (7,200 L)
Duration of operation per stage	2 h
Total time of operation/day	12 h
Minimum NaSCN recovery	98%
Minimum NaSCN concentration in product	3.5%
NaSCN concentration in final reject	<0.25%
Recommended range of flux	20–45 L/m <sup>2</sup> h
Membrane type	PERMA-250
Modular configuration	Spiral wound
Total membrane area requirement	90 m <sup>2</sup>
Dimension of each module	4" dia × 40" length
Effective area in each module	7.5 m <sup>2</sup>
Total number of spiral modules	12
Number of FRP housings	3

TABLE 42.8

Optimized Five-Stage Process Scheme for Feed Capacity of 8 m<sup>3</sup>/day (Second Cycle of Operation Onwards [Steady State])

Stage	Feed Solution (Liters) and Source	Demineralized Water Added (L)	Total Feed Volume	Permeate Volume (L) and Recovery	Reject Volume (L)	Flux (L/m <sup>2</sup> h)
I	8,000 Fresh feed	4,000 Fresh DM water	12,000	7,200 60%	4,800	40
II	4,800 Reject of Stage I	7,200 Permeate of Stage IV, cycle 1	12,000	7,200 60%	4,800	40
III	4,800 Reject of Stage II	7,200 Permeate of Stage V, cycle 1	12,000	7,200 60%	4,800	40
IV	4,800 Reject of Stage III	7,200 Fresh DM water	12,000	7,200 60%	4,800	40
V	4,800 Reject of Stage IV	7,200 Fresh DM water	12,000	7,200 60%	4,800	40

The design (for the first cycle of operation) was made as simple as possible to enable easy understanding and effortless operation as shown in Table 42.8. The total membrane area required for processing a feed of 12 m<sup>3</sup> in 2 h was also stipulated from the simulation program. It is a well-known fact that the area required is a function of the flux [14]. Figure 42.11 shows the variation of area with the average flux for a five-stage process. Flux between 20 and 45 L/m<sup>2</sup> h is within the acceptable range, while a rate below 20 L/m<sup>2</sup> h would be uneconomical and a value higher than 45 L/m<sup>2</sup> h is preferentially avoided to minimize membrane fouling. The membrane area required for every two hourly stage, in the present case, was found to vary from 180 to 80 m<sup>2</sup> as the flux increased from 20 to 45 L/m<sup>2</sup> h. Thus, the area required to obtain a permeate of 7.2 kg in 2 h at a flux of 40 L/m<sup>2</sup> h is 90 m<sup>2</sup>. Five stages would require a total operation time of 10 h. It may be noted that the same membrane area of about 90 m<sup>2</sup> can be utilized to operate each stage individually. As per the standard modular configurations (Table 42.7) available with the supplier (Permionics Membranes Pvt. Ltd., Baroda, India), the spiral membrane module of 4" diameter × 40" length was chosen, which gives an effective area of 7.5 m<sup>2</sup> each. Hence 12 such modules would provide an area of 90 m<sup>2</sup>.

## 42.2.6.1 Material Balance

The material balance for the first cycle of operation in the present study is shown in Figure 42.12. The present material balance shows a total input of 12 m<sup>3</sup> of 10% NaSCN feed containing 3% impurities. A total amount of 18.4 m<sup>3</sup> of DM water is added for dilution of feeds during the five stages from cycle 2 onwards. The output product is 21.6 kg of 3.6% NaSCN, which is free of color and contains only 0.06% of impurities since a dilution of 1:1.5 is employed from Stage II onwards. The other output is a final reject quantity of 4.8 m<sup>3</sup> containing <0.1% NaSCN and 4.7% impurities for disposal. The total NaSCN recovery is 99.4% and impurity rejection 94.2%.

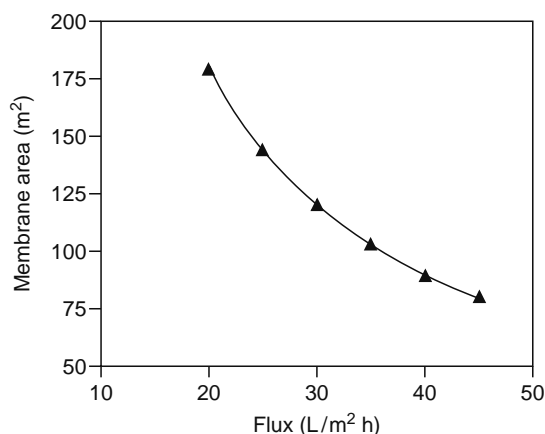


FIGURE 42.11 Variation of membrane area requirement per stage with average flux.

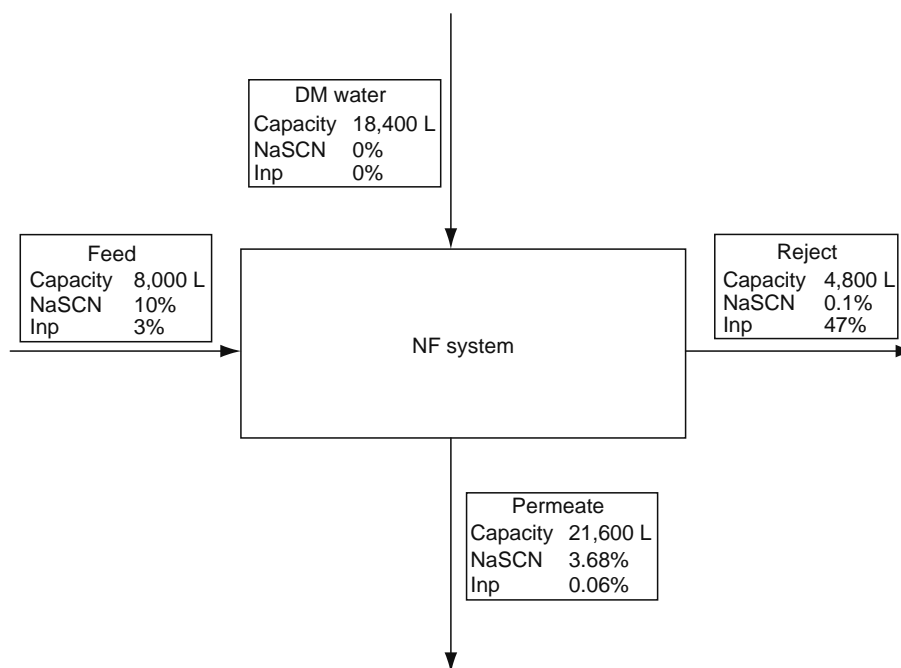


FIGURE 42.12 Overall material balance diagram for commercial nanofiltration system.

## 42.2.7 ECONOMIC ESTIMATION

### 42.2.7.1 Capital Investment

The two most important as well as expensive equipments in an NF system are the membrane assembly and the high-pressure system pump [189]. Most of the equipment shown in Figure 42.10 are listed in Table 42.9. These include membrane assembly, static mixer, prefilter assembly, besides fiber-reinforced plastic (FRP) tanks for storage of feed, permeate, and reject. The accessories that are not shown in Figure 42.10, but which form an integral part of the NF system are the low- and high-pressure pumps besides piping and instrumentation. The cost of each equipment was estimated in Indian rupees, but presented in U.S. dollars assuming an exchange rate of Rs 50 per U.S. dollar.

NaSCN solution being highly corrosive, the material for tanks and membrane housings was FRP, while piping and other contacting parts were made from stainless steel 316 L. The FRP feed tank (1 no.), permeate tanks (2 nos), and reject tank (1 no.) of 15 m<sup>3</sup>, 25 m<sup>3</sup>, and 15 m<sup>3</sup>, 5 m<sup>3</sup> capacities respectively, were purchased at the rate of \$216 per cubicmeter. The total capital investment for the NF system came to \$38,000 excluding expenditure for site preparation. The space required for installation of the NF system was 10 × 8 m.

TABLE 42.9

List of Equipment and Capital Cost for Commercial Nanofiltration Plant

Description	Capacity/Size	Quantity	Material of Construction	Unit Price (\$)
Prefilter assembly	75 L/min	01	MS epoxy	1,600
PERMA-250 membranes, pressure vessels, piping and skid	4" × 40"	01 set	—	9,700
Static mixer	2 m long	01	SS316L	800
System pump (high pressure)	50 L/min	01	SS316L	6,000
Feed transfer pump	75 L/min	01	PP	700
Permeate recycle pump	100 L/min	01	PP	1,000
Reject recycle pump	200 L/min	01	PP	1,200
Storage tanks for feed, permeate, and reject	5–25 m <sup>3</sup>	05	FRP	13,000
Piping, instrumentation	—	01 set	SS316L	4,000
Total				38,000

### 42.2.7.2 Operating Cost

Power cost for running a high-pressure pump of reasonable capacity and periodic membrane replacement account for a major proportion of the operating costs in NF [190]. Other contributors to the operating cost include consumables such as dosing chemicals for pretreatment of feed before NF, cleaning chemicals and utilities such as DM water, etc. The basis for calculation was a membrane life span of 2 years taking into consideration a 11 h/day period of operation. The number of working days per annum was assumed to be 325. From calculations, the power consumed by the high-pressure pump was 3,1736.25 kWh per year amounting to \$2540 per annum. The feed transfer pump, permeate, and reject recycle pump were expected to incur annual power consumptions of 6303.7, 1212.25, and 775.8 kWh, respectively. Hence the total power consumed was 40,028 kWh, which costs \$10 per day and \$3200 per year.

#### 42.2.7.2.1 Membrane Replacement

The cost of 12 modules (1 module of 7.5 m<sup>2</sup> effective area costing \$600) was \$7200. The membrane life is expected to be 2 years for 11 h duration of operation per day.

#### 42.2.7.2.2 Dosing Chemicals for Feed Pretreatment

The dosing chemicals such as antiscalant, SMBS (to consume free chlorine), and HCl used cost \$3 on a daily basis.

#### 42.2.7.2.3 Cleaning Chemicals

Cleaning agents, such as citric acid, EDTA, and TSP, and preservatives such as sodium metabisulfite costed \$2 per week.

#### 42.2.7.2.4 Utilities

Demineralized water for feed dilution and membrane storage, besides raw water for cleaning purpose, constitutes the main utilities. Raw water costs \$0.18 per cubicmeter while DM water is three times costlier. The quantity of raw water required is 0.5 m<sup>3</sup>/day and that of DM water is 19 m<sup>3</sup>/day. Other consumables, such as pump oil and spares, were negligible compared to the above costs and are not included. Existing Labor for conventional purification equipment was expected to operate NF plant. The total operating cost was determined to be \$11,700 per annum. Table 42.10 gives the total operating cost for the commercial NF plant.

## 42.2.8 CONCLUSIONS

Nanofiltration appears to be a promising process to recover impurity-free sodium thiocyanate from aqueous industrial process solution due to removal of color and most impurities in a single step at a reasonably high rate. Among the membranes tested, PERMA-250 was found to exhibit the optimum performance in terms of flux and impurity rejection with the permeate generated being practically colorless. PERMA-250 also showed sufficient affinity for sodium thiocyanate, which enabled the permeate to be enriched in NaSCN and the feed to be completely stripped off the same compound. Under the same operating conditions PERMA membranes gave 5–6 times higher flux compared to ordinary polyamide membrane of similar MWCO owing to greater sorption of water. A five-stage process design involving initial and intermittent dilution of the feed with recycle of the fourth and fifth stage permeates was ideal in achieving objectives including >98% NaSCN recovery in the permeate and <0.25% NaSCN in the final reject for disposal. Simulation using Excel functions enabled determination of output characteristics such as overall material balance, permeate and reject compositions, percentage recovery, expected fluxes, and most significantly the membrane area requirements for input characteristics such as feed capacity, stage dilution ratio, NaSCN

**TABLE 42.10**  
**Operating Cost Estimate for Commercial NF Plant**

Type of Cost	Details	Cost/Day (\$)	Cost/Year (\$)
Power	2 Pumps-1 Hp 1 Pump-2 Hp 1 Pump-12.5 Hp	10	3,200
Dosing chemicals	Anti-scalant, SMBS HCl	3	1,150
Cleaning chemicals	EDTA, citric acid TSP	2	400
Membrane replacement	PERMA-250 spiral modules (9 nos)	10	3,600
Utilities	DM water Raw water	10	3,350
Total		35	11,700

enrichment factor, and feed pressure. The commercial plant incurred a capital investment of \$38,514, while the operating cost was \$11700 per annum. The life of the PERMA-250 membrane was expected to be 2 years for a 12 h period of operation per day. Maintenance of the NF membrane through daily washing with citric acid and TSP followed by storage in aqueous solution of sodium metabisulfite was necessary to extract maximum life.

## ACKNOWLEDGMENTS

The authors acknowledge the encouragement given by Dr. J.S. Yadav, director and Dr. K.V. Raghavan, former director of Indian Institute of Chemical Technology (IICT), Hyderabad, India during the course of this project. The constant support of Dr. A.A. Khan, Dr. M. Ramakrishna, Dr. D.H.L. Prasad, and Dr. K. Babu Rao, scientists of the Chemical Engineering Division of IICT, Mr. Satyajai Mayor, managing director of Permionics Membranes Pvt. Ltd., Vadodara, India, is gratefully acknowledged. Mr. K.B.S. Saibabu of Chemical Engineering Design group and Mr. Murthy of Mechanical Engineering Division are thanked for their help during process design. The authors would like to thank Elsevier publications for granting permission to use a figure and few lines from one of their publications. The authors would like to extend their thanks to Dr. Chakravorty, Genesis Membranes Pvt. Ltd. for having enabled us to reproduce the figure pertaining to the module configurations. Finally, the efforts of Mr. G. Suryanarayana Murthy and Ms. D. Suhanya, Research Assistants at Membrane Separations Group, IICT are acknowledged.

## REFERENCES

1. Porter, M.C., *Handbook of Industrial Membrane Technology*, Noyes Publications, NJ, 1990, p. 61.
2. Porter, M.C., *Handbook of Industrial Membrane Technology*, Noyes Publications, Park Ridge, NJ, 1990, p. 156.
3. Kessler, S.B. and Klien, E., Dialysis. *Membrane Handbook*, Part III, Ho, W.S. and Sirkar, K.K., Eds., Van Nostrand Reinhold, Park Ridge, NJ, 1992, p. 11.
4. Mulder, M., *Basic Principles of Membrane Technology*, Kluwer Academic, Dordrecht, The Netherlands, 1996, p. 23.
5. Schafer, A.I., Fane, A.G., and Waite, T.D., *Nanofiltration Principles and Applications*, Elsevier Advanced Technology, Oxford, United Kingdom, 2005.
6. Bessarabov, D. and Twardowski, Z., Industrial application of nanofiltration—New perspectives, *Membr. Technol.*, 9, 6, 2002.
7. Ho, W.S.W. and Sirkar, K.K., *Membrane Handbook*, Kluwer Academic, Dordrecht, The Netherlands, 1991.
8. Richard, W.B., *Membrane Technology and Applications*, 2nd edition, John Wiley & Sons, West Sussex, England, 2004.
9. van Rijn, C.J.M., *Nano and Micro Engineered Membrane Technology*, Elsevier, The Netherlands, 2005.
10. Baker, R.W. et al., *Membrane Separation Systems: Recent Developments and Future Directions*, Noyes Publishing, Park Ridge, NJ, 1990.
11. Hillis, P., *Membrane Technology in Water and Waste Water Treatment*, Royal Society of Chemistry, London, 2000.
12. Hilal, N. et al., A comprehensive review of nanofiltration membranes: Treatment, pretreatment, modelling, and atomic force microscopy, *Desalination*, 170, 281, 2004.
13. Noble, R.D. and Stern, S.A., *Membrane Separations and Technology—Principles and Applications*, Elsevier, Amsterdam, The Netherlands, 1995.
14. Yaroshchuk, A.E., Rejection mechanisms of NF membranes, *Membr. Technol.*, 100, 9, 1998.
15. Peeters, J.M.M. et al., Retention measurements of nanofiltration membranes with electrolyte solutions, *J. Membr. Sci.*, 145(2), 199, 2004.
16. Koros, W.J., Ma, Y.H., and Shimadzu, T., Terminology for membranes and membrane processes, *Pure Appl. Chem.*, 68, 1479, 1996.
17. Eykamp, W., Ultrafiltration. In: *Membrane Separation Systems: A Research Needs Assessment*, US Department of Energy, Office of Energy Research. Report DOE/ER/30133-H1 April 1990; 7-13-7-17.
18. Robinson, R.A. and Stokes, R.H., *Electrolyte Solutions*, Academic Press, New York, 1955.
19. Mariñas, B.J. and Urama, R.I., Modeling concentration-polarization in reverse osmosis spiral wound elements, *J. Environ. Eng.*, 122(4), 292, 1996.
20. Jacangelo, J.G., Basic concepts for the use of membrane technology in drinking water treatment, *Proceedings of the American Water Works Association Workshop on GAC, Membranes and the ICR*, Cincinnati, OH, 1996.
21. Hong, S. and Elimelech, M., Chemical and physical aspects of natural organic matter (NOM) fouling of nanofiltration membranes, *J. Membr. Sci.*, 132, 159, 1997.
22. Jucker, C. and Clark, M.M., Adsorption of aquatic humic substances on hydrophobic ultrafiltration membranes, *J. Membr. Sci.*, 97, 37, 1994.
23. Ridgway, H.F., Microbial adhesion and biofouling of reverse osmosis membranes. In: *Reverse Osmosis Technology, Applications for High Purity Water Production*, Pakekh, B.S. and Dekker, M., Eds., Marcel Dekker, New York, 1988, p. 429.
24. Strathmann, H., Production of microporous media by phase inversion processes. In: *Material Science of Synthetic Membranes*, Lloyd, D.R., Ed., American Chemical Society, ACS Symposium Series 269, Washington, DC, 1985, p. 165.
25. Kesting, R.E., Phase inversion membranes. In: *Material Science of Synthetic Membranes*, Lloyd, D.R., Ed., American Chemical Society, ACS Symposium Series 269, Washington, 1985, p. 131.
26. Petersen, R.J., Composite reverse osmosis and nanofiltration membranes, *J. Membr. Sci.*, 83, 81, 1993.
27. Nunes, S.P. and Peinemann, K.V., *Membrane Technology in the Chemical Industry*, Wiley-VCH, Weinheim, NY, 2001.

28. Conlon, W., Pilot field test data for prototype ultra low pressure reverse osmosis elements, *Desalination*, 56, 203, 1985.
29. Eriksson, P., Nanofiltration extends the range of membrane filtration, *Environ. Prog.*, 7, 58, 1988.
30. Cadotte, J. et al., Nanofiltration membranes broaden the use of membrane separation technology, *Desalination*, 70, 77, 1988.
31. Rautenbach, R. and Groschl, A., Separation potential of nanofiltration membranes, *Desalination*, 77, 73, 1990.
32. Bhattacharya, D. and Williams, M., Separation of hazardous organics by low pressure reverse osmosis membranes-phase II, US Environmental Protection Agency, 1990.
33. Simpson, J., Kerr, C., and Buckley, C., The effect of pH on the nanofiltration of the carbonate system in solution, *Desalination*, 64, 305, 1987.
34. <http://www.chemeng.mcmaster.ca/graduate/CourseOutlines/742/Lecture4.ppt> (last accessed June 24, 2005).
35. Gill, W.N. and Bansal, B., Hollow fibre reverse osmosis systems: Analysis and design. *AIChE J.*, 19, 823, 1973.
36. Bansal, B. and Gill, W.N., Theoretical and experimental study of radial flow hollow fibre reverse osmosis. I. Industrial waste treatment, *AIChE Symp. Ser.*, 70, 136, 1974.
37. Taylor, J.S. and Jacobs, E.P., *Water Treatment Membrane Processes*, Chapter 9, McGraw-Hill, New York, 1996.
38. Cheryan, M., *Ultrafiltration Handbook*, Technomic Publishing, Lancaster, PA, 1986.
39. Furukawa, D.H. and Burton, F.L., Membrane technologies for water and wastewater treatment, EPRI TechCommentary, TC-107698, 1997.
40. Nunes, S.P., Recent advances in the controlled formation of pores in membranes, *Trend Polym. Sci.*, 5, 187, 1997.
41. Reuvers, A.J. and Smolders, C.A., Formation of membranes by means of immersion precipitation. Part II: The mechanism of formation of membranes prepared from the system cellulose acetate–acetone–water, *J. Membr. Sci.*, 34, 45, 1987.
42. Bulte, A.M.W. et al., Membranes of semicrystalline aliphatic polyamide nylon 4,6: Formation by diffusion-induced phase separation, *J. Appl. Polym. Sci.*, 56, 13, 1993.
43. Gaides, G.E. and McHugh, A.J., Gelation in an amorphous polymer: A discussion of its relation to membrane formation, *Polymer*, 30, 2118, 1989.
44. Wijmans, J.G., Baaij, J.P.B., and Smolders, C.A., The mechanism of formation of microporous or skinned membranes produced by immersion precipitation, *J. Membr. Sci.*, 14, 263, 1983.
45. Pinnau, I. and Koros, W.J., A qualitative skin layer formation mechanism for membranes made by dry/wet phase inversion, *J. Polym. Sci. B Polym. Phys.*, 31, 419, 1993.
46. Fibiger, R.F. et al., Novel polyamide reverse osmosis membranes, US Patent 4769148, 1988.
47. Fibiger, R.F. et al., Novel polyamide reverse osmosis membranes, US Patent 4859384, 1989.
48. Cadott, J.E. and Walker, D.R., Novel water softening membranes, US Patent 4812270, 1989.
49. Wheeler, J.W., Process for opening reverse osmosis membranes, US Patent 5262054, 1993.
50. Mickols, W.E., Method of treating polyamide membranes to obtain high flux, US Patent 5755964, 1998.
51. Nunes, S.P., Sforca, M.L., and Peinmann, K.V., Dense hydrophilic composite membranes for ultrafiltration, *J. Membr. Sci.*, 106, 49, 1995.
52. Zhao, Z-P., Li, J., Zhang, D-X., Chen, C-X., Nanofiltration membrane prepared from polyacrylonitrile ultrafiltration membrane by low-temperature plasma. I. Graft of acrylic acid in gas, *J. Membr. Sci.*, 232, 1, 2004.
53. Bhattacharyya, D. and Williams, M.E., Introduction and definitions in reverse osmosis. In: *Membrane Handbook*, Ho, W.S.W. and Sirkar, K.K., Eds., Kluwer Academic, Dordrecht, The Netherlands, 1991.
54. Belfort, G. and Ulbricht, M., Surface modification of ultrafiltration membranes by low temperature plasma. I. Treatment of polyacrylonitrile, *J. Appl. Polym. Sci.*, 56, 325, 1995.
55. Mukherjee, P., Jones, K.L., and Abitoye, J.O., Surface modification of nanofiltration membranes by ion implantation, *J. Membr. Sci.*, 254, 303, 2005.
56. Lajimi, R.H. et al., Change of the performance properties of nanofiltration cellulose acetate membranes by surface adsorption of polyelectrolyte multilayers, *Desalination*, 163, 193, 2004.
57. Belfer, S. et al., Surface modification of commercial composite polyamide reverse osmosis membranes, *J. Membr. Sci.*, 139, 175, 1998.
58. Belfer, S., Purinson, Y., and Kedem, O., Surface modification of commercial polyamide reverse osmosis membranes by radical grafting: An ATR–FT-IR study, *Acta Polym.*, 49, 574, 1998.
59. Nyström, M. and Väisänen, P., Contact angle measurements of protein adsorption onto membrane polymer films, *Acta Polytech. Scand., Chem. Technol. Ser.*, N273, 5, 2000.
60. Nyström, M., Fouling of unmodified and modified polysulfone ultrafiltration membranes by ovalbumin, *J. Membr. Sci.*, 44, 183, 1989.
61. Nabe, A., Staude, E., and Belfort, G., Surface modification of polysulfone ultrafiltration membranes and fouling by BSA solutions, *J. Membr. Sci.*, 133, 57, 1997.
62. Belfer, S. et al., Surface characterization by FT-IR-ATR spectroscopy of polyethersulfone membranes—unmodified, modified and protein fouled, *J. Membr. Sci.*, 172, 113, 1997.
63. Freger, V., Gilron, J., and Belfer, S., TFC polyamide membranes modified by grafting of hydrophilic polymers: An FT-IR/AFM/TEM study, *J. Membr. Sci.*, 209, 283, 2002.
64. Kaeselev, B., Pieracci, J., and Belfort, G., Photoinduced grafting of ultrafiltration membranes: Comparison of poly(ether sulfone) and poly(sulfone), *J. Membr. Sci.*, 194, 245, 2001.
65. Sergeeva, T.A. et al., Molecularly imprinted polymer membranes for substance-selective solid-phase extraction from water by surface photo-grafting polymerization, *J. Chromat. A*, 907, 89, 2001.
66. BCquet, S. et al., From ultrafiltration to nanofiltration hollow fiber membranes: A continuous UV-photografting process, *Desalination*, 144, 9–14, 2002.

67. Ferjani, E. et al., Bulk and surface modification of cellulose diacetate based RO/NF membranes by polymethylhydrosiloxane: Preparation and characterization, *Desalination*, 146, 325, 2002.
68. Wilbert, M.C., Pellegrino, J., and Zydney, A., Bench-scale testing of surfactant-modified reverse osmosis/nanofiltration membranes, *Desalination*, 115(1), 15, 1998.
69. Baier, R.E., Substrata influences on adhesion of microorganisms and their resultant new surface properties. In: *Adsorption of Microorganisms to Surfaces*, Bitton, G. and Marshall, K.C., Eds., John Wiley & Sons, 1980, p. 59.
70. Fletcher, M. and Loeb, G.I., The influence of substratum characterization on the attachment of a marine pseudomonad to solid surfaces, *Appl. Env. Microbiol.*, 37, 67, 1979.
71. Chen, V., Fane, A.G., and Fell, C.J.D., The use of anionic surfactants for reducing fouling of ultrafiltration membranes: Their effects and optimization, *J. Membr. Sci.*, 67, 249, 1992.
72. Bruggen, V.B. et al., The use of nanofiltration for the removal of pesticides from ground water: An evaluation, *Water Sci. Technol. Water Supply*, 1, 99, 2001.
73. Bruggen, V.B. et al., Application of nanofiltration for the removal of pesticides, nitrate and hardness from ground water: Retention properties and economic evaluation, *J. Membr. Sci.*, 193, 239, 2001.
74. Kiso, Y. et al., Rejection properties of non-phenylic pesticides with nanofiltration membranes, *J. Membr. Sci.*, 171, 229, 2000.
75. Kiso, Y. et al., Rejection properties of pesticides with a hollow fiber NF membrane (HNF-1), *Desalination*, 143, 147, 2002.
76. Kettunen, R. and Keskitalo, P., Combination of membrane technology and limestone filtration to control drinking water quality, *Desalination*, 131, 271, 2000.
77. Pervov, A.G. et al., RO and NF membrane systems for drinking water production and their maintenance techniques, *Desalination*, 132, 315, 2000.
78. Thanuttamavong, M. et al., Rejection characteristics of organic and inorganic pollutants by ultra low-pressure nanofiltration of surface water for drinking water treatment, *Desalination*, 145, 257, 2002.
79. Koyuncu, I. and Yazgan, M., Application of nanofiltration and reverse osmosis membranes to the salty and polluted surface water, *J. Environ. Sci. Health, A* 36(7), 1321, 2001.
80. Seidel, A., Waypa, J., and Elimech, M., Role of charge (Dorman) exclusion in removal of arsenic from water by a negatively charged porous nanofiltration membrane, *Environ. Eng. Sci.*, 18(2), 105, 2001.
81. Vroenhoeck, E. and Waypa, J., Arsenic removal from drinking water by a "loose" nanofiltration membrane, *Desalination*, 130, 265, 2000.
82. Hafiarle, A., Lemordant, D., and Dhahbi, M., Removal of hexavalent chromium by nanofiltration, *Desalination*, 13, 305, 2000.
83. Koyuncu, I., An advanced treatment of high-strength opium alkaloid processing industry wastewaters with membrane technology: Pretreatment, fouling and retention characteristics of membranes, *Desalination*, 155, 265, 2003.
84. Tang, A. and Chen, V., Nanofiltration of textile wastewater for water reuse, *Desalination*, 143, 11, 2002.
85. Bes-Pia, A. et al., Comparison between nanofiltration and ozonation of biologically treated textile waste water for its reuse in the industry, *Desalination*, 157, 81, 2003.
86. Brehant, A., Bonnelyeb, V., and Perez, M., Comparison of MF/UF pretreatment with conventional filtration prior to RO membranes for surface seawater desalination, *Desalination*, 144, 353, 2002.
87. Teng, C.K., Hawlader, M., and Malek, A., An experiment with different pretreatment methods, *Desalination*, 156, 51, 2003.
88. Vial, D., Doussau, G., and Galindo, R., Comparison of three pilot studies using Microza membrane for Mediterranean seawater pretreatment, *Desalination*, 156, 43, 2003.
89. Pervov, A. et al., A new solution for Caspian seawater desalination: Low pressure membrane, *Desalination*, 157, 377, 2003.
90. Pontie, M. et al., Seawater nanofiltration (NF): Fiction or reality? *Desalination*, 158, 277, 2003.
91. Vellenga, E. and Tragardh, G., Nanofiltration of combined salt and sugar solutions: Coupling between retentions, *Desalination*, 120, 211, 1998.
92. Horst, V.H.C. et al., Use of nanofiltration for concentration and demineralization in the dairy industry: Model for mass transport, *Journal of Membrane Science*, 104, 205, 1995.
93. Alkhatim, H.S. et al., Treatment of whey effluents from dairy industries by nanofiltration membranes, *Desalination*, 119, 177, 1998.
94. Lakshminarayan, R.P., Cheryan, M., and Rajagopalan, N., Consider nanofiltration for membrane separations, *Chem. Eng. Progress*, 90, 68, 1994.
95. Kelly, P.M., Horton, B.S., and Burling, H., Partial demineralization of whey by nanofiltration, *New Applied Membrane Processes*, International Dairy Federation, Belgium, 1991, pp. 130–140.
96. Durham, J. et al., Process for recycling of nutrients from food process streams, PCT WO 9904903, 1999.
97. Schmidt, M. et al., Nanofiltration of process solutions highly contaminated with low-molecular organic compounds, *Filtr. Sep.*, 10, 245, 1996.
98. Fritsch, J. and Zimmermann, B., Recycling of caustic cleaning solution with nanofiltration, *Filtr. Sep.*, 12, 248, 1998.
99. Rosler, H.W. and Yacubowicz, J., Novel membrane materials allow separation tasks under extreme process conditions, *Chem. Tech.*, 26, 200, 1997.
100. McGrath, S., The Talosave brine recovery process for treatment of ion exchange regenerant in sugar refineries, *Publ. Tech. Pap. Proc. Ann. Meet. Sugar Ind. Technol.*, 57, 299, 1998.
101. Cartier, S., Theoleyre, M.A., and Decloux, M., Treatment of sugar decolorizing resin regeneration waste using nanofiltration, *Desalination*, 113, 7, 1997.
102. Cueille, G. et al., Industrial waste brine treatment in the cane sugar refining process, *Filtr. Sep.*, 34, 25, 1997.
103. Wadley, S. et al., Modeling of nanofiltration applied to the recovery of salt from waste brine at a sugar decolorization plant, *J. Membr. Sci.*, 102, 163, 1997.

104. Yacubowicz, H. and Yacubowicz, J., Nanofiltration: Properties and uses, *Filtr. Sep.*, 42(7), 16, 2005.
105. Brockmann, M. et al., Sanitary water from anaerobically pretreated wastewater from processing of brewers' yeast, *AWT Abwassertech.*, 49, 18, 1998.
106. Timmer, J.W.K., Horst, V.H.C., and Robbertsen, T., Transport of lactic acid through reverse osmosis and nanofiltration membranes, *J. Membr. Sci.*, 85, 205, 1993.
107. Timmer, J.M.K., Kromkamp, J., and Robbertsen, T., Lactic acid separation from fermentation broths by reverse osmosis and nanofiltration, *J. Membr. Sci.*, 92, 185, 1994.
108. Han, I.S. and Cheryan, M., Nanofiltration of model acetate solutions, *J. Membr. Sci.*, 107, 107, 1995.
109. Han, I.S. and Cheryan, M., Downstream processing of acetate fermentation broths by nanofiltration, *Appl. Biochem. Biotechnol.*, 57, 19, 1996.
110. Timmer, J.M.K., Speelmans, M.P.J., and Horst, V.H.C., Separation of amino acids by nanofiltration and ultrafiltration membranes, *Sep. Purif. Technol.*, 14, 133, 1998.
111. Schaefer, T. et al., Nanofiltration of dye wastewater, *Filtr. Sep.*, 13, 9, 1999.
112. Sojka-Ledakowicz, J. et al., Membrane filtration of textile dyehouse wastewater for technological water reuse, *Desalination*, 119, 1, 1998.
113. Bowen, R.W. and Mohammad, W.A., A theoretical basis for specifying nanofiltration membranes for dye/salt/water streams, *Desalination*, 117, 257, 1998.
114. Bowen, R.W. and Mohammad, W.A., Diafiltration by nanofiltration: Prediction and optimization, *AIChE J.*, 44, 1799, 1998.
115. Achwal, W.B., Treatment of dyehouse water by nano-filtration, *Colourage*, 45, 39, 1998.
116. Wu, J., Eiteman, M., and Lew, E.S., Evaluation of membrane filtration and ozonation processes for treatment of reactive-dye wastewater, *J. Environ. Eng. (Reston, Va.)*, 124, 272, 1998.
117. Rozzi, A. et al., Ozone, granular activated carbon, and membrane treatment of secondary textile effluents for direct reuse, *Biol. Abwasserreinig. (Treatment of Wastewaters from Textile Processing)*, 9, 25, 1997.
118. Van't Hul, J.P., Racz, I.G., and Reith, T., The application of membrane technology for reuse of process water and minimization of waste water in a textile washing range, *J. Soc. Dyers Colour*, 113, 287, 1997.
119. Bonomo, L. et al., Possibilities of treatment and reuse of wastewater in textile industrial settlements of Northern Italy, *Proceedings of 68th Water Environ. Fed. Ann. Conf. Expo.* 3, 539, 1995.
120. Aloy, M. and Vulliermet, B., Membrane technologies for the treatment of tannery residual floats, *J. Soc. Leather Technol. Chem.*, 82, 140, 1998.
121. Cassano, A., Drioli, E., and Molinari, R., Recovery and reuse of chemicals in unhairing, degreasing and chromium tanning processes by membranes, *Desalination*, 113, 251, 1997.
122. Cassano, A. et al., Quality improvement of recycled chromium in the tanning operation by membrane processes, *Desalination*, 108, 193, 1997.
123. Ahn, K.H. et al., Application of nanofiltration for recycling of paper regeneration wastewater and characterization of filtration resistance, *Desalination*, 119, 169, 1998.
124. Manttari, M., Nuortila-Jokinen, J., and Nystrom, M., Influence of filtration conditions on the performance of NF membranes in the filtration of paper mill total effluent, *J. Membr. Sci.*, 137, 187, 1997.
125. Afonso, M.D. and de Pinho, M.N., Nanofiltration of bleaching pulp and paper effluents in tubular polymeric membranes, *Sep. Sci. Technol.*, 32, 2641, 1997.
126. Manttari, M., Nuortila-Jokinen, J., and Nystrom, M., Evaluation of nanofiltration membranes for filtration of paper mill total effluent, *Filtr. Sep.*, 34, 275, 1997.
127. Bryant, P. and Basta, J., Process for treating wastewater, PCT WO 9839258, 1998.
128. Afonso, M.D. and de Pinho, M.N., Treatment of bleaching effluents by pressure-driven membrane processes—a review, *Environ. Sci. Technol. (Membrane Technology: Applications to Industrial Wastewater Treatment)*, 1, 63, 1995.
129. Geraldes, V. and de Pinho, M.N., Process water recovery from pulp bleaching effluents by an NF/ED hybrid process, *J. Membr. Sci.*, 102, 209, 1995.
130. Rosa, M.J. and de Pinho, M.N., The role of ultrafiltration and nanofiltration on the minimisation of the environmental impact of bleached pulp effluents, *J. Membr. Sci.*, 102, 155, 1995.
131. Twardowski, Z. and Ulan, J.G., Nanofiltration of concentrated aqueous salt solutions, US Patent 5858240, 1995.
132. Hagg, M.B., Membranes in chemical processing—a review of applications and novel developments, *Sep. Purif. Methods*, 27, 51, 1998.
133. Maycock, K., Twardowski, Z., and Ulan, J., A new method to remove sodium sulfate from brine, *Mod. Chlor-Alkali Technol.*, 7, 214, 1998.
134. Lin, K.F., Bromide separation and concentration using semi-permeable membranes, US Patent 5158683, 1998.
135. Danziger, R.S., Purification of liquids contaminated by filamentary molecules, PCT WO 9723279, 1997.
136. Hoffmann, A. et al., Generation of supersaturations in nanofiltration. Determination of dimensioning data for a new crystallization process, *Chem. Ing. Tech.*, 69, 831, 1997.
137. Barfknecht, S., Method and device for separation of metal ions from contaminated wash water, Ger. Offen. DE 19729493, 1999.
138. Hammer, J., Richter, A., and Kraus, W., Method and device for treating wastewaters from a chemical mechanical polishing process in chip manufacturing, PCT WO 9849102, 1998.
139. Katselnik, P. and Morcos, S.Y., Reduction of nickel in plating operation effluent with nanofiltration, *Plat. Surf. Finish.*, 85, 46, 1998.
140. Eriksson, P.K., Lien, L.A., and Green, D.H., Nanofiltration for removal of surplus water in dump leaching, *Tailings Mine Waste 96, Proceedings of 3rd International Conference*, 1996, p. 451.

141. Green, D.H., Column-treatment system with nanofiltration stage for removal of metal ions after acidic leaching of copper ores, US Patent 5476591, 1995.
142. Green, D.H., Copper recovery from lixivant solutions in ore leaching, PCT WO 9530471, 1995.
143. Abolmaali, B., Yassine, I., and Capone, P., Water recovery from an aluminum can manufacturing process using spiral wound membrane elements, *Proceedings of WEFTEC '96 Annu. Conf. Expo.*, 69(5), 407, 1996.
144. Eriksson, P.K., Lien, L.A., and Green, D.H., Membrane technology for treatment of wastes containing dissolved metals, *Extr. Process. Treat. Minimization Wastes 1996, Proceedings of 2nd International Symposium*, 1996, p. 649.
145. Kyburz, M., Acid preparation by reverse osmosis and nanofiltration, *Filtr. Sep.*, 5, 13, 1995.
146. Mok, K.W., Pickering, P.J., and Broome, J.E.V., Method and apparatus for recovery and purification of lithium from lithium battery waste, PCT WO 9859385, 1998.
147. Ikeda, K., Kimura, S., and Ueyama, K., Characterization of a nanofiltration membrane used for demineralization of underground brackish water by application of transport equations, *Maku*, 23, 266, 1998.
148. Bryant, P. and Basta, J., Process for treating wastewater, PCT WO 9839258, 1998.
149. Durand-Bourlier, L. and Laine, J.M., Use of NF and EDR technology for specific ion removal: Fluoride, *Proceedings of the Membrane Technology Conference*, 1997, p. 1.
150. Natarajan, P., State-of-the-art techniques in reverse osmosis, nanofiltration and electrodialysis in drinking-water supply, *Water Supply*, 14(3/4, 20th International Water Supply Congress and Exhibition, 1995), 308, 1996.
151. Ratanatamskul, C. et al., Effect of operating conditions on rejection of anionic pollutants in the water environment by nanofiltration especially in very low pressure range, *Water Sci. Technol.*, 34(9, Water Quality International '96 art 5), 149, 1996.
152. Muntisov, M. and Trimboli, P., Removal of algal toxins using membrane technology, *Water*, 23, 34, 1996.
153. Vrouwenvelder, H.S. et al., Biofouling of membranes for drinking water production, *Desalination*, 118, 157, 1998.
154. Henigin, P. and Eymann, U., Method for treatment of landfill leachate, Ger. Offen. DE 19728414, 1997.
155. Peters, T.A., Purification of landfill leachate with reverse osmosis and nanofiltration, *Desalination*, 119, 289, 1998.
156. Heine, W. and Mohn, J., Membrane separation of liquid mixtures such as landfill leachate, Ger. Offen. DE 19702062, 1998.
157. Maleriat, J.P. et al., Study of a combined process using natural flocculating agents and crossflow filtration for the processing of an aged landfill leachate, *Proceedings of 7th World Filtr. Congr.*, 2, 507, 1996.
158. Urase, T. et al., Effect of high concentration of organic and inorganic matter in landfill leachate on the treatment of heavy metals in very low concentration level, *Water Sci. Technol.*, 36(12, Water Quality Conservation in Asia), 349, 1997.
159. Haertel, G. and Poetzschke, J., Potentials and perspectives of membrane separation technology, *Umwelt-Technol. Aktuell.*, 8, 453, 1997.
160. Wichterey, E. and Klos, D., Treatment of wastewaters containing inorganic and organic pollutants, Ger. Offen. DE 19605580, 1996.
161. Bersillon, J.L. and Cote, P., State-of-the-art techniques in reverse osmosis, nanofiltration and electrodialysis in drinking-water supply, *Water Supply*, 14(3/4, 20th International Water Supply Congress and Exhibition, 1995), 304–306, 1996.
162. Peters, T.A., Purification of landfill leachate by membrane filtration with permeate yield over 95%, *Umwelt-Technol. Aktuell.*, 57, 130, 1996.
163. Peters, T.A., Effective treatment of landfill leachate. Clear water yields of more than 95% with DT module technique for reverse osmosis and nanofiltration, *Umwelt-Technol. Aktuell.*, 26, 42, 1996.
164. Linde, K. and Jönsson, A.S., Nanofiltration of salt solutions and landfill leachate, *Desalination*, 103, 223, 1995.
165. Kharaka, Y.K., Ambats, G., Presser, T.S., and Davis, R.A., Removal of selenium from contaminated agricultural drainage water by nanofiltration membranes, *Applied Geochemistry*, 11, 797, 1996.
166. Hilal, N., Mohammad, A.W., Atkin, B., and Darwish, N.A., Using atomic force microscopy towards improvement in nanofiltration membranes properties for desalination pre-treatment: A review, *Desalination*, 157, 137, 2003.
167. Nunes, S.P. and Peinemann, K.V., *Membrane Technology in the Chemical Industry*, John Wiley & Sons, Germany, 2001, pp. 1–53.
168. Tay, J., Liu, J., and Sun, D.D., Effect of solution physico-chemistry on the charge property of nanofiltration membranes, *Water Res.*, 36, 585, 2002.
169. Bowen, W.R. and Mohammad, A.W., Diafiltration by nanofiltration: Prediction and optimization, *AIChE J.*, 44, 1799, 1998.
170. Schaep, J. et al., Modeling the retention of ionic compounds for different nanofiltration membranes, *Separ. Purif. Technol.*, 22–23, 169, 2001.
171. Bowen, W.R., Mohammed, A.W., and Hilal, N., Characterization of nanofiltration membranes for predictive purposes: Use of salts, uncharged solutes and atomic force microscopy, *J. Membr. Sci.*, 126, 91, 1997.
172. Bowen, W.R. and Welfoot, J.S., Modeling the performance of membrane nanofiltration: Critical assessment and model development, *Chem. Eng. Sci.*, 57, 1121, 2002.
173. Matsuura, T., Progress in membrane science and technology for seawater desalination—a review, *Desalination*, 134, 47, 2001.
174. Schaep, J. and Vandecasteele, C.J., Evaluating the charge of nanofiltration membranes, *J. Membr. Sci.*, 188, 129, 2001.
175. Afonso, M.D., Hagemeyer, G., and Gimbel, R., Streaming potential measurements to assess the variation of nanofiltration membrane surface charge with the concentration of salt solutions, *Separ. Puri. Tech.*, 22, 529, 2001.
176. Kawasaki, S. and Kohara, N., Process for recovering thiocyanate, EP 0 599 491 A1, 1993.
177. Kawasaki, S. et al., Process for removing colored components from solvent for polyacrylonitrile, European Patent EP0556003, 1997.
178. Kawasaki, S. et al., Process for recovering thiocyanate, US Patent 5344569, 1994.
179. Capelle, N. et al., Purification of heterocyclic drug derivatives from concentrated saline solution by nanofiltration, *J. Membr. Sci.*, 196, 125, 2002.
180. Lin, W.X., Ying, A.-L., and Wang, W.-N., Nanofiltration of L-phenylalanine and L-aspartic acid aqueous solutions, *J. Membr. Sci.*, 196, 59, 2002.

181. Stern, S.A. and Noble, R.D., *Membranes Separations Technology: Principles and Applications. Membrane Separation and Technology Series-2*, Elsevier, Amsterdam, the Netherlands, 1995.
182. Douglas, R.M., *Encyclopedia of Separation Technology*, Kirk Othmer Series, John Wiley & Sons, New York, 1997.
183. Amjad, Z., *Reverse Osmosis: Membrane Technology, Water Chemistry and Industrial Applications*, Van Nostrand Reinhold, New York, 1993.
184. Lin, W.X., Cheenghong, Z., and Pingkai, O., The possibility of separating of saccharides from NaCl solution by using nanofiltration in diafiltration mode, *J. Membr. Sci.*, 204, 271, 1992.
185. Shapiro, S. and Gurvich, Y., *Analytical Chemistry*, MIR Publishers, Moscow, 1972.
186. Rautenbauch, R. and Albrecht, R., *Membrane Processes*, John Wiley & Sons, New York, 1989.
187. Noronha, M., Mavrov, V., and Horst, C., Application of the process simulation tool NF-PROJECT for efficient process development—optimization of two-stage NF processes for treatment of spent water, *Desalination*, 152, 253, 2002.
188. Whu, J.A., Baltziz, B.C., and Sirkar, K.K., Modeling of nanofiltration-assisted organic synthesis, *J. Membr. Sci.*, 163, 319, 1999.
189. Owen, G., Bandi, M., and Howell, J.A., Economic assessment of membrane processes for water and waste water treatment, *J. Membr. Sci.*, 102, 77, 1995.
190. Davidson, J., *Process Pump Selection—A Systems Approach*. Institute of Mechanical Engineers, Alden Press, Oxford, England, 1986.



---

# 43 Future Progresses in Membrane Engineering

*Enrico Drioli and Enrica Fontananova*

## CONTENTS

43.1	Membrane Engineering for Process Intensification .....	1131
43.2	Fundamental Studies on Membranes Engineering .....	1132
43.3	Reverse Osmosis in Seawater and Brackish Water Desalination .....	1132
43.4	Membrane-Based Gas Separation .....	1134
43.5	Catalytic Membrane Reactors .....	1135
43.6	Membrane-Based Artificial Organs .....	1137
43.7	Contributions of Membrane Technologies to the Life in the Space and in Other Planets .....	1139
43.8	Nanostructured Materials .....	1139
43.9	Membranes in Electronic Devices .....	1141
43.10	Membrane Contactors .....	1142
43.11	Conclusions .....	1143
	References .....	1143

### 43.1 MEMBRANE ENGINEERING FOR PROCESS INTENSIFICATION

It is well understood today that our society has to face the challenge of modifying the traditional industrial growth to a sustainable growth, if we want to continue developing for generations. In principle, adverse environmental impact can be notably reduced by optimizing the existing activities. Present design methods are effectively devoted, in most cases, to manage wastes better, to introduce methods for pollution abatement, and to realize cleaner processes for cleaner products. Nevertheless, these positive effects are expected to be offset by the ongoing growth. Traditional environmental management and pollution prevention will not suffice in the long run; newer approaches, which are radically innovative and integrated, are needed. The chemical and engineering community are already paying significant attention to the quest for technologies that would lead us to the goal of technological sustainability.

A promising example with a lot of interest by process engineers is the strategy of process intensification. It consists of innovative equipment, design, and process development methods that are expected to bring substantial improvements in chemical and any other manufacturing and processing, such as decreasing production costs, equipment size, energy consumption, waste generation, and improving remote control, information fluxes, and process flexibility.

In this frame, an interesting and important case is the continuous growth of modern membrane engineering whose basic aspects satisfy the requirements of process intensification [1]. Membrane operations, with their intrinsic characteristics of efficiency and operational simplicity, high selectivity and permeability for the transport of specific components, compatibility between different membrane operations in integrated systems, low energetic requirement, good stability under operating conditions and environment compatibility, easy control and scale-up, and large operational flexibility, represent an interesting answer for the rationalization of chemical productions.

Many membrane operations are practically based on the same hardware (materials), only differing in their software (methods). The basic properties of membrane operations make them ideal for industrial production: they are simple in concept and operation; they are modular and easy to scale-up; and they are low in energy consumption with a remarkable potential for a more rational utilization of raw materials, and recovery and reuse of by-products.

Practically, there is a lot of opportunities for membrane separation processes in all areas of the modern industry. The most interesting developments for industrial membrane technologies are related to the possibility of integrating various membrane operations in the same industrial cycle, with overall important benefits in terms of product quality, plant compactness,

environmental impact, and energetic aspects. At present, redesigning important industrial production cycles by combining various membrane operations suitable for separation and conversion units, thus realizing highly integrated membrane processes, is an attractive opportunity because of the synergic effects that can be attained [2].

### 43.2 FUNDAMENTAL STUDIES ON MEMBRANES ENGINEERING

A continuous research work on membrane properties and fundamental aspects of transport phenomena in the various membrane operations is important for the future of membrane science and technology. There is a need for both basic and applied research to develop new membranes with improved properties and new membrane processes. These research efforts must take into account the studies done in other areas such as supramolecular chemistry, molecular imprints materials, nanotechnology, nonlinear optics, studies on biological membranes and biological phenomena, etc.

Progress in better understanding of fouling phenomena and their prevention, improving of membrane selectivity, and development of new enantioselective membranes, are some examples of sectors where basic research can contribute.

More progresses on anticipating and predicting relationship between membrane chemical properties, their morphology and configuration, with the overall membrane phenomena, are still necessary, as well as, the role of interfacial phenomena and the influence of the properties and phenomena in the solution upstream and downstream the membrane surfaces.

Computational strategies will be key tools for the understanding of properties and behavior of materials to exploit the potential use of novel highly complex composite systems, new molecules and new multifunctional materials, also in membrane technology.

The possibility to design, using molecular dynamics tools, new organic or inorganic materials having selectivity for different chemical species similar to the palladium for hydrogen or to the perovskite for oxygen, might be an interesting area for future research activities.

### 43.3 REVERSE OSMOSIS IN SEAWATER AND BRACKISH WATER DESALINATION

Desalination of seawater and brackish water has been at the origin of the research efforts on reverse osmosis (RO). Today, the scarcity of potable water resource is in fact one of the main worldwide problem. Membrane technology had contributed and can further contribute in the future for the resolution of water scarcity emergency. Membrane technology is nowadays well recognized as the most convenient approach in desalination, producing daily more water than any thermal systems. More progresses can be anticipated in terms of overall costs reduction and quality improvement, by the growing integration of different membrane operations in the same desalination system. Microfiltration (MF) and ultrafiltration (UF) are becoming standard in the feeds pretreatment alternative to the traditional sand filters, active charcoal, and similar.

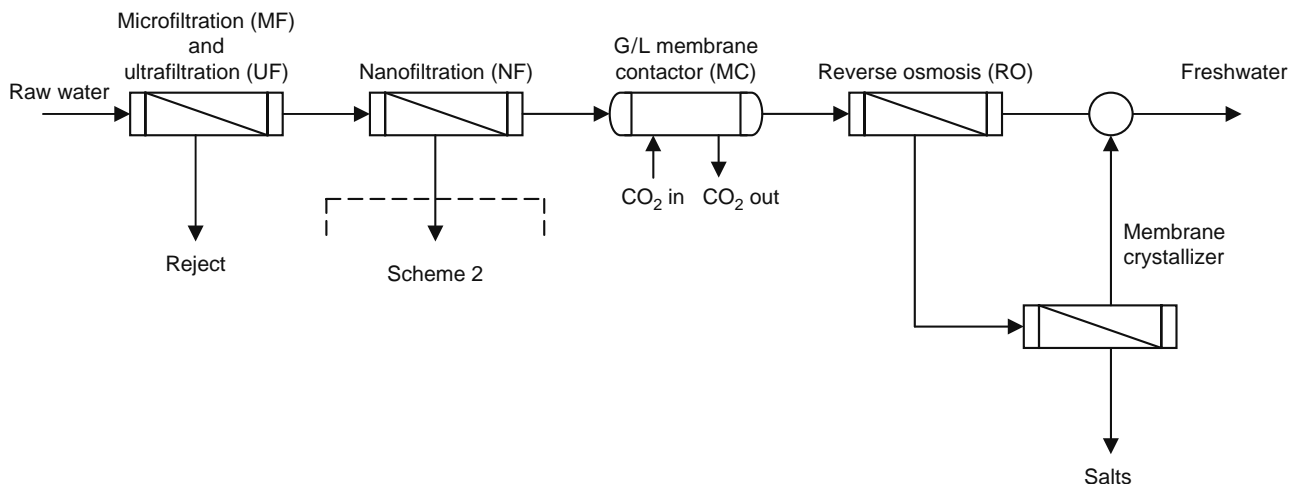
MF is a low energy-consuming technique that can be used to efficiently remove suspended solids and to lower COD/BOD (chemical oxygen demand/biological oxygen demand) and silt density index (SDI) [3,4]. UF is able to retain suspended solids, bacteria, macromolecules, and colloids thus reducing the potential of fouling and biofouling; despite of the larger pressure gradient with respect to MF, this membrane separation method remains competitive against conventional pretreatments. The introduction of nanofiltration (NF) pretreatment step leads to significant improvement in the reliability of RO; hardness is strongly reduced, as well as the most part of multivalent ions; monovalent species are also retained by 10%–50% depending on the membrane properties. As consequence, the osmotic pressure of the RO feed stream is decreased, thus allowing the unit to operate at high recovery factors without scaling problems.

Membrane contactors (MCs) represent another interesting frontier in the application of membrane technology in seawater desalination. Gas–liquid application for addition/extraction of selected gasses or operation like membrane crystallization has been recognized in some new experimental works, as important ways for improve efficiency and get some advantages for the overall desalination processes [5,6].

The increase of the low values of the recovery factor in the RO step by the introduction of membrane contactors stages on the brines of both NF, if used, and RO, has been recently proposed in literature (Figure 43.1). The use of gas–liquid membrane contactors can lead to a better and specific control of the gases dissolved in the feeds, thus preventing corrosion problems, reducing posttreatment operations, and providing optimal conditions for possible selective crystallization. Membrane contactors, in the form of membrane crystallizers, have been also recently tested as an innovative application in reducing the polluting charge and recovery some valuable salts of commercial relevance from the high concentrated brine of NF or RO plants in desalination installations (Figure 43.1) [5,6].

Presently, about 48% of all desalination facilities discharge their concentrate waste stream into surface waters or the ocean. This disposal method represents currently the most-effective and less-expensive option for both smaller and larger systems located near coastal regions. However, the promulgation of more and more stringent environmental protection regulations will reduce progressively this opportunity. In particular, the study of alternative design pathways for brine concentration is encouraged as viable opportunity to obtain value from saline waste streams, with consequent benefits in terms of overall costs reduction. In this respect, a membrane crystallization step for recovery of commercial solid substances that are present in

Scheme a



Scheme b

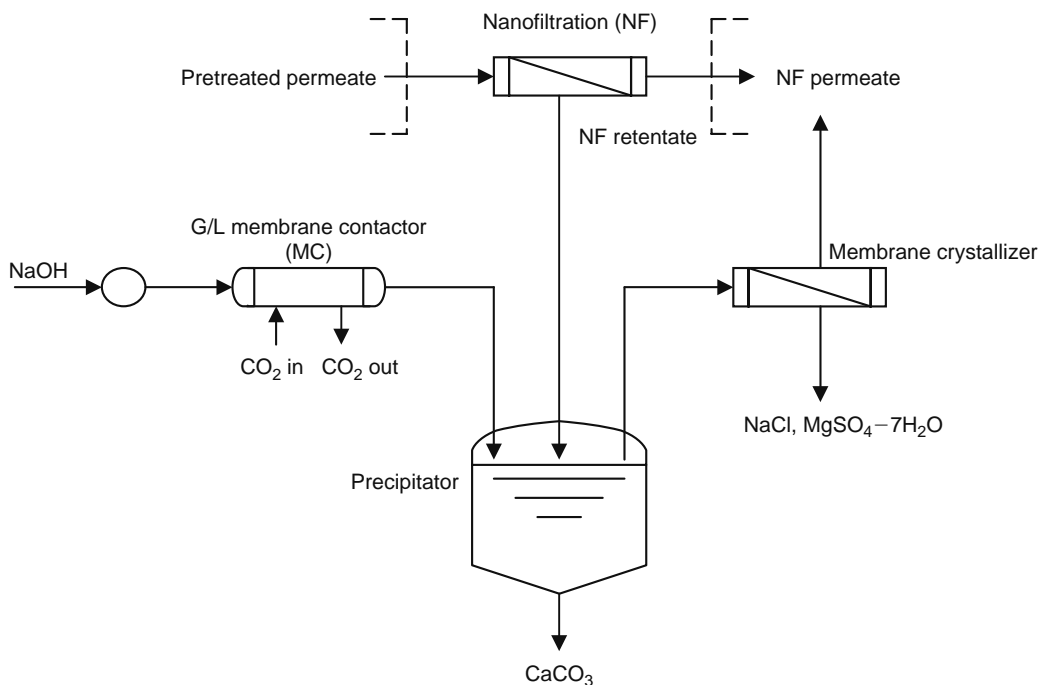


**FIGURE 43.1** Integrated membrane system proposed for seawater desalination. (Adapted from Drioli, E., Curcio, E., Criscuoli, A., and Di Profio, G., *J. Membr. Sci.*, 239, 27, 2004.)

the concentrated streams of the desalination plants, can improve the whole desalination process. The spontaneous precipitation of calcium carbonate from NF retentate has resulted in the formation of both NaCl and MgSO<sub>4</sub> · 7H<sub>2</sub>O salts using a membrane-based crystallization unit. In particular, it has been showed that 8.4 kg of MgSO<sub>4</sub> · 7H<sub>2</sub>O can be obtained per cubic meter of NF reject. When a membrane crystallizer follows an RO stage, the highly concentrate brine does not represent waste but rather the mother liquor in which sodium chloride crystals could nucleate and grow. The presence of the NF as pretreatment allows increasing the water recovery of the RO unit up to 50%. Moreover, introduction of a membrane crystallizer leads to a 100% recovery and elimination of the brine disposal problem, representing the pure crystals produced a valuable product (Figure 43.1).

The progress made in membrane-based desalination has lead to the substitution of evaporation plants with RO systems in different part of the world. For example, the United States holds the second position in worldwide desalination capacity (15.2% of the world production) and the 78% of their production come from RO treatments. Mediterranean countries, including Spain, Malta, Cyprus, and Israel, have also reverted from traditional multistage flash (MSF) to RO during the past two decades. The water production by reverse osmosis desalination plants passed from 36% of the global desalting capacity in 1996 to 42%

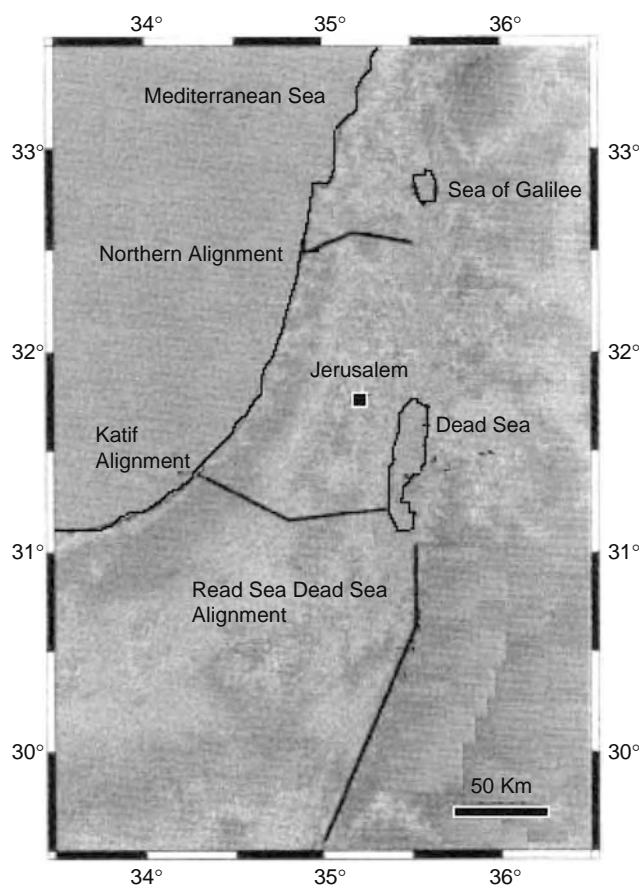


**FIGURE 43.2** The three alignments suggested for the realization of a seawater reverse osmosis (SWRO) desalination plant between Israel and the Hashemite Kingdom of Jordan. (From <http://www.mfa.gov.il/mfa>.)

in the 2000; the opposite trend was evident for the thermal plants. In particular, MSF processes passed from the 54% in 1996 to the 44% in 2000. In 2002, total installed or contracted desalting capacity based on RO processes reached the value of MSF-based plants at 43.5% of the world-installed capacity [7]. Currently the water production by membrane techniques has exceeded that of the traditional thermal systems, thanks to the construction of new systems. One of the Europe's largest seawater reverse osmosis (SWRO) plant was realized in the 2002 at Carboneras in Spain; this plant has a capacity of 120,000 m<sup>3</sup>/day. Moreover, many large plants are under construction. Particularly, in April 2003 began the realization on the South Israel (Ashkelon) of a SWRO plant which, once fully completed, will be the largest in the world. This plant alone will contribute to 100 million m<sup>3</sup>/year; the design will use advanced SWRO technology and state-of-the-art energy recovery systems to reduce operating costs and achieve one of the lowest water prices for this kind of operation (\$0.527/m<sup>3</sup>). A more ambitious project is the realization of a desalination plant between Red Sea and Dead Sea, using the process of hydrostatically supported reverse osmosis to provide a desalinated seawater (Figure 43.2). Hydrostatic energy potential of 300 m elevation difference between Red Sea and Dead Sea will be used for desalination by hydrostatically supported SWRO. On completion, this plant will produce 26 m<sup>3</sup>/s of water.

The need for even more cost-effective and efficient systems for water recovery was, and continues to be, the driving force for the research and development in RO technology.

#### 43.4 MEMBRANE-BASED GAS SEPARATION

The membrane-based gas separation (GS) processes are characterized by lower energy consume and capital investments compared to traditional gas separation systems. Both porous and nonporous membranes can be used in GS. Generally, porous membranes exhibit high level of gas flux but low selectivity. On the contrary, dense membranes generally provide high selectivity and low flux values compared to porous ones [8]. In a porous membrane, gas with different size can be separated; in a dense membrane, even gas having similar size can be separated. Membrane-based gas separation can be used as a single separation unit, or as part of an integrated separation system.

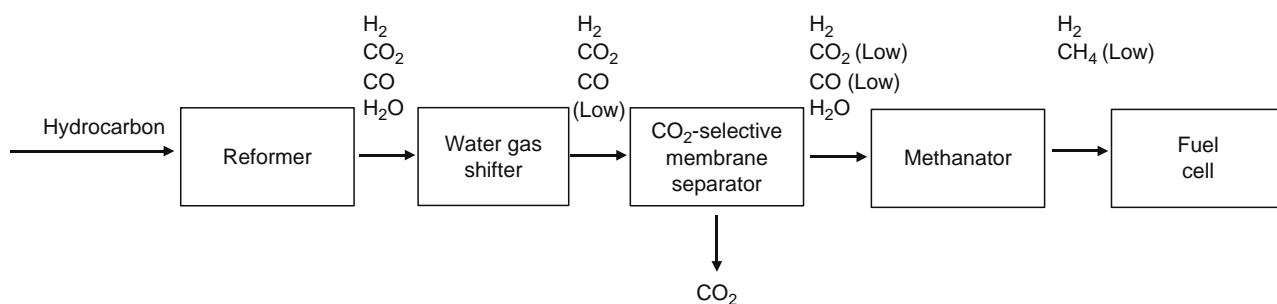
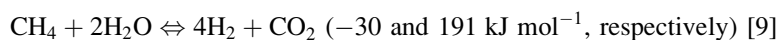


**FIGURE 43.3** One of the integrated system proposed in a U.S. Patent, ExxonMobil property. (Adapted from U.S. Patent No. 6 579 331 B1.)

Theoretical infinite selectivity can be achieved for hydrogen separation by Pd or Pd-alloy membranes. Hydrogen is one of the most important gases for industrial applications and its production is principally based on steam reforming of methane. The reaction is carried out at high temperature, about above 1000 K, because of the equilibrium of the endothermic reactions involved in the process:



and



Many studies demonstrate that Pd-based membranes with ideally infinite selectivity for H<sub>2</sub> can be used to increase the equilibrium conversion of steam reforming of methane by H<sub>2</sub> removal [10,11]. The driving force in this process is the partial pressure difference.

The high cost, limited lifetime, and low permeability are relevant limits of Pd and Pd-alloy membranes. To overcome these drawbacks, many studies have been carried out for the preparation of supported metallic membranes in which a thin metallic layer is supported on a thicker sublayer. However, the preparation technology of metallic membranes is still today not sufficiently mature and more work is necessary to produce defect free and stable membranes at acceptable costs.

Hydrogen separation can also be carried out using electrochemical method in an electrolysis cell. By applying a direct current to a proton-conducting membrane, hydrogen can be electrochemically dissociated at the anode, transported through the membrane as hydrated and protons, and recovered at the cathode. In this process, the electrochemical potential difference provides the driving force, and the separation rate can be easily controlled acting on the applied current [12].

In fuel cells systems, as reported in recent patents [13,14], membranes will be present not only as PEM (proton-exchange membrane), which allows protons to pass from the anode to the cathode where they are combined with oxygen and electrons to produce water, but also for the production and purification of the H<sub>2</sub> (Figure 43.3). This system provides a CO<sub>2</sub>-selective membrane process for the purification and water gas shift reaction of a reformed gas, generated from on-board reforming of a fuel, e.g., hydrocarbon, gasoline, diesel, methanol, or natural gas, to hydrogen for fuel cell vehicles.

Membranes have interesting application also in oxygen separation. In many gas-fired power plants for electricity generation, the oxygen for combustion is produced by very expensive cryogenic air separation techniques. This technology requires large plants to cool air to several 100° below zero to separate the component gases. Nitrogen and oxygen are then distributed to customers in liquid form by tanker trucks. About noncryogenic air separation, membrane technology offers interesting opportunities. Recent advances in the development of ion-transport membranes using dense mixed-conducting ceramic membranes to separate oxygen from air [15] will contribute to the complete replacing of cryogenic air separation techniques.

Perovskite-structured oxides with high electronic and oxygen ion conductivities could be used as a membrane alternative to solid electrolytes for oxygen separation. In such materials, both oxygen ions and electronic defects are transported in an internal circuit in the membrane material.

Perovskite membranes are interesting systems not only for their possible applications (e.g., fuel cells, oxygen generators, oxidation catalysts) but also for the fundamental fascination of fast oxygen transport in solid-state ionic.

### 43.5 CATALYTIC MEMBRANE REACTORS

Catalytic membrane reactors (CMRs) are an interesting example of integrated system in which molecular separation and chemical conversions are combined in one unit.

The heterogenization of catalysts in membrane is particularly suitable for catalyst design at the atomic and molecular level. One of the main advantages of the membrane reactors, compared to traditional reactors, is the possibility to recycle easily the catalyst. Moreover, the selective transport properties of the membranes can be used to shift the equilibrium conversion (e.g., esterification reaction), to remove selectively products and by-products from the reaction mixture, to supply selectively the reagents (e.g., oxygen for partial oxidation reactions).

The scientific literature on CMRs is significant today; however, practically only few large-scale industrial applications have been reported so far because of the relatively high price of membrane units. However, current and future advancements in membrane engineering might significantly reverse this trend. CMRs are today successfully applied in small-scale operations, but for their use on large industrial scale, additional efforts mainly related to the optimization of membrane materials, modules manufacturing and reactors design, are required.

The application of CMRs appears of particular interest in several areas such as hydrogen production, oxidation reactions, and enantiomeric productions.

A special category of membrane reactors exists when the membrane defines the reaction volume, e.g., by providing a contacting zone for two immiscible phases (phase-transfer catalysis) excluding solvents and thus making the process environmentally more attractive.

The first applications of CMRs have concerned high temperature reactions. The employed inorganic membranes, characterized by higher chemical and thermal stability with respect to polymeric membranes, still today suffer from some important drawbacks: high cost, limited lifetime, difficulties in reactor manufacturing (delamination of the membrane top-layer from the support due to the different thermal expansion coefficients).

On the other hand, the use of polymeric membranes in CMRs is increasing in interest [16]. The cost of polymeric membranes is generally lower in comparison with inorganic ones, and the preparation protocols allow a better reproducibility; moreover, the relatively low operating temperatures are associated with a less stringent demand for materials used in the reactor construction [16].

In general, polymeric membranes are less resistant to high temperatures and aggressive chemicals than inorganic or metallic membranes. However, polymeric materials resistant under rather harsh conditions, namely polydimethylsiloxane, Nafion, Hyflon, polyvinylidene fluoride, are today available. Moreover, many reactions of relevant interest in fine chemical synthesis or in water treatment take place under mild conditions.

For biological applications, synthetic membranes provide an ideal support for catalyst immobilization due to their wide available surface area per unit volume; enzymes that are retained in the reaction side do not pollute the products and can be continuously reused. Biocatalytic membrane reactors can also be used in production, processing, and treatment operations. The trend toward environmentally friendly technologies makes these units particularly attractive because of their ability to operate at moderate temperature and pressure, and reduce the formation of by-products. Enzymes, compared to inorganic catalysts, generally permit greater stereospecificity, and higher reaction rates under milder reaction conditions. Relevant applications of biocatalytic membranes reactors include production of new or better foodstuffs, in which desired nutrients are not lost during thermal treatment; novel pharmaceutical products with well-defined enantiomeric compositions; wastewater treatment. The catalytic action of enzymes is extremely efficient, selective and highly stereospecific when compared with chemical catalysts; moreover, immobilization procedures have been proven to enhance the enzyme stability. In addition, membrane bioreactors are particularly attractive in terms of eco-compatibility because they do not require additives, are able to operate at moderate temperature and pressure, and reduce the formation of by-products. Potential applications have been at the origin of important developments in various technology sectors, mainly concerning: induction of microorganisms to produce specific enzymes, techniques of enzymes purification, bioengineering techniques for enzyme immobilization, and design of efficient productive cycles.

One of the most interesting aspects of catalyst heterogenization in membranes is the effect of the membrane environment on the catalyst activity. Membrane composition (hydrophobic or hydrophilic characteristics of the membrane material, presence of chemical groups with acid or basic properties, etc.) and membrane structure (dense or porous, symmetric or asymmetric) can positively influence the catalyst performance, not only by the selective sorption and diffusion of reagents or products, but also influencing the catalyst activity by electronic (electron-donating and electron-withdrawing groups) and conformational effects (stabilization of the transition states). These effects are similar to those occurring in biological membranes.

A membrane-induced structure-reactivity trend that may be exploited to achieve selective processes has been recently observed in polymeric catalytic membranes prepared embedding polyoxotungstates, W(VI)-oxygen anionic clusters having interesting properties as photocatalysts, in polymeric membranes [17]. These catalytic membranes have been successfully applied in the photooxidation of organic substrates in water providing stable and recyclable photocatalytic systems.

Membrane reactors using biological catalysts can be used in enantioselective processes. Methodologies for the preparation of emulsions (sub-micron) of oil in water have been developed and such emulsions have been used for kinetic resolutions in heterogeneous reactions catalyzed by enantioselective enzyme (Figure 43.4). A catalytic reactor containing membrane immobilized lipase has been realized. In this reactor, the substrate has been fed as emulsion [18]. The distribution of the water organic interface at the level of the immobilized enzyme has remarkably improved the property of transport, kinetic, and selectivity of the immobilized biocatalyst.

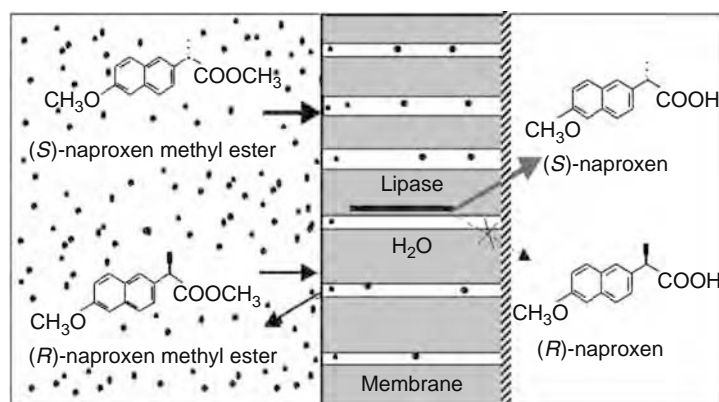


**FIGURE 43.4** Scheme of the *S*- and *R*-naproxen isomer production in the enzyme-emulsion membrane reactor. (From Li, N., Giorno, L., and Drioli, E., *Ann. N.Y. Acad. Sci.*, 984, 436, 2003.)

An innovative potential application of membrane technology in catalysis and in CMRs might be the possibility to produce catalytic crystals with a well-defined size, size distribution, and shape by membrane crystallization [19,20] (Figure 43.5). Membrane crystallization is particularly attractive for the preparation of heat-sensitive catalysts such as enzymes.

#### 43.6 MEMBRANE-BASED ARTIFICIAL ORGANS

The progress made in the last years in membrane science and technology has a positive fall out, not only in separation industrial processes but also in biotechnology and medical applications.

In particular, membrane bioartificial organs are promising means of treating acute organs failure in alternative to transplantation this is not an option for many patients.

Membrane, with appropriate permeability characteristics, as well as, physicochemical properties, is used in bioartificial organs as selective barriers to compartmentalize isolated cells while allowing the transport of nutrients and metabolites to cells and the transport of catabolites and specific metabolic products to blood. Moreover, the membrane avoids the contact between immune system components with xenogenic cells to prevent immunological response and rejection of xenograft.

Currently, the main areas of interest in membrane bioartificial organs include the bioartificial kidney, the bioartificial pancreas, and the bioartificial liver. Very interesting is also the study of artificial membrane retina, where an artificial membrane is used to convert the light signals to electric signals through the structural change of the membrane [21]. Membrane technology has also relevant potentiality in neural engineering [22] for the development of brain-implantable biomimetic devices.

Cytocompatibility is a key issue for membrane in bioartificial organs. In this respect, the development of new materials with physicochemical properties that provide improved blood/cell compatibility is strictly related to the progress in this promising

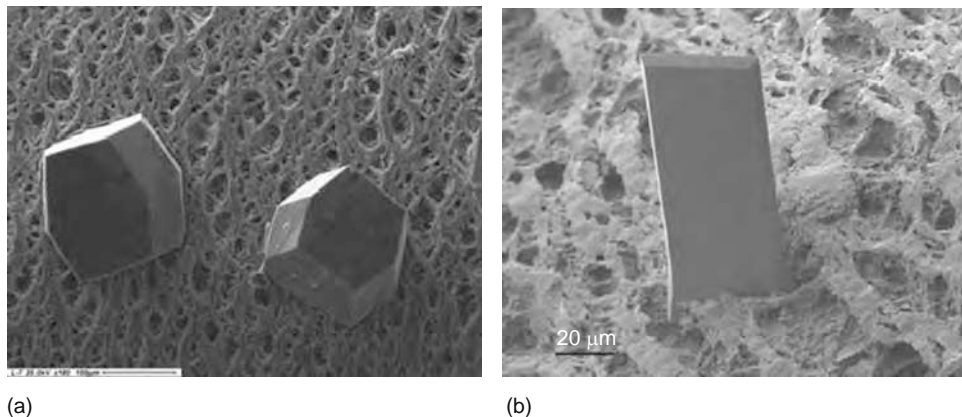


**FIGURE 43.5** Lysozyme (a) (Reprinted from Di Profio, G., Curcio, E., and Drioli, E., *J. Cryst. Growth*, 257, 359, 2003. With permission from Elsevier.) and trypsin (b) (Adapted from Drioli, E., Curcio, E., and Di Profio, G., *Chem. Eng. Res. Des.*, 83(A3), 223, 2005.) crystals grown on PP microporous hydrophobic membrane.

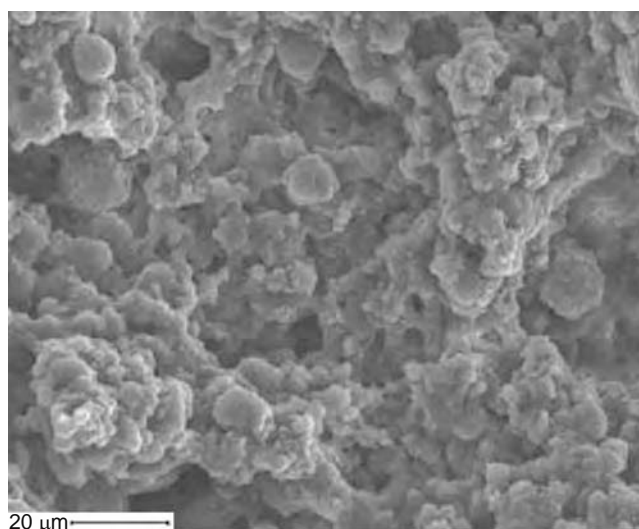


**FIGURE 43.6** Liver cells after 48 h of culture on microporous PEEK-WC membranes. (Reprinted from De Bartolo, L., Morelli, S., Rende, M., Gordano, A., and Drioli, E., *Biomaterials*, 25, 3621, 2004. With permission from Elsevier.)

area. Polymer-based materials have numerous applications in medicine for their relative inertness and possibility of controlled degradation to harmless by-products.

A recent study has shown that membranes made of a modified polyetheretherketone (PEEK-WC) are interesting materials for biomedical applications [23,24]. The cytocompatibility of PEEK-WC membranes was evaluated by culturing hepatocytes isolated from rat liver (Figure 43.6). The properties of PEEK-WC membranes were compared to polyurethane membranes prepared using the same technique, and commercial membranes (made of Nylon, polyethersulphone, and polyester). The results have shown that PEEK-WC membranes promoted hepatocyte adhesion most effectively and metabolic activities of cells cultured on these membranes improved significantly.

The interesting results obtained, not only with PEEK-WC but also with other materials, encourage further research work to better understand and improve the potentialities of membranes in biomedical applications.

In cell encapsulation, ultrathin polymeric membranes microcapsules are used for the immunoprotection of transplanted cells. The membrane must allow the selective passage of some molecules but must act as a barrier to others. As a consequence, a careful material design is fundamental.

Membrane capsules containing dopamine-secreting cells have been investigated for treating of Parkinson's disease. Immunoprotective membrane cell transplants are also being used in the treatment of other nervous system disorders [25].

Although the interesting results obtained in many studies, the lack of clinical-grade polymers and the difficulties in the production of uniform capsules with excellent repeatability and reproducibility, still limits the clinical applications of this technology [26].

Membrane emulsification has been recently proposed for the preparation of stable and uniform-sized microcapsules [27]. Membrane emulsification is a technology that allows to obtain uniform emulsions at low energy input compared to the emulsion prepared using high-pressure homogenizers and rotor/stator systems; therefore, it is very useful for the preparation of emulsions containing labile compounds such as bioactive molecules sensitive to shear stress [28].

Membranes have been also used in the antisolvent solidification process wherein a liquid medium containing organic or inorganic compounds which have to be solidified, is forced through a membrane into one or more antisolvent. Alternatively, one or more antisolvent can be forced through a membrane into a liquid medium containing the compounds, which are to be solidified, yielding a composition comprising these organic or inorganic compounds [29].

For many industrial applications, the particle size of the solidified compounds is very important. This issue is of particular interest in the area of pharmaceutical product development. For example, in low dosage forms it might be difficult to obtain a good homogeneity if the particle size is too large. Moreover, a large particle size can make the pharmaceutical compound difficult to process into a pharmaceutical end product. The particle size also influences the ease of segregation in a mixing process, which takes place before tableting. The controllability of the particle size is also important because a wide variation in particle size of the pharmaceutical compounds can lead to insufficient control of its concentration. Moreover, if the pharmaceutical compounds are prepared in a crystalline form, the purity, crystal size distribution, and polymorphy of the crystals can be very important. For example, differences in crystal structure can lead to a difference in physicochemical parameters such as stability, rate of dissolution, melting point, etc., which frequently are strongly influenced by the crystal forms of a polymorphous compound.

By using a membrane for the dosing of the antisolvent to the liquid medium containing the compounds of interest or vice versa for dosing the liquid medium in the antisolvent, an improved solidification process can be obtained.

This patented device allows to obtain a controlled solidification process, in many cases crystallisation, yielding a composition comprising solid particles which are in general nonagglomerated and which have an improved quality (e.g., an improved shelf life) [29]. Moreover, with this process higher product yields can be achieved. In other words, the antisolvent solidification process can allow a more efficient use of (starting) materials or solvents and, therefore, a decrease in energy consumption can be achieved compared to conventional evaporative or antisolvent processes [29]. Furthermore, the process can easily be scaled-up to a higher volume and enables a robust control of the particle size [29].

### 43.7 CONTRIBUTIONS OF MEMBRANE TECHNOLOGIES TO THE LIFE IN THE SPACE AND IN OTHER PLANETS

Membrane technology is also an ideal technology for application in the space because process intensification strategy is a more imperative request in the space than on the Earth, today. Volumetric efficiency, optimal remote control, energy, and waste saving are fundamental aspects in the space. Membranes could efficiently solve some of the problems of life in the space such as energy production and water and air purification, fulfilling these requirements.

Recently different research projects on membrane technology have been funded by NASA. In one of these, researchers are working for the production of rocket fuel from the Martian atmosphere using membrane-based gas separation [30]. The Martian atmosphere is composed mainly of 95% CO<sub>2</sub> (95%) that mixed with H<sub>2</sub> yields, when heated, methane, a useful propellant for rockets or rovers. This process, called Sabatier process, gives water as by-product that can be electrolyzed into oxygen, for breathing, and hydrogen, which can be used to produce another round of methane. However the Martian atmosphere is not pure enough for the Sabatier process, and CO<sub>2</sub> must be separated from the other atmospheric components, mostly nitrogen and argon, before its processing. In this project, specialized polymers engineered to increase CO<sub>2</sub> solubility are used for membrane preparation, and tested in a special chamber that simulates the Martian environment. The researchers want to design a device that produces CO<sub>2</sub> pure at 99.8% at a rate of 2.5 L/min.

These membranes could be also used to remove CO<sub>2</sub>, which is a waste product of human metabolism, from the atmosphere of a self-contained spacecraft. Moreover, these or similar membranes could also offer possible solutions to the problem of the CO<sub>2</sub> control emission also in the Earth.

Another important international project in which membranes are proposed as interesting tools for space life-support systems is the Space2Tex [31]. The Space2Tex project has been originally conceived within the framework of the European Space Agency's Technology Transfer Program, inspired by the MELiSSA (Micro-Ecological Life Support System Alternative) research activities on membrane bioreactors. MELiSSA has been conceived as a microorganisms and higher plants-based ecosystem intended as a tool to gain understanding of the behavior of artificial ecosystems, and for the development of the technology for a future regenerative life-support system for long-term manned space missions, e.g., a lunar base or a mission to Mars [32].

The Space2Tex project aims at developing a novel concept of compact high efficiency and cost-effective wastewater treatment plant for water recycling in textile finishing. The project final objective is the application of membrane bioreactors for the biodegradation of textile-finishing pollutants, often hardly biodegradable, in small wastewater system plants to be inserted end-of-pipe of textile-processing plants, with the final aim of 100% water recycling in micro-ecological space life-support systems.

It is important to note that the new membranes and membrane systems that have been, or will be developed for the life in the space in the next years could also help people to live in the Earth. Because of the more and more rapid growth of the worldwide population, the Earth is becoming a sort of big spacecraft where billions of people live together, and the problems of the life in the Earth are becoming very similar to the problem of the life in the space.

### 43.8 NANOSTRUCTURED MATERIALS

Development of innovative materials with improved properties is a key issue for the application of membrane technology in industrial processes. Significant progresses have been made in the study and realization of new organic and inorganic membranes with controlled structure.

The ability to control pore sizes is an important topic for membrane technology development. Membranes with controlled morphology can be used not only in separation process but also in chemical conversion supplying highly ordered and confined geometries for chemical reactions.

Nanoscale control of membrane architecture can further extend the field of application of membrane technology. With regard to this aspect, nanotechnologies have been used to create membrane structures by the typical methods used for electronic component construction using lasers and etching. Track etch membrane technology is an example of industrial application of track etching technique (Figure 43.7) [33].

In these membranes, pore size, shape, and density can be varied in a controlled way and, as a consequence, a membrane with the required transport and retention characteristics can be produced.

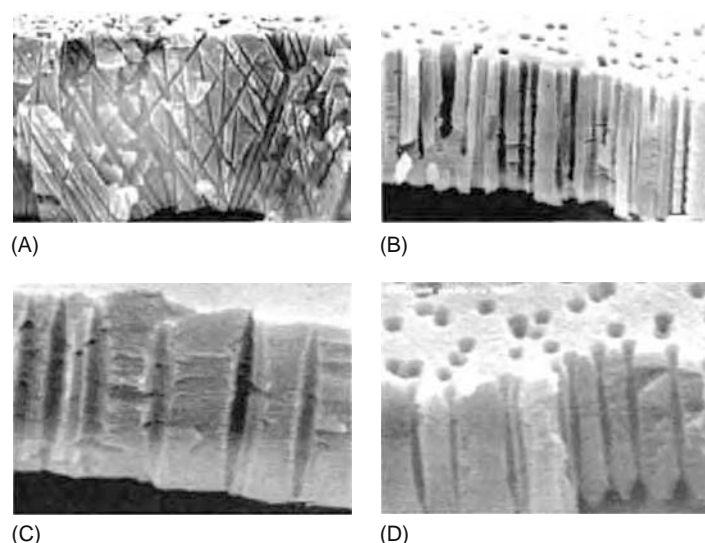


**FIGURE 43.7** Examples of porous structures produced in thin polymeric films using various methods of irradiation and chemical treatment. (Reprinted from Apel, P., *Radiat. Meas.*, 34, 559, 2001. With permission from Elsevier.) (A) Cross section of a polycarbonate membrane with cylindrical nonparallel pore channels; (B) polypropylene membrane with slightly conical parallel pores; (C) polyethylene terephthalate membrane with cigar-like pores; and (D) polyethylene terephthalate membrane with “bow-tie” pores.

Microporous alumina membranes electrochemically grown by anodizing of aluminium can be also produced with an excellent controlling of pore size distribution and porosity [34].

Membrane made of precisely sized nanotubes also hold great potential for filtration and separation processes. The nanometer-scale sized and hollow-, cylindrical-shaped nanotubes suggest that they may be used as membranes with pores on the order of 1–100 nm.

Nanotube membranes prepared via the template method are also of particular interest [35]. For example, gold nanotube membranes have been successfully synthesized using a template-based electroless plating technique [36] (Figure 43.8). Human serum albumin, which acts as an enantiomer selector, was immobilized on the inner surface of the nanotubes through a reactive thiol, obtaining a bio-nano device for chiral resolution. However, for large-scale application of nanotubes membranes improving in their preparation technique are request (lower costs, higher stability and reproducibility, etc.).

Preparation of membranes by phase separation performed on mould having a micrometer-sized surface profile has been also reported for the production of membranes with microstructure structure [37].

Self-assembling is another innovative research field in membrane technology. Self-assembly process consists in the regular assembly of small molecular entities into larger supramolecular structures exhibiting new functions that can not be exhibited by



**FIGURE 43.8** Gold nanotube synthesized by using a 50 nm polycarbonate membrane template. (Reprinted from Shao, P., Ji, G., and Chen, P., *J. Membr. Sci.*, 255, 1, 2005. With permission from Elsevier.)

the isolated units. The interaction between subunits is generally due to noncovalent bonds, such as hydrogen bonds, van der Waals interactions, and electrostatic forces. Recently, Massachusetts Institute of Technology researchers have patented stable macroscopic membranes formed by the self-assembly of amphiphilic peptides, peptides with alternating hydrophobic and hydrophilic residues [38]. The membranes result stable in aqueous solution, serum, ethanol, and are highly resistant to heat, alkaline and acidic pH, chemical denaturants, and proteolytic digestion. They are also noncytotoxic. Potential uses include biomaterial applications such as slow-diffusion drug delivery systems and artificial skin and separating filters. The invention further provides scaffolds comprising the self-assembling peptides and methods of using the scaffolds including for cell culture, tissue engineering, and tissue repair.

### 43.9 MEMBRANES IN ELECTRONIC DEVICES

Membranes applications in sensors and microelectromechanical systems (MEMS) are increasing in importance in our society. The development of new device able to give rapid detection of chemical and biological species is central to many areas of life science and industrial production. In particular, conducting polymeric materials show major potentiality in this field, and are replacing classical inorganic semiconductor materials because of their better selectivity and rapid measurements, low cost, and easy manufacture for their preparation as films [39]. Moreover, appropriate molecular design of polymer properties can increase the efficiency of the system.

Membrane technology has enormous potentiality in gas detection, ion-selective sensors, biochemical analyzes, medical applications, and quality control on industrial manufacturing processes, food and beverages. Polymeric membranes are used in sensor device, either participating in sensing mechanism or immobilizing the substance responsible for sensing. Membranes are applied today also for mimic natural sense organs. An electronic tongue using membranes based on conducting polymers (polypyrrole and polyaniline) and a lipid-like material components (stearic acid) has been already realized [40]. The device is able to distinguish salt, sweet, bitter, and acidic solutions.

Very promising can be the use in sensors field of molecular imprinted membrane [41,42], where the memory of a specific substance is imprinted in a polymeric material.

Membranes fabricated using the MEMS technology are finding an increasing number of applications in sensors, actuators, and other sophisticated electronic device. However, the new area of application of MEMS is creating new materials demands that traditional silicon cannot fulfill [43]. Polymeric materials, also in this case, are the optimal solution for many applications. Microfabrication of polymeric films with specific transport properties, or micromembranes, already exists, and much work is in progress [44–50].

Membranes made or filled with ferromagnetic materials have special features making them useful to MEMS applications. In a recent work [51] a micro-magnetic membrane for biological separation has been proposed. Magnetic beads have been engineered to bind to specific biological system (molecules, proteins, viruses, bacteria) and mixed with the biological solution of interest (Figure 43.9). After the binding process, the solution is passed through a nanoporous membrane with cylindrical pores partially filled with ferromagnetic material. An external magnetic field is applied parallel to the membrane surface to magnetize the ferromagnetic cylinders perpendicular to the wires' long axis. Inside the pores, the biological system, bound

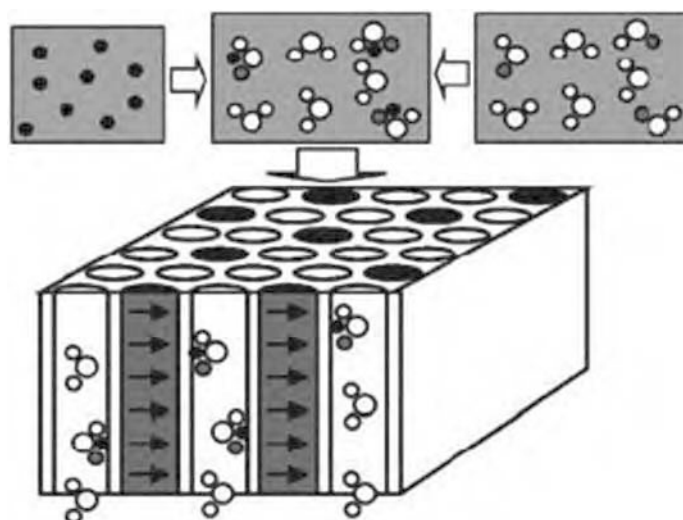


**FIGURE 43.9** Magnetic membrane proposed for biological separation. (Reprinted from Barbic, M., *J. Magn. Magn. Mater.*, 249, 357, 2002. With permission from Elsevier.)

to the magnetic bead, is trapped on the walls of the capillaries while the unbound units are passed through. The trapped particles can later be released simply by removing the external magnetic field. The magnetic forces depend inversely on the diameter of the ferromagnetic wires, and, therefore, smaller the pore diameter, stronger the magnetic field gradients and magnetic forces will be [52].

This method is well suited to be implemented into the microfluidic and MEMS designs.

### 43.10 MEMBRANE CONTACTORS

In the field of membrane technology, membrane contactors (MCs) represent a very important branch of new devices having a wide range of applications with a high charge of innovation. Membrane contactors are expected to play a decisive role in the design of alternative production systems appropriate for a sustainable growth [53,54]. Membrane contactors are systems where the membrane function is to facilitate diffusive mass transfer between two contacting phases (liquid–liquid, gas–liquid, gas–gas, etc.) without dispersion of one phase within another. This is accomplished by passing the fluids on opposite sides of a microporous membrane. By controlling the pressure difference between the fluids, one of them is immobilized in the pores of the membrane so that the fluid–fluid interface is located at the mouth of each pore (Figure 43.10).

In a membrane contactor, generally, microporous hydrophobic membranes are used to promote mass transfer between phases.

These membrane systems, mainly provided in the form of low cost hollow fibres, offer a high interfacial area, significantly greater than most traditional absorbers, between two phases to achieve high overall rates of mass transfer. Furthermore, whereas the design of the conventional devices is restricted by limitations in the relative flows of the fluid streams, membrane contactors give an active area which is independent of the liquid fluid dynamics.

Membrane crystallization has been recently proposed as one of the most interesting and promising extension of the membrane contactors concept [19,20]. This innovative technology uses the evaporative mass transfer of volatile solvents through microporous hydrophobic membranes to concentrate feed solutions above their saturation limit, thus attaining a supersaturated environment where crystals may nucleate and grow (Figure 43.5) [19,20]. In addition, the presence of a polymeric membrane increases the probability of nucleation with respect to other locations in the system (heterogeneous nucleation).

Membrane distillation	Contacting phases Phase I: Liquid Phase II: Liquid gas vacuum	Driving force $X_1^I$ $X_1^{II}$ $\Delta X_1 = \Delta T_1 - \Delta P_1$ (Partial pressure gradient)	Limit to mass transfer $T^I$ $T^{II}$ Temperature polarization
Osmotic membrane distillation	Contacting phases Phase I: Liquid Phase II: Liquid	Driving force $X_1^I$ $X_1^{II}$ $\Delta X_1 = \Delta T_1 - \Delta P_1$ (Partial pressure gradient)	Limit to mass transfer $c^I$ $c^{II}$ Concentration polarization
Membrane crystallization	Contacting phases Phase I: Liquid solid Phase II: Liquid	Driving force $X_1^I$ $X_1^{II}$ $\Delta X_1 = \Delta T_1 - \Delta P_1$ $\Delta X_1 = \Delta C_1 - \Delta P_1$	Limit to mass transfer $T^I$ $T^{II}$ $c^I$ $c^{II}$ Temperature polarization Concentration polarization
Gas–liquid membrane contactors	Contacting phases Phase I: Gas Phase II: Liquid	Driving force $X_1^I$ $X_1^{II}$ $\Delta X_1 = P_1 - HC_1$	Limit to mass transfer $p^I$ $c^I$ $c^{II}$ Resistance in liquid or in membrane phase
Membrane emulsifiers	Contacting phases Phase I: Liquid Phase II: Liquid	Driving force $X_1^I$ $X_1^{II}$ $\Delta X_1 = \Delta P$	Limit to mass transfer $c^I$ $c^{II}$ Resistance in liquid or in membrane phase
Phase–transfer catalysis	Contacting phases Phase I: Liquid Phase II: Liquid	Driving force $X_1^I$ $X_1^{II}$ $\Delta X_1 = \Delta C_1$	Limit to mass transfer $c^I$ $c^{II}$ Resistance in liquid or in membrane phase

FIGURE 43.10 Different examples of membrane contactors.

Membrane contactor offers potential solution in a wide range of gas/liquid and liquid/liquid applications: gas adsorption and stripping, liquid/liquid extraction, dense gas extraction, fermentation and enzymatic transformation, pharmaceutical applications, protein extraction, wastewater treatment, chiral separations, semiconductor manufacturing, carbonation of beverages, metal ion extraction, protein extraction, and VOCs removal from waste gas [55].

Membrane crystallizers, membrane emulsifiers, membrane strippers and scrubbers, membrane distillation systems, membrane extractors, etc. can be devised and integrated in the production lines together with the other existing membranes operations for advanced molecular separation, and chemical transformations conducted using selective membranes and membrane reactors, overcoming existing limits of the more traditional membrane processes (e.g., the osmotic effect of concentration by reverse osmosis).

A number of commercial applications of MCs have been already successfully realized. A bubble-free membrane-based carbonation line, using Liqui-Cel equipment, is in operation by Pepsi in West Virginia since 1993. MCs are also used in beer production: the CO<sub>2</sub> removal stage is followed by nondispersive nitrogenation to obtain a dense foam head. Another important field of application of MC is the production of ultrapure water for semiconductor manufacturing.

### 43.11 CONCLUSIONS

Membrane science and technology is expected to play an increasingly important role in the future for various industrial sectors. The availability of new membrane with tailor-made properties and new membrane processes offers important tools for the design of alternative production systems appropriate for a sustainable growth.

The traditional membrane separation processes (reverse osmosis, micro-, ultra- and nanofiltration, electrodialysis, pervaporation, etc.), already largely used in many different applications, are today combined with new membrane systems such as CMRs and membrane contactors. Membranes are applied not only in traditional separation processes such as seawater desalination but also in medicine, bioengineering, microelectronics, the life in the space, etc.

The biological systems well represent what are the new trends in membrane technology. The integration of membrane operations allows in prospective the possibility to redesign important industrial processes. Petrochemical plants, complex artificial organs such as the brain, etc. can be more and more conceived as based on integrated membrane systems simulating the analogous biological ones. The possibility to produce self-repairing membranes is also an interesting possibility.

Despite its success and undoubtedly great potential, membrane technology is still quite far from fulfilling all the expectations of its role in intensification of a large variety of processes. Actually, membrane-based hybrid separation methods cannot be proven to be significantly better than conventional techniques, and the use of catalytic membranes is just recently becoming effective for large-scale industrial applications. To overcome these barriers, more systematic analyzes of possible advantages or drawbacks due to the introduction of a membrane stage instead of a conventional unit, clear protocols and comparison indexes for the choice of the best membranes and optimal operative conditions, accurate modelling for an easy scale-up or scale-down, and significant multidisciplinary research efforts are needed.

However, these efforts need to be combined with new research works in the process dynamics and in the study of advanced control systems applied to integrated membrane systems. These multidisciplinary studies will offer interesting opportunities for the future development of membrane engineering.

### REFERENCES

1. Drioli, E., Process intensification using membrane systems, *Clean Tech. Environ. Policy*, 5, 3, 2003.
2. Drioli, E. and Romano, M., Progress and new perspectives on integrated membrane operations for sustainable industrial growth, *Ind. Eng. Chem. Res.*, 40, 1277, 2001.
3. Ebrahim, S., Bou-Hamed, S., Abdel-Jawad, M., and Burney, N., Microfiltration system as a pretreatment for RO units: Technical and economic assessment, *Desalination*, 109, 165, 1997.
4. Bonnelye, V., Sanz, M.A., Durand, J.-P., Plasse, L., Gueguen F., and Mazounie, P., Reverse osmosis on open intake seawater: Pre-treatment strategy, *Desalination*, 167, 191, 2004.
5. Drioli, E., Curcio, E., Criscuoli, A., and Di Profio, G., Integrated membrane system for recovery of CaCO<sub>3</sub> NaCl and MgSO<sub>4</sub> · 7H<sub>2</sub>O from nanofiltration retentate, *J. Membr. Sci.*, 239, 27, 2004.
6. Drioli, E., Criscuoli, A., and Curcio, E., Integrated membrane operations for seawater desalination, *Desalination*, 147, 77, 2002.
7. IDA news July/August 2002; Vol. 11 Issue 78.
8. Wijmans, J.G. and Baker, R.W., The solution-diffusion model: A review, *J. Membr. Sci.*, 107, 1, 1995.
9. Rostrup-Nielse, J.R., in: Anderson, J.R. and Boudard M. (Eds.) *Catalysis Science and Technology*, Vol. 5, Springer-Verlag: New York, 1984.
10. Barbieri, G., Violante, V., Di Maio, F.P., Criscuoli, A., and Drioli, E., Methane steam reforming analysis in a palladium-based catalytic membrane reactor, *Ind. Eng. Chem. Res.*, 36(8), 3369, 1997.
11. Tong, J. and Matsumura, Y., Effect of catalytic activity on methane steam reforming in hydrogen-permeable membrane reactor, *Appl. Catal. A*, 286, 226, 2005.

12. Lee, H.K., Choi, H.Y., Choi, K.H., Park, J.H., and Lee, T.H., Hydrogen separation using electrochemical method, *J. Power Sources*, 132, 92, 2004.
13. U.S. Patent No. 6 579 331, CO<sub>2</sub>-Selective membrane process and system for reforming a fuel to hydrogen for a fuel cell, 2003.
14. U.S. Patent No. 6 841 280, Fuel cell power plant, 2005.
15. Yantovski, E., Gorski, J., Smyth, B., and Elshof, J., Zero-emission fuel-fired power plants with ion transport membrane, *Energy*, 29, 2077, 2004.
16. Vankelecom, I.F.J. and Jacobs, P.A., Polymeric membranes in catalytic reactors, *Catal. Today*, 56, 147, 2000.
17. Bonchio, M., Carraro, M., Scorrano, G., Fontananova, E., and Drioli, E., Heterogeneous photooxidation of alcohols in water by photocatalytic membranes incorporating decatungstate, *Adv. Synth. Catal.*, 345, 1119, 2003.
18. Li, N., Giorno, L., and Drioli, E., Effect of immobilization site and membrane materials on multiphasic enantioselective enzyme membrane reactors, *Ann. N.Y. Acad. Sci.*, 984, 436–452, 2003.
19. Di Profio, G., Curcio, E., and Drioli, E., Membrane crystallization of lysozyme: Kinetic aspects, *J. Cryst. Growth*, 257, 359, 2003.
20. Di Profio, G., Curcio, E., and Drioli, E., Trypsin crystallization by membrane-based techniques, *J. Struct. Biology*, 150, 41, 2005.
21. Nakanishi, H., Artificial retina membranes, *Prog. Surf. Sci.*, 49, 107, 1995.
22. Berger, T.W. and Baudry, M., Brain-implantable biomimetic electronics as the next era in neural prosthetics, *Proc. IEEE*, 89, 7, 993, 2001.
23. De Bartolo, L., Morelli, S., Bader, A., and Drioli, E., The influence of polymeric membrane surface free energy on cell metabolic functions, *J. Mat. Sci.: Mat. Med.*, 12, 959, 2001.
24. De Bartolo, L., Morelli, S., Rende, M., Gordano, A., and Drioli, E., New modified polyetheretherketone membrane for liver cell culture in biohybrid systems: Adhesion and specific functions of isolated hepatocytes, *Biomaterials*, 25, 3621, 2004.
25. De Bartolo, L., Giorno, L., and Drioli, E., in: D. Bhattacharyya and D.A. Butterfield (Eds.) *Membrane Bioreactors for Biotechnology and Medical Applications in New Insights into Membrane Science and Technology: Polymeric and Biofunctional Membranes*, Elsevier Science B.V.: Amsterdam, 2003, p. 187.
26. <http://www.nature.com/naturemedicine> (accessed June 2005).
27. Liu, R., Ma, G.H., Meng, F.-T., and Su, Z.-G., Preparation of uniform-sized PLA microcapsules by combining Shirasu Porous Glass membrane emulsification technique and multiple emulsion-solvent evaporation method, *J. Controll. Rel.*, 103, 31, 2005.
28. Giorno, L., Li, N., and Drioli, E., Preparation of oil-in-water emulsions using polyamide 10 kDa hollow fiber membrane, *J. Membr. Sci.*, 217, 173, 2003.
29. EU Patent No. WO2004096405, Antisolvent solidification process, 2004.
30. [http://www.nasa.gov/lb/vision/earth/technologies/03dec\\_membranes.html](http://www.nasa.gov/lb/vision/earth/technologies/03dec_membranes.html) (accessed February 2008).
31. <http://www.euratex.org/content/research/space2tex-04.pdf> (accessed February 2008).
32. <http://www.estec.esa.nl/ecls/melissa/melissa.html> (accessed June 2005).
33. Apel, P., Track etching technique in membrane technology, *Radiat. Meas.*, 34, 559, 2001.
34. Bocchetta, P., Sunseri, C., Chiavarotti, G., and Di Quarto, F., Microporous alumina membranes electrochemically grown, *Electrochim. Acta*, 48, 3175, 2003.
35. Aranda, P. and García, J.M., Porous membranes for the preparation of magnetic nanostructures, *J. Magn. Magn. Mater.*, 249, 214, 2002.
36. Shao, P., Ji, G., and Chen, P., Gold nanotube membranes: Preparation characterization and application for enantioselective separation, *J. Membr. Sci.*, 255, 1, 2005.
37. Vogelaar, L., Barsema, J.N., van Rijn, C.J.M., Nijdam, W., and Wessling, M., Phase Separation Micromolding—PSM, *Adv. Mater.*, 15, 1385, 2003.
38. U.S. Patent No. 6 800 481, Stable macroscopic membranes formed by self-assembly of amphiphilic peptides and uses therefor, 2004.
39. Adhikari, B. and Majumdar, S., Polymers in sensor applications, *Prog. Polym. Sci.* 2004; 29, 699–766.
40. Riul, A., Gallardo Soto, A.M., Mello, S.V., Bone, S., Taylor, D.M., and Lattoso, L.H.C., An electronic tongue using polypyrrole and polyaniline, *Synth. Met.*, 132, 109, 2003.
41. Piletsky, S.A., Panasyuk, T.L., Piletskaya, E.V., Nicholls, I.A., and Ulbricht, M., Receptor and transport properties of imprinted polymer membranes: A review, *J. Membr. Sci.*, 157, 263, 1999.
42. Donato, L., Figoli, A., and Drioli, E., Novel composite poly(4-vinylpyridine)/polypropylene membranes with recognition properties for (S)-naproxen, *J. Pharm. Biomed. Anal.*, 37, 1003, 2005.
43. Huber, R. and Singer, N., Out with the old in with the new, *Mater. Chem.*, 5, 36, 2002.
44. Grosjean, C., Yang, X., and Tai, Y.-C., A practical thermopneumatic valve, *IEEE*, 17(21), 147, 1999.
45. Pornsin-Sirirak, N., Liger, M., Tai, Y.-C., Ho, S., and Ho, C.-M., Flexible parylene-valved skin for adaptive flow control, *Proceedings of the Fifteenth IEEE International Conference on Micro Electro Mechanical Systems*, 2002, pp. 101–104.
46. Hsu, Y.-J., Chang, Y.-H., Chai, Y.-L., and Chen, G.-J., The influence of residual stress and membrane thickness on the performance of Fe–Ni–Cr/Invar bimetal freestanding membrane for microdevices, *Sens. Actuators, A*, 101, 160, 2002.
47. Shearwood, C., Harradine, M.A., Birch, T.S., and Stevens, J.C., Applications of polyimide membranes to MEMS technology, *Microelectron. Eng.*, 30, 547, 1996.
48. Chung, G.-S., Fabrication and characterization of micro-heaters with low-power consumption using SOI membrane and trench structures, *Sens. Actuators, A*, 112, 55, 2004.
49. Yua, A.B., Liua, A.Q., Zhang, Q.X., Alphones, A., Zhua, L., and Shacklock, A.P., Improvement of isolation for MEMS capacitive switch via membrane planarization, *Sens. Actuators, A*, 119, 206, 2005.
50. Dücső, C., Vázsonyi, E., Szabó, I., Bárszónyi, I., Gardeniens, J.G.E., and Van den Berg, A., Porous silicon bulk micromachining for thermally isolated membrane formation, *Sens. Actuators, A*, 60, 235, 1997.

51. Barbic, M., Magnetic wires in MEMS and bio-medical applications, *J. Magn. Magn. Mater.*, 249, 357, 2002.
52. Häfeli, U. Shütt, W., Teller, J., and Zborowski, M. (Eds.), *Scientific and Clinical Applications of Magnetic Carriers*, Plenum Press: New York, 1997.
53. Criscuoli, A., Curcio, E., and Drioli, E., Polymeric membrane contactors, *Recent Res. Devel. Polym. Sci.*, 7, 1, 2003.
54. Drioli, E., Curcio, E., and Di Profio, G., State of the art and recent progresses in membrane contactors, *Chem. Eng. Res. Des.*, 83(A3), 223, 2005.
55. Gabelman, A. and Hwang, S.-T., Hollow fibre membrane contactors, *J. Membr. Sci.*, 159, 61, 1999.



# Index

## A

- Acid caseinate in food industry, production of, 598–603; *see also* Food industries, EDBM applications in
- Acid digestion process, 947
- Acidified milk, 645
- Acid recovery, membrane in, 974
- Aciplex membranes, 794–796
- Actinides recovery, by PEHFSD technique
  - Am(III) extraction, 1067
  - Pu(IV) extraction, 1066–1067
  - U(VI) extraction, 1065–1066
- Actinides separation
  - bulk liquid membranes, 889–890
  - emulsion liquid membranes, 890–894
  - grafted membranes, 907–909
  - hollow fiber supported liquid membranes, 903–904
  - polymer inclusion membranes, 904–907
  - and removal of, 939–943
  - supported liquid membranes, 894
    - acidic extractants, 894–897
    - neutral donor, 897–902
  - track-etched membranes, 904
- Activated process, 71
- Activated surface diffusion, 291
- Active sites, 47
- ADMF, *see* Acidified milk
- Adsorbable organic halogens, 982
- Adsorptive membrane geometry and operation modes, 51–52
- Adsorptive membranes preparation
  - in affinity chromatography
    - microporous membrane modification, 34–35
    - phase inversion process, 34
  - affinity ligands
    - biospecific ligands, 44
    - combinatorial synthetic, 45
  - materials used in
    - acrylate- and methacrylate-based polymers, 33
    - cellulose, 28–29
    - chitin and chitosan, 29
    - dextran, 29–30
    - EVAL hollow fiber membranes, 31
    - inorganic supports, 33
    - polyacrylamide gels, 30–31
    - polyamides and nylon, 30
    - polyethylene and polypropylene membranes, 31
    - polysulfone and polystyrene, 32
- membrane activation and ligand coupling, reactions, 40
  - aldehyde and acetal functional groups, 43
  - amino groups, 43–44
  - carboxyl groups, 42–43
  - hydroxyl groups, 40–42
- monolithic stationary phases, 25
  - polymeric, 36–38
  - silica monoliths, 36
- particle-loaded membranes
  - dispersion of particles in, 40
  - in sheet form, 38–39
  - spacer molecules, 45–46
- Adsorptive processes, separation efficiency in, 47
- ADUF, *see* Ammonium diuranate filtrate
- Affinity column bed
  - geometry of, 26
  - mass transfer in, 47
- Affinity columns, mass transfer in
  - axial diffusion, 48
  - flow patterns, 48
  - matrix and active sites, interaction with, 51
  - RTD of, 49–50
  - separation efficiency, 47
  - variance, 50
- Affinity ligands, classification of, 44; *see also* Ligands
- Affinity membrane chromatography
  - advantages of, 46–47
  - applications of
    - recombinant protein G isolation, 54
  - membrane preparation in
    - microporous, 34
    - modification techniques, 34–35
  - principle of, 27
  - using immobilized metal ions, 45
- Affinity purification, 54
- Aggressive gases, membrane for recovery of, 101
- AGMD, *see* Air gap membrane distillation
- Air gap membrane distillation, 526–528
- Air purification, using ceramic filters, 160
- Air separation, membrane for
  - high-purity nitrogen production, 98
  - high-purity oxygen, 99–100
  - oxygen-enriched air production, 98–99
- Alcohol dehydration, 291
  - using zeolite A, 292–293
  - using zeolite MOR and T (OFF structure), 293
- Allentown Water Treatment Plant, 960
- Alum recovery, DMP application for, 946–947
  - fundamentals of, 953–955
  - membrane structure role in, 957–958
  - modeling protocol of, 955–957
  - from WTR, 963
- Americium, extraction of, 941–943
- Ammonium diuranate filtrate, 832–833
- Ammonium molybdophosphate, 829
- AMP, *see* Ammonium molybdophosphate
- Anion-exchange chromatography, 54–55
- AOX, *see* Adsorbable organic halogens
- Apple juice in food industry, production of, 603–606; *see also* Food industries, EDBM applications in
- Applications, membranes of, *see* Membrane applications
- Aroma compounds, recovery of, 127–128
- Asymmetric membranes, 450–452; *see also* Drug delivery, membranes in
- Attenuated total reflection (ATR)-Fourier transform infrared (FTIR) spectroscopy, 332
- Au(I) extraction from cyanide media, by PEHFSD technique, 1062–1063
- Average residence time, 50
- AWTP, *see* Allentown Water Treatment Plant
- Axial dispersed plug flow model
  - Kozeny–Carman equation, 49
  - Peclet number, 48
- Azimuthal Reynolds number, 215

**B**

- Bacillus cereus*, 646  
 Ballard Advanced Materials (BAM), 797  
 BAM membranes, 797–799  
 BAT, *see* Best Available Technology  
 Batch filtration system, schematic representation of, 156  
 Batch system membrane plant  
   for fermentation broth microfiltration, 163  
 Beer industry, membrane separation/application  
   role in, 553–556  
   alcohol removal, 576–577  
   economic prospects of, 577–578  
   factors affecting  
     composition, 556–558  
     membrane characteristics, 558  
     membrane fouling, 558–560  
     process parameters, influence of, 560–565  
   filtration of, 568–573  
   permeate flux in, 566–568  
   RO role and microbiological quality control in, 577  
   spent beer recovery, 573–576  
 Best Available Technology, 1001  
 Beverage processing, using ceramic membranes, 161–162  
 Bioaffinity separation, 54  
 Biocatalytic membrane reactors, 171–172  
 Bioindustries, BPM in  
   lactic acid, production and isolation of, 617–620  
   phospholipids, production of, 620–623  
 Biological membranes, importance and usages of, 495  
 Biomimetic membranes, 80  
 Biomolecule purification methods, 25  
 Biospecific ligands, 44  
 Biot number, 715  
 Bipolar membrane, 582–583  
   electrodialysis and  
     EDBM configurations, 588–589  
     H<sup>+</sup> and OH<sup>-</sup> generation, 584  
     water dissociation, catalysts role in, 587–588  
     water dissociation in, 584–587  
   parameters of, 591–593  
 BLM, *see* Bulk liquid membrane  
 Block copolymers, separation mechanism in, 78  
 Blood oxygenator, 671  
   CFD methods in, 685–688  
   design of, 676–677  
     hemoglobin, oxygen binding to, 682–685  
     lumped parameter, value of, 685  
     non-newtonian blood rheology, effects of, 682  
     water, oxygenation and deoxygenation of, 677–682  
   future prospects of, 688  
   history of, 673–676  
 BO, *see* Blood oxygenator  
 Boiler plant, schematic diagram of, 18  
 Boiler water degasification system, 18  
 Borsig envelope-type membrane module, 89  
 BPM, *see* Bipolar membrane  
 Breakthrough curve, visual representation of, 47  
*Brevundimonas diminuta*, 410  
 Brownian diffusion model, 196  
 Brownian motion, 50–51  
 Bubble BOs, 673; *see also*  
   Blood oxygenator  
 Bulk liquid membrane, 885, 889–890

**C**

- Caffeine/SC CO<sub>2</sub> separation  
   by molecular-sieving mechanism  
     drawback of, 185  
     solute permeability, 184  
   schematic representation of, 182–183  
   solute rejection rate, 183  
   through adsorption mechanism, 183–184  
 Cake depolarization, mechanisms of, 222  
 Calcium alginate membranes, in theophylline permeation, 444–446  
 Capillary liquid membrane systems, 391–392  
 Carbamoyl methyl phosphonate, 899  
 Carbamylation reactions, 43–44  
 Carbonaceous removal, membrane bioreactor in, 1012  
 Carbon dioxide (CO<sub>2</sub>) removal  
   membrane modules for  
     from biogas, 95–97  
     from exhaust gas, 96–97  
     in life support systems, 98  
     from natural gas, 94–95  
 Carbon dioxide hydrogenation, 299–300  
 Carbon molecular sieving membranes, 67  
   production process of, 80–81  
   regeneration, importance in, 80–81, 83  
   separation properties for  
     permeance and selectivity, 81–82  
 Carbon nanotubes, template-synthesized, 694–695  
 Carbonylation reaction  
   with carbonyldiimidazoles, 42  
   schematic representation of, 41  
 Carboxymethyl dextran hydrogel, 476  
 Cardopolymers, 79  
 Carrier facilitated transport, 710  
 CAS, *see* Conventional activated sludge process  
 Catalytic membrane reactors, 1135–1137  
   biocatalytic membrane reactors, 171–172  
   as contactor, 296  
   in flow-through configuration, 297  
   gas–liquid–solid membrane contactors, 170–171  
   high-temperature configurations of, 172  
   roles of membrane in, 169–170  
 Catalytic zeolite-membrane reactors  
   in fine chemicals industry  
     enzyme immobilization, 305  
     selective liquid-phase hydrocarbon oxidation, 305–306  
   for selectivity enhancement  
     *i*-butene, 303–304  
     thermal treatment, 305  
     VOC degradation, 304  
 Cation-exchange membranes, 55  
 CED, *see* Cohesion energy density  
 Cell membrane, electroporation in; *see also* Electroporation  
   biophysical basis of, 746–747  
   factors affecting efficiency  
     biological factors, 748  
     electrodes and pulsing medium, 749  
     field strength and pulse shape, 748  
     post electroporation incubation, 748  
     pulsing and incubation medium, 748  
   mechanical breakdown model, 747–748  
   pore model, 747  
   principle of, 745–746  
   resealing characteristics, 748  
   resting and induced transmembrane potential, 746  
   threshold value, 747

- Cell plasma membrane, 742
  - electroporation, 745–749
  - fluid mosaic model, 744
  - membrane proteins, 744
  - molecular transport, 745
  - permeability barrier, 745
  - phospholipid bilayer in, 743–744
  - physical organization of, 744–745
- Celulose
  - commercially available, 29
  - description of, 28
  - membranes, 29
- Ceramic ion-conducting membranes, 152
- Ceramic ion-selective membranes, 1076
- Ceramic membrane disks, and membrane holder, 153–154
- Ceramic membranes
  - applications of
    - in catalytic membrane reactors, 169–173
    - gas separation, 166–167
    - liquid processing, 160–162
    - liquid–solid separation, 163–164
    - membrane emulsification, 165–166
    - nanofiltration, liquid media, 164–165
    - ozonation, 166
    - pervaporation and vapor permeation, 167–169
    - pharmaceuticals and bioproducts recovery, 162–163
    - products manufacturing and recycling, 163–164
    - waste liquids and gases, treatment of, 158–160
    - waste oils, recovery of, 164
  - characteristics of, 863
  - commercially available
    - competitiveness of, 156–157
    - modules and disks, 153–154
    - modules arrangement, 154–156
  - dense membrane structure, 145–146
  - ionic transport mechanism, 152
  - mass transfer and separation properties, 146
    - gas and vapor separation, 151–152
    - ion-conducting membranes, 152
    - liquid filtration, 147–150
  - membrane elements
    - filtration mode, 153, 155
    - geometrical and structural characteristics of, 140–142
  - multichannel, 141
  - porous structure
    - bottleneck geometry, 145
    - inorganic, 142, 144
    - micropores, 145–146
- Ceramic oxygen-transporting membrane, 88
- Cetyl-trimethyl-ammonium bromide, 660
- CFD, *see* Computational fluid dynamics
- CFLME, *see* Continuous flow liquid membrane extraction
- CFMF, *see* Crossflow microfiltration
- CFP, *see* Creeping film process
- Chemical industry waste treatment, membrane application in, 823–824
- Chemical process industries
  - mode of consumption of NRS in, 107–108
- Chemi-thermomechanical pulp mills, 993
- Chiral crown ether, 55
- Chitin, 29
- Chitosan membranes, 29
- Chromatographic separation and columns
  - based on membrane (*see* Membrane chromatographic system)
  - disadvantages of, 47
  - packed beds, 25–26
  - pressure drop problem, 26
  - types of interactions involved in, 53
  - using flat sheet membranes, 27
- Chromium recovery, by SLM technique, 1060–1061
- Cibacron blue, 45
- Cibacron Blue F3GA dye membranes, 53–54
- CICMs, *see* Ceramic ion-conducting membranes
- Classical bed chromatography, active sites in, 47
- CLMs, *see* Contained liquid membranes
- Clostridium sporogenes*, 644
- Clostridium tyrobutyricum*, 644
- CMAS, *see* Completely mixed activated sludge
- CM-dextran hydrogel, *see* Carboxymethyl-dextran hydrogel
- CMP, *see* Carbamoyl methyl phosphonate
- CMPO, *see* Octyl(phenyl)-*N,N*-diisobutylcarbamoylmethylphosphine oxide
- CMRs, *see* Catalytic membrane reactors
- CMS membranes, *see* Carbon molecular sieving membranes
- Coagulation systems, for pretreatment process, 335
- Coating technique, for membrane modification, 34–35
- Cohesion energy density, 239
- Colon drug delivery systems, 452–454; *see also* Drug delivery, membranes in
- Column chromatography, 25
- Combinatorial synthetic ligands, 45
- Commercial Parr autoclave, 271–272
- Competitive pertraction system, 380
- Completely mixed activated sludge, 1011
- Composite cellulose membranes, 29
- Composite ionomer membranes
  - CREAFILTER membranes, 810
  - electrolyte-filled microporous membrane, 809–810
  - heteropolyacid additive, 806–807
  - hydrophilic fillers and ormosil networks, 801–804
  - phosphate and phosphonate additives, 807–809
  - recast membranes, properties of, 805–806
- Composite membranes
  - of cellulose and acrylamide polymer, 31
  - fabrication techniques, 118
  - support layer, importance in, 117–118
- Composite nylon membranes, 30
- Computational fluid dynamics, 685
- Concanavalin A (ConA), 475
- Concentration polarization, 1105
  - at membrane surface, 326–327
  - of permeants, 114
- Configurational diffusion, *see* Activated surface diffusion
- $\beta$ -Conglycinin protein, 614
- Conical nanotubes, 704–706
- Contact angle
  - interface between liquid and solid substrate, 8
  - for materials in water, 9
- Contained liquid membranes, 1024
- Continuous beds, *see* Monolithic stationary phases
- Continuous flow liquid membrane extraction, 360
- Continuously stirred reactor, 48
- Conventional activated sludge process, 1008
  - membrane bioreactor in, 1011–1012
- Copper recovery, by PEHFSD technique, 1059–1060
- Cordierite monolith, EDX mapping of, 272–273
- Corrugated membrane
  - effect of pulsations on oxygen transfer, 209
  - and pulsatile flow, 209
- Coupling reagents activation method, 42–43
- CP, *see* Concentration polarization
- CPI, *see* Chemical process industries
- CPS, *see* Competitive pertraction system
- Creeping film process, 387
- Critical flux
  - back transport mechanism, 196
  - different mechanisms, coefficient of, 196
  - hydrodynamic techniques, 198
  - stepped TMP increase protocols, determination of, 197

Cross-flow filtration, 158  
 Crossflow filtration system, in beer filtration, 570  
 Cross-flow membrane emulsification, 165  
 Crossflow microfiltration, 636, 639, 643, 647, 650  
 in beer industry, 558–560  
 Cross-flow operation mode, modules, 155  
 CSTR, *see* Continuously stirred reactor  
 CTAB, *see* Cetyl-trimethyl-ammonium bromide  
 CTMP, *see* Chemi-thermomechanical pulp mills  
 Curtis azide rearrangement, 42–43  
 Cyanogen bromide reaction, 40–41  
 Cyclic *trans*-2,3-carbonate method, 40–41  
 Cystinuria, 693

## D

DAF, *see* Dissolved air flotation  
 Dairy industry  
 cleaning and sanitation in, 657–660  
 membrane applications in  
 cheese manufacturing, 640–646  
 cheese whey, pretreatment of, 639  
 development and limitations of, 660–663  
 lactose and minerals, recovery of, 649  
 microorganisms, removal of, 646–648  
 milk fat, fractionation of, 649–651  
 milk, standardization of, 648–649  
 whey proteins, concentration of, 637–639  
 membrane performance in  
 energy consumption, 656–657  
 fouling and flux prediction, 651–656  
 microfiltration role in, 636  
 RO and nanofiltration role in, 637  
 ultrafiltration role in, 636–637  
 Dairy wastewater treatment, 609–611; *see also*  
 Food industries, EDBM applications in  
 Damköhler number, 715, 718  
 DBOA, *see* *N,N*-di-*n*-butyloctanamide  
 DCMD, *see* Direct contact membrane distillation  
 Dead-end operation mode, 154–155; *see also* Ceramic membranes  
 Dean flow-enhanced membrane filtration, 200  
 Dean numbers, 199  
 Decontamination factor, 828, 844  
 Dehydration of organics, *see* Organics, dehydration of  
 DF, *see* Decontamination factor  
 DHDECMP, *see* Dihexyl-*N,N*-diethyl  
 carbomoyl methyl phosphonate  
 Diafiltration, 1104  
 Dialkyl amides, in actinide separation, 900–901  
 Diazotization activation, 43–44  
 DIDPA, *see* Di-*iso*-decyl phosphoric acid  
 Diethylenetriamine-*N,N,N',N',N''*-pentaacetic acid, 892  
 Differential-algebraic nonlinear optimization, 1033  
 Diffusion  
 dialysis  
 application of, 958–960  
 and radioactive waste treatment, 838–839  
 process  
 multicomponent, 113–114  
 single-component, 113  
 transport equation through membrane, 114  
 selectivity, definition of, 116  
 Diffusivity, in pervaporation, 291  
 Dihexyl-*N,N*-diethyl carbomoyl methyl phosphonate, 839  
 Di-*iso*-decyl phosphoric acid, 899  
 Di-1(1-methylheptyl) phosphoric acid, 892  
 Direct coating, 118  
 Direct contact membrane distillation  
 heat and mass transfer in, 516–524  
 models and parameters in, 525  
 Direct flow filtration, in pharmaceutical industry, 410–411  
 Direct membrane cleaning, 849  
 Direct methanol fuel cells, 304, 307  
 membrane requirements for, 773–774  
 Direct observation through the membrane  
 particle deposition pattern, 195, 207  
 Dispersion, 49–50  
 Dissolved air flotation, 997  
 Dissolved organic carbon, 947  
 Distillation and membrane separations, 108  
 DLS, *see* Dynamic light scattering  
 DMC, *see* Direct membrane cleaning  
 DMFCs, *see* Direct methanol fuel cells  
 DMHPA, *see* Di-1(1-methylheptyl) phosphoric acid  
 DMP, *see* Donnan membrane process  
 DNLP, *see* Differential-algebraic nonlinear optimization  
 DOC, *see* Dissolved organic carbon  
 Donnan dialysis, and radioactive waste treatment,  
 838–839, 947, 976  
 Donnan effect, in NF membranes, 1104  
 Donnan membrane process, 945, 947–950, 976  
 in WTR coagulants recovery, 947  
 applications and modeling protocols of, 955–957  
 assumptions of, 953  
 concentration of, 949–950  
 Donnan equilibrium conditions, 950–951  
 fundamentals of, 948–949  
 future perspective of, 977  
 importance of, 976–977  
 kinetics and transport equations of, 951–953  
 membrane structure in, 957–958  
 techniques in, 960–962  
 Donnan-steric pore model, 1112  
 DOTM, *see* Direct observation through the membrane  
 Drinking and domestic water processing; *see also* Water  
 purification systems  
 ceramic membranes for, 161  
 membrane processes, problems in, 160  
 Drug delivery, membranes in, 428–431  
 drug diffusion coefficient measurement, 438–446  
 future perspectives of, 461–464  
 implantable delivery systems, 459–461  
 mechanism of, 431–438  
 oral administration, 446–454  
 responsive membranes in, 488–489  
 transdermal administration, 454–458  
 Dry gel method, 274  
 DSPM, *see* Donnan-steric pore model  
 DTPA, *see* Diethylenetriamine-*N,N,N',N',N''*-pentaacetic acid  
 Dual-mode model, 75–76  
 Du Pont membrane, 874  
 Dyes, 45  
 Dye-zeolite systems, 311  
 Dynamic light scattering, 438

## E

Ebonex ceramic electrodes, 1072–1073  
 ECF, *see* Elemental chlorine free  
 ECM, *see* Extracellular matrix  
 E-curve, 49–50  
 EDBMs, *see* Electrodialysis with bipolar membranes  
 EDC, *see* 1-ethyl-(3-3-dimethylaminopropyl) carbodiimide hydrochloride  
 EDR, *see* Electrodialysis reversal

- EDTA, *see* Ethylenediaminetetraacetic acid
- EIW, *see* Electrically ionized water
- Electrically assisted membrane process  
and effluents types, 1077–1078  
future of, 1078–1079
- Electrically ionized water, 1078
- Electrocatalytic membranes, for organic pollutants decomposition,  
case study, 1081–1083
- Electrochemical disinfection, 1074
- Electrochemical oxidation, for organic pollutants  
removal, 1072–1074
- Electrochemical reactions, electrofiltration process, 226
- Electrochemical reduction, for metal ions, 1074
- Electrochemical treatment, of waste, 1072  
direct anodic oxidation, 1073  
indirect oxidation, 1073–1074
- Electrodialysis (ED), 1075–1076  
principle of, 836–837  
process in pulp and paper industry, 1000–1001
- Electrodialysis reversal, 1075–1076
- Electrodialysis with bipolar membranes, 582; *see also*  
Bipolar membrane  
applications of, 593–594  
case studies of, 624–627  
cell design and process configuration in, 590–591  
characteristics of, 589–590  
configurations, 588–589  
in food industry  
acid caseinate, 598–603  
apple juice, enzymatic reaction in, 603–606  
dairy wastewater, purifying of, 609–611  
passion fruit juice, deacidification in, 606–609  
soybean protein fraction, fractionation of, 614–615  
soy protein, 594–598  
STW, protein extraction in, 615–617  
whey protein, separation of, 611–614  
history of, 623–624  
principle of  
catalyst role in, 587–588  
EDBM configurations, 588–589  
H<sup>+</sup> and OH<sup>-</sup> generation, 584  
water dissociation in, 584–587  
usage of, 623
- Electrofiltration, 1074–1075  
electric field, filtration enhancement, 225  
pressure-driven membrane filtration, 224  
schematics of, 225
- Electrokinetic, 225–226
- Electrolyte-filled microporous membrane, 809–810
- Electromembrane processes principles;  
*see also* Electrodialysis  
with bipolar membranes  
bipolar membrane and electrodialysis, principle of, 584–589  
BPM technology, parameters of, 591–593  
conventional electrodialysis, principle of, 583–584  
ion-exchange membranes, 582–583
- Electromembranes, 1072
- Electronic devices, membranes applications in, 1141–1142
- Electropermeabilization, *see* Electroporation
- Electrophoretic mobility, 225
- Electroporation, 742  
applications of  
cell fusion and hybridoma technology, 750  
cells electroloading, 751–752  
electro cell manipulation, 751  
electrochemotherapy (ECT), 752  
electroinsertion of proteins, 753–754  
electroporative gene delivery, 753  
electrotransfection, 750  
ex vivo applications, 755  
food sterilization, 755  
overcoming chemoresistance, 750–751  
radio-electrochemotherapy (RECT), 752  
radioiodine incorporation into tumor cells, 754  
therapeutic applications, 750  
transdermal drug delivery, 755  
transgenic plants and animals, 755  
in vivo applications, 753  
water sterilization, 754  
in cell membrane (*see* Cell membrane, electroporation in)  
devices  
cuvettes and electrodes, 749–750  
electric pulse generators, 749
- Electroremediation, 1077
- Electroseparation, definition of, 1072
- Electrosorption, 1076–1077
- Electrosorption cell, 1080
- Electrosorption membranes, for wastewater treatment,  
case study, 1079–1081
- Elemental chlorine free, 992
- ELM, *see* Emulsion liquid membranes
- EMB, *see* Extractive membrane bioreactor
- Emulsion liquid membranes systems and process, 709, 890–894  
and actinides transport, 890–894  
advantages and disadvantages of, 710  
applications of  
for acids and bases separation, 728  
for anions separation, 727  
biochemicals separation, 732  
commercial applications of, 727, 733  
for metal ions separation, 724–727  
mixtures separation, 729–731  
demulsification, methods for  
chemical treatment, 723  
physical treatments, 723–724  
emulsification, components of  
carriers, 719  
diluents, 718–719  
internal phase, 719  
surfactant, 718  
model parameters  
Biot number, 715, 718  
Damköhler number, 718  
emulsion globule size, 712, 715–717  
internal droplet size, 712  
models for type 1 facilitation, 711–713  
models for type 2 facilitation, 712, 714–715  
permeation and settling, parameters of  
composition, 720–721  
membrane leakage, 722–723  
swelling, 721–722  
process of  
demulsification, 723–724  
emulsification, 718–719  
permeation and settling, 719–723  
theory and mechanism  
type 1 facilitation, 710  
type 2 facilitation, 710–711
- Emulsion pertraction  
modeling, 1029–1036  
technology, 824, 1058–1061
- Entrainment swelling, *see* Swelling, in ELM systems
- Enzymatic membrane reactors, 171–172
- Enzyme-emulsion membrane reactor, 1136–1137
- Epoxide activation, 42
- EPP, *see* Emulsion pertraction technology

Essential oils/SC CO<sub>2</sub> separation, 185  
 1-Ethyl-(3-(3-dimethylaminopropyl) carbodiimide hydrochloride, 474  
 Ethylendiamine tetraacetic acid, 849, 855, 897, 1114  
 Ethylenevinyl alcohol membranes, usages of, 428  
 ETS-10, 278, 293, 307  
 EVAL, *see* Polyvinyl alcohol-co-ethylene  
 EVAL hollow fiber membranes, 31  
 Ex situ hydrothermal synthesis, zeolite membrane  
   crystal growth mechanisms, 276–277  
   preferential orientation, 275  
   seeds, 274–275  
 Externally regulated delivery systems, 428–429;  
   *see also* Drug delivery, membranes in  
 Extracellular matrix, 456, 459–460, 475, 746  
 Extractive membrane bioreactor, 1018

## F

Facilitated transport, 74, 80, 109, 248, 373, 391, 710–714, 887;  
   *see also* Membrane contactors  
 Facilitated transport membranes, and gas separation, 79  
 Feed recirculation modules stage, schematic representation of, 157  
 Ferric salts recovery, 963–965  
 FHA, *see* Fuel handling area  
 Fick's law, 68  
 Film BOs, 673; *see also* Blood oxygenator  
 Fixed-site carriers membranes  
   carrier mobility in, 74, 79  
   facilitated transport of CO<sub>2</sub> in, 75  
 Flat-sheet devices, 347; *see also* Membrane extraction  
 Flat sheets membrane module, 500  
 Flat-sheet supported liquid membrane, 886  
 Flemion membranes, 789–794  
 FLM, *see* Flowing liquid membrane  
 Flow channel spacers  
   CFD simulations, 206  
   flux vs. transmembrane pressure, 204  
   net-type spacers  
   cost estimation for filtration, 205  
   geometrical characteristics of, 203  
   spacer geometry, characteristics of, 204  
   turbulence promoters  
   corrugated membranes, 208–210  
   flux-time profiles, with HB, RB, and NB modes, 208  
   helical baffle, schematics of, 207  
   helical inserts, 206–208  
 Flowing liquid membrane modules, 389  
 Fluid mosaic model, of plasma membrane, 744  
 Fluorinated ionomers, partially  
   Ballard Advanced Materials (BAM) ionomers, 797–799  
   FuMA-Tech membranes, 796–797  
   radiation-grafted membranes, 799–801  
 Flux enhancement  
   effect of gas velocity, 223  
   with vertical hollow fibers, 222  
 Food industries, EDBM applications in  
   acid caseinate, 598–603  
   apple juice, 603–606  
   dairy wastewater, purifying of, 609–611  
   fruit juice, 606–609  
   soybean protein fraction, fractionation of, 614–615  
   soy protein, 594–598  
   soy tofu whey, protein extraction, 615–617  
   whey protein, separation of, 611–614  
 Food processing  
   membrane distillation and applications, 540–544

  using ceramic membranes  
   pasteurization and sucrose crystallization, 162  
   valuable milk components, fractionation, 161  
 Fouling, 147, 155–157, 161, 164; *see also* Membrane fouling;  
   Reverse osmosis technology  
   definition of, 1105  
   Donnan exclusion and, 963  
   effect of spacers on permeate flux, 335  
   empirical models in, 655  
   flux prediction and, 651–652  
   layers and effect of humic acid on, 329–330  
   limitations of, 194–195  
   at membrane surface, 326–327  
   methods to control membrane, 197–198  
   prevention of, 1112  
   in radioactive waste treatment, 848–  
   resistance, modifications for improvement, 1109–1110  
   resistance of hydrophilic and hydrophobic membranes, 336  
   schematics  
   for Pore construction and blocking, 195  
 Four-component condensation reaction, 43–44  
 Free volume diffusion model, 76  
 FSC membranes, *see* fixed-site carriers membranes  
 FSSLM, *see* Flat-sheet supported liquid membrane  
 Fuel cell applications, membrane requirements  
   automotive applications  
   cooling requirements, 762  
   humidification requirements, 762–766  
   catalyst utilization and interfacial aspects, 770–773  
   for direct methanol fuel cells, 773  
   methanol crossover, 774  
   water permeation, 774  
   porous structure and permeability requirements, 768–770  
   portable applications (H<sub>2</sub>-fuelled PEMFC), 767–768  
   specific conductivities of electrolytes in, 761–762  
   stationary application  
   chemical and electrochemical degradation, 766–767  
   mechanical degradation, 766  
   thermal degradation, 766  
 Fuel cells  
   market predictions for, 94  
   structure of, 760–761  
   working principle of, 93  
 Fuel handling area, 934  
 Fuel reprocessing, perfluorinated membrane in, 938–939  
 FuMA-Tech membranes, 796–797

## G

Gaseous stream treatment, membrane contactors in  
   advantages of, 1053  
   designing of, 1052–1053  
   performance of, 1047–1052  
   principles of, 1042–1047  
 Gases, solubility and diffusivity of  
   in natural rubber, 70  
 Gas-liquid contact, use of, 12–13  
 2D-Gas model, 72  
 Gas separation membranes  
   carbon molecular sieving membranes  
   regeneration, 83  
   separation mechanism for, 80  
   separation properties for, 81–83  
   development of, 66  
   industrial application of, 91  
   aggressive gases, recovery of, 101  
   air separation, 98–99

- CO<sub>2</sub> removal, 94–98
  - hydrocarbon separation, 100
  - hydrogen recovery, 91–94
  - natural gas dehydration, 101
  - VOC recovery, 100
  - inorganic membrane, 67
    - modified, 85–86
    - structure and morphology, 85
    - transport mechanisms in, 84
  - ion-conducting (*see* Ion-conducting membranes)
  - mixed matrix membranes/nanocomposites
    - with CMS and nanoparticles, 84
    - composition of, 83
  - module design
    - flat sheet plate and frame/envelope type, 89
    - flow patterns, 88
    - hollow fiber membranes and membrane contactors, 90
    - spiral-wound membrane, 89
  - polymeric membranes
    - composite, 74
    - gas sorption isotherms for, 76
    - transport mechanisms (*see* Gas transport mechanisms)
  - Gas transport mechanisms; *see also* Facilitated transport
    - facilitated transport, 74
    - Fick's law, 68
    - ion-conductive transport, 73
    - Knudsen diffusion, 71
    - molecular sieving, 72–73
    - selective surface flow, 71–72
    - solution diffusion, 69–71
    - through fuel cell, 87
    - through porous membranes, 151–152
  - GDL, *see* Gluconodelta-lactone
  - Gentle sterilization method, in milk processing, 646
  - Glassy polymer membrane, hydrocarbon separation and removal
    - aromatic/alicyclic, and aliphatic
      - aromatic/alicyclic, separation of, 257
      - aromatic isomers, separation of, 257–258
      - diffusion, component of, 258–260
      - sorption, component of, 260–262
    - olefins and paraffins
      - chemical composition, effect of, 249–254
      - gases mixture, time dependence of, 256
      - permeability coefficients of, 249–250
      - permeability, diffusion and sorption coefficients, 250–251
      - permeation process, kinetics of, 256
      - polyphenylene oxides, 252
      - pressure dependence of, 254–255
      - separation of, 248
      - temperature dependence of, 255–256
      - unsaturated bonds, effect of, 248
  - Glassy polymers
    - flux and selectivity in, 76
    - solubility in, 75
  - Globulins 7 S protein, 614
  - Gluconodelta-lactone, 645
  - Glycerin dehydration, 121
  - Glycinin protein, 614
  - Gold nanotube membranes, 699, 1140
  - Gore-Select membranes, 786–789
  - Grafted membranes, 907–909
  - Grafting polymerization, 35
  - Groundwater treatment, by NF membranes, 1110
- H**
- Heaviside step function, 50
  - Heavy water reactors moderator, 874
  - HEDPA, *see* 1-hydroxyethane-1,1-diphosphonic acid
  - HEH(EHP), *see* Mono-2-ethylhexyl 2-ethylhexylphosphonate
  - Helium recovery, 101
  - HFC, *see* Hollow fiber contactor
  - HFCLM, *see* Hollow-fiber contained liquid membrane
  - HFLM, *see* Hollow-fiber liquid membrane
  - HFSLM, *see* Hollow fiber supported liquid membrane
  - HHT, *see* High heat treatment
  - HI, *see* Hydrophobicity index
  - High-Energy Accelerators Research Organization, 874
  - High heat treatment, 641
  - High milk protein powders, 648–649
  - High-purity nitrogen
    - applications, 98
    - membrane designs for producing, 99
  - High-purity oxygen, 99–100
  - High shear devices
    - rotating systems
      - boundary layer, radial gradient, 216
      - rotating disk dynamic membrane systems, 215–216
    - vibratory systems
      - vibrating flat sheet membrane module, 217
      - vibrating submerged hollow fiber membrane, 218
      - vibratory hollow fiber membranes, 217–218
      - vibratory shear-enhanced process, 216–217
  - High-temperature catalytic membrane reactors
    - configurations of, 172
    - integrated distributor/extractor membrane reactor, 173
  - HLM, *see* Hybrid liquid membrane
  - HMPP, *see* High milk protein powders
  - Hollow fiber contactor, 939
  - Hollow-fiber contained liquid membrane, 385–386
  - Hollow fiber devices, 347–348; *see also* Membrane extraction
  - Hollow-fiber liquid membrane modules, 390–391
  - Hollow fiber membranes
    - alternative configurations for, 90
    - module, 500–501
  - Hollow fiber module, 1107–1108
  - Hollow fiber supported liquid membrane, 885–886, 903–904
  - Hot gas filtration, using ceramic filters, 160
  - HPBI, *see* 3-phenyl-4-benzoyl-5-isoxazolone
  - H2-separating membrane technology, for CO<sub>2</sub> capture, 97
  - HTM, *see* Hydrogen transport membrane
  - HTTA, *see* 2-thenoyl trifluoroacetone
  - Hybrid liquid membrane, 372; *see also* Liquid membranes
    - model of, 374–379
    - modules, 388
  - Hydrocarbon permeation in glassy and rubbery polymers
    - kinetic factor of permeability
      - CED, diffusion coefficient of, 239
      - diffusing molecules, effective sizes of, 237
      - diffusion coefficients, concentration dependencies of, 240
      - polybutadiene, diffusion coefficients of, 238
    - thermodynamic factor
      - dual-mode sorption model, 234, 237
      - gases and vapors, physical properties of, 235
      - glassy polymers, solubility coefficient of, 236
      - Henry's solubility coefficient, 236
      - natural rubber, solubility coefficient of, 235
  - Hydrocarbon separation and removal, industrial
    - aromatic, alicyclic, and aliphatic, 264
    - gases and vapors, 262
    - process of, 263
  - Hydrodynamic techniques, 198
  - Hydrogel membranes
    - preparation of, 478
    - production and usages of, 474–476
    - properties of, 473

- responsive membranes, 476–478, 488–489
- theories for, 479–488
- Hydrogen applications
  - in fuel cells, 93–94
  - in transport sector, 94
- Hydrogen-fuelled PEMFC, 767
- Hydrogen recovery
  - membrane system for
    - Pd membrane and MMMs, 93
    - performance of, 92
- Hydrogen transport membrane, 173
- Hydrophilic membrane applications
  - in esterification reactions, 121
- Hydrophilic perfluoromembranes, 79
- Hydrophilic polymers
  - dehydration applications, 121
- Hydrophobically modified water-soluble polymer (HMWSP), 226
- Hydrophobic chromatography, 55
- Hydrophobicity index, 290
- Hydrophobic/organophilic polymers
  - dissolved organics removal, 123–127
- 1-Hydroxyethane-1,1-diphosphonic acid, 896
- Hyflon AD
  - permeability and selectivity, 79
  - structure of, 78
- Hyflon ion, 783–784
- H-ZSM-5 membrane
  - direct in situ hydrothermal synthesis, 274
  - esterification reactions, 299

## I

- IAEA, *see* International Atomic Energy Agency
- IDA, *see* Iminodiacetic acid
- IDF, *see* International Dairy Federation
- IEMs, *see* Ion-exchange membranes
- ILM, *see* Immobilized liquid membrane
- Iminodiacetic acid, 45
- Immobilized dyes, as pseudo-affinity ligands, 45
- Immobilized liquid membrane, 372
- Immunoaffinity techniques, 53
- IMR, *see* Inert membrane reactor
- INCT, *see* Institute of Nuclear Chemistry and Technology
- Industrial plant, for tannery effluents treatment, 1088, 1098–1099
- Industrial solvents, dehydration of, 294
- Industrial waste management, membrane application in, 823–825
- Inert membrane reactor, 296
- Inorganic membrane reactors, 295
  - applications of, 296–297
  - classification of, 296
- Inorganic membranes
  - applications in catalytic reactors, 169
    - biocatalytic membrane reactors, 171–172
    - gas–liquid reactions, 170–171
    - high-temperature catalytic membrane reactors, 172–173
  - for gas separation, 67–68, 84
  - modified, 85–86
  - preparation using supercritical fluids, 189
  - supercritical fluid separation, 181
  - transport regimes in, 85
- Inorganic supports, 33
- In situ copolymerization
  - for membrane modification, 35
- In situ hydrothermal synthesis, zeolite, 274
- Institute of Nuclear Chemistry and Technology, 849

- Insulin delivery
  - membranes in, 429–431
  - responsive membranes in, 488–489
- Integrated Pollution Prevention and Control, 1001
- Interdiffusion coefficient, variation of, 969–971
- Interfacial polymerization
  - thin layer deposition, 118
- International Atomic Energy Agency, 856
- International Dairy Federation, 648
- Ionac MC 3470 transport property, heterogeneity on, 972
- Ion-conducting membranes, 152
  - oxygen-conductive membranes, 87–88
  - Pd membranes
    - hydrogen permeation through, 87
    - preparation methods, 86
  - proton-conducting polymeric membranes, 87
- Ion-exchange chromatography, 54
- Ion-exchange membranes, 582; *see also* Electromembrane processes
  - principles
    - in electrodialysis, 582–583
- Ion transport membrane, 99
- IPPC, *see* Integrated Pollution Prevention and Control
- Isobutane dehydrogenation, 298
- ITM, *see* Ion transport membrane

## J

- JAERI, *see* Japan Atomic Energy Research Institute
- Japan Atomic Energy Research Institute, 838

## K

- Kaowool 700 Grade Paper, 1079
- KEK, *see* High-Energy Accelerators Research Organization
- Knudsen diffusion, in microporous inorganic membrane, 71
- Knudsen flow, 71
- Kozeny–Carman equation, 49

## L

- Lactobacillus* sp., 617–618
- Large volume parenteral, 424
- Layered bulk liquid membrane modules, 387
- Levonorgesterol, 460
- LIE, *see* Liquid ion exchange
- Ligand–ligate complexes, 45
- Ligands
  - classification of, 44
  - coupling reactions, polymers containing
    - amino groups, 43–44
    - carboxyl groups, 42–43
    - hydroxyl groups, 40–42
  - coupling, supports for, 44
  - and ligates, 45
- Light water reactor, 836, 838, 874
- Liquid filtration
  - nanofiltration with ceramic membranes, 164–165
  - in porous media
    - Donnan exclusion, 148
    - in nonaqueous liquids, 150
    - permeation flux, 147
    - retention mechanisms, 149
    - solvent flux, 148
    - transport of solute, 148–149
- Liquid–gas contact system
  - mass transfer resistance in, 10

- Liquid ion exchange, 947
- Liquid–liquid contact  
use of liquid–liquid extraction, 13
- Liquid–liquid extraction, 9, 346, 372
- Liquid membranes  
classifications of, 885–886  
extraction techniques  
three-phase liquid membrane extraction techniques, 349–350  
two-phase liquid membrane extraction systems, 350  
integrity of, 909–910  
stability of, 909–910  
theory of, 372–374  
transport  
classification of, 887–889  
numerical model, 379–385
- Liquid–phase inversion method, *see* Wet-phase inversion method
- Liquid radioactive wastes, 824, 850, 856, 862, 866, 872
- Liquid radioactive waste treatment, membrane  
application in, 824  
<sup>137</sup>Cs liquid wastes, 927–928  
future prospects of, 931  
<sup>125</sup>I liquid wastes, 924–926  
membrane distillation, 866–872  
membrane performance, radiation influence, 920–923  
microfiltration, 866  
nanofiltration, 854  
radiological protection, 928–930  
reverse osmosis, 850–854  
ultrafiltration, 854–857  
and complexation method in, 860–863  
pilot plant experiments, 863–866  
radionuclides removal, 858–860
- LLE; LLX, *see* Liquid–liquid extraction
- LMPS, *see* Low-moisture part-skim
- LNG, *see* Levonorgestrel
- Loose reverse osmosis, *see* Nanofiltration
- Low-active liquid waste, electro dialysis for, 937–938
- Low-moisture part-skim, 645–646
- LRWs, *see* Liquid radioactive wastes
- LVP, *see* Large volume parenteral
- LWR, *see* Light water reactor
- M**
- MABR, *see* Membrane-aerated biofilm reactor
- MALDI-MS, *see* Matrix-assisted laser desorption ionization mass spectroscopy
- MASE, *see* Membrane-assisted solvent extraction
- Mass transfer resistance, 10
- Matrix-assisted laser desorption ionization mass spectroscopy, 332
- MBR, *see* Membrane bioreactor
- MC, *see* Membrane contactors
- MCH, *see* Microcrystalline chitosan
- MCM-41 and MCM-48, 278
- MD, *see* Membrane distillation
- MDF, *see* Medium density fiberboard
- Mechanical pulp mill effluents, membranes usages in, 993
- Mediated electrochemical oxidation, 1073
- Medium density fiberboard, 1000
- Membralox membranes, in radioactive waste treatment, 858–859
- Membrane activation, reactions for  
polymers containing  
amino groups, 43–44  
carboxyl groups, 42–43  
hydroxyl groups, 40–42
- Membrane-aerated biofilm reactor, 1018
- Membrane applications  
in actinides separation (*see* Actinides separation)  
in beer industry (*see* Beer industry, membrane separation/application role in)  
in blood oxygenator (*see* Blood oxygenator)  
in dairy industry (*see* Dairy industry)  
in drug delivery (*see* Drug delivery, membranes in)  
electrically enhanced membrane processes (*see* Electrically assisted membrane process; Water purification, by ceramic membranes)  
in electroporation (*see* Cell membrane, electroporation in; Electroporation)  
ELM (*see* Emulsion liquid membranes systems)  
in food and bio-industries (*see* Bipolar membrane; Electrodialysis with bipolar membranes)  
in gaseous stream treatment (*see* Gaseous stream treatment, membrane contactors in)  
industrial tannery effluents treatment (*see* Membrane bioreactor; Reverse osmosis pilot plant, for tannery effluents treatment)  
in industrial waste management, 823–825  
liquid radioactive waste, treatment of (*see* Liquid radioactive waste treatment, membrane application in)  
in membrane engineering, 1131–1132 (*see also* Reverse osmosis technology)  
in metallic pollutants treatment (*see* Metallic pollutants treatment, membrane-assisted solvent extraction)  
in nanofiltration technology (*see* Nanofiltration; Nanofiltration membranes)  
nanotube membranes (*see* Nanotube membranes, for bioseparations)  
in organic hybrid liquid membrane (*see* Organic hybrid liquid membrane)  
in pharmaceutical industry (*see* Pharmaceutical industry, membrane application in)  
proton-conducting membranes, for fuel cells (*see* Fuel cell applications, membrane requirements; Perfluorinated sulfonic acid membranes)  
in pulp and paper industry (*see* pulp and paper industry)  
in radioactive nuclear plant waste (*see* Radioactive nuclear plant waste, membrane application in)  
radioactive waste, treatment of (*see* Radioactive wastes, treatment of) strip dispersion technique  
(*see* Pseudo-emulsion based hollow fiber strip dispersion; Strip dispersion technique)  
in wastewater treatment (*see* Wastewater treatment)  
water treatment residuals, DMP in coagulants recovery (*see* Water treatment residuals, DMP in coagulants recovery)
- Membrane-assisted solvent extraction, 350  
in metallic pollutants treatment, 1023  
emulsion pertraction processes, modeling, 1029–1036  
future perspectives of, 1036–1037  
nondispersive solvent extraction modeling, 1024–1029
- Membrane-based gas separation, 1134–1135
- Membrane bioartificial organs, 1137–1139
- Membrane bioreactor, 196, 982  
biological unit and membrane module of, 159  
pilot plant, for tannery effluents treatment, 1089–1090  
biological oxygen demand (BOD<sub>5</sub>) evolution, 1091–1092  
chemical oxygen demand (COD) evolution, 1091  
chromium and sulfide elimination, 1093–1094  
nitrogen evolution, 1092–1093  
phosphorus concentration in, 1094  
suspended solids and volatiles, in permeate, 1091–1092  
potential applications of, 159–160  
in pulp and paper industry, 996–998  
role in chemical industry, 823  
in wastewater treatment, 1007  
advantages of, 1008, 1019–1020  
mechanisms of, 1014–1018  
membrane-aerated biofilm reactor, 1018–1019  
operating principle of, 1008–1009  
performance of, 1009–1014

- Membrane chromatographic system  
 advantages of, 46–47  
 applications of  
   cation-exchange membranes, 55  
   immunoglobulin preparation, 55  
   ion-exchange chromatography, 54  
   proteins, purification and analysis, 53  
   supercoiled plasmid DNA separation, 54  
 commercially available supports in, 51–52  
 loading capacity, 46  
 membrane layers, 27  
 stationary phase, 26
- Membrane contactors, 4, 1142–1143  
 applications of, 7  
   absorption of gaseous species, 12–13  
   air/gas streams, treatment and conditioning, 13  
   in liquid–liquid extraction, 13–14  
   ozonation, 166  
   VOC separation, 12  
 commercial installations  
   for carbonation and deoxygenation, 19  
   central ultrapure water degasification system, 17  
   for liquid–liquid extraction, 20  
   membrane degasifier system, 17–18  
   for osmotic distillation, 19  
   semiconductor plant ultrapure water production process, 16  
   in water purification systems, 17–18  
 commercial installations of, 15  
 definition of, 1041–1042  
 designs  
   module, CO<sub>2</sub> removal, 90–91, 97  
   parallel-flow and transverse-flow, 14  
   variation with baffle, 15  
 in gaseous stream treatment  
   advantages of, 1053  
   designing of, 1052–1053  
   performance of, 1047–1052  
   principles of, 1042–1047  
 mass transfer process in  
   mass transfer coefficients, 11  
   mass transfer resistance, 10–11  
 membranes used in, 8  
 principle of operation  
   capillary force, 8–9  
   liquid–gas interface, 9–10  
 rectangular, 15  
 supercritical fluid, 187
- Membrane contactor technology, benefits of, 10
- Membrane degasification, 17
- Membrane distillation, 13, 867  
 plant effluent  
   chemical composition of waste in, 869  
   radiochemical composition of, 869
- Membrane electrode assembly (MEA), in fuel cells, 760–761, 766
- Membrane emulsification, 1138  
 advantages of, 165  
 application areas of, 166
- Membrane engineering, 1131–1132
- Membrane extraction with a sorbent interface  
 technique, 360
- Membrane fabrication methods, 116–117
- Membrane filtration  
 concentration polarization boundary layer, 194  
 constant flux mode, 195  
 module cost, 198  
 performance enhancement, Methods of, 197
- Membrane flow channel equipped, schematics of, 210
- Membrane fouling, 195, 504, 566, 1014–1015, 1074, 1105;  
*see also* Membrane bioreactor  
 analytical strategies  
   bacterial cells passage, through membrane pores, 331  
   cell adhesion kinetics assessment, 331  
   concentration polarization measurement, 332  
   flux decline, models for, 332–333  
   fouling layer measurement, 331  
   gel-layer thickness variations, 333–334  
   membrane surface deposits, analysis of, 332  
   microbial adhesion, hydrodynamic studies on, 331  
   pore blockage and cake formation, 334  
 effect of spacers on permeate flux, 335  
 and gas separation processes, 338–339  
 humic acids fouling, 329–330  
 hydrodynamic methods, 197–198  
 inorganics, proteins, and colloids fouling, 330  
 in membrane separation of beer, 558–560  
 microbiological fouling, 327–329  
 minimization methods for  
   critical flux, control of, 336–337  
   hydrophilic membranes resistance, 336  
   membrane cleaning, by cleaning agents, 337  
   membrane surface modification, 336  
   pretreatment process, of feed water, 334–335  
   spacer thickness effects, 335  
 transition from reversible adsorption, to irreversible fouling, 330
- Membrane gas separation  
 driving force of, 66  
 potential and limitations of, 66  
 recycled gas, system design, 91
- Membrane materials, for gas separation, *see* Gas separation membranes
- Membrane module  
 ceramic membrane  
   filtration mode, 153, 155  
   transmembrane pressure, 154  
 composite membranes, 117–118  
 in membrane distillation, 535–538  
 pervaporation, 118–119  
 role in chemical industry waste treatment, 823–824  
 selection of, 119
- Membrane processes  
 flow channel spacers  
   net-type spacers, geometrical characteristics of, 203–206  
   tubular membrane, 206–210  
 limitations and enhancement  
   concentration polarization and fouling, 194–195  
   critical flux and sustainable flux, 195–197  
   methods to control, 197–198  
 membrane fouling, 195  
 pressure-driven, 195  
 pulsed flow  
   hydrodynamic characteristics of, 210–212  
   pulsatile flow-enhanced, 212–214  
   transmembrane pressure backshock technique, 214–215  
 secondary flow  
   Dean flow, characteristics of, 198–199  
   membrane performance, enhancement of, 199–201  
   Taylor flow, characteristics of, 201–202  
   Taylor flow, membrane filtration, 202–203  
 two-phase flows  
   gas–liquid mixture, 218–223  
   solid–liquid, by particle addition, 223–224
- Membrane proton conductivity, and interaction with water, 774–776
- Membrane(s), 195; *see also* Membrane applications; Membrane processes;  
 Membrane technologies; specific membranes  
 bioseparation, ultrafiltration in  
 bioseparation engineering in, 497–498

- clarification and macromolecular fractionation in, 509–511
- concentration process in, 504–505
- desalting in, 505–509
- membranes in, 499–502
- ultrafiltration in, 498–499
- cell technology, 938–939
- classification of, 427–428
- distillation, 513–514
  - air gap membrane distillation, 526–528
  - direct contact membrane distillation, 515–525
  - in food processing, 540–544
  - future perspectives of, 544
  - historical perspectives of, 514–515
  - membrane module for, 535–538
  - membranes in, 533–535
  - osmotic membrane distillation, 531–532
  - sweeping gas membrane distillation, 529–531
  - transmembrane flux enhancement in, 538–539
  - vacuum membrane distillation, 528–529
- element types of, 500
- extraction
  - apparatus for, 357–361
  - applications of, 361–362
  - liquid membrane extraction techniques, 349–350
  - membrane devices for sample preparation, 347–349
  - sample preparation and techniques of, 346–347
  - solid/polymeric membrane extraction techniques, 350
  - theory and principles of, 351–357
- gas permeability measurements, 769–770
- importance in industrial processes, 1071–1072
- separation processes, 1102–1103
  - industrial applications, 4
- Membrane separation systems, module design for, 387–393
- Membrane technologies, 3, 409–410
  - and applications of
    - bioartificial organs, 1137–1139
    - catalytic membrane reactors (CMRs), 1135–1137
    - electronic devices, 1141–1142
    - membrane-based gas separation, 1134–1135
    - membrane contactors (MCs), 1142–1143
    - in nanotechnology, 1139–1141
    - seawater desalination, 1132–1134
    - in space and other planets, 1139
  - and desalination, 1132–1134
  - direct flow filtration, 410–411
  - tangential flow filtration, 411–415
- Membrane transfer coefficient, 11
- MEMS, *see* Microelectromechanical systems technology
- MEO, *see* Mediated electrochemical oxidation
- MESI technique, *see* Membrane extraction with a sorbent interface technique
- Metal affinity chromatography, applications of, 54
- Metal ion removal, from wastewaters, 710–711
- Metal ion transport, mechanism of, 888–889
- Metallic pollutants treatment, membrane-assisted solvent extraction, 1023
  - emulsion pertraction processes, modeling, 1029–1036
  - future perspectives of, 1036–1037
  - nondispersive solvent extraction modeling, 1024–1029
- Methyl-*tert*-butyl ether, 295, 299
- Methyl tertiary-butyl ether, 1012
- MF, *see* Microfiltration
- MF ceramic Membralox membranes, in dairy industry, 663
- MFGM, *see* Milk fat globule membrane
- MHS, *see* Multimembrane hybrid systems
- Microchemical systems, 309
- Microcrystalline chitosan, 857
- Microelectromechanical systems technology, 1141
- Microfiltration, 844, 1102–1103, 1132
  - Microfiltration membrane
    - process in pulp and paper industry, 985–986
    - and radioactive waste treatment, 836
  - Micropollutant removal, membrane bioreactor in, 1011–1012
  - Microporous hollow fiber membrane
    - in membrane contactor, 8
  - Microporous membrane BOS, 673; *see also* Blood oxygenator
  - Microporous membrane liquid-liquid extraction, 350
    - mass transfer of, 354
  - Microporous membranes
    - single-gas transport through, 280–282
    - transport mechanisms in, 69
  - Microtechnologies, membranes in, 464
  - Milk fat globule membrane, 649
  - Milk microfiltrate WPI, 646
  - MIP, *see* Molecular imprinted network
  - Mixed liquor suspended solids, 996, 1008
  - Mixed matrix membranes
    - with CMS and nonporous nanoparticles, 84
    - with microporous filler, 83
    - molecular separation by, 83
  - Mixed office waste, 998
  - MLSS, *see* Mixed liquor suspended solids
  - 3M membranes, 784, 786
  - MMLLE, *see* Microporous membrane liquid-liquid extraction
  - 3M modules, 52
  - Molecular imprinted network, 462
  - Molecular imprinting technique,
    - principle of, 38
  - Molecular imprinting technique, principle of, 38
  - Molecular sieving
    - molecular size, 72
    - temperature effects on, 73
  - Molecular weight cut-off, 410, 636, 835; *see also* Nominal molecular weight cut-off
  - Mono-2-ethylhexyl 2-ethylhexylphosphonate, 890
  - Monolithic molecularly imprinted polymers, preparation of, 38
  - Monolithic stationary phases, 27
    - preparation of, 35
      - organic polymer monoliths, 36–38
      - silica monoliths, 36
  - Monolith membrane elements, 141; *see also* Ceramic membranes
  - Mosaic Systems, 52
  - MOW, *see* Mixed office waste
  - MTBE, *see* Methyl-*tert*-butyl ether; Methyl tertiary-butyl ether
  - Multichannel ceramic membranes, 141
  - Multimembrane hybrid systems, 388–389
  - Multistage chromatography, 55
  - Municipal carbonaceous removal, membrane bioreactor in, 1009–1010
  - MWCO, *see* Molecular weight cut-off
  - MWPI, *see* Milk microfiltrate WPI
- N**
- NaA zeolite membrane
  - etherification reactions, 299
  - optical fiber coated with, SEM images of, 311
  - pervaporation performance for, 292
  - synthesis on  $\alpha$ -alumina tubular supports, 308
  - XRD spectra of, 272
- Nafion 117 alum recovery, kinetic treatment, 968–969
- Nafion membrane, 304–305, 762, 769, 772, 774, 777, 782, 794, 806, 810, 874, 963
- Nafion 117 transport property, heterogeneity on, 972
- Nanocomposites, separation efficiency, 83
- Nanofiltration
  - applications of, 1110–1111
  - with ceramic membranes, 164–165

- commercial nanofiltration plant operations
    - cycle 1, 1118–1119
    - cycle 2, 1120
    - membrane cleaning and storage, 1120
  - coupling with SCF extraction, 185–186
  - definition, given by IUPAC, 1104
  - future research in, 1111–1112
  - history of, 1102
  - liquid radioactive waste treatment by, 854
  - membrane materials, 1106–1107
  - membrane modification, 1108–1110
  - membrane modules, 1107–1108
  - membrane process, in pulp and paper industry, 986
  - radioactive waste treatment by, 833
  - sodium thiocyanate extraction in acrylic
    - fiber industries(case study)
      - commercial nanofiltration plants, 1118–1120
      - concentration vs. conductivity analysis, 1115
      - economic estimation, 1122–1123
      - materials required, 1114
      - membrane cleaning and maintenance, 1115–1116
      - membranes and their preparation, 1114
      - nanofiltration procedure, 1115
      - performance analysis, of different membranes, 1116–1117
      - pilot-scale nanofiltration system, 1114
      - process description, 1112–1113
      - scope and objectives, 1113
      - simulation and design, 1120–1121
    - synthesis of membranes, 1107–1108
    - theory of, 1102–1103
      - Donnan effect, 1104
      - sieving effect, 1104
  - Nanofiltration membranes
    - commercial types and characteristics, 1107
    - polymers, chemical structures of, 1106
  - Nanoporous proton-conducting membranes, 810
  - Nanostructured materials and membrane
    - technology, 1139–1141
  - Nanotechnologies, membranes in, 464
  - Nanotube membranes, for bioseparations
    - amino acids separation, by apoenzymes, 702–704
    - antibody-functionalized membranes, for enantiomeric separations, 698–699
    - DNA-functionalized nanotube membranes, for DNA separations, 699–702
  - Nanotubes, template synthesis of, 694–695
  - NASA and membrane technology projects, 1139
  - Natural gas
    - dehydration using membranes, 101
    - sweetening, 96
  - Natural organic matter, 825, 946
  - NCN, *see* Noncasein nitrogen
  - NDM, *see* Nonfat dry milk
  - NDSX, *see* Nondispersive solvent extraction technology
  - NF, *see* Nanofiltration
  - NF membranes, surface modification of
    - for improving fouling resistance, 1109–1110
    - for improving performance, 1109
  - NMR, *see* Nuclear magnetic resonance
  - NMWC0, *see* Nominal molecular weight cut-off
  - N,N*-di-*n*-butyloctanamide, 892
  - Noble gases separation, in radioactive waste, 875
  - NOM, *see* Natural organic matter
  - Nominal molecular weight cut-off, 504
  - Noncasein nitrogen, 645
  - Nondispersive solvent extraction, 939
    - modeling of, 1024–1029
  - Nondispersive solvent extraction technology, 1059–1060
  - Nonfat dry milk, 642
  - Nonporous membrane BOs, 673; *see also* Blood oxygenator
  - NP-PCMs, *see* Nanoporous proton-conducting membranes
  - Nuclear Energy Agency of the Organisation for
    - Economic Co-operation and Development, 873
  - Nuclear industry waste treatment, membrane application in, 824–825
  - Nuclear magnetic resonance technique, 332, 438
  - Nuclear technology, future of membrane processes in
    - application of, 873–875
    - liquid radioactive waste processing, 872–873
  - Nutrient removal, membrane bioreactor in, 1010–1011
  - Nylon membranes, 30
- ## O
- OCC, *see* Old corrugated containers
  - Octyl-phenyl acid phosphate, 896
  - Octyl(phenyl)-*N,N*-diisobutylcarbamoylmethylphosphine oxide, 899, 900
  - OECD/NEA, *see* Nuclear Energy Agency of the Organisation for
    - Economic Co-operation and Development
  - OHLM, *see* Organic hybrid liquid membrane
  - Old corrugated containers, 998
  - OMD, *see* Osmotic membrane distillation
  - OPAP, *see* Octyl-phenyl acid phosphate
  - Optical sensors, 310–311
  - Ordered microporous structures, 278
  - Organic compounds/SC CO<sub>2</sub> separation, 185
  - Organic dehydration, with zeolite membranes, 294
  - Organic hybrid liquid membrane, 372
    - applications of, 393–398
    - membrane usage in, 392–393
    - theory of, 372–374
  - Organic–organic separations, 129–131
    - azeotropic mixture, 128, 131
    - parameters influencing membrane polymer selection in, 128
  - Organic polymer monoliths
    - preparation of, 36
    - polymethacrylate-based monoliths, 37–38
    - polystyrene-based monoliths, 37
  - Organics
    - dehydration of, 122–123
      - glycerin, 121
      - Poly(vinyl alcohol) for, 120
    - removal from aqueous phase
      - by hydrophobic membranes, 123–127
      - by liquid–liquid separator, 127
    - removal from water, 294–295
  - Organic separation, 295
  - Organosilicon polymers
    - effect of chemical structure of, 241
    - hydrocarbon/nitrogen permselectivity, 243
    - mass transfer properties of, 242
    - permeability coefficients, dependence of, 242
  - Organosilicon polymers, effect of chemical structure of, 241
  - Osmotic distillation, 13
  - Osmotic evaporation, *see* Osmotic distillation
  - Osmotic membrane distillation, 514–515, 531–532
  - Osmotic pressure, 1104
  - Osmotic swelling, *see* Swelling, in ELM systems
  - OTM, *see* Oxygen transport membrane
  - Oxygen-conductive membranes, 87–88
  - Oxygen-enriched air, 98
  - Oxygen-ion conducting membranes
    - membrane concepts for, 146
  - Oxygen separation and membrane technology, 1135
  - Oxygen transport membrane, 173

## P

- PAA, *see* Polyacrylic acid
- Packed beds, chromatographic column  
diffusion process, 46  
drawback of, 25  
pressure drop and bed height, 25–26
- Parallel-flow design, 14–15; *see also* Membrane contactors
- Particle-loaded fiber module, 52–53
- Particle-loaded membranes, 40  
with embedded C8 hydrophobic adsorbents, 55  
preparation of  
in cast form, 38–39  
disadvantages of, 39  
phase inversion, 40
- Passiflora edulis f. flavicarpa*, 606
- Passive transport, 109
- PBI, *see* Poly(2,20-[mphenylene]-5,50-bibenzimidazole)
- PCDCs, *see* Pressure-controlled delivery capsules
- PDMS, *see* Poly(dimethyl)siloxane
- PE, *see* Polyethylene
- Peclet number, definition of, 48
- PEHFSD, *see* Pseudo-emulsion based hollow fiber strip dispersion
- PEI, *see* Polyethyleneimine
- PEMEAS (Celanese) membranes, 811–814
- PEMFCs, *see* Polymer electrolyte membrane fuel cells
- Penicillin acylase enzyme, 419
- Perfluorinated membranes  
application of, 938–939  
mechanically reinforced  
Aciplex membranes, 794–796  
Flemion membranes, 789–794  
Gore-Select membranes, 786–789
- Perfluorinated polymers, 78
- Perfluorinated sulfonic acid membranes, 776  
commercial membranes, trade name, 776–777  
DuPont nafion membranes, performance of, 777–780  
Nafion PFSA membranes, 777  
PFSA monomers and polymers, synthesis of, 780–782  
properties of, 776  
short side chain perfluorinated sulfonic acid membranes, 782–786
- Perfluorosulfonylfluoride ethyl propyl vinyl ether, 780–782
- Perfusion chromatography, particles for, 26
- Periodate oxidation, of polysaccharide supports, 42
- PERMA membranes  
PERMA-250, 1114, 1116–1117, 1120, 1123–1124  
PERMA-400, 1114, 1116
- Permeance, 68
- Permeants, concentration polarization and permeation, 114–115
- Permeation  
concentration polarization and, 114–115  
gas, 151  
measurements, 273–274
- Perovskite membranes, 1135
- Pervaporation  
applications of  
aroma compounds, recovery of, 127–128  
in biotechnology industry, 128  
dehydration of organics, 120–123  
effluent treatment, 123–127  
organic–organic separations, 128–131  
ideal membrane for  
characteristics of, 116  
methods to prepare, 117  
mechanism, classification of, 109  
potential applications and advantages, 108  
problems in industrial use of  
membrane fouling, 119  
salt ingress, 120
- PSCF model (*see* Preferential sorption-capillary flow model)
- selectivity in, 115–116
- solute transport in  
chemical potential gradient, 109  
preferential sorption–capillary flow model, 109–110  
solution diffusion model, 110–114  
solution diffusion model (*see* Solution diffusion model)
- turbulence rates, membrane surface, 115
- PFR, *see* Plug flow reactor
- PFSA, *see* Perfluorinated sulfonic acid
- Pharmaceutical industry, membrane application in  
direct flow filtration, 410–411  
enzymes and antibiotics, 419–423  
future prospects of, 425  
ingredients of, 423–424  
parenterals solution, 424  
plasma fractionation, 415–419  
tangential flow filtration, 411–415
- Phase inversion, 29, 116  
in membrane formation, 34  
technique in NF membranes, 1107–1108  
for UF and RO processes, 117
- Phase separation process, 189–190
- PHEMA, *see* Polyhydroxy 2-ethyl methacrylate
- Phenol removal, from wastewaters, 710
- 3-phenyl-4-benzoyl-5-isoxazolone, 895
- Phosphocaseinate, 643
- Photomechanical wave drug delivery devices, 458;  
*see also* Drug delivery, membranes in
- PHWR, *see* Heavy water reactors moderator
- PIM, *see* Polymer inclusion membranes
- Plate and frame systems, 1107–1108
- PLGA, *see* Poly(lactic acid-co-glycolic acid)
- Plug flow reactor, 48
- Plutonium, separation and extraction of, 940–941
- PMMA, *see* Poly(methyl methacrylate)
- PNIPAAm, *see* Poly(*N*-isopropylacrylamide)
- Polishing loop degasification system, 17
- Polyacrylamide gels  
advantage in chromatographic processes, 31  
synthesis of, 30
- Polyacrylamide monoliths, preparation of, 37
- Polyacrylic acid, 447, 857
- Polyamides, 29–30
- Polycarbonates  
permeabilities and selectivities for, 70, 78  
structures of characterized families of, 77
- Polydimethylsiloxane, hydrocarbon activity, 243
- Poly(dimethyl)siloxane  
for organics removal, 123–127
- Polyetheretherketone (PEEK-WC) membranes, 1138
- Polyetherurethane-urea membranes, 33
- Polyethylene, 535  
and polypropylene membranes, microporous surface modification, 31
- Polyethyleneimine, 836, 857–858
- Poly(glycidyl methacrylate-co-ethylene dimethacrylate), 38
- Poly(GMA-co-EDMA)-based monoliths, 38
- Polyhydroxy 2-ethyl methacrylate, 541
- Polyimides  
Matrimid, 79  
permeabilities and selectivities of, 78  
structures of characterized families of, 77
- Poly(lactic acid-co-glycolic acid), 461

- Polymer electrolyte membrane fuel cells  
 design and working, 760–761  
 uses of, 761
- Polymeric membranes  
 aminated, facilitated transport of CO<sub>2</sub>, 80  
 basic transport mechanism through, 75  
 block copolymers, 78–79  
 cardopolymers, 79  
 fixed-site carrier polymers, 79–80  
 flux and selectivity, 76  
 gas sorption isotherms for, 76  
 preparation by  
 phase separation process, 189–190  
 wet-phase inversion method, 189  
 selectivity and permeability, relationship between, 84  
 T<sub>g</sub> of, 76
- Polymer inclusion membranes, 904–907  
 in actinide separation, 904–907
- Polymer membranes, with inorganic acid  
 impregnation, 810–814
- Polymethacrylate-based monoliths, preparation of  
 poly(GMAco-EDMA) monoliths, 38  
 polymerization mixture, 37
- Poly(methyl methacrylate), 429
- Poly(2,20-[mphenylene]-5,50-bibenzimidazole), 810–811
- Poly(*N*-isopropylacrylamide), 474
- Polypropylene, 535
- Polystyrene, 32
- Polystyrene-based monoliths, preparation of, 37
- Polysulfone and polyethersulfone, 32
- Polytetrafluoroethylene, 535, 866  
 microporous composite membranes, 33  
 structure of, 32
- Polyvinyl alcohol, 541  
 cross-linking with maleic anhydride, 120–121  
 for organics dehydration, 120
- Polyvinyl alcohol-co-ethylene, 31
- Polyvinyl chloride membranes, 33
- Poly(vinylidene fluoride), 447, 535, 867
- Polyvinylpyrrolidone, 857
- Polyvinyltrimethylsilane, 875
- Porous support, zeolite membranes, 270–271, 306–307
- Posttreatment processes, zeolite membranes, 277
- PP, *see* Polypropylene
- PPCN, *see* Phosphocaseinate
- Preferential sorption-capillary flow model  
 forces acting on permeants, 109–110  
 limitations of, 110
- Pressure-controlled delivery capsules, 454
- Pressurized heavy water reactors, 831
- Pretreatment processes, zeolite membranes, 277
- Procion Red HE-3B, 53–54
- α-1-Protease inhibitor protein, 417
- Protein immobilization  
 EVAL hollow fiber membranes for, 31  
 polymeric supports for, 43  
 reactions for, 44
- PSCF model, *see* Preferential sorption-capillary flow model
- PSEPVE, *see* Perfluorosulfonyl fluoride ethyl  
 propyl vinyl ether
- Pseudo-biospecific ligands, in membrane  
 chromatography, 44
- Pseudo-emulsion based hollow fiber strip dispersion, 824  
 advantages of, 1058  
 application of  
 actinides extraction, 1065–1068  
 in metal separation, 1059–1065  
 working function of, 1058–1159
- PTFE, *see* Polytetrafluoroethylene
- Pulp and paper industry, 981–982  
 case studies of membrane application  
 with biological treatment, 995–998  
 in board, recycling paper mill and deinking,  
 998–999  
 in coating and MDF effluents treatment, 1000  
 freshwater treatment, 999–1000  
 in paper and pulp mill, 989–995  
 electro dialysis in, 1000–1001  
 future perspectives of membrane application, 1001  
 membrane modules and filters, importance in, 986–988  
 membrane processes in  
 microfiltration membranes in, 985–986  
 ultrafiltration and nanofiltration membranes in, 986  
 membrane separation features in  
 membrane properties, 983–984  
 solution and filtration properties, 984–985
- Pulsed flow  
 pulsatile flow-enhanced  
 cake-resistance reduction, 213  
 collapse-tube pulsation generator, 214  
 mechanisms of, 212  
 pressure waveforms, 213  
 pulsatile flow, hydrodynamic characteristics of  
 plasma flux, flow deflector-equipped channel, 210  
 pulsed pressure gradient, 212  
 simulated waveforms, 211  
 between two points, 211  
 transmembrane pressure backshock technique, 214–215
- PUREX process and radioactive waste treatment, 840
- PV, *see* Pervaporation
- PVA, *see* Polyvinyl alcohol
- PVC membranes, 33
- PVD, *see* Polyvinylpyrrolidone
- PVDF, *see* Poly(vinylidene fluoride)
- PVTMS, *see* Polyvinyltrimethylsilane

## R

- Radiation-grafted membranes, 799–801
- Radiation-initiated grafting, of polymer films, 118
- Radioactive nuclear plant waste, membrane application in  
 electro dialysis in, 937–938  
 NDSX in separation and removal of actinides, 939–943  
 perfluorinated membrane in, 938–939  
 ultrafiltration and reverse osmosis, 933–936
- Radioactive wastes  
 characteristics of, 861  
 MD distillation advantages for, 867  
 origin of, 920  
 sources and characteristics of, 828  
 treatment of  
 chemical, sorption and ion exchange, 829  
 complexation ultrafiltration, 834–836  
 diffusion and donnan dialysis, 838–839  
 electrodeionization, 838  
 electro dialysis, 836–838  
 evaporation, 828  
 liquid membranes, 839–840  
 membrane methods, 844–850  
 membrane processes, 829–831  
 microfiltration, 836  
 nanofiltration, 833  
 osmotic concentrator, 836  
 polymeric membranes, 840  
 precipitation ultrafiltration, 834

- RO, 831–833
    - ultrafiltration, 833–834
    - uranyl nitrate, production of, 840
  - Radioimmunoassay liquid waste treatment, 924–926
  - Radionuclides removal, in liquid radioactive waste treatment, 858–860
  - Recovery, isolation, purification, and polishing scheme, 497
  - Residence time distribution, 49
  - Responsive hydrogel membranes, 476–478
    - in drugs delivery, 488–489
  - Reverse osmosis, in radioactive waste treatment
    - <sup>137</sup>Cs contaminated water, 927–928
    - <sup>125</sup>I liquid wastes treatment, 924–926
    - membrane performance, radiation influence, 920–923
    - radiological protection, 928–930
  - Reverse osmosis membranes, 185
  - Reverse osmosis pilot plant, for tannery effluents treatment, 1094
    - Osmonics reverse osmosis membrane, 1096–1098
    - Toray reverse osmosis membrane, 1096–1098
  - Reverse osmosis technology, 844, 1102–1103
    - and desalination, 1132–1134
    - in waste streams treatment, 934–937
  - RIA, *see* Radioimmunoassay
  - RIPP scheme, *see* Recovery, isolation, purification, and polishing scheme
  - RO, *see* Reverse osmosis
  - Robeson plot, 67
  - Rotating disc modules, 387
  - RTD, *see* Residence time distribution
  - RTD measurement, 50
  - Rubbery polymer membrane
    - hydrocarbon separation and removal from aqueous solutions
      - application of, 246–247
      - PTMSP, aging effects of, 247
    - hydrocarbon separation and removal from gas mixture
      - block copolymer plasticization, 244
      - organosilicon polymers, chemical composition effect of, 240–243
      - organosilicon polymers, chemical structure effect of, 241
      - organosilicon polymers, mass transfer properties of, 242
      - plasticization effects, 243–245
      - polytrimethylsilylpropyne, gas mixtures, 246
      - temperature dependence of, 245
      - thermal effect of, 245–246
- S**
- Sabatier process, 1139
  - SBR, *see* Sequenced batch reactor
  - Scanning electron microscopy, 331–332
  - SC CO<sub>2</sub>, *see* Supercritical carbon dioxide
  - Schiff base formation reaction, 43
  - Schroeder's paradox, 772
  - SDI, *see* Silt density index
  - Seawater desalination, membrane system for, 1133
  - Seawater reverse osmosis plant, 1134
  - Seawater treatment, by NF membranes, 1110
  - Secondary flow
    - Dean vortices
      - coiled helical tube, Dean flow, 199
      - Dean flow, characteristics of, 198–199
      - Dean generator test cell, configuration of, 200
      - enhancement of membrane performance, 199–201
      - permeation flux-time profiles for filtration, 200
    - Taylor flow
      - axial rotatory membrane module, 201
      - Characteristics of, 201–202
      - membrane filtration with, 202–203
      - rotation speed for filtration, 202
  - Selective surface flow
    - mechanism of, 71–72
    - selective adsorption, 72
  - Self-regulated delivery systems, 428–429; *see also* Drug delivery, membranes in
  - SEM, *see* Scanning electron microscopy
  - Semiconductor plant ultrapure water production process, 16
  - Separation factor for gases, 68
  - Sequenced batch reactor, 998
  - SGMD, *see* Sweeping gas membrane distillation
  - Short interfering RNA and electroporation, 753
  - SHP, *see* Super high permeation
  - Sieving effect, in NF membranes, 1104
  - Silicalite-1 membranes
    - for catalyst retention, 306
    - hydrophilic acid-proof, 294
    - organic separations by, 295
    - preparation of, 310
    - SEM images of, 275–276
    - Si/Al ratio, 290
  - Silica monolithic supports, 33
    - preparation of, 36
  - Silica nanotubes
    - chemical and biochemical extractions by, 696–697
    - differential functionalization in, 695–696
    - in drug detoxification, 697
  - SIL-1 microcrystals
    - monolayer assembly of, 275
    - SEM analysis of, 276
  - Silt density index, 998
  - Simple-pass modules stage, 155–156
  - Simulated milk ultrafiltrate, 650
  - Simulated oxygenator, schematics of, 209
  - Single-cell electroporation, 755–756
  - Single-gas permeation experiments, 273
  - Single-gas permeation, on zeolite membranes
    - qualitative model of, 280
      - hydrocarbon permeance, 281–282
      - thermal effects, 281
    - quantitative model of, 282
  - siRNA, *see* Short interfering RNA
  - SLM, *see* Supported liquid membrane
  - SLMSD, *see* Supported liquid membrane with strip dispersion
  - Small volume parenteral, 424
  - SMUF, *see* Simulated milk ultrafiltrate
  - Sodium polyacrylate (NaPAA), 863
  - Solid-phase extraction, 346
  - Solid-phase microextraction, 346
  - Solid/polymeric membrane extraction techniques, 350
  - Solids retention time, 1008
  - Solute rejection, 1105
  - Solution-diffusion mechanism, 69
    - activated process, 71
    - thermodynamic parameter, 70
  - Solution diffusion model
    - assumptions in, 110
    - diffusion process
      - multicomponent, 113–114
      - single-component, 113
      - transport equation through membrane, 114
    - sorption process
      - in amorphous and cross-linked polymers, 112
      - concentration of component, 111
      - in semicrystalline polymer, 112–113
      - solubility, permeants, 110–111
      - sorption isotherms, 111–112
  - Sorption selectivity
    - definition of, 115

- SOTE, *see* Standard oxygen transfer efficiency
- Soybean protein fraction fractionation, in food industry, 614–615;  
*see also* Food industries, EDBM applications in
- Soy protein in food industry, production of, 594–598; *see also* Food industries, EDBM applications in
- Soy tofu whey  
and protein extraction in, 615–617 (*see also* Food industries, EDBM applications in)
- Space, membrane technology application in, 1139
- Spacer molecule, 27  
enzyme immobilization, 46  
molecular interactions, 46
- Space2Tex project, 1139
- SPE, *see* Solid-phase extraction
- Specific flux, 1105
- Spiral-wound membrane  
module design, 89  
for natural gas sweetening, 96
- Spiral wound module, 203, 1107–1108
- SPME, *see* Solid-phase microextraction
- SRT, *see* Solids retention time
- Stacked column, visual representation of, 49
- Standard oxygen transfer efficiency, 1012
- Strip dispersion technique, 1057–1058
- Strontium recovery, by strip dispersion technique, 1061–1062
- STW, *see* Soy tofu whey
- Submerged hollow fiber membrane system, 221
- Sulfate and sulfite pulp mill effluents, membranes in, 990–992
- Supercritical carbon dioxide  
assisted ultrafiltration, 188  
in membrane preparation, 188  
inorganic membranes, 189  
polymeric materials, 189–190  
membrane reactor with, 186–187  
and organic membranes, 182  
properties of, 181  
in supercritical extraction  
of caffeine, 182–185  
coupling with nanofiltration, 185–186  
of essential oils and organic compounds, 185  
transfer mechanisms in, 181
- Supercritical fluid membrane contactors, 187
- Supercritical fluids, 181; *see also* Supercritical carbon dioxide membrane reactors with  
free and fixed catalyst, 186  
synthetic activity of, 187
- Super high permeation, 874
- Supported liquid membrane, 346, 894, 1024, 1057  
in actinides separation, 839, 886, 894  
acidic extractants, 895–897  
basic extractants, 902–903  
neutral donors, 897–902  
analyte trapping in, 353–354  
principles and chemistry of, 351–353
- Supported liquid membrane with strip dispersion, 824, 1058
- Surface water treatment, by NF membranes, 1110
- SVP, *see* Small volume parenteral
- Sweeping gas membrane distillation, 529–531
- Swelling, in ELM systems, 721–722
- SWM, *see* Spiral wound module
- SWRO, *see* Seawater reverse osmosis
- Synthetic hydrogels, synthesis of, 474
- Synthetic membranes, phases of, 428
- T**
- Tangential flow filtration, 411–415
- TBP, *see* Tributyl phosphate
- TCF, *see* Total chlorine free
- TEM, *see* Track-etched membranes
- Temperature polarization, 115
- Tetrafluoroethylene, 535
- Tetrahydrofuran, 294
- TFE, *see* Tetrafluoroethylene
- TFF, *see* Tangential flow filtration
- 2-Thenoyl trifluoroacetone, 895
- Thermally accelerated short time evaporation, 514
- Thermodynamic network analysis, 381
- Thermomechanical pulp plant, 993
- Thermostatic sweeping gas membrane distillation, 531
- THF, *see* Tetrahydrofuran
- Thiocarbamylation reactions, 43–44
- THMFP, *see* Trihalomethane formation potential
- TMP, *see* Thermomechanical pulp plant;  
Transmembrane pressure
- TNA, *see* Thermodynamic network analysis
- TOA, *see* Tri-*n*-octyl amine
- Total chlorine free, 992
- Tracer impulse method, 50
- Track-etched membranes, 904
- Track etch membrane technology, 1139
- Transfer coating, 118
- Transglutaminase enzyme, 663
- Transmembrane flux, 1104  
enhancement, in membrane distillation, 538–540
- Transmembrane pressure, 410, 500, 560–562, 1104  
and flux profiles for, 195
- Transport through membranes  
concentration polarization and permeation, 114–115  
PV process (*see* Pervaporation)
- Transverse-flow design, 14–15; *see also* Membrane contactors
- Triazine activation method  
for polysaccharides, 42  
schematic representation of, 41
- Triazine dyes, 46
- Triazine-linked dyes, 45
- Tributyl phosphate, 839, 899
- 2,2,4-Trifluoro-5-trifluoromethoxy-1,3-dioxole, 535
- Trihalomethane formation potential, 947
- Tri-*n*-octyl amine, 394–395, 714, 892–893, 902
- Tritium removal, in nuclear waste, 873–874
- TSGMD, *see* Thermostatic sweeping gas membrane distillation
- TTD, *see* 2,2,4-trifluoro-5-trifluoromethoxy-1,3-dioxole
- Tubular membrane module, 500–501
- Tubular module, 1107–1108
- Two-phase flows  
gas–liquid mixture  
bubbling enhanced flux for, 220  
bubbling with submerged membrane systems, 221–223  
filtration with tubular membranes, 218  
in tubular duct, 219  
vibratory shear-enhanced process (VSEP) system, 221  
solid–liquid, by particle addition  
fiber diameter, effect of, 223  
fluxes and the mass transfer coefficients, 223–224  
tubular membrane, schematics of, 224
- Two-step composite membrane process, 947
- U**
- UF, *see* Ultrafiltration
- UHT, *see* Ultra-high temperature-treated
- Ultrafiltration, 1102–1103, 1132–1133  
in liquid radioactive waste treatment, 854–857, 860–863  
pilot plant experiments, 863–866  
radionuclides removal, 858–860

- in protein bioseparation
  - bioseparation engineering in, 497–498
  - clarification and macromolecular fractionation in, 509–511
  - concentration process in, 504–505
  - desalting in, 505–509
  - membranes in, 499–502
  - ultrafiltration in, 498–499
- in pulp and paper industry, 986
- in radioactive waste treatment, 833–834
- SC CO<sub>2</sub>-assisted, 188
- separation process, 498–499
  - theory of, 502–504
- systems, functions of, 933–936
- techniques of, 947
- Ultra-high temperature-treated, 641
- Ultrapure water degasification system, central, 17
- Ultrasound membrane filtration systems, 226–227
- Umbite, 307
- Uniform transmembrane pressure, 645–647, 656
- Uranium, separation and extraction of, 940–941
- Uranous nitrate solution, usages of, 938–939
- UTMP, *see* Uniform transmembrane pressure
- U(VI) and Pu(IV) recovery, from oxalate supernatant waste, 1067–1068

## V

- Vacuum membrane distillation, 528–529
- Vapor transport
  - through ceramic membranes, 151–152
- Variance, 50
- Vibrating shear enhanced processing filter, 988
- Vibratory shear-enhanced process, 216–217
- VMD, *see* Vacuum membrane distillation
- VOC, *see* Volatile organic compounds
- Volatile organic compounds
  - recovery using membranes, 100
  - removal of dissolved, 12
- Volume reduction factors, 828, 832, 938
- Volume reduction ratio, 643
- VRFs, *see* Volume reduction factors
- VRR, *see* Volume reduction ratio
- VSEP, *see* Vibrating shear enhanced processing filter; Vibratory shear-enhanced process

## W

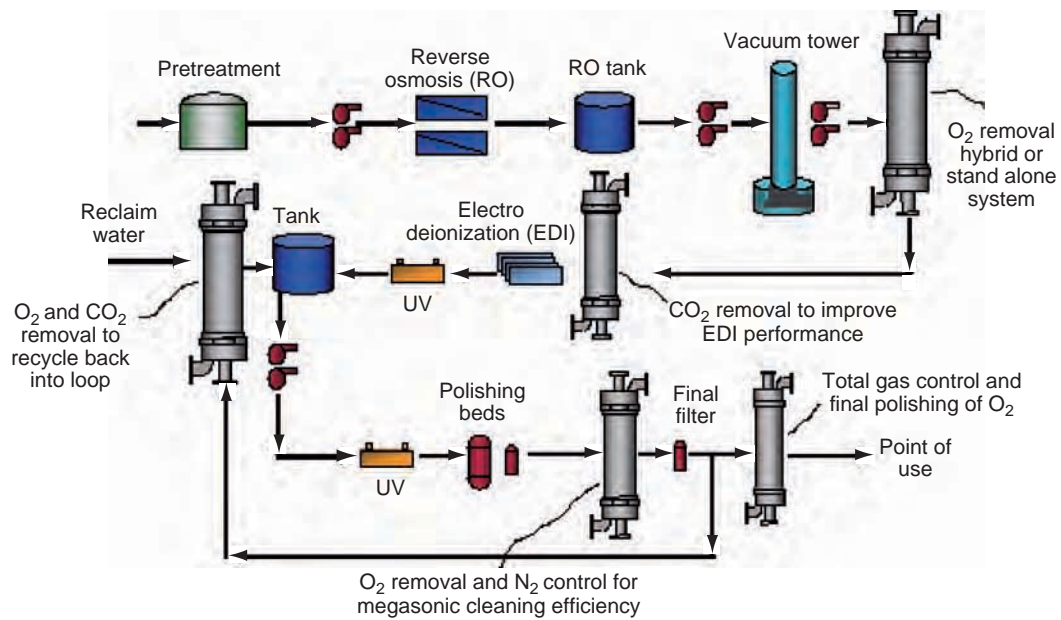
- Waste liquids treatment
  - air purification and hot gas filtration, 160
  - cross-flow filtration, 158–159
  - membrane bioreactor, 159–160
- Waste streams, radionuclides removal in, 907
- Wastewater treatment
  - membrane bioreactor in, 1007
    - advantages of, 1008, 1019–1020
    - mechanism of performance of, 1014–1018
    - membrane attached biofilms, 1018–1019
    - operating principle of, 1008–1009
    - performance of, 1009–1014
  - by NF membranes, 1110
- Water purification, by ceramic membranes
  - electrostatically driven pollutants
    - electrodialysis, 1074–1076
    - electrofiltration, 1074–1075
    - electroremediation, 1077
    - electrosorption, 1076–1077

- pollutants modification
  - electrochemical disinfection, 1074
  - electrochemical oxidation, 1072–1074
  - electrochemical reduction, 1074
- Water purification systems
  - ceramic membranes for, 161
  - for drinking and domestic water, 160–161
  - electrically enhanced membrane processes for, 1072–1081
  - PTFE matrix use, 33
  - pulsed electric field (PEF) technology, 754
  - RO for, 577
- Water removal in acid solutions
  - with zeolite MOR, 293
  - with zeolite T, 294
- Water treatment residuals
  - DMP in coagulants recovery, 947–948
    - applications and modeling protocols of, 955–957
    - assumptions of, 953
    - concentration of, 949–950
    - conditions of Donnan equilibrium, 950–951
    - fundamentals of, 948–949
    - future perspective of, 977
    - importance of, 976–977
    - kinetics and transport equations of, 951–953
    - membrane structure in, 957–958
    - techniques in, 960–962
- Wet-phase inversion method, 189
- Wet process phosphoric acid, 891, 893
- Whey protein concentrate, 617, 639
- Whey protein isolate, 639
- Whey protein separation, in food industry, 611–614; *see also* Food industries, EDBM applications in
- WPC, *see* Whey protein concentrate
- WPI, *see* Whey protein isolate
- WPPA, *see* Wet process phosphoric acid
- WTR, *see* Water treatment residuals

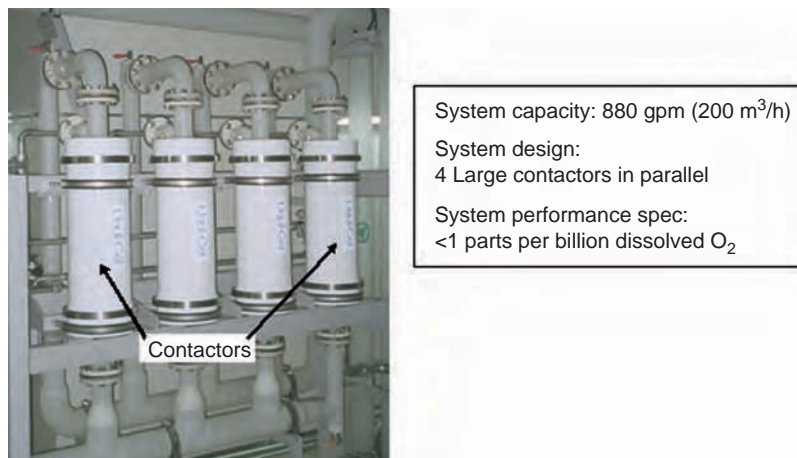
## Z

- Zeolite A
  - for alcohol dehydration, 292–293
  - industrial solvents, dehydration of, 294, 309
  - Si/Al of, 290
- Zeolite-based microreactor
  - fabrication approach, 310
  - and zeolite growth, 309
- Zeolite-based microsensors
  - chemical microsensors, 310
  - dye-zeolite systems, 311
  - optical sensors, 310–311
- Zeolite-based microseparators
  - methods for manufacturing, 310
- Zeolite-coated IDCs, 311
- Zeolite-membrane reactors
  - advantages of, 295
  - alternative supports and configurations for, 306
    - monoliths, 307–308
    - zeolite nanoparticles, 308
  - applications, 297
    - challenges for industrial, 308–309
    - conversion enhancement by catalyst poisons/inhibitors removal, 300–301
    - conversion enhancement by product removal, 298–300
    - hydroisomerization of alkanes, 303
    - microchemical systems, 309–311
      - as reactant distributors, selectivity enhancement, 301
      - selectivity enhancement, 301–302

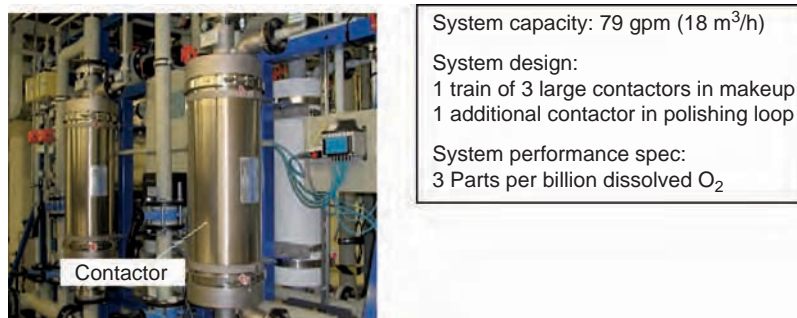
- catalytic (*see* Catalytic zeolite-membrane reactors)
- cyclohexane, catalytic dehydrogenation of, 298
- Zeolite membranes, 67
  - applications, gas separation, 283
    - competitive adsorption, 285–286
    - hydrogen separation, syngas production, 298
    - molecular sieving and preferential adsorption, 284–285
  - disadvantage of, 288
  - in esterification reactions, 299
  - experimental techniques to assess
    - permporometry, 273–274
    - SEM and SEM-EDX, 271–272
    - single-gas permeation experiments, 273
    - XPS and XRD, 272
  - gas separation mechanism, 278
    - conceptual schemes for, 279–280
    - multicomponent permeation, 282–283
    - single-gas permeation, 280–282
    - variables influencing, 279
  - membrane area, increasing, 277–278
  - pervaporation using, 286
    - alcohol dehydration, 291–293
    - aromatics separation, 288
    - diffusion, 289, 291
    - distribution of publications about, 288–289
    - factors influencing performance, 287
    - hydrophobicity and hydrophilicity, 290
    - organic dehydration, 294
    - organic separations, 295
    - removal of organics from water, 294–295
    - water removal in acid solutions, 293–294
  - quality enhancement, pre- and posttreatments for, 277
  - reaction–product separation by, 298
  - supported NaA, XRD spectra of, 271–272
  - synthesis
    - commercial Parr autoclave, 271–272
    - ex situ hydrothermal growth
      - methods, 274–277
    - inside porous support, 270
    - in situ crystallization, 274
    - template removal, 271
- Zeolite micromembranes, 309
- Zeolite-related materials, 278
- ZSM-5 coatings, 307



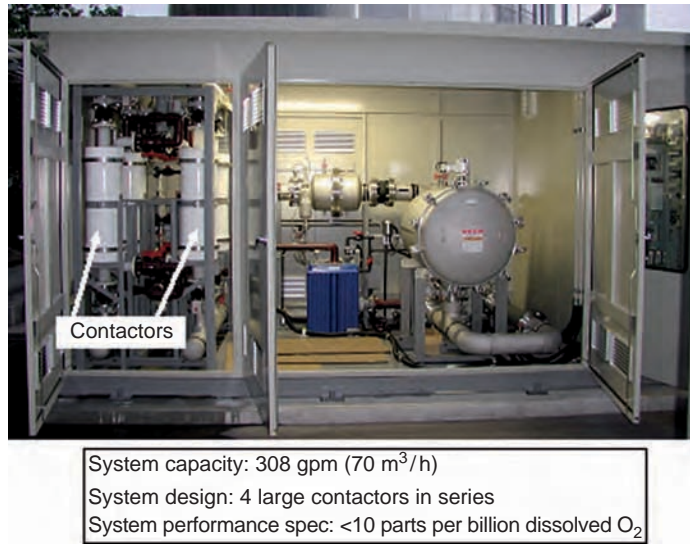
**COLOR FIGURE 2.6** Part of semiconductor plant ultrapure water production process.



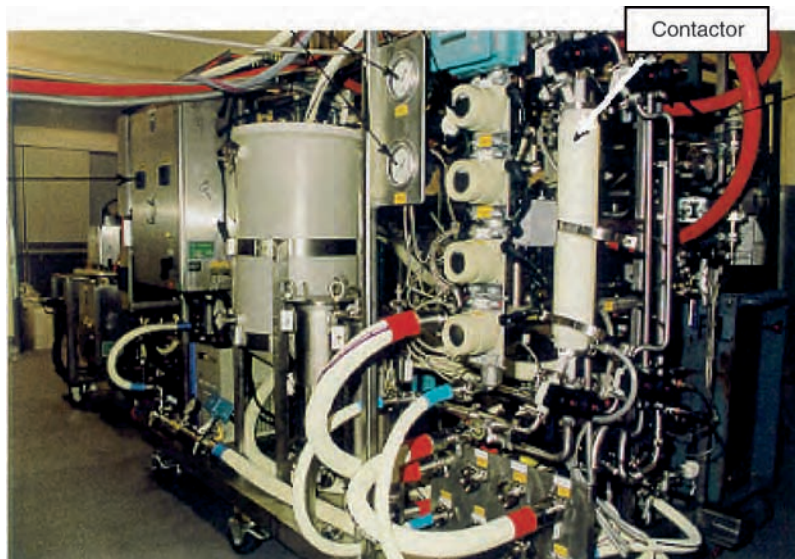
**COLOR FIGURE 2.9** Polishing loop degasification system.



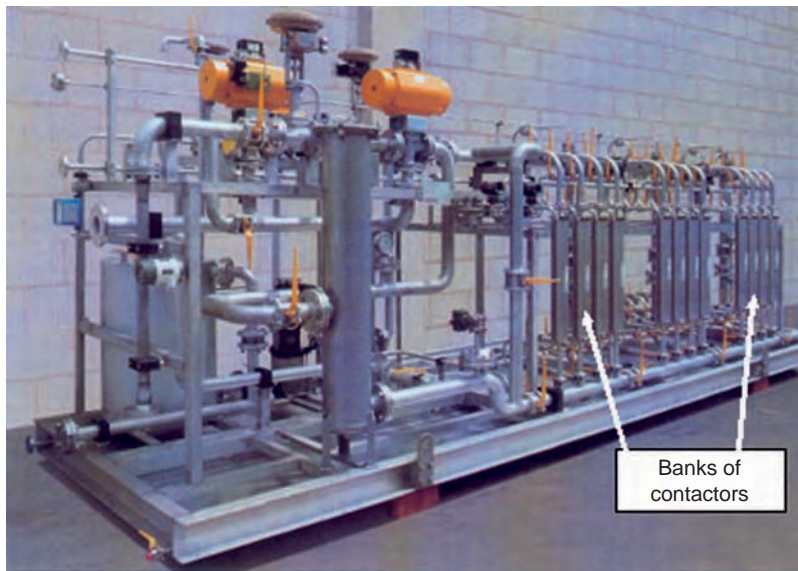
**COLOR FIGURE 2.10** Small-scale ultrapure water supply system.



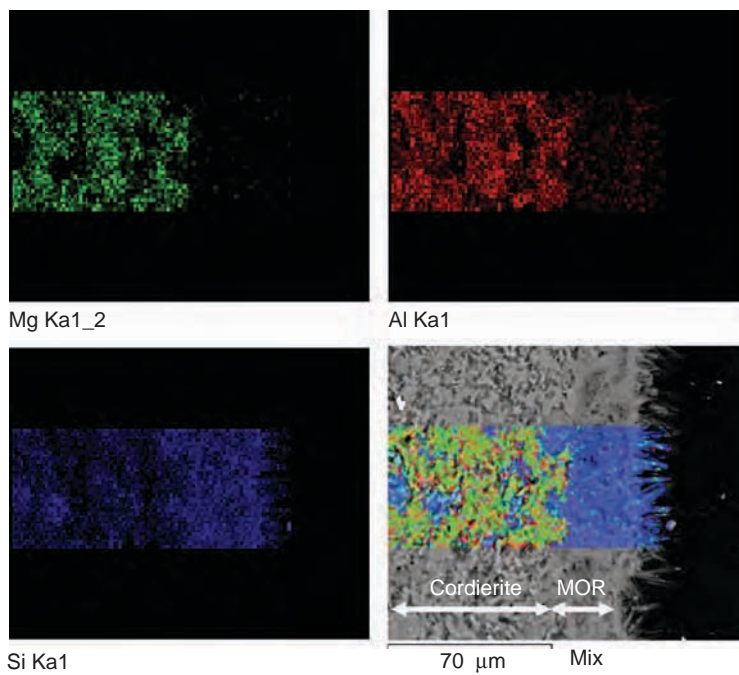
**COLOR FIGURE 2.13** Boiler water degasification system using membrane contactors.



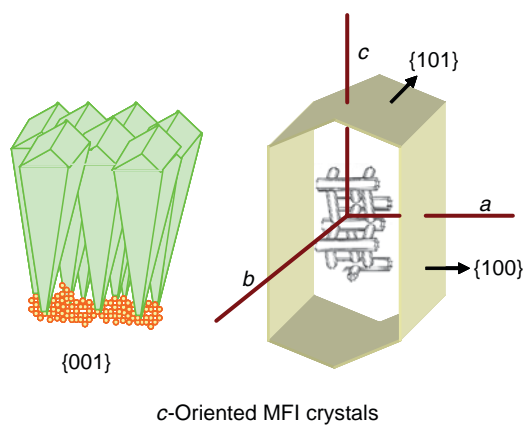
**COLOR FIGURE 2.15** Membrane contactor for fruit juice concentration using membrane distillation process.



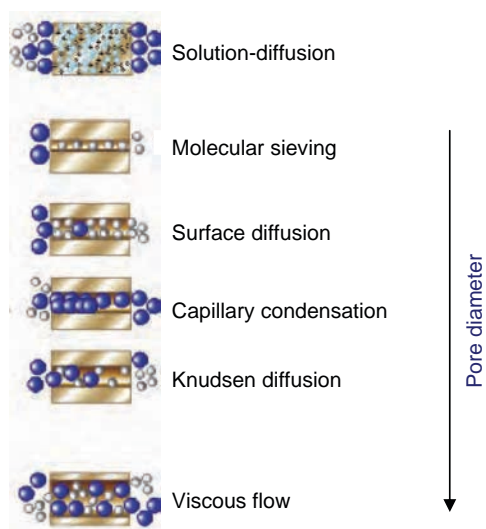
**COLOR FIGURE 2.16** Membrane contactors for liquid-liquid extraction.



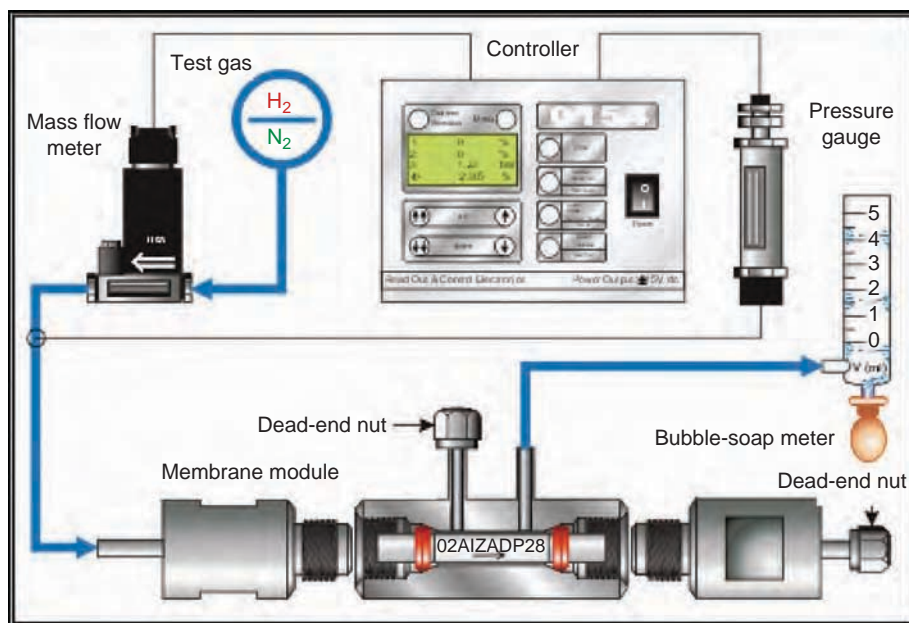
**COLOR FIGURE 10.4** EDX mapping of the cross section of a cordierite ( $\text{Mg}_2\text{Al}_4\text{Si}_5\text{O}_{18}$ ) monolith coated with a mordenite layer ( $\text{Si}/\text{Al} = 10$ ).



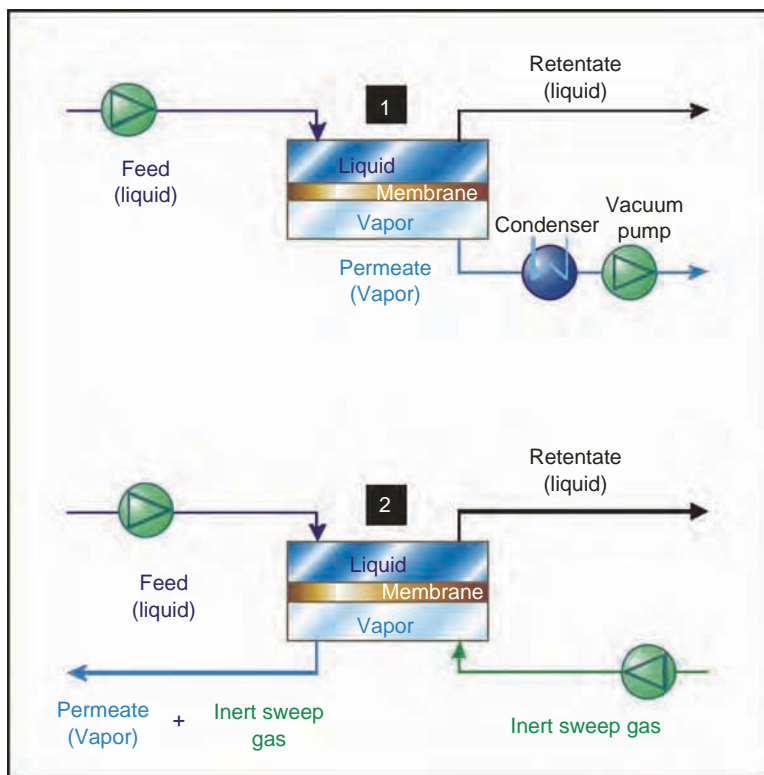
**COLOR FIGURE 10.8** Schematic representation of a *c*-oriented MFI zeolite crystal.



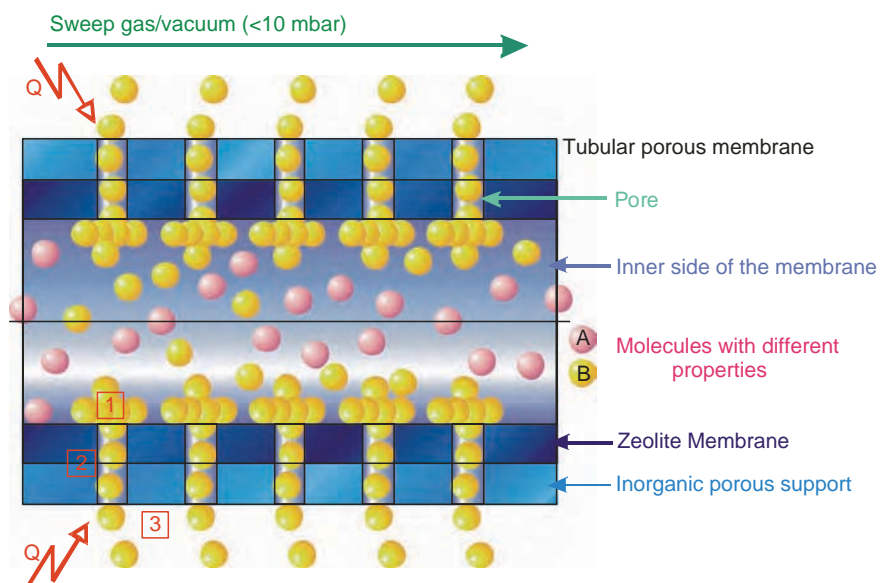
**COLOR FIGURE 10.12** Transport mechanisms in porous materials.



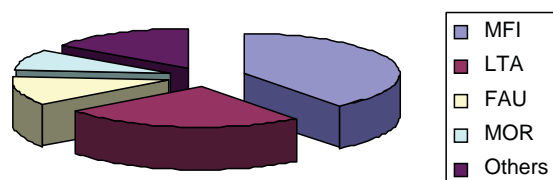
**COLOR FIGURE 10.13** Experimental system for the calculation of single-gas permeances on zeolite tubular membranes.



COLOR FIGURE 10.17 Schematic diagram of pervaporation.



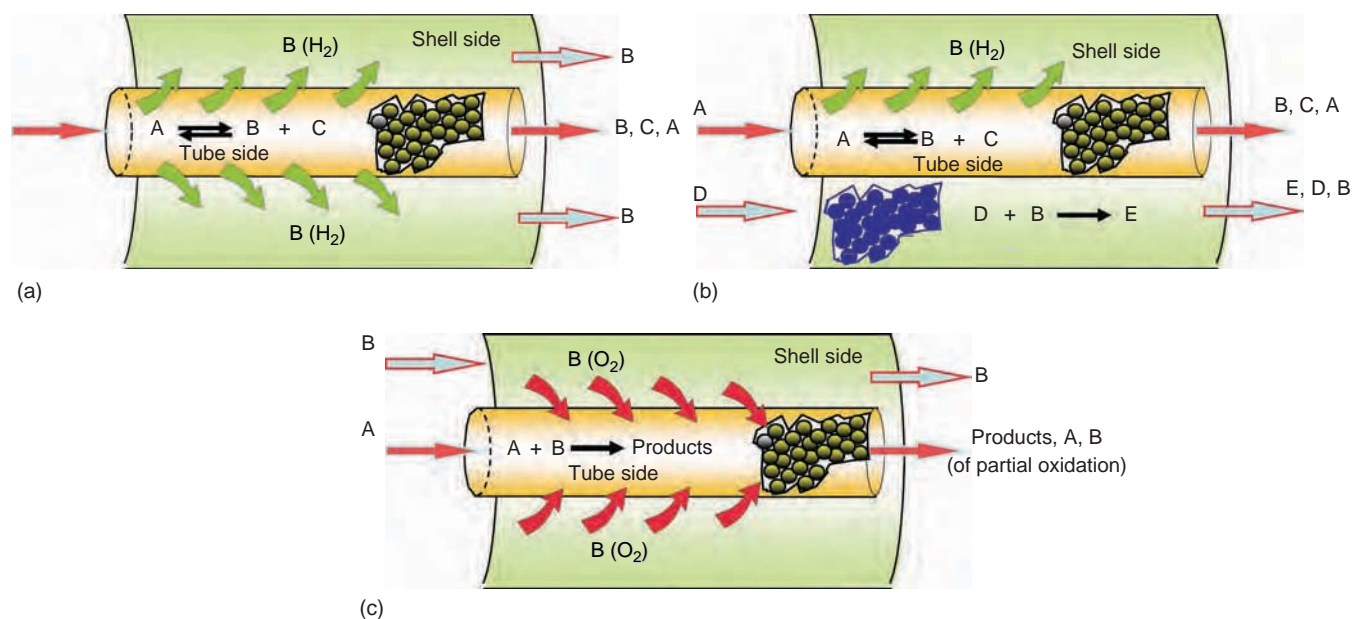
COLOR FIGURE 10.18 Steps involved in pervaporation: (1) adsorption, (2) diffusion, and (3) desorption.



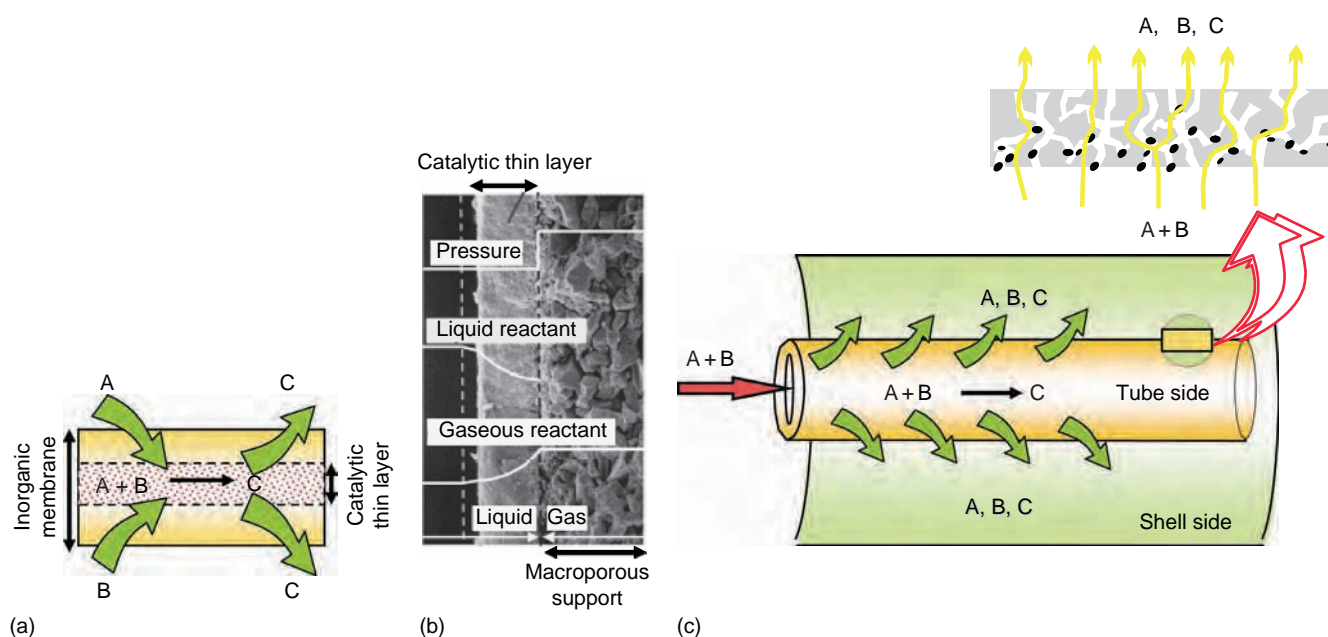
COLOR FIGURE 10.19 Distribution of publications about zeolite membranes in pervaporation during the last 10 years. (From ISI Web of Knowledge. Web of Science.)



**COLOR FIGURE 10.20** Transport through intercrystalline and intracrystalline pathways.



**COLOR FIGURE 10.21** Traditional applications of inorganic membrane reactors for (a) conversion enhancement by product removal, (b) permeation of products and reaction coupling, and (c) selectivity enhancement by reactant distribution.



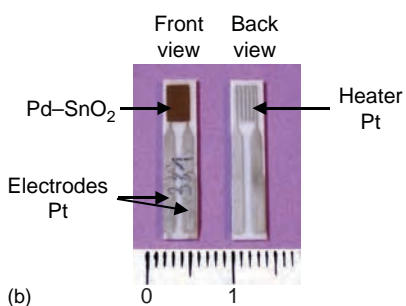
**COLOR FIGURE 10.22** Applications of catalytic membrane reactors as (a) contactors using opposing reactant mode, (b) interfacial contactors for triphasic reactions, and (c) efficient gas–solid contactor using forced flow mode.

Reactor Type	Reactor Configuration	Reactant Conversion <sup>a</sup> (%)	Equilibrium Displacement <sup>b</sup> (%)
Fixed bed reactor		49.4	—
Inert zeolite membrane reactor		56.9	2.4
Catalytic zeolite membrane reactor		63.1	5.6

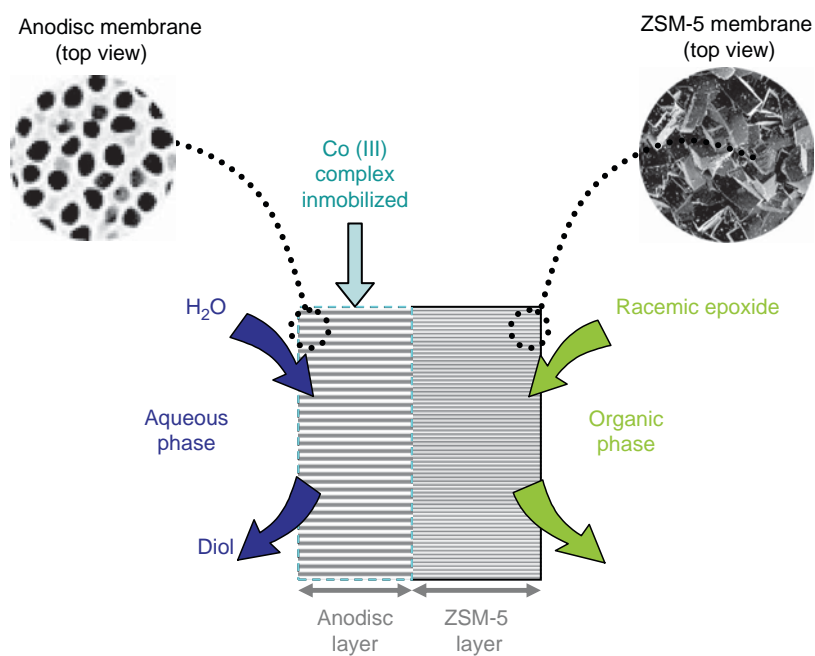
<sup>a</sup> Equimolar feed (ethanol/acetic acid) at 359 K

<sup>b</sup> Quaternary feed in equilibrium at 338 K

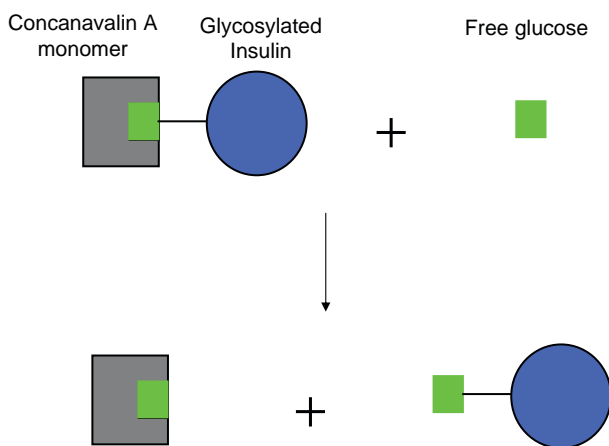
**COLOR FIGURE 10.23** Ethanol esterification with acetic acid: comparison performances of different reactor types.



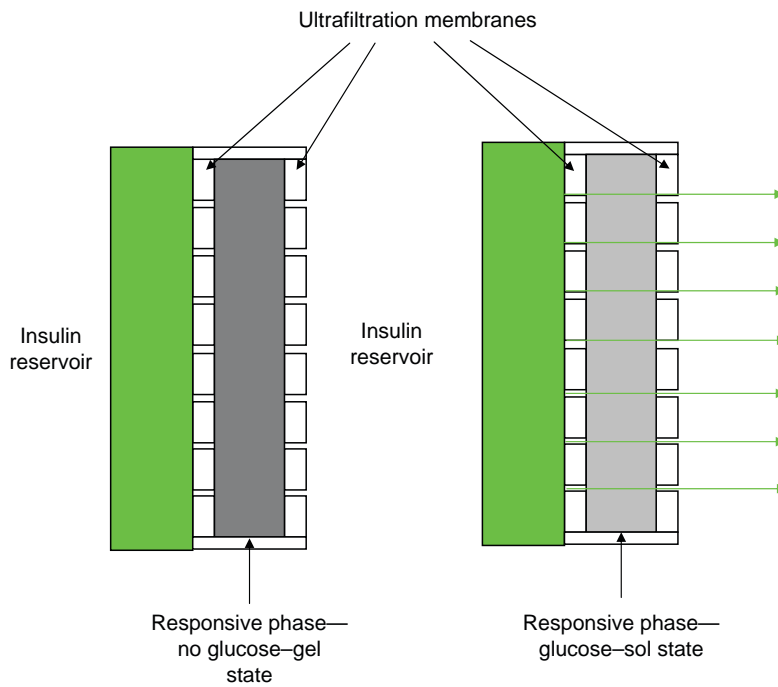
**COLOR FIGURE 10.25** SnO<sub>2</sub> sensors modified with zeolitic filters: (b) Front and back view of the as-received SnO<sub>2</sub> sensors.



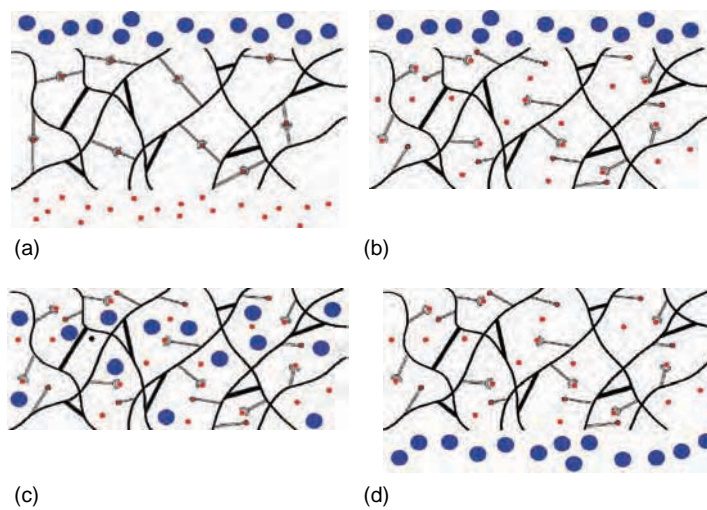
**COLOR FIGURE 10.26** ZSM-5/Anodisc membrane system used in the enantioselective asymmetric hydrolysis of racemic epoxides. (Adapted from Choi, S.D. and Kim, G.J., *Catal. Lett.*, 92, 35, 2004.)



**COLOR FIGURE 16.1** Displacement of ConA bound glycosylated insulin by free glucose.



**COLOR FIGURE 16.5** Diagram showing the structural elements of a responsive sol/gel release system.



**COLOR FIGURE 16.6** Mode of action of a glucose responsive hydrogel based on ligand–receptor interactions (bold lines denote covalent links). (a) Gel porosity reduced by affinity cross-links that exclude large molecules, e.g., insulin (blue), (b) glucose (red) diffuses in and competitively displaces affinity cross-links, (c) insulin is able to diffuse into the more highly porous gel, and (d) insulin diffuses through the gel providing the concentration gradient and glucose concentration is maintained.



(a)

(b)

**COLOR FIGURE 21.37** Organic acid production in France. (From Eurodia Co.)

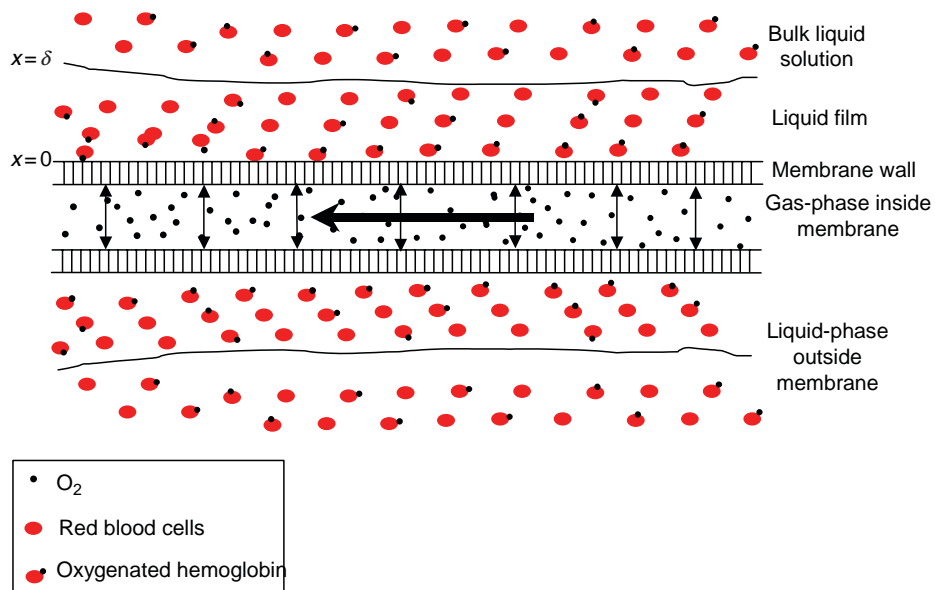


**COLOR FIGURE 21.38** Acetic acid production in Germany. (From Eurodia Co.)

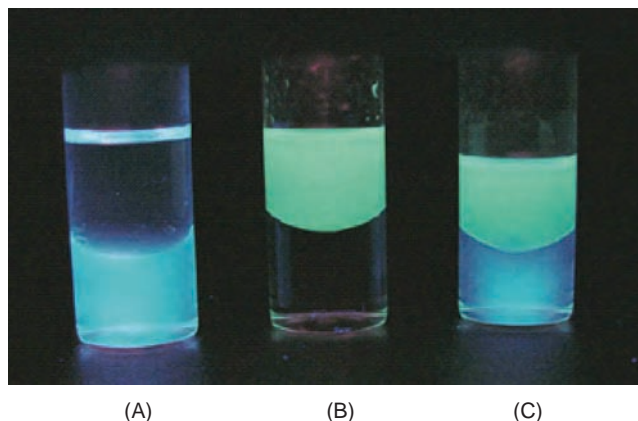


(a) (b)

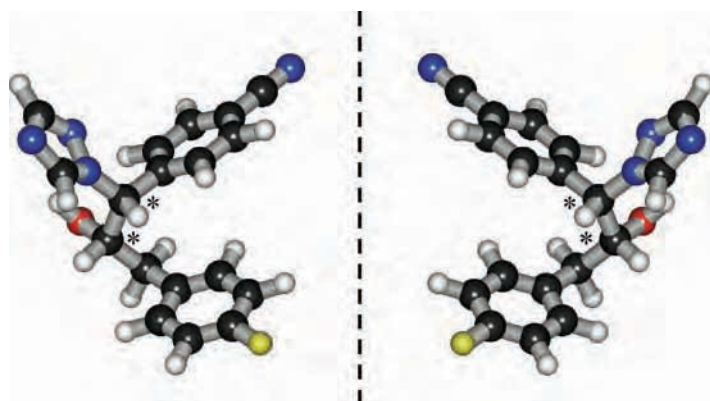
**COLOR FIGURE 21.41** Electrodesialysis stacks. (a) Aqualyzer EDC (conventional ED) and (b) aqualyzer EDBP (EDBMs). (From Eurodia Co.)



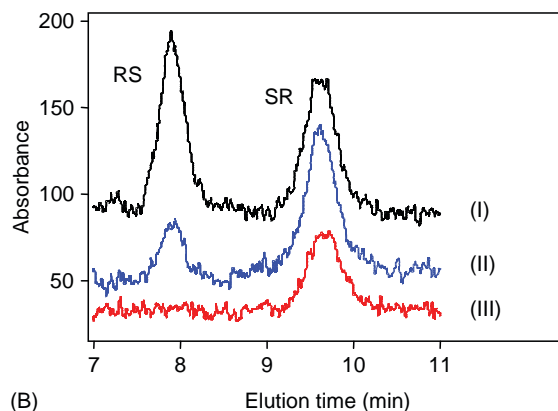
**COLOR FIGURE 23.11** Schematic representation of liquid film at the surface of a hollow fiber. (From Wickramasinghe, S.R. and Han, B., *Chem. Eng. Res. Des.*, 83(A3), 256, 2005. With permission.)



**COLOR FIGURE 24.3** Photographs of vials containing nanotubes modified with two different fluorophores in two different solvent medium. (A) Cyclohexane (upper) and water (lower) under UV light excitation after addition of 10 mg of nanotubes with dansylamide on inner and C<sub>18</sub> on outer surfaces, (B) quinineurethan on inner and no silane on outer surfaces, (C) 10 mg of both (A) and (B) nanotubes. 200 nm diameter nanotubes were used. (From Mitchell, D.T., Lee, S.B., Trofin, L., Li, N., Nevanen, T.K., Söderlund, H., and Martin, C.R., *J. Am. Chem. Soc.*, 124, 11864, 2002. With permission.)

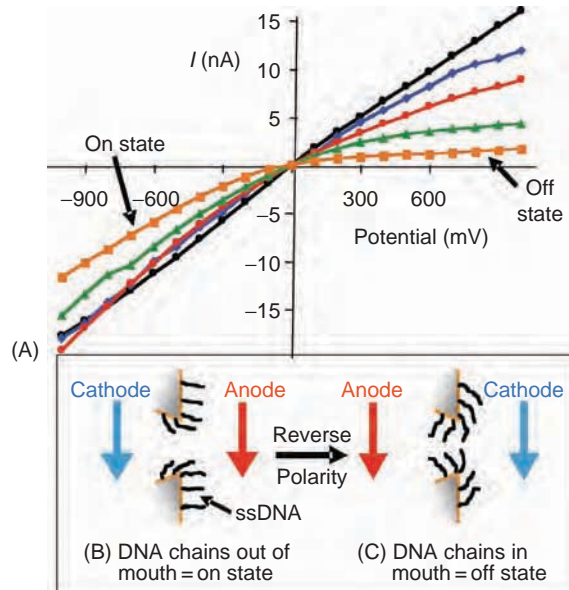


(A)

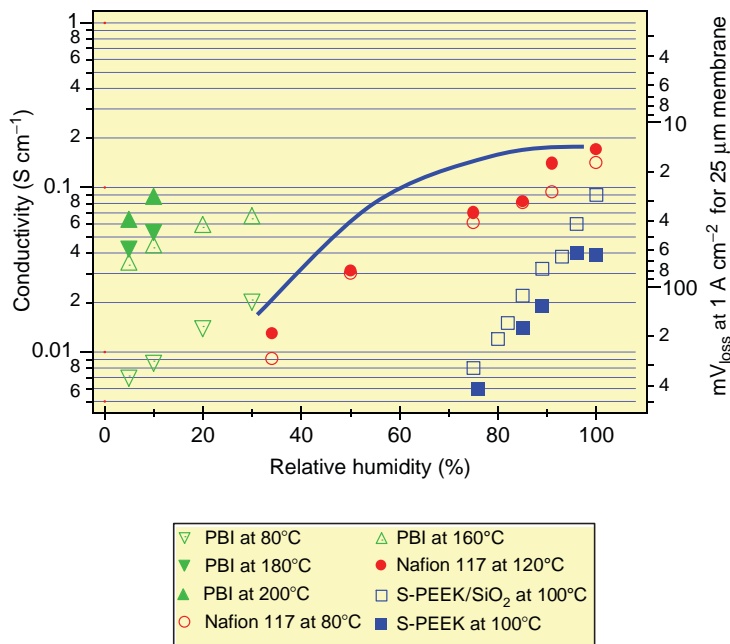


(B)

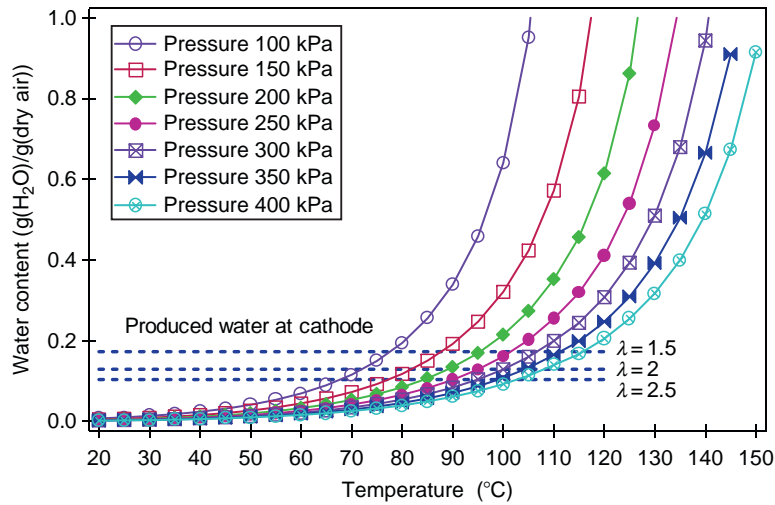
**COLOR FIGURE 24.5** Enantioseparations. (A) 3-Dimensional structures of the RS enantiomer (left) and the SR enantiomer (right) of the drug FTB. The black, white, blue, red, and yellow balls are carbon, hydrogen, nitrogen, oxygen, and fluorine, respectively, and \* denotes the chiral centers. The geometry optimization was done by ab initio calculation with minimal basis set in HyperChem 6.03. The drug is in clinical trials by Hormos Medical Corp., Turku, Finland. (From Lee, S.B., Mitchell, D.T., Trofin, L., Li, N., Nevanen, T.K., Söderlund, H., and Martin, C.R., *Science*, 296, 2198, 2002. With permission.) (B) Chiral HPLC chromatograms for racemic mixtures of FTB before (I) and after (II, III) extraction with 18 mg/mL of 200-nm Fab-containing nanotubes. Solutions were 5% dimethylsulfoxide in sodium phosphate buffer, pH 8.5. (From Mitchell, D.T., Lee, S.B., Trofin, L., Li, N., Nevanen, T.K., Söderlund, H., and Martin, C.R., *J. Am. Chem. Soc.*, 124, 11864, 2002. With permission.)



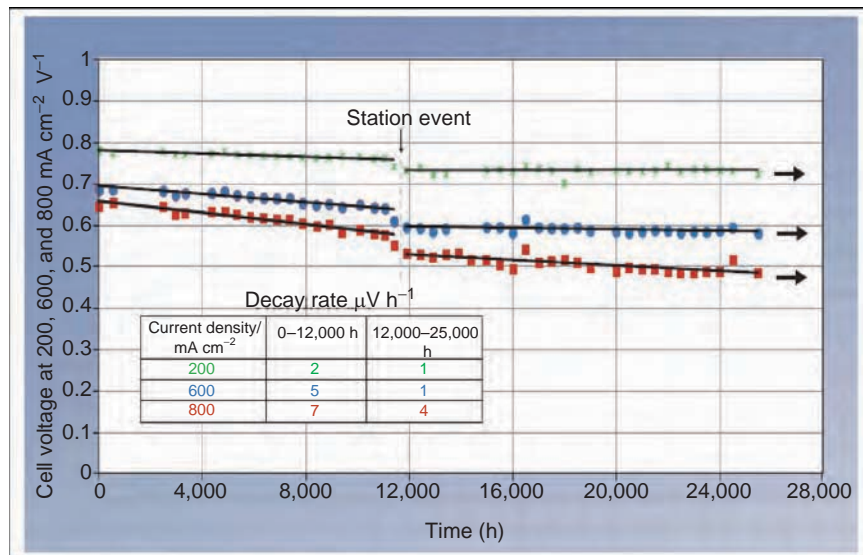
**COLOR FIGURE 24.13** (A) I–V curves for nanotubes with mouth diameter 40 nm containing no DNA (black) and attached 12-mer (blue), 15-mer (red), 30-mer (green), and 45-mer (orange) DNAs. (B,C) Schematics showing electrode polarity and DNA chain positions for on (B) and off (C) states. (From Harrell, C.C., Kohli, P., Siwy, Z., and Martin, C.R., *J. Am. Chem. Soc.*, 126, 15646, 2004. With permission.)



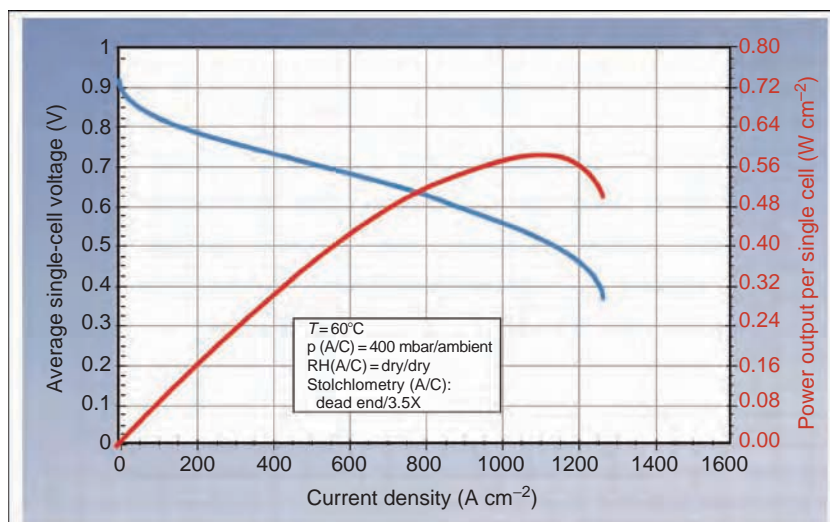
**COLOR FIGURE 27.4** Conductivity of different membranes as a function of humidity. Requirements for an advanced membrane. (Data from Alberti, G. et al. *Solid State Ionics*, 145, 249, 2001; Ma, Y.L., Wainright, J.S., Litt, M.H., and Savinell, R.F., *J. Electrochem. Soc.*, 151, A8, 2004; Wainright, J.S., Litt, M.H., and Savinell, R.F., in W. Vielstich, H.A. Gasteiger, and A. Lamm (Eds.), *Handbook of Fuel Cells: Fundamentals, Technology and Applications*, J. Wiley & Sons, Chichester, 2003.)



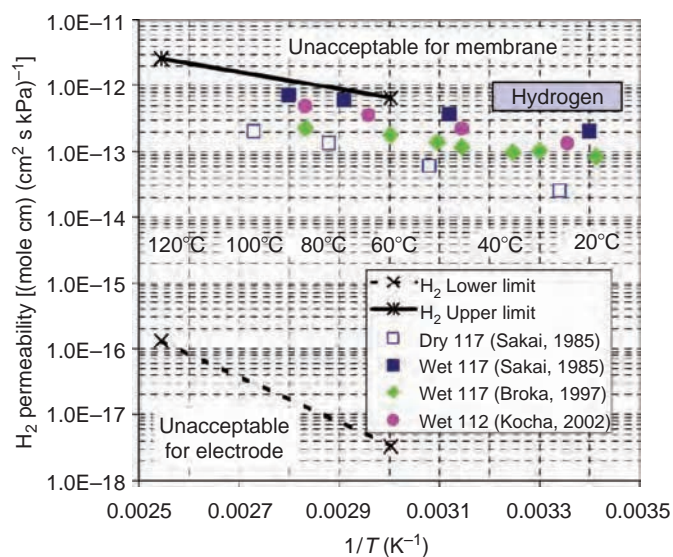
**COLOR FIGURE 27.6** Water content required for 50% RH in air for advanced membranes versus temperature for different air pressures. The dashed lines indicate the water produced for different air stoichiometries (ZSW measurements: Internal publication).



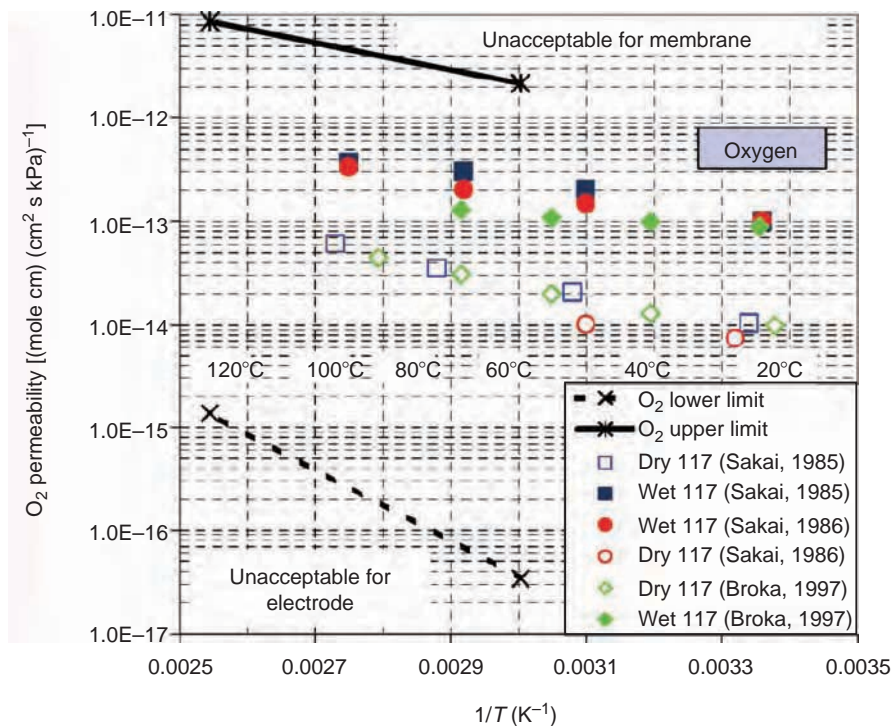
**COLOR FIGURE 27.8** Long-term tests. (From W.L. Gore & Associates, Elkton, Maryland.)



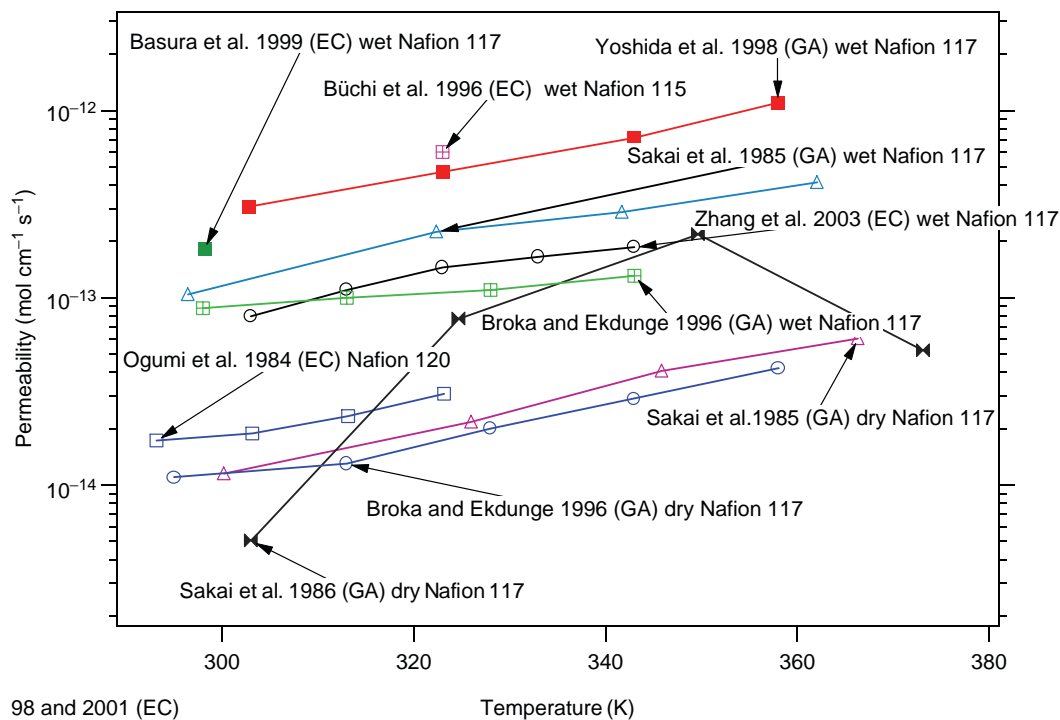
**COLOR FIGURE 27.9** Performance of the Gore 58 series in completely dry conditions. (From W.L. Gore & Associates, Elkton, Maryland.)



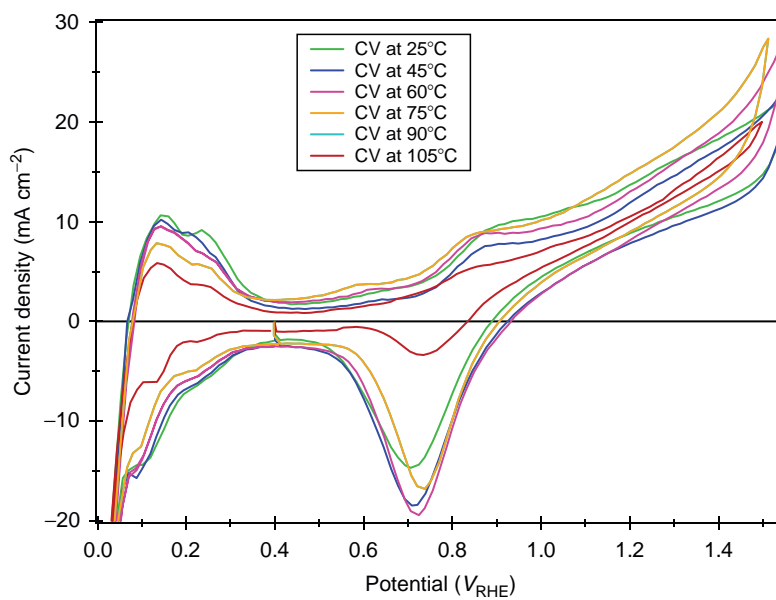
**COLOR FIGURE 27.11** H<sub>2</sub> permeability as a function of temperature and RH. Upper limit (solid line) defined by crossover losses (assuming no contribution from O<sub>2</sub> crossover), lower limit (dotted line) defined by electrode ionomer film-transport requirements, and data are for wet and dry Nafion 1100 EW-based membranes. (Reproduced from Gasteiger, H.A. and Mathias, M.F., in *Proceedings of the Symposium on Proton Conducting Membrane Fuel Cells III*, 2003. The Electrochemical Society of America. With permission from The Electrochemical Society, Inc.)



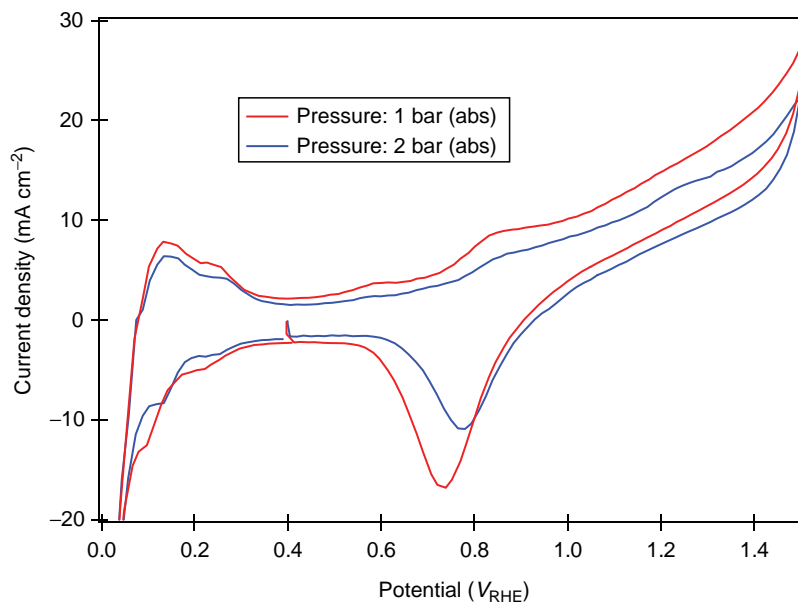
**COLOR FIGURE 27.12** O<sub>2</sub> Permeability as a function of temperature and RH. Upper limit (solid line) defined by crossover losses (assuming no contribution from H<sub>2</sub> crossover), lower limit (dotted line) defined by electrode ionomer film transport requirements, and data are for wet and dry Nafion 1100 EW-based membranes. (Reproduced from Gasteiger, H.A. and Mathias, M.F., in *Proceedings of the Symposium on Proton Conducting Membrane Fuel Cells III*, 2003. The Electrochemical Society of America. With permission from The Electrochemical Society, Inc.)



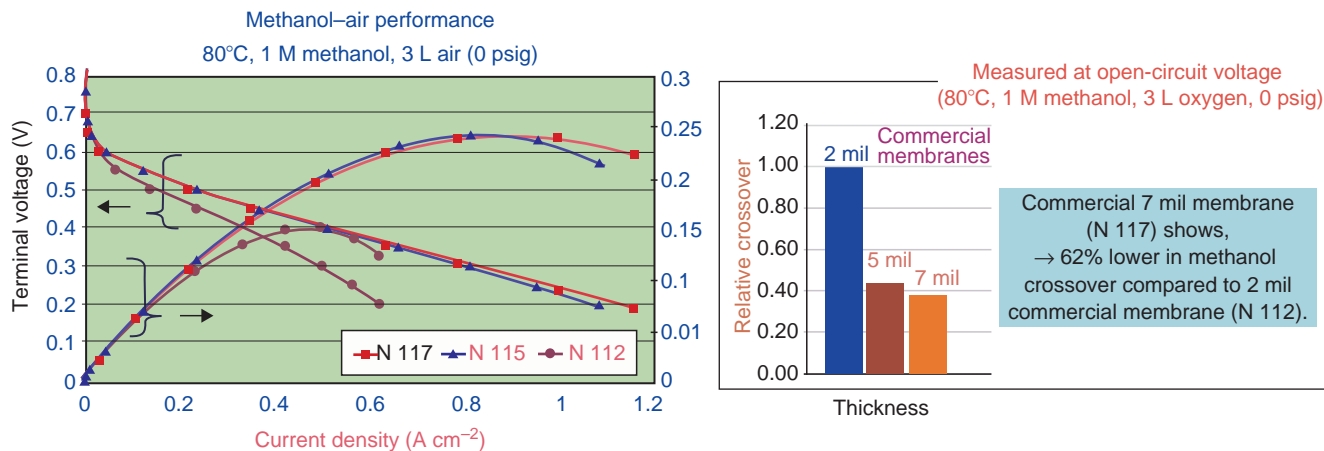
**COLOR FIGURE 27.13** O<sub>2</sub> permeability as a function of temperature measured using an electrochemical method (microelectrodes, EC) and a gas permeation (gas analysis, GA) method. Permeability calculated for a partial pressure gradient of 100 kPa. (From Vielstich, W., Gasteiger, H.A., and Lamm, A. (Eds.), *Handbook of Fuel Cells: Fundamentals, Technology and Applications*, J. Wiley & Sons, Chichester, 2003; Masten, D.A. and Bosco, A.D., in Vielstich, W., Gasteiger, H.A., and Lamm, A. (Eds.), *Handbook of Fuel Cells: Fundamentals, Technology and Applications*, J. Wiley & Sons, Chichester, 2003; Gasteiger, H.A. and Mathias, M.F., in *Proceedings of the Symposium on Proton Conducting Membrane Fuel Cells III*, The Electrochemical Society of America, 2003; Gasteiger, H.A., Panels, J.E., and Yan, S.G., *J. Power Sources*, 127, 162, 2004; Alberti, G., Casciola, M., Massinelli, L., and Bauer, B., *J. Membr. Sci.*, 185, 73, 2001; Ma, Y.L., Wainright, J.S., Litt, M.H., and Savinell, R.F., *J. Electrochem. Soc.*, 151, A8, 2004; Watanabe, M., Satoh, Y., and Shimura, C., *J. Electrochem. Soc.*, 140, 3190, 1993; Ge, S.H., Li, X.G., and Hsing, I.M., *J. Electrochem. Soc.*, 151, B523, 2004; Ge, S.H., Li, X.G., and Hsing, I.M., *Electrochim. Acta*, 50, 1909, 2005.)



**COLOR FIGURE 27.14** CVs of a commercial MEA with a 25  $\mu\text{m}$  thick membrane as a function of temperature. Scan rate  $50 \text{ mV s}^{-1}$  (ZSW measurements: Internal publication).

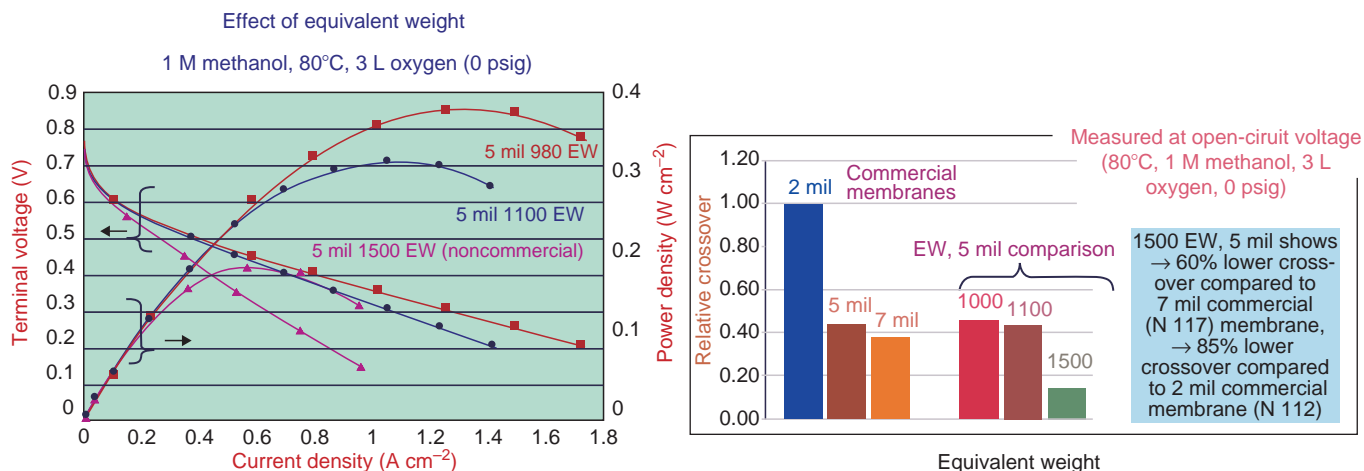


**COLOR FIGURE 27.16** CVs of a commercial MEA at  $90^\circ\text{C}$  for 1 and 2 bar (abs) pressure. Scan rate  $50 \text{ mV s}^{-1}$  (ZSW measurements: Internal publication).



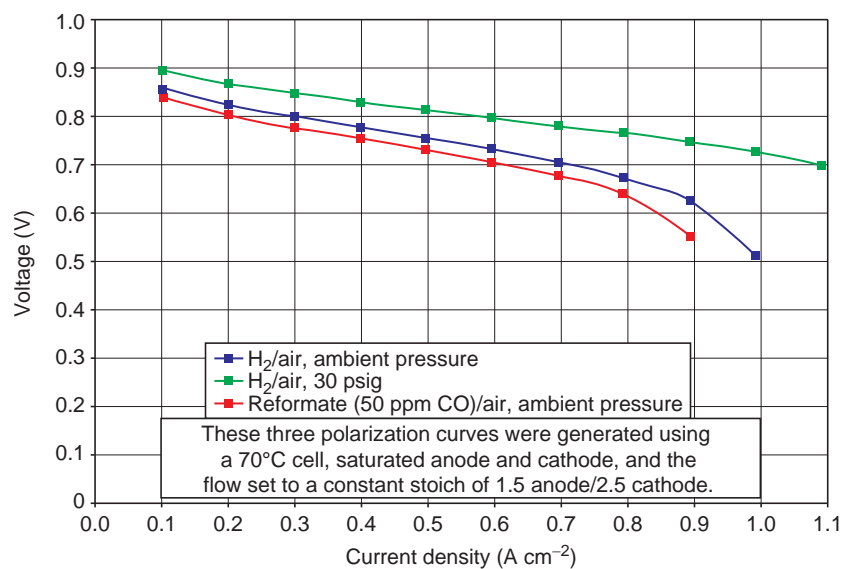
→ It appears, 2 mil membrane experiences a serious mass-transport limitation as a result of high methanol and water crossover to the cathode particularly when operating with air.

**COLOR FIGURE 27.23** Comparison of DMFC performance of Nafion 117, Nafion 115, and Nafion 112. (From DuPont 2002.)

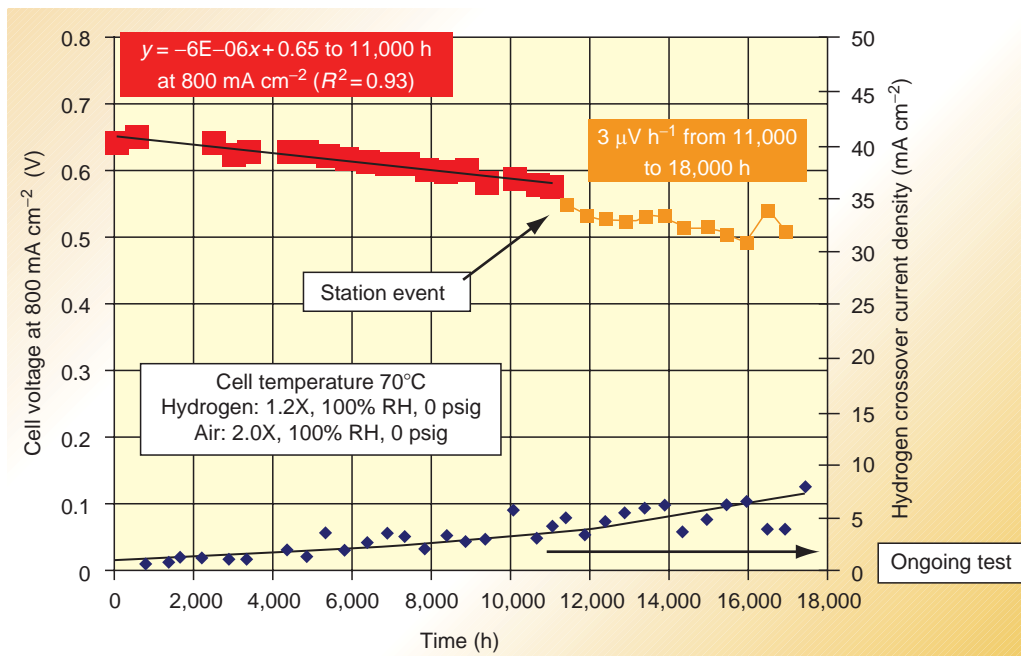


→ The peak power density of  $380\ mW\ cm^{-2}$  obtained with 5 mil 980 EW membrane (NE105) using DuPont MEA technology

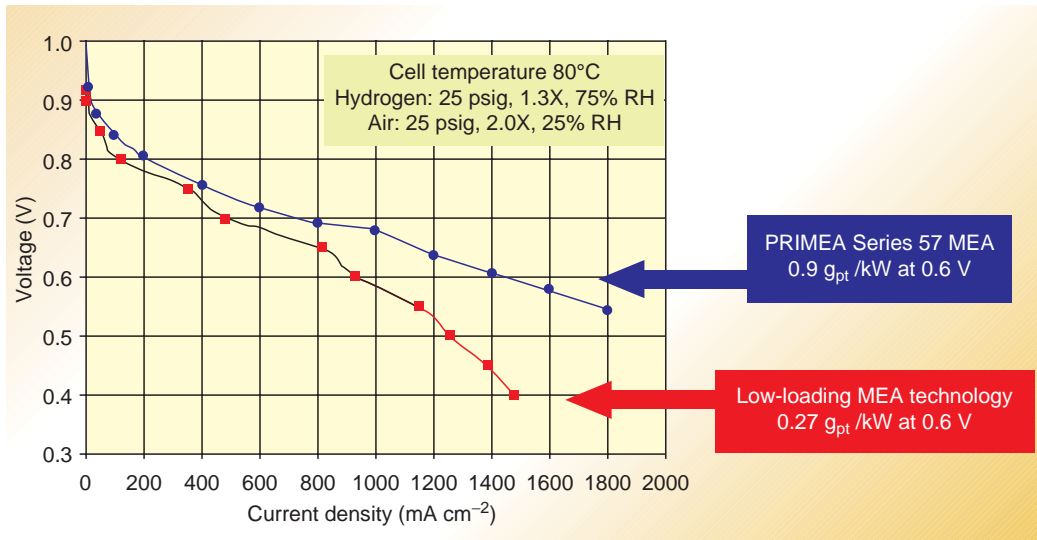
**COLOR FIGURE 27.24** Comparison of DMFC performance of 5 mil membranes with different EWs. (From DuPont 2002, www2.dupont.com.)



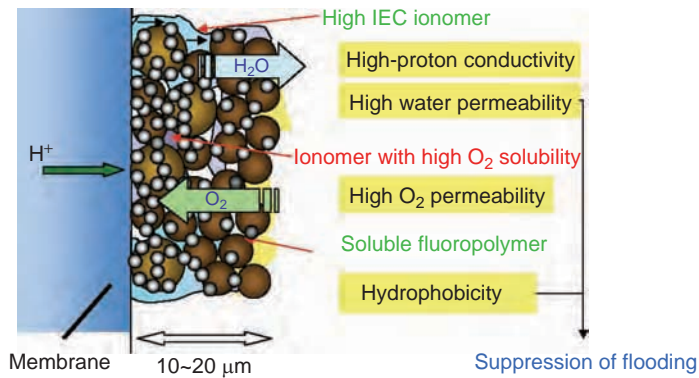
**COLOR FIGURE 27.36** Typical performance data for 3M seven-layer MEAs. (From 3M, www.3m.com.)



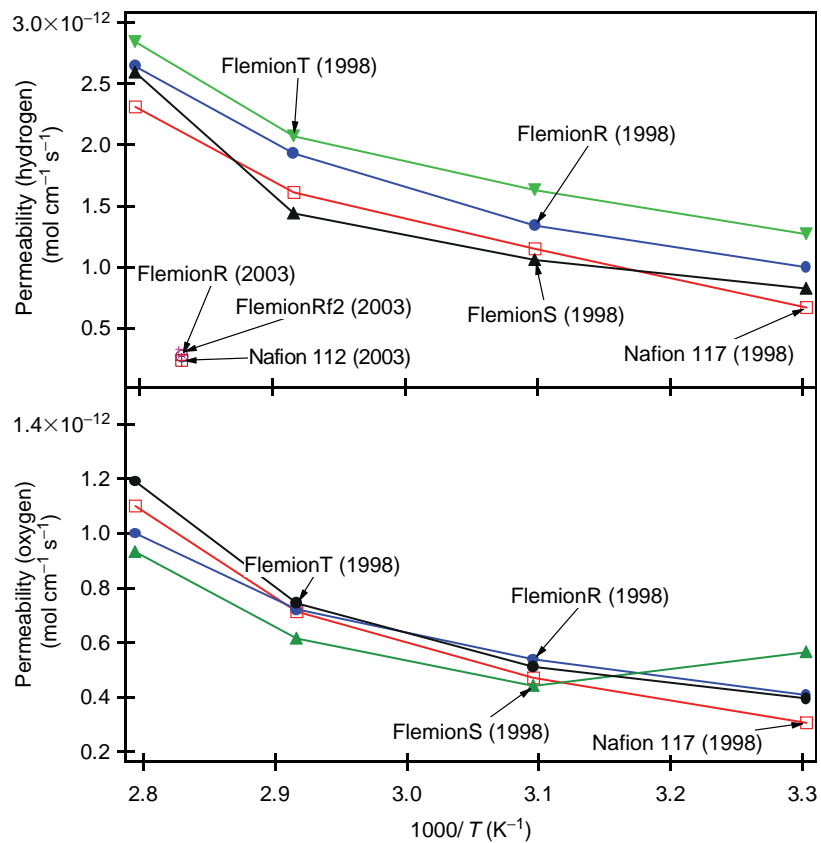
**COLOR FIGURE 27.39** PRIMEA Series 56 MEA validation life test. Hydrogen fuel—high current density (800 mA cm<sup>-2</sup>). (From W.L. Gore & Associates, Elkton, Maryland.)



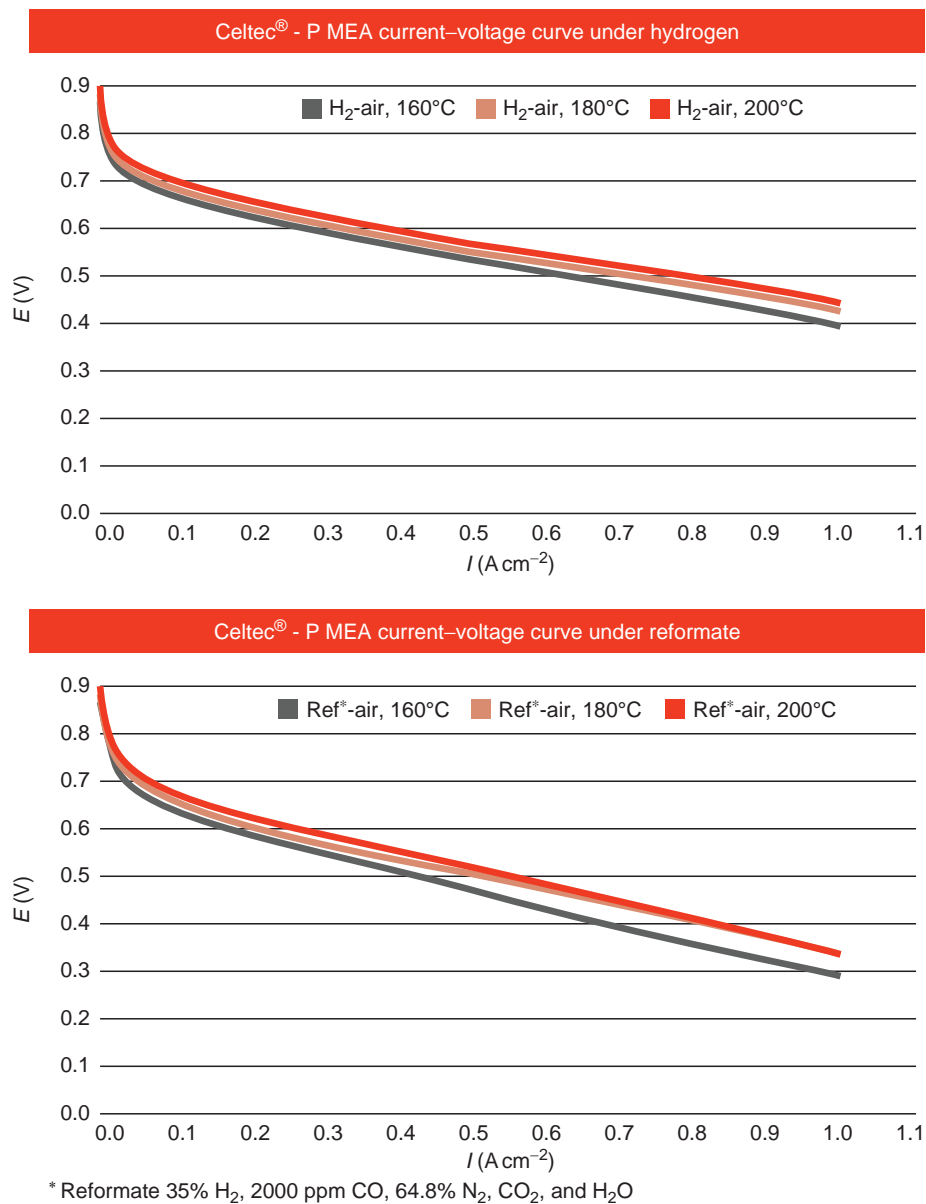
COLOR FIGURE 27.40 PRIMEA Series 57 low-loading MEA. (From W.L. Gore & Associates, Elkton, Maryland.)



COLOR FIGURE 27.44 Pictorial depiction of the development activities of Asahi Glass. (From Yamada, K. et al. *Abstracts of the 2003 Fuel Cell Seminar*. 2003.)



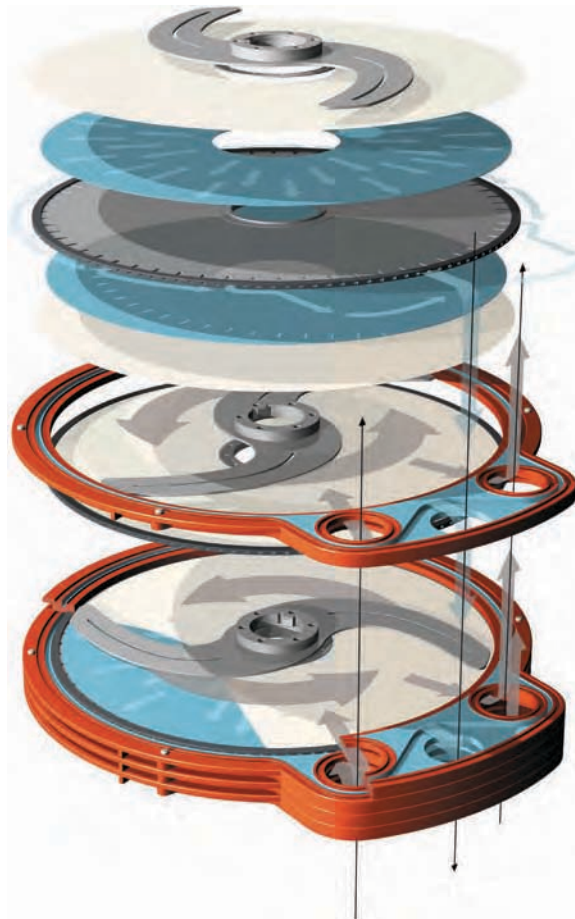
**COLOR FIGURE 27.46** Oxygen and hydrogen permeabilities of Flemion membranes in comparison with Nafion membranes. (From Pasaogullari, U. and Wang, C.Y., *Electrochim. Acta* 49, 4359, 2004; Stonehart, P., *Berichte der Bunsengesellschaft für Physikalische Chemie* 94, 913, 1990.)



**COLOR FIGURE 27.72** Celtec P MEA, active cell area: 45 cm<sup>2</sup>, air:λ = 2; 0 bar, H<sub>2</sub>:λ = 1.2; 0 bar, humidification: none. (From Celanese AG, www.celanese.com.)



**COLOR FIGURE 30.4** Three-stage RO plant for radioactive waste processing at Institute of Atomic Energy in Swierk.



**COLOR FIGURE 35.3** Principle of the CR filter. (From Kreutzman, E. and Sutela, T., *Ippta J.*, p. 15, 2004; Courtesy of Metso Paper. With permission.)



(a)



(b)

**COLOR FIGURE 36.2** The MEMBRIGHT process from Brightwater Engineering (United Kingdom) showing (a) a typical plant and (b) the membrane module.

(From the Foreword) “... *comprehensive discussion of membrane applications in the chemical, food, and pharmaceutical industries, in biotechnology, and in the treatment of toxic industrial effluents. The applications of membranes in different areas are described by scientists and engineers who not only are experts in membrane science and technology, but also have extensive experience in the specific field of membrane application...*”

—Heiner Strathmann, University of Stuttgart, Germany

During the past two decades, membrane technology has grown into an accepted unit of operation for a wide variety of separations in industrial processes and environmental applications. Written by prominent researchers and professionals from all over the world, the **Handbook of Membrane Separations: Chemical, Pharmaceutical, Food, and Biotechnological Applications** covers the full spectrum of membrane technology and discusses its advancement and applications.

#### Features

- Explores chemical, pharmaceutical, food processing, and biotechnological applications of membrane processes ranging from selective separation to solvent and material recovery
- Presents in-depth knowledge of membrane separation mechanisms, transport models, membrane permeability computations, membrane types and modules, and membrane reactors
- Provides background information on the various membrane components and processes to evaluate their potential application
- Deals with membrane applications in industrial waste management and environmental engineering

